# Supramolecular Chemistry

***Second Edition***

*Supramolecular Chemistry, 2nd edition* J. W. Steed and J. L. Atwood
© 2009 John Wiley & Sons, Ltd ISBN: 978-0-470-51233-3

# Supramolecular Chemistry

*Second Edition*

**Jonathan W. Steed**

**Department of Chemistry, Durham University, UK**

**Jerry L. Atwood**

**Department of Chemistry, University of Missouri, Columbia, USA**

WILEY

A John Wiley and Sons, Ltd, Publication

This edition first published 2009
© 2009, John Wiley & Sons, Ltd.

*Registered office*
John Wiley & Sons Ltd, The Atrium, Southern Gate, Chichester, West Sussex, PO19 8SQ, United Kingdom

For details of our global editorial offices, for customer services and for information about how to apply for permission to reuse the copyright material in this book please see our website at www.wiley.com.

The right of the author to be identified as the author of this work has been asserted in accordance with the Copyright, Designs and Patents Act 1988.

All rights reserved. No part of this publication may be reproduced, stored in a retrieval system, or transmitted, in any form or by any means, electronic, mechanical, photocopying, recording or otherwise, except as permitted by the UK Copyright, Designs and Patents Act 1988, without the prior permission of the publisher.

Wiley also publishes its books in a variety of electronic formats. Some content that appears in print may not be available in electronic books.

Designations used by companies to distinguish their products are often claimed as trademarks. All brand names and product names used in this book are trade names, service marks, trademarks or registered trademarks of their respective owners. The publisher is not associated with any product or vendor mentioned in this book. This publication is designed to provide accurate and authoritative information in regard to the subject matter covered. It is sold on the understanding that the publisher is not engaged in rendering professional services. If professional advice or other expert assistance is required, the services of a competent professional should be sought.

The publisher and the author make no representations or warranties with respect to the accuracy or completeness of the contents of this work and specifically disclaim all warranties, including without limitation any implied warranties of fitness for a particular purpose. This work is sold with the understanding that the publisher is not engaged in rendering professional services. The advice and strategies contained herein may not be suitable for every situation. In view of ongoing research, equipment modifications, changes in governmental regulations, and the constant flow of information relating to the use of experimental reagents, equipment, and devices, the reader is urged to review and evaluate the information provided in the package insert or instructions for each chemical, piece of equipment, reagent, or device for, among other things, any changes in the instructions or indication of usage and for added warnings and precautions. The fact that an organisation or Website is referred to in this work as a citation and/or a potential source of further information does not mean that the author or the publisher endorses the information the organisation or Website may provide or recommendations it may make. Further, readers should be aware that Internet Websites listed in this work may have changed or disappeared between when this work was written and when it is read. No warranty may be created or extended by any promotional statements for this work. Neither the publisher nor the author shall be liable for any damages arising herefrom.

*Library of Congress Cataloging-in-Publication Data*
Steed, Jonathan W., 1969-
Supramolecular chemistry / Jonathan W. Steed, Jerry L. Atwood. – 2nd ed.
p. cm.
Includes bibliographical references and index.
ISBN 978-0-470-51233-3 (cloth) – ISBN 978-0-470-51234-0 (pbk. :
alk. paper) 1. Supramolecular chemistry. I. Atwood, J. L. II. Title.
QD878.S74 2008
547'.1226--dc22
2008044379

A catalogue record for this book is available from the British Library.

ISBN: 978-0-470-51233-3 (Hbk)
ISBN: 978-0-470-51234-0 (Pbk)

Set in 10/12 pt Times by Thomson Digital, Noida, India
Printed in the UK by Antony Rowe Ltd, Chippenham, Wiltshire

*In loving memory of Joan Edwina Steed, 1922–2008*

# Contents


**About the Authors** xxi
**Preface to the First Edition** xxiii
**Preface to the Second Edition** xxv
**Acknowledgements** xxvii

**1 Concepts** 1

**1.1 Definition and Development of Supramolecular Chemistry** 2
1.1.1 What is Supramolecular Chemistry? 2
1.1.2 Host–Guest Chemistry 3
1.1.3 Development 4

**1.2 Classification of Supramolecular Host–Guest Compounds** 6

**1.3 Receptors, Coordination and the Lock and Key Analogy** 6

**1.4 Binding Constants** 9
1.4.1 Definition and Use 9
1.4.2 Measurement of Binding Constants 11

**1.5 Cooperativity and the Chelate Effect** 17

**1.6 Preorganisation and Complementarity** 22

**1.7 Thermodynamic and Kinetic Selectivity, and Discrimination** 26

**1.8 Nature of Supramolecular Interactions** 27
1.8.1 Ion–ion Interactions 27
1.8.2 Ion–Dipole Interactions 27
1.8.3 Dipole–Dipole Interactions 28
1.8.4 Hydrogen Bonding 28
1.8.5 Cation–π Interactions 32
1.8.6 Anion-π Interactions 33
1.8.7 $\pi$–$\pi$ Interactions 33
1.8.8 Van der Waals Forces and Crystal Close Packing 35
1.8.9 Closed Shell Interactions 36

**1.9 Solvation and Hydrophobic Effects** 38
1.9.1 Hydrophobic Effects 38
1.9.2 Solvation 39

**1.10 Supramolecular Concepts and Design** 41
1.10.1 Host Design 41
1.10.2 Informed and Emergent Complex Matter 42
1.10.3 Nanochemistry 44

**Summary** 45

**Study Problems** 45

**Suggested Further Reading** 46

**References** 47

## 2 The Supramolecular Chemistry of Life 49

**2.1 Biological Inspiration for Supramolecular Chemistry** 50

**2.2 Alkali Metal Cations in Biochemistry** 50
2.2.1 Membrane Potentials 50
2.2.2 Membrane Transport 53
2.2.3 Rhodopsin: A Supramolecular Photonic Device 60

**2.3 Porphyrins and Tetrapyrrole Macrocycles** 61

**2.4 Supramolecular Features of Plant Photosynthesis** 63
2.4.1 The Role of Magnesium Tetrapyrrole Complexes 63
2.4.2 Manganese-Catalysed Oxidation of Water to Oxygen 68

**2.5 Uptake and Transport of Oxygen by Haemoglobin** 70

**2.6 Enzymes and Coenzymes** 74
2.6.1 Characteristics of Enzymes 74
2.6.2 Mechanism of Enzymatic Catalysis 77
2.6.3 Coenzymes 79
2.6.4 The Example of Coenzyme $B_{12}$ 80

**2.7 Neurotransmitters and Hormones** 83

**2.8 Semiochemistry in the Natural World** 85

**2.9 DNA** 86
2.9.1 DNA Structure and Function 86
2.9.2 Site-Directed Mutagenesis 91
2.9.3 The Polymerase Chain Reaction 92
2.9.4 Binding to DNA 93
2.9.5 DNA Polymerase: A Processive Molecular Machine 97

**2.10 Biochemical Self-Assembly** 99

**Summary** 102

**Study Problems** 102

**References** 103

## 3 Cation-Binding Hosts 105

**3.1 Introduction to Coordination Chemistry** 106
3.1.1 Supramolecular Cation Coordination Chemistry 106
3.1.2 Useful Concepts in Coordination Chemistry 106
3.1.3 EDTA – a Classical Supramolecular Host 112

**3.2 The Crown Ethers** 114
3.2.1 Discovery and Scope 114
3.2.2 Synthesis 116

**3.3 The Lariat Ethers and Podands** 118
3.3.1 Podands 118
3.3.2 Lariat Ethers 120
3.3.3 Bibracchial Lariat Ethers 121

**3.4 The Cryptands** 122

**3.5 The Spherands** 125

**3.6 Nomenclature of Cation-Binding Macrocycles** 127

**3.7 Selectivity of Cation Complexation** 129
3.7.1 General Considerations 129
3.7.2 Conformational Characteristics of Crown Ethers 130
3.7.3 Donor Group Orientation and Chelate Ring Size Effects 132
3.7.4 Cation Binding by Crown Ethers 135
3.7.5 Cation Binding by Lariat Ethers 140
3.7.6 Cation Binding by Cryptands 142
3.7.7 Preorganisation: Thermodynamic Effects 144
3.7.8 Preorganisation: Kinetic and Dynamic Effects 147

**3.8 Solution Behaviour** 149
3.8.1 Solubility Properties 149
3.8.2 Solution Applications 149

**3.9 Synthesis: The Template Effect and High Dilution** 153
3.9.1 The Template Effect 153
3.9.2 High-Dilution Synthesis 157

**3.10 Soft Ligands for Soft Metal Ions** 160
3.10.1 Nitrogen and Sulfur Analogues of Crown Ethers 160
3.10.2 Nitrogen and Sulfur Analogues of Cryptands 163
3.10.3 Azamacrocycles: Basicity Effects and the Example of Cyclam 164
3.10.4 Phosphorus–Containing Macrocycles 167
3.10.5 Mixed Cryptates 168
3.10.6 Schiff Bases 170
3.10.7 Phthalocyanines 172
3.10.8 Torands 173

**3.11 Proton Binding: The Simplest Cation** 173
3.11.1 Oxonium Ion Binding by Macrocycles in the Solid State 174
3.11.2 Solution Chemistry of Proton Complexes 177

**3.12 Complexation of Organic Cations** 180
3.12.1 Binding of Ammonium Cations by Corands 181
3.12.2 Binding of Ammonium Cations by Three-Dimensional Hosts 183
3.12.3 Ditopic Receptors 184
3.12.4 Chiral Recognition 185
3.12.5 Amphiphilic Receptors 193
3.12.6 Case Study: Herbicide Receptors 194

**3.13 Alkalides and Electrides** 195

**3.14 The Calixarenes** 197
3.14.1 Cation Complexation by Calixarenes 198
3.14.2 Phase Transport Equilibria 204
3.14.3 Cation Complexation by Hybrid Calixarenes 206

**3.15 Carbon Donor and $\pi$-acid Ligands** 208
3.15.1 Mixed C-Heteroatom Hosts 209
3.15.2 Hydrocarbon Hosts 211

**3.16 The Siderophores** 213
3.16.1 Naturally Occurring Siderophores 213
3.16.2 Synthetic Siderophores 215

**Summary** 217

**Study Problems** 217

**Thought Experiment** 218

**References** 219

**4 Anion Binding** 223

**4.1 Introduction** 224
4.1.1 Scope 224
4.1.2 Challenges in Anion Receptor Chemistry 225

**4.2 Biological Anion Receptors** 227
4.2.1 Anion Binding Proteins 228
4.2.2 Arginine as an Anion Binding Site 229
4.2.3 Main Chain Anion Binding Sites in Proteins: Nests 230
4.2.4 Pyrrole-Based Biomolecules 231

**4.3 Concepts in Anion Host Design** 232
4.3.1 Preorganisation 232
4.3.2 Entropic Considerations 233
4.3.3 Considerations Particular to Anions 234

**4.4 From Cation Hosts to Anion Hosts – a Simple Change in pH** 236
4.4.1 Tetrahedral Receptors 236
4.4.2 Shape Selectivity 238
4.4.3 Ammonium-Based Podands 239
4.4.4 Two-Dimensional Hosts 240
4.4.5 Cyclophane Hosts 246

**4.5 Guanidinium-Based Receptors** 248

**4.6 Neutral Receptors** 251
4.6.1 Zwitterions 253
4.6.2 Amide-Based Receptors 253
4.6.3 Urea and Thiourea Derivatives 255
4.6.4 Pyrrole Derivatives 257
4.6.5 Peptide-Based Receptors 258

**4.7 Inert Metal-Containing Receptors** 259
4.7.1 General Considerations 259
4.7.2 Organometallic Receptors 261
4.7.3 Hydride Sponge and Other Lewis Acid Chelates 268
4.7.4 Anticrowns 271

**4.8 Common Core Scaffolds** 276
4.8.1 The Trialkylbenzene Motif 277
4.8.2 Cholapods 278

**Summary** 281

**Study Problems** 281

**Thought Experiments** 282

**References** 282

**5 Ion Pair Receptors** 285

**5.1 Simultaneous Anion and Cation Binding** 286
5.1.1 Concepts 286
5.1.2 Contact Ion Pairs 287
5.1.3 Cascade Complexes 289
5.1.4 Remote Anion and Cation Binding Sites 291
5.1.5 Symport and Metals Extraction 295
5.1.6 Dual-Host Salt Extraction 298

**5.2 Labile Complexes as Anion Hosts** 299

**5.3 Receptors for Zwitterions** 303

**Summary** 304

**Study Problems** 304

**References** 305

**6 Molecular Guests in Solution** 307

**6.1 Molecular Hosts and Molecular Guests** 308
6.1.1 Introduction 308
6.1.2 Some General Considerations 308

**6.2 Intrinsic Curvature: Guest Binding by Cavitands** 310
6.2.1 Building Blocks 310
6.2.2 Calixarenes and Resorcarenes 311
6.2.3 Dynamics of Guest Exchange in Cavitates 320
6.2.4 Glycoluril-Based Hosts 323
6.2.5 Kohnkene 326

**6.3 Cyclodextrins** 327
6.3.1 Introduction and Properties 327
6.3.2 Preparation 331
6.3.3 Inclusion Chemistry 331
6.3.4 Industrial Applications 335

**6.4 Molecular Clefts and Tweezers** 336

**6.5 Cyclophane Hosts** 340
6.5.1 General Aspects 340
6.5.2 Cyclophane Nomenclature 341
6.5.3 Cyclophane Synthesis 342
6.5.4 Molecular 'Iron Maidens' 345
6.5.5 From Tweezers to Cyclophanes 346
6.5.6 The Diphenylmethane Moiety 347
6.5.7 Guest Inclusion by Hydrogen Bonding 353
6.5.8 Charge-Transfer Cyclophanes 357

**6.6 Constructing a Solution Host from Clathrate-Forming Building Blocks: The Cryptophanes** 358
6.6.1 Construction of Containers from a Curved Molecular Building Block 358
6.6.2 Complexation of Halocarbons 361
6.6.3 Competition with Solvent 363
6.6.4 Complexes with Alkyl Ammonium Ions and Metals 364
6.6.5 Methane and Xenon Complexation 365
6.6.6 An 'Imploding' Cryptophane 366
6.6.7 Hemicryptophanes 367

**6.7 Covalent Cavities: Carcerands and Hemicarcerands** 370
6.7.1 Definitions and Synthesis 370
6.7.2 Template Effects in Carcerand Synthesis 373
6.7.3 Complexation and Constrictive Binding 373
6.7.4 Carcerism 375
6.7.5 Inclusion Reactions 376
6.7.6 Giant Covalent Cavities 379

**Summary** 381

**Study Problems** 381

**Thought Experiment** 382

**References** 382

**7 Solid-State Inclusion Compounds** 385

**7.1 Solid-State Host-Guest Compounds** 386

**7.2 Clathrate Hydrates** 387
7.2.1 Formation 387
7.2.2 Structures and Properties 388
7.2.3 Problems and Applications 391

**7.3 Urea and Thiourea Clathrates** 393
7.3.1 Structure 393
7.3.2 Guest Order and Disorder 394
7.3.3 Applications of Urea Inclusion Compounds 398

**7.4 Other Channel Clathrates** 399
7.4.1 Trimesic Acid 399
7.4.2 Helical Tubulands and Other Di-ols 401
7.4.3 Perhydrotriphenylene: Polarity Formation 403

**7.5 Hydroquinone, Phenol, Dianin's Compound and the Hexahost Strategy** 406

**7.6 Tri-*o*-thymotide** 410
7.6.1 Inclusion Chemistry 410
7.6.2 Synthesis and Derivatives 412
7.6.3 Applications 413

**7.7 Cyclotriveratrylene** 414
7.7.1 Properties 414
7.7.2 Synthesis 414
7.7.3 Inclusion Chemistry 416
7.7.4 Network Structures 418

**7.8 Inclusion Compounds of the Calixarenes** 419
7.8.1 Organic-Soluble Calixarenes 419
7.8.2 Fullerene Complexation 423
7.8.3 Water-Soluble Calixarenes 426

**7.9 Solid-Gas and Solid-Liquid Reactions in Molecular Crystals** 429
7.9.1 The Importance of Gas Sorption 429
7.9.2 Gas Sorption by Calixarenes 431
7.9.3 Gas Sorption by Channel Hosts 434
7.9.4 Gas Sorption by Coordination Complex Hosts 435

**Summary** 437

**Study Problems** 438

**References** 438

**8 Crystal Engineering** 441

**8.1 Concepts** 442
8.1.1 Introduction 442
8.1.2 Tectons and Synthons 443
8.1.3 The Special Role of Hydrogen Bonding 447
8.1.4 Hydrogen Bond Acidity and Basicity 452

**8.2 Crystal Nucleation and Growth** 453
8.2.1 Theory of Crystal Nucleation and Growth 453
8.2.2 NMR Spectroscopy as a Tool to Probe Nucleation 455
8.2.3 Crystal Growth at Air–Liquid Interfaces 456
8.2.4 Chirality Induction: The Adam Effect 458
8.2.5 Dyeing Crystal Interfaces 462
8.2.6 Hourglass Inclusions 464
8.2.7 Epitaxy: Engineering Crystals 467
8.2.8 Crystals as Genes? 469
8.2.9 Mechanochemistry and Topochemistry 470

**8.3 Understanding Crystal Structures** 476
8.3.1 Graph Set Analysis 476
8.3.2 Etter's Rules 478
8.3.3 Crystal Deconstruction 481
8.3.4 Crystal Engineering Design Strategies 482

**8.4 The Cambridge Structural Database** 484

**8.5 Polymorphism** 487
8.5.1 The Importance of Polymorphism 487
8.5.2 Types of Polymorphism 489
8.5.3 Controlling Polymorphism 492

**8.6 Co-crystals** 493
8.6.1 Scope and Nomenclature 493
8.6.2 Designer Co-crystals 494
8.6.3 Hydrates 497

**8.7 $Z' > 1$** 498

**8.8 Crystal Structure Prediction** 500
8.8.1 Soft *vs*. Hard Predictions 500
8.8.2 Crystal Structure Calculation 501
8.8.3 The CCDC Blind Tests 504

**8.9 Hydrogen Bond Synthons – Common and Exotic** 505
8.9.1 Hydrogen Bonded Rings 505
8.9.2 Hydrogen Bonds to Halogens 510
8.9.3 Hydrogen Bonds to Cyanometallates 511
8.9.4 Hydrogen Bonds to Carbon Monoxide Ligands 512
8.9.5 Hydrogen Bonds to Metals and Metal Hydrides 514
8.9.6 CH Donor Hydrogen Bonds 517

**8.10 Aromatic Rings** 519
8.10.1 Edge-to-Face and Face-to-Face Interactions 519
8.10.2 Aryl Embraces 522
8.10.3 Metal-π Interactions 523

**8.11 Halogen Bonding and Other Interactions** 524

**8.12 Crystal Engineering of Diamondoid Arrays** 526

**Summary** 530

**Study Problems** 531

**Thought Experiment** 532

**References** 532

**9 Network Solids** 537

**9.1 What Are Network Solids?** 538
9.1.1 Concepts and Classification 538
9.1.2 Network Topology 539
9.1.3 Porosity 542

**9.2 Zeolites** 543
9.2.1 Composition and Structure 543
9.2.2 Synthesis 547
9.2.3 MFI Zeolites in the Petroleum Industry 548

**9.3 Layered Solids and Intercalates** 550
9.3.1 General Characteristics 550
9.3.2 Graphite Intercalates 553
9.3.3 Controlling the Layers: Guanidinium Sulfonates 554

**9.4 In the Beginning: Hoffman Inclusion Compounds and Werner Clathrates** 556

**9.5 Coordination Polymers** 561
9.5.1 Coordination Polymers, MOFs and Other Terminology 561
9.5.2 0D Coordination Clusters 562
9.5.3 1D, 2D and 3D Structures 564
9.5.4 Magnetism 568
9.5.5 Negative Thermal Expansion 570
9.5.6 Interpenetrated Structures 571
9.5.7 Porous and Cavity-Containing Structures 575
9.5.8 Metal-Organic Frameworks 578
9.5.9 Catalysis by MOFs 583
9.5.10 Hydrogen Storage by MOFs 583

**Summary** 586

**Study Problem** 587

**References** 587

**10 Self-Assembly** 591

**10.1 Introduction** 592
10.1.1 Scope and Goals 592
10.1.2 Concepts and Classification 594

**10.2 Proteins and Foldamers: Single Molecule Self-Assembly** 598
10.2.1 Protein Self-Assembly 598
10.2.2 Foldamers 599

**10.3 Biochemical Self-Assembly** 600
10.3.1 Strict Self-Assembly: The Tobacco Mosaic Virus and DNA 600
10.3.2 Self-Assembly with Covalent Modification 602

**10.4 Self-Assembly in Synthetic Systems: Kinetic and Thermodynamic Considerations** 604
10.4.1 Template Effects in Synthesis 604
10.4.2 A Thermodynamic Model: Self-Assembly of Zinc Porphyrin Complexes 606
10.4.3 Cooperativity and the Extended Site Binding Model 610
10.4.4 Double Mutant Cycles – Quantifying Weak Interactions 615
10.4.5 Probability of Self-Assembly 616

**10.5 Self-Assembling Coordination Compounds** 620
10.5.1 Design and Notation 620
10.5.2 A Supramolecular Cube 621
10.5.3 Molecular Squares and Boxes 624
10.5.4 Self-Assembly of Metal Arrays 637

**10.6 Self-Assembly of Closed Complexes by Hydrogen Bonding** 641
10.6.1 Tennis Balls and Softballs: Self-Complementary Assemblies 641
10.6.2 Heterodimeric Capsules 646
10.6.3 Giant Self-Assembling Capsules 646
10.6.4 Rosettes 651

**10.7 Catenanes and Rotaxanes** 653
10.7.1 Overview 653
10.7.2 Statistical Approaches to Catenanes and Rotaxanes 655
10.7.3 Rotaxanes and Catenanes Involving π–π Stacking Interactions 656
10.7.4 Hydrogen Bonded Rotaxanes and Catenanes 666
10.7.5 Metal and Auxiliary Linkage Approaches to Catenanes and Rotaxanes 669
10.7.6 Molecular Necklaces 677

**10.8 Helicates and Helical Assemblies** 678
10.8.1 Introduction 678
10.8.2 Synthetic Considerations 681
10.8.3 [4 + 4] Helicates 682
10.8.4 [6 + 6] Helicates 683
10.8.5 Self-Recognition and Positive Cooperativity 684
10.8.6 Cyclic Helicates 686
10.8.7 Anion-Based Helices 687
10.8.8 Hydrogen-Bonded Helices 687

**10.9 Molecular Knots** 691
10.9.1 The Topology of Knots 691
10.9.2 Trefoil Knots 693
10.9.3 Other Knots 696
10.9.4 Borromean Rings 697

**Summary** 700

**Study Problems** 701

**Thought Experiment** 702

**References** 702

**11 Molecular Devices** 707

**11.1 Introduction** 708
11.1.1 Philosophy of Molecular Devices 708
11.1.2 When Is a Device Supramolecular? 708

**11.2 Supramolecular Photochemistry** 710
11.2.1 Photophysical Fundamentals 710
11.2.2 Mechanisms of Energy and Electron Transfer 713
11.2.3 Bimetallic Systems and Mixed Valence 715
11.2.4 Bipyridine and Friends as Device Components 716
11.2.5 Bipyridyl-Type Light Harvesting Devices 718
11.2.6 Light-Conversion Devices 725
11.2.7 Non-Covalently Bonded Systems 726

**11.3 Information and Signals: Semiochemistry and Sensing** 730
11.3.1 Supramolecular Semiochemistry 730
11.3.2 Photophysical Sensing and Imaging 731
11.3.3 Colorimetric Sensors and the Indicator Displacement Assay 738
11.3.4 Electrochemical Sensors 742

**11.4 Molecule-Based Electronics** 746
11.4.1 Molecular Electronic Devices 746
11.4.2 Molecular Wires 746
11.4.3 Molecular Rectifiers 750
11.4.4 Molecular Switches 752
11.4.5 Molecular Logic 756
11.4.6 Towards Addressable Molecular Devices 760

**11.5 Molecular Analogues of Mechanical Machines** 762

**11.6 Nonlinear Optical Materials** 765
11.6.1 Origins of Nonlinear Optical Effects 765
11.6.2 Second-Order Nonlinear Optical Materials 768
11.6.3 Third Harmonic Generation Nonlinear Optical Materials 771

**Summary** 771

**Study Problems** 771

**References** 772

**12 Biological Mimics and Supramolecular Catalysis** 777

**12.1 Introduction** 778
12.1.1 Understanding and Learning from Biochemistry 778
12.1.2 Characteristics of Biological Models 779

**12.2 Cyclodextrins as Enzyme Mimics** 780
12.2.1 Enzyme Modelling Using an Artificial Host Framework 780
12.2.2 Cyclodextrins as Esterase Mimics 782
12.2.3 Functionalised Cyclodextrins 783

**12.3 Corands as ATPase Mimics** 785

**12.4 Cation-Binding Hosts as Transacylase Mimics** 788
12.4.1 Chiral Corands 788
12.4.2 A Structure and Function Mimic 790

**12.5 Metallobiosites** 792
12.5.1 Haemocyanin Models 793
12.5.2 Zinc-Containing Enzymes 795

**12.6 Haem Analogues** 798
12.6.1 Models of Oxygen Uptake and Transport 798
12.6.2 Cytochrome P-450 Models 803
12.6.3 Cytochrome c Oxidase Models 807

**12.7 Vitamin $B_{12}$ Models** 808

**12.8 Ion Channel Mimics** 809

**12.9 Supramolecular Catalysis** 813
12.9.1 Abiotic Supramolecular Catalysis 813
12.9.2 Dynamic Combinatorial Libraries 817
12.9.3 Self-Replicating Systems 819
12.9.4 Emergence of Life 823

**Summary** 825

**Study Problems** 825

**Thought Experiment** 826

**References** 826

**13 Interfaces and Liquid Assemblies** 829

**13.1 Order in Liquids** 830

**13.2 Surfactants and Interfacial Ordering** 831
13.2.1 Surfactants, Micelles and Vesicles 831
13.2.2 Surface Self-Assembled Monolayers 837

**13.3 Liquid Crystals** 839
13.3.1 Nature and Structure 839
13.3.2 Design of Liquid Crystalline Materials 846
13.3.3 Supramolecular Liquid Crystals 848
13.3.4 Liquid Crystal Displays 851

**13.4 Ionic Liquids** 852

**13.5 Liquid Clathrates** 854

**Summary** 858

**Study Problems** 858

**References** 859

**14 Supramolecular Polymers, Gels and Fibres** 861

**14.1 Introduction** 862

**14.2 Dendrimers** 862
14.2.1 Structure and Nomenclature 862
14.2.2 Preparation and Properties of Molecular Dendrimers 866
14.2.3 Dendrimer Host–Guest Chemistry 869
14.2.4 Supramolecular Dendrimer Assemblies 872
14.2.5 Dendritic Nanodevices 874

**14.3 Covalent Polymers with Supramolecular Properties** 876
14.3.1 Amphiphilic Block Copolymers 876
14.3.2 Molecular Imprinted Polymers 879

**14.4 Self-Assembled Supramolecular Polymers** 880

**14.5 Polycatenanes and Polyrotaxanes** 883

**14.6 Biological Self-Assembled Fibres and Layers** 885
14.6.1 Amyloids, Actins and Fibrin 885
14.6.2 Bacterial S-Layers 887

**14.7 Supramolecular Gels** 888

**14.8 Polymeric Liquid Crystals** 893

**Summary** 894

**Study Problems** 895

**References** 895

**15 Nanochemistry** 899

**15.1 When Is Nano Really Nano?** 900

**15.2 Nanotechnology: The 'Top Down' and 'Bottom Up' Approaches** 900

**15.3 Templated and Biomimetic Morphosynthesis** 902

**15.4 Nanoscale Photonics** 905

**15.5 Microfabrication, Nanofabrication and Soft Lithography** 907

**15.6 Assembly and Manipulation on the Nanoscale** 912
15.6.1 Chemistry with a Microscope Tip 912
15.6.2 Self-Assembly on Surfaces 914
15.6.3 Addressing Single Molecules 918
15.6.4 Atomic-Level Assembly of Materials 920

**15.7 Nanoparticles** 921
15.7.1 Nanoparticles and Colloids: Definition and Description 921
15.7.2 Gold Nanoparticles 922
15.7.3 Quantum Dots 925
15.7.4 Non-Spherical Nanoparticles 927

**15.8 Endohedral Fullerenes, Nanotubes and Graphene** 927
15.8.1 Fullerenes as Hosts 928
15.8.2 Carbon Nanotubes 931
15.8.3 Graphene 935
15.8.4 Afterword – Damascus Steel 935

**Summary** 936

**Thought Experiment** 937

**References** 937

**Index** 941

# About the Authors

**Jonathan W. Steed** was born in London, UK in 1969. He obtained his B.Sc. and Ph.D. degrees at University College London, working with Derek Tocher on coordination and organometallic chemistry directed towards inorganic drugs and new metal-mediated synthesis methodologies. He graduated in 1993, winning the Ramsay Medal for his Ph.D. work. Between 1993 and 1995 he was a NATO postdoctoral fellow at the University of Alabama and University of Missouri, working with Jerry Atwood. In 1995 he was appointed as a Lecturer at Kings College London and in 1998 he was awarded the Royal Society of Chemistry Meldola Medal. In 2004 he joined Durham University where he is currently Professor of Inorganic Chemistry. As well as *Supramolecular Chemistry* (2000) Professor Steed is co-author of the textbook *Core Concepts in Supramolecular Chemistry and Nanochemistry* (2007) and more than 200 research papers. He has published a large number of reviews, book chapters and popular articles as well as two major edited works, the *Encyclopaedia of Supramolecular Chemistry* (2004) and *Organic Nanostructures* (2008). He has been an Associate Editor of *New Journal of Chemistry* since 2001 and is the recipient of the Vice Chancellor's Award for Excellence in Postgraduate Teaching (2006). His interests are in supramolecular sensing and molecular materials chemistry.

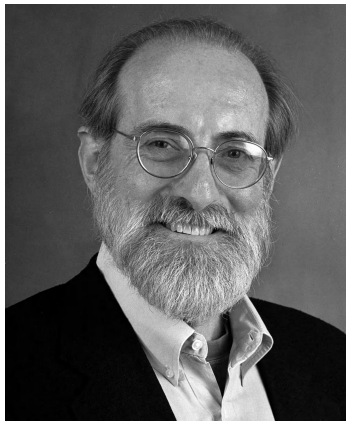

**Jerry L. Atwood** was born in Springfield MO, USA in 1942. He attended Southwest Missouri State University, where he obtained his B.S. degree in 1964. He carried out graduate research with Galen Stuckey at the University of Illinois, where he obtained his Ph.D. in 1968. He was immediately appointed as an Assistant Professor at the University of Alabama, where he rose through Associate Professor (1972) to full Professor in 1978. In 1994 he was appointed Professor and Chair at the University of Missouri – Columbia. Professor Atwood is the author of more than 600 scientific publications. His research interests revolve around a number of themes in supramolecular chemistry including gas storage and separation and the control of confined space. He has also worked on the self-assembly of non-covalent capsules, liquid clathrate chemistry, anion binding and fundamental solid state interactions, and is a world-renown crystallographer. He co-founded the journals *Supramolecular Chemistry* (1992) and *Journal of Inclusion Phenomena* (1983). He has edited an enormous range of seminal works in supramolecular chemistry including the five-volume series *Inclusion Compounds* (1984 and 1991) and the 11-volume *Comprehensive Supramolecular Chemistry* (1996). In 2000 he was awarded the Izatt-Christensen Prize in Supramolecular Chemistry

# Preface to the First Edition

Supramolecular chemistry is one of the most popular and fastest growing areas of experimental chemistry and it seems set to remain that way for the foreseeable future. Everybody's doing it! Part of the reason for this is that supramolecular science is aesthetically appealing, readily visualised and lends itself to the translation of everyday concepts to the molecular level. It might also be fair to say that supramolecular chemistry is a very greedy topic. It is highly interdisciplinary in nature and, as a result, attracts not just chemists but biochemists, biologists, environmental scientists, engineers, physicists, theoreticians, mathematicians and a whole host of other researchers. These supramolecular scientists are people who might be described as goal-orientated in that they cross the traditional boundaries of their discipline in order to address specific objectives. It is this breadth that gives supramolecular chemistry its wide allure, and sometimes leads to grumbling that 'everything seems to be supramolecular these days'. This situation is aided and abetted by one of the appealing but casual definitions of supramolecular chemistry as 'chemistry beyond the molecule', which means that the chemist is at liberty to study pretty much any kind of interaction he or she pleases – except some covalent ones. The situation is rather reminiscent of the hubris of some inorganic chemists in jokingly defining that field as 'the chemistry of all of the elements except for some of that of carbon'.

The funny thing about supramolecular chemistry is that despite all of this interest in doing it, there aren't that many people who will actually teach it to you. Most of today's practitioners in the field, including the present authors, come from backgrounds in other disciplines and are often self-taught. Indeed, some people seem as if they're making it up as they go along! As university academics, we have both set up undergraduate and postgraduate courses in supramolecular chemistry in our respective institutions and have found that there are a lot of people wanting to learn about the area. Unfortunately there is rather little material from which to teach them, except for the highly extensive research literature with all its jargon and fashions. The original idea for this book came from a conversation between us in Missouri in the summer of 1995. Very few courses in 'supramol,' existed at the time, but it was clear that they would soon be increasingly common. It was equally clear that, with the exception of Fritz Vögtle's 1991 research-level book, there was nothing by way of a teaching textbook of the subject out there. We drew up a contents list, but there the idea sat until 1997. Everybody we talked to said there was a real need for such a book; some had even been asked to write one. It finally took the persuasive powers of Andy Slade from Wiley to bring the book to fruition over the summers of 1998 and 1999. We hope that now we have written a general introductory text for supramolecular chemistry, many more courses at both undergraduate and postgraduate level will develop in the area and it will become a full member of the pantheon of chemical education. It is also delightful to note that Paul Beer, Phil Gale and David Smith have recently written a short primer on supramolecular chemistry, which we hope will be complementary to this work.

In writing this book we have been very mindful of the working title of this book, which contained the words 'an introduction'. We have tried to mention all of the key systems and to explain in detail all of the jargon, nomenclature and concepts pertaining to the field. We have not tried to offer any kind of comprehensive literature review (for which purpose JLA has co-edited the 11 volumes of *Comprehensive Supramolecular Chemistry*). What errors there are will be, in the main, ones of over-simplification in an attempt to make accessible many very complicated, and often still rapidly evolving, topics. To the many fine workers whose insights we may have trivialised we offer humble apology. We hope that the overwhelming advantages will be the excitement of the reader who can learn about any or all aspects of this hydra-like field of chemistry either by a tobogganing plunge from cover to cover, or in convenient, bite-sized chunks.

# Preface to the Second Edition

Since the publication of the first edition of *Supramolecular Chemistry* in 2000 the field has continued to grow at a tremendous pace both in depth of understanding and in the breadth of topics addressed by supramolecular chemists. These developments have been made possible by the creativity and technical skill of the international community and by continuing advances in instrumentation and in the range of techniques available. This tremendous activity has been accompanied by a number of very good books particularly at more advanced levels on various aspects of the field, including a two-volume encyclopaedia that we edited.

In this book we have tried to sample the entire field, bringing together topical research and clear explanations of fundamentals and techniques in a way that is accessible to final year undergraduates in the chemical sciences, all the way to experienced researchers. We have been very gratified by the reception afforded the first edition and it is particularly pleasing to see that the book is now available in Russian and Chinese language editions. For a short while we attempted to keep the book current by updating our system of key references on a web site; however it has become abundantly clear that a major overhaul of the book in the form of a refreshed and extended second edition is necessary. We see the strengths of the book as its broad coverage, the care we have tried to take to explain terms and concepts as they are encountered, and perhaps a little of our own personal interpretation and enthusiasm for the field that we see evolving through our own research and extensive contact with colleagues around the world. These strengths we have tried to build upon in this new edition while at the same time ameliorating some of the uneven coverage and oversimplifications of which we may have been guilty.

The original intent of this book was to serve as a concise introduction to the field of supramolecular chemistry. One of us (JWS) has since co-authored a short companion book *Core Concepts in Supramolecular Chemistry and Nanochemistry* that fulfils that role. We have therefore taken the opportunity to increase the depth and breadth of the coverage of this longer book to make it suitable for, and hopefully useful to, those involved at all stages in the field. Undergraduates encountering Supramolecular Chemistry for the first time will find that we have included careful explanations of core concepts building on the basics of synthetic, coordination and physical organic chemistry. At the same time we hope that senior colleagues will find the frontiers of the discipline well represented with plenty of recent literature. We have retained the system of key references based on the secondary literature that feedback indicates many people found useful, but we have also extended the scope of primary literature references for those wishing to undertake more in-depth reading around the subjects covered. In particular we have tried to take the long view both in temporal and length scales, showing how 'chemistry beyond the molecule' continues to evolve naturally and seamlessly into nanochemistry and molecular materials chemistry.

We have added a great deal to the book in this new edition including new chapters and subjects (*e.g.* supramolecular polymers, microfabrication, nanoparticles, chemical emergence, metal-organic frameworks, ion pairs, gels, ionic liquids, supramolecular catalysis, molecular electronics, polymorphism, gas sorption reactions, anion-$\pi$ interactions… the list of exciting new science is formidable). We have also extensively updated stories and topics that are a part of ongoing research with new results published since 2000. The book retains some of the 'classics' which no less striking and informative for being a little long in the tooth these days. As before we apologise to the many fine colleagues whose work we did not include. The objective of the book is to cover the scope of the field with interesting and

representative examples of key systems but we cannot be comprehensive. We feel this second edition is more complete and balanced than the first edition and we have really enjoyed putting it together. We hope you enjoy it too.

*Jonathan W. Steed, Durham, UK*
*Jerry L. Atwood, Columbia, Missouri, USA*

# Acknowledgements

Our thanks go to the many fine students, researchers and colleagues who have passed through our groups over the years, whose discussions have helped to both metaphorically and literally crystallize our thinking on this rapidly evolving field. Many colleagues in both Europe and the USA have been enormously helpful in offering suggestions and providing information. In particular we are grateful to Jim Tucker, Mike Hannon, Jim Thomas and the late Fred Armitage for their help in getting the ball rolling and constructive comments on the first edition. The second edition has benefited tremendously from input by Kirsty Anderson and Len Barbour, and we are also very grateful to Len for the brilliant X-Seed which has made the crystallographic diagrams much easier to render. David Turner also provided some excellent diagrams. We thank Graeme Day for useful information on crystal structure calculation and a number of colleagues for providing artwork or additional data, particularly Sir Fraser Stoddart, John Ripmeester, Peter Tasker, Travis Holman and Bart Kahr. Beth Dufour, Rebecca Ralf and Hollie Budge, Andy Slade, Paul Deards, Richard Davies and Gemma Valler at Wiley have worked tirelessly to bring the book to the standard and accessibility it needs to have. JWS is very grateful to Durham University for providing a term of research leave which made this book so much easier to write, and we are both as ever indebted to the many fine co-workers who have passed through our labs over the years who make chemistry such an enjoyable subject to work in.

# About the Front Cover

The front cover shows two views of the Lycurgus cup – a 4$^{th}$ century Roman chalice made of dichroic glass impregnated with nanoparticles made of gold-silver alloy. When viewed under normal lighting conditions the cup appears green but if light is shone through the glass the nanoparticles impart a gorgeous crimson colour. The chemistry of metallic nanoparticles remains a highly topical field in supramolecular chemistry. (Images courtesy of the British Museum, London, UK).

# Website

Powerpoint slides of all figures from this book, along with the answers to the problems, can be found at http://www.wiley.com/go/steed

*Supramolecular Chemistry, 2nd edition* J. W. Steed and J. L. Atwood
© 2009 John Wiley & Sons, Ltd ISBN: 978-0-470-51233-3

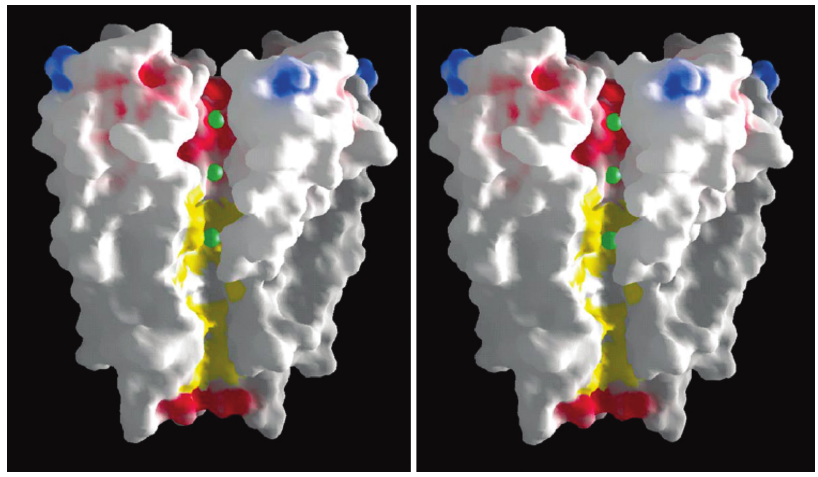

**Figure 2.7** Cutaway stereoview of the X-ray crystal structure of the $K^+$ channel of *Streptomyces lividans*. The upper and lower ends of the channel are regions of high negative charge density while the central portion comprises hydrophobic amino acid side chains. Positively charged regions are on the outer surface, while the spheres represent $K^+$ ion positions. (Reproduced with permission from [2] MacKinnon).

**Figure 2.26** (a) paired male and female *Bombyx Mori* silkworm moths (image courtesy of www.wormspit.com), (b) jasmine blossom.

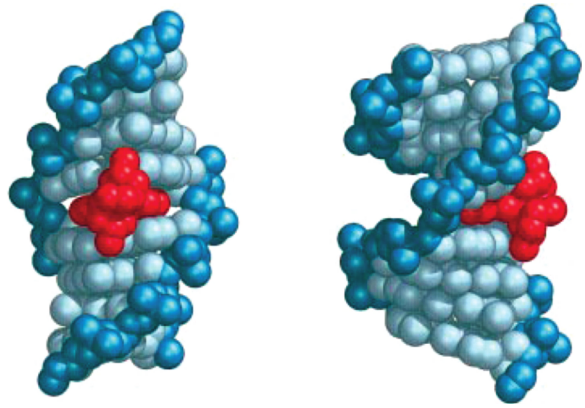

**Figure 2.37** Two views of the crystal structure of $[Rh(R, R\text{-}Me_2trien)(phi)]^{3+}$ bound within an eight-base-pair oligonucleotide. (Reproduced with permission from [18] © 1999, American Chemical Society).

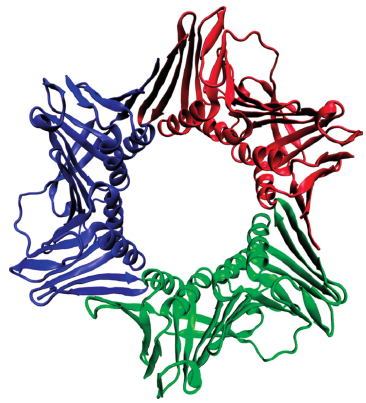

**Figure 2.39** A DNA clamp protein – a trimer of the protein Proliferating Cell Nuclear Antigen (PCNA). The three different trimer units are shown in different colours (image courtesy of www.wikipedia.org).

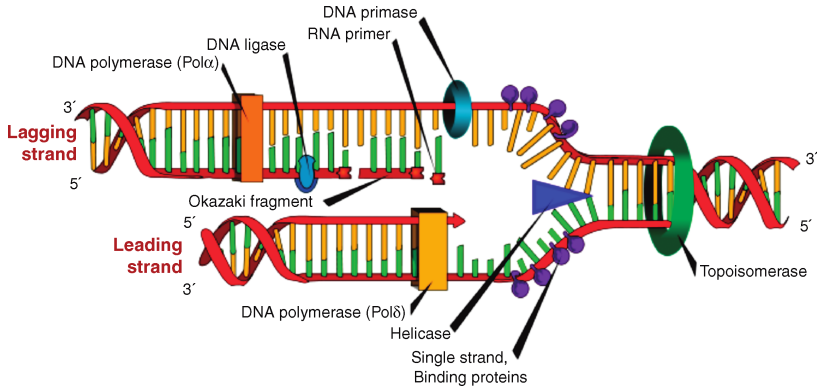


**Figure 2.40** The DNA replication fork comprising a number of cooperating enzymes. (image courtesy of www.wikipedia.org).

**Figure 7.1** 'Burning snowballs' of methane clathrate hydrate (image courtesy of the US Geological Survey).

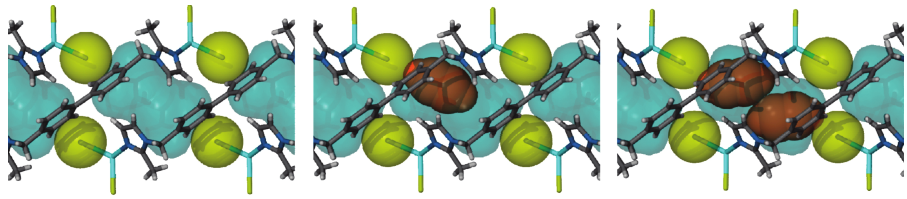

(a) (b) (c)

**Figure 7.49** X-ray crystal structures of **7.68** (a) apohost, (b) 1:1 inclusion compound with acetylene (1 bar) and (c) 1:2 acetylene complex (8 bar). The cavity volume is shown as a van der Waals survace – note that each cavity is discrete. Chloride ligands are shown as spheres and the acetylene molecules are shown in space-filling mode (pictures courtesy of Prof. L. J. Barbour, Stellenbosch University).

**Figure 8.8** Very large crystals such as this sample of KDP ($KH_2PO_4$) used for laser frequency doubling are produced by careful nucleation control at the metastable boundary between an unsaturated and supersaturated solution (image courtesy of the Lawrence Livermore National Laboratory).

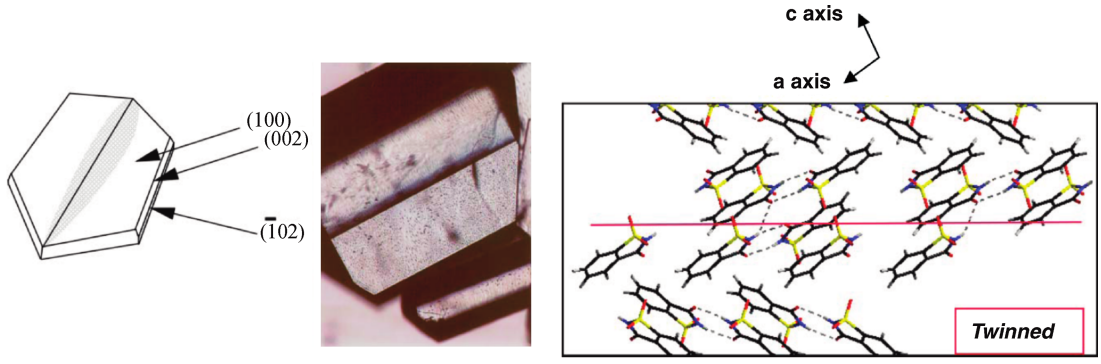


(a) (b)

**Figure 8.16** (a) Optical micrograph and schematic diagram of a twinned crystal grown in the presence of indigo at high supersaturation. The crystal is *ca*. 70 mm in length. (b) The $\{10\bar{2}\}$ twin interface in saccharin showing the new three centre C=O···H–N hydrogen bond which joins dimers across the plane (reproduced by permission from The Royal Society of Chemistry).

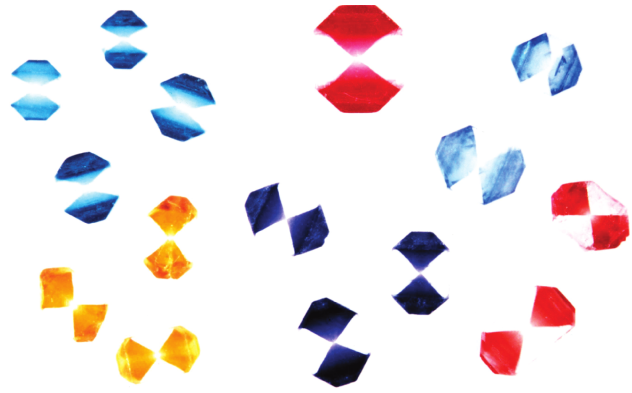

**Figure 8.19** Hourglass inclusion compounds of $K_2SO_4$ with a range of coloured dyes. (Courtesy of Prof. B. Kahr and Dr. J. A. Subramony.)

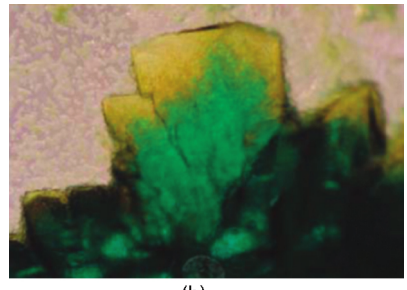

(b)

**Figure 8.22** (b) The green monomer **8.16** (bottom) is able to template the epitaxial growth of an olive-yellow daughter phase (top) of the dinuclear complex **8.15**.[24]

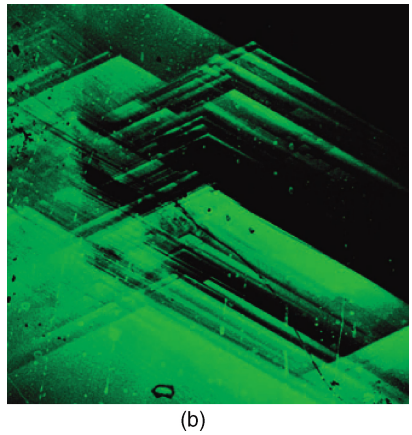

(b)

**Figure 8.23** (b) Confocal laser scanning microscopy image of potassium hydrogen phthalate with occluded dichlorofluorecein showing details of luminescence that has developed in the fast growing slopes of the (010) growth hillock. The vertices of the chevron-shaped hillock 'fossils' mark dislocation cores (reproduced by permission of The Royal Society of Chemistry).

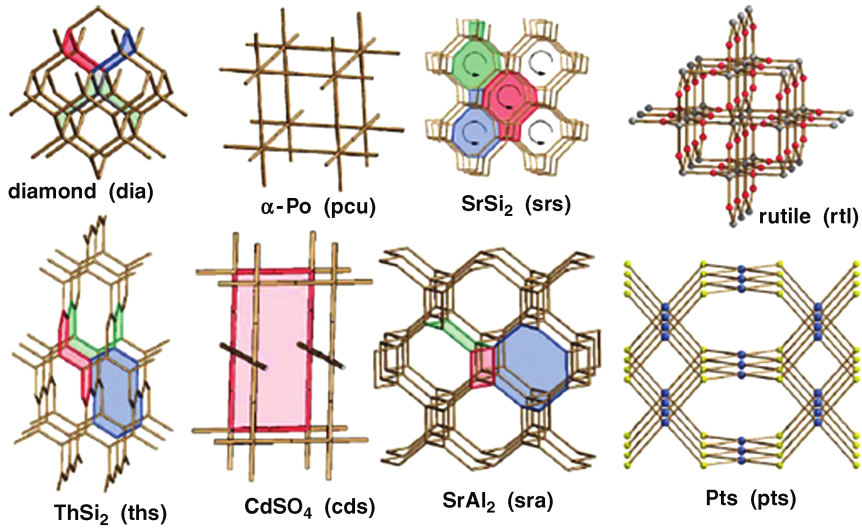


**Figure 9.4** Common nets exhibited by simple materials along with their generic names. Characteristic rings are shaded. The $SrSi_2$ structure is a (10,3)-a net (reproduced with permission from The Royal Society of Chemistry).

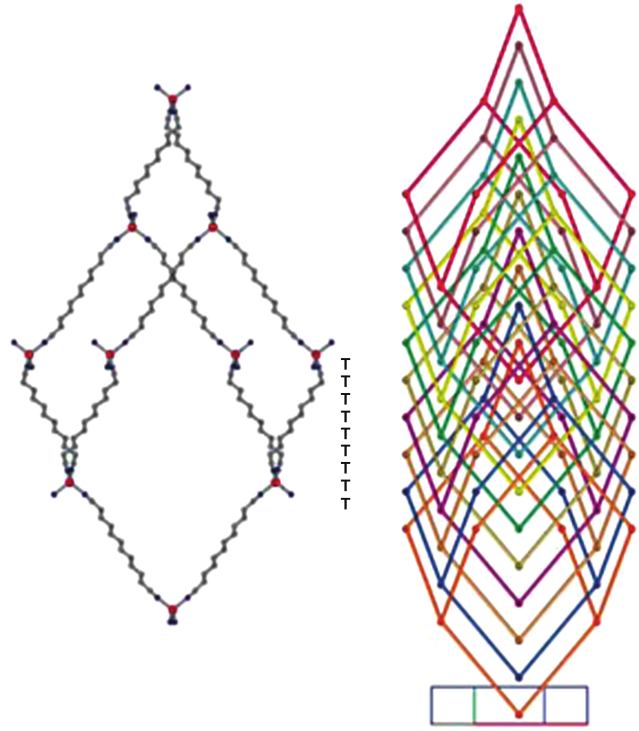


**Figure 9.35** The adamantoid cage and schematic of the tenfold interpenetration in [Ag(1,12-dodecanedinitrile)$_2$]$NO_3$ – all of the torsion angles of the ligand are *trans* (T) maximising its length (Copyright Wiley-VCH Verlag GmbH & Co. KGaA. Reproduced by permission).

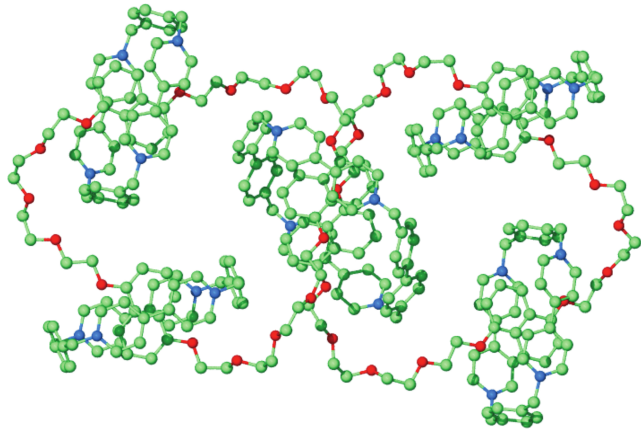

**Figure 10.61** X-ray crystal structure of the [7]catenane analogue of olympiadane.[64]

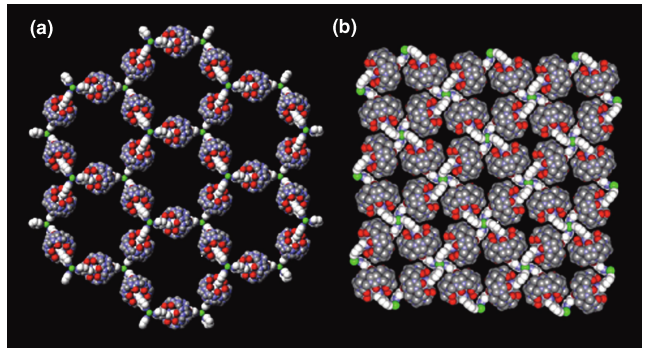


**Figure 10.71** Molecular necklace type coordination polymer rotaxanes (a) hexagonal 2D polyrotaxane net and (b) square-grid shaped 2D polyrotaxane net (reproduced by permission of The Royal Society of Chemistry).

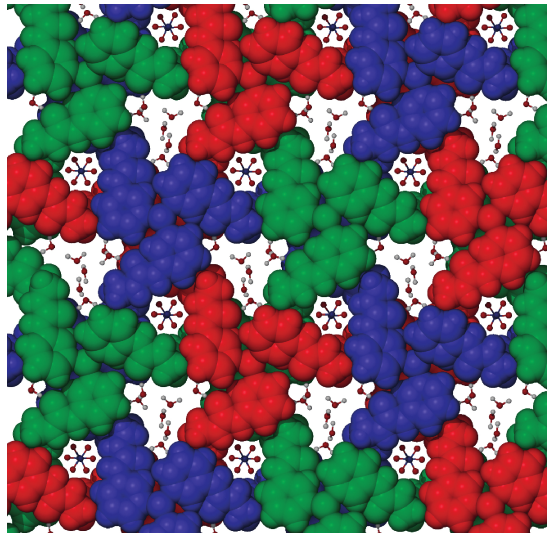

**Figure 10.93** A coordination polymer Borromean weave containing water guests in the open cavities and supported by saturated hydrogen bonding to nitrate anions.[113]

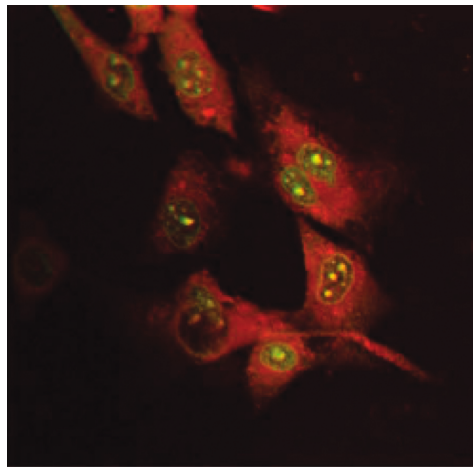

**Figure 11.21** Confocal fluorescence microscope image showing the cellular localisation behaviour of the europium complex **11.33** in living cells, revealing the staining of the nucleolus inside the cell nucleus (reproduced by permission of The Royal Society of Chemistry).

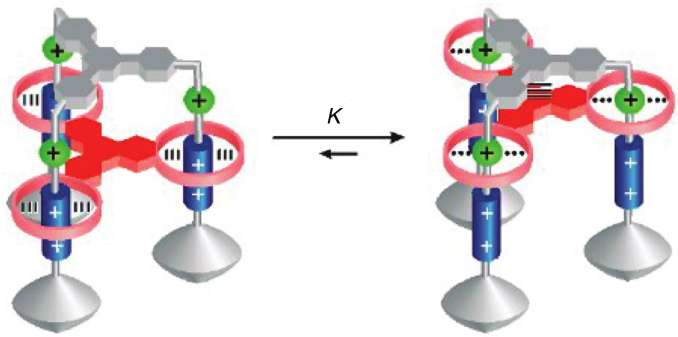


**Figure 11.42** Components and schematic of the 'molecular elevator' (image courtesy of Prof. Sir J. F. Stoddart).[68]

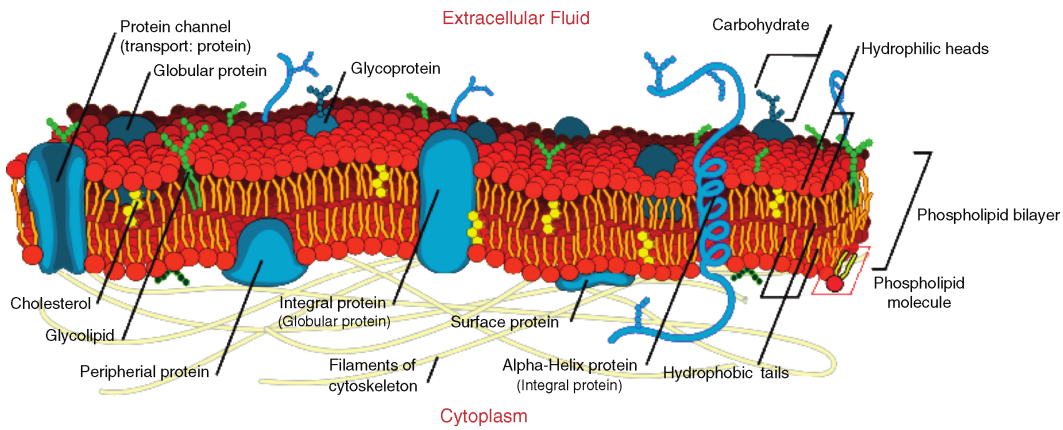


**Figure 13.7** The fluid mosaic model of biological cells. (image courtesy of www.wikipedia.org).

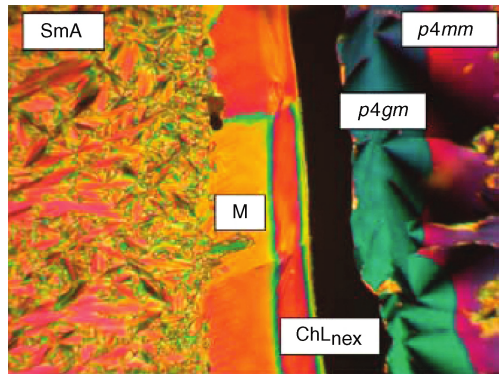


**Figure 13.21** Contact region at 78 °C showing the phase sequence smectic-A (fan texture), M (unidentified mesophase), hexagonal channelled layer pahse (ChLhex), square columnar phases p4gm and p4mm (from left to right) upon increasing concentration of **13.18** (reproduced by permission of The Royal Society of Chemistry).

(a) (b)

**Figure 15.6** (a) an opal bracelet and (b) the iridescent colours of the Madagascan sunset moth. The colouration in both come from light interference patterns caused by nanostructured materials.

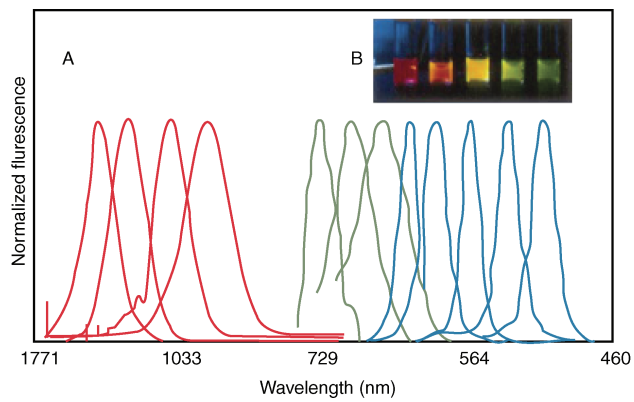


**Figure 15.25** (a) Size- and material-dependent emission spectra of several surfactant-coated semiconductor nanocrystals (quantum dots) in a variety of sizes. The blue series (right) represents different sizes of CdSe nanocrystals with diameters of 2.1, 2.4, 3.1, 3.6 and 4.6 nm (from right to left). The green series (centre) is of InP nanocrystals with diameters of 3.0, 3.5 and 4.6 nm. The red series (left) is of InAs nanocrystals with diameters of 2.8, 3.6, 4.6, and 6.0 nm. (b) A true-colour image of the fluorescence of a series of silica-coated core (CdSe)-shell (ZnS or CdS) nanocrystals (reproduced from [39] with permission from AAAS).

# 1 Concepts

*'Mankind is divisible into two great classes: hosts and guests.'*

Max Beerbohm (b. 1872), *Hosts and Guests*

## 1.1 Definition and Development of Supramolecular Chemistry

Lehn, J.-M., 'Supramolecular chemistry and self-assembly special feature: Toward complex matter: Supramolecular chemistry and self-organization', *Proc. Nat. Acad. Sci. USA*, 2002, **99**, 4763–4768.

### 1.1.1 What is Supramolecular Chemistry?

Supramolecular chemistry has been defined by one of its leading proponents, Jean-Marie Lehn, who won the Nobel Prize for his work in the area in 1987, as the 'chemistry of molecular assemblies and of the intermolecular bond'. More colloquially this may be expressed as 'chemistry beyond the molecule'. Other definitions include phrases such as 'the chemistry of the non-covalent bond' and 'non-molecular chemistry'. Originally supramolecular chemistry was defined in terms of the non-covalent interaction between a 'host' and a 'guest' molecule as highlighted in Figure 1.1, which illustrates the relationship between molecular and supramolecular chemistry in terms of both structures and function.

These descriptions, while helpful, are by their nature noncomprehensive and there are many exceptions if such definitions are taken too literally. The problem may be linked to the definition of organometallic chemistry as 'the chemistry of compounds with metal-to-carbon bonds'. This immediately rules out Wilkinson's compound, $RhCl(PPh_3)_3$, for example, which is one of the most important industrial catalysts for organometallic transformations known in the field. Indeed, it is often the objectives and thought processes of the chemist undertaking the work, as much as the work itself, which determine its field. Work in modern supramolecular chemistry encompasses not just host-guest systems but also molecular devices and machines, molecular recognition, so called 'self-processes'

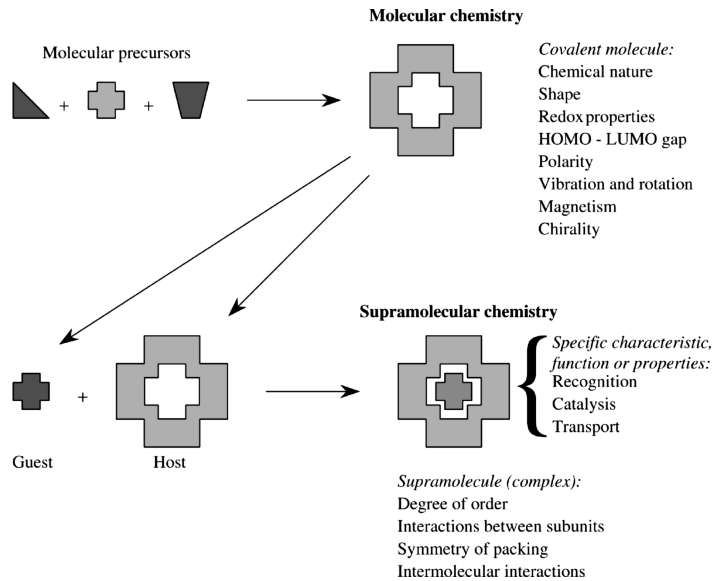


**Figure 1.1** Comparison between the scope of molecular and supramolecular chemistry according to Lehn.[1]

*Supramolecular Chemistry, 2nd edition* J. W. Steed and J. L. Atwood
© 2009 John Wiley & Sons, Ltd ISBN: 978-0-470-51233-3

such as self-assembly and self-organisation and has interfaces with the emergence of complex matter and nanochemistry (Section 1.10). The rapid expansion in supramolecular chemistry over the past 25 years has resulted in an enormous diversity of chemical systems, both designed and accidentally stumbled upon, which may lay some claim, either in concept, origin or nature, to being supramolecular. In particular, workers in the field of supramolecular photochemistry have chosen to adopt a rather different definition of a supramolecular compound as a group of molecular components that contribute properties that each component possesses individually to the whole assembly (covalent or non-covalent). Thus an entirely covalent molecule comprising, for example, a chromophore (light-absorbing moiety), spacer and redox centre might be thought of as supramolecular because the chromophore and redox centre are able to absorb light, or change oxidation state, whether they form part of the supermolecule or not (see Chapter 11). Similarly, much recent work has focused on the development of self-assembling synthetic pathways towards large molecules or molecular arrays. These systems often self-assemble using a variety of interactions, some of which are clearly non-covalent (*e.g.* hydrogen bonds) and some of which possess a significant covalent component (*e.g.* metal–ligand interactions, see Chapter 10). Ultimately these self-assembly reactions and the resulting self-organisation of the system rely solely on the intrinsic information contained in the structure of the molecular components and hence there is an increasing trend towards the study and manipulation of intrinsic 'molecular information'. This shift in emphasis is nothing more than a healthy growth of the field from its roots in host–guest chemistry to encompass and inform a much broader range of concepts and activities.

### 1.1.2 Host–Guest Chemistry

Kyba, E. P., Helgeson, R. C., Madan, K., Gokel, G. W., Tarnowski, T. L., Moore, S. S. and Cram, D. J., 'Host-guest complexation .1. Concept and illustration', *J. Am. Chem. Soc.*, 1977, **99**, 2564–2571.

If we regard supramolecular chemistry in its simplest sense as involving some kind of (non-covalent) binding or complexation event, we must immediately define what is doing the binding. In this context we generally consider a molecule (a 'host') binding another molecule (a 'guest') to produce a 'host–guest' complex or supermolecule. Commonly the host is a large molecule or aggregate such as an enzyme or synthetic cyclic compound possessing a sizeable, central hole or cavity. The guest may be a monatomic cation, a simple inorganic anion, an ion pair or a more sophisticated molecule such as a hormone, pheromone or neurotransmitter. More formally, the host is defined as the molecular entity possessing *convergent* binding sites (*e.g.* Lewis basic donor atoms, hydrogen bond donors *etc.*). The guest possesses *divergent* binding sites (*e.g.* a spherical, Lewis acidic metal cation or hydrogen bond acceptor halide anion). In turn a binding site is defined as a region of the host or guest capable of taking part in a non-covalent interaction. The host–guest relationship has been defined by Donald Cram (another Supramolecular Chemistry Nobel Laureate)[2] as follows:

> *Complexes are composed of two or more molecules or ions held together in unique structural relationships by electrostatic forces other than those of full covalent bonds … molecular complexes are usually held together by hydrogen bonding, by ion pairing, by π-acid to π-base interactions, by metal-to-ligand binding, by van der Waals attractive forces, by solvent reorganising, and by partially made and broken covalent bonds (transition states)… High structural organisation is usually produced only through multiple binding sites… A highly structured molecular complex is composed of at least one host and one guest component… A host–guest relationship involves a complementary stereoelectronic arrangement of binding sites in host and guest… The host component is defined as an organic molecule or ion whose binding sites converge in the complex… The guest component as any molecule or ion whose binding sites diverge in the complex…*

This description might well be generalised to remove the word 'organic', since more recent work has revealed a wealth of inorganic hosts, such as zeolites (Section 9.2) and polyoxometallates (Section 9.5.2), or mixed metal-organic coordination compounds (*e.g.* Section 5.2), which perform similar functions and may be thought of under the same umbrella. The host–guest binding event may be likened to catching a ball in the hand. The hand, acting as the host, envelops the ball providing a physical (steric) barrier to dropping it (disassociation). This analogy falls down at the electronic level, however, since there is no real attractive force between hand and ball. Host and guest *molecules and ions* usually experience an attractive force between them and hence a stabilising binding free energy. The analogy does serve to introduce the term 'inclusion chemistry', however (the ball is included in the hand), hence the inclusion of one molecular in another.

One key division within supramolecular host–guest chemistry in its general sense relates to the stability of a host–guest complex in solution. The field of clathrate, or more generally, inclusion, chemistry, relates to hosts that are often only stable in the solid (crystalline) state and disassociate on dissolution in a solvent. Gas hydrates, urea clathrates and a wide variety of crystalline solvates (Chapter 7) fall into this category. On the other hand, molecular hosts for ions such as the crown ethers, cryptands and spherands (Chapter 3), or hosts for neutral molecules such as the carcerands and cryptophanes (Chapter 6), display significant binding both in the solid state and in solution. We should also note that there exist purely liquid-phase phenomena, such as liquid crystals and liquid clathrates, that have no direct solid-state analogies (Chapter 13).

### 1.1.3 Development

Supramolecular chemistry, as it is now defined, is a young discipline dating back to the late 1960s and early 1970s. However, its concepts and roots, and indeed many simple (and not-so-simple) supramolecular chemical systems, may be traced back almost to the beginnings of modern chemistry itself. An illustrative (although necessarily subjective and non-comprehensive) chronology is given in Table 1.1. Much of supramolecular chemistry has sprung from developments in macrocyclic chemistry in the mid-to-late 1960s, particularly the development of macrocyclic ligands for metal cations. Four systems of fundamental importance may be identified, prepared by the groups of Curtis, Busch, Jäger and Pedersen, three of which used the Schiff base condensation reaction of an aldehyde with an amine to give an imine (Section 3.10.6). Conceptually, these systems may be seen as a development of naturally occurring macrocycles (ionophores, hemes, porphyrins *etc.*). To these may be added the work of Donald Cram on macrocyclic cyclophanes (which dates back to the early 1950s) and, subsequently, on spherands and carcerands, and the tremendous contribution by Jean-Marie Lehn who prepared the cryptands in the late 1960s and has since gone on to shape many of the recent developments in the field.

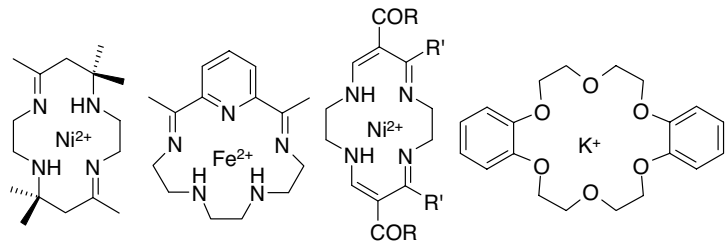


Curtis 1961 **1.1** Busch 1964 **1.2** Jäger 1964 **1.3** Pedersen 1967 **1.4**

**Table 1.1** Timeline of supramolecular chemistry.

1810 – Sir Humphry Davy: discovery of chlorine hydrate

1823 – Michael Faraday: formula of chlorine hydrate

1841 – C. Schafhäutl: study of graphite intercalates

1849 – F. Wöhler: $\beta$-quinol $H_2S$ clathrate

1891 – Villiers and Hebd: cyclodextrin inclusion compounds

1893 – Alfred Werner: coordination chemistry

1894 – Emil Fischer: *lock and key* concept

1906 – Paul Ehrlich: introduction of the concept of a *receptor*

1937 – K. L. Wolf: the term *Übermoleküle* is coined to describe organised entities arising from the association of coordinatively saturated species (*e.g.* the acetic acid dimer)

1939 – Linus Pauling: hydrogen bonds are included in the groundbreaking book *The Nature of the Chemical Bond*

1940 – M. F. Bengen: urea channel inclusion compounds

1945 – H. M. Powell: X-ray crystal structures of $\beta$-quinol inclusion compounds; the term 'clathrate' is introduced to describe compounds where one component is enclosed within the framework of another

1949 – Brown and Farthing: synthesis of [2.2]paracyclophane

1953 – Watson and Crick: structure of DNA

1956 – Dorothy Crowfoot Hodgkin: X-ray crystal structure of vitamin $B_{12}$

1959 – Donald Cram: attempted synthesis of cyclophane charge transfer complexes with $(NC)_2C{=}C(CN)_2$

1961 – N.F. Curtis: first Schiff's base macrocycle from acetone and ethylene diamine

1964 – Busch and Jäger: Schiff's base macrocycles

1967 – Charles Pedersen: crown ethers

1968 – Park and Simmons: *Katapinand* anion hosts

1969 – Jean-Marie Lehn: synthesis of the first cryptands

1969 – Jerry Atwood: liquid clathrates from alkyl aluminium salts

1969 – Ron Breslow: catalysis by cyclodextrins

1973 – Donald Cram: spherand hosts produced to test the importance of preorganisation

1978 – Jean-Marie Lehn: introduction of the term 'supramolecular chemistry', defined as the 'chemistry of molecular assemblies and of the intermolecular bond'

1979 – Gokel and Okahara: development of the lariat ethers as a subclass of host

1981 – Vögtle and Weber: podand hosts and development of nomenclature

1986 – A. P. de Silva: Fluorescent sensing of alkali metal ions by crown ether derivatives

1987 – Award of the Nobel prize for Chemistry to Donald J. Cram, Jean-Marie Lehn and Charles J. Pedersen for their work in supramolecular chemistry

1996 – Atwood, Davies, MacNicol & Vögtle: publication of *Comprehensive Supramolecular Chemistry* containing contributions from many key groups and summarising the development and state of the art

1996 – Award of the Nobel prize for Chemistry to Kroto, Smalley and Curl for their work on the chemistry of the fullerenes

2003 – Award of the Nobel prize for Chemistry to Peter Agre and Roderick MacKinnon for their discovery of water channels and the characterisation of cation and anion channels, respectively.

2004 – J. Fraser Stoddart: the first discrete Borromean-linked molecule, a landmark in topological synthesis.

As it is practised today, supramolecular chemistry is one of the most vigorous and fast-growing fields of chemical endeavour. Its interdisciplinary nature has brought about wide-ranging collaborations between physicists, theorists and computational modellers, crystallographers, inorganic and solid-state chemists, synthetic organic chemists, biochemists and biologists. Within the past decade Supramolecular chemistry has fed into very exciting new research in nanotechnology and at the interface between the two lies the area of *nanochemistry* (Chapter 15). The aesthetically pleasing nature of supramolecular compounds and the direct links established between the visualisation, molecular modelling and practical experimental behaviour of hosts and their complexes has fuelled increasing enthusiasm in the area to the extent that it is now a full member of the pantheon of scientific disciplines.

## 1.2 Classification of Supramolecular Host–Guest Compounds

Vogtle, F., *Supramolecular Chemistry*, John Wiley & Sons, Ltd: Chichester, 1991.

One of the first formal definitions of a supramolecular cage-like host–guest structure was proposed by H. M. Powell at the University of Oxford in 1948. He coined the term 'clathrate', which he defined as a kind of inclusion compound 'in which two or more components are associated without ordinary chemical union, but through complete enclosure of one set of molecules in a suitable structure formed by another'. In beginning to describe modern host–guest chemistry it is useful to divide host compounds into two major classes according to the relative topological relationship between guest and host. *Cavitands* may be described as hosts possessing permanent intramolecular cavities. This means that the cavity available for guest binding is an intrinsic molecular property of the host and exists both in solution and in the solid state. Conversely, *clathrands* are hosts with extramolecular cavities (the cavity essentially represents a gap between two or more host molecules) and is of relevance only in the crystalline or solid state. The host–guest aggregate formed by a cavitand is termed a *cavitate*, while clathrands form *clathrates*. We can also distinguish a third situation in which two molecules associate using non-covalent forces but do not fit the descriptions of 'host' and 'guest'. Under these circumstances we talk about the self-assembly of a mutually complementary pair (or series) of molecules. The distinction between the two host classes and self-assembly is illustrated schematically in Figure 1.2.

A further fundamental subdivision may be made on the basis of the forces between host and guest. If the host–guest aggregate is held together by primarily electrostatic interactions (including ion–dipole, dipole–dipole, hydrogen bonding *etc*.) the term *complex* is used. On the other hand, species held together by less specific (often weaker), non-directional interactions, such as hydrophobic, van der Waals or crystal close-packing effects, are referred to by the terms *cavitate* and *clathrate*. Some examples of the use of this nomenclature are shown in Table 1.2. The distinctions between these classes are blurred and often the word 'complex' is used to cover all of these phenomena. Within these broad classifications a number of intermediate types exist; indeed, it is often very much a matter of opinion as to exactly what the classification of a given material might be. The nomenclature should act as a conceptual framework helping the chemist to describe and visualise the systems being handled, rather than a restrictive and rigid series of 'phyla'.

## 1.3 Receptors, Coordination and the Lock and Key Analogy

Behr, J. P., *The Lock and Key Principle. The State of the Art –100 Years on*, John Wiley & Sons, Inc.: New York, 1994.

Host–guest (or receptor–substrate) chemistry is based upon three historical concepts:

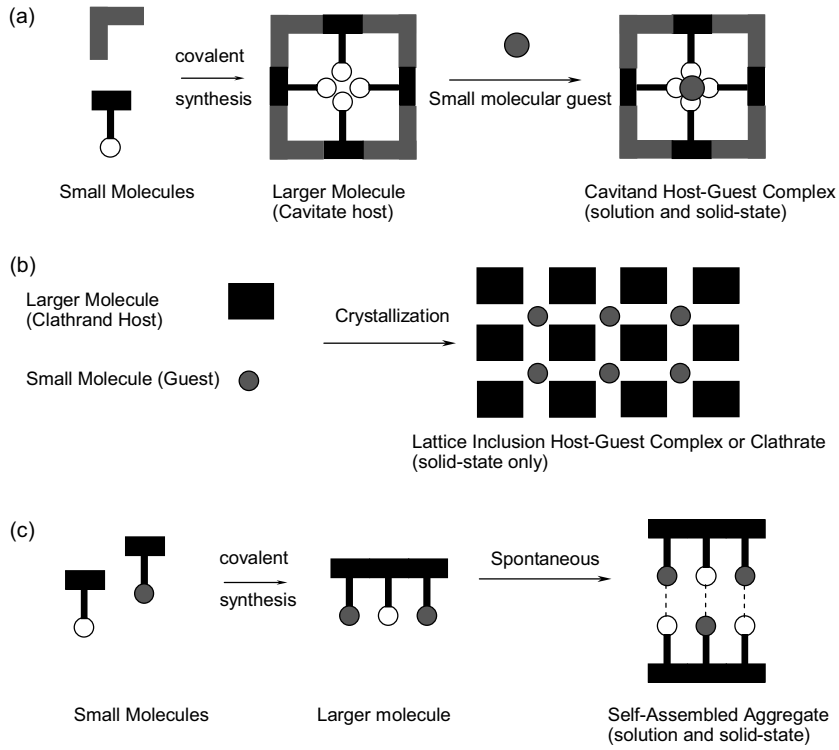


**Figure 1.2** Schematic illustrating the difference between a cavitate and a clathrate: (a) synthesis and conversion of a cavitand into a cavitate by inclusion of a guest into the cavity of the host molecule; (b) inclusion of guest molecules in cavities formed between the host molecules in the lattice resulting in conversion of a clathrand into a clathrate; (c) synthesis and self-assembly of a supramolecular aggregate that does not correspond to the classical host-guest description.

1. The recognition by Paul Ehrlich in 1906 that molecules do not act if they do not bind, '*Corpora non agunt nisi fixata*'; in this way Erlich introduced the concept of a biological receptor.
2. The recognition in 1894 by Emil Fischer that binding must be selective, as part of the study of receptor–substrate binding by enzymes. He described this by a *lock and key* image of steric fit in which the

**Table 1.2** Classification of common host–guest compounds of neutral hosts.

| Host | Guest | Interaction | Class | Example |
|---|---|---|---|---|
| Crown ether | Metal cation | Ion–dipole | Complex (cavitand) | $[K^+([18]crown–6)]$ |
| Spherand | Alkyl ammonium cation | Hydrogen bonding | Complex (cavitand) | Spherand$\cdot(CH_3NH_3^+)$ |
| Cyclodextrin | Organic molecule | Hydrophobic/ van der Waals | Cavitate | ($\alpha$–cyclodextrin)$\cdot$ ($p$–hydroxybenzoic acid) |
| Water | Organic molecule, halogen *etc.* | Van der Waals/ crystal packing | Clathrate | $(H_2O)_6\cdot(CH_4)$ |
| Calixarene | Organic molecule | Van der Waals/ crystal packing | Cavitate | ($p$–$t$–butylcalix[4]arene)$\cdot$ (toluene) |
| Cyclotriveratrylene (CTV) | Organic molecule | Van der Waals/ crystal packing | Clathrate | (CTV)$\cdot$0.5(acetone) |

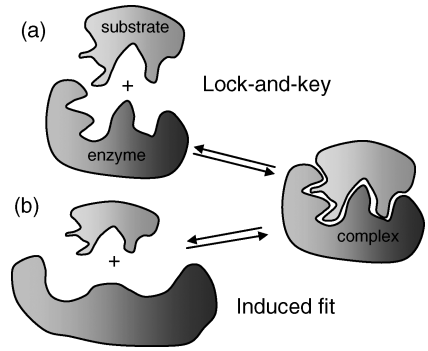


**Figure 1.3** (a) Rigid lock and key and (b) induced fit models of enzyme–substrate binding.

guest has a geometric size or shape complementarity to the receptor or host (Figure 1.3a). This concept laid the basis for *molecular recognition*, the discrimination by a host between a number of different guests.

3. The fact that selective binding must involve *attraction* or mutual affinity between host and guest. This is, in effect, a generalisation of Alfred Werner's 1893 theory of coordination chemistry, in which metal ions are coordinated by a regular polyhedron of ligands binding by dative bonds.

These three concepts arose essentially independently of one another and it was to be many years before the various disciplines in which they were born grew together to give birth to the highly interdisciplinary field of supramolecular chemistry. Ehrlich, for example, was working on the treatment of a range of infectious diseases. As part of his work he noticed that the dye methylene blue has a surprising affinity for some living cells, staining them an intense blue (his tutor Robert Koch had used methylene blue (**1.5**) to discover the tubercle bacillus, and Ehrlich had a ready supply of this synthetic dye from Farbwerke Hoechst, who had been manufacturing it since 1885). 'If only certain cells are coloured,' reasoned Ehrlich, 'then may there not be dyestuffs which colour only the carriers of illnesses and at the same time destroy them without attacking the body's own cells?' Ehrlich eventually went on to develop the arsenic-based anti-syphilis drug Salvarsan (arsphenamine, **1.6**) in 1910,[3] one of the most effective drugs known for that disease. In the process he became the founder of modern chemotherapy.

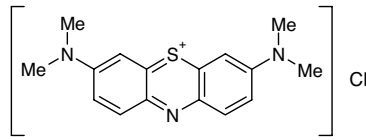


methylene blue

**1.5**

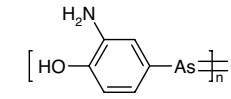


Salvarsan (arsphenamine)
n = typically 3 or 5

**1.6**

The marrying of the fields of coordination chemistry, chemotherapy and enzymology was finally spurred on by the advent of modern instrumental and synthetic techniques, and not least by the dramatic developments in organic synthesis, which was born as a discipline in itself in 1828 with Friedrich Wöhler's synthesis of urea from ammonium cyanate. In the course of the development of supramolecular chemistry, enormous progress has been made on quantifying the details of receptors with an affinity for guests which fit inside them. The lock and key image especially has suffered

successive waves of modification by the concepts of cooperativity, preorganisation and complementarity, solvation and the very definition of 'molecular shape' as we will see in the following sections. In particular, in enzyme catalysis, the lock-and-key image has been replaced by the 'induced fit' theory of Daniel Koshland[4] in which both enzyme and substrate (host and guest) undergo significant conformational changes upon binding to one another (Figure 1.3b). It is these conformational changes that allow the enzymatic catalytic rate acceleration since the substrate is commonly more like the reaction transition state in its bound form than in its unbound form. The occurrence of a conformational change upon guest binding is in fact a very common phenomenon both in biological chemistry, where it lies at the heart of 'trigger' processes such as muscle contraction and synaptic response, and in supramolecular chemistry.

## 1.4 Binding Constants

### 1.4.1 Definition and Use

Connors, K. A., *Binding Constants*, John Wiley & Sons, Ltd: Chichester, 1987.

The thermodynamic stability of a host-guest (*e.g.* metal–macrocycle) complex in a given solvent (often water or methanol) at a given temperature is gauged by measurement of the binding constant, $K$. Strictly the binding constant is dimensionless, but it is often calculated approximately using concentrations and thus has units of $dm^3\ mol^{-1}$, or $M^{-1}$, for a 1:1 complex. The binding constant is also known by the terms formation constant, $K_f$, association constant, $K_a$ or stability constant, $K_s$. In biological systems the dissociation constant, $K_d$, is commonly used. This quantity is the reciprocal of the binding constant and has units of concentration. The $K_d$ value is sometimes useful because it is a direct measure of the concentration below which a complex such as a drug-receptor complex will dissociate. The binding constant is the main method by which host-guest affinity in solution is assessed and so it is of fundamental importance in supramolecular chemistry and so it is worth spending some time looking into its proper definition and usage. Ignoring activity effects, the binding constant is merely the equilibrium constant for the reaction shown in Equation 1.1 (*e.g.* between a metal, M, and host ligand, L, in water):

$$M(H_2O)_n^{m+} + L \rightleftharpoons ML^{m+} + nH_2O \tag{1.1}$$

$$K = \frac{[ML^{m+}]}{[M(H_2O)_n^{m+}][L]} \tag{1.2}$$

Thus a large binding constant corresponds to a high equilibrium concentration of bound metal, and hence a more stable metal–macrocycle complex. Typical binding constants for crown ethers and alkali metal cations in water are in the range $10^1$–$10^2$. In methanol, this increases up to $10^6$ for $[K([18]crown-6)]^+$.* The binding constant for $K^+$ and [2.2.2]cryptand is about $10^{10}$. Some other examples are given in Table 1.3.

* Take care with square brackets. In equations square brackets are used to denote 'concentration of', however coordination chemists also use square brackets to denote a coordination complex ion, thus in a mathematical equation '$[ML^{m+}]$' means the 'concentration of the chemical species $ML^{m+}$'. If $ML^{m+}$ is a coordination complex ion, then it should be written outside an equation '$[ML]^{m+}$', *i.e.* a chemical entity comprising a metal of charge m+ and a ligand, L. The square brackets are useful because they always denote the ligands directly bound to the metal so, for example, $[Co(1,2\text{-diaminoethane})_2Cl_2]Br$ contains two $Cl^-$ ligands bound to Co(III) with a bromide counter anion balancing the overall charge, whereas $[Co(1,2\text{-diaminoethane})_2ClBr]Cl$ contains both Co–Cl and Co–Br bonds and a chloride counter anion.

**Table 1.3** Binding constants for a range of complexation processes.

| Guest | Host | Solvent | $K_{11}/M^{-1}$ | $\Delta G°/kJ\ mol^{-1}$ |
|---|---|---|---|---|
| $Na^+$ | $ClO_4^-$ | $H_2O$ | 3.2 | −3 |
| Iodine | Hexamethylbenzene | $CCl_4$ | 1.35 | −0.8 |
| Tetracyanoethylene | Hexamethylbenzene | $CH_2Cl_2$ | 17 | −7.1 |
| 7,7,8,8-Tetracyanoquinodimethane | Pyrene | $CH_2Cl_2$ | 0.94 | ~0.0 |
| Salicylic acid | Caffeine | $H_2O$ | 44 | −9.7 |
| Hydrocortisone | Benzoate ion | $H_2O$ | 2.9 | −2.5 |
| Methyl *trans*-cinnamate | Imidazole | $H_2O$ | 1.0 | 0.0 |
| *p*-Hydroxybenzoic acid | $\alpha$-Cyclodextrin | $H_2O$ | 1130 | −17.6 |
| Caffeine | Caffeine | $H_2O$ | 19 | −7.1 |
| Phenol | Dimethylformamide | $C_6H_6$ | 442 | −15.0 |
| $K^+$ | [18]crown-6 | $H_2O$ | 100 | −11.4 |
| $K^+$ | [18]crown-6 | Methanol | $10^6$ | −34.2 |
| $K^+$ | [2.2.2]cryptand | Methanol | $10^{10}$ | −57.0 |
| $Fe^{3+}$ | enterobactin | $H_2O$ | $10^{52}$ | −296 |

If a sequential process involving the binding of more than one metal ion is involved, then two $K$ values may be measured for the 1:1 and 1:2 complexes, respectively: $K_{11}$ and $K_{12}$ (*e.g.* binding of two $Na^+$ ions by dibenzo[30]crown-10).

$$M(H_2O)_n^{m+} + L \overset{K_{11}}{\rightleftharpoons} ML^{m+} + nH_2O \tag{1.3}$$

$$M(H_2O)_n^{m+} + ML^{m+} \overset{K_{12}}{\rightleftharpoons} M_2L^{(2m)+} + nH_2O \tag{1.4}$$

$$K_{12} = \frac{[M_2L^{(2m)+}]}{[M(H_2O)_n^{m+}][ML^{m+}]} \tag{1.5}$$

In these circumstances, an overall binding constant, $\beta_{12}$ may be defined for the overall process, the individual $K$ values are then known as the stepwise binding constants:

$$\beta_{12} = K_{11} \times K_{12} \tag{1.6}$$

$$\text{Or, more generally, } \beta_{xn} = \frac{[M_xL_n]}{[M]^x[L]^n} \tag{1.7}$$

Magnitudes of binding constants can vary widely, so they are often reported as log $K$, hence:

$$\log \beta_{12} = \log(K_{11} \times K_{12}) = \log K_{11} + \log K_{12} \tag{1.8}$$

The subscript numbers in stepwise binding constant notation refer to the ratio of one complexing partner to another, thus in a multi-step process the association of the host with the first guest might be denoted $K_{11}$, while the association of the resulting 1:1 complex with a further guest to produce a 1:2

complex has an equilibrium constant $K_{12}$ *etc.* Strictly speaking it is only possible to take a logarithm of a dimensionless quantity (*i.e.* logs can only come from a number, not something with units) but we have to remember that the strict definition of a binding constant is based on the activities of the chemical species, not their concentrations. The activity ($a$) of a chemical species, $i$, is its effective concentration for the purposes of mass action, $a_i = \gamma_i C_i / C_\Theta$ where $C_i$ is the concentration of $i$, $C_\Theta$ is equal to 1 mol dm$^{-3}$ if $C_i$ is given in mol dm$^{-3}$ and $\gamma_i$ is the *activity coefficient*, a factor that accounts for deviations from ideal behaviour. In approximate assessment of binding constants in supramolecular chemistry we make the approximation that $\gamma_i = 1$ and, activity (dimensionless) ≈ concentration.

Because binding constants are thermodynamic parameters, they are related to the free energy of the association process according to the Gibbs equation: $\Delta G^o = -RT \ln K$. (R = gas constant, 8.314 J K$^{-1}$ mol$^{-1}$, T = temperature in Kelvin) Thus the general affinity of a host for a guest under specific conditions (solvent, temperature *etc.*) may be given either in terms of $K$ or $-\Delta G^o$ values. In energy terms, complexation free energies may range from magnitudes of 20 to 100 kJ mol$^{-1}$ (5 to 25 kcal mol$^{-1}$; 1 kJ = 4.184 kcal) for alkali metal cation complexes. A large $K$ value of about $10^{10}$ corresponds to a $-\Delta G^o$ of about 57 kJ mol$^{-1}$ (13 kcal mol$^{-1}$). Some very general examples of the magnitudes of binding constants and their corresponding complexation free energies are given in Table 1.3.

Binding constants may also be defined in terms of the rate constants ($k$) of the complexation and decomplexation reactions:

$$M(H_2O)_n^{m+} + L \underset{k_{-1}}{\overset{k_1}{\rightleftharpoons}} ML^{m+} + nH_2O \tag{1.9}$$

$$K = \frac{k_1}{k_{-1}} \tag{1.10}$$

## 1.4.2 Measurement of Binding Constants

J. Polster and H. Lachmann, *Spectrometric Titrations*, VCH: Weinheim, 1989.

In principle, binding constants may be assessed by any experimental technique that can yield information about the concentration of a complex, [Host·Guest], as a function of changing concentration of the host or guest. In practice the following methods are in common use. In every case a concentration range must be chosen such that there is an equilibrium between significant amounts of bound and free host and guest, limiting the range of binding constants that can be measured by a particular technique. If binding by the target host is too strong then a competing host is sometimes added in order to reduce the apparent (measured) binding constant according to the difference in guest affinity between the two hosts. The true affinity can then be extrapolated from a knowledge of the binding constant of the guest for the host with the lower affinity.

### *Potentiometric Titration*

In the case of macrocycles that are susceptible to protonation (*e.g.* the cryptands with their basic tertiary amine nitrogen bridgeheads), the protonation constants (and hence p$K_a$ values) may be determined readily using pH (glass) electrodes to monitor a simple acid–base titration. Initially this will give the acid dissociation constant (p$K_a$) of the ligand's conjugate acid, HL$^+$).[5] Addition of a metal cation will perturb the macrocycle's basicity (ability to bind one or more protons) by competition between the metal ion and H$^+$ for the ligand lone pair(s) and hence will affect the shape of the titration curves.

$$K_a = \frac{[H^+][L]}{[HL^+]} \qquad HL^+ \underset{+\,H^+}{\overset{K_a\ -\,H^+}{\rightleftharpoons}} L \underset{-\,M^+}{\overset{K_{11}\ +\,M^+}{\rightleftharpoons}} ML^+ \underset{-\,M^+}{\overset{K_{12}\ +\,M^+}{\rightleftharpoons}} M_2L^+ \textit{ etc.}$$

**Scheme 1.1** Competing equilibria in a potentiometric titration.

Analysis of the various equilibria by a curve-fitting computer program (such as *Hyperquad*) along with knowledge of the ligand's p$K_a$ allows the determination of the amount of uncomplexed ligand and hence the concentration of the complex and the stability constants for the metal complexation reaction, Scheme 1.1

### *Nuclear Magnetic Resonance Titration*

If the exchange of complexed and uncomplexed guest is slow on the nuclear magnetic resonance (NMR) time scale, then the binding constant may be approximately evaluated under the prevailing conditions of concentration, temperature solvent *etc.* by simple integration of the NMR signals for bound and unbound host or guest. Most host–guest equilibria are fast on the (relatively slow) NMR spectroscopic time scale, however, and the chemical shift observed for a particular resonance (that is sensitive to the complexation reaction) is a weighted average between the chemical shift of the free and bound species. In a typical NMR titration experiment, small aliquots of guest are added to a solution of host of known concentration in a deuterated solvent and the NMR spectrum of the sample monitored as a function of guest concentration, or host:guest ratio. Commonly, changes in chemical shift ($\Delta\delta$) are noted for various atomic nuclei present (*e.g.* $^1$H in $^1$H NMR) as a function of the influence the guest binding has on their magnetic environment. As a result, two kinds of information are gained. Firstly, the location of the nuclei most affected may give qualitative information about the regioselectivity of guest binding (is the guest inside the host cavity?). More importantly, however, the shape of the titration curve (a plot of $\Delta\delta$ against added guest concentration, *e.g.* Figure 1.4) gives quantitative information about the binding constant. NMR spectroscopic methods are useful for binding constants in the range 10–$10^4$ $M^{-1}$. Such titration curves are often analysed by computer least-squares curve fitting (*e.g.* by a program such as EQNMR[6]) using Equation 1.14 to determine optimum values of $\delta_{mn}$ (chemical shift of each species present where mn is the ratio of host, H, and guest, G) and $\beta_{mn}$ (stepwise binding constant). The isotherm shown in Figure 1.4a fits a stoichiometry model involving both 1:1 and 1:2 host:guest complexes with log $\beta_{11}$ = 2.3 and log $\beta_{12}$ = 4.5. The plot also shows the relative percentage amounts of each species present in the solution for a given host and guest concentration.

$$\delta_{calc} = \sum_{m=1}^{m=i} \sum_{n=0}^{n=j} \frac{\delta_{mn}\beta_{mn}m[G]^m[H]^n}{[G]_{total}} \tag{1.11}$$

### *Method of Continuous Variation (Job Plots)*

A key aspect of such calculations is the use of the correct stoichiometry model (*i.e.* the ratio of host to guest, which must be assumed or determined). There is a strong bias in the supramolecular chemistry literature towards the fitting of data to 1:1 stoichiometries, and it is a common mistake to neglect higher aggregates. Binding stoichiometry may be confirmed in most kinds of titration experiments that allow the concentration of complex to be determined by making up a series of solutions with varying host:guest ratios such that the total concentration of host and guest is a constant. Monitoring the

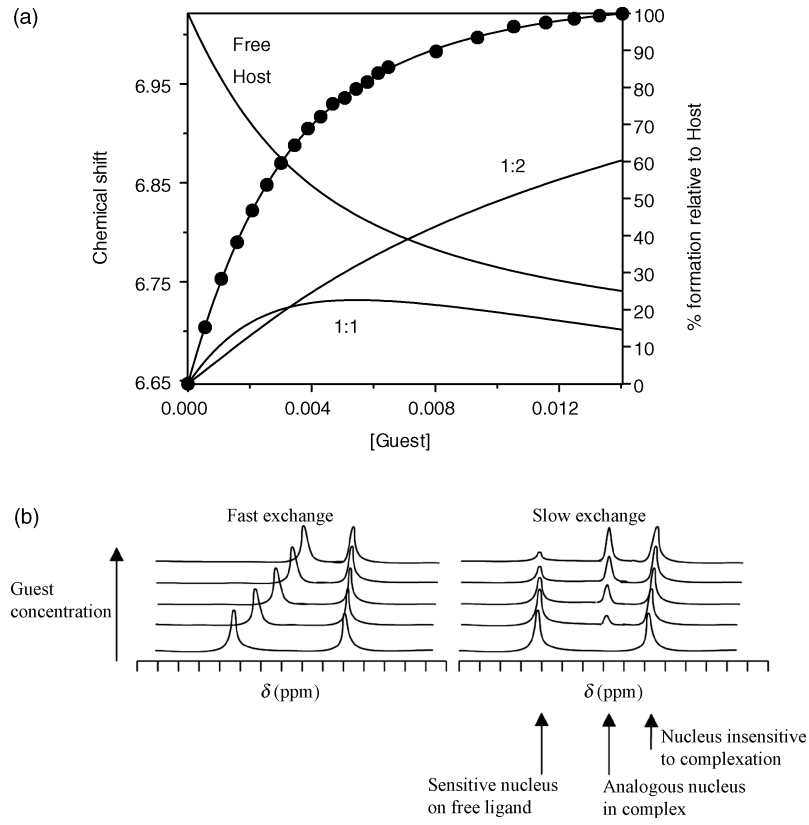


**Figure 1.4** (a) NMR titration plot (isotherm) and corresponding speciation plots for a system undergoing fast equilibration on the NMR time scale, with log $\beta_{11} = 2.3$ and log $\beta_{12} = 4.5$. (b) Schematic NMR spectra of slowly equilibrating mixtures of free host, guest and host–guest complex.

changing concentration of the host–guest complex in these samples allows a plot of [Complex] against ([Host]/([Host] + [Guest])) to be constructed. For a 1:1 complex, this kind of representation (referred to as a Job plot) should give a peak at 0.5 (Figure 1.5), a peak at 0.66 would correspond to a 2:1 stoichiometry and so on. The concentration of the complex is generally taken to be related to an observable quantity such as $\Delta\delta$ according to Equation 1.12. In a spectrophotometric experiment absorbance at a properly chosen wavelength is usually directly proportional to complex concentration.

$$[\text{Complex}] \propto \Delta\delta \times \text{mole fraction of host} \tag{1.12}$$

### *Fluorescence Titration*

Fluorescence titration measurements are based on the proportion of fluorescence intensity to fluorophore concentration (concentration of fluorescent species in solution; this is often a fluorescent guest, G). For a 1:1 complex with host, H, with stability constant $K_{11} = [\text{HG}]/[\text{H}][\text{G}]$ the fluorescence intensity $F$ is given by:

$$F = k_{\text{G}}[\text{G}] + k_{11}[\text{HG}] \tag{1.13}$$

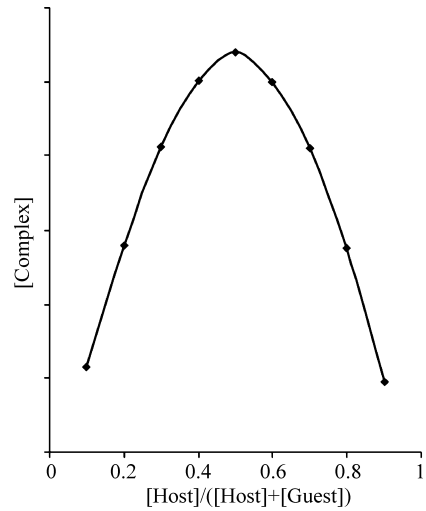


**Figure 1.5** Job plot for a 1:1 host–guest complex.

where $k_G$ and $k_{11}$ represent proportionality constants for the guest and the 1:1 host–guest complex respectively. In the absence of host the fluorescence intensity, $F_o$, is given by:

$$F_o = k_G^o G_{total} \tag{1.14}$$

where $G_{total} = [G] + [HG]$.

Combining these two relationships gives Equation (1.15), which provides the basis for most fluorimetric methods for stability constant ($K_{11}$) determination:

$$\frac{F}{F_o} = \frac{k_G/k_G^o + (k_{11}/k_G^o)K_{11}[H]}{1 + K_{11}[H]} \tag{1.15}$$

This equation is greatly simplified for cases where either the guest or host–guest complex are non-fluorescent (*i.e.* the fluorescence is 'turned on' by complexation, or in the case of quenching by the host), in which case either $k_G$ or $k_{11}$ become zero. For example, for $k_G = k_G^0$ and $k_{11} = 0$, we obtain:

$$\frac{F_o}{F} = 1 + K_{11}[H] \tag{1.16}$$

A simple plot of $F_o/F$ against [H] from titration of the quenching host into a guest solution should yield a straight line of slope $K_{11}$. Common fluorescent guests such as 8-anilino-1-naphthalenesulfonate (ANS, **1.7**) may be used to probe complexation ability of various hosts in this way.

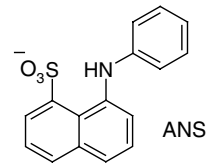


**1.7**

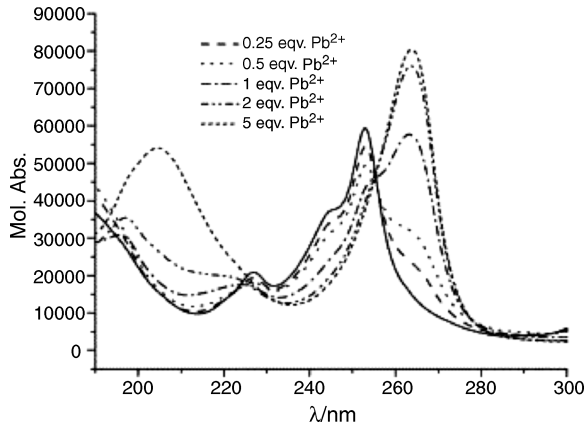


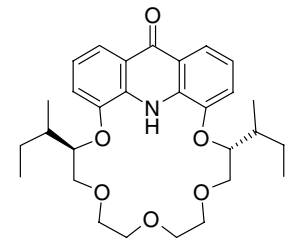


**1.8**

**Figure 1.6** UV-monitored titration of a diisobutyl-substituted acridono-18-crown-6 ligand **1.8** with $Pb^{2+}$ showing an isosbestic point at 271 nm (solid line represents free ligand spectrum, reproduced from [7] with permission from Elsevier).

### *UV-Vis Spectrophotometric Titration*

UV-Vis spectroscopic titration (or spectrophotometric titration) involves monitoring the intensity of a electronic absorption band at a particular wavelength that is characteristic of either the complex or free host or guest and is closely analogous to fluorescence titration methods. A plot is generated of absorbance intensity *vs.* concentration of added guest to a solution of constant host concentration. Software such as the program *Specfit*® can then be used, in conjunction with an appropriate stoichiometry model, to extract the binding constant(s). Both fluorescent and UV-Vis spectroscopic methods have the advantage over NMR methods that they are more sensitive and hence lower concentrations of host and guest can be used. Unlike fluorescence methods, the observation of one or more clear isosbestic points is common in absorption spectroscopic titrations. An isosbestic point is where the observed absorption intensity is constant throughout the titration. The observation of an isosbestic point is good evidence for the conversion of free host into complex without the involvement of significant intermediate species. Figure 1.6 shows the observed UV-Vis spectra during a titration of a diisobutyl-substituted acridono-18-crown-6 ligand **1.8** with $Pb^{2+}$. The isosbestic point occurs at at 271 nm.[7]

### *Calorimetric Titration*

Calorimetric titration, also known as isothermal titration calorimetry (ITC), involves careful measurement of the heat (enthalpy) evolved from a carefully insulated sample as a function of added guest or host concentration. The gradient of the ITC curve can be fitted to determine the binding constant and hence $\Delta G_{complex}$. Integration of the total area under the ITC plot gives the complexation enthalpy ($\Delta H_{complex}$) and hence the technique can give a measurement of all thermodynamic parameters of the system since $\Delta G_{complex} = \Delta H_{complex} - T\Delta S_{complex}$. ITC is useful for determination of binding constants that range from *ca.*$10^2 - 10^7$ $M^{-1}$. ITC has been used in an interesting case study to probe solvent and counter-cation effects on the binding of anions such as chloride to calix[4]pyrrole, **1.9** (Section 4.6.4).[8] Figure 1.7 shows the ITC data and resulting fit for the binding of $NBu_4^+Cl^-$ by **1.9** in nitromethane, giving $K_{11}$ = 19,200 $M^{-1}$, $\Delta G$ = 11.3 kJ $mol^{-1}$, $\Delta H$ = 8.55 kJ $mol^{-1}$ and $\Delta S$ = −9.1 J $K^{-1}$ $mol^{-1}$.

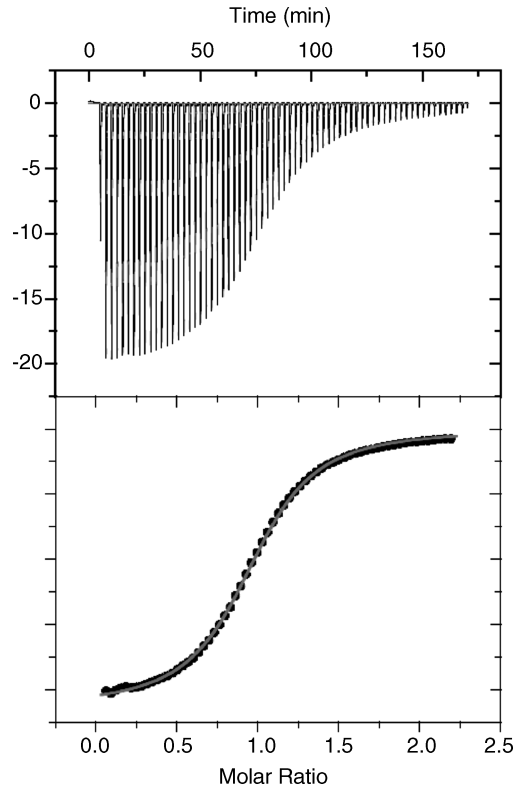


**1.9**

**Figure 1.7** ITC data at 25 °C for the binding of $NBu_4^+Cl^-$ by **1.9** in nitromethane – the top plot represents the raw data with the calorimetric response in μcal $s^{-1}$ for each addition of $NBu_4^+Cl^-$ while the lower plot is the titration isotherm fitted to a 1:1 model with kcal per mol $NBu_4^+Cl^-$ added *vs.* mole ratio of $NBu_4^+Cl^-$ to **1.9**. (Reproduced with permission from [8] © 2006, American Chemical Society).

### *Extraction Experiments*

The distribution (or partition) coefficient, $K_d$, of a metal cation between an aqueous (aq) and organic (org) phase may also be used to assess the selectivity of a given host for a range of metal cations under standard conditions, using the equilibrium constants ($K$) for the following processes (Equations 1.17–1.20) (for metal picrate (Pic) salt, water (aq) and water-saturated chloroform (org) phases, 25 °C).

$$[M^+ \cdot Pic^-]_{org} + [Host]_{org} = [M^+ \cdot Host \cdot Pic^-]_{org} \quad K_{11} \text{ (binding constant)} \tag{1.17}$$

$$[M^+]_{aq} + [Pic^-]_{aq} + [Host]_{org} = [M^+ \cdot Host \cdot Pic^-]_{org} \quad K_e \text{ (extraction constant)} \tag{1.18}$$

$$[M^+]_{aq} + [Pic^-]_{aq} = [M^+ \cdot Pic^-]_{org} \quad K_d \text{ (distribution coefficient)} \tag{1.19}$$

$$K_{11} = K_e / K_d \tag{1.20}$$

The concentration of picrate anion (and hence necessarily $M^+$ by charge balance) is determined by measurement of the electronic absorbance (380 nm) of each layer. The host is assumed to be essentially insoluble in the aqueous layer. The technique is of relatively low precision but is quick and lends itself readily to the screening of a wide range of compounds. It is suitable for measurement of binding free

energies in the range 25–70 kJ mol$^{-1}$ (*i.e.* binding constants of *ca.* $10^4$–$10^{12}$). Binding energies in excess of 70 kJ mol$^{-1}$ are assessed by competition with hosts of known binding energy.

## 1.5 Cooperativity and the Chelate Effect

Hancock, R. D., 'Chelate ring size and metal ion selection', *J. Chem. Ed.*, 1992, **69**, 615–621; Ercolani, G., 'Assessment of cooperativity in self-assembly', *J. Am. Chem. Soc.*, 2003, **125**, 16097–16103.

Much of the emphasis in the construction of supramolecular host molecules concerns bringing about summative or even multiplicative interactions. This means that we can construct a stable host–guest complex using (often weak) non-covalent interactions if we ensure that there are as many as possible of these interactions stabilising the complex. The small amount of stabilisation energy gained by any one such interaction when added to all the other small stabilisations from the other interactions (*summative*) results in a significant binding energy and hence complex stability. In some cases, the interaction of the whole system is synergically greater than the sum of the parts (multiplicative). When two or more binding sites (A and B) on a host cooperate in this fashion to bind to a guest the phenomenon is termed *cooperativity*. If the overall stability of the complex is greater than the sum of the energies of the interaction of the guest with binding groups A and B individually then the result is *positive cooperativity*. On the other hand, if unfavourable steric or electronic effects arising from the linking of A and B together into one host cause the overall binding free energy for the complex to be less than the sum of its parts then the phenomenon is termed *negative cooperativity*. Binding site cooperativity in a supramolecular host-guest interaction is simply a generalisation of the *chelate effect* found in classical coordination chemistry.

In energy terms the cooperativity arising from the chelate effect, or more generally from the interaction of a two-binding-site guest (A–B), with a bidentate host can be expressed in terms of the overall binding free energy $\Delta G_{AB}{}^{o}$ which is equal to the sum of the intrinsic binding free energies of each component A and B ($\Delta G_A{}^{i}$ and $\Delta G_B{}^{i}$) plus a factor arising from the summation or connection of A and B ($\Delta G^{s}$), Equation 1.21.[9]

$$\Delta G_{AB}{}^{o} = \Delta G_A{}^{i} + \Delta G_B{}^{i} + \Delta G^{s} \tag{1.21}$$

The intrinsic binding energy represents the energy group A or B imparts to the rest of the molecule assuming there are no unfavourable strain or entropy components introduced into the binding by the linking of the group with the rest of the molecule, *i.e.* Equation 1.22 (and similarly for component B)

$$\Delta G_A{}^{i} = \Delta G_{AB}{}^{o} - \Delta G_B{}^{o} \tag{1.22}$$

we can thus write Equation 1.23 which shows that the connection energy is equal to the sum of the separate affinities of the isolated ligands A or B minus the binding free energy of the connected molecule.

$$\Delta G^{s} = \Delta G_A{}^{o} + \Delta G_B{}^{o} - \Delta G_{AB}{}^{o} \tag{1.23}$$

Equation 1.23 can be used to give an empirical measure of the cooperativity, since equilibrium constants ($K$) for the binding of A, B and A-B by a host can be measured and related to the Gibbs free energy according to $\Delta G^{o} = -RT \ln K$. If $\Delta G^{s}$ is negative then the binding sites A and B exhibit unfavourable negative cooperativity. A positive value for $\Delta G^{s}$ implies a favourable positive cooperativity.

The chelate effect is well known in coordination chemistry and relates to the observation that metal complexes of bidentate ligands (such as 1,2-diaminoethane, en) are significantly more stable than closely

related materials that contain unidentate ligands (such as ammonia). For example, in the reaction shown in Equation 1.24, the value of the equilibrium constant for the replacement of ammonia with 1,2-diaminoethane indicates that the 1,2-diaminoethane chelate complex is more than $10^8$ times more stable.

$$[Ni(NH_3)_6]^{2+} + 3NH_2CH_2CH_2NH_2 \xrightarrow{\log K = 8.76} [Ni(NH_2CH_2CH_2NH_2)_3]^{2+} + 6NH_3 \quad (1.24)$$

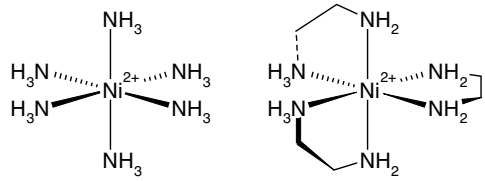

$[Ni(NH_3)_6]^{2+}$ $[Ni(en)_3]^{2+}$

**1.10** **1.11**

The special stability of chelate complexes in solution may be traced to both thermodynamic and kinetic effects. Thermodynamically, reaction of a metal with a chelating ligand results in an increase of the number of free particles (four on the left-hand side of Equation 1.24, seven on the right) and hence a favourable entropy contribution ($\Delta S^o$) to the overall free energy of the reaction ($\Delta G^o$), given by $\Delta G^o = \Delta H^o - T\Delta S^o$. In addition, clever design of the macrocycle to maximise conformational and electrostatic aspects of ligand–metal interactions can result in a favourable enthalpy of reaction as well. The entropic contribution is reinforced further by a statistical aspect, since in order for the chelate complex to dissociate, both of the metal–donor atom bonds must be broken simultaneously. Finally, kinetic effects are involved in the formation of the chelate complex. It is likely that the reaction of the metal with a ligand, L, proceeds at a similar rate to the binding of the first donor atom of a chelating ligand, L-L. The binding of the second donor atom of L-L proceeds much more rapidly, however, because in its 'tethered' state it has a much higher effective concentration than a second molecule of unidentate L.

While an experimental fact in solution coordination chemistry, the nature of the chelate effect has been the topic of much debate in the literature. The first problem concerns the definition of the stability constants; the second stepwise stability constant $\beta_{12}$ for the binding of two unidentate ligands (when calculated using concentrations instead of activities) does not have the same dimensions as the first stability constant for the bidentate ligand with which it is being compared. As a result, the influence of the solvent concentration is neglected. When this difference is taken into account by converting concentrations as mole fractions (*i.e.* concentration in mol $dm^{-3}$/concentration of solvent), the chelate effect almost disappears. Furthermore, measurements of gas phase stability also indicate little difference between comparable chelate and non-chelate complexes. Nevertheless it is a fact that, in the solution phase at least, chelate ligands will almost invariably displace their monodentate analogues.

The stabilisation afforded by the chelate effect is highly dependent on the size of the chelate ring (Figure 1.8). Five-membered rings, as in metal complexes of 1,2-diaminoethane, are often the most

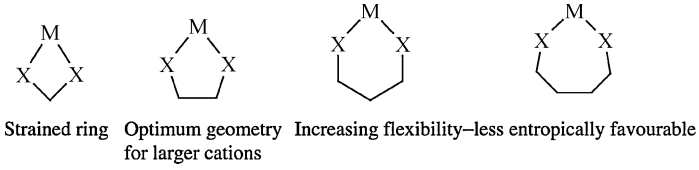


**Figure 1.8** Ring size dependence of the stabilisation offered by the chelate effect.

stable by far because they contain the least amount of ring strain, particularly for larger cations. Four-membered rings (*e.g.* chelating acetate) are highly strained, while as the chelate rings size increases the statistical likelihood of two donor atoms pointing directly at the metal becomes increasingly less probable, resulting in an unfavourable entropy. The strain energy in the chelate ring is dependent on the size of the metal cation, however. For very small cations such as $Li^+$ and $Be^{2+}$, six-membered chelate rings are common because the small cation results in cation–donor bond lengths similar to those found in unstrained six-membered ring molecules such as cyclohexane.

In supramolecular chemistry, the thermodynamic stability of a host–guest complex may be enhanced by the operation of a chelate effect giving rise to positive cooperativity. The ligand donor atoms are generalised to host binding sites (of whatever nature) and the metal is generalised to the guest (which indeed often is a metal cation, although guests may also be anions or neutral species). The operation of the chelate effect is observed in the binding of metal cations by *podands* — chain-like hosts with a number of donor atoms situated at intervals along their length as in **1.12** (see Section 3.3.1) and, more generally, positive binding site cooperativity is similarly observed in hydrogen bonded complexes such as receptor **1.13** which selectively binds citrate anion through multiple hydrogen bonding interactions.[10] Another good example of cooperativity is seen in the drug-receptor complex **1.14** formed between the new generation antibiotic vancomycin and proteins that are used in the synthesis of bacterial cell walls.[9] The proteins end in the sequence D-alanine-D-alanine which form numerous hydrogen bonded and hydrophobic contacts to the drug (Figure 1.9).

In addition to cooperativity between two or more host binding sites in binding a single guest we can also recognise both positive and negative cooperativity in the binding of multiple guests by a single host, multiple ligands by a single metal or in multi-component self-assembly processes. Multi-component self-assemblies are complicated by the occurrence of both intra- and inter-molecular associations, however, and simple binding models are not appropriate. This issue is of considerable relevance in highly topical self-assembled, multi-component metal complexes and we will look at models for these processes further in Section 10.4. Cooperativity in cases where the binding of a first guest influences (particularly enhances) the affinity of a host for a second guest at a remote site is termed an *allosteric effect*. A good example is shown in Scheme 1.2.[11] Here a binding of Ru(II) to the bipyridyl portion of the host changes its conformation by rotation about the pyridyl-pyridyl bond to create a cavity suitable for chelating an alkali metal cation such as $Na^+$. Similarly binding of $Na^+$ to the polyether site predisposes (*preorganises* – see Section 1.6) the bipyridyl portion for Ru(II) binding. The strength of

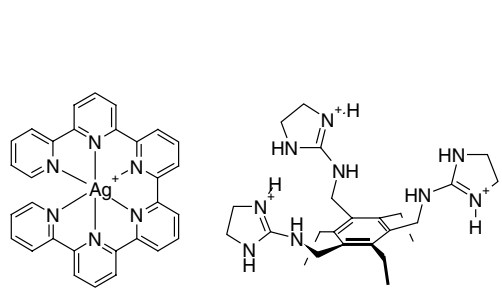

**1.12**



**1.13**

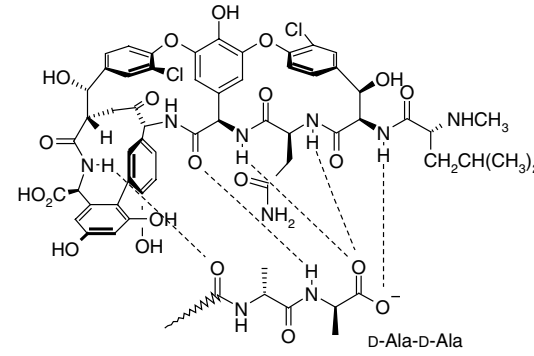


**1.14**

**Figure 1.9** Supramolecular host–guest complexation stabilised by positive cooperativity between binding sites: $Ag^+$ binding by **1.12**, a host for citrate anion (**1.13**) and a drug-receptor complex formed by vancomycin (**1.14**).

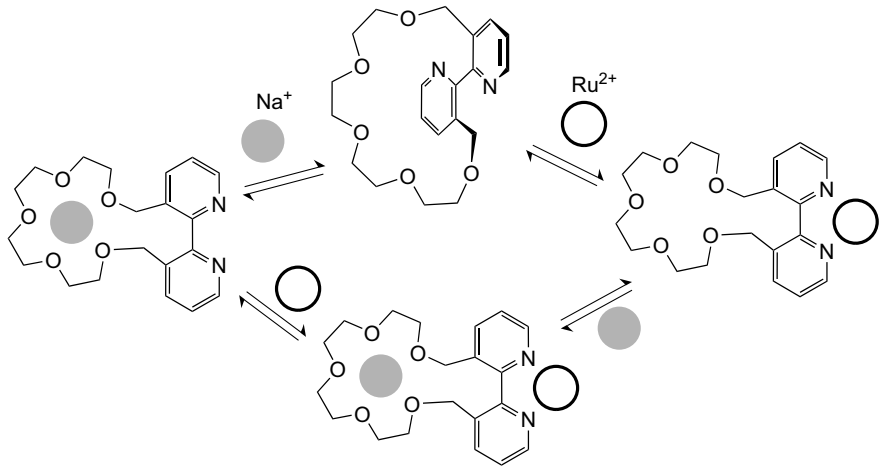


**Scheme 1.2** Allosteric (cooperative) enhancement of $Na^+$ binding by preorganisation of the polyether binding site by Ru(II), and *vice versa*.[11]

the sequential binding of the two metal cations can be quantified by the binding constants $K_{11}$ and $K_{12}$. The allosteric effect means that $K_{12}$, the affinity for the second cation, is always greater than the $K_{11}$ binding constant for that same cation alone, in the absence of the other metal. Allosteric effects are very important in biological systems, particularly in the case of the bonding of $O_2$ by haemoglobin (see Section 2.5).

Cooperativity may be recognised by the deviation from well-defined statistical relationships. Consider again the interaction of two binding sites –A and –B capable only of interaction with one another to give a species –A·B– in a reaction with the microscopic interaction equilibrium constant $K_{inter}$ (*i.e.* the equilibrium constant for the individual reaction step). We can examine the equilibria shown in Scheme 1.3 for a metal, M, with *m* identical binding sites of type –B (for example *m* would be the metal's coordination number) involved in a series of equilibria binding a number of ligands, L, each with a unique binding site –A.

On statistical grounds it can be shown that Equation 1.25 holds true. Equation 1.25 implies that the binding constant for each added ligand is less than the previous one. In fact successive equilibrium

$$M + L \overset{K_1}{\rightleftharpoons} ML$$

$$ML + L \overset{K_2}{\rightleftharpoons} ML_2$$

$$\downarrow$$

$$ML_{i-1} + L \overset{K_i}{\rightleftharpoons} ML_i$$

$$\downarrow$$

$$ML_{m-1} + L \overset{K_m}{\rightleftharpoons} ML_m$$

**Scheme 1.3** Equilibrium constants ($K$) for multiple ligands (L) binding to a single metal (M) *via* a binding site on the ligand termed 'A' interacting with a binding site on the metal termed 'B'.

constants decrease by a factor of at least a half as more ligands are added because of the increasing likelihood of displacing a ligand if there are more of them. This effect is evident for example, in the stability constants for the successive reaction of $[Ni(H_2O)_6]^{2+}$ with six molecules of $NH_3$: log $K_{1-6}$ = 2.80, 2.24, 1.73, 1.19, 0.75, 0.03.

$$K_i = K_{\text{inter}}(m - i + 1)/i \tag{1.25}$$

$$\frac{K_{i+1}}{K_i} = \frac{i(m-i)}{(i+1)(m-i+1)} \tag{1.26}$$

From Equation 1.25 we can derive Equation 1.26. The quantity $K_{i+1}/K_i$ may be used as a measure of cooperativity. If the statistical relationship shown in Equation 1.26 holds true the system is non-cooperative. If $K_{i+1}$ / $K_i$ is higher than would be expected from Equation 1.26 the system exhibits positive cooperativity, whereas if it is lower the system exhibits negative cooperativity and the binding of one ligand inhibits the binding of the next. Experimentally, cooperativity is often assessed by graphical methods based on a parameter $r$ (Equation 1.27), known as the *occupancy*, *i.e.* the average number of occupied binding sites, in this case on the metal, M.

$$r = \frac{\sum_{i=1}^{m} i\beta_i[\text{L}]^i}{1 + \sum_{i=1}^{m} \beta_i[\text{L}]^i} \tag{1.27}$$

Where $\beta_i$ represents the stepwise stability constants and [L] is the concentration of *free* ligand. If the system is non-cooperative (*i.e.* Equation 1.26 holds true) then Equation 1.27 becomes Equation 1.28:

$$r = \frac{mK_{\text{inter}}[\text{L}]}{1 + K_{\text{inter}}[\text{L}]} \tag{1.28}$$

Equation 1.28 can be put into two alternate linear forms known as the Scatchard (1.29) and Hill (1.30) equations.

$$\frac{r}{[\text{L}]} = -K_{\text{inter}}r + mK_{\text{inter}} \tag{1.29}$$

$$\log\left(\frac{r}{m-r}\right) = \log[\text{L}] + \log K_{\text{inter}} \tag{1.30}$$

A Scatchard plot is thus a plot of $r$/[L] as a function of $r$ and appears as a straight line for non-cooperative systems, a convex curve for negative cooperativity and a concave curve for positive cooperativity. A Hill plot is a plot of $\log[r/(m - r)]$ *vs.* log[L]. Cooperativity results in two straight lines connected by a S-shaped curve. The value of the slope in the central region of the curve is called the Hill coefficient ($n_{\text{H}}$). A value of $n_{\text{H}} > 1$ indicates positive cooperativity, while systems exhibiting negative cooperativity have $n_{\text{H}} < 1$. Hill and Scatchard plots for the binding of ammonia to $Ni^{2+}$ are shown in Figure 1.10. The value of the Hill coefficient of 0.59 and the convex shape of the curve indicates that the process exhibits negative cooperativity, as exemplified in the binding constants which are lower even than would be expected from a statistical effects. A word of warning, however, Cooperativity can *only* be assessed in this way for *intermolecular* processes involving the binding of multiple guests to a single host (*e.g.* multiple metal ions to a protein, multiple ligands to a metal). Multimolecular self-assembly that mixes

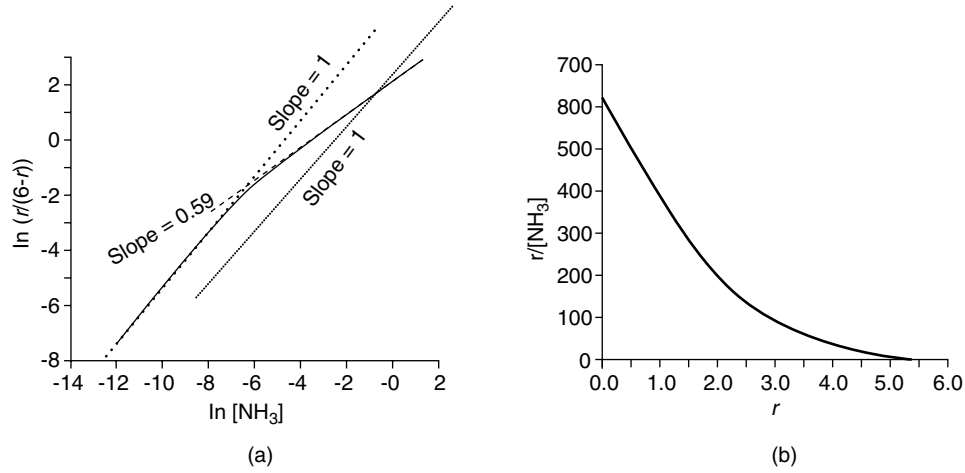


**Figure 1.10** (a) Hill plot and (b) Scatchard plot for the successive intermolecular connections of ammonia to bivalent nickel to give $[Ni(NH_3)_i]^{2+}$, the concentration of the free ligand [L] is computed by using the known stability constants. $[Ni]_{total} = 1 \times 10^{-3}$ M; $[NH_3]_{total}$ varies between $10^{-5}$ and 1 M. (Reproduced from [12] by permission of the Royal Society of Chemistry).

intra- and intermolecular processes requires a different treatment (Section 10.4) and this distinction has resulted in many erroneous claims of positive cooperativity in the literature.[12]

## 1.6 Preorganisation and Complementarity

Cram, D. J., 'Preorganisation – from solvents to spherands', *Angew. Chem., Int. Ed. Engl.* 1986, **25**, 1039–1134.

Many supramolecular host–guest complexes are even more stable than would be expected from cooperative / chelate effects alone. The hosts in these species are usually macrocyclic (large ring) ligands that chelate their guests, again *via* a number of binding sites. Such compounds are stabilised additionally by what is traditionally termed the *macrocyclic effect*. This effect relates not only to the chelation of the guest by multiple binding sites, but also to the *organisation* of those binding sites in space prior to guest binding (*i.e. preorganisation*) such that binding energy is not expended in the guest having to 'wrap' the host about itself in order to benefit from the most chelation. Furthermore the enthalpic penalty associated with bringing donor atom lone pairs into close proximity to one another (with consequent unfavourable repulsion and desolvation effects) has been 'paid in advance' during the synthesis of the macrocycle. This makes macrocycles difficult to make but stronger complexing agents than analogous non-macrocyclic hosts (podands). Some of the 'tricks' in macrocycle synthesis are discussed in Section 3.9 The macrocyclic effect makes cyclic hosts such as *corands* (*e.g.* crown ethers) up to a factor of $10^4$ times more stable than closely related acyclic *podands* with the same type of binding sites. The macrocyclic effect was first elucidated by Cabbiness and Margerum in 1969 who studied the Cu(II) complexes **1.15** and **1.16**.[13] Both ions benefit from the stability associated with four chelating donor atoms. However, the macrocyclic complex **1.15** is about $10^4$ times more stable than the acyclic analogue **1.16** as a consequence of the additional preorganisation of the macrocycle.

Thermodynamic measurements on the analogous (unmethylated) $Zn^{2+}$ complexes reveal that the stabilisation by macrocyclic preorganisation has both enthalpic and entropic contributions (Table 1.4).

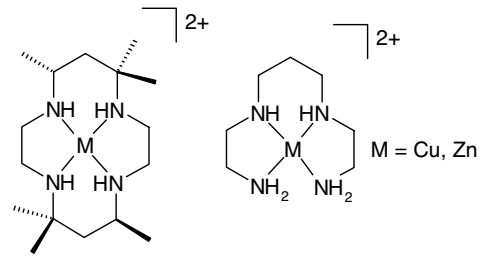


**1.15** **1.16**

The enthalpic term arises from the fact that macrocyclic hosts are frequently less strongly solvated than their acyclic analogues. This is because they simply present less solvent-accessible surface area. As a result there are fewer solvent–ligand bonds to break than in the extended, acyclic case. Entropically, macrocycles are less conformationally flexible and so lose fewer degrees of freedom upon complexation. In general, the relative importance of the entropic and enthaplic terms varies according to the system studied although the enthalpy is frequently dominant as a result of additional factors such as lone pair repulsions. Bicyclic hosts such as *cryptands* (Section 3.4) are found to be even more stable than monocyclic *corands* for much the same reasons. Historically this further additional stability is referred to as the *macrobicyclic effect* (Figure 1.11) and simply represents the more rigid, preorganised nature of the macrobicycle. The macrocyclic and macrobicyclic effects make an important contribution to hosts for alkali metal binding, (Scheme 1.4 and Section 3.7).

The macrocyclic and macrobicyclic effects are simply manifestations of increasing *preorganisation*. We can say that if a host molecule does not undergo a significant conformational change upon guest binding, it is *preorganised*. Host preorganisation is a key concept because it represents a major (in some cases decisive) enhancement to the overall free energy of guest complexation. Neglecting the effects of solvation, the host guest binding process may be divided very loosely into two stages. First, there is an activation stage in which the host undergoes conformational readjustment in order to arrange its binding sites in the fashion most complementary to the guest and at the same time minimising unfavourable interactions between one binding site and another on the host. This is energetically unfavourable, and because the host must remain in this binding conformation throughout the lifetime of the host–guest complex, this energy is never paid back. Following rearrangement, binding occurs which is energetically favourable because of the enthalpically stabilising attraction between mutually complementary binding sites of host and guest. The overall free energy of complexation represents the difference between the unfavourable reorganisation energy and the favourable binding energy. If the reorganisation energy is large, then the overall free energy is reduced, destabilising the complex. If the host is preorganised, this rearrangement energy is small.

The corollary of preorganisation is in the guest binding kinetics. Rigidly preorganised hosts may have significant difficulty in passing through a complexation transition state and so tend to exhibit slow guest binding kinetics. Conformationally mobile hosts are able to adjust rapidly to changing conditions,

**Table 1.4** Thermodynamic parameters for $Zn^{2+}$ complexes of **1.15** and **1.16** (298 K).

| | **1.15** | **1.16** |
|---|---|---|
| Log $K$ | 15.34 | 11.25 |
| $\Delta H^{o}$ (kJ mol$^{-1}$) | –61.9 | –44.4 |
| $-T\Delta S^{o}$ (kJ mol$^{-1}$) | –25.6 | –19.8 |

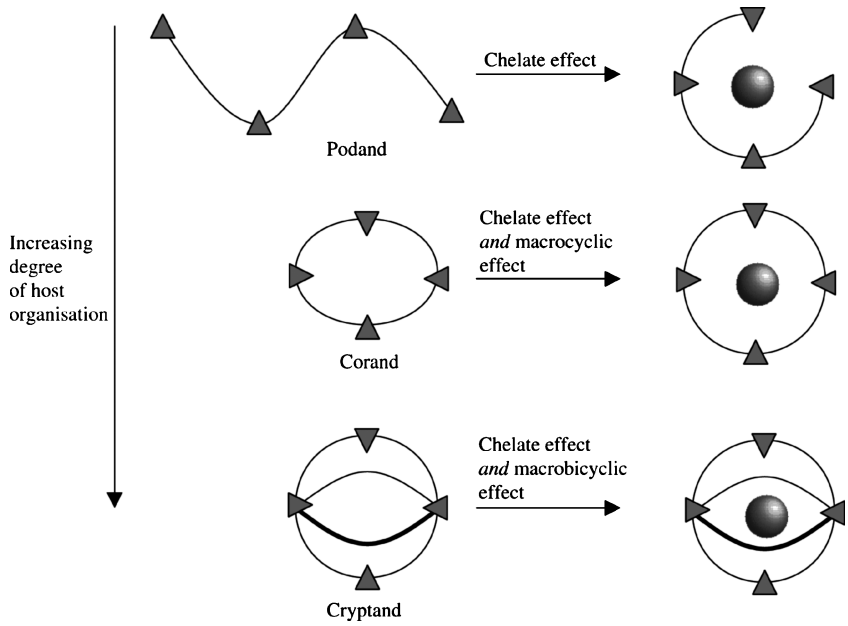


**Figure 1.11** The chelate, macrocyclic and macrobicyclic effects.

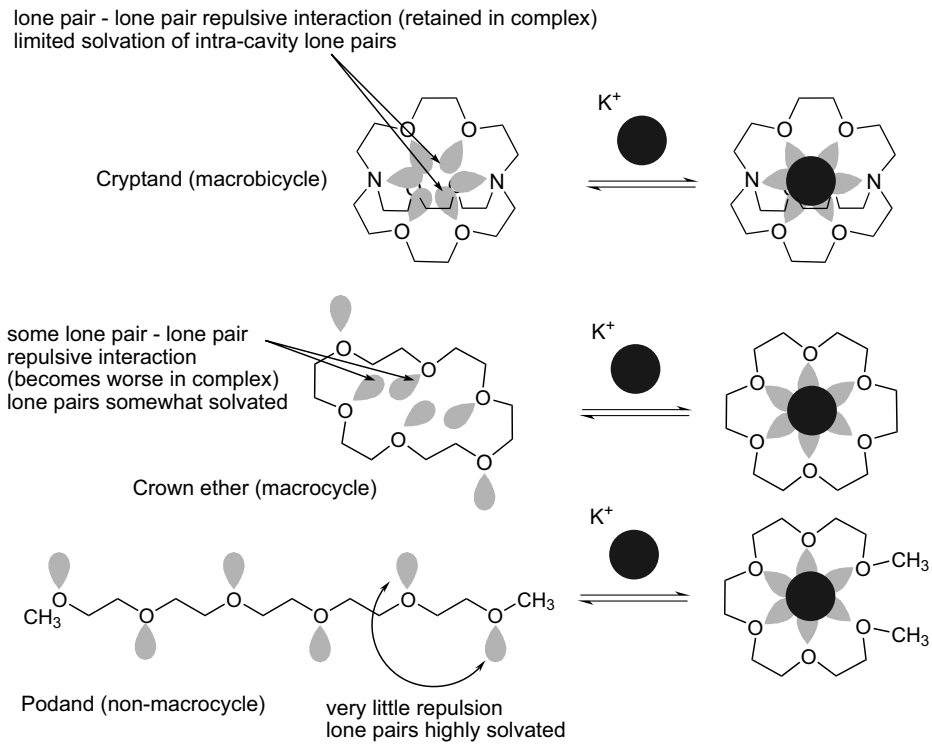


**Scheme 1.4** Comparison of preorganisation effects in $K^+$ binding by a macrobicycle, macrocycle and non-preorganised podand pentaethyleneglycol dimethyl ether.

and both complexation and decomplexation are rapid. Solvation enhances the effects of preorganisation since the solvation stabilisation of the unbound host is often greater than the case when it is wrapped around the guest, effectively presenting less surface area to the surrounding medium.

In addition to the degree of host preorganisation, the other principal factor in determining the affinity of a host for a guest is *complementarity*. In order to bind, a host must have binding sites that are of the correct electronic character (polarity, hydrogen bond donor/acceptor ability, hardness or softness *etc.*) to complement those of the guest. Hydrogen bond donors must match acceptors, Lewis acids must match Lewis bases and so on. Furthermore, those binding sites must be spaced out on the host in such a way as to make it possible for them to interact with the guest in the binding conformation of the host molecule. If a host fulfils these criteria, it is said to be *complementary*. The principle of complementarity has been summed up by Donald Cram: 'To complex, hosts must have binding sites which cooperatively contact and attract binding sites of guests without generating strong nonbonded repulsions.'

The combined effects of preorganisation and complementarity are startlingly illustrated by a comparison of the binding constants under standard conditions for the alkali metal complexes shown in Figure 1.12. All of the hosts bind through six ether oxygen atoms. The fairly hard (non-polarisable) oxygen donors are complementary to fairly hard alkali metal cations such as $K^+$. However, the stability constants range over nearly 14 orders of magnitude, reflecting the increasing preorganisation of the oxygen atom donor array. The amine nitrogen atoms in some hosts do not significantly enhance the binding because the softer amine is not complementary for alkali metal cations. Thus replacing two

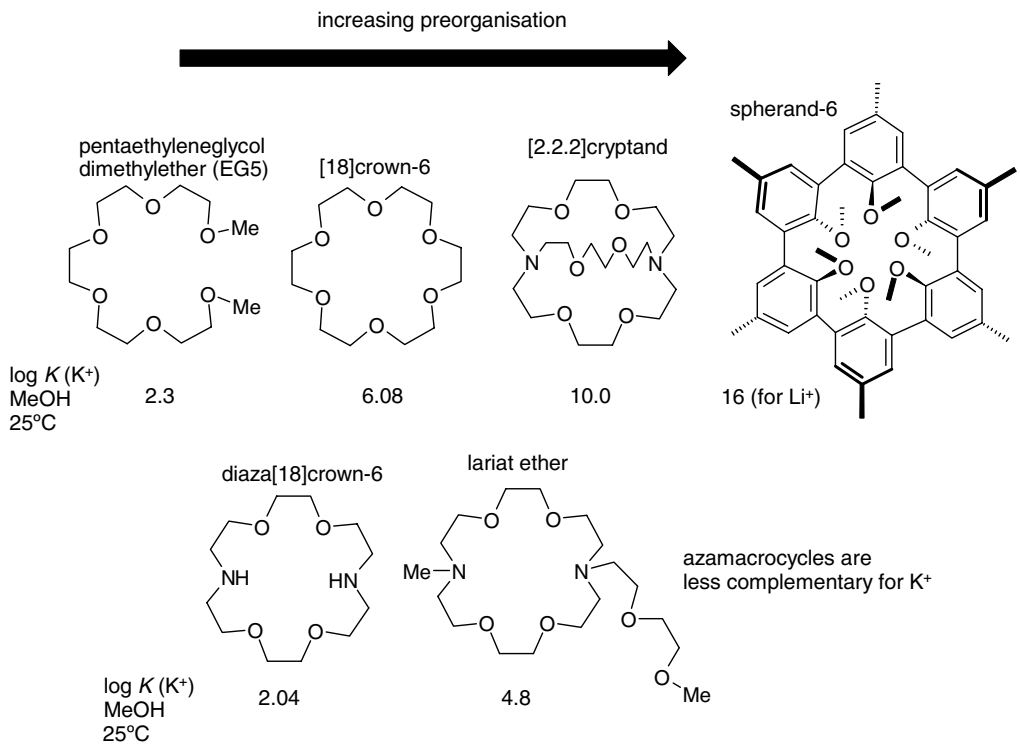


**Figure 1.12** Comparison of the effects of preorganisation and complementarity on the magnitudes of the binding constant of polyether hosts for alkali metal cations. The figure for $Li^+$ is given for the highly preorganised spherand-6 since it is too small to accommodate $K^+$.

oxygen atoms in [18]crown-6 with two secondary amine nitrogen atoms in diaza[18]crown-6 lowers the binding constant to below the value found for the podand EG5.

## 1.7 Thermodynamic and Kinetic Selectivity, and Discrimination

Schneider, H.-J. and Yatsimirsky, A. K., 'Selectivity in supramolecular host-guest complexes', *Chem. Soc. Rev.*, 2008, **37**, 263–277.

The goal of supramolecular host design, both in nature (enzymes, transport proteins *etc.*) and in artificial systems, is the achievement of selectivity; some kind of differentiation of different guests. In the blood, the iron haem transport protein haemoglobin is fine-tuned to selectively take up $O_2$ in the presence of $N_2$, water and $CO_2$, and even substances such as CO, which normally bind very strongly to iron. We can readily assess the affinity of a host for a particular receptor by its binding constant (Section 1.4). In thermodynamic terms, selectivity is simply the ratio of the binding constant for one guest over another:

$$\text{Selectivity} = \frac{K_{\text{Guest1}}}{K_{\text{Guest2}}} \tag{1.31}$$

This kind of selectivity tends to be the most easy to achieve because it is highly susceptible to manipulation by intelligent application of concepts such as the lock and key analogy, preorganisation and complementarity, coupled with a detailed knowledge of the host–guest interactions. So, we can say that [18]crown-6, with a binding constant for $K^+$ of $10^6$ $M^{-1}$, is 100-fold selective for $K^+$ over $Na^+$, which it binds with a binding constant of only *ca.* $10^4$ $M^{-1}$ under the same conditions. There is another kind of selectivity, however, which relates to the rate of transformation of competing substrates along a reaction path. This is *kinetic selectivity* and is the basis for directing the flow of directional processes such as supramolecular (enzymatic) catalysis and guest sensing and signalling. In this sense, it is the guest that is transformed *fastest*, rather than the one that is bound the strongest, that the system is said to be selective for. Indeed, in such time-resolved processes, large binding constants are inhibitory to the system since kinetics are slowed down. Many biochemical enzymes are kinetically selective and examination of their structures reveals that while they are perfectly complementary for the desired (sometimes transitory) state of the guest at any given instant, they are not generally preorganised in a rigid way since this would preclude rapid catalysis. In artificial systems, the engineering of time-resolved selectivity (as in the design of enzyme mimics, Chapter 12) is a much more difficult process since it requires the adaptation of the host to the changing needs of the guest as the system proceeds along its reactive pathway.

We should also distinguish between guest selectivity and inter-guest discrimination. While thermodynamic selectivity relates to the magnitude of observed binding constants, discrimination is applied to the magnitude of other observable results of often highly specific host-guest interactions. Good examples are fluorescent or colorimetri molecular sensing. The guest that is bound most strongly is not necessarily the guest that gives the largest change in colour or in fluorescent emission intensity. This is because the changes in light absorption or emission may result from a particular, guest-specific host-guest interaction, rather than being directly proportional to binding affinity. Thus a host or sensing ensemble may effectively *discriminate* between two potential guests even if their binding constants are similar. The concept of guest discrimination is particularly interesting in the context of binding patterns by arrays of different hosts (for a fuller discussion see Section 11.3.3).[14]

## 1.8 Nature of Supramolecular Interactions

Anslyn, E. V. and Dougherty, D. A., *Modern Physical Organic Chemistry*, University Science Books, Sausalito, CA, USA, 2006, *pp.* 162–168.

In general, supramolecular chemistry concerns non-covalent bonding interactions. The term 'non-covalent' encompasses an enormous range of attractive and repulsive effects. The most important, along with an indication of their approximate energies, are explained below. When considering a supramolecular system it is vital to consider the interplay of all of these interactions and effects relating both to the host and guest as well as their surroundings (*e.g.* solvation, ion pairing, crystal lattice, gas phase *etc.*).

### 1.8.1 Ion–ion Interactions

Ionic bonding is comparable in strength to covalent bonding (bond energy = 100–350 kJ $mol^{-1}$). A typical ionic solid is sodium chloride, which has a cubic lattice in which each $Na^+$ cation is surrounded by six $Cl^-$ anions (Figure 1.13a). It would require a large stretch of the imagination to regard NaCl as a supramolecular compound but this simple ionic lattice does illustrate the way in which an $Na^+$ cation is able to organise six complementary donor atoms about itself in order to maximise non-covalent ion–ion interactions. Note that this kind of lattice structure breaks down in solution because of solvation effects to give species such as the labile, octahedral $Na(H_2O)_6^+$.

A much more supramolecular example of ion–ion interactions is the interaction of the *tris*(diazabicyclooctane) host (**1.17**), which carries a 3+ charge, with anions such as $[Fe(CN)_6]^{3-}$ (Figure 1.13b).[15]

### 1.8.2 Ion–Dipole Interactions

The bonding of an ion, such as $Na^+$, with a polar molecule, such as water, is an example of an ion–dipole interaction, which range in strength from *ca.* 50 – 200 kJ $mol^{-1}$. This kind of bonding is seen both in the solid state and in solution. A supramolecular analogue is readily apparent in the structures of the complexes of alkali metal cations with macrocyclic (large ring) ethers termed crown ethers

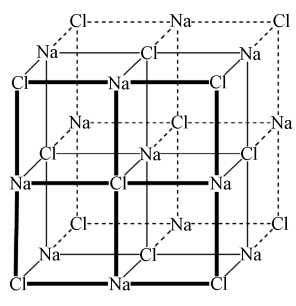


(a)

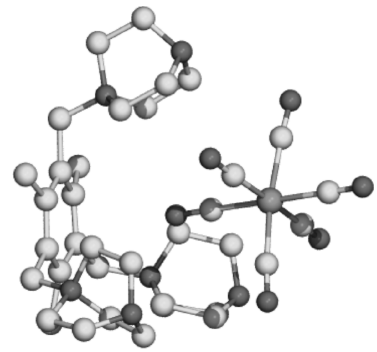

(b)

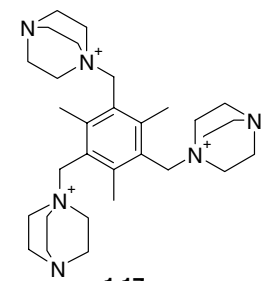

**1.17**

**Figure 1.13** (a) The NaCl ionic lattice. (b) Supramolecular ion–ion interactions exemplified by the interaction of the organic cation **1.17** with $[Fe(CN)_6]^{3-}$.

(Chapter 3) in which the ether oxygen atoms play the same role as the polar water molecules, although the complex is stabilised by the chelate effect and the effects of macrocyclic preorganisation. The oxygen lone pairs are attracted to the cation positive charge.

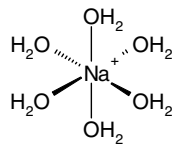


**1.18**

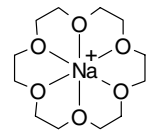


$Na^+$ crown ether complex

**1.19**

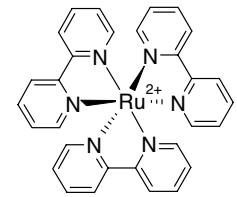


bpy = 2,2'-bipyridyl

$[Ru(bpy)_3]^{2+}$ **1.20**

Ion–dipole interactions also include coordinative bonds, which are mostly electrostatic in nature in the case of the interactions of nonpolarisable metal cations and hard bases. Coordinate (dative) bonds with a significant covalent component, as in $[Ru(bpy)_3]^{2+}$, are also often used in supramolecular assembly and, as we will see in Chapters 10 and 11, the distinction between supramolecular and molecular species can become rather blurred.

## 1.8.3 Dipole–Dipole Interactions

Alignment of one dipole with another can result in significant attractive interactions from matching of either a single pair of poles on adjacent molecules (type I) or opposing alignment of one dipole with the other (type II) (Figure 1.14) with energies in the range 5–50 kJ $mol^{-1}$. Organic carbonyl compounds show this behaviour well in the solid state and calculations have suggested that type II interactions have an energy of about 20 kJ $mol^{-1}$, comparable to a moderately strong hydrogen bond. The boiling point of ketones such as acetone (56 ºC), however, demonstrates that dipole–dipole interactions of this type are relatively weak in solution.

## 1.8.4 Hydrogen Bonding

Jeffrey, G. A., *An Introduction to Hydrogen Bonding*, Oxford University Press: Oxford, 1997.

Hydrogen bonding has tremendous effects on molecular properties. It is the strong hydrogen bonding in water that makes its boiling point of 100 ºC some 160 ºC higher than the heavier $H_2S$, simply

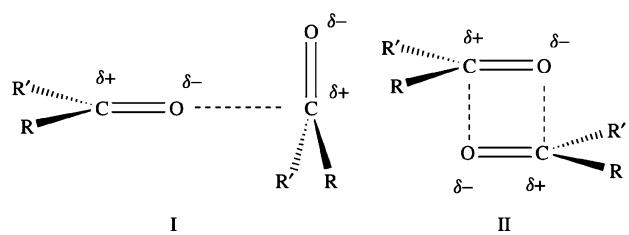


I II

**Figure 1.14** Dipole–dipole interactions in carbonyls.

because of the more polar nature of the O–H bonds. Similarly at room temperature (298 K) butanone gas ($C_4H_8O$) which has a hydrogen bonding carbonyl (C=O) functionality is a factor of $1.7 \times 10^4$ more soluble in water than the non-polar gaseous butane ($C_4H_{10}$). Conversely the inhibition of firefly luciferase activity (the reaction that causes the firefly's glow) by butane is a factor of 74 times more efficient than butanone in water. The increased solvation of the butanone prevents it from blocking the enzyme hydrophobic binding site.

A hydrogen bond may be regarded as a particular kind of dipole–dipole interaction in which a hydrogen atom attached to an electronegative atom (or electron withdrawing group) is attracted to a neighbouring dipole on an adjacent molecule or functional group. Hydrogen bonds are commonly written D–H··A and usually involve a hydrogen atom attached to an electronegative atom such as O or N as the donor (D) and a similarly electronegative atom, often bearing a lone pair, as the acceptor (A). There are also significant hydrogen bonding interactions involving hydrogen atoms attached to carbon, rather than electronegative atoms such as N and O (electronegativities: C: 2.55, H: 2.20, N: 3.04, O: 3.44). Because of its relatively strong and highly directional nature, hydrogen bonding has been described as the 'masterkey interaction in supramolecular chemistry'.[1] Normal hydrogen bonds typically range in strength from *ca*. 4–60 kJ mol$^{-1}$, although certain highly acidic compounds such as $HF_2^-$ have hydrogen bond energies up to 120 kJ mol$^{-1}$. An excellent example of hydrogen bonding in supramolecular chemistry is the formation of carboxylic acid dimers (**1.21**), which results in the shift of the $\nu$(OH) infrared stretching frequency from about 3400 cm$^{-1}$ to about 2500 cm$^{-1}$, accompanied by a significant broadening and intensifying of the absorption. Typically hydrogen bonded O···O distances are 2.50–2.80 Å in length, though interactions in excess of 3.0 Å may also be significant. Hydrogen bonds to larger atoms such as chloride are generally longer, and may be weaker as a consequence of the reduced electronegativity of the larger halide acceptor, although the precise strength of the hydrogen bonds is greatly dependent on its environment. Hydrogen bonds are ubiquitous in supramolecular chemistry. In particular, hydrogen bonds are responsible for the overall shape of many proteins, recognition of substrates by numerous enzymes, and (along with π-π stacking interactions) for the double helix structure of DNA (Sections 2.9 and 10.3).

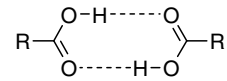


**1.21**

Hydrogen bonds come in a wide range of lengths, strengths and geometries and can be divided into three broad categories, the properties of which are listed in Table 1.5. A strong interaction is somewhat similar in character to a covalent bond, whereby the hydrogen atom is close to the centre-point of the donor and acceptor atoms. Strong hydrogen bonds are formed between a strong acid and a good hydrogen bond acceptor, for example in the $H_5O_2^+$ ion or in complexes of 'proton sponge' (Section 4.7.3), which are practically linear with the hydrogen atom between the two electronegative atoms. Moderate strength hydrogen bonds are formed between neutral donor and neutral acceptor groups *via* electron lone pairs, for example the self-association of carboxylic acids, or amide interactions in proteins. Moderate hydrogen bond interactions do not have a linear geometry but are slightly bent. Hydrogen bonds commonly deviate from linearity and their angular distribution is influenced by statistical factors. A 'conical correction' for statistical effects often appears in the analysis of hydrogen bond angle distributions, particularly from searches of the Cambridge Structural Database (Section 8.4). A linear hydrogen bond requires a fixed position of the hydrogen atom in relation to the acceptor, whereas non-linear hydrogen bonds have many possible positions that form a conical shape around the linear position. Larger bond angles result in a larger cone, and therefore there are more possible positions for the bond

**Table 1.5** Properties of hydrogen bonded interactions (A–H = hydrogen bond acid, B = hydrogen bond base).

| | Strong | Moderate | Weak |
|---|---|---|---|
| A—H···B interaction | Mainly covalent | Mainly electrostatic | Electrostatic |
| Bond energy (kJ $mol^{-1}$) | 60–120 | 16–60 | <12 |
| Bond lengths (Å) | | | |
| H···B | 1.2–1.5 | 1.5–2.2 | 2.2–3.2 |
| A···B | 2.2–2.5 | 2.5–3.2 | 3.2–4.0 |
| Bond angles (°) | 175–180 | 130–180 | 90–150 |
| Relative IR vibration shift (stretching symmetrical mode, $cm^{-1}$) | 25% | 10–25% | <10% |
| $^{1}$H NMR chemical shift downfield (ppm) | 14–22 | <14 | ? |
| Examples | Gas phase dimers with strong acids/bases | Acids | Minor components of bifurcated bonds |
| | Proton sponge | Alcohols | C—H hydrogen bonds |
| | HF complexes | Biological molecules | O—H···π hydrogen bonds |

to occur in. In the case of hydrogen bonds between neutral species, it is generally accepted that there is a direct correlation between hydrogen bond strength (in terms of formation energy) and the crystallographically determined distance between hydrogen bond donor and acceptor. Distances tend to be shorter in 'charge assisted' hydrogen bonds involving ions. The strength of similar hydrogen bonds can be very different between various systems and is not necessarily correlated with the Brønsted acidity of the proton (hydrogen) donor. It depends on the type of electronegative atom to which the hydrogen atom is attached and the geometry that the hydrogen bond adopts. Scales of hydrogen bond acidity and basicity exist that partially quantify these effects.[16] A single, strong hydrogen bond per molecule may be sufficient to determine solid-state structure and exert a marked influence on the solution and gas phases, although hydrogen bonding is much more significant in non-polar solvents than in water, where hydrogen bond donors and acceptors are highly solvated and hydrophobic interactions tend to dominate. Weaker hydrogen bonds play a role in structure stabilisation and can be significant when large numbers act in concert. They tend to be highly non-linear and involve unconventional donors and acceptors such as C–H groups, the π-systems of aromatic rings or alkynes or even transition metals and transition metal hydrides (Section 8.9).

While C–H donor hydrogen bonds are at the weaker end of the energy scale of hydrogen bonds, the presence of electronegative atoms near the carbon can enhance significantly the acidity of the C—H proton, resulting in a significant dipole. An elegant example of C—H···N and C—H···O hydrogen bonds is the interaction of the methyl group of nitromethane with the pyridyl crown ether shown in Figure 1.15.[17]

The types of geometries that can be adopted in a hydrogen bonding complex are summarised in Figure 1.16. These geometries are termed *primary hydrogen bond interactions*, this means that there is a direct interaction between the donor group and the acceptor group. There are also *secondary interactions* between neighbouring groups that must be considered. The partial charges on adjacent atoms can either increase the binding strength by virtue of attraction between opposite charges or decrease the affinity due to repulsion between like charges. Figure 1.17 shows two situations in which arrays of hydrogen bond donors and acceptors are in close proximity. An array of three donors (DDD) facing

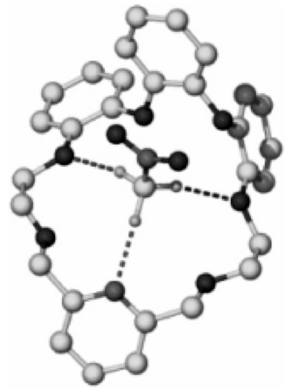

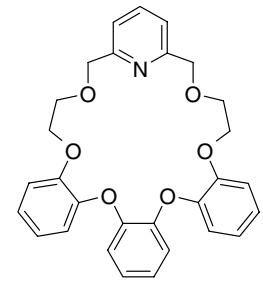


**1.22**

**Figure 1.15** X-ray crystal structure showing C—H···N (2.21Å) and C—H···O (2.41Å, average) hydrogen bonding in a complex of crown ether **1.22** with nitromethane.[17]

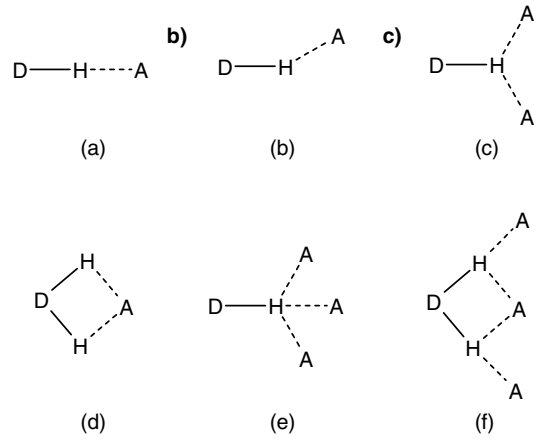


**Figure 1.16** Various types of hydrogen bonding geometries; (a) linear (b) bent (c) donating bifurcated (d) accepting bifurcated (e) trifurcated (f) three centre bifurcated.

three acceptors (AAA) (Figure 1.17a) has only attractive interactions between adjacent groups and therefore the binding is enhanced in such a situation. Mixed donor/acceptor arrays (ADA, DAD) suffer from repulsions by partial charges of the same sign being brought into close proximity by the primary interactions (Figure 1.17b).

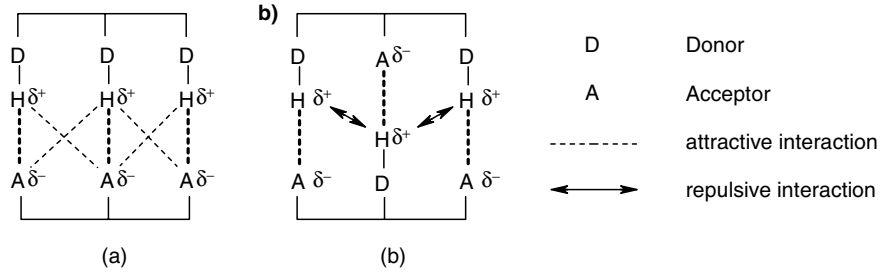


**Figure 1.17** (a) Secondary interactions providing attractions between neighbouring groups between DDD and AAA arrays (primary interactions in bold) and (b) repulsions from mixed donor/acceptor arrays (ADA and DAD).

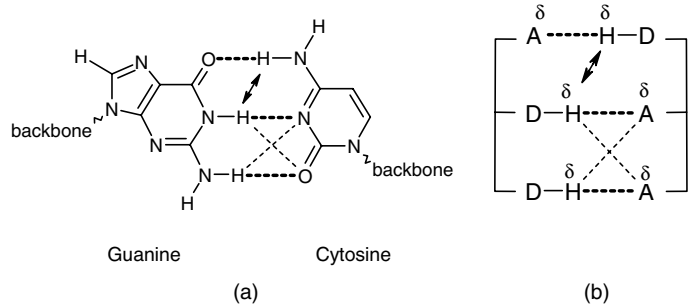


**Figure 1.18** (a) Primary and secondary hydrogen bond interactions between guanine and cytosine base pairs in DNA and (b) a schematic representation.

A real-life example of hydrogen bonding is the double helix of DNA. There are many hydrogen bond donors and acceptors holding base pairs together, as illustrated between the nucleobases cytosine (C) and guanine (G) in Figure 1.18. The CG base pair has three primary interactions (*i.e.* traditional hydrogen bonds) and also has both attractive and repulsive secondary interactions.

## 1.8.5 Cation–π Interactions

Ma, J. C., and Dougherty, D., 'The cation-$\pi$ interaction', *Chem. Rev.*, 1997, **97**, 1303–1324.

Transition metal cations such as $Fe^{2+}$, $Pt^{2+}$ *etc.* are well known to form complexes with olefinic and aromatic hydrocarbons such as ferrocene $[Fe(C_5H_5)_2]$ and Zeise's salt $[PtCl_3(C_2H_4)]^-$. The bonding in such complexes is strong and could by no means be considered non-covalent, since it is intimately linked with the partially occupied *d*-orbitals of the metals. Even species such as $Ag^+ \cdots C_6H_6$ have a significant covalent component. The interaction of alkaline and alkaline earth metal cations with C=C double bonds is, however, a much more non-covalent 'weak' interaction, and is suggested to play an important role in biological systems. For example, the interaction energy of $K^+$ and benzene in the gas phase is about 80 kJ $mol^{-1}$ (Figure 1.19). By comparison, the association of $K^+$ with a single water molecule is similar at 75 kJ $mol^{-1}$. The reason $K^+$ is more soluble in water than in benzene is related to the fact that many water molecules can interact with the potassium ion, whereas only a few bulkier benzene molecules can fit around it. The interaction of nonmetallic cations such as $RNH_3^+$ with double bonds may be thought of as a form of X—H $\cdots$ $\pi$ hydrogen bond.

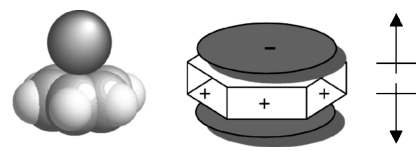


**Figure 1.19** Schematic drawing of the cation–π interaction showing the contact between the two. The quadrupole moment of benzene, along with its representation as two opposing dipoles, is also shown.

## 1.8.6 Anion-π Interactions

Berryman, O. B., Bryantsev, V. S., Stay, D. P., Johnson, D. W. and Hay, B. P., 'Structural criteria for the design of anion receptors: The interaction of halides with electron-deficient arenes', *J. Am. Chem. Soc.*, 2007, **129**, 48–58.

Cation-$\pi$ interactions (see Section 1.8.5) have been known for many years, however it is only relatively recently that there has been interest in anion-π interactions. Intuitively, the interaction of an anion with π-electron density seems like it should be repulsive and indeed the affinity of the aromatic ring containing cryptand **1.23** for halides rapidly falls off in the order $F^- >> Cl^- > Br^- \sim I^-$ because of anion-π repulsions in the case of the larger halides, with all except $F^-$ showing a constant anion-ring centroid distance of *ca.* 3.7 Å.[18] However, there is a charge difference between an overall neutral aromatic ring and an anion and therefore in principle the possibility exists for an electrostatic attraction. Work by Kochi[19] has shown that anions form stable charge transfer complexes with a variety of electron deficient aromatic compounds such as **1.24**. The formation constants for the anion-aromatic complexes are in the range 1–10 $M^{-1}$ and there is a linear correlation between the energy of the charge transfer band in the electronic spectrum and the formal reduction potential of the aromatic compound. This is referred to as a Mülliken correlation and provides strong evidence for the charge transfer nature of the interaction. The charge transfer also results in strong red or yellow colourations for the complexes and a number have been characterised by X-ray crystallography. The crystal structures reveal that the anion sits in a offset fashion at the edge of the aromatic rings rather than above the centroid with anion–carbon distances as short as 2.93 Å for tetrachloro *o*-quinone and $Br^-$, shorter than the sum of the a van der Waals radii (3.55 Å). Similar short anion-carbon contacts have been noted for organometallic calixarene derivatives such as **4.34** (see Chapter 4) where the aromatic ring bears a significant positive charge. Anion-$\pi$ interactions have also been implicated as controlling elements in self-assembly reactions of Ag(I) complexes with π-acidic aromatic rings.[20]

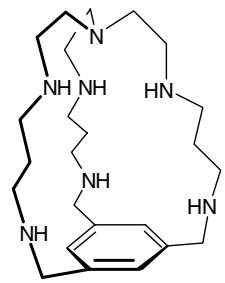


**1.23**

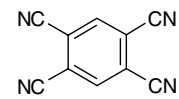


**1.24**

## 1.8.7 π–π Interactions

Hunter, C. A., Lawson, K. R., Perkins, J. and Urch, C. J., 'Aromatic interactions', *J. Chem. Soc., Perkin Trans. 2* 2001, 651–669.

Aromatic $\pi-\pi$ interactions (sometimes called $\pi-\pi$ stacking interactions) occur between aromatic rings, often in situations where one is relatively electron rich and one is electron poor. There are two general types of $\pi$-interactions: face-to-face and edge-to-face, although a wide variety of intermediate geometries are

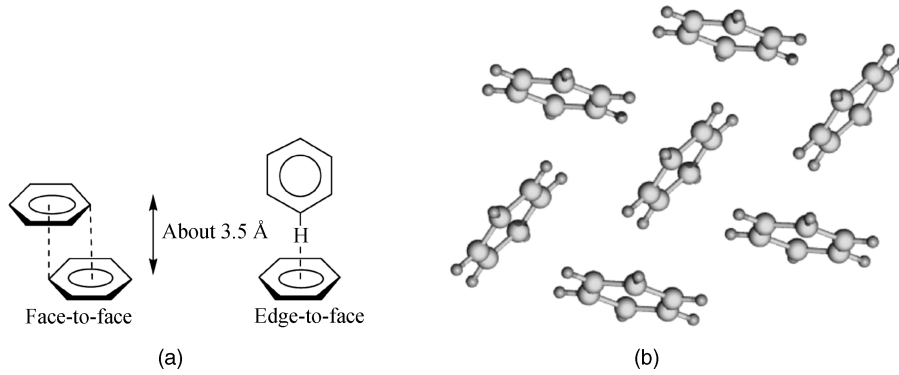


**Figure 1.20** (a) Limiting types of π–π interaction. Note the offset to the face-to-face mode (direct overlap is repulsive). (b) X-ray crystal structure of benzene showing herringbone motif arising from edge-to-face interactions.

known (Figure 1.20a). Face-to-face $\pi$-stacking interactions are responsible for the slippery feel of graphite and its useful lubricant properties. Similar $\pi$-stacking interactions between the aryl rings of nucleobase pairs also help to stabilise the DNA double helix. Edge-to-face interactions may be regarded as weak forms of hydrogen bonds between the slightly electron deficient hydrogen atoms of one aromatic ring and the electron rich $\pi$-cloud of another. Strictly they should not be referred to as $\pi$-stacking since there is no stacking of the $\pi$-electron surfaces. Edge-to-face interactions are responsible for the characteristic herringbone packing in the crystal structures of a range of small aromatic hydrocarbons including benzene (Figure 1.20b).

Sanders and Hunter have proposed a simple model based on competing electrostatic and van der Waals influences, in order to explain the variety of geometries observed for $\pi$–$\pi$ stacking interactions and to predict quantitatively the interaction energies. Their model is based on an overall attractive van der Waals interaction (Section 1.8.8), which is proportional to the contact surface area of the two $\pi$-systems. This attractive interaction dominates the overall energy of the $\pi$–$\pi$ interaction and may be regarded as an attraction between the negatively charged $\pi$-electron cloud of one molecule and the positively charged $\sigma$-framework of an adjacent molecule. The relative orientation of the two interacting molecules is determined by the electrostatic repulsions between the two negatively charged $\pi$-systems (Figure 1.21).

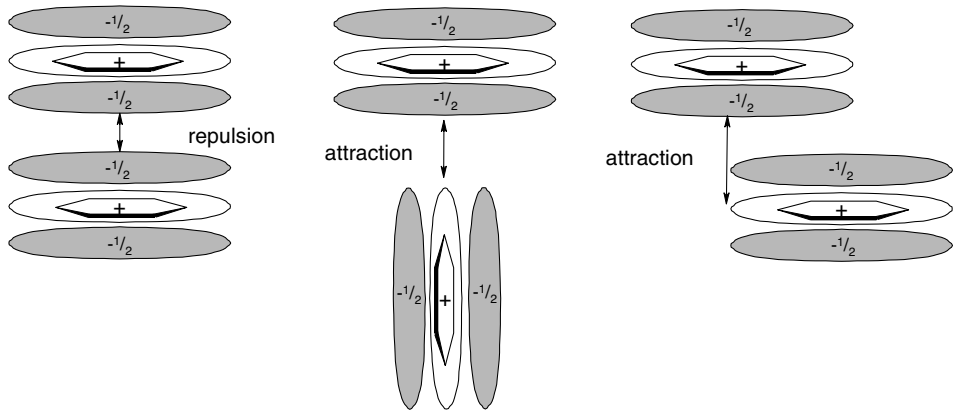


**Figure 1.21** Interacting $\pi$-quadrupoles.

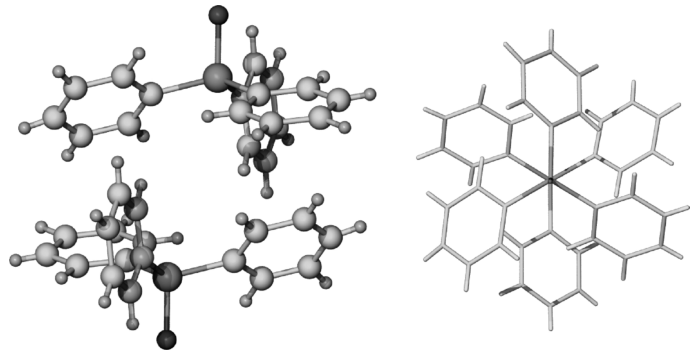

**Figure 1.22** Sixfold edge-to-face phenyl embrace in $ClGePh_3$.[23]

Sanders and Hunter stress the importance of the interactions between individual pairs of atoms rather than molecules as a whole and, while their approach has been relatively successful, there is still a great deal of current debate over the nature of $\pi$–$\pi$ stacking interactions. In particular, work involving substituent effects suggests that London dispersion forces might play a more important role than electrostatic interactions.[21] $\pi$-stacking interactions are of considerable interest and importance in the crystal structures of both organic and coordination compounds and have a marked influence on solution binding *via* the hydrophobic effect (Section 1.9.1). Edge-to-face $\pi$-interactions give rise to common motifs such as the sixfold phenyl embrace often found in compounds containing three or more aromatic rings, such as metal complexes of $PPh_3$ (Figure 1.22). A survey of $\pi$-interactions in crystalline coordination compounds found that a slipped (parallel displaced) interaction is the most common with the vector between the ring centroids forming an angle of about 20° and aromatic ring centroid – centroid distances of up to 3.8 Å. This parallel-displaced structure is thought to have a contribution from $\pi$-$\sigma$ attractive interactions that increases with increasing offset.[22]

## 1.8.8 Van der Waals Forces and Crystal Close Packing

Kitaigorodskii, A. I., *Organic Chemical Crystallography* (Originally published in Russian by Press of the Academy of Sciences of the USSR, Moscow, 1955). Consultants Bureau: New York, 1961.

Van der Waals interactions arise from the polarisation of an electron cloud by the proximity of an adjacent nucleus, resulting in a weak electrostatic attraction. They are nondirectional and hence possess only limited scope in the design of specific hosts for selective complexation of particular guests. In general, van der Waals interactions provide a general attractive interaction for most 'soft' (polarisable) species with an interaction energy proportional to the surface area of contact. In supramolecular chemistry, they are most important in formation of 'inclusion' compounds in which small, typically organic molecules are loosely incorporated within crystalline lattices or molecular cavities, *e.g.* the inclusion of toluene within the molecular cavity of the *p-tert*-butylphenol-based macrocycle, *p-tert*-butylcalix[4]arene (Section 6.2.2 and Figure 1.23).[24] Strictly, van der Waals interactions may be divided into dispersion (London) and exchange–repulsion terms. The dispersion interaction is the attractive component that results from the interactions between fluctuating multipoles (quadrupole, octupole *etc.*) in adjacent molecules. The attraction decreases very rapidly with distance ($r^{-6}$ dependence) and is additive with every bond in the molecule contributing to the overall interaction energy. The exchange–repulsion defines molecular shape and balances dispersion at short range, decreasing with the twelfth power of interatomic separation.

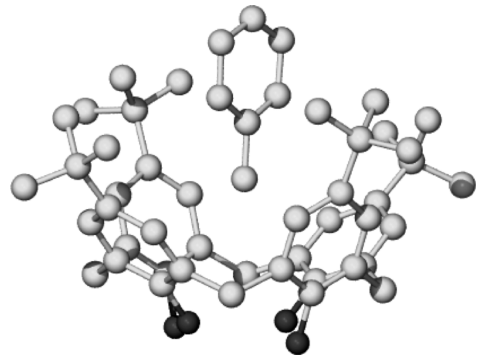

**Figure 1.23** X-ray crystal structure of a typical van der Waals inclusion complex *p-tert*-butylcalix[4]arene·toluene.[24]

In examination of solid state (*i.e.* crystal) structures the need to achieve a close packed arrangement is also a significant driving force. This has been summed up in the truism 'Nature abhors a vacuum', but, according to the close packing theory of Kitaigorodsky, it is simply a manifestation of the maximisation of favourable isotropic van der Waals interactions. Kitaigorodsky's theory tells us that molecules undergo a shape simplification as they progress towards dimers, trimers, higher oligomers, and ultimately crystals. This means that one molecule dovetails into the hollows of its neighbours so that a maximum number of intermolecular contacts are achieved, rather like the popular computer game *Tetris*. Very few solid-state structures are known to exhibit significant amounts of 'empty' space. Those which do (*e.g.* zeolites, Section 9.2) possess a very rigid framework that is able to resist implosion under what amounts effectively to an enormous pressure differential between atmospheric pressure and the empty crystal pore or channel. Such materials often exhibit very interesting and useful properties in catalysis and separation science.

## 1.8.9 Closed Shell Interactions

Pyykkö, P., 'Strong closed-shell interactions in inorganic chemistry', *Chem. Rev.*, 1997, **97**, 597–636.

Atoms with unfilled electron shells form strong, covalent bonds. Ions generally have closed valence electron shells but experience strong attractions between oppositely charged pairs. We would not intuitively expect closed shell atoms of neutral or like charges to form significant interactions, however in some cases they do. These interactions are termed closed shell interactions and include secondary bonding interactions,[25] metalophilic interactions[26] and halogen bonding.[27] Closed shell interactions are broadly comparable in strength with moderate strength hydrogen bonds and are thought to arise from electron correlation effects, significantly strengthened by relativistic effects in heavy elements, particularly gold (where they are termed *aurophilic interactions*). Thus closed shell interactions are most pronounced for heavy metals with examples reported for electron configurations from $d^8$ to $d^{10}s^2$, and the heavier halogens with halogen bonding strength decreasing in the order I > Br > Cl >> F. Structural studies have shown that halogen bonds of type D···X–C (where D is an electron-pair donor and X is a halogen electron pair acceptor) have a well-defined, linear geometry (160–180°) with D···X distances considerably less than the sum of the van der Waals radii of D and X. The most obvious example is the $I^-\cdots I_2$ interaction found in the $I_3^-$ ion which has an energy of *ca.* 200 kJ $mol^{-1}$, and indeed halogen bonds have been known since the discovery of $Me_3N\cdots Br_2$ in 1896. The geometries adopted by halogen bonding are influenced by 'polar flattening', the anisotropic distribution of electron density about halogen and some other polarisable atoms, however they represent a genuine attractive interaction (see further discussion in Section 8.4)

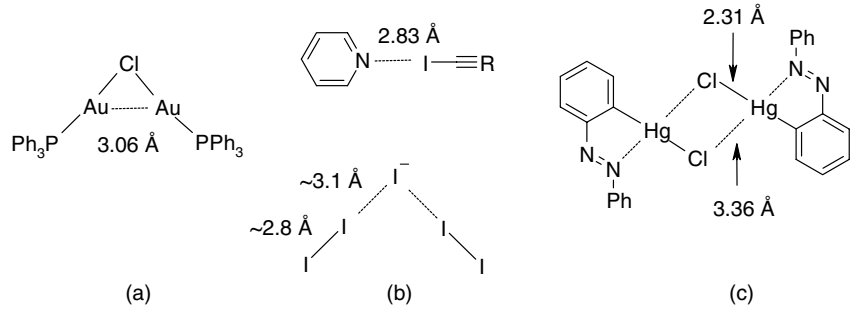


**Figure 1.24** Examples of closed shell interactions (a) Aurophilic interactions in $[Au_2(\mu\text{-}Cl)(PPh_3)_2](ClO_4)$, (b) halogen bonding in pyridine···I–CCR and $I_5^-$ and (c) secondary bonding in $[\{HgCl(C_6H_4N_2Ph)\}_2]$.

Aurophilic interactions experience significant relativistic shortening and the Au···Au distances which are in the range 2.8–3.0 Å are typically shorter than silver(I) analogues. The relativistic factor comes from the fact that electrons moving near highly charged nuclei have a velocity close to that of the speed of light and therefore experience a relativistic mass that is larger than their resting mass. The increased mass causes a decrease in the orbital radius and hence a decrease in atomic radius that is particularly pronounced for gold. Aurophilic interactions are ubiquitous in linear, 2-coordinate Au(I) complexes with many examples having the 'A-frame' geometry as in $[Au_2(\mu\text{-}Cl)(PPh_3)_2](ClO_4)$, Au···Au = 3.06 Å, Figure 1.24.[28] Interestingly in the compound $[Au_2(dmpm)_3](ClO_4)_2$ which exhibits an Au···Au distance of 3.05 Å, it proved possible to measure a Raman vibrational stretching band for the Au···Au bond at 79 $cm^{-1}$. The energy of this band *increases* to 165 $cm^{-1}$ on UV irradiation suggesting that aurophilic interaction is strengthened in the excited state.[29]

Secondary bonding (a term coined by Alcock in 1972) is a closed shell interaction of type X–A···X′ where X is commonly a heavier halogen or chalcogenide element (Cl, Br, S *etc.*). Secondary bonds closely resemble hydrogen bonds except that A is often a multi-valent heavy atom such as Hg, Tl, Sn, Pb, Sb, Bi, Se or Te instead of hydrogen. The X–A bond is a normal covalent bond and while the A···X′ is a closed shell interaction involving donation of a non-bonding lone pair on X′ into an antibonding $\sigma^*$ orbital of the X–A bond, Figure 1.25. Secondary bonding is a very significant interaction in determining the solid state structures of heavy element compounds.

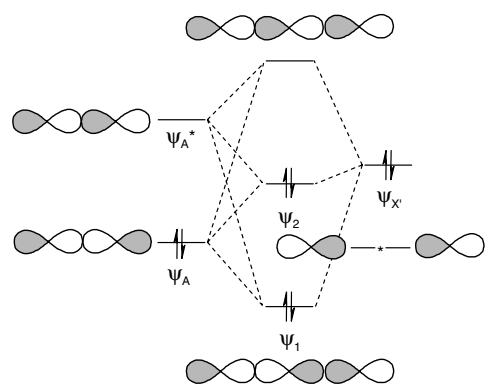


**Figure 1.25** Molecular orbital description of secondary bonding and related interactions showing the $n \rightarrow \sigma^*$ interaction.

# 1.9 Solvation and Hydrophobic Effects

## 1.9.1 Hydrophobic Effects

Southall, N. T.; Dill, K. A and Haymet, A. D. J., 'A view of the hydrophobic effect', *J. Phys. Chem. B*, 2002, **106**, 521–533.

Although occasionally mistaken for a force, hydrophobic effects generally relate to the exclusion from polar solvents, particularly water, of large particles or those that are weakly solvated (*e.g. via* hydrogen bonds or dipolar interactions). The effect is obvious in the immiscibility of mineral oil and water. Essentially, the water molecules are attracted strongly to one another resulting in a natural agglomeration of other species (such as non-polar organic molecules) as they are squeezed out of the way of the strong inter-solvent interactions. This can produce effects resembling attraction between one organic molecule and another, although there are in addition van der Waals and $\pi$–$\pi$ stacking attractions between the organic molecules themselves. The hydrophobic effect is very important in biological systems in the creation and maintenance of protein and polynucleotide structure and in the maintenance of phospholipid bilayer cell walls. Hydrophobic effects are of crucial importance in the binding of organic guests by cyclodextrins and cyclophane hosts in water (Chapter 6) and may be divided into two energetic components: enthalpic and entropic. The enthalpic hydrophobic effect involves the stabilisation of water molecules that are driven from a host cavity upon guest binding. Because host cavities are often hydrophobic, intracavity water does not interact strongly with the host walls and is therefore of high energy. Upon release into the bulk solvent, it is stabilised by interactions with other water molecules. The entropic hydrophobic effect arises from the fact that the presence of two (often organic) molecules in solution (host and guest) creates two 'holes' in the structure of bulk water. Combining host and guest to form a complex results in less disruption to the solvent structure and hence an entropic gain (resulting in a lowering of overall free energy). The process is represented schematically in Figure 1.26.

As an example, consider the binding of the guest *p*-xylene by the cyclophane host **1.25** (part of a class described in more detail in Section 6.5). The binding constant in water is $9.3 \times 10^3\,M^{-1}$. At 293K, the complexation free energy, $\Delta G^o$, is –22 kJ mol$^{-1}$ which divides into a favourable enthalpic stabilisation, $\Delta H^o = -31$ kJ mol$^{-1}$, and an unfavourable entropic component, $T\Delta S^o = -9$ kJ mol$^{-1}$. In this case it is the enthalpic contribution to the hydrophobic binding that dominates. The enthalpic contribution is too great to result from attractive forces between host and guest (which experience only weak $\pi$-stacking

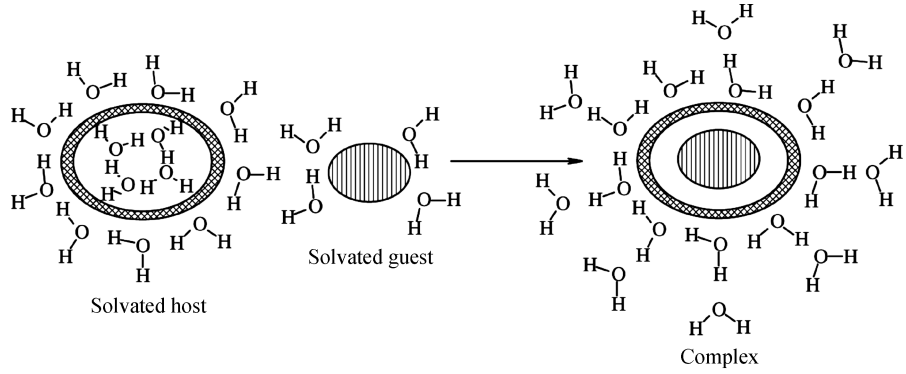


**Figure 1.26** Hydrophobic binding of organic guests in aqueous solution.

and van der Waals interactions) and thus must arise from specific solvent–solvent forces. In methanol solvent, the enthalpic component is reduced greatly as a result of weaker solvent–solvent interactions.

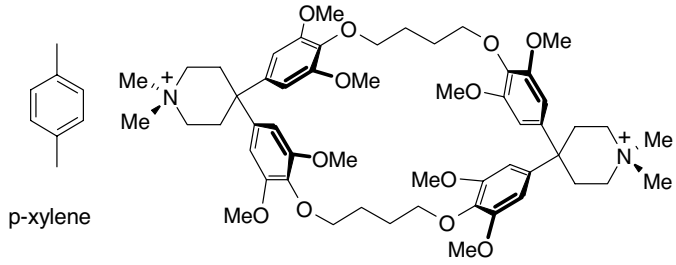


**1.25**

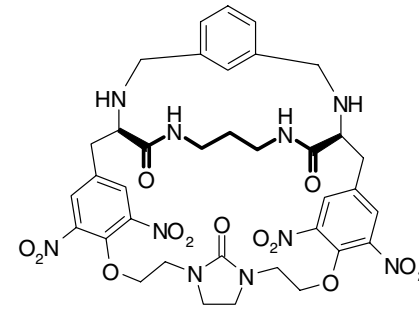


**1.26**

## 1.9.2 Solvation

Smithrud, D. B., Sanford, E. M., Chao, I., *et al.*, 'Solvent effects in molecular recognition', *Pure Appl. Chem.*, 1990, **62**, 2227–2236.

The importance of solvent in supramolecular chemistry can hardly be overstated. In the solid state solvent is often included as a guest in the crystal lattice and usually mediates the nucleation and deposition of a crystalline (or otherwise) compound from solution. In solution all complexation phenomena are in competition with solvation interactions and the solvent is almost invariably in a huge molar excess. Polar solvents, particularly water, compete very effectively for binding sites, particularly hydrogen bonding functionality, making hydrophobic (or solvophobic) effects of paramount importance. In non-polar solvents and in the gas phase specific host-guest dipolar and hydrogen bonding interactions are much more significant. It is thus essentially meaningless to discuss the magnitude of binding constants without mention of solvent and impossible to compare binding constants or even relative affinity across different solvent media. Indeed a common 'trick' to differentiate the affinity of a host for various guests is to lower the apparent binding constants by moving to a more competitive (generally more polar) solvent. Thus binding constants that are too high to measure in one solvent become lower and hence experimentally accessible in a more competitive one. An example of the influence of solvent of binding constant is shown in Table 1.6. Binding is clearly enhanced in non-polar solvents with a dramatic maximum value for 1,1,2,2-tetrachloroethane coming from the fact that this solvent is too large to enter the macrobicyclic cavity and hence it does not compete for the guest binding site.

So far we have regarded the host-guest binding process as being the interaction of a more-or-less preorganised host with a naked guest. In reality both host and guest are highly solvated in solution and the solvation stabilisation of the free host may well be significantly different from its interactions to solvent in the complexed state, particularly if there is a significant conformational change (induced fit) on binding. A fuller picture of both the energetics and kinetics of the complexation process must take into account the desolvation of both host and guest upon binding and the resolvation of the resulting complex, often with release of free solvent and consequent formation of solvent-solvent interactions, Figure 1.27.

Unfortunately specific solvation effects are very difficult to understand, although molecular mechanics simulations have recently gone some way towards modelling complexation phenomena

**Table 1.6** Influence of solvent on the binding constant of host **1.26** for the neutral organic molecule imidazole (298 K).

| Solvent | Solvent type | $K_{11}$ ($M^{-1}$) |
|---|---|---|
| $CH_2Cl_2$ | Non-polar | 240 |
| $CHCl_3$ | Non-polar | |
| | H-bond acidic | 490 |
| $CH_3CCl_3$ | Non-polar | 8161 |
| $CHCl_2CHCl_2$ | Non-polar | |
| | Larger size | 128,000 |
| tetrahydrofuran (THF) | Non-polar, coordinating | 29.0 |
| 2-Me-THF | Non-polar, coordinating | 77.0 |
| 2,5-$Me_2$-THF | Non-polar, coordinating | 185 |
| 2,2-$Me_2$-THF | Non-polar, coordinating | 156 |
| 2,2,5,5-$Me_4$-THF | Non-polar, coordinating | |
| | Sterically hindered | 1067 |
| tetrahydropyran | Non-polar, coordinating | 104 |
| 1,4-dioxane | Non-polar, coordinating | 87 |
| *tert*-butyl methyl ether | Non-polar, coordinating | 566 |
| *iso*-propanol | Polar, protic | 13 |
| *tert*-butyl alcohol | Polar, protic | 66 |
| acetonitrile | Polar, aprotic, coordinating | No association |

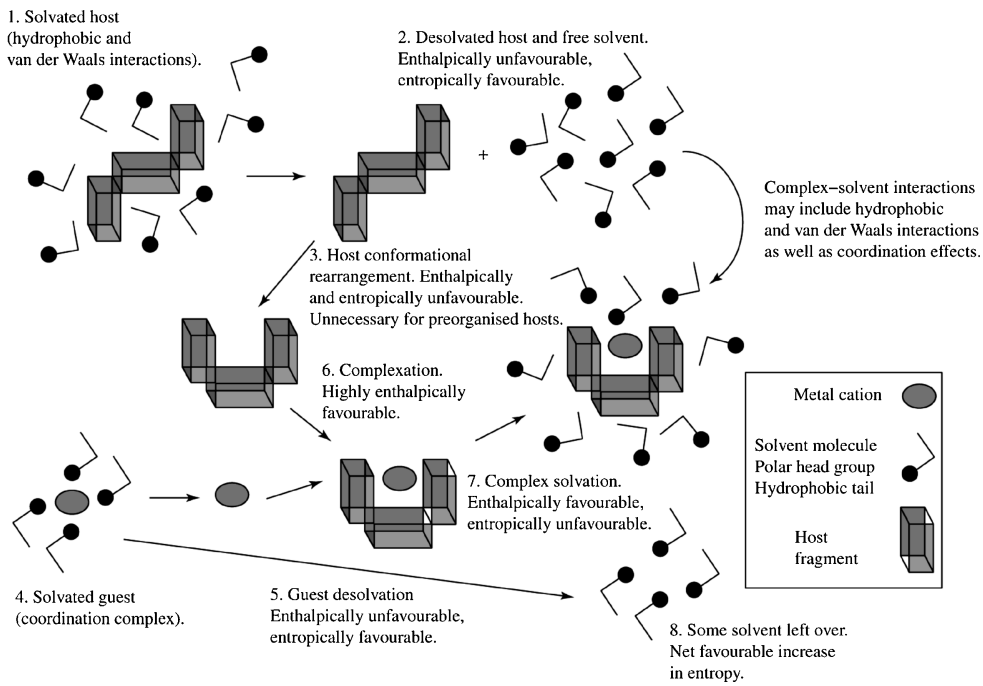


**Figure 1.27** Solvation considerations during the host-guest complexation of a metal cation.

in solution. For example a molecular dynamics study of halide anion inclusion complexes of a macrotricyclic tetrahedral host **1.27** compared halide binding in 'dry' and 'wet' forms of an ionic liquid solvent. In the 'dry' ionic liquid the uncomplexed halides are surrounded by 4–5 1-butyl-3-methylimidazolium cations whose binding mode changes from hydrogen bonding to facial coordination going from $F^-$ to $I^-$. In the wet solvent the first shell organic ionic liquid cations are all displaced by water molecules, while other halides exhibit a mixture. The solvation of the host and its halide complexes mainly involves $PF_6^-$ anions in the 'dry' medium, and additional water molecules in the 'wet' ionic liquid. The calculations predict that the anion binding selectivity is different in the two different media. In the 'dry' ionic liquid, $F^-$ is preferred over the other halides but in aqueous solution **1.27** is selective for $Cl^-$. In the 'wet' ionic liquid, there is no $F^-$ / $Cl^-$ selectivity, highlighting the importance of even small amounts of water on the complexation selectivity.[30]

An experimental comparison of the effect of 'wet' and 'dry' solvent has been carried out for host **1.28** which is capable of binding 2-aminopyrimidine (APy) to give a 1:1 complex **1.28**·APy. The binding constant in dry chloroform is up to $2.4 \times 10^4\ M^{-1}$, although this decreases significantly with temperature. Saturation of the chloroform with water does not result in a significant diminution of the host-guest affinity, as measured by the overall complexation free energy. This is because the competition for the binding sites by the water (which decreases the enthalpic contribution to the binding) is compensated by a more favourable entropy term associated with the release of water upon organisation of the complex (*cf.* the hydrophobic effect in neat water). A fortuitous case of cancellation of enthalpic and entropic effects.[31]

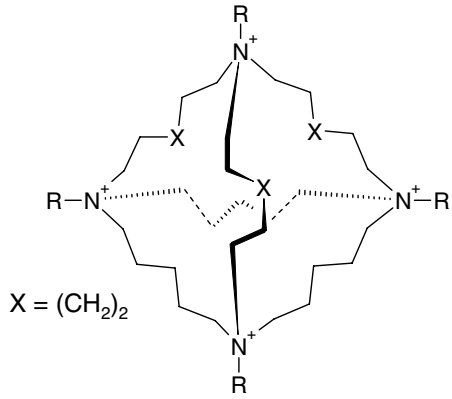


**1.27**

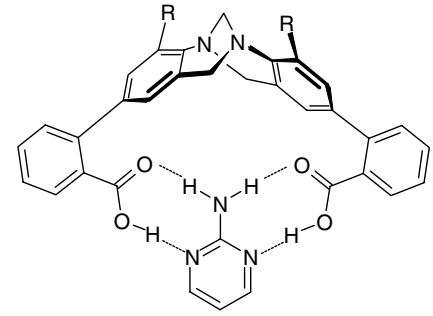


**1.28**.AMP

## 1.10 Supramolecular Concepts and Design

### 1.10.1 Host Design

Lehn, J.-M. 'Perspectives in supramolecular chemistry—from molecular recognition towards self-organisation', *Pure Appl. Chem.*, 1994, **66**, 1961–1966.

In order to design a host that will selectively bind a particular guest, we make use of the chelate and macrocyclic effects as well as the concept of complementarity (matching of host and guest steric and electronic requirements) and, crucially, host preorganisation.

The first step in host design is a clear definition and careful consideration of the target. This leads immediately to conclusions about the properties of the new host system. If a metal cation is to be the guest (Chapter 3), then its size (ionic radius), charge density and 'hardness' (Section 3.1.2) are important (*e.g.* soft donor atoms such as sulfur are suited to the binding of soft guests such as $Hg^{2+}$, $Ag^{+}$ and $Pb^{2+}$). For anion complexation (Chapter 4), these factors also affect spherical anions such as chloride, bromide *etc.*, but for nonspherical anionic guests, other factors such as shape, charge and hydrogen bond donor characteristics come into play. Organic cations and anions may require hosts with both hydrophilic and hydrophobic regions, while neutral molecule guests may lack specific 'handles' such as polar groups that can strongly interact with the host.

Having defined parameters such as the required host size, charge, character of the donor atoms *etc.*, the intellectual process of ligand tailoring can begin. The key concept in this process is organisation. Host–guest interactions occur through binding sites. The type and number of binding sites must be selected in a fashion that is most complementary to the characteristics of the binding sites of the guest (recall the definition of a guest as the partner with divergent binding sites), and these binding sites must be arranged on a (usually) organic scaffold or framework of suitable size to accommodate the guest. Binding sites should be spaced somewhat apart from one another to minimise repulsions between them, but arranged so that they can all interact simultaneously with the guest. The more favourable interactions there are, the better. The most stable complexes are generally obtained with hosts that are preorganised for guest binding, thus where there is no entropically and enthalpically unfavourable rearrangement on binding that reduces the overall free energy of complexation. Such hosts are ideally 'sinks' for their guests in which binding is entirely irreversible. This kind of complexation is ideal, for example, for the removal of toxic metal ions from polluted water. Hosts that bind guests less strongly (*i.e.* there is some equilibrium between bound and unbound species) find applications as sensors and carriers in which event sequences such as 'bind–detect–release' or 'bind–transport–release' are needed.

The nature of the organic framework of the host itself, whether lipophilic or hydrophilic, plays a fundamental role in host behaviour. This determines the solubility characteristics of the host and its complexes. The thickness of the ligand and the ease of access to the binding pocket, cavity or cleft affect both thermodynamic stability and binding kinetics. Addition of side arms may enhance lipophilicity (*e.g.* long alkyl chains) or encourage interaction with some external entity such as a polymer support or biomolecule. Such hosts are used to transport radioactive isotopes to targeted regions of the human body for medical radioimaging purposes or to develop artificial 'enzyme mimics' (Chapter 12).

Overall, the thorough application of these very broad principles has been generalised into what has been referred to as 'complete coordination chemistry', encompassing both supramolecular and classical (Werner) inorganic coordination chemistry.

## 1.10.2 Informed and Emergent Complex Matter

Lehn, J.-M., 'Toward complex matter: Supramolecular chemistry and self-organization', *Proc. Nat. Acad. Sci. USA* 2002, **99**, 4763–4768.

We saw in Figure 1.2c that supramolecular chemistry is not just about solid state or solution host-guest chemistry but increasingly emphasises self-assembly and the construction of multi-nanometre scale devices and ultimately materials based on nanometre-scale components (a nanometre is $10^{-9}$ of a metre). Strict supramolecular self-assembly (Chapter 10) involves the spontaneous formation of a multi-component aggregate under thermodynamically controlled conditions based on information encoded within the individual building blocks (referred to as 'tectons') themselves. The aggregate might comprise only one kind of molecule (as in the multiple copies of the same protein that comprise

the coat of many viruses such as the tobacco mosaic virus) or more than one type. In the latter case the different components are usually mutually complementary. Strict self-assembly implicitly carries with it the notion of reversibility of inter-component bond formation in that the final aggregate is the most thermodynamically stable structure under the prevailing conditions. This means that there is an inbuilt error-checking mechanism – malformed aggregates are less stable than the true minimum energy structure and decompose and are reassembled correctly if sufficient time is allowed to pass. Self-assembly processes may be regarded as the result of a series of supramolecular templated steps that build the aggregate. In turn, the interactions and synergy of self-assembled components, leading to the emergence of collective behaviour and properties, may be regarded as *self-organisation*. The hierarchical sequence of *templation* leading to *self-assembly* leading to *self organisation* represents a supramolecular information concept in which all the information needed to produce a complex, functioning device or material with some measure of sophisticated responsiveness to external stimuli is contained in the molecular components themselves.

When we talk of the *emergence* of a self-organised system we are talking very specifically about complex properties arising over time as a result of non-linear and perhaps unpredictable interactions between the molecular components. *Emergence* is a powerful, if controversial topic[32] that is part of the field of complexity science and cuts across a very broad range of disciplines. Emergence is in some sense the opposite of *convergence*, another possible outcome of templation and self-assembly, in which a single stable structure results from the interactions of the molecular components. A good example of an emergent structure in the everyday world is the complex network of tunnels and vents that regulate the environment within a termite mound (Figure 1.28). The mound is not planned by the termites and does not arise from a predictable template. It emerges from the individual, synergic efforts of the individual termites over time. From a chemical point of view it is possible to exert a high degree of control over the structure and shape and hence information content of small molecules (*i.e.* around 1 nm or less size) using chemical synthetic techniques. Self-organisation then leads to multi-nanometre scale structures and systems that, because of their complexity and large number of components, cannot be made in a linear one-step-at-a-time fashion. Emergent structures and properties arising from the self-assembly and self-organisation of molecules on a multi-nanometre scale are ubiquitous in Biochemistry (*e.g.* self-replication and enzymic catalysis) and are increasingly being studied by chemists in artificial, abiotic (= non biochemical) systems.

**Figure 1.28** A termite mound in Australia's Northern Territory. Termite mounds are classic examples of Natural emergent structures.

### 1.10.3 Nanochemistry

Ozin, G. and Arsenault, A. *Nanochemistry*, Royal Society of Chemistry: Cambridge, 2005.

We can refer to the synthesis and study of chemical systems with features and functionality on the multi-nanometre length scale as *nanochemistry* and materials with features of size of the order of 1–100 nm as *nanomaterials*. Very broadly there are two approaches to the nanoscale dimension – 'synthesising-up' and 'engineering-down'. The engineering down approach includes the latest in modern techniques for producing electronic components and originates in a bulk sense. Engineering down to the nanoscale (*nanotechnology*) involves doing the same sorts of things that an engineer or artisan does on a macroscopic scale but using specialised techniques in order to miniaturise. In contrast the synthesising-up approach (*nanochemistry*) is modelled on biology, particularly biological self-assembly, and aims to produce nanoscale functional components (perhaps with molecular device or molecular scale computing applications in mind) by chemical synthesis. Indeed the very first reports of functional molecular computing using supramolecular species have already begun to appear.[33] Geff Ozin of the University of Toronto, one of the leading proponents of nanochemistry and the synthesis of nanomaterials has defined nanomaterials as materials whose properties change according to their size, or the size of their components. An excellent example is gold *nanoparticles*. Nanoparticles are tiny fragments of a material such as metallic gold. They are typically more or less spherical in shape (Figure 1.29) and may have a regular, faceted crystalline morphology and structure (in which case they are referred to as *nanocrystals*). Nanoparticles are typically 2–30 nm in radius and very interestingly often exhibit very intense colours. You may already have seen such colours in red or purple suspensions of gold colloids. The colour arises from a visible absorption termed a *surface plasmon resonance* absorption and it arises from the collective motion of free electrons around across the surface of the nanoparticle. Crucially the wavelength of this absorption (and hence the observed colour) depend on the size of the nanoparticle.

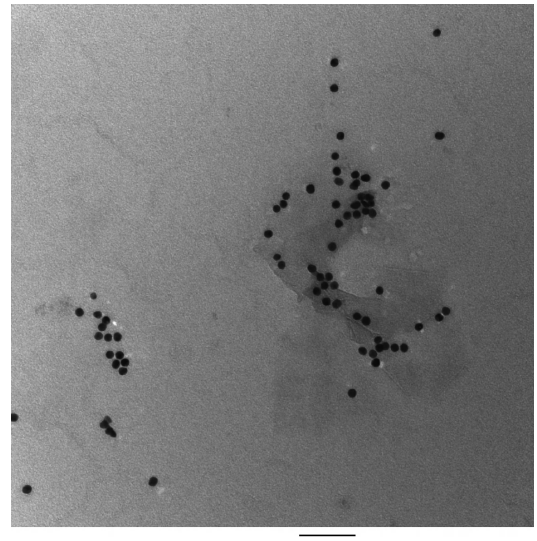

**Figure 1.29** TEM micrograph showing gold nanoparticles. Note the regular shape and uniform size distribution. Scale bar = 100 nm.

We can also include in the definition of nanochemistry molecular systems exhibiting designed or emergent nanometer-scale features, functionality or properties. For example, interlocked molecules termed *catenanes* can exhibit complex nanoscale molecular motions somewhat analogous to the mechanical interlocking of gears (Section 11.5). As we will see in Chapter 15 there are also hybrid systems coupling molecular hosts to nanomaterials such as nanoparticles. It is also possible to carry out nanochemistry using a variety of scanning probe microscopy based techniques such as Scanning Tunnelling Microscopy (STM) and Atomic Force Microscopy (AFM). Because they operate on the nanometer scale these techniques give unique insight into molecular behaviour. In addition scanning probe microscope tips may be used to carry out molecular manipulations and redox chemistry. Tips may even be modified by attaching a probe molecule and using molecular recognition to examine a surface. Chemical reactions may even be carried out by physically pushing individual molecules into close mutual proximity using an STM tip.[34] Chemical assembly thus represents one facet of the preparation and study of nanoscale materials and there is a continuum of increasing complexity and decreasing predictability and control between molecular and materials properties. Within this continuum we can make a useful distinction between situations where an observed property is an emergent consequence of the interactions between molecules or ions and where it is a distinctive molecular property. In this book we aim to show the full series of steps from the grass roots of simple intermolecular interactions through to emergent nanomaterials and nanochemical systems.

## Summary

- Supramolecular Chemistry involves the chemistry of the non-covalent bond.
- Non-covalent bonds include ionic and dipolar interactions, hydrogen bonds, aromatic interactions ($\pi-\pi$, cation-$\pi$ and anion-$\pi$), closed shell interactions and van der Waals interactions.
- Supermolecules generally comprise a host component with convergent binding sites and a guest component with divergent binding sites.
- In solid-state host-guest or clathrate compounds the guest is included within a gap in the packing of host molecules.
- Self-assembling systems do not involve hosts and guests but rather self-complementary molecules or complementary partners (tectons).
- The affinity of a host for a guest is measured by the binding constant; selective hosts have a high binding constant for one particular guest.
- Supramolecular chemistry makes use of 'generalised' coordination chemistry and binding cooperativity.
- The traditional picture of 'lock-and-key' binding is generally less appropriate than an induced-fit approach.
- Perhaps the most important concepts in supramolecular host design and preorganisation and complementarity, which encapsulate more traditional concepts such as the macrocyclic effect.
- Solvation and desolvation effects are of tremendous importance in assessing binding equilibria.
- Modern supramolecular chemistry is progressing towards concepts such as molecular information content and intermolecular interaction algorithms, leading to the self-organisation of increasingly complex, informed matter with emergent properties that arise spontaneously in the multi nanometre length scale.

## Study Problems

1.1 Thermodynamic parameters for the reaction of $Cu^{2+}_{(aq)}$ with various ligands are given below (aqueous solution, 25 ºC). Use these data to calculate the binding constants (log $K$) for the resulting 1:1 metal-to-ligand complexes. Explain the differences in stability observed.

| Ligand | $\Delta H^{o}$ (kJ mol$^{-1}$) | $T\Delta S^{o}$ (kJ mol$^{-1}$) |
|---|---|---|
| 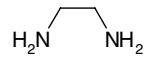 | −105 | 7.1 |
| 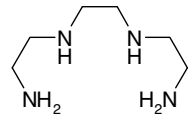 | −90.4 | 24.3 |
| 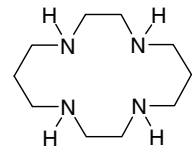 | −76.6 | 64.0 |

1.2 Give a concise definition of the term 'supramolecular chemistry'. Explain the distinction between molecular and supramolecular interactions. Illustrate your answer with examples of supramolecular interactions and discuss their relative importance.

1.3 Draw up a relative scale of the strengths of non-molecular interactions using the information given in Section 1.8. Correlate this with a second scale of the importance of these interactions in supramolecular design of host for metal cations, taking into account factors such as directionality, ease of incorporation into host frameworks, and propensity of binding enhancement *via* multiple binding sites. Would this ranking change if you were to design hosts for anions or neutral organic molecules? What interactions might be important in designing a host for the following species: methane, benzene, methanol, phenol, ammonia, $Cl^{-}$, $Na^{+}$ and $Ni^{2+}$?

1.4 Using the timeline given in Table 1.1 suggest what may be some of the most important discoveries in supramolecular chemistry. Why do you think it has taken so long for the topic to evolve as a separate discipline?

## Suggested Further Reading


Atwood, J. L. and Steed, J. W. (eds), *Encyclopedia of Supramolecular Chemistry*, Marcel Dekker, New York, NY, USA, 2004.

Atwood, J. L. and Steed, J. W. (eds.), *Organic Nanostructures*, Wiley-VCH: Weinheim, 2008.

Anslyn, E. V. and Dougherty, D. A., *Modern Physical Organic Chemistry*, University Science Books: Sausalito, California, USA, 2006.

Balzani, V., Credi, A. and Venturi, M. *Molecular Devices and Machines: A Journey into the Nanoworld*, Wiley-VCH: Weinheim, 2003.

Cragg, P. J., *Practical Supramolecular Chemistry*, John Wiley & Sons, Ltd., Chichester, UK, 2006.

Desiraju, G. R. (ed.), *The Crystal as a Supramolecular Entity*, John Wiley & Sons, Ltd., Chichester, UK, 1996.

Haiduc, I. and Edelmann, F. T., *Supramolecular Organometallic Chemistry*, Wiley-VCH, Weinheim, Germany, 1999.

Lehn, J.-M., *Supramolecular Chemistry*, VCH, Weinheim, Germany, 1995.

Lehn, J.-M., Atwood, J. L., Davies, J. E. D., MacNicol, D. D. and Vögtle, F. (eds), *Comprehensive Supramolecular Chemistry*, Pergamon, Oxford, UK, 1996.

Ozin, G. A. and Arsenault, A. C., *Nanochemistry*, The Royal Society of Chemistry, Cambridge, UK, 2005.

Schneider, H.-J. and Yatsimirski, A. K., *Principles and Methods in Supramolecular Chemistry*, Wiley-VCH, Weinheim, Germany, 2000.
Sessler, J. L., Gale, P. A. and Cho, W.-S., *Anion Receptor Chemistry*, Royal Society of Chemistry: Cambridge, 2006.
Schalley, C. A. (ed.), *Analytical Methods in Supramolecular Chemistry*, Wiley-VCH: Weinheim, 2007.
Steed, J. W., Turner, D. R. and Wallace, K. J., *Core Concepts in Supramolecular Chemistry and Nanochemistry*, John Wiley & Sons, Ltd., Chichester, UK, 2007.

## References

1. Lehn, J.-M., *Supramolecular Chemistry*. 1 ed.; VCH: Weinheim, 1995;
2. Cram, D. J., Preorganisation – from solvents to spherands. *Angew. Chem., Int. Ed. Engl.* 1986, **25**, 1039–1134.
3. Lloyd, N. C.. Morgan, H. W., Nicholson, B. K., Ronimus, R. S., The Composition of Ehrlich's Salvarsan: Resolution of a century-old debate. *Angew. Chem. Int. Ed.* 2005, **44**, 941–944.
4. Koshland, D. E., The Key-Lock Theory and the Induced Fit Theory. *Angew. Chem., Int. Ed.* 1995, **33**, 2375–2378.
5. Bencini, A., Bianchi, A., Garcia-España, E., Micheloni, M., Ramirez, J. A., Proton coordination by polyamine compounds in aqueous solution. *Coord. Chem. Rev.* 1999, **188**, 97–156.
6. Hynes, M. J., EQNMR: A computer program for the calculation of stability constants from nuclear magnetic resonance chemical shift data. *J. Chem. Soc., Dalton Trans.* 1993, 311–312.
7. Szalay, L., Farkas, V., Vass, E., Hollósi, M., Móczár, I., Pintér, Á., Huszthy, P., Synthesis and selective lead(II) binding of achiral and enantiomerically pure chiral acridono-18-crown-6 ether type ligands. *Tetrahedron Asymmetry* 2004, **15**, 1487–1493.
8. Sessler, J. L., Gross, D. E., Cho, W.-S., *et al.*, Calix[4]pyrrole as a chloride anion receptor: Solvent and countercation effects. *J. Am. Chem. Soc.* 2006, **128**, 12281–12288.
9. Williams, D. H., Westwell, M. S., Aspects of weak interactions. *Chem. Soc. Rev.* 1998, **27**, 57–63.
10. Metzger, A., Lynch, V. M., Anslyn, E. V., A synthetic receptor selective for citrate. *Angew. Chem., Int. Ed. Engl.* 1997, **36**, 862–865.
11. Rebek Jr., J., Binding forces, equilibria, and rates—new models for enzymic catalysis. *Acc. Chem. Res.* 1984, **17**, 258–264.
12. Hamacek, J., Borkovec, M., Piguet, C., Simple thermodynamics for unravelling sophisticated self-assembly processes. *Dalton Trans.* 2006, 1473–1490.
13. Cabbiness, D. K., Margerum, D. W., Macrocyclic effect on the stability of copper(II) tetramine complexes. *J. Am. Chem. Soc.* 1969, **91**, 6540–6541.
14. Folmer-Andersen, J. F., Kitamura, M., Anslyn, E. V., Pattern-based discrimination of enantiomeric and structurally similar amino acids: An optical mimic of the mammalian taste response. *J. Am. Chem. Soc.* 2006, **128**, 5652–5653.
15. Garratt, P. J., Ibbett, A. J., Ledbury, J. E., O'Brien, R., Hursthouse, M. B., Malik, K. M. A., Molecular design using electrostatic interactions. 1. Synthesis and properties of flexable tripodand tri- and hexa-cations with restricted conformations. Molecular selection of ferricyanide from ferrocyanide. *Tetrahedron* 1998, **54**, 949–968.
16. Laurence, C.; Berthelot, M., Observations on the strength of hydrogen bonding. *Persp. Drug Disc. Des.* 2000, **18**, 39–60.
17. Weber, E., Franken, S., Puff, H., Ahrendt, J., Enclave inclusion of nitromethane by a new crown host—X-ray crystal-structure of the inclusion complex and host selectivity properties. *J. Chem. Soc., Chem. Commun.* 1986, 467–469.
18. Ilioudis, C. A., Tocher, D. A., Steed, J. W., A highly efficient, preorganized macrobicyclic receptor for halides based on CH··· and NH···anion interactions. *J. Am. Chem. Soc.* 2004, **126**, 12395–12402.
19. Rosokha, Y. S., Lindeman, S. V., Rosokha, S. V., Kochi, J. K., Halide recognition through diagnostic 'anion-π' interactions: Molecular complexes of Cl-, Br-, and I- with olefinic and aromatic π receptors. *Angew. Chem., Int. Ed.* 2004, **43**, 4650–4652.
20. Schottel, B. L., Chifotides, H. T., Shatruk, M., *et al.*, Anion-$\pi$ interactions as controlling elements in self-assembly reactions of Ag(I) complexes with $\pi$-acidic aromatic rings. *J. Am. Chem. Soc.* 2006, **128**, 5895–5912.
21. Kim, E.-I., Paliwal, S., Wilcox, C. S., Measurements of molecular electrostatic field effects in edge- to-face aromatic interactions and CH-p interactions with implications for protein folding and molecular recognition. *J. Am. Chem. Soc.* 1998, **120**, 11192.
22. Janiak, C., A critical account on π-π stacking in metal complexes with aromatic nitrogen-containing ligands. *J. Chem. Soc., Dalton Trans.* 2000, 3885–3896.

23. Prince, P. D., McGrady, G. S., Steed, J. W., Weak interactions induce asymmetry in the crystal structures of triaryl derivatives of group 14 elements. *New J. Chem.* 2002, **26**, 457–461.
24. Andreetti, G. D., Ungaro, R., Pochini, A., Crystal and molecular structure of cyclo{quarter[(5-t-butyl-2-hydroxy-1, 3-phenylene)methylene]} toluene (1:1) clathrate. *J. Chem. Soc., Chem. Commun.* 1979, 1005–1007.
25. Alcock, N. W., Countryman, R. M., Secondary bonding .1. Crystal and molecular-structures of $(C_6h_5)_2 I_x$ (X=Cl, Br, or I). *J. Chem. Soc., Dalton Trans.* 1977, 217–219.
26. Laguna, A., Fernández, E. J., López-de-Luzuriaga, J. M., 'Aurophilic interactions', in *Encyclopedia of Supramolecular Chemistry*, Atwood, J. L., Steed, J. W., eds. Marcel Dekker: New York, 2004; Vol. 1, *pp.* 82–87.
27. Metrangolo, P., Resnati, G., 'Halogen bonding', in *Encyclopedia of Supramolecular Chemistry*, Atwood, J. L., Steed, J. W., eds. Marcel Dekker: New York, 2004; Vol. 1, *pp.* 628–635.
28. Jones, P. G., Sheldrick, G. M., Uson, R., Laguna, A., μ-Chloro-bis(triphenylphosphine)digold(I) perchlorate dichloromethane solvate. *Acta Crystallogr., Sect. B* 1980, **36**, 1486–1488.
29. Leung, K. H.; Phillips, D. L.; Mao, Z.; Che, C. M.; Miskowski, V. M.; Chan, C. K., Electronic excited states of $[Au_2(dmpm)_3](ClO_4)_2$ (dmpm= bis(dimethylphosphine)methane) *Inorg. Chem.* 2002, **41**, 2054–2059.
30. Chaumont, A., Wipff, G., Halide anion solvation and recognition by a macrotricyclic tetraammonium host in an ionic liquid: a molecular dynamics study. *New J. Chem.* 2006, **30**, 537–545.
31. Adrian, J. C., Wilcox, C. S., Chemistry of synthetic receptors and functional-group arrays .15. Effects of added water on thermodynamic aspects of hydrogen-bond-based molecular recognition in chloroform. *J. Am. Chem. Soc.* 1991, **113**, 678–680.
32. Goldstein, J., Emergence as a construct: history and issues. *Emergence: Complexity and Organization* 1999, **1**, 49–72.
33. Collier, C. P., Wong, E. W., Belohradsky, M., *et al.*, Electronically configurable molecular-based logic gates. *Science* 1999, **285**, 391–394.
34. Hla, S. W., Bartels, L., Meyer, G., Rieder, K. H., Inducing all steps of a chemical reaction with the scanning tunneling microscope tip: Towards single molecule engineering. *Phys. Rev. Lett.* 2000, **85**, 2777–2780.

# 2 The Supramolecular Chemistry of Life

*'Nature that fram'd us of four elements,*
*Warring within our breasts for regiment,*
*Doth teach us all to have aspiring minds:*
*Our souls, whose faculties can comprehend*
*The wondrous Architecture of the world……'*

Christopher Marlowe (1564–1593), *Conquests of Tamburlaine*

## 2.1 Biological Inspiration for Supramolecular Chemistry

Nelson, D. L. and Cox, M. M., *Lehninger Principles of Biochemistry.* 4th ed.; W. H. Freeman: New York, 2004.

Much of the inspiration and origins of supramolecular chemistry comes from the chemistry found in living biological systems. Sometimes incredibly complex, sometimes elegantly simple, Nature has evolved an enormous amount of highly specific, hierarchical, selective and cooperative chemistry that enables living systems to maintain themselves in a dynamic equilibrium with their environment and to feed, respire, reproduce and respond to external stimuli. In biological chemistry, the supramolecular hosts are the receptor sites of enzymes, genes, antibodies of the immune system, and ionophores. The guests are substrates, inhibitors, co-factors, drugs or antigens. These components variously exhibit supramolecular properties such as molecular recognition, self-assembly, self-organisation, self-replication and kinetic and thermodynamic complementarity. The vast majority of these properties rely upon supramolecular interactions such as coordination (ion–dipole) bonds, hydrogen bonds and π–π stacking discussed in Section 1.8. Biological systems are, therefore, supramolecular systems *par excellence.* A great deal of effort in supramolecular chemistry has been expended in attempts to model or mimic biological processes such as the catalysis of organic chemical reactions by enzymes, or the selective transport of metal cations or molecular substrates such as $O_2$. As part of this process, our understanding of biological systems has grown enormously, but it is also fair to say that the molecular and supramolecular chemistry of human endeavour, as they stand now, are still a long way away in scale, scope and functionality from their biochemical analogues. The fact that Nature exhibits such a rich and efficient natural supramolecular chemistry is, however, an enormous encouragement and motivation to continue to seek ever more sophisticated abiotic (nonbiological) analogues and indeed to attempt to develop synthetic systems capable of carrying out transformations or possessing properties not found naturally. In this chapter, we give a brief and highly selective overview of some of the more important biological chemistry of relevance to supramolecular chemists by way of a very brief introduction to the extensive synthetic systems that we will be looking at in the rest of this book. Subsequent chapters will deal with the ways in which synthetic and model systems mimic these biological processes and how insight has been gained into biochemistry by the study of supramolecular compounds, as well as the enormous diversity of entirely non-biological supramolecular chemistry.

## 2.2 Alkali Metal Cations in Biochemistry

### 2.2.1 Membrane Potentials

Energy is vital to life. Plants get energy from sunlight (photosynthesis), humans get energy from food, which we oxidise to $CO_2$ and water. Energy is used in respiration, a process by which energy from food is transformed and stored as the chemical bond energy of ATP (adenosine triphosphate). Strictly, ATP has a 4– ionic charge, balanced by alkaline and alkaline earth metal cations. In biological notation this is often omitted. ATP is capable of long-term energy storage and is transported to any areas where energy is needed to drive endergonic (energy-consuming) reactions such as muscle contraction. The energy is released from ATP by a class of enzymes called ATPases, of which $Na^+/K^+$-ATPase is perhaps the most important example. One mole of ATP releases 35 kJ of energy, according to the

*Supramolecular Chemistry, 2nd edition* J. W. Steed and J. L. Atwood
© 2009 John Wiley & Sons, Ltd ISBN: 978-0-470-51233-3

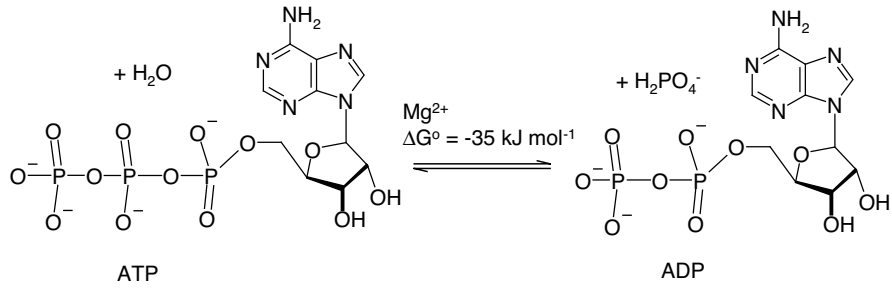


**Scheme 2.1** Energy-releasing dephosphorylation of ATP to ADP and dihydrogen phosphate. $Mg^{2+}$ acts as a catalyst for the reaction.

reaction shown in Scheme 2.1. Note that while the ATP molecule is relatively complex, it is only the triphosphate tail that is changed during the course of the reaction. Breaking of the terminal phosphate ester P—O bond gives the dihydrogen phosphate anion ($H_2PO_4^-$, often referred to as 'inorganic phosphate', $P_i$) and adenosine diphosphate, ADP.

The $Na^+/K^+$-ATPase enzyme is an example of a *transmembrane* enzyme, *i.e.* an enzyme that exists in the phospholipid membrane (wall) of a biological cell. As part of the process of consuming ATP, the $Na^+/K^+$-ATPase enzyme transports the alkali metal cations $Na^+$ and $K^+$ from one side of the cell membrane to the other. Effectively, the enzyme scavenges $Na^+$ from the inside of the cell and transports it to the outside, against the prevailing concentration gradient. Simultaneously, $K^+$ is transported into the cell. Thus, in the intracellular fluid there is a high concentration of $K^+$; outside there is a high concentration of $Na^+$ (Table 2.1). This uneven distribution of alkali metal cations across the cell membrane is a highly important and necessary feature and results in a transmembrane electrical potential, rather like a battery. This potential difference across the cell is used, amongst other things, in information transfer in nerve cells (Figure 2.1).

The actual amount of charge separation across a cell membrane is very small (the number of $M^+$ ions is equal on either side of the membrane). Such a potential difference could, in principle, have been set up by separating $Na^+$ and $Cl^-$ across a membrane. However, such an actual separation of oppositely charged ions would require much more energy because of the large electrostatic forces between such ions. In fact, the resulting chemical potential arising from the different identities of the alkali metal ions ($Na^+$ and $K^+$) is sufficient to generate the required signal.

The most important requirement for utilisation of this kind of ionic diffusion as a means to information transfer is the maintenance of the non-equilibrium ionic concentration gradient. This is a relatively unstable state – it requires energy to counteract the natural entropy-increasing flow back to equilibrium. This is best illustrated by the *pump storage* model. Ions are actively 'pumped' through

**Table 2.1** Some examples of biochemical $Na^+$ and $K^+$ distributions.

| | Concentration/mmol $kg^{-1}$ | |
|---|---|---|
| Location | $K^+$ | $Na^+$ |
| Human intracellular fluid (*e.g.* erythrocytes) | 92 | 11 |
| Human extracellular fluid (*e.g.* blood plasma) | 5 | 152 |
| Squid nerve (inside) | 300 | 10 |
| Squid nerve (outside) | 22 | 440 |

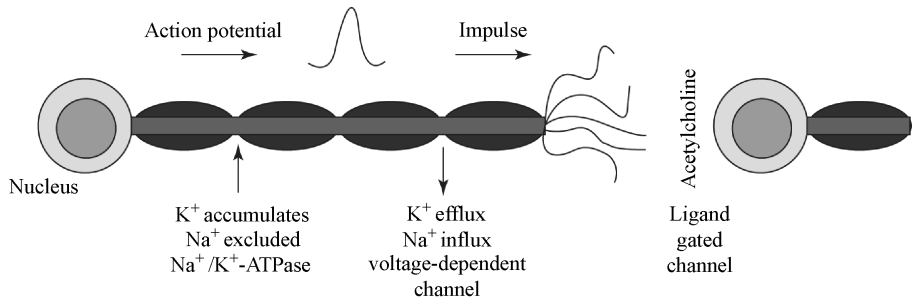


**Figure 2.1** Mode of signal transduction of nerve system. Under concentration gradients, generated by $Na^+/K^+$-ATPase, opening of an ion channel causes the passive efflux of $K^+$ and the influx of $Na^+$ resulting in a small burst of electrical current (nerve impulse) and a change in the membrane potential. At the end of the nerve cell (axon) the electrical signal is transformed into a chemical signal by triggering the ejection of a hormone such as acetylcholine (Section 2.7). The hormone, in turn, triggers the opening of a ligand-gated ion channel in the next nerve axon and restarts the nerve impulse as an electrical current by allowing passive flow of $K^+$ and $Na^+$ across the next membrane.

the biological membrane against the concentration gradient until a stationary, non-equilibrium state is reached. Stimulation results in the rapid, passive flow of ions back to equilibrium *via* the operation of *gate functions* (Figure 2.2).

The importance of maintaining precise concentration gradients is highlighted by the severe effects of metabolic disorders involving alkali metal cations. For example, high sodium intake is linked intimately with the development of high blood pressure; on the other hand, aged

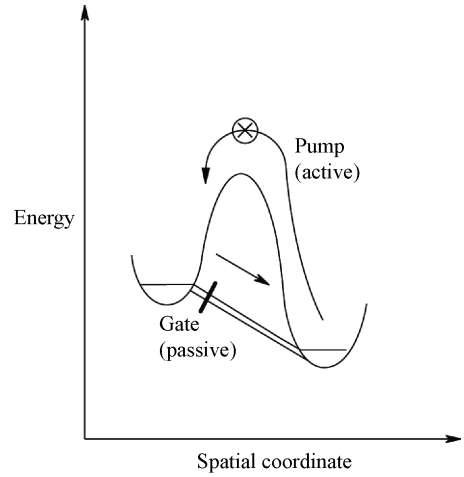


**Figure 2.2** The pump storage model. Metal ions are actively pumped by $Na^+/K^+$-ATPase (an energy-consuming process) from regions of low concentration to regions of high concentration against the concentration gradient until a dynamic non-equilibrium state is reached in which active pumping is balanced by accidental diffusion. Upon activation by the appropriate hormone, selectively gated ion channels open allowing the passive (and therefore rapid) flow of ions back towards equilibrium, resulting in current flow.

organisms have some difficulty in preventing the excretion of the very labile $K^+$ because of disturbed membrane permeabilities.

## 2.2.2 Membrane Transport

So how does an alkali metal get from the inside of the cell to the outside? A cell membrane consists of hydrophilic (water soluble) phosphate head groups attached to a long lipid (fatty) tail and is thus an example of an amphiphile (Section 13.2.1). In the body's aqueous environment, the hydrophilic head groups are attracted to the surrounding medium (*e.g. via* hydrogen bonding and dipolar interactions) while the organic tail is repelled. This results in a bilayer arrangement in which the organic components are all hidden away from the solvent while the hydrophilic portions face out. Anything that is to pass through the cell wall must therefore be able to pass this lipophilic (fat-soluble) region (Figure 2.3).

Sodium and potassium cations are not at all lipophilic. They cannot effectively diffuse through the cell wall unless something makes them lipophilic or a nonlipophilic pathway is created for them. There are two main possible methods of such passive cation transport along a concentration gradient: transport by some kind of lipophilic carrier, or controlled passage through a hydrophilic channel in the membrane (Figure 2.4).

Transport of metal ions *via* the carrier mechanism involves a carrier ligand that is able both to bind selectively to the metal cation and to shield it from the lipophilic region of the membrane. Such ion carriers are termed *ionophores*. The natural products valinomycin (**2.1**) and nonactin (**2.2**) are among the best known. Valinomycin was first isolated from the bacterium *Steptomyces fulvissimus* in 1955, and was established in 1967 to catalyse the exchange of $K^+$ and $H^+$ across the membrane of mitochondria within cells *via* a carrier mechanism without affecting $Na^+$ concentration. Chemically, valinomycin is a cyclic depsipeptide made up of a threefold repetition of four amino acid residues: L-valine (Val), D-hydroxyisovaleric acid (Hyi), D-valine and L-lactic acid (Lac) (**2.3**). Hydrogen bonding of type N–H···O=C to both ester and amide carbonyl groups plays an important role in the conformation of valinomycin, where it helps the peptide chain wrap around the metal cation, contributing to its degree of preorganisation and stabilising the bound conformation. Valinomycin and nonactin are both selective for $K^+$ because they are able to fold in on themselves in order to produce an approximately octahedral array of hard (*i.e.* non-polarisable, according to the hard and soft acids and bases (HSAB) theory; see Section 3.1.2) carbonyl oxygen atom donors exactly suited to fit an ion of the size of $K^+$. Rubidium and caesium are too large, whereas the ionophore cannot contract tightly enough to bind to $Na^+$. The X-ray crystal structure of the $K^+$ complex of valinomycin is shown in Figure 2.5. It can

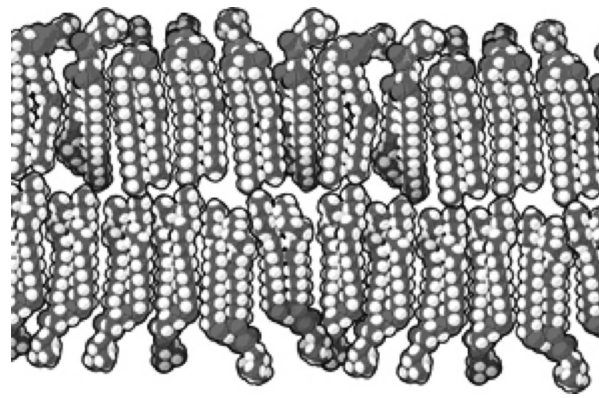

**Figure 2.3** Schematic diagram of a phospholipid biological membrane (5–6 nm in width).

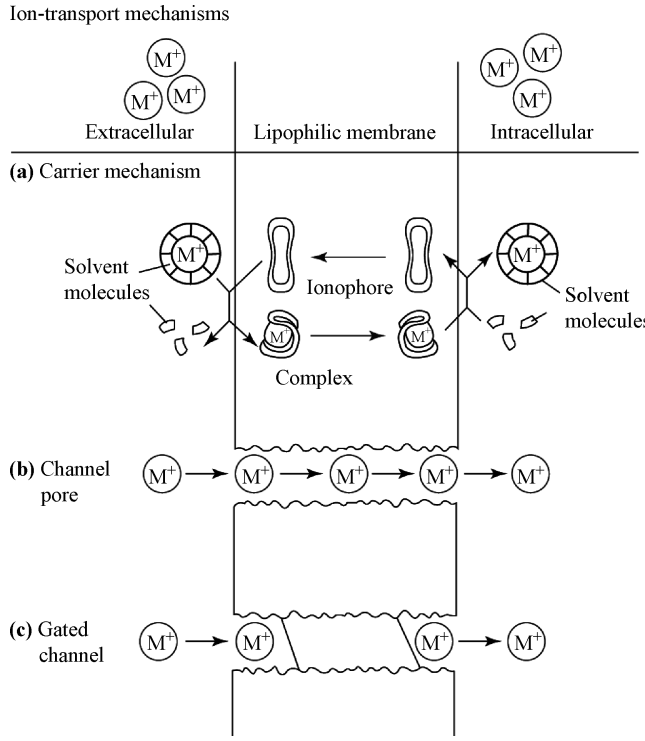


**Figure 2.4** (a) Carrier, (b) channel and (c) gated channel mechanisms of ion transport across a biological membrane. The carrier encapsulates the alkali metal cation, stripping away most or all of the water molecules bound to it. The carrier then presents a lipophilic surface, moving across the membrane and releasing the ion back into aqueous solution at the other end. The channel is, primarily, an aqueous hole running through the membrane. Ions can traverse swiftly through the channel without losing their solvent sphere throughout most of their journey, as long as the gate (activated by potential changes or hormones) is open and the ion can pass through the selectivity filter (which discriminates between $Na^+$ and $K^+$). (Reproduced by permission of John Wiley & Sons, Ltd).

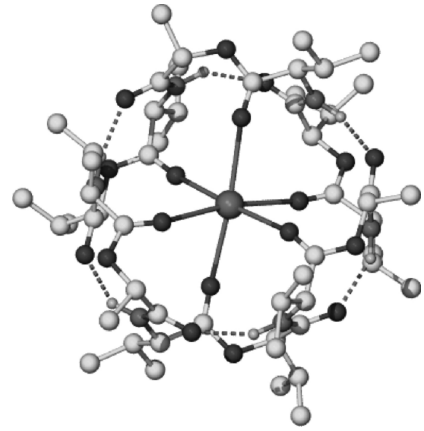

**Figure 2.5** X-ray crystal structure of the $K^+$ complex of valinomycin. For a summary of the technique of X-ray crystallography, see Box 2.1.

**Box 2.1** X-ray Crystallography of Supramolecular Compounds

Massa, W. and Gould, R. O., *Crystal Structure Determination*. 2nd ed.; Springer: Heidelberg, 2004.

The primary objective of an X-ray diffraction experiment is to obtain a detailed picture of the contents of the crystal at the atomic level, as if you were viewing it through an extremely powerful microscope. Experimentally this process consists of a series of intensity measurements of X-ray beams diffracted from a small, single crystal sample. In the best case the experiment results in a detailed knowledge of the positions of all the atoms in the molecule and hence detailed knowledge of the molecular structure as a whole, including bond lengths, angles and intermolecular contacts. The experiment also gives insight into thermal motion in the solid state. These results are of particular importance to supramolecular chemists because they give direct information on intermolecular interactions such as hydrogen bonding and ion–dipole interactions, as well as the steric fit of a receptor and a substrate (host and guest). Because X-ray crystallography relies upon diffraction by the electron density in the crystal, however, it is not very good at locating hydrogen atoms accurately (after all, they have only one electron each). These are important in hydrogen bonding studies and, if extremely precise information is required, they are usually located using single crystal neutron diffraction (see Box 8.1).

So, why don't we just use a very powerful microscope and view atoms directly? The answer is that atoms are simply too small. The wavelength of visible light falls between 400 and 700 nm. In comparison, a typical bond distance between two atoms (*e.g.* carbon) is about 0.15 nm, so we need radiation of a much smaller wavelength, comparable to that of the interatomic separations: X-ray radiation. The problem with radiation of very short wavelength is that it is impossible to manufacture a lens powerful enough to refocus it. This is referred to as the phase problem. Another way of describing the phase problem is that crystal structure determination calculations require information about the amplitude of diffracted X-rays (the so-called structure factor amplitude, F) which is proportional to the square root of the observed X-ray intensity. Unfortunately F can be both positive and negative and there is no way of directly determining the sign of F from a measurement of intensity, *i.e.* $F^2$ because $|-F|^2$ is the same as $|+F|^2$. This loss of $+/-$ phase information is the phase problem. The phase problem is solved by developing a mathematical model of the structure based on clues from the experimental data and chemical intuition. This is used to calculate the molecules' X-ray diffraction patterns. The calculated prediction is compared with the observed experimental data and improved by least-squares refinement. The experiment is complete when the agreement between calculated and observed data is as good as possible. This agreement is measured by the *R* (residual) factor and the standard uncertainties (errors, often referred to as estimated standard deviations) on the individual bond lengths and angles. For a good structure determination, the R factor should be around 5 % or less.

### *A Typical Experiment*

1. Prepare single crystal sample (slow evaporation, recrystallisation *etc.*):
   - Homogeneous single crystal without defects or cracks.
   - Size 0.1–0.8 mm edge length, ideally spherical or at least equidimensional.
2. Examine under optical microscope to check for imperfections.
3. Preliminary X-ray photographs (polaroid film or electronic area detector).
   - Check crystal quality.
   - Determine unit cell dimensions and symmetry information (the unit cell is the basic building block of the crystal).
4. Collect intensity data (1000–100 000 data points depending on molecular size).
5. Develop an approximate model of the structure (referred to as *solving* the structure).
   - Application of Patterson or Direct methods to 'guess' approximate phases.
   - Stereochemistry of molecule in outline.
   - Bond lengths to ± 0.1Å (1Å (Ångstrom) = $10^{-10}$ m = 0.1 nm).

(*continued*)

**Box 2.1** (*Continued*)

6. Refine structure by least squares method.
   - Optimise model (set of atom coordinates and thermal parameters) to get best fit.
   - Bond lengths to ± 0.005Å.
   - Precise stereochemistry.
7. Convert coordinates to tables of bond lengths and angles, and draw picture.
8. Deposit the results in CIF format in the Cambridge Structural Database (CSD, Section 8.4)

This process becomes more complicated as the size of the molecule or array to be studied increases. Most supramolecular compounds are of a size intermediate between traditional 'small molecules' and large biomolecules such as proteins and it is usually possible to obtain precise information on them fairly readily. As the size of the molecule of molecular assembly increases, however, the number of data measured and parameters that must be fitted rises dramatically. This complexity is often accompanied by increasing problems in obtaining good-quality crystalline samples. Large molecules, particularly those encountered in supramolecular chemistry that contain cavities or are of awkward shapes and fit together poorly, often contain occluded solvent molecules. These can diffuse out of the crystal lattice during the X-ray experiment causing loss of crystallinity and hence loss of diffraction intensity. They can also move around resulting in a 'smeared' (disordered) averaged electron density, which is difficult to model. Even in cases where solvent is not present, poorly packed crystals result in weak diffraction. The X-ray crystallography of even higher molecular weight samples, such as proteins, is much more complicated, requiring the collection of a number of closely related sets of data, often from many crystals. In protein work, problems are encountered with X-ray damage to the sample, weak diffraction, and difficulty in identifying the various molecular fragments. Both supramolecular and protein crystallography have been revolutionised by the advent of area detectors such as charge-coupled device (CCD) instruments (Figure 2.6) (X-ray detectors that are capable of measuring many data points simultaneously), which enhance vastly both the speed and sensitivity of the experiment. Moreover synchrotron sources such as Diamond in the UK are becoming relatively accessible and are able to obtain single crystal X-ray data on extremely small samples often only a few tens of microns in size. In addition modern X-ray diffraction work, especially that involving hydrogen bonded or solvated supramolecular species, is generally carried out at very low temperatures (100–150 K) to reduce atomic motion and prevent diffusional solvent loss.

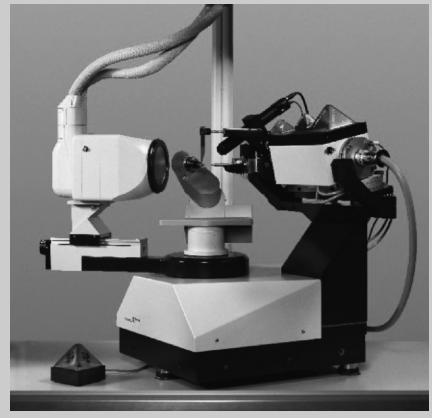

**Figure 2.6** A modern CCD diffractometer. Note the circular area detector on the left, which acts as a very sensitive electronic, reusable equivalent of photographic film, allowing many data points to be collected simultaneously. (Photograph courtesy of Nonius.).

be seen clearly that the interaction of the hydrophilic carbonyl oxygen atoms with the central $K^+$ ion causes the lipophilic *iso*-propyl groups to point outwards thus exposing a primarily hydrocarbon coated outer sheath to the surrounding medium. The remaining amide functionalities act to 'zip up' the molecule *via* intramolecular hydrogen bonds, ensuring the $K^+$ ion is encased entirely in a lipophilic exterior as it crosses the membrane. Both valinomycin and nonactin are potent antibiotics because of their ability to perturb transmembrane ionic balance in bacteria.

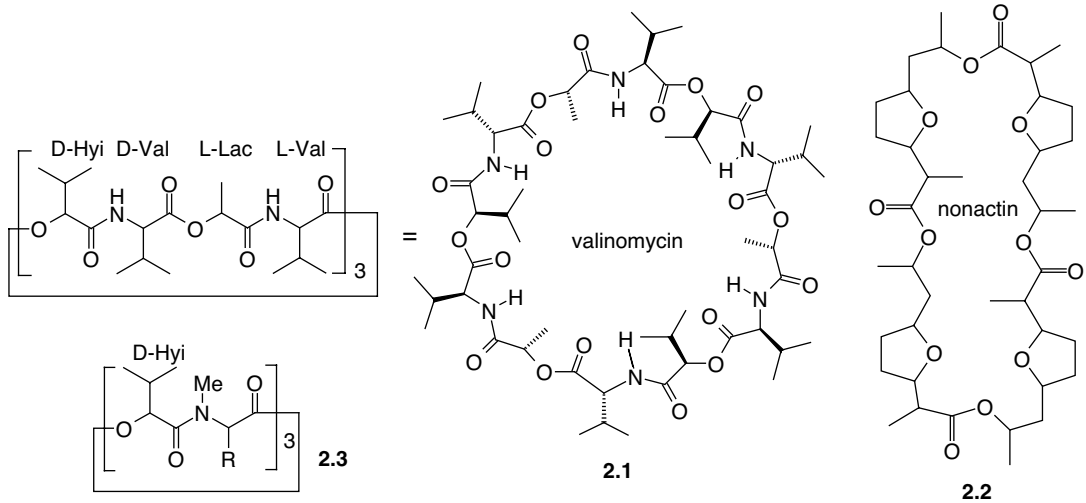


Enniatin A: R = *N*-methyl-L-isoleucine
Enniatin B: R = *N*-methyl-L-valine
Enniatin C: R = *N*-methyl-L-leucine
Baeuvericin: R = *N*-methyl-L-phenylalanine

Related closely to valinomycin are the enniatins (**2.3**), which are made up of only half the number of amino acid binding units (see Box 2.2 for amino acid structure). The enniatins transport alkali metal cations and alkaline earth metal ions, although they are much less selective than valinomycin. Note that the amide nitrogen atoms are methylated, precluding the possibility of hydrogen bonding. Binding constants for a range of naturally occurring ionophores are given in Table 2.2. Note that many of the ionophores bind strongly to $K^+$ while only monesin actually binds $Na^+$ with any selectivity. We will return to the origins of the high affinity of these ligands for $K^+$ and the factors affecting selectivity in general in the next chapter.

**Table 2.2** Log $K_{11}$ values for alkali metal ion binding by naturally occurring ionophores in methanol solvent at 25 °C.

| Ligand | $Li^+$ | $Na^+$ | $K^+$ | $Rb^+$ | $Cs^+$ |
|---|---|---|---|---|---|
| Valinomycin | <0.7 | 0.67 | 4.90 | 5.26 | 4.42 |
| Monactin | <0.3 | 2.60 | 4.38 | 4.38 | 3.30 |
| Enniatin B | 1.28 | 2.42 | 2.92 | 2.74 | 2.34 |
| Nigericin | – | 4.7 | 5.6 | 5.0 | – |
| Monensin | 3.6 | 6.5 | 5.0 | 4.3 | 3.6 |

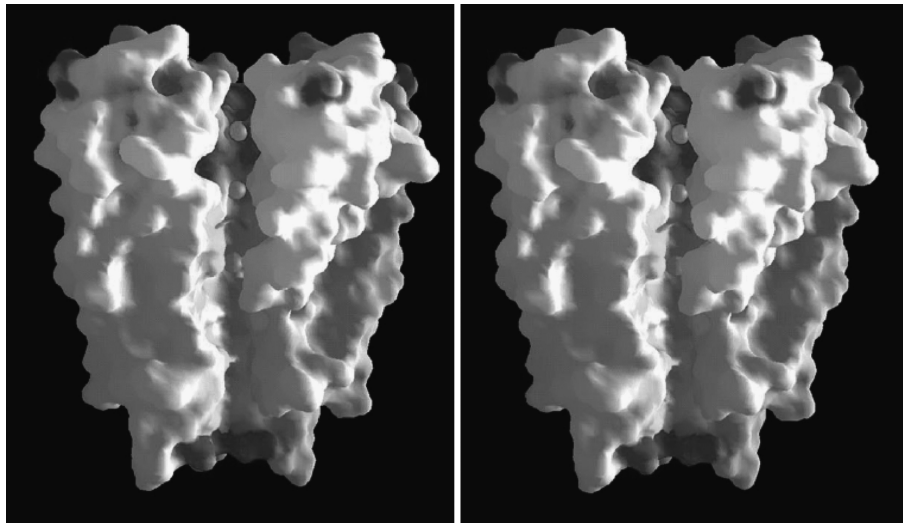

**Figure 2.7** Cutaway stereoview of the X-ray crystal structure of the $K^+$ channel of *Streptomyces lividans*. The upper and lower ends of the channel are regions of high negative charge density while the central portion comprises hydrophobic amino acid side chains. Positively charged regions are on the outer surface, while the spheres represent $K^+$ ion positions. (Reproduced with permission from [2] MacKinnon). See plate section for colour version of this image.

While important, the sequential desolvation–complexation–transport–decomplexation mechanism of ionophore-mediated cation transport is far too slow for effective use in the generation of nerve impulses. In contrast, passage of ions through ion channels results in transport close to the diffusion limits (about $10^8$ ions per channel per second). The X-ray crystal structure determination on the $K^+$ channel from the microorganism *Streptomyces lividans*[2] reveals the basis for both the remarkable ion throughput rate and the vital $10^5$-fold selectivity of the channel for $K^+$ over $Na^+$ (Figure 2.7). Both ends of the ion channel are surrounded by negatively charged amino acid residues, which have the effect of raising the local concentration of cations. The majority of the pore consists of a wide tunnel (18Å in length), opening out into a central cavity of about 10Å in diameter at the centre of the pore. Potassium cations can traverse both tunnel and cavity without shedding their hydration sphere. It has been suggested that the large central cavity overcomes the electrostatic destabilisation resulting from the low dielectric constant of the bilayer simply by surrounding the ion with polarisable water. The pore then narrows into a selectivity filter lined with polar carbonyl oxygen atoms, prearranged for binding a metal ion with the radius of $K^+$. Rubidium, which is only slightly bigger (see Box 3.1), also passes readily through the channel. Most importantly, the ring of metal cation binding sites is held open in a 'spring-loaded' fashion by the aryl moieties of tryptophanyl and tyrosyl residues positioned like a cuff of the selectivity filter (see Box 2.2 for amino acid structures). The binding site is thus kept open so that it cannot contract sufficiently to bind to $Na^+$, hence the origin of its selectivity.

Just as there are cation channels, there are also trans-membrane channels involved in the transport of biologically important anions such as $Cl^-$. The crystal structure of the CIC chloride channel from *Salmonella typhimurium* was reported in 2002.[3] Along with the determination of the *Streptomyces lividans* potassium channel structure, this work won a share of the 2003 Nobel prize in chemistry for Roderick MacKinnon (Howard Hughes Medical Institute, New York, USA). Chloride channels catalyse the flow of chloride across cell membranes and play a significant role in functions such as

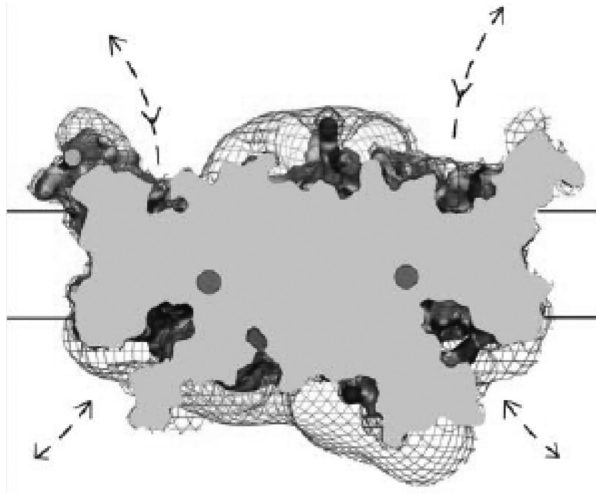

**Figure 2.8** Surface electrostatic potential map of the ClC chloride channel dimer. The channel is sliced in half to show the pore entryways (but not the full extent of their depth) on the extracellular (above) and intracellular (below) sides of the membrane (represented by horizontal lines. The $Cl^-$ ions are shown as spheres and dashed lines highlight the pore entryways. (reproduced with permission from Reference 3).

the regulation of pH, volume homeostasis, organic solute transport, cell migration, cell proliferation and differentiation. In skeletal muscle, ClC chloride channels stabilise the resting membrane potential while in the kidney they act in conjunction with a $Na^+$, $K^+$, $Cl^-$ co-transporter and $K^+$ channels to produce transepithelial fluid and electrolyte transport. The structure of the CIC chloride channel is based on two identical subunits and the channel functions as a dimer. In contrast to the $K^+$ channel structure, each subunit has its own individual aqueous pore and chloride selectivity filter (Figure 2.8). In the $K^+$ channel the pore occurs at the interface between four protein subunits. The anion binding region is surrounded by positively charged N-terminus regions of the protein, complementary to $Cl^-$. The channel also conducts $Br^-$ well, however, like $Rb^+$ and $Cs^+$, bromide is not a significant bulk biological anion. Another chloride channel of interest to supramolecular chemists is the *cystic fibrosis transmembrane conductance regulator* (CFTR). The CFTR is found in the epithelial (*i.e.* surface) cells of a range of major organs, particularly the lungs and skin. Like the CIC channel its role is chloride ion transport, in this case from out of the epithelial cell to the surrounding mucus. This process causes an electrical gradient and the movement of $Na^+$ ions in the same direction to balance the charge ($Na^+$ / $Cl^-$ *symport*). This results in the absorption of water by the mucus maintaining the correct level of fluidity. In the genetic disease cystic fibrosis (CF) mutations in the CFTR reduces the ability of the affected cells, predominantly epithelial cells lining the lung and other mucosal surfaces, to transport chloride effectively with consequences for fluid transport. Defective fluid transport leads to an underhydration of mucus secretions which then obstructs organ passages and causes the widespread and serious organ malfunction associated with the disease. The development of artificial chloride channels to treat the disease is of considerable interest in supramolecular chemistry (Section 12.8).[4]

The crystal structure of $Na^+/K^+$-ATPase, the enzyme responsible for maintaining $Na^+/K^+$ non-equilibrium in most eucaryotic organisms was determined 2007.[5] The enzyme is difficult to purify since it is membrane-bound and has a high molecular mass (294 kDa). It is a heterodimer made up of

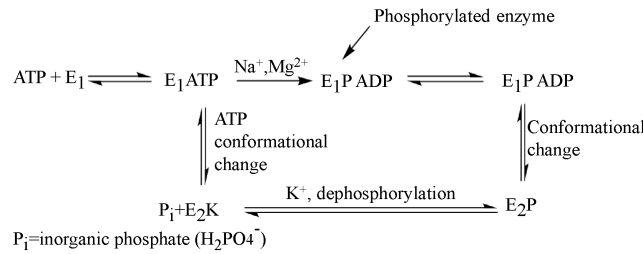


**Scheme 2.2** Mechanism of the enzymatic action of ATPase.

two pairs of a large ($\alpha$) and small ($\beta$) peptide, *i.e.* $(\alpha\beta)_2$. Each $\alpha\beta$ pair is active. The $\beta$-peptide is a glycopeptide with a molecular weight of about 50 000 Da which is a special feature of $K^+$-counter-transporting ATPases. Its job is the routeing of the $\alpha$-subunit to the plasma membrane and binding of the $K^+$ ions. The $\alpha$-peptide is a membrane-spanning protein with a molecular weight of about 100 000 Da, and exists in different conformations in the presence of $Na^+$ (conformation $E_1$) or $K^+$ ($E_2$). It is involved in $Na^+$-dependent phosphorylation of the $\beta$-carboxyl group of an aspartic acid residue, a process that also requires $Mg^{2+}$. Conversely, loss of the phosphate requires $K^+$. The overall process is:

$$3\,Na^+_{ic} + 2K^+_{ec} + ATP^{4-} + H_2O \xrightarrow{Mg^{2+}} 3\,Na^+_{ec} + 2K^+_{ic} + ADP^{3-} + HPO_4^{2-} + H^+ \qquad (2.1)$$

(ic = intracellular, ec = extracellular)

The mechanism of the enzymatic action of the ATPase, in isolation from its transport function, may be considered as shown in Scheme 2.2.

The system may be regarded as involving a $Na^+/Mg^{2+}$ co-catalysed phosphorylation step and a $K^+$ catalysed dephosphorylation. Each phosphorylation/dephosphorylation step involves a 'pseudorotation' of an $Mg^{2+}$-stabilised 5-coordinate intermediate, resulting in transport of the alkali metal cations. The cation transport ability of the enzyme is a direct result of the enzymatic reactivity of the protein. There are three binding sites with high $Na^+$ affinity and two with $K^+$ affinity (occupied by $Rb^+$ in the crystal structure determination). The structure (which is of the $E_2K$ state of the system) reveals that carboxy end of the $\alpha$-subunit is held in a pocket in between transmembrane helices and acts as an unusual regulating element that controls sodium affinity and may be influenced by the membrane potential.

## 2.2.3 Rhodopsin: A Supramolecular Photonic Device

Pepe, I. M., 'Rhodopsin and phototransduction', *J. Photochem. Photobiol. B-Biology* 1999, **48**, 1–10.

Supramolecular alkali metal cation transport is also of importance in other signal generating processes, such as the stimulation by visible light of rod and cone cells in the retina of the eye. The rod cells responsible for black and white vision are better understood and bear all of the characteristics of a functional supramolecular device. The structure of a typical rod is shown in Figure 2.9a. The light-harvesting portion of a rod cell contains a photosensitive reddish pigment called rhodopsin (commonly known as *visual purple*). This comprises a complex protein (opsin) conjugated with a simple aldehyde of vitamin A (carotene) called retinine. The absorption spectrum of rhodopsin is sensitive to the kinds of wavelengths that occur at low lighting levels, and on photoexcitation the connection between the opsin and retinine components (an azomethine function, $C{=}NH^+$) undergoes a simple *cis* to *trans* isomerism forming bathorhodopsin. This results in the degradation of cyclic guanosine monophosphate

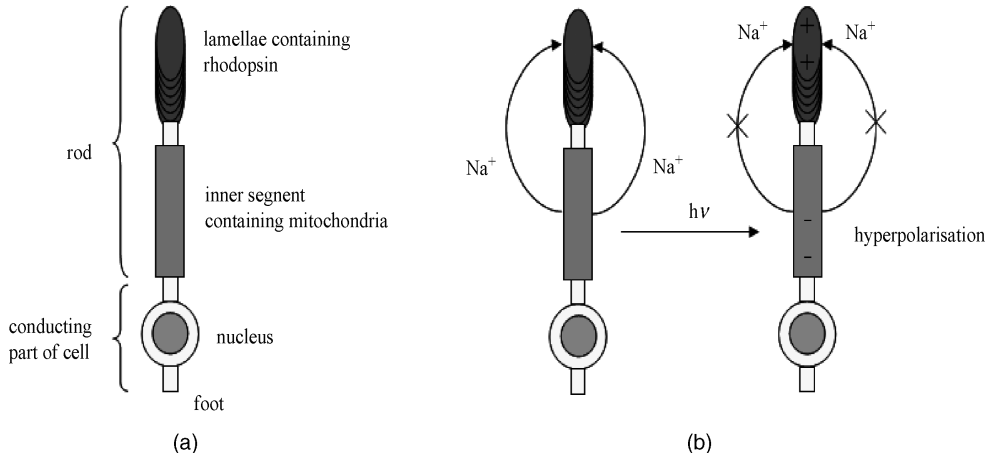


**Figure 2.9** (a) Light-responsive rod cell from the human retina. The photoresponsive pigment rhodopsin is located in the outer lamellae. The foot makes contact with the optic nerve. (b) Operation of the rod cell.

(cGMP), which is necessary to the maintenance of the ever-present energy-consuming flow of $Na^+$ ions that comprise the cell's 'dark current', and hence $Na^+$ transmembrane channels close. This, in turn, causes a marked hyperpolarisation within the cell and leads to amplification of the original light signal and the generation of a nerve impulse (Figure 2.9b).

Rhodopsin absorbs light at 498 nm while the three pigments responsible for trichromatic colour vision in the cone cells absorb at 425, 530, and 560 nm. Interestingly the chromophore in these receptors is the same compound – a protonated Schiff base of 11-cis-retinal. Logically, therefore, the absorption wavelength of these pigments must be related to their supramolecular environment within their protein home. Interestingly recent calculations show that the main role of the protein binding pocket is to stabilise the pigments as they undergo the isomerisation reaction to bathorhodopsin and it is the counter anion that has by far the most significant effect on the pigment absorption maximum.[6]

Examples such as this show the importance of alkali metal cation binding and transport in biochemistry, and a great deal of effort has been expended in supramolecular chemistry in attempts to understand natural cation binding and transport of the ionophore and channel type and to develop artificial systems capable of similar selectivities and reactivities. We will take a close look at many of these compounds in Chapter 3.

## 2.3 Porphyrins and Tetrapyrrole Macrocycles

Macrocyclic (large-ring) ligands are common in biochemistry, and are able to bind even substitutionally labile metal ions by virtue of the chelate and macrocyclic effects. This stabilisation is especially important for alkali metal cation binding, in a similar way to ionophores such as valinomycin and nonactin. Tetrapyrrole macrocycles are also important in binding to both transition and main group metal ions in an enormous variety of situations in which strong, size-selective complexation is required. Tetrapyrroles possess extensive redox chemistry because the conjugated ring framework itself may be readily reduced. Common examples are:

- chlorophylls, which contain otherwise labile $Mg^{2+}$, and are important as energy harvesters in photosynthesis;
- cobalamins, the active form of vitamin $B_{12}$, which involves a partially conjugated 'corrin' ring system (Figure 2.10);

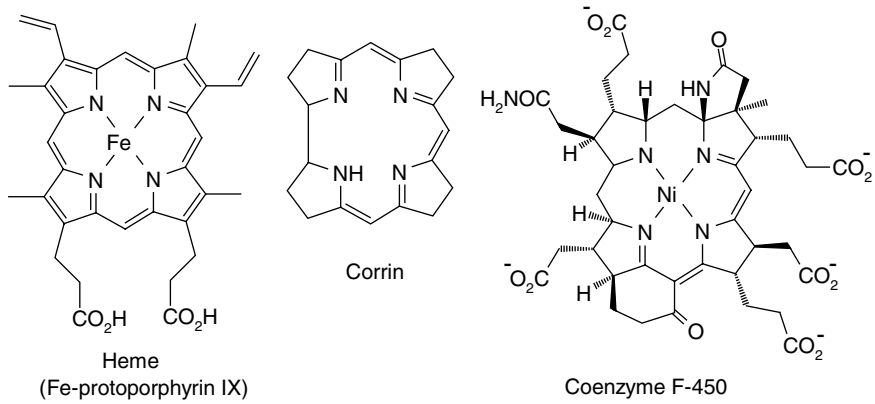


**Figure 2.10** Biological tetrapyrrole macrocyclic compounds.

- haem complexes, which consist of an iron centre and a subsitiuted porphyrin ligand, as in iron protoporphyrin IX (Figure 2.10), the active $O_2$ binding site found in haemoglobin; haems are also found in a variety of enzymes such as cytochromes, which rely upon $O_2$ as a substrate;
- a porphyrinoid nickel(II) complex, coenzyme F450 (Figure 2.10c), found in methane-producing microorganisms; the independence of the function of this species from proteins makes it a good candidate for 'first-hour' catalysis, *i.e.* the origins of life.

Tetrapyrrole macrocycles such as haems and corrin exhibit a number of special features that make them extremely important:

- The underlying planar (or near-planar) ring system is very stable.
- As tetradentate chelate ligands that, after deprotonation, carry a single (corrin) or double negative charge, the tetrapyrrole can bind even highly labile metal ions. The complex can dissociate only if all metal ligand bonds are broken at the same time (*cf.* chelate and macrocyclic effects).
- Macrocyclic ligands are usually quite selective with regard to the ionic radius of the metal ion they will bind (those that are bound preferentially are those that fit the cavity). Tetrapyrroles are especially selective in this regard because of their rigidity, which arises from the conjugated network of double bonds.
- Most tetrapyrroles contain a conjugated π-system. The Hückel rule for aromatic systems is obeyed for porphyrins which feature 18 π-electrons in the inner 16-membered ring (aromatic systems contain $4n + 2$ π-electrons; for fully conjugated tetrapyrroles $n = 4$). This goes some way to account for the thermal stability of the ring system. It also often results in intense colours, hence the designation 'pigments' for many tetrapyrrole-containing biological species. Furthermore, it means that the oxidation and reduction products that form part of biological processes can be quite stable because of delocalisation of the resulting charges.
- The macrocycle contains four coordinating atoms in a planar arrangement, leaving two available sites on an octahedral metal centre available to bind the substrate and a regulating ligand.
- Tetrapyrroles are able to distort to give a 'domed' (rather than planar) coordination environment for large metal ions such as high-spin Fe(II). Reversible stabilisation of this high-spin state is vital in the action of haemoglobin. In contrast, a planar tetrapyrrole system gives a high ligand field splitting and hence low-spin complexes.

In the ensuing sections we will examine some porphyrin and tetrapyrrole complexes in greater detail.

# 2.4 Supramolecular Features of Plant Photosynthesis

Allen, J. P. and Williams, J. C., 'Photosynthetic reaction centers', *FEBS Lett.* 1998, **438**, 5–9.

## 2.4.1 The Role of Magnesium Tetrapyrrole Complexes

Photosynthesis is the process by which organic matter (reduced carbon) is produced from $CO_2$ and water by a process of uphill (energy-consuming) catalysis using sunlight — a readily available, clean, though rather 'diluted', form of energy.

$$H_2O + CO_2 \underset{\text{respiration (downhill catalysis)}}{\overset{\text{photosynthesis (uphill catalysis)}}{\rightleftharpoons}} 1/n(CH_2O)_n + {}^3O_2 \quad \Delta H = +470\,\text{kJ mol}^{-1} \tag{2.2}$$

Photosynthesis is carried out by green plants and certain kinds of bacteria and algae, and may involve the oxidation of other substrates such as $H_2S$ or $H_2$ instead of water, depending on the conditions under which the organism evolved. In green plants, the photosynthetic output is about 1 g of glucose per hour per 1 $m^2$ of leaf surface area. Although this represents a relatively inefficient utilisation of the available radiation energy (<1 per cent) the global turnover is tremendous: about 200 billion tons of carbohydrate equivalents $(CH_2O)_n$ are produced from $CO_2$ each year (Equation 2.3).

Sunlight available at the Earth's surface includes the wavelength range visible to the human eye (380–750 nm), but there is also a significant contribution from light of longer wavelengths (and therefore lower energy) up to about 1000 nm. Efficient photosynthetic transformation of light of this range of energies requires a number of different pigments (*i.e.* light receptors or chromophores), each sensitive to a particular part of the spectrum. These pigments include chlorophyll *a* and bacteriochlorophyll *a* (Figure 2.11) as well as a number of related receptors, all based on tetrapyrrole macrocycles both with and without a metal cation guest. The pigments are positioned in a highly folded photosynthetic membrane with a large surface area and therefore a high cross-section for photon capture.

Chlorophylls contain a fully conjugated tetrapyrrole π-system (18 π electrons) with a low-energy $\pi$–$\pi^*$ transition. The extinction coefficient is high (about $10^5\,M^{-1}\,cm^{-1}$) at both long- and short-wavelength ends of the spectrum. The complementary colours blue (after short-wavelength absorption) and yellow (after long-wavelength absorption) combine to give the characteristic green colour of fresh leaves ($\lambda_{max}$ 455 and 630 nm). Bacteriochlorophylls have two partially hydrogenated pyrrole rings and their absorption is consequently shifted to longer wavelengths, reaching the near infrared (IR) region. Carotenoids and open chain tetrapyrrole molecules, such as phycobilins, complement the chlorophyll pigments so that a broad range of absorption is covered (Figure 2.12). At the end of each growth period non-green catotenoid pigments become visible (resulting in autumn colours) as the relatively unstable chlorophylls decompose (*e.g.* phycoerythrin, $\lambda_{max}$ 455, 510 and 555 nm; phycocyanin, 595 nm).

Because of the relatively slow rate of light absorption in diffuse sunlight, the majority (>98 per cent) of pigments are used as light-harvesting or antenna devices, absorbing and transferring energy to the actual reaction centres. This means that there has to be efficient, spatially-orientated transfer of the absorbed energy. This energy transfer is made possible by a well-defined antenna network of pigments that are able to funnel the light energy in an energy transfer 'cascade' (Figure 2.13a). Essentially, the energy transfer proceeds *via* overlap of the emission bands of the source with the absorption bands of the acceptor (Figure 2.13b).

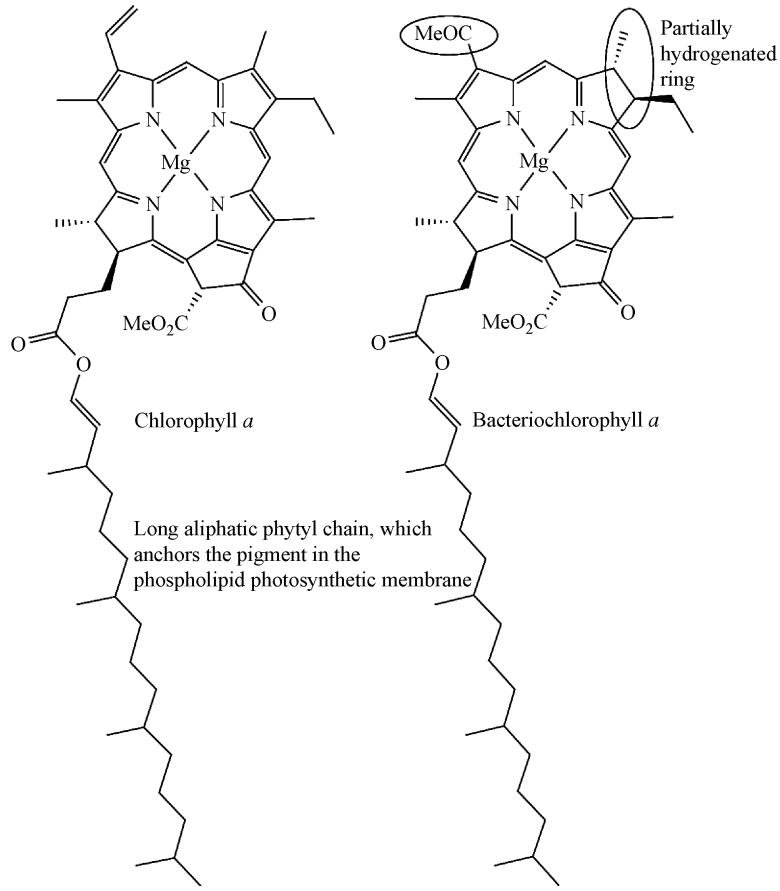


**Figure 2.11** Structures of chlorophyll *a* and bacteriochlorophyll *a*.

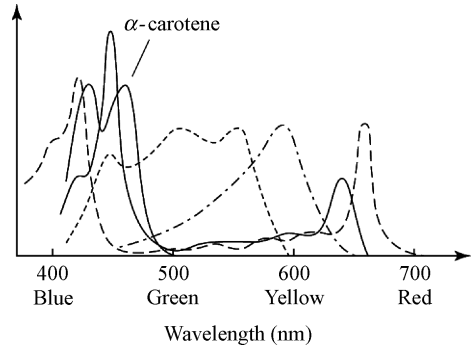


**Figure 2.12** Absorption spectra of various pigments from algae and plants: chlorophyll *a* (----), chlorophyll *b* (–––) $\alpha$-carotene (–––), phycocyanin (–·–·), phycoerythrin (- -). (Reproduced by permission of John Wiley & Sons, Ltd).

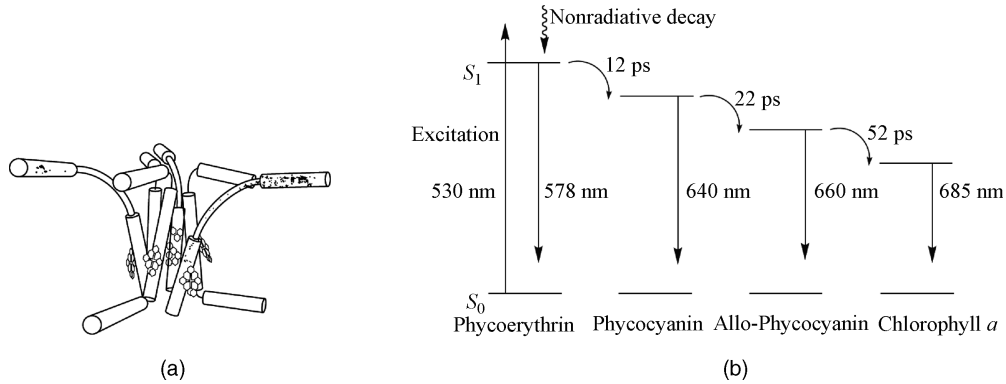


**Figure 2.13** (a) Spatially-orientated antenna network of light-harvesting pigments. (Reproduced by permission of John Wiley & Sons, Ltd). (b) Energy-transfer cascade for antenna pigments in light-harvesting complexes of the algae *Porphyridium cruetum*.

The role of the coordinated $Mg^{2+}$ ion in chlorophylls is to contribute to the arrangement of the pigments. Pigments are anchored spatially in their correct place, to some extent, by the long phytyl side chain, buried deep in the photosynthetic membrane. However, in order to fix the pigment firmly, the free axial coordination site of the normally square pyramidal $Mg^{2+}$ is bound to polypeptide side chain ligands, giving two points of anchorage of the pigment and hence a well-defined spatial orientation. In the case of the photosynthetic reaction centres of purple bacteria this is a histidine nitrogen atom. $Mg^{2+}$ is particularly suited to this role for the following reasons:

- high natural abundance (consistent with this noncatalytic 'bulk' function);
- lack of redox activity (redox activity at the metal is incompatible with interpigment electron transfer);
- strong tendency for penta- or hexacoordination;
- suitable ionic radius;
- small spin-orbit coupling constant (spin-orbit coupling results in the formation of long-lived triplet excited states by intersystem crossing, resulting in light- or heat-producing processes competing with chemical reactions).

The X-ray crystal structure of ethyl chlorophyllide (in which the phytyl group is replaced with a simple ethyl substituent) (Figure 2.14) shows the tendency of the $Mg^{2+}$ towards a 5- or 6-coordinate environment. The axial site of the polypyrrole-bound $Mg^{2+}$ ion is bound to a water molecule, which, in turn, hydrogen bonds to the carbonyl group on adjacent molecules, forming a hydrogen-bonded solid-state polymer. This is a good example of solid-state supramolecular organisation, but this kind of direct linkage probably does *not* occur in the real system.

The energy collected by light-harvesting antennae systems and funnelled to the photosynthetic reaction centre is used to produce a spatial charge separation. In other words, an electron is promoted to an excited state and used to effect a chemical reduction before it has the chance to undergo a biochemically useless radiative decay back to its ground state. In simple reaction centres, such as that of the purple bacteria *Rhodopseudomonas viridis*, the excited electron is transferred to an external acceptor. In higher evolved organisms, the 'hole' left behind is also utilised to oxidise a substrate by the involvement of an external donor. Ultimately this results in the production of $O_2$ from water (Figure 2.15).

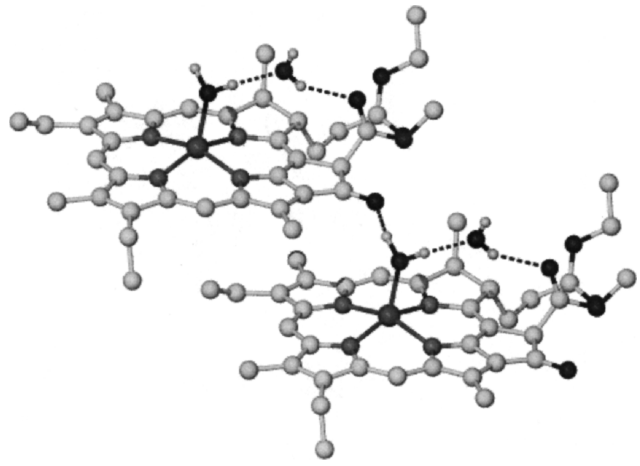

**Figure 2.14** X-ray crystal structure of ethyl chlorophyllide show in the 5-coordinate $Mg^{2+}$ ion.[7]

In *Rps. viridis*, the reaction centre is situated in a polyprotein complex that spans the photosynthetic membrane. It consists of a nearly $C_2$ symmetric arrangement in which a bacteriochlorophyll dimer, $(BC)_2$, sits on the symmetry axis. Electronic excitation of this dimer (called $P_{960}$–a pigment with a long-wavelength absorption maximum at 960 nm) results in an electronically excited state. This is termed *primary charge separation*. Following this excitation, one energetically elevated electron is transferred to the primary acceptor, a monomeric bacteriochlorophyll, before radiative decay can occur. The reduced monomeric BC molecule transfers an electron in turn to the secondary acceptor, a bacteriopheophytin (BP; a bacteriochlorophyll molecule without a coordinated metal centre). This is known as *secondary charge separation* and results in the spatial removal of the electron from its source (Scheme 2.3). The absence of the metal centre makes the molecule easier to reduce since the ionic bond to the $Mg^{2+}$ ion from the dianionic ligand leaves a significant amount of electron density on the ligand. In effect, replacing the $Mg^{2+}$ ion with protons results in a more covalent situation. The electron is then transferred from the BP radical anion to a *para*-quinone, $Q_a$, such as menaquinone (**2.4**), reducing it to a semiquinone radical anion. This in turn reduces a more labile quinone, $Q_b$, such as ubiquinone (**2.5**), *via* a high-spin, six-coordinate iron(II) centre. $Q_b$ is not bound tightly to the

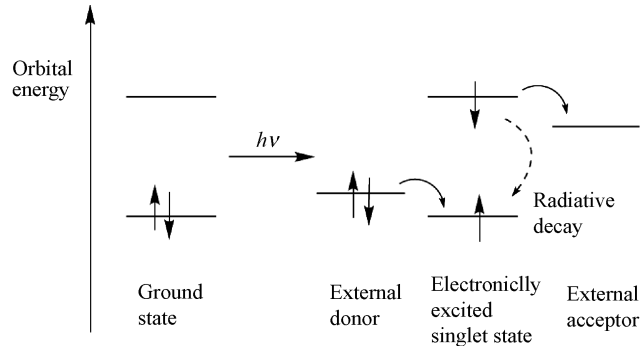


**Figure 2.15** Fate of the photoexcited electron and the resulting positive hole.

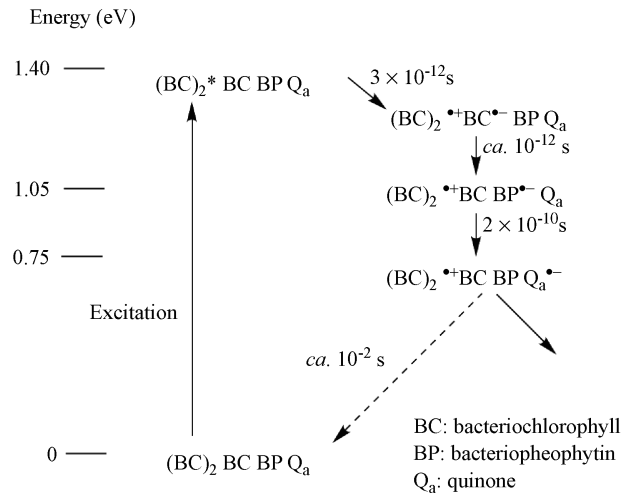


**Scheme 2.3** Charge separation at the photosynthetic reaction centre of *Rps. viridis*.

protein, but exchanges with quinones in the 'quinone pool' of the membrane. The resulting electron gradient finally gives rise to a coupled $H^+$ gradient and photosynthetic phosphorylation (ATP synthesis) takes place. In higher organisms, further 'dark' reactions take place resulting in the reduction of $CO_2$ (this is known as the Calvin cycle):

$$4e^- + 4H^+ + CO_2 \longrightarrow 1/n\,(CH_2O)_n + H_2O \tag{2.3}$$

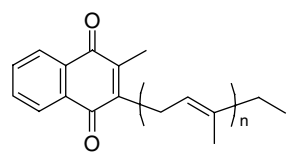


menaquinone ($n = 9$)

**2.4**

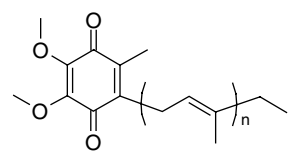


ubiquinone ($n = 10$)

**2.5**

In *Rps. viridis*, the radical cation, $(BC)_2^{\bullet+}$, which remained after the initial charge separation is reduced after a relatively long time through regulated electron flow *via* one or more haem centres of cytochrome proteins. In higher organisms, this hole is the beginning of substrate oxidation, which requires an additional photosynthetic system including a manganese containing oxidation catalyst (Section 2.4.2).

The key feature of photosynthesis is the ability to carry charge spatially away from an excited state reaction centre before the usually highly efficient and biochemically useless recombination can take place. In photosynthetic systems, charge separation occurs about $10^8$ times faster than recombination, a ratio that is impossible to reach in 'normal' chemical reactions. This phenomenon is achieved by the spatial anchoring of the components at particular orientations to one another within a non-polar region of the membrane anchored protein, thus preventing free diffusion and allowing a vectorial uphill chemical reaction.

## 2.4.2 Manganese-Catalysed Oxidation of Water to Oxygen

In higher plants, there are two coupled, separately excitable photosystems (PS), labelled PS I and PS II. PS I is based around a pigment ($P_{700}$) with an absorption at 700 nm; which receives an excitation from PS II and, ultimately, goes on to reduce $CO_2$. PS II resembles the simpler bacterial photosynthetic reaction centre (Scheme 2.3), but is based around a higher-energy absorbing pigment, $P_{680}$. Promotion of an electron in PS II, and its use in ATP synthesis, results in a strongly oxidising hole being left behind. The high energies involved mean that this hole may be used to oxidise tyrosine to a tyrosine radical cation (+0.95 V), which in turn oxidises a hydroquinone (plastohydroquinone, $PQH_2$) to the quinone form (PQ). The reactive PQ oxidises water in a four-electron redox step, catalysed by the so-called OEC (oxygen-evolving complex), which is an enzyme containing four Mn centres. In the process, four protons are transferred from the outside of the membrane to the inside, resulting in a proton gradient. The overall reaction is:

$$2H_2O + 2PQ + 4H^+_{out} \xrightarrow{4h\nu,\ [Mn]_x\ cat.} {}^3O_2 + 2PQH_2 + 4H^+_{in} \qquad (2.4)$$

Overall, PS II consists of the following necessary elements (those involved directly with water oxidation are shown in **bold**):

~200 Antenna chlorophylls
~50 Carotenoids
1 Reaction centre, $P_{680}$
2 Chlorophylls
2 Pheophytins (primary acceptor)
2 **Plastoquinones**
2 **Tyrosine residues** (primary donor)
4 **Mn centres**
1 **$Ca^{2+}$** (role still relatively obscure, but may be related to structure stabilisation or regulation)
several **$Cl^-$**
1 Cytochrome $b_{559}$

It is well established, however, that the OEC contains four Mn centres in one 33 kDa subunit. Extended X-ray absorption fine structure (EXAFS) measurements indicate Mn—Mn distances of 2.70 and 3.30Å, suggesting, respectively, oxide and carboxylate bridges linking pairs of metal centres. Supporting evidence comes from an extensive number of small structural model compounds such as **2.6** that mimic these properties successfully. During the process of oxidation of two water molecules to $O_2$, the $Mn_4$ cluster passes through a total of five different states, referred to as $S_0$ to $S_4$, during the course of a few hundred milliseconds. Structural changes are small between each of the five states, consistent with a low activation energy, but there are significant changes in oxidation state.

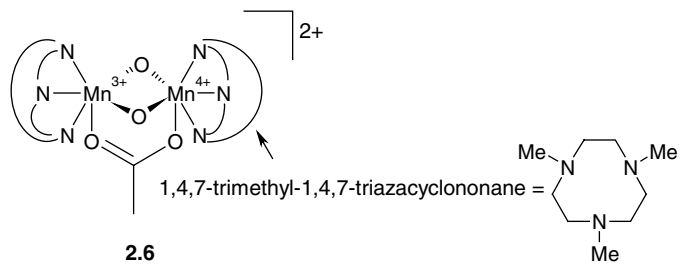


**2.6**

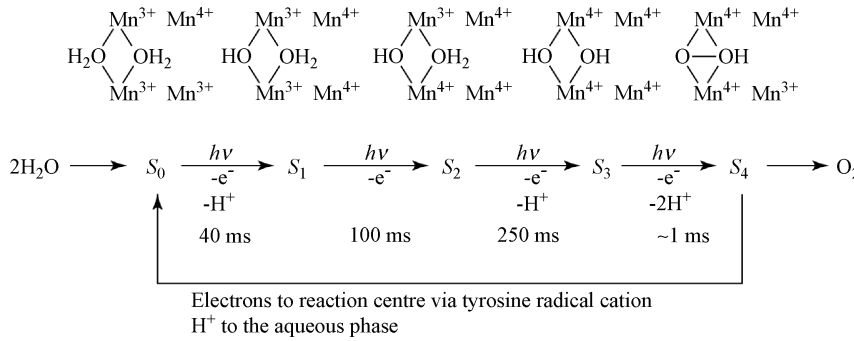


**Figure 2.16** Changes in manganese oxidation state in the conversion of water to $O_2$.

Figure 2.16 represents one possibility for the changes occurring in the five *S* states. Evidence from EXAFS spectroscopy confirms a change in oxidation state going from $S_0$ to $S_1$ and to $S_2$, but there are conflicting reports concerning the change to $S_3$. It may involve oxidation of a histidine ligand instead of a Mn centre. There is good evidence from EPR spectroscopy that the $S_2$ state involves a single unpaired electron, consistent with an odd total number of electrons and antiferromagnetic coupling.

The very short-lived $S_4$ state contains a peroxide $O_2^{2-}$ ligand and one of the Mn(IV) centres may have been reduced back to Mn(III) to give back the odd number of electrons observed for $S_2$ ($S_4$ has two electrons fewer than $S_2$, and so if $S_2$ is odd, $S_4$ must also be odd). The fact that the system involves an odd number of unpaired electrons is important since oxygen must be released in its triplet $^3O_2$, state, *i.e.* with an even number of unpaired electrons. A match between the catalyst and the oxygen might result in irreversible binding, as is the case with the reactions of most transition metals with $O_2$. Luckily, the spin flipping required to make the two systems compatible is a formally forbidden, and hence slow, process. This 'spin inhibition' is similar to that for the reaction of $H_2$ and $O_2$, which does not proceed without a bond breaking catalyst or radical initiator.

$$\underset{S=1}{\overset{\uparrow\downarrow}{H-H}} + \underset{}{\overset{\uparrow\downarrow}{H-H}} + \underset{}{\overset{\uparrow\downarrow\uparrow\uparrow}{O=O}} \longrightarrow \underset{S=0}{\overset{\uparrow\downarrow\uparrow\downarrow}{H-O-H}} + \underset{}{\overset{\uparrow\downarrow\uparrow\downarrow}{H-O-H}} \tag{2.5}$$

$$\underset{S=0}{2H_2O} + \underset{S=1/2}{(Mn-Mn)^{n+}} \longrightarrow \underset{S=1}{{}^3O_2} + \underset{S=3/2}{(Mn-Mn)^{(n-4)+}} + 4H^+ \tag{2.6}$$

So, what makes manganese so suitable as an oxidation catalyst? This question may be summarised by the following points:

- It is known that fresh manganese dioxide, $MnO_{2-x}{\cdot}nH_2O$, a nonstoichiometric mixed-valent (+IV, +III) system, acts as a good heterogeneous catalyst for the decomposition of $H_2O_2$ to $O_2$ and water.
- Manganese was readily bioavailable in seawater at the time of the evolution of photosynthesis (about $3 \times 10^9$ years ago) and now abounds on the sea bottom in the form of oxidic manganese nodules with about 20 per cent Mn content.
- Manganese has a large variety of stable or metastable oxidation states (+II, +III, +IV, +VI, +VII).
- Manganese exhibits labile binding of ligands.
- Manganese has a strong preference for high-spin states because of small *d* orbital splitting.

In the four-electron oxidation of water to $O_2$, the polymanganese system acts as (i) an electron reservoir, accumulating charge in an exactly controlled fashion at physiologically high redox potential and (ii) as a non-$^3O_2$-retaining catalyst.

The role of the essential $Cl^-$ ions may be that of temporary ligands for the Mn centres in between $O_2$ release and water binding. Usually this role is fulfilled by the solvent, but in this case the solvent (water) is also the substrate. $Cl^-$ is unlikely to be oxidised itself ($E^\circ$ +1.36 V for oxidation to $Cl_2$) but more sensitive peptide residues may be damaged if the $Cl^-$ were not present to prevent their binding.

## 2.5 Uptake and Transport of Oxygen by Haemoglobin

Dioxygen, $O_2$, is a vital part of the metabolism of higher organisms that respire aerobically. It is used to metabolically oxidise sugars such as glucose and sucrose (Equation 2.7) with an associated release of energy. The energy from this controlled 'cold combustion' is used in ATP synthesis.

$$C_6H_{12}O_6 + 6O_2 \longrightarrow 6CO_2 + 6H_2O + \text{Energy} \tag{2.7}$$

Oxygen is produced biogenically by higher plants (Section 2.4.2) and must initially have been a waste product arising from the need to replace the photoexcited electron in the photosynthetic reaction centre. In the primeval oceans, water would have been by far the most abundant electron source. Unfortunately, $O_2$ is a highly reactive and, to primitive organisms, highly toxic gas. Initially, oxgen was scavenged from the atmosphere by reduced metal ions such as Fe(II) and Mn(II), but about two billion years ago, following the deposition of large amounts of metal oxide sediments, the $O_2$ content began to rise in the primitive atmosphere from levels of less then one per cent (as it is on lifeless planets and moons today) to 21 per cent of the atmospheric volume. As a result, most primitive organisms would have perished by radical degradation mechanisms and oxidation of metalloenzymes. Only the newly evolved aerobic organisms that had begun to appear as a result of this surplus of high-energy compound would have survived. Today, only a few anaerobic organisms survive: those that live in ecological niches such as the deep ocean, where atmospheric $O_2$ cannot penetrate, and those that were able to develop defence mechanisms against $O_2$ and its partially reduced radical products.

In order for aerobic organisms to utilise the reactive $O_2$ in what is effectively the reverse of photosynthesis, it is necessary for the $O_2$ to be taken up and transported to the cell mitochondria where respiration with 'food' (*i.e.* sugars) occurs without reacting irreversibly or causing radical or oxidative damage along the way. A very sophisticated oxygen uptake and transport protein, haemoglobin, has evolved to carry out this task. Haemoglobin is a tetrameric protein (RMM = 64.5 kDa) containing four myoglobin units (RMM = 17.8 kDa). Each myoglobin unit contains an iron–porphyrin coordination complex called haem or Fe-protoporphyrin IX (Figure 2.10), which is bound to the protein by a coordination interaction between an axial site of the octahedral Fe(II) centre and a nitrogen atom from the proximal protein histidine residue. It is the ability of the iron centre to bind $O_2$ *reversibly* that is the key to this vital biological system. The remaining axial site on the iron atom is available for oxygen binding, although it may be occupied by a loosely bound water molecule in its resting state.

The main problem with the reaction of metal centres with $O_2$ is its tendency to react irreversibly with oxidation of the metal centre, to form either *cis* dioxo species or μ-oxo bridged binuclear complexes (Scheme 2.4a). However, in cases where there is a strong driving force towards lower oxidation states, the reaction is somewhat reversible, *e.g.* reaction with Vaska's compound (Scheme 2.4b). The role of the haem centre in haemoglobin is to ensure not only that is $O_2$ binding reversible, but that both its complexation and release occur rapidly and at the correct concentrations. These concentrations, or partial pressures, must correspond to those found in the lung and intracellular medium, respectively.

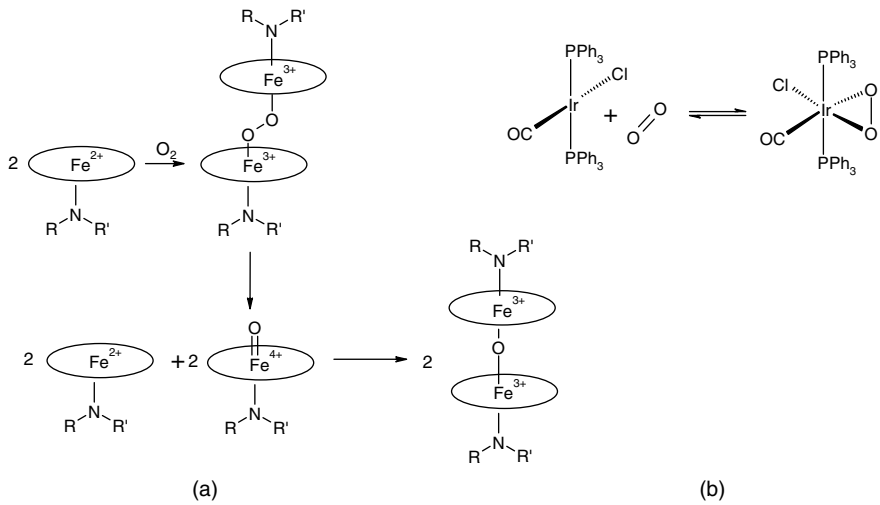


**Scheme 2.4** (a) Irreversible μ-oxo dimer formation in nonprotein iron porphyrin complexes. (b) A rare example of reversible $O_2$ binding in a simple inorganic complex. The formally Ir(III)/$O_2^{2-}$ complex is destabilised by the π-acceptor properties of the phosphine and CO ligands.

Furthermore, $O_2$ binding must occur selectively amongst other atmospheric components such as water, $N_2$, $CO_2$ and even excellent ligands for Fe(II) such as CO. Haemoglobin is thus an excellent example of a functional and selective supramolecular receptor.

Before $O_2$ binding, the haem units contain high-spin Fe(II) centres of valence electron configuration $(t_{2g})^4(e_g)^2$, resulting in a paramagnetic species with four unpaired electrons (Figure 2.17a). The Fe(II) centre is thought to be located significantly out of the plane of the porphyrin unit, a conformational characteristic known as 'doming', and is orientated towards the proximal (closest) histidine residue of the surrounding protein. This is a consequence of the large size of high-spin Fe(II) compared with the dimensions of the porphyrin ring (ionic radius = 0.78Å). The binding of $O_2$ (in its triplet ground state) has been the subject of much controversy centred around two opposing viewpoints: the Pauling and Weiss models. According to the Weiss model (which is now generally accepted), $O_2$ binding is accompanied by a single electron transfer to give a doublet superoxide ligand ($^2O_2^{\bullet-}$) and a low-spin Fe(III) centre. The smaller ionic radius for Fe(III) (high spin, 0.65Å; low spin, 0.55Å) results in a much better fit for the porphyrin, and no porphyrin 'doming' (Scheme 2.5). The Weiss model maintains that the Fe(III) centre is now low-spin $(t_{2g})^5$. This should result in paramagnetism both from the one remaining unpaired electron on the Fe(III) centre and the unpaired electron of the superoxide ligand. In fact the oxygenated haem system is found experimentally to be diamagnetic (this clearly rules out a high-spin Fe(III) centre, which would have five unpaired electrons). Weiss suggested a strong degree of spin correlation between the low-spin Fe(III) and $^2O_2^{\bullet-}$ unpaired electrons, resulting in virtual diamagnetism for the low-spin case. The transition from high to low spin is explained by the increase in crystal field splitting energy as the Fe centre moves into the plane of the haem unit on $O_2$ binding. This is termed the *trigger* mechanism. The alternative explanation, put forward by Pauling, suggests that a spin cross-over occurs such that $O_2$ is bound by a low-spin Fe(II) centre in the singlet form $^1O_2$ in the more conventional synergic fashion. Both components are diamagnetic and hence the complex as a whole is diamagnetic (Figure 2.17b). Again, the transition form high to low spin is explained by the trigger mechanism. The Weiss model is favoured by the observation of the infrared ν(O—O) stretch at 1100 $cm^{-1}$, consistent with $O_2^{\bullet-}$ rather than the higher wavenumber expected for the double bonded $^1O_2$. Furthermore, replacement of the iron centre in the haem with cobalt to give coboglobin (which

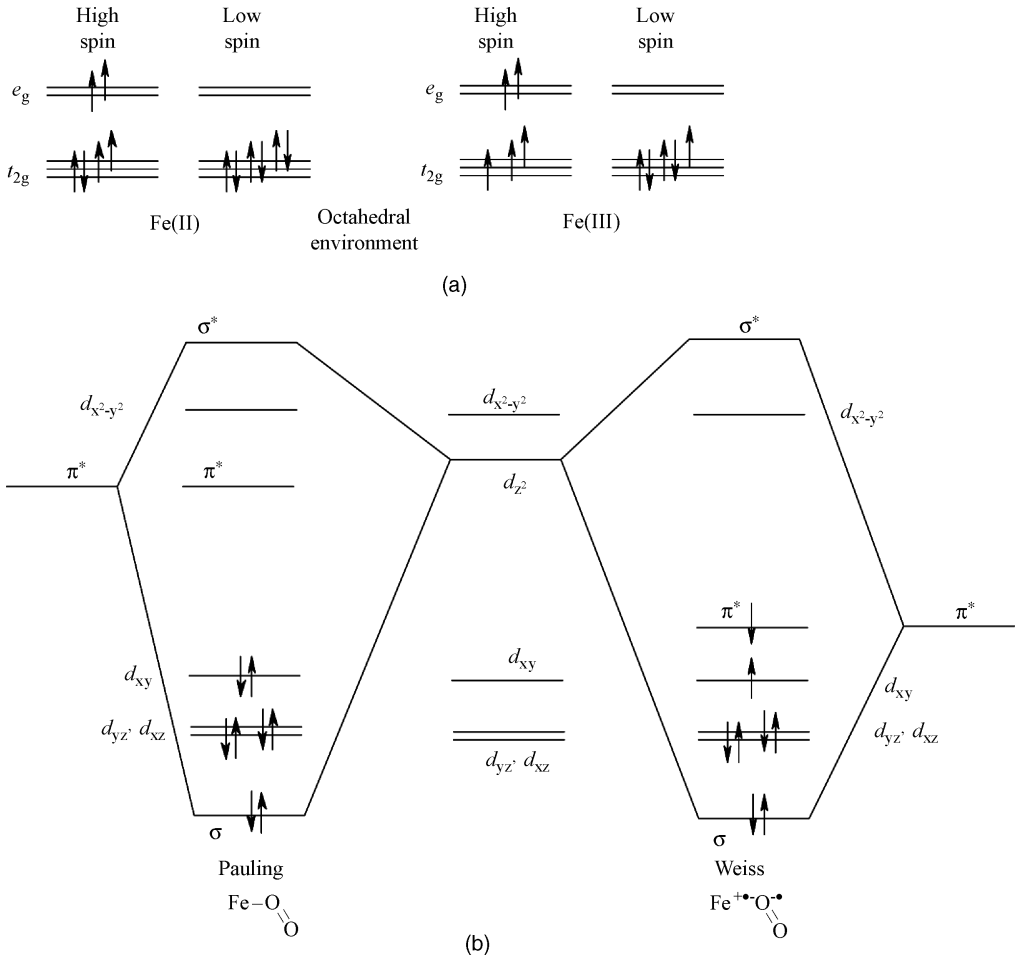


**Figure 2.17** (a) Crystal field orbital descriptions for high- and low-spin iron(II) and iron(III). (b) Ligand field description of the Pauling and Weiss models for oxygen binding by haemoglobin. The Weiss model involving superoxide binding to an iron(III) centre was eventually proven to be correct.

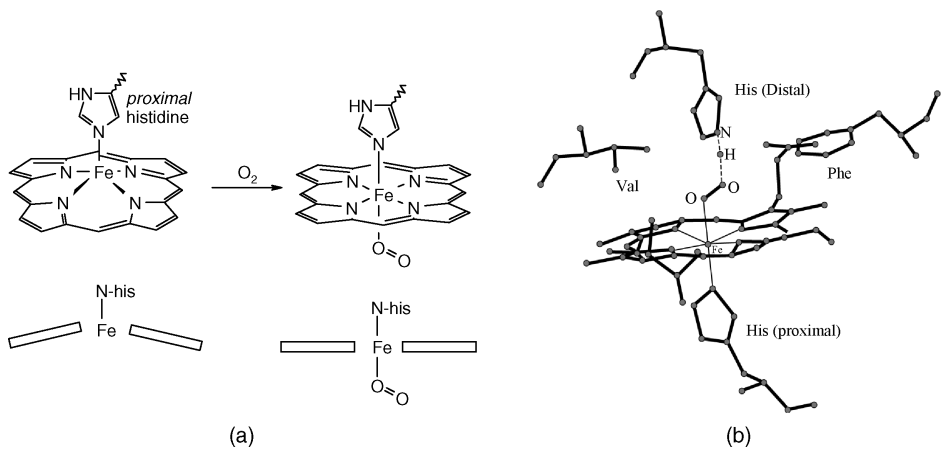


**Scheme 2.5** (a) Porphyrin doming relaxes upon $O_2$ binding. (b) Oxygenated haem showing immediate protein environment including stabilising hydrogen bonds (reproduced with permission from Reference 1).

gives a system with one extra electron) gives EPR spectroscopic data that suggests that this extra electron resides on the oxygen. This results in the formulation Co(III)—$O_2^{\bullet -}$, which is in agreement with the Weiss model. X-ray photoelectron spectroscopy also suggests iron has an oxidation state of approximately 3.2 and hence the correct oxidation state of iron is thus the +3 state.

Evidence for the trigger mechanism comes from the X-ray crystal structure of a 'picket fence porphyrin' model compound. In this species (containing a 2-methyl imidazole ligand in one axial site as a model for the proximal histidine residue) the deoxy form is found to have a doming corresponding to the Fe ion being 0.399Å out of the plane formed by the four porphyrin N atoms. $O_2$ binding causes the Fe to move to a position only 0.086Å out of the macrocycle (N) plane. An extensive range of porphyrin-based model compounds have been prepared to help understand the mechanism of operation of haemoglobin. These compounds are discussed in Section 12.6.1. It is surprising, however, that the binding of a weak ligand such as $O_2$ should induce a spin cross-over from high to low spin at the metal centre. Indeed, porphyrin ligands usually induce a large ligand field, resulting in complexes always being of low spin. Thus the high-spin situation (which is vital for $^3O_2$ binding if forbidden spin cross-overs are to be avoided) is something of an anomaly that can be explained only by the porphyrin doming and consequent weakening of the ligand field. The relatively light pull from the incoming $O_2$ thus makes all the difference in energy terms between the strained, high-spin deoxygenated state and the low-spin oxygenated state. The porphyrin doming thus represents an example of enzymatic *entatic state*, in which the role of the bulk protein environment is to maintain the active site in a state of high energy, part way along the desired reaction coordinate. Metalloproteins in general are found very rarely with the metal ion in a relaxed, regular coordination environment, but are often balanced finely between two high-energy states requiring only small external influences to effect the cross-over from one to another.

It is well known that gases such as CO or readily adsorbed salts such as $CN^-$ are extremely toxic. This is because they bind irreversibly to the Fe in haemoglobin preventing oxygen transport and resulting in rapid suffocation. CO in particular is a much better π-acceptor than $O_2$ and hence is bound very much more strongly. The affinity of protein-free haem model systems for CO is much greater than for $O_2$, as expected: $K_{CO}/K_{O_2} = 25\,000$. In haemoglobin, however, this ratio is reduced to a more favourable 200 enabling the human body to at least tolerate small quantities of CO. This phenomenon is explained by the protein conformation restricting access to the iron binding site such that the geometry of the binding pocket is more suited to the bent $O_2$ mode of binding than the linear CO form (Figure 2.18). In the oxygenated haem, the $O_2$ molecule is bound through only one O atom with an Fe—O—O angle of about 120° (O—O distance 1.89Å) as a consequence of the remaining lone pair on the binding O atom. The haem-$O_2$ interaction is stabilised by hydrogen bonding of the unbound $O_2$ to a distal histidine NH functionality.

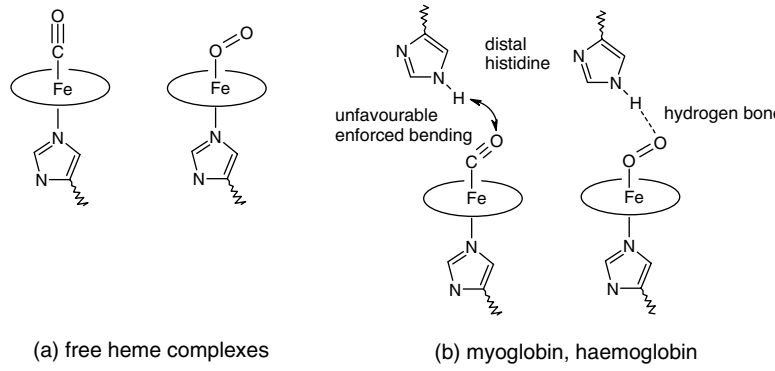


**Figure 2.18** Improved selectivity for $O_2$ over CO is enforced by the protein environment.

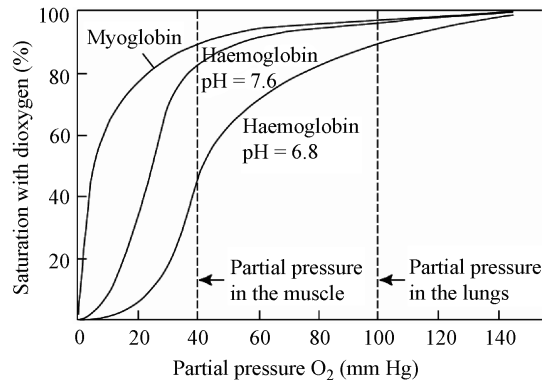


**Figure 2.19** Oxygen saturation curves for myoglobin and haemoglobin and different pH values. (Reproduced by permission of John Wiley & Sons, Ltd).

One final point concerns the incorporation of four myoglobin units into the overall haemoglobin protein. Clearly myoglobin alone is quite capable of $O_2$ uptake and transport, so why is it necessaryto incorporate it into a tetrameric protein? The answer lies in the mutual interactions of the four myoglobin units in haemoglobin. This has the effect of synergically modifying the $O_2$ uptake and decomplexation characteristics to make them more suitable for the $O_2$ partial pressures found in the lungs and muscle. The behaviour of myoglobin and haemoglobin (Figure 2.19) shows that, without these cooperative characteristics, myoglobin would not be able to release $O_2$ where it is needed in oxygen-deficient tissue such as muscle.

This cooperative behaviour relates to the enhancement of binding at one haem site if another is oxygenated or, if one haem centre loses its $O_2$, lowered oxygen affinity at the other iron centres. Long-range influences on binding at one site by binding at another of this type are termed *allosteric* effects and the sigmoidal binding profile is characteristic of their occurrence (see Section 1.5). The result is an all-or-nothing type of behaviour in that as soon as $O_2$ levels are high enough to induce binding at one site (*i.e.* in the lung) all sites are quickly saturated. Upon $O_2$ release in the muscle, decomplexation of all four sites follows rapidly upon release of $O_2$ from any one of them. The mode of operation of this allosteric effect has been described by a 'spring loaded' model in which the haemoglobin as a whole alternates between two states termed *tense* (T) and *relaxed* (R). Hence each haem may be either oxy or deoxy and T or R. Binding of $O_2$ to the domed deoxy T form causes a reduction in doming to give a strained oxy T form. Strain is released by movements of the proximal histidine residue to give a straighter Fe—N bond. This results in a movement of the protein backbone, which is transmitted to the remaining myoglobin units, encouraging $O_2$ binding.

## 2.6 Enzymes and Coenzymes

### 2.6.1 Characteristics of Enzymes

Kim, D. H., 'Supramolecular aspects of enzymes', in *Comprehensive Supramolecular Chemistry*, J.L. Atwood, J.E.D. Davies, D.D. MacNicol and F. Vögtle (eds), Pergamon: Oxford, 1996, vol. 4, 503–526.

Enzymes are of vital importance and interest in biochemistry. It is enzymes that catalyse essentially all biological processes and, as we will see in Chapter 12, they have stimulated a wealth of interest from supramolecular chemists. Enzymes are dynamic macromolecules with a molecular weight

generally in excess of 10 000 Da. They are made up of polypeptide chains, which in turn are polymers of the protein amino acids (Box 2.2). The polypeptide chains are folded into a unique conformation giving a globular structure incorporating surface clefts and crevices. Substrate binding in enzymatic catalysis occurs within one of these clefts, termed the *active site* which often contains a metal ion. The initial binding is a thermodynamically controlled equilibrium process and is highly selective, usually proceeding on an induced fit basis. Binding occurs by three-dimensional contact between enzyme and substrate, and involves hydrophobic effects, hydrogen bonding, salt bridges (ion–ion) and other forms of intermolecular interaction. Bound substrates experience chemical transformation, sometimes at rates approaching the diffusion limit (the reaction occurs as fast as the substrate reaches the enzyme in accordance with the local concentration gradient and thermal fluctuation; about $10^8$ $s^{-1}$ $M^{-1}$). A key concept behind this rate enhancement in enzymatic catalysis is that of the *entatic state*. Bound substrates are held in a way that distorts them making them more like the transition state for the reaction the enzyme catalyses thus lowering the activation barrier for the reaction.

Enzyme structure may be divided into primary, secondary, tertiary and quaternary features, Figure 2.20. The primary structure is the sequence of amino acid residues on the polypeptide chain and is determined by the way in which the enzyme is synthesised. The secondary structure relates to ordering of the chains into discrete units or segments such as α-helices and β-sheets, while tertiary structure is the way in which the secondary structural features arrange themselves to produce the full globular protein. This occurs *via* hydrogen bonding, stacking interactions and hydrophobic forces, and often involves the participation of water molecules buried deep within the enzyme, where they fill small cavities and act as a 'glue' holding secondary features together. In many cases more than one protein strand is involved in a fully functioning enzyme system and the supramolecular association

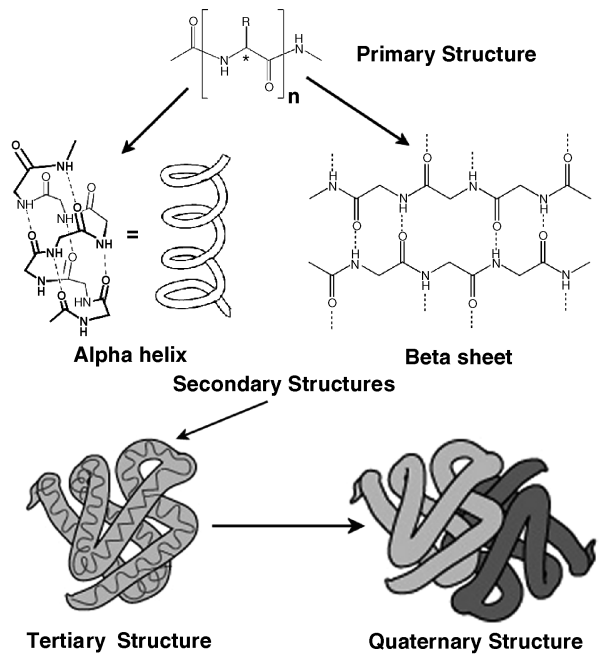


**Figure 2.20** Enzyme structure can be divided into primary (amino acid sequence), secondary (chain folding), tertiary (full 3D conformation) and quaternary (association of more than one protein chain) features.

**Figure 2.21** Eduard Buchner – father of enzyme chemistry.

of more than one protein molecule is termed quaternary structure (*e.g.* haemoglobin, a tetramer of four myoblobin units). It is the enzyme tertiary and quaternary structure that is responsible for the organisation of the binding site(s); it is also the most flexible component of the enzyme structure, allowing the binding site to deform in response to guest binding. Enzyme tertiary and quaternary structure is well-defined, however, and enzymes are ordered so highly that they can be crystallised. The way in which tertiary and quaternary structure is encoded within the primary amino acid sequence is a complicated and, as yet, unsolved mystery—one that challenges supramolecular chemists to address. Hydrophobic effects, resulting in an overall globular shape, are important, as are steric effects, which may be responsible for most of the organisation. Specific, directional hydrogen bonds then determine which of a small number of globular conformations is the one favoured.

Some of the earliest work on enzymes was by German chemist Eduard Buchner (Figure 2.21) working at Berlin University who in 1897 discovered that yeast extracts that without any living yeast cells were still able to ferment sugar. Buchner named the enzyme that brought about sucrose fermentation *zymase*. His work won him the 1907 Nobel Prize in Chemistry. In line with Buchner's ideas enzymes are generally named according to the reaction they carry out with the suffix *-ase* being added to the name of the substrate. Hence $Na^+/K^+$-ATPase is an enzyme that uses ATP and lactase is an enzyme that cleaves lactose. Enzymes can also be named after the type of reaction they catalyse, for example DNA polymerase forms polymeric DNA.

There exists a bewildering variety of protein-based enzymes ranging in size from a mere 62 amino acid residues for monomer of 4-oxalocrotonate tautomerase[8] to a whopping 2500 residues for fatty acid synthase.[9] According to the International Union of Biochemistry and Molecular Biology nomenclature for enzymes each enzyme is described by a sequence of four numbers preceded by 'EC'. The first number broadly classifies the enzyme based on its mechanism. The first-level general categories are listed below (see http://www.chem.qmul.ac.uk/iubmb/enzyme/ for the complete nomenclature).

- EC 1 *Oxidoreductases*: catalyze oxidation/reduction reactions
- EC 2 *Transferases*: transfer a functional group (*e.g.* a methyl or phosphate group)
- EC 3 *Hydrolases*: catalyze the hydrolysis of various bonds
- EC 4 *Lyases*: cleave various bonds by means other than hydrolysis and oxidation
- EC 5 *Isomerases*: catalyze isomerisation changes within a single molecule
- EC 6 *Ligases*: join two molecules with covalent bonds

## 2.6.2 Mechanism of Enzymatic Catalysis

The overall process of enzyme catalysis may be represented by Equation 2.8, where E, S and P represent enzyme, substrate and product, respectively. Note that the enzyme is regenerated after the reaction, as required in a catalytic process.

$$E + S \underset{k_{-1}}{\overset{k_1}{\rightleftharpoons}} ES \xrightarrow{k_{cat}} P + E \tag{2.8}$$

$$k_1/k_{-1} = K_{11} \tag{2.9}$$

The specificity and selectivity of a particular enzyme for competing substrates depends on both rate constants $k_1$ and $k_{-1}$ for each substrate (and hence on the equilibrium constant), and $k_{cat}$. This is usually expressed as an overall specificity constant, $k_{cat}/K_{11}$. Thus, the most specific enzymes carry out their catalysis rapidly, without the need for particularly strong binding. Many enzymes adhere to Michaelis-Menten kinetic parameters (named after Leonor Michaelis and Maud Menten who first described a model of enzyme reactivity crucially dependent on the existence of the ES complex shown in Equation 2.8). In the Michaelis-Menten model, the rate of catalysis ($V$ – defined as the number of moles of product formed per second) increases with increasing concentration of substrate, S. For a constant enzyme concentration, $V$ is linearly proportional to the concentration of S (denoted [S]) *when [S] is small*. At high [S] (*i.e.* when S is in vast excess compared to the enzyme concentration), $V$ is nearly independent of [S]. This gives a plot of $V$ against [S] of the type shown in Figure 2.22a. Combining experimental observation with mathematical principles gives the famous Michaelis-Menten equation, Equation 2.10.

$$V = V_{max} \frac{[S]}{[S] + K_M} \tag{2.10}$$

The quantities $K_M$ and $V_{max}$ are important parameters that can be used to characterise and understand enzymatic reactivity. The $K_M$ value is the *Michaelis constant* which is defined as the substrate concentration at which the reaction rate is half of its maximal value. Hence $K_M$ (which varies considerably) is

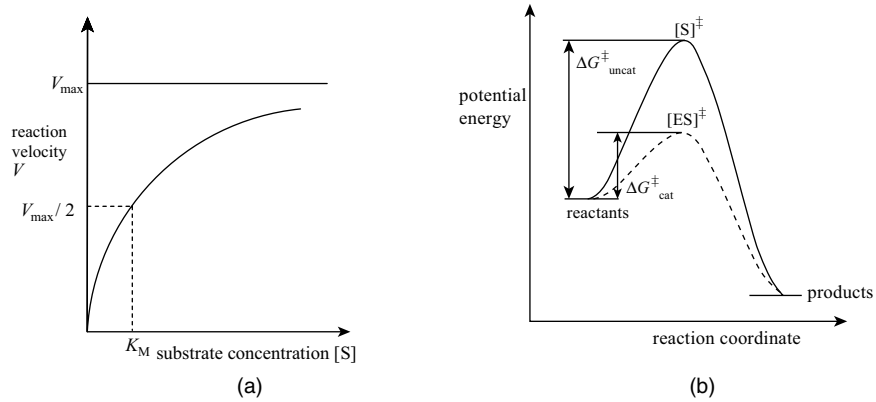


**Figure 2.22** (a) a plot of reaction velocity $V$ agains substrate concentration [S] for an enzyme that obeys Michaelis-Menten kinetics. $V_{max}$ is the maximum reaction velocity and $K_M$ is the Michaelis constant (b) Chemical reactions profiles for catalysed (⋯) and uncatalysed reactions (——).

a measure of the relative affinity of an enzyme for its substrate –the *higher* the $K_M$ value the *lower* the affinity for the substrate. The $V_{max}$ parameter describes the maximum rate of product formation under conditions of high substrate concentration (*i.e.*, a large excess over the concentration of enzyme) where all of the active sites of an enzyme are occupied. The $V_{max}$ and $K_M$ values can be determined by varying the concentration of S and looking at the amount of product formed. This information can be expressed as a Lineweaver-Burk plot, namely $1/V$ *vs.* $1/[S]$. This graph gives a straight line with a *y*-axis intercept of $1/V_{max}$ and a slope of $K_M/V_{max}$. The *x*-axis intercept gives $1/K_M$. This kind of plot can give a significant amount of information about the mechanism of enzyme inhibition by specific compounds.

There are exceptions to Michaelis-Menten behaviour. For example allosteric enzymes which instead of a hyperbolic curve in a $V$ versus [S] graph yield a sigmoidal plot (the behaviour is rather like non-catalytic allosteric proteins, such as haemoglobin, Section 2.5. This type of curve can indicate *co-operative binding* of the substrate to the enzyme. We have discussed cooperativity in Section 1.5 (see also Section 10.4.3). In addition, regulatory molecules can further alter the activity of allosteric enzymes.

The key to an understanding of the way in which enzymes are able to achieve such large rate accelerations in the reactions they catalyse may be found in the insight of Linus Pauling, who stated in 1948 that 'enzymes are molecules that are complementary in structure to the transition states of the reactions they catalyze'. This simple, but profound, assertion relates to the overall transition state theory in chemical reactions, as exemplified by the type of reaction coordinate profile shown in Figure 2.22b. The job of the enzyme catalyst is to lower the energy of the activated enzyme substrate complex $[ES]^{\ddagger}$ and hence the free energy of activation, $\Delta G^{\ddagger}_{cat}$ relative to the energy of the activated substrate, $[S]^{\ddagger}$, in the uncatalysed reaction. The enzyme must, therefore, be more complementary to the activated substrate than it is to the ground-state species. Indeed, the non-covalent forces involved in substrate binding should be sufficient to distort the substrate such that it proceeds some distance from left to right along the reaction coordinate. In other words, it becomes more like the transition state, hence lowering the activation energy required to form $[ES]^{\ddagger}$. This is a further manifestation of the induced fit model (Section 1.3). Not only does the enzyme undergo a conformational change on substrate binding, but so does the substrate (Figure 1.3b). This conformational change should result in strain at the scissile bond (the one that is to be broken in the catalysed reaction). As an example, the transition state in the deamination reaction of adenosine triphosphate is stabilised by around 73.2 kJ $mol^{-1}$ at 310K. Despite the power of this approach, transition state stabilisation is not the only possibility when it comes to explanation of enzymatic rate enhancements. One other topical factor is *dynamical effects.* Rate enhancement from dynamical effects means that the enzyme has evolved to optimise a particular vibrational mode that moves the substrate to the transition state or moves the transition state towards the product. Dynamical effects are controversial and computational analysis does not support their having a significant role, however the idea is an interesting alternative.[10]

Another factor, in addition to transition-state stabilisation, that contributes to enzymatic acceleration is effective concentration. In general, in nonenzymatic chemistry, intramolecular reactions (such as cyclisation) are much faster than their bimolecular analogues because of statistical effects; for example, the intramolecular reaction of phenyl succinate is about $10^5$ times faster than the bimolecular reaction of acetate with phenyl acetate at 1 M concentration of all species (Scheme 2.6). The ratio $k_1/k_2$ is termed the effective molarity and its value of $10^5$ M is clearly much larger than a real concentration (neat acetic acid is about 17 M), even though it notionally represents the acetic acid concentration required to achieve the same rate as the intramolecular equivalent. Compared to bimolecular reactions, unimolecular processes result only in a loss of internal rotational entropy and so may be favoured by as much as 54–59 kJ $mol^{-1}$ on entropic grounds. In enzymes, if the binding of the substrate with the enzyme is strong enough, then the ES complex acts as if it were one molecule, thus intramolecular-type rate accelerations of the order of $10^9$ are observed. In effect, the entropic 'price' required for bringing together two reactants is 'paid for' by the substrate binding, not during the reaction itself.

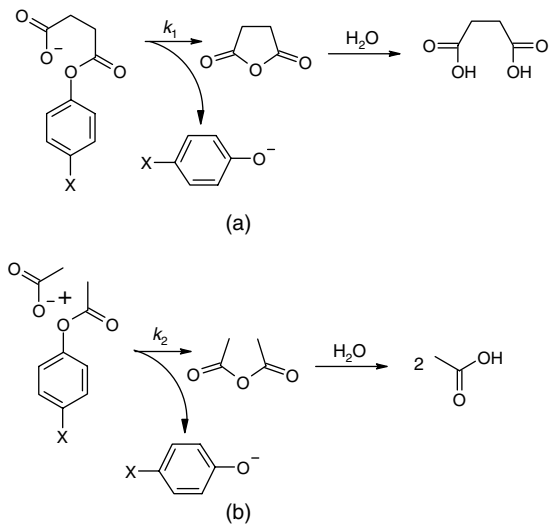


**Scheme 2.6** Intramolecular reactions **(a)** are much faster than bimolecular equivalents **(b)**.

A final key factor in enzymatic rate acceleration is also the desolvation of the bound substrate, again 'paid for' in energy terms at the complexation stage. The enzyme functional groups and surface interactions effectively replace the water molecules formerly surrounding the substrate. It is often the case that the reactive group attached to the enzyme is one of these solvating moieties, and hence the reactants are brought within one another's first solvation sphere to form a contact pair with high affinity and are held in that way for long enough for the reaction to occur. This process is referred to as *spatiotemporal theory.*

Clearly, enzymes have evolved to carry out these special tasks in a highly selective fashion, and each enzyme family is very different from the others, despite their common amino acid building blocks, according to their particular task. One feature that enzymes share is that they are all very large and complicated molecules. This factor alone almost prohibits any opportunity for a full understanding of enzyme function in model systems since small-molecule models simply cannot begin to approach the complexity of the real species. So, is this large size really necessary, or is it an evolutionary accident? It is possible that the size of enzymes is simply the minimum needed to achieve the required binding site cleft geometry and orientation through the use of folded peptide interactions. Furthermore, the binding site must possess some controlled, well-defined flexibility to accommodate the movements of the substrate as it undergoes chemical transformations. This is one of the reasons why it is constructed using malleable protein tertiary structure. Also perhaps of importance is the large number of functional groups on the enzyme surface remote from the binding site. These may serve to trap potential substrates and enhance their rate of diffusion towards the active site. Often, the very largest enzymes are the most specific, having other polypeptides as their substrates. It has been estimated that an interacting surface area of at least 10 $nm^2$ is required for such interactions to be of significance. It is likely that small proteins with molecular weights of less than 10 000 Da and total surface areas of under 15 $nm^2$ simply do not have the available contact area to be effective.

## 2.6.3 Coenzymes

While many enzymes can function by themselves, others work in a modular way with a coenzyme. A coenzyme is a non-enzyme 'helper molecule' that forms one constituent of a biological catalysis system. In order to function, the full system requires the *coenzyme*, an *apoenzyme* and a *substrate.* A chemical

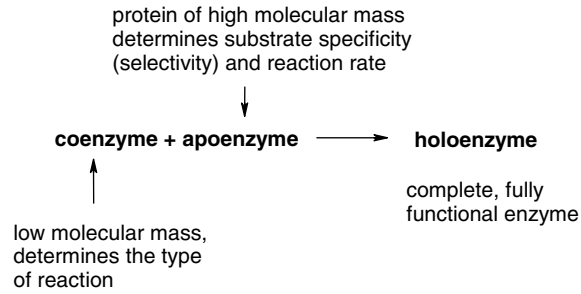


**Scheme 2.7** Modular construction of holoenzymes.

reaction occurs between the coenzyme and the substrate while they are both bound by the apoenzyme. A combined apoenzyme and coenzyme is termed a *holoenzyme* and this is the active species (Scheme 2.7).

Common examples of coenzymes include ATP (the biological energy storage molecule) and NADH (the reduced form of the biological electron carrier) which are a ubiquitous feature of all living systems suggesting that these molecules emerged very early in evolutionary terms. Interestingly the nucleotide adenosine is found in coenzymes that are involved in the catalysis of a broad range of fundamental metabolic reactions such as the transfer of methyl, acyl, and phosphoryl groups, and redox reactions. It has been suggested that this prevalence makes adenosine a chemical fossil remnant of the RNA world in which catalysis was carried out by ribonucleic acid enzymes (ribozymes) rather than proteins, which evolved to bind a restricted set of nucleotides. Adenosine-based coenzymes might have acted as interchangeable adaptors that allowed ribozymes to link to different coenzymes without major modification to existing adenosine-binding regions. We will return to the RNA world theory in Section 12.9.4.

Coenzymes can be either inorganic species such as coenzyme F450 and or purely organic as in coenzyme A (**2.7**), the coenzyme that carries acyl groups in the synthesis and oxidation of fatty acids, and is responsible for oxidation of pyruvate in the citric acid cycle. Vitamins are commonly coenzymes or their precursors. Coenzyme A is vitamin $B_5$ and we will look in detail at cobalamin, vitamin $B_{12}$, by way of an example in the next section. Some examples of vitamin and non-vitamin coenzymes are shown in Table 2.3.

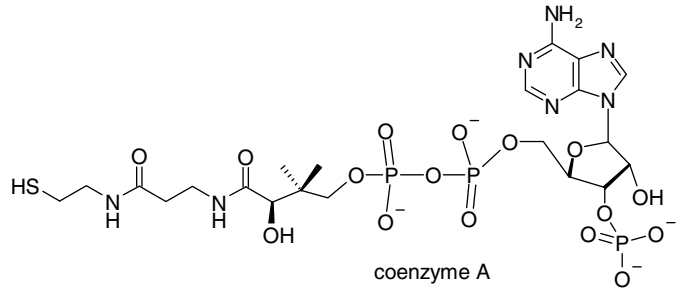


**2.7**

## 2.6.4 The Example of Coenzyme $B_{12}$

To give an example of how a coenzyme functions we will look at the example of coenzyme $B_{12}$ which has proved a popular target for model studies over many years. Coenzyme $B_{12}$ and its derivatives such as vitamin $B_{12}$ are also based on tetrapyrrole macrocycles, Figure 2.10. The structures of these

**Table 2.3** Role and distribution for some vitamin and non-vitamin coenzymes (adapted from http://en.wikipedia.org/wiki/Coenzyme).

| **Vitamins and derivatives** | | | | |
|---|---|---|---|---|
| Coenzyme | Vitamin | Additional component | Chemical group(s) transferred | Distribution |
| $NAD^+$ and $NADP^+$ | Niacin ($B_3$) | ADP | Electrons | Bacteria, archaea and eukaryotes |
| Coenzyme A | Pantothenic acid ($B_5$) | ADP | Acetyl group and other acyl groups | Bacteria, archaea and eukaryotes |
| Tetrahydrofolic acid | Folic acid ($B_9$) | Glutamate residues | Methyl, formyl, methylene and formimino groups | Bacteria, archaea and eukaryotes |
| Menaquinone | Vitamin K | None | Carbonyl group and electrons | Bacteria, archaea and eukaryotes |
| Ascorbic acid | Vitamin C | None | Electrons | Bacteria, archaea and eukaryotes |
| Coenzyme F420 | Riboflavin ($B_2$) | Amino acids | Electrons | Methanogens and some bacteria |

| **Non-vitamins** | | |
|---|---|---|
| Coenzyme | Chemical group(s) transferred | Distribution |
| Adenosine triphosphate | Phosphate group | Bacteria, archaea and eukaryotes |
| S-Adenosyl methionine | Methyl group | Bacteria, archaea and eukaryotes |
| 3'-Phosphoadenosine -5'-phosphosulfate | Sulfate group | Bacteria, archaea and eukaryotes |
| Coenzyme Q | Electrons | Bacteria, archaea and eukaryotes |
| Cytidine triphosphate | Diacylglycerols and lipid head groups | Bacteria, archaea and eukaryotes |
| Nucleotide sugars | Monosaccharides | Bacteria, archaea and eukaryotes |
| Glutathione | Electrons | Some bacteria and most eukaryotes |
| Coenzyme M | Methyl group | Methanogens |
| Coenzyme B | Electrons | Methanogens |
| Methanofuran | Formyl group | Methanogens |

compounds are shown in Figure 2.23 and are all based on cobalt(III) complexes of the corrin ring, which, when acting as a ligand, possesses a single negative charge. The remaining charge on the cobalt is balanced by an integral phosphate residue and a substituent, X, which is the enzymatic 'business end' of the molecule. In the active form of the coenzyme, this substituent is a carbanion. Coenzyme $B_{12}$ and its derivatives are, therefore, the only naturally occurring true organometallic compounds.

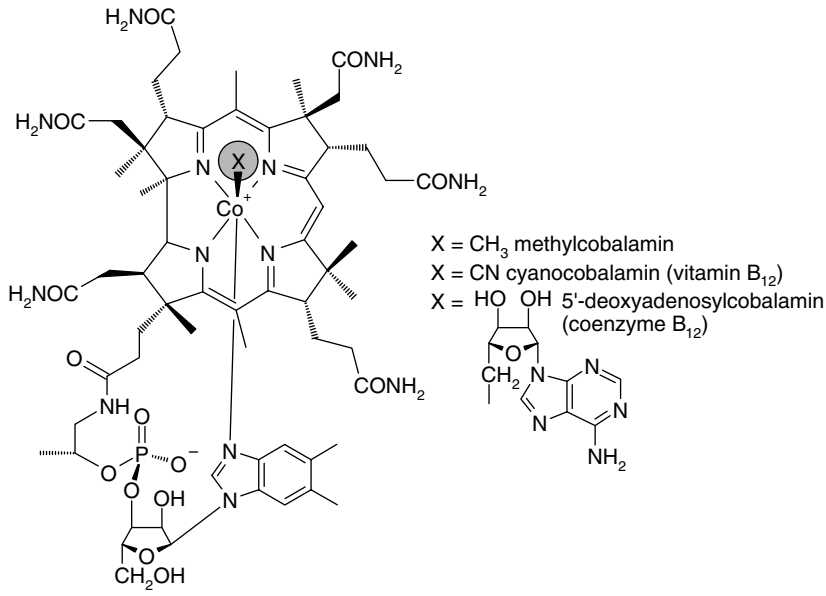


**Figure 2.23** Coenzyme $B_{12}$ and its derivatives.

Remarkably the Co—C bond is very stable under physiological conditions (pH 7, oxygenated aqueous solution).

The modular nature of holoenzyme catalysis allows coenzyme $B_{12}$ to be used in a variety of biological reactions with different apoenzymes. These reactions can involve homolysis of the Co—C bond to give an alkyl radical resulting in radical induced rearrangements, redox reactivity *via* reduction to Co(II) and Co(I), and alkylations. The nature of the coenzyme determines the type of the reaction, while the nature of the apoenzyme determines the selectivity of the reaction in terms of the substrate and the regiospecificity.

The $B_{12}$ class compounds are required in only very small amounts, consistent with the poor bioavailability of cobalt, and are used mainly by microorganisms, which can also synthesise them. In mammals, the $B_{12}$-dependent methylmalonyl–CoA mutase system is of particular importance, however. It is required for amino acid metabolism in the liver and its absence, as a result of genetic defects, is lethal. Indeed, as early as the 1920s it was observed that extracts from animal livers could cure otherwise lethal pernicious anaemia. The presence of cobalt was detected in these liver extracts and this led to

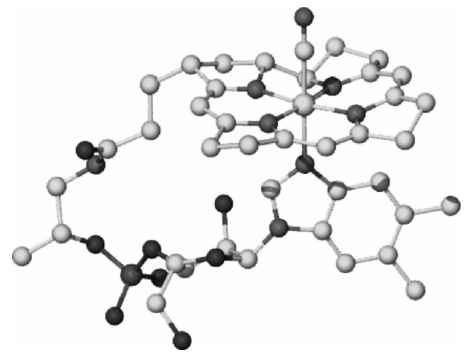

**Figure 2.24** X-ray crystal structure of vitamin $B_{12}$ (substituents omitted for clarity).

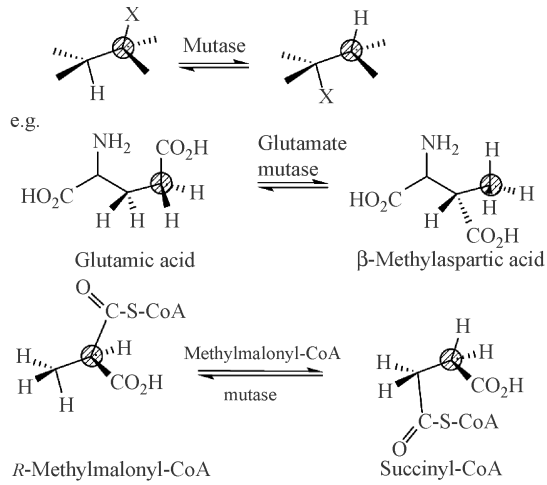


**Scheme 2.8** 1,2-Shifts by coenzyme $B_{12}$ mutases.

a great deal of work to isolate this unusual cobalt-containing compound, which is present in blood in concentrations of about 0.01 mg $L^{-1}$. Using chromatographic methods and a great deal of perseverance, cyanocobalamin was finally isolated in pure form in 1948. The $CN^-$ group is not part of the active form of the complex, but is an artefact of the isolation procedure. However, the cyano derivative is still therapeutically useful and the new isolated material was named vitamin $B_{12}$. The X-ray crystal structure of this rather large 'small molecule' (RMM 1350 Da) (Figure 2.24) earned the 1964 Nobel Prize in Chemistry for Dorothy Crowfoot-Hodgkin. The structure demonstrated a bent, 'butterfly' shape of the corrin ring, which is a consequence of its small size (15-atom ring instead of the usual 16 in porphyrins). This distortion is of relevance to the reactivity of the coenzyme and represents an entatic state structure.

The biochemistry of coenzyme $B_{12}$ generally revolves around either mutase enzyme activity, involving functional group migration, notably by stereospecific 1,2-shifts (Scheme 2.8), or methylation by methionine synthetase. The general mechanism for the mutase activity is a radical-based one and has been established by EPR spectroscopy to be of the general form shown in Scheme 2.9.

## 2.7 Neurotransmitters and Hormones

D.A. Dougherty, 'Is the brain ready for physical organic chemistry?', *J. Phys. Org. Chem.*, 1998, **11**, 334–340.

In addition to the bioinorganic chemistry involving metal cations in various forms, there exists a vast amount of biological chemistry that, in a supramolecular sense, involves molecular species and anions as the guests. While the detail of this chemistry is beyond the scope of this book, we must mention in passing the role of two particular classes of biological guest, namely hormones and neurotransmitters, which, broadly speaking, act as messengers and activating agents. Hormones such as the human sex hormones, oestrogen and testosterone, and the pregnancy hormone, progesterone, are household names. A range of testosterone derivatives, the anabolic–androgenic steroids, are capable of altering human physical performance significantly and as a result are highly topical within the context of their illegal use in competitive sports. Similarly, levels of neurotransmitters such as dopamine and acetylcholine may have dramatic effects on brain chemistry and hence behaviour, and

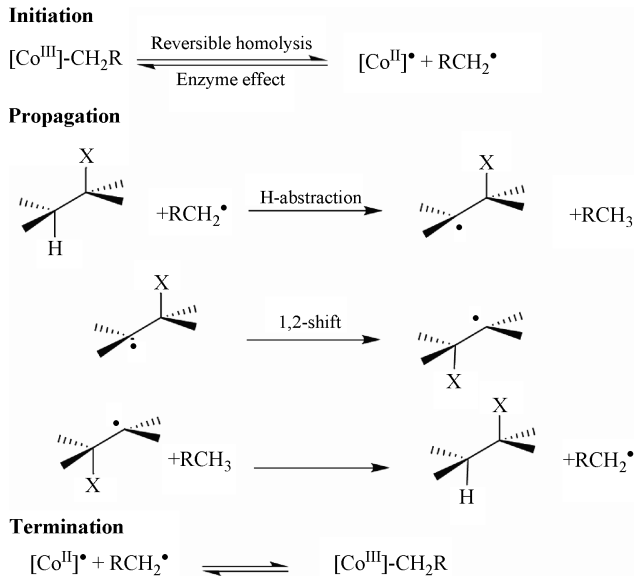


**Scheme 2.9** Radical mechanism for mutase activity.

imbalances are implicated in a number of mental disorders such as schizophrenia and Parkinson's disease, highlighting the chemical nature of even our very thought processes.

To illustrate the supramolecular biological role of such molecular species we will look at the mode of action of acetylcholine (ACh, **2.8**) in particular since this example highlights the profound effect that the non-covalent binding of a small molecular guest may have on a biological system.

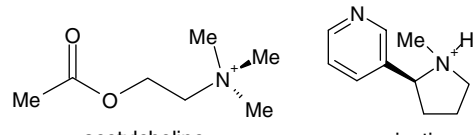


Acetylcholine is a key neurotransmitter molecule. Nerve pulses are passed on from nerve fibre to nerve fibre across the synapses (the gaps between nerve cells, about 30–40 nm thick) by transfer of acetylcholine from one nerve cell to the next. The role of acetylcholine is to bind to, and hence open, a gated sodium ion channel (*cf.* Section 2.2), which forms part of the nicotinic acetylcholine receptor protein (nAChR). This large transmembrane protein is composed of five subunits (two labelled $\alpha$, and the others labelled $\beta$, $\delta$, $\gamma$, Figure 2.25) with similar amino acid sequences, which encircle a central channel. Acetylcholine binds to the two $\alpha$-subunits, causing a conformational change in the channel external region, which allows access to $Na^+$ ions located in the synapse. These then flow rapidly into the cell in accordance with the prevailing concentration gradient, resulting in a current flow. The binding of the agonist acetylcholine to its receptor is highly selective and involves cation–$\pi$ interactions (Section 1.8.5) between the quaternary ammonium moiety and a particular tryptophan amino acid residue. Interestingly, acetylcholine activity is affected severely by nicotine (**2.9**), which also possesses a quaternary ammonium residue, and it is likely that this is the basis for nicotine addiction in smokers. Once the membrane has depolarised and the neural current has been generated, acetylcholine is removed by another acetylcholine-binding protein, acetylcholine esterase, which hydrolyses the ester functionality preventing the molecule from binding to nAChR.

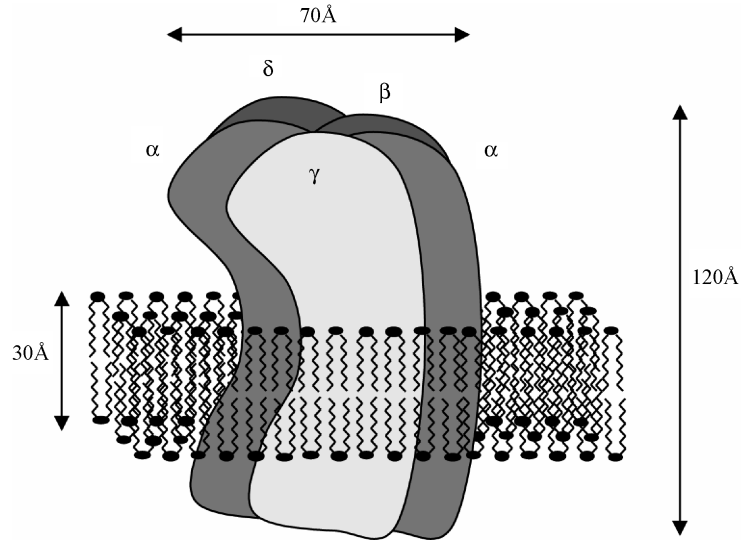


**Figure 2.25** The membrane-bound nicotinic acetylcholine receptor (nAChR).

The competition for nAChR binding by acetylcholine and nicotine illustrates the key role of selectivity in binding in supramolecular chemistry. Because nAChR is not fully selective, it is also able to bind the interfering nicotine. The fact that nicotine, like acetylcholine, possesses a quaternary ammonium moiety that is implicated in its binding mechanism highlights the dependence of biological processes on ostensibly weak supramolecular interactions.

## 2.8 Semiochemistry in the Natural World

Schulz, S. (ed.), 'The chemistry of pheromones and other semiochemicals I, and II', *Top. Curr. Chem.*, 2004 vol. 239 and 2005 vol. 240.

Semiochemistry is the chemistry of signalling and sensing and, like the binding of neurotransmitters and hormones, a great deal of sensing and signalling in the natural world makes use of chemical recognition events, usually between a chemical messenger molecule such as a hormone or pheromone and a protein-based receptor. Hormones are responsible for intercellular signalling in the body where they are involved in the regulation of cell function. Pheromones can be used by insects as well as reptiles and mammals to induce particular kinds of behaviour or to signal information such as the whereabouts of food or sexual availability. There are numerous classes of pheromone including aggregation, alarm and epideictic (signal the presence of insect eggs) pheromones; releaser, primer, territorial, trail and sex pheromones. The sense of smell is also based on molecular recognition with odourants dissolving in nasal mucus where they bind to and activate odourant binding proteins or, in insects, chemosensory proteins (isolated for the first time as recently as 1999[11]) generating a nerve signal to the brain.

A good example of a pheromone is bombykol, (10E,12Z)-hexadeca-10,12-dien-1-ol (**2.10**), a pheromone which is used by the female silkworm moth to attract a mate (Figure 2.26a). Its predominantly hydrocarbon structure makes it water insoluble and thus it remains localised near the source. Bombykol was one of the first pheromones to be isolated (in 1959) and is used in minute quantities to confuse male moths as to the location of females and thus control numbers.

(a) (b)

**Figure 2.26** (a) paired male and female *Bombyx Mori* silkworm moths (image courtesy of www.wormspit.com), (b) jasmine blossom. See plate section for colour version of this image.

Another particularly sweet smelling example of a small molecule messenger is methyl jasomate, the principal scent component (*ca.* 2.5 per cent) of jasmine oil. Methyl jasmonate (**2.11**) can be detected by scent in very small quantities, indeed it takes some 10,000 flowers to make just 1 g of the oil (Figure 2.26b), and is used as a perfume in detergents and is also a flavour ingredient in black tea. Methyl jasmonate has two chiral centres and therefore exists as four stereoisomers. The fact that only one, Methyl (+)-epijasmonate, (3R,7S)-(+)-methyl 3-oxo-2-(2-(Z)-pentenyl)cyclopentane-1-acetate, has any significant odour, highlights the remarkable specificity of the molecular shape recognition by odour proteins (which are themselves chiral, of course). When a plant is attacked by an insect it produces higher levels of methyl jasmonate, which build up in the damaged parts of the plant. It is thought that the damage activates a lipase enzyme causing the release of linolenic acid (the precursor of jasmonic acid) and activation of proteinase inhibitor genes. The resulting proteinase is ingested by the insect and interferes with its digestive system, preventing further feeding. Methyl jasmonate is more volatile than the strongly hydrogen bonding jasmonic acid and hence can signal the occurrence of insect attack to nearby undamaged plants stimulating the production of defensive chemicals. Methyl jasmonate may also act as an attractant for insect predators.[12]

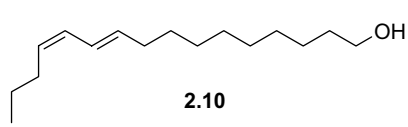


**2.10**
Bombykol

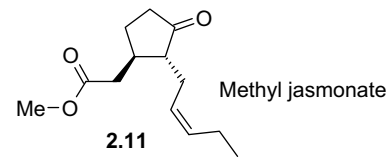


**2.11**

## 2.9 DNA

### 2.9.1 DNA Structure and Function

Calladine, C. R., Drew, H. R., Luisi, B. and Travers, A. *Understanding DNA: The Molecule and how it Works*, Academic Press: New York, 3rd ed., 2004.

DNA (deoxyribonucleic acid) is well known as the molecule that bears all of the genetic information necessary to construct and operate a living organism. The cell nuclei of all eucaryotic organisms contain DNA and each cell contains all the genetic code needed to assemble the entire organism – a remarkable duplication of information. The amount of information involved requires the individual DNA

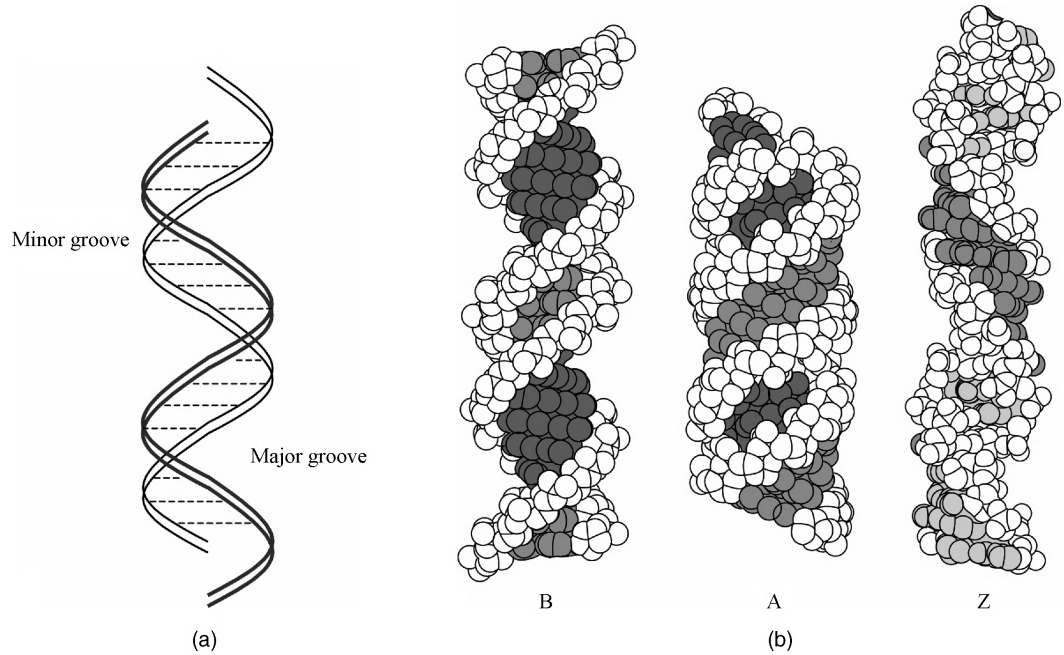


**Figure 2.27** (a) The DNA double helix. Dotted lines represent hydrogen bonded base–pair interactions; (b) Idealised views of the three most common forms of DNA: B, A and Z. Structures B and A have right-handed helicity with 10 and 11 phosphate residues per turn, respectively. The Z form is left-handed with 12 phosphates per turn. (Reproduced with permission from Academic Press).

strands to be extremely long. Each cell contains about 3 cm of DNA. The fact that this vast molecule fits within a cell of width around $10^{-5}$ m is because the DNA molecule is very thin, having a diameter of just $2 \times 10^{-9}$ m. In its resting state, DNA has a double helical structure that involves two identical strands linking together *via* hydrogen bonding and π–π stacking interactions (Figure 2.27a). The real (but idealised) structure of DNA in its common forms is shown in Figure 2.27b. The driving force for this assembly is thought to be the fact that the double helical structure enables the hydrophobic portions of the molecule (the nucleobases) to avoid the aqueous solvent by stacking in the centre of the helix. The helical structure offers the best possible optimisation of inter-nucleobase interactions while minimising empty space in the interior.

The basic components of DNA are *nucleotides*, molecules that contain a nucleobase (either adenine (A), thymine (T), cytosine (C) or guanine (G)) attached to a sugar and a phosphate tail (Figure 2.28). The A and T components are known as *purines*, while the C and G nucleobases are called *pyrimidines*. Polymerisation of these nucleotides *via* the sugar–phosphate residues forms the backbone of a DNA single strand (**2.12**). The genetic information on DNA is stored as a large number of three-letter 'words'. These 'words' comprise triplets of nucleobases (*e.g.* GCC, CAG, ATC *etc.*). Each 'word' is translated biochemically into one of the 20 protein amino acids (Box 2.2) according to Table 2.4.

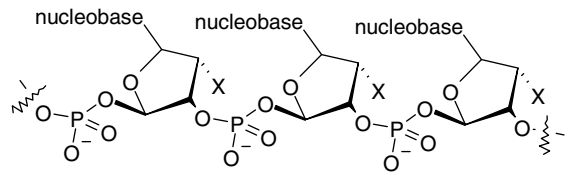


**2.12**

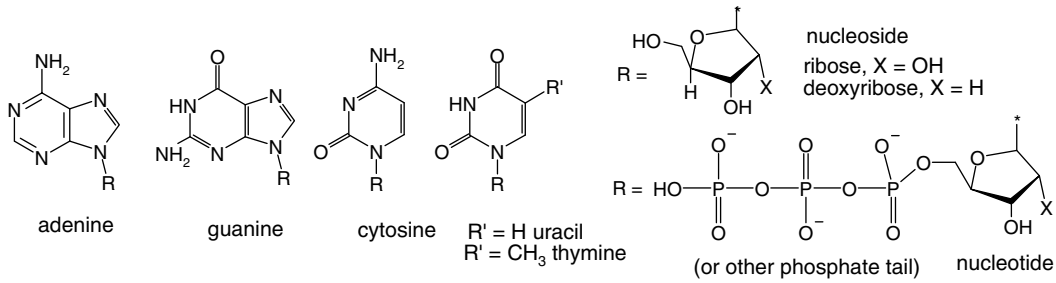


**Figure 2.28** A nucleotide comprises a nucleobase attached to a sugar (to give a nucleoside) and a phosphate tail.

**Table 2.4** The genetic code.

| First base | Second base | | | | Third base |
|---|---|---|---|---|---|
| | T | C | A | G | |
| **T** | Phe | Ser | Tyr | Cys | T |
| | Phe | Ser | Tyr | Cys | C |
| | Leu | Ser | STOP | STOP | A |
| | Leu | Ser | STOP | Trp | G |
| **C** | Leu | Pro | His | Arg | T |
| | Leu | Pro | His | Arg | C |
| | Leu | Pro | Gln | Arg | A |
| | Leu | Pro | Gln | Arg | G |
| **A** | Ile | Thr | Asn | Ser | T |
| | Ile | Thr | Asn | Ser | C |
| | Ile | Thr | Lys | Arg | A |
| | Met (START) | Thr | Lys | Arg | G |
| **G** | Val | Ala | Asp | Gly | T |
| | Val | Ala | Asp | Gly | C |
| | Val | Ala | Glu | Gly | A |
| | Val | Ala | Glu | Gly | G |

Each sequence of three bases in DNA may be translated into one of the 20 protein amino acids in an amino acid chain (Box 2.2). Each chain begins with the start code ATG corresponding to the amino acid methionine (Met). The information stored in DNA is used to encode the synthesis of all of the

**Box 2.2** The Protein Amino Acids

The protein amino acids are the basic building blocks for all peptide chains (amino acid polymers and oligomers) and protein chains (a protein is a large polypeptide), which make up the structure of an enormous number of biological molecules including enzymes. The chains are held together by peptide links (amide

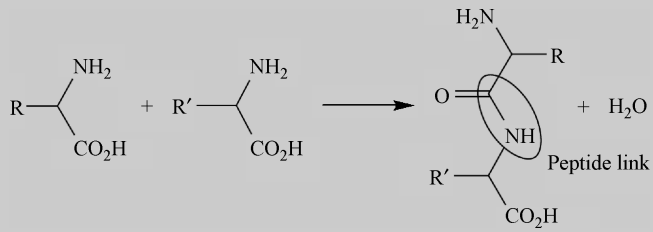


**Scheme 2.10** Condensation reaction between acid and amine parts of amino acids.

bonds), formed by intermolecular condensation reactions between the acid and amine parts of the amino acids, as shown in Scheme 2.10.

The 20 primary protein constituents are shown in Figure 2.29. The R-groups are termed side chains and determine the identity of the amino acid. Amino acids are chiral molecules, and in higher organisms the range of proteins found is limited to L-α-amino acids. In bacteria and fungi, a much wider range of amino acids is found. Amino acids are synthesised entirely enzymatically by a class of enzymes termed aminotransferases (Scheme 2.11) which use the key amino acid glutamic acid as their substrate. Glutamic acid represents the main nitrogen transfer molecule in amino acid synthesis. It is itself synthesised from ammonium ions and α-ketoglutarate by an enzyme called *glutamate dehydrogenase* which uses NADPH as a coenzyme. Glutamic acid is thus the gateway between inorganic and organic nitrogen in biochemistry. The formation of peptides and proteins from amino acids is more complicated, requiring both transfer RNA and messenger RNA; in higher organisms, this takes place within a particular part of the cell (the ribosome)

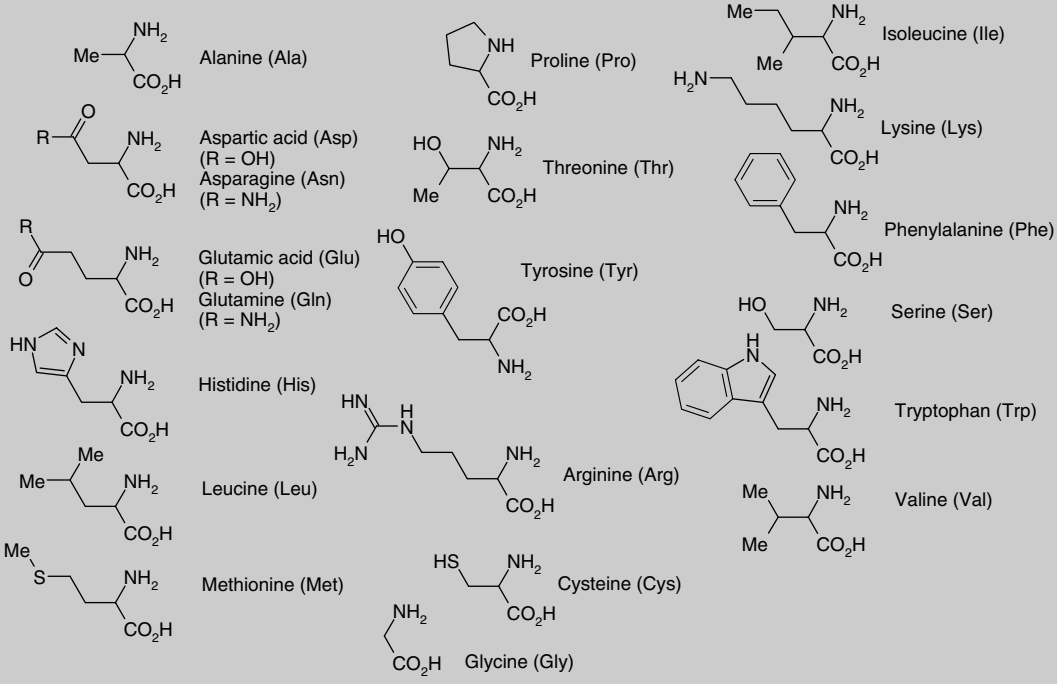


**Figure 2.29** The 20 primary protein amino acids.

(*continued*)

**Box 2.2** (*Continued*)

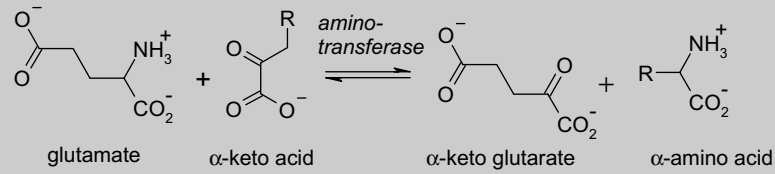


**Scheme 2.11** Aminotransferase catalysed amino acid synthesis.

by cleavage of protein precursors, thus limiting the range of available amino acids. In lower organisms, peptides arise from non-ribosomal enzymatic processes, which are less discriminating. All are α-amino acids except for proline, which is a cyclic α-imino acid.

proteins required by the organism for its biological function. This process is illustrated in Figure 2.30. The intranuclear DNA is used to template the synthesis of messenger RNA (ribonucleic acid), a direct copy of the DNA code but with an extra oxygen atom that enables it to escape the cell nucleus *via* small holes in the nuclear membrane. The RNA is carried to a portion of the cell called the ribosome, the cell's protein factory. The code carried by the RNA is used to assemble very specific combinations of 20 different amino acids (the protein amino acids) to form biological proteins such as enzymes and triggering and transport proteins, which carry out all of the organism's biochemistry. The double-helical state of DNA represents a resting state. When the genetic information is read out the double helix unwinds and is used to assemble a complementary molecule of RNA containing a copy of the genetic code. The RNA in turn assembles the encoded protein by binding whichever amino acids correspond to the sequence of 'words' of the code. This amino acid sequence determines the structure and function of the resulting protein when the amino acids are polymerised and the protein assembles *via* secondary and tertiary interactions (Section 2.6.1).

Within the DNA double helix, the hydrogen-bonded pairs are of a very specific type termed Watson–Crick base pairs (after James Watson and Francis Crick who first described the structure of

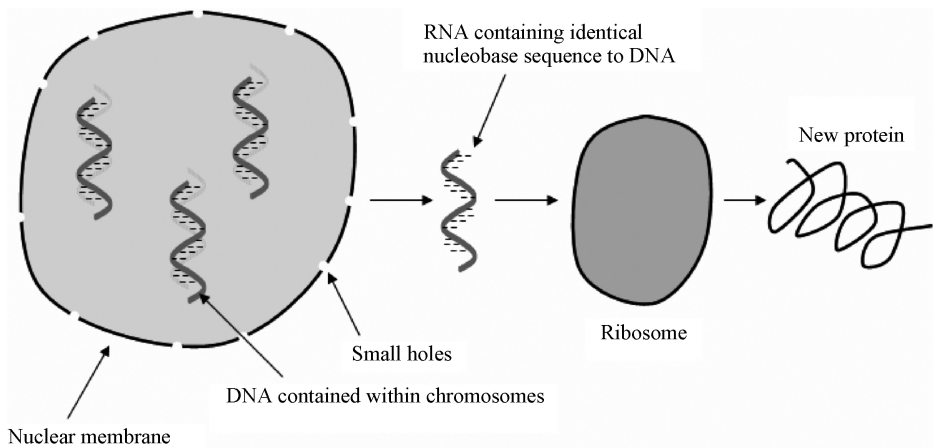


**Figure 2.30** Transformation of the genetic code from DNA to the ribosome for protein synthesis *via* messenger RNA.

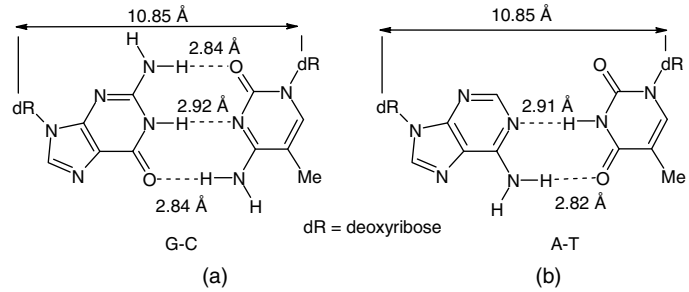


**Figure 2.31** Watson–Crick base pairing. (a) C–G and (b) A–T. The presence of three hydrogen bonds in the G-C pair makes it more stable than A-T.

DNA in 1952). This interaction takes the form of very specific, mutually complementary hydrogen bonds between either adenine and thymine, or guanine and cytosine (in RNA, thymine is replaced by the very similar uracil). No other combinations exist and it is this ability of each nucleic acid to recognise its complementary partner that is the basis for the mode of operation of DNA.

The A–T and C–G hydrogen bonded base pairing is shown in Figure 2.31. In both cases, more than one hydrogen bond is responsible for the mutual recognition of the complementary bases and the geometry is such that the overall lengths of the two pairs are equal. The hydrogen bond lengths of 2.8–2.9Å are typical of medium-strength N—H···O/N hydrogen bonds. The fact that the G-C pair has three hydrogen bonds while the A-T has only two means that G-C rich regions of the DNA strand are more stable that A-T regions. The role of base pairing and π–π stacking in assembling the DNA double helix is an excellent example of supramolecular self-assembly, and enables DNA to replicate itself as well as passing on its encoded genetic information to transfer RNA. The self-assembly takes the form of a cascade process in which the additive contributions from the formation of each successive base pair gradually overcome the entropic penalty associated with the loss of the degrees of freedom of the two separate strands. DNA self-assembly is discussed in detail in Section 10.3.1.

Nucleobases are also capable of engaging in an alternative type of hydrogen bonding interaction termed *Hoogstein base pairing*, which involves the five-membered rings of either the adenine or guanine residues (Fig. 2.32). Hoogstein hydrogen bonding sites are located on the external surface of the DNA molecule are thus accessible to DNA binding agents.

## 2.9.2 Site-Directed Mutagenesis

Smith, M., 'Synthetic DNA and biology (Nobel Lecture)', *Angew. Chem., Int. Ed. Engl.* 1994, **33**, 1214–1221.

The 1993 Nobel Prize for Chemistry was shared by Michael Smith of the University of British Columbia, Canada, and Kary B. Mullis of La Jolla, California, USA, for the development of site-directed mutagenesis and the polymerase chain reaction (PCR), two techniques for manipulating DNA. Site-directed mutagenesis enables the reprogramming of the genetic code held within DNA in order to produce protein variations with new properties. Applications are in the protein engineering of tailored antibodies to attack specific areas such as tumour cells, the production of more stable proteins for technical applications, and potentially the cure of hereditary diseases such as cystic fibrosis. The method has also been applied to the genetic engineering of crops to produce faster-growing and disease-resistant strains. This new technology has been at the centre of the recent controversy over GM (genetically modified) foods because of public

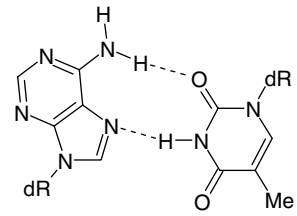


**Figure 2.32** Hoogstein base pairing between adenine and thymine.

and media fears over the possibility of modified proteins possessing unpredictable properties, especially in the long term, and/or competing with 'natural' varieties.

The site-directed mutagenesis process involves the preparation of oligonucleotide fragments that incorporate the desired mutation. The mutation takes the form of an alteration of one of the genetic code words, *e.g.* alteration of CAC to GAC causes the replacement of a histidine amino acid residue by aspartic acid. This mutated oligonucleotide is introduced to a segment of viral DNA to which it binds in the same place as an unmutated analogue. This is because the interstrand complementarity is capable of tolerating a small number of base pair mismatches. The mutated oligonucleotide is then incorporated into a copy of the original DNA by the enzyme DNA polymerase, which forms the phosphate–sugar backbone, linking nucleotide fragments together. The resulting mutant DNA is then introduced to a suitable bacterial host organism in which it is multiplied, producing copies of itself and, when present in sufficient quantity, synthesises (expresses) the desired mutated protein. Such mutations occur all the time in nature as random events, and are a fundamental part of the theory of evolution. Most natural mutations are fatal to the organism, but controlled, designed mutagenesis may be highly beneficial. The process is summarised in Figure 2.33.

## 2.9.3 The Polymerase Chain Reaction

Mullis, K. B., 'The polymerase chain-reaction (Nobel Lecture)', *Angew. Chem., Int. Ed. Engl.* 1994, **33**, 1209-1213.

The polymerase chain reaction (PCR) is another extremely important recent development in DNA chemistry. PCR enables the synthesis of large amounts of a particular piece of DNA or oligonucleotide fragment, starting with just a small sample. The technique is used widely in forensic science in which amounts of DNA large enough to analyse may be replicated from small traces of blood or tissue. The PCR process is of vital importance to the HUGO (Human Genome) project, which in 2001 determined every single DNA code in human genetic material.[13, 14] It also offers unique possibilities such as the production of large quantities of the DNA of extinct species from traces that may be found in fossil remains. This application inspired the science fiction of recreating dinosaurs in the novel *Jurassic Park*, although the rebirth of extinct species is not possible with the current technology.

PCR works by the synthesis of two short oligonucleotides that bind correctly to opposite strands of the DNA to be replicated. This allows the DNA polymerase enzyme to begin to assemble copies of the two strands, resulting in two new DNA strands. Heating the sample causes the unwinding of the resulting double helices and provides four fresh strands that can be used as the templates for the formation of four more strands. The procedure is repeated 20–60 times over the course of a few hours either

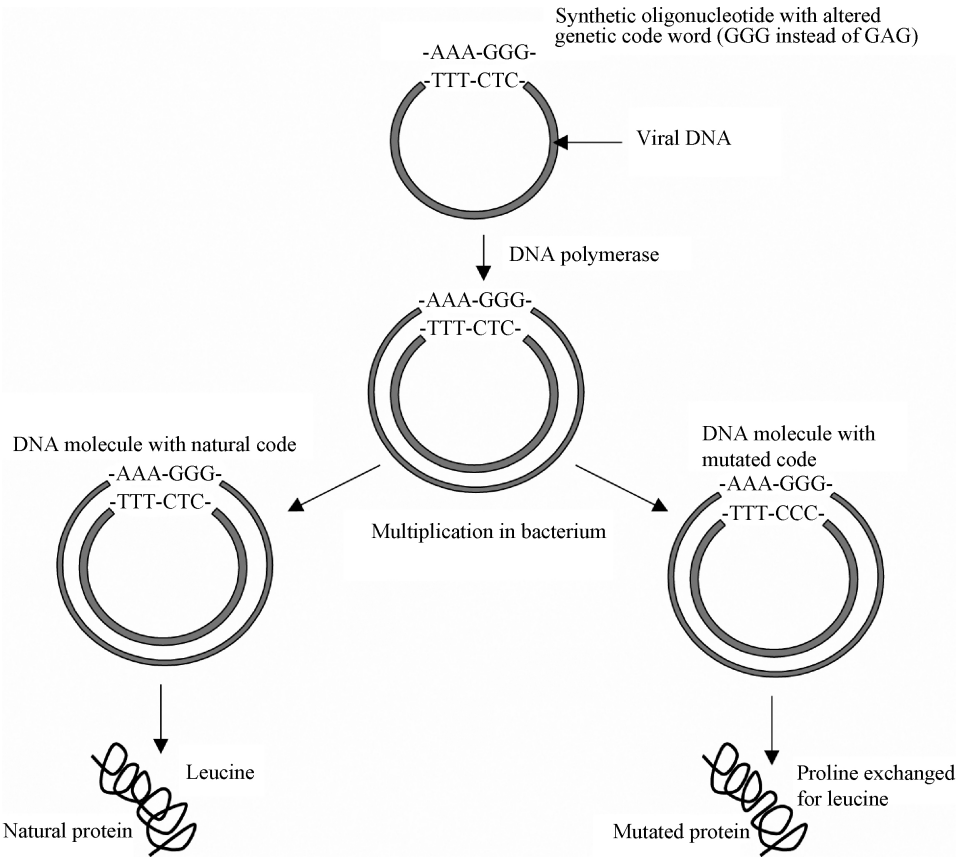


**Figure 2.33** Site-directed mutagenesis.

manually, or, usually, by an automated cycling apparatus. This results in $2^{20}$–$2^{60}$ ($10^6$–$10^{19}$) copies of the original fragment (Figure 2.34).

## 2.9.4 Binding to DNA

Metcalfe, C. and Thomas, J. A., 'Kinetically inert transition metal complexes that reversibly bind to DNA', *Chem. Soc. Rev.* 2003, **32**, 215–224.

A number of cancers are highly susceptible to treatment by platinum complexes, which act by binding to tumour DNA. Almost all active antitumour agents contain Pt(II) in a square planar geometry with two *cis* primary or secondary amines and two more weakly-bound ligands such as chloride or carboxylates. Related octahedral Pt(IV) complexes with additional axial ligands are also active and are believed to be reduced to Pt(II) species with loss of the axial ligands *in vivo* (*i.e.* in a real living system).

Two of the most important platinum anticancer drugs are cisplatin (**2.13**) and carboplatin (**2.14**). Cisplatin is effective against testicular tumours, ovarian carcinoma and some other types of cancer, but relatively inactive against breast and lung cancers; it is also a very toxic compound. Side effects include loss of high-frequency hearing, neuropathy and nausea. Kidney damage may also result, but is minimised

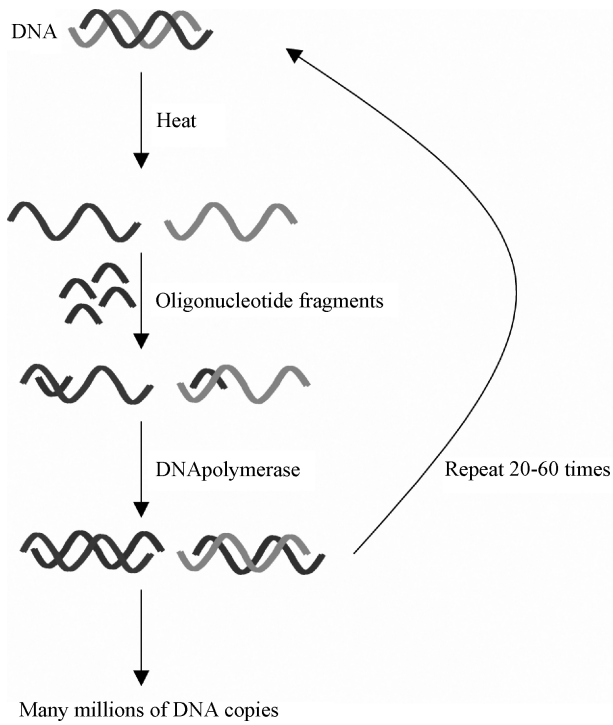


**Figure 2.34** Operation of the PCR technique.

by hydration of patients to ensure that any unused drug is washed swiftly through the body. Carboplatin is a more recent drug, and is less toxic. Notably, it doesn't cause loss of high-frequency hearing.

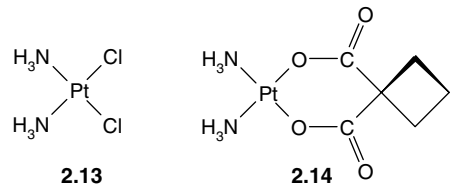


**2.13** Cisplatin

**2.14** Carboplatin

The mode of operation of many inorganic anticancer drugs appears to be their ability to bind to DNA. A major target of platinum in the body is guanine residues exposed in the major groove of certain types of DNA. The drug is injected directly (to avoid hydrolysis on the acidic gastric juices). A significant fraction binds to plasma proteins and is then excreted rapidly *via* the kidneys. The remainder is transported in the blood and passes through the cell membrane in neutral form. The chloride or carboxylate ligands are lost (there is a lower intracellular $Cl^-$ concentration) forming $[Pt(NH_3)_2Cl(H_2O)]^+$; the positive charge results in attraction to the negatively charged DNA, ultimately allowing the '$(NH_3)_2Pt^{2+}$' unit to bind to the DNA. It is possible that this involves the formation of a bridge across a DNA strand, disrupting the base pairing that holds together the DNA double helical structure (Figure 2.35). This in turn causes a 'kink' in the DNA that is not recognised by DNA repair enzymes in tumour cells. *Trans*-$[PtCl_2(NH_3)_2]$ cannot form a DNA cross-link with the same geometry, which may account for its inactivity.

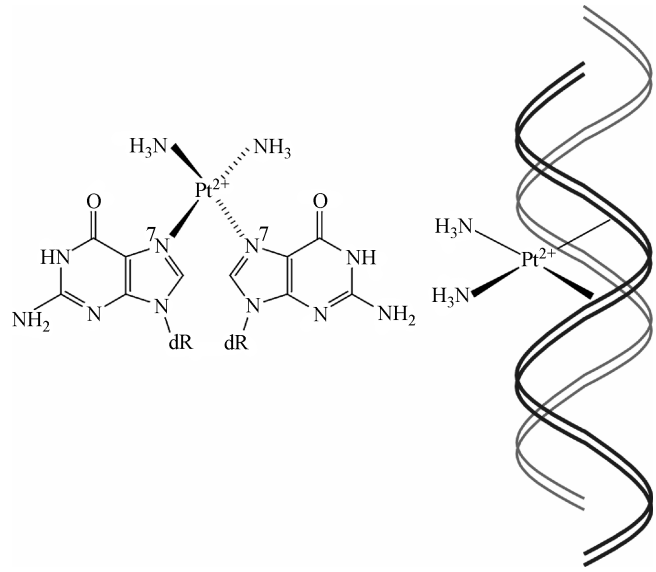


**Figure 2.35** Platinum binding to DNA.

A model for the DNA–Pt interaction is the $Pt(NH_3)_2^{2+}$ complex of the guanosine dinucleotide d(pGpG), which contains two guanine bases linked by a sugar–phosphate backbone. The X-ray crystal structure of this material (Figure 2.36) shows the platinum interaction with adjacent guanine N(7) donors. Additional stabilisation comes from hydrogen bonding from the ammonia ligands to a phosphate oxygen atom. A crystal structure of cisplatin binding to DNA itself has also been reported.[15]

Binding by coordinative bonds to transition metals is far from being the only way of targeting the DNA molecule. A range of coordination compounds termed 'intercalators' are known, which are able to bind to DNA exclusively *via* a combination of electrostatic and $\pi$–$\pi$ stacking interactions. Early work showed that square planar Pt(II) complexes containing planar aromatic heterocyclic ligands such as 2,2′-bipyridyl were able to bind to DNA by partially inserting (intercalating) the aromatic ligand between π-stacked nucleobases on the major groove side. Similar intercalation was observed for chiral octahedral species such as $[Ru(phen)_3]^{2+}$ (phen = 1,10-phenanthroline) (**2.15**) and, significantly,

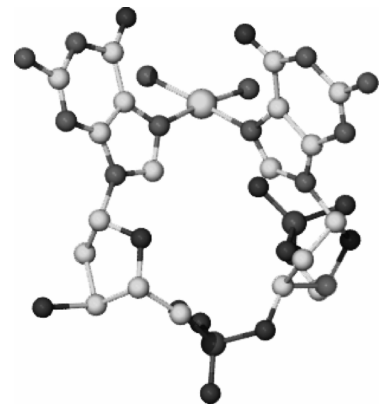

**Figure 2.36** X-ray crystals structure of *cis*-$Pt(NH_3)_2^{2+}$[d(pGpG)].[16]

some preference was observed for the intercalation of the right-handed Δ-isomers into right-handed DNA.

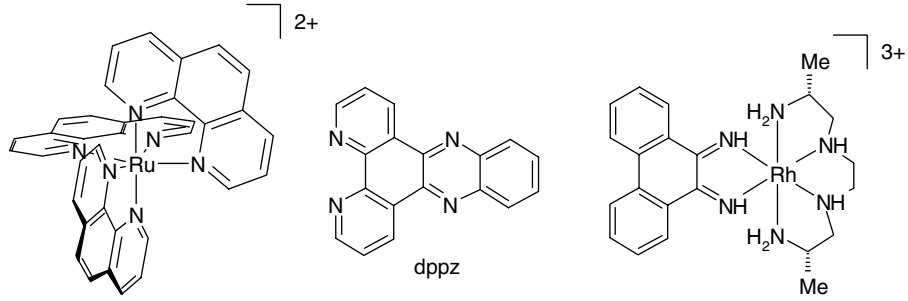


Δ-[Ru(phen)$_3$]$^{2+}$ **2.15**

**2.16**

[Rh(*R,R*-Me$_2$trien)(phi)]$^{3+}$ **2.17**

The affinity of intercalators for DNA can be enhanced markedly by increasing the surface area of the intercalating ligands, thus the analogous complexes with the large-surface-area dppz ligand (**2.16**) show binding constants of more than $10^6\,M^{-1}$. Any ambiguity in the nature of the binding of intercalators to DNA was removed by Jacqueline Barton of the California Institute of Technology, USA, who carried out a crystal structure determination of the complex of another intercalator, [Rh(*R*, *R*–Me$_2$trien)(phi)]$^{3+}$ (**2.17**), bound to the central 5′-TGCA-3′ site of an eight-base-pair oligonucleotide. The structure shows clearly the π-ligand intercalating in the place of a single nucleobase (Figure 2.37), engaging in a number of hydrogen bonded contacts between the axial portions of the amine ligand and adjacent guanine residues. Remarkably, the structure, including hydrogen bonds, was predicted by Barton's group, and represents the successful targeting of the 5′-TGCA-3′ site by the designer intercalator. Consistent with this elegant piece of molecular design, the binding constant of $9 \times 10^7\,M^{-1}$ is very high. Bimetallic chiral DNA intercalators based on two dppz units have also been prepared which slowly intercalate into DNA based on a threading mechanism. The presence of a second dppz moiety results in particularly high DNA affinity but the synthesis of such chiral species is demanding.[17] The application of coordination complex DNA intercalating agents is still in its infancy, but potential uses include fluorescent tagging in diagnosis and probing of damage and repair processes, and targeted sensitisation to oxidative or photolytic cleavage.

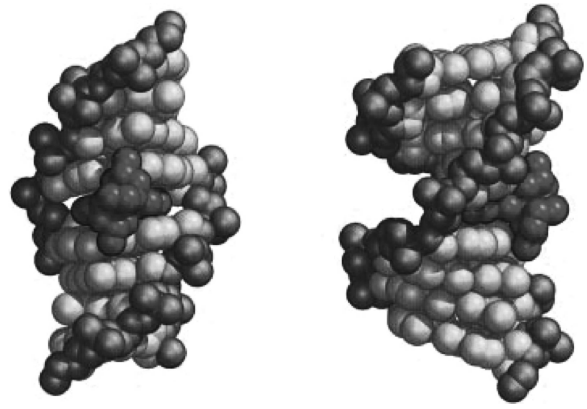

**Figure 2.37** Two views of the crystal structure of [Rh(*R*,*R*-Me$_2$trien)(phi)]$^{3+}$ bound within an eight-base-pair oligonucleotide. (Reproduced with permission from [18] © 1999, American Chemical Society). See plate section for colour version of this image.

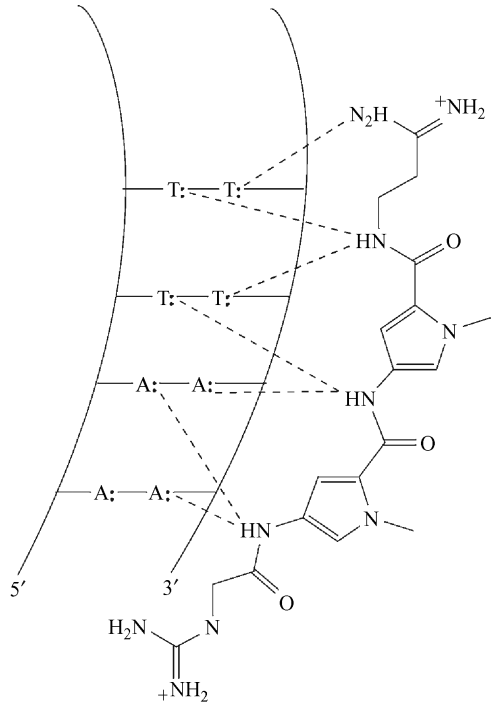


**Figure 2.38** Hydrogen bonding of netropsin with the 5′-AATT-3′ region of DNA.

DNA is also bound by a range of well-known and wholly organic peptides. Antibiotics such as the ionophore nonactin, as well as the natural products netropsin and distamycin A, are capable of binding within the DNA major groove in a sequence specific fashion *via* the formation of multiple hydrogen-bonded interactions. The peptides are essentially crescent shaped and lie within AT rich sequences forming bifurcated hydrogen bonds with the adenine N3 and thymine O2 (Figure 2.38). Binding free energies are in the region of 53 kJ $mol^{-1}$. The synthetic malleability of the peptide framework in antibiotics of this type allows extensive tuning and a range of synthetic derivatives has been produced.

The search for modern anticancer drugs occupies a great deal of medicinal supramolecular chemistry. DNA binding agents that act by coordination interaction and/or by combinations of Hoogstein type hydrogen bonding and π–π stacking (DNA intercalation) are seen as one of the most promising avenues of current research.

## 2.9.5 DNA Polymerase: A Processive Molecular Machine

Keck, J. L. and Berger, J. M., 'DNA replication at high resolution', *Chemistry & Biology* 2000, **7**, R63–R71.

Cell division involves the replication of the cellular DNA. The DNA double helix is separated into the two individual strands and each one is used as a template to assemble nucleotide-by-nucleotide, a complementary strand resulting in a copy of the original DNA double helix. The enzyme that does this job, DNA polymerase, is one of the most accurate and remarkable pieces of molecular machinery

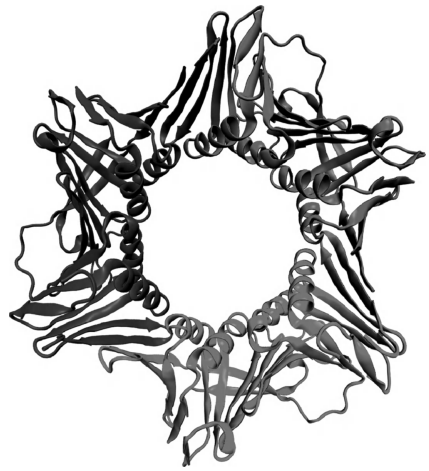

**Figure 2.39** A DNA clamp protein – a trimer of the protein Proliferating Cell Nuclear Antigen (PCNA). The three different trimer units are shown in different colours (image courtesy of www.wikipedia.org). See plate section for colour version of this image.

in the whole of biochemistry. The incoming DNA strand is threaded through a giant circular aperture (termed the *DNA clamp* – Figure 2.39) like a thread through a needle, making a giant biomolecular rotaxane (see Section 10.7). *DNA Polymerase* forms part of a larger system of molecular machinery termed the *replication fork*, Figure 2.40 which involves a number of cooperating enzymes. While DNA polymerase enzymes are at the business end of growing the two new DNA strands, other enzymes such as *topoisomerase*, *helicase* and *DNA primase* are involved in splitting the incoming strand, and priming it ready for the polymerase to get to work.

The DNA replication process begins at *origin* points in the parent DNA strand which are targeted by DNA binding proteins resulting in the separation of the strands and the initiation of the replication fork complex *via* the *helicase* enzyme. The origin points tend to be A-T rich regions because of

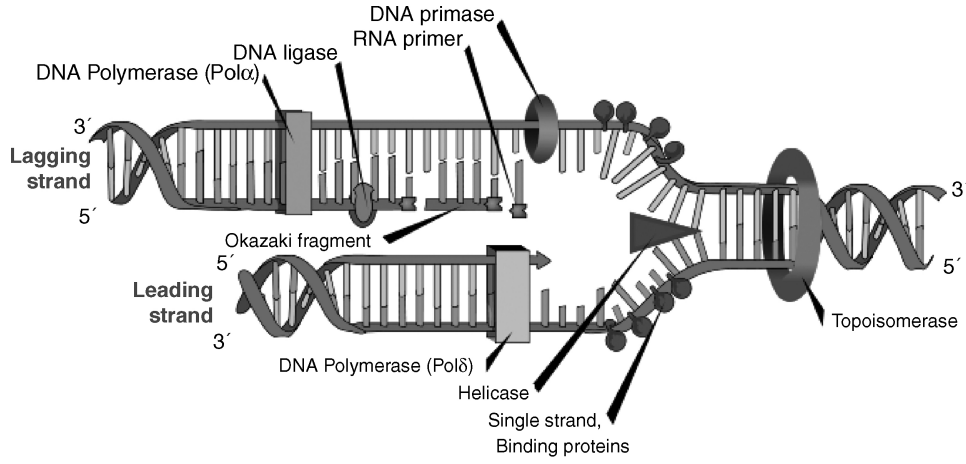


**Figure 2.40** The DNA replication fork comprising a number of cooperating enzymes (image courtesy of www.wikipedia.org). See plate section for colour version of this image.

the weaker hydrogen bonding between adenine and thymine (Figure 2.31). The two resulting single strands are termed the *leading* and *lagging* strands. The leading strand at the replication fork is the one that is synthesised in the 5′,3′ direction. The DNA polymerase then begins to synthesise DNA on the leading strands using the free 3′ OH group donated by a single RNA primer. The entire replication fork then moves along the incoming parent DNA adding nucleobases to each new strand as it goes in a remarkable example of *processive catalysis*. Continuous synthesis of new DNA occurs in the direction in which the replication fork is moving. It is not possible to synthesise DNA in the 3′→5′ direction on the lagging strand in this way and so the lagging strand is processed in short segments termed *Okazaki fragments*. Using the lagging strand as a template *primase* builds RNA primers in small groups which are then polymerised by DNA polymerase *via* the free 3′ OH groups in the 5′→3′ direction. These RNA primers are then replaced by new deoxyribonucleotides that are, in turn, linked by *DNA ligase* to give a completed section of the lagging strand.

The replication fork exhibits some fascinating dynamics during the replication process. As the DNA is unwound by the *helicase* enzyme the parent DNA ahead of the fork rotates building up twists that would ultimately cause tension and hence halt the replication process. This problem is solved by yet another enzyme, *DNA topoisomerase*. *DNA topoisomerase I* breaks a single phosphate backbone linkage in the double strand allowing the two parent strands to move around one another and prevent twisting. Another topoisomerase, *DNA topoisomerase II*, can cut the backbone on both strands to remove knots and entanglements that sometimes occur in natural DNA. We will look at some DNA knots in more detail in Section 10.9 (see also Figure 10.86 for an SEM image of a DNA knot). The DNA conformation is also carefully controlled during replication by single-strand binding proteins that bind to the DNA and prevent it from folding back on itself and forming a variety of secondary structures until a second strand is synthesised and the double helix re-formed. Clamp proteins such as the one illustrated in Figure 2.39 help the DNA polymerase to maintain contact with the DNA. The clamp can release *via* a conformational change once the end of the chain is reached.

Despite the beauty and high fidelity of the copying process, the DNA polymerase system can only copy the DNA it is given and while its small size means that it is tempting to see a DNA molecule as a perfect, highly efficient code for building an organism, in fact a great deal of our DNA is useless 'junk' DNA that is simply good at getting itself copied and serves no useful purpose. Junk DNA even includes the complete genomes of ancient viruses that have permanently spliced themselves into the host genetic code for a free ride – why build your own body when another organism can do it for you?[19]

Processive catalysis of this kind involves extremely sophisticated molecular machinery including both RNA and protein components suggesting that it emerged relatively late in evolutionary terms. Processive catalysis is now a target for the design of artificial supramolecular machines and an interesting recent example is discussed in Section 10.7.3.

## 2.10 Biochemical Self-Assembly

Lindsey, J. S., 'Self-assembly in synthetic routes to molecular devices. Biological principles and chemical perspectives: a review', *New J. Chem.*, 1991, **15**, 153–180.

The double-helical structure of DNA and the ability of the molecule to unravel in order to template the formation of copies of itself and transcribe RNA is clearly connected intimately with the supramolecular interactions that bind the two nucleotide strands together. It is the information encoded within the individual nucleobases that 'tells' the molecule to form a double helix. This is an

example of the much more general phenomenon of self-assembly, which is of enormous importance in modern supramolecular chemistry. Self-assembling systems may be thought of very generally as comprising two or more elements that may associate reversibly in such a way that the resulting aggregate represents the most thermodynamically stable structure available to the system under the prevailing conditions. Strictly, all of the information needed to form the final aggregate must be present (encoded) in the reacting components. It is this thermodynamic stability, coupled with the error checking enabled by the reversibility of the equilibration process, which is responsible for the structure and complexity of many biological systems and molecular devices. In addition to the templated recognition if incoming nucleotides in DNA replication, examples include the translation of messenger and transfer RNA into protein in the ribosome, as well as virus structures (which are often beautifully symmetrical as a result of the self-assembly of a number of identical protein subunits to give a coat or capsid protecting the viral genetic material), enzyme and protein folding, light harvesting in the phycobilisome, and photo-induced ion pumping across membranes by bacteriorhodopsin. It is noteworthy, however, that in general living organisms as a whole are far from thermodynamic equilibrium and require a constant input of energy in order to maintain homeostasis.

As an example of protein self-assembly, take the protein ribonuclease, a 124-residue protein containing four disulfide (—S—S—) bonds. Reduction of these linkages gives a reduced protein containing eight SH groups that is entirely denatured (*i.e.* enzymatically inactive). Reoxidation of the protein in the presence of urea (which acts as a denaturing agent by virtue of its versatile hydrogen-bonding ability) results in a mixture of scrambled (incorrectly folded) proteins containing most (if not all) of the 105 possible combinations of disulfide bonds. Addition of β-mercaptoethanol causes the disulfide bonds to break slowly and reform in an equilibrium process; if the urea is removed and β-mercaptoethanol added, the proteins unscramble to give the native ribonuclease with full enzymatic activity, (Figure 2.41). The conclusion is that the native protein represents the structure with the lowest Gibb's free energy, and that all the information required to assemble the protein is encoded into the amino acid sequence.

As an example of information encoding, consider the iron-storage protein ferritin. The protein comprises 24 identical subunits that, together, form a nearly spherical shell of octahedral symmetry. Why 24 subunits, and why octahedral symmetry? Examination of the individual subunits

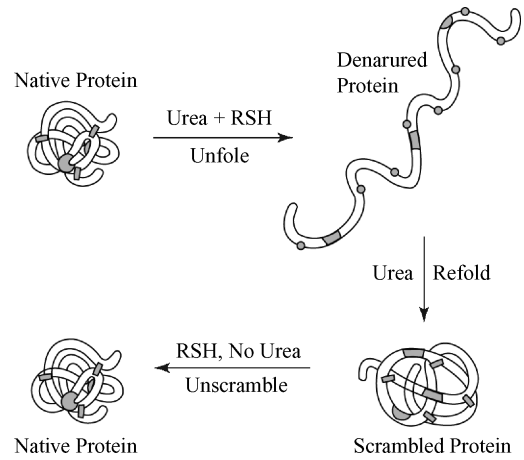


**Figure 2.41** Denaturing and self-reassembly of ribonuclease. The correct folding occurs only when disulfide bond formation is made reversible by the addition of β-mercaptoethanol (RSH) allowing the system to equilibrate (Reproduced from Section Key Reference by permission of The Royal Society of Chemistry).

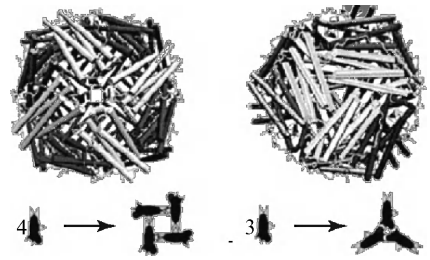


**Scheme 2.12** Representations of the structure of human H chain ferritin viewed down the four- and three-fold symmetry axes (left and right respectively). The interactions about the fourfold axis are at 90º and are based on four subunit tetramers. Protein trimers arranged at 60 degrees to one another form the three-fold axis. (Reproduced with permission from Reference 20).

reveals that as a result of the distribution of their binding sites, there are two possible modes of aggregation. One involves a lock and key interaction of each subunit at 90º to its neighbour resulting in a four-subunit tetramer of four-fold symmetry; the other involves a lock and key interaction between three subunits positioned 60º apart to give a three-fold symmetric moiety. Crucially, therefore, if the protein is to satisfy simultaneously all of its binding sites, the resulting aggregate must possess both three- and four-fold symmetry axes. The only way in which this can be achieved is by the formation of a 24-subunit cluster with octahedral symmetry (Scheme 2.12).

Other examples of biochemical self-assembly include the dimerisation of the human immunodeficiency virus 1 (HIV-1) protease, an enzyme that is essential for the assembly and infectivity of the AIDS virus. Viruses represent particularly fascinating examples of biochemical self-assembly in which numerous protein sub-units, encoded by viral RNA, self-assemble reversibly to form protective hollow coatings termed *capsids*. Capsids are often highly symmetrical and can either be *pseudo*-spherical (as in the icosahedral *rhinovirus*, cause of the common cold), crystalline arrays (as in the structure of *cypovirus* which holes up in pores of a crystalline protein called polyhedrin recently studied by X-ray crystallography[21]), or tubular as in the tobacco mosaic virus. The mechanism of formation of this remarkable species is treated in Chapter 10 by way of introduction to the rapidly growing field of synthetic self-assembly and its potential applications in the formation of molecular machines and devices. We conclude this chapter with a TEM image of another self-assembled virus, *rotavirus*, Figure 2.42. The rotavirus RNA is sheathed within a three-layered icosahedral protein capsid up to 76.5 nm in diameter. Despite its beautiful appearance rotavirus is

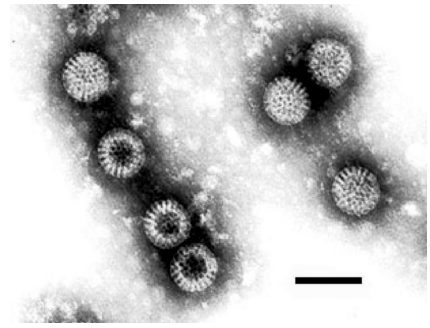

**Figure 2.42** Electron microscope image of the highly symmetrical icosahedral *rotavirus* (scale bar = 100 nm).

a killer, causing severe diarrhea in children. Current supramolecular research is actively engaged in using hollow capsids such as this example with the RNA stripped out to make entirely artificial polymers and nanoparticles using the capsid as a nanosized container, or to study the operation of single molecules of enzyme included within the emptied protein-based shell.[22]

## Summary

- Biological systems are fundamentally supramolecular in nature and provide much of the underlying inspiration for supramolecular synthesis in terms of the desire to mimic biological process such as enzyme catalysis, self-assembly and ion transport.
- Biology also provides useful molecular and nanoscale fragments that can be incorporated into abiotic molecular recognition, *e.g.* nucleobases, porphyrins and viral capsids.
- Alkali metal transport in biochemistry is a vital process in maintenance of cell membrane potentials of use, for example, in nerve signal transduction and is at the core of some of the early work on artificial ionophores that mimic natural ion carriers such as valinomycin. Ionophore mediated ion transport is much slower than transport through cation and anion ion channel proteins, however.
- Porphyrin type macrocycles clearly illustrate supramolecular principles, binding tightly to metal ion guests by virtue of their rigid preorganisation and complementary donor atoms. Porphyrins have their own redox and photochemistry which is modulated by bound metals making them a key component in biological electron and energy transfer processes.
- Oxygen transport by haemoglobin involves a myoglobin tetramer with each unit containing an iron(III) porphyrin superoxide complex in the bound state. Oxygen is reversibly bound and released with high selectivity and cooperative allosteric interactions between the four myoglobin sub-units. The protein framework limits poisoning by interfering $O_2$ analogues such as CO and prevents irreversible oxo-bridged dimer formation.
- Enzymes are Nature's catalysts, facilitating all of the chemical reactions of metabolism. They bind a specific substrate in an *entatic state* moving it along the reaction coordinate towards the reaction transition state thus lowering the reaction activation energy. Enzymes are generally made of proteins and contain an active site, often based around a metal ion.
- A great deal of biochemical signalling and semiochemistry involves the specific molecular recognition of tiny amounts of molecular messengers such as neurotransmitters, hormones and pheromones.
- Extremely sophisticated biological machinery based on specific non-covalent molecular recognition is involved in biological processes such as DNA replication, the transcription of the genetic code and in RNA-mediated protein synthesis at the ribosome. This biochemical molecular machinery has recognisable mechanical features.
- Application of molecular recognition principles allows the design of small molecules able to interact with biological systems for use, *e.g.* as anticancer drugs.
- Biochemical self-assembly proceeds by fundamental supramolecular principles and can lead to structures of startling complexity including DNA and viral capsids.

## Study Problems

2.1 Using the information given in Table 2.1, calculate the potential difference (in mV) across a squid nerve cell.

2.2 Calculate the energy required to hold the $Na^+$ and $Cl^-$ ions 5 nm apart in $1.0 \times 10^{-5}$ moles of NaCl. What is the analogous electrostatic potential energy between 1 mole of $Na^+$ and $Cl^-$

situated 1000 km apart? (Electrostatic energy = $q_1q_2/4\pi\varepsilon_0 r$; unit charge = $1.602 \times 10^{-19}$ C, $\varepsilon_0 = 8.854 \times 10^{-12}$ F m$^{-1}$).

2.3 Using Table 2.2, give the amino acid sequence coded by the following nucleobase sequence starting from base 1:

ATGTTCCATAGCAAGTAG
1 2 3

Repeat the process starting from bases 2 and 3. Note that the amino acid sequence assembled depends crucially on the starting point or 'reading frame'. Addition of a single nucleobase somewhere in the middle of the sequence alters the code entirely. This is known as a 'frame shift mutation'. Try inserting a C after the ATG 'start' code and repeat the protein assembly.

2.4 Discuss the significance of biological transmembrane potential differences. How are such potential differences created and maintained?

2.5 The daily recommended dietary allowances (RDA) for a number of different metals are given below. Account for these differences by a brief explanation of the functions of these different elements in human biochemistry.

| Element | US RDA/mg day$^{-1}$ |
|---|---|
| K | 2000–5500 |
| Na | 1100–3300 |
| Ca | 800–1200 |
| Mg | 300–400 |
| Fe | 10–20 |
| Co | 0.2 |

## References


1. Kaim, W., Schwederski, B., *Bioinorganic Chemistry: Inorganic Elements in the Chemistry of Life*. John Wiley & Sons, Ltd: Chichester, 1994;
2. Doyle, D. A., Cabral, J. M., Pfuetzner, R. A., *et al.*, The structure of the potassium channel: Molecular Basis of $K^+$ conduction and selectivity. *Science* 1998, **280**, 69–77.
3. Dutzler, R., Campbell, E. B., Cadene, M., Chait, B. T., MacKinnon, R., X-ray structure of a CIC chloride channel at 3.0 angstrom reveals the molecular basis of anion selectivity. *Nature* 2002, **415**, 287–294.
4. Davis, A. P., Sheppard, D. N., Smith, B. D., Development of synthetic membrane transporters for anions. *Chem. Soc. Rev.* 2007, **36**, 348–357.
5. Morth, J. P., Pedersen, B. P., Toustrup-Jensen, *et al.*, Crystal structure of the sodium-potassium pump. *Nature* 2007, **450**, 1043–U6.
6. Sekharan, S., Sugihara, M., Buss, V., Origin of spectral tuning in rhodopsin – It is not the binding pocket. *Angew. Chem., Int. Ed.* 2007, **46**, 269–271.
7. Chow, H.-C., Serlin, R., Strouse, C. E., Crystal and molecular structure and absolute configuration of ethyl chlorophyllide a-dihydrate. Model for the different spectral forms of chlorophyll a. *J. Am. Chem. Soc.* 1975, **97**, 7230–7237.
8. Chen, L. H., Kenyon, G. L., Curtin, F., *et al*., 4-Oxalocrotonate tautomerase, an enzyme composed of 62 amino acid residues per monomer. *J. Biol. Chem.* 1992, **267**, 17716–17721.
9. Smith, S., The animal fatty acid synthase: one gene, one polypeptide, seven enzymes. *FASEB J.* 1994, **8**, 1248–1259.
10. Olsson, M. H. M., Parson, W. W., Warshel, A., Dynamical contributions to enzyme catalysis: Critical tests of a popular hypothesis. *Chem. Rev.* 2006, **106**, 1737–1756.
11. Angeli, S., Ceron, F., Scaloni, A., *et al.*, Purification, structural characterisation, cloning and immunocytochemical localisation of chemoreception proteins from Schistocerca gregaria. *Eur. J. Biochem.* 1999, **292**, 745–754.

12. Sabelis, M. W., Janssen, A., Kant, M. R., Ecology – The enemy of my enemy is my ally. *Science* 2001, **291**, 2104–2105.
13. Lander, E. S. *et al. Nature* 2001, **409**, 860–921.
14. Venter, J. C. *et al.*, The sequence of the human genome. *Science* 2001, **291**, 1304–1351.
15. Takahara, P. M.. Rosenzweig, A. C., Frederick, C. A., Lippard, S. J., Crystal-structure of double-stranded DNA containing the major adduct of the anticancer drug Cisplatin. *Nature* 1995, **377**, 649–652.
16. Sherman, S. E., Gibson, D., Wang, A. H. J., Lippard, S. J., Crystal and molecular-structure of Cis-[$Pt(NH_3)_2$(D(Pgpg))] the principal adduct formed by Cis-Diamminedichloroplatinum(II) with DNA. *J. Am. Chem. Soc.* 1988, **110**, 7368–7381.
17. Onfelt, B., Lincoln, P., Norden, B., Enantioselective DNA threading dynamics by phenazine-linked $[Ru(phen)_2dppz]^{2+}$ dimers. *J. Am. Chem. Soc.* 2001, **123**, 3630–3637.
18. Erkkila, K. E., Odom, D. T., Barton, J. K., Recognition and reaction of metallointercalators with DNA. *Chem. Rev.* 1999, **99**, 2777–2795.
19. Ridley, M., *Genome: The Autobiography of a Species in 23 Chapters*. Fourth Estate: Glasgow, 2000.
20. Caulder, D. L., Raymond, K. N., Supermolecules by Design. *Acc. Chem. Res.* 1999, **32**, 975–982.
21. Coulibaly, F., Chiu, E., Ikeda, K., *et al.*, The molecular organization of cypovirus polyhedra. *Nature* 2007, 446, 97–101.
22. Comellas-Aragones, M., Engelkamp, H., Claessen, V. I., *et al.*, A virus-based single-enzyme nanoreactor. *Nature Nanotechnology* 2007, **2**, 635–639.

# 3 Cation-Binding Hosts

*'Now spurs the lated traveller apace*
*To gain the timely inn.*
*Ourself will mingle with society*
*And play the humble Host.'*

William Shakespeare (1564–1616), *Macbeth*

# 3.1 Introduction to Coordination Chemistry

## 3.1.1 Supramolecular Cation Coordination Chemistry

Lehn, J.-M., 'Supramolecular chemistry – scope and perspectives molecules, supermolecules, and molecular devices', *Angew. Chem. Int. Ed. Engl.*, 1988, **27**, 89–112; Cram, D. J., 'The design of molecular hosts, guests, and their complexes (Nobel Lecture)', *Angew. Chem. Int. Ed. Engl.*, 1988, **27**, 1009–1020; Pedersen, C. J., 'The discovery of crown ethers (Nobel Lecture)', *Angew. Chem. Int. Ed. Engl.*, 1988, **27**, 1021–1027.

The examples of natural ionophores, such as valinomycin, nonactin and the enniatins discussed in Chapter 2, have provided an enormous impetus to supramolecular chemists to synthesise artificial ionophore mimics and model compounds capable of exhibiting selective complexation and transport, not only of alkali metal cations but also the majority of the *s*, *p d* and *f* block metals and nonmetallic cations such as $NH_4^+$ and organic ammonium salts. A particular challenge has been the enantiospecific binding of chiral species such as protonated amino acids. Cation complexation chemistry has effectively given birth to the whole field of molecular recognition (the area of chemical research involving the selective binding by hosts that are structurally and electronically preprogrammed for complexation of particular guests). An enormous and diverse range of ligands (hosts for metal ions) has been prepared, exhibiting both remarkable selectivities and useful reactivity properties. In this chapter, we will survey some of the most common classes of ligand and use these as examples in the discussion of the basis for their molecular recognition properties. We will then look at the application of these concepts to more complex or specialised systems.

## 3.1.2 Useful Concepts in Coordination Chemistry

Housecroft, C.E. and Sharpe, A.G., *Inorganic Chemistry*, 3rd edn., Prentice Hall: Upper Saddle River, 2007.

We saw in Section 1.3 how Alfred Werner formulated the modern concept of coordination chemistry, which supramolecular chemistry generalises to a 'complete coordination chemistry'. Prior to Werner's time the 'chain' theory of coordination compounds was popular. The chain and Werner formulations of '$Co(NH_3)_4Cl_3$' and '$Co(NH_3)_3Cl_3$' are shown in Figure 3.1. While both theories predict that '$Co(NH_3)_4Cl_3$' will exhibit one labile chloride ion per molecule, the chain theory also predicts that '$Co(NH_3)_3Cl_3$' will have one labile chloride, while Werner's theory ultimately correctly predicted that the chloride is not labile in this case.

The study of supramolecular complexes of metal cations is really nothing more than the coordination chemistry of relatively labile (*i.e.* ligand substitution is relatively rapid under ambient conditions) metal ions and relatively elaborate, usually chelating or multidentate ligands (see Section 1.5).[1] It is therefore worth spending a little time reviewing some basics of coordination chemistry before looking at specific supramolecular systems. Experts read no further!

### *Complex Compound or Coordination Compound*

A complex compound is compound formed between reactants of which the valencies are already formally saturated, *e.g.* $CoCl_2 + 2\ Et_4N^+Cl^- \rightleftharpoons (Et_4N)_2[CoCl_4]$. All three compounds are stable individually. We generally use square brackets to denote the coordination complex.

*Supramolecular Chemistry, 2nd edition* J. W. Steed and J. L. Atwood
© 2009 John Wiley & Sons, Ltd ISBN: 978-0-470-51233-3

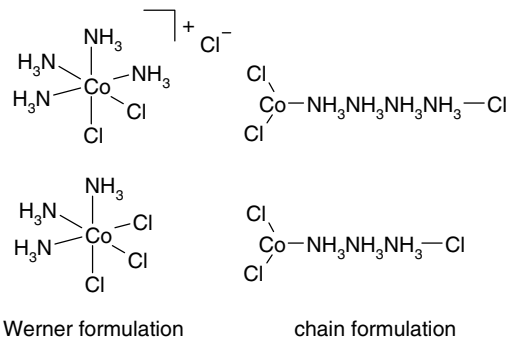


**Figure 3.1** Werner and historical chain formulations of '$Co(NH_3)_4Cl_3$' and '$Co(NH_3)_3Cl_3$'.

### *Ligand*

A ligand* is an ion or a molecule which is bonded to the central atom(s) in a complex compound. In the example above chloride is the ligand in $(Et_4N)_2[CoCl_4]$. Generally ions or molecules which act as ligands are Lewis bases (electron donors; often lone pair donors) and are capable of independent existence. Ligands can often bind through more than one donor atom or group and the number of such donors is referred to as the ligand's denticity (= the number of 'teeth' it has that can 'bite' onto the metal). Chloride is a monodentate ligand, 1,2-diaminoethane is bidentate *etc.* In cation supramolecular chemistry we call relatively elaborate, multidentate ligands 'hosts'.

### *Oxidation State*

The oxidation state of an element in a compound is the resultant charge on the central atom(s) when the attached groups (ligands) are removed in their closed electron shell configurations (*e.g.* in $[CoCl_4]^{2-}$ the chloride ligands would be removed as $Cl^-$ because this has a closed valence electron shell containing 8 electrons). For example: $[CoCl_4]^{2-}$ can be dismantled to give four chloride ions $Cl^-$ and a cobalt(II) ion, $Co^{2+}$. The oxidation state of the chlorine is thus –1, or (-I) and that of cobalt is +2, or (II). These are usually written as Cl(-I) and Co(II).

### *Bonding*

Bonding in coordination complexes ranges from entirely ionic ion-dipole type interactions in which a ligand lone pair of electrons forms a dative bond to a positively charged metal cation to entirely covalent in which there is significant orbital overlap between metal and ligand valence orbitals. Most compounds are somewhere in between and hence have at least some non-covalent component to the interaction. The degree of covalency will be determined by the metals charge and size and the nature of the ligand. Small, highly charged metal ions, and those with closed valence shells such as $Na^+$ or $Al^{3+}$, tend to form more ionic compounds. The coordination number and geometry of the complex is then dependent on the number of ligands that can pack around the small metal centre. As a result coordination geometries can be highly irregular and dependent on the geometry of the ligand, particularly if it is a macrocycle or constrained in some way. As a result matching the metals' coordination geometry

* From the Latin *ligare*, to bind. For an interesting discussion of the use and spread of this term see: Brock, W. H., Jensen, K. A., Jørgensen, C. K., Kauffman, G. B., The origin and dissemination of the term 'ligand' in chemistry. *Polyhedron* 1983, **2**, 1–7.

tendencies is less important in host design for these kinds of metals. In contrast metals in lower oxidation states or those with unfilled sub-shells such as the transition metals tend to form more covalent complexes with well-defined coordination geometries and a preference for more polarisable ligands. A detailed discussion of the bonding in transition metal complexes can be found in the key reference.

### *Coordination Number*

In solid state chemistry where there are often a number of equal short interatomic contacts, the simplest definition of coordination number is the number of nearest neighbours. In coordination chemistry (solid, solution and gas phases) a more practical definition of coordination number is the number of atoms or ligating groups (such as a C=C double bond) bound to a metal. Thus in $[CoCl_4]^{2-}$ the coordination number is four. The majority of coordination complexes are either 4- or 6-coordinate. For 6-coordinate the most important geometrical arrangement is the octahedron (or *pseudo*octahedron if the six ligands are different from one another). This term implies that the six ligands lie on the cartesian axes at 90° to one another. Drawing imaginary lines from each ligand to those adjacent gives an 8-sided 3D polyhedron; an octahedron. Arbitrarily we refer to the top and bottom sites as axial and the middle four as equatorial. In reality these sites are indistinguishable in a complex in which all the ligands are the same. The other possible 6-coordinate geometry is the trigonal prism, as in $[ZrMe_6]^{2-}$ and $[Re(S_2C_2Ph_2)_3]$. For 4-coordinate complexes there are two geometries with approximately equal occurrence: square planar and tetrahedral. Square planar complexes are not common outside transition metal chemistry ($ICl_4^-$ is one example) and are mostly found in complexes of Rh(I), Ir(I), Ni(II), Pd(II), Pt(II) and possibly Cu(II). $[NiCl_4]^{2-}$ is tetrahedral, whereas $[Ni(CN)_4]^{2-}$ is square planar. Other coordination numbers are also encountered such as linear 2-coordinate Ag(I) in $[Ag(NH_3)_2]^+$. The reaction of a bidentate ligand such as 1,2-diaminoethane with $Ag^+$ does not lead to a chelate complex, but instead to a linear two coordinate coordination polymer. One reason for this is that bidentate ligands can not exist in *trans* arrangements unless they are extremely long and flexible, *i.e.* they cannot span 180°. Coordination numbers for the large lanthanoid metal ions ($La^{3+}$ – $Lu^{3+}$) are commonly 8–12. Thus the ability of multidentate macrocycles to bind lanthanoid cations can be combined with additional water coordination in their use as Magnetic Resonance Imaging (MRI) contrast agents (Section 11.3.2).

### *Nomenclature*

Connelly, N. G. (ed.) *Nomenclature of Inorganic Chemistry IUPAC Recommendations 2005*, Royal Society of Chemistry: Cambridge, 2005.

In both names and formulae of *salts* (*i.e.* ionic compounds) cations precede anions. When writing the formulae of binary compounds the usual rule is to write the more electropositive element first. So we have $SiF_4$ not $F_4Si$. An 'element seniority sequence', which differs slightly from the electronegativities has been drawn up by IUPAC, which explains why we have $H_2O$ but $NH_3$. Coordination entities are named by writing the ligands in alphabetical order with appropriate numerical prefixes, followed by the central atom and its oxidation state. The numerical prefixes are ignored when establishing the alphabetical order. Thus, tri**b**romo precedes **i**odo. Although the alphabetical order is used for names, when writing *formulae* the sequence is: 1. Central atom, 2. Anionic ligands, 3. Neutral ligands, and the formula of the coordination entity is enclosed in square brackets. Some deviation is allowed if it is desired to convey specific structural information.

The names of *anions* usually end in –ide if there are monatomic or homopolyatomic, or –ate for heteropolyatomic anions and coordination compounds. Anionic ligands usually end in –o. Thus $Cl^-$ is chloride, $I_3^-$ is triiodide and $SO_4^{2-}$ is sulfate but become, chloro, triiodo and sulfato if they are coordinated as ligands. The names of complex anions are not always derived from the familiar name

of the element. Thus iron anions are ferrates, silver anions are argentates, gold anions are aurates, lead anions are plumbates, and tin anions are stannates. *Cations* or *neutral compounds* are not given any special ending, but coordinated water is referred to as aqua (previously aquo) and coordinated ammonia is referred to as ammine.

The IUPAC rules generally use numerical prefixes derived from Greek. Latin prefixes (*e.g.* uni instead of mono) were used and will be encountered in older literature. Some of the higher number prefixes revert to Latin, so that nona is used in preference to ennea. The multiplicative prefixes are necessary to avoid ambiguity, for example, bis(methylamine) is $(CH_3NH_2)_2$ but dimethylamine is $(CH_3)_2NH$. Italics are used for geometrical and structural prefixes *e.g. cis-, trans-, fac-, mer-* but not for other prefixes (bis, tris, tetrakis *etc.*). Note that the geometrical and structural prefixes are used with a hyphen, but numerical prefixes are not. Bridging atoms are designated with Greek μ. The Greek letter κ (kappa) is used to designate which atom of a polyatomic ligand is coordinated to the metal atom. So $[(NH_3)_5CoONO]^{2+}$ is the pentaamminenitrito–κO-cobalt(III) ion and $[(NH_3)_5CoNO_2]^{2+}$ is the pentaamminenitrito–κN-cobalt(III) ion. The old names for these ions were pentaamminenitritoco balt(III), and pentaamminenitrocobalt(III) respectively.

| | Greek derived prefix | multiplicative | Latin prefix |
|---|---|---|---|
| 1. | mono | prefixes | uni |
| 2. | di | bis | bi |
| 3. | tri | tris | tri (ter) |
| 4. | tetra | tetrakis | quadri |
| 5. | penta | pentakis | quinque |
| 6. | hexa | hexakis | sexa |

### *Synthesis*

Generally transition metal coordination compounds are prepared simply by mixing a solution of the central (metal) ion *in a suitably receptive state* with the ligand. Not all ions undergo rapid reactions (*e.g.* complexes of the inert Cr(III) and Co(III) which are often prepared from Cr(II) and Co(II)). In many cases of first row transition metals the hydrated metal ions are readily available and water may be replaced by more strongly complexing ligands. In some cases a solid product can only be isolated if a large counter ion (*e.g.* $BPh_4^-$ or $NEt_4^+$) is used. This is because the lattice energy is proportional to $1/r_A + r_C$ (where $r_A$ and $r_C$ are the anion and cation radii, respectively) but the solvation energy is proportional to $1/r_A + 1/r_C$ so if either $r_A$ or $r_C$ are small the solvation energy will tend to be large and the salt will be soluble. *e.g.* $(NEt_4)_2[CoCl_4]$ is insoluble. Complexes of macrocyclic and Schiff base ligands are often made by template synthesis methods where the host ligand is prepared in the presence of the metal guest, see Section 3.9.

### *Hard and Soft Acid and Base Theory*

The idea of hard and soft acids and bases (HSAB) is a development of the concept of Lewis acids and bases, so that acids are electron acceptors and bases are electron donors.

- Hard acids: the acceptor atom is of high positive charge, small size, and does not have easily excited outer electrons, *i.e.* non-polarisable. Examples: $H^+$, $Na^+$, $Ca^{2+}$, high oxidation states of the transition metals.

- Soft acids: the acceptor atom is of low positive charge, large size, and has several easily excited outer electrons, *i.e.* it is polarisable. Examples: $Pt^{2+}$, $Rh^{+}$, $Tl^{+}$, $Hg^{2+}$, low oxidation states of the transition metals.
- Hard bases: the donor atom is of low polarisability, high electronegativity, hard to reduce, and associated with empty orbitals of high energy and hence inaccessible. Examples: $F^{-}$, ligands with oxygen or to some extent nitrogen donor atoms.
- Soft bases: the donor atom is of high polarisability, low electronegativity, easily oxidised and associated with empty, low-lying orbitals. Examples: $I^{-}$, $R_3P$, $R_2S$, $H^{-}$.

The *Principle* of Hard and Soft Acids and Bases states that hard acids form more stable complexes with hard bases and soft bases form more stable complexes with soft acids. In orbital terms hard molecules have a large gap between the highest occupied molecular orbital (HOMO) and lowest unoccupied molecular orbital (LUMO), and soft molecules have a small HOMO-LUMO gap. In recent years it has been possible to correlate the hardness with the electronic properties of the atoms involved. Thus, if the enthalpy of ionisation (I) and the electron affinity (A) are known the so-called absolute hardness ($\eta$) and absolute electronegativity ($\chi$) can be found from: $\eta = (I - A) / 2$ and $\chi = (I + A) / 2$. For example, the first and second ionisation enthalpies of sodium are 5.14 and 47.29 eV. Thus for $Na^{+}$, $I = +47.29$ and $A = +5.14$, so $\eta = (47.29 - 5.14) / 2 = 21.1$. Similarly for silver the first and second ionisation enthalpies are 7.58 and 21.49eV, so for $Ag^{+}$ we have, $\eta = (21.49 - 7.58) / 2 = 6.9$.

There is no sharp dividing line between the classes and the class depends on the oxidation state. High oxidation states will have more hard character than low oxidation states; Cu(II) is hard whereas Cu(I) is soft. The Leden-Chatt triangle (Figure 3.2) is a useful way to remember the soft metal ions. The division is far from perfect, however! An interesting example of the HSAB principle is given by the reaction: $LiI + CsF \rightarrow LiF + CsI$. This proceeds from left to right as predicted by HSAB but contrary to Pauling's electronegativity which gives more energy for large electronegativity differences. It is worth noting that while the HSAB theory deals predominantly with electronic (ionic and covalent) effects it has been suggested that there is also a significant steric component based on donor atoms' size.[2]

### *Optical isomerism in Coordination Chemistry*

Optical isomerism occurs when a molecule contains neither a centre of symmetry (inversion centre, *i*) nor a mirror plane (*m*) or other reflection operation such as improper rotation ($S_n$). The molecule is thus chiral and will rotate the plane of polarised light if present as a pure enantiomer. Chiral molecules exist in left and right handed forms (isomers) usually labelled with a relative configuration *d* or *l* (from the Latin *dextro-* and *laevo-* meaning right and left relative to the configuration of glyceraldehyde). Chiral molecules can also be denoted + or – according to their direction of rotation of plane polarised light. Note there is not relationship betweel the *d* or *l* relative configuration and the rotation of plane polarised light. In organic compounds we can usually discover whether a molecule is chiral by looking for a carbon atom with four different substituents and we can assign its absolute handedness (*R* or *S* according to the Cahn-Ingold-Prelog rules; it takes a combination of structural and optical rotation measurements to tie together the (+/−) optical rotation properties with the absolute configuration).

| | | | | |
|---|---|---|---|---|
| Co | Ni | **Cu** | Zn | Ga |
| Rh | **Pd** | **Ag** | **Cd** | In |
| **Ir** | **Pt** | **Au** | **Hg** | **Tl** |

**Figure 3.2** The Leden-Chatt triangle with copper at the apex. A useful way to remember some of the soft metal ions.

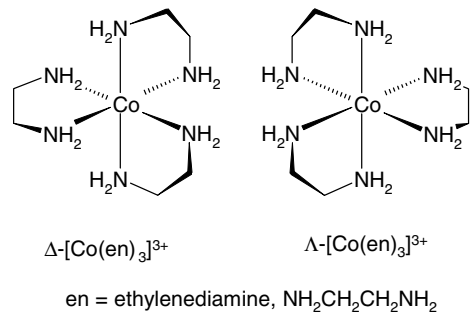


**Figure 3.3** Optical isomers of $[Co(en)_3]^{3+}$.

The Cahn-Ingold-Prelog rules work for inorganic compounds too but coordination complexes often have coordination numbers greater then four and may exhibit helical chirality, for example, denoted Δ and Λ (or *P* and *M* in the Cahn-Ingold-Prelog system). The formal condition for chirality is that the molecule should not have an improper axis of rotation (*i.e.* a rotation + reflection axis, $S_n$; $S_1$ = mirror, $S_2$ = *i*) of any order (including 1). In coordination chemistry optical activity is common when chelate rings are present and hence is common in supermolecules. Hence, $[M(L\text{-}L)_3]$ and *cis*-$[M(L\text{-}L)_2X_2]$ complexes (where L-L = didentate chelate) are chiral, although *trans*-$[M(L\text{-}L)_2X_2]$ is not, *e.g.* $[Co(H_2NCH_2CH_2NH_2)_3]^{3+}$, Figure 3.3.

Enantiomers have identical physical and chemical properties to one another except the direction in which they rotate plane polarised light (clockwise or anticlockwise). They may be separated by interaction with a second chiral species. This gives two diastereoisomers (if the two chiral centres are the same we can describe the diastereoisomers as optically pure *meso* ΔΛ and the racemic or *rac* form which itself occurs as two pairs of enantiomers, ΔΔ and ΛΛ) which do differ in their physical properties (*e.g.* have different NMR spectra, can be separated by achiral chromatography *etc.*). For example, Scheme 3.1 shows the experimental resolution of $[Co(en)_3]^{3+}$ using tartrate.

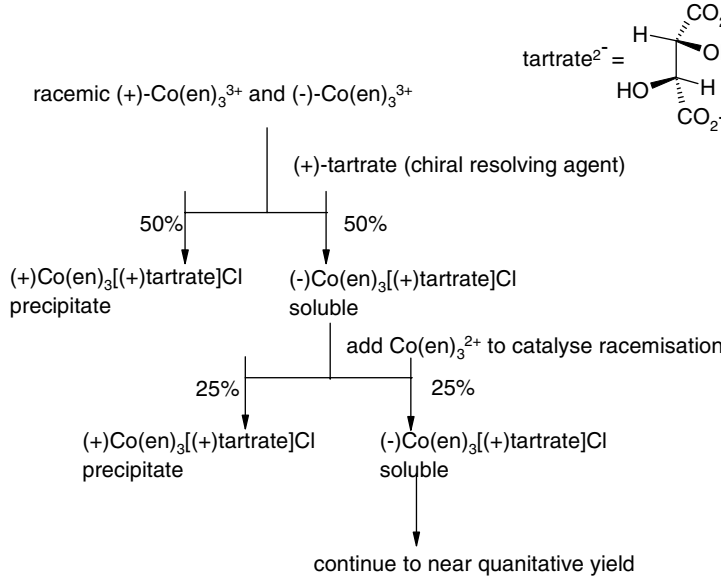


**Scheme 3.1** Experimental resolution of $[Co(en)_3]^{3+}$ using optically pure +-tartrate.

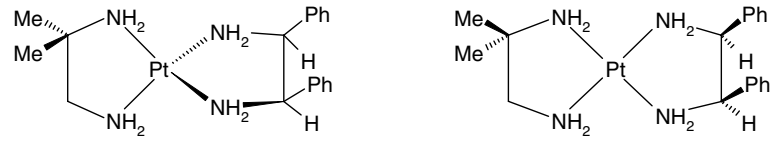


**Figure 3.4** Use of chirality to establish the square planar geometry of Pt(II).

One of the most elegant uses of optical activity was the experiment by Mills and Quibell which demonstrated the square planar geometry of Pt(II). They prepared the Pt(II) complex of isobutylenediamine and *meso*-stilbenediamine and found that it was chiral. If the geometry at platinum is tetrahedral the complex has a mirror plane and so is not chiral, Figure 3.4.

Enantiomers may be distinguished by their influence on the rotation of plane polarised light. This is measured by a type of electronic spectroscopy called *circular dichroism*. The ability of the complex to rotate plane polarised light is given in terms of an optical rotation given in degrees at a particular wavelength (see Box 6.2). X-ray crystallography may also distinguish enantiomers as long as there are 'heavy' atoms present (usually heavier than Na, although specialist experiments can distinguish enantiomers of organic compounds as well). This is a special type of crystallographic experiment termed *absolute structure determination* and makes use of a property of crystals termed *anomalous dispersion*.[3]

## 3.1.3 EDTA – a Classical Supramolecular Host

Ethylenediamine tetraacetic acid ($H_4EDTA$) in its deprotonated form, $EDTA^{4-}$, is an extremely common, chelating ligand that is able to bind to most metal centres. It represents an excellent illustration of how a supramolecular host is nothing more than a classical multidentate ligand. It may be deprotonated up to four times to give $EDTA^{4-}$ which acts as a multiply chelating ligand. EDTA titrations are used for the analytical determination of metal ion concentrations (*e.g.* $Mg^{2+}$ and $Ca^{2+}$ in a 24 hour urine sample). This is possible because $EDTA^{4-}$ binds so strongly to most metal ions that essentially 100% of the ion is bound to the ligand. A dye such as the murexide ion is used as an indicator and hence the reaction shown in Equation 3.1 takes place. Decomplexation of the metal-bound indicator causes a change in the energy of the indicator HOMO and hence a change in the electronic absorption energy and hence colour. This kind of indicator displacement assay is a useful sensing method (Section 11.3.3).

$$[M{\cdot}\text{indicator}]^{n+} + EDTA^{4-} \rightarrow [M(EDTA)]^{(4-n)-} + \text{free indicator} \qquad (3.1)$$

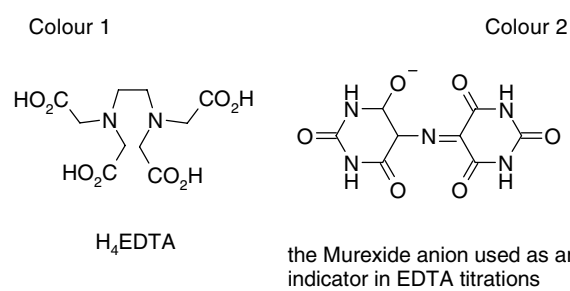

**Table 3.1** Stability constants (Log *K*) in aqueous solution for metal complexes of $EDTA^{4-}$.

| | | | | | |
|---|---|---|---|---|---|
| $Mg^{2+}$ | 8.7 | $Zn^{2+}$ | 16.7 | $La^{3+}$ | 15.7 |
| $Ca^{2+}$ | 10.7 | $Cd^{2+}$ | 16.6 | $Lu^{3+}$ | 20.0 |
| $Sr^{2+}$ | 8.6 | $Hg^{2+}$ | 21.9 | $Sc^{3+}$ | 23.1 |
| $Ba^{2+}$ | 7.8 | $Pb^{2+}$ | 18.0 | $Ga^{3+}$ | 20.5 |
| $Mn^{2+}$ | 13.8 | $Al^{3+}$ | 16.3 | $In^{3+}$ | 24.9 |
| $Fe^{2+}$ | 14.3 | $Fe^{3+}$ | 25.1 | $Th^{4+}$ | 23.2 |
| $Co^{2+}$ | 16.3 | $Y^{3+}$ | 18.2 | $Ag^{+}$ | 7.3 |
| $Ni^{2+}$ | 18.6 | $Cr^{3+}$ | 24.0 | $Li^{+}$ | 2.8 |
| $Cu^{2+}$ | 18.8 | $Ce^{3+}$ | 15.9 | $Na^{+}$ | 1.7 |

Binding constants as Log *K* values for the equilibrium: $M^{n+} + EDTA^{4-} = [M(EDTA)]^{(n-4)+}$ are given in Table 3.1. They cover over 23 orders of magnitude from 1.7 for the relatively large, low charge and labile $Na^{+}$ to 25.1 for the highly charged, complementary $Fe^{3+}$. Significant factors are the cations' charge and ionic radius. For example for $Na^{+}$, $Ca^{2+}$ and $Lu^{3+}$ the ionic radius is very similar but the charge increases, Table 3.2.

If we look at the data for the alkaline earths we see that $Mg^{2+}$ is anomalous because the value is lower than we would expect from charge and radius considerations, Table 3.3. This reflects the high degree of solvation of the small, polarising $Mg^{2+}$ and that fact that it is too small to form an optimum chelate geometry. Moreover the hard $Mg^{2+}$ is not particularly complementary to the softer tertiary amine nitrogen donors. As a result the complex is 7-coordinate with an open face that interacts with an additional aquo ligand (Figure 3.5). In contrast the smaller Co(III) ion is able to coordinate optimally to six $EDTA^{4-}$ donor atoms, while the larger Ni(II) interacts with an aquo ligand instead of an EDTA donor atom. Note that the divalent $Ni^{2+}$ and $Mg^{2+}$ are insufficiently polarising to form stable complexes with the fully deprotonated $EDTA^{4-}$.

**Table 3.2** Correlation of ionic charge with affinity for $EDTA^{4-}$.

| | $Na^{+}$ | $Ca^{2+}$ | $Lu^{3+}$ |
|---|---|---|---|
| radius (Å) | 0.95 | 0.99 | 0.93 |
| log *K* (EDTA) | 1.7 | 10.7 | 20.0 |

**Table 3.3** correlation of ionic radius with affinity for $EDTA^{4-}$; $Mg^{2+}$ is anomalous.

| | $Mg^{2+}$ | $Ca^{2+}$ | $Sr^{2+}$ | $Ba^{2+}$ |
|---|---|---|---|---|
| radius (Å) | 0.65 | 0.99 | 1.13 | 1.35 |
| charge/radius | 3.07 | 2.02 | 1.77 | 1.48 |
| log *K* ($EDTA^{4-}$) | 8.7 (7 coord.) | 10.7 | 8.6 | 7.8 |

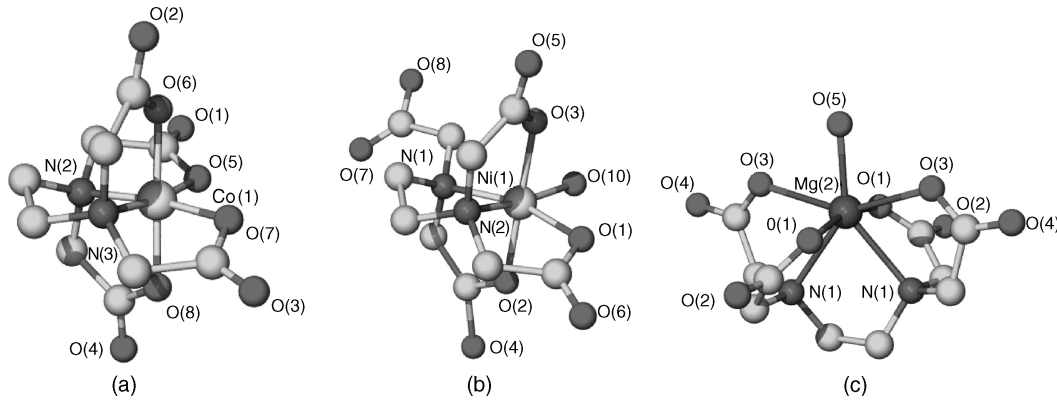


**Figure 3.5** X-ray molecular structures of (a) $[Co(EDTA)]^-$, (b) $[Ni(HEDTA)(H_2O)]^-$ and (c) $[Mg(H_2O)(HEDTA)]^-$.

## 3.2 The Crown Ethers

G. W. Gokel, *Crown Ethers*, Royal Society of Chemistry: Cambridge, 1990.

### 3.2.1 Discovery and Scope

The crown ethers are among the simplest and most appealing macrocyclic (large ring) ligands, and are ubiquitous in supramolecular chemistry as hosts for both metallic and organic cations. They consist simply of a cyclic array of ether oxygen atoms linked by organic spacers, typically —$CH_2CH_2$— groups. While the metal binding ability of unidentate ethers such as the common solvent diethyl ether is very poor, the crown ethers are much more effective by virtue of the chelate effect and the partial preorganisation arising from their macrocyclic structure (Section 1.5).

The discovery of the crown ethers in 1967 gained a share of the 1987 Nobel Prize for Chemistry for Charles Pedersen, a chemist working at the American du Pont de Nemours company. Oddly, however, Pedersen's initial synthesis of the first crown ether, dibenzo[18]crown-6 (**3.4**) was accidental. In trying to carry out the synthesis of the linear di-ol (**3.3**), which he hoped might act as a ligand for the catalytic vanadyl ion, Pedersen carried out the reaction shown in Scheme 3.2. The starting material was the catechol (1,2-dihydroxybenzene) derivative (**3.1**), in which one of the hydroxyl groups is protected by a tetrahydropyran ring to prevent its reaction. Unknown to Pedersen, his starting material was slightly contaminated by some free catechol (**3.2**). The resulting product was a mixture of the desired compound (**3.3**) along with a small amount of dibenzo[18]crown-6, formed in only 0.4 % yield. It is a tribute to Pedersen's skills that he was able to isolate and characterise this small amount of by-product.[4]

Pedersen's interest was aroused by the interesting solubility properties of (**3.4**), and by its high degree of crystallinity (suggesting a molecular compound rather than a polymer). The compound dissolved sparingly in methanol, but its solubility was enhanced significantly on addition of alkali metal salts. Pedersen soon synthesised the compound in much better yield. He found that it dissolved inorganic salts like $KMnO_4$ in organic solvents such as benzene to give it a purple colouration (this was termed 'purple benzene'). Pedersen also became aware of the crown ether's ability to dissolve the alkali metals themselves to give interesting blue solutions of what are now known to be alkalide and electride salts

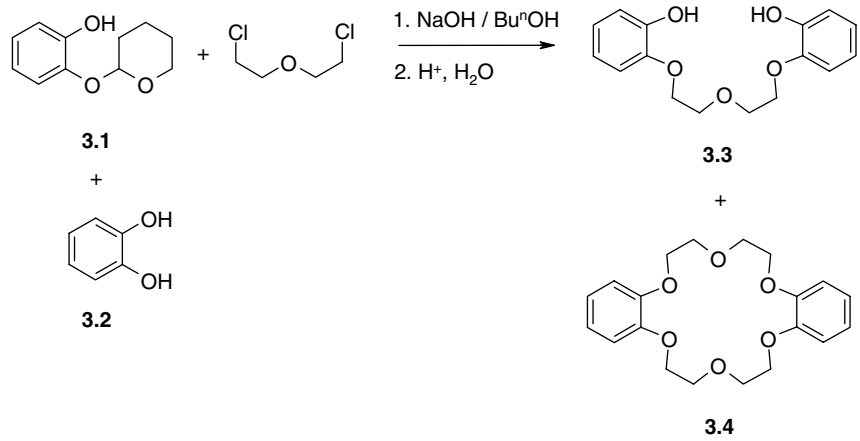


**Scheme 3.2** Accidental synthesis of the first crown ether, dibenzo[18]crown-6.[4]

(Section 3.13). He eventually concluded that 'the potassium ion had fallen into the hole at the centre of the molecule' (Figure 3.6), at the time a bold and highly imaginative statement. Events were quickly to prove him to be entirely correct. This initial result led rapidly to the synthesis of a related family of species (Figure 3.2) to which Pedersen gave the name 'crown ethers' because of the crown-like shape of the capsular complex between **3.4** and $K^+$.

Since the early work of Pedersen, the crown ethers have become very popular in cation complexation chemistry. Their versatile binding ability and their almost infinite synthetic malleability have led to an enormous variety of functionalised and derivatised crowns and crown analogues with varying selectivity for an enormous variety of guest species, Figure 3.7. The analogy of the $K^+$-binding ability of **3.4**

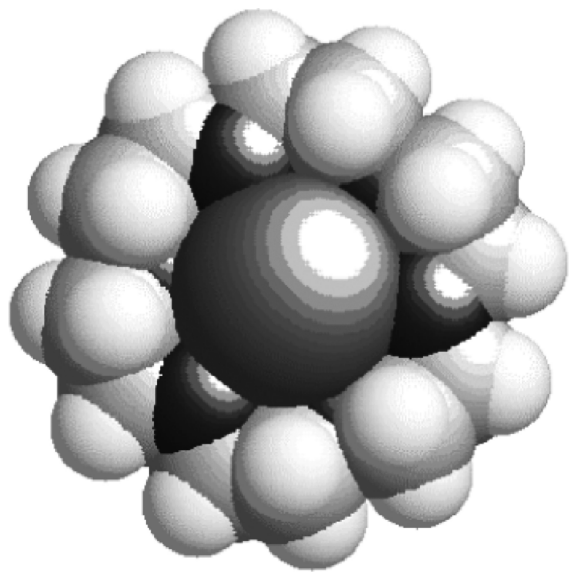

**Figure 3.6** Space-filling diagram of the complex between [18]crown-6 (**3.4**) and $K^+$.

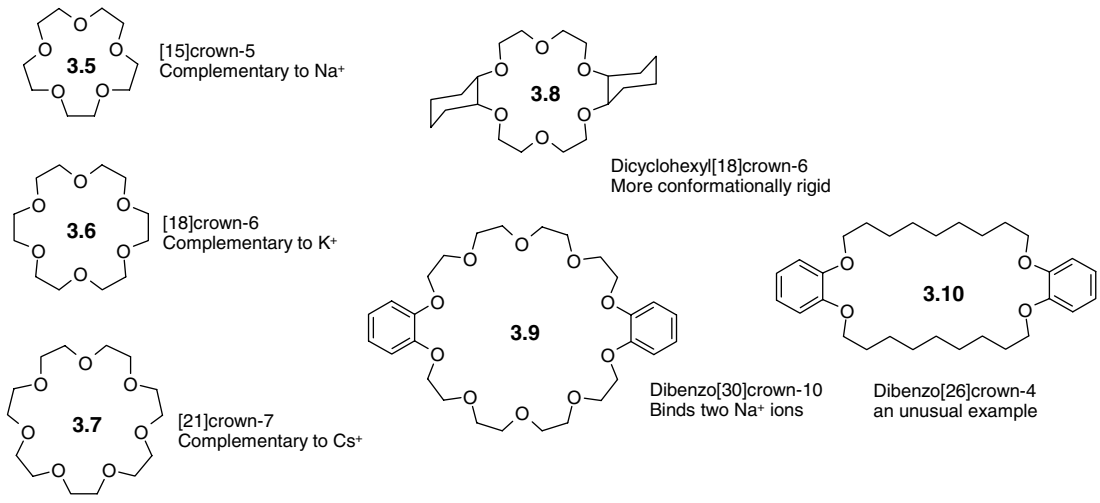


**Figure 3.7** Some common crown ethers.

and the metal complexes of the ionophores such as valinomycin and nonactin discussed in Section 2.1 is immediately apparent and extensive studies have been made of the crown ethers as models for ionophore behaviour.

## 3.2.2 Synthesis

D. Parker, *Macrocycle Synthesis: A Practical Approach*, OUP, Oxford, 1996.

Pedersen described a total of six different methods of crown ether synthesis in his original work. These still form much of the basis for modern crown ether preparations (Scheme 3.3). Most new crown ethers are prepared by either method (a) or (b). All of the methods shown in Scheme 3.3 are examples of the Williamson ether synthesis, although it was an example of method (c) that led to the original preparation of dibenzo[18]crown-6. In fact, dibenzo[18]crown-6 may be prepared in much better yield (about 80 per cent yield, versus 45 per cent) *via* method (b). Furthermore, the unreacted catechol may cause problems in the separation of the [1 + 1] and [2 + 2] cycloaddition products in (c). The method shown in scheme (d) was used by Pedersen only for the preparation of macrocycle **3.10**. Method (e) (intramolecular cyclisation) is not a particularly viable one in general terms because of the nonavailability of the starting materials and usually poor yields. For example, [18]crown-6 (**3.6**) may be prepared by this method in 1.8 % yield, although excellent yields have been obtained for oligoethyleneglycol [$HO(CH_2CH_2O)_nH$] cyclisations by slow addition of *p*-toluenesulfonyl chloride to a suspension of alkali metal hydroxide, which acts as the base. In general, increasing use of the tosylate (*p*-toluenesulfonate, $MeC_6H_4SO_2^-$, $Ts^-$) function as a leaving group instead of chloride has often led to increasingly better yields.

Method (f) is a catalytic reduction to produce saturated cyclohexyl rings from the corresponding arenes. In the case of dibenzo[18]crown-6 this can, in principle, result in up to five isomers of dicyclohexyl[18]crown-6 (**3.8**), of which only the first four have been isolated (Figure 3.8). The different configurations of these materials (which are noninterconvertable) result in a wide variation of their binding ability. Their affinity for $Na^+$ in methanol, for example, ranges over about 1.5 orders of magnitude, the *cis-syn-cis* isomer being the most effective.

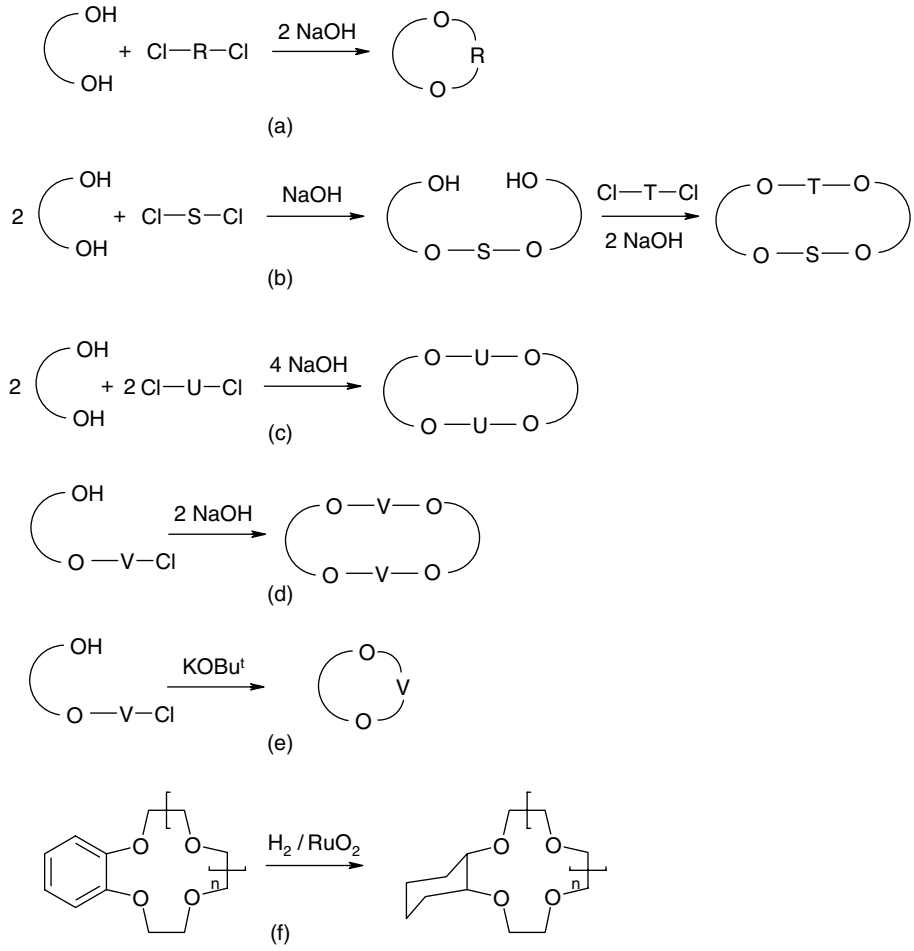


**Scheme 3.3** Methods for synthesising the crown ethers (R – V are organic linker groups).

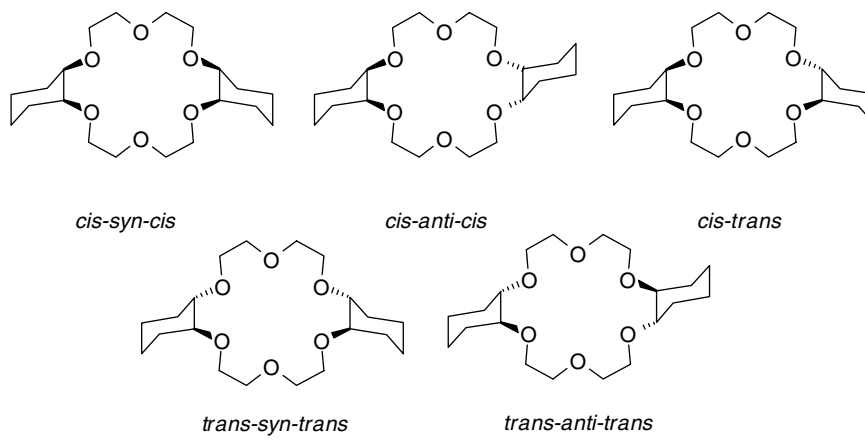


**Figure 3.8** Isomers of dicyclohexyl[18]crown-6.

# 3.3 The Lariat Ethers and Podands

## 3.3.1 Podands

Gokel, G. W. and Murillo, O. 'Podands', in *Comprehensive Supramolecular Chemistry*, J. L. Atwood, J. E. D. Davies, D. D. MacNicol and F. Vögtle (eds), Pergamon: Oxford, 1996, vol. 1, 1–33.

Acyclic hosts with pendant binding sites are termed *podands*. The simplest podands are simply acyclic analogues of the crown ethers such as pentaethyleneglycol dimethylether (**3.11**), analogous to [18]crown-6, or its di-ol analogue (**3.12**).

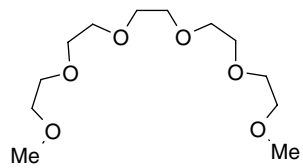


**3.11**

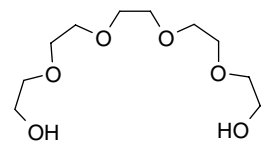


**3.12**

Podand hosts generally exhibit less cation affinity than their cyclic analogues, as a result of their lack of preorganisation (Section 1.6), but they may adopt similar wrapping conformations to the crown ethers in the presence of suitable metal cations, such as the highly charged lanthanoids (Figure 3.9). The extra flexibility of podand hosts, however, also allows them to engage in multiple bridging and helical binding modes unknown for the crown ethers (Figure 3.10).

As early as 1972, podand $Ca^{2+}$ carriers with transmembrane ionophore-type behaviour were reported by the Eidgenössische Technische Hochschule (ETH) group of Simon in Zürich.[5] These hosts (*e.g.* **3.13**) rely on the polar amide groups for their binding ability, and the fact that the long ester arms are flexible and able to bend back on themselves to simultaneously coordinate the metal cation.

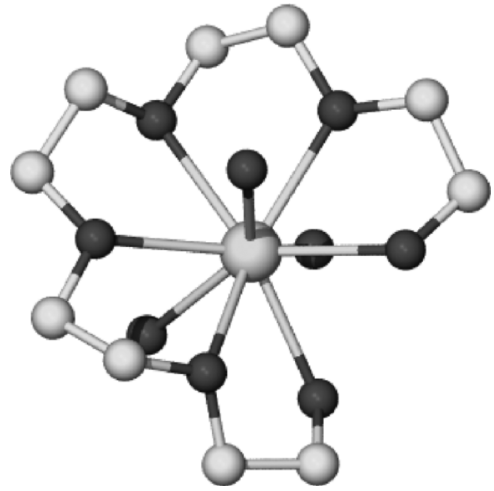

**Figure 3.9** X-ray molecular structure of the europium(III) podand complex $[Eu(H_2O)_3(\mathbf{3.12})]^{3+}$.

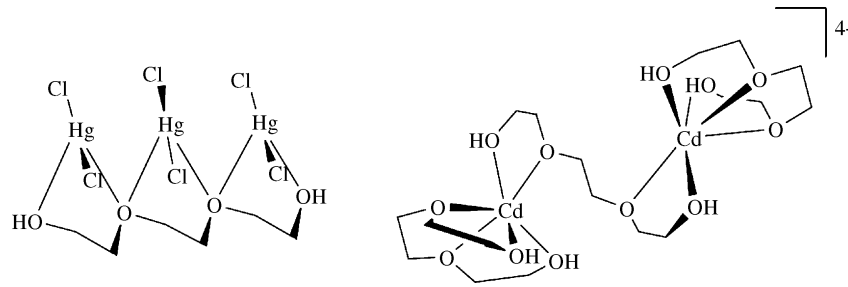


**Figure 3.10** Alternative coordination modes of the simple podand trioxyethylene glycol.

Also, the aliphatic chains contribute greatly to the lipophilicity of the compound, hence its membrane transport ability.

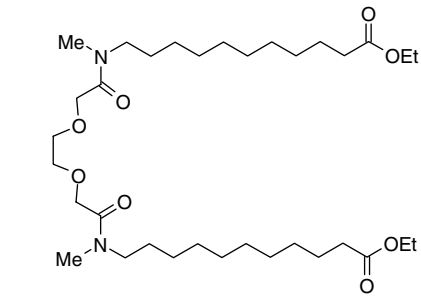


**3.13**

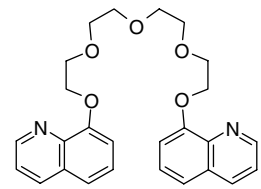


**3.14**

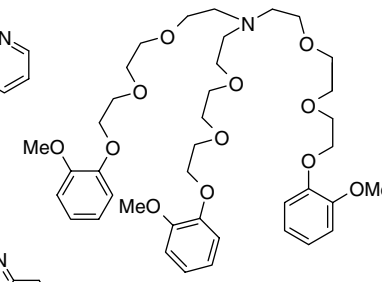


**3.17**

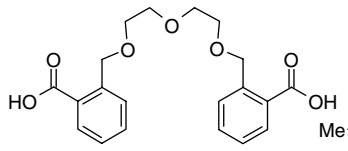


**3.15**

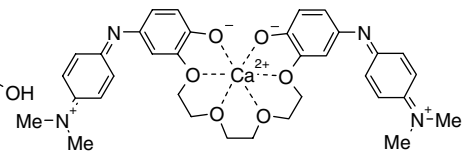


**3.16**

The term 'podand' was coined by Vögtle and Weber in 1979,[6] whose early work involved quinoline-terminated podands such as **3.14**, which are able to form stable crystalline compounds with a wide variety of alkali metal salts as well as transition metals and even uranyl nitrate, $UO_2(NO_3)_2.6H_2O$. As part of their work on podands, these researchers also formulated the important *end group concept*. One of the problems with podands is their high degree of flexibility, allowing them to adopt non-binding open conformations. If the podand is terminated by a rigid functionality (*e.g.* aryl, ester, amide), however, binding is enhanced by the extra degree of organisation given to the podand host by the rigidifying endgroup. A good example of this concept is **3.15**, in which the conjugated benzoic acid moieties provide a rigid, planar and partially preorganised binding cleft, especially in conjunction with the short diethyleneglycol bridge. The rigid-end-group host **3.16**, which is terminated by quinone monoimine groups, was studied as a possible means of sensing the presence of cations by changes in the UV–visible absorption spectrum of the host (a *chromoionophore*). This zwitterionic podand, binding *via* two anionic oxygen donors, gave large spectral changes in the presence of divalent cations. Extending the podand concept to three dimensions gives tripodal

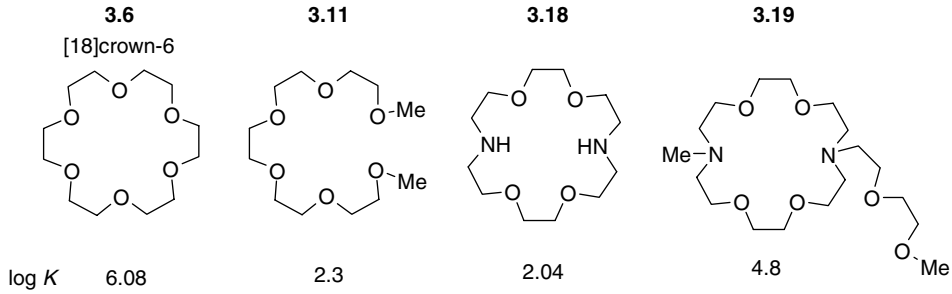


**Figure 3.11** Binding constants (log $K$) for $K^+$ binding by simple podand, crown and lariat ether compounds in methanol at 25 °C.

molecules, such as **3.17**, which are able to encapsulate their guests more fully. Again, the rigid-end-group philosophy is applicable since tripodal hosts are often highly flexible as a consequence of inversion at the bridgehead nitrogen atoms.

## 3.3.2 Lariat Ethers

Gokel, G. W., 'Lariat ethers - from simple sidearms to supramolecular systems,' *Chem. Soc. Rev.* 1992, **21**, 39–47.

The term 'lariat ether' refers to a crown ether or similar macrocyclic derivative with one or more accompanying appendages designed to enhance metal cation complexation ability by giving some three-dimensionality to the binding (*cf.* **3.17**). The compounds may be regarded as a crown type macrocycle with a podand side-arm. The name comes from the Spanish *la reata*, meaning 'the rope', and suggests the concept of the macrocycle representing the loop of a lasso and the podand side-arm representing the rope by which it is held. They thus combine the higher rigidity and preorganisation of macrocyclic compounds with the additional stability and flexibility (which leads to fast cation-binding kinetics) of podand complexation. A comparison between the binding ability of some simple podand, crown and lariat ether compounds is shown in Figure 3.11. Clearly [18]crown-6 is a much more effective ligand for $K^+$ than the podand pentaethyleneglycol dimethylether (**3.11**) (the $K^+$ complex is almost four orders of magnitude more stable). At first sight, the lariat ether **3.19** seems to lie somewhat in between the binding ability of the cyclic and acyclic compounds. However, the affinity for $K^+$ is also regulated by the character of the donor atoms. A more direct comparison between the azacrowns **3.18** and **3.19** suggests that it is the three-dimensional binding by the lariat ether (Figure 3.12) that is the more effective of the two, although the greater amine basicity in **3.19** also enhances the binding constant (*cf.* *N*,*N*′-di-*n*-butyldiaza[18]crown-6, log $K$ = 3.8). The number of donor atoms (eight as opposed to six) is also a key consideration.

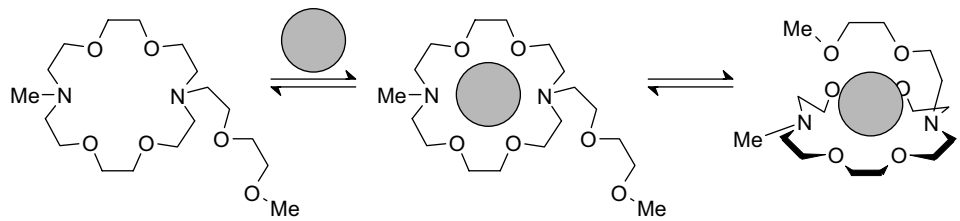

**Figure 3.12** Metal complexation by a lariat ether.

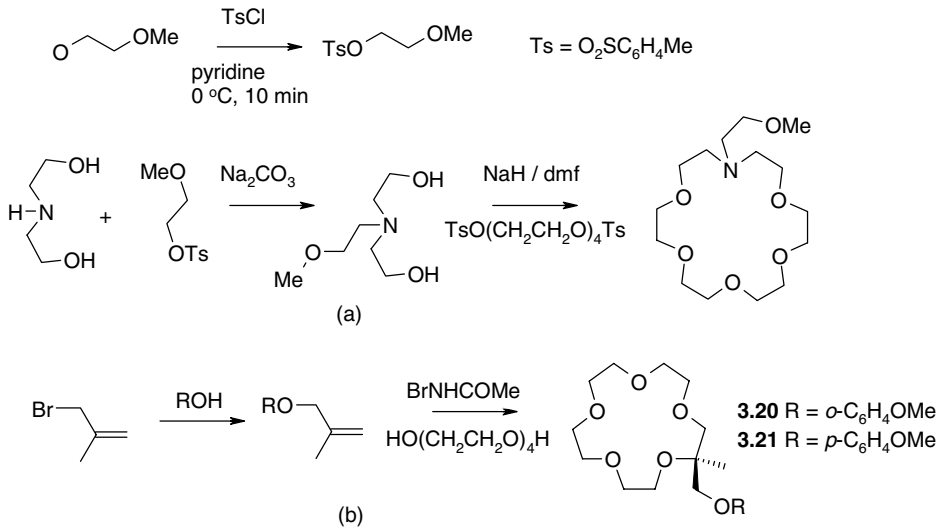


**Scheme 3.4** Syntheses of **(a)** N-pivot and **(b)** C-pivot lariat ethers **3.20** and **3.21**.[7]

Compound **3.19** makes use of a tertiary amine nitrogen atom as a pivot where the podand side chain is attached to the crown ether ring. However, effective lariat ethers may also be synthesised by use of the carbon backbone as the point of attachment, as in **3.20**. Example syntheses of both types of compound are shown in Scheme 3.4.[7] Interestingly, while **3.20** may be readily prepared in excess of 70 per cent yield, the analogous *para* isomer **3.21**, which is sterically incapable of coordinating both side-arm donors to the same metal cation, is produced in only 30 per cent yield, highlighting the mechanism of the reaction, which involves binding of the reactants to the metal cation during the transition state. The synthesis proceeds under kinetic control, using the metal ion to organise the reactants. This is referred to as the *kinetic template effect* and is discussed in detail in Section 3.9.

## 3.3.3 Bibracchial Lariat Ethers

The lariat ether concept may be readily extended to produce so-called bibracchial lariat ether (BiBLE) hosts, which have two podand side-arms, thus displaying even more three-dimensional binding coverage of the metal ion guest's surface. A wide range of N-pivot BiBLE ligands has been prepared by Gokel *et al*. according to the convenient, although relatively low-yielding, method outlined in Scheme 3.5.[8]

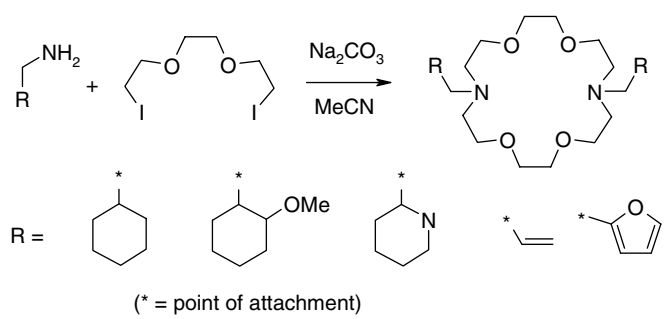


**Scheme 3.5** Simultaneous four-bond coupling to produce BiBLE ligands.[8]

## 3.4 The Cryptands

Lehn, J. -M. *Supramolecular Chemistry: Concepts and Perspectives*, VCH: Weinheim, 1995.

Shortly after Pedersen's work, Jean-Marie Lehn, then a young researcher at the University of Strasbourg, decided to design three-dimensional analogues of the crown ethers. In this way it was anticipated that metal ions could be encapsulated entirely within a crown-like host with consequent gains in cation selectivity and enhancements in ionophore-like transport properties. Accordingly, the bicyclic *cryptands* (named because of their ability to spherically surround or 'entomb' a metal cation, as in a crypt; from the Greek *kruptos* meaning 'hidden') and an ever-increasing range of related compounds were synthesised using the high-dilution technique (Section 3.9.2), the majority in remarkably high yields (Scheme 3.6). The first and most important member of the series is [2.2.2]cryptand (**3.22**), which is sold commercially under the trade name *Kryptofix*®. Because it is based on a similar sized ring to [18]crown-6, this host also exhibits selectivity for $K^+$ over the other alkali metals. The binding of $K^+$ by [2.2.2]cryptand in methanol is, however, some $10^4$ times stronger than its crown analogue. Similarly, [2.2.1]cryptand (**3.23**) is selective for $Na^+$. The key to the dramatically enhanced metal cation binding ability of cryptands over crown ethers is the pre-organised, three-dimensional nature of their cavity, which enables *spherical recognition* of the $M^+$ ion to take place.

High-dilution syntheses, while highly versatile, do not readily enable large quantities of material to be prepared, and often involve many steps, particularly the final reductive decarbonylation with diborane. Since the early work of Lehn, a wide variety of synthetic procedures has been developed to prepare an enormous range of cryptands of varying degrees of sophistication, including chiral species and those containing three different bridges. Many of these follow a stepwise approach, which may be summarised as follows:

1. building up two linear chains possessing suitable reactive groups at each chain end;
2. cyclisation reaction of these two chains leading to a corand (crown ether-like macrocycle);
3. addition of a third chain to the corand to give a macrobicyclic compound.

Because of the length and tedium of such approaches, much simpler routes, often taking advantage of the *template effect* (Section 3.9.1), have been devised, which, in many simple cases, can be remarkably effective. Such alternative syntheses of **3.22** and related compounds are shown in Scheme 3.7.

The synthetic versatility of azacrowns (crown ethers with some oxygen atoms replaced with NH functionalities), such as **3.18**, has made possible the synthesis of an enormous range of

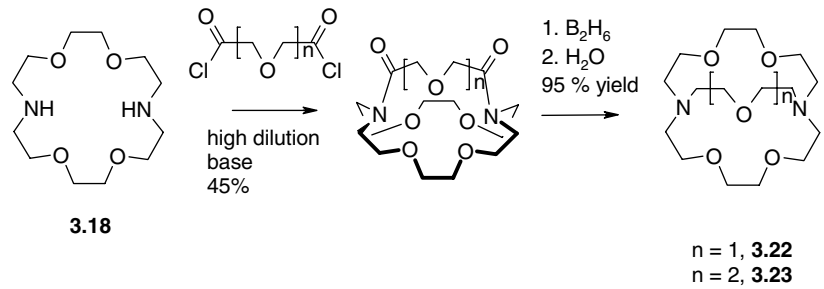


**3.18**

**Scheme 3.6** High dilution synthesis of [2.2.1]cryptand (n = 1) and [2.2.2]cryptand (n = 2).[9]

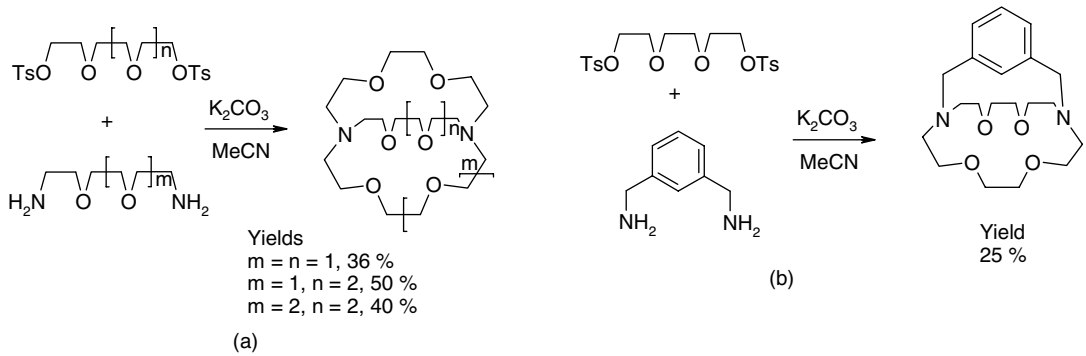


**Scheme 3.7** Simple template synthesis of selected cryptands with yields.

cryptands, many with very unusual cation and anion binding properties. Some examples are shown in Figure 3.13.

A particularly novel class of cryptand are the *sepulchrates*, which arise from a Co(III) templated condensation of various capping groups with *tris*(chelate) complexes of bidentate ligands. The first example, reported in 1968 by Boston and Rose, involved the reaction of *tris*(dimethylglyoximato) cobalt(III) with the highly Lewis acidic boron trifluoride etherate (Scheme 3.8). The fact that Co(III) is a highly inert metal ion (see Chapter 10, Box 10.1) means that it is very likely that the cryptate complex is formed as a consequence of the ability of the metal ion to hold the ligand in an orientation similar to the geometry of the final product. Work by Alan Sargeson of the Australian National University has resulted in a range of related complexes derived for 1,2-diaminoethane. Sargeson coined the name 'sepulchrates' for the nitrogen-capped metal compounds and 'sarcophagines' for the analogous *C*-bridged species because the sequestered, metal complex is highly stable

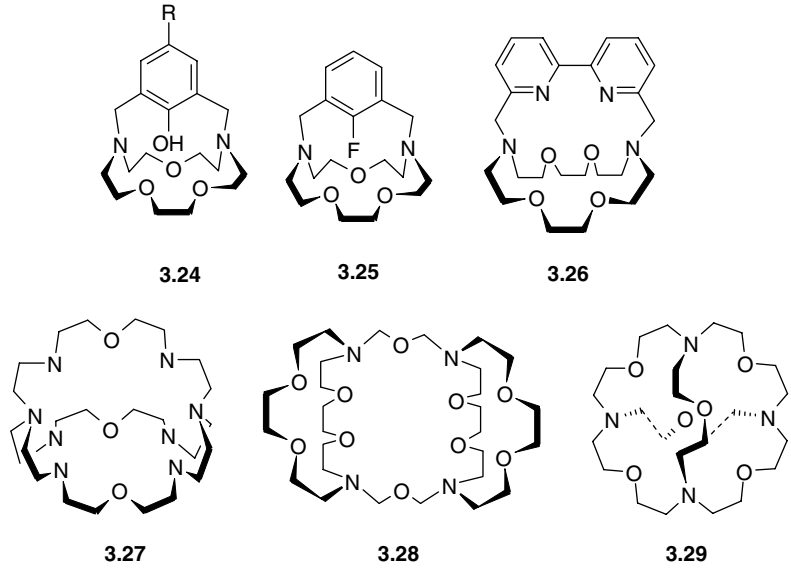


**Figure 3.13** Some examples of cryptands.

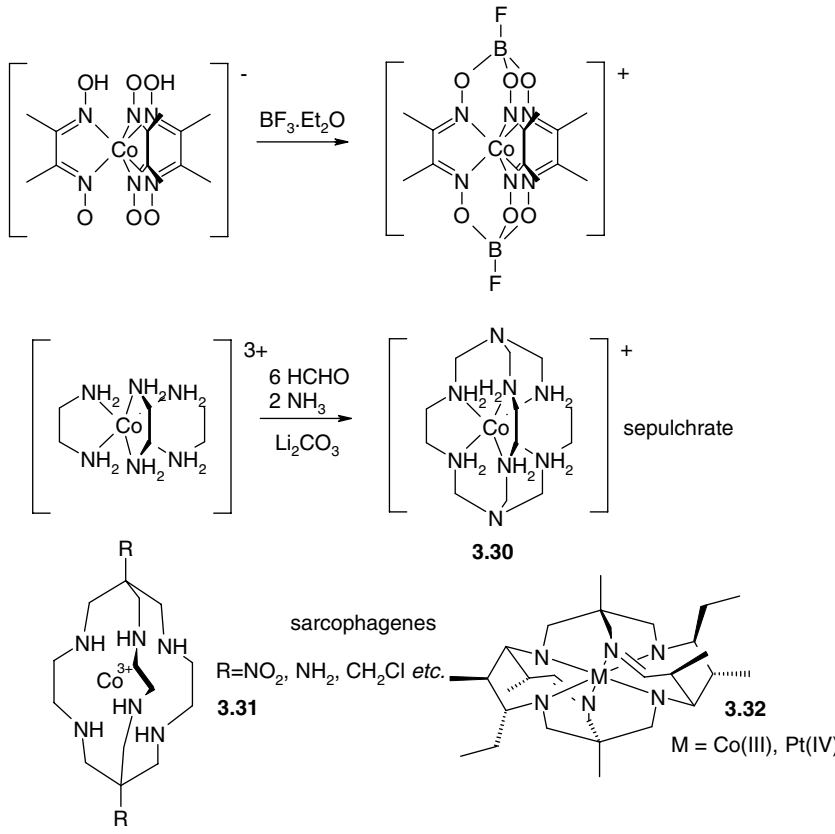


**Scheme 3.8** Sepulchrates and sarcophagenes.

and unreactive. This work has been extended to remarkably regio- and stereoselective preparations of Co(III) and Pt(IV) sarcophagines such as **3.32** by a Schiff base condensation technique. Schiff base macrocycles are described further in Section 3.10.6. The X-ray structure of one such compound is shown in Figure 3.14.

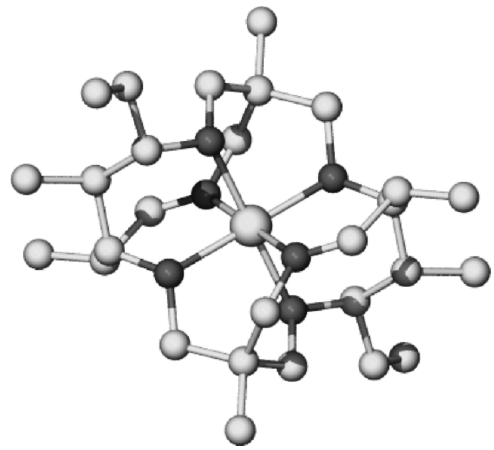

**Figure 3.14** X-ray molecular structure of the Pt(IV) sarcophagine **3.32**.[10]

## 3.5 The Spherands

Maverick, E. and Cram, D. J., 'Spherands: Hosts preorganised for binding cations', in *Comprehensive Supramolecular Chemistry*, J. L. Atwood, J. E. D. Davies, D. D. MacNicol and F. Vögtle (eds), Pergamon: Oxford, 1996, vol. 1, 213–243.

In addition to Pedersen and Lehn, the 1987 Nobel Prize for Chemistry was shared by a third supramolecular chemist, Donald Cram, for his development of a further type of macrocyclic cation host: the spherands. While the crown ethers and even the cryptands are relatively flexible in solution, Cram realised that if a rigid host could be designed, which had donor sites that were forced to converge on a central binding pocket even before the addition of a metal cation, then strong binding and excellent selectivities between cations should be observed. Using space-filling molecular models (termed Corey–Pauling–Koltun or CPK models, Figure 3.15), Cram and co-workers designed the rigid, three-dimensional spherands **3.33** and **3.34**, whose cation-binding oxygen atoms are preorganised in an octahedral array, ready to receive a metal ion.

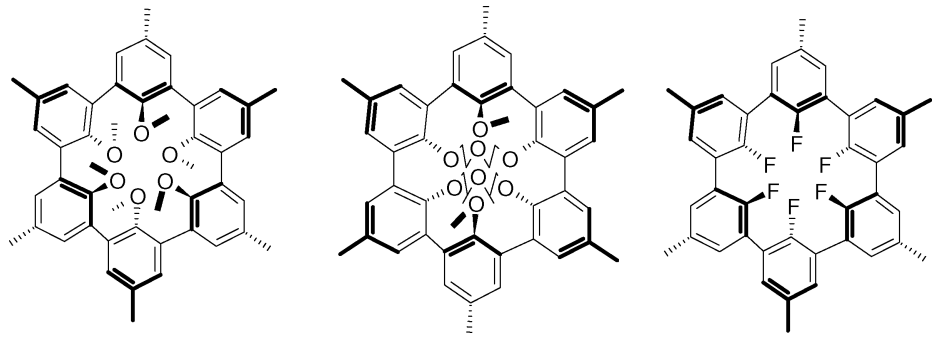

**3.33** **3.34** **3.35**

In the case of compound **3.33**, three of the aryl rings are pointing upwards (out of the page) and three downwards. This results in the anisyl oxygen atoms being fixed in a nearly perfect octahedral array, while the *p*-methyl and anisyl methyl groups present a lipophilic surface to the solvent. This host selectively binds small cations such as $Li^+$ and, to a lesser extent, $Na^+$, in its cavity. Indeed, **3.33** is one of the strongest complexants known for $Li^+$. All other cations are excluded because they are simply too big to fit within the binding pocket. Spherand **3.34** has a binding pocket of similar size, formed from the tethering of the rings in pairs with diethylene glycol linkages, resulting in four rings being down and two up. The analogous fluoro compound **3.35**, along with an octameric analogue,

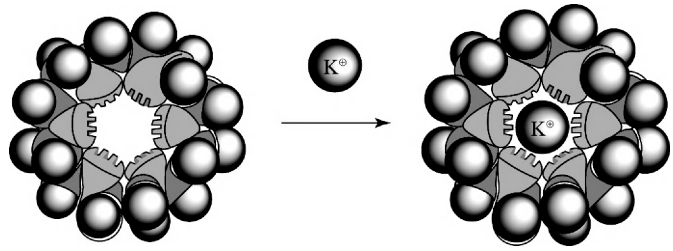


**Figure 3.15** CPK models of crown ether and spherand complexes were used in early supramolecular design. Modern computational techniques, such as molecular mechanics have, to some extent, replaced such tactile representations. (Reproduced by permission of John Wiley & Sons, Ltd).

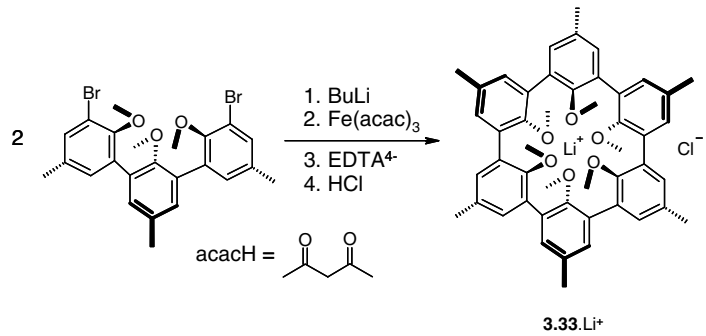


**3.33**.Li+

**Scheme 3.9** Synthesis of spherand **3.33** as its $Li^+$ complex (spheraplex).

have also been synthesised. While X-ray crystallography confirms that the hosts possess very similar cavities to **3.33**, the fluoro species display no metal ion binding properties. Apparently the intrinsic affinity of fluoro substituents for alkali metal cations is so low that even incorporation of multiple binding sites into a highly organised host cannot bring the binding on to a measurable scale. Interestingly, however, a definite interaction of cation guest with a fluoro substituent is observed for cryptand **3.25**, both in the solid state by X-ray crystallography and in solution by $^{19}F$ NMR spectroscopy.

In order to achieve the final cyclisation step in the spherand syntheses, a new synthetic ring-closure procedure was developed, which proceeds according to Equation 3.2 (acac = acetylacetonato, $CH(COMe)_2^-$). The aryl lithium compound produced by action of butyl lithium is oxidised by the Fe(III) complex to give an aryl biradical, which then undergoes a template cyclisation about the $Li^+$ ion (see Section 3.9.1 for an explanation of the template effect). In the case of **3.33**, this method resulted in the isolation of the complex in 28 % yield from the reaction shown in Scheme 3.9.

$$\text{Ar–Br} \xrightarrow{\text{BuLi}} \text{Ar–Li} \xrightarrow{\text{Fe(acac)}_3} \text{Ar–Ar} \tag{3.2}$$

By way of comparison, acyclic podand hosts analogous to compound **3.33** have been produced in order to assess the importance of the rigid preorganisation afforded by a cyclic host. Comparison of the closely related podand **3.36** (which is estimated to possess over 10 000 possible conformations, only two of which can bind cations in a convergent manner) and **3.33** (which is locked in only one conformation) shows that the spherand binds $Li^+$ more than $10^{12}$ times more effectively. This highlights the importance of preorganisation effects in host design.

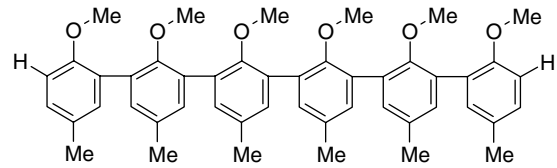


**3.36**

Cross-fertilisation between the crown ethers (or, more generally, corands), cryptands, spherands and podands has produced an enormous range of hybrid hosts such as cryptaspherands and hemispherands, many exhibiting all the useful features of the parent materials (Figure 3.16).

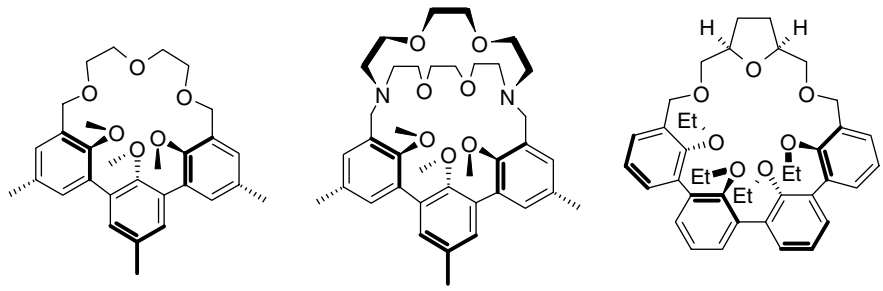


**Figure 3.16** Hybrid cation hosts.

## 3.6 Nomenclature of Cation-Binding Macrocycles

The naming of crown ethers is relatively simple, although for historical reasons it is only unambiguous if the exclusive use of ethylene glycol (—$OCH_2CH_2O$—) linkages is assumed; in more complicated cases, the name is usually accompanied by a pictorial representation.

1. The first number in the crown name designates the number of atoms in the ring (usually given in square brackets).
2. The second number gives the number of oxygen (or other donor) atoms.
3. Substituents are denoted with a prefix such as benzo-, dicyclohexano- *etc.*

For example, dibenzo[18]crown-6 is a crown ether with an 18-membered macrocyclic ring containing six oxygen atoms with two benzo substituents. A more generalised system of nomenclature for such neutral organic ligands was developed by Vögtle and Weber,[6] and later modified by Cram,[12] in which any monocyclic system such as a the crown ether is termed a *corand* (originally *coronand*). Open chain molecules such as **3.3** and **3.11** are called *podands*; bicyclic or oligocyclic systems are termed *cryptands* (Figure 3.17); and rigid, *p*-methylanisole-based systems are given the name *spherand*. In general, for purely oxygen donor ligands, the historical crown nomenclature is retained.

Figure 3.18 shows examples of podands, corands and cryptands. Under this system, all of the crown ethers belong to the general class of corands. The name of [18]crown-6 (**3.6**) becomes $18\langle O_6 2_6 \text{corand-}6\rangle$, meaning an 18-membered ring monocyclic (*i.e.* corand) compound containing six oxygen atoms linked by six spacers containing two carbon atoms each to give a total of six donor atoms.

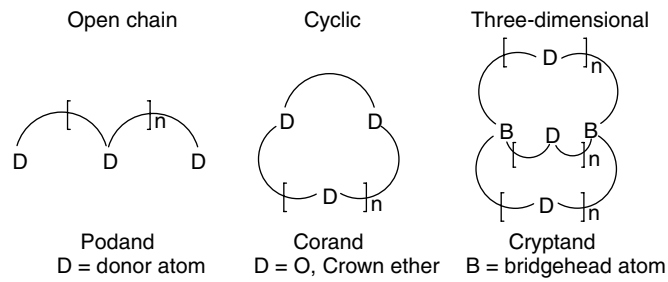


**Figure 3.17** Classes of cyclic and acyclic ligands.

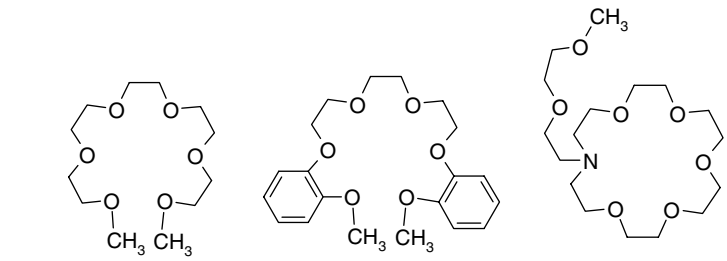

**3.11** **3.40** **3.41**

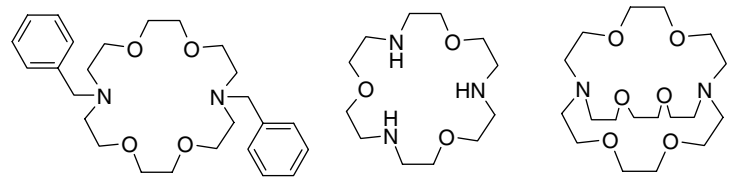

**3.42** **3.43** **3.23**

**Figure 3.18** Podands **3.11** and **3.40**, corands **3.41**–**3.43** and cryptands **3.23** related to [18]crown-6. Compounds **3.41** and **3.42** are members of a hybrid corand–podand family termed *lariat ethers*. Lariat ethers with two podand arms such as **3.42** are termed BiBLE's (bi-bracchial lariat ethers).

This is sometimes abbreviated to [18]-$O_6$. Similarly, the azacorand compound **3.43** is called $18\langle O_3N_32_6$corand-6$\rangle$. A similar system of nomenclature, also common in the literature, especially for corands containing multiple nitrogen or sulfur donors, considers the corand as a large, substituted cycloalkane, hence the suffix '-ane' is used along with numbers denoting the ring size and donor atoms. Thus, $18\langle N_62_6$corand-6$\rangle$ (**3.44**) is denoted [18]ane-$N_6$ and its sulfur homologue, [18]ane-$S_6$. Other names, often descriptive, are also common in the literature. Compound **3.44** is often called hexacyclen (because of its resemblance to 1,2-diaminoethane, often abbreviated as 'en'). Azacorand analogues of crown ethers such as **3.45**, in which the ether oxygen atoms are replaced entirely by NH functions, were developed separately as ligands for transition metals and thus often have unusual names. Thus corand **3.45** is referred to as cyclam. It could also be referred to as tetraza[14]crown-4 or, more systematically, $14\langle N_42_23_2$corand-4$\rangle$. Similarly, there are trivial names such as sarcophagenes and sepulculrates **3.30**–**3.32**, named by analogy with the cryptands.†

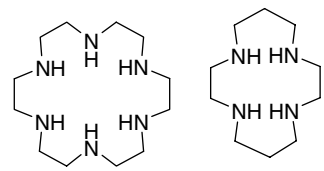

**3.44** **3.45**

† The way in which new nomenclature enters the literature can be somewhat haphazard. The dangerously explosive macrocycle $Se_4N_4$ has been referred to as *phaetodigitogenic*, a term coined by Woolins *et al*., then of Imperial College London, which essentially implies that the compound explosively removes fingers!

The cryptands, which present a more spherical, rather than crown-like structure, have a somewhat different nomenclature. Each host is denoted by a series of numbers indicating the number of donor atoms in each of the bridges between the bridgehead atoms. Thus **3.22** and **3.23** are termed [2.2.2]cryptand and [2.2.1]cryptand, respectively. An enormous variety of cryptands have been synthesised, with bridges originating from carbon as well as nitrogen atoms, bridged by S, N and various other donor atoms and moieties and containing multiple bridges (*e.g.* the 'soccer ball' cryptand, **3.29**). The nomenclature of these species is often highly appealing, although nonrigorous.

All of these ligands have been synthesised with the binding of metal cation guests in mind, and thus the nomenclature must distinguish between the free (uncomplexed) ligand and the metal complex. This is achieved by use of the ending *-and* to mean uncomplexed ligand, and the ending *-ate* for the metal complex. Thus metal complexes of podands are termed *podates*, corand complexes are called *corates*, and cryptand complexes are called *cryptates*. In formula terms, this is sometimes denoted by the mathematical symbol '$\subset$', meaning 'part of the set of'. Thus the corand $18\langle O_6 2_6$corand-6$\rangle$ forms the corate $[K^+ \subset 18\langle O_6 2_6$corand-6$\rangle]$, shown in Figure 3.6.

However, it has been pointed out that this nomenclature, which is in general usage, is misleading since the suffix *-ate* is usually used for anions (*cf.* acetate, sulfate), whereas many of the host–guest complexes referred to are cations. It has been proposed that this should be replaced by the suffix *-plex* to give *coraplex*, *spheraplex etc.*[12] In this book the most commonly used terms will be employed in order to avoid confusion with the literature as far as possible. In most cases, despite the bewildering variety of terms in use, the nomenclature is often highly descriptive, and lends itself readily to educated guesswork on the part of the uninitiated!

## 3.7 Selectivity of Cation Complexation

### 3.7.1 General Considerations

Martell, A. E., Hancock, R. D., Motekaitis, R. J., 'Factors affecting stabilities of chelate, macrocyclic and macrobicyclic complexes in solution,' *Coord. Chem. Rev.* 1994, **133**, 39–65.

The thermodynamic selectivity of a given host for a particular cation represents the ratio between the host's affinity for a given metal (*e.g.* $K^+$) and other guest cations. Strong but selective binding is the basis of molecular recognition. Thus a successful host exhibits a strong affinity for one particular guest and a much lower affinity (as measured by the binding constant, Section 1.4) for other cations. Note that there is an important distinction between the thermodynamic stability of a complex (the *static complex stability*) and kinetic behaviour during the complex formation and decomposition (decomplexation) reactions (*dynamic complex stability*) (Section 3.7.8). Designing a synthetic host that will be highly selective for a given cation is a very complicated task because the selectivity is governed by an enormous number of factors, some of the most important of which are listed below:

- size complementarity between cation and host cavity;
- electronic complementarity between the cation and host binding sites (*cf.* HSAB, Section 3.1.2);
- electrostatic charge;
- solvent (polarity, hydrogen bonding and coordinating ability);
- degree of host preorganisation;
- enthalpic and entropic contributions to the cation–host interaction;

- cation and host free energies of solvation;
- nature of the counter-anion and its interactions with solvent and the cation;
- cation binding kinetics; and
- chelate ring size and donor group orientation.

Amongst these, the size match (*cf.* the selectivity of valinomycin for $K^+$, Section 2.1) is an important and readily envisaged factor, but it is not necessarily dominant. Solvation and preorganisation also play a very important part, as well as effects such as chelate ring size and donor group orientation.[13] In addition care should be taken to compare like with like, thus comparing stabilities of ammine ($NH_3$) complexes with macrocyclic ligands possessing tertiary amine donors is invalid because of the enhanced basicity of tertiary amines compared to ammonia.

## 3.7.2 Conformational Characteristics of Crown Ethers

Wolf, R. E., Hartman, J. A. R., Storey, J. M. E., Foxman, B. M., Cooper, S. R., 'Crown thioether chemistry – structural and conformational studies of Tetrathia-12-Crown-4, Pentathia-15-Crown-5, and Hexathia-18-Crown-6 – implications for ligand design', *J. Am. Chem. Soc.* 1987, **109**, 4328–4335.

Before we consider in detail the binding of metal cations it is worth looking at the conformations and coordination preferences (and hence degree of preorganisation) for crown ether type macrocycles themselves. The O–C–C–O and C–C–O–C bonds around the crown ether typically adopt either *gauche* or *anti* torsional angles to minimise steric interactions in the eclipsed *synperiplanar* and *anticlinal* conformations. In order to form a cyclic molecule a crown-type macrocycle must have eight *gauche* torsion angles (Figure 3.19). If those *gauche* angles occur at O–C–C–O bonds then the oxygen atoms will point into the centre of the ring and hence will be preorganised for metal ion binding. Conversely, if they occur at C–C–O–C bonds then the donor atoms will point out of the ring, reducing the degree of preorganisation. The conformation adopted by [18]crown-6 in the solid state derived by X-ray crystallographic measurements is shown in Figure 3.20. Two of

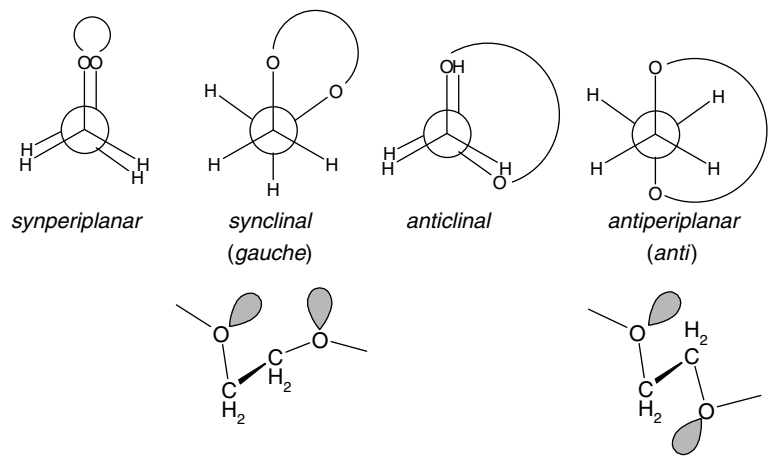


**Figure 3.19** Torsion angles in crown ether complexes.

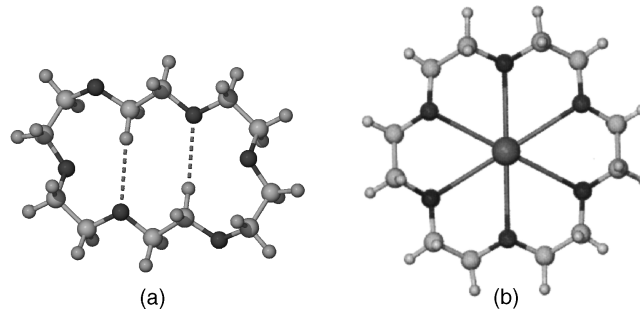


**Figure 3.20** Comparison of the X-ray crystal structures of (a) free [18]crown-6 showing intramolecular CH···O hydrogen bonds with (b) the potassium complex of [18]crown-6.

the oxygen atoms point out of the ring (allowing the formation of a pair of intramolecular CH···O hydrogen bonds) and the remainder are inside, with four *gauche* O–C–C–O angles, generally in the range 65–75º, close to the optimum calculated value of 72º for 1,2-dimethoxyethane. In contrast, it is a general observation that in the sulfur analogues (thiacrowns) the vast majority of the sulfur donors point out of the ring. For [12]ane-$S_4$ and [15]ane-$S_5$ all of the sulfur atoms point out of the ring while for [18]ane-$S_6$ there are two gauche S–C–C–S angles allowing two sulfur atoms to point into the ring (Figure 3.21). Examination of mixed oxygen and sulfur crown ethers shows that there is an overwhelmingly strong affinity for the *gauche* placement of C–S bonds while there is a strong antipathy for *gauche* C–O bonds.

These observations may be explained by examination of 1,4-interactions at these bonds. In the case of *gauche* C–C bonds in fragments of type E–C–C–E (E═N, O, F; Figure 3.22a) there is a weakly attractive 1,4-interaction between the E atoms as a result of dispersion forces (electron attraction to the adjacent nucleus). This is termed the *attractive gauche effect* and contrasts to the case of the thiacrowns where the larger size of the sulfur atoms results in unfavourable electron-electron repulsions (the *repulsive gauche effect*). Turning to *gauche* C–E bonds, the shorter length of the C–O bond means that there are unfavourable steric interactions between the methylene hydrogen atoms (Figure 3.22b). These repulsions are not significant in the case of thiacrowns because of the longer C–S bonds. These two effects at *gauche* C–C and C–E bonds *reinforce* one another and together account for the observed conformation preferences. Thus while many oxygen-donor crown ethers are relatively preorganised and coordinate to a single metal ion, thiacrowns will often form bridged complexes as in the coordination polymer [{CuCl($\mu$-[18]ane-$S_6$)}$_n$], Figure 3.23.

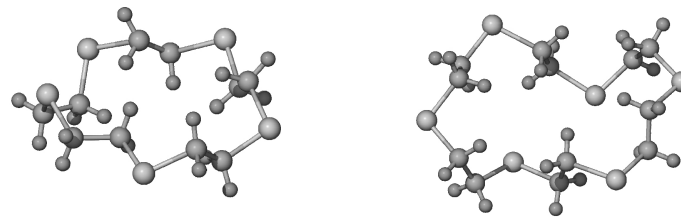


**Figure 3.21** X-ray crystallographically-derived structures of (a) [15]ane-$S_5$ and (b) [18]ane-$S_6$.

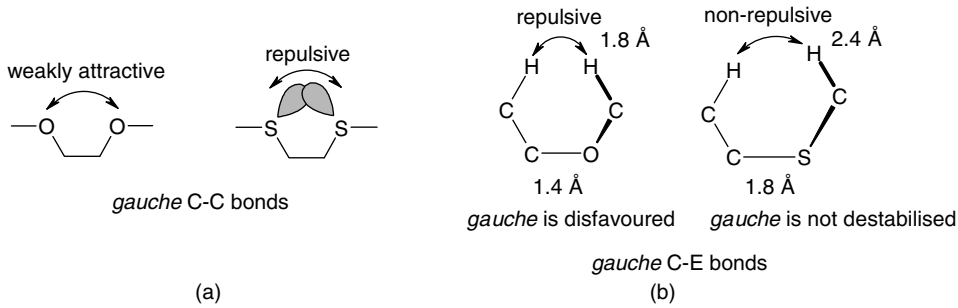


**Figure 3.22** 1,4-interactions in in *gauche* C–C–E–C and E–C–C–E units (E═O, S) in crown ether and thiacrown complexes.[14]

## 3.7.3 Donor Group Orientation and Chelate Ring Size Effects

Hay, B. P., Hancock, R. D., 'The role of donor group orientation as a factor in metal ion recognition by ligands', *Coord. Chem. Rev.* 2001, **212**, 61–78.

A key criterion for a complementary host for metal cations is that the host geometry should allow the metal to bond to all of the donor atoms or groups of the ligand at the optimal metal–ligand distance. Moreover in metal–donor atom bonds that have some degree of covalency there must be the correct alignment of the ligand orbitals (*e.g.* lone pair orbitals) and metal orbitals in order to achieve optimum bond strength. Similarly in ionic metal–ligand bonds the orientation of the ligand dipoles with respect to the metal ion must be in such a way as to result in optimum electrostatic interaction. For $sp^3$ hybridised amine nitrogen donors the strongest interaction with metals occurs when the M–N–X angle has a value of 109.5° and the M–N–C–X torsion angle has a value of ±60 or 180°. This corresponds to the M–N axis being coincident with the orientation of the amine lone pair. Any deviation from this angle weakens the M–N interaction, thus a 10° compression of the M–N–C angle weakens the bonding interaction by *ca.* 2.9 kJ mol$^{-1}$. For ether oxygen atoms the optimum interaction occurs when the metal ion aligns with the ether dipole yielding a trigonal planar oxygen. The M–O–C angles are 123.5° with the metal ion laying in the plane of the C–O–C moiety. This means that M–O–C–X torsion angles are optimal at 0 and ±120°. The interaction becomes weaker as the deviation from this orientation increases, thus a 30° displacement of $Na^+$ from the C–O–C plane results in a loss in energy of *ca.* 4 kJ mol$^{-1}$, Figure 3.24. This result will come as a surprise to anyone

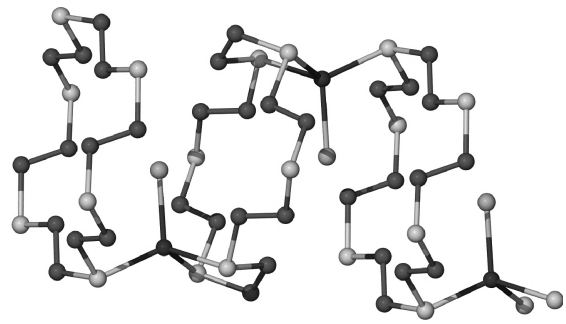

**Figure 3.23** X-ray crystal structure of [{CuCl($\mu$-[18]ane-$S_6$)}$_n$]}, a coordination polymer in which two different [18]ane-$S_6$ conformers, one bis(bidentate) and one bis(monodentate) bridge Cu(I) centres (H atoms omitted for clarity).

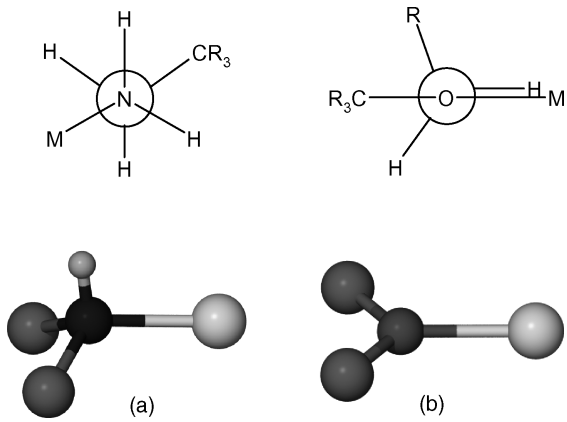


**Figure 3.24** Optimal amine and ether donor group orientations. Note that metal-ether interactions are optimal with a planar $C_2$–O–M unit.

familiar with the structures of crown ether complexes since distortions are common with the $C_2$–O–M unit being frequently pyramidal rather than planar. This kind of distortion arises because of strain induced by the crown ethers' cyclic structure and is atypical of ether ligands generally.

When multiple donor groups are included within a ligand framework then the constraints of the ligand backbone can result in an inability of all of the donor groups to simultaneously form optimal interactions with a metal centre. We can represent the donor group orientations as lines drawn along the vectors of optimal metal ion approach. In a perfectly preorganised ligand these vectors will overlap at a single point at the optimal M–L bond length. The more widely the vectors diverge from this situation the less preorganised the ligand will be. Some examples of the optimal donor group orientation for ethylene diamine, propylene diamine and dimethoxy ethane are shown in Figure 3.25, while Figure 3.26 shows the donor group orientations in the macrocycles [14]ane-$N_4$ (cyclam) and [18]crown-6 in its $D_{3d}$ conformation before and after $Ni^{2+}$ and $K^+$ binding, respectively. In each case, there is some degree of induced fit as the molecule adjusts itself to the demands of the metal guest. This process results in more favourable M–L interactions at the expense of increased strain in the macrocycle itself. Figure 3.26b in particular shows

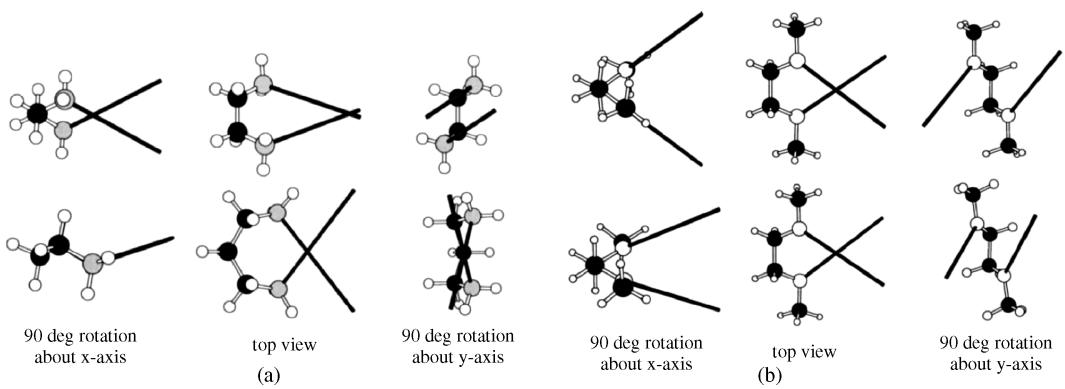


**Figure 3.25** (a) Three views of ethylene diamine (top) and 1,3-propylene diamine (bottom) and (b) Three views of 1,2-dimethoxyethane (dme) before (top) and after (bottom) $Na^+$ complexation. The 5 Å long, vector attached to each oxygen illustrates the optimal line of approach for the metal ion (reproduced from [13] with permission from Elsevier).

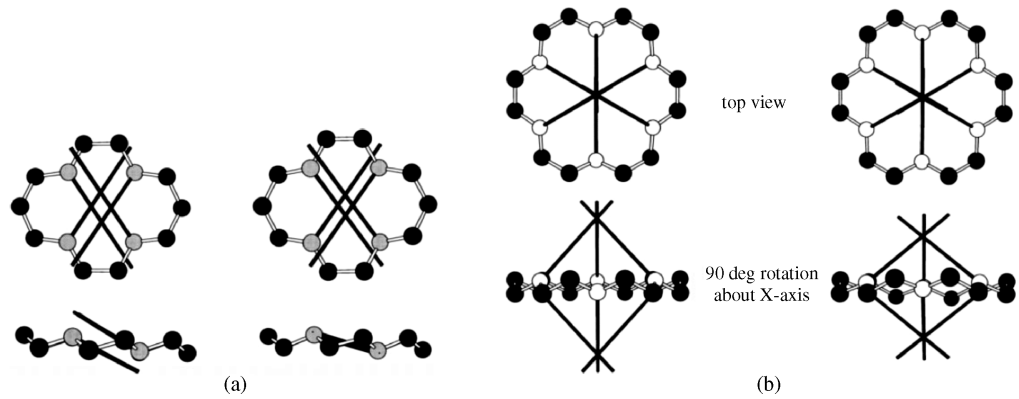


**Figure 3.26** (a) Donor group orientation vectors in the ++−− conformer of [14]ane-$N_4$ before (left) and after (right) coordination to Ni(II) and (b) donor group orientation vectors in the $D_{3d}$ conformer of 18-crown-6 before (left) and after (right) $K^+$ coordination (reproduced from [13] with permission from Elsevier).

just how far out of the crown ether plane the donor group vectors converge (far from the optimal $K^+$–O distance). Of course these pictures of donor group orientation rely on static models or crystallographic structural data and we must remember that in reality macrocycles such as cyclam and [18]crown-6 possess a considerable degree of flexibility and are highly mobile in solution. One interesting point to note about Figure 3.25 is the difference between ethylene diamine (which forms 5-membered chelate rings with metals) and propylene diamine (which forms 6-membered rings). In the case of the 5-membered chelate ring (top) the optimal line of metal ion approach vectors cross at a much longer M–L bond length than in the 6-membered ring analogue. It transpires that this is a general result and hence ligands that form *five* membered chelate rings form stronger interactions with larger metal ions, *i.e.* those that form long M–L bonds, while six-membered rings favour smaller metal ions. Size mismatches lead to increases in the strain energy of the chelate ring, estimated by molecular mechanics calculations to be up to *ca.* 25 kJ $mol^{-1}$ thus a rule of host ligand design is that '*the complexes of large metal ions are destabilised more than those of small metal ions by an increase in chelate ring size from five to six membered*'. We can see this effect in the binding of the large Pb(II) by tetraazamacrocycles of varying ring size. Aqueous binding constants for Pb(II) binding by [*n*]ane-$N_4$ ($n$ = 12 – 16) are log $K_{11}$ = 16.0, 13.6, 10.8, 10.2 and 9.6, respectively. It seems counter-intuitive that the affinity for a large metal ion *decreases* as the ring size goes up but every addition of another $-CH_2-$ group converts a 5-membered chelate ring in the complex into a less stable, more strained six-membered ring, Figure 3.27.

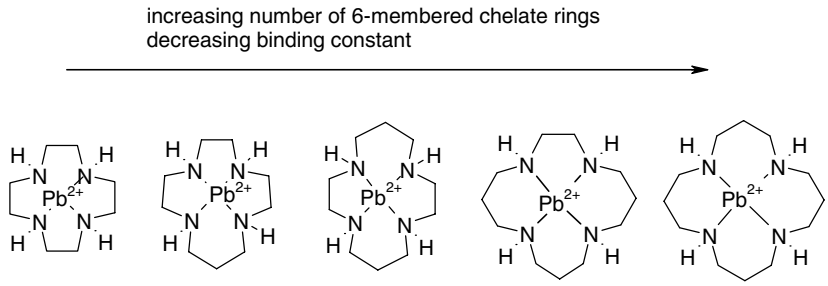


**Figure 3.27** Binding constants for the large metal ion Pb(II) decrease by over six orders of magnitude as the ring size increases in tetraazamacrocycles as a result of the conversion of 5-membered chelate rings (suitable for large metal ions) into six-membered chelate rings (suitable for small metal ions).

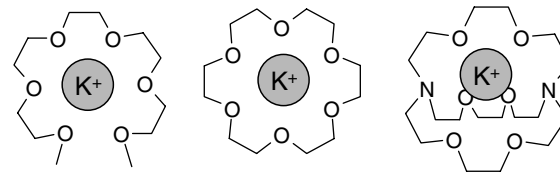


| | [K⁺-**3.11**] | [K⁺-**3.6**] | [K⁺-**3.23**] |
|---|---|---|---|
| log *K* (MeOH, 25 °C) | 2.0 | 6.1 | 10.0 |

**Figure 3.28** Stabilities of podand (acyclic), crown ether (macrocyclic) and cryptand (macrobicyclic) complexes of $K^+$.

## 3.7.4 Cation Binding by Crown Ethers

The interaction of $K^+$ with a weak, monodentate base such as dimethyl ether (as measured by its binding constant) is almost negligible. We have seen, however, that etheric macrocycles display significant affinity for alkali metal cations. The origins of this difference in behaviour may be traced to the chelate and macrocyclic preorganisation effect commonly observed in coordination chemistry (Section 1.6). The fact that all six donor atoms are joined together in a ligand such as [18]crown-6 greatly contributes to the stability of $[K([18]crown\text{-}6)]^+$ in comparison to $[K(OMe_2)_6]^+$ on enthalpic, entropic and statistical grounds. The macrocyclic effect is very apparent in these systems. Compare the stability of $[K([18]crown\text{-}6)]^+$ and [K(**3.11**)]$^+$ (Figure 3.28). Both of these species benefit from chelate stabilisation but the macrocyclic species is still some $10^4$ times more stable in methanol solution. This extra stabilisation is a consequence of macrocyclic preorganisation. The [2.2.2]cryptand complex is still more stable, as a consequence of macrobicyclic preorganisation.

For an explanation of these preorganisation effects, we must break down the enthalpic and entropic contributions to the stability of complexes such as [$K^+ \subset$ **3.11**] and [$K^+ \subset$ **3.6**]. At 298 K, we find the parameters given in Table 3.4. From these data, it is clear that both enthalpic and entropic contributions favour the stability of the macrocyclic complex. In this case the dominant effect is the enthalpy, although this is not true in every system.

For highly flexible macrocycles, such as the crown ethers, the variation of binding constant for a given macrocycle going down the group I cations often exhibits *plateau selectivity*. By this we mean that the binding constants do not exhibit a smooth rising and falling trend across a series of guests, such as the alkali metal cations, but have a similar affinity for several metal ions. For example, the binding constants may be similar for smaller metal cations and decrease as the cation radius increases, resulting in poor discrimination between $Na^+$ and $K^+$. Alternatively, binding constants may increase with cation radius to give a plateau at $Rb^+$ and $Cs^+$. This may be attributed to the two-dimensional nature of the complexation that enables the crown ligands to accommodate a wide variety of metal cations, irrespective to some extent of ionic radius. So how important is the match of cation radius

**Table 3.4** Thermodynamic contributions to the stabilities of podate and crown ether complexes of $K^+$.

| Complex | $\Delta G^o$(J mol$^{-1}$) | $\Delta H^o$(J mol$^{-1}$) | $\Delta S^o$(J K$^{-1}$ mol$^{-1}$) |
|---|---|---|---|
| [$K^+ \subset$ **3.11**] | −11 368 | −36 400 | −84 |
| [$K^+ \subset$ **3.6**] | −34 842 | −56 000 | −71 |

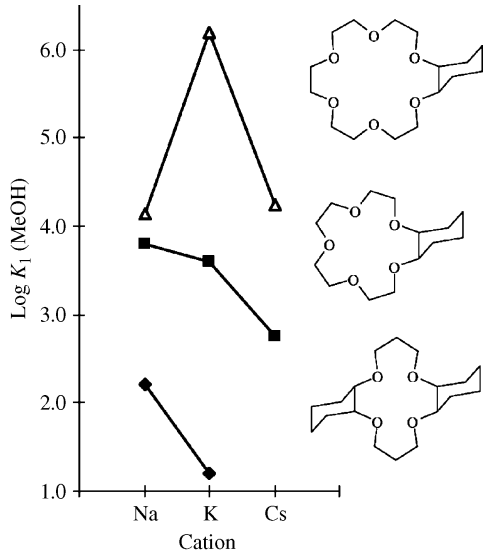


**Figure 3.29** Variation of binding constant as a function cation radius for cyclohexyl crown ethers.

with host cavity radius in simple ligands such as the crown ethers? Figure 3.29 and Figure 3.30 show the variation of binding constant with cation diameter for crown ethers of different ring size; Table 3.5 compares metal ionic radius with crown cavity size as estimated from examination of CPK molecular models. Additional metal cations are included for comparison.

Figure 3.30 shows evidence of plateau selectivity by the larger crown ethers because of their highly flexible nature. Also, it is clear the $K^+$ is bound much more strongly than the other cations by 18-membered macrocycles, as expected from cavity size fit arguments. A number of other features of Figure 3.29 and Figure 3.30 are less readily explained. In fact, [18]crown-6 and its derivatives bind all of the cations more strongly than the other hosts. Moreover, $K^+$ is the most strongly bound of all of the metal cations. Within

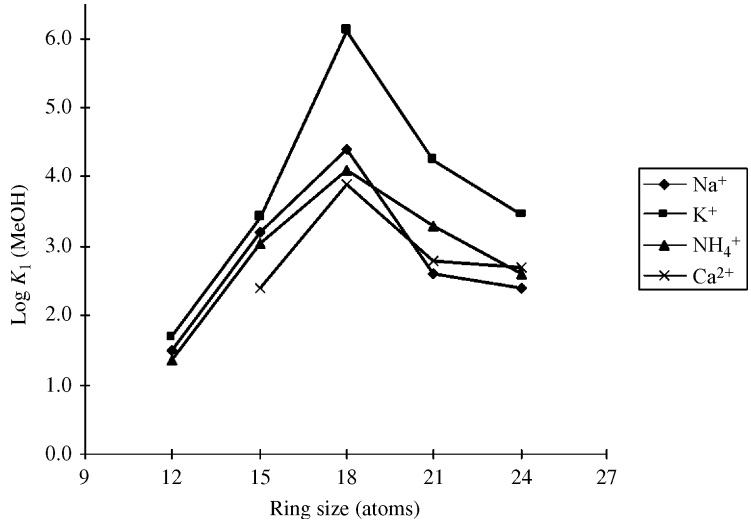


**Figure 3.30** Variation of binding constant as a function of crown ring size for various cations.

**Table 3.5** Comparison of the diameters of different crown ethers with the ionic diameter of various metal cations.

| Cation | Diameter (Å)[a] | Crown ether | Cavity diameter (Å) |
|---|---|---|---|
| $Li^+$ | 1.36 | [12]crown-4 | 1.20–1.50 |
| $Na^+$ | 1.90 | [15]crown-5 | 1.70–2.20 |
| $K^+$ | 2.66 | [18]crown-6 | 2.60–3.20 |
| $Cs^+$ | 3.38 | [21]crown-7 | 3.40–4.30 |
| $Cu^+$ | 1.92 | | |
| $Ag^+$ | 2.52 | | |
| $Mg^{2+}$ | 1.44 | | |
| $Ca^{2+}$ | 2.20 | | |
| $La^{3+}$ | 2.34 | | |
| $Lu^{3+}$ | 2.00 | | |
| $Zr^{4+}$ | 1.72 | | |

[a]Assuming most common coordination number.

this limited data set, it would seem that, rather than a size-based selectivity trend, we are seeing two much more general principles:

1. All crown ethers are selective for $K^+$.
2. [18]crown-6 and its derivatives are selective for all cations!

If this were true of all supramolecular systems, the prospects for designed selectivity would be bleak indeed. In order to explain these phenomena, we must look at the interplay of all of the factors listed at the beginning of this section. In this case the most relevant are:

- *Size match between host cavity and guest cation*. In fact, the flexible [18]crown-6 is a reasonably good size match for all of the alkali metal cations, although it is optimum for $K^+$.
- *Number of donor atoms*. In general, supramolecular interactions are additive, hence we would expect the larger crown ethers to bind more strongly to metal cations as long as all of the donor atoms can fit around the metal. This contributes to the plateau selectivity seen for most cations on the right-hand side of Figure 3.20.
- *Solvation of cation and ligand*. The solvation free energy increases in the order $K^+ < Na^+ < Ca^{2+}$, hence less energy is required to (partially) desolvate $K^+$ in order to bind it.
- *Chelate ring size (ligand bite angle)*. In the complexed species for hosts with ethenyl (two-carbon) bridges, five-membered chelate rings are formed (Figure 3.31a). The small bite angle of the

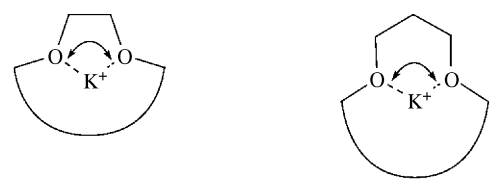


(a) Five-membered chelate ring, bite angle about 60º

(b) Six-membered chelate ring, bite angle about 60º

**Figure 3.31** Ligand bite angles for (a) two-carbon and (b) three-carbon linked crown ethers.

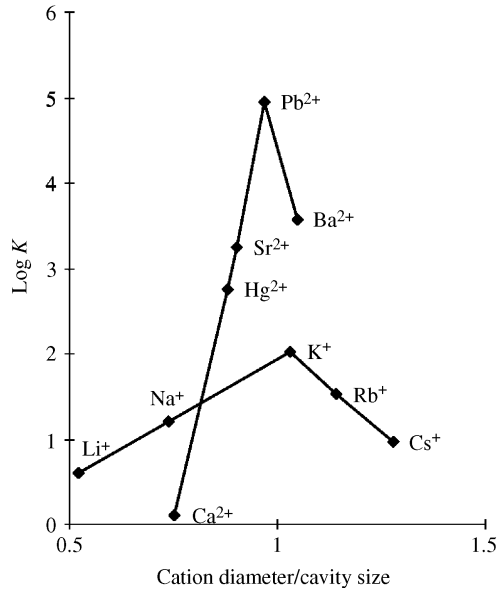


**Figure 3.32** Relationship between binding constants (log *K*) and cation size for mono- and divalent metal complexes of *cis-syn-cis*-dicyclohexyl[18]crown-6 (water, 25 ºC).

ethylenedioxy unit is suitable for larger cations such as $K^+$. Smaller metals, particularly $Li^+$, are less suited to spanning the distance between one donor atom and the next, and hence do not complex as strongly. This is evident in the greater affinity of dicyclohexyl[14]crown-4 for $Na^+$ (Figure 3.29) (*cf.* [12]crown-4, Figure 3.20, and Section 3.7.3).

Another important consideration not addressed in Figure 3.30 is the effect of cation charge. Clearly $Ca^{2+}$ is bound only weakly by a large variety of crown ethers. However, this has much to do with its small size and large hydration energy. The much larger $Ba^{2+}$ exhibits a log *K* value of 7.0 for complexation by [18]crown-6 in methanol (*cf.* 6.10 for $K^+$). A comparison of mono- and divalent cation association constants for *cis-syn-cis*-dicyclohexyl[18]crown-6 is shown in Figure 3.32, which suggests that for well-matched cations and cavities, in the absence of large hydration effects, the formal positive charge on the cation is a dominant factor.

Larger crown ethers exhibit selectivity for $Rb^+$ and $Cs^+$. Crown ethers based on tribenzo[21]crown-7 are slightly selective for $Rb^+$ as measured by the water/chloroform distribution coefficients of their nitrate salts (Figure 3.33). The $Rb^+$ selectivity is attributed to the ligand's conformational preferences. Examination of M—O bond lengths for the $Na^+$, $Rb^+$ and $Cs^+$ complexes shows that in the case of $Rb^+$ a heptadentate conformation is achieved relatively easily with Rb—O distances covering a narrow range (2.98–3.09 Å), whereas in the $Na^+$ case a broader range is encountered (2.43–2.63 Å), suggesting steric strain in adapting the large crown to the small cation.

Surprisingly, on moving to very large crown ethers such as dibenzo[24]crown-8 (**3.46**) and dibenzo[30]crown-10 (**3.47**), we again see good selectivity for $K^+$, which actually increases with increasing macrocycle size. Log $K_{11}$ (methanol, 25ºC) for dibenzo[24]crown-8 is 3.49, and for dibenzo[30]crown-10 is 4.60. This is a result of the ability of the large, flexible crown ether to 'wrap' around the metal cation, effectively enclosing it almost entirely within an organic sheath

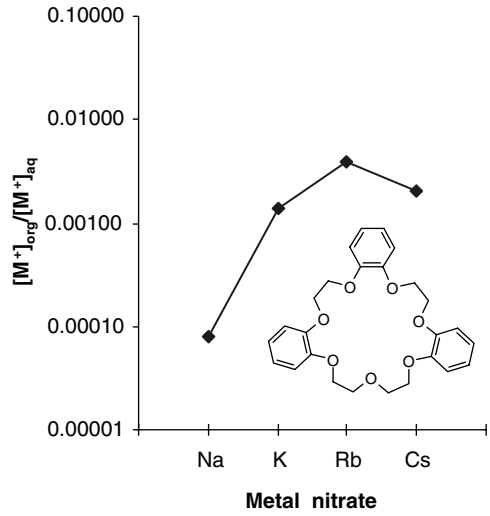


**Figure 3.33** Competitive extraction of alkali metal nitrates by tribenzo[21]crown-7.

(*cf.* valinomycin, Section 2.2). The X-ray crystal structure of $[K([30]crown\text{-}10)]^+$ is shown in Figure 3.34. Indeed, even the enormous dibenzo[60]crown-20 is fully able to bind effectively to $K^+$, with a binding constant (log $K_{11}$) of 3.90. For small cations such as $Na^+$, the binding constant with dibenzo[30]crown-10 is much smaller (log $K_{11} = 2.0$): the macrocycle is simply too large to effectively encapsulate $Na^+$. Interestingly, however, a 2:1 complex is also formed in which two $Na^+$ ions reside in the cavity in a deep nesting fashion reminiscent of 1:1 complexes with smaller crown ethers.

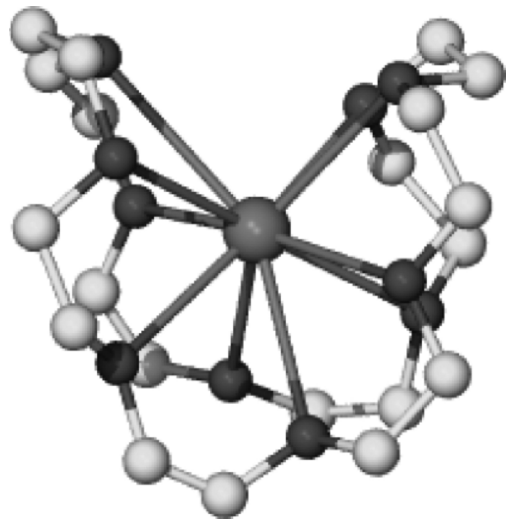

**Figure 3.34** Structure of $[K([30]crown\text{-}10)]^+$ showing the ability of the macrocycle to adopt a wrapping conformation to encapsulate the metal cation.

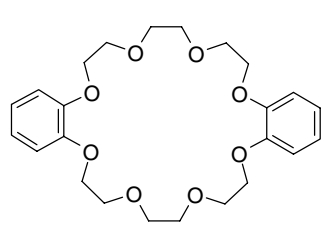

3.46

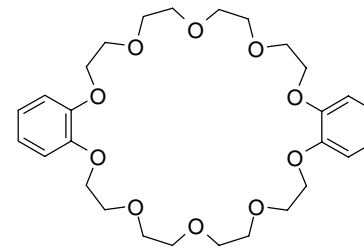

3.47

## 3.7.5 Cation Binding by Lariat Ethers

The lariat ethers consist simply of a crown ether type ring with a pivoting, podand side arm designed to bring some three-dimensionality to cation complexation, while still retaining the fast kinetics expected for highly flexible corand systems (Section 3.3.2). They thus combine characteristics of podands, corands and cryptands. Representative binding constants for N-pivot polyether side-arm lariat ethers of various side-arm chain length are shown in Table 3.6. The N-pivot macrocycles tend to be more able to direct their side arm towards the guest since the pivot atom is directed towards the metal cation, and as a result side-arm binding is more pronounced in these systems than in their

**Table 3.6** Binding constants (log $K_{11}$) for lariat ethers in methanol at 25 °C.

| | Log $K_{11}$ | | | |
|---|---|---|---|---|
| Host | $Na^+$ | $K^+$ | $NH_4^+$ | $Ca^{2+}$ |
| 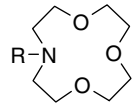 3.48 | | | | |
| R = $CH_2CH_2OMe$ | 3.25 | 2.73 | 3.06 | – |
| R = $(CH_2CH_2O)_2Me$ | 3.60 | – | | – |
| R = $(CH_2CH_2O)_3Me$ | 3.64 | 3.85 | 3.29 | – |
| R = $(CH_2CH_2O)_4Me$ | 3.76 | – | | – |
| R = $(CH_2CH_2O)_5Me$ | 3.73 | 4.34 | 3.49 | – |
| 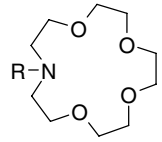 3.49 | | | | |
| R = H | 1.70 | 1.60 | 2.99 | – |
| R = $CH_2CH_2OMe$ | 3.88 | 3.95 | 3.14 | 3.75 |
| R = $(CH_2CH_2O)_2Me$ | 4.54 | 4.68 | 3.19 | 4.06 |
| R = $(CH_2CH_2O)_3Me$ | 4.32 | 4.91 | 3.38 | 3.84 |
| R = $(CH_2CH_2O)_4Me$ | 4.15 | 5.28 | 3.48 | 3.78 |
| R = $(CH_2CH_2O)_5Me$ | 4.19 | 4.91 | 3.49 | 3.80 |

**Table 3.6** (*Continued*)

| Host | Log $K_{11}$ | | | |
|---|---|---|---|---|
| | $Na^+$ | $K^+$ | $NH_4^+$ | $Ca^{2+}$ |
| 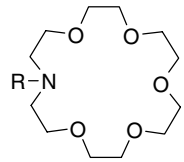 **3.50** | | | | |
| R = H | 2.69 | 3.98 | – | 3.96 |
| R = $CH_2CH_2OMe$ | 4.58 | 5.67 | 4.21 | 4.34 |
| R = $(CH_2CH_2O)_2Me$ | 4.33 | 6.07 | 4.75 | 4.23 |
| R = $(CH_2CH_2O)_3Me$ | 4.28 | 5.81 | 4.56 | 4.11 |
| R = $(CH_2CH_2O)_4Me$ | 4.27 | 5.86 | 4.40 | 4.13 |
| R = $(CH_2CH_2O)_5Me$ | 4.22 | – | 4.04 | 4.11 |
| 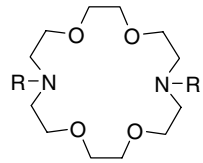 **3.51** | | | | |
| R = H | 1.5 | 1.8 | – | – |
| R = $CH_2CH_2OMe$ | 4.75 | 5.46 | – | 4.48 |
| R = $CH_2CO_2Et$ | 5.51 | 5.78 | – | 6.78 |

C-pivot analogues. Table 3.6 shows that in all cases the lariat ether effect (stability enhancement by binding by both side arm and ring) is obvious in comparison to cases where R = H. This is particularly striking in the case of the BiBLE ligands of type **3.51**, in which even for the monoether chains (R = $CH_2CH_2OMe$) the binding constant for $K^+$ is about $10^4$ times the corand analogue. The trend of increasing side-arm chain length results in a very slight enhancement of $Na^+$ binding for small ring compounds of type **3.48**. The same is true of the [15]crown-5 derivatives up to two side-arm donor atoms but affinity is then constant at log $K_{11}$ = *ca.* 4.2 for side chains with up to five donor atoms. The trend may also be observed for $K^+$ complexes of types **3.49** and **3.50** where $K^+$ binding reaches a maximum at log $K_{11}$ = *ca.* 6 for eight donor atoms (corand + side chain), the inference being that further donor atoms are 'noneffective' donors, *i.e.* not sterically able to coordinate to the metal cation. Just as with metals, the ammonium cation may also bind to crown ether type ligands, binding proceeding *via* N—$H^+$ ⋯ O hydrogen bonds (Section 3.12). In the case of the lariat ethers, the results for $NH_4^+$ binding are striking since they seem to be almost constant for all receptors of types **3.48** and **3.49** but suddenly increase by an order of magnitude for **3.50** type hosts. This may be explained with the aid of molecular models, which predict that the mode of $NH_4^+$ binding is a tripodal mode of hydrogen bonding of three of the hydrogen atoms with two donor atoms of the corand ring and one from the side arm. It is only sterically feasible for the fourth NH hydrogen atom to hydrogen bond in the [18]crown-6 derivatives, thus enhancing the binding (Figure 3.35).

Thermodynamic parameters derived from calorimetry for metal ion binding by a range of aza-oxa lariat ethers and BiBLE's with amide side-arms (**3.52** and **3.53**) is shown in Table 3.7. Coordination occurs *via* the macrocycle and amide oxygen atom. The longer chain side arms **3.52b** and **3.53b** are

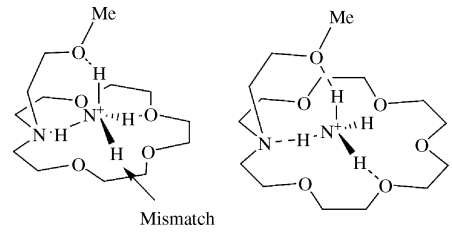


**Figure 3.35** Steric constraints on $NH_4^+$ hydrogen bonding interactions with lariat ethers.

more flexible than **3.52a** and **3.53a**. The ligands are relatively preorganised in comparison to larger, all-oxygen crown ethers, with all donor atoms pointing into the macrocycle cavity. Of particular interest is the complexation entropy, $\Delta S$. There is a significant favourable (positive $T\Delta S$) contribution in each case from the change in translational entropy of liberated solvent molecules, particularly for highly solvated cations such as $Li^+$. The entropic contributions are markedly less favourable for the more flexible **3.53b** compared to **3.53a** as a result of loss of ligand flexibility. Interestingly the binding constant data reveal a distinct lack of selectivity across the metal ions listed; however, this masks significant compensating enthalpy and entropy effects. Binding of cations that are too large or too small for the cavity may result in significant conformational changes. In general, however, significant affinity for the small $Li^+$ and $Ca^{2+}$ is observed, consistent with the formation of six-membered rings and the higher charge in the case of $Ca^{2+}$.[15]

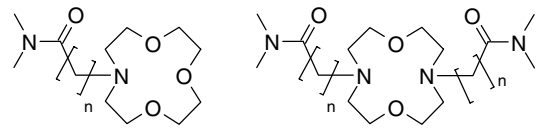

**3.52a** n = 1
**3.52b** n = 2

**3.53a** n = 1
**3.53b** n = 2

## 3.7.6 Cation Binding by Cryptands

In contrast to the crown ethers, the three-dimensional cryptands display *peak selectivity*. The macrobicyclic cavities are more rigid and restricted so that they are unable to constrict sufficiently

**Table 3.7** Thermodynamic data for amide lariat ethers (methanol, 25 °C).[15]

| Ligand | | $Li^+$ | $Na^+$ | $K^+$ | $Rb^+$ | $Ca^{2+}$ | $Sr^{2+}$ | $Ba^{2+}$ |
|---|---|---|---|---|---|---|---|---|
| **3.52a** | Log *K* | 2.71 | – | – | – | 2.72 | – | – |
| | $-\Delta H$ | 3.00 | 20.80 | 13.10 | – | 6.80 | 11.90 | 19.10 |
| | $T\Delta S$ | 12.40 | – | – | 8.70 | – | – | – |
| **3.53a** | Log *K* | 5.38 | 4.72 | 3.85 | 3.08 | > 5.5 | > 5 | 4.94 |
| | $-\Delta H$ | 12.70 | 26.00 | 25.70 | 22.70 | 46.60 | 35.80 | 33.0 |
| | $T\Delta S$ | 17.90 | 0.80 | –3.80 | –5.20 | – | – | –4.90 |
| **3.53b** | Log *K* | 2.99 | 3.01 | 3.03 | 3.08 | 4.10 | 4.36 | 3.30 |
| | $-\Delta H$ | 23.80 | 37.60 | 30.60 | 11.00 | 45.90 | 19.90 | 44.50 |
| | $T\Delta S$ | −6.80 | −20.50 | −13.40 | 6.50 | −22.60 | −4.90 | −25.70 |

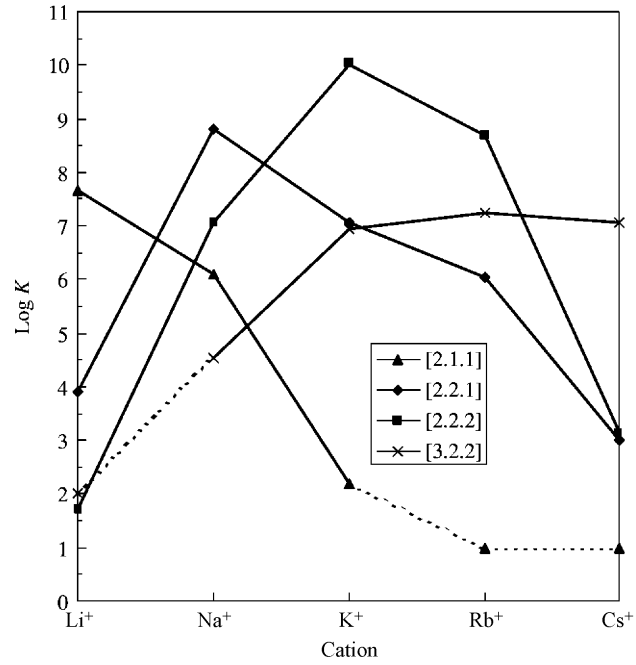


**Figure 3.36** Binding constants for various cryptands with alkali metal cations in methanol (dotted lines are estimates).

to bind cations that are too small for the cavity; nor can they expand to accommodate cations with radii much greater than the optimum size fit. Furthermore, the three-dimensional cryptand cavity is much more preorganised for cation binding, meaning that there is less entropically, and often enthalpically, unfavourable conformational rearrangement that must take place in order to adopt the optimum complex geometry. Thus the binding constant for [2.2.2]cryptand is at a maximum for $K^+$ salts in methanol (log $K_{11}$ = 10.5), whereas the smaller [2.2.1]cryptand is selective for $Na^+$ (log $K_{11}$ = 9), and [2.1.1]cryptand for $Li^+$ (log $K_{11}$ = 8.05). For [2.2.2]cryptand the $K^+/Na^+$ selectivity is about $10^3$, whereas for [18]crown-6 under the same conditions the discrimination is less than $10^2$ (Figure 3.36).

A striking illustration of the rigidifying, preorganising effects of the three-dimensional cavity of the cryptands may be seen in the data given in Figure 3.37. Clearly, even though the size match is

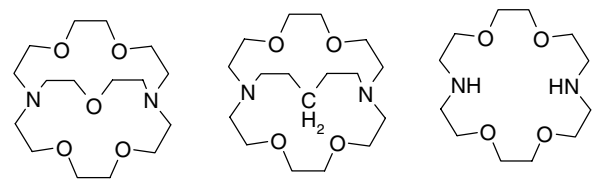


| | **3.22** | **3.54** | **3.18** |
|---|---|---|---|
| Log $K_{11}$ ($K^+$) | 7.0 | 5.4 | 2.0 |

**Figure 3.37** Comparison of the $K^+$ binding constant for cryptand and corand hosts (MeOH, 25ºC).

not perfect, the three-dimensional cavity and seven donor atoms of [2.2.1]cryptand gives very strong $K^+$ binding, some five orders of magnitude larger than its diaza[18]crown-6 analogue (**3.18**), which has only six binding sites and a two-dimensional cavity. Notably, however, the hydrocarbon-bridged cryptand **3.54**, which also has six identical donor atoms to **3.18** binds $K^+$ more than $10^3$ times more strongly, despite the fact that the lipophilic bridge might be expected to cause repulsive interactions with the strongly hydrophilic cation. Clearly, the preorganisation of the three-dimensional host is the dominant factor. Preorganisation as a key factor in host guest affinity is discussed more fully in the next section.

Examination of the cryptates of the alkaline earth metal cations shows similar trends to those observed for the crown ethers. The small [2.1.1]cryptand is ineffective at binding any of the divalent ions $Mg^{2+}$–$Ba^{2+}$ (log $K_{11}$ in water is about 2.5 for $Mg^{2+}$, dropping to $<2$ for $Ba^{2+}$). Increasing the cavity size to [2.2.1]cryptand results in a peak selectivity at $Sr^{2+}$, although the log $K_{11}$ value of 7.35 is only marginally larger than the stabilities of the $Ca^{2+}$ and $Ba^{2+}$ complexes. $Mg^{2+}$ is hardly bound at all in aqueous solution, because of its particularly large hydration energy. [2.2.2]Cryptand is an extremely effective ligand for $Ba^{2+}$ and a comparison of the $Ba^{2+}$ log binding constant of 9.5 with that for $K^+$ in water (log $K_{11} = 5.4$) shows clearly the effect of the dipositive charge of the alkaline earth metal. Strontium is bound significantly more weakly (log $K_{11} = 8.0$) and the stability continues to fall with values of 4.4 and $<2$ observed for $Ca^{2+}$ and $Mg^{2+}$ respectively.

## 3.7.7 Preorganisation: Thermodynamic Effects

Cram, D. J., 'Preorganisation - from solvents to spherands,' *Angew. Chem., Int. Ed. Engl.* 1986, **25**, 1039–1134.

Table 3.8 gives a summary of binding free energies of alkali metal picrates with a variety of different hosts. As may be seen from this small sample of binding data, the families of compounds generally fall into the following order when arranged according to the $-\Delta G^o$ with which they bind their most complementary guests: spherands > cryptaspherands > cryptands > hemispherands > corands > podands > solvents. The difference in the $-\Delta G^o$ values for $Li^+$ binding by spherand **3.33** and podand **3.36** of 17 kcal $mol^{-1}$ (71 kJ $mol^{-1}$) corresponds to a difference in binding constant, $K$, of more than 12 log units. Also, as the order is descended, peak selectivity gives way to plateau selectivity until, for podand **3.36**, no selectivity is observed at all. The binding free energies shown in Table 3.8 are influenced significantly by the number and nature of the donor atoms, ranging from six in spherand **3.33** to nine in **3.38**. The stability might be expected to increase with number of binding sites in an additive fashion as the energy of each coordination interaction contributes to the binding. However, the trend is clearly dominated by the degree of preorganisation.

A comparison of the X-ray crystal structures of spherand **3.33** and its highly stable spheraplex **3.33**·$Li^+$ reveals that in both instances the host has the same conformation (Figure 3.38). Host **3.33** is entirely preorganised for metal binding and no enthalpically unfavourable conformational change is required upon complexation. Furthermore, the six anisole oxygen atoms are, in the free host, buried deeply within an unsolvated pocket formed by the hydrophobic host backbone. There is thus no desolvation step associated with these donor atoms when the metal cation is complexed.

Compare the preorganisation shown in Figure 3.39 with the free and complexed forms of [18]crown-6, Figure 3.20. Clearly the crown ether must undergo considerable rearrangement (and desolvation in solution) in order to bind the host cation. Similar rearrangements are needed for [2.2.2]cryptand (Figure 3.39), whereas the anisyl residues of the cryptaspherands are partially preorganised, although the cavity is filled by the methylene groups of the cryptand portion of the molecule.

**Table 3.8** Binding free energies (kcal mol$^{-1}$; 1 kcal = 4.184 kJ) for alkali metal picrates under standard conditions. The values of the metal ions most complementary to each host are highlighted in bold.

| | | $-\Delta G°$ (kcal mol$^{-1}$) | | | | |
|---|---|---|---|---|---|---|
| Host | Family | $Li^+$ | $Na^+$ | $K^+$ | $Rb^+$ | $Cs^+$ |
| 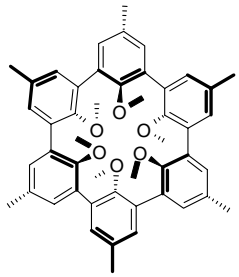 | Spherand (**3.33**) | >**23** | 19.2 | ⋘6 | – | – |
| 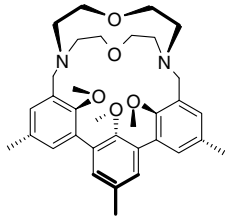 | Cryptaspherand (**3.55**) | 18.8 | **20.6** | 15.0 | 13.3 | 10.4 |
| 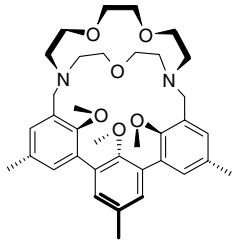 | Cryptaspherand (**3.56**) | 13.4 | **21.0** | >19.9 | 20.4 | 16.4 |
| 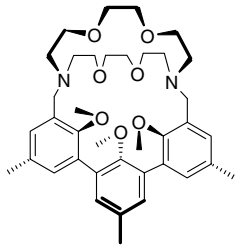 | Cryptaspherand (**3.38**) | 9.9 | 13.5 | 19.0 | 20.3 | **21.7** |
| 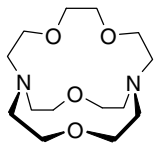 | Cryptand (**3.57**) | **16.6** | – | – | – | – |
| 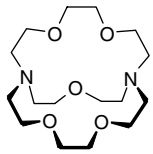 | Cryptand (**3.22**) | 10.0 | **17.7** | 15.3 | 12.7 | – |

(*continued*)

**Table 3.8** (*Continued*)

| Host | Family | $-\Delta G°$ (kcal mol$^{-1}$) | | | | |
|---|---|---|---|---|---|---|
| | | $Li^+$ | $Na^+$ | $K^+$ | $Rb^+$ | $Cs^+$ |
| 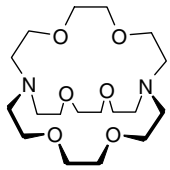 | Cryptand (**3.23**) | – | 14.4 | **18.0** | 16.8 | 10.3 |
| 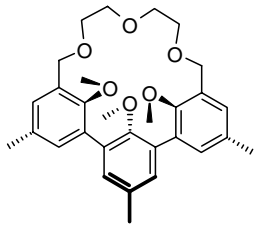 | Hemispherand (**3.37**) | 7.0 | **12.2** | 11.9 | 10.4 | 9.0 |
| 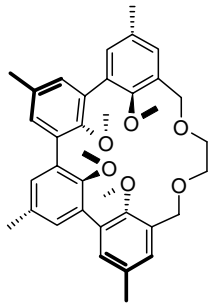 | Hemispherand (**3.58**) | 7.2 | **13.5** | 10.7 | 8.4 | 7.1 |
| 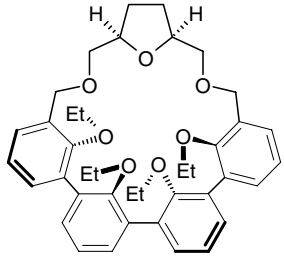 | Hemispherand (**3.39**) | 6.5 | 7.1 | **11.6** | 11.4 | 10.8 |
| 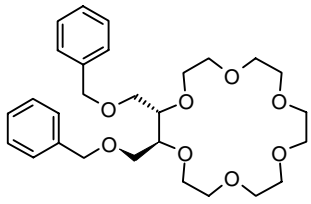 | Corand (lariat ether) (**3.59**) | 6.3 | 8.4 | **11.4** | 9.9 | 8.5 |
| 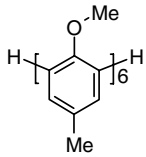 | Podand (**3.36**) | <6 | <6 | <6 | <6 | <6 |

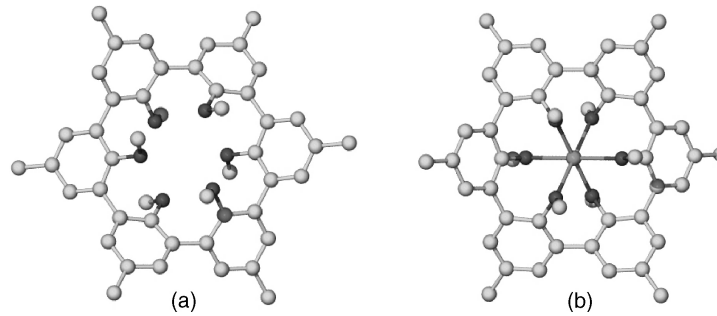


**Figure 3.38** Comparison of the X-ray molecular structures of (a) the free spherand **3.33** and (b) its $Li^+$ spheraplex.[16]

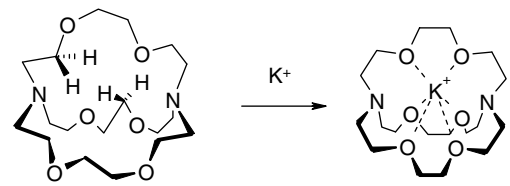


**Figure 3.39** Conformational rearrangement of [2.2.2]cryptand upon binding to $K^+$.

The entropically, and often enthalpically, unfavourable degree of host rearrangement is even more pronounced in podand hosts such as **3.33** and *Kryptofix-5* **3.60**, which adopt extended conformations in the free state. The degree to which **3.60** has to rearrange in order to wrap itself about a $Rb^+$ cation is evident from the X-ray crystal structure of the $Rb^+$ podaplex (Figure 3.40).

## 3.7.8 Preorganisation: Kinetic and Dynamic Effects

The enhanced stability of complexes for which the host is already preorganised for binding bears some conceptual resemblance to transition state theory in organic chemistry, which states that the more closely a reactant resembles the transition state for a reaction, the faster that reaction will proceed as a consequence of the reduced activation energy needed to go from reactant to reactive transition state. The distinction is that so far, we have discussed preorganisation in the context of the thermodynamic stability of the resulting host–guest complexes. However, host preorganisation and degree of flexibility do have a marked effect on the rates of complexation and decomplexation reactions.

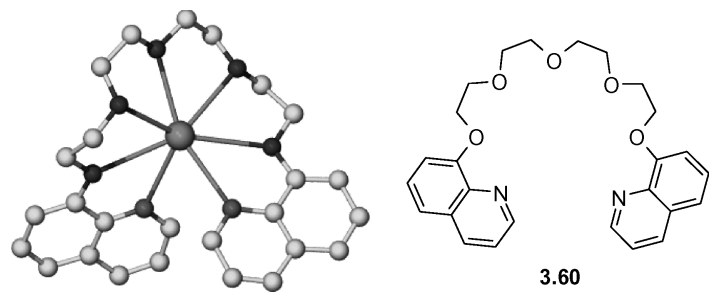

**3.60**

**Figure 3.40** X-ray crystal structure showing the wrapping of the podand *Kryptofix-5* (**3.60**) around an $Rb^+$ cation.

**Table 3.9** Complexation and decomplexation rate constants of picrate salts for representative compounds under standard conditions.

| | **3.33** | | **3.61** | | **3.62** | |
|---|---|---|---|---|---|---|
| | capsular | | nesting | | perching | |
| | $k_1$ | $k_{-1}$ | $k_1$ | $k_{-1}$ | $k_1$ | $k_{-1}$ |
| Guest | ($M^{-1}\,s^{-1}$) | ($s^{-1}$) | ($M^{-1}\,s^{-1}$) | ($s^{-1}$) | ($M^{-1}\,s^{-1}$) | ($s^{-1}$) |
| $Li^+$ | $8 \times 10^4$ | $<10^{-12}$ | | | | |
| $Na^+$ | $4 \times 10^5$ | $2 \times 10^{-7}$ | | | | |
| $K^+$ | | | $2 \times 10^9$ | 14 | | |
| $(CH_3)_3CNH_3^+$ | | | | | $3 \times 10^{12}$ | $7 \times 10^2$ |

The equilibrium constant, $K$, is related to the rates for the complexation ($k_1$) and decomplexation ($k_{-1}$) reactions by the equation $K = k_1/k_{-1}$ (Section 1.4). The forward and reverse complexation rate constants for three types of complex are given in Table 3.9. In general, it is found that the rates of both the forward and reverse reactions decrease in the order perching > nesting > capsular.

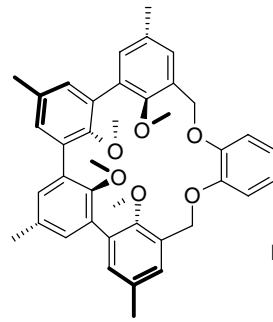

**3.61**

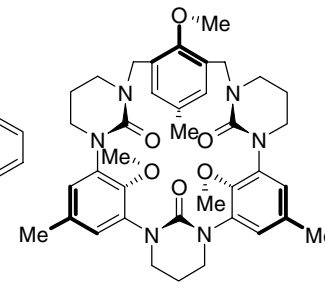

**3.62**

In a perching complex in which the guest rests on top of a host binding surface as in the *t*-butylammonium complex of **3.62** (Figure 3.41), the disruption to the cation solvation shell upon binding is relatively minimal. Disruption increases moving to a partially embedded (nesting) complex and is at a maximum in capsular complexes. Thus the free cation in perching complexes most resembles the complexation transition state, hence resulting in a fast reaction. In spheraplexes of **3.33**, examination

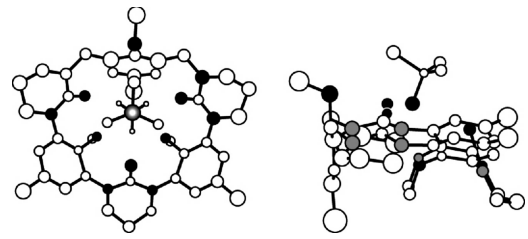

**Figure 3.41** X-ray crystal structure of the tetrabutylammonium hemispheraplex of **3.62**. (Reproduced from [12] by permission of The Royal Society of Chemistry).

of CPK models indicates that in the transition state for the complexation reaction (as the guest enters the cavity) there is space for only one solvent molecule (or perhaps the phenolate oxygen of the picrate anion) with the remainder of the cation surrounded by a hydrocarbon bubble formed from the host preorganised cavity and anisyl methyl groups. Thus slow kinetics would be expected for complexation by **3.33** since the cation has to desolvate almost entirely (a process that is enthalpically unfavourable and leads to a high-energy transition state) before it can regain enthalpy by complexation. In fact it is a general phenomenon that the more rigidly preorganised a host is for cation binding, the slower the kinetics of the process are. More flexible hosts, such as the corands and especially podands, should be able to move smoothly from solvation to host complexation without the need to pass through unstable desolvated intermediates.

Table 3.9 shows that all of the complexation rates are very fast on the human time scale and cannot even be followed by $^1$H NMR spectroscopy (effectively, reactions occur immediately upon mixing). Decomplexation rates for more flexible hosts are also fast on the human time scale, but may be accessible by $^1$H NMR, while for spheraplexes the reverse reaction is very slow even on the human time scale at 25 °C.

The interplay of complex stability and cation exchange kinetics is very important in the uses of supramolecular cation hosts. On the basis of their behaviour, we may distinguish between *cation receptors* (slow kinetics, large stability constants) and *cation carriers* (fast kinetics, lower stability). In the next section we will see how fast exchange kinetics make cation carriers highly useful in applications such as phase transfer catalysis.

## 3.8 Solution Behaviour

### 3.8.1 Solubility Properties

Crown ethers such as [18]crown-6 are remarkable in that, in the absence of guests, they are soluble in a wide range of solvents, from water to alkanes. Indeed, on a lipophilicity scale based on the partition of solutes between octanol and water, [18]crown-6 has a value of exactly zero, indicating a perfect balance between hydophilicity and lipophilicity. A comparison of the X-ray crystal structure of the free host compared to its complex with $K^+$ (Figure 3.20) gives us a clue as to the reason for this versatile behaviour. In the $K^+$ complex, all of the oxygen atoms are directed inwards (recall the definition of a host as a chemical entity with convergent binding sites in the complex), resulting in an entirely hydrophobic exterior, analogous to membrane transport ionophores such as valinomycin (Section 2.2). However, in the free ligand, two of the oxygen atoms are directed outwards, presenting a much more polar exterior. In fact corands such as [18]crown-6 are highly flexible in solution, allowing them to present either an entirely hydrophilic surface, thus masking their lipophilic ethylene backbone, or an entirely hydrophobic exterior, with oxygen lone pairs directed inwards in a fashion preorganised for cation complexation (Figure 3.42). Similar, albeit reduced, flexibility is displayed by the cryptands. The spherands, however, are much more rigid.

### 3.8.2 Solution Applications

The versatile solubility properties of the crown ethers and cryptands are important in two of their major applications, phase transfer catalysis and anion activation. Phase transfer catalysis involves the transport of guest species from one phase to another. The two phases in question are usually two immiscible liquids (liquid–liquid phase transport). In practice, this usually means the use of a

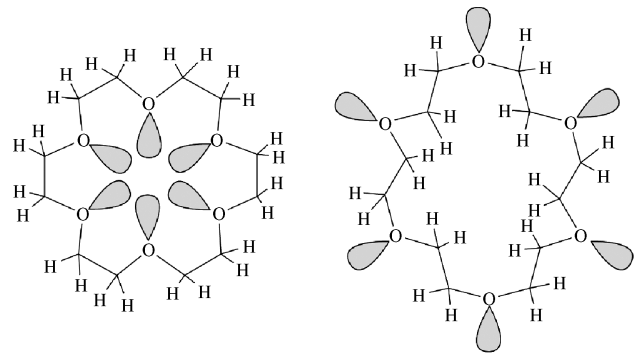


**Figure 3.42** Solution behaviour of [18]crown-6, (a) in an organic solvent such as dichloromethane (the crown resembles a droplet of water in oil), and (b) extreme representation of the structure in a hydrophilic medium (droplet of oil in water).

suitable host to promote the solubility of inorganic salts in nonpolar media. Thus a reaction between an hydrophilic inorganic salt and a lipophilic organic substrate is catalysed by the supramolecular host species by allowing the reactants to mix homogeneously within the organic phase.

Complexation of inorganic cations such as alkaline or alkaline earth metals by macrocyclic polyethers produces large, lipophilic cationic metal–macrocycle complexes that are readily soluble in nonpolar solvents such as benzene, toluene and haloalkanes. In order to maintain charge balance, the cationic complex has an associated counter anion. In an immiscible two-phase liquid system, such as a mixture of chloroform and water, the anion is necessarily pulled into the organic phase as the cationic complex crosses the phase boundary. A simple illustration of this principle is obtained by addition of a chloroform solution of [18]crown-6 to an aqueous solution of potassium picrate (potassium 2,4,6-trinitrophenolate). The yellow colour of the picrate anion is transported rapidly into the contiguous (physically in contact) chloroform phase upon agitation (Figure 3.43).

Once in the organic phase, reactive anions are able to react chemically with substances in the organic phase in a homogeneous fashion, rather than just at the phase boundary or interface. This activation results in enormous reaction rate enhancements and generally makes the difference between an excellent (often quantitative) yield and no appreciable reaction occurring at all. This is a true catalytic process because only a small amount of crown or cryptand is required. Once the reaction has taken place the crown may return to the organic–water interface to pick up more reactant and drop off inorganic by-products. Thus the net equilibrium concentration of inorganic salt in the organic phase is not necessarily large, but the fact that the anion (*e.g.* $MnO_4^-$) is continually reacting causes the crown-mediated diffusion of fresh salt across the interface in accordance with the concentration gradient (the concentration of inorganic salt in the organic layer is always much lower than in the aqueous phase).

Another intriguing aspect of reaction catalysis by macrocyclic cation hosts is the ‘naked anion’ effect. In a conventional anion reaction, such as an organic nucleophilic substitution, the activity of the anionic nucleophile is reduced by coordination or ion pairing with the cation (its counter ion). The activation energy for the reaction is thus increased by the amount of energy necessary to break the anion–cation association. In the presence of a crown ether or especially cryptand, the cation is sequestered within a lipophilic sheath, bringing about a large physical separation of anion and cation. As a result, the anion does not have nearly so significant an interaction with the cation. This has the

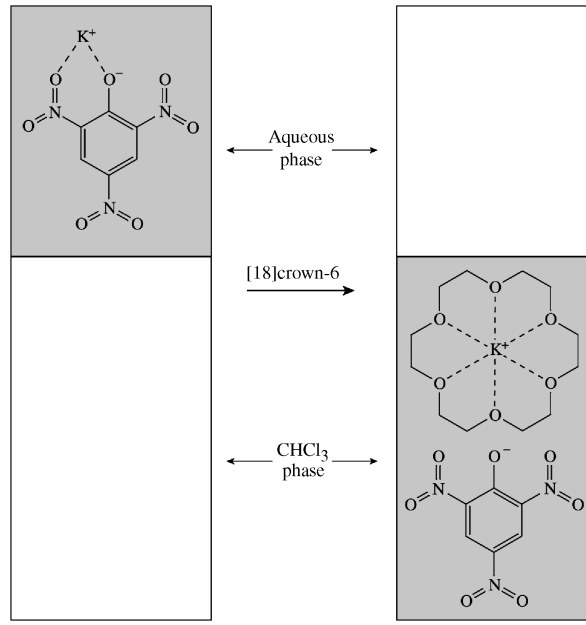


**Figure 3.43** Phase transfer catalysis by a crown ether.

effect of lowering the activation energy for the reaction because there is no longer any contribution to the activation energy from the anion–cation association.

In principle, macrocyclic complexing agents may be used to enhance any reaction in which ions, ionic intermediates or highly polar species are involved. Important examples include:

- nucleophilic substitution;
- reactions with carbanions;
- C—C bond formation (*e.g.* Darzens or Knoevenagel condensation);
- addition;
- eliminations;
- carbene generation;
- reduction (especially with electride salts, Section 3.13); and
- rearrangements (Favorskii, Cope).

The use of crown ethers and cryptands in phase transfer catalysis and anion activation are illustrated in the following case studies.

### *Oxidation of Organic Substrates by $KMnO_4$*

Addition of lipophilic crown ethers to inorganic salts such as potassium permanganate, potassium dichromate *etc.* which are normally insoluble in nonpolar solvents, enables them to smoothly oxidise organic substrates in quantitative yields (Scheme 3.10). In the absence of the macrocycle, yields are extremely poor.

### *Reaction of Potassium Salts with Benzyl Chloride in Acetonitrile*

The general reaction of anions ($A^-$) with benzyl derivatives is shown in Scheme 3.11.

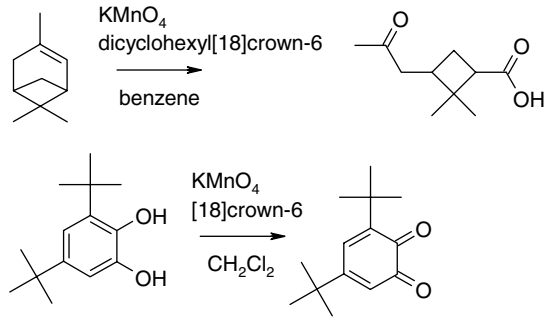


**Scheme 3.10** Transfer of the usually insoluble $MnO_4^-$ ion into organic solvents by [$K^+ \subset$ crown ether] complexes results in quantitative oxidation of the organic substrates.

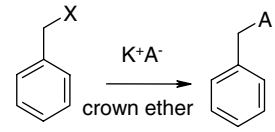


**Scheme 3.11** Reaction of potassium salts with benzyl chloride in acetonitrile (X = Cl, A = anion, *e.g.* acetate).

Table 3.10 shows that the rate of this simple nucleophilic substitution is enhanced dramatically as a result of the participation of a crown ether, which acts to disassociate the $K^+$ cation from the relatively strongly coordinating acetate anion, thus freeing the anion to act as a nucleophile. Table 3.11 demonstrates that in protic media, where the binding by the crown ether is weaker, large differences in reaction rate are observed for various anions according to their ability to complex $K^+$. Thus the soft $I^-$ is associated weakly with $K^+$, in addition to being weakly solvated, and reacts quickly. Fluoride is ion-paired closely with $K^+$, and strongly solvated, and reacts slowly. In an organic solvent, the potassium ion is much more strongly complexed by the crown ether and as a result all the anions react at more similar rates; indeed, the smaller, more mobile $F^-$ with its high negative charge density is now more nucleophilic than $I^-$.

### *Formation of a 'Naked' Carbide Ligand*

Individual carbon atoms are very uncommon ligands for transition metals. The synthesis of a molybdenum complex containing a single $C^{\bullet -}$ radical anion, uncomplexed to any other metals or functional

**Table 3.10** Dependence of reaction rate with A = $CH_3CO_2^-$ on added crown ether (leaving group, X = Cl).

| Crown ether | Reaction half-life (h) |
|---|---|
| None | 685 |
| [18]Crown-6 | 3.5 |
| Dibenzo[18]crown-6 | 9.5 |
| Dicyclohexano[18]crown-6 | 1.5 |

**Table 3.11** Nucleophilicity of various anions ($A^-$) in the presence of [18]crown-6 (leaving group, X = *p*-toluenesulfonate).

| Nucleophile | Relative rate | Relative rate in protic media |
|---|---|---|
| $N_3^-$ | 10.0 | 100 |
| $CH_3CO_2^-$ | 9.6 | 5 |
| $CN^-$ | 2.4 | 1250 |
| $Br^-$ | 1.3 | 80 |
| $Cl^-$ | 1.3 | 10 |
| $I^-$ | 1.0 | 1000 |
| $F^-$ | 1.4 | 1 |
| $SCN^-$ | 0.3 | 625 |

groups, was achieved by the sequestering of $K^+$ counter ions by benzo[15]crown-5 or [2.2.2]cryptand, according to Scheme 3.12.[17] The X-ray crystal structure of the product shows clearly the isolation of the $K^+$ cation (Figure 3.44).

## 3.9 Synthesis: The Template Effect and High Dilution

### 3.9.1 The Template Effect

Gerbeleu, N. V., Arion, V. B. and Burgess, J., *Template Synthesis in Macrocyclic Chemistry*, John Wiley & Sons, Ltd: Chichester, 1999.

A look at the original synthesis of dibenzo[18]crown-6 (Scheme 3.2) suggests a possible side reaction that might have resulted in the crown ethers never being discovered at all. The fortuitous macrocycle dibenzo[18]crown-6 that gave birth to modern supramolecular chemistry might never have formed

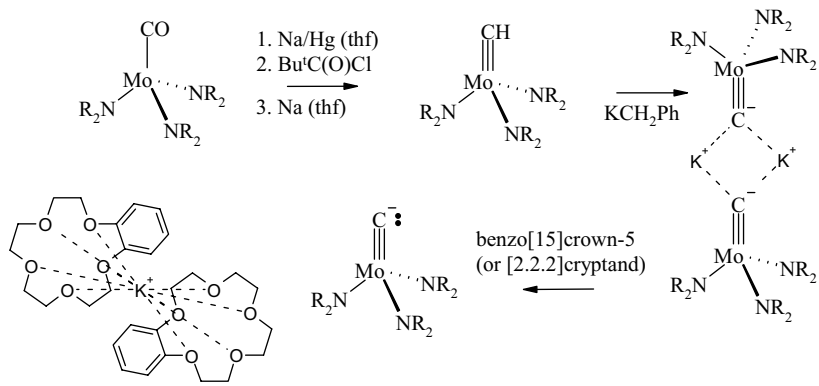


**Scheme 3.12** Formation of a 'naked' carbide complex by complexation of $K^+$ with benzo[15]crown-5 or [2.2.2]cryptand.

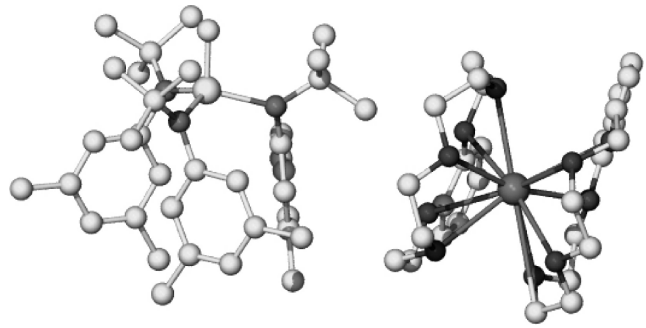

**Figure 3.44** X-ray crystal structure of the molybdenum carbide complex. The coordinating $K^+$ ion is sequestered by two benzo[15]crown-5 ligands.

if the reaction had taken a different course, leading to polymeric (polycondensation) products. The conflicting possibilities are illustrated for the closely related [18]crown-6 in Scheme 3.13.

The fact that the macrocyclic crown ethers are the major products is not because they are the most thermodynamically stable. In fact it is no coincidence that 18-membered crowns are selective for $K^+$, and it is a potassium salt of the carbonate base that is most commonly used in their synthesis. Indeed, exchanging $K_2CO_3$ for an organic base such as triethylamine does result in the formation of predominantly polymeric product. This crucial difference between the behaviour of the two classes of base lies in the ability of the $K^+$ ion to organise the reactants about itself to give a reaction intermediate (probably resembling **3.63**) that is preorganised to form a cyclic product. The functional groups —OH and —Cl are brought into close proximity to one another by coordination to the potassium cation (*via* the chelate effect) and cyclise

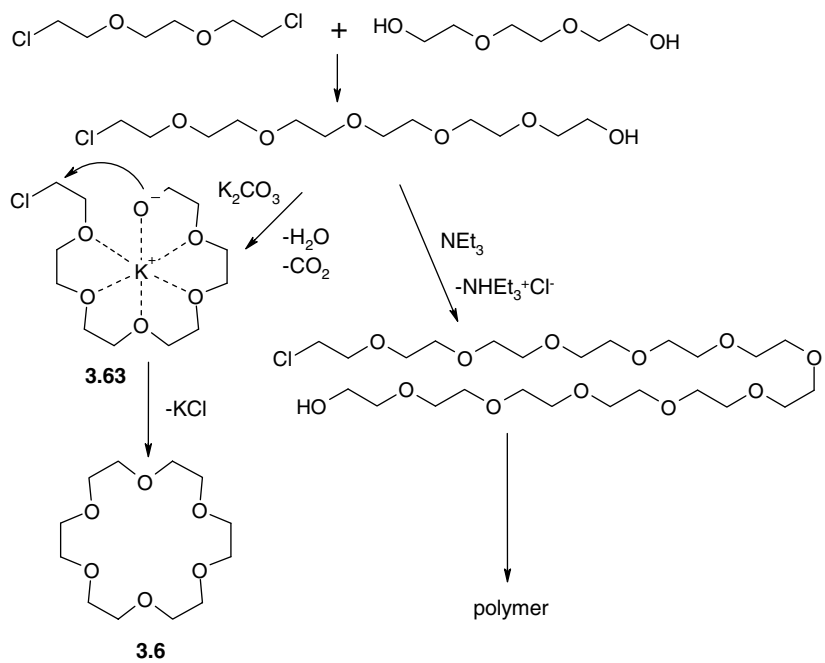


**Scheme 3.13** Possible pathways leading to cyclic and acyclic products in the synthesis of [18]crown-6.

readily. The organic base is unable to bring about the formation of this intermediate and the reaction takes an intermolecular, rather than intramolecular, pathway. The $K^+$ ion is thought of as a template for the reaction, and the formation of macrocyclic compounds in this way is termed the *template effect*, or, more rigorously, the *kinetic template effect*. In fact, this is a form of catalysis in which the metal cation acts to stabilise the cyclic intermediate, thus dramatically increasing the rate of formation of the cyclic product. The template effect is thus a kinetic effect and the macrocycle is a kinetic product. In simple terms, if we want to induce the formation of a host that is selective for an alkali metal about the size of $K^+$, we use $K^+$ as a pattern to induce its formation. The template effect is used widely in macrocyclic synthesis, including the synthesis of macrobicyclic compounds, knots, interlocking rings (catenanes) and many other examples. Alkali metals, alkaline earth, transition metal and lanthanide cations may all exhibit template behaviour. In many early syntheses particularly involving thiols, $Cs^+$ proved to be particularly effective as a template and the yield enhancement of cyclic products obtained was called the *caesium effect*. The caesium effect is now believed to be due to ion pairing between thiolate anions and the $Cs^+$ cation leaving a 'naked' base that results in a faster raction that favours cyclic products for the same reason that cyclisation reactions are favoured by fast intrinsic rations rates under high dilution conditions (Section 3.9.2, *cf.* also the naked anion effect, Section 3.8.2).

In order to recognise a template effect two tests must be applied:

1. Organisation of other molecular components by the template.
2. Accompanying chemical reactions must include significant spatial, topological or geometric control.

Figure 3.45 shows the results of kinetic studies of the template synthesis of benzo[18]crown-6 according to the reaction shown, as a function of the templating cation. Clear rate enhancements

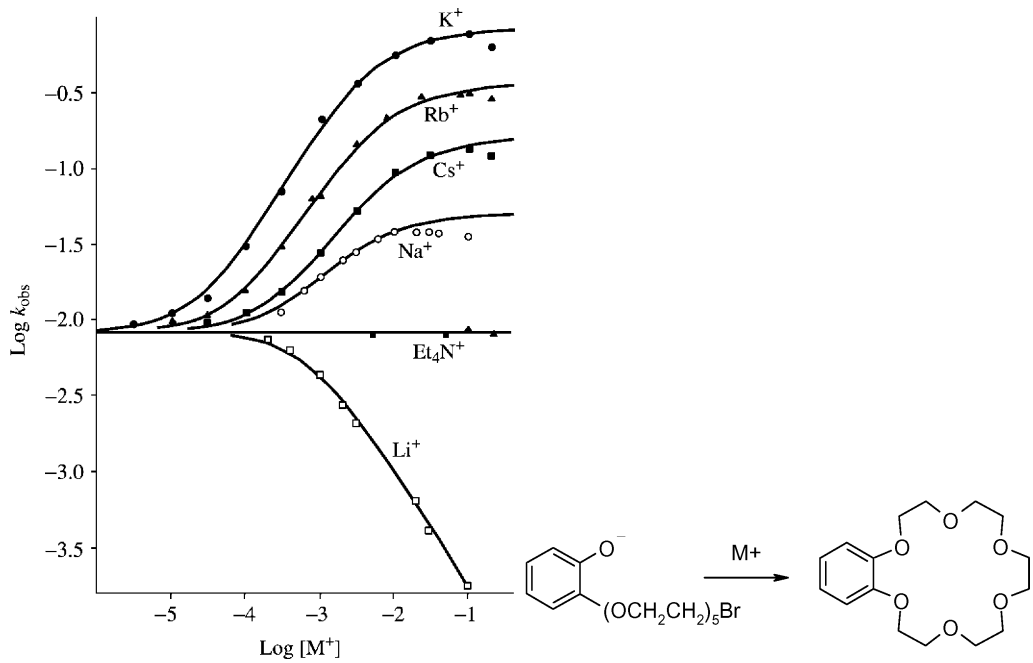


**Figure 3.45** Kinetic studies of the template effects of metal ions on cyclisation to form benzo[18]crown-6. (© Wiley-VCH Verlag GmbH & Co. Reproduced with permission).

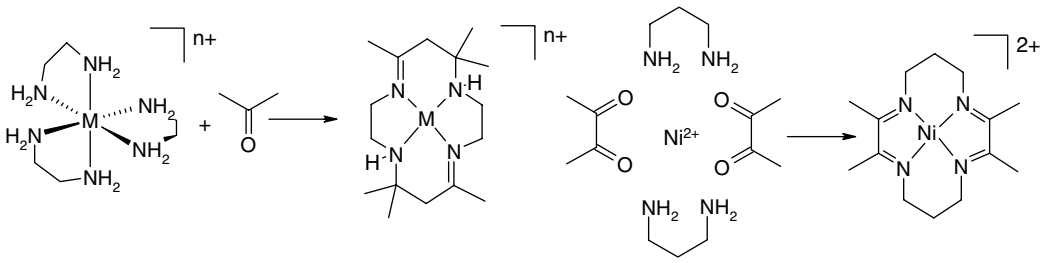

**Scheme 3.14** Thermodynamic template synthesis of two tetrazamacrocycles.

(relative to the untemplated reaction in the presence of $NEt_4^+$) are seen with increasing concentration of all alkali metal ions except $Li^+$, which tends to form very strongly bound ion pairs with the phenoxide ion, thus inhibiting its reactivity. As anticipated, $K^+$, which is most complementary to the crown cavity, gives the most effective enhancement. Analogous cyclisation with alkyl chain analogues removes the organisational effects of the cations, resulting in decreases in the rate of formation of cyclic products (and hence their yield) compared to reactions in the absence of alkali metal cations in every case. This retardation is a result of ion pairing.

In discussing the kinetic template effect, it is important to distinguish it from another effect termed the *thermodynamic template effect*. The kinetic template effect involves the actual formation of ligands about the metal centre. On the other hand, the thermodynamic template effect concerns the ability of a metal cation to pick out a ligand complementary to it from an equilibrating mixture of products, thus driving the equilibrium over to the product thus stabilised. One of the first examples of the thermodynamic template effect concerns the condensation of acetone with *tris*(ethylenediamine)nickel(II) salts according to Scheme 3.14. Similar results may be obtained for other metals and ketones. Evidence for this being a thermodynamic effect comes from the following observations:

- The reactivity depends on the lability of the metal ion, indicating that condensation of the amino groups requires their disassociation from the metal ion—substitutionally inert Co(III) salts do not react at all.
- Unsymmetrical ketones produce less branched products under basic conditions (Claisen–Schmidt condensation) again suggesting the absence of the metal ion.
- The ligands may be produced without a metal ion being present.

In addition to the very common use of metal ions as templates (so-called *exo-templates*) macrocycle formation may also occasionally be templated by *endo-templates*. This kind of templation involves a kind of covalently bound molecular scaffolding holding the macrocycle together during the synthesis until ring formation is complete. The endo-templated synthesis of 1,5,9-triazacyclododecane is shown in Scheme 3.15. Further examples of the thermodynamic template synthesis of Schiff base macrocycles are shown in Section 3.10.6, while kinetic templating of phosphorus macrocycles is described in Section 3.10.4. More unusual template effects, such as those involving

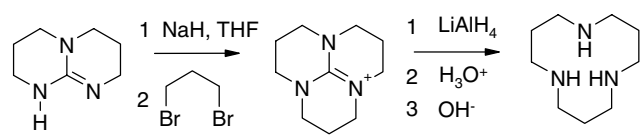

**Scheme 3.15** Endo-templated synthesis of 1,5,9-triazacyclododecane.

catenane and rotaxane synthesis and the beginnings of self-replicating, systems are discussed in Chapters 10 and 12.

## 3.9.2 High-Dilution Synthesis

Illuminati, G. and Mandolini, L., 'Ring closure reactions of bifunctional chain molecules', *Acc. Chem. Res.*, 1981, **14**, 95–102.

In the absence of a suitable template, the synthesis of macrocyclic ligands is much more difficult and high-dilution conditions must be employed. By 'high dilution', we mean that small quantities of reactants are used in a large volume of solvent. A typical apparatus for carrying out this kind of procedure is shown in Figure 3.46. Reactants are added dropwise at a very slow rate from each of the dropping reservoirs (this may be done automatically with an electronically controlled syringe pump) and mixed in the large round-bottomed flask at the bottom.

The rationale for this approach is that in dilute solutions the formation of a cyclic product by intramolecular reaction (*i.e.* one end of a molecule bumping into itself) is more likely, and hence faster, than formation of a polymer, which requires a collision between two separate reactants (an intermolecular reaction) (Figure 3.47). If we compare the rates of cyclisation ($r_c$) of a reactant X—Y, $r_c = k_c \cdot [X—Y]$, with polymerisation, $r_p = k_p \cdot [X—Y]^2$, we derive the expression:

$$\frac{r_c}{r_p} = \frac{k_c\,[X-Y]}{k_p\,[X-Y]^2} = \frac{k_c}{k_p\,[X-Y]} \tag{3.3}$$

where $k_c$ and $k_p$ are the cyclisation and polymerisation rate constants. Thus the quantity $r_c/r_p$ increases with decreasing concentration of reactant X—Y, suggesting that $r_c$ will dominate over $r_p$ in dilute solutions.

It follows from this argument that the faster the reaction, the better this approach will work since, if the reaction is intrinsically faster than the rate of addition of the reactants (large $k_c$ and $k_p$ values), then the concentration of the reactants will always be small and will not build-up during the course of the reaction. High-dilution conditions have been used in a large number of macrocyclic and macrobicyclic

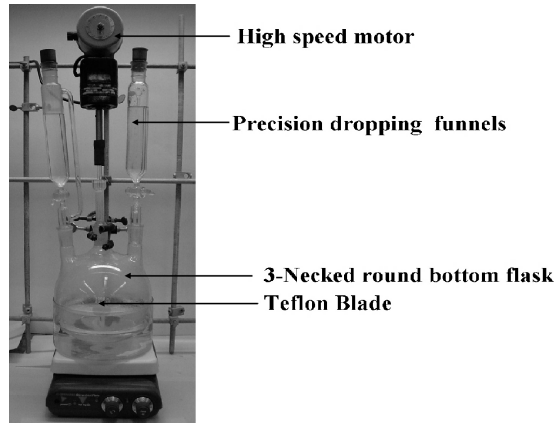


**Figure 3.46** Apparatus to achieve high-dilution conditions in macrocyclisation reactions.

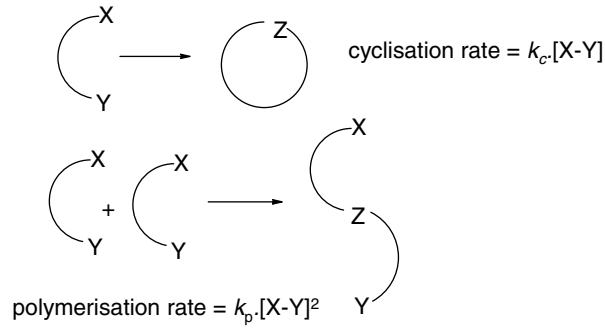


**Figure 3.47** Macrocyclic synthesis by high-dilution methods.

syntheses, including many of the original cryptand preparations (Scheme 3.6). In particular, the reaction of an amine with an acid chloride occurs sufficiently rapidly as a result of the electron withdrawing and resonance stabilisation effect of the carbonyl groups. Its use in the high-dilution synthesis of a simple azacrown is shown in Scheme 3.16.

Interestingly there are macrocyclisation strategies that do not always require high dilution conditions. A particularly important synthetic method that works under relatively concentrated conditions (allowing the ready preparation of large quantities of material) is the Richman Atkins reaction,[19] developed in 1974 shortly after the first crown ether and cryptand syntheses (Scheme 3.17). This method involves conversion of primary amines to sulfonamides (*e.g. p*-toluene sulfonamide) in a dipolar, aprotic solvent such as dimethyl formamide (DMF) which results in an increase in the acidity of the amine and hence ready deprotonation as well as protection of the nitrogen atom from further reaction. The deprotonated tosylamide then displaces a leaving group such as a halide or tosylate from a complementary reactant to give a tosylated macrocycle. Detosylation with sulfuric acid generally affords the desired polyamine in excellent yield. The reaction benefits from the conformational constraints of the reactants which

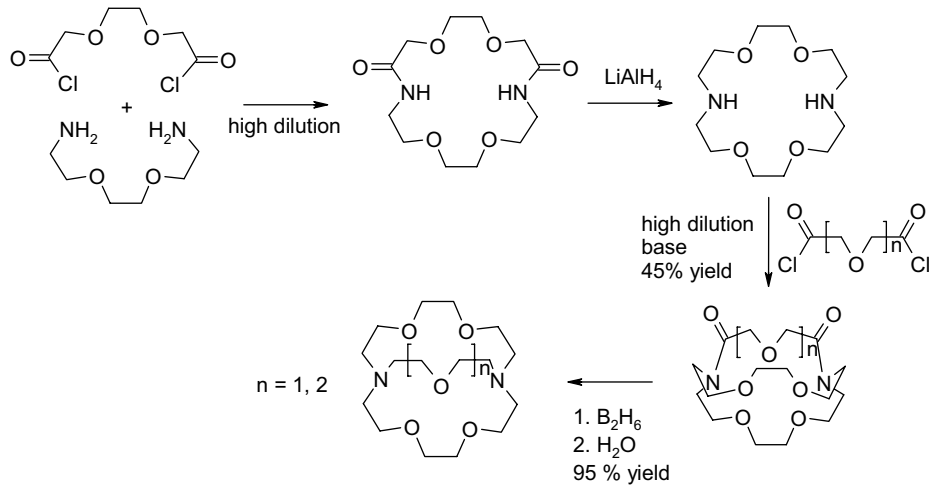


**Scheme 3.16** High-dilution synthesis of diaza[18]crown-6 and thence [2.2.2] and [2.2.1]cryptands. Note the use of acid chloride groups to enhance reaction rate.[9]

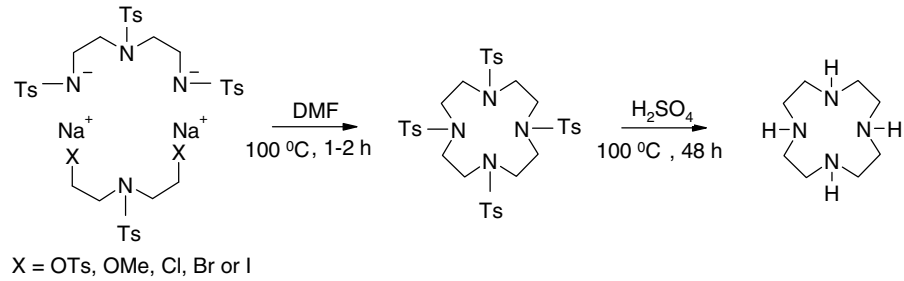


**Scheme 3.17** Richman–Atkins synthesis of 1,4,7,10-tetraaza-cyclododecane followed by deprotection of the secondary amine groups (80 per cent yield, OTs = $OSO_2C_6H_4CH_3$).[19]

promote cyclisation as well as the fact that sulfonamides are excellent leaving groups, resulting in an intrinsically fast reaction.

A wide variety of particularly interesting cryptands, especially containing larger cavities, have been synthesised by combined intra- and intermolecular reactions. The most common of these is the [2 + 2] cyclococondensation reaction in crown ether or cryptand synthesis, in which, often by accident, two pairs of reactants come together to make a macrobicycle or macrotricycle instead of a [1 + 1] reaction as shown in Scheme 3.17. For the crown ethers this is exemplified by reaction (c) in Scheme 3.3. In the case of cryptands the behaviour is illustrated diagrammatically in Scheme 3.18a. Generally [2 + 2] cyclococondensation reactions result from situations in which the conditions of the reaction (rate and concentration) are balanced between polymerisation and cyclisation, or in circumstances where the [1 + 1] cyclisation product is sterically strained or otherwise disfavoured. An example is the simultaneous formation of tetraoxo[24]ane-$N_8$ along with the monomer dioxo[12]ane-$N_4$ (Scheme 3.18b).[20] In its diprotonated form the larger macrocycle binds $ATP^{2-}$ Log $K$ = 4.66 in water.

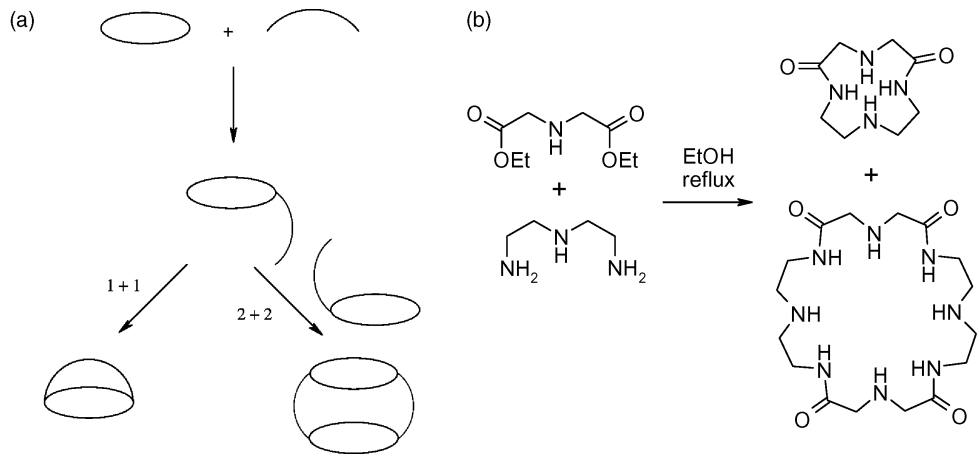


**Scheme 3.18** (a) Schematic representation of [1 + 1] and [2 + 2] cyclococondensation in the cryptands, (b) formation of tetraoxo[24]ane-$N_8$ in 6% isolated yield as a byproduct of the coupling reaction that leads to dioxo[12]ane-$N_4$.[20]

## 3.10 Soft Ligands for Soft Metal Ions

So far, most of the metal ion complexes we have looked at have been complexes of hard, nonpolarisable metal ions such as the alkali metal cations. The binding in such complexes is primarily electrostatic in nature, with the host donor atoms arranging themselves about the surface of the cation sphere such as to minimise intra-host steric repulsions and optimise host-cation interactions. There is relatively little directional preference or covalency in the bonding and the resulting metal ion coordination geometry and coordination number is greatly dependent on host conformational preferences (Box 3.1). In general, ligands that are effective at binding hard metal cations display only limited affinity for softer metal ions such as $Ag^+$ and many lower oxidation state transition metals, especially from the second and third rows of the *d*-block. In this section we will examine a range of common host ligands for these softer kinds of metal cations.

**Box 3.1** Selective binding of Alkali Metal Cations

Properties of alkali metal cations:

- Hard, nonpolarisable spheres (see Section 3.1.2).
- Little fixed preference for particular coordination geometries.
- Relatively high free energies of hydration.
- Affinity for highly charged, nonpolarisable bases.

These features make the design of suitable ligands that can displace water and bind both strongly and selectively to these freely diffusing cations a difficult task. The only basis for selectivity between alkali metal cations is ionic size (Figure 3.48).

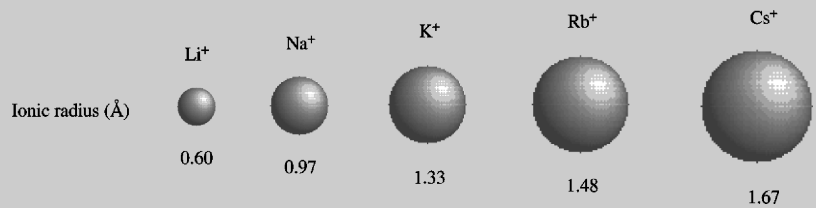


**Figure 3.48** Size of alkali metal cations.

### 3.10.1 Nitrogen and Sulfur Analogues of Crown Ethers

Incorporation of one or more softer donor atoms (*e.g.* N, S *etc.*) results in dramatic changes in both binding ability of the ligand and geometry of the resulting complexes. We have already seen the radical conformational differences that arise from substituting S for O (Section 3.7.2). Table 3.12 shows the vastly enhanced binding of the soft $Ag^+$ (and corresponding drop in affinity for $K^+$) as soon as hard ether oxygen donors are exchanged for S or N. Clearly the soft $Ag^+$ has a strong affinity for S-donors, with the binding increasing in the order S > NH > O while for the intermediate $Pb^{2+}$ the order is NH > O > S. In contrast, the binding constants for hard cations such as $K^+$, $Ba^{2+}$ and the intermediate $Tl^+$ decrease with decreasing donor atom electronegativity: O > NH > S. This is reasonable from the

**Table 3.12** Comparative binding constants (log $K_{11}$) for hard and soft metal ions with various ligands.

| | Ligand | | | | | | |
|---|---|---|---|---|---|---|---|
| Cation | [18]crown-6 | **3.64** | **3.18** | [15]crown-5 | **3.66** | **3.67** | **3.68** |
| $K^+$ (methanol) | 6.10 | 1.15 | 2.04 | – | – | – | – |
| $K^+$ (water) | 2.10 | – | <1 | 0.74 | – | 1.0 | – |
| $Ag^+$ (methanol) | 4.58 | – | – | – | – | – | – |
| $Ag^+$ (water) | 1.60 | 4.34 | 7.80 | 0.94 | 5.0 | 5.85 | 8.95 |
| $Tl^+$ (water) | 2.27 | 0.93 | 1.1 | 1.23 | 0.8 | – | – |
| $Ba^{2+}$ (water) | 3.78 | – | 2.51 | – | – | 1.0 | – |
| $Pb^{2+}$ (water) | 4.27 | 3.13 | 6.9 | 1.85 | 1.65 | 5.85 | 5.67 |

point of view of the magnitude of the cation–dipole interactions, which form the basis of the binding, but the very large drop on going from O to N (*e.g.* from [18]crown-6 to diaza[18]crown-6, **3.18**) is striking given the similar gas-phase affinities of $K^+$ for N and O bases. Clearly solvation and conformational effects must also play a large part, perhaps linked to the hydrogen bond donor ability of the NH group.

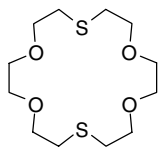


**3.64**

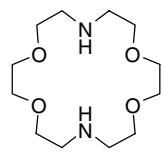


**3.18**

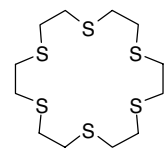


**3.65**

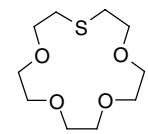


**3.66**

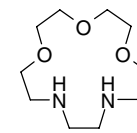


**3.67**

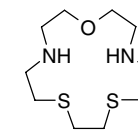


**3.68**

Thermodynamic data for the binding of the soft $Ag^+$ by a range of macrocycles and macrobicycles in methanol is given in Table 3.13. The data confirms that in enthalpic terms Ag forms the strongest interactions with S and NMe donors, then with NH donors and is bound much more weakly by O donors. [18]crown-6, [18]ane-$S_2O_4$ and [18]ane-$N_2S_4$ all have unfavourable $\Delta S$ terms that suggest significant conformational rearrangement, consistent with the conformational effects discussed in Section 3.7.2.

**Table 3.13** thermodynamic parameters for $Ag^+$ binding by various ligands in methanol at 25 °C

| Ligand | Log $K$ | $-\Delta H$ (kJ mol$^{-1}$) | $T\Delta S$ (kJ mol$^{-1}$) |
|---|---|---|---|
| [18]ane-$N_4S_2$ | 14.1 | 77 | 3.3 |
| [18]ane-$N_4O_2$ | 11.2 | 59.5 | 4.4 |
| [18]ane-$N_2O_4$ | 10.0 | 51.4 | 5.7 |
| [18]ane-$N_2S_4$ | 13.7 | 83.2 | −5.0 |
| [18]ane-$S_2O_4$ | 10.3 | 64.0 | −5.3 |
| [18]crown-6 | 4.58 | 38.3 | −12.1 |
| [2.2.1]cryptand | 14.4 | 81.9 | 0.1 |
| [18]ane-$(NMe)_2N_2O_2$ | 13.4 | 84.3 | −7.8 |
| [18]ane-$(NMe)_2N_2S_2$ | 14.6 | 102.1 | −18.7 |

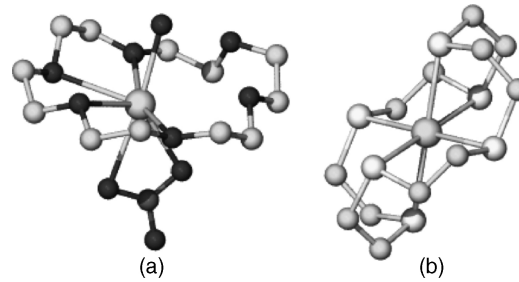


**Figure 3.49** X-ray molecular structures of the $Ag^+$ complexes of (a) [18]crown-6 and (b) its sulfur analogue (nitrate salts).

The entropic term is particularly unfavourable for NMe donor groups despite the significant enthalpy term. This phenomenon may relate to steric interactions involving the bulky NMe groups and the face that tertiary amines are less solvated than secondary amines, leading the the release of fewer methanol molecules upon binding.

The X-ray crystal structures shown in Figure 3.49 make a striking illustration of the distinction between nondirectional electrostatic binding in $[Ag([18]crown\text{-}6)]^+$ and the dative covalent nature of the forces in the thiacorand analogue $[Ag([18]ane\text{-}S_6)]^+$. In $[Ag([18]crown\text{-}6)]^+$, the crown ring is only slightly distorted from a planar conformation and occupies the equator of the complex, with water and the nitrato anion in the axial positions. On the other hand, $[Ag([18]ane\text{-}S_6)]^+$ exhibits a more recognisable octahedral coordination geometry similar to conventional Werner coordination complexes. [18]Ane-$S_6$ (**3.65**) also binds soft transition metal ions such as $Pd^{2+}$. In this case, the crown is sufficiently flexible to accommodate the square planar coordination preference of the palladium ion with four short Pd—S bonds (2.31 Å) and two much longer axial interactions (3.27 Å).

Transition metal cations are also not bound strongly by crown ethers. Indeed, because of the relatively small ionic radii of many transition metal cations, they are often not bound at all by larger crown ethers such as [18]crown-6, and instead form hydrogen-bonded second-sphere complexes as their hexaquo ions (Figure 3.50a). This is consistent with studies by Christensen *et al.* in 1971[21] who suggested that, for the alkali metals, cation diameter to host cavity size ratios of 0.75–0.90 are favourable for direct ion–crown ether binding. Thus, for [18]crown-6 (cavity diameter, 2.6–3.2 Å, depending on conformation) ratios of 0.61–0.75, 0.83–1.02 and 1.03–1.27 are obtained for $Na^+$, $K^+$ and $Cs^+$, respectively, consistent with the observed selectivities. Likewise, for [15]crown-5 (cavity diameter, 1.7–2.2 Å) a ratio of 0.89–1.15 is obtained for $Na^+$ and reflects the size match for that ion. Thus most first-row divalent transition metal ions such as $Co^{2+}$, $Ni^{2+}$ and $Zn^{2+}$ are too small to be included within [18]crown-6, but fit snugly into [15]crown-5. In these systems, multiple hydrogen-bonded interactions from both axial and equatorial aqua ligands result in highly crystalline solid-state supramolecular polymers (polymers held together by nonmolecular interactions, usually hydrogen bonds) that have been isolated in the solid state for a range of $M^{2+}(ClO_4)_2$ salts (M = Co, Ni, Cu, Zn). In aqueous solution, however, the hydrogen bonding interactions are broken down readily resulting in highly fluxional (rapidly exchanging) systems. In the case of $Cu^{2+}$, a second compound may be isolated, which does evince some first-sphere coordination of the macrocycle (Figure 3.50b). Smaller crown ethers such as [15]crown-5 and [12]crown-4 will bind transition metal cations (Figure 3.50c and d). For [15]crown-5, seven coordinate species are commonly isolated with the crown ether occupying the equatorial plane of the metal centres

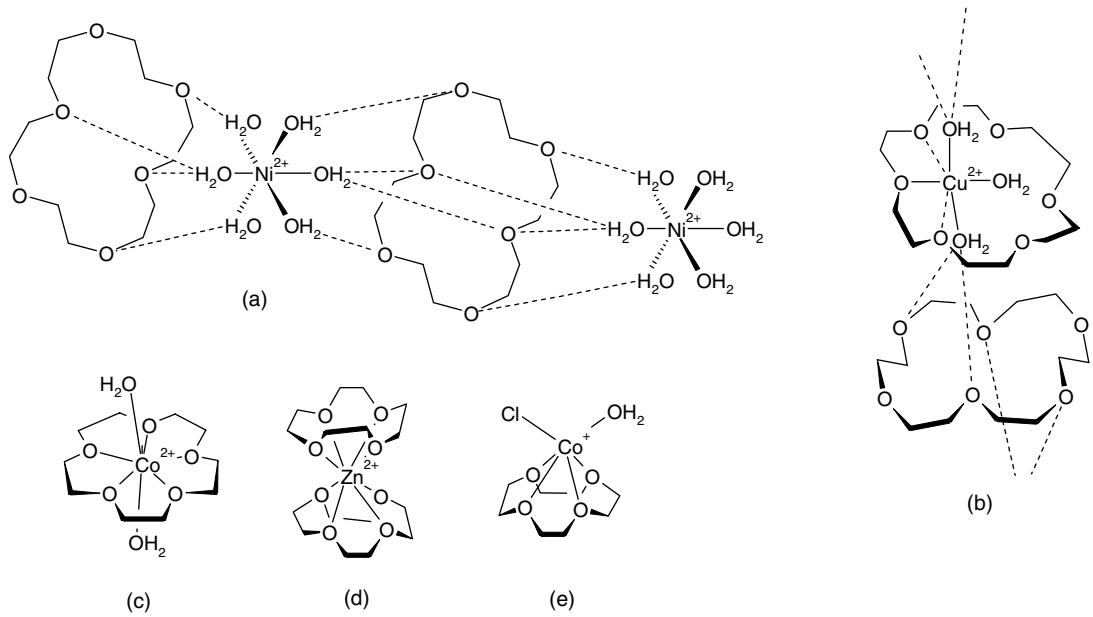


**Figure 3.50** Products arising from the reactions of transition metal dications with [18]crown-6, [15]crown-5 and [12]crown-4 in aqueous or alcohol solution.

with axial aqua ligands. In the case of [12]crown-4, products are highly dependent on the nature of the counter-anion and metal cation with both 2:1 (sandwich) and 1:1 (perching) complexes being isolated, as well as hydrogen-bonded polymers involving metal hexaquo ions, as observed for [18]crown-6.[22]

Unlike oxygen-donor crown ethers, thiacrowns are very suited to binding transition metal ions, and indeed their excellent ligating properties they can stabilise interesting an unusual oxidation states by virtue of the additional stability of the chelate and macrocyclic effects. Thus thioethers have been used to stabilise silver and gold complexes in the very rare +2 oxidation state as in the Ag(II) and Au(II) mononuclear complexes $[Au([9]aneS_3)_2]^{2+}$ and $[Ag([18]ane\text{-}S_6)]^{2+}$. The crystal structure of the Au(II) species shows a Jahn-Teller tetragonally distorted geometry, consistent with the $d^9$ electron configuration.[23]

Synthetically is it relatively challenging to prepare heavier analogues of the thiacrowns containing Se and Te donors. The macrocycle [16]ane-$Se_4$ is known and forms complexes with Ru(II) that can be oxidised to Ru(III) and isolated.[24] Tellurium-containing macrocycles are limited to mixed Te/S donors such as [$n$]ane-$S_2Te$ ($n$ = 9, 11 and 12).[25]

## 3.10.2 Nitrogen and Sulfur Analogues of Cryptands

As for corands, replacing oxygen for NH or S donor functionalities in the cryptands alters dramatically the complexation behaviour of otherwise similarly sized hosts. Thus incorporation of two NMe groups into [2.2.2]cryptand gives **3.70**, which displays a binding constant for $Ag^+$ (log $K$) of 11.5, even in water. The corresponding figure for $K^+$ is only 2.7 (compared to 10.5 for **3.23**), while $Tl^+$ exhibits somewhat intermediate behaviour, with a log $K$ value of

**Table 3.14** Binding constants for $Ag^+$, $K^+$ and $Tl^+$ for various cryptands.

| | Log $K_{11}$ | | | |
|---|---|---|---|---|
| Ligand | $Ag^+$ | $K^+$ | $Tl^+$ | Solvent |
| **3.23** | 9.6 | 5.4 | 6.3 | $H_2O$ |
| | 12.22 | 10.49 | – | MeOH |
| **3.69** | 10.8 | 4.2 | 6.3 | $H_2O$ |
| **3.70** | 11.5 | 2.7 | 5.5 | $H_2O$ |
| **3.71** | 13.0 | 1.7 | 4.1 | $H_2O$ |
| **3.72** | 12.7 | – | 3.9 | $H_2O$ |
| **3.73** | 12.39 | 6.92 | – | MeOH |

5.5. The affinity of a range of heterocryptands for these representative metal ions is shown in Table 3.14.

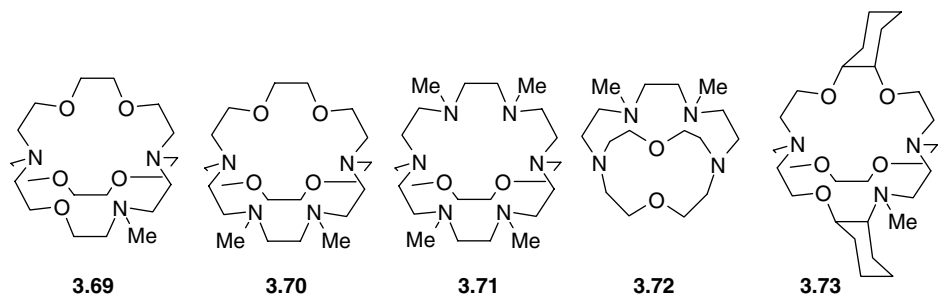

**3.69** **3.70** **3.71** **3.72** **3.73**

The series **3.23** and **3.69** to **3.71** is particularly interesting since it shows a smooth change in binding constant as oxygen atoms are sequentially replaced by nitrogen. The increased affinity for $Ag^+$ confirms the strong nature of the $Ag^+$—N interaction, which contains a significant covalent component. On the other hand, $K^+$ binds in a purely ionic fashion and is much more stabilised by oxygen donors. Clearly $Tl^+$ shows $K^+$-like behaviour in that the stability decreases with increasing proportion of nitrogen. The more polarisable character of the $Tl^+$ ion is clear from the magnitude of the values and the more gradual change, however. Comparison of the binding data for $Ag^+$ between **3.71** and the smaller **3.72** shows that the affinity for the [2.1.1]cryptand analogue (**3.72**) is almost as great as the larger host, despite the fact that compound **3.71** has six N-donors (complementary to $Ag^+$) instead of four. This observation has been attributed to a closer size match of $Ag^+$ and **3.72**. Overall, it is clear that the $Ag^+$ affinity for most of the cryptands shown, even those with few nitrogen atoms such as **3.73**, is extremely high, even in a highly competitive solvent such as water. This may generally be attributed to the more inert character of $Ag^+$ compared to $K^+$, covalency in the Ag—N interactions, and the lower solvation free energy of $Ag^+$, coupled with the plasticity of its coordination sphere.

## 3.10.3 Azamacrocycles: Basicity Effects and the Example of Cyclam

Nitrogen-containing macrocycles are highly complementary for first row transition metals as in the examples shown in Section 1.6. Common azamacrocycles include cyclen ([12]ane-$N_4$) and cyclam (**3.45**) and many have a history that significantly pre-dates the crown ethers. Unlike the crown ethers which do not have donor atom substituents, the binding constants of azamacrocycles such as cyclam are greatly affected by N-alkylation. Alkylated amines are significantly more basic than ammonia, for

**Table 3.15** Comparison of the binding constants (log $K_{11}$) of cyclam and tetramethyl cyclam for various transition metals (water, 25 °C).[26]

| Metal ion | Cyclam | Tetra-N-methylcyclam | Ionic radius (Å) |
|---|---|---|---|
| Cu(II) | 27.2 | 18.3 | 0.65 |
| Ni(II) | 22.2 | 8.6 | 0.69 |
| Co(II) | 12.7 | 7.6 | 0.72 |
| Zn(II) | 15.5 | 10.4 | 0.74 |
| Cd(II) | 11.7 | 9.0 | 0.97 |
| Pb(II) | 11.3 | (~7.5) | 1.21 |

example (one of the origins of the macrocyclic effect is the fact that the macrocycle backbone increases the basicity of the donor atoms). At first sight this seems surprising since the basicities (as measured by the p$K_a$ values) of trimethylamine and ammonia in water are quite similar; however, aqueous solvation effects mask the intrinsic donor ability. Thus the ammonium ion is highly stabilised by hydrogen bonds to solvent in water, whereas $Me_3NH^+$ engages in far fewer hydrogen bonds and is somewhat hydrophobic. Hydrogen bonding to solvents is also destabilised by steric effects. In comparison gas phase basicities can be assessed independently of solvation effects by mass spectrometry. The result is a clear increase in basicity upon replacing H with an alkyl group for $H_2O$, $H_2S$, $NH_3$ and $PH_3$. This increase arises from the increase in the inductive electron release by the methyl group.

We would therefore expect to increase the basicity of macrocyclic ligands such as cyclam by methylation of the nitrogen atoms. Table 3.15 shows that the reverse is true, however. Tetramethyl cyclam binds metal ions *less* strongly than its secondary amine analogue because the complexation energy must over come the unfavourable steric repulsions between the methyl groups themselves and also between the methyl groups and the methylene groups of the macrocycle backbone

Cyclam, or 1,4,8,11-tetraazacyclotetradecane, was first synthesised, inadvertently, by van Alphen in 1937 through the reaction of 1,3-bis-(2-aminoethyl)-aminopropane with 1,3-dibromopropane. The first major studies of the ligand by Bosnich *et al*. used X-ray crystallography to elucidate different conformations of the metal complexes of the macrocycle.[27] Their synthesis was similar to van Alphen's procedure, but did not involve a template method and as a result yields were unimpressive. They showed that five out of the possible ten different metal-complex conformers exist in the solid-state (Figure 3.51).

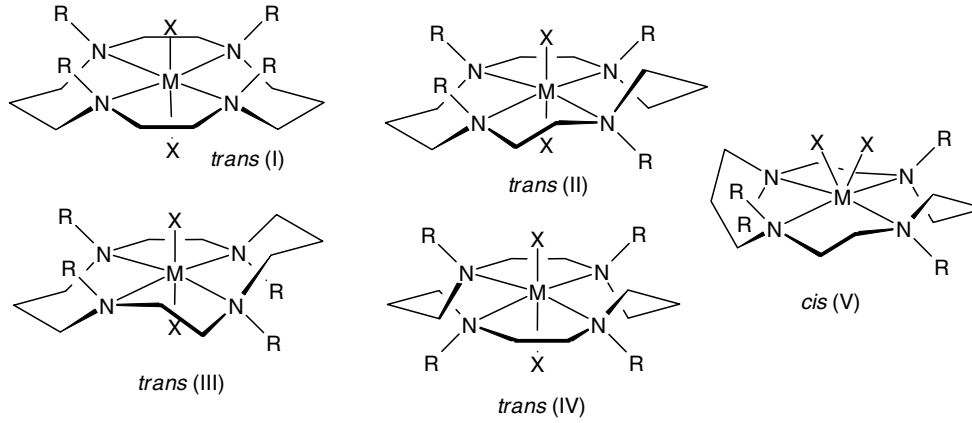


**Figure 3.51** The five most stable conformers of cyclam (M= transition metal, X=coordinating anion, R = H, Me *etc.*).

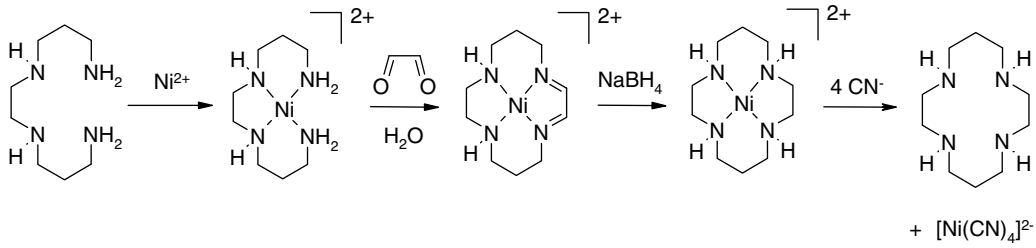


**Scheme 3.19** Template synthesis of cyclam (**3.45**).

These five conformers are the most stable structures because they have the least amount of repulsion between the donor atoms and the least amount of bond strain. They are given *cis*- and *trans*-assignments, based on the arrangement of the axial ligands about the bound metal ion. It has recently been suggested based on an extensive analysis of the Cambridge Structural Database (CSD) that the terms *folded* and *planar*, respectively, are more appropriate.[28] The most common form is the *trans*(III), which is the standard conformer for octahedral complexes and is similar to the familiar chair conformation of cyclohexane. By analogy the boat conformation of cyclohexane corresponds to the *trans*(I) form. This latter geometry is more predominant in square-planar and five-coordinate complexes.

The standard synthesis for cyclam was developed by Barefield and Wagner in 1976.[29] They used similar starting materials to the van Alphen procedure but the cyclisation yield is improved through the use of a nickel(II) template. Glyoxal completes the macrocycle by a Schiff base condensation reaction. The resulting imine functionalities are reduced with sodium borohydride to leave the complexed macrocycle. The metal ion is then removed by reaction with cyanide and the free ligand extracted with chloroform (Scheme 3.19). Yields are typically in the region of 60%.

An advantage of cyclam, like other tetraamines, is that it encircles the metal ion helping to satisfy the cation's coordination requirements and in some cases, stabilising uncommon oxidation states. The axial sites on these complexes are left unhindered so further chemistry can be conducted on the metal involving the coordination of anionic or neutral ligands. Cyclam forms very stable complexes with transition metals with log $K_{11}$ values of 27.2, 22.2, and 15.5 for Ni(II), Cu(II) and Zn(II), respectively. The four-nitrogen system of cyclam can be a versatile biological mimic and has been used to investigate the properties of metal centres in biological porphyrins in cases where the conjugation and planarity of the porphyrin system are not important factors. Cyclam derivatives are not troubled by the disadvantages of lengthy syntheses and low solubilities in conventional solvents, which are common problems with porphyrin complexes.

An interesting cyclam derivative has been prepared by Fabbrizzi *et al*. incorporating a pendant tris(2-aminoethyl)amine (tren) derived podand and a 1,4-xylyl spacer (**3.74**). The cyclam moiety binds to Ni(II) while the tren group includes Cu(II). The system behaves as a redox-driven anion translocation switch. Addition of chloride in MeCN solution results in chloride binding to the free axial site at the copper centre. Upon oxidation of the dimetallic complex, the Ni(II) changes to Ni(III) and the chloride reversibly shifts to this centre. Based on free energy measurements, this translocation has been hypothesised as being an entropy-driven intramolecular redox process involving a Cu–Cl–Ni chloride-bridged intermediate rather than an outer-sphere process, Figure 3.52.[30]

Cyclam derivatives such as **3.75** with hydroxypropyl side arms engage in a lariat ether-like coordination of one hydroxyl group to give square pyramidal complexes that hydrogen bond to anions

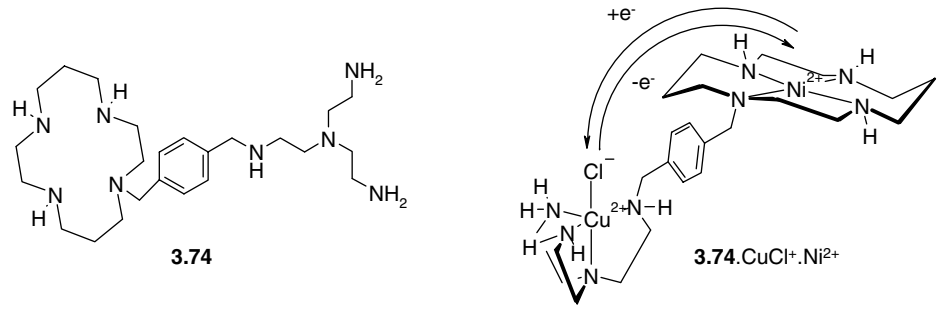


**Figure 3.52** Redox-driven chloride translocation in a mixed Cu/Ni complex of **3.74**.

(Section 5.1.4). However such is the affinity of transition metals for nitrogen donors that even if these compounds are derivatised to give macrotricyclic cryptands (**3.76**), Cu(II) and Ni(II) still only form 1:1 complexes rather than a 2:1 complex taking advantage of the mixed O/N donor array.[31] In contrast the analogous all-nitrogen macrocycles (**3.77**) form 2:1 complexes.

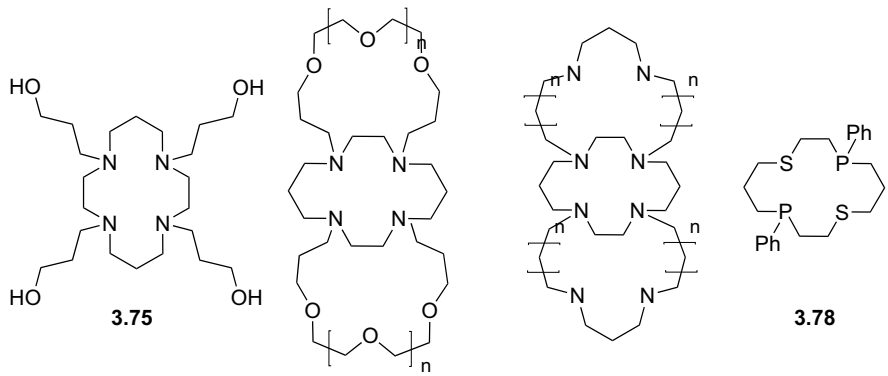


## 3.10.4 Phosphorus–Containing Macrocycles

Unidentate phosphines such as $PPh_3$ are ubiquitous ligands in catalysis and in the coordination chemistry of low oxidation state transition metal complexes. As π-acids they are able to form stable covalent bonds (Box 3.2) and their synthetic versatility means that the phosphine substitutent can be used to tune the complex's electronic properties, geometry and solubility *etc.* While bidentate phosphines such as diphenylphosphinoethane (dppe) and linear and tripodal tridentate phosphines such as bis(2-diphenylphosphinoethyl)phenylphosphine are also well-known, macrocyclic phosphines are particularly rare as a consequence of the difficulty in synthesising them. Mixed P/S-macrocycles such as Ph[9]ane-$PS_2$ and $Ph_2$[l4]ane-$P_2S_2$ (**3.78**) have been prepared by high dilution reaction of a dithiol with a dibromoalkane. The slow inversion at phosphorus means that the P atoms are chiral centres but treatment of the initial diastereoisomeric mixture with acetone allows the selective isolation of the *meso* form. Ligand **3.78** is an excellent ligand

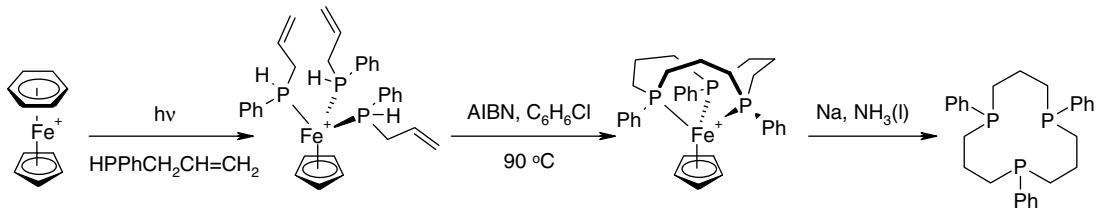


**Scheme 3.20** Template synthesis of the triphosphine macrocycle $Ph_3$[12]ane-$P_3$.[33]

for Pt(II) and Rh(III), giving respectively square planar $[Pt(Ph_2[l4]ane\text{-}P_2S_2)]^{2+}$ and octahedral *trans*-$[RhCl_2(Ph_2[l4]ane\text{-}P_2S_2)]^{+}$. The formation of the *trans* Rh(III) complex contrasts to the structure of the *cis*-dichloro form of the thiacrown complex *cis*-$[RhCl_2([l4]ane\text{-}S_4)]^{+}$ in which the thioether crown is in a folded conformation.[32] More recent work by Peter Edwards's group at Cardiff University UK has resulted in the isolation of several purely phosphorus-containing macrocycles by a novel template method. Photolysis of $[Fe(\eta^5\text{-}C_5H_5)(\eta^6\text{-benzene})]^{+}$ allows substitution of the benzene by three allylphosphine ligands. The vinyl groups can then by cyclised in a radical process while coordinated to the Fe(II) centre to give an iron complex of the triphosphine macrocycle $Ph_3$[12]ane-$P_3$ in a reasonable 30 % yield. Treatment with sodium in liquid ammonia gives free $Ph_3$[12]ane-$P_3$, Scheme 3.20.[33]

## 3.10.5 Mixed Cryptates

The combination of hard and soft donor atoms within a single receptor allows it either to complex a wide variety of metal ions or, more interestingly, to bind simultaneously soft and hard metals. For example, mixed S,N,O-cryptands (Figure 3.53) are able to bind both soft cations, such as $Rh^{+}$, and Lewis acid alkali metal ions to give cryptates containing both a redox active metal centre and a Lewis acid site that may be of interest in the supramolecular binding and activation of small organic substrates such as CO. The presence of the CO ligand in **3.79** indicates a possible model for such a process, in which the CO is bound to the low oxidation state transition metal in a stable, synergic fashion (Box 3.2) and activated by coordination to the alkali metal cation.

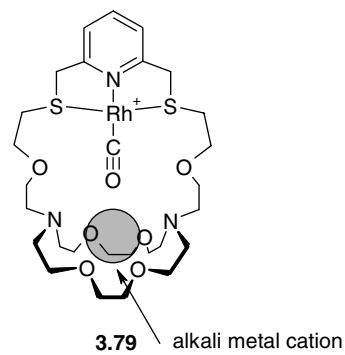


**Figure 3.53** A CO substrate is sandwiched between a redox-active transition metal and a Lewis acidic alkali metal cation by a cryptand with both hard and soft donor sites.

**Box 3.2** The Synergic Effect

Low oxidation state complexes are usually stabilised by $\pi$–acid ligands such as CO, $PR_3$ (phosphines), olefins *etc*. The use of the word 'acid' here refers to Lewis acidity, *i.e.* electron acceptance. Binding to $\pi$–acid ligands occurs in a synergic fashion that comprises two components:

1. Donation of electron density from the ligand to an unoccupied metal *p*- or *s*-orbital in a $\sigma$-fashion (*i.e.* the electron density maximum lies along a line joining the two atomic centres—the inter-atomic vector) (Figure 3.54a).
2. Metal-to-ligand back-bonding (Figure 3.54b). Donation of electron density from a filled metal *d*-orbital to an unoccupied, antibonding ligand orbital of $\pi^*$ character (as in CO) or $\sigma^*$ character with some *d* component (as in $PR_3$). Back-bonding occurs in a $\pi$–fashion in which two maxima in metal–ligand bonding electron density occur on either side of the interatomic vector. This has the effect of strengthening the M—L bond but weakening the bonds within the ligand itself (*e.g.* the C≡O bond in CO) because the back donation occurs into an antibonding ligand orbital, thus reducing the overall bond order.

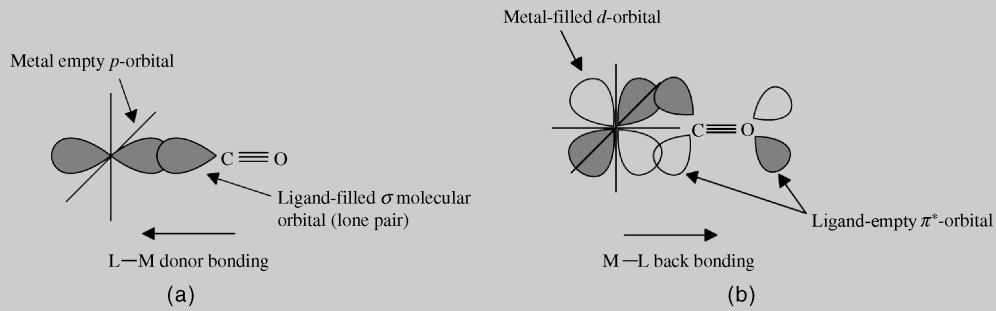


**Figure 3.54** Synergic bonding in CO (a) donation of electron density from ligand to unoccupied metal *p*- or *s*-orbital and (b) metal-to-Ligand backbonding.

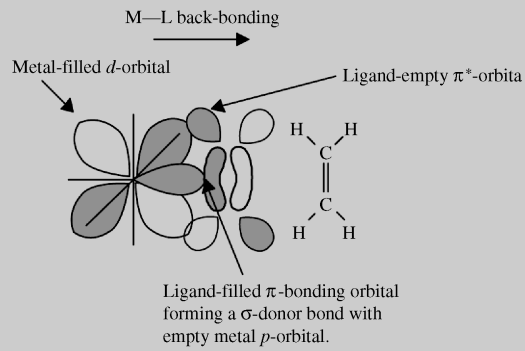


**Figure 3.55** Dewar Chatt Duncanson bonding model in metal alkene complexes.

These two components reinforce each other and are said to be 'synergic'. This bonding model is consistent with Pauling's electroneutrality principle (which does not allow the build-up of charge on any particular atom) because charge that is donated by the $\pi$-acid ligand's lone pair is returned to it by back-bonding. In the case of alkene compounds, this bonding model is known as the Dewar Chatt Duncanson model (Figure 3.55):

(*continued*)

**Box 3.2** (*Continued*)

1. forward donation from the olefin $\pi$-bonding orbital to an empty metal *p*-orbital;
2. back donation from filled metal *d*-orbital into olefin antibonding orbital.

This has the following observable effects in alkenes such as ethene:

- Weakening of the C = C and consequent donation into $\pi^*$-orbital. The C = C distance in $[PtCl_3(C_2H_4)]^-$, a typical synergic complex, is 1.37 Å (*cf.* free ethene, 1.34 Å).
- Lowering the vibrational stretching frequency. In the above example $\nu$(C = C) is 1520 $cm^{-1}$ (*cf.* $\nu$(C = C) in free ethene, 1623 $cm^{-1}$).
- Displacement of H atoms 16° away from the metal centre from their position in planar ethene as a consequence of partial rehybridisation to $sp^3$ carbon atoms.

## 3.10.6 Schiff Bases

A vast range of Schiff base macrocycles and macrobicycles exist and have been of great importance in macrocyclic coordination chemistry, particularly of the transition metals, from the very beginning of supramolecular chemistry. The key Schiff base condensation reaction involves simply the reaction of an amine with an aldehyde to eliminate (condense) water and give an imine. If desired, the product may be reduced (*e.g.* with $NaBH_4$) to give an amine or a secondary amine-based macrocycle (Scheme 3.21).

We have already looked at three key Schiff base macrocycles (Figure 3.56), which were amongst the first artificial metal macrocycle compounds to be synthesised. These compounds are generally formed by thermodynamic template effects because, unless water is removed during the course of the reaction, the condensation is reversible, allowing complexation to sequester the most stable metal–product

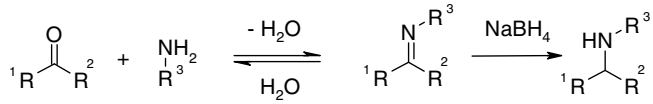


**Scheme 3.21** The Schiff base condensation and the reduction of the product to give an amine.

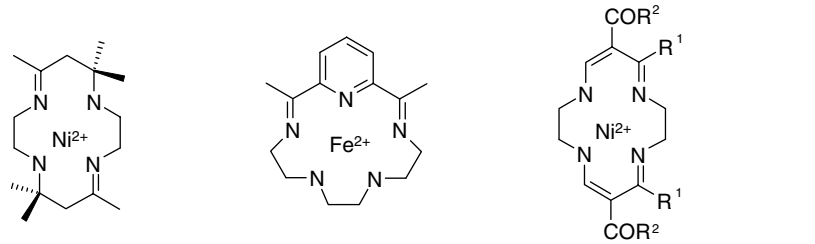


Curtis 1961

Aldol condensation of acetone and $[Ni(en)_3]^{2+}$

Busch 1964

Fe(II) templated condensation of 2,6-diacetylpyridine with diethylene tetramine.

Jäger 1964

Metal templated reaction of β-ketoiminato complexes with 1,2-diaminoethane (en)

**Figure 3.56** The original Schiff base macrocycles.

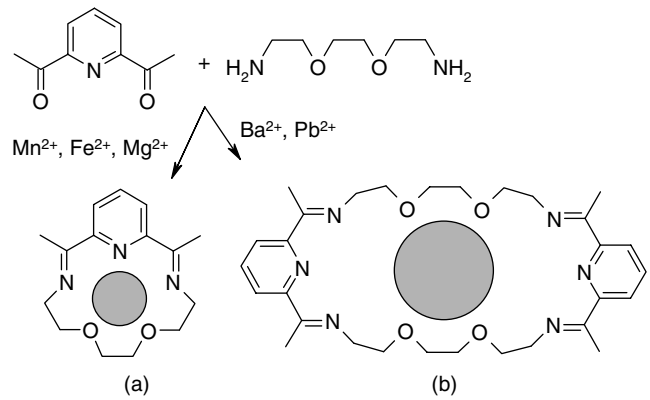


**Scheme 3.22** Schiff base reactions (a) 1:1 cyclocondensation templated by small metal ions; (b) larger macrocycles are obtained with larger templates.

compounds (Section 3.9.1). Templating metal ions may be used to control the size of the macrocycle formed. Thus small cations such as $Mn^{2+}$, $Fe^{2+}$ and $Mg^{2+}$ can result in the formation of 1:1 condensation products as in Scheme 3.22a, while larger 2:2 macrocycles may be selected through the use of cations such as $Pb^{2+}$ and $Ba^{2+}$ (Scheme 3.22b). One disadvantage of the template procedure, however, is that if the metal-free macrocycle is desired (*e.g.* for further complexation experiments or as part of a more elaborate synthesis), the templating cation must be removed. A number of ways have been devised in which to accomplish this, of which the most common are extraction of the macrocycle into an organic solvent (for weakly coordinating metal ions such as the alkaline or alkaline earth cations) or exchange of the macrocycle for very strongly coordinating ligands such as $CN^-$ (as in the synthesis of cyclam, Scheme 3.19).

Despite these drawbacks, however, Schiff base condensation reactions are extremely versatile and high yielding, and have been applied to the preparation of an enormous range of metallomacrocyclic and macrobicycic compounds, as well as open-chain podand analogues. Indeed, interaction of transition metals with the imine nitrogen is particularly strong as a result of back-bonding interactions with the C=N $\pi^*$ antibonding orbital. Schiff base type condensation reactions are also found in a great deal of polypyrrole-based macrocyclic chemistry as discussed in the next section. A particularly striking recent example of the use of a Schiff base macrocycle is the activation of the normally inert uranium(VI) uranyl cation ($UO_2^{2+}$) by the dipyrrolylmethane based tetraimine **3.80**.[34] The uranyl

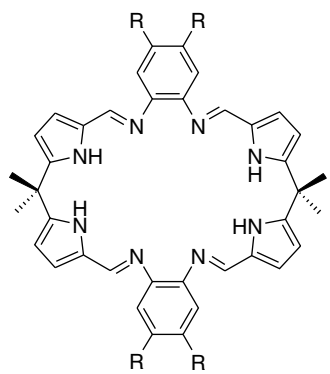

**3.80**

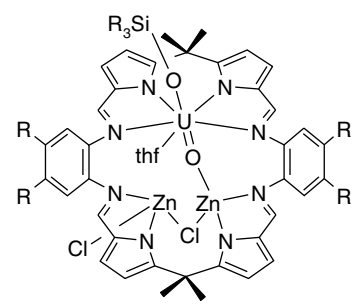


**3.81**

cation is the predominant form of uranium in the environment where its solubility makes it a problematic contaminant, leading to many attempts to bind and extract it, *e.g.* using calixarene sulfonates (Section 3.14).[35] It is also extremely chemically robust, however the rigid, well-defined macrocyclic framework of ligand **3.80** allows it to be activated by a metal ion simultaneously bound within the macrocycle. The uranyl ion undergoes a single electron reduction on reaction with a trialkylsilyl amide to give a uranium(V) complex containing a monofunctionalised $[O{=}U^{\cdots}OR]^{+}$ unit in **3.81**, isolated in the presence of transition metal cations such as Fe(II) and Zn(II).

## 3.10.7 Phthalocyanines

The phthalocyanines are important industrial dyes closely related to the porphyrins whose importance in biological systems can hardly be overstated (discussed in Section 2.3). The first report of a phthalocyanine as an unidentified blue by-product (in fact metal-free phthalocyanine) was reported in 1907. Later in 1927, two researchers from Switzerland accidentally synthesised copper phthalocyanine (**3.82** R = H, known as phthalocyanine blue), copper naphthalocyanine and copper octamethylphthalocyanine (**3.82** R = Me) from the attempted conversion of 1,2-dibromobenzene into phthalonitrile. They found that these complexes were very stable but did not fully characterise these blue materials. The later accidental discovery of these compounds at Scottish Dyes Ltd. (a fore-runner of ICI) resulted in their exploitation in the dyes industry. The colour of the phthalocyanine complexes is readily varied by change in the substituents R and the nature of the embedded metal, thus phthalocyanine green is compound **3.82** with R = Cl. Commercial phthalocyanine dyes used in the fabrics and paper industries are made water soluble by appending sulfonate groups and they can be used in organic solvents by choosing tetraalkylammonium counter cations in charged complexes.

Both porphyrins and phthalocyanines are prepared by template Schiff base type condensation rections. For example, the use of a large template is evident in the synthesis of the superphthalocyanine **3.83**, in which five repeat units are organised about the pentagonal bipyramidal $UO_2^{2+}$ core, instead of four as in more traditional phthalocyanine complexes such as **3.82**. Smaller templates result in the formation of the trimeric subphthalocyanine **3.84**. The reversible nature of the condensation reaction means that both **3.83** and **3.84** can be converted into normal tetrameric phthalocyanine, **3.85**, Scheme 3.23.

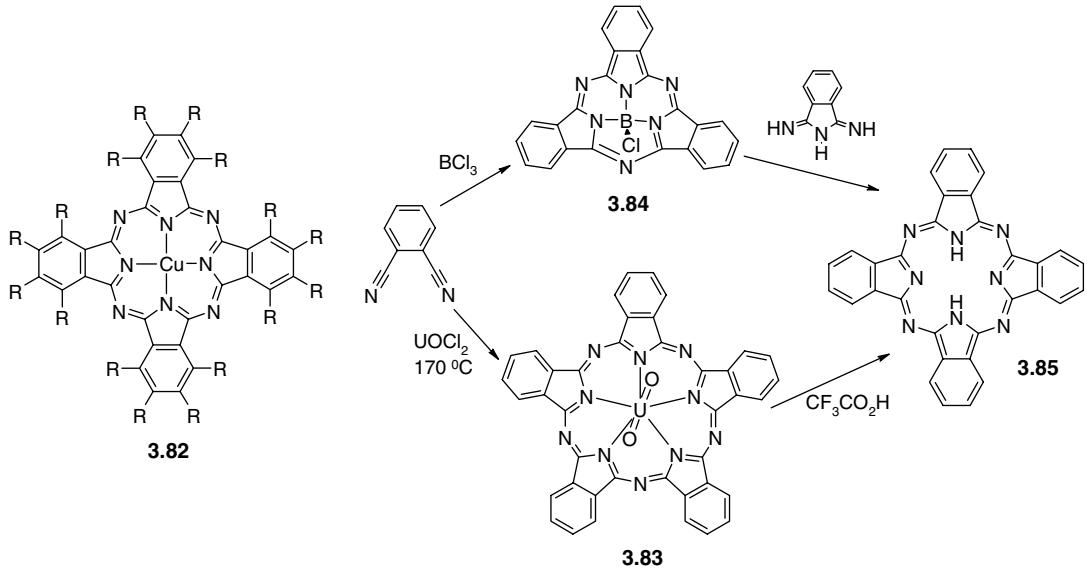


**Scheme 3.23** Template synthesis of the phthalocyanines.

## 3.10.8 Torands

Bell, T. W. 'Torands', in *Encyclopedia of Supramolecular Chemistry*, Atwood, J. L. and Steed, J. W. (eds), Dekker: New York, 2004, vol. 2, *pp.* 1508–1515.

The *torands* (from 'torus' and 'ligand') are a series of extremely rigid ligands based on fused aromatic rings. The two best known torands are **3.86** and **3.87**. Their extreme rigidity means that even though they are only two-dimernsional hosts compound **3.86** bind extremely strongly to a wide range of metals. The relatively soft electronic character of the pyridyl-derived donor atoms suggests that transition metals should be strongly bound and indeed they are, however even alkali metal cations that do not normally show a strong affinity for pyridyl donors are extremely strongly complexed. Indeed the affinity constant of **3.86** for $Na^+$ in water saturated chloroform is over $10^{14}$ making it comparable to the equally preorganised spherand-6. The expanded torand **3.87** binds to organic cations, particularly guanidinium *via* NH···N interactions. Host **3.87** is particularly complementary to guanidinium because of the match between the threefold symmetry of host and guest which allows the formation of a total of six charge-assisted hydrogen bonds. The presence of the *n*-butyl substituents means that the torands are reasonably soluble in organic solvents. Their main drawback, however, is the relative difficulty of their synthesis.

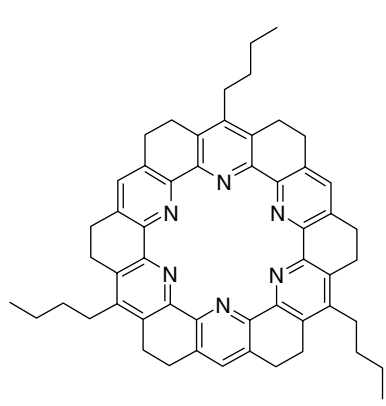

**3.86**

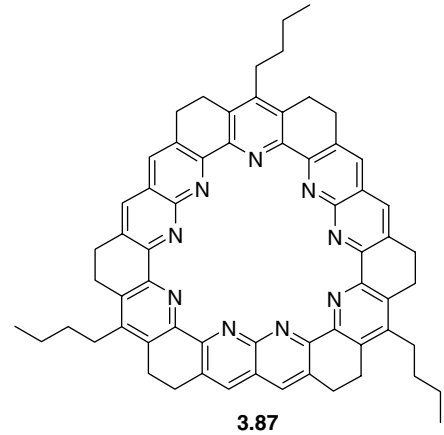

**3.87**

# 3.11 Proton Binding: The Simplest Cation

Ratcliffe, C. I., Irish, D. E., 'The nature of the hydrated proton,' in *Water Science Reviews 3*, Franks, F., ed. Cambridge University Press: Cambridge, 1988; *pp* 1–78.

The proton, $H^+$, usually in some hydrated form, $H(H_2O)_n^+$ ($n = 1 - 20+$) is one of the simplest cations and is fundamental to chemical and biological processes. Indeed the transfer of a proton from one atom to another has been described as '*The most general and important reaction in chemistry*'. Interactions to protons in the gas phase, in solution and in the solid state all take the form of more or less non-covalent interactions, often strong charge-assisted hydrogen bonds (*i.e.* hydrogen bonds between ions). Protonolysis equilibria are intimately involved in supramolecular systems, often in competition with metal ion binding in aqueous solution (*cf.* potentiometric methods for binding constant determination, Section 1.4.2) and supramolecular hosts have been developed that can bind protons either *via* hydrogen

bonding or protonation reactions of amines allowing insight into the structural and solution chemistry of this unique cation.

## 3.11.1 Oxonium Ion Binding by Macrocycles in the Solid State

Junk, P. C., 'Crown ethers as stabilising ligands for oxonium ions', *New J. Chem.*, 2008, **32**, 762–773.

Interaction of [18]crown-6 with aqueous acid almost invariably results in isolation of crystalline solids of the cation $H_3O^+$·[18]crown-6. The reaction also works in less polar media, thus interaction of [18]crown-6 with HCl gas in toluene in the presence of a little moisture results in the formation of an ionic liquid clathrate layer (Section 13.5) with the composition $(H_3O)$[[18]crown-6][$HCl_2$]·3.8$C_6H_5Me$, from which crystals of composition [$H_3O \subset$ [18]crown-6]($HCl_2$) (**3.88**) may be isolated upon standing. Reaction of this liquid clathrate layer with two equivalents of water gives a further crystalline product ($H_5O_2$)[$H_3O \subset$ [18]crown-6]$Cl_2$ (**3.89**), which is also deposited from the clathrate layer. The liquid clathrate formation is a consequence of the large [$H_3O \subset$ 18-crown-6]$^+$ cation and smaller halide anions, resulting in favourable cation–π interactions with the toluene solvent, coupled with a low lattice energy. Both of these compounds contain the oxonium cation $H_3O^+$ bound within the crown ether by hydrogen-bonding interactions to the crown oxygen atoms (Figure 3.57a). The higher oxonium ion $H_5O_2^+$ is situated externally to the cavity in **3.89**. Examination of a wide range of related systems has revealed a strong selectivity of [18]crown-6 for $H_3O^+$. The $H_3O^+$ cation, which is the simplest member of the family of oxonium cations, $H^+(H_2O)_n$, is estimated to fall between sodium and potassium in effective ionic radius. It exhibits both a size and topological (three-fold symmetry) match with [18]crown-6 and inclusion is driven by the formation of three bifurcated O—H ··· O hydrogen bonds. The ion is fully capable of sitting entirely within the macrocycle cavity. However, a survey of a range of [$H_3O \subset$ 18-crown-6]$^+$-containing species revealed that the oxygen atom is situated between 0.007 and 0.87 Å out of the crown ether mean plane, highlighting the flexibility of the interactions and the macrocycle. Interestingly, interaction of solid-state structures of [18]crown-6 containing (unprotonated) water are entirely different as a consequence of the different symmetry constraints of the $C_{2v}$ guest, and the longer length of the hydrogen bonds, which are not charge-assisted. The structures of [18]crown-6·4$H_2O$, [18]crown-6·8$H_2O$ and [18]crown-6·12$H_2O$ contain similar $D_{3d}$ crown ethers, hydrogen-bonded to four water molecules, two above and two below the mean crown plane (Figure 3.57b).[36]

The elegant match of $H_3O^+$ for [18]crown-6 suggests that the crystallisation of crown ether and cryptand complexes from acidic liquid clathrate media might represent a straightforward

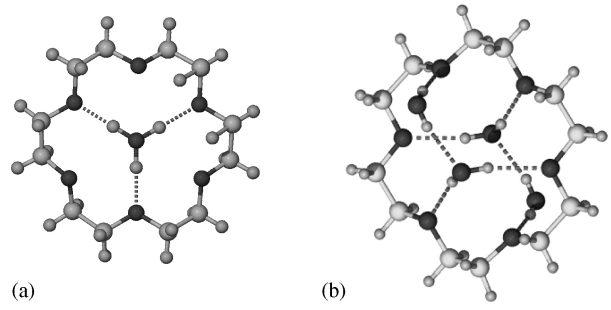


**Figure 3.57** (a) X-ray crystal structure of the [$H_3O \subset$ [18]crown-6]$^+$ cation (b) The [$(H_2O)_4$[18]crown-6] in [18]crown-6 tetrahydrate.[36]

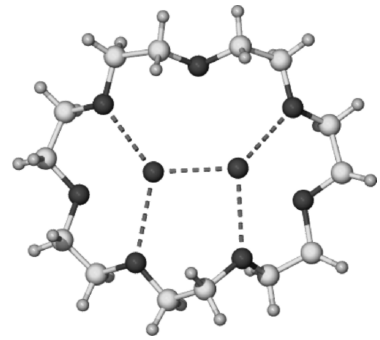

**Figure 3.58** Complexation of $H_5O_2^+$ by [21]crown-7 from a liquid clathrate medium.[37]

method for systematic isolation of various forms of the oxonium ion according to the size of the crown ether and the topological fit of the hydrogen bonding network. Liquid clathrate formation is observed upon bubbling HCl gas through toluene solutions of a large range of crown ethers in the presence of trace amounts of moisture. The solutions may be induced to crystallise by addition of an enormous variety of metal-containing species, which interact with the excess chloride to give large inorganic haloanions. In particular, transition metal carbonyls react to give anions of type $[M(CO)_5Cl]^-$, $[M(CO)_4Cl_3]^-$, $[M(O)Cl_4(H_2O)]^-$ *etc.* (M = Mo, W). In this way, oxonium ion complexes of a wide range of crown ethers have been isolated. In cases where there is a genuine size and symmetry match between crown and oxonium ion, some selectivity for particular oxonium ions has been observed, particularly amongst larger crown ethers. Thus [21]crown-7 and dibenzo[24]crown-8 both encapsulate $H_5O_2^+$ (Figure 3.58), while dibenzo[30]crown-10 includes two isolated $H_3O^+$ ions. Smaller crown ethers such as [15]crown-5 and [12]crown-4 give highly variable behaviour depending on the nature of the anion. The oxonium ions are intercalated between crown ether molecules with the crown–crown spacing, and hence oxonium ion identity, being subject to a variety of crystal packing considerations. $H_7O_3^+$ and $H_9O_4^+$ species have been isolated in this way.[37]

A range of oxonium ion crown ether complexes have also been isolated from solutions of metallic gold in the very strong aqueous acid *aqua regia* (gold dissolved in a 4 : 1 mixture of hydrochloric and nitric acids), a mixture believed by Roger Bacon to be the 'Elixir of Life'! *Aqua regia* is an oxidising acidic solvent and has been known since the Middle Ages as the only reagent capable of dissolving metallic gold (its invention has been attributed to the alchemist Gerber, the 'father of modern chemistry,' who died in 803 CE). Under these conditions the gold is oxidised to Au(III) and thus oxonium ion crown ether complexes are isolated as their tetrachloroaurate(III), $[AuCl_4]^-$, salts. This work resulted in the isolation of $H_3O^+$, $H_5O_2^+$, $H_7O_3^+$ and $H_{11}O_6^+$ complexes all hydrogen bonding strongly to the crown ethers. In particular a dibenzo[30]crown-10 derivative proved a good match for $H_7O_3^+$, while the very large $H_{11}O_{16}^+$ ion was isolated threading through a dibenzo[18]crown-6 derivative. The smaller crown ethers again give sandwich compounds in which $H_5O_2^+$ and $H_7O_3^+$ ions alternate with the crown ether hydrogen bond acceptors. The structure of $[(H_7O_3)(15\text{-crown-}5)][AuCl_4]$ was determined by single crystal neutron diffraction (Figure 3.59).[38] Unlike X-ray crystallography, neutron diffraction (see Chapter 8, Box 8.1) is a precise way to locate hydrogen atoms, which are of obvious importance to oxonium ion structures. The structure shows a chain of three water molecules exhibiting very short O···O distances. While most O–H bonds are relatively close to the value for water itself (*ca.* 0.95 Å), one proton situated in between the closest pair of oxygen atoms exhibits a remarkably elongated O–H bond length

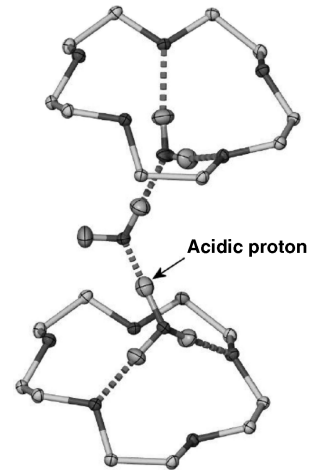


**Figure 3.59** Single crystal neutron structure of $[(H_7O_3)(15\text{-crown-}5)][AuCl_4]$ showing two crown ether repeats sandwiching an $H_7O_3^+$ ion.[38]

(1.12 Å) and a very short OH···O distance (1.32 Å), consistent with 'strong' hydrogen bonding (see Section 1.8.4).

Proton binding by azacrowns and cryptands is also possible, although in these cases the proton invariably forms a covalent interaction with one of the nitrogen atoms, in some cases hydrogen bonding to water molecules. Thus the hydrated $H^+$ complex of [18]ane-$O_5N$ contains an N-protonated H[18]ane-$O_5N^+$ cation hydrogen bonding with a cavity-included water molecule. A particularly interesting example comes from the deep blue liquid clathrate formed from the interaction of [2.2.2]cryptand with HCl gas in toluene in the presence of $CoCl_2$. Upon prolonged standing a crystalline material of formula $\{[2.2.2]\text{cryptand-}2H^+\cdot[CoCl_4]^{2-}\}_2\cdot C_6H_5Me$ is isolated. The cryptand is protonated at the bridgehead nitrogen atoms and the protons are situated inside the macrobicyclic cavity. This species contains linear stacks of type anion···cation···arene···cation···anion, clearly demonstrating a cation–π stacking interaction (*cf.* Section 1.8.5) that serves to insulate the protonated cryptand cations from one another (Figure 3.60). Evidence for the formulation of this as an attractive interaction comes from the compressed nature of the cryptand, which exhibits an N ··· N interbridgehead distance of 6.36 Å, markedly shorter than in the structure of the same complex with chloride anion (6.87 Å), which does not include toluene.[39]

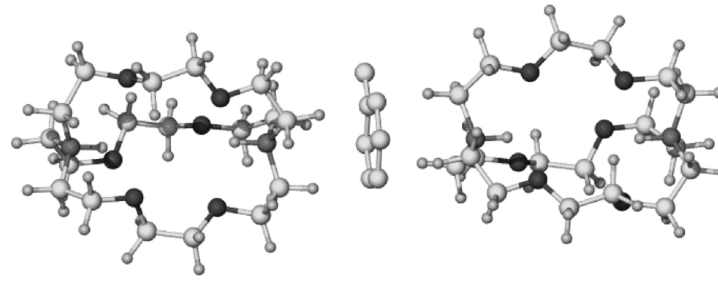

**Figure 3.60** Cation–π interactions in $\{[2.2.2]\text{cryptand-}2H^+\cdot[CoCl_4]^{2-}\}_2\cdot C_6H_5Me$.[39]

## 3.11.2 Solution Chemistry of Proton Complexes

Bencini, A., Bianchi, A., Garcia-España, E., Micheloni, M., Ramirez, J. A., 'Proton coordination by polyamine compounds in aqueous solution,' *Coord. Chem. Rev.* 1999, **188**, 97–156.

The solution concentration of protons (the pH or potence hydrogen, equal to –log [$H^+$] in dilute solutions) is readily determined through potentiometric measurements using a glass electrode. Such measurements are generally reliable in the range $2.5 < pH < 10.5$ corresponding to $H^+$ concentrations of *ca.* $10^2$–$10^{11}$. At high pH the glass electrode suffers from interference by alkali metal cations while the acidic end is subject to liquid junction potential effects. Other techniques such as calorimetry and spectrophotometry can give information outside this range. Solution binding of $H(H_2O)_n^+$ by [18]crown-6 in dry $CDCl_3$ has been observed by $^1H$ NMR spectroscopy[40] suggesting a 1:2 $H^+$ : crown ether ratio, however in supramolecular chemistry we are very often dealing with the protonation of amine based hosts and we will focus on amine macrocycles as a representative systems.

As discussed in Section 3.10.3, in the gas phase the basicity of simple amines follows the order $NMe_3 > NHMe_2 > NH_2Me > NH_3$ because of the electron donating effect of the methyl (Me) groups. In solution, however, we can define a basicity constant as the equilibrium constant for the reaction shown in Equation 3.4. Note it is important to specify temperature, solvent (usually water) and solution ionic strength, $I$.[‡] Basicity constants are related to the acid dissociation constants ($K_a$) of the base's conjugate acid *via* the dissociation constant of water, $K_w = 10^{-14}$ at 25 °C. Thus $K_b \times K_a = K_w$.

$$R_3N_{(aq)} + H^+_{(aq)} \underset{}{\overset{K_b}{\rightleftharpoons}} R_3NH^+_{(aq)} \tag{3.4}$$

In aqueous solution the basicity constant values, log $K_b$, for ammonia and methylated amines are 10.77 ($NHMe_2$), 10.63 ($NH_2Me$), 9.82 ($NMe_3$) and 9.28 ($NH_3$), thus the basicity order is $NHMe_2 \approx NH_2Me > NMe_3 > NH_3$. This change compared to the gas phase can be explained by the better solvation of the hydrogen bond donor ammonium ions by water. In macrocyclic systems intrinsic basicity and solvation effects are superimposed on two additional factors, namely the repulsion between neighbouring protonated $NH^+$ groups that are sometimes forced into close proximity by the structure of the macrocycle, its preorganisation, and stabilising intramolecular $NH^+\cdots N$ hydrogen bonding effects. Hydrogen bonding effects are illustrated by a comparison of the cyclic [9]ane-$N_3$ with the acyclic diethylenetriamine (Table 3.16, entries 1 and 2). The macrocycle is almost $10^3$ times more basic for the first protonation step because the resulting $NH^+$ group forms a bifurcated intramolecular hydrogen bond to both unprotonated N atoms, as shown in the X-ray crystal structure of the tri-N-methyl derivative, Figure 3.61. However addition of a second and third proton is relatively unfavourable because of the breaking of this hydrogen bond and the resulting proximity of the charged $NH^+$ groups. In contrast the linear chain analogue protonates at the ends first where the two resulting positive charges are well separated and it is only at the third protonation step that significant repulsions are introduced.

Unfavourable intramolecular repulsions between $NH^+$ groups are highly dependent on the distance between the protonation sites and thus the introduction of a longer, propylenic spacer generally increases the second and subsequent basicity constants as well as influencing the first by increased electron donation. Compare entries 3 and 4 in Table 3.16. The effect is also evident in the linear

[‡] The ionic strength is a function of the total concentration of all ions of whatever charge and is defined as: $I = \frac{1}{2} \sum_{i=1}^{n} c_i z_i^2$, where $c_i$ is the molarity concentration of ion $i$, $z_i$ is the charge of that ion. For a 1:1 electrolyte such as sodium chloride, the ionic strength is equal to the concentration, but for multiply chanrged ions as in $MgSO_4$ the ionic strength is four times higher. In general multivalent ions contribute strongly to the ionic strength.

**Table 3.16** Basicity constants for some representative polyamines.

| Entry | Compound | Log $K_1$ | Log $K_2$ | Log $K_3$ | Log $K_4$ |
|---|---|---|---|---|---|
| 1 | 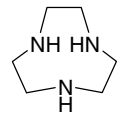 | 12.6 | 7.55 | 2.53 | |
| 2 | 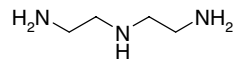 | 9.84 | 9.02 | 4.23 | |
| 3 | 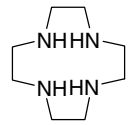 | 10.38 | 9.71 | 2.05 | <1 |
| 4 | 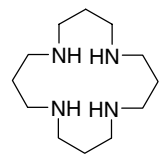 | 10.85 | 9.80 | 7.21 | 5.69 |
| 5 | 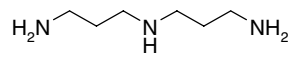 | 10.65 | 9.57 | 7.69 | |
| 6 | 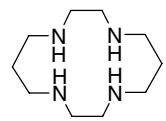 | 11.58 | 10.62 | 1.61 | 2.41 |
| 7 | 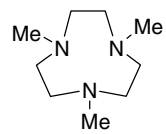 | 11.7 | 5.1 | ~0.4 | |
| 8 | 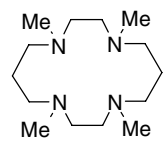 | 10.10 | 9.35 | 3.45 | 2.7 |

amines (compare entries 2 and 5). For cyclam (Section 3.10.3) the combination of two-carbon and three carbon linkers and the ability to form two intramolecular hydrogen bonds results in very striking behaviour (entry 6) with ready uptake of two protons followed by very significant lack of basicity at the remaining two N atoms. A third protonation would result in breaking hydrogen bonds and placing two protons next to one another separated only by a two-carbon linkage. The fact that the third protonation step is even more unfavourable than the fourth is ascribable to a conformational rearrangement fron an *in* to an *out* conformation at this stage.

*N*-methylation changes secondary amines into tertiary amines. While inductive effects might mean an increase in the amine gas phase basicity, the low solvation of tertiary amines generally means that methylation reduces solution basicity (compare entries 1 and 7). In addition to solvation effects, it is thought that steric effects may favour the *out* conformer. In the case of tetramethylcyclam (entry 8)

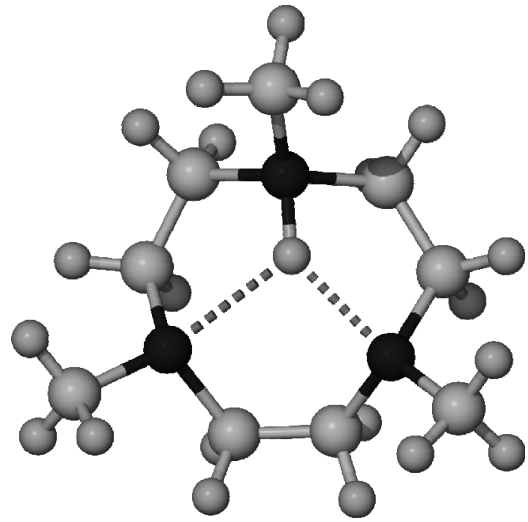

**Figure 3.61** X-ray molecular structure of mono-protonated $Me_3$[9]ane-$N_3$ ($ClO_4^-$ salt) showing the stabilising intramolecular hydrogen bond.

the anomalously low value for the third protonation is not evident suggesting methylation favours the conformational change that occurs at the third protonation stage.

A key question very often in protonation studies is the location of the protonation site in multifunctional polyamines. This cannot be directly assessed by basicity data and other evidence must be sought that can give information on the protonation regiospecificity. A useful tool in this regard is $^1$H and particularly $^{13}$C NMR spectroscopy. Figure 3.62 shown the changes in the $^1$H and $^{13}$C NMR spectra of azacyclophane **3.90**. The very significant shift in the $^{13}$C resonance assigned to CB1 strongly suggests that protonation is initially at the benzylic amines, a conclusion supported by the low entropy and high enthalpy terms associated with the process which are consistent with a high degree of hydrophobicity of the protonation site.

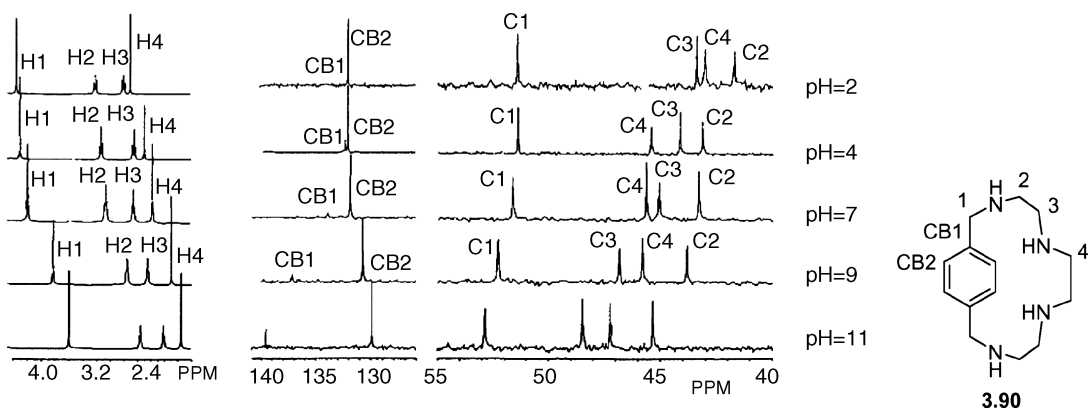


**Figure 3.62** $^1$H and $^{13}$C NMR spectra of macrocycle **3.90** as a function of pH. (Reproduced from Section Key Reference with permission from Elsevier).

Finally, we look briefly at macrobicycles. The two cryptands [1.1.1]cryptand (**3.91**) and azacyclophane (**3.92**) have been prepared as proton binding hosts. Compound **3.91** behaves as a diprotic base and each bridgehead nitrogen can exist in both *in* (*i*) and *out* (*o*) forms with the lone pair either pointing into the cavity (*i*) or outside it. The log $K_b$ values for the $io^+$ and $o^+o^+$ forms are very low at 7.1 and *ca.* 1, respectively. In contrast the internally protonated complexes $ii^+$ and $i^+i^+$ show extremely strong basicity (log *K* 17.8 and ~8, respectively) coupled with very slow exchange between intra-cavity protons and the surrounding medium. The intracavity N–$H^+$ group is stabilised by hydrogen bonding to the three ether oxygen atoms. Compound **3.92**, which only exhibits an *in* form, is also highly basic with the log *K* values for $H^+$·**3.92** being 10.21 and 10.43 (R = H and Me, respectively) again with exchange between intra-cavity and extra-cavity protons. In the absence of stabilising $NH^+\cdots O$ interactions, the intra cavity proton is stabilised by an $NH\cdots\pi$ interaction.[41] Gas phase measurements suggest that $HNMe_3^+$ interacts approximately equally well with both benzene and a water molecule. The fact that the N-methylated compound is more basic that the secondary amine analogue is good evidence for the low importance of solvent in the first protonation step. Interestingly an analogous hydrocarbon macrobicycle *in*-[$3^{4,10}$][7]metacyclophane (**3.93**) that is not expected to exhibit this kind of stabilising interaction has also been synthesised.[42] The $^1$H NMR spectrum exhibits a resonance at *ca.* –4 ppm for the bridgehead CH proton consistent with its postion in the shielding region of the aromatic ring (see Box 3.3). While no X-ray crystal structure has been determined, infrared spectroscopic evidence suggests remarkable C–H bond compression as a result of a repulsive C–H···arene interaction, with the vibrational IR absorption of the C–H bond occurring at 3325 $cm^{-1}$, dramatically shifted from the typcal value of ca. 2900 $cm^{-1}$. Other such molecular 'iron maidens' are discussed in Section 6.5.4.

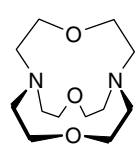


**3.91**

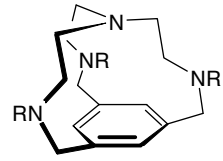


**3.92** R = H, Me

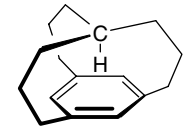


**3.93**

## 3.12 Complexation of Organic Cations

So far, we have discussed only the complexation of metal cations, which rely primarily on cooperative ion–dipole or Lewis acid/base interactions for stability. However, non-metal cations can also interact with corands and cryptands as in the tetrahedral recognition of the ammonium cation ($NH_4^+$) by the 'soccer ball' cryptand **3.29** (Figure 3.63). While this recognition only occurs *via* hydrogen bonding ($N^+$—H ··· N type), the effect on the ammonium ion is such as to increase its p*K*a value by six units, thus the cryptate is a million times less likely to deprotonate than its uncomplexed analogue. The binding of organic cations, particularly ammonium species *via* hydrogen bonding, as well as electrostatic interactions, is also of significant interest, not least because these more complicated cations can be chiral, thus posing the question, *can a chiral host recognise one enantiomer over another* (see Section 3.12.4)?

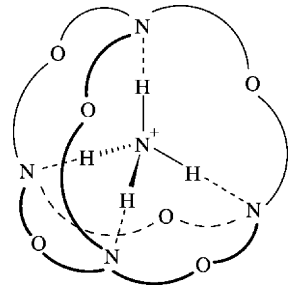

**Figure 3.63** Tetrahedral recognition of $NH_4^+$ by the 'soccer ball' cryptand (**3.29**).

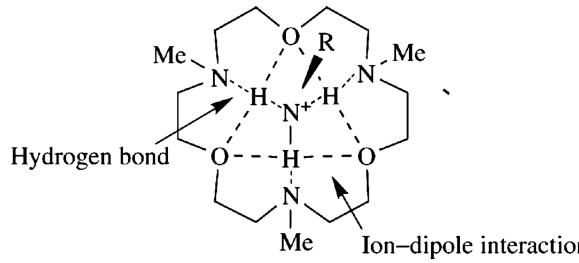


**Figure 3.64** Perching geometry in alkyl ammonium ion complexes of $Me_3$[18]ane-$O_3N_3$ held together by charge-assisted hydrogen bonds.

## 3.12.1 Binding of Ammonium Cations by Corands

The binding of ammonium and alkyl ammonium cations by [18]crown-6 and C-backbone substituted derivatives proceeds *via* three $N^+$—H ⋯ O hydrogen bonds to give a perching complex, although [18]crown-6 binds $K^+$ more strongly than $NH_4^+$, a reflection of the relatively hard character of the ether oxygen atoms. The analogous triaza corand [18]ane-$O_3N_3$ (**3.43**) and it trimethyl analogue form a sterically nearly identical triple array of $N^+$—H ⋯ N hydrogen bonds (Figure 3.64) and is selective for alkyl ammonium ions over $K^+$, although this may be a reflection of the decrease in $K^+$ affinity as much as increase in affinity for the ammonium species.

Table 3.17 shows the complexation free energies for various ammonium ions with three corand receptors. It is immediately apparent that $NH_4^+$ is bound more strongly than either of its alkylated analogues, and methylammonium is bound more strongly than *t*-butylammonium, with a particularly large difference between $NH_4^+$ and $CH_3NH_3^+$ complexes of **3.95** and **3.96** (10 kJ mol$^{-1}$).

**Table 3.17** Complexation free energies for corand receptors with ammonium ions.

| | $-\Delta G°$ (kJ mol$^{-1}$) | | |
|---|---|---|---|
| Host | $NH_4^+$ | $CH_3NH_3^+$ | $(CH_3)_3CNH_3^+$ |
| **3.94** | 43.9 | 37.7 | 34.7 |
| **3.95** | 39.7 | 31.4 | 28.9 |
| **3.96** | 37.2 | 28.9 | 26.8 |

This difference suggests that steric effects may be important in all hosts. In particular, low binding free energies are observed for alkylammonium complexes of **3.96**. This low affinity is attributed to unfavourable steric interactions between the methyl groups of the host with those of the guest. In the X-ray crystal structure of **3.96**·$(CH_3)_3CNH_3^+$, the methyl groups of the guest contact those of the host in the seven and 12 o'clock positions (Figure 3.65).

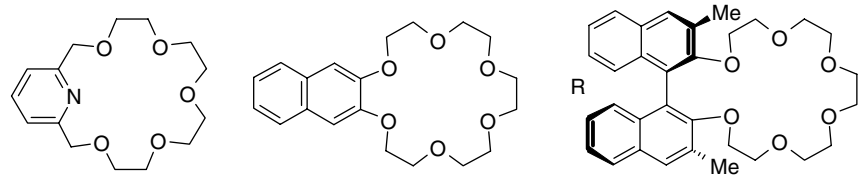


**3.94** **3.95** **3.96**

Addition of negatively charged functional groups, such as carboxylates, on to the carbon backbone of [18]crown-6 enhances alkyl ammonium cation binding by reinforcement of the hydrogen bonding network with electrostatic attractions between the $–NH_3^+$ residue and the anionic $–CO_2^-$ moiety. Thus receptors such as **3.97a** bind strongly to primary ammonium salts, and indeed are selective for them over secondary and tertiary species. This phenomenon is termed *central discrimination* (Figure 3.66), because it involves selectivity arising from the central corand core of the macrocycle, and allows recognition of primary ammonium salts of biological importance such as noradrenaline and norephendrine over their *N*-methylated analogues. Variation of the side chains, X, gives rise to a range of receptors that may be tuned to selectively bind particular primary ammonium ions by virtue of specific interactions (hydrogen bonding, electrostatic, π-stacking, van der Waals *etc.*) with the substituents on the R group of the guest. This kind of discrimination is termed *lateral discrimination* (Figure 3.66) and, in a well-designed host, is complementary to the central discrimination.

In the case of secondary ammonium ions, $R_2NH_2^+$, the tripodal, perching motif observed in Figure 3.65 is no longer feasible. However, binding is observed to small corands such as diaza[12]crown-4 *via* two $N^+$—H ⋯ N hydrogen bonds. Complexation of larger ammonium cations, such as the guanidinium ($C(NH_2)_3^+$) and imidazolium ($N_2C_3H_5^+$) ions, may be accomplished by increasing the size of the receptor. Note that in the above examples based on 18-membered corands, the central

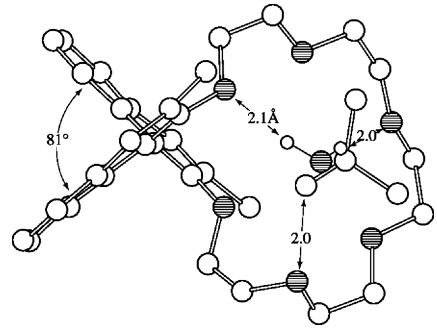


**Figure 3.65** X-ray crystal structure of **3.96**·$(CH_3)_3CNH_3^+$ showing the unfavourable steric interactions between the methyl groups of host and guest. (© Wiley-VCH Verlag GmbH & Co. Reproduced by permission).

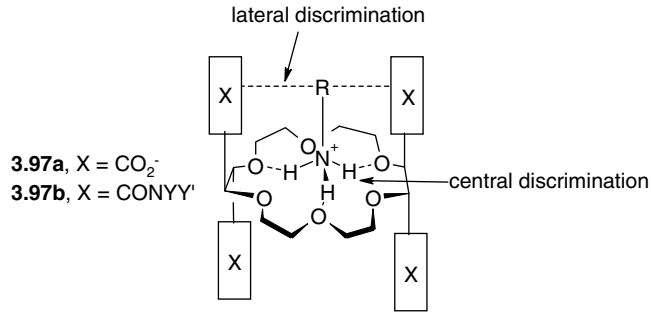


**Figure 3.66** Lateral and Central discrimination.

binding site is able to adopt a three-fold symmetry, complementary to that of the pseudo-three-fold symmetry axis of the $RNH_3^+$ group. The receptor is thus symmetry-complementary to the guest. In the same way, larger hosts based upon [27]crown-9 such as **3.98** complement the threefold symmetry of guanidinium.

## 3.12.2 Binding of Ammonium Cations by Three-Dimensional Hosts

As noted for metal cation binding, three-dimensional bicyclic hosts bind more strongly to alkyl ammonium cations than their corand analogues. Table 3.18 contains binding free energy data for a range of three-dimensional hosts with ammonium and alkylammonium ion guests. In particular, the complexation of cryptaspherand **3.38** for $NH_4^+$ is very strong, suggesting the complex to be of the capsular type, with the protons of the $NH_4^+$ cation orientated towards the nitrogen atoms of the cryptand portion of the molecule and the anisole oxygen atoms. Consistent with this, the X-ray crystal structures of the $K^+$ and $Cs^+$ cryptaspheraplexes of **3.38**, which display similar binding free energies, show that they are also capsular. The much lower free energies of the hemispheraplexes of **3.99** suggest that these materials are not capsular, and indeed CPK molecular models suggest a strained nesting structure. Models of the $NH_4^+$ complexes of **3.100** and **3.101** suggest that both are perching, consistent with the low free energies of complexation.

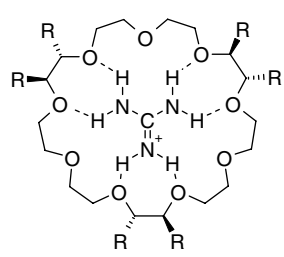

**3.98** R = $CO_2^-$

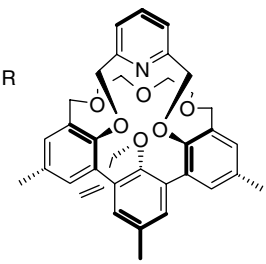

**3.99**

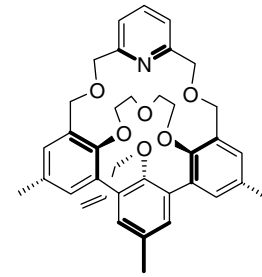

**3.100**

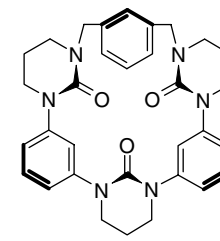

**3.101**

Ammonium cations may also be bound by cation-$\pi$ interactions by large cyclophanes such as **3.102** (calixarene-derivatives – see Section 3.14). The rigid, deep-cavity tetrahydroxy receptor **3.102a** is able to selectively bind tetramethylammonium ions with $K_{11} > 10^4$ $M^{-1}$ in chloroform solution,

**Table 3.18** Complexation free energies for spherand-type receptors with ammonium ions.[12]

| Host | $-\Delta G°$ (kcal mol$^{-1}$) | | |
|---|---|---|---|
| | $NH_4^+$ | $CH_3NH_3^+$ | $(CH_3)_3CNH_3^+$ |
| **3.38** | 20.2 | – | – |
| **3.62** | 14.4 | 14.4 | 13.2 |
| **3.99** | 12.7 | 11.9 | 11.7 |
| **3.100** | 9.2 | 8.4 | 8.3 |
| **3.33** | 9.9 | 8.2 | 7.7 |
| **3.101** | 7.0 | 7.4 | 8.6 |

however the methoxy derivative **3.102b** is a much poorer receptor suggesting an anion-induced allosteric effect, with acetate anion being the most effective, presumably hydrogen bonding to the OH groups.[43] The complex is thus, strictly an ion-pair receptor and we will see similar examples in Section 5.1.4.

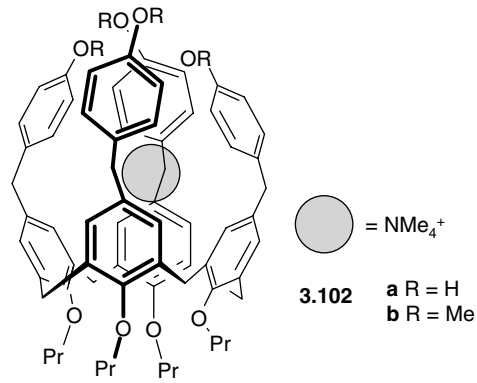


**3.102** **a** R = H
**b** R = Me

## 3.12.3 Ditopic Receptors

A ditopic receptor is a receptor that possesses two remote guest guest binding regions (possibly comprising one or more converging binding sites). Hosts with three binding pockets are thus termed *tritopic* and those with many are called *polytopic* receptors. In principle, because two or more recognition events are taking place, the affinity of a ditopic host for a bifunctional guest should be greater than that for a monotopic analogue and there is the possibility of positive cooperativity between the binding regions (Section 1.5). Furthermore, the possibilities for selective molecular recognition may be extended greatly by the placement and spacing of receptor binding sites.

In 1980, Lehn synthesised the ditopic hosts **3.103**, which are capable of *linear molecular recognition* of diammonium cations according to the length of the guest spacer groups. $^1$H NMR measurements indicate that for guests $NH_3^+(CH_2)_nNH_3^+$, relatively little selectivity is exhibited by the smaller host **3.103a**. However, hosts **3.103b**, **3.103c** and **3.103d** give maximum chemical shift changes for the guest chain protons on binding guests of chain length n = 5, 7 and 10, respectively (Figure 3.67) in comparison to both longer- and shorter-chain analogues. Large chemical shift changes are expected if the guest is within the molecular cavity because the guest aliphatic chain

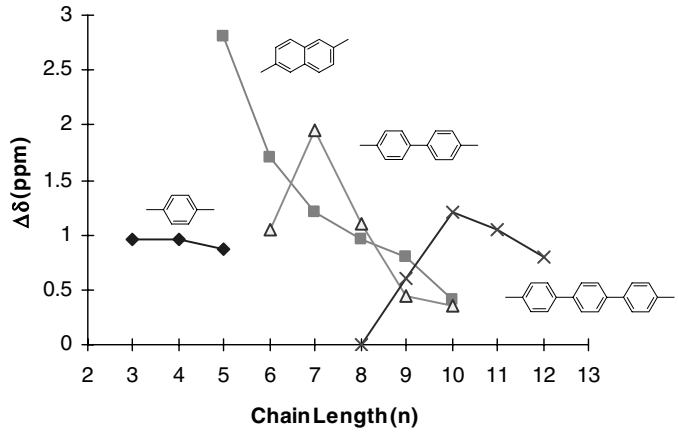


**Figure 3.67** Largest upfield shift Δδ as a function of guest chain length, n, for hosts **3.103a–d**.

then falls within the shielding region of the ring current generated by the aromatic spacer groups, R (Box 3.3).

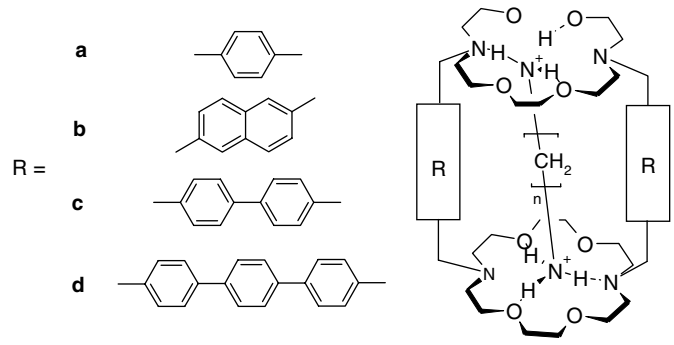


**3.103**

A particularly interesting result was obtained by measurement of NMR spectroscopic relaxation times for host and guest. These results showed that sterically complementary host–guest pairs show very similar molecular motions in solution (strong dynamic coupling), and these motions are significantly slowed down in comparison to those of the free host. As the host–guest fit becomes less complementary, the motions become *anisodynamic* with the guest motion speeding up while those of the host remain about the same. In cases of particularly bad fit (*e.g.* **3.103d**, n = 8) the host motions slow down even more, while those of the substrate speed up. This is interpreted as involving binding external to the cavity, *via* one guest —$NH_3^+$ group and one host corand ring. This effectively increases the host molecular mass, slowing down its motion. The extra-cavity guest is free to flex.

## 3.12.4 Chiral Recognition

Davis, A. P. 'Chiral guest recognition', in *Encyclopedia of Supramolecular Chemistry*, Atwood, J. L. and Steed J. W. (eds), Dekker: New York, 2004, *pp.* 236–244.

In biochemical systems, enantiospecific receptor–substrate binding is of the utmost importance. As a result, there is a great deal of interest in the application of chiral supramolecular compounds as

**Box 3.3** NMR Spectroscopy of Supramolecular Compounds

Keeler, J., *Understanding NMR Spectroscopy*, John Wiley & Sons, Ltd: Chichester, 2005.

A discussion of the fundamentals of the NMR technique is beyond the scope of this work, but may be found in the key reference. However, there are one or two aspects of NMR that are of particular interest to supramolecular chemists, as well as the obvious general need for a technique for characterising new chemical compounds. We have already seen in Section 1.4 the use of the NMR spectroscopic titration technique for the measurement of host–guest association constants in dilute solutions. However, more information may be gained from NMR spectroscopy than just binding constants.

### *Aromatic Ring Current Effects*

Even a simple comparison of the guest spectrum in the presence and absence of host can reveal some very unusual features, particularly in cases where either host or guest contain an aromatic ring. In the presence of a magnetic field, the delocalised $\pi$-electrons in benzene derivatives or higher aromatics such as porphyrins represent a circulating charge which basic electromagnetic theory tells us will produce a magnetic field that opposes the externally applied field, $B_0$. This is responsible for the effective deshielding of the C—H protons of benzenoid compounds since these protons are located in the region of the induced field that is aligned with $B_0$. However, in cases where a guest is included within an aromatic host (usually a cyclophane, Section 6.5), the guest is often situated directly above the aryl ring in its shielding region, resulting in very large chemical shift changes to higher field (*i.e.* towards lower chemical shift) (Figure 3.68). The degree to which various guest nuclei are affected can give good qualitative information about the relative orientations of host and guest and the regioselectivity of the binding.

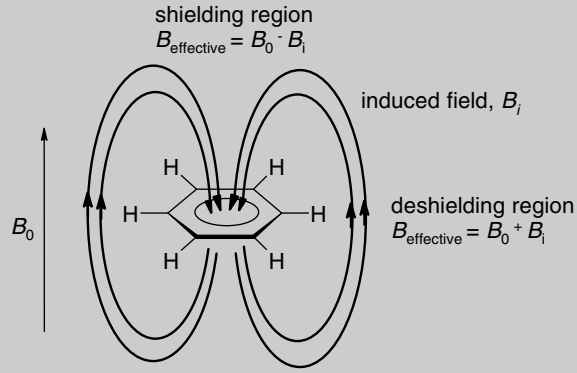


**Figure 3.68** Aromatic ring current effects.

### *Nuclear Overhauser Effect*

More quantitative information about host–guest proximity may be obtained by application of the nuclear overhauser effect (NOE). Very simply, the NOE involves the saturation of the spin of one nucleus by continuous irradiation, and monitoring the resulting intensity enhancements of the NMR resonances of adjacent atoms. The idea is that the irradiation of one nucleus causes it to become excited to a nonequilibrium distribution of spin states. Relaxation of this excited state situation occurs by dipole–dipole spin-lattice transfer of the excess energy, resulting in enhancement of the intensity of signals for nuclei physically close to the irradiated nucleus, irrespective of whether they are actually bonded. NOE intensity enhancements may be anywhere

from zero to 200 % more than the original intensity, and observation of an NOE effect is a good indication that nuclei are spatially close. For example in the semiclathrate compound **3.104**, nuclei $H_a$ and $H_b$ are very close together. If the resonance of $H_a$ is saturated, the intensity of the $H_b$ signal is increased by 45 %, while more distant protons are essentially unaffected. As a result, the stereochemistry of the molecule may be assigned with reasonable confidence. An example in a true host–guest system is described in Section 3.14.1.

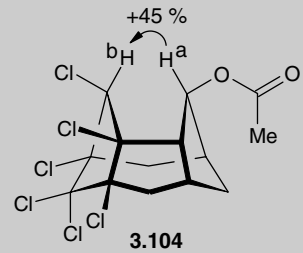


**3.104**

### *Coupling*

Through-bond spin–spin coupling in NMR spectroscopy is a result of the influence on the effective magnetic field at a particular nucleus by those adjacent to it. In general, coupling observations are very useful at giving bond connectivity information. No coupling would be expected between host and guest species in supramolecular compounds because they are not bonded together covalently. However, if there is an interaction between host and guest that can result in shared electron density, then observation of splitting of host signals by the spin state of the guest or vice versa may occur. This is particularly noticeable when nuclei that give large couplings are involved, *e.g.* $^{19}F$.

### *Guest Exchange Dynamics*

In cases where guest binding is of a suitable energy (about 20–100 kJ $mol^{-1}$), it is possible to observe exchange between free and bound guest by the *coalescence* method. If guest exchange is kinetically slow on the NMR time scale (complex lifetime $>$ *ca.* $10^{-2}$–$10^{-3}$ s), then separate peaks for bound and free guest are observed. Raising the temperature of the NMR probe causes the exchange rate to increase, which is reflected in the NMR spectrum by a broadening of the resonances for the two distinct species. When the exchange rate becomes comparable to the frequency separation between the two signals, peak coalescence occurs and the two resonances merge to give a single broad peak (assuming no spin–spin coupling is present). After this point, (the coalescence temperature, $T_c$), further warming results in a resharpening of the spectrum. At $T_c$, the rate of guest exchange is given by Equation 3.5.

$$k_c = \pi\delta\nu/\sqrt{2} \tag{3.5}$$

where $\delta\nu$ is the resonance frequency separation between the NMR peaks under slow exchange conditions.

If separate peaks for bound and free guest are not observed at room temperature, sometimes guest exchange can be slowed down sufficiently by lowering the temperature in the NMR probe. Temperatures as low as –90 °C may be reached in conventional deuterated solvents such as $CD_2Cl_2$ or $CO(CD_3)_2$, and in special cases even lower temperatures may be achieved through the use of freons such as $CF_2Cl_2$.

Given a measurement of guest exchange rate, application of the Eyring equation (3.6) allows the activation free energy $\Delta G^*$ of the complexation process to be determined.

$$k_c = \chi \frac{k_B T}{h} e^{-\Delta G^*/RT} \tag{3.6}$$

(*continued*)

**Box 3.3** (*Continued*)

where $\chi$ is a transmission coefficient usually assumed to be 1, $k_B$ is the Boltzmann constant ($1.3805 \times 10^{-23}$ J K$^{-1}$), $h$ is Planck's constant ($6.6256 \times 10^{-34}$ Js), and T is the temperature in Kelvin.

To take a very simple example of the method, the methyl region of the $^1$H NMR spectrum of *N*,*N*-dimethylformamide (DMF) at various temperatures is shown in Figure 3.69. The coalescence of the two methyl groups is caused by the gradual increase of the rate of rotation about the C—N bond, which has some double bond character. It could just as easily correspond to the flipping of a DMF guest within an unsymmetrical carcerand host (Section 6.7). In this case, the coalescence temperature is 120ºC (393 K) and the frequency separation is 9.5 Hz (corresponding to a very small chemical shift difference at 60 MHz), hence applying Equation 3.5, we obtain $k_c = 21$ s$^{-1}$. Plugging this value into Equation 3.6 gives $\Delta G_{393}^{*} = 87.5$ kJ mol$^{-1}$. The error is typically about $\pm 1$ kJ mol$^{-1}$.

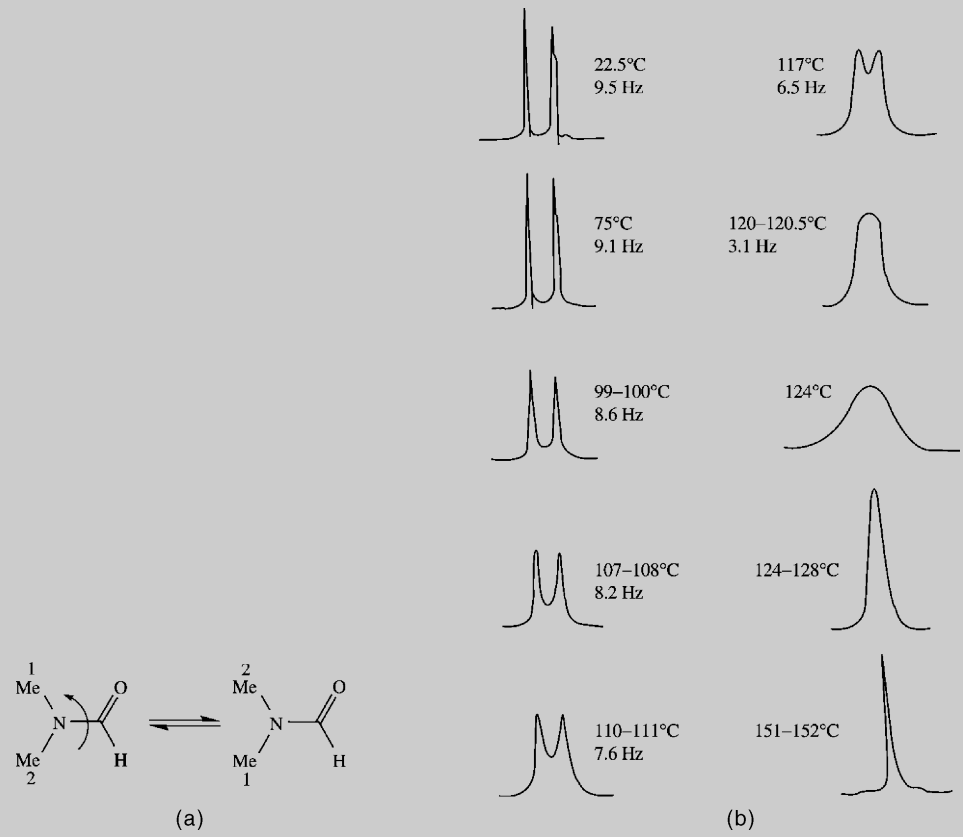


**Figure 3.69** (a) DMF methyl exchange mechanism. (b) $^1$H NMR spectroscopic signals for the methyl protons of DMF recorded at various temperatures. With slow site exchange at low temperatures, two signals are observed. As the temperature is raised to the coalescence temperature of 120 ºC, the signals broaden and merge. (© Wiley-VCH Verlag GmbH & Co. Reproduced by permission).

### *Diffusion Ordered Spectroscopy (DOSY)*

Diffusion-ordered spectroscopy (DOSY)[45] is a NMR spectroscopic technique that separates the NMR signals of different compounds according to their diffusion coefficient (*D*, their rate of diffusion in a particular medium). A series of spin echo spectra is measured with different pulsed field gradient strengths, and the signal decays are fitted to give diffusion coefficients for each compound present. In 2D DOSY this

gives a series of diffusion-weighted one-dimensional spectra that allows particular resonances to be assigned to species with a particular diffusion coefficient. The technique is useful for analysing mixtures of compounds of different size and hence different diffusion rates. Thus, for example, a mixture of monomer and self-assembled dimer will have very different diffusion rates. The effect of complexation on diffusion coefficient is readily apparent from Figure 3.70. The calixarene host **3.105** readily dimerises to form the capsule $(\mathbf{3.105})_2$. The capsule binds the cobaltocinium cation but ferrocene is not complexed. DOSY can measure diffusion coefficients for species with molecular weights uf up to *ca.* 10,000 Da relatively easily. It is however, limited to species with relatively long $T_2$ (spin-spin) relaxation times, which can cause difficulties with large molecules that can have low diffusion coefficients and short $T_2$ values. Solvation can also play a siginifcant role and hence neutral and charged system cannot be readily compared since ions are often much more highly solvated.

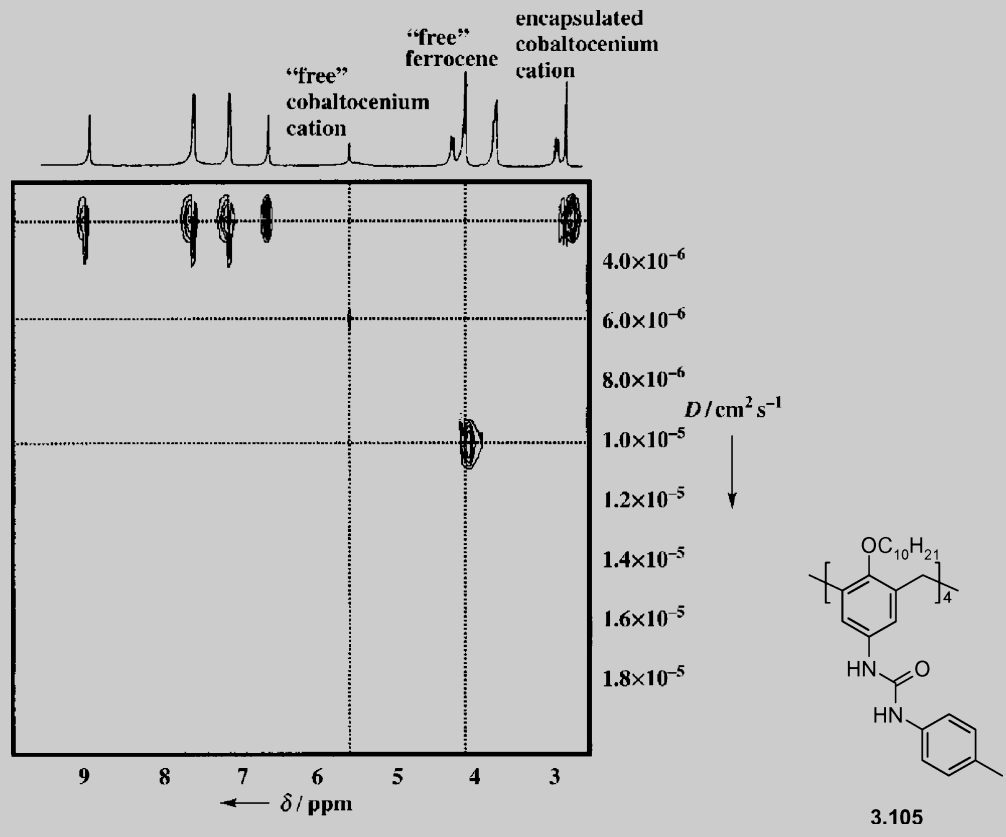


**Figure 3.70** DOSY spectrum (400 MHz, 298 K) of a mixture of $(\mathbf{3.105})_2$, ferrocene and cobaltocinium. The peak at 2.72 ppm corresponds to the encapsulated cobaltocinium ion and has the same diffusion coefficient as the resonances assigned to $(\mathbf{3.105})_2$. (© Wiley-VCH Verlag GmbH & Co. Reproduced by permission).

enzyme mimics and models (Chapter 12) as well as in abiotic chiral catalysis, which might ultimately find application in the synthesis or separation of chiral pharmaceuticals for example. A general rule in chiral recognition is known as the *three point rule* which has been formulated by Pirkle as 'Chiral recognition requires a minimum of three simultaneous interactions between the [receptor] and at least one of the enantiomers, with one of these interactions being stereochemically dependent.' In practice,

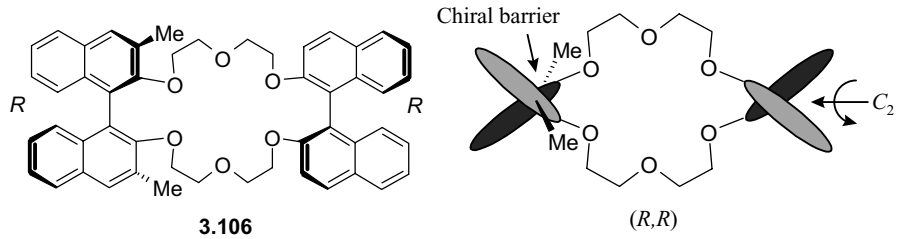


**Figure 3.71** Example of a chiral barrier host.

however, this type of design does not lead to very efficient enantioselectivity and the most successful chiral receptors possess a complicated array of functional groups and steric barriers strongly differentiating the mode of interaction of the two enantiomers. Broadly speaking, rigidity and the presence of bulky groups are key features.

In As early as 1978, Cram's group designed and resolved the chiral corand **3.106**.[47] While **3.106** does not possess specific asymmetric carbon atoms, it is chiral by virtue of the relative orientations of the two binapthyl (binap) moieties. The presence of the two methyl substituents prevents rotation about the bond between the two napthalene groups on the left hand side of the host, resulting in a twisted conformation, termed a *chiral barrier* (Figure 3.71). The design of *R*,*R*-**3.106** is such that it possesses a $C_2$ symmetry axis passing horizontally through the two bonds between the pairs of napthalene residues, making both binding faces equivalent (*i.e.* nonsided, with respect to perching, tripodal guests). This means that chiral recognition must take place regardless of which side of the host the guest binds.

The chiral recognition ability of **3.106** was assessed by two-phase liquid–liquid extraction experiments of racemic mixtures of amino acid and ester guests. These experiments resulted in the selective extraction of the D-enantiomers in every case. The process can be quantified by the measurement of *chiral recognition factors* (the concentration of D-enantiomer divided by concentration of L-enantiomer, extracted into the organic phase), which ranged from a high of 31 for $C_6H_5CH(CO_2Me)NH_3^+$, down to a low of 2.3 for $C_6H_5CH(CO_2H)NH_3^+$ (the protonated form of phenylglycine – a synthetic amino acid). The basis of the chiral recognition lies in unfavourable steric interactions between the bulky substrate substituents and the protruding methyl substituents of the host (Figure 3.72).

The chiral resolving ability of hosts *R*,*R*-**3.106** and its *S*,*S*-enantiomer were investigated further by the construction of an enantiomer-resolving machine, pictured in Figure 3.73. The basis of the device is a W-shaped tube with a chloroform solution of host in the bottom of each side of the 'W'. The *S*,*S*-enantiomer

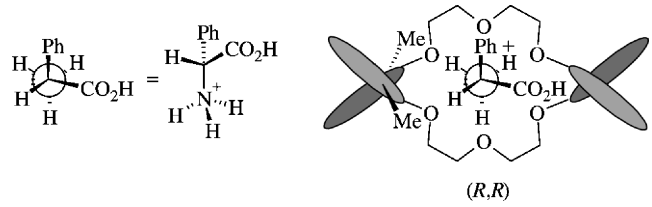


**Figure 3.72** Selective binding of the D-enantiomer of the phenylglycinate cation by **3.106**. In the L-enantiomer, the carboxylic acid group is brought into close proximity with a methyl substituent of the host.

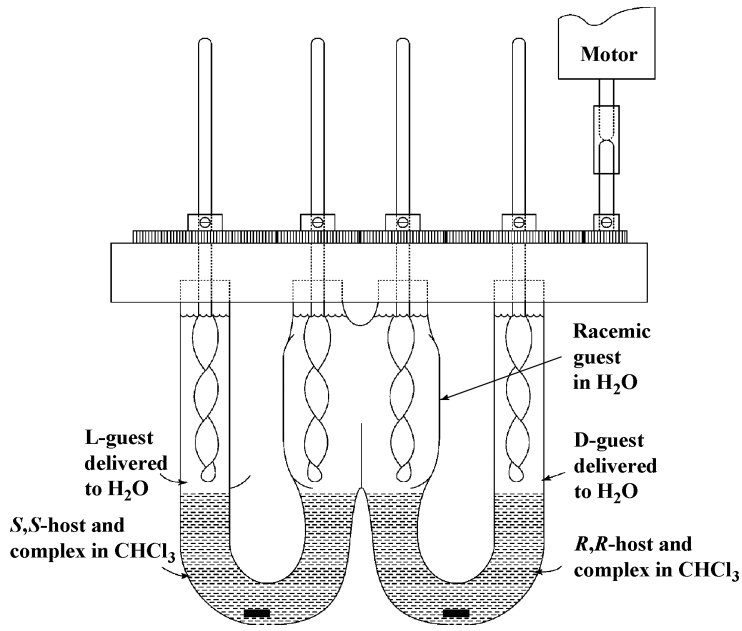


**Figure 3.73** The enantiomer-resolving machine. (Reprinted with permission from [48] © 1979 American Chemical Society).

is on the left, the *R,R*-enantiomer is on the right. The central reservoir contains an aqueous solution of racemic guest, which is stirred mechanically to begin the experiment. At each of the left- and right-hand water–chloroform phase boundaries, enantioselective binding occurs with the D-guest being transported through the right-hand chloroform phase and ending up in the aqueous phase on the top right-hand side of the 'W'. The L-guest is transported selectively to the left-hand side of the apparatus. The concentration gradient is maintained by continuous removal of 86–90 % enantiomerically pure guests from the left- and right-hand aqueous layers, while fresh racemate is added to the central reservoir.[48]

With this success, Cram's group went on to construct the first chiral chromatographic column by attaching the *R,R*-enantiomer of host **3.106** to a polymeric resin support *via* the end of one of the napthalene groups. This chiral immobile phase was used as the chromatographic packing and racemic solutions of chiral guests passed down the column. Because the binding of the D-enantiomer is stronger than that of the L-guest, the L-form passed through the column more quickly and it proved possible to collect it separately from the D-form. Separation factors obtained in this way paralleled the liquid–liquid extraction experiments, ranging from 26 to 1.4.

This technique is now used extensively to assess enantiomeric excesses in organic reactions and separate small quantities of enantiomers. Closely related chiral corands are particularly useful in assessing the optical purity of amino acids, although modern chiral columns for HPLC may cost in excess of US$ 2000.

Pyridine-based crown ethers such as **3.107** have also been extensively studied. *R,R*-**3.107** binds the *R* enantiomer of [$\alpha$-(1-naphthyl)ethyl]ammonium some 12 kJ mol$^{-1}$ more strongly than the *S* enantiomer. The reason is evident from the stereoviews shown in Figure 3.74. The napthyl substituent on the *R* enantiomer avoids the bulky phenyl group of the receptor on the same face as the bound cation, while there is a steric clash in the *S* enantiomer.[49]

Another key group of chiral hosts capable of organic cation recognition are the cyclophanes **3.108**. These chiral receptors are able to bind a variety of aromatic quinoline-based and related guests with cationic species being bound more strongly as a result of cation-$\pi$ interactions, Table 3.19. Interestingly, while the guests bound are achiral, inclusion within the chiral receptors results in the observation of

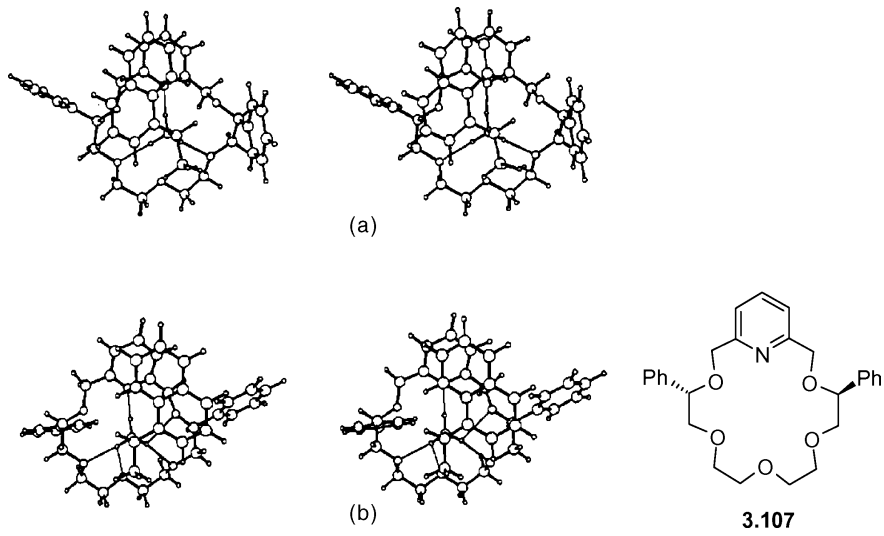


**Figure 3.74** Stereoviews of the interaction of [α-(1-naphthyl)ethyl]ammonium with *R,R*-**3.107** (a) *R* enantiomer (good fit) and (b) *S* enantiomer (mismatch). (Reproduced with permission from [49] © 1991 American Chemical Society).[§]

induced circular dichroism (ICD) in the guest spectra. In the case of **3.108b** in particular ICD effects allowed the determination of the relative host–guest orientations for the included species.[50]

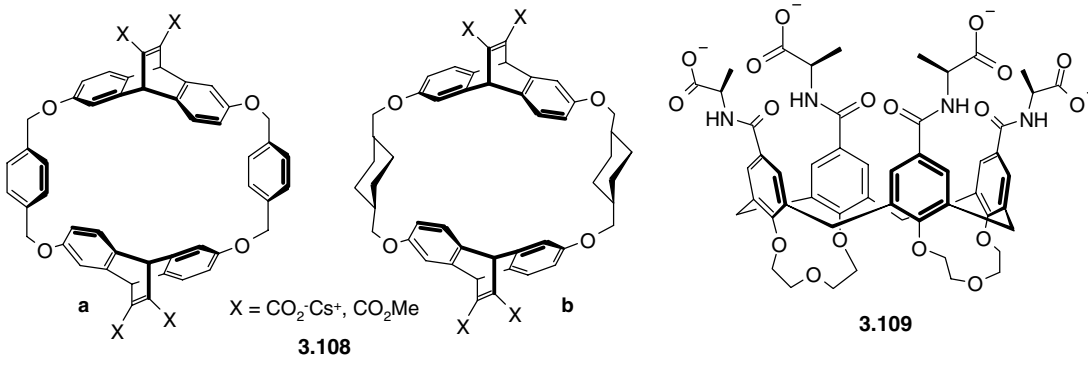


The chiral cavitands **3.109** have been developed by combining the amino acid residue L-alanine with macrocyclic cavitands (calixarenes – Section 3.14).[51] These ammonium ion receptors are able to complex a range of amino acids and their methylester hydrochloride salts, all of which contain an $-NH_3^+$ functionality capable of interaction with the carboxylate residues of the host. In general amino acids are bound only very weakly in aqueous solution, while association constants with the chiral methyl esters range from 620 $M^{-1}$ for L-tryptophan methylester to 110 $M^{-1}$ for L-alanine methylester. The methylester of glycine is not bound at all. Receptors related to **3.109** with variable four peptide loops arrayed around a central calixarene core have been used to bind to the surfaces of proteins. The

[§] To view a stereoview hold the page flat, perpendicular to your eyes. Cross your eyes so that the two pictures merge in the middle and then try to focus on the merged image. You might find it useful to move the page slowly towards you while keeping your focus constant.

**Table 3.19** Free energy of complexation, ($-\Delta G^{o}$ / kcal mol$^{-1}$) of neutral and cationic guests (iodide salts) by chiral receptor **3.108** (20 °C, borate buffer, pD = 9, $CDCl_3$ solution).[50]

| Guest | X = $CO_2^-Cs^+$ | X = $CO_2Me$ |
|---|---|---|
| 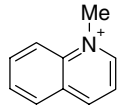 | 7.6 | 3.5 |
| 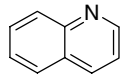 | 5.4 | 0.0 |
| 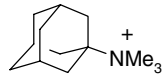 | 6.7 | 2.1 |

receptors have a surface area of *ca.* 450 Å$^2$ and one such compound acts as a potent inhibitor of chymotrypsin (a digestive enzyme responsible for peptide cleavage) by binding to the surface of the protein. Protein binding kinetics resemble several of the natural protein proteinase inhibitors.[52]

## 3.12.5 Amphiphilic Receptors

An *amphiphilic* receptor is one that combines two or more forms of guest recognition, resulting in a synergic enhancement of the binding. Amphiphilic receptors that combine polar or charged sites with a hydrophobic residue (which shields the polar sites from solvation and enhances electrostatic attraction) are termed *speleands*, and their cryptate complexes are called *speleates*. One such speleate **3.110**, combines a corand 18-membered $N_3O_3$ polar binding group with the hydrophobic pocket of a cyclotriveratrylene (CTV)-derived scaffold. The macrocycle CTV is commonly known for the enclathration of neutral guests (Section 6.6) but in this case, affords hydrophobic recognition of the methyl group of a methylammonium cation, while the corand fragment hydrogen bonds with the tripodal ammonium head group.[53]

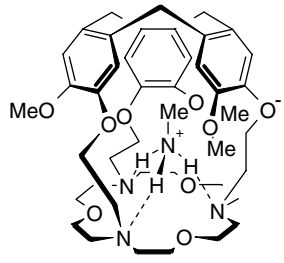

**3.110**

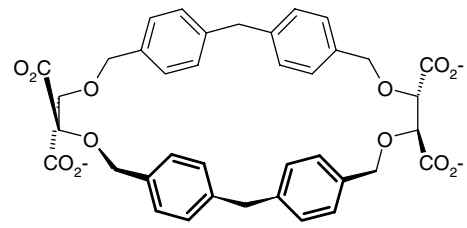

**3.111**

Another speleate, **3.111**,[54] makes use of an enlarged corand with oxygen donor sites, assisted by podand-like, anionic carboxylate functionalities, coupled to a hydrophobic region produced by four central aryl rings. The conceptual resemblance to **3.118** (Figure 3.66) is clear. In water at neutral pH compound **3.111** complexes a wide range of organic ammonium salts. The fact that the hydrophobic binding cavity is in the shielding region of the host aromatic rings results in large upfield shifts of the guest $^1$H NMR resonances. In particular, **3.111** is an effective receptor for the neurotransmitter

acetylcholine. The interest in this guest arises as a consequence of the desire to learn more about the transmission of neural impulses by modelling the interaction between the neurotransmitter and natural neuroreceptor. As with the simpler, related dibenzo[30]crown-10, host **3.111** also binds the methylviologen dication (**3.113**) with a binding constant in excess of $10^5\,M^{-1}$.

## 3.12.6 Case Study: Herbicide Receptors

Colquhoun, H., Stoddart, J. F. and Williams, D. 'Chemistry beyond the molecule', *New Scientist*, 1 May 1986, 44–48.

The redox-active ammonium ions diquat (**3.112**) and paraquat (methylviologen, **3.113**) are particularly interesting guests because of their properties as electron carriers, their use in electron transfer and photochemical energy storage processes, and their practical applications as herbicides.

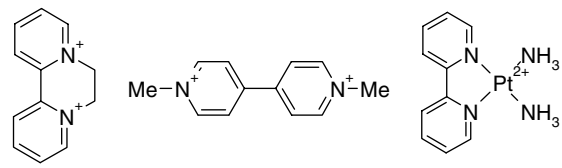


diquat **3.112** paraquat **3.113** **3.114**

We have already seen (Section 3.7.4) how the conformationally flexible dibenzo[30]crown-10 (**3.47**) is capable of wrapping around a metal ion such as $K^+$ to form a 1:1 complex. With **3.112**, a 'U'-shaped wrapping conformation is also observed, which enables the crown to act as an amphiphilic receptor engaging in ion–dipole interactions between the ether oxygen and with the quaternary nitrogen atoms as well as donor–acceptor $\pi$-stacking interactions involving the electron-rich benzo substituents and the electron-deficient diquat aromatic rings. The complex is also markedly stabilised by weak C—H $\cdots$ O hydrogen bonds from the carbon atoms adjacent to the charged nitrogens. Interestingly, a very similar complex is formed with the coordination complex $[Pt(bpy)(NH_3)_2]^{2+}$ (**3.114**), in which N—H $\cdots$ O hydrogen bonds from the ammine ligands enhance the ion–dipole and $\pi$-stacking stabilisations. In effect, the crown ether acts as a second-sphere ligand for the Pt(II) centre, much as in the case of Figure 3.50a. The X-ray crystal structure of the Pt(II) species is shown in Figure 3.75a.

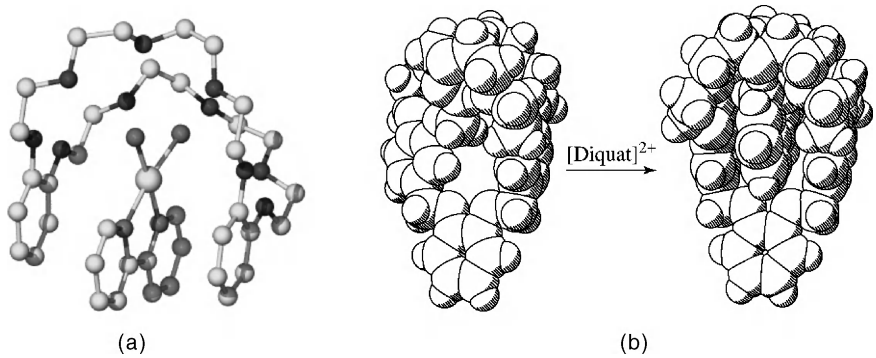


**Figure 3.75** (a) X-ray crystal structure of the bipyridyldiammineplatinum(II) cation with dibenzo[30]crown-10. (b) X-ray crystal structures of free and diquat-complexed **3.115** showing the preorganisation of the host for diquat binding. (© Wiley-VCH Verlag GmbH & Co. Reproduced with permission).

The novel conformation of dibenzo[30]crown-10 shown in Figure 3.75a has led to the synthesis of more preorganised cryptand hosts with similar complexation properties. Incorporation of a third catecholate bridge gives host **3.115** (derived from dibenzo[30]crown-10), which is fully preorganised for diquat binding.[55] This preorganisation (Figure 3.75b), and the three-dimensional cryptand nature of **3.115**, is reflected in the binding constant (acetone, 25 °C) for diquat, which is $>9 \times 10^5\ M^{-1}$, compared to $1.7 \times 10^4\ M^{-1}$ for dibenzo[30]crown-10.

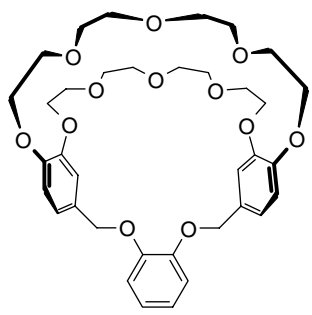

**3.115**

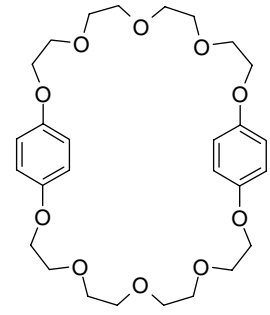

**3.116**

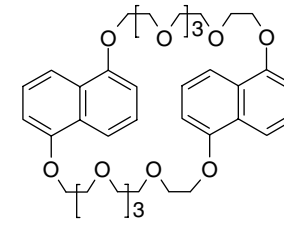

**3.117**

In contrast to diquat, the herbicide paraquat (**3.113**), is not complementary to hosts such as dibenzo[30]crown-10 (**3.47**) and **3.115** because of the greater distance between its two $N^+$ centres, and is not bound by them. However, it does bind to **3.116** and **3.117**. In the former case, a red, 1:1 complex results ($K = 730\ M^{-1}$, acetone, 25 °C). The intense colour arises as a result of a charge transfer absorption at 436 nm. X-ray crystallography again demonstrates the preorganisation of **3.116** for binding paraquat (**3.113**). In the case of host **3.117**, a 2:1 complex is formed with guest cations both inside and outside the host ring, engaging in stacked $\pi$–$\pi$ charge transfer interactions. This charge transfer chemistry has been used extensively in the construction of interlinked molecules termed *catenanes*, in which one corand-type ring is threaded through another to give a supramolecular species that cannot be disassociated, except by the breaking of covalent bonds. The synthesis of catenanes and related chemistry is described in Chapter 10.

## 3.13 Alkalides and Electrides

Dye, J. L., Redko, M. Y., Huang, R. H., Jackson, J. E., 'Role of cation complexants in the synthesis of alkalides and electrides', *Adv. Inorg. Chem.*, 2007, **59**, 205–231.

As early as 1969, Pedersen was intrigued by the intense blue colour observed upon dissolution of small quantities of sodium or potassium metal in coordinating organic solvents in the presence of crown ethers. Indeed, the history of alkali metal (as opposed to metal cation) solution chemistry may be traced back to an 1808 entry in the notebook of Sir Humphry Davy, concerning the blue or bronze colour of potassium–liquid ammonia solutions. This blue colour is attributed to the presence of a solvated form of free electrons. It is also observed upon dissolution of sodium metal in liquid ammonia, and is a useful reagent for 'dissolving metal reductions', such as the selective reduction of arenes to 1,4-dienes (Birch reduction). Alkali metal solutions in the presence of crown ethers and cryptands in etheric solvents are now used extensively in this context. The full characterisation of these intriguing materials had to wait until 1983, however, when the first X-ray crystal structure of an electride salt (a cation with an electron as the counter anion) was obtained by James L. Dye and

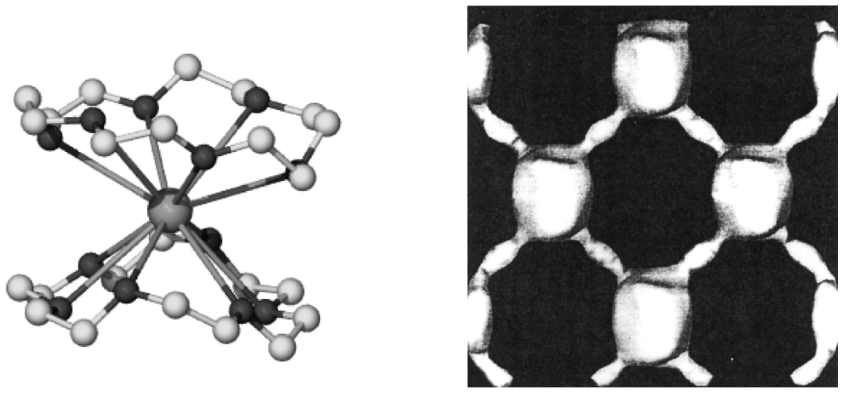


**Figure 3.76** (a) The X-ray crystal structure of $[Cs([18]crown\text{-}6)_2]^+ \cdot e^-$, the first electride complex. (b) cavities and channels in the structure in the *a–b* plane. (Reprinted with kind permission from Elsevier).

co-workers at the University of Michigan (Figure 3.76). This highly air- and moisture-sensitive material, $[Cs([18]crown\text{-}6)_2]^+ \cdot e^-$, was shown to contain a $Cs^+$ cation sandwiched between two [18]crown-6 hosts. The electron is trapped within nearly spherical lattice cavities about 2.4 Å in diameter, with shortest electron–electron distances of 8.68 Å. As a result of this long distance, the solid is not an electrical conductor, (conductivity $\simeq 10^{-10}\ \omega^{-1}\,cm^{-1}$ at 200 K).

Since X-ray crystallography cannot observe the lone electron directly (Box 2.1), it is questionable whether it is really situated at such a distance from the $Cs^+$ cation. If true, this would represent a very extreme example of the naked anion effect (Section 3.8.2). An alternative explanation localises the electron on the $Cs^+$ cation, which would also account for the observed low conductivity. However, convincing evidence for the separation of cation and electron comes from the nearly isostructural sodide ($Na^-$) and kalide ($K^-$) analogues of $[Cs([18]crown\text{-}6)_2]^+ \cdot e^-$. In these, species the alkali metal anions are situated in the same localised cavities as their electride analogues.

Alkali metal anions and electride complexes are formed simply by dissolution and crystallisation of the alkali metal and crown ether or cryptand in nonpolar, but coordinating, solvents such as tetrahydrofuran (thf) or dimethyl ether. The only caveat is that air, moisture, protic solvents and any kinds of dirt or impurities must be rigorously excluded because of the extreme sensitivity of the products. The sodide $[Na^+([2.2.2]cryptand)] \cdot Na^-$ is stable for a few hours at room temperature, whereas the electride $[Li^+([2.2.2]cryptand)] \cdot e^-$ decomposes rapidly above 230 K. At the time of their discovery, the idea of alkali metal anions was sufficiently novel that a distinguished London professor set about changing $Na^-$ to $Na^+$ in an innovative undergraduate examination paper, before being enlightened by a junior colleague.

A more interesting electride, $[K([2.2.2]cryptand)]^+ \cdot e^-$ is formed by the reaction of [2.2.2]cryptand with potassium metal in diethyl ether at –50°C. In this material, the X-ray crystal structure shows that the $[K([2.2.2]cryptand)]^+$ cations are separated by large dumbbell-shaped cavities in which pairs of electrons reside, some 5.3 Å apart. Each pair of cavities is connected with adjacent cavities *via* channels 7.8 and 8.4 Å long (Figure 3.77). The structures of the alkalide anion analogues $[K([2.2.2]cryptand)]^+ \cdot M^-$ have also been reported,[57] and show that the alkali metal anions also occupy the cavities proposed for the electrons, with a short $K^- \cdots K^-$ distance of 4.90 Å, rising to 6.38 Å in the caeside ($Cs^-$) analogue, suggesting the existence of the surprising dimers $M_2^{2-}$. Because of the interconnected nature of its cavities, $[K([2.2.2]cryptand)]^+ \cdot e^-$ exhibits a significant (though not metallic) molar conductivity of about 10 $\omega^{-1}\,cm^{-1}$, vastly greater than its isolated analogue, $[Cs([18]crown\text{-}6)_2]^+ \cdot e^-$.

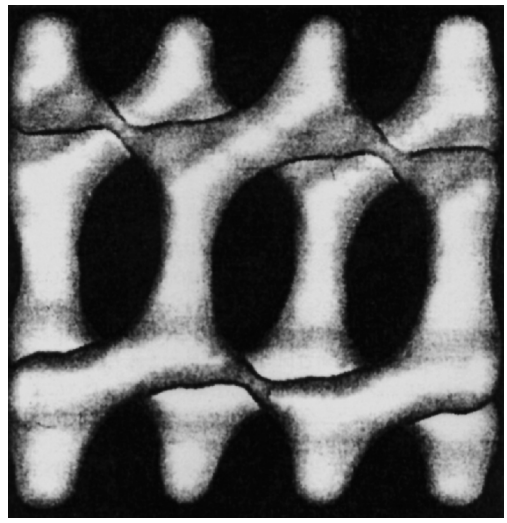

**Figure 3.77** Channel structure of the cryptand electride $[K([2.2.2]cryptand)]^{+}\cdot e^{-}$. (Reprinted with kind permission from Elsevier).

This highlights the effects of the topological structure of the host cation and its crystalline framework on the electrical and magnetic properties of the electron guests. The formation of these interesting species is crucially dependent on the ability of the macrocyclic hosts to isolate the alkali metal cations within a deep, lipophilic sheath, thus presenting a steric barrier to the recombination of cation and electron. The overall complexation free energy for the organic host–cation complex must outweigh the (fortunately low) ionisation energy of the alkali metal atom.

Much more recently the caeside salt $[Li([2.1.1]cryptand)]^{+}Cs^{-}$ has been reported. The material contains as one-dimensional zigzag chain of $Cs^{-}$ anions situated 6 Å apart, shorter than the 7 Å sum of the van der Waals radii. The material has interesting properties including low band gap semiconductivity that result from the overlap of the adjacent $Cs^{-}$ wave functions.[58]

## 3.14 The Calixarenes

Gutsche, C. D., *Calixarenes*, Royal Society of Chemistry: Cambridge, 1989; Gutsche, C. D., *Calixarenes 2*, Royal Society of Chemistry: Cambridge, 1997.

The calixarenes are a popular and versatile class of macrocycle formed from the condensation of a *p*-substituted phenol (*e.g. p-tert*-butylphenol) with formaldehyde. Since they contain bridged aromatic rings, they are formally members of the cyclophane family (Section 6.5). In cyclophane nomenclature they are termed 'substituted [1.1.1.1]metacyclophanes'. The descriptive name 'calixarene' was coined by C. David Gutsche (Washington University, USA) because of the resemblance of the bowl-shaped conformation of the smaller calixarenes to a Greek vase called a *calix crater* (Figure 3.78). The number of phenolic residues is denoted by a number in square brackets. Thus the most common cyclic tetramer with *p-t*-butyl substituents is termed *p-t*-butyl-calix[4]arene (**3.118**). It is easy to understand why this appealing nomenclature has found wide acceptance within the field when it is compared to the Chemical Abstracts systematic name for **3.118**, $[19.3.1.1^{3,7}1^{9,13}1^{15,19}]$octacosa-1(25),3,5,7(28),9,11,

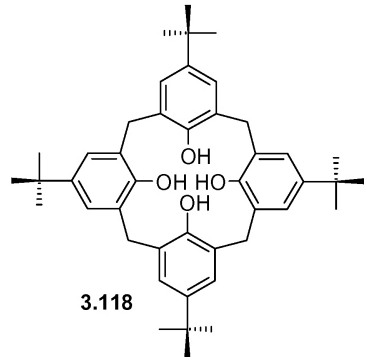


3.118

**Figure 3.78** *p-t-butyl*-calix[4]arene (**3.118**) resembles a *calix crater* vase in shape.

13,(27),15,17,19(26),21,23-dodecaene. The history of the development of the calixarenes is reviewed in Box 3.4.

## 3.14.1 Cation Complexation by Calixarenes

Ikeda, A. and Shinkai, S. 'Novel Cavity design using calix[n]arene skeletons: towards molecular recognition and metal binding', *Chem. Rev.*, 1997, **97**, 1713–1734.

The calixarenes are extremely versatile host frameworks and, depending on their degree of functionalisation, may act as hosts for cations, anions and neutral molecules, as we will see in Chapters 4 and 5.

**Box 3.4** Historical Development of the Chemistry of the Calixarenes

Work as early as 1872 on the reaction between phenol and formaldehyde had resulted in the formation of various polymeric tar- or cement-like materials that had resisted characterisation by the crude techniques of the time (chiefly elemental analysis). In 1902, a gifted and, by then, very wealthy chemist, Leo Bakeland, turned his attention to the reaction in the hope of finding a commercial use for the hard intractable phenol–formaldehyde resin. By carrying out the reaction in the presence of very carefully controlled amounts of base, Bakeland was able to produce a much more homogeneous and appealing material, which he called Bakelite, thought to consist of a highly cross-linked polymer of phenol moieties, joined by —$CH_2$— and —$CH_2OCH_2$— bridges both *ortho*- and *para*- to the phenolic hydroxyl groups. He filed a patent for his process on 18 February 1907, thus beginning the age of modern synthetic plastics. The use of Bakelite plastics underwent an exponential growth, with moulded Bakelite objects entering every aspect of modern life up until their replacement in recent times by petrochemical-derived materials. Despite the enormous amount of study on Bakelite materials, however, many details of their actual chemical composition are still unknown.

In 1942, as part of a study of the Bakelite process, Alois Zinke (University of Graz, Austria) decided to simplify the reaction by examination of the condensation of *p*-substituted phenols, particularly, *p-tert*-butylphenol, with formaldehyde. Zinke was able to isolate a crystalline product of empirical formula $C_{11}H_{14}O$ and, because the substituted phenol can only react at the *ortho* position (the hydroxyl group is *ortho* and *para* directing) and based on current literature precedent, he postulated a cyclic tetrameric structure (**3.118**). Annoyingly, however, cryoscopic molecular weight measurements on the acetate derivative suggested that the product was actually of much higher molecular mass. This was ascribed to

contamination by mixed species, and later work on the product from *p*-1,1,3,3-tetramethylbutylphenol gave a molecular weight entirely consistent with a tetrameric formulation. Further evidence for a teterameric structure came from a rational, step-by-step synthesis of *p*-methyl derivative in 1956 by B.T. Hayes and R. F. Hunter, researchers at the Research and Development Department of Bakelite Ltd. Their final cyclisation step (Scheme 3.24) was effected under high dilution conditions to give the product **3.119** in unstated, though presumably low, yield.

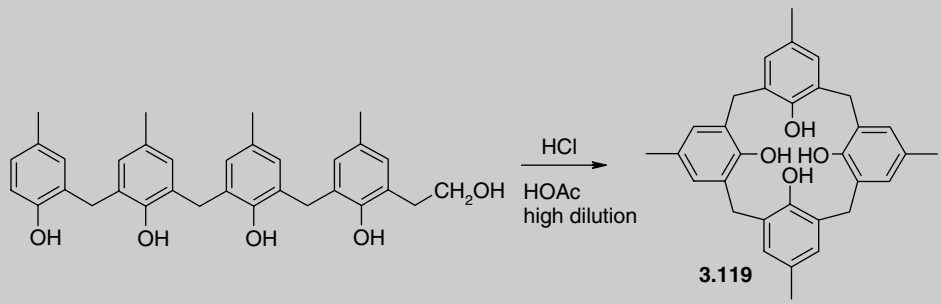


**Scheme 3.24** Cyclisation step of the Hayes and Hunter synthesis of *p*-methylcalix[4]arene.

In 1955 a British chemist named John Cornforth interested in the cyclic structures as possible tuberculostatic substances repeated the Zinke syntheses but was able to isolate two products of similar but distinct melting points, from both the *t*-butyl and 1,1,3,3-tetramethylbutyl reactions. A combination of preliminary X-ray crystallographic evidence and molecular weight determinations led Cornforth to agree with Zinke and assign tetrameric structures to all four of his materials. He suggested, from examination of CPK molecular models, that the observation of two compounds of each type was due to restricted rotation about the bonds joining the phenolic nuclei to the methene bridges, resulting in the formation of diastereoisomers. Today these diastereoisomers are known as the cone, partial cone, 1,2-alternate and 1,3-alternate conformers (Figure 3.79). Of these, the cone conformer is by far the most common because it is stabilised by a cyclic network of intramolecular hydrogen bonds between the hydroxyl groups at the lower rim of the molecule. In fact, evidence from $^1$H NMR spectroscopy shows that the molecular models significantly overestimate the rotational barriers.

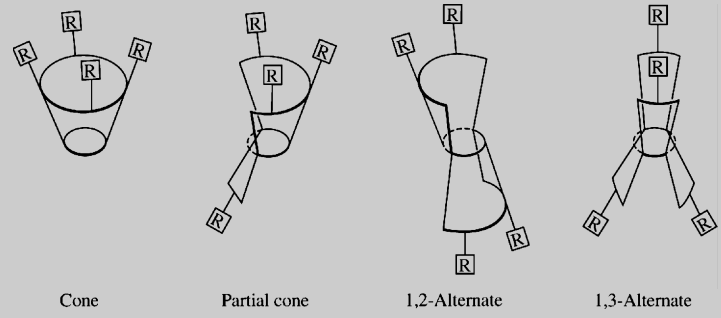


**Figure 3.79** Conformers of *p-tert*-butylcalix[4]arene. Cornforth originally suggested that restricted rotation about the aryl–methene bonds should result in these materials being noninterconvertable. In fact, interconversion is slow on the NMR time scale at room temperature (about 150 $s^{-1}$) but readily observed at 60ºC. (Reproduced by permission of The Royal Society of Chemistry.)

(*continued*)

**Box 3.4** (*Continued*)

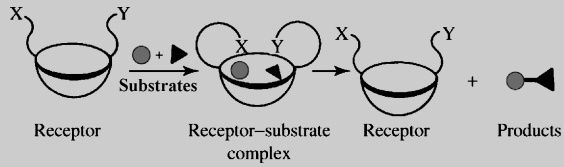


**Figure 3.80** Proposal for the use of calixarenes as enzyme mimics. (Reproduced with permission of The Royal Society of Chemistry.)

It was not until 1972 that C. David Gutsche revived the chemistry of these cyclic oligophenol products in the hope of producing a range of cavity-containing substances suitable for the construction of enzyme mimics, particularly using the basket-like cone conformation (Figure 3.80). After assuming that his experiments had also produced a range of cyclic tetrameric products, the appearance of some anomalies in the literature caused Gutsche to examine more closely the various reports of calixarene synthesis. Careful recrystallisation of the crude condensation products produced a sharp melting material with an osmometric molecular weight of 1330 Da, consistent with a cyclic octamer. The mass spectrum of the trimethylsilyl derivative also suggested an octameric structure. The mystery was finally solved by an X-ray crystal structure that showed that the high melting materials of Cornforth are indeed cyclic octamers—calix[8]arenes. Indeed, it is now known that the base-catalysed reaction of *p*-alkylphenols with formaldehyde rarely gives pure cyclic tetramers, although many of Zinke's products were indeed such. Mixtures of products of cyclic tetramers, hexamers and octamers are common. Odd-numbered calixarenes are less common, although both calix[5]- and calix[7]arenes are now well known. Careful chromatographic work has now isolated species all the way up to calix[20]arenes. The past two decades have seen an explosion in calixarene chemistry. The calixarene framework, with its fascinating hydrophobic cavity, has been used as the basis for a vast range of host materials for cations, anions and neutral molecules as well as its original applications as an enzyme mimic.

As hosts for cations, the phenolic oxygen atoms at the calixarene lower rim (Figure 3.81) have the potential to act in a similar way to the anisole residues of the spherands, either in the original hydroxyl form or as alkyl ether derivatives. This kind of behaviour has been observed for the methyl ether of the parent *p*-*t*-butylcalix[4]arene (compound **3.121**) upon reaction with a mixture of sodium benzoate, one

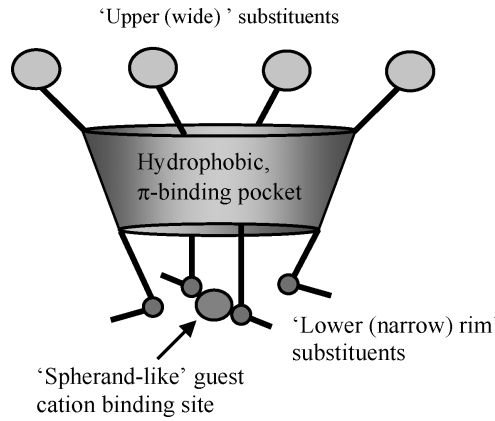


**Figure 3.81** Anatomy of a calix[4]arene in the cone conformation. The terms 'upper' and 'lower' rim are historical, but in common usage. The alternatives 'wide' and 'narrow' have the advantage of being orientation-independent.

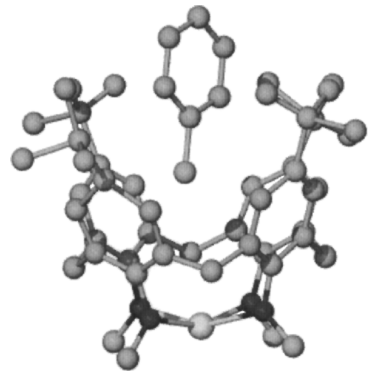

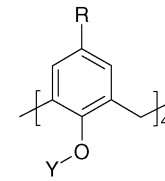


R = H, Y = Me, **3.120**
R = *t*-Bu, Y = Me, **3.121**
R = H, Y = *n*-Pr, **3.122**

**Figure 3.82** X-ray structure of the $Na^+$ complex of the tetramethyl ether of calix[4]arene (**3.121**).[59]

equivalence of water and trimethyl aluminium. The resulting complex contains an $Na^+$ cation coordinated by all four oxygen atoms of the calixarene tetraether. The exposed face of the nesting $Na^+$ cation is bound to a methyloxyaluminate anion arising from the other components in the reaction mixture (Figure 3.82). Interestingly, the calixarene hydrophobic cavity also contains a guest molecule of toluene. The host thus serves as a simultaneous receptor for cations and neutral molecules.[59]

Although Figure 3.82 clearly indicates that binding of $Na^+$ by **3.121** occurs in the cone conformation, this is by no means the most stable solution conformation for the methyl ether because there no longer exists the cyclic hydrogen-bonded network at the calixarene lower rim, which stabilises the cone conformer. In fact the calixarene isomerism in **3.120** and **3.121** is very solvent-dependent, and all isomers may be present in equilibrium. For example, in $CDCl_3/CD_3CN$ (10:1 v/v) solution at –50 °C, calixarene **3.120** exists as a 69:31 mixture of partial cone and cone isomers. In general, the percentage of cone isomer increases linearly with the solvent polarity. This is consistent with the fact that the cone isomer is a more polar species than the partial cone isomer, since all of the oxygen atoms lie on the same side of the molecule. Thus, in nonpolar solutions the partial cone form, which is not preorganised for lower-rim $M^+$ binding, predominates. Addition of $MClO_4$ (M = Li, Na) to **3.120** in a chloroform/methanol (4:1) solution results in the observation of $^1H$ NMR spectra consistent with $M^+$ complexes of both cone and partial cone **3.120**. However, when M = $K^+$ or $Ag^+$, large chemical shift changes, associated with the partial cone and 1,3-alternate isomers, are observed. This change is a result of the fact that the harder, more oxophilic $Li^+$ and $Na^+$ ions binding to the lower-rim oxygen atoms, which are to some degree preorganised for convergent $M^+$ complexation in the cone and partial cone isomers. $Ag^+$ and $K^+$ bind to both the oxygen atoms and engage in cation–π interactions with the aromatic rings (Figure 3.83). Addition of alkyl ammonium cations $RCH_2NH_3^+$ results in binding in the cone conformation. This may result either from cation–π interactions with the aromatic rings, or hydrophobic inclusion of the organic tail of the guest.

Work with *N*-methyl pyridinium iodide indicates clearly that the complexation process is able to induce conformational rearrangement with the fraction of cone **3.120** increasing from 31 % to 67 % upon addition of this guest. Replacing the methyl substituent with an *n*-propyl group entirely prevents conformational rearrangement, resulting in rigid, isolable conformers. The geometry of the complex of the *n*-propyl ether analogue **3.122** with *N*-methyl pyridinium iodide was probed with NOE NMR spectroscopy. This type of $^1H$ NMR experiment examines the transfer of magnetisation (*i.e.* spin excitation) from one proton to those nearby (Box 3.3). Because this is a through-space effect, the degree of magnetisation transfer (as measured by the enhancement of NMR peak intensities) is a good measure of the spatial proximity of one hydrogen nucleus (*e.g.* on the host) to another (*e.g.* on

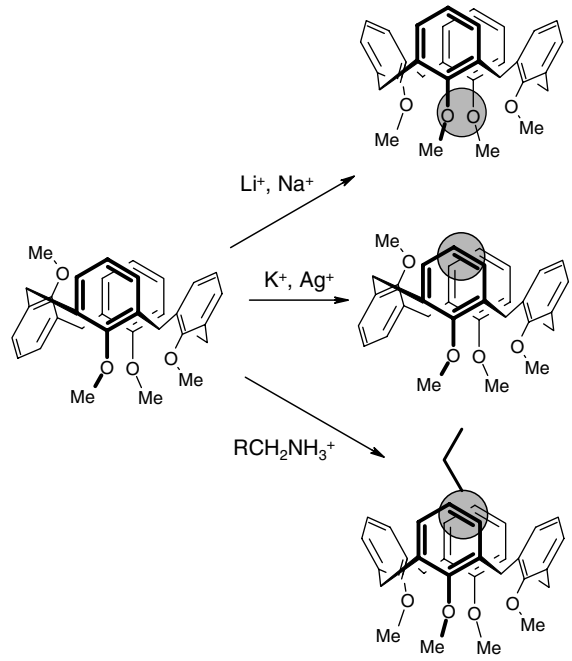


**Figure 3.83** Conformational aspects of cation inclusion by **3.120**.

the guest). The results (Figure 3.84) suggest the interaction of the nitrogen atom of the pyridinium cation with the $\pi$-electron density of the calixarene rings.

For $Ag^+$, complexation *via* the calixarene aromatic rings has been firmly established for both the partial cone and cone conformations of the immobile tetra-*n*-propyl ethers by X-ray crystallography.[60] In both cases, the $Ag^+$ cation is sandwiched between two distal (opposite sides of the molecule, as opposed to proximal, meaning adjacent to one another) calixarene rings, which are nearly mutually perpendicular giving a pinched cone conformation. The exposed face of the cation is coordinated to a triflate anion in both cases. For the partial cone case, the $Ag^+$ ion also interacts with one of the anisole oxygen atoms, which is inverted with respect to the other three at the lower rim (Figure 3.85).

The parallel ring geometry observed in both X-ray crystal structures may also be achieved in the 1,3-alternate conformation, and it has been shown by NMR spectroscopy that $K^+$ and $Ag^+$ binding also

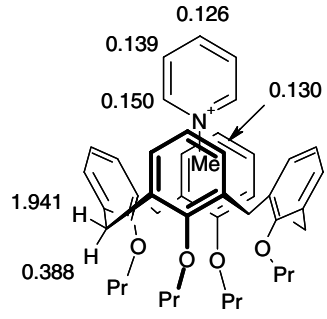


**Figure 3.84** NOE peak intensities upon excitation of the *meta*-aryl protons of the calixarene cavity in **3.122**.

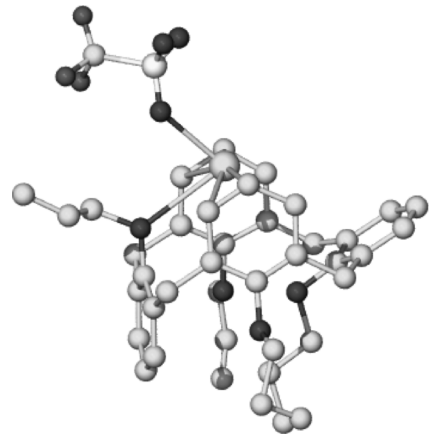

**Figure 3.85** X-ray crystal structure of the $Ag^+$–$\pi$ complex of **3.122**.[60]

occurs in this isomer. In this instance, the two sides of the host are equivalent and an interesting and very rapid cation tunnelling effect is observed with a coalescence temperature of about –70 °C, in which the $Ag^+$ ion passes through the annulus of the calixarene (Figure 3.86). In the substituted calixcrown calix[4]arene-bis-crown-5 (**3.123a**) this effect is slow in the case of alkali metal ions, even at room temperature. Integration of peak intensities for free and complexes host gives log $K_{11}$ values (25 °C) of 3.8 for $K^+$ and 2.9 for $Rb^+$. The presence of two crown-like loops allows the incorporation of a second $K^+$ cation, with log $K_{12}$ of 2.7. The host is able to bind $NH_4^+$, but no affinity whatsoever is observed for substituted alkyl ammonium salts, consistent with a capsular geometry for the complexes. The analogous calix[4]arene-bis-crown-6 (**3.123b**) is highly selective for $Cs^+$ as a result of the preorganisation of the calixarene backbone and $Cs^+\cdots\pi$ interactions (factor of $2 \times 10^3$ over $Na^+$)[61] and has been extensively studied with a view to the selective extraction of radioactive $^{134}Cs^+$ and $^{137}Cs^+$ from highly alkaline nuclear waste streams. This kind of metal extraction chemistry is explored in the next section.

Finally, an interesting hybrid between $Na^+$–O binding and $Na^+$–$\pi$ interactions is seen in the 2:1 complex between $NaPF_6$ and the the related hexahomooxacalix[3]arene as a lower-rim diethylamide derivative (**3.124**). The homooxacalixarenes contain $–CH_2OCH_2–$ bridges in place of the shorter methylene linkers in conventional calixarenes and are sometimes byproducts of calixarene synthesis. Compound **3.124** contains a large 18-membered ring annulus somewhat similar to [18]crown-6 and is able to complex two $Na^+$ ions to give a complex displaying both lower rim oxygen coordination and a second combined oxygen and $\pi$-coordinated $Na^+$ ion within the calixarene bowl. The two $Na^+$ ions are

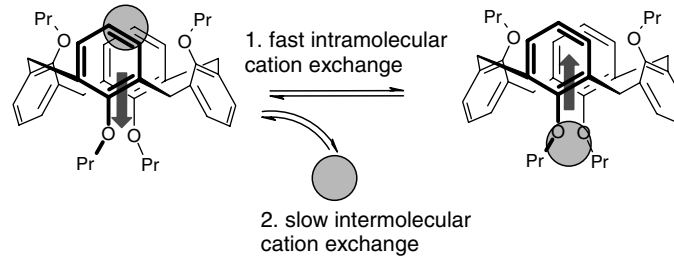


**Figure 3.86** $Ag^+$ tunnelling in a 1,3-alternate calixarene. This fast intramolecular effect is distinguishable from intermolecular processes by $^1H$ NMR spectroscopy.

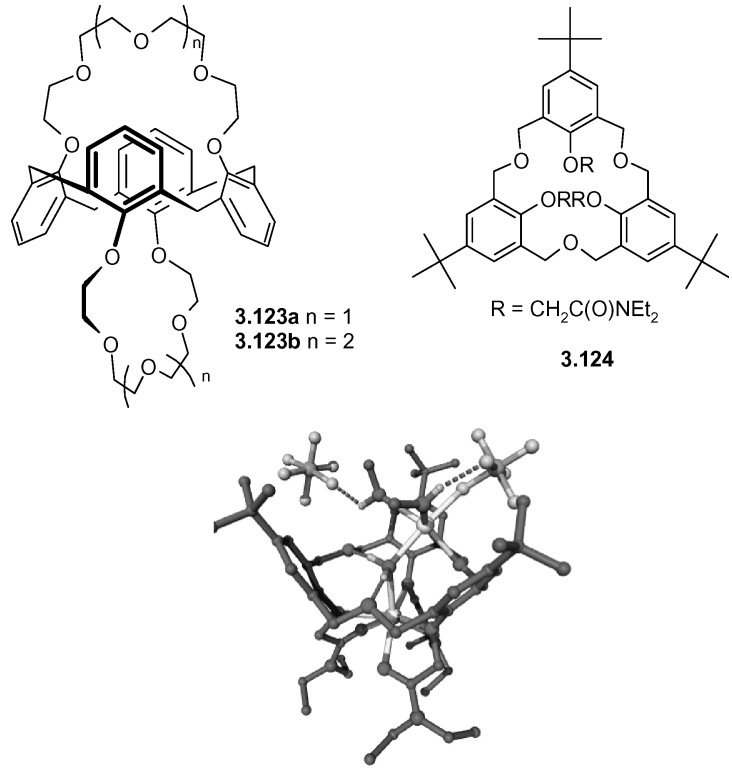


**Figure 3.87** X-ray structure of the disodium complex of **3.124** showing the two different $Na^+$ environments and the intra-cavity bridging water molecule.[62]

bridged by a water molecule leading to the suggestion that the structure is a mimic of biological alkali metal cation transport, Figure 3.87.[62]

## 3.14.2 Phase Transport Equilibria

The parent *p*-*t*-butylcalix[n]arenes (n = 4, 6, 8) are almost completely insoluble in water. However, their resemblance to crown ethers and spherands makes them interesting from the point of view of applications as phase transfer catalysts (Section 3.8.2). Table 3.20 shows the selectivity of calixarene **3.118** and its hexameric and octameric homologues for the extraction of various metal hydroxides into an organic receiving phase such as chloroform. Fortunately, in aqueous base the calixarenes are sufficiently soluble to act as phase transfer catalysts as a consequence of deprotonation of one of their phenolic hydroxyl groups. This solubility contrasts to [18]crown-6, which is much more effective in neutral solution.

Table 3.20 indicates that all of the calixarenes are especially good at transporting $Cs^+$, but show very little affinity or variation amongst the other metal cations, including the more highly charged $Ba^{2+}$. Table 3.20 also gives the approximate diameter of the hole between the oxygen atom of the calixarene lower rim, which, by analogy with Figure 3.82, might be expected to be the principal binding site for the metal cations. In fact, none of the metal cations seems to fit the anulus diameter, although in the

**Table 3.20** Selective phase transport of metal cations by calixarenes from basic aqueous solution. The data represent the rate of cation transport (flux) across the phase boundary in moles $s^{-1}\,m^2 \times 10^8$.

| Metal salt | Cation diameter | *p-t*-butylcalix[n]arene | | |
|---|---|---|---|---|
| | | n = 4 | n = 6 | n = 8 |
| Lower rim anulus diameter (Å) | | 1.0 | 2.4 | 4.8 |
| LiOH | 1.52 | – | 10 | 2 |
| NaOH | 2.04 | 2 | 22 | 9 |
| KOH | 2.76 | <0.7 | 13 | 10 |
| RbOH | 3.04 | 6 | 71 | 340 |
| CsOH | 3.40 | 260 | 810 | 996 |
| $Ba(OH)_2$ | 2.70 | 1.6 | 3.2 | – |

case of the methyl ether at least, the calixarene is clearly flexible enough to incorporate $Na^+$. So, what is the origin of the special selectivity for the relatively soft, polarisable $Cs^+$? Although the caesium cation is too large to bind within the square of the four oxygen atoms of the calix[4]arene, it fits beautifully within the calixarene cavity, stabilised by extensive cation–$\pi$ interactions as shown in the X-ray crystal structure of the nonbutylated $Cs^+$ calix[4]arene mono-anion complex (Figure 3.88). Here, the large alkali metal cation is situated symmetrically within the calixarene bowl-shaped cavity, with Cs—C distances in the range 3.55–4.12 Å. This work was published by Jack Harrowfield, then of the University of Western Australia, under the delightfully alliterative title 'Calixarene Cupped Caesium: A Coordination Conundrum'.[63] Clearly, the large, soft $Cs^+$ cation is both sterically and electronically compatible with encapsulation in the calixarene cavities, with the larger, more flexible calixarenes wrapping around the cation. It is interesting to compare these results with the intracavity $K^+$ intermediate suggested for *bis*(calixarene) host (**3.126**) in the next section.

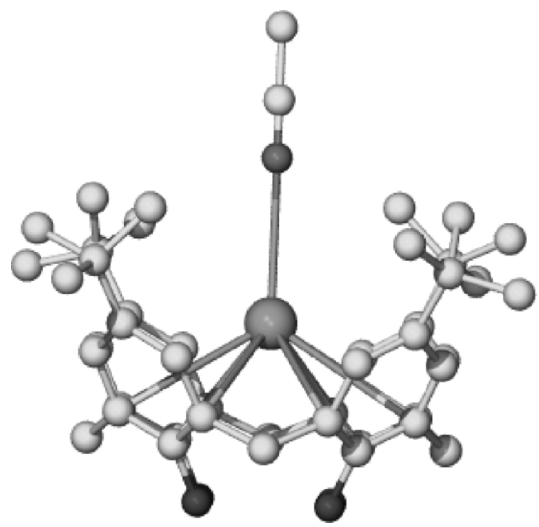

**Figure 3.88** Calixarene coordination of $Cs^+$ *via* the aryl rings and MeCN.[63]

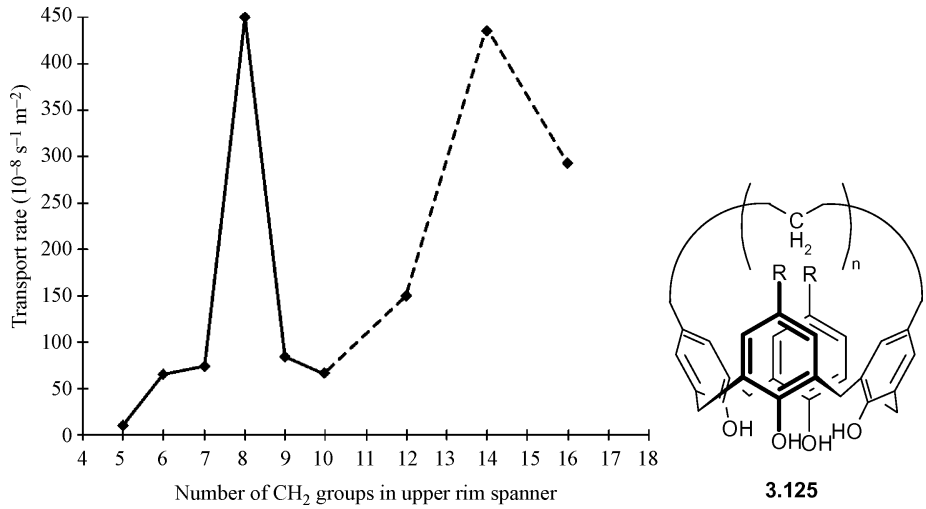


**Figure 3.89** Liquid–liquid phase transport rate of $Cs^+$ (flux) as a function of chain length (n) in hosts **3.125** ($CH_2Cl_2$—$CCl_4$/$CsOH_{aq}$). Dotted lines indicate the absence of data for n = 11, 13 and 15.

Intracavity complexation of $Cs^+$ has also been suggested by work on upper-rim bridged calix[4]arenes (**3.125**). Studies on the effect of the length of the upper-rim bridge on the transport phenomena give maxima at n = 8 and 14 $CH_2$ groups (Figure 3.89). The transport rate at n = 8 is equivalent to that obtained for *p-t*-butylcalix[4]arene itself [$(437 \pm 83) \times 10^{-8}$ mol $s^{-1}$ $m^{-2}$]. X-ray crystallographic results show that the amount of distortion in the phenolic oxygen atoms is small for $n < 8$ and negligible for $n > 8$, thus these results are interpreted in terms of the effects on the calixarene cavity size itself, with n = 8 being optimum. The flexibility of the unsubstituted calixarene and those with $n \geq 14$ also enable strong complexation. Other bridges induce unfavourable distortions on the calixarene cavity.

## 3.14.3 Cation Complexation by Hybrid Calixarenes

By combining the lower-rim cation binding properties of calixarenes with ethene glycol linkages similar to those found in crown ethers, a large macrotricyclic *bis*(calixarene) cage (**3.126**), which exhibits a great deal of selectivity for potassium, has been synthesised.[64] The $K^+$ binding constant is $4 \times 10^4$ in chloroform/methanol, and the selectivity for potassium over all other alkali metal iodides is in excess of $10^2$. Molecular mechanics simulations suggest that complexation occurs *via* a two-stage mechanism in which the intermediate involves an intracavity $K^+$–$\pi$ complex (Scheme 3.25). This is of interest as a model system for $K^+$ transport by gated ion channels (Section 2.2).

With the larger *bis*(calix)crown (**3.127**),[65] two dynamic processes are observed. The intermolecular association/disassociation equilibrium in which the complex equilibrates with the uncomplexed ligand and free metal cation is slow on the NMR time scale. The complex also exhibits a faster intramolecular vibration of the metal cation from one binding site to another (Scheme 3.26). Compound **3.127** is also interesting because the mechanism of this fast, intramolecular cation shuttling process may have important implications on the analogous movement of metal cations through transmembrane ion channels (Section 2.2).

As with the hosts mentioned earlier, other hybrid host molecules have been synthesised which combine the advantages of the rigid, readily available calixarene framework with the binding

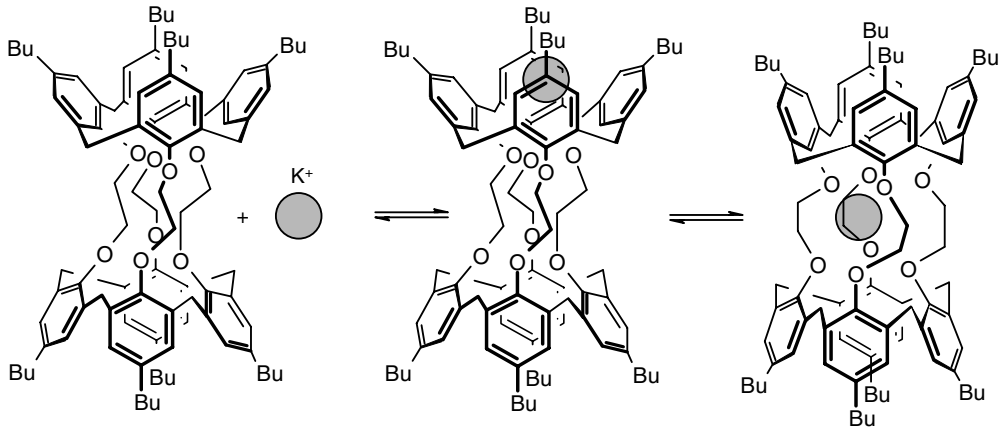


**Scheme 3.25** Potassium ion complexation by the *bis*(calixarene) cage host **3.126**.[64]

properties of hosts such as the cryptands and spherands. Solution extraction experiments with alkali metal picrates give the following binding energies ($-\Delta G°$ in kcal mol$^{-1}$, ±0.2) for calixspherand **3.128**: $Na^+$, 13.6; $K^+$, 14.0; $Rb^+$, 12.0; $Cs^+$, 9.8. The fact that the metal cation is bound in an encapsulating fashion is evidenced by the complexation rates, with $Rb^+$ and $Cs^+$ complexing fully in less than six hours, whereas times in excess of 48 hours are required for the $Na^+$ complex, suggesting that full desolvation is a necessary preliminary to binding since the hydration free energy of $Na^+$ is greater than $Rb^+$ and $Cs^+$. The calixcrown species **3.129** is an effective ionophore for larger alkali metal cations, with $-\Delta G°$ values of 11.3, 10.6 and 7.8 kcal mol$^{-1}$ for $K^+$, $Rb^+$ and $Cs^+$, respectively. The ligand also exhibits a selectivity factor (ratio of binding constants) of about

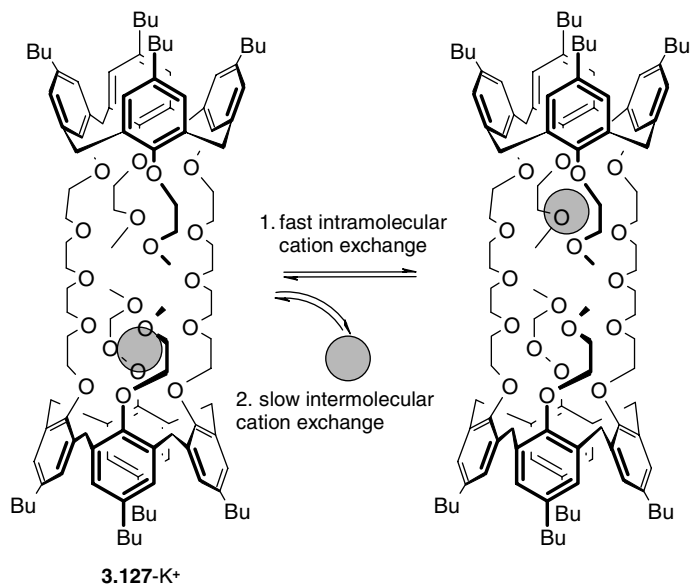


**Scheme 3.26** Intra- and intermolecular metal exchange processes in **3.127**.[65]

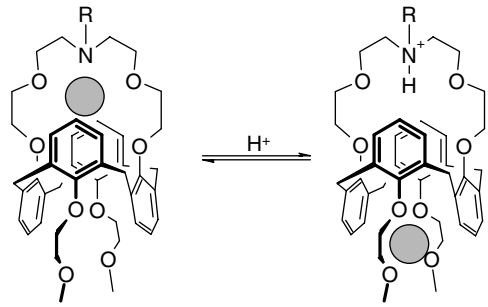


**3.131**

**Figure 3.90** Metal 'pumping' by a molecular syringe.[66]

2000 for $K^+$ over $Na^+$. In contrast, a smaller sodium-selective ionophore **3.130** has been developed, which has been incorporated into ion-selective electrodes. These devices demonstrate a remarkable reverse selectivity for $Na^+$ over $K^+$ with selectivity factors of up to $10^{5.3}$ for both cone and partial cone isomers.

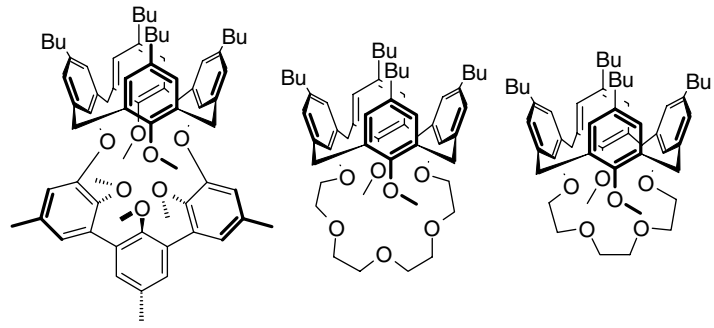


**3.128** **3.129** **3.130**

An interesting prototype for a molecular device analogous to a syringe has been constructed from the unsymmetrical calixarene **3.131**. The affinity of $Ag^+$ for the nitrogen atom donor of the crown is such that an overall log $K_{11}$ value of 9.78 is observed in $CD_2Cl_2/CD_3OD$ solution, with the $Ag^+$ cation residing in the crown portion of the molecule. On protonation of the basic nitrogen atom however (Figure 3.90), the crown $Ag^+$ binding is switched off, effectively 'pumping' the cation through the annulus of the calixarene to the lower binding site. Deprotonation 'sucks' the $Ag^+$ ion back up again.[66]

## 3.15 Carbon Donor and $\pi$-acid Ligands

Gokel, G. W., Barbour, L. J., Ferdani, R., Hu, J. X., 'Lariat ether receptor systems show experimental evidence for alkali metal cation-π interactions', *Acc. Chem. Res.* 2002, **35**, 878–886.

Soft metal ions are not restricted to complexation by heteroatom donors. Their electron-rich nature and large, uncontracted orbitals allow some very interesting complexation behaviour with $\pi$-acid ligands at the boundary between supramolecular and organometallic chemistry. A large range of transition metals

form covalent complexes with alkene, alkyne and aryl ligands stabilised by synergic back-bonding (Box 3.2). Even in the absence of covalent, synergic bonding, the noncovalent cation-$\pi$ interaction (Section 1.8.5) plays a significant role as a supramolecular force. We have already seen the significant role played by cation-π interactions in the complexation of $Ag^+$ and the larger alkali metal cations by the calixarene carbocyclic rings (Section 3.14). In the following section, we will examine this kind of complexation as a more general phenomenon.

## 3.15.1 Mixed C-Heteroatom Hosts

The allyl lariat ether (Section 3.3) **3.132** forms complexes with both $K^+$ and $Ag^+$ (which are of similar ionic radius, Table 3.5). In the case of the $K^+$ complex, as may be expected, the potassium ion is too large to fit snugly within the aza[15]crown-5 ring and lies somewhat above the donor atom plane. The exposed face of the metal atom is occupied by a $PF_6^-$ anion. Similar coordination to the crown is exhibited by $Ag^+$ but instead of an anion, the exposed face of the metal ion is coordinated to the allyl side chain of an adjacent molecule to give an infinite polymer in the solid state (Figure 3.91).

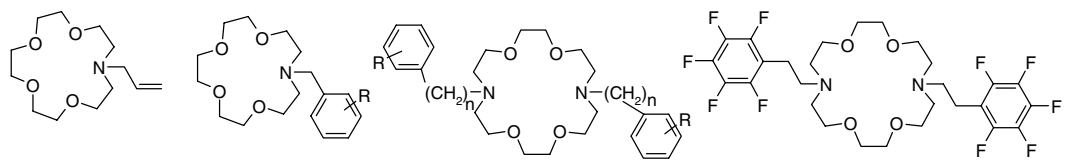

**3.132** **3.133** **3.134a** n = 1 **3.134b** n = 2 **3.135**

R = 2-$NO_2$, 4-$NO_2$, 2-CN, 4-CN, 2-Cl, 4-Cl, H, 2-OMe, 4-OMe

A study of the selectivity of lariat aza[15]crown-5 (**3.133**) and BiBLE (bi-brachial lariat ether) diaza[18]crown-6 derived ligands (**3.134**) containing variously substituted arene rings showed that the $Ag^+$ complex stability decreased as a function of the electron-withdrawing ability of the substituents, R, as measured by the substituents' Taft $\sigma^0$ inductive constant (a parameter measuring the electron-withdrawing

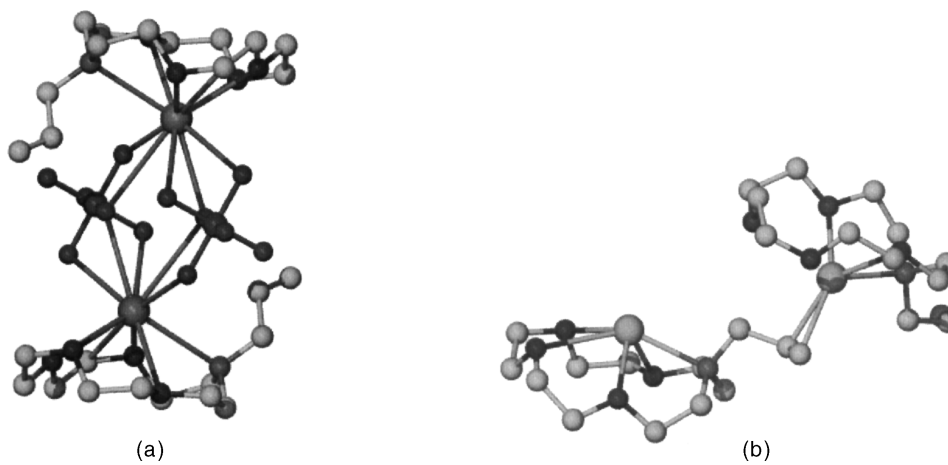

(a) (b)

**Figure 3.91** Contrast between bonding of (a) the hard $K^+$ ion and (b) soft $Ag^+$ ($PF_6^-$ salts) by the lariat ether **3.132**. The Ag—C distances are 2.36–2.39 Å.[68]

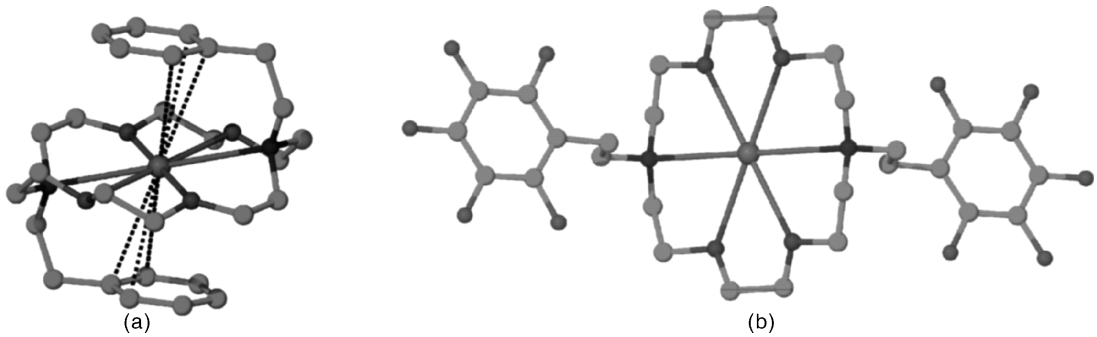


**Figure 3.92** Crystallographically determined structures of $K^+$ complexes of BiBLEs (a) *N,N′*-bis(phenylethyl)diaza[18]crown-6 showing the double $K^+\cdots\pi$ interaction and (b) *N,N′*-bis(pentafl uorophenylethyl)diaza[18]crown-6 which exhibits an extended conformation distancing the $C_6F_5$ substitutents from the metal cation.[69]

ability of *p*-substituents of benzoic acid derivatives by their effect on the acid's p$K_a$ value).[67] Silver cation binding constants (log *K*) ranged from 2.47 (R = *o*-$NO_2$) to 4.22 (R = *o*-OMe) for ligands of type **3.133**, and 3.17 to 6.30 for compound **3.134a** with the same substituents. This trend has been attributed both to through-bond inductive effects on the electron density at the nitrogen atom and $Ag^+$–$\pi$ interactions in solution. The log *K*:$\sigma^0$ correlation is much less precise for $Li^+$ and $Na^+$, consistent with that fact that these metals interact much less strongly with nitrogen and have little affinity for direct cation-$\pi$ interactions.

Extensive work by George Gokel of the University of Missouri, USA, has shown that lariat ethers and BiBLEs equipped with longer, more flexible alkene, alkyne and aromatic groups at least as long as 3-butenyl can engage in intramolecular cation-π interactions. Moreover not only soft metal ions such as $Ag^+$ can bind to these hosts, but alkali metals such as $Na^+$ and $K^+$ also form scorpion-like cation-π interactions with the lariat side arms. A good representative example of an very large body of work is the KI complex of *N,N′*-bis(phenylethyl)diaza[18]crown-6 (**3.134b**, R = H). The free ligand adopts an extended conformation in the solid state, but upon binding $K^+$ the X-ray crystal structure (Figure 3.92a) shows that the two phenyl groups are situated either side of the crown-coordinated $K^+$ ion and interact with strong $K^+\cdots\pi$ interactions. In contrast the electron deficient aryl rings of the bis(pentafluorophenyl) analogue (**3.135**) do not interact at all with crown-coordinated alkali metal cations, Figure 3.92b).

In solution, the interactions of $Ag^+$ and especially alkali metal cations, with alkenes and other π-systems are relatively weak. Low oxidation state transition metals cations and neutral atoms such as Cr(0), Mn(I), Fe(II), Ru(II) and Rh(III) often exhibit much stronger interactions, forming fully covalent $\pi$-arene and $\pi$-alkene complexes. While most of these fascinating materials are outside the scope of this book, it is noteworthy that these kinds of interaction are beginning to be used in the design of geometrically and electronically selective cation hosts, with the very high binding ability expected from the formation of complexes with a significant amount of covalent character. In particular, a class of *tris*(pyrazolyl) and pyridyl ligands such as **3.136**, termed *coelenterands* (from the Greek for 'hollow stomach') have been prepared.[70] The coelenterands possess two possible coordination modes (Figure 3.93). The tripodal chelating mode resembles conventional ligands such as the *tris*(pyrazoyl)borates and their *tris*(pyrazolyl)methane analogues. The encapsulating mode is rare, but reaction of the Ru(II) dimethylsulfoxide (dmso) precursor [$RuCl_2(dmso)_4$] with **3.136** results in the isolation of a fully encapsulating complex on addition of $ZnCl_4^-$ as the counter anion. The X-ray crystal structure shows the Ru(II) cation deeply embedded within the ligand's erstwhile 'empty stomach' with a rather short Ru—ring centroid distance of 1.58 Å (compared to normal values in organometallic complexes of

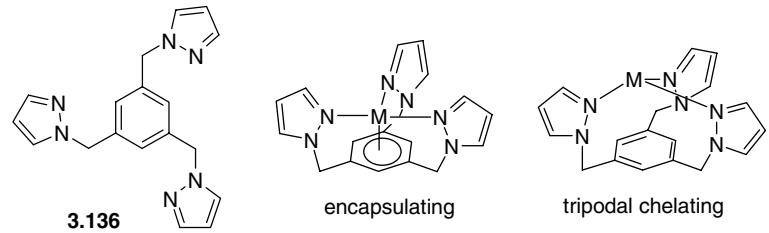


**Figure 3.93** Coordination modes of the coelenterands.[70]

about 1.67–1.70 Å), suggesting a chelate reinforcement of the Ru—C binding. Evidence from $^{13}C$ NMR spectroscopy suggests that the complex is stable in solution over extended periods.

## 3.15.2 Hydrocarbon Hosts

The presence of heteroatom donors is not essential to cation-π complexation, and indeed a number of purely hydrocarbon π—C—donor ligands have been prepared. Ligand **3.137** is synthesised in 90% yield by cyclisation of the precursor diketone under high dilution conditions in order to minimise the formation of polymeric by-products (Scheme 3.27).

The distance between facing pairs of double bonds was shown by X-ray crystallography to be 5.11 Å, suggesting excellent preorganisation for $Ag^+$, which typically forms bonds to alkenes with Ag—C distances in the range 2.4–2.6 Å. Reaction of **3.137** with $Ag[CF_3SO_3]$ (the trifluoromethane sulfonate or triflate anion is a common, readily available anion, which coordinates only weakly to metal centres) gives a complex $[Ag(\mathbf{3.137})]^+$ in good overall yield (Figure 3.94). The X-ray crystal structure of this material shows a square planar $Ag^+$ coordination geometry, unique for a $d^{10}$ metal ion. Remarkably, the $^{13}C$ NMR spectrum of this species exhibits significant $^{13}C$—Ag coupling and the complex proved highly stable to air, light and heat, under conditions that generally destroy Ag–π complexes. The analogous di- and trimeric macrocycles have also been prepared, but only tetrameric **3.137** is large enough to encompass a metal cation within its cavity. Similar compounds are also found for hosts composed of aryl rings. In particular, [2.2]paracyclophane (**3.138**), [3.3]paracyclophane (**3.139**) and [2.2.2]paracyclophane (**3.140**) form interesting organometallic complexes with a variety of low oxidation state metals. The nomenclature and chemistry of cyclophanes is discussed in more detail in Section 6.5.

One of the most effective ligands for complexation of Ag(I) is the highly preorganised diphenylmethane-derived cyclophane **3.141**. This compound incorporates a norbornyl bridgehead and alkene 'walls' making the cavity extremely rigid, while the aromatic π-surface is complementary to

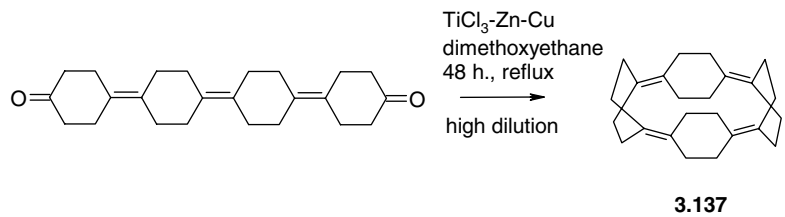


**Scheme 3.27** Synthesis of an unsaturated hydrocarbon macrocycle.

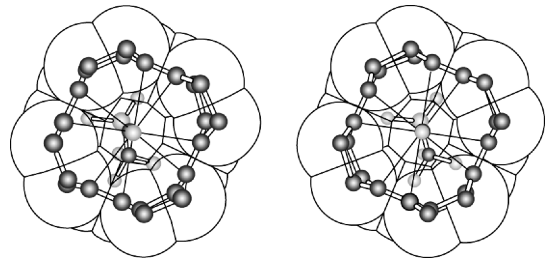

**Figure 3.94** Stereoview of the highly symmetrical $Ag^+$ complex of **3.137**. (Reproduced by permission of John Wiley & Sons, Ltd).

the soft Ag(I). In binding $AgCF_3SO_3$ in competition with control compound **3.142** which lacks the norbornyl group, only signals attributable to $[Ag(\mathbf{3.141})]^+$ are observable by NMR spectroscopy, implying that this small difference results in an increase of a factor of at least $10^2$ $M^{-1}$ in the binding constant.[71]

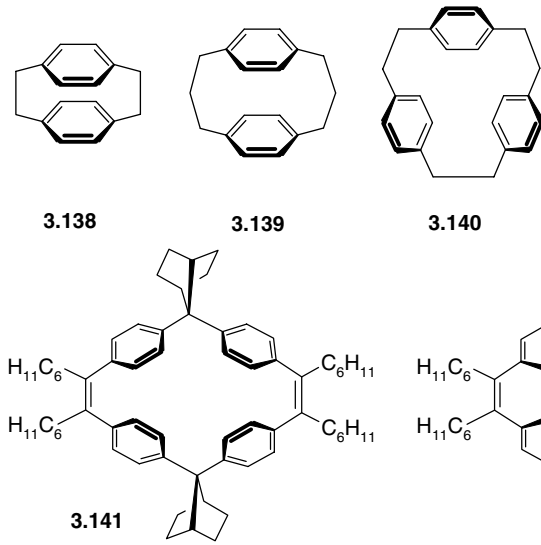


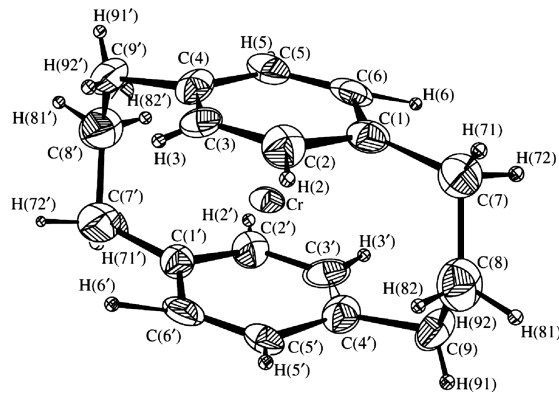


**Figure 3.95** X-ray crystal structure of the $Cr^+$ complex of paracyclophane **3.139**. (© Wiley-VCH Verlag GmbH & Co. Reproduced by permission).

Both **3.138** and **3.139** react with metallic chromium in the vapour phase according to a method called metal–atom ligand–vapour synthesis,[72] in which high-temperature vaporised metal atoms and gaseous ligand are co-condensed on to a liquid-nitrogen or liquid-helium cooled surface, and then warmed gradually until reaction takes place. The resulting complexes contain zero-valent chromium encapsulated (sandwiched) between the facing aryl rings. While the complexes themselves are too reactive to be crystallised, oxidation to the analogous $Cr^{+}$ complexes with iodine allowed crystals of both compounds to be obtained (Figure 3.95).[73]

## 3.16 The Siderophores

### 3.16.1 Naturally Occurring Siderophores

Albrecht-Gary, A. M., Crumbliss, A. L., 'Coordination chemistry of siderophores: Thermodynamics and kinetics of iron chelation and release,' in *Metal Ions in Biological Systems*, 1998, **35**, 239–327.

Iron has a crucial biochemical role in an enormous range of cell redox processes in plants, bacteria and higher organisms. In terms of bioavailability, however, iron leaves much to be desired since in its most common naturally occurring oxidation state, Fe(III) (rust), is highly insoluble in aqueous solution. At a physiological pH of 7.4, the solubility of $[Fe(H_2O)_6]^{3+}$ is about $10^{-18}$ mol dm$^{-3}$. Vast regions of the Pacific ocean are essentially sterile because of a lack of bioavailable iron and one of the more creative and controversial plans to tackle global warming has been to seed the ocean with iron to promote microorganism growth on a vast scale thereby sequestering atmospheric $CO_2$. Trials involving addition of iron compounds to the water do indeed result in a rapid flourishing of marine phytoplankton but this is short-lived since the iron does not remain in solution for long enough. Optimum microorganism growth requires an intracellular concentration in the region of $10^{-7}$ mol dm$^{-3}$, a factor of about a hundred billion times more concentrated than the solubility-limited concentration of Fe(III). As a result, plants and bacteria require highly effective iron-complexing ligands in order to mobilise $Fe^{3+}$ and deliver it to the cell. These naturally occurring ligands are termed *siderophores* (from the Greek meaning 'iron bearer'), and may be regarded as essential microorganism growth promoters. The sideophores were discovered as early as 1911, but it was not until 1951 that the first natural sideophore, mycobactin (**3.143**) was isolated, as its aluminium complex.

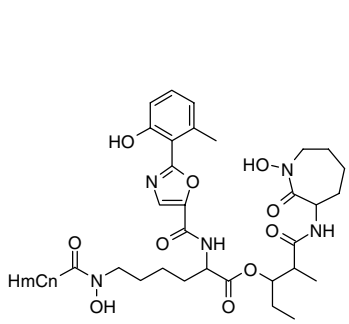


**3.143**
Mycobactin
n >12

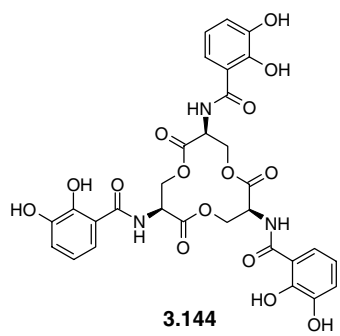


**3.144**
Enterobactin

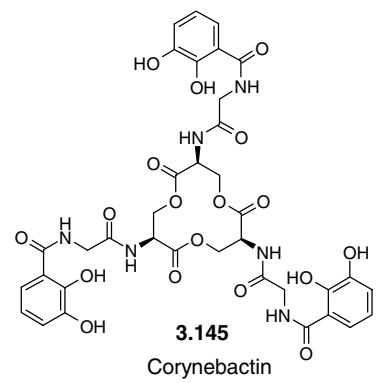


**3.145**
Corynebactin

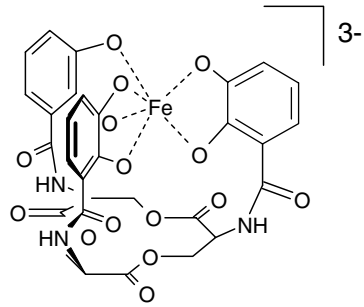


**Figure 3.96** Trigonal prismatic coordination of $Fe^{3+}$ in $[Fe(enterobactin)]^{3-}$.

Siderophores such as mycobactin (**3.143**) and enterobactin (**3.144**) are essentially three-armed podands, binding through deprotonated hydroxyl groups. The ligands have an overall 6– charge, making them complementary to highly charged cations; the hard character of the phenolate or catecholate moieties bind strongly to the hard $Fe^{3+}$. Indeed, enterobactin has an $Fe^{3+}$ stability constant of $10^{52}$, making it the most effective natural iron chelating agent known.[74] It is so effective at binding iron that at pH 7 no competition is observed from the well-known sequestering agent, ethenediamine tetraacetate ($EDTA^{4-}$, Section 3.1.3). It has been demonstrated by the isolation of a number of siderophores from bacteria and the roots of plants, especially those growing in alkaline soils, that the *o*-dihydroxybenzene (catechol) moiety is a common feature to effective iron chelators. Enterobactin, with its three catecholate arms, is able to envelop $Fe^{3+}$ in a trigonal prismatic, six-coordinate geometry (Figure 3.96).

Enterobactin was originally isolated from bacterial cultures of *Salmonella typhimurium* or *Escherichia coli* by lengthy extraction and chromatographic purification procedures giving yields in the region of 15 mg of product per litre of nutrient solution. Understandably, the exacting nature of this procedure has led to the development of a number of laboratory procedures to produce enterobactin synthetically. The most efficient of these makes use of the template effect (Section 3.9.1) involving the trimerisation of bulky triphenylmethyl substituted L-serine derivative about a tin atom (Scheme 3.28).

Enterobactin is a chiral compound by virtue of the three asymmetric carbon atoms adjacent to nitrogen. Use of the opposite enantiomer D-serine starting material gives enantioenterobactin, the mirror image of **3.144**. Interestingly, growth of bacteria in the presence of enantioenterobactin showed that no growth promotion occurred. Indeed, growth was inhibited because the non-natural siderophore kept the iron within the culture medium, preventing its assimilation by the bacteria. The natural form of **3.144** is a highly effective growth promoter.

In biochemical systems $[Fe(enterobactin)]^{3-}$ enters the bacterial cell through an outer membrane protein, the structure of the *E. coli* version of which has recently been determined.[74] The catechetol functionalities are crucial to this transport but the trilactone ring can be replaced with many other

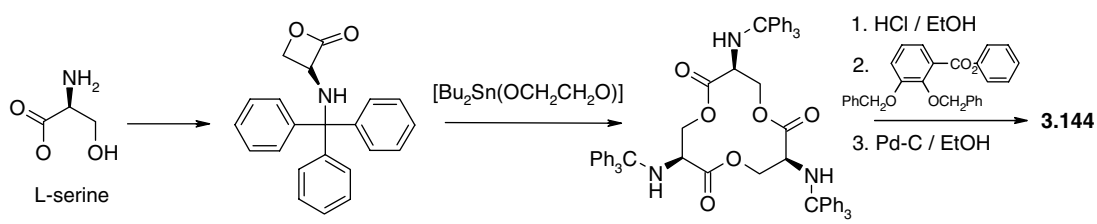


**Scheme 3.28** Template synthesis of enterobactin.

scaffolds. When it has crossed into the cell the complex moves to the cytoplasm *via* the ATP binding cassette transporter. The mechanism of this process is common across a wide range of ferric siderophores and has a number of key features: (i) binding of the ferric complex by the periplasmic binding protein, (ii) interaction of the binding protein with the cytoplasmic membrane spanning protein, and (iii) transport of the ferric siderophore across the cytoplasmic membrane by hydrolysis of ATP in a membrane bound protein (*cf.* $Na^+/K^+$-ATPase, Section 2.2). The structure of the periplasmic enterobactin binding protein is not known but binding studies show that it is very highly specific for enterobactin with $K_d = 30$ nM, corresponding to a binding constant of $3.3\times10^7$.

For many years it was thought that enterobactin's the trilactone ring was unique. However, in 1997 another natural sideophore *corynebactin* (**3.145**) was isolated from Gram-positive *Corynebacterium glutamicum* and *Bacillus subtilis*.[74] *Corynebactin* incorporates a threonine trilactone and incorporates glycine spacers which have the effect of elongating the three chelating arms. *Corynebactin* also binds Fe(III) very strongly indeed, but modeling studies indicate that instead of forming a D-helical ferric structure as in enterobactin, it has L handedness. Both the incorporation of a glycine spacer and the methylation of the trilactone ring (a change from serine to threonine) favour the L conformation. This significant difference may affect the mechanism of its biochemical iron transport.

## 3.16.2 Synthetic Siderophores

Vögtle, F., *Supramolecular Chemistry*, John Wiley & Sons, Ltd: Chichester, 1991.

The enormous iron complexing ability of enterobactin has led to the synthesis of a number of synthetic podand and cryptand analogues. In particular, the tricatecholate mesitylene derivative **3.146** bears a close structural resemblance to **3.144** and, moreover, does not feature its hydrolysis-prone ester linkages, making it an easier ligand to handle. As expected, given its close relationship with **3.144**, the synthetic host **3.146** (MECAM) is also a strong iron complexant. However, the $Fe^{3+}$ binding constant for compound is only $10^{46}$, some million times lower than enterobactin itself, suggesting immediately a strong structural basis for enterobactin's particularly effective complexing properties. The smaller mesityl spacer group in MECAM presumably results in a more strained complex geometry. The complex $[Fe(MECAM)]^{3-}$ was tested in *E. coli* culture and, despite its lower $Fe^{3+}$ affinity, it is able to bind to the *E. coli* enterobactin receptor systems and promote the growth of the organism.

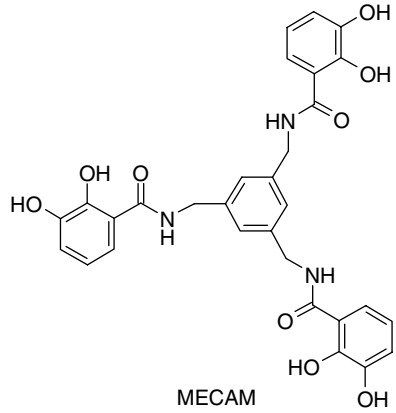


MECAM

**3.146**

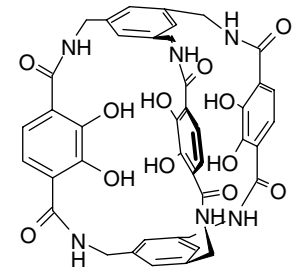


**3.147**

**Table 3.21** p*M* values and binding constants for $Fe^{3+}$ chelate ligands in aqueous solution.

| Ligand | p*M* | log *K* |
|---|---|---|
| Enterobactin | 35.5 | 52 |
| MECAM | 29.1 | 46 |
| $EDTA^{4-}$ | 12.2 | 25.1 |

Catechol is a only a weak acid and, as a 6– anion, the host conjugate base is susceptible to protonation, resulting in a significant pH dependence on its $Fe^{3+}$ complexation ability. For example, under slightly acidic conditions (pH 5) there is significant competition for $Fe^{3+}$ by $EDTA^{4-}$ (a stronger acid in its protonated form), which can be detected by UV–visible spectroscopy. For this reason, in order to be able to distinguish usefully between the metal binding ability of different siderophores, a p*M* scale has been introduced for these ligands. The p*M* value is defined by analogy with pH by the following relationship:

$$pM = -\log[Fe(H_2O)_6{}^{3+}] \tag{3.7}$$

Thus a large positive p*M* value corresponds to a low equilibrium concentration of aqueous $Fe^{3+}$, and hence effective metal complexation by the ligand. Crucially, the p*M* value is measured under standard conditions in aqueous solution with 1 μM total $Fe^{3+}$ concentration, 10 μM total ligand concentration at pH 7.4. Some example p*M* values are given in Table 3.21.

Despite the enormous success of **3.14** and its synthetic analogue **3.146**, we have seen that in other systems podand hosts are intrinsically less effective than their cyclic analogues (Section 3.2.1). Accordingly, the macrobicyclic ligand **3.147** and a wide variety of related hosts with spacer units of varying size (*e.g.* triphenylmethane caps, bipyridyl binding sites) have been synthesised. Consistent with the rigid, preorganised structure of **3.147**, it displays an enormous $Fe^{3+}$ binding constant under physiological conditions of about $10^{59}$, making it the most effective $Fe^{3+}$ complexant yet known.[75]

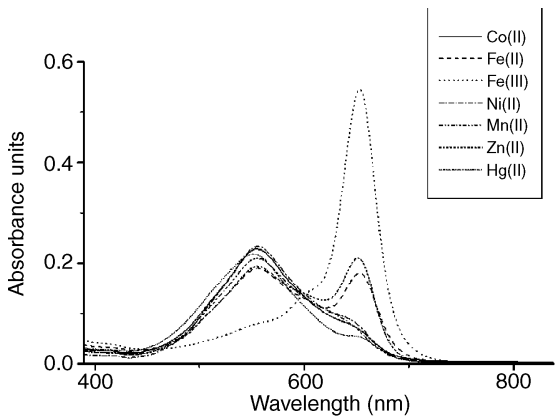


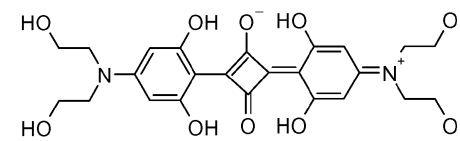


**3.148**

**Figure 3.97** Fe(III) specific colorimetric sensing by squarine-based siderophore **3.148**. (Reproduced by permission of The Royal Society of Chemistry).

Ligand **3.147** is part of the class of *siderands* (synthetic siderophores), and displays further useful properties such as stability towards oxidation of the catechol binding sites and hydrolysis resistance. This represents one of the few examples where man-made molecules are more effective than their natural precursors.

Finally, recently a simple, synthetic dye-based siderophore has been developed that can colorimetrically detect Fe(III).[76] The compound (**3.148**) is based on the four-membered ring squaric acid and binds two equivalents of Fe(III) with $K_{11} = 8.9\times10^7$ and $K_{21} = 1.4\times10^6$ in DMSO solution. While not nearly as significant as the binding by the macrobicyclic systems, Fe(III) binding promotes a planar structure facilitating the stacking of the receptors to give 'H'-aggregates involving the overlap of the electron deficient squarine part with adjacent aromatic rings. The result is a change from blue to purple and a gives rise to a readily observed absorption at 651 nm, Figure 3.97.

## Summary

- Supramolecular chemistry involves a generalisation of the principles of coordination chemistry and was first applied to hosts for metal cations.
- Schiff base macrocycles and phthalocyanines are readily prepared and pre-date crown ethers and cryptands but are more suitable for binding transition metals or softer main group ions.
- Preorganisation and Complementarity are of crucial importance in determining the binding constant as exemplified by the extremely high binding constants observed for spherands and torands. The detailed factors governing selectivity are complex, however, and include chelate ring size, donor group orientation, hard/soft acid/base effects and solvation.
- Template and high dilution methods are vital to produce reasonable yields of macrocycles, which are generally much more preorganised for cation binding than comparable *podands*
- Hosts such as crown ethers and cryptands are useful as phase transfer agents and mimics of biological membrane transporting ionophores.
- Crown ethers bind well to organic ammonium cations and oxonium ions by charge-assisted hydrogen bonding interactions, as well as metal cations. In some cases they can be used to resolve chiral ammonium salts.
- The high affinity of crown ethers and cryptands for alkali metal cations will cause the metals themselves to disproportionate into cations and alkalide anions or electride salts.
- The calixarenes have become extremely popular and versatile cation complexing agents and supramolecular scaffolds.
- Iron(III) binding siderophores exhibit some of the highest binding constants known for metal ions, with artificial hosts being just as effective as natural systems.
- NMR spectroscopy is a tremendously powerful tool for monitoring weaker host-guest binding processes.

## Study Problems

3.1 How many structural isomers are there of dibenzo[18]crown-6? Draw them.

3.2 Hydrogenation of the isomer of dibenzo[18]crown-6, originally synthesised by Pedersen using $H_2$/Pd, gives the saturated dicyclohexyl[18]crown-6. Excluding enantiomers, this material has five isomers, of which the *cis-syn-cis* isomer (isomer A) is shown below. The other isomers are called *cis-anti-cis*, *trans-syn-trans*, *trans-anti-trans* and *cis-trans*. Draw these isomers and assign the names to the structures.

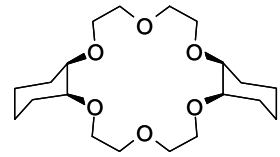

cis-syn-cis-dicyclohexyl[18]crown-6

3.3 Look at your answers to question 3.2. Are these isomers interconvertible by bond rotations? Which of them are chiral? You will probably find that building a molecular model will help you answer these questions.

3.4 Define the term 'binding constant'. The logarithms of the binding constants for the complexation of $Na^+$ by the various isomers of dicyclohexyl[18]crown-6 that have been synthesised so far are 4.08, 3.68, 2.99 and 2.52 for the *cis-syn-cis*, *cis-anti-cis*, *trans-syn-trans* and *trans-anti-trans* isomers, respectively (MeOH, 25 °C). Suggest reasons for this large variation. The corresponding binding constant for [18]crown-6 is 4.32. How does this fit in with your ideas?

3.5 The logarithms of the $K^+$ binding constants ($M^{-1}$, MeOH 25 °C) for three hosts are shown below. Explain this large variation.

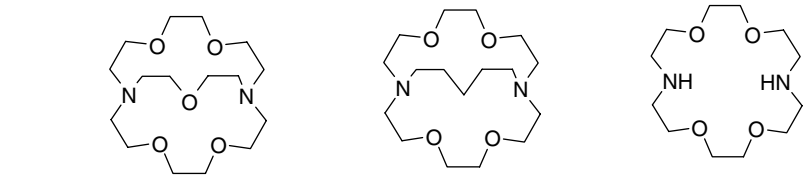

log $K_1$ ($K^+$) 9.0 5.4 2.0

3.6 Make brief explanatory notes on the following concepts. Source material may be found in both Chapters 1 and 3: (a) the template effect; (b) the chelate and macrocyclic effects; (c) the high dilution technique in macrocyclic synthesis; and (d) preorganisation and complementarity.

3.7 Compare and contrast the properties of the following classes of host molecule. Include in your answer information on selectivity, solubility and binding kinetics: (a) naturally occurring ionophores; (b) podands; (c) corands; (e) lariat ethers; (f) cryptands; (g) calixarenes; and (h) spherands. You may find it helpful to present the information in the form of a comparative table.

3.8 From your answers to question 3.6 or otherwise, suggest artificial systems that mimic (a) some of the properties of the natural ionophores and (b) features of transmembrane ion channels.

## Thought Experiment

A number of structural subunits are shown below. From your reading of this chapter, suggest structural modifications or appropriate functional groups that might be appended to make each host type serve as (a) a host for metal cations and (b) a host for organic ammonium ions. Using the concepts of preorganisation, solvation, enthalpic and entropic effects and complementarity, suggest what the selectivity sequence of your hosts might be for the following guest series:

(a) $Na^+$, $K^+$, $Rb^+$, $Cs^+$

(b) $RNH_3^+$ (R = Me, Et, *t*–Bu ,$PhC(CO_2^-)$)

(c) $NH_3^+R'NH_3^+$ (R′ = $CH_2$,$C_2H_4$, *o* – $C_6H_4$,*p* – $C_6H_4$)

In each case consider whether the guest complexation will be of the capsular, nesting or perching type, or some other arrangement. Use this information to guess qualitatively the rate of guest complexation and decomplexation in each case.

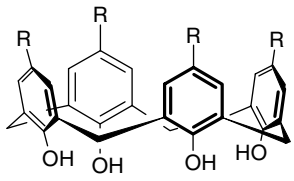


calix[4]arene

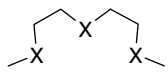


X = O, NH, S

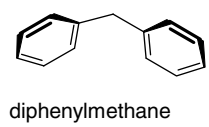

diphenylmethane

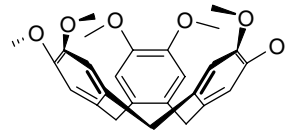

CTV

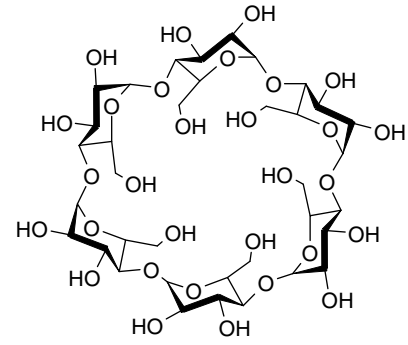

α-cyclodextrin

## References


1. Dance, I., What is Supramolecular? *New. J. Chem.* 2003, **27**, 1–2.
2. Hancock, R. D., Marsicano, F., Parametric correlation of formation constants in aqueous solution. 2. Ligands with large donor atoms. *Inorg. Chem.* 1980, **19**, 2709–2714.
3. Clegg, W., *X-ray Crystallography*. Oxford University Press: Oxford, 1998.
4. Pedersen, C. J., Cyclic polyethers and their complexes with metal salts. *J. Am. Chem. Soc* 1967, **89**, 7017–7036.
5. Ammann, D., Pretsch, E., Simon, W., Calcium ion-selective electrode based on a neutral carrier. *Analytical Letters* 1972, **5**, 843–850.
6. Vogtle, F., Weber, E., Multi-dentate acyclic neutral ligands and their complexation. *Angew. Chem., Int. Ed. Engl.* 1979, **18**, 753–776.
7. Nakatsuji, Y., Nakamura, T., Okahara, M., Dishong, D. M., Gokel, G. W., The effect of sidearm heteroatoms and aquaternary methyl-group at the pivot position in lariat ethers. *Tetrahedron Lett.* 1982, **23**, 1351–1352.
8. Gatto, V. J., Arnold, K. A., Viscariello, *et al.*, Syntheses and binding-properties of bibrachial lariat ethers (BiBLEs) – survey of synthetic methods and cation selectivities. *J. Org. Chem.* 1986, **51**, 5373–5384.
9. Dietrich, B., Lehn, J.-M., Sauvage, J. P., Diazapolyoxamacrocycles and macrobicycles. *Tetrahedron Lett.* 1969, 2885–2888.
10. Brown, K. N., Geue, R. J., Hambley, T. W., Sargeson, A. M., Willis, A. C., Stereospecific template synthesis of a new class of cage complexes: An example of self assembly. *Chem. Commun.* 1996, 567–569.
11. Vögtle, F., *Supramolecular Chemistry*. John Wiley & Sons, Ltd: Chichester, 1991.
12. Cram, D. J., Preorganisation – from solvents to spherands. *Angew. Chem., Int. Ed. Engl.* 1986, **25**, 1039–1134.
13. Hay, B. P., Hancock, R. D., The role of donor group orientation as a factor in metal ion recognition by ligands. *Coord. Chem. Rev.* 2001, **212**, 61–78.
14. Wolf, R. E., Hartman, J. A. R., Storey, J. M. E., Foxman, B. M., Cooper, S. R., Crown thioether chemistry - structural and conformational studies of Tetrathia-12-Crown-4, Pentathia-15-Crown-5, and Hexathia-18-Crown-6 – implications for ligand design. *J. Am. Chem. Soc.* 1987, **109**, 4328–4335.
15. Kataky, R., Matthes, K. E., Nicholson, P. E., Parker, D., Buschmann, H. J., Synthesis and binding-properties of amide-functionalized polyaza macrocycles. *J. Chem. Soc., Perkin Trans. 2* 1990, 1425–1432.
16. Trueblood, K. N., Knobler, C. B., Maverick, E., Helgeson, R. C., Brown, S. B., Cram, D. J., Spherands, the 1st ligand systems fully organized during synthesis rather than during complexation. *J. Am. Chem. Soc.* 1981, **103**, 5594–5596.
17. Peters, J. C., Odom, A. L., Cummins, C. C., A terminal molybdenum carbide prepared by methylidyne deprotonation. *Chem. Commun.* 1997, 1995–1996.
18. Illuminati, G., Mandolini, L., Masci, B., Template Effects .4. Ion-pairing of aryloxide ions with alkali cations in 99-percent $Me_2SO$ - influence on the rate of formation of Benzo-18-Crown-6 and of other Williamson-type reactions. *J. Am. Chem. Soc.* 1983, **105**, 555–563.

19. Richman, J. E., Atkins, T. J., Nitrogen analogs of crown ethers. *J. Am. Chem. Soc.* 1974, **96**, 2268–2270.
20. Kimura, E., Kuramoto, Y., Koike, T., Fujioka, H., Kodama, M., A study of new bis(macrocyclic polyamine) ligands as inorganic and organic anion receptors. *J. Org. Chem.* 1990, **55**, 42–46.
21. Christensen, J. J., Hill, J. O., Izatt, R. M., Ion binding by synthetic macrocyclic compounds. *Science* 1971, **174**, 459.
22. Steed, J. W., McCool, B. J., Junk, P. C., Hydrogen bonded polymers and oligomers from metal salts and 18-crown-6. *J. Chem. Soc., Dalton Trans.* 1998, 3417–3423.
23. Shaw, J. L., Wolowska, J., Collison, D., *et al.*, Redox non-innocence of thioether macrocycles: Elucidation of the electronic structures of mononuclear complexes of gold(II) and silver(II). *J. Am. Chem. Soc.* 2006, **128**, 13827–13839.
24. Levason, W., Quirk, J. J., Reid, G., Smith, S. M., Synthesis, spectroscopic and redox properties of ruthenium complexes with selenoether macrocycles: crystal structures of cis-[$RuCl_2$([16]ane$Se_4$)] and trans-[RuCl($PPh_3$)([16]ane$Se_4$)]$PF_6$ ([16]ane$Se_4$ = 1,5,9,13-tetraselenacyclohexadecane). *J. Chem. Soc., Dalton Trans.* 1997, 3719–3724.
25. Hesford, M. J., Levason, W., Matthews, M. L., Orchard, S. D., Reid, G., Synthesis, characterisation and coordinating properties of the small ring $S_2$Te-donor macrocycles [9]ane$S_2$Te, [11]ane$S_2$Te and [12]ane$S_2$Te. *Dalton Trans.* 2003, 2434–2442.
26. Martell, A. E., Hancock, R. D., Motekaitis, R. J., Factors affecting stabilities of chelate, macrocyclic and macrobicyclic complexes in solution. *Coord. Chem. Rev.* 1994, **133**, 39–65.
27. Bosnich, B., Poon, C. K., Tobe, M. L., Complexes of cobalt(III) with a cyclic tetradentate secondary amine. *Inorg. Chem.* 1965, **4**, 1102–1109.
28. Donnelly, M. A., Zimmer, M., Structural analysis of all the nickel 14-membered tetraaza macrocycles in the Cambridge structural database. *Inorg. Chem.* 1999, **38**, 1650–1658.
29. Barefield, E. K., Wagner, F., Hodges, K. D., Synthesis of macrocyclic tetramines by metal-ion assisted cyclization reactions. *Inorg. Chem.* 1976, **15**, 1370–1377.
30. Fabbrizzi, L., Gatti, F., Pallavicini, P., Zambarbieri, E., Redox-driven intramolecular anion translocation between transition metal centres. *Chem. Eur. J.* 1999, **5**, 682–690.
31. Channa, A., Steed, J. W., Anion and cation binding by a pendant arm cyclam and its macrobicyclic derivatives. *Dalton Trans.* 2005, 2455–2461.
32. Champness, N. R., Frampton, C. S., Reid, G., Tocher, D. A., Mixed phosphathia macrocyclic chemistry - synthesis and characterization of [M($Ph_2$[14]ane$P_2S_2$)]$^{2+}$ (M = Pd or Pt) and [$RhCl_2$($Ph_2$[14]ane$P_2S_2$)]$^+$ ($Ph_2$[14]ane$P_2S_2$ = 8,12-Diphenyl-1,5-Dithia-8,12-Diphosphacyclotetradecane). *J. Chem. Soc., Dalton Trans.* 1994, 3031–3037.
33. Edwards, P. G., Malik, K. M. A., Ooi, L.-l., Price, A. J., Iron complexes of facially capping triphosphorus macrocycles. *Dalton Trans.* 2006, 433–441.
34. Arnold, P. L., Patel, D., Wilson, C., Love, J. B., Reduction and selective oxo group silylation of the uranyl dication. *Nature* 2008, **451**, 315–317.
35. Nagasaki, T., Kawano, K., Araki, K., Shinkai, S., Kinetic-studies of calixarene-based cyclic and noncyclic super-uranophiles. *J. Chem. Soc., Perkin Trans. 2* 1991, 1325–1327.
36. Albert, A., Mootz, D., Formation and crystal structures of the hydrates of 18-crown-6. *Zeit. Naturforsh. Teil. B* 1997, 615–619.
37. Atwood, J. L., Junk, P. C., Synthesis and X-ray crystal structures of oxonium ion complexes of 21-crown-7 and dibenzo-30-crown-10. *J. Chem. Soc., Dalton Trans.* 1997, 4393–4399.
38. Calleja, M., Mason, S. A., Prince, P. D., Steed, J. W., Wilkinson, C., Single crystal neutron and X-ray diffraction studies of $(H_7O_3)$·$AuCl_4$·15-crown-5. *New J. Chem.* 2001, **25**, 1475–1478.
39. MacGillivray, L. R., Atwood, J. L., Structural reorganisation of the doubly protonated [222]cryptand through cation-pi and charge-charge interactions: synthesis and structure of its [$CoCl_4$].0.5$C_6H_5CH_3$ salt. *Angew. Chem., Int. Ed. Engl.* 1996, **35**, 1828–1830.
40. Calleja, M., Johnson, K., Belcher, W. J., Steed, J. W., Oxonium ions from aqua regia: Isolation by hydrogen bonding to crown ethers. *Inorg. Chem.* 2001, **40**, 4978–4985.
41. Ilioudis, C. A., Bearpark, M. J., Steed, J. W., Hydrogen bonds between ammonium ions and aromatic rings exist and have key consequences on solid-state and solution phase properties. *New J. Chem.* 2005, **29**, 64-67.
42. Pascal, R. A., Grossman, R. B., Vanengen, D., Synthesis of in- 3(4,10) 7 metacyclophane – projection of an aliphatic hydrogen toward the center of an aromatic ring. *J. Am. Chem. Soc.* 1987, **109**, 6878–6880.
43. Arduini, A., Giorgi, G., Pochini, A., Secchi, A., Ugozzoli, F., Anion allosteric effect in the recognition of tetramethylammonium salts by calix[4]arene cone conformers. *J. Org. Chem.* 2001, **66**, 8302–8308.
44. Friebolin, H., *Basic One- and Two-Dimensional NMR Spectroscopy*. 2nd ed., VCH: Weinheim, 1993.
45. Cohen, Y., Avram, L., Evan-Salem, T., Frish, L., 'Diffusion NMR in supramolecular chemistry'. in *Analytical Methods in Supramolecular Chemistry*, Schalley, C. A., ed. Wiley-VCH: Weinheim, 2007, *pp.* 163–219.
46. Cohen, Y., Avram, L., Frish, L., Diffusion NMR spectroscopy in supramolecular and combinatorial chemistry: an old parameter - new insights. *Angew. Chem. Int. Ed.* 2005, **44**, 520–554.

47. Peacock, S. C., Domeier, L. A., Gaeta, F. C. A., Helgeson, R. C., Timko, J. M., Cram, D. J., Host-guest complexation .13. High chiral recognition of amino esters by dilocular hosts containing extended steric barriers. *J. Am. Chem. Soc.* 1978, **100**, 8190–8202.
48. Newcomb, M., Toner, J. L., Helgeson, R. C., Cram, D. J., Host-guest complexation .20. Chiral recognition in transport as a molecular-basis for a catalytic resolving machine. *J. Am. Chem. Soc.* 1979, **101**, 4941–4947.
49. Huszthy, P., Bradshaw, J. S., Zhu, C. Y., Izatt, R. M., Lifson, S., Recognition by new symmetrically substituted chiral diphenyl-butylpyridino-18-crown-6 and di-tert-butylpyridino-18-crown-6 and asymmetrically substituted chiral dimethylpyridino-18-crown-6 ligands of the enantiomers of various organic ammonium perchlorates. *J. Org. Chem.* 1991, **56**, 3330–3336.
50. Forman, J. E., Barrans, R. E., Dougherty, D. A., Circular-dichroism studies of molecular recognition with cyclophane hosts in aqueous-media. *J. Am. Chem. Soc.* 1995, **117**, 9213–9228.
51. Sansone, F., Barboso, S., Casnati, A., Sciotto, D., Ungaro, R., A new chiral rigid cone water soluble peptidocalix[4]arene and its inclusion complexes with alpha-amino acids and aromatic ammonium cations. *Tetrahedron Lett.* 1999, **40**, 4741–4744.
52. Park, H. S., Lin, Q., Hamilton, A. D., Protein surface recognition by synthetic receptors: A route to novel submicromolar inhibitors for alpha-chymotrypsin. *J. Am. Chem. Soc.* 1999, **121**, 8-13.
53. Canceill, J., Collet, A., Gabard, J., Kotzybahibert, F., Lehn, J. M., Speleands –macropolycyclic receptor cages based on binding and shaping subunits – synthesis and properties of macrocycle-cyclotriveratrylene combinations. *Helv. Chim. Acta* 1982, **65**, 1894–1897.
54. Dhaenens, M., Lacombe, L., Lehn, J. M., Vigneron, J. P., Binding of acetylcholine and other molecular cations by a macrocyclic receptor molecule of speleand type. *J. Chem. Soc., Chem. Commun.* 1984, 1097–1099.
55. Allwood, B. L., Kohnke, F. H., Stoddart, J. F., Williams, D. J., A Macrobicyclic receptor molecule for the diquat dication. *Angew. Chem., Int. Ed. Engl.* 1985, **24**, 581–584.
56. Atwood, J. L., Davies, J. E. D., MacNicol, D. D., Vögtle, F., *Comprehensive Supramolecular Chemistry*. Pergamon: Oxford, 1996, Vol. 1, p. 500.
57. Dye, J. L., Electrides – ionic salts with electrons as the anions. *Science* 1990, **247**, 663–668.
58. Ichimura, A. S., Huang, R. H., Xie, Q. S., Morganelli, P., Burns, A., Dye, J. L., One-dimensional zigzag chains of Cs-: The structures and properties of Li+(cryptand[2.1.1])Cs- and Cs+(cryptand[2.2.2])Cs. *J. Phys. Chem. B* 2006, **110**, 12293–12301.
59. Bott, S. G., Coleman, A. W., Atwood, J. L., Inclusion of both cation and neutral molecule by a calixarene - structure of the [para-tert-butylmethoxycalix[4]arene-sodium-toluene]+cation. *J. Am. Chem. Soc.* 1986, **108**, 1709–1710.
60. Ikeda, A., Tsuzuki, H., Shinkai, S., Nmr Spectroscopic and X-ray crystallographic studies of calix[4]arene $Ag^+$ complexes - influence of bound $Ag^+$ on $C_{2v}$-$C_{2v}$ interconversion in cone-calix[4]arenes. *J. Chem. Soc., Perkin Trans. 2* 1994, 2073–2080.
61. ArnaudNeu, F., Asfari, Z., Souley, B., Vicens, J., Binding properties of calix[4]-bis-crowns towards alkali cations. *New J. Chem.* 1996, **20**, 453–463.
62. Cragg, P. J., Allen, M. C., Steed, J. W., A 'toothpaste tube' model for ion transport through trans- membrane channels. *Chem. Commun.* 1999, 553–554.
63. Harrowfield, J. M., Ogden, M. I., Richmond, W. R., White, A. H., Calixarene-cupped cesium – a coordination conundrum. *J. Chem. Soc., Chem. Commun.* 1991, 1159–1161.
64. Matthews, S. E., Schmitt, P., Felix, V., Drew, M. G. B., Beer, P. D., Calix[4]tubes: A new class of potassium-selective ionophore. *J. Am. Chem. Soc.* 2002, **124**, 1341–1353.
65. Ohseto, F., Shinkai, S., Metal vibration in an ionophoric biscalix[4]arene. *Chem. Lett.* 1993, **22**, 2045–2048.
66. Ikeda, A., Tsudera, T., Shinkai, S., Molecular design of a 'molecular syringe' mimic for metal cations using a 1,3-alternate calix[4]arene cavity. *J. Org. Chem.* 1997, **62**, 3568–3574.
67. Gustowski, D. A., Gatto, V. J., Mallen, J., Echegoyen, L., Gokel, G. W., Direct correlation of cation binding strengths to Hammett parameters in substituted *N*-benzylaza-15-crown-5 lariat ether and *N,N'*-dibenzyl-4,13-diaza-18-crown-6 BiBLE derivatives. *J. Am. Chem. Soc.* 1987, **52**, 5172–5176.
68. Arya, P., Channa, A., Cragg, P. J., Prince, P. D., Steed, J. W., *C*-donor lariat ether 'Scorpionates'. *New. J. Chem.* 2002, 440–447.
69. Gokel, G. W., Barbour, L. J., Ferdani, R., Hu, J. X., Lariat ether receptor systems show experimental evidence for alkali metal cation-pi interactions. *Acc. Chem. Res.* 2002, **35**, 878–886.
70. Hartshorn, C. M., Steel, P. J., Coelenterands: a new class of metal-encapsulating ligands. *Angew. Chem. Int. Ed. Engl.* 1996, **35**, 2655–2657.
71. Martinez, A. G., Barcina, J. O., Heras, M. D. C., Cerezo, A. D., Salvador, M. D. T., Complexation behavior of a highly preorganized 7,7-diphenylnorbornane-derived macrocycle: Towards the design of molecular clocks. *Chem. Eur. J.* 2003, **9**, 1157–1165.

72. Timms, P. L., The use of free atoms of transition-metals in chemical synthesis. *Proc. Royal Soc. Ser. A* 1984, **396**, 1–19.
73. Benn, R., Blank, N. E., Haenel, M. W., Klein, J., Koray, A. R., Weidenhammer, K., Ziegler, M. L., Structural investigations on ($\eta^{12}$-[3.3]paracyclophane)chromium(0) and its cation in ($\eta^{12}$-[3.3]paracyclophane)chromium(I) triiodide. *Angew. Chem., Int. Ed. Engl.* 1980, **19**, 44–45.
74. Raymond, K. N., Dertz, E. A., Kim, S. S., Enterobactin: An archetype for microbial iron transport. *Proc. Nat. Acad. Sci. USA* 2003, **100**, 3584–3588.
75. Stutte, P., Kiggen, W., Vogtle, F., Large molecular cavities bearing siderophore type functions. *Tetrahedron* 1987, **43**, 2065–2074.
76. Wallace, K. J., Gray, M., Zhong, Z. L., Lynch, V. M., Anslyn, E. V., An artificial siderophore for the detection of iron(III). *Dalton Trans.* 2005, 2436–2441.

# 4 Anion Binding

*'A man ought warily to begin [deficit] charges which, once begun, will continue.'*

Francis Bacon (1561–1626), *Essays* (*Of Expenses*), 1625

# 4.1 Introduction

## 4.1.1 Scope

Sessler, J. L., Gale, P. A. and Cho, W.-S., *Anion Receptor Chemistry*, Royal Society of Chemistry: Cambridge, 2006.

The field of non-covalent anion coordination chemistry as we know it today may be traced back to a report by C. H. Park and H. E. Simmons of the du Pont de Nemours Company in 1968, concerning the halide complexation properties of a series of macrobicyclic hosts termed *katapinands* (**4.1**).[1] The katapinands (named from the Greek *katapino*, meaning to swallow up or engulf) are able to bind halide ions within their macrobicyclic cavity when protonated at the bridgehead nitrogen atoms. This encapsulation behaviour (Figure 4.1), later confirmed by X-ray crystal structure determination, was the first example of anion binding by a macrocyclic host, and preceded the discovery of the cryptates (Section 3.4) by several years. In fact, Simmons and Park's paper, submitted on 13 November 1967, was the second major contribution to the then unborn field of supramolecular chemistry to come out of the laboratories of the du Pont Company. Seven months earlier, on 13 April, Charles Pedersen had submitted his landmark work on the cation-binding behaviour of dibenzo[18]crown-6, which marked the beginning of modern supramolecular chemistry.

Interest and developments in non-covalent anion coordination chemistry continued sporadically throughout the 1970s and early 1980s, with the synthesis of several hosts of crucial conceptual importance (mainly of cryptand type, analogous to the katapinands) by the groups of Franz P. Schmidtchen of the Technical University of München, Germany, and Jean-Marie Lehn.[2] It was not until the late 1980s, however, that anion complexation became a popular topic as a new generation of chemists began to address this relatively unconquered frontier; even the 1996 *Comprehensive Supramolecular Chemistry* devotes only one chapter fully to anion binding.[3] Perhaps with some degree of prophecy, Lehn in 1992 described the field of supramolecular anion coordination chemistry as '*a full member of the field of supramolecular chemistry*'. In 2006 Sessler, Gale and Cho published a major review that forms the key reference to this chapter. The huge amount of activity they detail in their book would seem to bear him out. Indeed, the challenge of anion complexation chemistry has spawned an enormous variety of imaginative host molecules, which exercise the skill of the chemist both in their synthesis, the scale of their architecture and in their modes of anion binding.

The applications of cation-binding ligands are legion; from mimics of biological ion transport to mining and the extraction of metals and as selective catalysts. Similarly it is worth spending a moment to look at real world issues of interest to anion supramolecular chemists. Simple inorganic anions are ubiquitous in the natural world; chloride is a major component of the oceans and it is the dominant anion in biological extra-cellular fluid. Nitrate (from $N_2$ oxidation) and sulfate from burning organo sulfur compound containing fossil fuels) are key components in acid rain and roadside particulate matter. Hydrogen carbonate and carboxylates are also key biological anions, while carbonates, phosphates and silicates are the major anions in biomineralised materials such as the exoskeletons of radiolarian, and in bone. Phosphates and nitrates in fertilisers are beneficial to agriculture but also major pollution hazards since such bioavailable sources of phosphorus and nitrogen are often *biolimiting*, *i.e.* rate of microorganism growth is limited by the amount of these elements that are present. Excess fertilisers, for example in fresh water lakes from agricultural runoff, causes a process termed *eutrophication*; the uncontrolled growth of large floating masses of algae that deplete local dissolved oxygen

*Supramolecular Chemistry, 2nd edition* J. W. Steed and J. L. Atwood
© 2009 John Wiley & Sons, Ltd ISBN: 978-0-470-51233-3

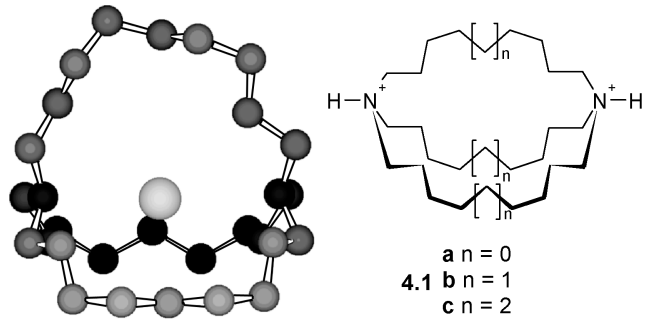


**4.1** **a** n = 0
**b** n = 1
**c** n = 2

**Figure 4.1** Minimised structure of the chloride complex of 1,11-diazabicyclo[9.9.9]nonacosane; katapinand **4.1b**.

levels, killing fish and damaging the aquatic ecosystem. Other anthropogenic anions are also major pollutants, *e.g.* the highly soluble and mobile $^{99}TcO_4^-$ and $ClO_4^-$. Technetium-99 is a $\beta$-emitter with a half-life of 213,000 years and is a product of the nuclear fuel cycle, formed in *ca.* 6 % fission yield and can leach from nuclear waste storage facilities. Perchlorate was used extensively as an explosive and rocket propellant. Recent concerns revolve around its extensive contamination of the Colorado river in the USA, affecting the drinking water supplies of *ca.* 15 million people. Its toxicity data effects are still under debate. Naturally occurring polluting anions such as arsenate are also a problem, contaminating wells in developing countries such as Bangadesh. Anions are crucial in biological systems – perhaps this is why imbalances in their concentration have such serious effects. Between 70 and 75 per cent of enzyme substrates and cofactors are anions, very often phosphate residues (as in ATP and ADP) or as inorganic phosphate ($H_2PO_4^-$). Chloride anion is the major extracellular anion, and it is responsible for the maintenance of ionic strength. A protein called the cystic fibrosis transmembrane conductance regulator (CFTR) protein acts both as a transmembrane chloride channel and as a regulator of other ion channels (Section 2.2). Mutations in the genes that code for this protein result in impaired chloride transport and chloride ion transmembrane balance, giving rise to the lethal genetic disease cystic fibrosis.

### 4.1.2 Challenges in Anion Receptor Chemistry

Despite the early discovery of the katapinands, non-covalent anion coordination chemistry was relatively slow to develop in comparison with the development of hosts for cations and even neutral molecules. While it is generally true that anion hosts obey the same rules that govern the magnitude of binding constants and host selectivity in cation hosts (primarily based on preorganisation, complementarity, solvation and size and shape effects), their application is made much more difficult because of some of the intrinsic properties of anions, listed below.

- Anions are relatively large and therefore require receptors of considerably greater size than cations. For example, one of the smallest anions, $F^-$, is comparable in ionic radius to $K^+$ (1.33Å versus 1.38Å). Other selected anion radii are shown in Table 4.1.
- Even simple inorganic anions occur in a range of shapes and geometries, *e.g.* spherical (halides), linear ($SCN^-$, $N_3^-$), planar ($NO_3^-$, $PtCl_4^{2-}$), tetrahedral ($PO_4^{3-}$, $SO_4^{2-}$), octahedral ($PF_6^-$, $Fe(CN)_6^{3-}$) as well as more complicated examples as in the case of biologically important oligophosphate anions.

**Table 4.1** Properties of some common anions and cations (ionic radii in part from Reference 4).

| Ion | Radius (Å) | $\Delta G_{hydration}$ (kJ mol$^{-1}$) | p$K_a$ (298K) |
|---|---|---|---|
| $F^-$ (6 coord.) | 1.33 | −465 | 3.3 |
| $Cl^-$ (6 coord.) | 1.81 | −340 | Low |
| $Br^-$ (6 coord.) | 1.96 | −315 | Low |
| $I^-$ (6 coord.) | 2.20 | −275 | Low |
| $ClO_4^-$ | 2.50 | −430 | – |
| $NO_3^-$ | 1.79 | −300 | −1.4 |
| $CO_3^{2-}$ | 1.78 | −1315 | 6.4, 10.3 |
| $SO_4^{2-}$ | 2.30 | −1080 | Low, 2.0 |
| $PO_4^{3-}$ | 2.38 | −2765 | 2.1, 6.2, 12.4 |
| $H_2PO_4^-$ | 2.00 | −465 | 2.1, 6.2, 12.4 |
| $PdCl_6^{2-}$ | 3.19 | −695 | – |
| $Na^-$ | 2.2 | n/a | – |
| $Cs^-$ | 3.5 | n/a | – |
| $Li^+$ (6 coord.) | 0.76 | −475 | – |
| $Na^+$ (6 coord.) | 1.02 | −365 | – |
| $K^+$ (6 coord.) | 1.38 | −295 | – |
| $Cs^+$ (6 coord.) | 1.67 | −250 | – |
| $Ca^{2+}$ (6 coord.) | 1.00 | −505 | – |
| $Zn^{2+}$ (6 coord.) | 0.74 | −1955 | – |
| $Al^{3+}$ (6 coord.) | 0.54 | −4525 | – |
| $La^{3+}$ (6 coord.) | 1.03 | −3145 | – |
| $NH_4^+$ | 1.48 | −285 | 9.3 |

- In comparison to cations of similar size, anions have high free energies of solvation and hence anion hosts must compete more effectively with the surrounding medium, *e.g.* $\Delta G_{hydration}(F^-) = -465$ kJ mol$^{-1}$, $\Delta G_{hydration}(K^+) = -295$ kJ mol$^{-1}$. Other solvation free energies are given in Table 4.1.
- Many anions exist only in a relatively narrow pH window, which can cause problems especially in the case of receptors based upon polyammonium salts where the host may not be fully protonated in the pH region in which the anion is present in the desired form.
- Anions are usually coordinatively saturated and therefore bind only *via* weak forces such as hydrogen bonding and van der Waals interactions, although they can form dative bonds.

In considering the differential or selective binding of one anion or another, the intrinsic properties of anions mean that we are not on a 'level playing field'; it is considerably easier to bind some anions than others. In general, in the absence of specific chemical recognition between anion and host, anion binding selectivity, particularly in solvent extraction experiments or in the detection of anions by membrane-based ion selective electrodes, follows the order of anion hydrophobicity. This order is termed the *Hofmeister series*, or lyotropic series and was first outlined in 1888 from experiments based on the

**Table 4.2** The Hofmeister Series

| Weakly hydrated (hydrophobic) | Strongly hydrated (hydrophilic) |
|---|---|
| **Anions:** organic anions $> ClO_4^- > I^- > SCN^- > NO_3^- > ClO_3^- \cdots$ | |
| $> Br^- > Cl^- >> F^-, IO_3^- > CH_3CO_2^-, CO_3^{2-} > HPO_4^{2-}, SO_4^{2-} >$ citrate$^{3-}$ | |
| **Cations:** $N(CH_3)_4^+ > NH_4^+ > Cs^+ > Rb^+ > K^+ > Na^+ > H^+ > Ca^{2+} > Mg^{2+}, Al^{3+}$ | |

ability of various ions to 'salt out' proteins from water. The Hofmeister series is shown in Table 4.2, where the left-hand side represents anions that dissolve and denature proteins in concentrated salt solutions, and the right-hand side represents precipitation of proteins. The series is thought to be related to the ordering of the water solvent by the various species and is also correlated with the anion hydration energy.[5]

It is, of course, impossible to accurately consider the binding of an anion or a cation in isolation. Electrostatic forces are so strong that ions are never far away from an oppositely charged counter-ion and hence any neutral molecule capable of acting as a host for anions also acts as a host for the counter-cation. Any cationic molecule that acts as a host for anions is *in competition with* the counter-cation, particularly in non-polar solvents where ion pairing can be very significant. In this chapter we will deal with both neutral and cationic anion binding systems in which relatively little attention is paid to the counter-ion and it is generally assumed that counter ion effects are, if not negligible, at least constant within the system under study. In Chapter 5 we will consider hosts that explicitly and selectively bind both ions of an ion pair.

## 4.2 Biological Anion Receptors

Mangani, S. and Ferraroni, M., 'Natural anion receptors: anion recognition by proteins', in *Supramolecular Chemistry of Anions*, Bianchi, A., Bowman-James, K. and Garcia-España, E. (eds), Wiley: New York, 1997, 63–78.

Before embarking upon a discussion of the design and preparation of artificial anion hosts it is worthwhile looking briefly at the way in which Nature carries out the task of anion complexation and transport. At least 14 mitochondrial anion transport systems have been identified to date including systems involving flux of ADP, ATP, citrate, phosphates, glutamate, fumarate, maleate, oxaloacetate and halides. Glutamate (Chapter 2, Figure 2.29) in particular plays the central role in mammalian nitrogen flow, serving as both a nitrogen donor and nitrogen acceptor, and is a key ingredient in aminotransferase-catalysed amino acid synthesis. A key result, the structure of a chloride channel protein, was reported in 2002 and, along with earlier work on potassium channels, led to the award of a share of the 2003 Nobel Prize in Chemistry to Roderick MacKinnon (Section 2.2). In biochemical anion binding, the enzyme or protein host is always part of a functioning biological system, *e.g.* in biocatalysis or anion transport. Thus natural anion binding systems must not only have high affinity for their target anion and low affinity for other species present in the cell or extracellular fluid (thermodynamic selectivity), but must also complex and release their substrates rapidly and at the appropriate time (kinetic selectivity, Section 1.7). This has the result that anion binding proteins tend not to be rigidly preorganised macrocyclic or macrobicyclic systems, but much more flexible thread-like species, relying on tertiary interactions to assemble them into anion bonding conformations. The lack of preorganisation is made up for by a large number of enthalpically stabilising protein–anion interactions.

### 4.2.1 Anion Binding Proteins

Work by Florante Quiocho at Rice University, Texas, USA, has resulted in the crystallographic characterisation of two bacterial periplasmic anion transport proteins termed phosphate binding protein (PBP) and sulfate binding protein (SBP).[6] The function of the proteins is to bind tightly to the anion once it has crossed the bacterial cell membrane by passive diffusion. The structures of the two proteins are remarkably similar to one another. In each case, the anions are bound within a cleft some 8 Å deep, formed by the intersection of two protein globular domains, folded in a similar way to one another. The crucial difference between the two structures, which gives rise to their almost complete selectivity for their respective substrates (selectivity factor of about $10^4$), is the arrangement of hydrogen bonding residues at the protein binding site. In the case of PBP, the protein responds to the fact that both $HPO_4^{2-}$ and $H_2PO_4^-$ are capable of acting as hydrogen bond donors as well as acceptors. The crystal structure determinations of this protein all include well-resolved, bound $HPO_4^{2-}$, which is held in place by a total of 12 hydrogen bonding interactions with N/O $\cdots$ O distances between 2.62 and 2.92Å. Seven are from NH groups from the protein main chain or arginine side chain residues, four are from OH groups (two serine and two threonine), and one involves an oxygen atom from a carboxylate anion (Asp56), which acts as a hydrogen bond acceptor. It is this hydrogen bond accepting group that is the key to the selectivity of the protein; this group is absent in SBP. The sulfate anion in the SBP structure is held in place by a total of seven hydrogen bonds from backbone NH, serine OH and tryptophan NH groups, all of which act as hydrogen bond donors (Figure 4.2). Replacement of the hydrogen bond donor serine130 with cysteine (SH instead of OH), alanine ($CH_3$ substituent) or glycine (no substituent) by site-directed mutagenesis reduces the affinity of the protein for sulfate. In the case of cysteine, the reduction in affinity is by a factor of about 3200 as a result of unfavourable steric interactions. The other replacements (which result in the loss of one of the seven hydrogen bonds) both reduce affinity by 100 and 15 times, respectively, corresponding to the loss of a hydrogen bond of about 7 kJ $mol^{-1}$.

More recently the high resolution X-ray crystal structure of the sulfate complex of DNA helicase RepA has also been reported. This study reveals a total of six hydrogen bonding interactions between anion and protein with a seventh interaction to a water molecule. The sulfate anions are occupying the active sites where the product phosphate residues usually bind. Sulfate binding induces significant conformational changes in the enzyme suggesting a structural change to an 'open' form upon binding and hydrolysis of the nucleotide 5′-triphosphate substrate that could be essential for DNA duplex-unwinding activity.[7]

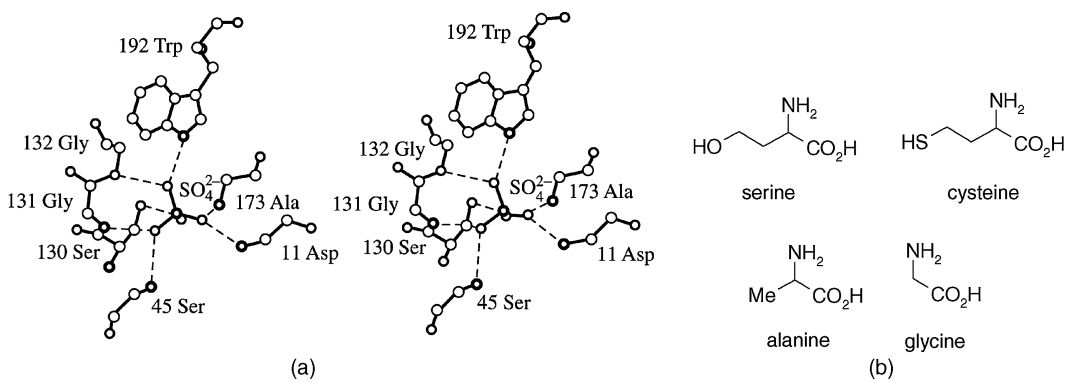


**Figure 4.2** (a) Stereoview of the SBP–sulfate interactions in *Salmonella typhimurium* (reproduced from [8] with permission from Elsevier); (b) Structures of serine, cysteine, alanine and glycine.

The biological recognition of phosphate and sulfate has also been the subject of a survey of the Cambridge Structural Database (Section 8.4). This study reveals that the average hydrogen bonding S = O ··· H angle of 127.9º is some 9 degrees larger than in the analogous phosphate interaction. Also, sulfonyl hydrogen bonding interactions are clustered much more densely about this value than are phosphoryl analogues. The former also tend towards a nearly eclipsed geometry in contrast to the phosphoryl preference for gauche interactions.

### 4.2.2 Arginine as an Anion Binding Site

Of particular importance in anion binding proteins and enzymes is the arginine residue, which contains a guanidine group. Guanidinium, the protonated form of guanidine, is an excellent anion binding site because it remains protonated over an extremely wide pH range ($pK_a$ = 13.5 for the parent $CN_3H_6$) and can participate in double hydrogen bonds with carboxylates, phosphate, sulfate *etc.*, as well as a unique interaction with two anions termed the *arginine fork* motif (Figure 4.3).

Important arginine-containing biological systems include superoxide dismutase (a Cu, Zn enzyme that catalyses the transformation of superoxide ($O_2^-$) into hydrogen peroxide and dioxygen), and citrate synthase. It has been proposed that argentine-based proteins are able to use the argentine fork motif to recognise particular loops and bulges in RNA and indeed RNA-binding regions in proteins such as the human immuno-deficiency (HIV) virus tat protein exhibit argentine-rich regions.

The 2.5-Å resolution crystal structure of another arginine-based system, *Yersinia* protein tyrosine phosphatase (PTPase), has been determined in the presence of tungstate anion. Protein tyrosine phosphatases, along with kinases, regulate phosphorylation levels necessary for cell growth, signalling and differentiation. *Yersinia* is the bacterium responsible for the bubonic plague, and secretes a PTPase that suppresses host immune cells. The protein structure shows the sequestration of the $WO_4^{2-}$ guest within a network of 12 hydrogen bonds ranging in length from 2.7 to 3.4 Å. Notably, four of these hydrogen bonds arise from the guanidinium moieties of arginine residues within the enzyme, highlighting the importance of these functionalities in biological systems. Tungstate is often used as a model for other tetrahedral anions, and the presence of a heavy atom like tungsten also makes the process of solving protein structures much easier. The structure of the tungstate complex differs from that of the native protein in that a 10-residue loop has moved an average of 3.3Å in order to encapsulate the bound anion. If such a conformational change is also observed on binding a phosphotyrosine substrate, the structures give an excellent insight into the mechanism of proton transfer during the proposed hydrolysis steps undergone by the enzyme–substrate complex.

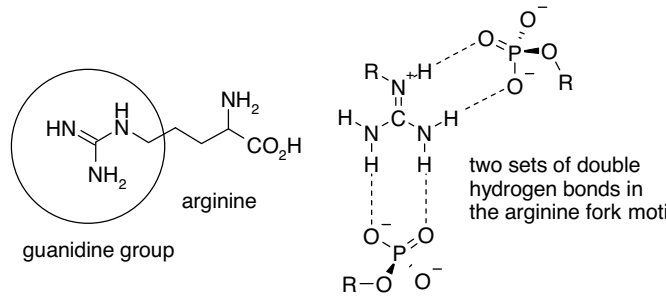


**Figure 4.3** The amino acid arginine and the 'arginine fork' binding mode with phosphate anion residues.

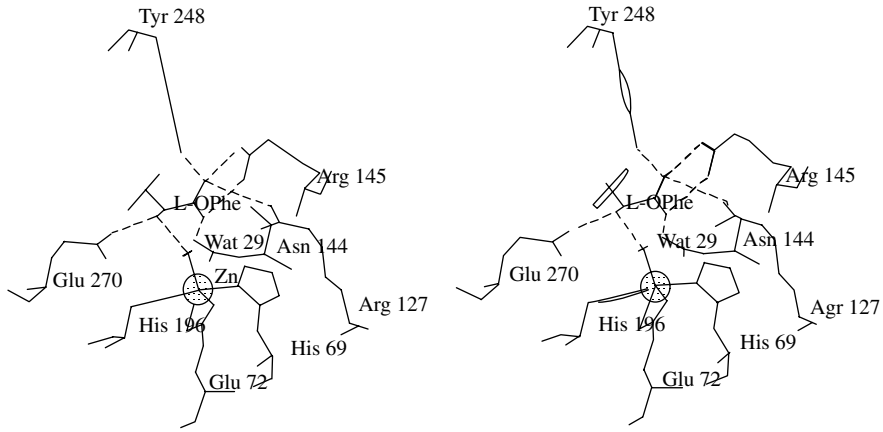


**Figure 4.4** Stereoview of the binding of L-phenyllactate to CPA. (© Wiley-VCH Verlag GmbH & Co. Reproduced by permission).

Another enzyme that uses an arginine residue to bind its anionic substrate is carboxypeptidase A (CPA). The role of this zinc-containing enzyme is the hydrolytic cleavage of the terminal peptide or ester bond at the carboxylate end of polypeptide or ester substrates bearing $\beta$-aromatic side chains on the last residue. The binding of the carboxylate anion portion of a substrate is carried out by a positively charged arginine residue (Arg145) forming a 'salt bridge' of two identical, charge-assisted hydrogen bonds, as shown in Figure 4.3. There also exists additional hydrogen bonding to other residues including a tyrosine (Tyr248), giving a total of two hydrogen bonds per carboxylate oxygen atom. The participation of the tyrosine represents a good example of induced fit, since this residue moves from its location 14 Å away in the native enzyme upon substrate binding. The $\beta$-aromatic ring of the substrate is bound within a carefully tailored hydrophobic pocket, and is a necessary part of the enzyme selectivity. The crystal structure of the active site of the enzyme with bound L-phenyllactate (which acts as an inhibitor to the enzyme function) is shown in Figure 4.4. In the binding of the real polymeric substrate, further binding sub-sites closer to the enzyme surface also play a role.

### 4.2.3 Main Chain Anion Binding Sites in Proteins: Nests

Watson, J. D., Milner-White, E. J., 'A novel main-chain anion-binding site in proteins: the nest. A particular combination of $\phi$ and $\psi$ values in successive residues gives rise to anion-binding sites that occur commonly and are found often at functionally important regions', *J. Mol. Biol.* 2002, **315**, 171–182.

Protein backbones are made up of polyamide residues from polymerisation of amino acids. Amides are good hydrogen bond donors and hence interact strongly with anions and polar functionality with a partial negative charge such as the oxygen atoms of carbonyls. Anions are bound strongly by amides in proteins at the nitrogen terminus of an $\alpha$-helix where usually two or three free amide NH groups occur that are not involved in holding the helix together. In addition to this common feature, systematic analysis of protein crystal structures by James Milner-White of the University of Glasgow, UK, has revealed another common anion-binding site, namely the 'nest' motif. The nest involves alternating three consecutive residues with particular main chain dihedral angles such as to give a three amide NH pocket in which especially the first and third amide groups can hydrogen bond to

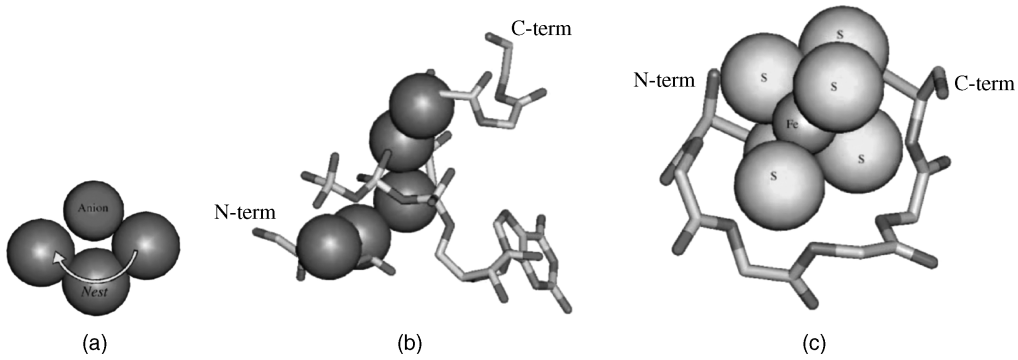


**Figure 4.5** (a) the positions of the three amide NH atoms in the anion-binding nest motif found in a wide range of functional anion binding proteins, (b) the five-amide compound nest in the P-loop of p21 *ras* – a nucleotide triphosphate binding protein and (c) a six-amide compound nest surrounding the iron sulfur core in ferredoxin. (Reproduced from Section Key Reference with permission from Elsevier).

the anion (or negatively polarised) guest. Typical nest geometries are shown in Figure 4.5. A search of 67 well defined and mutually different protein structures revealed a total of 323 nests showing that the motif is a very common one. The nest motif can expand to give compound nests comprising four or more residues with alternating torsional characteristics that organise the NH groups into a pocket surrounding a central binding site. Among many functionally important nests is the P-loop; a glycine-rich sequence that binds to triphosphate anions in many ATP and GTP binding proteins. The P-loop comprises five amide NH units, shown in spacefilling mode in Figure 4.5b, forming a feature described as a 'giant anion hole'. Nests are also features of the oxyanion hole found in serine proteases, they form the second coordination sphere of $Ca^{2+}$ in the trigger protein calmodulin, and some of the longest extended nest features bind to iron-sulfur anions in iron sulfur proteins such as ferredoxin. The geometries of some functional anion-binding nests are shown in Figure 4.6.

## 4.2.4 Pyrrole-Based Biomolecules

In 1992 the X-ray crystal structure of porphobilinogen deaminase was solved, an enzyme that is involved with the biosynthesis of a linear tetrapyrrole precursor to protoporphyrin IX, found in haemoglobin

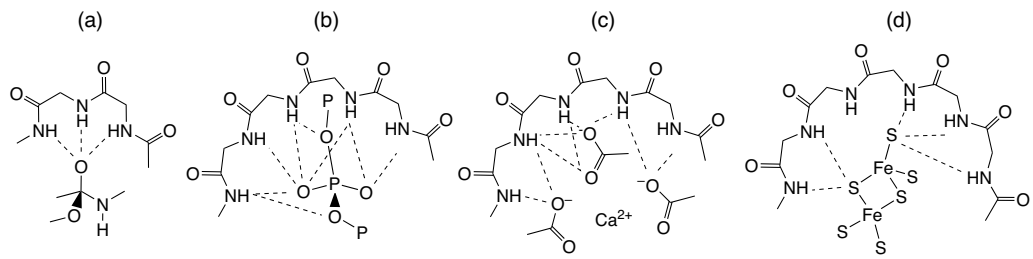


**Figure 4.6** Hydrogen bonding in functional nests (a) oxyanion hole in serine protease binding the substrate tetrahedral intermediate, (b) P-loop showing the β-phosphate (middle phosphate residue) of GTP bound to a compound nest, (c) $Ca^{2+}$ binding in calmodulin. The calcium is bound to three carboxylate oxygen atoms which are in turn bound to bound to a five-amide compound nest (d) the cysteine-bound $Fe_2$ unit in spinach ferredoxin.

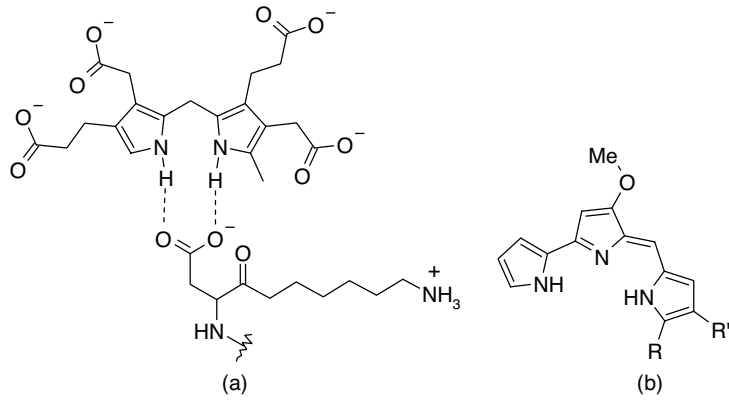


**Figure 4.7** (a) interaction of a dipyrromethane-based cofactor in porphobilinogen deaminase with an aspartic acid-derived side chain. The carboxylate residues of the co-factor are stabilised by protein arginine residues. (b) general structure of the prodigiosins (R, R′ = alkyl).

(Section 2.5).[10] The key aspect of this structure is the interaction of a dipyrromethane unit in the enzyme's co-factor through the pyrrolic NH groups to a carboxylate side chain of an aspartic acid residue (Figure 4.7a). The co-factor carboxylate side chains also binds to enzyme arginine groups. If the aspartic acid residue is replaced by glutamte the enzyme loses essentially all activity suggesting that this interaction is particularly important.

The dipyrromethane moiety is also a core component of the prodigiosins, a family of naturally occurring tripyrrolic red pigments (Figure 4.7b). Prodigiosins have very promising immunosuppressive and anti-cancer properties and have proven to be an inspiration for recent research into a range of artificial analogues with extensive anion-binding properties but more flexibility and versatility than cyclic analogues such as porphyrins (and their expanded homologues) and calixpyrroles (Section 4.6.4).

## 4.3 Concepts in Anion Host Design

Schmidtchen, F. P., 'Reflections on the construction of anion receptors - Is there a sign to resign from design?', *Coord. Chem. Rev.* 2006, **250**, 2918–2928.

### 4.3.1 Preorganisation

In Chapter 1, we defined a host as a molecule possessing convergent binding sites, and a guest as one possessing divergent binding sites. We would also like a host to exhibit selectivity or discrimination between one guest and another. In the case of anion coordination chemistry, this definition is still helpful, but we run into some trouble on two accounts. Firstly, the large size and high polarisability of anions means that non-directional forces such as dispersion interactions play a significant role in anion binding. Also, as a charged particle, an anion intrinsically experiences an electrostatic attraction to molecules, even if they are not positively charged, simply because there is a charge difference between the negatively charged anion and an electrically neutral molecule. This means that a significant contribution to anion binding comes from dispersion and electrostatic interactions, which are non-directional, and so in some sense the whole host is a binding site, although some regions of the host will interact more strongly with the anion than others. The second problem concerns the definition of binding sites on the anion itself. The coordinatively saturated nature of anions and in some cases the lack (with the exception of anions such

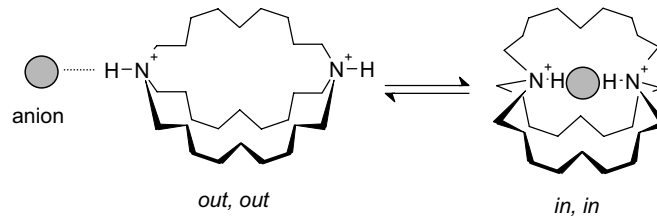


**Scheme 4.1** Conformational change in the katapinands on anion binding.

as $H_2PO_4^-$) of specific hydrogen bonding functionality, means that species, such as halides especially, behave approximately like spherical charges and have a highly versatile coordination geometry without specific binding sites.

The generalised definition of a host as a convergent entity allows us to rule out metal ions as anion hosts, even though they display a great deal of selectivity in their interactions with anions (*cf.* the HSAB theory, Section 3.1), simply because there is generally only one binding site for an individual anion per metal and the metal ion sites are divergent (nobody would seriously propose the $Na^+$ ion in NaCl as an anion binding host, even though $Na^+$ is selective for $Cl^-$ over $I^-$ with a binding constant of over $10^{300}$ based solely on Coulombic considerations, and in the cubic NaCl lattice a $Cl^-$ ion is octahedrally surrounded by six $Na^+$ ions, Figure 1.9). Clearly, however, the bicyclic katapinands (**4.1**) are classifiable as anion hosts. They bind their anionic guest species *via* two converging $N^+$—H $\cdots$ $X^-$ hydrogen bonds (the $NH^+$ groups are the binding sites) and display a size-based selectivity according to the dimensions of the host (as determined by the chain length, *n*). The [8.8.8]-bridged katapinand (**4.1a**) exhibits no significant anion binding; the analogous [9.9.9] host (**4.1b**) exhibits binding constants of the order of $10^2\,M^{-1}$ for $Cl^-$ in water/trifluoroacetic acid solvent, with a modest selectivity for chloride over bromide of a factor of about 8, while [10.10.10] (**4.1c**) binds $Cl^-$, $Br^-$ and $I^-$ with little selectivity. The katapinands are not preorganised hosts, however, and undergo a major conformational change on anion binding, corresponding to a rearrangement from an *out*, *out* geometry, to an *in*, *in* conformer (Scheme 4.1). This is, in effect, the same sort of process undergone by the crown ethers on cation binding in aqueous solution.

Given these observations, it is clearly important to know to what degree the bicyclic nature of the katapinand contributes to its anion binding ability. Does the three-dimensional host structure help to organise the two binding sites, or does the driving force for the organisation of the binding *in,in* conformation come from the interaction with the $Cl^-$ anion? This is tantamount to asking how important is preorganisation in anion complexation chemistry. The low binding constants observed for the katapinands suggests that as with cation binding, preorganisation (or the lack of it in the katapinands) it is of significant importance and should be incorporated into host design.

## 4.3.2 Entropic Considerations

As with all host-guest systems, in designing an anion-binding host both preorganisation, and complementarity are of crucial importance, particularly with regard to maximising the enthalpically favourable interaction between anion and receptor. Entropic effects are also of fundamental importance and go beyond the mere 'release of high energy solvent' paradigm. For example isothermal titration calorimetric measurements (Section 1.4.2) show that the binding of oxoanions to polyammonium hosts in water essentially enthalpically neutral and all of the driving force is entropic. In the key reference to Section 4.3 Schmidtchen breaks down the entropic contribution to anion binding into

two components, $\Delta S_{obs} = \Delta S_{intrinsic} + \Delta S_{solv}$. The solvation effects ($\Delta S_{solv}$) are essentially not subject to molecular design; however, the chemist may have some hope to control $\Delta S_{intrinsic}$ which may itself be broken down into a number of factors for easier understanding: $\Delta S_{intrinsic} = \Delta S_{trans+rot} + \Delta S_{vibration} + \Delta S_{conformation} + \Delta S_{configuration}$. The $\Delta S_{trans+rot}$ component refers to the change in translational and rotational entropy of the host and guest upon association. While a matter of debate, this term is essentially constant for the kinds of artificial host-guest systems we are concerned with and so is not subject to design. The remaining terms are highly important in design terms. The $\Delta S_{vibration}$ term refers to the generation of vibrational entropy on association, $\Delta S_{conformation}$ refers to the freezing of internal rotations upon association and $\Delta S_{configuration}$ is related to the different possible geometrical arrangements of the binding partners.

The vibrational and conformational terms are closely related. If a flexible host interacts loosely with a flexible guest such that internal rotations are relatively unimpeded and vibrations associated with the bonds between host and guest have low force constants then the entropic cost of binding is small, resulting in a favourable situation – the generation of low frequency motions increases entropy and hence augments affinity. Conversely, in the case of very tight binding internal rotations are severely restricted (and in fact become high frequency vibrations) and bonding vibrations increase in frequency and decrease in amplitude. This situation results in a decrease in entropy and lowered affinity. Thus strong but relatively unselective binding (*e.g.* for sequestration or extraction) will correspond to a favourable association entropy, while tight, structure-specific binding will give a less favourable association entropy more appropriate in situations involving anion catalysis, region-/stereoselective binding or self-assembly. These considerations are subject to interference from the additional $\Delta S_{configuration}$ component, however. It is possible for a given host-anion complex to bring in a number of different, distinct orientations with significant barrier to interconversion yet of comparable relative energy even though many techniques such as NMR spectroscopy mask this possibility by rapid averaging under ambient conditions. A full discussion of entropic considerations in design is given in the key reference.

## 4.3.3 Considerations Particular to Anions

The design of preorganised, complementary anion binding hosts exhibiting maximum complexation free energy and selectivity must follow from an appreciation of some of the fundamental characteristics of anions. Listed below are some of the issues that are important to anion binding in particular.

### *Negative Charge*

The negative charge suggests that both neutral, and especially positively charged, hosts will bind anions. Unfortunately electrostatic interactions are non-directional and so all anions will be attracted to hosts on an electrostatic basis, forming a solvated ion pair in solution. Affinity would be expected to increase with anion net charge. If a positively charged host is chosen, there will be a significant degree of competition with the existing counter anions, thus any observed binding constant really represents a relative selectivity factor for the binding of one anion over the other. Commonly counter cations such as $NBu_4^+$ that are thought to interact only weakly with anions are chosen, however even these exhibit significant ion pairing. For example, a 1 mM solution of tetrabutylammonium chloride in $CH_2Cl_2$ is less that 20 % dissociated at 22 °C.[11] Moreover many tetrabutylammonium salts are very hydroscopic and extremely difficult to dry and can even decompose in the absence of water. One possible solution is the use of cryptand complexes of potassium salts of target anions, however this is not widespread and has its own purity concerns.

### *Lewis Basicity*

The vast majority of anions are Lewis bases, although there are some exceptions that do not have lone pairs (*e.g.* $AlH_4^-$, $B(C_6H_5)_4^-$, *closo*-$B_{12}H_{12}^{2-}$) or are only very weak bases (*e.g.* $B(C_6F_5)_4^-$). This property suggests that hosts containing Lewis acidic atoms, such as organo boron, mercury or tin compounds, or metal cations in general, might make the basis of a suitable host by formation of coordinate bonds. This is the basis of the *anticrown* hosts, which resemble the crown ethers with Lewis basic oxygen replaced by Lewis acidic binding sites (Section 4.7.4). Lewis acid–base coordinate interactions have a high degree of directionality and so make a good basis for the design of selective hosts. The property of Lewis basicity also makes anions suitable as hydrogen bond acceptors, as in halide binding by katapinands, in which charge-assisted N—H $\cdots$ Cl hydrogen bonds are responsible for a large amount of the complexation ability of the hosts.

### *High Polarisability*

Anions are highly polarisable and so van der Waals interactions will be significant. While non-directional, these are related to the contact surface area of host and anion, and so three-dimensional encapsulation of the anion should enhance binding of all anions capable of fitting within the host.

### *Solvation*

Anions generally have high solvation energies and so, to an even greater degree than cation binding, the medium in which solution–anion complexation experiments are carried out will strongly influence binding constant measurements. Binding constants for monovalent inorganic anions of about $10^2$–$10^3$ in water represent strong binding, whereas strong binding is achieved much more readily in non-polar solvents, such as chloroform, because of the anions' solvophobic properties. Binding constants are expected to increase on changing solvent in the order $H_2O < DMSO < MeCN < CHCl_3 < CCl_4$, although interesting enthalpy–entropy compensation effects may be observed in the complexation of all kinds of guests (see, for example, Section 1.9).

### *Coordination Number*

Another question that is of potential importance concerns the coordination number and geometry of a bound anion. In the search for complementary hosts for metal cations, metal binding is much stronger in cases where the coordination number and geometry of the metal matches that of the ligand (octahedral, tetrahedral, square planar *etc.*). The importance is diminished significantly in cases such as alkali metal cations, in which there is no strong coordination preference. In crystalline NaCl, the chloride is in a regular, octahedral six-coordinate environment. In contrast, in the case of the katapinands the encapsulated chloride may be thought of as two-coordinate since it engages in two N—H $\cdots$ Cl hydrogen bonds. In fact, a wide variety of anion coordination geometries are known, with the number of interactions an anion is able to form increasing with its size. Artificial halide hosts may bind *via* two to six interactions in acyclic and cyclic structures, while larger, multi-atom anions may form anything from zero to three hydrogen-bonded interactions per terminal atom. The structure of the protein PBP (Section 4.2.1) with its 12 hydrogen bonds, three to each phosphate oxygen atom, thus represents an excellent example of the maximisation of coordination number in order to obtain the maximum stabilisation.

## 4.4 From Cation Hosts to Anion Hosts – a Simple Change in pH

Garcia-España, E., Diaz, P., Llinares, J. M. and Bianchi, A., 'Anion coordination chemistry in aqueous solution of polyammonium receptors', *Coord. Chem. Rev.* 2006, **250**, 2952–2986.

### 4.4.1 Tetrahedral Receptors

By far the most obvious way in which to address the binding properties of anions is to combine electrostatic attraction for a positively charged host with the anions' Lewis basic character, which should enable then to act as hydrogen bond acceptors. This is exactly the strategy that led to Park and Simmons' original success with the katapinands. There exists an enormous variety of cryptands designed for complexation of metal ions by virtue of the Lewis basic nature of their tertiary nitrogen bridgeheads and polyether or secondary amine chains. A simple change in solution pH should result in the protonation of these amine functionalities, according to their relative basicities (Section 3.11), to give a katapinand-like host for anions. The only factors of real importance are that the cryptand should be large enough to incorporate the anion (*i.e.* as large as [2.2.2]cryptand or bigger), and that there are not so many repulsions between the protonated nitrogen atoms that the host is incapable of converging, or is rendered too weakly basic and does not protonate at all. This simple approach is beautifully illustrated by the macrotricyclic cryptand **3.29**, which may be regarded as arising from four fused triaza[18]crown-6 rings. Compound **3.29** has been termed a 'soccer ball' molecule because of its nearly perfect spherical shape. The presence of the four nitrogen bridgeheads on this molecule make it a highly versatile example of a tetrahedral receptor. In addition to its Lewis basic properties, which enable it to bind strongly to cations, in its tetraprotonated form it is also capable of binding anions such as $Cl^-$, acting *via* the formation of four hydrogen bonds supported by electrostatic interactions with the ether oxygen atoms. Thus, depending on the pH of the medium, the neutral host may bind cations, especially ammonium ($NH_4^+$); in its diprotonated state, it binds neutral molecules, particularly water; and in its tetraprotonated state, it binds anions such as $Cl^-$ (Figure 4.8). Unlike the katapinands, the protonated soccer ball **3.29**-$4H^+$ has an extremely high affinity for $Cl^-$ (log $K_{11} > 4$, methanol/water) and the selectivity for $Cl^-$ over $Br^-$ is a factor of about 50.[12] Such affinities and selectivities represent significant achievements in anion complexation chemistry (especially of monovalent anions), where host–guest affinities are dramatically less than those observed for cation binding. The X-ray crystal structure of **3.29**-$4H^+ \subset Cl^-$ (Figure 4.9) shows that the N—H $\cdots$ $Cl^-$ hydrogen bonded distances are 3.09 Å, comparable to the katapinand structure (3.10 Å), clearly indicating that both hosts are geometrically complementary to chloride. The greater affinity of **3.29**-$4H^+$

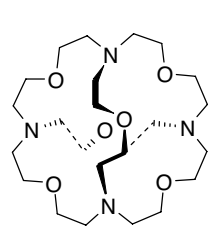

**3.29**

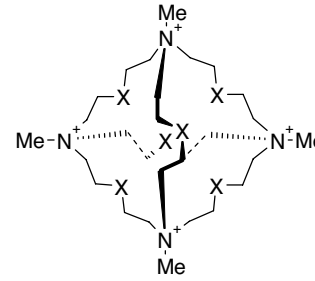

X = O, **4.2**
X = $(CH_2)_2$, **4.3**

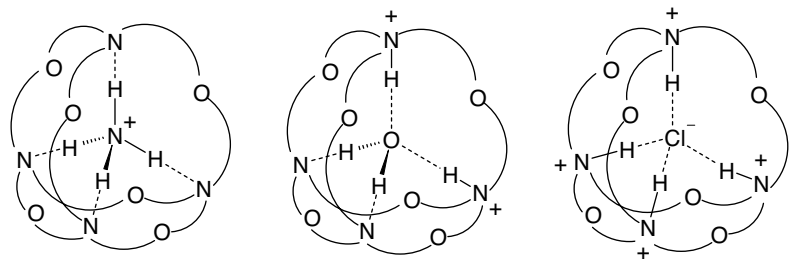

**Figure 4.8** Tetrahedral recognition: the 'soccer ball' cryptand as a receptor for ammonium ion, water or chloride, depending on the pH of the medium.

therefore must rest with its much more preorganised nature, its greater positive charge and the greater number of binding sites. The lower affinity for $Br^-$ is related to the non-optimal match between the longer N—H ⋯ Br hydrogen bond distances and the cavity dimensions.

The soccer ball cryptate is clearly an excellent match for its target anion in terms of preorganisation, size, charge and hydrogen bonding functionality. It is not clear, however, from a comparison of soccer ball and katapinand hosts, which of these factors is the most important in determining anion binding affinity and selectivity. As early as 1977, some evidence was gained on the influence of hydrogen bonding by Schmidtchen by the preparation of **4.2**, the *N*-methyl analogue of **3.29**, and a closely related hydrocarbon-bridged species (**4.3**). The addition of the methyl group in both cases causes the hosts to adopt an outward conformation (otherwise the methyl groups would be forced into close proximity with one another at the centre of the molecule). This makes the tetracationic cavity much larger than in **3.29**-$4H^+$ and as a result the highest binding constants are observed for bromide and iodide (log $K$ = 2.25 in water). The X-ray crystal structure of the iodide complex is shown in Figure 4.9(b) and reveals that the iodide anion is situated centrally in the tetrahedral macrotricyclic cage, some 4.54Å from the cationic nitrogen centres.

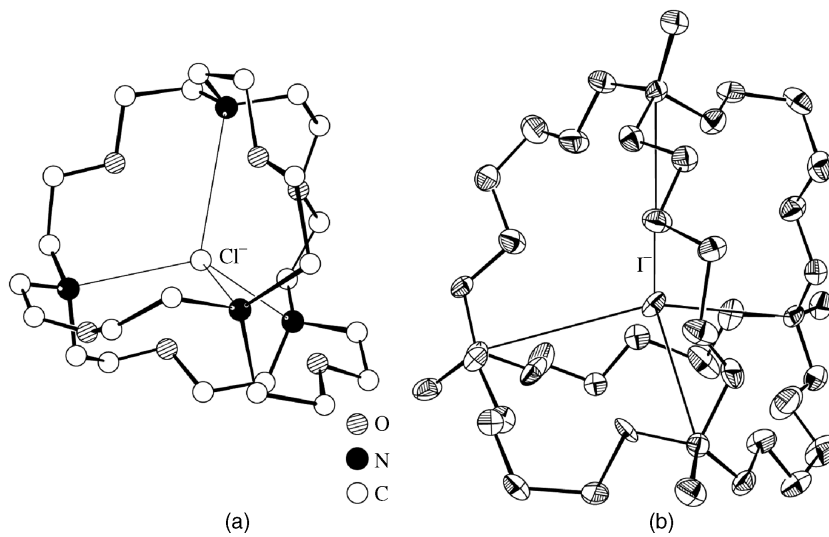


**Figure 4.9** (a) X-ray crystal structure of the 'soccer ball' chloride cryptate **3.29**-$4H^+ \subset Cl^-$ and (b) structure of the iodide cryptate of **4.3**. (Reproduced by permission of The Royal Society of Chemistry).

## 4.4.2 Shape Selectivity

Dietrich, B. Guilhem, J. Lehn, J.-M., Pascard, C. and Sonveaux, E., 'Molecular recognition in anion coordination chemistry', *Helv. Chim. Acta.*, 1984, **67**, 91–104.

In the case of the tetrahedral receptors discussed in Section 4.4.1, the halide coordination geometries (as determined by their shortest intermolecular contacts or hydrogen bonded distances) may be described as tetrahedral. In the preceding sections, we have already mentioned halide coordination numbers ranging from two to six. So, is there any evidence for preferred halide coordination geometries, or are coordination environments imposed on the halides by the preorganisation and topology of the host? Huge insight into this question and other factors affecting anion binding selectivity is obtained by the

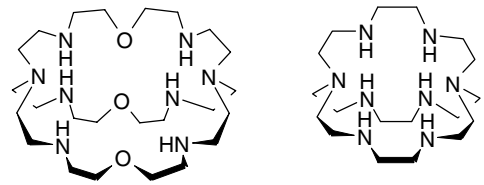

*bis*(tren) **4.4** **4.5**

binding characteristics of the cylindrical macrobicycle *bis*(tren) (**4.4**) and the smaller analogue (**4.5**). The X-ray crystal structures of the complexes of hexaprotonated *bis*(tren) (**4.4**-6H$^+$) with $F^-$, $Cl^-$, $Br^-$ and $N_3^-$ (azide) are shown in Figure 4.10, along with the structure of the fluoride cryptate of (**4.5**-6H$^+$). Note that the tertiary bridgehead nitrogen atom is not protonated because its basicity is reduced dramatically as a consequence of its proximity to the protonated secondary amines in each case.

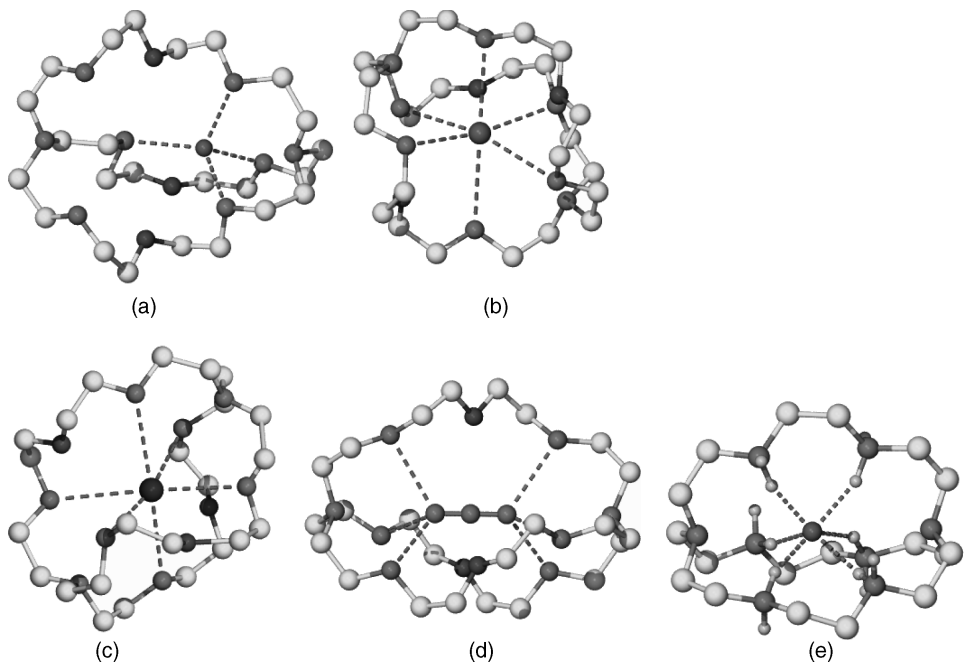


**Figure 4.10** X-ray structures of the *bis*(tren) (**4.4**-6H$^+$) cryptates of (a) $F^-$, (b) $Cl^-$, (c) $Br^-$ and (d) $N_3^-$; (e) structure of the $F^-$ complex of **4.5**-6H$^+$.

The solution binding constants in water for halide binding by protonated *bis*(tren) are (log *K*) 4.19, 3.0, 2.6 and 2.15 for $F^-$, $Cl^-$, $Br^-$ and $I^-$, respectively. In addition to fluoride, azide is also bound very strongly (log $K = 4.30$). Surprisingly, the order of halide binding constants follows their hydration energies with the most highly solvated (fluoride) also bound the most strongly (an anti-Hofmeister selectivity order). This is even more remarkable given the crystal structure of the compound (Figure 4.10a), which shows that $F^-$ is a very poor fit for the long, cylindrical *bis*(tren) cavity. The $F^-$ anion is situated far to one side of the macrocycle, in an approximately tetrahedral arrangement, with mean N ⋯ F hydrogen bonding distances of 2.72Å. The larger chloride and bromide ions (Figure 4.10b and c) are situated much more symmetrically in the cavity, interacting with six NH groups, with mean $N \cdots Cl^-$ distances of 3.19–3.39Å and $N \cdots Br^-$ distances of 3.33–3.47Å. Note that these distances are much longer than the optimum $N \cdots Cl^-$ contacts found for **4.1b** and **3.29**-$6H^+$ of about 3.10Å. Consistent with this observation, the binding of chloride, bromide and iodide is much weaker than fluoride. The best fit to the cylindrical cavity in terms of shape and topological match is the cylindrical azide anion (Figure 4.10d), which is bound the most strongly. The $N \cdots N_3^-$ distances are of optimum length and fall into a narrow range of 2.81–3.02Å, indicating symmetrical binding arising from good complementarity. The overall selectivity sequence of **4.4** for monovalent anions is in the order $ClO_4^-$, $I^-$, $Br^-$, $Cl^- < CH_3CO_2^- < HCO_2^- < NO_3^-$, $NO_2^- < F^-$, $N_3^-$. This trend does not appear to show significant correlation with anion size or hydration energy series, or with the Hofmeister series (Section 4.1.2). In fact, the binding in **4.4** is composed of a combination of electrostatic contributions, in which anions with a relatively high charge density such as $F^-$ are bound strongly, and a topological (*i.e.* shape as opposed to size) complementarity favouring azide (which also has a high negative charge density). The electrostatic factors become apparent as soon as the affinity for multiply charged species such as $P_2O_7^{4-}$ (log $K = 10.30$), $ATP^{4-}$ and $ADP^{3-}$ are examined. All of these anions are bound very strongly, the 4− species more so than 3−. When all of these factors come together (size and shape complementarity, strong electrostatic interactions and multiple hydrogen bonds), extremely strong binding is observed. The small host **4.5**-$6H^+$ is a perfect match for fluoride (Figure 4.10e), binding in a distorted trigonal prismatic geometry with $N \cdots F^-$ distances in the range 2.76–2.86Å and a binding constant in water, log *K*, of 11.2.[15]

## 4.4.3 Ammonium-Based Podands

Hossain, A., Liljegren, J. A., Powell, D., Bowman-James, K., 'Anion binding with a tripodal amine', *Inorg. Chem.* 2004, **43**, 3751–3755.

Even simple protonated tripodal amines such as tren (2,2′,2″-*tris*(aminoethyl)amine, **4.6**) itself exhibit interesting anion-binding geometries. The X-ray crystal structure of tren·HBr (Figure 4.11a) shows the bromide anion interacting with all three terminal amine groups, one of which is protonated.[16]

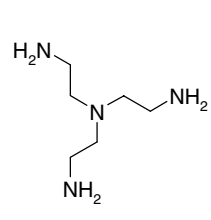


tren

**4.6**

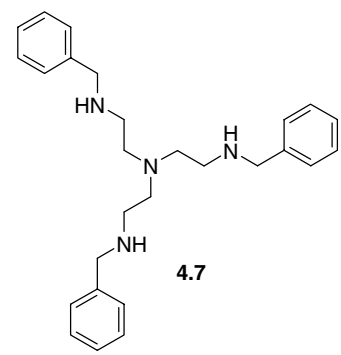


**4.7**

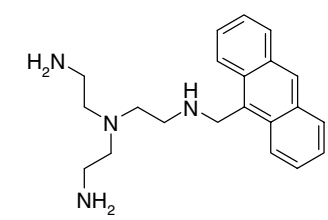


**4.8**

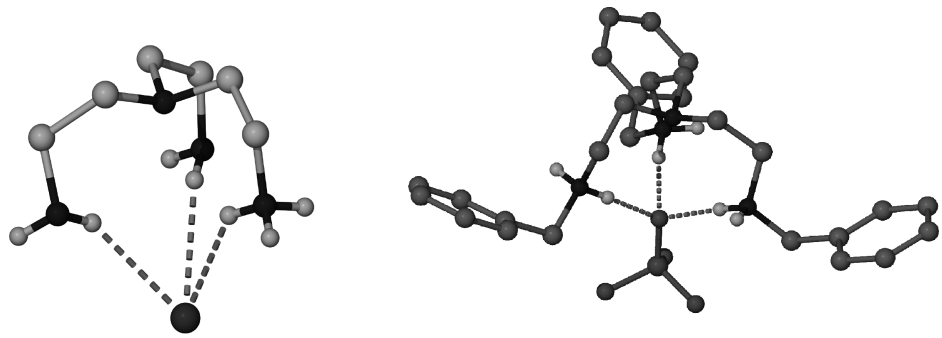


**Figure 4.11** X-ray crystal structures of (a) tren·HBr and (b) the trischelate unit in **4.7**-$4H^+ \cdot 4H_2PO_4^-$.

Similar tripodal complexes are formed by triprotonated tren with $HPO_4^{2-}$ and $SO_4^{2-}$.[17] Work by Kristin Bowman-James at the University of Kansas, USA, has resulted in a tren-derived solution phase host **4.7**. The tetraprotonated form of **4.7** exhibits a trischelate interaction with $H_2PO_4^-$ (Figure 4.11b). Despite the lack of preorganisation, the binding constants of the triprotonated form (as the triflate salt) for $H_2PO_4^-$ and $HSO_4^-$ (in non-competitive chloroform solvent) are significant ($\log K > 3$) while other anions are bound with long $K < 2$. It is suggested that the residual acidic protons on the $HSO_4^-$ and $H_2PO_4^-$ anions can protonate the bridgehead nitrogen atom resulting in ion-pairing. These interesting results with **4.7** build on earlier work on **4.8** which acts as a fluorescent sensor for anions. The receptor is triprotonated at pH 6 and addition of $HPO_4^{2-}$ results in a 145 % increase in the fluorescence intensity of the anthracenyl chromophore, a phenomenon also seen in the sensing of metal complexes (Section 11.3.2) termed *chelation enhanced fluorescence* (CHEF).[18]

### 4.4.4 Two-Dimensional Hosts

Boudon, S., Decian, A., Fischer, J., Hosseini, M. W., Lehn, J.-M. and Wipff, G., 'Structural and anion coordination features of macrocyclic polyammonium cations in the solid, solution and computational phases', *J. Coord. Chem.*, 1991, **23**, 113–135.

The anion coordination behaviour of a large range of azacorand type macrocycles such as **4.9**–**4.14** (nitrogen analogues of the crown ethers) has been studied in aqueous solution. Binding and protonation constant measurements may be made readily by potentiometric titration (Section 1.4.2). Frequently, a variety of differently protonated species are present and the anion binding experiment is a summation of the contributions from a variety of different solution equilibria. As a result, the titration data must be deconvoluted by regression calculation into each of the different components present, often resulting in large errors. Because water is such a strongly solvating medium with a high dielectric constant, generally only interactions between multiply charged species are significant. As formal charge increases, however, extremely thermodynamically stable complexes are formed.

Hexacyclen (**4.9**), [18]ane$N_6$, the aza analogue of [18]crown-6, has been shown by potentiometric titration to be an extremely strong diprotic acid in its hexaprotonated form, meaning that for most practical purposes in all but very acidic solutions, it exists as the tetraprotonated form **4.9**-$4H^+$. This is a general kind of observation for macrocycles of type **4.14** in which the nitrogen atoms are separated by only two carbon atoms. Protonation of all of the nitrogen atoms results in severe electrostatic repulsions

between the $NH_2^+$ groups and dramatically lowers p$K_a$ values compared to acyclic analogues, which almost invariably adopt a linear, all-*anti* conformation when fully protonated to minimise repulsion between the cationic groups. In solution, hexacyclen binds nitrate in preference to halide anions, but X-ray crystallographic results indicate that none of these anions is included within the macrocycle. Halides adopt a perching geometry with $N \cdots Cl^-$ distance of 3.07–3.28Å, while in the X-ray crystal structure of **4.9**-$4H^+ \cdot 2Cl^- \cdot 2NO_3^-$, the nitrate anions interact with the host indirectly *via* included water molecules. Crystals of **4.9**-$6H^+ \cdot 2Cl^- \cdot 4NO_3^-$ do show direct interaction with the nitrate anions *via* one hydrogen bond each. Clearly the hexacyclen cavity, similar in size to [18]crown-6, but partially filled by the NH protons, is much too small to include anions. Antonio Bianchi (University of Florence, Italy) and Enrique Garcia-España (University of Valencia, Spain) have investigated much larger rings up to [36]ane$N_{12}$. Such large-ring species are able to act as hosts for large inorganic anions such as $[PdCl_4]^{2-}$ and $[Fe(CN)_6]^{4-}$, which can be included within the macrocyclic cavity, as exemplified by the X-ray crystal structure of $H_{10}$[30]ane$N_{10}^{10+}$ with $[PdCl_4]^{2-}$ guest (Figure 4.12). The term 'supercomplexes' was adopted for these complexes of metal complexes. The elegant simplicity of this structure is belied by the complexity of the solution behaviour of the multiple protonation states of the amine.

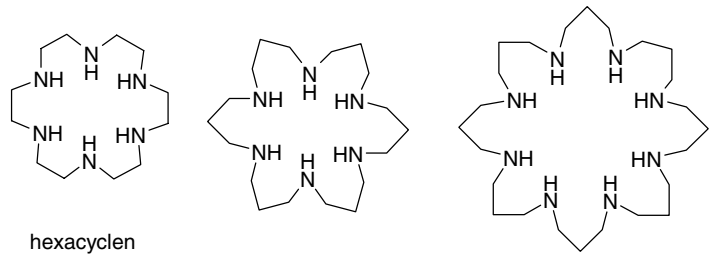

hexacyclen

**4.9** **4.10** **4.11**

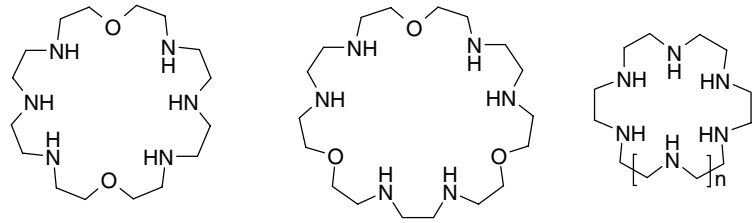

**4.12** **4.13** **4.14**

n = 2 - 7

These workers have also studied the complexation of $[Fe(CN)_6]^{4-}$ by a range of large-ring azacorands. The speciation diagram (solution composition as a function of pH) for the behaviour of this anion with [27]ane$N_9$ is shown in Figure 4.13. As this diagram reveals, species all the way from tetraprotonated to octaprotonated macrocycle are present and indeed the macrocycle may retain four protons even at a fairly basic pH of 9 or higher. The hexacyanoferrate(II) anion is interesting because, in addition to potentiometry, its complexation may be monitored by cyclic voltammetry (Box 4.1). The Fe(II)/Fe(III) redox couple in this species is highly reversible and sensitive to the iron atom's second coordination sphere. The shifts in redox potential as a function of pH are also plotted in Figure 4.13. The diagram indicates clearly that the anion becomes progressively more difficult to oxidise as the state of protonation of the host–increases. It is more difficult to pull an electron away from the more positively charged host-guest complexes. Also, the potential does not increase smoothly, but changes

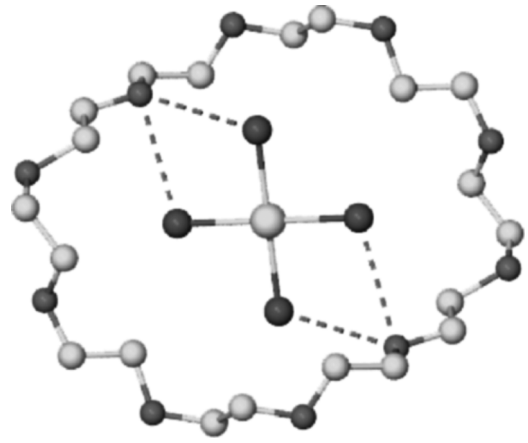

**Figure 4.12** X-ray crystal structure of the $[PdCl_4]^{2-}$ complex of $H_{10}[30]aneN_{10}^{10+}$, showing the anion inclusion.[19]

in a stepped fashion in accordance with the peaks in the concentrations of the various solution species. Stepwise binding constants for the various solution species are given in Table 4.3.

The table shows firstly that binding constants for all of the complexes formed are very high in aqueous solution (compared to complexes of univalent anions), consistent with the highly charged nature of the interacting species. Secondly, there is a distinct increasing stability as the charge on the macrocycle increases, consistent with the electrostatic nature of the interactions. Finally, it is also noteworthy that the most stable compounds are formed with the smallest macrocycle, where the positive charge is more concentrated (fewer intervening non-protonated NH groups). Host–anion interactions are of the charge assisted $N^+$—$H\cdots NCFe^-$ type, and no complexes are formed with macrocycles with fewer than four protons, the minimum required for charge neutralisation.

In order to avoid the problem of increasing difficulty in fully protonating macrocycles like hexacyclen and higher analogues, which have two carbon bridges between the nitrogen atoms, a number of

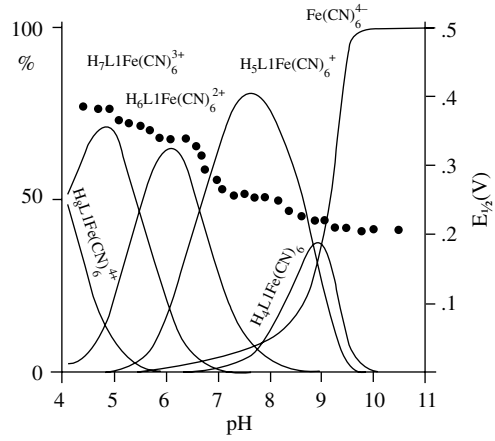


**Figure 4.13** Distribution (speciation) diagram (——) for the system $H^+/[Fe(CN)_6]^{4-}/[27]aneN_9$ and the Fe(II)/Fe(III) redox potential (*E*/*V*) (•) versus pH. (Reproduced with permission from [20] © 1987 American Chemical Society).

**Table 4.3** Binding constants (log $K$) for the stepwise formation of 'supercomplexes' between **4.14** (n = 3–5) and $[Fe(CN)_6]^{4-}$ according to the reactions shown.[20]

| | Log $K$ | | |
|---|---|---|---|
| Reaction | n = 3 | n = 4 | n = 5 |
| (**4.14**)-4$H^+$ + $[Fe(CN)_6]^{4-}$ = $[H_4$(**4.14**)$Fe(CN_6)]$ | 4.06 | 3.69 | 3.61 |
| (**4.14**)-5$H^+$ + $[Fe(CN)_6]^{4-}$ = $[H_5$(**4.14**)$Fe(CN_6)]^+$ | 5.63 | 4.78 | 4.66 |
| (**4.14**)-6$H^+$ + $[Fe(CN)_6]^{4-}$ = $[H_6$(**4.14**)$Fe(CN_6)]^{2+}$ | 7.60 | 6.23 | 5.72 |
| (**4.14**)-7$H^+$ + $[Fe(CN)_6]^{4-}$ = $[H_7$(**4.14**)$Fe(CN_6)]^{3+}$ | 9.33 | 7.92 | 6.93 |
| (**4.14**)-8$H^+$ + $[Fe(CN)_6]^{4-}$ = $[H_8$(**4.14**)$Fe(CN_6)]^{4+}$ | — | 9.03 | 8.07 |

**Table 4.4** Variation of p$K_a$ with spacer length in macrocycles of type $H_m$[4n]ane$N_4^{m+}$ (n = 2–4; m = 3 and 4).

| Host | n | p$K_{a3}$ | p$K_{a4}$ |
|---|---|---|---|
| **4.15a** | 2 | 1.7 | <1 |
| **4.15b** | 3 | 6.9 | 5.4 |
| **4.15c** | 4 | 10.6 | 8.9 |

alternatives have been prepared. Macrocycles such as **4.10** and **4.11** allow protonated nitrogen atoms to separate further by use of propenyl spacers, while **4.12** and **4.13**, which are less conformationally flexible, use ether groups to space out positive charge. This strategy proved successful in that the fully protonated species all exhibit p$K_a$ values above 7. The dependence of p$K_a$ upon spacer length is exemplified by the series [4n]ane$N_4$ (n = 2–4, **4.15**), which shows the p$K_a$ variation given in Table 4.4. For **4.10**–**4.13**, anion binding behaviour is similar in type to that observed for compounds of type **4.14**, however, with binding constants increasing with anion charge. For anions of the same charge, structural effects were observed in which anions that matched the symmetry of the macrocycles were bound most tightly (*e.g.* three-fold axis of $SO_4^{2-}$ with **4.13**-6$H^+$; four-fold symmetry of squarate, $C_4O_4^{2-}$, with **4.11**-8$H^+$). Also, larger anions tend to complex more strongly with the larger macrocycle, **4.11**-8$H^+$. Interestingly, binding constants for multiply charged anions such as ATP are significantly higher than analogous acyclic reference compounds such as spermine, $H_2N(CH_2)_3NH(CH_2)_4NH(CH_2)_3NH_2$, indicating a significant anion binding macrocyclic effect, analogous to that found for the crown ethers as cation hosts. The ATP and ADP binding ability of macrocycles such as **4.12** has been used as the basis for an artificial ATP producing system (Section 12.3).

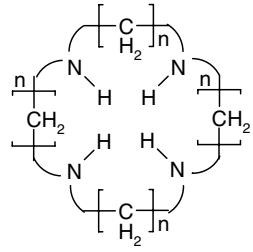

**4.15**

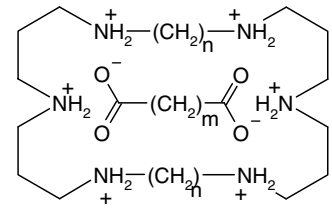

**4.16** (n = 7 and 10)
with α,ω-dicarboxylic acid guest

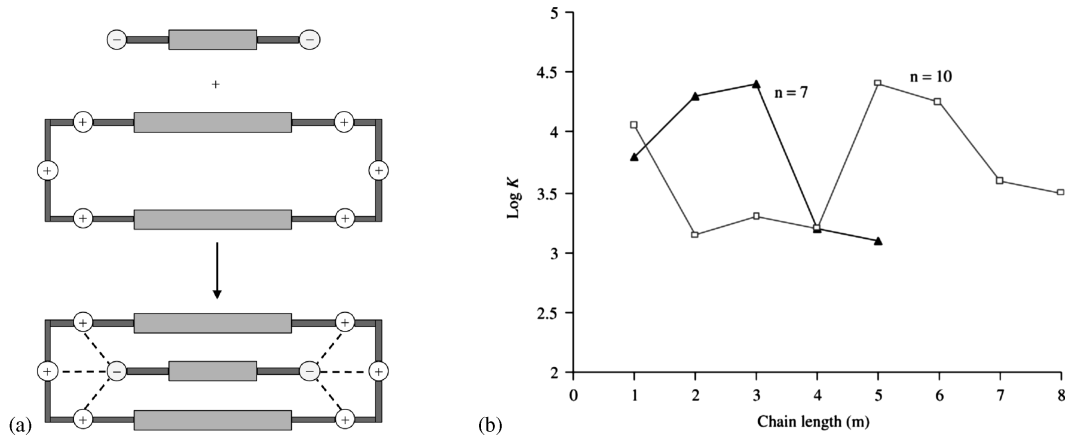


**Figure 4.14** (a) Length-based recognition of $\alpha,\omega$-dicarboxylic acids by monocyclic hosts **4.16**. (b) Binding constants for hosts **4.16** as a function of dicarboxylate guest spacer length, *m*.

The ability of monocyclic azacrown type hosts to recognise anions on a size and shape fit basis has been investigated further by the preparation of hosts of type **4.16** that contain two-binding-domains. It was anticipated that the ditopic hosts **4.16**, which possess a cavity of varying size, dependent on the length of the spacer, $(CH_2)_n$, would exhibit selectivity for $\alpha,\omega$-dicarboxylic acids $^{-}O_2C(CH_2)_mCO_2^{-}$ according to the length of the acid (determined by the length of the $(CH_2)_m$ group). Those dianionic guests that best fit the cavity should be bound the strongest. Observed binding constants for compounds **4.16** with $n = 7$ and 10 as a function of guest length, *m*, are shown in Figure 4.14. Modest peak selectivities are observed, signifying the dimensional matching of the host and guest, despite the relative flexibility of both partners.[21]

Another interesting class of anion receptors based upon protonated nitrogen atoms are the expanded porphyrin macrocycles such as **4.17** (diprotonated sapphyrin) and compound **4.18**. The tetrapyrrole porphyrin macrocycles are excellent hosts for metal cations such as $Fe^{2+}$ and $Mg^{2+}$ (*e.g.* haemoglobin and chlorophylls, Sections 2.3–2.5); however, their cavity dimensions are too small to accommodate anions. Conversely, expanded porphyrins such as **4.17** comprising five or more pyrrole residues present a rigid macrocyclic cavity about 5.5Å in diameter, in which (particularly when protonated) the NH

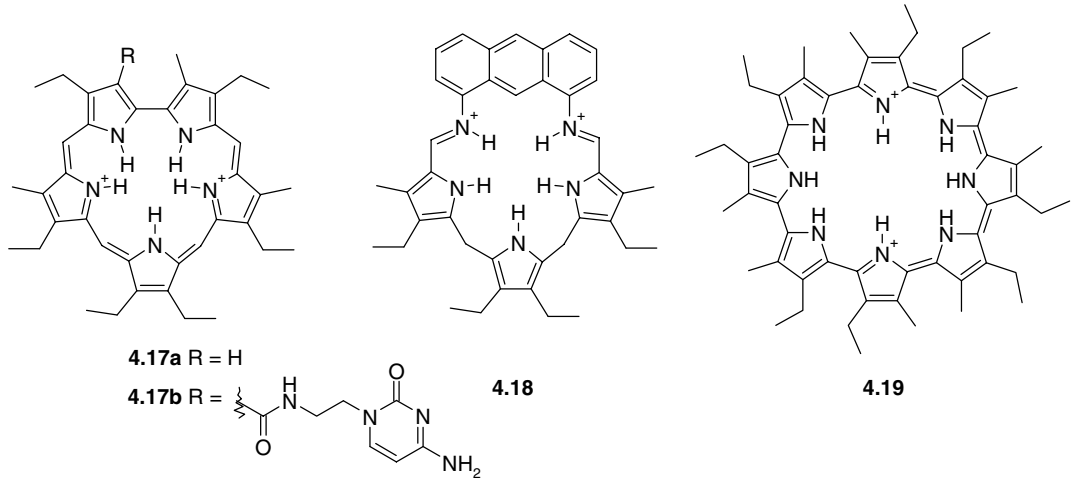

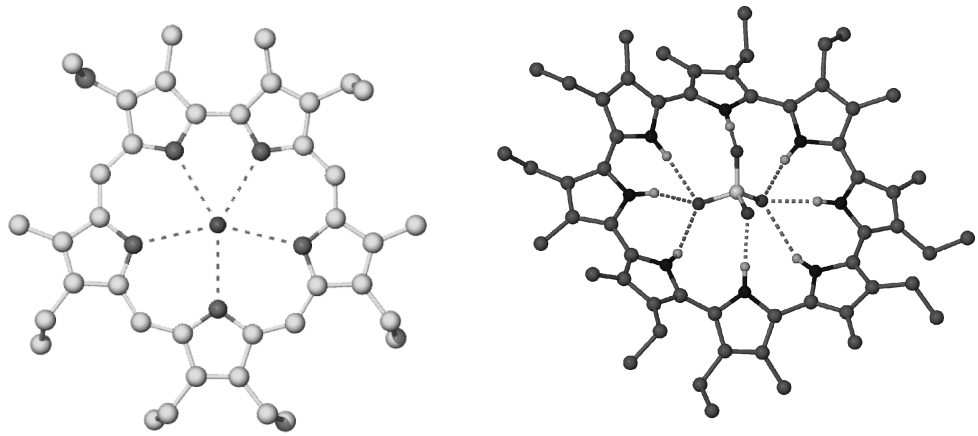


**Figure 4.15** (a) X-ray crystal structure of the diprotonated expanded porphyrin host sapphyrin (**4.17**) with encapsulated fluoride. The fluoride anion lies entirely within the plane of the macrocycle.[22] (b) $SO_4^{2-}$ binding by diprotonated octaphrin.[23]

groups are suitable for anion complexation. Diprotonated sapphyrin (**4.17**) forms an extremely stable complex with fluoride ($\log K = 5.0$) in methanol solution. The excellent fit of the anion within the sapphyrin cavity is demonstrated by X-ray crystallography (Figure 4.15a) with five short, symmetrical N···F distances in the range 2.67–2.79 Å.[22] The fact that this very large macrocycle is ideally suited to the encapsulation of the smallest anion is a clear indication of the problems faced in preparing hosts large enough to bind effectively to anions. In contrast, the analogous structure with chloride shows binding of two chloride anions above and below the plane of the macrocycle, due to poor fit. The binding constant for chloride is lower by a factor of more than $10^3$. Phosphate residues of organophosphates and polyphosphates are also bound with a single P—$O^-$ bond perching just above the plane of the macrocycle, and sapphyrin is useful in phosphate transport.

In order to prepare chloride-selective macrocycles based on the polypyrrole motif, non-aromatic expanded porphyrins have been designed which possess a much larger cavity. Compound **4.18** has been shown by X-ray crystallography to exhibit a good fit to chloride, binding through four N—H···$Cl^-$ hydrogen bonds with N···Cl distances of 3.11–3.25Å. The host–chloride complex may be detected by fast atom bombardment (FAB) mass spectrometry, suggesting that it is associated in the gas phase. Solution binding constants in $CH_2Cl_2$ (note the much less polar solvent, which is required because of the lower solubility of the macrocycle in more polar media) are $2 \times 10^5\ M^{-1}$ for $Cl^-$ and $1.4 \times 10^4$ for $F^-$. The expanded porphyrin systems were also studied by anion transport experiments from one aqueous layer to another *via* a $CH_2Cl_2$ liquid membrane (Figure 4.16). These experiments show that **4.18** is a much better fluoride carrier than **4.17**, but does not carry $Cl^-$ nearly as effectively. This is consistent with the stronger binding to $Cl^-$ (and stronger binding of $F^-$ by **4.17**), which means that the anion is not readily released after transport (*cf.* cation receptors and cation carriers, Sections 3.8.2 and 3.14.2). The initial anion flux, $\Phi$, (defined as the number of moles of anion transported per unit time) is 5.03 µmol $h^{-1}$ for $F^-$ and 1.56 µmol $h^{-1}$ for $Cl^-$. Furthermore, addition of $Cl^-$ was found to inhibit $F^-$ transport. In the absence of the macrocycle, the flux is negligible. A gradual neutralisation of the pH on both sides of the experiment was also noted, consistent with a *symport* mechanism in which $H^+$ and halide anion are carried simultaneously in the same direction (*cf.* transport of $Na^+$ and $K^+$ across cell membranes *via antiport*, Section 2.2; see also Section 5.1.5).

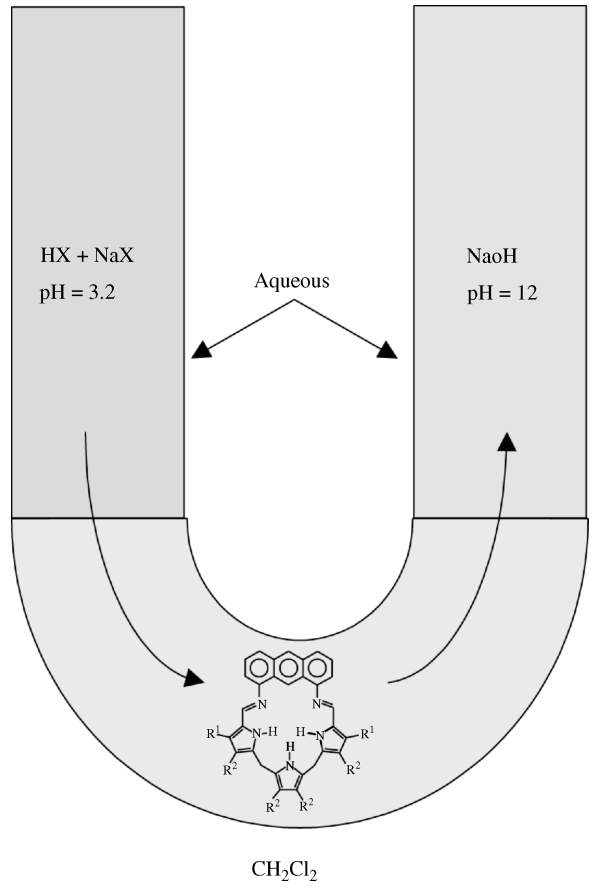


**Figure 4.16** Simultaneous transport of $H^+$ and $Cl^-$ (symport) through a liquid $CH_2Cl_2$ membrane (X = F, Cl).

In order to recognise and transport nucleotide anions sapphyrin has been derivatised with a lariat-type side arm bearing a cytosine derivative, complementary to guanosine monophosphate (5′-GMP) but not to its cytosine or adenosine analogues (5′-CMP and 5′-AMP). Simultaneous recognition of the phosphate anion group and the guanosine nucleobase resulted in the selective transport of 5′-GMP by a factor of 8 – 100.[24] Expanding the ring size still further gives cyclo[n]pyrroles (n = 6–8); pyrrole-based macrocycles with 6-8 pyrrole units linked by a single bond, and able to encapsulate increasingly larger anions. Thus in the neutral form of cyclo[8]pyrrole (**4.19**) binds hydrogen sulfate in DMSO with log $K = 5.8 \times 10^3\ M^{-1}$. This binding probably reflects protonation of the neutral macrocycle by the acidic anion and indeed an X-ray crystal structure has been obtained of diprotonated octaphyin binding $SO_4^{2-}$, Figure 4.15b.[23]

## 4.4.5 Cyclophane Hosts

A range of cyclophanes (compounds containing a bridged aromatic ring – for a full discussion of cyclophane chemistry see Section 6.5) with protonated nitrogen functionalities have been used with great success as anion binding hosts. In particular, the diphenylmethane moiety is commonly used

as a spacer in the construction of cyclophane hosts for both anions and neutral molecules in order to impart curvature and increase the size of the host walls while retaining rigidity. Macrocycle **4.20** binds anions such as 1-anilino-8-naphthalenesulfonate (ANS), which is used as a fluorescent probe in order to measure host–ANS affinity spectrophotometrically. Binding of ANS relies on hydrophobic and π–π stacking interactions, as well as electrostatic interactions and hydrogen bonds, since neutral molecules are also strongly bound.

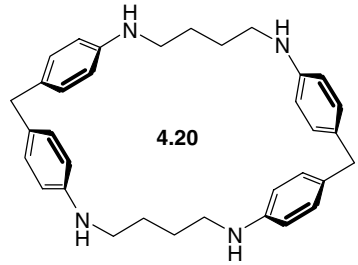


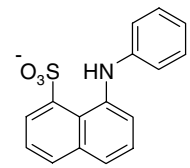


Extending the host to three dimensions gives **4.21**, which is an effective host for terephthalate dianion. The X-ray crystal structure of the complex shows that the anion is encapsulated entirely by the bicyclic host system, held in place by N—H···O hydrogen bonds, hydrophobic and van der Waals interactions and π–π stacking. On terephthalate complexation, the two bridgehead nitrogen atoms move in towards the guest by some 1.8 Å, indicating some induced fit. The host also binds nucleosides with log $K = 4$–5. Other bicyclic cyclophane hosts such as **4.22** and **4.23** bind anionic guests when protonated. Compound **4.23** in particular was shown by pH-metric titration and NMR spectroscopic data to form 1:1 complexes with a range of anions with log $K$ values ranging from 2.5 to 6.0 for mono- and divalent anions. Surprisingly, however, the X-ray crystal structure of the material (as the nitrate salt) shows that the anions are situated externally to the cavity, even though in solution even the host–guest exchange kinetics indicate encapsulation.[25] This highlights the care that must be taken in comparing solid state crystallographic data to solution phase results.

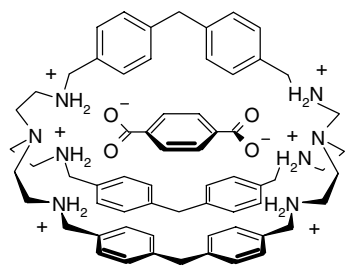

**4.21**.terephthalate$^{2-}$

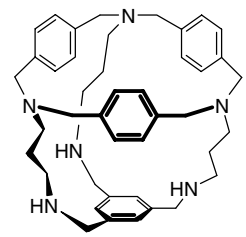

**4.22**

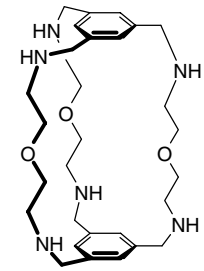

**4.23**

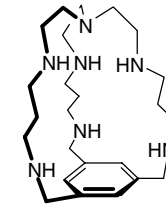

**4.24**

A smaller, tren-capped analogue of **4.23**, compound **4.24**, has been developed which has been shown by X-ray crystallography to include halides within the cavity. In aqueous solution the protonated cryptand is strongly selective for $F^-$ with log $K = 9.54$ compared to the value for $Cl^-$ of 4.19 and essentially no binding for bromide and nitrate. While not as significant as the tremendous affinity for $F^-$ observed for the hexaprotonated form of octazazcryptand **4.5**, this large, peak selective anion affinity is remarkable since it results from three NH···$F^-$ interactions and three intrinsically weaker CH···$F^-$ interactions, highlighting the preorganisation of the rigid, cyclophane cryptand. The lack of affinity for larger halides is attributed to repulsive anion···π interactions.[26]

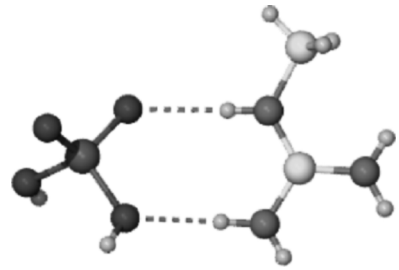

**Figure 4.17** X-ray crystal structure of methylguanidinium dihydrogen phosphate.

## 4.5 Guanidinium-Based Receptors

Schmuck, C., 'How to improve guanidinium cations for oxoanion binding in aqueous solution? The design of artificial peptide receptors', *Coord. Chem. Rev.* 2006, **250**, 3053–3067.

The guanidinium ion has proved to be a very popular motif in the design of anion complexation hosts. Interest in it was sparked by its common occurrence as part of arginine residues in naturally occurring anion binding hosts (Section 4.2.2). The native guanidinium ion has a p$K_a$ of 13.5, meaning that it is protonated and therefore positively charged and an effective hydrogen bond donor, over a wide pH range. In the solid-state, methylguanidinium forms a 1:1 complex with dihydrogen phosphate, indicating clearly its bidentate hydrogen bonding coordination mode (Figure 4.17). In an attempt to take advantage of this behaviour in a macrocyclic host, Lehn's group prepared the macromonocycles **4.25** and **4.26**.[27] The 3+ charge and three-fold symmetry of **4.25** in particular suggests that this host should bind strongly to $PO_4^{3-}$. Because of the low Brønstead acidity of the protonated guanidinium moieties, the host should remain protonated under the highly basic conditions required for the existence of $PO_4^{3-}$. Surprisingly, the observed log *K* values are only 2.4 and 1.7 for **4.25** and **4.26**, respectively. It was suggested initially that this may arise from the low charge density of the guanidinium moiety, implying weak electrostatic interactions, although this would be surprising given its biological ubiquity. It is also possible that the macrocycles are both too small to accommodate the large phosphate anion and too inflexible to direct their guanidinium moieties towards an anion in a perching geometry. The high degree of solvation of the guanidinium ion in polar solvents is probably also detrimental to strong binding, although this is less of a factor in other work involving this moiety.

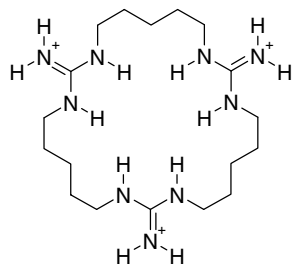

**4.25**

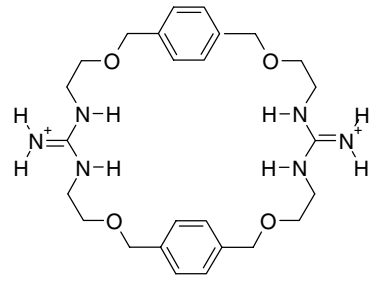

**4.26**

Despite these disappointing results, a great deal of activity has focused on guanidinium-based hosts. The majority of recent systems are acyclic, however, analogous to podand hosts for cations. These species combine ease of synthesis (no high dilution required) and the fast complexation/decomplexation

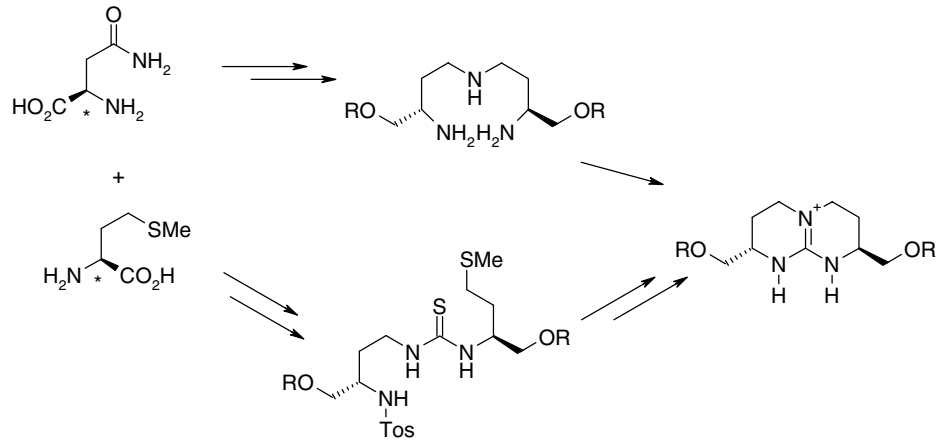

**Scheme 4.2** Synthesis of chiral guanidinium hosts starting from chiral amino acids either *via* cyclisation of an open chain triamine or unsymmetrically substituted thiourea.[29]

kinetics observed in biological systems, at the expense of preorganisation. Simple bis(guanidinium) compounds, such as **4.27**, exhibit excellent cooperative binding of phosphodiesters ($R_2O_2PO_2^-$) with association constants in acetonitrile of about $5 \times 10^4\,M^{-1}$. The hosts also act as catalysts for transesterification reactions (exchange of one R group for another in esters $-C(O)OR$), with rate enhancements of up to 300-fold compared with the uncatalysed reaction.

A breakthrough in guanidinium-based anion hosts came with the synthesis of the bicyclic derivative **4.28** by Schmidtchen in 1980.[28] The presence of the hydrocarbon backbone reduces dramatically the solvation of the guanidinium moiety and increases its lipophilicity, resulting in complexes with *p*-nitrobenzoate guest, for example, with association constants of the order of $1.4 \times 10^5\,M^{-1}$ in chloroform. Interestingly, $C_2$ symmetric chiral derivatives may be prepared starting from chiral amino acids *via* the procedure shown in Scheme 4.2.[29]

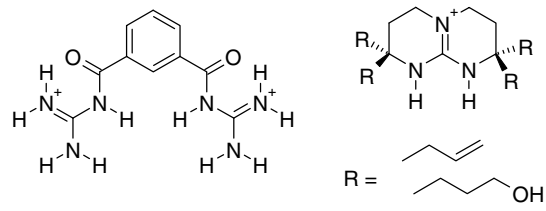

**4.27** **4.28**

The chiral derivative **4.29** is able to extract *N*-acetyltryptophan (an amino acid derivative) from a racemic aqueous solution into chloroform with a modest 17 per cent diastereomeric excess (*de*). Binding comes from a combination of guanidinium–anion hydrogen bonding and π–π stacking. In a clever piece of molecular design, one of the naphthoate residues was replaced by an aza[18]crown-6 derivative **4.30**, allowing ditopic recognition of both the carboxylate and $NH_3^+$ functionalities of underivatised amino acids such as tryptophan and phenylalanine. In this instance *de* values of 80 per cent were obtained for the L-isomers.[30] Molecular modelling studies indicate that the guanidinium group contributes about half the total binding energy, with a further third from the binding of the $NH_3^+$ group

by the crown ether and the remainder from π–π stacking interactions. Further such zwitterion-binding compounds are described in Chapter 5, Section 5.3.

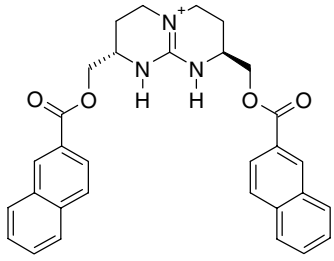

**4.29**

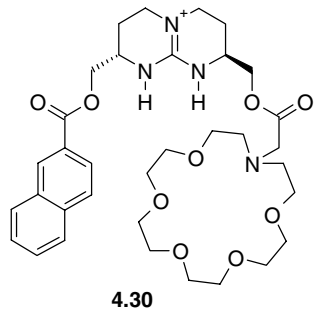

**4.30**

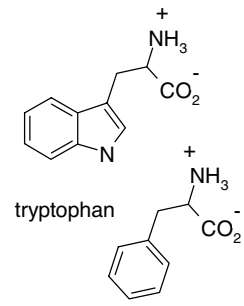


phenylalanine

Bicyclic guanidinium derivatives have also been incorporated into bis(guanidinium) receptors capable of recognising tetrahedral oxoanions, particularly polyphosphate residues of important biological molecules. The flexibility of receptor **4.31** allows the two guanidinium arms to swing into a mutually perpendicular arrangement in order to effectively complex polyphosphates even in water.

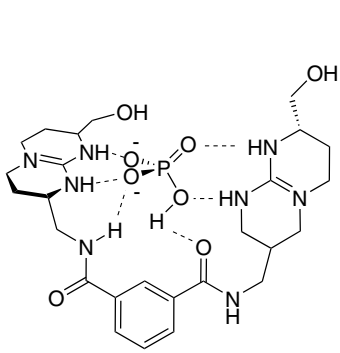

**4.31**.$HPO_4^{2-}$

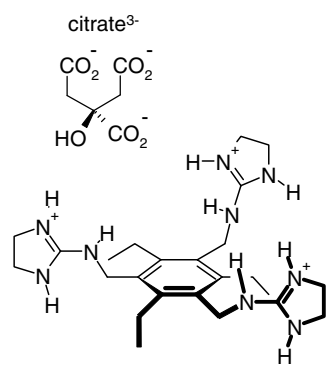


**4.32**

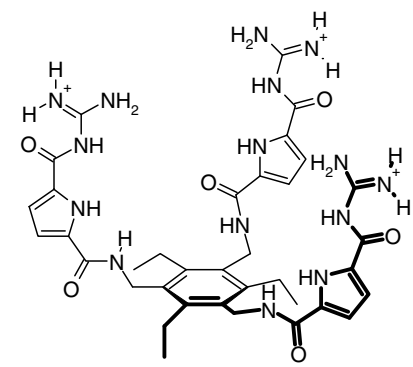

**4.33**

A seminal paper by Eric V. Anslyn of the University of Texas – Austin, USA, in 1997[31] described a tripodal tris(guanidinium) receptor capable of selective binding to the biologically important citrate anion even in pure water, with $K = 6.9 \times 10^3$ $M^{-1}$. The X-ray crystal structure of the complex is shown in Figure 4.18. The importance of ion pairing is highlighted by the fact that this affinity drops to below $10^2$ $M^{-1}$ in the presence of buffer salts. The role of the ethyl groups is to preorganise the podand into a '3-up and 3-down' arrangement producing an anion-chelating conformation in which all of the hydrogen bond donors can converge on the guest because hexasubstitution of the central aryl ring results in a steric preference for alternation of the substituents, overcoming the mutual repulsion of the cationic guanidinium groups. The energetic preference for alternation about a hexasubstituted aryl ring imparts *ca.*15 kJ $mol^{-1}$ additional binding energy to the complex.

The binding of citrate by **4.28** has been investigated by the i*ndicator* d*isplacement* a*ssay* (IDA) method (*cf.* EDTA titrations, Section 3.1.3). Binding of an organic dye indicator with comparable structure to citrate competes with the substrate for the same binding site. The binding of the indicator

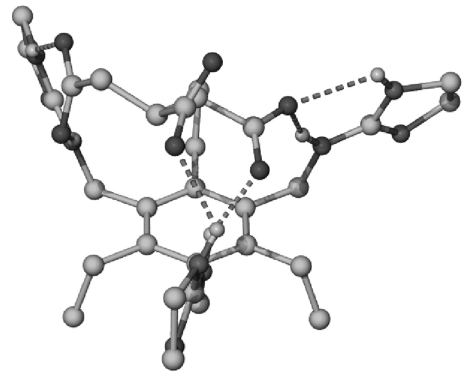

**Figure 4.18** X-ray crystal structure of the citrate complex of **4.32**.[31]

by the receptor results in a characteristic electronic absorption maximum ($\lambda_{max}$), indicative of the microenvironment of the receptor. Upon addition of the citrate anion the indicator is displaced into free solution resulting in a change the wavelength of the absorption maximum as a result of its enhanced solvation. The process is particularly effective when the indicator is chemically related to the target guest species and the sensitivity of the system can be tuned by close attention to the relative affinity of the host for indicator and analyte. The process of choosing an appropriate indicator is made easier by references such as the Sigma-Aldrich Handbook of Stains, Dyes, and Indicators.[32] In Section 11.3.3 we will explore how such assays can be used to produce electronic microarray sensors.

This work has been extended by Carsten Schmuck (Würtzburg, Germany) to tripodal receptors bearing guanidinocarbonyl pyrrole binding sites.[33] The guanidinocarbonyl pyrroles have several key advantages. Firstly, the p$K_a$ of values of such acyl guanidinium groups is *ca.* 7–8, lower than simple guanidiniums. While this runs the risk of deprotonation in basic media, it also suggests that the formation of stronger, more acidic hydrogen bonding is likely (although hydrogen bond acidity and Brønstead acidity are not quite the same thing, see Section 1.8.4!). Secondly the amide NH group provides an additional hydrogen bond donor site, thirdly the binding group is rigidly planar, limiting the reduction of conformational entropy upon binding and representing preorganisation for planar carboxylate anions and finally additional secondary interactions can be introduced to further enhance selectivity. The resulting guanidinocarbonyl pyrrole tripod **4.33** is remarkably successful, selectively binding citrate in aqueous buffer in the presence of over 1000-fold excess chloride with $K > 10^5$ M$^{-1}$. This receptor can be used for naked eye detection of citrate by an indicator displacement assay with carboxyfluorescin dye.

The tripodal, trialkylbenzene-based core has proved to be an extremely versatile scaffold in both cation and particularly anion supramolecular chemistry and we will return to it in more detail in Section 4.8.1.

## 4.6 Neutral Receptors

Antonisse, M. M. G. and Reinhoudt, D. N., 'Neutral anion receptors, design and application', *Chem. Commun.*, 1998, 443–448.

All of the hosts examined in Sections 4.4 and 4.5 possess a formal positive charge, which assists in their anion complexing ability through the formation of non-directional electrostatic interactions. Despite the strong binding by charged hosts, there are two potential disadvantages to the use of cations as anion

complexing agents. Firstly, the non-directional nature of electrostatic forces means that *all* anions are bound with some degree of strength, which can reduce anion selectivity. What selectivity there is must be a result of additional interactions, such as hydrogen bonds, size fit *etc.*, which often represent proportionately small contributions to the overall binding and can be swamped by the electrostatic forces. As well as being non-selective, each cationic host must have a counter anion, incorporated at the time of synthesis, in order to fulfil the requirement of overall electroneutrality. These counter anions generally interfere with binding of the target anion, and observed binding constants are ratios of the affinity for one anion over the other, rather than representing absolute host guest affinity. This competition is demonstrated readily by $^1$H NMR spectroscopy using the organometallic host **4.34**. Compound **4.34** is a 6+ species and was synthesised as a hexakis trifluoromethane sulfonate ($CF_3SO_3^-$) salt. Titration with NaBr in aqueous solution results in a smooth binding curve corresponding to the replacement of the intracavity and extracavity $CF_3SO_3^-$ anions with $Br^-$. However, if the experiment is repeated in such as way that $NaCF_3SO_3$ is also added to give a constant ionic strength (Section 3.11.2), the $Br^-$ binding is severely inhibited at the beginning of the experiment because of the presence of a large excess of $CF_3SO_3^-$. Binding begins as the balance shifts towards $Br^-$, but inhibition is noted all of the way up until the concentration of added $CF_3SO_3^-$ is zero (Figure 4.19).

As a result of both the non-directional electrostatic binding and inter-anion competition, it is more difficult to incorporate selectivity into charged hosts. This issue has brought about significant research into the synthesis of neutral anion binding compounds. The work has been spurred on by the knowledge that neutral hosts should exhibit much better membrane transport properties because of their more lipophilic nature, as in biological systems. The corollary, of course, is that a neutral host does not interact solely with an anion, but in fact must bind both the anion and its counter-cation and so is formally a host for an ion pair. In this section we will examine some of the chemistry of neutral receptors where the effects of the counter cation are ignored or constant. Chapter 5 deals with hosts with explicit binding sites for the simultaneous binding of both anions and cations.

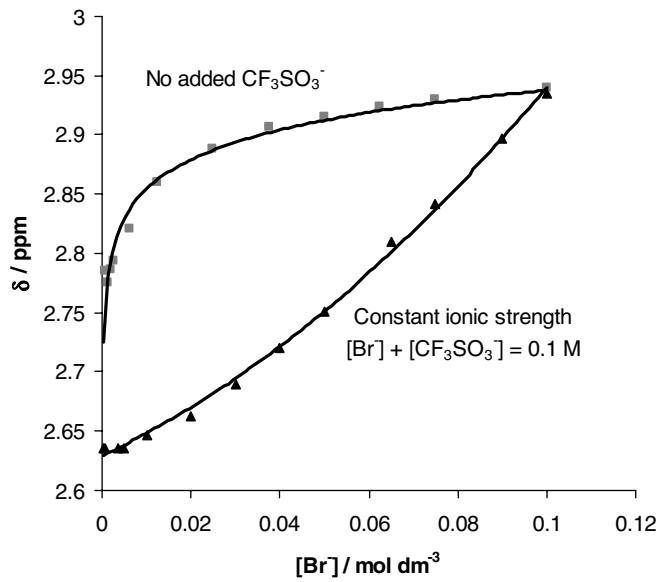


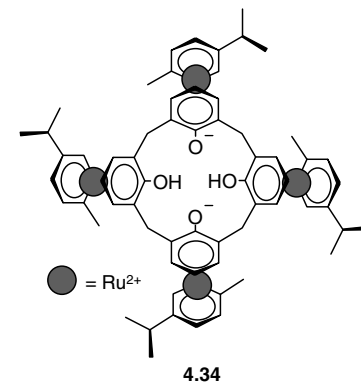


**4.34**

**Figure 4.19** $^1$H NMR titration data for **4.34** with $Br^-$ and with a mixture of $Br^-$ and $CF_3SO_3^-$ at constant ionic strength.

## 4.6.1 Zwitterions

A zwitterion is a neutral molecule containing both positive and negative charge (*e.g.* the amino acids phenylalanine and tryptophan in which the acid —$CO_2H$ group is acidic enough to protonate its own $NH_2$ functionality). The majority of biological anion binding proteins and enzymes are zwitterionic, having positively charged regions in which the anion binding occurs, coupled to negatively charged carboxylates, which impart overall electrical neutrality, facilitating the proteins' membrane solubility. Receptors that bind zwitterions as guests are treated in Chapter 5, however there exist a few zwitterionic host molecules for anions in which the cation binding is external to the cavity and these represent an interesting bridge between charged and neutral receptors.

In a conceptually simple exercise in preparing neutral host molecules Schmidtchen *et al*. reacted a tricyclic tetramine with borane ($B_2H_6$) in tetrahydrofuran (THF) to give a tetrakis ($BH_3$) adduct **4.35**.[34] The overall charge is neutral, but the host still possesses a significant amount of positive charge on the nitrogen atoms as a result of the $^+N—B^-$ dipolar bonds, which exert directionality, encouraging anions to enter the cavity in a similar way to the methylated host **4.3**. Host **4.35** binds a wide variety of anions in its molecular cavity and is able to transport them into chloroform solution. By analogy with biological systems, zwitterion **4.36** was also prepared along the same lines. The anionic carboxylate portions of the molecule are prevented from entering the cavity by the rigidity of the aryl spacers. As a result, the compound is highly water-soluble, consistent with a lack of intramolecular ion pairing of the charged $CO_2^-$ groups with the quaternary ammonium functionalities, and again binds anions readily. Association constants for halides and $CN^-$ in water of (300–600) $\times$ $10^3$ $M^{-1}$ are observed.

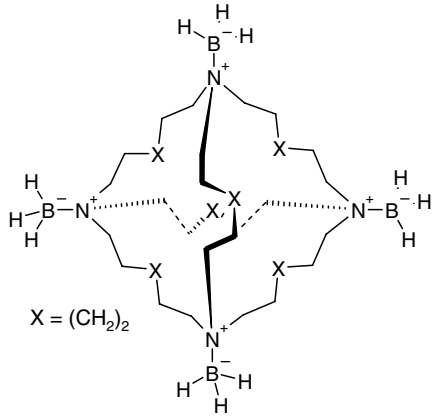


**4.35**

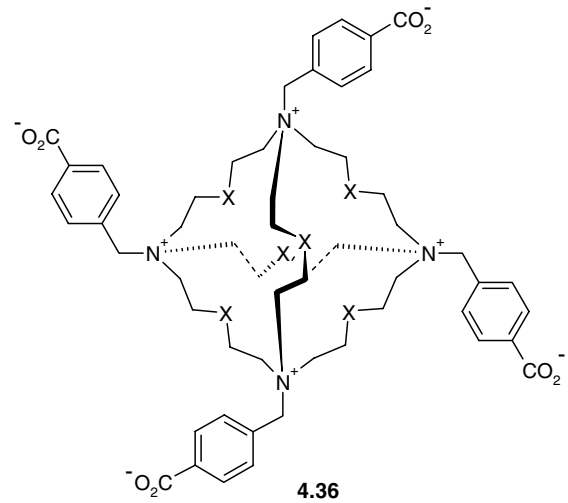

**4.36**

## 4.6.2 Amide-Based Receptors

Kang, S. O., Begum, R. A. and Bowman-James, K., 'Amide-based ligands for anion coordination', *Angew. Chem. Int. Ed.* 2006, **45**, 7882–7894.

The secondary amide group, –C(O)NHR, is ubiquitous in protein structures where hydrogen bonding from the amide NH group to the carbonyl oxygen atom is responsible for much of the secondary structure of proteins such as α-helices and β-sheets. The electron withdrawing effect of the carbonyl oxygen

atom make the amide NH group a strong and directional hydrogen bond donor. Moreover amides are generally readily synthesised from the reaction of a carboxylic acid or acid chloride with an amine and hence amides were among the first neutral anion hosts. Perhaps one of the most important contributions to amide-based anion host chemistry are the compounds of type **4.37** first prepared by Bob Crabtree at Yale University, USA in 1997.[35] The bromide salt of **4.37a** shows both amide NH groups hydrogen bonding to $Br^-$. The low solubility of **4.37a** meant that solution studies in $CH_2Cl_2$ were carried out on alklyated analogues such as **4.37b** which selectively binds $Cl^-$ among the halides and acetate, with log $K = 4.8$. Interestingly the sulfonamide analogue, **4.37c** forms both 1:1 and 2:1 complexes with $F^-$ and acetate and is relatively unselective, perhaps reflecting a lowered degree of preorganisation. Almost simultaneously with the Crabtree work, Brad Smith at Notre Dame, USA, reported the very highly preorganised boronic acid derivative **4.38**.[36] The Lewis acidic boron atom forms an adduct with the lone pairs of the carbonyl oxygen atoms, inhibiting molecular rotation in the host by forming a cyclic framework. This means, among other considerations, that less rotational entropy is lost on binding. The complex binds strongly to acetate as a result of cooperative polarisation effects arising from the bound boronate group and the binding constant for acetate is *ca.* 20 times that of **4.38a** in DMSO solution. Binding in these systems can be enhanced by addition of additional anion-binding functionality, as in **4.39**.[37] This modification significantly enhances binding, particularly for oxyanions such as dihydrogen phosphate with all four amide NH groups interacting with the polyatomic anions. Hosts **4.40** and **4.41** are again based on the tren motif (Section 4.4.3), which presents three N–H bonds convergently towards a central binding site. In the case of **4.40**, binding is aided by the presence of stacking interactions with the napthyl rings, while in **4.41**, the three ferrocenyl moieties act as redox sensors to detect anion binding as well as providing stabilisation by the Lewis acidity of the metal and C—H $\cdots$ anion interactions. This species binds $H_2PO_4^-$ with an impressive binding constant of $1.4 \times 10^4\,M^{-1}$ in acetonitrile despite its fundamentally flexible nature. We will examine such redox sensors in more detail in Section 11.3.4.

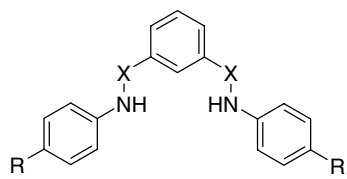

**4.37a** R = H, X = CO
**4.37b** R = n-Bu, X = CO
**4.37c** R = H, X = $SO_2$

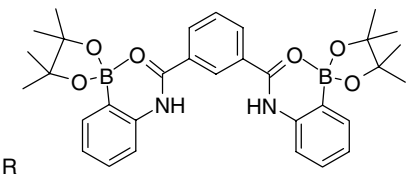

**4.38**

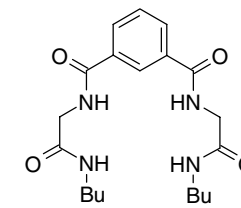

**4.39**

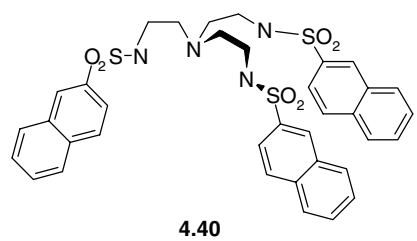

**4.40**

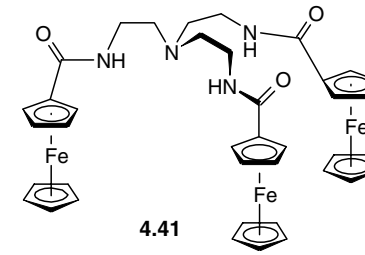

**4.41**

The range and versatility of amide anion binding hosts is very extensive. Macrocyclic amides have also been reported, such as **4.42** which forms a remarkable sandwich compound with sulfate in the solid state. Sulfate binding is enhanced by protonation of the tertiary amine groups and the host is thus a hybrid between amide and ammonium binding sites. The triethylbenzene scaffold has been used to prepare

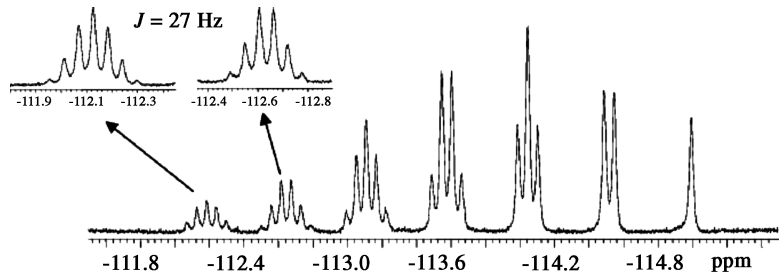


**Figure 4.20** $^{19}$F NMR spectrum of **4.44** · $(n\text{-Bu})_4N^+F^-$ 0.5:1 after heating at 150 °C for 1 h in DMSO-$d_6$ followed by storage at 25 °C for 10 d. The resonances from left to right correspond to anion cryptates with respectively 0, 1, 2, 3, 4, 5 and 6 NH protons replaced by deuterium. The observed multiplicity follows the standard formula multiplicity = 2n$I$ + 1 where n is the number of $^1$H nuclei remaining and $I$ is the nuclear spin quantum number of $^1$H, *i.e.* ½. (Reproduced with permission from [38] © 2004 American Chemical Society).

a threefold symmetric macrobicyclic amide (**4.43**) that acts as a host for the acetate anion. The binding constant of 770 $M^{-1}$ in $MeCN/CD_2Cl_2$ is surprisingly low, however. In contrast very significant binding of $F^-$ is observed for amide cryptands such as **4.44** (log $K$ = 5.90). Fluoride exchange is slow on the $^{19}$F NMR spectroscopic timescale and the strong interaction is exemplified in the observation of a septet due to coupling of the $F^-$ ion with the six equivalent amide NH protons. Interestingly, on action of heat over time the basicity of fluoride is enough to catalyse H/D exchange with the DMSO-$d_6$ solvent resulting in the gradual replacement of the amide NH protons with deuterium. As a quadrupolar nucleus deuterium does not exhibit significant coupling with $^{19}$F and hence the line multiplicity is reduced by one for each deuterium atom, until the fully deuterated sample exhibits only a $^{19}$F NMR singlet resonance, Figure 4.20.

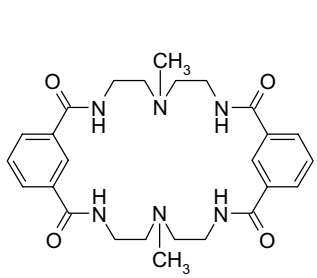

**4.42**

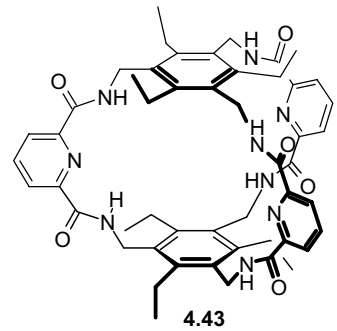

**4.43**

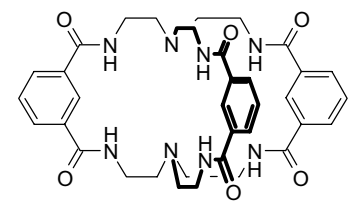

**4.44**

## 4.6.3 Urea and Thiourea Derivatives

Amendola, V., Esteban-Gomez, D., Fabbrizzi, L. and Licchelli, M., 'What anions do to N-H-containing receptors', *Acc. Chem. Res.* 2006, **39**, 343–353.

Urea and thiourea themselves have been known since 1940 as channel-forming clathrate compounds. Their channel forming ability is related to the strong hydrogen bonding ability of the urea NH groups. In urea clathrates urea molecules self-associate by NH···O=C interactions. Interactions to thiourea are even stronger as a result of the increased hydrogen bond basicity of the thiourea sulfur atom (it is a better hydrogen bond base because of the longer C=S bond which makes the sulfur atom more available even

though it is less electronegative than oxygen). Like amides, urea derivatives are extremely useful in the construction of anion hosts. The steric bulk and rigidity of multifunctional anion receptors means that urea self-association is not significant and hence their strong hydrogen bonding results in high anion affinities. Moreover ureas are very readily synthesised by reaction of an isocyanate with an amine and hence are very versatile anion binding sites. For example, a rigid urea-based molecular 'cleft' host (**4.45**) has been prepared, which is able to chelate carboxylate, phosphate, sulfonate and similarly shaped anions. Anion affinity depends on the Brønsted basicity and charge of the guest; the greater the better, although the variation is not very large. Even the very simple urea derivative **4.46** interacts strongly with fluoride, acetate and benzoate to give a bright yellow colour in the case of oxoanions (absorption at *ca.* 370 nm), log *K* values 7.38, 6.61 and 6.42, respectively in acetonitrile solution. Addition of further equivalents of the basic fluoride results in deprotonation for give complexes of $HF_2^-$ and a new absorption band at 475 nm. Indeed deprotonation in the presence of basic anions, particularly in thiourea derivatives where the sulfur can stabilise the resulting negative charge) is a significant issue in these types of host and should always be considered as a possible explanation for significant spectral changes on interaction with anions.

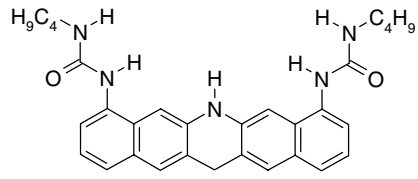

**4.45**

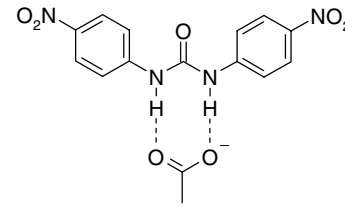

**4.46**.acetate

In the design of hosts of these types, the imagination of the chemist is limited only by his or her synthetic ability, and a great many hybrid hosts bearing hydrogen binding functionalities or various macrocyclic and macrobicyclic scaffolds are known. A good example is the calix[6]arene thiourea derivative **4.47**, which uses the large calixarene to organise spatially the three thiourea moieties in a three-fold symmetrical arrangement.[39] The host binds halides moderately well in chloroform but is particularly effective for the complexation of the threefold symmetric trianion benzene-1,3,5-tricarboxylate

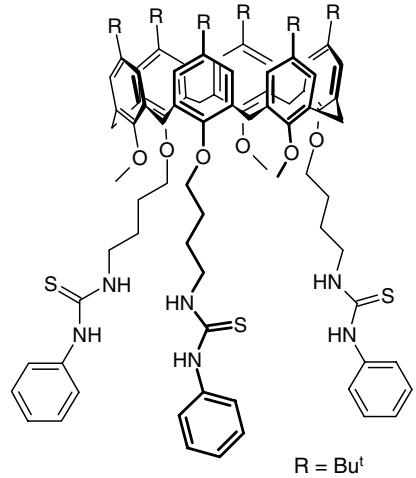

R = Bu$^t$

**4.47**

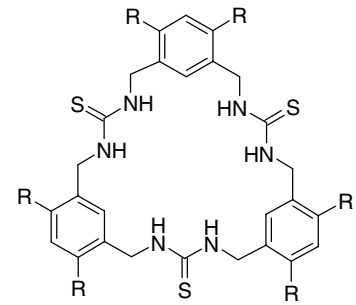

**4.48a** R = H
**4.48b** R = $C_2H_5$

(the trianion of trimesic acid), which is complexed with an association constant of $2 \times 10^5\,M^{-1}$ in chloroform. The topological (symmetry) complementary is confirmed by the 10–100-fold weaker binding of the 1,2,4- and 1,2,3-substituted isomers, despite the flexibility of the three arms of the host. Just as with amides, tripodal, macrocyclic and macrobicyclic derivatives have all been prepared. For example the threefold symmetric tris(urea) macrocycles **4.48**. The less flexible compound **4.48b** forms the strongest complexes with anions and is selective for acetate ($K = 5300\,M^{-1}$ in DMSO) over dihydrogen phosphate and chloride. The selectivity order is slightly different for the more flexible **4.48a** with the binding constant following the order $H_2PO_4^- > CH_3CO_2^- > Cl^-$, however affinities are $< 10^3\,M^{-1}$.

## 4.6.4 Pyrrole Derivatives

Sessler, J. L., Camiolo, S., Gale, P. A., 'Pyrrolic and polypyrrolic anion binding agents', *Coord. Chem. Rev.* 2003, **240**, 17–55.

Calix[4]pyrroles such as **4.49** (named because of their resemblance to calix[4]arenes) possesses only a very small cavity, too small to encapsulate all but the smallest anions. Despite this, compound **4.49** can form four hydrogen bonds to anions, which adopt a perching mode on what would be its lower rim, if the calixarene analogy is maintained. The compound is especially appealing since it is readily obtained in one step from condensation of pyrrole and acetone. It has been shown to complex fluoride in $CH_2Cl_2$ with a binding constant of $1.7 \times 10^4\,M^{-1}$ and a selectivity over chloride of a factor of 50 (Figure 4.21). Interestingly, the structure of the free macrocycle shows that it adopts a 1,3-alternate conformation and hence anion complexation induces a conformational rearrangement. Derivatives of both the methyl and cyclohexyl derivatives of calix[4]pyrrole have been attached to silica gels and used as the stationary phase in high pressure liquid chromatographic (HPLC) separations of anions. This medium allows the separation of mixtures of (i) AMP, ADP and ATP, (ii) aromatic carboxylates, and (iii) oligonucleotides of varying chain length (Figure 4.22) under isochratic conditions.*

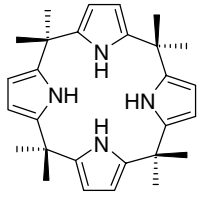

**4.49**

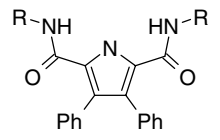

R = alkyl, nitrophenyl *etc.*

**4.50**

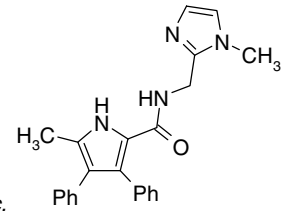

**4.51**

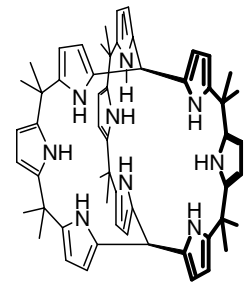

**4.52**

While interesting neutral alternatives to the unsaturated expanded porphyrin derivatives, calix[n]pyrroles (n = 4, 5, 6, 8) are relatively limited in their scope for anion binding because of the constraints of the cavity size. Nevertheless pyrroles linked by an $sp^3$ hybridised carbon atom are of considerable interest because of their resemblance to the anti-cancer agents the prodigiosins (Section 4.2.4), moreover pyrrole anion-receptor chemistry is synthetically versatile and hence a range of acyclic pyrroles and hybrid amidopyrroles such as **4.50**–**4.52** have been developed, particularly by the groups of

* isochratic– a chromatographic technique involving one eluent (solvent medium) throughout. The method does not separate early eluters very well, while late eluters are spread out too much. The alternative is the gradient technique involving two or more eluents, gradually changed from weak to strong solvent.

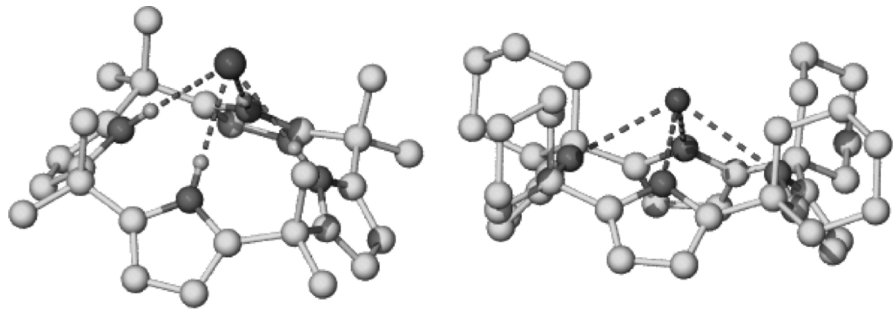


**Figure 4.21** X-ray structures of (a) the chloride complex of **4.49** and (b) the fluoride complex of the analogous cyclohexyl derivative, showing the better fit of the $F^-$ anion.

Jonathan Sessler at the University of Texas, Austin, USA and Phil Gale at the University of Southampton, UK. The elegant cryptand **4.52** is in fact too small to bind even $F^-$ within the cavity and NMR spectroscopic studies reveal that it forms a 1:1 fluoride complex in which the anion interacts with six of the nine pyrrole-derived units. In contrast chloride forms a 2:1 complex (anion:host) with a binding constant, $\beta_{12}$ of $3.1 \times 10^6\ M^{-2}$ in dichloromethane. Of particular interest is the imidazole-functionalised amidopyrrole **4.50** which was designed as a synthetic prodigiosin mimic. The imidazole acts as a basic site for $H^+$ binding while chloride binds to the amidopyrrole unit to give a receptor capable of binding and transporting HCl in a symport fashion. The X-ray crystal structure suggests the hydrochloride complex exists as a dimer with the ionic groups shielded within a lipophilic exterior. The compound is effective at $H^+$ and $Cl^-$ release from vesicles (Section 5.1.5) which act as models for biological cells.

## 4.6.5 Peptide-Based Receptors

In recent years anion receptors based on peptides (oligomers of amino acids) have become of increasing interest, not least because of their resemblance to biological receptors. The archetypal example is the antibiotic vancomycin illustrated in Section 1.5. Vancomycin binds to the L-Lys-D-Ala-D-Ala

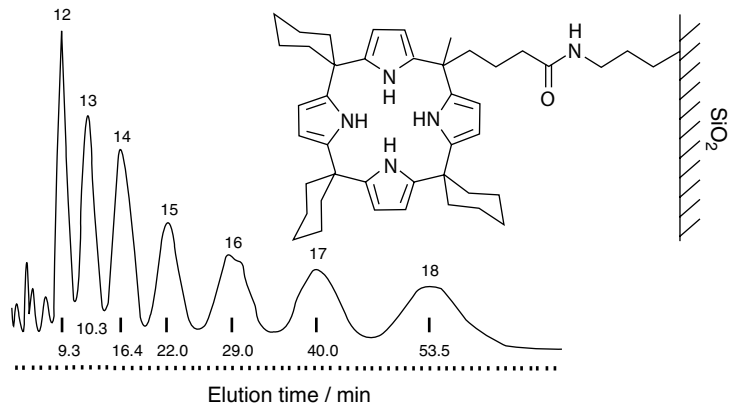


**Figure 4.22** Separation of oligodeoxythymidylate fragments containing 12–18 nucleotide sub-units ($dT_{12-18}$) on calixpyrrole modified silica gel column. (Reproduced by permission of The Royal Society of Chemistry).

carboxylate anion terminus of bacterial cell wall peptides and has been characterised crystallographically as an acetate complex. The synthetic, cyclic hexapeptide **4.53** has been synthesised from L-α-aminoxy acid building blocks. The small cavity binds very strongly to chloride and is highly selective over the smaller $F^-$ ($K_a$ in chloroform = 11,880 *vs.* 30 $M^{-1}$!).[41] In contrast the cysteine-based macrocycle **4.54** is fluoride selective with $K_a$ = 418 $M^{-1}$ in acetonitrile solution. Other anions are bound more weakly according to the order of their polarisability.[42]

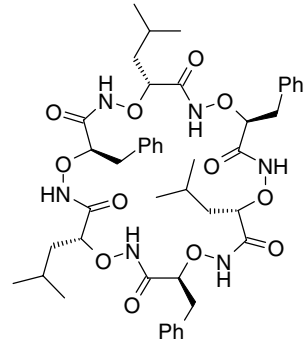

**4.53**

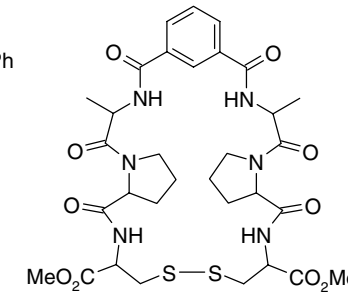

**4.54**

## 4.7 Inert Metal-Containing Receptors

### 4.7.1 General Considerations

Beer, P. D., Hayes, E. J., 'Transition metal and organometallic anion complexation agents', *Coord. Chem. Rev.* 2003, **240**, 167–189.

Anion receptors based on metal centres are a well established class of anion binding compound and can be classified into three broad categories, listed below.

1. Those in which an inert or labile metal centre plays a structural role
2. Those in which an inert or labile the metal is a key component of the anion binding site
3. Those in which an inert or labile metal acts as part of a redox, luminescent or colorimetri reporter or sensing group

Of course there are examples of compounds that fall into more than one group (*e.g.* compound **4.55**, Scheme 4.3), in which the ferrocene-derived unit acts as both a colorimetri reporter for $F^-$ binding and a structural element[43]). We will consider complexes of labile metal centres (*i.e.* situations in which the rate of metal exchange with bulk solution is comparable to the rate of anion exchange) separately as ion par receptors in Chapter 5. In the case of inert complexes (either because the metal itself has an inert electron configuration as in Co(III), Ru(II) or Pt(II) complexes, or because the metal is held by several strong coordinate bonds by a chelate ligand) we can regard the metal as being an integral part of a single, stable receptor and consider the compound in the same way as organic anion hosts. For example, in compound **4.56** two thiourea-derived terpyridyl ligands are held together in a well-defined way by an inert chelate complex of a (low spin $d^6$) ruthenium(II) centre, Scheme 4.4. This host, developed by Andrew Hamilton at Yale University in 1997, was among the first examples of what is

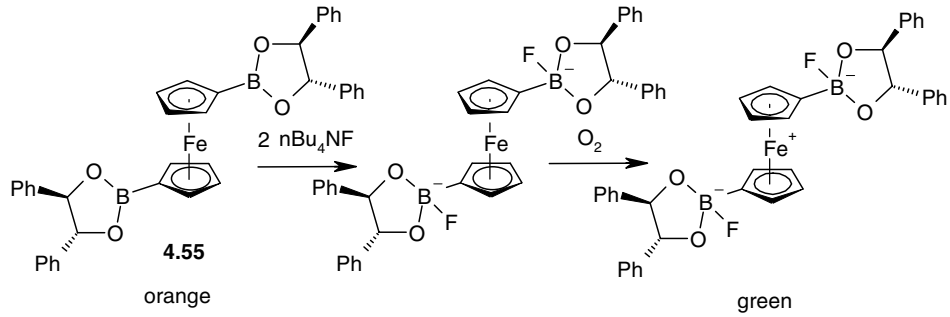


**Scheme 4.3** Iron as a structural and sensing element in **4.55**. Fluoride binding to the boronic acid derived groups results in a lowering of the ferrocene-derived core's oxidation potential, allowing aerial oxidation of the Fe(II) centre to Fe(III) with concomitant colour change from orange to green.

becoming an increasing trend towards coordination compounds in which the host geometry is defined by metal coordination. The compound binds long dicarboxylates, particularly pimelate.[44]

In contrast, labile coordination compounds are not true anion hosts in the conventional sense. Instead they fall into the category of self-assembly (*cf.* Chapter 10) and are frequently a templated multi-component array of anions, cations and anion-binding ligands. The ensemble may be thought of as a multi-component self-assembly of ligands that, like the urea-containing terpyridines in **4.56**, contain both anion and cation binding functionality. An illustration of the boundary between labile and inert complexes comes from the arene ruthenium(II) derivatives **4.57** and **4.58**. The presence of the bidentate bispyrrole ligand makes complex **4.57** inert and binds a number of anions *via* hydrogen bonding interactions to the bispyrrole NH functionalities.[45] In contrast, while **4.58** binds effectively to chloride, nitrate and hydrogen sulfate, the monodenate pyridyl ligands are displaced over a period of hours by $Cl^-$ which moves from binding to the amine NH groups to direct coordination to the semi-labile metal centre. Compound **4.58** represents an interesting example in which one metal centre, ruthenium(II), is used as a structural element, while another, iron(II), acts as a redox reporter group.[46]

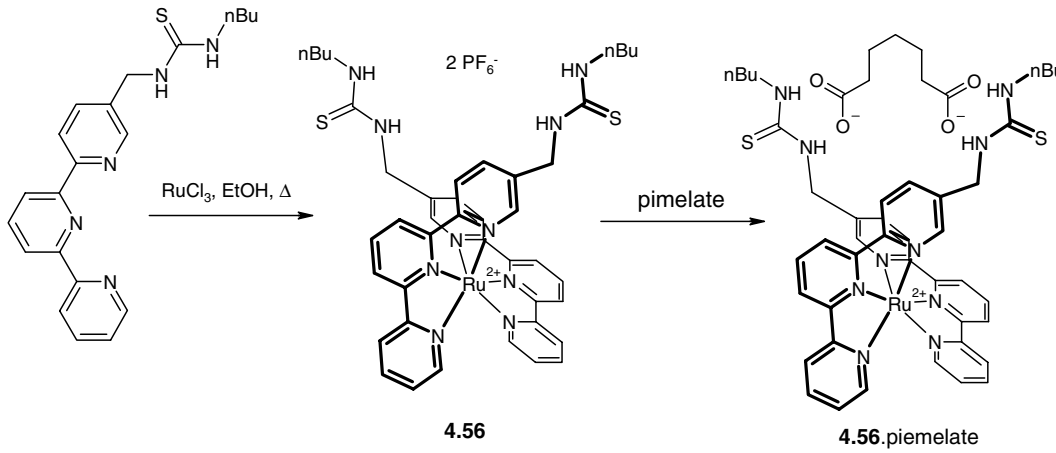


**Scheme 4.4** Use of an inert Ru(II) centre to organise an anion chelate ligand.

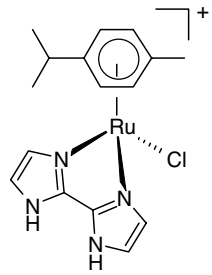


**4.57**

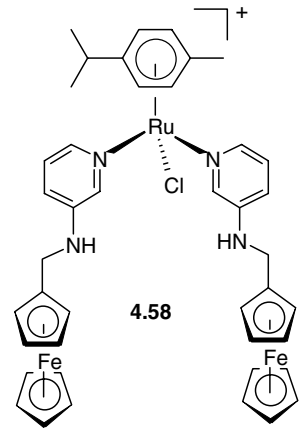


**4.58**

## 4.7.2 Organometallic Receptors

Lenthall, J. T. and Steed, J. W., 'Organometallic cavitands: Cation–π interactions and anion binding *via* π-metallation', *Coord. Chem. Rev.* 2007, **251**, 1747–1760.

Incorporation of organometallic fragments into anion receptors can result in interesting redox chemistry with potential applications in electrochemical sensing arising from the ability of the organometallic ligands to stabilise a variety of (generally lower) oxidation states. The covalent nature of the M–C bonds usually results in complexes that are relatively inert and hence the metal also acts as a structural element, while frequent positive charge associated with metal complexes increases ligand hydrogen bond acidity and is intrinsically attractive to anions.

In 1989, Paul Beer and co-workers from the University of Oxford, UK, prepared the bis(cobaltocenium) receptor **4.59**. This organometallic macrocycle possesses a dipositive charge arising from the Co(III) centres, and so is capable of binding anions purely on the basis of electrostatic interactions. Beer and co-workers quickly realised that much greater anion affinity and selectivity could be achieved, however, by adding hydrogen bonding functionality to the anion affinity exerted by the positively charged metal cation alone, and so prepared a range of amide hosts such as bis(amide) **4.60**. The X-ray crystal structure of this material shows interactions to $Br^-$ anions *via* N—H $\cdots$ $Br^-$ and C—H $\cdots$ $Br^-$ hydrogen bonds (Figure 4.23). Consistent with these interactions, $^1$H NMR spectroscopy reveals large downfield shifts of the NH protons (several ppm) on titration with various anions in dipolar aprotic solvents, such as DMSO and MeCN. The use of aprotic solvents is vital because the acidic NH proton is exchanged for deuterium, resulting in loss of the NMR signal for this nucleus, in $D_2O$. Along with $^1$H NMR spectroscopy, cyclic voltammetry (Box 4.1) also provides an excellent 'handle' to observe guest binding because of the redox potential shifts induced in the Co(III)/Co(II) redox couple by the identity and proximity of the guest anions (which effectively forms the metal's second coordination sphere). Redox potential shifts ($\Delta E_{1/2}$) of the Co(III)/Co(II) couple in **4.60** of 85 mV were observed in the presence of $Cl^-$ (Figure 4.24), while $H_2PO_4^-$ gave shifts of 240 mV. The cobaltocinium moiety thus contributes directly to anion binding *via* positive charge and Lewis acidity and also allows the electrochemical detection of the anion binding process.[47]

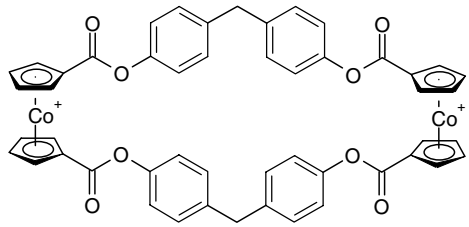

4.59

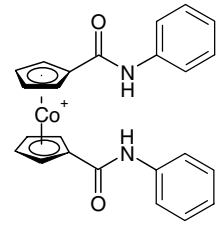

4.60

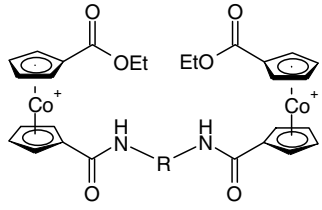

R = $(CH_2)_2$, $(CH_2)_3$, $(CH_2)_4$, diphenylmethane

4.61

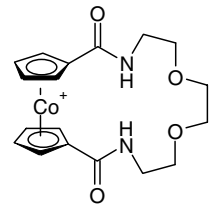

4.62

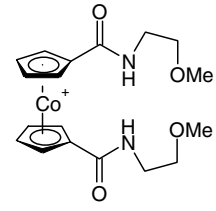

4.63

Given this excellent way of studying anion recognition by a combination of NMR spectroscopy and electrochemistry, Beer and co-workers went on to design the bis(cobaltocenium) hosts **4.61** and the macrocycle **4.62**. Compounds **4.61** display halide binding behaviour, which decreases sharply as the length of the spacer group R increases, consistent with a chelate effect of the two NH groups (Table 4.5). Comparison of the cyclic receptor **4.60** with its acyclic analogue **4.63** revealed a distinct macrocyclic effect for chloride binding in DMSO, with **4.62** exhibiting a binding constant of 250 $M^{-1}$, compared to only 20 $M^{-1}$ for **4.63**.

As with cation binding hosts, it is also possible to use calixarene frameworks (Section 3.14) to organise anion binding moieties. Addition of a cobaltocinium bis(amide) moiety to the upper rim of a calix[4]arene with *p*-toluenesulfonate functionalities to enhance solubility results in a rigid host **4.64**

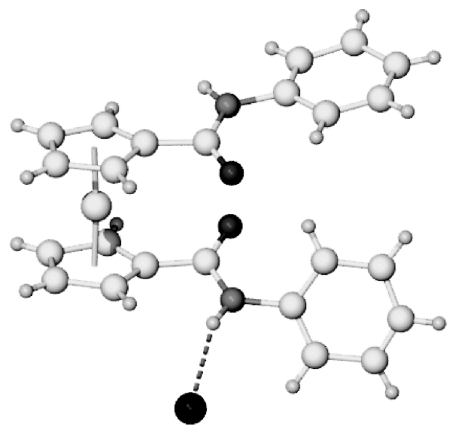

**Figure 4.23** X-ray crystal structure of the bromide complex of **4.60**.

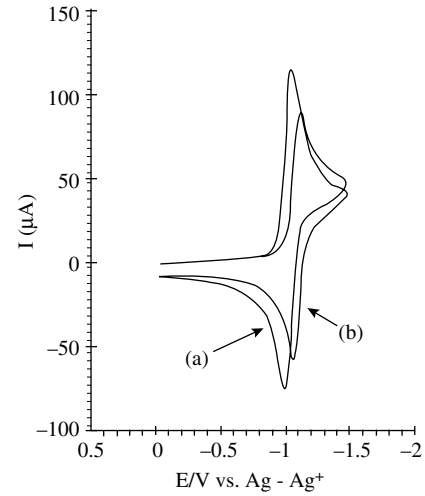


**Figure 4.24** Cyclic voltammetric waves for **4.60** (a) in the absence and (b) in the presence of $Cl^-$. (Reproduced with permission from Reference 47).

in which the positioning of the two amide NH groups is well suited for carboxylate anion complexation. The binding constant for acetate in DMSO solution is 41,500 $M^{-1}$, compared to a chloride affinity of only 70 $M^{-1}$. The X-ray crystal structure of the chloride complex showing N—H $\cdots$ $Cl^-$ hydrogen bonds is shown in Figure 4.25.

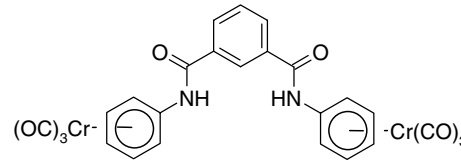


**4.65**

Organometallic fragments can have a significant effect on the properties of more conventional host fragments. For example Gale and co-workers have taken the simple step of attaching $Cr(CO)_3$ groups to the isophthalamide host **4.37a** to give **4.65**. The electron withdrawing $Cr(CO)_3$ groups increase the acidity of the NH protons. $^1$H-NMR titrations in $CD_3CN$ demonstrate that the new, more sterically hindered host has a selectivity for chloride over other anionic guests, with log $K > 4$. Selectivity for chloride over dihydrogen phosphate is high.[48]

**Table 4.5** Halide binding constants ($M^{-1}$, MeCN) as a function of spacer length in **4.61**.

| Spacer | Binding constant $K$ / $M^{-1}$ | | |
|---|---|---|---|
| | $Cl^-$ | $Br^-$ | $I^-$ |
| —$(CH_2)_2$— | 2500 | 330 | 450 |
| —$(CH_2)_3$— | 1300 | 270 | 275 |
| —$(CH_2)_4$— | 280 | 260 | 100 |

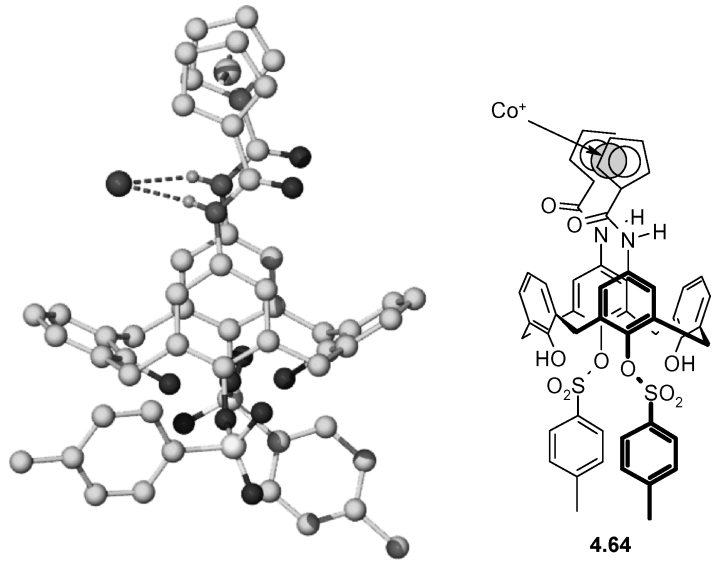


**Figure 4.25** X-ray structure of the chloride complex of calixarene receptor **4.64**.

Work by K Travis Holman and Jerry Atwood at the University of Missouri, USA has resulted in a tricationic host **4.66** based on the macrocycle cyclotriveratrylele (CTV, Section 7.7), which exhibits a deep anion binding pocket surrounded by three metal centres. A guest $PF_6^-$ anion fits neatly into the cavity, stabilised by C—H $\cdots$ F interactions, which may be differentiated from symmetry-related, non-interacting protons on the other side of the metallated aryl ring by $^1$H NMR spectroscopy. The X-ray crystal structure of this material is shown in Figure 4.26.

The preparation of **4.66** was based upon the ruthenium calix[4]arene and CTV derivatives **4.34** (Figure 4.19) and **4.67**, which form very simple electrostatic anion complexing agents and discriminate on a size-selective basis even in the very coordinating solvent, water.[50] Thus, anions that fit

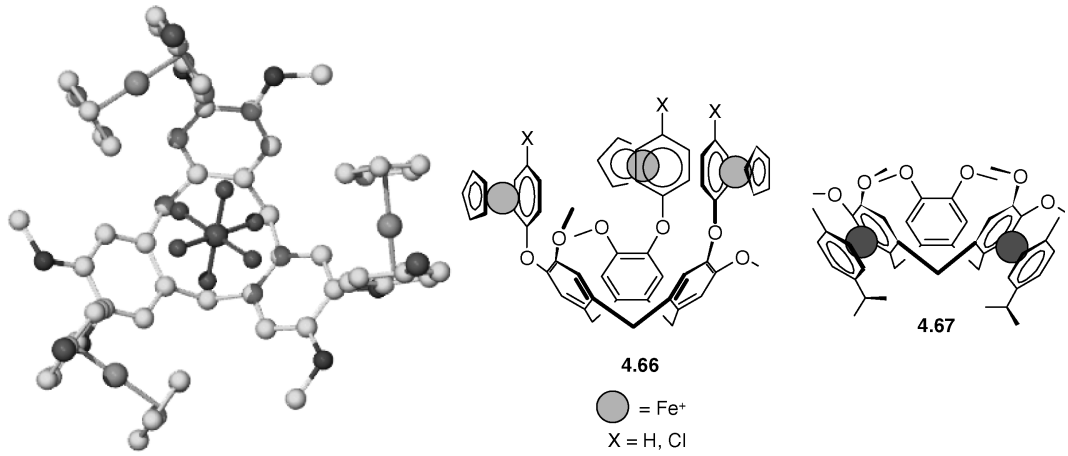


**Figure 4.26** X-ray crystal structure of the $PF_6^-$ complex of the tricationic podand-type host **4.73** and structural formulae of **4.66** and **4.67**.[49]

neatly within the macrocyclic cavity experience the maximum electrostatic interactions with the surrounding metal cations. The presence of the methyl-4-*iso*propylbenzene (*p*-cymene) ligands serves to enhance the solubility in organic media. The analogous tetrametallic calix[4]arene exhibits a binding constant for $Cl^-$ of 551 $M^{-1}$ in water, compared to values of 133, 51 and 49 $M^{-1}$ for $Br^-$, $I^-$ and $NO_3^-$. Acetate, sulfate and $H_2PO_4^-$ are not complexed at all, an observation that is consistent with the larger size of these anions and the high hydration energies of sulfate and phosphate. The researchers concluded that at least two metal ions attached to adjacent aryl rings are needed to bring about anion complexation, thus the X-ray crystal structure of the trimetallic $[(Cp^*Ir)_3(p\text{-}t\text{-butylcalix[5]arene-H})]^{5+}$ ($Cp^* = C_5Me_5^-$) includes one $BF_4^-$ anion deep within the large cavity, close to the two adjacent (pentamethylcyclopentadienyl)Ir(III) groups.[51] The CTV derivative **4.67** has a much wider, shallower bowl and shows a preference of large tetrahedral oxoanions that are not strongly solvated, such as $^{99}TcO_4^-$. Binding of this anion, which is of interest as a product from the nuclear fuel cycle, was established by partition experiments between aqueous solution and nitromethane in presence of competing guests such as halides, sulfate, nitrate *etc.*).

The chemistry used in the synthesis of **4.66** can be used to cap molecules of this type with a second CTV type unit to give extended analogues of cryptophanes.[49] The cryptophanes are cage-like molecules in which two CTV units are covalently linked together and generally bind neutral guests *via constrictive binding*, *i.e.* guest exchange is kinetically slow for example on the NMR spectroscopic timescale (Section 6.6). Demetallation then gives the free cryptophane. More recently Holman has gone on to prepare a remarkable hexametallic cryptophane derivative $[(Cp^*Ru)_6((\pm)\text{-cryptophane-E})]^{6+}$ (**4.68**).[52] The presence of the $Cp^*Ru$(II) centres on the surface of the cage expands the cavity size and renders it suitable for anion inclusion. The X-ray crystal structures of both salts demonstrate encapsulation of $CF_3SO_3^-$ and $SbF_6^-$, respectively, Figure 4.27. The complementarity of this organometallic cage structure for large

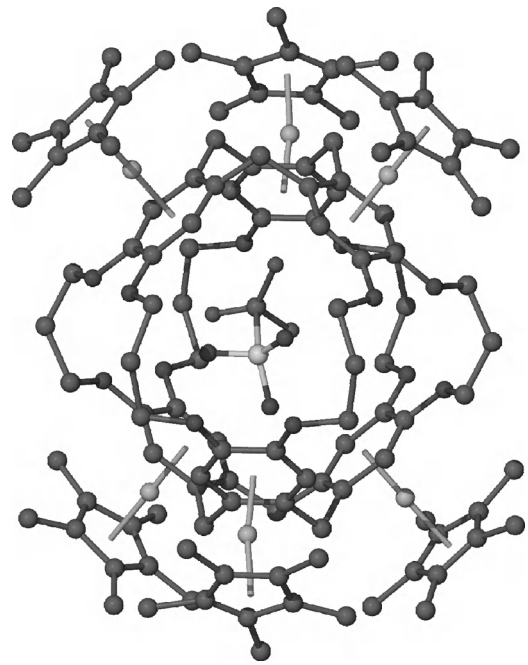

**Figure 4.27** Crystal structure of $[(Cp^*Ru)_6((\pm)\text{-cryptophane-E})]^{6+}$ **4.68**, showing inclusion of a triflate anion within the cage structure.[52]

anions is shown by the close anion-arene contacts, which represent significant anion-π interactions (Section 1.8.6). For $[\mathbf{4.68}\cdot SbF_6]^{5+}$ the 'axial' fluorine atoms display close contacts with all six aryl rings with closest distances F···C 2.97 Å and F···centroid 3.08 Å. $^1$H NMR spectroscopy reveals a simple spectrum highlighting the three fold symmetry of the host. Competition for the cavity is observed between triflate and competing $PF_6^-$ or $SbF_6^-$ anions; however, equilibrium is only achieved after weeks. There is also a very interesting solvent dependence such that in nitromethane solution the triflate cryptate is the only species present with distinct $^{19}$F NMR signals observed for bound and free anion. In $CD_2Cl_2$, however, over a period of *ca.* 3 weeks the signals for the anion inclusion compound are joined by signals assigned to a solvent-occupied cryptophane. Isolation of this mixture and redissolution in nitromethane results in slow conversion back to the anion cryptate and allows the determination of the *constrictive binding energy* $\Delta G^{\ddagger} = 75$ kJ mol$^{-1}$ (the steric activation barrier to guest decomplexation) considerably larger than the value of 56 kJ mol$^{-1}$ determined for $CDCl_3$ binding by cryptophane-E in dichloroethane.

**Box 4.1** Cyclic Voltammetry of Supramolecular Compounds

Kaifer, A. E. 'Electrochemical techniques', in *Comprehensive Supramolecular Chemistry*, J. L. Atwood, J. E. D. Davies, D. D. MacNicol and F. Vögtle (eds), Pergamon: Oxford, 1996, 499–535**.**

The cyclic voltammetric experiment is an interfacial electrochemical technique (*i.e.* monitoring of processes occurring near the electrode surface) that involves measurement of current flow as a function of applied potential. The potential is swept from a resting potential, $E_i$ (measured against a reference such as the saturated calomel electrode or the potential of the Fe(II)/Fe(III) couple in ferrocene), at a constant rate (usually 10–500 mV s$^{-1}$) to a limiting potential, $E_s$, and then returned to its initial value, giving a profile such as that shown in Figure 4.28a. Any reversible redox processes that occur during the course of the potential sweep will give a characteristic voltammogram of the type shown in Figure 4.28(b). The experimental set up is shown in

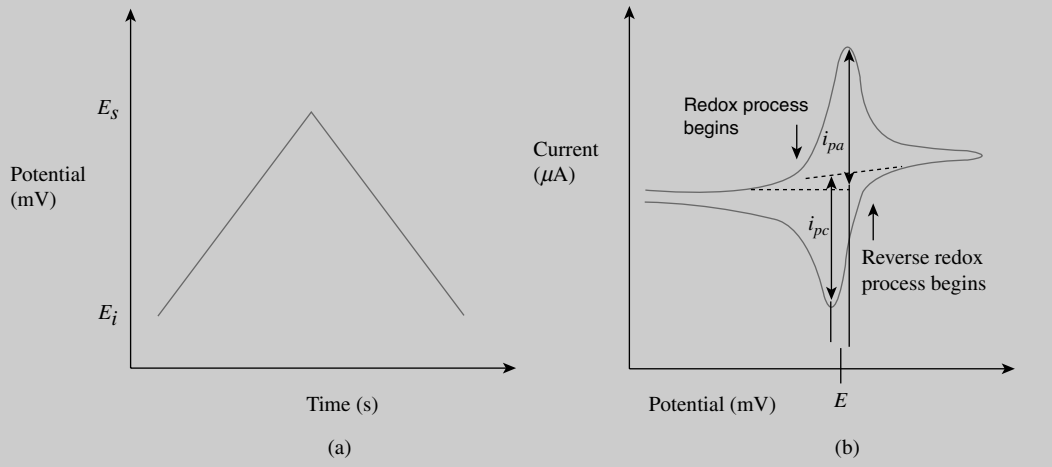


**Figure 4.28** (a) Potential versus time profile in a cyclic voltammetric experiment. (b) The resulting current versus potential trace (voltammogram) for a reversible redox process. $i_{pa}$ = current for anodic peak, $i_{pc}$ = cathodic (assuming scan to positive potential), $E$ = electrode potential, usually very close to the formal redox potential for the redox process under study.

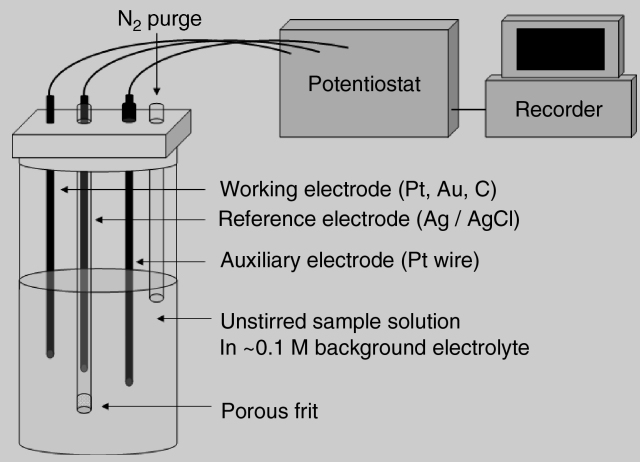


**Figure 4.29** Schematic diagram of the experimental apparatus for a cyclic voltammetric experiment.

Figure 4.29. In a cell used for electroanalytical measurements there are always three electrodes immersed in an electrolyte solution (the medium through which charge transfer can take place by the movement of ions), which is usually deoxygenated by passage of an inert gas prior to the beginning of the measurement. The *working electrode* is the electrode at which the electrochemical process being investigated takes place. The *reference electrode* is the electrode with a constant potential that is used as the reference standard against which the potentials of the other electrodes in the cell are measured. Finally the *auxiliary electrode* serves as a sink for electrons so that current can be passed from the external circuit through the cell. Note that the sample is not stirred during the measurement, and hence only material near the electrode surface is reduced or oxidised. This enables the experiment to be repeated many times as fresh reactants diffuse to the electrode from the bulk solution.

The cyclic voltammetric experiment can give a great deal of information about the redox activity of a compound and the stability and accessibility of its reduced or oxidised forms. For a fully chemically reversible process, $i_{pa}$ must equal $i_{pc}$, *i.e.* all of the material oxidised at the electrode surface on the forward scan must be re-reduced on the reverse scan (or vice versa). If this condition does not hold true, then the process may be partially reversible ($i_{pc} < i_{pa}$) or irreversible ($i_{pc} = 0$). Observation of processes that are not fully reversible implies decomposition or chemical reaction of the reduced or oxidised species and the ratio of $i_{pa}$ to $i_{pc}$ will show a strong dependence on scan rate since the reverse current is related to the lifetime of the redox-generated material. Note that processes that are chemically reversible (in the sense that the reduced and oxidised species are both stable) may not be *electrochemically* reversible (a term that relates to the relative rates of forward and back electron transfer). Electrochemically reversible processes are characterised by a separation between the forward and reverse potential peaks of exactly 59 mV.

More importantly from a supramolecular chemist's point of view, the redox potential $E$ is influenced significantly by the electronic environment about the redox centre. Thus, in an anion binding experiment, a large anion binding constant will result in the charged anionic guest spending (on average) a large amount of time close to the redox centre (*e.g.* in the case of a metallocene host in its second coordination sphere as an ion pair). This will significantly perturb the metal centre's redox potential, making it more difficult to reduce and/or easier to oxidise. The binding is thus reflected in a shift in the potential, $\Delta E$, typically between 0 and 250 mV.

Cyclic voltammetric measurements may also be used to assess the relative mutual affinity of the reduced and oxidised forms of a host and guest by a titration method. For example, take the binding of an anionic guest,

(*Continued*)

**Box 4.1** (*Continued*)

G, to a host (H) containing copper, which may exist as either Cu(II) or Cu(I). Titrating guest G with a sample of H and monitoring the cyclic voltammogram after each addition, will yield a titration curve of $E_{1/2}$ versus concentration of G, which may be analysed using Equation 4.1.

$$E_{1/2}\,(\mathbf{H}) = E_{1/2} + \frac{RT}{2nF}\ln\left[\frac{1 + K_{Cu(I)}[G]}{1 + K_{Cu(II)}[G]}\right] \tag{4.1}$$

where $K_{Cu(I)}$ and $K_{Cu(II)}$ are the binding constants of G with the Cu(I) and Cu(II) forms, respectively, R is the gas constant, T is the absolute temperature, F is the Faraday constant, and n is the number of electrons involved in the redox process (one in this case). A rather simpler measurement consists of simply recording the $E_{1/2}$ value before and after the addition of a large excess of a guest, G, to a host (H) solution. This may then be analysed by means of Equation 4.2. Even more simply, for cases in which strong binding is observed, separate redox peaks will be observed for both bound and unbound species in solution as in NMR spectroscopic titrations (*cf.* Section 1.4.2).

$$E_{1/2}\,(\mathbf{H}) = E_{1/2}\,(\mathbf{HG}) + \frac{RT}{nF}\ln\left[\frac{K_{Ox}}{K_{Red}}\right] \tag{4.2}$$

## 4.7.3 Hydride Sponge and Other Lewis Acid Chelates

Melaimi, M. and Gabbai, F. P., 'Bidentate group 13 Lewis acids with ortho-phenylene and peri-naphthalenediyl backbones', *Adv. Organomet. Chem.*, 2005, **53**, 61–99.

One of the most obvious ways to bind anions is to incorporate functionality into a host that forms a direct (possibly covalent) coordination interaction to the anionic guest. Since most anions are Lewis bases then Lewis acid functionality is an appropriate choice. Both metal ions and non-metals such as organoboron compounds can act as Lewis acids and for convenience we discuss both together here. In the case of organoboron derivatives the electron deficient nature of trivalent boron means that strong dative bonds are formed with most Lewis bases. Tetravalent silicon compounds can also interact with anions by expanding their coordination sphere to give five- or even six-coordinate *hypervalent* compounds (compounds formally possessing more than 8 valence electrons in their outer shell[53]). Metallic main group elements can also expand their coordination sphere forming various closed-shell interactions with anions which represents a kind of *secondary bonding* (Section 1.8.9).

Proton sponge, 1,8-bis(dimethylamino)naphthalene (Figure 4.30a) has been known since 1968 as an extremely effective proton chelating agent. The protonation of one of the $NMe_2$ groups serves to significantly reduce the repulsion between the two nitrogen atoms in the free host, and consequently enhances greatly the basicity of the diamine. The N—$H^+$—N hydrogen-bonded bridge is almost symmetrical (Section 8.1.3).[54] If the two amines are replaced by $BMe_2$, groups a highly electron-deficient anion host, termed 'hydride sponge' **4.69** is created, which demonstrates a marked ability to abstract hydride from almost all other hydride sources (*e.g.* $HBEt_3^-$). The interaction energy between the $H^-$ guest and the diboron ligand has been estimated to be at least 71 kJ $mol^{-1}$ by variable-temperature NMR spectroscopic experiments. An X-ray crystal structure of the complex shows that the hydride ligand is coplanar with the boron atoms and napthalene ring, although it is situated asymmetrically between the two boron atoms within the three-centre, two-electron bond with the two B—H distances being 1.49 and 1.20Å in the KH complex (Figure 4.30b).

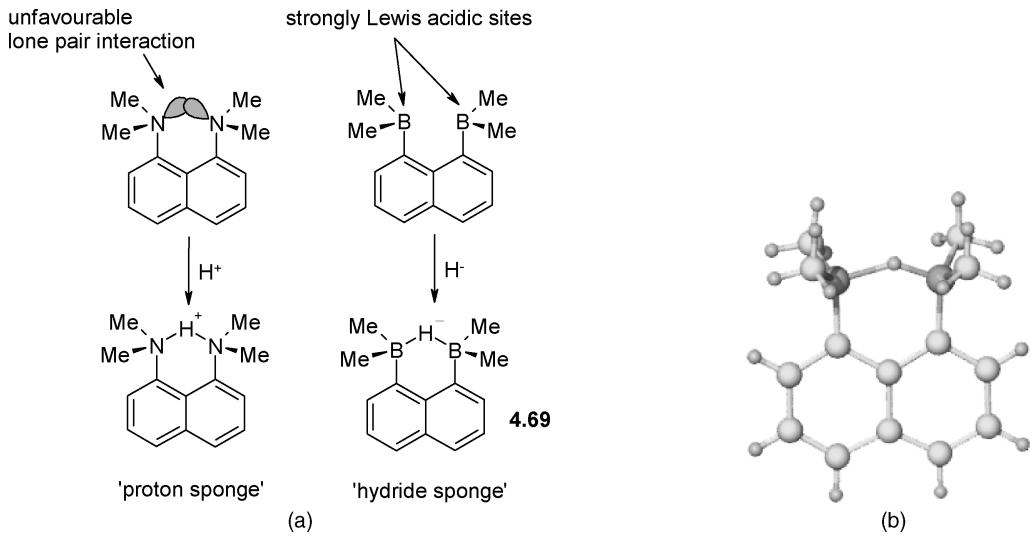


**Figure 4.30** (a) Comparison of 'proton sponge' and 'hydride sponge'. (b) X-ray crystal of the anion in the KH complex of hydride sponge **4.69.**

In fact, the discovery of **4.69** (and indeed the majority of supramolecular chemistry), was preceded by the observation in 1967 that the much more flexible bidentate Lewis acid $F_2BCH_2CH_2BF_2$ (**4.70**) is capable of chelating methoxide ion to give five-membered rings as shown in Scheme 4.5.

Following the discovery of hydride sponge by Howard Katz of the AT & T Bell Laboratories, New Jersey, USA,[56] a number of other Lewis acid chelates such as **4.71**–**4.76** have been prepared, all of which show a strong affinity for anions. Binding occurs by virtue of the anions Lewis base character and rigid, geometric preorganisation. All of the di-boron and related compounds **4.71**–**4.77** form chelate complexes. Compound **4.71** chelates $Cl^-$ in a distinctly out-of-plane fashion because of the large size of $Cl^-$ compared to the B ⋯ B separation in the rigid napthelenyl system. Despite this mismatch, the chelate effect is evident and the complex is significantly more stable than the model analogue $PhBCl_3^-$. The extended compound **4.72** was designed to offer a much larger chelate 'bite' angle and displays a distinct chelate coordination to the complementary neutral molecule 5-methylpyrimidine (binding constant 130 $M^{-1}$ compared to 70 $M^{-1}$ with a single boron-containing analogue). The organometallic cation **4.73** is ideally suited to form a neutral chelate complex with anions, although in the free state it is not preorganised for anion binding since the two $B(Pr^i)_2$ substituents adopt an *anti* conformation. The compound may be obtained anion free (eliminating inter-anion competition effects) by reduction to the neutral Co(II) analogue. Oxidation of this neutral precursor $[Co(C_5H_4B(Pr^i)_2)_2]$ with $[Fe(C_5H_5)_2][PF_6]$, $Cu(OH)_2$ or $C_2Cl_6$ in non-polar solvents gives a range of complexes of formula **4.73**·X (X = $PF_6$, OH or Cl). Only the

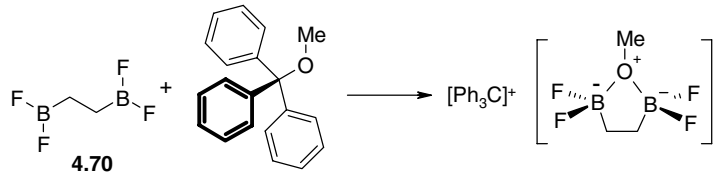


**Scheme 4.5** Anion chelate behaviour.[55]

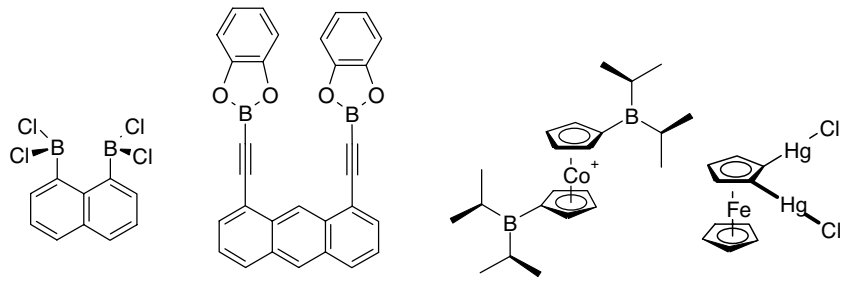


**4.71** **4.72** **4.73** **4.74**

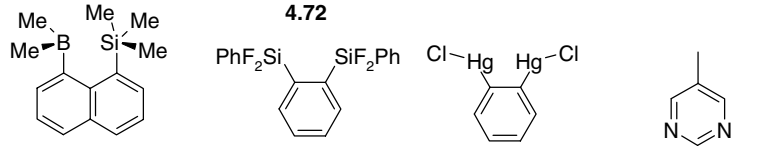


**4.75** **4.76** **4.77** 5-methylpyrimidine

hydroxy derivative is a chelated compound with the two $B(Pr^i)_2$ substituents rotated into a *syn* conformation. The chloride adduct contains a chloride anion attached to only one boron centre, while the $PF_6$ complex is a salt. It seems likely that this is a result of the strong Lewis basicity of hydroxide and its small size, which can fit conveniently between the two substituted cyclopentadienyl rings (Figure 4.31).[57]

One of the most remarkable boronic acid derivatives is the very rigid bis(bora)-*p*-*t*-butylcalix[4]arene derivative **4.78** developed by Matt Davidson at the University of Bath, UK. The host binds fluoride very strongly in chloroform with log $K_{11} = 6.3$. The fluoride is exclusively chelated in between the two boron atoms since fluoride binding to the outside of the host would result in unfavourable steric repulsions between the phenyl groups, Scheme 4.6. While relatively weak, the fluorescence of the phenyl groups may be used to monitor binding; addition of tetrabutylammonium fluoride almost completely quenches the fluorescence.[58]

Compounds **4.75** and **4.76** formally contain tetravalent silicon, which is not electron-deficient. It is, however, a strong Lewis acid, and on reaction with $F^-$, five-coordinate silicon compounds are obtained. In the case of **4.75**, the fluoride anion is localised mainly on the boron atom, although it does display dynamic behaviour involving hopping between boron and silicon. Compound **4.76** as the KF adduct contains two five-coordinate silicon atoms that chelate the $F^-$ anion. The coordination sphere of the $K^+$ counter-ion is completed by a molecule of [18]crown-6 (Figure 4.32a).

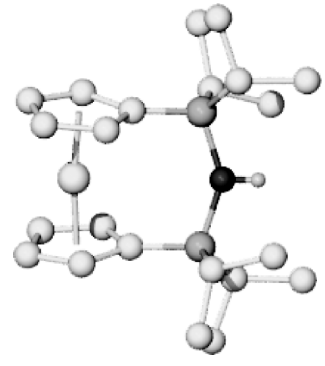

**Figure 4.31** X-ray structure of **4.73**·OH showing the symmetric chelation of the hydroxide anion.[57]

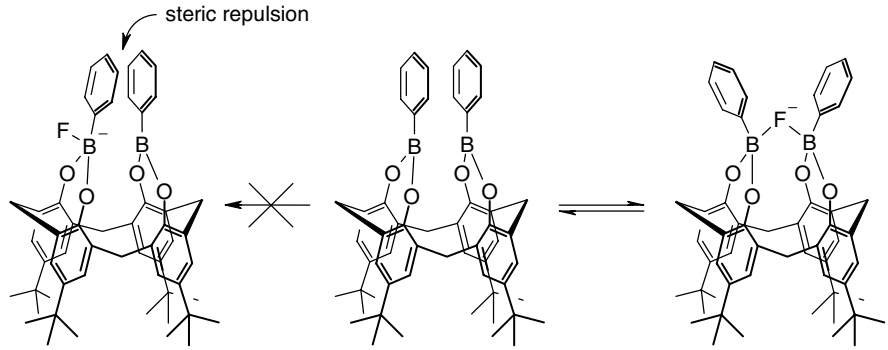


**4.78**

**Scheme 4.6** Fluoride binding by the bis(bora)-*p*-*t*-butylcalix[4]arene derivative **4.78**.[58]

As with the formally saturated silicon compounds, the dimercury compound **4.77** is readily able to expand its coordination sphere and forms an adduct with halides. In solution, $^{199}$Hg NMR spectroscopic results suggest a 1:1 complex is formed with chloride in which the two Hg centres chelate the anion in a similar way to the hydride sponge type hosts. The X-ray crystal structure of the material, however, shows a 2:1 adduct in which a single additional chloride anion is bound by two hosts, with covalent Hg—Cl bonds of 2.93Å and secondary interactions of 3.17Å (Figure 4.32b). An organometallic, ferrocene-derived analogue of **4.77**, compound **4.78**, behaves in a similar way, forming 2:1 complexes with two different organic chloride salts. In the presence of DMSO solvent, however, a neutral 1:1 complex is generated with the DMSO binding to both Hg(II) centres *via* the oxygen atoms.[59]

## 4.7.4 Anticrowns

Wedge, T. J. and Hawthorne, M. F., 'Multidentate carborane-containing Lewis acids and their chemistry: mercuracarborands', *Coord. Chem. Rev.* 2003, **240**, 111–128; Wuest, J. D., 'Multiple coordination and activation of Lewis bases by multidentate Lewis acids', *Acc. Chem. Res.*, 1999, **32**, 81–89.

The bidentate coordination behaviour of Lewis acid anion chelating ligands such as **4.69**–**4.78** suggests that very strong anion binding might be achieved with those Lewis acid groups as part of a macrocyclic

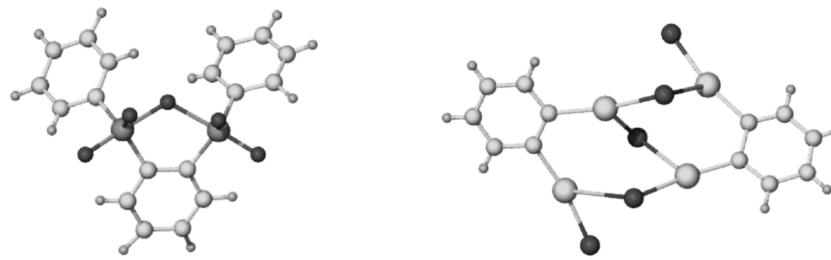


**Figure 4.32** (a) Structure of the anion in the KF adduct of compound **4.76**. Bridging Si—F distances are 1.898 and 2.065Å, compared to terminal Si—F distances of 1.60–1.65Å. (b) X-ray crystal structure of the 2:1 *o*-phenylenedimercurial receptor **4.77** with $Cl^-$.

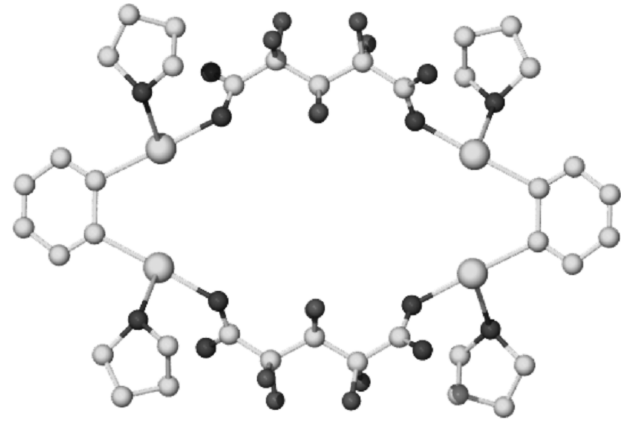

**Figure 4.33** X-ray structure of **4.79** showing the included THF molecules.

ring. A crown ether analogue made up from electron acceptor residues, as opposed to Lewis bases in the conventional crown ethers, can be thought of as an 'anticrown' because of its opposite complexation behaviour—affinity for Lewis basic anions instead of Lewis acids such as alkali metal cations. As part of a macrocyclic ring system, anticrowns should benefit from stabilisation of the complex by the macrocyclic effect and the chelate effect, as well as enhanced preorganisation.

Starting from an oxo-bridged analogue of the *o*-phenylenedimercurial residue **4.77**, a tetrametallic anticrown **4.79** has been prepared by reaction with perfluoro glutaric acid. The incorporation of the perfluoroalkyl chain is somewhat unconventional, yet this is the only 'mercuracycle' that could be prepared after much endeavour with a variety of fluorinated and non-fluorinated $\alpha,\omega$-dicarboxylic acids, most other reactions resulting in intractable polymers. It is possible that, unlike alkali metal templating in crown ether synthesis, a suitable 'antitemplate' is not present in most of these reactions. The X-ray crystal structure of **4.79** reveals that the macrocycle binds THF molecules as guests, which are coordinated to the Lewis acid mercury sites (Figure 4.33). It is not yet known whether these THF molecules play an intimate role in the formation of the anticrown, which is prepared in 81 per cent yield. Anion complexation behaviour of **4.79** has not been reported.

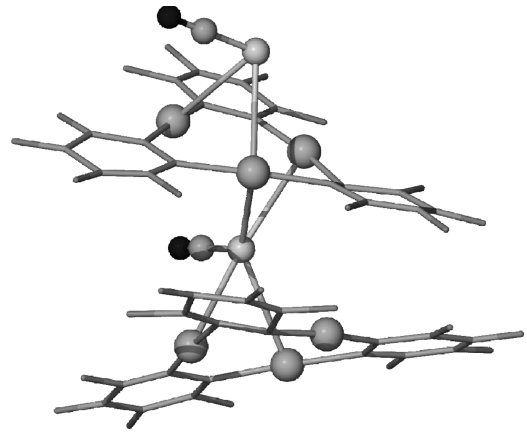

**Figure 4.34** Sandwich polymer of the $SCN^-$ complex of **4.80** (Hg and SCN atoms shown as spheres).[60]

Following the preparation of **4.79**, a number of other cyclic mercury crown compounds have been synthesised, which do exhibit halide complexation behaviour. Compound **4.80**, forms a 1:1 polymer with bromide in the solid state in which the $Br^-$ anions perch above the $Hg_3$ plane. The Hg—Br distances of 3.07–3.39Å are considerably longer than normal Hg—Br covalent bonds (about 2.54Å).[61] The compound also binds $SCN^-$ with similarly long bonds as shown in Figure 4.34.[60] The analogous chloride complex has a 3:2 stoichiometry suggesting a triple-decker sandwich of type [**4.80** ··· Cl ··· **4.80** ··· Cl ··· **4.80**]$^{2-}$.

Compound **4.81** adopts a 1:2 host:guest stoichiometry, in which the two chloride anions perch above and below the $Hg_5$ plane, one anion bridging quadruply and the other interacting with three Hg centres. The tetra carborane derivative **4.82** is the only compound that actually encapsulates an anion in crown ether-like fashion. Chloride fits well into the centre of the [12]mercuracarborand-4 ring with Hg—Cl distances of 2.94Å (Figure 4.35). The analogous iodide species has a doubly perching 1:2 stoichiometry, consistent with the larger size of $I^-$.[62] Analogous [9]mercuracarborand-3 ionophores such as **4.83** have been incorporated into ion selective electrodes where they are highly halide selective but suffer from problem of saturation because of the very strong binding affinities. This issue can be ameliorated by addition of a competing thiol ligand such as 1-decanethiol into the membrane cocktail. The small size of the 9-membered ring means that halides adopt a perching geometry in a 2:1 stoichiometry with one halide on either face. The apparent chloride binding constant is reduced from log $\beta_{12}$ = 13.4 (no 1-decanethiol) to log $\beta_{12}$ = 5.67 with the addition of a 1:4 molar ratio of the thiol.[63] This experiment highlights that it is not always high binding constants that make for a useful host. It is its ability to discriminate between potential guests under the desired conditions.

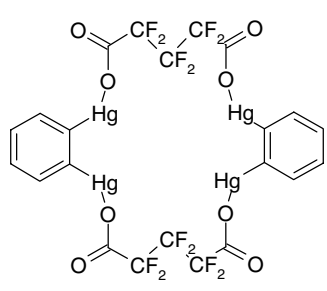

**4.79**

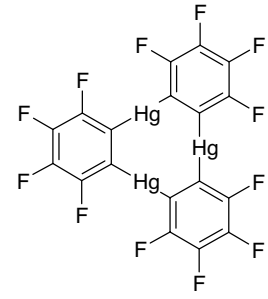

**4.80**

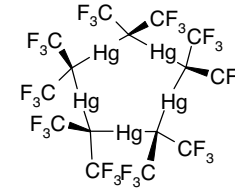

**4.81**

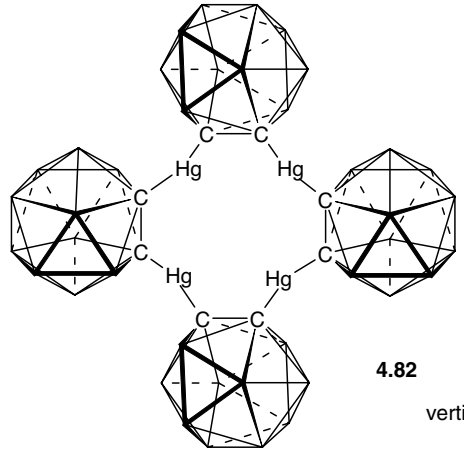

**4.82**

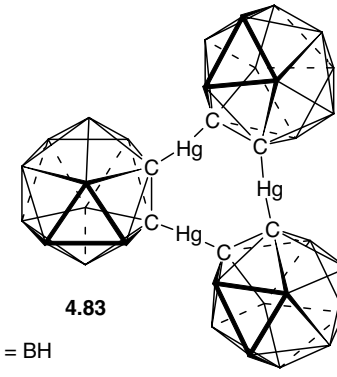

**4.83**

vertices = BH

[12]mercuracarborand-4

[9]mercuracarborand-3

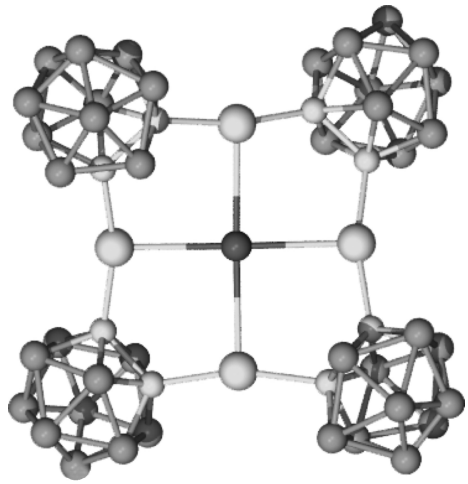

**Figure 4.35** Chloride inclusion within the carborane-based mercura[12]crown-4.

Just as with silicon and mercury, tin(IV) is also able to expand its coordination sphere from four- to five-coordinate in displaying Lewis acid behaviour. Armed with this knowledge, Martin Newcomb and co-workers of Texas A&M University, USA, prepared a range of anticrown and anticryptand stannacycles **4.84**–**4.86** somewhat resembling katapinands. Compound **4.84** binds chloride in acetonitrile; however, the binding constant is only twice that of open-chain analogues and is independent of ring size, suggesting little cooperativity to the binding. The macrobicyclic compounds **4.85** have been characterised by X-ray crystallography as the fluoride ($n = 6$) and chloride ($n = 8$) derivatives. In the former case, the fluoride anion is approximately symmetrically bridging between the two tin atoms, with Sn—F distances of 2.12 and 2.28Å (Figure 4.36a). This host binds strongly to fluoride ($K_{11} = 10^4\,M^{-1}$) and does not interact with chloride at all, presumably because of a size fit mismatch. In the $Cl^-$ complex of the larger host, the chloride is coordinated within the macrobicycle to only one tin centre (Sn—Cl distances 2.61 and 3.39 Å), suggesting that the cavity is too large for the anion. The tendency towards linear bridging, if present, is not strong enough to bring about any induced fit (Figure 4.36b). Interestingly however, even at −100ºC, in solution the $Cl^-$ anion is hopping rapidly back and forth between the two metal centres. The binding constant is very low and comparable to that of a single Sn centre in acyclic systems.

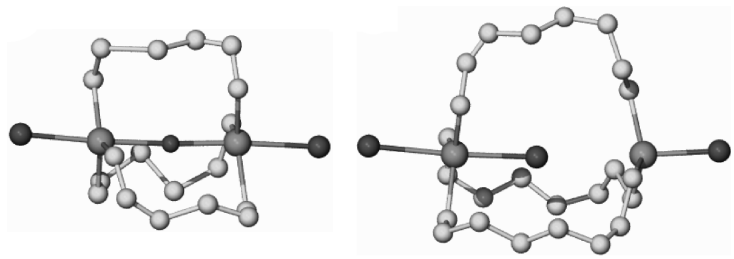


**Figure 4.36** X-ray crystal structures of (a) host **4.85** ($n = 6$) with $F^-$ and (b) compound **4.85** ($n = 8$) with $Cl^-$.[64]

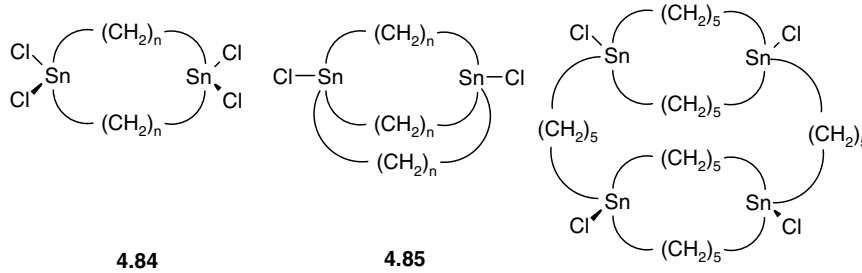


**4.84**
$n$ = 8, 10, 12

**4.85**
$n$ = 6, 8

**4.86**

Consistent with the greater number of Sn atoms and the greater organisation of the host in **4.86**, chloride affinity is increased dramatically, with a binding constant of 500 $M^{-1}$ in chloroform. While it seems that in general chloride interactions with tin-based macrocycles are not particularly strong, it must be remembered that these species also contain only katapinand-like alkyl spacers. There seems to be great scope for the incorporation of greater numbers of binding sites and increased host rigidity, which may well result in dramatic enhancements to host performance.

In recent years a very unusual form of *inverse crown* compound has been developed by Robert Mulvey of Glasgow University, UK.[65] Reaction of ferrocene or its heavier group 18 homologues ruthenocene, or osmocene with amide base sodium-magnesium tris(diisopropylamido) gives a homologous series of deprotonated metallocene tetra-anion derivatives [{$M(C_5H_3)_2$}$Na_4Mg_4$(*i*-$Pr_2N)_8$] (M = Fe, Ru or Os; **4.87**). The inverse crown structure has a 16-membered $[(NaNMgN)_4]^{4+}$ ring that resembles an inverse crown ether 'host' containing a metallocenetetraide $[M(C_5H_3)_2]^{4-}$ 'guest' core. The metallocenes are deprotonated selectively from the 1, 1′, 3, and 3′-positions. These materials are somewhat labile and highly reactive and therefore do not really fall into the category of host-guest structures, nevertheless they bear a striking casual resemblance to inverted crown ethers with the metal atoms comprising the macrocycle and the organometallic anions playing the role of the guest anion, Figure 4.37.

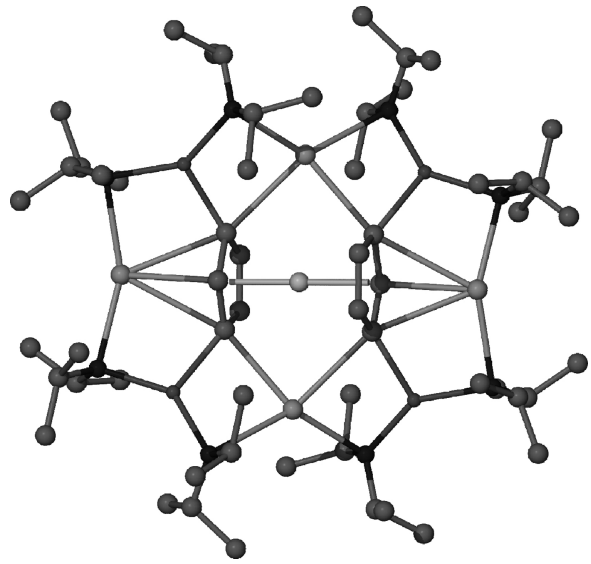

**Figure 4.37** X-ray crystal structure of the inverse crown [{$Fe(C_5H_3)_2$}$Na_4Mg_4$(*i*-$Pr_2N)_8$].[65]

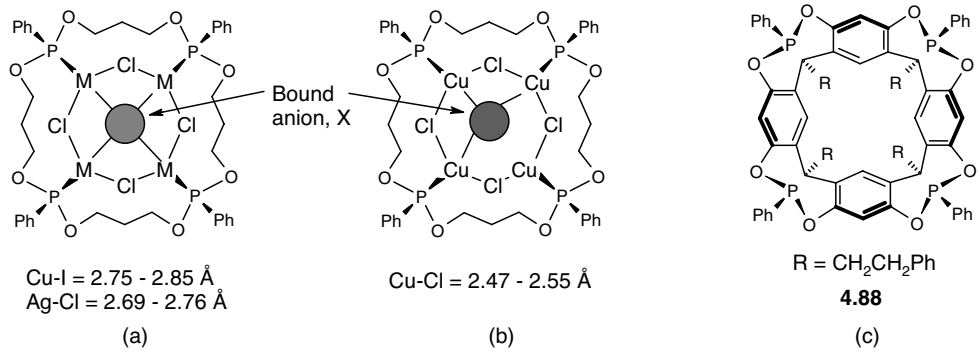


**Figure 4.38** Anion coordination geometry for complexes of **4.88** (a) M = Cu, X = I; M = Ag, X = Cl and (b) M = Cu, X = Cl (c) molecular structure of ligand **4.88**.[66]

Variable-temperature NMR spectroscopic studies indicate that the crown structure is retained in solution with the compounds existing as two distinct inter-converting conformers with 'W' and 'Z' shapes in benzene solution.

Other Lewis acidic metal cations supported on various organic scaffolds may be used in similar ways to the 'anticrown' compounds to bind anions. Ligand **4.88** readily complexes the monovalent coinage metals, M = Cu(I), Ag(I) and Au(I), to give tetrametallic complexes in which the upper rim of the [4]resorcarene bowl (Section 6.2.2) is decorated with a $M_4Cl_4$ ring (M = Cu, Ag; the Au(I) compound does not adopt a bridging chloride motif). This results in a central cavity of extremely rigid, well-defined dimensions into which anions may be included by long-range lateral interactions with the two-coordinate metal centres, just as for the mercuracarborane crown-type hosts discussed in Section 4.7.4. The anion interactions for the various structures are summarised in Figure 4.38. In the case of large anions such as $I^-$ or the larger metal $Ag^+$, the central anion adopts a symmetric $\mu_4$-bridging coordination-mode interaction approximately equally with all four metal centres. The structure is so rigid, however, that with the smaller $Cu^+$ the small chloride is not able to stretch to fill the cavity and adopts an unsymmetrical $\mu_3$-bridging mode.

## 4.8 Common Core Scaffolds

Supramolecular hosts for all guests including anions come in a wide variety of designs depending on the binding affinity of purpose of the compound. We have seen in Section 4.7 how there are certain popular classes of anion binding functionality the crop up time and time again in a variety of anion binding compounds because of the high intrinsic affinity of these groups for anions. Similarly, there are a number of common cores or frameworks that impart particular spatial or preoganisational features of host compounds irrespective of the particular binding functionality that is appended onto that core. Good examples are the calixarenes and cyclodextrins (Sections 3.14 and 6.3) which act as a 'molecular scaffold' in a plethora of different supramolecular systems. The synthetic versatility of the calixarenes in particular enables them to act as a framework that can support and organise a very broad range of binding, signalling or other functional appendages. In this section we highlight two other useful scaffolds that have proven highly versatile in anion binding applications; the flexible trialkylbenzene motif and the very rigid, preorganised cholesterol framework.

## 4.8.1 The Trialkylbenzene Motif

Hennrich, G. and Anslyn, E. V., '1,3,5-2,4,6-functionalized, facially segregated benzenes – Exploitation of sterically predisposed systems in supramolecular chemistry', *Chem. Eur. J.* 2002, **8**, 2218–2224.

The trialkylbenzene core, particularly derived from 1,3,5-tri(bromomethyl)-2,4,6-triethylbenzene[67] has been extensively used to make tripodal receptors for both cations and anions. For example the imidazoline receptor **4.89** has a high affinity for $NH_4^+$ and is selective for this cation over $K^+$.[68] The steric preference of *ca.* 10–15 kJ mol$^{-1}$ for alternating the position of substitutents around a hexasubstituted effectively preorganises receptors to adopt a geometry in which the three ethyl groups are on one face of the arene ring and the three binding groups are on the other. While there is no actual alternation in the trimethyl derivatives, the methyl substituents still reduce the tendency to adopt a non-cofacial arrangement of the binding groups. We have already seen triethylbenzene-derived anion hosts based on guanidinium and amide groups as in **4.31**–**4.33**. Indeed triethyl benzene derivatives form basis for a very broad range of anion hosts such as the boronic acid **4.90** and including those containing metal centres such as **4.91**. An array of such hosts attached to polystyrene beads form the basis for a fluorescent 'electronic tongue' able to distinguish certain beverage components or bioanalytes based on their recognition signature pattern as part of a dye displacement assay (see Section 11.3.3).[69] A similar core has been used to produce a range of CH hydrogen bond donor systems such as **4.92** that also bind effectively to anions, for example $K_a = 1.1 \times 10^6$ for $Cl^-$ binding by **4.92** in 9:1 MeCN: DMSO. The electron withdrawing

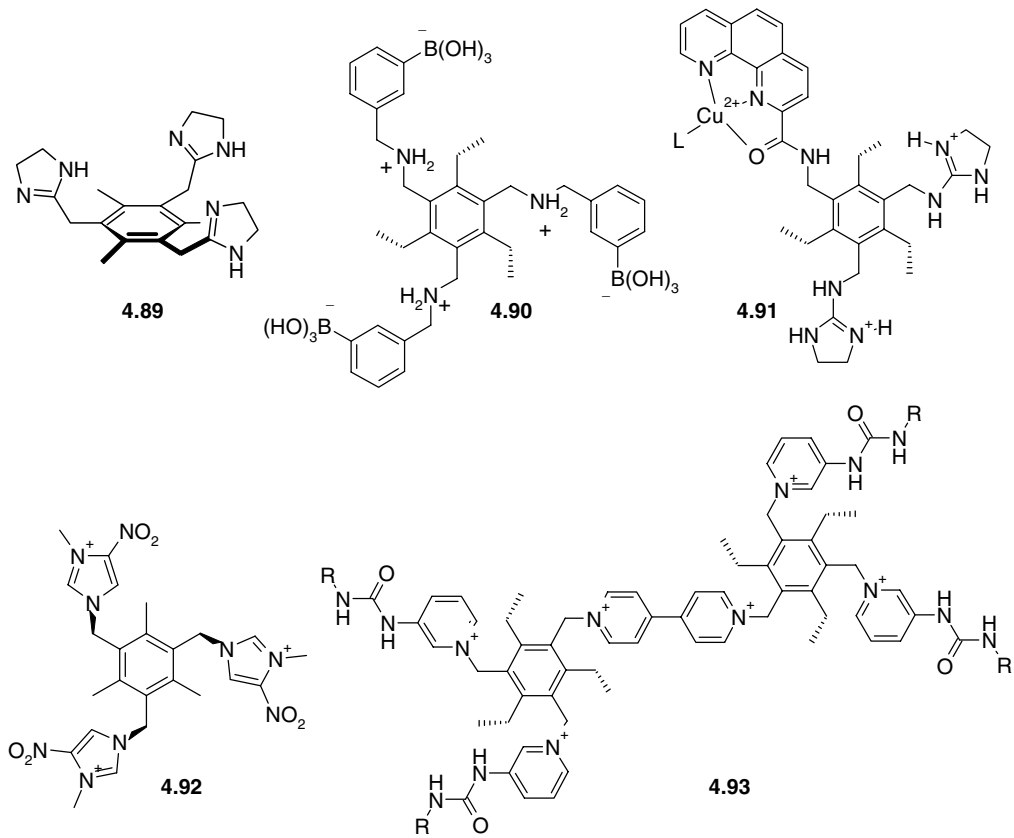

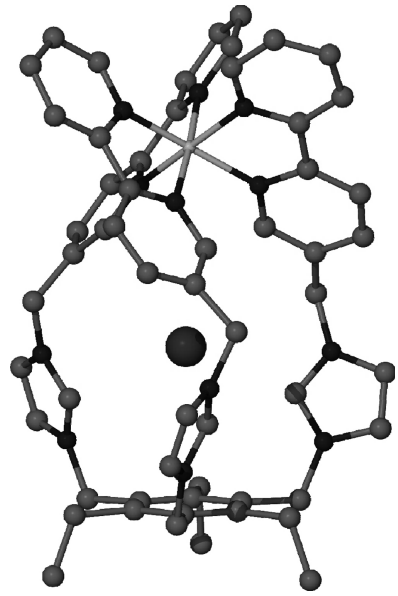

**Figure 4.39** X-ray crystal structure of the Fe(II) complex a 2,2′-bipyridyl derived tris(imidazolium) receptor including $Br^-$ solely by CH···$Br^-$ hydrogen bonds.[72]

nitro groups enhance the hydrogen bond acidity of the imidazolium CH groups.[70] The triethylbenzene core has been used as the basis for a ditopic receptor (**4.93**) based on 4,4′-bipyridinium (viologen). The compound binds up to two equivalents of acetate or one equivalent of dicarboxylates such as malonate to the urea groups without giving rise to a significant colour change. Addition of further anion, however, results in binding to the viologen linker and the production of an intense violet colour due to anion···host charge transfer interactions.[71] Work by Luigi Fabbrizzi at the University of Pavia, Italy, has resulted in the synthesis of a particularly interesting cryptand in which the open top of a tripodal imidazolium anion host related to **4.92** is closed off by the binding of three 2,2′-bipyridyl substituents to an Fe(II) centre. The complex binds $Cl^-$ and $Br^-$ in acetonitrile solution with log $K > 7$ and the X-ray crystal structure shows that halides are bound solely by an array of six CH···anion interactions, Figure 4.39.[72]

## 4.8.2 Cholapods

Davis, A. P., 'Anion binding and transport by steroid-based receptors', *Coord. Chem. Rev.* 2006, **250**, 2939–2951.

The *cholapods* represent a large series of anion receptors, generally of a podand type, incorporating a variety of geometries and binding functionality all based on the cholesterol framework (**4.94**). The cholapod series have been pioneered by Anthony Davis of Bristol University, UK, who has used bile acids such as cholic acid (**4.95**) (readily available from the digestive tracts of vertebrates) to produce a range of receptors that benefit from the high degree of rigidity and stereochemically well-defined nature of the cholesterol backbone. A particularly attractive feature of cholapod chemistry is the differentiation of the various sites of binding group attachment allowing the synthesis of highly unsymmetrical but uniquely tailored receptors. The framework is also chiral allowing for the possibility of differentiation between enantiomeric guests.

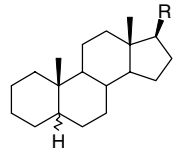


**4.94**

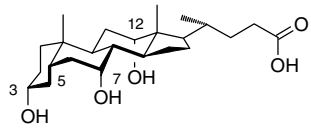


**4.95**

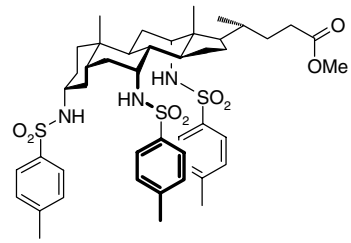


**4.96**

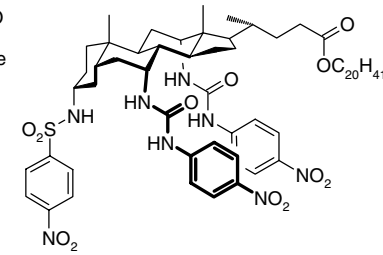


**4.97**

Among the first cholapods was the *p*-toluenesulfonamide **4.96**. This receptor exhibits relatively restricted rotation about the C–N bonds, making it quite preorganised for chloride and the association constant for $Cl^-$ binding in chloroform is 92,000 $M^{-1}$, an order of magnitude larger than the affinity for $Br^-$ which is too large for the rigid binding pocket. This degree of preorganisation is remarkable for a podand host. Davis' group went on the refine the design of the cholapods by adding thiourea functionalities (giving more hydrogen bonds) and placing electron withdrawing substituents such as nitrophenyl groups on the ureas, resulting in a second generation host **4.97**. This unsymmetrical derivative incorporates a $C_{20}H_{41}$ tail for solubility in organic solvents and binds chloride in chloroform with a staggering binding constant of $10^{11}$ $M^{-1}$, greater than any other reported for an abiotic, electroneutral anion receptor! This example represents a near-optimal combination of multiple, strongly hydrogen bond acidic binding sites, rigidly preorganised in an environment where they are relatively unsolvated,

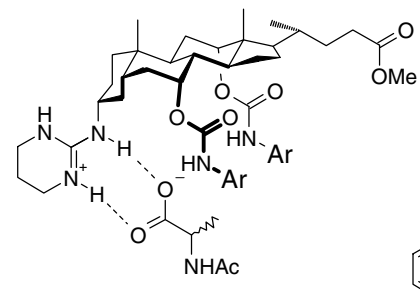


**4.98**
(with chiral amino acid derived guest)

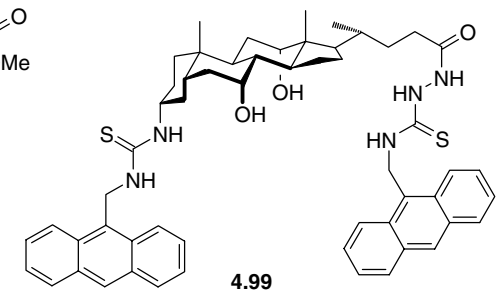


**4.99**

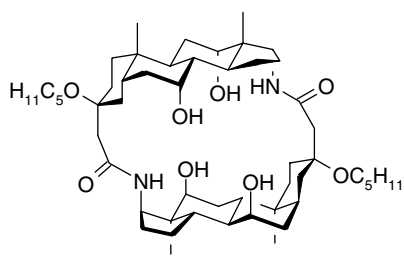


**4.100**

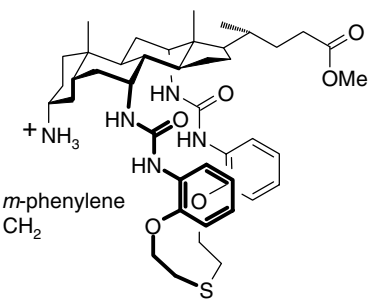


**4.101a** S = *m*-phenylene
**4.101b** S = $CH_2$

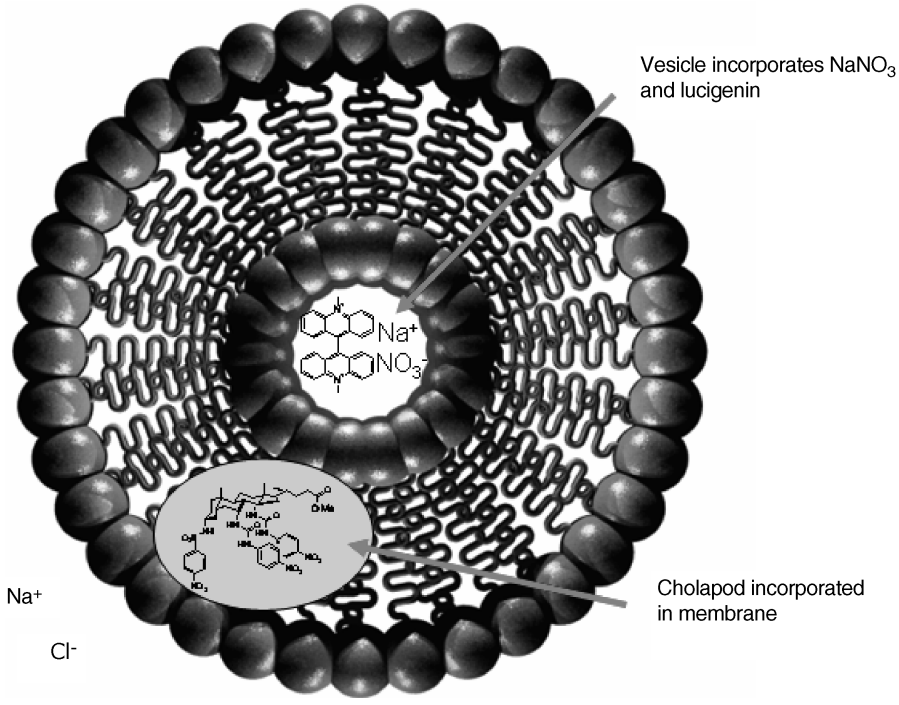


**Figure 4.40** Chloride transport by a lipid vesicle membrane-incorporated cholapod. Chloride flux from outside to inside the vesicle quenches the fluorescence of the lucigenin dye in the interior of the system.

both because of the restricted space within the cholapod binding cavity and the relatively uncompetitive nature of the solvent – chloroform is a particularly bad hydrogen bond acceptor. Such large affinities are difficult to measure by spectroscopic means and Davis' group have used the solvent extraction technique first developed by Cram for assessing the (also very preorganised) spherands (Section 3.5). In principle there is no upper limit on this technique imposed by issues such as spectrometer sensitivity and hence even very large affinities can be assessed by increased dilution (Section 1.4.2).

As any effective 'core' should, the steroid framework can support a wide variety of functional groups, thus in addition to neutral anion receptors, cationic guanidinium derivatives have been prepared such as **4.98**, able to distinguish between enantiomers of carboxylates. Fluorophores have also bee appended as in **4.99** which binds dicarboxylates (*e.g.* glutamate $K_a = 6 \times 10^6$ $M^{-1}$ in the competitive MeOH/water 1:1) accompanied by a modest decrease in fluorescence intensity. Macrocyclic derivatives such as **4.100** and **4.101** also exist. Interestingly, the small cryptand **4.100** is an example of anti-preorganisation, with the cavity too small to bind effectively to halides., giving 1:1 complex formation, with binding constants of 3320, 990 and 250 $M^{-1}$ to fluoride, chloride and bromide, respectively. The nature of the spacer 'S' in **4.101** is crucial in determining selectivity with **4.101a** being chloride selective, while **4.101b** is acetate selective.

The high chloride affinity and selectivity afforded by cholapods such as **4.97** suggests that they may be of use in the treatment of cystic fibrosis (Section 4.1) by acting as artificial chloride transporters. Chloride transport has been measured in an artificial vesicle system† in which the fluorescent dye lucigenin is incorporated into the inner aqueous pore of the vesicle in the presence of a background

† For a description of vesicles see Section 13.2.

salt ($NaNO_3$) and the membrane-soluble cholapod. Sodium chloride is then introduced into the outer aqueous phase. The fluorescence of lucigenin is quenched by the presence of chloride and hence if the cholapod (under suitably controlled conditions) is able to transport chloride across the vesicle membrane then an initially observed fluorescence should be 'turned off' as the experiment proceeds (Figure 4.40). The tests revealed that the methyl ester analogue of **4.97** is indeed a very efficient chloride transporter.

## Summary

- Anions require receptors of greater size than cations and they occur in a range of shapes and geometries. Anions have high free energies of solvation and hence anion hosts must compete more effectively with the surrounding medium. Many anions exist only in a relatively narrow pH window and are usually coordinatively saturated.
- Anion hydrophobicity is quantified by the *Hofmeister series.*
- Biological anion binding proteins and naturally occurring receptors such as the prodigiosins provide much of the inspiration for anion receptor chemistry.
- Key anion binding moieties are strong hydrogen bonding groups such as guanidinium, ureas, amides and pyrroles.
- Both charged and neutral anion binding hosts are common. Charged hosts must compete with the counter cation while neutral hosts are effectively ion-pair binding hosts.
- Macrocycles such as cryptands and azacrowns can readily bind anions upon protonation.
- Metal-based receptors provide excellent frameworks for anion host organisation and can act as reporter groups in electrochemical and luminescent anions sensing applications.
- Lewis acids based on boronic acid derivatives or main group elements such as mercury, tin and silicon form strong bonds to anions with considerable covalency, exemplified by *hydride sponge* and the *anticrowns.*
- Careful control of preorganisation and hydrogen bond acidity can result in very high binding constants as in the *cholapods.*

## Study Problems

4.1 According to Table 1, the free energy of hydration of anions decreases with increasing anionic radius. Despite this, the smallest, most highly solvated anions are bound most strongly by most host species. Explain this observation.

4.2 The strongest binding constants for any type of guest are often observed when hosts are rigid and preorganised for guest binding. Explain why these features are not exhibited by anion binding proteins and enzymes discussed in Section 4.2. How does this relate to the use of $[24]N_6O_2$, (**4.9**) as an artificial ATPase enzyme, as described in Section 12.3?

4.3 Anion binding by katapinand hosts such as diazabicyclo[9.9.9]nonacosane is much weaker than in the related azacryptand bis(tren) (**4.4**). What relevance does the phenomenon of *in*, *out* isomerism have on this observation?

4.4 Assuming a completely rigid tetrahedral arrangement of nitrogen bridgehead groups for the protonated 'soccer ball' cryptand (**3.29**), shown in Figure 4.5 with N ⋯ N nonbonded contacts of 4.65Å, calculate how sterically complementary the host is for $NH_4^+$ (non-protonated), $H_2O$ (diprotonated) and the halides $Cl^-$, $Br^-$ and $I^-$ (tetraprotonated). Explain qualitatively how this complementarity might be modified in the real host, which is somewhat flexible. (Assume O—H

and N—H bond distances are 1.00Å and that hydrogen bonds are linear and are at optimum distance at the 0.5Å less than the van der Waals separation of hydrogen and acceptor. Van der Waals radii: 1.10Å for H, 1.40Å for O, 1.50Å for N, 1.80Å for Cl, 1.95Å for Br and 2.15Å for I.)

4.5 Explain why tetrapyrrole macrocycles feature highly as cation binding hosts in biological systems (Chapter 2) while 'expanded porphyrins' such as (**4.14**) are more suited to anion binding.

4.6 Suggest experimental techniques for assessing the affinity of a host for a particular anion in solution. Which of these techniques might be appropriate for (a) podand (**4.40**), (b) diboryl hosts such as 'hydride sponge' (**4.69**) and (c) zwitterions such as (**4.35**).

## Thought Experiments

List similarities and differences in the design of selective supramolecular hosts for anions and cations. What are the key considerations in each case? Build on these ideas by suggesting reasons why the supramolecular chemistry of anions has developed more slowly than that of cations.

The p$K_a$ values for $H_3PO_4$ are 2.1, 6.2 and 12.4. From your reading of this chapter, or otherwise, suggest possible hosts types that may be selective for the anions $H_2PO_4^-$, $HPO_4^{2-}$ and $PO_4^{3-}$. What might be key considerations in the host design process?

# References


1. Park, C. H., Simmons, H. E., Macrobicyclic amines .3. Encapsulation of halide ions by in,in-1,(K+2)-diazabicyclo K.L.M alkane-ammonium ions. *J. Am. Chem. Soc.* 1968, **90**, 2431–2432.
2. Schmidtchen, F. P., Berger, M., Artificial organic host molecules for anions. *Chem. Rev.* 1997, **97**, 1609–1646.
3. 'Comprehensive supramolecular chemistry'. in 1 ed., Atwood, J. L., Davies, J. E. D., MacNicol, D. D., Vögtle, F., eds, Pergamon: Oxford, 1996, Vol. 2, *pp.* 519–552.
4. Shannon, R. D., Revised effective ionic radii and systematic studies of interatomic distances in halides and chalcogenides. *Acta Crystallogr., Sect. A* 1976, **32**, 751–767.
5. Jencks, W. P., *Catalysis in Chemistry and Enzymology*. McGraw Hill: New York, 1969, *pp.* 351–364.
6. Quiocho, F. A., Atomic Structures of periplasmic binding-proteins and the high-affinity active-transport systems in bacteria. *Phil. Trans. Royal Soc. Ser. B, Biol. Sci.* 1990, **326**, 341–352.
7. Xu, H., Strater, N., Schroder, W., Bottcher, C., Ludwig, K., Saenger, W., Structure of DNA helicase RepA in complex with sulfate at 1.95 angstrom resolution implicates structural changes to an 'open' form. *Acta Crystallogr. Sect. D-Biol. Cryst.* 2003, **59**, 815–822.
8. Pflugrath, J. W., Quiocho, F. A., The 2-a resolution structure of the sulfate-binding protein involved in active-transport in salmonella-typhimurium. *Journal of Molecular Biology* 1988, **200**, 163–180.
9. Bianchi, A., Bowman-James, K., Garcia-España, E., *Supramolecular Chemistry of Anions*. Wiley-VCH: New York, 1997.
10. Louie, G. V., Brownlie, P. D., Lambert, R., *et al.*, Structure of porphobilinogen deaminase reveals a flexible multidomain polymerase with a single catalytic site. *Nature* 1992, **359**, 33–39.
11. Alunni, S., Pero, A., Reichenbach, G., Reactivity of ions and ion pairs in the nucleophilic substitution reaction on methyl p-nitrobenzenesulfonate. *J. Chem. Soc., Perkin Trans. 2* 1998, 1747–1750.
12. Graf, E., Lehn, J.-M., Anion cryptates-highly stable and selective macrotricyclic anion inclusion complexes. *J. Am. Chem. Soc.* 1976, **98**, 6403–6405.
13. Metz, B., Rosalky, J. M., Weiss, R., [3] Cryptates – X-ray crystal-structures of chloride and ammonium ion complexes of a spheroidal macrotricyclic ligand. *J. Chem. Soc., Chem. Commun.* 1976, 533–534.
14. Schmidtchen, F. P., Müller, G., Anion inclusion without auxiliary hydrogen bonds: X-ray structure of the iodide cryptate of a macrotricyclic tetra-quaternary ammonium receptor. *J. Chem. Soc., Chem. Commun.* 1984, 1115–1116.
15. Dietrich, B., Dilworth, B., Lehn, J.-M., *et al.*, Anion cryptates: Synthesis, crystal structures, and complexation constants of fluoride and chloride inclusion complexes of polyammonium macrobicyclic ligands. *Helv. Chim. Acta* 1996, **79**, 569–587.
16. Ilioudis, C. A., Hancock, K. S. B., Georganopoulou, D. G., Steed, J. W., Insights into supramolecular design from analysis of halide coordination geometry in a protonated polyamine matrix. *New J. Chem.* 2000, **24**, 787–798.
17. Ilioudis, C. A., Georganopoulou, D. G., Steed, J. W., Insights into supramolecular design 2: Analysis of anion coordination geometry of oxoanions in a protonated polyamine matrix. *CrystEngComm* 2002, **4**, 26.

18. Huston, M. E., Akkaya, E. U., Czarnik, A. W., Chelation enhanced fluorescence detection of non-metal ions. *J. Am. Chem. Soc.* 1989, **111**, 8735–8737.
19. Bencini, A., Bianchi, A., Dapporto, P., *et al.*, $[PdCl_4]^{2-}$ inclusion into the deca-charged polyammonium receptor $(H_{10}[30]aneN_{10})^{10+}$ ($[30]aneN_{10}$ = 1,4,7,10,13,16,19,22,25,28-deca-azacyclotriacontane). *J. Chem. Soc., Chem. Commun.* 1990, 753.
20. Bencini, A., Bianchi, A., Garciaespana, E., *et al.*, Anion coordination chemistry. 2. Electrochemical, thermodynamic, and structural studies on supercomplex formation between large polyammonium cycloalkanes and the 2 complex anions hexacyanoferrate(Ii) and hexacyanocobaltate(Iii). *Inorg. Chem.* 1987, **26**, 3902–3907.
21. Hosseini, M. W., Lehn, J. M., Anion coreceptor molecules - linear molecular recognition in the selective binding of dicarboxylate substrates by ditopic polyammonium macrocycles. *Helv. Chim. Acta* 1986, **69**, 587–603.
22. Shionoya, M., Furuta, H., Lynch, V., Harriman, A., Sessler, J. L., Diprotonated sapphyrin: A fluoride selective halide anion receptor. *J. Am. Chem. Soc.* 1992, **114**, 5714–5722.
23. Seidel, D., Lynch, V., Sessler, J. L., Cyclo[8]pyrrole: A simple-to-make expanded porphyrin with no meso bridges. *Angew. Chem., Int. Ed.* 2002, **41**, 1422–1425.
24. Kral, V., Sessler, J. L., Furuta, H., Synthetic sapphyrin cytosine conjugates - carriers for selective nucleotide transport at neutral Ph. *J. Am. Chem. Soc.* 1992, **114**, 8704–8705.
25. Dietrich, B., Guilhem, J., Lehn, J.-M., Pascard, C., Sonveaux, E., 11. Molecular recognition in anion coordination chemistry. Structure, binding constants and receptor-substrate complementarity of a series of anion cryptates of a macrobicyclic receptor molecule. *Helv. Chim. Acta* 1984, **67**, 91–104.
26. Ilioudis, C. A., Tocher, D. A., Steed, J. W., A highly efficient, preorganized macrobicyclic receptor for halides based on CH··· and NH···anion interactions. *J. Am. Chem. Soc.* 2004, **126**, 12395–12402.
27. Dietrich, B., Fyles, D. L., Fyles, T. M., Lehn, J. M., Anion coordination chemistry – polyguanidinium salts as anion complexones. *Helv. Chim. Acta* 1979, **62**, 2763–2787.
28. Schmidtchen, F. P., Synthesis of symmetrically substituted bicyclic guanidines. *Chem. Ber.-Recl.* 1980, **113**, 2175–2182.
29. Metzger, A., Peschke, W., Schmidtchen, F. P., A Convenient access to chiral monofunctionalized bicyclic guanidinium receptor groups. *Synthesis-Stuttgart* 1995, 566–570.
30. Galán, A., Andreu, D., Echavarren, A. M., Prados, P., de Mendoza, J., A receptor for the enantioselective recognition of phenylalanine and tryptophan under neutral condtions. *J. Am. Chem. Soc* 1992, **114**, 1511–1512.
31. Metzger, A., Lynch, V. M., Anslyn, E. V., A synthetic receptor selective for citrate. *Angew. Chem., Int. Ed. Engl.* 1997, **36**, 862–865.
32. Green, F. J., *Sigma-Aldrich Handbook of Stains, Dyes, and Indicators*. Aldrich Chemical Co.: Milwaukee, WI, USA, 1990.
33. Schmuck, C., Schwegmann, M., A Molecular flytrap for the selective binding of citrate and other tricarboxylates in water. *J. Am. Chem. Soc.* 2005, **127**, 3373–3379.
34. Worm, K., Schmidtchen, F. P., Schier, A., Schafer, A., Hesse, M., Macrotricyclic borane-amine adducts – the first uncharged synthetic host compounds without Lewis-acid character, for anionic guests. *Angew. Chem., Int. Ed. Engl.* 1994, **33**, 327–329.
35. Kavallieratos, K., deGala, S. R., Austin, D. J., Crabtree, R. H., A readily available non-preorganized neutral acyclic halide receptor with an unusual nonplanar binding conformation. *J. Am. Chem. Soc.* 1997, **119**, 2325–2326.
36. Hughes, M. P., Smith, B. D., Enhanced carboxylate binding using urea and amide-based receptors with internal Lewis acid coordination: A cooperative polarization effect. *J. Org. Chem.* 1997, **62**, 4492–4499.
37. Kondo, S., Hiraoka, Y., Kurumatani, N., Yano, Y., Selective recognition of dihydrogen phosphate by receptors bearing pyridyl moieties as hydrogen bond acceptors. *Chem. Commun.* 2005, 1720–1722.
38. Kang, S. O., VanderVelde, D., Powell, D., Bowman-James, K., Fluoride-facilitated deuterium exchange from DMSO-d(6) to polyamide-based cryptands. *J. Am. Chem. Soc.* 2004, **126**, 12272–12273.
39. Scheerder, J., Engbersen, J. F. J., Casnati, A., Ungaro, R., Reinhoudt, D. N., Complexation of Halide Anions and Tricarboxylate Anions by Neutral Urea-Derivatised p-tert-Butylcalix[6]arenes. *J. Org. Chem.* 1995, **60**, 6448–6454.
40. Gale, P. A., Sessler, J. L., Kral, V., Calixpyrroles. *Chem. Commun.* 1998, 1–8.
41. Yang, D., Li, X., Sha, Y., Wu, Y. D., A cyclic hexapeptide comprising alternating alpha-aminoxy and alpha-amino acids is a selective chloride ion receptor. *Chem. Eur. J.* 2005, **11**, 3005–3009.
42. Huang, H., Mu, L. J., He, J. Q., Cheng, J. P., A cystine-bearing pseudo-cyclopeptide as a new amphi-receptor. *Tetrahedron Lett.* 2002, **43**, 2255–2258.
43. Aldridge, S., Bresner, C., Fallis, I. A., Coles, S. J., Hursthouse, M. B., Multidentate Lewis acids: synthesis, structure and mode of action of a redox-based fluoride ion sensor. *Chem. Commun.* 2002, 740–741.
44. Hamilton, A. D., Linton, B., Formation of artificial receptors by metal-templated self-assembly. *Chem. Rev* 1997, **97**, 1669–1680.
45. Ion, L., Morales, D., Pérez, J., *et al.,* Ruthenium biimidazole complexes as anion receptors. *Chem. Commun.* 2006, 91–93.
46. Wallace, K. J., Daari, R., Belcher, W. J., Abouderbala, L. O., Boutelle, M. G., Steed, J. W., Oxo-anion binding by metal containing molecular 'clefts'. *J. Organomet. Chem.* 2003, **666**, 63–74.
47. Beer, P. D., Transition metal receptor systems for the selective recognition and sensing of anionic guest species. *Acc. Chem. Res.* 1998, **31**, 71–80.
48. Camiolo, S., Coles, S. J., Gale, P. A., Hursthouse, M. B., Mayer, T. A., Paver, M. A., Hydrogen bonding networks and anion coordination in ($h^6$-arene)$Cr(CO)_3$ complexes: metal carbonyls as hydrogen bond acceptors. *Chem. Commun.* 2000, 275–276.

49. Holman, K. T., Orr, G. W., Steed, J. W., Atwood, J. L., Deep cavity CpFe(arene) (+) derivatized cyclotriveratrylenes as anion hosts. *Chem. Commun.* 1998, 2109–2110.
50. Staffilani, M., Hancock, K. S. B., Steed, J. W., *et al.*, Anion binding within the cavity of $\pi$-metalated calixarenes. *J. Am. Chem. Soc.* 1997, **119**, 6324–6335.
51. Steed, J. W., Juneja, R. K., Atwood, J. L., A water-soluble bear trap exhibiting strong anion complexation properties. *Angew. Chem., Int. Ed. Engl.* 1995, **33**, 2456–2457.
52. Fairchild, R. M., Holman, K. T., Selective anion encapsulation by a metalated cryptophane with a $\pi$-acidic interior. *J. Am. Chem. Soc.* 2005, **127**, 16364–16365.
53. McGrady, G. S., Steed, J. W., 'Hypervalent compounds'. in *Encyclopedia of Inorganic Chemistry 2*, King, R. B., ed. John Wiley & Sons, Ltd: Chichester, 2005, Vol. 3, *pp.* 1938–1961.
54. Mallinson, P. R., Smith, G. T., Wilson, C. C., Grech, E., Wozniak, K., From weak interactions to covalent bonds: A continuum in the complexes of 1,8-bis(dimethylamino)naphthalene. *J. Am. Chem. Soc.* 2003, **125**, 4259–4270.
55. Shriver, D. F., Biallas, M. J., Observation of the chelate effect with a bidentate Lewis acid, $F_2BCH_2CH_2BF_2$. *J. Am. Chem. Soc.* 1967, **89**, 1078.
56. Katz, H. E., Hydride Sponge: Complexation of 1,8-naphthalenediylbis(dimethylborane) with hydride, fluoride and hydroxide. *J. Org. Chem* 1985, **50**, 5027–5032.
57. Herberich, G. E., Fischer, A., Wiebelhaus, D., Bis(boryl)metallocenes. 1. 1,1′-bis(diisopropylboryl)cobaltocenium cation: A novel anion-binding ligand. *Organometallics* 1996, **15**, 3106–3108.
58. Arimori, S., Davidson, M. G., Fyles, T. M., Hibbert, T. G., James, T. D., Kociok-Kohn, G. I., Synthesis and structural characterisation of the first bis(bora)calixarene: a selective, bidentate, fluorescent fluoride sensor. *Chem. Commun.* 2004, 1640–1641.
59. Venkatasubbaiah, K., Bats, J. W., Rheingold, A. L., Jakle, F., Rational synthesis and complexation behavior of the bidentate lewis acid 1,2-bis(chloromercury)ferrocene. *Organometallics* 2005, **24**, 6043–6050.
60. Tikhonova, I. A., Dolgushin, F. M., Yanovsky, *et al.*, Crown compounds for anions. A polymeric complex of cyclic trimeric perfluoro-o-phenylenemercury with thiocyanate anion containing an infinite helical chain of alternating molecules of mercury-containing macrocycle and SCN- ions. *J. Organomet. Chem.* 1996, **508**, 271–273.
61. Shur, V. B., Tikhonova, I. A., Yanovsky, A. I., *et al.*, Compounds for anions – unusual complex of trimeric perfluoro-o-phenylenemercury with the bromide anion having a polydecker sandwich structure. *J. Organomet. Chem.* 1991, **418**, C29–C32.
62. Yang, X. G., Knobler, C. B., Zheng, Z. P., Hawthorne, M. F., Host-guest chemistry of a new class of macrocyclic multidentate lewis-acids comprised of carborane-supported electrophilic mercury centers. *J. Am. Chem. Soc.* 1994, **116**, 7142–7159.
63. Radu, A., Bakker, E., Shifting the measuring range of chloride selective electrodes and optodes based on the anticrown ionophore [9]mercuracarborand-3 by the addition of 1-decanethiol. *Chemia Analityczna* 2005, **50**, 71–83.
64. Blanda, M. T., Horner, J. H., Newcomb, M., Macrocycles containing tin - preparation of macrobicyclic Lewis acidic hosts containing 2 tin atoms and Sn-119 Nmr-studies of their chloride and bromide binding-properties in solution. *J. Org. Chem.* 1989, **54**, 4626–4636.
65. Andrikopoulos, P. C., Armstrong, D. R., Clegg, *et al.*, A homologous series of regioselectively tetradeprotonated group 8 metallocenes: New inverse crown ring compounds synthesized *via* a mixed sodium-magnesium tris(diisopropylamide) synergic base. *J. Am. Chem. Soc.* 2004, **126**, 11612–11620.
66. Xu, W., Vital, J. J., Puddephatt, R. J., Selective anion inclusion in calix[4]arene complexes driven by face-bridging mu-4 halide binding. *J. Am. Chem. Soc.* 1993, **115**, 6456–6457.
67. Wallace, K. J., Hanes, R., Anslyn, E., Morey, J., Kilway, K. V., Siegel, J., Preparation of 1,3,5-tris(aminomethyl)-2,4,6-triethylbenzene from two versatile 1,3,5-tri(halosubstituted) 2,4,6-triethylbenzene derivatives. *Synthesis-Stuttgart* 2005, 2080–2083.
68. Oh, K. S., Lee, C. W., Choi, H. S., Lee, S. J., Kim, K. S., Origin of the high affinity and selectivity of novel receptors for NH4+ over K+: Charged hydrogen bonds vs cation-$\pi$ interaction. *Org. Lett.* 2000, **2**, 2679–2681.
69. Wright, A. T., Anslyn, E. V., Differential receptor arrays and assays for solution-based molecular recognition. *Chem. Soc. Rev.* 2006, **35**, 14–28.
70. Ihm, H., Yun, S., Kim, H. G., Kim, J. K., Kim, K. S., Tripodal nitro-imidazolium receptor for anion binding driven by (C-H)+... X- hydrogen bonds. *Org. Lett.* 2002, **4**, 2897–2900.
71. Dickson, S. J., Wallace, E. V. B., Swinburne, A. N., *et al.*, Intramolecular binding site competition as a means of tuning the response of a colorimetri anion sensor, *New J. Chem.,* 2008, **32**, 786–789.
72. Amendola, V., Boiocchi, M., Colasson, B., Fabbrizzi, L., Douton, M.-J. R., Ugozzoli, F., A Metal based tris-imidazolium cage that provides six C-H hydrogen bond donor fragments and includes halides and pseudohalides. *Angew. Chem. Int. Ed.* 2006, **45**, 6920–6924.

# 5 Ion Pair Receptors

*'Kingdoms are clay; our dungy earth alike*
*Feeds beast as man; the nobleness of life*
*Is to do thus; when such a mutual pair*
*And such a twain can do't, in which I bind.'*

William Shakespeare (1564−1616), *Antony and Cleopatra*, I. i. 33, 1623.

# 5.1 Simultaneous Anion and Cation Binding

## 5.1.1 Concepts

Sessler, J. L., Gale, P. A. and Cho, W.-S., 'Anion receptor chemistry', Royal Society of Chemistry: Cambridge, 2006, ch. 6, *pp.* 259–293.

We have already seen in Section 4.7 a description of supramolecular complexes comprising an inert metal ion that is part of a host able to bind labile anions. In this context we defined an inert complex as one in which the rate of metal exchange with bulk solution is negligible, or at least much lower than the rate of anion exchange. This is perhaps a more demanding definition that Henry Taube's original description of an inert metal ion and one in which reactions are not complete immediately on mixing.* In contrast hosts that bind simultaneously to labile (metal) cations and labile anions may be thought of as hosts for cation + anion ion pairs. Such hosts usually have two or more binding regions, one complementary for cation binding and one complementary to anions. In some cases the binding of one ion (usually the cation) creates the binding site for the other; *e.g.* a metal cation may bind to a macrocycle and then the anion subsequently interacts with the bound cation. Such compounds are termed *cascade complexes*. Of course any neutral molecular receptor necessarily binds ion pairs because of the requirement of overall charge neutrality, but we will concern ourselves here only with systems in which specific provision is made to design cation and anion receptor regions within the receptor. The design and synthesis of ion pair receptors is a significant growth area in supramolecular chemistry, spurred not least because of the importance of natural biological systems able to simultaneously transport oppositely charged ions such as $H^+$ and $Cl^-$ across membranes, a process termed *symport*.[1]

In solution, broadly speaking, we can distinguish three different kinds of ion pairs. In polar solvents, particularly in aqueous media, solvation energy overcomes the electrostatic mutual attraction of ion pairs and hence the predominant species are solvent-separated ion pairs. This ion solvation is particularly advantageous in organic synthesis, for example, where dipolar, aprotic solvents such as dimethyl formamide or acetonitrile are used to effectively solvate cations, leaving reactive anions relatively free to undergo reactions such as nucleophilic substitution with a subtrate (*cf.* the *naked anion effect*, Section 3.8.2). In less polar media, ions are often poorly solvated and form either contact ion pairs, in which an individual pair of oppositely charged ions are directly bonded *via* electrostatic interactions, or aggregated contact ion pairs in which a number of ions form a small cluster which is itself solvated by the surrounding medium. In bonding anions and cations in non-polar media there can therefore be a considerable enthalpic cost associated with breaking the bonds in contact ion pairs. Finally we will also consider zwitterions, single overall neutral molecules with both positive and negative parts. The classic examples of zwitterions are amino acids in which the carboxylic acid group generally protonates the amine functionality, Figure 5.1. We have already discussed examples of zwitterionic receptors for anions in Sections 4.4 and 4.6.1.

Faced with the challenge of ion pair binding, there are three basic ion pair receptor designs; contact ion pair receptors (including cascade complexes) in which the anion and cation are bound as a contact ion pair, ditopic receptors with individual, well-separated anion and cation binding sites, and zwitterion receptors, Figure 5.2. We will discuss some examples of each type of complex in the following sections.

* Henry Taube, Canadian-born US chemist (1915−2005) winner of the 1983 Nobel Prize for chemistry for his work on the kinetics and mechanism of inorganic electron transfer reactions in solution.

*Supramolecular Chemistry, 2nd edition* J. W. Steed and J. L. Atwood
© 2009 John Wiley & Sons, Ltd ISBN: 978-0-470-51233-3

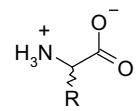

**Figure 5.1** Zwitterionic structure of an amino acid.

## 5.1.2 Contact Ion Pairs

Definitive evidence for the binding of individual contact ion pairs is relatively rare despite the fact that contact ion pair binding avoids the necessity for energetically unfavourable separation of opposite charges. Among the most striking examples of contact ion pair receptors synthesised in recent times are a series of macrobicycles such as **5.1** and **5.2** prepared by Bradley D. Smith and co-workers at the University of Notre Dame, USA.[2] The larger receptor **5.1** is able to simultaneously bind $Na^+$ within the crown ether cavity and $Cl^-$ by hydrogen bonding to the amide NH groups. In the absence of $Na^+$, the chloride binding constant in DMSO/MeCN solution is only 50 $M^{-1}$, however this is enhanced to 410 $M^{-1}$ in the presence of $Na^+$. The large size of receptor **5.1** means that, in the solid state at least, there is space for a molecule of chloroform which hydrogen bonds to the $Cl^-$ anion, hence this represents binding of a solvent-separated ion pair. In contrast, the smaller receptor **5.2** is a genuine contact ion pair receptor. In the absence of metal cations, chloride affinity is 35 $M^{-1}$ in DMSO solution. This value does not increase significantly in the presence of $Na^+$, but in the presence of $K^+$ the affinity rises to 460 $M^{-1}$. The X-ray crystal structure suggest a reason for this selectivity, with the $K^+$ ion doming out of the plane of the dizaz[18]crown-6 ring to optimised the $K^+\cdots Cl^-$ interaction, while the $Na^+$ ion is situated more in the ring plane, resulting in unfavourable interactions between the chloride anion and oxygen lone pairs. The crystal structures of **5.1** · NaCl and **5.2** · KCl are shown in Figure 5.3. In addition to binding alkali metal halide salts, receptor **5.2** is also able to distinguish between various monoalkylammonium salts by binding them as contact ion-pairs. The affinity for linear *n*-propylammonium chloride is at least 2 orders of magnitude greater than that for *n*-propylammonium acetate.[3] The *m*-phenylene diamide anion binding group is analogous to receptor **4.37** (Section 4.6.2). Receptors have also been synthesised in which this anion binding moiety has been replaced by an alternate bis(amido)pyrrole functionality. The additional NH hydrogen bond donor results in a modest enhancement of the chloride affinity. Related work has resulted in the synthesis of **5.3**, an analogue of **5.2**, in which an inert ferrocene-derived linker serves to act as an electrochemical reporter group. The binding constants

(a) (b) (c)

**Figure 5.2** Schematic diagram of the three different types of simultaneous ion pair receptors. (a) cascade receptor, (b) ditopic receptor and (c) zwitterion receptor.

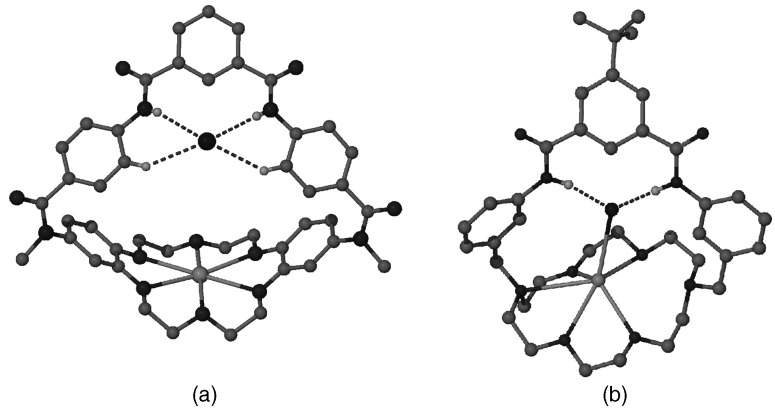


**Figure 5.3** X-ray crystal structures of (a) **5.1** · NaCl and (b) **5.2** · KCl.

for $Br^-$ in the presence of $Na^+$ is significant at 16,100 $M^{-1}$ in chloroform/acetonitrile 95:5 v/v − note the less polar solvent medium in comparison to DMSO). Cyclic voltammetric measurements (Box 4.1) show that the oxidation potential of the Fe(II)/Fe(III) redox couple is shifted by up to 107 mV on $Cl^-$ binding by the free host, but this rises to 153 mV in the presence of $K^+$, a very significant change in these kinds of systems. In addition to these crown ether-based compounds, the *m*-phenylene diamide unit has also been appended to calixarene-based systems, to give the calix[4]diquinone **5.4**. The receptor was designed using molecular modelling to give an optimum fit for the KCl ion pair. In the absence of $K^+$ the receptor displays essentially no affinity for $Cl^-$ but when one equivalent of $K^+$ is added the $Cl^-$ affinity is in excess of $10^4$ $M^{-1}$ in the moderately competitive solvent acetonitrile.[4]

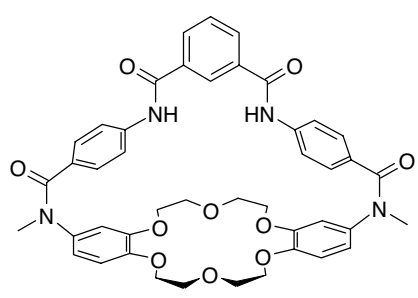


**5.1**

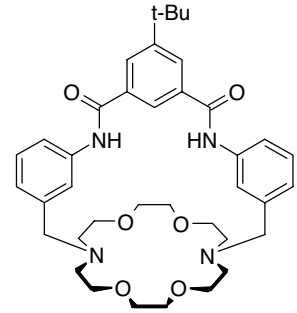


**5.2**

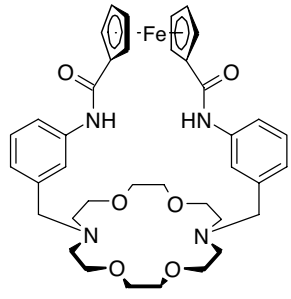


**5.3**

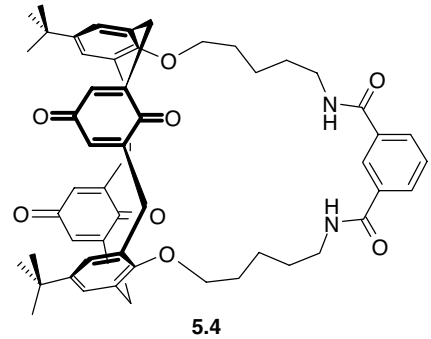


**5.4**

## 5.1.3 Cascade Complexes

Hancock, R. D. and Martell, A. E., 'Ligand design for selective complexation of metal-ions in aqueous-solution', *Chem. Rev.* 1989, **89**, 1875–1914.

Cascade complexes represent the earliest simultaneous receptors with extensive work dating back to the 1970s.[5] Typically, more than one metal ion (cation) coordinates to a particular ligand (classically a Schiff base or macrocyclic heteroalkane) in a well-defined geometry. The anion then coordinates to the metal centre, possibly with additional hydrogen bonding or other interactions to the receptor framework. For example, the macrocycle [24]ane-$N_2S_4$ (Scheme 5.1) is able to coordinate two copper(II) ions, on each tridentate SNS chelate binding domain. Since Cu(II) is typically four- or five-coordinate the remaining coordination sites are available for anion-binding, in this case with the azide ($N_3^-$) counter ions. The X-ray crystal of the complex shows that two azide anions bridge across the two metal ions while the remaining two bind in a terminal fashion, one to each copper centre, Scheme 5.1.[6] Cascade receptors often find applications as models for enzyme active sites,[7] and copper complexes are of particular interest because of the naturally occurring *haemocyanins*; di-copper respiratory proteins that perform a similar role to haemoglobin in most molluscs and some arthropods. Deoxy-haemocyanin is colourless and contains two copper(I) sites coordinated by nitrogen atoms from histidine residues. Binding of $O_2$ results in oxidation to copper(II) linked in a cascade fashion by a $\mu$-$\eta^2$:$\eta^2$-$O_2^{2-}$ anion (*i.e.* both oxygen atoms of the $O_2^{2-}$ ligand are bridging the same two metal centres), accompanied by a colour change to blue, hence the haemocyanins are blue pigments, Figure 5.4. Haemocyanins are a significant target for modelling using synthetic cascade compounds and further haemocyanin models are discussed in Section 12.5.1.

One of the earliest Schiff base macrocycles to exhibit a haemocyanine-like structure was the copper(II) perchlorate complex of **5.5** which binds readily to azide or hydroxide.[8] The azide complex exhibits two square pyramidal copper binding domains with the basal plane occupied by one pyridyl nitrogen atom and two imine functionalities as well as a terminal azide ligand. The apices of the two pyramidal coordination polyhedra are linked by a single bridging azide anion. Continuing the biomimetic theme, manganese(II) cascade complexes of the unsymmetrical **5.6** have

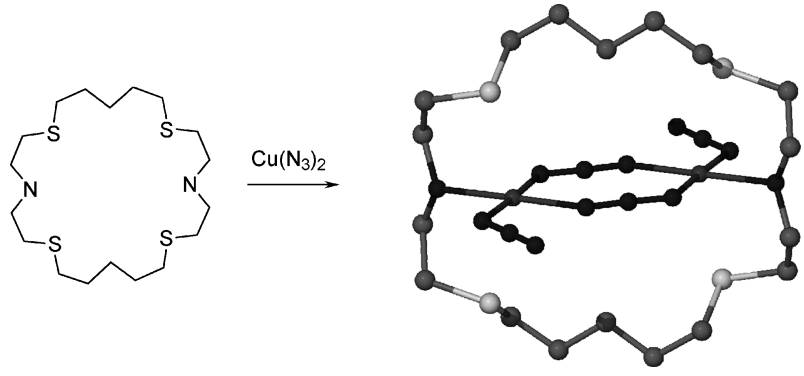


**Scheme 5.1** Macrocyclic receptor **5.4** is able to coordinate two Cu(II) ions that, in turn, bind two azide anions bridging across the two metal centres to give the Cu(II) azido complex [$Cu_2$(**5.4**)($\mu$-$N_3$)$_2$($N_3$)$_2$].

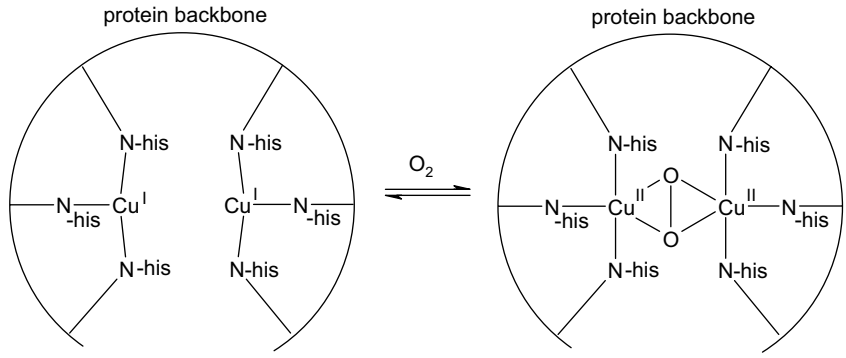


**Figure 5.4** Dioxygen binding by haemocyanin.

been used as functional models for the manganese catalase enzyme, a dimetalloenzyme which catalyses the disproportionation of hydrogen peroxide into dioxygen and water. The asymmetry is highlighted by the X-ray structure of the Mn(II) complex of the deprotonated ligand [$Mn_2$(**5.6**-H)($MeCO_2$)$_2$(NCS)] (**5.7**) with one Mn(II) centre being in a distorted square pyramidal environment while the other is distorted octahedral. In functional terms these asymmetric complexes are less efficient catalysts than symmetric analogues suggesting that equivalent manganese centres are required in the real enzyme.[7] A great many cascade complexes are based on such bimetallic Schiff base derivatives. For example the sterically hindered di-vanadyl complex (vanadyl = $VO^{2+}$) **5.8** binds alkoxide ions (and related compounds bind hydroxide), while the copper analogue binds oxide, $O^{2-}$, in a 2:1 sandwich fashion with the oxide ion interacting simultaneously with all four copper(II) centres.[9]

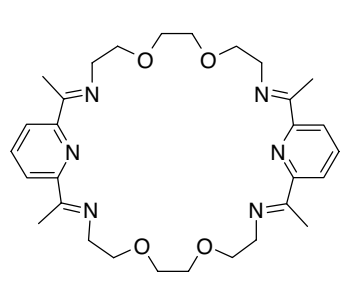

**5.5**

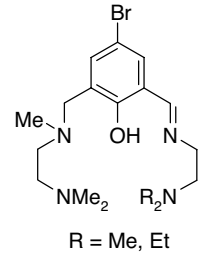


R = Me, Et

**5.6**

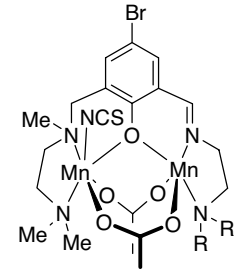


**5.7**

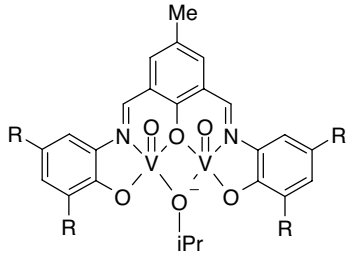


R = $^t$Bu

**5.8**

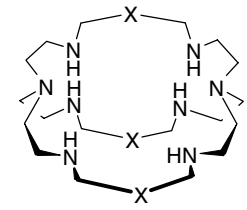


**5.9**

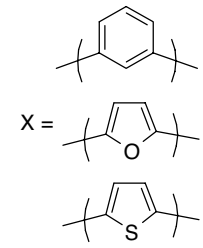


Macrobicyclic cascade cryptands have also been prepared such as the series of bis(tren) derived (tren = tris(2-aminoethyl)amine, see Section 4.4.3) compounds **5.9**. The di-nickel(II) and di-copper(II) complexes of the cages with various spacers all bind a metal cation into each tren unit. These metal

complexes have been shown to accommodate azide and bromide within the cavity, each bound linearly between the two metal centres. The highest binding constant (observed in aqueous solution at approximately neutral pH) is for the di-copper complex of the thiophene-bridged compound, binding azide, $\log K_{11} = 6.75$.[10]

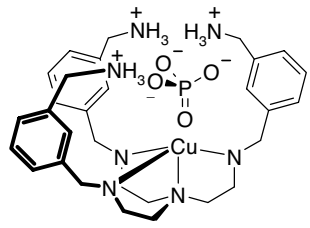

**5.10**.$H_3PO_4$

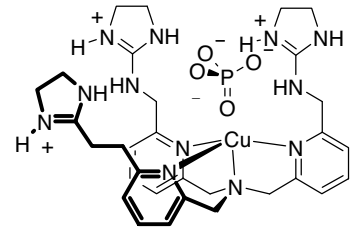

**5.11**.$H_3PO_4$

Recently two novel cascade complexes capable of complexing hydrogen phosphate anion, $HPO_4^{2-}$ in water have been reported by Eric Anslyn and co-workers at the University of Texas, Austin, USA. Both are based on tetrahedral copper(II) anion binding sites with additional charge-assisted hydrogen bonding to the tripodal peripheral groups. Complex **5.10** is protonated at neutral pH and binds $HPO_4^{2-}$ with $K_a = 2.5 \times 10^4\ M^{-1}$ in water. The affinity for the more rigidly preorganised **5.11** is slightly lower at $1.5 \times 10^4\ M^{-1}$ but the host is more phosphate-selective. Detailed thermodynamic studies reveal that phosphate binding in the case of **5.10** is entirely entropically driven, while the equilibrium in the case of **5.11** is enthalpy driven. This data can be rationalised in terms of the fact that solvent organisation around the guanidinium groups in **5.11** is much lower than around the more exposed ammonium groups and so binding of the anion to **5.10** leads to entropically favourable solvent release.[11]

## 5.1.4 Remote Anion and Cation Binding Sites

One of the first ion pair receptors was the 21-membered crown ether **5.12**, prepared by M. T. Reetz of the University of Marburg, Germany in 1991, which possesses a Lewis acidic boronate centre. Ligand **5.12** is capable of dissolving stoichiometric amounts of KF in dichloromethane at room temperature to give a KF adduct in which the $K^+$ ion is bound by the crown ether ring while the $F^-$ anion forms a dative bond with the boron centre out of the plane of the crown ether. Ligand **5.12** fails to dissolve either KCl or KBr as a consequence of the weaker nature of the B-Cl and B-Br bonds.

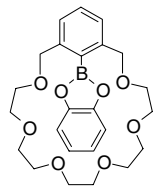

**5.12**

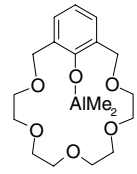

**5.13**

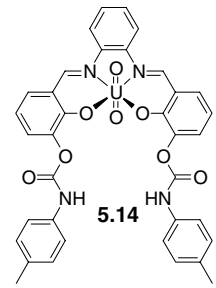

**5.14**

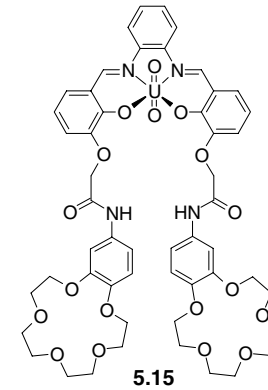

**5.15**

KI and KSCN are dissolved by **5.12** but without complexation of the boron atom. The stabilisation of the $K^+$ ion by the crown ether moiety is apparently sufficient in these cases.[12] Similarly, the 18-membered phenolic crown ether analogue can be metalated (= exchange of a proton for a metal ion; in this case the OH proton) with trimethylaluminium to give **5.13** which forms a ditopic complex with LiCl in solution and in the solid state.

A ditopic receptor that makes use of both the Lewis acidity of a uranyl ($UO_2^{2+}$) metal centre and additional hydrogen bonding interactions *via* pendant arms has been prepared (**5.14**).[13] The high affinity of actinide metals such as uranium for oxoanions means that the metal centre is complementary to phosphates. Uranium commonly adopts a pentagonal bipyramidal coordination geometry, meaning that there is a vacant coordination site for anion interaction. Within the complex, phosphate anions may also accept hydrogen bonds from the NH groups and donate them to the aryl ether oxygen atoms. In fact a 1:2, host:guest complex is formed with $H_2PO_4^-$ Figure 5.5), with one phosphate bound strongly to the metal centre and the other hydrogen-bonded to the first. In the absence of the *p*-tolyl blocking groups, similar 2:2 complexes are obtained in which the second phosphate is complexed by a further host molecule. This system has been elaborated to give the crown ether derivative **5.15** in which phosphate ions bind to the uranyl centre while $K^+$ cations are bound by the crown ether moieties.[14] Strictly complex **5.14** could be regarded as an example of a contact ion pair receptor as discussed in Section 5.1.2, however there exists a number of other such Schiff base complexes in which the anion and cation binding sites are not in contact. For example the salen-based receptor **5.16** reacts with $NiSO_4$ to give a complex in which the OH groups become deprotonated while the morpholine groups become protonated. The ligand complex readily extracts $CuSO_4$ into chloroform solution, for example, with essentially 100 % efficiency. Macrocyclic analogues of this system such as **5.17** have been prepared which exhibit significant co-operativity between anion and cation binding.[15]

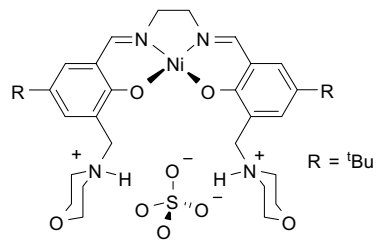


**5.16**.$SO_4$

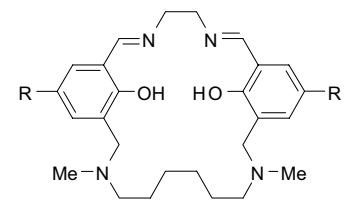


**5.17**

Ditopic receptors can also comprise more conventional combinations of anion and cation binding functionality. We have already seen in Section 4.5 guanidinium based zwitterion receptor **4.30** that takes advantage of crown ether groups to bind on to the ammonium residues of zwitterionic amino acids while the anion-binding guanidinium residue interacts with the carboxylate anion portion (Figure 5.1). Similarly, the tripodal tris(amido-benzo[15]crown-5) receptor **5.18** exhibits cooperative binding with $Cl^-$, $I^-$ and $ReO_4^-$ anions in conjunction with a crown ether unit that complexes $Na^+$ ions. $Na^+$ binding improves the receptor's affinity for $ReO_4^-$ by a factor of 20 in comparison to $Cl^-$ and $I^-$ anions under conditions that mimic aqueous waste streams of environmental significance in the nuclear fuel industry where the binding of the highly labile pertechnetate anion ($^{99}TcO_4^-$) is of concern.[16] Perrhenate represents a commonly accepted non-radioactive model for pertechnetate. Compound **5.18** is representative of a range of cation-binding crown ethers derivatised with anion binding functionality such as amides and ureas of the types as discussed in Chapter 4. For example the ureido-derived benzo[15]crown-5 ligand **5.19** forms a 2:1 sandwich complex with NaCl in which the $Na^+$ ion is bound

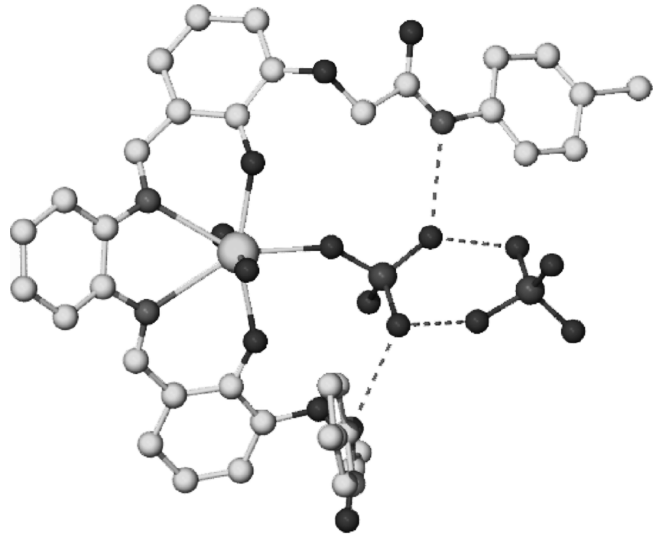

**Figure 5.5** Structure of the 1:2 complex of **5.14** with $H_2PO_4^-$.

between two crown ether moieties while the $Cl^-$ ion interacts with the urea groups. In contrast the same ligand forms a 2:2 complex with $NaNO_3$ in which an $NaNO_3$ contact ion pair is sandwiched between a crown ether on one side and a urea group on the other, Figure 5.6.[17] In contrast, the larger dibenzodiaza[30]crown-10 derivative **5.20** wraps around a single $K^+$ ion with $K_{11} = 5600\ M^{-1}$ in acetonitrile solution. $K^+$ binding preorganises the two thiourea groups for binding oxyanions, with the affinity for diphenyl phosphate being enhanced by a factor of 19 compared to the binding constant in the absence of $K^+$.[18] Similarly transition metal ion pair receptors have been prepared by derivatising common aza-macrocycles such as cyclam (Section 3.10.3) with hydrogen bonding groups. Thus cyclam can be transformed into tetra(hydroxypropyl)cyclam (**5.21**) by a Michael addition (Scheme 5.2). Ligand **5.21** forms a 1:1 complex with copper(II) acetate in which the copper(II) ion is bound within the macrocycle in a square pyramidal fashion, with one of the hydroxypropyl groups in the apical position. This

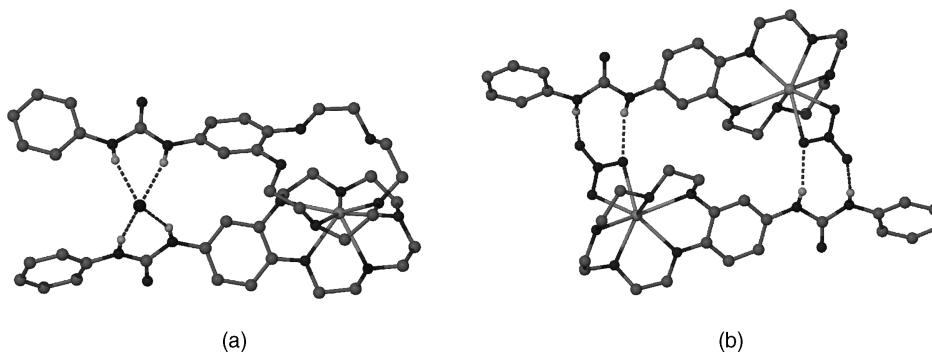


**Figure 5.6** X-ray crystal structures of **5.19** (a) 2:1 complex with NaCl and (b) 2:2 contact ion pair complex with $NaNO_3$.[17]

coordinated hydroxyl group along with two further hydroxypropyl arms then hydrogen bonds to an acetate anion (Scheme 5.2).[19]

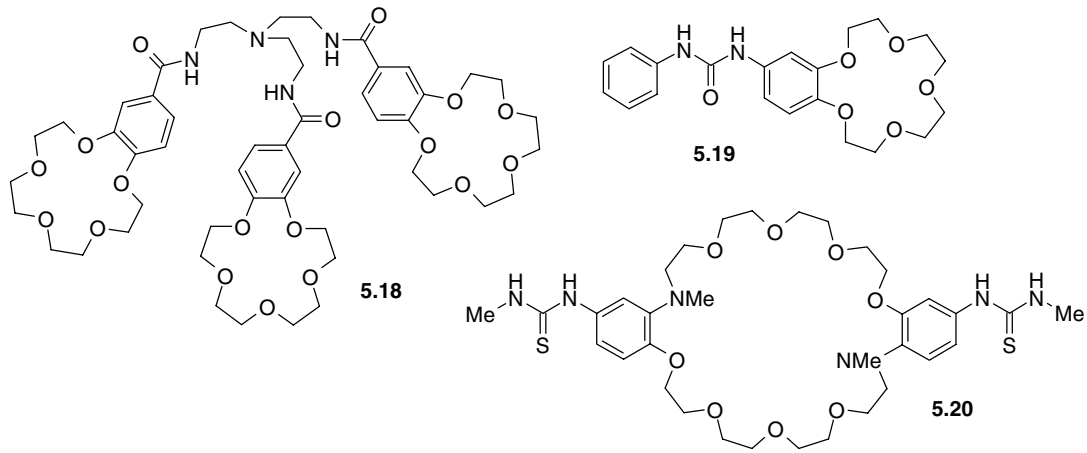


Moving away from metal cations, a resorcarene-based receptor for $NMe_4^+Cl^-$ has been designed by positioning amide groups at the top of a [4]resorcarene scaffold derived from the highly versatile Mannich reaction.† The hydrophobic resorcacene cavity hosts the tetramethylammonium cation (for which it is highly selective among other alkylammonium ions) while the chloride anion is held at the neck of the bottle-shaped cavity, Figure 5.7a. In the second generation host (**5.22b**) the phenyl groups serve to isolate both ions from the surrounding medium thus in chloroform solution the complex is thermodynamically and kinetically stable on the NMR spectroscopic time scale (the anion exchange rate constant $\ll 60\ s^{-1}$ at 300 K). Addition of methanol increases the anion exchange rate but does not destroy the complex.[20] An interesting variation on this theme has been reported by Rebek Jr. and co-workers from the Scripps Institute, USA. Rebek recognised that certain self-assembled dimeric capsules (discussed in detail in Chapter 10) such as $(\mathbf{5.23})_2$ are able to bind anions within their internal cavity space, often in conjunction with solvent molecules such as chloroform that act to fill the cavity space and solvate the bound anion. Similarly, other dimeric capsules such as $(\mathbf{5.24})_2$ bind tightly to

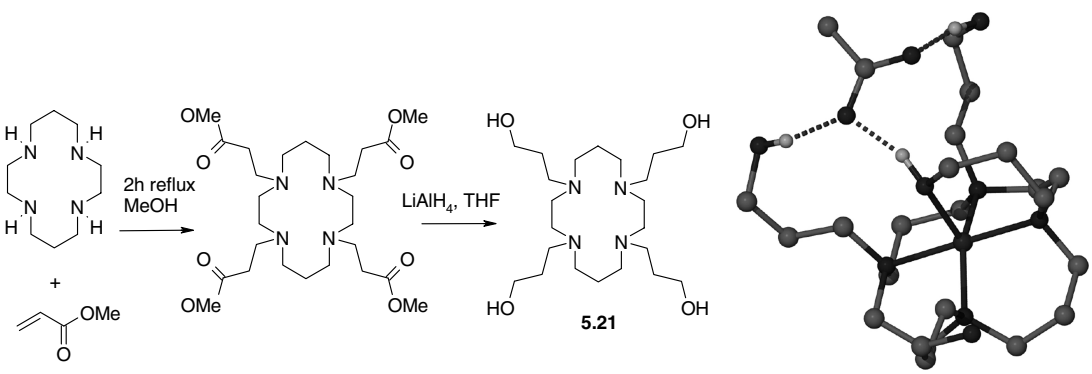


**Scheme 5.2** Synthesis of tetra(hydroxypropyl)cyclam (**5.21**) *via* Michael addition followed by reduction, and X-ray crystal structure of its 1:1 copper(II) acetate complex.[19]

† The multi-component condensation of a non-enolisable aldehyde such as formaldehyde, a primary or secondary amine and an enolisable carbonyl compound or, in this case, a resorcarene, to give an aminomethylated product. In effect the reaction adds an $R_2NCH_2$-group onto the aromatic ring.

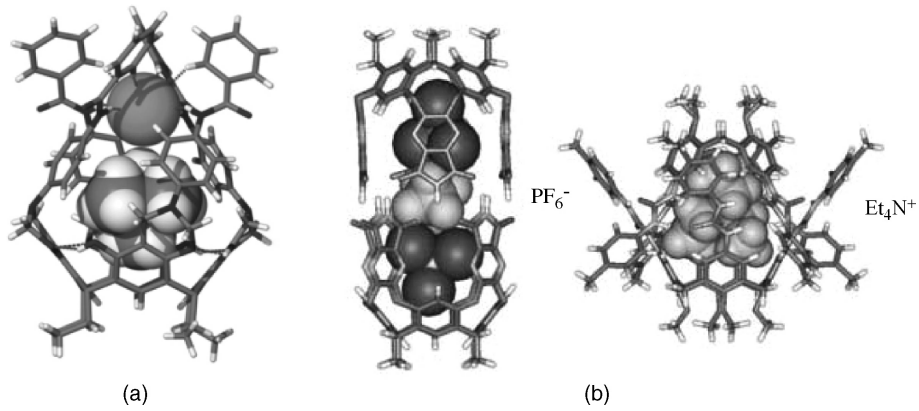


**Figure 5.7** (a) X-ray crystal structure of the $NMe_4Cl$ complex of **5.22b**. The guest ions are shown as van der Waals spheres (reproduced by permission of The Royal Society of Chemistry). (b) Molecular model of the capsular ion pair ($\mathbf{5.23}_2 \cdot PF_6^- \cdot 2CHCl_3$)($\mathbf{5.24}_2 \cdot NEt_4^+$) (© Wiley-VCH Verlag GmbH & Co. Reproduced with permission).

tetraalkylammonium cations such as $NEt_4^+$. Rebek's group were thus able to prepare a capsular ion pair of formula ($\mathbf{5.23}_2 \cdot PF_6^- \cdot 2CHCl_3$)($\mathbf{5.24}_2 \cdot NEt_4^+$), Figure 5.7b.[21]

A very large self-assembled calixarene-based ion pair binding complex (**5.25**) has been prepared by J. T. Davis and co-workers of the University of Maryland, USA.[22] In wet chloroform solution (water is necessary to avoid non-specific aggregation) the guanosine substituents self-assemble to give the well known G-quartet motif commonly found in biological alkali-metal binding systems.[23] This also creates an anion binding site by preorganising the amide groups. The dimer is readily able to extract NaCl from water into the organic phase, Figure 5.8.

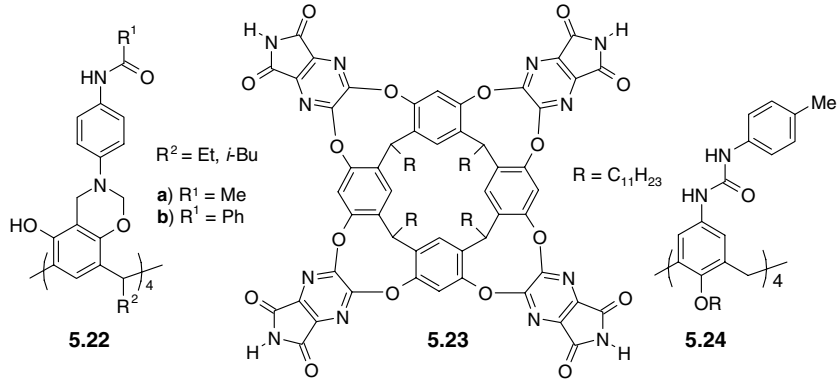


## 5.1.5 Symport and Metals Extraction

We have already seen in Section 2.2 how the transport of both anions and cations is a vital part of biochemistry. We will examine supramolecular models of biological ion channels in detail in Chapter 12 but here we focus on some simple ion transport systems (ionophores) relevant to simultaneous anion and cation binding. Because of the need to maintain overall and local charge neutrality during any transport process the transport of individual ions across a biological or artificial membrane never occurs in isolation. There are two kinds of primary transport processes. Ion exchange or *antiport*, occurs when chemically different ions of like charge such as $Na^+$ and $K^+$ are simultaneously transported in

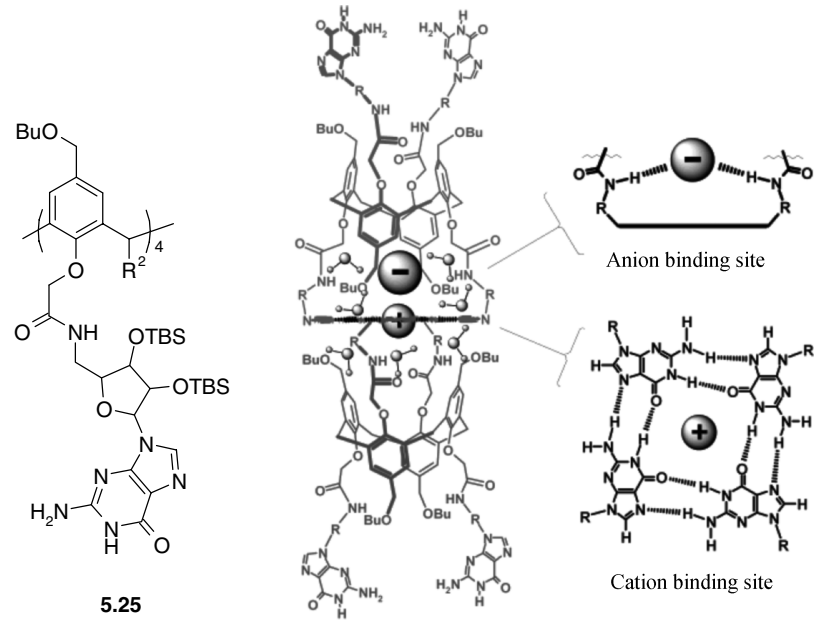


5.25

**Figure 5.8** Self-assembled dimer of **5.25** with $Na^+$ binding by a guanosine tetramer motif (G-quartet) and $Cl^-$ binding by amide functionalities. Remaining space if filled by water molecules. (Reproduced with permission from [22] © 2003 American Chemical Society).

*opposite directions*. Conversely, *symport* is when two ions of opposite charge such as $H^+$ and $Cl^-$ are simultaneously transported in the *same direction*. In biochemistry antiport of $Na^+$ and $K^+$ is responsible for the maintenance of transmembrane electrical potentials, whereas symport of $H^+$ and $Cl^-$ is responsible for the acidity of the stomach, for example. Both processes result in no *net charge separation*. Clearly hosts capable of simultaneously (and selectively) binding anions and cations have the potential to be useful in *symport* processes. We have already seen an example of $H^+$ and halide anion symport by expanded porphyrin systems in Section 4.4.4. The simple pyrrole **5.26** is a mimic for the naturally occurring prodigiosin (Section 4.2.4). Compound **5.26** is able to bind HCl by protonation of the basic imidazole nitrogen atom.[24] The **5.26**·HCl complex forms a '2 + 2' dimer in the solid state with each chloride ion bound by three hydrogen bonds; two from the pyrrole and amide NH groups of one receptor and one from the imidazolium group of another. An interesting feature is that all the hydrophilic functionality is inside the dimer; whereas, the exterior projects lipophilic groups. The abilities of **5.26** to co-transport $H^+$ and $Cl^-$ across bilayer membranes has been studied using 200 nm diameter vesicles composed of a phosphocholine derivative/cholesterol mixture. Chloride leakage from the vesicles (efflux) can be measured using a chloride-selective electrode. No chloride efflux is observed when both the inside and outside of the vesicle are acidic. At pH 7.2 some moderate efflux is observed, but

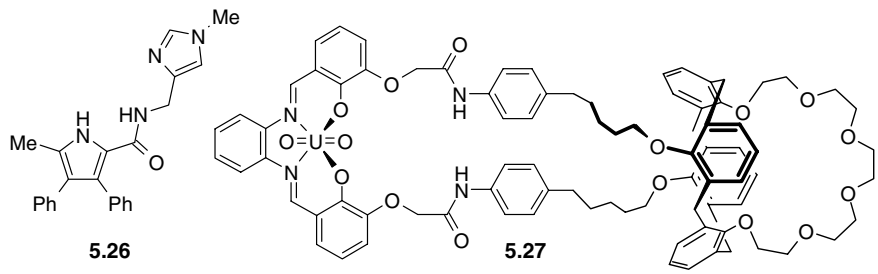

5.26 5.27

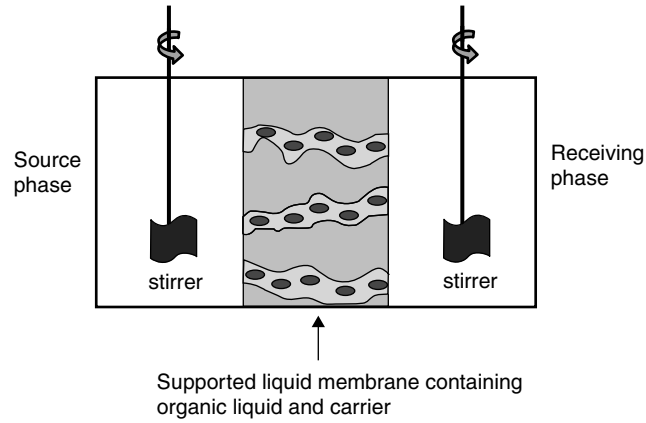


**Figure 5.9** A supported liquid membrane (SLM) a porous polymer membrane whose pores are filled with the organic liquid and a carrier, set in between the aqueous source phase and the aqueous receiving phase, which are being gently stirred.

the greatest $Cl^-$ transport rate is found when there is a pH gradient with the inside of the vesicle being more acidic than the outside. The chloride electrode results can be corroborated by examining the change in fluorescence of an acid sensitive dye such as Oregon Green®. Symport systems such as this have the potential to act as deacidifying drugs for treatment of drug-resistant tumours, for example.

We will look briefly at metal salt symport. Salt-binding ligand systems are very important as overall neutral ligands in metal salt extraction and metals recovery. In terms of alkali metals, radioactive $^{137}Cs$ is of tremendous interest in the nuclear industry. Host **5.27** is a rigid calix-crown analogue of **5.15** and has been assessed for its ability to co-transport $Cs^+$ as the $Cl^-$ and $NO_3^-$ salts. The calix-crown framework is highly $Cs^+$ selective and has been extensively studied in connection with extraction of $^{137}Cs^+$.[25] Addition of the uranyl-salen functionality gives a preorganised anion binding pocket. Salt transport has been assessed using a supported liquid membrane (SLM, Figure 5.9). A much higher flux is observed for CsCl than $CsNO_3$ despite the fact that $Cl^-$ is much more hydrophilic than nitrate (see the Hofmeister series, Table 4.2). Monofunctional control compounds do not give nearly as fast a rate of transport confirming the efficacy of the ion-pair binding properties of the host.[26]

Extraction of valuable and increasingly rare transition metals such as copper by hydrometallurgy, *e.g.* from ores or mixtures is also of significant current interest.[27] Conventional metal extraction processes use either cation exchange reagents, anion exchange hosts or solvating reagents in order to extract metals ion water-immiscible solvents in order to concentrate them and purify them from other metals. One of the most famous examples is the use of a solvating reagent is the extraction of uranyl cation ($UO_2^{2+}$) from nitric acid in the nuclear industry by tributyl phosphate in which both the tributyl phosphate, and a nitrate anion participate in inner sphere coordination to the uranium metal. Cation extractants are part of traditional and heavily used industrial metal extraction methods. A typical flow chart for extraction of copper using phenolic oxime ligands as cation extractants is shown in Figure 5.10, along with the associated chemical equations. These kinds of processes currently account for around a third of the world's copper production.‡

Conventionally attendant anions are not transported in ion exchange processes. However, current interest in the design of salt extractants explicitly incorporates both anion and binding functionality

‡ As an interesting historical aside, copper production, initially as bronze, a copper-tin alloy, dates back over 10,000 years, with a copper pendant found in northern Iraq dating back to 8700 BCE. Roman copper extraction represents one of the earliest examples of biotechnology. Copper ore, chiefly naturally occurring chalcopyrite ($CuFeS_2$), is not efficiently attacked by sulfuric acid, but the copper can be leached out of it if first oxidized by long exposure to the atmosphere in contact with naturally occurring *thiobacillus thiooxidans* and *thiobacillus ferrooxidans* bacteria.

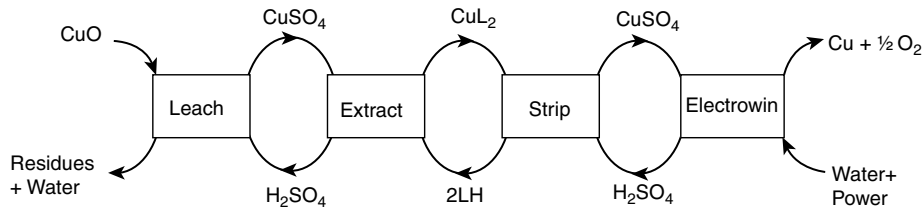


| | | | |
|---|---|---|---|
| $CuO + H_2SO_4$ | $\rightleftharpoons$ | $CuSO_4 + H_2O$ | Leach |
| $CuSO_4 + 2LH_{(org)}$ | $\rightleftharpoons$ | $CuL_{2(org)} + H_2SO_4$ | Extraction |
| $CuL_{2(org)} + H_2SO_4$ | $\rightleftharpoons$ | $CuSO_4 + 2LH_{(org)}$ | Strip |
| $CuSO_4 + H_2O$ | $\rightleftharpoons$ | $Cu + ½\,O_2 + H_2SO_4$ | Electrowin |
| $CuO$ | $\rightleftharpoons$ | $Cu + ½\,O_2$ | Overall |

LG =

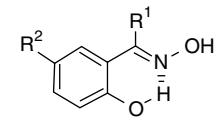


**Figure 5.10** Steps and materials balance for copper production using phenolic oximes as cation exchange solvent (reprinted from [27] with permission from Elsevier).

in di- and tritopic host systems, binding MX or $MX_2$ (M = divalent metal, X = mono- or divalent anion), respectively. Binding of the anion(s) and cation(s) is generally co-operative, a factor that can be exploited to enhance selectivity and binding strength. Binding can be controlled by changes in pH to protonate the ligand and recover the salt after extraction. Typical extractants are based on Schiff base motifs, as in complex **5.16**$\cdot SO_4$. For example, ligands such as **5.28** are very effective extractants for copper, nickel or zinc salts, but the structure of the complex formed depends strongly on the anion affinity for the bound metal ion and the metal coordination geometry requirements. Weakly coordinating anions such as nitrate approach the axial sites of the $N_2O_2$-plane in copper(II) complexes to generate a tetragonally distorted octahedron. The wrapping of two ligands about a single copper(II) centre ensures the metal is isolated from the solvent and hence soluble in water-immiscible phases. Because the salicylaldoxime is zwitterionic the assembly is overall charge-neutral. The X-ray crystal structure of the copper(II) nitrate complex of **5.28** is shown in Figure 5.11.

## 5.1.6 Dual-Host Salt Extraction

The anion- and cation-binding portions of an ion pair binding system do not necessarily have to be covalently linked together and indeed it is synthetically usually much more straightforward and cheaper

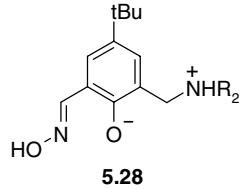


**5.28**

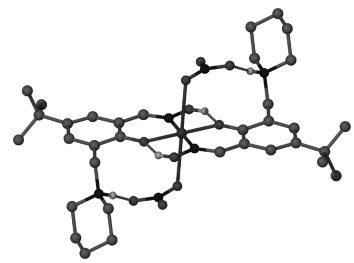

**Figure 5.11** X-ray crystal structure of the $Cu(NO_3)_2$ complex of the zwitterionic salicylaldoxime **5.28** showing the axial binding of $NO_3^-$ to copper supported by hydrogen bonding interactions.[27]

**Table 5.1** Extraction constants ($K_{ex}$) of $K^+$ salts of various anions either by dicyclohexano[18]crown-6 (**5.30**) alone or by the dual-host system dicyclohexano[18]crown-6/***N,N′***-diphenylthiourea.

| | $K_{ex}$ | | |
|---|---|---|---|
| Anion | **5.30** | **5.29/5.30** | $K_{ex}$ with **5.29**/$K_{ex}$ |
| $NO_3^-$ | 194.1 | 354.5 | 1.8 |
| $Br^-$ | 75.4 | 256.4 | 3.4 |
| $Cl^-$ | 4.2 | 66.7 | 15.9 |
| $MeCO_2^-$ | No extraction | 3.1 | – |

to prepare separate anion- and cation hosts, particularly given the plethora of compounds that are commercially available. Ion pair extraction or transport using separate anion and cation hosts is referred to as the *dual-host* approach and it relies on careful choice of anion and cation host such that there is an efficient synergy between them. To take a simple example, the combination of the simple ***N,N′***-diphenylthiourea (**5.29**) with dicyclohexano[18]crown-6 (**5.30**) results in very efficient synergistic extraction of potassium salts into nitrobenzene solution. The extraction data in Table 5.1 shows that in all cases the presence of the thiourea **5.29** enhances the salt extraction, giving a greater apparent extraction constant, $K_{ex}$ (where $K_{ex} = [\mathbf{5.30}\cdot K^+\cdot X^-]_{org} / [\mathbf{5.30}]_{org}[K^+]_{aq}[X^-]_{aq}$ and org and aq refer to the organic and aqueous phases, respectively).

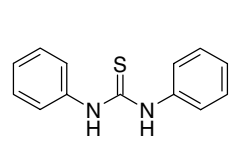


**5.29**

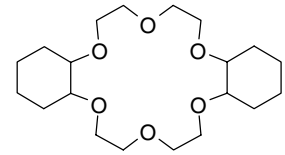


**5.30**

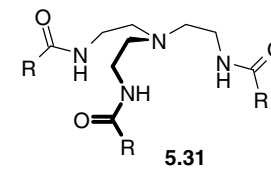


**5.31**

Dual-host approaches have also been used to good effect for $CsNO_3$ extraction. Nitrate is a common anion found upon nitric acid extraction of $^{137}Cs^+$ in the nuclear industry. $Cs^+$ is conveniently complexed by a large crown ether such as tetrabenzo[24]crown-8 while simple tripodal amide hosts of type **5.31** (where R is a long alkyl group to impart lipophilicity) are effective at binding $NO_3^-$. Extraction efficiency of $Cs^+$ from water into 1,2-dichloroethane was found to be enhanced by a factor of up to 4.4 in the presence of the anion host.[28]

## 5.2 Labile Complexes as Anion Hosts

Rice, C. R. 'Metal-assembled anion receptors', *Coord. Chem. Rev.*, 2006, **250**, 3190–3199.

In the previous sections in this chapter we have seen a range of discrete host molecules exhibiting anion and cation binding sites within the same molecule. In Section 4.7 we discussed inert coordination complexes in which a series of ligands form a complex with a metal ion that is long-lived in the timescale of anion binding processes involving the complex. The role of the metal ion is thus a structural one, holding the complex together and effectively preorganising several ligands that each contain (usually) a single anion binding functionality. We now complete that discussion by looking at labile complexes in which a series of ligands interact simultaneously with one or more labile metal cations and labile anions.

Such complexes form a precursor to a full discussion of the vast and highly topical field of self-assembly (Chapter 10). We consider them here since they resemble structurally the types of compounds discussed in Section 4.7, but unlike metal-based anion receptors the simple thermodynamic equilibrium between host, anion and complex is not the only process occurring in solution. In fact multiple equilibria are occurring covering all possible combinations of interaction between anions, cations and ligands. These systems have the appeal that the formation of particular metal coordination complexes are thus subject to thermodynamic anion templating (*cf.* the thermodynamic template effect in macrocycle synthesis, Section 3.9.1) and vice versa.

One very simple example is the ligand **5.32** that contains a single pyridyl functionality and a urea anion binding group. In the presence of the labile $d^{10}$ Ag(I) cation and nitrate anion the complex $[Ag(\mathbf{5.32})_2(S)]NO_3$ (S = solvent molecule) forms. The labile nature of the complex may be demonstrated by addition of excess nitrate which results initially in conversion to a dinitrate complex, $[Ag(\mathbf{5.32})_2(S)](NO_3)_2$ in which each urea group binds a single anion and, ultimately, binding of nitrate at the Ag(I) centre itself, Scheme 5.3.[29] While $[Ag(\mathbf{5.32})_2(S)]NO_3$ is a discrete complex that exists in both solution and the solid-state, the combination of $Ag^+$, **5.32** and other anions such as $CF_3SO_3^-$ gives hydrogen bonded polymers in the solid state in which anions bridge between $[Ag(\mathbf{5.32})_2]^+$ complexes rather than being bound by a single complex in a pincer-like fashion.

The related monodentate ligands **5.33** and **5.34** form $ML_4$ type complexes with the relatively inert platinum(II). The complex $[Pt(\mathbf{5.33})_4]^{2+}$ adopts a 1,2-alternate conformation (by analogy with the calixarenes, Section 3.14) giving two anion-binding pockets that can bind planar anions such as nitrate and acetate in a 1:2 ratio. Acetate displays a positive allosteric effect with $K_{12}$ being more than twice $K_{11}$. Tetrahedral anions are bound in a 1:1 ratio, however, and it is likely the complex can adopt a variety of conformations in solution. Related to $[Pt(\mathbf{5.33})_4]^{2+}$ is $[Pt(\mathbf{5.34})_4]^{2+}$. Like the complex with **5.33**, X-ray diffraction results show that the chloride complex adopts a 1,2-alternate conformation with a

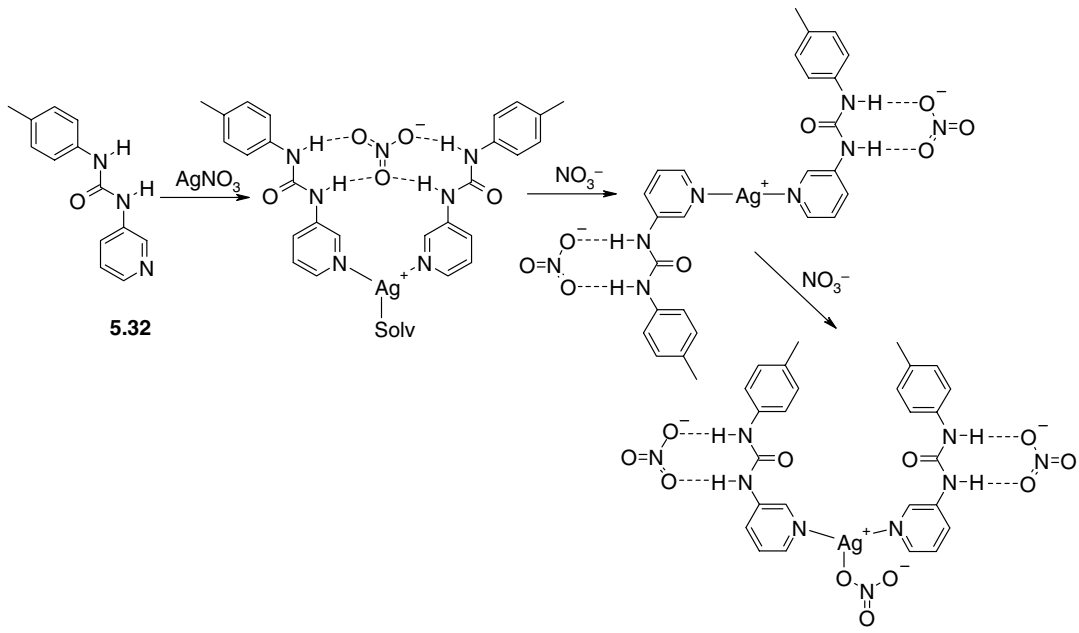


**Scheme 5.3** Self-assembly of a labile nitrate-binding Ag(I) complex of **5.32** and its evolution in the presence of excess nitrate.[29]

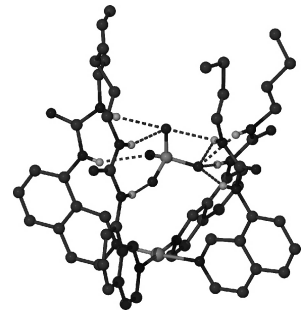

**Figure 5.12** X-ray crystal structure of [Pt(**5.34**)$_4$]($SO_4$) showing the interaction of $SO_4^{2-}$ with all four urea groups in a 'cone' conformation.[30]

binding constant of 11,700 $M^{-1}$ in DMSO solution, however with $SO_4^{2-}$ the anion is bound by all four urea groups in a cone conformation (Figure 5.12) and the binding constant is in excess of $10^5$ $M^{-1}$.[30]

Very simple pyrazole ligands such as 3,5-dimethylpyrazole (**5.35a**) can also form anion binding coordination complexes when organised into a *fac* geometry in 3:1 complexes with octahedral meta centres to give [Re(CO)$_3$(**5.35a**)$_3$]$^+$, or by tetrahedral metal centres to give [ZnCl(**5.35b**)$_3$]$^+$. The rhenium complex binds $Cl^-$ with $K_{11}$ = 6385 $M^{-1}$ in acetonitrile solution,[31] while the zinc complex of the closely related *t*-butylpyrazole (**5.35b**) binds anions in the selectivity sequence [$Cl^-$, $ClO_4^-$, $NO_3^-$] > [$Br^-$, $I^-$, $CF_3SO_3^-$] ⩾ [$BF_4^-$, $PF_6^-$].[32]

A very interesting example of the templation of a labile complex by choice of anion is the formation of helical bimetallic complexes by ligand **5.36**. Compound **5.36** contains two bidentate *S,N* binding domains (*i.e.* regions where a metal ion can bind) as well as a single amide anion binding functionality on each ligand. Reaction with the labile Co(II) results in the formation of a triple helical dinuclear complex [$Co_2$(**5.36**)$_3$]$^{4+}$ (a helicate, Section 10.8) that can exist as a mixture of isomers, either with all of the three amino acid groups at the head of the molecule (HHH) or a head-to-head-to-tail arrangement, HHT with one pointing the other way. With $Co(ClO_4)_2$ the HHH:HHT ratio is 1:3, however, if the complex is refluxed with nitrate anion the system converts almost exclusively to the HHH isomer, Figure 5.13a. This rearrangement occurs because the nitrate anion forms a strong, threefold hydrogen bonded interaction with the three amide NH groups of the amino acid functionalities in this isomer − in effect the nitrate anion organises its own binding pocket in a variation of the thermodynamic template effect.[33] The rearrangement from low to high symmetry is particularly evident from the reduction in the number of resonances for the H3 and H3′ protons in the $^1$H NMR spectrum of the complex upon addition of nitrate, Figure 5.13b.

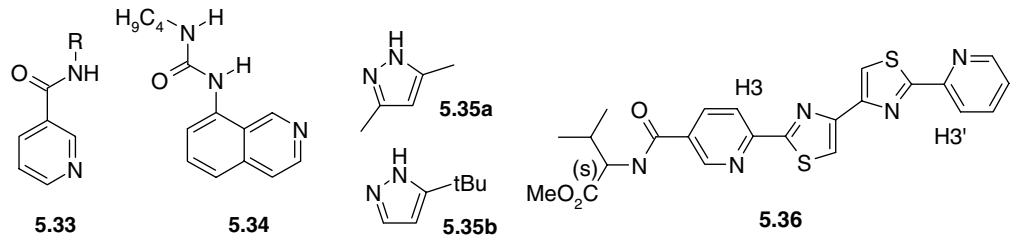


Anion templating is a formidable approach to the construction of large coordination complexes, cages and polyhedra by self-assembly using relatively simple ligands and we will examine some anion templated systems as part of our discussion of self-assembly in Chapter 10. For example, a

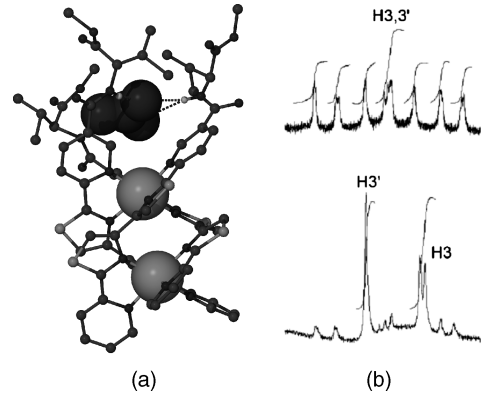


**Figure 5.13** X-ray crystal structure of the HHH isomer of $[Co_2(\mathbf{5.36})_3]^{4+}$ binding nitrate (the nitrate anion and metal centres are shown as large spheres) (b) partial $^1$H NMR spectra of $[Co_2(\mathbf{5.36})_3]^{4+}$ as the perchlorate salt (top) and after $NO_3^-$ addition (bottom) (reproduced by permission of The Royal Society of Chemistry).

luminescent tetra-gold(I) metallomacrocycle **5.37** is templated according to the series of reactions shown in Scheme 5.4 in which $AgNO_3$ or $AgCF_3SO_3$ is used to remove $Cl^-$ from the intermediate. Interestingly if reaction is carried out using tetrahedral anions such as $ClO_4^-$ then a trimeric macrocycle **5.38** that includes the perchlorate anion in the centre but no 4,4′-bipyridine is observed instead. It is not yet known whether the anion plays a templating role but this seems highly likely.[34] Anion templating is also a highly significant factor in the synthesis of metallacages and clusters of type $[M_2Ni_4(atu)_8X]^{3+}$ (M = Ni, Pd) based on the deprotonated form of amidothiourea (atu). The cluster forms an octahedral cage around the encapsulated halide anion but no cluster is formed in the presence of a range of other anions. The formation of the cage is accompanied by a significant

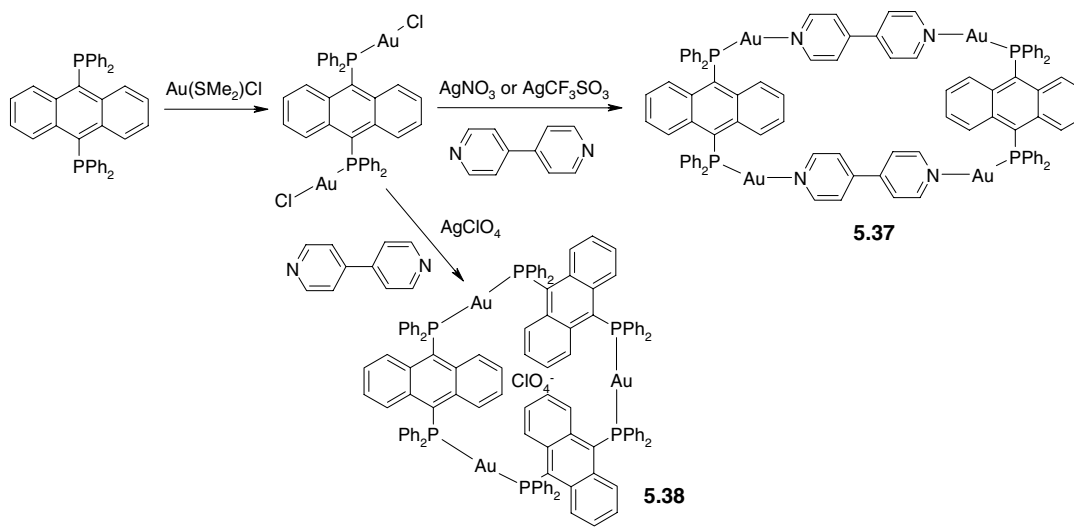


**Scheme 5.4** Anion templated self-assembly of gold(I) phosphine macrocycles.[34]

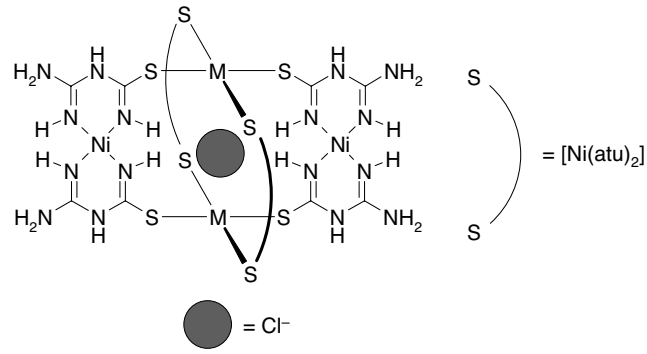


**Figure 5.14** Chloride anion templated metallacages based on amidothiourea (Hatu) (M = Ni, Pd).[35]

colour change from orange to green, a property that has been used for colorimetri detection of chloride, Figure 5.14.[35]

## 5.3 Receptors for Zwitterions

We saw in Section 4.6.1 the use of zwitterionic hosts for anions in which the counter-cation is non-specifically bound on the outside of the molecule. We now turn to zwitterionic guests where the guest has both cationic and anionic parts. We have already described in Section 5.1.1 the zwitterionic structure of amino acids and amino acid binding has been a major part of the interest in the construction of hosts for zwitterions. An excellent example is compound **4.30** (Section 4.5) which is

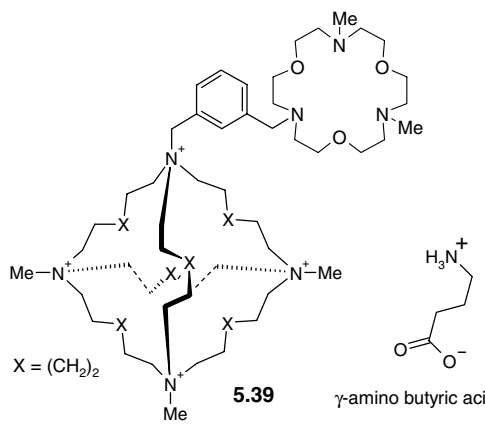


**5.39**



γ-amino butyric acid (GABA)

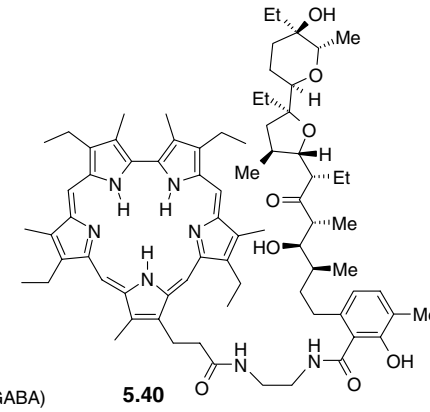

**5.40**

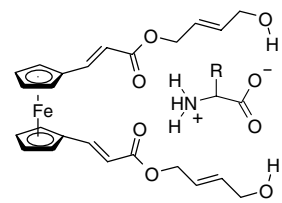

**5.41**

a logical extension of a guanidinium anion-binding host, with an added crown ether cation binding group. Macrobicyclic cages of the type described in Section 4.6.1 can be adapted to give specific anion and cation binding functionality in a similar way, as in the crown ether derivative **5.39**. This host binds the zwitterionic neutrotransmitter γ-amino butyric acid (GABA) with the carboxylate end being bound within the cationic cage while the ammonium terminus hydrogen bonds to the oxygen atoms of the triaza[18]crown-6 derivative.[36] Neutral amino acid receptors based on expanded porphyrin anion-binding functionality have been used to transport amino acids across U-tube model membranes (see Section 4.4.4). The sapphyrin-lasalocid conjugate **5.40** binds carboxylate groups of amino acids in a perching fashion in the expanded porphyrin cavity, while the ammonium end interacts with the side-arm. The compound exhibits different transport rates according to the identity of the amino acid with L-Phe being transported *ca.*1000 more rapidly than L-Tyr. Also interestingly the L-enantiomer is carried about twice as rapidly as the D-isomer, suggesting a degree of modest enantioselectivity, albeit not correlated with the binding constants. The enantioselective transport may be related to the rate of decomplexation.[37] Finally, a more recent report deals with a ferrocene-based receptor **5.41** able to recognise Gly and Gln at pH 8.0.[38] Binding constants were determined by cyclic voltammetry (see Box 4.1) in water/acetonitrile which gave binding constants of $1.54 \times 10^6$ and $8.9 \times 10^5$ $M^{-1}$ for these two amino acids, respectively. Anion binding occurs by hydrogen bonding to the terminal hydroxyl functionalities while the ammonium head group interacts with the ester carbonyl groups.

## Summary

- Ion pairs commonly exist as *solvent separated ion pairs* in polar media but may form *contact ion pairs* or aggregates in less polar solvents.
- Ion pair receptors contain a cation and an anion binding region, often a combination of common binding motifs, and can bind both contact or separated ion pairs to give an overall neutral complex.
- Ion pair receptors are useful in mimicking biological *symport* processes − the simultaneous transport of oppositely charged ions in the same direction.
- Ion pair receptors are also common used in the extraction of metal salts in refining or purification processes.
- A *cascade receptor* is a host that binds one of more metal ions which, in turn, bind anions. They are of interest in the modelling of biological metal-based active sites − *metallobiosites.*
- *Dual host salt extraction* involves the simultaneous extraction of a cation and anion by two separate receptors, one complementary to each ion.
- Binding of one ion may be used to template the self-assembly of a complex of an oppositely charged ion and labile ligands.
- Ion pair receptors can bind zwitterions such as amino acids.

## Study Problems

5.1 Calculate the $K_{ex}$ values for the following $K^+$ salts (0.01 M) a 1.0 mM crown ether salt extraction system (a) in the absence of a urea-based anion binding host and (b) in its presence, from the table below and hence calculate the improvement factor $K_{ex}$ with anion host/$K_{ex}$ without anion host. The [$K^+$] back extracted represents the concentration of $K^+$ moving into the organic phase, as measured by back-extraction.

| | [$K^+$] back extracted (mM) | |
|---|---|---|
| Anion | crown | crown + anion host |
| $NO_3^-$ | 0.66 | 0.78 |
| $Br^-$ | 0.43 | 0.72 |
| $Cl^-$ | 0.04 | 0.40 |
| $MeCO_2^-$ | No extraction | 0.03 |

# References


1. Neubert, R., Ion-pair transport across membranes. *Pharmaceutical Research* 1989, **6**, 743–747.
2. Mahoney, J. M., Beatty, A. M., Smith, B. D., Selective recognition of an alkali halide contact ion-pair. *J. Am. Chem. Soc.* 2001, **123**, 5847–5848.
3. Mahoney, J. M., Davis, J. P., Beatty, A. M., Smith, B. D., Molecular recognition of alkylammonium contact ion-pairs using a ditopic receptor. *J. Org. Chem.* 2003, **68**, 9819–9820.
4. Lankshear, M. D., Cowley, A. R., Beer, P. D., Cooperative AND receptor for ion-pairs. *Chem. Commun.* 2006, 612–614.
5. Motekaitis, R. J., Martell, A. E., Murase, I., Cascade halide binding by multiprotonated bistren and copper(II) bistren cryptates. *Inorg. Chem.* 1986, **25**, 938–944.
6. Agnus, Y., Louis, R., Weiss, R., Bimetallic copper(I) and copper(II) macrocyclic complexes as mimics for type-3 copper pairs in copper enzymes. *J. Am. Chem. Soc.* 1979, **101**, 3381–3384.
7. Fenton, D. E., Metallobiosites and their synthetic analogues – a belief in synergism – 1997–1998 Tilden Lecture. *Chem. Soc. Rev.* 1999, **28**, 159–168.
8. Drew, M. G. B., McCann, M., Nelson, S. M., Binuclear macrocyclic copper(II) complexes as receptors for small bridging ligands - X-ray crystal and molecular-structure of a mu-azido complex. *J. Chem. Soc., Chem. Commun.* 1979, 481–482.
9. Mukherjee, S., Weyhermuller, T., Bothe, E., Chaudhuri, P., Structural, magnetochemical and electrochemical studies of dinuclear complexes containing the $[(VO)\text{-}O\text{-}V]_2$, $[(VO)\text{-}O\text{-}IV]_2$, $Cr_2(III)$, $Mn_2(III)$ and $Fe_2(III)$ cores of a potentially pentadentate phenol-containing ligand with (O,N,O,N,O)-donor atoms. *Eur. J. Inorg. Chem.* 2003, 1956–1965.
10. Amendola, V., Fabbrizzi, L., Mangano, C., Pallavicini, P., Zema, M., A di-copper(II) bis-tren cage with thiophene spacers as receptor for anions in aqueous solution. *Inorg. Chim. Acta* 2002, **337**, 70–74.
11. Tobey, S. L., Anslyn, E. V., Energetics of phosphate binding to ammonium and guanidinium containing metallo-receptors in water. *J. Am. Chem. Soc.* 2003, **125**, 14807–14815.
12. Reetz, M. T., Niemeyer, C. M., Harms, K., Crown ethers with a Lewis acidic center - a new class of heterotopic host molecules. *Angew. Chem., Int. Ed. Engl.* 1991, **30**, 1472–1474.
13. Rudkevich, D. M., Verboom, W., Brzozka, *et al.*, Functionalised $UO_2$ salenes: neutral receptors for anions. *J. Am. Chem. Soc.* 1994, **116**, 4341–4351.
14. Rudkevich, D. M., Brzozka, Z., Palys, M., Visser, H. C., Verboom, W., Reinhoudt, D. N., A difunctional receptor for the simultaneous complexation of anions and cations; Recognition of $KH_2PO_4$. *Angew. Chem., Int. Ed. Engl.* 1994, **33**, 467–468.
15. Plieger, P. G., Tasker, P. A., Galbraith, S. G., Zwitterionic macrocyclic metal sulfate extractants containing 3-dialkylaminomethylsalicylaldimine units. *Dalton Trans.* 2004, 313–318.
16. Beer, P. D., Hopkins, P. K., McKinney, J. D., Cooperative halide, perrhenate anion-sodium cation binding and pertechnetate extraction and transport by a novel tripodal tris(amido benzo-15-crown-5) ligand. *Chem. Commun.* 1999, 1253–1254.
17. Barboiu, M., Vaughan, G., van der Lee, A., Self-organized heteroditopic macrocyclic superstructures. *Org. Lett.* 2003, **5**, 3073–3076.
18. Tozawa, T., Misawa, Y., Tokita, S., Kubo, Y., A regioselectively bis(thiourea)-substituted dibenzo-diaza-30-crown-10: a new strategy for the development of multi-site receptors. *Tetrahedron Lett.* 2000, **41**, 5219–5223.
19. Channa, A., Steed, J. W., Anion and cation binding by a pendant arm cyclam and its macrobicyclic derivatives. *Dalton Trans.* 2005, 2455–2461.
20. Atwood, J. L., Szumna, A., Anion-sealed single-molecule capsules. *Chem. Commun.* 2003, 940–941.
21. Hayashida, O., Shivanyuk, A., Rebek Jr., J., Molecular encapsulation of anions in a neutral receptor. *Angew. Chem., Int. Ed.* 2002, **41**, 3423–3426.

22. Kotch, F. W., Sidorov, V., Lam, Y. F., Kayser, K. J., Li, H., Kaucher, M. S., Davis, J. T., Water-mediated association provides an ion pair receptor. *J. Am. Chem. Soc.* 2003, **125**, 15140–15150.
23. Williamson, J. R., Raghuraman, M. K., Cech, T. R., Mono-valent cation induced structure of telomeric DNA - the G-quartet model. *Cell* 1989, **59**, 871–880.
24. Gale, P. A., Light, M. E., McNally, B., Navakhun, K., Sliwinski, K. E., Smith, B. D., Co-transport of $H^+/Cl^-$ by a synthetic prodigiosin mimic. *Chem. Commun.* 2005, 3773–3775.
25. Sachleben, R. A., Urvoas, A., Bryan, J. C., Haverlock, T. J., Hay, B. P., Moyer, B. A., Dideoxygenated calix[4]arene crown-6 ethers enhanced selectivity for caesium over potassium and rubidium. *Chem. Commun.* 1999, 1751–1752.
26. Rudkevich, D. M., Mercerchalmers, J. D., Verboom, W., Ungaro, R., Dejong, F., Reinhoudt, D. N., Bifunctional recognition – simultaneous transport of cations and anions through a supported liquid membrane. *J. Am. Chem. Soc.* 1995, **117**, 6124–6125.
27. Tasker, P. A., Tong, C. C., Westra, A. N., Co-extraction of cations and anions in base metal recovery. *Coord. Chem. Rev.* 2007, **251**, 1868–1877.
28. Kavallieratos, K., Danby, A., Van Berkel, *et al*., Enhanced of $CsNO_3$ extraction in 1,2-dichloroethane by tris (2-aminoethyl)amine triamide derivatives *via* a dual-host strategy. *Anal. Chem.* 2000, **72**, 5258–5264.
29. Turner, D. R., Smith, B., Spencer, E. C., *et al*., Anion binding by Ag(I) complexes of urea-substituted pyridyl ligands. *New J. Chem.* 2005, **29**, 90–98.
30. Bondy, C. R., Gale, P. A., Loeb, S. J., Metal-organic anion receptors: Arranging urea hydrogen-bond donors to encapsulate sulfate ions. *J. Am. Chem. Soc.* 2004, **126**, 5030–5031.
31. Nieto, S., Pérez, J., Riera, L., Riera, V., Miguel, D., Pyrazole complexes as anion receptors. *Chem. Eur. J.* 2006, **12**, 2244–2251.
32. Renard, S. L., Kilner, C. A., Fisher, J., Halcrow, M. A., Supramolecular anion binding by the $ZnCl(Hpz(t)Bu)_3^+$ cation (Hpz(t)Bu=5-tert-butylpyrazole). *J. Chem. Soc., Dalton Trans.* 2002, 4206–4212.
33. Harding, L. P., Jeffery, J. C., Riis-Johannessen, T., Rice, C. R., Zeng, Z. T., Anion control of the formation of geometric isomers in a triple helical array. *Dalton Trans.* 2004, 2396–2397.
34. Lin, R., Yip, J. H. K., Zhang, K., Koh, L. L., Wong, K. Y., Ho, K. P., Self-assembly and molecular recognition of a luminescent gold rectangle. *J. Am. Chem. Soc.* 2004, **126**, 15852–15869.
35. Vilar, R., Mingos, D. M. P., White, A. J. P., Williams, D. J., Anion control in the self-assembly of a cage coordination complex. *Angew. Chem., Int. Ed.* 1998, **37**, 1258–1261.
36. Schmidtchen, F. P., Tetazac – a novel artificial receptor for binding omega-amino carboxylates. *J. Org. Chem.* 1986, **51**, 5161–5168.
37. Sessler, J. L., Andrievsky, A., Sapphyrin-Lasalocid conjugate: A novel carrier for aromatic amino acid transport. *Chem. Commun.* 1996, 1119–1120.
38. Debroy, P., Banerjee, M., Prasad, M., Moulik, S. P., Roy, S., Binding of amino acids into a novel multiresponsive ferrocene receptor having an ene backbone. *Org. Lett.* 2005, **7**, 403–406.

# 6 Molecular Guests in Solution

*'I envy not in any moods*
*The captive void of noble rage,*
*The linnet born within the cage,*
*That never knew the summer woods.'*

— Alfred, Lord Tennyson (1809–1892), *In Memoriam*

# 6.1 Molecular Hosts and Molecular Guests

## 6.1.1 Introduction

The host-guest binding of a neutral (usually organic) molecule may occur *via* its physical imprisonment either as part of a solid-state network, forming a solid-state inclusion compound (clathrate), or a metal-organic framework complex (see Chapters 7 and 9, respectively), or within the cavity of a solution species such as a *cavitand* (a molecule such as a calixarene possessing a permanent and intrinsic guest-binding cavity). In general, the binding of neutral, non-polar organic molecules in non-polar solvents by the majority of cavitands is relatively weak because there is no significant enthalpic gain from strong host–guest interactions. Solid-state complexes are widespread, however, because of the need to pack efficiently in the crystal lattice – unfilled holes are relatively unstable and hence very uncommon because there is a loss of stabilisation from the van der Waals interactions between all molecules. In solution, interactions between the guest and the host may be either very limited (*e.g.* van der Waals interactions) or of significant stability (*e.g.* hydrogen bonds). Significant binding of polar or charged molecular guests is observed in many hosts, with binding of alkyl ammonium cations being particularly common. In non-polar solvents such binding often takes the form of specific host-guest dipole–dipole or hydrogen-bond interactions, often with *charge assistance* (*i.e.* the interaction is strengthened by ion–dipole interactions). Hydrophobic portions of the guest are sequestered within hydrophobic portions of the host. In water, polar groups on the host and guest are highly solvated and hence organic guest binding relies much more on the hydrophobic effect. In order to achieve molecular guest complexation in solution as well as in the solid state, it is necessary for the host to possess a permanent, intrinsic cavity, or to organise or self-assemble (Chapter 10) several components in solution in order to produce one. In this chapter, we will examine a variety of individual host molecules that possess intrinsic curvature, allowing them to include guest species in a capsular manner to give complexes that are stable, in principle, in all phases of matter (solid, solution and gas phase). Just as with cation and anion complexation, solution binding constants (Section 1.4) can be measured and the information used to derive structure–function relationships useful in host design. We will examine the more classical field of solid state clathrate or lattice inclusion chemistry in Chapter 7 and the highly topical solid state inclusion compounds formed by robust, infinite coordination network solids in Chapter 9.

## 6.1.2 Some General Considerations

Schneider, H. J., 'Mechanisms of molecular recognition - investigations of organic host guest complexes', *Angew. Chem., Int. Ed. Engl.* 1991, **30**, 1417–1436.

Broadly speaking the same kinds of supramolecular interactions that govern ion binding are also relevant to molecular complexation but there is a significant change of emphasis and importance. The concept of cooperativity between binding sites is still relevant, however what constitutes the binding sites themselves can be more difficult to recognise. The larger surface area of molecular guests means that, depending on solvent, van der Waals and hydrophobic/solvophobic interactions become much more important at the expense of point interactions such as hydrogen bonding and dipolar interactions. For example, Figure 6.1 shows a number of systems that illustrate nicely that strong complexation

*Supramolecular Chemistry, 2nd edition* J. W. Steed and J. L. Atwood
© 2009 John Wiley & Sons, Ltd ISBN: 978-0-470-51233-3

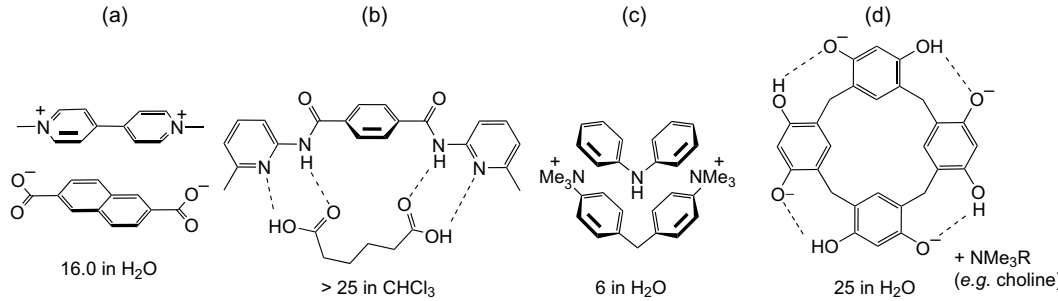


**Figure 6.1** Interactions between open, extended surfaces with the relevant solvent and interaction energy ($-\Delta G$/kJ mol$^{-1}$).

can readily occur at open, extended receptor surfaces. Note that the receptor combination that relies primarily on hydrogen bonding interactions (Figure 6.1b) achieves strongest complexation in chloroform, a non-polar solvent, while the remaining systems benefit from the hydrophobic effect in water. While surface interactions are significant, however, three-dimensional preorganisation of the receptor usually leads to substantial increases in affinity. This is in principle because spherical particles (guests) in a hemispherical cavity, experience four times as much dispersive binding force as on a planar surface. Moreover this factor increases to six with a cylindrical cavity and approximately eight with a fully encompassing spherical cavity. As a result hosts, or host components, that have some kind of intrinsic curvature so that they can wrap around guests, are enduringly popular, as we will see in the next section. There are some exceptions to this rule, however, generally arising from negative preorganisation or unfavourable solvation effects in the three-dimensional host. For example, the binding constants for the binding of the fluorescent guest 8-anilinonapthalene sulfonate (ANS) by the cyclic diphenylmethane derivative **6.1** and the bicyclic, potentially 3D-encapsulating analogue **6.2** are $2.0\times10^5$ M$^{-1}$ and $0.4\times10^5$ M$^{-1}$, respectively in water.

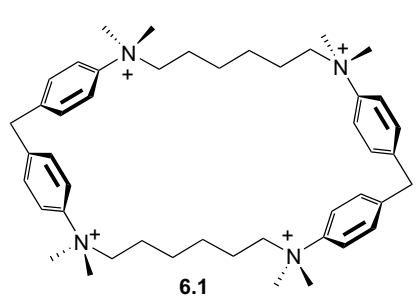

**6.1**

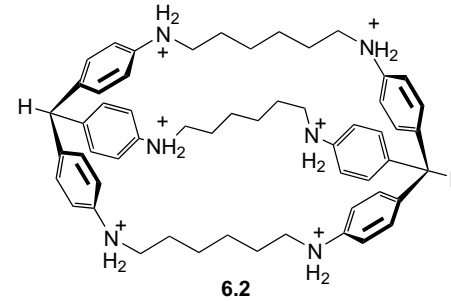

**6.2**

Broadly speaking the important types of interaction in molecular host-guest complexes are listed below.

1. **Hydrophobic binding.** The hydrophobic effect can have both enthalpic and entropic components, although the classical hydrophobic effect is entropic in origin (Section 1.9.1). Studies on the associations between planar aromatic molecules show an approximately linear relationship between the interaction energy and their mutual contact surface area with slope 64 dyn cm$^{-1}$, very close to the macroscopic surface tension of water (72 dyn cm$^{-1}$). Hence, in the absence of specific host or guest interactions with the solvent the hydrophobic effect can be calculated solely from the energy required to create a free surface of 1 Å$^2$ which amounts to $7.2 \times 10^{-12}$ J or 0.43 kJÅ$^{-2}$ mol$^{-1}$.

2. **Electrostatic interactions involving permanent charges (salt bridges).** According to the Bjerrum model the binding constant between two ions $A^+$ and $B^-$ can be described in terms of the product of the ionic charges $z_A \cdot z_B$ and the mean effective distance between the ions. These parameters along with the dielectric permittivity (ε) determine the magnitude of the Bjerrum function *Q(b)*. The binding constant is then given by: $K = \frac{4\pi N}{1000}\left[\frac{|Z_A Z_B|}{\varepsilon kT}\right]^3 \cdot Q(b)$. This equation predicts a linear dependence of ln *K* with $z_A$ and $z_B$ which is obeyed for many simple inorganic ions. Significant deviations are noted for more complex organic ions, however. The effect of the medium is such that decreases in dielectric constant lead to significant increases in association as a result of decreased dielectric shielding.
3. **Induced dipolar interactions.** The electron clouds in many (especially large) organic molecules are readily polarised resulting in the formation of induced dipoles that can interact, resulting in complex stabilisation. Both cations and anions can induce dipoles in aromatic molecules, for example.
4. **π-π Interactions and charge transfer.** Edge-to-face and face-to-face (stacking) π–π interactions are discussed in Section 1.8.7. Stacking interactions between an electron poor and electron rich partner can result in the transfer of electron density from the HOMO of the donor to the low-lying LUMO of the acceptor. The viologens (*N,N′*-disubstituted-4,4′-bipyridyl derivatives) for example are particularly electron-poor and form charge transfer complexes of the type shown in Figure 6.1a, as evident from the observation of charge transfer transitions in their UV-Vis absorption spectra.
5. **Hydrogen bonding.** A typical hydrogen bonded complex is shown in Figure 6.1b. Hydrogen bonding in neutral molecule complexes is most significant in non-polar solvents where the polar hydrogen bonding donor and acceptor groups are relatively unsolvated.

## 6.2 Intrinsic Curvature: Guest Binding by Cavitands

### 6.2.1 Building Blocks

Individual host molecules possessing an intrinsic cavity that is present in both the solid state and in solution are termed *cavitands*. A cavitand is defined as a molecular container with an enforced, concave surface. The molecular cavity is generally open at one end. Inclusion of guest species within a cavitand results in a *cavitate* (or *caviplex*). Molecules or fragments that possesses intrinsic curvature (*i.e.* are structurally bent or curved) may be used to bind guest molecules in both solution as well as the solid state since dissolution of the host does not result in disappearance of the cavity. Intrinsically curved molecular building blocks that are reasonably synthetically accessible are relatively uncommon, and as a result cavitand hosts and a wide range of related species tend to fall into loose families. These families may be grouped according to the kinds of building blocks used to impart curvature and hence achieve a concave binding pocket. A range of examples of synthetically accessible cavitands and curved precursors that have been used to host molecular guests are shown in Figure 6.2. In addition to intrinsically curved species, there exists a vast range of hosts that may be broadly termed cyclophane hosts, which make use of bridged aryl rings as container walls with a wide variety of flexible or angled spacers that enable the host to close in on itself. The following sections present a brief overview of the intracavity inclusion chemistry of some important hosts in both aqueous and non-aqueous media and the concepts that result from such studies.

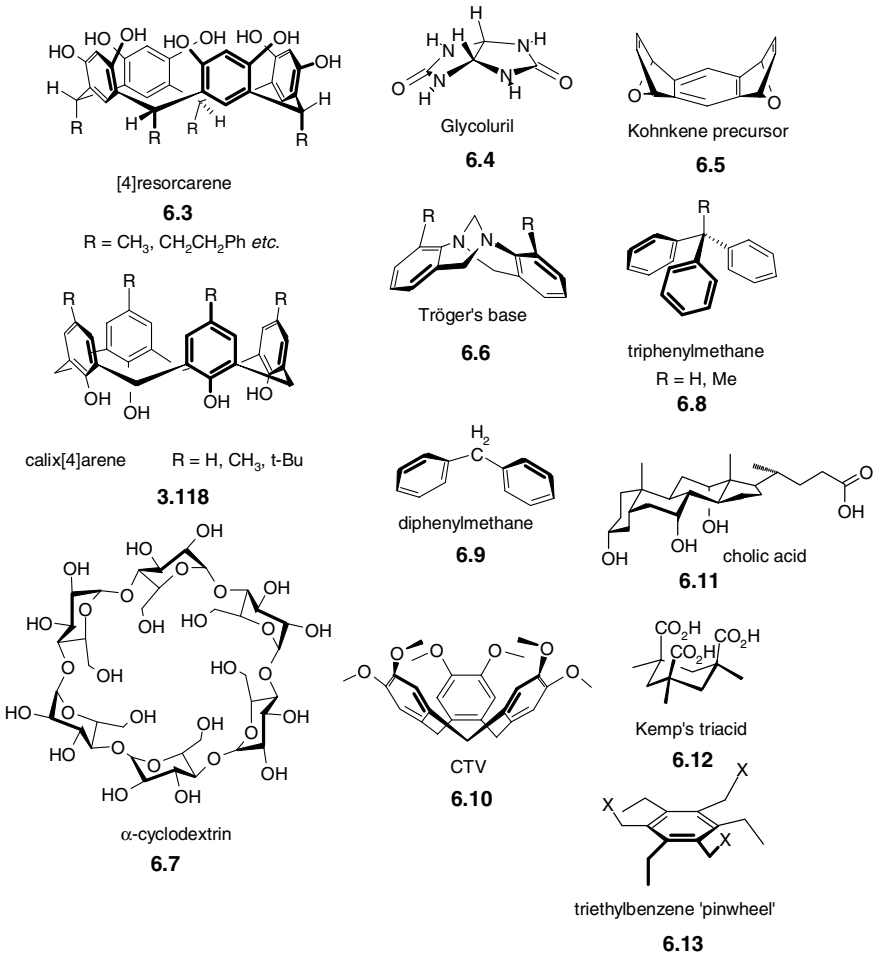


**Figure 6.2** Range of curved building blocks and structural types.

## 6.2.2 Calixarenes and Resorcarenes

Stibor, I. and Lhoták, P. 'Calixarenes and their Analogues: molecular complexation', in *Encyclopedia of Supramolecular Chemistry*, Atwood, J. L., Steed, J. W., eds. Marcel Dekker: New York, 2004; vol. 1, *pp.* 628–635.

The synthesis and nomenclature of calixarenes such as **3.118** has already been in introduced (Section 3.14 - For an introduction to calixarenes and the history of their development see Box 3.4) in the context of their widespread applications as hosts for cations, generally binding to metals through their phenolic oxygen atoms. Closely related are the *resorcarenes* (or *calixresorcarenes*), such as **6.3**, which are prepared in similar fashion to the calixarenes by condensation of resorcinol (3-hydroxyphenol) with aldehydes, as shown in Scheme 6.1.[1] In this case, acid-catalysed conditions are used and the preparation does not work with formaldehyde itself because of polymerisation reactions occurring from the 2-position. A wide range of other aldehydes are highly effective, however, and commonly acetaldehyde (giving methyl 'feet' to the resorcarene bowl) or 2-phenylethanal (resulting in enhanced

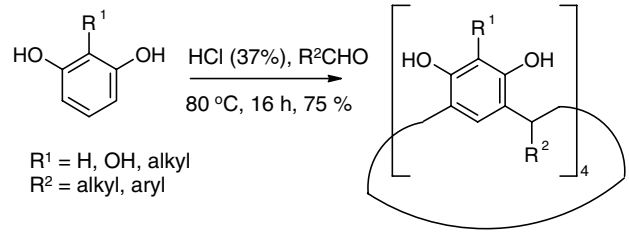


**Scheme 6.1** Typical synthesis of [4]resorcarenes.

solubility of the product in organic solvents) are used. Both calix[4]arenes and [4]resorcarenes possess a bowl-shaped conformation in their most stable forms. In the case of [4]resorcarenes, this bowl is wider and shallower than in the calixarene analogues as a consequence of the presence of the 'upper rim' hydroxy substituents, which stabilise the bowl by intramolecular hydrogen bonding. Both calixarenes and resorcarenes bearing small substituent groups are relatively conformationally mobile, adopting partial cone, 1,2-alternate and 1,3-alternate conformations as well as the cone form (Figure 3.79). Indeed, resorcarenes are significantly more conformationally mobile with free energy activation barriers $\Delta G^{\ddagger}$ for conformational interconversion of 18.4 kJ mol$^{-1}$ for [4]resorcarenes with $R^1 = n$-hexyl and $R^2 = H$. This may be compared with values in the range 63–67 kJ mol$^{-1}$ in $CDCl_3$ for calix[4]arenes, where the cyclic lower-rim intramolecular hydrogen bonding is much stronger than the analogous upper-rim interactions in compounds such as **6.3** (Figure 6.3). In both cases, however, it is generally the cone conformation that is the only one to exhibit significant binding of organic guest molecules. A typical solid-state structure of cone *p-t*-butylcalix[4]arene (**3.118**) binding toluene is shown in Figure 1.23 (note that it is the aliphatic methyl end of the toluene that is extended into the cavity). Solid state $^2$H and $^{13}$C NMR results indicate that the toluene is static at 129 K but at 180 K is undergoing rapid 180 ° flips about its molecular $C_2$ axis with an activation energy of 34 kJ mol$^{-1}$.[2]

Intracavity inclusion of a wide range of aromatic guest molecules in a similar 1:1 fashion has been observed for numerous calix[n]arenes and while the cavity is somewhat chlorophobic, there is an absence of specific host-guest interactions, with space-filling and the consequent gain in van der Waals interactions being the main driving force. Thus a long molecule such as an alkane will curl up to fill space rather than adopt the sterically more favourable all-*trans* conformation. In the case of *p-iso*-propyl calix[4]arene, which forms a 1:1 complex with *p*-xylene, heating in the solid state results in loss of half of the guest molecules to form a cage-like 2:1 structure in which the two guest methyl substituents are

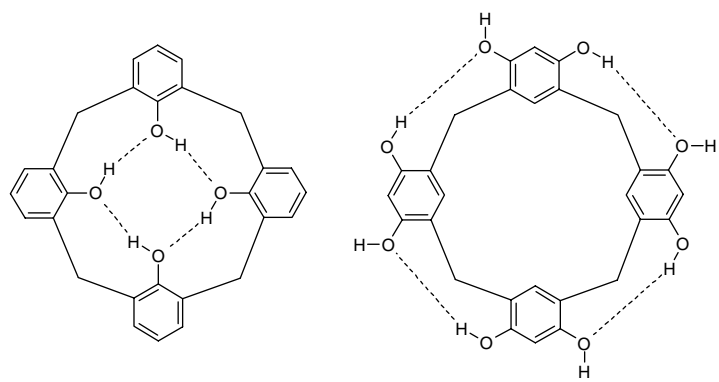

**Figure 6.3** Upper- and lower-rim intramolecular hydrogen-bonding interactions in calix[4]arenes and [4]resorcarenes, which stabilise the cone conformations.

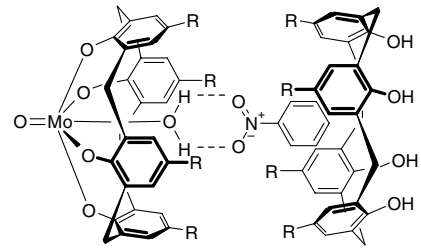

**Figure 6.4** Capsule of [MoO(*p*-*t*-butylcalix[4]arene–4H)]·(*p*-*t*-butylcalix[4]arene)·$H_2O$·$NO_2Ph$ (R = *t*-Bu).[3]

each complexed by different calixarenes. A similar arrangement is observed for the anisole complex of **3.118**, although the anisole guest molecules are highly disordered. A related encapsulating behaviour is also observed for the Mo(VI) derivative of the tetraanion of **3.118**, [MoO(*p*-*t*-butylcalix[4]arene-4H)], which forms an amazing solid state complex with free **3.118**, a water molecule and nitrobenzene (Figure 6.4).[3] In every case, the closest contacts are between the $CH_3$ groups and the aromatic rings with a distance of about 3 Å from the upper-rim alkyl substituents of the host to the guest aryl ring. The calixarene phenolic groups can be extensively derivatised, forming complexes with oxophilic metals as in the Mo(VI) example above and with non-metals. The double-cone structure of the silicon derivative **6.14** inspired M. Wais Hosseini and co-workers from the University of Strasbourg, France, to prepare (solid-state) inclusion polymers termed *koilates* (from the Greek word κοιλοσ meaning hollow) based on linear extended guests such as hexadiyne (Figure 6.5). The double calixarenes (*koilands*) exhibit a natural tendency to stack bowl-to-bowl in their solid state structures and hence combining a long linear guest with the double receptor gives a 1:1 inclusion polymer. Unfortunately, however, the koilate is too unstable to exist in solution.[4]

A wide range of such solid-state inclusion complexes is formed by both calix[4]arenes and [4] resorcarenes with aromatic and aliphatic guests (haloalkanes, acetone, dmf, dmso *etc*.), generally stabilised by weak interactions of the C—H ··· $\pi$ type. Calix[5]arenes also possess a well-defined cavity and form similar complexes, whereas the higher calixarenes such as calix[6]arene and calix[8]arenes (calixarenes all the way up to calix[20]arene have been prepared and isolated chromatographically by the group of C. David Gutsche[5]) form much less defined cavities and often do not exhibit the formation of such well-defined nesting or encapsulated species. One exception to this

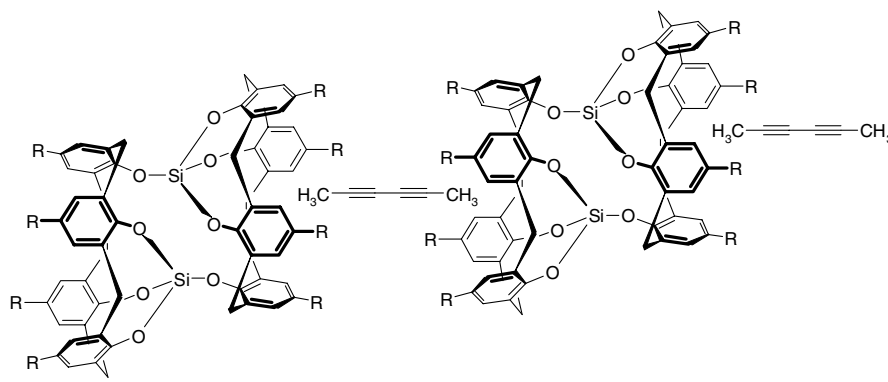

**Figure 6.5** Combination of a double calixarene *koiland* (**6.14**) with a long, linear guest such as hexadiyne gives an inclusion polymer or *koilate* (two repeat units shown).[4]

rule, however, is the inclusion of the fullerenes within calixarenes and cyclotriveratrylene (CTV, **6.10**), see Section 7.8.2. Despite these interesting complexation modes observed in the solid-state, however, there is little evidence for significant binding of neutral, underivatised calixarenes to the majority of molecular guests in non-aqueous solution. The calix[4]arene cavities are relatively small and too conformationally mobile to offer significant solvophobic protection, while the absence of strong host–guest interactions means that there is little enthalpic stabilisation of the complexes. An exception is the complexation of amines by alkylcalix[4]arenes, which gives binding constants in $CD_3CN$ of the order of $10^4\,M^{-1}$. This complexation is thought to occur by a two-stage mechanism involving initial protonation of the amine by one of the acidic calixarene phenolic groups, followed by binding of the guest cation by the resulting calixarene anion. The complex is thus stabilised significantly by ionic interactions. Similarly, even neutral calixarenes can form stable complexes with a variety of organic ammonium cations in solution. For example the *N*-methylpyridinium cation is bound by methoxy derivatives of a range of calix[n]arenes (n = 4, 6 and 8) in a 10:1 mixture of $CDCl_3$:$CD_3CN$, with interaction energies in the range 4.3–5.7 kJ $mol^{-1}$. It is likely that the ammonium cations interact with the polar lower rim of the calixarene rather than the hydrophobic cavity. What affinity calixarene do have for truly neutral molecular guests is highly solvent dependent, with the choice of a solvent that it not bound by the cavity being crucial. Thus in $CCl_4$ for example (a solvent that does not enter the cavity), binding constants of up to 230 $M^{-1}$ have been observed for small guests such as nitromethane by the rigidified, preorganised calix[4]arene **6.16**. One remarkable example of a calixarene binding a gaseous guest, $NO_2$, has been reported by Dimitry Rudkevich of the University of Texas Arlington, USA. Nitrogen dioxide is a gas of particular interest because of its environmental effects and hence there is significant research into its sequestration. Bubbling $NO_2$ into chloroform solutions of both cone and 1,3-alternate conformers of *O*-hexyl-*p*-*t*-butylcalix[4]arenes gives an immediate colour change from colourless to deep purple as a consequence of the formation of charge-transfer calixarene complexes of the highly reactive $NO^+$ cation arising from disproportionation of two molecules of $NO_2$ into $NO^+$ and $NO_3^-$. Over a period of hours the calixarenes are chemically nitrated, however the $NO^+$ complexes can be stabilised by adding a Lewis acid, $SnCl_4$. Treatment with alcohols re-generates the calixarene host unchanged.[6] Related work on other *O*-alkyl analogues gives binding constants in excess of $5 \times 10^5\,M^{-1}$ for $NO^+$ binding as the $SbF_6^-$ salt in $CD_2Cl_2$ and an X-ray crystal structure shows the $NO^+$ ion deeply embedded in the calixarene cavity, Figure 6.6.[7] Other interesting supramolecular chemistry of gases in solid hosts is covered in more detail in Section 7.9, while gas binding by molecular hosts has been recently reviewed.[8]

In aqueous solution, water-soluble calixarenes have the potential to bind much more strongly to organic guests than in lipophilic media because of the hydrophobic effect (Section 1.9). Unfortunately, *p*-alkylcalixarenes are not water-soluble and must be derivatised in order to take them up into aqueous

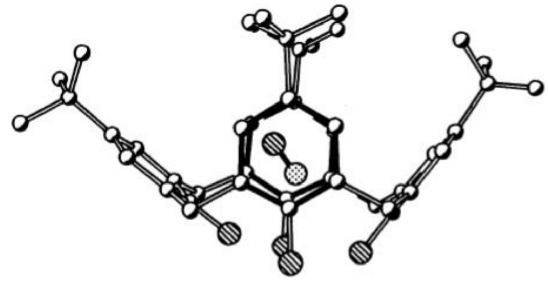

**Figure 6.6** X-ray crystal structure of the $NO^+$ complex of *O*-propyl-*p*-*t*-butylcalix[4]arene, propyl groups and hydrogen atoms removed for clarity (Copyright Wiley-VCH Verlag GmbH & Co. KGaA. Reproduced by permission).

solution. This has been most simply achieved by sulfonation of the upper-rim substituents to give a range of *p*-sulfonatocalix[n]arenes (**6.15a–e**), generally as the sodium salts, which are highly water-soluble.

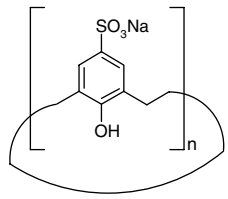


n = 4, **6.15a**
n = 5, **6.15b**
n = 6, **6.15c**
n = 7, **6.15d**
n = 8, **6.15e**

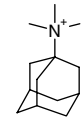


adamantyltrimethylammonium

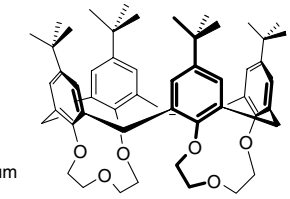


**6.16**

Compound **6.15a** proves to be very acidic in aqueous solution, consistent with the protonation of amine guests by **3.118**, with a first p$K_a$ value of about 3.3, compared to p$K_a$ of >11 for the remaining three phenoxy protons. It is generally accepted that this acidity arises as a consequence of the stabilisation of the deprotonated phenoxy anion, by intramolecular hydrogen bonding. Compound **6.15a** forms strong complexes in aqueous solution with cationic organic molecules, the binding constant for the adamantyltrimethylammonium cation, for example, being 21 000 $M^{-1}$. It is also able to bind neutral molecules such as toluene, although the binding constant is only 7.0 $M^{-1}$. Solid-state complexes of **6.15a–c** all form bilayer structures in which the hydrophobic calixarene portion alternates with hydrophilic layers comprising water molecules, $Na^+$ ions and the calixarene sulfonate functions. These structures closely resemble naturally occurring clay minerals, as we will see in Section 7.8. Other water-solubilising substituents such as aminomethyl and carboxyethyl functionalities have also been appended to calixarenes, as in compounds **6.17** and **6.18**, which were studied in dilute acid or base, respectively. Complexation studies with aromatic compounds such as durene and napthalene in water gave binding constants in the range $6 \times 10^2 - 1.5 \times 10^4\ M^{-1}$. Similar studies on the larger-cavity derivative **6.19** with a range of aromatic guests from durene to chrysene give a linear correlation of binding constant with the number of aromatic rings in the guest, with the binding for the four-ring chrysene being $7.0 \times 10^4\ M^{-1}$.

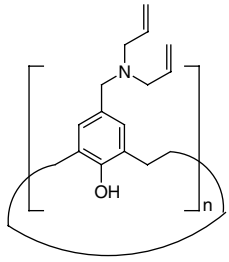


n = 4, 6 and 8, **6.17**

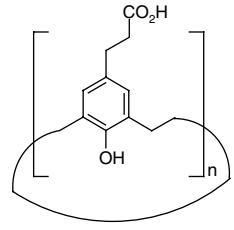


n = 4, 6 and 8, **6.18**

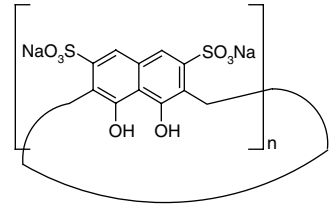


n = 4, **6.19**

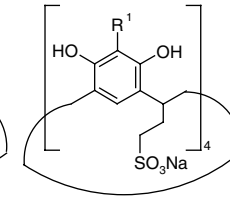


$R^1$ = H, **6.20a**
Me, **6.20b**
OH, **6.20c**

Sulfonated [4]resorcarenes have also been prepared, and their ability to bind a range of sugars and cyclohexanols in aqueous solution has been examined. This work followed from an observation that monolayer assemblies of alkyl derivatives of [4]resorcarenes can detect ribose at concentrations down to $4 \times 10^{-5}$ M at aqueous solution-electrode interfaces. Binding constants for hosts **6.20a–c** are given in Table 6.1. The primary point of interaction is of the guest organic moieties with the apolar region of the host with no hydrogen bonds between host and guest, consistent with the fact that no binding is observed in organic media for lipophilic resorcarene hosts where the main driving force for complexation is

**Table 6.1** Binding constants for sulfonated resorcarenes with various alcohol guests.

| | | $K/M^{-1}$ | | |
|---|---|---|---|---|
| Guest | number | **6.20a** | **6.20b** | **6.20c** |
| Bu$^t$OH | **6.21** | 4.2 | 19 | 24 |
| 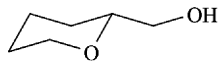 | **6.22** | 30 | 200 | 92 |
| 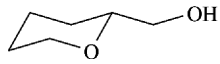 | **6.23** | 29 | 180 | 160 |
| | **6.24** | 16 | 125 | 64 |
| 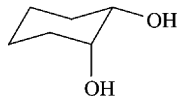 | **6.25** | 14 | 80 | 80 |
| 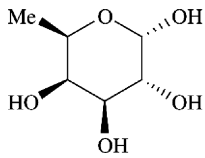 | **6.26** | 1.8 | 6.0 | 8.4 |
| 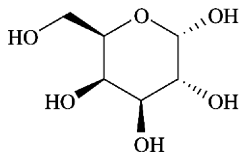 | **6.27** | ~0 | ~0 | ~0 |

hydrogen bonding. Both derivatives **6.20b** and **6.20c** bind guests more strongly than the parent compound, despite the different polarities of their substituents and the degree to which they donate electrons into the aryl rings. It seems that relatively hydrophobic guests such as **6.21** bind preferentially **6.20b** to **6.20c**, whereas the opposite is true for the hydrophilic **6.26**. The highly hydrophilic **6.27** is not bound at all. Overall, the results suggest significant C—H $\cdots$ $\pi$ interactions from the guest to the host electron-rich aryl rings (both $CH_3$ and OH substituents are electron donating).

While the native calixarenes and resorcarenes do not generally posses significant solution affinity for organic molecules, their binding ability may be enhanced markedly by elaboration of the cavity. Synthesis of deeper cavities has the dual effect of increasing the degree of guest shielding from solvent and often results in rigidification of the host, increasing its degree of preorganisation and preventing the cavity from collapsing in on itself. For example, work by Cram *et al*.[9] has resulted in the preparation of a range of multiply bridged [4]resorcarenes such as **6.28** and **6.29**, which exhibit significantly reduced conformational mobility in solution. The substituents, X, are excellent functional groups for even further elaboration of these materials. The presence of a rigid molecular cavity means that compounds **6.28** and **6.29** invariably crystallise with an intracavity guest, and a large range of X-ray structures have been undertaken by Cram's group with guests such as $SO_2$, $CS_2$, $CH_3C{\equiv}CH$, MeCN and $CH_2Cl_2$.

Cavitand **6.29** has a vase-shaped cavity that is large enough to accommodate $Me_2NCHO$ in the solid state. In solution, the most effective host is the dimethylsilyl derivative (**6.28e**), which has a tall, narrow cavity suitable for inclusion of linear guests such as those listed above. Compound **6.28e** is prepared readily from the octol [4]resorcarene **6.3** by treatment with $SiMe_2Cl_2$. The X-ray crystal structure of the $CS_2$ complex of **6.28e** is shown in Figure 6.7, indicating clearly the neat fit of the linear

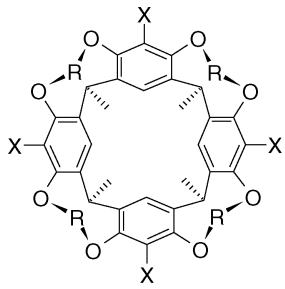

**6.28**

**a** X = H, R = $CH_2$
**b** X = Br, R = $CH_2$
**c** X = $CH_2SH$, R = $CH_2$
**d** X = $CH_2Cl$, R = $CH_2$
**e** X = H, R = $SiMe_2$

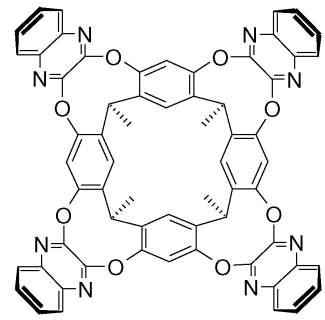

**6.29**

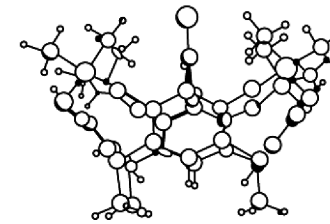

**Figure 6.7** X-ray crystal structure of host **6.28e** with $CS_2$ guest. (Copyright Wiley-VCH Verlag GmbH & Co. KGaA. Reproduced by permission).

guest, threaded through the narrow aperture formed by the host methyl substituents. In non-polar solvents ($CDCl_3$, $C_6D_6$), the free energy of complexation, $-\Delta G°$, for this complex is around 8 kJ $mol^{-1}$.

Calixarenes may also be transformed into effective solution hosts by other ways of elaborating the upper rim. The readily available nature of the calixarene framework has resulted in the synthesis of a number of hosts that use the calixarene as a spacer and rigid, three-dimensional anchor or molecular platform upon which to build other binding groups. This is analogous to the chemistry of the calix-crowns described in Section 3.14. One particularly good example of this approach is the addition of 2,4-diaminotriazine groups on to two opposite calixarene aryl moieties to give the receptor **6.30**. Functionalisation of the lower rim with bulky alkyl ether chains forces the two triazine moieties to position themselves parallel to each another. In this preorganised conformation, they act as an effective hydrogen-bonding receptor for barbiturates.[11] Remarkably, closely related chiral derivatives of **6.30** form chiral helical molecular capsules in both solution and in the solid-state involving three bifunctionalised calixarenes and six 5,5′-diethylbarbituric acid guests (Figure 6.8). Spontaneous non-covalent chiral resolution is observed.[12]

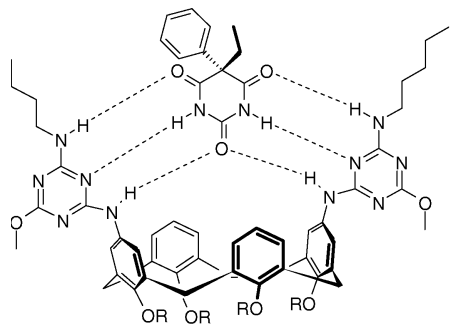

**6.30** R = $CH_2CH_2OEt$

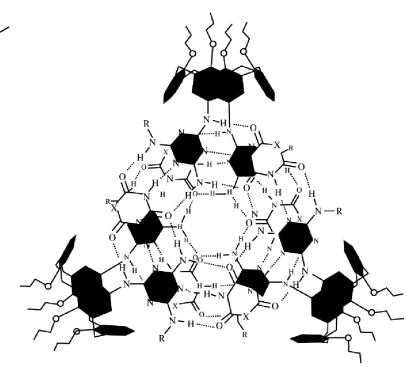

**Figure 6.8** Structure of the chiral nine-molecule assembly formed by three compounds of type **6.30** with resolved diethylbarbituric acid derivatives. (Copyright Wiley-VCH Verlag GmbH & Co. KGaA. Reproduced by permission).

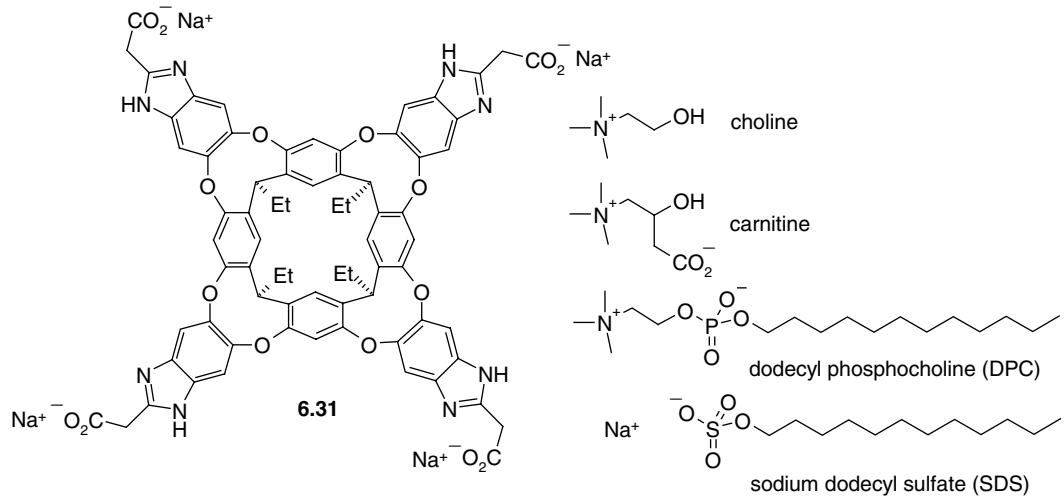


Closely related to **6.29** is the [4]resorcarene **6.31**. The peripherial carboxylate groups impart water solubility and the compound is able to bind strongly to biologically relevant guests such as choline in aqueous solution with $K_a$ in excess of $10^4$ $M^{-1}$ with slow exchange between bound and free guests on the NMR spectroscopic time scale (for reasons explained in Section 6.2.3). The cation-π interactions of the trimethylammonium group with the resorcarene aromatic rings are a significant factor in the complexation and, in contrast, the related carnitine is much more weakly bound ($10^2$ $M^{-1}$) because of the anionic residue. While large ammonium cations are not bound at all, the trimethylammonium head group in dodecyl phosphocholine (DPC) should be able to fit inside the receptor, however it is the doedcyl chain that is included. Analogous results are observed with other surfactants such as sodium dodecyl sulfate (SDS – an anionic surfactant that is used in household products such as toothpastes, shampoos, shaving foams and bubble baths for its thickening effect and its ability to create a lather) are similar with significant upfield shifts in the $^1$H NMR spectra of the complexes indicating that around eight of the twelve carbon atoms are included in the cavity, Figure 6.9.[13] The inclusion of the alkyl chain is driven by the burial of the hydrophobic surface (some 230 Å$^2$) and consequent release of intra-cavity water, attractive van der Waals interactions with the cavity and

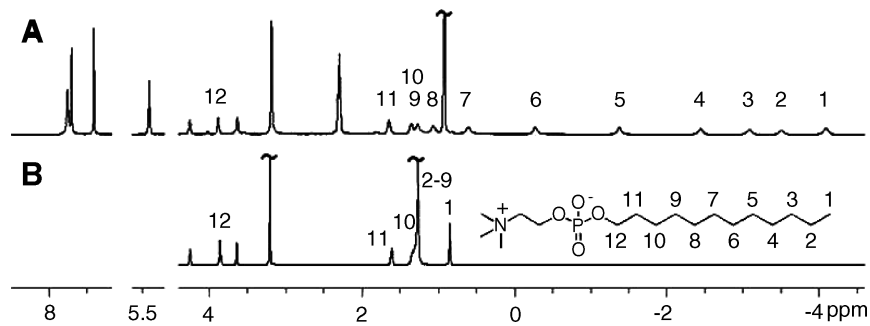


**Figure 6.9** (a) $^1$H NMR spectrum of the DPC complex of **6.31** showing the upfield (to negative ppm) chemical shifts of the included $CH_3$– and $CH_2$– groups of the DPC dodecyl chain (see Box 3.3 for a discussion of the effect of inclusion on chemical shift), (b) reference spectrum of DPC in the absence of host showing the numbering scheme. (Reprinted from [13] with permission from AAAS).

the fact that the alkyl chain of volume 126 Å$^3$ is an excellent fit to the cavity which has a volume of 225 Å$^3$. This ratio represents a packing efficiency of *ca.* 56 % which is an almost ideal ratio (see also cavity occupancy factor, Section 6.6.5). The hydrophobic inclusion affinity is sufficient to overcome unfavourable *gauche* interactions along the chain that result when it is coiled from the favourable all-*trans* conformation into a compressed, helical conformation in order to include the maximum number of methylene groups. Each *gauche* interation destabilises the conformer by *ca.* 2.5 kJ mol$^{-1}$ and there are around five in the bound complex (see Section 3.7.2 for an explanation of *trans* and *gauche* conformations).

Elaboration of the calixarene upper rim with more extensive functionality gives a class of highly 'multivalent' (sometimes co-operative, see Section 1.5) receptors, *i.e.* receptors capable of multiple interactions with large guest species, particularly biomolecules. The role of the calixarene is simply that of a scaffold for the multiple binding functionality. Good examples are a series of carbohydrate derived receptors prepared by Rocco Ungaro and co-workers, of the University of Parma, Italy as in hosts such as **6.32**. In addition to acting as biological energy sources, carbohydrates are increasingly recognised as fundamental substrates for specific receptors in biological processes such as intercellular communication, cell trafficking, immune response, infections by bacteria and viruses, and the growth and metastasis (transmission from an original site to elsewhere in the body *via* blood vessels or the lymphatic system, for example) of tumour cells. All these processes occur due to binding of the carbohydrate residues present on cell surfaces by carbohydrate receptors. In general individual carbohydrate groups are only weakly bound and hence these recognition events depend on the simultaneous complexation of several identical glycoside (carbohydrate precursor) residues, exposed at the substrate surface, by proteins that possess a number of equivalent binding sites. This is an aspect of multivalency that is sometimes called the glycoside cluster effect. Receptor **6.32** is water soluble, but tends to aggregate to form micelles or vesicles (Chapter 13). It binds strongly to lectin proteins such as Concanavalin A (ConA) in the way shown in Figure 6.10.[14] Elaboration of the calix[n]arene framework with guanidinium functionalities gives **6.33a** (n = 4, 6 or 8). Electrophoretic mobility shift assay measurements* show that these hosts bind strongly to both linear and plasmid (cyclic) DNA and can also deliver DNA into cells (transfection). The calix[4]arene derivative binds to DNA through guanidinium–phosphate electrostatic interactions and condenses a single DNA filament into a tightly coiled knot through intramolecular hydrophobic interactions

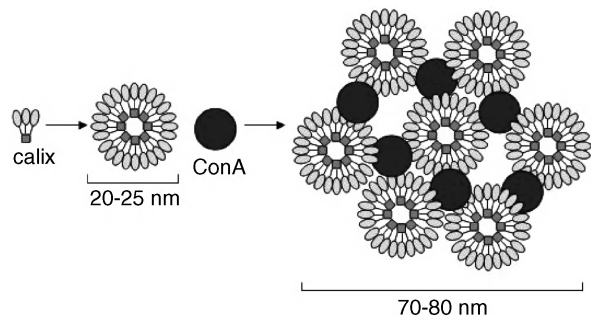


**Figure 6.10** Aggregation and lectin binding by multivalent calixarene carbohydrate-based receptors such as **6.32**.[14]

* The electrophoretic mobility shift assay is a technique commonly used to analyze interactions of DNA with proteins or other DNA-binding ligands. When subjected to electrophoresis (migration under an electric field), free DNA will migrate differently than a DNA-protein complex. When a protein binds to a DNA fragment it hinders the fragment's movement through a gel and so bound DNA is shifted higher on the gel plate compared to unbound DNA.

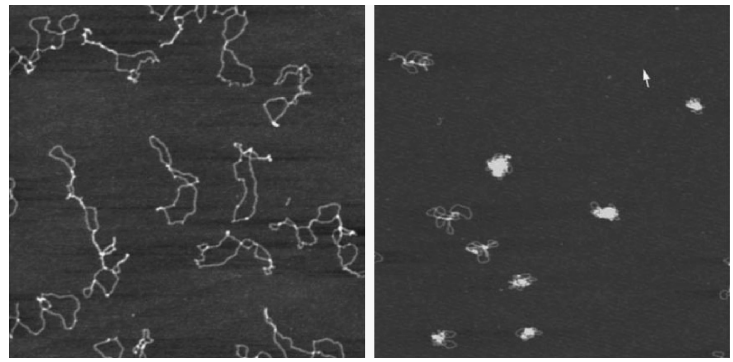

**Figure 6.11** AFM images of (left) 1 nM supercoiled plasmid DNA (left) and (right) condensed blobs of 1 nM supercoiled plasmid DNA in the presence of 1 mM of calixarene **6.33a** (n = 4). Each image is 2 × 2 μm. (Reproduced by permission of The Royal Society of Chemistry).

of the liphophilic chains at the calixarene lower rim. Atomic force microscope (AFM) images of the DNA are shown in Figure 6.11.

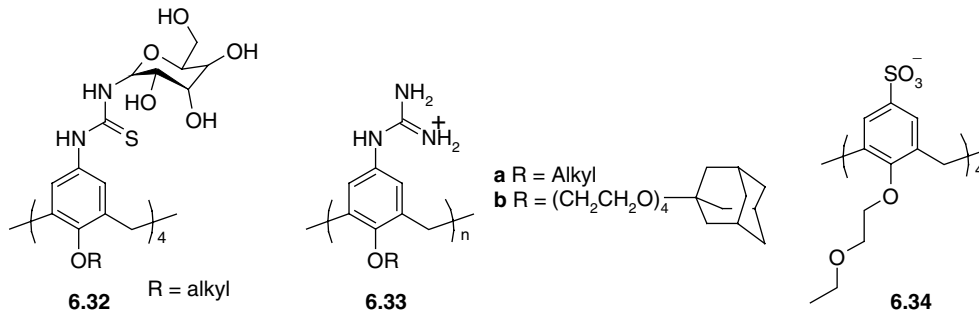


In a remarkable example of multiple host-guest association the related calixarene **6.33b**, which possesses long polyethyleneglycol tails terminated by a hydrophobic adamantyl group, has been assembled on a cyclodextrin functionalised gold surface. The cyclodextrin binds to the gold *via* a thioether linkage forming a self-assembled monolayer (SAM – see Section 13.2.2). Cyclodextrins (discussed in Section 6.3), like calixarenes, have a hydrophobic cavity suitable for binding the adamantyl terminus of **6.33b** with a binding constant of around $10^4$ $M^{-1}$ in water. By immobilising the cyclodextrins on a gold surface, this affinity increases to a striking $10^{15}$ $M^{-1}$ as measured by surface plasmon resonance (see Section 13.2.2), giving a surface-anchored calixarene held by host-guest chemistry that cannot be removed even by a vast excess of free cyclodextrin. In a final elaboration, the surface anchored calixarene was used to form an egg-shaped closed capsule by adding the complementary sulfonate **6.34**, Figure 6.12. The capsule could only be disrupted by adding excess KCl which weakens the electrostatic interactions between the two components.[14] The basis for this capsule chemistry is discussed in Section 10.6.

## 6.2.3 Dynamics of Guest Exchange in Cavitates

In the complexes examined so far in complexation of cations (Chapter 3), anions and neutral species, the overall message that has come across has suggested that capsular complexes, in which the guest

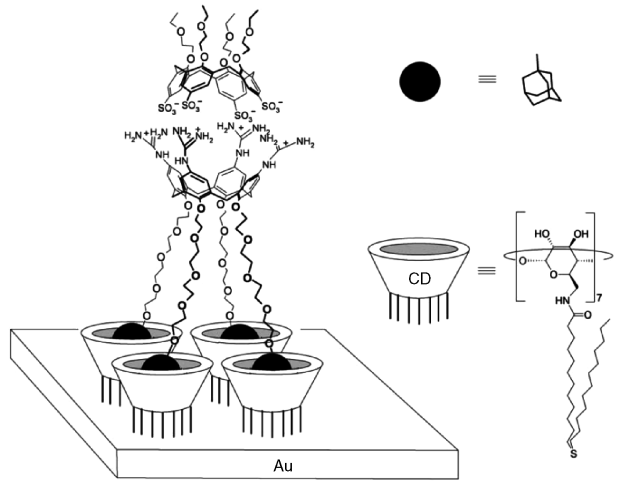


**Figure 6.12** The molecular capsule **6.33b**·**6.34** held by interactions to cyclodextrins as a self-assembled monolayer on gold. (Reproduced by permission of The Royal Society of Chemistry).

(ion or molecule) is encased entirely within an essentially closed host, exhibit characteristically high binding constants and slow guest exchange with those in the outside medium. This was well established by comparing the binding of alkali metal cations by the two-dimensional crown ethers with complexation by the three-dimensional spherands. We will see later (Section 6.7) that this observation is also borne out in neutral molecule binding by a comparison of the calixarenes and resorcarenes with spherical hemicarcerands, and especially carcerands, in which there is no measurable guest exchange at all. In the case of neutral molecules, the reason for the tight binding within the three-dimensional hosts is steric imprisonment as opposed to favourable enthalpic attraction.

It is interesting to speculate, however, upon the mechanism of guest entry and exit from 'open' container molecules (cavitands) such as *p-t*-butylcalix[4]arene (**3.118**). A guest that exhibits a good fit within the calixarene bowl must enter and exit through the open top of the host, as part of an exchange process. Since the guest fits the host cavity, there clearly is not enough room for more than one guest to enter or leave a cavity at a time. To put this another way, the mechanism for guest exchange must be a disassociative one: the original guest must leave the cavity before a new guest can enter. This implies that there must be some kind of intermediate stage in which the host is empty. The host, in effect, contains a vacuum at this stage. Energetically, this is a highly unfavourable situation since the van der Waals interactions between the guest and host surfaces are lost without any compensating interaction (as in the old saying 'Nature abhors a vacuum'). Consequently the activation energy required for such guest exchange should be extremely high and hence the guest exchange kinetics should be slow. In fact, we know that for open, flexible hosts such as calix[4]arene, guest exchange (with other guests and with solvent) is extremely rapid under ambient conditions. So, how do we explain this apparent contradiction? The answer lies in the host's ability to distort temporarily in order to avoid presenting an empty cavity. Host distortion is concerted with guest exit, and hence the guest exchange transition state is only mildly energetically unfavourable as a consequence of small increases in bond strain. Upon entry of the new guest, the host can, of course, relax back to its previous conformation. In the case of the calixarenes, this distortion takes the form of a 'pinch' from $C_{4v}$ to $C_{2v}$ symmetry (Scheme 6.2).[15] This feature becomes of critical importance when the host is rigid, or when such conformational change is associated with a large enthalpic destabilisation. Indeed, it is interesting to speculate upon guest exchange rates in a theoretical host that is entirely rigid. Would guest exchange become impossible

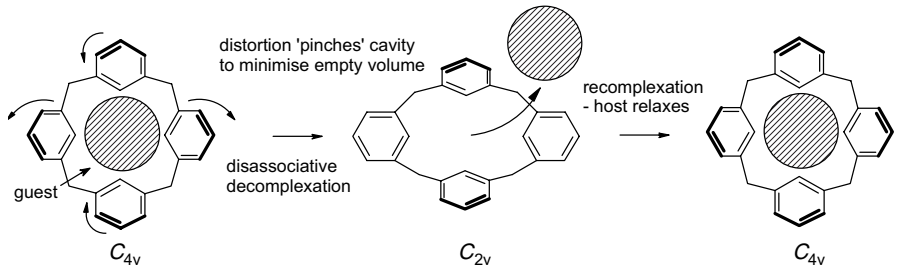


**Scheme 6.2** Cavity volume is minimised during the decomplexation process for flexible hosts such as unmodified calix[4]arenes.

because of the resulting vacuum? The effect would be akin to trying to empty a bottle of milk by up-ending it. The milk is unable to rush out in accordance with the force of gravity because of the vacuum that would be left behind. Air is unable to get in to fill the vacuum because the milk is in the way. The result is (at best) a very turbulent, slow exit for the milk.

A rigid host has been designed in order to test this theory.[16] The host is based on [4]resorcarene (**6.3**) with the resorcarene upper rim elaborated with a rigid network of hydrogen bond donors and acceptors (**6.35**). The hydrogen-bonding moieties result in a deep, open cavity of $C_{4v}$ symmetry, somewhat resembling a whisky tumbler in shape (Figure 6.13). The host is able to adopt both $C_{4v}$ and $C_{2v}$ conformations, but the presence of the cyclic hydrogen-bonding network strongly favours the $C_{4v}$ form.

Large guests such as adamantane fit snugly within this molecular tumbler, giving an $^1$H NMR spectroscopic signal at –1 ppm, consistent with the shielding effects expected from the host aromatic rings. Crucially, separate signals are observed for bound and free adamantane guest, indicating that guest exchange is slow on the NMR time scale. Such an observation is contrary to expectation because the cavity is open and unobstructed, but is consistent with the difficulty in removing guest or solvent from the cavity without leaving a vacuum. In fact, guest exchange does occur slowly by a flower-like opening out of the hydrogen-bonded substituents, breaking the hydrogen-bonded network. Dynamic NMR measurements indicate a large activation barrier of 71 kJ mol$^{-1}$ for the guest exchange process, and it is thought that this energy barrier is associated directly with the loss of the enthalpic stabilisation of the hydrogen bonds. These results suggest that for all 'open' cavitand hosts, neutral organic guest binding in solution may be enhanced dramatically by the construction of rigid concave surfaces with a single, relatively narrow exit and entry aperture. We will come across another example in which guest removal causes host 'implosion' later on in Section 6.6.6.

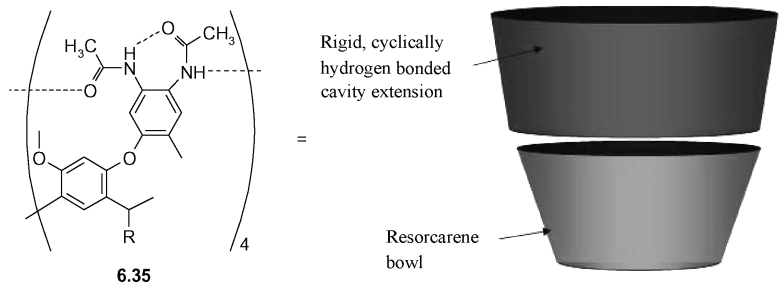


**6.35**

**Figure 6.13** The 'whisky tumbler' shape of **6.35** which possesses an upper rim rigidified by intramolecular hydrogen bonding interactions.[16]

## 6.2.4 Glycoluril-Based Hosts

Kim, K., Selvapalam, N., Ko, Y. H., Park, K. M., Kim, D., Kim, J., 'Functionalized cucurbiturils and their applications', *Chem. Soc. Rev.* 2007, **36**, 267–279.

Glycoluril (**6.4**), because of its curved backbone and versatile derivatisation chemistry, has been used as a fundamental building block in the synthesis of a number of curved 'barrel-shaped' hosts, molecular clips and three-dimensional capsules that form *via* self-assembly (Section 10.6.1). The curvature of diphenylglycoluril is illustrated by the 'molecular clip' derivative **6.36**, which is able to act as a host to aromatic guests such as resorcinol in which the two resorcinol hydroxyl groups point downwards into the molecular cleft in order to hydrogen bond with the host carbonyl oxygen atoms.[17] Binding constants of up to $10^5$ $M^{-1}$ in chloroform have been observed. The structure of the host is shown in Figure 6.14.

Molecular clips such as **6.36** have been elaborated into molecular 'baskets' such as **6.37**. The naphthalene derivative **6.37** can exhibit several conformations that interconvert slowly on the NMR spectroscopic time scale, of which only the *anti-anti* isomer is suitable for guest inclusion, but the *syn-anti* predominates. The compound shows allosteric binding (Section 1.5) of alkali metal cations and aromatic molecular guests because the binding of metals such as $K^+$ to the azacrown ether portion of the molecule converts it exclusively to the *anti-anti* conformation. Thus binding of a second $K^+$ ion is *ca.* 100 times more favourable than the first. In the presence of $K^+$ the affinity for molecular guests such as 1,3-dinitrobenzene increases by a factor of 2–6 depending on solvent.[17] Related baskets can self-assemble into spherical vesicles or tube-like structures depending on the influence of 1:1 or 1:2 alkali metal cation binding.

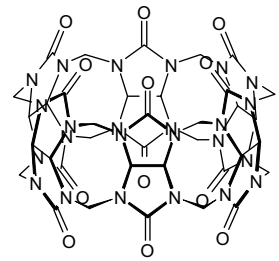

Cucurbituril
**6.38**

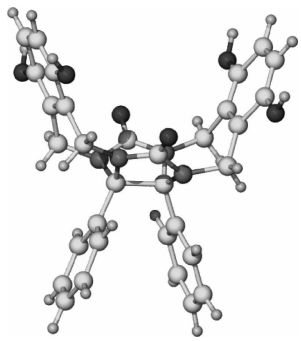

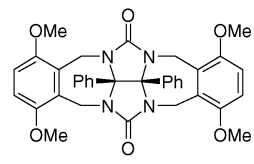

**6.36**

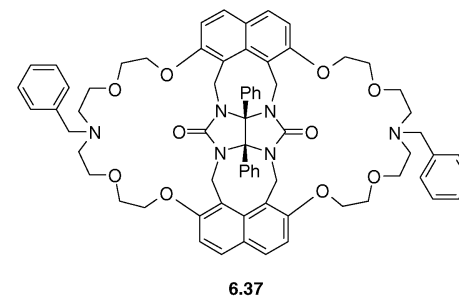

**6.37**

**Figure 6.14** X-ray structure of glycoluril-based host **6.36** showing the intrinsic curvature.[17]

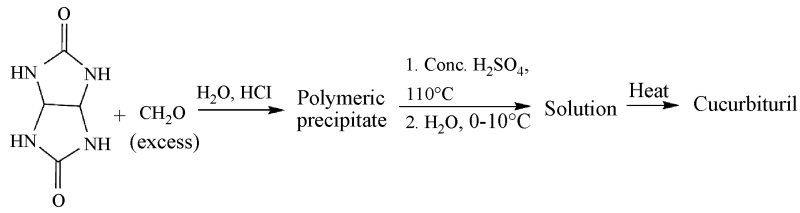


**Scheme 6.3** Synthesis of cucurbituril.

The most well known glycoluril-based host is cucurbituril (**6.38**). Cucurbituril (pronounced 'kyu ker bit yur eel') is named because of the resemblance of the barrel-shaped molecule to a gourd or pumpkin of the *Cucurbitaceae* family, particularly the jack-o-lantern, *Cucurbita pepo.* Compound **6.38** has been known since 1905, although its full characterisation had to wait until the work of William Mock from the University of Chicago, USA, who characterised it by X-ray crystallography and other techniques in the early 1980s. The compound is readily prepared by condensation of glycoluril with formaldehyde. This gives an initial substance that remains poorly characterised, but is probably a cross-linked aminal type polymer. The material is highly intractable and, in efforts to solubilise it, Behrend, who carried out the original 1905 work, treated it with hot, concentrated sulfuric acid, which slowly dissolved it. The resulting solution was diluted with cold water and subsequently boiled, eventually giving a crystalline precipitate, later shown to be **6.38** (Scheme 6.3).

The clean formation of this remarkable hexamer is thought to occur *via* a templated reaction (Section 3.9.1) in which oxonium ions (probably $H_3O^+$) hydrogen bond to the carbonyl oxygen atoms at the top and bottom of the molecule. Cucurbituril is the hexameric member of a whole family of cucurbit[n]urils comprising anywhere from 5 to 11 glycoluril sub-units. No other glycoluril oligomers are found in the reaction shown in Scheme 6.3, although in 1992 Stoddart's group were able to prepare a closely analogous pentamer, named decamethylcucurbit[5]uril, from dimethylglycoluril under milder acid conditions.[18] However, in 2000 the group of Kim were able to modify the original reaction conditions to produce cucurbit[n]urils (CB[n]) where $n = 5 - 9$.[19] The lower reaction temperature in this case suggests that the hexamer is the thermodynamic product and the other homologues are kinetically trapped. As soon as it was prepared, it was recognised that not only was curcubituril remarkably chemically robust, but that it also formed a variety of crystalline complexes with metal salts and dyestuffs. Systematic surveys have shown that the molecule is an effective host for protonated polyamines and metal ions in aqueous solution and the solid state, but not for neutral organic molecules. This inclusion chemistry arises from the presence of the barrel-shaped cavity that is approximate 6 Å deep, and the coordinating ability of the ring of carbonyl oxygen atoms. The pentameric decamethylcucurbit[5]uril has a narrower cavity and does not exhibit extensive inclusion chemistry. Cucurbit[10]uril is initially isolated as a remarkable inclusion complex with cucurbit[5]uril,[20] Figure 6.15, but free cucurbit[10]uril can be isolated by displacing the smaller cucurbituril guest with melamine diamine followed by removal of the new guest through acylation and repeated washing.[21] Inverted cucurbit[n]urils *i*CB[n] are also known in which one glycoluril unit is attached to the macrocycle in a concave fashion. Some cavity properties of the CB[n] and *i*CB[n] families are shown in Table 6.2.

Because cucurbituril does not possess aromatic rings, it might be anticipated that the complexation-induced shifts in guest NMR spectra might be less than those observed in benzenoid derivatives (*cf.* Box 3.3). In reality, however, the aliphatic framework also results in a significant shielding effect. The $^1$H NMR spectrum of 1,5-diaminopentane in $HCO_2H$-$D_2O$ solution, which exhibits two multiplets at $\delta$ 3.17 and 1.77 ppm in the absence of **6.38**, exhibits two new signals at $\delta$ 2.73

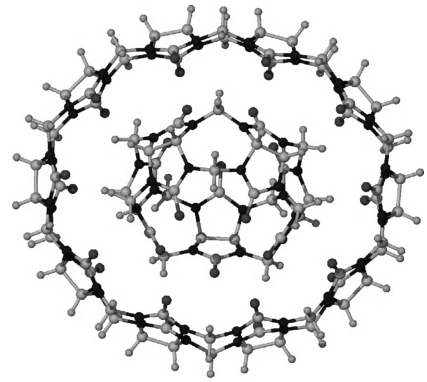

**Figure 6.15** X-ray structure of the inclusion complex cucurbit[10]uril· cucurbit[5]uril.[20]

and 0.77 ppm, which replace those of the free guest as cucurbituril is added. Eventually a stable 1:1 host–guest adduct is formed in which the amine (which is diprotonated by the formic acid) is threaded through the host cavity. Guest exchange is slow on the $^1$H NMR time scale. For a series of diamine guests, $NH_2(CH_2)_nNH_2$ (n = 1–10), in the same medium the highest binding constants occurred for $n = 5$ and 6, corresponding to hydrophobic inclusion of the alkyl chain while allowing hydrogen bonding of the $—NH_3^+$ groups to the carbonyl oxygen atoms (Figure 6.16). Note that there is a symmetry match between the three-fold symmetry of the ammonium substituent and the six-fold symmetry of **6.38**, allowing the formation of three bifurcated, charge-assisted $N^+—H\cdots O$ hydrogen bonds.

Cucurbit[6]uril and increasingly its higher homologues have been used extensively in a variety of host-guest chemistry and nanostructure assemblies. Of particular appeal are rotaxanes and molecular necklaces, mechanically interlocked assemblies of molecules based on CB[6]. Efficient synthesis of 1D, 2D and 3D polyrotaxanes and molecular necklaces (cucurbituril beads linked by a macrocyclic molecule 'string') has been achieved by a combination of self-assembly and coordination chemistry. We discuss rotaxanes and molecular necklaces in Section 10.7, and cucurbil-based systems are summarised in a recent review.[23]

**Table 6.2** Dimensions of the CB[n] and *i*CB[n] families (reproduced by permission of The Royal Society of Chemistry).

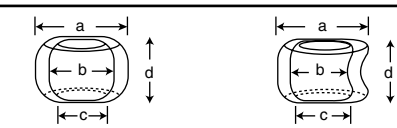


CB[*n*]: $n$ = 5,6,7,8,10 /CB[*n*]: $n$ = 6,7

| | | CB[5] | CB[6] | CB[7] | CB[8] | [a]CB[10] | *i*CB[6] | *i*CB[7] |
|---|---|---|---|---|---|---|---|---|
| Outer diameter/Å | a | 13.1 | 14.4 | 16.0 | 17.5 | 18.7–21.0 | 13.3–14.4 | 14.9–16.0 |
| Cavity/Å | b | 4.4 | 5.8 | 7.3 | 8.8 | 10.7–12.6 | 4.2–5.8 | 5.7–7.3 |
| | c | 2.4 | 3.9 | 5.4 | 6.9 | 9.0–11.0 | 3.9–5.5 | 5.4–6.1 |
| Height/Å | d | 9.1 | 9.1 | 9.1 | 9.1 | 9.1 | 9.1 | 9.1 |
| Cavity volume/Å$^3$ | — | 82 | 164 | 279 | 479 | 870 | — | — |

(a) determined from cucurbit[10]uril· cucurbit[5]uril.[20]

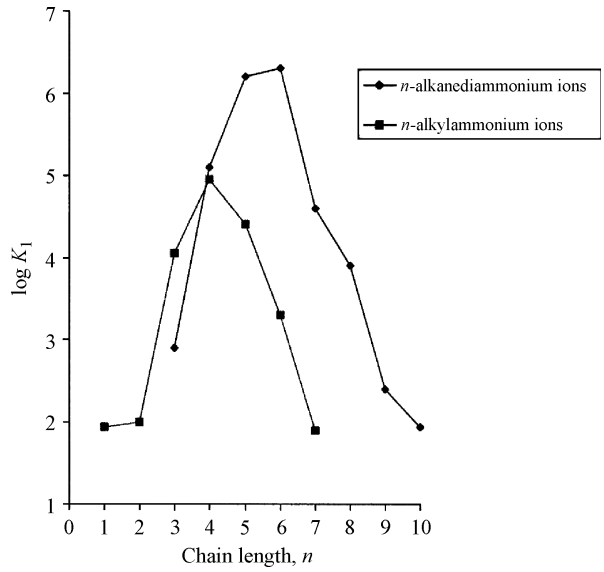


**Figure 6.16** Relationship between binding constant with cucurbituril and chain length for protonated amines, $NH_2(CH_2)_n$, and diamines, $NH_2(CH_2)_nNH_2$, in $HCO_2H$-$D_2O$.

## 6.2.5 Kohnkene

Mathias, J. P. and Stoddart, J. F., 'Constructing a molecular LEGO set', *Chem. Soc. Rev.*, 1992, **21**, 215–225.

In the mid 1980s, J. Fraser Stoddart and Franz Kohnke, then from the University of Sheffield, UK, developed another rather less studied curved building block **6.5**, which is derived from the reaction of 1,2,4,5-tetrabromobenzene with furan (Scheme 6.4). Kohnkene (**6.39**), which was named after its creator, is a very rigid structure, and possesses a small elliptical cavity that is unsuitable for inclusion of molecular guest species. However, the molecule may be deoxygenated to give dideoxykohnkene

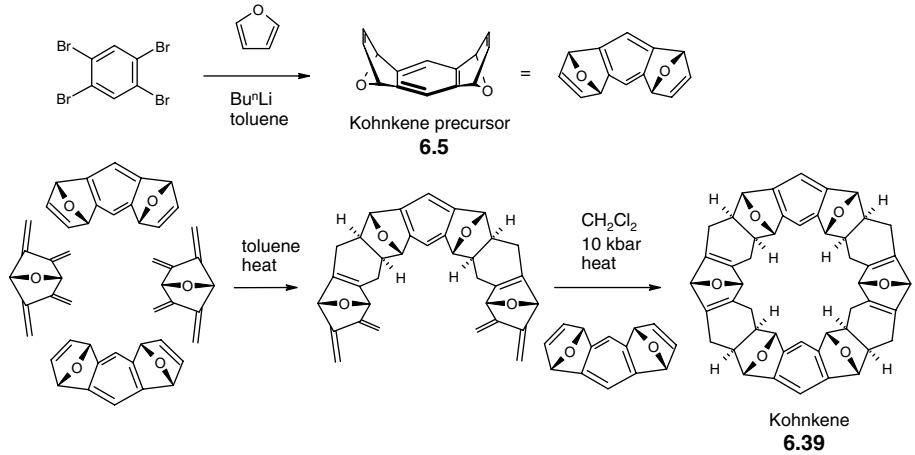


**Scheme 6.4** Synthesis of Kohnkene by multiple Diels–Alder addition.

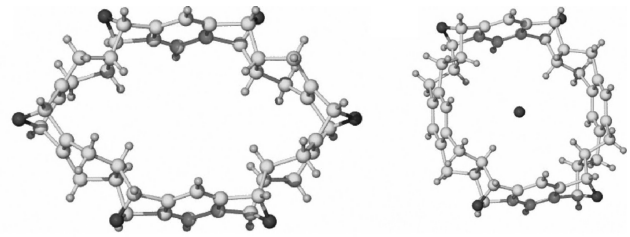


**Figure 6.17** X-ray structures of (a) kohnkene and (b) dideoxykohnkene, showing the included water molecule in the latter.

(**6.40**), which has a rather more square cavity, just the right size to include a single water molecule (Figure 6.17). This example highlights in particular the enormous difficulty and ingenuity required to prepare molecular cage compounds with even a small cavity, a difficulty that increases with cavity size. Stoddart and other co-workers have extended their general approach to form a versatile molecular tool kit that they term 'molecular LEGO' after the children's building blocks, which has enabled them to produce varying sizes of kohnkene-type rings, molecular 'waves' (arising from anti-Diels–Alder additions) and even the cage compound (**6.41**), which they named trinacrene, after the old name, Trinacria, for Franz Kohnke's native Sicily.

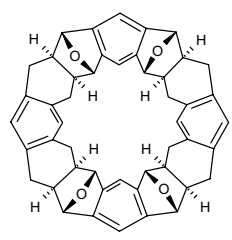

dideoxykohnkene
**6.40**

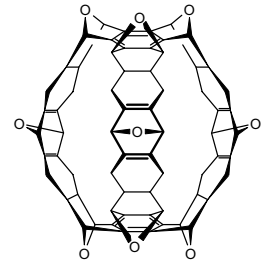

Trinacrene
**6.41**

## 6.3 Cyclodextrins

Szejtli, J. 'Introduction and overview of cyclodextrin chemistry', *Chem. Rev.*, 1998, **98**, 1743–1753.

### 6.3.1 Introduction and Properties

The chemistry of the calixarenes and cavitands (Section 6.2.2) demonstrates clearly that as a molecular cavity becomes more rigid (and therefore preorganised) and deeper, its ability to complex organic guest species in solution is enhanced. As we have seen in the glycoluril-based hosts (Section 6.2.4), linked aromatic rings (cyclophanes) are not the only way to introduce rigidity into a host design. Indeed the most common, most studied and cheapest commercially available hosts, the cyclodextrins, are fully saturated and rely upon a combination of intramolecular hydrogen bonding and a sharp radius of curvature in order to introduce rigidity. Cyclodextrins as a class are enormously important host compounds, with a wide variety of industrial uses in the food, cosmetics and pharmaceuticals sectors, generally as

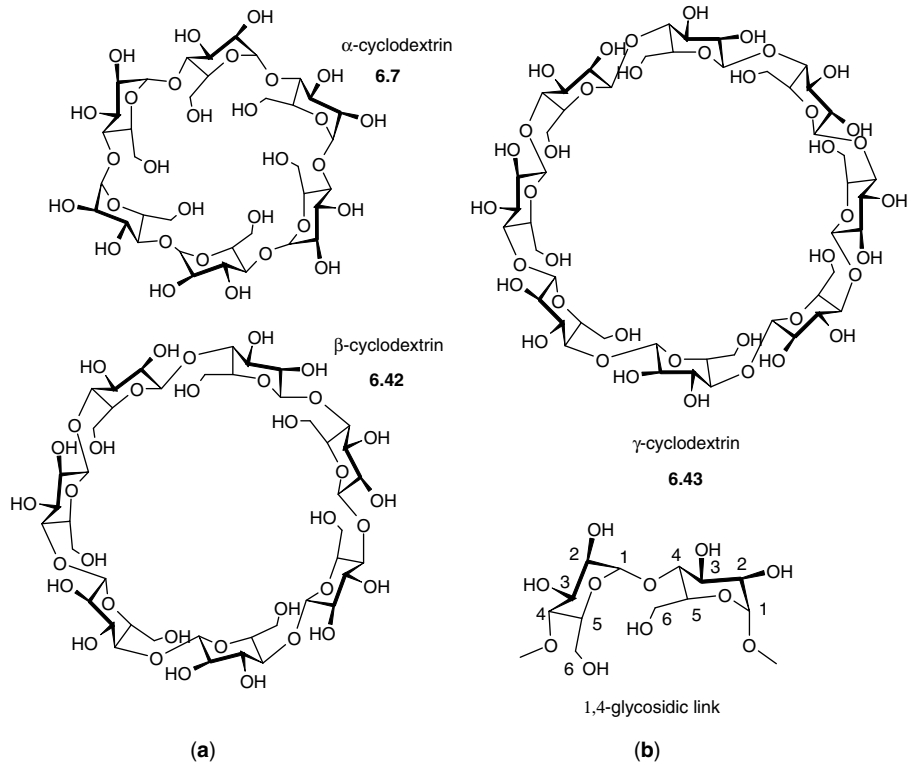


**Figure 6.18** (a) The three most important cyclodextrins. (b) The 1,4-glycosidic link that joins adjacent D-glucopyranoside units.

slow-release and compound-delivery agents. They are also of significant importance as enzyme mimics (Section 12.2). They have the particular advantage of being entirely nontoxic over a wide dosage range. So important are they that an entire volume of *Comprehensive Supramolecular Chemistry* is devoted to them.[24] Industrial production of the most important member of the cyclodextrin family, $\beta$-cyclodextrin (**6.42**), is about 1500 tons per year, and its price is just a few US dollars per kilogram.

Cyclodextrins are cyclic oligosaccharides comprising (usually) six to eight D-glucopyranoside units (Figure 6.18a), linked by a 1,4-glycosidic bond (Figure 6.18b). The three most important members of the cyclodextrin family are $\alpha$-cyclodextrin ($\alpha$-CD, **6.7**), $\beta$-cyclodextrin ($\beta$-CD, **6.42**) and $\gamma$-cyclodextrin ($\gamma$-CD, **6.43**), which possess, respectively, six, seven and eight glucopyranoside units. Several other (minor) cyclodextrins are known, including $\delta$-cyclodextrin and ε-cyclodextrin (nine and ten units, respectively), and the five-membered pre-$\alpha$-cyclodextrin. The $\alpha$, $\beta$, $\gamma$ nomenclature serves to distinguish the different ring sizes of the homologous series and is essentially historical in nature. It is very widely used, however, despite the fact that it does not distinguish the ring size explicitly. This is unsurprising, since systematic names for the cyclodextrins are extremely cumbersome. Other terms for $\beta$-cyclodextrin include cyclomaltoheptose, cycloheptaglucan and cycloheptaamylose, with analogous terms for the other members of the family. The cyclodextrin portion of the name comes from dextrose, an early synonym for glucose. Other cyclic oligosaccharides derived from mannose and galactose are also known, but are much less studied.

The shape of a cyclodextrin is often represented as a tapering torus or truncated funnel and, like the upper and lower rims of calixarenes, there are two different faces to the cyclodextrins, referred to as the primary and secondary faces. The primary face is the narrow end of the torus, and comprises the

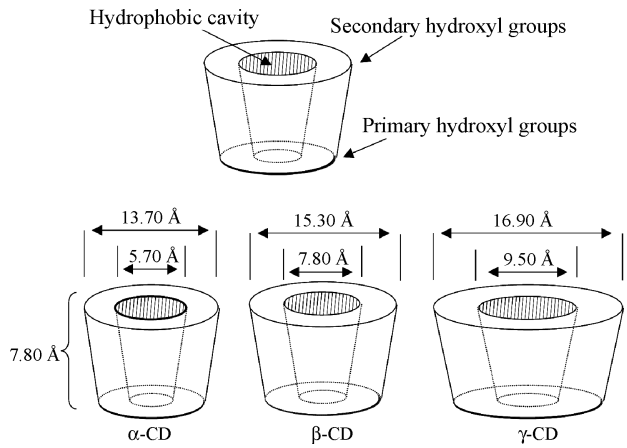


**Figure 6.19** Anatomy of the cyclodextrins.

primary hydroxyl groups. The wider secondary face contains the —$CH_2OH$ groups. The six-membered D-glucopyranoside rings are linked edge to edge, with their faces all pointing inwards towards a central hydrophobic cavity of varying dimensions. It is this cavity, coupled with the water solubility derived from the hydrophilic alcohol functionalities, that gives the cyclodextrins their unique complexation ability in aqueous solution. A functional scheme of cyclodextrin anatomy, along with the cavity sizes is shown in Figure 6.19. Important parameters are given in Table 6.3.

**Table 6.3** Characteristics of $\alpha$-, $\beta$- and $\gamma$-Cyclodextrins.

| | $\alpha$ | $\beta$ | $\gamma$ |
|---|---|---|---|
| Number of glucose units | 6 | 7 | 8 |
| Ring size | 30 | 35 | 40 |
| Internal cavity centre diameter (Å) | 5.0 | 6.2 | 8.0 |
| Solubility in water (g $L^{-1}$,25ºC) | 145 | 18.5 | 232 |
| $\Delta H^o$ solution (kJ $mol^{-1}$) | 32.1 | 34.7 | 32.3 |
| $\Delta S^o$ solution (J $K^{-1}$ $mol^{-1}$) | 57.7 | 48.9 | 61.4 |
| $[\alpha]_D$25ºC | 150.5 | 162.0 | 177.4 |
| Cavity volume ($Å^3$) | 174 | 262 | 427 |
| Cavity volume in 1 g cyclodextrin ($cm^3$) | 0.10 | 0.14 | 0.20 |
| Crystalline water (wt. %) | 10.2 | 13.2–14.5 | 8.13–17.7 |
| p$K_a$ (25ºC, by potentiometry) | 12.33 | 12.20 | 12.08 |
| Rate of hydrolysis by *A. oryzae* $\alpha$-amylase | Negligible | Slow | Rapid |
| Common guests | Benzene, phenol | Napthalene, 1-anilino-8-napthalenesulfonate | Anthracene, crown ethers, 1-anilino-8-napthalene-sulfonate |

In general, the cyclodextrins form a relatively smooth series from $\alpha$- to $\gamma$-CD in terms of their physical and chemical properties, although very large cyclodextrins such as $\delta$-CD begin to deviate because they are less rigid than the smaller hosts and, as a consequence, exhibit much poorer guest complexation ability. One important exception to a smooth change in properties, however, is the cyclodextrins' water solubility (Table 6.3), which is significantly less for the odd-numbered $\beta$-CD than for $\alpha$- and $\gamma$-CD (as determined by refractometry; the measurement of the solution refractive index). The solubility of the odd-numbered $\delta$-CD is also less than for $\alpha$- and $\gamma$-CD, although the deviation is less marked. This relative insolubility of $\beta$-CD has important consequences on its applications as a solution host. A number of explanations have been put forward for this anomalous behaviour. Examination of the enthalpy and entropy of hydration show that both are less favourable for $\beta$-CD than for the smaller and larger analogues. This has been attributed to the interruption of the hydrogen-bonded structure of water by aggregated $\beta$-CD. The reasoning is that the six- and eight-fold symmetries of the other cyclodextrins are more compatible with the solvent cage, which has an even number of hydrogen-bond donors and acceptors. It has also been suggested that the intramolecular hydrogen bonds on the secondary face of $\beta$-CD are responsible for its low solubility, limiting the interactions with solvent water. The analogous hydrogen-bonded network is incomplete in $\alpha$-CD because of strain, whereas $\gamma$-CD is more flexible. Indeed, methylation of the secondary hydroxyl groups increases $\beta$-CD solubility.

All of the cyclodextrins crystallise from water as hydrates containing varying amounts of water, depending on crystallisation conditions. In each case, the semi-polar cyclodextrin cavity is filled with water molecules, which are of relatively high energy as a consequence of their limited interactions with the walls of the cyclodextrin cage. In solution, it has been suggested that a large contribution to the complexation of guest species is the expulsion of these high-energy water molecules from the cavity as part of an overall hydrophobic effect. While probably significant, this contribution seems to involve lowering of an unfavourable term (desolvation of the host) rather than comprising a real driving force in its own right, as we will see. The water distribution in various forms of the crystalline hydrates is summarised in Table 6.4. Note that the solid-state cavity volume is limited for larger cyclodextrins by inclusion of glucose residues from adjacent hosts. Each cyclodextrin crystallises in a variety of forms (denoted by Roman numerals for well-characterised cases). In general, the structures of the cyclodextrin hosts themselves do not vary greatly from one form to another, and the differences lie in the distribution of the water molecules. $\alpha$-CD adopts an elliptically distorted, irregular shape in forms I and III, with two glucose units rotated about their glycosidic linkage to present the primary hydroxyl side inwards towards the cavity, making the cavity volume smaller. The form II hydrate is more regular.

**Table 6.4** Solid-state cyclodextrin hydrates.

| | $\alpha$ | $\beta$ | $\gamma$ | $\delta$ |
|---|---|---|---|---|
| Number of water molecules (form) | 6 (I) | 12 (I) | 19 | 13.75 |
| | 6 (II) | 11 (II) | 14.1 | |
| | 7.57 (III) | | 15.7 | |
| Number of water molecules in cavity (form) | 2 (I) | 7.3 (I) | 7.1 of 14.1 | Two glucose units occupy cavity; water distributed in open space on primary face |
| | 1 (II) | 6.3 (II) | Two glucose units also occupy cavity | |
| | 2.57 (III) | | | |

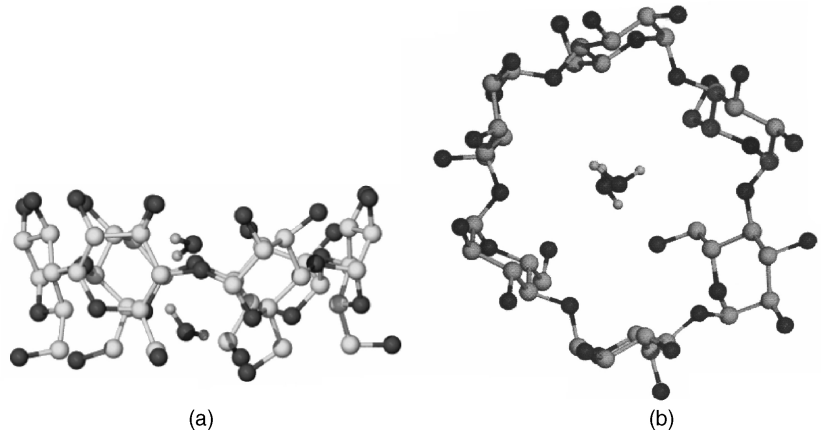


**Figure 6.20** Two views of the X-ray crystal structure of form I of $\alpha$-CD hydrate.

Both forms of the $\beta$-CD have similar host geometries, which are much more regular than $\alpha$-CD, with the occupancies of some of the disordered water sites being higher in form I. The structure of $\beta$-CD hydrate form I is shown in Figure 6.20. The structure of $\gamma$-CD closely resembles that of $\beta$-CD, and again there is complex disorder of the water molecules. Both hosts exhibit a regular array of intramolecular hydrogen bonds on the primary face with O···O contacts in the range 2.70–3.00 Å. The structure of $\delta$-CD is distorted into a boat-like shape, giving it a shallower cavity.

## 6.3.2 Preparation

Plant photosynthesis produces two main products: starch and cellulose. Cellulose is an insoluble, resilient structure-forming component of cells. In contrast, starch is essentially an energy store. It is readily solubilised and converted into biochemically usable forms, and it is from these that cyclodextrins are prepared. Starch comprises two glucose polymers, both consisting of hundreds, or even thousands, of D-glucopyranoside residues: amylose and ramified amylopectin. Amylose contains only 1,4-glycosidic linkages, while the ramified amylopectin also contains 1,6-bonds. Degradation of starch with a variety of enzymes in the presence of water gives rise to the dextrins, which result from the hydrolysis of glycosidic linkages. Dextrins are used in the food, textile and paper industries, and are consumed in the production of bread, beer *etc.* If dextrins are degraded by the glucosyltransferase enzyme, the primary product of the chain splitting (a linear oligosaccharide) undergoes intramolecular cyclisation, without the involvement of water, to give the cyclodextrins. Individual cyclodextrins are isolated from the mixture by complexation with non-polar guests such as toluene (Figure 6.21), which results in dramatic decreases in solubility. Industrially produced cyclodextrins are generally over 99 per cent pure.

## 6.3.3 Inclusion Chemistry

Connors, K. A., 'The stability of cyclodextrin complexes in solution', *Chem. Rev.*, 1997, **97**, 1325–1357.

Generally, interaction of a cyclodextrin with an apolar guest molecule in water results in the formation of 1:1 molecular inclusion compounds, in which the guest in included within the cyclodextrin cavity. Higher equilibria involving the formation of 1:2 complexes, or multiple aggregates involving more than one cyclodextrin, are common, and often exist simultaneously. The driving force for guest inclusion

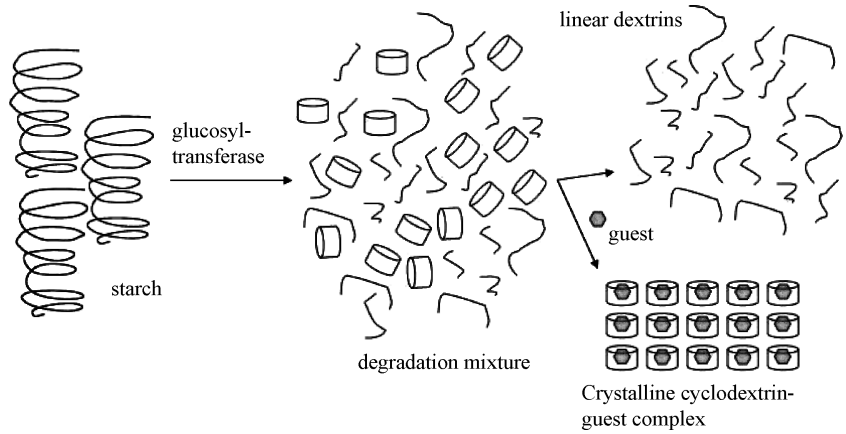


**Figure 6.21** Isolation of the cyclodextrins by glucosyltransferase degradation of starch.

involves a number of contributions, the importance of which is still a matter of some debate. The subject has been discussed in depth in the key reference for this section. Chiefly the factors of importance are:

- steric fit;
- release of high-energy water;
- hydrophobic effects;
- van der Waals interactions;
- dispersive forces;
- dipole–dipole interactions;
- charge-transfer interactions;
- electrostatic interactions; and
- hydrogen bonding.

Table 6.3 shows that, in general, the size of guest that may be accommodated increases as the size of the cyclodextrin becomes larger, although there is some flexibility in the host structures and size fit is not a rigid criterion. Release of high-energy water and the hydrophobic effect (Section 1.9), comprise two energetic components: enthalpic gain as high-energy solvent molecules rejoin the bulk and, entropic gain as two holes in the solvent (host and guest) are reduced to one (complex). The classical hydrophobic effect involves a clearly negative $\Delta S^{o}$, but this is not always the case for cyclodextrin complexes because the cavity is not really non-polar. It has a variety of functionalities and is better described as 'semi-polar'. Nonetheless, non-classical hydrophobic effects may well be highly important. In addition to size fit and solvation effects, solid and solution complexes are often stabilised by additional enthalpically favourable interactions, such as hydrogen bonds between the guest and the primary or secondary cyclodextrin hydroxyl groups and dipolar interactions. Connors (key reference to this section) has developed a generalised model for cyclodextrin complexation in solution, which gives the overall complexation free energy, $\Delta G_{comp}$, as comprising the following terms:

$$\Delta G_{comp} = \Delta G_{intrasolute} + \Delta G_{solvation} + \Delta G_{genmed} \tag{6.1}$$

The term $\Delta G_{intrasolute}$ describes host–guest interactions and must have a favourable or, at worst, zero contribution. It involves contributions from hydrogen bonding, dipolar and van der Waals forces. $\Delta G_{solvation}$ describes solvent effects (hydrophobic, solvent rearrangement). This may be favourable or

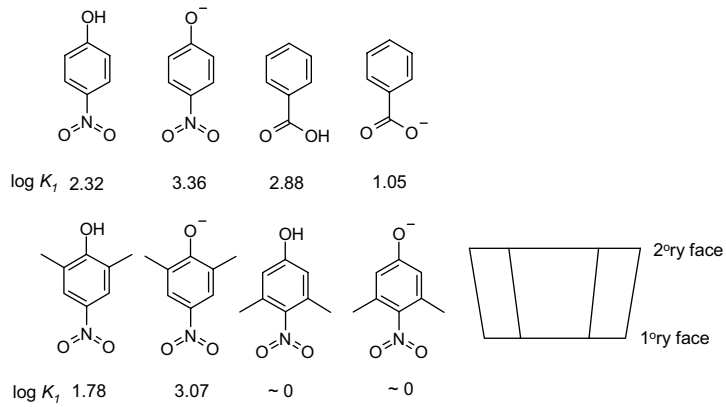


**Figure 6.22** Guests and their binding constants for $\alpha$-cyclodextrin in water.

unfavourable, but is usually unfavourable. This term represents the difference between the solvation free energy of the complex and that of the individual host and guest. If the water within the free cyclodextrin hosts is of high energy, this will tend to make $\Delta G_{\text{solvation}}$ more favourable (or less unfavourable). $\Delta G_{\text{genmed}}$ is a general medium effect, which represents the creation of a solvent cavity, when a solute is dissolved. This term depends on the surface area of the cavity and solvent surface tension. The implication of this relationship is that significant complexation must be driven by favourable contributions from both $\Delta G_{\text{intrasolute}}$ and $\Delta G_{\text{genmed}}$. Binding constants for $\alpha$-cyclodextrin with charged and uncharged guests are shown in Figure 6.22. Clearly, the 4-nitrophenolate anion is bound much more strongly than the analogous neutral compound. The guest is included with the hydrophobic nitrophenyl substituent within the cavity with the phenolate moiety situated at the larger secondary hydroxyl face, and thus hydrophobic interactions are the same for the two guests (*cf.* binding constants for dimethyl nitrophenol derivatives; the bulky 2,5-dimethyl derivative does not fit in the narrow primary hydroxyl region of the cyclodextrin, whereas significant binding is observed for the 2,6-dimethyl analogue where the methyl substituents are situated at the wider secondary face). The additional stabilisation comes from a boost in induced dipole–dipole and van der Waals forces, which arise from the enhanced polarisability of the anion in which the negative charge is delocalised throughout the molecule. This sequence is in direct contrast to the results for benzoic acid and its conjugate base, in which the anion is bound more weakly because the site of ionisation in this guest is also the binding site (*i.e.* the carboxylate residue).

On complexation of aliphatic guests of type $CH_3(CH_2)_nX$, binding is found to be much stronger in cases where X is a polar group, such as COOH or OH, than when X = $CH_3$, again suggesting a significant enthalpically favourable host–guest interaction such as a dipole–dipole or hydrogen-bonding interaction with the host rim.

Interestingly, the fact that the complexation may be detected in solution, *e.g.* by monitoring of NMR spectroscopic shifts, circular dichroism or the observation of a catalytic effect, does not mean necessarily that crystalline or solid-state inclusion complexes may be isolated. In the solid, the hydrophobic repulsion between guest and solvent is absent, and thus if there are no significant attractive interactions, there may be much less complexation driving force. It is not uncommon for stable solution complexes to crystallise as a fine dispersion of isolated host and guest crystals. However, a large range of stable crystalline inclusion complexes have been isolated and, even in the absence of significant favourable host–guest interactions, solid-state complexation may be driven by the need to avoid empty space in the crystalline structure. Guests are required because the cyclodextrin torus cannot collapse in on itself.

Solid-state cyclodextrin complexes generally fall into three broad categories – channel, cage and layer – depending on the orientations of the cyclodextrin moieties and the connectivity between one

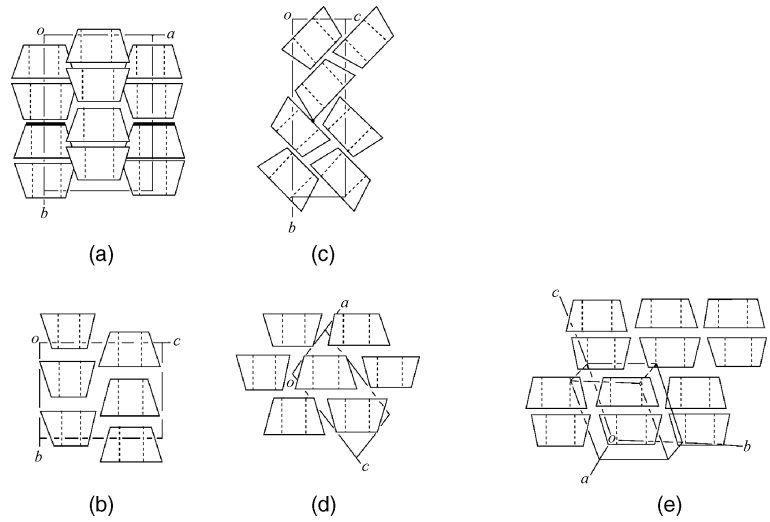


**Figure 6.23** Schematic representation of the packing of cyclodextrin structures. (a) Head-to-head channel type; (b) head-to-tail channel type; (c) cage type; (d) layer type; and (e) layer type composed of $\beta$-CD dimers. (Reproduced from [24] with permission of Elsevier).

cavity and the next. Further subdivisions are observed depending upon the relative orientations of the primary and secondary faces. The possible packing modes are illustrated in Figure 6.23.

Cage-type structures are observed when the guest molecule is small enough to be enclosed fully within the cyclodextrin cavity. This results in a 'herring-bone' arrangement of cyclodextrin molecules. The $\alpha$-CD cavity is large enough to accommodate benzene with its long axis parallel to the pseudo-six-fold symmetry axis, and small organic molecules such as methanol, 1-propanol and 3-iodopropanoic acid, which all crystallise in a cage-type arrangement. Similar encapsulation is observed for $I_2$ and krypton. The $\beta$-CD cavity is large enough to accommodate benzene with its long axis perpendicular to the pseudo-seven-fold symmetry axis. $\beta$-CD also forms cage-like complexes with small guests such as benzyl alcohol (Figure 6.24). There is no evidence that $\gamma$-CD forms cage-type compounds other than with water. This behaviour is a consequence of the inclusion of glucose residues from adjacent molecules on the secondary face, which significantly reduces the cavity volume in the cage arrangement.

With larger guest molecules that do not fit the cavity, all three principal cyclodextrins are capable of forming channel structures in which the cyclodextrin cavities line up in order to produce an extended hydrophobic channel into which guests can be threaded in a similar way to urea clathrates

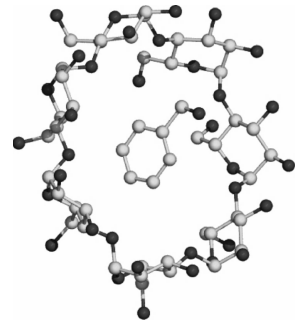

**Figure 6.24** Cage arrangement for $\beta$-CD · benzyl alcohol.[25]

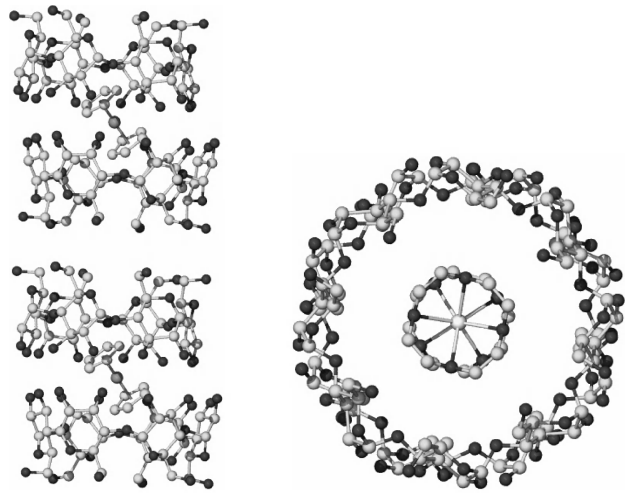


**Figure 6.25** Channel structures of (a) the $\alpha$-CD complex of ferrocene[26] and (b) the 'Russian doll' $\gamma$-CD complex of $[Na([12]crown\text{-}4)_2]^+$.[27]

(Section 7.3). Such structures are observed for the $\alpha$-CD complex of the indicator methyl orange, in which the guest spans three cyclodextrin cavities, and with ferrocene (Figure 6.25a) and the $\gamma$-CD complex of the much larger $[Na([12]crown\text{-}4)_2]^+$ (Figure 6.25b). The inclusion of $Na^+$ within a pair of crown ethers, which are in turn included within a pair of cyclodextrin cavities, has been termed a 'Russian doll' complex by analogy with the traditional Russian *matrioshka* wooden dolls that nest one inside the other. The presence of the chloride counter-ion necessitates the alternation of the metal-crown guest encapsulated by two $\gamma$-CD complexes with a further $\gamma$-CD that has a molecule of free [12]crown-4 included within it, to give an overall stoichiometry of $\{(\gamma\text{-CD})_3 \subset Na([12]crown\text{-}4)_2 \cdot Cl \cdot [12]crown\text{-}4\}$.[27]

## 6.3.4 Industrial Applications

Del Valle, E. M. M., 'Cyclodextrins and their uses: a review', *Process Biochemistry*, 2004, **39**, 1033–1046.

Cyclodextrins have a large range of industrial applications. The market for them is growing as a consequence of their unique inclusion properties and decomplexation kinetics in conjunction with their stability, non-toxicity and relative cheapness. Cyclodextrins are the main active ingredient in Procter and Gamble's deodorising product *Febreze*, for example, where their complexation ability binds molecules responsible for household odours. The principal areas of interest are summarised in Figure 6.26. Some 1,649 research papers were published with the word 'cyclodextrin' in the title in 2006 alone.

The distribution of new research given in Figure 6.26 is not representative of current cyclodextrin applications, however. About 80–90 per cent of cyclodextrin production (mainly $\beta$-CD) is for the food industry, where cyclodextrins are favoured because of their high-temperature stability during food processing. One of the most prevalent use of cyclodextrins is as a process aid in the removal of cholesterol from animal products such as eggs and dairy products. The cholesterol is bound as a guest in the cyclodextrin cavity which is typically successful in removing *ca*. 80 per cent of this unwanted component. Complexation of expensive flavour oils and spices, such as apple, citrus fruits, cinnamon,

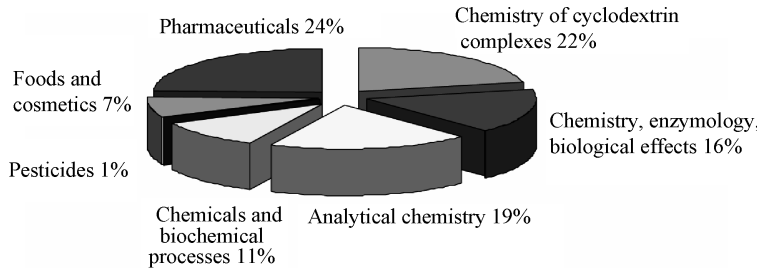


**Figure 6.26** Distribution of papers on cyclodextrin chemistry and applications.

garlic, ginger, menthol, spearmint and thyme, by cyclodextrins dramatically reduces the amounts that need to be added to foods in order to achieve the required flavour strength. Complexation by the cyclodextrin makes the flavourings much more resistant to oxidation, photochemical degradation, thermal decomposition or loss by sublimation. To take just one illustrative example, the amount of onion flavouring required for spiced ewe cheese may be reduced from 550 g per hundred portions to 10 g if the flavouring is complexed with $\beta$-cyclodextrin. Similar stabilisation is achieved for food colourings and pigments, which are apt to decompose photolytically or upon pH changes. To make cyclodextrins even more attractive to food manufacturers, cyclodextrins also impart benefits such as ease of handling and weighing (dry powder as opposed to volatile oil), reduced packaging and storage costs, and reduction of microbial contamination.

In addition to their uses in the food industry, the cyclodextrins are also of application in the pharmaceuticals industry as drug-delivery systems. As in the food industry, the cyclodextrins may act as protecting agents, preventing premature drug metabolism thus allowing, for example, oral rather than intravenous delivery. They may also modify the drug's solubility and biological transport properties, increasing specificity for the target site. Cyclodextrins may also enhance the solubility of poorly soluble drugs without the need to chemically modify the drug itself to include hydrophilic residues, which may interfere with membrane transport of the drug. Finally, cyclodextrin complexation is known to relieve local irritation or drug-induced damage, and to mask unpleasant or bitter tastes.

The other major area of cyclodextrin application is in analytical chemistry, particularly in chromatographic methods such as thin-layer chromatography, gas chromatography, capillary electrophoresis and high-pressure liquid chromatography (HPLC). Again, the role of cyclodextrins is as complexants for the analytes under study. The presence of cyclodextrins (and their derivatives) either as additives to the mobile phase, or chemically bonded to the stationary phase, may improve the separation efficiency and speed of analysis and lead to separations of closely related compounds and isomers, particularly enantiomers. HPLC separation of enantiomers using chiral columns is generally extremely expensive because of the high cost of the stationary phase (US$1000–2000 per column). In contrast, use of a much cheaper ODS (octadecyldimethylsilica) achiral column with $\beta$-cyclodextrin additive in the mobile phase enables the chiral resolution of barbiturates in human serum, for example.[28]

## 6.4 Molecular Clefts and Tweezers

Hamata, M., 'Chiral molecular tweezers', *Acc. Chem. Res.* 2004, **37**, 862–873.

Molecular clips and tweezers are two closely related types of compound. Molecular tweezers represent a simple kind of receptor in which two guest-binding domains usually comprising flat,

aromatic groups, are positioned by a relatively rigid tether (in a more or less preorganised fashion) on either side of the proposed binding site. The guest is then held between the two 'pincers' of the host. In general, aromatic rings or alkynes are used as rigid spaces in order to hold the host pincers at the required distance apart, typically about 7 Å in the case of aromatic guests that π-stack with aromatic binding sites. The spacer and nature of the binding sites should also prevent self-association. The types of tweezers have been expanded greatly since the original definition and terms such as tweezers or clips are used almost interchangeably in a descriptive way. We have already seen a molecular clip based on Tröger's base in action in Section 1.9.2 where we noted the interesting effects of solvation on its binding ability. The molecular tweezers concept originated in 1978 with Howard Whitlock[29] of the University of Wisconsin, USA, exemplified in molecular tweezers **6.44**, which rely upon a combination of $\pi$–$\pi$ stacking and ion–dipole interactions for guest binding. Whitlock's work was inspired by the observation, in 1970, that the hydrolysis of aspirin in water is inhibited by caffeine, suggesting some kind of binding of the drug by the caffeine. Whitlock anticipated that this binding might be studied using better defined systems such as host **6.44** with guests such as the potassium salt of 1,3-dihydroxy-2-naphthoate (KDN). The distance between the two theophylline pincers in **6.44** is held fairly rigidly by a six-carbon diyne spacer, which allows some pivoting at the $sp^3$ methylene linkers (Scheme 6.5). The complex studied between **6.44** and KDN is highly insoluble and so could not be studied by NMR spectroscopy. Instead, the binding constant was measured by the assessment of partition coefficients by UV–Visible spectroscopy between phosphate-buffered aqueous solution and dichloroethane. This gave respectable binding constants in the region of $10^4$.

The molecular tweezers concept has been extended by Zimmerman[30] to the double recognition of guests *via* $\pi$–$\pi$ stacking pincers with a hydrogen bonding core. The compounds incorporate a rigid backbone that enforces a *syn* conformation hence increasing preorganisation and 'turning off' the kind of conformational mobility shown in Scheme 6.5. Host **6.45** binds 9-alkyl adenines such as 9-propyladenine (9PA) with binding constants of up to $1.2 \times 10^5\ M^{-1}$ in chloroform. Replacement of the $-CO_2H$ group with the analogous methyl ester ($CO_2Me$) disrupts the hydrogen-bonding complementarity and reduces dramatically the complex stability in chloroform. Similarly, dimethylation of the primary amine (N6) group again reduces the complex stability because it eliminates the stabilising NH···O hydrogen bonds.

Very rigid tweezers such as **6.46** and **6.47** based on methylene-bridged 6-membered rings have been produced by the Klärner group.[31] Molecular models of the geometries of these compounds are shown in Figure 6.27. While **6.46** really is a very rigid molecule, **6.47** behaves much more like a pair of tweezers

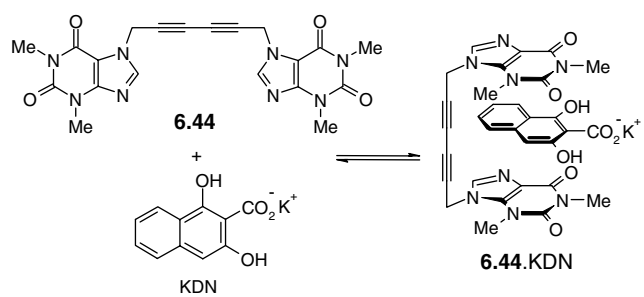


**Scheme 6.5** Conformational change in molecular tweezers **6.44** upon aromatic guest binding.[29]

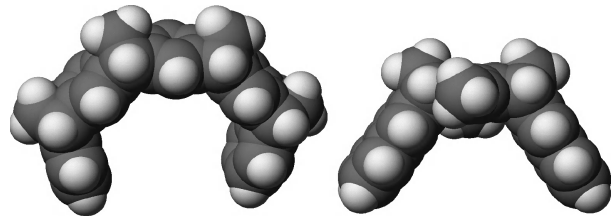

**Figure 6.27** Optimised geometries of molecular tweezers **6.46** and **6.47**. Tweezers **6.47** are *ca.*10 Å wide at the tips but can close up upon guest binding. [31]

and contracts from an approximately 10 Å separation in the free state to 7.6 Å in the 1:1 complex formed with 1,4-dinitrobenzene.

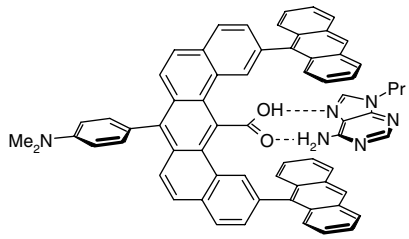

**6.45**.9PA

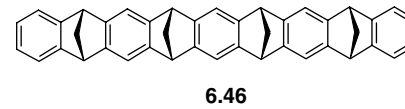

**6.46**

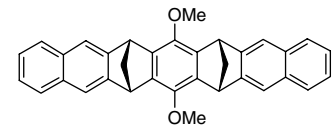

**6.47**

Work by Rebek has resulted in the production of a versatile series of rigid clip hosts such a **6.48**–**6.50**.[32] These molecules are prepared readily from the conformationally rigid Kemp's triacid and various aromatic diamines (Scheme 6.6). The key feature of these hosts is the rigidity of the framework, which organises the materials into convergent 'C'-shaped receptors. This rigidity is a consequence of

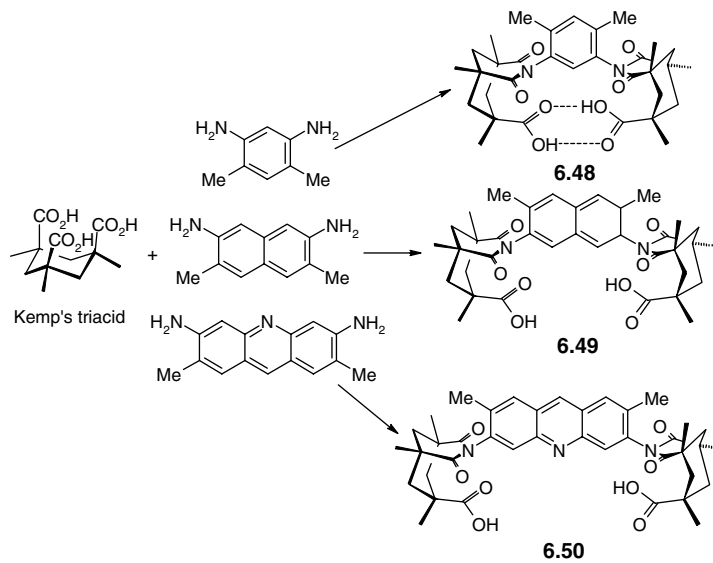

**6.48**

**6.49**

**6.50**

**Scheme 6.6** Synthesis of Kemp's triacid derived molecular clips.

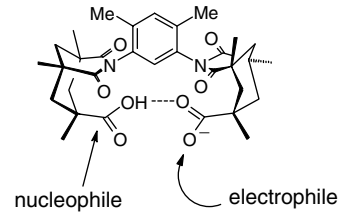


**Figure 6.28** Approach trajectories for nucleophilic and electrophilic attack on the molecular clip **6.48**.

the presence of methyl substituents on the cyclohexane rings, which prevent epimerisation of the axial carboxyl groups, and the methyl groups on the aryl spacers, which prevent rotation about the N—Ar bonds. If not inhibited, both of these processes would result in isomerisation to divergent receptors. Host **6.48** shows interesting reactivity patterns as a result of the inhibition of electrophilic attack (*e.g.* alkylation by diazomethane, $CH_2N_2$) on the carboxylate functions because of intramolecular pair-wise hydrogen bonding. Nucleophilic attack on the carboxyl carbon atom is not inhibited because the incoming nucleophile does not need to insert itself between the two arms of the pincer in order to react (Figure 6.28).

The larger tweezers **6.49** and **6.50** do not undergo intramolecular hydrogen bonding and the two pincers communicate only *via* solvent molecules. The cleft is therefore available for substrate binding and studies have focussed on biologically relevant guests with a view to applications as a model for biological (enzyme) catalysis. In particular, the related imide tweezer host **6.51** is able to extract adenine, and even carbohydrates such as adenosine and deoxyadenosine, from aqueous solution and transport them across liquid organic membranes.

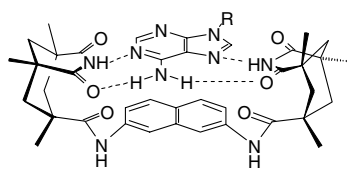


**6.51**.adenine

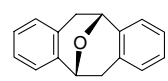


**6.52**
Kagan's ether

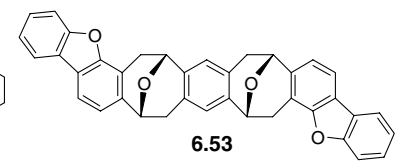


**6.53**

Extensive recent work by Mike Harmata of the University of Missouri–Columbia, USA, has focussed on the Kagan's ether scaffold, **6.52**. Kagan's ether has a bent shape suitable for forming molecular clips/tweezers, and is chiral. Using an 'inside out' synthetic approach Harmata's group were able to prepare a number of tweezers containing two Kagan's ether units and resolve then into a single diastereoisomer during the synthesis. While derivatives terminated with benzo groups do not bind aromatic guests, extending the tweezers as in the dibenzofuran derivative **6.53** does result in effective binding of electron deficient guests such as trinitrobenzene. The $C_2$ chiral curved shape of **6.53** is shown in Figure 6.29a. Harmata's group probed the chiral recognition properties of **6.53** by eluting it through a chiral a (3*R*,4*S*) Whelk-O 1 silica-based chromatography column (Figure 6.29b) using high pressure liquid chromatography (HPLC). Since the column is chiral then the enantiomer of **6.53** that binds most strongly to the chiral guest (which resembles trinitrobenzene for which the host has a known affinity) will elute more slowly than the 'wrong' enantiomer. Separation factors for the enantiomers of **6.53** (corresponding to enantioselectivity) range from 1.21 to 1.75 depending on solvent and hence the host is capable of modest chiral differentiation. The enantioselectivity is somewhat solvent dependent because the diastereomeric host-guest complexes are stabilised to different extents by different solvent media.

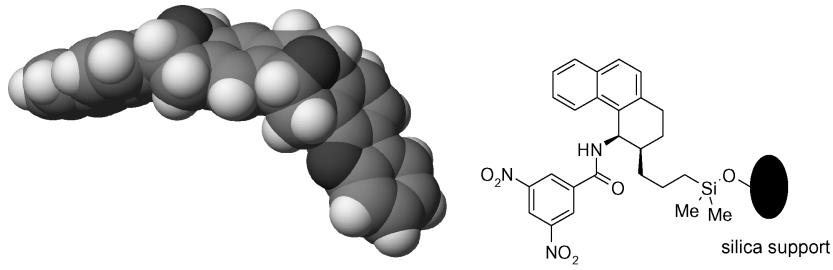


**Figure 6.29** (a) molecular model of the chiral tweezers **6.53**, (b) the chiral guest that forms part of the π-acidic stationary phase, a (3*R*,4*S*) Whelk-O 1 silica-based chromatography column.

By carrying out the chromatographic analysis at different temperatures a van t'Hoff analysis is possible which demonstrates that enantiodifferentiation is enthalpic in nature with the all-*S* enantiomer of the host binding more strongly by *ca*. 0.5 kcal $mol^{-1}$ (2 kJ $mol^{-1}$)

## 6.5 Cyclophane Hosts

Gleiter, R. and Hopf, H. (eds), *Modern Cyclophane Chemistry*, Wiley-VCH: Weinheim, 2004.

### 6.5.1 General Aspects

The term 'cyclophane' literally means any organic molecule containing a bridged aromatic ring. Thus specific cyclophanes such as the calixarenes and resorcarenes that we encountered in Section 6.2 fall under this category. They have been treated separately partly because they possess a number of properties unique to the presence of multiple benzenoid rings and partly because they have been studied so extensively. The chemistry of aromatic rings and their evolution towards cyclophanes with interesting electronic and structural properties has long aroused interest (Figure 6.30). We will focus primarily on the supramolecular aspects of cyclophanes as host-guest systems and the following

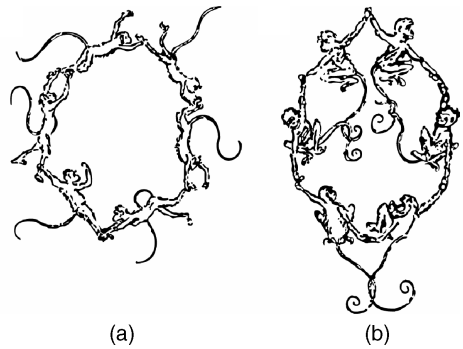


**Figure 6.30** Illustration from a spoof issue of *Berichte der Durstigen Chemischen Gesellschaft* (Berlin, 1886) showing (a) monkeys grasping one another's limbs, an image that originally inspired Kekulé's structure of benzene and (b) a facetious benzene 'tautomer' in which the monkeys are allowed to use their tails instead of their feet for bonding. The purported effect was termed a 'caudal residual affinity'.

sections serve to illustrate lessons from the much wider variety of synthetic cyclophane hosts that have been designed to bind organic molecules in aqueous and non-aqueous media. By definition, cyclophane hosts must contain at least one macrocyclic ring and thus must achieve closure by some means of curvature. This curvature is often based upon the kinds of intrinsically curved components shown in Figure 6.2, and hybrid hosts containing such fragments are common. Cyclophane hosts commonly bind both neutral molecules and organic cations, and there is sometimes even some ambiguity as to whether a guest is protonated by, for example, a hydrogen bond acid host or vice versa, resulting in charge-assisted binding. Cyclophanes may or may not contain a molecular cavity large enough to host guest species, but in some cases cavities are unnecessary to achieve high binding affinity as long as binding sites exhibiting stereoelectronic (steric and electronic) complementary to the guest and are properly positioned (preorganised) on the surface of the host. Thus cyclophanes can exhibit capsular or nesting types of binding, or even apolar surface interactions, often leading to aggregation. Cavities are frequently encountered however, because of the entropic and enthalpic gains associated with spherical or three-dimensional encapsulation of the guest by a host with convergent binding sites.

## 6.5.2 Cyclophane Nomenclature

Powell, W. H., 'Phane nomenclature. Part I: phane parent names', *Pure Appl. Chem.*, 1998, **70**, 1513–1545, and Favre, H. A., Hellwinkel, D., Powell, W. H., Smith, H. A., Tsay, S. S. C., 'Phane nomenclature. Part II. Modification of the degree of hydrogenation and substitution derivatives of phane parent hydrides – (IUPAC Recommendations 2002). *Pure and Applied Chemistry* 2002, **74**, 809–834. online: http://www.chem.qmul.ac.uk/iupac/phane and http://www.chem.qmul.ac.uk/iupac/phane2 (Accessed October 2007)

Cyclophane chemistry can be traced back at least as far as 1899 when Pellegrin prepared [2.2]metacyclophane.[33] In general, any aromatic ring bridged by at least one aliphatic *n*-membered bridge with $n \geq 0$ is termed a cyclophane (a contraction of *cyclophe*nylene alk*ane*). The number of atoms, *n*, in each bridge is denoted in square brackets in front of the name 'cyclophane', starting with the longest one along with a designator (ortho-, meta- or para- or numbers in brackets) indicating the substitution pattern of the aromatic ring(s). For multibridged arenes the number of equal bridges can be indicated as a subscript to the number of carbon atoms they contain. Thus compound **6.54**, originally prepared independently by Brown and Farthing (1949)[34] and Cram and Steinberg (1951)[35] is denoted [2.2]paracyclophane. Calix[4]arenes (such as **3.118**) are, formally, substituted [1.1.1.1]metacyclophanes, while cyclotriveratrylene (**6.10**) is a hexamethoxy [1.1.1]orthocyclophane. The presence of heteroatoms gives rise to related names, *e.g.* nitrogen-containing bridged aromatic rings are termed *azacyclophanes.* Some examples are shown as **6.55** – **6.57**.

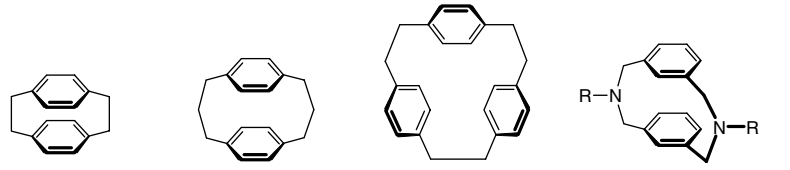


[2.2]paracyclophane **6.54** | [3.3]paracyclophane **6.55** | [2.2.2]paracyclophane **6.56** | diaza[3.3]metacyclophane **6.57**

The International Union of Pure and Applied Chemistry (IUPAC) produced a set of rules for the definition of highly complex ring systems. Under these guidelines a cyclophane (i) has a 'mancude'

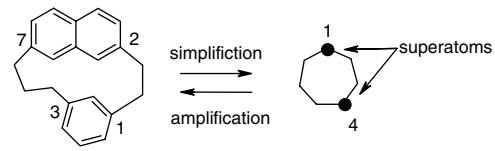


[3]metacyclo[2](2,7)naphthalenophane

1(2,7)-naphthalena-4(1,3)-benzenacycloheptaphane

**Figure 6.31** Application of the Vogtle/Neumann and IUPAC nomenclature for cyclophanes.

ring system (maximum number of non-cumulative double bonds), or an assembly of mancude ring systems, and (ii) atoms and/or unsaturated chains as alternate components of a large ring. In the IUPAC rules each aromatic ring is collapsed to a single atom ('superatom') that together with the remaining backbone is named as an alicyclic ring system (= aliphatic ring) with the *–ne* ending replaced by *–phane*. The superatoms are then designated by prefixes derived from the names of the parent arenes by changing the terminal *–e* to an *–a*, thus 'benzene' becomes 'benzena–'. The arene position is denoted using the ring position of the superatom. An example is shown in Figure 6.31 in which the [3]metacyclo[2](2,7)naphthalenophane collapses to a cycloheptaphane alicyclic ring. Under the IUPAC nomenclature this becomes 1(2,7)-naphthalena-4(1,3)-benzenacycloheptaphane.

## 6.5.3 Cyclophane Synthesis

Breitenbach, J., Boosfield, J. and Vögtle, F., 'Some general synthetic strategies towards macrocyclic systems', in *Comprehensive Supramolecular Chemistry*, J.L. Atwood, J.E.D. Davies, D.D. MacNicol and F. Vögtle (eds), Pergamon: Oxford, 1996, **2**, 29–67.

Cyclophane synthesis necessarily involves the closure of medium- to large-sized rings and is therefore always problematic because of competing oligomerisation and polymerisation reactions. It is beyond the scope of this work to present a detailed treatment of the numerous procedures for preparing cyclophanes, but an excellent overview may be found in the key reference and literature.[36] Some common techniques and particular 'tricks' in this advanced form of organic synthesis are worth referring to, however, and a few important reactions in cyclophane (and macrocyclic) synthesis are listed below:

1. *Nucleophilic substitutions involving sulfur, and sulfur extrusion reactions.* Sulfur is much more reactive than oxygen as a consequence of the greater acidity of the SH functionality. Intermediate thioethers may be oxidised to the corresponding S=O or $SO_2$ derivatives, and pyrolysis results in sulfur extrusion to give the corresponding C— C bonded species, such as **6.58** (Scheme 6.7).
2. *Amine-aldehyde condensations.* Sometimes known as a Schiff base condensation, the reaction of dialdehydes with diamines has been used extensively in the preparation of macrocyclic ligands for metal cations. Reduction of the resulting imine (C═N) group with $NaBH_4$ gives the corresponding aliphatic amine (Section 3.10.6).
3. *Conversion of* ω*-hydroxy acids into lactones via the Mitsonobu reaction* (Scheme 6.8). Ring size and degree of oligomerisation is dependent on temperature and additives.
4. *Carbon–carbon bond forming reactions* such as Wurtz coupling and 1,6-elimination, *e.g.* synthesis of [2.2]paracyclophane (Scheme 6.9). Here the lack of templation means that competing cyclisation and polymerisation is a significant problem.
5. *Amide formation via* reaction of amines with an acid chloride as in the synthesis of various cryptands (Scheme 3.6).
6. Copper-catalysed alkyne coupling (Scheme 6.10).

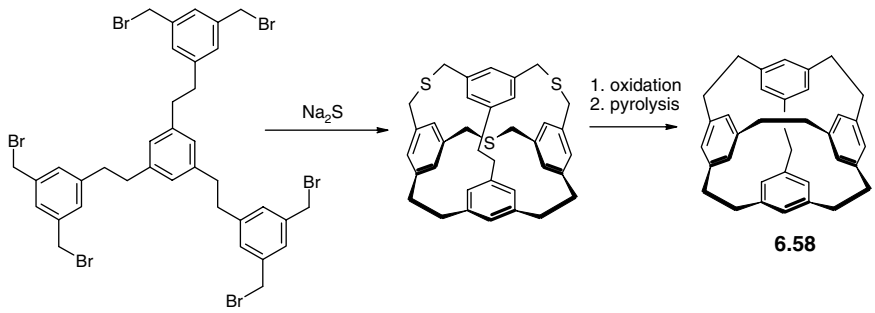


**Scheme 6.7** Macrocycle synthesis *via* sulfur extrusion.

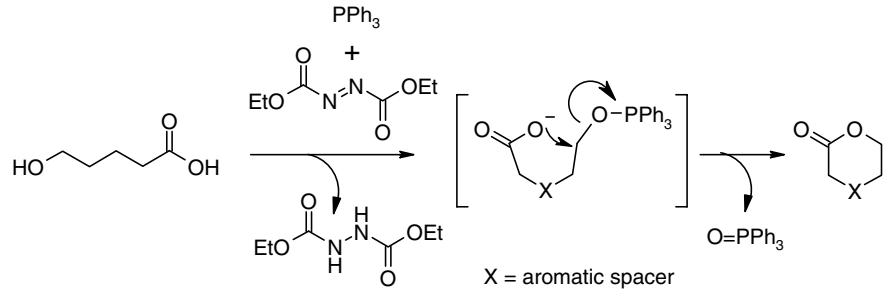


**Scheme 6.8** Conversion of *ω*-hydroxy acids into lactones *via* the Mitsonobu reactions.

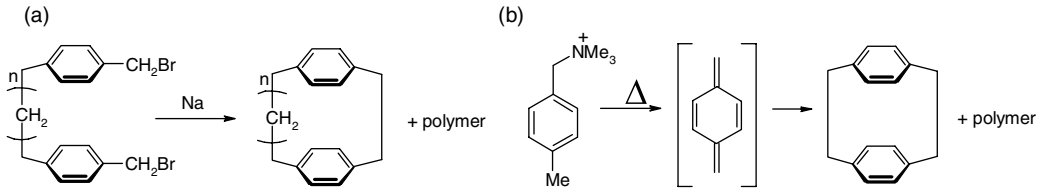


**Scheme 6.9** Preparation of a simple cyclophane *via* (a) Wurtz coupling and (b) 1,6-elimination.

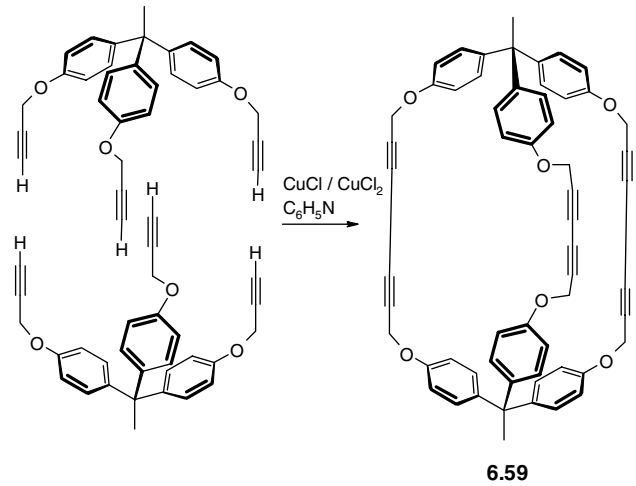


**Scheme 6.10** Copper-catalysed alkyne coupling.

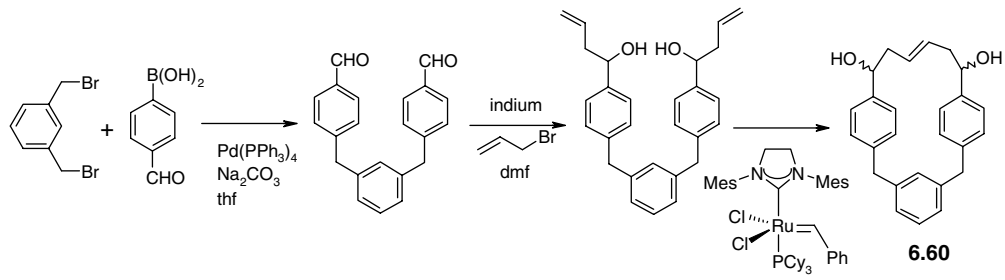


**Scheme 6.11** Suzuki-Miyaura cross-coupling and alkene ring closing metathesis reactions.[37]

7. *Alkene metathesis*. The alkene metathesis reaction won the 2005 Nobel prize in chemistry for Grubbs, Schrock and Chauvin and has become tremendously widely used across all branches of synthetic chemistry including macrocycle synthesis. The reaction involves the metathesis (exchange) of the carbon atoms from one double bond with those of another, hence it is particularly useful for marcocyclisation by linking together two pendant alkene groups. In the example shown in Scheme 6.11 the alkenes are installed by palladium-catalysed Suzuki-Miyaura cross-coupling, followed by alkylation. The alkene ring-closing metathesis reaction is then used to cyclise the product to give cyclophane **6.60**.[37]

As far as azacyclophanes are concerned the very powerful Richman Atkins method (Section 3.9.2) is very commonly used.[39] Aza$_n$[3$^n$]cyclophanes such as **6.57** may also be prepared by *N*-alkylation of diethyl phosphoramidates using bis(bromomethyl) arenes in the presence of base. This process results in the formation of (diethoxyphosphoryl)(aza)$_n$[3$^n$]cyclophanes. The diethoxyphosphoryl groups are then readily cleaved by acid to give secondary amine azacyclophanes, Scheme 6.12.[38] Of primary importance in all aspects of cyclophane synthesis are template effects and the use of high-dilution synthesis (Section 3.9; advanced template effects in self-assembly are discussed in Chapter 10). High dilution may even be achieved by the use of *heterogeneous dilution*, in which either products or one of the reactants are insoluble in the reaction medium. Dilution is achieved because reactions take place only at phase boundaries, or because the product is removed by precipitation. Cyclophane synthesis also benefits from the *caesium effect* and the *rigid group principle*. The caesium effect relates to the observation of significant yield enhancements when CsF, $Cs_2CO_3$ or CsOH are used as bases in cyclisation reactions, and is probably a manifestation of the kinetic template effect coupled with the relatively high solubility of caesium salts and the lack

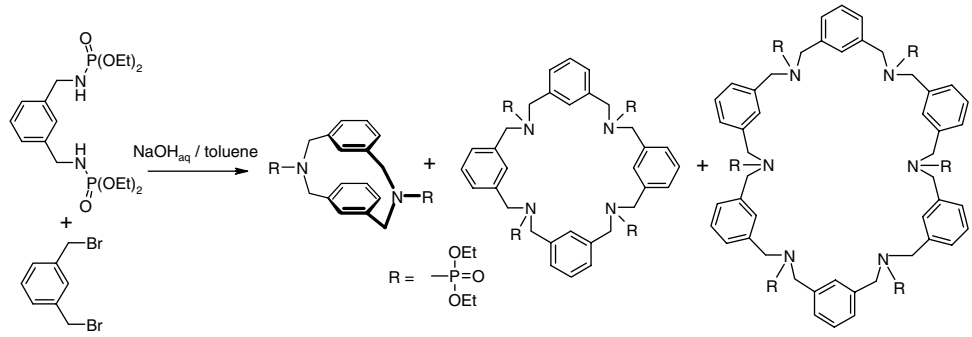


**Scheme 6.12** Synthesis of azacyclophanes by *N*-alkylation of diethyl phosphoramidates.[38]

of ion pairing between the relatively oft $Cs^+$ and oxoanions. The rigid group principle states that as the chain length of the starting material shortens, and hence the degrees of freedom available to the reacting system lessen, the faster cyclisation will occur. This is simply a statistical effect — as the number of possible reactant conformations rises, the less likely the occurrence of a suitable conformation for ring closure becomes. Introduction of rigid groups such as aryl rings, alkynes *etc.* should raise the yield of cyclic products. This is a kind of synthetic analogy to the preorganisation principle and is also manifested in the rigid end group principle in complexation by podands (Section 3.3.1).

## 6.5.4 Molecular 'Iron Maidens'

Pascal, R. A., 'Molecular 'iron maidens': Ultrashort nonbonded contacts in cyclophanes and other crowded molecules', *Eur. J. Org. Chem.* 2004, 3763–3771.

As supramolecular chemists our interest in cyclophanes comes from their ability to complex guest species within the macrocyclic portion of the molecule and from the ridigifying effect of the aromatic ring. Before we look at the host-guest chemistry of larger cyclophanes, however, we will spent a moment in a brief digression into the weird world of molecular 'iron maidens'; highly sterically strained cyclophanes that exhibit bonding way outside the normal realm of chemistry. We saw in Section 3.15.2 how [2.2]- and [3.3]paracyclophane are just about able to host a neutral chromium metal atom under extreme conditions. [2.2]Paracyclophane exhibits a significant degree of boat-shaped out of plane deformation of the aryl rings as a consequence of steic strin with interesting consequences on its electronic structure. But, what happens as the cyclophanes get smaller still? We touched briefly in Section 3.11.2 on the azacyclophane **3.92** which is just large enough to host a proton, and compared it to the smaller hydrocarbon macrobicycle *in*-[$3^{4,10}$][7]metacyclophane (**3.93**). Cyclophane **3.93** is synthesised by sulfur extrusion (*cf.* scheme 6.7) from a larger precursor. This size reduction results in the *endo* CH bond becoming highly compressed because of a repulsive interaction with the aromatic ring. The CH bond is sterically crushed up against the arene and its IR frequency rises from a typical value of *ca.*

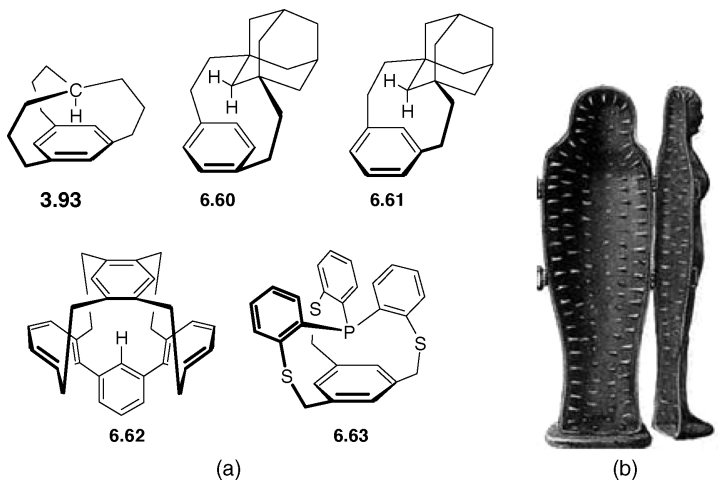


**Figure 6.32** (a) 'iron maiden' cyclophanes exhibiting severe steric compression and (b) the real thing – a medieval iron maiden torture device.

2900 $cm^{-1}$ for aliphatic CH stretches to 3325 $cm^{-1}$. This means the bond is getting in effect stronger since IR frequency is related to the square root of the bond force constant. It is this 'crushing' that gives these kinds of compound their 'iron maiden' nickname after the medieval torture device (defined by *Webster's New International Dictionary*, 2nd ed. as 'an iron frame in human form hinged to admit a victim, who, as the frame closed, was impaled on the spikes which stud the interior'), Figure 6.32. The world record holders for steric compression are the adamantine-derived cyclophanes **6.60** and **6.61**. In the case of **6.60** X-ray crystallography shows that the *endo* CH bond is just 1.64 Å above the ring centroid and occurs in the $^{1}H$ NMR spectrum of the compound at –4.08 ppm. Moving to the *meta* derivative **6.61** the *endo* CH proton is displaced from the ring centroid (the CH···Ar distance is longer at 2.02 Å) but there is a staggeringly short contact to an individual carbon atom of 1.98 Å. For comparison a C–C single bond is 1.55 Å long! Steric compression is also exhibited by the 'cappedophanes' such as **6.62** where the *endo* CH resonance occurs at δ 3.67 ppm, far upfield of the usual position of *ca.* 7ppm for aryl CH protons. Steric compression is also known for heteroatoms as in **6.63**. This compound exhibits the shortest P···centroid distance known of 2.90 Å and exhibits significant $^{31}P$-$^{13}C$ coupling to the basal aromatic ring in its $^{31}P$ NMR spectrum.

### 6.5.5 From Tweezers to Cyclophanes

The features shared by all of the successful molecular tweezer hosts detailed in Section 6.4 are a reasonably high degree of structural rigidity coupled with multipoint binding, generally taking the form of synergic π–π stacking and hydrogen bonding effects, resulting in guest encapsulation. If we examine the chemistry of cation-binding hosts (Chapter 3), the association of rigid preorganisation and high binding constants is clear, with binding affinity increasing from podands to corands to cryptands and spherands. The effectiveness of the molecular tweezers may be linked to the enhancement of podand binding by the rigid end group concept of Vögtle and Weber (Section 3.3.1), which enhances preorganisation. Clearly, however, moving from podand-like tweezers to true cyclophanes, in which the binding pocket is part of an overall cyclic structure, should result in further binding enhancements by additional host preorganisation and entropic gains in binding affinity associated with the lowering of the degrees of host conformational freedom.

By analogy with the tweezer concept used for **6.44**, the [8.8]paracyclophane **6.64** containing two hexadiyne bridges was prepared by Whitlock in 1980.[40] Multipoint binding is incorporated by an ion-pairing interaction between the carboxylate anion and the positive charge of a 2-naphthylmethyltriethylammonium cation guest. The binding constant for this apparently complementary pair is only 55 $M^{-1}$, however. Molecular modelling studies show that the cavity is too small for the guest and it simply does not fit within. Furthermore, an open conformation may be adopted that does not offer significant π–π stacking interactions. In response to this problem, a number of other hosts, such as **6.65**, were designed with larger cavities, which also incorporated additional preorganising bridges and hydrogen bond acceptor sites in some instances. Unfortunately, binding constants for **6.65** in $CHCl_3$ for a variety of guests were also low. In this case, the cavity is too large for effective guest binding, resulting in disruption of the double π–π stacking motif. It is through such apparent failures as these that Whitlock was able to recognise the importance of the key interactions of the system and the overall host–guest complementarity.

As a compromise, host **6.66** was designed. This species uses a napthyl spacer and incorporates a hydrogen-bond accepting pyridyl moiety at the core of its bonding pocket. One of the hexadiyne bridges has also been replaced by a shorter *p*-xylyl spacer, which results in additional edge-to-face π–π interactions. The association constant of this host for *p*-nitrophenol is much larger: $9.6 \times 10^{4}\ M^{-1}$ in $CD_2Cl_2$ solution. Intracavity complexation is strongly suggested by unusual $^{1}H$

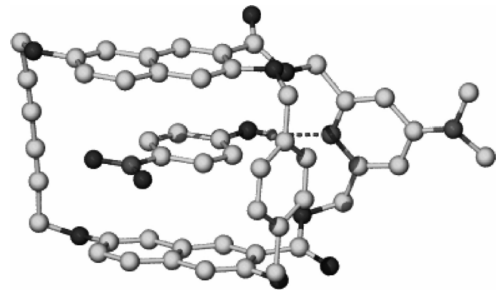

**Figure 6.33** X-ray crystal structure of the *p*-nitrophenol complex of **6.66**. Note the C—H $\cdots$ $\pi$ and, OH $\cdots$ N hydrogen bonds and the $\pi$–$\pi$ stacking interactions.[41]

NMR chemical shifts for the guest, and was confirmed by an X-ray crystal structure determination (Figure 6.33).

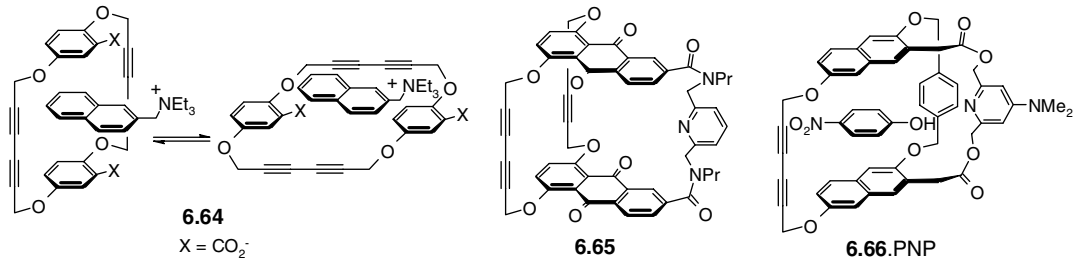


## 6.5.6 The Diphenylmethane Moiety

One of the most important breakthroughs in the search for synthetic hosts capable of binding organic molecules in (particularly aqueous) solution came in the development of the cyclophane **6.67** (1,6,20,25-tetraaza[6.1.6.1]paracyclophane) by Koga and co-workers in 1980.[42] This compound makes use of the diphenylmethane moiety in order to provide curvature on two sides of the approximately rectangular macrocyclic cavity. The two diphenylmethane fragments are linked by flexible aliphatic amine spaces. At pH $<$ 2 in aqueous solution, host **6.67** is water-soluble as a consequence of the protonation of the nitrogen atoms. Significant shifts are noted in the $^1$H NMR spectrum of the molecules in the presence of a range of organic molecules, particularly aromatic guests such as 8-anilino-1-napthalenesulfonate (ANS), the binding of which can be followed readily by fluorescence spectroscopy, and 2,10-dihydroxynapthalene. Such evidence of interaction had been observed in other systems before 1980, but the main advance in the chemistry of **6.67** was the discovery that the addition of durene (1,2,4,5-tetramethylbenzene) to a solution of the host caused the formation of a crystalline solid, which was analysed by X-ray crystallography. The crystal structure of **6.77**·durene is shown in Figure 6.34. This structure provided the first definitive evidence of the inclusion of the organic guest in the centre of the macrocyclic cavity, just as suggested by simple model building. It was hence possible to design an entirely artificial cavity that could complex organic guests in water. The durene molecule is bound *via* both edge-to-face and offset face-to-face π–π stacking interactions, with the shortest C $\cdots$ C distance being 3.59 Å from a durene methyl group to a host aryl carbon atom. Compound **6.67** was also important because it established NMR spectroscopy as *the*

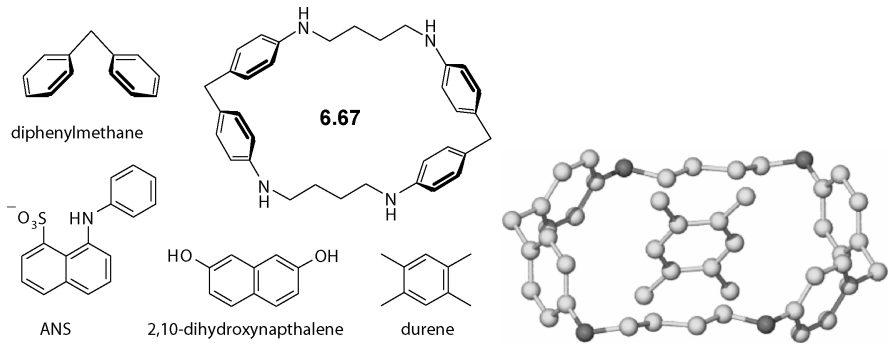


**Figure 6.34** Molecular host and guests and X-ray structure of the 1:1 **6.67**·durene complex showing the intracavity complexation of durene.[42]

tool of choice for the study of host–guest complexation in solution. Because of the magnetic anisotropy of the aryl rings, large $^1$H NMR chemical shift changes are observed on guest complexation. Furthermore, the magnitude of the chemical shift change is related to the proximity of the guest protons to the aromatic rings of the host (and *vice versa*) and their relative orientations (Box 3.3). $^1$H NMR spectral changes associated with the complexation of 2,10-dihydroxynapthalene by **6.67** are shown in Figure 6.35. The $^1$H NMR evidence suggests strongly that guest inclusion occurs in the orientation shown in Figure 6.35 and found in the crystalline state in the case of durene guest (Box 6.1).

While conceptually an extremely important leap forward, host **6.67** left a great deal of room for improvement and a huge number of new and more effective or tailored diphenylmethane-based systems have been prepared by a number of different groups. Particular problems to be addressed with **6.67** include:

1. The need to work in strongly acidic solutions. Solubility at neutral pH would be useful in studies on physiological systems.
2. The proximity of the polar amine groups needed for water solubility and the guest binding site makes it difficult to decouple ion-pairing (salt-bridge) effects from hydrophobic binding. Positioning the polar groups remote from the binding site would improve the analysis of selectivity patterns.
3. The polymethylene linkers between the two diphenylmethane moieties are very flexible leading to a poorly preorganised host. Spacers that are more rigid should result in greater selectivity.
4. The host is achiral. Incorporation of chirality would give access to studies on chiral recognition and asymmetric catalysis.

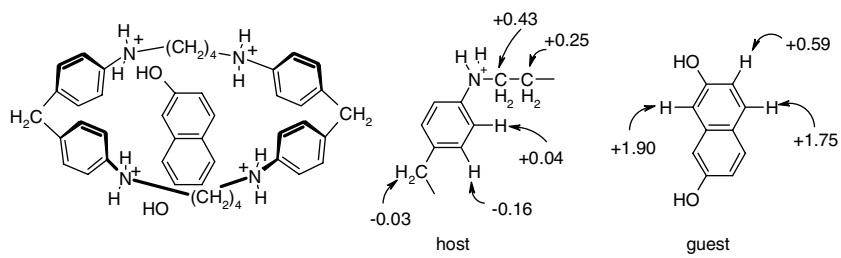


**Figure 6.35** $^1$H NMR chemical shift changes (ppm) upon interaction of **6.67** (0.025 M) with 2,10-dihydroxynapthalene in dilute HCl solution. The chemical shift changes are good evidence for the axial type inclusion shown (*cf.* Box 6.1).

Water solubility at neutral pH was achieved readily by peralkylation of the NH functionalities to give $NMe_2^+$ groups, which are charged and hence water-soluble, independent of pH. A further improvement came in the synthesis of **6.68**, which possesses solubilising groups remote from the cavity,[43] while Diederich introduced a versatile class of *spiro* compounds, such as **6.69**.[44] Improvements in host rigidity and preorganisation have been made by Kearney *et al*. (1993) and Webb and Wilcox (1993) through the introduction of bridged anthracene **6.70**[45] and Tröger's base-building blocks (**6.71**), and hybrids of the two as in **6.72**.[46] In each case the enhanced preorganisation and rigidity results in more effective guest binding.

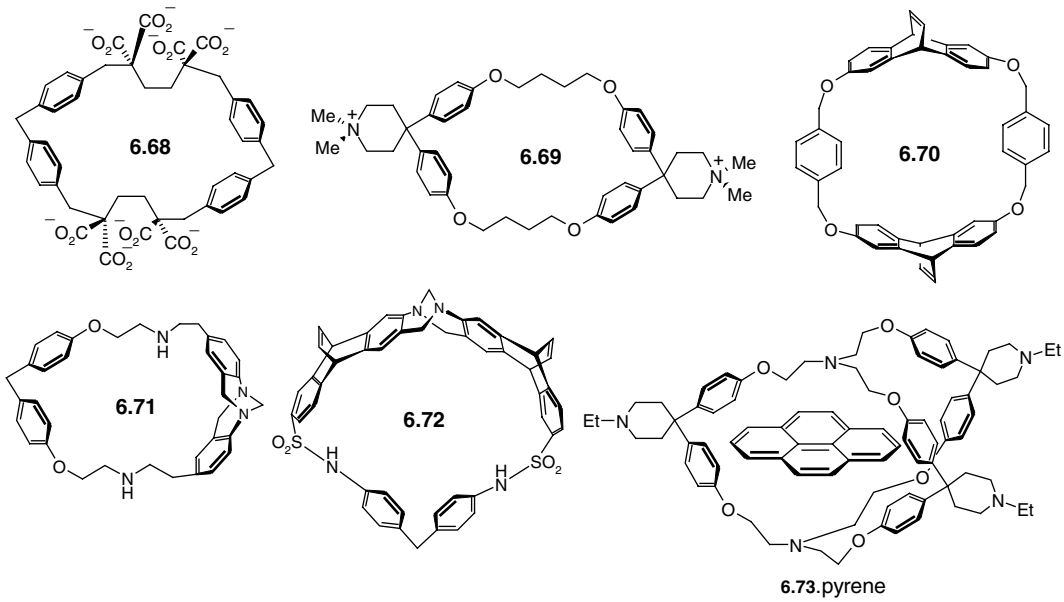


With all of the hosts based on the diphenylmethane moiety, and indeed with most cyclophane hosts in general, binding of organic guests in aqueous solution is dependent primarily on the hydrophobic effect. Organic molecules are naturally insoluble in water and seek refuge in the non-polar host cavity if it is sterically feasible for the guest to fit within the host. Binding constants tend to follow the order of guest lipophilicty as measured by the guest octanol/water partition coefficient. For example, a derivative of **6.69** binds perylene with an association free energy of –40.2 kJ $mol^{-1}$, corresponding to $K$ of about $10^7$. Association constants of this host with a range of guests have been studied and tend to follow the order of guest insolubility in water. In addition to hydrophobic effects, binding constants generally increase the more the surface area of the guest is covered by the host, and binding energies may be regarded as comprising an additive series of hydrophobic interaction terms. Binding of aliphatic guests has been less well studied, but data appear to indicate that binding is generally weaker. Stronger binding of alkylammonium cations is sometimes observed, with binding constants being enhanced by cation–$\pi$ interactions.

Since coverage of hydrophobic surfaces is of such importance in determining guest binding in water, Diederich *et al*. have prepared a three-dimensional host **6.73** capable of binding non-polar guests such as pyrene (shown) in a three-dimensional fashion, analogous to cation binding by cryptands.[47] Host **6.73** is soluble in a wide range of solvents from polar to non-polar, and pyrene binding was examined calorimetrically in each of them. In general, solvation (solvophobic) effects arise from two quite

different sources. Firstly, marrying of two lipophilic surfaces within a polar medium such as water results in a gain in overall entropy of the system, favouring guest binding. The second effect is termed the 'cohesive' effect and relates to the hydrogen-bonded attraction of one water (solvent) molecule to another. The guest-host interaction results in the formation of only one hole in the solvent instead of two, and hence an energy gain. The Diederich group calorimetric studies demonstrate that the cohesive term dominates. Complexation free energy was found to exhibit a linear correlation with solvent polarity. Binding constants from $6 \times 10^6$ in water/DMSO (99:1) to $9 \times 10^0$ in $CS_2$ were observed, with a linear increase in complexation free energy as a function of solvent polarity. Solvent polarity was quantified by the empirical Dimroth–Reichardt $E_T(30)$ parameter ($E_T$ = transition energy of the Dimroth–Reichardt betaine, in kcal $mol^{-1}$), which is related to macroscopic properties such as dielectric constant, dipole moment, cohesion and polarisability.[48]

Care must be taken in evaluating aqueous solution association constants, however, since guest binding can be in significant competition with host aggregation (*i.e.* binding of one host by another). The host molecules themselves possess large lipophilic surfaces and, above certain critical concentrations (termed the *critical aggregation concentration*, CAC), will aggregate to form micelle-like species of high molecular weight and poorly defined mutual orientations (like microscopic globules of oil in water). Such aggregation interferes significantly with host–guest association. Actual CAC values may be in the range $10^{-5}$ to $10^{-1}$ M, and a plot of host $^1$H NMR spectral changes for the representative **6.74** as a function of increasing host concentration is shown in Figure 6.36. Clearly, below the CAC of about $10^{-2}$ M, the spectrum is independent of concentration and this represents the best concentration range in which to measure guest association. At higher concentrations, large spectral changes associated with aggregation are observed, even in the absence of guest species.[49]

An interesting recent development in cyclophane chemistry are the *dendrophanes*, cyclophane-based dendrimers (Section 14.2). The dendrimer substituents impart water solubility allow intra-cavity apolar binding of organic guests in aqueous solution. The large cyclophane cores mean that guests can enter and exit the dendrimer core because the dendritic brances are relatively well spaced apart. Two dendrophanes developed by Francois Diederich at the ETH in Switzerland are shown in Figure 6.37.[50] The diphenylmethane based compound Figure 6.37a contains a small cavity suitable for guests such

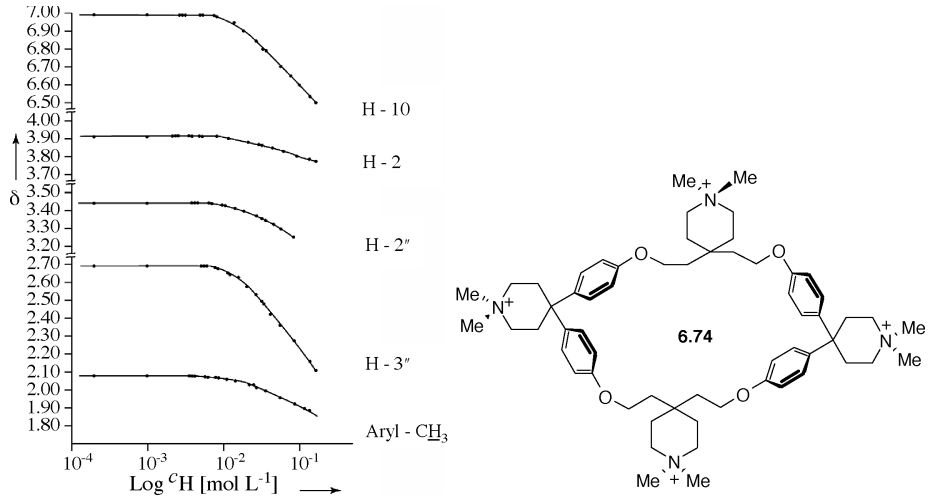


**Figure 6.36** Chemical shift of various protons for host **6.74** as a function of host concentration. (Copyright Wiley-VCH Verlag GmbH & Co. KGaA. Reproduced by permission).

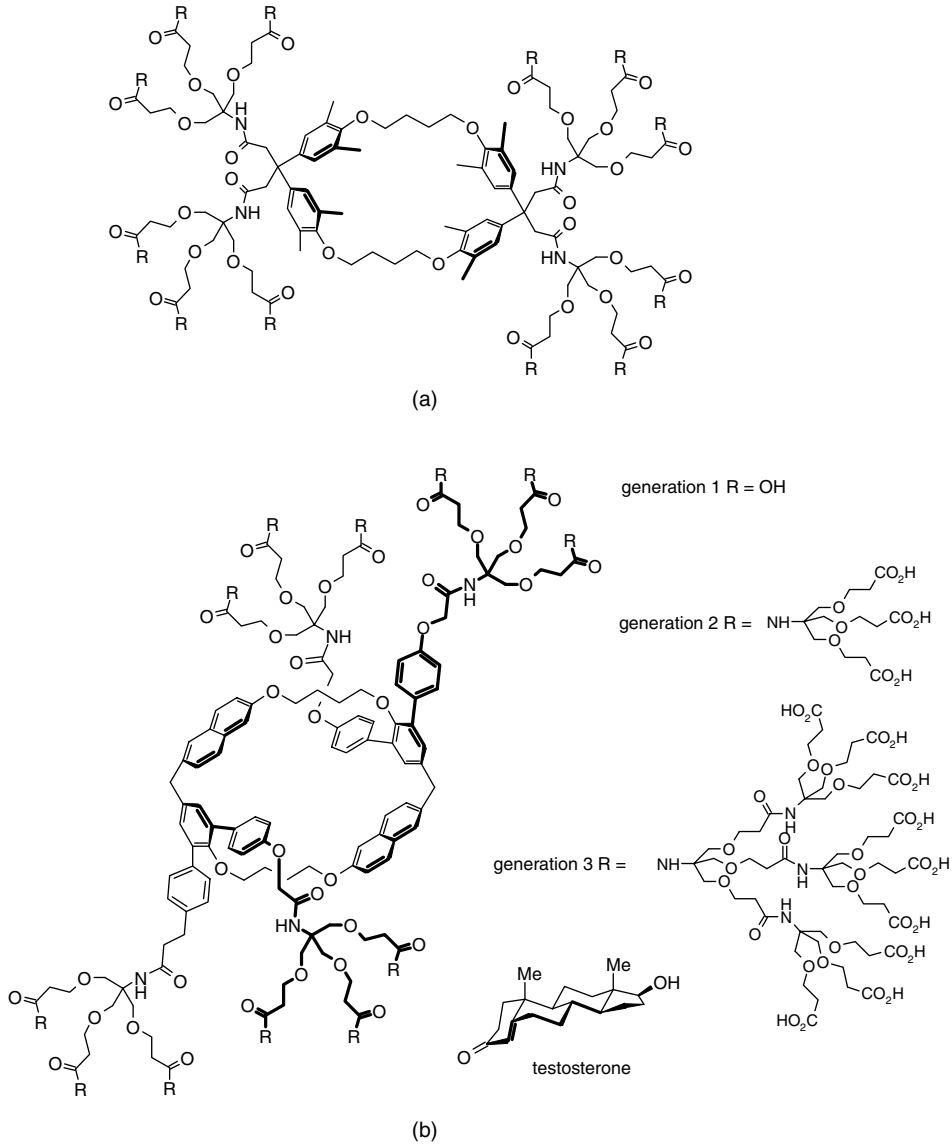


**Figure 6.37** (a) small cyclophane core dendrophane for complexation of small aromatic guests such as benzene, (b) large core dendrophane for binding steroids such as testosterone.[50]

as benzene while the larger analogue (Figure 6.37b) is suitable for binding larger steroidal molecules such as testosterone. In both cases three generations of dendrimers have been synthesised with the dendritic branches becoming larger and more densely packed with each generation. Synthesis of a fourth generation compound proved impossible. Careful studies on these dendrophanes revealed the following conclusions:

1. The preorganised macrocycle binding sites remain effective at all dendrimer generation levels and hence binding is not inhibited by hydrophobic collapse of the dendritic branches.

2. The micropolarity around the dendrophane core is reduced with increasing dendrimer generation. In the third generation material the polarity is roughly equivalent to that of ethanol, as measured by the fluorescent polarity probe 6(*p*-toluidino)naphthalene-2-sulfonate (closely related to ANS).
3. The kinetics of guest exchange are fast because the dendrimer branches are held well apart by the large cores.

Further developments in dendrophane chemistry should lead to intra-cavity catalysis in aqueous solution, although these are very complex molecules that can represent a considerable synthetic challenge, particular in achieving pure materials at higher dendrimer generations.

**Box 6.1** Solution Structure by NMR Spectroscopy

Schneider, H.-J., Rudiger, V., 'The use of complexation induced proton NMR chemical shifts for structural analysis of host-guest complexes in solution', *Chem. Eur. J.* 2000, **6**, 3771–3776.

There exist a number of useful NMR spectroscopic measurements for extracting structural information in solution and NMR spectroscopy is now a strong alternative to crystallography for determining protein structure. In protein work nuclear Overhauser enhancement (NOE) effects, coupling constants and relation times are commonly employed. In supramolecular chemistry binding-induced chemical shift changes upon host-guest association of the type shown in Figure 6.35 are also very useful. These changes are termed *complexation induced shifts* (CIS) and they can be used to give a significant amount of information about the structure of a host-guest complex in solution, in conjunction with either *ab initio* or semi-empirical computational molecular modelling methods and other data. In general CIS values provide specific information about functional group interactions (hydrogen bonds, π-stacking *etc.*), while NOE data is useful for locating which protons are close together in space. CIS measurements are usually undertaken at 100 % complexation in the presence of excess guest. The kind of qualitative structural information available from NMR data is analogous to the results of X-ray crystal structure determination but, unlike crystallography, the method is applicable in solution. The disadvantage of the method is that it requires many more assumptions than crystallography, not least an accurate knowledge of host and guest molecular connectivity and complexation stoichiometry. NMR structure determination software such as 'SHIFT' is generally parameterised using known crystallographic or structural data and measured CIS on a broad range of host-guest systems. This gives classical equations describing anisotropy ($\Delta\chi$) and linear electric field effects (LEF). Other effects such as strain effects or the effects of square electric fields can be added as refinements but are generally small in supramolecular systems. As input the software requires a model in the form of starting 3D structural coordinates for the host guest complex (obtained crystallographically or computationally) and chemical shift information for a number of nuclei in the free host and guest compounds. Chemical shift information is then calculated for the host guest complex described by the model using the empirical equations and compared to the experimentally observed CIS. The conformation of the host-guest complex is then adjusted either by hand, or in a more sophisticated automated approach such as genetic algorithm methods[51] to give maximum agreement between observed and calculated CIS. While host-guest complexes are generally present in solution in an equilibrating mixture of many possible conformers, a conformation of a particular residue that gives a significantly better agreement than other conformers may be regarded as being dominant. An example of the results of NMR structure determination is shown in Table 6.5 for a diphenylmethane based host binding napthalene-2-sulfonate. The calculations clearly indicate that the axial mode of binding is the favoured form in solution. In general the combination of as much data as possible, particularly CIS and NOE measurements, leads to the most accurate results. An interesting recent twist on NMR structure determination has been its application to the early stages of crystal nucleation (see Section 8.2.2).

**Table 6.5** Calculated and observed chemical shift data for a diphenylmethane based host binding napthalene-2-sulfonate.

| Geometry | Proton | $\Delta\chi_{arom}$ | LEF | $\Delta\chi_{arom}$ + LEF (= $CIS_{calc}$) | $CIS_{experimental}$ |
|---|---|---|---|---|---|
| Axial | 1 | 0.10 | −0.07 | 0.03 | 0.10 |
| | 2 | 0.14 | −0.03 | 0.11 | 0.45 |
| | 3 | −0.14 | −0.02 | −0.16 | −0.15 |
| | 4 | −0.53 | 0.03 | −0.50 | −0.60 |
| | 5 | −0.40 | 0.00 | −0.04 | −0.90 |
| | 6 | −0.95 | 0.02 | −0.93 | −1.25 |
| *Pseudo*equatorial | 1 | 0.01 | −0.10 | −0.09 | |
| | 2 | −0.03 | −0.05 | −0.02 | |
| | 3 | 0.01 | −0.01 | 0.0 | |
| | 4 | 0.12 | 0.03 | 0.09 | |
| | 5 | −0.01 | −0.04 | −0.05 | |
| | 6 | −0.42 | 0.00 | −0.42 | |

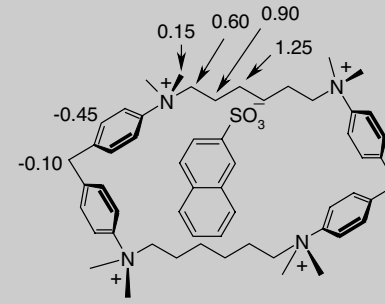


## 6.5.7 Guest Inclusion by Hydrogen Bonding

The linear dependence of binding constant on solvent polarity observed for complexation of non-polar guests by hosts such as **6.73** is, in part, related to the absence of specific enthalpically stabilising host–guest interactions. However, we have already seen the use of a combination of π–π stacking interactions and hydrogen bonding to enhance the enthalpic stability of the host–guest complex in the binding of *p*-nitrophenol by **6.66**. This sophisticated host is extremely effective because it is both highly stereoelectronically complementary to its target guest and rigidly preorganised. Additional stabilisation comes from the multipoint combination of interactions. Similarly, the molecular tweezer host **6.43** binds guest species *via* hydrogen bonding fairly strongly in non-polar media. Indeed, significant interference with the binding thermodynamics is observed in the presence of water due to competing solvation of the host binding sites (Section 1.9.2). Hence, guest binding by cyclophanes in non-polar media requires a very different host design strategy: one in which there is an active host–guest attraction (Figure 6.38).

One of the most effective early designs for guest inclusion in apolar media *via* hydrogen bonding was reported by Chang and Hamilton at the University of Pittsburgh.[52] Recognising the possibility of multiple interactions offered by the barbiturate family (**6.75**) (which are interesting guests in their own right, finding widespread clinical use as sedatives and anticonvulsants), these workers designed the complementary macrocyclic host **6.76** and its acyclic analogue **6.77** (*cf.* later work on the calixarene-based **6.30**). The results were highly gratifying. NMR solution complexation studies in chloroform indicated clearly the selective binding of barbital (**6.75b**) ($K = 1.37 \times 10^6\,M^{-1}$) over the more bulky (**6.75d**) ($K = 6.80 \times 10^2\,M^{-1}$), and highlighted the greater efficacy of the preorganised macrocyclic host (for barbital, $K = 2.08 \times 10^4\,M^{-1}$). Similar results were obtained with closely related hosts with dicarboxylic acid guests, with the binding strength being dependent on the length of the dicarboxylic

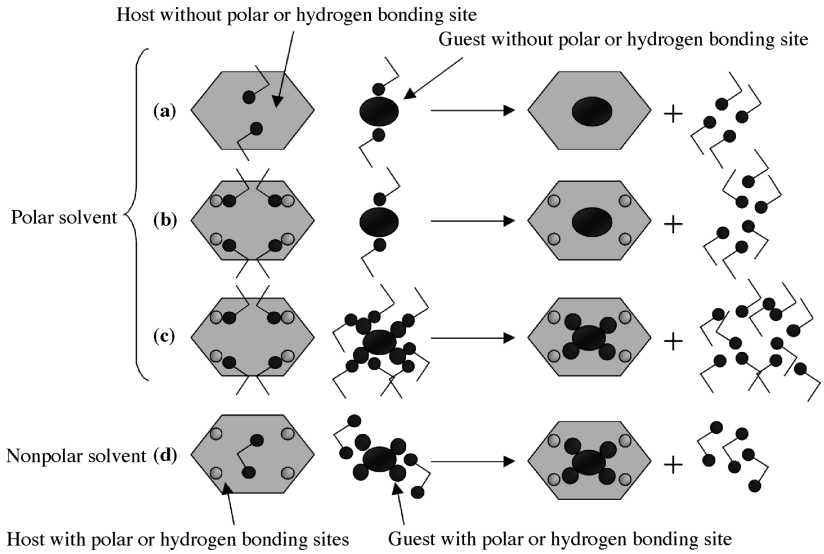


**Figure 6.38** Polar and non-polar guest binding in polar and non-polar media by various host types. (a) Hydrophobic host cavity binding non-polar guest: small enthalpic gain because of ready desolvation and van der Waals attractions; large entropic gain because of hydrophobic effect. (b) Host cavity with polar sites binding non-polar guest: less stable complex because of unfavourable desolvation of host functional groups. (c) Host cavity with polar sites binding polar guest: more stable complex because unfavourable desolvation of host functional groups is balanced by interactions with the guest. (d) Host cavity with polar sites binding polar guest in non-polar solvent: stable complex because of favourable host–guest interactions; no solvophobic stabilisation.

acid molecule. This concept has been utilised in the development of a prototype redox sensor for dicarboxylic acids (Section 11.3.4).

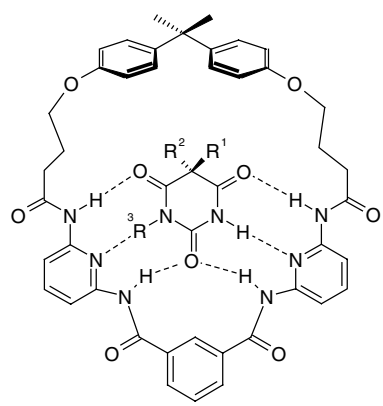

**6.75** in **6.76**

**a** $R^1 = R^2 = R^3 = H$
**b** $R^1 = R^2 = Et$, $R^3 = H$
**c** $R^1 = Et$, $R^2 = Ph$, $R^3 = H$
**d** $R^1 = Et$, $R^2 = Ph$, $R^3 = Me$

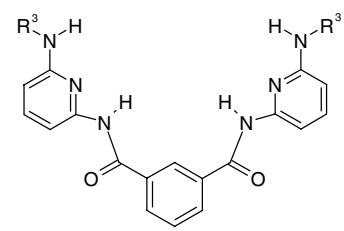

**6.77**

$R^3 = CO(CH_2)_2Me$

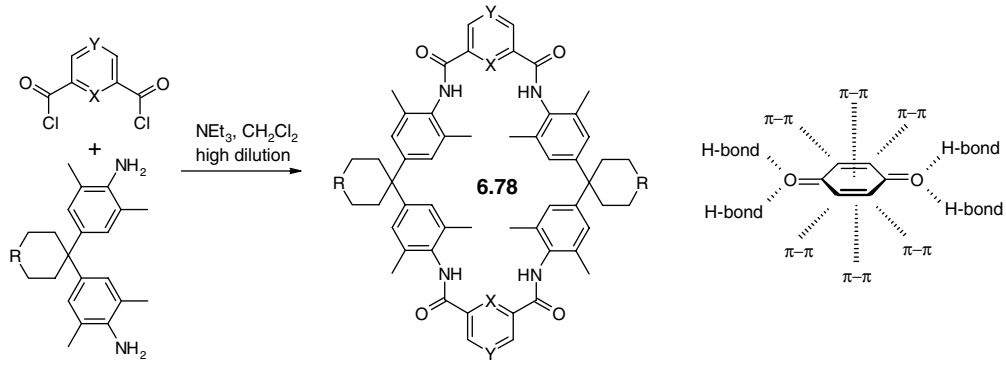


**Scheme 6.13** Design and synthesis of quinone receptor **6.78** (X/Y = CH or N, R = $CH_2$,[53] R = $N^+Me_2Cl^-$ [54]).

Work by Chris Hunter of the University of Sheffield, UK, has applied multiple hydrogen bond and multiple π–π stacking recognition to the binding of the hydrogen-bond acceptor *p*-benzoquinone, resulting in the design and synthesis of receptor **6.78**, which incorporates a complementary set of four hydrogen bond donors (NH groups; one for each quinone lone pair), and diphenylmethane-based π-surfaces (Scheme 6.13).[53] Preparation of **6.78** is complicated by the formation of large yields of the analogous cyclic trimer and tetramer and even a [2]catenane in which two molecules of **6.78** are interlocked mechanically (Section 10.7). Adopting a stepwise process allows the macrocycle to be isolated in acceptable yield, however. Binding constants for hosts **6.78** with *p*-benzoquinone are in the range 230 – 1800 $M^{-1}$ in $CDCl_3$ solution, depending on X and Y.

Strong binding of the quinone guest is observed, as exemplified by $^1$H NMR shifts of up to 2.5 ppm for the amide protons, characteristic of hydrogen bonding to the quinone. Larger substituted quinones such as tetramethylquinone, which do not fit the cavity, are not bound at all. The characteristic reduction potential of the quinone is also shifted to more positive potential by about 200 mV, reflecting the strong polarising effect of the amide NH bonds. The binding mode of the quinone has been established by NMR structure determination[51] (Box 6.1) and is shown schematically in Figure 6.39. Functionalising the compound with water-soluble dimethylammonium groups allows this type of compound to function

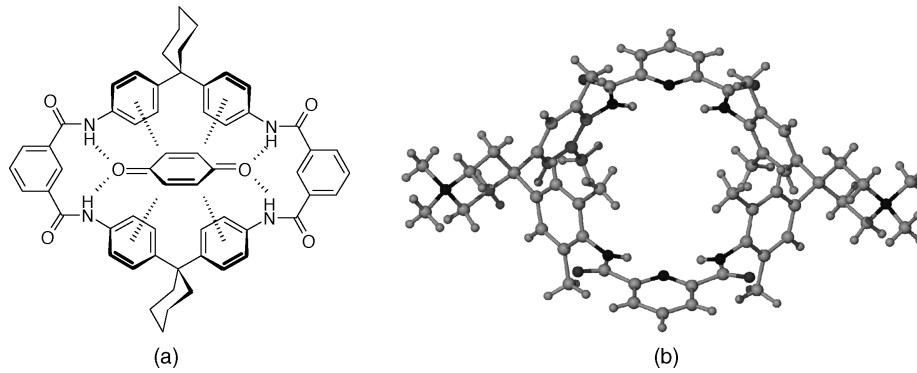


**Figure 6.39** (a) Binding of *p*-benzoquinone by **6.78** (R = $CH_2$, substituents omitted for clarity), (b) X-ray crystal structure of **6.78**.[54]

**Table 6.6** Binding constants ($/M^{-1}$) of hydrogen-bonding guests by host **6.78** (R = $NMe_2Cl^-$).[54]

| Guest | *K* (water) | *K* (chloroform) |
|---|---|---|
| 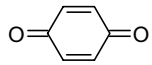 | <5 | 230 |
| | 94 | 850 |
| 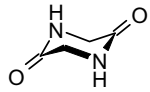 | 71 | $1.0\times10^6$ |
| 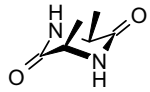 | 760 | — |

in aqueous solution. So with R = $N^+Me_2Cl^-$, **6.78** may be used to complex organic guest species in water (*cf.* hydrophobic recognition demonstrated in other diphenylmethane-based species). The binding constant for *p*-quinone in water proved to be <5 $M^{-1}$ however, while in chloroform a value of 230 $M^{-1}$ is obtained. Increasing the number of hydrogen bonding groups on the guest gives dramatic increases in the binding constants measured both in water and chloroform (Table 6.6), with a remarkable binding constant of $10^6$ $M^{-1}$ for glycine anhydride in chloroform. This affinity is a result of additional NH···π interactions as shown in the X-ray crystal structure, Figure 6.39b. The further increase in affinity in water moving to the dimethyl analogue is a result of the hydrophobic effect.

Related endo-acidic cyclophanes have been prepared by Weber. Compound **6.79** forms a wide range of hydrogen bonded complexes in varying ratios from 1:1 (benzoquinone, benzene, cyclohexane, toluene and diazabicyclooctane), 1:2 (DMSO, propionic acid and methanol) to 1:4 (acetic acid and acetone). The carboxylic acid group can orientate both into and outside the cavity.[55] A hydrogen bonding approach has also been adopted for the complexation of hydrogen bond donors such as 1,3,5-trihydroxybenzene (THB, phloroglucinol). Based on a modular acid chloride–amine condensation approach, Vögtle's group were able to prepare a range of enormous cylindrical, triply bridged cyclophanes such as **6.79**.[56] Host **6.79** exhibits a binding constant of $1.1 \times 10^4$ $M^{-1}$ in $CH_2Cl_2$ solution with

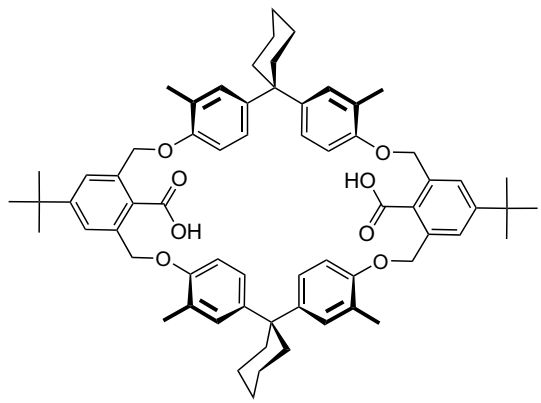

**6.79**

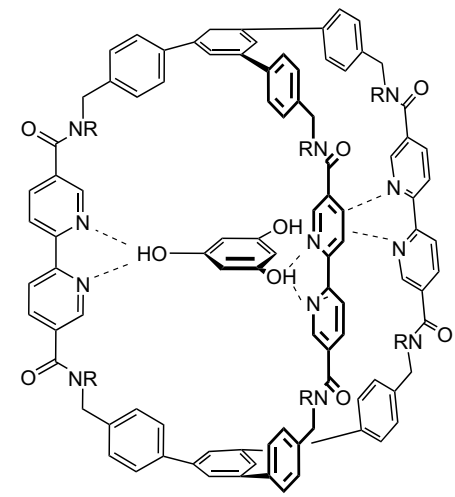

**6.80**.THB

complexation proceeding *via* bifurcated O—H···N hydrogen bonds, assisted by weaker Ar—H···N interactions. Smaller derivatives proved to be useful complexing agents for metal centres such as $Ru^{2+}$ (*cf.* $[Ru(2,2'\text{-bipyridyl})_3]^{2+}$), while those possessing catechol (*o*-dihydroxybenzene) units made effective siderands for complexation of iron (*e.g.* **3.147**, Section 3.16.2).

## 6.5.8 Charge-Transfer Cyclophanes

Benniston, A. C., 'Cyclophanes: endoacidic, endobasic and endolipophilic cavities', in *Encyclopedia of Supramolecular Chemistry*, Atwood, J. L. and Steed J. W. (eds), Dekker: New York, 2004, vol. 1, *pp.* 424–431.

In addition to cyclophane hosts based on hydrophobic and hydrogen bonding recognition, a wide range of cyclophanes and cages have been prepared based on charge-transfer interactions. In Section 3.12.6 we came across a series of electron-rich cyclophanes – benzo crown ether derivatives able to form attractively coloured charge transfer complexes with the herbicide paraquat (*N,N'*-dimethyl-4,4'-bipyridinium) and related electron deficient pyridinium type compounds. The host-guest interactions arise from face-to-face charge transfer π-stacking (*cf.* Section 8.10.1) and CH···O hydrogen bonding. We can readily turn the polarity of this interaction on its head to give an electron deficient paraquat-derived cyclophane **6.81** capable of binding electron rich aromatic guests such as derivatives of *p*-dimethoxybenzene. Compound **6.81**, prepared by the group of Sir J. Fraser Stoddart of Northwestern University, USA, is perhaps one of the most famous cyclophanes in supramolecular chemistry. It is known as the 'blue box' because of Stoddart's colour coding system of filled blue circles for electron deficient and red for electron rich aromatic rings, Figure 6.40. Blue is an appropriate choice because of the violet-blue colour of the radical cation formed upon one-electron reduction of many paraquat derivatives; a colour that gives them the name 'viologens'. The blue box has proved to be an amazingly versatile component of many supramolecular assemblies, notably catenanes and roxtaxanes, and we will return to a full discussion of these fascinating systems in Chapter 10. It forms host-guest complexes with a wide range of electron-rich guests, it has extensive redox chemistry involving both one- and two-electron reduction of both paraquat moieties (Scheme 6.14a), and useful photophysical properties making it a handy probe of electron transfer theory, a useful photosynthesis mimic, and a component of light and redox-activated molecular devices (Chapter 11). The blue box has been developed further by incorporation of extra recognition sites as in the chiral **6.82**. Compound **6.82** is capable of shape-selective

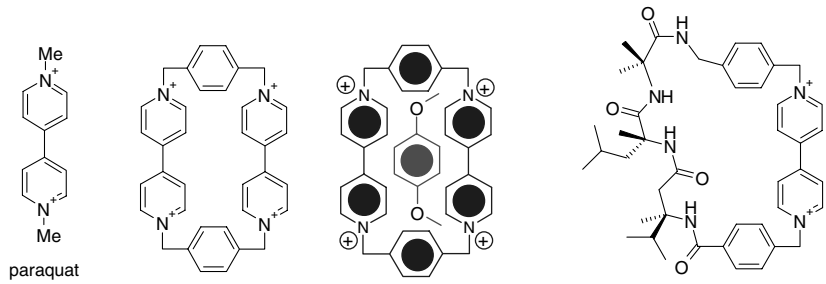


**Figure 6.40** Paraquat, the electron deficient 'blue box' developed by Stoddart and co-workers and a later derivative. Electron deficient aromatic rings are coloured blue, red is used for electron rich rings, neutral hydrocarbons are coloured black while green is used for other moieties such as tetrathiafulvalene.

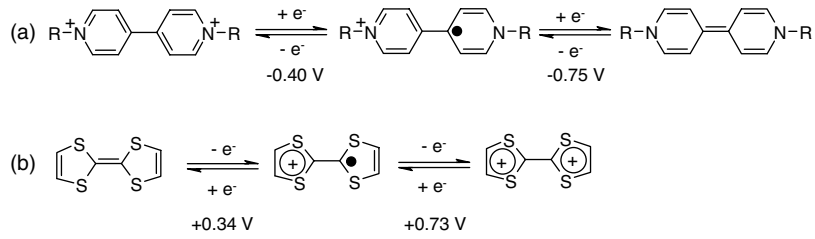


**Scheme 6.14** Redox chemistry of (a) viologens and (b) tetrathiafulvalene.

molecular recognition of a single enantiomer of DOPA [3-(3,4-dihydroxyphenyl)-DL-alanine].[57] DOPA resolution is important because L-DOPA is used as a drug in the management of Parkinson's disease.

Another very versatile cyclophane component capable of forming charge-transfer compounds is the tetrathiafulvalene (TTF) moiety. Like paraquat, TTF has an extensive redox chemistry summarised in Scheme 6.14b, however TTF is an electron donor not an electron acceptor. This redox activity means that it has been incorporated into a range of organic molecular electronic devices (Chapter 11). In terms of cyclophane chemistry, TTF-derived cyclophanes and cages are well known and have interesting properties.[58] To take one example, a TTF linked derivative of based on the classic diphenylmethane cyclophane has been prepared (**6.83**). In the solid state **6.83** incorporates a total of four chloroform guests, two in the cavity and two at the edge. It forms weak charge transfer complexes with the electron acceptor tetracyanoquinodimethane (TCNQ) although it is not known if the TCNQ guest resides within the cavity in solution.

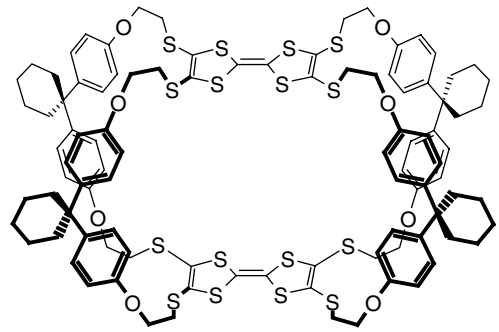

**6.83**

## 6.6 Constructing a Solution Host from Clathrate-Forming Building Blocks: The Cryptophanes

Collet, A., Dutasta, J.-P., Lozach, B. and Canceil, J. 'Cyclotriveratrylenes and cryptophanes: their synthesis and applications to host–guest chemistry and to the design of new materials', *Top. Curr. Chem.*, 1993, **165**, 103–130.

### 6.6.1 Construction of Containers from a Curved Molecular Building Block

The very versatile and readily prepared saucer-shaped building block cycloveratrylene (CTV, **6.10**) has an extensive classical inclusion chemistry, although strangely in the case of small guests this behaviour

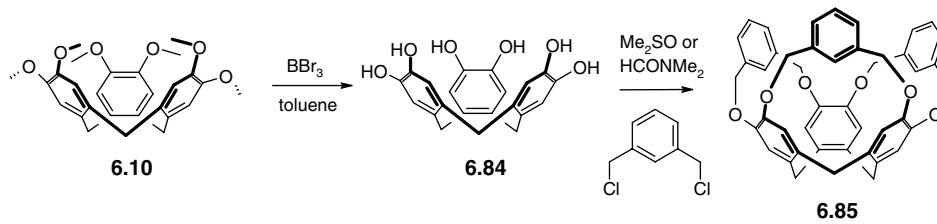


**6.10** **6.84** **6.85**

**Scheme 6.15** Synthesis of CTV-based cavitands.[60]

is not linked to its intrinsic molecular cavity (Section 7.7). As far as neutral guest binding is concerned, however, CTV does not generally exhibit significant solution binding ability, which is consistent with the channel nature of its solid-state inclusions. For large guests such as buckminsterfullerene ($C_{60}$), and the analogous complex with the spherical carborane, *o*-$C_2B_{10}H_{12}$, there is intra-cavity binding in the solid and significant solution binding in non-aqueous solvents, although $^1$H NMR titration data in the carborane case do not fit a 1:1 model.[59] The general lack of solution-binding ability of CTV is unfortunate since the molecule is prepared readily and the methoxy substituents offer a great deal of scope for further elaboration of the molecular cavity. Furthermore, the curvature inherent in the saucer-shaped structure is a potentially valuable property in the construction of encapsulating hosts. The reason CTV itself is such a poor host may be traced to the shallowness of the cavity. The wide aperture of the CTV bowl means that the cavity does not provide a significant refuge for organic compounds from polar solvent media. At the same time, the aryl rings are capable of only weak π-stacking or π-hydrogen bonding interactions with guests. In order to achieve significant solution complexation of guests other than those that, like $C_{60}$, are highly complementary to CTV, it is clearly necessary to elaborate the molecular cavity. This has been carried out by Cram to produce a range of CTV-based *cavitands* (Scheme 6.15).[60]

Cavitand **6.85** and pyridyl and phenanthroline-bridged analogues possess deep, permanent cavities capable of binding neutral molecules such as $CH_2Cl_2$ in both solution and the solid state. In uncomplexed **6.85**, the *m*-xylyl bridges are highly mobile; however, this mobility is reduced significantly upon guest complexation. Molecular mechanics calculations suggest that the cavitate **6.85**·$CH_2Cl_2$ is more stable than the free host by 57.3 kJ mol$^{-1}$, although this large value should not be confused with a solution binding constant, since it does not take account of competitive effects of the medium.

Clearly, deepening the CTV cavity to form cavitands is highly effective in enhancing the solution binding characteristics of the basic CTV motif. However, we saw in the case of the cryptands (Chapter 3) that host–guest affinity is enhanced even further by the formation of a closed, three-dimensional shell that can entirely encapsulate the guest species. The three-dimensionality confers preorganisation, serves to protect the guest from the solvent medium, and slows down guest exchange kinetics. A range of three-dimensional CTV-based hosts have been prepared by André Collet (Lyon, France), in which two CTV-type cavities face one another and are linked covalently by —$(CH_2)_n$—, —$CH_2$—CH=CH—$CH_2$— or —$CH_2$—C≡C—$CH_2$— bridges (n = 3–8). Aryl-bridged analogues have also been prepared by capping of $CpFe^+$ based podand anion-binding hosts such as **4.66** (Section 4.7.2). These capsular hosts have been given the name *cryptophanes* by analogy with the cryptands (the *-phane* ending comes from the fact that they belong to the class of [1.1.1]orthocyclophanes; see Section 6.5.2 for cyclophane nomenclature). Cryptophanes exist in two distinct varieties with *anti* **6.85** and *syn* **6.86** orientations of the substituent groups on the two hemispheres, generally exhibiting $D_3$-*anti* or $C_{3h}$-*syn* symmetry. The cryptophanes have been named chronologically in the order of their discovery, thus cryptophane-A and cryptophane-B are the *anti/syn* derivatives with X = —$(CH_2)_2$— bridges, while in cryptophane-E

and -F, X = $-(CH_2)_3-$. Cryptophanes-C and -D have $—(CH_2)_2—$ bridges like cryptophane-A/B, but lack OMe groups on one hemisphere. The face-to-face geometry is highly reminiscent of the solid-state $\gamma$-phase inclusion compounds of CTV itself (Section 7.7).

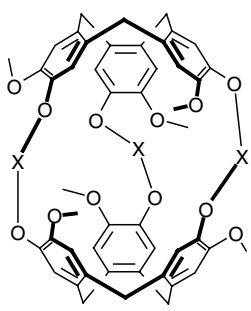

$D_3$-*anti*

**6.86**

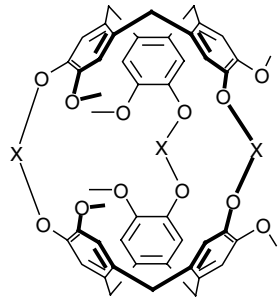

$C_{3h}$-*syn*

**6.87**

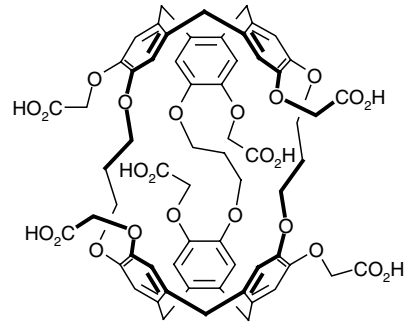


**6.88**

X = -$(CH_2)_n$-, -$CH_2$-CH=CH-$CH_2$-, alkyne, $C_6H_4$

Cryptophane synthesis is accomplished by one of two methods. Initial procedures employed a covalent template effect in which one CTV-derived bowl preorganised the cyclisation of the second under high dilution conditions (Scheme 6.16a). More recently, a much more straightforward procedure has been developed in which cryptophanes are formed directly in a double trimerisation reaction (Scheme 6.16b).

Yields of various cryptophanes obtained by these routes are shown in Table 6.7. Clearly, the direct method results universally in poorer yields, presumably because it represents a triple ring-closure of large rings as part of a three-component self-assembly, without significant template assistance. This is in significant competition with polymer formation. However, it is generally the method of choice because it does not require high-dilution conditions (Section 3.9.2), meaning that much larger quantities of product can be prepared at a time, and it is much more straightforward. More interestingly, method (b) results in a very different *anti/syn* ratio than the template procedure. In method (a) the *anti/syn* ratio favours *anti* configurations for bridges with even numbers of carbon atoms, and *syn* for odd numbers. The fact that changing a double bond from *cis* to *trans* has the same effect suggests a bridge-induced orientational preference in the immediate precursor. The direct approach always gives *anti* preferentially. It is likely that this preference arises from the fact that in method (b), the two CTV-derived portions cyclise in a concerted fashion, with both rings forming simultaneously.

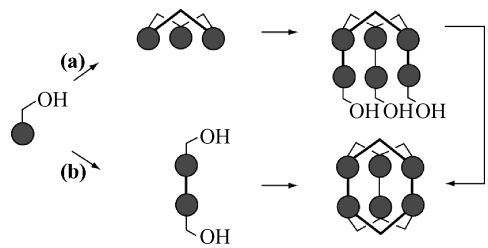


**Scheme 6.16** Strategies for cryptophane synthesis. (Reproduced with permission from Section Key Reference).

**Table 6.7** Yields (%) for cryptophanes prepared by methods shown in Scheme 6.16.

| | Template procedure (a) | | Direct method (b) | |
|---|---|---|---|---|
| Bridge O—X—O | *anti* | *syn* | *anti* | *syn* |
| —$(CH_2)_2$— | 80 | 0 | 5 | 0 |
| —$(CH_2)_3$— | 27 | 50 | 17 | 3 |
| —$(CH_2)_4$— | – | – | 8 | 2 |
| —$(CH_2)_5$— | 21 | 43 | 12 | 6 |
| —$(CH_2)_6$— | 18 | 9 | 8 | 2 |
| —$(CH_2)_7$— | – | – | 5 | 1 |
| —$(CH_2)_8$— | 60 | 20 | 0 | 0 |
| —$CH_2$—CH=CH—$CH_2$—(*E*) | 34 | 5 | 5 | 1 |
| —$CH_2$—CH=CH—$CH_2$—(*Z*) | 25 | 50 | 10 | 8 |
| —$CH_2$—C≡C—$CH_2$— | 43 | 20 | 0 | 0 |

## 6.6.2 Complexation of Halocarbons

Consistent with their encapsulating nature, cryptophanes possess remarkable binding ability for small, tetrahedral molecules such as methane and halogenated derivatives. The $^1$H NMR spectrum of cryptophane-E in the presence of two equivalents of $CHCl_3$ is shown in Figure 6.41. The spectrum is recorded in deuterated 1,1,2,2-tetrachloroethane, which is too large to fit within the cavity. Sharp, distinct peaks for the included and extracavity $CHCl_3$ molecules are readily observed at room temperature. As the temperature is raised to 340K, they gradually broaden as guest exchange becomes fast on the NMR time scale. The upfield chemical shift of the included guest is a characteristic consequence of the shielding effects of the aromatic rings. Observation of slow exchange is consistent with the need of the guest to make its way through the restricted host windows. Line shape analysis gives activation energies for guest exchange of 54–63 kJ mol$^{-1}$ for this host. At 300 K, the binding

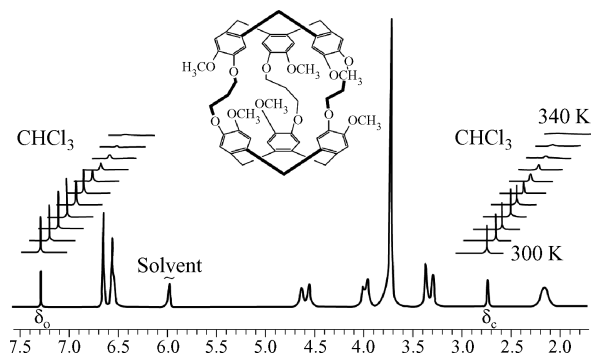


**Figure 6.41** $^1$H NMR spectrum of cryptophane-E (**6.86**, X = $(CH_2)_3$) in the presence of two equivalents of $CHCl_3$; solvent: $(CDCl_2)_2$, $\delta_c$ is assigned to bound $CHCl_3$, $\delta_o$ corresponds to $CHCl_3$ outside the cavity. (Reproduced with permission from [61] © 1986 American Chemical Society).

constant is 470 $M^{-1}$, which is remarkably strong given the intrinsically weak nature of the binding forces, especially since hydrophobic effects are not in operation in the non-polar solvent medium. This is highlighted by the much larger binding constant of 7700 $M^{-1}$ for $CHCl_3$ in water by the closely related water-soluble host **6.88**, in which the OMe substituents have been replaced by hydrophilic $OCH_2CO_2H$ groups.

The complexation free energies of cryptophane-E for various neutral guests is shown in Figure 6.42. As might be expected from their three-dimensional nature, the hosts show peak selectivities, with a good correlation of cavity host size with guest van der Waals volume. Thus, the smaller cryptophane-C with —$(CH_2)_2$— bridges is apparently selective for smaller guests such as $CH_2Cl_2$, whereas the larger $CHCl_3$ is bound more tightly by cryptophane-E, which possesses —$(CH_2)_3$— bridges. This simple size fit notion breaks down, however, if the complexation free energies are broken down into their respective enthalpic and entropic contributions. This may be done from a van t'Hoff plot (ln $K$ against 1/T). The parameters for $CH_2Cl_2$ and $CHCl_3$ binding by cryptophane-C and the larger cryptophane-E are shown in Table 6.1.

Clearly, the fact that the smaller cryptophane-C is selective for $CH_2Cl_2$ is not a question of a match between the host's small cavity and the guest's size after all. The enthalpy of the interaction of $CHCl_3$ with this host is much more significant, despite its small size. However, $CHCl_3$ binding

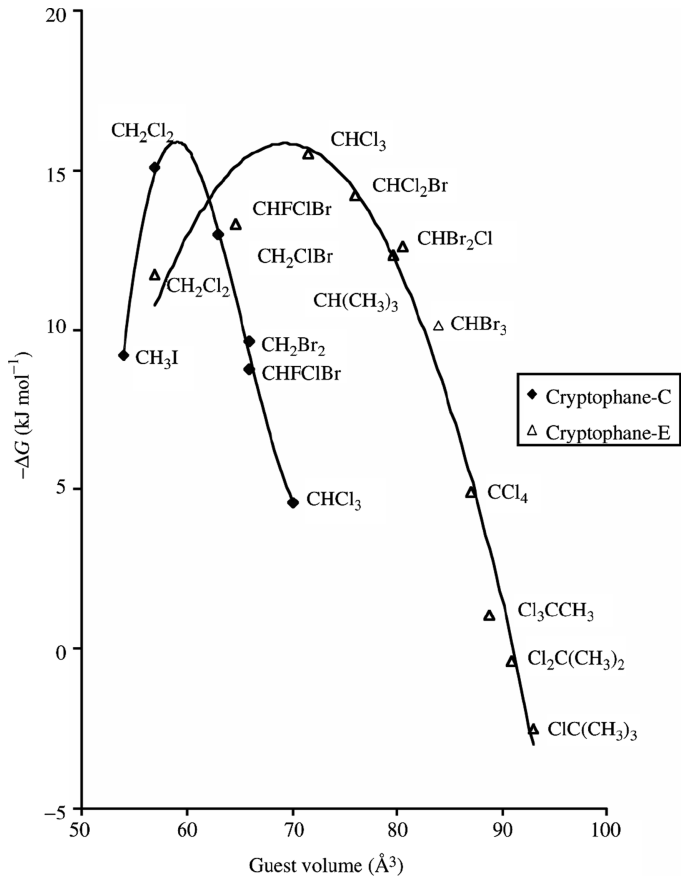


**Figure 6.42** Complexation free energy of cryptophane-C and -E for various guests at 300 K (reproduced with kind permission from Springer Science + Business Media from Section Key Reference © 1993).

**Table 6.8** Thermodynamic parameters for guest binding by cryptophanes in $(CDCl_2)_2$ at 300 K.

| Host | Guest | $\Delta G^o$/kJ mol$^{-1}$ | $\Delta H$/kJ mol$^{-1}$ | $\Delta S$/J K$^{-1}$ mol$^{-1}$ |
|---|---|---|---|---|
| Cryptophane-C | $CH_2Cl_2$ | −15.1 | −16.3 | −4 |
| | $CHCl_3$ | −6.7 | −26.8 | −67 |
| Cryptophane-E | $CH_2Cl_2$ | −11.7 | +4.2 | +25 |
| | $CHCl_3$ | −15.5 | −25.1 | −29 |

is destabilised dramatically by the entropy contribution, which gives an unfavourable –T$\Delta S$ contribution to the complexation free energy of +20.1 kJ mol$^{-1}$ at 300 K. This arises from the fact that the $CHCl_3$ is probably too good a fit to the cavity and it is held very rigidly, thus reducing drastically its' degrees of freedom. On the other hand, $CHCl_3$ is also bound strongly by cryptophane-E and in the larger host has room to move around somewhat, significantly diminishing the entropic destabilisation. The X-ray crystal structure of the $CHCl_3$ complex of cryptophane-E is shown in Figure 6.43.

The cryptophanes were originally designed in order to solve the long-standing problem of the separation of enantiomers of one of the simplest chiral compounds, fluorochlorobromomethane, CHFClBr. This tetrahedral molecule is of a suitable size to fit within a cryptophane cavity, and the intrinsic chirality of the *anti* $D_3$ cryptophanes means that the possibility of chiral recognition exists. Using a partially resolved sample of (±)-CHFClBr Collet's group monitored the complexation by an resolved sample of (+)-cryptophane-C. Separate peaks were observed for the guest signals of the two diastereomeric host–guest complexes, (+)-host, (+)-guest and (+)-host, (−)-guest. Integration revealed that the sample was in 4.5 per cent enantiomeric excess and, in conjunction with circular dichroism data, gave the optical rotation (Box 6.2) of the guest $[\alpha]_D^{25} = 1.6 \pm 0.5^o$, a piece of information that had been sought for a century.

### 6.6.3 Competition with Solvent

Initial studies on the complexation ability of cryptophanes were carried out in $CDCl_3$ solvent with closely related guests such as $CH_2Cl_2$, and gave very small binding constants in the region of 1–2 M$^{-1}$. Clearly, therefore, there is a profound solvation effect upon guest encapsulation. In the case of guest binding in water, this is a positive reinforcement of the binding by the host by hydrophobic effects. However, if the solvent is an effective competitor for the host cavity, binding constants are greatly reduced, as is the case of $CH_2Cl_2$ binding in $CDCl_3$. This is to be expected given the high affinity of the cryptophane hosts for both of these species (Figure 6.42) and results in the observation of an equilibrium constant that is a concentration-weighted measure of the relative affinity of the host for guest

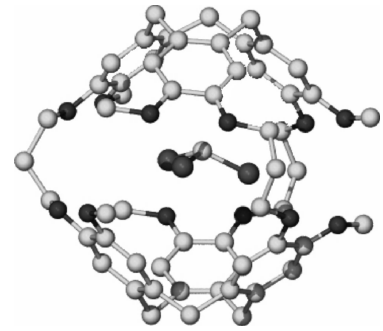

**Figure 6.43** X-ray crystal structure of the $CHCl_3$ complex of cryptophane-E.

and solvent. Thus the observed complexation equilibrium constant, $K$, is given by the expression in Equation 6.1, where [S] = solvent molar concentration (activity); $K_s$ = equilibrium constant for solvent binding $K_{11}$ = guest binding constant.

$$K = K_{11}\,(1 + K_s[S]) \tag{6.1}$$

In this case, it is clear that $K \approx K_{11}$ *only* when $K_s[S] << 1$. Generally, for organic solvents [S]≃10M and hence $K_s$ must be $<10^{-2}$. In the case of cryptophane-C, the observed binding constant for $CH_2Cl_2$, $K$, in $CDCl_3$ is 2.6 $dm^3\,mol^{-1}$. For $CDCl_3$ at room temperature, [S] = 12.4 mol $dm^{-3}$. Measurements in non-competitive solvents such as $(CDCl_2)_2$ show that $CDCl_3$ is bound with $K_s$ = 10 $dm^3\,mol^{-1}$. Application of Equation 6.1 gives $K_{11}$ for $CH_2Cl_2$ of around 325 $M^{-1}$. The effect of the medium is clearly of paramount importance.

### 6.6.4 Complexes with Alkyl Ammonium Ions and Metals

One of the most remarkable features of cryptophanes is their ability to complex organic ammonium cations highly effectively in non-polar media. Tetramethylammonium ($NMe_4^+$) is bound by cryptophane-E with an association constant of 250 000 $M^{-1}$ in $(CDCl_2)_2$. In contrast, the neutral guest $CClMe_3$, which has a similar size, is hardly bound at all. Clearly, there is a much more significant interaction with the cationic guest. The strong binding is also reflected with a number of other alkyl ammonium cations, with binding dropping off as the size of the alkyl groups increases. The strong binding of the cation may be a consequence of its much more hydrophilic nature. If the host cavity represents a more polar 'solvation shell' than the highly non-polar solvent, then a favourable enthalpy term will be generated. Notably, similar sized anions such as $BF_4^-$ are not bound at all. Also, it is interesting to compare the cation-binding ability of the cryptophanes with that of speleands (Section 3.12.5), which are also based upon a CTV framework. In that case, however, the primary component of the host–guest interaction involves directional hydrogen bonds.

No evidence exists to suggest that unfunctionalised cryptophanes bind to metal cations; however, a functionalised cryptophane (**6.89**) with endo-carboxylate has been shown to extract metal ions, particularly $Ca^{2+}$ and $Sr^{2+}$ from aqueous solution into chloroform.[62] The compound is also very efficient at extracting trivalent lanthanide ions such as $Eu^{3+}$ and a DFT model suggests that the $Eu^{3+}$ cation is a good fit to the cavity of the triply deprotonated cryptophane, forming a sixfold trigonal prismatic binding site, Figure 6.44. The cavity volume of the neutral receptor is tiny at only 28 $Å^3$, however it does have some flexibility of the bridges and hence its ability to bind alcohol guests was also examined. The compound proved able to bind strongly to methanol, $K$ = 7500 $M^{-1}$ in $CDCl_2CDCl_2$, weakly to ethanol (41 $M^{-1}$) and

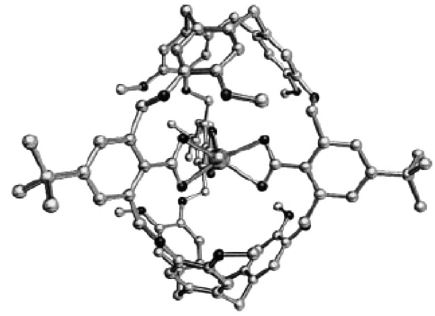

**Figure 6.44** DFT minimised structure of the triply deprotonated **6.89** binding $Eu^{3+}$ (Copyright Wiley-VCH Verlag GmbH & Co. KGaA. Reproduced by permission).

not at all to isopropanol. The complexation induced upfield chemical shift change of the methanol methyl froup of $\Delta\delta = 1.76$ ppm confirms intra-cavity binding.

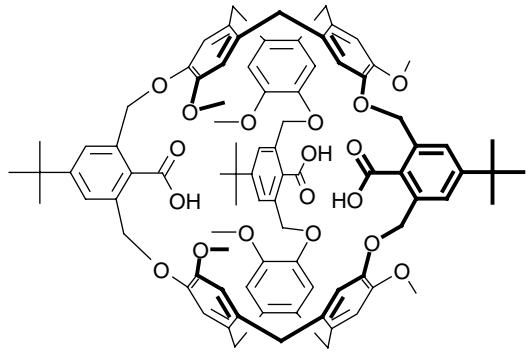

*$C_{3h}$-syn*

**6.89**

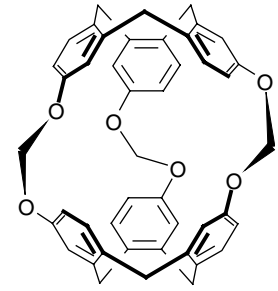

*$D_3$-anti*

**6.90**

## 6.6.5 Methane and Xenon Complexation

Taking the binding of neutral molecules to extreme, Collet and co-workers have also investigated the binding ability of the small cryptophane-A for methane. Methane is a small molecule of fundamental importance, not least because of its occurrence as natural gas and in coal and oil deposits. Since methane is highly symmetrical, uncharged, non-polar and capable of interacting with its environment only *via* weak van der Waals forces, it is extremely difficult to bind. These drawbacks are exacerbated by its extreme volatility, which makes it difficult to study methane binding in solution. In fact, cryptophane-A is found to be highly effective at binding methane, with complexation free energies at 300 K comparable to those of the same host with $CHCl_3$, despite the large disparity in their overall molecular volumes. Methane binding is both enthalpically and entropically favoured in $(CDCl_2)_2$, with $\Delta H^o = -6.7$ kJ mol$^{-1}$ and $\Delta S^o = +17$ J K$^{-1}$ mol$^{-1}$. The binding constant is 130 M$^{-1}$ and the encapsulated methane has a reasonably long residence half-life of 9 ms at 199 K, meaning that separate peaks for free and complexed guest may be observed by $^1$H NMR spectroscopy at this temperature. Free methane resonates at about 0.2 ppm, while the bound $CH_4$ molecule gives a signal at –4.4 ppm. At 298 K, an averaged signal is observed. Molecular modelling of the structure shows that the mean $C_{guest} \cdots C_{host}$ distance is about 4.5 Å, *i.e.* 20 per cent larger then the sum of the van der Waals radii. This distance corresponds closely with the maximum attractive forces in a van der Waals attraction potential and may be one reason for the extraordinary stability of the complex.

The ratio between the cavity and guest size in terms of their molecular volumes may be expressed in terms of the cavity occupancy factor (ρ). A ρ value of 1 represents a completely filled cavity. Occupancy factors for various cryptophanes and guests are shown in Table 6.9.

**Table 6.9** Occupancy factors (ρ) for cryptophane complexes.[a]

| Guest | Cryptophane-A | Cryptophane-C | Cryptophane-E |
|---|---|---|---|
| $CH_4$ | 0.35 | — | — |
| $CH_2Cl_2$ | 0.70 | 0.70 | 0.65 |
| $CH_2Br_2$ | 0.80 | — | — |
| $CHCl_3$ | 0.89 | 0.89 | 0.81 |

[a] using cavity volumes of 81.5 Å$^3$ for cryptophanes A and C and 89.0 Å$^3$ for E.

Clearly, methane is a much poorer fit to the cavity than the haloalkanes. However, it is interesting to compare the ρ value obtained (0.35) with various other 'states of matter' of methane. Gaseous methane, for example, has a ρ of $0.77 \times 10^{-3}$ at 1 atm pressure and 298 K. At its critical point (45.6 atm, 190.6 K, the temperature and pressure at which there is no longer any distinction between liquid and gas), ρ rises to 0.17, while solid methane at 0 K exhibits a ρ value of 0.67. In occupancy terms, then, the intracavity environment is akin to a supercritical fluid. Translated to the macroscopic scale, one molecule of methane in the cavity of cryptophane-A is equivalent to one mole of methane in 49 mL, exerting a pressure of 610 atm at 298 K. In contrast, for $CHCl_3$ the occupancy factor of 0.89 is akin to a very densely packed crystal, and indeed the entropic and enthalpic changes on binding are similar to those that occur in the formation of crystalline organic compounds.

Binding of the Noble gas xenon is also of interest in cryptophane chemistry. Supramolecular complexes of xenon have tremendous potential applications as biosensors for future magnetic resonance imaging (MRI) applications based on laser-polarised (LP) xenon. LP xenon NMR spectra exhibit very clear discrimination between signals for bound and free xenon atoms and hence can be used for chemical-shift imaging for biological applications. The beauty of xenon is that it is not naturally occurring *in vivo* and hence xenon NMR does not suffer from interference with the surroundings. Attaching bound xenon to a biospecific carrier allows the target area to be imaged. The small cryptophane-A does bind xenon in $CDCl_2CDCl_2$ solution with $K = 3900\ M^{-1}$, rising to $6900\ M^{-1}$ in water if a water soluble carboxylate derivative is used. The cavity size of cryptophane-A is not optimal for xenon, however, which has a van der Waals volume of 42 $Å^3$ giving $\rho = 0.44$. The optimal occupancy factor is about 0.55 according to measurements made on a variety of capsular compounds by Rebek Jr.[63] and hence even stronger binding is obtained using the tiny methylene-bridged cryptophane-1.1.1 (**6.90**), with $\rho = 0.52$.[64] The binding constant in $CDCl_2CDCl_2$ is $10{,}000\ M^{-1}$ and xenon exchange dynamics are significantly slowed compared to the xenon complex of cryptophane-A. The $^{129}Xe$ NMR spectrum of the complex has a sharp resonance at 31.1 ppm, shifted dramatically from free xenon at 190 – 230 ppm as a consequence of ring current effects.

### 6.6.6 An 'Imploding' Cryptophane

Cavity-containing molecules such as cryptophanes are generally much more stable when occupied by a guest species both in the solid state and in solution because of the favourable van der Waals interactions between the host cavity walls and any guest molecule and indeed as we saw in Section 6.2.3 there can be a significant energy barrier to guest removal when the guest is not replaced by a new cavity-filling molecule in a concerted fashion. In the case of the flexible calixarenes we showed that the calixarene can adopt a pinched $C_{2v}$ conformation in order to minimise free space in the absence of guest. For the more rigid cryptophanes the required conformational change is more extreme! Figure 6.45 shows a remarkable conformational equilibrium in a crytophane ester related to **6.89** reported by K. Travis Holman from Georgetown University, USA.[65] The cryptophane exists as an *anti* isomer with approximate $D_3$ symmetry and includes a molecule of tetrahydrofuran (THF) in the cavity as well as three other THF molecules in the solid state. Thermogravimetric analysis (TGA, Box 9.1) indicates that while loss of the extra-cavity THF is facile, the intra-cavity solvent is not lost until the sample is heated to over 120 °C, way above the normal boiling point of pure THF, Figure 6.45c. Holman's group were able to crystallographically characterise the fully desolvated form of the compound by recrystallising the heated material in chloroform. They showed it to be a remarkable 'imploded' atropisomer in which one of the CTV bowls adopts the very rare saddle-twist conformation. The activation energy barrier for the molecule to isomerise back to the bowl conformer is 99 kJ $mol^{-1}$ and hence the process is very slow at room temperature, allowing

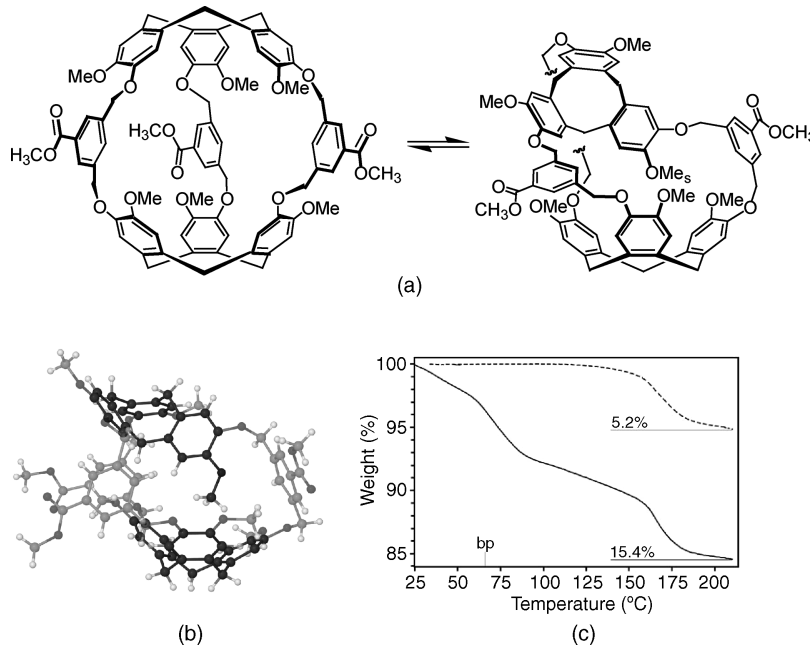


**Figure 6.45** (a) conformational 'implosion' of a cryptophane ester upon guest removal, (b) X-ray molecular structure of the 'imploded' atropisomer and (c) TGA trace showing the facile loss of the three lattice THF molecules from the cryptophane·$(thf)_4$ complex (solid line) and the very reluctant loss of the intra-cavity thf molecule from cryptophane·thf. The boiling point of pure thf is also marked.[65] (Figures courtesy of Prof. K. T. Holman).

the isolation of this conformer. The implosion process upon guest removal *via* a dramatic activation barrier to form a conformer that is *ca.* 15 kJ $mol^{-1}$ higher in energy highlights the importance of van der Waals interactions in cavity-containing compounds.

## 6.6.7 Hemicryptophanes

Closely analogous to the cryptophanes are the hemicryptophanes with a cavity superstructure based on only one CTV fragment. The compounds are conceptually analogous to the hemispherands (Section 3.7.7), but the nomenclature is somewhat inconsistent with the hemicarcerands (discussed in the next section) where two bowl shaped units are present. Hemicryptophane **6.93** is prepared by reacting the tri-ol cyclotriguaiacylene **6.91** over several steps to produce the trialdehyde **6.92**. Intramolecular capping/cyclisation (route 'a', Scheme 6.16), gives the hemicryptophane **6.93**, Scheme 6.17. The hemicryptophane can exist as two different steroisomers, depending on whether the P=S bond points *into* or *out* of the cavity. Only one of the isomers can be isolated, shown by X-ray crystallography to be the outward isomer, which contains a toluene guest molecule. In addition to being a neutral guest (toluene) receptor this molecule also possesses basic imine functionalities and hence can also act as a ditopic receptor and simultaneously bind cations. A related hemicryptophane **6.94** also acts as a ligand for vanadyl ion ($VO^{2+}$). The ligands have been resolved into optically pure stereoisomers according to the ligand skeletal helicity (*M* or *P*). The synthesis proceeds in a similar way to the synthesis of **6.93** but in reverse with the CTV-derived saucer-shaped fragment being formed last. The

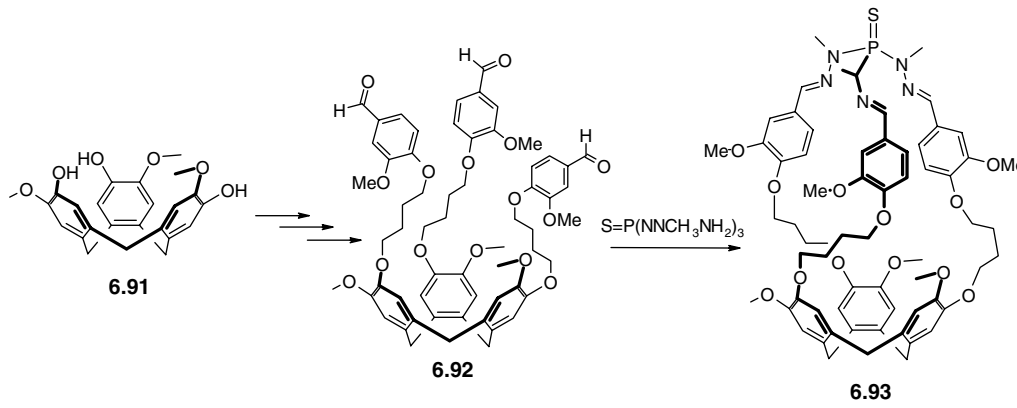


**Scheme 6.17** The synthesis of hemicryptophane **6.93**.[67]

*R* stereocentres are installed stereospecifically early in the synthesis but when the final cyclisation occurs to give the CTV fragment a compound of either *M* or *P* helicity can result and hence two diastereoisomers are produced, either *M*-(*R,R,R*)-**6.94** or *P*-(*R,R,R*)-**6.94**. Similarly starting from the *S* enantiomer of the backbone the diastereomeric pair *M*-(*S,S,S*)-**6.94** and *P*-(*S,S,S*)-**6.94** are also accessible (for a discussion on *M* and *P* helicity see Section 10.8). It is possible to separate disatereomeric pairs such as *M*-(*R,R,R*)-**6.94**/*P*-(*R,R,R*)-**6.94** by column chromatography and thus obtain all four isomers in pure form. The optical purity can be established by circular dichroism spectroscopy, Box 6.2. The resulting chiral ligands as their vanadyl complexes are proposed as biomimetic chiral catalysts.[66]

**Box 6.2** Circular Dichroism Spectroscopy

Circular dichroism spectroscopy (CD) is a type of electronic spectroscopy (*i.e.* it probes electronic transitions in the UV-visible region of the electromagnetic spectrum) that measures the difference in absorbance and hence difference in molar extinction coefficient ($\Delta\varepsilon$) between enantiomers of chiral compounds. Unlike conventional electronic spectroscopy which uses linearly polarised light (all of the wave vectors propagate in the same plane), CD uses circularly polarised light in which the electric field vector has a constant length, but rotates about its propagation direction and so it forms a helix in space while propagating. This helix can be a left or right handed helix and so we refer to left or right circularly polarised light. When light interacts with a molecule then the electric field component causes the electron charge to be linearly displaced. The magnetic field component causes charge circulation. As a result there is a helical displacement of charge when light interacts with a molecule. If the light is circularly polarised then it is itself chiral and hence will interact differently with the left or right enantiomers of a chiral molecule with the two types of circularly polarised light being absorbed to different extents. In the CD experiment a resolved chiral molecule is subjected to equal amounts of left and right hand circularly polarised light usually in solution. One 'handedness' of light is absorbed more than another at a given wavelength and it is this wavelength-dependent difference that gives the CD spectrum. Thus, examination of Figure 6.46 reveals that the CD spectrum is a plot of the difference in molar extinction coefficient, $\Delta\varepsilon$ (obtained from the difference in measured absorbance *via* the Beer-Lambert law) over a range of wavelengths.

If, in two separate experiments, the CD spectra of two resolved, pure enantiomers are measured then they should be equal and opposite in the sign of Δε and this represents a good test as to whether the resolution has been successful. Of course if we measure the CD spectrum of a racemic micture then there is no net absorbance; the rotation of the two enantiomers present in the solution cancel one another out. Choosing a wavelength where Δε is large allows measurement of the *specific rotation* of the compound. Single wavelength measurements can be made using a polarimeter.

The specific rotation of a compound ($[\alpha]$ / deg cm$^2$ g$^{-1}$) is defined as the observed angle of optical rotation when plane polarised light is passed through a sample of path length 1 decimeter (10 cm) and a sample concentration 1 g per decilitre (100 mL). The value is accompanied by the temperature in °C as a superscript and the wavelength of the light used to make the measurement as a subscript. A subscript 'D' means the wavelength of the sodium-D line (589 nm). In solution specific rotation is given by Equation 6.2, where $l$ is the path length in decimetres and $c$ is the concentration of the compound in g per 100 mL. The sign of the rotation (±) is always given, as is the solvent used to make the measurement. The observed rotation $\alpha$ is obtained directly from the absorbance difference (or Δε).

$$[\alpha]_{\lambda}^{T} = \frac{100\alpha}{l \times c} \tag{6.2}$$

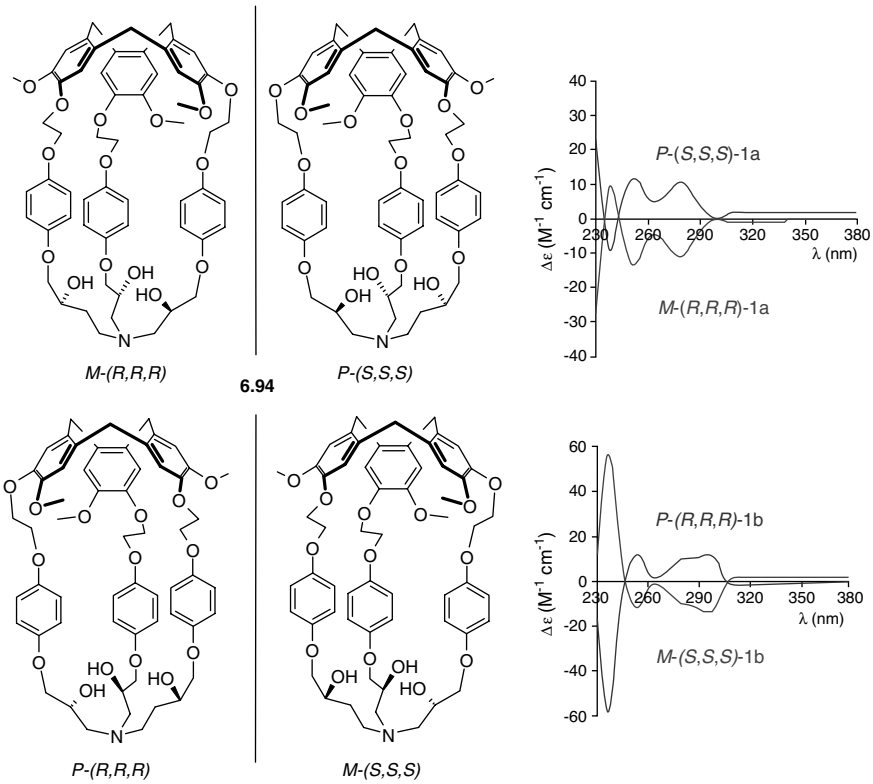


**Figure 6.46** The four isolated isomers of hemicryptophane **6.94** showing the two pairs of enantiomers along with their respective circular dichroism spectra (reprinted with permission from [66] © 1996 American Chemical Society).

## 6.7 Covalent Cavities: Carcerands and Hemicarcerands

Jasat, A. and Sherman, J.C., 'Carceplexes and Hemicarceplexes', *Chem. Rev.*, 1999, **99**, 931–967.

### 6.7.1 Definitions and Synthesis

A *carcerand* is defined as a closed molecular container or capsule without portals of significant size through which guests can either enter or leave (from the Latin *carcer* meaning 'prison'). Guest molecules within a carcerand are therefore permanently trapped or 'incarcerated' within the internal volume, unless covalent bond breakage within the host occurs. A carcerand that contains a guest giving an incarcerated host–guest complex is termed a *carceplex*. Given this definition, it is necessary also to employ another term, *hemicarcerand*, which describes closed molecular containers from which guests *can* enter and exit with a measurable activation barrier. In the presence of guest species, hemicarcerands form *hemicarceplexes*. Good examples of hemicarcerands are the cryptophanes (Section 6.6), which are able to reversibly entrap relatively small guests such as methane, haloalkanes *etc*. Much of the interest in this kind of three-dimensional inclusion chemistry stems from the possibility of stabilisation of reactive species within the host cavity, drug delivery and intracavity catalysis. All of these applications require the hemicarcerands' ability to (selectively) bind and expel guest species in response to external conditions. Carcerands themselves are not capable of these kinds of applications, although uses in the field of molecular electronics, sensing and molecular devices might be envisaged.

While the cryptophanes are highly successful hosts for binding single molecules, their overall cavity volume (80–90 $Å^3$) is too small to bind simultaneously two guest species in order to admit the possibility of intracavity reactivity and catalysis. Work by Cram *et al*.[68] has focused upon the larger [4]resorcarenes related to **6.3**. Adopting a similar strategy to cryptophane synthesis, Cram was able to couple the upper rims of two resorcarene bowls **6.95** and **6.96** under high-dilution conditions to give a pseudo-spherical cavity-containing capsule (**6.97**, Scheme 6.18).

Carcerand **6.97** was designed by Cram's group, just as they had designed the spherands, with the aid of CPK molecular models. In his Nobel Prize address, writing just two years after the preparation of **6.97**, Cram describes his interest in the host–guest chemistry of this new capsule:

> *The first question to be answered was: what guest compound would be trapped inside during the shell closure? This question is akin to asking whether two soup bowls closed rim-to-rim under the surface of a kettle of stew would net any stew. The answer was that [**6.97**] 'contained' essentially every kind of component of the medium present during ring closure.*[10]

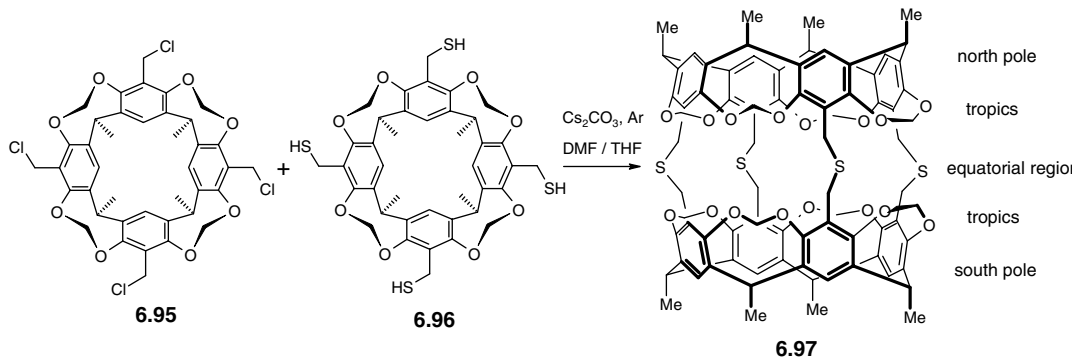


**Scheme 6.18** Synthesis of the first carcerand.[68]

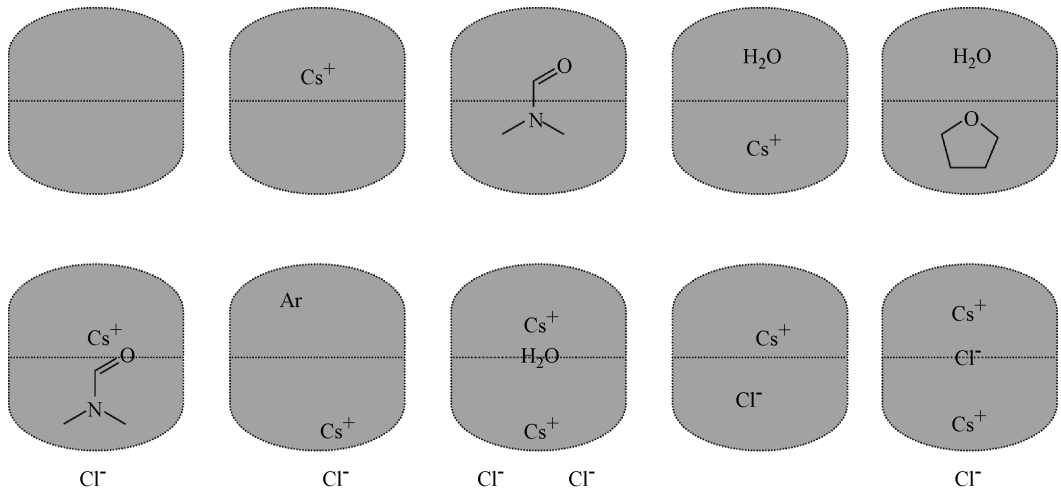


**Figure 6.47** Carceplexes formed in the preparation of **6.97** (denoted by grey oval).

The reaction product from Scheme 6.18 proved to be extremely insoluble in all solvents, and as a result its characterisation was a painstaking procedure. Impurities and unreacted starting materials were extracted by treatment of the product mixture with the most powerful solvents of every type (polar, non-polar, hydrogen bonding, dipolar aprotic *etc.*). The remaining product (various carceplexes – *i.e.* host–guest complexes – of **6.97**) was analysed by elemental analysis for the elements C, H, S, O, N, Cl and Cs, all of which proved to present in varying amounts, the ratio between Cs and Cl being stoichiometric. A solid-state infrared spectrum revealed the presence of the reaction solvent, dimethyl formamide, from observation of the characteristic C=O band. Analysis of the mixture by mass spectrometry (fast-atom bombardment) revealed the presence of all of the carceplexes shown in Figure 6.47. No peaks were found at molecular masses higher than the heaviest carceplex, and no other peaks were observed. Clearly, once ring closure occurs any species present in the inner region of the forming carcerand are completely unable to escape, even argon gas!

Cram's group found that careful drying of the hydrated complexes followed by reflux in $D_2O$ results in the substantial replacement of the incarcerated water by the deuterated analogue, suggesting that the portals on the sides of the carcerand are large enough to permit the diffusion of small molecules such as water through the cavity walls, although it is possible that even this process involves exchange of $D^+$ for $H^+$ ions. The elemental analysis data indicated that about five per cent of the mixture consisted of the free carcerand, 60 per cent encapsulated $Cs^+$, 45 per cent contained $Me_2NCHO$, 15 per cent THF and only one to two per cent $Cl^-$. This distribution is consistent with the affinity of calix[4]arene type molecules for $Cs^+$ (Section 3.14) and suggests that formation of **6.97** involves an $S_N2$ linear transition state in which the $Cs^+$ is coordinated to the sulfur (Equation 6.3).

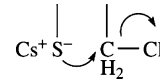


(6.3)

The problems with carcerand solubility were soon overcome by exchange of the methyl 'feet' for a range of groups such as *n*-pentyl, *n*-undecyl, 2-phenyl ethyl *etc.* to give carceplexes soluble in organic solvents with solvent molecule guests, in yields as high as 32 per cent. Related compounds with acetal bridges ($OCH_2O$) between the hemispheres such as **6.98**, have been prepared from $CH_2Br_2$ and tetrol **6.99** (Scheme 6.19). Use of longer alkyl chains up to $(CH_2)_4$ results in elongated capsules whose bridges

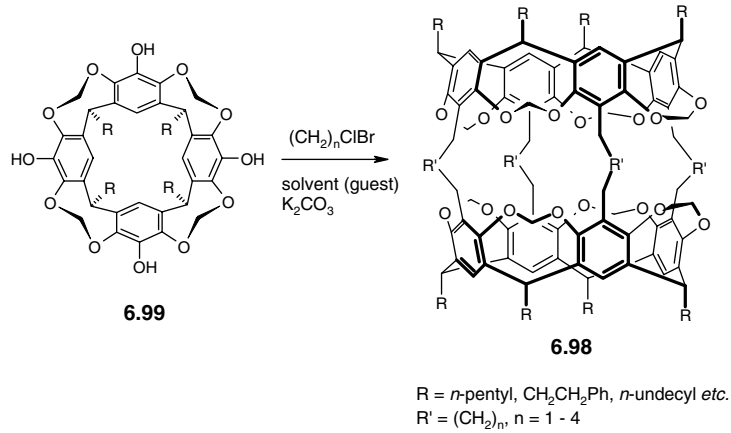


**Scheme 6.19** Preparation of $(CH_2)_n$-bridged carcerands and hemicarcerands from tetrol **6.99**.

are flexible enough to allow the passage of some small guest species under forcing conditions, forming hemicarceplexes. The rigidifying acetal spacers at the upper rim of each bowl (termed the 'tropical' regions by analogy with planetary geography) may also be altered to $OCH_2CH_2O$ groups, giving a wider, shallower curvature to each hemisphere. All of these multiple ring-closure steps involve the simultaneous assembly of seven molecules (including the guest), yet despite this carcerand **6.98** is formed in up to an amazing 87 per cent yield.

Even in the presence of $(CH_2)_4$ bridges, however, complexes **6.98** are still reluctant to allow passage of guest molecules in and out of their cavities. As a result, true hemicarceplexes active for host–guest chemistry involving multiple guest exchange and intracavity reactivity have a specific portal engineered into one side of the compound. Thus, reaction of the triol **6.100** with dihalides $X(CH_2)_nX$ gives the triply bridged hemicarceplex **6.101**, which has one distinct open portal, allowing ready guest access (Scheme 6.20).

Since the preparation of **6.97**, an enormous range of carcerand and hemicarcerand species have been prepared based upon both [n]resorcarenes and calix[n]arenes (n = 4,5), all of which exhibit interesting binding behaviour and intra-cavity reactivity, as we will see in the next sections.

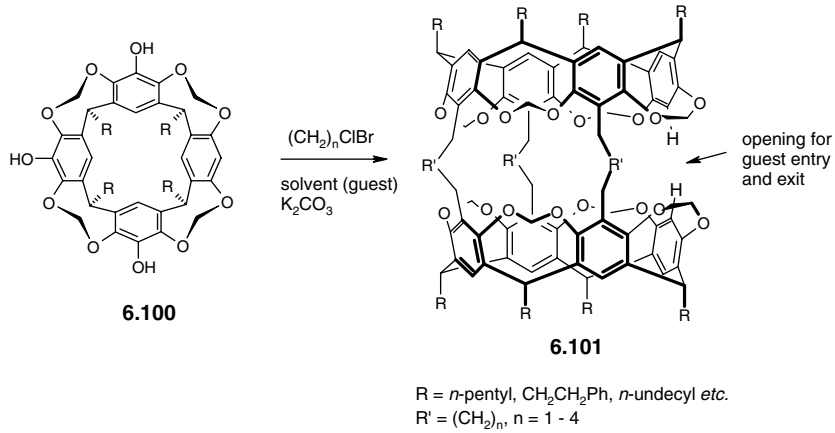


**Scheme 6.20** Reaction of a resorcarene triol with dihaloalkanes to give a hemicarcerand with a portal for guest exchange.

## 6.7.2 Template Effects in Carcerand Synthesis

The excellent yields obtained for the preparation of many carceplexes and hemicarceplexes is entirely contrary to expectation based on the statistical coming together of so many reactants and the closure of so many rings. It is clear that their formation is not statistical at all, and that a templated mechanism is in operation. Indeed, studies on the ring closure of a large range of capsular compounds of this type confirm that they are formed only in the presence of a suitable templating guest. Attempts to prepare carceplexes in solvents that are too large to fit within the cavity are unsuccessful. The templating ability of an enormous range of potential guests has been quantified by the measurement of *template ratios* for the synthesis of carcerand **6.98** ($n = 1$, R = $CH_2CH_2Ph$). These studies were aided by the fact that *N*-methylpyrrolidinone (NMP) proves to be an extremely poor solvent for the synthesis of this compound. Therefore, competition experiments were carried out in which equal amounts of two potential guests compete for the intra-cavity place during the synthesis of **6.98** in NMP solution. This situation results in the formation of two distinct carceplexes of **6.98**, one with each of the competing guests. Analysis of the resultant mixture by $^1$H NMR spectroscopy gives the ratio between the two carceplexes by integration of the guest signals. Formation of one carceplex in preference to another suggests that the guest within the favoured carceplex is better able to stabilise the intermediate in the final closure of the carcerand. This reaction step is termed the *guest-determining step* (GDS) because the guest cannot escape after this stage. The range of template ratios extends over a factor of $10^6$ with pyrazene proving to be the most effective template. In the case of pyrazene, a high template ratio correlates well with a high reaction yield (75 per cent); however, there are some exceptions to the rule of high yields from good templates. The template ratio also correlates well with the relative stability constants of the various carceplexes ($K_{rel}$). This observation suggests that the guests impart similar effects on the overall complex free energy as they do on the transition state activation energy. Example template ratios and $K_{rel}$ values are given in Table 6.10. In general, guest size and shape are important. However, the large disparity in the results for the closely related 1,3- and 1,4-dioxane suggest that specific directional effects are involved as well. These may well take the form of non-covalent interactions between the guest and the walls of the cavity as it forms. Thus, guests that can achieve the maximum number of van der Waals and C—H $\cdots$ $\pi$ interactions with the cavity walls make the most effective templates.[69]

## 6.7.3 Complexation and Constrictive Binding

Guest binding by carcerand-type hosts is characterised by the guest exchange rate with the external medium. True carceplexes exhibit virtually no guest exchange. Slow guest exchange (hours–days) is characteristic of hemicarceplexes, whereas binding of very small molecules, such as $O_2$, that are in rapid exchange (on the NMR spectroscopic time scale) results in what are strictly termed complexes rather than hemicarceplexes. Hemicarcerands are characterised by *constrictive binding*. The constrictive binding energy represents the magnitude of the sterically-imposed activation energy barrier to guest entry into the cavity during the exchange process and arises from the instability of the guest exchange transition state which involves significant bond strain as the guest squeezes through the wall of the hemicarcerand. Clearly as the guest gets smaller, or the portal through which it must pass gets larger, the constrictive binding energy, which is generally much larger than the intrinsic binding energy (as measured by the conventional binding constant), decreases, Figure 6.48. Constrictive binding is related to the steric energy barrier that keeps a rotaxane 'threaded' (Section 10.7) and is quite distinct from the intrinsic binding energy – the complexation free energy for the guest binding reaction. As with the cryptophanes, the complexation behaviour of carcerands is readily monitored by $^1$H NMR spectroscopy, where the magnetic anisotropy of the aryl rings that form the cavity walls

**Table 6.10** Template ratios for the formation of **6.98** (n = 1, R = $CH_2CH_2Ph$) by a variety of guest species, and relative stabilities of the resulting carceplexes in nitrobenzene-$d_5$. Values normalised to NMP = 1.[69]

| Guest | Template ratio | $K_{rel}$ |
|---|---|---|
| Pyrazene | 1 000 000 | 980 000 |
| 1,4-Dioxane | 290 000 | 240 000 |
| Pyridine | 34 000 | 7100 |
| Benzene | 2400 | 540 |
| 1,3-dioxane | 200 | 140 |
| Dimethyl acetamide | 20 | 8.9 |
| NMP 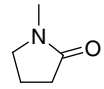 | 1 | 1 |

gives rise to large chemical shift changes (usually upfield) for the resonances assigned to guest species. As the guest, penetrates deeper into the cavity, this effect becomes more pronounced and $\Delta\delta(=\delta_{free} - \delta_{entrapped})$ values of 2–4.5 ppm are common, depending on the degree of guest penetration into the resorcarene hemispheres. The infrared spectra of trapped species are also significantly perturbed. In the case of carceplexes formed between **6.98** and dimethyl formamide (DMF) or dimethyl

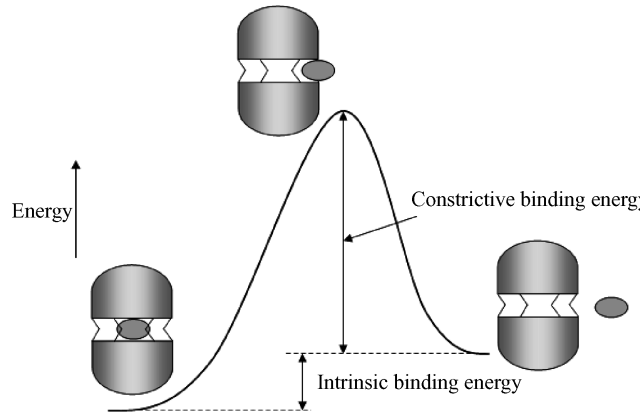


**Figure 6.48** Constrictive binding energy – the activation energy for guest enty to the cavity.

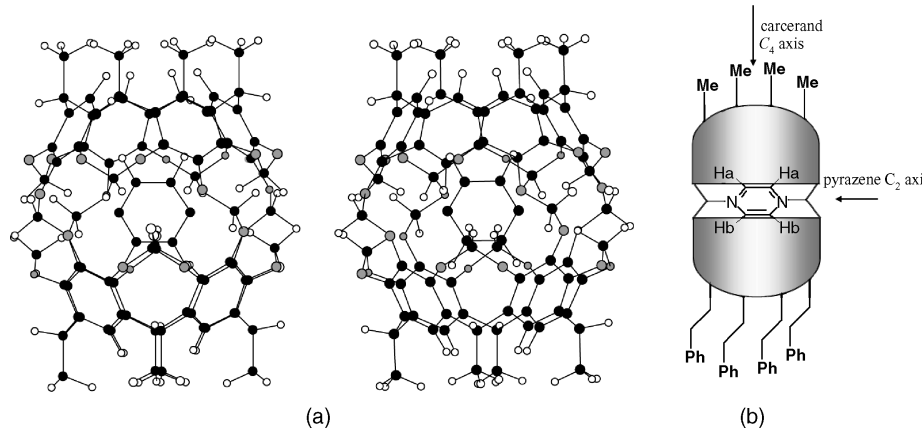


**Figure 6.49** (a) X-ray crystal structure (stereoview) of the pyrazene carceplex of **6.98** (reprinted with permission from [70] © 1996 The American Chemical Society) and (b) cartoon view of an asymmetric analogue of the complex in which the different 'feet' render $H_a$ and $H_b$ inequivalent, allowing the rate of rotation about the pyrazene N–N $C_2$ axis to be measured.

acetamide (DMA) the characteristic  stretching frequencies are intermediate between those commonly observed for the liquid and gas phases of the pure molecules (*cf.* methane within the interior of cryptophane-A, Section 6.6.5).

The X-ray crystal structure of the pyrazene carceplex of **6.98** is shown in Figure 6.49a. Pyrazene has one of the largest template ratios known, suggesting favourable guest–host interactions. This is clearly evident in the structure with the guest nitrogen atoms engaging in C—H $\cdots$ N hydrogen bonds with the host methylene bridges. In addition, C—H $\cdots$ $\pi$ interactions are observed from the other host methylene bridges to the pyrazene $\pi$-system, and the pyrazene protons to the host aryl rings. These interactions have the effect of slowing down the intracavity rotation of the pyrazene along its N—N axis. Using an asymmetric carcerand having extracavity methyl substituents on one hemisphere and 2-phenylethyl groups of the other (Figure 6.49b), it is possible to measure the rate of this rotation which proves to have a large energy barrier of 80 kJ mol$^{-1}$. The structure of the pyrazene complex also displays the excellent fit of the pyrazene guest. In the carceplex, the two hemispheres of the host are rotated 21 degrees with respect to one another about the pseudo-$C_4$ axis, but are essentially parallel, enabling full conjugation of the interbowl oxygen atoms with the aromatic rings. In contrast, the structure of the DMA derivative is distorted 5.2 degrees from a parallel arrangement as a result of the steric bulk of the larger guest.

## 6.7.4 Carcerism

Carcerand hosts are not limited to resorcarene derivitaves. David Reinhoudt's group (Twente, Netherlands) have prepared the mixed [4]resorcarene–calix[4]arene host **6.102** again arising from face-to-face coupling of the two different bowl-shaped macrocyclic hemispheres (Scheme 6.21).[71] While the intramolecular cavities in the resorcarene-based carcerands are essentially spherical or elongated curved-ended cylinders, the cavity in **6.102** is more egg-shaped, making it highly unsymmetrical, with the wider, shallower resorcarene cavity forming the base of the egg and the deeper, narrower calix[4]arene forming the tip.

The preparation of **6.102** is carried out in a variety of solvents, such as DMF, DMA, dimethylsulfoxide (DMSO) and ethyl methyl sulfoxide, at 80ºC and the yield of the carcerand is virtually quantitative.

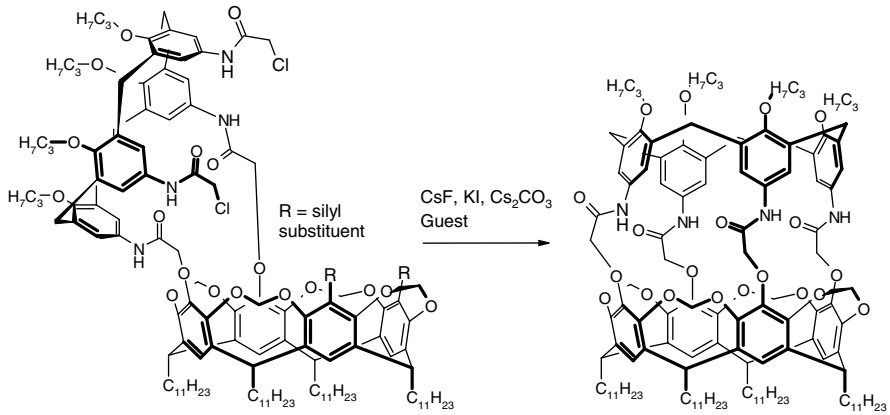


**6.102**

**Scheme 6.21** Synthesis of the egg-shaped carcerand **6.102**.[71]

However, in larger potential guest solvents (too large to fit the cavity), yields decreased markedly. For example, 1,5-dimethyl-2-pyrrolidinone gives only five per cent yield of the capsule. In the case of small guests such as DMF, rotation about the $C_2$-type axis is rapid, with only one species being observed. However, larger guests such as DMA exhibit highly hindered rotation, with rotational barriers in the range 53–73 kJ $mol^{-1}$. This restricted rotation results in the existence of two orientational isomers – a new type of stereoisomersim. Reinhoudt and co-workers proposed the term *carceroisomerism* (*carcersim* for short) to describe this phenomenon (Figure 6.50).

## 6.7.5 Inclusion Reactions

Warmuth, R., Yoon, J., 'Recent highlights in hemicarcerand chemistry', *Acc. Chem. Res.* 2001, **34**, 95–105.

The robust, well-shielded cavity found in hemicarcerands offers tremendous scope for the use of these hosts as micro-reaction vessels in order to protect reactive species from bimolecular decomposition by isolating them from the outside medium. Furthermore, the unique intracavity environment with its fluid-like properties in which guest species are, formally, in a very condensed state at very high pressures, may well result in unique inclusion reactivity. Indeed, the inner volume of carcerands and hemicarcerands has been described as a 'new phase of matter' distinct from solid, liquid and gas. A number of elegant demonstrations have been made of the potential of inclusion reactions, and there is clearly a great deal of scope for their use as molecular reaction vessels.

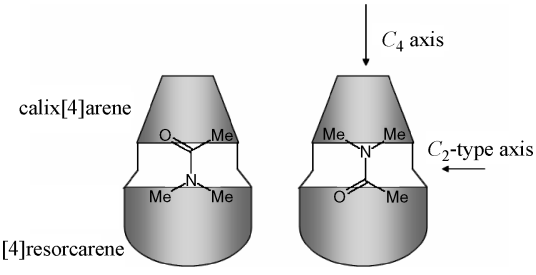


**Figure 6.50** 'Carcerism' in DMA complexes of hybrid carcerands.[71]

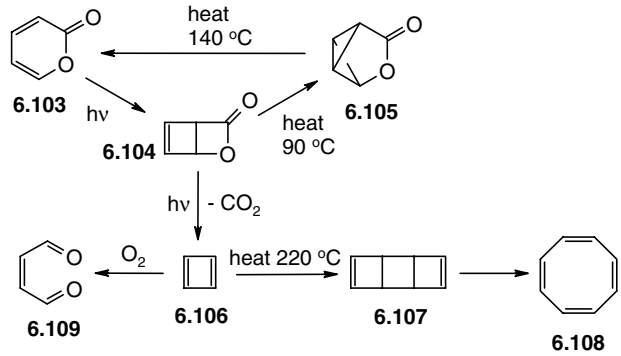


**Scheme 6.22** Intracavity preparation and reactions of cyclobutadiene.[72]

One of the simplest demonstrations of the effect incarceration has on a guest's reactivity is the measurement of the basicity of included amine ligands. Solutions of pyridine in $CDCl_3$ may be shown by $^1$H NMR spectroscopy to be readily protonated by $CF_3CO_2D$. An analogous reaction of the pyridine hemicarceplex of the 'open' portal hemicarcerand **6.101** results in the pyridine remaining unprotonated. This means that incarcerated pyridine is a much weaker base than the free molecule. This difference is explained most reasonably by the fact that the host has only a very limited ability to solvate the pyridinium ion and will sterically inhibit the formation of pyridinium–trifluoroacetate contact ion pairs.

A much more dramatic use of hemicarcerands is Donald Cram's 1991 landmark preparation of the highly unstable molecule cyclobutadiene (**6.106**) within the cavity of **6.101**.[72] Prior to this work, cyclobutadiene had only been observed frozen in an inert gas matrix at 8 K after photolysis of $\alpha$-pyrone (**6.103**). Upon warming, the cyclobutadiene dimerises rapidly, ending up as cyclooctatetraene (**6.108**). Cram and co-workers carried out all of the chemistry shown in Scheme 6.22 within the cavity of **6.101**. Careful control of conditions enabled them to cycle through the photolysis of $\alpha$-pyrone (which was included by reflux with the free host) to give the lactam **6.104**, rearranged lactam **6.105** and back to $\alpha$-pyrone once more. The hemicarceplex of the normally reactive **6.104** proved to be stable for two weeks in the solid state at room temperature. Most remarkably, irradiation of the hemicarceplex of **6.104** with a 75-W xenon arc lamp for 30 min gave incarcerated cyclobutadiene (**6.106**) at room temperature. The new guest exhibits an $^1$H NMR signal at $\delta$ 2.27 ppm and proved to be highly stable within the protected hemicarcerand environment. The $CO_2$ formed as a by-product is ejected from the cavity. By analogy with the upfield shift caused in the spectrum of incarcerated benzene, Cram calculated that the chemical shift of free cyclobutadiene should be about 5.2–5.7 ppm. The observation of sharp signals confirms that cyclobutadiene has a singlet ground state.

The reactivity of the incarcerated cyclobutadiene was probed by warming the NMR sample to 220ºC for 5 min. This resulted in the formation of free cyclooctatetraene (**6.108**), clearly from ejection of the cyclobutadiene from the cavity and its subsequent dimerisation *via* **6.107**. Reaction with $O_2$ (which is able to enter the cavity of **6.101** gave incarcerated malealdehyde (**6.109**).

For some time, the taming of cyclobutadiene remained the only major achievement in the application of host container molecules to the stabilisation of reactive species. However, the stabilisation of 1,2,4,6-cycloheptatriene (**6.110**)[73] and the even more reactive *o*-benzyne (**6.111**) have both now been achieved by the group of Ralph Warmuth (Rutgers, New Jersey, USA). Bother of these compounds are important synthetic intermediates. Cyclobutadiene is unstable as a consequence of its need to produce 90-degree bond angles from $sp^2$ hybrid orbitals, which have an optimum at 120º. In contrast, benzyne is aiming for 120-degree angles from *sp* orbitals, which have an optimum angle of 180º. The stabilisation of *o*-benzyne was achieved within the four-bridged hemicarceplex **6.98** (n = 4), which does not possess a

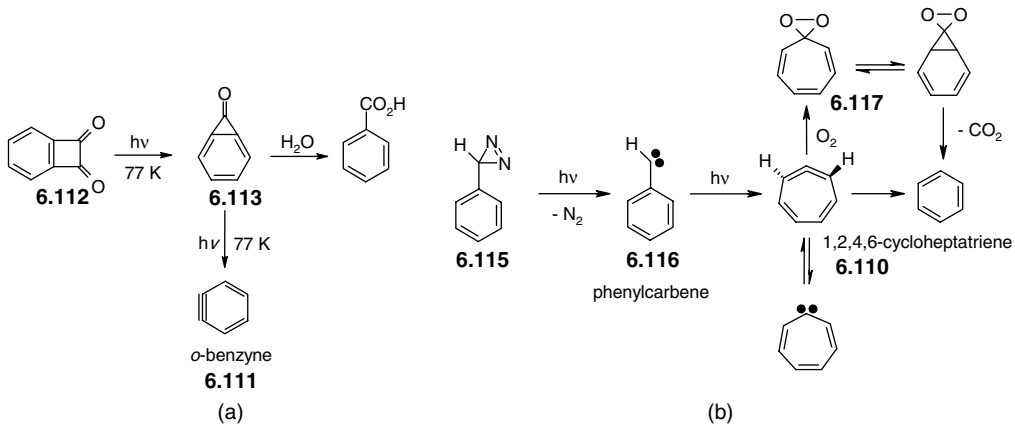


**Scheme 6.23** Intra-cavity preparation of (a) *o*-benzyne and (b) 1,2,4,6-cycloheptatriene.

specific portal for guest inclusion. Benzocyclobutenedione (**6.112**) was incarcerated in 35 per cent yield by heating of **6.98** in the pure guest. Photolysis at 77 K gave the carceplex of the cyclopropenone **6.113**. This material is apparently indefinitely stable and has been characterised by X-ray crystallography. In the presence of water, it reacts slowly to give incarcerated benzoic acid. Further photolysis at 77 K gives the desired *o*-benzyne, which is stable enough for its $^{1}$H and $^{13}$C NMR spectra to be measured at –75 ºC and –98 ºC respectively (Scheme 6.23a). The $^{1}$H NMR spectrum shows two signals for the two unique pairs of *o*-benzyne protons at $\delta$ 4.99 and 4.31 ppm. Interestingly, on warming to room temperature, the guest is still unable to escape its prison, but instead reacts with the walls of the carcerand in a Diels–Alder addition to give a benzo-bridged 1,4-cyclohexadiene product (**6.114**). Intra-cavity preparation of 1,2,4,6-cycloheptatriene according to the route outlined in Scheme 6.23b is also complicated by undesirable innermolecular rections of phenylcarbene (**6.116**) with the acetyl bridges of the hemicarcerand. This problem is minimised by deuteration. It is then possible to produce and isolate the hemicarceplex of the normally highly unstable 1,2,4,6-cycloheptatriene. Within the cavity the molecule is stable up to 60 ºC and does not react with water or methanol, which are able to enter the cavity, however exposure to oxygen gives benzene *via* **6.117**. The cavity also significantly slows the equilibrium between **6.110** and its planar carbene analogue. The enantiomerisation rate of the chiral **6.110** was measured using a chiral hemicarcerand and the barrier found to be in excess of 80 kJ mol$^{-1}$.

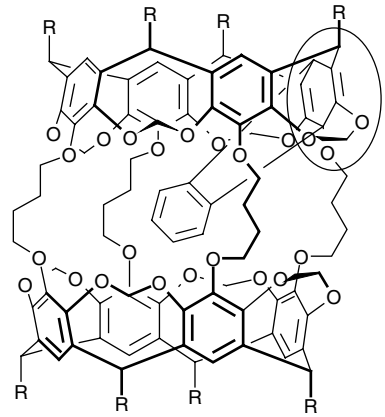

**6.114**

While extremely elegant, the preparations of reactive compounds such as cyclobutadiene and *o*-benzyne within hemicarcerand cavities *via* photolysis suggest that the possibilities for the use of the host materials to accomplish other intracavity chemistry might be limited by the need to accommodate chemical reagents in the host cavity in the event of the reaction not proceeding by photolysis. Interestingly however, Cram *et al*. have also carried out a range of quantitative oxidations and reductions within **6.98** (n = 4) upon incarcerated quinones and related species. The redox reagents were materials such as $SmI_2$ and $Ce(NH_4)_2(NO_3)_6$, which have no chance of entering the cavity. Nonetheless, the redox reactions proceeded extremely smoothly (in the case of nitrobenzene giving the unusual *N*-phenylhydroxylamine instead of aniline) with electron, proton and water transfer occurring through the walls of the host.[74]

## 6.7.6 Giant Covalent Cavities

While the properties of the hemicarceplexes are striking, they are fundamentally limited in the size of inner-space offered by the two [4]resorcarene bowls. Two alternative strategies exist for expanding the bowl size; either construction of face-to-face duplexes using larger [n]resorcarenes or calix[n]arenes, or incorporating more calixarene-type macrocycles into the compound. Both of these approaches have been realised. The first [5]resorcarene-based carcerand (**6.118**) was prepared by the group of John C. Sherman (University of British Columbia, Canada) in 2002.[75] The new carcerand exhibits $C_5$ symmetry and is prepared without the characteristic 'feet' of other carcerands. The cavity is large enough to include two DMF or DMA guests which do not exchange with other guests such as nitrobenzene even over periods of weeks.

The linking together several [4]resorcarene cavities reprents an, in principle, more straightforward approach to truly giant cavities, if only for the ready availability of [4]resorcarene building blocks. Using a protecting group approach in which pairs of hydroxyl groups in [4]resorcanene **6.99** are reacted at a time, Sherman's group have prepared the three-bowl macrocycle **6.119**. Exploitation of template in which more than one guest is involved in the final GDS then allows this compound to be capped to give the trimer carceplex **6.120**, Figure 6.51. The compound is large enough to host three DMF guest molecules and a wide variety of other compounds.[76] The largest carcerand-type molecule prepared to date is an $–NHCH_2CH_2NH–$ bridged carcerand hexamer with an internal cavity volume of *ca*. 1700 Å$^3$ (Figure 6.52). The hexamer is prepared in excellent yield in an astounding 18-component one-pot synthesis starting from [4]resorcarene tetraaldehyde **6.122** and 1,2-diaminoethane followed by reduction of the unstable imine bonds.[77] It is the unstability of the imine bonds in the intermediate that allow the reaction to proceed *via* a self-assembly process (Chapter 10), hence the remarkable yield for such a complex, multi-component process.

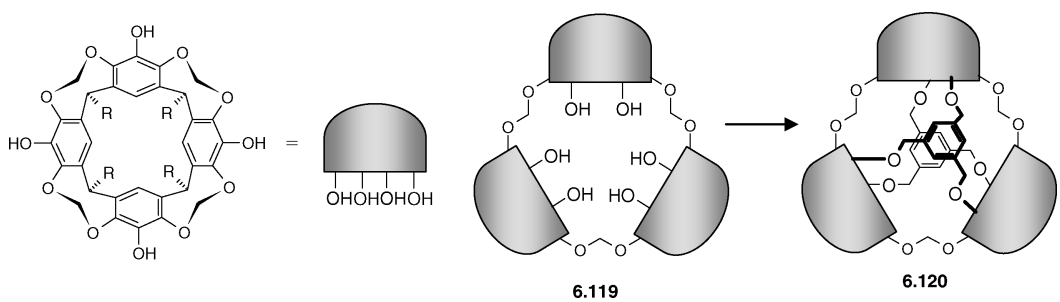


**Figure 6.51** Synthesis of a trimeric carcerand from a resorcarene trimer precursor.[76]

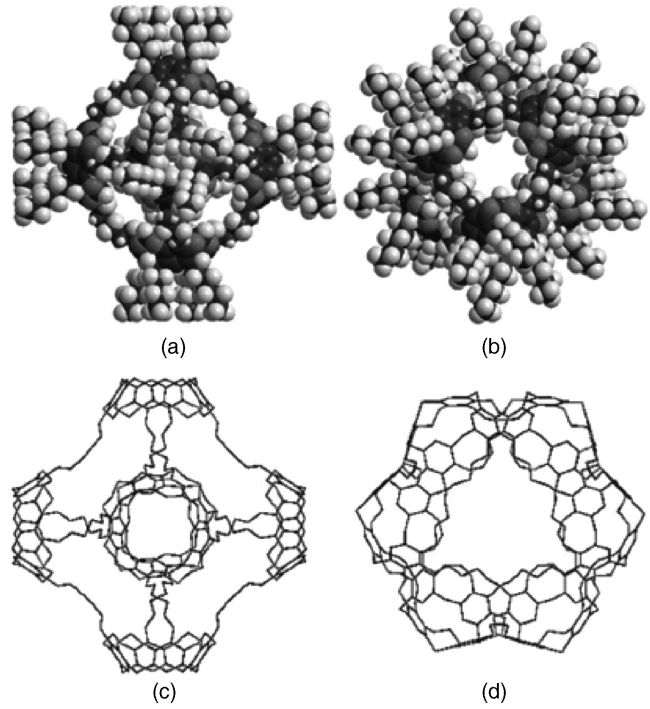


**Figure 6.52** Molecular models viewed along the $C_4$ (a and c) and $C_3$ (b and d) axes of the 1700 Å$^3$ resorcarene hexamer formed in an 18-component, one-pot synthesis. (Copyright Wiley-VCH Verlag GmbH & Co. KGaA. Reproduced by permission).

The portals in the compound evident in Figure 6.52a are *ca.* 8Å in diameter allowing relatively facile guest exchange. Related hexa-resorcarenes have been prepared by a stepwise approach related to that shown in Figure 6.51 and shown to be templated by, and to complex, seven DMSO guest molecules as well as form mixed-guest complexes.[78] The compounds are closely related to a series of hydrogen-bonded self-assembled resorcarene hexamers and we will return to these non-covalent capsules in Chapter 10.

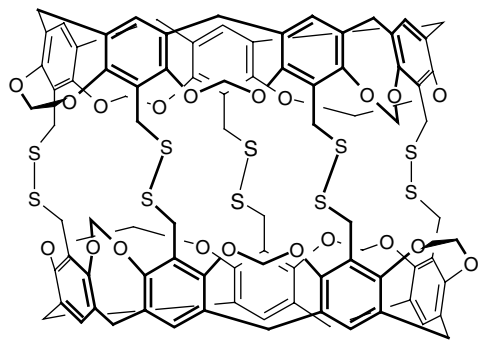

[5]carceplex

**6.118**

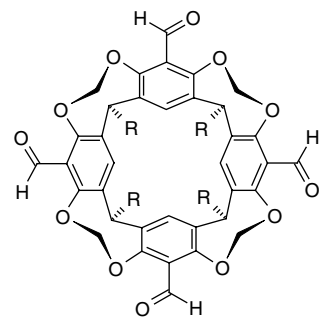

R = $C_5H_{11}$

**6.122**

## Summary

- Molecular guest binding in solution generally involves hosts such as the calixarenes or cyclodextrins that have intrinsically curved surfaces or cavities and is highly dependent on solvent. In non-polar solvents strong, polar interactions such as hydrogen bonding dominate whereas in polar media, particularly water, solvophobic binding is of much more importance.
- The cyclodextrins in particular are of considerable commercial importance in applications such as food additives, drug delivery and analytical separations because of their complexing ability in water and in the solid state, non-toxicity and chirality.
- Synthetic organic chemistry has now evolved to the point where extremely sophisticated, designed cavity-containing molecules of the cyclophane type can be prepared and their solubility and binding properties tuned extremely precisely.
- The construction of large, sterically restricted cavities gives rise to *constrictive binding* as in the cryptophanes and hemicarcerands, allowing such hosts to be used as molecular reaction vessels and in the stabilisation of reactive species. These tightly controlled inner phases of matter give rise to interesting phenomena such as *carcerism* and opportunities to permenantly entrap probe such as $^{129}Xe$ for medical imaging applications.
- The optimum occupancy factor in host cavities is around 55 per cent.

## Study Problems

6.1 The binding constant of cryptophane-A for methane is 130 $M^{-1}$ in $(CHCl_2)_2$, a solvent that is not bound by the cavity. Calculate the binding constant in $CHCl_3$ if $K_s$ for this solvent is 10 $M^{-1}$ and the density of liquid $CHCl_3$ is 1.48 g $cm^{-3}$ at 25 ºC.

6.2 A large carcerand has a cavity volume of 120 $Å^3$. If the molecular volume of methane is 28.5 $Å^3$, calculate the occupancy factor, ρ, for a 1:1 methane carceplex of this host. What host volume would result in an occupancy factor of 0.67, equivalent to solid methane? Calculate the notional pressure of one molecule of methane in a cavity of this size. Do you think that such a carceplex is likely to form?

6.4 Explain why carcerism is not observed for small carcerands based purely on [4]resorcarenes, such as **6.98**.

6.5 Explain the incorporation of the methyl substituents in the Kemp's triacid based molecular tweezers shown in Scheme 6.6 in terms of the principle of preorganisation discussed in Chapter 1.

6.6 Name the following cyclophanes, along with compounds **6.58** and **6.67**:

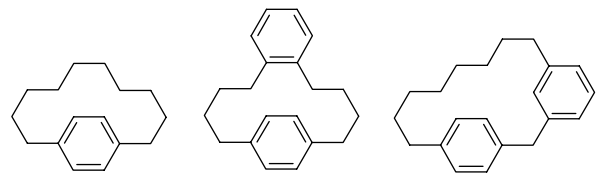

6.7 Suggest a possible synthetic route to the [4]resorcarene **6.100**.

## Thought Experiment

From your reading of Section 6.7, guess possible values for the template ratios for the synthesis of **6.98** in NMP in the presence of the following guests. Consider the influence of molecular size and shape, as well as host–guest interactions such as C— H hydrogen bonds, $\pi$–$\pi$ stacking *etc*.

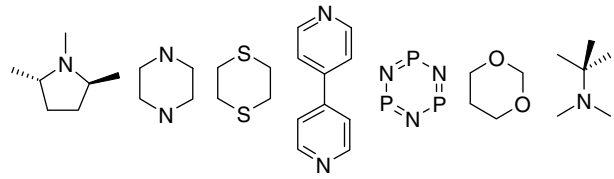

# References


1. Moran, J. R., Ericson, J. L., Dalcanale, E., Bryant, J. A., Knobler, C. B., Cram, D. J., Vases and kites as cavitands. *J. Am. Chem. Soc.* 1991, **113**, 5707–5714.
2. Brouwer, E. B., Enright, G. D., Ratcliffe, C. I., Ripmeester, J. A., Udachin, K. A., 'Dynamic structures of host-guest systems'. in *Calixarenes 2001*, Asfari, Z., Böhmer, V., Harrowfield, J., Vicens, J., eds. Kluwer: Dordrecht, 2001, *pp.* 296–311.
3. Corazza, F., Floriani, C., Chiesi-Villa, A., Guastini, C., The oxo-molybdenum(VI) group over a calixarene-oxo surface—calix[4]arene complexing inorganic and organic functionalities. *J. Chem. Soc., Chem. Commun.* 1990, **640**.
4. Hajek, F., Graf, E., Hosseini, M. W., Delaigue, X., DeCian, A., Fischer, J., Molecular tectonics .1. The first synthesis and X-ray analysis of a linear koilate obtained by self-assembly of linear koilands and hexadiyne. *Tetrahedron Lett.* 1996, **37**, 1401–1404.
5. Stewart, D. R., Gutsche, C. D., Isolation, characterization, and conformational characteristics of p-tert-butylcalix[9-20]arenes. *J. Am. Chem. Soc.* 1999, **121**, 4136–4146.
6. Zyryanov, G. H., Kang, Y., Stampp, S. P., Rudkevich, D. M., Supramolecular fixation of $NO_2$ with calix[4]arenes. *Chem. Commun.* 2002, 2792–2793.
7. Rathore, R., Lindeman, S. V., Rao, K., Sun, D., Kochi, J. K., Guest penetration deep within the cavity of calix[4]arene hosts: The tight binding of nitric oxide to distal (cofacial) aromatic groups. *Angew. Chem., Int. Ed.* 2000, **39**, 2123–2127.
8. Rudkevich, D. M., Progress in supramolecular chemistry of gases. *Eur. J. Org. Chem.* 2007, 3255–3270.
9. Cram, D. J., Stewart, K. D., Goldberg, I., Trueblood, K. N., Complementary solutes enter nonpolar preorganized cavities in lipophilic noncomplementary media. *J. Am. Chem. Soc.* 1985, **107**, 2574.
10. Cram, D. J., The design of molecular hosts, guests and their complexes (Nobel Lecture). *Angew. Chem. Int. Ed. Engl.* 1988, **27**, 1009–1020.
11. van Loon, J. D., Heida, J. F., Verboom, W., Reinhoudt, D. N., Calix[4]Arenes as Building-Blocks for Molecular Receptors. *Recl. Trav. Chim. Pays-Bas* 1992, **111**, 353–359.
12. Prins, L. J., Huskens, J., de Jong, F., Timmerman, P., Reinhoudt, D. N., Complete asymmetric induction of supramolecular chirality in a hydrogen-bonded assembly. *Nature* 1999, **398**, 498–502.
13. Trembleau, L., Rebek, J., Helical conformation of alkanes in a hydrophobic cavitand. *Science* 2003, **301**, 1219–1220.
14. Baldini, L., Casnati, A., Sansone, F., Ungaro, R., Calixarene-based multivalent ligands. *Chem. Soc. Rev.* 2007, **36**, 254–266.
15. Arduini, A., Fabbi, M., Mantovani, M., *et al.*, Calix[4]arenes blocked in a rigid cone conformation by selective functionalization at the lower rim. *J. Org. Chem.* 1995, **60**, 1454–1457.
16. Rudkevich, D. M., Hilmersson, G., Rebek, J., Intramolecular hydrogen bonding controls the exchange rates of guests in a cavitand. *J. Am. Chem. Soc.* 1997, **119**, 9911–9912.
17. Rowan, A. E., Elemans, J. A. A. W., Nolte, R. J. M., Molecular and supramolecular objects from glycoluril. *Acc. Chem. Res.* 1999, **32**, 995–1006.
18. Flinn, A., Hough, G. C., Stoddart, J. F., Williams, D. J., Decamethylcucurbit[5]uril. *Angew. Chem., Int. Ed. Engl.* 1992, **31**, 1475–1477.
19. Kim, J., Jung, I.-S., Kim, S.-Y., *et al.*, New curcurbituril homologues: syntheses, isolation, characterisation and X-ray crystal structures of curcurbit[n]uril (n = 5, 7 and 8). *J. Am. Chem. Soc.* 2000, **122**, 540–541.

20. Day, A. I., Blanch, R. J., Arnold, A. P., Lorenzo, S., Lewis, G. R., Dance, I., A cucurbituril-based gyroscane: A new supramolecular form. *Angew. Chem., Int. Ed.* 2002, **41**, 275–277.
21. Liu, S. M., Zavalij, P. Y., Isaacs, L., Cucurbit[10]uril. *J. Am. Chem. Soc.* 2005, **127**, 16798–16799.
22. Kim, K., Selvapalam, N., Ko, Y. H., Park, K. M., Kim, D., Kim, J., Functionalized cucurbiturils and their applications. *Chem. Soc. Rev.* 2007, **36**, 267–279.
23. Kim, K., Mechanically interlocked molecules incorporating cucurbituril and their supramolecular assemblies. *Chem. Soc. Rev.* 2002, **31**, 96–107.
24. Atwood, J. L., Davies, J. E. D., MacNicol, D. D., Vögtle, F., *Comprehensive Supramolecular Chemistry*. 1 ed., Pergamon: Oxford, 1996, Vol. 3.
25. Harata, K., Uekama, K., Otagiri, M., Hirayama, F., Ohtani, Y., The structure of the cyclodextrin complex .18. Crystal-structure of beta-cyclodextrin benzyl alcohol (1-1) complex pentahydrate. *Bull. Chem. Soc. Jpn.* 1985, **58**, 1234–1238.
26. Odagaki, Y., Hirotsu, K., Higuchi, T., Harada, A., Takahashi, S., X-ray structure of the alpha-cyclodextrin ferrocene (2-1) inclusion compound. *J. Chem. Soc.-Perkin Trans. 1* 1990, 1230–1231.
27. Kamitori, S., Hirotsu, K., Higuchi, T., Crystal and molecular-structure of double macrocyclic inclusion complexes, gamma-cyclodextrin.12-crown-4.nacl, a model for the transport of ions through membranes. *Bull. Chem. Soc. Jpn.* 1988, **61**, 3825–3830.
28. Eto, S., Noda, H., Noda, A., Chiral Separation of barbiturates and hydantoins by reversed-phase high-performance liquid-chromatography using a 25 or 50 mm short ods cartridge column *via* beta-cyclodextrin inclusion complexes. *J. Chromatogr.* 1992, **579**, 253–258.
29. Chen, C. W., Whitlock, H. W., Molecular tweezers – simple-model of bifunctional intercalation. *J. Am. Chem. Soc.* 1978, **100**, 4921–4922.
30. Zimmerman, S. C., Rigid molecular tweezers as hosts for the complexation of neutral guests. *Top. Curr. Chem.* 1993, **165**, 71–102.
31. Klärner, F. G., Panitzky, J., Blaser, D., Boese, R., Synthesis and supramolecular structures of molecular clips. *Tetrahedron* 2001, **57**, 3673–3687.
32. Rebek, J., Molecular Recognition with model systems. *Angew. Chem., Int. Ed. Engl.* 1990, **29**, 245–255.
33. Pellegrin, M. M., Contribution à la étude de la réaction de Fittig. *Recl. Trav. Chim. Pays-Bas* 1899, **18**, 457–465.
34. Brown, C. J., Farthing, A. C., Preparation and structure of di-p-xylylene. *Nature (London)* 1949, **164**, 915.
35. Cram, D. J., Steinberg, H., Macro rings. I. Preparation and spectra of the paracyclophanes. *J. Am. Chem. Soc.* 1951, **73**, 5691.
36. Diederich, F., *Cyclophanes*. The Royal Society of Chemistry: Cambridge, UK, 1991,
37. Kotha, S., Mandal, K., Suzuki-Miyaura cross-coupling and ring-closing metathesis: A strategic combination for the synthesis of cyclophane derivatives. *Eur. J. Org. Chem.* 2006, 5387–5393.
38. Takemura, H., Wen, T., Shinmyozu, T., A new synthetic method for (Aza)(n)[3(n)]cyclophanes by diethyl phosphoramidates. *Synthesis-Stuttgart* 2005, 2845–2850.
39. Ilioudis, C. A., Steed, J. W., Organic macrocyclic polyamine-based receptors for anions. *J. Supramol. Chem.* 2001, **1**, 165.
40. Jarvi, E. T., Whitlock, H. W., Synthesis and Characterization of 1,8,15,22-tetraoxa[8.8]-paracyclophane-3,5,17,19-tetrayne-10,25-dicarbox ylic acid - novel water-soluble and donut-shaped molecule. *J. Am. Chem. Soc.* 1980, **102**, 657–662.
41. Whitlock, B. J., Whitlock, H. W., Concave functionality – design criteria for non-aqueous binding sites. *J. Am. Chem. Soc* 1990, **112**, 3910.
42. Odashima, K., Itai, A., Iitaka, Y., Koga, K., Host-guest complex formation between a water soluble polyparacyclophane and a hydrophobic guest molecule. *J. Am. Chem. Soc.* 1980, **102**, 2504.
43. Vögtle, F., Merz, T., Wirtz, H., Large carbocyclic cavities for the selective inclusion of organic guest molecules in aqueous-solution. *Angew. Chem., Int. Ed. Engl.* 1985, **24**, 221–222.
44. Diederich, F., Dick, K., New water-soluble macrocycles of the paracyclophane type - aggregation behavior and host-guest-interaction with hydrophobic substrates. *Tetrahedron Lett.* 1982, **23**, 3167–3170.
45. Kearney, P. C., Mizoue, L. S., Kumpf, R. A., Forman, J. E., McCurdy, A., Dougherty, D. A., Molecular recognition in aqueous-media - new binding-studies provide further insights into the cation-$\pi$ interaction and related phenomena. *J. Am. Chem. Soc.* 1993, **115**, 9907–9919.
46. Webb, T. H., Wilcox, C. S., Enantioselective and diastereoselective molecular recognition of neutral molecules. *Chem. Soc. Rev.* 1993, **22**, 383–395.
47. Ferguson, S. B., Sanford, E. M., Seward, E. M., Diederich, F., Cyclophane arene inclusion complexation in protic solvents – solvent effects versus electron-donor acceptor interactions. *J. Am. Chem. Soc.* 1991, **113**, 5410–5419.
48. Reichard, C., *Solvents and Solvent Effects in Organic Chemistry*. 3rd ed., VCH: Weinheim, 2003,
49. Diederich, F., Complexation of neutral molecules by cyclophane hosts. *Angew. Chem., Int. Ed. Engl.* 1988, **27**, 362–386.
50. Diederich, F., Felber, B., Supramolecular chemistry of dendrimers with functional cores. *Proc. Natl. Acad. Sci. U. S. A.* 2002, **99**, 4778–4781.

51. Hunter, C. A., Packer, M. J., Complexation-induced changes in H-1 NMR chemical shift for supramolecular structure determination. *Chem. Eur. J.* 1999, **5**, 1891–1897.
52. Chang, S. K., Hamilton, A. D., Molecular Recognition of biologically interesting substrates - synthesis of an artificial receptor for barbiturates employing 6 hydrogen-bonds. *J. Am. Chem. Soc.* 1988, **110**, 1318–1319.
53. Hunter, C. A., Molecular recognition of para-benzoquinone by a macrocylcic host. *Chem. Commun.* 1991, **749**.
54. Allott, C., Adams, H., Bernad, P. L., Hunter, C. A., Rotger, C., Thomas, J. A., Hydrogen-bond recognition of cyclic dipeptides in water. *Chem. Commun.* 1998, 2449–2450.
55. Weber, E., Helbig, C., Seichter, W., Czugler, M., A new functional cyclophane host. Synthesis, complex formation and crystal structures of three inclusion compounds. *J. Incl. Phenom. Macrocycl. Chem.* 2002, **43**, 239–246.
56. Seel, C., Vogtle, F., Molecules with large cavities in supramolecular chemistry. *Angew. Chem., Int. Ed. Engl.* 1992, **31**, 528–549.
57. Chen, G. Y., Lean, J. T., Alcala, M., Mallouk, T. E., Modular synthesis of $\pi$-acceptor cyclophanes derived from 1,4,5,8-naphthalenetetracarboxylic diimide and 1,5-dinitronaphthalene. *J. Org. Chem.* 2001, **66**, 3027–3034.
58. Jeppesen, J. O., Nielsen, M. B., Becher, J., Tetrathiafulvalene cyclophanes and cage molecules. *Chem. Rev.* 2004, **104**, 5115–5131.
59. Blanch, R. J., Williams, M., Fallon, G. D., Gardiner, M. G., Kaddour, R., Raston, C. L., Supramolecular complexation of 1,2-dicarbadodecaborane(12). *Angew. Chem., Int. Ed. Engl.* 1997, **36**, 504–506.
60. Cram, D. J., Weiss, J., Helgeson, R. C., Knobler, C. B., Dorigo, A. E., Houk, K. N., Design, synthesis, and comparison of crystal, solution, and calculated structures within a new family of cavitands. *J. Chem. Soc., Chem. Commun.* 1988, 407–409.
61. Canceill, J., Lacombe, L., Collet, A., New cryptophane forming unusually stable inclusion complexes with neutral guests in a lipophilic solvent. *J. Am. Chem. Soc.* 1986, **108**, 4230–4232.
62. Roesky, C. E. O., Weber, E., Rambusch, T., Stephan, H., Gloe, K., Czugler, M., A new cryptophane receptor featuring three endo-carboxylic acid groups: Synthesis, host behavior and structural study. *Chem. Eur. J.* 2003, **9**, 1104–1112.
63. Mecozzi, S., Rebek, J., The 55% solution: A formula for molecular recognition in the liquid state. *Chem. Eur. J.* 1998, **4**, 1016–1022.
64. Fogarty, H. A., Berthault, P., Brotin, T., Huber, G., Desvaux, H., Dutasta, J. P., A cryptophane core optimized for xenon encapsulation. *J. Am. Chem. Soc.* 2007, **129**, 10332–10333.
65. Mough, S. T., Goeltz, J. C., Holman, K. T., Isolation and structure of an 'imploded' cryptophane. *Angew. Chem. Int. Ed.* 2004, **43**, 5631–5635.
66. Gautier, A., Mulatier, J. C., Crassous, J., Dutasta, J. P., Chiral trialkanolamine-based hemicryptophanes: Synthesis and oxovanadium complex. *Org. Lett.* 2005, **7**, 1207–1210.
67. Gosse, I., Dutasta, J. P., Perrin, M., Thozet, A., A thiophosphorylated hemicryptophane: structure of the toluene inclusion complex. *New J. Chem.* 1999, **23**, 545–548.
68. Cram, D. J., Karbach, S., Kim, Y. H., Baczynskyj, L., Kalleymeyn, G. W., Shell closure of 2 cavitands forms carcerand complexes with components of the medium as permanent guests. *J. Am. Chem. Soc.* 1985, **107**, 2575–2576.
69. Chapman, R. G., Olovsson, G., Trotter, J., Sherman, J. C., Crystal structure and thermodynamics of reversible molecular capsules. *J. Am. Chem. Soc.* 1998, **120**, 6252–6260.
70. Fraser, J. R., Borecka, B., Trotter, J., Sherman, J. C., An asymmetric carceplex and new crystal-structure yield information regarding a 1-million-fold template effect. *J. Org. Chem.* 1995, **60**, 1207–1213.
71. Timmerman, P., Verboom, W., Vanveggel, F., Vanhoorn, W. P., Reinhoudt, D. N., An organic-molecule with a rigid cavity of nanosize dimensions. *Angew. Chem., Int. Ed. Engl.* 1994, **33**, 1292–1295.
72. Cram, D. J., Tanner, M. E., Thomas, R., The taming of cyclobutadiene. *Angew. Chem., Int. Ed. Engl.* 1991, **30**, 1024–1027.
73. Warmuth, R., Marvel, M. A., 1,2,4,6-cycloheptatetraene: Room-temperature stabilization inside a hemicarcerand. *Angew. Chem., Int. Ed.* 2000, **39**, 1117–1119.
74. Robbins, T. A., Cram, D. J., Through-shell oxidation and reduction reactions of guests in a hollow container single-molecule. *J. Am. Chem. Soc.* 1993, **115**, 12199–12199.
75. Naumann, C., Place, S., Sherman, J. C., Synthesis and characterization of a disulfide-linked C-5-symmetric [5]carceplex. *J. Am. Chem. Soc.* 2002, **124**, 16–17.
76. Makeiff, D. A., Sherman, J. C., Template effect where 1-3 molecules drive formation of a trimer carceplex. *Chem. Eur. J.* 2003, **9**, 3253–3262.
77. Liu, X. J., Liu, Y., Li, G., Warmuth, R., One-pot, 18-component synthesis of an octahedral nanocontainer molecule. *Angew. Chem., Int. Ed.* 2006, **45**, 901–904.
78. Makeiff, D. A., Sherman, J. C., A six-bowl carceplex that entraps seven guest molecules. *J. Am. Chem. Soc.* 2005, **127**, 12363–12367.

# 7 Solid-State Inclusion Compounds

*'Stone walls do not a prison make nor iron bars a cage.'*

Richard Lovelace (1618–1658), *To Althea, From Prison*

## 7.1 Solid-State Host-Guest Compounds

The formation of solid-state clathrate, or cage, compounds (Section 1.2) has been known since the discovery of the chlorine clathrate hydrate, an inclusion compound between $Cl_2$ gas and water–ice, by Sir Humphrey Davy in 1811. The term *clathrate* was coined by H. M. Powell in 1945 from the Latin *clathratus* meaning 'to fit with bars'.[1] Originally the term applied to inclusion compounds of hydroquinone and was specific to cases where the guest is held in a cage-like cavity in the host solid. It has gradually broadened to include most aspects of molecular solid-state inclusion chemistry and is almost interchangeable with the term 'solid-state inclusion compound'. As with many aspects of supramolecular chemistry, it required the advent of modern X-ray diffraction techniques (Box 2.1) before chemists fully understood these inclusion compounds. The realisation that clathrates essentially involve the physical imprisonment of the guest molecule either within a host cavity or, more commonly, within voids in the crystal in between hosts, has inspired modern supramolecular design of molecular hosts that can imprison neutral guests in both the solid state and solution and, indeed, carry out chemistry within the host matrix or cavity. However, there are two crucial differences between the kind of molecular host-guest chemistry we discussed in Chapter 6 and the more traditional solid-state clathrate chemistry:

1. The host in a clathrate is the entire (usually crystalline) solid and the guest binding cavity does not need to be an intrinsic property of the individual host molecules.
2. Clathrates can often be *non-stoichiometric* corresponding to cases in which not all of the voids in the crystal are filled by guests.

While often involving weak interactions and hence low association constants, the solid-state inclusion chemistry of molecular guests has many important applications, including the separation of mixtures of closely related compounds and enantiomers, storage of gases and toxic substances, stabilisation of reactive compounds, slow release of drugs under physiological conditions, and control of reaction pathways by inclusion within molecular reaction vessels or channels (topochemistry). Solid-state inclusion chemistry is closely related to crystal engineering (Chapter 8) and is by definition an example of the formation of co-crystals (crystals containing more then one kind of molecule), a subject of increasing topicality in the pharmaceuticals industry, which we will return to in Section 8.6.

A host molecule capable of forming a clathrate does not always do so, particularly if crystallised in the absence of a suitable guest. In common usage the pure, cavity-free crystal can be referred to as the '$\alpha$-phase'. The same molecule crystallised in a different crystal form that *does* contain a cavity but empty of guest molecules is referred to as the $\beta_0$-phase or *apohost*. The *apohost* is often a rather unstable and elusive crystal form because of the void space within it and hence its low density. Apohosts are usually therefore metastable and readily revert to the $\alpha$-form. Indeed so elusive can they be that the research students of one well-respected inclusion chemist once placed a spoof advertisement in a local newspaper entitled 'Wanted: $\beta_0$ phase'! Addition of guests to the apohost gives the clathrate. Clathrates are referred to by a bewildering variety of names depending on the preferences of the researchers; the terms 'clathrate', 'inclusion compound', '*pseudo*polymorph', 'solvate', 'solvatomorph' and 'co-crystal' all mean more or less the same thing – a crystal comprising more than one kind of discrete molecule. These different host guest phases have the same host crystal structure as the $\beta_0$ phase and are termed the $\beta_1$, $\beta_2$…$\beta_n$ phases. A good example is tetragonal urea ($\alpha$-phase) and the various hexagonal urea inclusion compounds ($\beta_n$ phases), Section 7.3. If a further crystal form is isolated than additional greek letters are used; $\gamma$-phase *etc.* Characterisation of

*Supramolecular Chemistry, 2nd edition* J. W. Steed and J. L. Atwood
© 2009 John Wiley & Sons, Ltd ISBN: 978-0-470-51233-3

these solid state crystal forms can be a challenging task since differences can be subtle and the full arsenal of single crystal and powder diffraction methods, thermochemical methods such as DSC and TGA, guest sorption and loss experiments, optical microscopy and other techniques must be brought to bear.

We will look at the precise meanings of these various terms used to describe solid inclusion compounds in Section 8.5. For the moment we will begin our study of clathrates with a survey of some of the more interesting channel and cage-like clathrate-forming materials, and trace the growth of the field into more sophisticated designer inclusion compounds and recent interest in gas sorption. We will take up the wider topic of crystal design and synthesis, including co-crystals in the next chapter, and conclude solid state materials chemistry in chapter 9 with a look at coordination polymers and other network structures.

## 7.2 Clathrate Hydrates

Ripmeester, J. A., Ratcliffe, C. I. and Udachin, K. A., 'Clathrate hydrates', in *Encyclopedia of Supramolecular Chemistry*, Atwood, J. L. and Steed, J. W. (eds), Dekker: New York, 2004, **1**, 274–279.

### 7.2.1 Formation

Clathrate hydrates are inclusion compounds formed by the enclosure of a small guest molecule within a hydrogen bonded cage of solid-state water. Clathrate hydrates are co-crystals and are thus distinct from ice, which is made of pure water, and hence can have different physical properties to ice such as a different melting point. The classic example of a clathrate hydrate is the 'burning snowball' of methane clathrate hydrate. The combustion of the methane in the clathrate is self-sustaining, Figure 7.1. Many

**Figure 7.1** 'Burning snowballs' of methane clathrate hydrate (image courtesy of the US Geological Survey). See plate section for colour version of this image.

relatively non-polar compounds that do not hydrogen bond with water are capable of forming clathrate hydrates. Historically the first hydrate species to be isolated was formed when an aqueous solution of chlorine was cooled below 9.0 ºC, giving a solid compound of formula $Cl_2 \cdot 10H_2O$. The material was discovered by Sir Humphrey Davy in 1810 and its formula was confirmed by Michael Faraday in 1823. The compound was of unknown structure at the time, however early researchers rapidly found a large range of hydrates with guests such as $SO_2$, discovered by de la Rive in 1829; $Br_2$ by Alexeyeff in 1876; alkanes, including methane, by Villard in 1888; noble gases by de Forcrand in 1923; $H_2S$, $CS_2$, $N_2O$ and many others. In all of these cases, the hydrate-forming guest is imprisoned within a lattice void in the water crystal and does not engage in any strong interactions (hydrogen bonding, dipole–dipole *etc.*) with the water host matrix. Compounds such as alcohols, acids and ammonia, which are capable of such stronger interactions, do not generally form hydrates, although a few examples are known in which anions (*e.g.* $F^-$) are incorporated within the host framework without causing its collapse. This type of inclusion is a typical example of enclathration and is quite distinct from the formation of stoichiometric metal salt hydrates such as $NiCl_2{\cdot}6H_2O$, which actually contains the discrete octahedral coordination complex $[Ni(H_2O)_6]^{2+}$.

Solid clathrate hydrates are formed under very specific conditions of temperature and pressure. It is one of their most important and remarkable properties that they are often stable solids well above the 0 ºC melting point of the most common form of pure ice (symbol Ih, meaning ice-hexagonal). Indeed, some gas hydrates are stable up to 31.5 ºC. This property was noted by Davy, who commented on his chlorine (then called oxymuriatic gas) hydrate:

> *It is generally stated in chemical books, that oxymuriatic gas is capable of being condensed and crystallised at low temperature; I have found by several experiments that this is not the case. The solution of oxymuriatic gas in water freezes more readily than pure water, but the pure gas dried by muriate of lime [anhydrous calcium chloride] undergoes no change whatever at a temperature of 40 below 0º of Fahrenheit.*

This high degree of thermal stability is currently a significant problem in the natural gas industry. Transport of natural gas (primarily methane) in pipelines from sources in regions of permafrost or low temperature conditions on the sea bed (*e.g.* Alaska, Siberia and the North Sea), to its end-use point is plagued by blockages caused by the formation of clathrate hydrates. In addition, formation of clathrate hydrates at drill heads is a major problem. Millions of dollars are spent annually in addressing this issue through expedients such as drying and warming the gas and addition of large quantities of kinetic and thermodynamic hydrate formation inhibitors (Section 7.2.3).

## 7.2.2 Structures and properties

'Normal' ice, Ih, does not possess any cavities capable of including guest molecules. However, in the presence of hydrate-forming species, a template reaction occurs in which polyhedral cavities are formed about the guest according to guest size. These cavities are composed almost exclusively of fused five- and six-membered hydrogen-bonded rings (Figure 7.2), and are denoted by superscripts according to the numbers of each type of ring present in the cage (Figure 7.3). Almost all clathrate hydrates form one of two basic structures, termed type I and type II. Type I clathrates arise from the fusion of two $5^{12}$ and six $5^{12}6^2$ cavities (*i.e.* two cavities comprising twelve 5-membered rings and six comprising twelve 5-membered rings and two 6-membered rings), while the much larger type II unit cell (the crystallographic unit cell is the basic structural repeat unit or building block of the crystal) possesses sixteen $5^{12}$ and eight $5^{12}6^4$ cages. There are only around six exceptions to these two basic

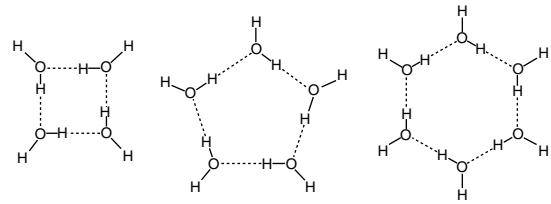

**Figure 7.2** Hydrogen bonded rings of water molecules found in clathrate hydrate structures. Four-membered rings are only found in structure H.

types, out of more than 100 clathrate-forming compounds. These exceptions are bromine, dimethyl ether, ethanol, ammonium and alkyl amine salt hydrates (low-symmetry structures III–VII) and molecules approximately the size of methyl cyclohexane or larger (structure H – a material that is now known to be naturally occurring and remarkably stable[2, 3]). Structure H is unique in being the only structure to include four-membered rings of water molecules (a special case is dimethylether which forms 'structure T' hydrate which possesses $5^{12}6^3$, $5^{12}6^2$ and $4^15^{10}6^3$ cages). More recently, Udachin and Ripmeester have also reported a very unusual new 'complex' structure containing features related to structure H and structure II (composition: 1.67 choline hydroxide · tetra–*n*–propylammonium fluoride · 30.33 $H_2O$).[4] The properties of the three main structural types and cages are summarised in Figure 7.3. The bromine clathrate hydrate is unique in being the only one to form a 15-hedral cage, $5^{12}6^3$, which generally has an unfavourable strain relative to the other three cavities.

In general, small guests occupy the small $5^{12}$ type cavities. The small difference between the size of this cavity in structures I and II can have a significant effect on which structural type is adopted. Thus the smallest guest, argon (radius 1.92 Å) occupies the smaller $5^{12}$ cavity of structure II, as do $N_2$ and $O_2$. Methane and $H_2S$ (radii 2.18 and 2.29 Å, respectively), while still small enough to fit within the $5^{12}$ cavities, form structure I hydrates. Helium, hydrogen and neon are small enough to diffuse through the

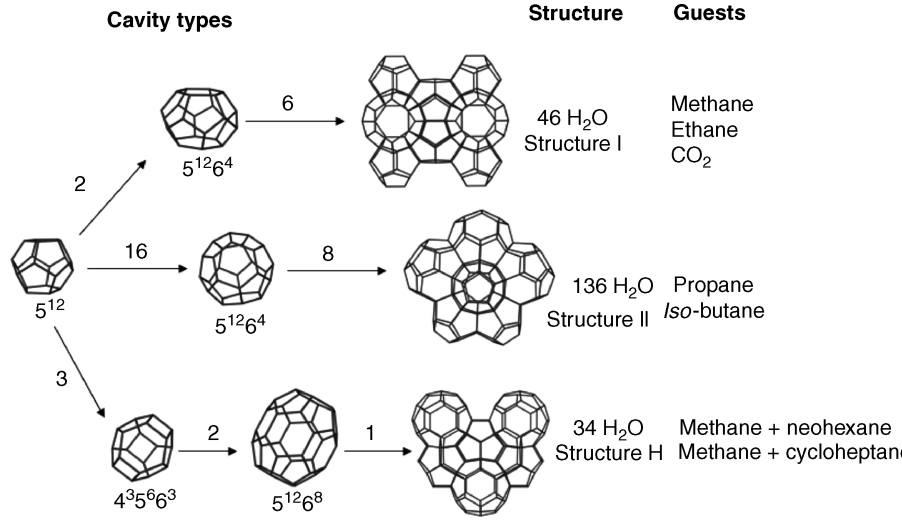


**Figure 7.3** Cavity types found in structures I, II and H clathrate hydrates and the numbers of each that goes into each structure unit cell along with number of water molecules and typical guests. Each vertex denotes a water molecule; connecting lines represent hydrogen-bonded contacts.

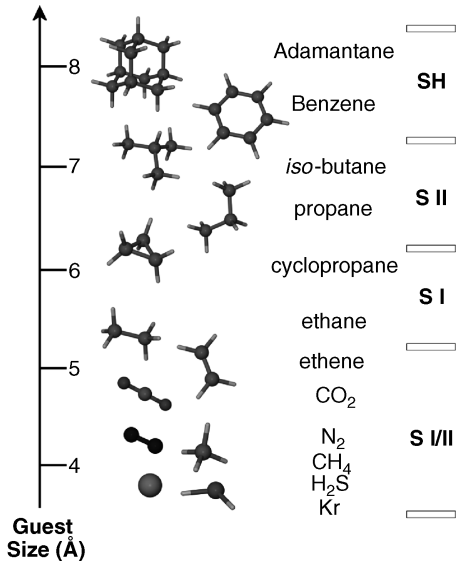


**Figure 7.4** Comparison of guest sizes and cavities occupied as simple hydrates.

hydrogen bond 'bars' of the cage and do not form hydrates. The larger $5^{12}6^2$ cage found in structure I hydrates is large enough to entrap molecules of diameter up to about 6.0 Å (*e.g.* ethane, $CO_2$) and plays the main structure-stabilising role in almost all structure I hydrates, being the preferred site for most guests. The $5^{12}6^4$ cavity will encompass molecules as large as 6.6 Å, such as propane and *iso*-butane. Even *n*-butane may be accommodated over a limited temperature and pressure range if a small co-guest is available to fill the $5^{12}$ cavities. The range of guest sizes and their effect on structural type adopted is summarised in Figure 7.4. While it is possible to fill all of the cavities with the appropriate sized guest molecules, in reality some cages remain empty and real hydrates have more water than the ideal composition. For example, the original chlorine clathrate hydrate was determined (after some controversy) to have an empirical formula $Cl_2 \cdot 10H_2O$, compared to the ideal $7\frac{2}{3}$ water molecules for a type I structure with only the $5^{12}6^2$ cavities occupied. In the vast majority of cases only a maximum of one guest molecule occupies any given cage. Under high pressure small guests particularly hydrogen can form hydrates with up to two guest molecule in the small cage and four in the large cage of hydrate structure II.[5]

Since the mole fraction of water in clathrate hydrate structures is usually in excess of 85 %, it is worthwhile to compare the effect the guest molecules have on the hydrate physical properties in comparison to ice. Data from solid-state $^1H$ NMR line width measurements indicates that at temperatures below 50 K, the hydrate structures, like ice, are rigid. Above this temperature, individual water molecules within hydrate structures begin to undergo reorientation and translational diffusion. At 273 K, the diffusion rate is more than 100 times that of ice. Fixed-site reorientation occurs approximately every 10 μs, compared to 21 μs in ice. This rapid diffusion also has an effect on the material's bulk dielectric constant which is about half that of ice. Far infrared data (i.e. low wavenumber), however, suggests that the hydrogen bonds are of similar strength to those in ice. Indeed, the hydrogen bond lengths as determined in the X-ray crystal structures are only 1 % longer than those of Ih in the unstrained $5^{12}$ cages. Another notable difference between hydrates and Ih is their thermal conductivity, which is higher for Ih by a factor of about five. It has been suggested that this arises as a consequence of phonon scattering as a consequence of anharmonic guest vibrations and rotations. This phenomenon

may also be linked to the observation that the coefficient of thermal expansion is generally significantly greater for hydrate structures than ice.

## 7.2.3 Problems and Applications

Sloan, E. D., 'Fundamental principles and applications of natural gas hydrates', *Nature* 2003, **426**, 353–359.

With the growth of the oil and gas industry in the USA, it was realised as early as 1934 that the blocking of gas pipelines at temperatures where normal water would not freeze was being caused by clathrate hydrate formation. The combination of water and hydrocarbons at low temperature, and often increased pressure, are ideal conditions for hydrate formation. Much understanding of this phenomenon has been gained since that time, but as drilling and transportation conditions become more extreme, clathrate hydrate formation continues to be a major problem and is still a very active area of research.

Gas deposits being forced from a natural reservoir are saturated with water. As the gas expands into separators or wellheads, its temperature drops resulting in solid hydrate formation, blocking pipelines and processing equipment. Hydrate formation also robs the oil of its lighter, less viscous fractions, resulting in the formation of heavy oil and tar sands. Indeed decomposition of *in situ* hydrates might make the extraction of such deposits much easier as a consequence of the decreased viscosity of the crude oil on redissolution of the low-molecular-weight hydrocarbons.

The oil and gas industry has developed a number of methods for combating the problems of hydrate formation, both in terms of treatment of the gas and equipment and in process design, in order to minimise hydrate-forming conditions and the consequences of hydrate deposition. Indeed, it is estimated that between 5 % and 8 % of the total process cost is in addressing the hydrate problem (about US$1 billion per annum). Among the most important methods are:

- drying the natural gas;
- heating the gas to temperatures above the hydrate melting point;
- lowering the gas pressure to below the hydrate formation point;
- influencing the hydrate formation phase diagram by injection of large quantities of inhibitors such as methanol, glycol or salt solutions, although these latter may often be corrosive (these are known as thermodynamic inhibitors); and
- reducing the rate of hydrate formation through the use of *low dosage hydrate inhibitors* – small quantities of polymeric organic materials, which inhibit the nucleation of hydrate crystals (i.e. they act as kinetic inhibitors) such as PVP (polyvinylpyrrolidinone, **7.1**).

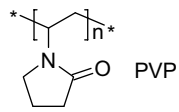


**7.1**

In addition to post-extraction problems, the presence of a gas hydrate layer in the earth during drilling may also have catastrophic effects. Gas hydrates and their decomposition due to sudden changes in pressure or temperature have been known to cause problems such as casing damage, uncontrolled gas release, blowouts, fires and gas leakage outside the casing. As a result, extensive geological surveys are carried out to determine hydrate distribution, volume, reservoir temperature, pore pressures, rock

porosities and permeabilities. Particularly large natural hydrate layers may occur in sediment either below permafrost, or beneath the ocean floor. Action is generally taken to either prevent hydrate decomposition or promote its decomposition in a controlled, manageable fashion.

While natural gas hydrate formation is currently regarded as an expensive nuisance by the petroleum industry, as natural fossil fuels run out it may be that hydrates of methane could become a valuable fuel source. Calculation of density of methane within methane hydrate, $CH_4 \cdot 6H_2O$, suggests that the hydrate corresponds with a highly compressed form of the gas (184 times the amount of methane is stored by hydrates than the equivalent gas volume at standard temperature and pressure), despite its stability at relatively low pressures. The lattice energy of methane hydrate is such that about only 10 % of the energy available from combustion of the methane would be required to decompose the hydrate. This is illustrated strikingly by the fact that methane hydrate will support its own combustion (Figure 7.1).

Estimates place the world reserves of natural gas hydrates as being in the region of $5 \times 10^{13}\,m^3$ on land, mostly in the permafrost regions of Alaska and Siberia, as well as a further $5–25 \times 10^{15}\,m^3$ of gas in the oceans, particularly around Central America. This figure is around twice that of the total fossil fuel reserve; this is an enormous wealth of energy which will become increasingly important as fossil fuels run out. Indeed, in the Russian Federation the enormous gas hydrate deposit at Messoyakha has been used as a natural gas source since 1971.

In addition to the use of existing hydrates, it has also been suggested that clathrate hydrates could find applications in storage and separation technology. Bardhun showed in 1962 the viable application of hydrates in desalination of sea water, while hydrates have also been investigated as a method for the storage and transport of methane without the use of high-pressure containers.

Methane hydrate deposits in permafrost regions are not only potential fuel reserves but are also associated with aspects of global warming. It is postulated that increasing global temperatures may be speeding up the release of methane from these reservoirs, which in turn speeds up the heating process. Methane is ten times worse as a greenhouse gas than carbon dioxide and catastrophic methane release from clathrate hydrate deposits may have been responsible for the 4–8 °C temperature rise over a brief geological time interval of just 1000 years called the Late Palaeocene Thermal Maximum (LPTM). Other environmental phenomena are also being blamed on hydrate deposits. Some deep-sea deposits cause massive slippage when they decompose and it is thought that these could be the cause of some large tidal wave events. It is even suggested that gases given off when hydrates decompose could be behind the Bermuda Triangle phenomenon, although this has not been proven. Not all hydrate deposits have a negative consequence, some deep-sea hydrate deposits act as habitats for bacteria which thrive off of methane. Clathrate hydrates are also now thought to exist (from spectroscopic data) extra-terrestrially on Mars, Saturn, Neptune and Uranus and even form parts of comets. Indeed, it has been suggested that $CO_2$ clathrate may exist in winter at the Martian poles, an observation which may be circumstantial evidence of extraterrestrial life.

A use of hydrates in synthetic systems is in the separation of gases by the differences in the formation conditions of their respective hydrates. For example, it is possible to separate hydrofluorocarbons and nitrogen in this manner. Pollutant streams can also be cleared up in a similar fashion and it has been shown that hydrates are able to recover carbon dioxide from a mixture of $CO_2$, $O_2$ and $N_2$ in high yields. Perhaps the most striking recent results in the promise of clathrate hydrates in hydrogen storage applications. Up to 4 % by weight hydrogen can be included at modest pressures by tuning clathrate hydrate composition to allow the hydrogen guests to enter both larger and smaller cages using water-soluble hydrate promoters and various small gaseous guests.[6] We will return to hydrogen storage later in Section 7.9 (and in the context of artificial metal organic frameworks in Chapter 9, Section 9.5.10).

## 7.3 Urea and Thiourea Clathrates

Harris, K. D. M., 'Fundamental and applied aspects of urea and thiourea inclusion compounds', *Supramol. Chem.* 2007, **19**, 47–53.

### 7.3.1 Structure

The common organic molecule, urea (**7.2**), and its sulfur analogue, thiourea (**7.3**), both form solid-state clathrates with long-chain hydrocarbons such as *n*-alkanes. Urea is able to act as a host by virtue of strong intermolecular hydrogen bonding interactions between the acidic protons of the $NH_2$ groups and the oxygen or sulfur atoms of adjacent molecules. This results in the formation of a chiral, helical hollow tube of urea molecules of minimum van der Waals diameter 5.5–5.8 Å, into which guests of small cross-section can fit. This helical arrangement, termed hexagonal- or β-urea, allows each urea molecule to hydrogen bond with all of its NH protons, maximising intermolecular interactions. This means that each oxygen (or sulfur) atom must accept a total of four hydrogen bonds. The thiourea channels are similar but larger and with more variation in their diameter, allowing inclusion of branched hydrocarbons although not small *n*-alkanes (Figure 7.5). While hexagonal urea may generally be regarded as comprising fairly smooth tunnel-like channels, the thiourea host channels are more 'cage-like'.

Because the urea molecules do not have any 'spare' hydrogen bonding functionality, they present only a smooth face to the included guests, resulting in weak binding. Inclusion compounds are frequently non-stoichiometric, and there are substantial guest translational and vibrational motions in the solid state, usually leading to substantial guest disorder in crystals of urea inclusion compounds. Thus, irrespective of the guest identity, the average hexagonal symmetry of the lattice is retained.

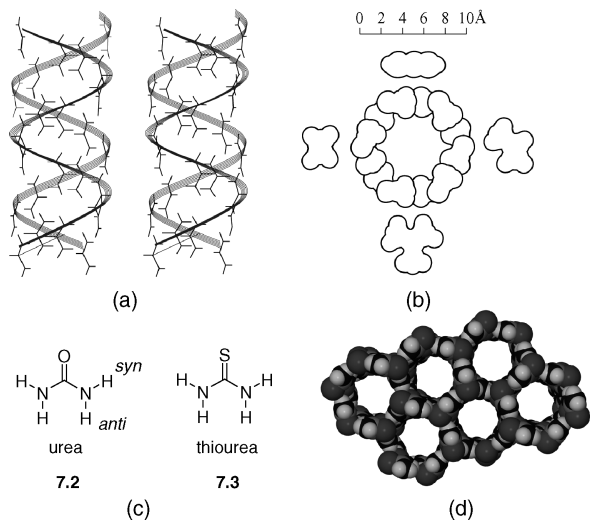


**Figure 7.5** (a) Stereoview of one urea host channel. The chiral ribbons are defined by the *anti*-N—H ⋯ O hydrogen bonds and are interlinked by the *syn*-N—H ⋯ O hydrogen bonds. (Reprinted from [9] with permission from AAAS) (b) Van der Waals cross-section of the cavity in the urea channel compared with the size of *n*-octane (left), benzene (top), 3-methylheptane (right) and 2,2,4-trimethylpentane (bottom), (c) chemical structures of urea and thiourea, (d) packing of urea channels to give the honeycomb-like structure of hexagonal urea.

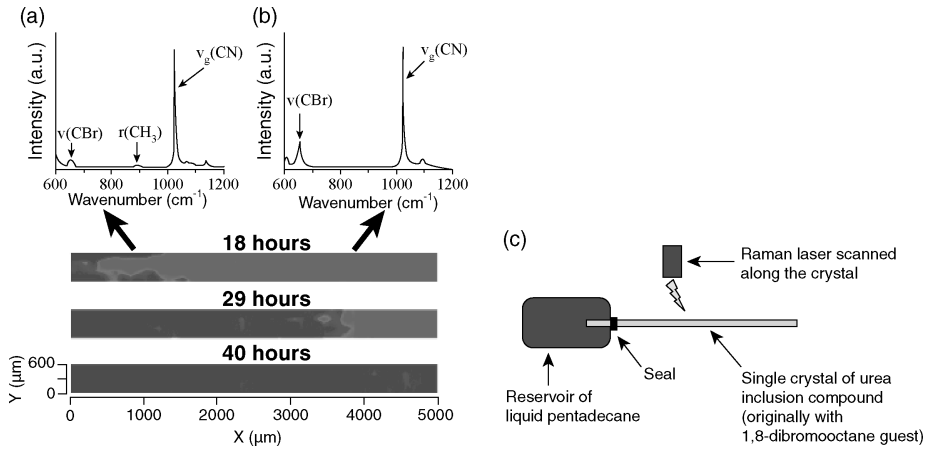


**Figure 7.6** Raman spectra recorded during the replacement of 1,8-dibromooctane guests with the alkane pentadecane within a single crystal of urea. Spectrum (a) is taken from the interface region and shown features for both guests and for the host lattice, and indicates a significant proportion of the 1,8-dibromooctane guests are in the unfavourable *gauche* conformation. Spectrum (b) is taken from a region containing only dibromooctane. The lower figures show the variation in composition for the imaged region of the crystal at different times after commencement of the transport process (lighter coloured regions are rich in dibromooctane) (Reproduced with permission. Copyright American Chemical Society) (c) schematic diagram of the instrumental configuration.

Urea channel clathrates are truly porous materials in the sense that guests may be exchanged for others guest species in the solid state without the collapse of the urea framework.[7] This porosity can be demonstrated elegantly in real time by observing the displacement of one guest by another. Figure 7.6 shows the real-time monitoring of guest diffusion in a urea single crystal by Raman spectroscopy. The original guest, 1,8-dibromooctane (**7.5**) is being replaced by pentadecane (**7.4**) by diffusion from the end of the crystal over a period of several days. The crystal is orientated such that the channels are parallel with the long axis of the needle-shaped crystal. The directional diffusion is achieved by the setup shown in Figure 7.6c. In the interface region the Raman spectrum shows that a significant proportion of the 1,8-dibromooctane molecules adopt the normally unfavourable *gauche* end group conformation reflecting interaction with the incoming pentadecane.[8] So, the urea host lattice is stable to guest exchange as long as it is continuously filled by *some kind* of guest. However, in the absence of guest molecules (*e.g.* guest removal by external vacuum) the host framework changes into tetragonal- or α-urea which is close packed and does not include guests.

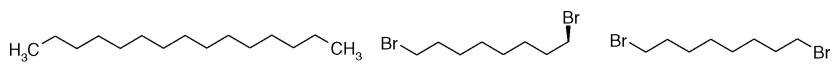


pentadecane **7.4** *gauche* 1,8-dibromooctane **7.5** *trans* 1,8-dibromooctane

## 7.3.2 Guest Order and Disorder

One of the main interests in urea inclusion compounds is their potential application in the separation of linear and branched hydrocarbons in the petroleum industry. Because the channel diameter is only slightly larger than the van der Waals diameter of a linear hydrocarbon, only a small amount of branching can be tolerated. Whether a particular urea inclusion compound will form or not may be assessed simply by comparison of the channel size with the diameter of the guest. For example, benzene is

found to be marginally wider than the channel, and inclusion is quite difficult (Figure 7.5b). Interestingly however, increasing chain lengths allow the toleration of larger, more branching end groups. Thus, 1-phenyloctane does not form an inclusion compound, but the much longer 1-phenyleicosane does. Equilibrium vapour-phase measurements suggest that the enthalpy of complexation increases by approximately 10.0 kJ $mol^{-1}$ for each —$CH_2$— group added to a linear chain, and hence the additional stabilisation gained upon complexation of the longer guest outweighs the unfavourable steric interactions with the phenyl end group. In general, alkane guest molecules display one-dimensional ordering in urea channels. They are ordered along the urea channel direction in the sense that they all have the same orientation, but the line of guests in one channel may freely slip along the channel axis relative to the guests in another. This one dimensional ordering is characterised by the observation of diffuse scattering lines in the X-ray diffraction pattern instead of discrete Bragg peaks. If the guests have a more anisotropic shape then they can distort the urea channels and give rise to two dimensional ordering. The example of the *p*-didecylbenzene inclusion compound of urea was studied by T. R. Welberry of the Australian National University.[10] This compound gives remarkable circular X-ray diffuse scattering features that arise from partial two-dimensional ordering. The elongated shape profile of the aromatic guest viewed along the channel axis (Figure 7.7b) slightly distorts the urea channels such that they pack best when orientated in the same direction (Figure 7.7c). This distortion results in domains

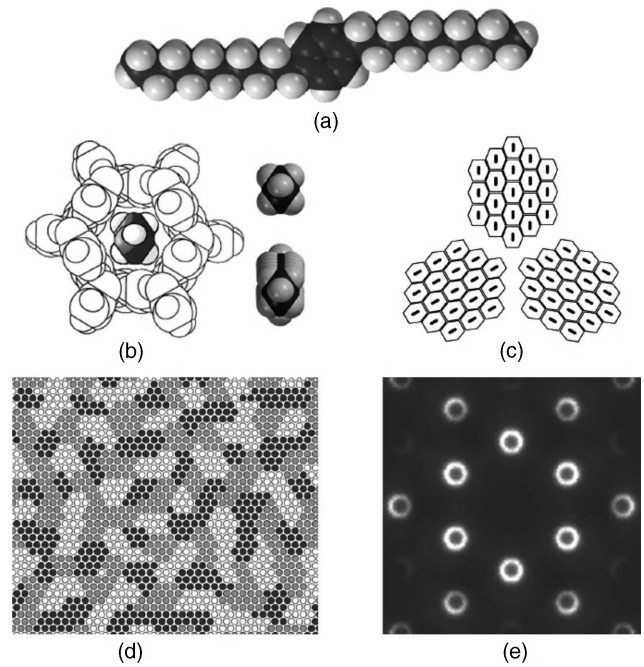


**Figure 7.7** (a) Space-filling model of the *p*-didecylbenzene molecule. (b) Urea channel containing the 'footprint' of an n-alkane molecule, together with a comparison of the 'footprints' of an n-alkane and the more elongated didecylbenzene molecule. (c) Exaggerated schematic view of three different orientations of the distorted urea network when containing the didecylbenzene molecules. (d) Portion of distribution of three 'footprint' orientations as calculated from Monte Carlo simulation. The three shades of grey represent the three orientations shown in (c). (e) Diffraction pattern calculated from the distribution shown in (d) and strongly resembling the experimental one (reproduced by permission of The Royal Society of Chemistry).

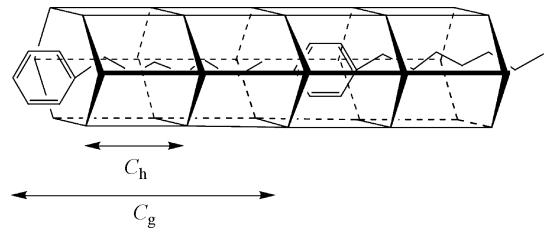


**Figure 7.8** Host and guest repeat distances in urea inclusion compounds are not necessarily the same.

within the crystal in which all of the guests are aligned along with interfaces where stacking faults occur giving a domain with a different orientation. The hexagonal shape of the channel means that three possible orientations are possible (Figure 7.7d). Using this model a calculated diffraction pattern can be derived that agrees closely with experiment (Figure 7.7e).

The ordering of the guests in urea channels can be assessed by looking at the ratio between the crystallographic repeat distances of host and guest parallel to the channel axis. By 'repeat distance', we mean the distance an imaginary observer would have to travel in the crystal along a certain direction before the environment (in terms of the surrounding molecules) is identical to the one the observer started from. The host arrangement repeats itself every 11.02 Å, a quantity termed $c_h$ (the $c$ arises simply from the fact that the channel is aligned with the crystallographic $c$ unit cell direction). A *commensurate* structure is defined as one in which the guest exhibits a repeat distance, $c_g$, that is the same as the host, or bears a simple relationship to it (Figure 7.8). That is, for a commensurate structure, the relationship $pc_h \approx qc_g$ holds true when $p$ and $q$ are small integers. There is no simple relationship between host and guest lattices in incommensurate structures.

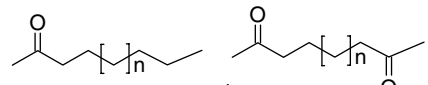


**7.6** n = 1, **a** n = 2, **b** n = 3, **c** **7.7**

The ordering effects of inclusion compound formation on guest behaviour are best illustrated by the case of long-chain alkanones and alkanediones (**7.6** and **7.7**).[11] In general, a study of more than 100 such guests suggests that, unlike alkane analogues, many of them display an X-ray diffraction pattern that suggests significant three-dimensional ordering, as opposed to order along the channel axis only. This observation implies both inter-channel interactions between the guests, and regular head-to-head or head-to-tail packing along the channel axis. However, calculations suggest that the dipole–dipole interactions of $C^{\delta+}{=}O^{\delta-} \cdots C^{\delta+}{=}O^{\delta-}$ type are too weak to effect such an inter-channel ordering, and indeed in some cases (*e.g.* **7.6b** and **7.6c**) only one-dimensional ordering is found by X-ray diffraction and solid-state $^{13}C$ NMR spectroscopic measurements. The key to understanding this problem lies in the commensurate structures formed by compounds (**7.7a–c**). The difference between the commensurate dione and incommensurate alkanone phases is clearly demonstrated by the X-ray diffraction photographs of the urea complexes of **7.6c** (Figure 7.9a) and **7.7c** (Figure 7.9b). In the former case, the presence of the disordered guest is indicated only by diffuse lines in the layers marked 'g'. In contrast, a strong diffraction pattern with $3c_g = 4c_h = 44.0$ Å is clearly visible for the commensurate complex in Figure 7.9b.

The origins of these effects were identified by a full X-ray crystal structure determination, which shows remarkable hydrogen bonding interactions between certain urea NH groups and the carbonyl

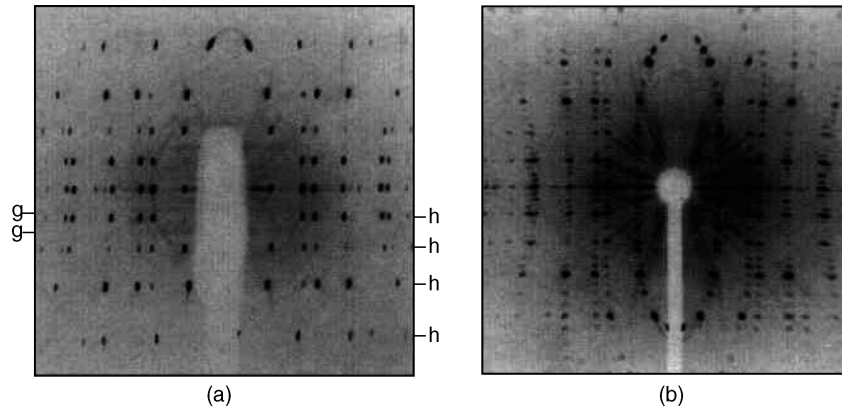


**Figure 7.9** (a) X-ray diffraction channel oscillation photograph of 2-decanone-urea showing host lattice diffraction (*h*) and diffuse horizontal bands in the region of the guest diffraction pattern (*g*); (b) X-ray diffraction photograph of 2,9-decandione-urea showing the commensurate relationship $3c_g = 4c_h = 44.0$ Å. (Reprinted from [9] with permission from AAAS).

oxygen atoms of the guest (Figure 7.10). In fact, in the structures of all the alkanone and alkanedione complexes, suitably placed host molecules are able to tilt out of the plane of the channel wall, presenting one of their —$NH_2$ groups to hydrogen bond with the guest. In the case of the alkanediones (**7.7**), the double hydrogen-bonded interaction is strong enough to result in a three-dimensionally ordered commensurate structure at room temperature. For incommensurate-structure-forming guests of type **7.6**, such as 2-decanone, cooling to –85 ºC also results in a similar commensurate structures.

The exact position of the hydrogen-bonding urea molecules is crucially dependent upon chain length. The case of 2,10-undecanedione is particularly interesting. For odd-numbered chain-length diones of which 2,10-undecanedione is an example, the two carbonyl functionalities are on the same side of the molecule in the extended all-anti conformation of the chain. This results in the formation of a different commensurate structure with $2c_g = 3c_h = 33.0$ Å, with concomitant contraction of the channel width as a consequence of hydrogen bonding interactions with one side only. This lower symmetry structure exhibits remarkable ferroelastic properties (ferroelastic materials have distinct domains of ordered

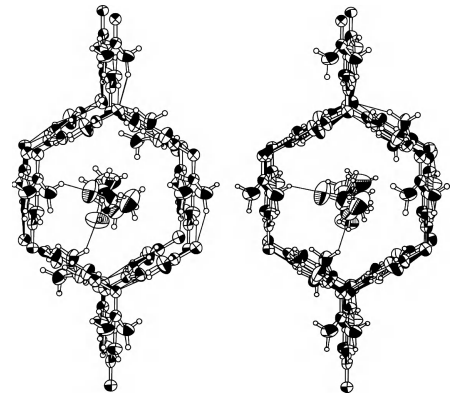

**Figure 7.10** Channel axis stereoview of 2,9-decanedione-urea showing hydrogen bonding between guest carbonyl functionalities and 'tilted' urea donors. (Reprinted from [12] with permission from Elsevier).

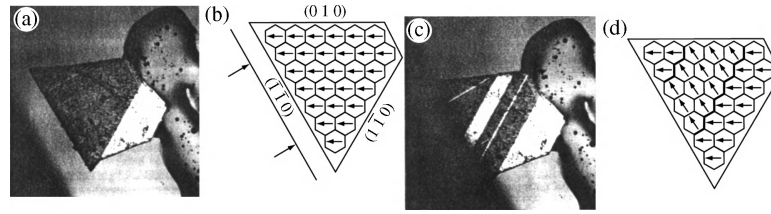


**Figure 7.11** Irreversible stress-induced phase reorientation in 2,10-undecandione-urea. (a) Crystal before stress. (b) Schematic of crystal before stress; arrows represent carbonyl dipoles for guests in one layer. (c) Crystal under uniform stress from bottom left of picture. (d) Schematic of stressed crystal. (Reproduced by permission from Macmillan Publishers Ltd).

molecules that may be switched on application of an external mechanical stress). Small mechanical stresses can reorientate bulk domains within the crystal corresponding to the effective concerted 60 degrees rotation of groups of guests in adjacent channels, resulting in the formation of striking parallel streaks if the crystal is viewed under polarised light (Figure 7.11). If the applied stress is gentle enough, the reorientated domain will relax back to its original orientation in a few seconds. Greater stresses lead to permanent effects, although even these may be reversed simply by rotating the crystal through 60 degrees and reapplying the pressure.

### 7.3.3 Applications of Urea Inclusion Compounds

We have already mentioned the linear channel of urea inclusion compounds which makes them applicable in the separation of linear and branched hydrocarbons. The larger channels in thiourea are suited to the intriguing application of these inclusion compounds in carrying out chemical reactions within the host matrix. The rigorous steric constraints of the host impose a great deal of stereo- and regioselectivity on the course of the reaction, which might otherwise be difficult to control under normal conditions. The channel structure of urea compounds immediately suggests their suitability for the selective formation of long, straight-chain polymers. In particular, as early as 1960, Brown and White published the inclusion polymerisation of 2,3-butadiene, 2,3-dichlorobutadiene, cyclohexadiene and related compounds. In most cases, crystalline polymers with high melting points were isolated, suggesting long-chain materials with a narrow molecular weight band, clearly formed in a highly controlled fashion.

Recently the ability of urea inclusion compounds to line up molecules in their channels has also suggested their possible application as X-ray dichroic filters. Visible light dichroic filters (polaroid sheets) are commonplace. The dichroic filter selectively attenuates (reduces the intensity of) radiation with polarisation parallel to a certain axis in the filter material while allowing radiation with perpendicular polarisation to pass through with much less absorption. Dichroic filters for X-rays are difficult to achieve but have technological applications in areas such as magnetic X-ray scattering. X-rays are absorbed strongly by heavy, multi-electron atoms such as bromine and a urea inclusion compound of 1,10-dibromodecane has been shown to act as an X-ray dichroic filter. X-ray radiation polarised parallel to the C–Br bond is absorbed preferentially over radiation polarised perpendicular to it. However the efficiency is reduced by the tendency of the C–Br bonds to undergo reorientation under ambient conditions (*cf. gauche* **7.5**). A much more efficient material is the designer thiourea inclusion compound of 1-bromoadamantane. In this material all of the C–Br bonds are aligned with the channel axis and do not reorientate under ambient conditions. The compound achieves almost the theoretical maximum X-ray attenuation ratio.[13]

# 7.4 Other Channel Clathrates

## 7.4.1 Trimesic Acid

Kolotuchin, S. V., Thiessen, P. A., Fenlon, E. E., Wilson, S. R., Loweth, C. J. and Zimmerman, S. C., 'Self-assembly of 1,3,5-benzenetricarboxylic (trimesic) acid and its analogues', *Chem. Eur. J.*, 1999, **5**, 2537–2547.

Trimesic acid, or 1,3,5-benzenetricarboxylic acid (TMA, **7.8**), is capable of forming a variety of complexes *via* hydrogen bonding to the carboxylic acid residues or ionisation to form salt complexes. The crystal structure of the guest-free α-trimesic acid is also known and exhibits mutual triple catenation of pleated hexagonal networks of hydrogen-bonded TMA molecules. The α-TMA structure is tightly packed but contains small cavities able to include halogens at interstitial sites to give complexes of formula TMA · $^1/_6$ $Br_2$ and TMA · $^1/_{12}$ $I_2$.[14] Of particular interest, however, are the structures of the trimesic acid monohydrate networks. Crystallisation of **7.8** from water without careful control of temperature gives two types of hydrate crystal, TMA · $2H_2O$ and TMA · $\frac{5}{6}$ $H_2O$ in addition to cubes of unsolvated TMA. Addition of picric acid (2,4,6-trinitrophenol) results in yellow needles of composition TMA · $H_2O$ · $\frac{2}{9}$ (picric acid). Surprisingly, given their diverse compositions, the structures of these three hydrates are very closely related. The core unit in each case is a rectangular arrangement of two pairs of TMA molecules to give a two-dimensional series of rectangular cavities in the host structure. Each network is linked to adjacent rectangular units in the same plane by hydrogen bonding to a water molecule. The overall host layer stoichiometry is TMA · $H_2O$, hence the term monohydrates (Figure 7.12a).

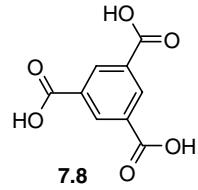


**7.8**

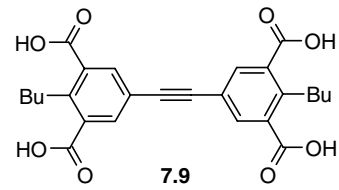


**7.9**

In both TMA · $H_2O$ · $\frac{2}{9}$ (picric acid) and TMA · $2H_2O$ the monohydrate layers are situated directly above one another forming infinite rectangular channels into which the guest molecules (water or picric acid) are included without any specific interactions between guest and channel. The guest dispositions and stoichiometry are determined by the relationship between guest size and layer thickness. There is considerable disorder in the guest portion of each structure and X-ray photographs contain strong diffuse

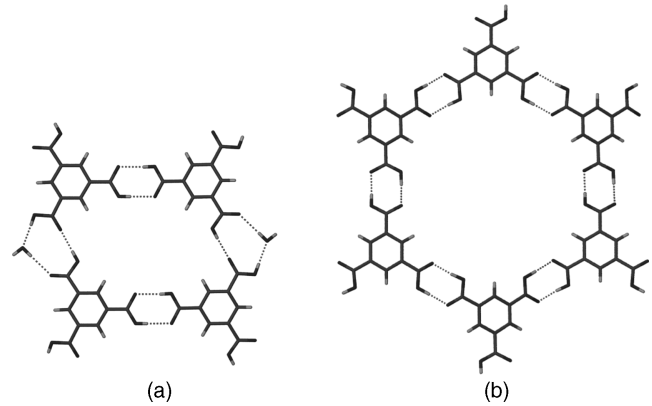


**Figure 7.12** (a) Part of a planar layer of TMA hydrate showing the rectangular channel and (b) the hexagonal clathrate structure that TMA forms when in the presence of large, templating guests.

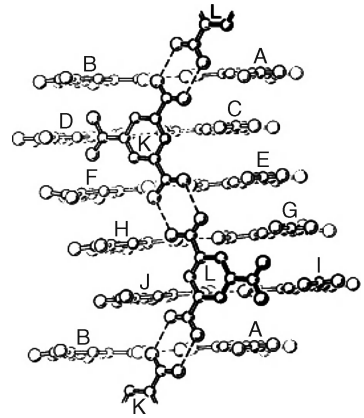


**Figure 7.13** Offset layer packing in TMA · $H_2O$ · [0.2TMA]. TMA molecules A-J form the host framework while K and L are the guests (reproduced with permission from IUCr).

scattering, suggesting the guest molecules are partially ordered (*cf.* one-dimensional ordering in urea clathrates). While the picric acid complex is stable, TMA · $2H_2O$ rapidly loses water upon exposure to the atmosphere, consistent with the open nature of the channels.

The structure of TMA · $\frac{5}{6}$ $H_2O$ is based on the same rectangular host network. The peculiar stoichiometry may be explained by expanding the formula to 6TMA · $5H_2O$ and rewriting as 5TMA · $5H_2O$ · TMA, or by analogy with the picric acid structure, TMA · $H_2O$ · [0.2TMA]. In fact the monohydrate host framework contains an infinite zigzag chain of hydrogen-bonded TMA guests, resulting in an offset of one layer with respect to the next to give zigzag channels (Figure 7.13). The structure is perfectly ordered and stable and there is no significant interaction between the guest TMA chain and the host layers perpendicular to it.

Interestingly, TMA inclusion chemistry is not limited to the formation of rectangular channels. In the presence of large guest species, such as linear and branched long-chain hydrocarbons, paraffins, long-chain alcohols *etc.*, a hexagonal host channel is formed involving a two-dimensional 'chicken wire' uninterrupted TMA motif (Figure 7.12b). The resulting 14 Å diameter channels are filled with guest molecules and may take two, three or even five host layers before the pattern repeats itself. The structure of 2TMA · [*n*–tetradecane] which is of this type is shown in Figure 7.14.[16] An expanded 'chicken wire' structure is found for the inclusion complex of TMA with pyrene and methanol or ethanol, formula $TMA_2$ · pyrene · 2ROH. In this material two of the three carboxylic acid residues form

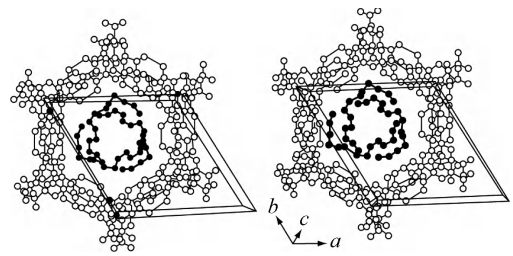


**Figure 7.14** Stereoview of 2TMA · [*n*–tetradecane] viewed along the crystallographic *c* axis. The *n*-tetradecane molecules are highly disordered. The host structure repeats every three layers. (Reproduced with kind permission from Springer Science + Business Media from [16] © 1987).

8-membered hydrogen bonded rings as in Figure 7.12b, while the remaining carboxylic acid interacts with an alcohol solvent molecule which, in turn, bridges to the next layer of TMA molecules. The pyrene is included within the large cavity. In a nice piece of molecular engineering, Steve Zimmerman at the university of Illinois, USA, has replaced this alcohol linked hydrogen bonded unit with a covalent alkyne spacer in compound **7.9**. Compound **7.9** forms hexagonal 'chicken wire' complexes in which the covalent link replaces a carboxylic acid dimer. molecules of THF are included within the channels, along with the butyl groups of the host.

## 7.4.2 Helical Tubulands and Other Di-ols

Bishop, R., 'Designing new lattice inclusion hosts', *Chem. Soc. Rev.* 1996, **25**, 311–319.

Closely related to urea and thiourea channel host structures (Section 7.3) are the helical tubuland channel structures formed by a large family of alicyclic diols such as **7.10**–**7.12**. Crystallisation of **7.10** in the presence of an enormous variety of solvents and other potential guest molecules results in the formation of channel-type structures in which the walls of the trigonal channels (Figure 7.15) comprise two helical threads of diol molecules hydrogen-bonded together about a common 'spine' of three-fold screw symmetry ($3_1$; rotation through 120º accompanied by translation along the rotation axis, Box 8.2).

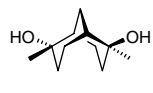


**7.10**

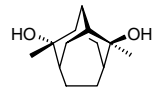


**7.11**

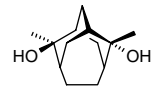


**7.12**

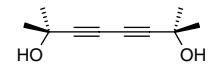


**7.13**

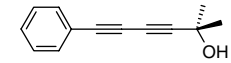


**7.14**

The channel structure may incorporate most guest species capable of fitting within the space available, with the exceptions of phenols and other strongly hydrogen bonding species that adopt non-channel hydrogen-bonded co-crystalline structures. In the tubular species, the diol:guest ratio is usually 3:1 (with guests such as acetonitrile, thiophene, dioxane *etc.*), but a number of nonstoichiometric inclusion compounds are also known, depending on the guest length in comparison to the length of the channel $(\mathbf{7.10})_3$ repeat unit. While strongly hydrogen bonded, the channel walls have considerable flexibility and in the presence of various guests the unit cell dimensions perpendicular to the channel direction may vary by 5 % or so (11.89–12.47 Å, acetonitrile to dioxane) as the structure flexes to incorporate larger guests.

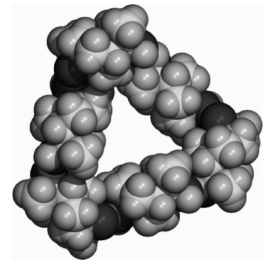

**Figure 7.15** Space-filling diagram of the hexagonal channel structure of **7.10** showing channels of trigonal cross-section and edge length 6.30 Å.

The alicyclic diol motif (**7.10**) may be subject to considerable structural variation resulting in the production of channels of highly varying dimensions (*e.g.* **7.11** and **7.12**). Broadly, the helical tubuland family falls into two categories: hosts with narrow channels that may exist even without the presence of guests, and those with much larger channels that collapse upon removal of the guest species. The smaller structures have an unobstructed cross-sectional area (UCA— the area of channel viewable when looking down the channel axis— this represents the minimum area of the channel since there are indentations at some points) of about 1.2–9.9 $Å^2$, while the large channels fall in the range 19.8–34.0 $Å^2$.

A wide range of other alcohols and di-ols are known to form clathrates, in part because of the need to satisfy the highly directional nature of the OH···O hydrogen bonding (discussed further in Section 8.9.1), which can leave lattice gaps that must be filled by guest molecules. We will discuss the traditional phenol-type clathrates based on molecules such as hydroquinone in Section 7.5. In the context of the 'self-inclusion' of TMA · $H_2O$ · [0.2TMA] one other recently reported di-ol system, the dialkyne **7.13** channel host, is of interest. Like the helical tubulands, alkyne **7.13** forms hydrogen-bonded trimeric rings giving a helical host channel capable of including $CCl_4$ and benzene in a commensurate fashion. Most interestingly, however, the same host framework can also be obtained by sublimination in which compound **7.13** acts as the guest molecule as well, Figure 7.16. This material represents a pure phase of **7.13** in which different molecules of the di-ol play different roles. While any pure crystalline compound can be trivially thought of as being 'self-included' in the sense that any one molecule is surrounded by other molecules of the same type, this pure phase of **7.13** is the only known compound that obeys a strict definition of self-inclusion as involving a molecular crystal in which the identical host framework is precedented by at least one other structure with a different guest.[17] The term *isoskeletal* may be used to describe related structures with the same host framework but different guests as in (**7.13**)$_6$·G (where G = 2 $CCl_4$, 2 $C_6H_6$ or **7.13**). While the benzene and $CCl_4$ clathrates of **7.13** are commensurate with each guest occupying the broad part of the host channel, in the self-included structure the guest is disordered over two positions and is twice the length of the channel repeat distance. It is likely that guests within a channel are ordered but guests in adjacent channels can be either aligned or slipped by half a molecule length. Surprisingly, a similar host structure is formed by **7.14** in which a trimeric edge-to-face π-interaction motif replaces one of the hydrogen bonded trimers.

The bulky end groups and 'thin' acetylenic spacer in hosts such as **7.13** are an example of the 'wheel and axel' concept in inclusion compound design. The dictates of crystal close packing suggest that

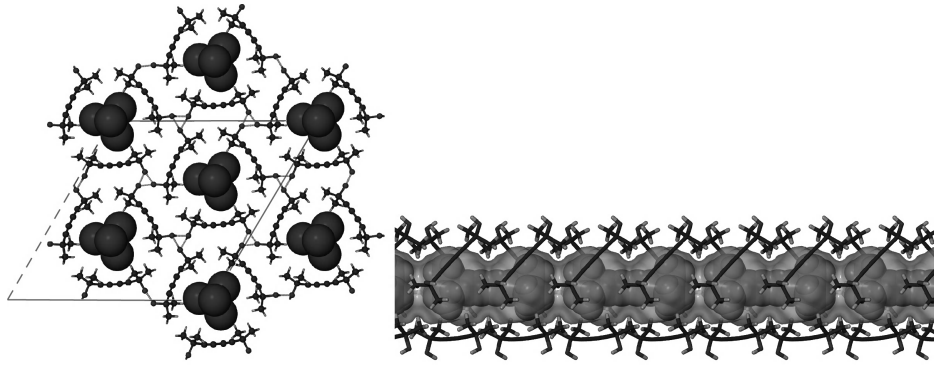


**Figure 7.16** Channel inclusion compounds of di-ol **7.13** with either (a) $CCl_4$ or (b) the host molecule itself as guests.

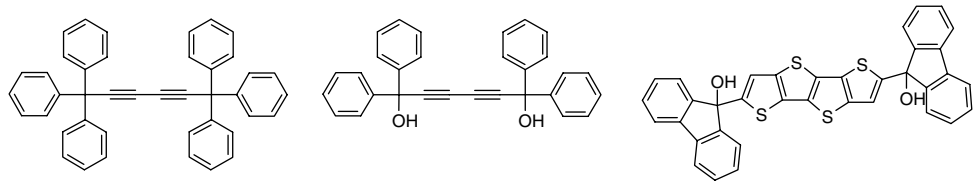


**Figure 7.17** 'Thin' and 'flat' spacers in both di-ols and purely awkwardly shaped molecules that act as hosts according to the 'wheel and axel' concept.

even in the absence of specific, strong attractive interactions, the general effect of dispersion/van der Waals forces will be such as to induce molecules to fill as much space as possible. This leads inevitably to the observation that the density of organic crystals is reasonably constant (about 1.4–1.6 g $cm^{-3}$). Organic molecules are frequently unsymmetrical and of irregular shape, but despite this they are able to pack reasonably regularly, the majority exhibiting good crystallinity without the inclusion of solvent molecules. This efficient packing arises because of their conformational flexibility and the 'soft' nature of van der Waals interactions, coupled with the molecules' generally convex shape, which, to a rough first approximation, is essentially spherical. The observation of solvent inclusion in the formation of many clathrate hosts is very often a result of the fact that these clathrate-formers are of sufficiently irregular (often concave) shape (*e.g.* the calixarenes discussed in Chapter 3) that they are unable to pack efficiently and must incorporate small 'space-filler' molecules to fill these gaps. The wheel and axel concept takes advantage of this simple observation by the deliberate synthesis of molecules with awkward shapes. Wheel and axel hosts based on thin acetylenic or flat oligothiophene spacers[18] are shown in Figure 7.17. The combination of the wheel and axel concept and two alcohol functionalities is particularly powerful because of the directionality of the hydrogen bonding in alcohols as we have already discussed; however, purely awkwardly shaped wheel and axel hosts are also effective simply because of the need to fill in the empty cleft between the two bulky 'wheels'.

## 7.4.3 Perhydrotriphenylene: Polarity Formation

Hulliger, J., 'Polarity formation: Markov chain model', in *Encyclopedia of Supramolecular Chemistry*, Atwood, J. L. and Steed, J. W. (eds.), Dekker: New York, 2004, vol. 2, *pp.* 1120–1128.

Perhydrotriphenylene (PHTP, **7.15**) is a chiral, $D_3$ symmetric, saturated organic compound that forms hexagonally arranged stacks in the solid state (rather like a honeycomb), leaving isolated channels some 15 Å apart into which guest molecules are included. Guests are generally long, linear species such as hydrocarbons, alcohols, esters, ethers and acids, which match the long channels, but branched and bulky guests are also included. Host–guest interactions are minimal (van der Waals type). Because of the non-functionalised nature of the hydrocarbon, host and guest molecules often exhibit extensive disorder and incommensurate, or one-dimensional ordered packing, as in urea inclusions (Section 7.3). This gives a channel unit cell dimension for the guest, $c_g$, which is a multiple of the host unit cell, $c_h$, depending on the length of the guest. PHTP is of particular interest because of its ability to include hyperpolarisable guest species to form crystals with overall bulk polarity. This results in PHTP inclusions exhibiting interesting nonlinear optical, and electro-optical properties (Section 11.6). The apparent crystallographic disorder arising from the one-dimensional guest ordering results in significant structural problems in characterising PHTP inclusion compounds, and it was only in 1997 that Hans-Beat Bürgi, from the University of Berne in Switzerland, was able to fully structurally characterise a PHTP inclusion compound that exhibited polar order and bulk crystal polarity. The material studied was an inclusion compound of (±)-PHTP

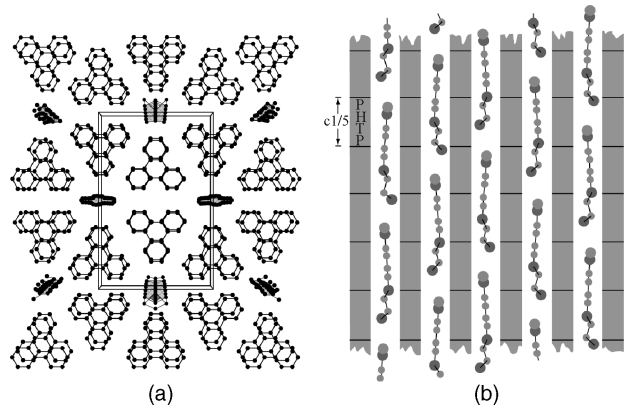


**Figure 7.18** (a) Projection of the structure of $[(\pm)\text{–PHTP}]_5[\text{NPP}]$ along the channel axis. (b) Schematic drawing of the channel of NPP guest molecules. The guests interact *via* N—H ⋯ $O_2$N hydrogen bonds and are ordered within each channel. The guest positions from one channel to the next differ by integer multiples of $c_g/5$. (Reproduced with permission from [19] © 1997 American Chemical Society).

with 1-(4-nitrophenyl)piperazine, (NPP, **7.16**) of formula $[(\pm)\text{–PHTP}]_5[\text{NPP}]$, which exhibits second harmonic generation, electro-optical and pyroelectric effects, all arising from bulk crystal polarity. The 5:1 host:guest ratio is a direct consequence of the relative lengths of the host repeat unit ($c_h$ = 4.73 Å) and the guest ($c_g = 5\ c_h$). A projection of the packing of the host–guest complex along the channel axis is shown in Figure 7.18a and a view of the guest arrangement is shown in Figure 7.18b.

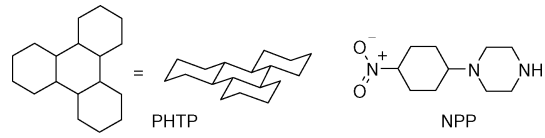


The key question in the structure of $[\text{PHTP}]_5[\text{NPP}]$ concerns the origin of the nonlinear polarisation properties of the crystal. Such properties could easily arise from polar stacking of either guests or hosts, but the question is which, and why should the molecules stack in a noncentrosymmetric fashion? Bulk crystal polarity could arise from spontaneous resolution of the (+)- and (−)-forms of the host into discrete enantiomeric crystals (*cf.* Section 8.2.4). However, the host crystal lattice is centrosymmetric and there is disorder between (+)-PHTP and (−)-PHTP within the same crystal. Detailed analysis of the packing in the host reveals that this takes the form of individually polar, homochiral stacks (*i.e.* only one enantiomer in each stack) of either (+)- or (−)-forms. These stacks are distributed randomly throughout the crystal. The van der Waals interaction energy of interactions between pairs of either the (+)−(+), (−)−(−) or (+)−(−) forms is approximately equal so the random distribution is unsurprising. Importantly, the host lattice is, on average, nonpolar as a result of the cancellation of (+) stacks by an equal number of (−) stacks. The polarity must, therefore, come from the guest molecules. Again it is easy to envisage a polar chain of guest molecules arranged in a donor— acceptor— donor— acceptor (… DADA …) fashion according to the hydrogen bonding donor ability of the NH group and acceptor ability of the $NO_2$ group. In contrast D–D and A–A interactions, in which a molecule in the chain is reversed, should be unfavourable. Such DADA chains would be individually polar but, since the chains are separated from each other by 15 Å, it is difficult

to imagine cooperative guest–guest interactions between channels resulting in the alignment of all of the chains in the same direction. Indeed chain–chain interactions should lean towards cancellation of polarity.

Examination of the channel dimensions reveals that it is not possible for a molecule of NPP to invert itself once the full three-dimensional channel has formed, and so the orientation of the NPP chains must be determined during the crystal growth. If the crystal has a bulk polarity, this must mean that there is a driving force positioning more than 50 % of the chains in the same direction and therefore a driving force exposing (for example) an $NO_2$ group more often than the opposite end of the guest molecule at the entrance of the growing channel. In fact, the overall polarity is a result of the different probability of the various …DA… …DD… and …AA… guest–guest interactions (Figure 7.19). The complementary …DADA… motif is, of course the most favourable, resulting in individual polar chains. The evidence indicates that these chains run for about 100 Å before a 'mistake' occurs, resulting in the incorporation of either a …DD… (*i.e.* N—H···H—N) or …AA… (*i.e.* $NO_2 \cdots O_2N$) defect, which has the effect of reversing the chain polarity. The key point is that it is less likely that an …AA… defect will occur than a …DD… type. This is because the interaction between the two $NO_2$ groups is repulsive, whereas there is some attraction from the proton of one NH group to the nitrogen of another NH moiety. As a result, as the channels assemble, the operation of statistics dictates that there will be more $NO_2$ end groups at the channel entrance than NH moieties.

This growth mechanism is termed the *Markov growth model* and it allows the appearance of spontaneous bulk crystal polarity independent of the initial state at the point when the crystal is seeded. The Markov model states that the most efficient way to engineer polarity is in isolated chains (the isolation provided by hosts such as PHTP reduces the tendency towards antiparallel stacking of polar chains) containing guests A–R (where R is a fragment undergoing no particular inter-fragment interactions) where $E_{AR} \approx E_{RR} \approx 0$ and $E_{AA} \gg 0$, *i.e.* the A-A interaction is strongly repulsive. Under these circumstances *ca.* 95 % of the functional groups at the surface will be of only one type within six growth steps.

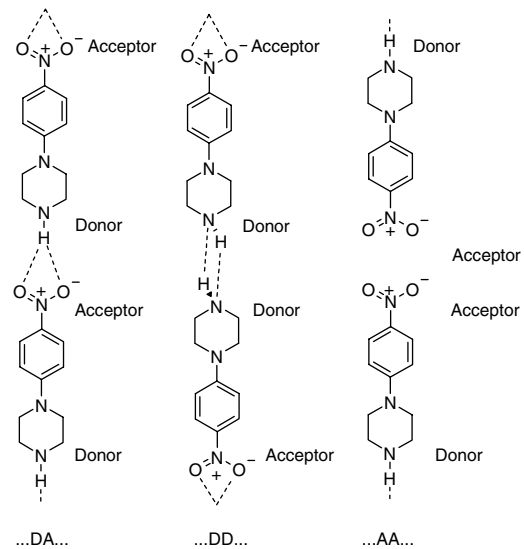


**Figure 7.19** Possible guest arrangements in PHTP inclusion channels. While the …DA… interaction is by far the most likely, the occurrence of a greater number of …DD… defects than …AA… results in overall crystal polarity.

The $[PHTP]_5[NPP]$ inclusion compound is particularly rich in the information available on guest and host low-dimensional ordering from diffuse scattering and the advent of modern synchrotron radiation techniques has allowed a detailed analysis of these phenomena in this system.[20]

## 7.5 Hydroquinone, Phenol, Dianin's Compound and the Hexahost Strategy

Mak, T. C. W. and Bracke, B. R. F. 'Hydroquinone clathrates and diamondoid host lattices', in *Comprehensive Supramolecular Chemistry*, Atwood, J. L., Davies, J. E. D., MacNicol, D. D. and Vögtle, F. (eds), Pergamon: Oxford, 1996, vol 6, 23–60.

Hydroquinone (**7.17**), phenol (**7.18**) and Dianin's compound (**7.19**) all act as hosts *via* the formation of hexagonal, cyclic hydrogen bonded rings (*cf.* Figure 7.2). This stable solid-state arrangement of the phenolic hydroxyl groups has the immediate consequence of causing the bulky aryl substituents to adopt an alternating up–down pattern around the core hexagonal ring, forming a cavity lined with aryl moieties. In the crystal, these cavities all interlock (Figure 7.20), to give a closed cage into which a variety of molecular guests are accommodated.

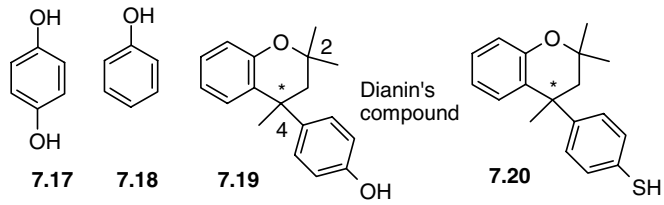


Hydroquinone exists in three forms in the solid state, labelled α, β and γ, of which only the β-form forms clathrates. β-Hydroquinone clathrates have the general formula $3C_6H_4(OH)_2 \cdot xG$ where G is a guest species and $x$ is a site occupancy factor depending on reaction conditions. For full occupancy of every cage, $x = 1$, but for many guest species, $x$ may be less then 1 (*e.g.* G = Xe, $x = 0.866$; G = $H_2S$, $x = 0.874$) and a stable clathrate still results. The six-membered rings and cavity dimensions are capable of significant distortion in response to guest dimensions. Thus small, spherical guests such as Xe and $H_2S$ form high-symmetry type I (space group $R\bar{3}$) cages. With methanol, $SO_2$ and HCl, the symmetry is lowered to $R3$ (no longer centrosymmetric), giving a type II clathrate in which the cage length is increased to accommodate the longer guest. One example of a type III clathrate

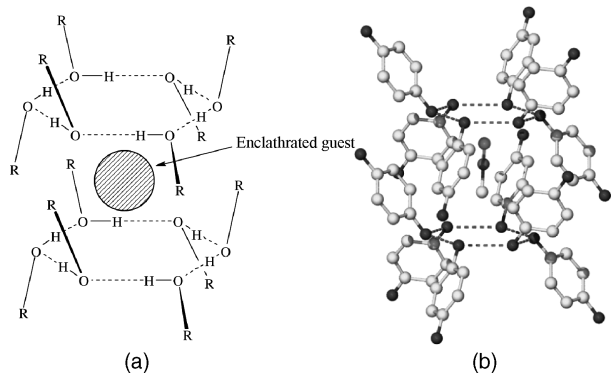


**Figure 7.20** (a) Schematic diagram showing the hydroquinone cage structure. (b) Structure of the β-hydroquinone lattice cavity with methylisocyanide guest.

(MeNC guest) is also known in which three different guest orientations are observed (symmetry *P*3). Also, buckminsterfullerene ($C_{60}$) forms a very-high-symmetry 3:1 structure $3(C_6H_4(OH)_2) \cdot C_{60}$ with hydroquinone, resembling the topology of metallic polonium. The dimensions of the cavities in the hydroquinone lattice (about 10 Å) correspond closely with the size of $C_{60}$ and the electron-rich nature of hydroquinone complements the electron-deficient $C_{60}$. The interplane distance between the $C_{60}$ surface and the hydroquinone aryl ring is 3.1 Å, suggesting optimum π–π stacking. Reaction of six equivalents of hydroquinone with pure $C_{70}$ in benzene gives brownish-red crystals of composition $9(C_6H_4(OH)_2) \cdot 2C_{70} \cdot 2C_6H_6$, which adopt a much more complicated structure in order to optimise the differing steric requirements of the rugby ball-shaped $C_{70}$ molecule and the hydroquinone packing.

Recent interest has focussed on hydrogen storage by clathrates (for applications in hydrogen-powered fuel cell vehicles) and β-quinone has been studied in this regard by molecular dynamics simulations. The computational results suggest that up to four hydrogen molecules per cage may be included, perhaps by diffusion of the small gas molecules into the empty metastable host structure at low temperature. At a loading of one hydrogen molecule per cage the hydrogen is distributed evenly round the cavity. At two molecules per cage there is preferential occupation near the hydroxyl ring crowns of the cavity while higher loadings leads to occupation of the interstitial sites (the hydroxyl rings) between cages by a single $H_2$ molecule with the remaining molecules occupying the equatorial plane of the cavity.[21]

Dianin's compound is named after the Russian chemist, A. P. Dianin, who first isolated it in 1914 by condensation of phenol and mesityl oxide, incidentally preparing several clathrate compounds of the host with common solvents. Dianin's compound is a chiral molecule (the asymmetric carbon is marked with an asterisk) and in the solid state adopts a geometry of the type shown in Figure 7.21(a) with one enantiomer 'up' and the other 'down'. Indeed, the resolved *S*-enantiomer does not form clathrates by itself at all. Of all the phenolate hosts, Dianin's compound is one of the most versatile, and is known to include, amongst a wide range of organic and inorganic guests, argon, glycerol, small carbohydrates, and notably $SF_6$, which is used widely as an insulating gas in the electrical industry. This suggests possible applications for **7.19** in the storage and transport of volatile species. Dianin's compound also includes a wide variety of solvents and related molecules. For the majority of clathrates, including aromatic guests, the host:guest ratio is 6:1, consistent with the hexameric structure. Larger solvent molecules such as butanol, ethanol or acetone form 3:1 adducts in which two molecules occupy the hexameric cages, while methanol forms a 2:1 species. Only piperidine forms a 1:1 adduct. The structure of the guest-free complex, showing the hexagonal arrangement of the host, is shown in Figure 7.21 along with a schematic of the resulting cavity dimensions.

Investigation of the dynamics of included molecules shows that small molecules such as ethanol (two per cage) are undergoing rapid liquid-like motion, even at low temperature in the solid state. On the

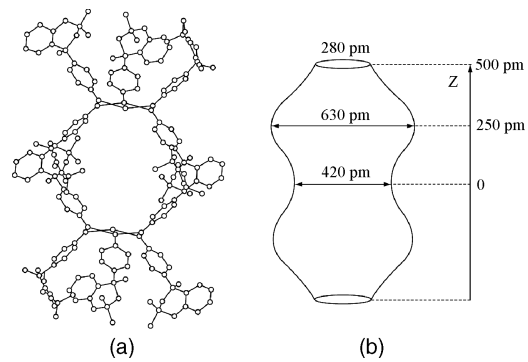


**Figure 7.21** (a) The structure of unsolvated Dianin's compound (front and back of the central cavity omitted for clarity). (b) Schematic diagram of the host cavity; the cage height is 11.0 Å. (Reprinted with permission from [22]).

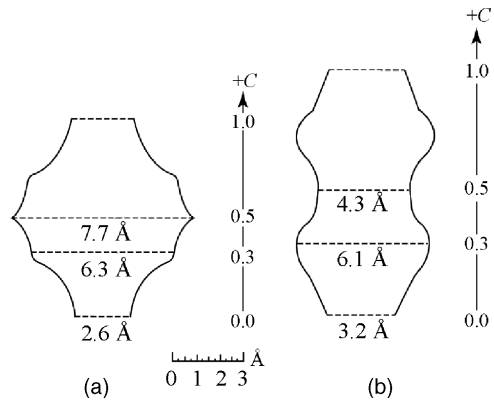


**Figure 7.22** Sections through the van der Waals surface of the cavity in (a) **7.22** and (b) **7.21**. (Reproduced by permission of The Royal Society of Chemistry).

other hand, $CCl_4$, which fits the cage quite well, is held relatively rigidly. As with clathrate hydrates, the thermal conductivity of the guest-filled host is extremely low.

The inclusion ability of **7.19** is sufficiently robust that it can tolerate a variety of substitutions and still retain (modified) clathrate-forming ability. A wide variety of analogues have been prepared, which exhibit different size and shape cavities by the following modifications:

1. Perturbation of the substitution pattern at the C(2) and C(4) positions.
2. Changing the OH group for other hydrogen bonding functionalities such as $NH_2$ and SH.
3. Replacement of the etheric oxygen with S, Se, $SO_2$ *etc.*
4. Addition of substituents to the fused aromatic ring.

Use of strategy 1 enabled David MacNicol of the University of Glasgow, UK,[23] to produce a host with a much wider central cavity (7.10 Å, versus 4.20 Å), by removal of one of the C(2) methyl groups. Removal of the C(4) methyl group results in an entirely different structure that does not exhibit clathrate behaviour. Replacement of OH with $NH_2$ in accordance with strategy 2 again results in a loss of clathrate behaviour. The thiol analogue (**7.20**), however, behaves very similarly to Dianin's compound itself when crystallised from $CCl_4$, giving a 6:1 complex with a slightly wider and elongated cavity in accordance with the longer S—H $\cdots$ S hydrogen bond lengths and S–C bonded distances compared to the hydroxyl analogue. Incorporation of sulfur according to strategy 3 resulted in a particularly effective host (**7.21**) able to encapsulate small molecules in a 3:1 fashion (*i.e.* two guests per cavity) and larger guests as 6:1 clathrates. The host is even able to retain the volatile (and highly toxic) dimethyl mercury, $Hg(CH_3)_2$, under high vacuum for several days. Finally, addition of methyl groups to various ring positions according to strategy 4 results in a range of interesting hosts with varying cavity sizes. In particular, host **7.22** displays a remarkably different cavity from the parent **7.19** and **7.21**, ranging from 2.60 to 7.70 Å wide, in a lantern shape (Figure 7.22). Compound **7.23** does not exhibit clathrate behaviour, however.

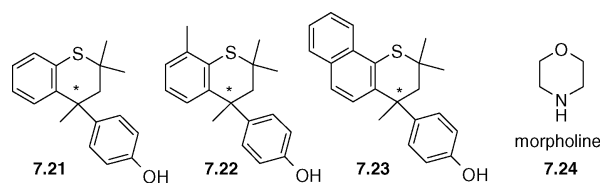

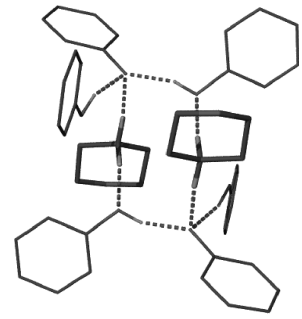

**Figure 7.23** The hexameric hydrogen bonding in the Dianin's complex of morpholinium cation (only the phenol residues of Dianin's compound shown for clarity).[24]

Work by Len Barbour at the Stellenbosch University, South Africa, has examined the inclusion of morpholine (**7.24**) by Dianin's compound. Two guests are bound in their protonated form (morpholinium) with concomitant deprotonation of two of the Dianin's host molecules per cavity. Despite this dramatic change the overall structure is disrupted very little. The guest $NH_2^+$ groups participate in hydrogen bonding to reform a hexmeric ring, albeit of a different composition to that found in classical Dianin-type compounds, Figure 7.23.[24] Barbour has also ingeniously used the chirality of Dianin's compound and its thiol analogue (**7.20**) in order to further tune the cavity size. A 1:1 mixture of racemic **7.19** and **7.20** form separate, pure host networks and the pure, resolved *R* or *S* forms of each compound do not form clathrates. However, synthesis of one enantiomer of **7.19** and co-crystallising it with the opposite enantiomer of **7.20** results in a mixed cage host with an alternating $(SH\cdots OH\cdots)_3$ hydrogen bonded ring. The dimensions of the cavity are intermediate between those of the pure hosts.

The hydrogen bonded hexagonal structure of phenol-derived hosts such as hydroquinone and Dianin's compound has inspired a number of covalently bonded analogues, generally based on a six-membered aromatic ring, that can dimerise in the solid state to form interdigitated cavities closely analogous to the spontaneously formed hydrogen-bonded structures. These designer clathrates were termed the *hexahosts* by MacNicol. One of the first hexahosts was the hexakis(thioether) **7.25** which forms cavities very much like those formed by hydroquinone. The long C–S bonds are necessary to give sufficient space for the aryl rings to adopt the required conformation. A later development is the *piedfort unit*,* a dimer of compounds such as **7.26**, Figure 7.24.[25] In this case the interdigitated dimer has no space in the centre of the assembly where the triazine derivatives overlap, but still includes guests such as dioxane in lattice voids.[25]

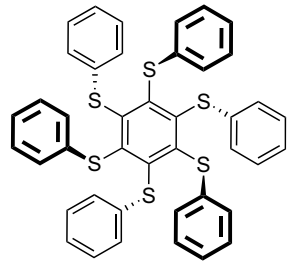

**7.25**

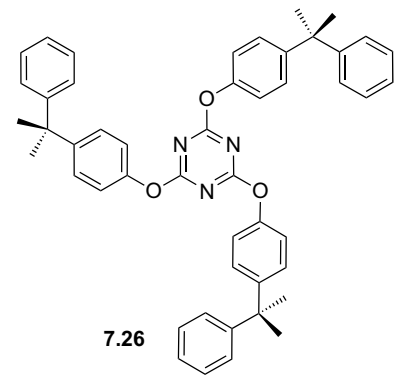

**7.26**

* The name *piedfort* comes from a type of specially struck coin which is much thicker and heavier than normal, often exactly twice the normal weight. The word is derived from French and literally means heavy weight.

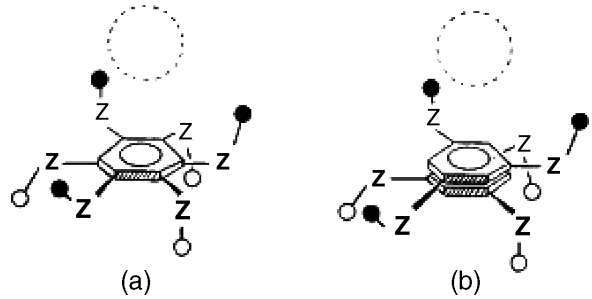


**Figure 7.24** A comparison of a typical hexa-host *(A)* with its Piedfort analogue *(B),* composed of two trisubstituted aromatic rings juxtaposed. The light dotted circle is symbolic of the projected guest binding region in each case. (Reproduced by permission of The Royal Society of Chemistry).

## 7.6 Tri-*o*-thymotide

Arad-Yellin, R., Green, B. S., Knossow, M. and Tsoucaris, G., 'Enantiomeric selectivity of host lattices', in *Inclusion Compounds*, J. L. Atwood, J. E. D. Davies and D. D. MacNicol (eds), Academic Press: New York, 1984, vol. 3, 278–284.

### 7.6.1 Inclusion Chemistry

Tri-*o*-thymotide (TOT, **7.27**) is known to form a very large range of solid-state inclusion compounds, of which more than 140 have been isolated. A particularly remarkable feature of TOT host–guest chemistry is the enormous range of crystal symmetries adopted by its clathrates with at least 12 distinct crystal-packing modes. The reason for this enormous diversity is not yet known, but apparently arises as a consequence of the ability of TOT to enclathrate an enormous variety of guest shapes and sizes including guests with linear, planar or globular backbones. Only linear, highly-branched guests are not enclathrated effectively. For example, guests as diverse as 9-methylanthracene (**7.28**) and pentacarbonyl-4-aminopyridyltungsten (**7.29**) are readily encapsulated, although *trans*-2-bromocyclohexan-1-ol (**7.30**) does not form a clathrate. Clathrates are also formed, with some difficulty, with small guests such as methanol, and while a clathrate is formed with $I_2$, 90 % of the cavities are void of guests.

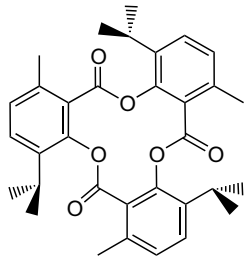


**7.27**

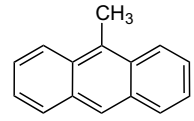


**7.28**

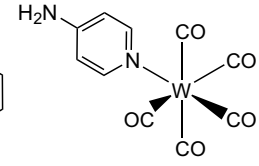


**7.29**

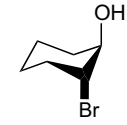


**7.30**

In solution, $^1$H NMR spectroscopic results indicate that TOT exists in two distinct, equlibrating conformations (each of which is present in two enantiomeric forms): the more predominant propeller form, and the minor 'helical' form that has one $C{=}O$ group orientated in the opposite direction from

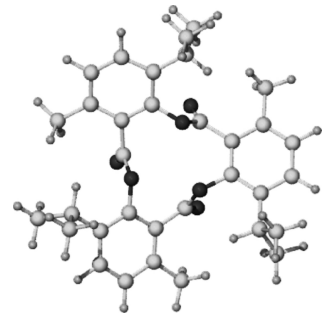

**Figure 7.25** X-ray molecular structure of the (−)-(*M*) configuration of TOT.

the other two. It is only the chiral propeller form that is observed in the crystalline state, adopting the (−)-(*M*) conformation (or the enantiomeric (+)-(*P*) conformation of opposite helicity – for a discussion of helicity see Section 10.8.1) shown in Figure 7.25. Dissolution of a chiral crystalline sample, and measurement of its optical rotation as a function of time as the sample racemises (equilibrates between the (−)-(*M*) and (+)-(*P*) conformations), enables the optical rotation of the pure enantiomer to be measured. Extrapolation of the plot to time = 0 gives a large optical rotation $[\alpha]_{546}^{20}$ of 88.75 ± 0.16° in $CHCl_3$ (for a discussion of optical rotation see Box 6.2).

The most common form of TOT clathrate crystallises as discrete $C_2$ symmetric cavities in the chiral space group $P3_121$, implying that the (−)-(*M*) and (+)-(*P*) forms separate spontaneously as crystallisation occurs. This property of TOT has been used in an ambitious model experiment designed to test the theory that the parity-violating energy difference (the violation of parity or symmetry in elementary particles), with autocatalytic amplification (in the case of TOT during crystallisation) is responsible for the observed chirality of modern biomolecules. The experiment did not find any evidence to support the theory, with equal amounts of each enantiomeric crystal being isolated.[26]

The chirality of the TOT crystal form allows some differentiation between chiral guests. The lattice cavity, which contains the guest molecule, is formed by a total of eight TOT hosts arranged in pairs related by a two-fold rotation axis. The cavity surface is lined by hydrogen atoms and two carbonyl oxygen atoms. The carbonyl substituents generally do not take part in direct host–guest hydrogen bonds (the only exception is 2-hydroxycyclopenten-1-one, which forms a strong hydrogen bond to a C=O group), and host–guest interactions are of the van der Waals type. Cavity volume, and hence unit cell parameters, show an approximately linear correlation with guest molecular volume. The clathrates are generally highly thermally stable, despite the fact that cage occupancy factors are usually between 0.65 and 0.75, meaning that 25 to 35 % of the cages (host: cage ratio of 2:1) are empty, depending on the guest and crystallisation conditions. This is a surprising observation, since thermal stability is not usually associated with empty lattice voids. *Trans*-dimethyloxirane and 2-bromobutane form cage clathrates with TOT and these chiral guests are included with enantiomeric excesses of 47 and 35 %, respectively, indicating a significant, but not overwhelming, chiral selectivity on guest complexation.

In addition to cage structures, TOT may also form channel clathrates (space group symmetries $P6_1$, $P6_2$ or $P3_1$) in the presence of long, linear guest molecules such as $Me(CH_2)_nX$ (X = OH, Br, I; n = 4–7, 16, 18). Host:guest ratios are ill-defined and depend on guest length, and the structures are incommensurate, rather like urea clathrates (Section 7.3). The host channels arise from the arrangement of 12 TOT molecules that form the channel repeat unit. Two sequences of six molecules form a double-helix structure (Figure 7.26).

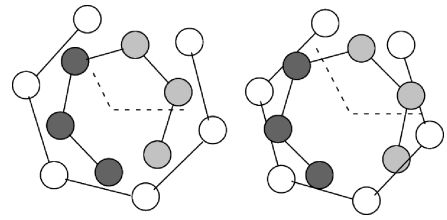

**Figure 7.26** Stereoview along the crystallographic *c* axis showing the centres of the 12 TOT molecules that make up the host channel. The *a* and *b* unit cell axes are represented by dotted lines. (Reproduced with permission from [27]).

## 7.6.2 Synthesis and Derivatives

Early work on TOT clathrates was hampered by the relatively low yield of the host when prepared directly from *o*-thymotic acid (**7.31**) as a consequence of the formation of a linear dimer and other open-chain condensation products arising from the acid catalysed decarboxylation of **7.31**. More recent work has resulted in the synthesis of **7.27** in 84 % yield *via* trimerisation of **7.31** at 100 ºC in neat $POCl_3$.[28] The guest-free host is recovered by desolvation under reduced pressure and elevated temperature. The TOT framework presents a number of possibilities for structural modification, including change of R-groups and the ester linker **7.32**. However, small changes in structure can have a dramatic effect on the hosts' clathrate-forming ability. Even the simple exchange of the methyl and *iso*propyl substituents on TOT to give tri-*o*-carvacrotide results in a complete absence of clathrate formation. In contrast, tris-3-(2-butyl)-6-methylsalicylide **7.33** forms over 30 clathrates, all of the cage type. This host is of interest because it bears chiral substituents on the aromatic rings (marked with an asterisk), offering even greater potential of discrimination between chiral guests. However, structural studies reveal disorder between the *R* and *S* forms in the solid state, rather than spontaneous resolution. Substitution of the TOT ring with various halogen atoms again results in an absence of clathration behaviour.

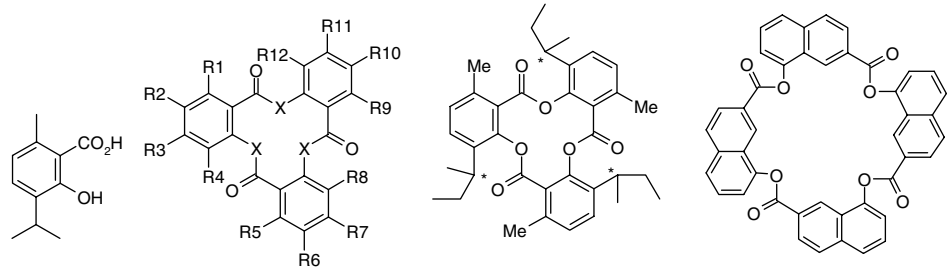


**7.31** **7.32** **7.33** **7.34**

Substitution of the ester functionality for sulfur (X = S) to give trithiosalicydes results in compounds displaying no clathrate forming behaviour. A range of trislactams (**7.32**, X = NMe or $NCH_2Ph$) have been prepared (generally *via* stepwise procedures), and their inclusion behaviour studied. Unlike TOT itself, the lactams adopt almost exclusively the helical conformation in solution and there is free exchange between helix and the minor propeller forms. The trislactams include guests such as toluene and ethanol. Only one derivative (X = 2 × NMe and 1 × $NCH_2Ph$; $R^4 = R^8 = R^{12}$ = Me) exhibits spontaneous resolution in the solid state akin to TOT, forming a clathrate with toluene, in which the helical host crystallises with wide channels occupied by disordered guests.

Cyclisation of 1-hydroxy-2-napthoic acid in dry toluene in the presence of phosphorous pentoxide as a dehydrating agent gives a small yield of a cyclic tetramer, termed tetra-1-napthoid (**7.34**). Host **7.34** forms a number of 1:2 clathrates with small molecules such as $CHCl_3$ and benzene, which are very unstable with respect to desolvation. Complexes of 2-bromobutyric acid and napthalene are much more stable. A charge transfer complex with tetracyanoethylene (TCNE) is also known in which the electron-poor TCNE accepts electron density from the electron-rich aryl rings of the macrocycle.

## 7.6.3 Applications

Tri-*o*-thymotide has been used extensively in solid-phase reaction chemistry, in which guest molecules trapped within the TOT lattice undergo reaction either photolytically or with small molecules such as $O_2$, HCl and HBr, which can perfuse through the solid matrix *via* narrow, keyhole-shaped channels between TOT molecules. The reactions are carried out in a fine TOT powder in order to enhance reaction kinetics (by increased surface area and smaller particle size allowing rapid perfusion), in a solvent in which the clathrate is completely insoluble. The advantages of such solid-phase syntheses are high specificity and regio- and enantioselectivity. The approach is analogous to inclusion reactions carried out in zeolite supports (Section 9.2), but has the distinction that the TOT cavity is chiral and possesses no active sites that may interfere with reactivity. To take just one example, photooxygenation of the prochiral (*Z*)-2-methoxybut-2-ene (**7.35**) with singlet oxygen in solution to give the racemic allylic hydroperoxide (**7.36**), does not result in the observation of any enantioselectivity. However, compound **7.35** forms a cage clathrate with TOT, which resolves spontaneously into crystals of the (+)-(*P*) and (−)-(*M*) types. Irradiation of the separated crystals in the presence of $O_2$ and a photosensitiser results in an inclusion reaction, again forming **7.36** in the solid state. Dissolution of the product crystals and measurement of the optical rotation of the sample after the TOT host has racemised gives the specific rotations shown in Scheme 7.1. This is clear evidence of transfer of the chirality of the TOT host lattice to the photooxygenation product. In making this measurement it is of course important to wait until the TOT has entirely racemised in solution to ensure that no measured optical rotation (and therefore enantiomeric excess) is due to the TOT host itself.[29]

In addition to inclusion reactions, TOT has been applied in the separation of enantiomers by enantioselective complex formation. Enantiomeric excesses (*ee*) of guests within a single TOT clathrate crystal grown from a racemic guest solution are generally in the range 2–60 % in cage-type clathrates. This kind of *ee* is inadequate for industrial purposes, which require at least 80 % in a single recrystallisation step. However, *ee* values can be improved by 'chirality ampification'. If a solution of racemate is seeded with small crystals containing some excess of one enantiomer, the crystals grow to produce samples with *ee* values in excess of 90 %.

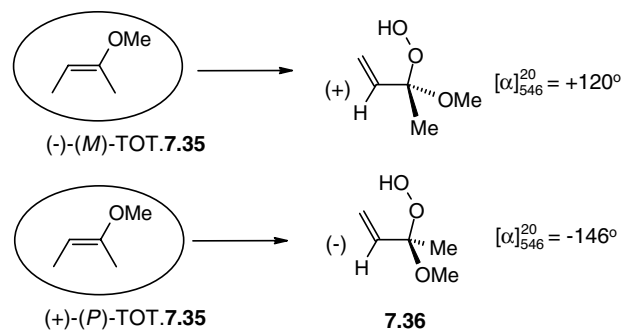


**Scheme 7.1** Transfer of chirality by inclusion reaction.[29]

# 7.7 Cyclotriveratrylene

Collet, A., 'Cyclotriveratrylenes and cryptophanes: their synthesis and applications to host-guest chemistry and to the design of new materials', *Top. Curr. Chem.* 1993, **165**, 103.

## 7.7.1 Properties

Cyclotriveratrylene (CTV, **7.37**) has proved to be both a highly versatile host in its own right and a key bowl-shaped, or shallow saucer-shaped, building block for the construction of a large range of hosts capable of complexing neutral molecules and even anions in solution as well as in the solid state (Sections 6.6 and 4.7.2). The utility of CTV arises from the significant conformational preference of the central nine-membered cyclononatriene-derived ring for a crown conformation, which causes the three aryl rings to all point 'up' in the same direction. Variable-temperature $^1$H NMR spectroscopic studies have shown that conformational inversion (*via* a saddle intermediate with one aryl ring 'up' and two 'down') is slow on the NMR time scale. The conformational immobility is observed clearly in the inequivalence of the geminal (attached to the same carbon atom) protons of the methylene bridge, which appear as an AB quartet. The slow rate of inversion has also been established by measurement of the racemisation rate of the chiral CTV-$d_9$ derivative **7.38**, which gave an energy barrier to inversion of 110.9 kJ mol$^{-1}$. This means that the inversion half-life is around one month at 20ºC, but less than 0.1 s at 200ºC. The bowl or crown conformation is common to almost all CTV-related compounds except for **7.39**, in which the metastable saddle conformation is a consequence of the peculiar synthesis of the molecule, and the 2,5-dimethylthiophene derivative **7.40**, in which unfavourable steric interactions between adjacent methyl groups force the adoption of a saddle ($C_2$ symmetric) conformation (Figure 7.27). We also saw a striking 'imploded' cryptophane CTV derivative in Section 6.6.6.

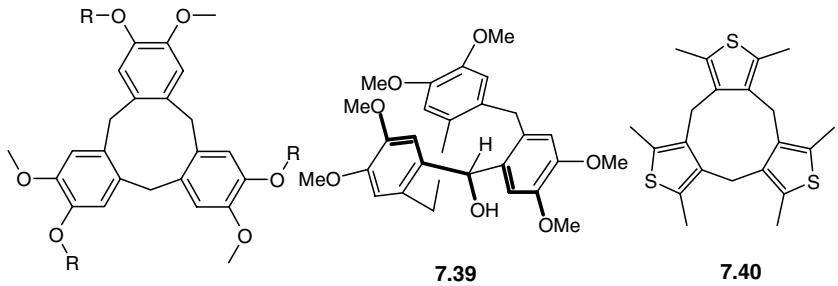


R = $CH_3$ **7.37**
R = $CD_3$ **7.38**

**7.39** **7.40**

## 7.7.2 Synthesis

Cyclotriveratrylene was first prepared by Gertrude Robinson in 1915 (Scheme 7.2). Robinson was interested in following up earlier work on the synthesis of anthracene derivatives and concluded that her product (empirical formula, $C_7H_{10}O_2$, was 2,3,6,7-tetramethoxy-9,10-dihydroanthracene (**7.43**), the dimer of the intermediate veratryl cation (**7.42**). During the 1950s, CTV was again reformulated erroneously as a hexamer (**7.44**) and it was not until 1963 that the onset of a variety of modern techniques established a trimeric formula.

Cyclotriveratrylene is formed in over 70 % yield by the condensation of the veratryl cation (**7.42**), whether it is produced from veratryl alcohol (**7.41**) or directly from veratrole (1,2-dimethoxybenzene) and formaldehyde in aqueous acid. In organic solvents such as acetic acid in the presence of a

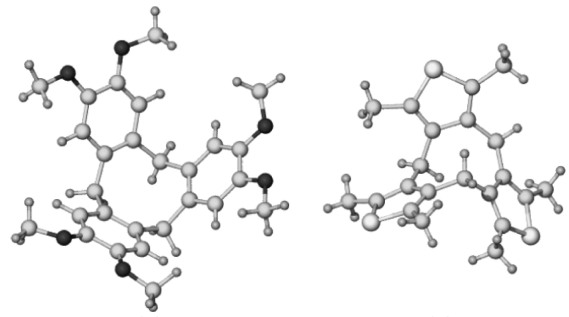


**Figure 7.27** (a) Bowl-shaped conformation of CTV (**7.37**) and (b) saddle conformation of the related **7.40** which arises from unfavourable steric interactions between the methyl substituents.

Lewis acid such as $SnCl_4$ or benzene/$BF_3$/ether, significant amounts of the analogous tetramer cyclotetraveratrylene (CTTV, **7.45**) are produced. CTTV does not possess a bowl conformation and adopts a saddle shape, although it is capable of forming a limited range of lattice inclusion compounds involving hydrogen bonding to the methoxy substituents.[30] Cyclisations such as that shown in Scheme 7.2 are reasonably tolerant of replacement of the methoxy substituents by other functional groups in the 3- and 4-positions. However, it is vital that the 4-position be occupied by an electron-donating group in order to stabilise the positive charge in the veratryl cation intermediate (**7.42**), although novel Lewis acids such as scandium triflate can give excellent yields of unusual derivatives such as **7.46** (Scheme 7.3), a useful intermediate on the way to cryptophane synthesis.[31] The facile formation of the cyclic trimer (as opposed to polymers and higher oligomers) is an interesting aspect of this chemistry, and it is not known whether this is a result of thermodynamic equilibration (possibly driven by insolubility of the product), or the result of a kinetic template effect.

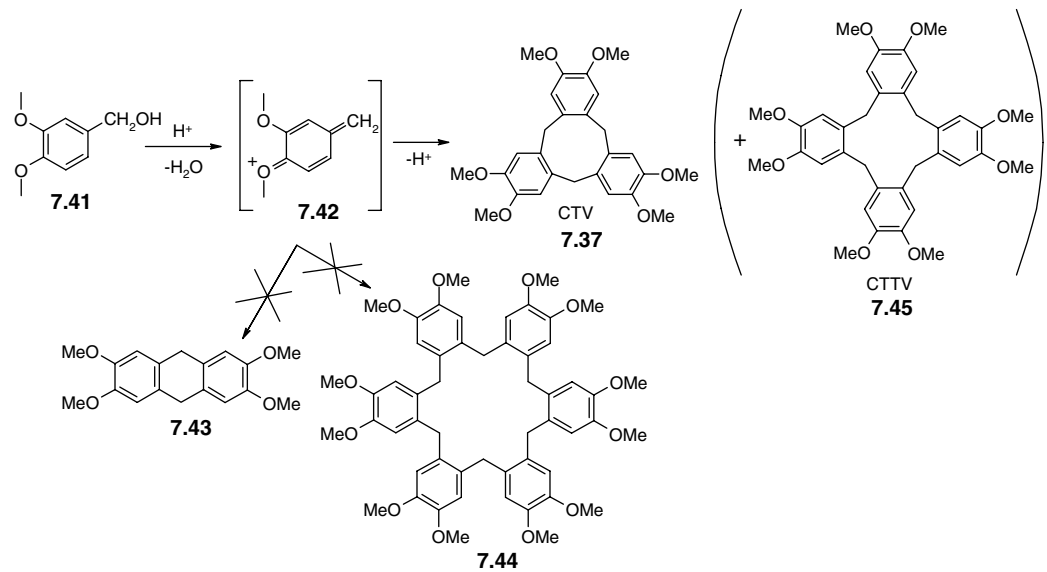


**Scheme 7.2** Robinson's synthesis of CTV, initially assumed to be the dimer (**7.43**), and later hexamer (**7.44**). While neither of these compounds is formed, manipulation of the reaction conditions, *e.g.* using a Lewis acid such as $SnCl_4$, does give the tetramer, CTTV (**7.45**).

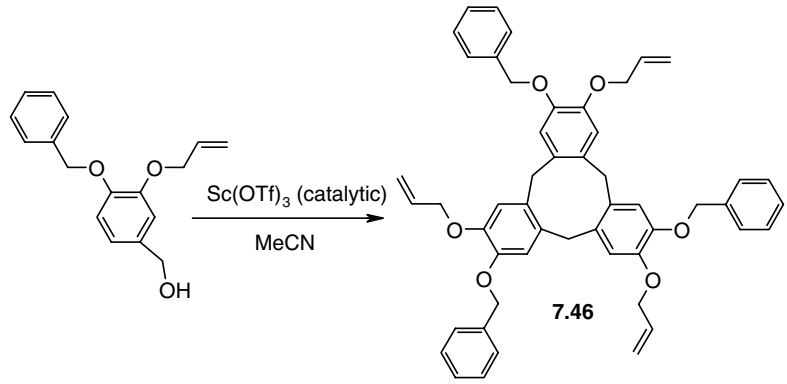


**Scheme 7.3** Scandium triflate catalysed synthesis of novel CTV derivatives.[31]

## 7.7.3 Inclusion Chemistry

It was recognised relatively early on that CTV forms solid-state inclusion compounds with a wide variety of small neutral molecules such as benzene, toluene, water, acetone and $CS_2$. Based on the correlation of IR spectroscopic data and crystallographic unit-cell parameters, CTV clathrates are divided into two distinct phases, designated α and β with small differences in their solid-state properties. Early X-ray crystallographic work showed that in the α phase at least, CTV molecules stack one within the other, rather like a pile of saucers, to give a characteristic crystallographic *b* unit cell dimension (9.6–9.7 Å for the α-phase and 8.1–8.3 Å for the β-phase). It is this characteristic 'self-inclusion' that makes the attractive saucer-shape of the cavity unusable for the inclusion of guests, and all CTV inclusion compounds isolated up until 1994 possess guest species only in channels running between stacks of CTV molecules. The structural characterisation of two β-phase complexes[32] finally resolved the nature of the difference between the two classes of compound. The differences in the spectroscopic parameters were found to result from a twist of one of the methoxy groups in response to the hydrogen bond donor/acceptor properties of the guest. In the language of modern crystal engineering (Chapter 8), CTV is solely a hydrogen-bond acceptor, with little donor ability. In the presence of hydrogen-bond donor guests (even weak hydrogen-bond acids such as benzene), the guest protons hydrogen bond with the methoxy oxygen atoms. If the guest is incapable of acting as a hydrogen-bond acid in this way, however, the CTV molecule distorts in order to present the weakly hydrogen-bond donating $OCH_3$ protons in order to interact with the guest acceptor.

Shortly after the first β-phase structures, a third clathrate phase, termed the γ-phase, was reported by Ibragimov *et al*.[33] The compound is of formula $(CTV)_4 \cdot$ acetone, and contains an acetone molecule sandwiched between a pair of CTV bowls facing each another in order to create a capsule-like space. As with the β-phase clathrates, the nature of the host–guest interaction involves $OCH_3 \cdots OCMe_2$ hydrogen bonds (Figure 7.28). The solid-state structure of $(CTV)_4 \cdot$ acetone is remarkable since it both demonstrates intracavity inclusion and represents a noncovalent analogue of the capsular CTV-based cryptophanes (Section 6.6). More recently a further example CTV·0.25EtOH has been reported.[34] These intrabowl inclusion compound with simple, small molecule guests are relatively unusual for CTV, with $CTV \cdot (DMSO)_2 \cdot (H_2O)_2$ which contains an intra-cavity DMSO molecule being the only other known example.[34] However, for more unusual spherical guests such as buckminsterfullerene ($C_{60}$) and 1,2-dicarbadodecaborane(12) (*o*-carborane, **7.47**), intracavity 'ball-and-socket' inclusion compounds have been known since 1994.[35, 36] Intra-cavity inclusion is also observed extensively in CTV-based coordination networks, as we will see in the next section. In the case of $C_{60}$, there is both a steric and electronic complementarity between host and guest. The radius of curvature of the

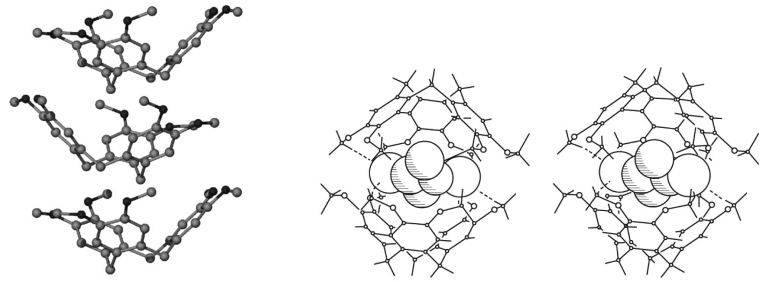


**Figure 7.28** (a) Stacking in the α-phase of CTV; (b) stereoview of the X-ray crystal structure of the γ-phase CTV clathrate, $(CTV)_4 \cdot$ acetone (acetone guest disordered) (reproduced with kind permission from Springer Science + Business Media from [33] © 1999).

wide CTV cavity is similar to that of the large fullerene sphere. In addition, the CTV aryl rings are very electron-rich as a consequence of the electron-donating effect of the methoxy substituents. This complements the electron-deficient nature of $C_{60}$, allowing the formation of solution charge-transfer complexes. The solution interaction can be monitored by UV–visible spectroscopy which indicates the formation of micelle-like aggregates.[37] Confirmation of the intracavity inclusion has been demonstrated for both carborane and fullerene complexes by X-ray crystallography in the solid state. In the case of $C_{60}$, a six-membered ring is positioned directly above the CTV three-fold rotation axis, giving a good symmetry match. For the carborane complex the compound is stabilised by C—H $\cdots \pi$ interactions of 2.18 and 2.56 Å from the acidic carborane C— H protons to the CTV rings. Significantly, the much more electron-rich B— H hydrogen atoms are repelled by the CTV aryl rings (shortest B—H $\cdots \pi$ distance, 2.77 Å) (Figure 7.29).

In addition to these complementary species, the electron-rich nature of the CTV veratrole rings enable it to form a range of unusual inclusion complexes with cyclopentadienyl-arene iron(II) cations.[38] Generally, the smaller $C_5H_5$ ring sits within the CTV cavity and the acidic protons of the coordinated ring engage in C—H $\cdots \pi$ hydrogen bonds with the electron-rich CTV aryl moieties. The principal interaction is of a charge transfer type, with face-to-face stacking of the $C_5H_5$ ring with one of the CTV aryl residues. This results in the formation of noncentrosymmetric two-dimensional polar frameworks in the solid state.

A variety of CTV derivatives have been synthesised using both standard and solventless methodologies with other substituents at the rim of the CTV bowl (*e.g.* ethyl, propyl, allyl or propargyl) Crystal structures of the hexa(ethyl), tri(ethyl) and tri(propargyl) analogues have been determined, and show either intra-cavity host-guest binding or self-stacking motifs.[34]

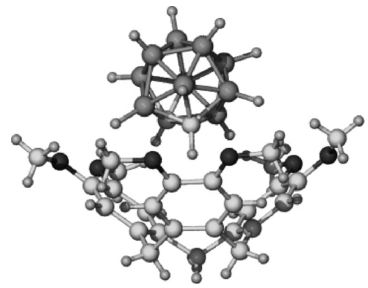

**Figure 7.29** X-ray crystal structure of the 1,2-dicarbadodecaborane(12) cavity inclusion complex with CTV.[36]

## 7.7.4 Network Structures

Hardie, M. J., Ahmad, R. and Sumby, C. J., 'Network structures of cyclotriveratrylene and its derivatives', *New J. Chem.* 2005, **29**, 1231–1240.

Work particularly by Colin Raston (University of Western Australia) and Michaele Hardie (Leeds University, UK) has dramatically expanded the range of CTV inclusion compounds in recent years. Following on from the intra-cavity inclusion of 1,2-dicarbadodecaborane(12) (**7.47**) into the CTV cavity, these workers have shown that CTV forms numerous complex networks structures with alkali and alkaline earth metal salts with both neutral carboranes and carborane anions, particularly non-coordinating, strong CH hydrogen bond donors such as $CB_{11}H_6Br_6^-$ (**7.48**). Examples with neutral **7.47** as a co-guest are shown in Scheme 7.4,[39] Structure **7.53** is of the ball-and-socket type with the carborane within the CTV bowl, stabilised by CH···π interactions, while the water molecule hydrogen bond to the CTV oxygen atoms. In contrast, in **7.50** the cavity is occupied by DMF. A common motif is the chelation of the alkali metal cations by one or two CTV oxygen atoms to form 5-membered rings as in **7.49**. Co-crystals with carborane anions include $[Na(CTV)(H_2O)(CB_{11}H_6X_6)]\cdot(CF_3CH_2OH)_8$ (**7.54**) in which the sodium ion is chelated by two CTV ligands as well as interacting with a water molecule and the carborane anion, forming a a single B–Cl–Na interaction (the bromo complex is isostructural). As with the neutral *o*-carborane, the $CB_{11}H_6X_6$ anion occupies the CTV cavity of the CTV host, stabilised by a CH···π hydrogen bond, Figure 7.30a. The potassium complex with $CB_9H_5Br_5^-$ anion and trifluoroethanol guest molecules, $[K(CTV)_2](CB_9H_5Br_5)(CF_3CH_2OH)_2$ (**7.55**) exhibits a 1D chain structure with $K^+$ ions linking pairs of face-to face CTV molecules. The eight coordinate $K^+$ ions are each bound by four chelating CTV ligands which act as hosts for the trifluoroethanol guests, Figure 7.30b. The guests show both hydrophobic binding with the $CF_3$ group in the cavity or OH···π interactions. In the latter case the CTV host also shows a rotation of one methoxy group to give an out-of plane $CH_3$ group, a similar conformation observed with

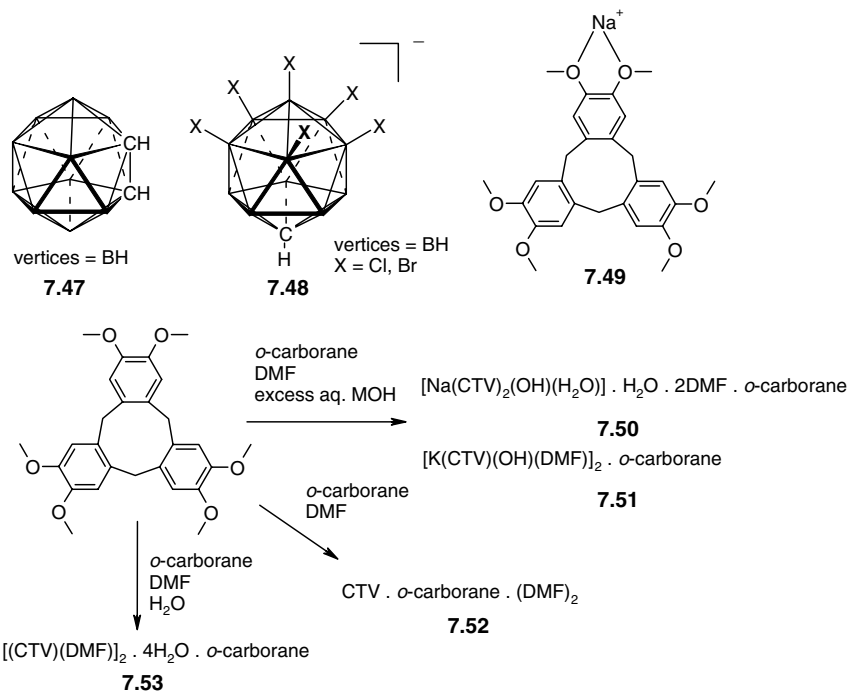


**Scheme 7.4** Supramolecular networks from co-crystallisation of CTV and *o*-carborane.[39]

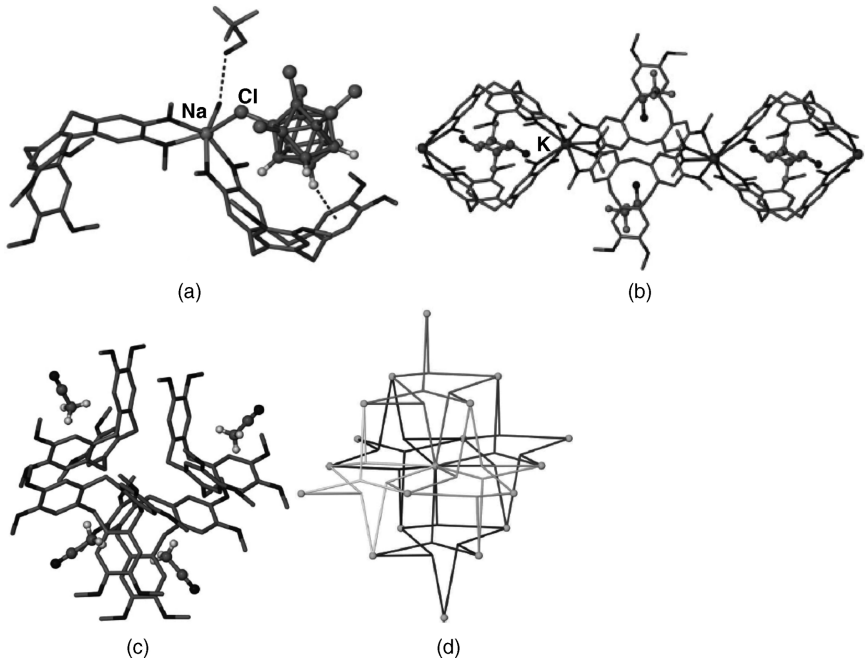


**Figure 7.30** CTV co-crystals with carborane anions (a) Portion of the X-ray crystal structure of [Na(CTV)($H_2O$)($CB_{11}H_6Cl_6$)]·($CF_3CH_2OH$)$_8$ (**7.54**) showing the $Na^+$ coordination sphere and intra-cavity position of the carborane anion, (b) the 1D chain in K(CTV)$_2$]($CB_9H_5Br_5$)($CF_3CH_2OH$)$_2$ (**7.55**) and (c) back-to-back tetramer in [Sr($H_2O$)$_8$][($CH_3CN$)(CTV)]$_4$($H_2O$)$_4$[Co($C_2B_9H_{11}$)$_2$]$_2$ (**7.56**) and (d) the resulting six vertex sharing adamantoid cage structure – each sphere represents the position of a $Sr^{2+}$ ion, while the 3-connected nodes are situated at the centre of a CTV molecule. (Reproduced by permission of The Royal Society of Chemistry)

β-phase CTV clathrates. It is not just alkali metals that form complexes; alkaline earths are also bound as in the strontium complex [Sr($H_2O$)$_8$][($CH_3CN$)(CTV)]$_4$($H_2O$)$_4$[Co($C_2B_9H_{11}$)$_2$]$_2$ (**7.56**) which contains a cobalticarborane anion. The CTV forms a second sphere ligand to the $Sr^{2+}$ aquo cation, hydrogen bonding to the coordinated water. The CTV cavity is occupied by the methyl groups of the acetonitrile ligands and the [($CH_3CN$)(CTV)]$_4$ unit takes the form of a striking tetrahedral, back-to-back tetramer, Figure 7.30c. This tetramer, *via* the hydrogen bonding to the strontium cations, extends into a 3D adamantoid hydrogen-bonded network (of α-polonium topology – Section 9.1) in which each giant adamantoid cage shares a vertex with five others, Figure 7.30c.

## 7.8 Inclusion Compounds of the Calixarenes

Asfari, Z., Bohmer, V., Harrowfield, J. and Vicens, J. (eds.), *Calix 2001*, Kluwer, Dordrecht, 2002.

### 7.8.1 Organic-Soluble Calixarenes

Ripmeester, J. A., Enright, G. D., Ratcliffe, C. I., Udachin, K. A., Moudrakovski, I. L., 'What we have learned from the study of solid *p*-tert-butylcalix[4]arene compounds', *Chem. Commun*. 2006, 4986–4996.

We saw in Chapter 1 (Figure 1.23) the formation of a simple 1:1 inclusion compound of toluene by *p-t*-butylcalix[4]arene (**3.118**) originally reported in 1979. As a reminder you may want to take a look at

Box 3.4 for some of the early history of this compound. Calixarenes are predisposed to form clathrates because their intrinsic molecular cavity (which is also preserved in solution as we saw in Chapter 6) automatically creates a void space in a crystal which is generally filled by available solvent molecules. Because this is a molecular cavity open on only one face then calixarenes typically form cage-type clathrates. The larger calix[5]arene behaves similarly with the large cavity allowing face-on inclusion of toluene, or inclusion of larger molecules such as tetralin, for example.[40, 41] Such compounds have formed the basis for the extensive interest in calixarene chemistry since its popularisation by Gutsche in the late 1970s. While there is a superficial resemblance between cavitand inclusion compounds in solution and in the solid state, the factors governing their stability are really quite different. In solution often only a single interaction is dominant and often only pair-wise interactions between host and guest must be considered, along with the significant influence of solvation factors. In the solid state multiple interactions relevant to the whole lattice as well as kinetic factors are of much greater importance. The interest in calixarenes in particular has spurred a range of detailed studies into their clathrates over the past 10–15 years and significant progress has been made, not least in the diffusion of volatile guests in these apparently non-porous materials. In this section we set the scene for some of the basic inclusion chemistry of calixarene hosts in the solid state. We will then go on to look at some of the particularly exciting developments in calixarene solid-gas and solid-liquid host guest reactions, and single crystal transformations in Section 7.9 within the context of other compounds displaying related behaviour.

The original X-ray crystal structure of the high-symmetry, fourfold symmetric *p-t*-butylcalix[4]arene inclusion complex with toluene (Figure 1.23) proved to be extensively disordered and the final residual (*R*-factor, Box 2.1) was relatively high. Extensive studies by solid-state $^{13}C$ and $^{2}H$ NMR spectroscopy, along with TGA and DSC (Box 9.1) have provided a great deal of information about the local dynamics of the inclusion compound. Below 250 K the material undergoes a phase change to a lower symmetry structure in which fourfold rotation of the toluene guest is replaced by twofold flips of 180 degrees each about the C–Me axis. Further cooling results in a static structure, Figure 7.31a. The lowered symmetry is evident in additional satellite Bragg reflections in the diffraction pattern, but only with molybdenum radiation! The larger domain size required by copper radiation is apparently larger than the domains in the crystal

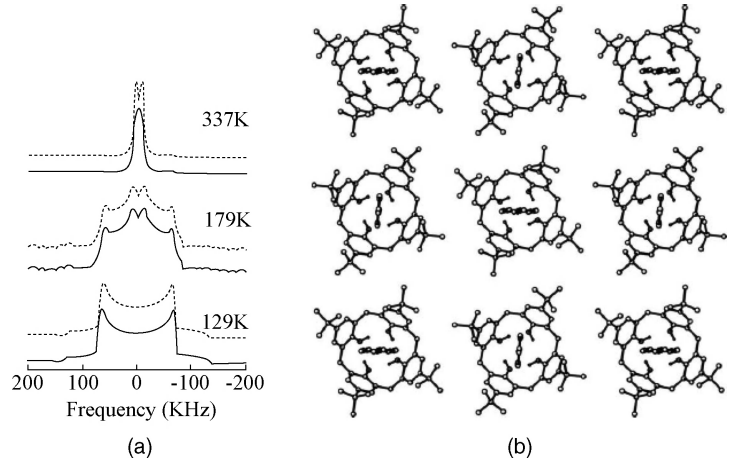


**Figure 7.31** (a) $^{2}H$ solid-state NMR lineshape of *p-t*-butylcalix[4]arene with included toluene-$d_8$ as a function of temperature. The dotted lines are the theoretical fit for static aromatic rings (129 K), twofold flips of the aromatic ring (179 K), and fourfold rotation (337 K). (b) Improved, ordered X-ray crystal structure at low temperature showing the different toluene orientations, pinched cavity shape and different *t*-butyl group orientations (reproduced by permission of The Royal Society of Chemistry).

**Table 7.1** Inclusion compounds of *p-t*-butylcalix[4]arene (reproduced by permission of The Royal Society of Chemistry).

| Structural type or characteristic | Guest(s) |
|---|---|
| Dense guest-free ($\alpha$) | — |
| Open guest-free ($\beta'_o$) and guest–host | Xe, $CO_2$ |
| Simple inclusion, 1 : 1 ($\beta_1$) axially symmetric, *P4/n*; $a = 12.55$, $c = 13.77$ Å | Pentane, benzene, pyridine, 1-chlorobutane, 1-bromobutane, 1-butanol, 1,3-dichloropropane, fluorobenzene, *n*-butylamine, phenol, 1,2,3,5-tetrafluorobenzene, acetone |
| Simple inclusion, 1 : 1 distorted<br>*P2/c*; $a = 17.81$, $b = 13.9$, $c = 17.81$ Å, $\beta = 90.04^\circ$<br>*Pna*$2_1$; $a = 29.4$ $b = 12.48$, $c = 12.72$ Å<br>*P2/c*; $a = 18.03$, $b = 27.11$, $c = 18.10$ Å, $\beta = 90.566^\circ$ | Mesitylene<br>Nitrobenzene<br>1,3,5-Trifluorobenzene<br>Tolune (low temp.) |
| Simple inclusion, 1 : 2 ($\beta_2$) axially symmetric *P4/nnc*, $a = 12.88$, $c = 25.10$ Å | Anisole, *n*-hexane, 1-octanol, dodecane, *p*-dichlorobenzene, toluene (high temp.), pentane (high temp.), *n*-butylamine (high temp.) |
| Simple inclusion, 1 : 2, distorted<br>$P2_1/n$; $a = 12.70$, $b = 27.12$, $c = 12.79$ Å, $\beta = 90.649^\circ$<br>$p\bar{1}$; $a = 12.66$, $b = 12.89$, $c = 14.59$ Å, $\alpha = 112.1$, $\beta = 103.3$, $\gamma = 90.492$ | Azobenzene, menthol |
| Inclusion/intercalation | Tetradecane |
| Self inclusion and intercalation | 1,2,4,5-Tetrafluorobenzene, dodecylamine |
| Self inclusion and $\pi$ stacking | Hexafluorobenzene |
| Inclusion and H-bonding | *n*-Butylamine; *n*-Butylamine and $H_2O$; diaminobutane |
| H-Bonding, secondary coordination | Isopropylamine, $Ag^+$ ; *n*-butylamine, $H_2O$ |

and hence averaging between ordered domains increases the apparent symmetry. Using molybdenum radiation a greatly improved model is obtained, Figure 7.31b. These experiments highlight the highly mobile nature of the solid inclusion compound. Also evident is some up-down disorder of the toluene methyl group. Some 95 % of the time the methyl group points down into the cavity, engaging in CH···$\pi$ interactions, but 5 % of the guests are inverted, although this proportion is sample dependent suggesting it is fixed during crystallisation. A wide range of guest species are known for *p-t*-butylcalix[4]arene (Table 7.1) and the proportions of these different orientation isomers gives some insight into the complexation properties of the cavity. Chlorobenzene has 100 % of the chloro substituents pointing out of the cavity suggesting a chlorophobic cavity and stabilising aryl CH···$\pi$ interactions, while phenol has an almost equal mixture of in and out OH groups reflecting the stabilising OH···$\pi$ interactions. For aliphatic guests no disorder is apparent suggesting that the long, thin guests are able to reorientate in the solid to adopt the most stable geometry. There is a consistent trend with the end group (X) preference for the intra-cavity site decreasing in the order $CH_3 > CH_2 > CH \approx OH > Cl \approx Br$ for compounds of type $X(CH_2)_3Y$.

Heating the 1:1 *p-t*-butylcalix[4]arene·toluene complex ($\beta_1$ phase) at *ca.* 140 °C results in loss of half of the toluene to give a 1:2 toluene:calixarene complex ($\beta_2$ phase) in which the toluene is sandwiched between pairs of calixarenes. Despite the fact that this transformation requires a significant movement of one layer of calixarenes relative to another the process occurs as a single-crystal-to-single-crystal transformation implying relatively little stress between the domain boundaries as the change occurs, Figure 7.32. Powder X-ray diffraction results suggest that during the transformation from the $\beta_1$ to the $\beta_2$ phase crystals exist in which domains of both phases are mixed together. Such mixed-phase 'hybrid' crystals were first identified in 1957 by Ubbelohde[42] but they have been essentially unrecognised in organic systems with the possible exception of the recent report of two intergrown aspirin polymorphs.[43]

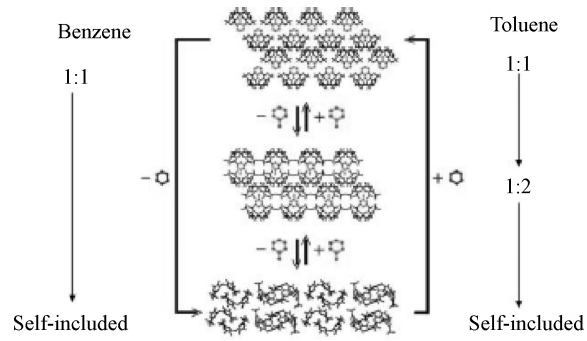


**Figure 7.32** Single crystal transformations between the 1:1 and 1:2 toluene inclusion complexes of *p-t*-butylcalix[4]arene. The transformation of the the toluene or benzene clathrates to the guest-free α-form causes crumbling of the crystal (reproduced by permission of The Royal Society of Chemistry).

Further heating of the calixarene toluene or benzene inclusion compounds or recrystallisation after refluxing in a high boiling solvent such as tetradecane, causes loss of all of the guests to give a dense, self-included α-phase in which the calixarene cavity is filled by a neighbouring *t*-butyl group, accompanied by cracking of the crystal. Heating the α-phase to 253 °C or high temperature vacuum sublimation produces a very interesting open guest free apohost ($\beta_0$ phase). In this particular case the apohost has sufficient stability to allow the facile inclusion of guest molecules such as xenon and $CO_2$ gas (for $^{129}$Xe NMR studies). The transformations for *p-t*-butylcalix[4]arene are summarised in Figure 7.33.

Studies on this common host molecule have revealed a wealth of information about the organic solid state generally and have highlighted the need to combine crystallographic measurements with other techniques such as TGA/DSC and particularly techniques such as solid-state NMR spectroscopy that give information about local, short-range interactions, rather than averaged structure over large regions. These insights have provided a springboard for much modern solid-gas and solid-liquid chemistry of relevance not just to calixarenes (which are a prime example) but to many organic solids that we will encounter this work shortly in Section 7.9. Readers who want to continue the story at this point should skip ahead now!

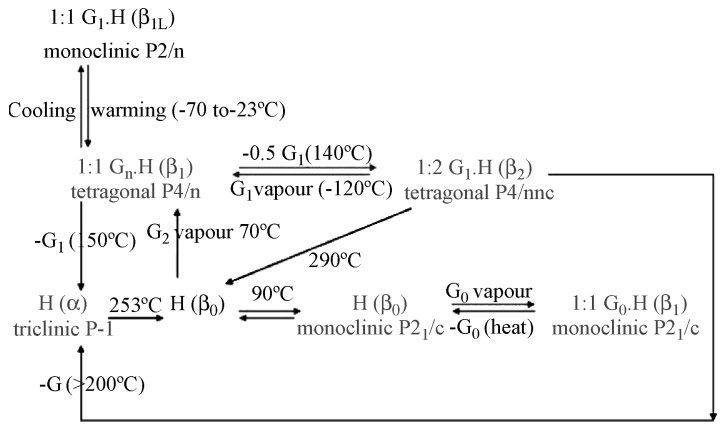


**Figure 7.33** Summary of the solid-state phase behaviour of of *p-t*-butylcalix[4]arene. The a-phase is the dense pure host with no lattice voids, the $b_0$ phase contains voids but they are unfilled by guests and the $\beta_1$ and $\beta_2$ phases are host guest complexes with guest:host ratios of 1:1 and 1:2, respectively (reproduced by permission of The Royal Society of Chemistry).

## 7.8.2 Fullerene Complexation

Makha, M., Purich, A., Raston, C. L. and Sobolev, A. N., 'Structural diversity of host-guest and intercalation complexes of fullerene $C_{60}$', *Eur. J. Inorg. Chem.* 2006, 507–517.

The 1985 discovery of the fullerenes – closed three-dimensional molecules made up solely from carbon – represents one of the most striking and appealing discoveries in chemistry in recent years and earned the 1996 Nobel Prize in chemistry for Robert F. Curl, Jr and Richard E. Smalley from Rice University, Houston, USA, and Harold W. Kroto from the University of Sussex, UK, for their work in this area (Box 7.1). Fullerenes, especially buckminsterfullerene ($C_{60}$, 'buckyball') and $C_{70}$, have proved enormously popular throughout many areas of chemistry, not least in supramolecular chemistry. Fullerenes have made appearances as both hosts and guests. As hosts, they exhibit intercalation behaviour somewhat analogous to graphite, and can also include species such as helium and metals within their closed cavity (Section 15.8). As guests, they represent a large, electron-deficient template capable of forming a variety of charge transfer compounds with electron donors such as ferrocene and TTF derivatives as well as van der Waals inclusion compounds, particularly in the solid state. We have already seen the ability of $C_{60}$ to form inclusion compounds with the electron-rich, saucer-shaped macrocycle CTV (Section 7.7.3) and with hydroquinone (Section 7.5). Fullerenes in general form inclusion compounds with aromatic macrocycles, and larger calixarenes such as *p-t*-butylcalix[8]arene and *p-t*-butylcalix[6]arene may be used in the purification of fullerenes $C_{60}$ and $C_{70}$ from the complex soot mixture formed by carbon arc vaporisation of graphite. The key to the procedure lies in the ability of the larger calixarenes to selectively complex fullerenes in toluene solution, resulting in crystallisation of the well defined 1:1 complex *p-t*-butylcalix[8]arene · $C_{60}$ and the 1:2 complexes *p-t*-butylcalix[6]arene · $(C_{60})_2$ and *p-t*-butylcalix[6]arene · $(C_{70})_2$.[44] Treatment of these solid inclusion complexes with chloroform decomposes the products to give precipitates of the purified fullerenes and chloroform solvated calixarenes, stabilised by C—H $\cdots\pi$ interactions, which are strengthened by the high acidity of the chloroform C— H group (Figure 7.34). The solid-state structure of the fullerene–calixarene complexes shows the encapsulation of the fullerenes by the electron-rich hosts (Figure 7.35). This work has sparked research into a wide variety of fullerene host–guest complexes, and a number of X-ray structures are now known of fullerene complexes with various calixarenes, hexahomooxacalix[3]arene (1:1) (**7.57**), tryptycene (1:2) (**7.58**), octaphenylcyclotetrasiloxane (1:1) (**7.59**) and porphyrins *etc.* Perhaps one of the most striking is the enormous eight molecule asymmetric unit in the ternary co-crystal $(\text{calix[5]arene})_4 \cdot (C_{60})_5 \cdot (\text{toluene})_2$ which contains both ball-and-socket $C_{60}$ molecules included into the calix[5]arene cavity and a double calixarene-sandwiched $C_{60}$ molecule, Figure 7.35b.[45] Discrete 1:1

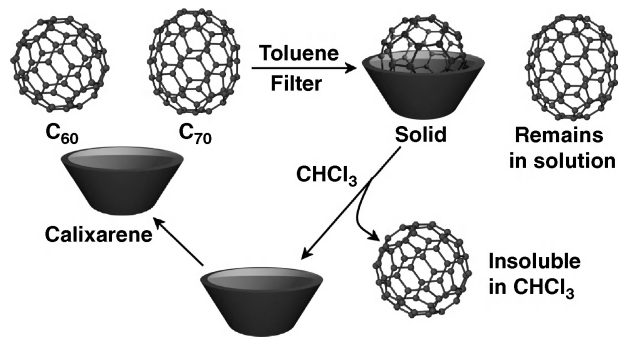


**Figure 7.34** *p-t*-Butylcalix[8]arene-based purification of a mixture and $C_{60}$ and $C_{70}$.[44]

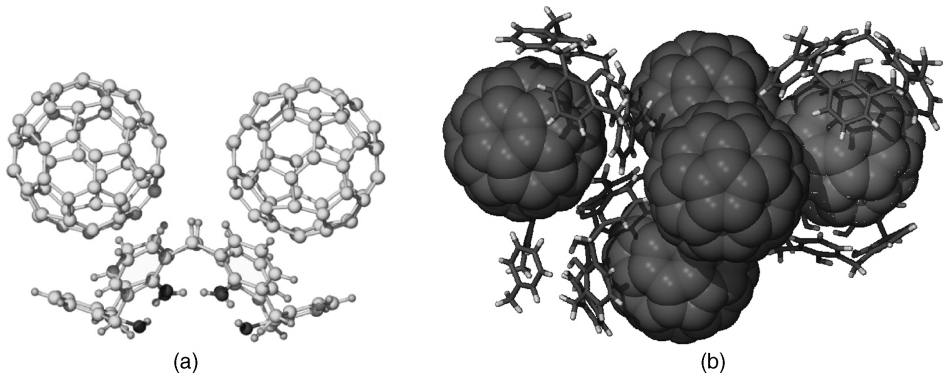


**Figure 7.35** X-ray crystal structures of (a) calix[6]arene$(C_{60})_2$[47] and (b) the symmetry-unique portion of the unit cell in $(\text{calix[5]arene})_4 \cdot (C_{60})_5 \cdot (\text{toluene})_2 - C_{60}$ shown in spacefilling mode.[45]

and 2:1 complexes with γ-cyclodextin have also been reported,[46] and the large cyclodextrin may be used to solubilise both $C_{60}$ and $C_{70}$ in water. Concentrations are only of the order of $10^{-4}$ M, giving a slight yellow colour to the solution, in contrast to the deep reds and purples of fullerenes in aromatic solvents such as benzene and toluene. Modelling suggests that the five-fold axis of the fullerenes is orientated parallel to the pseudo-eight-fold axis of the cyclodextrin.

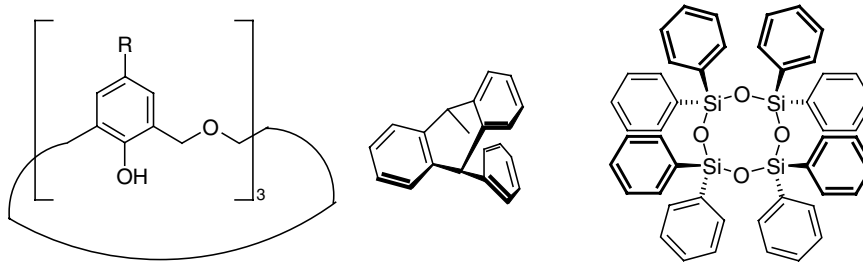


hexahomooxacalix[3]arene **7.57** tryptycene **7.58** octaphenyldisiloxane **7.59**

**Box 7.1** Discovery of the Fullerenes

Kroto, H. W. '$C_{60}$: Buckminster Fullerene, the celestial sphere that fell to earth', *Angew. Chem. Int. Ed. Engl.*, 1992, **31**, 111–129.

Before 1985, six crystalline forms of carbon were known: two forms of graphite, two forms of diamond, and chaoit and carbon (VI) discovered in 1968 and 1972, respectively. In addition a number of almost pure amorphous forms exist, such as polyacetylene (**7.60**) and cumulene (**7.61**) and recently a number of interesting nanostructured forms of carbon have been produced (Section 15.8). The year 1985 marked the discovery of the fullerenes, which represent the only truly pure molecular form of carbon, are produced under very extreme conditions as carbon vapour condenses in an atmosphere of an inert gas such as helium. Harold Kroto's interest in this chemistry originated with microwave spectroscopic studies of the atmosphere of stars and interstellar dust clouds. Kroto wanted to try to reproduce in the laboratory spectra of carbon

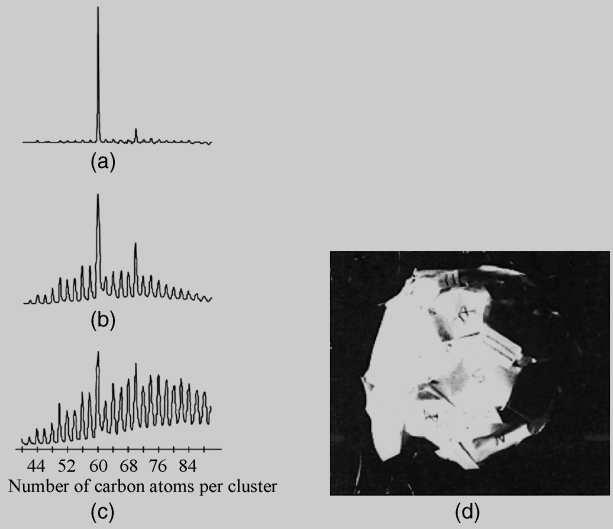


**Figure 7.36** (a–c) Mass spectra of fullerene mixtures produced by vaporisation of graphite. The size distribution is affected dramatically by increasing the amount of 'chemical boiling', allowing equilibration to the thermodynamic minimum energy structure, $C_{60}$. (d) First model of $C_{60}$ produced by Smalley from paper hexagons and pentagons (Copyright Wiley-VCH Verlag GmbH & Co. KGaA. Reproduced by permission).

nitrogen compounds termed cyanopolyynes (**7.62**) he had detected in space in 1975–78. He contacted Richard Smalley, who had instrumentation for the vaporisation of metal atoms to study metal clusters by mass spectrometry, and together they applied the method to graphite. The resulting mass spectrum (Figure 7.36) proved very exciting since it showed a number of peaks identifiable with carbon clusters, but the peaks corresponding to $C_{60}$, and $C_{70}$ stood out amongst the rest, implying that these clusters were somehow of greater stability.

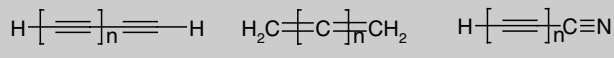


polyacetylene **7.60** cumulene **7.61** cyanopolyynes **7.62**

The researchers were initially at a loss to explain the special stability of the peak at mass/charge 720, corresponding to $C_{60}$ and it was only after the realisation that this might be a closed cluster that the team spent the evening trying to fit together hexagonal pieces of paper and joining jelly beans with toothpicks. A key factor, fortunately realised by the researchers from a model 'star-dome' owned by Kroto, was that pentagonal faces might also be needed. They were finally able to achieve the elegant, spherical 60-vertex solid (a truncated icosahedron), which is the structure of $C_{60}$, through the use of 12 pentagons and 20 hexagons (Figure 7.36d). The molecule has exactly the same structure as Kroto's stardome, as well as a European football, and the geodesic domes of the architect R. Buckminster Fuller. The new molecule was named buckminsterfullerene after him, and a paper was written immediately. The closely related $C_{70}$ is a cylindrical-shaped molecule with identical ends to $C_{60}$, but with an extra row of hexagons about the middle. In fact, 12 pentagons are needed to close any solid figure— hexagons alone cannot do it (a geometric fact known as Euler's Law).

The discovery of the fullerenes was received with a mixture of enthusiasm and hostility. The molecules existed only in the mass spectrometer and some researchers were dubious. Final proof came in 1990 with the isolation of macroscopic amounts of $C_{60}$. This allowed the $^{13}C$ NMR spectrum of the compound to be recorded. As predicted, it proved to be a single line (at $\delta$ 143 ppm) – all of the carbon atoms in $C_{60}$ are equivalent.

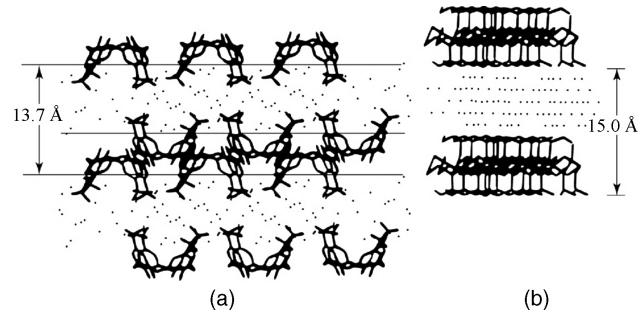


**Figure 7.37** Comparison of the X-ray crystal structure of (a) *p*-sulfonatocalix[4]arene with (b) the naturally occurring clay mineral sodium vermiculite. (Reproduced with permission from [49]).

## 7.8.3 Water-Soluble Calixarenes

Atwood, J. L., Barbour, L. J., Hardie, M. J. and Raston, C. L., 'Metal sulfonatocalix[4,5]arene complexes: bi-layers, capsules, spheres, tubular arrays and beyond', *Coord. Chem. Rev.* 2001, **222**, 3–32.

In Chapter 6 we briefly discussed the solution-phase inclusion properties of the water-soluble calixarene sulfonates. While the small cavity of calix[4]arene sulfonate and the flexibility of the larger calixarenes makes them relatively uninteresting hosts in solution, their solid state chemistry is rich and varied. Solid calix[n]arene sulfonates (**6.15a–c**, n = 4 –6) all form bilayer structures in which the hydrophobic calixarene portion alternates with hydrophilic layers comprising water molecules, $Na^+$ ions and the calixarene sulfonate functions. These structures closely resemble naturally occurring clay minerals (Figure 7.37, and see Section 9.3). In the solid state *p*-sulfonatocalix[4]arene (**6.15a**) complexes strongly to a water molecule that is embedded within the calixarene cavity. This structure provided the first solid-state evidence for O—H $\cdots\pi$ hydrogen bonds from water to aryl rings, a phenomenon thought to stabilise protein tertiary structure.[48] The intra-cavity water molecule donates both of its protons to hydrogen bonds to opposite faces of the calixarene cavity with O—H $\cdots$ $\pi$–centroid separations of 2.38 and 2.50 Å (Figure 7.38). *Ab initio* calculations on the interaction of water with benzene suggest a stabilising interaction energy of 14.2 kJ $mol^{-1}$.

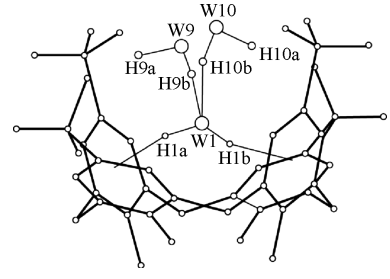


**Figure 7.38** Inclusion of water by water-soluble *p*-sulfonatocalix[4]arene (**6.15a**). (Reprinted by permission from Macmillan Publishers Ltd).

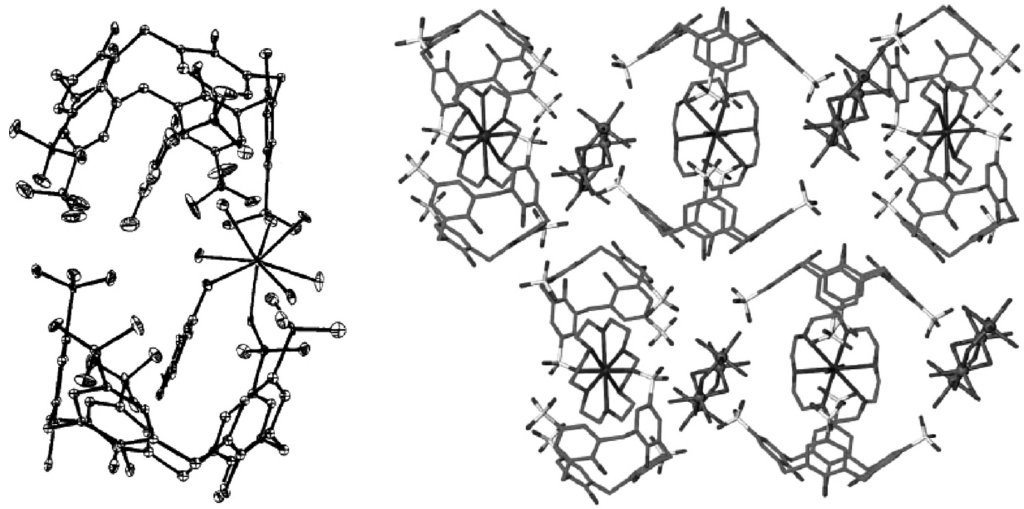

**Figure 7.39** X-ray crystal structure of (a) $Na[Eu(H_2O)_9]_2[Eu(pyridine\text{-}N\text{-}oxide)(H_2O)_5(calix[5]arene\text{-}p\text{-}sulfonato)_2]\cdot pyridine\text{-}N\text{-}oxide\cdot 17.5H_2O$[50] (b) $[Rh_4(\mu\text{-}OH)_6(H_2O)_{12}][X{+}2H_2O\cdot X\cdot 8H^+]\cdot 33H_2O$ where X = ($p$-sulfonatocalix[4]arene)$_2$(Na([18]crown-6)]$^{7-}$ (reprinted from the Section Key Reference with permission from Elsevier).

*p*-Sulfonatocalix[4 and 5]arenes have a particular rich chemistry as ligands for oxophilic metal centres, *e.g.* the *p*-sulfonatocalix[5]arene complex $Na[Eu(H_2O)_9]_2[Eu(pyridine\text{-}N\text{-}oxide)(H_2O)_5(calix[5]arene\text{-}p\text{-}sulfonato)_2]\cdot pyridine\text{-}N\text{-}oxide\cdot 17.5H_2O$ in which a $Eu^{3+}$ ion binds two calix[5]arenes together in a face to face arrangement. One europium-bound and one free pyridine-*N*-oxide ligand occupy the calixarene cavities (Figure 7.39a).[50] Calixarene sulfonates also form a huge range of complexes as second-sphere ligands for metal macrocycle compounds, *e.g.* forming 'superanion' complexes such as ($p$-sulfonatocalix[4]arene)$_2$(Na([18]crown-6)$(H_2O)_2]^{7-}$. An example is shown in Figure 7.39b. Hydrated structures of *p*-sulfonatocalix[8]arene have also been reported showing either pleated double cone or circular conformations.[51]

The presence of particular metal ligand combinations can induce the assembly of vast spherical and tubular structures as alternatives to the common bilayer packing. *p*-Sulfonatocalix[4]arene is able to form a vesicle-like structure with both an internal and external aqueous phase,[52] in which the hydrophilic upper-rim sulfonate groups point outwards, stabilised by interactions to metal cations. The recipe for this assembly, which produces a capsule with an internal volume of 1700 Å$^3$, involves a three-component system consisting of the pentasodium salt of the calixarene, a lanthanide metal ion nitrate such as $La(NO_3)_3\cdot 6H_2O$, and pyridine-*N*-oxide, which is added as a co-ligand for the oxophilic lanthanide cation. These capsule-forming components are added in the ratio 2:1:2. If the recipe is changed to a 2:1:8 ratio, however, an infinite, helical tubular assembly of comparable width is formed. These reactions are summarised in Scheme 7.5, and the structures of sphere and tube are shown in Figure 7.40 and Figure 7.41. The amazing metallocalixarene assembly shown in Figure 7.40 bears a resemblance to a Platonic solid (Section 10.6.3), the great rhombicubeoctahedron (rhombitruncated cubeoctahedron), although it is distorted from the regular geometry.

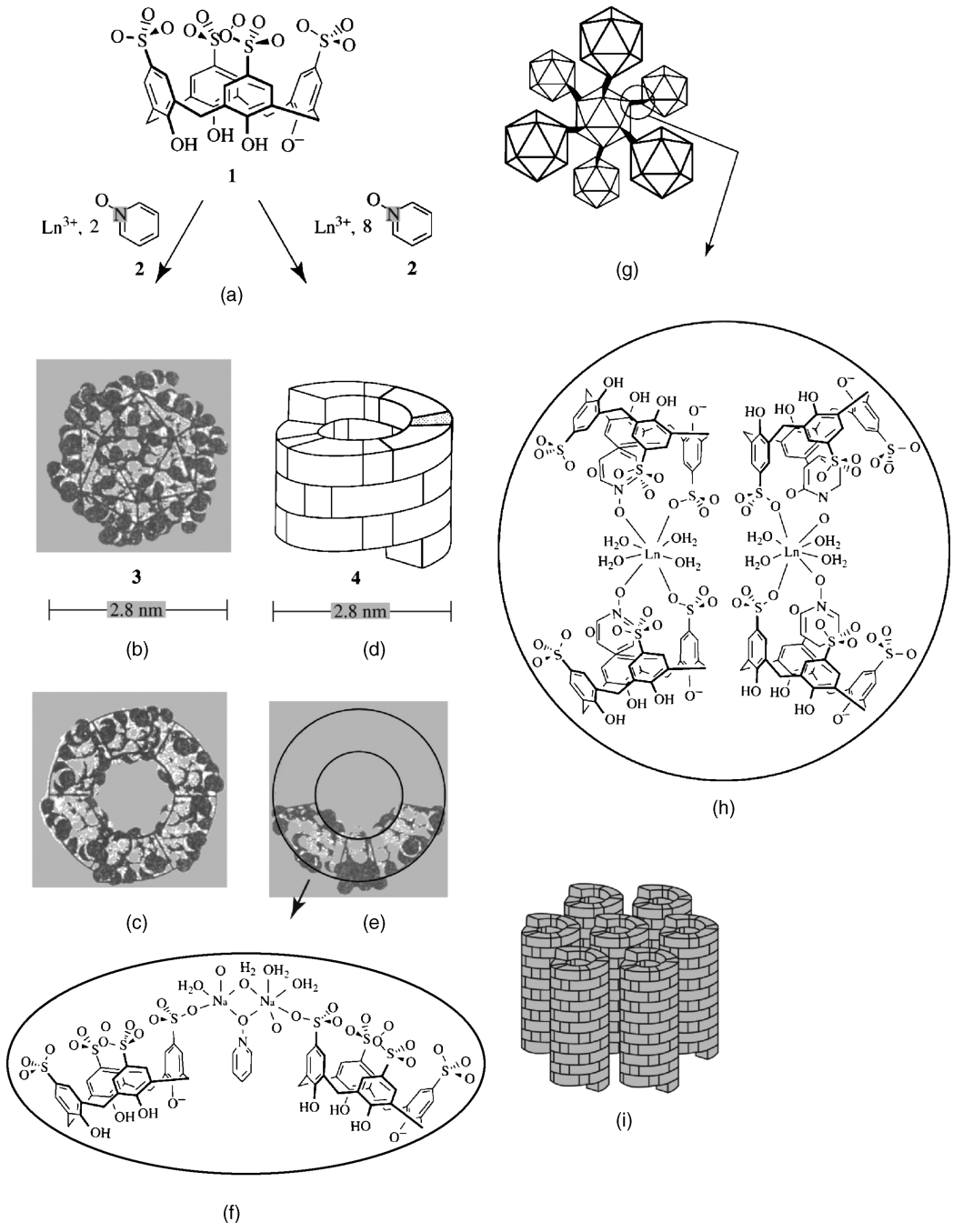


**Scheme 7.5** Schematic representation of the organisation of the *p*-sulfonatocalix[4]arene spherical (**a–c**) and tubular (**d–f**) assemblies. Formation of higher aggregates by intersphere and intertube association are shown in (**g–i**). (Reproduced with permission from Reference 52).

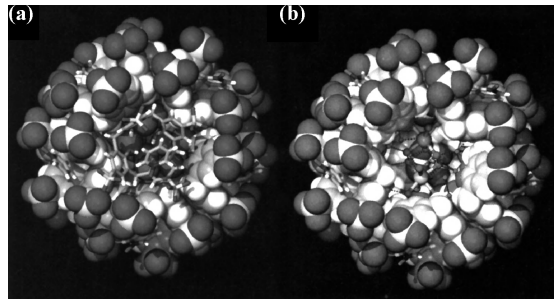


**Figure 7.40** Structure of the spherical lanthanide *p*-sulfonatocalix[4]arene assembly (a) partial space-filling view along the *pseudo*-fivefold axis. Pyridine-*N*-oxide and one calixarene are shown in stick mode. $SO_3$ groups line the surface of the sphere, aryl rings define the hydrophobic shell and the polar core comprises 30 water molecules and two $Na^+$ ions. (b) cut away view showing an $[Na(H_2O)_6]_2$ cluster within the core. (Reprinted with permission from AAAS from [52]).

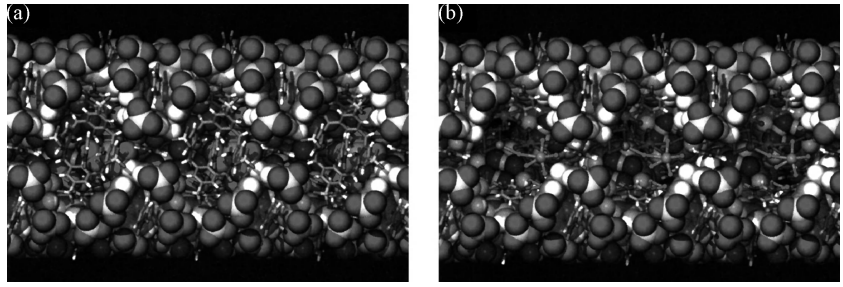


**Figure 7.41** Structure of the tubular lanthanide *p*-sulfonatocalix[4]arene assembly (a) partial space-filling view perpendicular to the tube showing six turns of the helix. *p*-Sulfonatocalix[4]arene anions shown in stick mode mark two helix turns. Helix turns involve π-stacking between calixarenes and pyridine-*N*-oxide guests (also shown as sticks). (b) cutaway view showing hydrated $Na^+$ and $La^{3+}$ ions within the cylindrical channel. (Reprinted with permission from AAAS from [52]).

## 7.9 Solid-Gas and Solid-Liquid Reactions in Molecular Crystals

Dalgarno, S. J., Thallapally, P. K., Barbour, L. J. and Atwood, J. L., 'Engineering void space in organic van der Waals crystals: calixarenes lead the way', *Chem. Soc. Rev.* 2007, **36**, 236–245.

### 7.9.1 The Importance of Gas Sorption

Gas diffusion into solids is of tremendous technological interest. Solid materials able to selectively absorb particular gases could be used to effect important separations such as the separation of hydrogen and $CO_2$ from mixtures formed in the industrially important transition metal catalysed water-gas shift reaction, Equation 7.1. Along with the high temperature steam reforming of methane (Equation 7.2), this process is a main source of hydrogen production. While carbon dioxide is a low energy, relatively useless byproduct, CO and particularly hydrogen are valuable industrial feedstocks. Hydrogen is of particular and increasing potential importance in 'green' hydrogen fuel cell powered vehicles since

the only byproduct of its combustion is water. We have already mentioned briefly the use of clathrate hydrates in hydrogen storage. The US Department of Energy has set a minimum target for a hydrogen storage material to be able to store 6 % by weight of hydrogen by 2010, increasing to as much as 9 % by weight in the next decade. This is an ambitions target because of the very low molecular mass of hydrogen meaning that many moles of the gas are needed per mole of host material – the target rules out conventional metal gas cylinders, for example. A number of candidate materials are being explored with this application in mind including ammonia storage, amine borane complexes, metal hydrides, carbon nanotubes, metal-organic frameworks, polymers, glass microspheres, imidazolium ionic liquids, phosphonium borate and clathrate-forming materials. Of particular interest to supramolecular chemists are metal organic frameworks which we will encounter in the next chapter, and clathrates. We will also explore carbon nanotubes briefly in Chapter 15.

$$CO + H_2O \rightleftharpoons^{\text{cat.}} CO_2 + H_2 \tag{7.1}$$

$$CH_4 + H_2O \underset{>700°C}{\overset{\text{Ni cat.}}{\rightleftharpoons}} CO + 3H_2 \tag{7.2}$$

In addition to the intrinsic importance of gases for energy and environmental reasons, gas sorption studies are used to study and characterise the materials properties of porous materials and provide evidence for the existence of permanent voids or channels. (Sorption is the the taking up and holding of one substance by another. Sorption includes the processes of chemical absorption and physical adsorption). Porous materials are classified on the basis of their pore sizes as being either:

- microporous – channel diameter $< 2$ nm,
- mesoporous – channel diameter between 2 nm and 50 nm or,
- macroporous – diameter more than 50 nm.

The plot of the amount of gas absorbed *versus* pressure is termed the gas sorption isotherm. Pressure ($P$) is usually given as a fraction $P/P_0$ where $P$ is the gas partial pressure and $P_0$ is the saturation pressure of the gas. Typically, adsorption isotherms are measured using nitrogen or $CO_2$ in cases when a long time is needed for nitrogen saturation, and are grouped into types I – VI, Figure 7.42.[53] The kinds of microporous host materials we have discussed so far in this chapter are characterised by a type I isotherm involving rapid uptake at low values of $P/P_0$ ($< 0.1$) with little or no hysteresis upon desorption. Analysis of the gas sorption isotherm by the Brunauer-Emmett-Teller (BET) method allows calculation of available surface area (in $cm^2$ per gram of material) and accessible cavity volume.[53]

As well as surface area and pore size measurements, gas sorption can be used as a probe. Particularly absorption of xenon allows the examination of the pore structure by $^{129}Xe$ solid-state NMR spectroscopy. The chemical shift of the xenon nuclei is sensitive to their location within the cavity or pore and so xenon absorbed onto the pore walls will have a different chemical shift to subsequent layers of xenon atoms situated near the centre of the pore. A recent development is double quantum filtering which makes it possible to distinguish xenon atoms close to other xenon (as in a doubly occupied cavity) from adsorption at different sites in a singly occupied cavity. For example, Dianin's compound is able to include two Xe atom per cavity. Crystallisation of Dianin's compound from mesitylene (a molecule too large to fit the cavity) in the presence of one atmosphere of $^{129}Xe$ gives a material displaying two peaks in the magic angle spinning $^{129}Xe$ NMR spectrum at $\delta$ 134 and 154 ppm. If the experiment is repeated under 3 atmospheres of xenon then only the peak at 154 ppm remains. In the spectrum of the material obtained at one atmosphere, the double quantum filtering experiment eliminates the signal at 134 ppm which is due to cavities containing only a single xenon atom and confirms that the signal at 154 ppm can be assigned to a doubly occupied cavity, Figure 7.43.[54]

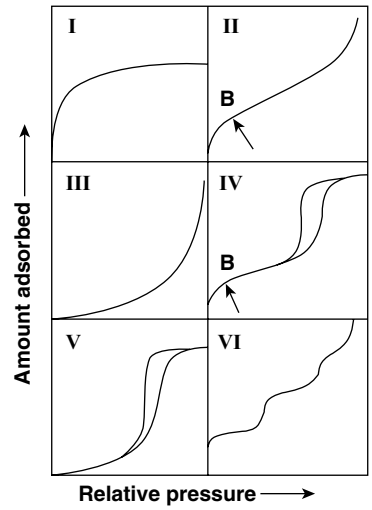


**Figure 7.42** Types of gas sorption isotherm – microporous solids are characterised by a type I isotherm. Type II corresponds to macroporous materials with point 'B' being the point at which monolayer coverage is complete. Type III is similar to type II but with adsorbate-adsorbate interactions playing an important role. Type IV corresponds to mesoporous industrial materials with the hysteresis arising from capillary condensation. The limiting adsorption at high $P/P_0$ is a characteristic feature. Type V is uncommon. It is related to type III with weak adsorbent-adsorbate interactions. Type VI represents multilayer adsorption onto a uniform, non-porous surface with each step size representing the layer capacity (reproduced by permission of IUPAC).

## 7.9.2 Gas Sorption by Calixarenes

So how can solid-state clathrates absorb gases? While the time- and space-averaged structure of solid-state inclusion compounds observed by X-ray crystallography may appear highly ordered and static, we saw in Section 7.8.1 that in fact the solid state is a mobile, dynamic phase capable of significant guest diffusion, including diffusion of gases such as xenon into the cavity-containing *p-t*-butylcalix[4]arene $\beta_0$ phase. What is surprising about this process is that, unlike metal-organic frameworks, there are no

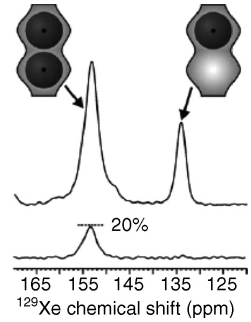


**Figure 7.43** (top) $^{129}$Xe CP-MAS NMR solid-state spectra for a the xenon clathrate of Dianin's compound obtained at 1 atmosphere pressure; (bottom) the DQ filtered spectrum showing only the resonance due to the doubly occupied cavity. (Reproduced by permission of The Royal Society of Chemistry).

obvious continuous holes or channels even in materials such as the calixarene $\beta_0$ phase – its xenon and $CO_2$ complexes are cage-type clathrates. So, while it is easy to imagine a guest occupying the cavity it is hard to explain why guest ingress is so facile. The answer to this problem is poorly understood but must in some way relate to the opening up of transient apertures in the host structure as a consequence of either guest-induced or intrinsic thermal motion, allowing the guest to 'hop' from site to site from regions of high guest concentration to regions of low guest concentration.

Diffusion into crystals can be demonstrated by treatment of the empty *p-t*-butylcalix[4]arene $\beta_0$ apohost (grown by sublimation) with liquid vinyl bromide ($CH_2$=CHBr). The solid calixarene is insoluble in vinyl bromide but it is known that if the calixarene is crystallised from solution with guests like vinyl bromide it forms a 1:1 host guest complex. Interestingly this same kind of host-guest compound also forms in a single-crystal-to-single-crystal phase transition over a period of about fifteen minutes when the solid, guest free calixarene is immersed without dissolution in the liquid vinyl bromide. A crystal used for determining the apohost structure can be placed back on a diffractometer and gives the X-ray crystal structure of the 1:1 calixarene vinyl bromide host-guest complex. In X-ray crystallographic terms the electron-rich bromine atom of the guest is very easy to resolve in the presence of only carbon, hydrogen and oxygen. X-rays interact with electrons (Box 2.1) and so vinyl bromide with its hefty bromine is a very easy guest to follow. While diffusion into crystals is well known in proteins (the method of isomorphous replacement involves soaking protein crystals in solutions containing heavy metal ions – the metals diffuse into the protein crystal and help crystallographers to solve the crystal structure of the original metal-free protein) proteins aren't close packed solids. Crystalline bio-molecules are generally awash with large water-filled channels which the metal ions can easily diffuse into. In contrast, diffusion of a largish molecule like vinyl bromide through a, non-porous, close-packed solid *without disrupting the regular crystalline structure* is difficult to imagine, particularly since the guest binding only involves van der Waals forces. If this kind of non-porous solid-state diffusion can happen with calixarenes the implication is that it can happen with very many other materials. The proposed mechanism for this phenomenon involves 'a highly synchronised process whereby neighboring host molecules at the advancing phase boundary cooperate with one another, not only to relay the guest through the lattice, but also to maintain continuity of the material such that the crystal does not fracture'.[55]

The structure of the host crystal before and after treatment with vinyl bromide is shown in Figure 7.44 and Hybrid crystals can be isolated by stopping the process part-way. Guest absorption by the calixarene was also monitored by DSC which showed surprisingly that the process is *endothermic*, and hence

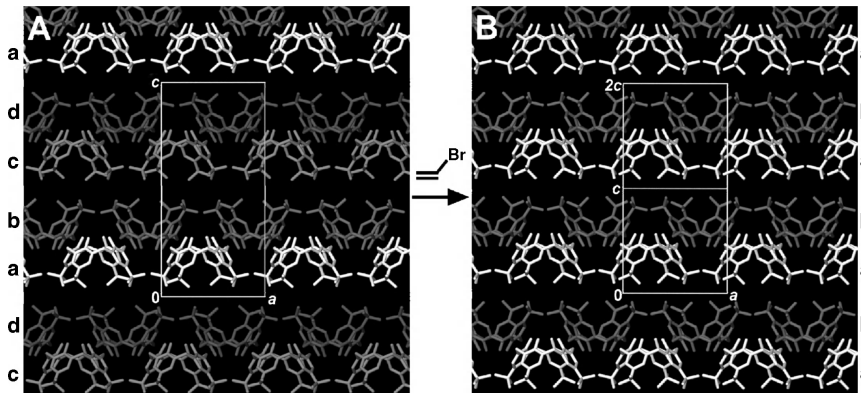


**Figure 7.44** X-ray crystal structure of the host portion of *p-t*-butylcalix[4]arene (A) guest-free crystal showing a, b, c, d… repeating layers and (B) after exposure to vinyl bromide showing an a, b, a, b… repeat pattern arising from a shift of *ca.* 6Å between layers b and c (reprinted with permission from AAAS from [55]).

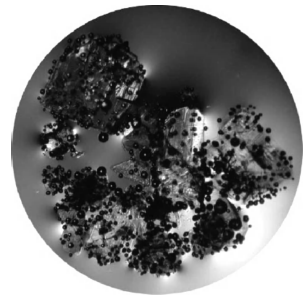

**Figure 7.45** Immersing sublimed crystals of the apparently guest-free $\beta_0$ phase of *p-t*-butylcalix[4]arene results in the immediate displacement of bubbles of air from the crystal lattice as the air molecules are replaced by nitrobenzene guest (reproduced by permission of The Society of Chemistry).

entropy driven. This is a surprising observation since the filling of empty cavities should be an enthalpically favourable process. However, the observation is explained by visual observation of the crystals during the absorption of the liquid guest – immersing the sublimed crystal into liquid nitrobenzene, a guest readily bound like vinyl bromide, results in the immediate formation of large bubbles of gas at the crystal surface (escaping air), Figure 7.45. So, as soon as the sublimed crystal is removed from vacuum it rapidly absorbs gases in the form of air. This observation suggests that empty organic hosts might be very suitable candidates for gas sorption materials and as we will see this indeed proves to be the case.

Gas sorption by solids can be measured either volumetrically by recording the drop in pressure when the solid is exposed to a fixed volume of gas at a known pressure, or gravimetrically by measuring the mass increase of the sample as the gas enters the host cavities. Commercial gas sorption apparatus exists that can carry out the latter measurements precisely on relatively little material at controlled pressure and over a range of temperatures, allowing the extraction of both kinetic and thermodynamic parameters. Volumetric measurements on *p-t*-butylcalix[4]arene indicate that the apohost material absorbs $O_2$ and $N_2$ to some extent, with $O_2$ being favoured. Hydrogen is only absorbed at high pressure but $CO_2$ is absorbed extremely effectively. At one atmosphere pressure $CO_2$ occupancy is 80 %, rising to 100 % at the relatively low pressure of three atmospheres Thus the material is able to readily purify a $H_2$ / $CO_2$ mixture. Acetylene is absorbed even more effectively than $CO_2$ with complete filling of the cavities even at one atmosphere pressure. The compound also proves to be more effective at methane absorption at room temperature than other modern materials such as metal organic frameworks and single-walled carbon nanotunes.[56]

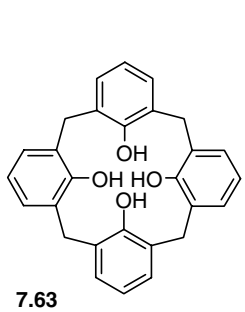


**7.63**

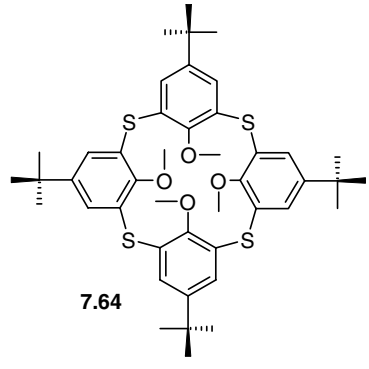


**7.64**

Related behaviour is exhibited by the dealkylated analogue, calix[4]arene (**7.63**). This material can also be sublimed to give a guest-free host but in this case the empty host forms an unusual trimer motif which is almost spherical and packs in a hexagonal close packed array with just a small interstitial void

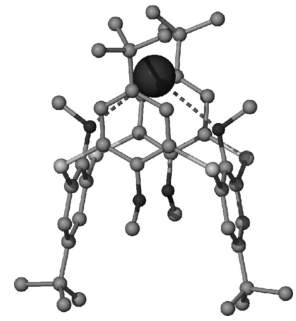

**Figure 7.46** Binding of a single water molecule to **7.64** prevents occupation of the second binding site by acting as a brace (H atoms omitted, water molecule shown as a large sphere).[57]

space of 153 $Å^3$ (i.e. in between groups of trimers and outside any molecular cavity). The interstitial cavity is just large enough to house small tetrahedral molecular such as methane or volatile freons such as $CF_3Br$. Gas incorporation can be achieved by heating the 3:1 acetone solvate of the host under pressure with the gas, causing rearrangement from the solvate structure to the trigonal motif with stoichiometric gas incorporation. Unlike the gases in *p-t*-butylcalix[4]arene, the interstitial gases in **7.63** are extremely difficult to remove with the methane clathrate not decomposing until some 320 °C above the normal boiling point of methane.

Other aspects of small molecule diffusion in crystals have been explored using the thiacalixarene **7.64**. The calixarene adopts a 1,3-alternate conformation and is essentially box-like in shape. Sublimation of the compounds gives a guest-free $\beta_0$ phase with small voids in between pairs of oxygen atoms just large enough to accommodate a water molecule. Immersing the sublimed crystals in water indeed results in the incorporation of water guest in the lattice. The water sits in between pairs of aryl rings hydrogen bonding to the two ether oxygen atoms, Figure 7.46. Interestingly, while each host has two essentially equivalent water binding sites, only one of them is ever occupied to give a stoichiometric 1:1 inclusion compound. It appears that ingress of the water into the host cleft requires one face to open out, consequently pinching the other face together. Once one water molecule has bound, it effectively acts as a brace, preventing the ingress of a second one. What is remarkable about the diffusion of water into this compound at all, however, is that there are no channels linking the water binding cavities together and the vast majority of the crystal is highly hydrophobic (it is insoluble in water of course). This experiment provides further evidence for the ability of small guests to 'hop' or diffuse through apparently non-porous organic crystals.[57]

## 7.9.3 Gas Sorption by Channel Hosts

In contrast to the intuitively surprising gas sorption by the apparently non-porous calixarenes, gas diffusion into channel-containing hosts is predictable and does indeed occur. A good example is the trigonal tris(*o*-phenylenedioxy)cyclotriphosphazene (**7.65**) which forms a hexagonal array of microporous channels about 5 Å in diameter. Unlike urea channels, upon removal of solvent such as benzene, the porous host phase is stable in the absence of guests up to 150 °C forming an apohost or $\beta_0$ phase, as in the calixarene compounds discussed in the last section, with *ca.* 25 % void space. This robustness has led to the description of this material as being one of the first *organic zeolites*, by analogy with the robust, porous aluminosilicate zeolites (Chapter 9). For gas sorption studies one of the best guests to start with is iodine. Iodine is a solid at room temperature bu readily sublimes under ambient conditions.

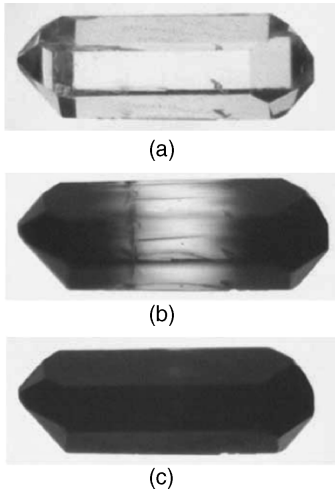


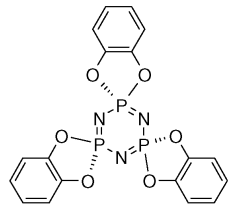


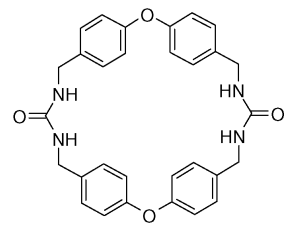


**Figure 7.47** Inclusion of iodine vapour into the THF inclusion compound of **7.65**. (a) initial state, ($b_0$ early stage with only the ends of he crystal stained by iodine and (c) final state with channels fully occupied. The inclusion of iodine from both ends implies counter-diffusion of thf and $I_2$. (Copyright Wiley-VCH Verlag GmbH & Co. Reproduced by permission).

Its relatively small size means that it can penetrate most porous materials and its intense purple colour gives an immediate visual indication of inclusion. Iodine vapour inclusion into a single crystal of **7.65** upon exposure of the tetrahydrofuran (THF) inclusion compound of the host to iodine vapour is readily apparent from the darkening of the ends of the crystal as the iodine enters, Figure 7.47.[58] The fact the darkening occurs from both ends simultaneously implies a counter-diffusion mechanism in which THF diffuses out past the incoming $I_2$ within the same channel. The resulting iodine inclusion compound has interesting properties as an electrical conductor with conductivity along the iodine chains being a factor of up to 30 greater than perpendicular to them. Crystals of **7.65** have also been used to store both methane and carbon dioxide with up to 60 % and 100 % occupation of the channels, respectively. For methane the storage capacity is 2.4 weight % at 195 K, dropping to 0.6 weight % at ambient temperature and pressure.[59] This kind of reduced sorption at high temperature is characteristic of most gas sorption materials and corresponds to a greater thermal energy of the guests compared to the interaction energy with the host. Nevertheless this figure is comparable to zeolites and an improvement over some materials that require high pressures to reach saturation.

A designed channel clathrate capable of gas sorption has been prepared based on the urea macrocycle **7.66**. The macrocycles stack up in a tube with their cavities aligned, initially filled with acetic acid hydrogen-bonded dimers. The acetic acid can be removed to give an apohost and re-adsorbed from the vapour phase re-forming the original host-guest compound. The compound also adsorbs $CO_2$ and the $CO_2$ sorption isotherm confirms type I microporous behaviour (Section 7.9.1). BET analysis gives a surface area of 316 $m^2\ g^{-1}$ at 0 °C, comparable to microporous zeolites, and a total pore volume of 0.059 $cm^3\ g^{-1}$ for pores less than 6.5 Å.[60]

## 7.9.4 Gas Sorption by Coordination Complex Hosts

Work by Leonard Barbour at Stellenbosch University, South Africa, has resulted in a coordination compound-based macrocyclic host (**7.67**) with a continuous channel conceptually analogous to **7.66**

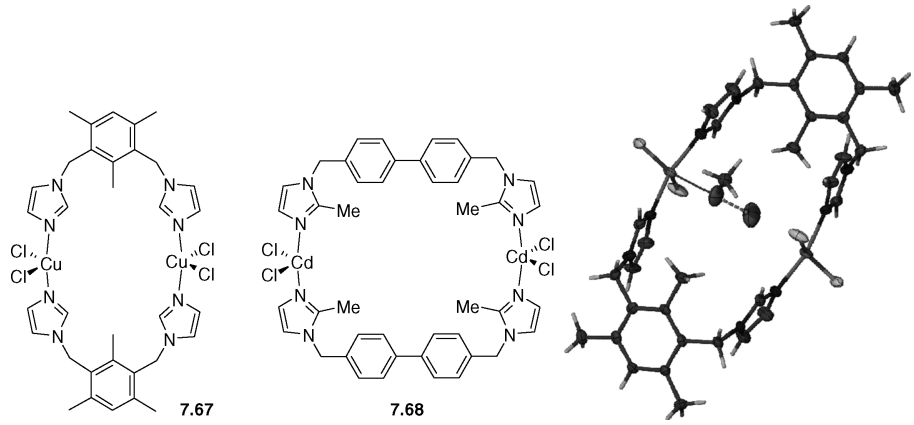


**Figure 7.48** Structures of imidazole-derived metallomacrocycles and crystal structure of the water/methanol inclusion complex of **7.67**.[61]

has been prepared from a bis imidazole ligand. The as-synthesised material includes water and methanol in the metallomacrocyclic cavity, however this solvent can be removed under relatively mild conditions *via* a single-crystal-to-single-crystal transformation, to give an empty apohost of essentially identical structure with discrete unoccupied voids of 108 $Å^3$ but no channel allowing access to them. However, despite the apparent absence of pores, the material is permeable to a wide range of gases including $H_2$, $O_2$, $N_2$, CO, $CH_4$, $CO_2$ and $I_2$.[61]

Barbour's group have designed a system allowing them to obtain X-ray crystallographic data under moderate pressures of gas (up to at least 80 atm). This apparatus has allowed them to structurally characterise the $CO_2$ inclusion complex of **7.67** and, remarkably to correlate the ingress of $CO_2$ into the structure modelled by molecular dynamics calculations, with the intrinsic thermal motion of the crystal as evidenced by the thermal ellipsoids modelled in the crystallographic experiment (Figure 7.48). Those atoms that experimentally have the largest anisotropic thermal motion in the crystal structure are also those that are calculated to move the most to open up a transient channel to allow guest ingress.

Barbour's group have gone on to prepare an expanded metallomacrocycle (**7.68**) and monitor its uptake of acetylene (HC≡CH) in a similar way to $CO_2$ uptake by **7.67**. Once again the guest-free material may be obtained and volumetric acetylene uptake experiments indicate that at one atmosphere pressure each cavity is occupied by a single acetylene molecule. Increasing the pressure to *ca.* 8 atmospheres gives double occupancy with two acetylene molecules per cavity. X-ray crystal structures have been obtained for the empty, singly and doubly occupied host-guest compounds, Figure 7.49. In the single occupied compound the H-bond acid acetylene interacts with one of the chloride ligands, forming a linear CH···Cl hydrogen bond on one side of the cavity. However, significant re-orientation is needed to accommodate the second acetylene molecule and the CH···Cl interactions become more bent.

The ability of coordination compounds to bind to ligands through specific metal-ligand interactions, however, means that gas sorption can also occur in apparently non-porous compounds that do not contain empty cavities. An example has been reported in which a sulfur dioxide guest undergoes a single-crystal-to-single-crystal gas-solid reaction with a square planar platinum-containing coordination compound (**7.69**) to give the square pyramidal adduct **7.70** (Scheme 7.6).[62] When the colourless organoplatinum crystals are subjected to sulfur dioxide for a minute or so, a beautiful orange colour develops, spreading from the outside of the crystal inwards as the square planes of the platinum molecules transform to the square pyramids of the $SO_2$ adduct. Even though the total volume of the crystal unit cell increases by *ca.* 25% during the whole process, the crystal remains perfectly

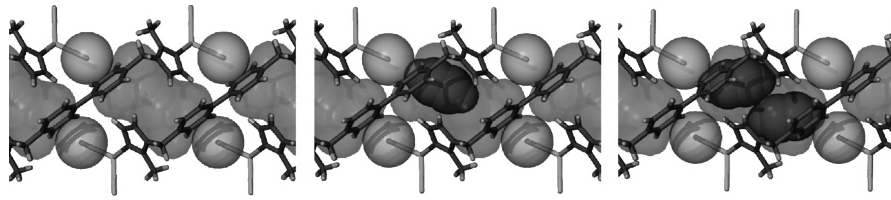


**Figure 7.49** X-ray crystal structures of **7.68** (a) apohost, (b) 1:1 inclusion compound with acetylene (1 bar) and (c) 1:2 acetylene complex (8 bar). The cavity volume is shown as a van der Waals survace – note that each cavity is discrete. Chloride ligands are shown as spheres and the acetylene molecules are shown in space-filling mode (pictures courtesy of Prof. L. J. Barbour, Stellenbosch University). See plate section for colour version of this image.

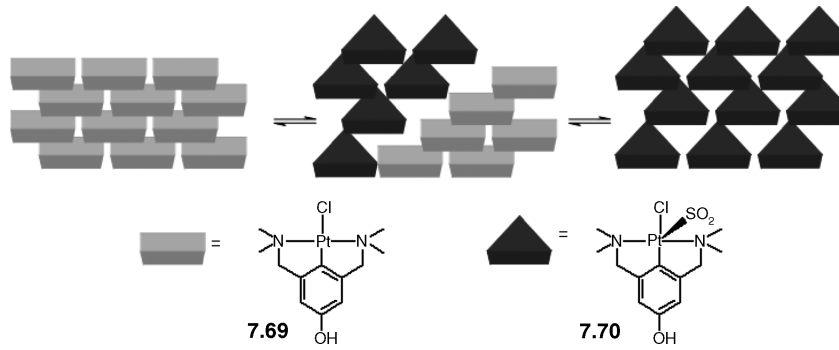


**Scheme 7.6** Single-crystal-to-single-crystal transformation of **7.69** to **7.70** by absorption of gaseous $SO_2$.[62]

three-dimensionally ordered, with one organoplatinum molecule patiently waiting for its $SO_2$ partner while its neighbours expand, pushing the entire structure outwards. If the swelled crystal is exposed to an inert gas then the $SO_2$ desorbs, with the crystal relaxing back down to its former colourless, $SO_2$ free state. The process may be cycled several times without loss of crystallinity. This kind of gas-sensitive material might form the basis for a crystalline optical switch because of the colour changes between the 'off' ($SO_2$ free) and 'on' ($SO_2$ present) states or by virtue of the size changes. Such switches would have applications in gas sensing, for example. The question of course arises as to why these crystals reversibly absorb a gas when so many others crumble or simply do not react as solids? The answer is not yet clear but must reside in the interactions between one organoplatinum molecule and the next. The crystalline framework is held together by a linear string of hydrogen bonds able to tolerate a considerable degree of deformation. Moreover the flat organoplatinum molecule may be able to tilt to accommodate the stress associated with the $SO_2$-induced expansion.

## Summary

- Solid state host-guest compounds or clathrates are examples of co-crystals where the host packs in such a way as to leave a gap in the crystal lattice suitable for inclusion of the guest.

- Clathrates are the original host-guest compounds with chlorine clathrate hydrate – a compounds in which a water hydrogen bonded network hosts a molecule of $Cl_2$ – being known since 1810.
- Common hosts such as urea or *p-t*-butylcalix[4]arene can exist as various crystal phases, some if which do not contain cavities. The crystal form of the pure host without cavities is called the $\alpha$–phase. The $\beta_0$ (apohost) phase contains unfilled cavities while the $\beta_{1\text{-}n}$–phases have the same host structure but contain different guests. Such structures are sometimes referred to as *pseudopolymorphs*. Further pure phases ($\gamma$–phase) or clathrates ($\gamma_{1\text{-}n}$–phases) may also exist in some cases, as in tri-*o*-thymotide. Apohosts are usually relatively unstable but allow the inclusion of interesting guests such as gases.
- Clathrates are useful for the control of the stereo- and regiospecificity of intra-cavity chemical reactions and can be used to engineer materials properties such as a polarity leading to non-linear optical materials, and ferroelastic or ferroelectric behaviour.
- Hydroquinone and phenol based clathrates including Dianin's compound are based upon cages made up of 6-membered hydrogen bonded rings of hydroquinone and are subject to considerable synthetic variation.
- The $\alpha$- and $\beta$-phases of CTV both contain guests but the guests do not reside in the saucer-shaped cavity. More recent reports of a $\gamma$-phase and exotic inclusion compounds with $C_{60}$ and carboranes as well as network structure show that they CTV cavity does include guests, however.
- There has been a great deal of detailed recent work on calix[4]arene type inclusion compounds showing phenomena such as diffusion of gases and liquids through the apparently non-porous structures and even diffusion of water through a close-packed hydrophobic crystal. Some of these transformations involve considerable movements of the host packing arrangement but can still proceed as single-crystal-to-single crystal transformations.
- A particular topical area in inclusion chemistry gas gas soption and separation. Gases of interest include $H_2$ (for application in fuel cells), methane and $CO_2$. Recent developments in crystallography allow crystal structures to be obtained routinely under significant gas pressure.

## Study Problems

7.1 Assuming the $5^{12}$ cavities in structure I clathrate hydrates to be approximately spherical (radius 3.91 Å), calculate the occupancy factor and notional pressure for a methane molecule included in such a cavity. How does this compare with a $5^{12}6^2$ cavity (radius 4.33 Å)? Which cavity do you think methane is most likely to occupy?

7.2 Calculate the percentage weight loss (as measured by TGA analysis) of 1:1, 2:1 and 3:1 inclusion compounds of tetraphenylene ($C_{24}H_{16}$), urea ($CO(NH_2)_2$) and *p-t*-butylcalix[4]arene ($C_{44}H_{56}O_4$) with the following guests: water, $CHCl_3$, benzene, $C_{60}$. How useful would TGA be in studying the host–guest chemistry of each of these complexes?

## References

1. Palin, D. E., Powell, H. M., Hydrogen bond linking of quinol molecules. *Nature* 1945, **156**, 334–335.
2. Ripmeester, J. A., Tse, J. S., Ratcliffe, C. I., Powell, B. M., A new clathrate hydrate structure. *Nature* 1987, **325**, 135–136.
3. Lu, H. L., Seo, Y. T., Lee, J. W., *et al*., Complex gas hydrate from the Cascadia margin. *Nature* 2007, **445**, 303–306.
4. Udachin, K. A., Ripmeester, J. A., A complex clathrate hydrate structure showing bimodal guest hydration. *Nature* 1999, **397**, 420–423.
5. Mao, W. L., Mao, H. K., Goncharov, A. F., *et al.*, Hydrogen clusters in clathrate hydrate. *Science* 2002, **297**, 2247–2249.
6. Lee, H., Lee, J. W., Kim, D. Y., *et al.*, Tuning clathrate hydrates for hydrogen storage. *Nature* 2005, **434**, 743–746.

7. Barbour, L. J., Crystal porosity and the burden of proof. *Chem. Commun.* 2006, 1163–1168.
8. Marti-Rujas, J., Desmedt, A., Harris, K. D. M., Guillaume, F., Direct time-resolved and spatially resolved monitoring of molecular transport in a crystalline nanochannel system. *J. Am. Chem. Soc.* 2004, **126**, 11124–11125.
9. Hollingsworth, M. D., Brown, M. E., Hillier, A. C., Santarsiero, B. D., Chaney, J. D., Superstructure control in the crystal growth and ordering of urea inclusion compounds. *Science* 1996, **273**, 1355–1358.
10. Welberry, T. R., Diffuse X-ray scattering and strain effects in disordered crystals. *Acta Crystallogr., Sect. A* 2001, **57**, 244–255.
11. Brown, M. E., Hollingsworth, M. D., Stress-induced domain reorientation in urea inclusion-compounds. *Nature* 1995, **376**, 323–327.
12. Hollingsworth, M. D., Harris, K. D. M., 'Urea, thiourea and selenourea'. in *Comprehensive Supramolecular Chemistry*, Atwood, J. L., Davies, J. E. D., MacNicol, D. D., Vögtle, F., eds. Pergamon: Oxford, 1996, Vol. 6, *pp* 177–237.
13. Chao, M. H., Kariuki, B. M., Harris, K. D. M., Collins, S. P., Laundy, D., Design of a solid inclusion compound with optimal properties as a linear dichroic filter for X-ray polarization analysis. *Angew. Chem., Int. Ed.* 2003, **42**, 2982–2985.
14. Herbstein, F. H., Kapon, M., Reisner, G. M., Trimesic acid, its hydrates, complexes and polymorphism .8. interstitial complexes of alpha-trimesic and (the hypothetical) gamma-trimesic acid. *Acta Crystallogr. Sect. B-Struct. Commun.* 1985, **41**, 348–354.
15. Herbstein, F. H., Marsh, R. E., Crystal-Structures of Trimesic acid, its hydrates and complexes .2. trimesic acid monohydrate-2/9 picric acid and trimesic acid 5/6 hydrate. *Acta Crystallogr. Sect. B-Struct. Commun.* 1977, **33**, 2358–2367.
16. Herbstein, F. H., Structural parsimony and structural variety among inclusion complexes (with particular reference to the inclusion-compounds of trimesic acid, N-(para-tolyl)-tetrachlorophthalimide, and the Heilbron complexes). *Top. Curr. Chem.* 1987, **140**, 107–139.
17. Lloyd, G. O., Alen, J., Bredenkamp, M. W., de Vries, E. J. C., Esterhuysen, C., Barbour, L. J., Solid-state self-inclusion: The missing link. *Angew. Chem., Int. Ed.* 2006, **45**, 5354–5358.
18. Mazaki, Y., Hayashi, N., Kobayashi, K., An even odd effect in inclusion properties and crystal-structures of a new host series based on linearly condensed polythiophenes. *J. Chem. Soc., Chem. Commun.* 1992, 1381–1383.
19. Konig, O., Burgi, H. B., Armbruster, T., Hulliger, J., Weber, T., A study in crystal engineering: Structure, crystal growth, and physical properties of a polar perhydrotriphenylene inclusion compound. *J. Am. Chem. Soc.* 1997, **119**, 10632–10640.
20. Weber, T., Estermann, M. A., Burgi, H. B., Structural complexity of a polar perhydrotriphenylene inclusion compound brought to light by synchrotron radiation. *Acta Crystallogr. Sect. B-Struct. Commun.* 2001, **57**, 579–590.
21. Daschbach, J. L., Chang, T. M., Corrales, L. R., Dang, L. X., McGrail, P., Molecular mechanisms of hydrogen-loaded beta-hydroquinone clathrate. *J. Phys. Chem. B* 2006, **110**, 17291–17295.
22. Atwood, J. L., Davies, J. E. D., MacNicol, D. D., Vögtle, F., *Comprehensive Supramolecular Chemistry*. Pergamon: Oxford, 1996, Vol. 6, p. 619.
23. Hardy, A. D. U., McKendrick, J. J., Macnicol, D. D., Alteration of cage geometry by systematic structural modification of a clathrate host molecule. *J. Chem. Soc., Perkin Trans. 2* 1979, 1072–1077.
24. Lloyd, G. O., Bredenkamp, M. W., Barbour, L. J., Enclathration of morpholinium cations by Dianin's compound: salt formation by partial host-to-guest proton transfer. *Chem. Commun.* 2005, 4053–4055.
25. Jessiman, A. S., Macnicol, D. D., Mallinson, P. R., Vallance, I., Inclusion compound design - the Piedfort concept. *J. Chem. Soc., Chem. Commun.* 1990, 1619–1621.
26. Bonner, W. A., Enantioselective autocatalysis. V. The spontaneous resolution of tri-o-thymotide. *Orig. Life Evol. Biosph.* 1999, **29**, 317–328.
27. Atwood, J. L., Davies, J. E. D., MacNicol, D. D., Vögtle, F., *Comprehensive Supramolecular Chemistry*. Pergamon: Oxford, 1996, Vol. 6, p. 247.
28. Gnaim, J. M., Green, B. S., Aradyellin, R., Keehn, P. M., Improved preparation of the clathrate host compound triortho-thymotide and related trisalicylide derivatives. *J. Org. Chem.* 1991, **56**, 4525–4529.
29. Gerdil, R., Barchietto, G., Jefford, C. W., Heterogeneous Chirality Transfer on Photooxygenation. *J. Am. Chem. Soc.* 1984, **106**, 8004–8005.
30. Zhang, H. M., Steed, J. W., Atwood, J. L., Inclusion chemistry of cyclotetraveratrylene. *Supramol. Chem.* 1994, **4**, 185–190.
31. Brotin, T., Roy, V., Dutasta, J. P., Improved synthesis of functional CTVs and cryptophanes using Sc(OTf)(3) as catalyst. *J. Org. Chem.* 2005, **70**, 6187–6195.
32. Steed, J. W., Zhang, H. M., Atwood, J. L., Inclusion chemistry of cyclotriveratrylene and cyclotricatechylene. *Supramol. Chem.* 1996, **7**, 37–45.
33. Ibragimov, B. T., Makhkamov, K. K., Beketov, K. M., Polymorphism of crystalline inclusion complexes and unsolvated hosts. Part 8. Endocyclic modification of the cyclotriveratrylene host-guest complex with acetone. *J. Incl. Phenom. Macrocycl. Chem.* 1999, **35**, 583–593.
34. Ahmad, R., Hardie, M. J., Synthesis and structural studies of cyclotriveratrylene derivatives. *Supramol. Chem.* 2006, **18**, 29–38.

35. Steed, J. W., Junk, P. C., Atwood, J. L., Barnes, M. J., Raston, C. L., Burkhalter, R. S., Ball-and-socket nanostructures - new supramolecular chemistry based on cyclotriveratrylene. *J. Am. Chem. Soc.* 1994, **116**, 10346–10347.
36. Blanch, R. J., Williams, M., Fallon, G. D., Gardiner, M. G., Kaddour, R., Raston, C. L., Supramolecular complexation of 1,2-dicarbadodecaborane(12). *Angew. Chem., Int. Ed. Engl.* 1997, **36**, 504–506.
37. Atwood, J. L., Barnes, M. J., Gardiner, M. G., Raston, C. L., Cyclotriveratrylene polarisation assisted aggregation of $C_{60}$. *Chem. Commun.* 1996, 1449–1450.
38. Holman, K. T., Steed, J. W., Atwood, J. L., Intra-cavity inclusion of CpFeII(arene) (+) guests by cyclotriveratrylene. *Angew. Chem., Int. Ed. Engl.* 1997, **36**, 1736–1738.
39. Hardie, M. J., Raston, C. L., Wells, B., Altering the inclusion properties of CTV through crystal engineering: CTV, carborane, and DMF supramolecular assemblies. *Chem. Eur. J.* 2000, **6**, 3293–3298.
40. Juneja, R. K., Robinson, K. D., Orr, G. W., Dubois, R. H., Belmore, K. A., Atwood, J. L., Inclusion of multiring compounds by P-tert-butylcalix[5]arene. *J. Incl. Phenom. Mol. Recogn. Chem.* 1992, **13**, 93–96.
41. Perrin, M., Lecocq, S., Crystal and Molecular-structures of para-(1,1,3,3-tetramethylbutyl)calix[5]arene and its 1-1 complex with toluene. *J. Incl. Phenom. Mol. Recogn. Chem.* 1991, **11**, 171–183.
42. Ubbelohde, A. R., Thermal transformations in solids. *Q. Rev. Chem. Soc.* 1957, **11**, 246–272.
43. Bond, A. D., Boese, R., Desiraju, G. R., On the polymorphism of aspirin: Crystalline aspirin as intergrowths of two 'polymorphic' domains'. *Angew. Chem., Int. Ed.* 2007, **46**, 618–622.
44. Atwood, J. L., Koutsantonis, G. A., Raston, C. L., Purification of $C_{60}$ and $C_{70}$ by selective complexation with calixarenes. *Nature* 1994, **368**, 229–231.
45. Atwood, J. L., Barbour, L. J., Raston, C. L., Supramolecular organization of $C_{60}$ into linear columns of five-fold, Z-shaped strands. *Cryst. Growth Des.* 2002, **2**, 3–6.
46. Andersson, T., Nilsson, K., Sundahl, M., Westman, G., Wennerstrom, O., $C_{60}$ embedded in gamma-cyclodextrin – a water-soluble fullerene. *J. Chem. Soc., Chem. Commun.* 1992, 604–606.
47. Atwood, J. L., Barbour, L. J., Raston, C. L., Sudria, I. B. N., $C_{60}$ and $C_{70}$ compounds in the pincerlike jaws of calix[6]arene. *Angew. Chem., Int. Ed.* 1998, **37**, 981–983.
48. Atwood, J. L., Hamada, F., Robinson, K. D., Orr, G. W., Vincent, R. L., X-Ray diffraction evidence for aromatic $\pi$-hydrogen bonding to water. *Nature* 1991, **349**, 683–684.
49. Atwood, J. L., 'Cation complexation by calixarenes'. in *Cation Complexation by Macrocycles*, Inoue, Y., Gokel, G., eds. Dekker: New York, 1991.
50. Steed, J. W., Johnson, C. P., Barnes, C. L., *et al.*, Supramolecular chemistry of p-sulfonatocalix[5]arene - a water-soluble, bowl-shaped host with a large molecular cavity. *J. Am. Chem. Soc.* 1995, **117**, 11426–11433.
51. Perret, F., Bonnard, V., Danylyuk, O., Suwinska, K., Coleman, A. W., Conformational extremes in the supramolecular assemblies of para-sulfonato-calix[8]arene. *New J. Chem.* 2006, **30**, 987–990.
52. Orr, G. W., Barbour, L. J., Atwood, J. L., Controlling molecular self-organisation: formation of nanometre scale spheres and tubules. *Science* 1999, **285**, 1050.
53. Sing, K. S. W., Everett, D. H., Haul, R. A. W., *et al.*, Reporting physisorption data for gas solid systems with special reference to the determination of surface-area and porosity (Recommendations 1984). *Pure Appl. Chem.* 1985, **57**, 603–619.
54. Brouwer, D. H., Alavi, S., Ripmeester, J. A., A double quantum Xe-129 NMR experiment for probing xenon in multiply-occupied cavities of solid-state inclusion compounds. *Phys. Chem. Chem. Phys.* 2007, **9**, 1093–1098.
55. Atwood, J. L., Barbour, L. J., Jerga, A., Schottel, B. L., Guest transport in a non-porous organic solid *via* dynamic van der Waals cooperativity. *Science* 2002, **298**, 1000–1002.
56. Thallapally, P. K., Kirby, K. A., Atwood, J. L., Comparison of porous and nonporous materials for methane storage. *New J. Chem.* 2007, **31**, 628–630.
57. Thallapally, P. K., Lloyd, G. O., Atwood, J. L., Barbour, L. J., Diffusion of water in a nonporous hydrophobic crystal. *Angew. Chem. Int. Ed.* 2005, **44**, 3848–3851.
58. Hertzsch, T., Budde, F., Weber, E., Hulliger, J., Supramolecular-wire confinement of $I_2$ molecules in channels of the organic zeolite tris(o-phenylenedioxy)cyclotriphosphazene. *Angew. Chem., Int. Ed.* 2002, **41**, 2281–2284.
59. Sozzani, P., Bracco, S., Comotti, A., Ferretti, L., Simonutti, R., Methane and carbon dioxide storage in a porous van der Waals crystal. *Angew. Chem., Int. Ed.* 2005, **44**, 1816–1820.
60. Dewal, M. B., Lufaso, M. W., Hughes, A. D., Samuel, S. A., Pellechia, P., Shimizu, L. S., Absorption properties of a porous organic crystalline apohost formed by a self-assembled bis-urea macrocycle. *Chem. Mat.* 2006, **18**, 4855–4864.
61. Dobrzanska, L., Lloyd, G. O., Raubenheimer, H. G., Barbour, L. J., Permeability of a seemingly nonporous crystal formed by a discrete metallocyclic complex. *J. Am. Chem. Soc.* 2006, **128**, 698–699.
62. Albrecht, M., Lutz, M., Spek, A. L., van Koten, G., Organoplatinum crystals for gas-triggered switches. *Nature* 2000, **406**, 970–974.

# 8 Crystal Engineering

*'Whether on crystal rocks ye rove, / Beneath the Bosom of the sea*
*Wand'ring in many a coral grove, / Fair nine, forsaking Poetry*
*How have you left the ancient love / That bards of old enjoy'd in you!*
*The languid strings do scarcely move! / The sound is forc'd, the notes are few.'*

William Blake (1757–1827), *To the Muses.*

# 8.1 Concepts

## 8.1.1 Introduction

Braga, D., Brammer, L., Champness, N. R., 'New trends in crystal engineering', *Cryst. Eng. Comm.* 2005, **7**, 1–19.

The crystallisation process is, by definition, a self-assembly process in the sense that the component molecules or ions encounter and recognise one another, usually in solution, and pack together as close as possible to their optimum orientation in the time available, according to their intrinsic steric and electronic properties. The resulting aggregate, as an assembly, then goes on to accrete further molecules or ions faster than the dissociation of those already comprising the aggregate, ultimately resulting in an ordered nucleus of more than transient stability. This nucleus continues to grow by adding molecules from solution to produce the whole crystal. We must be clear, however, about the distinction between crystal self-assembly and solution self-assembly (which is discussed fully in Chapter 10).

- Crystallisation is fundamentally a non-equilibrium phenomenon in which both kinetic and thermodynamic aspects contribute to the eventual structure. The final structure is a function in many cases of crystallisation conditions, and polymorphs (crystals made from the same molecules but with different packing arrangements) are common. Structures that form faster may well predominate over structures that are most stable.
- Solution self-assembly is a thermodynamically controlled equilibrium reaction in which components are able to sift through a variety of possible structures until they find the one of the maximum stability. There is effectively infinite time available for the reaction and 'mistakes' in the assembly process may be rectified by decomplexation and recomplexation steps.

The emerging science of crystal engineering can be thought of as a kind of synthetic chemistry of crystals; i.e. the design and understanding of the way in which molecules crystallise to produce new materials with controlled and understood structure. Molecular and crystal synthesis are distinguished from one another by both scale and diversity. In terms of scale, atoms and molecules are microscopic entities possessing quantum mechanical properties. Crystals are macroscopic objects exhibiting long-range order and bulk properties (electrical conductivity, heat capacity *etc.*). In terms of diversity, the covalent bond is a complicated, yet well-studied interaction, with high strength over a short range, directionality and synthetic malleability. The synthesis of crystals is a much more difficult process to control since it involves manipulation of a synergistic whole of long- and short-range interactions. Some interactions fall off rapidly with distance (induction and dispersion depend on the sixth power of distance between the interacting partners), while others such as hydrogen bonds and dipolar interactions may be effective at very long range. It is not surprising, therefore, that while the structured synthesis of complex covalent molecules (natural products, carcerands *etc.*) has been achieved, the ability to predict and perhaps hence control the structures of all but the most simple crystals is still largely unrealised, although there continues to be significant progress towards this goal.

*Supramolecular Chemistry, 2nd edition* J. W. Steed and J. L. Atwood
© 2009 John Wiley & Sons, Ltd ISBN: 978-0-470-51233-3

The field of crystal engineering was given an identity by von Hippel, who described its fundamentals in detail under the term 'molecular engineering' in 1962.[1] Modern crystal engineering may be traced back to the early 1960s when it was developed initially as a method for understanding the regioselectivity and product distribution in solid-state molecular reactions in species such as $\alpha,\beta$-unsaturated acids and *p*-quinones, a field termed *topochemistry*.[2] It has developed rapidly, however, especially with the advent of modern crystallographic techniques (initially four-circle diffractometers in the early 1970s and latterly CCD and area detector technology for small molecule crystallography, Box 2.1) and now encompasses many aspects of solid-state intermolecular interactions, structure prediction, control and rationalisation, as well as the synthesis of novel molecular building blocks and crystalline molecular materials. This kind of 'soft' materials chemistry has applications in a variety of areas such as non-linear optical materials, pharmaceutical formulation, drug delivery mechanisms and gas storage and separation. Crystal engineering, as it is now practised, may be broken down into two main components: analysis and synthesis. Some of the main proponents of modern crystal engineering, Dario Braga and Fabrizia Grepioni of the University of Bologna, Italy, and Gautam Desiraju of the University of Hyderabad, India, have summarised the interplay between these two pursuits in the following way:

> *Reason and imagination come into play simultaneously in the quest for new functionalised solids, while experiment and computation are of equal significance in the prediction and design of crystal structures.*[3]

Crystal engineering is, therefore, the design and preparation of a crystalline material based on a knowledge, or at least consideration, of the steric, electronic, topological and intermolecular bonding capabilities of the constituent building blocks. These considerations have been termed 'intermolecular valence' by analogy with conventional atomic valence. Coupled with this design must come a knowledge of the kinetics and thermodynamics of crystal nucleation phenomena, the requirements of crystal close packing and the relative importance of the multiplicity of interactions that go together to assemble the crystalline entity. The field has thus come a long way from the rather diffuse origins of the study of the morphology (external appearance) of crystals that marked the beginnings of crystallography (Figure 8.1)!

## 8.1.2 Tectons and Synthons

Desiraju, G. R., 'Supramolecular synthons in crystal engineering – a new organic synthesis', *Angew. Chem., Int. Ed. Engl.* 1995, **34**, 2311–2327.

In molecular chemistry, the fundamental building block is the atom. Atoms interact with other atoms *via* the formation of covalent bonds to give molecules. Small molecules, in turn, undergo reactions to form larger molecules. Often these reactions involve particular chemical groups. When synthetic organic chemists look at the ways in which they can assemble a molecule *via* covalent bonds they use a process termed *retrosynthetic analysis*, or *retrosynthesis*. Retrosynthesis consists of identifying particular bonds in the final target molecule that can be formed by a known chemical reaction of two or more molecular precursors (a *synthetic operation*). The covalent bond can be thought of as being between two component *synthons,* a term originally coined by E. J. Corey.* The

* US organic chemistry Elias James Corey (b. 12 July 1928) winner of the 1990 Nobel Prize in Chemistry particularly for the development of retrosynthetic analysis.

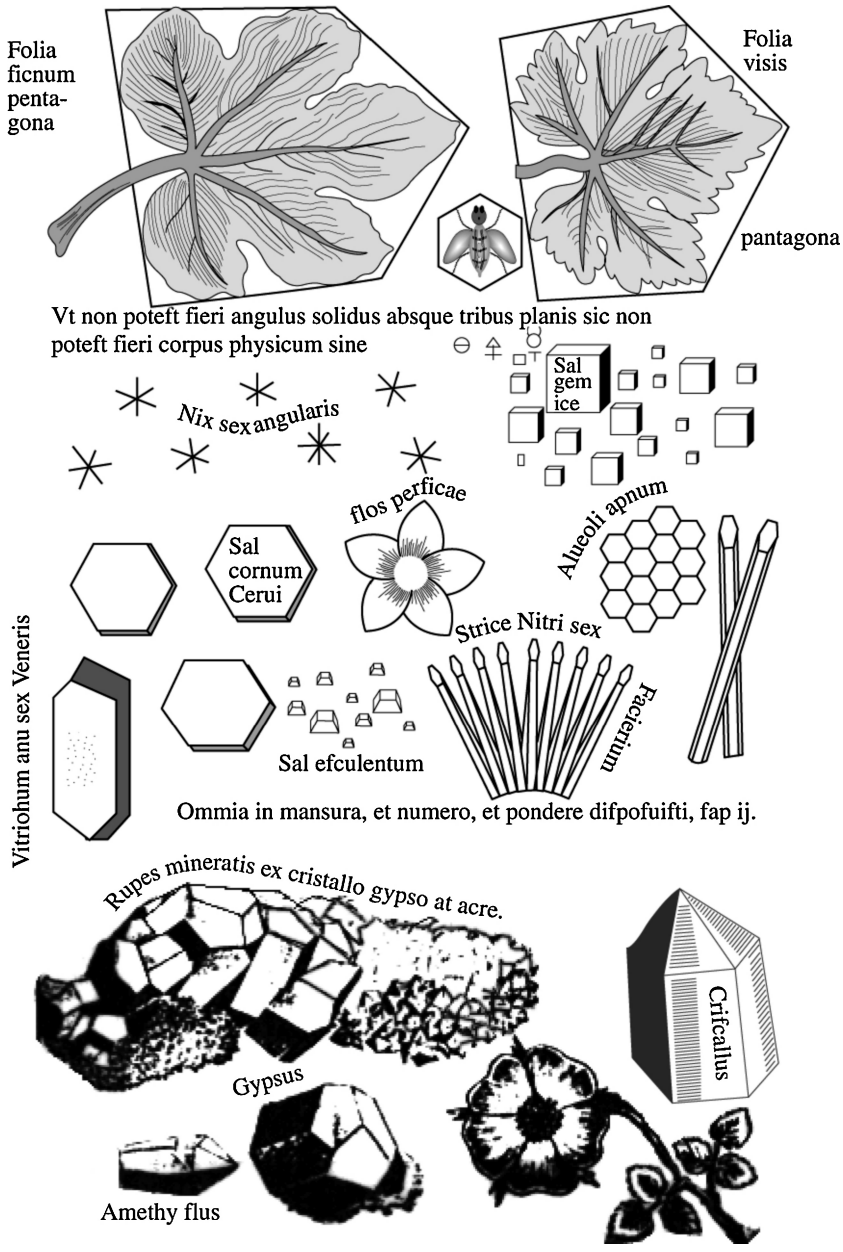


**Figure 8.1** Illustration showing the occurrence of regular Platonic shapes in crystalline solids and natural forms. The illustration is by Scotsman, William Davidson (called 'Davissone'), who was among the first to allude to crystallography, '*a new subject which, so far as I know, none before me has elaborated*'. (From W. Davisonne, *Les Elements de la Philosophie de l'Art du Feu, ou Chemie*, Paris 1657.)

synthons may not be particularly readily available or stable by themselves and often the new bond is formed by a chemical reaction between *synthetic equivalents* to the synthons. In the example shown in Scheme 8.1 retrosynthetic analysis of phenylacetic acid (**8.1**) suggests it can be broken down into the synthons $PhCH_2^+$ and $CO_2^-$. Neither of these synthons is stable by itself and so

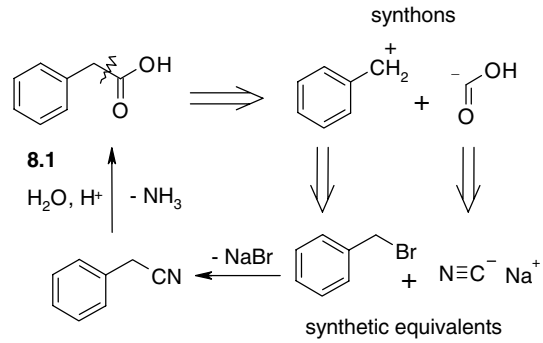


**Scheme 8.1** Retrosynthesis in synthetic organic chemistry to determine suitable synthons and hence prepare the target molecule from suitable synthetic equivalents. The retrosynthetic steps are indicated by open arrows.

the bond is formed by reaction of two much more readily handled synthetic equivalents, benzyl bromide and the cyanide anion. These reactants form phenyl acetonitrile which is then hydrolysed to give the desired product.

Put very simply, self-assembly in all phases of matter represents the supramolecular equivalent of this view of molecular chemistry. The building blocks are now molecules instead of atoms, and are termed *tectons*. The molecules interact with one another *via* the formation of non-covalent bonds (Section 1.8) to give crystalline solids, and solution and gas phase aggregates. The non-covalent bond linking these tectons can be thought of as a *supramolecular synthon* if it reliably and reproducibly forms the same kind of supramolecular interaction between tectons with particular kinds of functional groups. The concept of the supramolecular synthon was first described by Gautam Desiraju in 1995 and is a very powerful way of designing supramolecular aggregates. While in principle the concept applies to any phase of matter, it is usually only used in the solid state as a way of understanding and designing crystalline molecular materials (*i.e.* crystalline solids made up from the non-covalent packing of discrete molecules, as opposed to ionic solids such as NaCl or giant covalent lattices such as diamond). Figure 8.2 shows some examples of common supramolecular synthons. Hydrogen bonded supramolecular synthons are perhaps the most common and obvious, but supramolecular synthons are known involving other interactions such as halogen bonding and π-interactions. For example, the nitro/iodo supramolecular synthon has been used to assemble a non-linear optical organic crystal from 4-iodo-4′-nitrobiphenyl.[4] The directionality of the I···$O_2$N interaction causes all of the 4-iodo-4′-nitrobiphenyl molecules to line up giving non-centrosymmetric tapes. Overall crystal non-centrosymmetry is necessary for non-linear optical activity (Section 11.6) and hence the non-centrosymmetric tapes are prevented from forming an overall centrosymmetric anti-parallel arrangement by the chiral twisted conformation adopted by the biphenyl units. In contrast, the structure of 4-nitroiodobenzene contains the same iodo/nitro synthon but is centrosymmetric because of antiparallel packing of the planar tapes, Figure 8.3.

In crystal engineering, more than any other aspects of supramolecular chemistry, the synergistic interplay of intermolecular non-covalent interactions must be considered as a single interrelated entity. In the absence of any one dominant interaction (as is usually the case), this makes crystal structure analysis and prediction extremely difficult. The various kinds of non-covalent interactions have been summarised in Section 1.8. In general, most of these intermolecular bonds are of electrostatic origin. For crystal engineering purposes, what matters most is their distance dependence and their directionality. Medium range forces, particularly van der Waals interactions, define molecular shape and contribute favourably to the overall crystal stability as well as providing a

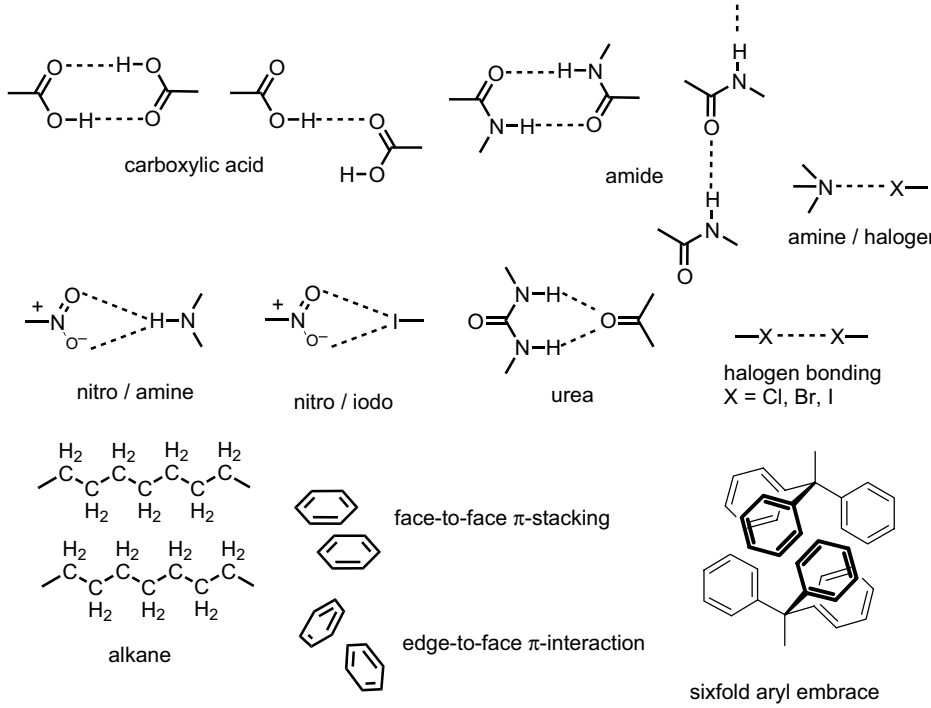


**Figure 8.2** Common supramolecular synthons – commonly occurring interactions between functional groups on different molecules in crystals that can sometimes be used in a predictive fashion to engineer crystal structures.

driving force towards close packing. Longer-range forces such as hydrogen bonds are much more highly directional and may even acquire some covalent character. Very-long-range ionic forces, such as those between metal cations and heteroatoms, exert very specific controls and constraints on crystal structure.

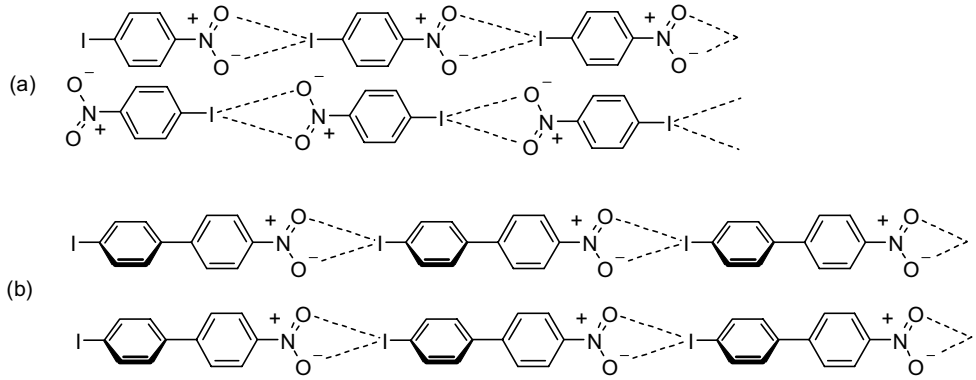


**Figure 8.3** Crystal packing using the nitro/iodo supramolecular synthon (a) antiparallel, centrosymmetric packing in 4-nitroiodobenzene, (b) non-linear optical active parallel arrangement of polar stacks in 4-iodo-4′-nitrobiphenyl.[4]

## 8.1.3 The Special Role of Hydrogen Bonding

Jeffrey, G. A., *An Introduction to Hydrogen Bonding*, Oxford University Press: Oxford, 1997.

Hydrogen bonding has been described as the 'masterkey interaction in supramolecular chemistry', and this observation is especially true in crystal engineering studies. It is characterised by both high-strength (typically up to 60 kJ $mol^{-1}$, although with some examples being significantly stronger) and distinct directionality. George Jeffrey of the University of Pittsburg, USA, has made a lifetime study of hydrogen bonds and classifies them into three general categories: strong, medium and weak, according to the energy of the interaction. General properties of the three classes of hydrogen bond are given in Table 1.5. These three divisions are mainly for convenience since, as we will see in the ensuing sections, there is very much a 'continuum of hydrogen bonds' with the weakest strong bond being of comparable energy to the strongest medium bond, and so on. Since its original description by Pauling in 1939[5] the concept of the hydrogen bond has gradually become more relaxed and has broadened to include ever weaker interactions as long as there is some electrostatic character. At their weakest these weak hydrogen bonds have considerable dispersive-repulsive components and become indistinguishable from van der Waals interactions. It has been suggested[6] that given this diversity the term *hydrogen bridge* might be more appropriate, recognising an interaction without borders with significant variation in its relative covalent, electrostatic and van der Waals components. It seems unlikely that the term 'hydrogen bond' will disappear anytime soon, however. In crystals, and in supramolecular systems generally, weaker and stronger interactions often act in concert and it is often unclear from an examination of the overall crystalline structure which interaction, if any, is structure-defining. This is particularly apparent in the structure of the 6:1 cyclohexanedione·benzene 'cyclamer', $(\mathbf{8.2})_6{\cdot}C_6H_6$,[7] which was adopted as the logo for the journal *CrystEngComm* (Royal Society of Chemistry, UK, 1999). The beautiful cyclic structure is held together by very short, medium-strength O–H···O=C hydrogen bonds with O ··· O 2.579 Å, which are apparently structure dominating. However, the cyclamer (specifically a cycla-6-mer because it comprises six host residues) is only formed in the presence of a benzene guest. The benzene engages in six very long C—H ··· O interactions of 3.00 Å, in which the C—H bonds point directly at the *syn* lone pair of the ketone oxygen atom. Crystallisation from thiophene, pyridine, alcohols or chloroform gives rise to a linear structure, which does not enclose guest molecules. This leads to the intriguing possibility that there is little preference between cyclic and linear chain structures for ketone **8.2** and the weak interactions to the benzene are strong enough to cause the observed change in solid-state behaviour.

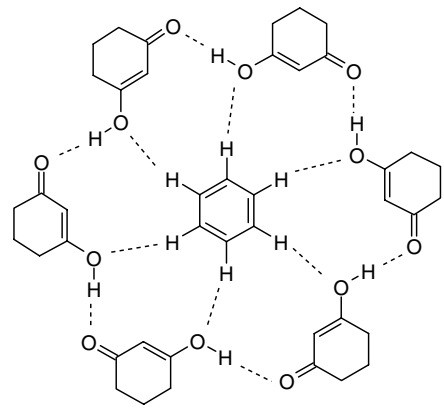

$(\mathbf{8.2})_6{\cdot}C_6H_6$

**Box 8.1** Single Crystal Neutron Diffraction

Single crystal X-ray diffraction and single crystal neutron diffraction are both good techniques for the study of molecular and crystal structure in the solid state; both operate on similar principles. Indeed, the same software may be used to carry out refinements against both neutron and X-ray diffraction data. Unlike X-ray work, which is carried out in most modern universities and many industrial labs, neutron diffraction is an uncommon and highly expensive technique. The only source of neutrons available is a nuclear reactor or spallation source. The velocity of fast neutrons is slowed down such that their wavelength corresponds to about 1 Å, comparable to the separation between atoms in crystals. After collimation, a more or less monochromatic neutron beam is obtained, suitable for the diffraction experiment. Alternative *quasi*-Laué methods on instruments such as LADI and VIVALDI at the Institut Laue Langevin, Grenoble, France, and LMX at ISIS in the UK use a range of wavelengths from *ca.* 1–5 Å. Unfortunately, the intensity (flux) of the neutrons is very low compared to X-rays, and hence neutron diffraction often requires very large crystalline samples (1–5 mm; *cf.* 0.02–0.5 mm for modern CCD X-ray facilities) and long data collection times. With these experimental difficulties, it is unsurprising that relatively few neutron diffraction experiments are undertaken. However, neutron diffraction has one very great advantage over X-ray diffraction in that because neutron scattering depends on the atomic nuclei and not the electron density as in X-ray methods, light atoms, particularly hydrogen, are readily located (although commonly deuterium is substituted for hydrogen; the neutron scattering cross section of $^{2}H$ is about twice that of $^{1}H$ in magnitude and deuteration reduces background from the significant inelastic scattering of neutrons by $^{1}H$ – one more experimental complication). Clearly, in hydrogen bonding studies, where the accurate location of hydrogen atoms is of paramount importance, only a neutron diffraction experiment can give precise information on hydrogen atom locations. Furthermore, the atomic coordinates located in a neutron diffraction experiment are not affected by the incorporation of hydrogen atom electron density into covalent bonds, which shifts the apparent atomic position towards the atom to which the H atom is bound, artificially shortening the X—H bond distance. Typically, a good neutron diffraction experiment can give X—H bond distances to a precision of ±0.002 Å and angles to ± 0.01º. This may be compared to the best low-temperature X-ray data, in which errors are at least an order of magnitude higher, even in the absence of atoms heavier then C or O.

In the early days of structural studies involving hydrogen bonds of type X—H···X using X-ray crystallography (Box 2.1), the hydrogen atom could not be located because the technique relies upon the location of electron density, of which there is very little for hydrogen atoms. Location of hydrogen atoms using X-rays still remains a problem, even with modern low-temperature data, especially in the presence of many-electron atoms such as transition metals. A much more accurate and precise way to locate hydrogen atoms is the complementary technique of single crystal neutron diffraction, which is extremely effective at locating H atom positions (Box 8.1). Unfortunately, this method is both time-consuming and expensive since the only know neutron sources are either nuclear reactors or pulsed spallation sources,[†] and neutron detector technology is not very sensitive as a result of the non-charged nature of the neutron. As a result, knowledge of hydrogen atom positions has historically been sparse and crystallographers have traditionally adopted a criterion based on the non-bonded X···X distance for hydrogen bond location (where X = non-hydrogen atom). In general, the presence of a hydrogen bond is assumed when the non-hydrogen atom separation (which can be determined quite precisely by X-ray work) is less than the sum of the van der Waals radii of the two putatively hydrogen bonded non-hydrogen atoms. The van der Waals radii for the elements of interest are about 1.10 Å for hydrogen, 1.40 Å for oxygen, 1.50 Å for nitrogen, 1.80 Å for chloride, 1.95 Å for bromide and 2.15 Å for iodide. Therefore, hydrogen bonded N···X distances involving an N-H···X interaction, for example, are expected to be less than 2.90, 3.00,

[†] Spallation occurs in a particle accelerator when a high-energy proton bombards a heavy atomic nucleus, resulting in some neutrons being knocked out or 'spalled'.

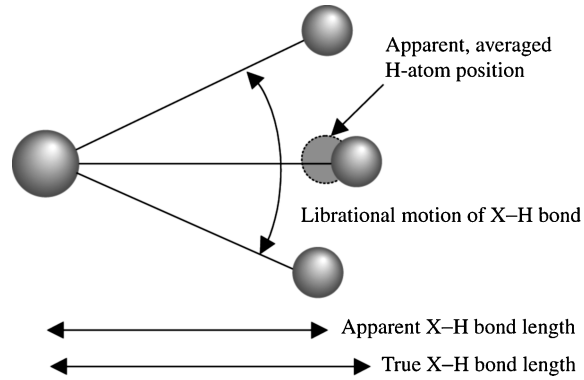


**Figure 8.4** Librational shortening of covalent bonds.

3.30, 3.45 and 3.65 Å for X = O, N, Cl, Br and I, respectively. With the advent of modern X-ray detectors and cryocrystallography (low temperature diffraction studies, generally in the range 100–250K), it is now possible to locate hydrogen atoms and refine their positions to within ±0.02 Å. The resulting hydrogen atom coordinates are affected strongly by the librational (bending) motion of the X—H bond (Figure 8.4) and are artificially shortened by the polarisation of the hydrogen atom electron density towards the atom to which it is bonded. However, when these effects are taken into account it becomes possible to develop much more reliable tests of hydrogen bonds based on both the directionality of the X—H vector and the H···X distance as well as the X···X distance. The results of these studies show that the X···X distance criterion is relatively insensitive to hydrogen bond strength, and is particularly bad at highlighting multi-centre interactions in which the hydrogen atom interacts with two or more acceptors.

### *Strong Hydrogen Bonds*

Strong hydrogen bonds in the crystalline state are associated most commonly with strong acids such as HF as in the $HF_2^-$ ion, or with the hydrated proton (oxonium ion), $H_3O^+$, $H_5O_2^+$, $H_7O_3^+$, or more generally, $H^+(H_2O)_n$ (n = generally 1–6, although in the gas phase in mass spectrometers, clusters with n > 20+ have been detected). In chapter 3 we discussed oxonium ion binding by crown ethers (Section 3.11.1). The example shown in Figure 3.59 shows the single crystal neutron structure of an $H_7O_3^+$ ion sandwiched between two molecules of [15]crown-5. The neutron data show clearly that the bonds to the acidic hydrogen atom in between all significantly longer than the other O–H bond lengths. The elongated covalent O–H bond correlates to a short O···O distance of 2.44 Å and a near-linear O-H···O angle of 178.5°. Strong hydrogen bonds are also observed in complexes of proton sponge (**8.3**), in which the proton is shared more or less equally between two $NMe_2$ groups held in mutual close proximity. In this case, the presence of the proton actually reduces unfavourable lone pair-lone pair interactions, and the strength of the hydrogen bond is assisted by interactions between the nitrogen lone pair and the proton's naked positive charge.

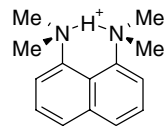


H+ complex of 'proton sponge'

**(8.3)**.$H^+$

The strong hydrogen bond is characterised by an X—H—X (X = F, O, N) angle of close to 180° and a short X···X distance, and is accompanied by a lengthening of the covalent X—H distance, such

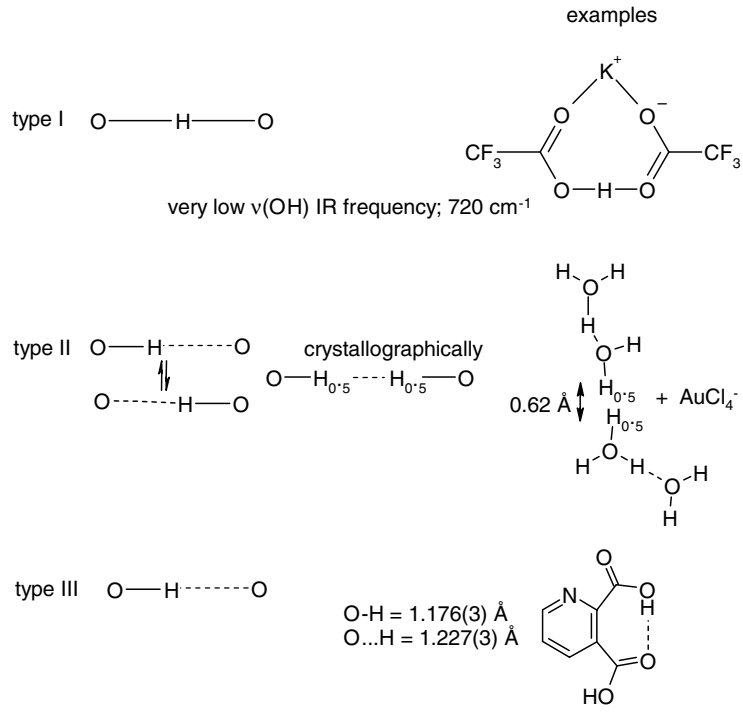


**Figure 8.5** Symmetry of proton environments in representative strongly hydrogen bonded complexes.

that the proton is shared almost equally between the two electronegative atoms. In fact, there are only a few cases in which the proton appears to be genuinely equidistant between the two acceptor atoms (type I, Figure 8.5). More commonly, crystallographic disorder can result in apparently equidistant protons (type II) or, in the case of very unsymmetrical species, the individual positions are resolved (type III). In general, however, the proton is on a very flat potential energy surface and its precise position is influenced strongly by the overall crystal field environment.

### *Medium Hydrogen Bonds*

Medium-strength hydrogen bonds are by far the most common type encountered for hydrogen attached to electronegative atoms (particularly oxygen), and are ubiquitous in biological systems, particularly in the stabilisation of protein tertiary structure. Hydrogen bonded distances may vary over more than 0.5 Å, and X—H ⋯ X angles range between about 178° and 140°. Analyses of hydrogen bonds found in the Cambridge Structural Database (Section 8.4) show that the most common X—H ⋯ X angle (ϕ) observed is generally in the region of about 155°. This observation arises from statistical considerations. Out of all of the possible hydrogen bonded geometries or orientations by which a donor, X—H, may approach an acceptor, only one is at exactly 180°, and thus a hydrogen-bonded angle of exactly 180° is statistically highly unlikely. As this angle is allowed to deviate from precise linearity to give a 'cone of approach' of the X—H donor, the number of possibilities increases with the sine of the angle. Thus distributions of hydrogen bond angle reach a maximum at an angle that is a combination of this conical factor and the tendency towards highest strength at 180°. If a conic correction is applied to take account of this statistical factor, then the most common angle becomes 180°, corresponding to the line of most

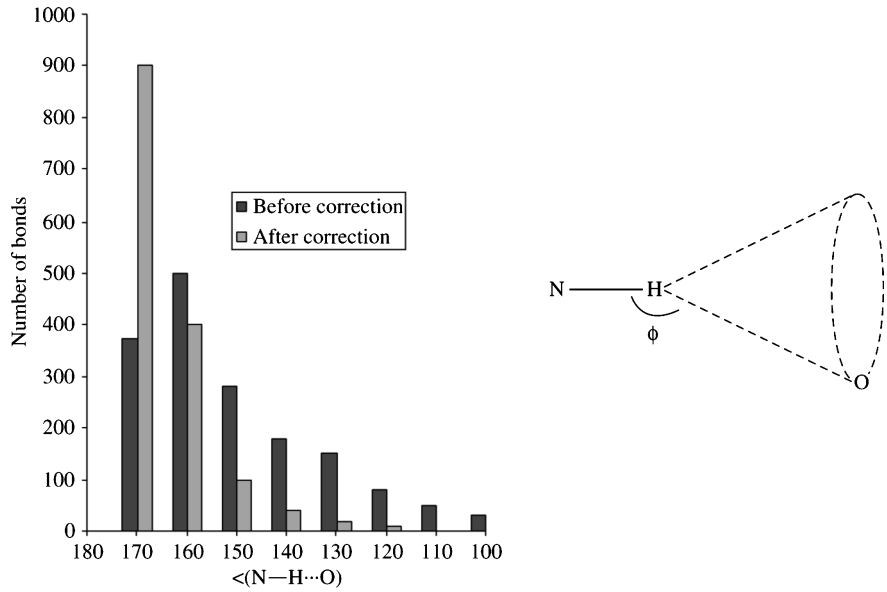


**Figure 8.6** Distribution of 1509 N—H ··· O = C hydrogen bonds before and after application of a conic correction factor.[8]

interaction. This the observed distribution and its conical correction is illustrated in Figure 8.6 for a database analysis of N—H ··· O=C hydrogen bonds.[8]

The requirement that the conically corrected X—H ··· X angle should tend to 180° is only true in the case of two centre hydrogen bonds in which there is only a single acceptor atom. In fact, about 20 to 25 % of moderate-strength hydrogen bonds are three-centred, or 'bifurcated', either symmetrically (with two equal H ··· X distances to two acceptors) or unsymmetrically. For amines the tendency towards bifurcation decreases in the order $R_3N^+$—H < $R_2HN^+$—H < $RH_2N^+$—H < $H_3N^+$—H < $R_2N^+_{sp2}$—H, which is the inverse of the hydrogen bond lengths. This means, simply, that bifurcated bonds occur when there is more space about the donor. Trifurcated four-centre bonds are also known. Multicentre bonding tends to increase hydrogen bond distances significantly, and to reduce the X—H ··· X angle typically to 90–140°. It also makes the interaction much more difficult to detect when the hydrogen atom is not located experimentally. See Section 1.8.4 for a further discussion of hydrogen bonding.

### *Weak Hydrogen Bonds*

The area of weak hydrogen bonds encompasses both poor donors such as C—H bonds (the C—H bond can act as a hydrogen bond acid in cases in which the carbon is attached to an electronegative group or is otherwise acidic, such as arenes, acetylenes, ethers, chloroalkanes *etc.*) and poor acceptors such as π-electron density and heavy atoms (Br, S, Se *etc.*). Distances and angles may cover wide ranges and the low fall-off of electrostatic interactions with distance ($r^{-1}$ dependence) means that even very long separations in the region of 4 Å cannot be discounted. Good structural data, coupled with a detailed analysis of the geometry of the system as a whole, are required. In the absence of strong interactions, weak hydrogen bonds can dominate the structure entirely as in the CH···N≡C interactions found in the 1:1 co-crystal of 1,3,5-tricyanobenzene with hexamethylbenzene (Figure 8.7).[9]

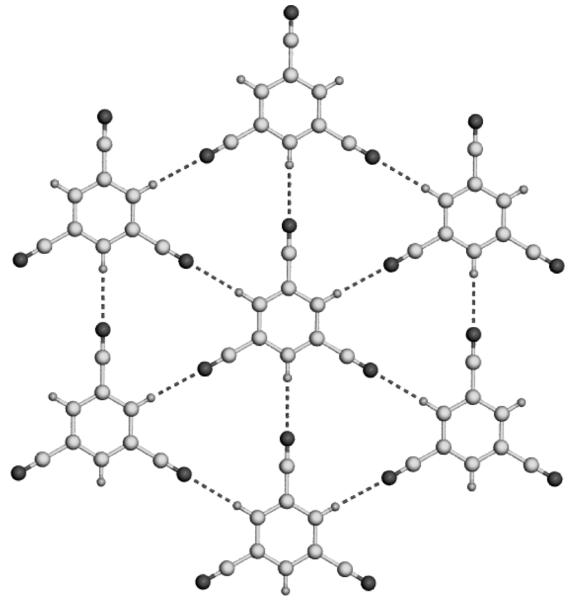

**Figure 8.7** Hexagonal network of 1,3,5-tricyanobenzene in the 1:1 complex with hexamethylbenzene.[9]

## 8.1.4 Hydrogen Bond Acidity and Basicity

Laurence, C., Berthelot, M., 'Observations on the strength of hydrogen bonding,' *Persp. Drug Disc. Des.* 2000, **18**, 39–60.

When we talk about relative strengths of hydrogen bonding as we did in the previous section it is important to understand and be able to predict the origins of different hydrogen bonding strength according to chemical group, allowing for the fact that hydrogen bond energies may be very different in solution, where solvation plays a major role, and in the solid state or gas phase. The Brønsted acidity or basicity of a particular proton donor or acceptor is readily qualified by its p$K_a$ in aqueous solution (Section 3.11.2). As we discussed in Section 1.8.4, however, hydrogen bond acidity and basicity is not the same as Brønsted acidity or basicity. In a hydrogen bond the proton is not lost as it is in a proton donation reaction and similarly a hydrogen bond base does not simply accept a proton, but a whole molecule hence and the affinity of hydrogen bond donors or acceptors is influenced by steric factors (the accessibility of the donor and acceptor groups) as well as electronic factors such as electronegativity and hybridisation. Extensive work, particularly by the groups of Robert W. Taft[10] (University of California Irvine, USA) and Michael H. Abraham[11] (University College London, UK), has resulted in quantified scales of hydrogen bond acidity and basicity (as well as other solute-solvent interaction parameters). Abraham's work has focussed on the definition of a quantity log $K_A^H$ which represents hydrogen bond acidity in $CCl_4$ (an essentially non-hydrogen bonding solvent) against a series of reference bases. Taft's work has been expanded by Lawrence and Berthelot (University of Nantes, France) to give a p$K_{HB}$ scale for hydrogen bond bases where 1.364 p$K_{HB}$ = $-\Delta G_{HB}$ (/kcal mol$^{-1}$).[12] Experimentally p$K_{HB}$ represents the equilibrium constant (log $K$) for the 1:1 complexation of a reference hydrogen bond donor, 4-fluorophenol, with hydrogen bond acceptors, again in carbon tetrachloride at 298 K. The way in which the scale is defined is consistent with the definition of p$K_a$

**Table 8.1** Representative $pK_{HB}$ values for hydrogen bond bases.[12]

| **C** | $pK_{HB}$ | **N** | $pK_{HB}$ | **O** | $pK_{HB}$ | **F** | $pK_{HB}$ |
|---|---|---|---|---|---|---|---|
| Ethylenic: | −0.8 | Nitrile: | 0.9 | Alcohol: | 0.8 | Fluoroalkane: | 0.0 |
| Aromatic: | −0.5 | Pyridine: | 1.9 | Ether: | 1.0 | | |
| Acetylenic: | −0.2 | Amine: | 2.1 | Ketone: | 1.2 | | |
| | | | | Amide: | 2.3 | | |
| | | | | Sulfoxide: | 2.6 | | |
| | | | | Phosphine oxide: | 3.5 | | |
| | | | | Amine oxide: | 6.0 | | |
| | | | | $NBu_4^+MeCO_2^-$: | 5.6 | | |

| **P** | | **S** | | **Cl** | |
|---|---|---|---|---|---|
| Phosphine: | *ca.* 0.8 | Thioether: | 0.3 | Chloroalkane: | −0.3 |
| | | Thioamide: | 1.3 | $NBu_4^+Cl^-$: | 4.3 |

| **Se** | | **Br** | |
|---|---|---|---|
| Selenoether: | *ca.* 0.2 | Bromoalkane: | −0.3 |

| **I** | |
|---|---|
| Iodoalkane: | −0.4 |
| $NBu_4^+I^-$: | 2.8 |

and so the most basic compounds and the strongest hydrogen bond acceptors have the largest $pK_a$ and $pK_{HB}$ values, respectively. Extensive tables of log $K_A^H$ and $pK_{HB}$ values are given in the references.[12, 13] Some representative $pK_{HB}$ values are given in Table 8.1. Perhaps the most striking is the very high hydrogen bond basicity of sulfoxides and particularly amine oxides in comparison to known strong Brønsted bases such as pyridine. This high basicity stems from the accessibility of the oxygen atom and the zwitterionic character of the $R_2S^+–O^-$ and $R_2N^+–O^-$ bonds. It is even higher than the basicity of acetate because of the delocalisation of the acetate negative charge over two oxygen atoms.

## 8.2 Crystal Nucleation and Growth

Davey, R. J., Allen, K., Blagden, N., *et al.*, 'Crystal engineering – nucleation, the key step', *Cryst. Eng. Comm.* 2002, 257–264.

### 8.2.1 Theory of Crystal Nucleation and Growth

In examining a crystalline structure as revealed by diffraction experiments it is all too easy to view the crystal as a static entity and focus on what may be broadly termed attractive intermolecular interactions (dipole–dipole, hydrogen bonds, van der Waals *etc.*, as detailed in Section 1.8) and neglect the actual mechanism by which a crystal is formed, *i.e.* the mechanism by which these interactions act to assemble the crystal from a non-equilibrium state in a super-saturated solution. However, it is very often nucleation phenomena that are ultimately responsible for the observed crystal structure and hence we were careful to draw a distinction between solution self-assembly and crystallisation at the beginning of this chapter. For example paracetamol, when crystallised from acetone solution gives the stable monoclinic crystal form I, but crystallisation from a molten sample in the absence of solvent

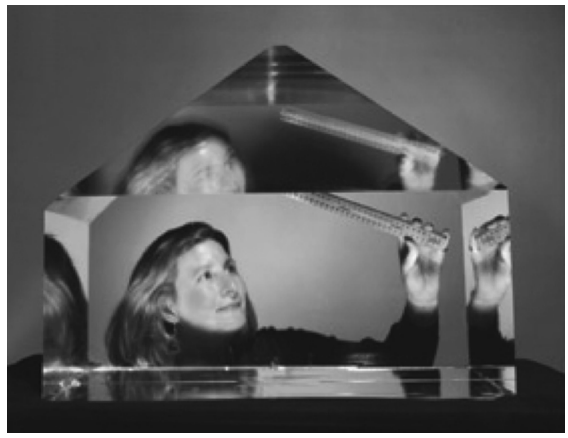

**Figure 8.8** Very large crystals such as this sample of KDP ($KH_2PO_4$) used for laser frequency doubling are produced by careful nucleation control at the metastable boundary between an unsaturated and supersaturated solution (image courtesy of the Lawrence Livermore National Laboratory). See plate section for colour version of this image.

results in the orthorhombic metastable (*i.e.* kinetically stable but not the most stable form overall) layer structure, form II. Crystal nucleation results in the formation of a new solid-solution interface which is unfavourable in free energy terms. The free energy available to form this new interface depends on the supersaturation (the amount of material dissolved over and above that which can be dissolved in the solvent under normal circumstances), and the nucleus will only be viable if this penalty is recoverable from the free energy gain of creating the bulk crystalline material. Within a supersaturated solution there is a steady-state distribution of aggregates of molecules linked by recognisable supramolecular synthons.[‡] Depending on the supersaturation (which can to some extent be controlled by the experimenter) there will be a critical nucleus size, above which these assemblies can grow, and below which they are unstable. The more supersaturated the solution is the smaller the size of this stable nucleus, hence the easier crystal nucleation becomes, resulting in the formation of numerically more crystals. A key point to bear in mind is that, unlike most of chemistry in which the laws of statistical probability are strictly obeyed because of the very large numbers of molecules involved, crystal nucleation can sometimes occur only a very few times in a given crystallisation experiment (sometimes only once giving rise to very large single crystals, Figure 8.8) and hence it is difficult to predict and control. A detailed treatise of crystal growth phenomena is beyond the scope of this work, and a more rigorous discussion may be found in the literature[14, 15] and the key reference to this section; however, the basic aspects are discussed below.

Classically, the process by which crystals are deposited involves the initial clustering of solutes in supersaturated solution into stable or transient assemblies (nucleation) followed by growth once the assembly has reached a critical size. The process is shown below:

1. Formation of aggregates from tecton A.

$$A + A = A_2$$
$$A_2 + A = A_3 \ldots$$

[‡] Instead of supramolecular synthons, in nucleation work it is more common to talk about a *growth unit* defined as the essential building block that transfers structural information from the solution to the crystal surface. The relationship between supramolecular synthons, which come from observation of complete crystal structures, and growth units, is at present poorly understood.

2. Build-up or coalescence of clusters.
   $A_n + A = A_{n+1}$
   $A_n + A_m = A_{m+n} \ldots$
3. Formation of a critical nucleus $A_n^*$ and its growth.
   $A_{n-1} + A = A_n^*$
   $A_n^* + A = A_{n+1} \ldots$
4. Molecular accretion on macroscopic crystal surfaces ($\Omega$).
   $\Omega + A = \Omega A$

Below the critical nucleus $A_n^*$ sub-critical particles may form and redissolve according to statistical fluctuations in thermal energy. Once the critical (spherical) nucleus size has been reached, accretion proceeds in a fashion that has been likened to a radical chain reaction. Growing crystals have been shown by light scattering experiments to be surrounded by a partially ordered solution layer, which may be several micrometres thick. The resulting crystal structure and morphology (crystal shape) are dependent on the thermodynamics of the system (including the non-covalent intermolecular interactions), the kinetics, and mass and heat transport effects. The free energy required to form the critical nucleus, $\Delta G^*$, may be positive or negative under the conditions of the crystallisation and is frequently lowered by interactions with the reaction vessel surfaces or the presence of even very small concentrations of impurities. Low levels of impurities may also act to inhibit crystal growth on one or more faces. This is the basis for the action of kinetic growth inhibitors of gas hydrate formation in the natural gas industry (Section 7.2.3). A number of elegant experiments have been carried out to probe various aspects of crystal growth and molecular recognition at crystal surfaces and interfaces and we will examine some interesting cases in the sections below.

## 8.2.2 NMR Spectroscopy as a Tool to Probe Nucleation

Spitaleri, A., Hunter, C. A., McCabe, J. F., Packer, M. J., Cockroft, S. L., 'A $^1$H NMR study of crystal nucleation in solution', *CrystEngComm* 2004, **6**, 489–493.

A key question in crystal nucleation concerns the structure of the self-assembled aggregate that results in crystal nucleation and the growth units that form along the way towards a critical nucleus. It is very difficult to probe these early assembly processes however in the case of relatively simple compounds NMR spectroscopy can yield useful information. We saw in Chapter 6 (Box 6.1) how $^1$H NMR spectroscopy can be used as a tool to probe the solution structure of a host-guest compound of, for example, a cyclophane host. We also saw how cyclophanes (like a wide range of other compounds) can undergo aggregation in solution as manifest in concentration-dependent NMR chemical shift changes. At its simplest this aggregation results in the formation of dimers or other short oligomers. It is just this kind of weak association in solution, however, that must begin the nucleation process. Therefore solution NMR structure determination methods which make use of concentration-dependent chemical shift changes can be used to gain insight into crystal nucleation processes. This approach is at a relatively early stage but as NMR instrumentation increases in sophistication and computing resources improve it could become a significant tool in the future, particularly in cases where association constants and solubility constraints allow a large range of 'aggregation space' (*i.e.* large range of concentrations of all of the possible solution species) to be sampled. Figure 8.9a shows the chemical structure of sulfamerizine, a conformationally flexible drug molecule that exists in two crystal polymorphs depending on crystallisation solvent. Sulfamerizine exhibits concentration dependent behaviour in its $^1$H NMR spectrum as the sample is diluted which can be fitted to a dimerisation model with $K_a = 16\ M^{-1}$ in

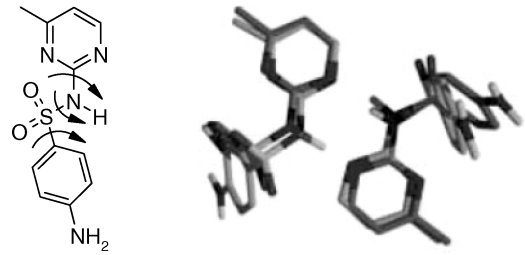


**Figure 8.9** (a) chemical structure of sulfamerizine showing possible rotateable bonds and (b) overlay of the structure of sulfamerizine dimers found in the crystal structure with the solution dimer structure from NMR spectroscopy (reproduced by permission of The Royal Society of Chemistry).

acetonitrile giving a maximum of 32 % dimer formation within solubility constraints. The structure of the solution dimer was determined using genetic algorithm methods and gave good agreement with the observed chemical shift changes during the dilution. Figure 8.9b shows an overlay of the solution dimer and the final crystal structure obtained from the same solvent. They are very similar, both exhibiting an 8-membered hydrogen bonded ring synthon. The rms (root mean square) average deviation between solution and crystal structure is just 0.30 Å. Thus the same dimer that predominates in the very early stages of nucleation is conserved in the eventual crystal structure.

## 8.2.3 Crystal Growth at Air–Liquid Interfaces

Weissbuch, I., Addadi, L., Berkovitch-Yellin, Z., Gati, E., Lahav, M., Leiserowitz, L., 'Spontaneous generation and amplification of optical-activity in α-amino-acids by enantioselective occlusion into centrosymmetric crystals of glycine', *Nature* 1984, **310**, 161–164.

Work by Lahav at the Weizmann Institute of Science, Israel, has focused upon attempts to gain insight into the structure of transient solution assemblies, which may form the nuclei for crystal growth. In particular, the crystallisation of the achiral amino acid $\alpha$-glycine (**8.4**) has been examined. The structure of pure glycine is shown in Figure 8.10(a) and comprises centrosymmetric layers (*i.e.* layers related by an inversion centre; inversion centres exchange *R* and *S* chirality in chiral compounds). Pure $\alpha$-glycine crystallises in the bipyramidal morphology shown in Figure 8.10(b). Interestingly, addition of resolved, chiral amino acids causes distinct changes in crystal morphology (Figure 8.10c–e). For example, addition of resolved *R*-enantiomers causes the formation of pyramidal crystals with an (010) basal face. (In crystallographic nomenclature the Miller indices (010) denote a plane parallel to the unit cell axes *a* and *c* and cutting the *b* axis once every unit cell. The $(0\bar{1}0)$ plane simply faces the opposite direction; the symbol $\bar{1}=-1$.) The analogous *S*-enantiomers result in pyramids with an $(0\bar{1}0)$ basal face. The difference between the two can be distinguished by eye. This effect is attributed to the inclusion (occlusion) of the chiral amino acid within the growing $\alpha$-glycine crystal. Chromatographic measurements indicate that about 0.3 % of the chiral amino acid is included within the glycine crystal. In glycine, the (010) and $(0\bar{1}0)$ faces are chiral and are related by an inversion centre. The chiral amino acid is only occluded on one face of the growing glycine crystal for steric reasons. If an *S*-enantiomer were to approach the (010) face, for example, the orientation of the amino acid side chain (of the 'wrong chirality') would cause overwhelming steric repulsion with the surface of the glycine crystal. On the other hand, the *S*-guest is a good match for the $(0\bar{1}0)$ face. Indeed, occlusion of the chiral amino acid retards the growth of the occluded face and hence alters the crystal morphology. If glycine crystals are grown

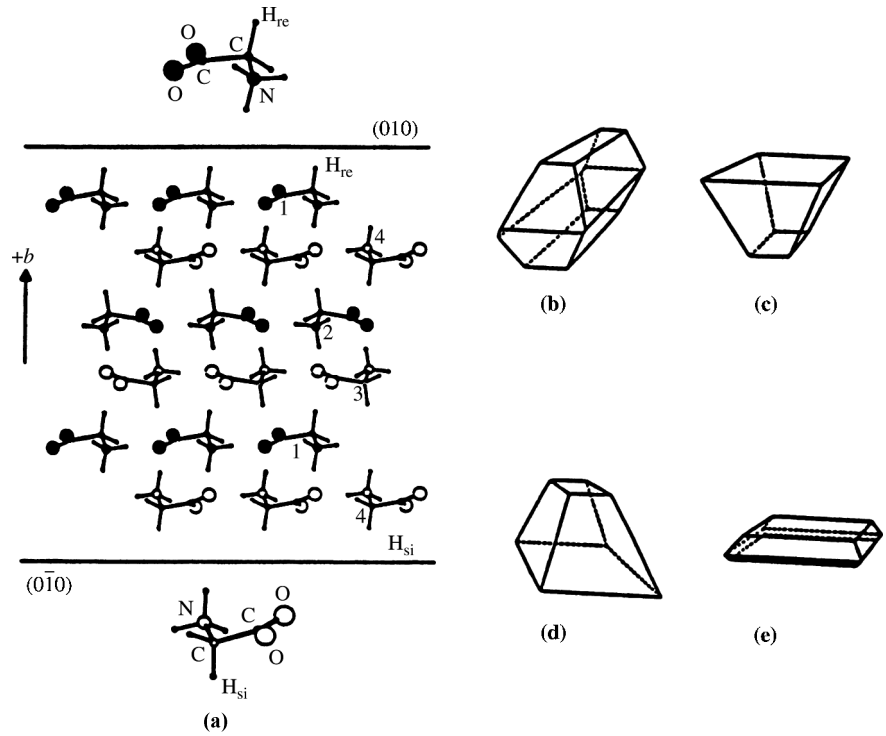


**Figure 8.10** (a) Crystal packing in α-glycine. (b) Crystal morphology for pure racemic $\alpha$-glycine. (c)–(e) crystal grown in the presence of (*R*), (*S*) and racemic hydrophobic amino acid derivatives as additives, respectively. (Reproduced with permission from [16]).

from an unresolved mixture of *R*,*S*-amino acids, then the growth of both faces is retarded, resulting in the formation of plate-like crystals.

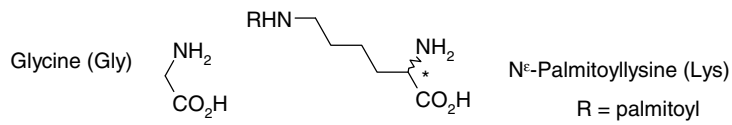


**8.4** **8.5**

If the chiral amino acids contain a hydrophobic residue (such as $N^{\varepsilon}$-palmitoyl-(*R*,*S*)-lysine, **8.5**) then the orientation and morphology of the glycine crystals may be templated. The hydrophobic portions of the $N^{\varepsilon}$-palmitoyllysine protrude from the aqueous phase, forming a two-dimensional monolayer at the air–water interface. The $\alpha$-glycine crystals are less dense than water and hence grow in this region. In the presence of resolved $N^{\varepsilon}$-palmitoyl-(*R*)-lysine, the $\alpha$-glycine crystals grow with their (010) faces upwards, whereas the *S*-enantiomer causes the formation of $\alpha$-glycine crystals with (0$\bar{1}$0) faces upwards. A racemic mixture of both enantiomers of the templating amino acid gives a random mixture of individual crystals with one or the other face upwards. Note the contrast to crystals grown in the absence of template, which are bipyramidal. Examination of the crystal packing of the solid-state structures of (*R*,*S*)-lysine and $\alpha$-glycine shows that they are very similar, suggesting that the growth of the $\alpha$-glycine is nucleated by the lysine residues. The chirality of the lysine determines the orientation of the first layer

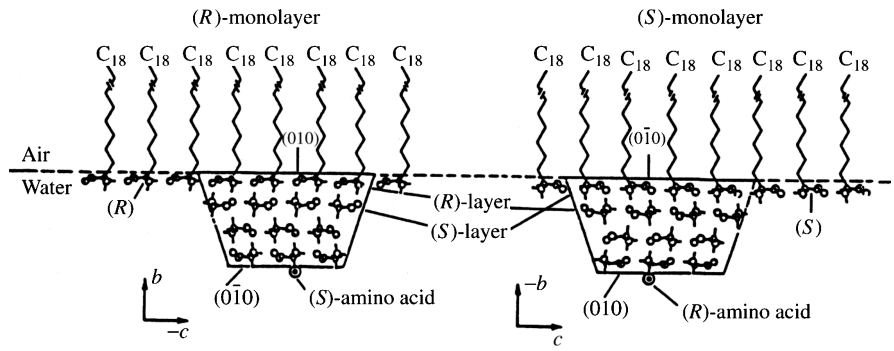


**Figure 8.11** Formation of pyramidal crystals of α-glycine attached to the $N^{\varepsilon}$-palmitoyl-(*R*,*S*)-lysine monolayers. (Reproduced with permission from [16]).

of the $\alpha$-glycine crystal. The observation of mixed crystals in the racemic case suggests the spontaneous organisation of the $N^{\varepsilon}$-palmitoyl-(*R*,*S*)-lysine monolayer into isolated *R* and *S* domains (Figure 8.11). More information on the formation of surface monolayers may be found in Chapter 13.

The interesting part about this phenomenon is that if one face of a growing glycine crystal is blocked during growth (*e.g.* by floating at an air–water interface), then the glycine crystals will occlude only one enantiomer from a racemic mixture in solution (the one that matches the exposed face) with the solution becoming enriched in the other. This is effectively a partial resolution of the two chiral amino acids. Furthermore, the effect is amplified if the chiral amino acids remaining in solution act, like $N^{\varepsilon}$-palmitoyl-(*R*,*S*)-lysine, as templates to the growth of further orientated glycine crystals. If the solution is rich in a templating *R*-enantiomer, for example, then this will begin crystal growth with the (010) face upwards and hence result in the occlusion of further *S*-enantiomer on the growing (0$\bar{1}$0) face in solution. Hence the solution will become even more enriched in *R*-enantiomer. This amplification mechanism has been used to carry out separations of chiral amino acids. It has also been suggested that it may form the basis for a model of the resolution of chiral amino acids under prebiotic conditions, which must have led ultimately to the incorporation of chial amino acids in the first evolving life. This primoridal 'Adam effect' is discussed further in the next section.

## 8.2.4 Chirality Induction: The Adam Effect

McBride, J. M., Tully, J. C., 'Did life grind to a start?', *Nature* 2008, **452**, 161–162.

As discussed in Section 8.2.1 crystal nucleation phenomena are of particular interest because, unlike most chemical reactions, which are the result of the actions of upwards of about $10^{20}$ individual molecules, nucleation involves only a very few events – sometimes only one. This means that unlike most chemistry, it is not subject to the statistical certainty that accompanies a very large sample size. This is of especial relevance to the concept of chirality in chemistry and biochemistry. Why, for example, do the vast majority of natural biological molecules exist as only one optical isomer? The human body readily absorbs only one glucose enantiomer, but relatively wealthy dieters may sweeten their food with 'inverted' sugars of opposite chirality to the naturally occurring forms, which are not absorbed by the body. Similarly, all amino acids in biochemical proteins of higher organisms are of L-handedness. Can this be linked to a primordial 'Adam effect', in which all life is derived from one single initial chiral event or molecule that templated the whole of evolution?

We have already seen the effect of chiral templates on the growth of $\alpha$-glycine crystals in the previous section. In the absence of templates, the formation of crystals of a racemic mixture of molecules that are individually chiral generally gives centrosymmetric structures in which both enantiomers are present, related by an inversion centre (see Box 8.2). If a chiral compound is resolved deliberately so that only one enantiomer is present, it must perforce crystallise in a chiral crystal symmetry form (chiral space group) corresponding to whichever enantiomer is present in solution. The crystal cannot contain an inversion or reflection symmetry element because inversion and reflection symmetry automatically reverse chirality. There are particular chemical systems, however, that adopt chiral crystal structures even though the compound in solution is not chiral. The solid-state chirality is a result of the way in which the molecules are packed together rather than the presence of individual molecular chiral centres. In such cases, the chirality of the crystal nucleus must determine the chirality of the macroscopic crystal. Because crystal nucleation is not statistically predictable, this may lead to surprising effects such as spontaneous resolution *i.e.* formation of crystals of a single enantiomeric form even though either D or L (*dextrorotatory* or *laevorotatory*) forms are equally likely.

Spontaneous resolution has been demonstrated ingeniously for crystals of $NaClO_3$ by J. Michael McBride and Randall Carter of Yale University, USA.[17] $NaClO_3$ is an achiral species in solution, but in the solid state it forms crystals in the chiral, cubic space group $P2_13$. The handedness of an individual crystal may be measured by its rotation of polarised light ($\pm 3.6°mm^{-1}$ at wavelength 546 nm). If a purified supersaturated solution of $NaClO_3$ is allowed to crystallise without any disturbance, it was shown as early as 1898 that in a sample of some 3137 crystals from 46 separate crystallisations, 50.08 % of the crystals were of D-handedness and the remainder were L, *i.e.* there is no statistical preference for one enantiomorphic form over the other, as would be expected. Following up on results by Kondepudi, however, McBride and Carter carried out the same experiment in a *stirred* solution. Nucleation is sufficiently unlikely in this system that they were able to obtain a sample in which a single crystal (of L-handedness) was growing towards the magnetic stirrer bar. The researchers made a video recording of this process and caught on camera the precise moment at which the growing crystal was first struck by the stirrer bar. Within 30 seconds of this event, more than 5000 daughter crystals had begun to form in the solution. All of these crystals were of L-handedness. The clear implication is that the impact of the stirrer bar sends a shower of crystallites of L-handedness into the supersaturated solution that act as secondary nuclei for the growth of daughter crystals, which are of the same handedness as the parent. No crystals of D chirality were observed. Video images are shown in Figure 8.12. The implication is that the one microscopic nucleation event that determined the handedness of the parent crystal results in the same chirality for the entire sample despite the fact that each form is equally likely.

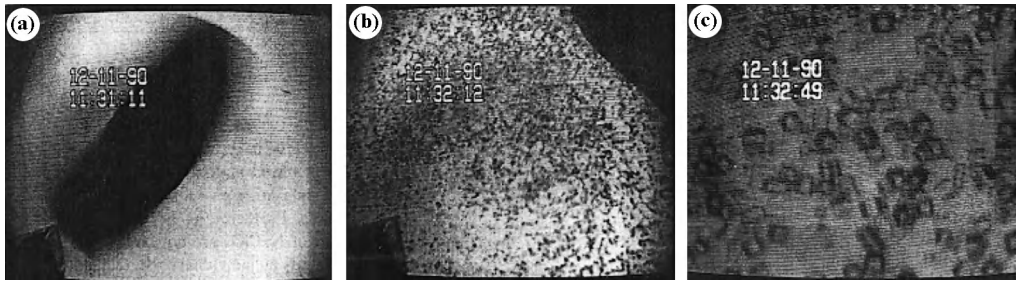


**Figure 8.12** Video images of a magnetically stirred crystallisation of $NaClO_3$ solution. (a) First contact between the stirrer bar and the growing parent crystal of L-handedness. (b) The daughter crystals formed within one minute of impact – note that the tip of the parent crystal is not damaged visibly by the contact with the stirrer bar. (c) Magnified image of the daughter prisms. (Copyright Wiley-VCH Verlag GmbH & Co. Reproduced by permission).

In 2005 further work on this system showed that crystals of a single enantiomeric form of sodium chlorate could be obtained from a slurry of mixed handedness crystals in a near-equilibrium saturated solution. In the presence of a slight excess of one crystal form in the crystalline solid part of the slurry stirring the mixture resulted in complete conversion of the sample to the chiral form of the whichever enantiomer is present in slight excess. The process requires the addition of glass beads, implying a mechanochemical role in the stirring process (*cf.* Section 8.2.9). The precise mechanism of the process is not known but one theory suggests that the grinding of the crystals against the glass beads accelerates up the net dissolution of the minor population of crystals. Once this material is dissolved the compounds can re-crystallise as the mirror image form and feed the growth of the major population. This mechanism is interesting because it could have played a role in the early evolution of life, *e.g.* the grinding of crystalline solids against sand grains on a sea shore and indeed a similar effect has been demonstrated for a chiral amino acid derivative, the imine of 2-methyl-benzaldehyde and phenylglycinamide. Unlike $NaClO_3$, this compound is chiral in solution as well as in the solid state, however in the presence of base it slowly converts from one enantiomer to the other. Stirring a slurry of this crystalline compound with glass beads under slightly basic conditions also results in enhancement of the population of a single crystal enantiomer.[18]

**Box 8.2** Molecular and Crystal Symmetry

In molecules, there are five symmetry elements: identity, mirror planes, proper rotation axes, improper rotation axes and inversion. A full explanation of these symmetry elements and their corresponding operators may be found in any standard chemistry textbook, and are shown diagramatically in Figure 8.13.

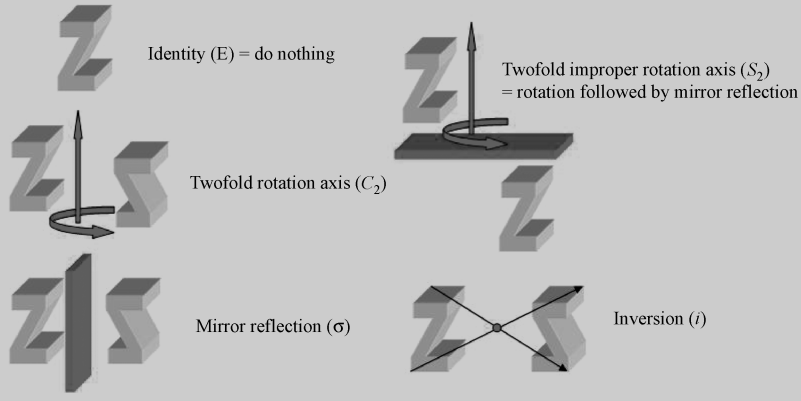


**Figure 8.13** Molecular symmetry operations.

Molecules in crystals may display all of these kinds of symmetry; and in addition, such molecular symmetry may relate one molecule to another within a crystal (although in practice inversion results in much better packing than rotation, and mirror symmetry is never observed *between* two molecules in real crystals, only relating one half of a molecule to the other[19]). Thus, a mirror plane, improper rotation or an inversion centre will relate one enantiomer to another in a crystal containing a racemic mixture of two chiral molecules. These are 'point' symmetry operators and are all that is necessary to describe the symmetry of a single molecule in various spectroscopic applications. Together, they give rise to the 36 molecular symmetry point groups (*e.g.* water, $C_{2v}$).

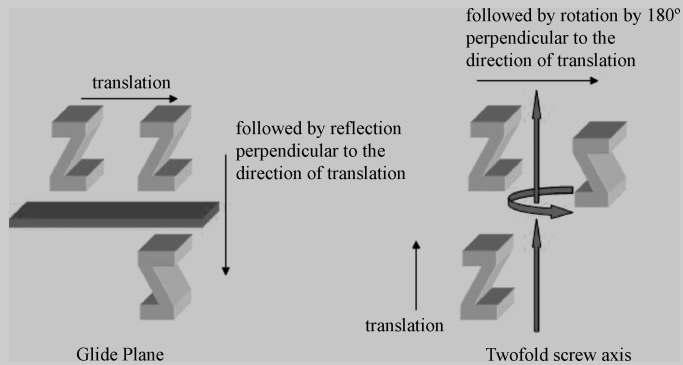


**Figure 8.14** Translational symmetry operations in crystals. A screw axis, symbol $n_m$, involves a translation by a fraction of *m/n* of the unit cell length followed by a rotation of 360/*n* degrees thus a twofold screw axis, $2_1$, involves a 180° rotation.

In crystallography, we are concerned with translational symmetry as well as point group symmetry, and this means that we must add two additional translational symmetry operators (Figure 8.14):

- screw axis (rotation + translation)
- glide plane (reflection + translation).

To make matters even more complicated, it is much more convenient in crystallography to use an entirely different system of symmetry symbols, termed the Herman–Maugin (as opposed to Schoenflies) notation (Table 8.2).

Combining the five point group symmetry operators with the two translational symmetry operators gives a total of exactly 230 different possible combinations, called the crystallographic *space groups*. Every crystal

**Table 8.2** Symmetry notation in the Schoenflies and Herman–Maugin systems commonly used in spectroscopy and crystallography, respectively.

| Operation | Spectroscopy | Crystallography |
|---|---|---|
| Proper rotation | $C_2$ | 2 (number of times you get coincidence) |
| | $C_3$ | 3 |
| | $C_4$ | 4 |
| | $C_6$ | 6 |
| Improper rotation | $S_6$ | $\bar{3}$ |
| | $S_4$ | $\bar{4}$ |
| | $S_3$ | $\bar{6}$ |
| Reflection | σ | *m* |
| Inversion | *i* | $\bar{1}$ |
| Screw axis | – | $n_m$ (180° rotation followed by translation by $\frac{m}{n}$ of the unit cell length parallel to the rotation axis, *e.g.* $2_1$ 180° rotation plus a half cell translation) |
| Glide plane | – | *a, b, c, n, d* (reflection + translation a half cell in indicated direction, *e.g.* *a* is a translation in the x direction) |

(*continued*)

**Box 8.2** (*continued*)

belongs to one of these space groups, just as every molecule belongs to a point group. The simplest (least symmetric) point group (possessing only the identity operator) is $C_1$. The lowest symmetry crystallographic space group is the primitive, triclinic space group $P1$. Most crystal unit cells (the basic building blocks of the crystal) contain not one, but several molecules, related to one another by the space group symmetry. The unique, non-symmetrical portion of the unit cell is termed the *asymmetric unit*. Application of space group symmetry on the asymmetric unit generates the entire unit cell. Repeating the unit cell infinitely in all three directions (by translation) gives the entire crystal structure.

Crystal engineering would be an extremely complicated discipline if all 230 space groups were common. In practice however, just two space groups, $P2_1/c$ and $P\bar{1}$ account for more than 60 % of the *ca.* 400 000 crystal structures known in the Cambridge Structural Database at the time of writing; together with a few other groups, they comprise the vast bulk of known structures (Table 8.3). Crystallographers and crystal engineers have essentially no control over space group and space group occurrence frequencies represent the intrinsic packing tendencies of molecules. Note the common occurrence of two-fold screw axes ($2_1$–corresponding to the herringbone packing mode as observed for crystalline benzene for example, Fig. 1.20b). This is an energetically efficient way to pack molecules together since bumps in one molecule align with troughs in adjacent molecules. Inversion symmetry is also common (more so for organometallic compounds, which tend to have less effort put into the resolution of chiral compounds), but with the exception of the two-fold rotation ($C_2$ or 2) in $C2/c$, other molecular (non-translational) symmetry elements are generally absent, indicating clearly that these forms of relating one molecule to another do not generally result in efficient crystal packing.

**Table 8.3** Common space groups (and hence forms of crystal packing in molecular crystals).

| Space group | Symmetry elements (in addition to identity) | Relative frequency of occurrence in the CSD (%) | |
|---|---|---|---|
| | | Organic compounds | Organometallic compounds |
| $P2_1/c$ | Screw, glide | 100 | 100 |
| $P\bar{1}$ | Inversion | 44.6 | 59.1 |
| $P2_12_12_1$ | Screw | 45.7 | 12.0 |
| $P2_1$ | Screw | 29.2 | 6.8 |
| $C2/c$ | Two-fold rotation, glide, inversion | 16.0 | 22.1 |
| $Pbca$ | Inversion, glide | 12.2 | 9.9 |
| $Pna2_1$ | Screw, glide | 4.7 | 4.1 |
| $Pbcn$ | Inversion, glide | 2.2 | 2.7 |
| $P1$ | None | 4.0 | 1.7 |

## 8.2.5 Dyeing Crystal Interfaces

Davey, R. J., Williams-Seton, L., Lieberman, H. F., Blagden, N., 'Stabilizing a solid-solid interface with a molecular-scale adhesive', *Nature* 1999, **402**, 797–799.

Another very intriguing piece of work that gives insight into the crystal nucleation process has been carried out on the simple sulfonamide saccharin (**8.6**) by Roger Davey of the University of Manchester, UK. Saccharin is one of the oldest known artificial sweeteners; about 300 times as sweet as sucrose

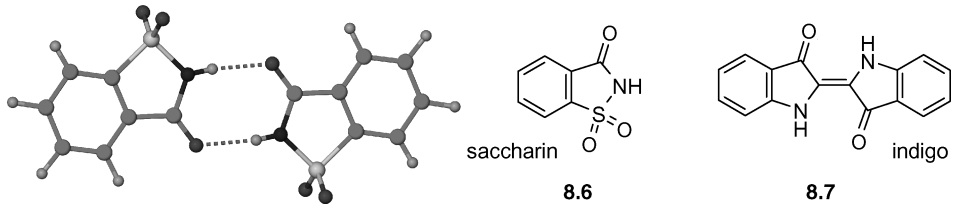


**Figure 8.15** Centrosymmetric 8-membered hydrogen bonded amide ring supramolecular synthon found in the crystal structure of saccharin.

but with an unpleasant bitter aftertaste. The crystal structure of saccharin occurs in the common centrosymmetric space group $P2_1/c$ and is based on the amide dimer synthon, Figure 8.15. Davey's group noticed that when crystallised from acetone solution some saccharin crystals proved to be twinned, *i.e.* comprised two joined crystals in this case along the $\{10\bar{2}\}$ plane. Surprisingly the twinned crystals occurred *less* frequently at higher supersaturation. Twinning is generally considered to be a fault or imperfection in crystal packing and thus would be expected to occur *more* frequently at higher supersaturations as crystals nucleate and grow more quickly, allowing less time for their formation. Crystallisation from ethanol solution generally was found to result in very little twinning, however addition of the difunctional blue dye molecule indigo (**8.7**) resulted in a dramatic increase in the formation of twins in ethanol, and remarkably the interface between the two crystals of the twin was dyed blue, Figure 8.16. In acetone solution saccharin exists as solvated monomers whereas in ethanol it exists as solvated monomers and hydrogen bonded dimers of the type shown in Figure 8.15. The twinning is favoured by the occurrence of monomers, not dimers and only occurs during crystal nucleation. Careful modelling studies showed that the $\{10\bar{2}\}$ twin plane is stabilised by the formation of a three-centre hydrogen bond (Figure 8.16b). Looking at the interface surface there are two possibilities. If the fundamental growth unit is monomeric (as in acetone) then the nucleus has a $\{10\bar{2}\}$ interface terminated by the amide and sulfoxide functionalities. Addition of further monomers can then result in the formation of the three centre hydrogen bond and hence give rise to twinning. On the other hand if the crystal nucleates by the aggregation of only dimers then the surface is terminated only by non-polar benzo substituents and so no twinning results. Hence we can see in this relatively simple example that

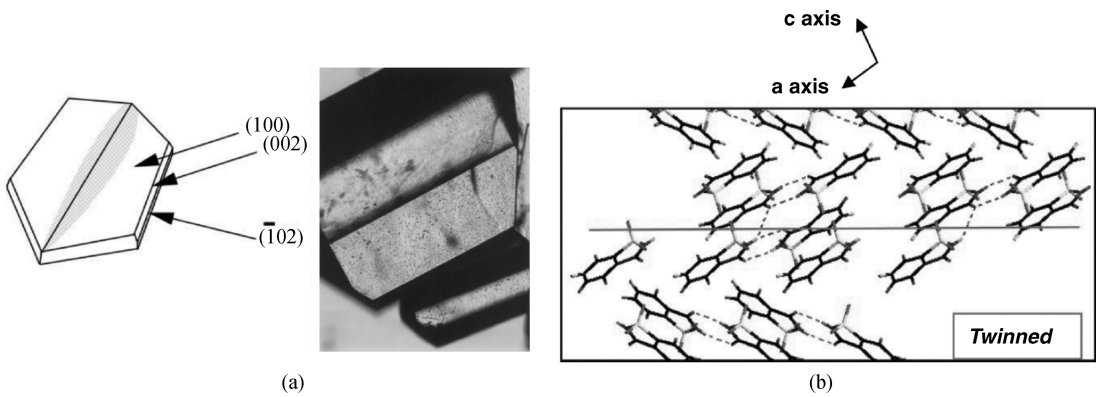


**Figure 8.16** (a) Optical micrograph and schematic diagram of a twinned crystal grown in the presence of indigo at high supersaturation. The crystal is *ca.* 70 mm in length. (b) The $\{10\bar{2}\}$ twin interface in saccharin showing the new three centre C═O···H–N hydrogen bond which joins dimers across the plane (reproduced by permission from The Royal Society of Chemistry). See plate section for colour version of this image.

the nature of the growth unit (monomer or dimer) is intimately linked to the final crystal morphology. So where does the indigo dye fit in? The indigo acts effectively as a catalyst for the formation of twins and the fact that it is only incorporated at the twin boundary (giving rise to a distinctive blue line) implies that it is only involved at the nucleation stage. Unlike the saccharin which is structurally resembles, the indigo is symmetrical and so no matter which side it joins to the growing nucleus the other face of the indigo molecule is available to hydrogen bonding to the sulfoxide oxygen atoms and act to modify the assembly of growth units to create nuclei incorporating the twin plane defect, even in ethanol solutions consisting mostly of dimers.

## 8.2.6 Hourglass Inclusions

Kahr, B., Gurney, R. W., 'Dyeing crystals', *Chem. Rev.* 2001, **101**, 893–951.

We saw in the previous section how an accidental match between the surface of the growing crystal nucleus and the structure of an impurity such as indigo can result in the incorporation of the impurity in a specific way into the growing crystal. The often beautiful, faceted shapes of crystals make it tempting to think of them as pure, perfectly ordered materials but in fact crystals contain many defects and dislocations and can readily incorporate impurities particularly of molecules that have some structural similarity to the parent crystal. The result is the formation of non-stoichiometric phases in which one crystal lattice can template the formation of another. In cases where the two components are not separated into clearly observable domains, this can result in significant confusion and apparent disorder, since the results of crystal structure determinations give an averaged structure over all of the unit cells of the crystal. This kind of behaviour was responsible for the apparent observation of so-called 'bond-stretch isomerism' in the late 1980s (Box 8.3). When the phenomenon is more well-defined however, it can result in mixed crystals with very interesting properties, particularly in inorganic semiconductor systems. One particularly visually appealing case of mixed crystallisation is the hourglass inclusions (HI).

Hourglass inclusions are formed by the inclusion of small amounts of water-soluble organic dye molecules such as the aryl sulfonates **8.8** and **8.9** within an inorganic lattice such as $K_2SO_4$ or $KH_2PO_4$. The inclusion of the dye, which is non-stoichiometric and usually present in about one in a thousand unit cells, is readily apparent because of the colour it imparts to specific regions of the inorganic crystal, resulting in a characteristic hourglass shape (Figure 8.17). Unlike the indigo inclusion in saccharin, however, dye inclusion occurs throughout the growing crystal. The hourglass shape arises from the fact that only certain crystal faces provide a match between the parent lattice spacing and the structure of the dye.

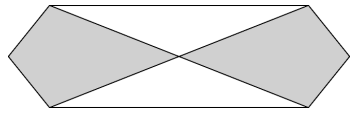

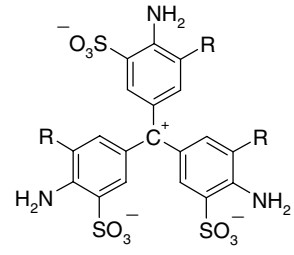


**8.8**

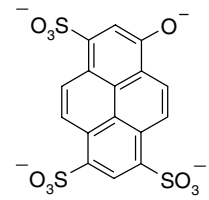


**8.9**

**Figure 8.17** Schematic drawing of the characteristic coloured and colourless regions of an hourglass inclusion compound. (Reprinted with permission from [21] © 1994 American Chemical Society).

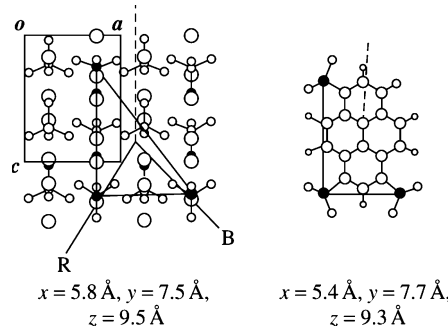


**Figure 8.18** Lattice match between $K_2SO_4$ and dye **8.9**. (Reproduced with permission from Reference 21).

The inclusion of dichroic fuchsia (**8.8**) into the lattice of potassium sulfate was first reported by H. E. Buckley in 1934, although hourglass inclusions were known as early as 1854. The advent of modern structure determination techniques has enabled their thorough characterisation and the design of new dye inclusions. Dichroic fuchsia is incorporated on to the growing {110} face of the $K_2SO_4$ crystal because of a close match in the disposition of the $SO_3^-$ functionalities of the dye with the sulfate positions in the crystal lattice. The rigid inorganic lattice causes the dye molecule to be deposited and held in a well-defined orientation and it cannot deposit on to lattice faces that it does not fit. Measurement of the polarised absorption spectra for HI crystals held in known orientation enabled Bart Kahr and co-workers from The University of Washington, Seattle, USA, to match observed and calculated absorbances, confirming the site-match model for the incorporation of the dye into the inorganic matrix. Armed with a knowledge of the dimensions and geometry of the site at which the dye molecule is included, Kahr went on to select a further dye, **8.9**, which exhibits an even better fit to the inorganic lattice (Figure 8.18). Gratifyingly, this dye molecule was also included, resulting in the first designer HI. More recent work has since resulted in the inclusion of a large range of coloured dyes (Figure 8.19) that are absorbed on to various faces of the growing salt crystals depending on the match between the positions of the sulfonate groups of the dye and the sulfonate ion arrangement in the lattice.

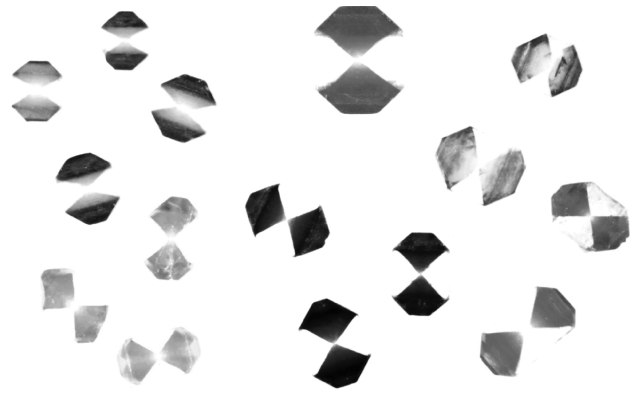

**Figure 8.19** Hourglass inclusion compounds of $K_2SO_4$ with a range of coloured dyes. (Courtesy of Prof. B. Kahr and Dr. J. A. Subramony.) See plate section for colour version of this image.

**Box 8.3** Bond Stretch Isomerism

Gibson, V. C. and McPartlin, M., 'Bond Stretch Isomerism: Fact or Artefact?', *J. Chem. Soc., Dalton Trans.*, 1992, 947–956.

Bond stretch isomerism was originally defined as the existence of two well-separated energy minima along a simple bond stretch coordinate. Hypothetical examples such as **8.10** have been proposed, and indeed hexamethyl(Dewar)benzene (**8.11**) is a real example, which is symmetrically forbidden to convert to the more stable Kekulé form. Except for special cases such as this, however, bond-stretch isomers were thought not to exist in separable isolable forms under ambient conditions. That all changed with the isolation and characterisation of a number of compounds such as $[Mo(O)Cl_2(PMe_2Ph)_3]$ (**8.12**), originally reported in 1970. These compounds apparently occurred in two forms of very different colour, blue and green, and the colours were originally thought to represent *cis* and *trans* geometrical isomers.

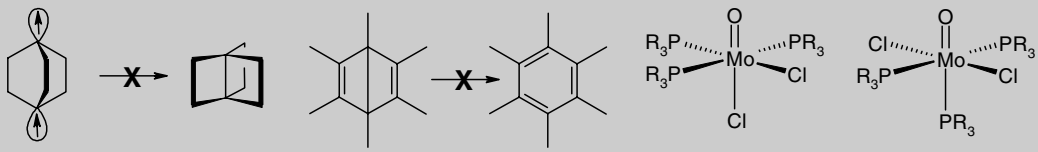


X-ray crystallographic results upon related complexes, however, showed that both blue and green forms were very likely to be *cis* isomers (the green form of **8.12** proved difficult to crystallise, but the analogous green $PEt_2Ph$ complex proved to be *cis*). The two materials were little different from each other, except for a small difference in the phosphine ligands and the remarkable observation that in the green forms in several different analogues the Mo=O bond distance was dramatically longer (1.801 Å) than in the blue form (1.676 Å). After much careful work and supporting spectroscopic evidence, it was suggested that these materials corresponded to bond-stretch isomers. The study of these materials and related species such as $[NbECl_3(PMe_3)_3]$ (E=O or S), which also exhibited coloured forms with anomalously different bond lengths, became topical in the late 1980s and early 1990s. However, some researchers were not convinced by this strange effect since there was no obvious chemical or crystal packing explanation for it, although theoretical extended Hückel calculations supported the proposals. Very careful re-examination of the composition of blue and green

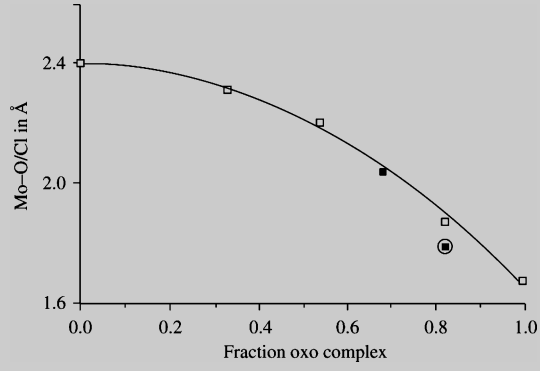


**Figure 8.20** Mo—O/Cl distance as a function of oxygen site occupancy in compounds of type **8.12**. (Reprinted with permission from Section Key Reference © 2001 American Chemical Society).

forms of $PMe_3$ derivatives of **8.12** revealed that the *green* forms could, in fact, be separated into a minor yellow fraction, identified as $[MoCl_3(PMe_2Ph)_3]$ and the pure *blue* compound with the shorter bond length, which is the genuine *cis*-**8.12**. Co-crystallisation of the yellow trichloro species with the blue material gives a crystal of a green colour, and the observed Mo=O bond distance is actually a weighted average of the relative occupancies of chloride (true Mo—Cl = 2.4 Å) and oxide in the Mo—O/Cl site. The contamination is clearly visible in the elongation of the anisotropic thermal ellipsoid for the contaminated oxide site and a graph of 'observed' Mo=O distance against fractional chloride occupancy can be constructed based on deliberately contaminated samples (Figure 8.20). Similar co-crystallisation was found to be the culprit of apparent bond-stretch isomerism in the $[NbECl_3(PMe_3)_3]$ system as well, which proved to contain traces of $[NbCl_4(PMe_3)_3]$. Bond-stretch isomerism is now generally accepted to be an artefact of mixed crystals, but the controversy did serve to highlight the useful point that homogeneous crystals need not be pure compounds and may be regarded as 'solid solutions'. We will return to this concept in Section 8.6.

## 8.2.7 Epitaxy: Engineering Crystals

MacDonald, J. C., Dorrestein, P. C., Pilley, M. M., Foote, M. M., Lundburg, J. L., Henning, R. W., Schultz, A. J., Manson, J. L., 'Design of layered crystalline materials using coordination chemistry and hydrogen bonds', *J. Am. Chem. Soc.* 2000, **122**, 11692–11702.

The match of parts of one kind of molecule onto a crystal face composed of different molecules can be used as a tool to grow composite crystals will well defined and chemically distinct regions sharing a common crystal lattice. The templated growth of a *daughter* crystal on the surface of a *parent* is termed *epitaxial growth* (from the Greek *epi* 'above' and *taxis* 'in ordered manner') and is of considerable importance in nanotechnology and in semiconductor fabrication where it is the key method of high crystalline quality growth for many semiconductors, including technologically important materials as silicon-germanium, gallium nitride, gallium arsenide and indium phosphide. Work by John MacDonald of Northern Arizona University, USA, has focussed on the deliberate engineering of composite crystals by this kind of templated growth. The work focussed on five bis(imidazolium 2,6-pyridinedicarboxylate) metal(II) trihydrate complexes containing either $Mn^{2+}$, $Co^{2+}$, $Ni^{2+}$, $Cu^{2+}$ or $Zn^{2+}$ (**8.13**). The pure complexes all crystallise in the same way with the same crystal structure (they are *isomorphous*[§]). The crystal packing is dominated by strong ionic hydrogen bonds between the 2,6-pyridinedicarboxylate anions and the imidazolium cations, forming two-dimensional layers. The ligand and imidazolium structure can be thought of as a host that is able to accommodate any one of the five metal guest cations, or a mixture of them. Changing the metal cations allows the electronic, magnetic and photophysical properties of the crystals to be tuned. So, crystal growth from solutions containing two or more different metal complexes produces mixed crystals in which mixtures of the different metal complexes are incorporated in the same relative molar ratio present in solution. Epitaxial growth of crystals from one metal complex on the surface of a seed crystal that contains a different member of the series results in composite crystals with well-defined regions containing different metals within the same ligand and imidazolium

[§] Crystals are *isomorphous* if they have the same space group and unit-cell dimensions, and the types and the positions of atoms in each crystal are the same except for a replacement of one or more atoms in one structure with different types of atoms in the other. *Isostructural* crystals have the same structure, but not necessarily the same cell dimensions nor the same chemical composition, and have a comparable variability in the coordinates of the atoms to that of the cell dimensions and chemical composition. For more information on crystallographic terms see the International Union of Crystallography (IUCr) online dictionary: http://reference.iucr.org/dictionary.

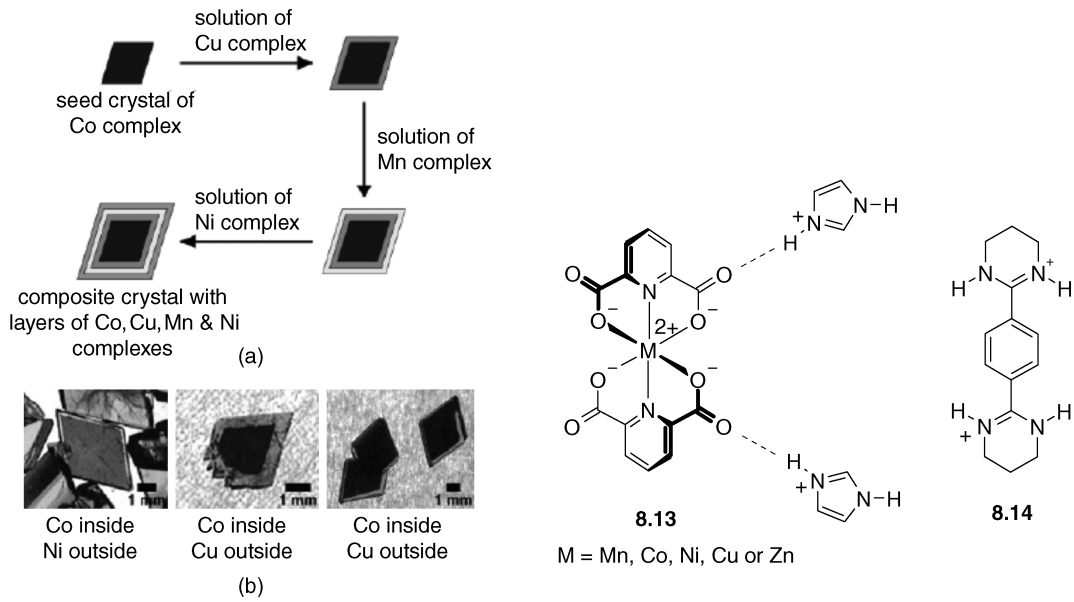


**Figure 8.21** (a) Illustration of a hypothetical composite crystal in which successive layers of different metal complexes of type **8.13** are added sequentially to the surface of a seed crystal. (b) Actual crystals composed of an inner region of $Co^{2+}$ and outer regions of $Ni^{2+}$ or $Cu^{2+}$ (reprinted with permission from Section Key Reference © 2000 American Chemical Society).

framework, Figure 8.21. Analogous work by Mir Wais Hosseini in Strasbourg has resulted in up to third generation composite crystals with alternating layers of red $[Fe(CN)_6]^{3-}$ and colourless $[Ru(CN)_6]^{3-}$ with cation **8.14**.[23] Interestingly, as we saw for the hourglass inclusions, it is not necessary for the parent and daughter phase to be strictly isomorphous. There just has to be a match of one part of the molecule to one of the crystal faces. In the equilibrating system shown in Figure 8.22 the equilibrium is shifted from the green monomer to the olive-yellow dinuclear complex as crystallisation proceeds. While the pure compounds have very different crystal structures, the green crystals are able to act as a parent for the epitaxial growth of an olive yellow daughter phase of the dinuclear complex because of the similarity of the *N*,*N*′,*N*″-trimethyltriazacyclononane ends of the two molecules.[24]

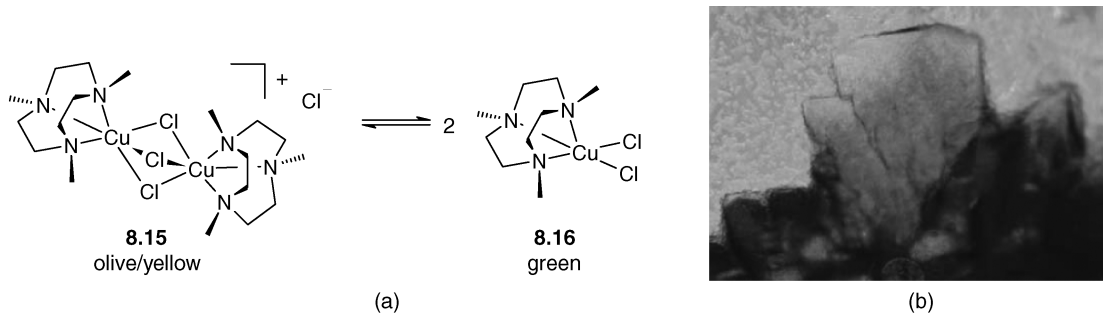


**Figure 8.22** (a) Equilibrium in copper(II) complexes of *N*,*N*′,*N*″-trimethyltriazacyclononane. (b) The green monomer **8.16** (bottom) is able to template the epitaxial growth of an olive-yellow daughter phase (top) of the dinuclear complex **8.15**.[24] See plate section for colour version of this image.

## 8.2.8 Crystals as Genes?

Bullard, T., Freudenthal, J., Avagyan, S. and Kahr, B., 'Test of Cairns-Smiths crystals-as-genes hypothesis', *Faraday Discuss.* 2007, **136**, 231–245.

Imperfections in crystals arising as a consequence of their growth mechanism have been the subject of a very imaginative proposal originally made by A. G. Cairns-Smith[25] for genetic information transfer in pre-biotic times – a kind of primitive precursor to modern biological information transfer by DNA and RNA. Cairns-Smith postulated that genetic information originated as imperfections in a mineral material. Following natural selection eventually some kind of nucleic acid type compound would have taken over from the primary mineral genes that were then discarded as mere scaffolds. Indeed it has been demonstrated that montmorillonite clay particles can catalyse the condensation of nucleotides.[26] Cairns-Smith argued that crystals with imperfections such as screw dislocations running through their structure could split apart and act as seeds for the growth of numerous daughter crystals all bearing the same pattern of dislocations. The daughter crystals could, in turn give rise to granddaughters which would again inherit the dislocation pattern and so on, Figure 8.23. Until recently this appealing hypothesis had not been subjected to any kind of experimental test. However Bart Kahr and co-workers have devised a method based on relatives of the hourglass inclusion crystals (Section 8.2.5), namely potassium hydrogen phthalate with included fluorescent dyes. While potassium hydrogen phthalate is not a candidate for the kinds of crystals that were abundant around the time of the beginning of life (minerals such as clays are more likely candidates), it does represent a system that is amenable to studying the crystals-as-genes hypothesis. The dye molecules are included to a different degree on different faces of 'growth hillocks' of the crystal as it forms. The growth hillocks represent a fossil record of the crystal growth process and these fossils can be 'dug up' by imaging using confocal laser scanning microscopy. The apex of each growth hillock represents the position of a screw dislocation and hence the dyes represent a way of mapping the 'genetic information' represented by these screw dislocation imperfections. Kahr's group produced offspring from the parent crystals by cleaving them with a razor blade and using the resulting fragments as seeds to produce daughter crystals. Mapping

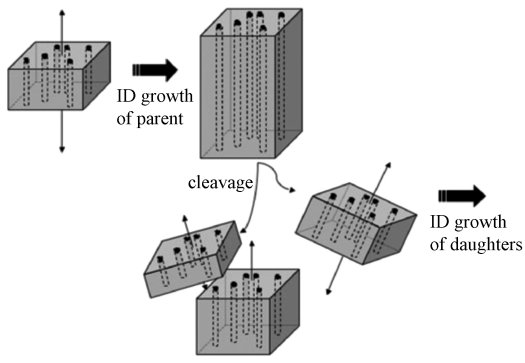


(a)

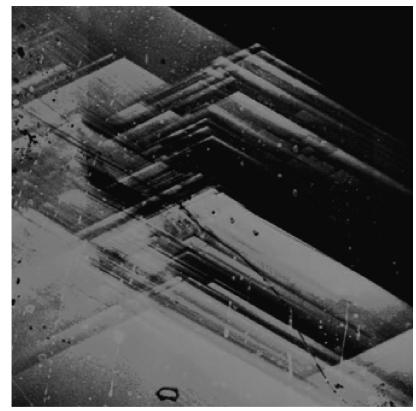

(b)

**Figure 8.23** (a) The transfer of imperfections in crystals *via* cleavage and subsequent growth. (b) Confocal laser scanning microscopy image of potassium hydrogen phthalate with occluded dichlorofluorecein showing details of luminescence that has developed in the fast growing slopes of the (010) growth hillock. The vertices of the chevron-shaped hillock 'fossils' mark dislocation cores (reproduced by permission of The Royal Society of Chemistry). See plate section for colour version of this image.

the pattern of screw dislocations in the daughter crystals showed that the dislocations were indeed transmitted from parent to daughter. However large numbers of new dislocations were also observed ('mutations') and the overall conclusion was that in this system the dislocation pattern was not faithful enough to transfer information from one generation to the next. However there is still a great deal of work to do on this popular concept.

## 8.2.9 Mechanochemistry and Topochemistry

Garay, A. L., Pichon, A., James, S. L., 'Solvent-free synthesis of metal complexes', *Chem. Soc. Rev.* 2007, **36**, 846–855.

To complete our discussion of insights into crystal nucleation and growth we turn to the very topical field of mechanochemistry – the synthesis of new crystalline materials by grinding their precursors in the solid state. Mechanochemistry in the form of manual grinding or automatic ball milling can be used as a means of inducing chemical reactions in between solid precursors to give microcrystalline powders of new chemical compounds or it can induce crystal phase changes, polymorphism or the formation of co-crystals (Section 8.6) with more than one molecular component. Strictly the term mechanochemistry should be used for processes involving the breaking or formation of chemical bonds, whereas more generally grinding or milling can induce other processes as well. Mechanochemical syntheses are of particular interest because they are both atom efficient and generate very little waste from purification procedures. Detailed studies of mechanochemical reactions, particularly by atomic force microscopy (AFM), give fascinating insights into the mobility of molecules in the solid state. As an example of solid-state reactivity, mechanochemistry is linked to the origins of the field of crystal engineering in topochemistry (Section 8.1.1). While the *topochemical postulate* suggests that (light induced) chemical reactions in solids require particular spatial mutual orientation of the reactants and close proximity of the reacting functional groups in the crystal, mechanochemistry, on the other hand, is reliant upon significant molecular movement and migration in crystalline solids. We will see that there is evidence that both of these factors are true, albeit with molecular migration being the most common. To begin with, however, we will look at some practicalities of mechanochemical synthesis.

Visual observation of the mechanochemical synthesis of simple coordination complexes such as $[Ni(phenanthroline)_3]^{2+}$ highlights just how efficient and striking this method is. Just a few strokes of grinding of pale green Ni(II) salts with white phenanthroline using a simple pestle and mortar produces a very sudden purple streak of colour attributed to the product, that follows the line of applied pressure. Within a minute the transformation is complete.[27] Despite the simplicity of the pestle and mortar approach, more consistent and reliable results are obtained by using a programmable ball mill. Ball mills also do not require manual effort and are capable of delivering more power at the sample. There are two common types of ball mill; the shaker mill and planetary mill, Figure 8.24. Each design is based on ball bearings either impacting or rubbing against the solid sample enclosed in the vessel with the shaker (or 'mixer') mill generally delivering higher power, while the planetary design is suitable for larger quantities. The sample container can be pre-cooled for low temperature grinding and any number of solid components can be ground together, or can be 'kneaded' in the presence of a drop of solvent. The impact of the ball on the sample can induce reactions in a variety of ways including local heating, reduction in particle size, improved mass transport, inducing crystal dislocations and local melting. In some cases mixing two organic solids together results in a *eutectic* mixture with a melting point below ambient and hence the solids temporarily melt until reaction is complete at which point they re-solidify.[28] The most important factor is mass transport, however – grinding is a little like stirring and the effects of localised

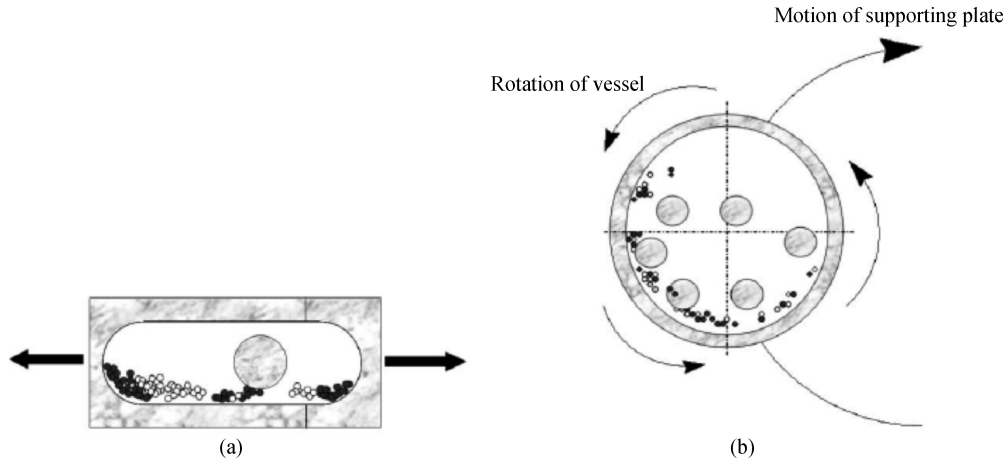


**Figure 8.24** (a) Shaker mill and (b) planetary mill (reproduced by permission of The Royal Society of Chemistry).

heating by impact may not be all that important. Indeed grinding represents a way of promoting a reaction without heating. One recent study has highlighted the importance of the glass transition temperature** of a material compared to the milling temperature. Decreasing the milling temperature tends to make molecular solids more amorphous while milling above $T_g$ can result in crystal-to-crystal transformation between polymorphs. This observation implies that localised heating is not responsible for these changes since equilibrium thermodynamics are not appropriate for describing the process.[29]

A nice example of grinding-induced crystal engineering is the formation of a hydrogen bonded co-crystal between ferrocene dicarboxylic acid and 1,4-diazabicyclo[2.2.2]octane (DABCO). The ferrocene dicarboxylic acid exists in the solid as a hydrogen bonded dimer based on two repeats of the carboxylic acid dimer synthon (solid A). Grinding with DABCO (solid B) gives rise to a new solid, C, in which the carboxylic acid dimers have been broken and replaced by an acid-amine synthon, Figure 8.25.[30]

Identification of the products of a mechanochemical reaction can be difficult and is primarily by powder X-ray diffraction (PXRD, Box 8.4). If the crystal structure of the product is known then its PXRD pattern can be calculated from the single crystal data and compared to the PXRD pattern of the mechanochemically synthesised material. If the mechanochemical reaction results in a new compound or new crystal form then the PXRD pattern will be clearly different to that of the starting materials but can yield little structural information. One possible tactic is to use crystallites of the mechanochemically prepared material to seed solution crystallisation of single crystals of the new phase suitable for structure determination using single crystal methods (Box 2.1). This approach was adopted successfully to characterise 'solid C' shown in Figure 8.25. Alternatively, using modern structure solution and Rietveld refinement methods it can be possible to solve and refine the structure purely from powder data, however this can be a very difficult task and can become impossible for flexible molecule or those with more than one component. There are particular problems with solving powder structures from samples prepared mechanochemically since the grinding process results in a loss of crystallinity and peak broadening due to induced stresses in the crystallites degrading the quality of the PXRD data.

** A glass transition represents a change in the physical properties of an amorphous (*i.e.* non-crystalline) material from liquid-like or rubbery behaviour to solid-like (a 'glassy state'). The transition occurs at a characteristic glass transition temperature, $T_g$, which is the temperature below which molecules have little relative mobility. The effect can be appreciated by cooling a length of rubber tubing in liquid nitrogen for example. Once cooled below its glass transition temperature the rubber shatters on impact like glass, instead of bending as it would at room temperature.

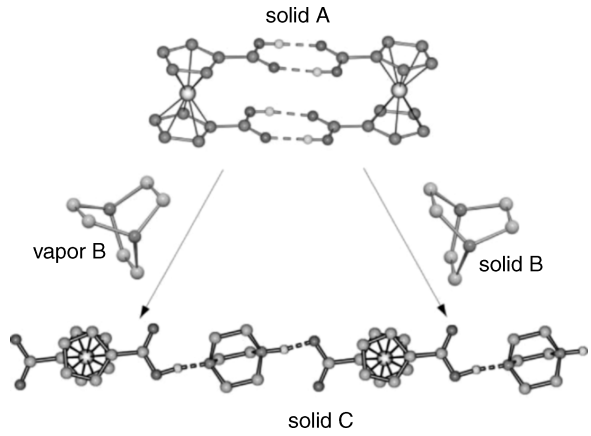


**Figure 8.25** Solid-solid or solid-vapour synthesis of a hydrogen bonded co-crystal between ferrocene dicarboxylic acid and 1,4-diazabicyclo[2.2.2]octane (reproduced by permission of The Royal Society of Chemistry).

Higher quality samples may be prepared by mechanochemical *initiation* of a reaction by grinding for a few minutes. The solid-state reaction is subsequently allowed to proceed to completion over a period of hours or days without further grinding resulting in the formation of larger, better quality crystallites. The fact that, once initiated, solid state reactions can proceed without grinding suggests that a great deal of molecular movement is possible in the solid state. This observation has been confirmed by extensive AFM and scanning near-field optical microscopy (SNOM) by Gerd Kaupp of the University of Oldenburg, Germany who has shown that mechanochemically induced molecular migration can be used to carry out a wide variety of solid state reactions in essentially 100% yield.[31] A particularly interesting demonstration of molecular migration is 'nanoscratching'.[32] This technique involves scratching the surface of a molecular crystal with the corner of a cube-shaped AFM tip. In cases where the crystal structure is interlocked scratching results in merely abrasion without molecular migration and the pile up of debris in front of the scratch direction. However, nanoscratching of compounds crystallising with anisotropic layers results in the facile migration of molecules along the resulting cleavage planes in between the layers. This migration is anisotropic and only occurs along the cleavage plane direction. The migration pattern can reveal information about the underlying structure. Figure 8.26 shows

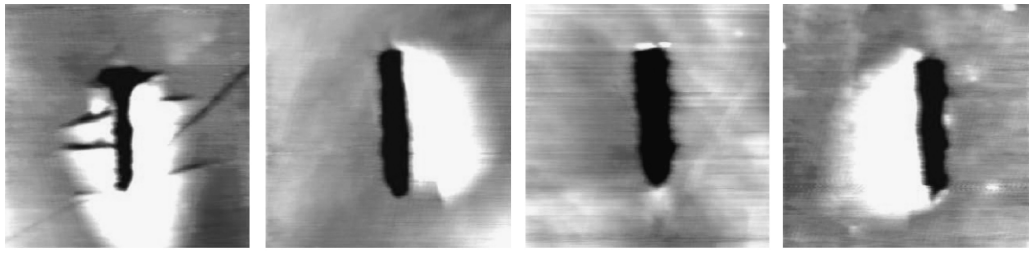


**Figure 8.26** Nanoscratching of a crystal of thiohydantoin (**8.17**). The light areas represent areas of molecular migration. Each scratch is *ca.* 5μm long. (a) 0° to the long axis or [001] direction the horizontal fissures show the direction of the cleavage planes and these is molecular migration in front and to either side of the scratch direction, (b) 90° molecular migration occurs only to the right of the scratch, consistent with the cleavage plane direction, (c) 180° there is only abrasion, no molecular migration and (d) 270° molecular migration occurs only on the left, opposite to 'b' (reproduced by permission of The Royal Society of Chemistry).

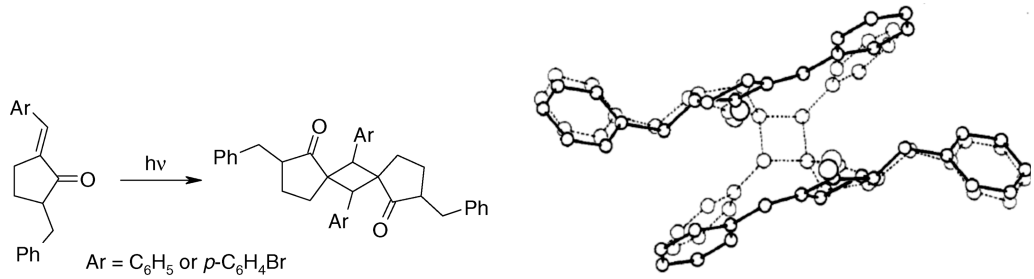


**Figure 8.27** (a) Topotactic, single crystal solid-state photodimerisation of 5-benzyl-2-benzylidene-cyclopentanone. (b) Superposition of the structures of the starting material and dimersied product (reprinted with permission from [33] © 1981 American Chemical Society).

AFM images arising from nanoscratching crystals of thiohydantoin (**8.17**). The molecule crystallises in hydrogen bonded sheets with strong hydrogen bonded interactions in the 2D plane of the sheet but weaker inter-sheet interactions, allowing the formation of cleavage planes.

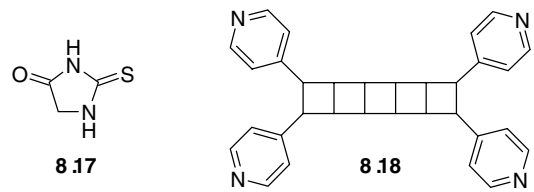


In contrast there are a few solid-state reactions that are genuinely topotactic with minimal movement during the conversion of starting materials to product. An example authenticated by AFM studies is the photodimerisation of 5-benzyl-2-benzylidene-cyclopentanone, Figure 8.27.[33] The double bonds in the starting material are 3.8 – 4.2 Å apart depending on the identity of the substituent and move together on formation of the centre 4-membered ring without significant change in the overall crystal packing arrangement.

Recent work by Len MacGillivray of the University of Iowa, USA, has used topochemistry to produce an impressive range of new solid compounds by the addition of hydrogen bonded templates in order to bring about the designer orientations of photochemically reactive molecules in the solid state.[34] A simple example is the use of resorcinol (1,3-dihydroxybenzene) to position two molecules of trans-1,2-bis (4-pyridyl)ethylene with their double bonds overlapping at *ca.* 4 Å as required by the topochemical postulate. Upon photolysis the product *rctt*-tetrakis(4-pyridyl)cyclobutane is formed stereospecifically and in 100 % yield, Scheme 8.2. In the absence of the resorcinol template trans-1,2-bis(4-pyridyl)ethylene is

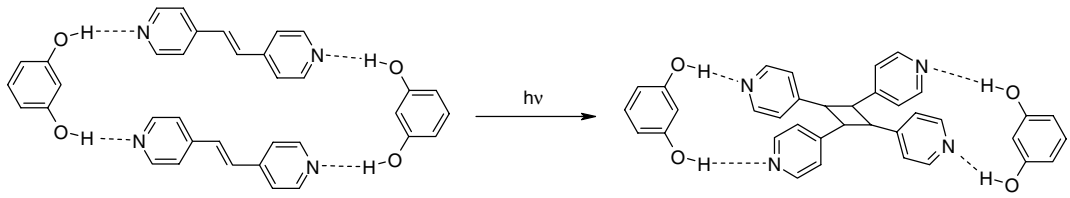


**Scheme 8.2** Solid state topochemical photocyclisation induced by resorcinol template positioning of the trans-1,2-bis(4-pyridyl)ethylene reactants within the crystal.[34]

photostable. MacGillivray and co-workers have gone on to produce striking 'ladderane' structures such as **8.18** consisting of up to five fused four-membered rings by multiple photocyclisaton reactions in crystals containing between templated poylene precursors.[35] The ladderane motif is ordinarily very difficult to synthesise artificially but occurs naturally as a core structural feature of ladderane lipids, which are integral components in the microbiological conversion of ammonium and nitrite ions to dinitrogen gas.

**Box 8.4** Powder X-ray Diffraction (PXRD)

Evans, J. S. O., 'X-ray and neutron powder diffraction' in *Encyclopedia of Supramolecular Chemistry*, Atwood, J. L. and Steed, J. W. (eds), Dekker: New York, 2004, vol. 2, *pp.* 1592–1598.

The diffraction of X-rays (and neutrons) by powders is governed by exactly the same physics as in the case of single crystals. The difference is that the X-ray beam interacts with many, randomly orientated crystallites instead of a single, three-dimensionally ordered array of molecules. The result is a loss of 3D information and the compression of the diffraction pattern into one dimension. Powder diffraction is thus an information poor technique in comparison to single crystal work. The advantage, of course, is that it is not necessary to undergo the often difficult process of preparing a suitable single crystal. The actual appearance of a powder diffraction pattern is of a cone of diffraction corresponding to each reflection that obeys the Bragg diffraction condition ($n\lambda = 2d \sin \theta$). Recorded on a photographic plate or electronic area detector the pattern appears as a series of concentric circles (termed *Debye-Scherrer rings*) of varying intensity. If the crystallite shape is highly anisotropic then the X-ray intensity will vary around the circle because the crystallites tend to line up in particular directions (a phenomenon termed *preferred orientation*). Commonly powder X-ray diffractometers are based on a point detector such as a scintillation counter and hence the pattern is captured as a one-dimensional cross sectional slice through the two dimensional concentric circle pattern, giving a PXRD pattern that is a plot of X-ray intensity against diffraction angle, $2\theta$. Under these circumstances preferred orientation can be a problem and care is taken during sample preparation to ensure random alignment of the crystallites. The contrast between single crystal and powder patterns is shown schematically in Figure 8.28 .

Two common geometries are used for collecting powder diffraction data, either the 'reflection' or Bragg-Brentano method (Figure 8.29a) which uses a flat plate sample holder made either of glass or, ideally, of an

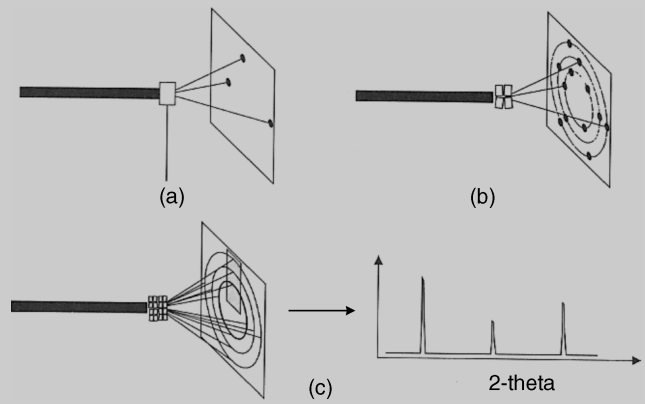


**Figure 8.28** Schematic diagram showing (a) diffraction from a single crystal, (b) from four crystals at different orientations with respect to the incident beam and (c) from a polycrystalline powder giving rise to a pattern of concentric cones of diffraction, often presented as a one-dimensional plot of intensity *vs* diffraction angle (reproduced by permission of The Royal Society of Chemistry).

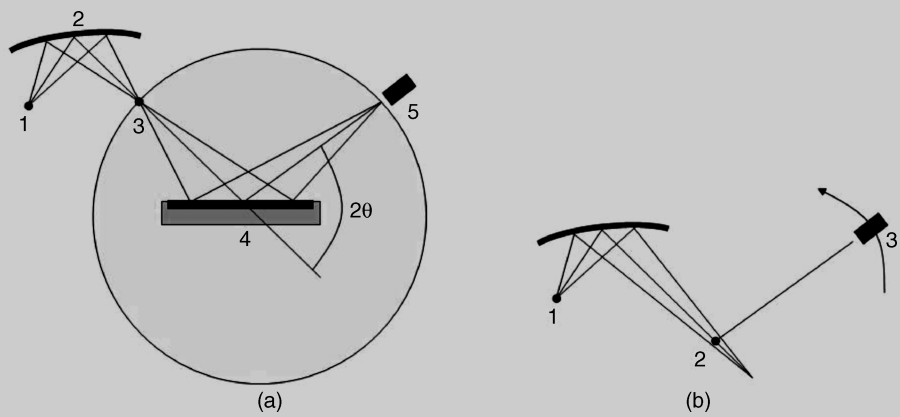


**Figure 8.29** Typical geometries in laboratory PXRD instruments (a) Bragg-Brentano, (b) capillary (not to scale).

orientated silicon wafer (aligned to give zero background), or the 'transmission' method (Figure 8.29b) in which the sample is placed in a thin walled glass capillary. In the Bragg-Brentano method an X-ray line source is placed at position 1 (Figure 8.29a) and passed through a curved Johannsen monochromator (typically Ge (111)) to give an effective, monochromatic line source at position 3. The sample, typical area 100 $mm^2$, is placed at 4 and diffracted X-rays detected by a scintillation counter at position 5. Often an additional graphite monochromator is placed between the sample and detector to give only a 2:1 mixture of Cu-K$\alpha_1$ and Cu-K$\alpha_2$ radiation ($\lambda$ = 1.540569 and 1.544493 Å, respectively).

An X-ray powder diffraction pattern is a useful characteristic 'fingerprint' of a particular crystal form of a compound and libraries exist such as the International Centre for Diffraction Data's Powder Diffraction File (PDF) containing known common diffraction patterns, particularly for simple inorganic materials. Moreover the data in the Cambridge Structural Database allows the calculation of the theoretical powder diffraction pattern for any of the *ca.* 400,000 compounds in it for which 3D atomic coordinates are known. More often than not, however, PXRD patterns of new materials are encountered and there are significant limitations on the use of PXRD patterns to determine structure *ab initio.* It is generally only possible to undertake a structure determination using powder data for single-component crystals of small molecules, with few conformational degrees of freedom. Structure solution and refinement is assisted by high quality data with relatively narrow peaks. Narrow peak widths, particularly of the type obtained from a synchrotron X-ray source, allow much better deconvolution of overlapping data than conventional laboratory instruments. To give some idea of the problem a typical unit cell of volume 3400 $Å^3$ that would be readily studied by single crystal methods would give rise to *ca.* 5500 reflections between 0 and 90° 2θ using copper-$K_\alpha$ radiation. With typical peak widths of 0.15° (at full width, half maximum, FWHM) this means that there is only about a tenth of the space needed to fully resolve every peak even if they were evenly spaced. In order to determine a structure by powder diffraction it is first necessary to *index* the pattern and hence determine unit cell dimensions from observed peak positions. Space group symmetry is then determined from systematic absences in a similar way to single crystal data. A starting model is then needed comprising approximate atomic coordinates and peak shape function is needed. Obtaining this model is termed *structure solution* and the process can be challenging. Various methods can be used including direct methods or Patterson solution as for single crystal methods, but these techniques are hampered by the dearth of reliable intensities for non-overlapping Bragg peaks in the powder pattern. Other direct space methods involving varying the position of a known structure or structural fragment such as Monte Carlo, simulated annealing or genetic algorithms are also very powerful. A recent development is charge flipping.[36] These methods are fascinating but outside of the scope of this book. The most common peak shape function is the *pseudo*-Voigt

(*continued*)

**Box 8.4** (*continued*)

(a mixture of Gaussian and Lorentzian contributions). The initial model is refined to give the final structure using the powerful technique of Rietveld refinement. This uses the least squares method to vary the atomic coordinates, thermal and unit cell parameters to maximise the agreement between calculated and observed intensity *over the whole pattern*, not just the peak maxima. The final quality of the structure is assessed by agreement (or *residual*) factors such as $R_{wp}$ (residual weighed powder based on the entire pattern) or $R_{Bragg}$ (based on the observed and calculated intensities of the Bragg peaks). Often a good quality assessment can be made by a visual inspection of a superimposed plot of the observed and calculated PXRD patterns, Figure 8.30.

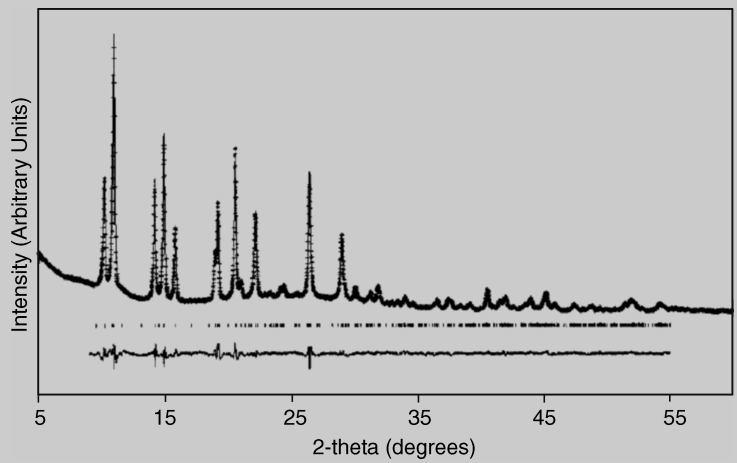


**Figure 8.30** Rietveld refinement of the non-linear optically active inclusion compound 4-(4-dimethylaminophenylazo)-1-methyl-pyridinium[$MnCr(oxalate)_3$]·0.6MeCN. The experimental PXRD pattern is shown as crosses superimposed on a solid line representing the final calculated pattern. The difference between the two is the lower line, which should ideally be flat. The 'tick marks' represent the positions of the individual Bragg peaks – the overlap particularly at high 2θ is evident. In this case $R_{wp} = 1.45$ % and $R_{Bragg} = 2.74$ % representing good agreement (reprinted with permission from [37] © 2001 American Chemical Society).

## 8.3 Understanding Crystal Structures

### 8.3.1 Graph Set Analysis

Bernstein, J., Davis, R. E., Shimoni, L. and Chang, N.-L., 'Patterns in hydrogen bonding: functionality and graph set analysis in crystals', *Angew. Chem., Int. Ed. Engl.*, 1995, **34**, 1555–1573.

Having discussed the occurrence of individual hydrogen bonds, and the importance of their interconnectivity within the context of molecular shape in determining solid-state structure, it is important to develop a language to describe the way in which hydrogen-bonded networks are assembled in crystals. In particular, such a language can help with the identification of related families of crystal geometries, topologies and connectivity in chemically very different structures.

Such a system of nomenclature and analysis—graph set analysis—has been applied to hydrogen bonds by Margaret C. Etter (University of Minnesota, USA), and extended by Joel Bernstein (Ben-Gurion University, Israel) and Raymond Davis (University of Texas, Austin, USA). Using graph set analysis, all hydrogen-bonded crystal structures may be reduced to combinations of four simple patterns designated chains (**C**), rings (**R**), intramolecular hydrogen bonded patterns (**S**, for 'self') and other finite patterns

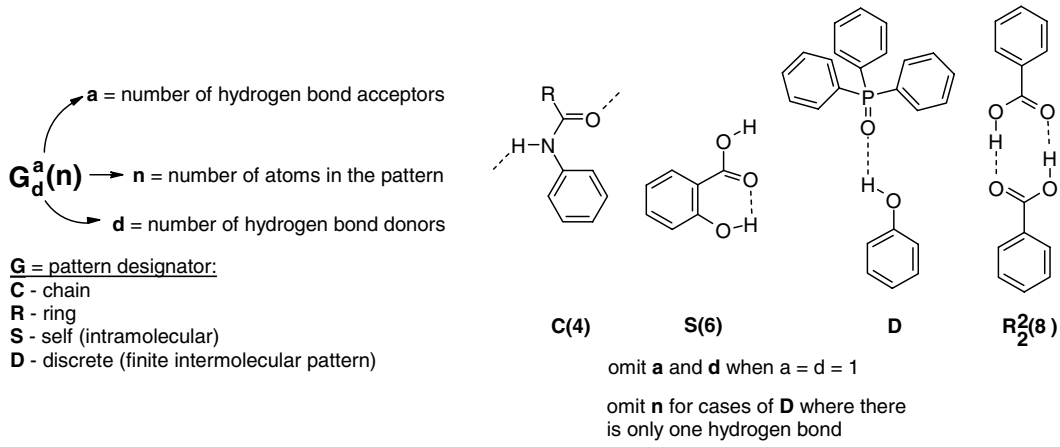


**Figure 8.31** The composition of the graph set descriptor with illustrative examples.

(**D**, for 'discrete'). To these fundamental designators is added a subscript denoting the number of hydrogen bond donors in the pattern (**d**) and a superscript denoting the number of acceptors (**a**). The total number of atoms (**n**), including H, in the pattern is termed the *degree* of the pattern and is given in brackets after the pattern designator. This gives a total graph set descriptor $\mathbf{G_d^a(n)}$ (Figure 8.31).

This nomenclature is readily apparent in simple cases where there is only one type of (symmetry unique) hydrogen bond and one kind of pattern. A structure containing only one type of hydrogen bond is referred to as a *motif* and will have one or more graph set descriptors associated with it. In more complex cases, where there is more than one motif in the structure, it is possible to assign graph set descriptors for each motif individually as if the others were not present. Such descriptors are termed *first-level* graph sets and collectively form the *unitary graph set*, given the symbol $\mathbf{N_1}$.

The most interesting cases frequently arise from the interaction of more than one motif. Take a structure such as the amino acid $\alpha$-glycine ($NH_3^+CH_2CO_2^-$) in which there are two unique hydrogen bonds, *a* and *b* (Figure 8.32). In additional to the first-level graph sets describing *a* and *b* individually, we also have a binary graph set, $\mathbf{N_2}$, involving both *a* and *b*. In the case of glycine there are, in fact, two choices

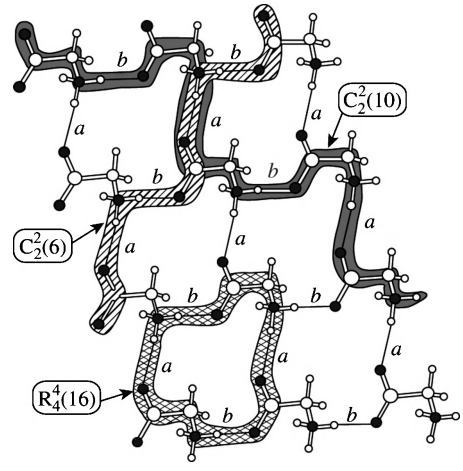


**Figure 8.32** Graph set assignments for the binary level of $\alpha$-glycine. (Copyright Wiley-VCH Verlag GmbH & Co. KGaA. Reproduced by permission).

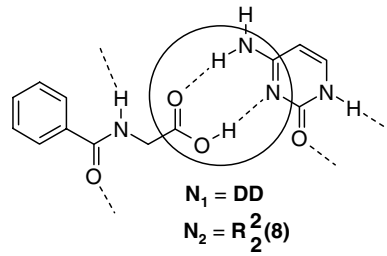


**Figure 8.33** The first-level graph set for this ring is **DD**. The descriptor $\mathbf{R_2^2(8)}$ is a second-level graph set.

for hydrogen-bonded chains involving hydrogen bonds *a* and *b*, namely $\mathbf{C_2^2(6)}$ referred to as the *basic* binary graph set, and $\mathbf{C_2^2(10)}$, which is a *complex* graph set because it has a higher value of *n* for the same two hydrogen bonds. However, neither of these two binary graph sets describes the most obvious feature of the system, the ring, which is denoted $\mathbf{R_4^4(16)}$.

In a system involving three hydrogen bonds *a*, *b* and *c* there will be three binary (second-level) graph sets that contain more than one kind of hydrogen bond (these can even be the same type of bond in two symmetry unique forms; they do not have to be chemically different), $\mathbf{N_2}(ab)$, $\mathbf{N_2}(ac)$ and $\mathbf{N_2}(bc)$. We will also have a third-level graph set, $\mathbf{N_3}(abc)$, and so on. The relationship between first- and second-level graph sets is illustrated by the example shown in Figure 8.33, in which there are two quite distinct hydrogen bonds forming an eight-membered ring. It is tempting to apply immediately the descriptor $\mathbf{R_2^2(8)}$ to this portion of the structure; however, while correct, this is a second-level graph set because it involves two different hydrogen bonds. Formally, we must first recognise the presence of two distinct **D** motifs (one for each type of hydrogen bond), *i.e.* $\mathbf{N_1 = DD}$ before moving on to assign $\mathbf{N_2 = R_2^2(8)}$ (amongst other connectivity). Graph set analysis is potentially an extremely powerful tool in crystal engineering studies. Its unambiguous application, however, often depends on automated analysis by computer in more complicated cases. Automated graph set descriptor assignment up to the second level graph set is available in the *RPluto* software available free of charge from the Cambridge Crystallographic Data Centre (www.ccdc.cam.ac.uk). The software requires the user to make fundamental decisions such as what constitutes a hydrogen bond and from that point is able to define the first and second level graph sets automatically.

## 8.3.2 Etter's Rules

Etter, M. C., 'Encoding and decoding hydrogen bond patterns of organic compounds', *Acc. Chem. Res.*, 1990, **23**, 120–126.

In the light of the difficulty in predicting even simple crystal structures, it is unsurprising that few researchers in the crystal engineering field have dared to make detailed forecasts of solid-state behaviour. In the case of reasonably strongly hydrogen-bonded systems, however, in which there is a single interaction that dominates the crystal packing of regularly shaped small molecules, it is possible to make some predictions about the resulting crystal structures. Such a set of rules with some predictive ability has been laid down by Margaret Etter who made the following general statements concerning hydrogen bonded organic compounds:

1. All good proton donors and acceptors are used in hydrogen bonding.
2. Six-membered-ring intramolecular hydrogen bonds form in preference to intermolecular hydrogen bonds.

3. The best proton donors and acceptors remaining after intramolecular hydrogen bond formation form intermolecular hydrogen bonds to one another.

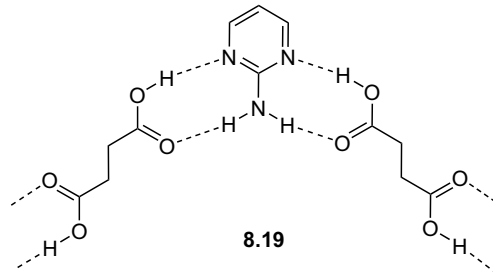

**8.19**

In the case of rule 1, a 'good proton donor' is one such as those found in carboxylic acids, amides, ureas, anilines, imides, phenols *etc.* The reasoning behind rule 2 is based on the same kind of ideas as the chelate effect in inorganic chemistry (Section 1.5) and is entropically favoured. Five- and seven-membered intramolecular hydrogen-bonded rings are also common, but it has not been established how well these more potentially strained systems compete with intermolecular hydrogen bond formation. Rule 3 may be illustrated by examination of the co-crystals formed between 2-aminopyrimidine and carboxylic acids. The best donors (acid OH) are paired with the best acceptors (ring N) *e.g.* (**8.19**). In addition to these general rules specific functional classes may also tolerate generalisations. These are listed below.

### *Nitroanilines*

1. Amino protons will hydrogen bond to nitro groups.
2. One or more intermolecular amino–nitro hydrogen bonds will form.
3. The aggregate patterns formed from intermolecular hydrogen bonds between substituents in *meta* and *para* positions will be acentric.
4. The amino–nitro interaction is usually a three-centre hydrogen bond, $\mathbf{R_1^2(4)}$ (**8.20**).
5. *Ortho*-substituted primary nitroanilines usually form two-centre intermolecular hydrogen bonds rather then three-centre, with graph set $\mathbf{R_2^2(6)}$ (**8.21**).

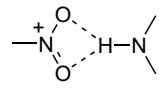

**8.20**

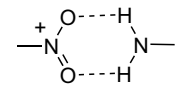

**8.21**

### *Diarylureas*

1. The NH hydrogen atoms tend to adopt an *anti* relationship to the carbonyl group and to form three-centre bonds to urea carbonyl groups, $\mathbf{C(4)[R_2^1(6)]}$ (**8.22**).
2. Co-crystals form in $\mathbf{R_2^1(6)}$ patterns (**8.23**) when there are strong *meta* substituted electron-withdrawing substituents, like $NO_2$ groups, on the aryl rings, and when the guest molecules have acceptor groups that are stronger than the internally hydrogen bonded urea carbonyl oxygen.
3. When co-crystals form, the NH protons form three-centre bonds to acceptor groups, $\mathbf{R_2^1(6)}$.
4. Nitro groups of *m*-nitro substituted diaryl ureas are not usually used as hydrogen bond acceptors for urea NH hydrogen atoms in the presence of guest molecules with good hydrogen bond acceptors.

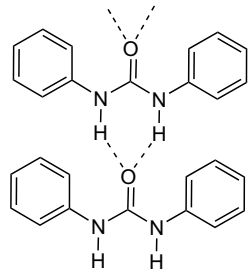

**8.22**

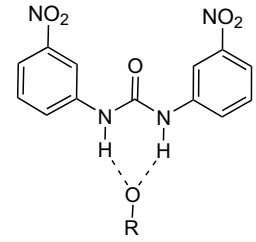

**8.23**

*Carboxylic Acid Co-crystals with 2-Aminopyrimidine*

1. Both NH protons and both ring nitrogen atoms are used in hydrogen bonds.
2. 2-Aminopyrimidine prefers to form hydrogen bonds to acids rather than to itself.
3. 2-Aminopyrimidine forms cyclic $\mathbf{R_2^2(8)}$ patterns with acids and with itself.
4. The two NH protons need not form hydrogen bonds to identical groups. Likewise for ring nitrogen atoms.
5. A ranking of proton-accepting ability consistent with these structures is N1 > N3 > acid carbonyl > N2 or N4 (see **8.24** and **8.25**).
6. Proton donor ranking is acid OH > NH(1) > NH(3) > NH(2).

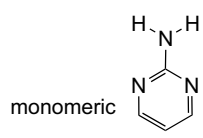


**8.24**

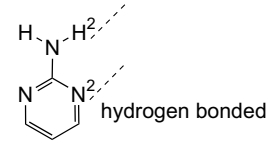


**8.25**

*Nucleotide Base Co-crystals*

1. Adenine (A) and cytosine (C) form co-crystals with many acidic organic compounds, but thymine and uracil do not.
2. Co-crystals of A and C with carboxylic acids give patterns with $\mathbf{R_2^2(8)}$ or $\mathbf{R_2^2(9)}$ graph sets (**8.26**).
3. Neutral *N*-acylamino acids complex with A or C in $\mathbf{R_2^2(8)}$ patterns (**8.27**).
4. Cyclic alternant —C(O)—NH— groups complex with A and C with preferred graph set $\mathbf{R_2^2(9)}$ $\mathbf{R_2^2(9)}$ (**8.28**).
5. Three-centred hydrogen bond contacts are frequently found with $\mathbf{N_1} = \mathbf{R_2^2(8)}$ and $\mathbf{N_2} = \mathbf{R_2^2(12)}$ (**8.29**).
6. A common motif for nucleotide base complexes involves two primary amines and two carbonyl groups in an $\mathbf{R_4^2(8)}$ or $\mathbf{C_2^1(4)}$ pattern.

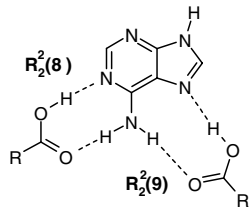


**8.26**

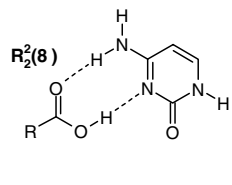


**8.27**

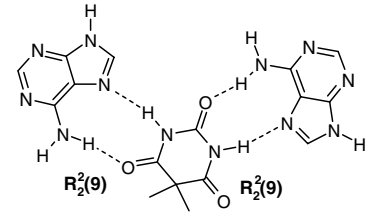


**8.28**

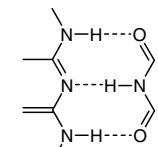

**8.29**

While empirical, Etter's work represented the first attempt to quantify some general rules about crystal packing. These rules have proved to be very useful and have inspired a number of follow-up studies on these kinds of system. For example, recent work by Ashwini Nangia at the University of Hyderabad, India, has focussed on diarylureas, in particular dipyridylurea.[38] Nangia and co-workers showed that the conventional urea tape motif (**8.22**) forms because the aryl groups are tilted out of the way of the carbonyl oxygen atom making it reasonably sterically unencumbered and allowing the approach of an adjacent urea group. In the presence of electron withdrawing substituents such as the $-NO_2$ group studied by Etter, or a pyridyl ring, the aryl CH atoms become more acidic and forces the molecule into a planar conformation by a double intramolecular CH···O hydrogen bonding interaction (remember intramolecular interactions are particularly favoured by Etter's rules). These hydrogen bonds then sterically restrict the oxygen atom forcing the urea NH group to interact either with guest molecules or with the pyridyl nitrogen atom, as in **8.30**, despite the fact that the hydrogen bond basicity of pyridine is much lower ($pK_{HB} = 1.9$) than ureas such as tetramethylurea ($pK_{HB} = 2.44$), see Section 8.1.4.

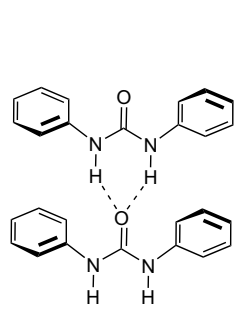

**8.22**- tilted aryl groups

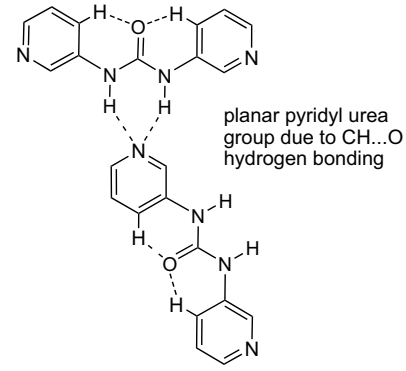


**8.30**

## 8.3.3 Crystal Deconstruction

Braga, D., Grepioni, F. and Desiraju, G. R., 'Crystal engineering and organometallic architecture', *Chem. Rev.*, 1998, **98**, 1375.

There is clearly a vast gap between a consideration of the processes by which molecules recognise one another beginning the crystal nucleation process, and an appreciation of the final effectively infinite crystal structure. Insights to the relationship between the two may be gained by the process of crystal deconstruction, illustrated schematically for a molecule of $Cr(CO)_6$ in Figure 8.34.[39]

This process involves taking an arbitrary reference molecule within the full crystal structure and gradually stripping away those molecules that surround it, initially to gain insight into the way in which it is enclosed in three dimensions by its nearest neighbours. The problem is then simplified further to two-dimensional and finally one-dimensional interactions. The analysis may proceed either *via* detailed examination of intermolecular distances and angles between nearest neighbours or by calculation of intermolecular interaction energies using computational atom–atom potential methods (Section 8.8). The ultimate aim is to identify pairs of molecules with the most important interacting geometries that may form the bases for key crystallographic symmetry operations and to understand the way in which they interact.

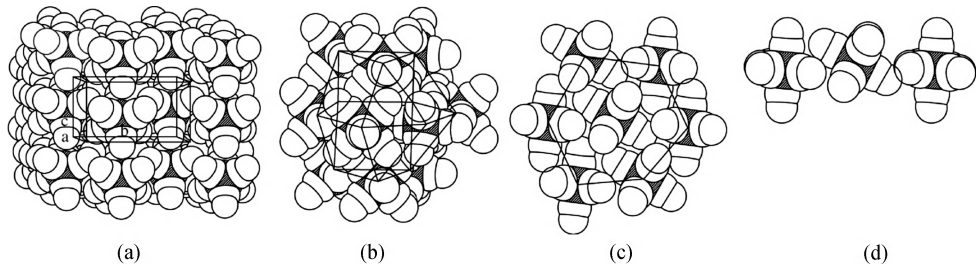


**Figure 8.34** The crystal structure decoding and deconstruction process for $Cr(CO)_6$ from (a) the full three-dimensional packing to (b) the 'enclosure shell' of first neighbours to (c) a molecular layer and finally (d) a molecular row. (Reprinted with permission from Section Key Reference © 1990 American Chemical Society).

### 8.3.4 Crystal Engineering Design Strategies

Crystal engineering design is the predictive branch of the topic. Strictly we are referring to 'soft' predictions in the sense that it is the occurrence of particular synthons, coordination network topologies, stoichiometries or structural features that is being designed rather than full prediction of the details of the crystal packing, symmetry and space group. It involves the use of knowledge of the optimum intermolecular interactions for the system in question, along with molecular shape, topology and electronic properties in order to select and prepare one or more components that will assemble spontaneously in the solid state into the desired crystal structure. The component(s) are ideally mixed in the appropriate ratio in a suitable solvent and allowed to crystallise by a variety of techniques, ranging from slow evaporation and slow cooling, through to more sophisticated methods such as convection, liquid–liquid diffusion or vapour diffusion. Alternatively solvothermal, solid-solid or solid-gas reactions may also be employed.

This kind of crystal design is more often a failure than a success, and crystal structure prediction, particularly 'hard' crystal structure prediction is still extremely difficult (Section 8.8). Generally, a large majority of the currently known host structures discussed in Chapter 7, for example, were discovered by accident rather than design. However, as our knowledge of the factors involved grows, in tandem with more powerful computational and modelling tools, more successes may be expected.

Consider a crystal made up of two separate molecular components (supramolecular tectons). At one end of the spectrum, this might be regarded as a host–guest complex or clathrate in which a crystalline network formed from one component acts as a host for the other component. Such a complex has the requirement that the host should form an approximately invariant network that is predominantly independent of the nature of the guest. This suggests that the host should, therefore, be able to accommodate a variety of guest species. A number of materials fitting this description have been described in Chapter 7 (*e.g.* trimesic acid, urea, helical tubulands, CTV *etc.*). Design of such materials is greatly facilitated if the host component may be subjected to a number of variations in molecular structure without disruption of the fundamental crystal packing motif (synthons), allowing structure tuning. Such manipulation is not feasible for urea (Section 7.3), for example, whereas the structures of the alicyclic diols that comprise the helical tubuland family (Section 7.4.2), may be modified widely. Simple design strategies that have been adopted for host networks include the choice of particularly unsymmetrical, or concave, molecules with awkward shapes that cannot close-pack efficiently, causing the inclusion of a second guest component on an approximate size fit basis as in the wheel and axel hosts (Section 7.4.2). It is fair to say, however, that there is little obvious link between molecular structure and crystal structure in many such systems.

At the other end of the two-component spectrum are tectons that possess mutually complementary shapes or functionality (*e.g.* hydrogen bond acid and base), which crystallise together preferentially

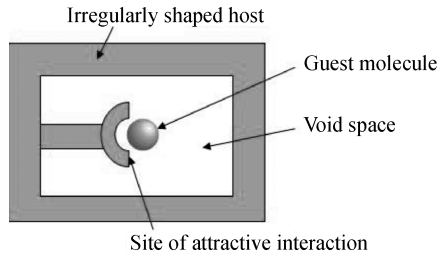


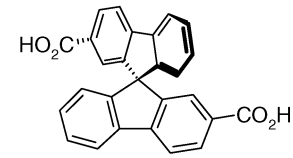


**8.31**

**Figure 8.35** The 'coordinato-clathrate' approach of Weber.[40]

when mixed, as opposed to forming isolated crystals of the pure components. In such cases, the distinction between host and guest is a highly subjective one at best, and the 'host–guest' terminology is not of great utility. Design strategies may be based on the electronic nature of the substituents (matching donor and acceptor; acid and base) or on their spatial distribution about the molecule.

The idea of awkward molecular shape and strongly interaction functionality as a crystal design tool has been developed by Weber *et al.*[40] into a 'coordinato-clathrate' approach in which not only does the guest posses an awkward shape and therefore pack poorly, but there is also a distinct site of guest binding (*e.g.* *via* hydrogen bonding) as shown in Figure 8.35. Specific examples include 9,9′-spirofluorene-2,2′-dicarboxylic acid (**8.31**), which interacts with guest molecules *via* hydrogen bonds to the carboxylic acid residues, but is prevented from crystallising as a pure substance by the awkward cross shape of the molecule.

From observation of the six-fold crystal packing geometry of phenol and hydroquinone clatharates, MacNicol has designed the 'hexahosts'. The crystal packing in hydroquinone results in the formation of an $(\text{up–down})_3$ arrangement of the aromatic rings (Section 7.5), leaving a cavity large enough to accommodate even guests such as $C_{60}$. By replacing the hydrogen bonded six-membered ring (**8.32**) with a covalent one, a range of hosts such as **8.33** have been prepared, which come together in the solid state in a fashion that mimics the hydroquinone inclusion ability.

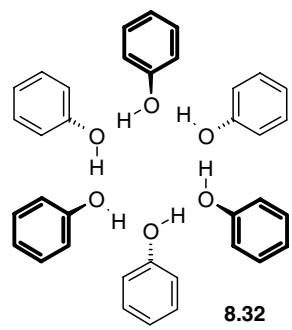

**8.32**

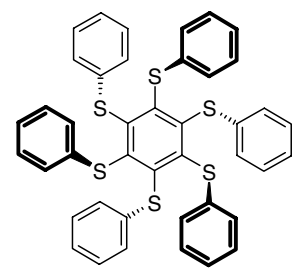

**8.33**

Other obvious design strategies include the matching of geometrically compatible hydrogen-bond donors and acceptors. These may be either mutually compatible, such as carboxylic acids, or donor acceptor pairs such as alcohols and alkyl amines. A particular area of interest is in the design of crystals that are non-centrosymmetric for applications in chiral separations (*cf.* tri-*o*-thymotide, Section 7.6) and nonlinear optics (doubling or trebling of the frequency of laser light by passing it through crystals capable of 'second harmonic generation', Section 11.6). An easy way to do this

is to incorporate a resolved asymmetric centre into the host material. Other methods include the templating of chiral lattices with chiral crystal additives or seeding with resolved crystals of one enantiomer. Design of polar chains as in 4-iodo-4′-nitrobiphenyl (Figure 8.3) is also a powerful strategy.

## 8.4 The Cambridge Structural Database

🗝 Allen, F. H., Taylor, R., 'Research applications of the Cambridge Structural Database', *Chem. Soc. Rev.* 2004, **33**, 463–475; Allen, F. H., 'The Cambridge Structural Database: a quarter of a million crystal structures and rising', *Acta Crystallogr., Sect. B* 2002, **58**, 380–388.

The Cambridge Structural Database (CSD) maintained by the Cambridge Crystallographic Data Centre (www.ccdc.cam.ac.uk) is a means of collating all of the structural data (single crystal and powder X-ray crystallographic and neutron) on 'small molecules' (*i.e.* not biological macromolecules) containing 'organic carbon' (*i.e.* at least one C–H bond as in organics, organometallics, coordination compounds *etc.*). It is complemented by the Brookhaven Protein Data Bank (PDB), the Nucleic Acids Databank (for oligonucleotides), the Inorganic Crystal Structure Database (ICSD) and the Metals Crystallographic Data File (CRYSTMET). Information in the CSD is classified according to its dimensionality and the CSD contains 1D, 2D and 3D information. The 1D information consists of text fields such as bibliographic information, compound name, parameters such as crystal unit cell, notes and a unique *refcode* that identifies each structure unambiguously. The 2D information is the chemical connectivity of the molecule stored in such a way as to allow full 2D connectivity searching. The 3D information comprises the atomic coordinates giving the full molecular and crystal structure of the compound. For crystal engineering studies, the CSD is an invaluable tool, particularly because of this 3D crystal structure information. The database now contains 436 436 structures (Jan 2008) dating back as far as 1923, and it is estimated that this will grow to more than half a million by the year 2010. Quite apart from the ease in finding individual structures compared with manual reading of the literature, the large sample size of the database means that statistical analysis of intermolecular interactions and structural motifs may be carried out. There is thus the possibility of discovering new scientific facts by search and analysis of the database. These facts may well be entirely unrelated to the original rationale of the workers who undertook the actual structure determinations examined. This added value is possible because the crystallographic experiment always gives a full molecular structure in terms of 'hard' (numerical) data, which may be further manipulated and analysed without the need for prior interpretation. This application was first realised in the *structure correlation* principle of Bürgi and Dunitz who used the CSD to establish experimental evidence for a variety of fundamental reaction pathways, notably in organic nucleophilic substitution reactions.[41] The structure correlation principle holds that the distribution of static structures observed in the CSD as a result of the proximity of neighbouring functional groups in the crystal parallels the bond elongations and deformations that occur during chemical reactions. In the use of the CSD in supramolecular chemistry, for example, analysis of the distribution of hydrogen atom positions relative to non-bonding heteroatoms can reveal optimum hydrogen-bonded geometries and highlight the effects produced by substituent groups. In this way a database approach has been adopted by Mascal[42] to infer the commonplace existence of C—H ⋯ N hydrogen bonding. Statistical analysis of the H ⋯ N distance ($r$) and C—H ⋯ N angle ($\alpha$) (Figure 8.36) revealed a wealth of interactions with $r < 2.45$ Å (the sum of the van der Waals radii of H and N) and $120 < \alpha < 180°$. The distribution of the angle, α, is centred around 155–160° as anticipated before conical correction (Figure 8.6) and a large number of low values of $r$ (as low as 2.05 Å) were observed (*cf.* Figure 1.15).

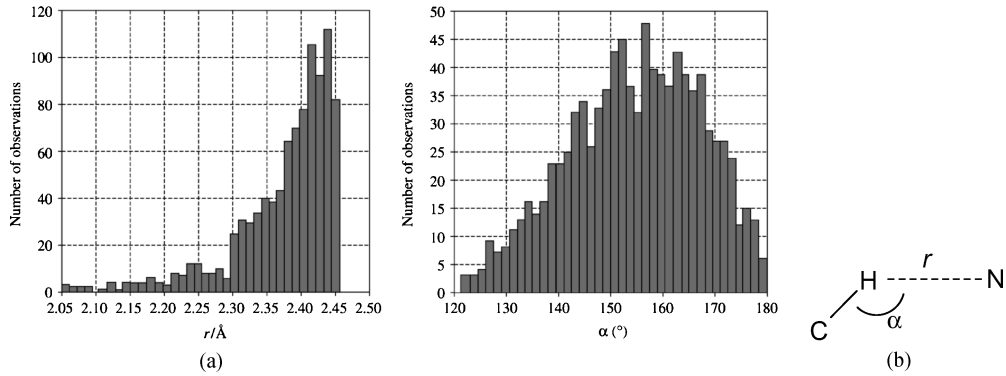


**Figure 8.36** Histograms (a) for C—H ⋯ N hydrogen bonding interactions as in (b). (Reproduced by permission of The Royal Society of Chemistry).

This kind of information is incorporated into the CSD knowledgebase *IsoStar* which stores collated information about intermolecular interactions in the form of scatterplots. These scatterplots such as the example shown in Figure 8.37 show information about the distribution of a contact functional group (an O-H donor group in Figure 8.36) around a specific central group (in this case an aliphatic ester carbonyl group). Isostar brings together knowledge from the CSD, the PDB and from calculations of theoretical interaction energies obtained using *ab initio* intermolecular perturbation theory.

The CSD has been used to classify the occurrence and connectivity of crystal hydrates[43, 44] (Section 8.6.3), symmetry and space group frequency (as in the sub-database CSDSymmetry),[45] frequencies of 'low symmetry' packing where there is more then one molecule in the asymmetric unit (Section 8.7)[46] and the occurrence of polymorphism (Section 8.5),[47] CSD-based tables for bond length distributions for organic and coordination compounds have been derived[48, 49] and efforts are currently underway to develop an automated library of such parameters called *Mogul*.[50]

The CSD was controversially used by Braga *et al*.[51] in conjunction with *ab initio* calculations to call into question the generality of the 'strength-length analogy' in which short intermolecular contacts are taken

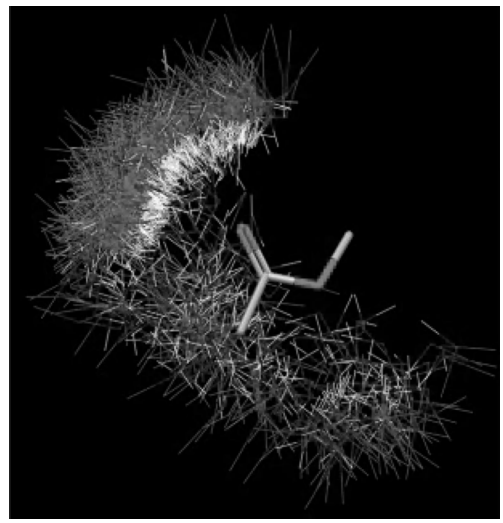

**Figure 8.37** IsoStar scatterplot, using CSD data, showing the distribution of alcohol OH contact groups around an aliphatic ester central group (image courtesy of the CCDC).

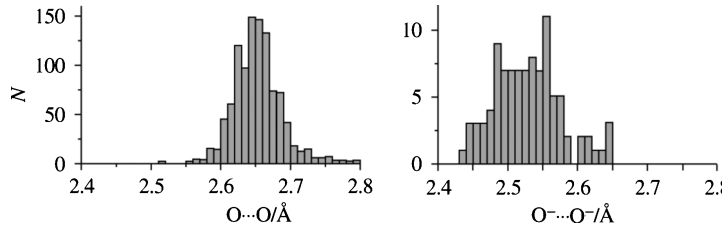


**Figure 8.38** Histograms of O ⋯ O separations in carboxylic acid derivatives for interactions of type O—H ⋯ O and O—H$^-$ ⋯ O$^-$. (Reproduced by permission of The Royal Society of Chemistry).

to imply strong intermolecular interactions (Section 8.1.3). Analysis of hydrogen-bonded O ⋯ O separations for neutral species such as carboxylic acids gives a distribution centred around 2.652 ± 0.001 Å. In contrast, inter-anion O ⋯ O separations of type O—H$^-$ ⋯ O$^-$ are much shorter (mean value 2.528 ± 0.005 Å) (Figure 8.38). However the short inter-anion interaction was suggested to be a repulsive one from the theoretical computational results. The short distance was suggested to arise from the electrostatic attraction to the counter-cations in all the anionic systems overcoming the intrinsic anion–anion repulsion, a phenomenon termed *charge compression*.[52] While the CSD statistics on the length distribution are clear, other workers have argued against the interpretation of the results and have demonstrated that the ionic interaction / contact exhibits all of the formal characteristics of a hydrogen bond both in solution and in the solid state.[53, 54] Thus the CSD can generate controversial research even on questions as fundamental as the nature of the hydrogen bond. Further calculations suggest that the strength-length correlation is subject to significant variation with different distributions evident in charge···charge and neutral···neutral isolated pairs, and certainly care must be taken in comparing distances in different structures.[55]

Much earlier in the history of the CSD in 1979, with a follow-up in 1985, a cautionary note on short intermolecular interactions was also sounded by Stan Nyburg.[56] Analysis of non-bonded, non-hydrogen-bonded

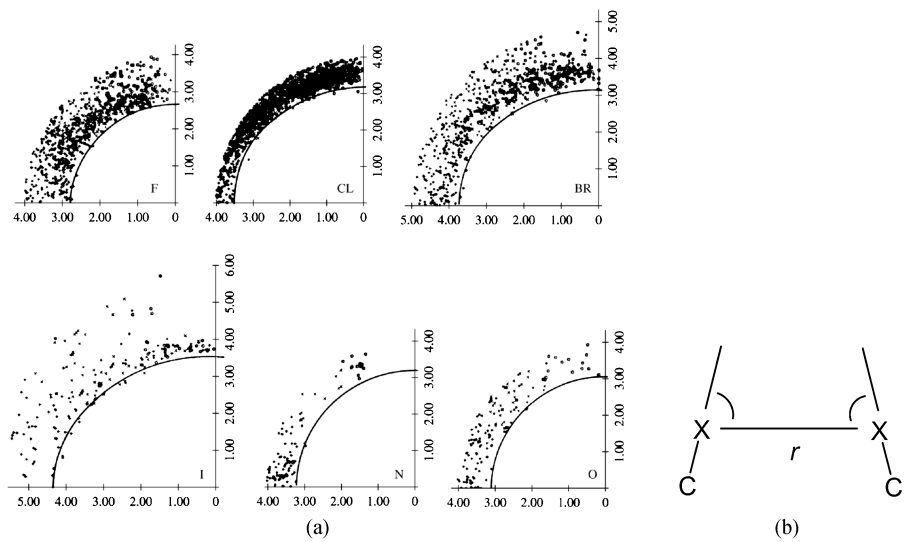


**Figure 8.39** (a) Polar scatterplots for N, O and halide non-bonded contacts. (b) The X ⋯ X distance ($r$) is shown on the axes while $\mu_1$ is measured clockwise from the vertical. (Reprinted with permission from IUCr).

X ⋯ X contacts (X = N, O, F, Cl, Br, I, S, Se) showed that while the contacts to the relatively non-polarisable N, O and F gave a reasonably hemispherical distribution of the X ⋯ X distance ($r$) as a function of the angle $\mu_1$ for cases where $\mu_1 \approx \mu_2$, the larger atoms Cl, Br, I, S and Se gave a much more elliptical shape, a phenomenon described as 'polar flattening' (Figure 8.39). This was interpreted in terms of non-spherical van der Waals radii with the van der Waals radius of the atom in the direction of the C—X bond (*i.e.* $\mu \approx 90°$) being smaller than that perpendicular to it (*i.e.* $\mu \approx 0°$). Short contacts between halogen atoms in fact arise from the specific attractive halogen bonding interactions (Section 1.8.9) and, while anisotropic electron distributions are a reality in these types of system, Allen *et al.* stated in 1997 that 'calculations … indicate that the anisotropic electron distribution around Cl causes a decreased repulsive wall and an increased electrostatic attraction for electronegative atoms, in the forward direction'.[57] In a more recent theoretical study Zou *et al.* concluded that 'the so-called 'polar flattening effect', although helpful to our understanding of the experimentally observed halogen-bonded geometries, is completely unimportant for describing the electron-accepting propensities of the halogen-containing molecules'.[58]

## 8.5 Polymorphism

Bernstein, J., *Polymorphism in Molecular Crystals*. Clarendon Press: Oxford, 2002.

### 8.5.1 The Importance of Polymorphism

Polymorphism is the ability of a chemical compound to exist in more than one crystal packing arrangement in the solid state and hence exhibit different packing of the molecules and generally different crystal unit cell dimensions *etc.* Different polymorphs can be produced according a wide variety of influences on crystallisation conditions such as solvent, temperature, humidity and the presence of seeds or additives. Crystallisation method is also of crucial importance, *e.g.* if crystals are obtained by cooling or evaporating a solution, from a melt or by sublimation. Solid crystals can also change form, sometime irreversibly, as a function of temperature, pressure, humidity changes or just time. In cases where the compound is an element such as sulfur, in which the $S_8$ rings can crystallise in both monoclinic or rhombic forms depending on temperature, we refer to the phenomenon as allotropy. Strictly this phenomenon is crystal allotropy since other forms of sulfur that are not based on $S_8$ rings such as amorphous plastic sulfur or other ring discrete sizes are sulfur allotropes but have different molecular structure, and hence are unrelated to polymorphism. To take another example diamond, graphite and $C_{60}$ are all allotropes of carbon but differ in their molecular structures and so are not polymorphs. The first description of polymorphism is generally thought to have been made in 1832 by Friedrich Wöhler (the father of organic synthesis – Section 1.3) and Justus von Liebig when they examined the crystallisation of benzamide (**8.34**).[††] Benzamide initially forms silky needle-shaped crystals on cooling an aqueous solution but over time these are replaced by rhombic crystals. A modern reinvestigation of the compounds has shown that there are three polymorphs for benzamide. Rapid cooling gives the monoclinic form II which is the least stable. The form Wöhler and Liebig observed is a centrosymmetric form III which is dominated by π-stacking interactions, while the most stable form is monoclinic form I which has optimal hydrogen bonding interactions.[59]

The topic of polymorphism is of tremendous and increasing academic and industrial importance in modern crystal chemistry and crystal engineering. The industrial interest stems from the pharmaceutical industry and has stimulated wide-ranging academic study. Legally, a molecule (termed an *active pharmaceutical ingredient*, API) with particular biological activity *in vivo* can be patented as a new invention. Moreover, particular crystal forms of that molecule (polymorphs) can be separately patented as distinct inventions. If particular polymorphs are patented after the original API patent then upon the

[††] Although there was an earlier report by Mitscherlich in 1822 (E. Mitscherlich, *Ann. Chim. Phys.* 1822, **19**, 350–419).

expiry of the API patent, rival generic drug companies are prevented from marketing their own versions of the drug because they infringe the patent on the solid form. In a famous case GlaxoSmithKline defended its patent for the polymorph type II of ranitidine hydrochloride, the active ingredient in *Zantac*, a stomach acid production inhibitor, against competitors when the patent on polymorph type I had already expired. Conversely, if a rival discovers a new solid form of an API they can separately patent this new polymorph and secure exclusive rights over other companies when the API patent expires. The reason the particular solid forms count as new inventions is that different polymorphs exhibit different physical properties such as electrical or thermal conductivity, filtering, drying, flow, tabletting, dissolution and processing characteristics and hence can have different bioavailability. The different properties of particular polymorphs of the same compound can also result in profound problems for drug manufacturers. In one famous case Abbott Laboratories introduced the anti-AIDS drug ritonavir in 1996. After 18 months on the market a previously unknown polymorph was suddenly detected during manufacture. The reasons for the change were unknown but were presumably due to some subtle alteration in manufacturing conditions or even seeding by microscopic particles of the second polymorph. The new form proved to be thermodynamically more stable than the original polymorph. In this regard it obeys the classic *Ostwald's step rule* conceived by Wilhelm Ostwald which states that in general it is not the most stable, but the *least* stable polymorph that crystallises first with increasingly more stable forms crystallising out in steps. Abbott chemical engineers were unable to stop the formation of the new polymorph and it rapidly came to be the major solid form coming off the production lines. Unfortunately the new, more stable form was only half as soluble as the first and so patients were not getting enough into their bloodstreams. As a result sales of the drug had to be discontinued at tremendous cost. Despite frenzied efforts to find conditions under which the original polymorph could be reliably produced only mixtures of the two forms were formed from then on and eventually the drug was reformulated as a liquid gel capsule containing the pre-dissolved API, annoyingly requiring refrigeration.

While relatively few compounds have known polymorphs in the CSD (*ca.* 5 %), Walter McCrone famously stated that 'every compound has different polymorphic forms, and that, in general, the number of forms known for a given compound is proportional to the time and money spent in research on that compound'.[60] It is certainly true that pharmaceuticals that have a very large amount of time and money spent on them can by highly polymorphic. The anti-cholesterol drug atorvastatin (lipitor) has up to 15 forms including hydrates and salts *etc*. The record holder for well-characterised pure forms is 5-methyl-2-[(nitrophenyl)amino]-3-thiophenecarbonitrile (**8.38**), known as ROY, which has six polymorphs with colours varying between red, orange and yellow (hence the name) arising from different molecular conformations.

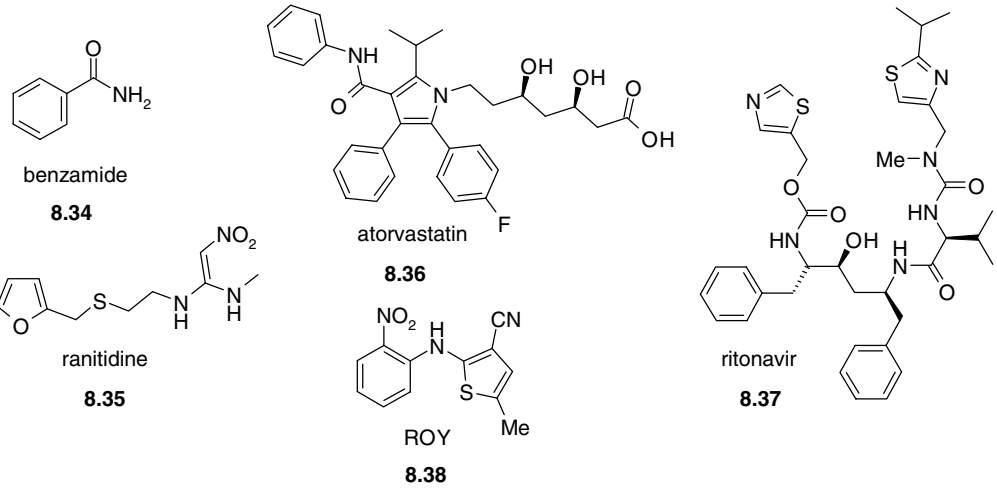

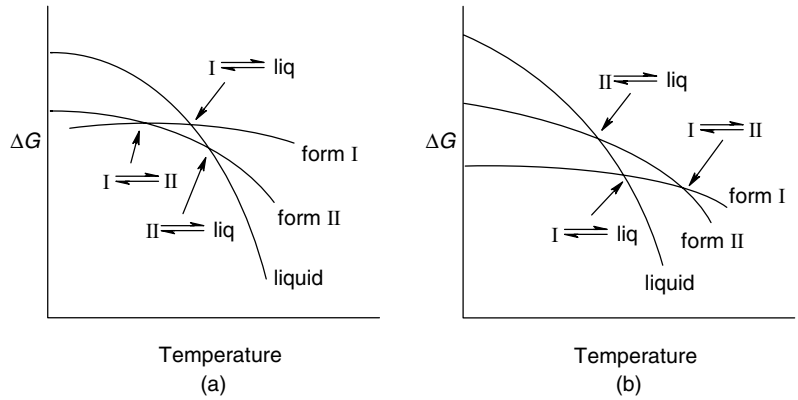


**Figure 8.40** Free energy *vs.* temperature diagrams for two polymorphs (forms I and II) showing free energy crossing points (a) enantiotropic system; (b) monotropic system.

## 8.5.2 Types of Polymorphism

Strict definition of what constitutes polymorphism and its particular sub-types is difficult and surrounded by issues of legal interpretation within patent law. Generally we regard as polymorphic solids that are different in crystal structure but identical in the liquid or vapour states. Hence crystals containing molecules with different atomic arrangements can be classed as polymorphs if the molecules concerned interconvert rapidly in the melt or in solution to give the same equilibrium mixture. In thermodynamic terms there are two basic kinds of polymorphism; *enantiotropic* and *monotropic*. Figure 8.40 shows free energy *vs.* temperature plots for the two kinds of system. In the monotropic case (Figure 8.40b) the free energy plot for the various polymorphs do not cross before the melting point of all the polymorphs is reached. As a result any transition from one polymorph to another will be irreversible. In the case of an enantiotropic system the free energy plot contains a crossing point before the melting points of the polymorphs and hence it may be thermodynamically (if not kinetically) possible to convert reversibly between the two polymorphs by heating and cooling.

The polymorphism literature is also rife with a wide variety of terms that are sometimes loosely used. In this section we will try to give some definitions that reflect current common usage and are as rigorous as possible but some of these terms are a mater of some (rather futile) debate at present. Useful schematic summaries is given in Figure 8.41 and Figure 8.42.

***Pseudo*polymorphism (solvatomorphism)**: a *pseudo*polymorph is not a polymorph at all. A *pseudo*polymorph of a pure material is one in which that material is crystallised with an additional molecule, usually of water or some other solvent – a solid state host guest compound or *molecular complex*. Hence the *pseudo*polymorph contains a different molecule in addition to the one found in the pure crystal, hence it is strictly a co-crystal. The term *pseudo*polymorph is a synonym for *hydrate* (when the co-crystallised guest is water) or *solvate* (when the guest is a solvent molecule other than water). *Pseudo*polymorphs are also sometimes referred to as *solvatomorphs.* A variety of *pseudo*polymorphs of a compound can exist each with different solvent molecules occupying a cavity in the host crystal. We discussed these kinds of compounds, also known as clathrates or inclusion compounds, in Chapter 7. In order for *pseudo*polymorphs to form it has been shown that multiple interactions such as both strong and weak hydrogen bonding between solvent molecule and solute are often required in order to retain the solvent molecule in the growing crystal nucleus,[61] although as with urea, this is not always the case.

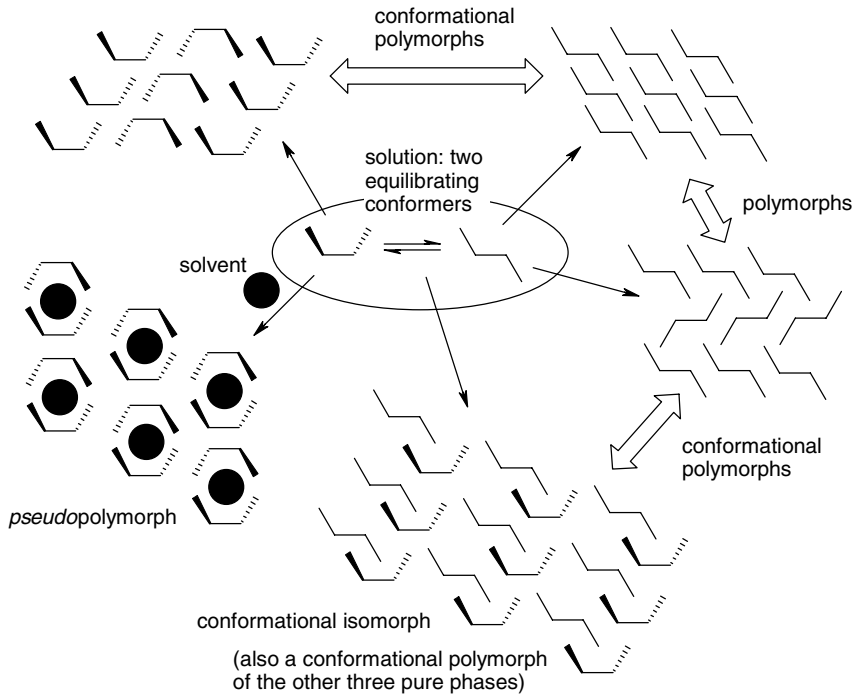


**Figure 8.41** Schematic illustrating the relationship between various types of polymorph.

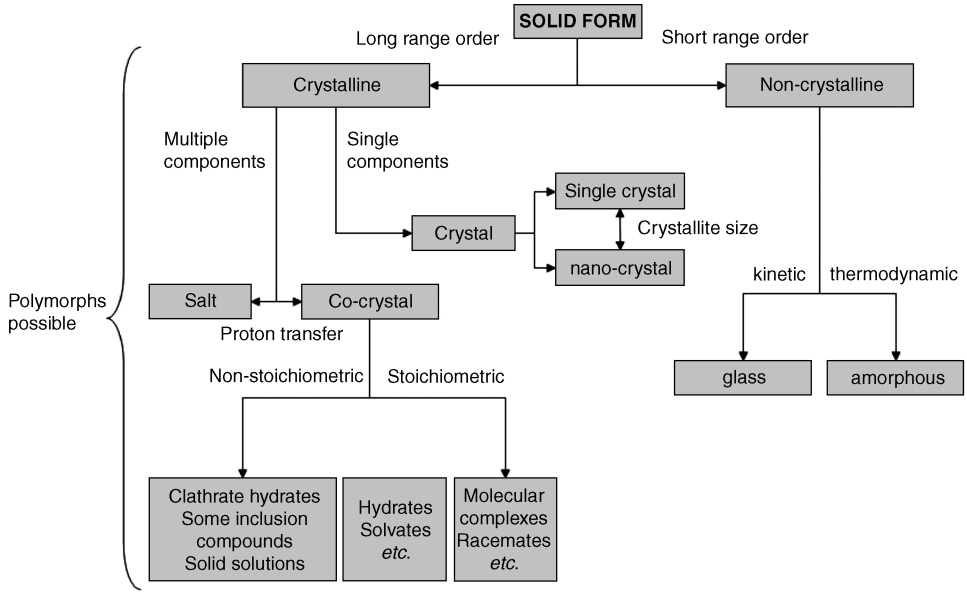


**Figure 8.42** Classification scheme for molecular solids (adapted from Section Key Reference).

**Conformational polymorphs**: conformational polymorphs are different pure crystal forms of the same substance that differ in one or mode bond rotations in the molecular structure. The implication is that these two or more conformers are in rapid equilibrium under the conditions under which the crystal formed and hence usually represent rotations about single bonds. If this were not the case the different conformers would be distinct isomers and would be formally different chemical substances and hence not polymorphs. Crystal packing interactions can stabilise particular conformers that are relatively unstable in solution and hence crystals can contain sometimes surprising conformational isomers. A remarkable example is trans-1,4-diethynylcyclohexane-1,4-diol which has two forms (A and B). Each crystal contains three molecules in the asymmetric unit. Form A comprises two molecules of conformer **8.39a** (equatorial OH groups) and a third diaxial molecule (**8.39b**). Form B is the opposite with two diaxial OH and one diequatorial. Form B is 3% more efficiently packed than form A (higher density) but the O–H···O hydrogen bonds in form A are shorter. This is a commonly observed difference. Forms A and B are thus conformational polymorphs of one another. In this case they are also *conformational isomorphs*; conformation isomorphism occurs when two or more conformers occur in the *same* crystal structure. Interestingly enough compound **8.39** also crystallises as a monohydrate (a *pseudo*polymorph, form C) of the diequatorial conformer. A trimeric O-H···O hydrogen-bonded helical spine is the dominant recurring pattern in all three crystalline forms, somewhat reminiscent of the helical tubulands (Section 7.4.2). Finally all three of forms A, B and C all form in a single crystallisation mixture and hence they are also *concomitant polymorphs*!

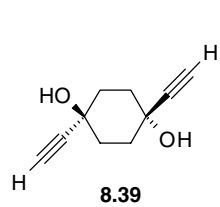


**8.39**

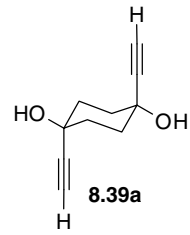


**8.39a**

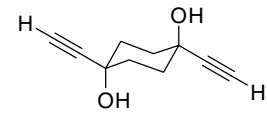


**8.39b**

**Concomitant polymorphs**: concomitant polymorphs are polymorphic forms of a substance that crystallise out at the same time from the same crystallisation mixture. Here 'at the same time' does not necessarily mean that the crystals form at exactly the same instant, just that they can be observed co-existing at some point during the crystallisation process. We have already come across concomitant polymorphs in the early example of benzamide where forms I and II are concomitant. Many more interesting and beautiful examples are covered in a recent review.[62]

**Disappeared polymorph**: in a very engaging article published in 1995 entitled 'Disappearing Polymorphs' Dunitz and Bernstein described anecdotal evidence for crystal forms that have been isolated and characterised but proved difficult to reproduce.[63] We have already encountered one such example in the case of ritonavir in which the original soluble form 'disappeared' and could no longer be isolated because of the appearance of a second, more stable form. In this case the original form did not completely disappear but it could no longer be isolated pure and free of the new polymorph. This kind of occurrence is sufficiently common for the slightly unfortunate term 'disappeared polymorph' to catch on in a few papers in the literature. Dunitz and Bernstein put forward some reasonable explanations for difficulties in reproducing particular polymorphs, namely that the appearance of kinetic or *metastable* crystal forms is highly subject to experimental conditions particularly nucleation phenomena which, as we saw in Section 8.2, are not subject to the same statistical predictability as most other phenomena in chemical science because they involve relative few events. Thus seeding by microscopic nuclei of a newly discovered more stable polymorph form could make metastable polymorphs (which we expect

to crystallise first according to Ostwald's rule of stages) very elusive. Indeed in cases where extreme precautions have been taken to eliminate possible seeding most 'disappeared' polymorphs have been reproduced. Thus, while difficulties in isolating metastable forms is a reality there is nothing unscientific about the phenomenon and no polymorphs truly 'disappear'.

**Supramolecular isomerism**: Supramolecular isomerism has been defined by Zaworotko[64] as the 'existence of more than one type of network superstructure for the same molecular building blocks,' and hence he adds that it 'is therefore related to structural isomerism at the molecular level.' In cases where the molecular building blocks are capable of forming more than one type of supramolecular synthon then supramolecular isomerism is identical to polymorphism. Zaworotko defines another kind of supramolecular isomerism, however, in which the same building blocks exhibit different network architectures or superstructures. We will see examples of this phenomenon in chapter 9, particularly regarding interpenetrated networks.

### 8.5.3 Controlling Polymorphism

Until very recently controlling the polymorphic form of crystalline compounds has been very difficult with research being essentially empirical variation of classical factors such as concentration and degree of supersaturation, temperature, time, pH and identity of the crystallisation solvent. These kinds of approaches are embodied in the *polymorph screening* process that every new candidate drug molecule must now undergo. Typically an empirical high throughput screening approach is adopted with multiple crystallisation wells reflecting systematic variation of solvent, supersaturation *etc.* being analysed by rapid *in situ* techniques such as Raman spectroscopy. These studies are supported by examination of the structures of known forms of the drug for telltale signs of potential polymorphism such as unsatisfied hydrogen bond donors and the output of crystal structure prediction software (Section 8.8) to assess likely synthons and packing motifs.

Recent work has turned to some more exotic methods aimed at influencing the formation of particular polymorphic forms as opposed to empirically screening for them. Work by Allan Myerson at the Illinois Institute of Technology, USA, has shown that glycine crystals can be induced to nucleate on functionalised metallic square islands. The glycine crystal size is controlled by the dimensions of the islands with small metallic islands promoting the formation of the *metastable* $\beta$-polymorph while large islands tend to give the more stable $\alpha$-form.[65] Myerson has also been involved with the use of intense pulses of near-infrared light to influence glycine polymorphism with different polymorphs arising depending on whether the light is circularly or linearly polarised. The infrared radiation is thought to influence the aggregation of the glycine molecule as they begin to cluster very early in the nucleation process.[66] Crystal growth on organic polymer surfaces can also influence polymorphism, as in the two forms of the pain reliever acetaminophen and a number of related APIs or API precursors such as ROY (**8.38**). One form grows in the presence of polymer surfaces such as nylon and polyvinyl chloride (PVC) while other polymers such as cellulose favour the other form.[67] The polymer surfaces, or *heteronuclei*, act to seed particular polymorphs by interacting with specific arrangements of the solute molecule that in turn nucleate the crystal in a similar way to the templation discussed in Section 8.2. Other interesting work by Mike Ward from the University of Minnesota, USA, has been based on the knowledge that the outcome of a particular crystallisation is decided very early on in the process, as soon as critical nuclei form containing tens to hundreds of molecules. Since the nuclei of different polymorphs are of different sizes the Minnesota researchers carried out crystallisations within the confines of porous materials – polymer blocks with cylindrical channels *ca.* 30 nm in diameter. In this way they were able to selectively produce just one of the six ROY polymorphs.[68]

# 8.6 Co-crystals

## 8.6.1 Scope and Nomenclature

Stahly, G. P., 'Diversity in single- and multiple-component crystals. The search for and prevalence of polymorphs and cocrystals', *Cryst. Growth Des.* 2007, **7**, 1007–1026.

Perhaps more than any other term in crystal engineering, the word *co-crystal* (or, more commonly in the US, *cocrystal*) has continued to generate controversy over its meaning and definition and such is the confusion that some advocates have suggested its abandonment entirely and the adoption of the phrase *multi-component molecular crystal*. The basic concept behind a co-crystal is clear however, it is a crystalline solid containing more than one kind of molecule. Co-crystals are thus distinct from salts which comprise separate anions and cations because it is impossible to separate a salt into the pure anions and pure cations – electrostatic charge balance considerations mean that each ion must always be partnered by an oppositely charged counter-ion. This is not the case for co-crystals where the different molecules found together in the crystal are distinct, separate and separable chemical substances. Thus *pseudo*polymorphs, hydrates, solvates and all solid-state host guest compounds discussed in Chapter 7 are all examples of co-crystals. As with polymorphism, co-crystals are of considerable interest within the pharmaceutical industry. By deliberately (or otherwise) crystallising a pharmaceutical API with another molecule it is possible to modify the physical properties of the resulting crystalline solid compared to crystals of the pure API. The API co-crystal may therefore have improved solubility, processing stability or tabletting characteristics compared to the pure compound. An example is the use of cyclodextrins as drug delivery agents (Section 6.3.4) although cyclodextrins also affect the solution properties of the drug. As with polymorphism much of the controversy arises from the legal and patent issues surrounding co-crystals. While the formation of a salt of an API (such as protonating an amine with citric acid to produce a more soluble citrate salt) is not a patentable *inventive step*, the formulation or discovery of a co-crystal is potentially patentable. There is thus a great deal of interest in distinguishing between co-crystals of a neutral base such as an amine with a neutral acidic molecule such as citric acid, and a salt formed by proton transfer from the citric acid to the amine.[69] The distinction between salt and co-crystal here essentially revolves around the movement of a single proton and thus a crystal of a particular such acid/base compound may be a salt at one temperature and a co-crystal at another! Conceptually any crystal with more than one separable molecular component may be thought of as a co-crystal. We can distinguish, however, between the common phenomenon of the accidental inclusion of a common solvent molecule such as water within the crystal and the deliberate, designed or crystal-engineered introduction of a co-crystallising substance into a crystallisation mixture. We also note that while commonly co-crystals are ordered with a well-defined stoichiometric ratio between the two or more components, there also exist non-stoichiometric inclusion compounds such as the clathrate hydrates and some urea inclusion compounds, and *solid solutions*[‡‡] in which there is an essentially random distribution of one molecule within a crystal of another (*cf.* hourglass inclusions, Section 8.2.6). A particularly common and interesting kind of co-crystal is one in which two enantiomers of the same chiral molecule co-crystallise to give a racemic crystal. Because enantiomers commonly do not interconvert in solution under ambient conditions (usually high

[‡‡] A *solid solution* is a solid mixture of one or more compounds within a 'solvent' of another solid crystalline compound. For the mixture to be considered a solid solution the crystal structure of the solvent must remain essentially unchanged upon the addition of the solute(s) and the whole mixture must remain as a single homogeneous phase. We can distinguish two types of inclusion within the solvent crystal: *substitutional* in which the solute molecule replaces a solvent molecule in the lattice, or *interstitial* in which the solute molecule fits into a space in between solvent particles. The properties of the solvent material are affected by the formation of solid solutions because the process results in distortions in the crystal lattice and disrupts the overall homogeneity of the host material.

energy covalent bond breaking and re-forming is required) then a crystal of two enantiomers is formally a co-crystal. It is rarely regarded as such, however, because the two kinds of molecule have the same chemical structure apart from being mirror images and commonly crystallise in a space group that involves a symmetry operation such as inversion that relates one enantiomer to another, thus $Z' = 1$. A summary of the classification of crystal forms is given in Figure 8.42.

## 8.6.2 Designer Co-crystals

Aakeröy, C. B., Salmon, D. J., 'Building co-crystals with molecular sense and supramolecular sensibility', *Cryst. Eng. Comm.* 2005, **7**, 439–448.

A simple example of designer co-crystals comes from the combination of alcohols with amines. An alcohol may be regarded as ideally donating one hydrogen bond and accepting two (one for each lone pair), while an amine is perfectly complementary to it, donating two hydrogen bonds and accepting one. Furthermore, alcohols are generally Brønsted acids, and amines are bases, so there is a high degree of mutual affinity. Mixtures of alcohols and amines, therefore, tend to form *saturated hydrogen-bonded* (SHB) co-crystals. Saturated hydrogen bonding occurs when every possible acidic proton and every hydrogen bond acceptor lone pair is involved in hydrogen bonding. In a study of 1,4-diaminobenzene co-crystals with phenol (1:2) and various diols (1:1), supported by CSD analyses of other SHB species, Bernstein *et al.* observed two common packing modes: a hexagonal 'chicken wire' structure and a 'ladder' structure, composed of only D-type graph set motifs (level one), Figure 8.43.[70] The level-two graph sets of both forms illustrate the complexity of graph

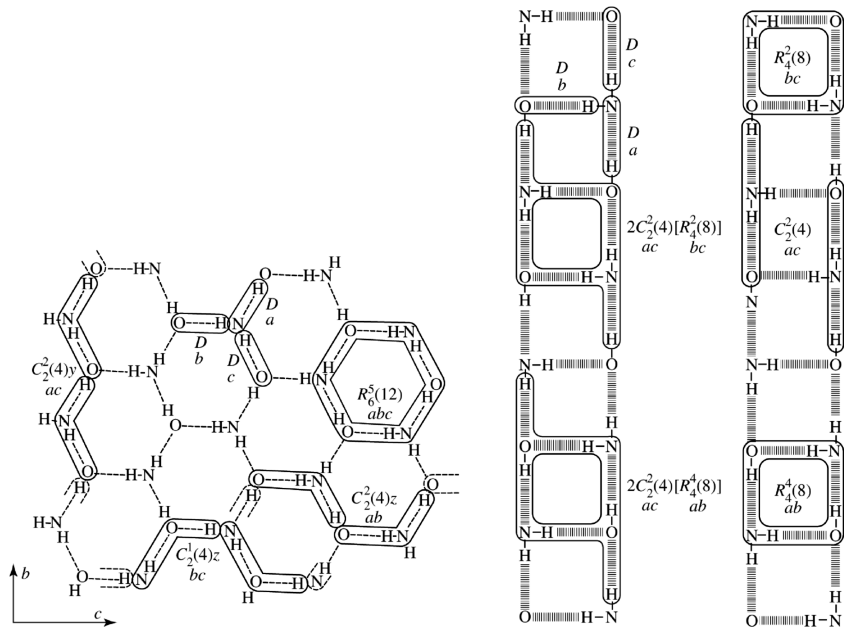


**Figure 8.43** (a) Chicken wire and (b) ladder motifs for saturated hydrogen bonded structures. The *a*, *b* and *c* designations are assigned in order of increasing hydrogen bond length. (Reprinted with permission from IUCr).

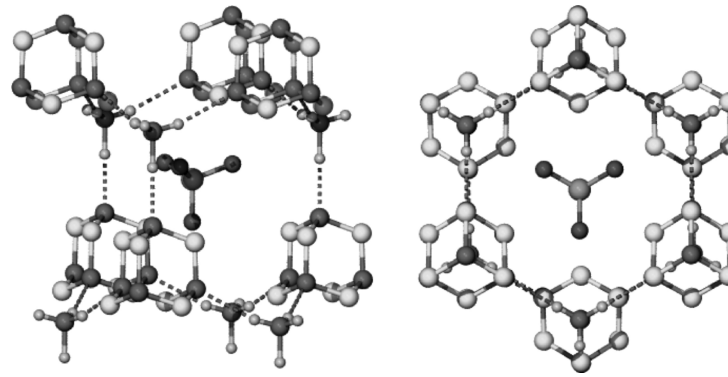

**Figure 8.44** Two representations of the super-wurtzite structure of $[NH_4 \cdot \mathbf{8.40}]BF_4$ showing the included $BF_4^-$anion.[71]

set analysis even for what are, chemically, relatively straightforward systems. The richness of the deceptively simple connectivity is clear.

Complementarity between number of hydrogen bond donors and number of lone pairs is also exhibited by the crystal structure of the ammonium tetrafluoroborate complex of urotropin (**8.40**, $N_4(CH_2)_6$) which is an example of a co-crystal between a salt and a neutral molecule. The $NH_4^+$ donor is perfectly complementary to the four tetrahedrally arranged tertiary amines of the urotropin acceptor. However, despite the tetrahedral nature of the urotropin building block, a diamondoid structure does not result (*cf.* Section 8.12) and the resulting complex has a super-wurtzite (ZnS) structure in which the $Zn^{2+}$ is replaced by $NH_4^+$ and the $S^{2-}$ by urotropine. The hexagonal ice-like cages of $NH_4^+$ ions act as hosts for the tetrahedral $BF_4^-$ anions (Figure 8.44).[71] The N ⋯ N hydrogen bond distances of 3.0 Å are relatively short for N—H ⋯ N interactions (as a result of charge assistance and the contracting effect of the $BF_4^-$ anion). A related 3:2 co-crystal of the high explosive cyclotetramethylenetetranitramine (HMX) and ammonium perchlorate is used as a convenient rocket propellent. The co-crystal renders the effective oxidant perchlorate water insoluble making dessicants and motor seals redundant.

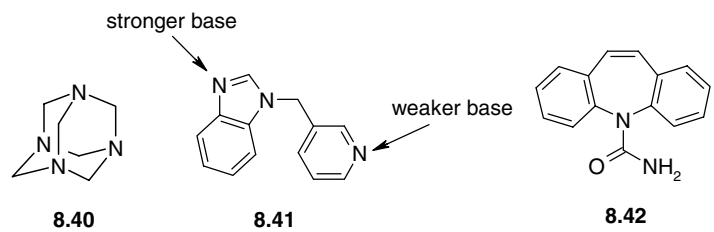


**8.40** **8.41** **8.42**

In an attempt to go beyond binary co-crystals (i.e. those containing two chemically distinct components) Christer Aakeröy (Kansas State University, USA) has designed the 'ditopic supramolecular coupling reagent' **8.41**. The compound contains two hydrogen bond basic sites, of which one, the imidazole nitrogen atom, is a significantly stronger base than the other and this basicity can be tuned by the addition of appropriate substituent groups. The compound does not contain any strong hydrogen bond acids and hence would be expected to form co-crystals with good hydrogen bond donors. Crystallisation of this supramolecular reagent from 1:1 mixtures of various acids gives ternary co-crystals with the stronger

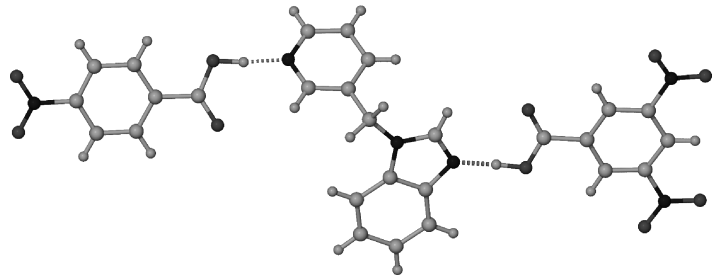

**Figure 8.45** Ternary co-crystal of the 'ditopic supramolecular coupling reagent' **8.41** with two benzoic acid derivatives. The stronger 3,5-dinitrobenzoic acid interacts with the stronger imidazole base while the 'second best' acid, 4-nitrobenzoic acid interacts with the 'second best' pyridyl base.

acids forming OH···N interactions to the imidazole acceptor and weaker acids interacting with the pyridyl group. Figure 8.45 shows the 1 : 1 : 1 co-crystal of **8.41** with 4-nitrobenzoic acid and 3,5-dinitrobenzoic acid. In neither case does any proton transfer take place to give salts.

Within the arena of pharmaceutical co-crystals, there are relatively few co-crystallising agents (and few common solvents) that are pharmacologically acceptable in drug formulations and hence there are well-defined limitations on the range of compounds that can be used. However, pharmaceuticals contain a range of common functional groups such as amides that form well-defined and extensively studied supramolecular synthons, including *heterosynthons*, *i.e.* synthons formed between different chemical groups. Outside hydrates, systematic pharmaceutical co-crystal research is still at an early stage, however it is clear from many studies that APIs can readily form co-crystals. A typical example is carbamazepine (**8.42**) an anticonvulsant and mood stabilising drug, used primarily in the treatment of epilepsy and bipolar disorder. Carbamazepine exists as four pure polymorphs and two solvates and in each case the compound crystallises with the amide dimer synthon (Figure 8.46a).[72] Because carbamazepine is a primary amide this leaves a peripheral hydrogen bond donor and acceptor pair unsatisfied as a result of the geometric constraints of the rest of the molecule and hence hydrogen bond acceptor solvents such as acetone and DMSO are commonly included to act as acceptors to the remaining amide NH proton and to fill the void between the adjacent amide dimer pairs. Similarly non-solvent co-crystal formers with hydrogen bond acceptor groups such as saccharin (Figure 8.46b) and nicotinamide can also play this role. In the presence of a variety of carboxylic acids such as formic, acetic, butyric and trimesic acids, the amide homosynthon can be broken to give the supramolecular

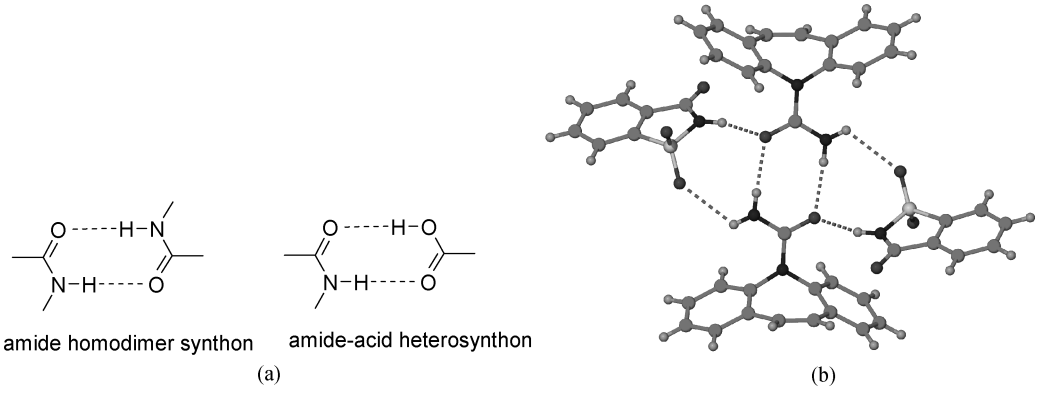


**Figure 8.46** (a) Amide supramolecular homo- and heterosynthons found in co-crystals of carbamazepine (**8.42**) and (b) X-ray crystal structure of the carbamazepine-saccharin co-crystal.[72]

amide-acid heterosynthon (Figure 8.46a). The saccharin co-crystal exhibits potentially pharmacologically useful superior dissolution characteristics compared with one of the pure anhydrous polymorphs.

## 8.6.3 Hydrates

Infantes, L., Fabian, L., Motherwell, W. D. S., 'Organic crystal hydrates: what are the important factors for formation', *CrystEngComm* 2007, **9**, 65–71.

The self-assembled structure of water and the way it interacts with dissolved solutes and with hydrophobic surfaces continues to be highly topical and the journal *Science* ranked the study of water among the top 10 breakthroughs in 2004. There exist a number of high quality fundamental solid-state structural studies that have described water clusters, chains and sheets in various crystalline solids with the analysis of water in the single crystal neutron structure of vitamin $B_{12}$ coenzyme representing a classic in the field.[73] Interest in water channels in biological systems has been particularly stimulated by the award of the 2003 Nobel Prize in Chemistry to Peter Agre of the Johns Hopkins school of Medicine, USA, for his work on the *aquaporins*, channel proteins that allow water to cross biological membranes while completely excluding protons in the form of $H_3O^+$. Water transport is very rapid and is mediated by so-called functional water. There have been a number of X-ray structure reports of water in a plethora of environments, of possible relevance to the structure of ice and the nature of water interactions with solutes, particularly biomolecules and it is clear that the occurrence of small clusters of water or extended infinite hydrogen bonded chains, ribbons, sheets and networks is common. A particularly interesting example involving ligand **10.19** is discussed in Section 10.5.3 There is also interest in the pharmaceuticals industry in the effect of hydrate formation on physical properties such as solubility, dissolution profile and crystal mechanical strength. Some basic rules have been suggested for the formation of hydrates; it is possible that they arise from the presence of excess hydrogen bond donors in crystals, they are more common in ionic compounds and are very rare for hydrophobic compounds with an increasing polar surface being correlated with increasing degree of hydrate formation. Of particular importance in hydrate formation is the sum of the average donor and acceptor counts (*i.e.* the count per molecule of numbers of strong hydrogen bond donor and acceptor contacts). The absolute difference of the sum of average hydrogen bond donor contacts and the sum of the average acceptor contacts is also positively correlated with hydrate occurrence. Within hydrate crystals the environment a given water molecule finds itself in is dependent on the ratio of hydrogen bonds donors to acceptors. The presence of relatively few donors tends to result in water acting as a hydrogen bond donor, typically donating two hydrogen bonds and accepting one. In the presence of excess donors water tends to be a hydrogen bond acceptor, although this situation is much rarer.

Water motifs have been classified systematically using a system of nomenclature somewhat analogous to graph set analysis (Section 8.3.1).[43] in this scheme water structures are discussed in terms of particular classes, listed below.

**D** discrete chains
**R** discrete rings
**C** infinite chains in 1 dimension involving no rings
**T** infinite tapes in 1 dimension involving rings
**L** infinite layers in 2 dimensions

In addition about 4% of compounds were unclassified (U or network, N) showing cross-linking within rings. The D and C patterns prove to be by far the most common, accounting for 61 % and

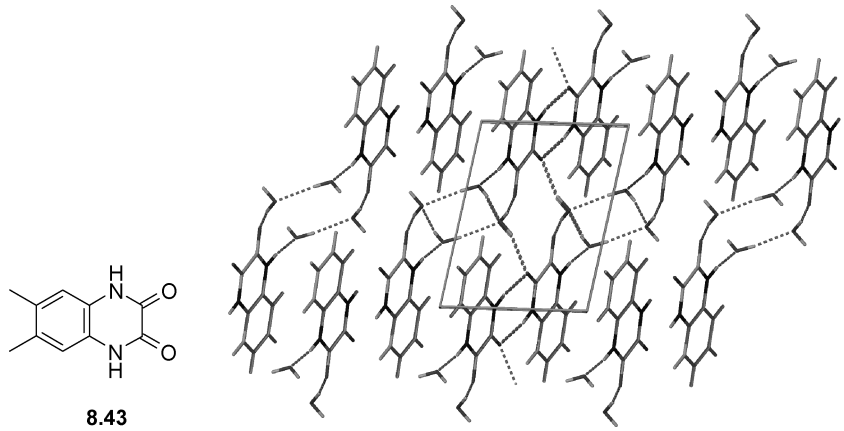


**8.43**

(a) (b)

**Figure 8.47** (a) The dimethyl 1,4-dihydroquinoxaline-2,3-dione host **8.43** and (b) the two-dimensional water sheet composed of pentagonal and octagonal units in the crystal structure of **8.43**·6$H_2O$ (view down the crystallographic *b* axis; unit cell edges shown).[74]

20 % of the hydrate structures in the CSD, respectively. These letter descriptors are supplemented by numbers reflecting the numbers of water molecules involved. Thus one of the simplest and most common patterns, D2, comprises simply two water molecules hydrogen bonded together. Unlike graph set nomenclature the scheme is independent of hydrogen atom positions and was designed to better illustrate the extended structure. Further analysis has also been undertaken showing how these water structures interact with other functional groups and the reader is referred to the original literature for further information.[44]

Work by Neil Champness of the University of Nottingham, UK, has resulted in a strategy for encouraging the formation of extended water arrays in molecules such as **8.43** that contain a 1,4-dihydroquinoxaline-2,3-dione core.[74] These host compounds incorporate a hydrophilic oxalamide-based end functionality that acts as a hydrogen bond acceptor. There is also a hydrophobic aromatic ring region that does not interact strongly with water and hence is thought to encourage the formation of discrete water clusters as opposed to three-dimensional networks. A systematic study was undertaken, albeit with relatively few examples which resulted in the formation of hydrates with zero-, one- and two-dimensional arrays of water. In the case of **8.43**·6$H_2O$ there is a two-dimensional water sheet composed of pentagonal and octagonal units sandwiched between the molecules of **8.43**, Figure 8.47. While studies such as this are encouraging, in general it is fair to say that comparative studies on water in crystals are hampered by the serendipitous nature of the occurrence of hydrates and the unpredictability of their structures.

## 8.7 $Z' > 1$

Steed, J. W., 'Should solid-state molecular packing have to obey the rules of crystallographic symmetry?', *Cryst. Eng. Comm.* 2003, **5**, 169–179.

The parameter $Z'$ is used to denote the number of molecules or *formula units* in the asymmetric unit of a crystal structure, *i.e.* the number of molecules that cannot be related to one another by the symmetry operations defined by the crystal space group. Of course, $Z'$ is therefore crucially dependent on the somewhat subjective definition of what constitutes the 'formula unit'. Strictly $Z'$ is defined as the number of formula units in the unit cell divided by the number of independent general positions. The

complexity of the asymmetric unit derives from the fact that the molecules within the asymmetric unit are free to associate themselves in three-dimensional space, unlike the asymmetric units themselves which are compelled to tessellate *via* particular symmetry operators (to form one of the 230 space groups). Around 8.8% of structures in the CSD crystallise with $Z' > 1$ with values ranging from $1\ ^1/_{12}$ to 32. Even numbers of $Z'$ are more common than odd numbers and the number of structures with $Z' > 4$ is almost negligible. Certain classes of compound, particularly chiral molecules such as nucleosides, nucleotides, steroids and other natural products show a greater tendency to form high $Z'$ structures. Strong intermolecular interactions such as the highly directional O-H···O interaction have been implicated in the formation of high $Z'$ structures, although there are also many high $Z'$ structures known which arise from only weak interactions (*e.g.* the rhenium(I) complex $[Re(MeCN)Cl_2(NO)(PMe_3)_2]$, $Z' = 11$ which is held together predominantly by C-H···O and C-H···Cl hydrogen bonds).

Broadly high $Z'$ structures can arise from frustration between two or more competing, directional interactions (*e.g.* optimisation of hydrogen bonds vs. optimal shape packing) either during the nucleation process or as a dominant contribution to the bulk structure. A classic example is the combination of the presence of a resolved chiral centre with a synthon with a strong tendency towards inversion symmetry such as carboxylic acid or amide dimers, Figure 8.2. The result is frustration between the centrosymmetic packing tendency of the synthon and the need to adopt a chiral space group because of the molecular chirality. The result is an overwhelming tendency to give crystals with $Z' = 2$.[75] High $Z'$ structures are also of significant interest because of the insights they may give into the crystal nucleation process. Some high $Z'$ structures represent metastable polymorphs or even fixed 'fossil relics' of the nucleation process, particularly when the nucleation growth unit (Section 8.2) itself contains more than one molecule. Techniques such as Differential Scanning Calorimetry (DSC) or variable temperature X-ray crystallography can be used to probe high $Z'$ structures for polymorphic behaviour.

The observation of $Z' > 1$ may be regarded as a special case of co-crystallisation where the two components are the same as one another. Thus research on high $Z'$ structures is closely related to co-crystals, solvates, hydrates *etc*. Figure 8.48 shows the X-ray crystal structure of a remarkable

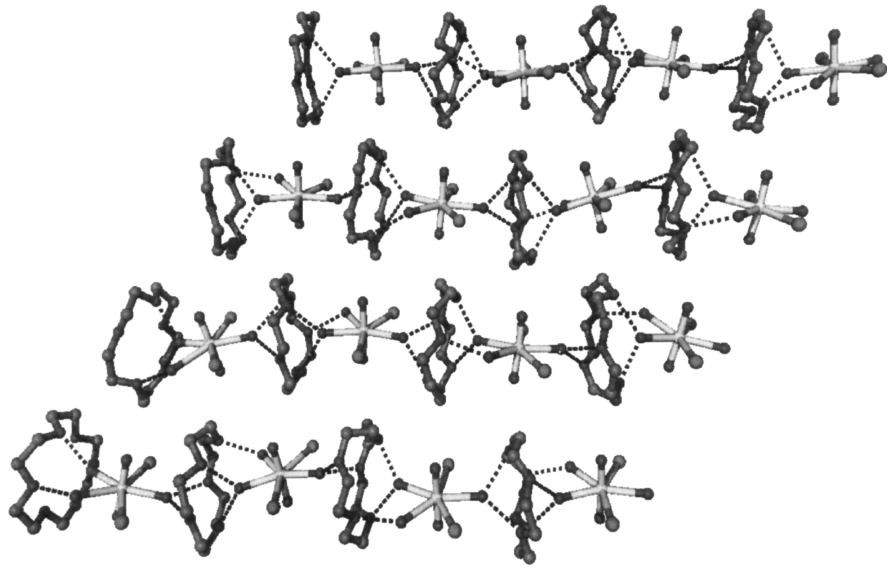

**Figure 8.48** The symmetry unique portion of the infinite co-crystal hydrogen-bonded chain structure of $[UO_2Cl_2(H_2O)_3]_{16}\cdot([15]\text{crown-5})_{16}$.[76]

$Z' = 16$ hydrogen bonded co-crystal between the neutral uranyl complex $[UO_2(H_2O)_3]$ and [15]crown-5. The asymmetric unit contains a total of 32 independent molecules.[76] Up-to-date information and a database of high $Z'$ structures is maintained online at http://www.dur.ac.uk/zprime.

## 8.8 Crystal Structure Prediction

### 8.8.1 Soft *vs.* Hard Predictions

In Section 8.3.4 we made the point that much of crystal engineering concerns empirical approaches using chemical concepts such as supramolecular synthons and accumulated experience concerning intermolecular interactions in order to design or engineer particular features of crystal structures. This kind of prediction might be termed a 'soft' prediction in the sense that while there are sometimes successes in the designed 'synthesis' of crystals incorporating particular supramolecular synthons or structural features, or the preparation of materials with given coordination network topologies or stoichiometries there is no attempt to undertake full prediction of the details of the crystal packing, symmetry and space group. Such prediction because of the precision required might be described as 'hard' predictions and it is notoriously difficult to achieve. In 1988 Maddox famously described the ongoing inability to predict the structure of molecular solids from a knowledge of their chemical structure as a 'continuing scandal'.[77] Since that time there has been significant progress in hard crystal structure prediction, much of it by the use of ever more sophisticated and intensive computational methods and hence the term *crystal structure calculation* is perhaps more appropriate. Crystal structure calculation is a task that is severely complicated by the occurrence of polymorphism, solvates/co-crystals and crystal structures with $Z' > 1$. It requires a good knowledge of the most stable or most likely molecular structure which in itself can be difficult for conformationally flexible molecules, particularly since crystal packing effects can stabilise conformers that are relatively unstable in solution. The relative stability of a series of candidate crystal structures is also not only potentially dependent on lattice energy but also at real temperatures (*i.e.* above 0 K) on lattice entropy considerations such as molecular vibration. Moreover, as we have seen in Section 8.2 crystal structure is highly dependent on nucleation and growth kinetic factors and morphological considerations (very anisotropic shapes such as thin plates are less likely to be stable). Despite these difficulties the prediction of crystal structure is a much sought-after goal. Ultimately all the materials properties of molecular solids stem from their crystal structure and hence the ability to know *ab initio* what polymorphic forms are to be expected, and what their solubility, hardness, magnetic and optical properties are likely to be before even synthesising a molecule would be highly desirable. There is now a tremendous amount of data available on crystal structures, particularly from the Cambridge Structural Database (Section 8.4), which forms an invaluable tool for organisation and statistical analysis of experimental structure data for comparison with prediction and calculation. Despite the fact that, in general, crystal structures are not predictable, a number of attempts, some of them increasingly successful, have been made to address the problem from a computational standpoint. Crystal structure calculation is particularly useful in tandem with additional data from other (usually experimental) sources. Complementary experimental and theoretical techniques in crystal structure prediction are shown in Table 8.4.

In addition to purely 'synthon-based' and 'brute force calculation' approaches to crystal structure prediction there are other intelligent methods of deriving crystal packing models by analysis of known crystal structure. One such method is the *Derived Crystal Packing Model*.[79] The derived crystal packing model aims to resolve issues such as twinning, epitaxial growth of one phase on another, polymorphism and concomitant polymorphism by extraction of periodic fragments from a known crystal structure – the *mother phase*. These periodic fragments are then used to generate new theoretical daughter phases

**Table 8.4** Complementary experimental and theoretical techniques in crystal structure prediction.[78]

| Experimental | Theoretical |
|---|---|
| Studies of nucleation | Cambridge Structural Database |
| Studies of morphology | First principles calculations on sample systems |
| Systematic search for polymorphs | Empirical methods |
| Standardised dissolution studies | Crystal potentials |
| X-ray crystallography | Lattice dynamics |
| Single crystal (Box 2.1) | Search of crystal potential hypersurfaces |
| Powder and Rietveld refinement | Monte Carlo methods |
| Thermochemistry | Molecular dynamics |
| DSC (see Box 9.1) | |
| TGA (see Box 9.1) | |
| Vapour pressure measurements | |
| Solid-state NMR | |
| Ultramicroscopy | |
| Scanning electron microscopy (SEM) | |
| Tunnelling electron microscopy (TEM) | |
| Atomic force microscopy (AFM) | |

by applying likely crystallographic symmetry operations to these periodic fragments. Lattice energy differences between daughter phases depend on interactions between periodic fragments. If the interactions *within* the periodic fragment are strong compared to the interactions between them then daughter phases will have similar energies to one another and to the mother crystal. They should also derive from similar growth units during nucleation. The daughter phases may thus represent structural models for real polymorphs. They may help with the understanding and modelling of epitaxy or twinning or feed into the crystal structure calculation process.

## 8.8.2 Crystal Structure Calculation

Price, S. L., 'The computational prediction of pharmaceutical crystal structures and polymorphism', *Adv. Drug Deliv. Rev.* 2004, **56**, 301–319.

A flow chart describing typical steps in modern crystal structure calculation is shown in Figure 8.49. Starting from a molecule of known connectivity (2D structure) an accurate 3D structure is calculated using a quantum mechanical energy optimisation procedure. For flexible molecules this may mean considering a number of possible conformers and examination of the Cambridge structural database for known related compounds to guide conformer choice. Once a candidate 3D molecular structure is established trial crystal structures are randomly generated. The most convenient approach is to use the most common crystal symmetry elements (inversion, screw axes, glide planes and translation, Box 8.2) to generate likely-looking dimers or small clusters of molecules (this is referred to as the 'cluster method'). For simplicity it is generally assumed that $Z' = 1$ (although successful structure calculations with more than one molecule in the asymmetric unit have been carried out) and that the structure is likely to be in one of the more common

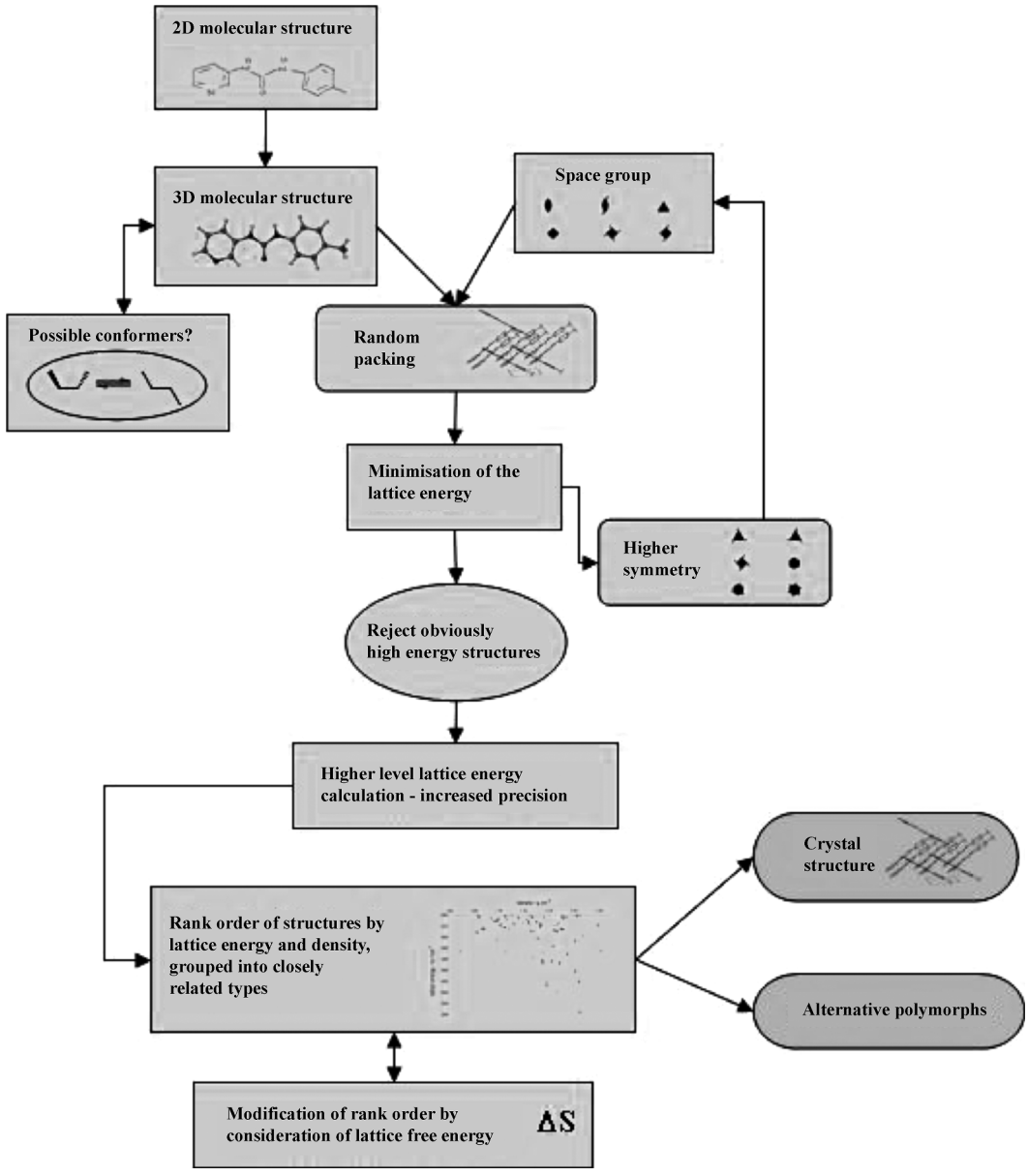


**Figure 8.49** A typical procedure for crystal structure calculation.

space groups (Table 8.3). With modern computing power tens or even hundreds of thousands of trial structures can be generated and assessed. It is possible, however, to reduce the number of possibilities by rejecting those that have very unlikely packing arrangements or very high energies based on a low-level preliminary lattice energy calculation. The main stage in the crystal structure calculation is then the lattice energy minimisation procedure. This procedure yields the lattice energies for all of the trial structures, notionally at zero Kelvin. True lattice energies may be verified experimentally by measurement of the heat of sublimation of the crystal, allowing minimisation procedures to be parameterised.[80] This procedure

gives the lowest energy possible crystal structures ranked by increasing lattice energy. If the procedure is successful then the observed structure for 'known' cases should be within *ca.* 5 kJ mol$^{-1}$ of the lowest energy structure and other structures of similar energy may represent possible undiscovered polymorphs. Lattice energy differences between polymorphs in real structures are typically very small, of the order of 0.05 – 0.5 kJ mol$^{-1}$.

In terms of lattice energy minimisation methods one of the most common approaches is the atom–atom potential method. Parameters for the individual potentials between atom pairs (*e.g.* H ⋯ H, C ⋯ H, C ⋯ C, C ⋯ Cl *etc.*) for both hydrogen-bonded and non-hydrogen-bonded situations have been empirically derived and fine-tuned, and reproduce well the experimental heats of sublimation. Differences between one structure and another arising from entropic effects are taken to be negligible. The interaction energies of atom pairs within clusters of molecules are calculated *via* the summation of the energetic potential between each atom pair, in principle out to infinity, but in practice to a predefined cut-off. Construction of stable clusters or aggregates is made simpler when dominant strong interactions are present.

One of the most successful modern implementations is the PIXEL method developed by Angelo Gavezzotti of the University of Milan, Italy.[81] PIXEL is based on integral sums over the molecular electron density to obtain coulombic, polarisation, dispersion and repulsion lattice energies. The program incorporates improved treatment of overlap repulsion and lattice energy minimisation based on the Symplex algorithm. The method is in principle applicable for most of the periodic table using relatively few parameters. A key aspect of the method is the treatment of intermolecular interactions as effects of the whole molecular electron density, an approach that is physically more justifiable than a pure atom-atom potential method. Results for the crystal structure calculation of naphthalene using UNI,[80] an older atom-atom potential method, and the PIXEL method are shown in Figure 8.50. While both methods reproduce

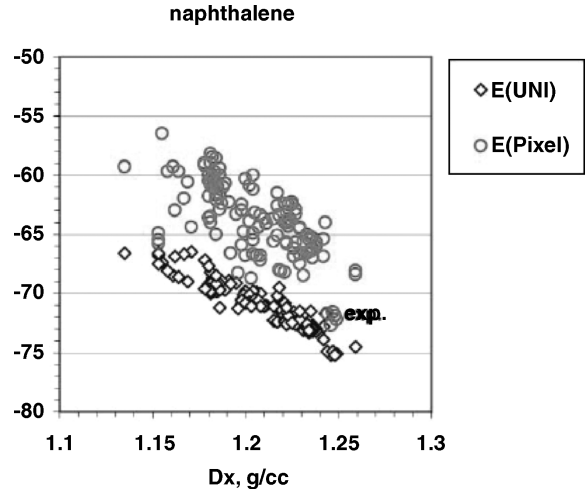


**Figure 8.50** A comparison of the performance of atom–atom potentials using the UNI method[80] and PIXEL potentials in the description of the energy landscape for 133 naphthalene crystal structures. The experimental crystal structure is represented by a cluster of 5 points representing very similar structures with different unit cell settings. Energies are given on the abscissa in kJ mol$^{-1}$. The plot shows the usual way of representing the results of crystal structure calculations with the expectation that the most stable structure should be at the lowest energy and exhibit the highest density. (Reproduced with permission from The Royal Society of Chemistry).

the experimental crystal structure there is a clear difference between the experimental structure (represented by a group of five circles that refer to essentially the same structure with different unit cell settings) and other candidates. The UNI method gives much poorer energy resolution. Figure 8.50 also illustrates the way in which the results of crystal structure calculations are generally presented with the expectation that the most stable structure should be at the lowest energy and exhibit the highest density.

Recent refinements on the atom–atom potential method include the development of accurate anisotropic model intermolecular potentials from *ab initio* electron distributions of the molecules. The non-spherical features in these charge distributions reflect features of real molecules such as lone pair and π-electron density, and therefore are much more effective at representing key interactions such as hydrogen bonding.

Calculations using empirical force-field methods are only as good as the force field and that data against which it has been parameterised and currently crystal structure calculation based on these methods is sporadic in its successes. Some methods reproduce certain classes of structures well if they are specifically parameterised for them but there is not one general overall method that is consistently successful over a broad range of compounds. Perhaps the method that currently comes closest is the 'hybrid' method developed by Markus Neumann of Avant-garde materials simulation. Instead of using an empirical force field this method uses *ab initio* density functional theory (DFT) to calculate the lattice energy – the method is therefore extremely computationally intense. Because DFT calculations use the independent electron approximation, they do not incorporate long-range dispersive interactions (van der Waals interactions) which result from electron correlation effects. These interactions play an important role in molecular crystals. As a result in the hybrid method DFT calculations are supplemented by an empirical van der Waals correction factor.[83] In the 2007 CCDC blind crystal structure prediction tests (see next section) the hybrid method implemented in the program VASP (Vienna *ab initio* simulation program) correctly calculated the experimental structures of all four test crystals! This unprecedented success came at the cost of 250,000 CPU hours computing time, however.

Empirical atom–atom potential methods that involve sifting a large number of possible structures are examples of 'static' methods. They are generally reasonably successful, especially when supported by additional experimental data from the kinds of techniques outlined in Table 8.4 although of course they cannot take account of crystal nucleation and growth kinetic effects. An alternative 'dynamic' approach uses Monte Carlo or molecular dynamics methods. These methods begin with a large number of molecules in random orientations – a large enough sample to be analysed statistically. Intermolecular interactions are calculated using empirical potential methods (similar to the atom–atom potential approach). The whole assembly is allowed to evolve in time, by solving the classical equations of motion for each molecule or averaged over a large configurational space. The final result is a predicted, ordered equilibrium state, which should correspond to the crystal structure. Dynamic methods are highly intensive of computing time and the problem worsens exponentially as the number of molecules in the sample increases. In principle dynamic methods are much more versatile than static approaches, however, since they could be used to explore the entire phase space of the system as a function of temperature, pressure *etc.*

## 8.8.3 The CCDC Blind Tests

Neumann, M. A., Leusen, F. J. and Kendrick, J., 'A major advance in crystal structure prediction', *Angew. Chem. Int. Edit.,* 2008, **47**, 2427–2430.

The state of the art in crystal structure calculation is tested every few years in the crystal structure prediction blind tests organised by the Cambridge Crystallographic Data Centre (CCDC). As of the

time of writing there have been four blind test exercises starting in 1999 with the results of the fourth test being announced in summer 2007. More complete data is available for the third test in 2005 which involved 18 international research groups, the vast majority working on lattice energy minimisation approaches. The tests have evolved to cover 3–4 molecules whose crystal structure is known to the test administrators but is unpublished and unknown to the participants. Participants are given 2D diagrams of the test compounds and asked to submit three predictions for the most likely crystal structure of each. In recent years there has been no restriction on possible space group of the target crystal structures and both $Z' = 1$ and $Z' = 2$ structures are allowed. The test compounds are chosen to contain either straightforward atom types or those which are computationally more challenging, and to cover a range of flexibility with more flexible molecules being more difficult. In the third test success rates as measured by the correct structure being in the list of three predictions submitted were not especially high with only one successful prediction for any of the three molecules. The most rigid molecule was particularly challenging because it had $Z' = 2$ and there was no success in predicting the structure of the flexible molecule. In contrast, in the fourth test which involved four 'blind' molecules, the results indicate that the computationally intensive *ab initio* DFT hybrid method[83] discussed in the previous section was successful *in every case*! This method is based on a very precise calculation of lattice energy ranking. The fact that this method has proved so successful suggests that lattice entropy effects, which are neglected in the method, are relatively unimportant in determining crystal structure energy ranking.

## 8.9 Hydrogen Bond Synthons – Common and Exotic

Braga, D., Grepioni, F. and Desiraju, G., 'Crystal engineering and organometallic architecture', *Chem. Rev.*, 1998, **98**, 1375–1405.

Consistent with its place as the 'masterkey interaction' in supramolecular chemistry, more crystal engineering studies have been carried out with hydrogen-bonded systems than with any other kind of interaction. It is impossible to do justice to the scope of hydrogen-bonded systems in a general work such as this, and hence the following sections contain only a few illustrative examples of the use of strong and moderately strong hydrogen bonds in crystal engineering. Many of the examples involve metal–organic species which display the full range of possible interactions observed in organic and coordination compounds. In general, the intermolecular interactions and concepts of intermolecular valence are closely related for organic and metal-organic systems because the metal atom is not situated on the periphery of the supramolecular synthon and hence plays little part in the crystal assembly. Metal-based systems do have the advantage, however, that a wider variety of shapes and topologies are frequently encountered. Further reading may be found in the references.

### 8.9.1 Hydrogen Bonded Rings

Allen, F. H., Motherwell, W. D. S., Raithby, P. R., Shields, G. P., Taylor, R., 'Systematic analysis of the probabilities of formation of bimolecular hydrogen-bonded ring motifs in organic crystal structures', *New J. Chem.* 1999, **23**, 25–34.

Hydrogen bonded rings are among the most beautiful and most versatile supramolecular synthons in crystal engineering. A systematic survey of the CSD was undertaken in 1999 to determine the tendency of particular functional groups to form hydrogen bonded ring dimer synthons as opposed to other motifs

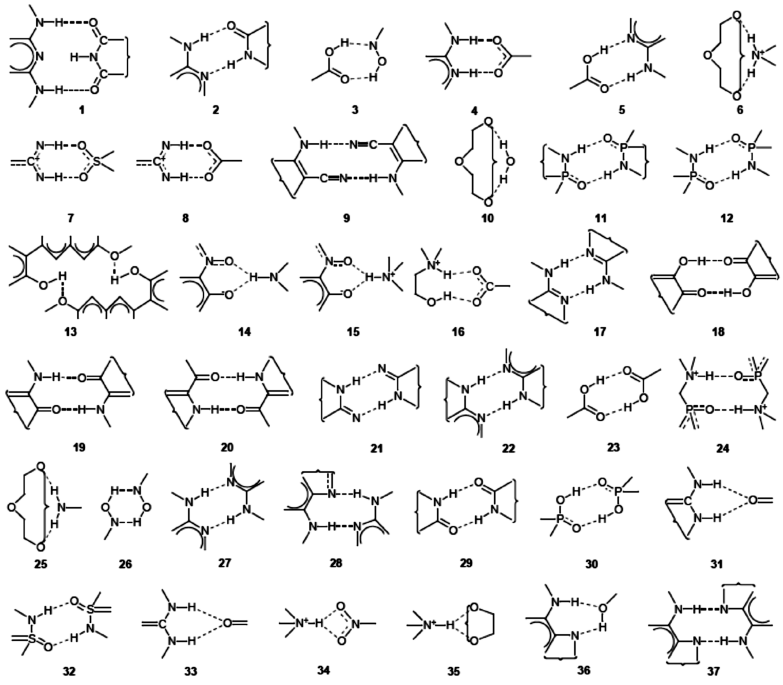

(a)

| Motif | Graph set | $P_m$(%) |
|---|---|---|
| 1 | R2,2(12) | 97 |
| 2 | R2,2(8) | 91 |
| 3 | R2,2(7) | 90 |
| 4 | R2,2(8) | 82 |
| 5 | R2,2(8) | 76 |
| 6 | R2,2(10) | 58 |
| 7 | R2,2(8) | 54 |
| 8 | R2,2(8) | 51 |
| 9 | R2,2(12) | 47 |
| 10 | R2,2(10) | 45 |
| 11 | R2,2(8) | 43 |
| 12 | R2,2(8) | 41 |
| 13 | R2,2(20) | 39 |
| 14 | R2,1(6) | 39 |
| 15 | R2,1(6) | 39 |
| 16 | R2,2(9) | 37 |
| 17 | R2,2(8) | 37 |
| 18 | R2,2(10) | 36 |
| 19 | R2,2(10) | 36 |
| 20 | R2,2(10) | 35 |
| 21 | R2,2(8) | 35 |
| 22 | R2,2(8) | 33 |
| 23 | R2,2(8) | 33 |
| 24 | R2,2(10) | 32 |
| 25 | R2,2(10) | 32 |
| 26 | R2,2(6) | 27 |
| 27 | R2,2(8) | 26 |
| 28 | R2,2(9) | 24 |
| 29 | R2,2(8) | 24 |
| 30 | R2,2(8) | 21 |
| 31 | R1,2(6) | 18 |
| 32 | R2,2(8) | 17 |
| 33 | R1,2(6) | 17 |
| 34 | R2,1(4) | 16 |
| 35 | R2,1(5) | 16 |
| 36 | R2,2(7) | 16 |
| 37 | R2,2(10) | 16 |

(b)

**Figure 8.51** (a) The first 37 of 75 hydrogen bonded dimer ring motifs in the 1999 version of the CSD with greater than 12 occurrences, ranked in decreasing order of probability of occurrence and (b) percentage probability of formation of ring motifs 1–37 ($P_m$ = number of motifs observed / number that could have possibly occurred) along with their graph set descriptors (reproduced with permission from The Royal Society of Chemistry).

such as discrete or chain structures. A total of 75 dimer synthons with 12 or more occurrences were found, of which the first 37 are shown in Figure 8.51, ranked in order of probability of occurrence and hence synthon robustness. There is in general a strong tendency towards the formation of hydrogen bonded rings with some functional groups almost invariably forming these kinds of synthon. There is significant interference from other functional groups however. The most robust motifs 1 and 2 are analogous to the mutual recognition of nucleotides in DNA and their robustness is well recognised in crystal engineering and in supramolecular chemistry, in particular complexes formed between melamine and cyanuric acid and their derivatives (see Section 10.6.4). Synthon 8 is found in biological structures involving arginine and aspartic and glutamic acids. Motifs 6 and 10 are components of crown ether complexes of ammonium ions (Section 3.12.1). Cyclic amide and carboxylic acid dimers are among the most frequently occurring motifs but it is surprising that the carboxylic acid dimer (synthon 23) only has a probability of *ca.* 33 %, with chain formation being a significant competitor (see Figure 8.2). The low probability is due to the presence of other competing functional groups such as co-crystallised water or ionic carboxylate groups in partially deprotonated polycarboxylic acids. When the effects of these competing groups are removed and the search repeated only for neutral carboxylic acids with no competing NH or OH donors the probability of forming the ring synthon increases to *ca.* 95 % for monocarboxylic acids and 85 % for dicarboxylic acids. The lower value for diacids reflects the competing formation of the intramolecular S(7) ring in 1,2-dicarboxylic acids.

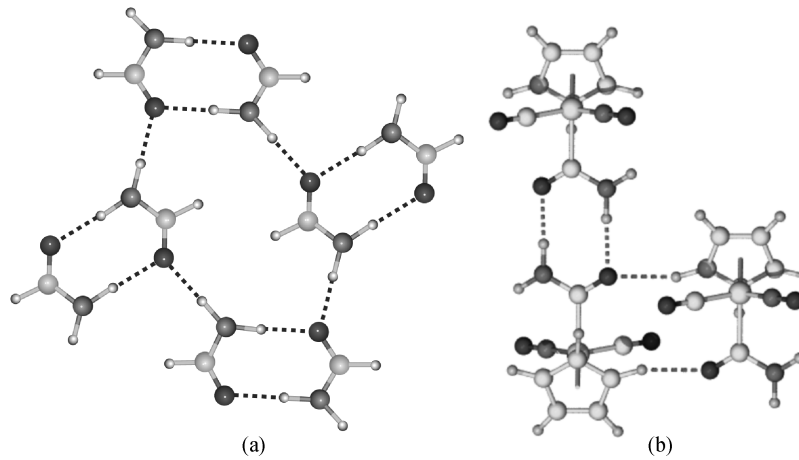


**Figure 8.52** Structures of (a) formamide and (b) $[Mn(C_5H_5)(CO)(NO)(CONH_2)]$.

Amide dimers (motif 29) are also commonly occurring synthons although their percentage of dimers formed is low for the same reasons as carboxylate dimers. The amide moiety is particularly interesting from a crystal engineering point of view. Not only does it possess acidic NH groups capable of acting as hydrogen bond donors, and a hydrogen bond acceptor C═O group, but the amide —CHO proton is also highly acidic compared to other C—H protons because of the inductive effect of the nearby oxygen and nitrogen atoms. This frequently results in the occurrence of relatively strong C—H ⋯ X interactions. An interesting example of both continuity of hydrogen-bonded motifs, as well as the effects of substitution, is observed in the comparison of the crystal structures of formamide ($H_2NCHO$) and $[Mn(C_5H_5)(CO)(NO)(CONH_2)]$ (Figure 8.52). Both structures conserve the cyclic, eight-membered hydrogen-bonded ring similar to those seen for the carboxylic acid dimer structures; however, in formamide, the second NH proton allows a cross-linked chain structure to form. This link is absent in the managanese compound, which also lacks the acidic C—H proton. Instead, an additional C—H ⋯ O interaction is formed from the $C_5H_5$ ligand to the amide C═O group.

Alcohols, ROH, possess one hydrogen bond donor proton and two accepting lone pairs, and thus generally cannot form saturated hydrogen-bonded structures (hydrogen bond interactions to every acidic proton and every lone pair). As a result, there are generally only two interactions to each oxygen atom: one hydrogen bond donating and one accepting. This results in the formation of either infinite chains, as in the helical tubuland structures (Section 7.4.2), or rings. While hydrogen bonded dimers are known, they occur only 1.9 % of the time and are highly strained. More commonly ring structures usually comprise either four or six OH groups (Figure 8.53).

In the case of quinones and phenols such as Dianin's compound (Section 7.5), the six-membered ring is prevalent and results in significant clathrate-forming ability. The motif is sufficiently robust, and its inclusion-forming abilities sufficiently common, that it has been used as the model for a range of covalent hosts according to the 'hexahost strategy', *e.g.* (Section 8.3.4) in which the hydrogen-bonded ring is replaced by covalent bonds. A number of bulky organometallic complexes replicate these ring motifs with the size of ring being dependent loosely on the steric properties of the remainder of the alcohol. Thus $[Mo(CO)_2(\eta^5\text{-}C_5H_5)(\eta^3\text{-}C_7H_{10}OH)]$ forms four-membered rings in which all of the OH groups are directed inwards, leaving the bulky organometallic groups to form weaker interactions on the periphery of the molecule, while the $Fe_2$ dimer $[Fe_2(CO)_4(C_5H_4C_2H_4OH)_2]$ forms a six-membered hydrogen bonded ring (Figure 8.54).

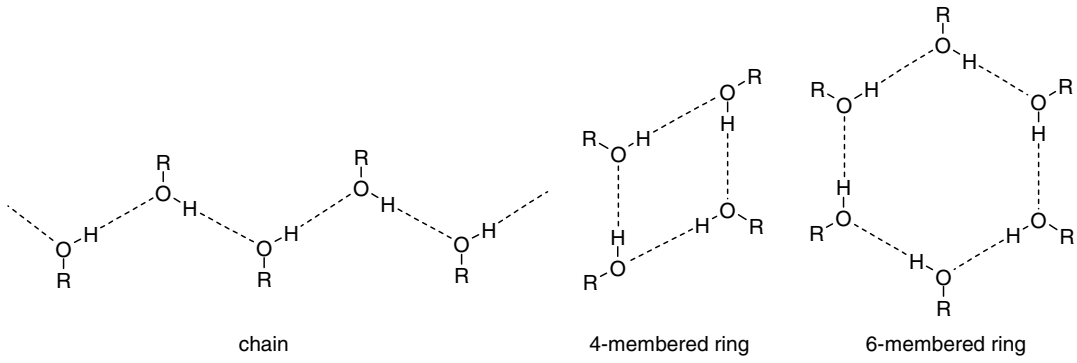


**Figure 8.53** Common hydrogen bonded geometries for alcohols, ROH.

Carol Brock of the University of Kentucky, USA, has undertaken a systematic study of the hydrogen bonding in alcohols[84] and vicinal di-ols.[85] While the monoalcohol work was undertaken using the CSD in 1994 its conclusions have stood the test of time. Brock postulated that because alcohols are both good hydrogen bond donors and acceptors than chain or ring structures of the type shown in Figure 8.53 (along with trimers) should predominate, as opposed to discrete aggregates in which some OH protons are not engaged in hydrogen bonding. The data revealed that full OH···O bonding was indeed observed in 67 % of cases. In cases where the substituent of the OH group is relatively 'thin' then the molecules involved in OH···O interactions can be related to one another by $2_1$ screw symmetry or glide planes (see Box 8.2 for an explanation of crystallographic symmetry operations), Figure 8.55a. As the substituents get bulkier then it is not sterically possible to fit the three oxygen atoms together to form an OH···OH···OH interaction in which the O···O distances must be *ca*. 2.8 Å,

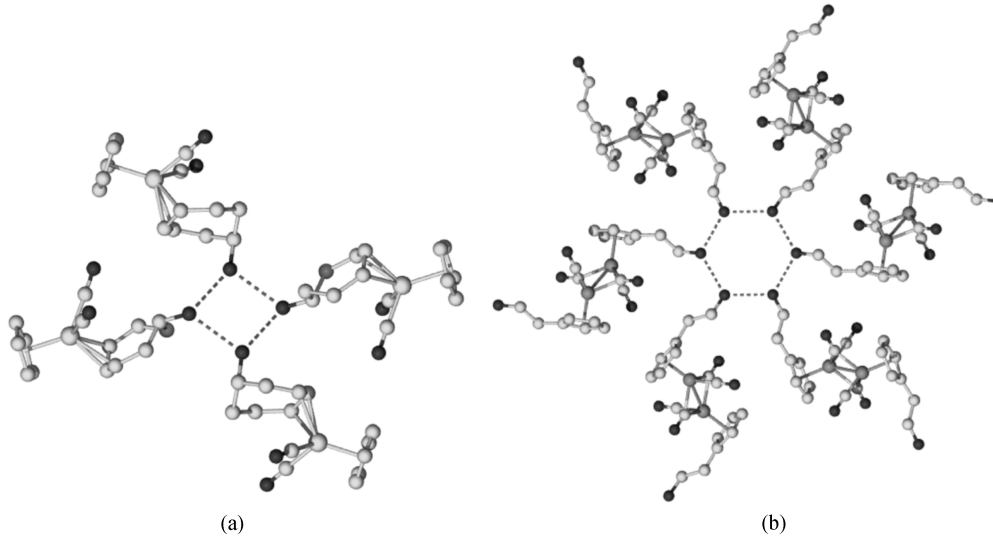


**Figure 8.54** Four- and six-membered hydrogen bonded ring structures in (a) $[Mo(CO)_2(\eta^5\text{-}C_5H_5)(\eta^3\text{-}C_7H_{10}OH)]$ and (b) $[Fe_2(CO)_4(C_5H_4C_2H_4OH)_2]$.

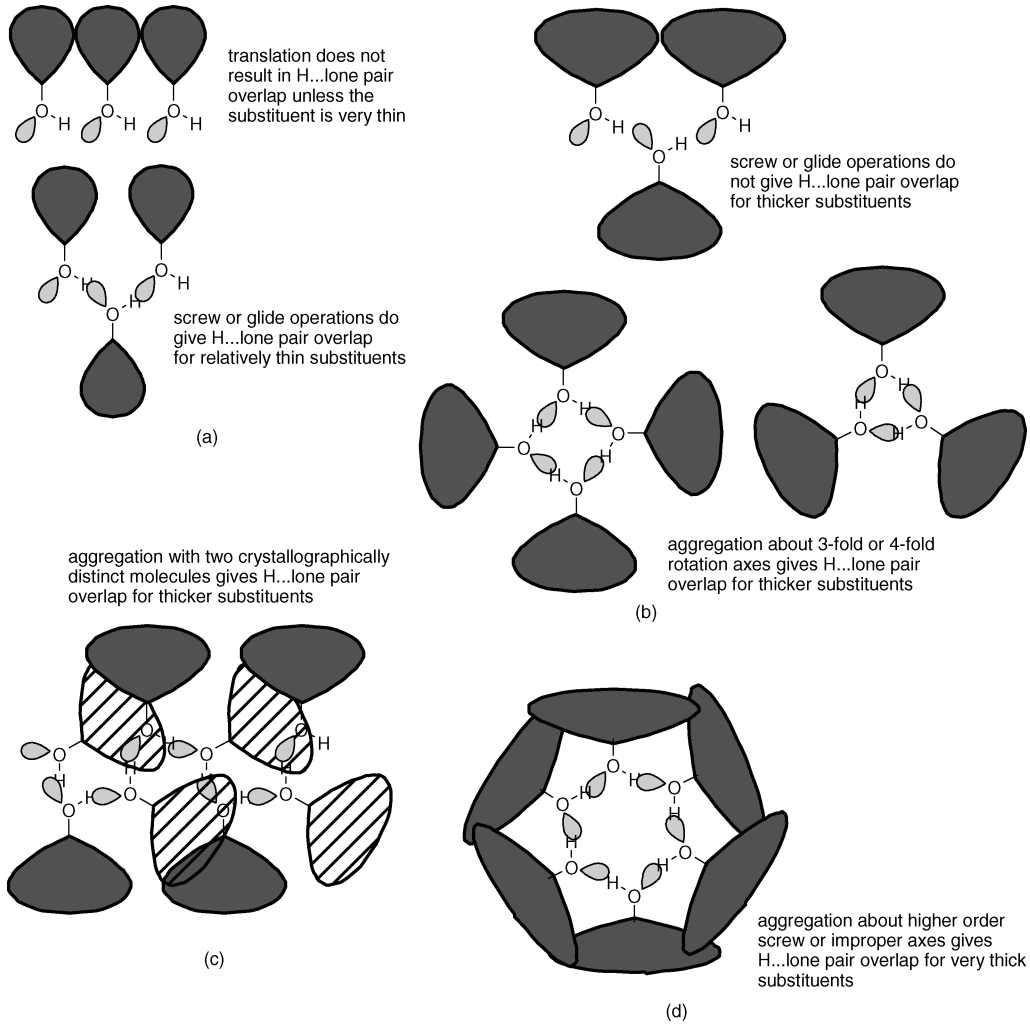


**Figure 8.55** Ways of packing monoalcohols with variable thickness of substituent (a) thin substituents pack by translation or by $2_1$ screw or glide operations, (b) with thicker substituents rings are favoured, (c) thicker substituents may also pack with more than one molecule in the asymmetric unit and (d) very thick substituents result in packing about higher order screw or improper rotation axes.[84]

and so either cyclic trimers, tetramers or hexamers must form (Figure 8.55b – a pentamer is unlikely because there is no fivefold symmetry operation in crystallography) or the number of molecules in the crystallographic asymmetric unit must increase, i.e. $Z' > 1$ (Figure 8.55c, see Section 8.7 for an explanation of $Z'$). If the substituents become very large then packing about higher order screw axes such as $3_1$ or $4_1$ or improper rotation axes such as $\bar{3}$ or $\bar{4}$ become favoured (Figure 8.55d). Using this reasoning Brock was able to predict that monoalcohols exhibiting full hydrogen bonding (*i.e.* complete chains or rings) should either adopt $Z' > 1$ structures more frequently than the CSD average (they do: 51 % *vs.* 8 %) and/or exhibit a tendency towards higher symmetry space groups (they do: 32 % *vs.* 1 %). Brock's analysis also proved similar for di-alcohols, with the $R_2^2(10)$ motif between two di-ols being the most common.

## 8.9.2 Hydrogen Bonds to Halogens

Kovacs, A. and Varga, Z., 'Halogen acceptors in hydrogen bonding', *Coord. Chem. Rev.* 2006, **250**, 710–727.

While hydrogen bonding to organic halogens is generally extremely weak, halide ions and metal-coordinated halides are very effective hydrogen bond acceptors with $F^-$ and $Cl^-$ in particular having very high hydrogen bond basicity because of their high negative charge density and steric accessibility (Section 8.1.4). Hydrogen bonds to isolated $Cl^-$ ions in the solid state can act to dominate crystal packing with primary interactions such as OH···$Cl^-$ and NH···$Cl^-$ being supplemented by multiple CH···$Cl^-$ bonds until the anion is completely surrounded. For a given donor type, the H···F distances are generally much shorter than distances to other halides with hydrogen-bond distances typically increasing by more than 0.5 Å moving from from $F^-$ to $Cl^-$. The distance increases by a further 0.15 Å from $Cl^-$ to $Br^-$ and by a further 0.25 Å to $I^-$. CH donors interact very strongly to $Cl^-$ with strong of the C-H donors such as chloroform having an average H···Cl separation of only 2.39 Å (average C···Cl separation 3.42 Å) Hydrogen bonds to heavier halide ions are also significant, albeit with decreasing hydrogen bond basicity going down the group. Hydrogen bonding to metal halides is almost as strong as to halide ions and is significantly more directional. There are significant differences in the acceptor properties of metal fluorides compared to $F^-$ with distances to coordinated fluoride being significantly longer than to $F^-$. In contrast isolated and coordinated iodide behave quite similarly. Metal fluorides are also atypical of other metal halides as hydrogen bond acceptors with metal fluorides exhibiting typical H···F–M angles of 120–160°; significantly larger than H···X–M angles which are typically 90-130° for X = Cl, Br, I. Indeed while metal fluorides exhibit very strong hydrogen bonds on account of the high electronegativity of fluorine, they exhibit markedly less directional preference in the H···X–M angle then other metal halide acceptors. The origins of this effect are electronic. The coordinated fluoride ligand behaves essentially like an only slightly perturbed isolated $F^-$ ion and hence approach from almost any direction will result in a strong hydrogen bond. In contrast, negative electron density in the heavier metal halides is depleted on the face of the coordinated halide opposite (trans to) the metal, Figure 8.56a. This means that hydrogen bond donors

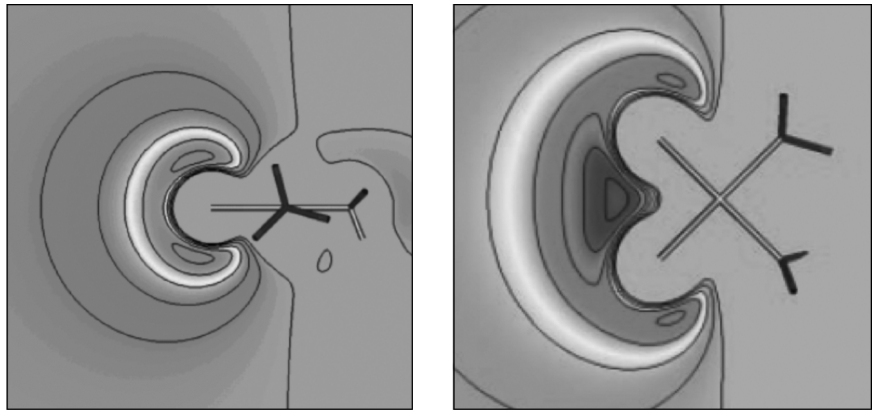

(a) (b)

**Figure 8.56** (a) Calculated negative electrostatic potential for a coordinated $Cl^-$ ligand in the model compound $PdClMe(PH_3)_2$ showing the distribution of the hydrogen bond acceptor electron density away from the Pd–Cl vector and (b) negative electrostatic potential for a coordinated $Cl^-$ ligands in the model compound *cis*-$PdCl_2(PH_3)_2$ showing the concentration of negative charge in between the two chloride ligands. Contours are at 10 kcal $mol^{-1}$ intervals (reprinted from [86] and [88] with permission from AAAS).

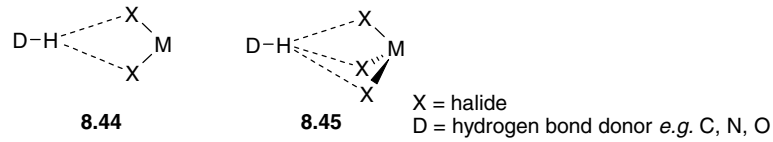


**8.44** **8.45**

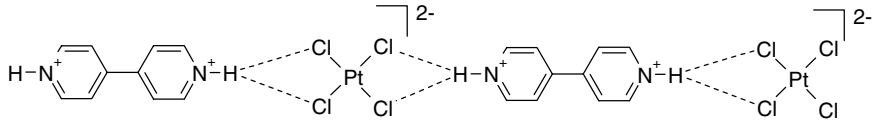


**8.46**

**Figure 8.57** Supramolecular synthons **8.44** and **8.45** formed to halometallate complexes along with the tape structure formed by 4,4′-bipyridinium tetrachloroplatinate(II) *via* an $R_1^2(4)$ hydrogen bonded synthon.[87]

tend to cluster towards the regions of higher electron density away from the X–M vector hence giving rise to a significantly bent H···X–M angle.[86] This directional preference has led to the development of two robust metal-halide supramolecular synthons (**8.44** and **8.45**) by A. Guy Orpen at the University of Bristol, UK.[87] These synthons are based on mutually *cis* dihalides or *fac* trihalides and a single hydrogen bond donor linked in the case of **8.44** by a bifurcated $R_1^2$ (4) synthon, and a similar trifurcated motif for **8.45**. The bi- or trifurcation in each case allows the donor to interact at the optimum, highly non-linear angle with more than one acceptor hence forming two or three optimum hydrogen bonds to strong acceptors, Figure 8.56b. Orpen's group has used this synthon to crystal engineer tape structures such as **8.46**, Figure 8.57.

In the context of hydrogen bonds to halides it is noteworthy that even main group fluorides such as the anions $PF_6^-$ and $BF_4^-$ which are traditionally thought of as non-coordinating can form multiple hydrogen bonds of non-negligible strength and current research in 'super-weak' non-coordinating anions tends towards halogenated carboranes $CB_{11}H_{11-n}X_n^-$ and fluorinated analogues of $BPh_4^-$ such as $B(3,5\text{-}C_6H_3(CF_3)_2)_4^-$ which lack these acceptor properties.

## 8.9.3 Hydrogen Bonds to Cyanometallates

Paraschiv, C., Ferlay, S., Hosseini, M. W., Bulach, V., Planeix, J.-M., 'Molecular tectonics: design of luminescent H-bonded molecular networks', *Chem. Commun.* 2004, 2270–2271.

As with metal-coordinated halides, metal-coordinated cyanide ligands are also good hydrogen bond acceptors because of both their residual negative charge and the highly sterically accessible linear shape of the M–C≡N unit. Moreover the M–CN bond is strong and relatively inert and hence $CN^-$ ligands can act as useful handles to arrange metal ions by hydrogen bonding. Work by Mir Wais Hosseini at the University of Strasbourg, France, has shown that the packing of both $Au(CN)_2^-$ and $M(CN)_4^{2-}$ anions can be controlled very successfully by hydrogen bonding interactions to bisamidinium dications of type **8.47**, Figure 8.58. If a short spacer such as $-CH_2CH_2-$ is used then the Au(I) ions are brought into close proximity resulting in Au···Au interactions and hence solid-state luminescence of the crystal.

Mike Ward of the University of Sheffield, UK, has taken advantage of hydrogen bonding from coordinated ruthenium(II) biimidazole complexes (**8.48**) to tectons such as $[Ru(2,2'\text{-bipyridyl})(CN)_4]^-$

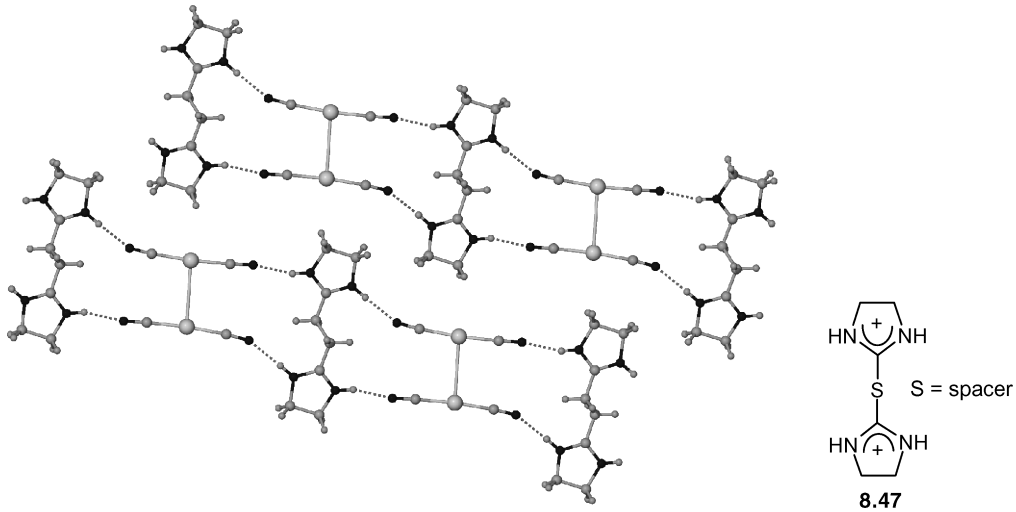


8.47

**Figure 8.58** Tecton **8.47** forms hydrogen bonds to helometallate anions such as $Au(CN)_2^-$ such that the Au···Au distance in the crystal is critically dependent on the size of the spacer, S. The X-ray crystal structure of the S = $CH_2CH_2$ analogue exhibits Au···Au interactions that result in solid-state luminescence.

(**8.49**), $[Co(CN)_6]^{3-}$ or $[Fe(CN)_6]^{3-}$.[89] The double biimidazole-NCRu hydrogen bond is evident in both the solid state and in $CDCl_3$ solution, where binding constants of over $10^3 - 10^5$ were measured. Interaction with hexacyanoferrate(III) brings about a photoinduced electron transfer process which entirely quenches the Ru(II) luminescence.

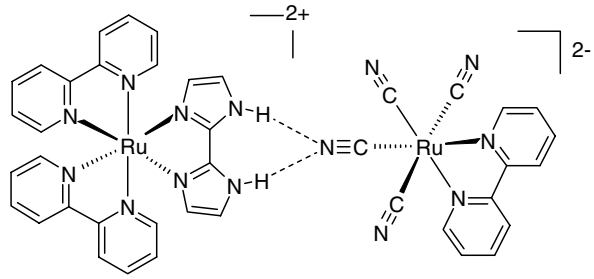


8.48 8.49

## 8.9.4 Hydrogen Bonds to Carbon Monoxide Ligands

Braga D. and Grepioni, F., 'Hydrogen bonding interactions with the CO ligand in the solid state', *Acc. Chem. Res.*, 1997, **30**, 81–87.

Carbon monoxide is a good ligand for low-oxidation-state metal centres as a result of its ability to act as a π-acid. The delocalisation of the oxygen lone pairs, however, make it a relatively poor

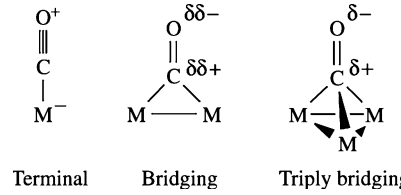


**Figure 8.59** Coordination modes of CO along with formal charges.

hydrogen bond acceptor, and in some cases (e.g. the $Mn_4$ cubeane **8.60**, Section 8.12) even benzene is preferred over CO as an acceptor. In the absence of better acceptors, however, hydrogen bonding to CO may be a significant factor in crystal organisation. The hydrogen bond basicity of coordinated CO increases on moving from a terminal to bridging to triply bridging mode (Figure 8.59), as the CO becomes more like a ketone (double bond) rather than triply bonded. This intermolecular hydrogen bonding may even have an effect on the molecular structure of malleable metal carbonyl species if there are two or more structures with varying occurrences of bridging CO close together in energy. The hydrogen-bonded interactions to CO favour the bridging mode in the solid state.

In the presence of strong ('hard') hydrogen-bond donors such as alcohols or carboxylic acids, CO rarely takes part in significant interactions and the hydrogen bond functionality generally binds with other strongly interacting moieties as outlined in Section 8.9.1 (*cf.* Etter's rules). In one case, the structure of $[Cr(CO)_3\{\eta^6\text{–}C_6H_4(C_5H_4MeOH)\}]$ (Figure 8.60), there is a synergic mixture of interactions in which the hydroxyl group forms a bifurcated hydrogen bond with two CO oxygen atoms, which is of comparable length to intermolecular C–H···O hydrogen bonds from the coordinated aryl group to the hydroxyl lone pair (2.29, 2.44 and 2.27 Å, respectively).[90] The case is rather different for 'soft' hydrogen-bond donors, such as C–H bonds, in which C–H···O=C hydrogen bonds are the most abundant interaction in organometallic systems. This has been the subject of a CSD search,[91] which gives a spread of intermolecular C···O distances of between 3.2 and 3.9 Å with C–H interactions to bridging CO being on average significantly shorter than to terminal CO (Figure 8.61).

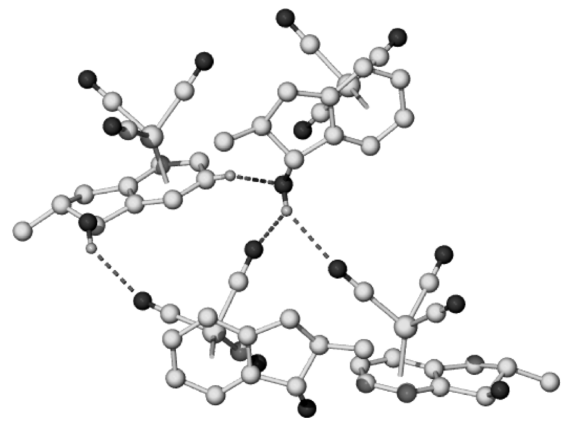

**Figure 8.60** X-ray crystal structure of $[Cr(CO)_3\{\eta^6\text{–}C_6H_4(C_5H_4MeOH)\}]$ showing O–H···O=C and C–H···O hydrogen bonds.[90]

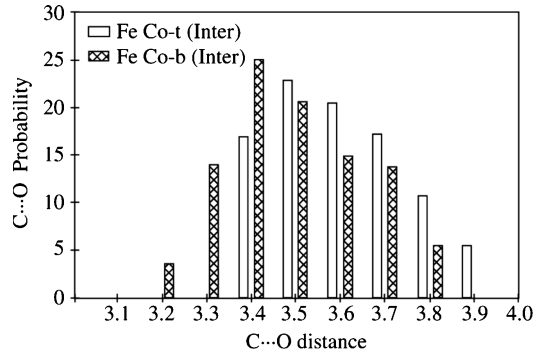


**Figure 8.61** Histogram of intermolecular C···O terminal and bridging distances for C–H···C=O bonded complexes in the CSD. Interactions to the more basic bridging CO ligands are significantly shorter. (Reprinted with permission from [91] © 1995 American Chemical Society).

## 8.9.5 Hydrogen Bonds to Metals and Metal Hydrides

Epstein, L. M., Shubina, E. S., 'New types of hydrogen bonding in organometallic chemistry', *Coord. Chem. Rev.* 2002, **231**, 165–181.

### *Direct Interactions to the Metal*

Metal atoms or ions are of a highly amphoteric character, and may act as both Lewis bases and Lewis acids depending on the identity of the metal, oxidation state, ancillary ligands *etc.* In organometallic chemistry, the interaction of the σ-electron density in a covalent bond, particularly a C–H bond, with an electron-deficient metal centre is a well-known phenomenon, termed agostic bonding (Figure 8.62a). A strong agostic interaction may be regarded as a three-centre, two-electron bond, and will result in a reduction in C–H bond order. Such interactions may be detected by:

- Reduced $^{1}J_{CH}$ $^{13}$C NMR coupling constant (which is related to the C—H σ-bonding electron density).
- High field $^{1}$H NMR chemical shift as a result of shielding by the electropositive metal centre (about 0–10 ppm like that of a metal hydride).

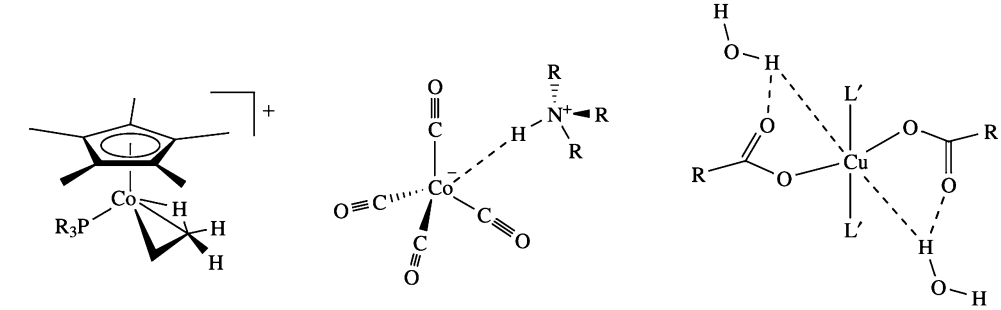


**Figure 8.62** Types of M···H interaction.[92]

- Reduced ν(CH) IR or Raman vibrational frequency as a consequence of lowered vibrational force constant.
- Short $T_1$ (spin lattice) NMR relaxation time, since spin polarisation may be readily transferred on to the metal centre.

Agostic bonds are commonly highly covalent, but in the weaker extreme bear many angular and distance characteristics that might classify them as a M···H–C hydrogen bonds. Such interactions with X—H bonds in general have been classified as *intermolecular pseudo-agostic* (IPA), and there is ample evidence in the CSD to support their existence.[92] One of the most characteristic IPA interactions concerns the simple salt $[R_3NH^+][Co(CO)_4^-]$ (Figure 8.62b). The sterically unhindered nature of the tetrahedral Co(−1) complex allows the close approach of the N–H group to form a charge-assisted $N^+$—H ··· $Co^-$ IPA hydrogen bond. A neutron diffraction study of the case when R = Et gives an N ··· Co distance of 3.666 Å and an H ··· Co contact of 2.611 Å. The bond is essentially linear. There is a crucial difference between agostic and IPA interactions, however. True agostic interactions are three-centre two-electron interactions involving a single electron pair occupying an orbital that is delocalised over C, H and metal atoms. In contrast IPA interactions are much more electrostatic in nature and are three-centre four-electron interactions in which a metal lone pair or metal electron density interacts with a D–H dipole. Agostic bonding was postulated to explain the close approach of a C–H group to Cu(II) in the coordination compound $[Cu(Hceph)_2]$ where ($H_2$ceph) is N-[2-hydroxy-1-(*S*)-methyl-2(*R*)-phenylethyl]-N-methylglycine; however, a detailed analysis revealed that this is a case in which an intramolecular CH···O hydrogen bond brings the CH bond into close proximity to the metal centre.[93] Such interactions are related to IPA interactions and are termed *intermolecular multicentre hetero-acceptor* hydrogen bonds (IMH) and relate to interactions of the usual donors of type X—H (X = O, N, C *etc.*) with M—X′, where M and X′ are electron-rich. Essentially, this interaction is a form of bifurcated hydrogen bond in which the metal and a coordinated heteroatom (X′) act as the two acceptors. An IMH interaction is formed in the Cu(II) species $[CuL_2L_2'] \cdot 2H_2O$ (L = the conjugate anion of *N*-acetyl-$\alpha$-alanine, L′ = *N*-methylimidazole) in which a water O—H group interacts simultaneously with the Cu(II) centre and a coordinated oxygen atom (O—H ··· O = 2.027 Å, O—H ··· Cu = 2.568 Å) (Figure 8.62c).

### *Interactions to Metal Hydrides*

In addition to the metal itself acting as a hydrogen bond acceptor, it has become increasingly clear that M—H fragments can act as both hydrogen bond donors and acceptors *via* the hydridic hydrogen atom, which usually bears a formal negative charge. As a non-traditional hydrogen bond donor, the hydrogen atom of the M—H fragment needs to be both sterically accessible and relatively electron-poor. Since the hydride ligand is solely a σ-donor, its electronic nature will depend on the electron density at the metal centre. This is determined largely by the metal oxidation state, with cationic metal ions withdrawing the most electron density. The effect is particularly pronounced when the hydride is in a doubly or even triply bridging coordination mode with more than one metal centre making demands on its electron density. In such instances, the M—H fragment is a 'soft' hydrogen bond donor and interacts frequently with soft acceptors such as CO, which is a common co-ligand in metal hydride compounds. The complex $[Os_3(CO)_{10}(\mu\text{–H})(\mu\text{–NCHCF}_3)]$ is an excellent example in which the hydride ligand (which is double bridging) forms a single, short $M_2H \cdots O{=}C$ interaction (2.594 Å) to a terminal carbonyl ligand on an adjacent cluster. Ionic hydride hydrogen bonds are found in $[Os(\eta^2\text{-H}_2)(CH_3CN)(dppe)_2](BF_4)_2$ in which the hydridic $H_2$ ligand forms an interaction to one of the $BF_4^-$ anions with an H···F distance of 2.4 Å, less then the sum of the van der Waals radii of H and F (2.7 Å).

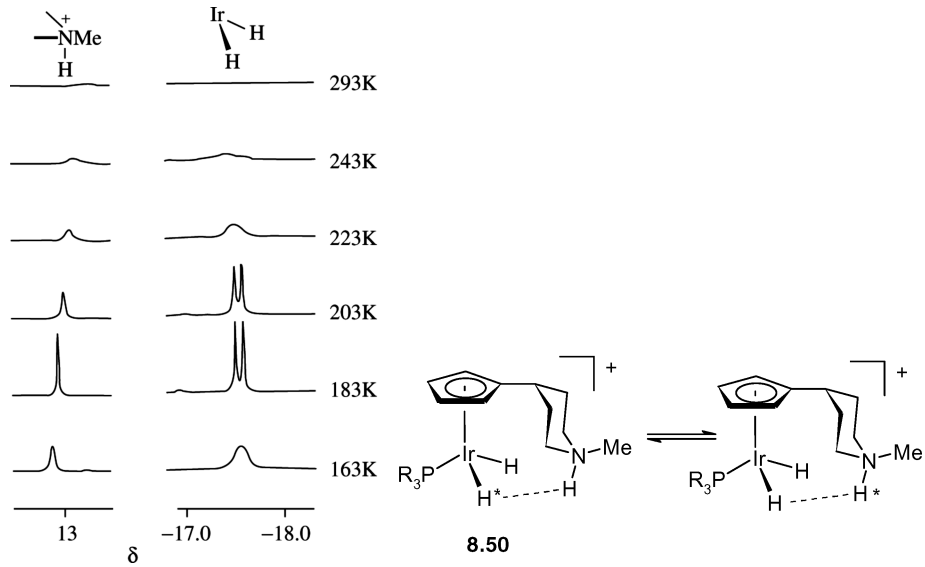


**Figure 8.63** Variable temperature $^1$H NMR spectra of the Ir—H and N—H regions in **8.50** showing the proton exchange process. (Reproduced with permission from The Royal Society of Chemistry).

An equally common situation is when the M—H fragment is electron-rich with the hydridic hydride ligand acting as a pseudo-halogen. In such circumstances, the hydride is capable of acting as a non-traditional hydrogen bond acceptor, forming hydrogen bonds of type M–H···H–X (X = electronegative atom such as O, N, C *etc.*). These hydrogen bonds, termed *dihydrogen bonds*, may be either intermolecular, or intramolecular, and have been observed structurally by X-ray and neutron diffraction and by experimental charge density analysis for a wide range of H—X functionalities and *s*-, *p*- and *d*-block hydrides. There is also significant evidence for dihydrogen bonding in solution as in the case of the Ir—H ··· H—N interaction in the iridium(III) dihydride **8.50**. Variable temperature $^1$H NMR spectroscopy allows the study of the exchange of the acidic and basic hydrogen atoms in this compound, possibly *via* a coordinated $H_2$ intermediate (Figure 8.63).[94] These results are of great interest in the study of the mechanism of activation of $H_2$ by metal catalysts. *Ab initio* calculations on a range of other strongly interacting M—H ··· H—X systems give the distances and interaction energies shown in Table 8.5.[95]

**Table 8.5** Calculated parameters for various M—H ··· H—X systems.[95]

| Complex | H ··· H distance (Å) | Interaction energy (kJ mol$^{-1}$) |
|---|---|---|
| $Mo(CO)_2(PH_3)_2(NO)(H)\cdots H—F$ | 1.378 | 46.4 |
| $Mo(CO)_2(NH_3)_2(NO)(H)\cdots H—F$ | 1.300 | 64.4 |
| $Mo(CO)_2(NH_3)_2(NO)(H)\cdots H—OH$ | 1.647 | 54.8 |
| $Re(C_5H_5)(CO)(NO)(H)\cdots H—OH$ | 1.770 | 45.6 |
| $Re(C_5H_5)(CO)(NO)(H)\cdots H—OCF_3$ | 1.458 | 41.0 |

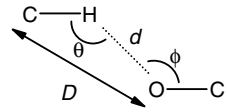


**Figure 8.64** Parameters characterising a CH···O interaction.

## 8.9.6 CH Donor Hydrogen Bonds

Desiraju, G. R., 'The C-H···O hydrogen bond: structural implications and supramolecular design', *Acc. Chem. Res.* 1996, **29**, 441–449; Nishio, M., 'CH/π hydrogen bonds in crystals', *CrystEngComm* 2004, **6**, 130–158.

The concept of the C–H bond as a hydrogen bond acid, capable of forming weak interactions with basic acceptors, particularly oxygen, was first suggested by Sutor in 1962. At the time, the idea met with significant resistance but in the light of numerous surveys of the CSD and the discovery of many characteristic C—H···O hydrogen-bonded compounds, the presence of the interaction is now generally accepted and C···O distances (*D*) anywhere between 3.0 and 4.0 Å are considered significant (Figure 8.64). In the special case of CH interactions to coordinated CO (Section 8.9.4), we saw that the C···O distance (*D*) was dependent on the basicity of the oxygen acceptor. While this is true, it is only one of three factors, along with the acidity of the C—H bond and the steric environment of the C—H proton, which determine *D*. Of these, it seems apparent that sterics play the dominant role, limiting *D* to a narrow range between 3.38 and 3.52 Å simply because of the trade-off between unfavouable steric interactions and van der Waals attractions in other parts of the molecule. In unencumbered systems, the C—H acidity is by far the most important factor, and it is only because the C—H acidity is averaged over a large sample size that the oxygen basicity effect is apparent in Figure 8.61. In fact, a comparison of the range of distances *D* with the C-acid p$K_a$ in DMSO reveals a significant correlation (Figure 8.65). Generally C···O distances increase linearly with p$K_a$, with the shortest distances, in the region of 3.1–3.2 Å, noted for unhindered, strongly acidic C—H bonds such as in $CHCl_3$ and $(CN)_2$=CHR

One of the most elegant weakly interacting complexes, 2-ethylyladamantan-2-ol (**8.51**) was studied by neutron diffraction in 1996 by Judith Howard of the University of Durham, UK, and collaborators.[96] This structure shows the mutual reinforcement to two strong O—H···O hydrogen bonds and two 'weak' C—H···O interactions from the acidic alkyne protons to give a cyclic tetramer. The neutron study determined the C—H···O distance, *d*, to be 2.070 Å, one of the shortest known (the C···O distance, $D$ = 3.135 Å). The OH groups, which do not all engage in O—H···O hydrogen bonds, form a further kind of weak interaction with the acetylenic π-electron density. The intermolecular interactions of the system as a whole are thus maximised (Figure 8.66).

Surprisingly, even very weak acids such as methyl groups may exhibit significant intermolecular hydrogen bonding interactions, as exemplified by the 1:1 co-crystal of 4-nitrobenzoic acid and 4-(*N*,*N*'-dimethylamino)benzoic acid (**8.52**), which forms a ribbon structure comprising alternating carboxylic acid dimer rings (*cf.* Section 8.9.1) and a further eight-membered ring in which the nitro group accepts two hydrogen bonds from the dimethylamino moiety.

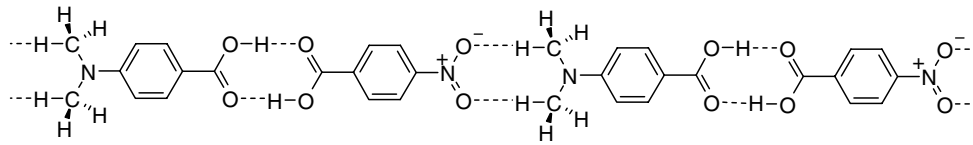

**8.52**

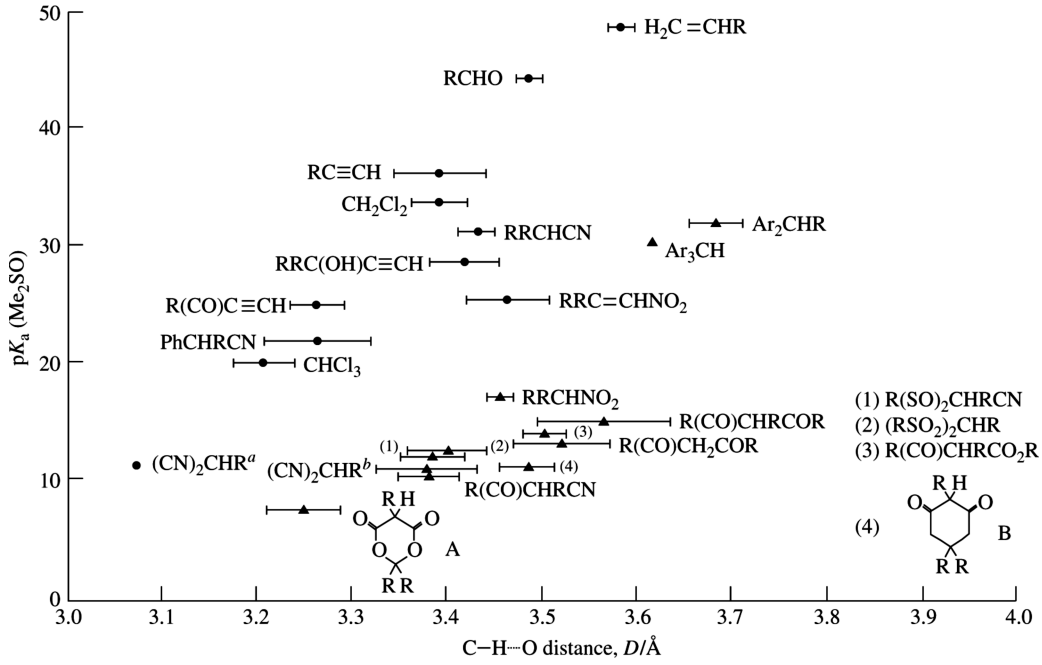


**Figure 8.65** Correlation of carbon acidity (p$K_a$ in DMSO) with hydrogen-bonded C···O distances ($D$). Points marked • are not sterically hindered, whereas in those marked ▲, the approach of the C—H and O groups is difficult. For $(CN)_2CHR$, the one unclathrated structure is marked 'A', while clathrates are marked 'B'. (Reproduced with permission from The Royal Society of Chemistry).

While the most prevalent, C—H···O hydrogen bonds are not the only form of weak hydrogen bond with crystal engineering potential. Carbon acid interactions of type C—H···N, C—H···Cl and C—H···$\pi$ as well as interactions to weak acceptors such as O—H···$\pi$ and N—H···$\pi$, have all been observed. A report by Roger Hunter of the University of Cape Town, South Africa,[97] describes the observation of a sandwich-like pair of C—H···$\pi$ interactions in which two molecules of $Ph_3PMe^+$

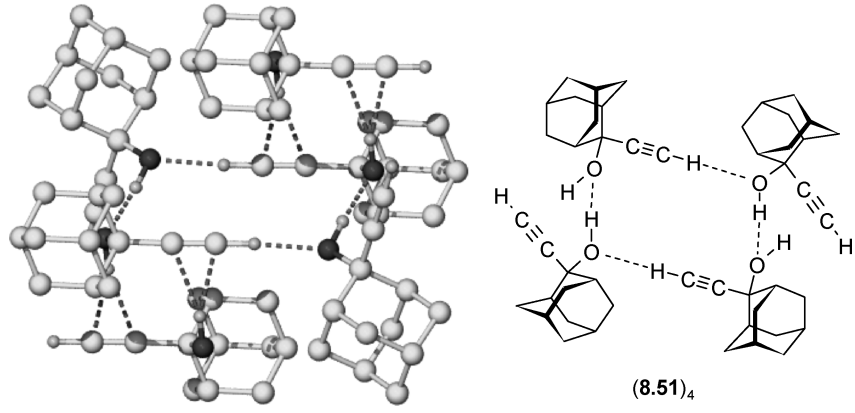


**Figure 8.66** Neutron diffraction structure and schematic drawing of **8.51** showing O—H···O, C—H···O and O—H···$\pi$ interactions.[96]

interact with furan ($C_4H_4O$) *via* the protons of the methyl groups (**8.53**). An accompanying search of the CSD gave shortest H $\cdots$ $\pi$ distances in the range 2.35–2.79 Å. The compound also shows C—H $\cdots$ N interactions to the CN groups of the accompanying cation ($D$ = 3.425 Å, $d$ = 2.46 Å, $\theta$ = 177°). Motohiro Nishio of the CHPI Institute, Tokyo, Japan, has undertaken an exhaustive survey of these very weak CH$\cdots\pi$ hydrogen bonds and shown that they are a ubiquitous form of soft hydrogen bonding interaction that permeates chemistry and biology. CH$\cdots\pi$ interactions stabilise inclusions compounds of organic guests such as toluene within calix[4]arenes, for example (Figure 1.23). Nishio has summarised some of the key characteristics of CH$\cdots\pi$ interactions, as listed below.

1. CH$\cdots\pi$ bonds work cooperatively. The weak directionality of CH$\cdots\pi$ interactions and the large surfaces offered by $\pi$ systems means that many aromatic compounds exhibit multiple such interactions. While they are individually weak their combined, cooperative effect can be very significant. The existence of CH$\cdots\pi$ interactions is manifest in the commonly higher melting points and facile crystallisation of aromatic compounds compared to aliphatic compounds of similar molecular weight.
2. The CH$\cdots\pi$ bond is statistically likely. The commonplace occurrence of relatively acidic CH groups and $\pi$-systems means that there are many possible interactions in a given compound or crystal and hence a high probability they will form.
3. The CH$\cdots\pi$ bond is effective in water. The CH$\cdots\pi$ interaction depends mostly on dispersion forces and hence, unlike electrostatic interactions, it is not damped by polar solvents. As a result the interaction is a significant contributor to the hydrophobic effect.

## 8.10 Aromatic Rings

### 8.10.1 Edge-to-Face and Face-to-Face Interactions

Hunter, C. A., Lawson, K. R., Perkins, J., Urch, C. J., 'Aromatic interactions', *J. Chem. Soc., Perkin Trans. 2* 2001, 651–669.

Our discussion of CH$\cdots\pi$ interactions in the previous section brings us directly onto another ubiquitous kind of synthon: $\pi$-$\pi$ stacking, the basis of which is discussed in Section 1.8.7. In the introductory discussion in Chapter 1 we delineated two basic types of $\pi$–$\pi$ interaction; edge-to-face (which are an example of C—H $\cdots$ $\pi$ interactions) and face-to-face interactions between aromatic rings (C $\cdots$ C). Strictly speaking the word 'stacking' only applies to face-to-face interactions and hence phrases such as *aromatic interactions* are now generally used to cover both kinds. Whether aromatic interactions are attractive or repulsive is highly dependent on the angle between the aromatic rings and their mutual offset distance, Figure 8.67. Thus a direct, non-offset, 0° face-to face overlap between two like aromatic rings is repulsive but becomes attractive as the offset increases. In contrast 90° edge-to-face CH$\cdot\cdot\pi$ interactions are attractive at zero offset but become repulsive as the CH 'edge' moves from the $\pi$-system to the CH edge of the adjacent molecule. The situation can be very different for co-crystals of different kinds of molecule however as we will see.

Aromatic interactions are very important in the stabilisation of molecular host-guest complexes of aromatic guests in solution (Chapter 6). While aromatic stacking interactions are of tremendous importance in biochemistry where they are responsible, for example, for porphyrin stacking giving rise to the vectorial energy transfer required for photosynthesis (Section 2.4), in terms of crystal engineering, aromatic interactions are relatively weak and only weakly directional. They are therefore difficult to predict and control, especially in the presence of other, stronger interactions. Intermolecular $\pi$–$\pi$

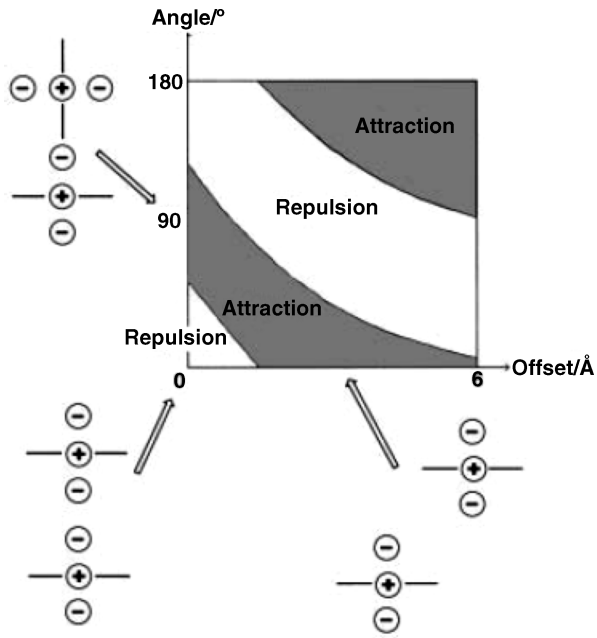


**Figure 8.67** Electrostatic interactions between π-charge distributions as a function of orientation (reproduced by permission of The Royal Society of Chemistry).

stacking interactions are of importance in the structures of aromatic molecules like benzene, where they give rise to the characteristic herringbone packing motif (Figure 1.20). Face-to-face π–π stacking interactions are responsible for the slippery feel (*superlubricity*) of graphite as one 'chicken wire' layer slides over another.[98] In the case of large, polycyclic aromatic hydrocarbons whose structures are somewhere between those of benzene and graphite, the importance of stacking interactions increases with the number of aromatic rings. Desiraju and Gavezzotti[99] have developed a predictive model for the structure of fused-ring aromatic hydrocarbons (FAH) based simply upon the 'stacking' and 'gliding' of hydrogen and carbon atoms in a molecule on the basis of their topological connectivity. In general, the structures of FAH molecules fall into four distinct classes based upon the length of their shortest crystallographic axis, and the tendency to adopt one of these types is determined simply by the relative contribution of carbon and hydrogen atoms to the molecular surface area. These four types are listed below, and illustrated by the representative examples, napthalene, pyrene, coronene and tribenzopyrene, in Figure 8.68.

1. Simple herringbone; nearest neighbours nonparallel; 5.4 Å $<$ shortest axis $<$ 8.0 Å.
2. Sandwich herringbone; herringbone motif is comprised of sandwich-like diads; shortest axis $>$ 8.0 Å.
3. $\gamma$-Type, interactions between parallel translated molecules; 4.6 Å $<$ shortest axis $<$ 5.4 Å.
4. $\beta$-Type; graphitic planes, shortest axis $<$ 4.2 Å.

Which crystal structure is adopted is based on the optimisation of C$\cdots$C interactions, which are at a maximum between parallel molecules stacked in an offset face-to-face fashion at van der Waals separation (glide interactions), and C$\cdots$H interactions, which are optimum in inclined molecules as a result of their electrostatic nature (stack interactions). The $\gamma$- and $\beta$-structures are adopted in cases

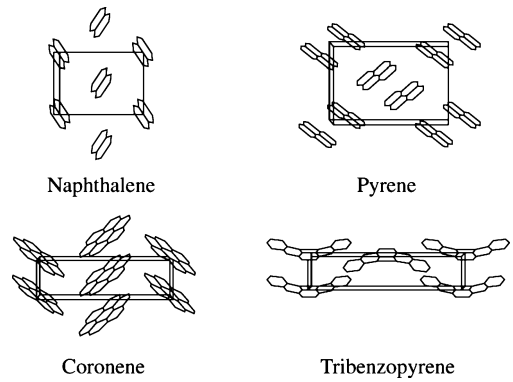


**Figure 8.68** The four basic aromatic packing types with the short axis vertical in each case. (Reproduced by permission of The Royal Society of Chemistry).

where it is important to maximise C···C interactions, while the herringbone motif maximises C···H interactions. Both interactions are important in the sandwich herringbone.

Face- and edge-stacking interactions are also important in the structures of aromatic organometallic compounds. The first aromatic organometallic molecule ever prepared, ferrocene, $Fe(C_5H_5)_2$, adopts a total of three different crystalline phases, all of which are of a herringbone motif because of the high content of hydrogen atoms on the surface area (Figure 8.69). The differences between the three phases (room-temperature disordered monoclinic, and low-temperature triclinic and orthorhombic) depend on the relative orientations of the two $C_5H_5$ rings. This in turn affects the directionality of the C—H···C interactions. Like ferrocene, the solid state structure of bis(benzene)chromium, $Cr(C_6H_6)_2$, is of an approximately herringbone type. Interestingly, however, if the electron-rich $Cr(C_6H_6)_2$ is co-crystallised with the electron-deficient $C_6F_6$, a red, charge-transfer complex $Cr(C_6H_6)_2{\cdot}C_6F_6$ is formed in which there is precise face-to-face overlap of the six-member rings of the two components, which are separated by 3.48 Å (Figure 8.70).[100]

Face-to-face aromatic stacking interactions are common in a wide range of organic charge-transfer compounds where there is a donor-acceptor interaction between an electron rich π-system and an electron

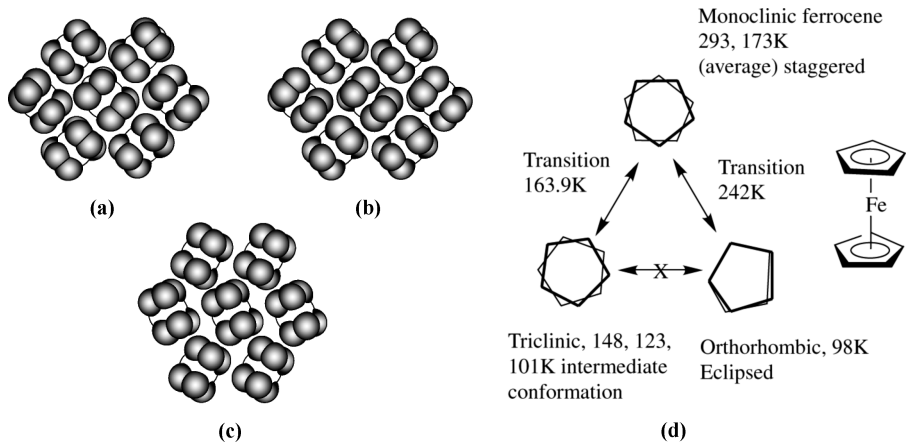


**Figure 8.69** Space-filling representation of the three polymorphic forms of ferrocene: (a) triclinic, (b) monoclinic, and (c) orthorhombic. (Reprinted with permission from [3] © 1998 American Chemical Society) (d) Phase behaviour of ferrocene.

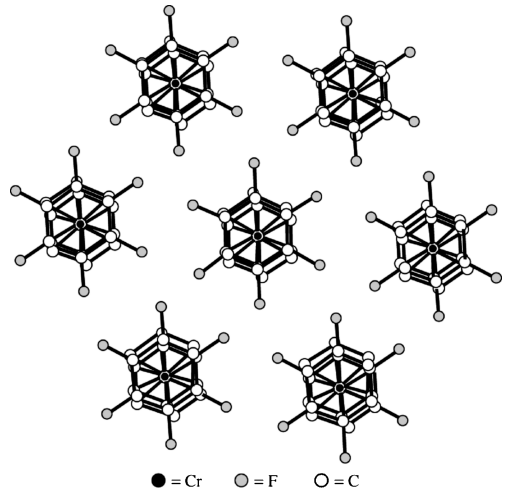


**Figure 8.70** Donor–acceptor direct $\pi$–$\pi$ stacking in $Cr(C_6H_6)_2 \cdot C_6F_6$. (Reproduced by permission of The Royal Society of Chemistry).

poor partner. Such compounds can display interesting properties such as intense colours, optical behaviour and interesting magnetism. Charge transfer interactions in co-crystals are very significant in determining the crystal packing mode and face-to-face stacking is very common, allowing maximum overlap of the donor highest occupied molecular orbital (HOMO) and acceptor lowest unoccupied molecular orbital (LUMO). Some typical face-to-face stacking geometries in charge transfer solids are shown in Figure 8.71.

## 8.10.2 Aryl Embraces

Dance, I., Scudder, M., 'The sextuple phenyl embrace, a ubiquitous concerted supramolecular motif', *J. Chem. Soc., Chem. Commun*. 1995, 1039–1040.

Edge-to-face CH···π interactions are individually weak but can be significant when acting in a cooperative fashion. A very common and relatively easily recognised example of this cooperative strength is the ubiquitous sixfold aryl embrace (6AE) supramolecular synthon (Figure 8.72a). The 6AE pattern, sometimes called a sixfold phenyl embrace, involves multiple CH···π interactions between pairs of compounds containing an $-EAr_3$ moiety; *i.e.* three aromatic rings linked to a central atom. This kind

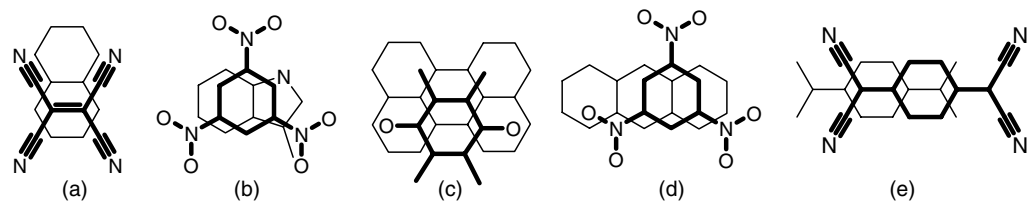


**Figure 8.71** Skeletal representations of face-to-face stacking in the X-ray crystal structures of some typical charge transfer complex co-crystals: (a) naphthalene·TCNE, (b) skatole·trinitrobenzene, (c) perylene·fluoroanil (d) anthracene·trinitrobenzene and (e) TCNQ·TMPD.

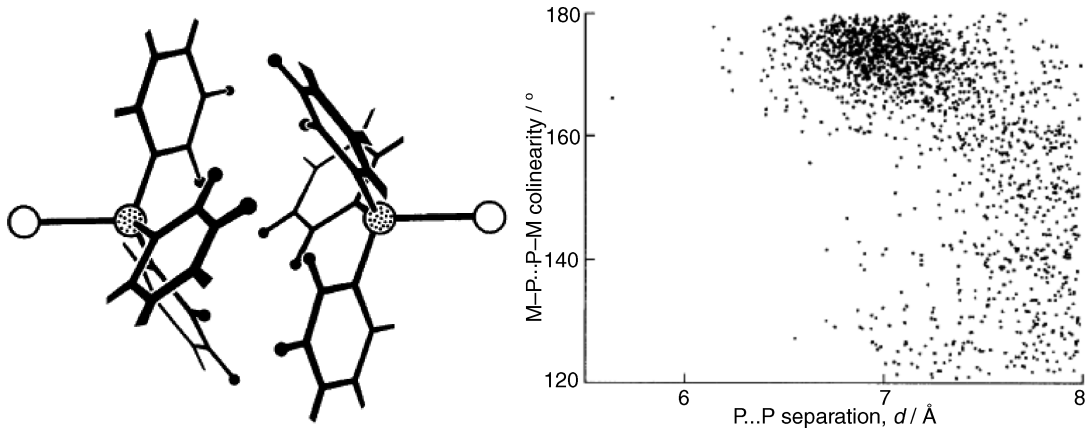


**Figure 8.72** (a) Sixfold aryl embrace in two X-$PPh_3$ moieties. Hydrogen atoms at the 2 and 3 positions of each ring (filled circles) are directed towards carbon atoms at the 2, 3, 4 and 5 positions of an opposite ring. The two X-P groups are approximately co-linear, (b) scatterplot of the geometry of the shorter intermolecular contacts for transition metal (M) compounds with $PPh_3$ ligands. The M–P···P–M colinearity is half the sum of the M–P–P and P–P–M angles; 1498 of the 1987 points occur in the domain 160–180° corresponding to collinear M–P···P–M vectors and correspond to 6AE interactions (reproduced by permission of The Royal Society of Chemistry).

of pattern occurs very frequently for example in metal complexes of triphenyl phosphine ($MPPh_3$) or in tetraphenyl phosphonium ($PPh_4^+$) salts. The motif is favoured when the central atom, E, is larger than carbon as in the example of $ClGePh_3$ in Figure 1.22. Figure 8.72b shows the results of a CSD search on metal $PPh_3$ complexes. The P···P separation in these compounds is typically much shorter than the average radius of $PPh_3$ and the M–P vectors are generally co-linear. This situation corresponds to the 6AE motif which is calculated by the atom-atom potential method to have an interaction energy of *ca.* 60 – 85 kJ $mol^{-1}$.

## 8.10.3 Metal-π Interactions

Petrukhina, M. A., 'Designed solvent-free approach toward organometallic networks built on directional metal-π-arene interactions', *Coord. Chem. Rev.* 2007, **251**, 1690–1698.

In Section 1.8.5 we introduced the cation-π interaction and examined its theoretical basis. Both metal cations and organic cations exhibit a significant interaction energy with aromatic rings, however cation-π interactions tend to lose out to interactions with smaller, electron donors such as water molecules because aromatic rings are relatively large and hence fewer of them can fit around a given cation. In crystals of alkali metal salts of aromatic organic compounds, however, cation-π interactions are relatively common, particularly if the compound is crystallised from a non-polar medium and under these circumstances the cation-π interaction can be of considerable importance in determining the overall crystal packing mode. Thus larger alkali metal cations such as $K^+$, $Rb^+$ and $Cs^+$ can form strong interactions to solvents such as toluene in the structure of $Cs[Al_2Me_6N_3]\cdot 2(p\text{-xylene})$, discussed in Section 13.5, which crystallised from an aromatic liquid clathrate mixture. The calixarenes with their extended aromatic cavities are also good at binding to metal cations even when crystallised from polar, competitive solvents. Recent work by Marina Petrukhina of Albany University, New York, USA, has

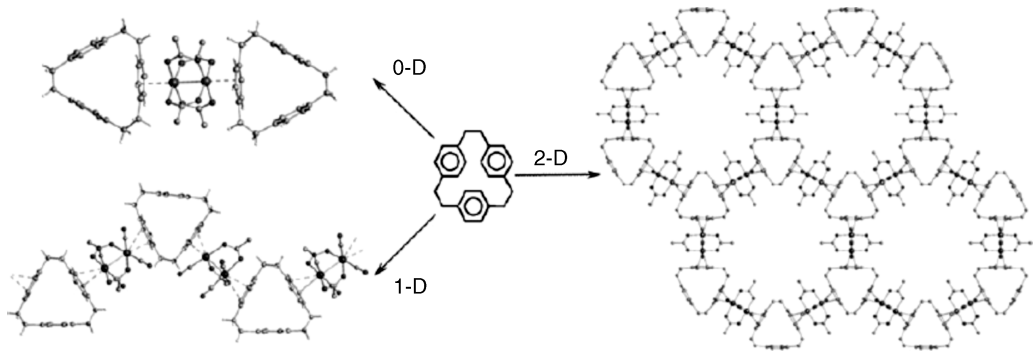


**Figure 8.73** Formation of discrete $[Rh_2(\mu\text{-}O_2CCF_3)_4([2.2.2]paracyclophane)_2]$, 1D $[Ru_2(m\text{-}O_2CCF_3)_4(CO)_4([2.2.2]paracyclophane)]_\infty$ or 2D $[\{Rh_2(\mu\text{-}O_2CCF_3)_4\}_3([2.2.2]paracyclophane)_2]_\infty$ (**8.55**) from gas phase deposition of volatile metal precursors and [2.2.2]paracyclophane (reprinted from Section Key Reference with permission of Elsevier).

focussed on a novel solvent-free synthetic approach to make full use of the potential of metal-π interactions as a crystal engineering tool. Sublimation-deposition reactions between volatile metal fragments and aromatic ligands are carried out in small glass ampoules at temperatures between 40 °C and 350 °C and some control over products is obtained by varying the ratio of reactants, temperature gradient, temperature and reaction time. Solid products deposit on cooler portions of the ampoule. The approach has the advantage that solvents and atmospheric components are completely eliminated allowing complexes between metals and the aromatic ligands to form exclusively. Suitable metal precursors are Rh(II), Ru(II) and Ru(II) lantern type $M_2(carboxylate)_4$ complexes, particularly the trifluoroacetate compound $[Rh_2(\mu\text{-}O_2CCF_3)_4]$ which forms complexes with a wide range of polycyclic aromatic hydrocarbons in this way, coordinating *via* the vacant axial sites, one on each of the two metal centres. Particularly striking are the $[Rh_2(\mu\text{-}O_2CCF_3)_4]$ or $[Ru_2(\mu\text{-}O_2CCF_3)_4(CO)_4]$ adducts of [2.2.2]paracyclophane (**8.54**) which, depending on conditions and metal complex forms either a discrete 2:1 complex $[Rh_2(\mu\text{-}O_2CCF_3)_4([2.2.2]paracyclophane)_2]$, a 1:1 1D chain $[Ru_2(\mu\text{-}O_2CCF_3)_4(CO)_4([2.2.2]paracyclophane)]_\infty$ or a 2:3 2D hexagonal grid $[\{Rh_2(\mu\text{-}O_2CCF_3)_4\}_3([2.2.2]paracyclophane)_2]_\infty$ (**8.55**), Figure 8.73. All of the complexes are based on coordination of the aromatic rings *via* one double bond of the arene rings in an $\eta^2$– fashion. The 2D hexagonal grid complex **8.55** has infinite channels running through the [2.2.2]paracyclophane cavities, however no gas sorption was detected except for a small amount of $CO_2$.

## 8.11 Halogen Bonding and Other Interactions

Metrangolo, P., Neukirch, H., Pilati, T., Resnati, G., 'Halogen bonding based recognition processes: A world parallel to hydrogen bonding', *Acc. Chem. Res.* 2005, **38**, 386–395.

In addition to classical and non-classical hydrogen bonds and π-stacking, there is ample evidence for the existence of other atom–atom interactions that may have crystal engineering potential. Such interactions are often weak, although they are shorter than the spherical van der Waals radii and are usually directional. The most common short contacts in crystals are observed involving polarisable atoms such as Cl, Br, I, S, Se *etc.*, suggesting that any attractive forces between them may be of the induced dipole type. Typical interactions involve closed shell bonding and include halogen bonding,

secondary bonding and metallophilic interactions (Section 1.8.9). Of these interactions it is principally halogen bonding, broadly defined as the non-covalent interaction between halogen atoms (Lewis acids) and neutral or anionic Lewis bases that has been used most extensively for crystal engineering. For example, helical tubuland hosts (Section 7.4.2) include molecules such as $CCl_4$ with Cl ⋯ Cl contacts of 3.54 Å, and $I_2$, which interacts with the oxygen atom of included ethanol. Desiraju has used CN ⋯ Cl interactions to produce molecular tapes in the solid state of type **8.56** ($R^1 = R^2 = Me$).[101] The N ⋯ Cl distances are remarkably short (3.10 Å) and fairly directional, with a C≡N ⋯ Cl angle of 137°. Note the absence of any other strong intermolecular interactions or potentially interacting groups. Replacement of one of the methoxy groups with an OH functionality ($R^1 = H$, $R^2 = n$–octyl) does not destroy the ribbon structure, although the N ⋯ Cl distances are markedly lengthened (3.4 Å) as a consequence of the need to accommodate stronger O—H ⋯ Cl hydrogen bonds.

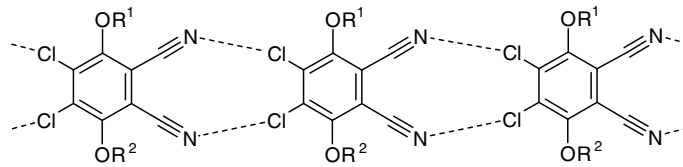


**8.56**

**a** $R^1 = R^2 = Me$
**b** $R^1 = H$, $R^2 = C_8H_{17}$

Dihaloalkane and arene derivatives have proved to be a rich source of crystal engineering because of the robustness of supramolecular synthons such as X···I–C≡C. The interaction energy of the N···I–C bonds in the 1:1 complex of 4,4′-bipyridyl and 1,4-diiodobenzene is 13.2 kJ $mol^{-1}$ with the N···I distance being 3.03 Å. The analogous complex with 1,4-diiodotetrafluorobenzene has an interaction energy of 24.3 kJ $mol^{-1}$ and an N···I distance of just 2.85 Å. Crystal engineering using halogen bonds has been particularly popularised in recent years by the group of Metrangolo and Resnati from the University of Milan, Italy, who have taken advantage of this increase of interaction energy upon fluorination to give highly reproducible structures based on α,ω-dihaloperfluoroalkanes and diamines or nitriles as in the structure of $ICF_2(CF_2)_6CF_2I{\cdot}NC(CH_2)_6CN$, Figure 8.74. These robust structures have been developed

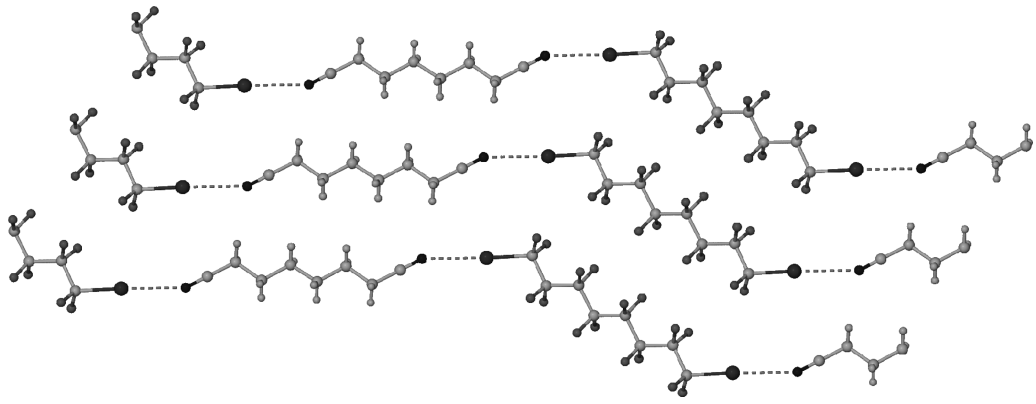

**Figure 8.74** X-ray crystals structure of $ICF_2(CF_2)_6CF_2I{\cdot}NC(CH_2)_6CN$ showing the CN···I synthon.

into square layer structures based on α,ω-dihaloperfluoroalkanes and the pentaerythritol derivative **8.57**, and into remarkable diamondoid networks with up to tenfold interpenetration and with potential for non-linear optical properties by combination of **8.57** and **8.58**.[102] Work by Desiraju has also resulted in materials with proven non-linear optical properties based on nitro-iodo halogen bonding (*cf.* Figure 8.3).[4]

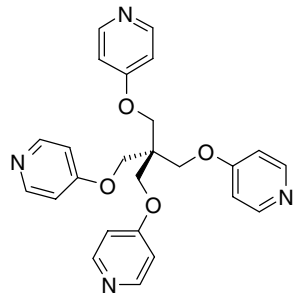

**8.57**

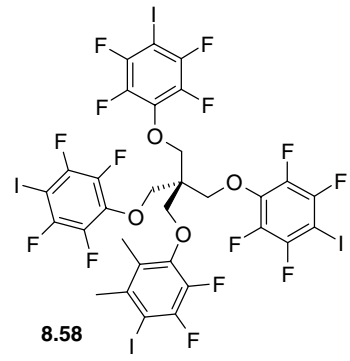

**8.58**

Halogen bonding is also found in the so-called double shell complexes of type $[M^{II}X_4\{M^I([18]crown\text{-}6)\}_4][TlX_4]_2$ ($M^I$ = Rb, Tl; $M^{II}$ = Zn, Cu, Mn, Co; X = Cl, Br, I). These elegant structures form a diamondoid array (Section 8.12) of $TlX_4^-$ tetrahedra that are held together by short halogen bonded X···X contacts, comparable to those found in the pure halogens. The diamondoid cavity holds four [18]crown-6 molecules, which are arranged tetrahedrally about a central inner cavity into which the $M^{II}X_4^{2-}$ anion or other guests are included. In the case of $TlI_4$, I···I distances are 3.69 Å, comparable to the short I—I···I—I distances in $I_2$ of 3.50 Å.

## 8.12 Crystal Engineering of Diamondoid Arrays

Zaworotko, M. J. 'Crystal engineering of diamondoid networks', *Chem. Soc. Rev.*, 1994, 283–288.

We saw in the preceding section the crystal engineering of diamondoid arrays arising *via* halogen bonding, from the use of tetrahedral building blocks. We complete this chapter by a brief discussion of what constitutes a diamondoid array and why they are not just interesting from a materials point of view but also very beautiful.

The crystal structure of diamond, the metastable allotrope of carbon, comprises $sp^3$ hybridised carbon atoms all interlinked mutually to form an infinite 'covalent molecular crystal', in which each atom is linked to four others *via* single covalent bonds. The crystal repeat unit is made up of building blocks resembling the organic molecule adamantane (Figure 8.75). Diamond is not a supramolecular compound *per se* because the bonding is covalent. However, if we were to try to analyse the diamond structure in the language of crystal engineering we might describe a carbon atom as being a 'self-complementary tecton with four tetrahedrally arranged binding sites'. Presumably, we could therefore obtain a diamond-like (diamondoid) crystal structure from any other tecton that also fits this criterion. Two such materials are the water molecule and potassium dihydrogenphosphate (KDP, $KH_2PO_4$). The water molecule has two hydrogen bond donor sites and two acceptors, which, together, result in diamondoid (cubic) polymorphs of normal hexagonal ice (Ih, Section 7.2). Similarly, the $H_2PO_4^-$ anion in KDP forms an even larger diamonoid network. While diamond, water and KDP are all related topologically, the relative sizes of the networks have significant consequences. Diamond is a very closely

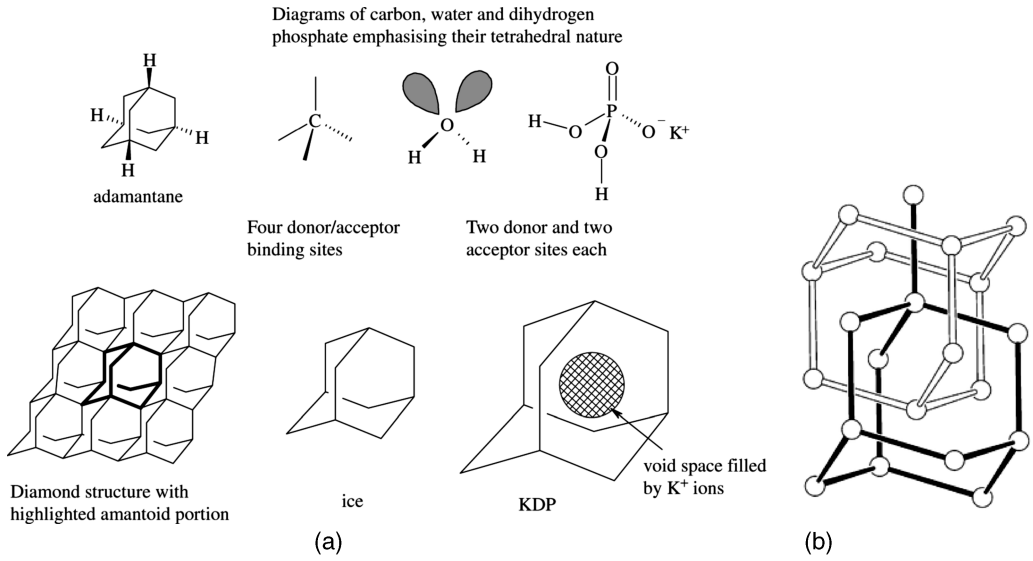


**Figure 8.75** (a) Diamondoid networks and their components. Normal ice Ih has a hexagonal arrangement but two diamondoid polymorphs are known. (b) twofold interpenetration of adamantoid cages in a diamondoid structure (reproduced by permission of The Royal Society of Chemistry).

packed network and is one of the hardest and highest melting substances known. Cubic ice is not packed efficiently, and this is responsible for its anomalously low density compared with liquid water. The diamondoid $H_2PO_4^-$ network in KDP is so large that significant void space occurs within each adamantoid cage unit. This is filled by the $K^+$ ions. Other large diamondoid networks fill such voids by *interpenetration* in which a second independent diamondoid framework runs through the voids in the first. We saw in the previous section a tenfold interpenetrated diamondoid structure comprising ten independent, interpenetrating networks!

Diamondoid crystals are of significant interest because of their ability to leave vacant space in the structure, resulting either in interpenetration or guest inclusion, and a significant amount of research is being directed towards preventing interpenetration in order to use diamondoid cavities. Also interesting is the fact that diamondoid structures, because they are based on building blocks of (approximately) tetrahedral symmetry, lack inversion centres and therefore crystallise in polar space groups. You can see from Table 8.3 that this property is relatively unusual and it can result in some useful properties such as ferroelectricity, piezoelectricity, pyroelectricity and non-linear optical activity. Indeed, a major use of KDP is as a non-linear optical material in tuning laser frequencies (Section 11.6). These features, coupled with the robustness of the diamondoid framework, have resulted in the study of increasingly larger diamondoid structures.

In designing ever larger diamondoid networks, it is important to retain the approximate $T_d$ symmetry of the building blocks. This may be achieved *via* a single self-complementary building block such as **8.59** which possesses four mutually complementary carboxylic acid groups, or by a modular approach, which uses a combination of a $T_d$ (or at least $S_4$) node such as the cubeane cluster $[Mn(CO)_3(\mu_3\text{-}OH)]_4$ (**8.60**) and a linear spacer (A-A) (Figure 8.76).

The self complementary **8.59** may be regarded as the logical three-dimensional progression of the topological zero-, one- and two-dimensional points, chains and sheets formed by benzoic acid, terephthalic acid and trimesic acid (Section 7.4.1), shown schematically in Figure 8.77. Adamantane-1,3,5,7-tetracarboxylic acid (**8.59**) forms a diamondoid network with cavities so large that close packing can

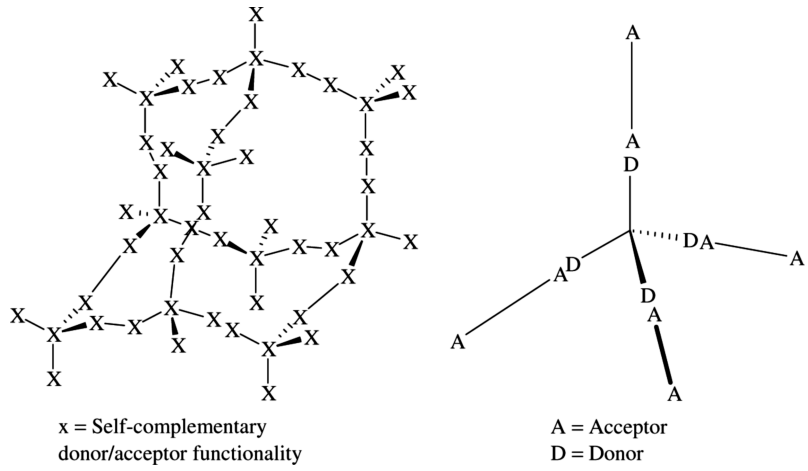


**Figure 8.76** Construction of diamondoid networks *via* self-assembly of self-complementary $S_4$ building blocks or modular self-assembly of mutually complementary $S_4$ nodes and linear spacers.

be achieved only by interpenetration (catenation) of a total of five entirely independent diamondoid networks (five-fold interpenetrated), leaving no room for guest inclusion. Interpenetration may be reduced by modification of the adamantane framework. The dione derivative **8.61** exhibits only three-fold interpenetration in order to make room for the carbonyl groups that protrude into the cavities. This is sufficient space to allow the incorporation of acetic acid guest molecules.

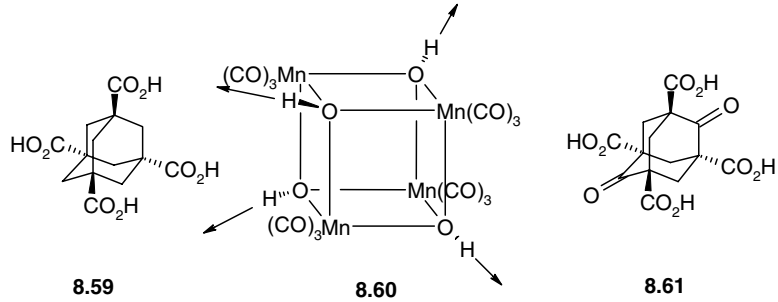

**8.59** **8.60** **8.61**

Truly enormous diamondoid structures have been prepared by Mike Zaworotko of the University of Southern Florida, USA, using the stable cubane cluster **8.60**. Compound **8.60** is a good illustration of a supramolecular tecton that is a rigid hydrogen bond donor of $S_4$ symmetry but possesses very little hydrogen bond acceptor capability (the oxygen atoms of the CO ligands are only very weakly basic, see Section 8.9.4). As a result, it interacts with an enormous range of hydrogen bond acceptors (even weak acceptors such as benzene), to give two-, three- and four-fold interpenetrated diamondoid networks (Table 8.6). While some of the hydrogen bonds are weak, it is the directionality that counts in the assembly of the system. Many hydrogen bonds are of a conventional O—H $\cdots$ N type. The O—H $\cdots$ $\pi$ interactions in the benzene derivative involve the close approach of the OH proton to three of the benzene carbon atoms in an allylic fashion.

Multiple hydrogen bonding interactions in tetrahedral building blocks have been employed by the group of Wuest to produce a remarkable tailored porous zeolite mimic, dubbed an 'organic zeolite' because it does not contain any inorganic components at all.[104] The pore-forming material is based on

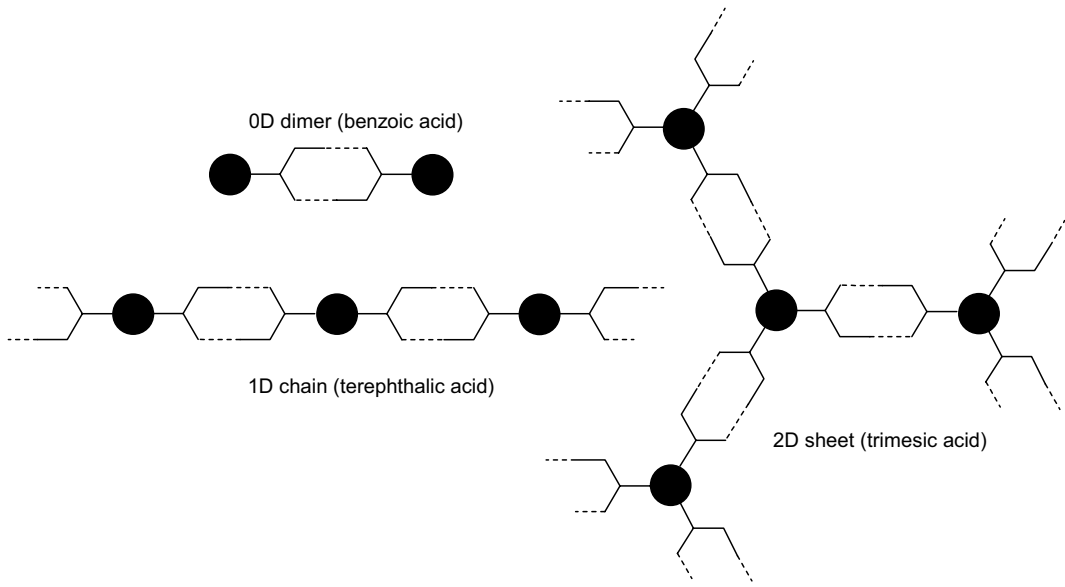


**Figure 8.77** Schematic diagram of zero-, one- and two-dimensional networks formed by the carboxylic acid cyclic dimer motif.

the one component self-assembly of the tetrahedral **8.62** into a cross-linked network of cavity-containing sheets. Each cavity is approximately square in shape, of side 11.8 Å, binding multiple guests such as dioxane, acetonitrile and water. The non-covalently linked organic structure is so robust that it is able to retain its structural integrity even after 66% of the guest molecules have been removed under vacuum. The formation of a porous structure by **8.62** is in contrast to other studies in the crystal engineering of tetrahedral building blocks, in which interpenetrated diamondoid networks are formed, precluding the formation of cavities. Examination of the monomer component **8.62** reveals that it is not fully self-complementary in the sense that it possesses an excess of hydrogen bond donor sites (—$NH_2$) over acceptor (=N—) It is possible, therefore, that the reason interpenetrated structures are not formed in

**Table 8.6** Diamondoid structures formed by modular self-assembly of **8.60** with a variety of hydrogen bond acceptors. The inter-cube distance is the distance from one molecule of **8.60** to the next and represents the diamondoid edge length.

| Acceptor, A–A | Inter-cube distance (Å) | Crystal system | Interpenetration (n-fold) |
|---|---|---|---|
| Benzene | 9.74 | Cubic | 2 |
| Napthalene | 10.40 | Tetragonal | 2 |
| $Me_2NCH_2CH_2NMe_2$ | 11.35 | Tetragonal | 2 |
| 1,4-Diaminobenzene | 11.79 (Re analogue) | Tetragonal | 2[a] |
| 2-Cl-pyrazene | 11.82 | Cubic | 3 |
| $Ph_2P(O)CH_2CH_2P(O)Ph_2$ | 13.53 | Tetragonal | 2[a] |
| 4,4′-Bipyridyl | 15.22 | Tetragonal | 4[a] |

[a]MeCN solvent included in microchannels.

this case is the driving force to form hydrogen bonds to these 'excess' amine protons, resulting in the incorporation of hydrogen bond acceptor guests. This suggests new strategies for the preparation of such porous materials and offers the possibility of fine-tuning by reaction at these hydrogen bond acid sites.

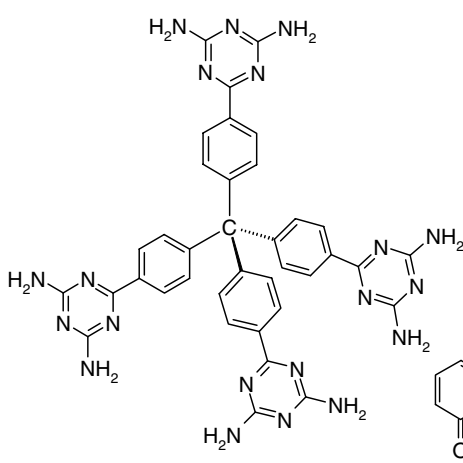

**8.62**

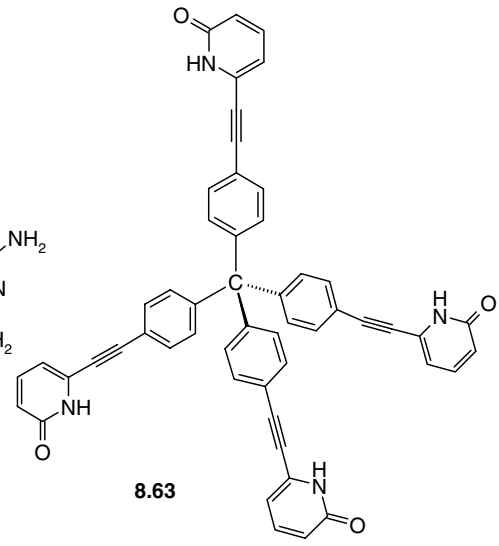

**8.63**

Wuest *et al*. have also prepared a related tetrahedral tecton **8.63**, which also produces a diamondoid polymeric framework. In this case, the solid-state network is seven-fold interpenetrated, with one diamondoid lattice filling much of the large cavities in those adjacent. It is possible that the interpenetration in this instance is a result of the self-complementary nature of the host, which contains an equal number of hydrogen bond donor and acceptor sites. However, even in this case small cavities exist, which are filled by two molecules of butyric acid per host formula unit. The formation of these kinds of framework materials opens entirely new possibilities for tailor-made porous materials with very large cavities, although it is unlikely that purely organic frameworks will ever rival aluminosilicate-based materials for sheer mechanical strength.

In addition to hydrogen bonding, diamondoid networks can also form purely from other well-recognised synthons such as the sixfold aryl embrace motif (Section 8.10.2). The copper(I) complex $[Cu\{P(C_6H_4\text{-}p\text{-}OMe)_3\}_3](ClO_4)$ exhibits a diamondoid structure linked entirely by multiple aryl embraces. The $ClO_4^-$ anions occupy the centres of the *pseudo*-adamantanoid cages from which the diamondoid network is formed. This extended network has been described as a super-HA6PE (hexagonal array of sixfold phenyl embraces).[105]

## Summary

- A *supramolecular synthon* represents a reproducible, frequently occurring kind of non-covalent interaction found in molecular crystal structures. It has predictive power and may be used in crystal design. Supramolecular synthons are distinct from *tectons*; the molecules or the building blocks of the crystal.
- Crystal formation depends not only on the interaction energy of a particular synthon but on a wide variety of other factors, particular crystal nucleation and growth kinetics and nucleus-solution interfacial energy. Other important factors are lattice enthalpy and lattice entropy, long range interactions

such as dipolar alignment, solute-solvent interactions and solution speciation under supersaturated conditions. All of these factors make crystal structure very difficult to control and predict. Crystallisation is thus distinct from much more straightforward solution phase self-assembly under thermodynamic control.

- Progress in crystal structure prediction has been significant in recent years with parallel synthon-based and crystal structure calculation based approaches. Calculations are now sometimes able to correctly determine crystal structure in an *ab initio* fashion but analysis of synthons can give significant qualitative insight.
- The goal of designable and predictable crystal structures has significant real world applications for example in the design of non-linear optical materials or those displaying interesting ferroelectric or magnetic behaviour and in the control of pharmaceutical crystal form.
- The understanding of hydrogen bonded motifs has been greatly helped by the development of *graph set theory* which allows a systematic approach to comparing hydrogen bonded patterns, which are among the most powerful supramolecular synthons.
- The vast number of crystal structures now deposited in the Cambridge Structural Database and recent software developments make systematic exploration of crystal packing trends another new, powerful tool.
- A particularly topical field within crystal engineering is the study of co-crystals which allow a great degree of freedom in tuning materials properties, particularly for applications in pharmaceutical formulation. The study of crystals with $Z' > 1$ represents an interesting special case in which a molecule is co-crystallised with itself.

## Study Problems

8.1 Suggest solid-state structures that might correspond to the following graph sets and molecules:
(a) $\mathbf{R_2^2(8)}$ (acetic acid)
(b) $\mathbf{R_6^6(12)}$ (phenol)
(c) $\mathbf{R_2^2(6)}$ (nitrobenzene + aniline 1:1)
(d) $\mathbf{R_1^2(4)}$ (nitrobenzene + phenol 1:1)
(e) $\mathbf{S_1^1(8)}$ ([4]resorcarene)
(f) $\mathbf{C(4)}$ (2-nitroacetanilide)
(g) $\mathbf{S(6)}$ (2-nitroacetanilide)

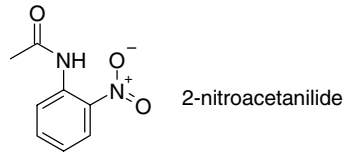

2-nitroacetanilide

8.2 Assign unitary and binary graph sets for the nucleobase pairings shown in Figure 2.31 and Figure 2.32. Is graph set analysis useful for distinguishing between Watson–Crick and Hoogstein base pairing?

8.3 Note down the key features distinguishing strong, medium and weak hydrogen bonds. Which do you think has the greatest crystal engineering potential?

8.4 Explain the fact that benzene adopts a herringbone packing motif (Figure 1.20), whereas higher aromatic hydrocarbons possess γ-type or graphitic interactions.

8.5 An OH bond is observed to have a bond length of 0.85 Å by X-ray crystallography at 298 K. The structure of the same compound at 100 K gives a distance of 0.92 Å for the same parameter. Explain this observation and, using simple trigonometry, estimate the angle through which the

OH bond is vibrating at 298 K (assume that vibration is negligible at 100 K). How would you obtain an accurate measurement of this bond length?

8.6 Rank the following hydrogen bond acids in order of the strength of their hydrogen bonds: MeOH, $Me_2P(O)OH$, $RCO_2H$, $CF_3OH$, $MeNH_2$, $Me_2NH$, PhOH, $PhNH_2$, $CH_2Cl_2$, $CHCl_3$, MeSH, $C_6H_6$, $Me(CH_2)_4Me$, MeOMe, $Me_2NH_2^+$, $H_3O^+$.

8.7 Suggest ways in which you might distinguish experimentally between the X—H bonds in alkanes, alcohols and amines that are (a) free, (b) engaged in agostic bonding or (c) forming an intermolecular pseudo-agostic interaction.

8.8 Predict the general form of the $^1H$ NMR spectrum of protons $H^1$—$H^4$ of the following compound (a) in static form; (b) when rotation about the Ir—$C_5$ vector is fast; and (c) when exchange of $H^1$ with $H^2$ is also fast.

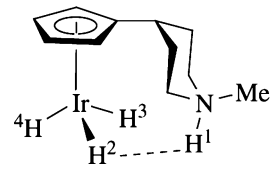


## Thought Experiment

Why has hydrogen bonding been described as the 'masterkey interaction in supramolecular chemistry'? Make a list of features that distinguish hydrogen bonding from other non-covalent interactions.

## References

1. von Hippel, A. R., Molecular designing of materials. *Science* 1962, **138**, 91.
2. Cohen, M. D., Schmidt, G. M. J., Topochemistry .1. Survey. *J. Chem. Soc.* 1964, 1996–2000.
3. Braga, D., Grepioni, F., Desiraju, G. R., Crystal engineering and organometallic architecture. *Chem. Rev.* 1998, **98**, 1375–1405.
4. Sarma, J. A. R. P., Allen, F. H., Hoy, *et al.*, Design of an SHG-active crystal, 4-iodo-4′-nitrobiphenyl: the role of supramolecular synthons. *Chem. Commun.* 1997, 101–102.
5. Pauling, L., *The Nature of the Chemical Bond and the Structure of Molecules and Crystals: An Introduction to Modern Structural Chemistry*. 1 ed., Cornell University Press: Ithaca, 1939,
6. Desiraju, G. R., Hydrogen bridges in crystal engineering: Interactions without borders. *Acc. Chem. Res.* 2002, **35**, 565–573.
7. Etter, M. C., Urbanczyklipkowska, Z., Jahn, D. A., Frye, J. S., Solid-state structural characterization of 1,3-cyclohexanedione and of a 6-1 cyclohexanedione-benzene cyclamer, a novel host guest species. *J. Am. Chem. Soc.* 1986, **108**, 5871–5876.
8. Taylor, R., Kennard, O., Versichel, W., The Geometry of the N-H ... O=C Hydrogen-bond .3. hydrogen-bond distances and angles. *Acta Crystallogr. Sect. B-Struct. Commun.* 1984, **40**, 280–288.
9. Reddy, D. S., Goud, B. S., Panneerselvam, K., Pilati, T., Desiraju, G., C-H···N mediated hexagonal network in the crystal-structure of the 1/1 molecular-complex 1,3,5-tricyanobenzene hexamethylbenzene. *J. Chem. Soc., Chem. Commun.* 1993, 663–665.
10. Taft, R. W., Gurka, D., Joris, L., Schleyer, P. V., Rakshys, J. W., Studies of hydrogen-bonded complex formation with P-fluorophenol .V. linear free energy relationships with OH reference acids. *J. Am. Chem. Soc.* 1969, **91**, 4801–4808.
11. Abraham, M. H., Scales of solute hydrogen-bonding – their construction and application to physicochemical and biochemical processes. *Chem. Soc. Rev.* 1993, **22**, 73–83.
12. Laurence, C., Berthelot, M., Observations on the strength of hydrogen bonding. *Persp. Drug Disc. Des.* 2000, **18**, 39-60.
13. Abraham, M. H., Grellier, P. L., Prior, D. V., Duce, P. P., Morris, J. J., Taylor, P. J., Hydrogen-bonding .7. a scale of solute hydrogen-bond acidity based on log K-values for complexation in tetrachloromethane. *J. Chem. Soc., Perkin Trans. 2* 1989, 699–711.

14. Hulliger, J., Chemistry and crystal growth. *Angew. Chem., Int. Ed. Engl.* 1994, **33**, 143–162.
15. Blagden, N., 'Crystal growth mechanisms'. in *Encyclopedia of Supramolecular Chemistry*, Atwood, J. L., Steed, J. W., Eds. Marcel Dekker: New York, 2004, Vol. 1, *pp.* 364–370.
16. Atwood, J. L., Davies, J. E. D., MacNicol, D. D., Vögtle, F., Eds. in *Comprehensive Supramolecular Chemistry*, Pergamon: Oxford, 1996, Vol. 6, *pp.* 888–889.
17. McBride, J. M., Carter, R. L., Spontaneous resolution by stirred crystallisation. *Angew. Chem., Int. Ed. Engl.* 1991, **30**, 293–295.
18. Noorduin, W. L., Izumi, T., Millemaggi, A., *et al.*, Emergence of a single solid chiral state from a nearly racemic amino acid derivative. *J. Am. Chem. Soc.* 2008, **130**, 1158–1159.
19. Brock, C. P., Dunitz, J. D., Towards a grammar of crystal packing. *Chem. Mater.* 1994, **6**, 1118–1127.
20. Davey, R. J., Allen, K., Blagden, N., *et al.*, Crystal engineering – nucleation, the key step. *Crystengcomm* 2002, 257–264.
21. Kelley, M. P., Janssens, B., Kahr, B., Vetter, W. M., Recognition of dyes by $K_2SO_4$ crystals – choosing organic guests for simple salts. *J. Am. Chem. Soc.* 1994, **116**, 5519–5520.
22. Kahr, B., Jang, S. H., Subramony, J. A., Kelley, M. P., Bastin, L., Dyeing salt crystals for optical applications. *Adv. Mater.* 1996, **8**, 941–944.
23. Dechambenoit, P., Ferlay, S., Hosseini, M. W., From tectons to composite crystals. *Cryst. Growth Des.* 2005, **5**, 2310–2312.
24. Steed, J. W., Goeta, A. E., Lipkowski, J., Swierczynski, D., Panteleon, V., Handa, S., Templated crystal nucleation: mixed crystals of very different copper(II) *N,N′,N″* -trimethyltriazacyclononane complexes. *Chem. Commun.* 2007, 813–815.
25. Cairns-Smith, A. G., *Genetic Takeover and the Mineral Origins of Life*. Cambridge University Press: Cambridge, 1982,
26. Ferris, J. P., Hill, A. R., Liu, R. H., Orgel, L. E., Synthesis of long prebiotic oligomers on mineral surfaces. *Nature* 1996, **381**, 59–61.
27. Nichols, P. J., Raston, C. L., Steed, J. W., Engineering of porous π-stacked solids using mechanochemistry. *Chem. Commun.* 2001, 1062–1063.
28. Cave, G. W. V., Raston, C. L., Scott, J. L., Recent advances in solventless organic reactions: towards benign synthesis with remarkable versatility. *Chem. Commun.* 2001, 2159–2169.
29. Descamps, M., Willart, J. F., Dudognon, E., Caron, V., Transformation of pharmaceutical compounds upon milling and comilling: The role of T-g. *Journal of Pharmaceutical Sciences* 2007, **96**, 1398–1407.
30. Braga, D., Giaffreda, S. L., Grepioni, F., *et al.*, Mechanochemical preparation of molecular and supramolecular organometallic materials and coordination networks. *Dalton Trans.* 2006, 1249–1263.
31. Kaupp, G., Solid-state molecular syntheses: complete reactions without auxiliaries based on the new solid-state mechanism. *CrystEngComm* 2003, **5**, 117–133.
32. Kaupp, G., Naimi-Jamal, M. R., Mechanically induced molecular migrations in molecular crystals. *Crystengcomm* 2005, **7**, 402–410.
33. Nakanishi, H., Jones, W., Thomas, J. M., Hursthouse, M. B., Motevalli, M., Static and dynamic single-crystal X-ray-diffraction studies of some solid-state photo-dimerization reactions. *J. Phys. Chem.* 1981, **85**, 3636–3642.
34. MacGillivray, L. R., From engineering crystals to engineering molecules: emergent consequences of controlling reactivity in the solid state using linear templates. *CrystEngComm* 2002, **6**, 37–41.
35. Gao, X. C., Friscic, T., MacGillivray, L. R., Supramolecular construction of molecular ladders in the solid state. *Angew. Chem., Int. Ed.* 2004, **43**, 232–236.
36. Coelho, A. A., A charge-flipping algorithm incorporating the tangent formula for solving difficult structures. *Acta Crystallogr., Sect. A* 2007, **63**, 400–406.
37. Evans, J. S. O., Benard, S., Yu, P., Clement, R., Ferroelectric alignment of NLO chromophores in layered inorganic lattices: Structure of a stilbazolium metal-oxalate from powder diffraction data. *Chem. Mat.* 2001, **13**, 3813-–3816.
38. Reddy, L. S., Basavoju, S., Vangala, V. R., Nangia, A., Hydrogen bonding in crystal structures of N,N′-bis(3-pyridyl)urea. Why is the N–H···O tape synthon absent in diaryl ureas with electron-withdrawing groups? *Cryst. Growth Des.* 2006, **6**, 161–173.
39. Braga, D., Grepioni, F., Tedesco, E., Orpen, A. G., Crystal construction and molecular recognition for $[Cr(CO)_6]$. *J. Chem. Soc., Dalton Trans.* 1995, 1215–1220.
40. Weber, E., Csoregh, I., Ahrendt, J., Finge, S., Czugler, M., Design of roof-shaped clathrate hosts - inclusion properties and X-ray crystal-structures of a free host and of inclusion-compounds with 1-Buoh and Dmf. *J. Org. Chem.* 1988, **53**, 5831–5839.
41. Murray-Rust, P., Burgi, H.-B., Dunitz, J. D., Chemical-Reaction Paths .5. SN1 reaction of tetrahedral molecules. *J. Am. Chem. Soc.* 1975, **97**, 921–922.
42. Mascal, M., Statistical analysis of C-H...N hydrogen bonds in the solid state: there *are* real precedents. *Chem. Commun.* 1998, 303–304.
43. Infantes, L., Motherwell, S., Water clusters in organic molecular crystals. *CrystEngComm* 2002, **4**, 454–461.

44. Infantes, L., Chisholm, J., Motherwell, S., Extended motifs from water and chemical functional groups in organic molecular crystals. *Crystengcomm* 2003, **5**, 480–486.
45. Pidcock, E., Motherwell, W. D. S., Cole, J. C., A database survey of molecular and crystallographic symmetry *Acta Crystallogr., Sect. B* 2003 **59**, 634–640.
46. Steed, J. W., Should solid-state molecular packing have to obey the rules of crystallographic symmetry? *CrystEngComm* 2003, **5**, 169–179.
47. van de Streek, J., Searching the Cambridge Structural Database for the 'best' representative of each unique polymorph. *Acta Crystallogr., Sect. B* 2006, **62**, 567–579.
48. Allen, F. H., Kennard, O., Watson, D. G., Brammer, L., Orpen, A. G., Taylor, R., Tables of bond lengths determined by X-ray and neutron-diffraction .1. Bond lengths in organic-compounds. *J. Chem. Soc., Perkin Trans. 2* 1987, S1–S19.
49. Orpen, G., Brammer, L., Allen, F. H., Kennard, O., Watson, D. G., Taylor, R., Tables of bond lengths determined by X-ray and neutron diffraction. Part 2. Organometallic compounds and co-ordination complexes of the *d*- and *f*-block metals. *J. Chem. Soc., Dalton Trans.* 1989, S1–S83.
50. Harris, S. E., Orpen, A. G., Bruno, J. J., Taylor, R., Factors affecting d-block metal-ligand bond lengths: Toward an automated library of molecular geometry for metal complexes. *Journal of Chemical Information and Modeling* 2005, **45**, 1727–1748.
51. Braga, D., Grepioni, F., Novoa, J. J., Inter-anion O-H$^{-}$...O$^{-}$ hydrogen bond like interactions: the breakdown of the strength-length analogy. *Chem. Commun.* 1998, 1959–1960.
52. Braga, D., D'Oria, E., Grepioni, F., Mota, F., Novoa, J. J., Rovira, C., O-H...O interactions involving doubly charged anions: Charge compression in carbonate- bicarbonate crystals. *Chem. Eur. J.* 2002, **8**, 1173–1180.
53. Mascal, M., Marjo, C. E., Blake, A. J., Breakdown of the hydrogen bond strength-length analogy: a revision. *Chem. Commun.* 2000, 1591–1592.
54. Steiner, T., Inter-anion O-H...O interactions are classical hydrogen bonds. *Chem. Commun.* 1999, 2299–2300.
55. D'Oria, E., Novoa, J. J., The strength-length relationship at the light of ab initio computations: does it really hold? *Crystengcomm* 2004, **6**, 367–376.
56. Nyburg, S. C., Faerman, C. H., A Revision of Vanderwaals Atomic radii for molecular-crystals - N, O, F, S, Cl, Se, Br and I bonded to carbon. *Acta Crystallogr. Sect. B-Struct. Commun.* 1985, **41**, 274–279.
57. Allen, F. H., Lommerse, J. P. M., Hoy, V. J., Howard, J. A. K., Desiraju, G. R., Halogen...O(nitro) supramolecular synthon in crystal engineering: A combined crystallographic database and ab initio molecular orbital study. *Acta Crystallogr. Sect. B-Struct. Commun.* 1997, **53**, 1006–1016.
58. Zou, J.-W., Jiang, Y.-J., Guo, M., Hu, G.-X., *et al.*, Ab initio study of the complexes of halogen-containing molecules RX (X=Cl, Br, and I) and $NH_3$: Towards understanding the nature of halogen bonding and the electron-accepting propensities of covalently bonded halogen atoms. *Chem. Eur. J.* 2005, **11**, 740–751.
59. Thun, J., Seyfarth, L., Senker, J., Dinnebier, R. E., Breu, J., Polymorphism in benzamide: solving a 175-year-old riddle. *Angew. Chem. Int. Ed.* 2007, **46**, 6729–6731.
60. McCrone, W. C., 'Polymorphism'. in *Physics and Chemistry of the Organic Solid State*, Fox, D., Labes, M. M., Weissberger, A., Eds. Interscience: New York, 1965, Vol. 11, *pp.* 726–767.
61. Nangia, A., Desiraju, G. R., Pseudopolymorphism: occurrences of hydrogen bonding organic solvents in molecular crystals. *Chem. Commun.* 1999, 605–606.
62. Bernstein, J., Davey, R. J., Henck, J. O., Concomitant polymorphs. *Angew. Chem., Int. Ed.* 1999, **38**, 3441–3461.
63. Dunitz, J. D., Bernstein, J., Disappearing Polymorphs. *Acc. Chem. Res.* 1995, **28**, 193–200.
64. Moulton, B., Zaworotko, M. J., From molecules to crystal engineering: Supramolecular isomerism and polymorphism in network solids. *Chem. Rev.* 2001, **101**, 1629–1658.
65. Lee, A. Y., Lee, I. S., Dettet, S. S., Boerner, J., Myerson, A. S., Crystallization on confined engineered surfaces: A method to control crystal size and generate different polymorphs. *J. Am. Chem. Soc.* 2005, **127**, 14982–14983.
66. Garetz, B. A., Matic, J., Myerson, A. S., Polarization switching of crystal structure in the nonphotochemical light-induced nucleation of supersaturated aqueous glycine solutions. *Phys. Rev. Lett.* 2002, **89**.
67. Price, C. P., Grzesiak, A. L., Matzger, A. J., Crystalline polymorph selection and discovery with polymer heteronuclei. *J. Am. Chem. Soc.* 2005, **127**, 5512–5517.
68. Ha, J. M., Wolf, J. H., Hillmyer, M. A., Ward, M. D., Polymorph selectivity under nanoscopic confinement. *J. Am. Chem. Soc.* 2004, **126**, 3382–3383.
69. Childs, S. L., Stahly, G. P., Park, A., The salt-cocrystal continuum: The influence of crystal structure on ionization state. *Molecular Pharmaceutics* 2007, **4**, 323–338.
70. Loehlin, J. H., Franz, K. J., Gist, L., Moore, R. H., Supramolecular alcohol-amine crystals and their hydrogen-bond patterns. *Acta Crystallogr. Sect. B-Struct. Commun.* 1998, **54**, 695–704.
71. Ermer, O., Eling, A., Molecular recognition among alcohols and amines – super-tetrahedral crystal architectures of linear diphenol-diamine complexes and aminophenolse. *J. Chem. Soc., Perkin Trans. 2* 1994, 925–944.

72. Almarsson, O., Zaworotko, M. J., Crystal engineering of the composition of pharmaceutical phases. Do pharmaceutical co-crystals represent a new path to improved medicines? *Chem. Commun.* 2004, 1889–1896.
73. Bouquiere, J. P., Finney, J. L., Lehmann, M. S., Lindley, P. F., Savage, H. F. J., High-resolution neutron study of vitamin-B12 coenzyme at 15-k - structure-analysis and comparison with the structure at 279-K. *Acta Crystallogr. Sect. B-Struct. Commun.* 1993, **49**, 79–89.
74. Oxtoby, N. S., Blake, A. J., Champness, N. R., Wilson, C., Water superstructures within organic arrays, Hydrogen-bonded water sheets, chains and clusters. *Chem. Eur. J.* 2005, **11**, 4643–4654.
75. Anderson, K. M., Afarinkia, K., Yu, H.-W., Goeta, A. E., Steed, J. W., When $Z'=2$ is better than $Z'=1$ - supramolecular centrosymmetric hydrogen bonded dimers in chiral systems. *Cryst. Growth Des.* 2006, **6**, 2109–2113.
76. Steed, J. W., Sakellariou, E., Junk, P. C., Smith, M. K., 15 crown-5: An unsymmetrical bifacial hydrogen-bond acceptor in crystal engineering. *Chem. Eur. J.* 2001, **7**, 1240–1247.
77. Maddox, J., Crystals from 1st principles. *Nature* 1988, **335**, 201–201.
78. Gavezzotti, A., Are crystal structures predictable? *Acc. Chem. Res.* 1994, **27**, 309–314.
79. Gervais, C., Coquerel, G., Simple model designed to generate new crystal structures derived from a mother phase, application to molecular compounds. *Acta Crystallogr. Sect. B-Struct. Commun.* 2002, **58**, 662–672.
80. Filippini, G., Gavezzotti, A., Empirical Intermolecular potentials for organic-crystals - the 6-exp approximation revisited. *Acta Crystallogr. Sect. B-Struct. Commun.* 1993, **49**, 868–880.
81. Gavezzotti, A., Calculation of lattice energies of organic crystals: the PIXEL integration method in comparison with more traditional methods. *Z. Kristall.* 2005, **220**, 499–510.
82. Gavezzotti, A., Towards a realistic model for the quantitative evaluation of intermolecular potentials and for the rationalization of organic crystal structures. Part II. Crystal energy landscapes. *Crystengcomm* 2003, **5**, 439–446.
83. Neumann, M. A., Perrin, M. A., Energy ranking of molecular crystals using density functional theory calculations and an empirical van der Waals correction. *J. Phys. Chem. B* 2005, **109**, 15531–15541.
84. Brock, C. P., Duncan, L. L., Anomalous space group frequencies for monoalcohols $C_mH_nOH$. *Chem. Mater.* 1994, **6**, 1307–1312.
85. Brock, C. P., Crystal packing in vicinal diols CnHm(OH)(2). *Acta Crystallogr. Sect. B-Struct. Commun.* 2002, **58**, 1025–1031.
86. Brammer, L., Bruton, E. A., Sherwood, P., Understanding the behaviour of halogens as hydrogen bond acceptors. *Cryst. Growth. Des.* 2001, **1**, 277–290.
87. Dolling, B., Gillon, A. L., Orpen, A. G., Starbuck, J., Wang, X. M., Homologous families of chloride-rich 4,4′-bipyridinium salt structures. *Chem. Commun.* 2001, 567–568.
88. Brammer, L., Swearingen, J. K., Bruton, E. A., Sherwood, P., Hydrogen bonding and perhalometallate ions: a supramolecular synthetic strategy for new inorganic materials. *Proc. Nat. Acad. Sci. USA* 2002, **99**, 4956–4961.
89. Derossi, S., Adams, H., Ward, M. D., Hydrogen-bonded assemblies of ruthenium(II)-biimidazole complex cations and cyanometallate anions: structures and photophysics. *Dalton Trans.* 2007, 33–36.
90. Braga, D., Grepioni, F., Sabatino, P., Desiraju, G. R., Hydrogen-bonding in organometallic crystals .1. from carboxylic-acids and alcohols to carbonyl-complexes. *Organometallics* 1994, **13**, 3532–3543.
91. Braga, D., Grepioni, F., Biradha, K., Pedireddi, V. R., Desiraju, G. R., Hydrogen-bonding in organometallic crystals .2. C—H...O hydrogen-bonds in bridged and terminal first-row metal-carbonyls. *J. Am. Chem. Soc.* 1995, **117**, 3156–3166.
92. Braga, D., Grepioni, F., Tedesco, E., Biradha, K., Desiraju, G. R., Hydrogen bonding in organometallic crystals .6. X-H---M hydrogen bonds and M---(H-X) pseudo-agostic bonds. *Organometallics* 1997, **16**, 1846–1856.
93. Thakur, T. S., Desiraju, G. R., Misassigned C–HCu agostic interaction in a copper(II) ephedrine derivative is actually a weak, multicentred hydrogen bond. *Chem. Commun.* 2006, 552–554.
94. Abad, M. M., Atheaux, I., Maisonnat, M., Chaudret, B., Control of proton transfer by hydrogen bonding in the protonated forms of the binucleophilic complex $[\{h^5\text{-}C_5H_4CH(NH_2)_4NMe\}Ir(PPh_3)H_2]$. *Chem. Commun.* 1999, 381–382.
95. Orlova, G., Scheiner, S., Kar, T., Activation and cleavage of H-R bonds through intermolecular H...H bonding upon reaction of proton donors HR with 18-electron transition metal hydrides. *J. Phys. Chem. A* 1999, **103**, 514–520.
96. Allen, F. H., Howard, J. A. K., Hoy, V. J., Desiraju, G. R., Reddy, D. S., Wilson, C. C., First neutron diffraction analysis of an O-H ... π hydrogen bond: 2-Ethynyladamantan-2-ol. *J. Am. Chem. Soc.* 1996, **118**, 4081–4084.
97. Hunter, R., Haueisen, R. H., Irving, A., The first water dependent liquid clathrate: X-ray evidence in the solid for a C—H...pi(heteroarene)..H-C interaction. *Angew. Chem. Int. Ed. Engl.* 1994, **33**, 566–568.
98. Dienwiebel, M., Verhoeven, G. S., Pradeep, N., Frenken, J. W. M., Heimberg, J. A., Zandbergen, H. W., Superlubricity of graphite. *Phys. Rev. Lett.* 2004, **92**, 126101.
99. Desiraju, G. R., Gavezzotti, A., From molecular to crystal-structure – polynuclear aromatic hydrocarbons. *J. Chem. Soc., Chem. Commun.* 1989, 621.
100. Aspley, C. J., Boxwell, C., Buil, M. L., Higgitt, C. L., Long, C., Perutz, R. N., A new combination of donor and acceptor: bis(h6- benzene)chromium and hexafluorobenzene form a charge-transfer stacked crystal. *Chem. Commun.* 1999, 1027.

101. Reddy, D. S., Panneerselvam, K., Pilati, T., Desiraju, G. R., Molecular tapes based on CN...Cl interactions. *J. Chem. Soc., Chem. Commun.* 1993, 661–662.
102. Metrangolo, P., Meyer, F., Pilati, T., Proserpio, D. M., Resnati, G., Highly interpenetrated supramolecular networks supported by N···I halogen bonding. *Chem. Eur. J.* 2007, **13**, 5765–5772.
103. Batten, S. R., Topology of interpenetration. *Crystengcomm* 2001, **3**, 67–72.
104. Brunet, P., Simard, M., Wuest, J. D., Molecular tectonics. Porous hydrogen-bonded networks with unprecedented structural integrity. *J. Am. Chem. Soc.* 1997, **119**, 2737–2738.
105. Scudder, M., Dance, I., A diamondoid supramolecular crystal lattice maintained entirely by sixfold phenyl embraces. *Crystengcomm* 2001, **3**, 46–49.

# 9 Network Solids

*'Laws are generally found to be nets of such a texture as the little creep through, the great break through, and the middle-sized are alone entangled in.'*

William Shenstone (1714–1763), *Essays on Men and Manners. On Politics.*

# 9.1 What Are Network Solids?

## 9.1.1 Concepts and Classification

Moulton, B. and Zaworotko, M. J., 'From molecules to crystal engineering: Supramolecular isomerism and polymorphism in network solids', *Chem. Rev.* 2001, **101**, 1629–1658.

So far we have been predominantly focused on the host-guest paradigm of supramolecular chemistry. In Chapters 3–6 we looked at discrete, solution phase hosts for various guests. In Chapter 7 we focused on (predominantly organic) molecular crystalline solids with guest binding cavities or channels and in the last chapter we developed this solid state chemistry into crystal engineering – designer solids based on supramolecular interactions. Now that we have seen that it is possible to understand and engineer molecular solids we turn to infinite solid-state networks where, formally, there are no discrete molecules and the entire solid is either all one molecule (as in diamond) or made up of relatively few infinite polymeric strands linked together by strong covalent, or more commonly, dative coordination bonds. Into this category fall naturally occurring inorganic materials such as zeolites as well as a vast range of coordination polymers – infinite coordination complexes in which metal ions are bridged by multidentate ligands into an infinite line or array. Some of these materials (*e.g.* zeolites) have cavities and are porous and so act as hosts for guests in the way we saw organic hosts do in Chapter 7. Others are not hosts but are still interesting from the point of view of materials design using supramolecular interactions or templating. In this chapter we progress from frameworks for capture, storage or transport that are often only stable in the presence of guests (*i.e.* clathration – the process of transforming a dense crystal form to an open structure containing the guest) to materials that take up guests reversibly without a major alteration in host structure (*i.e.* sorption – relatively facile diffusion of guests into a structure with permanent void space). At the interface between these extremes is nascent interest in host materials that respond to an external stimulus in a controlled fashion. This kind of dynamic 'smart' sorbent exhibits more complicated behaviour with significant changes at both the crystal and molecular levels.

In this chapter we begin with some relatively classical materials that are well-known and move on to the latest research in coordination polymers, particularly *metal-organic frameworks* that exhibit remarkable structural robustness in comparison to traditional clathrates, yet are highly amenable to design and modification, in contrast to the inorganic zeolites. In reaching this point we have come on a long journey following the science of non-covalent interactions, from solution host-guest chemistry, which has been traditionally the preserve of synthetic organic chemists or coordination chemists, through the physical organic chemistry of clathrates all the way to what is really a branch of modern materials science. This breadth of supramolecular chemistry is at once one of its most daunting yet exciting features.

For convenience we will classify network solids according to the dimensionality of their connectivity as listed below, where connectivity in this context refers to a strong covalent or coordination bond. Some examples are shown in Figure 9.1.

- 0D solids comprise discrete molecules – these are the kinds of compound we considered in the last chapter.
- 1D solids comprise infinite thread-like strands. The solid is then made up of the non-covalent packing of these strands.
- 2D solids are made up of sheet-like components that are infinite in two dimensions and pack together *via* non-covalent interactions in the third.

*Supramolecular Chemistry, 2nd edition* J. W. Steed and J. L. Atwood
© 2009 John Wiley & Sons, Ltd ISBN: 978-0-470-51233-3

- 3D solids are fully three-dimensionally interconnected covalent or coordination compounds in which the entire crystal is formally a single molecule.

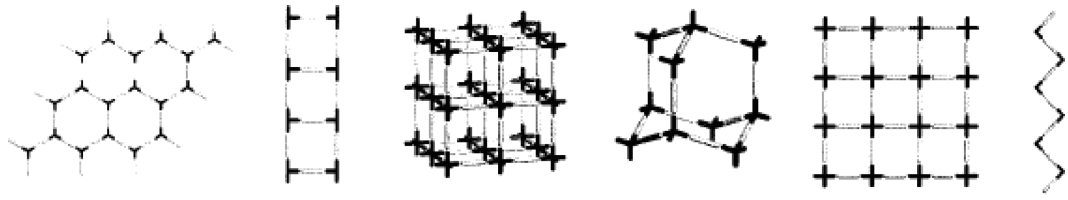


**Figure 9.1** Schematic representation of some of the simple network architectures structurally characterised for metal-organic polymers: (a) 2D honeycomb, (b) 1D ladder, (c) 3D octahedral, (d) 3D hexagonal diamondoid, (e) 2D square grid, and (f) 1D zigzag chain (reprinted from Section Key Reference © The American Chemical Society).

Within these categories we will also distinguish between materials that are either *porous* or *non-porous* according to strict definitions that we will discuss in Section 9.1.3, and whether or not individual networks are *interpenetrated* (in one, two or three dimensions) with other networks – *i.e.* whether they are mutually topologically entangled in such a way that they could not be separated without breaking bonds. We begin with a description of nomenclature that we will use to describe network topology.

## 9.1.2 Network Topology

Robson, R., 'A net-based approach to coordination polymers', *J. Chem. Soc., Dalton Trans.* 2000, 3735–3744.

Topology is a basic field of mathematics in which any network is reduced to a series of nodes (connection points) and connections. Networks are said to be topologically equivalent unless they cannot be deformed into one another without cutting or glueing. Thus the topology of networks depends on the way in which they are connected, not on the shape or size of the individual components. The science of topology began with Leonhard Euler's solution to the *seven bridges of Königsberg* problem. Königsberg (now Kaliningrad in Russia) was the capital of East Prussia and is built on the River Pregel at the junction with another river. The island of Kniephof is situated at the conflux of the two rivers. The island and different parts of the mainland are mutually linked by a total of seven bridges, Figure 9.2. The problem

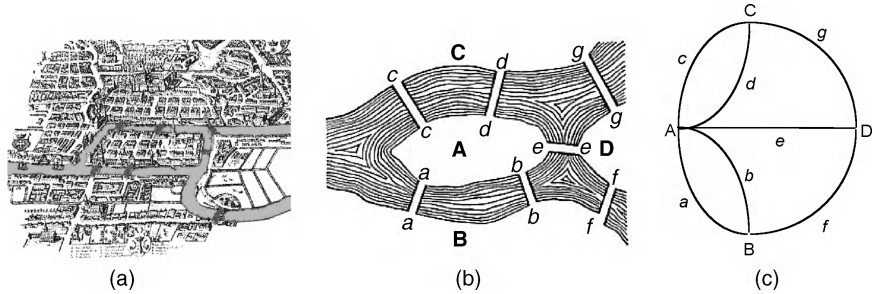


**Figure 9.2** (a) The City of Königsberg showing the seven bridges. The island of Kniephof is in the centre. (b) simplified map and, (c) topological representation where land masses are reduced to nodes and bridges are reduced to lines.

is to cross all seven bridges without crossing any one twice. In 1735, Euler presented the solution to the problem to the Russian Academy, proving that crossing all seven bridges without crossing a bridge twice is impossible. Euler's solution was based on his invention of graph theory, from which, in turn topology developed. He reasoned that every land mass muct have an even number of bridges allowing a traveller to get on and off again. In fact each land mass has an odd number.

As far as real network solids go, we can reduce chemical entities such as metal centres or small clusters of metals (termed *secondary building units* or SBUs) to nodes, and bridging ligands to connections. It then becomes possible to describe the topology of a chemical network material. In a famous book published in 1977 A. F. Wells identified a number of commonly occurring chemical network topologies[1] and many more are now known, although presumably more remain to be discovered. Network topologies may be described by two somewhat related sets of symbols or notation, and it is easy to become confused between them.

*Wells notation* takes the form $(n, p)$-net where $n$ and $p$ are integers that describe, respectively, the shortest route in terms of number of nodes to complete a circuit back to the starting place and the connectivity of a given node. Thus a (6,3)-net contains hexagonal holes (or, if irregular, holes that form a six-sided polygon; a 6-gon; $n = 6$) and each node is 3-connected ($p = 3$).

A *Schläfli symbol* describes the length of the shortest routes, in terms of number of nodes, from one node back to itself based on each pair of connections at the node. For example, the Schläfli symbol $6^3$ means that 6-gons are the shortest circuit of connecting nodes that can be formed, and that there are three of these circuits radiating out in different directions from each node. Similarly the symbol $4.8^2$ indicates that the shortest circuit back to a three-connected node is a 4-gon between one pair of connections and two 8-gons between the other two pairs. Some common network topologies and their Schläfli symbols are given below. Note how the hexagonal grid and 'brick wall' patterns are topologically identical – they are both $6^3$ (or (6,3) in Wells' system) networks. The two sets of symbols are not always the same, however. For a square grid based on a square planar metal centre node for example, the Wells nomenclature is (4,4). In the Schläfli nomenclature this network would be described as $4^4.6^2$ – there are four pairs of *cis* related connections giving four 4-gons (squares in the example shown in Figure 9.3 but there are also two pairs of *trans* related connections giving

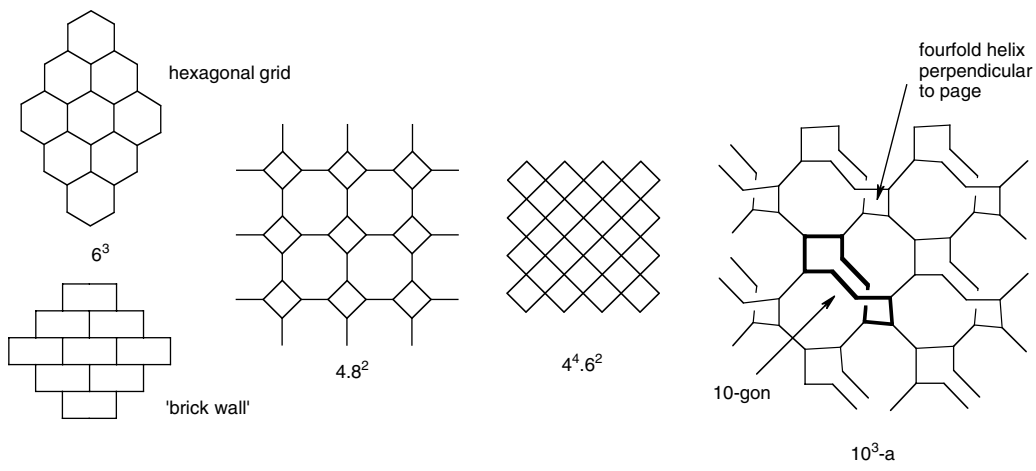


**Figure 9.3** Examples of network topologies along with their Schläfli symbols. The corresponding Wells symbols are (6,3), ($4,8^2$), (4,4) and (10,3)-a.

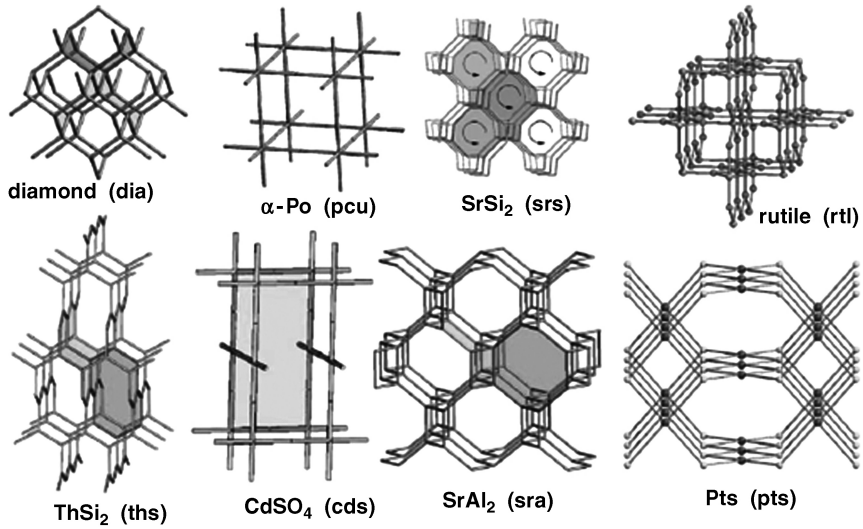


**Figure 9.4** Common nets exhibited by simple materials along with their generic names. Characteristic rings are shaded. The $SrSi_2$ structure is a (10,3)-a net (reproduced with permission from The Royal Society of Chemistry). See plate section for colour version of this image.

two 6-gons (rectangles). The Wells and Schläfli nomenclature can become complicated in three dimensions and for complex topologies, particularly when more than one topologically distinct type of node is present (the nets shown in Figure 9.3 are all examples of uninodal nets; nets with two, three or more types of node are termed binodal, trinodal *etc*.). For nets that are common, recognised types a trivial name based on the simplest representative member of the series is often adopted (Figure 9.4). For example diamondoid (4-connected tetrahedral centres, Section 8.12), α-polonium (or NaCl, with 6-connecting, octahedral centres), the NbO net (square planar 4-connecting centres with a 90° rotation along each connection); the PtS net (with a 1 : 1 ratio of tetrahedral and square planar nodes), the rutile net (octahedral and trigonal centres in a 1 : 2 ratio); the '$Pt_3O_4$' net (with square planar and trigonal nodes in a 3 : 4 ratio) and the $Ge_3N_4$ net (with tetrahedral and trigonal nodes in a 3 : 4 ratio).

Another interesting net is the cubic (10,3)-a (Wells) or $10^3$-a (Schläfli) net exhibited by $SrSi_2$. This may be regarded as a three-connected analogue of the four-connected, cubic diamondoid net. The 'a' refers to the most symmetrical variant of (10,3) nets identified by Wells. The (10,3)-a net is chiral with fourfold screw axes (Box 8.2) running through the structure. An nice example is the zinc(II) tripyridyltriazine (**9.1**) complex $[Zn(\mathbf{9.1})_{2/3}(SiF_6)(H_2O)_2(MeOH)] \cdot$ solvent. In this case the Zn(II) ions are each bound to two tripyridyltriazine ligands and so act as essentially linear connectors (the zinc coordination environment is completed by bonds to two water molecules, the $SiF_6^{2-}$ anion and a methanol molecule, none of which matter from a topological point of view). As a result it is the tripyridyltriazine ligands that we think of as being the 3-connected nodes. The network structure actually comprises eight interpenetrating (10,3)-a nets, four of each handedness. The environment about one of the fourfold helices is shown in Figure 9.5.

Recently there have been significant advances in mathematical tiling theory which have been applied to more rigorous descriptions of complex 3D (or 3-*periodic*) network topologies. The reader is referred to the literature for a complete description of these powerful new methods.[3, 4]

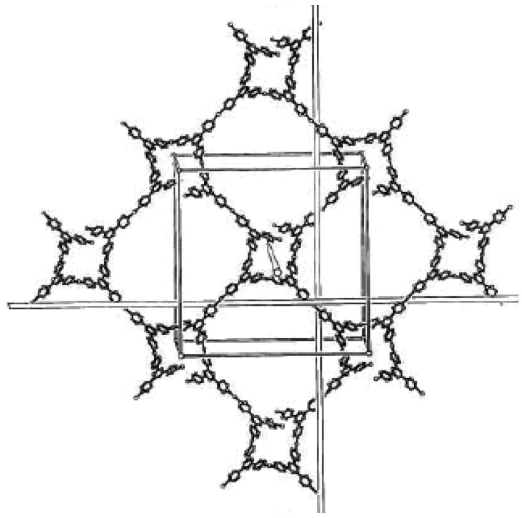

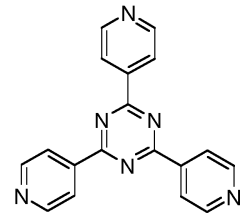

**9.1**

**Figure 9.5** The view along the fourfold helix in one of the eight interpenetrating (10,3)-a nets in $[Zn(\mathbf{9.1})_{2/3}(SiF_6)(H_2O)_2(MeOH)]\cdot$solvent. Helices are highlighted by imaginary poles running along the selected helical axes (reproduced with permission from The Royal Society of Chemistry).

## 9.1.3 Porosity

Barbour, L. J., 'Crystal porosity and the burden of proof', *Chem. Commun.* 2006, 1163–1168.

The presence or absence of 'porosity' in solids is of crucial interest in their ability to function as host materials for any substance, be it liquid, solid or gas under ambient conditions. Porous materials have very broad applications in catalysis, separations and sequestration applications and are an area of tremendous current interest. Len Barbour of the University of Stellenbosch, South Africa, identifies two key criteria (listed below) that must be fulfilled if a material is to be described as porous.

1. Permeability should be demonstrated (*e.g.* by gas sorption measurements, spectroscopic evidence of guest exchange or crystallography).
2. The term 'porous' should apply to a specific host phase and not simply to the host molecules as an amorphous or mutating collective. Therefore, in principle, the host framework should remain *substantially unaffected* by guest uptake and removal. This requirement means that we do not describe, for example, the close-packed, tetragonal $\alpha$-phase of urea as porous, however the description would be appropriate for an empty, hexagonal urea $\beta_0$ apohost phase (Section 7.3)

Given these requirements Barbour identifies three kinds of porosity in the current literature:

1. porosity 'without pores',
2. conventional porosity,
3. virtual porosity.

We have already seen in Section 7.9 a number of systems exhibiting porosity 'without pores'. This term applies to generally relatively soft solids such as molecular clathrates that can deform in such a way as to allow the ingress and egress of guest molecules without any obvious channel or port in the

conventional space-filling representation of the structure of the material. Porosity without pores is a real and useful phenomenon and the reader is referred to Section 7.9 for a description of some of the fascinating compounds exhibiting this kind of behaviour. In this chapter we will focus much more on conventional porosity. Conventional porosity requires the existence of permanent, linked gaps or holes in a solid with a minimum diameter of about 3 Å, and a size typically in the region 3–10 Å for microporous solids. In Section 7.9 we identified the various categories of micro- meso- and macroporous solids and the size ranges of the pores they possess. Note however that pore size, particularly in microporous solids, is somewhat dependent on how it is measured. The usual method involves choosing a 'probe' of arbitrary radius (*e.g.* 1.1 Å the radius of a hydrogen atom) and computationally rolling the probe around the van der Waals surface of the void space and measuring the volume swept out using software such as MSROLL. The result is clearly dependent on the choice of probe radius! Conventional porosity is exhibited by compounds such as zeolites and is of tremendous academic and industrial interest. The third category, virtual porosity, is not a category of porosity at all according to the definitions given above, but rather a warning to researchers to beware misleading pitfalls. Virtual porosity can come about by the appearance of a pore or cavity if a crystal structure is viewed in ball-and-stick mode but disappears if viewed in van der Waals space-filling mode. Virtual pores can also be created by artificially not showing a component that the naïve user designates as a 'guest' even if that guest is necessary for the maintenance of the structure, *e.g.* counter anions. Thankfully publications exhibiting this false, 'virtual' kind of porosity are rare!

## 9.2 Zeolites

Web site of the International Zeolite Association: http://www.iza-online.org/. This resource contains a comprehensive database of manipulable 3D zeolite structures.

### 9.2.1 Composition and Structure

Čejka, J., 'Zeolites: structures and inclusion properties', in *Encyclopedia of Supramolecular Chemistry*, Atwood, J. L., Steed, J. W., eds. Marcel Dekker: New York, 2004; Vol. 2, *pp.* 1623–1630.

Zeolites are naturally occurring and artificial porous aluminosilicates in which a generally anionic framework is balanced by cations, usually located within the solid cavities or channels, although by no means filling them. The global annual market for zeolites is several million tons and they have been phenomenally successful over a wide range of applications particularly in catalysis and separation science problems, especially in the petrochemicals industry. Key areas include adsorptive separation of hydrocarbons, purification of gases and liquids, and catalytic cracking of long-chain hydrocarbons to form more valuable short-chain homologues. Zeolites also have applications in ion exchange, particularly as a detergent additive (water softening), and the separation and extraction of gases and solvents, *e.g.* as 'molecular sieves' for dehydration of organic solvents. The general formula defined by the International Union of Pure and Applied Chemistry (IUPAC) for a zeolite takes the form:

| $[A_aB_bC_c]$ | $\{(Al_dM_eSi_f)O_g\}$ | $(xH_2O,\ yN)$ |
|---|---|---|
| Cations A, B, C | Framework composition | Occluded guests |

Each species is also denoted by a three-letter structure code that describes the framework topology (connectivity, channel dimensionality *etc.*). Examples are given in Table 9.1; common structures of some representative zeolites are shown in Figure 9.6.

**Table 9.1** Characteristics of some common zeolite framework topologies.

| Structure type code | Type of material: Name | Type of material: Formula | Framework composition | Channel system | Pore opening | Cage | Comments |
|---|---|---|---|---|---|---|---|
| AFI | $AlPO_4$-5 | $Al_{12}P_{12}O_{48}$ | $AlPO_4$-based<br>High silica | 1D | 12-rings<br>7.3 Å | None | |
| FAU | Faujasite | $M_{29}[Al_{58}Si_{134}O_{384}]\cdot 240H_2O$ | Aluminosilicate | 3D | 12-rings | *fau* | ABC stacking of puckered sodalite cage layers |
| | | (M = $Na_2$, Ca, Mg) | High silica | | 7.4 Å | *sod* | |
| | | | $AlPO_4$-based | | | d6R | |
| LTA | Linde type A | $\{Na_{12}[Al_{12}Si_{12}O_{48}]\cdot 27H_2O\}_8$ | Aluminosilicate | 3D | Eight-rings | *sod* | |
| | | | High silica | | 4.1 Å | $\alpha$ | |
| | | | $AlPO_4$-based | | | | |
| | | | $GaPO_4$-based | | | | |
| MEL | ZSM-11 | $Na_n[Al_nSi_{96-n}O_{192}]\cdot 16H_2O$ | High silica | 3D | Elliptical | None | Straight channels |
| | | (n < 16) | | | 10-rings<br>5.5 Å<br>(mean) | | |
| MFI | ZSM-5 | $Na_n[Al_nSi_{96-n}O_{192}]\cdot 16H_2O$ | High silica | 3D | Elliptical | None | One straight and one zigzag channel |
| | | (n < 27) | | | 10-rings<br>5.5 Å<br>(mean) | | |
| SOD | Sodalite | $Na_6[Al_6Si_6O_{24}]\cdot 2NaCl$ | Many combinations of Al, Si, P, Ga, Be, As and Zn | None | 6-rings only<br>2.8 Å | *sod* | ABC stacking of six rings |

Zeolites are generally regular crystalline materials, although defects such as non-bridging oxygen atoms, vacant sites or large pores are common, and often contribute to the reactivity of the materials. Silicon is the key element in the zeolite framework, with aluminium, as the $AlO_4^-$ anionic fragment, most easily substituted within the neutral $SiO_4$ sites. In every case the oxygen atoms are bridging. A wide range of other $TO_4$ species (termed the *primary building units*) may also be included (T = tetrahedral centre such as Ge, Ga, P, As *etc.*). In zeolites, Al/Si ratios are known from one to infinity, which corresponds to a minimum requirement that there should be no Al–O–Al bonds anywhere in the structure; only Al–O–Si and Si–O–Si are stable. Based on their aluminium to silicon ratio, zeolites are usually divided into two broad categories:

1. Zeolites with low or medium Si/Al ratio (Si/Al < 5).
2. Zeolites with high Si/Al ratio (5 < Si/Al).

Materials with very high Si/Al ratios (tending to infinity) are called all-silica molecular sieves, zeosils or porosils. If any aluminium is present, non-framework cations such as alkaline or alkaline earth metals

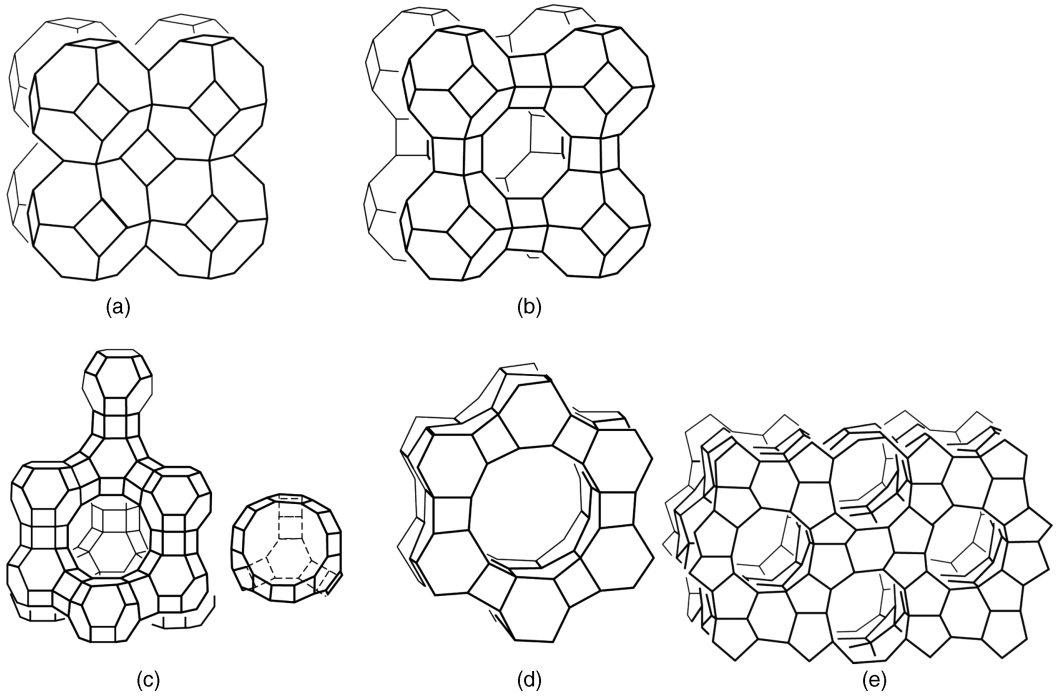


**Figure 9.6** Topologies of zeolite structure types. (a) Sodalite; (b) Linde type A; (c) faujasite (zeolite X and Y); (d) $AlPO_4$-5; and (e) ZSM-5. The vertices represent the positions of $AlO_4^-$ or $SiO_4$ tetrahedra while straight lines represent Si–O–Si or Si–O–Al linkages. (Reproduced with permission from [5]).

or organic tetraalkyl or tetraarylammonium ions are incorporated within the pores. Neutral organic molecules or solvent molecules and water may also be present depending on the synthesis method. The smaller cations may be exchanged in ion-exchange processes, while the organic species may be transformed into protons by calcination (heat treatment at about 500 ºC).

About 60 naturally occurring zeolites are known, of which bikitaite, $Li_2[Al_2Si_4O_{12}]\cdot 2H_2O$, heulandite, $Ca_4[Al_8Si_{28}O_{72}]\cdot 24H_2O$ and faujasite, $(Na_2, Ca, Mg)_{29}[Al_{58}Si_{134}O_{384}]\cdot 240H_2O$, are examples. The first naturally occurring zeolite, stilbite ($NaCa_2Al_5Si_{13}O_{36}\cdot 14H_2O$), was discovered by the Swedish mineralogist Crønsted about 250 years ago who found that the new mineral released water on heating, hence its name from the Greek *zeo* (to boil) and *lithos* (stone). Many of the more important zeolites, such as ZSM-5 used in the petrochemicals industry for gasoline production, are synthetic, however. Recent template syntheses using surfactants have given access to very interesting mesoporous (intermediate pore size) materials such as MCM-41 and MCM-48, which have much larger cavities than the traditional microporous materials. ZSM and MCM stand for Zeolite Socony Mobil and Mobil Catalytic Material respectively. They form part of a large series of three-letter code descriptions for particular series of materials, particularly those of industrial importance, which have a historical basis, but are still in common usage. A full listing is given on the web site of the International Zeolite Association cited at the beginning of this section. Much of the usefulness and chemistry of zeolites arises as a consequence of the presence of channels and cavities in the structures, which include metal cations (which counterbalance the charge of the anionic framework), water and a vast range of other guests. The beauty of zeolites is that the aluminosilicate cages are sufficiently robust that guest species may enter and leave the channels with no disruption of the host structure. As a result, zeolites are used as 'molecular sieves', separating catioic and molecular guests on a size or adsorption-selective basis, and as reaction vessels for high selective intrachannel and intracavity reactions.

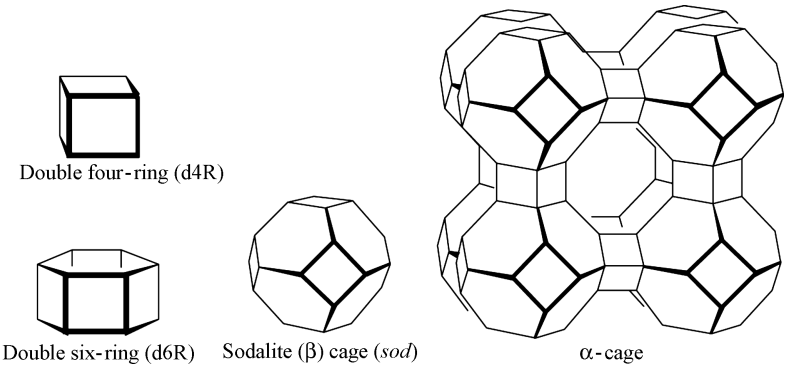


**Figure 9.7** Zeolite cage structures incorporated as *secondary building units*.

In general the tetrahedral primary building units form common structural features termed *secondary building units* (SBU – some examples are shown in Figure 9.7) that are linked together in different ways to give the overall zeolite structure. The inclusion chemistry of zeolites depends very much on the channel and pore size and on the size of the windows giving access to those solid state cavities. In the case of sodalite, the $\beta$-cages (Figure 9.7) are accessible only through four- and six-membered rings (that is comprising four or six tetrahedral atoms with their associated oxygen linkers) that are not large enough to admit the vast majority of guest species. In contrast, the Linde type A (LTA) topology, while still based on sodalite cages, contains additional double four-ring spacers. This results in $\alpha$-cages accessible by eight-rings and giving the material an overall three-dimensional channel structure. Extending the structure still further, in the faujasite type, sodalite cages are arranged in a tetrahedral fashion, exactly like the carbon atoms in diamond, joined by double six-rings. The result is the faujasite cage (*fau*), which comprises a three-dimensional 12-ring channel system. The framework is highly porous and ideal for a number of inclusion catalytic purposes.

In contrast to the SOD, LTA and FAU topologies, ZSM-5 and ZSM-11 are not based on the sodalite motif. They are complex structures with 10-ring aperture channels based on the 'six-ring wrap' motif in which the channel walls are made of a sheath of fused six-rings. The only difference between the two substances is the occurrence of an inversion centre in ZSM-5 and a mirror plane in ZSM-11. This results in one straight and one zigzag channel in ZSM-5 (Figure 9.8) and entirely linear channels for ZSM-11. The AFI type, typified by $AlPO_4$-5, is also based on channels. In pure aluminophosphate zeolites, the $Al^{3+}$ and $PO_4^{3-}$components strictly alternate to give a neutral cage framework and so there are only even-membered rings. The pore system is based on a one-dimensional channel with 12-ring openings.

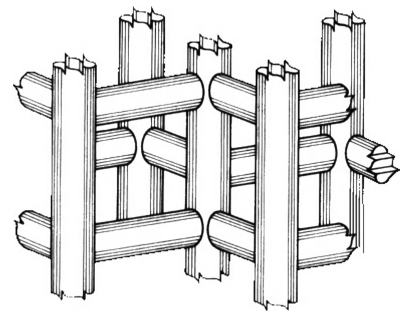

**Figure 9.8** Linear and zigzag channels in ZSM-5.

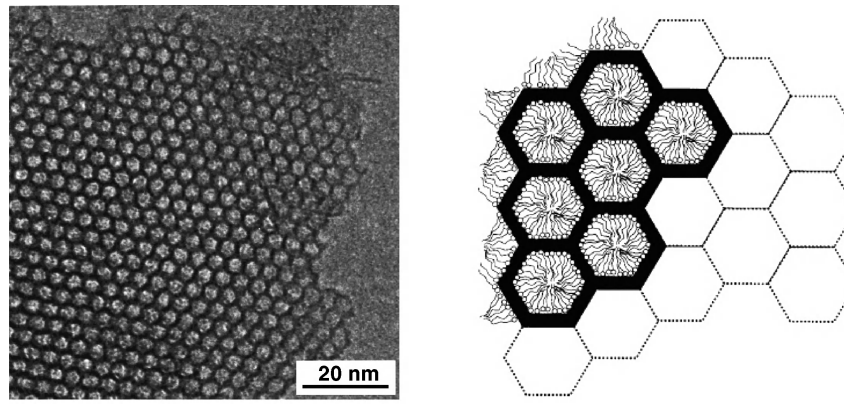


**Figure 9.9** (a) High resolution TEM image of calcined MCM-41 showing the hexagonal mesoporous structure, (b) schematic diagram of how the mesopores are templated using a surfactant (reprinted with permission from [6] © 2000 American Chemical Society).

The zeolites shown in Table 9.1 are all examples of microporous materials, so called because of their relatively small pore dimensions. In 1992, the M41S family of zeolites, of which MCM-41 and MCM-48 are members, were reported by Mobil. These species are templated by surfactant molecules such as alkyl trimethylammonium salts $NRMe_3^+$ ($R = C_nH_{2n+1}$; $n = ca.\ 12 - 22$) that form micelles in solution (Section 13.2.1), templating the formation of very large pores (mesopores) with the pore size depending on the length of R.[6] Zeolite MCM-41 has a one-dimensional hexagonal arrangement of open channels of dimensions 15–100 Å, readily observed by transmission electron microscopy, Figure 9.9. MCM-48 has a three-dimensional arrangement of pores about 30 Å in diameter, in a cubic arrangement. These mesoporous materials have opened up a new field in 'expanded' zeolite compounds over the past 15 years or so. Other approaches to these larger pore compounds include the preparation of delaminated zeolites from zeolite precursors and synthesis of pillared layered materials with spaced zeolite layers.[7]

## 9.2.2 Synthesis

In order to prepare zeolites of well-defined structural type, templating materials must be used which determine the pore size distribution. The overall mechanism of zeolite formation is thought to involve the gradual replacement of water of hydration about the templating cation by silicate or aluminosilicate units. Thus, the pore size is determined by the dimensions of the cation, subject to the formation of an at least metastable framework. Some examples of cations and the zeolite types templated are given in Table 9.2. A wide range of other factors such as the crystal deposition kinetics and Si/Al ratio must also be controlled. As a result, zeolite synthesis is commonly carried out in a solid gel phase, in which the framework building species are supplied continuously at a controlled rate by continuous dissolution. A general synthesis scheme is shown in Figure 9.10.

Control of pH is critical in the determination of the Si/Al ratio. As the pH increases, the ability of the silicate to condense decreases because of a decrease in the amount of Si–$O^-$species relative to Si–OH. The anionic form is necessary in order for the initial nucleophilic attack to take place. In contrast, the condensation rate of $Al(OH)_4^-$ remains constant and so aluminium-rich zeolites crystallise preferentially at high pH and vice versa. Zeolite synthesis also depends on a wide range of experimental parameters, including concentrations and degree of supersaturation, the source of the framework materials, solvent

**Table 9.2** Templating cations and the resulting zeolites.

| Cations | Zeolite type |
|---|---|
| $Na^+$ | Sodalite |
| $Na^+ + NMe_4^+$ | Faujasite, sodalite, zeolite-A (LTA) |
| $Na^+ + NPr_4^+$ | ZSM-5 |
| $Na^+$ + benzyltriphenylammonium | ZSM-11 |
| $Na^+$ + [15]crown-5 | High-silica faujasite |
| $C_nH_{2n+1}Me_3N^+$ ($n$ = 8–16) | MCM-41 |

(sometimes alcohols or glycols are used), gel dissolution rate, ageing, addition of seed crystals, temperature, agitation time, and pressure. The ideal parameters have been determined quite precisely by experimentation and zeolites may be prepared readily in large quantities.

## 9.2.3 MFI Zeolites in the Petroleum Industry

Marcilly, C., 'Zeolites in the petroleum industry', in *Encyclopedia of Supramolecular Chemistry*, Atwood, J. L., Steed, J. W., eds. Marcel Dekker: New York, 2004; Vol. 2, *pp.* 1599–1609.

The MFI class of channel zeolites, of which ZSM-5 is a member, are of enormous importance in the petrochemicals industry because of their shape-selective adsorption and transformation properties. The most well-known example is the selective synthesis and diffusion of *p*-xylene through ZSM-5, in preference to the *o*- and *m*-isomers. Calcined zeolites such as ZSM-5 are able to carry out remarkable transformations upon normally unreactive organic molecules because of 'super-acid' sites that exist

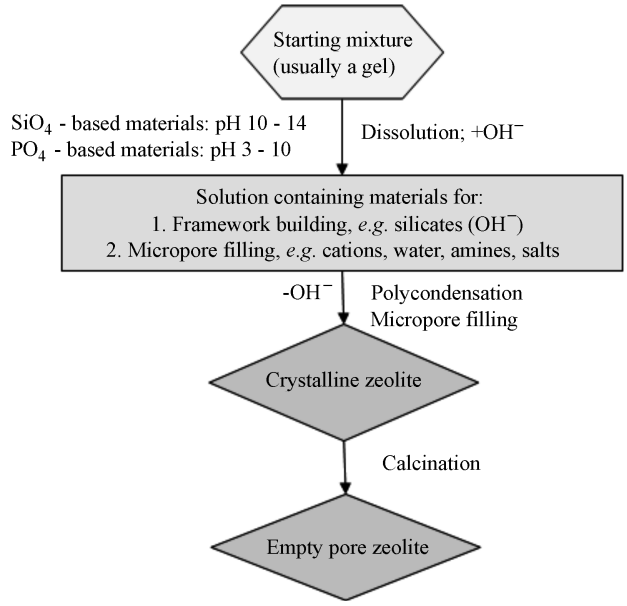


**Figure 9.10** Schematic diagram illustrating zeolite synthesis in the presence of a mineraliser (*e.g.* $OH^-$) in aqueous phase.

within the zeolite pores. In calcined zeolites, the negative charge of the framework is balanced only by protons, which reside either upon defect sites or on bridging oxygen atoms. In the empty zeolite cavity, the proton is unsolvated and is therefore extremely reactive. This has the result that even very weak bases such as aromatic hydrocarbons, and even *n*-alkanes and waxes, are protonated as they diffuse through the zeolite channels, forming reactive carbocations that may readily rearrange, forming a mixture of products. Intracavity synthesis of xylenes is carried out by reaction of toluene with methanol. The zeolite acidity results in electrophilic aromatic substitution of the aryl ring to give a mixture of *o*-, *m*- and *p*-xylenes, which are in a state of equilibration within the zeolite medium. Crucially it is only the *para* isomer that is able to diffuse readily through the zeolite channel, however, because of its linear, thread-like shape. The more bulky *ortho* and *meta* isomers are much less mobile in the zeolite interior, and hence are much more likely to reisomerise, forming an additional statistical amount of *p*-xylene, which again diffuses away. In this way, zeolites such as ZSM-5 are highly *para*-selective. This property is known as *diffusion selectivity*. In fact, the *para* isomer diffuses about 14 times faster than the *o*-isomer and about 1000 times faster than *m*-xylene (Figure 9.11a)

The zeolites' high acidity is also of crucial importance in the production of gasoline *via* the 'M-forming' process. In gasoline, linear *n*-alkanes are relatively undesirable compared to their branched counterparts because of their lower octane numbers. Separation of linear and branched materials increases the value of the gasoline. Better still, if linear materials can be converted into branched species,

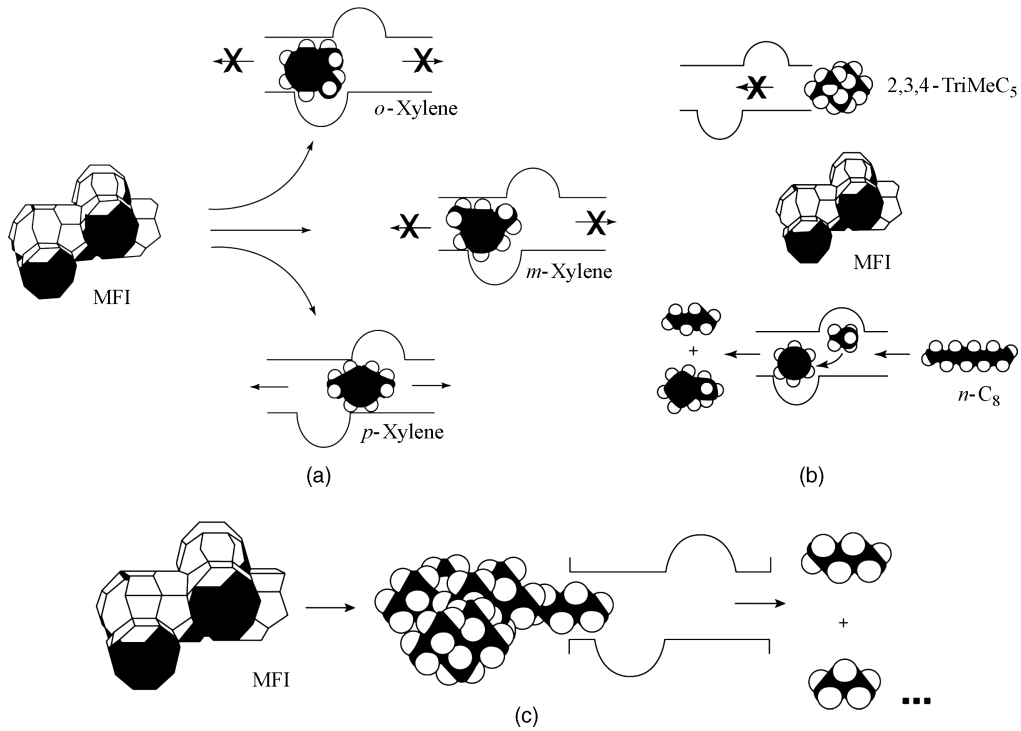


**Figure 9.11** (a) Diffusion shape selectivity in xylene isomerisation. (b) The M-forming process for gasoline upgrading by MFI-type zeolites; high-octane compounds such as 2,3,4-trimethylpentane are prevented from reacting by both transition state and diffusion selectivity; *n*-alkanes penetrate into the channels and are cracked; aromatics are alkylated with the light fragments from cracking. (c) Wax components are cracked into gasoline and liquid petroleum gas. (Reproduced with permission from [8]).

significant profit may be generated. Highly branched alkanes such as 2,3,4-trimethylpentane diffuse very slowly into the ZSM-5 channels. Furthermore, even if they do find themselves within the zeolite, the primary mechanism for alkane isomerisation involves hydride transfer to a zeolite cationic site. The transition state for this reaction is highly bulky and, as a result, only linear alkanes are able to undergo reaction. This is known as *transition state selectivity*. Both transition state selectivity and diffusion selectivity, therefore, result in valuable branched hydrocarbons being unchanged by the zeolite. On the other hand, linear species such as *n*-octane diffuse readily into the zeolite and react with the acid sites, resulting in their catalytic cracking to lighter fractions, readily separated from the mixture. Aromatics are alkylated by the cracking fragments and contribute to the gasoline product, resulting in little volume loss. Since the carcinogen, benzene, is the most reactive there is a desirable lowering of the benzene: toluene ratio in the product (Figure 9.11b).

Other larger zeolites of the FAU type are used in the cracking of long-chain waxes and paraffins, which are of low value because of their viscosity. The products of this process are gasoline and liquid petroleum gas, which is treated further with MFI-type zeolites as detailed above (Figure 9.11c).

## 9.3 Layered Solids and Intercalates

### 9.3.1 General Characteristics

O'Hare, D., 'Inorganic intercalation compounds', in *Inorganic Materials*, D.W. Bruce and D. O'Hare (eds), J. Wiley & Sons, Ltd: Chichester, 1996, 171–254.

Layered solids include materials such as graphite, cationic and anionic clay minerals, metal phosphates and phosphonates, and a range of other inorganic and coordination compounds. The first report of their occurrence seems to be the production of porcelain by the Chinese around AD 600–700. This occurs by the intercalation, or inclusion, of alkali metal ions in naturally occurring layered minerals such as feldspar or kaolin. A layered solid is characterised by a two-dimensional sheet arrangement in which the components of the sheet interact covalently (or are otherwise strongly bound), while the interactions from one sheet to the next are of a weak type, commonly van der Waals interactions. Some of the characteristics of layered solids are summarised in Figure 9.12, while examples of various classes of layered material are given in Table 9.3.

The layered arrangement makes these materials very interesting from the point of view of host–guest behaviour because ionic or molecular guest species may be inserted between one layer and another causing the layers to expand or swell. Guest intercalation is generally reversible, and it is an important characteristic of layered solids that, rather like zeolites, they can retain their layered host structure

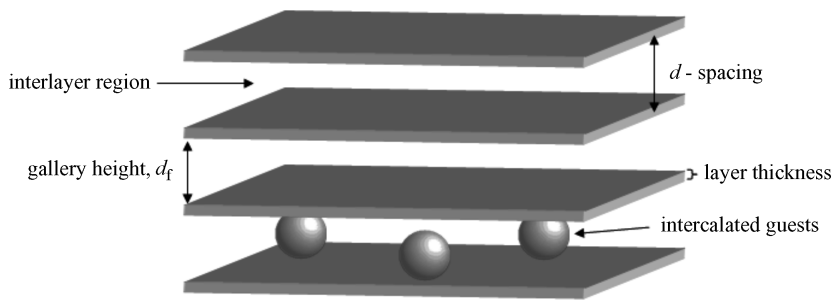


**Figure 9.12** Characteristics of layered solids.

**Table 9.3** Classes of layered solids.

| Layered material | Formula |
|---|---|
| (a) Uncharged layers | |
| (i) Insulators | |
| Clays | |
| Kaolinite, dickite | $Al_2Si_2O_5(OH)_4$ |
| Serpentine | $Mg_3Si_2O_5(OH)_4$ |
| Nickel cyanide | $Ni(CN)_2$ |
| (ii) Electrically conducting layers | |
| Graphite | C |
| Transition metal dichalcogenides | $MX_2$ (M = Ti, Zr, Hf, V, Nb, Ta, Mo, W; X = S, Se, Te) |
| Metal(IV) oxyphosphates | $MOPO_4$ (M = V, Nb, Ta) |
| (b) Charged layers | |
| (i) Anionic layers | |
| Clays | |
| Montmorillonite | $Na_x(Al_{2-x}Mg_x)(Si_4O_{10})(OH)_2$ |
| Saponite | $Ca_{x/2}Mg_3(Al_xSi_{4-x}O_{10})(OH)_2$ |
| Vermiculite | $(Na,Ca)_x(Mg_{3-x}Li_xSi_4O_{10})(OH_2)$ |
| Muscovite | $KAl_2(AlSi_3O_{10})(OH)_2$ |
| $\beta$-alumina | $NaAl_{11}O_{17}$ |
| Alkali transition metal oxides | $M^IXO_2$ ($M^I$ = alkali metal; X = Ti, V, Cr, Mn, Fe, Co, Ni) |
| (ii) Positively charged layers | |
| Hydrotalcite | $[Mg_6Al_2(OH)_6]CO_3 \cdot 4H_2O$ |

throughout successive intercalation and de-intercalation steps. Unlike zeolites, however, intercalate host layers are flexible and may bend to accommodate partial guest inclusion in some zones but not others.

Layered intercalate compounds generally form staged structures in which the stage number represents the ratio of guest layers to host layers. Thus a stage 1 complex has alternating layers of host and guest. A stage 2 complex has two host layers for every one guest layer, and so on. Fractional stages are also encountered, and are often found as intermediates, for example in the conversion of a stage 2 compound into a stage 1 material. Classically, a transformation of this kind *via* a fractional stage intermediate would require the departure of all of the guests from some of the layers, the collapse of the structure back to its guest-free *d*-spacing, and the repopulation of other layers. Such a model is unlikely, and is inconsistent with the observed facile interconversions. As a result a nonclassical model, the Daumas–Hérold model, was proposed for intercalate staging, which simply allows the density of guests to vary within a layer while recognising that unoccupied areas in one layer will tend to align with occupied areas in adjacent layers in order to minimise distortion of the entire structure and maximise electrostatic attraction. The difference between the two pictures of intercalation is shown in Figure 9.13; the Daumas–Hérold picture of interconversion of a stage 2 intercalate into a stage 1 material is given in Figure 9.14.

Historically, the chemistry of layered intercalates began in 1840 with the report that graphite was able to intercalate sulfuric acid between successive layers of its 'chicken wire' mesh. It was not until after the 1960s that serious interest was aroused by intercalates, following the realisation that guest intercalation may significantly alter the host's chemical, catalytic, electronic and optical properties. This is especially true when the host properties are dependent on its layered structure. In the case of graphite, for example, its use as a 'dry', low-temperature lubricant has come about because of the ease

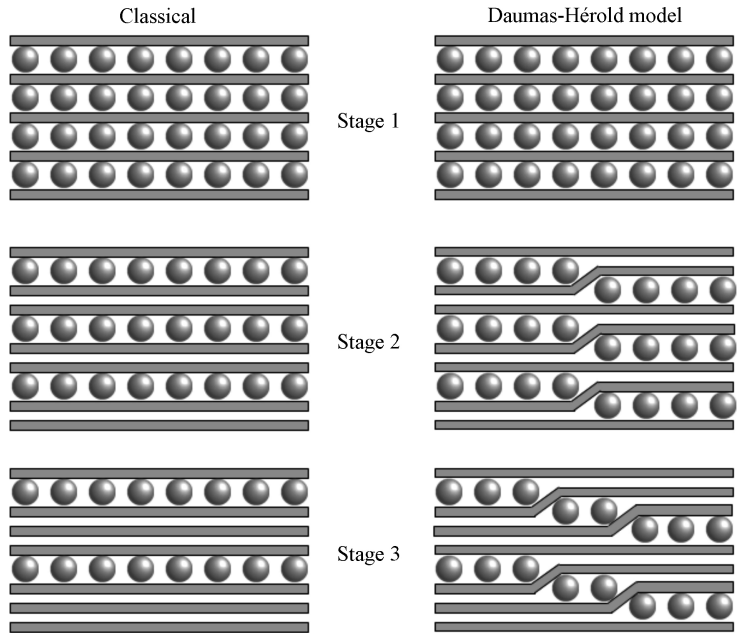


**Figure 9.13** Classical and Daumas–Hérold model of staging in intercalate compounds. The stage number represents the ratio of host to guest layers.

in which one carbon layer slides across another (you will probably have felt the slippery feel of a soft pencil lead, for example, which is really low-clay graphite). Interestingly, the lubricant properties of graphite depend crucially upon the presence of intercalated oxygen. In the absence of oxygen, which acts as a sort of molecular ball bearing, graphite becomes much less slippery. This proved to be a particular problem in the use of graphite lubricants in the space programme. Other intercalate materials, particularly clays, have applications as ion-exchange media for both cation and anion exchange. The most important applications of intercalates are as components in solid-state electrochemical devices, particularly in energy storage as in lithium ion batteries,[9,10] and their use in heterogeneous catalysis.[11] Both graphite and layered-metal chalcogenides intercalate alkali metals and have applications as electrodes for solid-state batteries. The lithium intercalate of $TiS_2$ is used commercially in battery applications requiring high-energy density, such as cellular phones, or high reliability, such as cardiac pacemakers. In the area of catalysis, clays were used extensively in the petrochemicals industry before the discovery of zeolites. Interest in pillared clays with pores in excess of 1 nm is reviving as a

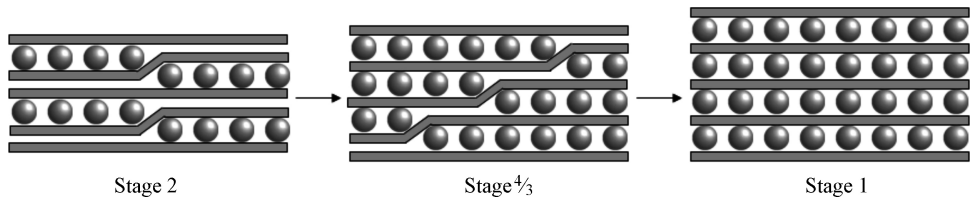


**Figure 9.14** Schematic representation of a stage 2 to stage 1 transformation *via* a stage $4/_3$ intermediate as additional guests are intercalated.

consequence of the inability of the small zeolite pores to crack very heavy crude oil fractions. There is also a rich catalysis of organic transformations within clay minerals. Furthermore, clays can take up neutral and charged organic species, and smectite clays are used for decolourising edible oils, clarifying alcoholic beverages, and removing acidic impurities from PVC. It is beyond the scope of this book to examine these areas in detail, and as representative examples we will look only at graphite intercalates at this stage. A much fuller discussion may be found in the references including the tremendous current interest in inorganic-organic hybrid nanocomposite materials, *e.g.* comprising inorganic and organic polymer layers.[12]

## 9.3.2 Graphite Intercalates

Enoki, T., Endo, M. and Suzuki, M., *Graphite Intercalation Compounds and Applications*. Oxford University Press: Oxford, 2003.

The structure of graphite (**9.2**), an allotrope of essentially pure carbon, is an infinite sheet comprising only six-membered rings with $sp^2$ hybridised carbon atoms. The sheets stack in weakly interacting layers about 3.35 Å apart, maximising C···C$\pi - \pi$ stacking interactions (*cf.* Section 8.10). Pure graphite is a semi-metal with a filled valence π-band immediately followed by an empty $\pi^*$-conduction band, with no band-gap of the type that characterises semiconductors. The $\pi - \pi$ interactions result in a slight overlap of the valence and conduction bands and hence there is a nonzero density of states at the Fermi level, right between the two bands. In terms of electronic properties, the Pauling electronegativity of carbon of 2.5 places it right in the middle of the first long period of the periodic table, suggesting that it may well be susceptible to loss and gain of electrons depending on the electron donor or acceptor nature of guest species that may fit between the layers. In fact, graphite forms intercalates with both metal atoms, in which the metal reduces the graphitic layers, and with fluoroanions, in which the graphite has been oxidised. Typical metal complexes include $LiC_6$, and $MC_8$ (M = K, Rb, Cs, Ca, Sr, Ba, Sm, Eu and Yb). Metal fluorides that form fluoroanion complexes, along with their reduction enthalpies, are summarised in Figure 9.15.[13] Clearly only those species that have reduction enthalpies more negative than –502 kJ mol$^{-1}$ can form full stage 1 intercalates. Partial (higher stage) materials form below –440 kJ mol$^{-1}$.

Interestingly, when $KC_8$, which has a 2 × 2 in-plane structure (**9.3**) is exposed to a CO or $O_2$ atmosphere, the guest is gradually lost, giving successive phases of $KC_{24}$, $KC_{36}$ and $KC_{48}$. Starting from $KC_{24}$, $KC_{36}$ and $KC_{48}$ are generated successively. This is seen as good evidence for the Daumas–Hérold model outlined in Section 9.3.1. Graphite also forms intercalates readily with $Br_2$, and with the interhalogens IBr and ICl, but not with $F_2$, $Cl_2$, $I_2$ or with sodium. The structure of the $Br_2$ intercalate shows undissociated $Br_2$ molecules sitting with each atom above a graphite hexagonal ring. It is likely that the Br–Br bond length, as well as those in IBr and ICl (2.27, 2.49 and 2.40 Å, respectively), represent a good match to the interhexagon separation, whereas $F_2$, $Cl_2$, $I_2$ (bond lengths 1.41, 1.99 and 2.67 Å, respectively) are either too large or too small. In the case of sodium, it seems that metallic radius of the sodium is too large for an effective $NaC_6$ arrangement, but too small for the common $MC_8$ structure of a range of other metals.

Research in graphite intercalates has paved the way for significant current interest in intercalation compounds of the fullerenes (Box 7.1) and carbon nanotubes, which represent 'wrapped up' versions of graphite sheets. Graphite intercalation compounds have been prepared with intercalated fullerenes and nanotubes. We will return to carbon nanotube chemistry in Chapter 15.

Also of current technological interest is *exfoliated graphite*, a form of graphite produced from intercalation compounds submitted to a thermal shock such as passing through a hot flame. The intercalate

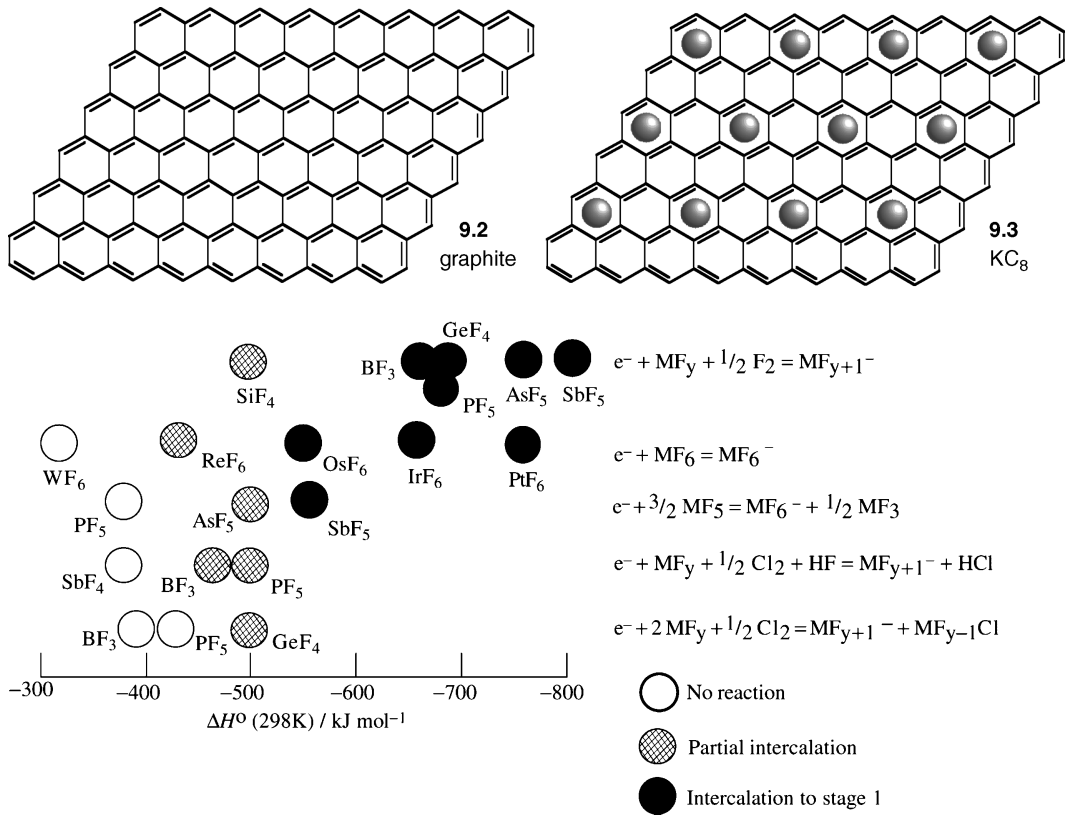


**Figure 9.15** Reduction enthalpy (kJ mol$^{-1}$ for the reaction shown) and degree of intercalation of fluoroanions with graphite.

is suddenly volatilised resulting in a tremendous expansion of the intercalated flakes in one direction. The result is a pure graphite snow with a worm-like morphology. Various consolidated materials are made from this exfoliated graphite by compression. Moderate compression leads to highly porous graphite 'foams'. Heavy compacting (and laminating) gives impervious and flexible graphite foils. These materials have numerous applications and a bright future as solid-state supports, and for uses in gasketing, adsorption, electromagnetic interference shielding, vibration damping, thermal insulation, electrochemical applications and stress sensing.[14]

## 9.3.3 Controlling the Layers: Guanidinium Sulfonates

Holman, K. T., Pivovar, A. M., Swift, J. A., Ward, M. D., 'Metric engineering of soft molecular host frameworks', *Acc. Chem. Res.* 2001, **34**, 107–118.

In the case of intercalates we have seen how the inclusion of guests swells the layers, such that the materials respond dynamically to the intercalation process. We now turn to a different approach in which a crystal engineering based design strategy has created rigid, well-defined materials based on ionic hydrogen-bonded solids in which polar guanidinium disulfonate layers – $(C(NH_2)_3^+)_2$

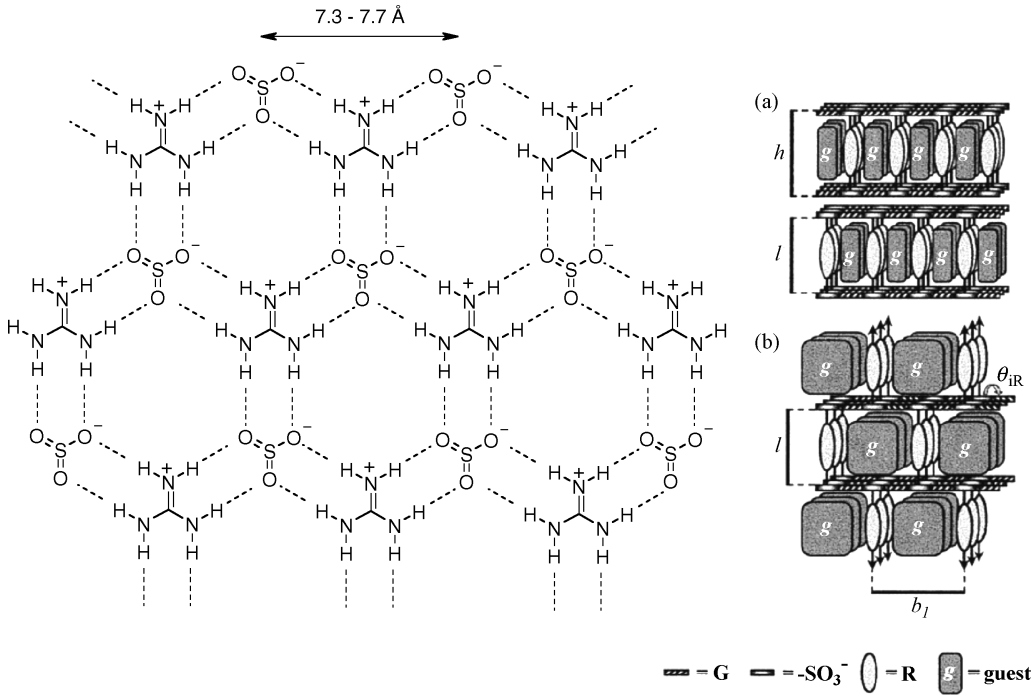


**Figure 9.16** Ionic guanidinium sulfonate layer in pillared guanidinium disulfonates along with the two main types of architecture (a) pillared discrete bilayer and (b) 'simple brick' (reprinted with permission from Section Key Reference © American Chemical Society).

($^{-}O_3SRSO_3^{-}$) – that link the solid structure together are held at a rigidly well-defined distance apart by the introduction of organic spacers (R) or 'pillars'. These material are mimics of pillared clays and the result is a rigid framework with relatively hydrophobic cavities linked by a strongly hydrogen bonded ionic layers. The rigidity of the compounds comes from the multiple, DD···AA charge assisted hydrogen bonded interactions between guanidinium and sulfonates. The size of the guanidinium ions results in a well defined S···S distance between the sulfonates of 7.3–7.7 Å, Figure 9.16. Two basic framework types are known; either a 2D bilayer structure or a 3D 'simple brick' structure resembling the $6^3$ net described in Section 9.1.2. These two types have been described as 'architectural isomers' and are *supramolecular isomers* of one another in the sense described in Section 8.5.2. Unlike zeolites, however, these infinite hydrogen bonded framework materials require the presence of guests to retain their structural integrity. Also unlike zeolites they are 'soft' and can deform to accommodate a wide variety of guests. They thus represent a 'first step' from clathrates towards robust infinite framework solids. The deformation takes the form of a concerted flexing of the layer at the N–H···O junctions, an angle termed the *inter ribbon puckering angle*, ($\theta_{IR}$ in Figure 9.16b) and it determined the spacing perpendicular to the guanidinium sulfonate ribbon ($b_1$).

The volume, height and shape of the cavity in GS inclusion compounds may be tightly controlled by the choice of spacer in the disulfonate. Figure 9.17 gives a series of disulfonates in order of increasing length ($l$) and the corresponding observed cavity volume of their host materials. Typical guest molecules range from solvents up to relatively large aromatics such as *p*-divinylbenzene. Depending on the size, shape and conformation of the spacer the host can either exhibit discrete cavities, 1D

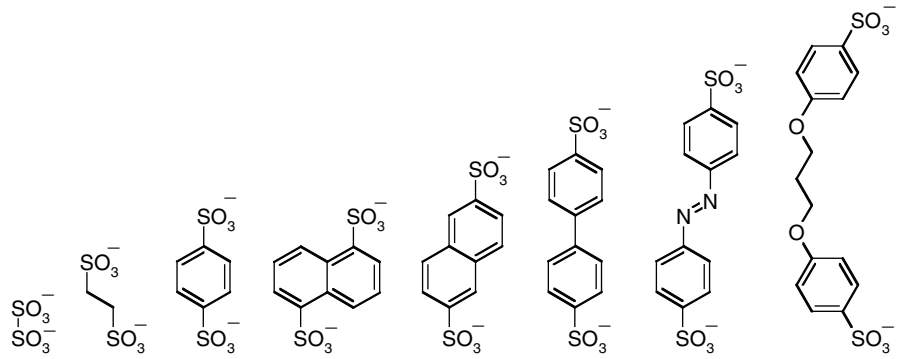


**Figure 9.17** Variation of cavity volume with disulfonate length in guanidinium sulfonates.

continuous channels or 2D interconnected layers of interconnected channels. In extreme cases as with biphenyldisfonate, the cavity can take up to up to 70 per cent of the crystal volume!

Related to guanidinium sulfonates are analogous cation phosphonate structures which can adopt either pillared or zeotype structures. Recently novel tubular morphologies have also been discovered for both classes of compound which may have promise for improving porosity in these types of material. At present, like the guanidinium sulfonates, few phosphonates, are really porous and removal of the guest template generally leads to the collapse of the structures.[15]

## 9.4 In the Beginning: Hoffman Inclusion Compounds and Werner Clathrates

Soldatov, D. V., Enright, G. D., Ripmeester, J. A., 'Polymorphism and pseudopolymorphism of the [Ni(4-methylpyridine)$_4$(NCS)$_2$] Werner complex, the compound that led to the concept of "organic zeolites"', *Cryst. Growth Des.* 2004, **4**, 1185–1194.

Either side of the border between network solids and clathrates are the very well known Werner clathrates such as **9.4** and Hoffman inclusion compounds such as **9.5**. Hoffman inclusion compounds are true infinite coordination polymers, while Werner clathrates are discrete Werner-type coordination compounds. Both classes of compound are amenable to synthetic design and manipulation and hence have been of enduring interest in the field. Both Hoffman- and Werner-type inclusion complexes result from lattice voids in the assembly of inorganic coordination compounds. Hoffman inclusion compounds have the general formula $M(NH_3)_2M'(CN)_4{\cdot}2G$ (where M is a first-row transition metal Mn–Zn or Cd; M′ is Ni, Pd or Pt; and G is a small aromatic molecule). The solid-state structure of these species consists of a 2D polymeric sheet in which the $CN^-$ ligands bridge between the square planar group 14 metal (M′) and the equatorial sites of the octahedral transition metal (M). This results in the ammonia ligands protruding above and below the plane of the sheet, forming lattice boxes suitable for the inclusion of small aromatic molecules such as benzene or thiophene. The structure of Hoffman's benzene clathrate $Ni(NH_3)_2Ni(CN)_4 \cdot 2C_6H_6$ is shown in Figure 9.18.

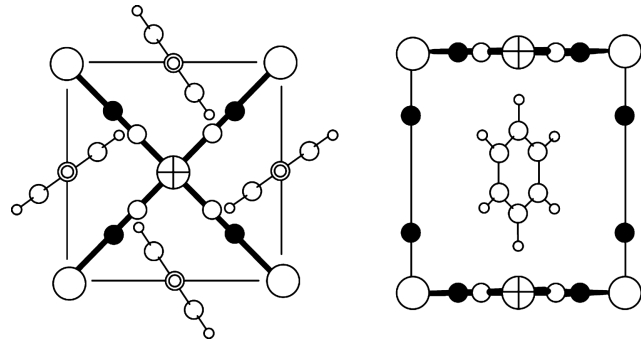

**Figure 9.18** X-ray crystal structure of Hoffman's benzene clathrate $Ni(NH_3)_2Ni(CN)_4 \cdot 2C_6H_6$ (left view perpendicular to the coordination polymer plane and right, parallel view. N atoms black circles, C atoms small open circles, Ni of $Ni(CN)_4^{2-}$ unit crossed larger circle, Ni of $Ni(NH_3)_2^{2+}$ unit large open circle).

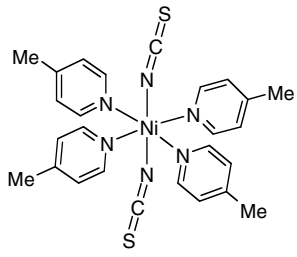

**9.4**

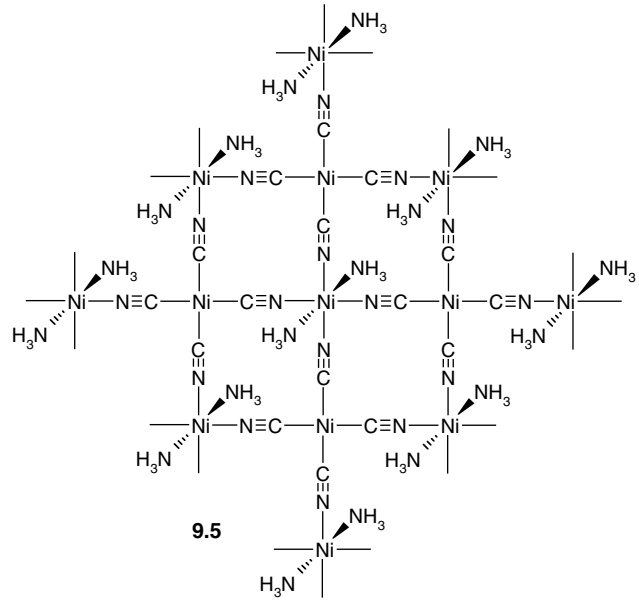

**9.5**

Werner clathrates are formed by a wide range of discrete Werner-type metal coordination complexes of type $MX_2A_4$ (M is a first-row transition metal Cr–Zn, Cd or Hg; X is $NCS^-$, $NCO^-$, $CN^-$, $NO_3^-$, $NO_2^-$, $Cl^-$, $Br^-$ or $I^-$; A is a neutral, substituted pyridine). As with Hoffman clathrates, small aromatic guests are accommodated, although the host material is not polymeric. In this case, the lattice void arises from the presence of the wide, flat pyridyl ligands. Werner clathrates have been used in separations applications such as the separation of *o*-, *m*- and *p*-isomers of disubstituted benzenes by chromatographic methods.[16] The original Werner host host [Ni(4-methylpyridine)$_4$(NCS)$_2$] (**9.4**) can form two kinds of inclusion compound, a $\beta$-phase with a 1:1 host guest ratio and a channel structure and a $\gamma$-phase with a 1:2 host guest ratio and a layer structure. The pure $\alpha$-phase can be obtained from nitromethane or ethanol while the $\gamma$-phase is formed by crystallisation from benzene but slowly transforms into the $\beta$-phase over time. In many cases guest removal results in the collapse of both materials to a pure,

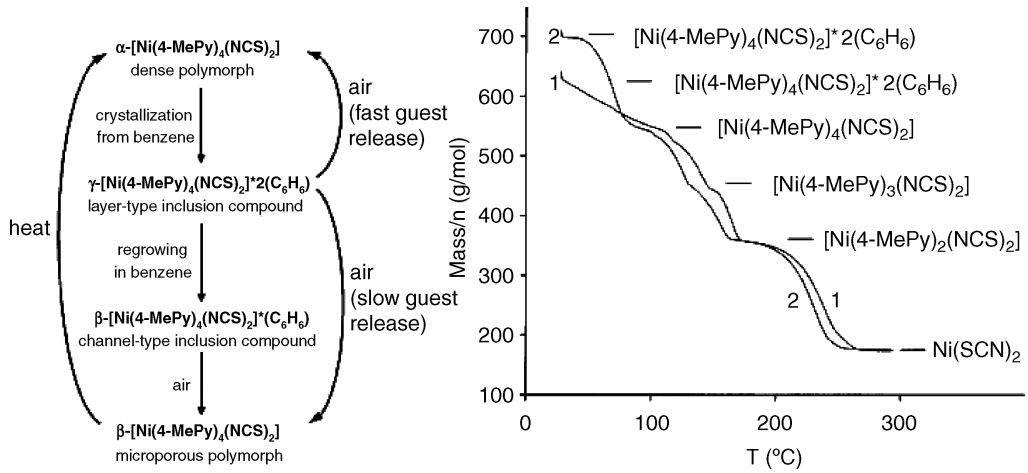


**Figure 9.19** (a) transformations between different polymorphs or pseudopolymorphs of **9.4**, (b) TGA thermograms of $\beta$-[Ni(4-MePy)$_4$(NCS)$_2$]·C$_6$H$_6$ (trace 1) and $\gamma$-[Ni(4-MePy)$_4$(NCS)$_2$]·2(C$_6$H$_6$) (trace 2) plotted as mass/*n vs.* temperature (*n* is the number of moles of each compound calculated from the mass of the final Ni(SCN)$_2$ product). Each experiment starts with crystals of an inclusion compound wetted with benzene (reprinted with permission from Section Key Reference © 2004 American Chemical Society).

dense $\alpha$-phase (Figure 9.19). In general, such inorganic clathrate complexes may be formed by a wide variety of coordination compounds, not just of the MX$_2$A$_4$ type, although these materials are noteworthy for their robustness and structural consistency. Formation occurs in any instance in which the complex is unable to pack efficiently (primarily due to shape) in the solid state and there is a reasonably conveniently sized solvent or other molecule present in the crystallisation medium to act as guest. Indeed, many such clathrates are isolated serendipitously. Werner clathrates provide stable and convenient model systems for systematic studies, and do have some zeolite-like properties, hence the use of the term *organic zeolites* to describe them. In terms of separation science do not generally compete with Zeolite separation methods (Section 9.2) but they *are* truly porous, however: one of the remarkable properties of **9.4** (first reported in 1957) and some analogues is that slow removal of guests can result in the formation of a microporous, guest-free apohost $\beta_0$-phase.

The process of guest release for the two types of inclusion compound of **9.4** can be followed by thermogravimetric analysis (TGA, Box 9.1). This reveals the 'clathrate-like' behaviour of the $\gamma$-phase (trace 2) and contrasts significantly with the zeolite-like behaviour of the microporous $\beta$-phase (trace 1), Figure 9.19b. The mass loss stages followed by both compounds after initial wetting in benzene are as follows:

1. evaporation of excess solvent,
2. release of guest benzene,
3. release of the first 4-methylpyridine ligand,
4. release of the second 4-methylpyridine ligand,
5. release of the remaining two 4-methylpyridine ligands to give [Ni(SCN)$_2$].

The important part is step 2, the guest release. For the clathrate $\gamma$-form this process occurs over a narrow temperature range bracketed by two plateaus corresponding to the initial ($\gamma$) and final ($\alpha$) phases. This behaviour is typical of clathrates. In contrast, for the $\beta$-phase, guest release is continuous over the entire temperature range until the host complex decomposes. This kind of desolvation behaviour in which guests slowly exit a channel that remains intact is characteristic of zeolites.

**Box 9.1** Thermogravimetric Analysis and Differential Scanning Calorimetry in the Study of Inclusion Compounds

The fact that guest molecules may in included within hosts, or host lattices in the solid state, automatically suggests that there must be some energy or stability associated with that inclusion. In solution inclusion, thermodynamics may be assessed by binding constants measurements (Section 1.4). In the solid state, there is not generally a complexation–decomplexation equilibrim taking place and so other methods must be used to assess both the stability and even stoichiometry of inclusion compounds. Two of the most common techniques are thermogravimetric analysis (TGA) and differential scanning calorimetry (DSC). Both are reasonably fast (minutes to a few hours), require only small amounts of sample (about 10 mg) and may be performed in the laboratory on equipment costing about US$20 000–30 000 (relatively inexpensive compared to techniques such as NMR spectroscopy and X-ray crystallography).

*Thermogravimetric Analysis*

In a TGA experiment, the mass of a solid sample is recorded as a function of steadily increasing temperature. As the experiment proceeds, the sample mass is expressed as a percentage of the initial mass, resulting in a trace that exhibits one or more plateaux, separated by slopes corresponding to the loss of guest molecules at various temperatures. If the formula mass of the host and guest is known, then the host–guest ratio may be obtained by comparison of calculated and observed weight loss for various stoichiometries. The temperature at which the guest is lost gives some indication of the stability of the host–guest complex, although the precise temperature at which guest loss occurs is dependent on the heating rate. TGA analysis often also contains slopes arising from host decomposition at higher temperatures. The TGA experiment is carried out in a flowing gas stream (usually $N_2$) to carry away the weight-loss products, and this may be fed into a second instrument such as an infrared spectrometer (TGA–IR) to aid with the characterisation of the emitted species.

The TGA slope for the Zn(II) coordination polymer $[Zn(H_2O)_2(tph)]_\infty$ ($H_2$tph=terephthalic acid, $p$–$C_6H_4(CO_2H)_2$) is shown in Figure 9.20a. Loss of coordinated water occurs in two distinct steps at 168 and

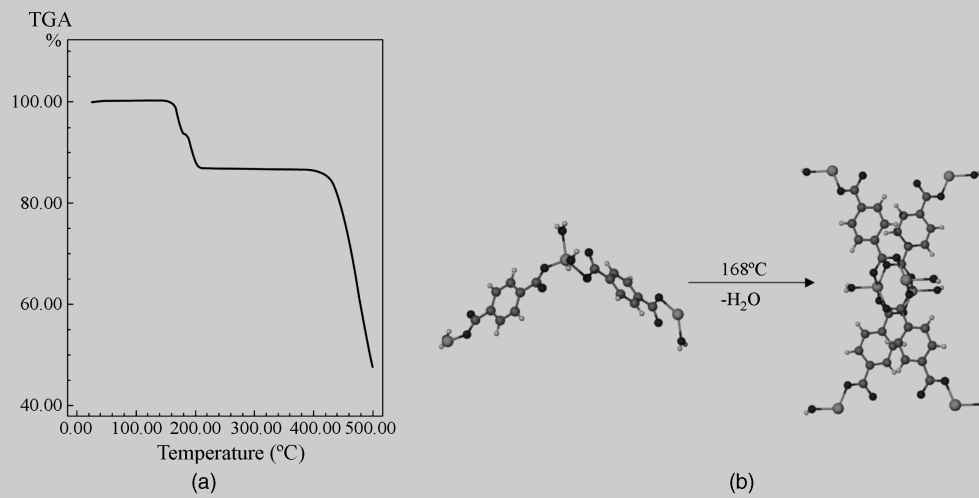


**Figure 9.20** (a) TGA trace for the dehydration of $[Zn(H_2O)_2(tph)]_\infty$. (b) X-ray crystal structures of the di- and monohydrates.[17]

(*continued*)

**Box 9.1** (*Continued*)

192ºC, corresponding to a weight loss of 6.8 per cent in each case. It has been suggested that loss of the first water molecule corresponds to a transformation from a linear, zigzag polymer based on distorted tetrahedral $Zn^{2+}$ into a multiply bridged structure involving trigonal bipyramidal zinc centres.[17]

*Differential Scanning Calorimetry*

The DSC technique involves measurement of the difference in power requirements between a sample and reference maintained at the same temperature as the sample while that temperature is scanned either up or down at rates of a few K $min^{-1}$. It is a calorimetric technique, which means that it deals with enthalpy differences. The advantage of DSC compared with TGA is that it is sensitive to phase changes that do not result in changes in mass (*e.g.* melting), and integration of peak area gives a quantitative measure of the enthalpy change, $\Delta H$, associated with processes being studied. Thus, if the sample is undergoing a phase change that is endothermic, such as melting, more power will be required in the sample chamber compared to the reference (which is of similar mass but does not undergo anomalous phase changes). This will result in a positive peak in the resulting DSC trace. Similarly, exothermic processes result in negative peaks, while a flat trace implies no difference between the behaviour of sample and reference. The TGA and DSC techniques are often used together in order to disentangle overlapping thermal events such as phase transitions and decomposition. The DSC trace for $[Zn(H_2O)_2(tph)]_\infty$ is shown in Figure 9.21, indicating clearly that the loss of water from the sample is endothermic, as is the final decomposition, which sets in a higher temperature.

Closely related to DSC is the much older technique of differential thermal analysis (DTA). DTA works on the simpler principle of measurement (*via* thermocouple) of temperature difference between a sample and reference as the same heating power is supplied to both. The DTA trace therefore represents a temperature effect, which is related only semiquantitatively to $\Delta H$. A combined DTA–TGA trace for the Werner clathrate (Section 9.4) $[Ni(NCS)_2(4\text{-phenylpyridine})_4]\cdot 4C_6H_6$ is shown in Figure 9.22. The DTA trace shows that all three thermal events observed are endothermic. The first is associated with loss of the benzene guest, while the second and third relate to loss of the coordinated 4-Phpy ligands. Note the high temperature (about 350 ºC) required to remove the enclathrated benzene. This is a clear indication of the thermal stability of the Werner clathrate family.[18]

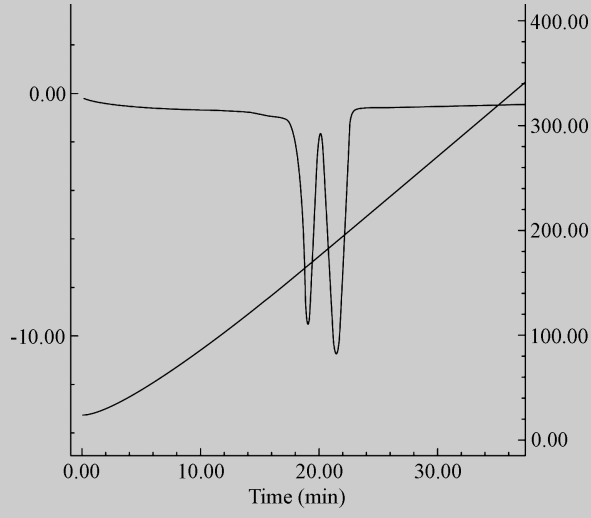


**Figure 9.21** DSC trace for $[Zn(H_2O)_2(tph)]_\infty$, the diagonal line charts the change in temperature (right hand axis, ºC) during the experiment.

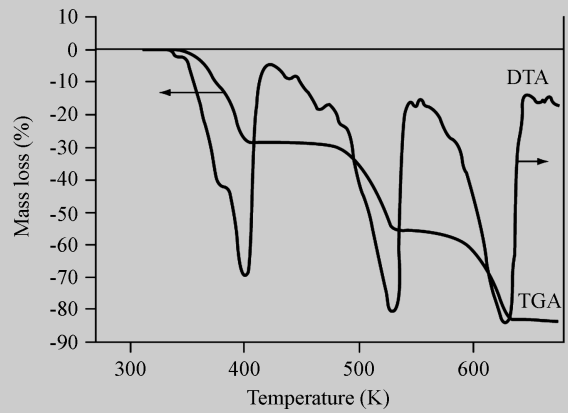


**Figure 9.22** DTA–TGA trace for $Ni(NCS)_2(4\text{-Phpy})_4 \cdot 4C_6H_6$ showing the endothemic loss first of benzene and then the 4-phenylpyridine ligands in two distinct stages. (Reprinted with permission from IUCr).

# 9.5 Coordination Polymers

## 9.5.1 Coordination Polymers, MOFs and Other Terminology

Yaghi, O. M., O'Keeffe, M., Ockwig, N. W., Chae, H. K., Eddaoudi, M. and Kim, J., 'Reticular synthesis and the design of new materials', *Nature* 2003, **423**, 705–714.

The term *coordination polymer* very broadly encompasses any extended structure based on metal ions linked into an infinite chain, sheet or three dimensional architecture by bridging ligands, usually containing organic carbon. More recently the term *metal organic framework* (MOF) has entered the literature. A metal organic framework is a kind of coordination polymer that is a three-dimensional, crystalline solid that is both robust and porous. The organic bridging ligands within MOFs are generally subject to some kind of synthetic choice and hence coordination polymers involving simple ligands such as cyanide are not generally considered MOFs. The chemistry of MOFs has benefited greatly from the introduction of concepts from zeolite chemistry, particular the secondary building unit (SBU) and there are now MOF frameworks with significant structural robustness with pores in the mesoporous domain (see Section 7.9 for an explanation of pore size classification). Another powerful concept is *reticular synthesis* (the synthesis of periodic repeating nets) leading to *isoreticular expansion* and *decoration*. Isoreticular expansion means the increasing of the length of a spacer while retaining the same network topology. Thus an isoreticular MOF (IRMOF) is (usually) an expanded version of a previously known MOF. This expansion generally leads to larger pore size and is a feature of the control allowed by synthetically designable building blocks. Decoration means replacing a vertex within a net with a series of vertices. In general the entire field of coordination polymer chemistry is of tremendous current interest, in the main because of the tremendous diversity (and hence tunability) and scope for design in the construction of new materials that are hybrids between metals and/or metal clusters and organic ligands within the context of designer materials chemistry. It is fair to say that the scope for the application of MOFs in gas separation and storage, particularly as

hydrogen storage materials (Section 7.9) is one of the principal driving forces in current research endeavour. However there are many other uses and areas of interest in coordination polymer chemistry. These include magnetism and magnetic spin crossover behaviour, non-linear optical activity, catalysis and negative thermal expansion. We will look briefly at each of these areas in the following sections. Before embarking upon a necessarily concise description of the metals, SBUs, ligands and structures encountered in modern coordination polymer chemistry we list below some useful terms that we will be encountering along the way.

- *Reticular*: (adjective) having the form of a (usually periodic) net.
- *Isoreticular*: Based on the same net (having the same topology).
- MOF-*n*: Metal-organic framework (where *n* is an integer assigned in roughly chronological order of discovery, *e.g.* MOF-5).
- IRMOF-*n*: Isoreticular MOF (with *n* an integer referring to a member of the series).
- *Interpenetration*: A term used to describe the mutual intergrowth of two or more networks in a structure where the networks are physically but not chemically linked.
- *Expansion*: Increasing the spacing between vertices in a network.
- *Decoration*: Replacing a vertex in a net by a group of vertices.
- SBU: Secondary building unit in the context of coordination polymer network synthesis (reticular chemistry) refers to the geometry of metal coordination cluster fragments units as defined by the points of extension (such as the carboxylate C atoms in most carboxylate MOFs).
- *Supramolecular isomerism*: the existence of more than one type of network superstructure for the same molecular building blocks (Section 8.5.2).

### 9.5.2 0D Coordination Clusters

There exist a vast number of discrete, polymetallic coordination clusters both of the metal-metal bonded type and linked by a tremendous variety of bridging ligands, notably carboxylates. Such compounds are not coordination polymers but oligomers and hence can be more soluble, more well-defined and easier to characterise than coordination polymers, for which they can serve as useful model systems. We will discuss discrete, self-assembled complexes of semi-protected metal ions that act as hosts in solution or as 3D capsules in the next chapter and we will not cover these systems in detail here except to note in passing a couple of examples that are of particular interest. One particularly prominent cluster is $Mn_{12}$-acetate,[19] the mixed-valence compound $[Mn^{III/IV}{}_{12}O_{12}(CH_3CO_2)_{16}(H_2O)_4]$ studied intensively since the early 1990s. This discrete cluster is a disk-like cluster with a cube-shaped $Mn^{IV}{}_4O_4$ core bridging to either Mn(III) ions, with bridging acetate at the periphery of the disk, Figure 9.23. The compound was one of the first and still most significant *single molecule magnets*. It has an $S = 10$ ground state ($S$ = total spin quantum number, corresponding to 20 unpaired electrons) and there is a significant barrier to magnetisation relaxation meaning that this molecule is a prototype component of a 'spin computer' because it can store digital information according to its magnetisation state. A large number of comparable clusters have since been discovered.[20]

Also of interest in the context of supramolecular chemistry is recent work on very large entirely inorganic spherical capsules based on the $(\text{pentagon})_{12}(\text{linker})_{30}$ type such as the polyoxomolybdate $[P_{12}\{Mo_2O_4(MeCO_2)\}_{30}]^{42-}$ (Figure 9.24, where P = the pentagonal cluster $\{(Mo)Mo_5O_{21}(H_2O)_6\}^{6-}$). These structures are examples of a general series of large, polymetallic cyclic structure obtained from

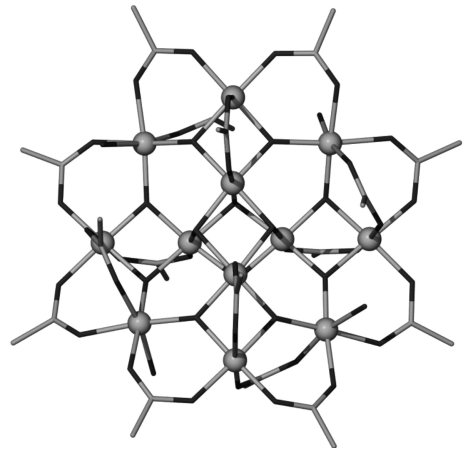

**Figure 9.23** Structure of $Mn_{12}$-acetate, a single molecule magnet (Mn ions shown as spheres).[19]

molybdenum 'blues' – partially reduced solutions of Mo(VI) oxides in the presence of templating agents. The characteristic blue colour arises from the presence of delocalised electrons. In the case of the spheres these entirely synthetic, abiotic containers can function as a kind of artificial biological cell (or a nano-chromatograph for the separation of metal ions).[21] The capsule size and shape can be tailored by careful choice of conditions and the largest such hollow sphere comprises 368 Mo atoms and has an internal cavity 2.5 nm wide and 4 nm long, containing about 400 structured water molecules in a confined environment. Metal cations are able to selectively diffuse in and out of the holes created by the carboxylate substituents with a significant dependence on the ability of the water confined within the capsule to coordinate to the cation. The confined environment of this 'inorganic cell' exhibits some remarkable properties while the polyoxomolybdate cell wall exhibits some features in common with cation transport through biological ion channels (*cf.* Section 2.2). The adaptation of the confined

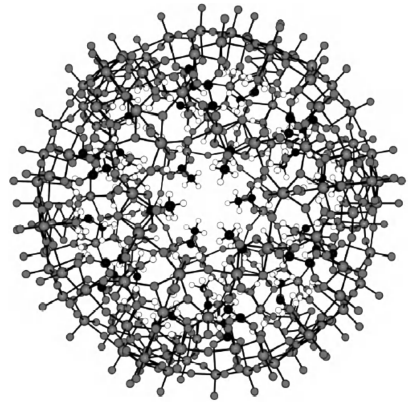

**Figure 9.24** The polyoxomolybdate nanocluster $[P_{12}\{Mo_2O_4(MeCO_2)\}_{30}]^{42-}$ (P = $\{(Mo)Mo_5O_{21}(H_2O)_6\}^{6-}$) that behaves as an artificial cell, showing the pore opening in the centre (reprinted from [21] with permission of Elsevier).

structured water to the ingress of metal ions suggests insights into the way in which a biological cell converts an incoming chemical signal into a response.

## 9.5.3 1D, 2D and 3D Structures

Moulton, B. and Zaworotko, M. J., 'From molecules to crystal engineering: Supramolecular isomerism and polymorphism in network solids', *Chem. Rev.* 2001, **101**, 1629–1658.

The transition from discrete complexes to coordination polymers can be seen as a logical progression as we change from semi-protected metal ions (*i.e.* those in which one face is blocked off by a spectator ligand such as ethylene diamine (en), acetylacetonate (acac) or [9]ane-$S_3$) to naked ones, and in doing so increase their potential for network connectivity. For example, using linear pyridyl type ligands such as 4,4′-bipyridyl (bpy) we can identify a progression from a 0D box as exemplified by $[\{Pd(en)(\mu\text{-bpy})\}_4]^{8+}$,[22] in which two cis-related sites are available on the metal centre, to a 1D chain-type coordination polymer, $[Zn(acac)_2(\mu\text{-bpy})]_n$,[23] in which two *trans* sites are available to propagate the chain, to a 2D grid using axially protected Co(II) with 4 equatorial sites, $[Co(bpy)_2(CF_3CO_2)_2]_n$,[24] and finally a 3D network structure based on the related pyrazene ($N_2C_4H_4$) with the rare octahedral Ag(I), $\{[Ag(pyrazene)_3](SbF_6)\}_n$ using unprotected metal ions (Figure 9.25).[25]

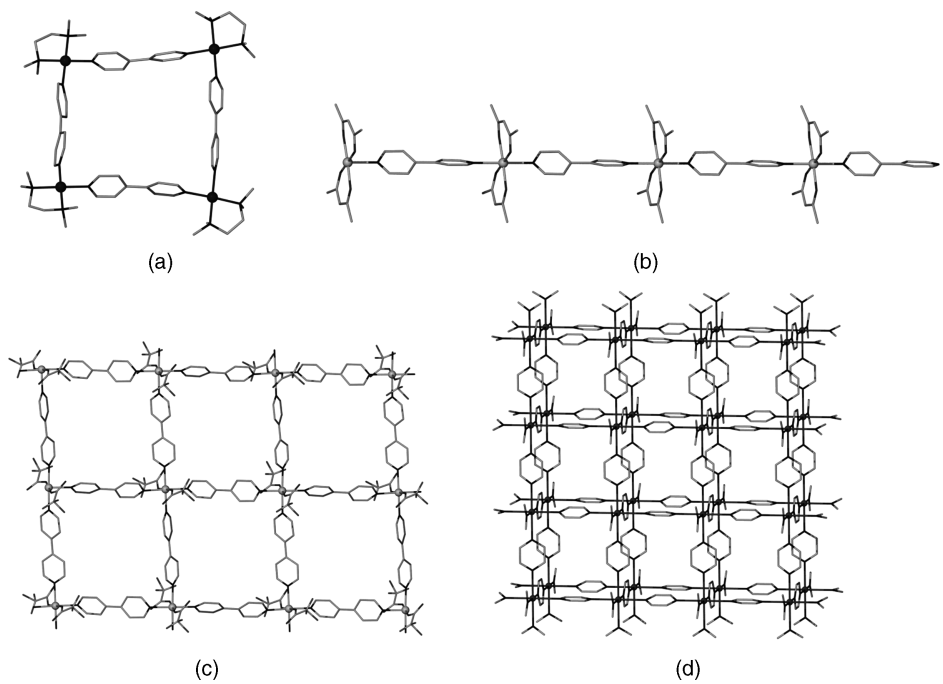


**Figure 9.25** Progression from 0D discrete self-assembled complexes to 1D, 2D and 3D architectures as the degree of 'protection' around the metal centre from spectator ligands is decreased, as exemplified by 4,4′-bipyridyl complexes (a) $[\{Pd(en)(\mu\text{-bpy})\}_4]^{8+}$,[22] (b) $[Zn(acac)_2(\mu\text{-bpy})]_n$,[23] (c) $[Co(bpy)_2(CF_3CO_2)_2]_n$,[24] and (d) the pyrazene complex $\{[Ag(pyrazene)_3](SbF_6)\}_n$.[25]

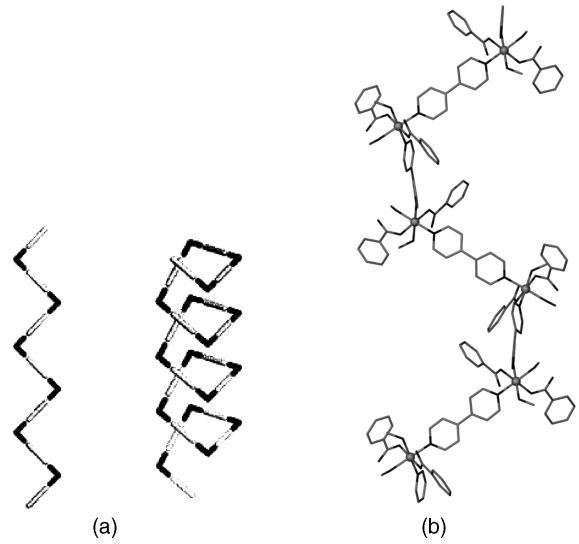


**Figure 9.26** (a) zig-zag and helical supramolecular isomers of 1D chains made up of a linear spacer (light grey) and a *cis* metal centre (black) (reprinted with permission from Section Key Reference © 2001 American Chemical Society). (b) chiral helical structure of [Ni(bpy)(benzoate)$_2$(MeOH)$_2$].

As we progress from 0D to networks the compounds become insoluble, but all are potentially capable of including guests depending on the lengths of the spacers, size of the nodes and degree of interpenetration.

In terms of 1D coordination polymers based on *cis* related coordination sites on a square planar or octahedral metal centre, they can adopt either zig-zag or helical chain architectures (as well as a discrete triangle, square or other box-like structure). The zig-zag and helical structures are supramolecular isomers of one another and fundamentally differ in that the helical structure is intrinsically chiral even if the building blocks that comprise it are not, Figure 9.26a. Zig-zag polymers are fairly common, while the helical structure is more unusual. A nice example of the latter is [Ni(bpy)(benzo ate)$_2$(MeOH)$_2$] which forms aligned helices in the solid state (Figure 9.26b) with void cavities of *ca.* 500 Å$^3$ able to accommodate nitrobenzene guests arranged in dimers. In many cases of chiral motifs within crystals both enantiomers are simultaneously present meaning that there is no overall crystal chirality. In this case, however, every individual crystal is chiral because the helices are aligned rather than antiparallel. Moreover, as we saw in Section 8.2.4, seeding may give rise to bulk chiral samples opening the possibility of chiral separations of guests.

Another kind of 1D coordination polymer is the ladder structure, this time made up of 3-connected nodes. One connector per node makes up a rung of the ladder and hence the polymer only propagates in one dimension producing a flat ribbon-like structure. With ligands like bpy the 3-connected node and bidentate nature of the ligand require a metal : ligand stoichiometry of 1:1.5 as in [Co(bpy)$_{1.5}$(NO$_3$)$_2$]·2CHCl$_3$ in which the chloroform guests reside in square cavities between the rungs. A good example of a simple expansion is the replacement of bpy with the extended 1,2-bi-4-pyridylethane which gives a closely related structure in which there is room for three chloroform molecules.

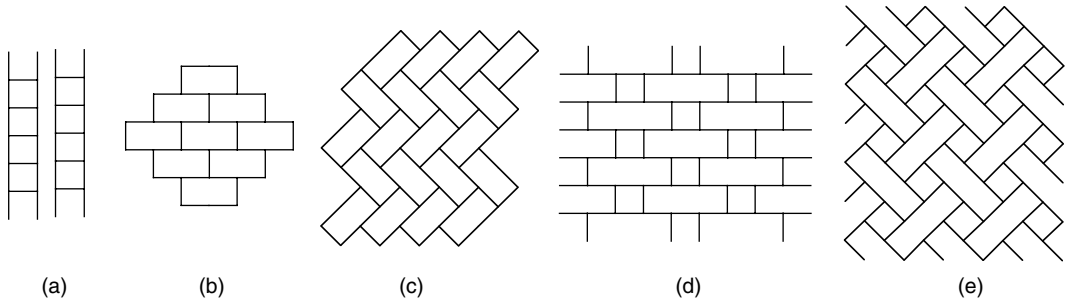


**Figure 9.27** Possible 3-connected networks (a) 1D ladder, (b) 'brick wall' (c) herringbone, (d) long and short brick and (e) basket weave. The latter two networks have yet to be realised in practice.

In terms of two dimensional coordination polymers the square grid (4,4) network is very common with square planar and axially-capped octahedral metal ions, as in $[M(bipy)_2(NO_3)_2]\cdot$guest (M = Co, Ni). Various types of compound within this series exist depending on grid shape (as opposed to topology), host:guest stoichiometry and the interactions of one 2D layer with the next. 2D nets can also be produced based on 3-connected nodes. The 'brick wall' (6,3) net is one example that has been realised. Examples of the related herringbone (6,3)-net are also known but the other theoretically possible networks (Figure 9.27d and e) have not yet been realised.

A particularly novel 2D net based on pentagons (which cannot tessellate in two dimensions) is also known. The net topology is $\left(5,^{3}_{4}\right)$ in Wells nomenclature, meaning that it is composed of 3- and 4-connected nodes linked by 5-gons. The pentagons are not regular and the 2D sheets have a wave-shape to them allowing them to tessellate. Chemically the compound is of formula $[(HMTA)_3(Cu_2(\mu\text{-}O_2CCH_2CH_3)_4)_5]_n$ (HMTA = hexamethylene tetramine).[26] The 3- and 4-connected nodes are both the HMTA ligands and the spacers are the linear $[Cu_2(\mu\text{-}O_2CCH_2CH_3)]_4$ bimetallic fragments. The fact that a bimetallic cluster is involved instead of a simple metal ion is an example of the use of an SBU. The tetrahedrally disposed nitrogen atoms on HMTA give the non-planarity to the sheets with all four being involved in bonding in the 4-connected nodes. One HMTA atom is unconnected in the 3-connected nodes which act to cap the sheets, Figure 9.28.

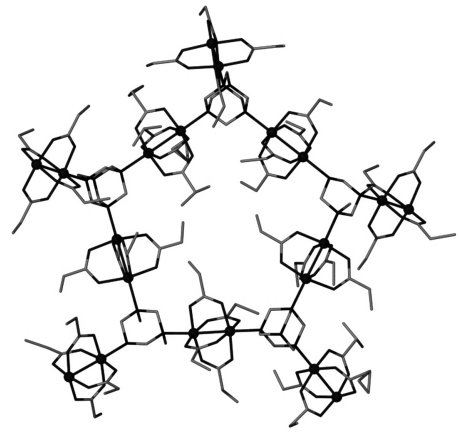

**Figure 9.28** A surprising $\left(5,^{3}_{4}\right)$-net based on irregular pentagons in the structure of $[(HMTA)_3(Cu_2(\mu\text{-}O_2CCH_2CH_3)_4)_5]_n$.[26]

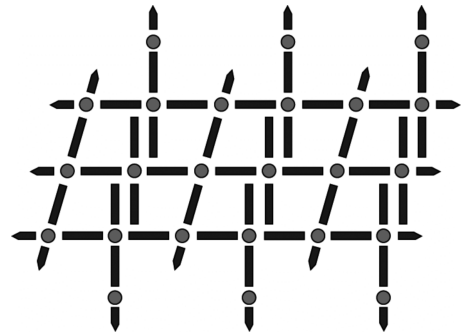

**Figure 9.29** NbO framework of $[Cu(1,2\text{-bi-4-pyridylethane})_2(NO_3)_2]_n$. (Reproduced with permission of The Royal Society of Chemistry).

Three-dimensional networks offer the most scope for the construction of robust frameworks and also in some ways are the most subject to design by the crystal engineer/materials chemist. For example a tetrahedral node and a linear spacer should give a diamondoid network and indeed diamondoids account for very many 3D networks. Similarly octahedral nodes and linear spacers should, sterics allowing, give an α-Po structure. Often steric constraints and the individual shape of metals and ligands cause surprises, however. As we will see a wide variety of other 3D structures are known, either synthesised by design or more commonly, serendipitously. For example the reaction of 1,2-bi-4-pyridylethane with with Cu(II) forms a surprising network $[Cu(1,2\text{-bi-4-pyridylethane})_2(NO_3)_2]_n$ (Figure 9.29). Cu(II) is a $d^9$ metal ion and exhibits a strongly Jahn–Teller distorted ground state geometry in which the octahedral metal centre exhibits much longer bonds to the axial ligands (nitrate), which protrude into the grid cavities, than the bipyridyl ligands. It is unclear why Cu(II) should adopt the NbO structure with this ligand in which the equatorial plane of the metal ion is rotated through 90° compared to two of its four nearest neighbours, but the difficulty in filling the larger cavities engendered by the expanded bipyridyl ligand is a possible reason. The cavities are also filled by twofold interpenetration and still exhibit 11 × 11 Å cavities filled by benzene and methanol guest molecules. In general the dimensionality and shape of the ligand plus the dimensionality of the *free coordination sites* on the metal or fragment such as an SBU should determine the network connectivity and dimensionality, Figure 9.30.

3D networks based on the lanthanides with their high coordination numbers (typically 7–11) are less predictable than those based on transition metals and the high oxophilicity of the lanthanide(III) ions means that they do not bind strongly to ligands such as pyridine derivatives. As a result lanthanide coordination networks are less common in the literature; however, they represent tremendous potential in terms of ever more complex topologies.

Another key factor in coordination polymer design is charge balance in the structure. Structures in which neutral ligands link together charged metal ions must involve some kind of counter ion to give overall electrical neutrality. Typically non-coordinating anions such as $BF_4^-$, $PF_6^-$ and $CF_3SO_3^-$ are common. These counter-anions (or in the more unusual case of anionic frameworks, counter cations) cannot be removed from a structure because of the very high strength of electrostatic forces even if they are apparently in a stack that resembles a channel (*cf.* 'virtual porosity', Section 9.1.3) and hence they fill the framework, reducing the tendency towards interpenetration or guest inclusion. They also can play a role in templating the observed shape and network topology. Charge neutral frameworks *e.g.* with divalent metals and dicarboxylate anions offer the greatest scope for overall porosity but can be difficult to synthesise because of the stronger metal-ligand bonds.

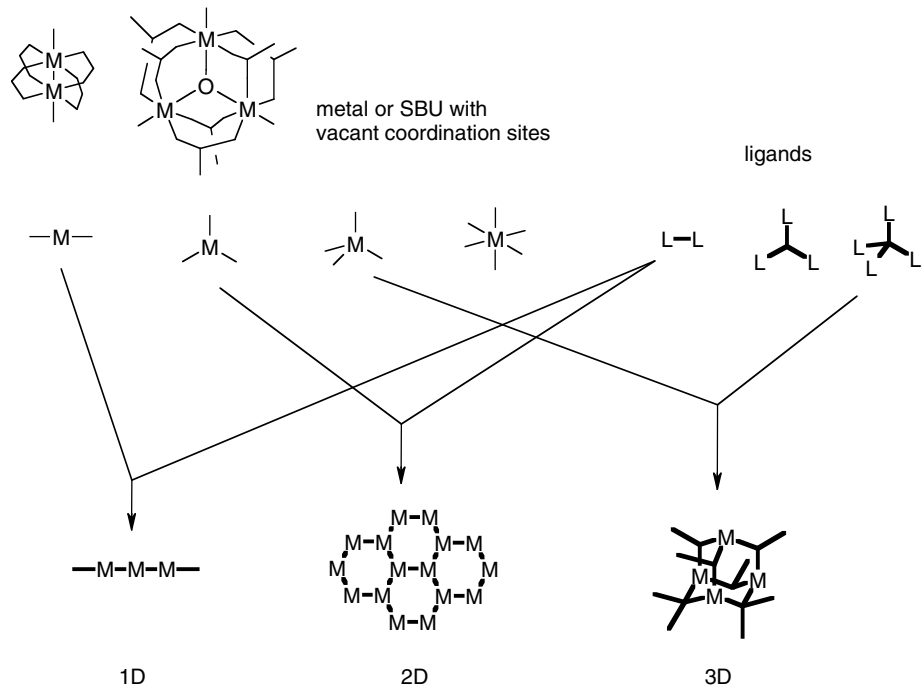


**Figure 9.30** The dimensionality of the coordination polymer is dependent upon the connectivity and shape of the ligands and the distribution of the vacant coordination sites on the metal or SBU.

## 9.5.4 Magnetism

Batten, S. R., Murray, K. S., Structure and magnetism of coordination polymers containing dicyanamide and tricyanemethanide. *Coord. Chem. Rev.* 2003, **246**, 103–130.

The first true coordination polymer ever isolated was Prussian blue, an intensely coloured blue compound produced accidentally by a painter and dye maker Heinrich Diesbach in Berlin in 1704.[28] This material is an α-Po network of formula $Fe(III)_4[Fe(II)(CN)_6]_3 \cdot nH_2O$ ($n$ = 14–16). The iron ions are

**Figure 9.31** The rutile structure α-M(**9.5**)$_2$ Metal atoms are shown in black, nitrogen atoms in grey, carbon in white (reproduced from Section Key Reference with permission from Elsevier).

bridged by the $CN^-$ ligands to give a cubic, three-dimensional structure. The blue colour comes about as a result of intervalence charge transfer interactions between the Fe(III) and Fe(II) ions, mediated by the short, multiple bonded cyanide ligands. Prussian blue has a long history as a pigment in monochrome printing processes, for example – its use in architecture is where the term 'blueprint' originates. It is also electrochromic, changing colour from blue to colourless upon reduction, it undergoes spin crossover (a change of spin state between low spin and high spin in response to changes in temperature or upon irradiation) and inclusion of other metals such as vanadium or chromium within the Prussian blue structure results in room temperature magnetic properties with proposed applications in areas such as data storage.

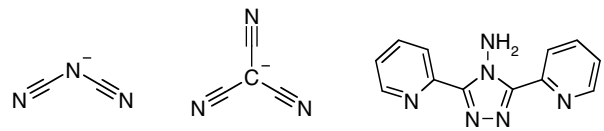


**9.5** **9.6** **9.7**

Inspired by the cyanide bridges in Prussian blue, a range of polynitrile ligand have been developed such as dicyanamide $N(CN)_2^-$ (**9.5**) and tricyanomethanide $C(CN)_3^-$ (**9.6**) and used in the construction of magnetic coordination networks. Binary compounds $\alpha$-M(**9.5**)$_2$ form an isostructural series (M = Cr, Mn, Fe, Co, Ni, Cu) which have a single rutile-like network (rutile is $TiO_2$) that involves $\mu_{1,3,5}$-bridging (*i.e.* coordination through all three nitrogen atoms) of the dicyanamides making them 3-connecting centres, while the metals are all 6-connecting with an octahedral geometry. In each case the individual metal ions have unpaired electrons and the dicyanamide ligands mediate spin-spin interactions between then resulting in different kinds of long-range magnetic order, namely ferromagnetism (parallel ordering of spins) in the case of Co, Ni and Cu while the Cr, Mn and Fe compounds are canted-spin antiferromagnets (antiparallel ordering of spins but with a net magnetic moment because the canting results in incomplete cancellation).

The discrete, mononuclear compound [Fe(**9.5**)$_2$(**9.7**)$_2$] displays the interesting phenomenon of *magnetic spin crossover*, $S = 2 \leftrightarrow S = 0$, which can be induced by both light and thermal activation.[29] Spin crossover is relatively common in Fe(II) compounds with nitrogen donor ligands and it occurs when the spin pairing energy of the *d* electrons (P) is approximately equal to the ligand field splitting energy, $\Delta_O$ that separates the upper, antibonding $e_g$ orbitals from the lower weakly bonding $t_{2g}$ set in octahedral transition metal compounds. Iron(II), which has six *d* electrons, at low temperatures adopts a diamagnetic ($S = 0$), low spin $(t_{2g})^6$ configuration, but at higher temperatures or when irradiated by a laser it crosses over to a metastable (large activation barrier to returning to the ground state) high spin state corresponding to the promotion to a high spin configuration with four unpaired electrons and $S = 2$, $(t_{2g})^4(e_g)^2$ (Figure 9.32). Spin crossover behaviour is also exhibited in a binuclear dicyanamide complex [Fe(L)($\mu_{1,5}$-**9.5**)Fe(L)]$^{3+}$ (where L = pentadentate polypyridyl ligand). In one particularly interesting example the magnetic spin crossover transition is linked to guest removal from an Fe(II) clathrate. The iron(II) complex **9.8** includes two molecules of diethyl ether in the solid state. Upon release of the solvent from the host crystal **9.8**·2$Et_2O$ undergoes a single-crystal-to-single-crystal transformation to a monosolvate **9.8**·$Et_2O$. While the disolvate is paramagnetic (high spin) at all temperatures, the monosolvate undergoes a reversible spin crossover conversion between paramagnetism and a diamagnetic state upon cooling.[30] The implication is that the closer proximity of the metals caused by the loss of solvent mediates the spin-crossover transition.

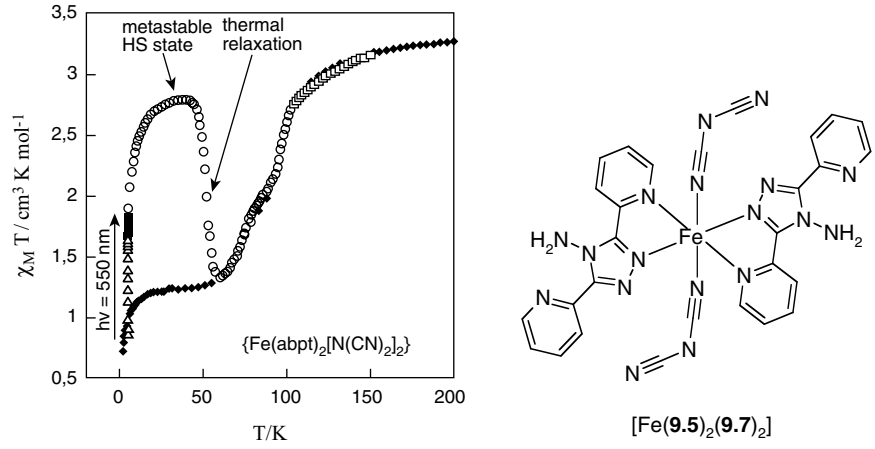


**Figure 9.32** Molecular structure and magnetic spin crossover behaviour of mononuclear dicyanamide complex [Fe(**9.5**)$_2$(**9.7**)$_2$]. Filled squares correspond to cooling to just above absolute zero, resulting in a drop in magnetic susceptibility corresponding to a high-spin to low-spin transition. The sample is then irradiated promoting it back to a metastable high spin state (open triangles). The sample undergoes thermal relaxation back to the low spin state before finally a thermally induced transition back to high spin occurs between *ca.* 60 – 100 K (open circles). (Reprinted with permission from [81] © 2001 American Chemical Society).

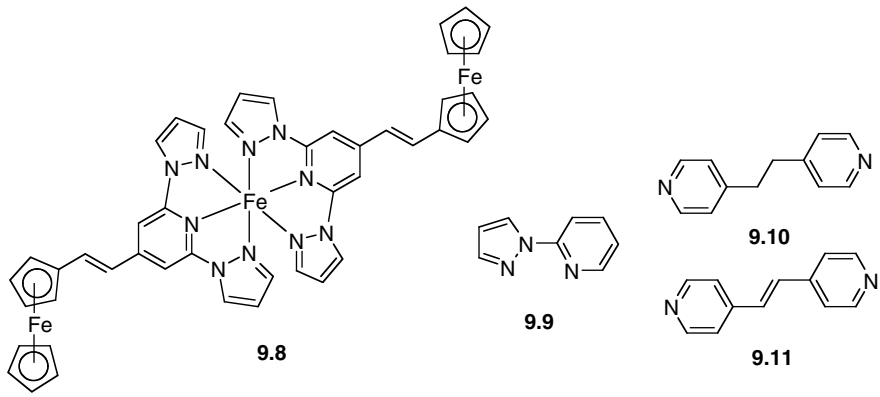


In terms of coordination polymers, in addition to Prussian blue, a range of spin crossover coordination polymers are known, many based on cyanide ligands. A series of iron(II) 1D coordination polymers have been reported, [Fe(**9.9**)$_2$(X)](ClO)$_2$·*n*EtOH (X = **9.10**, **9.11** or bpy).[31] Variable-temperature magnetic susceptibility measurements and Mossbauer spectroscopy reveal gradual spin transitions centred at *ca.* 170 – 190 K. Spin crossover in both coordination polymers and hydrogen bonded polymer materials such as [Fe(**9.5**)$_2$(**9.7**)$_2$] is of considerable interest in the context of magnetic data storage, in the same way as in the single molecule magnets discussed in Section 9.5.1.

## 9.5.5 Negative Thermal Expansion

Evans, J. S. O., 'Negative thermal expansion materials,' *J. Chem. Soc., Dalton Trans.* 1999, 3317–3326.

Negative thermal expansion (NTE) is a property of materials in which they become *smaller* with increasing temperature. It is a comparatively rare property and the general trend is for substances to

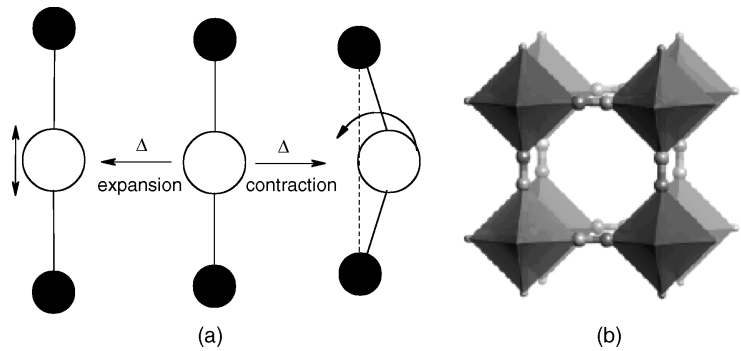


**Figure 9.33** (a) Schematic illustrating the different types of vibrational motion an M-L-M bridging unit undergoes with increasing temperature. The transverse 'guitar string' motion tends to lead to NTE behaviour. Solid circle = metal, open circle = ligand such as $O^{2-}$ or $CN^{-}$. (b) the structure of the Prussian Blue analogues $[M^{II}Pt^{IV}(CN)_6]$ (M = Mn, Fe, Co, Ni, Cu, Zn, Cd) as an example of the Prussian Blue family. The $M^{II}N_6$ octahedron is top left and bottom right while the $Pt^{IV}C_6$ octahedron is bottom left and top right (reprinted with permission from [33] © 2006 American Chemical Society).

expand on heating and contract on cooling. You can see this behaviour in the cracking of asphalt on a road for example – the asphalt expands in hot weather and then cracks as it shrinks again in winter. Thermal expansion can be a problem in some materials, causing wear, cracking and stress. However, a composite material that is just the right mixture of a positive thermal expansion material and a compatible negative thermal expansion material would not change size at all with temperature. Such a property would be of tremendous use in high precision optical mirrors, for example. This goal has spurred significant research into negative thermal expansion and the field has redoubled in importance recently with the observation that $ZrW_2O_8$ contracts over a temperature range in excess of 1000 K.[32] Negative thermal expansion is only of interest to relatively few supramolecular chemists and we will only touch upon it briefly. However it is interesting in the context of framework materials because the principal cause of NTE behaviour is changes in the bending or transverse 'guitar string' type vibrations of a M-L-M unit in a framework material with temperature, Figure 9.33. These structural changes must outweigh the natural tendency of bonds to lengthen with increasing temperature. Typically L in this context is an oxide ligand, but longer multiatomic ligands such as $CN^{-}$ also display this type of behaviour. Examples of coordination polymers exhibiting NTE include $[Ni(CN)_2]_n$ and the Prussian blue analogues $[M^{II}Pt^{IV}(CN)_6]$ (M = Mn, Fe, Co, Ni, Cu, Zn,Cd).[33] Perhaps the most striking material in this context is $Ag_3[Co(CN)_6]$ which exhibits tremendous positive thermal expansion in one direction due to weak $Ag^{+}\cdots Ag^{+}$ interactions that is transmitted by Co-CN-Ag-NC-Co linkages into a 'colossal' NTE along the crystal trigonal axis. Both the positive and negative thermal expansion are an order of magnitude greater than that observed in any other crystalline material.[34]

## 9.5.6 Interpenetrated Structures

Batten, S. R., 'Topology of interpenetration', *CrystEngComm* 2001, **3**, 67–72.

As we saw for hydrogen bonded diamondoid solids in Section 8.12 interpenetration is defined as the mutual interweaving of two or more independent, unconnected networks such that they cannot be separated without breaking bonds – they are topologically entangled. Thus a single polymer chain passing through a channel in a host net is not interpenetrated – it is simply a guest. We will return to

molecular interpenetration in the next chapter when we talk about the chemistry of catenanes. Two interpenetrated circles would resemble the magic trick involving 'magic rings' that apparently pass through one another to interlink, but, unlike the trick rings, interpenetrated chemical networks are inseparable. When only two networks are interpenetrated we describe the network as twofold interpenetrated. More generally networks can be *n*-fold interpenetrated with values of *n* up to 11 being known! Interpenetration is a beautiful phenomenon and it arises from the driving force towards close packing in solids. In networks with large void spaces such as expanded diamondoid nets (in which there is a very large hole in the middle of the adamantoid unit) the solid is unstable because there is a lack of van der Waals interactions at the surface of the cavity. If the cavity can be removed those interactions are restored. There are two ways in which the space can be filled; either through the inclusion of guests to give a potentially porous solid, or by interpenetration of additional, independent networks. From the point of view of designing porosity, therefore, interpenetration is a considerable hindrance.

The nomenclature for interpenetration takes the form *m*D→*n*D where *m*D is the dimensionality of the individual independent networks (in the present case coordination polymer networks) and *n*D is the dimensionality of the resultant interpenetrating system. The networks are also described as *parallel* or *inclined* depending on whether the interpenetrated polymers propagate in parallel directions or at a significant angle to one another. For networks which involve interpenetration between networks of different dimensions, then *m*D is replaced by *m*D/*p*D. For interpenetrating nets which have the same dimensionality but different topology, *m*D is replaced by *m*D/*m*D. For 2D inclined interpenetration, only a 3D entanglement is possible, so the →3D is redundant and omitted. Similarly, for 3D interpenetration, everything from the arrow onwards in the nomenclature is also not needed.

A survey of 301 interpenetrated structures in the CSD and ICSD was undertaken in 2004 which showed the distribution of structure types given in Figure 9.34. The 3D diamondoid net with its large adamantoid cavities proved to be by far the most common interpenetrated solid. For coordination polymers the highest degree of interpenetration is 10-fold and occurs for a silver(I) complex of 1,12-dodecanedinitrile. This simple ligand in fact forms three different diamondoid nets with Ag(I) of formula [Ag(1,12-dodecanedinitrile)$_2$]X with the $Ag^+$ ions acting as tetrahedral 4-connected nodes.[35] The degree of interpenetration depends on the anion with fourfold interpenetration in the $ClO_4^-$ salt, eightfold with $PF_6^-$ and $AsF_6^-$, and tenfold with $NO_3^-$. The eightfold structures are strictly an interpenetration of two normal fourfold interpenetrated diamondoid networks and have

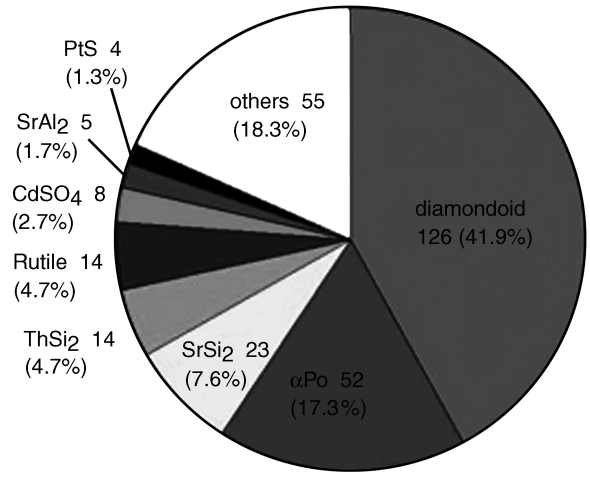


**Figure 9.34** Distribution of the topologies within the 301 interpenetrated structures observed in the CSD and ICSD (reproduced with permission of The Royal Society of Chemistry).

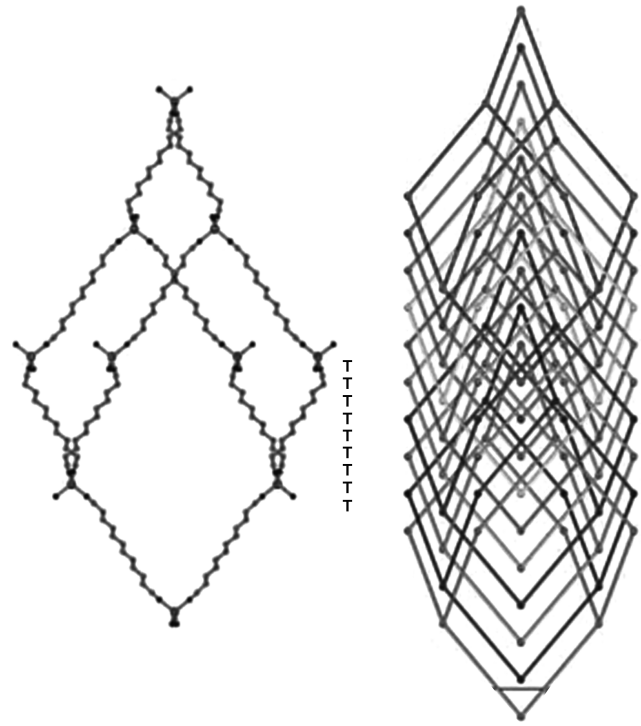

**Figure 9.35** The adamantoid cage and schematic of the tenfold interpenetration in [Ag(1,12-dodecanedinitrile)$_2$]$NO_3$ – all of the torsion angles of the ligand are *trans* (T) maximising its length (Copyright Wiley-VCH Verlag GmbH & Co. KGaA. Reproduced by permission). See plate section for colour version of this image.

been described as [4+4]-fold interpenetrated. The different anions cause changes in the torsion angles in the ligand, changing its length. Thus the nitrate compound has all *trans* torsions and the ligand adopts the conformation with the maximum length. In the [4+4] interpenetrated complex half of the ligand have two *gauche* torsions, one at each end, and in the fourfold structure all of the ligands have two *gauche* angles. The ten independent networks in the nitrate salt are shown in Figure 9.35.

The topologically simplest networks are 1D→1D parallel networks but few are known for coordination polymers. A hydrogen bonded example is the co-crystal of 4,4′-dipyridylpropane (**9.12**) and 4,4′-sulfonyldiphenol (**9.13**), Figure 9.36. One dimensional strands can also give rise to two dimensional

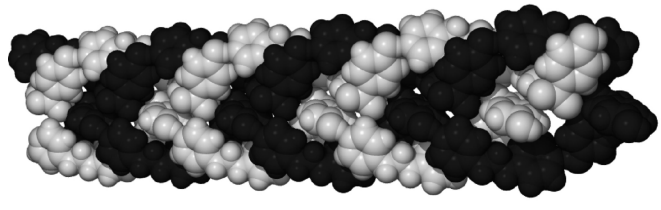

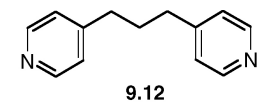


**9.12**

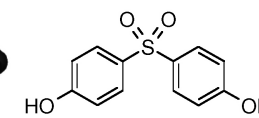


**9.13**

**Figure 9.36** 1D→1D parallel interpenetration of hydrogen bonded strands of 4,4'-trimethylenedipyridine **9.12** and 4,4'-sulfonyldiphenol **9.13**.

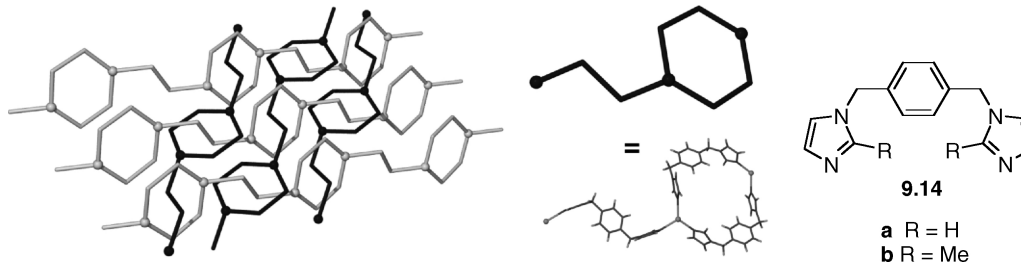


**Figure 9.37** 1D→2D inclined interpenetration in $[Ag_2(\mathbf{9.14a})_3](NO_3)_2$.[36]

sheets as in the Ag(I) complex of **9.14a** in which 1D strands are threaded through a metallomacrocyclic portion of an independent network to give 1D→2D inclined interpenetration, Figure 9.37.[36] Two dimensional sheets may interpenetrate in three different ways; either 2D→2D parallel, 2D→3D parallel and 2D→3D inclined. The first possibility can only occur if the mean planes of the topologically connected sheets are not offset in the direction perpendicular to the direction of their propagation. One particular nice example is a 'Borromean' 2D→2D parallel net of (6,3) topology with silver ions linked by ligand **9.14b** (Figure 9.38) and lined up by closed shell argentophilic interactions (Section 1.8.9).[37] We will return to the elegant Borromean motif, in which three mutually rings are topologically held together even though no two are interlinked, in the next chapter. Finally, a remarkable comprehensive, annotated and classified list of essentially all known interpenetrated structures is maintained by Stuart Batten at Monash University, Australia (http://www.chem.monash.edu.au/staff/sbatten/interpen/index.html).

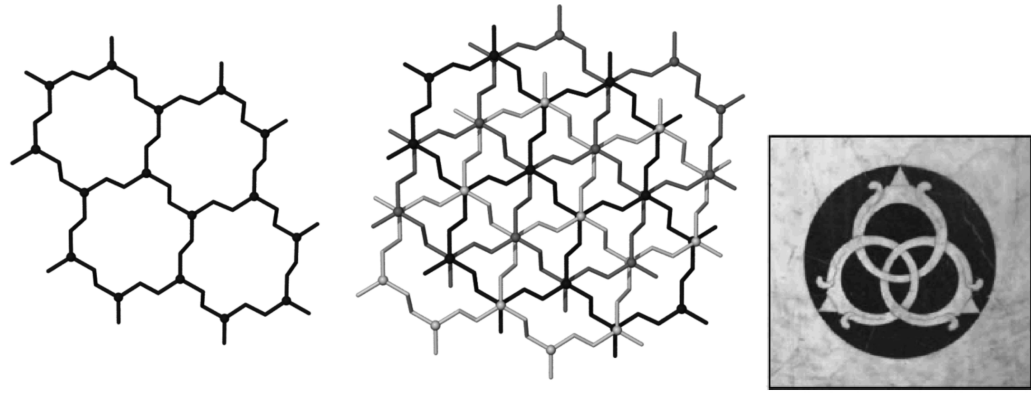


**Figure 9.38** (a) A 6,3-sheet of $[Ag_2(\mathbf{9.14b})_3](BF_4)_2$ and (b) the 2D→2D parallel Borromean interpenetrating network that it forms with the means planes of the 2D sheets coincidental. The Ag atoms (spheres) lie above each other, held by argentophilic interactions. (c) Borromean rings in black on white marble at the Cappella Rucellai in the Church of San Pancrazio, now the Marino Marini Museum, in Florence. The rings form part of the coat of arms of the Borromeo family and are also said to be a symbol of the Florentine de Medici family (photograph courtesy of Prof. L. J. Barbour).[37]

## 9.5.7 Porous and Cavity-Containing Structures

Yaghi, O. M., Li, H. L., Davis, C., Richardson, D. and Groy, T. L., 'Synthetic strategies, structure patterns, and emerging properties in the chemistry of modular porous solids', *Acc. Chem. Res.* 1998, **31**, 474–484.

As we have seen much of the interest in coordination polymers comes from their potential and actual porosity and hence zeolite-like properties – they are often described as 'organic zeolites'. In this chapter we have already encountered a number of compounds with channels and cavities but we have not so far addressed the issue of whether these are porous materials according to the strict definitions given in Section 9.1.3. In coordination polymer chemistry the rational design of microporous and channelled polymeric molecular or supramolecular materials is a challenging, but increasingly fruitful, area of research. Such materials may have key applications in the petrochemicals industry (*cf.* production of simple feedstocks such as methanol by zeolites), separation science and the environment, *e.g.* the destruction of volatile organic compounds (VOCs). The potential for directed chemical reactions within a solid matrix has already been demonstrated for urea inclusion compounds, while the attractive goal of enantiospecific syntheses within chiral frameworks has yet to be realised. To date, much use has been made of microporous silicas and aluminosilicates, such as zeolites, in these kinds of applications because of their thermal robustness (even in the absence of guest) and the malleability of the framework size by use of a templated synthetic approach. Because of the simple nature of the building blocks (tetrahedral fragments such as $SiO_4^{4-}$) the design of more versatile hosts, including chiral hosts, is not feasible by this method, however. Design of rigid ligands with divergent, carefully placed binding sites offers enormous potential for the synthesis of tailor-made porous materials. In principle, the construction of porous coordination polymers is as simple as choosing a combination of a ligand with more than one binding site that cannot chelate (divergent binding sites), and a metal centre that has complementary divergent coordination sites. The result should be a coordination polymer (*cf.* Figure 9.25). If the ligand is large enough, cavities will be left between one metal node and the next. The situation is not as simple as it seems, however. Metal–ligand interactions are often strong and hence non-labile. As a result, products may deposit rapidly as amorphous powders, and kinetic products of irregular structure are common. This kind of problem may be overcome partially through the use of diffusion, solvothermal (heating in water under pressure) and gel permeation synthetic and crystal growth techniques. Furthermore, the geometry of the metal–ligand interactions is not always easy to predict, and even if a pore structure is generated there is no guarantee that the pores will be accessible to guest molecules from outside the crystal *via* access channels. However, this is a necessary criterion for the use of such designer materials in ion exchange or inclusion reaction type applications. Moreover, as we saw in the last section, carefully designed pores may end up being filled by interpenetration instead of guest-containing channels or cavities. Despite these drawbacks, a great deal of progress has been made in the engineering of porous solids. A broad range of ligands such as 4,4′-bipyridyl (bpy) and expanded analogues such as **9.10–9.12**, carboxylates and other oxygen donors, nitriles, as well as more exotic bridges such as the tetrahedral $Ge_4S_{10}^{4-}$ (**9.15**), have been used as prototype divergent building block ligands.

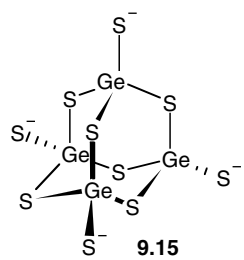


**9.15**

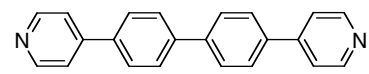


**9.16**

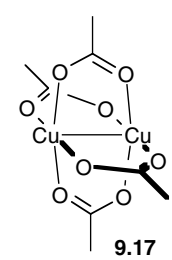


**9.17**

Bpy in particular forms an enormous variety of porous networks with the network geometry depending on the coordination requirements of the metal centre. Simple networks do not exhibit any interpenetration however, as the complexity increases, two-, three-, four- and six-fold interpenetrated structures are formed, although many still contain pores and channels that include the counter anions (Figure 9.39). The four-fold interpenetrated diamondoid $[Cu(bpy)_2](PF_6)$ contains $PF_6^-$ anions in interstitial sites of 6 Å width, which cannot be exchanged for other anions. In contrast, the more open (although still highly interpenetrated) $[Cu(bpy)_{1.5}](NO_3)\cdot 1.25H_2O$ exhibits anion exchange behaviour once the water is removed by heating. The small $NO_3^-$ can be exchanged for $SO_4^{2-}$ and $BF_4^-$.[38] Similarly in the extended structure $\{[Ag(\mathbf{9.10})]ClO_4\}_n$ the perchlorate anions can be exchanged for $PF_6^-$ by soaking in $NaPF_6$ solution, but not the other way around. The hexafluorophosphate structure is postulated to be more stable because of increased Ag···Ag interactions.[39] There is considerable debate about the mechanism of these anion exchange processes which could be either involve anions diffusing into and out of a solid microporous host or it could involve a solution-mediated dissolution and recrystallisation process. Strong evidence for the latter has been obtained for the anion exchange coordination polymers $\{[Ag(bpy)]BF_4\}_n$ and $\{[Ag(bpy)]NO_3\}_n$ using a combination of IR and $^1$H NMR spectroscopy, transmission electron (TEM) and atomic force (AFM) microscopies, and X-ray powder diffraction (PXRD) [40, 41] Hence reports of anion (as opposed to neutral guest) exchange *via* a solid-state mechanism in coordination polymers should be regarded with caution.

Both bpy and the extended bipyridyl ligand (**9.10**) have been used to produce square grid compounds, analogous to Hoffman-type inclusion compounds. The additional two carbon spacer in **9.10** apparently has the effect only of extending the grid dimensions in most cases with the exception of the NbO network

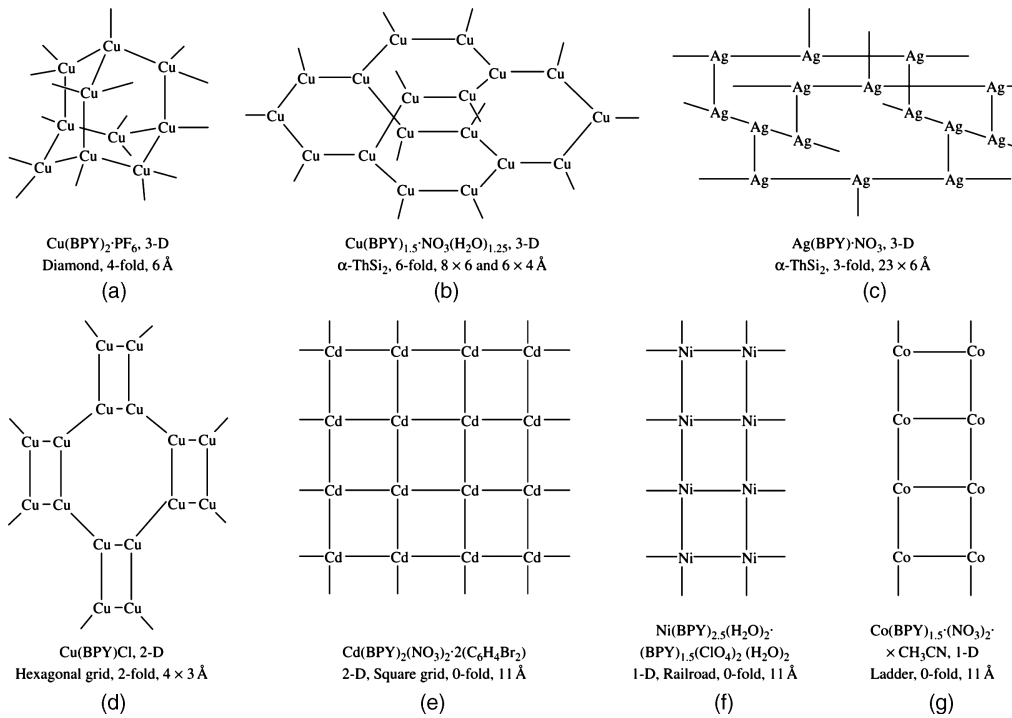


**Figure 9.39** Schematic representations of metal 4,4′-bipyridyl porous networks. Lines represent the bipyridyl ligand except for vertical lines in (c), which represent Ag···Ag bonds (2.977 Å long), and horizontal lines in (d) which represent Cu···Cu. The chemical formula, framework dimensionality, structure type, degree of interpenetration and pore aperture are listed under each representation. (Reproduced with permission from Reference 38).

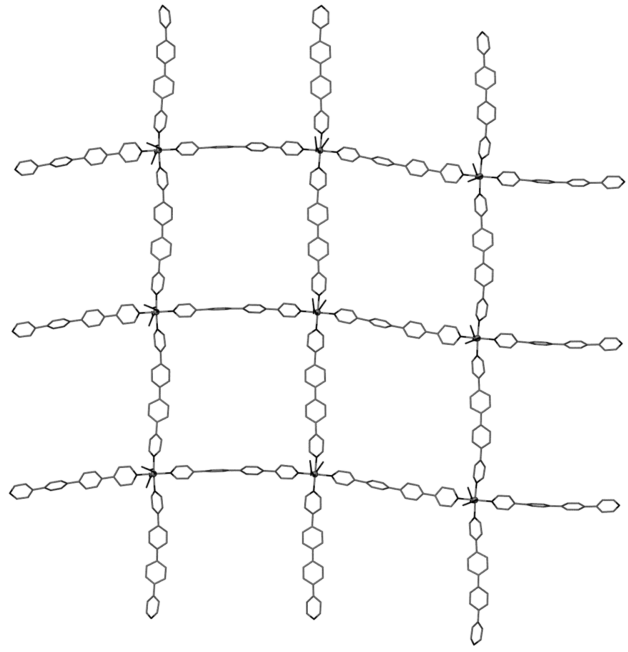

**Figure 9.40** 2D grid coordination polymer with included o-xylene guests based on the extended bipyridyl **9.16**.[42] (Reprinted with permission from [38] © 1996 American Chemical Society)

noted above. Very long bipyridyl ligands with up to two phenylene spacers (**9.16**) also produce 2D square grid coordination polymers with Ni(II) of formula $\{[Ni(\mathbf{9.16})_2(NO_3)_2]\cdot 4o\text{-xylene}\}_n$ with cavities of dimensions 20 × 20 Å occupied by the xylene guests and channels of cross-section 20 × 10 Å, surprisingly without interpenetration, Figure 9.40.[42] The coordination polymer is truly porous and can withstand guest removal. The framework is stable up to 300 °C because of the relative involatility of the larger ligand.

The dimensionality of bipyridyl-based networks can be reduced by selective blocking of metal coordination sites while the SBU concept can be used to reduce problems of interpenetration. A designer 1D coordination polymer results from the interaction of bipyridylpropane (**9.12**) with the dicopper tetraacetate 'paddlewheel' or 'lantern' SBU $Cu_2(OAc)_4$ (**9.17**) which has two vacant sites, one on each copper(II) ion parallel to the Cu–Cu axis. The result is a parallelogram-shaped grid structure arising from the crossing of 1D strands. A variety of guest molecules such as acetic acid dimers, methanol and ethylene glycol are included into the parallelogram cavities, Figure 9.41. The van der Waals nature of the interactions between the polymer strands, however, means that the host does not survive removal of the guests and so it cannot be regarded as truly porous. Interestingly, however, this material can be prepared by solid state mechanochemical grinding of the metal salt and ligands (Section 8.2.9).[43] Recent work has also shown that even 3D coordination polymers can be synthesised in this way. While mechanochemistry can degrade crystallinity on prolonged grinding, it appears that after a short period of grinding to initiate a reaction, solid-state synthesis of coordination polymer frameworks can continue without further agitation. In general mechanochemistry represents an interesting new approach to coordination polymer synthesis.[44]

While pyridyl-based coordination polymers are extremely synthetically versatile they are not generally particularly thermally robust as a consequence of the tendency of the pyridyl ligands to dissociate or decompose above *ca*. 250–300 °C. The volatility of the ligands is linked to the fact that they are neutral and hence stable in the free state. Moreover their neutrality means that even in the absence of interpenetration, coordination polymer frameworks are generally filled with counter-anions which,

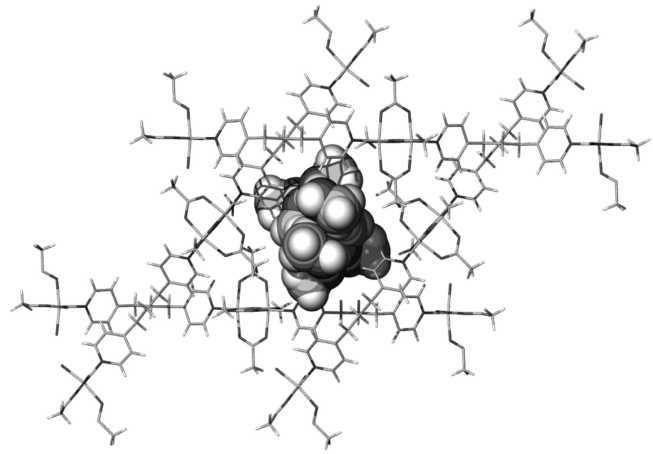

**Figure 9.41** Methanol guest inclusion by the 1D coordination polymer $[Cu_2(OAc)_4(\mu\text{-}\mathbf{9.12})]$ (guest shown in space-filling mode.[43])

as we have seen, are difficult to remove without dissolution of the framework. These issues suggest that thermally robust, involatile anionic ligands might make more zeolite-like coordination polymer frameworks. Just such an example comes from the reaction of $[Mn(O_2CCH_3)_2(H_2O)_4]$ with the inorganic ligand **9.15** which gives the elegant diamondoid solid $[NMe_4]_2[MnGe_4S_{10}]$, in which the $NMe_4^+$ counter ions are included as guests within the large pores in the diamondoid lattice. Heating the material up to 500 ºC in an analogous fashion to the preparation of zeolite frameworks (calcination) results in the decomposition of the alkylammonium cation to give the effectively guest-free porous material in which the framework charge is balanced by $H^+$. The compound is indefinitely stable because of its extremely robust inorganic architecture. The $NMe_4^+$ cations may be replaced by a variety of divalent metals. In the next section we will see how anionic ligands, in combination with the SBU concept, have finally led to robust, zeolite-like coordination polymers with large pores and highly versatile sorption properties.

## 9.5.8 Metal-Organic Frameworks

Rowsell, J. L. C., Yaghi, O. M., 'Metal-organic frameworks: a new class of porous materials', *Micropor. Mesopor. Mater.* 2004, **73**, 3–14; James, S. L., 'Metal-organic frameworks', *Chem. Soc. Rev.* 2003, **32**, 276–288.

A key result in the area of porous materials came in 1995 with the synthesis of the first MOF by the group of Omar Yaghi, then at Arizona State University, USA (now Michigan).[45] These researchers prepared **9.18**, a layered coordination polymer based on benzene 1,3,5-tricarboxylic acid (trimesic acid, **9.19**). The spacer units (S) are two pyridine ligands and the whole assembly comprises a two-dimensional sheet coordination polymer. Each sheet interacts with those above and below it by individually weak $\pi$–$\pi$ stacking interactions of the pyridine aromatic rings. Thermogravimetric analysis of the material indicates that it is able to reversibly release aromatic guest molecules from its channel-like pores at 190 ºC, yet the overall crystalline host structure is retained up to 350 ºC, as demonstrated by X-ray powder diffraction analysis and examination of the crystals by optical microscope. Addition of further guests to the guest-free structure results in their incorporation into the host channels. The overall mode of guest inclusion is reminiscent of Hoffman-type clathrates (Section 9.4) and the thermal robustness and reversibility of the binding suggested that these systems may prove to be of significant practical application.

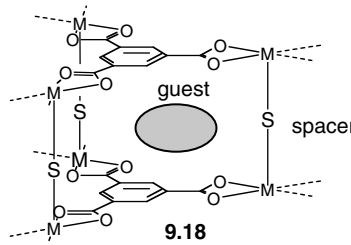


**9.18**

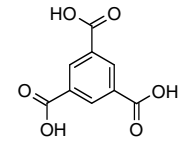

**9.19**

Four years later in 1999 Yaghi's group reported a 3D MOF termed MOF-5,[46] a compound that has subsequently formed the basis for a huge range of important MOFs and is produced commercially on a large scale. MOF-5 is based on an octahedral zinc(II) oxo-centred SBU (Figure 9.42) that occupies the vertices of a cubic lattice, and bridging terephthalate (1,4-benzene dicarboxylate) dianions, Figure 9.43. The compound is prepared *quasi*-solvothermally and the optimised conditions are very straightforward. An *N*,*N*-diethylformamide solution of $Zn(NO_3)_2{\cdot}4H_2O$ and terephthalic acid is heated at between 85° and 105 °C in a closed vessel to give crystalline MOF-5 in 90 % yield. The use of an octahedral SBU (which is formed under the conditions of synthesis) instead of an octahedral metal centre has the effects of markedly expanding the structure and because of its size it reduces the degree of interpenetration. The structure can be further expanded by the use of larger, linear dicarboxylates ligands to yield *isoreticular structures* (structures with nets of equivalent topology) termed IRMOFs, Figure 9.43. This series of MOFs exhibit square pore windows with diameters up to 19.1 Å while the internal pore diameters are up to 28.6 Å. The size of the MOFs can be controlled by choice of the length of the aromatic region of the dicarboxylate ligands. The calculated densities of the frameworks of materials are as low as 0.21g $cm^{-3}$ which represents the lowest density observed for any crystalline material (compare this number to 1.0 g $cm^{-1}$ for liquid water and about 1.5 g $cm^{-3}$ for normal organic solids). As the spacers become larger the SBU does not entirely prevent interpenetration and in a few cases doubly interpenetrating frameworks have been observed but repeating the syntheses at lower concentration gives analogous non-interpenetrated structures. This dependence on conditions highlights the role that solution speciation has on crystal nucleation. These IRMOF frameworks generally display remarkable stability even at high temperatures (~ 300 °C) and are stable even in the absence of guests and hence are truly porous. Indeed they are remarkably effective at storing gases such as methane after removal of guest solvent. The most effective framework, IRMOF-6, absorbs an amount of methane equivalent to 240 $cm^3$ per gram of MOF (if the methane were at standard

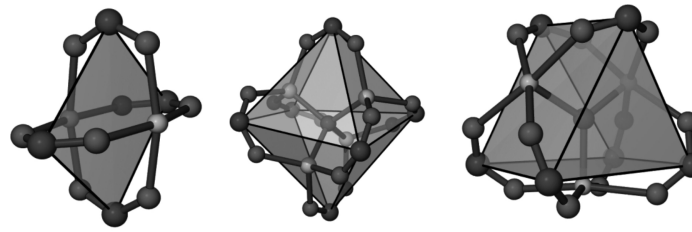


**Figure 9.42** Secondary Building Units (SBU) using carboxylates with rigid coordination geometries that replace metal ions as vertices in MOFs. (a) Paddlewheel or lantern structure as in **9.17**, (b) octahedral 'basic zinc acetate' SBU used in MOF-5 and (c) a trigonal prismatic oxo-centred trimer. The polyhedra use carboxylate carbon atoms as their vertices and the MOFs propagate *via* the linkers attached to these carbon atoms. The metal atoms are bound to only terminal ligands in addition to those shown.

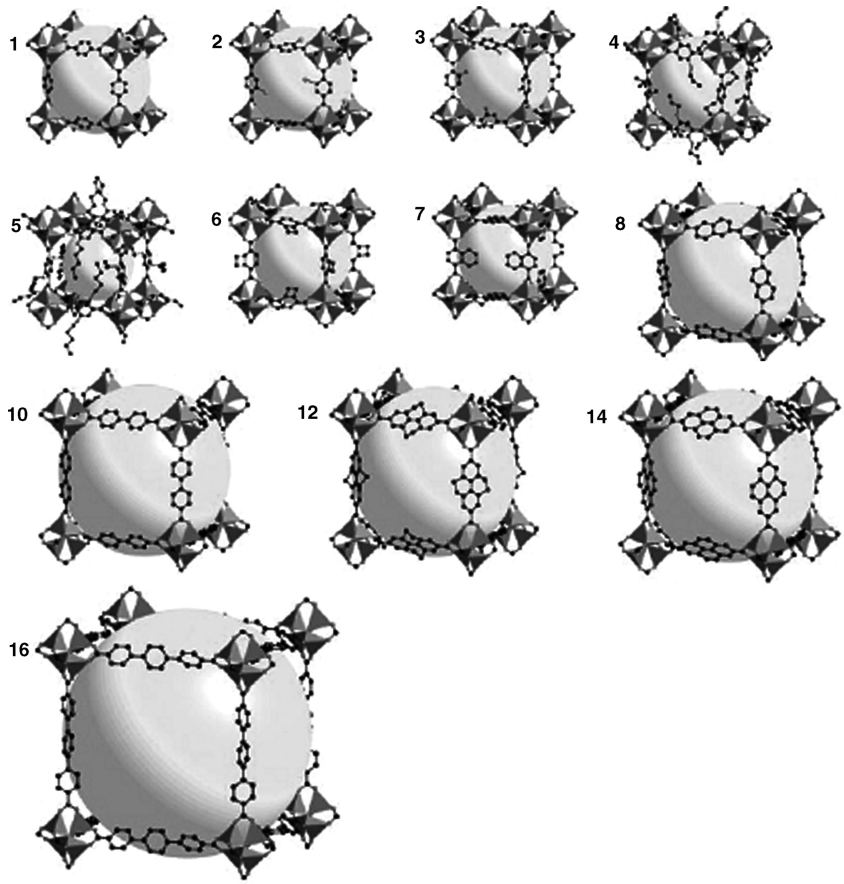


**Figure 9.43** Single crystal X-ray structures of IRMOF-*n* ($n = 1 - 7, 8, 10, 12, 14$, and 16), labelled respectively. MOF-5 is re-designated IRMOF-1 as part of this series. IRMOFs 9, 11, 13, and 15 are doubly interpenetrated. Zn(II) tetrahedral shown as polyhedra. The large spheres represent the largest van der Waals spheres that fit in the cavities without touching the frameworks (reprinted from [47] with permission from AAAS).

temperature and pressure). The methane is adsorbed at 298 K and under 36 atm pressure. This represents 70 per cent of the compression achieved in methane cylinders which operate at over 200 atm.

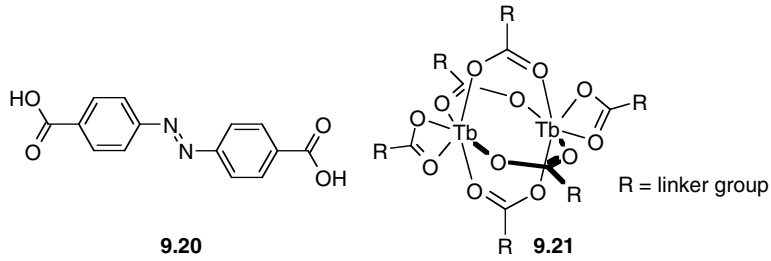


**9.20** **9.21**

The way in which SBU size affects interpenetration has been investigated systematically and theoretically for the terbium(III) SBU **9.21** with the extended dicarboxylate **9.20**. These components crystallise from DMSO to give MOF-9, a doubly interpenetrated cubic network with significant void space filled by DMSO molecules. The question arose as to whether the observed doubly interpenetrated network is the maximum degree of interpenetration possible given the size of the SBU. The compound can be described

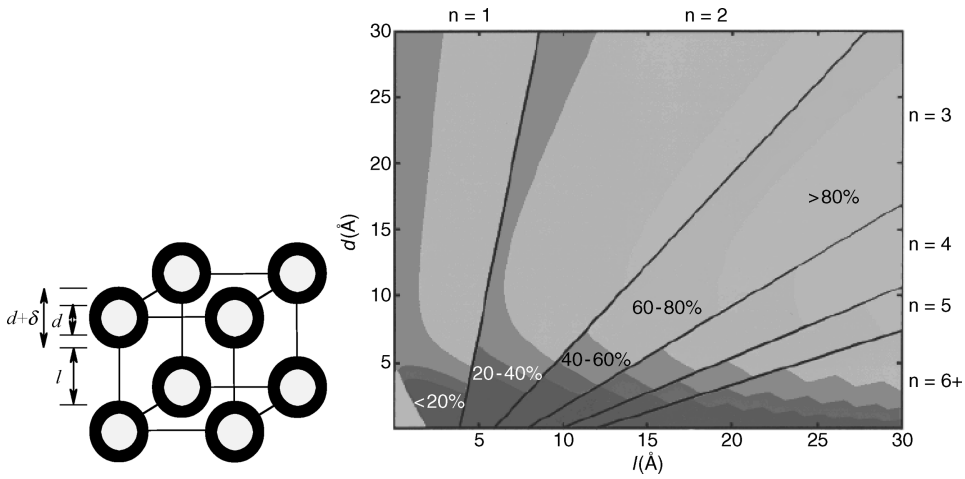


**Figure 9.44** Geometrical parameters used in equation 9.1 and free volume/interpenetration plot for compounds related to MOF-9. Interpenetration $n$ is plotted (total number of frameworks in a structure) as a function of $d$ (diameter of an SBU) and $l$ (length of linker) with the corresponding free volume expressed as percent of crystal volume shown in decreasing shades of darkness (darkest: <20 to lightest: >80%). The solid dark lines for $n$ =1 to $n$ = 6 + were obtained according to equation 9.1 (see text) and assuming a C connector with $\delta$ = 3.4 Å (van der Waals diameter of a C atom) and linkers with negligibly small diameter. For the volume calculation the SBUs diameter was considered $d$ and the volume of the linker was based on a cylinder of a diameter ($2r$) equivalent to that of a benzene ring (5 Å) and a length $l$. Thus, the free volume was calculated based on the following: Volume of the cell = $(d + l)^3$; volume occupied by SBUs/cell = $n(\pi/6)d^3$; and volume of the linkers/cell = $3n[(\pi r^2)]l$. (Reprinted with permission from [48] © 2000 American Chemical Society).

by a geometric model based on two interpenetrating cubic frameworks in which the vertices where the SBU are situated are approximated as large spheres. The maximum degree of interpenetration, $n$, is related to the diameter of the SBU, $d$, the length of the linker, $l$, and the van der Waals radius of the atom joining the SBU and linker, $\delta/2$ (Figure 9.44). The unit cell edge length $a = d + l$. For $n$ frameworks to interpenetrate with the centres of their SBUs aligned along a body diagonal, $n(d + \delta) = \sqrt{3}a$; thus,

$$n \leq \sqrt{3}\,\frac{d+l}{d+\delta}$$

This relationship can be used to predict the consequences of $d$ and $l$ for the percentage free volume in cubic structures that interpenetrate to the maximum possible degree given the bulk of the components, Figure 9.44. The conclusion is that the $n$ = 2 structure observed is indeed the most interpenetrated possible, *i.e.* it is *maximally interpenetrated* as a consequence of the size of the SBU.

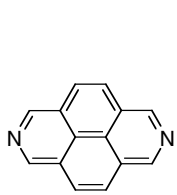


**9.22**

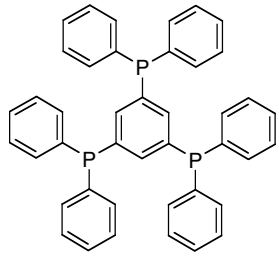


**9.23**

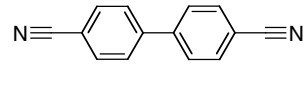


**9.24**

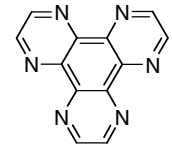


**9.25**

Interpenetration has also been reduced by the use of large bridging ligands, such as **9.22** in place of bpy, which reduces interpenetration from fourfold to threefold in the case of the diamondoid [Cu(**9.22**)]($PF_6$),[49] and in the case of the very bulky **9.23** where the framework [$Ag_4$(**9.23**)$_3$($CF_3SO_3$)$_4$] exists as a non-interpenetrated hexagonal structure with large 72 membered rings of width 16–18.4 Å.[50] Conversely, nitrile ligands such as **9.24** tend to increase interpenetration because they do not have much steric bulk at the metal centre, *e.g.* the ninefold interpenetrated structure of [Ag(**9.24**)$_2$]($PF_6$).

The remarkable porosity of zeolite-type compounds stems from the intrinsically robust nature of the Al-O-Si and Si-O-Si linkers and their relative chemical inertness (they don't react with oxygen when heated to very high temperatures, for example). Generally MOFs do not exhibit such thermal stability and linkers can be labile, and hence loss of crystallinity of guest removal or on heating. However, there are now a number of MOFs that undergo very little framework change upon adsorption or desorption of guests. Such frameworks can even be based on pyridyl type ligands, as in [$Ni_2$(bpy)$_3$($NO_3$)$_4$] which exhibits little structural change on removal of adsorbed ethanol from its 6 × 3 Å channels at 100 °C. If the empty framework is exposed to ethanol the original structure is regained. Interesting 'step' type adsorption behaviour that deviates from the type I isotherm (Section 7.11) observed for ethanol is observed for methanol vapour, however, in which initial adsorption is fast, corresponding to hydrogen bonding of the methanol guest to the nitrate anions, followed by a slower structural rearrangement of the adsorbed guests that allows additional methanol incorporation.[51] Another interesting material is the pyrazene (**9.27**) based MOF [$Cu_2$(**9.26**)$_2$(pyrazene)] which exhibits permanent one-dimensional channels of cross-section 4 × 6 Å. This compound has hydrogen bond basic oxygen atom sites that interact with guest water in the assynthesised material. The water can be removed without altering the framework and the empty host proves to selectively adsorb hydrogen bond acidic guests such as acetylene in preference to non hydrogen bond acids such as $CO_2$. Acetylene is a very useful chemical feedstock but is often contaminated with other gases such as $CO_2$. It is a highly reactive molecule which cannot be compressed above 20 atmospheres or it explodes even without oxygen, at room temperature. Hence safe materials for $C_2H_2$ separation and storage are of significant interest. The acetylene sorption capacity in [$Cu_2$(**9.26**)$_2$(pyrazene)] is 42 $cm^3$ (at stp) per gram of host material corresponding to one acetylene per framework formula unit. In comparison only 26 $cm^3$ $g^{-1}$ $CO_2$ is adsorbed.[52] Hydrogen bonding to the host non-coordinated oxygen atoms means that the acetylene molecules are held at a periodic distance from one another within the channels. This results in a 'confinement effect' which permits the stable storage of acetylene at a density 200 times the safe compression limit of the free gas at room temperature.

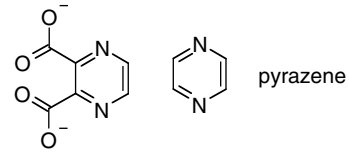


**9.26** **9.27**

As a general principle framework robustness is improved by the use of chelate ligands and a good match between metal and ligand hard/soft acid/base properties (Section 3.1) leading to high bond strength, as in lanthanide carboxylates, which often form some of the most stable MOF type materials. Chelating pyridyl type ligands such as **9.25** have been used in MOFs, as in [Ag(**9.25**)($ClO_4$)] · 2$NO_2$Me. This material undergoes reversible exchange of the nitromethane guests for atmospheric water without loss of framework integrity. It is this chelation or bridging within an SBU by multidentate carboxylates,

in combination with the use of rigid aromatic rings as spacers and their 3D connectivity, that makes the IRMOFs and compounds like them particularly robust and useful in porosity-dependent applications such as gas storage. In the final section in this chapter we will look at the particular interest surrounding the use of MOFs in catalysis and hydrogen storage.

## 9.5.9 Catalysis by MOFs

Horike, S., Dincă, M., Tamaki, K. and Long, J. R., 'Size-selective lewis acid catalysis in a microporous metal-organic framework with exposed $Mn^{2+}$ coordination sites', *J. Am. Chem. Soc.* 2008, **130**, 5854–5855.

It is a particularly attractive research goal to use MOFs as solid state catalysts in an analogous way to zeolites, with all the concomitant advantages of heterogeneous catalysis such as easy product and catalyst separation and with the added advantage of the tunability offered by MOFs, including framework chirality. However intra-cavity catalysis of many chemical reactions by MOFs is not trivial to achieve because it requires the incorporation of catalytically active sites in the MOF. The active site must be able to carry out the desired chemistry yet not react with the MOF ligands nor lose its activity upon prolonged exposure to other potential guest species. This is a significant challenge given the relatively reactive nature of MOFs compared to zeolite frameworks and the traditional kinds of MOFs that have coordinatively saturated metal centres accompanied by robust chelating ligands. Significant progress is beginning to be made in MOF catalysis, however, including enantioselective catalysis, and we highlight just one very interesting recent example here. The MOF $Mn_3[(Mn_4Cl)_3(BTT)_8(CH_3OH)_{10}]_2$ ($H_3BTT$ = 1,3,5-benzenetristetrazol-5-yl) is known to act as an effective $H_2$ sorbent because of its large pores. The material also has $Mn^{2+}$ ions exposed on the surface of the framework which might act as Lewis acid catalytic sites. The compound has been found to catalyze the cyanosilylation of aromatic aldehydes and ketones. It also carries out the Mukaiyama-aldol reaction – a reaction this is not quite so facile. Because the reaction occurs within the confines of the MOF framework cavities there is a significant degree of size-selectivity in the products obtained which is in line with the known cavity dimensions of the material. This aldehydes bearing smaller substituents such as phenyl and napthyl reacy readily because the product can fit within the zeolite, while aldehydes bearing larger substituents react only sluggishly, Figure 9.45.

## 9.5.10 Hydrogen Storage by MOFs

Rowsell, J. L. C. and Yaghi, O. M., 'Strategies for hydrogen storage in metal-organic frameworks', *Angew. Chem., Int. Ed.* 2005, **44**, 4670–4679.

We have already discussed the technological importance of hydrogen storage materials in Section 7.9, where we looked at clathrate-type organic frameworks in this context. We now return to the subject

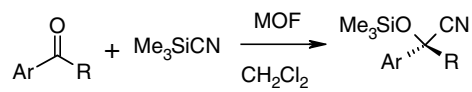


**Figure 9.45** MOF catalysed cyanosilylation reaction – when Ar is phenyl or napthyl the product can pass freely through the pores giving yields of over 90 per cent. When Ar = 4-phenoxyphenyl or biphenyl the yields are below 20 per cent because the molecules do not fit readily within the cavities.

with a case study on recent progress in hydrogen storage within MOFs. Hydrogen storage by intrinsically low density materials is of key importance as part of the emerging hydrogen economy. They are particularly crucial in 'green' hydrogen fuel cell based transport applications where there is a vital need to store sufficient hydrogen to power a vehicle over a reasonable journey length (taken to be *ca*. 300 miles or 480 km) without making the energy cost in transporting the storage apparatus (the hydrogen 'fuel tank') prohibitive.[53] The holy grail in this area is a material that meets the US DOE 2010 and, ultimately, 2015 energy density targets (including container and recharge/discharge apparatus). For 2010 these are 7.2 MJ $kg^{-1}$ and 5.4 MJ $L^{-1}$, which translates as 6.0 weight percent and a volumetric density of 45 kg hydrogen per cubic metre. The 2015 targets, the sort of levels that would be of serious interest to automobile manufacturers, are 9.0 weight percent and 81 kg hydrogen per $m^3$. For comparison mass density of elemental hydrogen is only 70.8 kg $m^{-3}$ as a liquid at 20 K (1 atm) and 5 kg of hydrogen gas occupies 56 $m^3$ under ambient conditions (ignoring container mass of course). Given the higher energy density of hydrogen as a fuel and the greater efficiency of fuel cells compared to conventional combustion engines only about 4–10 kg of hydrogen is actually needed and demonstration 'concept cars' have achieved the 2010 specifications using cylinders of hydrogen either under pressure or at cryogenic temperatures. The 2015 targets, however, are not within easy reach by these methods.

So, how do MOFs currently stack up in the hydrogen storage stakes, and what is their future potential? Current MOF research indicates that micro or mesoporous MOFs with significant interactions between the hydrogen and the channel walls are likely to be the most promising materials – adsorption of a second and subsequent layers of hydrogen is really quite weak and so homogeneous, very large diameter pores are not likely to be as useful and hence a large pore surface area is an important property. Moreover hydrogen storage with the H–H bond intact is likely to make for the best discharge and recharge efficiencies and speed. However, given the mass of the framework, and the low mass of the $H_2$ molecule storage of many moles of hydrogen per mole of framework is necessary and of course the best frameworks will make use of light atoms, particularly light metals, not heavy transition metals or lanthanides.

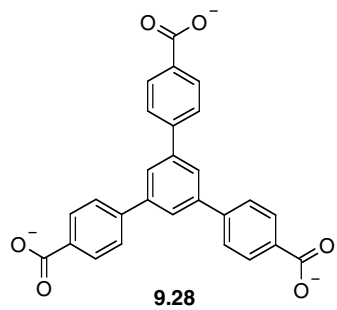

**9.28**

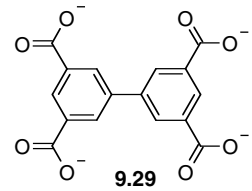

**9.29**

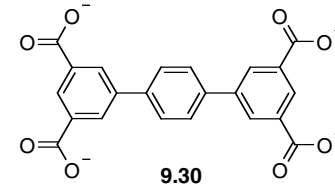

**9.30**

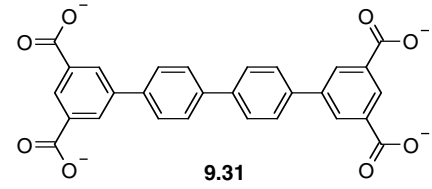

**9.31**

In terms of surface area MOFs have very promising properties. The largest currently known surface area for a microporous material is MOF-177, a material that uses the octahedral 'basic zinc acetate' SBU (Figure 9.42b) in conjunction with the tricarboxylate **9.28**. At 77 K this compound exhibits an $N_2$ adsorption-based monolayer-equivalent surface area of 4500 $m^2\ g^{-1}$ and a micropore volume of 0.69 $cm^3\ cm^{-3}$. The compound does not absorb as much hydrogen at lower pressures as other materials with smaller surface areas, however, possibly because of its structure comprising large cavities *ca*. 11 Å in diameter linked by narrower channels. This result highlights the need for a better understanding and careful engineering of surface structure and pore/channel shape as well as just surface area. At high pressure MOF-177 is extremely impressive, adsorbing 7.3 weight percent at 50 bar, Figure 9.46. The

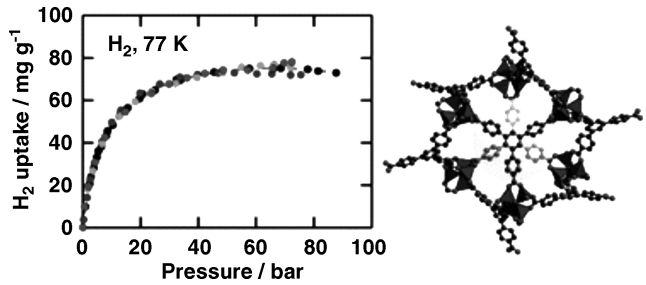


**Figure 9.46** Hydrogen adsorption isotherm at 77 K and X-ray crystal structure of MOF-177 (reproduced with permission of The Royal Society of Chemistry).

adsorption is best described by a micropore filling model and so the hydrogen fills much of the cavity (the estimated total capacity is *ca.* 11 weight per cent) as well as being surface adsorbed in the pores.[54] Among the IRMOF series, the best results are obtained for IRMOF-8 which stores up to 2.0 per cent by weight of hydrogen at 298 K and 10 atmospheres pressure. Hydrogen storage at ambient temperature is an ideal situation, however capacity increases as temperature goes down because of the longer residence time of adsorbed hydrogen on the micropore walls and hence for reasons of ease of measurement results are often reported at 77 K and one atmosphere pressure.

Optimal packing of hydrogen would be in a pore that equates to its diameter giving equivalent interactions all around. The kinetic diameter of hydrogen is larger than some gases at 2.89 Å, but this value is clearly much smaller than some of the pore sizes we have encountered and hence there is a possibility of 'wasted space' at monolayer coverage. Hence a highly segmented material with smaller pores is desirable. However, the thickness of the walls of the segment reduces the efficiency and hence a compromise must be reached. In a series of MOFs based on **9.29**–**9.31** of formula $[Cu_2(L)(H_2O)_2]$ (L = **9.29**–**9.31**) all based on the dicopper tetracarboxylate 'paddlewheel' SBU (Figure 9.42a) and with NbO topology, the Nottingham group led by Martin Schröder and Neil Champness showed that the largest pore material is not necessarily the best at hydrogen uptake. In these materials the pores are all of similar shape, occupying 63.3, 70.4 and 75.5 per cent of the crystals, respectively. The pore volumes calculated from the maximum amount of $N_2$ adsorbed are 0.680, 0.886 and 1.138 $cm^3\ g^{-1}$, respectively for the three materials. Hence there is a relationship between the ligand length and pore size. Hydrogen uptake results showed, however, that it is the intermediate pore size material based on **9.30** that exhibits the most hydrogen uptake, reaching a maximum value of 43.6 g $L^{-1}$, close to the 45 g $L^{-1}$ specified by the 2010 DOE target. Gravimetrically this corresponds to 2.52 weight percent at one atmosphere pressure and an impressive 6.06 weight percent at 20 atmospheres and 78 K, or 7.8 % at 60 atmospheres.[55] The efficacy of the intermediate material is attributed to a good balance between pore volume and surface area.

Another strategy for increasing hydrogen absorption by MOFs is to include metal atoms with vacant coordination sites that can specifically form σ-bonded $H_2$ complexes. Many SBU have coordination sites that are only occupied by weakly coordinating ligands that can be displaced by heating. This opens the possibility of chemisorption of $H_2$. A related development is the phenomenon of catalytic 'spillover'. Spillover involves the splitting of $H_2$ into hydrogen atoms by small particles of a finely divided metal catalyst such as platinum. If the catalyst is in good contact with the storage material then the hydrogen atoms are included in a way that is poorly understood but results in tangible benefits to their storage ability. For example, hydrogen uptake by MOF-5 and IRMOF-8 can be enhanced by a factor of 3.3 and 3.1, respectively (to nearly 2 wt % at 10 MPa and 298 K). The binding isotherms are fully reversible implying that the spillover hydrogen atoms are also readily recombined into $H_2$.[56]

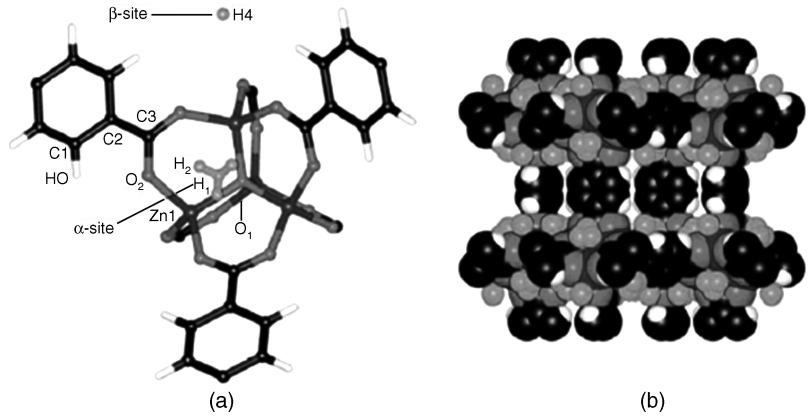


**Figure 9.47** (a) The location of the hydrogen absorption sites at 5 K relative to the framework atoms. The α-site is 100% occupied at 50 K, 30 K and 5 K The $H_2$ molecule is disordered over three possible orientations of which the atoms labelled H1 and H2 represent one possibility. The β-site is 98% occupied at 5 K. (b) Space-filling diagram of one of the framework cavities at 5 K showing the hydrogen positions (reproduced with permission of The Royal Society of Chemistry).

MOF hydrogen sorption chemistry has been dogged by a series of claims of high storage capacity followed by retractions or corrections and the variations in pressures, temperature and conditions make it difficult to compare results. Hydrogen sorption is extremely difficult to measure precisely and the slightest leaks or impurities in the gas significantly distort results because most contaminant gases are adsorbed more strongly than hydrogen. Indeed it is generally accepted as good practice to check $H_2$ sorption data by performing the analogous experiments with $D_2$. In addition to the systems already described, among the most impressive MOFs is one reported by the group of Férey (Versailles, France) who have produced the cubic zeotype MOF $[Cr_3F(H_2O)_2(\text{terephthalate})_3]\cdot nH_2O$ (n = *ca.* 25). The compound has a very large cell volume of *ca.* 702 000 $Å^3$ and exhibits a hierarchy of large pores. The nitrogen sorption derived pore volume is 2.0 $cm^3\ g^{-1}$ giving a surface area of *ca.* 5900 $m^2\ g^{-1}$. This interesting material adsorbs 4.5 weight per cent hydrogen at 77 K and 30 atmospheres, although it is not yet certain that this is a maximum value.[57]

The precise site(s) of hydrogen adsorption in MOF-5 has been probed by single crystal neutron diffraction by the group of Judith Howard (Durham, UK).[58] Neutrons are much better than X-ray at precisely locating hydrogen – Box 8.1. The results for data recorded at several temperature from 5 to 120 K are shown in Figure 9.47. Hydrogen sorption occurs at quite specific sites at low loading (1 atmosphere pressure) with the α-site near the SBU node being the most favoured.

## Summary

- Robust inorganic porous networks such as zeolites are of tremendous industrial interest in separation, storage and catalysis. As a result they have stimulated the preparation of a wider range of 'organic zeolites' that aim to mimic their porous and robust properties while allowing more extensive synthetic tenability.
- The term 'porosity' requires a demonstration of permeability and is applied to a particular solid form, not just to a particular chemical substance.

- Network topologies can be extremely complex exhibiting complexity such as interpenetration. They are commonly described either by analogy to known structures (diamondoid, α-Po, NbO *etc*.) or using either Wells or Schäfli symbols.
- Layered solids such as graphite are interesting in separation and sorption applications and can be doped to give interesting materials properties as in Li ion batteries. Their intercalation behaviour is best described by the Daumas-Hérold model.
- Coordination polymers are infinite network solids made up of metals and ligands. They can be either discrete or 1–3 D and can have interesting and tuneable magnetic and themal expansion properties.
- Prussian blue was the first coordination polymer and has found extensive applications as a dye and ink. It has inspired the related Hoffman clathrates which are also $CN^-$ bridged coordination polymers. In contrast Werner clathrates are based on discrete coordination complexes as the host but they do display some of the robustness of coordination polymers.
- Metal-organic frameworks are highly versatile and tuneable 3D coordination polymers that are stable at relatively high temperature (though not as much as zeolites) and can exist in an empty, guest-free state. They are able to include a wide variety of guests including gases such as hydrogen, $CO_2$ and methane. They can also act as catalysts.
- Hydrogen storage by metal-organic frameworks is highly topical. The DOE targets however require light materials with large void space and hence low density. Void space alone does not make a good hydrogen sorbing material and framework surface area is also a key criterion, as is the nature of the interaction of the hydrogen with the framework. Chemical activation *via* spillover can help in this regard.

## Study Problem

9.1 A MOF based on a cubic repeating structure is composed of octahedral SBUs of volume 300 $Å^3$ linked by a spacer ligand of length 10 Å and volume 200 $Å^3$. (a) calculate the percentage void space available within the crystalline framework. (b) assuming a van der Waals volume for $H_2$ of 15 $Å^3$ how many hydrogen atoms could potentially fit into such a material? (c) How would these parameters change if the spacer ligand is lengthened to 15 Å and a new IRMOF synthesised? Assume the volume of the new ligand is 300 $Å^3$.

## References


1. Wells, A. F., *Three-Dimensional Nets and Polyhedra*. Wiley-Interscience: New York, 1977.
2. Blatov, V. A., Carlucci, L., Ciani, G., Proserpio, D. M., Interpenetrating metal-organic and inorganic 3D networks: a computer-aided systematic investigation. Part I. Analysis of the Cambridge structural database. *Crystengcomm* 2004, **6**, 377–395.
3. Delgado-Friedrichs, O., O'Keeffe, M., Yaghi, O. M., Taxonomy of periodic nets and the design of materials. *Phys. Chem. Chem. Phys.* 2007, **9**, 1035–1043.
4. Friedrichs, O. D., Dress, A. W. M., Huson, D. H., Klinowski, J., Mackay, A. L., Systematic enumeration of crystalline networks. *Nature* 1999, **400**, 644–647.
5. Atwood, J. L., Davies, J. E. D., MacNicol, D. D., Vögtle, F., *Comprehensive Supramolecular Chemistry*. Pergamon: Oxford, 1996, Vol. 7, p. 226.
6. Kruk, M., Jaroniec, M., Sakamoto, Y., Terasaki, O., Ryoo, R., Ko, C. H., Determination of pore size and pore wall structure of MCM-41 by using nitrogen adsorption, transmission electron microscopy, and X-ray diffraction. *J. Phys. Chem. B* 2000, **104**, 292–301.
7. Ma, Y., Tong, W., Zhou, H., Suib, S. L., A review of zeolite-like porous materials. *Microporous and Mesoporous Materials* 2000, **37**, 243–252.
8. Atwood, J. L., Davies, J. E. D., MacNicol, D. D., Vögtle, F., eds. *Comprehensive Supramolecular Chemistry*, Pergamon: Oxford, 1996, Vol. 7, *pp.* 641–642.

9. Tirado, J. L., Inorganic materials for the negative electrode of lithium-ion batteries: state-of-the-art and future prospects. *Materials Science & Engineering R-Reports* 2003, **40**, 103–136.
10. Julien, C., Pereira-Ramos, J. P., Momchilov, A., *New Trends in Intercalation Compounds for Energy Storage*. Kluwer: Dordrecht, 2002.
11. Carrado, K. A., Synthetic organo- and polymer-clays: preparation, characterization, and materials applications. *Applied Clay Science* 2000, **17**, 1–23.
12. Sanchez, C., Julian, B., Belleville, P., Popall, M., Applications of hybrid organic-inorganic nanocomposites. *J. Mater. Chem.* 2005, **15**, 3559–3592.
13. Katinonkul, W., Lerner, M. M., Graphite intercalation compounds with large fluoroanions. *Journal of Fluorine Chemistry* 2007, **128**, 332–335.
14. Celzard, A., Mareche, J. F., Furdin, G., Modelling of exfoliated graphite. *Progress in Materials Science* 2005, **50**, 93–179.
15. Wu, Z. B., Tian, P., Liu, Z. M., Mao, Z. Q., Progress in porous phosphonates. *Prog. Chem.* 2006, **18**, 1092–1100.
16. Lipkowski, J., Pawlowska, M., Sybilska, D., Experimental-study of selectivity and column efficiency in clathrate chromatography using Werner complexes as clathrate host components .1. Relationship between selectivity of $Ni(Ncs)_2(4\text{-methylpyridine})_4$. Guest clathrate sorbents and composition of the mobile phase. *J Chromatogr.* 1979, **176**, 43–53.
17. Guilera, G., Steed, J. W., Topological control in coordination polymers by non-covalent forces. *Chem. Commun.* 1999, 1563–1564.
18. Lavelle, L., Nassimbeni, L. R., Niven, M. L., Taylor, M. W., Studies in Werner Clathrates .2. Structure and thermal-analysis of bis(isothiocyanato)tetrakis(4-phenylpyridine)nickel(II) benzene clathrate (1-4). *Acta Crystallogr. Sect. C-Cryst. Struct. Commun.* 1989, **45**, 591–595.
19. Lis, T., Preparation, structure, and magnetic-properties of a dodecanuclear mixed-valence manganese carboxylate. *Acta Crystallogr. Sect. B-Struct. Commun.* 1980, **36**, 2042–2046.
20. Stamatatos, T. C., Foguet-Albiol, D., Lee, S. C., *et al.*, 'Switching on' the properties of single-molecule magnetism in triangular Manganese(III) complexes. *J. Am. Chem. Soc.* 2007, **129**, 9484–9499.
21. Muller, A., Bogge, H., Henry, M., Coordination chemistry under confined conditions: a simplified illustrative view. *Comptes Rendus Chimie* 2005, **8**, 47–56.
22. Fujita, M., Sasaki, O., Mitsuhashi, T., *et al.*, On the structure of transition-metal-linked molecular squares. *Chem. Commun.* 1996, 1535–1536.
23. Qian, B. H., Ma, W. X., Lu, L. D., Yang, X. J., Wang, X., *catena*-Poly[[bis(acetylacetonato-κ-O-2,O′)zinc(II)]-$\mu$-4,4′-bipyridyl-κ-*N*-2 : *N*′]. *Acta Crystallogr. Sect. E.-Struct Rep. Online* 2006, **62**, M2818–M2819.
24. Zhang, Y. S., Enright, G. D., Breeze, S. R., Wang, S. N., Coordination polymers of cobalt(II): $[Co(4,4'\text{-bpy})_2(O_2CCF_3)_2]_n$ and $[Co(4,4'\text{-bpy})(O_2CCH_3)_2(H_2O)_2]_n$. *New J. Chem.* 1999, **23**, 625–628.
25. Carlucci, L., Ciani, G., Proserpio, D. M., Sironi, A., Novel networks of unusually coordinated silver(i) cations – the wafer-like structure of $[Ag(Pyz)_2][Ag_2(Pyz)_5](PF_6)_3{\cdot}2g$ and the simple cubic frame of $[Ag(Pyz)_3](SbF_6)$. *Angew. Chem., Int. Ed. Engl.* 1995, **34**, 1895–1898.
26. Moulton, B., Lu, J. J., Zaworotko, M. J., Periodic tiling of pentagons: The first example of a two- dimensional (5,(3)(4))-net. *J. Am. Chem. Soc.* 2001, **123**, 9224–9225.
27. Power, K. N., Hennigar, T. L., Zaworotko, M. J., X-ray crystal structure of $\{Cu[1,2\text{-bis}(4\text{-pyridyl})\text{ethane}]_2(NO_3)_2\}_n$: the first example of a coordination polymer that exhibits the NbO 3D network architecture. *Chem. Commun.* 1998, 595–596.
28. Dunbar, K. R., Heintz, R. A., 'Chemistry of transition metal cyanide compounds: modern perspectives'. in *Progress in Inorganic Chemistry*, Karlin, K. D., ed. John Wiley & Sons, Inc.: New York, 1997.
29. Moliner, N., Gaspar, A. B., Muñoz, M. C., Niel, V., Cano, J., Real, J. A., Light- and thermal-induced spin crossover in {Fe(abpt)2[N(CN)2]2}. synthesis, structure, magnetic properties, and high-spin T low-spin relaxation studies. *Inorg. Chem.* 2001, **40**, 3986–3991.
30. Nihei, M., Han, L. Q., Oshio, H., Magnetic bistability and single-crystal-to-single-crystal transformation induced by guest desorption. *J. Am. Chem. Soc.* 2007, 129, 5312–5313.
31. Matouzenko, G. S., Perrin, M., Le Guennic, B., *et al.*, Spin crossover behavior in a family of iron(II) zigzag chain coordination polymers. *Dalton Trans.* 2007, 934–942.
32. Barrera, G. D., Bruno, J. A. O., Barron, T. H. K., Allan, N. L., Negative thermal expansion. *J. Phys.-Condes. Matter* 2005, 17, R217–R252.
33. Chapman, K. W., Chupas, P. J., Kepert, C. J., Compositional dependence of negative thermal expansion in the Prussian blue analogues (MPtIV)-Pt-II(CN)(6) (M = Mn, Fe, Co, Ni, Cu, Zn, Cd). *J. Am. Chem. Soc.* 2006, **128**, 7009–7014.
34. Goodwin, A. L., Calleja, M., Conterio, M. J., *et al.*, Colossal positive and negative thermal expansion in the framework material Ag3[Co(CN)6]. *Science* 2008, **319**, 794–797.
35. Carlucci, L., Ciani, G., Proserpio, D. M., Rizzato, S., Three novel interpenetrating diamondoid networks from self-assembly of 1,12-dodecanedinitrile with silver(I) salts. *Chem. Eur. J.* 2002, **8**, 1520–1526.

36. Hoskins, B. F., Robson, R., Slizys, D. A., An infinite 2D polyrotaxane network in Ag-2(bix)$_3$(NO$_3$)$_2$ (bix = 1,4-bis(imidazol-1-ylmethyl)benzene). *J. Am. Chem. Soc.* 1997, **119**, 2952–2953.
37. Dobrzanska, L., Raubenheimer, H. G., Barbour, L. J., Borromean sheets assembled by self-supporting argentophilic interactions. *Chem. Commun.* 2005, 5050–5052.
38. Yaghi, O. M., Li, H. L., Davis, C., Richardson, D., Groy, T. L., Synthetic strategies, structure patterns, and emerging properties in the chemistry of modular porous solids. *Acc. Chem. Res.* 1998, 31, 474–484.
39. Pan, L., Woodlock, B., Wang, X., Lam, K.-C., Rheingold, A. L., Novel silver(I)-Organic Coordination Polymers: conversion of extended structures in the solid state as driven by argentophilic interactions. *Chem. Commun.* 2001, 1762–1763.
40. Thompson, C., Champness, N. R., Khlobystov, *et al.*, Using microscopic techniques to reveal the mechanism of anion exchange in crystalline co-ordination polymers. *J. Microsc.-Oxf.* 2004, **214**, 261–271.
41. Khlobystov, A. N., Champness, N. R., Roberts, C. J., Tendler, S. J. B., Thompson, C., Schroder, M., Anion exchange in co-ordination polymers: a solid-state or a solvent-mediated process? *Crystengcomm* 2002, 426–431.
42. Biradha, K., Hongo, Y., Fujita, M., Open square-grid coordination polymers of the dimensions 20 x 20 Å exhibiting remarkably stable and crystalline solids. *Angew. Chem. Int. Ed.* 2000, **39**, 3843.
43. Belcher, W. J., Longstaff, C. A., Neckenig, M. R., Steed, J. W., Channel-containing 1D coordination polymers based on a linear dimetallic spacer. *Chem. Commun.* 2002, 1602–1603.
44. Garay, A. L., Pichon, A., James, S. L., Solvent-free synthesis of metal complexes. *Chem. Soc. Rev.* 2007, **36**, 846–855.
45. Yaghi, O. M., Li, G., Li, H., Selective binding and removal of guests in a microporus metal-organic framework. *Nature* 1995, **378**, 703–706.
46. Li, H., Eddaoudi, M., O'Keeffe, M., Yaghi, O. M., Design and synthesis of an exceptionally stable and highly porous metal-organic framework. *Nature* 1999, **402**, 276–279.
47. Eddaoudi, M., Kim, J., Rosi, N., *et al.*, Systematic design of pore size and functionality in isoreticular MOFs and their application in methane storage. *Science* 2002, **295**, 469–472.
48. Reineke, T. M., Eddaoudi, M., Moler, D., O'Keeffe, M., Yaghi, O. M., Large free volume in maximally interpenetrating networks: The role of secondary building units exemplified by Tb-$_2$(ADB)$_3$[(CH$_3$)$_2$SO]$_4$·16[(CH$_3$)$_2$SO]. *J. Am. Chem. Soc.* 2000, **122**, 4843–4844.
49. Blake, A. J., Champness, N. R., Khlobystov, A. N., Lemenovskii, D. A., Li, W. S., Schroder, M., Crystal engineering: The effects of $\pi$-$\pi$ interactions in copper(I) and silver(I) complexes of 2,7-diazapyrene. *Chem. Commun.* 1997, 1339–1340.
50. Xu, X. L., Nieuwenhuyzen, M., James, S. L., A nanoporous metal-organic framework based on bulky phosphane ligands. *Angew. Chem., Int. Ed.* 2002, **41**, 764–767.
51. Fletcher, A. J., Cussen, E. J., Prior, T. J., Rosseinsky, M. J., Kepert, C. J., Thomas, K. M., Adsorption dynamics of gases and vapors on the nanoporous metal organic framework material Ni$_2$(4,4′-bipyridine)$_3$(NO$_3$)$_4$: Guest modification of host sorption behavior. *J. Am. Chem. Soc.* 2001, **123**, 10001–10011.
52. Matsuda, R., Kitaura, R., Kitagawa, S., *et al.*, Highly controlled acetylene accommodation in a metal-organic microporous material. *Nature* 2005, **436**, 238–241.
53. 'Hydrogen Posture Plan', United States Department of Energy, February 2004. http://www.eere.energy.gov/hydrogenandfuelcells/pdfs/hydrogen_posture_plan.pdf.
54. Furukawa, H., Miller, M. A., Yaghi, O. M., Independent verification of the saturation hydrogen uptake in MOF-177 and establishment of a benchmark for hydrogen adsorption in metal-organic frameworks. *J. Mater. Chem.* 2007, **17**, 3197–3204.
55. Lin, X., Jia, J. H., Zhao, X. B., *et al.,* High H-2 adsorption by coordination-framework materials. *Angew. Chem., Int. Ed.* 2006, **45**, 7358–7364.
56. Li, Y. W., Yang, R. T., Significantly enhanced hydrogen storage in metal-organic frameworks *via* spillover. *J. Am. Chem. Soc.* 2006, **128**, 726–727.
57. Férey, G., Mellot-Draznieks, C., Serre, C., *et al*., A chromium terephthalate-based solid with unusually large pore volumes and surface area. *Science* 2005, **309**, 2040–2042, correction 2005, **310**, 1119.
58. Spencer, E. C., Howard, J. A. K., McIntyre, G. J., Rowsell, J. L. C.; Yaghi, O. M., Determination of the hydrogen absorption sites in Zn$_4$O(1,4-benzenedicarboxylate) by single crystal neutron diffraction. *Chem. Commun.* 2006, 278–280.

# 10 Self-Assembly

*'On from room to room I stray*
*Yet mine host can ne'er espy*
*And I know not to this day*
*Whether guest or captive I.'*

Sir William Watson (1858–1936), *World-Strangeness*

# 10.1 Introduction

Lindoy, L. F., Atkinson, I., *Self-assembly in Supramolecular Systems.* Royal Society of Chemistry: Cambridge, 2000.

## 10.1.1 Scope and Goals

Whitesides, G. M., Grzybowski, B., 'Self-assembly at all scales', *Science* 2002, **295**, 2418–2421.

The synthesis of even small molecules by conventional organic or coordination chemistry may often be a tedious and repetitive process. With every new stage in the synthetic pathway, more and more product is lost, even in relatively high-yielding steps. The cost, both in materials and specialist endeavour, rises steeply. Indeed, entire chemistry-related disciplines such as chemical engineering have, as a primary goal, the task of simplifying chemical syntheses as much as possible. However, in the preparation of many speciality or fine chemicals this is often a very difficult task. Even more difficult is the extension of conventional chemistry to the preparation of intermediate and large-size molecules, assemblies and nanometre-scale (nanoscale) machines. Yet it is the preparation of such large aggregates that many supramolecular chemists believe will pave the way to the construction of new ultra-miniaturised components for computational, electronic and optical devices (Chapter 11). As a result, a great deal of work has gone into the development of preprogrammed systems in which small, readily prepared molecular components automatically converge to produce a much larger, more complicated aggregate. By the term 'preprogramming' we understand a chemical system in which the very nature of the molecular building blocks (in terms of size, shape, symmetry and the electronic properties of their binding sites) contains all the information necessary to selectively produce the desired superstructure. The supramolecular complex assembles itself. Thus we can define self-assembly as *the spontaneous and reversible association of molecules or ions to form larger, more complex supramolecular entities according to the intrinsic information contained in the molecules themselves.*

This kind of approach is potentially of central importance in bridging the gap between the scale of structures and components available within the molecular world and those available on the tens to hundreds on nanometer scale *via* current lithographic techniques (particularly in the electronics industry). Production of electronic devices on the molecular scale would enable dramatic increases in speed and computing power, as well as the enhanced versatility that comes from small space requirements. Indeed, already computer hard disks have a read head flying at only 25 nm or 200 atoms above the surface of the disk. In order to function, however, molecular bistable devices (switches) must be provided with the input/output infrastructure necessary for them to communicate with the outside world. Furthermore, they must be completely controllable, reversible and readable at the molecular level through millions of 'on–off' cycles. Current lithographic etching techniques result in the production of components of silicon wafers of sizes down to about 0.1 μm (*i.e.* 1000 Å or 100 nm). Already, even at that scale, problems are encountered with electron tunnelling and difficulty of heat dissipation, as well as more subtle effects such as quantum mechanical confinement of charge carriers, which results in each component having a different range of energy levels depending on its size. It is possible that fabrication of components by lithography is fundamentally limited to the tens of nanometre size scale. On the other hand, the *largest* well-characterised synthetic supermolecules to date are of the order of a few tens of nanometre in size, and have much more well-defined properties. Unfortunately, they lack the integrated suite of functionality requirements for practical device manufacture. This suggests

*Supramolecular Chemistry, 2nd edition* J. W. Steed and J. L. Atwood
© 2009 John Wiley & Sons, Ltd ISBN: 978-0-470-51233-3

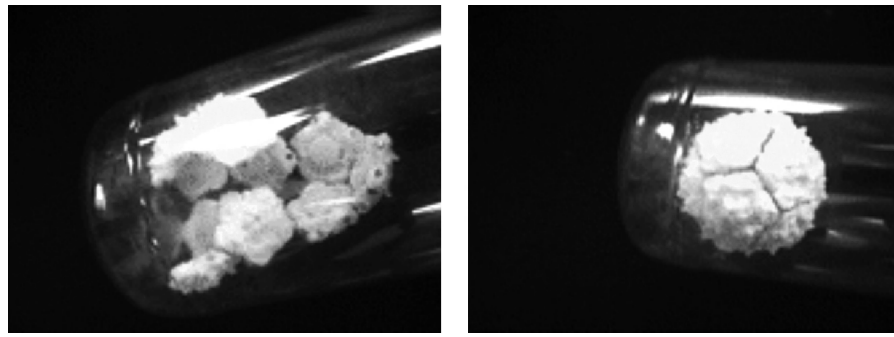

**Figure 10.1** Self-assembly of twelve autofabricated pentameric tiles linked by magnetic interactions inspired by the self-assembly of the protein capsid of the poliovirus (Copyright National Academy of Sciences, U.S.A.).

that there is a point in between the worlds of electronic engineering and chemical synthesis, on the size scale 10–1000 nm, in which well-defined, functional and networked supramolecules might form the basis for a new kind of electronic design. Precedent for this molecular engineering comes from the world of molecular biology (Chapter 2) in which functional molecular devices of sizes between 1 and 10 000 nm regulate all of the chemistry of life, and indeed there is no fundamental reason why artificial molecular devices may not similarly exist. The vast majority of such biochemical systems are self-assembling in order to economise on the amount of genetic information required to synthesise them. For example the coats or capsids of virus particles generally comprise multiple copies of the same protein that self-assemble into highly regular geometric arrangements. Figure 10.1 shows a macroscopic model that gives at least a cartoon-type insight into the principles that underlie complex processes such as viral self-assembly. The model uses tiles based on the pentameric shape of poliovirus intermediates in capsid assembly. The tiles interact with one another *via* magnets which simulate the supramolecular interactions involved in linking them together. Manual shaking of twelve such curved pentagonoids in a container results in the 'self-assembly' of a closed, dodecahedral structure in just 1–2 minutes.[1]

In order to bridge the gap between current electronic and chemical technology, two distinct approaches may be distinguished: 'engineering down' and 'synthesising up'. We have already seen that there is little room for manoeuvre in engineering down due to current technological limitations, and thus the challenge to chemical technology is to develop ways to 'synthesise up' into the required range of scale and functionality through the use of supramolecular techniques. We will look in more detail at the 'synthesising up' and 'engineering down' approaches to nanotechnology in Chapter 15. For the time being we will explore the unit chemical steps that have so far been explored in the synthesis of large scale supramolecular systems and show what has been achieved so far in terms of the programmed or templated self-assembly of functional multi-nanometre scale supramolecular aggregates.

Closely linked to the concept of self-assembly is the idea of self-replication: the ability of one molecule or entity to produce a copy of itself. The analogy to biological (asexual) reproduction is clear and the ability to self-replicate has been suggested to constitute a basic criterion of life. Abundant examples in nature demonstrate that self-replication is a feasible, and indeed commonplace, occurrence at the molecular level. Biological cell division involves the unwinding of the DNA double helix and the templated synthesis, *via* interstrand hydrogen bond base pairing, of a complementary copy of each single strand to generate two new double helices (Section 2.9.5). A single DNA strand contains all the information necessary to produce its complementary partner leading to self-replication of the

double helix without the prohibitively frequent introduction of mistakes or variations (mutations). By comparison, the conventional synthesis of even a small oligonucleotide by stepwise condensation of phosphate residues would be a monumental task. Indeed, the surmounting of this barrier to oligonucleotide production by the polymerase chain reaction (PCR) (a process by which small amounts of oligonucleotides template the formation of a large number of copies of themselves) earned the 1993 Nobel Prize in Chemistry for Kary B. Mullis for his work in this area (Section 2.9.3). Increasingly in biochemical and chemical systems the concept of dynamic or time-resolved self-assembly is being recognised leading to a temporal hierarchy. Generally speaking this concept means that in complex systems self-assembly occurs in a sequence of stages with the higher stages ($j$) not assembling until the self-assembly of a building block step ($j - 1$) is complete. The lifetime of each self-assembled stage ($\tau$) is inversely proportional to its position in the hierarchy, thus the highest stages are much longer lived than the stages below them, *i.e.* $\tau_j >> \tau_{j-1}$. The relevance of this kind of hierarchial self-organisation in biology is clear – the dimerisation of two nucleobases is individually short lived but a biological cell and thence an organism has an indefinitely long lifetime.

All of self-assembly is based on some kind of templating (*i.e.* information-based assembly). We have already seen the operation of the template effect in synthesis (Section 3.9.1), in which a metal cation is used as a simple spherical template for the assembly of macrocyclic organic ligands. In this chapter we will examine much more generalised applications of templates and the self-templation that constitutes self-assembly, including the synthesis of elaborate supramolecular structures such as molecular knots, catenanes and rotaxanes. The next chapter, Chapter 11, then deals with large-scale functional devices, while the efforts of the supramolecular chemistry community to produce biomimetic and artificial, abiotic (*i.e.* non-biological) self-replicating systems is discussed along with supramolecular (templated) catalysis in Chapter 12.

## 10.1.2 Concepts and Classification

Lindsey, J. S., 'Self-Assembly in synthetic routes to molecular devices: biological principles and chemical perspectives – a review', *New J. Chem.* 1991, **15**, 153–180.

Before embarking upon a survey of both natural and synthetic template-assembled and self-assembling systems, it is important to define and distinguish some of the language that will be required. Much of the terminology of supramolecular chemistry is still in a state of rapid change, and many terms are used either interchangeably or loosely with different terms being applied to very similar phenomena in chemistry and biochemistry in particular. Jean-Marie Lehn has distinguished a hierarchical order of the terms 'templating', 'self-assembly' and 'self-organisation'. Together, these terms cover the processes that enable preprogrammed molecular components or *tectons* (from the Greek tektōn, meaning builder, *cf.* Section 8.1.2) to come together spontaneously, in a well-defined way, to give assemblies presenting order in one, two or three dimensions and perhaps (although not necessarily) time. We have already discussed the template effect (Section 3.9.1) as a useful aid to synthesis through the involvement of temporary or permanent 'helper' species (*e.g.* an alkali metal cation). *Self-assembly* may or may not involve an actual template, such as a metal cation, and thus the template effect itself is not strictly an example of self-assembly, but has been classified by Lehn as 'the unit step in self-assembly processes that comprise several steps occurring spontaneously in a single operation'. Within self-assembly processes, we must distinguish *molecular self-assembly* and *supramolecular self-assembly.* Molecular self-assembly concerns the formation of covalent bonds as part of a special synthetic procedure. The assembly is subject to control by the reaction stereochemistry and the conformational features of the intermediates, *e.g.* the formation of amine–aldehyde condensation macrocycles, as in Scheme 3.21. Supramolecular self-assembly concerns the recognition-directed, reversible spontaneous association

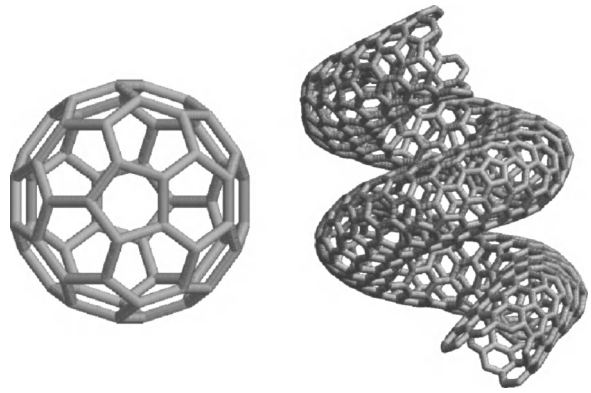

**Figure 10.2** Fullerenes such as $C_{60}$ and carbon nanotubes self-assemble covalently under extreme conditions.

of a limited number of tectons (components) under the intermolecular control of relatively labile, noncovalent interactions such as coordination interactions, hydrogen bonds and dipolar interactions. The reversibility of supramolecular self-assembly is key to the resulting systems' ability to sift through the available components to form the thermodynamically most favourable structure. This incorporates the potential for self-repair and correction of defects, as in biological systems. Fundamentally self-assembly is a *convergent* process in which a number of components assemble into, ideally, a single final, stable structure. Self-assembly is thus very distinct from chemical *emergence* which is a divergent process in which complexity evolves over time (Section 1.10.2). We will return to the interesting concept of emergence in chemical systems in Chapter 15.

An interesting borderline case between covalent and supramolecular self-assembly concerns the formation of fullerenes, such as $C_{60}$ and $C_{70}$, and related species such as extended carbon nanotubes (Figure 10.2) within a high-temperature carbon vapour. While strictly an example of irreversible covalent bond formation, the extreme conditions of the carbon vapour permit a certain amount of reversibility in the formation of even strong covalent bonds, allowing them to behave somewhat like weaker supramolecular interactions do under ambient conditions. This means that more stable closed structures such as $C_{60}$, which does not have any dangling bonds, are formed in preference to fragments of graphitic sheet, for example.

On a higher level, the term *self-organisation* incorporates both the interaction between constituent parts of self-assembled entities and the integration of those interactions leading to collective behaviour such as is found in phase changes, for example. Self-organisation admits the possibility of emergent behaviour that is a property arising from complex interactions between self-assembled entities.

In 1991 Lindsey introduced a definitive classification scheme for various types of self-assembly across biochemistry and chemistry which still remains the basis for the way in which we think about self-assembly today. Lindsay's scheme divides self-assembly into seven broad, overlapping classes.

### *Class 1. Strict Self-Assembly*

In a strict self-assembly process, the final product is produced entirely spontaneously when the components are mixed together in the correct ratios under a given set of conditions of temperature, pH, concentration *etc.* The product formation must be completely reversible and represent the thermodynamic minimum for the system. In essence, all the information necessary for the assembly to occur is coded into the constituent parts. The concept of strict self-assembly is rooted in the 'Thermodynamic Hypothesis' of Afinison who suggested that under physiological conditions the native structure of a protein is

the one in which the Gibbs free energy of the system is at its lowest.* Later work showed that this basic concept is not true of all proteins, some of which are assembled by entities such as chaperones.

### *Class 2. Irreversible Self-Assembly*

Irreversible self-assembly involves the formation of a product through a series of irreversible (usually covalent) bond-forming steps under kinetic control. There is no margin for self-correction and any 'mistakes' are fatal to the formation of the final assembly. This class of reaction is not of significant interest in supramolecular chemistry but is topical in organic synthesis as 'tandem' or 'domino' reactions.[2]

### *Class 3. Precursor Modification Followed by Self-Assembly*

This process involves precursors that cannot undergo self-assembly until they are chemically modified – they are thus in a kind of 'resting state' until activated by some trigger or change. An example is the biosynthesis of collagen, the fibrous protein that are the major components of skin and bone. Collagen forms long fibrous bundles outside the cell, called fibrils. It would be fatal to the cell if these fibrils self-assembled inside it and so the collagen precursor, procollagen, is prevented from doing so by end-capping amino acid chains termed 'propeptides'. Once synthesised the procollagen is secreted out of the cell where the capping propeptides are removed by proteolytic enzymes, triggering the self-assembly process (*cf.* prions and amyloids in Section 14.6.1).

### *Class 4. Self-Assembly with Postmodification*

This process involves the covalent 'locking in' of structures formed by reversible self-assembly. The irreversible, post-assembly step switches off the equilibrium process involved in the self-assembly. As we will see in the following sections, self assembly with covalent postmodification is involved in a range of biochemistry (*e.g.* insulin synthesis) and elegant abiotic supramolecular synthesis as in the formation of catenanes and knots.

### *Class 5. Assisted Self-Assembly*

In an assisted self-assembly process external factors that are not part of the final assembly are involved in mediating the assembly process rather like a catalyst. This concept became important with the recognition of the role played by molecular chaperones in protein folding. The chaperone does not influence the thermodynamics of the assembly process and thus it leaves the ratio of folded and unfolded polypeptide chains the same but it stabilises intermediates along the folding pathway, accelerating the folding rate. Chaperones are important in prevention of peptide aggregation and in refolding denatured proteins.[3]

### *Class 6. Directed Self-Assembly*

Directed self-assembly processes are those which involve a template, whether or not it ends up in the final structure. Typical examples are vesicle-directed biomimetic mineralisation strategies (Section 15.3)

### *Class 7. Self-Assembly with Intermittent Processing*

This class of self-assembly incorporates elements from all of the preceeding classes and involved complex processes in which there are sequential steps involving self-assembly and covalent or irreversible modification. In general such processes are only found in biology at the present state of the field.

---

* US biochemist Christian Anfinsen 1916–1995, winner of the 1972 Nobel Prize in Chemistry for 'his work on ribonuclease, especially concerning the connection between the amino acid sequence and the biologically active conformation'.

For the most part, in abiotic supramolecular chemistry which is overwhelmingly based on either metal-ligand coordination interactions or hydrogen bonding, we will be concerned only with classes 1 and 4, *i.e.* either strict self-assembly or self-assembly with postmodification. Even within these classes, however, we can distinguish some subtleties of the kinds of bonding that can be involved with often more than one kind of interaction, perhaps of different strength, being involved. Depending on the number and types of interaction we can classify self-assembly processes as either a *Single* or *Multiple Interaction Self-Assembly.* These descriptive terms pertain to the number of different kinds of interaction that are present within the assembled structure. Single interaction self-assemblies might depend only on metal ligand interactions, for example, while multiple interaction processes might involve metal-ligand interactions and hydrogen bonding. We can also subdivide multiple interaction self-assemblies based on the number of a particular type of interaction present. If the self-assembled system contains different categories of interaction (*e.g.* both metal-ligand bonds and hydrogen bonds) then the term *multimediated assembly* is used, whereas if the assembly contains two different metal coordination environments but no other types of interaction then we refer to it as a *unimediated assembly* because even though there are two distinct interactions, they are both metal-ligand interactions, Figure 10.3.

In general, in self-assembly, we can identify three main drivers that pervade a wide variety of chemical systems, particularly metal-ligand complexes:

1. Efficient self-assembly occurs when there is a match between the geometric or stereochemical preferences of the components, *e.g.* the coordination polyhedron of a metal ion and the possible binding site arrangement(s) on a ligand. These pairings are sometimes referred to as *incommensurate symmetry interactions* or *interactional algorithms*
2. All binding sites must be involved in the assembly.
3. Assemblies are influenced by the efficient packing of geometrical shapes in crystals or macroscopic materials.

Before we go on to discuss artifical self-assembly, particular the current intense interest in self-assembling coordination complexes, we will look for inspiration at how Nature does it!

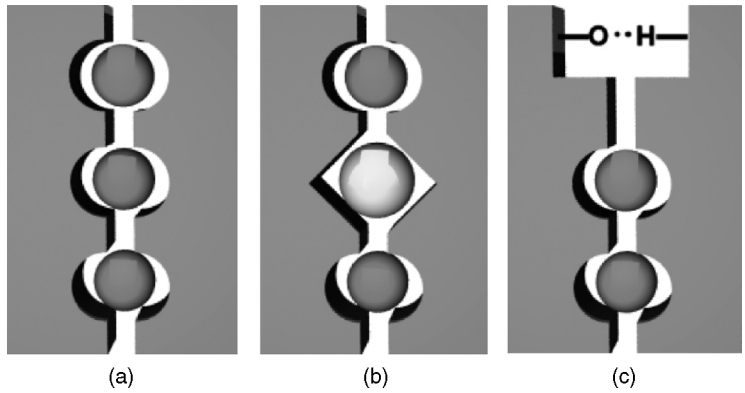


**Figure 10.3** (a) A single interaction assembly using one specific type of metal-ligand interaction, (b) A unimediated multiple interaction assembly, using two different metal-ligand interactions, (c) A multimediated multiple interaction assembly using both metal-ligand interactions and hydrogen bonding.

## 10.2 Proteins and Foldamers: Single Molecule Self-Assembly

### 10.2.1 Protein Self-Assembly

Okabayashi, H.-F., Ishida, M. and O'Connor, C. J., 'The self-assembly of oligo-peptides', in *Self-Assembly*, Robinson, B. H. (ed.), *pp.* 331–338, IOS Press: Amsterdam, 2003.

In a strict self-assembly process all of the interactions contribute to the overall free energy of the assembly and the final product will be the one with the lowest overall free energy. The sequence of events by which the assembly forms may well depend on the magnitude of the interactions, however, with the stronger or primary interactions (*e.g.* metal-ligand bonds) needing to form first before the structure is further stabilised by *secondary interactions* such as hydrogen bonding between partially assembled fragments. This process is termed *hierarchial assembly* and is a common feature in both abiotic and biological self-assembly. In proteins, the linear polypeptide sequence folds first into significant secondary structural features such as α-helices and β-sheets, held together by amide NH···O=C hydrogen bonding interactions and hydrophobic effects in aqueous solution. The repetition of these features within a particular strand is often termed *supersecondary structure*. The overall folding of each polymer strand gives the protein tertiary structure and is responsible for many of the protein's properties including the catalytic activity of enzymes which is often closely linked to the geometry and environment of the active site. Interactions between folded polymers to give self-assembled aggregates of a number of folded protein chains is termed the quaternary structure (Figure 2.20). For example, haemoglobin is made up from four separate myoglobin subunits (Section 2.5). Clearly the quaternary structure cannot assemble until the tertiary structure has formed, and so on. This hierarchical mechanism allows proteins to fold into their active conformations in a matter of minutes. For comparison, it is estimated that for a small 100 amino acid residue protein a random search for the lowest energy conformer would take about $10^{27}$ years. Such slow speeds are not biochemically viable – this figure is about $10^{18}$ times longer than the age of the universe! In abiotic systems we can also recognise some of these kinds of features. For example in the case of a metal helicate the primary structure involves the metal-ligand bonds with the secondary structure being the helical conformational folding. We might also recognise tertiary structure in the circular helicates (Section 10.8.6) The hierarchical nature of protein folding to give the precise conformation based on the information encoded into the primary sequence of amino acid residues is vital from a biological viewpoint. Errors in protein folding can have disastrous consequences. For example, many serious diseases such as BSE, CJD, Diabetes and Alzheimer's Disease are caused by the misfolding of proteins into toxic, aggregated β-sheet fibrils termed *amyloids*, Figure 10.4. The tightly packed β-sheet structure of amyloid fibres is characterised by two characteristic X-ray diffraction maxima at 4.7 and 10 Å, corresponding to the interstrand and stacking distances in β-sheets These represent cases where the biological self-assembly process has 'gone wrong' in some way. This might be due to the malign influence of an external agent such as a *prion* (**pr**oteinaceous **i**nfectious particle) which infects and propagates by refolding abnormally into a structure which is able to convert normal molecules of the protein into an abnormally structured form. The fact that normal proteins can be refolded in this way suggests that they may not represent true examples of strict self-assembly since the refolded form is in some way more stable (although the insolubility of amyloids is also a significant driving force). Indeed while many proteins do self-assemble, others require some kind of assistance in their folding in the form of other proteins called molecular chaperones that guide or catalyse the assembly process.

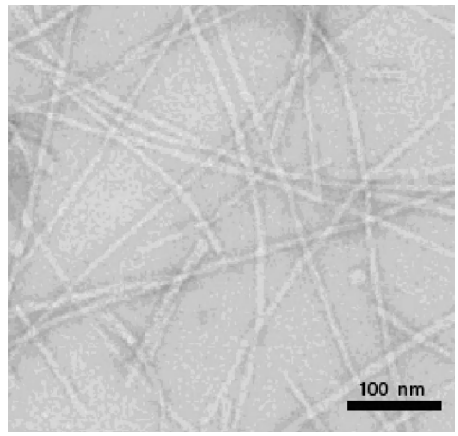


**Figure 10.4** Electron microscope image of negatively stained amyloid fibrils formed by islet amyloid polypeptide showing long, unbranching fibrils of 100 Å in diameter (reproduced with permission from [4]).

## 10.2.2 Foldamers

Goodman, C. M., Choi, S.. Shandler, S. and DeGrado, W. F., 'Foldamers as versatile frameworks for the design and evolution of function', *Nature Chem. Biol.* 2007, **3**, 252–262.

Given the importance of single molecule self-assembly in proteins it is natural that supramolecular chemists have tried to mimic this property in biological models and in artificial systems. Artificial or biomimetic molecules that self-assemble into a particular conformation are termed *foldamers* and they represent a popular area of current research not just as aids in our understanding of protein folding but also as artificial scaffolds used to place functional or sensing groups in a precise way relative to one another – a step towards chemical nanotechnology. Foldamers can be amino acid based short polypeptide sequences as in non-natural peptide oligomers such as aliphatic β-, γ-, and δ-peptides, which are significant because of their similarity to α-peptides (a β-peptide has the amine group on the second carbon atom of the chain instead of the first as in natural α-amino acid derived peptides, similarly a γ-peptide has the amine group on the third carbon atom and so on). Aromatic amides are particularly popular foldamer components because of the restricted rotation about the Ar–C(O)NH bond that is a result of the delocalisation of the amide lone pair, Scheme 10.1a. The conformation of the group can also be locked in by particular hydrogen bonding interactions, Scheme 10.1b.[5]

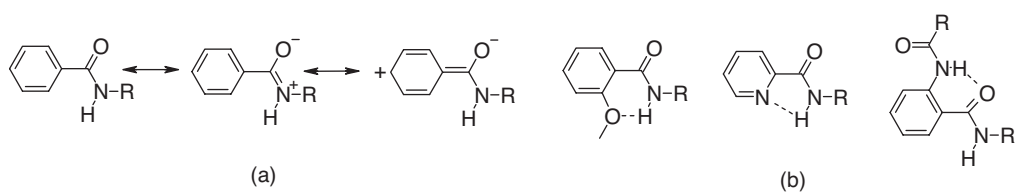


**Scheme 10.1** (a) resonance forms in aryl amides illustrating the restricted rotation of the Ar–C(O)NH bond because of the partial double bond character and (b) examples of hydrogen bonding motifs stabilising particular aryl amide conformers.

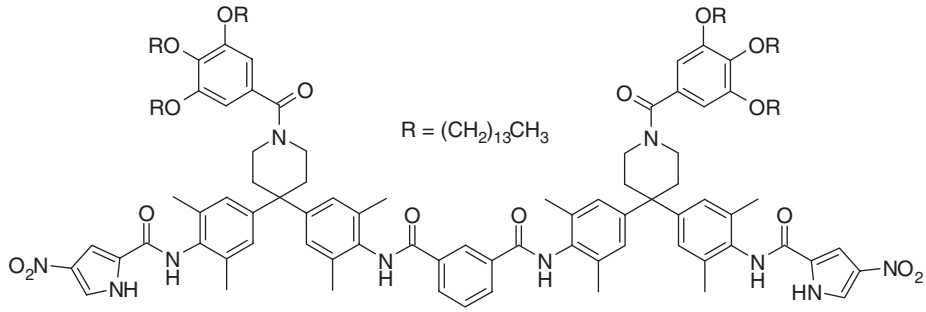


**10.1**

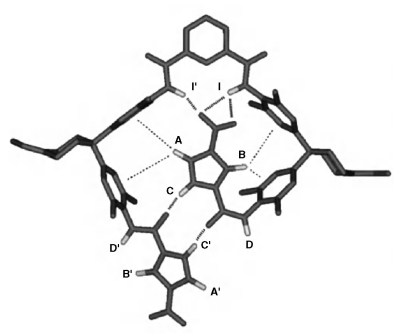


(a)

(b)

**Figure 10.5** (a) solution structure of the 'tailbiter' foldamer (**10.1**) (reproduced by permission of The Royal Society of Chemistry) and (b) Lucas Jennis' engraving of the wyrm Ouroboros that swallows its own tail, published on an alchemical emblem-book entitled *De Lapide Philisophico* (1625).

A particularly attractive aryl amide foldamer is 'talibiter' (**10.1**) named after the mythological wyrm Ouroboros that Kekulé claimed inspired his structure of benzene (Figure 10.5),[6] which folds back on itself in a spiral conformation such that the pyrrole unit on one end is close to the other end of the molecule. The solution conformation of the foldamer was determined using NMR spectroscopic methods as described in Box 6.1.

## 10.3 Biochemical Self-Assembly

### 10.3.1 Strict Self-Assembly: The Tobacco Mosaic Virus and DNA

Klug, A., 'The tobacco mosaic virus particle: structure and assembly', *Phil. Trans. Royal Soc. Ser. B, Biol. Sci.* 1999, **354**, 531–535.

We have already dealt with some general aspects of biochemical self-assembly in Section 2.10 including the remarkable formation of viral capsids. There are some biochemical examples, however, that translate readily into supramolecular chemical concepts and have been pivotal in defining the field. One such system is the tobacco mosaic virus, a virus that is very harmful to a variety of crops including tobacco, tomato, pepper, cucumbers and species such as ornamental flowers. This system consists of a helical virus particle measuring some 300 × 18 nm (Figure 10.6). A central strand of RNA is sheathed by 2130 identical protein subunits, each of which contains 158 amino acids. What is remarkable about

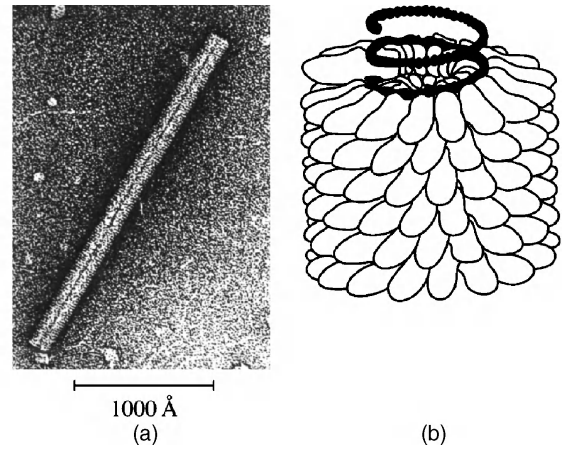


**Figure 10.6** (a) Electron micrograph and (b) Schematic representation of the tobacco mosaic virus. (Copyright Wiley-VCH Verlag GmbH & Co. KGaA. Reproduced by permission).

the virus, compared to a purely chemical entity, is that if it is decomposed into its component parts and these fragments are mixed under physiological conditions, then the virus particle is accurately self-reassembled and regains full functionality. The mechanism of this impressive piece of self-assembly is well established and consists of the formation of a disk-shaped module by the aggregation of two layers of the protein sheath subunits. The protein disk is transformed into two helix turns by threading a loop of RNA into the central hole of the disk. The process is repeated by threading additional disks until the viral particle is complete, (Figure 10.7).

The advantage of this convergent, modular approach to viral assembly, in which identical subunits are assembled into the complete entity, is that much less genetic information is required to program the formation of the assembly compared to coding the location of each residue individually. The formation of the tobacco mosaic virus serves to illustrate the role played in nature of noncovalent interactions. The entire self-assembly process is driven by nothing stronger than hydrogen bonding, electrostatic and solvophobic effects and other very weak interactions, all acting in concert. The final structure represents a thermodynamic product and is favoured by a high equilibrium constant of formation (formation constant). The self-assembly of the tobacco mosaic virus is thus an example of strict self-assembly in Lindsey's scheme. The weak nature of the interactions means that if a mistake is made during the assembly process, then it is rectified automatically because the process is reversible and the 'mistaken' product is simply not as stable as the correct arrangement.

The most famous example of a strict self-assembly process is the formation of the DNA double helix (Figure 2.27), by the spontaneous association (by hydrogen bonding) of complementary

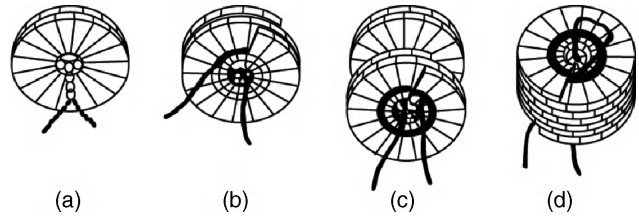


**Figure 10.7** (a)–(d) Stepwise self-assembly of the tobacco mosaic virus. (Copyright Wiley-VCH Verlag GmbH & Co. KGaA. Reproduced by permission).

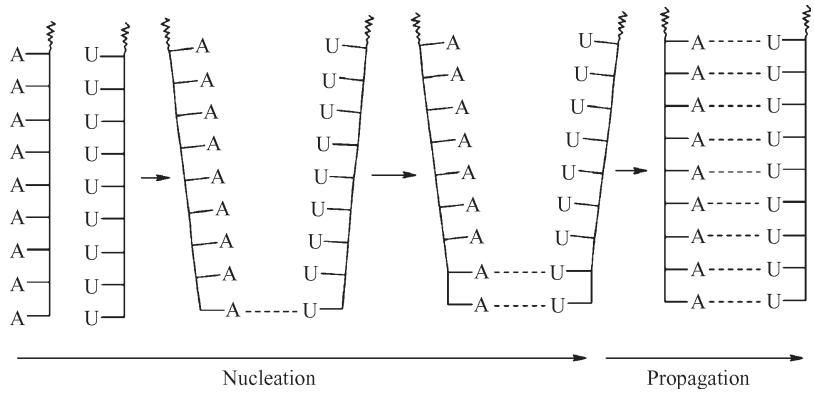


**Figure 10.8** Stages in the self-assembly of adenine–uracil nucleic acid double helices.

nucleobase pairs such as guanine and cytosine (Fig. 2.28). The thermodynamics of 'zipping up' the double-helical structure are of interest since the association of the two helical strands results in a thermodynamically unfavourable decrease in entropy, suggesting that there might be a significant thermodynamic barrier to be overcome. Studies on relatively small model systems such as the adenine- and uracil-based complementary pair of nucleic acids $(A)_{17}$ and $(U)_{17}$ show that the entwining of the two strands to form a double helix is a two-stage process consisting firstly of a nucleation phase followed by a cascade propagation sequence, which completes the process (Figure 10.8). The nucleation phase brings together the two strands and is dominated by the thermodynamically unfavourable entropy component, since the favourable enthalpy term arising from the formation of hydrogen bonds between a few base pairs is relatively insignificant. Once nucleation has occurred, the association of every new base pair results in further increases to the magnitude of the favourable enthalpy term with little change in entropy, resulting in a complete double helix (Figure 10.9).

## 10.3.2 Self-Assembly with Covalent Modification

The term 'self-assembly with covalent modification' is generally applied to systems in which the formation of covalent linkages is irreversible, particularly as in classes 3 and 4 in Lindsey's scheme. If the covalent bond formation occurs *after* the self-assembly (class 4) then, unlike a strict self-assembly, the final product does not necessarily need to be a thermodynamic minimum structure. On the other hand class 3 self-assembly does result in a thermodynamically stable structure once the covalent initiation step has taken place. Figure 10.10a shows a cartoon representation of the concept of precursor preprocessing. The interlocking of the two self-assembling components cannot occur until a covalent chemical change is carried out on the precursor of one of them. This may result in a change in size, shape or orientation, or the removal of a blocking effect. The two subunits are then free to self-assemble. Self-assembly with covalent modification may also involve post-assembly processing in which non-covalent interactions are used to assemble a precursor complex that is then fixed in the desired state by covalent modification, Figure 10.10b. This may be regarded as a kind of template effect, and indeed parts of the structure needed to template the initial self-assembly may subsequently be cleaved away if no longer required. An excellent biological example is the biosynthesis of the mammalian hormone, insulin. Insulin consists of two polypeptide chains (A and B)

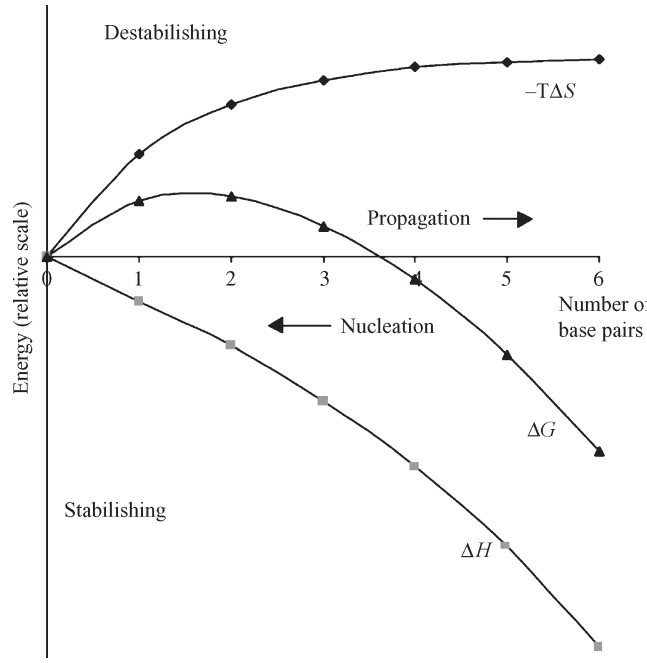


**Figure 10.9** Energetics of the self-assembly of nucleic acid double helices as a function of increasing number of base pairs.

linked by a pair of disulfide bridges. Reduction of these —S—S— bridges leads to the break-up of the insulin molecule. Unlike the tobacco mosaic virus, however, the individual polypeptide chains do not contain the information necessary to self-assemble and hence reoxidation does not result in the reformation of active insulin. In fact, insulin is synthesised from a much larger polypeptide, preproinsulin, by two post-translational processing steps. Preproinsulin is able to self-assemble, using noncovalent forces, into a conformation that places the A and B fragments of the nascent insulin in their correct relative orientations. The two strands are then linked together *via* the irreversible formation of the two disulfide linkages to give proinsulin. With the strands safely joined, the excess polypeptide can then be removed to form the final product (Figure 10.11).

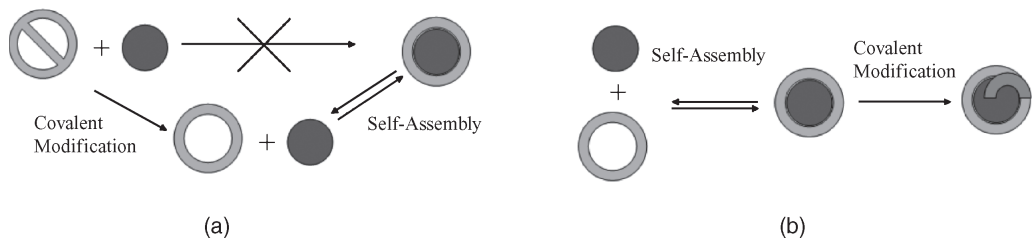


**Figure 10.10** (a) Combination of covalent preprocessing modification and self-assembly, (b) self-assembly followed by covalent postmodification.

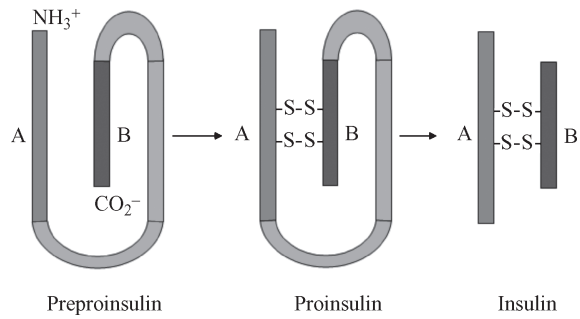


**Figure 10.11** Biosynthesis of insulin by self-assembly followed by covalent modification.

## 10.4 Self-Assembly in Synthetic Systems: Kinetic and Thermodynamic Considerations

### 10.4.1 Template Effects in Synthesis

Busch, D. H., Vance, A. L. and Kolchinski, A. G., 'Molecular template effect: historical view, principles and perspectives', in *Comprehensive Supramolecular Chemistry*, Atwood, J. L., Davies, J. E. D., MacNicol, D. D. and Vögtle, F. (eds), Pergamon: New York, 1996, vol. 9, 1–42.

In Section 3.9, we distinguished between the kinetic and thermodynamic template effects in macrocycle synthesis. Under the operation of a kinetic template effect, the distribution of the products of a cyclisation reaction is altered by the binding of the reactants in an enforced and relatively rigid geometry about the metal ion template. Crucially, the reaction should not be reversible under the prevailing conditions since the templated species is unlikely to be the most thermodynamically stable reaction product. Indeed, the cost of unfavourable interactions within the macrocycle must be borne during its synthesis. This is the origin of the enhancement of the metal ligand binding constant as a result of macrocyclic preorganisation (Section 1.6). The purpose of the synthetic template is to enable us to take advantage of this energetic 'pay in advance' gain in complexation ability. Effectively we are taking advantage of the self-assembly of a template complex followed by covalent postmodification to 'fix' the macrocycle.

The use of metal ions as kinetic synthetic templates is extremely widespread, and is an excellent way in which to bring about the organisation of a number of reacting components in order to direct the geometry of the product. Because some metal ions, such as the transition metals, often have preferred coordination geometries (*e.g.* tetrahedral, square planar, octahedral *etc.*), changes in metal ion may have a profound effect on the nature of the templated product. Metal-ion-templated syntheses may be classified more generally as examples of self-assembly with covalent postmodification. For example, the synthesis of the artificial siderophore **10.2** is effected by the use of an octahedral $Fe^{3+}$ template.[8] In this case, the macrobicyclic product is obtained as the $Fe^{3+}$ complex from which it is difficult to separate.

In contrast, use of metalloid elements, such as silicon, tin antimony or boron, which can form weak covalent bonds with oxygen, nitrogen or sulfur substituents during the course of the reaction, results in templated products that may be obtained metal-free by simple hydrolysis. These 'covalent template reactions' (the M—X bond is essentially covalent in these cases) also have the advantage that the

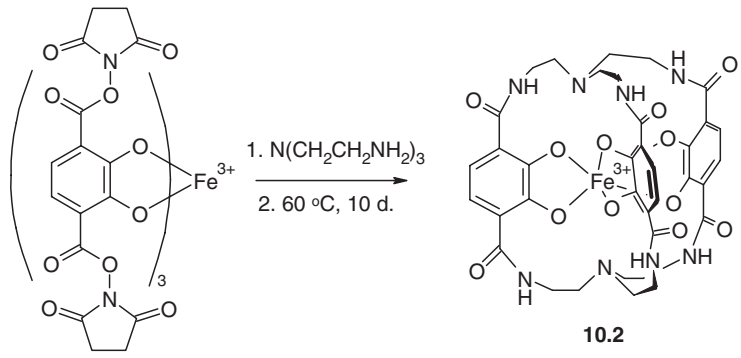


**10.2**

bound O, N or S remains relatively nucleophilic. The first example of this process was the condensation of tetrahedral silicon tetraisocyanate with glycol to give **10.3**. This spiro intermediate was then reacted with $C(=O)Im_2$ as a source of 'CO' to give the silyl macrocyclic complex **10.4**. Hydrolysis yields the free macrocycle **10.5** (Scheme 10.2).

Ions other than metal cations may also act as templating agents, for example in the synthesis of zeolites and mesoporous silicas by templating about alkali metal cations and large quaternary ammonium ions (Section 9.2.2). Similarly the synthesis of large polyoxovanadate cages is templated by the presence of ions such as $Cl^-$ or a combination of $NH_4^+$ and $Cl^-$.

In contrast, the thermodynamic template effect in macrocycle synthesis is a process by which the presence of a metal ion template stabilises thermodynamically, or removes (*e.g.* by precipitation) one particular (usually cyclic) product from an equilibrating mixture, driving the equilibrium towards this thermodynamic minimum. This leads us to the conclusion that any thermodynamically stabilising influence may drive an equilibrium mixture towards a particular product according to Le Chatalier's Principle (in an equilibrating situation, the system will react to diminish the effects of externally applied changes in conditions).

On the border between kinetic and thermodynamic synthetic template effects are processes involving stepwise self-assembly followed by covalent modification. Electrostatic forces may be readily employed in this kind of templating role, for example in the synthesis of more unusual kinds of cyclic molecules, including interpenetrated *catenane* compounds. Face-to-face $\pi$-stacking interactions between electron-rich and electron-poor aromatic rings have been used to induce the interpenetration of one aryl ring within a cavity formed by a separate macrocycle (Figure 10.12). If the resulting inclusion compound can be cyclised, the result is an interpenetrated catenane in which one macrocyclic ring is threaded irreversibly through another. Alternatively, addition of bulky end groups results in a *rotaxane*, a compound in which a thread-like guest is inserted irreversibly within a cyclic host. The initial inclusion *via* $\pi - \pi$ stacking interactions is an example of thermodynamic

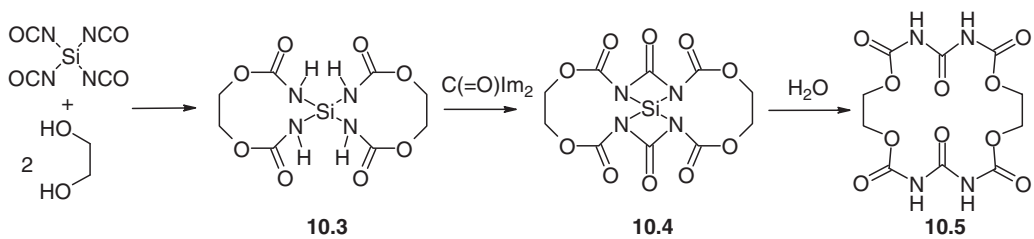


**10.3** **10.4** **10.5**

**Scheme 10.2** Covalent template synthesis of an 18-membered macrocycle.

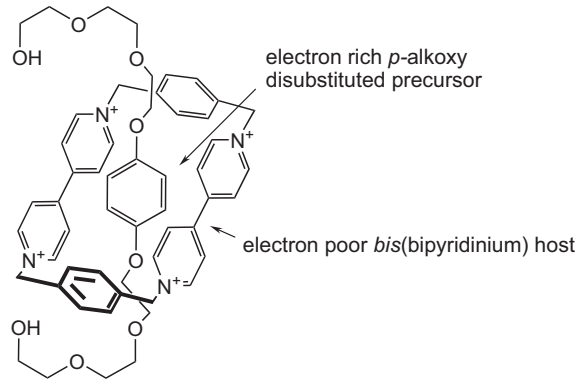


**Figure 10.12** Interpenetration of an electron-rich catenane or rotaxane precursor within an electron-poor macrocycle.

self-assembly, while the subsequent covalent cyclisation or capping reaction that fixes the components in place is controlled kinetically. This latter stage in catenane synthesis is carried out under high-dilution conditions, with assistance from weaker, extra-cavity $\pi - \pi$ stacking interactions. Once the second, kinetically controlled stage is complete, the templating interaction is no longer necessary, although it is not necessarily removed. The extensive chemistry of catenanes and rotaxanes is discussed in Section 10.7.

As we have seen in biological systems, hydrogen bonding is also a powerful templating factor. While an individual hydrogen bond may constitute a relatively weak interaction, arrays of hydrogen bonds arranged in a complementary fashion can stabilise large aggregates. Hydrogen-bonding interactions have been used in the development of the first self-replicating systems (Section 12.9.3). In these autocatalytic molecules, a self-complementary amide derivative is able to organise a ternary (three-component) complex under thermodynamic control between itself and two precursor components. These precursors are brought into close proximity to one another in a well-defined orientation within the ternary assembly and react to produce a copy of the templating molecule. Such systems again make use of a templating effect in which thermodynamic self-assembly is followed by kinetic covalent modification.

## 10.4.2 A Thermodynamic Model: Self-Assembly of Zinc Porphyrin Complexes

Chi, X. L., Guerin, A. J., Haycock, R. A., Hunter, C. A. and Sarson, L. D., 'The thermodynamics of self-assembly', *J. Chem. Soc., Chem. Commun.* 1995, 2563–2565.

There have been several approaches to modelling the thermodynamic self-assembly of coordination complexes and hydrogen bonded assemblies, often taking a specific set of compounds as a representative model. One of the earlier, successful models which gives a good feel for the factors involved is based on the zinc porphyrin complexes **10.6**–**10.8** (Figure 10.13). This systems represents an interesting test case to demonstrate the thermodynamics of the self-assembly of closed, cyclic oligomers (dimers, trimers tetramers *etc.*) as opposed to 'open' coordination polymers. Compounds **10.6**–**10.8** all self-assemble spontaneously from their constituent monomer units under thermodynamic control under well-defined conditions. Their formation is entirely equilibrium driven, since the $Zn^{2+}$—N(pyridyl) bond is relatively labile (rapidly and reversibly broken and reformed) in organic solvents ($CH_2Cl_2$, toluene *etc.*)

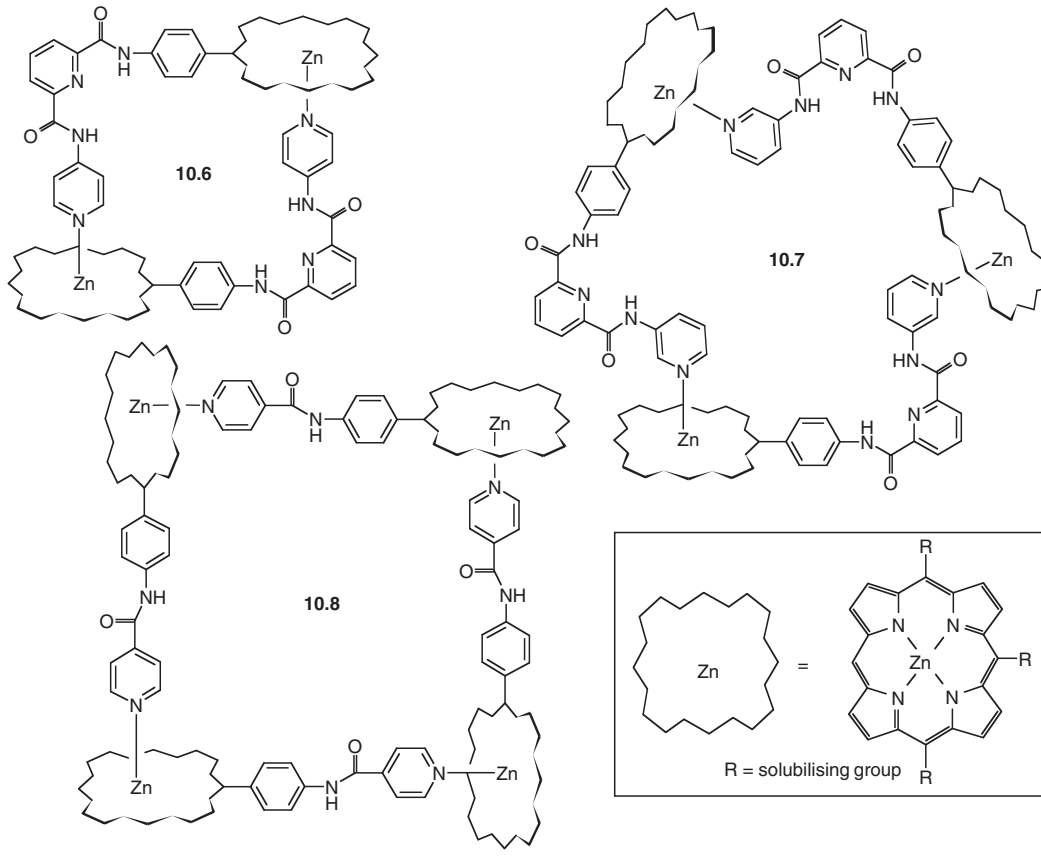


**Figure 10.13** Closed, cyclic, self-assembling zinc porphyrin oligomers.

at room temperature. This lability arises from the hard nature of the $Zn^{2+}$ centre (Section 3.1) and the lack of any significant covalent component to the bonding. Note, however, that the $Zn^{2+}$ ion is held very strongly within the porphyrin $N_4$ framework because of stabilisation by both the chelate and macrocyclic preorganisation effects of the porphyrin ring. The formation of the three closely related cyclic oligomers is in competition with polymer formation as outlined in Scheme 10.3.

The system as a whole may be characterised by the following quantities.

1. $$K_{\text{closed}} = \frac{[\text{cycle}]}{[\text{monomer}]^n} \tag{10.1}$$

The equilibrium constant for the self-assembly of the cyclic oligomer containing $n$ monomer units.

2. $$K_{\text{open}} = \frac{[n - \text{mer}]}{[(n-1) - \text{mer}][\text{monomer}]} \tag{10.2}$$

The equilibrium constant for the open (noncyclic) association of a monomer with a growing linear oligomer containing $n - 1$ monomer units. This is a difficult parameter to measure because strictly

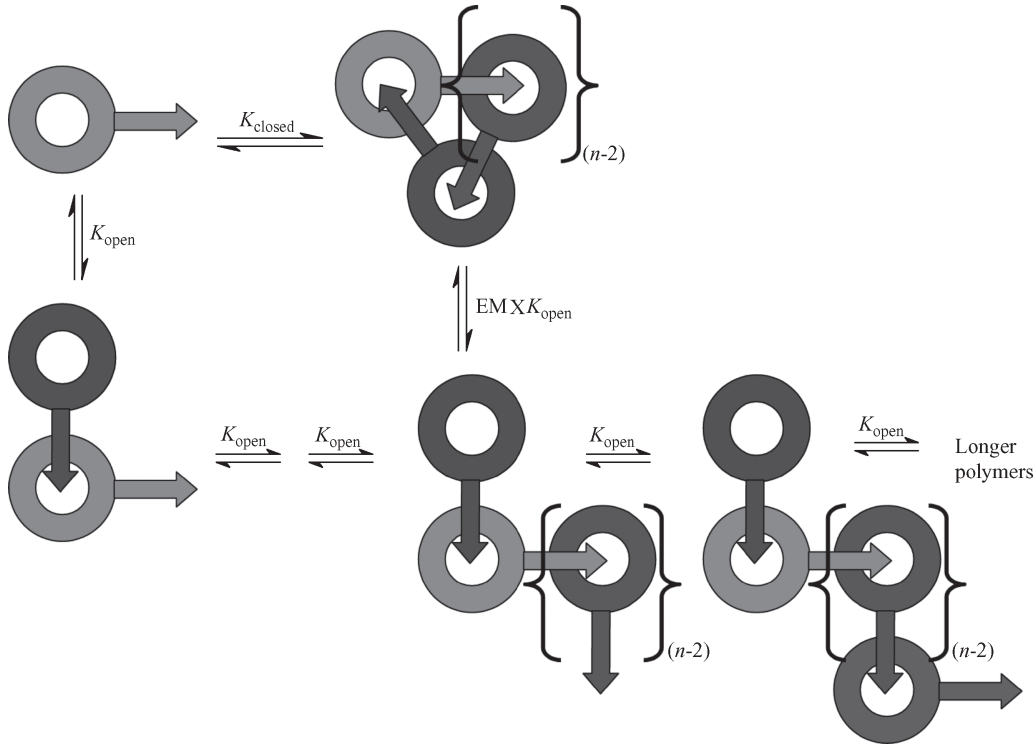


**Scheme 10.3** Competitive formation of open (polymeric) and closed (cyclic) zinc porphyrin species.

there should be a different value for each open association step. Furthermore, even the measurement of one such stepwise parameter is rendered extremely difficult by competing formation of the closed structure. However, $K_{open}$ may be approximated by measurement of the equilibrium constant for the association of a Zn(porphyrin) unit with pyridyl ligands incapable of assembling to form a closed structure. The association constant for these model, or reference species is denoted $K_{ref}$; $K_{ref} \approx K_{open}$.

3. Effective molarity, $EM = \dfrac{K_{closed}}{K_{open}^{n}} = \dfrac{K_{closed}}{K_{ref}^{n}}$ (10.3)

The effective molarity is a very useful parameter that represents the concentration at which polymer formation begins to compete with the self-assembly of closed oligomers, *i.e.* it is the upper limit at which the cyclic structure is stable.

4. Critical self-assembly concentration, $\text{csac} = [\text{monomer}]$, when $\dfrac{n[\text{cycle}]}{[\text{monomer}]^{n}} = 1$ (10.4)

$$\text{and } [\text{cycle}] = K_{closed}\,[\text{monomer}]^{n} \quad (10.5)$$

The csac is the minimum monomer concentration at which self-assembly of the closed structure begins. It is defined as the concentration at which the complex is half assembled, *i.e.* mole fraction of

**Table 10.1** Self-assembly parameters for cycles **10.6** – **10.8** (room temperature, $CH_2Cl_2$).

| Complex | $n$ | $K_{ref}$ ($dm^3\ mol^{-1}$) | csac (mol $dm^{-3}$) | *EM* (mol $dm^{-3}$) | $\varepsilon$ |
|---|---|---|---|---|---|
| **10.6** | 2 | $5.6 \times 10^{-3}$ | $3 \times 10^{-9}$ | 6 | 9.3 |
| **10.7** | 3 | $3.9 \times 10^{-3}$ | $2 \times 10^{-7}$ | 100 | 8.7 |
| **10.8** | 4 | $1.9 \times 10^{-3}$ | $33 \times 10^{-5}$ | 0.6 | 4.5 |

monomer units present in the form of the fully assembled complex is 0.5. Given a knowledge of *EM*, csac may be calculated from Equations (10.4) and (10.5), thus:

$$\text{csac} = \frac{1}{n^{1/(n-1)} K_{\text{closed}}^{1/(n-1)}} \tag{10.6}$$

Substituting into Equation (10.3) for $K_{closed}$ gives

$$\text{csac} = \frac{1}{n^{1/(n-1)} EM^{1/(n-1)} K_{\text{ref}}^{n/(n-1)}} \tag{10.7}$$

Data for the zinc macrocyclic compounds **10.6**–**10.8** are given in Table 10.1. This data shows clearly that the macrocycles consisting of fewer monomer units ($n$) are more stable than those with increasing $n$. We can explain this trend on entropic grounds by the greater decrease in the number of degrees of freedom as more and more monomer units aggregate. This factor fundamentally limits the number of monomer units that can come together to form a closed structure. In turn we can surmise that this number may be increased by designed decreases in the number of degrees of conformational freedom and preorganisation of the oligomeric units for cyclisation, *e.g.* by steric constraints or multiple binding interactions.

The experimental values of *EM* compare reasonably well with the theoretical maximum values, which may be obtained from Equation (10.8).[9]

$$EM_{\text{max}} = \exp\left(\frac{-\Delta S_{\text{ref}}}{R}\right) \tag{10.8}$$

For zinc pyridine reference complexes in toluene $\Delta S$ values are about 50 J $K^{-1}$ $mol^{-1}$, and hence the upper limit for *EM* is in the region of 400 mol $dm^{-3}$. For the trimer **10.7**, the experimental value (in $CH_2Cl_2$) of 100 mol $dm^{-3}$ is close to the theoretical maximum, which suggests that this system is nearly geometrically optimal (*i.e.* the monomer units are highly complementary). In contrast, factors such as ring strain may contribute to the lower value for the dimer **10.6**.

Taken together, the *EM* and the csac represent the concentration window over which the closed, self-assembled structure is thermodynamically stable. The wider this window, the more stable the complex is. Thus an overall efficiency of the self-assembly process ($\varepsilon$) may be defined in terms of csac and *EM*.

$$\varepsilon = \log\left(\frac{EM}{csac}\right) \tag{10.9}$$

hence

$$\varepsilon = \left[\frac{n}{n-1}\log(EM\ K_{\text{ref}})\right] + \frac{\log(n)}{n-1} \tag{10.10}$$

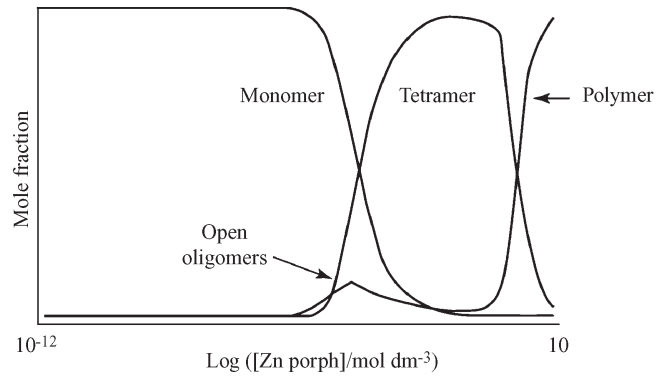


**Figure 10.14** Distribution of solution species for the self-assembling tetramer **10.8**. (Reproduced by permission of The Royal Society of Chemistry).

The lower limit of $\varepsilon$ for which self-assembly may be realistically studied is $\varepsilon \simeq 4$, since at this efficiency the self-assembled complex constitutes more than 90 % of the species present over a concentration range of only $10^2$ mol dm$^{-3}$. Even then, it is in equilibrium with significant amounts of oligomers. This may be readily appreciated from the speciation diagram for the tetramer **10.8** (Figure 10.14).

Given a knowledge of the binding enthalpy for a realistic reference system, $\Delta H_{\text{ref}}$, a theoretical estimate of the maximum $\varepsilon$ may be obtained by substituting Equation (10.8) into (10.10) to give:

$$\varepsilon_{\max} = \left( \frac{n}{n-1} \frac{\Delta H_{\text{ref}}}{2.303RT} \right) + \frac{\log(n)}{n-1} \tag{10.11}$$

Likewise, a minimum value for csac may also be obtained from Equations (10.7) and (10.8):

$$\text{csac}_{\min} = \frac{1}{n^{1/(n-1)}} \exp\left[ \frac{n\,\Delta H_{\text{ref}}}{(n-1)RT} - \frac{\Delta S_{\text{ref}}}{R} \right] \tag{10.12}$$

### 10.4.3 Cooperativity and the Extended Site Binding Model

Hamacek, J., Borkovec, M. and Piguet, C., 'Simple thermodynamics for unravelling sophisticated self-assembly processes', *Dalton Trans.* 2006, 1473–1490.

Given the beauty and elegance of some self-assembling processes it is tempting to attribute some magical properties that allow complex mixtures to sort themselves out into a multi-component single product. In reality the stability of self-assembled complexes is often just the result of additive supramolecular interactions coupled with the need to use all possible binding sites at minimum entropic cost. In some cases, but by no means all, assemblies are more stable than the sum of their individual interactions. This phenomenon is termed *positive cooperativity*. Alternatively the binding of a first component may destabilise the binding of a second component. In the case of multiple metal cations binding to a ligand or series of ligands this *negative cooperativity* may arise as a result of electrostatic repulsions between the ions. We discussed in Section 1.5 a variety of graphical tests such as Scatchard and Hill plots that can be used to identify positive or negative cooperativity in systems involving purely intermolecular equilibria. These methods derive from a model called the *site binding model* originally used to describe intermolecular protein ligand interactions. The situation is more complex for self-assembled compounds

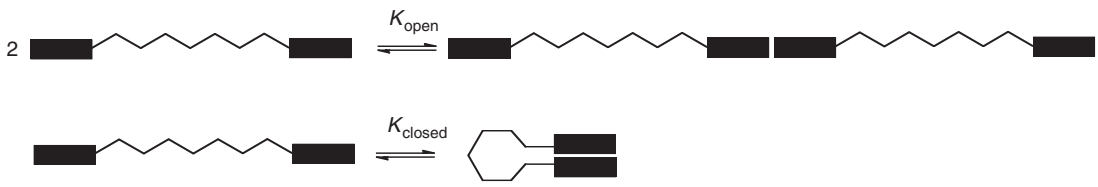


**Figure 10.15** Schematic showing competing intermolecular and intramolecular equilibria. The rectangles represent binding sites.

exhibiting both inter- and intramolecular equilibria and, apart from the treatment detailed in Section 10.4.2 (which does not explicitly consider metal–ligand complexation processes), it was not until 2003 that a proper description of their thermodynamics was derived by Gianfranco Ercolani at the University of Rome, Italy. Ercolani's model has since been extended to give the *extended site binding model* by Claude Piguet (Geneva, Switzerland).[10] We will briefly summarise these new thermodynamic treatments and look at some of their predictive implications. A more detailed explanation of the derivation of the models is given in the key reference.

### *Ercolani's Model*

In the previous section we came across the concept of effective molarity, *EM*, an empirical parameter that is used extensively (*e.g.* in polymer chemistry) to assess the relative efficiency of intra *versus* intermolecular complexation processes; $EM = K_{closed} / K_{open}$ (Equation 10.3 and Figure 10.15).

If we express *EM* in terms of free energies we obtain Equation 10.13 and we can recognise that $-RT\ln(EM)$ is an empirical correction factor when an intermolecular process is replaced by an intramolecular one. If we substitute into Equation 10.13 the separate enthalpy and entropy terms and recognise that in a strain free ring $\Delta H_{inter} \approx \Delta H_{intra}$ we get Equation 10.14.

$$-RT\ln(EM) = -RT\ln(K_{closed}) + RT\ln(K_{open}) = \Delta G_{closed} - \Delta G_{open} \tag{10.13}$$

$$-RT\ln(EM) = (\Delta H_{closed} - \Delta H_{open}) - T(\Delta S_{closed} - \Delta S_{open}) \approx -T(\Delta S_{closed} - \Delta S_{open}) \tag{10.14}$$

It is convenient to replace *EM* with the identical but theoretical parameter effective concentration ($c^{eff}$). Substituting this nomenclature change into Equation 10.14 we get Equation 10.15 and hence we can derive Equation 10.16 from the original definition of *EM* (Equation 10.3).

$$c^{eff} = e^{(\Delta S_{closed} - \Delta S_{open})/R} \tag{10.15}$$

$$K_{closed} = c^{eff} K_{open} = e^{(\Delta S_{closed} - \Delta S_{open})/R} K_{open} \tag{10.16}$$

The same approach can be applied not only to the bulk equilibrium constants (*K*) but also to the microscopic connection processes (given the symbol *k*). Recall that the macroscopic equilibrium constant is simply the sum of all the microscopic equilibrium constants. For example, if an acid ($H_2A$) has two non-equivalent ionisable protons there are two distinct but equivalent ways to remove a proton to produce $HA^-$ and hence there are two microscopic equilibrium constants ($k_1$ and $k_2$) for this deprotonation process. Thus the macroscopic acid dissociation constant, $K_a = k_1 + k_2$. Don't get confused between microscopic equilibrium constants and rate constants, both of which have the symbol *k*. So, in terms of

micro constants, Ercolani proposed that the overall assembly equilibrium constant ($\beta_{mn}$ where $m$ and $n$ are the numbers of metal (M) and ligand (L) components) for an equilibrium of the type shown in Equation 10.17 involving both intra- (closed) and intermolecular (open) association can be calculated by multiplying together the micro constants as in Equation 10.18.

$$m\,\mathrm{M} + n\,\mathrm{L} = [\mathrm{M_mL_n}] \tag{10.17}$$

$$\beta_{mn} = \omega_{mn} \prod_{closed} k_{closed} \prod_{open} k_{open} \tag{10.18}$$

The parameter $\omega_{mn}$ is what is called a degeneracy parameter. It corrects for the number of different ways that any particular microspecies $[\mathrm{M_mL_n}]$ can be formed. For example if we have a single octahedral metal with three bidentate 'binding domains' (*i.e.* region where a metal can bind), interacting with a single ligand with two chelate binding domains to form a 1:1 ML complex then $\omega_{11} = 6$. Each of the three metal binding sites can interact with either one of the ligand binding sites. The most stable assemblies are those in which all binding sites are occupied and these are the only ones we are concerned with, so in an assembly of ligands possessing $m$ binding sites between them with metals having in total $n$ coordination sites between them to give a complex $[\mathrm{M_mL_n}]$ (Equation 10.17) there is a total of $N$ components, where $N = m + n$. These components are linked by a total number of connections $C$ where $C = mn$. Of these connections $N - 1$ are intermolecular and $C - (N - 1) = C - N + 1 = mn - m - n + 1$ are intramolecular. If we substitute these numbers into Equation 10.18 we get Equation 10.19. Equation 10.19 also contains a symmetry parameter, $\sigma_{mn}$, that describes the change in degeneracy of the microspecies involved in the assembly process. In complexes such as helicates this may include the formation of enantiomers.

$$\beta_{mn} = \sigma_{mn} (k_{closed})^{mn-m-n+1} (k_{open})^{m+n-1} \tag{10.19}$$

Equation 10.19 allows us to calculate the overall stability constant for multi-component self-assembly processes provided we have a knowledge of the two micro constants $k_{open}$ and $k_{closed.}$ In general these are measured approximately by determining the macroscopic equilibrium constant for simple model reactions that mimic the more complex assembly. We can then determine the cooperativity of the system by examining whether the measured macroscopic stability constant for the assembly is greater than, less than or equal to that calculated from Equation 10.19, corresponding, to positive, negative and non-cooperative processes, respectively. An illustration of the operation of Equation 10.19 is shown in Figure 10.16. This process involves the self-assembly of two metals with two ligands to give a complex $[\mathrm{M_2L_2}]$. Imagine that the metals are tetrahedral ions such as Cu(I) and the ligands have two bidentate binding domains such as a quaterpyridine ligand. The first three processes are all intermolecular (open)

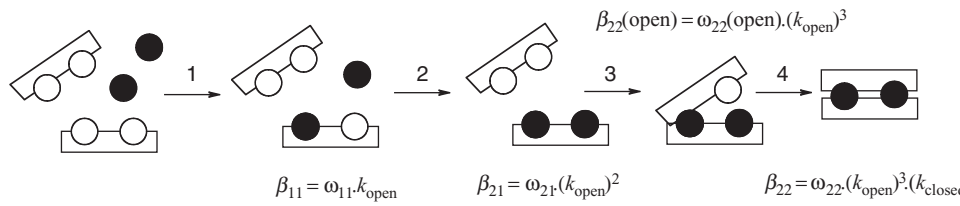


**Figure 10.16** Description of the formation of a $\mathrm{M_2L_2}$ complex by Equation 10.19.[10] Open circles represent ligand binding sites and closed circles represent metal ions.

processes corresponding to the binding of first one, then two metals to a single ligand and then the addition of the second ligand to one of the metals. The final step is an intramolecular ring closure process in which the dangling end of one ligand locks on to the vacant binding domain of the second metal. In Section 10.8.5 we will see Erolani's equation in action in assessing the cooperativity of a helicate system.

### *The Extended Site Binding Model*

While very powerful, Ercolani's model has two drawbacks. First, because only two microscopic affinities are used ($k_{open}$ and $k_{closed}$) only assemblies involving more or less equivalent binding sites can be treated. Secondly cooperativity, *i.e.* any deviations from statistical binding, are not clearly assigned to extra energy gains or losses arising from interactions between components that are not considered in the metal–ligand connections. These issues are addressed by adapting of Ercolani's model to give the *extended site binding model* which allows the assignment of the origin of cooperativity to the combination of intermetallic and interligand interactions such at metal-metal electrostatic repulsion and ligand-ligand interactions such as hydrogen bonding. The extended site binding model breaks down the free energy of formation of complex multi-component assemblies such as that described by Equation 10.17 into five distinct energetic terms, Equation 10.20.

$$\Delta G_{mn} = -RT\ln(\beta_{mn}) = -RT\ln(\sigma_{chir}\,\omega_{mn}) - \sum_{i=1}^{\boldsymbol{m\cdot n}} RT\ln(k_i) - \sum_{i=1}^{m\cdot n-m-n+1} RT\ln\left(c_i^{eff}\right) + \sum_{i<j}{}'' \left(\Delta E_{ij}^{MM}\right) + \sum_{k<l}{}''' \left(\Delta E_{kl}^{LL}\right) \tag{10.20}$$

This substantial equation requires some explanation and we will consider each of the five terms separately. The first term $-RT\ln(\sigma_{chir}\,\omega_{mn})$ represents the degeneracy of the microscopic state. The $\sigma_{chir}$ part refers to the generation of enantiomers; $\sigma_{chir} = 1$ when no enantiomers are generated and is equal to 2 when two enantiomers are formed. The $\omega_{mn}$ term is the degeneracy; the number of equivalent microspecies that contribute to the microscopic state as we saw in Ercolani's model.

The second term $-\sum_{i=1}^{m\cdot n} RT\ln(k_i)$ is the sum total of the microscopic free energies that arise from making metal-ligand connections *assuming all of those connections are intermolecular.* We will correct for this assumption in the third term. The total number of connections is $m{\cdot}n$ assuming all binding sites are occupied and there are no dangling bonds.

The third term $-\sum_{i=1}^{m\cdot n-m-n+1} RT\ln(c_i^{eff})$ is the entropic correction for the total of $m{\cdot}n - m - n + 1$ intramolecular connections in the $[M_mL_n]$ complex. Terms 2 and 3 correspond to Ercolani's model.

The fourth term $\sum_{i<j}{}''(\Delta E_{ij}^{MM})$ takes account of all intermetallic interactions that occur in the self-assembled complex $[M_mL_n]$. While this term will be heavily dependent on short range interactions between adjacent metals it can also include longer range interactions. If the interactions are of an electrostatic nature then we expect $\Delta E^{MM}$ to be inversely proportional to the distance between the metal ions.

Finally, the fifth term $\sum_{k<l}{}'''(\Delta E_{ij}^{MM})$ takes account of ligand-ligand interactions.

The overall equation is more conveniently used in its compact form, Equation 10.21, where $u_{ij}^{MM} = e^{-\frac{\Delta E_{ij}^{MM}}{RT}}$ and $u_{kl}^{LL} = e^{-\frac{\Delta E_{kl}^{LL}}{RT}}$.

$$\beta_{mn} = (\sigma_{chir}\,\omega_{mn})\prod_{i=1}^{mn}(k_i)\prod_{i=1}^{mn-m-n+1}(c_i^{eff})\times\prod_{i<j}{}''(u_{ij}^{MM})\prod_{k<l}{}'''(u_{kl}^{LL}) \tag{10.21}$$

For simple processes in which multiple metals bind to a single ligand $c^{eff} = 1$ and $u^{LL} = 1$ ($\Delta E^{LL} = 0$) and hence the extended site binding model reduces back the basic site binding model. Figure 10.17 shows

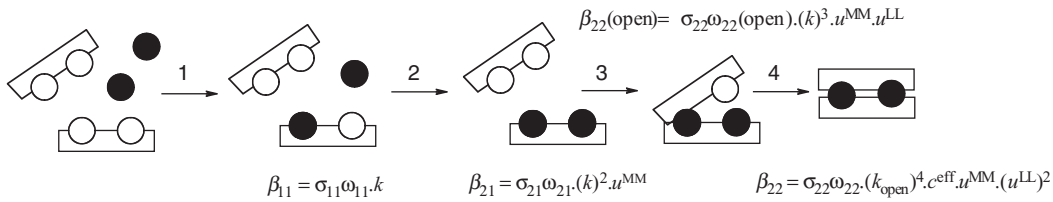


**Figure 10.17** Description of the formation of a $M_2L_2$ complex by Equation 10.21.

the same process as we examined in Figure 10.16 for Ercolani's model but now described in terms of the extended site binding model. The cooperativity in the extended site binding model depends on the metal-metal and ligand-ligand interaction terms, $\Delta E^{MM}$ and $\Delta E^{LL}$ and we can define an overall free energy deviation term $\Delta E_{dev}$ according to the sum of these contributions, Equation 10.22. If $\Delta E_{dev} > 0$ the process is negatively cooperative, if $\Delta E_{dev} < 0$ the process exhibits positive cooperativity and is non-cooperative for $\Delta E_{dev} = 0$.

$$\Delta E_{dev} = \sum_{i<j}{}'' (\Delta E_{ij}^{MM}) + \sum_{k<l}{}''' (\Delta E_{kl}^{LL}) \tag{10.22}$$

After all of this theory, it is time to get back to some real chemistry and so we will illustrate the workings of the extended site binding model by looking at the self-assembly of ligand **10.9** (L) with $Eu^{3+}$. The final assembly is a triple stranded bimetallic helicate (more on helicates in Section 10.8), $[Eu_2(\mathbf{10.9})_3]$ and the steps encountered during its formation are shown in Figure 10.18. Detailed kinetic and thermodynamic studies on this system have allowed the measurement of five macroscopic binding constants shown in Table 10.2.[11] The two metal binding sites are symmetric in the $C_{2v}$ ligand so only a single microscopic metal-ligand binding constant $k$ is required. The $c^{eff}$ will vary depending on the differing degrees of preorganisation in the various 'open' complexes but because of the limited data available an average value is used. The $\sigma_{chir}$ and $\omega_{mn}$ values for each product are given alongside the equilibria in the table. Fitting the observed data with these parameters according to Equations 10.21 and 10.22 leads to the $\Delta E_{dev}$ values and hence cooperativity given in Table 10.2. The fitting results give an expected unfavourable $\Delta E^{MM}$ of 10 kJ mol$^{-1}$ but balanced by a surprising attractive $\Delta E^{LL}$ of $-5$ kJ mol$^{-1}$ perhaps arising from a stabilising hydrogen bonded network of carboxylates in aqueous solution. The

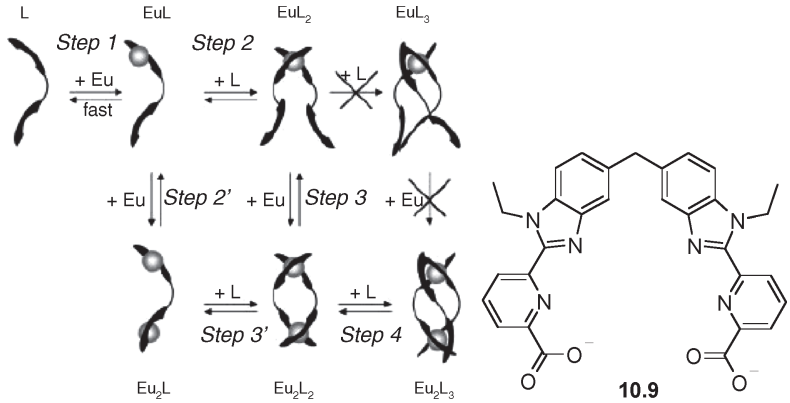


**Figure 10.18** Self-assembly of the europium triple helicate complex of ligand **10.9** (= L) (Copyright Wiley-VCH Verlag GmbH & Co. KGaA. Reproduced by permission).

**Table 10.2** Equilibria, binding constants, extended site binding model parameters and cooperativity for the formation of the Eu(III) complex of **10.9** (L).

| Equilibrium | steps | Measured equilibrium constant | $\sigma_{chir}$ | $\omega_{mn}$ | $\Delta E_{dev}$ product / kJ mol$^{-1}$ | cooperativity |
|---|---|---|---|---|---|---|
| $Eu^{3+} + L = [EuL]^{+}$ | step 1 | $\log \beta_{11} = 4.4$ | 1 | 6 | n/a | – |
| $2Eu^{3+} + L = [Eu_2L]^{4+}$ | steps 1+2′ | $\log \beta_{21} = 6.4$ | 1 | 9 | −5.1 | positive |
| $Eu^{3+} + 2\,L = [EuL_2]^{-}$ | steps 1+2 | $\log \beta_{12} = 9.3$ | 1 | 12 | 10.3 | negative |
| $2Eu^{3+} + 2\,L = [Eu_2L_2]^{2+}$ | steps 1–3 | $\log \beta_{22} = 16.0$ | 2 | 9 | 0.6 | ≈ none |
| $2Eu^{3+} + 3\,L = [Eu_2L_3]$ | steps 1–4 | $\log \beta_{23} = 26.1$ | 2 | 1 | −19.4 | positive |

metal-metal repulsion and ligand-ligand attraction compete with one another giving variously negative and positively cooperative steps, but the overall process is positively cooperative because of the long distance (9 Å) between metal sites and attractive ligand-ligand interaction.

### 10.4.4 Double Mutant Cycles – Quantifying Weak Interactions

Cockroft, S. L. and Hunter, C. A., 'Chemical double-mutant cycles: dissecting non-covalent interactions', *Chem. Soc. Rev.* 2007, **36**, 172–188.

While we are discussing cooperativity in self-assembly it is worth mentioning a useful tool for assessing the strength of particular intermolecular interactions based on the comparison of free energy changes in self-assembly of series of related compounds. The method is termed a *double mutant cycle* and, like the site binding model, was originally developed for use in proteins where a particular residue that takes part in a supramolecular interaction can be selectivity mutated to give a different residue which does not. The method was originally proposed by Fersht in 1984 for the evaluation of cooperativity in protein-substrate interactions[12] but has since been used in a number of ingenious ways in chemical self-assembling systems. The basis of the method is shown in Figure 10.19 and relies on four different self-assembling systems A–D (the 'native' compounds and three 'mutants'). The question to be addressed is what is the magnitude of the interaction between groups x and y when they are part of a complicated interacting whole (as in A in Figure 10.19)? We might imagine we could answer this question by comparing the stability of self-assembled system A which possesses the interaction x···y to D which does not. However, the issue is not that simple because of the effect the presence of groups x or y have on the strength of the other interactions holding the self-assembly together and the secondary interactions represented by the thin dashed lines in Figure 10.19 (*i.e.* cooperativity). The double mutant cycle overcomes these problems because these secondary interactions cancel out during the assessment and thus the free energy difference between any two parallel 'mutations' $\Delta\Delta G_{x\text{-}y} = (\Delta G_A - \Delta G_B) - (\Delta G_C - \Delta G_D) = (\Delta G_A - \Delta G_C) - (\Delta G_B - \Delta G_D)$ gives a measure of the interaction energy between x and y. In order for the double mutant cycle to work it must fulfil three criteria listed below:

1. The secondary interactions must be additive functions of the mutations
2. The double mutant serves as the reference state and so the individual mutations should be non-interacting.
3. Each member of the cycle should have the same conformation and any structural changes must be the same on both sides of the cycle.

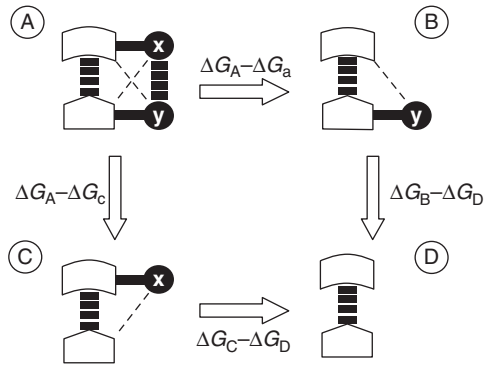


$$\Delta\Delta G_{xy} = (\Delta G_A - \Delta G_B) - (\Delta G_C - \Delta G_{D)}$$
$$= (\Delta G_A - \Delta G_C) - (\Delta G_D - \Delta G_{D)}$$

**Figure 10.19** General schematic representation of a supramolecular doublemutant cycle for measurement of the x–y interaction. The bold broken lines represent the major non-covalent interactions in the supramolecular complex, and the fine broken lines are the secondary effects that are cancelled in the cycle (reproduced by permission of The Royal Society of Chemistry).

The binding of guests within macrocycles or cryptands does not lend itself very readily to double mutant cycles because the structure of the host is an intimate part of the binding and any changes will strongly affect its preorganisation. More appropriate are receptors with pendant binding groups or 'molecular zippers' in which binding sites are arranged linearly along a backbone. For example, the molecular zipper system somewhat related to foldamer **10.1** shown in Figure 10.20 has been used to assess the magnitude of π-π interactions. The complex shown in 'A' is held together by both NH···O hydrogen bonds and edge-to-face π-π interactions. The mutations remove the contribution of the π-interactions by taking out the aromatic ring pendant groups on first one partner (single mutant B), then the other (single mutant C) and then both partners (double mutant D). The overall edge-to-face π-interaction energy is determined to be –1.2 kJ $mol^{-1}$ (strictly an average over the distribution of conformers in the system), showing how the method is sensitive to even small energy changes.

## 10.4.5 Probability of Self-Assembly

Gibb, C. L. D. and Gibb, B. C. 'Estimating the efficiency of self-assemblies', *J. Supramol. Chem.*, 2001, **1**, 39–52.

We can take thermodynamic stability to be a measure of the success of a self-assembly or of its design. If the self-assembled product is truly stable it should be produced in high yield as the end of the self-assembly reaction. Hence percentage yield is also a measure of success in self-assembly. However, by itself, the product yield only tells us what went right in the reaction, not what could have, and indeed did, go wrong. In fact a better measure of the operation of successful self-assembly is a comparison of product yield with the theoretical yield assuming only a statistical (*i.e.* unprogrammed and hence effectively random) distribution of products. If we can get a better yield than we would expect on statistical grounds then there must be some kind of driving force towards the self-assembled product and hence the product is thermodynamically favoured. So how likely is it for a particular complex to self-assemble, and what are the other possibilities? The answers to these questions depend on the number of components (*e.g.* metals and

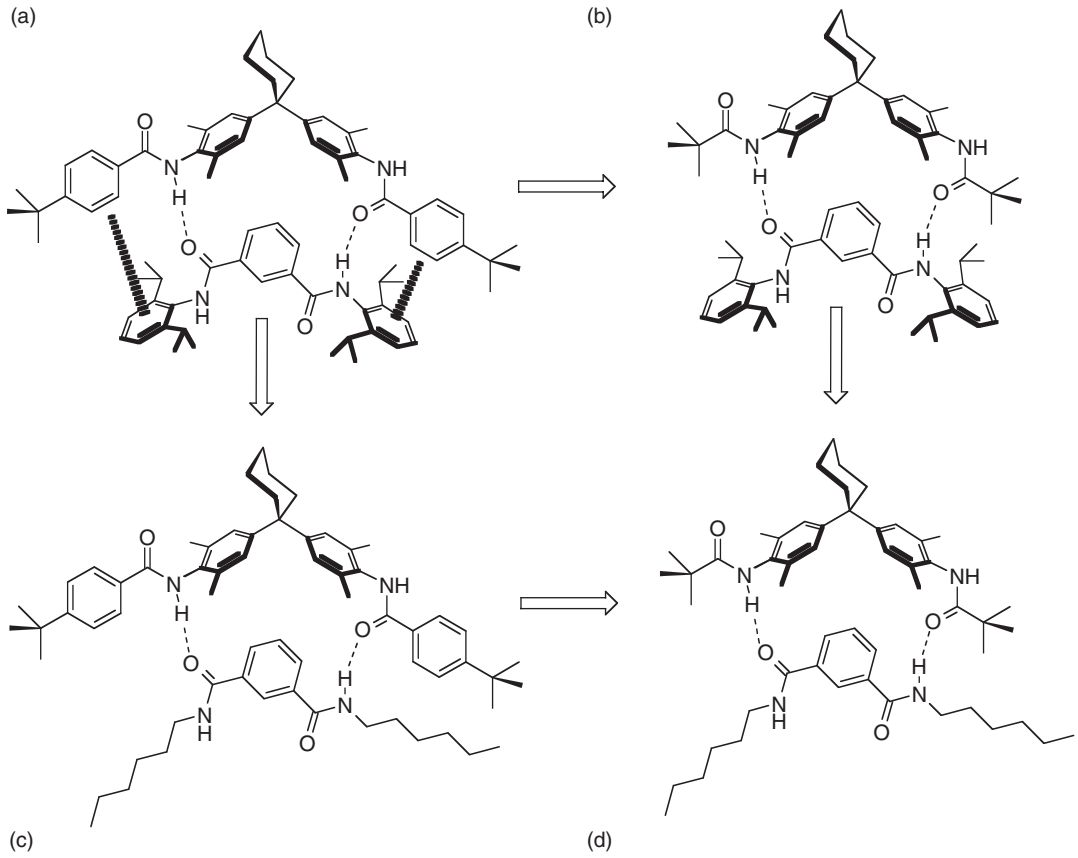


**Figure 10.20** A chemical double mutant cycle to assess the strength of edge-to-face π-π interactions (thick dashed wedges) in a molecular zipper complex; $\Delta\Delta G_{\pi\text{-}\pi} = \Delta G_A - \Delta G_B - \Delta G_C + \Delta G_D$.

ligands) and the topology of their connectivity. The number of possible products increases rapidly with the number of components and the degree of branching. Take the example shown in Figure 10.21. This system is an early example of a self-assembling hexametallic cage based on the labile ethylenediamine palladium(II) fragment, a very versatile linking moiety with two available coordination sites (initially occupied by nitrate ligands) situated 90° apart on the square planar metal centre. We will return to this useful fragment further on in Section 10.5. The report in 1995 of the reaction of six of these palladium(II) centres with four triangular tripyridyl triazine-based 'molecular panels' by the group of Makoto Fujita in Japan, really brought to prominence the self-assembly of closed, discrete molecular boxes using this 'panelling' approach.[13] What is the probability that the 10-component self-assembly needed to form the closed assembly shown will occur, and what other possible products are there? In answering these questions we need to make two assumptions. First we have to choose an arbitrary cut-off in terms of number of components, otherwise the possibilities are infinite. In this case we will confine ourselves to assemblies involving four ligands. Since each ligand has three pyridyl nitrogen atoms and each palladium has two available coordination sites the ligand and metal need to react in a 2 : 3 molar ratio in order to avoid any 'dangling bonds', *i.e.* unoccupied metal coordination sites or unbound pyridyl nitrogen atoms (the central

triazine nitrogen atoms are too sterically hindered to bind to a metal). So we will consider assemblies with up to four ligands and up to six metals. The second assumption is that all interactions are equally stable (*i.e.* we are dealing with a flat potential energy surface) and the only allowed motion is bond rotation within sub-units (excluding impossible rotations such as ligands passing through one another). This assumption results in a 'level playing field' and removes any bias towards particular conformers. In reality the intrinsic bias towards particular assemblies and conformers is what makes the assembly process successful and hence these factors form part of the actual measured yield. With the assumptions we are using the probability represents a worst case scenario in which the subunits are essentially devoid of any molecular programming. We can now calculate the mathematical probabilities ($\rho$) of each assembly forming as part of an 'assembly tree'. The assembly tree for the system in question is shown in Figure 10.21. The initiation of the self-assembly of the four ligand system shown in Figure 10.21 must involve one Pd(II) ion joining together two of the ligands to give the first 'bow-tie' shaped intermediate. If the four ligands are labeled A, B, C and D then the first intermediate is AB. The probability of this step is 1/1 and for

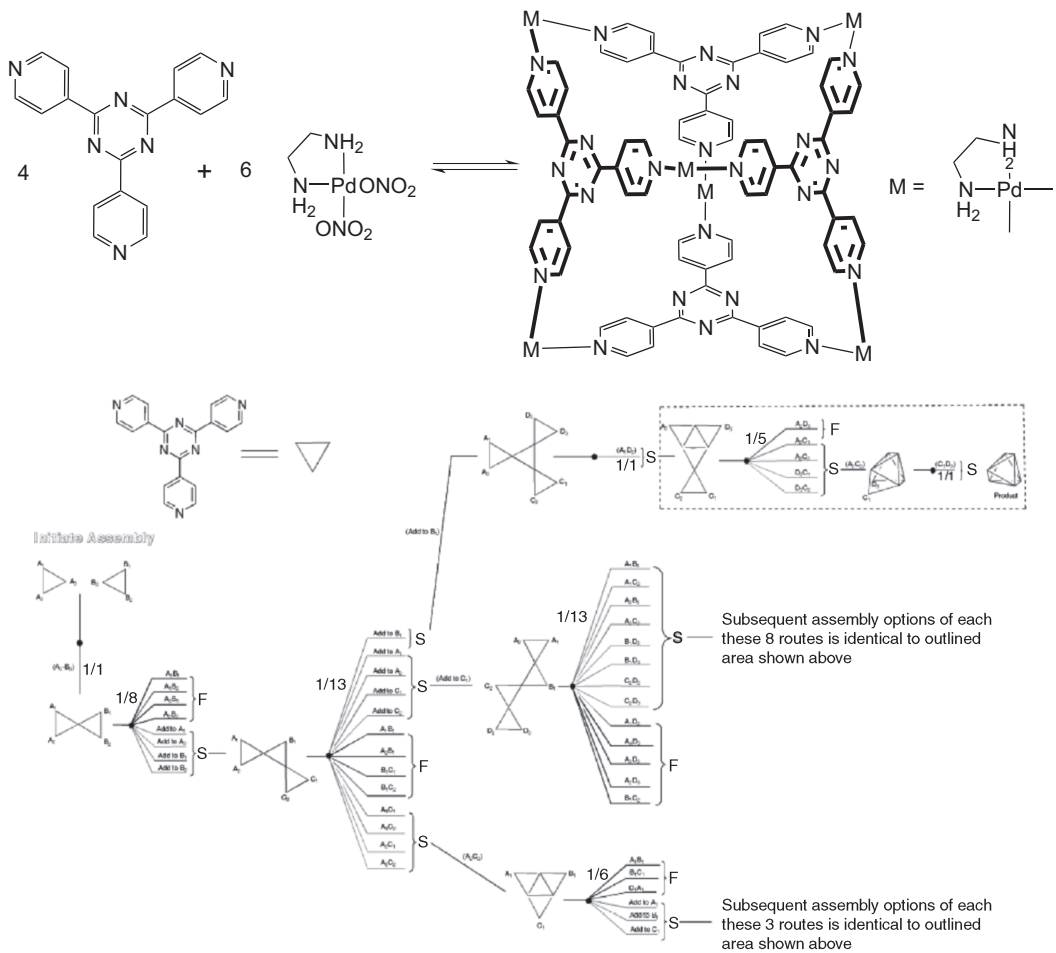


**Figure 10.21** A strict self-assembling hexametallic cage[13] and its assembly tree (reproduced with permission from [14]).

the purposes of this exercise we assume the process is irreversible, although in reality it is not. There are then eight possible next steps. Four of them are fatal to the formation of the target assembly because they involve a second metal ion bridging the same pair of ligands (A and B), a structural feature that is not part of the final assembly. These are labelled 'F' (fail). The other four are possible steps towards the target and represent the four different positions a third ligand (C) could add to the initial bow-tie intermediate. Thus at this second stage the probability of successfully (S) moving towards the target assembly is 4/8 or 0.5. If we analyse all of the possibilities as shown in the assembly tree (Figure 10.21) we find that the overall probability of obtaining the target assembly is $\rho = 0.1301$, *i.e.* 13 %. In reality the product is obtained in quantitative yield so the actual yield is 7.68 times better than the statistics suggest. This ratio between actual and statistical yield is referred to as the *assembly number*. The higher the assembly number is, the more efficient the self-assembly process is.

It is all very well to predict in a theoretical way as in the example above what kinds of species might be present within a self-assembling mixture. It would be useful, however, to be able to derive the speciation for a self-assembling system based on a knowledge of binding constants and concentration. An approach to this problem has been derived recently by Tom Fyles of the University of Victoria, Canada.[15] Fyles used the extended site binding model described in the previous section and applied it to the self-assembly of the molecular square **10.10** shown in Scheme 10.4, first reported by Fujita in 1990.[16] Fyles used inputs into the extended site binding model based on appropriate model compounds in order to derive a number of microscopic binding constant terms ($k$) for the association of square planar '$Pd(en)^{2+}$', 4,4′-bipyridine and $H^+/OH^-$ (en = 1,2-diaminoethane). This empirical approach diminishes generality but facilitates the practical application of the method. The result is a 2D map of speciation in the system with different maps produced for different concentrations. Figure 10.22b shows that the 4:4:0 square complex (where the numbers indicate the numbers of Pd : bipyridyl : $H^+$) predominates across a wide pH range at a 1:1 ratio of of Pd : bipyridyl at higher concentration. As concentration drops as in Figure 10.22a, the 'island of stability' for the self-assembled square becomes smaller. This palladium-based square and the '$Pd(en)^{2+}$' unit in general have proven to be extremely versatile building blocks in self-assembly and we now turn to a study of this and related chemistry from a more descriptive standpoint with emphasis on the factors governing their self-assembly and the resulting properties of such 'molecular containers'.

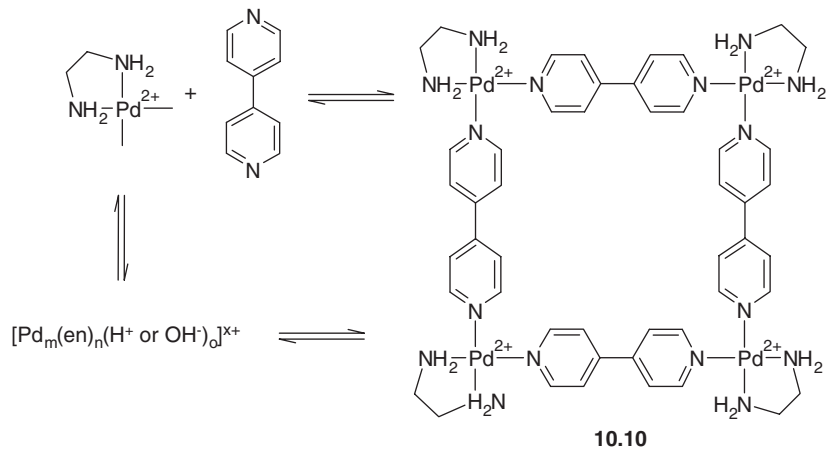


**Scheme 10.4** Self-assembly of molecular square **10.10** from '$Pd(en)^{2+}$' and 4,4′-bipyridine in competition with protonation reactions.

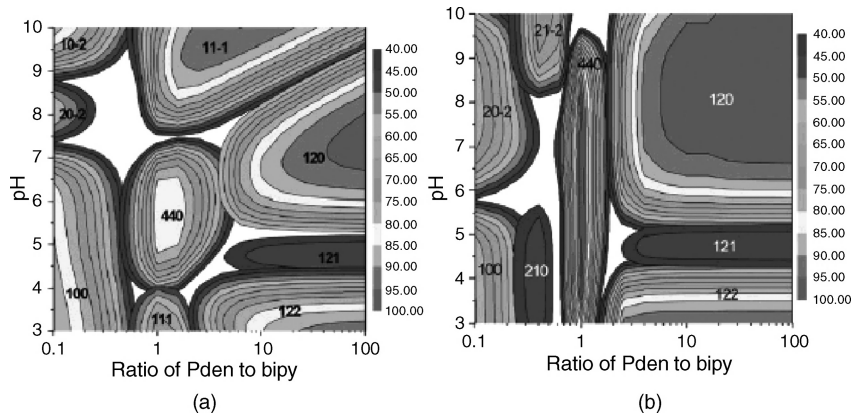


**Figure 10.22** Speciation maps for $Pd(en)^{2+}$ / 4,4′-bipyridyl mixtures at (a) 0.01 mM and (b) 5 mM total '$Pd(en)^{2+}$' concentration. The three numbers represent the numbers of '$Pd(en)^{2+}$', 4,4′-bipyridyl and $H^+$ components in the assembly, respectively. A −1 for the number of $H^+$ indicates $OH^-$. The molecular square **10.10** is species 440. (Reproduced by permission of The Royal Society of Chemistry).

## 10.5 Self-Assembling Coordination Compounds

Turner, D. R., Pastor, A.. Alajarín, M. and Steed, J. W., 'Molecular containers: Design approaches and applications', *Struct. Bond.* 2004, **108**, 97–168.

### 10.5.1 Design and Notation

Swiegers, G. F. and Malefetse, T. J., 'Classification of coordination polygons and polyhedra according to their mode of self-assembly', *Chem. Eur. J.* 2001, **7**, 3637–3643.

Generalising the results described in Section 10.4.2 for $Zn^{2+}$ porphyrinate complexes, we find that the design of self-assembling supramolecular assemblies based on any kind of directional interaction (covalent, coordinate or hydrogen bonding; ion–dipole or dipole–dipole interactions *etc.*) may be divided loosely into two categories: those that form polymeric species and those that form discrete aggregates. Both classes of compound are of interest: polymers in the context of areas such as tuneable zeolite mimics (Chapter 9), cyclic oligomers as hemicarcerand-type molecular reaction vessels, and both species in the area of nanoscale devices.

Makoto Fujita of Tokyo University, Japan, has pointed out that within the context of aggregates based upon transition metal coordination compounds (and by inference those involving other kinds of directional bonding), the type of aggregate produced is predictable and controllable by the nature of the building blocks. More precisely, we are interested in the divergent or convergent nature of the binding sites. Recall the definition of a host as a component consisting of convergent binding sites. Conversely, a guest possesses divergent binding sites (Section 1.1.2). This means that the resulting host–guest complex is a discrete, nonpolymeric species since the convergent host envelops the divergent guest. Extending this logic, if the convergent component cannot envelop the guest it will form a larger discrete aggregate until it is able to do so (Scheme 10.5a), since formation of discrete species is thermodynamically favourable within the appropriate concentration range. If, however, a divergent ligand is used, a discrete complex can arise only if the metal centre is protected in order to make it convergent (*e.g.* by a blocking ligand, Scheme 10.5b). Thus, more generally, discrete species are formed by any (complementary) convergent/divergent pair. Finally, in a two-component system, if both species are divergent, then a polymer must result (Scheme 10.5c).

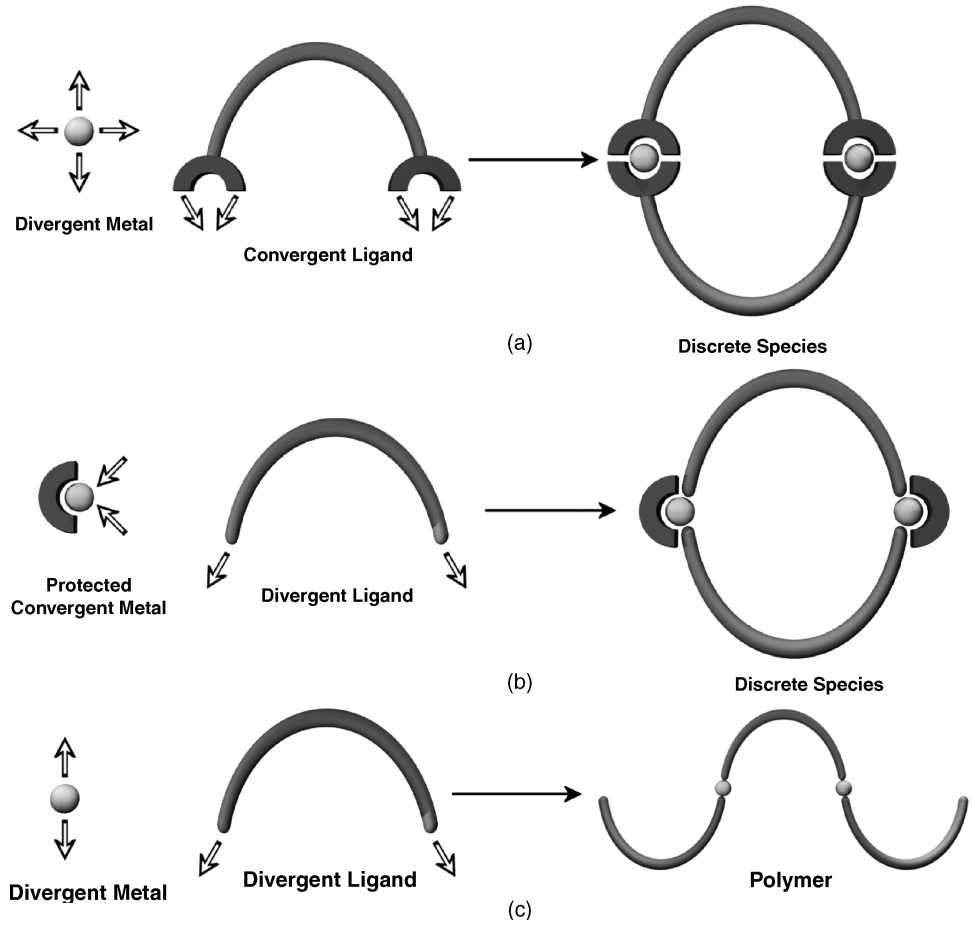


**Scheme 10.5** Design of capsular and polymeric self-assembling structures.

It is convenient to have a notation to describe the formation of self-assembled coordination compounds in terms of the shape of their components which can be *angular* (A) or *linear* (L) and whether they are electron *donors* (d) or acceptors (a). This simple notation is surprisingly powerful in providing a concise description of a variety of assemblies. Thus the hexametallic complex shown in Figure 10.21 becomes $A_6^{2a}\,A_4^{3d}$ because the six angular Pd(II) metal ions can accept two ligand donor interactions while the angular ligands can simultaneously donate to three metals. Some other examples of this notation in action are shown in Figure 10.23.

## 10.5.2 A Supramolecular Cube

Roche, S., Haslam, C.. Adams, H.. Heath, S. L. and Thomas, J. A., 'Self-assembly of a supramolecular cube', *Chem. Commun*. 1998, 1681–1682.

In 1998, Jim Thomas and co-workers at the University of Sheffield, UK, set out to prepare a self-assembling supramolecular cube by a combination of linear spacers, which would provide the cube edges, and pyramidal corners, which would constitute the vertices. Deconstruction of a cubic figure in this way reveals immediately that a ratio of eight corners to 12 edges is needed (Figure 10.24).

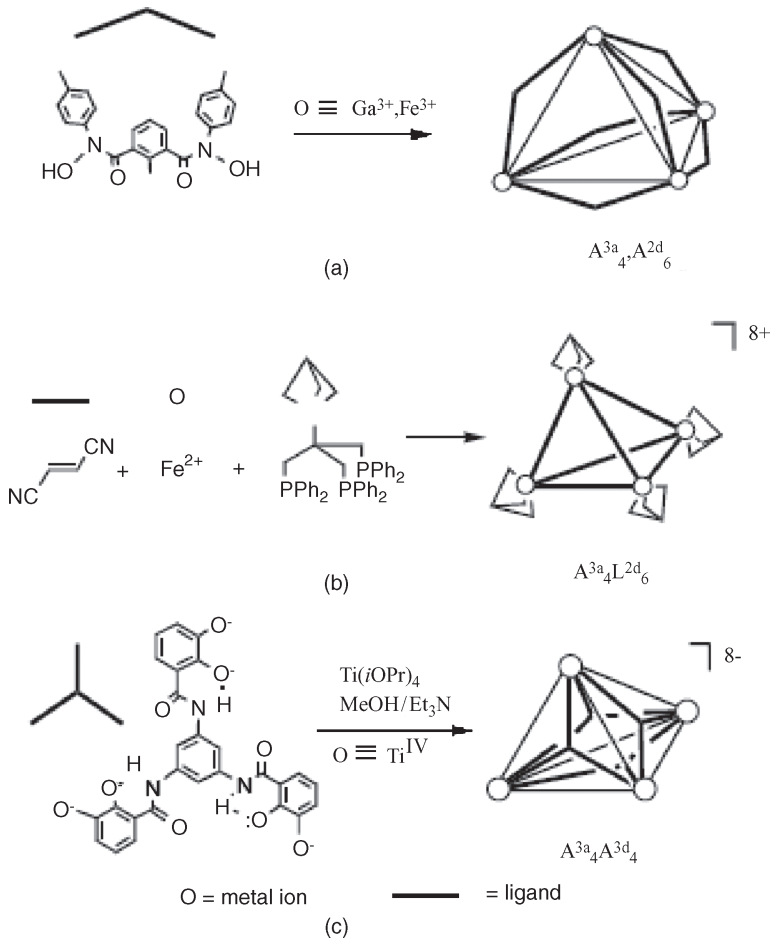


**Figure 10.23** Examples of self-assembled coordination polyhedra and their descriptors (Copyright Wiley-VCH Verlag GmbH & Co. KGaA. Reproduced by permission).

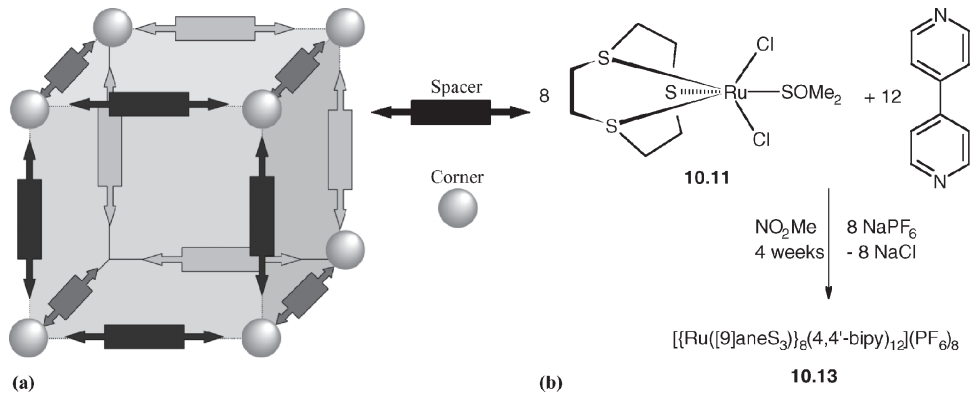


**Figure 10.24** (a) Components of a supramolecular cube. (b) Synthesis of a supramolecular cube.

As an 'edge', the divergent bridging ligand 4,4′-bipyridyl was chosen, while the corners were derived from the semilabile Ru(II) coordination complex $[Ru([9]ane\text{-}S_3)Cl_2(DMSO)]^{2+}$ (**10.11**). This is an example of strategy (b) in Scheme 10.5, since the chloride and DMSO (dimethyl sulfoxide) ligands in **10.11** are removed easily to give three convergent binding sites. The [9]ane-$S_3$ acts as a blocking group for the remaining three *fac* sites on the octahedral metal centre. Reaction of **10.11** with three equivalents of 4,4′-bipyridyl should result in the replacement of the labile Cl and DMSO ligands with three 4,4′-bipyridyl moieties to give $[Ru([9]ane\text{-}S_3)(4,4'\text{-bipyridyl})_3]^{2+}$ (**10.12**) because of the good donor strength and $\pi$-acceptor ability of the bipyridyl ligands, which stabilise Ru(II). More problematic is persuading four molecules of **10.12** to react with a further four equivalents of **10.11** to generate a closed, cuboidal molecule. While this is one possible course for the reaction, an enormous number of other oligomers and polymers can be formed, and in the absence of a template (*e.g.* a large, cubic anion) it is unclear why the desired cube $[\{Ru([9]ane\text{-}S_3)\}_8(\mu\text{-}4,4'\text{-bipyridyl})_{12}]^{16+}$ (**10.13**) should be formed. When the reaction is carried out (Figure 10.24b), a complex mixture of products is obtained initially. However, upon refluxing for a period of up to one month, the product distribution gradually simplifies, until eventually a single set of $^1$H NMR spectroscopic signals (an AA′BB′ pattern as expected for a single, symmetrical bipyridine environment) for the bipyridyl ligands is observed: the cubic structure has self-assembled (Figure 10.25).

This apparent anti-entropic production of an ordered, symmetrical molecule may be explained by the operation of a process of chemical 'natural selection' as for the square **10.10**. The self-assembly is not really anti-entropic because heat is being given out and the overall free energy change is still downhill. The simultaneous assembly of 20 components (eight corners and 12 edges) is, however, statistically highly unlikely, especially in the absence of a kinetic template. However, since Ru(II) – low spin $d^6$ – is a semilabile ion, bonds will be continuously (albeit slowly) breaking and reforming as the mixture equilibrates. Fragments of the cube coexist with monomer and polymer units, and occasionally minute quantities of the cubic product (**10.13**) will be formed. Unlike all of the open products,

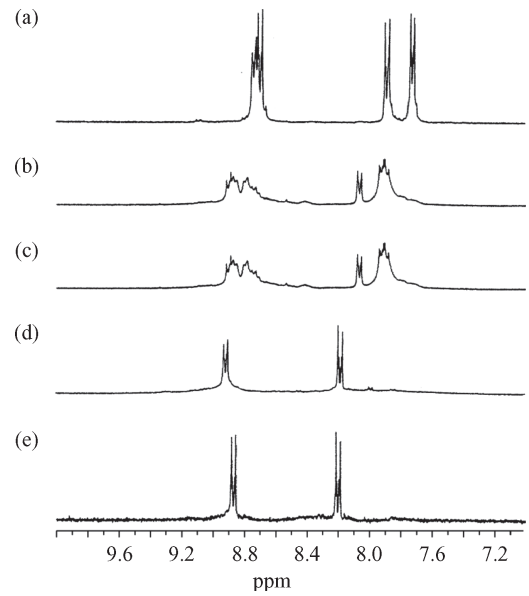


**Figure 10.25** $^1$H NMR spectra (bipyridyl region) of the products and reactants from Figure 10.24 (a) $[Ru([9]ane\text{-}S_3)(4,4'\text{-bipyridyl})_3]^{2+}$ (**10.12**), (b) after three days, (c) after one week, (d) after four weeks, (e) isolated product **10.13**. (Reproduced by permission of The Royal Society of Chemistry).

however, the closed, cubic molecule is significantly more thermodynamically stable and its formation is not very reversible since breaking down the cube requires distortion of the entire closed structure instead of the simple breaking of a single Ru—N bond. As a result, over an enormous period of time, the cubic structure is selected as the final product of the reaction. The entire process is only possible because Ru—N bond formation in *tris*(bipyridyl) complexes is reversible. Thomas *et al.* postulate that this reversibility is a result of unfavourable steric interactions between the *ortho*-C—H protons of the bipyridyl ligands. Without these slightly destabilising interactions, $Ru^{2+}$ would be too inert to self-assemble the cube structure within a viable time scale.

It is worth noting that this type of cube self-assembly is quite general, and similar cubic species such as $[\{Co(triazacyclononane)\}_8(\mu\text{-}CN)_{12}]^{12+}$ and $[\{Co(triazacyclononane)\}_4\{Cr(triazacyclononane)\}_4(\mu\text{-}CN)_{12}]^{12+}$ based on the Prussian blue motif of bridging $CN^-$ ions have also been produced. In these cases, intermediate squares could be isolated with DMSO molecules blocking unused coordination sites. Yet larger clusters of this type with two different kinds of metal have also been made by using a blocking ligand on only one of the mononuclear metal components. Reaction of capped Cr(III) with divergent Ni(II) gives the fourteen-metal cluster $[(Me_3trizazcyclononane)_8Cr_8Ni_6(CN)_{24}]^{12+}$ which incorporates a cube of eight capped Cr(III) ions that link *via* bridging cyanide ligands to six square-planar Ni(II) ions situated near the center of each cube face.[17]

## 10.5.3 Molecular Squares and Boxes

Fujita, M., Tominaga, M., Hori, A. and Therrien, B., 'Coordination assemblies from a Pd(II)-cornered square complex', *Acc. Chem. Res.* 2005, **38**, 369–378.

As we have already seen in the synthesis of **10.10** the concept of the special stability of closed, three-dimensional solid figures is not restricted to cubes. Extensive research has gone into the construction of self-assembling objects from two or more fragments that can mutually recognise each other, with a view to the construction of cavity-containing molecules and assemblies that are stable in solution. This research has been directed towards mimicking the solution complexation behaviour and supramolecular reactivity (*e.g.* protection of sensitive species from the external medium) of the carcerands, hemicarcerands and related species (Section 6.7). As with the production of nanoscale components, the self-assembling approach offers the distinct potential for engineering-up the production of extremely large cavities, capable of carrying out more complex chemistry and binding or protecting much larger (and perhaps more functional) guest species. In general it is possible to classify relatively rigid bridging ligands used in self-assembly into two broad classes; one-dimensional and two-dimensional. One-dimensional ligands such as 4,4′-bipyridine and extended analogues bridge between two metal centres and are topologically equivalent to straight lines, forming the edges of self-assembled structures. This kind of assembly process that we saw in the formation of **10.10** and cube **10.13** is termed *molecular scaffolding*. Ligands that bridge between more than two metal atoms can be considered two-dimensional and form the faces of the final structure. The assembly of polyhedral capsules using 2D ligands as in Figure 10.21 is termed *molecular paneling*.[18] Molecular paneling has given access to increasingly larger assemblies with significant void space because the faces defined by the ligands can be designed to be of increasing size. This has resulted in the self-assembly of cavities big enough to encapsulate larger guest species or more than one guest.

### *Molecular Scaffolding*

The work of Thomas *et al.* was preceded by the formation of a range of related molecular squares and triangles such as Fujita's molecular square (**10.10**), which is able to function as a solution host for aromatic guests such as naphthalene with a binding constant, $K_{11}$ of 1800 $M^{-1}$. Rigid spacers (edges)

like 4,4′-bipyridyl do not permit the formation of triangles, and their complex assemblies are restricted by the necessity of achieving bond angles at metal centres close to 90º (octahedral and square planar coordination geometries). In order to produce analogous closed coordination macrocycles with fewer than the eight components required for **10.10**, more flexible edge spacers are needed. For example, a range of triangular hosts (**10.14**) are produced by longer analogues of 4,4′-bipyridyl, while a simple cyclophane (bridged aryl ring) receptor (**10.15**) forms from the very flexible *α,α′-bis*(4-pyridyl)-*p*-xylene, in a four-component self-assembly. Note again the use of a protected, convergent metal fragment with divergent ligands (the ethylene diamine is the protecting group). Compound **10.15** is especially remarkable because, in addition to binding organic guest species as for **10.10**, it is also able to bind to itself to give an entirely self-assembling [2]catenane (a pair of interlinked rings, Section 10.7). The cyclic bimetallic compound **10.15** exists in a highly concentration-dependent equilibrium with the interlinked molecule **10.16**. At concentrations in excess of 50 mM, the catenane is the dominant species, whereas the single-ring cyclophane predominates at concentrations under 2 mM.

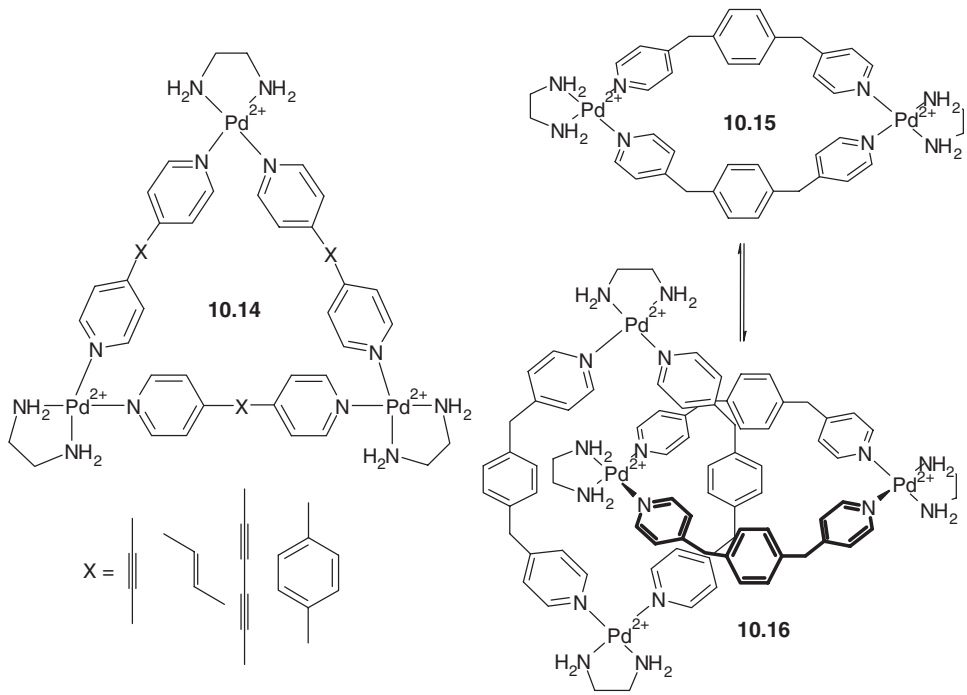


Formation of **10.16** is possible because of the lability of the Pd—N bonds holding the complex together. These bonds form and disassociate fairly readily under ambient conditions. Palladium(II) is much more labile than the Ru(II) ion we encountered in the molecular cube, for example. This results in the formation of an equilibrium-controlled (*i.e.* thermodynamic) product that is interlocked only at high concentration. Use of less labile metal ions can result in significantly more kinetically stable products. In this way, the propensity of the long *α,α′-bis*(4-pyridyl)-*p*-xylene ligand in **10.15** to form catenated species has been used to form a much more stable catenane that does not dissociate by M—N bond fission. Replacing palladium(II) with the much less labile platinum(II) results in the formation of the Pt(II) analogue of **10.16** from [Pt(en)$(NO_3)_2$] (en = ethylenediamine) only after prolonged reflux (as in the formation of the supramolecular cube from semilabile Ru(II)). Because Pt—N bonds are much more inert (Box 10.1) than Pd—N, the complex is long-lived and, even at high concentrations, does not dissociate in order to form the analogous Pt(II) catenated species. The Pt—N bonds can be dissociated, however, upon reflux at 100 ºC

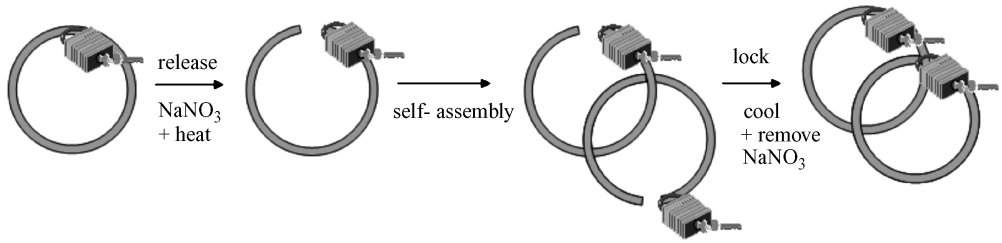


**Figure 10.26** Cartoon representation of the formation of the Pt analogue of **10.16** from the uncatenated monomer by a 'molecular lock' method.

in the presence of excess salt ($NaNO_3$). This feature of the chemistry has been utilised in the formation of platinum catenane species by a 'molecular lock' method (Figure 10.26).

Reflux of the monocycle with $NaNO_3$ 'unlocks' the ring by labilising the Pt—N bonds. Under these conditions, the system is under thermodynamic control and, at high concentrations, self-assembles into the [2]catenane. In reality, this process probably involves the breaking of a Pt—N bond, the threading of the resulting linear complex through the annulus of a second macrocycle as a result of hydrophobic influences, and reclosing the broken coordination bond. Cooling back to room temperature, and removal of excess salt, effectively locks the two catenated rings together because of the nonlability of the Pt—N bonds. The salt/heat treatment effectively represents the key to the lock. More information about metal-backbone catenanes of this type can be found in the literature,[19] while the extensive chemistry of other kinds of catenanes is explored further in Section 10.7.

While interesting, compounds **10.14** and **10.15** are essentially only two-dimensional (corand type) hosts, which, as we have already seen (Chapter 3), give weaker binding than their three-dimensional cryptand analogues and, more importantly from the point of view of intracavity chemistry, do not offer protection from the external medium above and below the cavity. The flexible spacer concept seen for compound **10.15** has been extended, however, to give a tripodal ligand, *α,α′,α″-tris* (4-pyridyl)-mesitylene, capable of taking part in a five-component self-assembly to give the cryptand analogue of **10.15**, compound **10.17**.[20] The three-dimensional host is prepared in water in yields in excess of 90 % only in the presence of a suitable large guest such as 2-phenylpropionic acid or 1-adamantanecarboxylic acid. Smaller, less polar guests such as *p*-xylene give much lower yields, while cationic guests do not template the complex formation. This kind of self-assembly, in which the information is carried by a guest molecule, corresponds to Lindsey's class 6 can be thought of as a kind of induced fit, in which the formation of the host is induced by the size of the guest. In principal, different guests could direct the formation of various oligomeric assemblies depending on guest size and properties. The effect is analogous to the kinetic template effect discussed in Chapter 3 because the products, once formed, are reasonably robust, and do not necessarily represent thermodynamic minima for the system. Furthermore, they do not require the continued presence of the templating molecule. By analogy with this chemistry, even larger three-dimensional hosts $[\{Pd(en)\}_{12}(\mathbf{10.18})_8]^{12+}$ (the smallest example of the series with X = nothing is shown in Figure 10.21) of diameter up to 4.6 nm have been prepared[13] and their existence in solution shown by light scattering experiments (in which visible light is scattered by large particles of dimensions comparable to its wavelength). Supermolecule $[\{Pd(en)\}_{12}(\mathbf{10.18a})_8]^{12+}$ is able to bind simultaneously four molecules of adamantane carboxylic acid within its cavity, although the structure is stable even in the absence of this guest. Remarkably, the binding process exhibits a distinct allosteric cooperative effect: titration of the solvated host with adamantane carboxylic acid guest reveals immediate 1:4 complexation with no intermediate formation of 1:1, 1:2 or 1:3 complexes. Thus a 1:1 mixture of host and guest contains signals only for free host (75 %) and 1:4 complex (25 %). This is attributed to the complex's increasing ability to bind guest molecules as the inclusion of the first guests renders the cavity more and more hydrophobic.

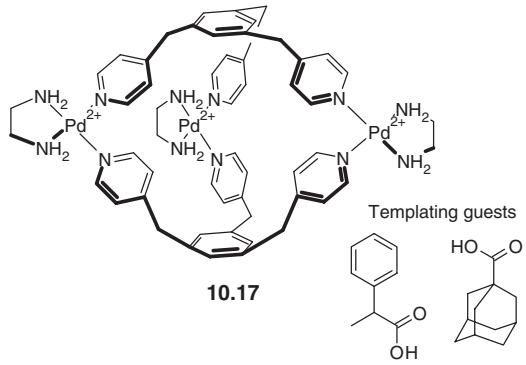


**10.17**

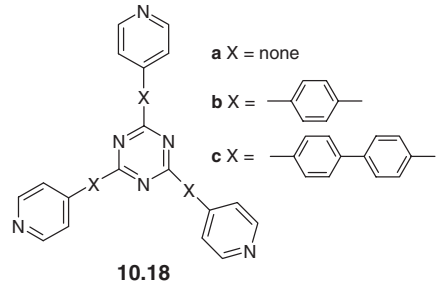


**10.18**

It is not always necessary to use protected metal ions, however, if there is a degree of templation or preorganisation in the ligand. For example, as part of the research into systems mimicking biological cavity-containing macromolecules, Atwood's group prepared the *exo*-bidentate ligand **10.19**, which was designed to exhibit water solubility, and possesses amide groups and aryl rings common in biological systems as well as divergent binding sites. Even in the absence of a terminating ligand such as ethylene diamine, this ligand self-assembles readily in the presence of $Cu(NO_3)_2$ to give the closed, cavity-containing assembly $[Cu_2(\mathbf{10.19})_4(H_2O)_4](NO_3)_4{\cdot}8H_2O$. The fact that a coordination polymer is not formed is apparently a result of a templating effect involving hydrogen bonding of axial water ligands to four nitrate anions, which are included within the giant cavity of the assembly. Most surprisingly of all, the solid state structure of the assembly contains a hydrogen-bonded cluster of 10 water molecules, an interesting, although unplanned feature within the context of the authors' aims at biological mimicking systems.[21]

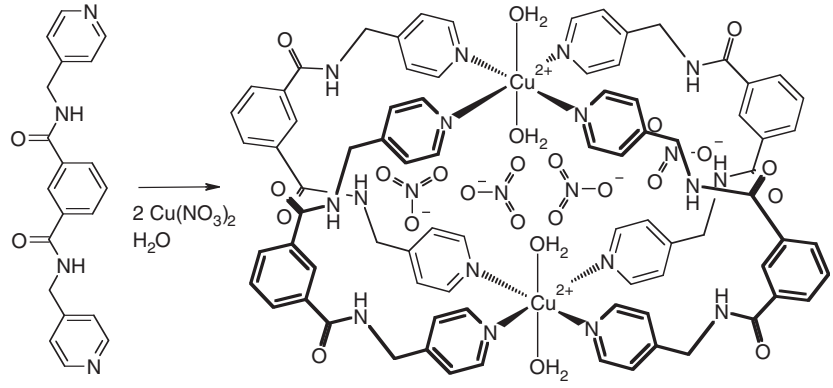


**10.19**

$[Cu_2(\mathbf{10.19})_4(H_2O)_4](NO_3)_4{\cdot}8H_2O$

More rigid, extended linear ligands have been used to form some remarkably large assemblies. A series of assemblies based on pyridyl pyrazenes have been investigated by Mike Ward and co-workers from Sheffield, UK. While ligands like **10.20** in some cases form only mononuclear complexes, anion templation can result in tetranuclear and even decanuclear assemblies such as $[Cd_{12}(\mathbf{10.20})_{18}](BF_4)_{24}$.[22] This remarkable complex, and its close related copper(II) analogue have remarkably large crystallographic unit cell dimensions, with the 29.4 × 29.4 × 92.8 Å primitive hexagonal unit cell comparable in size (and crystallographic challenge!) to a respectably sized protein. The structure contains four tetrafluoroborate anions that may play a templating role in the assembly and a helical arrangement of 1D bridging ligands, Figure 10.27. Work by Ken Raymond at Berkley has used a similar concept based on catechol (1,2-dihydroxybenzene) derived binding sites, which when doubly deprotonated, have a

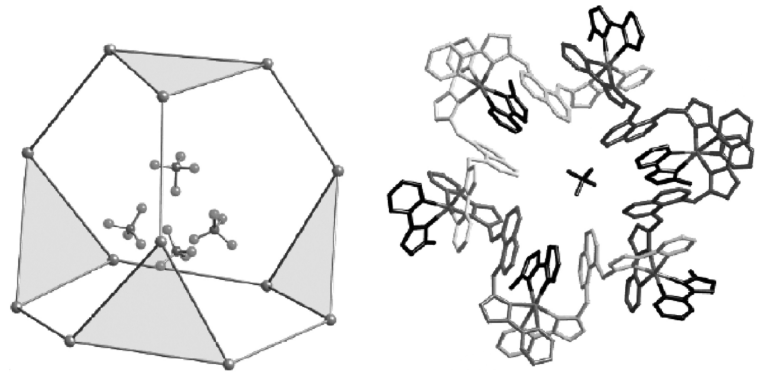


**Figure 10.27** The structure of $[Cd_{12}(\mathbf{10.20})_{18}](BF_4)_{24}$ showing (a) polyhedral metal cage and the four encapsulated $BF_4^-$ anions; (b) view down one of the $Cd_6$ *pseudo*hexagonal faces, emphasising the cyclic helical array of ligands and the presence of an anion in the centre of the face (reproduced with permission from [22] © 2006 American Chemical Society).

strong affinity for hard metals such as Fe(III) and Ga(III), forming very stable trigonal prismatic or octahedral arrangements (*cf.* siderophores, Section 3.16). The anionic nature of the ligands means that the assemblies are usually anionic and hence entrap cations. Ligand **10.21** forms chiral tetrahedral tetrametallic cages with Fe(III) and Ga(III) of formula $[M_4(\mathbf{10.21})_6]^{12-}$ with a cavity *ca*. 300–500 Å$^3$ into which a tetramethylammonium cation is encapsulated (Figure 10.28). The larger ligand **10.22** forms an analogous, larger cage with Ti(IV), $[Ti_4(\mathbf{10.22})_6]^{8-}$ but *only* in the presence of a tetraalkyammonium ion to act as a guest to the cage. If an alkali metal cation is used then a dimetallic triple helicate results for formula $[Ti_2(\mathbf{10.22})_3]^{4-}$.[23] Cages such as $[Ga_4(\mathbf{10.21})_6]^{12-}$ can also encapsulate a wide range of reactive organometallic compounds and the rigidity and chirality of the cavity means that the intra-cavity guest might be expected to catalyse enantio- or regiospecific organic transformations even if it is itself achiral. This goal has been realised with the encapsulation of the reactive cationic Ir(III) species $[Cp^*(PMe_3)Ir(Me)(\eta^2\text{-}C_2H_4)]^+$ (**10.23**). This kind of organometallic complex thermally activates C-H bonds under mild conditions. The process appears to involve dissociation of a labile ligand to give a sixteen valence electron cation $[Cp^*(PMe_3)Ir(Me)]^+$ (**10.24**), which then reacts with a C-H bond. The fact that both **10.23**

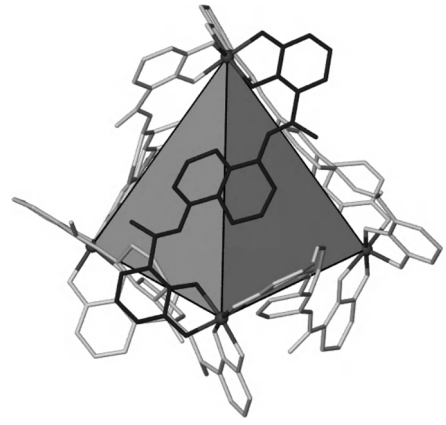

**Figure 10.28** Structure of the self-assembled cluster $[Ga_4(\mathbf{10.21})_6]$.[12–23]

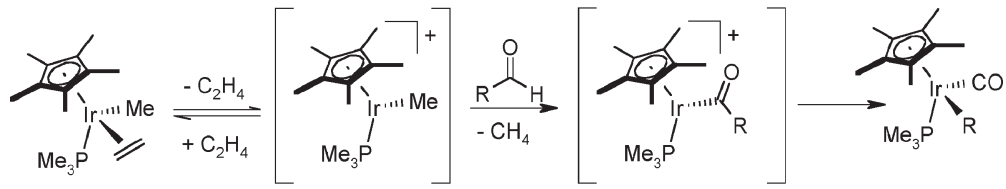


**Scheme 10.6** CH bond activation within a tetrahedral self-assembled cluster.[24]

and **10.24** are cationic is compatible with the overall negative charge of the cage.[24] Compound **10.23** is quantitatively encapsulated by $[Ga_4(\mathbf{10.21})_6]^{12-}$ resulting in the formation of diastereoisomers (observable by NMR spectroscopy) because of the chirality of the Ir(III) complex. Reaction of the encapsulated compound with a variety of aldehydes results in CH bond activation to give an alkyl carbonyl product **10.25** (Scheme 10.6) over a relatively long period with the diastereomeric ratio increasing from 60:40 to 70:30 with increasing aldehyde chain length until suddenly reactivity stops for chains longer than butyl. The cage is also capable of other interesting kinds of catalysis including the remarkable acid catalysed hydrolysis of orthoformates ($HC(OR)_3$ where R = alkyl or aryl) in extremely basic solution, pH = 11. The cavity is so effective at stabilising the protonated cationic intermediate that this reaction, which is facile at low pH but does not normally occur at all under basic conditions is markedly promoted.[25]

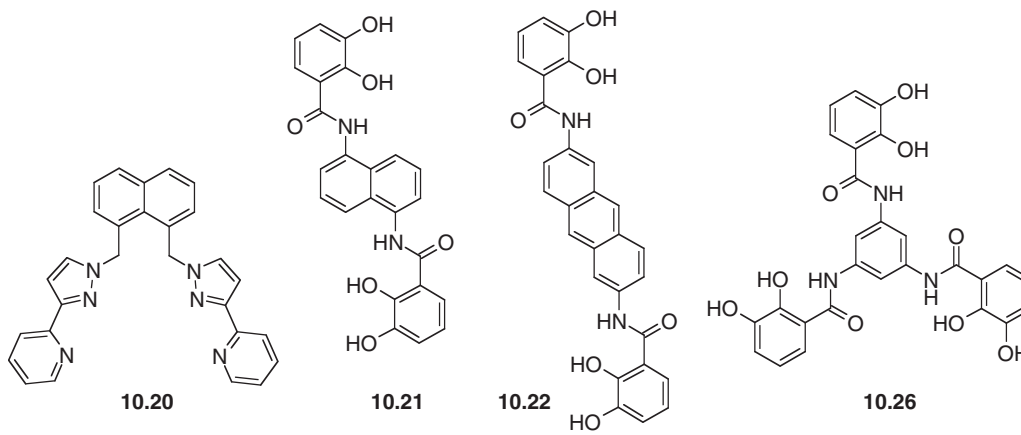


Extending these 1D ligands to 2D molecular panels is readily achieved using tripodal analogues such as **10.26**, the rigidity of which prevents any two catechol moieties from coordination to the same metal ion. The ligand forms tetrahedral cages with a variety of metal ions but is too small to contain a guest molecule. The $C_3$ symmetry of the ligand results in the cages being homochiral.

### *Molecular Paneling*

In 1999 the groups of Fujita and Stang were both able, independently, to induce the self-assembly of extremely large capsules. Applying the same principles used in his smaller square planar systems, Fujita reacted $[Pd(en)(NO_3)_2]$ with the triangular hexadentate ligand **10.27**, resulting in the formation of a hexahedron comprising six triangular ligands linked by 18 Pd(II) ions, Figure 10.29.[26] Note the matching of $6 \times 6 = 36$ donor atoms with $2 \times 18 = 36$ vacant coordination sites on the palladium(II) metals (on loss of the labile $NO_3^-$ ions). The internal volume of the capsule is some 900 Å$^3$, and contains a number of nitrate ions. The capsule highlights some of the problems associated with the X-ray

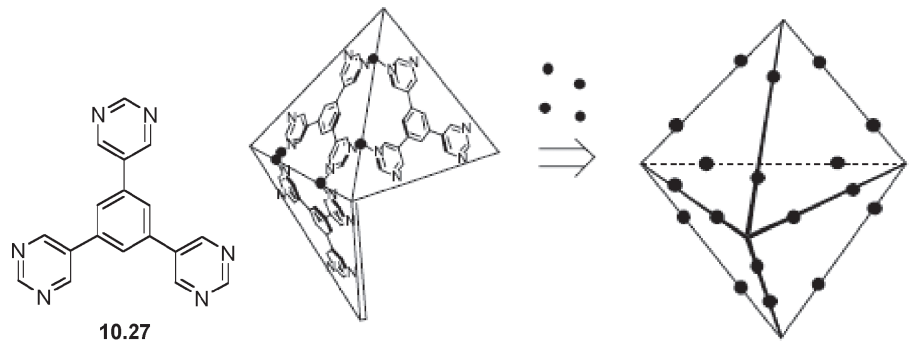


**Figure 10.29** Formation of a hexahedron from ligand **10.27** and 18 Pd(II) ions (reprinted with permission from Macmillan Publishers Ltd).

crystallography of supramolecular compounds: of a total 36 nitrate ions expected to be present, only 14 could be located experimentally, of which five were found in the cavity.

Two assemblies (**10.28** and **10.29**) produced by Stang, published directly after Fujita's paper in the journal *Nature*,[27] are also based on trigonal building blocks. Stang and co-workers again used a square planar metal ion, $Pt^{2+}$, with two labile ligands (trifluoromethane sulfonate) and two nonlabile ligands ($PPh_3$), this time in a *trans* geometry, to give a divergent metal unit. Convergence was achieved by addition of a second component (either a pyridyl-type ligand or a benzophenone derivative) possessing a 'V'-shape. The result was a cubeoctahedron (one of the Archimedian semiregular solids, Section 10.6.3) containing a total of 12 Pt(II) centres (Scheme 10.7). The calculated structure of the assembly is shown in Figure 10.30.

The smaller octahedron shown in Figure 10.21 is also formed by the molecular paneling approach, and while it has a smaller cavity than the assembly based on **10.27** it is still capable of a remarkable variety of inclusion phenomena (Figure 10.31). These include stabilisation of a highly reactive cyclic silanol oligomer, isolated from the surrounding media which prevents its hydrolysis. The capsule can stabilise *cis* isomers of stilbene derivatives (preventing conversion to the more stable *trans* isomer) by the formation of dimers within the cavity, akin to building a 'ship-in-a-bottle' (the dimer must form within

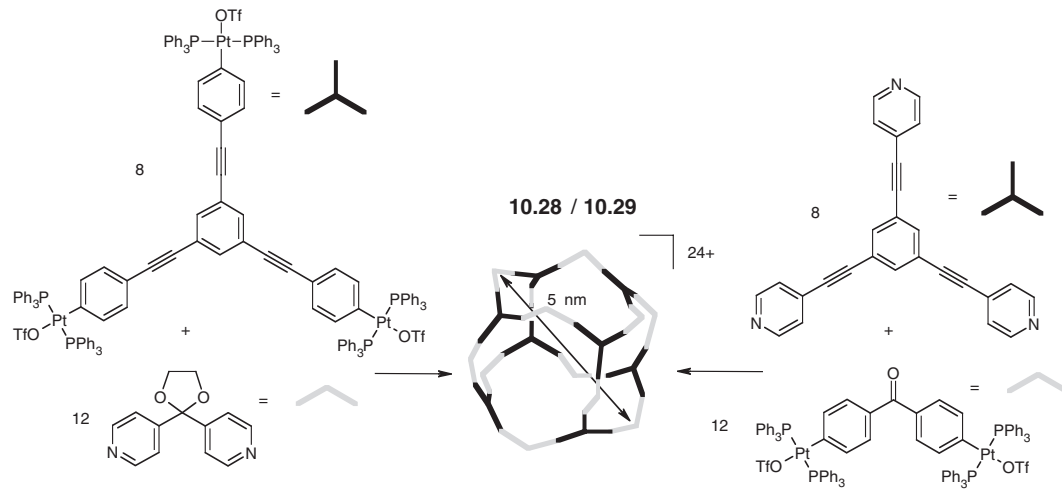


**Scheme 10.7** Self-assembly of nanoscopic cubeoctahedral **10.28** and **10.29** (conditions $CH_2Cl_2$, room temperature, 10 mins, yields > 98 %).[27]

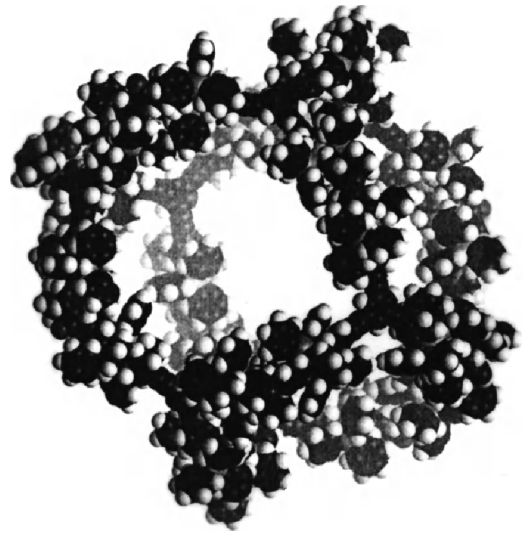

**Figure 10.30** Space-filling model of 10.29, the 12 Pt(II)-containing cubeoctahedron calculated by ESFF (extended systematic force field) methods. (Reprinted with permission from Macmillan Publishers Ltd).

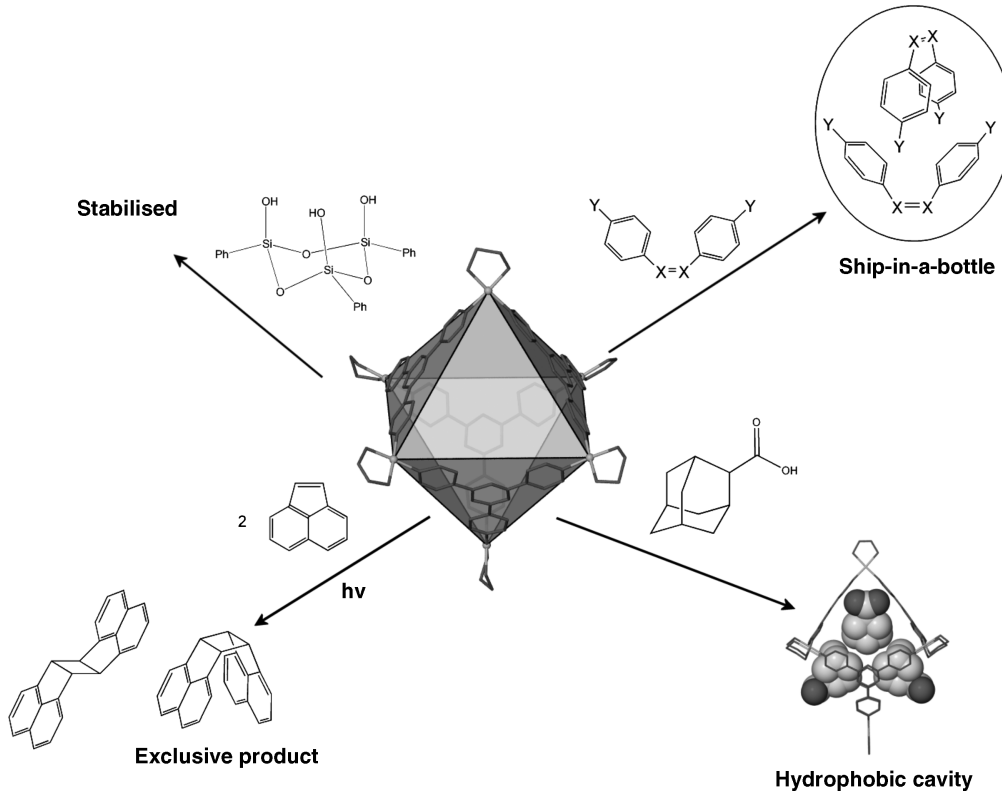


**Figure 10.31** Inclusion properties and reactivity of an octahedral capsule prepared by molecular paneling.[29]

the capsule as it is too large to enter 'pre-assembled'). Intracavity reactivity includes the stereoselective photodimerisation of olefins as only the *syn* isomer of the product is able to fit within the cavity. In the absence of the cage the reaction results in a mixture of the two isomers. Remarkably some of these reactions occur as single-crystal-to-single-crystal transformations upon irradiating a crystalline sample.[28]

Fujita's group has assembled a wide variety of cages of different shapes and sizes using the panelling approach. Some of the ligands used are **10.30–10.32** their resulting structures when self-assembled with the ubiquitous 'Pd(en)$^{2+}$' corner units are shown in Figure 10.32. An added refinement is the use of more than one type of ligand which allows finer control over the shape of the assembly, as in the reaction of pyrazene and **10.18a** which gives the trigonal box **10.33** which includes electron rich, planar aromatic guests such as **10.34**.

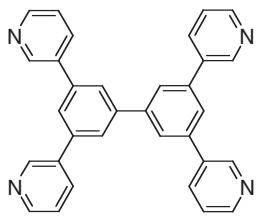

**10.30**

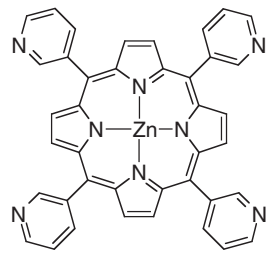

**10.31**

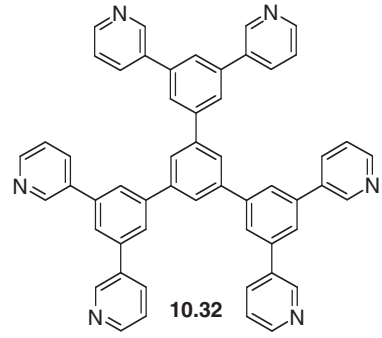

**10.32**

Finally, in a remarkable example of self-assembly followed by covalent post-modification, Harry Anderson in Oxford, UK, has produced an octaporphyrin 'nanocycle' based on a designer pyridyl template **10.36** which 'wraps' the linear 16-alkyne oligomer **10.35** into a circle allowing it to be covalently cyclised using palladium-catalysed alkyne coupling (Figure 10.33). The difference in complexation free energy for the template binding by the linear precursor **10.35** and the final nanocycle gives an estimate of the energy involved in bending the normally linear alkyne groups into this great circle. The $\Delta G_{\text{complexation}}$ values are −161 and −212 kJ mol$^{-1}$, respectively giving a strain energy of *ca.* 51 kJ mol$^{-1}$. It is not clear at present whether this is a mainly enthalpic or entropic barrier, *i.e.* does the linear porphyrin octamer **10.35** behave as a floppy chain resulting in an entropic cost associated with cyclisation around the template or as a rigid rod giving an enthalpic barrier. The UV-Vis spectrum of the nanocycle suggests that it is not particularly strained, however.[31]

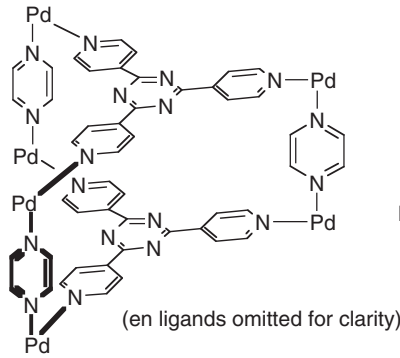


**10.33**

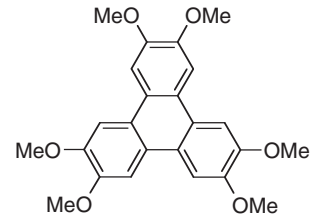

**10.34**

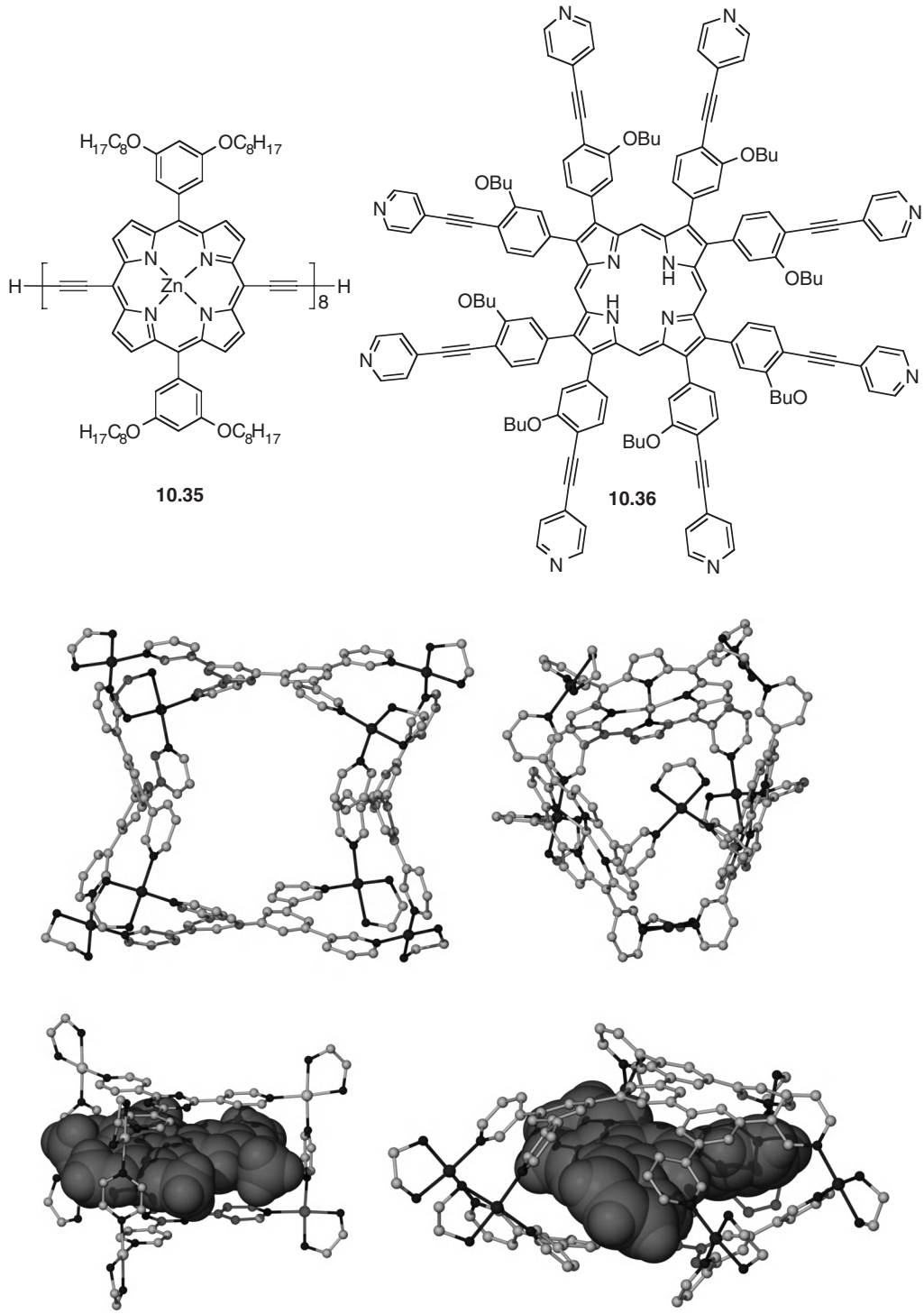


**Figure 10.32** Molecular panels and the structures formed with 'Pd(en)$^{2+}$' (aromatic guests shown as spacefilling representations).[30]

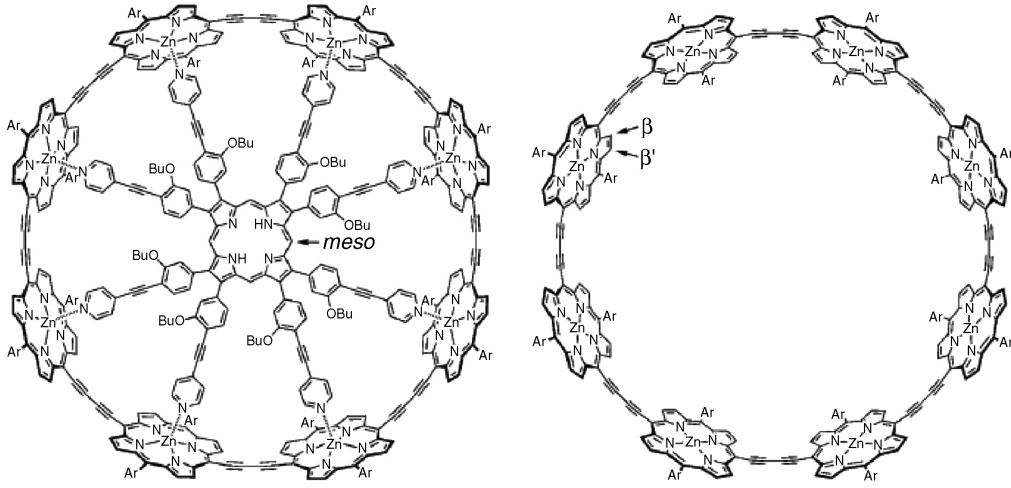


**Figure 10.33** Self-assembly followed by covalent modification results in the synthesis of an octaporphyrin nanocycle from a extended octapyridyl template (Copyright Wiley-VCH Verlag GmbH & Co. KGaA. Reproduced with permission).

### *Coordination Capsules*

In addition to capsules made from either molecular scaffolding or molecular panelling there have also been a number of impressive capsules made by assembling curved building blocks such as calixarenes with metal-containing bridges to give coordination complexes that are analogues of hemicarcerands (Section 6.7), but prepared by self-assembly. The obvious route to a metallo-hemicarcerand is linking together two bowl-shaped fragments with up to four metal ions and this has indeed been realised by reaction of the tetracarboxylate **10.37** with first row transition metals such as Co(II) or Fe(II) to give a capsule bridged by four 6-coordinate metal ions (**10.38**). In the solid state, in a variety of different structures of various salts of this type of capsule, the cavity is occupied generally by either water or neutral molecules such as $C_6H_5Br$. The $Sr^{2+}$ salt of the iron capsule contains a discrete water hexamer, Figure 10.34.[32]

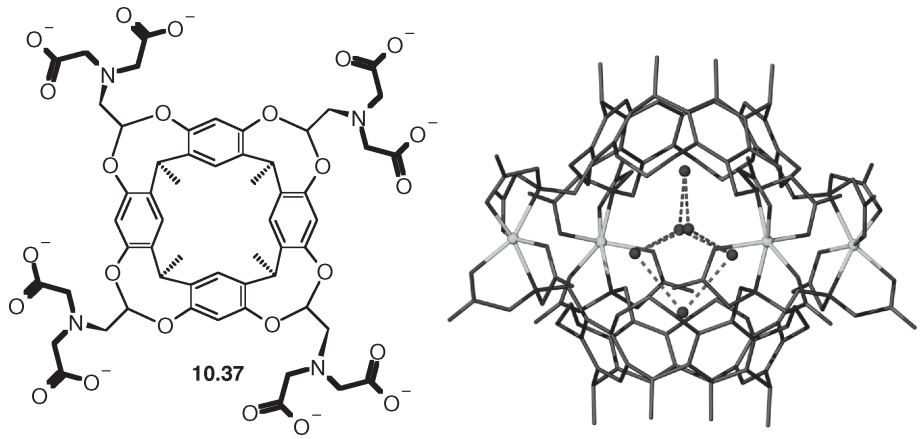


**Figure 10.34** Crystal structure of the $Sr^{2+}$ salt of the metallo-hemicarcerand **10.38**, assembled from two hemispherical octa-anionic ligands, **10.37**, and four Fe(II) ions. The cavity contains a discrete water hexamer.[34]

A number of other more fragile metallohemicarcerands have been characterised by sonic spray ionisation mass spectrometry (SSI-MS), a gentle mass spectroscopic technique that preserves compounds such as a palladium(II) diphenylphosphinopropane bridged resorcarene tetranitrile that fall apart under standard electrospray conditions.[33] The SSI source has two concentric capillaries. A solution of analyte is passed through the inner one and is nebulised without any applied potential by nitrogen gas flowing through the outer capillary. Fluid speeds are approximately the speed of sound, hence the name sonic spray.

Work by Paul Beer *et al*. in Oxford on dithiocarbamate-functionalised resorcarenes has resulted in resorcarene trimers termed 'molecular loops' and molecular tetrahedra composed of four resorcarene units. The molecular loops (pyridine-capped Cd(II) and Zn(II) complexes) can bind $C_{60}$ which fits neatly into the 16.4 Å wide central cavity.[35] The slightly larger tetrahedral tetramer which has a 19.4 Å edge length, compared to 19.1 Å for the loop, is bridged by square planar copper(III) ions, a very unusual oxidation state of copper that is obtained from iodine oxidation of an intermediate copper(II) complex. The solid-state structures of examples of the loop and tetrahedron are shown in Figure 10.35.

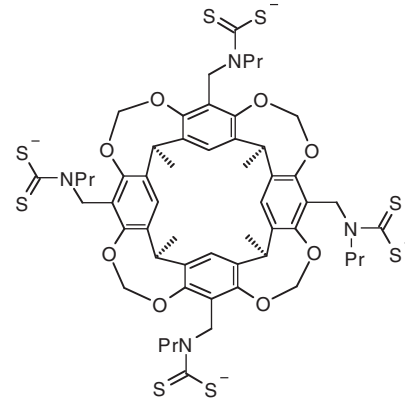

**10.39**

Resorcarene hexamers bridged either by 24 Cu(II) ions or 12 Ga(III) ions have also been prepared.[36, 37] These compounds are closely analogous to hydrogen-bonded resorcarene and pyrogallolarene hexamers (indeed the metal-bridged compounds can be prepared by substitution of $2H^+$ for $Cu^{2+}$) and we will look at these systems as a whole in Section 10.6.3.

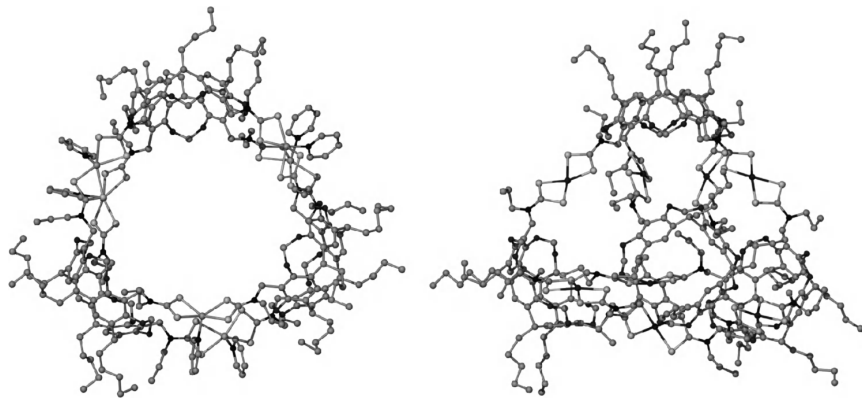

**Figure 10.35** X-ray molecular structures of a molecular loop and tetrahedron derived from the self-assembly of 10.39 with Zn(II) or Cu(III), respectively.[35]

**Box 10.1** Kinetic and Thermodynamic Stability

A coordination compound, such as **10.15** is said to be kinetically labile if, like the majority of transition metal complexes, it undergoes rapid ligand exchange reactions in solution. Labile complexes have been defined formally by Henry Taube (who won the 1983 Nobel Prize for his work in the area) as those that react completely within 1 min at 25 °C. The opposite of labile is *inert*. Inert and labile are terms that refer to a complex's kinetic stability. Inert complexes have a high activation energy barrier to reaction. For labile complexes, the reaction transition state is reached much more readily (*i.e.* $E_A$ is small). Kinetic stability (long lifetime under a certain set of conditions) is distinct from thermodynamic stability, which refers to the overall standard free energy for a reaction, $\Delta G_r^0$. If $\Delta G_r^0$ is large and negative, the reaction products are much more thermodynamically stable than the reactants, thus affecting the overall equilibrium position (Figure 10.36). Certain metals in certain electronic configurations have much slower rates of ligand exchange than others, *e.g.* octahedral Cr(III), electron configuration $3d^3$, Figure 10.37a. Consider a dissociative (D) reaction of an octahedral complex. This may be regarded as proceeding in two stages (Figure 10.36):

1. Loss of a ligand to form a square pyramidal, five-coordinate transition state (or possibly an intermediate if the compound is at a local minimum on the energy curve):

$$[M(H_2O)_6]^{n+} \rightarrow [M(H_2O)_5]^{n+} + H_2O \quad (10.23)$$

2. Reaction with another ligand (L) to generate an octahedral product:

$$[M(H_2O)_5]^{n+} + L \rightarrow [M(H_2O)_5L]^{n+} \quad (10.24)$$

The activation energy, the energy required to complete step 1, is made up of several factors, notably the M—$OH_2$ bond energy and any complex and solvent reorganisation energy in changing to the new structure. The latter will involve changes in the ligand field stabilisation energy (LFSE). This is the energy gained when the *d* electrons in the metal ion are in a nonspherical ligand environment (octahedral in this case). For example, for Cr(III) the $3d^3$ electron configuration gives an LFSE that is equal to three electrons stabilised by $^2/_5$ of the total ligand field splitting parameter, Δ. The square pyramidal reaction transition state is no longer octahedral and so does not give the same splitting of the valence *d* orbitals, resulting in a loss of LFSE and hence a high activation energy for the reaction. The larger the Δ value, the larger this loss will be, although it is tempered by the LFSE in the transition state/intermediate (square pyramidal in this case). The difference

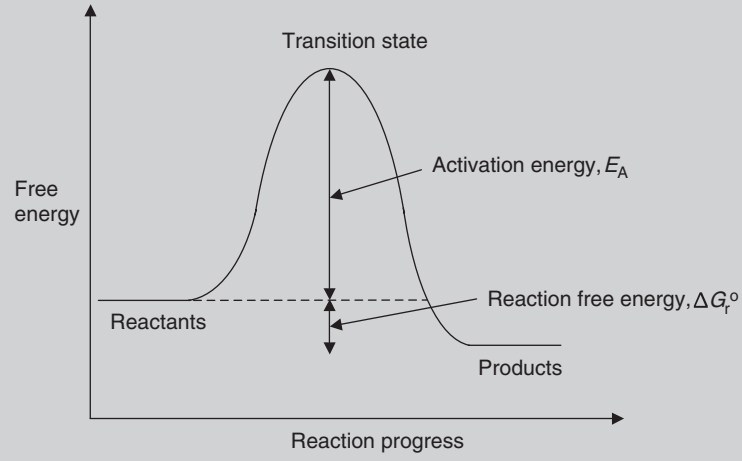


**Figure 10.36** Free energy changes during the course of a chemical reaction.

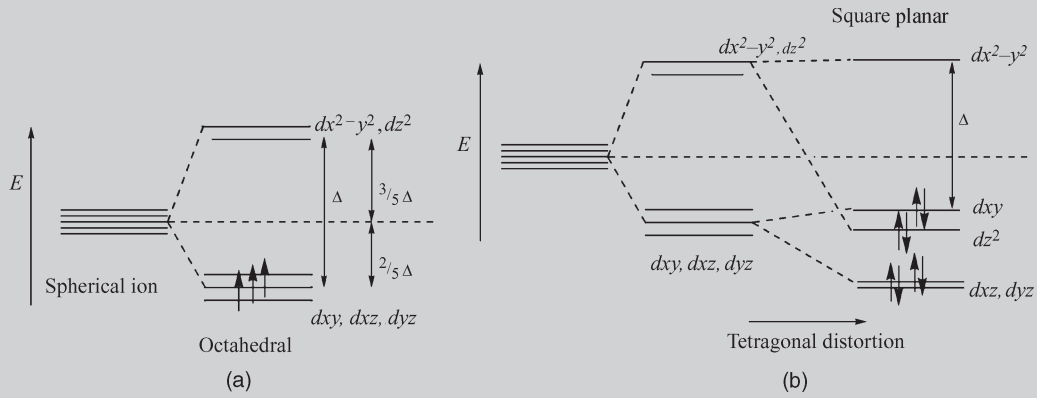


**Figure 10.37** (a) Orbital energy diagram for an octahedral $d^3$ metal ion. (b) Effect on the relative energies of metal of orbitals of moving from an octahedral to square planar ligand field by removal of axial ligands (tetragonal distortion).

between the LFSE in the ground state and the intermediate is termed the ligand field activation energy (LFAE), and it is this parameter that determines the overall reaction rate.

In compounds such as **10.15**, Pd(II) and Pt(II) both adopt square planar, rather than octahedral, geometries and hence their valence electrons occupy a different set of *d* orbitals (Figure 10.37b). The splitting pattern for square planar complexes may be thought of as arising from the removal of two axial ligands from an octahedron (an infinite tetragonal distortion). For a $d^8$ electron configuration as in Pd(II) or Pt(II), this results in a single empty, high-energy $dx^2 - y^2$ orbital. This configuration also results in a high LFSE and is therefore relatively inert, depending on the exact magnitude of the crystal field splitting energy, Δ. In fact Δ increases significantly on descending a group in the periodic table. Thus Ni(II) and Pd(II) are relatively labile, whereas the Δ value for Pt(II) is sufficiently large to dramatically slow down its ligand exchange reactions under ambient conditions.

## 10.5.4 Self-Assembly of Metal Arrays

Swiegers, G. F. and Malefetse, T. J., 'New self-assembled structural motifs in coordination chemistry', *Chem. Rev.* 2000, **100**, 3483–3537.

Moving away from closed capsules, a number of rack, ladder and grid structures have been produced *via* self-assembly (Figure 10.38) using linear 'rigid rod' multidentate bridging ligands, *e.g.* formation of the molecular ladder **10.40**. Again, the thermodynamic driving force results in the formation of discrete

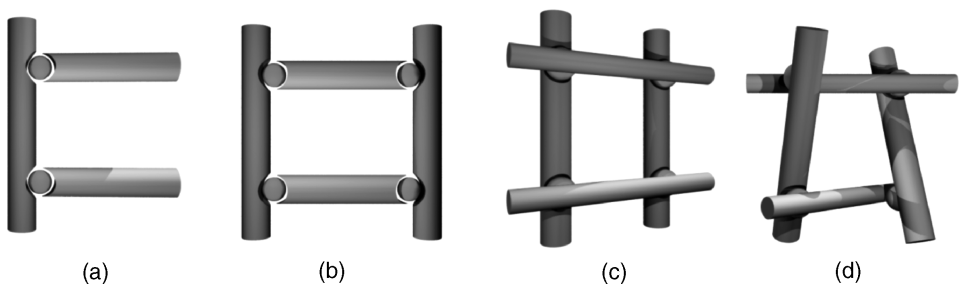


**Figure 10.38** Cartoon representations of (a) a [2]-rack, (b) a [2.2]-ladder, (c) a [2×2]-square grid and (d) a chiral [2×2]-grid. from 'rigid rod' ligands and metal ions.

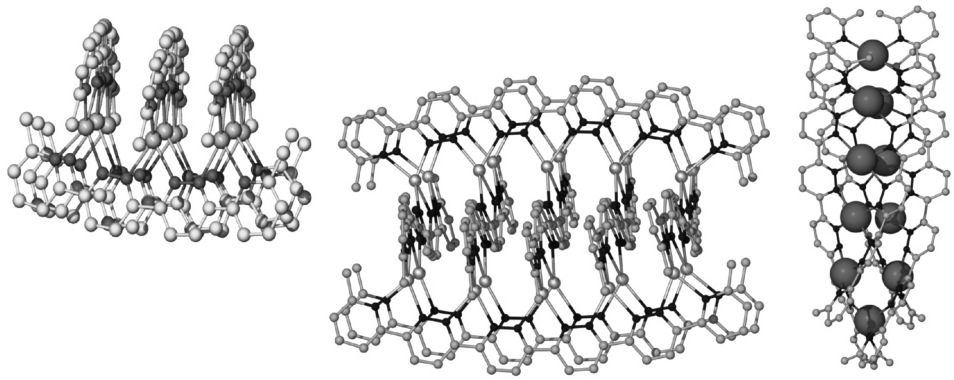


**Figure 10.39** X-ray molecular structures of (a) a [3×3] molecular grid, $[Ag_9(\mathbf{10.41})_6]^{9+}$, (b) a [4×5]-$Ag_{20}$ grid and (c) a decametallic quadruple helicate formed by **10.42** (Ag ions shown as large spheres).[38]

oligomeric entities, rather than polymers. In each case, the information for the assembly of the entire structure is coded into the individual components by virtue of the rigidity of the ligands and the number and positioning of donor sites, as well as the coordination geometry of the metal. Thus ligand **10.41** in the presence of 1.5 equivalents of $AgCF_3SO_3$ self-assembles in a 15-component reaction to give a [3×3] molecular grid, $[Ag_9(\mathbf{10.41})_6]^{9+}$. The $CF_3SO_3^-$ anion is used because it is a poor ligand for the soft $Ag^+$ and does not compete with the *N*-donors. Consistent with the grid structure, the $^{109}Ag$ NMR spectrum shows three distinct silver environments in ratio 4:4:1, assigned to the four metal ions on each corner, the four in the middle of each face and the central $Ag^+$, Figure 10.39a. ($^{109}Ag$ is a nucleus with a spin quantum number of ½ just like $^1H$, and high natural abundance, making $^{109}Ag$ NMR spectroscopy a very useful tool in studying assemblies of this metal.) Extending the grid concept further, ligand **10.42** might be expected to give a [5 × 5]-$Ag_{25}$ grid. However, the fact that the *cisoid* form of the ligand required by

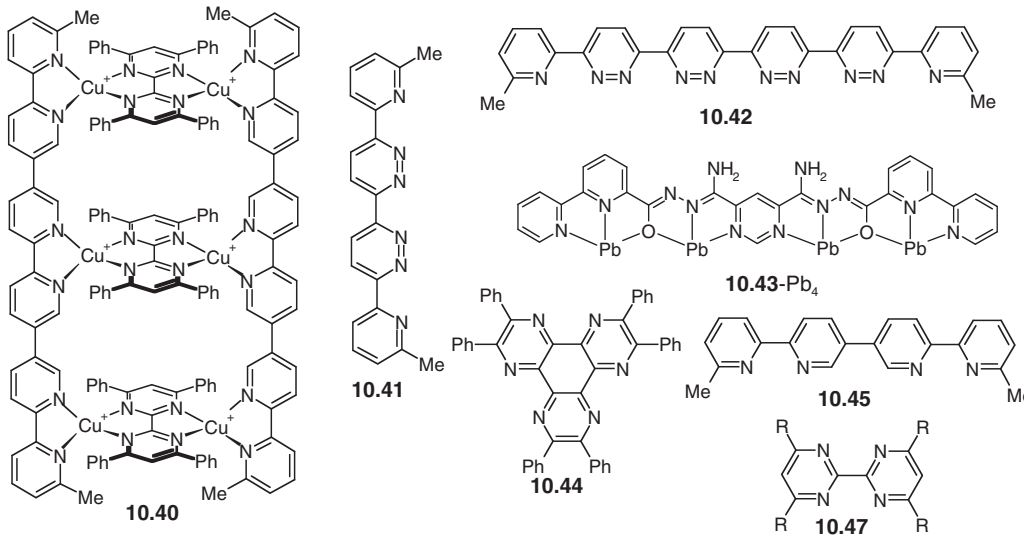

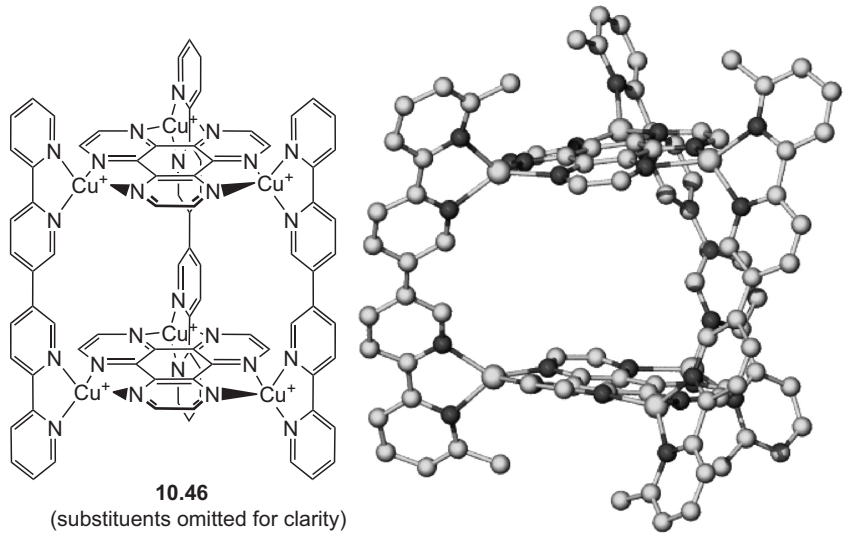


**Figure 10.40** X-ray crystal structure of the 'office block' **10.46** (substituents omitted for clarity).[40]

a regular grid is less stable and the non-planar 'doming' of larger grids caused by a slight mismatch in metal and ligand coordination preferences means that instead a remarkable [4×5]-$Ag_{20}$ grid is isolated, Figure 10.39b. However the structure is in fine balance with other self-assembled grid structures and at low temperature where the entropic contribution is less significant in solution the compound converts to a striking decametallic quadruple helicate, Figure 10.39c.[38] Use of 'compartmental' ligands in which binding domains are separated by spacers can result in interesting grids of grids. Ligand **10.43** in which two pairs of monoanionic tridentate binding domains are separated by a pyrimidine spacer, forms a [4×(2×2)]-$Pb_{16}$ complex $[Pb_{16}(\mathbf{10.43})_8(CF_3SO_3)_6(H_2O)_5]^{10+}$ with lead(II) in which four somewhat separated 2×2 grids are themselved linked into a 2×2 grid of grids.[39]

Lehn and co-workers have also looked at systems consisting of two different ligands, one rod-like in a similar way to **10.41**, and the other disc-like.[40] In this way, they were successful in assembling a cylindrical box resembling a molecular 'office building' with two 'floors' consisting of the *tris*(bidentate) **10.44** and three 6,6′′′′-dimethyl-2,2′:5′,3′′:6′′,2′′′-quaterpyridine **10.45** 'walls'. These ligand components are joined by six tetrahedral Cu(I) ions to give the assembly **10.46**. The X-ray crystal structure of this remarkable complex is shown in Figure 10.40. The top and bottom floors are too close together to allow significant guest inclusion.

Ligand **10.44** is an example of a ditopic ligand in the sense that it possesses two 2,2′-bipyridyl *binding domains*, each of which must chelate a different metal centre. Extending the number of binding domains, as for **10.41**, allows more metal ions to be linked together in a line. If the coordination spheres of these metal ions are completed by terminating ligands such a 2,2′-bipyridine itself, then molecular racks are generated in which a string of metals are linked by a single 1D bridging ligand. Replacing the terminator ligands with bridging bipyrimidine units such as **10.47** gives ladder structures as in **10.40**. Extending the concept still further, linear oligopyridyl ligands with as many as eight pyridine units have been developed and used in the construction by the self-assembly of multistorey office blocks (Figure 10.41). Note that in these structures, the thermodynamics of self-assembly of discrete structures has been aided by the presence of sterically bulky substituents on the periphery of the assembly, which discourages polymer-like aggregation.

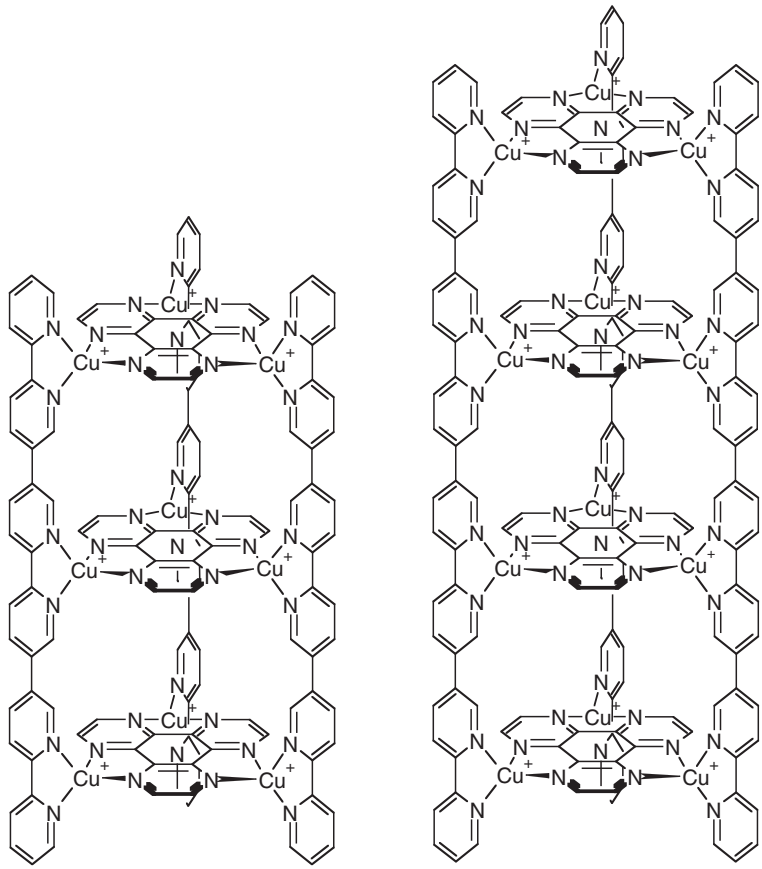

**Figure 10.41** Multistorey self-assembled structures (substituents omitted for clarity).[41]

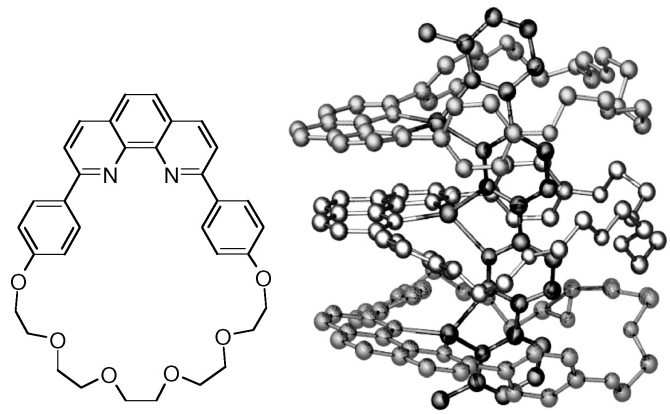

**10.48**

**Figure 10.42** A sheathed rack formed from Cu(I), **10.41** and **10.48** (each component is shaded differently for clarity).[42]

Combination of **10.41** with crown ether derivative **10.48** and Ag(I) gives a trimetallic 'sheathed rack' in which a rack of Ag(I) ions is threaded through the cavities of three heterocrowns (Figure 10.42). This complex is an example of a *pseudorotaxane* (strictly a [4]pseudorotaxane because there are four components – three loops and an axel) and we will return to these kinds of assemblies, which are precursors for the synthesis of complex interlocked molecules by postmodification techniques, in Section 10.7.

## 10.6 Self-Assembly of Closed Complexes by Hydrogen Bonding

### 10.6.1 Tennis Balls and Softballs: Self-Complementary Assemblies

Hof, F., Craig, S. L.. Nuckolls, C. and Rebek, J., 'Molecular encapsulation', *Angew. Chem., Int. Ed.* 2002, **41**, 1488–1508.

Coordination interactions are not the only way to use self-assembly to produce closed, capsular systems capable of binding guest species in solution. Work by Julius Rebek Jr (Scripps, USA)[43] has shown that multiple hydrogen-bonding interactions, because of their relatively weak, but directional, nature, are ideal for the strict self-assembly of closed spherical molecules and capsules. For example, component **10.49** consists of two intrinsically curved diphenylglycoluril units linked by a durene-based (1,2,4,5-tetramethyl benzene-based) spacer. In both solution and in the solid state, **10.49** self-assembles spontaneously to produce the tennis ball-shaped dimer $(\mathbf{10.49})_2$ shown in Figure 10.43. The formation of the dimer has been observed by:

- $^1$H NMR spectroscopy in $CDCl_3$ and $C_6D_6$ solution – the NH protons are shifted significantly downfield relative to model compounds that do not form dimeric capsules because of the electron-withdrawing presence of the carbonyl oxygen atoms hydrogen bonded to the NH protons.
- Mass spectrometry – in which a molecular ion peak for the dimer is seen under a variety of ionisation conditions.
- Vapour pressure osmometry – in which the molecular weight measured is that of the dimer.

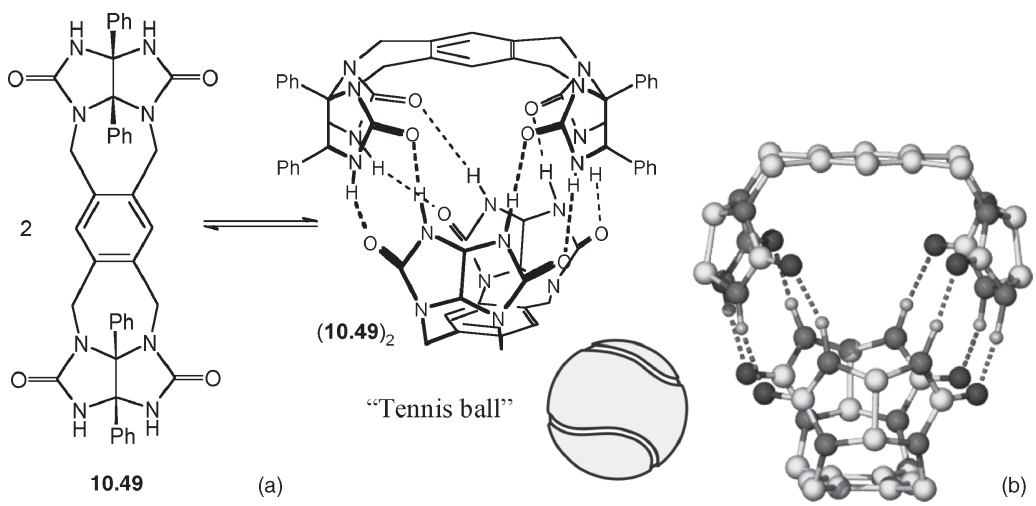


**Figure 10.43** (a) Self-assembly of two mutually complementary curved building blocks to produce a tennis ball shaped capsule – crystal structure shown in (b).[43]

- X-ray crystallography – which reveals a total of eight hydrogen bonds of N···O distances 2.78–2.89 Å.

Even with all of this evidence, the discovery of this material was so exciting that Rebek wanted to be completely certain that the dimer persisted in solution as well as the solid state. Because the two halves of the dimer are identical, it was difficult to be absolutely certain that the effects in the solution NMR spectra were indeed due to dimer formation. Rebek did not have any direct comparison with the individual monomer units under the same conditions. The final conclusive evidence for the formation of these fascinating assemblies came from their ability to encapsulate methane. Addition of methane to a solution of (**10.49**)$_2$ results in a shift of the $CH_4$ resonance from 0.23 ppm (free methane in $CDCl_3$) to –0.91 ppm, consistent with the location of the methane guest in the magnetic shielding region of the host aryl rings. Similar shifts were observed for a range of small-molecule guest species. This significant upfield shift is a consequence of the magnetic anisotropy of the aryl rings of the host durene-derived moiety. The encapsulated methane is in the shielding region of the ring current (see Box. 3.3).

The key features of **10.49** are its curvature, which is intrinsic to the glycoluril building blocks (Section 6.2.4), and its self-complementarity. The molecule possesses an exact match of four hydrogen bond donors and four acceptors. It was designed by analogy with the hexameric cucurbituril, which is able to bind simultaneously both alkali metal cations *via* its carbonyl oxygen array in a perching arrangement, and neutral guest molecules. (Binding constants up to 7140 $M^{-1}$ with furan guest in aqueous solution have been reported.)

As well as methane, the cavity formed by the dimer (**10.49**)$_2$ is sufficiently large to encapsulate small, neutral guests such as haloalkanes in much the same way as the cryptophanes (Section 6.6). Binding constant measurements by integration of the peaks for bound and unbound guest gave the $K_{11}$ values shown in Table 10.3. Temperature-dependent $^1$H NMR studies yielded thermodynamic parameters. These results show that guest binding is entropically unfavourable by 80–190 J $K^{-1}$ $mol^{-1}$, but the process is enthalpically favourable, giving an overall favourable free energy.

Rebek's group have gone on to design even larger self-assembling capsules using the glycoluril motif. In particular the dimers (**10.50**)$_2$ and (**10.51**)$_2$, termed 'softballs' because of their larger size compared to the tennis ball, form cavities capable of encapsulating large guests such as 1-adamantanecarboxylic acid and 1-ferrocenecarboxylic acid ($K_{11}$ = 770) and 280 $M^{-1}$, respectively, for (**10.50**)$_2$. Indeed, in the absence of large guests, in *p*-xylene solvent (a poor guest) the $^1$H NMR signals for **10.50** are broad, suggesting exchange between monomeric **10.50** and its dimer and hence the dimer formation is actually templated by the guest. Addition of guests results in a sharp signal once more. The addition of phenolic hydroxyl groups as in **10.51** renders the dimer formation an even more favourable process, with an additional eight hydrogen bonds (of type O—H···O═C) holding the two components together. Rebek referred to this improvement as a 'zippered' softball. Thermodynamic measurements on these large softball compounds indicate that, in contrast to (**10.49**)$_2$, guest encapsulation by these cavity-containing materials

**Table 10.3** Association constants for guest binding by (**10.49**)$_2$.

| Guest | $K_{11}$ (0°C, $CDCl_3$, $M^{-1}$) |
|---|---|
| $CHCl_3$ | 0.04 |
| $CF_4$ | 2.81 |
| $CH_2Cl_2$ | 4.00 |
| $C_2H_4$ | 278 |
| $CH_4$ | 303 |

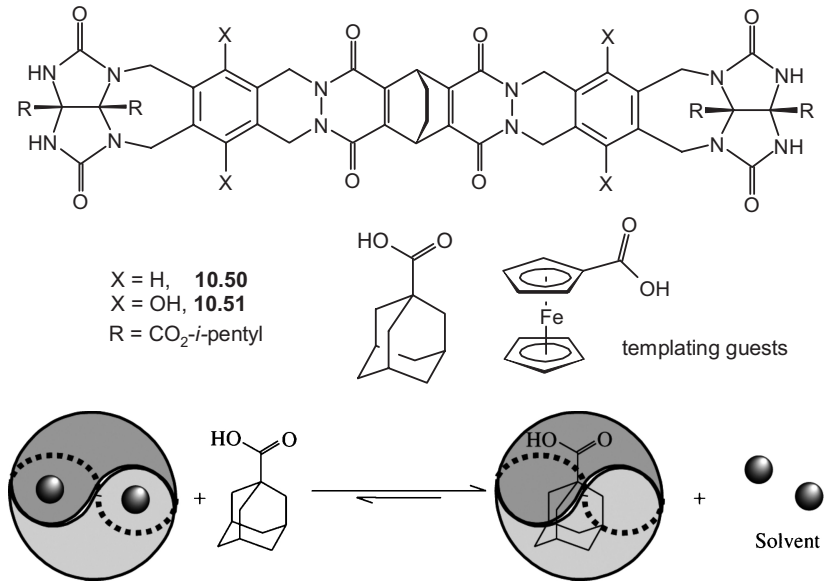


**Scheme 10.8** Guest encapsulation by 'softball' hosts is driven by entropic (solvophobic) effects.

is entropy-driven, with the large guest species displacing encapsulated solvent molecules (Scheme 10.8). In water, this would be equivalent to the hydrophobic effect, although most of the 'softball' chemistry has been carried out in aromatic solvents such as benzene and xylenes.

For such an entropy-driven encapsulation mechanism to be believable, it must result in a net gain in the number of free particles at the end of the encapsulation. This implies that there must be more than one solvent molecule displaced from the softball interior upon guest binding. The inclusion of multiple solvent molecules was established by dissolution of the softball in a mixture of two different, but closely related, solvents, $C_6D_6$ and $C_6D_5F$ and recording its NMR spectrum (hence the need for deuterated solvents). In either solvent alone, only one softball complex is observed. In the solvent mixture, three distinct host–guest species result, consisting of softballs containing either two benzene guests, two fluorobenzene molecules or one of each. Hence the softball is capable of encapsulating two solvent molecules.

The tennis ball and softballs were designed to be capsules that may act as 'reaction vessels' by analogy with the hemicarcerands of Cram *et al*. (Section 6.7). The advantage to the softballs is that they are prepared more readily since the key cavity-forming dimerisation step is self-assembling. In hemicarcerand synthesis, this is a kinetically controlled covalent bond forming step. Large softballs have been used as hosts for Diels–Alder reactions. The chamber of hosts such as (**10.51**)$_2$ is large enough for simultaneous encapsulation of *p*-quinone and cyclohexa-1,3-diene. Over the course of one day, the formation of the encapsulated addition product is observed (Scheme 10.9). Control experiments with non-dimerising hosts, or with dieneophile guests too large to fit the cavity, do not show any reaction. Unfortunately for catalytic applications, the formation of the addition product is plagued by self-inhibition (the addition product guest effectively blocks the cavity, preventing further host catalysis of the reaction).

It is interesting to speculate on the origins of the (stoichiometric) rate enhancement of these reactions inside the softball cavity. In more conventional forms of catalysis, such as reactions occurring at transition metal centres, the mode of catalysis often involves a significant statistical effect. The reactants are brought into close proximity to one another by simultaneous coordination to the metal. This increases

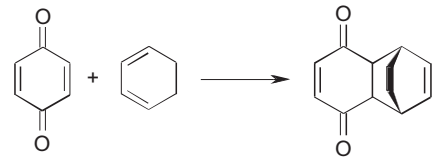

**Scheme 10.9** Softball host-catalysed Diels–Alder addition.[44]

dramatically their effective concentration and hence the rate of any bimolecular reaction between them. The same effect is also seen in the formation of ternary complexes in organic catalysis (Section 12.9). We can calculate very simply the effective concentration of guest species within the cavity in hosts such as (**10.51**)$_2$, using our knowledge of the cavity volume, which is about 300 Å$^3$. An example calculation for two molecules of deuterated benzene is shown below.

$$\text{Number of molecules of } C_6D_6 \text{ per cavity} = 2 \text{ (from } ^1\text{H NMR experiments)}$$

$$\text{Number of moles of } C_6D_6 \text{ per cavity} = \frac{2}{N_A} = \frac{2}{6.02 \times 10^{23}} = 3.32 \times 10^{-24}$$

$$\text{Concentration of } C_6D_6 \text{ in cavity} = \frac{\text{moles}}{\text{volume}} = \frac{3.32 \times 10^{-24} \text{ mol}}{300 \times (10^{-9} \text{ dm})^3} = 11.1 \text{ mol dm}^{-3}$$

This simple calculation tells us that the intracavity concentration of benzene is in excess of 10 M! By comparison, the concentration of pure liquid benzene is 11.2 M (this is readily obtained from the density of benzene, 0.874 g cm$^{-3}$, and its molar mass, 78.11 g mol$^{-1}$). The intracavity region is effectively neat benzene. If we take a figure from molecular modelling packages of 81 Å$^3$ for the molecular volume of benzene, then we can show that in liquid benzene, and in the cavity of doubly occupied softball hosts, about 55 % of the total volume is occupied and 45 % is empty. This observation has a great deal of potential as a design criterion, and competition experiments show that, in general, guests or combinations of guests that occupy about 55 % of the cavity volume are bound with the highest affinity. This figure may be increased by specific, enthalpically favourable interactions such as hydrogen bonds between the guests themselves or between guest and host. This observation is particularly interesting in the light of experiments involving the cryptophanes, where the highest binding affinities are noted for guests that are slightly too small to fit the host cavity.

A wide range of self-complementary hemispherical type molecules of varying shapes and sizes have been prepared along the lines of compounds of type **10.49**–**10.51**. Examples are **10.52**–**10.56** based on linkers such as glycoluril, urea or pyrrole-2,5-dione (as in **10.54**) and cores such as triphenylene, triethylbenzene (familiar from Section 4.8.1), calix[4]arenes and [4]resorcarenes. The trimeric **10.52** forms a dimer termed the 'jelly doughnut' because of its shape and central cavity capable of complexing small aromatic guests (which constitute the 'jelly' – or 'jam' for readers preferring British English).[45] The dimer (**10.54**)$_2$ encapsulates two aromatic molecules simultaneously. While two benzene and two toluene molecules are readily accommodated, two *p*-xylene guests are not. However the cylindrical cavity is *ca.* 20-fold selective for the benzene·*p*-xylene heteropair over two molecules of toluene (which is effectively an isomer). If there is more than one possible mutual arrangement of the two guests then the possibility of isomerism arises. This concept of a cavity with the same pairs of guests arranged in different mutual orientations that cannot readily exchange or change places has been termed *social isomerism* (Scheme 10.10) and represents a extension of the *carcerism* concept we encountered in covalent hosts in Section 6.7.4.[46] For smaller molecules such as chloroform and isopropyl chloride up the three guests can be accommodated

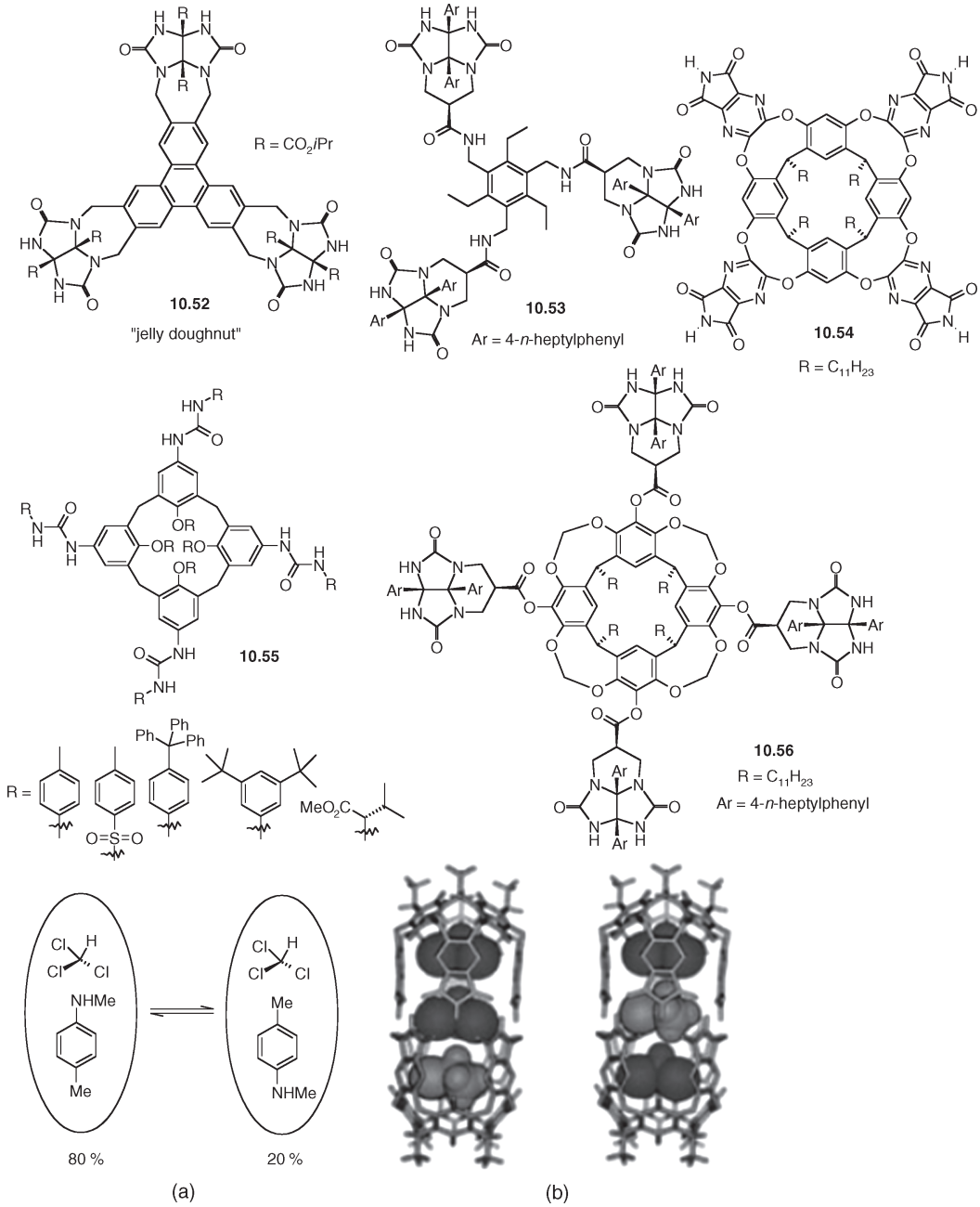


**Scheme 10.10** (a) 'social isomerism' in capsule $(\mathbf{10.54})_2$, (b) isomeric constellations in $(\mathbf{10.54})_2$. If the capsule holds a mixture of two chloroform and one $ClCH(CH_3)_2$ guest then two different isomeric arrangements are possible in which the $ClCH(CH_3)_2$ is in the middle or at one end (reproduced with permission from Reference 46).

at a time. If these guests are different (*e.g.* one molecule of isopropyl chloride and two molecules of chloroform) then there is considerable scope for social isomerism resulting in the possibility of *isomeric constellations* in which the guests are in different orientations and in a different order in the cylindrical cavity, Scheme 10.10b. The calixarene derivatives **10.55** for both homo- and heterodimers depending on the exact steric and electronic nature of the substituent groups. Larger analogous calix[6]arene-based tris(urea) based dimeric capsules have also been reported.[47] Host $(\mathbf{10.56})_2$ has a cavity volume of about 950 Å$^3$ and can encapsulate ion cryptate complexes to give a 'host within a host'.

## 10.6.2 Heterodimeric Capsules

Corbellini, F., van Leeuwen, F. W. B., Beijleveld, H., *et al.*, 'Multiple ionic interactions for noncovalent synthesis of molecular capsules in polar solvents', *New J. Chem.* 2005, **29**, 243–248.

In addition to self-complementary homodimers as we saw in the last section, it is possible to deliberately engineer capsules using mutually complementary components. One of the simplest approaches is to use ion pairing by combining anionic and cationic hemispheres. This has been done by David Reinhoudt's group (Twente, Netherlands) who have taken the anionic *p*-sulfonatocalix[4]arene and a calix[4]arene amidinium derivative to produce the heterocapsule **10.57**. A similar approach using a pyridinium-appended porphyrin gives **10.58**. Ion pairing with the counter ion prove to be very important in determining the observed association constant in polar media and can artificially reduce the measured dimerisation affinity, with can be up to $10^7$ $M^{-1}$ in water/methanol mixed solution after correction for counter-ion effects.

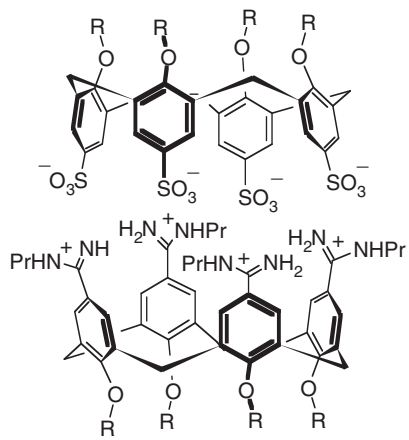

**10.57**

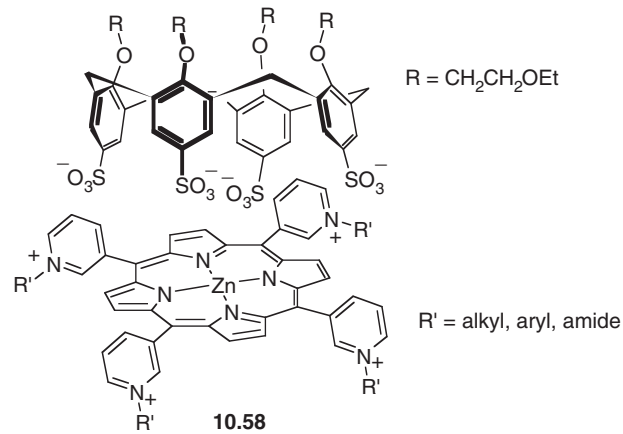


**10.58**

## 10.6.3 Giant Self-Assembling Capsules

Atwood, J. L., MacGillivray, L. R., 'Structural classification and general principles for the design of spherical molecular hosts', *Angew. Chem. Int. Ed.* 1999, **38**, 1018–1033.

The quest towards ever larger cavity systems, especially those stable in solution, has leaned increasingly more heavily upon self-assembly as a means towards synthesising assemblies capable of encapsulating large spatial volumes. Some of the largest cavities formed to date are based on the very

simple [4]resorcarene (**6.3**) and the related pyrogallol[4]arene (**10.59**) building blocks, as found in the covalently linked carcerands and hemicarcerands.

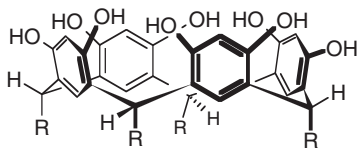


[4]resorcarene

**6.3**

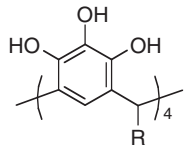


pyrogallol[4]arene

**10.59**

R= $CH_3$,$CH_2CH_2Ph$,*i*Bu *etc.*

Reaction of a [4]resorcarene with phenylethyl 'feet' with the unlikely template buckminsterfullerene ($C_{60}$) in propan-2-ol results in the isolation of a solid-state self-assembled hemicarcerand in which two resorcarene hemispheres are linked by an equator of eight propan-2-ol molecules (one for each upper-rim hydroxyl group) (Figure 10.44). These occluded solvent molecules effectively provide the glue that links the two halves of the capsule together. The $C_{60}$ template is also an integral part of the structure, isolating each capsule from the others. It is likely that the role of the $C_{60}$ is to interact with the aryl rings of the resorcarene 2-phenylethyl 'feet' *via* $\pi - \pi$ stacking interactions. The cavity volume comprises some 230 $Å^3$, which is large enough to contain several molecules of *o*-dichlorobenzene and propan-2-ol guests. Unfortunately, these guests are highly disordered in the solid state and the aggregate does not hold together in solution.[48]

While the role of the propan-2-ol in the capsule shown in Figure 10.44 is serendipitous, a number of designer heterocapsules of this type with linkers such as 4,4′-bipyridine and 2-aminopyrimidine have been prepared, Figure 10.45.[49, 50] These kinds of materials, and indeed [4]resorcarenes in general have found significant application as molecular containers, particularly in isolating and protecting

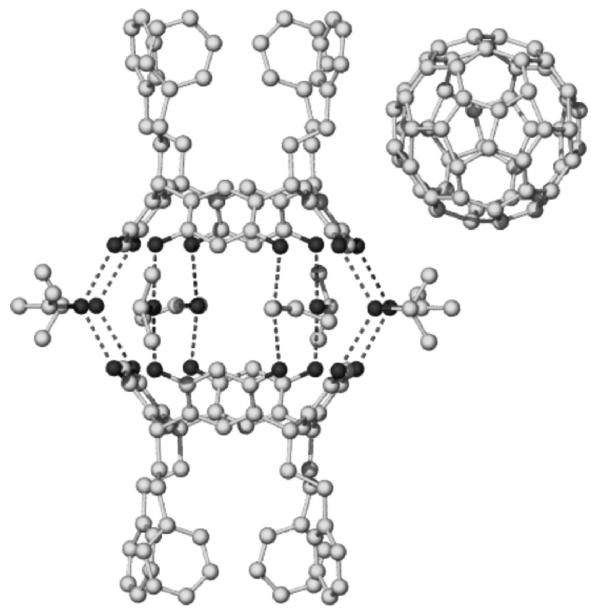

**Figure 10.44** X-ray crystal structure of the capsular, propan-2-ol linked *bis*([4]resorcarene) portion of the co-crystal of **6.3** (R = $CH_2CH_2Ph$) with $C_{60}$.[48]

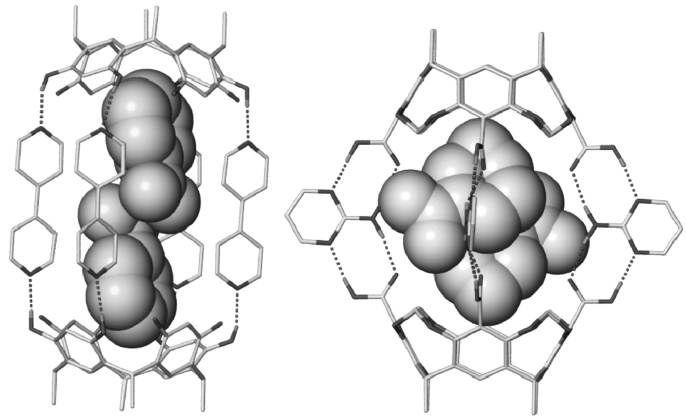


**Figure 10.45** Multi-component, hydrogen-bonded capsules (a) *C*-methyl[4]resorcarene 4,4′-bipyridine capsule with two included *p*-nitrobenzene guests,[49] (b) rigidified [4]resorcarene tetracarboxylic acid held together by 2-aminopyrimidine with two included *p*-nitrobenzene guests.[50]

photochemically active guests for *in situ* diffraction studies. Encapsulated photoactive guests are relatively dilute in crystals and hence require fewer photons to bring induce excited state formation, for example, allowing the study of excited states without excessive heating of crystals by lasers.[51, 52]

Work by Atwood and MacGillivray (1997) has resulted in a general formalism for the construction of large-volume hemicarcerand hosts by self-assembly, which is based on the fundamental geometric insights of the ancient Greek mathematicians and philosophers. Atwood and MacGillivray have pointed out that a great deal of synthetic effort is required in the designing of innate curvature into capsule components (Section 6.2). If non-curved components can be used to enclose three-dimensional space, potentially much simpler building blocks can be used, as in the synthesis of the supramolecular cube (**10.13**), which relies only upon readily prepared 'edges' and 'corners'. Contrast this result with the much more sophisticated (and difficult to prepare) tennis ball building block (**10.49**), which requires fewer components to encapsulate a finite volume of space because it already possesses the innate curvature of the glycoluril units. In fact, three-dimensional space may only be enclosed by 'flat' building blocks if they are equivalent (in terms of their potential connectivity, covalent or noncovalent) to regular shapes that tessellate in three dimensions. If only one such building block is used then the resulting supermolecule must be equivalent to one of the five Platonic solids (Figure 10.46), and hence the 'flat' building blocks must, in connectivity terms, be equivalent to either triangles, squares or pentagons. No other flat, regular figures will enclose three-dimensional space alone. This implies automatically that it is impossible to enclose three-dimensional space with fewer than four components (the minimum necessary to form a tetrahedron) unless those components are innately curved, as in **10.49**.

If two different components are used, then the possibilities become a little more varied. Combination of two regular two-dimensional figures in such a way as to enclose completely a three-dimensional space gives rise to the 13 Archimedian solids (Figure 10.47), and the isohedral bodies (prisms and antiprisms). Non-regular polygonal faces give rise to the 13 Catalan solids (named after Belgian mathematician, Eugène Catalan who first described them in 1865). Notice that the hexahedron prepared by Fujita based on **10.27** is a Johnson solid,[†] while the cubeoctahedra **10.28** and **10.29** correspond to structure (b) in

[†] A Johnson solid is a strictly convex polyhedron, each face of which is a regular polygon, which is not a Platonic solid, Archimedean solid, prism, or antiprism. Each face does not need to be the same polygon, and the same polygons do not need to join around each vertex.

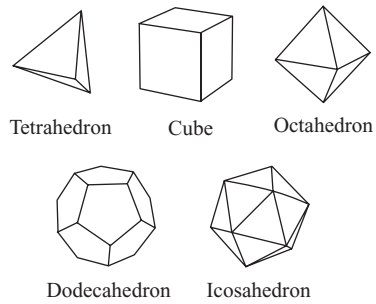


**Figure 10.46** The five Platonic solids. These are the only regular, three-dimensional solids that can be constructed from one type of two-dimensional shape.

Figure 10.47. Structure (j) (truncated icosahedron) is well known to the chemical community as buckminsterfullerene, $C_{60}$, comprising hexagons and pentagons. It has been well established, both chemically and geometrically, that the pentagons in the structure are necessary to effect three-dimensional closure, and without them only open, two-dimensional graphitic layers are formed. All fullerenes, and even the topical 'Bucky tubes' (Figure 10.2), that consist of fused hexagons are open at both ends unless pentagons are incorporated into the structure.

Atwood *et al.* have gone on to prepare a truly enormous molecular capsule along these principles, which conforms to the geometry of a snub cube (structure (f) in Figure 10.47). Reaction of six equivalents of the octol [4]resorcarene (with either methyl or undecyl 'feet') with eight water molecules results in

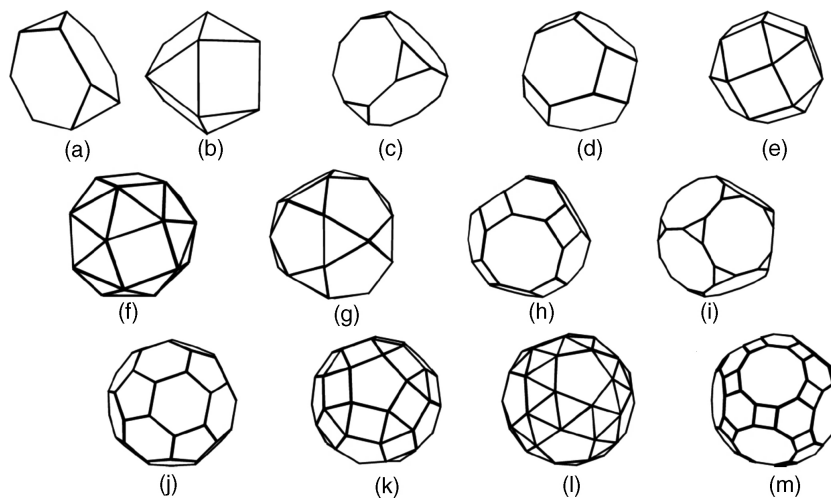


**Figure 10.47** The 13 Archimedian semiregular solids, constructed from combinations of two or more different two-dimensional figures. Note that, in addition to the triangles, squares and pentagons allowed in the Platonic solids, hexagons, octagons and decagons also make an appearance, but always in conjunction with other shapes. In particular, structure (j) corresponds to buckminsterfullerene, $C_{60}$, which requires pentagons to effect spatial closure, even though the structure consists predominantly of hexagons.

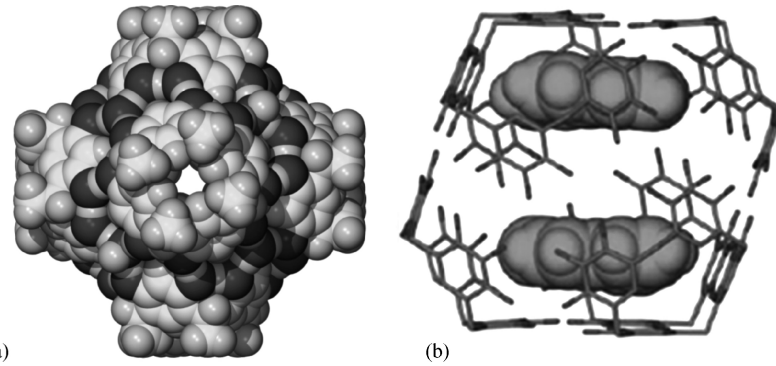


**Figure 10.48** (a) Space-filling view of the structure of the snub cube (f) formed from six [4]resorcarenes and eight water molecules.[53] (b) Crystal structure of the analogous pyrogallol[4]arene hexameric capsule containing two molecules of pyrene butyric acid (reproduced with permission from [54]).

self-assembly to form a chiral, spherical hexamer held together by 60 hydrogen bonds (Figure 10.48), in a topology somewhat resembling spherical viruses such as hepatitis B and the human rhinovirus (Section 2.10). In the case of the undecyl derivative, the structure is also maintained in solution, with the assembly resembling a small inverse micelle (Section 13.2.1). The snub cube has a cavity diameter of 17.7 Å and a volume of 1375 Å$^3$ (*cf.* 300 Å$^3$ for the largest 'softballs'). The chirality arises from the twisting of the resorcarene (square) faces by about 23 degrees with respect to the cuboid formed by the water molecules. In crystal engineering terms, the existence of four intramolecular hydrogen bonds within each resorcarene means that each is, in practice, a quadruple hydrogen bond donor. Because of the spherical nature of the capsule and their location in three-fold symmetric sites, each water molecule is capable of participating in only three hydrogen bonds and hence defines a triangular face. As a result, of the 64 acidic protons in the assembly (16 from water and $6 \times 8 = 48$ from calixarenes), only 60 are involved in hydrogen bonds within the capsule and the remaining four, situated in a tetrahedral array, link to neighbouring capsules. Of these 60, 36 are intermolecular interactions giving 2.6 hydrogen bonds per molecule holding the assembly together. Robust as this assembly is, the need for water incorporation increases the number of components and hence reduces stability. A closely analogous hexameric assembly is formed by the dodecahydroxyl compound pyrogallol[4]arene (**10.59**). In this case no water is required and the six components are held together by a total of 72 hydrogen bonds, 48 of which are intermolecular making an extremely robust assembly with a total of eight intermolecular hydrogen bonds per molecule. The *iso*-butyl compound is stable even in polar media such as 50:50 acetone/water.[55] The interior volume of the the capsule is a massive 1510 Å$^3$, large enough for up to 23 methanol molecules at 55 % packing occupancy – the ideal value for this kind of inclusion. NMR results indicate that *ca.* 18 molecules are actually included. The properties of the cavity in solution have been probed by use of a fluorescent reporter dye, pyrene butyric acid (**10.60**). The fluorescence of the dye is markedly increased upon encapsulation as a result of the lack of quenching by collision with solvent molecules. Moreover addition of a fluorescence quencher, dimethyl aniline, does not result in any diminution of the emission quantum yield. The X-ray crystal structure of the complex with **10.60** (Figure 10.48b) shows that two dye molecules are included but that the two pyrene groups are situated far apart. Consistent with this geometry being retained in solution no characteristic pyrene excimer emission (low energy emission

from a complex of an excited state pyrenyl moiety with a ground state pyrenyl group in close proximity) is observed (see Figure 11.3).[54]

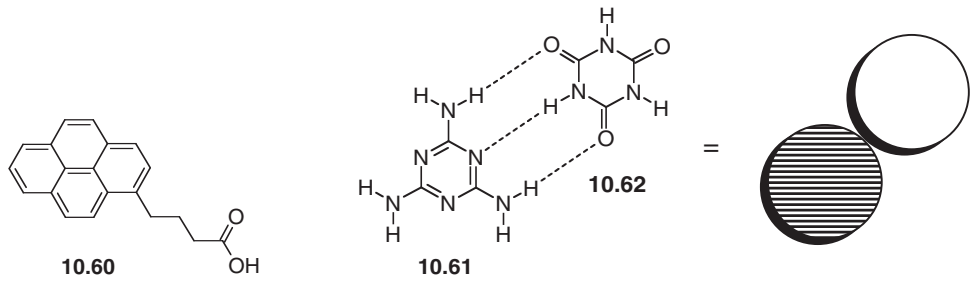


## 10.6.4 Rosettes

Whitesides, G. M., Simanek, E. E., Mathias, J. P., *et al.*, 'Noncovalent synthesis – using physical-organic chemistry to make aggregates', *Acc. Chem. Res.* 1995, **28**, 37–44.

We have already seen in Section 6.2.2 another approach towards self-assembled calixarene-based capsules comprising a melamine-derived calixarene and diethylbarbituric acid derivatives. Similar chiral assemblies, comprising three calixarenes can also be obtained from the calixarene and cyanuric acid.[56] The mutually complementary pair of disc-like molecules melamine (**10.61**) and cyanuric acid (**10.62**) can also form hydrogen-bonded rings ('rosettes') and chains ('tapes') in the solid state, as illustrated in Figure 10.49. This propensity has been used by the group of George Whitesides at the University of Harvard, USA to construct large structures and aggregates. These researchers recognised that in solution, the formation of the rosette structure is reasonably enthalpically favourable because it results in the formation of a total of 18 hydrogen bonds, corresponding to a $\Delta H$ in the region of $-100$ kJ mol$^{-1}$ in chloroform. This is balanced, however, by the extremely unfavourable entropy associated with bringing together six independent particles. Whitesides set out to prepare complexes in which rosette formation could be encouraged in solution by reduction in the unfavourable translational and rotational entropy components to the overall aggregation free energy. This was accomplished it two ways: *preorganisation* (*via* a linking group that tethers some of the components together) and *peripheral crowding* to disfavour the formation of the tape structures (Figure 10.50).

The preorganisation approach has proved to be particularly successful, with compounds such as **10.63** reacting with exactly three equivalents of cyanuric acid to give four-particle aggregates of molecular weight about 2.5 kDa. The aggregates are only poorly crystalline and decompose upon attempted mass spectrometry, making them difficult to characterise. Determinations of the degree of aggregation have relied primarily on solubilisation studies, gel permeation chromatography, vapour pressure osmometry and $^1$H NMR spectroscopy. In general, the stabilities of rosette aggregates are characterised by a simple parameter, $HB/(N - 1)$, somewhat related to the expression for $csac_{min}$ defined by Hunter (Equation 10.12; Section 10.4.2), where $HB$ is the number of hydrogen bonds enthalpically stabilising the assembly (18 per rosette) and $N$ is the number of free particles. The implication of this parameter is that increasing the number

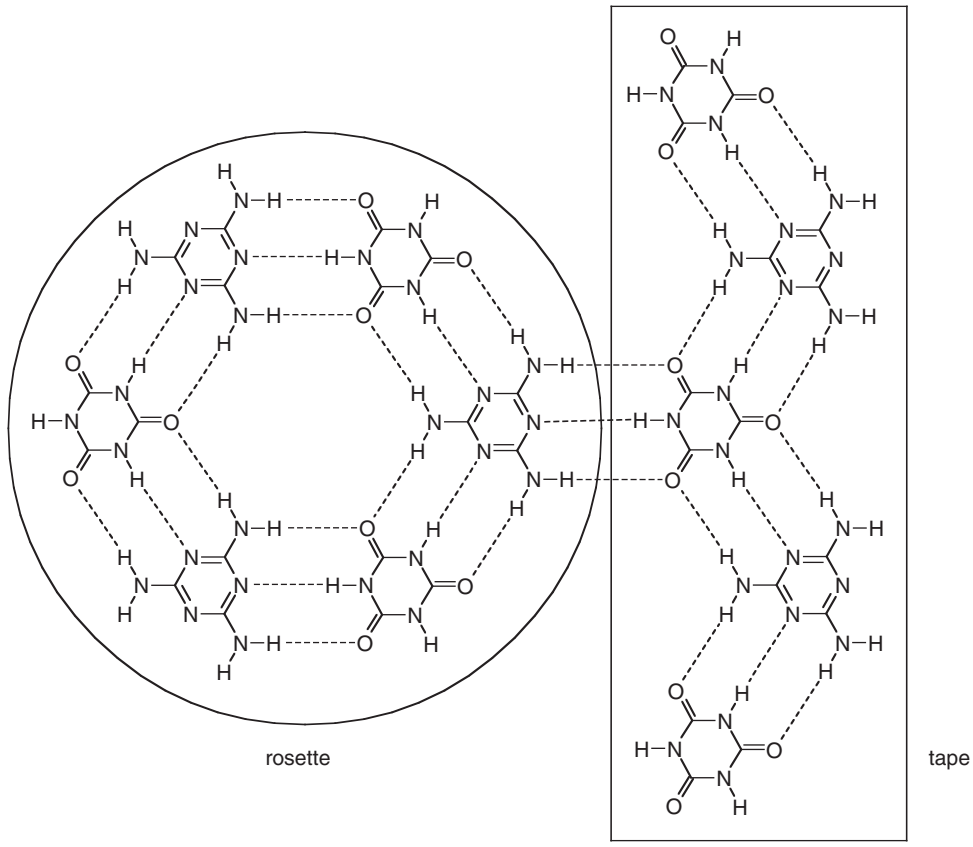


**Figure 10.49** Rosette and tape motifs in the solid-state structure of melamine·cyanuric acid.

of hydrogen bonds increases the enthalpic stabilisation of the complex, and increasing the number of free particles increases the entropic destabilisation. Thus for the moderately stable **10.63**·(**10.62**)$_3$ aggregate, $HB/(N - 1) = 6$. Other aggregates are represented schematically in Figure 10.51.

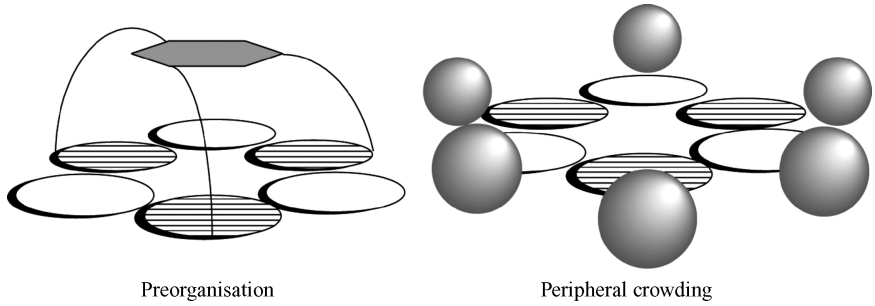


**Figure 10.50** Preorganisation and peripheral crowding approaches to solution stabilisation of rosette motifs.

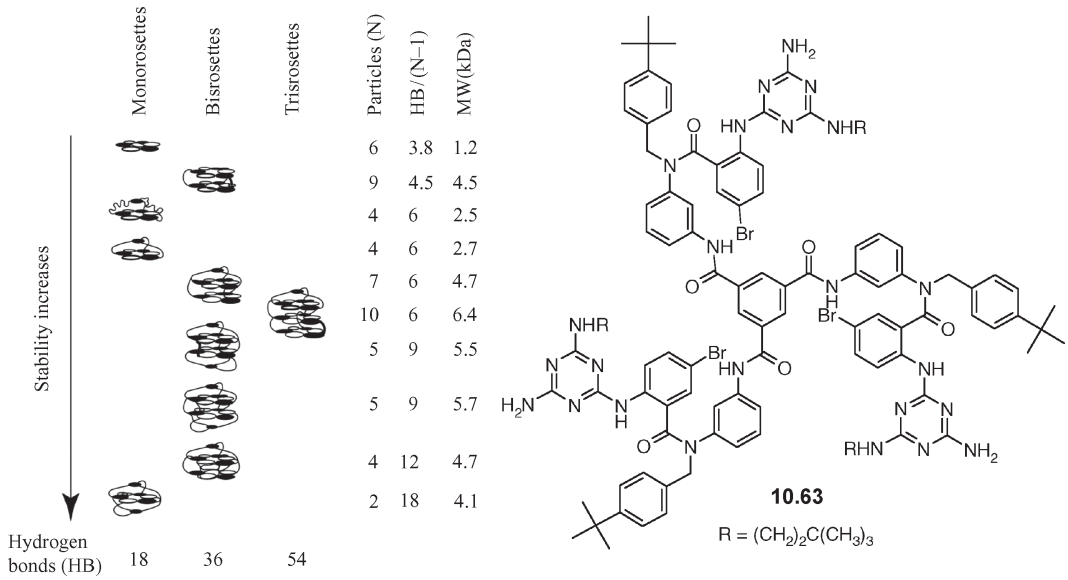


**Figure 10.51** Melamine·cyanuric acid derivatives arranged according to their relative stability as measured by the $HB/(N-1)$ parameter. (Reprinted with permission from Section Key Reference © 1995 American Chemical Society).

## 10.7 Catenanes and Rotaxanes

Raymo, F. M. and Stoddart, J. F. 'Interlocked macromolecules', *Chem. Rev.*, 1999, **99**, 1643–1666.

### 10.7.1 Overview

Breault, G. A.. Hunter, C. A. and Mayers, P. C., 'Supramolecular topology', *Tetrahedron* 1999, **55**, 5265–5293.

A catenane is a compound consisting of two or more rings that are interlocked mechanically without there being necessarily any chemical interaction between the two. Generally, the rings cannot be separated without breaking a chemical bond. Catenanes are named according to the number of interlocked rings, *e.g.* a [2]catenane consists of two interlocked rings (Figure 10.52). The 'ane' ending is by analogy with alk*ane*s and, generally, a catenane is taken to be an organic fragment, although it rarely consists solely of hydrocarbon moieties. The terms [n]caten*and* and [n]caten*ate* are also used, by analogy with crypt*and* and crypt*ate*, in circumstances where the interlocked ring system is capable of acting as a ligand for a metal centre. The catenand is the free ligand that forms a catenate complex in the presence of a metal centre.

Rotaxanes consist of a long, fairly linear molecule threaded through a macrocyclic ring, like cotton through the eye of a needle. Again, true rotaxanes cannot decompose back to a separate ring and chain without breaking chemical bonds, and hence the linear, chain part of the molecule is terminated frequently by bulky groups that are too large to fit through the cyclic fragment. Rotaxanes without such physical barriers, in which the 'thread' can slip out of the 'needle', are termed *pseudorotaxanes*. Pseudorotaxanes are frequently necessary precursors to both rotaxanes and catenanes. Typical synthetic procedures consist of the templated self-assembly of a pseudorotaxane (a kind of host-guest complex)

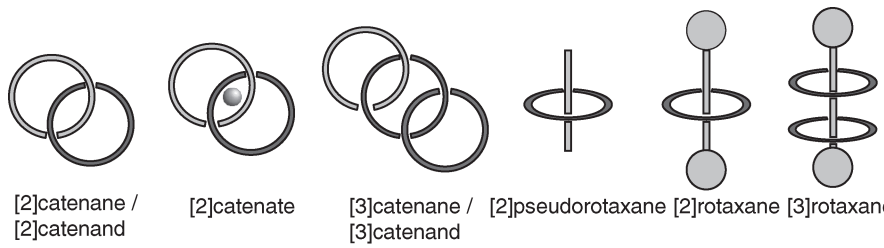


**Figure 10.52** Nomenclature of catenanes, rotaxanes and pseudorotaxanes.

*via* the intermediary of a metal ion, electrostatic or hydrogen bonding forces, followed by ring closure (catenanes) or termination at one or both ends with a bulky end group (rotaxanes) (Figure 10.53). Formation of these species is, to some extent, an academic curiosity, although as we saw in Chapter 2 they are models of some biological molecular machinery such as ATP synthase, which which couples the rotation of an axle in a wheel with the endergonic production of ATP, and DNA polymerisation by enzymes such as DNA polymerase III. However, the long-term possibilities for their application include the formation of sophisticated switchable molecular devices, development of materials with new physical properties, and surface immobilisation of catalytically photo or redox active species without the need to alter their properties by chemical modification.

The chemical composition of a catenane or rotaxane is identical to the two (or more) separate components, yet the threading of one component through another has important consequences for the physical and chemical properties of the resulting aggregate. This observation classes the formation of interlinked and threaded species as a form of isomerism (different from traditional chemical isomerism, such as *cis*/*trans* and *fac*/*mer*). Catenanes are termed 'topological' isomers of their separated ring components. In this context, we understand the topology of the aggregate to mean the number and type of crossing points if the structure is drawn out in two dimensions (*e.g.* on a piece of paper – this 2D representation is termed a *molecular graph*). We cannot draw a [2]catenane without at least two crossing points, whereas two separated macrocycles do not require any crossing points. The two structures are thus fundamentally different. Formally, they are *homeomorphic* (*i.e.* have the same form) without being *isotopic* (same structure and composition) and we say that their molecular graph is *non-planar* and their topology is *non-trivial*. Interestingly, following this strict definition, rotaxanes are not topological isomers of their individual components since, conceptually at least, the ring of the rotaxane can always be slipped over the end of the linear portion to give the separated constituents by infinitely expanding the ring. Chemically, while

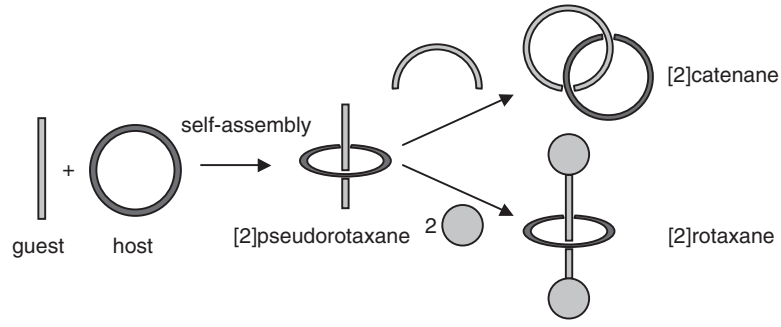


**Figure 10.53** Synthesis of catenanes and rotaxanes *via* host–guest chemistry.

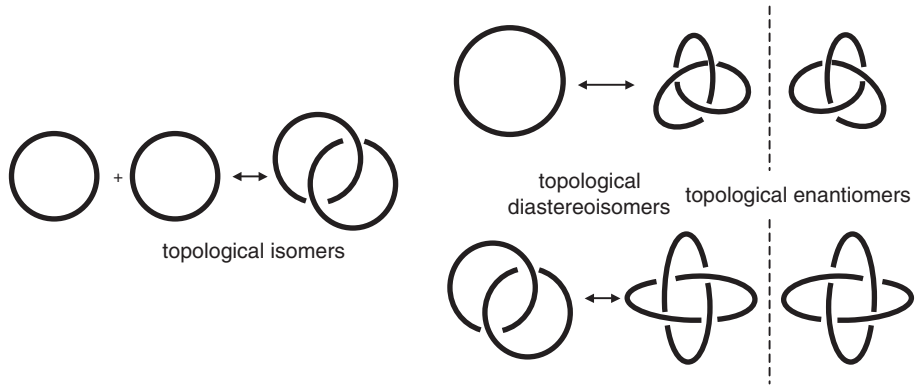


**Figure 10.54** Topological isomerism, diastereoisomerism and chirality as related to a [2]catenane, a trefoil knot and a doubly interlocked [2]catenane.

this is true for a pseudorotaxane, it cannot occur in practice for a true rotaxane because the stoppers (end groups) are too large. The difference between the real molecule and the topological definition is that, in topology, all of the components are infinitely stretchable as long as they are not broken. The existence of topological isomers also implies the existence of topological enantiomers in which a chiral catenane or other molecularly knotted system is chiral by virtue of its interlinkage as opposed to any intrinsic chirality of any of the components (Figure 10.54).

## 10.7.2 Statistical Approaches to Catenanes and Rotaxanes

Amabilino, D. B. and Stoddart, J. F. 'Interlocked and intertwined structures and superstructures', *Chem. Rev.*, 1995, **95**, 2725–2828.

There are two distinct approaches to catenane synthesis: the statistical approach, and approaches relying on self-assembly, so-called 'directed synthesis'. The statistical approach relies on the small chance that macrocyclisation may occur while a linear precursor is threaded through a macrocyclic component. Because this is a rather unlikely eventuality, it naturally results in low yields of interlinked product and is chiefly of historical interest. It was this kind of statistical approach that resulted in the first synthesis of a [2]catenane by Wasserman in 1960 (**10.64**), from cyclisation of the long-chain diester **10.65** while threaded through the annulus of a deuterated $C_{34}$ cycloalkane **10.66** (Scheme 10.11).[57] Although the overall yield of the catenation reaction was less than 1 %, the existence of the catenane was firmly established. The relatively polar [2]catenane product, along with other polar macrocyclisation reaction products and

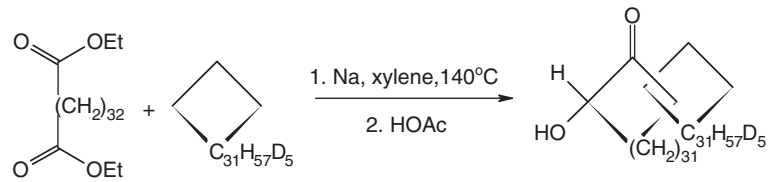


**10.65** **10.66** **10.64**

**Scheme 10.11** The first catenane synthesis *via* the statistical approach.[57]

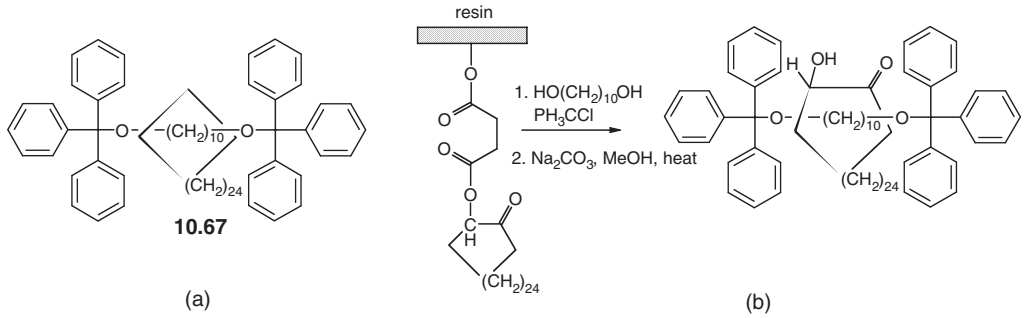


**Figure 10.55** Statistical rotaxane synthesis (a) product from solution and (b) analogue prepared in higher yield (6 %) on a solid support.

starting materials, was separated from 'free' cycloalkane. The acyloin ring was then cleaved and the nonpolar fraction collected. The presence of the deuterated macrocycle in this reaction fraction, it was argued, could arise only from a catenated product.

Statistical approaches have also been applied to rotaxane synthesis. Rotaxanes and pseudorotaxanes have been prepared by refluxing a range of cyclic hydrocarbons of between 11 and 39 —$CH_2$— groups with a linear triphenylmethyl-stoppered component at 120 ºC. At this elevated temperature, larger rings are occasionally able to 'slip' over the end of the triphenylmethyl stopper groups, forming low yields (less than 2 %) of rotaxanes (**10.67**) on cooling. At room temperature, the rotaxane containing the $C_{29}$ macrocycle is stable with respect to slippage back to the constituent components, whereas macrocycles with chain lengths of $C_{33}$ and upwards are extremely labile. It is possible to increase statistical yields by repetitive reaction with the cyclic component immobilised on a solid support. Covalently attaching a $C_{28}$ macrocycle to the surface of a resin and treating it with the dumb-bell components a total of 70 times gives a stable rotaxane that can be cleaved from the resin and purified to give an overall yield of 6 % (Figure 10.55).

## 10.7.3 Rotaxanes and Catenanes Involving π–π Stacking Interactions

Schalley, C. A., Beizai, K. and Vögtle, F., 'On the way to rotaxane-based molecular motors: Studies in molecular mobility and topological chirality', *Acc. Chem. Res.* 2001, **34**, 465–476.

Clearly the low yields obtained in the statistical approach to catenane and rotaxane synthesis suggest that a much more directed approach is very much needed, in which the chemist does not, in effect, rely on luck to thread molecular components together. The obvious strategy towards a directed rotaxane and catenane synthesis is to encourage the threading (self-assembly) of the reactants before the cyclisation or stoppering reaction that covalently fixes the array together. If the reactants are predominantly associated in solution as a self-assembled host–guest complex (*i.e.* relatively large binding constant), there is a much greater probability that they will be associated in the desired fashion when they react. Generally the pre-reaction host–guest complex is a pseudorotaxane and constitutes a self-assembled template for the covalent synthesis of the rotaxanes and catenanes proper (Figure 10.53).

We have already seen (Section 3.12.6) how strong π-stacking interactions occur with the aryl corands **3.116** and **3.117** and the herbicide paraquat (**3.113**) (*e.g.* **3.116** + **3.113**, $K_{11} = 730\ M^{-1}$ in $Me_2CO$), resulting in solid-state and solution incorporation of the electron-deficient guest within the corand ring. This inclusion of paraquat within the macrocycle is effectively the formation of a [2]pseudorotaxane, and this

system has formed the basis of extensive work by the group of Sir J. Fraser Stoddart (now at Northwestern University, USA) on the use of such interactions to generate a vast range of interpenetrated molecules. In the case of paraquat, it is the guest that is electron-deficient and the host that is electron-rich. Generally, the stability of the pseudorotaxanes increases with increasing chain length, thus for R=Me, $K_{11}(Me_2CO) = 17\ M^{-1}$, whereas for R = $H(OCH_2CH_2)_3$, $K_{11} = 2520\ M^{-1}$. Either approach is of great synthetic utility in the syntheses of rotaxanes and catenanes. Compare this assembly to Figure 10.12 in which a electron-rich podands of type $ROC_6H_4OR$ (R = Me, **10.68**; R = $H(OCH_2CH_2)_n$, n = 1–4, **10.69**) are incorporated into a rectangular box made up of two paraquat derivatives (**6.81**) to give another [2]pseudorotaxane. Compound **6.81** is famous as Stoddart's 'little blue box' (Section 6.5.8).

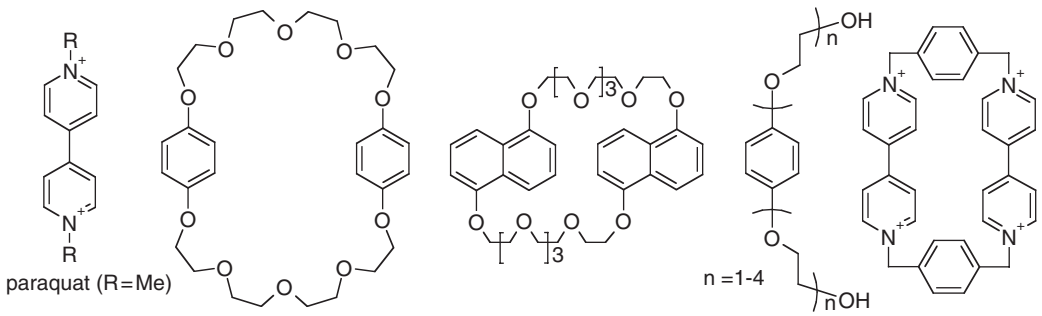


**3.113** **3.116** **3.117** **10.69** **6.81**

Based on the former approach, Stoddart *et al.* have constructed higher pseudorotaxanes such as the [3]pseutorotaxane **10.70** rather like threading beads on to a string. The tetracationic cyclophane is stabilised by π-stacking and charge-transfer interactions between the aryl rings, the 'solvation' of the positive charge on the 'blue box' by the crown oxygen atoms, and C—H ··· O hydrogen bonds from the relatively acidic aryl C—H protons to the crown oxygen atoms. The charge-transfer interactions give rise to a characteristic orange colour for all the complexes containing this kind of binding motif.

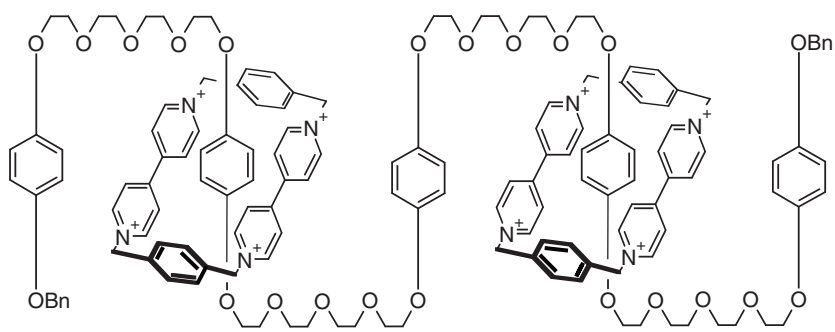


**10.70**

The most obvious way to prepare a rotaxane from a pseudorotaxane is to attach a bulky substituent group to the open end of the threaded molecule. The overall procedure is termed 'threading' (Figure 10.56). For example, reaction of the [2]pseudorotaxanes formed from di-ols **10.68** and **10.69** and bis(bipyridinium) receptor **6.81** with tri-*iso*-propylsilyl trifluoromethanesulfonate (triflate) in the presence of lutidine gives the corresponding tri-*iso*-propylsilylated [2]rotaxanes (**10.71**) in about

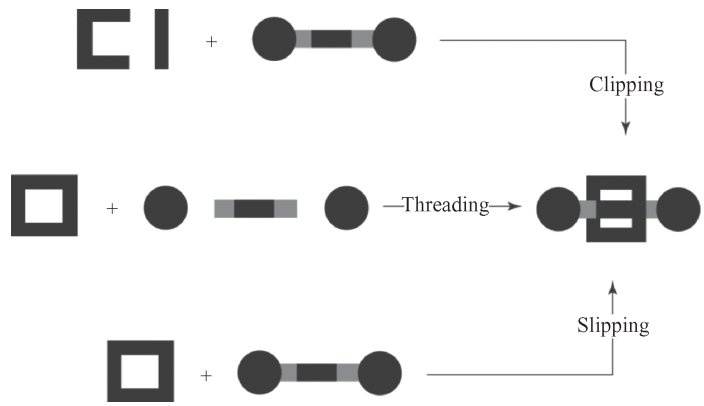


**Figure 10.56** Synthesis of rotaxanes *via* self-assembly of electron-rich and electron-poor aryl fragments. (Reproduced with permission from [58]).

21 % yield. The same compound can also be made by the 'clipping' route (Figure 10.56) in 14 % yield, using a preformed tri-*iso*-propylsilylated thread according to the reaction shown in Scheme 10.12. The final approach to rotaxanes, slipping, involves the use of a terminator group that is just small enough to pass through the macrocyclic ring upon careful heating/refluxing, but lacks sufficient energy to break through the conformational barrier at lower temperatures, as seen in the statistical approach to rotaxanes such as **10.67**.

A remarkable synthesis of [3]- and [4]rotaxanes has been achieved by Alan Rowan at the University of Nijmegen (Netherlands) using an alkene metathesis approach. Porphyrin-derived macrocycle **10.72** has a very strong affinity for bipyridinium derivatives such as **10.73** ($K_a > 10^6$ $M^{-1}$ in dichloroethane). Combining the two gives a [2]pseudorotaxane with a terminal alkene, ripe for alkene cross-coupling using Grubbs' catalyst. The coupling reaction gives only a 25 % yield of [3]rotaxane **10.74** and in an attempt to improve yields Rowan's group added an excess of macrocycle **10.72**. To their surprise this resulted in the formation of the [4]rotaxane **10.75** as well as **10.74**, implying that the thread **10.73** can bind two macrocycles before the coupling stage (Scheme 10.13).[59] The manganese(II) complex of the porphyrin-containing macrocycle **10.72** is a very good catalyst for epoxidation (addition of an oxygen

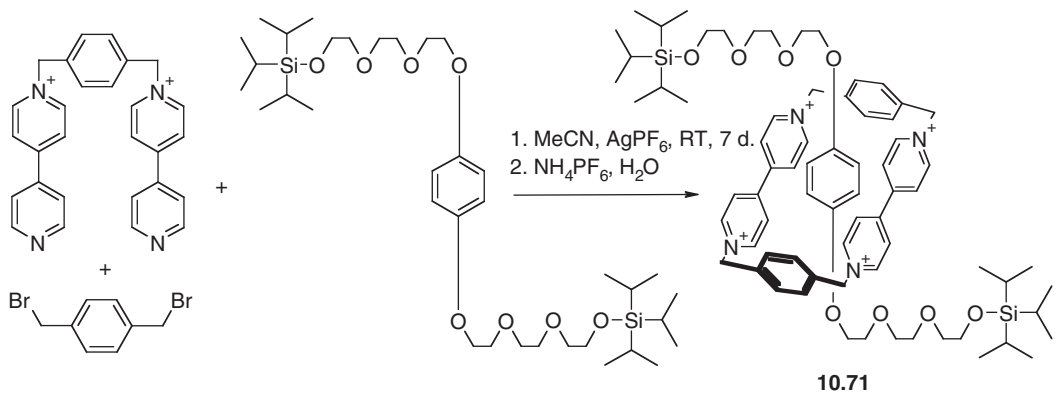


**Scheme 10.12** Synthesis of a [2]rotaxane *via* the clipping approach.

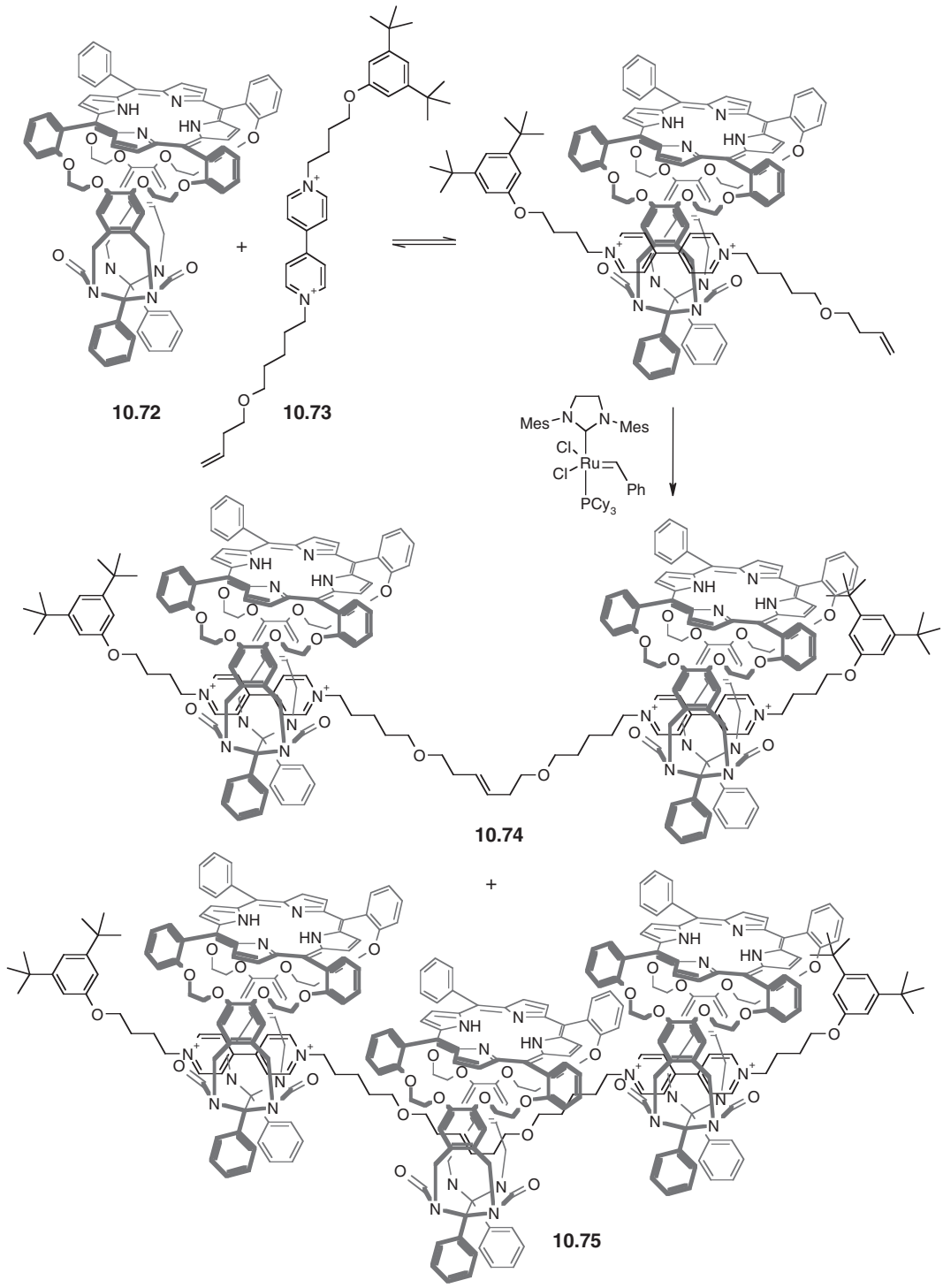


**Scheme 10.13** Synthesis of [3]- and [4]rotaxanes using alkene cross-coupling.[59]

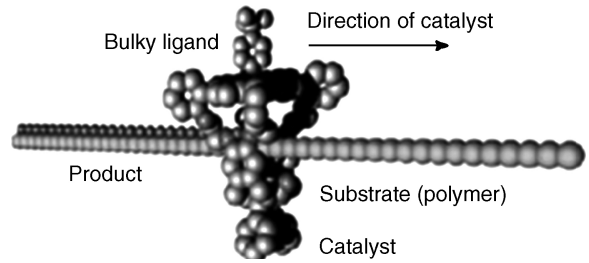


**Figure 10.57** Cartoon representation of the Mn(II) complex of **10.72** acting asa epoxidation processing catalyst (reprinted with permission from Macmillan Publishers Ltd).

atom to an alkene to give a three-membered C-O-C ring) of alkenes in the presence of oxidising agents such as iodsylbenzene (PhIO). The toroidal complex can act as a processing catalyst analogous to DNA polymerase (Section 2.9.5) which adds oxygen atoms to a threaded polybutadiene substrate. The process is shown schematically in Figure 10.57.[60] Rotaxanes are of considerable interest as molecular machines in this kind of way and we will return to this topic in the next chapter (Section 11.5).

By analogy with their use of charge-assisted $\pi$–$\pi$ stacking interactions in rotaxane synthesis, Stoddart's group prepared a [2]catenane by a planned template approach.[61] Again, the preparation involved the electron-deficient blue box **6.81** and followed a procedure in which the cation precursor was first threaded through the electron-rich crown ether **3.116** before ring closure to generate the [2]catenane **10.76** *via* a clipping approach (Scheme 10.14).

It is a tribute to the templating effect of the electronically matched pairs of reactants that the [2]catenane **10.76** is produced in 70 % overall yield. Even the analogous five-component self-assembly reaction in which **3.116** is reacted with two equivalents of 4,4′-bipyridyl and two equivalents of α,α′-dibromo-*p*-xylene proceeds in 42 % overall yield. The X-ray crystal structure of this compound (Figure 10.58) shows clearly the interlocking nature of the two rings, with the $\pi$-electron-rich quinone and $\pi$-electron-deficient bipyridinium rings stacked some 3.5 Å apart. Moreover, this same stacking interaction is seen between one [2]catenane molecule and the next within the solid-state structure, to give an infinite donor-acceptor array, reinforcing the evidence for the templated nature of the synthesis.

[2]Catenane **10.76** displays some very interesting dynamic properties, which may be followed by $^1$H NMR spectroscopy. In particular, at 81ºC the hydroquinone ring protons appear as a singlet signal

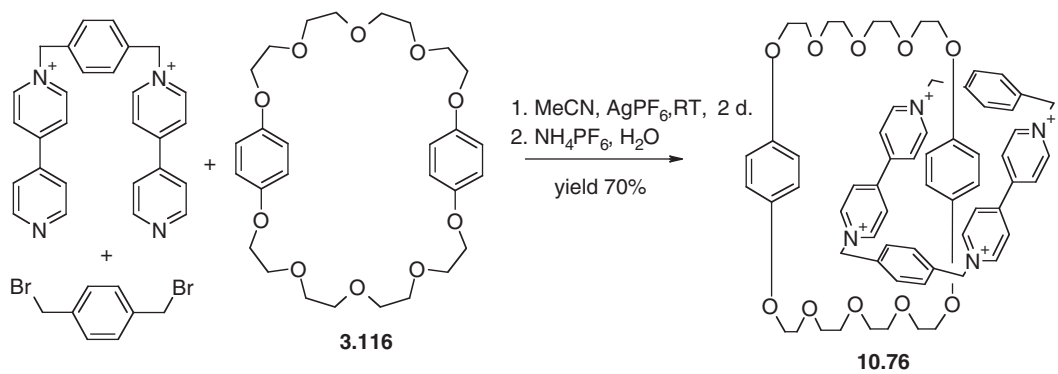


**Scheme 10.14** Template synthesis of the [2]catenane **10.76**.[61]

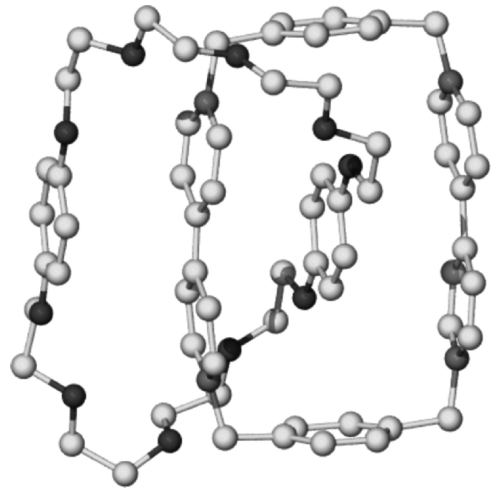

**Figure 10.58** X-ray crystal structure of the [2]catenane **10.76**.

at δ 4.57 ppm. At room temperature, slow circumrotation of the crown ether through the bipyridinium macrocycle (process I, Figure 10.59) results in two separate signals at δ 3.45 and 6.16 ppm, the former clearly affected significantly by the shielding effect of the inner surface of the bipyridinium cyclophane **6.81**. Using the coalesence method (Box 3.3), the energy barrier for the rotation can be calculated as 65.3 kJ $mol^{-1}$. The analogous circumrotation of the cyclophane through the crown ether may be monitored similarly (process II, Figure 10.59). Coalescence calculations give an energy barrier to rotation of 51.1 kJ $mol^{-1}$ with coalescence occurring at −45ºC in acetone solution. Two further processes termed rattling and rocking have also been identified.

The excellent synthetic results obtained for **10.76** can be compared with preparative yields obtained for various other $\pi$-donor crown ether ring sizes (Table 7.3). Clearly, the 34-membered ring is optimum, with yields dropping off very rapidly with smaller crowns as a function of poor fit. Lower yields are also observed for larger crowns as a result of increased conformational freedom. The greater flexibility of the rings is also reflected in the activation energy for ring rotation by process II, which was lowered by some 10.5 kJ $mol^{-1}$ for the larger crown ethers.

The electrochemistry of catenane **10.76** can be studied by cyclic voltammetry (Box 4.1). The compound possesses very different redox properties in comparison with the two isolated components.

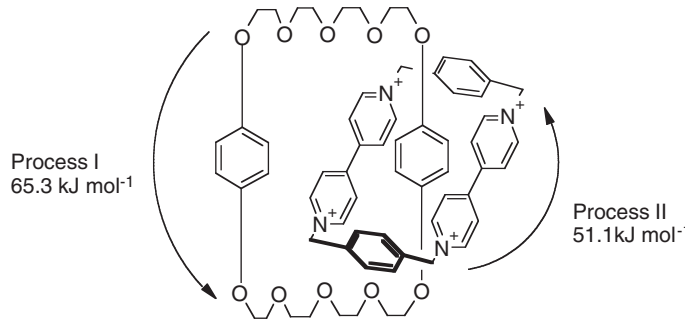


**Figure 10.59** Dynamic processes associated with [2]catenane **10.76**.

This difference is a direct result of the close π-stacking interactions. Electrochemical reduction of the bis(bipyridinium) cyclophane occurs in three distinct stages:

1. One-electron reduction of the more accessible, less stabilised bipyridinium moiety outside the crown ether cavity (this bipyridinium moiety acts as an acceptor to just one stabilising hydroquinone unit).
2. A second one-electron reduction corresponding to the bipyridinium moiety inside the cavity.
3. Finally, a two-electron reduction corresponding to the neutralisation of both bipyridinium rings.

In contrast, the bis(bipyridinium) macrocycle component (**6.81**) undergoes only two discrete two-electron reductions. The reason that four distinct reductions are not observed for **10.76** is that following the initial two reductions, the ring circumrotation process (process II, Figure 10.59) becomes fast on the cyclic voltammetric time scale and so the distinction between the 'inner' and 'outer' bipyridinium units is lost. The cyclic voltammetric waves are shown in Figure 10.60.

The self-assembling approach to catenane synthesis adopted by Stoddart *et al.* has proved to be extremely versatile, and since the preparation of **10.76** in 1989, these workers have been able to go on to construct [3]-, [4]- and even [5]- and [7]-catenanes using this methodology. Synthesis of [n]catenanes for values of $n > 2$ must necessarily be based upon larger-ring compounds that can accommodate portions of two interlocked rings within their cavities. Initial studies with this aim focused upon the dimer of **3.116**, tetrakis(*p*-phenylene)-[68]crown-20 (**10.77**). When the bis(bipyridinium) macrocycle is closed around it under relatively mild conditions similar to those shown in Scheme 10.14, only a [2]catenane (**10.78**) is produced, in a poor yield consistent with the large size of the crown ring (*cf.* Table 10.4). However, under 10 kbar pressure, a modest yield of the analogous [3]catenane (**10.79**) is obtained (Scheme 10.15). The low yields are a result of the high degree of flexibility of the 68-membered ring.[62]

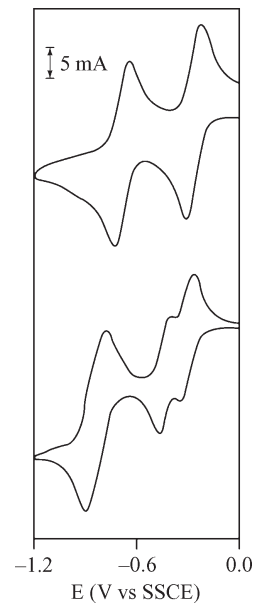


**Figure 10.60** Cyclic voltammograms of the cyclophane **6.81** (top) and [2]catenane **10.76** (bottom). (Reprinted with permission from [62] © 1995 American Chemical Society).

**Table 10.4** Yields of [2]catenanes produced *via* the type of reaction shown in Scheme 10.14 as a function of crown ether ring size.

| n | m | | Yield of [2]catenane (%) |
|---|---|---|---|
| 0 | 1 | [31]crown-9 | 10 |
| 1 | 1 | [34]crown-10 | 70 |
| 2 | 1 | [37]crown-11 | 55 |
| 2 | 2 | [40]crown-12 | 54 |
| 3 | 2 | [43]crown-13 | 40 |
| 3 | 3 | [46]crown-14 | 49 |

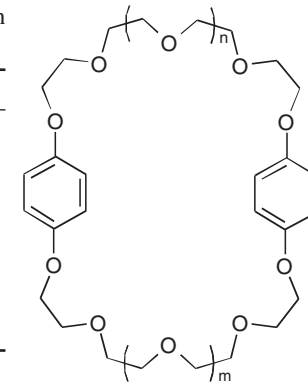

Like its smaller [2]catenane analogues, compound **10.78** exhibits some very interesting dynamic behaviour in which the smaller cationic cyclophane ring behaves like a molecular 'train', travelling around the four hydroquinone stations of the crown ring at a rate of 300 times per second, corresponding to an activation energy of 59.0 kJ mol$^{-1}$. If the [2]catenane is a molecular train, the [3]catenane **10.79** may be described as a molecular 'merry-go-round'. In solution, the symmetry of the crown ring is maintained indicating that even though both bipyridinium cyclophanes (**6.81**) are travelling around the crown ring (activation energy 57.0 kJ mol$^{-1}$), they do so in a concerted fashion, remaining at diametrically opposed hydroquinone stations.

Following the success of this work, Stoddart realised that in order to construct even larger catenanes, cyclophane **6.81** would have to be replaced by a larger acceptor ring capable of incorporating two hydroquinone units from separate crown ethers. A combination of a large-ring crown ether electron-donor and large cyclophane cations then allows access to ever larger catenanes and ultimately catenane polymers. The synthesis of a larger electron-acceptor was addressed by the preparation of the tetracationic cyclophane **10.80**, which simply replaces the *p*-xylyl spacer in **6.81** with a *p*-biphenyl group.

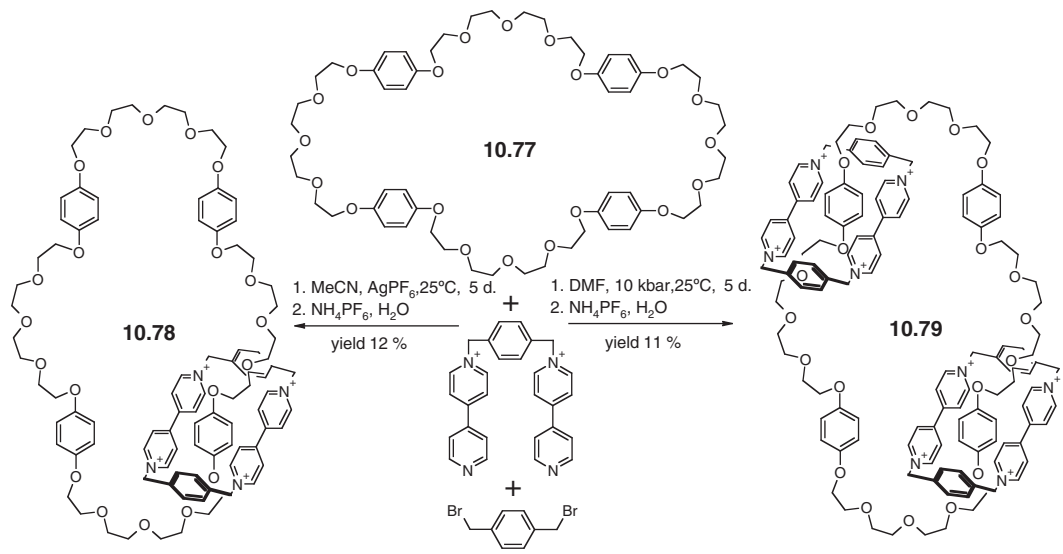


**Scheme 10.15** High-pressure synthesis of a [3]catenane.

Stoddart's group anticipated that a two-step process involving clipping of the precursors **10.81** and **10.82** around two molecules of **10.77** to give a [3]catenane centred upon **10.80**, followed by clipping on two molecules of **6.81**, would give the desired [5]catenane. Unfortunately, this ambitious scheme ended in failure, ascribed to the conformational mobility of crown ether **10.77**. Undeterred, they attempted the same strategy with the intermediate-sized crown ether **10.83**. Under atmospheric pressure, this reaction gave the intermediate [3]catenane **10.80**·(**10.83**)$_2$ in 3.5 % yield which they carried forward to the second stage. Under ultra-high pressure conditions, clipping **6.81** around this [3]catenane gave a 22 % yield of a [4]catenane and just a trace of the desired [5]catenane (**10.84**), Scheme 10.16. This low yield was frustrating, but encouraged the

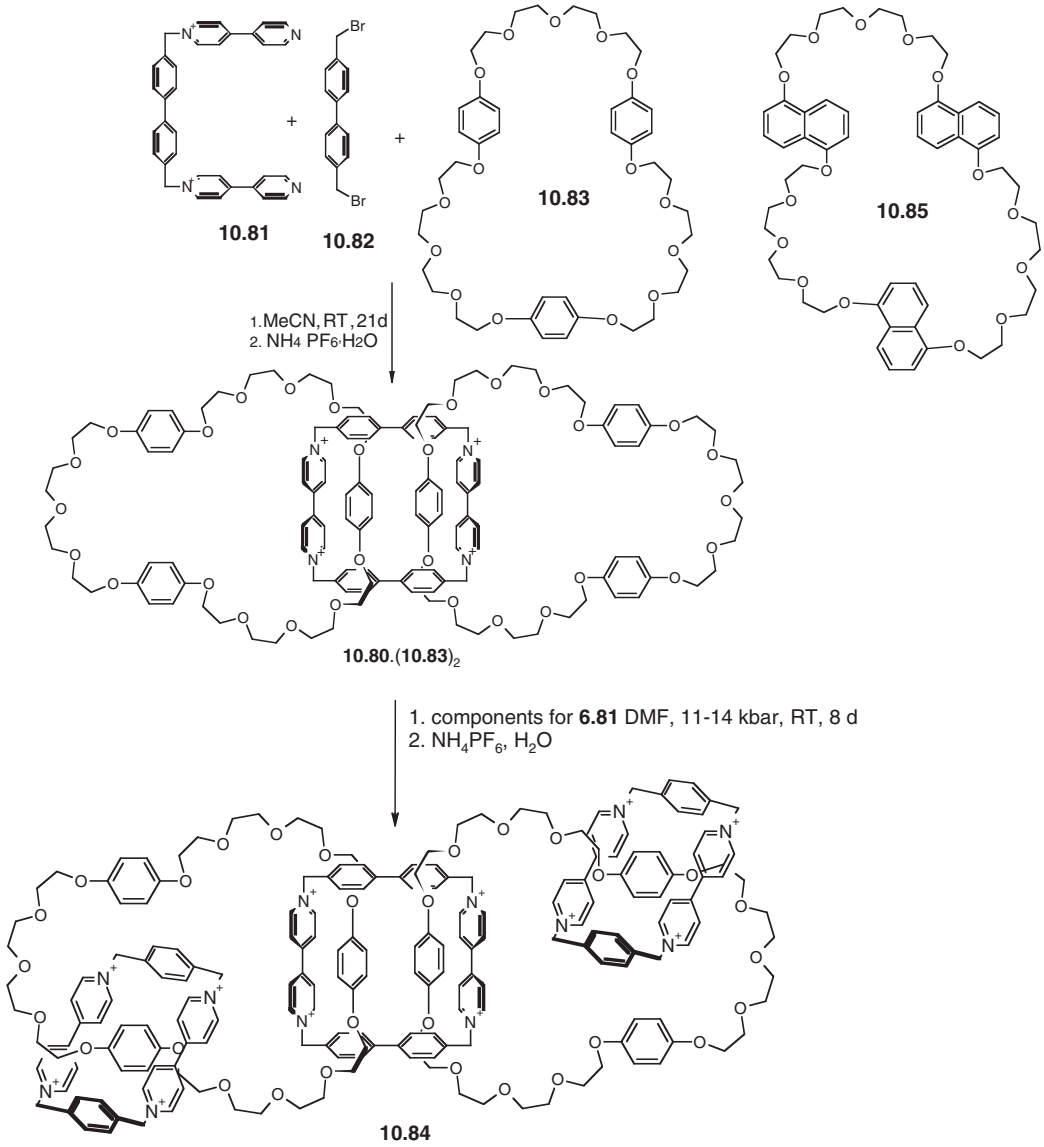


**Scheme 10.16** First synthesis of a [5]catenane.[63]

researchers to continue with their strategy to prepare macroscopic amounts of a [5]catenane. Their objective was finally achieved by yet another change of crown ether, this time substituting the aryl rings in **10.83** for the 1,5-dioxynapthalene analogue **10.85**. The strategy shown in Scheme 10.16 produced the expected [5]catenane in an acceptable yield of 5 % without the use of high pressure. The resulting molecule was dubbed 'olympiadane' because of its resemblance to the international Olympic Games symbol. The analogous [4]catenane was also produced in 31 % yield.[63]

Olympiadane was characterised by $^1$H NMR spectroscopy, which shows the molecule to be highly symmetric at 60 ºC due to fast interannular circumrotation of all the components. The spectrum is significantly broader at room temperature, while at 0 ºC the resonances assigned to the smaller cyclophanes (**6.81**) split into two signals corresponding to the freezing out of the rotation of these components. The mass spectrum of the [5]catenane is also highly definitive, with a clear peak at *m/z* 5072 corresponding to olympiadane in conjunction with seven, eight, nine and ten (of a possible 12) $PF_6^-$ anions and analogous peaks for the [4]catenane. Also, in a remarkable feat of supramolecular crystallography, the crystal structure of olympiadane has been determined by the group of David Williams at Imperial College, London, revealing a very compact structure. Remarkably Stoddart went on to prepare a [7]catenane by clipping four molecules of **6.81** to the intermediate **10.80**·(**10.83**)$_2$. The X-ray crystal structure of this enormous supermolecule was also determined by Williams, Figure 10.61.[64]

The charge-assisted $\pi - \pi$ stacking methodology has proved to be enormously versatile and has led to an enormous variety of catenated species. Of particular interest is the chiral bis([2]catenane) **10.86** arising from clipping two equivalents of the bis(pyridinium) precursor with the tetrabromo derivative **10.87** in the presence of crown ether **3.116**. Note that this compound is not a [3]catenane because it does not possess a central ring that interpenetrates with two others. It is simply a covalently linked pair of [2]catenanes. The chirality of the compound is readily evident in its $^1$H NMR spectrum, which gives a characteristic AB quartet for the diastereotopic $CH_2N^+$ protons of the octacationic cyclophane. Clearly there is little chance (on steric grounds) of the cyclophane cation rotating through the crown ether ring (process II), but the crown rotation (analogous to process I) is observed with an activation energy of 67.0 kJ mol$^{-1}$, very similar to the [2]catenane analogue **10.76**. At low temperature in acetone-$d_6$, NMR spectoscopy shows that **10.86** exists as two translational

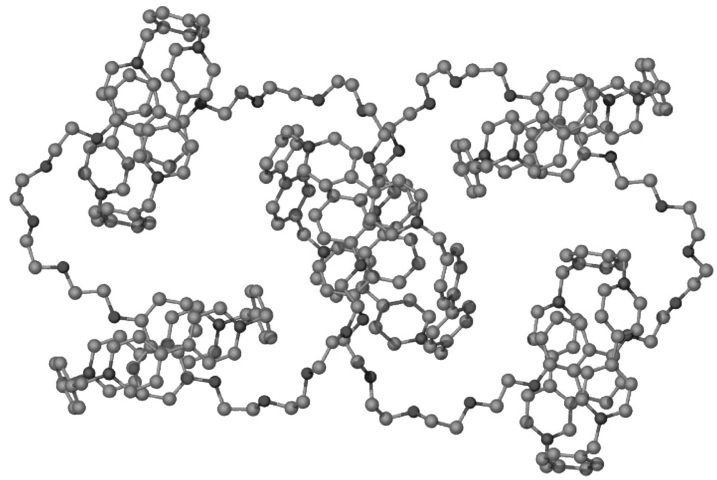

**Figure 10.61** X-ray crystal structure of the [7]catenane analogue of olympiadane.[64] See plate section for colour version of this image.

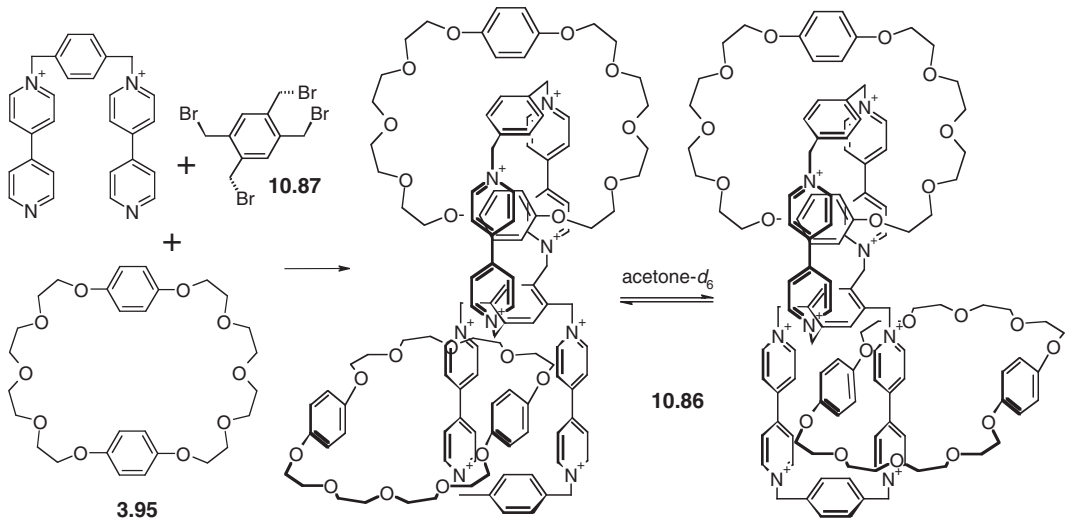


**Scheme 10.17** Synthesis and conformational equilibria of *bis*([2]catenane) **10.86**.[65]

isomers, each of equal population (Scheme 10.17).[65] Bis([2]catenane) **10.86** was prepared in 13 % yield from the one-step self-assembly of five components. Interestingly, the free octacationic cyclophane has not yet been isolated, clearly suggesting that the presence of the electron-rich crown ethers templates the reaction. In general, yields of these types of bis([2]catenanes) increase significantly when the length of the covalent spacer between the two rings of the cyclophane cation is increased.

A novel variant on the mechanical interlinking approach is to tether the two interlocked components together. This process results in a single knotted covalent molecule termed a *pretzelane* after the baked savory snack particularly popular in the US. Compound **10.88** is an example of a pretzelane (Figure 10.62) which is formed simultaneously with its dimer, a cyclic bis([2]catenane).[66] Use of a longer spacer between the two macrocycles gives exclusive formation of the pretzelane in 49 % yield. The pretzelane has both helical and plane chirality and hence exists as a mixture of two diastereoisomers, each of which has two enantiomers.

The versatility of this approach to interlocked molecules make it very attractive as a means towards nanoscale molecular machines in which the motions of the individual components are beginning to be translated into molecular logic operations and mechanical switches. We will return to this subject in the next chapter.

## 10.7.4 Hydrogen Bonded Rotaxanes and Catenanes

Kay, E. R. and Leigh, D. A., 'Hydrogen bond-assembled synthetic molecular motors and machines', *Top. Curr. Chem.* 2005, **262**, 133–177.

While attempting to prepare a simple amide-based macrocycle according to the reaction shown in Scheme 10.18, David Leigh (now of the University of Edinburgh, UK) and co-workers stumbled upon the [2]catenane **10.89** which is formed spontaneously. The two interpenetrated rings completely fill one another's cavity and the complex is held together by amide NH···O hydrogen bonding. These hydrogen bonds give a clue to the reason why catenane formation is so facile and occurs in reasonable yield. The assembling amide precursor is included within a second macrocycle by this same double

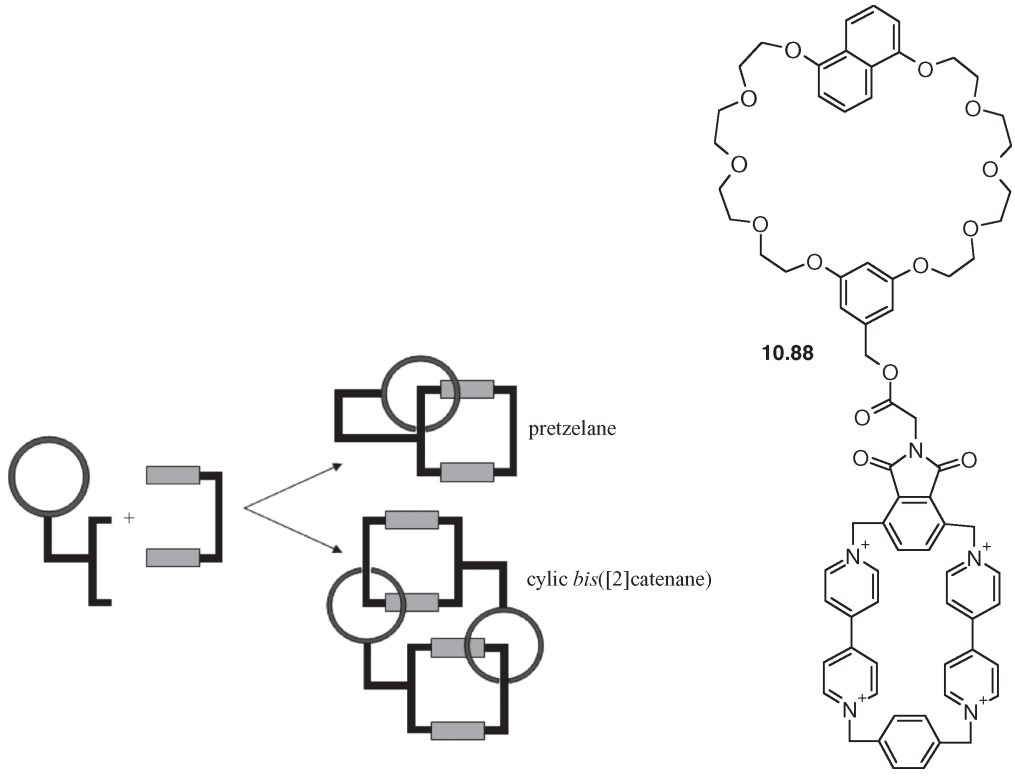


**Figure 10.62** Cartoon and 2D molecular representation of *pretzelane* **10.88** and the alternative bis([2]catenane).[66]

NH···O=C hydrogen bonding interaction causing cyclisation to occur on the included acid chloride. We saw a similar effect in Section 6.5.7 when we looked at amide-based macrocycles as hosts for *p*-quinone. This use of hydrogen bonding to template the formation of interlocked molecules has proved to be very useful and has also been applied to rotaxanes, as in the [3]rotaxane **10.90** which is synthesised under thermodynamic control using alkene metathesis (which causes the central double bond to break and re-form, allowing the macrocycles to thread on to the axel by a 'slipping' process).[67]

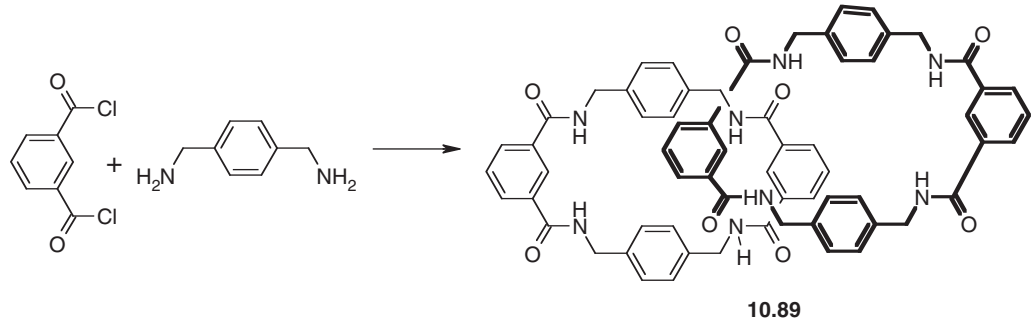


**Scheme 10.18** Accidental synthesis of an amide-based [2]catenane.[70]

Use of an asymmetric thread in conjunction with one of the macrocycles from **10.89** gives a bistable molecular machine, **10.91**. The hydrogen bonding is stronger to the succinamide diamide portion of the thread in the initial state in this complex. However photoexcitation of the naphthalimide followed by reduction of the resulting hole with an external donor makes a naphthalimide radical anion which is a much stronger hydrogen bonding site. As a result the macrocycle moves to the opposite end of the thread on the timescale of about 1μs. Following charge recombination over *ca.* 100 μs the system returns to the ground state and the macrocycle moves back to its original position. The ensemble somewhat resembles a molecular piston with the macrocycle shuttling back and forth about 10,000 times per second and generating $10^{-15}$ W of power per molecule![68]

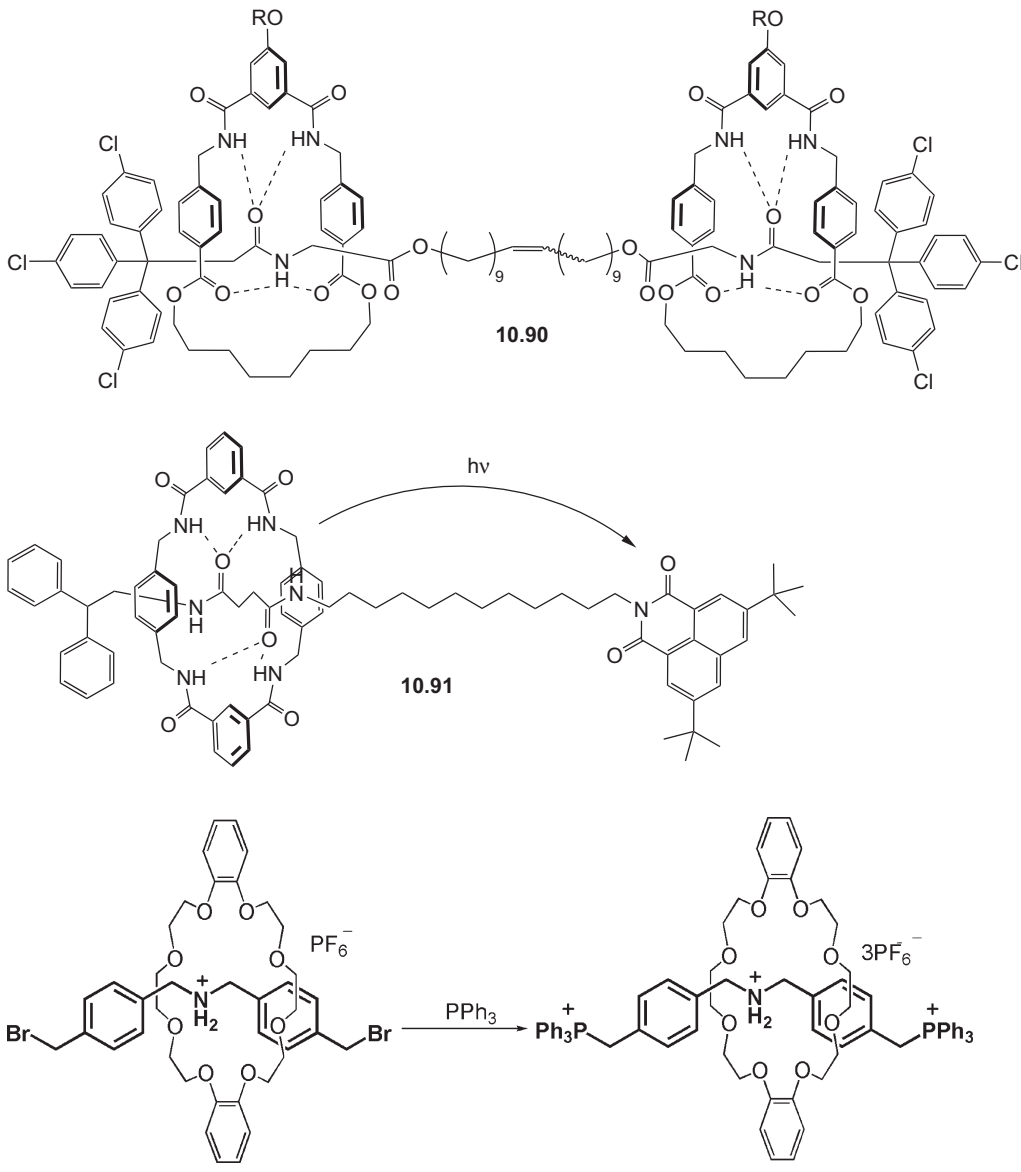


**Scheme 10.19** Formation of a rotaxane by capping a secondary ammonium guest.[69]

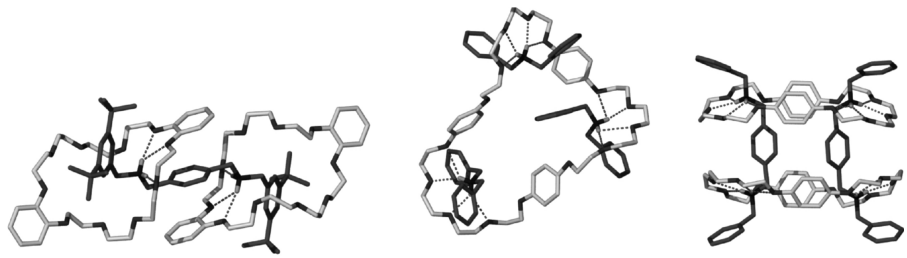


**Figure 10.63** Crown ether ammonium ion based rotaxane type hydrogen bonded complexes (a) [3]rotaxane, (b) three threads in one ring and (c) two threads linking two rings.

The hydrogen bonding of ammonium ions to crown ethers has also been used to assemble a range of rotaxanes and *pseudo*rotaxanes. The inclusion of a secondary ammonium thread into dibenzo[24]crown-8 followed by covalent capping to give a rotaxane is shown in Scheme 10.19.[69] This kind of approach can result in some interesting multiply threaded rotaxane type compounds, Figure 10.63.

## 10.7.5 Metal and Auxiliary Linkage Approaches to Catenanes and Rotaxanes

Lankshear, M. D. and Beer, P. D., 'Strategic anion templation', *Coord. Chem. Rev.* 2006, **250**, 3142–3160.

The beauty of the methodology of catenane synthesis pioneered by Stoddart and co-workers lies in its relative simplicity, high yields and versatility. By designing self-assembling host–guest systems, the reaction becomes preprogrammed towards catenane synthesis and the interpenetration brought about by self-assembly methods is fixed by covalent modification. The host–guest concept behind catenane synthesis may be generalised to the idea of an 'auxiliary linkage' in which there is no distinction between host and guest in the initial self-assembled complex, nor any distinction between the forces holding it together, which may be electrostatic, covalent, coordination interactions, hydrogen bonding *etc.* The auxiliary linkage is simply an organisational device that holds the reactants in the correct relative orientations or positions in order to give the desired catenated product (Figure 10.64) (*cf.* the synthesis of insulin by self-assembly with covalent modification, Section 10.3.2).

The earliest use of the auxiliary linkage approach was the employment of a steric barrier as an auxiliary linkage in the directed synthesis of hydrocarbon catenanes by Schill and Lüttringhaus. One of the most elegant examples of this approach is shown in Scheme 10.20.[71] The procedure involves the construction of a corand ring containing a primary amino substituent (**10.92**). The auxiliary linkage effect in this precursor is provided by a negative steric template that holds the two chloroalkane arms apart and forces them to point in opposite directions. The two arms are thus forced to attack the amino group from opposite directions resulting in the high-yield formation of the double ansa compound (**10.93**). Once this crucial cyclisation step has been accomplished, the auxiliary linkage is no longer necessary and is hydrolysed away with HBr in acetic acid to give the ketone (**10.94**). Finally, cleavage of the bond between the nitrogen atom and the aromatic ring liberates catenane **10.95**.

The existence of interlocked molecules such as **10.95** can be established by a variety of spectroscopic techniques. Most importantly, mass spectrometry provides very characteristic patterns for catenanes. The mass spectra for catenated species are very different from those of covalently linked precursors (such as **10.94**) but are more than the sum of their two individual components. Catenane mass spectra are characterised by the appearance of peaks at high $m/z$ corresponding to the parent species as well as fragments corresponding to the transfer of hydrogen atoms from one macrocycle to the functional

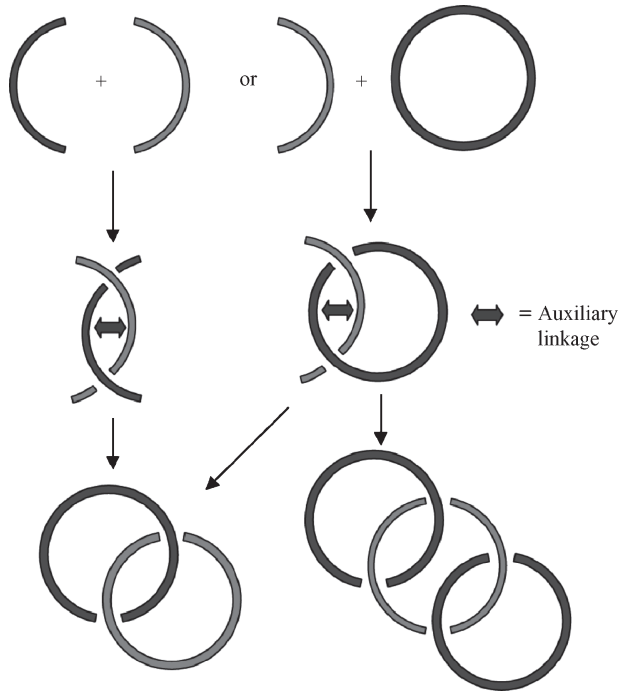


**Figure 10.64** The auxiliary linkage approach to the synthesis of [2] and [3]catenanes. The auxiliary linkage may be a covalent, coordinate or noncovalent bond.

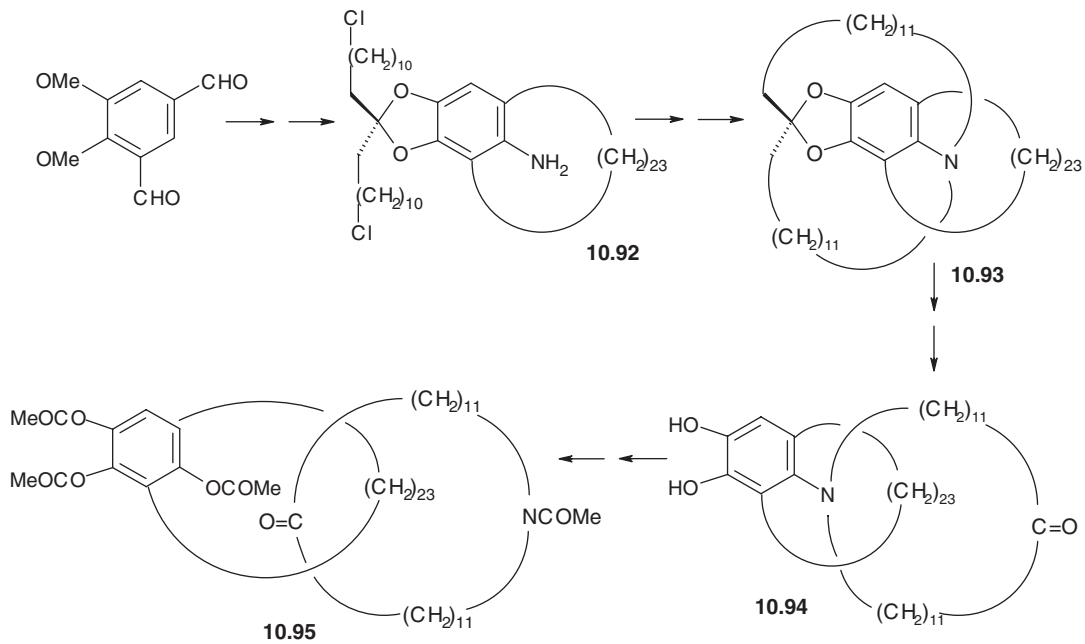


**Scheme 10.20** Directed synthesis of a [2]catenane by use of a negative templating steric barrier as an auxiliary linkage.[71]

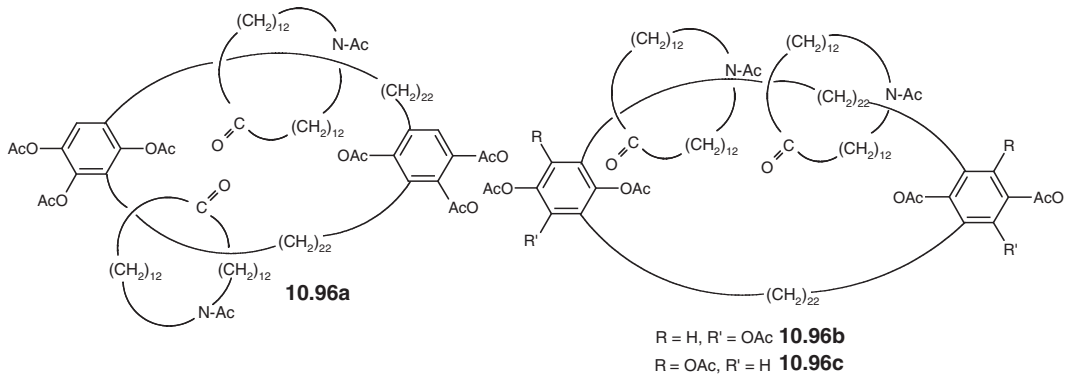


**Figure 10.65** [3]catenane translational isomers.[72]

group of the other. The first degradation process then seems to consist of disconnection of the two rings since there are then very few peaks until clear fragmentation peaks of the individual components, resembling the spectra of the individual macrocycles.

Generally, both $^{1}H$ and $^{13}C$ NMR spectroscopy reveal shifts to low field in resonances arising from nuclei within the interlocked structure. This shift has been attributed to van der Waals interactions between the two catenane components. Spin-lattice ($T_1$) relaxation time measurements in NMR spectra have also been used in related systems to establish that the motions of the interlocked rings are more restricted than the motions of the free species. Similar controlled methodology has been used to prepare a [3]catenane (**10.96**) that exists as a total of three isomers (Figure 10.65).[72] In addition to carcerism (Section 6.7.4) and topological isomerism that we have already encountered, this type of isomerism represents a further example of the way in which the mechanical arrangement of the fragments of a molecular aggregate can result in the formation of physically different compounds. The isomers differ in the placing of the nitrogen-containing rings with respect to one another, and in the substituents on the larger, central cyclophane ring. Compound **10.96a** proved sufficiently different in terms of polarity from the other two isomers that it could be separated from them chromatographically. The presence of the aryl rings prevents the mutual interconversion of **10.96a–c** under ambient conditions.

Attempts have also been made to carry out multiple sterically directed cyclisations on closely related systems with a view to generating multiply interlocked materials. Compound **10.97** was prepared and subjected to a triple ring closure reaction. Unfortunately, the inherent low yields of the crucial reaction steps resulted in immense difficulty in characterising the reaction products. Compound **10.97** is prepared in nine steps, and following multiple cyclisation, a total of only 1.7 % of product was obtained, which proved to be an isomeric mixture of three different interlocked species.

In general, because the molecule possesses two-fold symmetry, there are only two ways of connecting the chloro substituents 1–4 with amines 5 and 6: linking of 1 and 2 with 5 (and 3 and 4 with 6) or linking 1 and 3 with 5 (and 2 and 4 with 6). However, the various possibilities for topological isomerism and diastereoisomerism result in four different possible products (not counting enantiomers). The former connectivity results ultimately in [2]catenane formation, whereas the latter can produce a macrocyclic compound or a complicated knotted structure termed a trefoil knot, which was the original target of the synthesis (*cf.* Section 10.9) (Figure 10.66). A total of three products were obtained, and NMR spectroscopic results suggested that the precursor to the trefoil knot may have been produced as one of the products. The final steps to generate the noncovalently interlocked structures were not reported.[73]

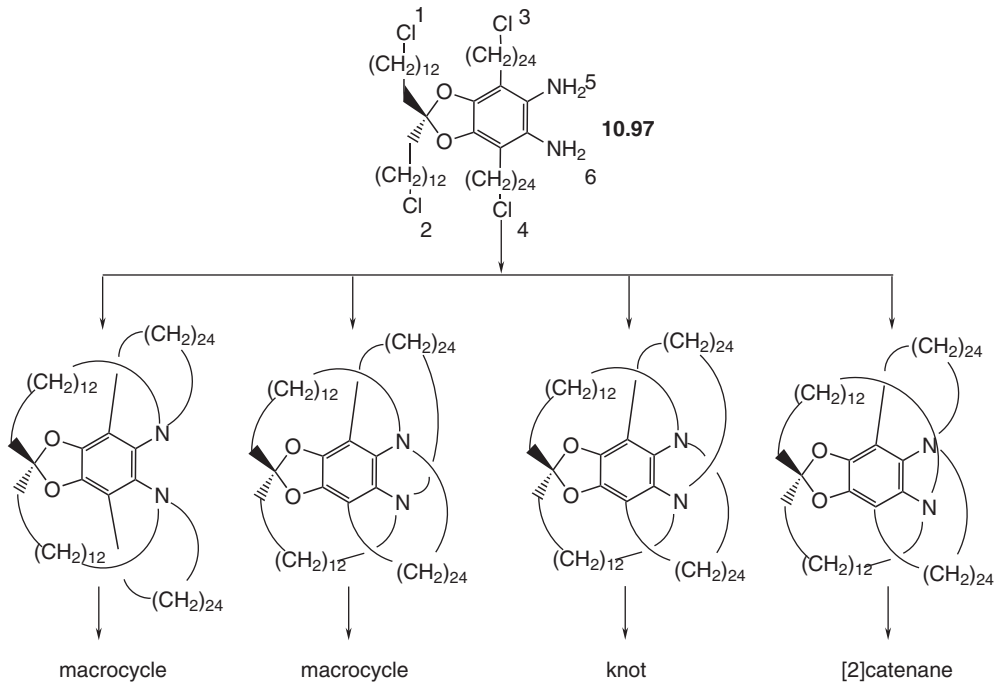


**Figure 10.66** Possible triply cyclised intermediates from **10.97**.[73]

In all cases examined so far, the precursors and resulting catenanes contain a number of functional groups necessary in order to 'direct' the synthesis. Since the beginning of catenane synthesis however, it had remained a goal, at least for the sake of academic interest, to prepare a purely hydrocarbon catenane consisting of two interlocked cycloalkanes. Clearly, with the severely limited strength of van der Waals interactions between alkane precursors, a purely statistical approach was unlikely to give appreciable yields. On the other hand, a directed approach was liable to result in the incorporation of a large number of functional groups that might be difficult to remove. This showcase feat of supramolecular chemistry was accomplished by a combination of statistical and then directed approaches (Scheme 10.21). Initially, the translationally isomeric [2]rotaxanes **10.98** were prepared by statistical slipping methods. The bulky triphenylmethyl (trityl) stoppers proved sufficient to prevent the unthreading of the rotaxanes at room temperature. The methylene groups alpha to the sulfonyl functionalities proved sufficiently acidic to deprotonate in the presence of alkyl lithium reagents and the resulting lithium salt was used to elaborate the rotaxanes with alkynyl substituents capable of undergoing cyclisation *via* Glaser coupling to give either a [2]rotaxane **10.99** or a [2]catenane **10.100**. Reduction of the resulting alkyne macrocycle and removal of the redundant blocking groups gave either the uncatenated macrocycles or the all-hydrocarbon catenane **10.101**.

The directed approach of Schill is a subtle manifestation of the auxiliary linkage approach, which, while extremely elegant, is highly intensive of synthetic effort and ultimately low-yielding because it relies on robust covalent linkages to force the reactants into a suitable conformation to optimise interlinked product formation. A more obvious and accessible example of an auxiliary linkage is coordination to a metal cation, in a variation of the kinetic template synthesis approach used in the simple macrocyclisation reactions studied in Chapter 3. This approach has been adopted with enormous success by Jean-Pierre Sauvage (Strasbourg, France). The Sauvage approach[75] relies upon the observation

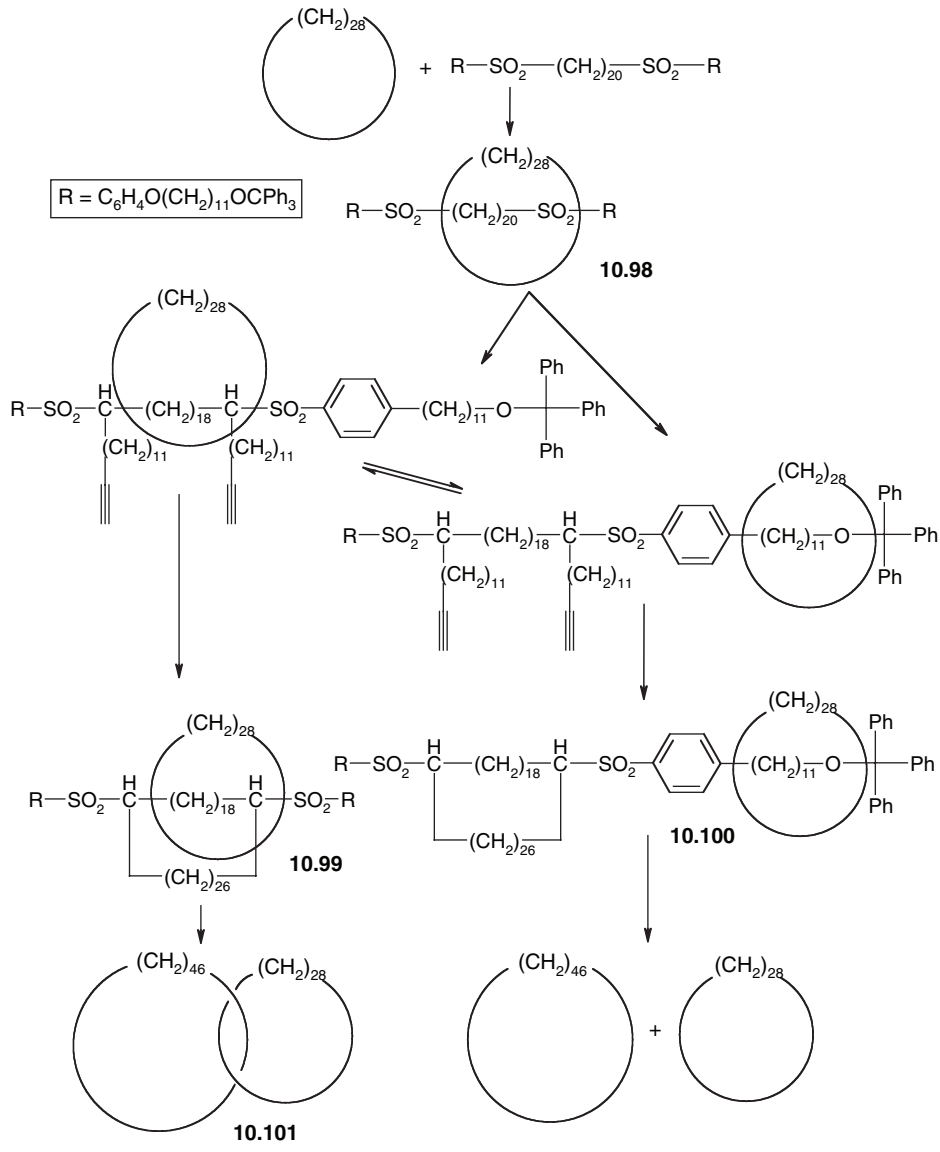


**Scheme 10.21** Statistical and directed synthesis of the first hydrocarbon catenane.[74]

(firmly established by a detailed NMR spectroscopic study) that transition metal ions such as Cu(I) generally adopt a tetrahedral coordination geometry and, in the presence of bidentate ligands such as a 1,10-phenanthroline derivative **10.102**, are able to organise those ligands in a mutually orthogonal fashion (Figure 10.67).

Sauvage realised immediately that functionalisation of the methoxy substituents and cyclisation with a long polyethylene glycol chain would inevitably result in catenanes under high-dilution macrocyclisation conditions. Deprotection of the anisole derivative **10.102** with pyridinium chlorohydrate gave a bis(phenol) compound that was cyclised with 1,14-diiodo-3,6,9,12-tetraoxatetradecane in dimethylformamide (DMF) to give directly the [2]catenane **10.103** in 27 % yield, along with a 20 %

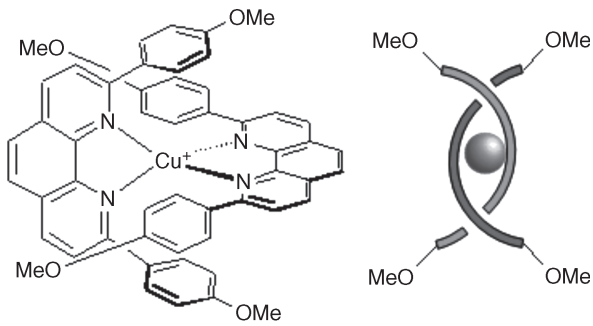


$[Cu(\mathbf{10.102})_2]^+$

**Figure 10.67** The 2:1 complex between 1,10-phenanthroline derivative **10.102** and Cu(I) along with cartoon schematic.[75]

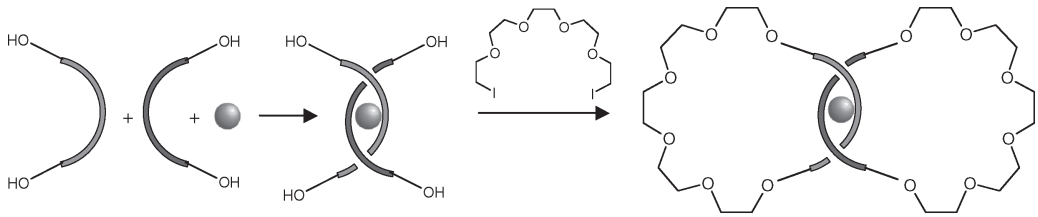


[2]catenate **10.103**

**Scheme 10.22** Metal templated synthesis of catenate **10.103**.[75]

yield of macrocycle **10.104** and polymeric products. In recognition of the fact that the two catenated phenanthroline units in **10.103** are acting as ligands for the Cu(I) centre, the complex as a whole was christened a *catenate*, by analogy with the cation *cryptates*. The free catenated ligand is thus referred to as a *catenand* (*cf. cryptand*) (Scheme 10.22).

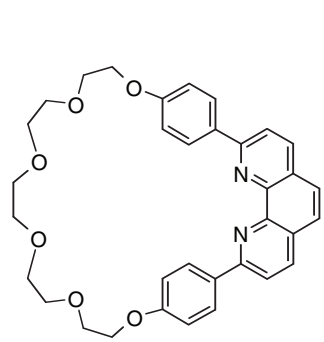


**10.104**

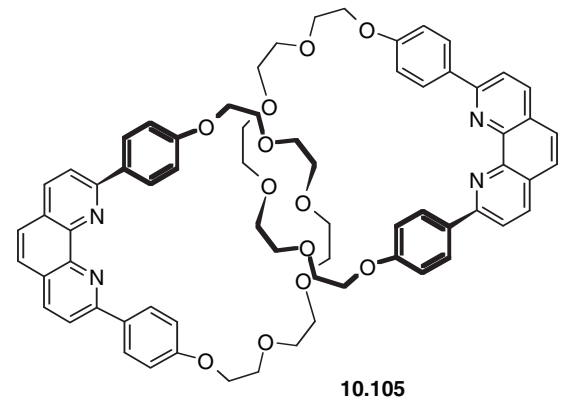


**10.105**

The yield of **10.103** is improved further by adopting a stepwise approach in which the preformed corand **10.104** is reacted with $[Cu(MeCN)_4]^+$ and one equivalent of the deprotected **10.102** to give an intermediate pseudorotaxane. Cyclisation as before gives the catenate **10.105** in an impressive 42 % yield.

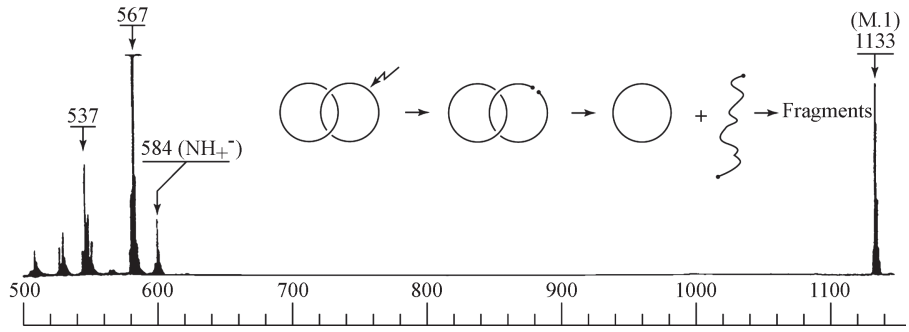


**Figure 10.68** Mass spectrum of catenand **10.105** showing molecular ion peak and fragmentation into the separated macrocycle. (Reprinted with permission from [76] © 1987 American Chemical Society).

As a final stage, the catenate was then treated with $CN^-$ (an excellent ligand for $Cu^+$) in order to remove the Cu(I) centre as $[Cu(CN_4)]^{3-}$ to give the free catenand, **10.105**. The catenand was characterised by mass spectrometry, with the molecular ion observed at *m*/*z* 1133. The mass spectrum shows the characteristic feature of catenands, namely that the the first fragmentation is ascribable to the decoupling of the two interlocked rings and so no fragmentation peaks are observed until the signal for uncatenated **10.104** at *m*/*z* 567 (Figure 10.68). Also of interest is the $^1$H NMR spectrum of the compound, which indicates that in the free state, without the Cu(I) centre to bind the two phenanthroline moieties together, the catenand undergoes a significant conformational change to relocate the bulky, electron-rich phenanthroline groups as far apart as possible, as indicated in the diagram of **10.105**. Both structures were confirmed by X-ray crystallography (Figure 10.69).

Interestingly, the kinetics of the metal decomplexation reaction from the catenate, both intrinsic and assisted by $CN^-$, as shown below, are particularly slow. Direct comparison of kinetic data for $[Cu(\mathbf{10.102})_2]^+$ and $[Cu(\mathbf{10.104})_2]^+$ (*i.e.* **10.103**) showed that the intrinsic decomplexation rate is 2500 times slower for the catenate than its open analogue, despite the fact that steric congestion around the metal centre is similar in both cases. The cyanide-assisted rate is 40 times faster in the uncatenated complex $[Cu(\mathbf{10.102})_2]^+$. This observation suggests that the presence of the polyether chain results in significant distortions as part of the decomplexation process, significantly raising the activation energy barrier.

Also of interest are the cyclic voltammetric (Box 4.1) properties of the two Cu(I) complexes, $[Cu(\mathbf{10.102})_2]^+$ and $[Cu(\mathbf{10.104})_2]^+$. The uncatenated bis(chelate) complex exhibits an entirely irreversible reduction at about −1.7 V (versus saturated calomel electrode reference, SCE), consistent with

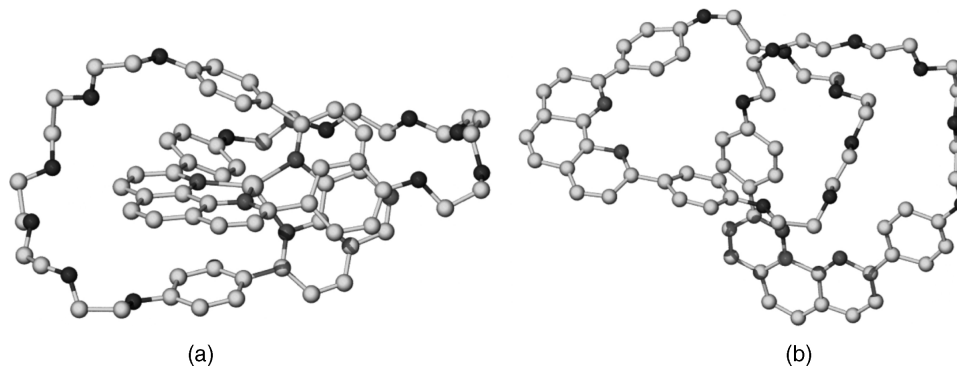


**Figure 10.69** X-ray crystal structures of (a) the catenate **10.103** and (b) the free catenand **10.105**.[76]

the decomposition of the complex to free **10.102** and copper metal when the Cu(I) centre is reduced to Cu(0). In contrast, an entirely reversible reduction wave at similar potential is seen for the catenate. This suggests that the fact that the complex is catenated (and therefore the two phenanthroline-binding domains cannot move apart from one another) stabilises the Cu(0) complex. Indeed, deep blue solutions of $[Cu(\mathbf{10.104})_2]^0$ are stable under argon for days. It is likely that the compound is only formally Cu(0); in reality, the added electron resides on one of the phenanthroline moieties to give an organic radical anion.

Sauvage and co-workers have gone on to prepare [3]- and [4]catenates such as **10.106** using a similar method with the greatly enlarged bis- and tris(phenanthroline) derivatives acting as the central macrocycles. Analogous systems have also been prepared with three larger chelating ligands around octahedral metal centres such as Fe(II) and Ru(II), resulting in three-component entanglements.[77] While these entanglements have yet to be transformed into complex interlocked compounds (but see Section 10.9 for a description of an 'open' trefoil knot produced in this way), an octahedral ruthenium(II) system has been used to produce a hetero-[2]catenane **10.107** based on a bis(phenanthroline) ligand on one ring and a bipyridyl on the other using ring-closing alkene metathesis.[78] Square planar metals such as Pd(II) have also been used as auxiliary linkages to template the formation of [2]rotaxanes as in **10.108**.[79] The bulky tetraphenylmethane-derived thread is linked to an open macrocycle precursor by coordination ot the Pd(II) centre. The ring is then closed by alkene metathesis followed by reduction of the resulting double bond. Once the rotaxane is formed the palladium(II) ion can be removed by addition of cyanide to give the free rotaxane. Yields for the complexation and decomplexation steps are almost quantitative while the combined macrocyclisation and reduction step proceeds in 69 % yield.

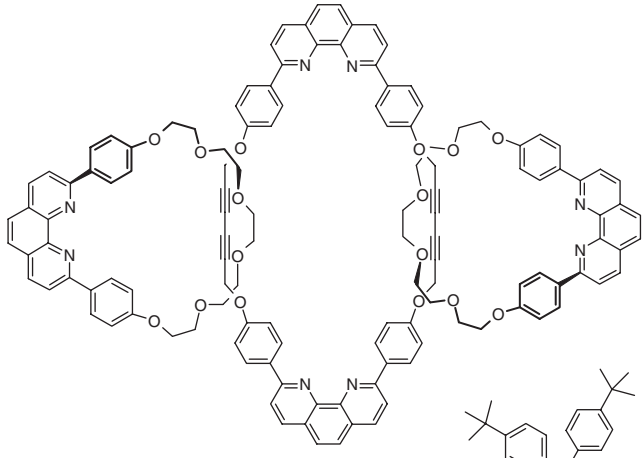

**10.106**

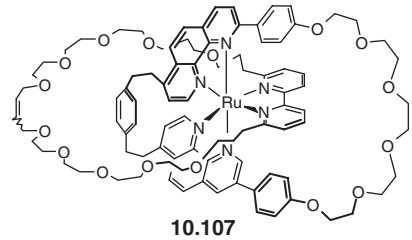

**10.107**

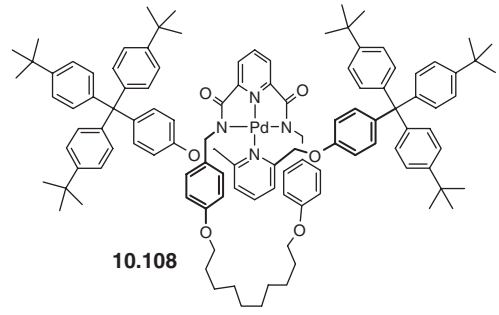

**10.108**

In addition to metal centres and covalent approaches, anions such as $Cl^-$ may also be used as templating auxiliary linkages.[80] Paul Beer and co-workers from the University of Oxford, UK, recognised that ion pairing in non-polar solvents such as acetone allowed the coordination of a neutral hydrogen bond donor such as **10.110** to the pyridinium salt **10.109**, with a binding constant

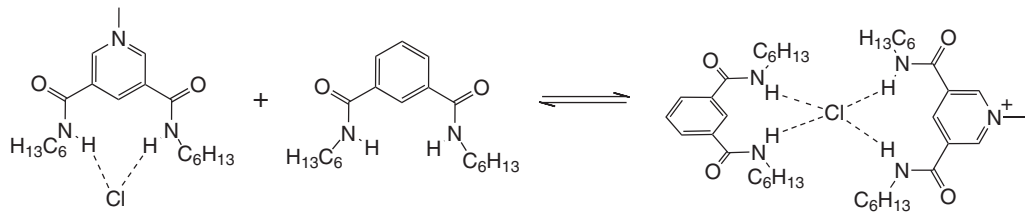

**10.109** **10.110**

**Scheme 10.23** Strong ion-pairing in the pyridinium salt in non-polar solvents allows the coordination of a neutral hydrogen bond donor and hence the creation of the precursor to a 'crossover' in a catenane using the chloride ion as an auxiliary linkage.[80]

of *ca.* 100 $M^{-1}$ (Scheme 10.23). This association creates a mutually orthogonal crossover point with the $Cl^-$ ion playing a role analogous to that of the Cu(I) centre in $[Cu(\mathbf{10.102})_2]^+$. Transferring this chemistry to cyclic species, Beer's group prepared a crown-ether derived macrocycle capable of interacting with the acidic pyridinium $-CH_3$ hydrogen bond donor and a pyridinium derivative capable of undergoing cyclication using ring closing metathesis once complexed. The result is [2]catenane **10.111**, formed in 45 % yield along with 5 % of a [3]catenane byproduct. The concept has also been used to prepare [2]rotaxanes similar to **10.108**. What is particularly interesting about these systems is that the templation is particularly effective even though the binding constants are not all that large. It is simply necessary to have a significant majority of the linked species in solution when the cyclication occurs.

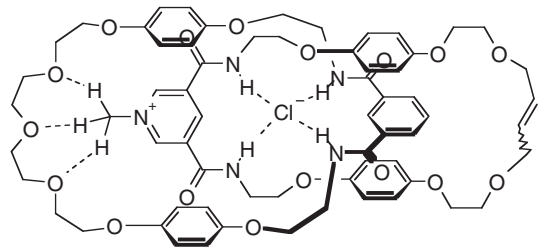

**10.111**

## 10.7.6 Molecular Necklaces

Kim, K., 'Mechanically interlocked molecules incorporating cucurbituril and their supramolecular assemblies', *Chem. Soc. Rev.* 2002, **31**, 96–107.

Before we leave catenanes we should mention one final class of compound, namely molecular necklaces, in which a number of marcocycles are looped onto a single central ring like beads onto a string. The concept is illustrated in Figure 10.70a and an example involving a metallomacrocycle threaded through three cucurbit[6]uril 'beads' (compound **6.38**, Section 6.2.4) is shown in Figure 10.70b. Because there is a total of four different rings this compound is described as a [4]molecular necklace or [4]MN. The large ring that forms the 'thread' is commonly linked using self-assembly of a coordination compound, in this case square planar platinum(II) ethylene diamine complex (*cf.* molecular squares and boxes, Section 10.5.3) and takes advantage of the affinity of cucurbituril for protonated diamine guests as in

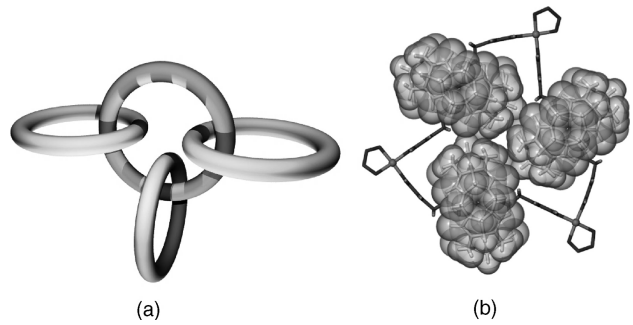


**Figure 10.70** (a) schematic representation of a [4]MN and (b) linking of three cucurbit[6]uril molecules around a platinum(II) based metallomacrocycle.[81]

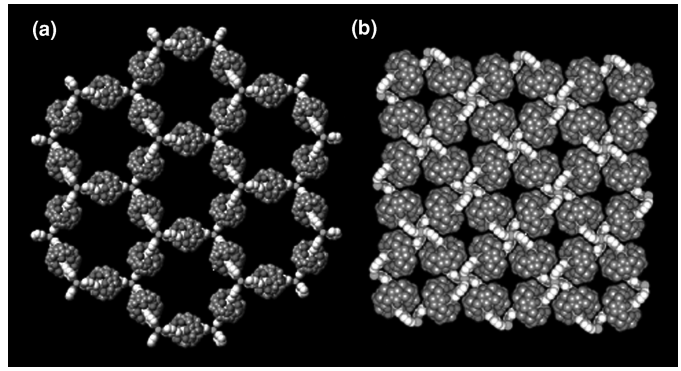


**Figure 10.71** Molecular necklace type coordination polymer rotaxanes (a) hexagonal 2D polyrotaxane net and (b) square-grid shaped 2D polyrotaxane net (reproduced by permission of The Royal Society of Chemistry). See plate section for colour version of this image.

the ligand **10.112** which links the Pt(II) centres together. Using the 3-pyridyl isomer of **10.112 t**he system can also be expanded to give a square 'string' able to bind four cucurbiturils (a [5]MN). A number of polymeric necklace-type systems are also known in which a coordination polymer network is ringed by cucurbiturils as in Figure 10.71.

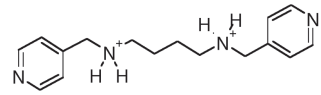

**10.112**

## 10.8 Helicates and Helical Assemblies

Piguet, C., Borkovec, M., Hamacek, J., Zeckert, K., 'Strict self-assembly of polymetallic helicates: the concepts behind the semantics', *Coord. Chem. Rev.* 2005, **249**, 705–726.

### 10.8.1 Introduction

The self-assembling double-helical structure of DNA has provided the inspiration for a further area of supramolecular self-assembly, namely the use of metal ions to template the assembly of organic threads into

multiple-helical structures. We have already come across lanthanide helicates based on **10.9** and studied the equilibria behind their self-assembly in Section 10.4.3. As well as being fascinating in their own right, helical coordination complexes have been used as the starting point for the effective preparation of a range of molecular knots such as trefoil knots. The fundamental defining property of a helical compound is the possession of chirality associated with the sense of a screw about a defined axis. The pitch of this screw is then the distance between one turn of the helix and the next (Figure 10.72). Helicate complexes consist almost invariably of molecular 'threads', which are extended, multidentate bridging ligands with more than one binding domain (*i.e.* more than one set of donor atoms capable of chelating different metal centres). An example of a binding domain might be a 2,2′-bipyridine (**10.113**) or 1,10′-phenanthroline (**10.114**) unit, thus a prototypical thread is 2,2′:6′,2″:6″,2‴-quaterpyridine (**10.115a**), which consists of two bipyridyl binding domains. Just as with cryptands and cryptates and catenands and catenates, helical metal compounds and their ligands are assigned analogous nomenclature. Thus molecular threads, such as **10.115a**, which can give rise to helical complexes are termed *helicands*, and the resulting helical metal complexes are *helicates*. In principle, there are three ways in which ligands such as **10.115a** can bind to a four-coordinate metal centre. They may form a mononuclear square planar 1:1 complex, a binuclear, nonhelical 2:2 complex, or a double-helical 2:2 complex, usually with tetrahedral coordination geometry about the metal. In the presence of a six-coordinate metal, triple-helical complexes may also be formed, if three helicands can fit about the metal centres (Figure 10.73). Alternatively, double helices may again result with the remaining metal coordination sites being taken up by additional ligands.

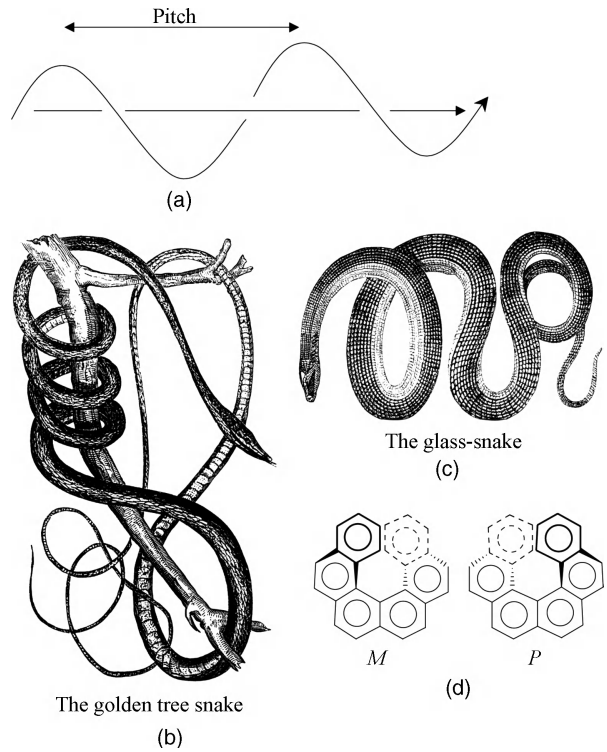


**Figure 10.72** (a) Helical screw about a defined axis. (b) *M*-helicity and (c) *P*-helicity, courtesy of the coils of the Mexican golden tree snake and North American glass snake, respectively. (Both are entirely harmless!) (Serpents from Johnson's Natural History, illustrated by S. G. Goodrich, Glidersleeve Press: NewYork, 1888.) (d) More conventional molecular helices.

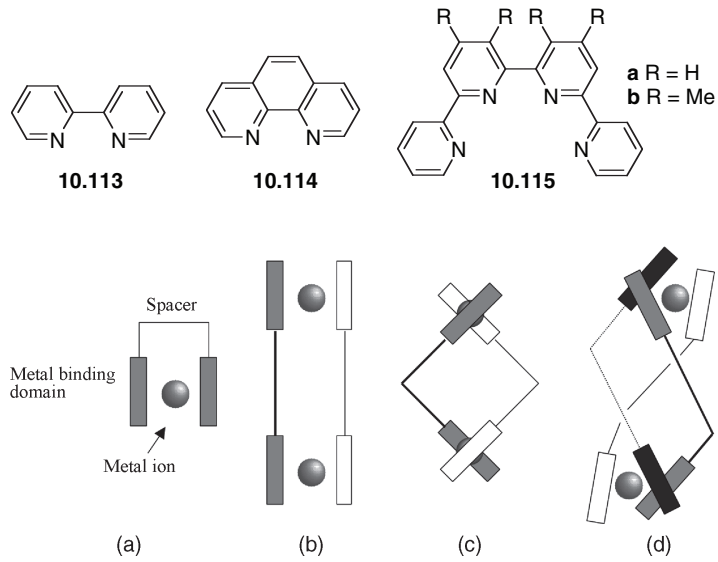


**Figure 10.73** Potential complexes formed by a two-domain helicand. (a) Mononuclear; (b) binuclear, nonhelical; (c) double-helical; and (d) triple-helical.

The relationship between the chiral single helix and the double-helical metal complexes is illustrated well by the 'Coup du Roi', in which the problem is to cut an apple into two homochiral components of the same helicity (Figure 10.74). The two chiral single helices of the same handedness (left, left or right, right) fit together to give a double helix. Single helices of opposite chirality cannot combine to form a double helix. Unlike apples, however, a key feature of double helicates is the chirality of the helical screw, which results in their occurrence as left-handed (*M*) and right-handed (*P*) forms (Figure 10.75). (The labels *M* and *P* follow the Cahn–Ingold–Prelog notation and represent simply 'minus' and 'plus'.[82]) Thus both single and double helices exist as enantiomeric pairs but, unlike the conventional combination of two chrial fragments, the double helix does not exist as two diastereoisomers because the heterochiral (left, right) combination of two single helices does not form a double helix.

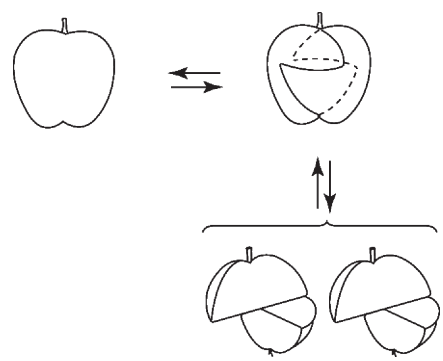

**Figure 10.74** The 'Coup du Roi': division of an apple into two homochiral fragments of the same helicity. (Reproduced from J.-M. Lehn, *Supramolecular Chemistry*, VCH: Weinheim, 1995.)

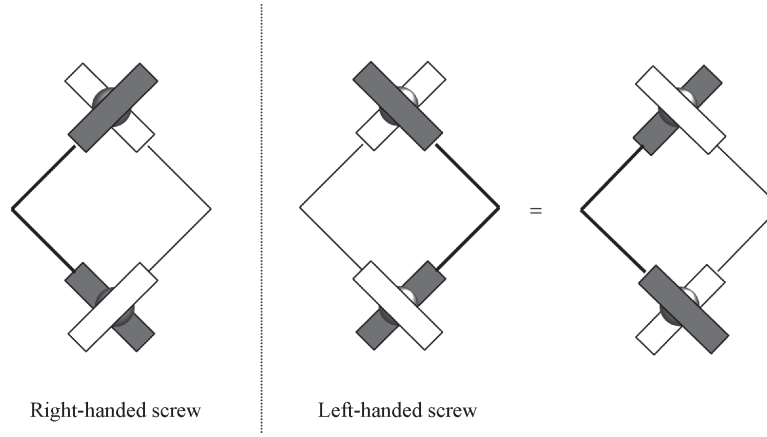


**Figure 10.75** Chirality in double helicates.

The chirality of metal helicates can be demonstrated experimentally by X-ray crystal structure determinations and in solution by NMR spectroscopy. Addition of chiral shift reagents such as $[Eu(tfc)_3]$ (tfc = 3-(trifluoromethylhydroxymethylene)-(+)-camphorato) to selected helicates results in the splitting of some of the ligand signals as a consequence of the formation of diastereomeric complexes with the shift reagent. Such splitting is not observed for the free ligands, which are achiral.

## 10.8.2 Synthetic Considerations

The vast majority of helicates are prepared by strict self-assembly and therefore represent thermodynamic minimum structures, as described by the extended site binding model, Section 10.4.3. This implies that all of the helix-forming information must be preprogrammed into the system, just as it is for DNA. In practice, this may be achieved by either metal-imposed or ligand-imposed constraints. By metal-imposed constraints, we mean fundamental properties such as the metal's preferred coordination number and coordination geometry, as well as other considerations such as optimum metal-to-ligand bond distances. Thus square planar metals such as Pd(II) and Pt(II) tend to give mononuclear non-helicate species in which all of the donor atoms of helicands such as **10.115** sit in the same plane, precluding helicity. On the contrary, tetahedral metals such as Cu(I) give double helicates because the spacer component between the ligands' binding domains is rarely flexible enough to allow the two domains to be situated essentially orthogonal to each another.

Ligand-imposed constraints consist of some degree of (usually steric) preorganisation of the ligand towards helicity. Thus the macrocyclic helicand **10.116** possesses inherent helicity because of the fixed relative orientations of the binapthyl substituents and forms a mononuclear double helicate cation $[Cu(\mathbf{10.116})]^+$. Similarly, ligand **10.117** is predisposed intrinsically towards helicity because of its rigid backbone consisting of fused six-membered rings. This factor brings the two terminal rings into close proximity, requiring helical distortion out of the ligand plane in order to avoid highly unfavourable steric interactions. Indeed, binding to sodium ions gives rise to various helical complexes.[83] In particular, the monosodium complex comprises a single-stranded helix that racemises slowly at room temperature. The substituted quaterpyridine ligand **10.115b** is somewhat predisposed towards helicity because of unfavourable steric interactions between the backbone methyl substituents. This encourages the two central pyridyl rings to orientate in a non-coplanar fashion, disfavouring square planar

coordination, although the ligand is capable of adopting a pseudo-planar geometry in the case of its Cu(II) complex. Chiral single helices may even be generated from unsubstituted polypyridyl ligands such as 2,2′:6′,2″:6″,2‴:6‴,2⁗-quinquepyridine **10.118** as a result of unfavourable steric interactions between the two termini. This is demonstrated clearly in the X-ray crystal structure of the Ag(I) complex [Ag(**10.118**)]$^+$ (Figure 10.76).

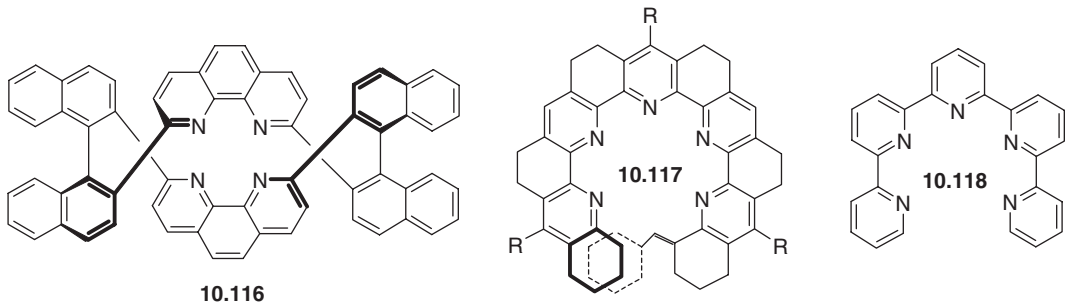


## 10.8.3 [4 + 4] Helicates

Interaction of the helicand **10.115b** (which is preorganised helically by virtue of steric repulsions between the methyl groups) with Cu(I) (generally in the form of relatively labile precursors such as $[Cu(MeCN)_4]^+$) rapidly produces the binuclear helicate $[Cu_2(\mathbf{10.115b})_2]^{2+}$, the X-ray molecular structure of which is shown in Figure 10.76b.[84] The binuclear $[Cu_2(\mathbf{115b})_2]^{2+}$ is an example of a [4 + 4] helicate in which [n + m] represents the coordination numbers of the two metal centres (four in each case). In this example, both the tetrahedral metal centre and the sterically preorganised ligand are predisposed towards helicate formation. The complex may thus be thought of as a complementary system for helicate formation. Unlike copper(I), copper(II) generally adopts a Jahn–Teller distorted octahedral or square pyramidal geometry less suited to helicate synthesis. Interesting results are therefore obtained upon stepwise oxidation of the Cu(I) centres in $[Cu_2(\mathbf{10.115b})_2]^{2+}$ to Cu(II). One-electron

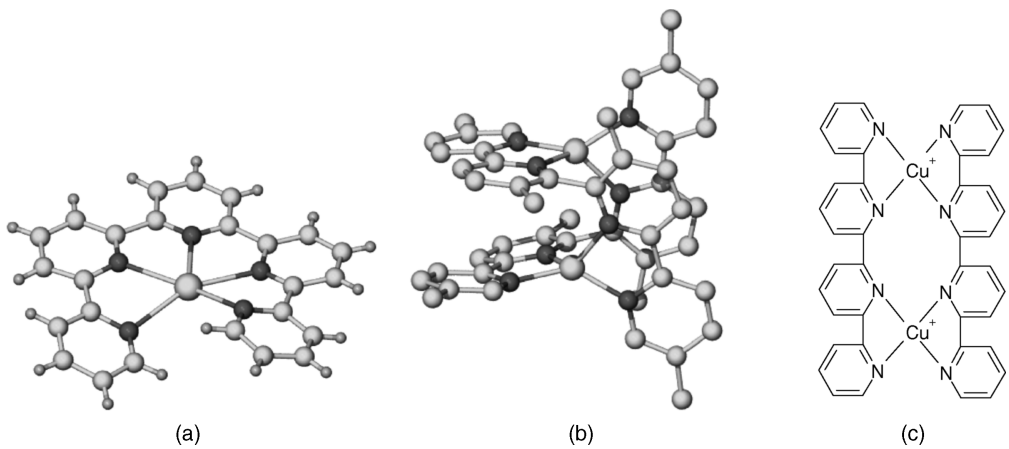


**Figure 10.76** (a) X-ray structure of the single helicate [Ag(**10.118**)]$^+$; (b) X-ray structure of the double helicate $[Cu_2(\mathbf{10.115b})_2]^{2+}$; (c) schematic representation of $[Cu_2(\mathbf{10.115b})_2]^{2+}$ emphasising connectivity.[84]

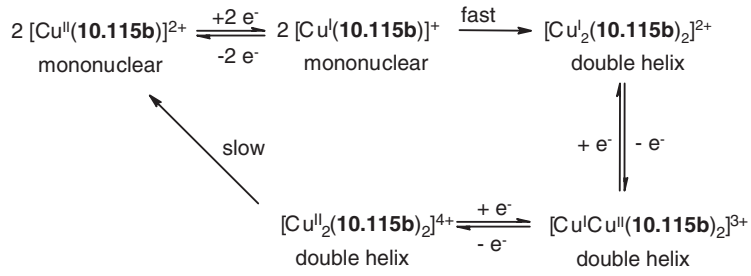


**Scheme 10.24** Helix formation as a function of copper oxidation state.

oxidation of the compound gives a mixed-valence Cu(I)–Cu(II) helicate. Upon further oxidation, the helicate decomposes to give a mononuclear Cu(II) species (Scheme 10.24).

Use of the less hindered (and less preorganised) helicand **10.115a** also gives a double helical Cu(I) complex, the tetrahedral coordination geometry of the metal ion being sufficient to template the helicate formation. Interestingly, however, the Cu ⋯ Cu separation (which corresponds to the pitch of the helices) in the non-methylated complex is 3.17 Å as opposed to 3.90 Å in $[Cu_2(\mathbf{10.115b})_2]^{2+}$. The analogous Ag(I) complex $[Ag_2(\mathbf{10.115a})_2]^{2+}$ gives a separation of 3.10 Å. These observations suggest that the role of the methyl groups is more to control the pitch of the helix than ligand preorganisation. Clearly, however, the presence of the methyl groups favours double-helix formation, since the mixed-valence intermediate $[Cu^ICu^{II}(\mathbf{10.115a})_2]^{3+}$ is not observable. The fact that the pitch of the silver complex of **10.115a** is shorter than the analogous Cu(I) species may be rationalised by likening the helix to a spring. Extending the metal–ligand bond distance to accommodate the larger metal ion results in tension perpendicular to the helical axis and hence a compensating compression in pitch along this axis.

## 10.8.4 [6 + 6] Helicates

The vast majority of double-helicate complexes involve four-coordinate metal centres, partly as a result of the fact that many helicand ligands involve bidentate binding domains. In such cases, six-coordinate metal ions tend to give triple helicates, as exemplified by ligand **10.119**, which gives a double helicate in the presence of the four-coordinate Cu(I), but a triple helicate with the six-coordinate Co(II). This behaviour may be regarded as a direct result of the different preprogramming of the two metal centres (Figure 10.77).

Formation of [6 + 6] double helicates is possible, however, if terdentate metal binding domains are used. A six-coordinate metal ion may thus bind to one domain from each helicand ligand. The simplest example of such a ligand is the attractively named 2,2′:6′,2″:6″,2‴:6‴,2⁗:6⁗,2⁗′-sexipyridine (**10.120**). In the presence of a wide variety of metal ions such as $Cd^{2+}$, $Fe^{2+}$, $Co^{2+}$, $Ni^{2+}$ and $Cu^{2+}$ a double helical 2:2 complex is formed. The X-ray molecular structure of the cadmium compound is shown in Figure 10.78.[85]

Ligand **10.120** is particularly versatile since it may be viewed as possessing two tridentate or three bidentate binding domains resulting in the formation of [6 + 6] or [4 + 4 + 4] double helicates and, as may be expected, the copper(II) [6 + 6] double helicate $[Cu_2(\mathbf{10.120})_2]^{4+}$ is capable of undergoing electrochemical reduction to give a [4 + 4 + 4] trimetallic double helicate based on tetrahedral copper(I), *via* a complicated series of intermediates. However, use of six-coordinate metal centres in conjunction with ligands that are more structured and possess two quite distinct bidentate binding domains gives rise to [6 + 6] triple helices. An excellent example of this approach has been reported by the group of Mike Hannon from the University of Birmingham, UK,[86] who prepared the bis(bidentate) imine ligand (**10.121**) *via* what they term an ‘inexpensive’ approach by straightforward

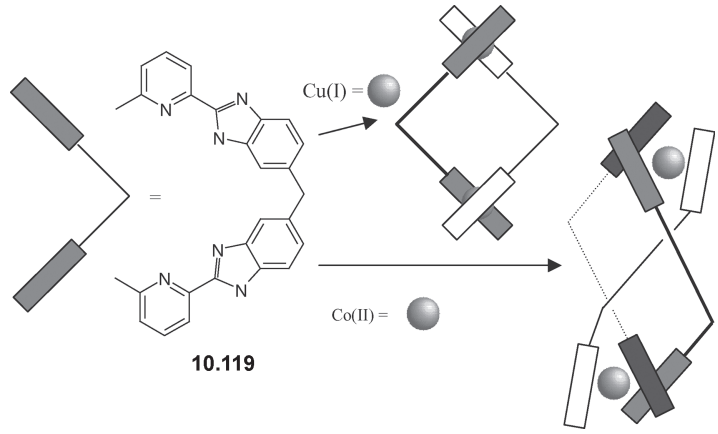


**Figure 10.77** Formation of double or triple helicates as a function of metal preprogramming.

mixing of commercially available starting materials as in Scheme 10.25. Reaction of **10.121** with Ni(II) in a 3:2 ratio gives the [6 + 6] triple helicate $[Ni_2(\mathbf{10.121})_3]^{4+}$ in more than 80 % yield.

## 10.8.5 Self-Recognition and Positive Cooperativity

We have already seen how a racemic mixture of chiral single helices forms a racemic mixture of two double-helicate enantiomers (Figure 10.74). Unlike the two half-apples in the 'Coup du Roi', however,

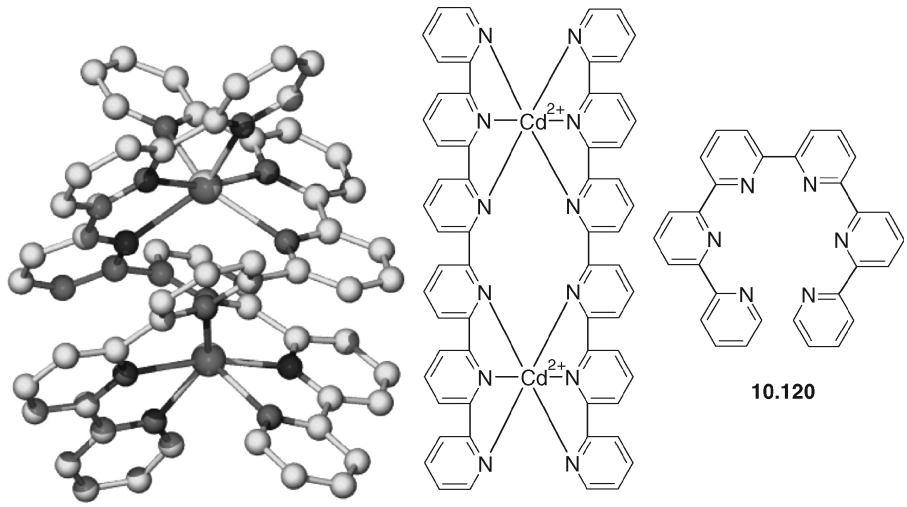


**Figure 10.78** X-ray crystal structure and schematic of the $Cd^{2+}$ [6 + 6] double helicate derived from **10.120**.[85]

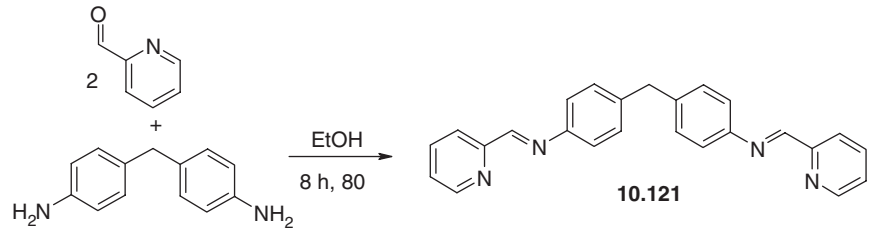


**Scheme 10.25** Formation of rigid helicands by an 'inexpensive' approach.[86]

helicand ligands are not necessarily chiral in their free state, implying no need for helices of the same chirality to find and recognise each another to form a double helicate. Indeed, helicands often develop their chirality only as part of the helicate structure. However, intrinsically chiral helicands may be prepared and resolved by the incorporation of asymmetric carbon centres as in **10.122**. In such instances, double-helix formation requires self-recognition by the two helicands. On the contrary, resolution of **10.122** into the enantiomer shown results in the formation of an enantiomerically pure right-handed double helicate.

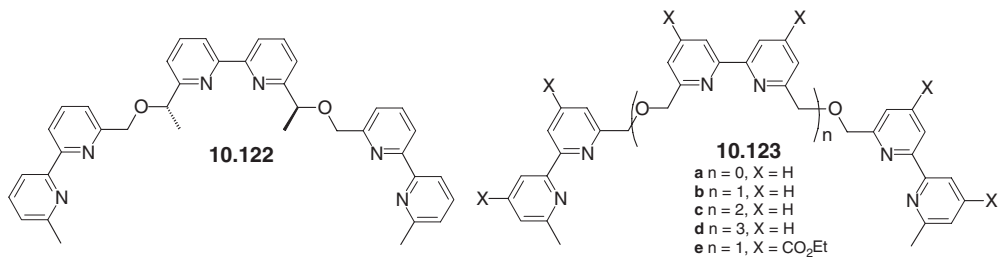


The question of self-recognition is also of relevance to the formation of multi-metallic helices containing two to five metal centres from the extended threads **10.123**. Interaction of Cu(I) with each ligand individually generates the expected [4 + 4], [4 + 4 + 4], [4 + 4 + 4 + 4] and [4 + 4 + 4 + 4 + 4] double helicates. Moreover, interaction of the metal ion with a mixture of all of the ligands again generates the homoleptic (same ligands within a given complex) helicates with virtually no trace of the generation of mixed species. As for nucleobase pairing, the zipping-up of helicates (*cf.* Figure 10.8) can demonstrate *positive cooperativity* in that once initiated, subsequent steps in the assembly are facilitated in a nonlinear process. The analysis of positive cooperativity in complex systems such as this which have both intermolecular and intramolecular steps in their self-assembly is discussed in Section 10.4.3. In this case the presence of clear isosbestic points in the spectrophotometric titration data indicate clearly the presence of only two species, and hence the clean generation of the helicates.

Some remarkable examples of positive cooperativity in helicate formation have also been reported by Ken Raymond from the University of California, Berkley, USA. Raymond's systems use the deprotonated 1,2-dihydroxy benzene dianion moiety as a basic ligating motif. Based on the identity and length of spacer units between two such binding domains, a large array of triple helices and coordination clusters (*cf.* Section 10.5.3) self-assemble selectively. In one example, a mixture of three such ligands in the presence of an appropriate ratio of $Ga^{3+}$ results in the selective formation of three individual, homoleptic triple helices (Scheme 10.26).[23]

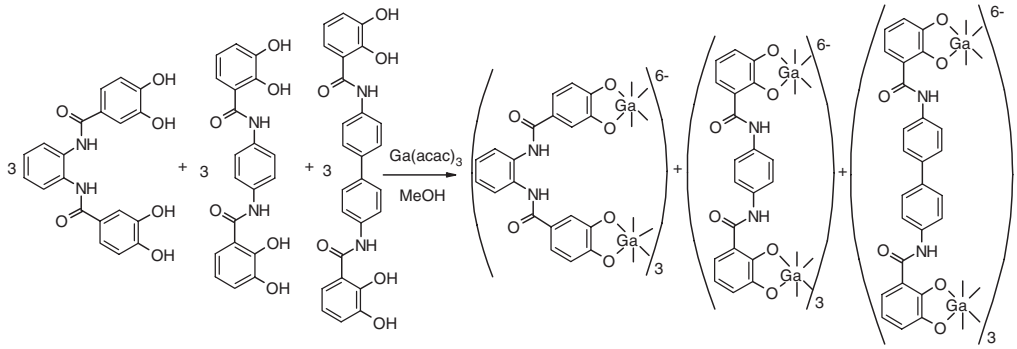


**Scheme 10.26** Positive cooperativity in the self-assembly of Ga(III) triple helicates.[23]

## 10.8.6 Cyclic Helicates

Work by Lehn[87] has shown that triple-helicate complexes are not the only possible result of the reaction of an octahedral metal centre with a *tris*(bidentate) ligand (three binding domains). In a remarkable reaction, Fe(II) combines with the *tris*(bipyridyl) ligand **10.124** to give a pentanuclear helicate Figure 10.79a. It is likely that the formation of this large cyclic complex is templated by the presence of chloride anions, one of which is included neatly within the centre of the nanoscale ring. In the presence of sulfate the related hexanuclear derivative is obtained. Lehn and co-workers have gone on to develop this chemistry by combining different types of binding domain within the same helicand.[88] Thus ligand **10.125** possesses a *bis*(bidentate) central binding domain similar to those observed in **10.41**, and four 2,2′-bipyridyl moieties, linked together as in ligands of type **10.123**. Each ligand is capable of binding in a bidentate fashion to a total of six metal centres and thus reaction with tetrahedral Cu(I) gives a high intertwined dodecanuclear complex of stoichiometry four ligands to twelve copper(I) centres, which exhibits a remarkable nanocyclic architecture based upon four double helices Figure 10.79b. The complex is obtained in essentially quantitative yield and has an external diameter of 28 Å. The internal cavity contains four $PF_6^-$ anions. Lehn and co-workers described the assembly of this compound as a 'double-subroutine self-assembly process' and the product combines four chiral double-helical sections into an object that is overall achiral. The bis(bidentate) pyrazole borate type ligand **10.126** also forms an anion-templated circular helicate structure comprising eight Co(II) ions, twelve ligands and a $ClO_4^-$ anion at the centre.[89]

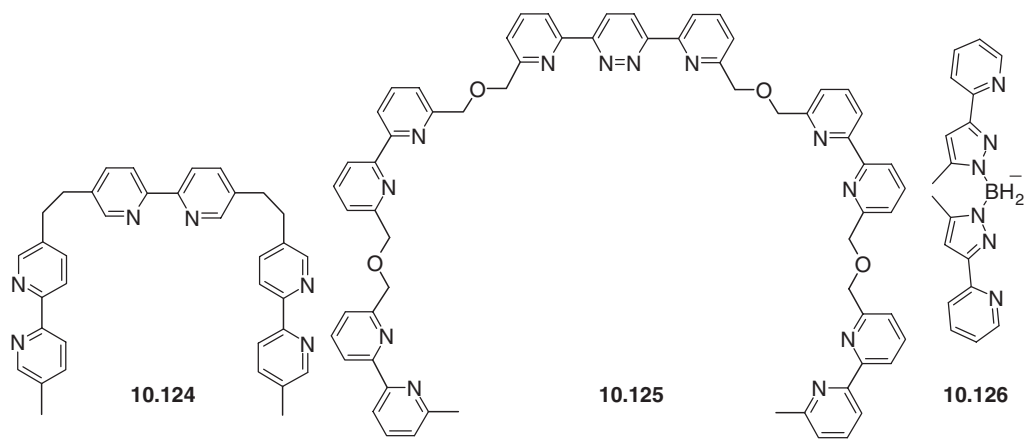


**10.124** **10.125** **10.126**

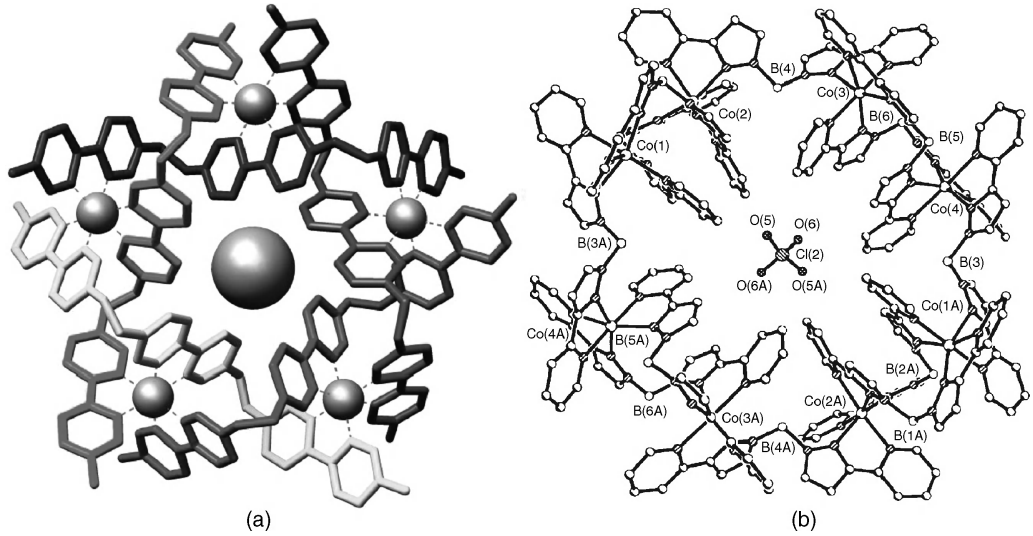


**Figure 10.79** X-ray molecular structures of cyclic helicates (a) pentanuclear species formed from **10.124** and templated by $Cl^{-}$[87]; (b) hexanuclear species formed from **10.126** and templated by $ClO_4^-$ (reproduced by permission of The Royal Society of Chemistry).

## 10.8.7 Anion-Based Helices

In addition to their role in templating metal helicates, hydrogen bonding interactions to anions can be used to form helical complexes in their own right. Just as with metals, the formation of binuclear helical systems versus mononuclear non-helical complexes is dictated by the size and shape of the anion and the steric requirements of the ligand. Thus the neutral anion host **10.127** forms a near-planar, non-helical 2:1 complex with $PF_6^-$, however, with the smaller fluoride a double helical 2:2 complex results, Figure 10.80.[90] Similarly the counter anion exerts a significant directing influence on Ag(I) coordination polymer structures of a dendritic extended bipyridine ligand. Smaller anions result in helical structures while cyclic dimers and ultimately lamellar structures result from increasingly larger anions.[91]

## 10.8.8 Hydrogen-Bonded Helices

Coordination interactions are, perhaps, the most common method of preparing synthetic helices. However, as we saw in the preceding section hydrogen bonding to anions is also a significant factor

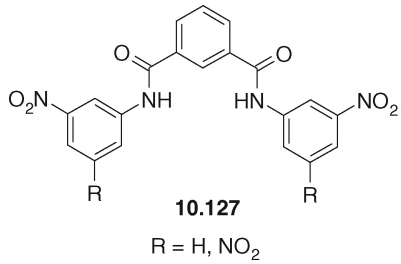


**10.127**

R = H, $NO_2$

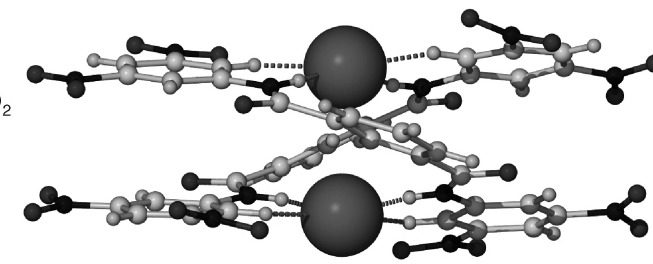

**Figure 10.80** Schematic of host **10.127** and X-ray crystal structure of its double helical 2:2 complex with fluoride ($F^-$ ions shown as large spheres).[90]

and the example of DNA suggests that hydrogen bonds may also be used to great effect in the formation of helical structures. The antibiotic gramicidin is another example of a naturally occurring hydrogen bonded helical structure.[92] Gramicidin, a component of one of the first commercial antibiotics, is a mixture of linear pentadecapeptides (*i.e.* 15 amino acid residues) called gramicidins A, B and C, of which gramicidin A is the major conponent (80 %). The mixture, termed gramicidin D, is obtained from the soil bacterial species *Bacillus brevis*. The amino acid sequence in the gramicidins is formyl-L-X-Gly-L-Ala-D-Leu-L-Ala-D-Val-L-Val-D-Val-L-Trp-D-Leu-L-Y-D-Leu-L-Trp-D-Leu-L-Trp-ethanolamine where X and Y depend upon the particular kind of gramicidin. The X group is either valine or isoleucine while the identity of Y determines which kind of gramicidin the compound is (in gramicidin A Y = tryptophanyl, in B, Y = phenylalaninyl and in C, Y = tyrosinyl). The amino acid stereochemistry (D or L) alternates along the chain and this allows the molecule to coil up into a β-helix inside a cell lipid bilayer. The length of the helix is about half of the 5 nm bilayer width but the molecule dimerises in a head-to-head fashion in lipid bilayers allowing it to span the membrane, Figure 10.81. The interior of the helix acts as a rudimentary ion channel (see Section 2.2) and this property is vital to its function as an antibiotic. The helical channel structure is known from solution and solid state NMR spectroscopic work. In the solid state X-ray crystallography on samples crystallised from organic solvents reveals a structure comprising left-handed, anti-parallel, double-stranded β-helices. The double helix is long enough to span the hydrophobic thickness of a lipid bilayer, and exhibit a central channel large enough to transport univalent cations.[93]

Lehn's group have designed an extremely novel helix-forming system based on the pairwise association of mutually complementary hydrogen-bonded units.[94] The complementary hydrogen-bonded units chosen were derivatives of 2,6-diaminopyridine (P) and uracil (U), which interact readily to form a hydrogen-bonded PU dimer (**10.128**).

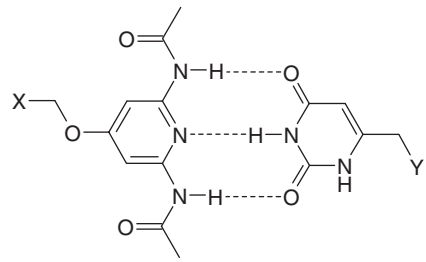


P **10.128** U

In cases where the substituents X and Y are long-chain alkyl esters or amides, liquid crystalline behaviour is observed (Section 13.3). While the individual components have no mesogenic properties, the aggregate forms a metastable columnar hexagonal type structure.

If, instead of isolating the PU dimer deep within an alkyl sheath in order to generate liquid crystalline behaviour, ditopic receptors of type PTP or UTU are synthesised (T = chiral spacer based on tartaric acid), then the self-assembly of a polymeric strand occurs. Addition of long alkyl groups to the backbone of the ditopic unit (UTU or PTP) results in various supramolecular polymers displaying liquid crystalline behaviour. Experimentally, this was realised by condensation of the complementary P and U groups with long-chain derivatives of either L-, D- or *meso*-(M) tartaric acid, which act as the spacer T (T = L, D or M), to give various isomers of the complementary ditopic receptors **10.129** (PTP) and **10.130** (UTU). These receptors self-assemble into polymeric strands $(PTP, UTU)_n$. In this instance, the chirality of the L- and D-isomers makes the individual polymeric strands chiral. Depending on the chirality at the 'T' group (L, D or M), various kinds of behaviour are observed. The resulting

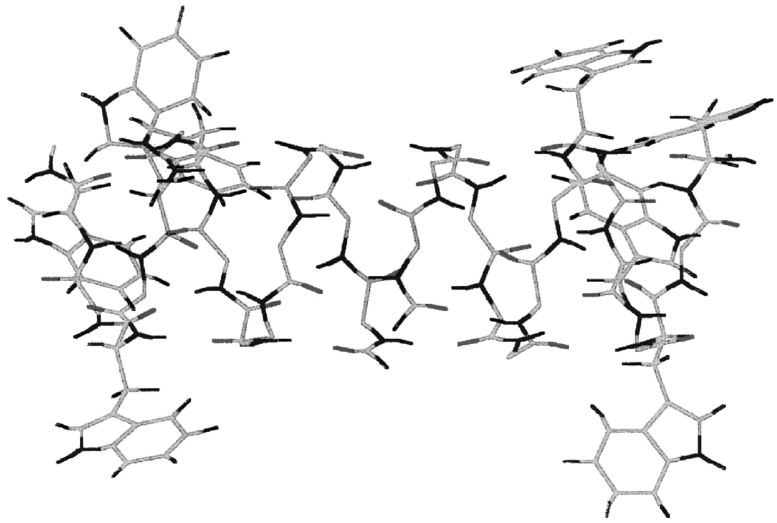

**Figure 10.81** β-helical structure of gramicidin A in a bilayer membrane as determined by NMR spectroscopy (reproduced with permission from [93]).

structures were analysed by X-ray fibre diffraction and electron microscopy. Most remarkably, the self-assembled resolved L-tartrate polymer (PLP, $ULU)_n$ (**10.131**) and its D-analogue self-organise *via* three intertwined strands into large triple helices, sheathed within the alkyl substituents on the tartrate-derived backbone (Figure 10.82). Conversely, the (PMP, $UMU)_n$ form gives three strands in a zigzag conformation. Both species display hexagonal columnar mesophase liquid crystalline behaviour. The L-, D-mixture exhibited spontaneous resolution into right- and left-handed helices, consistent with earlier observations on self-recognition (Section 10.8.5), resulting in spontaneous self-resolution.

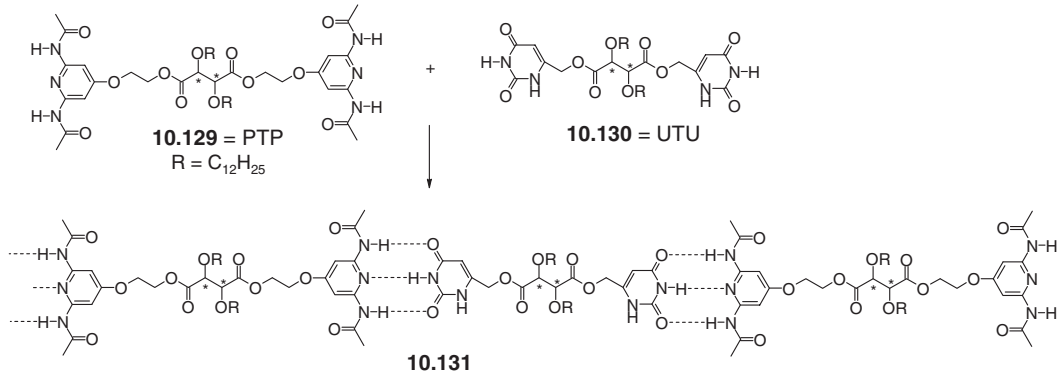


At high concentrations, the strands aggregate into large polymeric entities, initially *via* filament formation, followed by lateral, tree-like growth. Figure 10.82a–c shows electron microscope images of the various mixtures under these conditions. Note, especially, the opposite handedness of the L- and D-triple helices (right- and left-handed helices, respectively).

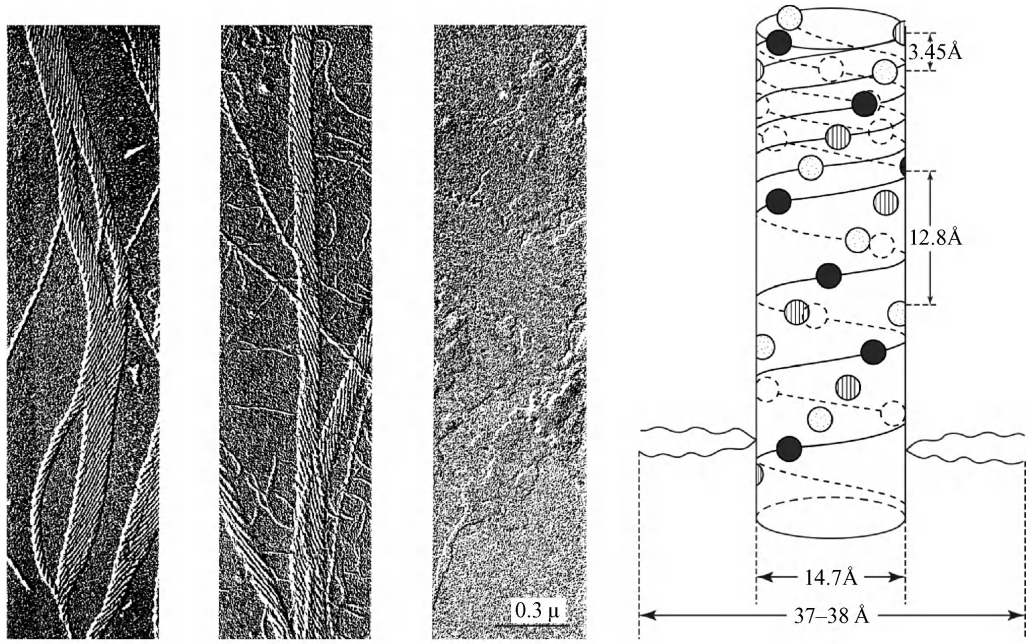


**Figure 10.82** (a) Electron microscope images of materials formed by PLP + ULU (right-handed helix), (b) PDP + UDU (left-handed) and (c) PMP + UMU (nonhelical). (d) Schematic representation of the model for the triple-helical organisation of three self-assembled homochiral polymer strands (PTP, $UTU)_n$ (T = L or D; not M). PU hydrogen-bonded pairs on the same strand are represented by circles of the same shading. Alkyl chains stick out of the side of the cylinder. (Reproduced with permission from J.-M. Lehn, *Supramolecular Chemistry*, VCH: Weinheim, 1995.)

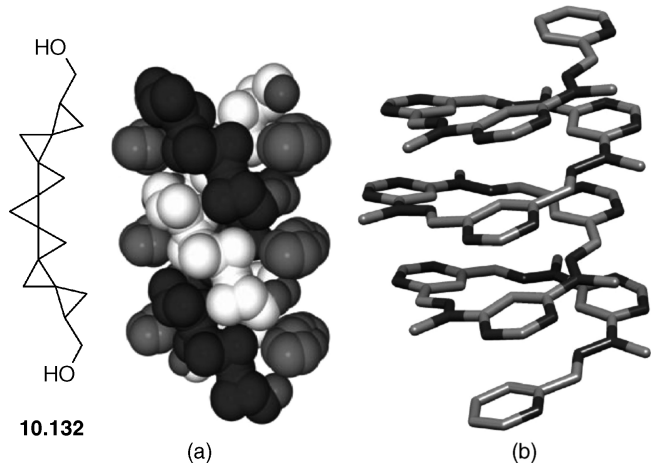


**Figure 10.83** Helical molecules (a) helical molecular and double helical crystal structure of the hydrogen bonded helix **10.132** (Copyright Wiley-VCH Verlag GmbH & Co. KGaA. Reproduced by permission) and (b) helical foldamer comprising $3^1/_3$ turns based on a hydrazone derivative.[96]

A remarkable example of an optically pure molecular single helix that forms a supramolecular double helix in the solid state has been reported. Cyclopropanation of an enantiomerically pure 1,1′-bis(dispiro-[2.0.2.1]heptylidene-methanol) gives the enantiomerically pure di-ol **10.132**. The intrinsic molecular chirality of the helix results in a substantial optical rotation $[\alpha]_D^{20}$ of $+691.2^{o}$. In the solid state two such helices come together by hydrogen bonding of the terminal alcohol units to give a supramolecular double helix, Figure 10.83a.[95] It is well established that particular heterocycles, notably series of directly connected pyridine and pyrimidine rings incorporated into a single molecule fold into extended helical structures (helical foldamers, *s.a.* Section 10.2.2). Lehn's group have reported a single helical foldamer shown in Figure 10.83b based on hydrazone, an isomorphic analogue of a pyridine group in such systems and much more readily incorporated from a synthetic standpoint. The example shown possesses $3^1/_3$ turns in the molecular helix and is held together by direct π-π stacking and hydrogen bonding.[96]

## 10.9 Molecular Knots

Lukin, O. and Vogtle, F., 'Knotting and threading of molecules: Chemistry and chirality of molecular knots and their assemblies', *Angew. Chem., Int. Ed.* 2005, **44**, 1456–1477.

### 10.9.1 The Topology of Knots

Chemical interest in knots dates back to a hypothesis of Lord Kelvin who suggested the atoms may be knotted forms of the aether – the undetectable substance postulated to form the medium through which light waves travel. This led the Scottish mathematician Tait to attempt a list of all possible knots and thus create a version of the periodic table of the elements. While Kelvin's theory turned out to be wrong, knot theory rapidly became assimilated into mathematics as part of the field of topology. It is ironic that 100 years after Kelvin's death (1907) cosmologists are again turning to knotted *superstrings* in attempts to explain the properties of fundamental sub-atomic particles.[97] Outside the chemical field, knots and interwoven figures have a long and distinguished history, often resulting in beautiful designs, such as the multiply interwoven lettering of the eighth century Celtic *Book of Kells*. The knot is the symbol of unbreaking links, as in the triply interlocked symbol of the powerful Italian Borromeo family, the Borromeo link, while the works of Dutch artist Cornelius Escher evoke superb (sometimes impossible) knotted geometric patterns, many of which are increasingly to be found in modern chemistry (Figure 10.84).

We have already encountered the field of chemical topology in our discussion of catenanes in Section 10.7.1. A [2]catenane is a *topological isomer* of two separated macrocycles and is characterised by having crossing points in its 2D graph set. We can distinguish topological isomers by imagining that the molecule of interest is placed on an infinitely flexible flat rubber sheet. The

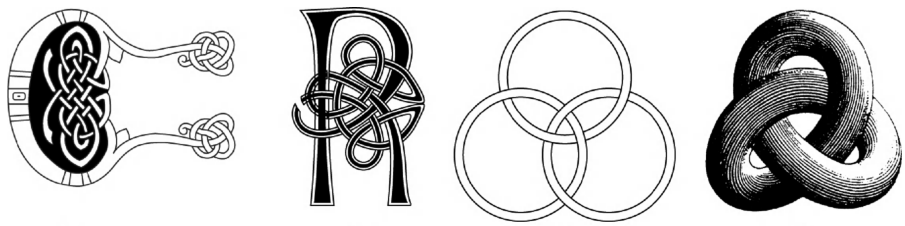


**Figure 10.84** (a) and (b) Interlocked lettering from the eighth century *Book of Kells*. (c) The Borromeo family symbol. (d) The trefoil knot as viewed by Dutch artist M. C. Escher. (Copyright Wiley-VCH Verlag GmbH & Co. KGaA. Reproduced by permission).

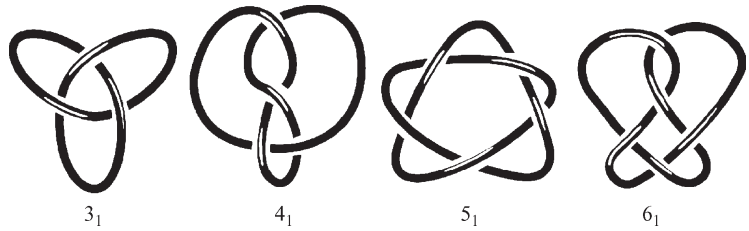


**Figure 10.85** The first four prime knots. The number denotes the number of crossings, while the subscript is the order of the knot. (Reprinted with permission from [98]).

sheet and object can be stretched or bent in any way but lines (bonds) cannot be broken and no line can pass through another. Thus a square, triangle and circle are topologically equivalent to one another and even a [2]rotaxane can in principle (albeit not in practice) be unthreaded by infinite expansion of the ring so that it fits over the stopper. A catenane is, however, fundamentally different and cannot be untangled in this way. A similar situation pertains for knots which represent a fascinating intellectual challenge for chemists and give access to new structural motifs with interesting properties.

The auxiliary linkage approach to the synthesis of catenanes such as **10.103** (Section 10.7.5) in combination with the expanding body of knowledge concerning the related helicates (Section 10.8) has enabled the high-yield synthesis of a range of multiply interpenetrated complexes termed *molecular knots*. Unlike catenanes, prime knots are based upon a single-stranded loop. Knots are therefore topological isomers of macrocycles (Figure 10.54). We have already seen the early attempt by Schill and co-workers to prepare a molecular trefoil knot from the auxiliary **10.97**, which, while possibly successful, was plagued by difficulties associated with low yields in the multiple cyclisation steps. In fact, the trefoil knot is the first of many prime knots, the first four of which are shown in Figure 10.85. In addition to the directed approach of Schill, a number of early statistical and semi-statistical approaches to knot formation were proposed and attempted, without significant yield of knotted products being obtained.

In the natural world, numerous knotted and entwined forms of DNA strands are known and have been imaged by electron microscopy (Figure 10.86).[99] Knotted proteins such as lactoferrin and ascorbinic acid

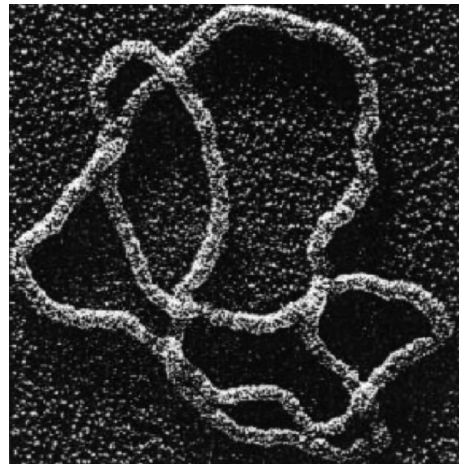

**Figure 10.86** Electron microscope image of a loose DNA knot (reproduced from [99] with permission from AAAS).

oxidase possess remarkable biological activity in comparison to analogous linear proteins, respectively in iron(III) transport and in enzymatic oxidation. Modern synthetic polymers often derive mechanical strength from their intertwined nature. On the other hand, molecular modelling studies by Wasserman at the DuPont company have led to the suggestion that the strain at knot cross-overs in polymer strands may result in the entrance to the knot being the mechanical weak points in some polymer materials.[100] Clearly, if large enough macrocycles can be prepared, then there is no reason why knots should not be chemically stable, in the same way that catenanes are.

## 10.9.2 Trefoil Knots

Following on from the preparation of [2]catenate **10.103** (Scheme 10.27a), Sauvage realised[101] that replacing the single Cu(I) core in $[Cu(\mathbf{10.102})_2]^+$ with a bimetallic double helicate would result in a precursor that, if it was stable enough to be cyclised, would immediately give a trefoil knot *via* a double auxiliary linkage approach (Scheme 10.27b).

Accordingly, the diphenol helicand (**10.133a**) was designed with a flexible —$(CH_2)_4$— linker between the two bonding domains. The ligand was prepared from 1,10-phenanthroline and $Li(CH_2)_4Li$ in several steps and then reacted with $[Cu(MeCN)_4]^+$ to give the helicate (**10.134a**). Following their catenane synthesis methodology, Sauvage then performed a double cyclisation reaction under high-dilution conditions to isolate the first synthetic trefoil knot (**10.135a**), after a lengthy chromatographic work-up, in 3 % overall yield. The knot was characterised by mass spectrometry and NMR spectroscopy. However, the closure of such a large ring (86-membered) is a statistically unlikely process, and a number of by-products were also present, all of them based on a chiral double helix. The definitive characterisation of the trefoil knot rested, therefore, on the removal of the metal centres with KCN to give the free ligands. Under these circumstances, only the knotted 86-membered ring possesses unconditional chirality, which was demonstrated. The other products, 86- and 43-membered macrocycles,

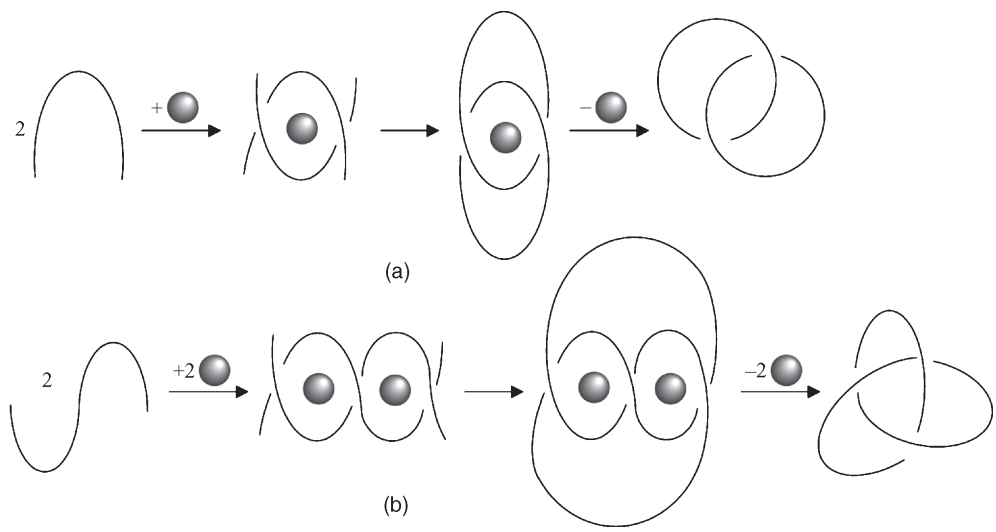


**Scheme 10.27** **(a)** Schematic diagram of the synthesis of a [2]catenane *via* the auxiliary linkage approach. **(b)** Extension of this approach to the formation of a trefoil knot *via* a bimetallic double helicate.[101]

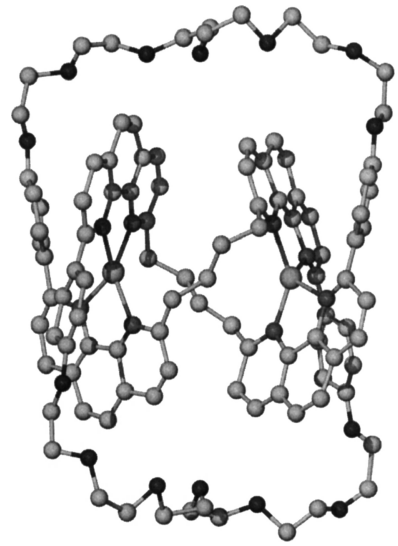

**Figure 10.87** X-ray molecular structure of the trefoil knot **10.135a**.[102]

are achiral in the absence of the helix-templating metals. The formation of the knot was confirmed later by an X-ray crystal structure determination (Figure 10.87).[102]

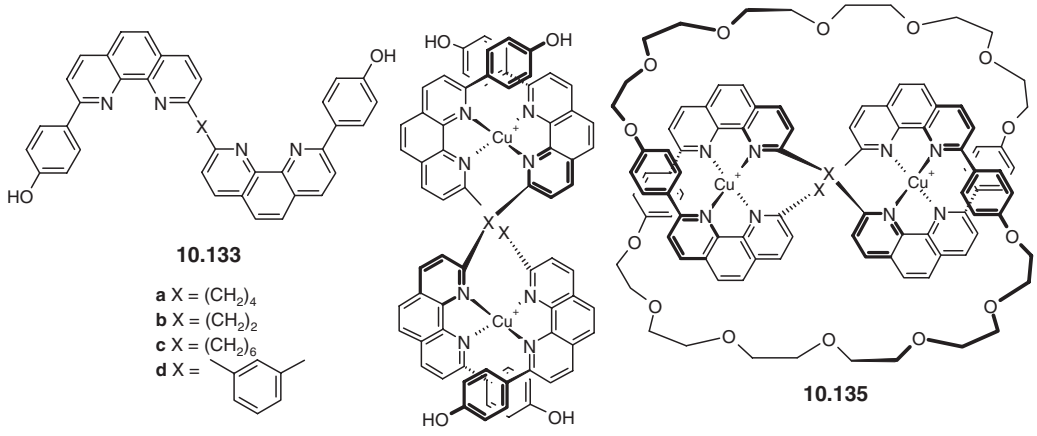


While ingenious, the low yield of **10.135a** left significant room for improvement. Particular problems identified were the competing formation of non-helical face-to-face 2 : 2 complexes during the helicate-formation step, and the spatial arrangement of the four reaction ends of **10.134**. Accordingly, Sauvage's group tried a number of other helicand ligands with a variety of spacers 'X' (**10.133b–d**) in the hope of improving overall yields. They also varied the length of the polyethyleneglycol chain used in the cyclisation step. Virtually all of the compounds tried yielded knots of type **10.135**. For **10.133b** and **10.133c**, yields were again low, the best being 8 %, obtained for X = $(CH_2)_6$ with a pentaethyleneglycol chain, to give an overall 84-membered knotted macrocycle. In contrast, yields of up to 24 % were obtained for the unknotted macrocyclic topological isomers. The more rigid ligand **10.133d** proved much more promising,

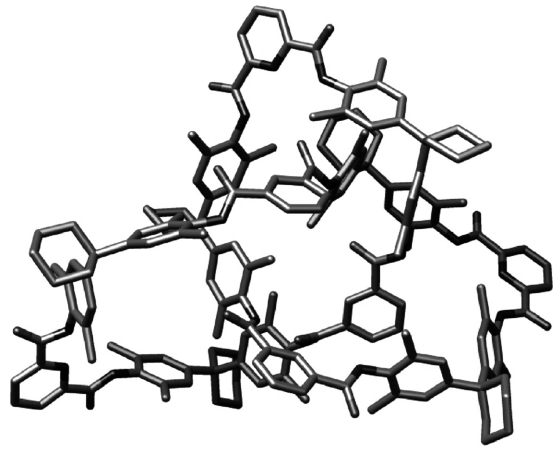

**Figure 10.88** X-ray crystal structure of a hydrogen-bonded trefoil knot produced in a one-pot synthesis.[104]

giving the trefoil knot **10.135d** in an overall 29 % yield after chromatography. This is a sufficient yield to allow the study of some of the knotted compound's properties and the full characterisation by NMR and FAB (fast atom bombardment—a relatively gentle ionisation technique) mass spectrometry. The reason for this greatly improved yield is not entirely clear, but it may well be related to the compound's compact geometry. The X-ray crystal structure of the precursor **10.134d** gives a Cu···Cu separation of 4.76 Å, compared to values of 6.30 and 7.00 Å for the knots with $(CH_2)_4$ and $(CH_2)_6$ spacers, respectively.

In principle a trefoil knot could also be templated using a single, octahedral metal centre and indeed this has been achieved by self-assembly of a linear tris(bidentate) strand about octahedral Zn(II). Thus reaction of the linear ligand **10.136** gives an 'open' trefoil knot based on a tris(bidentate) zinc centre. The knot has been characterised in solution and in the solid state and its formation is fully reversible, consistent with the principles of self-assembly. Thus, addition of chloride which coordinates to the $Zn^{2+}$ centre regenerates the free ligand **10.136**, while the trefoil knot re-forms upon removal of the chloride with $Ag^+$ (to give insoluble AgCl).[103]

A remarkable one-pot self-assembling synthesis of a 96-atom backbone trefoil knot was reported in 2000 by the group of Fritz Vögtle (Bonn, Germany). The knot comprises just twelve amide functionalities and is derived from essentially the same reaction discussed in chapter 6 as a synthesis of a *p*-quinone host (Scheme 6.13). The reaction is carried out under high dilution with a pre-formed diamide arising from the reaction of two diphenylmethane derived diamines with 2,6-pyridine dicarboxylic acid dichloride and gives the covalent knot in 20 % yield along with the 2+2 and 4+4 macrocycle products. The X-ray structure of this knot, which is templated *via* intramolecular hydrogen bonding without the use of a metal template, is shown in Figure 10.88.[104]

Finally, a trefoil knot has also been reported based on Stoddart's 'blue box' donor-acceptor stacking templating methodology (Section 10.7.3).[105]

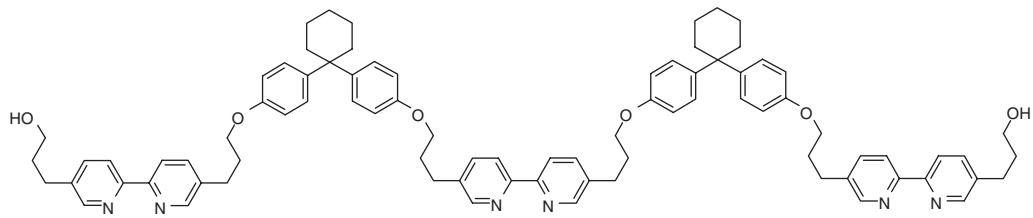


**10.136**

### 10.9.3 Other Knots

The potential exists of using the highly versatile helicate-based approach of Sauvage to continue to prepare more and more highly knotted and interlinked species. As a general rule, we can show that, in this approach, if the number of metal centres is even, then the number of crossings of the molecular loop will be odd. In this case, odd numbers of crossings are necessary in order to generate a knot. Thus two metal centres give the trefoil knot, four a pentafoil, six a heptafoil *etc.* On the other hand, odd numbers of metal centres will generate even numbers of crossings and give rise to doubly interlocked [2]catenanes (Figure 10.89).

Synthetically, Sauvage's group have been able to extend this work as far as three metal centres, giving rise to the (unconditionally chiral) doubly interlocked [2]catenate **10.137**.[106] The synthetic procedure is similar to those employed for the trefoil knots **10.135** and singly interlocked [2]catenane **10.103**, and involves a double high-dilution ring-closure of two 60-membered rings by $Cs_2CO_3$-catalysed reaction of the two diphenol precursor threads with $ICH_2(CH_2OCH_2)_6CH_2I$ in dimethyl formamide at 60ºC. Unsurprisingly, the reaction is not very clean. It is a tribute to the consummate skill of the researchers involved that, after extensive chromatographic work-up, a 2 % yield of the product was isolated and characterised by NMR spectroscopy and careful mass spectrometry. Similar careful work has resulted in the synthesis of some composite knots as diastereomeric mixtures, including a double trefoil.[107]

The scope of synthetic 'higher knots' is relatively limited at present because of the tremendous synthetic challenges involved. However, we have already seen that natural system forms knots readily and DNA is a particular good candidate as a knot template because of its double helical nature. The knot-forming tendencies of DNA have been exploited particularly by the group of Nadrian C. Seeman (New York, USA) to produce by design using both self-assembly and deliberate manipulation (*e.g.* by

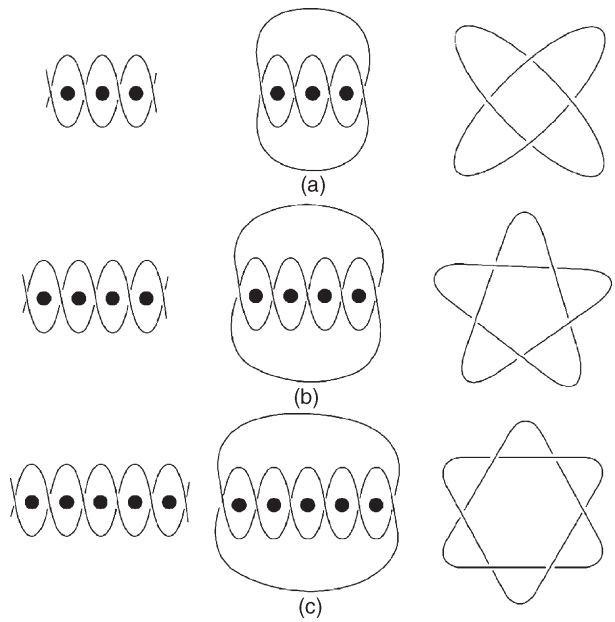


**Figure 10.89** Conceptual production of increasingly interlocked species through the use of multimetallic helicates. (a) Doubly interlocked [2]catenane from three metal centres. (b) Pentafoil knot from four metal ions. (c) Triply interlocked [2]catenane. (Reproduced with permission from [98]).

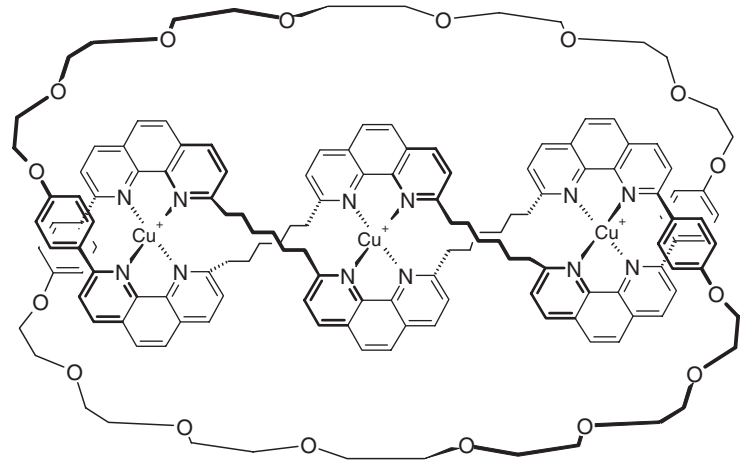

**10.137**

optical tweezers) DNA-based knotted and topologically complex structures. It is well established that DNA forms well-behaved right- (B-form) or left-handed (Z-form) double helical structures depending on the base sequence (*cf.* Section 2.9). Seeman's group designed and prepared a DNA single strand comprising a total of 104 nucleotide bases. The strand contains regions (A, A′, B and B′) with 11 or 12 complementary base pair sequences (*i.e.* A is complementary to A′, B is complementary to B′) that cause it to self-assemble into specifically either B- or Z-helices.[108] The sequences are linked by oligo-thymidine spacers. Self-assembly is induced and controlled by the concentration of $Mg^{2+}$ ions in conjunction with the inert $[Co(NH_3)_6]^{3+}$ resulting in the formation of a DNA macrocycle, a left- and a right-handed trefoil knot and a figure-of-eight knot (Figure 10.90). This work makes clever use of restriction enzyme cleavage strategies to confirm the topological properties of the products since conventional spectroscopic or diffraction methods are not useful in studying these very large assemblies. This basic approach has been used to give other very sophisticated DNA assemblies such as a cube, a truncated octahedron and even a Borromeo ring arrangement. We will look at other self-assembling strategies towards the enduringly popular Borromeo rings in the next section.[109]

Finally another interesting class of entanglement, *ravels*, distinct from knots has recently been recognised as at least a theoretical possibility. A ravel tangles a planar graph in the vicinity of a vertex whereas knots lie within cycles in the graph. The simplest kind of ravel is shown in Figure 10.91. It is postulated that ravels may be recognised in MOFs or DNA type structures in the future and they offer a tantalising new challenge to the synthetic chemist.[110]

## 10.9.4 Borromean Rings

Cantrill, S. J., Chichak, K. S., Peters, A. J. and Stoddart, J. F., 'Nanoscale Borromeo rings', *Acc. Chem. Res.* 2005, **38**, 1–9.

The three interlocked rings of the Borromeo symbol (Figure 10.84c) are an enduring and popular symbol of unity that features widely in heraldry and iconography. None of the three rings penetrates either of the other two in the way a catenane does, nevertheless they are topologically interlocked and cannot be separated without breaking one of the rings. However, if any one ring is removed the other two can be immediately separated intact. The Borromeo rings represent a particularly difficult

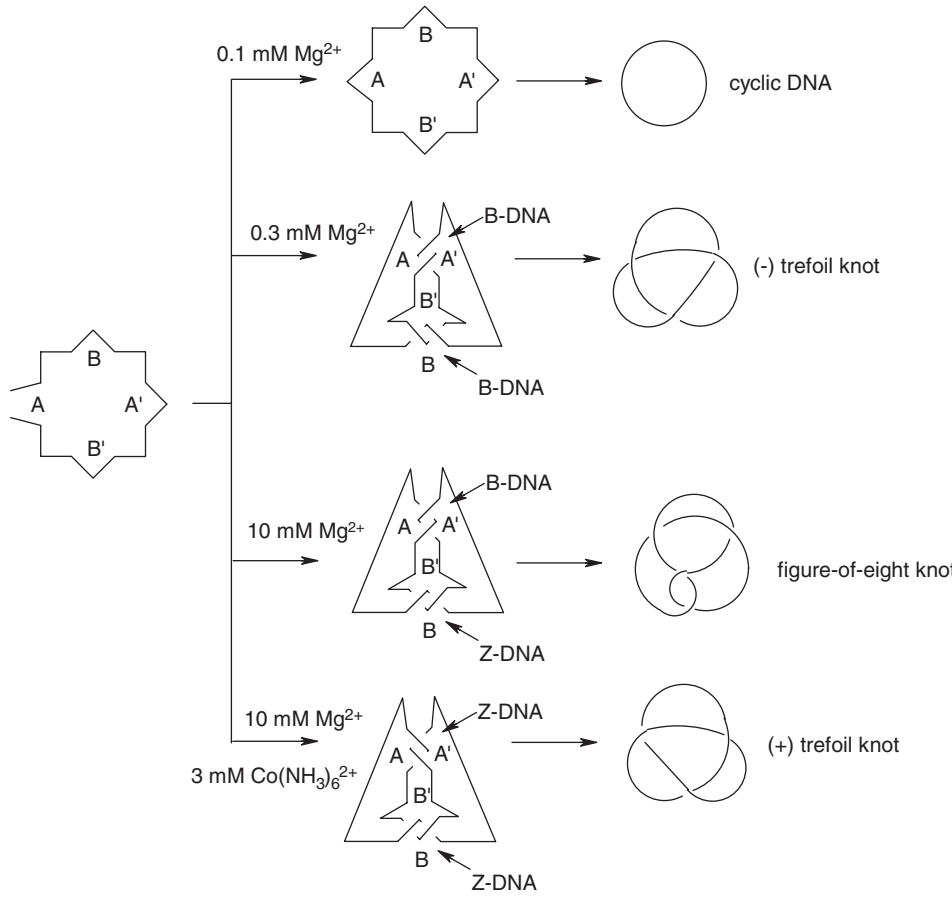


**Figure 10.90** Self-assembly of DNA knots.[108]

synthetic challenge since three separate macrocycles must be interlocked simultaneously. While DNA-based Borromeo rings were first synthesised in 1997,[109] it was not until 2004 that the self-assembly of a discrete artificial Borromeo ring compound (a zinc(II) based 'Borromeate') was realised by Stoddart's group at UCLA. The synthesis is based on the thermodynamic assembly of two kinds of error-checking,

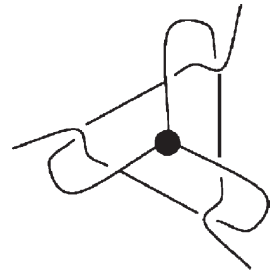

**Figure 10.91** The simplest kind of ravel based on a 3-connected vertex. While none of the three threads are knotted or catenated, pulling on all three of them simultaneously results in an entangled unit distinct from the analogous unravelled 3-connected node.[110]

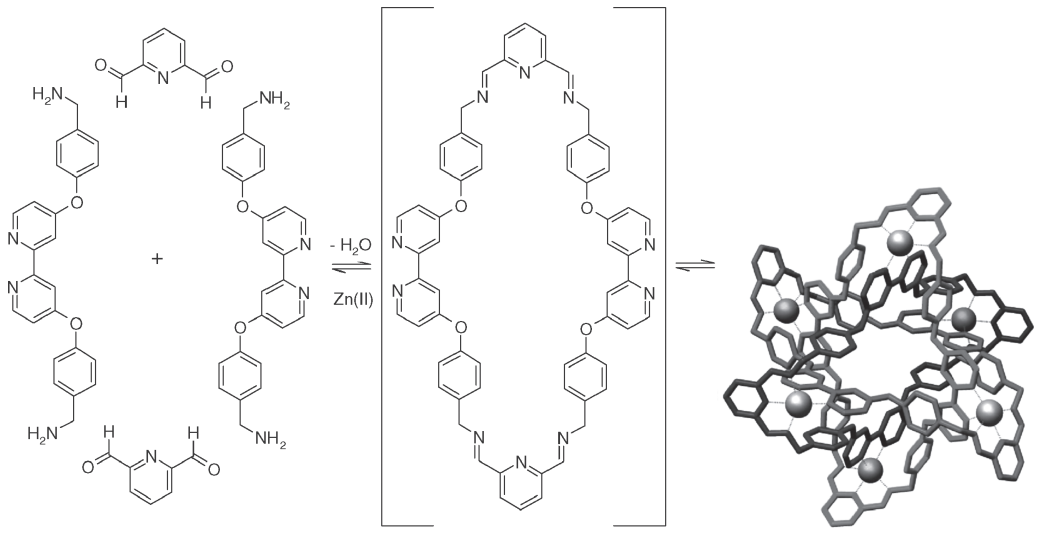


**Scheme 10.28** Self-assembly of a 2.5 nm wide Borromeo ring complex showing the product's X-ray molecular structure.[112]

reversible interaction – coordination of ligands to relatively labile $Zn^{2+}$ ions and reversible imine bond formation by Schiff base condensation, Scheme 10.28. The system was designed to give complete cross complementarity between the exo (bidentate) and endo (tridentate) sites in the final complex such that exo only matches with endo and *vice versa*. The use of $Zn^{2+}$ is important too since zinc(II) commonly forms five-coordinate complexes. The assembly proceeds in a remarkable 80 % yield in the final one-pot self-assembly step to give the hexanuclear Borromeate, which was characterised by X-ray crystallography, Scheme 10.28. There is some evidence for the templation of the assembly by a seventh Zn(II) ion situated at the centre of the assembly. Interestingly, while the Borromeo complex is the major product, carrying out the reaction with a 1:1 mixture of zinc(II) and copper(II) acetates gives a product of different topology – a tetrametallic *Solomon knot*, Figure 10.92. The Solomon knot can be isolated by careful crystallisation because it is less soluble then the Borromeo complex.[111]

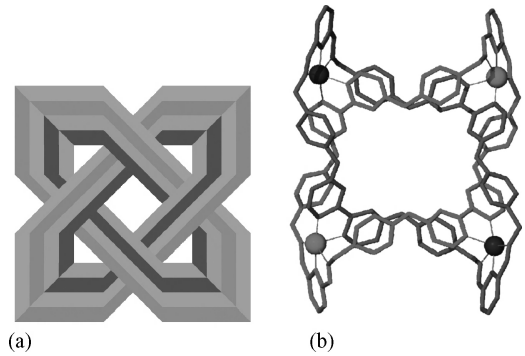


**Figure 10.92** (a) a stylistic rendering of a Solomon knot and (b) X-ray structure of the chemical Solomon's knot.[111]

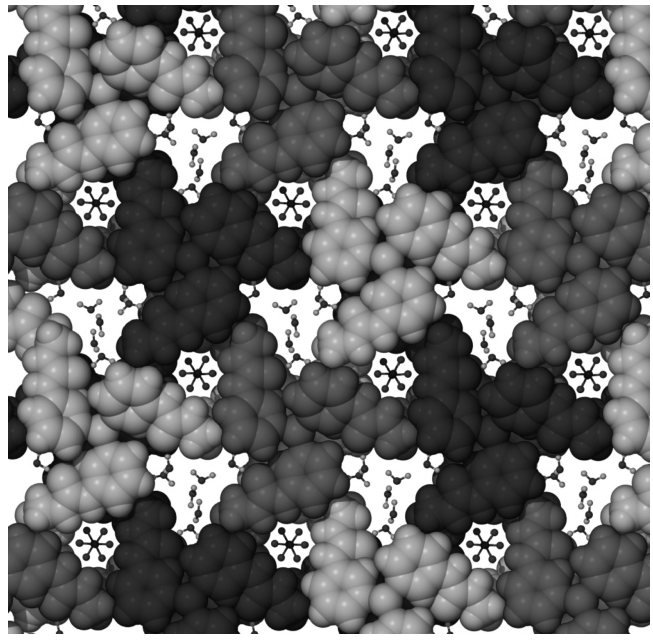

**Figure 10.93** A coordination polymer Borromeo weave containing water guests in the open cavities and supported by saturated hydrogen bonding to nitrate anions.[113] See plate section for colour version of this image.

In addition to DNA-based and discrete coordination complex systems, the Borromeo rings also make an appearance in a few coordination polymers. As discussed in Section 9.5.6 it is possible to isolate crystalline solids comprising three separate, distinct interlocked infinite coordination polymer mesh sheets in which the holes in one mesh are occupied by the strands of the other two sheets in a Borromeo fashion. Such motifs are termed 'Borromeo weaves'. In the last chapter we saw in Figure 9.38 a Borromeo weave linked together by argentophilic interactions. A Borromeo weave able to contain guests such as discrete water clusters or solvents such as methanol or acetonitrile, all supported by saturated hydrogen bonding to nitrate anions is shown in Figure 10.93.

## Summary

- Self-assembly is the *spontaneous and reversible association of molecules or ions (tectons) to form larger, more complex supramolecular entities according to the intrinsic information contained in the molecules themselves.*
- Fundamentally self-assembly is a *convergent* process in which a number of components assemble into, ideally, a single final, stable structure. Self-assembly is thus very distinct from chemical *emergence* which is a divergent process in which complexity evolves over time.
- Self-assembly can comprise a number of hierarchical levels, *j.* The lifetime of each self-assembled stage ($\tau$) is inversely proportional to its position in the hierarchy, thus the highest stages are much longer lived than the stages below them, *i.e.* $\tau_j >> \tau_{j-1}$.
- Self-assembly can be divided into a number of classes; 1. strict self-assembly, 2. irreversible self-assembly, 3. precursor modification followed by self-assembly, 4. self-assembly with post-modification, 5. assisted self-assembly, 6. directed self-assembly, 7. self-assembly with intermittent processing.

- Self-assembly within a molecule is akin to protein folding and is studied in synthetic *foldamers*.
- Self-assembly is of considerable importance in biochemistry where it helps us understand the structure of DNA and of viruses such as the tobacco mosaic virus.
- The thermodynamics of self-assembled systems are often characterized by positive co-operativity at the molecular level, however the thermodynamic analysis of co-operativity in self-assembly is complexes such as helicates is complicated by the occurrence of both inter- and intramolecular steps. It may be understood using the *extended site binding model*.
- Self-assembled capsules are of significant interest as molecular reaction vessels and in the control of confined 'inner space'.
- Self-assembly is a particular powerful tool in 'synthesising up' large scale nanostructures are topologically complex molecules such as molecular machines and topologically interlocked species.

## Study Problems

10.1 Predict the general form of the $^{109}$Ag spectrum for a grid complex consisting of 16 Ag(I) ions linked by eight of the octadentate ligands shown below. How many binding domains does this ligand possess? Would you expect this ligand to form helicate complexes? What would the $^{109}$Ag NMR spectra for the Ag equivalent of the ladder compound **10.40** and those shown in Figure 10.41 look like?

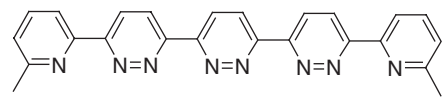


10.2 Consider a system containing only four individual molecules of $Pd(en)^{2+}$ and four individual molecules of 4,4′-bipyridyl. Assuming each fragment is rigid with N—Pd—N angles close to 90º, and ignoring rotamers, calculate the number of possible eight-component molecules that could self-assemble if the formation of each molecule was equally likely. Hence calculate the statistical probability of forming a molecular square. How does this probability change if (a) four-component assemblies and (b) two-, four- and six-component assemblies are also allowed? What effect would the presence of eight components of each type have? How many up to 10-component assemblies can you think of, starting from six individual molecules of $Pd(en)^{2+}$ and 4 individual molecules of 1,3,5-tri(4-pyridyl)triazine?

10.3 The binding constant for the binding of thread T by macrocycle M is 100 $M^{-1}$. Thread T undergoes cyclisation in 100 % yield to form a different macrocycle $T_c$. If the initial concentrations of T and M are is 0.1 mol $dm^{-3}$ calculate the amount of T bound by M at equilibrium and hence the yield of [2]catenane $T_cM$ formed compared to free $T_c$. Assume that the complexation of T by M is much faster than the cyclisation reaction of T to form $T_c$, that the decomplexation reaction is slow and that all of the T is eventually transformed into $T_c$. How would this calculation change if $T_c$ and M were identical? In this case you could plot the proportions of bound and free T as a function of reaction progress assuming an initial concentration of M of zero and hence estimate the relative yields of M and [2]catenane MM assuming M and MM are equally stable and reaction of T to form M is a fast unimolecular process that is not affected by binding to C.

10.4 A hemicarcerand has an internal cavity volume of 600 Å$^3$ and acts as a catalyst for the Diels–Alder coupling of 1,3-cyclohexadiene ($C_6H_8$) with *p*-quinone ($C_6H_4O_2$) (*cf.* Scheme 10.9). If the rate equation for the reaction follows the form rate = $k[C_6H_8][C_6H_4O_2]$, estimate the rate enhancement on moving from a solution containing 0.1 mol $dm^{-3}$ of each reactant in the absence of

catalyst to the catalysed rate using the effective concentrations within the hemicarcerand cavity. Why do you think that this kind of rate enhancement is unlikely to be achieved in practice?

10.5 Using a piece of cardboard and six pieces of string, build a topological model of compound **10.97**. By following the connectivity shown in Figure 10.66, tie the pieces of string together in pairs such as to make one of the various covalently interconnected products. Can you see where you would have to cut the string in order to give catenated or interlocked products?

## Thought Experiment

Given the reactants below (L = labile ligand), suggest possible closed cyclic oligomers that might form (a) if the $Cu^+$ ion is rigidly tetrahedral or (b) if the $Cu^+$ centre exhibits significant flexibility in its coordination geometry, and anions of various sizes are used to template the course of the reaction. Which system is more likely to form polymers? For some ideas, see S. W. Keller and S. Lopez, 'A two-dimensional geomimetic coordination polymer containing pentagonal cavities', *J. Am. Chem. Soc.*, 1999, **121**, 6306–6307.

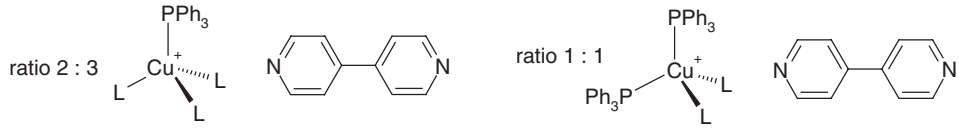


## References


1. Olson, A. J., Hu, Y. H. E., Keinan, E., Chemical mimicry of viral capsid self-assembly. *Proc. Natl. Acad. Sci. U. S. A.* 2007, **104**, 20731–20736.
2. McCarroll, A. J., Walton, J. C., Programming organic molecules: Design and management of organic syntheses through free-radical cascade processes. *Angew. Chem., Int. Ed.* 2001, **40**, 2225–2248.
3. Ellis, R. J., Hemmingsen, S. M., Molecular chaperones – proteins essential for the biogenesis of some macromolecular structures. *Trends Biochem.Sci.* 1989, **14**, 339–342.
4. Makin, O. S., Serpell, L. C., Structures for amyloid fibrils. *Febs Journal* 2005, **272**, 5950–5961.
5. Huc, I., Aromatic oligoamide foldamers. *Eur. J. Org. Chem.* 2004, 17–29.
6. Hunter, C. A.. Spitaleri, A.. Tomas, S., Tailbiter: a new amide foldamer. *Chem. Commun.* 2005, 3691–3693.
7. Philp, D.. Stoddart, J. F., Self-assembly in natural and unnatural systems. *Angew. Chem., Int. Ed. Engl.* 1996, **35**, 1155–1196.
8. McMurry, T. J., Raymond, K. N., Smith, P. H., Molecular recognition and metal-ion template synthesis. *Science* 1989, **244**, 938–943.
9. Anderson, H. L., Anderson, S., Sanders, J. K. M., Ligand-binding by butadiyne-linked porphyria dimers, trimers and tetramers. *J. Chem. Soc.-Perkin Trans. 1* 1995, 2231–2245.
10. Ercolani, G., Assessment of cooperativity in self-assembly. *J. Am. Chem. Soc.* 2003, **125**, 16097–16103.
11. Elhabiri, M., Hamacek, J., Bunzli, J. C. G., Albrecht-Gary, A. M., Lanthanide homobimetallic triple-stranded helicates: Insight into the self-assembly mechanism. *Eur. J. Inorg. Chem.* 2004, 51–62.
12. Carter, P. J., Winter, G., Wilkinson, A. J., Fersht, A. R., The use of double mutants to detect structural-changes in the active-site of the tyrosyl-transfer Rna-synthetase (bacillus-stearothermophilus). *Cell* 1984, **38**, 835–840.
13. Fujita, M., Oguro, D., Miyazawa, M., Oka, H., Yamaguchi, K., Ogura, K., Self-assembly of 10 molecules into nanometer-sized organic host frameworks. *Nature* 1995, **378**, 469–471.
14. Gibb, B. C., 'Strict self-assembly and self-assembly with covalent modification', in *Encyclopedia of Supramolecular Chemistry*, Atwood, J. L.. Steed, J. W., eds. Marcel Dekker: New York, 2004. Vol. 2, *pp.* 1372–1378.
15. Fyles, T. M., Tong, C. C., Predicting speciation in the multi-component equilibrium self-assembly of a metallosupramolecular complex. *New J. Chem.* 2007, **31**, 296–304.

16. Fujita, M., Yazaki, J., Ogura, K., Preparation of a macrocyclic polynuclear complex, $[(En)Pd(4,4'\text{-}Bpy)]_4(No_3)_8$, which recognizes an organic-molecule in aqueous-media. *J. Am. Chem. Soc.* 1990, **112**, 5645–5647.
17. Berseth, P. A., Sokol, J. J., Shores, M. P., Heinrich, J. L., Long, J. R., High-nuclearity metal-cyanide clusters: Assembly of a $Cr_8Ni_6(CN)_{24}$ cage with a face-centered cubic geometry. *J. Am. Chem. Soc.* 2000, **122**, 9655–9662.
18. Fujita, M., Umemoto, K., Yoshizawa, M., Fujita, N., Kusukawa, T., Biradha, K., Molecular paneling *via* coordination. *Chem. Commun.* 2001, 509–518.
19. Fujita, M., Self-assembly of [2]catenanes containing metals in their backbones. *Acc. Chem. Res.* 1999, **32**, 53–61.
20. Fujita, M., Nagao, S., Ogura, K., Guest-induced organization of a 3-dimensional palladium(II) cage-like complex - a prototype for induced-fit molecular recognition. *J. Am. Chem. Soc.* 1995, **117**, 1649–1650.
21. Barbour, L. J., Orr, G. W., Atwood, J. L., An intermolecular $(H_2O)_{10}$ cluster in a solid-state supramolecular complex. *Nature* 1998, **393**, 671–673.
22. Argent, S. P., Adams, H., Riis-Johannessen, T., *et al.*, Coordination chemistry of tetradentate N-donor ligands containing two pyrazolyl-pyridine units separated by a 1,8-naphthyl spacer: Dodecanuclear and tetranuclear coordination cages and cyclic helicates. *Inorg. Chem.* 2006, **45**, 3905–3919.
23. Caulder, D. L., Raymond, K. N., Supermolecules by Design. *Acc. Chem. Res.* 1999, **32**, 975–982.
24. Fiedler, D., Leung, D. H., Bergman, R. G., Raymond, K. N., Selective molecular recognition, C-H bond activation, and catalysis in nanoscale reaction vessels. *Acc. Chem. Res.* 2005, **38**, 351–360.
25. Pluth, M. D., Bergman, R. G., Raymond, K. N., Acid catalysis in basic solution: A supramolecular host promotes orthoformate hydrolysis. *Science* 2007, **316**, 85–88.
26. Fujita, M., Takeda, N., Umemoto, K., Yamaguchi, K., A Nanometre-sized hexahedral coordination capsule assembled from 24 components. *Nature* 1999, **398**, 794–796.
27. Stang, P. J., Olenyuk, B., Whiteford, J. A., Fechtenkotter, A., Self-assembly of nanoscale cuboctahedra by coordination chemistry. *Nature* 1999, **398**, 796–799.
28. Takaoka, K., Kawano, M., Ozeki, T., Fujita, M., Crystallographic observation of an olefin photodimerization reaction that takes place *via* thermal molecular tumbling within a self-assembled host. *Chem. Commun.* 2006, 1625–1627.
29. Fujita, M., Yoshizawa, M., Takeyama, Y., Kusukawa, T., Cavity-directed, highly stereoselective [2+2] photodimerization of olefins within self-assembled coordination cages. *Angew. Chem. Int. Ed.* 2002, **41**, 1347–1349.
30. Fujita, M., Tominaga, M., Hori, A., Therrien, B., Coordination assemblies from a Pd(II)-cornered square complex. *Acc. Chem. Res.* 2005, **38**, 369–378.
31. Hoffmann, M., Wilson, C. J., Odell, B., Anderson, H. L., Template-directed synthesis of a pi-conjugated porphyrin nanoring. *Angew. Chem., Int. Ed.* 2007, **46**, 3122–3125.
32. Fox, O. D., Dalley, N. K., Harrison, R. G., A metal-assembled, pH-dependent, resorcinarene-based cage molecule. *J. Am. Chem. Soc.* 1998, **120**, 7111–7112.
33. Gardner, J. S., Harrison, R. G., Lamb, J. D., Dearden, D. V., Sonic spray ionization mass spectrometry: a powerful tool used to characterize fragile metal-assembled cages. *New J. Chem.* 2006, **30**, 1276–1281.
34. Fox, O. D., Dalley, N. K., Harrison, R. G., Structure and small molecule binding of a tetranuclear iron(II) resorc[4]arene-based cage complex. *Inorg. Chem.* 1999, **38**, 5860–5863.
35. Fox, O. D., Drew, M. G. B., Beer, P. D., Resorcarene-based nanoarchitectures: Metal-directed assembly of a molecular loop and tetrahedron. *Angew. Chem., Int. Ed.* 2000, **39**, 136–140.
36. McKinlay, R. M., Thallapally, P. K., Atwood, J. L., Hexameric C-alkylpyrogallol[4]arene molecular capsules sustained by metal-ion coordination and hydrogen bonds. *Chem. Commun.* 2006, 2956–2958.
37. McKinlay, R. M., Cave, G. W. V., Atwood, J. L., Supramolecular blueprint approach to metal-coordinated capsules. *Proc. Natl. Acad. Sci. U. S. A.* 2005, **102**, 5944–5948.
38. Baxter, P. N. W., Lehn, J. M., Baum, G., Fenske, D., Self-assembly and structure of interconverting multinuclear inorganic arrays: A [4 x 5]-Ag-20(I) grid and an Ag-10(I) quadruple helicate. *Chem. Eur. J.* 2000, **6**, 4510–4517.
39. Onions, S. T., Frankin, A. M., Horton, P. N., Hursthouse, M. B., Matthews, C. J., Self-assembly of a unique hexadecanuclear [4 x (2 x 2)]-Pb-16 'grid of grids' type structure. *Chem. Commun.* 2003, 2864–2865.
40. Baxter, P., Lehn, J. M., Decian, A., Fischer, J., Multicomponent self-assembly – spontaneous formation of a cylindrical complex from 5 ligands and 6 metal-ions. *Angew. Chem., Int. Ed. Engl.* 1993, **32**, 69–72.
41. Lehn, J.-M., *Supramolecular Chemistry*. 1 ed., VCH: Weinheim, 1995.
42. Sleiman, H., Baxter, P. N. W., Lehn, J. M., Airola, K., Rissanen, K., Multicomponent self-assembly: Generation of rigid-rack multimetallic pseudorotaxanes. *Inorg. Chem.* 1997, **36**, 4734–4742.
43. Wyler, R., Demendoza, J., Rebek, J., A Synthetic cavity assembles through self-complementary hydrogen-bonds. *Angew. Chem., Int. Ed. Engl.* 1993, **32**, 1699–1701.
44. Rebek Jr, J., Conn, M. M., Self-assembling capsules. *Chem. Rev* 1997, **97**, 1647–1668.
45. Grotzfeld, R. M., Branda, N., Rebek, J., Reversible encapsulation of disc-shaped guests by a synthetic, self-assembled host. *Science* 1996, **271**, 487–489.

46. Rebek, J., Simultaneous encapsulation: Molecules held at close range. *Angew. Chem., Int. Ed.* 2005, **44**, 2068–2078.
47. Gonzalez, J. J., Ferdani, R., Albertini, E., *et al.*, Dimeric capsules by the self-assembly of triureidocalix[6]arenes through hydrogen bonds. *Chem. Eur. J.* 2000, **6**, 73–80.
48. Rose, K. N., Barbour, L. J., Orr, G. W., Atwood, J. L., Self-assembly of carcerand-like dimers of calix[4]resorcinarene facilitated by hydrogen bonded solvent bridges. *Chem. Commun.* 1998, 407–408.
49. MacGillivray, L. R., Diamente, P. R., Reid, J. L., Ripmeester, J. A., Encapsulation of two aromatics by a carcerand-like capsule of nanometre-scale dimensions. *Chem. Commun.* 2000, 359–360.
50. Kobayashi, K., Shirasaka, T., Yamaguchi, K., Sakamoto, S., Horn, E., Furukawa, N., Molecular capsule constructed by multiple hydrogen bonds: self-assembly of cavitand tetracarboxylic acid with 2-aminopyrimidine. *Chem. Commun.* 2000, 41–42.
51. Ma, B. Q., Zhang, Y. G., Coppens, P., Multiple conformations of benzil in resoreinarene-based supramolecular host matrixes. *J. Org. Chem.* 2003, **68**, 9467–9472.
52. Coppens, P., Zheng, S. L., Gembicky, M., Messerschmidt, M., Dominiak, P. M., Supramolecular solids and time-resolved diffraction. *Crystengcomm* 2006, **8**, 735–741.
53. MacGillivray, L. R., Atwood, J. L., A chiral spherical molecular assembly held together by 60 hydrogen bonds. *Nature* 1997, **389**, 469–472.
54. Dalgarno, S. J., Tucker, S. A., Bassil, D. B., Atwood, J. L., Fluorescent guest molecules report ordered inner phase of host capsules in solution. *Science* 2005, **309**, 2037–2039.
55. Atwood, J. L., Barbour, L. J., Jerga, A., Hydrogen-bonded molecular capsules are stable in polar media. *Chem. Commun.* 2001, 2376–2377.
56. Prins, L. J., De Jong, F., Timmerman, P., Reinhoudt, D. N., An enantiomerically pure hydrogen-bonded assembly. *Nature* 2000, **408**, 181–184.
57. Wasserman, E., The preparation of interlocking rings – a catenane. *J. Am. Chem. Soc.* 1960, **82**, 4433–4434.
58. Atwood, J. L., Davies, J. E. D., MacNicol, D. D., Vögtle, F., *Comprehensive Supramolecular Chemistry*. Pergamon: Oxford, 1996. Vol. 9, p 93.
59. Coumans, R. G. E., Elemans, J., Thordarson, P., Nolte, R. J. M., Rowan, A. E., Synthesis of porphyrin-containing [3]rotaxanes by olefin metathesis. *Angew. Chem., Int. Ed.* 2003, **42**, 650–654.
60. Thordarson, P., Bijsterveld, E. J. A., Rowan, A. E., Nolte, R. J. M., Epoxidation of polybutadiene by a topologically linked catalyst. *Nature* 2003, **424**, 915–918.
61. Ashton, P. R., Goodnow, T. T., Kaifer, *et al.*, A [2]Catenane Made to Order. *Angew. Chem., Int. Ed. Engl.* 1989, **28**, 1396–1399.
62. Amabilino, D. B., Stoddart, J. F., Interlocked and intertwined structures and superstructures. *Chem. Rev.* 1995, **95**, 2725–2828.
63. Amabilino, D. B., Ashton, P. R., Reder, A. S., Spencer, N., Stoddart, J. F., Olympiadane. *Angew. Chem., Int. Ed. Engl.* 1994, **33**, 1286–1290.
64. Amabilino, D. B., Ashton, P. R., Boyd, S. E., *et al.*, The five-stage self-assembly of a branched heptacatenane. *Angew. Chem., Int. Ed. Engl.* 1997, **36**, 2070–2072.
65. Ashton, P. R., Reder, A. S., Spencer, N., Stoddart, J. F., Self-Assembly of a chiral bis[2]catenane. *J. Am. Chem. Soc.* 1993, **115**, 5286–5287.
66. Liu, Y., Bonvallet, P. A., Vignon, S. A., Khan, S. I., Stoddart, J. F., Donor-acceptor pretzelanes and a cyclic bis[2]catenane homologue. *Angew. Chem., Int. Ed.* 2005, **44**, 3050–3055.
67. Hannam, J. S., Kidd, T. J., Leigh, D. A., Wilson, A. J., 'Magic rod' rotaxanes: The hydrogen bond-directed synthesis of molecular shuttles under thermodynamic control. *Org. Lett.* 2003, **5**, 1907–1910.
68. Alteri, A., Gatti, F. G., Kay, E. R., *et al.*, Electrochemically switchable hydrogen-bonded molecular shuttles. *J. Am. Chem. Soc.* 2003, **125**, 8644–8654.
69. Chiu, S. H., Rowan, S. J., Cantrill, S. J., Stoddart, J. F., White, A. J. P., Williams, D. L., Post-assembly processing of [2]rotaxanes. *Chem. Eur. J.* 2002, **8**, 5170–5183.
70. Johnston, A. G., Leigh, D. A., Pritchard, R. J., Deegan, M. D., Facile synthesis and solid-state structure of a benzylic amide [2]catenane. *Angew. Chem., Int Ed. Engl.* 1995, **34**, 1209–1212.
71. Logemann, E., Rissler, K., Schill, G., Fritz, H., Synthesis and spectra of 2 novel catenanes. *Chem. Ber.-Recl.* 1981, **114**, 2245–2260.
72. Schill, G., Rissler, K., Fritz, H., Vetter, W., Synthesis, isolation, and identification of translationally isomeric [3]catenanes. *Angew. Chem., Int. Ed. Engl.* 1981, **20**, 187–189.
73. Schill, G., Doerjer, G., Logemann, E., Fritz, H., Studies on the synthesis of molecules with knot structure fourfold bridged 5,6-diamino-1,3-benzodioxole derivatives. *Chem. Ber.-Recl.* 1979, **112**, 3603–3615.
74. Schill, G., Schweickert, N., Fritz, H., Vetter, W., [2]-[cyclohexatetraoctane][cyclooctacosane]catenane, the 1st hydrocarbon catenane. *Angew. Chem., Int. Ed. Engl.* 1983, **22**, 889–891.

75. Dietrich-Buchecker, C. O., Sauvage, J. P., Kern, J. M., Templated synthesis of interlocked macrocyclic ligands – the catenands. *J. Am. Chem. Soc.* 1984, **106**, 3043–3045.
76. Dietrich-Buchecker, C. O., Sauvage, J.-P., Interlocking of molecular threads: from the statistical approach to the templated synthesis of catenands. *Chem. Rev.* 1987, **87**, 795–810.
77. Durola, F., Russo, L., Sauvage, J. P., Rissanen, K., Wenger, O. S., Three-component entanglements consisting of three crescent-shaped bidentate ligands coordinated to an octahedral metal centre. *Chem. Eur. J.* 2007, **13**, 8749–8753.
78. Mobian, P., Kern, J. M., Sauvage, J. P., A [2]catenane constructed around a Ru(diimine)$_3^{2+}$ complex used as a template. *J. Am. Chem. Soc.* 2003, **125**, 2016–2017.
79. Fuller, A. M., Leigh, D. A., Lusby, P. J., Oswald, I. D. H., Parsons, S., Walker, D. B., A 3D interlocked structure from a 2D template: Structural requirements for the assembly of a square-planar metal-coordinated [2]rotaxane. *Angew. Chem., Int. Ed.* 2004, **43**, 3914–3918.
80. Beer, P. D., Sambrook, M. R., Curiel, D., Anion-templated assembly of interpenetrated and interlocked structures. *Chem. Commun.* 2006, 2105–2117.
81. Whang, D. M., Park, K. M., Heo, J., Ashton, P., Kim, K., Molecular necklace: Quantitative self-assembly of a cyclic oligorotaxane from nine molecules. *J. Am. Chem. Soc.* 1998, **120**, 4899–4900.
82. Cahn, R. S., Ingold, C., Prelog, V., Specification of Molecular Chirality. *Angew. Chem., Int. Ed.* 1966, **5**, 385–415.
83. Bell, T. W., Jousselin, H., Self-Assembly of a Double-Helical Complex of Sodium. *Nature* 1994, **367**, 441–444.
84. Lehn, J. M., Sauvage, J. P., Simon, J., *et al.*, Synthesis and metal-complexes of a conformationally restricted quaterpyridine – crystal-structure of its dimeric dinuclear Cu (I) complex, $[Cu_2(pqp)_2]^{2+}$. *Nouv. J. Chim. - New J. Chem.* 1983, **7**, 413–420.
85. Constable, E. C., Ward, M. D., Spontaneous assembly of a double-helical binuclear complex of 2,2′-6′,2″-6″,2‴-6‴,2⁗,6⁗,2⁗⁗-sexipyridine. *J. Am. Chem. Soc.* 1990, **112**, 1256–1258.
86. Hannon, M. J., Painting, C. L., Jackson, A., Hamblin, J., Errington, W., An inexpensive approach to supramolecular architecture. *Chem. Commun.* 1997, 1807–1808.
87. Hasenkopf, B., Lehn, J. M., Kneisel, B. O., Baum, G., Fenske, D., Self-assembly of a circular double helicate. *Angew. Chem., Int. Ed. Engl.* 1996, **35**, 1838–1840.
88. Funeriu, D. P., Lehn, J.-M., Baum, G., Fenske, D., Double subroutine self-assembly. spontaneous generation of a nanocyclic dodecanuclear Cu1 inorganic architecture. *Chem. Eur. J.* 1997, **3**, 99–104.
89. Jones, P. L., Byrom, K. J., Jeffery, J. C., McCleverty, J. A., Ward, M. D., A cyclic supramolecular complex containing eight metal ions, twelve bridging ligands, and an anion encapsulated in the central cavity. *Chem. Commun.* 1997, 1361–1362.
90. Coles, S. J., Frey, J. G., Gale, P. A., *et al.*, Anion-directed assembly: the first fluoride-directed double helix. *Chem. Commun.* 2003, 568–569.
91. Kim, H.-J., Zin, W.-C., Lee, M., Anion-directed self-assembly of coordination polymer into tunable secondary structure. *J. Am. Chem. Soc.* 2004, **126**, 7009–7014.
92. Cross, T. A., Arseniev, A., Cornell, B. A., *et al.*, Gramicidin channel controversy – revisited. *Nature Structural Biology* 1999, **6**, 610–611.
93. Marsh, D., Peptide models for membrane channels. *Biochem. J.* 1996, **315**, 345–361.
94. Gulikkrzywicki, T., Fouquey, C., Lehn, J. M., Electron-microscopic study of supramolecular liquid-crystalline polymers formed by molecular-recognition-directed self-assembly from complementary chiral components. *Proc. Natl. Acad. Sci. U. S. A.* 1993, **90**, 163–167.
95. de Meijere, A., Khlebnikov, A. E., Kozhushkov, S. I., *et al.*, Syntheses and properties of enantiomerically pure higher (n >= 7) [n-2]triangulanedimethanols and sigma-[n]helicenes. *Chem. Eur. J.* 2006, **12**, 5697–5721.
96. Schmitt, J. L., Stadler, A. M., Kyritsakas, N., Lehn, J. M., Helicity-encoded molecular strands: Efficient access by the hydrazone route and structural features. *Helv. Chim. Acta* 2003, **86**, 1598–1624.
97. Greene, B., *The Elegant Universe: Superstrings, Hidden Dimensions and the Quest for the Ultimate Theory*. Vintage: 2005.
98. Atwood, J. L., Davies, J. E. D., MacNicol, D. D., Vögtle, F., *Comprehensive Supramolecular Chemistry*. Pergamon: Oxford, 1996. Vol. 9, p. 44.
99. Wasserman, S. A., Dungan, J. M., Cozzarelli, N. R., Discovery of a predicted DNA knot substantiates a model for site-specific recombination. *Science* 1985, **229**, 171–174.
100. Saitta, A. M., Soper, P. D., Wasserman, E., Klein, M. L., Influence of a knot on the strength of a polymer strand. *Nature* 1999, **399**, 46–48.
101. Dietrichbuchecker, C. O., Sauvage, J. P., A Synthetic Molecular Trefoil Knot. *Angew. Chem., Int. Ed. Engl.* 1989, **28**, 189–192.
102. Dietrich-Buchecker, C. O., Guilhem, J., Pascard, C., Sauvage, J. P., Structure of a synthetic trefoil knot coordinated to 2 copper(I) centers. *Angew. Chem., Int. Ed. Engl.* 1990, **29**, 1154–1156.

103. Adams, H., Ashworth, E., Breault, G. A., Guo, J., Hunter, C. A., Mayers, P. C., Knot tied around an octahedral metal centre. *Nature* 2001, **411**, 763.
104. Safarowsky, O., Nieger, M., Fröhlich, R., Vögtle, F., A molecular knot with twelve amide groups – one-step synthesis, crystal structure, chirality. *Angew. Chem., Int. Ed.* 2000, **39**, 1616–1618.
105. Ashton, P. R., Matthews, O. A., Menzer, S., *et al.*, Molecular meccano, 27 – A template-directed synthesis of a molecular trefoil knot. *Liebigs Annalen-Recueil* 1997, 2485–2494.
106. Dietrich-Buchecker, C., Leize, E., Nierengarten, J. F., Sauvage, J. P., Vandorsselaer, A., Singly and doubly interlocked [2]-catenanes – influence of the degree of entanglement on chemical-stability as estimated by fast-atom-bombardment (Fab) and electrospray-ionization (Esi) mass spectrometries (Ms). *J. Chem. Soc., Chem. Commun.* 1994, 2257–2258.
107. Carina, R. F., DietrichBuchecker, C., Sauvage, J. P., Molecular composite knots. *J. Am. Chem. Soc.* 1996, **118**, 9110–9116.
108. Du, S. M., Stollar, B. D., Seeman, N. C., A synthetic DNA molecule in 3 knotted topologies. *J. Am. Chem. Soc.* 1995, **117**, 1194–1200.
109. Mao, C. D., Sun, W. Q., Seeman, N. C., Assembly of Borromeo rings from DNA. *Nature* 1997, **386**, 137–138.
110. Castle, T., Evans, M. E., Hyde, S. T., Ravels: Knot-free but not free. Novel entanglements of graphs in 3-space. *New. J. Chem.* 2008, **32**, 1484–1492.
111. Pentecost, C. D., Chichak, K. S., Peters, A. J., Cave, G. W. V., Cantrill, S. J., Stoddart, J. F., A molecular Solomon link. *Angew. Chem., Int. Ed.* 2007, **46**, 218–222.
112. Chichak, K. S., Cantrill, S. J., Pease, A. R., *et al.*, Molecular Borromeo rings. *Science* 2004, **304**, 1308–1312.
113. Byrne, P., Lloyd, G. O., Clarke, N., Steed, J. W., A 'compartmental' Borromeo sheet coordination polymer exhibiting saturated hydrogen bonding to anions and water cluster inclusion. *Angew. Chem.* 2008, **47**, 5761–5764.

# 11 Molecular Devices

*'The whole is greater than its part.'*

I. Todhunter, *The Elements of Euclid*, Macmillan: London, 1880 (from the original Greek).

## 11.1 Introduction

Balzani, V., Credi, A. and Venturi, M. *Molecular Devices and Machines*, Wiley-VCH: Weinheim, 2003.

### 11.1.1 Philosophy of Molecular Devices

The traditional goals of chemistry have centred on the idea of making molecules. If you can make molecules, then you can make new substances and materials, or make more of existing ones. Chemical substances – things like dyes and paints, metals and plastics, glass and ceramics, pharmaceuticals, synthetic textiles *etc.*– are useful things to have around. You can build things with them, wear them, change aesthetic and corrosion-resistance properties, consume them, make utensils and tools with them, and do whole host of other civilised things. In each case, only one main property of the chemical substance is being employed. This property can be something like colour (light absorption or emission), hardness and mechanical strength, cohesion and flexibility, therapeutic benefit (biochemical role), electrical or thermal conductance or insulating properties, and so on. Traditionally is has been left to the discipline of engineering, and latterly electronic engineering, to combine the bulk features of a number of different (chemical) substances, or at least mechanical components, in order to produce machines or devices.

We can define a machine as a functioning entity composed of a number of interacting components that collectively carry out a predefined task for (presumably) beneficial result. A machine, or device, differs from a chemical substance in that it is useful for what it *does*, rather than for what it *is*. Traditionally, because the components of a machine must be precisely orientated with respect to one another, and interact in a well-defined way, machines have been macroscopic structures that a human being can assemble through the use of keen eyesight and manual dexterity. In recent years, microscale machines (devices with components of the order of micrometres) have been produced in the electronics industry by other machines, which, metaphorically, have a vastly greater degree of manual dexterity and keener eyesight. Microscale machines take up less space, are subject to fewer external influences and, above all, are much faster and more sophisticated (in terms of the tasks they can perform) than their large ancestors. What has yet to be fully realised is the artificial production of nanoscale machines – machines the size of individual molecules – that have the potential to be yet faster and even more sophisticated. These kinds of nanoscale devices are exactly what Nature has evolved in living organisms and biochemical systems such as transport, signalling and recognition proteins, enzymes and the machinery of self-replication provide a lot if inspiration.

In Section 10.1, and throughout Chapter 10, we looked at methods by which large molecules or molecular-based systems on the nanometre scale might be assembled, or induced to self-assemble. Self-assembly addresses the fundamental problem of synthesising nanoscale structures in which components are placed in the correct orientations with respect to one another. In this chapter, we continue the theme of engineering large molecular structures, but with an emphasis on the properties of the individual components themselves and the ways in which they communicate, as a means towards the construction of molecular and supramolecular analogues of 'real world' devices, functioning on the nanometre scale.

### 11.1.2 When Is a Device Supramolecular?

So far we have focused on Lehn's definition of a supramolecular compound as one involving non-covalent interactions (Section 1.1). Such a definition is entirely appropriate to host–guest chemistry,

*Supramolecular Chemistry, 2nd edition* J. W. Steed and J. L. Atwood
© 2009 John Wiley & Sons, Ltd ISBN: 978-0-470-51233-3

and even to the templated and thermodynamic self-assembling systems discussed in Chapter 10. When we come to molecular devices, however, such a definition is not used by many workers in the field because the focus in the construction of supramolecular devices is on the functional interactions between the components rather than the chemical nature of their connectivity. This means that a 'supramolecular device' can be an entirely covalent molecule if it possesses characteristics of a supramolecular nature. Thus a supramolecular device may be defined as *a complex system made up of molecular components with definite individual properties*. These properties are intrinsic to a particular molecular component whether it is part of the device or not. Another way of saying this is that the *interaction energy* between the components of the supramolecular device must be small compared with other energy parameters relevant to the system. It does not matter, therefore, how the components are connected together in the device (covalently, hydrogen-bonded, coordination interaction *etc.*); all that matters is that each component should contribute something unique and identifiable with that component alone, within the system. If this rule does not hold true, and the functionality of the system is identifiable with the molecule as a whole, as opposed to the individual parts, then the complex is best thought of as a 'large molecule' and we will not consider it to be supramolecular.

Such a definition of a supramolecular device does not exclude the 'traditional' concept of host and guest or receptor and substrate. Molecular recognition events between host and guest may be an intrinsic part of the operation of a supramolecular device, which might, for example, be designed to bind and then signal the presence of a guest.

Common components within supramolecular devices as they are studied today are photochemically or redox active molecules, *i.e.* molecules capable of absorbing and/or emitting light and molecules capable of losing or gaining an electron. The definition of a supramolecular device made up from these components is illustrated in Figure 11.1. If light excitation of a molecule (♦↔•) results in the formation

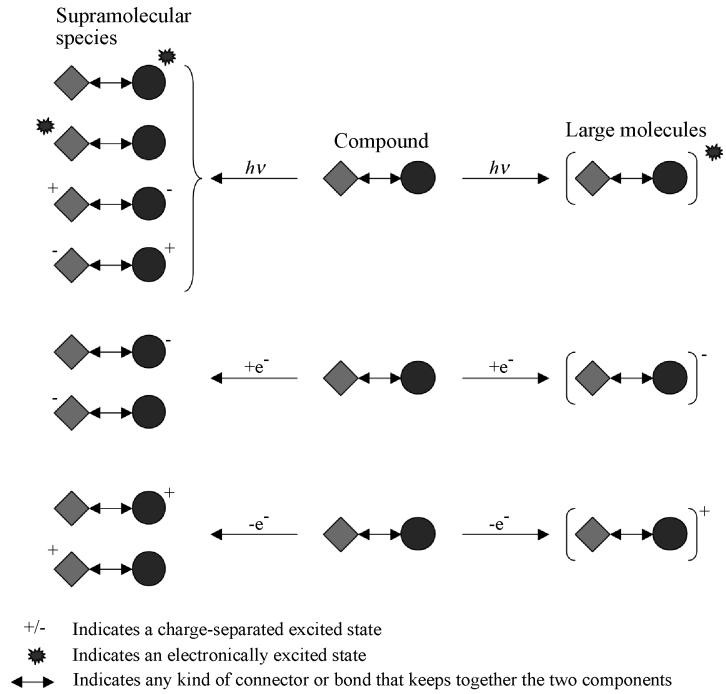


**Figure 11.1** Photochemical and electrochemical criteria used to classify a complex chemical species as a supramolecular device or a large molecule.

of excited states that are substantially localised on one of the two components (♦ or •) or causes electron transfer from one to the other, then the molecule is said to be supramolecular. If the excited state is substantially delocalised across both components, then the complex is best thought of as being simply a large single molecule. Analogous arguments apply to redox processes. Clearly a caveat of this line of reasoning is that the nature of the interaction between the two components would be expected to be dependent crucially on the nature of the connection between them (↔), be it a bridging ligand, rigid or mobile covalent spacer unit, or a non-covalent link.

## 11.2 Supramolecular Photochemistry

Balzani, V. and Scandola, F., *Supramolecular Photochemistry*, Ellis Horwood: Chichester, 1991.

### 11.2.1 Photophysical Fundamentals

Of all the ways in which to construct a supramolecular device, the use of photochemically active components is, perhaps, the most versatile. Light-induced processes are of fundamental importance in biochemical devices such as plant photosynthetic membranes (Section 2.4). Light-absorbing components (chromophores) are readily available and lend themselves to extensive synthetic modification, and light is readily introduced to a system that is in a variety of physical states (*e.g.* solid, liquid or gas) or media (solutions in various solvents). Light may be used to induce events such as charge separation, initiate catalysis, interrogate a system in sensing applications, or to bring about changes in the state of a bistable device (switching). Incorporation of photochemically active components within a supramolecular complex may be expected to perturb or modulate the photochemical behaviour of the chromophore(s), giving rise to a number of interesting and potentially useful effects such as energy migration, photoinduced charge separation, perturbations of optical transitions and polarisabilities, modification of ground- and excited-state redox potentials, photoregulation of binding properties, selective photochemical reactivity *etc.*

When a molecular chromophore is irradiated with electromagnetic radiation of a wavelength corresponding to the energy required to promote an electron to an accessible electronic excited state, energy is absorbed resulting in the promotion of an electron from a ground-state molecular orbital to one of higher energy. This is known as primary charge separation and results in a high-energy electron and a positively charged 'hole'. The energy of the excited-state electron can either be dissipated as heat by relaxation by the solvent (nonradiative decay), emitted radiatively (luminescence) or used to carry out a chemical reduction (Figure 11.2a). Luminescence involving direct radiative decay, in which the electron returns immediately to the ground state from a singlet excited state, is termed *fluorescence*. Fluorescent emissions are usually of lower energy than the absorbed energy because the electron is promoted into a vibrationally excited state from which it relaxes non-radiatively before fluorescing back to the electronic ground state (Figure 11.2a). This is the reason why many fluorescent dyes are able to absorb high-energy UV light and fluoresce in the visible region.

If the electron undergoes a change of spin state (intersystem crossing), then it accesses the triplet manifold of excited states. This transformation is formally forbidden because of the selection rule that there must not be a change in spin state during the transition, *i.e.* $\Delta S = 0$. This selection rule is a reflection of the fact that there is no component of electromagnetic radiation that interacts with electron spin. However the rule may be relaxed as a consequence of spin-orbit coupling. As a result of this selection rule, the triplet excited state, once formed, is long-lived and may undergo vibrational relaxation to a lower energy level before relaxing slowly *via* a back intersystem crossing, emitting a kind of luminescence, termed *phosphorescence*, of a lower frequency to the absorbed light. Fluorescent and phosphorescent processes may be distinguished by time-resolved spectroscopic measurements because

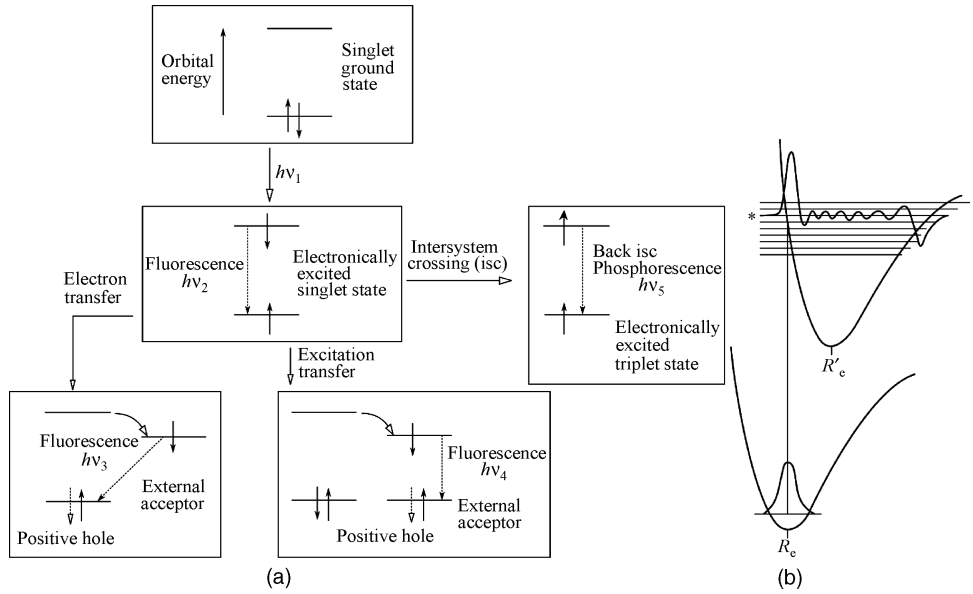


**Figure 11.2** (a) Possible radiative events following photoexcitation, (b) Photoexcitation of an electron into a vibrationally and electronically excited state. The electronic transition takes place within a stationary nuclear framework (Franck–Condon principle). Once the transition has occurred, the molecule experiences a new force field and bursts into vibration.

phosphorescence takes much longer to decay than fluorescence. In the presence of an external electron acceptor (low-lying empty orbital on an adjacent molecule or component), the excited-state electron may reduce the acceptor chemically, resulting in long-lived spatial charge separation (secondary charge separation). Eventual recombination is accompanied by emission of light of a different frequency, or by emission of heat. Finally, the energy from the excited state may be transferred to an external acceptor without electron transfer. This is termed *energy transfer* (ET). The resulting secondary excited state may then relax with emission of luminescence, again of a lower frequency to the original absorption. This process is the beginning of an energy transfer cascade as in photosynthesis.

In some cases excited state chromophores form supramolecular complexes either with ground state chromophores on the same molecule or one nearby resulting in the formation of an *excimer* (excited state dimer) or, if the two chromophores are different to one another an *exciplex*. Formally an excimer as defined as a dimer which is associated in an electronic excited state and which is dissociative in its ground state.[1] Formation of the pyrene excimer is illustrated in Figure 11.3.

The results of photoexcitation may be divided into three broad categories:

1. Re-emission of the absorbed energy as light (fluorescence or phosphorescence).
2. Chemical reaction of the excited state (secondary charge separation, isomerisation, disassociation *etc.*).
3. Non-radiative vibrational quenching of the excitation by solvent.

Within the context of supramolecular devices, re-emission of the radiation by luminescence is of interest in sensing and signalling applications, while chemical reactions are of interest in applications such as molecular switches and photocatalysis. Strictly speaking absorption and re-emission type processes are termed molecular 'photophysics' while light-induced chemical reactions or chemical processes are termed 'photochemistry'.

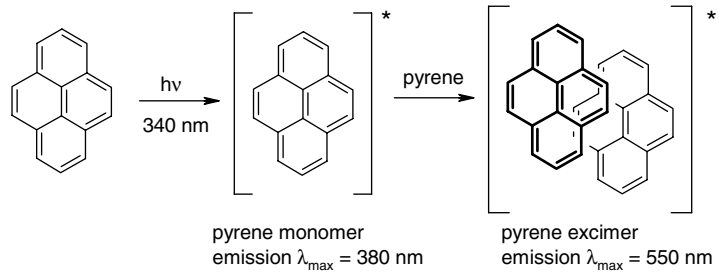


**Figure 11.3** The excited state of a chromophore such as pyrene can form a complex with a ground state molecule. If the result is an excited state dimer the complex is known as an *excimer*, while if the excited complex is formed between two different molecule it is termed and *exciplex*. Excimers and exciplexes emit at lower energy than the corresponding monomers.

Common chromophores are transition metal complexes that may be used either as a light-absorbing (sensitising) part of a supramolecular device or as a signalling and sensing component. In the case of a mononuclear transition metal complex, a simple molecular orbital (MO) description may be derived from linear combination of the orbitals of the metal and ligands. It is convenient, and usually a reasonable approximation, to discuss both the ground- and electronically excited-state electron configurations in terms of this orbital description. This is termed the 'localised molecular orbital approximation'. Individual MOs may be labelled M or L according to whether they are predominantly metal- or ligand-centred. An MO scheme for a mononuclear complex between a metal (M) and ligands (L) is shown in Figure 11.4.

In general, in complex ground states, the $\sigma_L$ and $\pi_L$ ligand orbitals are full. The $\pi_M$ orbitals (the $t_{2g}$ set in octahedral transition metal complexes) are at least partially filled (depending on the metal oxidation state) and the other orbitals are usually empty. Light absorption changes these populations. Metal-centred (MC)

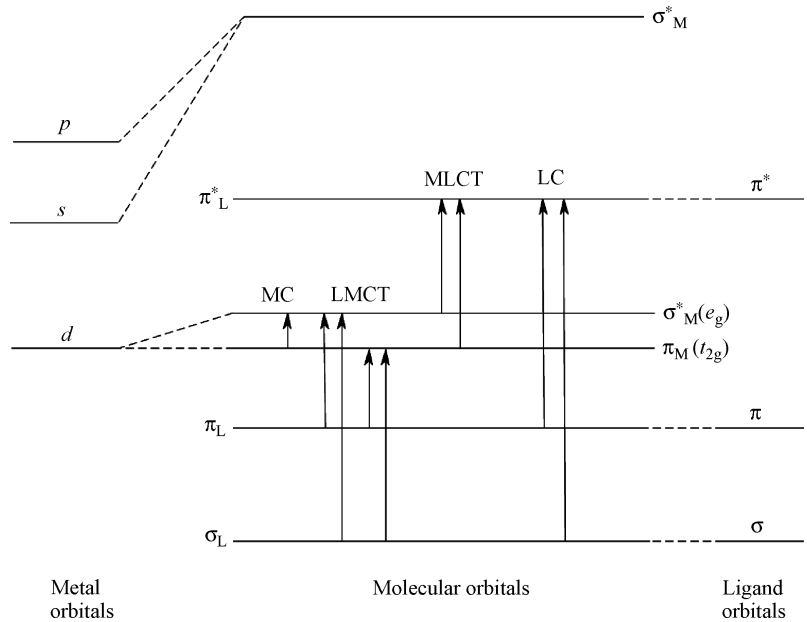


**Figure 11.4** Energy level diagram for an octahedral transition metal complex showing the various kinds of electronic transition. MC = metal-centred, LC = ligand-centred, MLCT = metal-to-ligand charge transfer, LMCT = ligand-to metal-charge transfer.

transitions, sometimes called *d–d* or ligand field transitions, are of low energy, often corresponding to the wavelength of visible light (transition metals are frequently highly coloured), and involve rearrangements of the metal *d*-electrons from the $t_{2g}$ to $e_g$ sets. Ligand-centred (LC) transitions are much higher in energy. The most common process is charge transfer (CT), which is strongly allowed since it involves a change in orbital angular momentum quantum number (*d*-electrons becoming *p*-electrons or vice versa). Metal-to-ligand charge transfer (MLCT) is particularly common since this involves promotion of electrons in the highest occupied molecular orbital (HOMO) to the lowest unoccupied molecular orbital (LUMO). The exact order of stability of the orbitals is highly dependent on the nature of the ligands and metal, and frequently the $\pi_L^*$ level comes below the metal-centred $e_g$ ($\sigma_M^*$) set, *e.g.* $[Ru(bpy)_3]^{2+}$ (bpy = 2,2′-bipyridyl). In some cases, oxidation or reduction leads to undesirable decomposition or metal–ligand disassociation, and it is a fundamental requirement for the incorporation of a chromophore into a supramolecular device that its redox and photophysical behaviour should be stable and reversible.

### 11.2.2 Mechanisms of Energy and Electron Transfer

The photoinduced transfer of energy (excitation) or electrons is of fundamental importance in molecular devices. Excitation transfer requires some kind of electronic interaction between donor and acceptor. It occurs *via* one of two mechanisms:[2]

1. The electron exchange (Dexter) mechanism which involves the overlap of wavefunctions of the donor and acceptor groups. This is a short-range excitation transfer mechanism that operates by exchange of electrons.
2. The coulombic (Förster) mechanism, a dipole-dipole mechanism that can operate over distances as long as 10 nm.

The difference between the mechanisms is illustrated in Figure 11.5. While the Dexter mechanism requires direct orbital overlap, the Förster mechanism involves energy transfer by non-radiative, long-range dipole-dipole coupling to an acceptor chromophore typically up to 10 nm away. Formally this energy transfer mechanism is called 'Förster resonance energy transfer' (FRET) after the German photophysicist Theodor Förster. Very often when both chromophores are fluorescent, the term 'fluorescence resonance energy transfer' is used, however the energy transfer is a non-radiative process and does not involve fluorescence hence the former description is preferred.

A significant challenge in the design of molecular devices is to extend the orbital overlap over a considerable distance to allow controlled, longer distance electron or Dexter-type energy transfer. The kinds of approaches that have been adopted use 'molecular wires' (Section 11.4.2) in which a conjugated $\pi$-system provides the necessary orbital overlap for efficient electron-exchange-type excitation transfer. An example is the linking of a $[Ru(bpy)_3]^{2+}$ type donor with a $[Os(bpy)_3]^{2+}$ acceptor by a rigid conjugated oligophenylene spacer, Figure 11.6a. The phosphorescence of the $[Ru(bpy)_3]^{2+}$ moiety (and of the oligophenylene spacer) is quenched by extremely rapid energy transfer to the osmium unit *via* the electron exchange mechanism despite the fact that the components are separated by 4.2 nm. Decreasing the number of oligophenylene spacer units increases the rate and efficiency of the excitation transfer process.[3]

In addition photoexcitation can also result in the transfer of an excited state electron to a distant acceptor group resulting in charge separation. This process can be understood within the framework of Marcus theory and subsequent more sophisticated theoretical treatments.[2, 5] The rate of electron transfer ($k_{el}$) drops with distance according to an attenuation factor $\beta^{el}$; $k_{el} \propto \exp(-\beta^{el} r_{AB})$ where $r_{AB}$ is the distance between donor and acceptor components A and B. When the donor and acceptor components are separated by a vacuum $\beta^{el}$ is estimated to be *ca.* 2 – 5 $Å^{-1}$. However when some kind of material substance is involved such as a bridge 'L' the electron transfer process can be

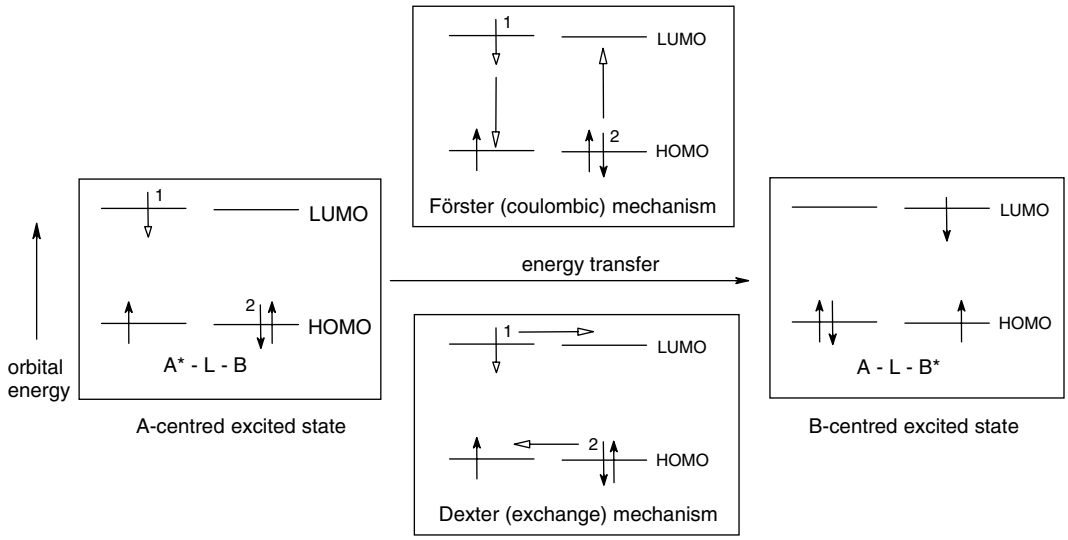


**Figure 11.5** Diagrammatic explanation of the coulombic and electron exchange energy transfer mechanisms (A and B are chromophore components and L is a bridging moiety or ligand).

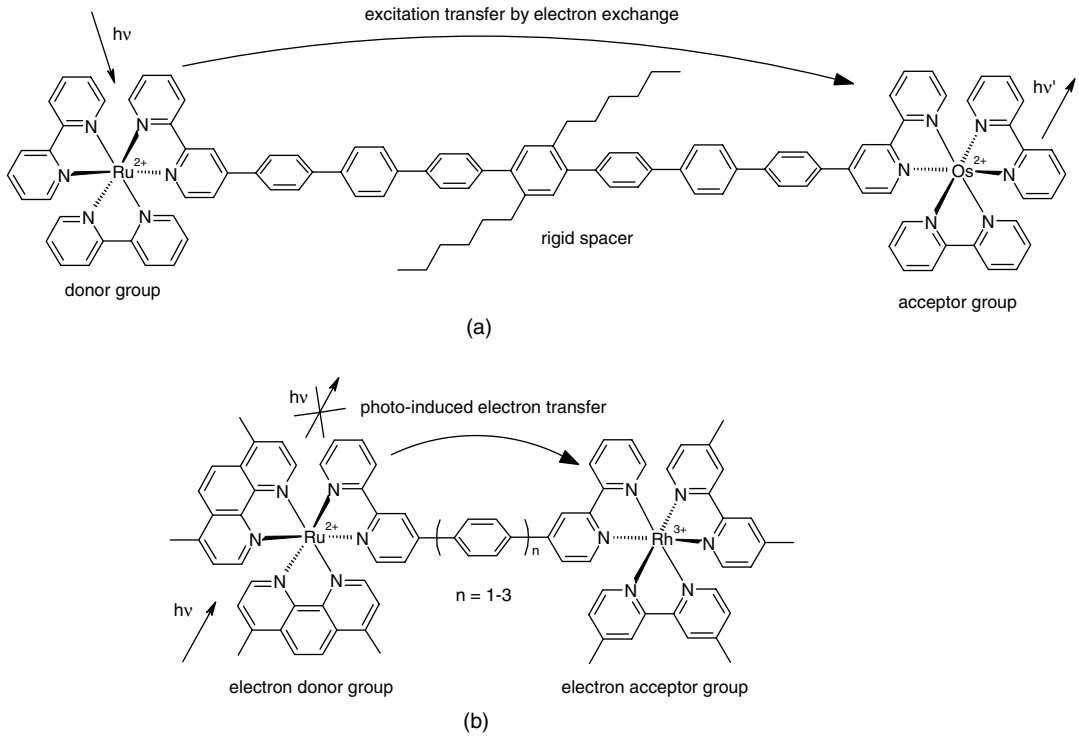


**Figure 11.6** (a) The triplet excitation transfer[3] between the ruthenium(II) donor and the osmium(II) acceptor in $[Ru(bpy)_3]^{2+}-(ph)_7-[Os(bpy)_3]^{2+}$ (b) photo-induced electron transfer from Ru(II) to Rh(III) across varying spacer lengths.[4]

mediated by mixing of the initial and final states of the system with virtual, high energy electron transfer states involving the intervening medium. This is referred to as the *superexchange mechanism* and has some similarities to the Dexter energy transfer mechanism. Similar systems to that shown in Figure 11.6a based on the more electron deficient Rh(III) of general formula $[(Me_2phen)_2Ru\text{-}bpy\text{-}(ph)_n\text{-}bpy\text{-}Rh(Me_2bpy)]^{5+}$ ($Me_2phen$ = 4,7-dimethyl−1,10-phenanthroline; ph = 1,4-phenylene; $n = 1-3$) have been used to study photo-induced electron (as opposed to energy) transfer as a function of spacer length, Figure 11.6b. For the compound with $n = 3$ the metal-metal distance is 2.4 nm. For all of the members of the series the typical metal-to-ligand charge-transfer luminescence of the ruthenium(II) moiety is quenched, meaning that efficient intramolecular photoinduced electron transfer from the excited ruthenium(II) moiety to the rhodium(III) unit takes place. The rate of the process decreases with spacer length but substituent effects indicate this it is also highly dependent on phenylene group mutual orientation highlighting the through-bond nature of the process, which proceeds by a superexchange mechanism.[4]

### 11.2.3 Bimetallic Systems and Mixed Valence

By definition, a supramolecular device comprises more than one component, and this may well involve two or more photophysically active or redox centres. The nature of the interaction between these components will depend strongly on the nature of the bridge between them. In the case of two interacting metal centres of the type discussed above, we can distinguish three classes of behaviour, denoted class I, II and III. If we consider the interaction between two valence-localised electronic isomers, in which the metal centres are of oxidation state +2 or +3 (*e.g.* $M_1^{II}\text{-}M_2^{III}$ and $M_1^{III}\text{-}M_2^{II}$), there exist particular equilibrium geometries (in terms of the primary coordination sphere M–L distances and interactions with the solvation sphere) for each 'isomer'. In a class I system, the two metal centres are essentially completely isolated and behave in a fashion analogous to the isolated mononuclear complexes. This situation is represented in Figure 11.7a. At the geometry of the electronic minima, each isomer may be considered to be an excited state of the other, separated by a reorganisational energy, $\lambda$. Broadly speaking, $\lambda$ represents the energy required to move the ligand and solvent atoms to their new equilibrium positions in response to a change in the metal oxidation state. At the crossing point, both electronic isomers have the same geometry and are of the same energy. Electron exchange between them is extremely unlikely, however, even if they acquire the necessary energy to reach the crossing point ($\lambda/4$ in this case).

In most cases, however, there is some electronic interaction between the two metal centres (Figure 11.7b). At the equilibrium geometries, the metal–metal interaction has little effect on the shape of the potential energy curve, but near the crossing point there is mixing of the zero order states (the isolated case represented in Figure 11.7a). This mixing is termed 'avoided crossing', and is a feature of class II mixed valence species. The systems are still valence-localised, and therefore are still supramolecular in the sense explained above, but new properties arising from the intervalence metal–metal interaction can be observed with, for example, an optical intervalence transition (IT) interconverting the two isomers. The energy for this kind of transition may be provided by irradiation.

Class III behaviour, as in the famous Ru(II)-Ru(III) Creutz–Taube ion, $[(NH_3)_5Ru(\mu\text{-pyrazene})Ru(NH_3)_5]^{5+}$, is outside the realm of supramolecular chemistry and corresponds to the situation in which no valence localisation can be observed (Figure 11.7c). In this case, there is significant metal–metal electronic coupling and the equilibrium geometries are significantly perturbed, corresponding to a single potential energy minimum for the complex in the case of very large coupling where $\lambda \approx H$ (the interaction energy). The properties of the fully delocalised $M_1^{II1/2}\text{-}M_2^{II1/2}$ system bear little resemblance to the mononuclear precursors or components. Class III systems are classified as 'large molecules'.

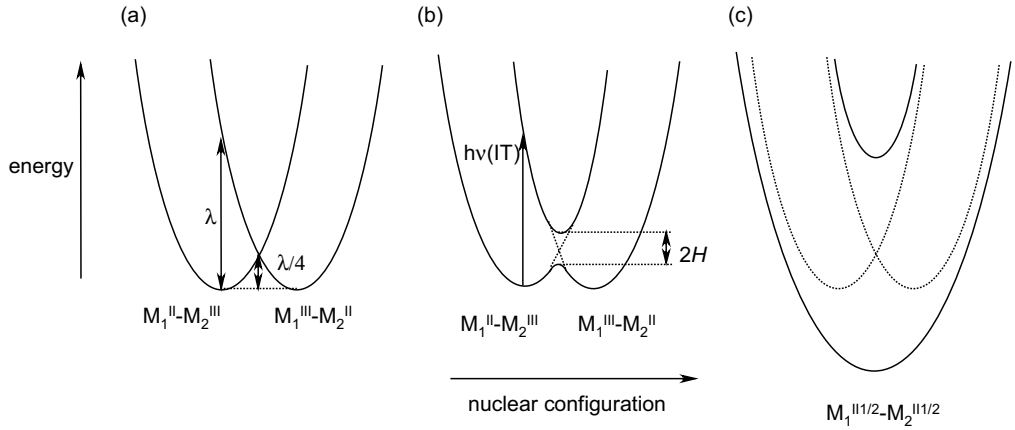


**Figure 11.7** Potential energy diagrams for a two-component mixed valence device with (a) negligible, (b) weak and (c) strong electronic coupling. The dashed curves represent unperturbed zero-order states. The horizontal axis represents generalised nuclear coordinates, including contributions from both ligand atom positions and solvent sphere.

## 11.2.4 Bipyridine and Friends as Device Components

One of the most common types of ligand in supramolecular photochemistry is the bidentate chelate 2,2′-bipyridine (bpy, **11.1**), which represents the first member of the homologous series of polypyridyls that includes 2,2′:6′,2″-terpyridine (tpy, **11.3**) and carries on up to the helicate-forming sexipyridine (**10.120**, Section 10.8) and beyond.

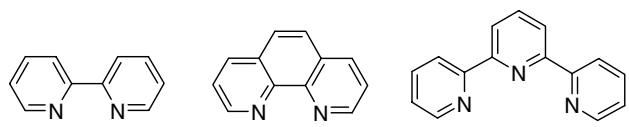


**11.1** **11.2** **11.3**

As molecules with extended $\pi$-systems, bpy, tpy and 1,10-phenanthroline (phen, **11.2**) are all capable of absorbing light, resulting in a $\pi$–$\pi^*$ transition. They are thus capable of sensitising coordinated metal ions by acting as light harvesters. Conversely, if the metal ion itself is photoexcited, then relaxation may occur by MLCT, in which the metal excited state reduces the ligand by charge transfer to the ligand-centred $\pi_L^*$ orbital.

In practice, metal complexes of bpy and phen, such as $[Ru(bpy)_3]^{2+}$ and $[Ru(phen)_3]^{2+}$, exhibit long-lived phosphorescent excited states, arising from ligand-centred triplet charge transfer states ($^3$MLCT). Lifetimes are of the order of $10^2$–$10^3$ ns in fluid solution at room temperature.

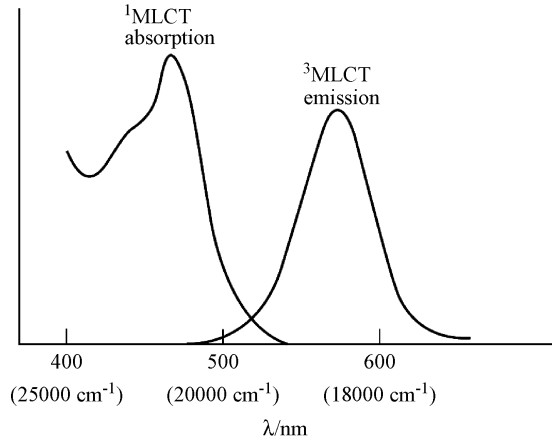


**Figure 11.8** Absorption and phosphorescence electronic spectra of $[Ru(bpy)_3]^{2+}$ (vertical axis: intensity, arbitrary units).

The phosphorescence spectrum of $[Ru(bpy)_3]^{2+}$ is shown in Figure 11.8. Much can be learned about the nature of photoexcited states by study of electrochemically reduced or oxidised species. Electrochemical oxidation of $[Ru(bpy)_3]^{2+}$ involves removal of a metal-centred electron at about +1.25 V to give a Ru(III) species (potential versus saturated calomel electrode (SCE) reference in MeCN). Replacement of one bpy by two chloride ligands lowers the potential to +0.32 V, while two CO $\pi$-acceptor ligands raise it to +1.9 V. Reduction is reversible and takes place on a $\pi_L^*$ orbital localised on a single ligand, keeping intact the inert $t_{2g}^6$ electron configuration at the metal. At −54ºC in DMF, up to six reduction waves may be observed between −1.33 and −2.85 V, corresponding to the sequential addition of one and then two electrons to each ligand. These electrochemical results tell us that if the orbital configuration is the same for the starting complex and its one-electron reduced form in both the ground and excited states (Koopman's theorem), then photoexcitation of $[Ru(bpy)_3]^{2+}$ must involve promotion of an electron from a metal-based HOMO to a ligand-based LUMO, *i.e.* MLCT, implying that the $\pi_L^*$ level is lower in energy than the metal $e_g$ set.

In contrast to the tris(bpy) and tris(phen) complexes, $[Ru(tpy)_2]^{2+}$ has a very short MLCT lifetime (about 250 ps) and does not luminesce. The main reason for this difference is that tpy is a less optimum ligand for Ru(II) because of its rather strained bite angle (*i.e.* the N-Ru-N bond angle). This structural feature results in a lower ligand field splitting energy (the energy difference between the metal-centred $e_g$ and $t_{2g}$ orbitals) and hence a smaller gap between the upper metal-centred (MC) level and the MLCT level ($\pi_L^*$; in Ru pyridyl compounds this level is below the $e_g$ set, not as shown in Figure 11.4). As a result, a convenient radiationless decay path is available *via* an activated crossing to an upper lying $^3$MC state. At 77 K, this decay pathway is frozen and $[Ru(tpy)_2]^{2+}$ exhibits similar luminescence to the bpy and phen analogues.

Unfortunately, despite its poor luminescent properties, tpy is a desirable ligand from a structural point of view in the design of supramolecular photochemical devices. Metal bis(tpy) complexes are achiral, which means that they do not give rise to undesirable mixtures of diastereoisomers when more than one metal centre is present, and as a bridging ligand, substituted tpy compounds are easier to make into rigid linear connectors than bpy or phen derivatives. Furthermore, substituted tpy compounds do not exhibit *fac*/*mer* isomerism as do their bidentate counterparts (Figure 11.9).

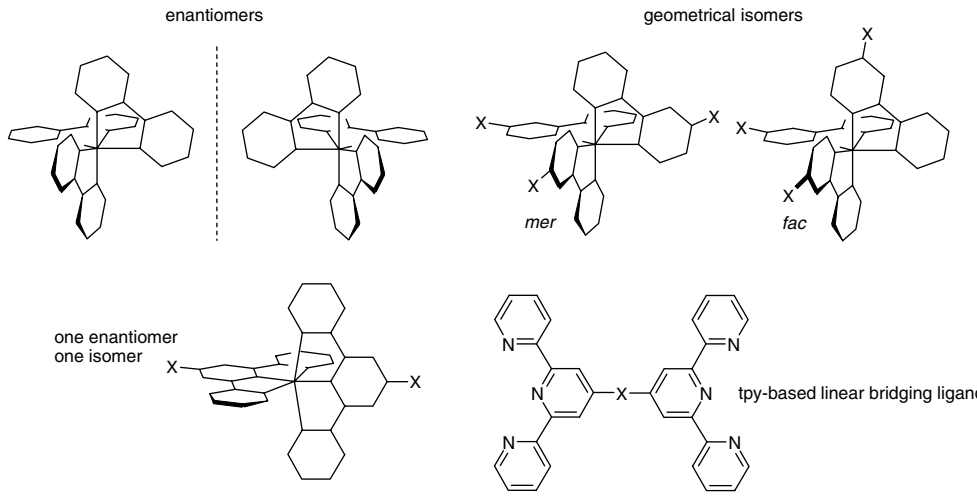


**Figure 11.9** Structural isomerism in homoleptic (same ligand) bpy and tpy complexes.

In order to take advantage of the simplicity of tpy chemistry, the ligand may be modified in two ways. Firstly, addition of electron acceptors to the 4′ position (X) increases the luminescence lifetime markedly (36 ns in the case of $SO_2Me$). On the other hand, sophisticated substitution of bpy- and phen-based units can also give linear bridging ligands, as in **11.4**.

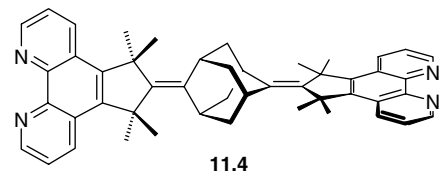

**11.4**

## 11.2.5 Bipyridyl-Type Light Harvesting Devices

Balzani, V., Juris, A., Venturi, M., Campagna, S. and Serroni, S., 'Luminescent and redox-active polynuclear transition metal complexes', *Chem. Rev.* 1996, **96**, 759–833.

Bpy-type ligands (including phen, tpy and a vast range of substituted derivatives) may be assembled with a number of different metal centres to give versatile photochemical devices *via* the *complexes as metals/complexes as ligands strategy* (Scheme 11.1). If we envisage the synthesis of a mononuclear

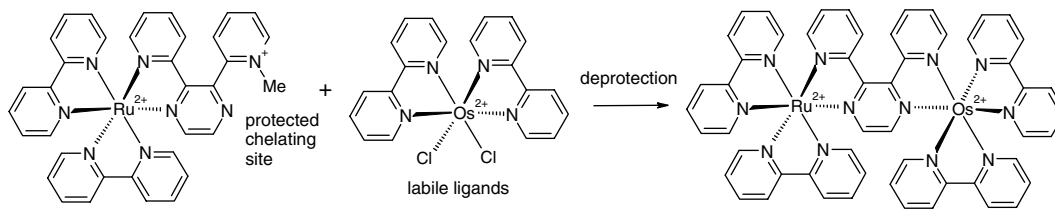


**Scheme 11.1** The complexes as metals/complexes as ligands strategy – a ruthenium(II) complex acts as a ligand for an osmium(II) complex.

metal complex as proceeding *via* the interaction of a metal ion with *n* ligands, then the assembly of multinuclear complexes may be carried out in an analogous fashion by replacing one or both of the metal (M) or ligands (L) with metal complexes with available binding sites.

The metal may be replaced by mono- or oligonuclear complexes with easily replaceable ligands such as $[Ru(bpy)_2Cl_2]$ (**11.5**), while the ligands may be replaced by mono- or oligonuclear complexes with uncoordinated lone pairs, as in (**11.6**). It is generally straightforward to prepare such unsaturated building blocks by simple control of reaction stoichiometry, since the complexes are relatively inert, or, if necessary, by protection *via N*-methylation of one of the nitrogen atoms.

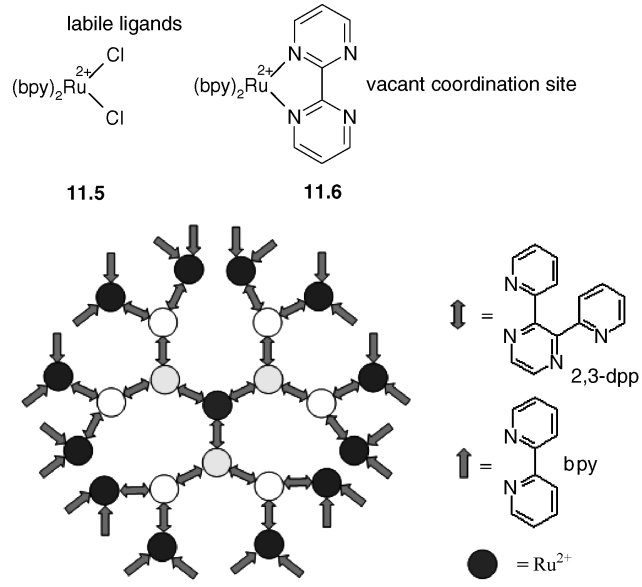


11.7

In this way, remarkable complexes have been built up, such as the 22-nuclear $[Ru\{(\mu\text{-}2,3\text{-dpp})[Ru(\mu\text{-}2,3\text{-dpp})Ru\{(\mu\text{-}2,3\text{-dpp})Ru(bpy)_2\}_2]_2\}_3]^{44+}$ (**11.7**). Compound **11.7** is an excellent example of the fact that metal complexes need to share the same bridging ligand in order to interact, thus the 12 peripheral $Ru^{2+}$ centres, which are not connected to one another in such a way as to allow electronic interaction between them, are all oxidised at the same potential in one single 12-electron process.

A typical class II mixed-valence compound based on the rigid bis(bpy) bridging ligand **11.8** has been synthesised by Vincenzo Balzani and co-workers from the University of Bologna, Italy.[6] This species may be prepared as the $Ru^{II}$-$Ru^{III}$, $Os^{II}$-$Os^{III}$ and $Ru^{II}$-$Os^{III}$ derivatives by a stepwise approach, as outlined above, starting with the less labile Os complexes in the mixed metal case. In each case, irradiation results in excitation of the $M^{II}$ centre, which acts as an electron donor. The $M^{II}$ centre is excited into a $^3$MLCT state of high energy, which then transfers its electron to the $M^{III}$ centre, resulting in the formation of an electronic isomer of the starting compound (Figure 11.10). In the case of the $Ru_2$ and $Os_2$ complexes of type **11.8a** and **11.8b**, the product is indistinguishable from the starting material, whereas the product from the mixed-metal **11.8c** is of type $Ru^{III}$-$Os^{II}$, which represents an excited state of the $Ru^{II}$-$Os^{III}$ ground state. The complex decays back to the ground state by thermal back-electron transfer. In each case, nuclear rearrangement is negligible because there is no change in the occupancy of the antibonding $e_g$ set of orbitals, which strongly affects M–L distances. The rate constant for the relaxation of the mixed metal system is appreciably slower than that any of the other processes, consistent with the lower driving force for

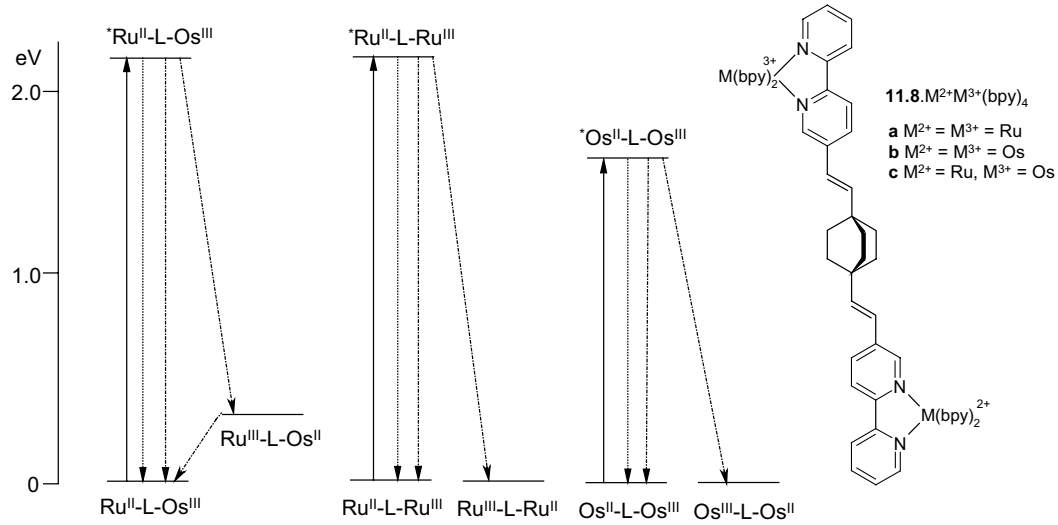


**Figure 11.10** Energy level diagrams for photoinduced electron transfer processed based on **11.8**, showing excitation (——), luminescence (- - - - ) and nonradiative decay (----).

the reaction. As supramolecular devices, these compounds represent the initial steps into charge separation and electronic switching.

One of the ultimate goals in the study of photoinduced electron transfer in polymetallic species of this type is the design of catalytic systems that can harness solar energy in order to carry out chemical reactions that are 'up hill' in energetic terms. The vast majority of such reactions (*e.g.* splitting of water into $H_2$ and $O_2$) are multi-electron processes. In natural photosynthesis, sophisticated antenna groups carry excitation to the reaction centre, which produces multiple high-energy electrons in order to bring about both the synthesis of $O_2$ from water and, more importantly, synthesis of reduced organic molecules from $CO_2$. Work in supramolecular photochemistry has therefore been directed to systems capable of multi-electron transfer, storage and catalysis. A schematic diagram of a simple example of such a process is shown in Figure 11.11. The two photosensitisers (PS) absorb light and transfer the resulting excited-state electrons to a central electron storage and reaction centre (SR). The SR component is capable of receiving two electrons, one from each PS group, and can therefore carry out a two-electron reduction upon multiple substrates to give a covalently bound product ($2\ Sub^+ \rightarrow Sub_2$). The resulting positive holes in the PS groups are filled by external sacrificial electron donors that are not, in themselves, sufficiently reducing to reduce $Sub^+$.

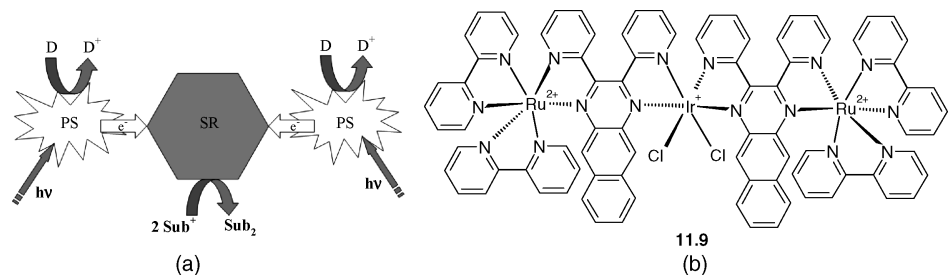


**Figure 11.11** (a) Schematic representation of a photochemical molecular device for photoinduced electron collection and multielectron catalysis. D = donor, PS = photosensitiser, SR = electron storage and reaction centre, sub = substrate. (b) a real prototype, compound **11.9**.[7]

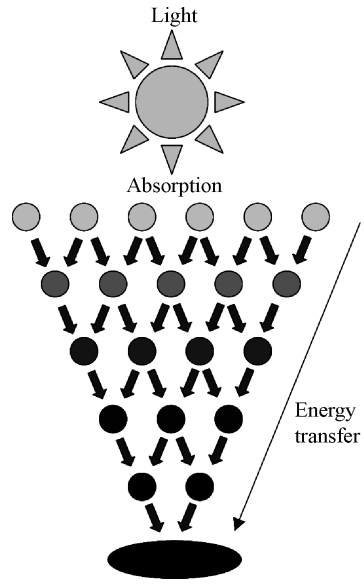


**Figure 11.12** Schematic representation of a supramolecular light-harvesting antenna device.

An example of a photochemical device capable of performing this kind of chemistry is compound **11.9**.[7] The PS groups are Ru(II) centres and the SR is an Ir(III) species. The complex as a whole is a class II mixed-valence compound. Photoabsorption and transmission by **11.9** is not very efficient, but it is able to catalyse the electrochemical reduction of $CO_2$ to formate *via* photoexcitation of the Ru(II) moieties and double electron transfer to the Ir(III) centre, transiently reducing it to Ir(I). The sacrificial donors are amines, such as dimethylaniline. The Ir(I) centre then reduces $CO_2$ to $HCO_2H$ in the presence of $H^+$. Extending this concept further, it should be possible to design large arrays of antenna components that gather energy and transfer excited electrons long distances *via* multiple 'hops' in order to concentrate them at a particular reaction centre. Current work on such systems includes photon-harvesting polymers with pendant chromophores and multiple porphyrin arrays. Dendrimer-based systems derived from metal polypyridyls are also of interest.

Using the complexes-as-metals/complexes-as-ligands strategy, polymetallic, cationic light harvesting molecules with dendritic type structure (for a discussion of dendrimer chemistry see Section 14.2) may be assembled reasonably easily. The 22-nuclear species **11.7** is an example of a third-generation dendrimer of this type and such species are excellent prototype supramolecular antenna devices capable of light-harvesting *via* an energy-transfer mechanism, analogous to biochemical photosynthetic membranes (Figure 11.12). Generally, dendritic multicentre metal complexes have been constructed based on Ru(II), Os(II) as well as Re(I) and other metal centres, using bridging ligands such as 2,3-dpp (as in **11.7**) and 2,5-dpp (**11.10**), and terminal ligands such as bpy (**11.1**) and biq (2,2′-biquinoline, **11.11**), Scheme 11.2.

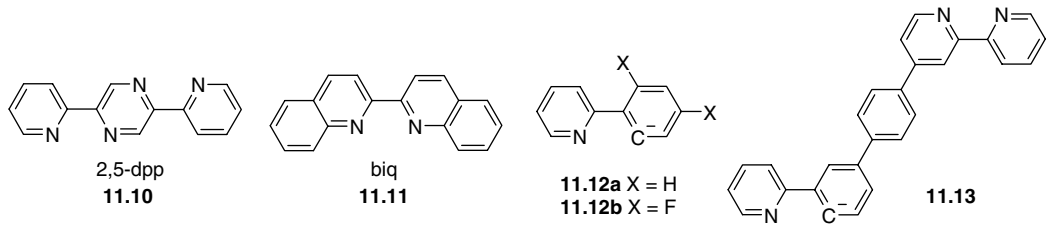

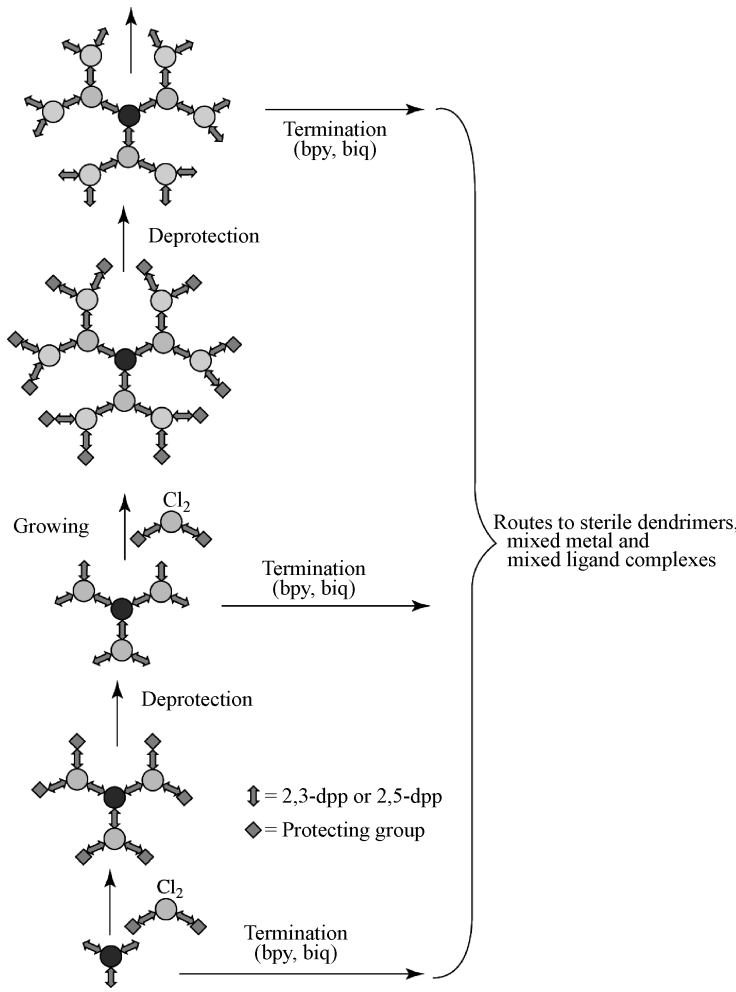


**Scheme 11.2** Dendrimer construction *via* the complexes-as-metals/complexes-as-ligands strategy – dendrimer generation increases ascending the diagram but growth is terminated by the horizontal processes.

The energy of the lowest MLCT state in each metal fragment (component) is readily predicted, and varies in a systematic fashion according to the identity of the metal and ligands. It is therefore possible to design electron- or energy-transfer cascade dendrimers by varying systematically the energy of the components' absorption from one generation to the next. Components with the lowest-energy MLCT bands (*e.g.* $Os(\mu\text{-}2,5\text{-}dpp)_3^{2+}$) are placed at the dendrimer core, and those with the highest energy absorptions terminate the dendrimer surface (*e.g.* $Ru(biq)_2(\mu\text{-}2,3\text{-}dpp)^{2+}$), resulting in controlled energy flow. Similarly, appropriate choice of fragment ordering can result in almost any combination of energy-transfer routes. All of the energy migration patterns for tetranuclear compounds shown in Figure 11.13 have been observed. Analogous systems containing six and ten components exhibit related, extended behaviour.

In extending these concepts to very large dendritic systems, it is likely that a wider range of metal ions and ligands will become necessary in order to give a smoothly graduated energy-transfer cascade.

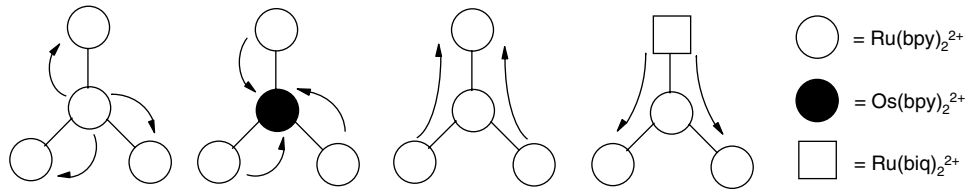


**Figure 11.13** Energy-transfer processes in tetranuclear (first-generation) complexes.

Metal ions such as Rh(III), Ir(III), Pd(II), Pt(II) and Pt(IV) may be used, although pyridyl-type ligands are less appropriate in these cases since they do not provide the required orbital energy levels. In such cases, combinations of pyridyl and N—C$^-$ carbanion ligands, such as deprotonated 2-phenylpyridine, are beginning to prove useful.

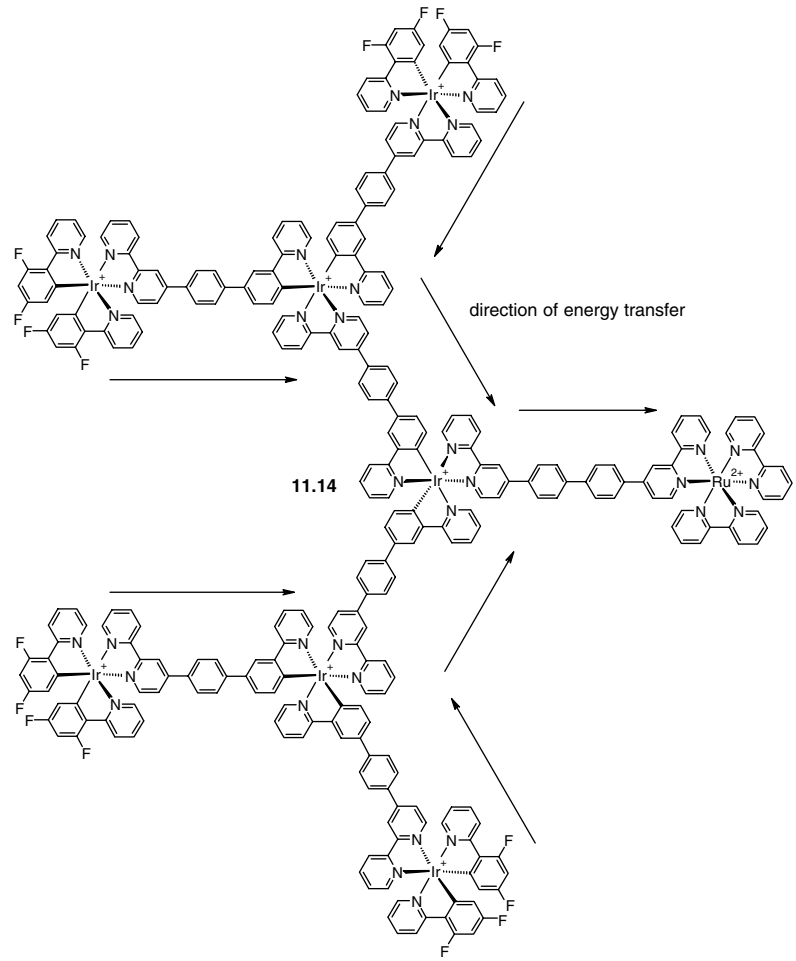


One example is the octanuclear iridium(III) compound **11.14** which uses the C,N-carbanion ligands **11.12** and **11.13**.[8] The periphery of the compound comprises fluorinated 2-phenylpyridine (**11.12b**) iridium units, linked *via* bridging ligand **11.13** to similar non-fluorinated iridium(III)

2-phenylpyridine centres. This iridium-based antenna array terminates in a ruthenium(II) tris(bpy) derived unit. All of the individual ruthenium and iridium based components absorb light and hence the absorption spectrum of the complex is roughly a sum of the absorption spectra of the individual fragments, which results in efficient light harvesting. However, in the emission spectrum, the maximum is observed at 630 nm which is a wavelength characteristic only of the ruthenium(II) component. What is happening is vectorial energy transfer from the periphery of the complex to the ruthenium(II) terminus. The synthesis of **11.14** is an interesting variant on the complexes as metals/complexes as ligands strategy in which palladium-catalysed Suzuki coupling is used to give the bridging ligand **11.13** from precursors that are already complexed to the metal centres.

Finally a particularly interesting strategy for creating long-lived charge-separated states as models for photosynthetic systems, in optoelectronics or as probes for DNA is the incorporation of more than one redox-active ligand within a ruthenium tris(bipy) complex. In the example shown in Figure 11.14 photoexcitation of one of the tetrathiafulvalene-derived dipyridophenazine (TTF-dppz) ligands results in electron transfer first to the ruthenium and then onto one of the other TTF-dppz substituents resulting in a charge-separated state TTF-dppz$^{-}$-Ru$^{2+}$-dppz-TTF$^{+}$ with a remarkably long lifetime of 2.3 μs, four orders of magnitude longer than the excited state of the ligand itself, because of the slow back-electron transfer from one ligand to another. [9]

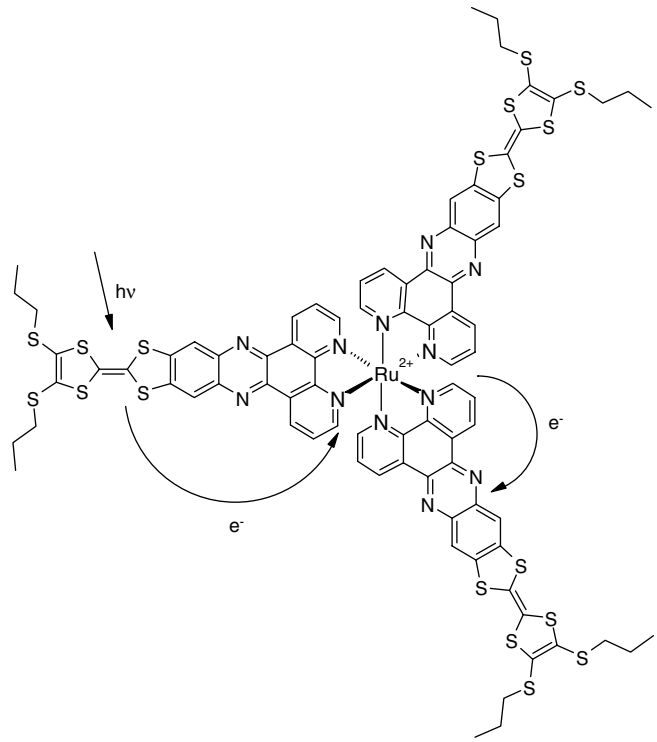


**Figure 11.14** A ruthenium(II) complex of an annulated donor–acceptor (D–A) ensemble, 4′,5′-bis (propylthio)tetrathiafulvenyl[i]dipyrido-[3,2-a:2′,3′-c]phenazine (TTF-dppz) exhibiting a long-lived charge-separated state TTF-dppz$^{-}$-Ru$^{2+}$-dppz-TTF$^{+}$ on photoexcitation.[9]

## 11.2.6 Light-Conversion Devices

Ward, M. D., 'Transition-metal sensitized near-infrared luminescence from lanthanides in d-f heteronuclear arrays', *Coord. Chem. Rev.* 2007, **251**, 1663–1677.

Taking advantage of the phenomenon of luminescence, it should be possible to design a photochemical device that is capable of absorbing light of one wavelength and re-emitting it at another. This simple task is performed by any luminescent species. In terms of tuneability of the wavelength of the emission and gathering the maximum amount of incident light, however, a supramolecular device offers the possibility of a modular approach. If we break the light conversion process down into a combination of absorbance (A), energy transfer (ET) and emittance (E) steps, then the functionality of the device must be of the A–ET–E type. An optimum device may be designed if the light absorber or antenna, light emitter and the degree of coupling between them may be tuned separately. The combination of coupled absorber and emitter thus produces a light-conversion device with optimal properties such as maximum light collection and emission at the desired wavelength.

In component terms, the bpy moiety offers significant scope as a light harvester, as we have seen earlier. The basic bpy motif is highly tuneable, and antenna (absorber) components might be produced from a range of biaryl and heterobiaryl moieties of the bpy type. Luminescent emitters might be metal ions such as the lanthanides Eu(III) and Tb(III), which offer an extensive manifold of *f*-electron states. The coupling between the A and E components could then occur *via* a metal–ligand interaction. This concept has been realised by the construction of lanthanide cryptates such as **11.15** and **11.16**.

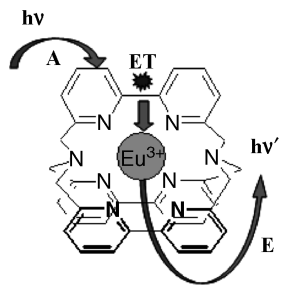


**11.15**

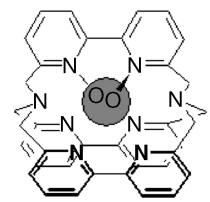

**11.16**

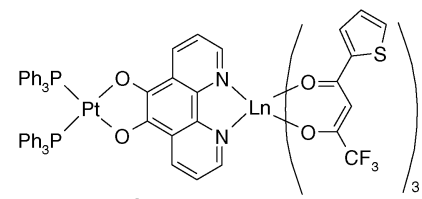


Ln = La, Gd, Nd, Yb, Er

**11.17**

Ordinarily, $Eu^{3+}$ is not luminescent in aqueous solution because excitation is quenched by solvent molecules without emission. Complexation by the tris(bipyridyl) cryptand ligand, however, protects the metal ion from the solvent, while simultaneously providing light-harvesting bpy units. The high charge of the $Eu^{3+}$ cation, coupled with the macrobicyclic stabilisation offered by the ligand, means that the complexes are highly stable. The complexes are brightly luminescent, with **11.16** especially exhibiting very efficient energy conversion of the order of about 60 % of the incident light. The presence of the *N*-oxide substituents stabilises the complex because of the hardness of the ligand, which matches that of the lanthanide ion, and increases ET coupling.[10]

A heterobimetallic *d-f* block metal strategy has also been used in the conversion of visible to near-infrared light in complexes such as **11.17** which can be readily prepared by the complexes-as-metals-complexes-as-ligands strategy. Excitation of the platinum(II) moiety at 520 nm in a variety of lanthanide derivatives of **11.17** results in each case in the characteristic lanthanide near-infrared emission.[11] These kinds of complexes are of potential in biological imaging because human tissue is relatively transparent at longer wavelengths (the light of an electric torch shone through

your hand appears red because the short wavelength blue light is absorbed) and in telecommunications since the emission wavelengths of particularly Pr(III) (*ca.* 1330 nm) and Er(III) (*ca.* 1550 nm) closely match the 'windows of transparency' in the silica waveguides used for fibre-optic data transmission.

### 11.2.7 Non-Covalently Bonded Systems

Ward, M. D. 'Photoinduced electron and energy transfer in noncovalently bonded supramolecular assemblies', *Chem. Soc. Rev.*, 1997, **26**, 365–375.

In the systems we have examined so far, coupled photoexcitation and electron transfer (eT) or energy transfer (ET) processes have occurred in strongly bonded systems, held together by covalent bonds or coordinate interactions with a significant degree of covalency. In these cases there is a well-defined spatial relationship between the light-absorbing group and the external donor or acceptor (termed a *quencher*, since it quenches the luminescent re-emission of the absorbed light by providing an alternative deexcitation pathway). An excellent example of the modularity of such covalent systems is **11.18**, a synthetic system that combines two of the key ingredients in natural photosynthesis: a metal porphyrin chromophore and a quinone quencher as an external electron acceptor. The two components are linked covalently by a long, $\pi$-conjugated bridge. Electron transfer along the bridge results in reduction of the quinone to a semiquinone and ultimately a hydroquinone.

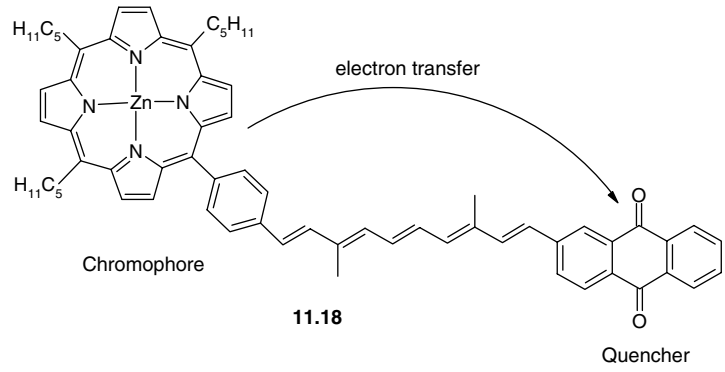


**11.18**

It is possible to design analogous modular (and therefore supramolecular) systems in which the components are joined by entirely noncovalent interactions such as hydrogen bonding. In this way, the concepts of self-assembly and molecular device design may be combined in order to provide a route into the preparation of much more sophisticated device arrays. The key is to construct functional components bearing mutually complementary and interacting binding sites. Such an approach can only be effective if non-covalent interactions can form an effective conduit for the eT or ET process; in order to test this possibility, two porphyrin-based systems **11.19** and **11.20** have been designed. Both systems involve photoexcitation of the Zn(II) porphyrin component, followed by electron transfer to the Fe(III) moiety, resulting in reduction to Fe(II). This electron transfer must occur *via* a hydrogen-bonded link in **11.19** or a covalent $\sigma$-bond framework in **11.20**. Remarkably, not only are both systems effective at carrying out this process, but the photoelectron transfer rate constants of $8.1 \times 10^9$ and $4.3 \times 10^9$ $s^{-1}$ for **11.19** and **11.20**, respectively, suggest that the familiar carboxylic acid double hydrogen bond is more effective at transmitting the excited electron than the $\sigma$-framework in **11.20**.

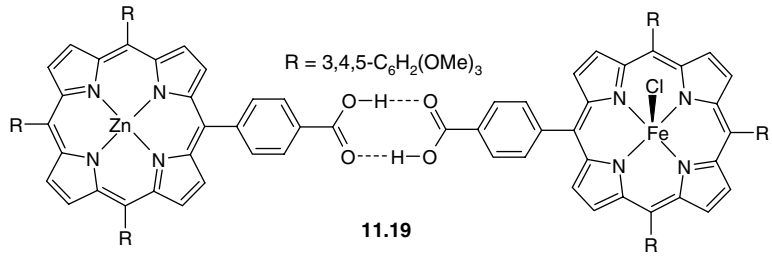


**11.19**

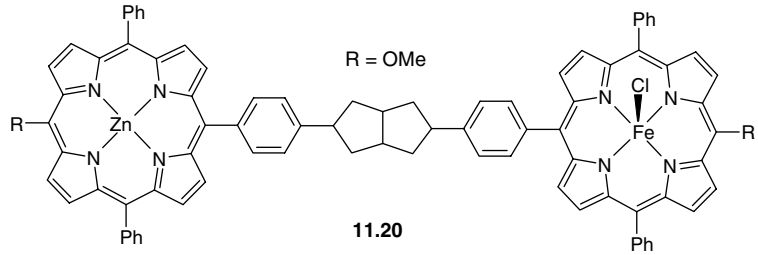


**11.20**

Consistent with the principles outlined in Chapter 1, strong hydrogen-bonded association may be achieved by multiple complementary interactions, as in the barbiturate-appended porphyrin system shown in **11.21** (*cf.* molecular rosettes, Section 10.6.4). This receptor binds a complementary dansyl (dimethylaminonapthalene-sulfonyl) group with an association constant in excess of $10^6$ $M^{-1}$. In this case, electron transfer is from the photoabsorbing dansyl group to the porphyrin acceptor; quenching is almost total, suggesting very fast electron transfer relative to the rate of fluorescence.[12]

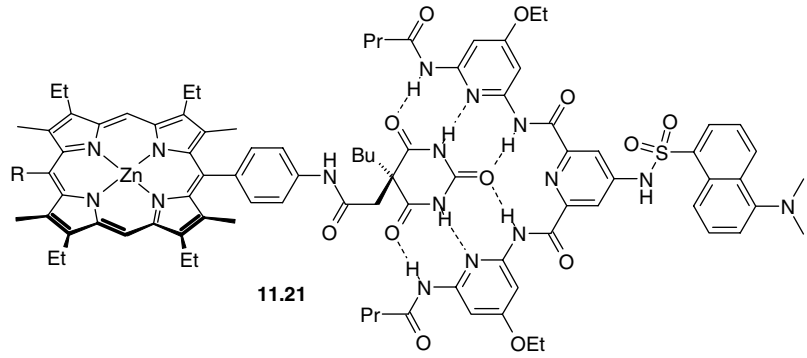


**11.21**

A remarkable example of a photon acceptor is **11.22**, which, instead of possessing a molecular chromophore, relies upon a nanoparticle of $TiO_2$ semiconductor about 2.2 nm in diameter.[13] The semiconductor particle is held in place by absorption of the alkyl chains of the diamidopyridine-based receptor to its surface. The nanocrystallite of $TiO_2$ has a small energy gap (band gap) between its valence electron states and its conduction band of empty orbitals. Photoexcitation at 355 nm can promote an electron from the valence to the conduction band, and the excited electron can then undergo electron transfer across the hydrogen-bonded connector to the viologen (4,4′-bipyridinium) acceptor. Control experiments show that the presence of the hydrogen bond is essential for electron transfer to take place, and without it through-space or collision-activated transfer does not occur.

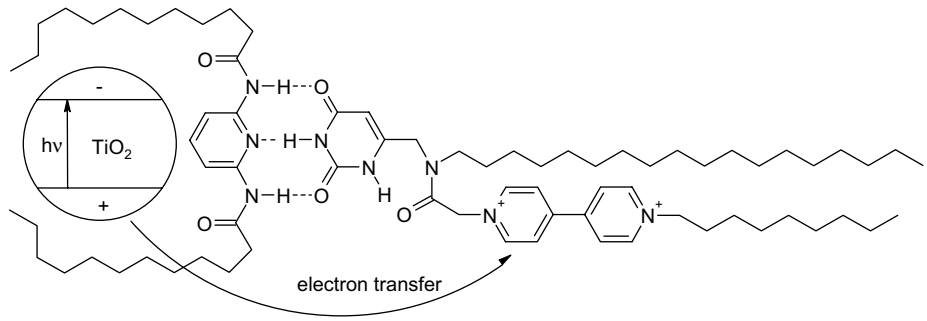


**11.22**

Even $\pi$-stacking interactions can be used to mediate electron transfer between components in photochemical devices. Compound **11.23** uses the intrinsic curvature of the glycoluril building block (Section 6.2.4) to position a quinone acceptor some 9 Å above a porphyrin chromophore in a U-shaped arrangement. In $CCl_4$ solution, the inner surface of the 'U' is filled with solvent molecules and the electron must traverse the very long through-bond pathway from chromophore to acceptor, resulting in very little electron-transfer quenching. In contrast, addition of an aromatic guest molecule such as hexyl-3,5-dihydroxybenzoate results in guest binding within the U-shaped cavity of the molecule, which acts as a solution host for aromatic guests. The guest is bound by a combination of $\pi-\pi$ stacking interactions and hydrogen bonds to the amide carbonyl groups at the bottom of the molecular cleft. Electron transfer can then be mediated *via* the $\pi$-system of the guest and, as a result, 75 % of the luminescence of the porphyrin fragment is quenched by electron transfer *via* the aromatic guest to the quinone acceptor (Figure 11.15). This kind of electron transfer *via* a $\pi$-stacked system is reminiscent of the electron-transfer processes within the DNA $\pi$-stacked double helix.

A particularly novel kind of two-component energy transfer device is the pH switched 'plug and socket' system shown in Scheme 11.3. When unbound there is no interaction between the binapthyl unit attached to the crown ether and the anthracene-appended secondary amine. However, protonation of the amine causes its complexation by the crown ether (as in Section 3.12.1) bringing the two chromophores into close proximity just like putting a plug into a socket. Energy transfer can then occur from the binapthyl group to the anthracenyl unit and hence irradiation of the binapthalene results in fluorescence of the anthracene-derived chromophore. If the methyl substituent is replaced by a bulky group such as phenyl then no complexation occurs because the plug does not fit the socket and hence no anthracenene fluorescence is observed on binapthalene excitation.[14] This concept has been further extended to give a three-molecule system in which if the two terminal molecules are a

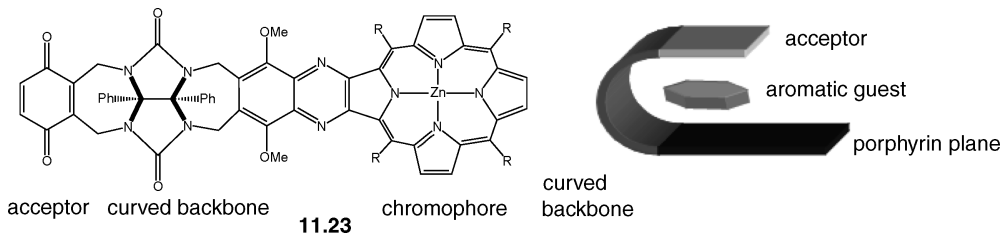


**11.23**

**Figure 11.15** Photochemical electron transfer mediated by $\pi$-stacking interactions with an aromatic guest.

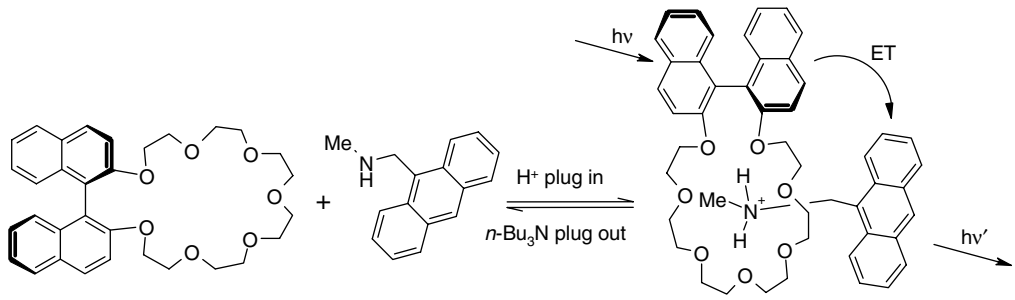


**Scheme 11.3** A supramolecular 'plug-and-socket' system.[14]

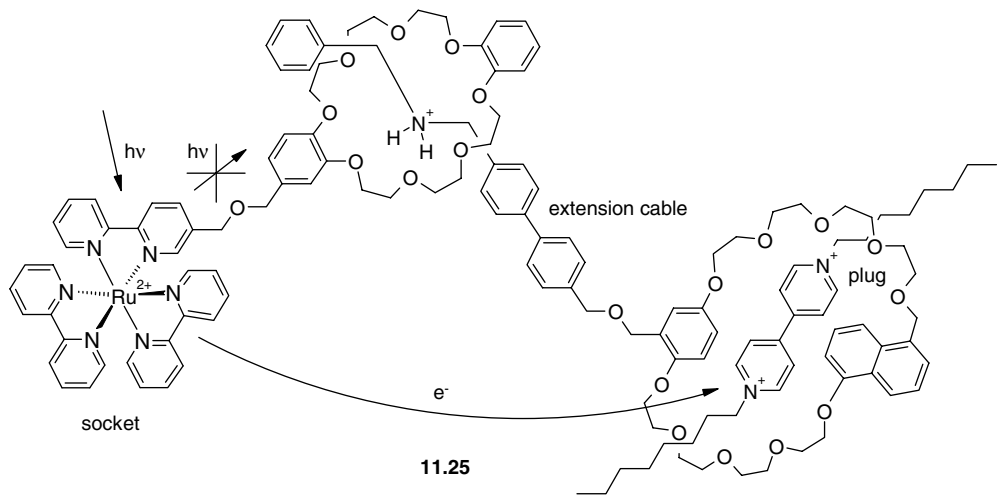


**Figure 11.16** A molecular extension cable as part of the 'plug and socket' concept.[15]

plug and socket, a central component is a molecular analogue of an 'extension cable'. The system is shown in Figure 11.16 with ammonium ion binding by the crown ether portion of the ruthenium(II) tris(bipyridyl) appended chromophore linking in a receptor site for a bipyridinium electron acceptor. Thus photoexcitation of the ruthenium-containing 'socket' results in electron transfer across the molecular extension cable to the bipyridinium 'plug'.[15]

Because of the sensitivity of fluorescence detection this kind of FRET process (Section 11.2.2) has also been used to study self-assembly mechanisms at extremely low concentrations, *e.g.* of resorcarene hexameric capsules. We have already seen the self-assembly of resorcarene hexamers in Section 10.6.3. This kind of self-assembly is generally studied by NMR spectroscopy in the millimolar range. Appending fluorophores to the resorcarene capsules enables much lower concentrations to be addressed. Rebek Jr. and co-workers (Scripps, USA) have tagged [4]resorcarenes with two different chromophores, namely pyrenyl (donor) and perylenyl (acceptor) groups. Mixing the two pure hexamers at nanomolar concentration results initially in observation only of the fluorescence of the donor. Over time, however, the self-assembled hexamers disproportionate to give mixed hexamers in which donor and acceptor are both present in the same assembly, resulting in the growth of acceptor emission by a FRET process,

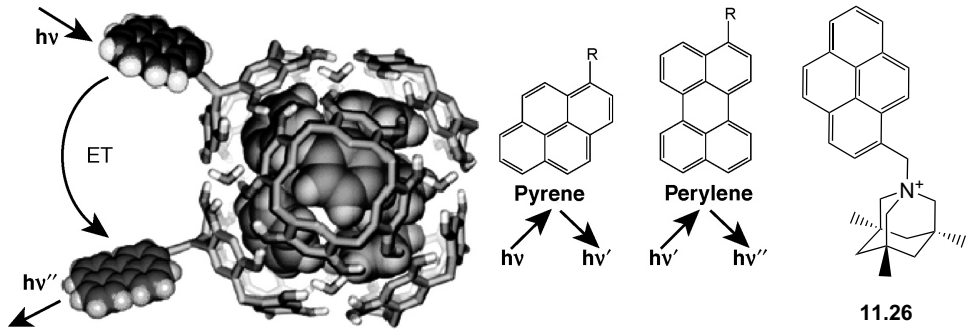


**Figure 11.17** Model showing the FRET process between pyrenyl donor and perylenyl acceptor in hexameric [4]resorcarene capsules containing benzene guests (reproduced from Reference 16) along with the structure of the fluorescent guest **11.26**.

Figure 11.17. The emission can be used to monitor the kinetics of capsule assembly showing it to be relatively fast under these dilute conditions (capsule half life *ca.* 10 mins depending on solvent). Addition of methanol to the chloroform solution to disrupt the hexamer assembly also results in loss of the FRET emission. FRET was also observed from the outside to the inside of the cavity using a fluorescent guest **11.26**.[16]

## 11.3 Information and Signals: Semiochemistry and Sensing

### 11.3.1 Supramolecular Semiochemistry

Fabbrizzi, L., Poggi, A., 'Sensors and switches from supramolecular chemistry', *Chem. Soc. Rev.* 1995, 197–202.

*Semiochemistry* is the name given to the area of supramolecular chemistry that is concerned with what might be termed, broadly, signalling devices. The term comes from 'semiotics,' meaning the study of signs or symbols and their use or interpretation. Thus, in biochemistry, a semiochemical is a substance such as a pheromone that conveys a signal from one organism to another. We looked briefly at biological semiochemistry, a process fundamentally based in molecular recognition, in Section 2.8. The most obvious area of application for semiochemistry is in the production of molecular sensor devices: compounds that can carry out the twin tasks of both molecular recognition and sensing. The basic concept of a molecular sensor is illustrated in Figure 11.18. The substrate (guest, analyte) must be attracted to a receptor portion of the sensor. This is a straightforward molecular recognition event, and the receptor can be any of the systems, such as crown ethers, cryptands, cavitands and so on, discussed in Chapters 3–6. The binding must be selective for the target substrate in the presence of a range of other potential guest species, depending on the system and its environment. The mere act of binding, however, is not enough. The receptor must also be in communication with a signalling unit that is responsive to the guest binding, which generates a signal in the form of an emission of electromagnetic radiation (photochemical sensing), a current (electrochemical sensing) or an otherwise externally measurable change (*e.g.* in colour or pH). This *transduction* implies automatically that the spacer that joins the signalling and receptor units together must permit communication between the two of them, and that the binding event must trigger intrinsically a change in the properties of the bound complex compared to the free

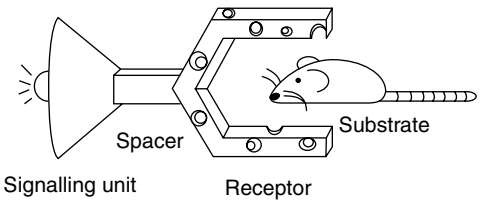


**Figure 11.18** Cartoon representation of a chemical sensor.

guest or receptor, which results in signal generation. Criteria for the construction of useful sensors may be summarised as:

- stability
- guest (analyte) selectivity
- guest affinity
- efficient signal transduction
- emission of detectable intensities of UV or visible radiation or other quantifiable signal
- kinetically rapid sensitisation
- ease of delivery to the target system
- availability.

One of the potential applications of these kinds of hosts is in analytical chemistry, in which the host is used to bind and recognise small quantities of analytes. If analyte concentration is particularly low, then high affinities are necessary in order to produce a measurable concentration of the complex and hence give a response. Unfortunately, high affinity and high selectivity are often antagonistic. Hosts that exhibit high binding constants often bind well to a wide variety of guest species, whereas hosts that are highly selective often exhibit low binding constants. This behaviour is frequently due to the fact that selectivity often arises from a strong, non-selective host–guest affinity (*e.g.* solvophobic binding or electrostatic attraction) coupled with a weaker repulsive interaction (*e.g.* unfavourable steric effects), which varies in magnitude according to the precise nature or geometry of the guest.

In its broadest sense, however, semiochemistry is more than just sensing. It also incorporates aspects of signal generation, processing, transfer, amplification, conversion and detection. In other words, all of the kinds of concepts associated with modern computers and electronic devices. The construction of molecular electronic devices is discussed in detail in Section 11.4. For the moment, we will concern ourselves with signal generation in chemical sensors. In other words how a supramolecular host-guest binding and recognition event can be transduced into a measurable output, be it either a change in colour and hence absorbance, a change in the intensity or wavelength of emitted light or a change in redox potential.

## 11.3.2 Photophysical Sensing and Imaging

Gunnlaugsson, T., Glynn, M., Tocci, G. M., Kruger, P. E., Pfeffer, F. M., 'Anion recognition and sensing in organic and aqueous media using luminescent and colorimetric sensors', *Coord. Chem. Rev.* 2006, **250**, 3094–3117.

When we come to the specific design of artificial molecules capable of signalling the presence of particular analytes to a human observer, it is not sufficient to have only molecular recognition, but also transduction of that recognition event in a process that ultimately leads to an observable signal. A particularly sensitive method of signal production is the emission of visible light; either visible to the human

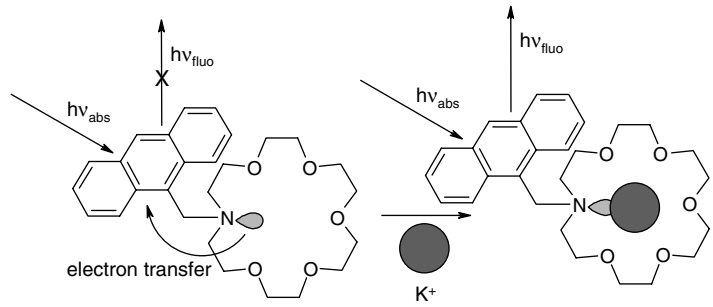


**11.27**

**Scheme 11.4** Cation sensing by anthracene-substituted azacorand **11.27**.[19]

eye, or more commonly to a sensitive detection device such as a fluorescence spectrometer. Fluorescence detection is particularly sensitive and can detect guests down to nanomolar concentrations.

An elegantly simple example of a modular fluorescent sensor system is the 'crown-anthracene' system (**11.27**) prepared by A. P. de Silva (Belfast, UK). This landmark sensor consists of an anthracene-based lariat ether (Section 3.3.2). The aza[18]crown-6 moiety acts as the receptor and is selective for $K^+$ amongst the alkali metal cations. The signalling unit is the anthracene moiety. Free anthracene exhibits strong fluorescence corresponding to the $\pi - \pi^*$ transition. In **11.27**, however, this fluorescence is quenched entirely as a result of electron transfer from the reducing nitrogen lone pair. The —$CH_2$— spacer is short enough to allow effective electron transfer to occur (Scheme 11.4). In the presence of $K^+$, however, this lone pair becomes involved in interactions to the metal centre as part of the binding by the macrocyclic ring. As a result, it is no longer available to quench the anthracene fluorescence on purely thermodynamic grounds (*i.e.* its oxidation potential is significantly lowered). As a result of $K^+$ binding, therefore, the anthracene fluorescence is 'switched on' and may be detected by an interrogatory irradiation and measurement of the resulting fluorescence intensity. This kind of sensor is called a PET (photon-induced electron transfer) sensor.[19]

A related anthracene-based ditopic sensor (**11.28**) has been constructed, which can recognise diammonium cations along the same lines as **3.103** (Section 3.12.3). Use of the anthracene-derived group as a spacer as in **11.27** gives fluorescent recognition of $H_3N^+(CH_2)_nNH_3^+$ guests as a function of spacer length.[20]

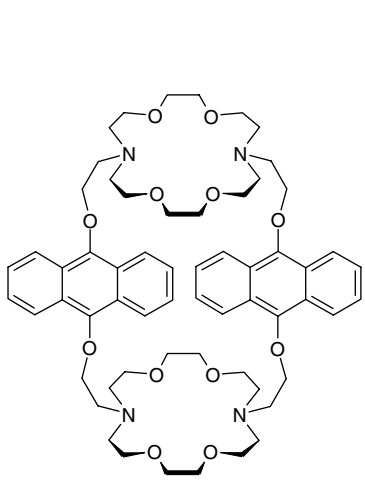

**11.28**

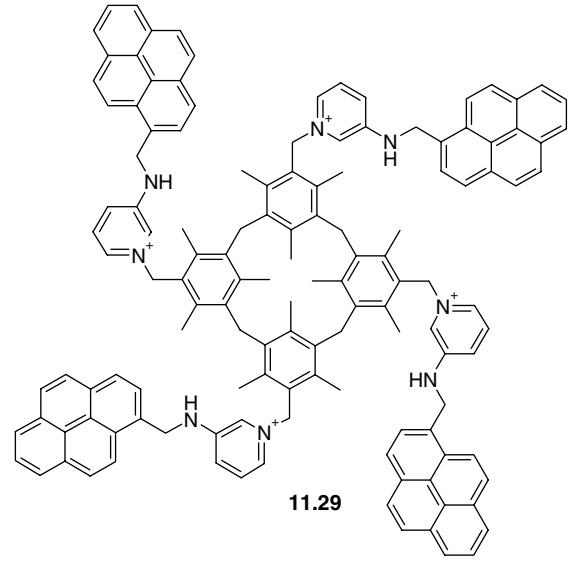

**11.29**

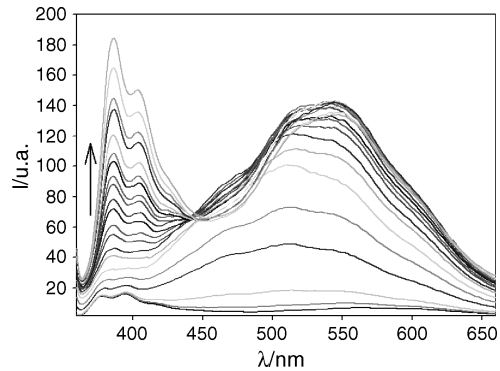


**Figure 11.19** Fluorescence spectra ($\lambda_{exc}$ = 343 nm) of **11.29** in $CH_3CN$ upon addition of increasing amount of $Cl^-$. The broad band at *ca.* 520 nm corresponds to pyrene excimer emission while the band at *ca.* 380 nm is from the pyrene monomer.[21]

A fluorescent 1,3-alternate calix[4]arene based sensor in which dual emission is 'switched on' according to the amount of chloride anion added has been prepared by Steed and Prodi (Durham, UK and Bologna, Italy). Compound **11.29** is a ditopic receptor containing two pairs of anion-binding aminopyridinium moieties and is able to bind a range of anions including chloride and particularly dicarboxylates. The characteristic pyrenyl fluorescence is quenched, however, by PET to the pyridinium acceptor. Addition of chloride (and only chloride!) reduces the acceptor ability of the pyridinium unit resulting in fluorescence. Moreover, the chloride binding between the two 'arms' brings the pyrenyl groups into close mutual proximity resulting in pyrene excimer formation with emission at *ca.* 500–550 nm (Figure 11.19). Addition of further chloride results in binding at the second site but due to negative allosteric effects (Section 1.5) excimer formation is not sterically feasible and hence emission at *ca.* 380 nm occurs, characteristic of a pyrene-derived monomer.[21]

The fluorescence properties of the $[Ru(bpy)_3]^{2+}$ moiety have also been used in a number of sensing applications, particularly in anion sensing, where it is possible to take advantage of the component's positive charge. A substituted bpy-based sensor for chloride has been developed by Paul Beer (Oxford, UK).[22] The hosts are based on an azacorand binding site, which can complex chloride *via* four N—H ··· Cl hydrogen bonds, with additional assistance from C—H ··· Cl bonds and the positive charge imparted by the $[Ru(bpy)_3]^{2+}$ derived units. Compound **11.30** was shown by $^1H$ NMR titration to complex chloride with an association constant of about $4 \times 10^4\ M^{-1}$ in DMSO, while $H_2PO_4^-$ was not bound at all, an observation attributed to the rigidity of the small macrocycle. The presence of two luminescent centres complicates the fluorescence sensing by **11.30** and so mixed electrophotosensors **11.31** were prepared. These compounds bind chloride with the same kind of affinity as **11.30** and, in the presence of one mole equivalent of chloride, significant enhancements (a factor of about three) are observed in the fluorescence emission spectra of **11.31b**.

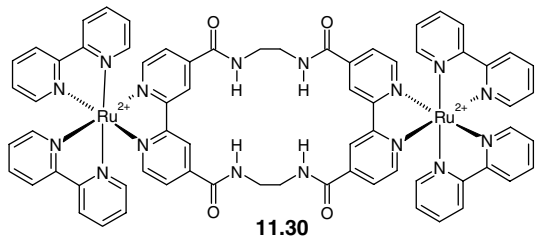

**11.30**

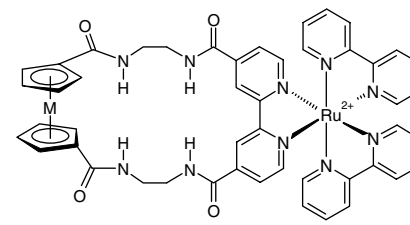

**11.31** **a** M = Fe
**b** M = $Co^+$

Sensitised lanthanide(III) complexes of macrocyclic podands such as **11.32** and **11.33** are particularly versatile luminescent sensors of cations, anions and pH and have been used extensively in biological systems.[23] While the lanthanide metal ions themselves are poor absorbers because the relevant *f-f* transitions are partially Laporte forbidden, their emission can be triggered by energy transfer from a sensitising aromatic group in a similar way to the energy conversion devices described in Section 11.2.6. Lanthanide ions have particularly long lived excited state lifetimes (typically $\mu$s for the near IR emission of $Yb^{3+}$, $Er^{3+}$ and $Nd^{3+}$ to ms for $Eu^{3+}$ and $Tb^{3+}$) because their emission, like their absorption, is Laporte forbidden. This long-lived emissive state allows time resolved methods to bring about extremely sensitive detection by introducing a delay before measuring to allow fluorescent processes to decay and eliminate interference from light scattering. This low background allows detection limits in the $10^{-12}$–$10^{-15}$ M range. In addition lanthanide emission peaks are very sharp compared to organic fluorophores (typically full width at half maximum less than 10 nm) because the core nature of *f* electrons means that they are not susceptible to broadening from changes in ligand field splitting arising from ligand vibrational motion. An example based on $Tb^{3+}$ showing broad ligand fluorescence and much sharper lanthanide emission is shown in Figure 11.20. Indeed, the metal-based emission profile is roughly similar for each lanthanide complex, although particularly for Eu(III) and Yb(III) complexes the relative intensity and overall form of the spectrum is dependent on coordination environment meaning that peak intensity ratio analysis can be used. There are three principal ways to utilise the emission of these types of compound, listed below, and their photophysics is summarised in Scheme 11.5.

1. Perturbation of the lanthanide singlet excited state, in which quenching by electron- or charge-transfer processes may be altered by the binding of analytes to the metal centre. For example the *N*-alkylphenanthridinium unit in **11.32** binds selectively to the electron-rich guanine-cytosine

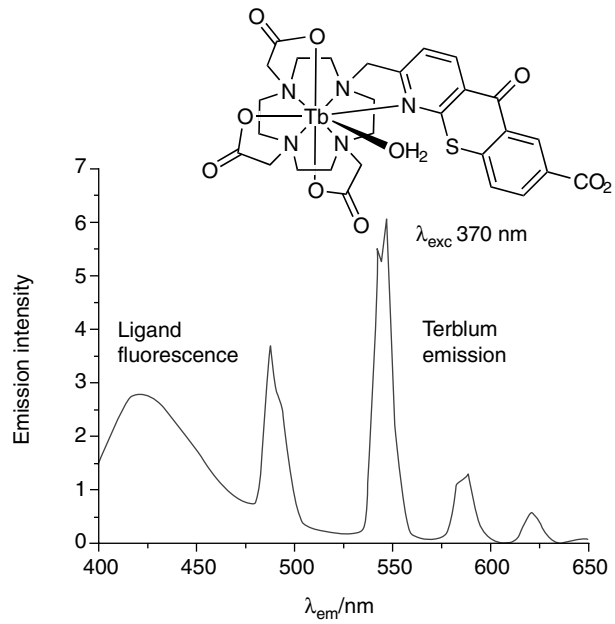


**Figure 11.20** The ligand fluorescence arising from the sensitiser is much broader than the lanthanide-based lines (reproduced by permission of The Royal Society of Chemistry).

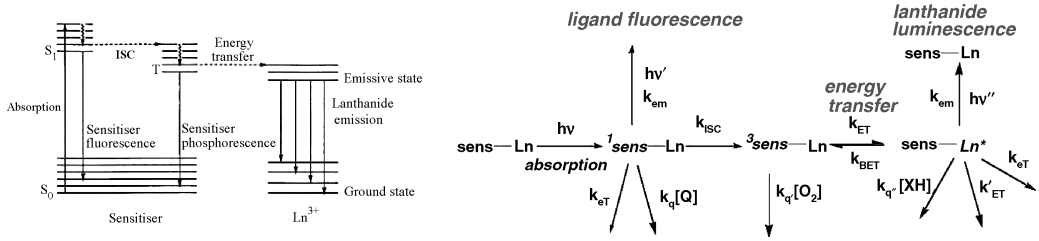


**Scheme 11.5** Photophysics of sensitised lanthanide sensors 'sens–Ln' such as **11.32** and **11.33**. Key: $k$ = rate constant, em = emission, eT = electron transfer, q = quenching, isc = inter-system crossing to triplet state, (B)ET = (back) energy transfer (reproduced with permission from Reference 24).

base pairs in DNA and oligonucleotides leading to quenching of the single fluorescence from the sensitiser $\pi$-system by a factor of up to 20. The energy transfer to the Eu(III) centre is also reduced and hence there is also a reduction in the metal-based emission.

2. Perturbation of the triplet excited state of a sensitising chromophore, *e.g.* by protonation or metal binding. This process alters the rate of forward or reverse energy transfer between metal and sensitising chromophore. In these systems the triplet state of the organic $\pi$-system is sensitive to quenching by collision with molecular oxygen, and hence when the oxygen quenching rate is similar to the energy transfer rate the emission intensity of the lanthanide and the emission lifetime are related to the amount of dissolved oxygen in solution.
3. The excited lanthanide ion itself may be quenched by intermolecular energy transfer to a nearby acceptor.

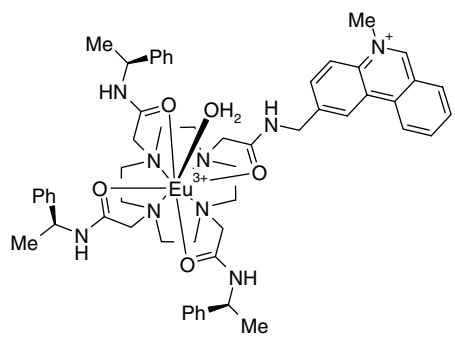


**11.32**

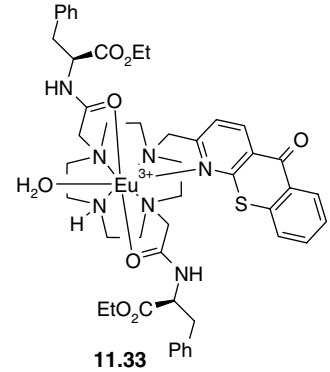


**11.33**

Lanthanide complexes such as **11.33** have been used as sensitive probes for biological cell imaging. Complex **11.33** is a ratiometric citrate sensor in which citrate replaces the bound water molecule (substitution of bound water is a general feature of anion sensing by these kinds of species). Citrate is a vital part of a number of biochemical pathways, notably the synthesis of fatty-acids, nitrogen metabolism and photorespiration. The form of the europium emission is dependent on local citrate concentration in biological media and the compound is taken up by living cells where it selectively stains the intranuclear cell nucleoli (sub-organelles of the cell nucleus). The bound complex can be imaged by fluorescence microscopy showing it is co-localised with conventional intra-nuclear stains such as 'SYTO-RNA-select', Figure 11.21. The emissive species is thought to be a protein-bound complex since cellular RNA quenches the emission. Finally, in these systems the presence of coordinated water molecules also allows them to find useful applications as MRI contrast agents.[23]

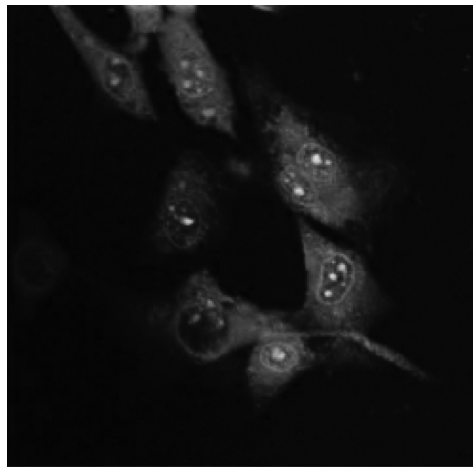

**Figure 11.21** Confocal fluorescence microscope image showing the cellular localisation behaviour of the europium complex **11.33** in living cells, revealing the staining of the nucleolus inside the cell nucleus (reproduced by permission of The Royal Society of Chemistry). See plate section for colour version of this image.

The development of compounds for measurement of the distribution and concentration of biologically important metal ions such as $Zn^{2+}$, $Ca^{2+}$ and $Mg^{2+}$ is of particular interest in sensor technology. Calcium and magnesium distributions across cell membranes are of great importance in various cellular triggering and regulating functions; zinc is a vital component of a number of key enzymes, such as carbonic anhydrase and zinc finger proteins, and influences DNA synthesis, apoptosis (programmed cell suicide, *e.g.* in formation of limbs and digits in embryos) and gene expression. It is of particular interest to be able to detect one of these cations in the presence of the others in tissue samples. The first ligand able to carry out this kind of function was TSQ (**11.34**), which acts as a selective fluorescent stain for $Zn^{2+}$ in the presence of $Ca^{2+}$ and $Mg^{2+}$.[25] Unfortunately, fluorescence intensity varies with the medium, and as the stoichiometry of the compounds is not at all clear, the system is far from ideal. An improved fluorophore is Zinquin (**11.35**). Zinquin is able to diffuse across lipophilic cell membranes because it is a neutral species. Once inside the cell, it is hydrolysed by esterase enzymes and complexes $Zn^{2+}$ as an anionic chelate ligand. Both 1:1 and 2:1 complexes are formed with binding constants of the order of $10^6$–$10^7$ $M^{-1}$ at physiological pH. This kind of affinity is sufficient for the detection of $Zn^{2+}$ within living cells, but will not allow interaction of Zinquin with tightly bound zinc in metalloenzymes and zinc finger proteins.

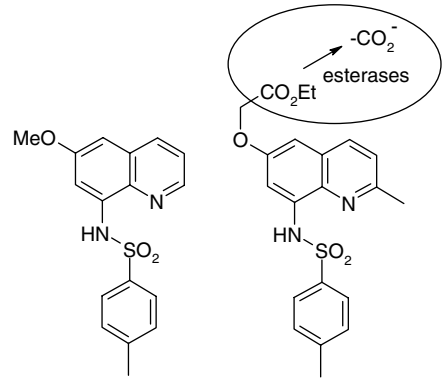


**11.34** **11.35**

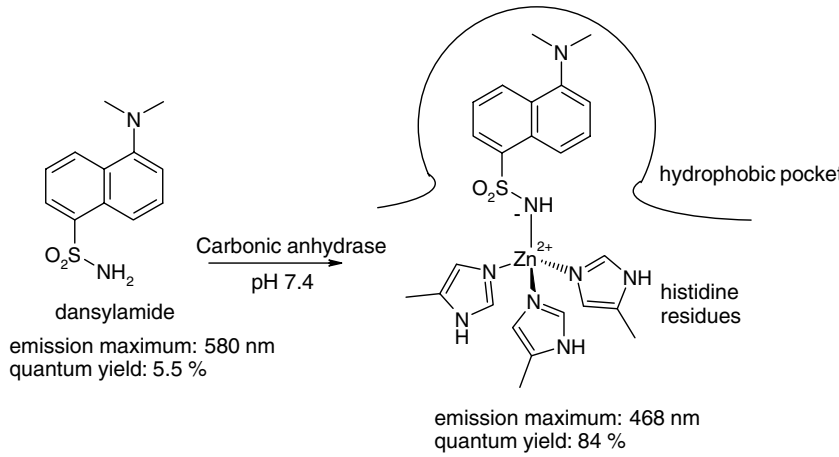


**Scheme 11.6** Fluorescence enhancement and blue-shift in dansylamide upon binding to carbonic anhydrase.[25]

The design of zinc sensors with much higher affinities was inspired by the observation that in the presence of the zinc-containing enzyme carbonic anhydrase (CA), the fluorescence intensity of the fluorophore dansylamide is enhanced dramatically and blue-shifted significantly (Scheme 11.6). This change is attributed to the incorporation and protection of the ligand within a highly hydrophobic enzyme pocket while binding to enzyme-bound $Zn^{2+}$, and deprotonation of the dansylamide (to give an $SO_2NH^-$ group), which also assists with binding to the zinc cation.

Based on this observation, Eiichi Kimura and co-workers from the University of Hiroshima, Japan, have designed an extremely effective zinc fluorophore, dansylamidoethylcyclen (**11.36**),[26] which takes advantage of the affinity of the deprotonated dansylamide group for $Zn^{2+}$ and the dramatic enhancement of fluorescence intensity noted on chelation of a metal centre by a chromophore with a number of amine arms appended. This latter factor is known as the CHEF (chelation-enhanced fluorescence) effect, and was first reported by the group of Czarnik in 1988.[27] The CHEF effect arises as a consequence of the extremely efficient quenching of the fluorescence of the fluorophore by the amine functionalities. Upon chelation (and therefore strong binding) to a metal centre, the amine lone pairs, which have a high effective concentration in the free state, are no longer available to quench the fluorescence, which is strongly 'turned on'.

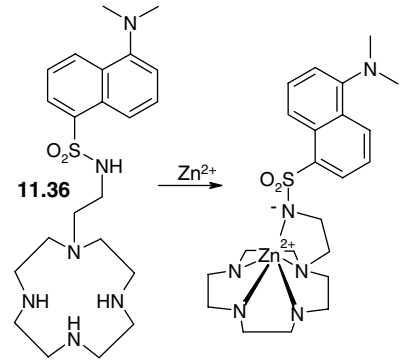


The cyclen ([12]aneN$_4$) binding site has a tremendous affinity for $Zn^{2+}$ and, in combination with the deprotonated dansylamide moiety, a five-coordinate, square pyramidal 1:1 complex is formed with

$Zn^{2+}$ with a binding constant of $10^{21}$ $M^{-1}$. Just as with the anthracene-based sensor **11.34**, the fluorescence of the dansylamine group is quenched partially by the nitrogen lone pair. However, protonation of receptor **11.36** to give **11.36**-$2H^+$ results in only a 20 % enhancement of the fluorescence intensity. In contrast, $Zn^{2+}$ complexation gives a five- to ten-fold enhancement depending on the wavelength, and a blue shift in emission maximum from 582 to 540 nm, in a similar way to the CA system. In contrast, copper(II) quenches the fluorescence completely because of the possibility of electron transfer to the partially filled metal *d*-shell. The fluorophore receptor **11.36** is capable of detecting $Zn^{2+}$ in the range 0.1–5 μM, with fluorescence intensity depending linearly upon concentration. Binding is unaffected by the presence of alkaline and alkaline earth metal ions, although $Cu^{2+}$ competes effectively with $Zn^{2+}$ (binding constant for $Cu^{2+} > 10^{30}$ $M^{-1}$). The ligand is so sensitive and effective that it is now marketed commercially.

## 11.3.3 Colorimetric Sensors and the Indicator Displacement Assay

Nguyen, B. T., Anslyn, E. V., 'Indicator-displacement assays', *Coord. Chem. Rev.* 2006, **250**, 3118–3127.

In the previous section we looked at examples of single molecules able to carry out both binding and transduce that binding into photophysical signalling of the presence of the bound analyte by means of luminescence. Perhaps conceptually an even simpler method of sensing is by bringing about a visual colour change, *i.e.* a change in the visible absorption spectral characteristics of the host or guest molecule upon binding. We have already seen a couple of examples of this kind of colorimetric sensing in Chapter 4, for example binding-induced redox potential changes in the ferrocene-based host shown in Scheme 4.3 that result in an orange-to-green colour change on $F^-$ binding. Similarly charge transfer interactions impart a purple colour to the viologen receptor **4.93** upon binding carboxylate anions. Colour changes are commonly brought about by covalent chemical reaction with analyte species. For example the reaction shown in Figure 11.22 between a nerve gas simulant and an orange oxime results in the formation of a yellow oximate adduct, a process useful in the colorimetric detection of a range of organophosphate nerve gases and their analogues. The sensor is proposed for use in the detection of chemical warfare agents such as sarin and soman.[28]

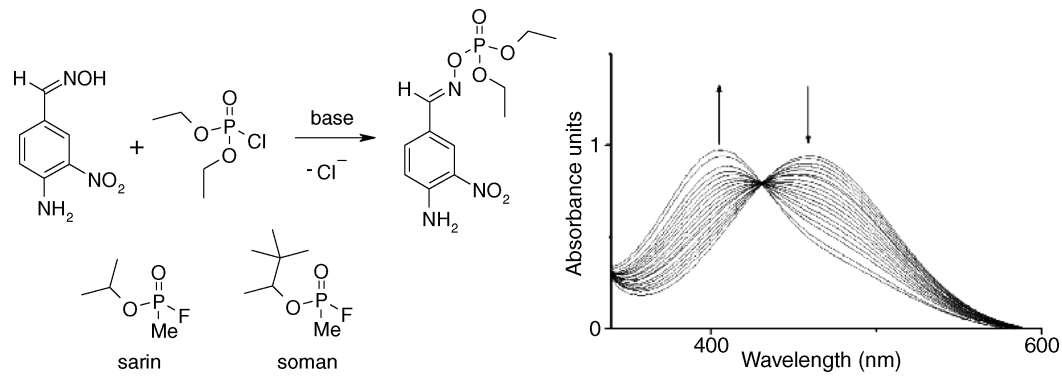


**Figure 11.22** Colorimetric detection of nerve gas agents by oximate formation. The spectra show the progress of the reaction by the disappearance of ther $n \rightarrow \pi^*$ band at 461 nm and the appearance of the product absorption at 413 nm through an isosbestic point indicating clean conversion (reproduced by permission of The Royal Society of Chemistry).

Hybrid amide-thiourea hosts based on *p-t*-butylcalix[4]arene have been prepared with coloured *p*-nitrophenyl (**11.37a**) or fluorescent 1-napthyl substituents (**11.37b**). In DMSO the host binds strongly to dicarboxylates, particularly adipate ($\log K = 2\times10^4\ M^{-1}$), accompanied by a colour change from yellow to red in the case of the nitrophenyl derivative. The colour change is reversible on addition of protic solvents such as methanol but is not observed for acetate or other basic, monovalent anions. While large chemical shift changes for the thiourea NH protons are observed for **11.37b** ($\Delta\delta$ up to *ca.* 3.5 ppm), the thiourea NH resonances for the more acidic **11.37a** disappear due to deprotonation. The fluorescence of the napthyl substituent in **11.37b** is significantly quenched in the absence of anions due to a PET process. Addition of dicarboxylates results in an increase of fluorescence emission intensity in a broad band from 410 – 600 nm. Addition of anion reduces the efficiency of the PET process.[29]

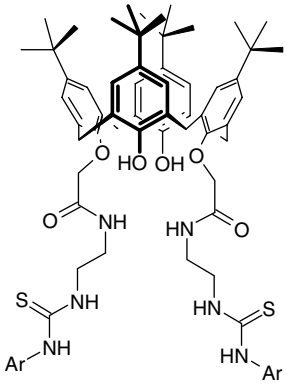


**11.37**

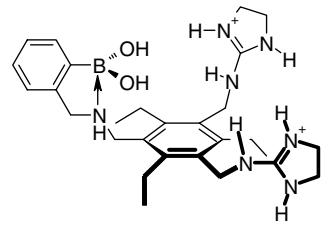

**11.38**

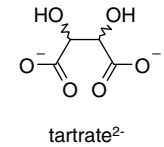


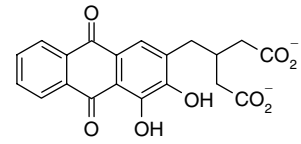

alizarin

While many hosts undergo subtle changes in their UV-Vis absorption spectrum upon guest binding (indeed computer fitting of such changes is a common way in which binding constants are determined, Section 1.4.2) it is difficult to engineer a clear and significant colour change that is visible to the naked eye in a single molecular sensor. A versatile alternative is to make use of a three-component system, namely host, a coloured guest as an indicator and the target analyte. The concept is a simple one: the indicator is bound by the host giving rise to a characteristic colour for that molecule in the solvent of choice. The indicator is chosen such that it binds to the host more weakly then the target analyte. Hence when the analyte is added, the indicator is released and the colour changes to the characteristic colour of the free indicator molecule. This kind of detection is termed an *indicator displacement assay* (IDA). Alternatively an indicator can be chosen that binds to the target guest and is then displaced by a stronger-binding host. We have already seen this latter kind of IDA in the displacement of the murexide ion by $EDTA^{4-}$ in EDTA titrations for the analysis of metals such as $Mg^{2+}$ and $Ca^{2+}$ (Section 3.1.3). The beauty of the indicator displacement assay is that it is synthetically relatively simple (no need to make a complicated host molecule with both binding and sensing functionality) and the indicator can be chosen such that the magnitude of its binding constant to either guest or host results in its displacement at the particular conditions and concentration of interest in the analysis being undertaken. A wide range of indicators is available, often with very high extinction coefficients allowing sensitive measurements at low concentrations, and are compiled in books such as *The Sigma-Aldrich Handbook of Stains, Dyes and Indicators*.[30]

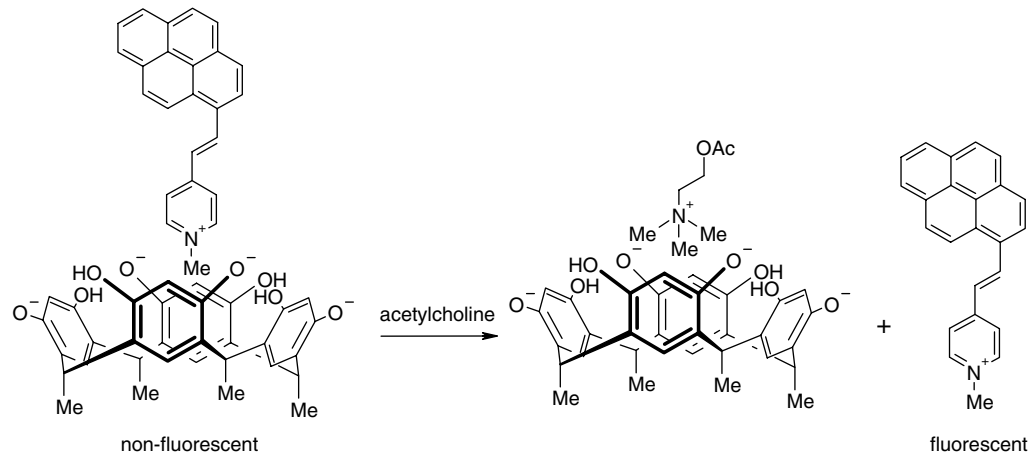


**Scheme 11.7** Fluorescent indicator displacement assay for acetylcholine developed by Inouye in 1994.[31]

Among the first modern indicator displacement assays in supramolecular chemistry was the fluorescence-based detection of the neurotransmitter acetylcholine developed by Inouye, Scheme 11.7.[31] The fluorescence of the pyrene derivative is quenched by binding to a deprotonated [4]resorcarene host. Addition of acetylcholine alone out of a wide range of related guests (*e.g.* serotonin, adrenaline, glutamic acid *etc.*) results in the displacement of the indicator and binding of the target analyte. Once free of the resorcarene the guest fluorescence is 'turned on'.

A good example of a colorimetric IDA is the combination of the 'pinwheel' receptor **11.38** (Section 4.8.1) with alizarin. The alizarin dye is displaced by tartrate, a common component of wines and grape juice and therefore a good target analyte. The carboxylates in the tartrate are bound by the guanidinium moieties while the boronic acid group binds to the di-ol (boronic acids form stable complexes with diols which displace the hydroxyl groups) to give a binding constant of $5.5\times10^4$ $M^{-1}$. The system has been used to assess the concentration of the related malate anion in Pinot Noir grapes. The ratio of receptor-to-indicator can be adjusted to give visual colour changes close to the point at which one equivalent of malate is added.

While these kinds of molecular sensing systems are readily prepared and highly appealing, it is rare that they are very highly selective for their target guests – the flexible nature of the binding site means that many related analytes are bound more or less equally well and indeed we can sometimes think of such flexible molecular receptors as being selective for particular *classes* of molecule instead of specific guests. Despite this lack of strong 'peak selectivity' *(cf.* the cryptands, Section 3.4) we can use what selectivity there is in each host as part of a *sensing array* able to *discriminate* between various analytes, even as part of complex mixtures. Here the concepts of *selectivity* and *discrimination* are very different from one another.[32] Selectivity refers to the ratio of binding constants of one guest over another by a particular host (Section 1.7). Discrimination refers to the ability of an assay or sensing method to detect and ideally quantify the amount of a particular analyte target (either specific molecule or ion, or class) within an unknown mixture. A particularly good way to discriminate between various analytes using relatively poorly selective hosts is to use pattern recognition. By taking a range of hosts with different selectivities a response pattern for particular mixtures can be developed, usually by training computer pattern recognition software on mixtures of known concentrations. The particular pattern is then characteristic of particular analytes. This kind of methodology has been used to great effect by the group of Eric V. Anslyn at the University of Texas, Austin, USA, using colorimetric sensing by

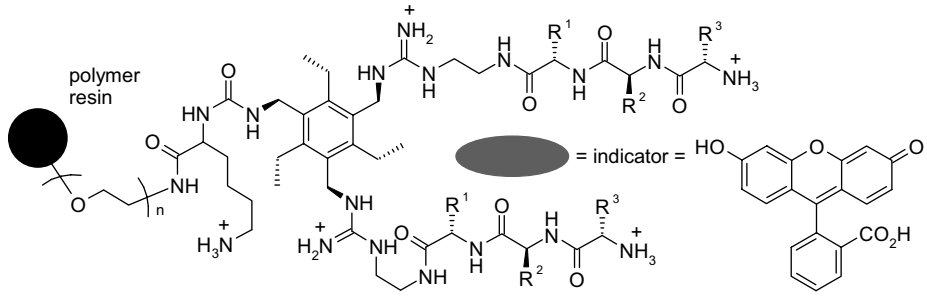


**Figure 11.23** A resin-bound peptide-based receptor used as part of an IDA-based pattern sensor with fluorescein.[33]

IDA. We will look at a particular example of a differential receptor system for the recognition of the nucleotides adenosine triphosphate (ATP), adenosine monophosphate (AMP), and guanosine triphosphate (GTP). Starting from the popular triethylbenzene 'pinwheel' core (Section 4.8.1) Anslyn's group attached one arm of the guanidinium tripodal anion binding unit to a polymer bead support to act as an anchor while analyte solution flows over the bead. The remaining two arms were then derivatised with a random array of amino acids to give short peptides, using combinatorial chemistry. This approach generated a library of 4913 different types of receptor-derivatised beads that differed only in the identity of the groups $R^1$, $R^2$ and $R^3$. Figure 11.23. The guanidinium heart of the receptor imparts strong but unselective anion binding of the phosphate tail of the nucleotide target analytes. The group hoped that the different peptide arms would have different affinities for the nucleobase and sugar portions of the analytes. Thirty of these beads were randomly selected and placed individually into micromachined wells in a $5 \times 7$ array in the presence of fluorescein indicator, Figure 11.24. The array also included five blank beads without any peptide chains. The analyte mixtures were allowed to flow over the beads, in some cases displacing the fluorescein where the analyte happened to be strongly bound by the particular bead. The colour change over time in each well was monitored using a CCD camera allowing a plot of the change in absorbance of *e.g.* the red channel over time. This method then gives 30 profiles of absorbance change over time for the 30 active receptor beads. The differences between each bead in response to a particular analyte are relatively subtle, however, it is

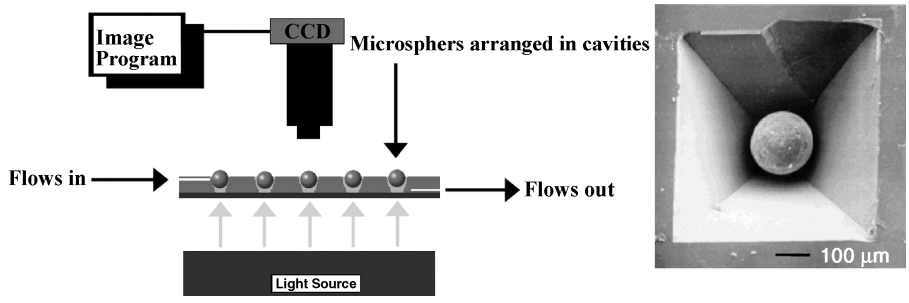


**Figure 11.24** A silicon wafer array, with micromachined pyramidal wells (detail shown right) for holding receptor derivatised beads. Fluid containing the experimental solution is added to the top of the array and flows through the bead matrix, and out of the bottom of the pyramidal wells holding the beads. Analyte binding by the differential receptors anchored to the beads gives a recognition pattern unique to each analyte mixture (reproduced with permission from [34] © 2001 American Chemical Society).

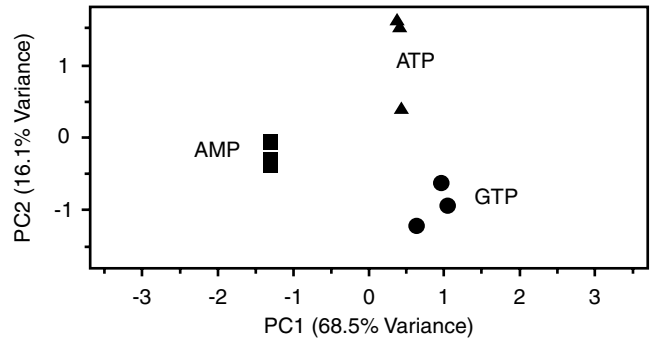


**Figure 11.25** The first two principal component axes in the data derived from the system shown in Figure 11.23. The clustering of the three target nucleotides into three distinct groups based on the array colorimetric response clearly evident (reproduced with permission from [35] © 2003 American Chemical Society).

possible to use principal component analysis (PCA) to disentangle to differences and discriminate between the analytes, Figure 11.25.

PCA or related pattern recognition techniques, allows patterns in large sets of overlapping data to be distinguished by plotting the data according to the maximum variance, *i.e.* in this case the maximum difference in response to the various analytes. PCA is extremely powerful at discriminating between a large numbers of very similar analytes in a complex mixture. The PCA method reduces the dimensionality of the data and summarises the most defining parts whilst simultaneously filtering out noise. For Anslyn's nucleotide assay, a Principle Component (PC) axis is calculated to lie along the line of the maximum variance in the original data over nine trials of different (known) sets of the nucleotides. Other PC axes lie along lines describing diminishing levels of variance. We can then derive a 'score plot' for the first two principle components. In this case there is clustering of individual analytes such as AMP, GMP and ATP allowing their mutual discrimination.

This kind of differential recognition represents a step on the way to the production of an 'electronic tongue' that mimics the sensation of taste in the sense that the simultaneous response pattern of the receptor array is specific for a particular set of stimuli. In mammals a real tongue recognises five distinct tastes categories, sweet (carbohydrate based), bitter (alkaloids), sour (acidity), salty (ionic) and umami (savoury-glutamate). The brain then disentangles these five simultaneous signals in conjunction with smell signals coming from the nasal receptors to give each food its characteristic taste. The development of electronic tongues and electronic noses is highly desirable because not only can they do the job of a human taster in distinguishing good tastes from bad but they can also be used to distinguish mixtures of compounds that humans would not be very suited to tasting such as narcotics or chemical warfare agents. We will return to sensor arrays when we look at molecularly imprinted polymers in Section 14.3.2.

## 11.3.4 Electrochemical Sensors

Beer, P. D., Bayly, S. R., 'Anion sensing by metal-based receptors', *Top. Curr. Chem.* 2005, **255**, 125–162.

In the same way as the molecular or supramolecular juxtaposition of a binding site and a chromophore can result in luminescent or colorimetric sensing of target substrates, so incorporation of a redox-active centre may allow electrochemical detection of binding. In Section 4.7.2, we examined a range of hosts for anions based on the Co(III)/Co(II) redox couple in cobaltocinium-based podands, corands

and calixarene-based hosts. In the case of these species, the presence of the $CoCp_2^+$ moiety ensures that the hosts are positively charged and therefore complementary to anions, as well as performing a role as a redox reporter group that enables anion binding to be detected by redox potential changes. This kind of chemistry may be carried out readily with the analogous neutral ferrocene derivatives in which the guest binding is thus separated from the function of the redox signalling group, which is effectively an observer of the complexation process. Work by Beer *et al*. has resulted in an intriguing sensor for neutral molecules based on calixarene inclusion (**11.39**).[36] The host comprises a calix[5]arene with three appended ferrocenyl reporter groups and it recognises dipolar solvent molecules such as MeCN, $Me_2S{=}O$ and $Me_2NCH{=}O$ which are bound *via* the calixarene lower rim by hydrogen-bonding interactions to the two remaining phenolic OH groups. The presence of the adjacent dipole results in small but consistent shifts in the redox potentials of the ferrocene groups, an effect that is absent in the presence of non-polar molecules such as toluene and $CH_2Cl_2$. Interestingly, the host exhibits two resolved oxidation waves, which correspond to the recognition by two of the three ferrocenyl moieties that the first has been oxidised. The resulting positive charge causes the second two centres to be oxidised at higher potential. The effect of polar guest binding is to merge the first and second redox waves, suggesting that the mechanism of guest detection is the disruption it causes on communication between the redox centres in the sensor.

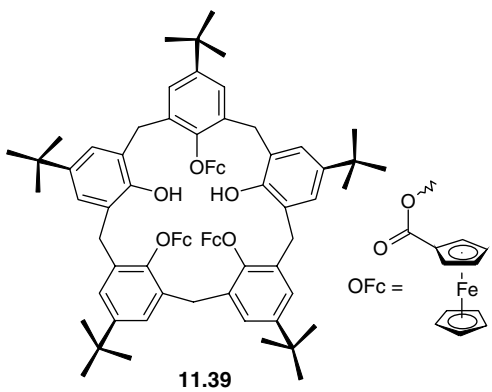


**11.39**

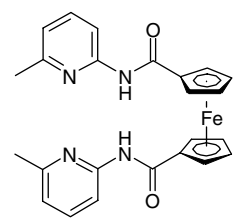


**11.40**

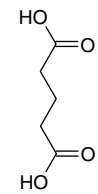


glutaric acid

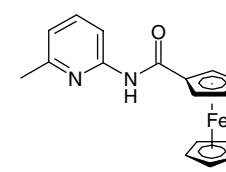


**11.41**

The binding of guest molecules by **11.39** is necessarily weak as a consequence of the weak binding sites employed. Much more significant electrochemical response to neutral molecule binding has been obtained by Jim Tucker of the University of Birmingham, UK, by incorporating the hydrogen bond recognition motifs developed by Hamilton (Section 6.5.7) within the ferrocenyl redox active host **11.40**.[37] Cyclic voltammetric and NMR spectroscopic measurements indicate the formation of a 1:1 complex between receptor **11.40** and glutaric acid in chloroform solution with a shift in redox potential on binding of –85 mV, compared to –20 mV for the control compound with only one pyridyl amide binding arm (**11.41**). The proposed binding mode, in which each carboxylate group forms a doubly hydrogen bonded $R_2^2(8)$motif with the pyridyl amide, is supported by the X-ray crystal structure of the 2:2 complex of **11.41** with glutaric acid (Figure 11.26).

Moutet and coworkers have produced rigid ferrocene-containing amide anion receptors such as **11.42**. The rigidity imparted by the cyclotriveratrylene scaffold means that, as with **11.39** two separate oxidation waves are observed on complexation of biologically interesting anions such as $H_2PO_4^-$ and $ATP^{2-}$ anions, with shifts of up to 260 mV in $CH_3CN/CH_2Cl_2$ mixtures.[38] The same group have also looked at the surprisingly simple receptor **11.43**. This compound electrochemically recognises dihydrogen phosphate and ATP anions. Dihydrogen phosphate induces a remarkable

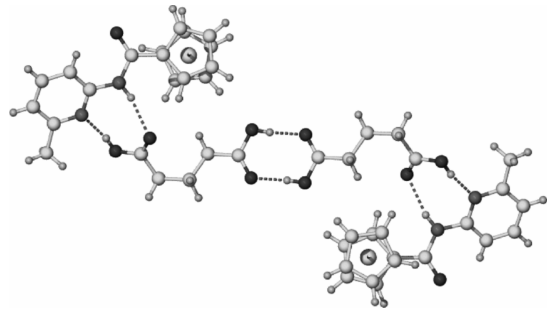

**Figure 11.26** X-ray crystal structure of the 2:2 complex of **11.41** with glutaric acid showing the matching of the guest and host hydrogen-bonding binding sites.[37]

shift of –470 mV in $CH_2Cl_2$ solution because of strong ion-pairing interactions.[39] Redox sensing of cations has also been extensively studied using metallocene-based sensors. For example compound **11.44** binds to $Ca^{2+}$ much more strongly in the reduced Co(II) state than the oxidised cobalticinium Co(III) form, resulting in an anodic shift of the redox potential of the Co(II)/Co(III) couple of 170 mV upon calcium binding.[40]

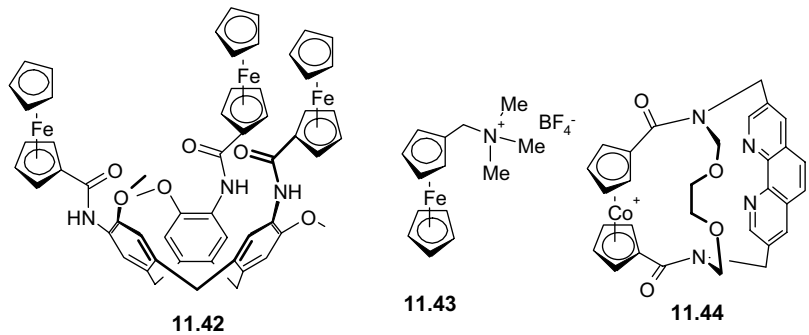


**11.42** **11.43** **11.44**

A particularly versatile series of compounds are the [12]metallacrown-3 derivatives and higher organometallic box-shaped and helicate structures such as those shown in Figure 11.27. The simple trimetallic complexes act as excellent receptors for alkali metal cations where their highly preorganised nature and polar oxygen ligating groups give them a high affinity for alkali metal halides,

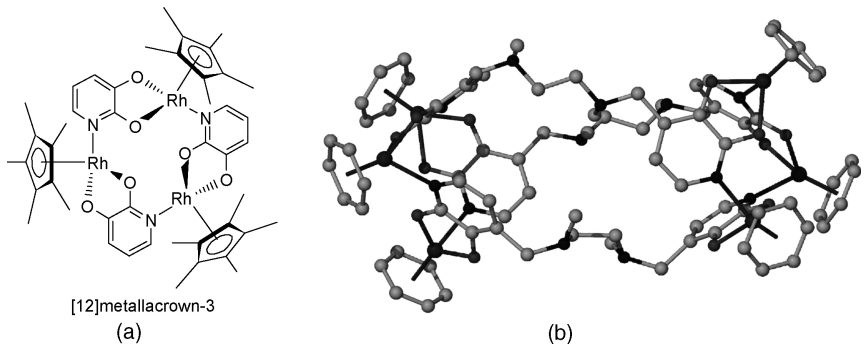


**Figure 11.27** (a) Structure of a [12]metallacrown-3 derivative and (b) X-ray molecular structure of an analogous hexanuclear complex based on ligands bridging two trimers.[41]

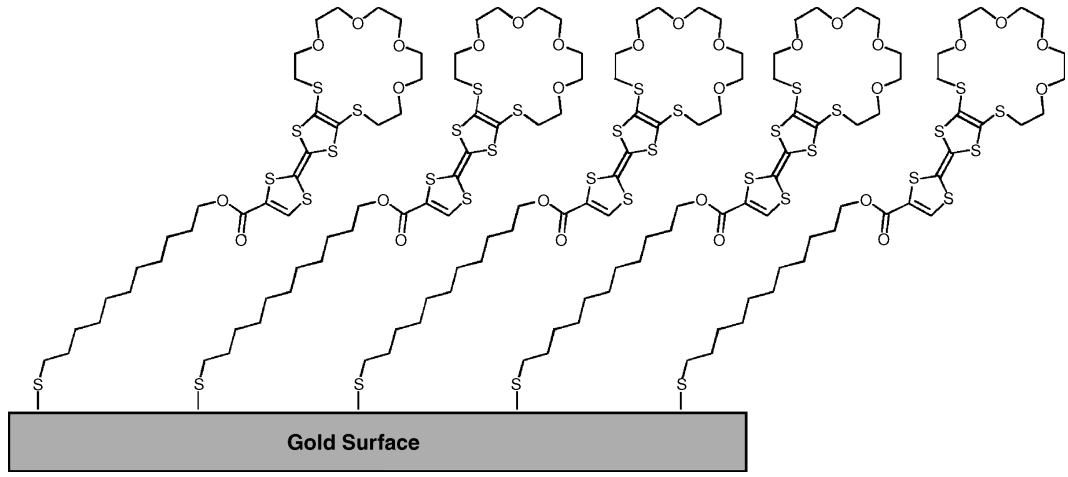


**Figure 11.28** A TTF derived molecular receptor self-assembled monolayer. [42]

comparable to the cryptands in non-polar solvents. The presence of electroactive metal fragments also results in effective cation sensing. The small cavity in the trimetallic species means that they are selective for $Li^+$ and $Na^+$ and thus while no change in the redox potential of the Rh(II)/Rh(III) couple is observed on addition of KCl, binding of LiCl results in a shift of + 300 mV. The $LiBF_4$ complex also electrochemically senses fluoride which binds strongly to the coordinated $Li^+$ giving a shift of –203 mV. These versatile, self-assembled compounds thus function as both cation and anion sensors.[41]

In addition to organometallic compounds, organic electro-active moieties such as tetrathiafulvalene (TTF) derivatives can be used in an electrochemical sensing context. Binding metal cations to TTF results in polarisation and hence a positive shift of the first oxidation potential. This effect has been incorporated into a thiacrown ether TTF derived monolayer sensor attached to a gold electrode surface, Figure 11.28. The monolayer exhibits a shift in the first oxidation potential of the TTF unit in the presence of metal cations. The monolayer is relatively insensitive to $Li^+$ and $K^+$, however moderate shifts of 45 and 50 mV are observed for $Na^+$ and $Ba^{2+}$ while $Ag^+$ binding results in a change of 90 mV. The soft $Ag^+$ ion would be expected to be bound strongly by the soft sulfur donor atoms near the TTF unit. The electrochemical response persists over 1000 cycles, indicating a stable monolayer.[42]

Another possible mechanism for making the transition from selective binding to signal generation is the incorporation of selective molecular receptors such as calixarenes or ionophores *etc.* into semiconductor devices. Devices such as ISFETs (ion-selective field-effect transistors) are capable of translating a molecular recognition event into an electrical signal. An ISFET consists of two n-type semiconductors (*i.e.* a semiconductor doped with excess electron-rich atoms), which act as source and drain, embedded within a p-type silicon bulk (Figure 11.29a). The conductivity in the channel between the two n-type regions is dependent on the electric field perpendicular to the surface of the bulk. Such devices may be used readily as pH sensors, in which the state of protonation of the SiOH groups at the surface determines the magnitude of the channel electric signal. If a chemically selective membrane is placed over an ISFET device, it may be used to recognise substrates other than $H^+$. The membrane is a hydrophobic layer containing host molecules capable of recognising a target analyte. Binding of the analyte (*e.g.* metal cations) within the membrane again results in a potential change that affects the channel conductivity, generating a signal. Such chemically modified ISFETs are termed CHEMFETs (Figure 11.29b). Membrane ionophores studied to date include crown ethers,

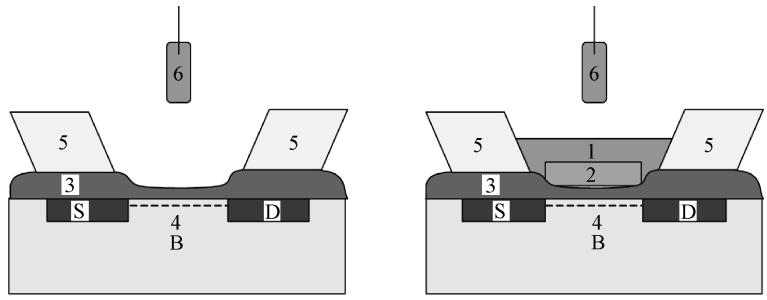


1. Hydrophobic membrane
2. Hydrogel
3. Gate oxide
4. Channel
5. Insulating resin
6. Reference electrode

S–Source
D–Drain
B–Bulk

(a) (b)

**Figure 11.29** Schematic diagrams of (a) ISFET and (b) CHEMFET devices.

cryptands, and variously modified calixarenes.[43] CHEMFET devices may be improved further by the addition of a hydrogel layer that eliminates interference by $CO_2$ by incorporation of a salt buffer.

## 11.4 Molecule-Based Electronics

### 11.4.1 Molecular Electronic Devices

Petty, M., *Molecular Electronics: From Principles to Practice*, Wiley: Chichester, 2008.

Molecular electronic devices are, conceptually at least, those that most resemble electronic and computer components. If individual electronic components that may be coupled together, such as wires, switches, rectifiers *etc.*, can be produced, then the conceptual basis exists to manufacturing molecule-sized (*i.e.* nanoscale) electronic devices with concomitant gains in speed, efficiency, capacity and reduced use of resources. The field of real world molecular computing is still in its infancy, although there have been some remarkable advances over the past five years. Chemically speaking, it is relatively straightforward to design and synthesise molecules that behave in an analogous way to individual electronic components, and we will look at a number of such examples in the sections below. However it is a far greater task to link such molecules together into a viable macroscopic device with input-output functionality, and the present state of the art still uses non-molecular (albeit often bordering on the nanoscale) read/write architecture as proof of principle of the functionality of the molecule-based components. We will look at recent progress in this regard in Section 11.4.6.

### 11.4.2 Molecular Wires

Ceccon, A., Santi, S., Orian, L., Bisello, A., 'Electronic communication in heterobinuclear organometallic complexes through unsaturated hydrocarbon bridges', *Coord. Chem. Rev.* 2004, **248**, 683–724.

The basic properties of a molecular wire are that it should connect to two components (generally an electron acceptor and an electron donor) and conduct an electrical signal or impulse between

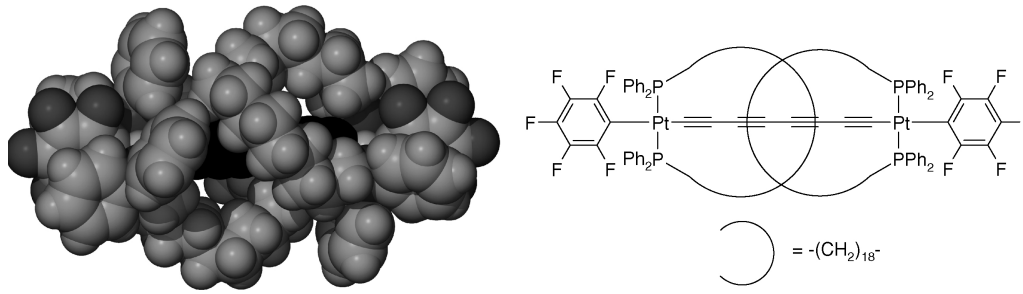


**Figure 11.30** An insulated molecular wire based on a platinum(II) polyalkyne surrounded by two long-chain diphosphines. The polyalkyne wire (shown dark in the middle of the structure) is barely visible within the insulation.[45]

them. On a molecular scale, this may amount to a single electron. The electrical signal may have to be carried over a significant spatial distance, for example across a biological cell membrane (about 5 nm). The problem is analogous to the transmembrane current flow required for the transmission of nerve impulses in biochemistry (Section 2.2). In biological cells, the problem is solved by channel- and ionophore-mediated ion transport. The molecular wire concept is analogous to the channel-mediated mechanism, since it is expected to involve a rapid current flow, but the ideal electronic device would result solely in electron flow rather than the flow of alkali metal cations. It is generally believed that electron transfer within a molecule can be enhanced by providing a series of conjugated bonds allowing orbital overlap over a considerable distance (*cf.* Figure 11.6). In early work Lehn's group addressed this problem by the preparation of a number of carotenoid type compounds such as **11.45**, termed *caroviologens* because of the presence of the viologen-like bipyridinium moieties.[44] Using a technique called linear dichrosism spectroscopy (LD)*, Lehn *et al*. showed that the caroviologens were able to span lamellar model membranes of dihexadecylphosphate (flat liquid bilayer membranes, *cf.* Section 13.2.1) of thickness comparable to the length of the molecular wires. The hydrophilic pyridinium groups serve to interact with the aqueous phase either side of the vesicle wall as well as being electroactive groups. Transmembrane conductivity experiments were carried out in solution dihexadecylphosphate vesicles. When small amounts of the zwitterion **11.45** were used, conductivity enhancements of four to eight times background were observed between a internal oxidising phase containing potassium ferricyanide, $K_3[Fe(CN)_6]$, and an external reducing phase of sodium dithionite (Figure 11.31). In real electronic devices, some degree of redundancy may be required in case of damage, and hence triple wires have been prepared representing three-stranded molecular cables. Ingenious analogues of insulating cable coatings have also been developed, for example by threading cyclodextrins onto the wire to 'sheath' these delicate caroviologens molecular wires by 'molecular insulation'. An fascinating alternative kind of molecular insulation involves inducing an aliphatic diphosphine ligand to wrap around a polyalkyne molecular wire, Figure 11.30.[45]

An alternative approach to molecular conductors has been pioneered by Marye Fox of the University of Texas, USA, using block copolymers comprising electron donor and acceptor units, separated

* LD is a spectroscopic technique that can be used with systems that are either intrinsically oriented, or can be oriented during an experiment by external forces. The technique gives information about conformation and orientation of structures within molecules. The linear dichroism of a sample is measured by orientating the sample along its axis and recording the difference in absorption of light linearly polarized parallel and perpendicular to the orientation axis. The LD signal is the difference in these two measurements (*cf.* circular dichroism, Box 6.2).

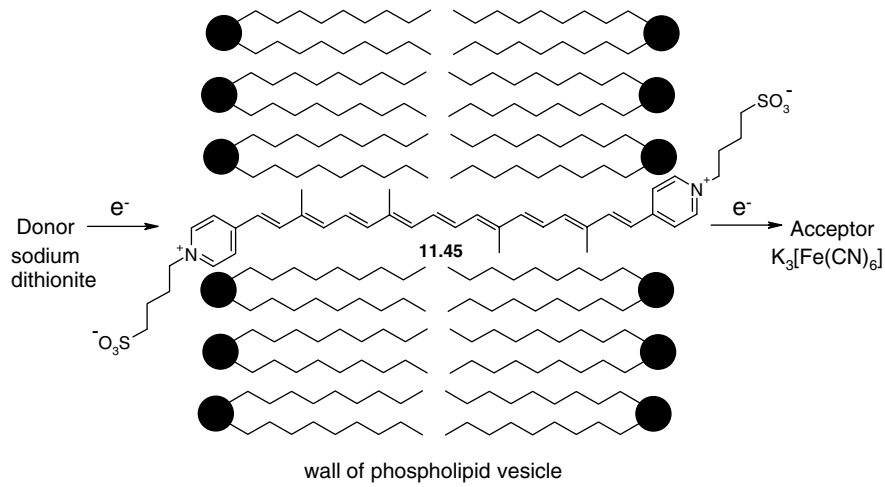


**Figure 11.31** Molecular conductivity through a phospholipid vesicle by caroviologen **11.45**.[44]

by conducting relays, as in **11.46**.[46] The block copolymers are prepared by ring opening metathesis polymerisation (ROMP), which allows highly monodisperse (narrow molecular weight range) materials to be prepared under mild conditions. The polymerisation is metal-catalysed and is an example of living polymerisation, *i.e.* once polymerisation is complete, addition of further monomer units (even structurally different ones) will restart the reaction. In this way, excellent control may be achieved over not only the overall polymer length, but the number of monomer units that comprise each polymer block. The polymers are also rigid (on the electron-transfer time scale), and hence display well-defined electrical characteristics and exhibit vectorial electron transfer from donor to acceptor. We will look at more block co-polymers in Section 14.3.1.

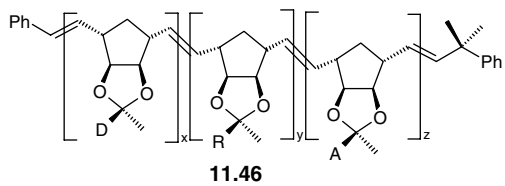


**11.46**

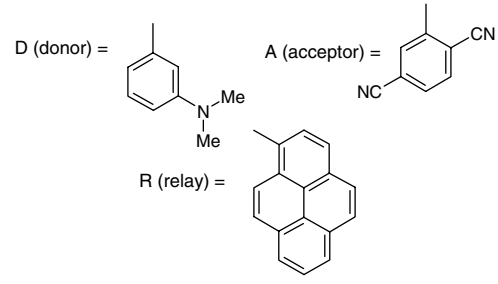


Interestingly, related polypeptide-based materials display differential electron-transfer rates depending on the orientation of the dipole of the peptide helix. This suggests that electron transfer in such systems may be controllable by externally applied potentials. Such results represent the beginning of the kind of long-range control and electron-transfer characteristics necessary for functional nanoscale optoelectronic devices.

As we saw in Figure 11.6 molecular wires are not limited to organic conductors. The incorporation of metal ions with their variable redox states and photochemical activity, not to mention widely tuneable electronic and geometric properties, gives ample scope for the synthesis of novel metal-containing molecular conductors. For example, the rigid rod oligomers **11.47a–c** all undergo two reversible

one-electron oxidations with the electrode potential separation between them increasing with decreasing bridge length (the separation is as much as 0.44 V in **11.47a**). The fact that two oxidation processes are noted (both formally transitions from Re(I) to Re(II)) indicates that the electronic environment about the second metal centre is influenced by the oxidation of the first *via* the conjugated polycumulene ligand. Indeed, in the case of **11.47a**, the mixed valence Re(I)/Re(II) species may be isolated and shown to be a class III mixed-valence compound (*i.e.* the 'extra' electron from the Re(I) side is delocalised fully over both metal centres).[47] These kinds of small molecule systems have been extended to form conducting metal–acetylide polymers such as **11.48**, which are also of interest for their electrical conductivity as well as nonlinear optical properties.

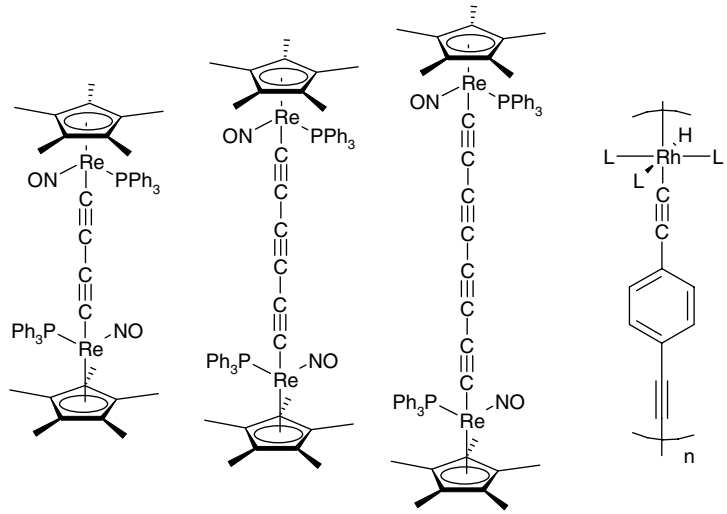


**11.47a** **11.47b** **11.47c** **11.48**

A fascinating series of fully conjugated porphyrin-based molecular wire has been reported by the group of Osuka (Kyoto, Japan).[48] The molecules are tape-like and exhibit extremely red-shifted absorption bands as a result of their extensively π-conjugated electronic systems which give rise to a low $\pi$–$\pi^*$ separation. The electronic absorption maximum for the dodecamer shown in Figure 11.32 is only *ca.* 3500 $cm^{-1}$, a similar energy to the vibration of an O–H bond! Understandably the compounds are also increasingly readily oxidised as the number of porphyrin units increases.

Finally the longest single molecular wire reported to date has been prepared by Martyn Bryce and coworkers from Durham University, UK. The rigid, conjugated molecule (Figure 11.33) is 7 nm long and is equipped with terminal thiol groups allowing it to dock between gold electrodes.[49] The central dipyridyl group can be protonated making it electron deficient and allowing coupling with an electron rich donor. This arrangement leads to the wire exhibiting rectification behaviour. We will look at molecular rectification in the next section.

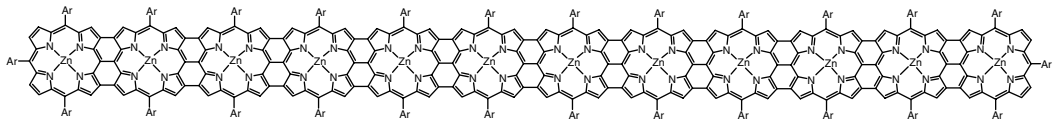

**Figure 11.32** A fully conjugated porphyrin-based molecular wire.[48]

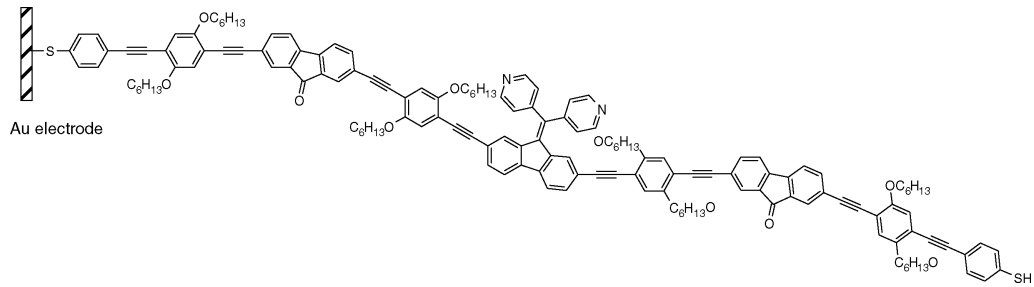


**Figure 11.33** A 7 nm long protonatable molecular wire.[49]

## 11.4.3 Molecular Rectifiers

Metzger, R. M., 'Unimolecular electrical rectifiers,' *Chem. Rev.* 2003, **103**, 3803–3834.

Electrical rectification by a single molecule was first seriously proposed in 1974 by Ari Aviram and Mark A. Ratner who proposed (but never synthesised) compound **11.49**. Their visionary ideas have since stood the test of experimental verification in other systems.[50] A rectifier is a device that allows only one-way flow of electrons. In bulk electronic devices, it is used to convert an alternating current into a direct current. Conventional rectifiers are made up of a contact between a p-type (electron-poor) and n-type (electron-rich) semiconductor. The rectifier operates by causing the build-up of an insulating layer in the contact region (Figure 11.34). When the p- and n-type junction is formed, electrons flow from donor to acceptor until the charge is neutralised within the contact region and no further current flow is possible. If an external voltage is applied to the rectifier, then one of two possible situations develops, depending on the polarity of the applied voltage. If the applied potential is such that the cathode (negatively charged electrode) is placed in contact with the n-type side and the anode in contact with the p-type side, the insulating layer will grow as a consequence of additional electron flow until, once again, no current flow is possible. Conversely, if the polarity is reversed, then the insulating layer will shrink, allowing current flow. If an alternating current is applied, the result is current flow only when the alternating cycle is of the correct polarity, *i.e.* the conversion of alternating current into direct current.

On a molecular level, exactly the same characteristics are required of supramolecular components and hence a molecular rectifier should comprise an electron donor and an electron acceptor, separated by an insulating spacer. Compounds **11.49** and **11.50** are based on $\sigma$-insulating framework, while donor–acceptor carotenoid derivatives such as **11.51** are separated by a more conducting $\pi$-system.

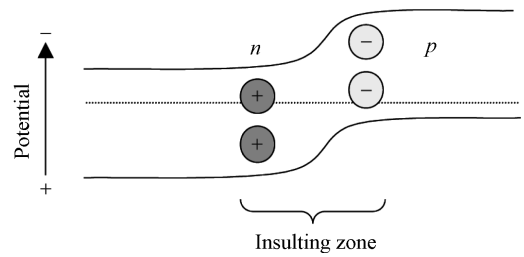


**Figure 11.34** Semiconductor p–n junction in a conventional rectifier.

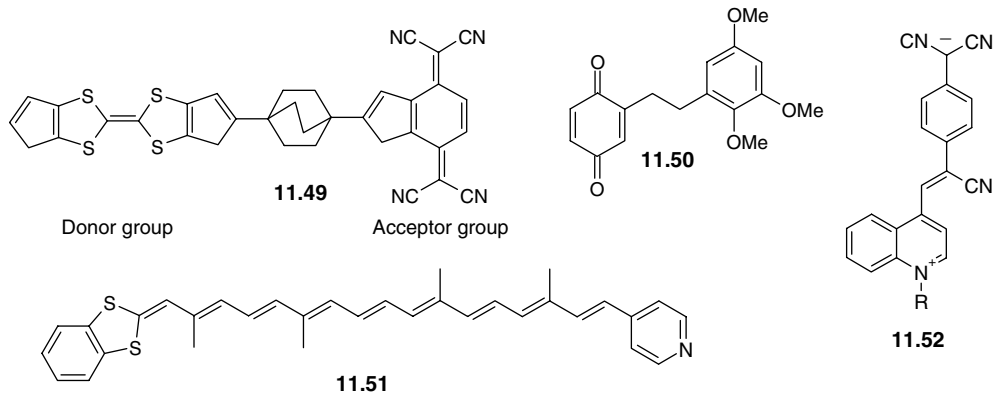


The operation of the molecular rectifiers may be explained with the help of Figure 11.35, which represents a molecule such as **11.49** attached *via* its donor and acceptor components to an anode and cathode with each possible polarity. The configuration shown in Figure 11.35a allows current to flow because the driving potential, V, required to overcome the insulating layer is relatively small, implying a small insulating layer. The required driving potential in Figure 11.35b is much larger, hence current flow is more difficult. The magnitude of V is determined by the relative energies of the donor and acceptor orbitals. In the case shown in Figure 11.35a, electrons from the cathode are transferred into acceptor orbital B as soon as the potential is large enough to cause overlap of donor and acceptor orbitals. Similarly, electrons are transferred from donor orbital C to the anode. Because the energy difference between B and C is small, electrons can

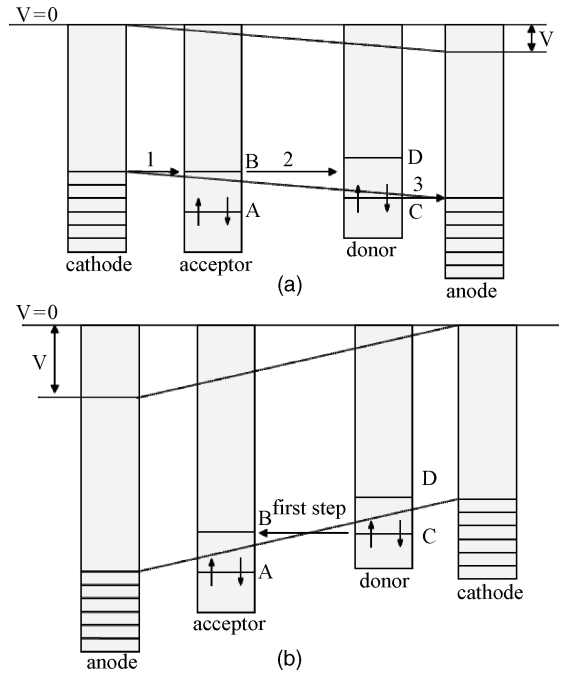


**Figure 11.35** Molecular rectification (a) Flow of electrons. (b) No current unless V is sufficiently large. Steps 1, 2 and 3 are tunnelling processes.

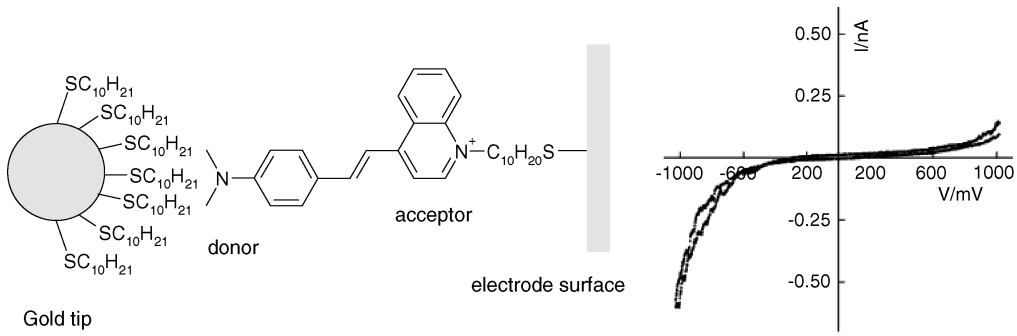


**Figure 11.36** A single molecule rectifier attached to a gold electrode surface and probed by a coated gold STM tip. The thickness of the coating allows control of the distance between the two gold electrodes. The resulting current-potential (I – V) curve is shown right (reproduced with permission from [52] © 2004 American Chemical Society).

tunnel through the insulating spacer. The electron from B tunnels into the donor manifold in an excited Franck–Condon state and decays back to the ground state, C, by radiationless relaxation, and the electrical circuit is closed. The process is irreversible as long as the energy of B is above that of C. In the reverse situation (Figure 11.35b), a continuous flow of electrons is achieved only if level D is below the Fermi level of the cathode, allowing electrons to flow from cathode to D. Similarly, the Fermi level of the anode would need to be below the level of A. The necessary potential to achieve this is much larger than in the former case. A great deal of work has been carried out on molecular rectifiers because they offer the possibility of being part of a molecular electronics system allowing very densely packed electronic circuitry.

There have been some impressive, relatively recent examples of molecular rectification. Compound **11.52** has proved to be an extremely efficient molecular rectifier, able to actually function as a rectification device by intramolecular tunnelling either as a monolayers or multilayer macroscopic film or on a nanoscopic level.[51] Switchable rectification has been demonstrated for a related dye shown in Figure 11.36. The electrical asymmetry can be chemically switched, off and then back on, by treatment with acid and base, respectively. Protonation disrupts the intramolecular charge-transfer axis, destroying the rectification effect.[52] Recent calculations, however, suggest that there may be relatively unpromising theoretical limits on the rectification possible by a single molecule.[53]

### 11.4.4 Molecular Switches

Otsuki, J., Akasaka, T. and Araki, K., 'Molecular switches for electron and energy transfer processes based on metal complexes', *Coord. Chem. Rev.* 2008, **252**, 32–56.

In principle any molecule able to exist in two reversible, switchable states can represents a molecular switch (bistable device) with potential to form part of molecular circuitry or act as molecular memory. An excellent component for switchable molecular devices is the 1,2-dithienylethene system, which has been exploited ingeniously by Lehn in a number of bistable systems.[54] The core switching element is the transformation of the dithienylethene unit between two stable states as a function of the wavelength of incident radiation (Scheme 11.8).

This switching ability is highly reversible simply by alternating between irradiation by ultraviolet (about 300 nm) and visible (>600 nm) light. Furthermore, the two states, 'open' and 'closed', have very different electronic properties. The closed state contains a fully conjugated $\pi$-system across the bridge, allowing effective electronic communication from substituent $R^1$ to $R^2$ *via* the delocalised $\pi$-system.

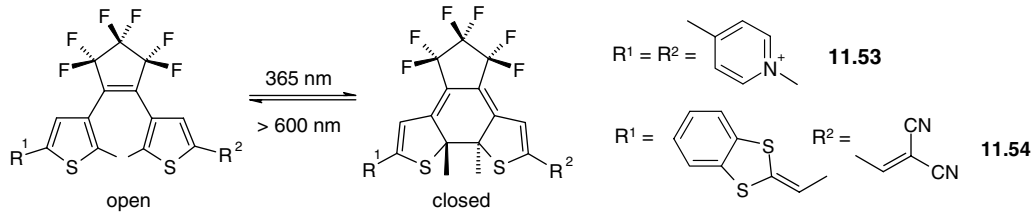


**Scheme 11.8** States of the bistable 1,2-dithienylethene switch unit.

The open state effectively insulates $R^1$ from $R^2$. Lehn's group have put this functional switching system to a number of different uses, highlighting its 'component' nature, which, by definition, must have intrinsic, transferable properties. In **11.53**, the two substituents linked by the switch are identical electroactive groups. In the closed form, compound **11.53** is easily reduced electochemically, whereas the open form is not. Thus we have a prototype switchable molecular wire. In the case of **11.54**, $R^1$ is an electron-donating group, while $R^2$ is an electron-poor acceptor. The resulting molecule in the closed form is an electronically communicating 'push–pull' system with marked nonlinear optical (NLO) properties, as characterised by a large hyperpolarisability ($\beta$ coefficient). Opening the switch by irradiation by visible light destroys the communication between the two ends of the molecule, and the hyperpolarisability is markedly decreased. An explanation of NLO properties may be found in Section 11.6.

Perhaps the most remarkable photoswitchable system based on this concept is that shown in **11.55** (Scheme 11.9), which represents a system that is both photo- and electroswitchable. As with **11.53**, the open BIS-OH form is electrochemically inert. Photoswitching to the closed form enables the molecule to be oxidised easily to the bis(quinone) BIS-Oq. The quinone form is photochemically inert and cannot revert back to an 'open' form until re-reduced. The system is of interest in the context of information storage applications. It represents a chemical approach to the EDRAW (erase direct read after write) mode

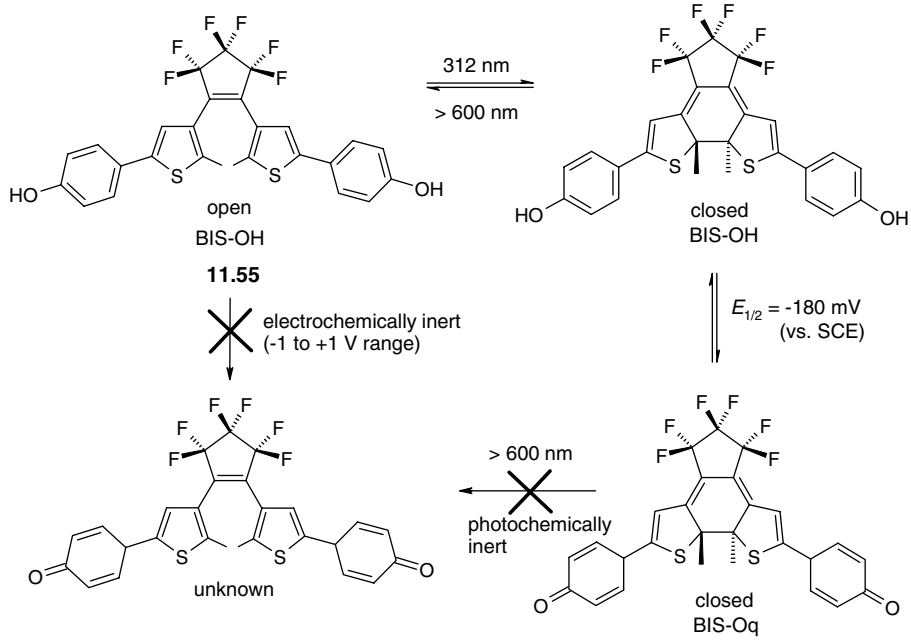


**Scheme 11.9** A photo- and electroswitchable system based on **11.55**.

of information storage in which information is written optically by irradiation with UV light and is then safeguarded by oxidation. The information may then be read many times without destruction before finally being erased after reductive unlocking (*cf.* the WORM (write once read many) type, in which information is written to media such as CD-ROM and may then be read a large number of times as required).

The 1,2-dithienylethene unit has also been used to link together metal tris(bipyridyl) moieties including an unsymmetrical Ru(II)/Os(II) complex. In the 'open' form luminescence from the MLCT state is observed with efficient energy transfer from ruthenium to osmium. However, the emission is quenched upon conversion to the closed form because of energy transfer to the photochromic 1,2-dithienylethene orbitals.[55]

Another example of a combined, switchable electro-optical molecular device is the couple **11.56** and **11.57**, which are readily interconverted electrochemically since oxidation of the hydroquinone moiety occurs before the oxidation of the Ru(II) centre. In the reduced hydroquinone form, the $Ru(bpy)_3^{2+}$ moiety is highly luminescent from its MLCT state, as described in Section 11.2. Electrochemical oxidation to the quinone form, however, results in complete switching off of the luminescence because of the quinone's ability to quench the MLCT state by extremely fast metal-to-ligand electron transfer. The quinone is an excellent electron acceptor, and indeed quinones play a significant role in charge separation in photosynthesis because of their low-lying $\pi^*$ acceptor orbitals (Section 2.4): hence the compound acts as an efficient bistable electrophotoswitch (Figure 11.37). Both oxidised and reduced forms of the compound are isolable and the redox couple is entirely reversible and stable. Luminescence quenching is complete.[56]

The mechanical nature of the connectivity between rotaxane and catenane components (Section 10.7) resembles strongly the mechanical connectivity in macroscopic machines and has inspired a great deal of work on photo-, redox- and pH-switchable systems. Initially, as part of attempts to produce [3]rotaxanes, long, terminated, dumb-bell-shaped threads were produced by Stoddart *et al*., incorporating two or more electron-rich aryl and biaryl residues. However, in most cases, only [2]rotaxanes resulted. The occurrence of a [2]rotaxane with two possible electron-rich binding sites raises the interesting possibility of the 'shuttling' of the 'blue box' macrocycle **6.81** (Section 6.5.8) back and forth between the two points of attachment, rather like a train on a railway line with two stations. As a result, the [2]rotaxane shown in Figure 11.38 was prepared *via* a threading approach in 19 % overall yield. Because the two 'stations' are different from each another, there is a significant energetic preference for the more electron-rich benzidine unit (nitrogen station). $^1$H NMR spectroscopy gives a ratio between the two translational isomers of 84:16 in $CD_3CN$ solution at –44ºC. However, protonation with trifluoroacetic acid decreases dramatically

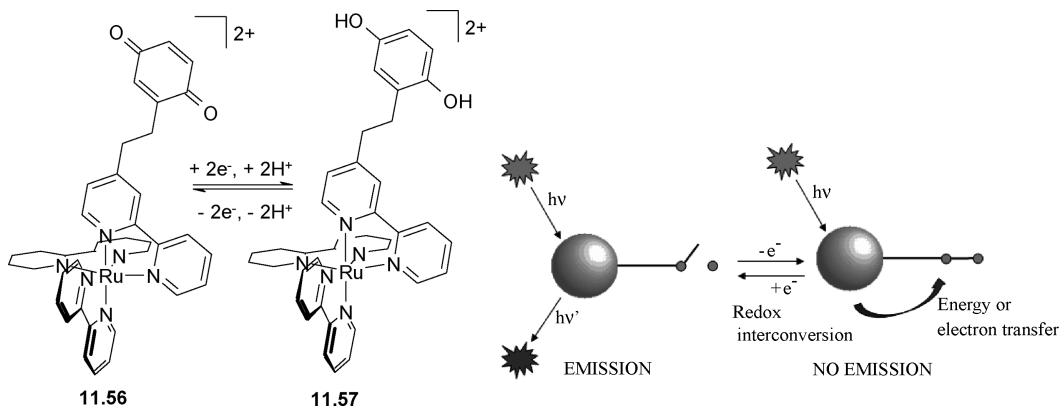


**Figure 11.37** Electrophotoswitching in a real system and cartoon representation.[56]

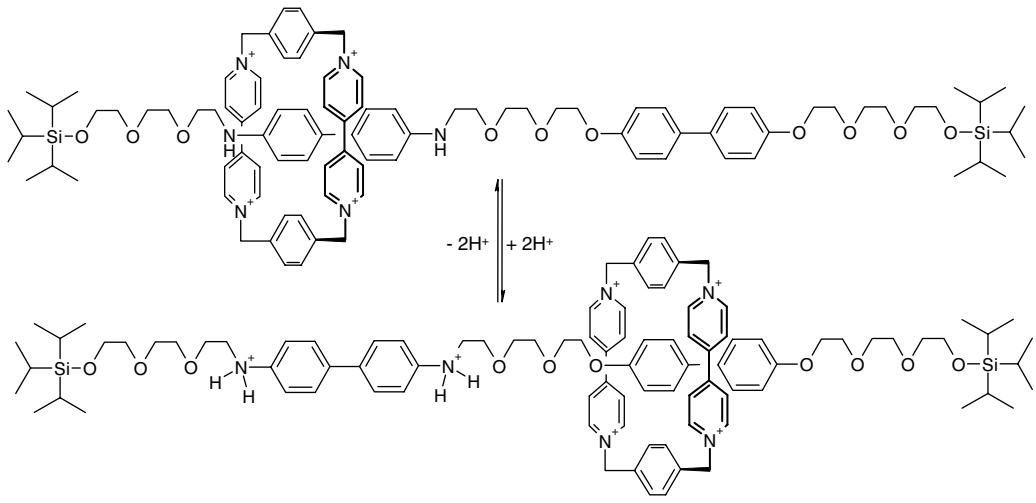


**Figure 11.38** A [2]rotaxane-based, pH- and redox-switchable molecular shuttle.

the electron density at the basic benzidine unit, causing the macrocycle to shunt completely to the 4,4′-biphenolate unit. A similar result is obtained by electrochemical oxidation of the benzidine station to the analogous radical cation. Both pH- and electrochemically driven processes are entirely reversible, giving a rotaxane-based molecular switch.

A great deal of work has gone into the production of further redox- and photoswitchable rotaxanes.[57] In particular, the use of photoactive terminator groups incorporating anthracene substituents, or redox active ferrocenyl groups, instead of Si(*i*-Pr)$_3$ groups, have been found to control the rate of charge recombination upon photoexcitation in rotaxane **11.58**. Photoexcitation by a laser pulse at 437 nm affords a radical ion pair by electron transfer from the electron-rich thread to the macrocyclic shuttle. In the case of the ferrocenyl derivative **11.59**, very long-lived charge-separated states, somewhat analogous to those occurring in photosynthesis, are observed. The photoexcited [2]rotaxane is quenched by rapid oxidation of the ferrocenyl stopper by the oxidised 4,4′-biphenol moiety. Charge recombination is very slow because of the repulsion of the cationic macrocycle away from the positively charged ferrocene-derived terminator group (Figure 11.39). In contrast, the analogous anthracenyl-stoppered analogue exhibits very rapid charge recombination.

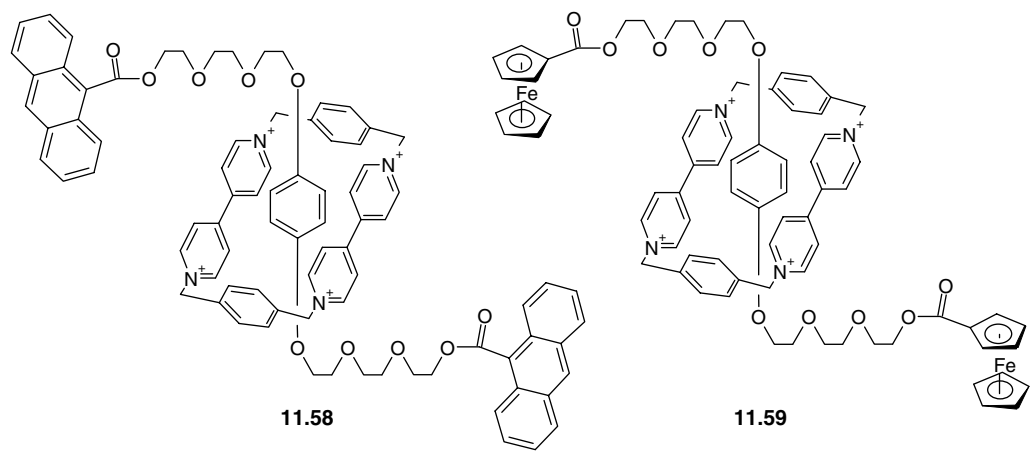


**11.58** **11.59**

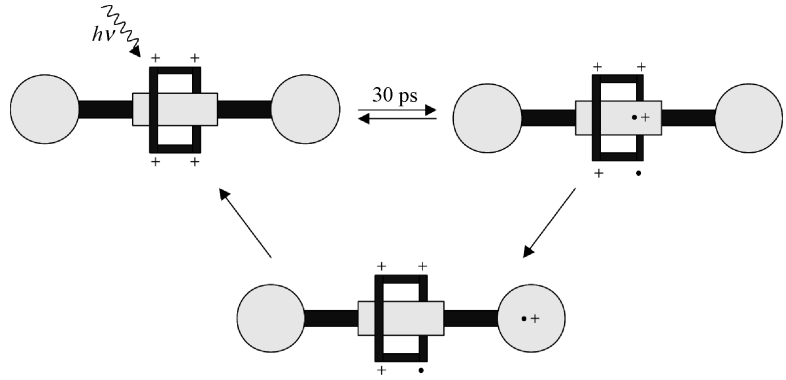


**Figure 11.39** Long-lived charge separation using **11.59**.

Work on pseudorotaxanes has resulted in a system that is switchable between two different colours (a chromophoric switch) as a function of the binding of two different rotaxane threads. The colour of the complex, which switches between red and purple, depends strongly upon which thread, **11.60** or **11.61** is bound. In the resting state of the switch, the more-electron rich 1,5-dioxynapthalene group of **11.60** is complexed preferentially, giving a purple colour to the complex in MeCN solution. Thread **11.60** is ditopic, however, and can act as a host for alkali metal cations, particularly $K^+$, by virtue of the appended [18]crown-6 ring. On binding of $K^+$ ions by the crown ether portion of **11.60**, there is immediate electrostatic repulsion between the thread and the cationic cyclophane paraquat macrocycle **6.81**. Because the complex is only a pseudorotaxane (there are no end stopper groups), this repulsion causes immediate dethreading, allowing complexation of the other thread, **11.61**, which imparts a red colour to the solution. The inference is that the presence of colourless $K^+$ salts may be detected by a simple visual examination of the solution (Scheme 11.10).

Just like the rotaxane-based shuttle shown in Figure 11.38, unsymmetrical catenanes can also undergo translational isomerism. A [2]catenane has been constructed based on a desymmetrised tetracationic cyclophane containing two different recognition sites, or 'stations': a bipyridinium unit and a *trans*-bis(pyridinium)ethylene moiety, **11.62**. This tetracationic cyclophane may be prepared interlocked with bis(*p*-phenylene)[34]crown-10 in the same fashion as the [2]catenane **10.76** (Section 10.7). The $^1$H NMR spectrum of the catenane in acetone shows that the smaller bipyridinium unit resides within the electron-rich crown component. Electrochemical reduction of **11.62** to produce a radical trication also occurs on the bipyridinium moiety because of its high $\pi$-acidity. The reduction reduces dramatically the electron-acceptor characteristics of the bipyridinium unit, however, and as a result it undergoes circumrotation to the outside of the crown, placing the now better $\pi$-accepting *trans*-bis(pyridinium)ethylene unit within the crown ether cavity. Upon reoxidation, the process is reversed (Scheme 11.11).[57]

## 11.4.5 Molecular Logic

Pischel, U., 'Chemical approaches to molecular logic elements for addition and subtraction', *Angew. Chem., Int. Ed.* 2007, **46**, 4026–4040.

In order to carry out sophisticated computation the molecular computers of tomorrow will need not just basic elements such as switches, memory and connectors but also more sophisticated components, particularly logic gates. A logic gate is an element of a computer that gives a particular output for a

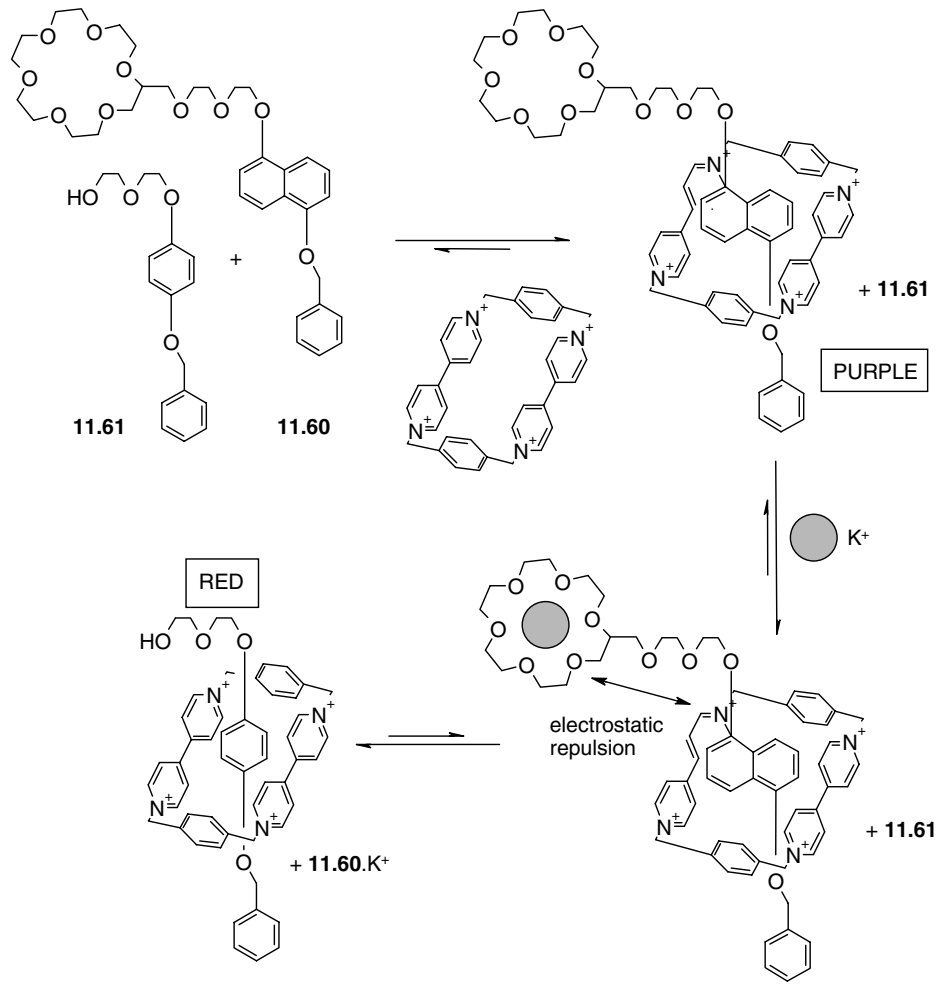


**Scheme 11.10** Pseudorotaxane-based, chemically driven chromophoric molecular switch.

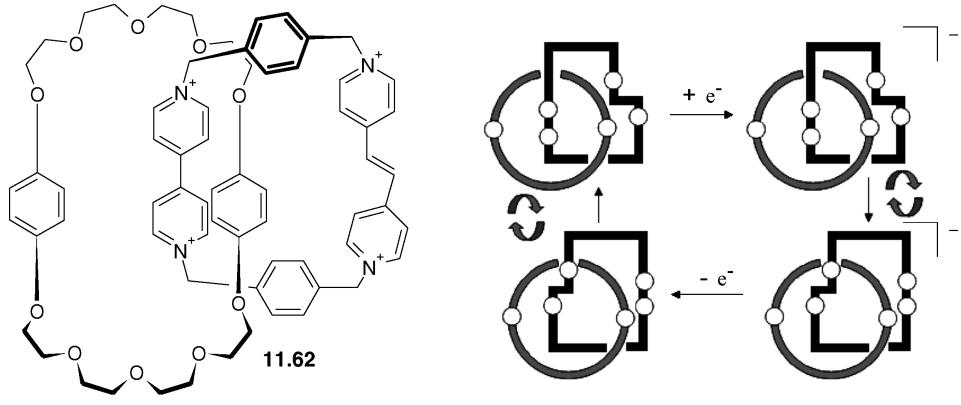


**Scheme 11.11** Electrochemically controlled movements of the ring components of a [2]catenane.[57]

**Table 11.1** Truth table and symbols for some common Boolean logic operations based on two inputs *P* and *Q*.

| | | **AND** | **OR** | **XOR** | **XNOR** | **NAND** |
|---|---|---|---|---|---|---|
| | | $P \wedge Q$ | $P \vee Q$ | $P \underline{\vee} Q$ | $P \underline{\wedge} Q$ | $P \overline{\wedge} Q$ |
| ***P*** | ***Q*** | | | 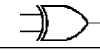 | 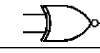 | 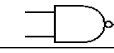 |
| 0 | 0 | 0 | 0 | 0 | 1 | 1 |
| 0 | 1 | 0 | 1 | 1 | 0 | 1 |
| 1 | 0 | 0 | 1 | 1 | 0 | 1 |
| 1 | 1 | 1 | 1 | 0 | 1 | 0 |

defined set of inputs. The output for any given logic gate depends on the binary input(s) and is usually presented in the form of a truth table, *e.g.* Table 11.1. The most important single-input logic gate is the NOT gate which inverts the input value (1 becomes 0 and vice versa). More interesting are the two-input gates such as the AND gate. For an AND gate both inputs have to be 'true' or have a binary value of '1' in order for the gate to give an output of '1'. These kinds of logic operations are usually termed 'Boolean' after Englishman George Boole (1815–1864), whose ideas were a key forerunner to the digital age. In current silicon-based computers, using positive logic, the value of '1' is generally assigned to a voltage above a certain threshold, while '0' is below that threshold. So if the threshold were 2 V then a potential of 3 V would be a '1' while 1 V would be a '0'. It is by no means certain that molecular computers would work in a similar way. In optical fibres, for example, propagating light signals of different wavelength do not interfere with one another and so massively parallel information transmission is possible. In contrast an electrical wire can only handle one signal at a time.

One of the first examples of a molecular device capable of Boolean logic operations, a molecular AND gate (**11.63**), was reported by A. P. de Silva (Belfast, UK) in 1993.[58] The receptor is based on the PET concept in that the anthracene derivative's fluorescence is quenched by both the lone pair of the tertiary amine nitrogen atom (*cf.* Scheme 11.14) and by the benzo crown ether. Protonation of the nitrogen atom ties up the amine lone pair preventing one of the two quenching mechanisms, while binding of $Na^+$ by the crown ether prevents the other. The compound thus is only fluorescent in the presence of *both* $H^+$ and $Na^+$. Here the proton and sodium cation are acting as the two inputs (0 for 'no ion', 1 for the presence of each ion) and the fluorescent signal is the output (0 unless both ions are present). The system works because of the basic principles governing binding selectivity; the amine is highly selective for $H^+$ while the crown ether is complementary to the hard $Na^+$.

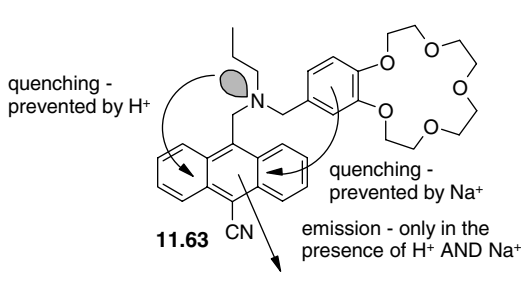


**11.63**

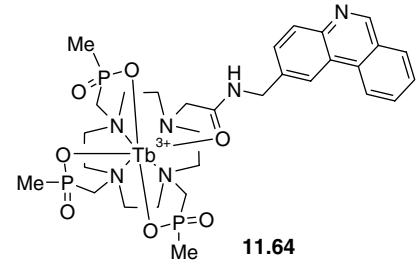


**11.64**

The opposite of the AND gate is the NAND operation. In the context of a luminescent device this logic corresponds to an emission only if neither one of two different chemical imputs are present. A good

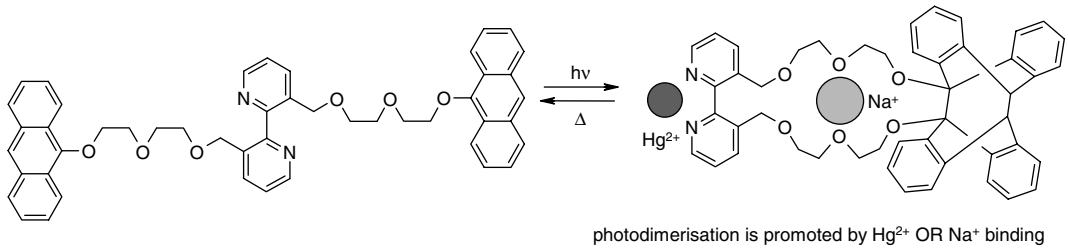


**Scheme 11.12** A molecular OR gate – the photodimerisation is promoted by either of the two metal ions.[60]

example is the phosphorescent lanthanide complex **11.64**, which when the phenanthridine sensitiser is excited at 304 nm emits a strong Tb(III) phosphorescence only in the *absence* of *both* $H^+$ and $O_2$. Otherwise $H^+$ protonates the phenanthridine while oxygen quenches the phenanthridine triplet donor.[59]

A molecular system showing OR logic is shown in Scheme 11.12. In this case the characteristic thermally reversible [4π+4π] photodimerisation of anthracene derivatives is promoted by the preorganisation brought about either by binding $Na^+$ in the crown ether-like binding site or by binding the softer Hg(II) by the bipyridyl unit.[60] The system has some similarities to the allosteric switch described in Section 1.5 (Scheme 1.2).

A molecular XOR gate has been assembled based on a pseudorotaxane comprising a good electron acceptor (a 2,7-diazapyrenium derivative, **11.66**) that interacts with the electron donating groups from the a naphthaleno crown ether (**11.65**), Scheme 11.13. This interaction is clearly observed in the UV-Vis spectrum as a broad band at 400 nm assigned to the low-energy charge transfer between the two components, and no fluorescence signal is observed because of charge transfer quenching. Addition of base (tributylamine) unthreads the pseudorotaxane and forms a complex **11.65**·$(tributylamine)_2$ showing a charge-transfer absorption around 550 nm and switching on the fluorescence of the crown ether. Subsequent addition of trifluoromethanesulfonic acid results in the neutralisation of the tributyl

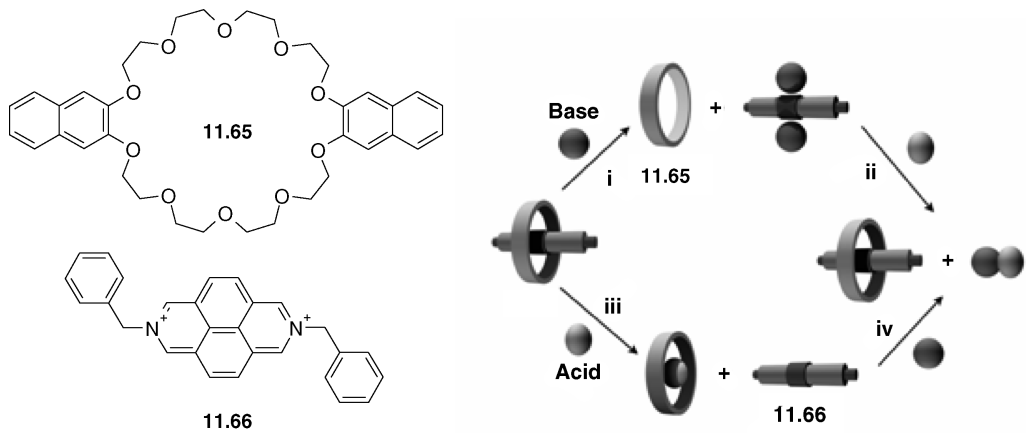


**Scheme 11.13** The unthreading and threading of the pseudorotaxane, corresponding to the XOR logic function. Unthreading to give either (i) a 'locked' thread or (iii) a locked ring followed by either (ii) or (iv) unlocking and rethreading to give $HN(CH_2CH_2CH_2CH_3)_3{}^+CF_3SO_3{}^-$. Acid = $CF_3SO_3H$, base = $N(CH_2CH_2CH_2CH_3)_3$.[61]

amine base and the re-formation of the pseudorotaxane, switching off emission once again. Providing the acid and base inputs in the opposite order also results in successive unthreading and re-threading with the acid protonating the crown ether giving fluorescence, followed by neutralisation by the base.[61]

## 11.4.6 Towards Addressable Molecular Devices

Flood, A. H, Stoddart, J. F., Stuerman, D. W. and Heath, J. R. 'Whence molecular electronics', *Science* 2004, **306**, 2055–2056.

While the systems we have looked at so far all exhibit some kind of chemical analogue of molecular electronic operations (even though they are really just simply well-defined chemical or photophysical reactions or processes) such individual switching or 'calculating' behaviour is not useful in the context of molecular machines or molecular electronic computing without some kind of input-output architecture that allows its interrogation and interaction with the outside world. Over the past decade or so work by Sir J. Fraser Stoddart (now at Northwestern University, USA) in collaboration with James Heath at Caltech has addressed this issue, combining molecular nanoscale devices with electronically addressable arrays. In 2007 the group reported a 160-kilobit molecular electronic memory assembled in a grid with a density of $10^{11}$ bits per square centimetre. The device has a pitch of 33 nm and a memory cell size of 0.0011 $\mu m^2$. Compare this to modern dynamic random access memory (DRAM) circuits which have 140 nm pitch wires and a memory cell size of 0.0408 $\mu m^2$. The molecular device has the basic characteristics of DRAM systems projected to be available in 2020 and is thus potentially a significant advance. The memory is based on rotaxane **11.67** in which the bipyridinium 'blue box' can move from the electron rich thtrathiafulvalene (TTF) unit to the napthalaene dioxy 'station' upon oxidation of the TTF, making it a poorer electron donor.[62] The molecule is amphiphilic with hydrophilic and hydrophobic ends allowing it to self-assemble into a surface monolayer. The final memory device comprises 400 phosphorus-doped silicon bottom-nanowire electrodes (16 nm wide, 33 nm pitch) crossed by 400 titanium top-nanowire electrodes of the same size that sandwich the rotaxane monolayer. Each digital 'bit' comprises an individual molecular switch tunnel junction (MSTJ) which is defined by a Si bottom nanowire and Ti top nanowire which allow it to be electronically addressed, and containing approximately 100 [2]rotaxane molecules This cross-wire geometry allows for good tolerance of defects because individually faulty cross 'bits' can be bypassed. The threshold for a 'good' bit was based on a minimum current ratio between a '1' and a '0' state of 1.5. While about 50 % of the bits exhibited some switching response, only 25 % passed this more stringent threshold.

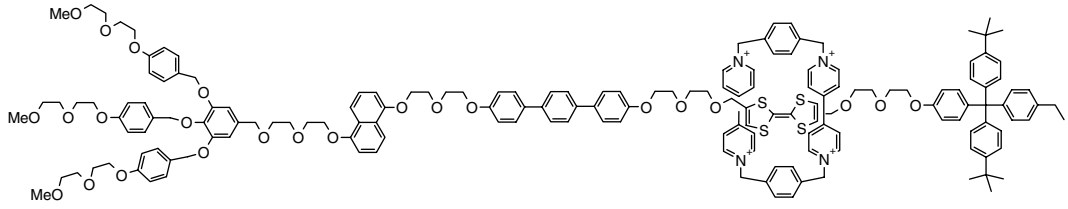


**11.67**

This remarkable molecular memory was preceded by two other related examples of addressable molecular electronics from the Stoddart and Heath groups in collaboration with Hewlett-Packard scientists. First in 1999 a [2]rotaxane based system was configured into molecular AND and OR logic gates,[63] then in 2000 a [2]catenane based molecular switch was reported.[64] The molecular basis for the operation of this switch is the same as in **11.67**, namely reorientation in response to reduction of

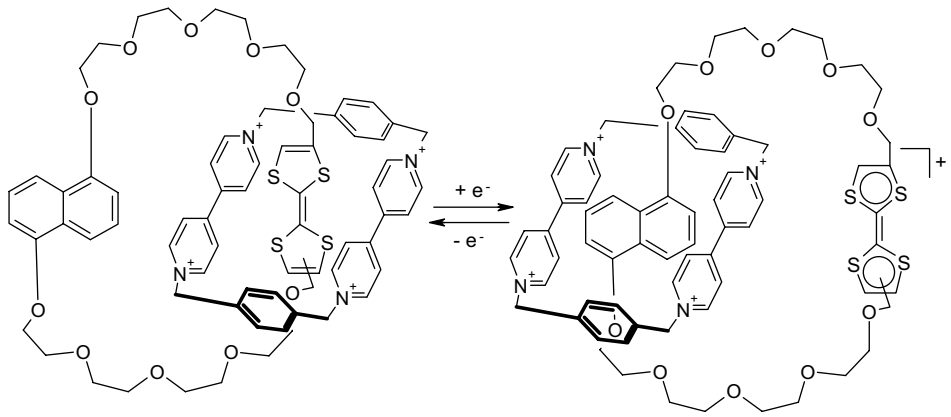


**Scheme 11.14** An electronically reconfigurable [2]catenane based molecular switch.[64]

the TTF unit (Scheme 11.14). The individual [2]catenane molecules were fabricated as part of a single monolayer with phospholipid counter anions between a silicon bottom electrode and a metallic top electrode. The switch opens at +2 V and closes at −2 V and can be interrogated as to whether it is in an 'on' or 'off' state (*i.e.* reduced or oxidised) through many cycles at 0.1 V.

Another addressed molecular electronic device made up from a single cobalt complex is the molecular transistor shown in Figure 11.40. The device exhibits electron transport through well-defined charge states of the single cobalt atom. The coupling between the metal ion and the electrodes is dependent on the length of the insulating spacers linking the complex to the electrode surface. Thus, depending on the length of the tethers the device that exhibits either single-electron transfer or a *Kondo resonance*, a particular kind of quantum mechanical resonance which correlates with a particular oxidation state observed in the solution phase redox chemistry of the cobalt complex.[65]

Finally, a very simple molecular electronic component is benzene-1,4-dithiol, which is readily used as a linker between gold electrodes in the same way as the cobalt terpyridine complex shown in Figure 11.40. Benzene dithiol has been used to demonstrate the thermoelectric effect in molecular electronic systems as a linker between a gold surface and the gold tip of a modified atomic force microscope. Thermoelectricity (termed the Seebeck effect) is the generation of an electrical potential

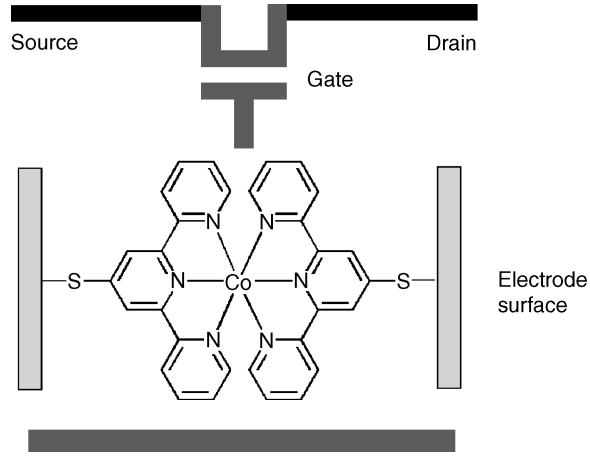


**Figure 11.40** A molecular transistor.[65]

difference directly from heat. While the effect has been known for over 200 years it is usually confined to metallic or semiconductor junctions.[66]

## 11.5 Molecular Analogues of Mechanical Machines

Kay, E. R., Leigh, D. A. and Zerbetto, F., 'Synthetic molecular motors and mechanical machines', *Angew. Chem., Int. Ed.* 2007, **46**, 72–191.

In addition to molecular electronic devices we should also mention molecular level analogues of mechanical devices within the context of molecular level machines. Such molecular devices include motors, ratchets, switches, shuttles, rotors and 'demons' and have very recently been comprehensively reviewed (key reference). As a result we will look at just a few examples by way of introduction to this extensive field. The key concept here is making molecules do some kind of mechanical work in response to some kind of energy input. An obvious analogy is the contraction of biological muscles powered by chemical energy from hydrolysis of ATP. Can we find a molecular analogue? One example is the behaviour of the extended terpyridyl ligand **11.68**.[67] In the free-state the compound adopts an extended conformation some 4 nm long. The imine functionalities make the ligand excellent for binding the soft $Pb^{2+}$ to give a 2:1 Pb:ligand complex which has a self-assembled coiled, helical structure only 0.72 nm long. The $Pb^{2+}$ can be removed by addition of tris(2-aminoethyl)amine (tren), a good chelating ligand for lead(II), which regenerates the extended free molecule **11.68**. Changes in pH by addition of trifluoromethane sulfonic acid protonates the tren, releasing the lead ions resulting in re-coiling. Raising the pH by adding triethylamine base deprotonates the tren, which then sequesters the lead(II) resulting in uncoiling, Figure 11.41. The work done in contracting the muscle is powered by the binding free energy of the ligand and Pb(II) ions. This energy is restored to the system by the acid-base neutralisation reactions.

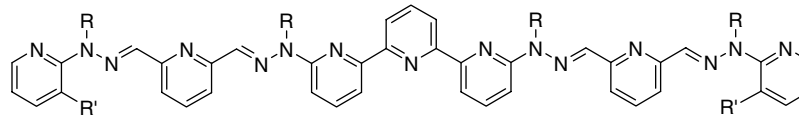


**11.68**

Changes in pH have also been used to power a molecular elevator developing a force of some 200 piconewtons per molecule.[68] The triple thread **11.70**, when protonated as shown, is readily

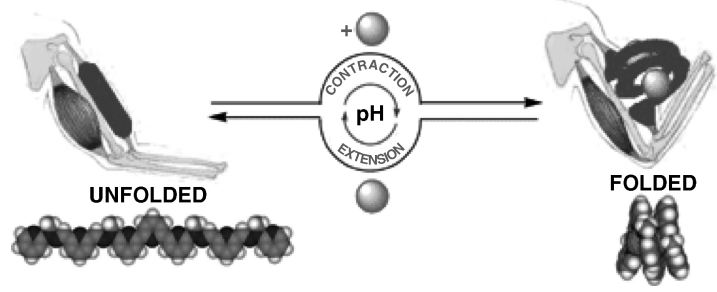


**Figure 11.41** A prototype pH triggered molecular muscle based on coiling of ligand **11.68** by $Pb^{2+}$. The binding of $Pb^{2+}$ is switched on or off according to the protonation state of the competitor ligand tren (reproduced by permission of The Royal Society of Chemistry).

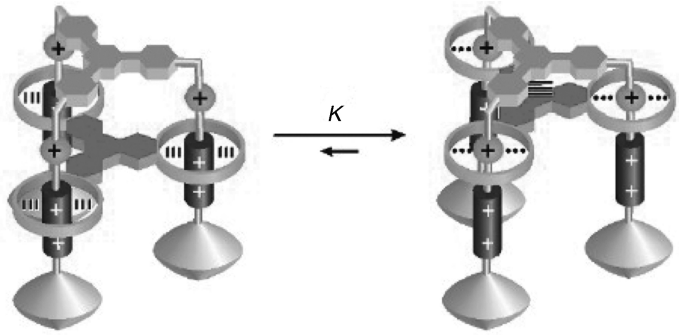


**Figure 11.42** Components and schematic of the 'molecular elevator' (image courtesy of Prof. Sir J. F. Stoddart).[68] See plate section for colour version of this image.

bound *via* $NH^+\cdots O$ hydrogen bonds into the crown ether moieties of the receptor **11.69**. The binding is irreversible and the molecule is a triple [2]rotaxane chemically synthesised by triple capping of a *pseudo*rotaxane intermediate. The protonated form of this molecular elevator is shown in Figure 11.42. Addition of base deprotonates the complex, breaking the stable $NH^+\cdots O$ hydrogen bonded arrangement and causing the triple ring to move some 0.7 nm to the bipyridinium stations, thus expanding the molecule. The process is reversed by addition of acid and mimics natural molecular motors such as myosin and kinesin, although the force generated is an order of magnitude higher.

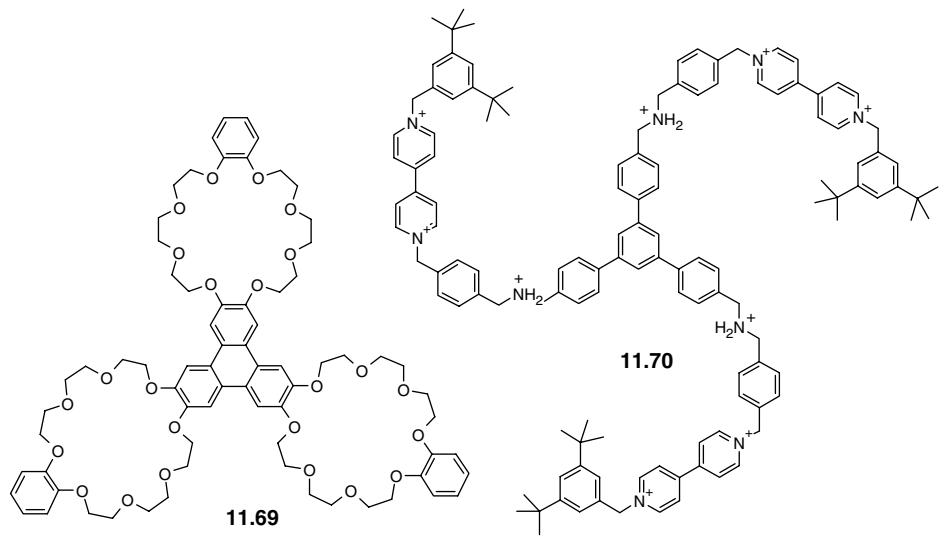


Instead of chemical energy as in changes in pH, molecular motions can also be powered by light. To give a simple example, photoirradiation of the anthracene chromophore in [2]rotaxane **11.71** results in shuttling of the ring from the ester to amide carbonyl as the C=O attached to the excited state chromophore becomes a better hydrogen bond acceptor. The lifetime of the system is 4.3 ns and during that time the ring moves back and forth some 3 Å.[69]

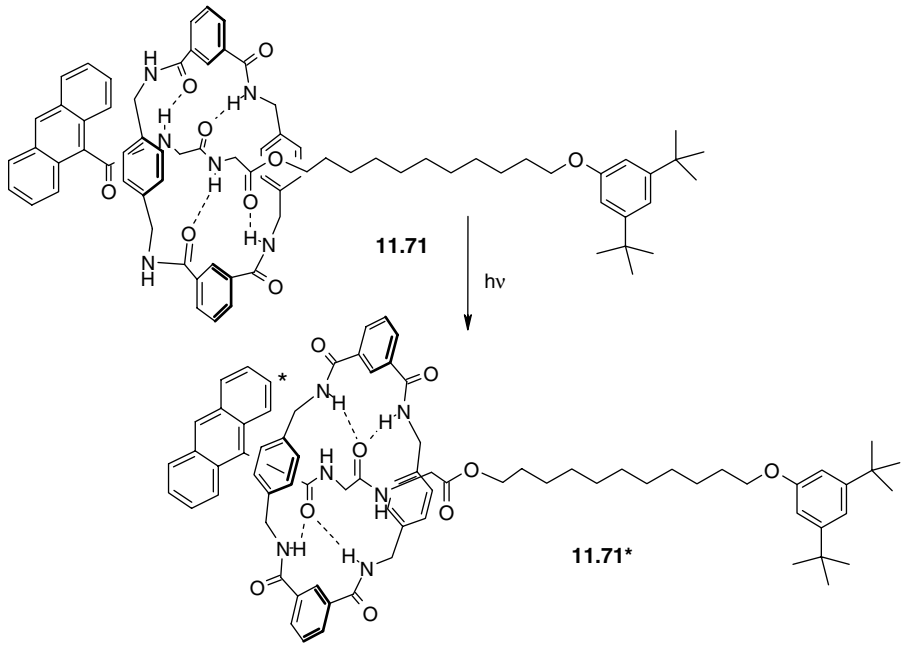


A long-term goal in research into molecular machines is the rectification of Brownian motion to give a system that imparts unidirectional motion based on ambient thermal fluctuations. Brownian motion (named in honour of the botanist Robert Brown) is the constant, random, fluctuation exhibited by small particles usually in a fluid medium. In terms of energy or motive force generation this motion is useless because it occurs randomly in every direction. If some way could be found to harness it such that the motion could be rectified, *i.e.* allowed in one direction only without the reverse motion being possible then we would have a way to obtain useful energy or force from useless ambient thermal energy. Such a process may be impossible and is closely related to the thought experiment concept of Maxwell's Demon that breaks the second law of thermodynamics (the entropy of an isolated system which is not in equilibrium will tend to increase over time, approaching a maximum value at equilibrium). Physicist James Clerk Maxwell envisaged a gas in a closed two-compartment system with a trapdoor in the middle operated by an intelligent 'sorting demon'. The gas is at ambient temperature and so contains a mixture of fast and slow moving particles. The demon opens the trapdoor when a fast moving particle approaches and closes it to bar the ingress of the slower particles to the second part of the chamber. The demon thus sorts the random mixture of particles into hot and cold sections which can be used to do useful work. In order to design a molecular device that might in practice harness Brownian motion to do useful work some kind of asymmetric energy surface is required. Such a device must also contain a randomising element and a source of energy input in order not to violate the second law of thermodynamics. Molecular machines that can undergo this kind of unidirectional motion are termed 'ratchets' and ratchet types of mechanism are thought to underlie many aspects of biological molecular machinery. Research into artificial molecular ratchets is in its infancy however there are some systems exhibiting this kind of irreversible molecular motion. Building on the kinds of rotaxane related to **11.71** David Leigh (Edinburgh, UK) has designed the compartmentalised Brownian molecular machine **11.72** that acts as an irreversible molecular switch. In **11.72** the macrocycle can sit at either one of two essentially equivalent 'stations' that differ only in the identity of the two 'stoppers'. As-synthesised the compound has the macrocycle 100 % situated on the left hand side. The distribution of the macrocycle across the two stations is not influenced by solvent or other external influences. It is determined by the time at

which the blocking trialkyl silyl group is hydrolysed away. As soon as this 'linking operation' is performed the system can move towards a 50–50 equilibrium distribution. Restoring the blocking group does not reset the machine to the original state however; the equilibrium distribution is now fixed. This kind of unidirectional behaviour is analogous to the motion of macroscopic mechanical devices such as clocks and, while it represents a very simple demonstration, hints at significant future possibilities. A key difference between mechanical motors and Brownian machines is that due to thermal noise the nanoscale Brownian system explores all possible motions and configurations of the system resulting in a uniquely chemical approach to controlling nanoscale motion.

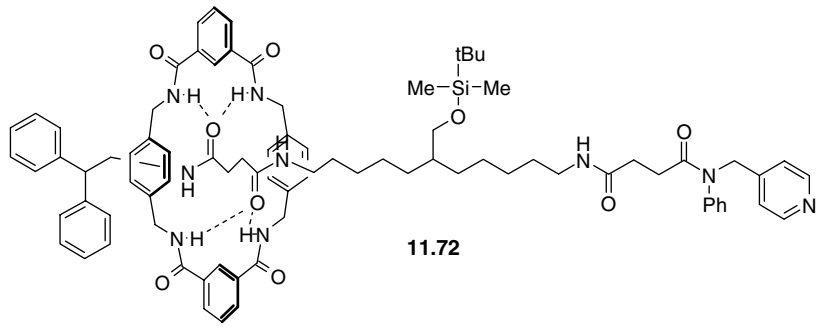


**11.72**

## 11.6 Nonlinear Optical Materials

Di Bella, S., 'Second-order nonlinear optical properties of transition metal complexes', *Chem. Soc. Rev.* 2001, **30**, 355–366.

The ability to manipulate the frequency, phase, polarisation or path of light has very important technological ramifications in areas such as production of tunable laser light and optical data storage. Currently, a great deal of research is being devoted to both organic and inorganic materials that exhibit nonlinear optical (NLO) effects, particularly second harmonic generation (SHG), which, put simply, causes a doubling in the frequency of incident light. This doubling is commonly used to produce blue light (wavelength of about 300 nm) from green light (wavelength 600 nm), for example. SHG materials such as potassium dihydrogen phosphate (KDP) are also used in wave mixing, in which light from two lasers of different frequencies is mixed, resulting in an 'added' output wave. The engineering of materials with desirable NLO properties is a major scientific challenge and, because it is subject to molecular design on a modular basis, has been addressed by supramolecular chemists. We have already seen some work on the crystal engineering of NLO materials in Section 8.1.2 and indeed the crystal engineering of materials showing NLO effects, particularly of polar coordination polymers, is now a major area of endeavour.[70] Before embarking on a discussion of NLO materials and their properties, it is worthwhile discussing briefly the origins of the effects and key features in their design. A full discussion may be found in the literature.[71]

### 11.6.1 Origins of Nonlinear Optical Effects

When electromagnetic radiation interacts with matter it causes the electron density in the material to oscillate at the same frequency as the incident light. Since the interaction of light and matter is a time-resolved process involving many photons, it should not be a surprise that the oscillation produced by

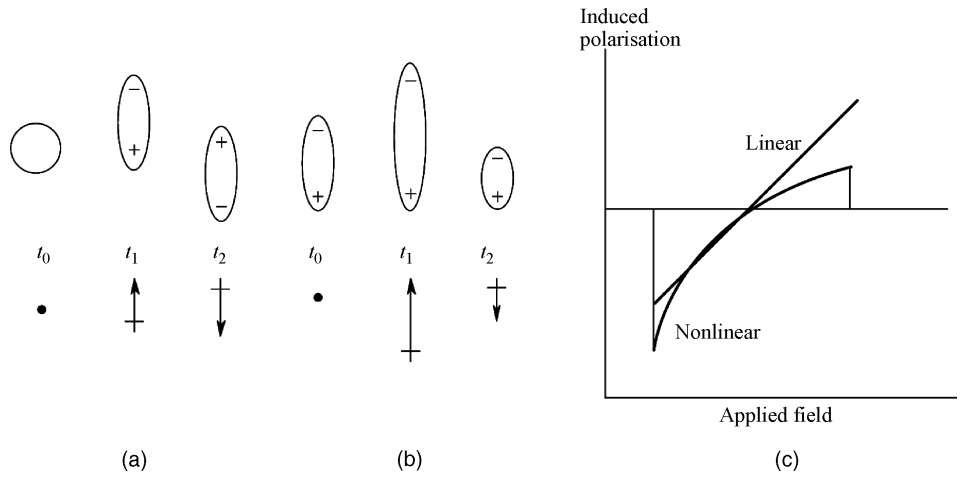


**Figure 11.43** Induced polarisation as a function of time. (a) Linear, (b) nonlinear and (c) graphical representation as a function of applied field.

interaction with one photon will affect the properties of the material 'seen' by the next. The presence of an oscillating charge results in some charge separation and the production of an oscillating induced dipole, with moment $\mu$, which is a function of the frequency of the incident light ($\omega$) and proportional to the magnitude of its electric field, **E** (Figure 11.43a). The magnitude of the induced dipole at a given **E** is determined largely by how easy it is to deform the electron density in a particular atom or molecule. The ease of deformation of the electron density is its polarisability. Because this may be different in different directions, polarisability is a tensor quantity, thus the overall molecular polarisation is given by:

$$\text{Polarisation} = \mu(\omega) = \alpha_{ij}(\omega)\mathbf{E}(\omega) \tag{11.1}$$

Here, $\alpha_{ij}(\omega)$ is the linear polarisability tensor at frequency $\omega$ and describes the linear variation of the induced dipole with the electric field. The resulting oscillation in the polarisation (oscillating dipole) is, in effect, a moving charge, and will therefore emit radiation of the same frequency as the oscillation. This gives rise to linear optical effects such as birefringence and refraction.

This equation describes the full picture only if the atomic or molecular potential is a classical harmonic potential. However, when a molecule is subjected to very intense fields, as in laser light, the material can become so polarised that its polarisability can change and hence the induced polarisation is a nonlinear function of field strength (Figure 11.43b). To take an example, consider the polar C=O bond in acetone. The electronegativity of oxygen means that the electron density will be polarised more easily towards O than C. The nonlinear polarisation has a diminished maximum in one direction and an enhanced maximum in the other. Once again, it is a tensor quantity because the incident light may come from any direction ($x$, $y$ or $z$) and induce a polarisation response in the $x$, $y$ or $z$ directions. This asymmetric polarisation response may be decomposed into a Fourier series containing a DC polarisation component ($\mu_0$) and components at the fundamental and second harmonic frequencies. This is commonly approximated by a Taylor expansion. Strictly, the expansion has an infinite number of terms, and becomes progressively more accurate as more terms are added. At high field strengths, the second and third terms become important.

$$\mu = \mu_0 + (\alpha_{ij})\mathbf{E} + \tfrac{1}{2}(\beta_{ijk})\mathbf{E}\cdot\mathbf{E} + \tfrac{1}{6}(\gamma_{ijk})\mathbf{E}\cdot\mathbf{E}\cdot\mathbf{E} + \cdots \tag{11.2}$$

The fundamental component ($\alpha\mathbf{E}$) is linear in $\mathbf{E}$ and represents the linear optical properties discussed above. The second ($\frac{1}{2}\beta\mathbf{E}\cdot\mathbf{E}$) third ($\frac{1}{6}\gamma\mathbf{E}\cdot\mathbf{E}\cdot\mathbf{E}$) and subsequent harmonic terms are nonlinear in $\mathbf{E}$ and give rise to NLO effects. The $\beta$ and $\gamma$ values are referred to, respectively, as the first and second hyperpolarisabilities. The second harmonic term gives rise to second harmonic generation (SHG), the third results in frequency tripling effects, and so on. Importantly, since only the time-averaged asymmetrically induced polarisation leads to second-order NLO effects, the molecule and crystal must be non-centrosymmetric, otherwise the effects will cancel one another. Third-order effects, however, may be observed in both centrosymmetric and non-centrosymmetric materials.

So, how does this effect that light has on matter result in the effects observed that the matter is having on the light (frequency doubling *etc.*)? In the case of the linear contribution, the oscillating charge re-emits light at the same frequency as its oscillation, which is the same frequency as the incident light. For the NLO contributions, the oscillation of the polarisation is anharmonic and contains an $\mathbf{E}\cdot\mathbf{E}$ contribution in the case of the second term. The electric field at a given point in time depends on the radiation frequency and the wave amplitude $\mathbf{E}_0$ in the following way:

$$\mathbf{E} = \mathbf{E}_0 \cos(\omega t) \tag{11.3}$$

Equation 11.2 can be rewritten:

$$\mu = \mu_0 + (\alpha_{ij})\mathbf{E}_0 \cos(\omega t) + \tfrac{1}{2}(\beta_{ijk})\mathbf{E}_0^2 \cos^2(\omega t) + \tfrac{1}{6}(\gamma_{ijk})\mathbf{E}_0^3 \cos^3(\omega t) + \cdots \tag{11.4}$$

The quantity $\cos^2(\omega t) = \frac{1}{2} + \frac{1}{2}\cos(2\omega t)$, and so the second-order oscillating polarisation induced by the electromagnetic radiation contains a component oscillating at $2\omega$, *i.e.* the frequency is doubled. This charge oscillating at double frequency will therefore re-emit radiation of double frequency in accordance with the magnitude of the second harmonic term. In effect, two photons of one frequency have combined to give one photon of double the frequency. Similarly, frequency-tripled contributions come from the third harmonic term, and so on.

In fact, this is really a special case of the combination of two (or more) photons where the energy of the two photons are the same. If light from two different laser sources is combined, then we have two electric fields, $\mathbf{E}_1$ and $\mathbf{E}_2$, and two frequencies, $\omega_1$ and $\omega_2$. The effect of SHG is now to add the two frequencies to give an emitted component, which is of a new frequency, $\omega_3 = \omega_1 + \omega_2$. In this way, tunable lasers with variable frequency, $\omega_3$, using NLO materials such as potassium dihydrogen phosphate (KDP) are now a reality. One of the problems with SHG, however, is that the amount of radiation of the desired frequency-doubled variety that is emitted is a very small proportion of the incident intensity. This depends on the magnitude of the $\frac{1}{2}(\beta)\mathbf{E}\cdot\mathbf{E}$ term. The intensity of the frequency-doubled light may be increased by increasing $\mathbf{E}$ (*i.e.* turning up the laser power), but it is still desirable to produce new materials that exhibit large hyperpolarisabilities ($\beta$ values) in order to increase the efficiency of the process.

So, how might we design a material that has a large hyperpolarisability coefficient? As chemists, we have some feel for the linear polarisability of a molecule. Organic molecules such as ethyne (acetylene) are more polarisable than ethane because of their $\pi$-electron clouds. Inorganic materials such as semiconductors, with their small HOMO-LUMO gap, are more polarisable than insulators. In general, we might say the polarisability is related to the extent of electron delocalisation, which in turn depends on the number of orbitals in the electronic system of interest, their hybridisation and the degree of interorbital coupling. For hyperpolarisability, the problem is less obvious. The anharmonic polarisation shows the largest deviation from the linear contribution at high degrees of distortion

of the electron cloud. This implies that we certainly will not get NLO effects from nonpolarisable molecules where the distortion is always small. In addition to this, we also need a large intrinsic anharmonicity (*i.e.* deviation of the potential from linearity and hence large $\beta$ value). In terms of molecular design, this means that we need an electron donor portion of the molecule and an electron acceptor. It will always be easier to polarise the molecular electron density towards the acceptor than the donor, and hence donor acceptor molecules, particularly organic ones, have some of the largest known $\beta$ values. However, large $\beta$ values are not enough in themselves for an effective SHG material. The criterion of overall non-centrosymmetric character must be observed (*i.e.* the crystalline material must crystallise in a polar space group) and there are also materials aspects. The material must be colourless, or only very palely coloured, so it does not absorb the laser light with consequent overheating or melting. It must also not be subject to radiation damage by the high light intensities involved. These properties are exhibited more commonly by inorganic compounds, which often have lower $\beta$ values, and hence the subject is still open for the design of improved NLO materials that possess the best of both organic and inorganic worlds.

### 11.6.2 Second-Order Nonlinear Optical Materials

The general electronic criteria for constructing an SHG device with a large $\beta$ seem to include the following:

- Large changes in dipole moment upon excitation.
- Large transition dipole moments.
- Small energy gap between the excited and ground states.

We have already come across several organic donor–acceptor molecules, such as the molecular rectifiers **11.49** – **11.52** and the asymmetric switch **11.54**. The large separation in these systems between an organic electron donor and an electron acceptor, coupled with the electronic communication between the two portions of the molecule (*via* a molecular wire), results in a polarisable and highly hyperpolarisable system that fulfils these criteria, and indeed these materials exhibit NLO behaviour. Using the molecular wires concept, Lehn has developed a number of 'push–pull polyenes' of various wire length based on either benzodithia or dimethylaminophenyl donor groups (D) and a variety of acceptor groups (A) (Figure 11.44). The longer-chain materials exhibit very large $\beta$ values but the problem remains to organise the molecules in space in a regular non-centrosymmetric fashion so that their NLO properties do not cancel out. (The $\beta$ value of a material may be measured by the electric-field-induced second harmonic generation experiment – EFISH. This solution phase technique allows for the vectorial extraction of the hyperpolarisability tensor along the molecular dipole direction and hence provides direct information on a molecule's intrinsic optical nonlinearity[72]) This spatial orientation can be achieved by incorporation of the longer-chain materials within a Langmuir–Blodgett monolayer-type film produced from a fatty acid. Fatty acids are examples of amphiphiles, and possess hydrophilic 'head' groups (—$CO_2H$) and a long hydrophobic tail. In water, they form surface layers or films in which the head groups all point into the aqueous layer, while the fatty chains protrude from the liquid surface into air in an ordered liquid array. Ordered liquids that behave in this way are described in Chapter 13. If the fatty acid is chosen such that it is approximately of the same length as the donor–acceptor material, with its hydrophobic molecular wire connector, then the NLO material is incorporated as a dispersion within the monolayer, with all the D and A groups all in the same non-centrosymmetric alignment. Monolayers produced in this way (Figure 11.45) exhibit marked NLO properties.

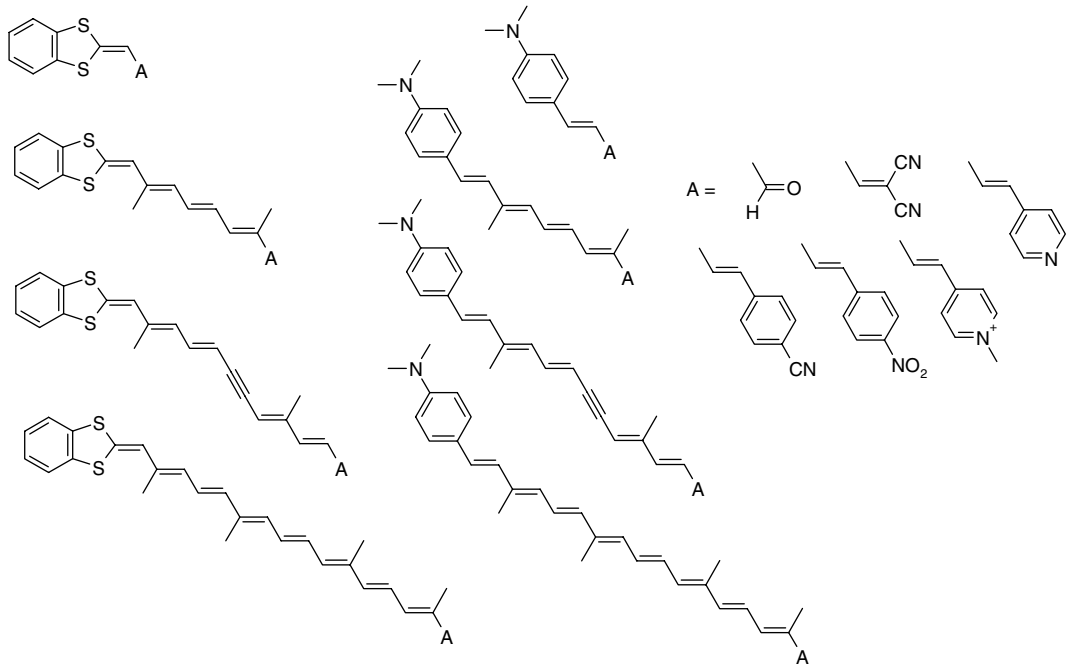


**Figure 11.44** Push–pull polyenes in which an organic electron donor and acceptor are connected by a molecular wire.

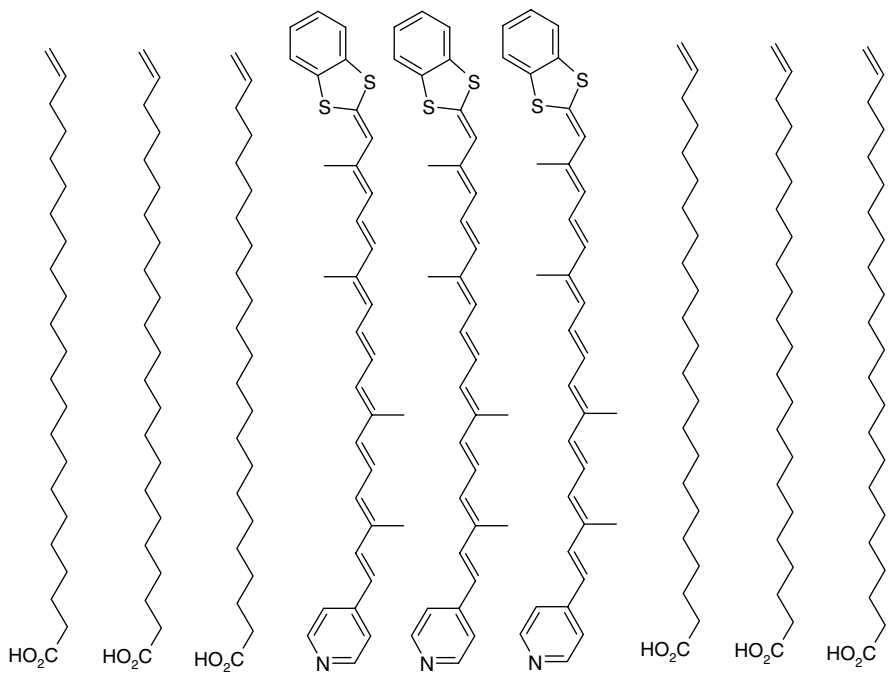


**Figure 11.45** Langmuir–Blodgett assembly of 'push–pull' NLO materials within a fatty acid matrix.

**Table 11.2** NLO data for compounds **11.73**[a].

| M | X | N | Isomer | Y | $\lambda_{CT}$ (nm) | $\mu$ ($\times 10^{-18}$ esu) | $\beta$ ($\times 10^{-30}$ esu) |
|---|---|---|---|---|---|---|---|
| Fe | H | 1 | E | $NO_2$ | 356/496 | 4.5 | 31.0 |
| Fe | H | 1 | Z | $NO_2$ | 325/480 | 4.0 | 13.0 |
| Fe | Me | 1 | E | $NO_2$ | 366/533 | 4.4 | 40.0 |
| Fe | H | 1 | E | CN | 324/466 | 4.6 | 10.0 |
| Ru | Me | 1 | E | $NO_2$ | 370/424 | 5.1 | 24.0 |
| Fe | Me | 2 | E,E | $NO_2$ | 382/500 | 4.5 | 66.0 |

[a]Measurements performed at 1.907 μm.

The same kinds of concepts may be applied to organometallic materials, where the presence of organometallic moieties such as metal carbonyls and metallocenes offers a great deal of scope for synthetic and electronic versatility. Metallocene derivatives such as **11.73** exhibit NLO properties as shown in Table 11.2. The β values are comparable to organic species of the same type, but do show additional behaviour due to mixing with metal states.[73]

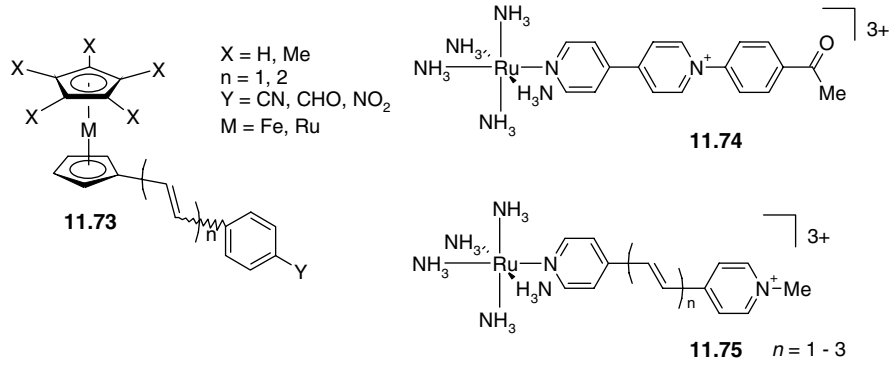


Examination of Table 11.2 shows clearly that NLO properties are enhanced by only a small increase in chain length. The presence of methyl substituents on the cyclopentadienyl ring also increases significantly both dipole moment and nonlinearity by making the donor component more electron-rich. *Trans* compounds are more nonlinear than *cis*, consistent with the greater distance between the two substituents and their enhanced coupling. The ruthenium compounds are less nonlinear than their iron counterparts, suggesting ruthenium is a poorer donor. This is borne out by the higher oxidation potential of ruthenium-containing metallocenes. Unfortunately, these compounds have charge-transfer absorptions in the visible region of the spectrum and this may limit their applications for UV or visible SHG, but uses in the telecommunications industry, where radiation of 0.8−1.5 μm is used, may be envisaged.

In remarkable work, Benjamin Coe of the University of Manchester, UK, has produced the first genuinely switchable NLO device. Coe and co-workers were able to show that the Ru(II) complex **11.74** exhibits a very large $\beta$ coefficient of 1112 $\times$ $10^{-30}$ esu associated with intense low-energy MLCT excitations. Furthermore, these $\beta$ values may be tuned by manipulation of the substituents on the bipyridinium portion of the molecule and exchange of the amine ligands for, for example, pyridyls. The key to the complexes' switching ability lies in the observation that the NLO behaviour of the system is reduced by approximately 10–20-fold by oxidation of the metal centre to Ru(III) by

aqueous, acidic hydrogen peroxide. The NLO behaviour is restored by re-reduction with hydrazine.[74] Coe has gone on to report related Ru(II) ammine donor-acceptor complexes **11.75** in which the d→π* metal-to-ligand charge-transfer bands unexpectedly blue-shift as the number of *E*-ethylene units (*n*) increases from 1 to 3. The $\beta$ coefficients for these complexes maximise at $n = 2$, unlike other known D-A polyenes in which the hyperpolarisability increases with *n*. This special behaviour arises from the particular orbital structure of the complexes promising a wealth of tunable NLO behaviour.[75]

### 11.6.3 Third Harmonic Generation Nonlinear Optical Materials

The factors affecting the preparation of SHG materials are reasonably well understood. In contrast, it is believed by some that the preparation of third harmonic generation materials by the conjugated olefin strategy, with sufficiently large $\gamma$ coefficients at sufficiently low cost, might be impossible. One somewhat successful approach has involved conjugated inorganic polyalkynes such as **11.76** (L = $PBu_3^n$) which possess extended delocalisation throughout the polymer chain.[76] The real and imaginary components of the second hyperpolarisability, $\gamma'$ and $\gamma''$ are 1552 and 344 × $10^{-36}$ esu, respectively.

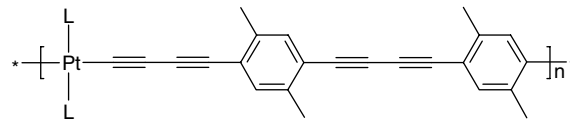


**11.76**

## Summary

- A supramolecular device comprises two or more components linked either covalently or non-covalently with distinct functions that are properties of the individual components.
- Supramolecular sensors comprise binding, transduction and actuator components either in a single molecule or as part of an indicator displacement assay.
- Pattern recognition leading to discrimination, as opposed to individual selectivity, is a powerful paradigm in sensor design.
- Molecules can display characteristics of electronic components such as the conduction of energy or electrons and are capable of simple Boolean logic functions.
- A frontier area in molecular electronics is the coupling of functional molecules with the appropriate input-output device architecture.
- Molecules are capable of doing mechanical work when stimulated by an appropriate energy source.
- Useful physical properties such as non-linear optical activity are subject to molecular design.

## Study Problems

11.1 A β-cyclodextrin host (H1; concentration $10^{-2}$ mol $dm^{-3}$) binds two nucleotide guests (A and B; $10^{-4}$ mol $dm^{-3}$) with weak binding free energies ($\Delta G_A$ = 10 kJ $mol^{-1}$, $\Delta G_B$ = 12 kJ $mol^{-1}$). Calculate the percentages of A and B complexed by the host at equilibrium. Express your result as a selectivity factor (= bound conc. of B / bound conc. of A). A second host (H2) under the same conditions exhibits much stronger binding free energies ($\Delta G_A$ = 30 kJ $mol^{-1}$, $\Delta G_B$ = 32 kJ $mol^{-1}$)

because of its higher positive charge. Calculate the bound concentrations and selectivity factor. Assuming the binding could be detected as part of an analytical measurement for the concentrations of A and B, which host would offer the best discrimination between the two analytes? What drawbacks would this host have in such an analytical application? Temperature = 25°C; gas constant, R = 8.314 J $K^{-1}$ $mol^{-1}$.

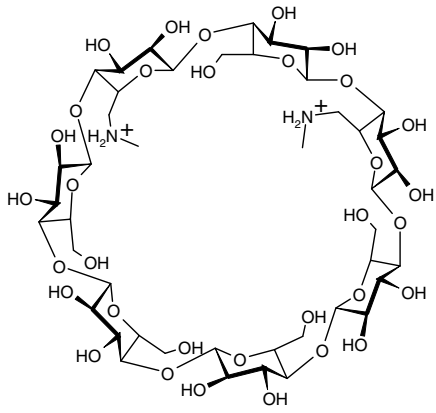

H1

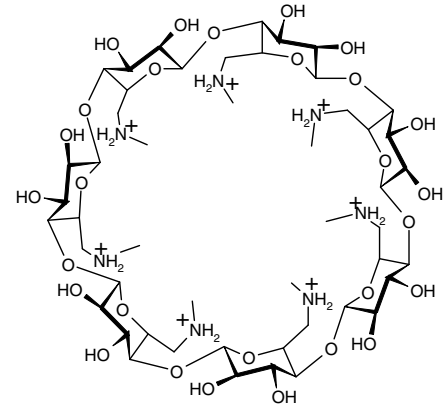

H2

11.2 Using the building blocks shown below, design a strategy using the complexes as metals/complexes as ligands strategy to prepare (a) a tetranuclear ruthenium complex and (b) a complex containing six $Os^{2+}$ and four $Ru^{2+}$ ions. If each metal centre can exist in two enantiomeric forms, how many diastereoisomers would each compound exhibit?

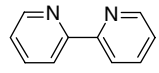

bpy

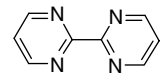

bpym

$[RuCl_2(bpy)_2]$ $[OsCl_2(bpy)_2]$ $[RuCl_2(MeCN)_4]$

a source of $Ru^{2+}$ or $Os^{2+}$ such as $[Ru(DMSO)_4Cl_2]$

11.3 A light-conversion device absorbs ultraviolet radiation at 200 nm with an absorption coefficient (ε) of 15 000 $dm^3$ $mol^{-1}$ $cm^{-1}$. A sample of concentration $2 \times 10^{-5}$ mol $dm^{-3}$ in an optical cell of path length 1.00 cm is irradiated for 15 min with 200 nm radiation of intensity $I_0 = 4 \times 10^{14}$ quanta $s^{-1}$. It re-emits this light in the visible region at 600 nm. Calculate the number of quanta absorbed at 200 nm during the course of the experiment and hence how many quanta are re-emitted at 600 nm assuming that the luminescence quantum yield is 0.1. (Hint: you will need the Beer-Lambert law and the definitions of absorbance and quantum yield.)

## References


1. Birks, J. B., Excimers. *Reports on Progress in Physics* 1975, **38**, 903–974.
2. Balzani, V., *Electron Transfer in Chemistry*. Wiley-VCH: Weinheim, 2001.
3. Welter, S., Salluce, N., Belser, P., Groeneveld, M., De Cola, L., Photoinduced electronic energy transfer in modular, conjugated, dinuclear Ru(II)/Os(II) complexes. *Coord. Chem. Rev.* 2005, **249**, 1360–1371.
4. Indelli, M. T., Chiorboli, C., Flamigni, L., De Cola, L., Scandola, F., Photoinduced electron transfer across oligo-p-phenylene bridges. Distance and conformational effects in Ru(II)-Rh(III) dyads. *Inorg. Chem.* 2007, **46**, 5630–5641.

5. Marcus, R. A., Sutin, N., Electron transfers in chemistry and biology. *Biochimica Et Biophysica Acta* 1985, **811**, 265–322.
6. Decola, L., Balzani, V., Barigelletti, F., *et al.*, Photoinduced energy and electron-transfer processes in supramolecular species - tris(bipyridine) complexes of Ru(II)/Os(II), Ru(II)/Ru(III), Os(II)/Os(III), and Ru(II)/Os(III) separated by a rigid spacer. *Inorg. Chem.* 1993, **32**, 5228–5238.
7. Molnar, S. M., Nallas, G., Bridgewater, J. S., Brewer, K. J., Photoinitiated electron collection in a mixed-metal trimetallic complex of the form $([(Bpy)_2Ru(Dpb)]_2IrCl_2(PF_6)_5$ (Bpy=2,2′-Bipyridine and Dpb=2,3-Bis(2-Pyridyl)Benzoquinoxaline). *J. Am. Chem. Soc.* 1994, **116**, 5206–5210.
8. Arm, K. J., Williams, J. A. G., Boronic acid-substituted metal complexes: versatile building blocks for the synthesis of multimetallic assemblies. *Chem. Commun.* 2005, 230–232.
9. Goze, C., Leiggener, C., Liu, S. X., *et al.*, Fused donor-acceptor ligands in Ru-II chemistry: Synthesis, electrochemistry and spectroscopy of $[Ru(bpy)_{3-n}(TTF\text{-}dppz)_n](PF_6)_2$. *Chemphyschem* 2007, **8**, 1504–1512.
10. Lehn, J.-M., *Supramolecular Chemistry*. 1 ed., VCH: Weinheim, 1995,
11. Shavaleev, N. M., Moorcraft, L. P., Pope, S. J. A., Bell, Z. R., Faulkner, S., Ward, M. D., Sensitised near-infrared emission from lanthanides using a covalently-attached Pt(II) fragment as an antenna group. *Chem. Commun.* 2003, 1134–1135.
12. Tecilla, P., Dixon, R. P., Slobodkin, G., Alavi, D. S., Waldeck, D. H., Hamilton, A. D., Hydrogen-bonding self-assembly of multichromophore structures. *J. Am. Chem. Soc.* 1990, **112**, 9408–9410.
13. Cusack, L., Rao, S. N., Fitzmaurice, D., Heterosupramolecular chemistry: Self-assembly of an electron donor ($TiO_2$ nanocrystallite)-acceptor (Viologen) complex. *Chem. Eur. J.* 1997, **3**, 202–207.
14. Ishow, E., Credi, A., Balzani, V., Spadola, F., Mandolini, L., A molecular-level plug/socket system: Electronic energy transfer from a binaphthyl unit incorporated into a crown ether to an anthracenyl unit linked to an ammonium ion. *Chem. Eur. J.* 1999, **5**, 984–989.
15. Ferrer, B., Rogez, G., Credi, A., *et al.*, Photoinduced electron flow in a self-assembling supramolecular extension cable. *Proc. Natl. Acad. Sci. U. S. A.* 2006, **103**, 18411–18416.
16. Barrett, E. S., Dale, T. J., Rebek, J., Assembly and exchange of resorcinarene capsules monitored by fluorescence resonance energy transfer. *J. Am. Chem. Soc.* 2007, **129**, 3818–3819.
17. Angeli, S., Ceron, F., Scaloni, A., *et al.*, Purification, structural characterisation, cloning and immunocytochemical localisation of chemoreception proteins from Schistocerca gregaria. *Eur. J. Biochem.* 1999, **292**, 745–754.
18. Sabelis, M. W., Janssen, A., Kant, M. R., Ecology –The enemy of my enemy is my ally. *Science* 2001, **291**, 2104–2105.
19. de Silva, A. P., Fox, D. B., Huxley, A. J. M., Moody, T. S., Combining luminescence, coordination and electron transfer for signalling purposes. *Coord. Chem. Rev.* 2000, **205**, 41–57.
20. Fages, F., Desvergne, J. P., Kampke, K., *et al.*, Linear molecular recognition - spectroscopic, photophysical, and complexation studies on alpha,omega-alkanediyldiammonium ions binding to a bisanthracenyl macrotricyclic receptor. *J. Am. Chem. Soc.* 1993, **115**, 3658–3664.
21. Filby, M. H., Dickson, S. J., Zaccheroni, N., *et al.*, Induced fit inter-anion discrimination by binding-induced excimer formation. *J. Am. Chem. Soc.* 2008, **130**, 4105–4113.
22. Beer, P. D., Szemes, F., Remarkable chloride over dihydrogen phosphate anion selectivity exhibited by novel macrocyclic bis[ruthenium(II) bipyridyl] and ruthenium(II) bipyridyl-metallocene receptors. *J. Chem. Soc., Chem. Commun.* 1995, 2245–2247.
23. Parker, D., Dickins, R. S., Puschmann, H., Crossland, C., Howard, J. A. K., Being excited by lanthanide coordination complexes: Aqua species, chirality, excited-state chemistry, and exchange dynamics. *Chem. Rev.* 2002, **102**, 1977–2010.
24. Pandya, S., Yu, J. H., Parker, D., Engineering emissive europium and terbium complexes for molecular imaging and sensing. *Dalton Trans.* 2006, 2757–2766.
25. Kimura, E., Koike, T., Recent development of zinc-fluorophores. *Chem. Soc. Rev.* 1998, **27**, 179–184.
26. Koike, T., Watanabe, T., Aoki, S., Kimura, E., Shiro, M., A novel biomimetic zinc(II)-fluorophore, dansylamidoethyl-pendant macrocyclic tetraamine 1,4,7,10-tetraazacyclododecane (cyclen). *J. Am. Chem. Soc.* 1996, **118**, 12696–12703.
27. Huston, M. E., Haider, K. W., Czarnik, A. W., Chelation-enhanced fluorescence in 9,10-bis(Tmeda)anthracene. *J. Am. Chem. Soc.* 1988, **110**, 4460–4462.
28. Wallace, K. J., Morey, J., Lynch, V. M., Anslyn, E. V., Colorimetric detection of chemical warfare simulants. *New. J. Chem.* 2005, **29**, 1469–1474.
29. Liu, S. Y., He, Y. B., Wu, J. L., *et al.*, Calix[4]arenes containing thiourea and amide moieties: neutral receptors towards alpha,omega-dicarboxylate anions. *Org. Biomol. Chem.* 2004, **2**, 1582–1586.
30. Green, F. J., *Sigma-Aldrich Handbook of Stains, Dyes, and Indicators*. Aldrich Chemical Co.: Milwaukee, WI, USA, 1990,
31. Inouye, M., Hashimoto, K., Isagawa, K., Nondestructive detection of acetylcholine in protic media – artificial-signaling acetylcholine-receptors. *J. Am. Chem. Soc.* 1994, **116**, 5517–5518.
32. Lavigne, J. J., Anslyn, E. V., Sensing a paradigm shift in the field of molecular recognition: From selective to differential receptors. *Angew. Chem., Int. Ed.* 2001, **40**, 3119–3130.

33. Wright, A. T., Anslyn, E. V., Differential receptor arrays and assays for solution-based molecular recognition. *Chem. Soc. Rev.* 2006, **35**, 14–28.
34. Goodey, A., Lavigne, J. J., Savoy, S. M., *et al*., Development of multianalyte sensor arrays composed of chemically derivatized polymeric microspheres localized in micromachined cavities. *J. Am. Chem. Soc.* 2001, **123**, 2559–2570.
35. McCleskey, S. C., Griffin, M. J., Schneider, S. E., McDevitt, J. T., Anslyn, E. V., Differential receptors create patterns diagnostic for ATP and GTP. *J. Am. Chem. Soc.* 2003, **125**, 1114–1115.
36. Beer, P. D., Gale, P. A., Chen, Z., Drew, M. G. B., New bis- and tris-ferrocenoyl and tris-benzoyl lower-rim substituted calix[5]arene esters: Synthesis, electrochemistry and X-ray crystal structures. *Supramol. Chem.* 1996, **7**, 241–255.
37. Carr, J. D., Lambert, L. l., Hibbs, D. E., Hursthouse, M. B., Malik, K. M. A., Tucker, J. H. R., Novel electrochemical sensors for neutral molecules. *Chem. Commun.* 1997, 1649–1650.
38. Reynes, O., Maillard, F., Moutet, J. C., Royal, G., Saint-Aman, E., Stanciu, G., Dutasta, J. P., Gosse, I., Mulatier, J. C., Complexation and electrochemical sensing of anions by amide-substituted ferrocenyl ligands. *J. Organomet. Chem.* 2001, **637**, 356-363.
39. Reynes, O., Moutet, J. C., Pecaut, J., Royal, G., Saint-Aman, E., (Ferrocenylmethyl)trimethylammonium cation: a very simple probe for the electrochemical sensing of dihydrogen phosphate and ATP anions. *New J. Chem.* 2002, **26**, 9–12.
40. Hall, C. D., Djedovic, N., The synthesis and complexation of a cobaltocenium-based redox-active cryptand containing the phenanthroline unit. *J. Organomet. Chem.* 2002, **648**, 8–13.
41. Rauchfuss, T. B., Severin, K., 'Supramolecular architectures based on organometallic half-sandwich complexes'. in *Organic Nanostructures*, Atwood, J. L., Steed, J. W., eds. Wiley-VCH: Weinhein, 2008, *pp.* 179–201.
42. Moore, A. J., Goldenberg, L. M., Bryce, M. R., *et al*., New crown annelated tetrathiafulvalenes: Synthesis, electrochemistry, self-assembly of thiol derivatives, and metal cation recognition. *J. Org. Chem.* 2000, **65**, 8269–8276.
43. Cobben, P., Egberink, R. J. M., Bomer, J. G., Bergveld, P., Verboom, W., Reinhoudt, D. N., Transduction of selective recognition of heavy-metal ions by chemically modified field-effect transistors (chemfets). *J. Am. Chem. Soc.* 1992, **114**, 10573–10582.
44. Arrhenius, T. S., Blancharddesce, M., Dvolaitzky, M., Lehn, J. M., Malthete, J., Molecular devices – caroviologens as an approach to molecular wires synthesis and incorporation into vesicle membranes. *Proc. Natl. Acad. Sci. U. S. A.* 1986, **83**, 5355–5359.
45. de Quadras, L., Bauer, E. B., Mohr, W., *et al*., sp carbon chains surrounded by $sp^3$ carbon double helices: Directed syntheses of wirelike $Pt(CC)_nPt$ moieties that are spanned by two $P(CH_2)_mP$ linkages *via* alkene metathesis. *J. Am. Chem. Soc.* 2007, **129**, 8296–8309.
46. Fox, M. A., Fundamentals in the design of molecular electronic devices: Long-range charge carrier transport and electronic coupling. *Acc. Chem. Res.* 1999, **32**, 201–207.
47. Bartik, T., Bartik, B., Brady, M., Dembinski, R., Gladysz, J. A., A step-growth approach to metal-capped one-dimensional carbon allotropes: Syntheses of C-12, C-16, and C-20 μ-polyynediyl complexes. *Angew. Chem., Int. Ed. Engl.* 1996, **35**, 414–417.
48. Tsuda, A., Osuka, A., Fully conjugated porphyrin tapes with electronic absorption bands that reach into infrared. *Science* 2001, **293**, 79–82.
49. Ashwell, G. J., Urasinska, B., Wang, C. S., Bryce, M. R., Grace, I., Lambert, C. J., Single-molecule electrical studies on a 7 nm long molecular wire. *Chem. Commun.* 2006, 4706–4708.
50. Aviram, A., Ratner, M. A., Molecular Rectifiers. *Chem. Phys. Lett.* 1974, **29**, 277–283.
51. Metzger, R. M., Chen, B., Hopfner, U., *et al*., Unimolecular electrical rectification in hexadecylquinolinium tricyanoquinodimethanide. *J. Am. Chem. Soc.* 1997, **119**, 10455–10466.
52. Ashwell, G. J., Tyrrell, W. D., Whittam, A. J., Molecular rectification: Self-assembled monolayers in which donor-($\pi$-bridge)-acceptor moieties are centrally located and symmetrically coupled to both gold electrodes. *J. Am. Chem. Soc.* 2004, **126**, 7102–7110.
53. Armstrong, N., Hoft, R. C., McDonagh, A., Cortie, M. B., Ford, M. J., Exploring the performance of molecular rectifiers: Limitations and factors affecting molecular rectification. *Nano Letters* 2007, **7**, 3018–3022.
54. Kawai, S. H., Gilat, S. L., Lehn, J. M., Dual-Mode Optical-electrical molecular switching device. *J. Chem. Soc., Chem. Commun.* 1994, 1011–1013.
55. Belser, P., De Cola, L., Hartl, F., *et al*., Photochromic switches incorporated in bridging ligands: A new tool to modulate energy-transfer processes. *Advanced Functional Materials* 2006, **16**, 195–208.
56. Goulle, V., Harriman, A., Lehn, J. M., An electro-photoswitch - redox switching of the luminescence of a bipyridine metal-complex. *J. Chem. Soc., Chem. Commun.* 1993, 1034–1036.
57. Balzani, V., Gomez-Lopez, M., Stoddart, J. F., Molecular machines. *Acc. Chem. Res.* 1998, **31**, 405–414.
58. Desilva, A. P., Gunaratne, H. Q. N., McCoy, C. P., A molecular photoionic and gate based on fluorescent signaling. *Nature* 1993, **364**, 42–44.

59. Parker, D., Senanayake, P. K., Williams, J. A. G., Luminescent sensors for pH, pO(2), halide and hydroxide ions using phenanthridine as a photosensitiser in macrocyclic europium and terbium complexes. *J. Chem. Soc., Perkin Trans. 2* 1998, 2129–2139.
60. McSkimming, G., Tucker, J. H. R., Bouas-Laurent, H., Desvergne, J. P., An anthracene-based photochromic system that responds to two chemical inputs. *Angew. Chem., Int. Ed.* 2000, **39**, 2167–2169.
61. Credi, A., Balzani, V., Langford, S. J., Stoddart, J. F., Logic operations at the molecular level. An XOR gate based on a molecular machine. *J. Am. Chem. Soc.* 1997, **119**, 2679–2681.
62. Green, J. E., Choi, J. W., Boukai, A., *et al*., A 160-kilobit molecular electronic memory patterned at $10^{11}$ bits per square centimetre. *Nature* 2007, **445**, 414–417.
63. Collier, C. P., Wong, E. W., Belohradsky, M., *et al*., Electronically configurable molecular-based logic gates. *Science* 1999, **285**, 391–394.
64. Collier, C. P., Mattersteig, G., Wong, E. W., *et al*., A [2]catenane-based solid state electronically reconfigurable switch. *Science* 2000, **289**, 1172–1175.
65. Park, J., Pasupathy, A. N., Goldsmith, J. I., *et al*., Coulomb blockade and the Kondo effect in single-atom transistors. *Nature* 2002, **417**, 722–725.
66. Reddy, P., Jang, S. Y., Segalman, R. A., Majumdar, A., Thermoelectricity in molecular junctions. *Science* 2007, **315**, 1568–1571.
67. Stadler, A.-M., Kyritsakas, N., Lehn, J.-M., Reversible folding/unfolding of linear molecular strands into helical channel-like complexes upon proton-modulated binding and release of metal ions. *Chem. Commun.* 2004, 2024–2025.
68. Badjic, J. D., Balzani, V., Credi, A., Silvi, S., Stoddart, J. F., A molecular elevator. *Science* 2004, **303**, 1845–1849.
69. Wurpel, G. W. H., Brouwer, A. M., van Stokkum, I. H. M., Farran, A., Leigh, D. A., Enhanced hydrogen bonding induced by optical excitation: Unexpected subnanosecond photoinduced dynamics in a peptide-based [2]rotaxane. *J. Am. Chem. Soc.* 2001, **123**, 11327–11328.
70. Evans, O. R., Lin, W. B., Crystal engineering of NLO materials based on metal-organic coordination networks. *Acc. Chem. Res.* 2002, **35**, 511–522.
71. Marder, S. R., 'Metal containing materials for nonlinear optics'. in *Inorganic Materials*, 2nd ed., Bruce, D. W., O'Hare, D., Eds. Wiley: Chichester, 1996, *pp* 121–169.
72. Cheng, L. T., Tam, W., Stevenson, S. H., Meredith, G. R., Rikken, G., Marder, S. R., Experimental investigations of organic molecular nonlinear optical polarizabilities .1. Methods and results on benzene and stilbene derivatives. *J. Phys. Chem.* 1991, **95**, 10631–10643.
73. Calabrese, J. C., Cheng, L. T., Green, J. C., Marder, S. R., Tam, W., Molecular 2nd-order optical nonlinearities of metallocenes. *J. Am. Chem. Soc.* 1991, **113**, 7227–7232.
74. Coe, B. J., Molecular materials possessing switchable quadratic nonlinear optical properties. *Chem. Eur. J.* 1999, **5**, 2464–2471.
75. Coe, B. J., Jones, L. A., Harris, J. A., *et al*., Syntheses and spectroscopic and quadratic nonlinear optical properties of extended dipolar complexes with ruthenium(II) ammine electron donor and N-methylpyridinium acceptor groups. *J. Am. Chem. Soc.* 2004, **126**, 3880–3891.
76. Guha, S., Frazier, C. C., Porter, P. L., Kang, K., Finberg, S. E., Measurement of the 3rd-order hyperpolarizability of platinum poly-ynes. *Optics Letters* 1989, **14**, 952–954.

# 12 Biological Mimics and Supramolecular Catalysis

*'Rules and models destroy genius and art.'*

William Hazlitt (1778–1830), *Round Table,* I, *On Taste*

## 12.1 Introduction

In this chapter we focus on supramolecular chemical reactivity. In particular this means predominantly the role supramolecular chemistry plays in accelerating or understanding chemical reactions. There are close parallels between artificial, abiotic supramolecular reactivity and biochemistry, for example in the study of enzymes, Nature's catalysts – described in Section 2.6. Synthetic catalysts can both model natural ones and allow the design of new, different kinds of reactions. Supramolecular catalysis sits somewhere between chemical catalysis (transition metal and organocatalysis) and biology. Some considerations within various kinds of catalysis are summed up in the chart shown in Figure 12.1.

### 12.1.1 Understanding and Learning from Biochemistry

Motherwell, W. B., Bingham, M. J., Six, Y., 'Recent progress in the design and synthesis of artificial enzymes', *Tetrahedron* 2001, **57**, 4663–4686.

Biological systems have provided much of the inspiration for the development of supramolecular chemistry. Many synthetic supramolecular systems have been designed to mimic the structure or function of more complex biological processes. Such artifical, abiotic (non-biological) molecules or reaction mimics are termed *models*. By this we mean that, on a smaller scale, the artificial systems resemble, and help chemists to understand some or all of the properties of the real, biological chemistry. The concept of a biological model has been summarised beautifully by Donald Cram in his Nobel Prize lecture:

> *Few scientists acquainted with the chemistry of biological systems at the molecular level can avoid being inspired. Evolution has produced chemical compounds exquisitely organised to accomplish the most complicated and delicate of tasks. Many organic chemists viewing the crystal structures of enzyme systems or nucleic acids and knowing the marvels of specificity of the immune system must dream of designing and synthesising simpler organic compounds that imitate working features of these naturally occurring compounds.*
>
> D.J. Cram, 'The design of molecular hosts, guests, and their complexes (Nobel Lecture)', *Angew. Chem., Int. Ed. Engl.*, 1988, **27**, 1009–1020.

The beginnings of supramolecular chemistry, long before sophisticated artificial hosts such as carcerands, cryptands or self-assembling devices and systems were conceived, may be traced back to Fischer's lock and key model of enzymatic catalysis (Section 1.3). This shape selection concept, coupled with Paul Erlich's work on antibodies, gives us the idea of a receptor. In biochemistry, receptor–substrate binding is of great importance and can be extremely selective. A classic example is the binding of bombykol to its receptor in the male silkworm moth, *Bombyx mori*. Bombycol is a sex attractant secreted by the female moth. The male becomes excited if exposed to air into which a solution of concentration $4.2 \times 10^{-18}$ M of bombycol has been introduced (Section 2.8). Similarly, ant trail marking pheromones are required in ridiculously small quantities. One milligram of the trail pheromone of the leafcutter ant, *Atta texana*, would be sufficient to guide a column of ants three times around the world.

Receptor–substrate binding is reversible, and is governed by thermodynamics. As discussed in Section 1.7, binding selectivity represents quantitatively a ratio of binding constants of a receptor

*Supramolecular Chemistry, 2nd edition* J. W. Steed and J. L. Atwood
© 2009 John Wiley & Sons, Ltd ISBN: 978-0-470-51233-3

| Biology – Enzymes | Chemistry – Lewis acid / transition metal |
|---|---|
| • High selectivity | • Somewhat selective |
| • High efficiency | • Somewhat efficient |
| • Little product inhibition | • Frequent product inhibition |
| **Interface – Catalytic antibodies** | **Supramolecular – cyclodextrins *etc.*** |
| • Selective | • Sophisticated |
| • Moderately efficient | • Relatively inefficient |
| • Hapten design is very difficult | • Biological models |
| • Elaborate techniques | • Longer term potential |

**Figure 12.1** A simplified picture of catalysis in biological, interfacial and chemical systems.*

for one substrate over another. However, in living systems, more than in any other aspect of supramolecular chemistry, mere binding is not enough. Binding of biochemical signallers such as hormones or neurotransmitters must be a prelude or trigger to events such as chemical dephosphorylation reactions, nerve impulses (membrane depolarisation), muscular contraction *etc.* Without the fully functioning system, the binding event is essentially useless. A large part of the role of substrate binding is often to induce a conformational change in the receptor that turns on a biochemical process. In effect, the binding energy of the substrate is being used to help the receptor achieve a conformational change as part of a triggering process which it does undergo alone. This is referred to as the *induced fit model*, and should be contrasted with the rigid lock and key picture (see Chapter 1, Figure 1.3).

In enzymes, which are biological chemical catalysts, fully functioning systems require kinetic selectivity in which the enzyme adapts in a time-resolved manner, to stabilise every point along the chemical reaction pathway. The achievement of this kind of 'living selectivity' is a far more daunting task than the mere influencing of an equilibrium, and it is fair to say that research into truly functional enzyme models is still in its infancy. However, it is possible to learn a great deal about the characteristics and mode of action of biological systems from models that mimic successfully some portion or another of the whole system. Furthermore, some abiotic functional systems do exist, particularly among receptors such as the cyclodextrins, which are capable of carrying out enzymatic type catalysis.

## 12.1.2 Characteristics of Biological Models

Kirby, A. J. 'Enzyme mimics', *Angew. Chem., Int. Ed. Engl.*, 1994, **33**, 551–553.

We can use the term 'model' in the context of understanding a more complex 'real' system in a number of ways. You will already be familiar with ball and stick models (either made of plastic or virtual on a computer screen) that scale up the size and bonds and atoms to macroscopic dimensions. While such conceptual models are useful, and indeed with the advent of powerful computers, high level computational calculations, *e.g.* involving density functional theory (DFT) can make detailed predictions, we need something more tangible if we are to experimentally test ideas about structural, physical and chemical characteristics in complex systems. We therefore turn to chemical models; real chemical compounds or systems that are simple enough to understand more fully than the 'real thing' but have characteristics that mimic the target system that they are designed to copy. Biological

* A hapten is a small molecule that reacts with a specific antibody but cannot induce the formation of antibodies unless bound to a carrier protein or other large antigenic molecule.

systems, particularly enzymes, show a number of characteristic features that need to be recreated in a model system, listed below.

1. Enzymes induce fast reaction rates under mild conditions.
2. Enzymes show a high degree of structural and chiral recognition of their substrates.
3. Each enzyme molecule catalyses the reaction of a huge number of substrate molecules without being destroyed itself (*i.e.* it has a high turnover number).
4. Enzymes are subject to competitive inhibition by compounds that bind to the enzyme but do not react themselves.

In addition to these features, it is desirable that enzyme mimics exhibit some properties not shared by biological enzymes, such as molecular weights less than about 2000–3000 Da, few chiral elements (to minimise the proliferation of diastereoisomers), stability to handling even at high temperatures, and solubility in a range of solvents as well as water. In attempting to model a biological molecule, it is unreasonable to expect to come up with an abiotic system (either by inspiration or blind providence) that can mimic simultaneously all of the structural, binding and catalytic features of the natural process. Nature has spent millions of years evolving highly complex biological processes, and artificial techniques and insight are not yet at a comparable level. As a result, several strategies may be adopted towards the final goal, from which we may distinguish two main approaches:

1. A system that shows efficient binding characteristics of the substrate or simplified analogue, or more properly of an analogue of the transition state of the biological reaction. This may be termed a *structural model*. Structural models in some sense 'look like' the real system and have structural similarities to it that can be probed, *e.g.* by crystallography or techniques such as EPR, Mossbaüer or X-ray photoelectron spectroscopy (XPS).
2. A (generally intermolecular) system that carries out the reaction concerned without the binding characteristics of the enzyme. This may be termed a *functional model*.

Both of these approaches should result in initial model systems, which, if they carry out the desired biological reaction at all, will do it much more slowly and less selectively than the natural enzyme and substrate. As the sophistication of the model system develops it should aspire towards the satisfaction of a number of basic requirements:

1. The model should provide a hydrophobic binding site for the substrate.
2. The model should afford hydrogen bonding and/or electrostatic binding sites that are complementary to those of the substrate.
3. Appropriate catalytic groups should be attached to the model.
4. The structure of the model should be well-defined and rigid.
5. The model should be water soluble and catalytically active under physiological conditions.

## 12.2 Cyclodextrins as Enzyme Mimics

Breslow, R. and Dong, S. D. 'Biomimetic reactions catalysed by cyclodextrins and their derivatives', *Chem. Rev.*, 1998, **98**, 1997–2011.

### 12.2.1 Enzyme Modelling Using an Artificial Host Framework

Of all the cavity-containing compounds, it is perhaps the cyclodextrins that provide the best basis for the construction of small(ish) molecule enzyme mimics. See Section 6.3 for an introduction to

the synthesis and structures of these versatile hosts. The general criteria for effective systems that can mimic the structure and/or function of biological enzymes are set out in Section 12.1.2. Broadly, these require a system to bind its substrate (guest) quickly, selectively and reversibly, generally in a non-covalent fashion, and to catalyse chemical reactions of that substrate. The goals of such chemistry are the better understanding of natural enzymes, development of industrial catalysts capable of carrying out hitherto unknown transformations with high activity and selectivity, and the artificial regulation of biochemical reactions. Within this context, the readily available cyclodextrins possess a number of features that make them attractive as potential enzyme mimics and models, notably the following.

- Water solubility at physiological pH—water is the medium in which most enzymes operate.
- Reversible, non-covalent guest-binding with the release of the guest being slower than binding, as with enzymes.
- Well-defined structures and guest-binding modes.
- A wide range of accessible derivatives.
- Juxtaposition of hydroxyl groups, which may take an active part in catalysis, and a hydrophobic cavity for guest-binding.
- A chiral molecular cavity, admitting the possibility of enantioselective binding and catalysis.
- Real catalytic activity.

Much of the interest in native, unfunctionalised cyclodextrins centres around the chemistry of the anion **12.1** in which one of the cyclodextrin —OH groups has been deprotonated. This deprotonation gives the cyclodextrin a reactive, nucleophilic functional group in close proximity to a hydrophobic binding cavity. Early work showed that esters bound within the cyclodextrin cavity could acetylate anionic $\beta$-cyclodextrin. The reaction rate proves to be about 100 times faster than the analogous hydrolysis of *m*-nitrophenyl acetate (**12.2**) in the absence of the cyclodextrin. Of course, this reaction is not catalytic and the rate enhancement is very modest by enzymatic standards. On the other hand, the molecular weight of the cyclodextrin complex is under 2000 Da, making it very much a 'small' molecule system, and the steps in the catalysis may be readily characterised. Furthermore, this reaction step is closely related to the action of serine protease enzymes in which an acyl group is transferred to a serine hydroxyl in the first enzymatic step.

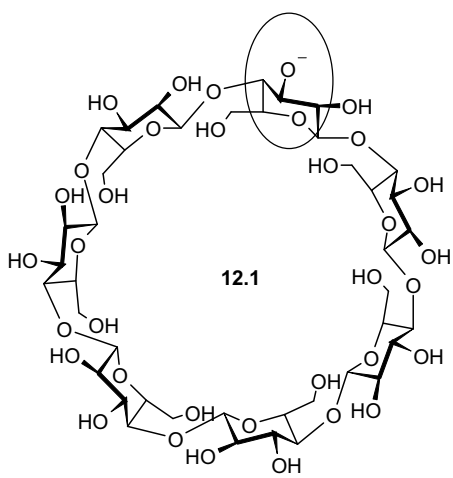

**12.1**

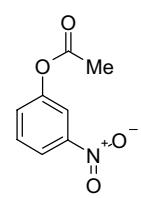

**12.2**

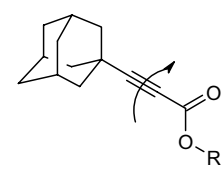

**12.3**

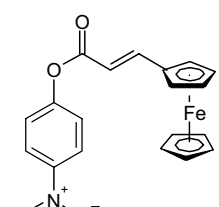

**12.4**

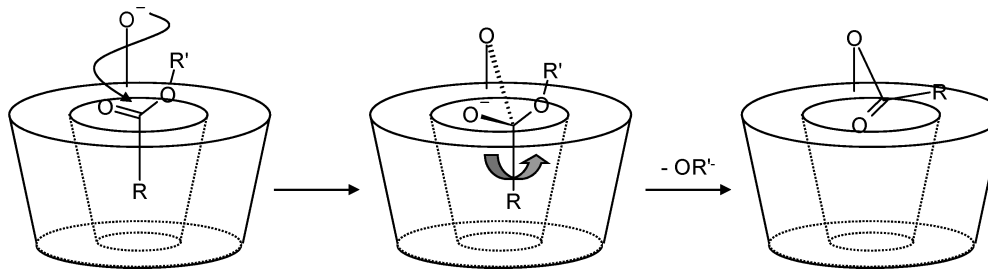


**Scheme 12.1** Acetylation of a cyclodextrin anion by a bound substrate *via* a tetrahedral intermediate.

Molecular models show that during the course of the acylation reaction, the bound substrate is pulled partially out of the cyclodextrin cavity in forming the tetrahedral reaction intermediate. In other words, the model enzyme is not exhibiting the required transition state selectivity. Furthermore, excessively rigid substrates experience difficulty in rotating while bound in order to accommodate the need of the cyclodextrin hydroxyl group to attach perpendicular to the substrate ester plane, and subsequently rotate to become incorporated into the plane of the new ester product (Scheme 12.1). These problems were addressed by examination of substrates, such as *p*-nitro derivatives in which the ester protrudes further from the cavity, and substrates with more rotational flexibility such as alkyne **12.3**. In these refined systems, much more enzyme-like rate accelerations of factors of up to 5 900 000-fold were observed for **12.4**, for example.

### 12.2.2 Cyclodextrins as Esterase Mimics

Cyclodextrins and their derivatives are already known to catalyse an enormous variety of biochemical and non-biochemical transformations. The basis of the catalysis by native (unmodified) cyclodextrins is the positioning of the reactive secondary hydroxyl groups directly at the entrance to the molecular cavity. One of the most effective reactions catalysed by cyclodextrins is the hydrolysis of aryl and phosphate esters (esterase activity). For example, the rate of hydrolysis of *p*-nitrophenol esters is increased by factors of up to 750 000 by $\beta$-CD. The mechanism of action of the cyclodextrin is shown in Scheme 12.2.[1]

A striking cyclodextrin rate acceleration is also seen in phosphate ester formation and hydrolysis by cyclodextrins in conjunction with lanthanide ions. The 3′,5′-cyclic monophosphate of adenosine (cAMP, **12.5**) is an important second messenger for cell-to-cell communication in biological systems. When a cell receives a stimulus (first messenger), compound **12.5** is formed from adenosine triphosphate (ATP, the basic energy storage and transport molecule). This reaction is catalysed by the adenylate cyclase enzyme. In turn, cAMP activates various other intracellular enzymes producing a cell response. The response is terminated by the hydrolysis of cAMP by phosphodiesterase, a phosphate ester hydrolysis enzyme (Scheme 12.3). The action of adenylate cyclase has been mimicked successfully under physiological conditions by a combination of $\beta$-CD and prasodymium(III) (other lanthanide(III) ions are also somewhat effective). Subsequent cleavage of **12.5** may be catalysed extremely effectively by γ-CD and cerium(IV). At physiological pH and 30°C, the half-life for the conversion of **12.5** into adenosine monophosphate (AMP) is only 6 s, compared to an uncatalysed half-life estimated at 3 million years! This difference represents a rate enhancement by a factor of $10^{13}$, and the mode of action probably involves the cyclodextrin acting as a ligand for the hard, oxophilic metal ions. Perhaps these entirely man-made enzyme mimics will open the way to a degree of artificial regulation of cell function?[2]

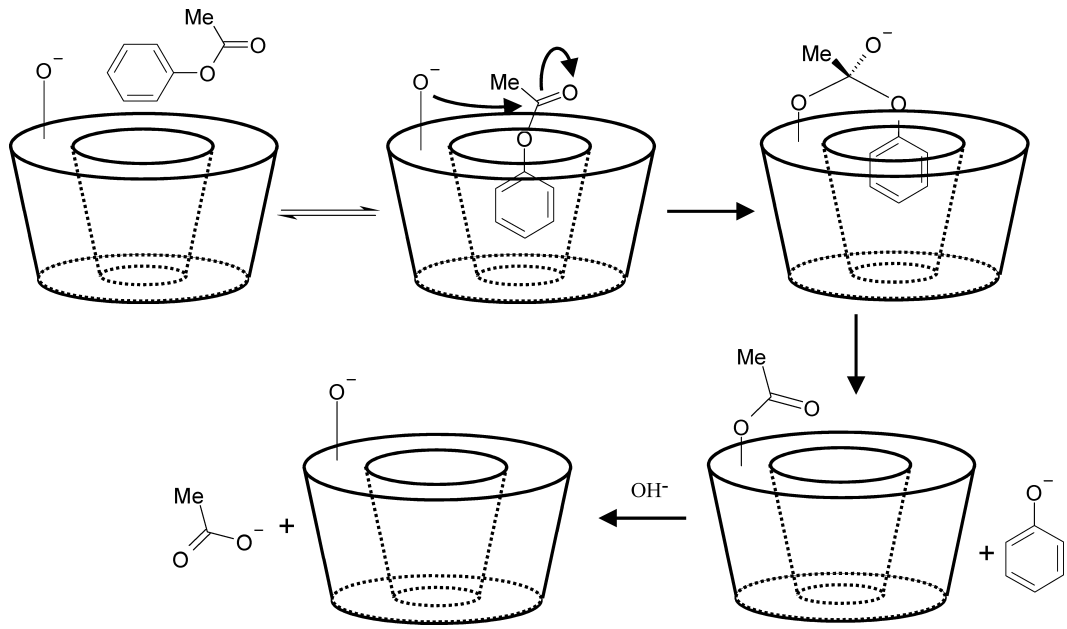


**Scheme 12.2** Mechanism of ester hydrolysis by $\beta$-cyclodextrin.[1]

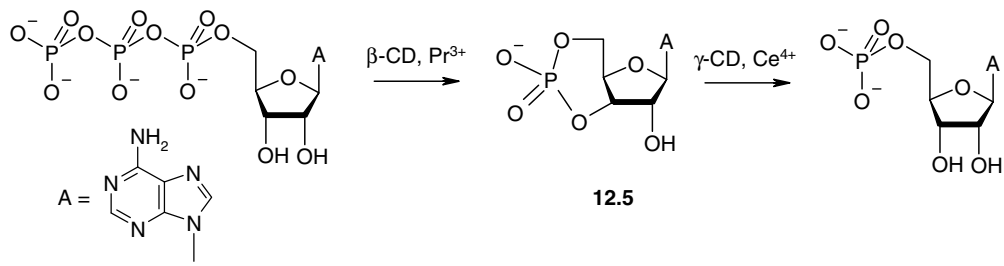


**Scheme 12.3** Adenylate cyclase/phosphodiesterase activity by cyclodextrin complexes.[2]

## 12.2.3 Functionalised Cyclodextrins

While the features of hydroxyl groups and hydrophobic cavity are a powerful combination in enzyme mimicking by cyclodextrins, they are essentially a fortuitous accident of the cyclodextrin structure. There is, in principle at least, a vastly greater range of cyclodextrin-based enzyme mimics in which the hydrophobic cavity is used as a component in a designed enzyme mimic containing other functional groups with model enzyme active sites. Indeed, the first compound ever referred to as an 'artificial enzyme' in the literature comprised a cyclodextrin with a copper(II) ion complexed to its secondary face by means of a pyridine dicarboxylate derived binding site (**12.6**).[3] This compound catalyses the hydrolysis of guest species that are not ligands for the metal centre and are not usually reactive towards hydrolysis by Cu(II) complexes. Extending this concept, compound **12.7** also proves to be a very effective hydrolytic catalyst. The *p*-nitroaryl substrate is bound within the cyclodextrin cavity and engages in interactions with the Ni(II) centre and cyclodextrin hydroxyl groups. Nucleophilic attack by the oxime ligand generates the hydrolysed product. The catalyst is regenerated as the product

is hydrolysed. Recent work on copper(II) dithiocarbamate derivatised α- and β-cyclodextrins such as **12.8** also gives good activity for the hydrolysis of *p*-nitrophenyl acetate at alkaline pH. The metal-free cyclodextrin catalysed rate is up to 165 times faster than the uncatalysed rate, but addition of Cu(II) further increases the activity by a factor of up to *ca.* 500 with the catalysed rate increasing with pH because basic conditions favour deprotonation of the copper-bound water molecule.[4]

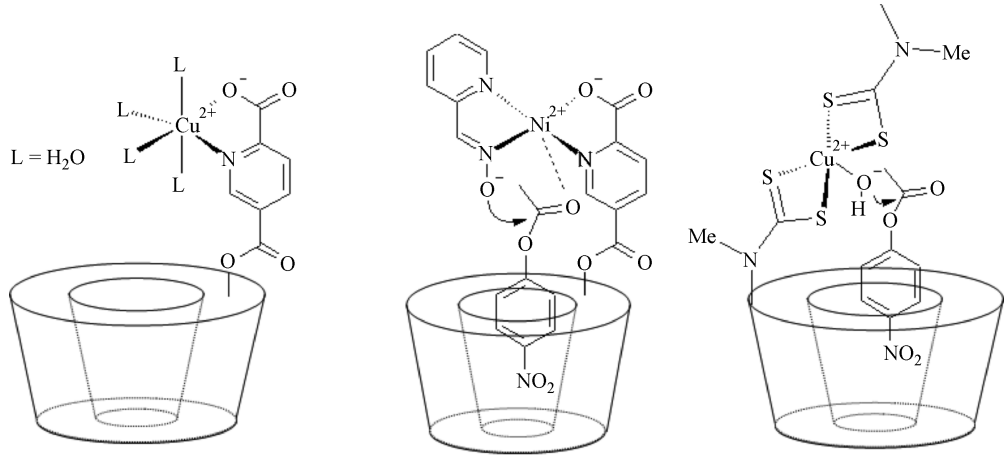


**12.6** **12.7** **12.8**

Cyclodextrins derivatised on the primary face have also been used as enzyme mimics, particularly as glyoxalase mimics. The function of glyoxalase enzymes is the isomerisation of α-keto aldehydes to hydroxy acids, a transformation that is accomplished through the involvement of thiolate moieties. The process has been mimicked by a β-cyclodextrin bearing an aminoethane thiol group on its primary face. The substrate is 2-naphthylglyoxal, which is rearranged to the corresponding hydroxy acid with moderate selectivity over cyclodextrin-free analogues, which represent control systems useful for comparison (Scheme 12.4).

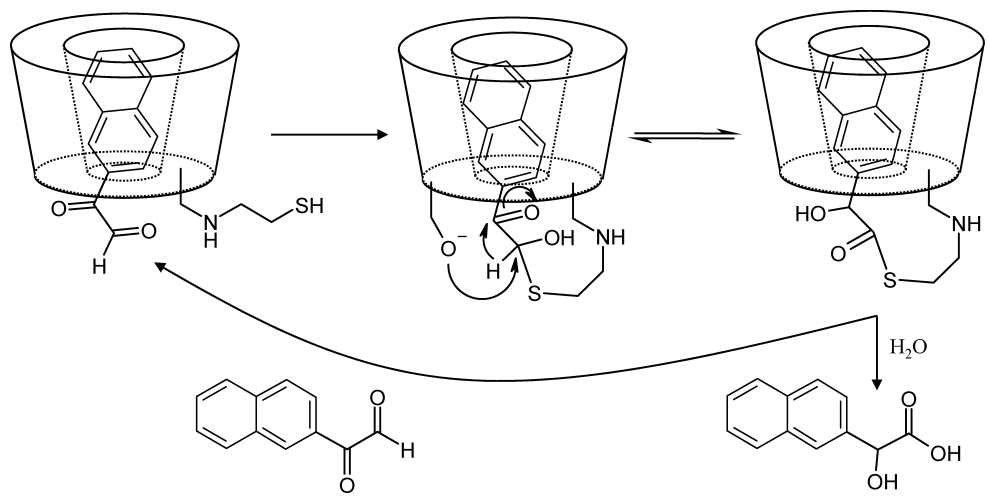


**Scheme 12.4** Glyoxalase mimics *via* derivitisation on the primary face.

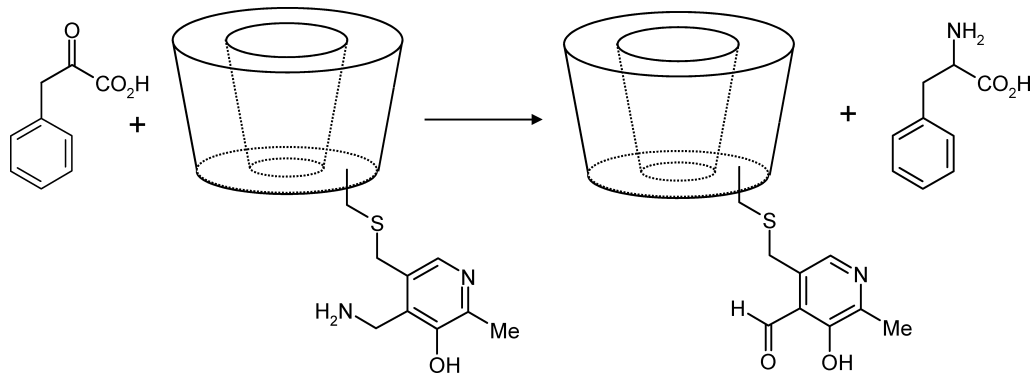


**Scheme 12.5** Transamination with a cyclodextrin and pyridoxamine cofactor.

In cases where the natural amino acid side chains of enzymes are insufficient to carry out a desired reaction, the enzyme frequently uses coenzymes. A coenzyme is bound by the enzyme along with the substrate, and the enzyme catalyses the bimolecular reaction between the coenzyme and the substrate (*cf.* Section 2.6.3). A simple model for $\alpha$-amino acid synthesis by transamination was developed by substituting $\beta$-cyclodextrin with pyridoxamine. Pyridoxamine is able to carry out the transformation of $\alpha$-keto acids to $\alpha$-amino acids even without the presence of the cyclodextrin, but with the cyclodextrin cavity as well, the enzyme model proves to be more selective and transaminates substrates with aryl rings bound strongly by the cyclodextrin much more rapidly than those having little affinity for the cyclodextrin. Thus (*p-tert*-butylphenyl)pyruvic acid and phenylpyruvic acid are transaminated respectively 15 000 and 100 times faster then pyruvic acid itself, to give (*p-tert*-butylphenyl)alanine and phenylalanine (Scheme 12.5).

## 12.3 Corands as ATPase Mimics

Hosseini, M. W., 'Supramolecular catalysis of phosphoryl anion transfer processes', in *Supramolecular Chemistry of Anions*, Bianchi, A., Bowman-James, K., Garcia-España, E., eds. Wiley: New York, 1997; *pp* 421–448.

Nucleotide polyphosphates, particularly adenosine tri- di- and monophosphates (ATP, ADP and AMP), are integral parts of the energy cycle for a vast range of biological processes, such as photosynthetic phosphorylation, oxidative phosphorylation, muscle contraction, and active transport. The role of ATP in providing the energy needed for the maintenance of cell transmembrane electric potentials has been outlined in Section 2.2. This energy comes from a class of enzymes termed ATPases ($Na^+/K^+$-ATPase in particular for cell membrane potentials). The key common function of ATPases is the hydrolysis of the terminal phosphate residue of the triphosphate tail of ATP to yield ADP and inorganic phosphate ($H_2PO_4^-$, $P_i$). This process releases about 35 kJ $mol^{-1}$ of energy and results in temporary phosphorylation of the enzyme.

A surprisingly effective model system for ATPase activity has been developed by Lehn, based on the large corand [24]$N_6O_2$ (**4.12**). We have already seen that, in the presence of acid, **4.12** may be protonated and exhibits significant affinity for multiply charged anions, with anion binding being accomplished through electrostatic and $N^+$—H$\cdots X^-$ hydrogen bonds (Section 4.4.4).

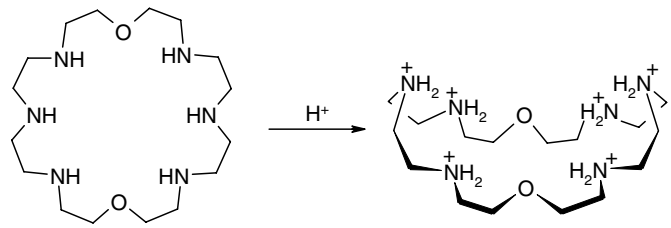


**4.12** **4.12**-6H$^+$

The X-ray crystal structure of the hexachloride salt of the protonated macrocycle shows that it adopts a cleft-like conformation as shown in the diagram, and modelling studies support the existence of this conformation in solution. The electrostatic nature of the anion binding by **4.12**-n$H^+$ means that it binds particularly strongly to multiply changed anions, and ATP, with its 4– charge, is bound in water at pH 4, with $\log K_{11} = 11$ for the hexaprotonated host.

Not only does **4.12** bind strongly to ATP despite being a flexible corand macrocycle, but it is also capable of accelerating the rate of its hydrolysis by a factor of about 100 over a wide pH range (2.5–8.5). The hydrolysis may be followed very conveniently by NMR spectroscopy using the $^{31}$P nucleus, which has a reasonably high receptivity and has a nuclear spin quantum number of $^1/_2$ (Figure 12.2), which

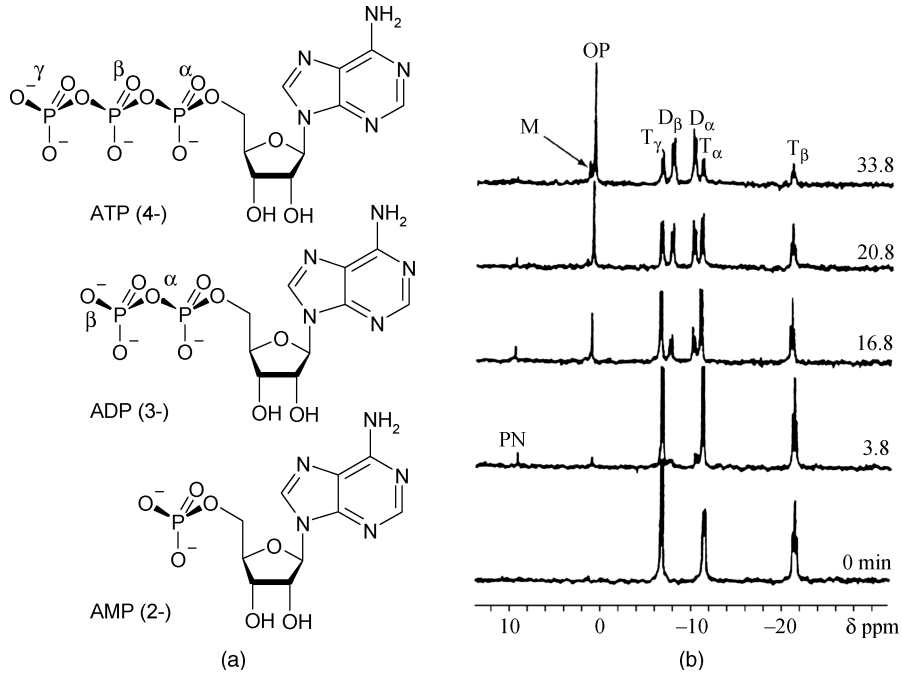


**Figure 12.2** (a)Deprotonated forms of ATP, ADP and AMP. (b) $^{31}$P NMR spectra of ATP hydrolysis by (**4.12**) at pH 7 as a function of time. $T_\alpha$, $T_\beta$ and $T_\gamma$ are the signals for the $\alpha$, $\beta$ and $\gamma$ phosphorus nuclei, respectively, of ATP. Analogous signals denoted D are from ADP. PN is the P—N bonded intermediate **12.9**, and the other signals are due to $H_2PO_4^-$ and $HPO_4^{2-}$ (reproduced by permission of John Wiley & Sons, Ltd).

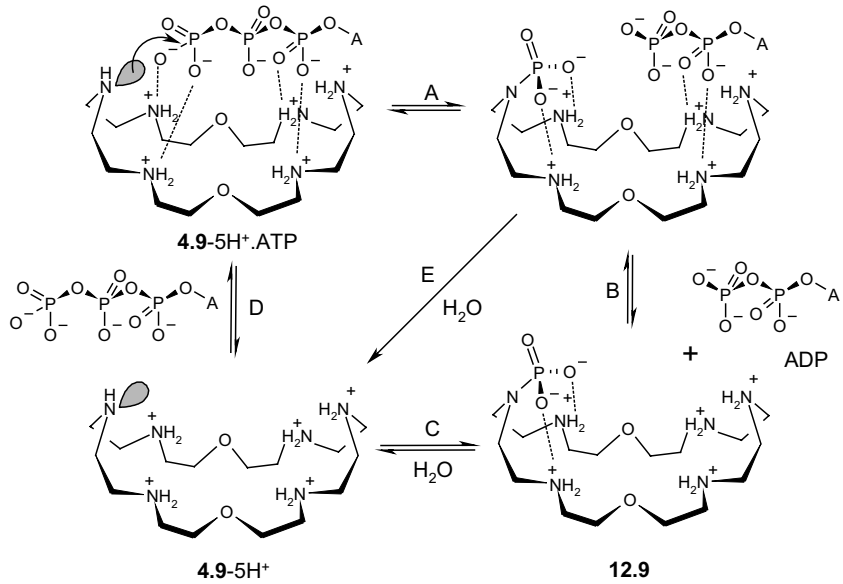


**Scheme 12.6** Mechanism of ATP hydrolysis by (**4.12**)-$5H^+$ (A = adenosine + sugar).

reveals the production of a phosphorylated macrocyclic intermediate. This suggests the overall mechanism shown in Scheme 12.6.

The beauty of the process is that, because ATP is complexed more strongly than ADP (ATP is more negatively charged), the catalytic cycle is readily established because fresh ATP can displace the ADP product from the host. Kinetic analysis shows that the concentration of ATP changes linearly with time in the initial stages of the reaction at a ATP : **4.12** ratio of 10:1, suggesting no product inhibition. The basic steps are as follows. Equilibrium A: the hexaprotonated macrocycle is relatively acidic and at pH 7 readily loses a proton from one of the central nitrogen atoms to yield a pentaprotonated host with one available lone pair as shown. Nucleophilic attack on the terminal ($\gamma$) phosphorus atom proceeds *via* a five-coordinate phosphorus intermediate, resulting in phosphorylation of the macrocycle and the formation of bound ADP. The reaction is rapid because the amine lone pair is positioned close to the terminal phosphate group by the pocket-like conformation of the macrocycle. The catalyst may be regenerated by decomplexation of the ADP (step B), followed by hydrolysis of the reactive intermediate **12.9** (which has been isolated), step C. Alternatively, reaction of the P—N bond in the ADP complex with water (step E) followed by displacement of ADP by ATP (step D) could also occur.

The overall rate of the reaction, which has a turnover of 0.064 $min^{-1}$, is much slower than natural ATPases (about $10^3-10^4$ $min^{-1}$), reflecting the much greater structural simplicity of the complex. Overall, however, the binding affinity is comparable to the natural system and the mechanism of operation is remarkably similar. Also related to the natural system is the effect of added metal ions, with $Ca^{2+}$ and $La^{3+}$ enhancing the reaction rate significantly. Natural ATPases require $Mg^{2+}$ and alkali metal cations to function. The effect of the metal ions is probably due to the formation of a ternary **4.12**·$M^{n+}$·ATP complex in which the metal coordinates to the uncomplexed ATP oxygen atoms, as well as acting as a Lewis acid and enhancing the nucleophilicity of coordinated water.

An interesting point concerns the reversibility of all of the reaction steps shown in Scheme 12.6. This implies that under certain circumstances, the system might change its behaviour from an ATPase mimic to ATP synthase-type behaviour. This has been achieved through the use of a phosphorylating cofactor, acetyl phosphate (AcP, $MeCO_2PO_3^{2-}$), and a divalent metal cation as a promoter ($Mg^{2+}$ or $Ca^{2+}$). Under

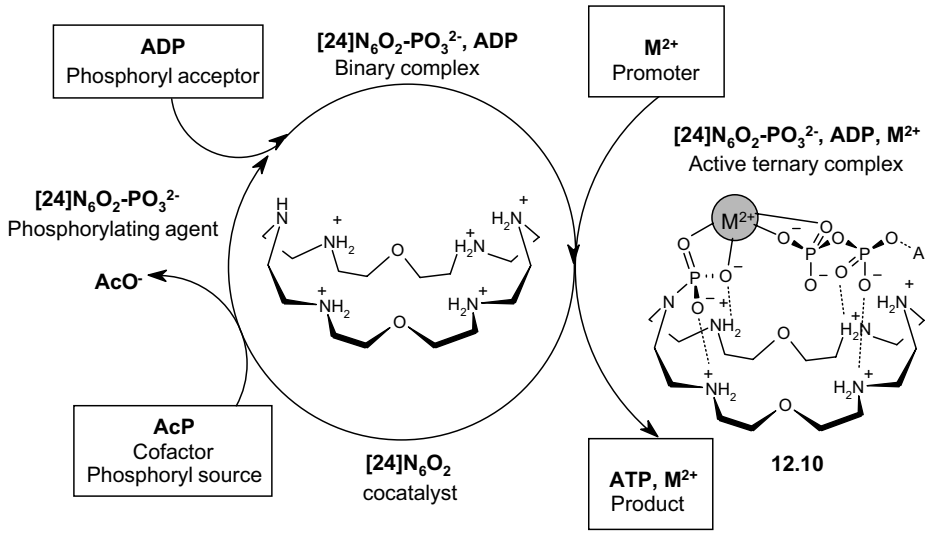


**Figure 12.3** ATP synthesis using 4.12.

these circumstances, about 35 % of the ADP may be converted back to ATP in the presence of a 10-fold excess of AcP. The synthesis is thought to proceed *via* **12.9** and ternary complex **12.10**, according to the cycle shown in Figure 12.3.

## 12.4 Cation-Binding Hosts as Transacylase Mimics

Cram, D. J. and Cram, J. M. *Container Molecules and their Guests*, Royal Society of Chemistry: Cambridge, 1994, 65–77.

### 12.4.1 Chiral Corands

We saw in Section 12.3.1 the use of the cyclodextrins as mimics for transacylases, a well-understood class of enzymes that perform the task of transferring an acyl group from one substrate to another (*e.g.* from an ester to water). Transacylase chemistry has also been addressed by Cram,[5] who used chiral corands, such as **12.11**, related to **3.106** bearing thiolate nucleophiles situated above and below the plane of the macrocycle. An acyclic analogue **12.12** was also prepared for comparison. The salient features of **12.11** are shown diagrammatically in Figure 12.4.

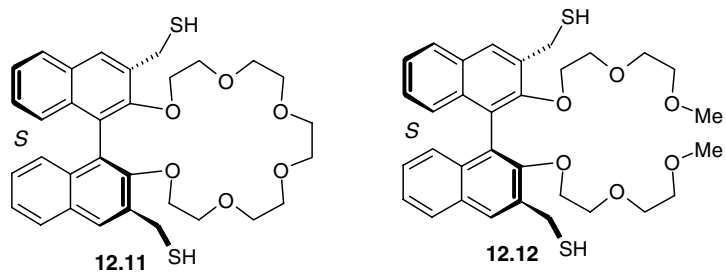

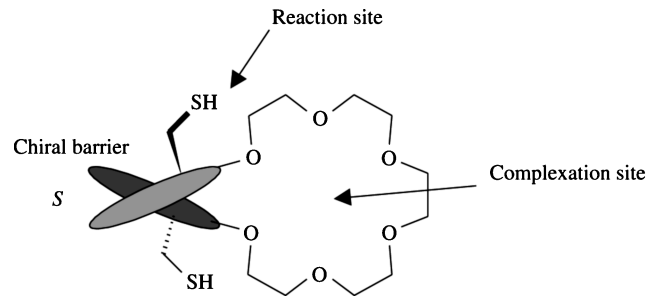


**Figure 12.4** Key features of chiral corand transacylase mimics.

As described in Section 3.12.4, corands of this type can bind primary ammonium cations *via* charge-assisted N—H···O hydrogen bonds. The host is complementary to the organic cation because of the matching of the three-fold symmetry of the $—NH_3^+$ group with the pseudo-six-fold arrangement of the corand binding sites (*cf.* Fig. 3.71). In the case of chiral guests, chiral recognition is observed as a consequence of steric interactions between the substituents on the naphthenyl groups ($-CH_2SH$ in **12.11** and **12.12**) and the substituents on the guest. Cram *et al*. examined the binding and reactivity of a number of esters of primary amino acids with **12.11** and **12.12**. The guests (of type $RCH(CO_2Ar)NH_3^+$) are bound in a perching fashion *via* their $NH_3^+$ substituents with complexation free energies in the order of 27 kJ $mol^{-1}$ in $CDCl_3$ saturated with $D_2O$ at 25°C. Guest binding was accompanied by transacylation, in which an acyl group is transferred from guest to the host thiol group as a result of nucleophilic attack by the thiol (Scheme 12.7). In each case, the resolved S-host was used, and it was found that in the intermediate the stabilisation of the S-host/L-amino ester pair was significantly greater than the S–D diastereoisomer. The system thus displays kinetic selectivity in the sense that the substrates of L-handedness react more quickly than those of D-chirality because the reaction transition state is more stable for the S–L pair. This kinetic selectivity depends strongly on the nature of the amino acid derivative, which determines the identity of the R group on the substrate. For small amino esters such as alanine derivatives (R = Me), the ratio $k_{S,L}/k_{R,L}$ is 1, *i.e.* no selectivity. The selectivity increases rapidly with the bulk of R, however, with rate selectivity factors of 6.4 for R = $Me_2CHCH_2$, 8.2 for R = $C_6H_5CH_2$ and 9.4 for R = $Me_3CH$.

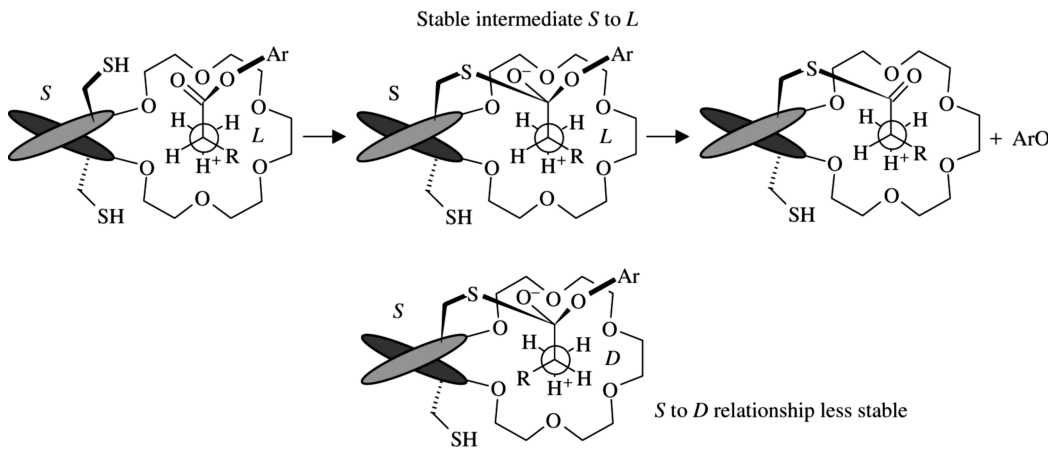


**Scheme 12.7** Transacylation step carried out by **12.11** (Ar = $p-C_6H_4NO_2$).

**Table 12.1** Rate acceleration factors and free energy differences for transacylation reactions of D-aminoesters by s-**12.11** and s-**12.12** (thiol present in 50-fold excess, 20% EtOH:80% $CH_2Cl_2$ v/v).

| Aminoester substrate ($Br^-$ salt) | $K_{\mathbf{12.11}}/k_{\mathbf{12.12}}$ | $\Delta(\Delta G^{\ddagger})$ (kJ mol$^{-1}$) |
|---|---|---|
| $Me_2CHCH_2CH(NH_3^+)CO_2Ar$ | >1170 | >17.6 |
| $C_6H_5CH_2CH(NH_3^+)CO_2Ar$ | 490 | 15.5 |
| $Me_2CHCH(NH_3^+)CO_2Ar$ | 160 | 12.5 |
| $MeCH(NH_3^+)CO_2Ar$ | >130 | >12.1 |
| $CH_2(NH_3^+)CO_2Ar$ | >130 | >12.1 |
| $C_4H_9N^+CO_2Ar$[a] | 0.8 | −0.4 |

[a] Proline ester salt.

Also of interest is the different behaviour observed in the comparison of the macrocycle **12.11** with the podand **12.12** (Table 12.1).

As in the case of all the primary aminoesters, the reactivity of **12.11**, in which organised substrate binding occurs, is $10^2-10^3$ times greater than in the non-preorganised podand, which is capable of only nonspecific binding. The $\Delta(\Delta G^{\ddagger})$ values represent the energetic lowering of the rate-limiting transition state relative to the equilibrium ground state. Only in the case of the secondary aminoester derived from proline is no rate acceleration observed. This substrate is not capable of tripodal binding. Apparently the tripodal perching binding mode lowers the reaction activation energy by about 10−20 kJ mol$^{-1}$. This binding-acceleration model is also supported by the fact that addition of $K^+$, which competes for the substrate binding site, results in a 500-fold inhibition of the acyl transfer reaction. Unfortunately, hydrolysis of the acylated host product proves to be very slow ($10^{-4}$ times the rate of transacylation) and so the system does not exhibit any catalytic turnover. It is best described therefore as a 'partial enzyme mimic'.

## 12.4.2 A Structure and Function Mimic

While the corand system described in the previous section is capable of mimicking the function (reactivity) of the transacylase class of enzymes, the binding sites and reactive moieties bear little resemblance to the natural systems. Compound **12.11** is thus not a *structural* mimic. The structure of a representative transacylase, chymotrypsin, is shown in Figure 12.5a. In addition to a hydrophobic binding site, the enzyme contains a nucleophilic serine hydroxyl group, a histidine imidazole residue and an aspartate carboxyl group, all preorganised by hydrogen bonds and other interactions. With this picture of the enzyme active site in mind, Cram used molecular CPK models, as he had for the spherands (Section 3.5), to design an 'ultimate' structural and functional mimic for chymotrypsin, compound **12.13**.

Compound **12.13**, which uses a spherand-based cation-binding site, is an extremely difficult compound to prepare, so its preparation was approached in stages. This approach had the advantage that at the completion of each stage of the assembly, the enzyme mimic activity of the molecule could be assessed in order to make sure that activity was maintained and enhanced, and assess the impact of each functional group individually. The binding site itself, hemispherand **3.62**, was first assembled and, as expected from its three-fold array of hydrogen bond acceptor carbonyl groups, binds $^tBuNH_3^+$ in chloroform with a complexation free energy of 55.2 kJ mol$^{-1}$, as discussed in Chapter 3 (see Figure 3.41 for the X-ray crystal structure of the **3.62**·$^tBuNH_3^+$ hemispheraplex). As a next step compound **12.14** was prepared and its reaction with the ester **12.15** (a substrate model) was examined (Scheme 12.8).

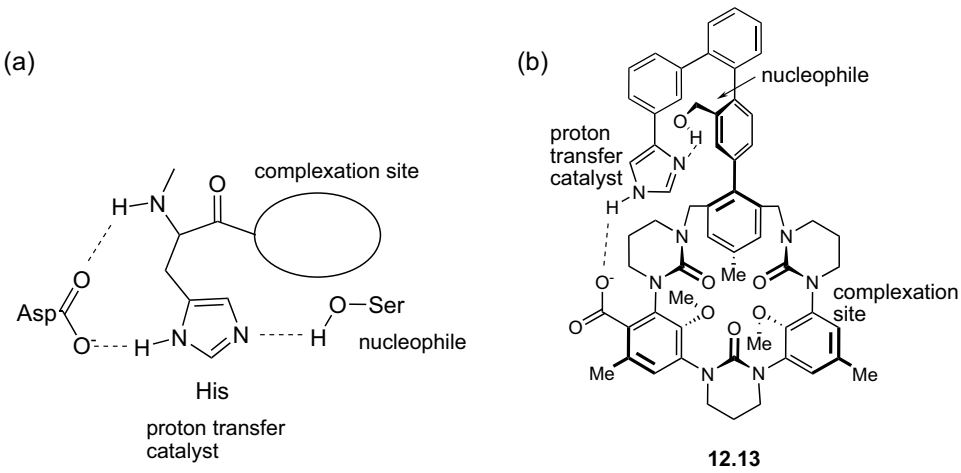


**Figure 12.5** (a) Active site of chymotrypsin and (b) a chymotrypsin mimic.

The formation of **12.16** proceeds $10^{11}$ times faster than the analogous reaction of a non-complexing model compound (3-phenylbenzyl alcohol) providing excellent evidence that the complexation by the hemispherand binding site is responsible for organising the reactants in the reaction transition state. The system also shows that the hydroxyl group was exhibits the hoped-for nucleophilicity. Addition of $Na^+$ reduces the reactivity by several orders of magnitude because of competition for the binding site. As a result of this successful step, a 30-stage synthesis of compound **12.17** was devised and, thanks to a great deal of hard work, about 0.5 g of the material was prepared. Compound **12.17** lacks only the carboxylate group that mimics the aspartate residue on the final molecule. Reaction of **12.17** with **12.15** (Scheme 12.9) proceeds extremely quickly, resulting in an initial product in which the imidazole is acetylated, compound **12.18** (reaction half-life, $t_{1/2} < 2$ min), followed by slower transfer to the hydroxyl group ($t_{1/2} = 4$ h). Imidazole acetylation is also noted for the real enzyme with nonspecific substrates. Again, addition of $Na^+$ results in a significant slowing of the overall reaction rate.

The final synthesis of target molecule **12.13** was never completed, but it seems that a systematic study of the reactivity of the compound with a range of acylating agents would produce a potent enzyme mimic. Clearly, however, the studies on **12.14** and **12.17** and a range of related compounds

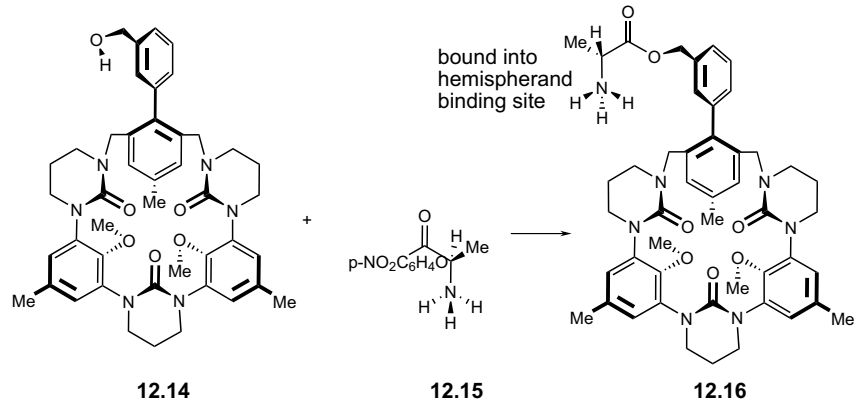


**Scheme 12.8** Partial model transacylase activity in a chymotrypsin mimic.

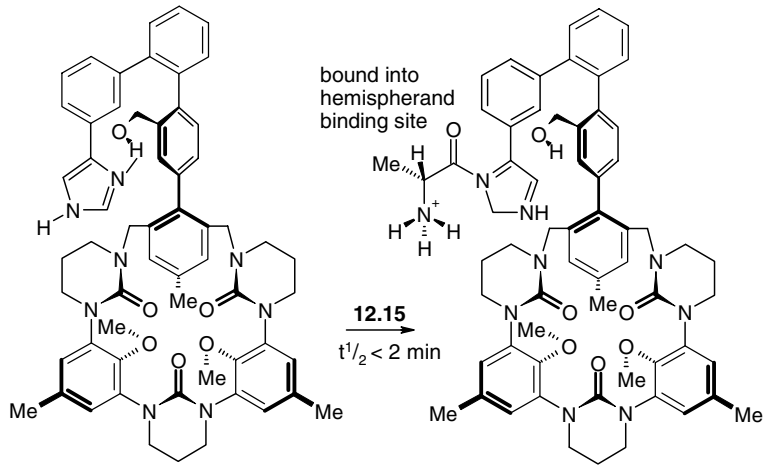


**Scheme 12.9** A more sophisticated chymotrypsin model.

demonstrate that enormous rate accelerations may be obtained by a combination of appropriate binding sites and reactive moieties. The complexity of preparing even these systems, which are relatively small compared to real enzymes, highlights the difficulties in creating real functional and structural enzyme mimics.

## 12.5 Metallobiosites

Fenton, D. E. 'Metallobiosites and their synthetic analogues—a belief in synergism', *Chem. Soc. Rev.*, 1999, **28**, 159–168.

Many biological proteins and enzymes are metalloproteins, *i.e.* they have a metal ion such as $Zn^{2+}$ or $Fe^{2+}$ at the core of their active site. The metal ion may play a Lewis acid or redox role, or act as a structure-stabilising, -templating or -regulation functionality. In effect, the metalloenzyme may be regarded as one enormous coordination compound in which the protein (organic) part of the biomolecule acts as a ligand for the metal centre. This structure suggests immediately that enzyme models may be developed by simulating the immediate coordination sphere around the metal ion, in much the same was as compounds such as **12.13** simulate an organic active site. Commonly, coordination compound models for the metal-containing sites in biological models (*metallobiosites*) are structural models, meaning that they mimic the structure of the enzyme active site, but not its function or catalytic activity. There is a great deal of interaction between information that may be gleaned from such simple model studies and more indirect studies on the real, natural systems. Structural models can suggest structural details such as conformations and bond lengths and angles, and provide comparative data for spectroscopic studies available from techniques such as such as electronic (UV–visible), Mossbaüer, EPR and extended X-ray absorption fine structure (EXAFS) spectroscopies. To take one example, the first enzyme to be crystallised was jack bean urease, a species that breaks down urea into ammonia and $CO_2$. The discovery that enzymes could be crystallised led to the award of the 1946 Nobel Prize in Chemistry to James B. Sumner. In 1975, the enzyme was shown to contain nickel by analysis of the UV–visible spectrum of the natural material. This data could be compared to the spectra of small,

well-characterised model coordination compounds and, as a result, it became readily apparent that the metal ion in the enzyme was an octahedral Ni(II) compound in a nitrogen-donor ligand environment. This structure was confirmed in 1995 by an X-ray crystal structure of a related urease from *Klebsiella aerogenes*. Models that attempt to mimic spectroscopic or magnetic properties of an enzyme of which the structure not known are termed *speculative* models. In contrast, a *corroborative* model tries to imitate directly known structural features of the metal coordination site in the natural material. This information usually comes from an enzyme crystal structure.

On a more sophisticated level, functional metallobiosite models may also, in principle, be prepared in the same conceptual fashion as applied to purely organic systems. Such systems are much more challenging and their success depends on the extent to which the enzyme activity is related to the nature of the metal first coordination sphere. It becomes, in general, almost exponentially more difficult to control the metallobiosite environment, the further the departure from the metal ion and its primary coordination sphere.

Metal ions often possess a number of coordination sites and, in a successful model, the identity of the donor groups at each site, regardless of whether it plays a direct part in the catalysis or biological function of the metal ion, must be well-defined and closely controlled. As a result, macrocyclic and chelating polydentate systems have been used frequently in metallobiosite models because they can contribute towards the mimicry of the (pre)organisation of the enzyme active site by virtue of their relative rigidity. The imine (Schiff base) macrocycles, such as those pioneered by Curtis, Busch and Jäger (Figure 3.56), have proved particularly useful because of the ability of these *N*-donor macrocycles to complex strongly to transition metal ions. Saturated azacorands have also been employed. Macrocycles are of particular interest in metallobiosite systems in which there are two metal ions that must be held at a relatively well-defined distance from each another. The dimensions of a macrocycle with two metal-coordination domains (*e.g.* ureases, which have two nickel centres about 3.7 Å apart) may then be used to regulate the metal–metal distance. A few examples of enzyme models based on macrocyclic and chelate ligands are discussed below.

### 12.5.1 Haemocyanin Models

Lewis, E. A., Tolman, W. B., 'Reactivity of dioxygen-copper systems', *Chem. Rev.* 2004, **104**, 1047–1076.

Of particular interest in enzyme modelling are copper-containing enzymes that bind or activate oxygen. Such naturally occurring systems are important in a range of biological processes including aromatic ring oxidations (*e.g.* tyrosinase), neurotransmitter biogenesis (dopamine $\beta$-monooxygenase) hydrogen peroxide generation (galactose oxidase), iron homeostasis (ceruloplasmin) and methane oxidation (particulate methane monoxygenase). Of particular importance is their role in haemocyanin, which we encountered briefly in Section 5.1.3. Haemocyanin is a metalloprotein involved in $O_2$ transport in arthropods and molluscs. Even the $O_2$ transport system of the giant squid, a creature that may weigh up to 150 kg, is based on haemocyanin rather than haemoglobin (Section 2.5). In the early 1980s, the structure of the active site of haemocyanin had not been determined, but it was believed from spectroscopic studies that it should contain the following features (some of which later proved to be incorrect, as we will see):

- two copper centres, each coordinated by three histidine units;
- an endogeneously bridging donor atom (perhaps a deprotonated oxygen from a tyrosine residue);
- strong antiferromagnetic coupling between the metal ions to give a diamagnetic complex;
- tetragonal Cu coordination environment ($\lambda_{max}$ 345 nm, $\varepsilon = 20\,000$, from UV–visible spectroscopy);

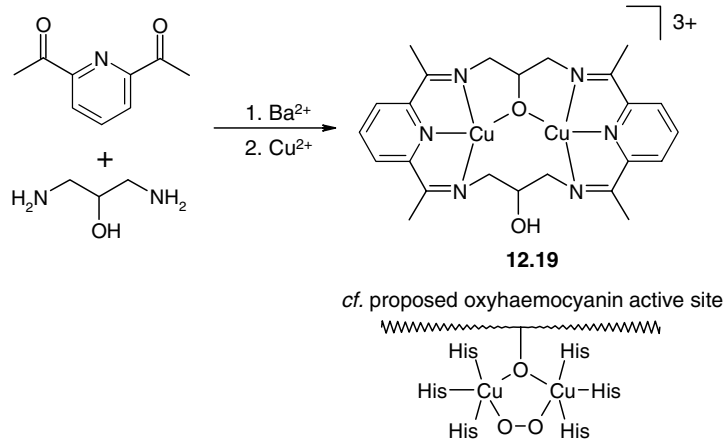


**Figure 12.6** Synthesis of a Schiff's base model for oxyhaemocyanin and comparison to the (incorrect) proposed natural system.[6]

- Cu···Cu 3.64 Å from EXAFS measurements;
- resonance Raman ν(O—O) 750 $cm^{-1}$ (suggesting possibly an $O_2^{2-}$ ligand).

In response to this data, work by David Fenton of the University of Sheffield, UK,[6] resulted in the bimetallic Cu(II) Schiff's base species **12.19**. This coordination complex, which is a speculative model, exhibits many of the expected features of the natural enzyme, such as a Cu···Cu separation of 3.64 Å, endogeneous alkoxo bridge and small antiferromagnetic coupling, Figure 12.6.

While an excellent approximation to the conventional wisdom, this model turned out to be a blind alley when the Xray crystal structure of deoxyhaemocyanin from the spiny lobster (*Panulirus interruptus*) was solved. This determination showed no endogeneous bridge, with the two Cu(I) centres each coordinated by three histidine residues separated by 3.7 Å. A further X-ray crystal structure of an oxygenated protein (oxyhaemocyanin, derived from *limulus polyphemus*) showed that the peroxide ($O_2^{2-}$) ligand in fact adopted an unusual $\mu$–$\eta^2$:$\eta^2$-bridging mode (Figure 12.7a). The revised structure was predicted by Kitajima in 1992 and was modelled successfully by the same group using sterically hindered tripodal ligands strongly resembling histidine residues, based on hydrotris(3,5-diisopropylpyrazolyl)borate (Figure 12.7b).[7] While oxygen bonding by this compound is irreversible, recent quantum computational calculations have focussed on this kind of model in order to explain the ability of haemocyanin to reversibly bind $O_2$. The calculated effective bond-order and localised

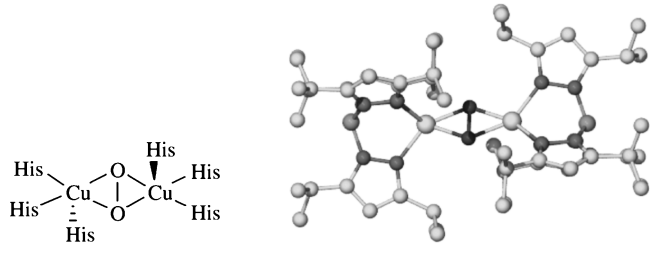


**Figure 12.7** (a) $\mu$–$\eta^2$:$\eta^2$-Bridging mode of coordinated peroxide in oxyhaemocyanin, (b) X-ray molecular structure of a dicopper hydro*tris*(3,5-diisopropylpyrazolyl)borate peroxide model.

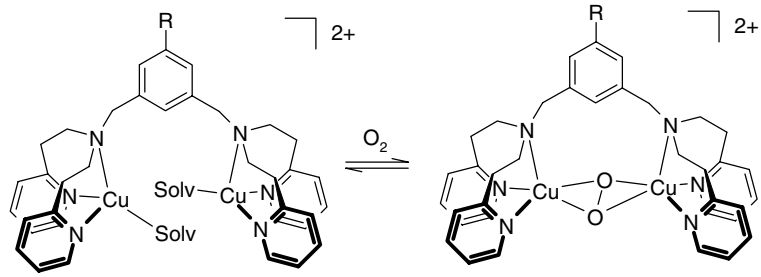


**Scheme 12.10** $O_2$ binding by a di-copper(I) model compound.[9]

electron density indicate that the copper-oxygen bonds exhibit an intermediate covalent-bonding character (half bonding), which is the origin of active control of oxygen transport by addition and dissociation of $O_2$ in haemocyanin coupled to enzyme conformational changes.[8] Experimental insights into the electronic effects governing the reversibility of the copper-oxygen linkage have been gained from the system shown in Scheme 12.10. The robustness of the system allows a systematic variation in the R substituent groups (R = H, *t*-Bu, OMe, F, CN, $NO_2$), which in turn affect the electronic properties of the copper(I) centres. The system reveals that the activation enthalpies for $O_2$ binding are low but there is a significant entropic penalty. For the fluoro complex and a methoxy analogue, interaction of the substituent with the metal inhibits oxygen binding. Comparing the nitro and *t*-Bu systems activation enthalpies for $O_2$ dissociation are lower and overall reaction enthalpies for peroxo complex formation are less favourable for the nitro-substituted system implying the electron donating substituent favours oxygen binding. Possibly direct interaction of the electrophilic $Cu_2O_2$ core with the arene ring may help to stabilise the peroxo complex. Alternatively there may be differences in the stabilities of the different conformers conformations of the complexes related to the flexibility of the benzylic linkages that influence the kinetic parameters.[9]

## 12.5.2 Zinc-Containing Enzymes

Hayashi, T. 'Zinc-containing enzymes and their models', in *Encyclopedia of Supramolecular Chemistry*, Atwood, J. L. and Steed, J. W. (eds), Dekker: New York, 2004, vol. 2, *pp.* 1631–1638.

We have already seen a number of models for the zinc(II) containing enzymes such as carbonic anhydrase in Section 11.3.2. Zinc is an essential component in biochemistry, and forms part of the active site of more then 100 enzymes, of which hydrolases (such as alkaline phosphatase and carboxypeptidase A), transferases (*e.g.* DNA and RNA polymerase), oxidoreductases (*e.g.* alcohol dehydrogenase and superoxide dismutase) and lysases (carbonic anhydrase) are the most common. In addition, the non-enzyme zinc finger proteins have an important regulatory function. In many of these systems, the non-redox-active $Zn^{2+}$ ion is present as a Lewis acidic centre at which substrates are coordinated, polarised and hence activated. Other roles of zinc include acting as a template and playing a structural or regulatory role.

Carbonic anhydrase (CA), in particular, has proved a popular target for the development of structural models. The role of this enzyme is to catalyse the simple, but very important, reaction of $CO_2$ fixation (Equation 12.1).

$$CO_2 + H_2O \rightleftharpoons HCO_3^- + H^+ \qquad (12.1)$$

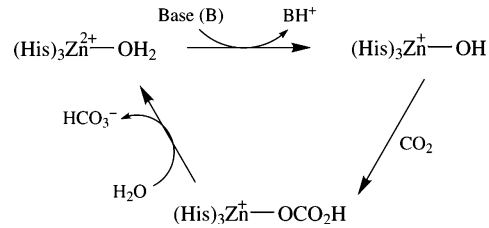


**Scheme 12.11** Key steps in the action of carbonic anhydrase.

The active site in various forms of the natural enzyme has been characterised by X-ray crystallography and comprises a tetrahedral $Zn^{2+}$ centre coordinated to three histidine residues and either a water molecule or hydroxide anion, depending on pH. The catalytic activity of the enzyme is based on the Lewis acidity of the $Zn^{2+}$ centre, which lowers the p$K_a$ of coordinated water from 14 to around 7. This enormous $10^7$-fold acidity enhancement is a result of the $Zn^{2+}$ ion being coordinated to neutral ligands (resulting in high positive charge), interaction with other acidic groups and the presence of an enzyme hydrophobic cavity (limiting solvation). The catalytic mechanism revolves around the steps shown in Scheme 12.11. The key step involves nucleophilic attack of the zinc-coordinated hydroxide on $CO_2$. This gives a five-coordinate intermediate containing a bidentate $HCO_3^-$ anion. The deprotonation of the water to form the much more nucleophilic hydroxide is, therefore, crucial.

A successful structural model for this process has been developed, which involves the tripodal tris(pyrazolyl)borate anion, resulting in the distorted tetrahedral species **12.20**. An analogue of the key hydrogen carbonate catalytic intermediate in which the $Zn^{2+}$ centre is five-coordinate is also known in the form of a bidentate nitrate analogue [Zn{$\eta^3$-HB(3-Phpz)$_3$}($\eta^2$-$NO_3$)].

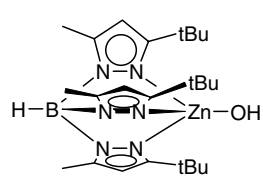


**12.20**

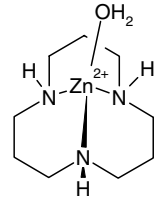


**12.21**

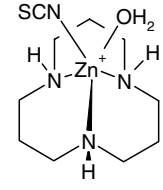


**12.22**

Work by Kimura *et al*. has centred around the macrocycle [12]ane-$N_3$, which also forms a tetrahedral zinc aquo complex **12.21**.[10] This species has the advantage of being dicationic as in the natural enzyme and does result in a significant enhancement to the acidity of coordinated water. Addition of $SCN^-$ results in the formation of a five-coordinate species **12.22** and ultimately a bis(thiocyanate). Such five-coordinate intermediates containing coordinated water or hydroxide and anions may be important steps in the operation of CA. Unlike the real system, however, neither **12.20** nor **12.21** contain a hydrophobic cavity, which is one of the important aspects of the enzyme's high acidity and nucleophilicity. In order to incorporate this feature, Paul Walton of the University of York, UK, has built up model hydrophobic cavities using Schiff's base chemistry along with a tripodal amine core, as in all *cis*-1,3,5-triaminocyclohexane (**12.23**). Condensation of this building block with a range of aldehydes, followed by reaction with $Zn^{2+}$, gives a range of tripodal ligands in which a hydrated zinc ion is situated at the bottom of a deep, hydrophobic well, as in **12.24**. The structure of the acetate complex of a related furan derivative show a marked structural correlation with the metal coordination environment in the bicarbonate form of the enzyme, Figure 12.8b.[11]

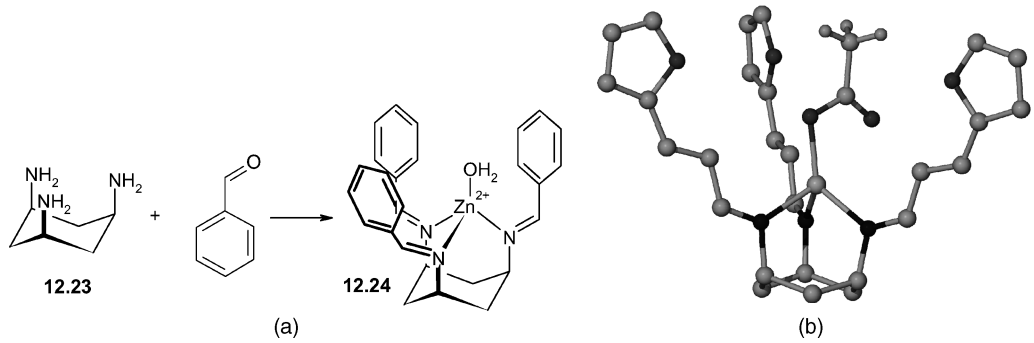


**Figure 12.8** (a) Synthesis of cyclohexane imine-based carbonic anhydrase mimics with a hydrophobic binding pocket, (b) X-ray molecular structure of the zinc(II) acetate complex of *cis*-1,3,5-tris [3-(2-furyl)prop-2-enylideneamino]cyclohexane showing the actate coordination, highly reminiscent of Zn-coordinated hydrogen carbonate in carbonic anhydrase.[11]

Work by the group of Stephen Lippard (MIT, USA) has focused on a different zinc-containing enzyme, $\beta$-lactamase. This enzyme hydrolyses the $\beta$-lactam ring in a series of antibiotics such as penicillin and cephalosporin derivatives nullifying their effect on pathogenic bacteria. Lippard's functional model is shown taking part in the hydrolysis of nitrocefin in Scheme 12.12. Nitrocefin is a chromogenic $\beta$-lactamase substrate that undergoes a color change from yellow to red as the amide bond in the $\beta$-lactam ring is hydrolyzed. It is thus an excellent way to follow the progress of the reaction. This process is accelerated some 2800-fold by the enzyme mimic compared to the uncatalysed rate at pH 7. The two zinc ions are involved in substrate binding while the bridging nitrate is replaced by hydroxide, which attacks the $\beta$-lactam ring.[12]

Finally, another well known zinc-containing enzyme is alcohol dehydrogenase – the enzyme in the liver responsible for metabolising alcohol to the corresponding acetaldehyde after a hard night out on the town. Oxidation of ethanol to acetaldehyde is catalyzed by alcohol dehydrogenase containing the coenzyme nicotinamide adenine dinucleotide ($NAD^+$; the ubiquitous biological electron carrier). The acetaldehyde is further oxidised to acetic acid and finally to $CO_2$ and water through the citric acid cycle. A number of metabolic effects from alcohol are directly linked to the production of an excess of both NADH and acetaldehyde and it is the aldehyde that is one of the major causes of alcohol toxicity. Acetaldehyde may also be involved in alcohol addiction. In the brain it seems to inhibit enzymes

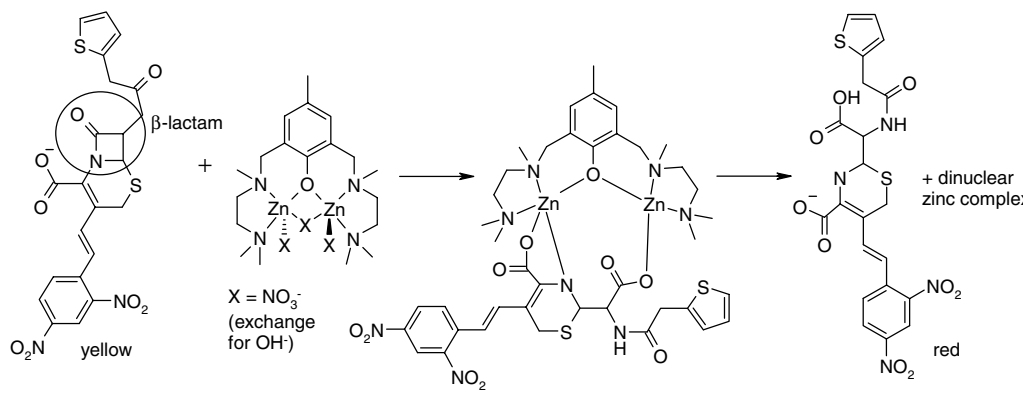


**Scheme 12.12** A functional model for $\beta$-lactamase.[12]

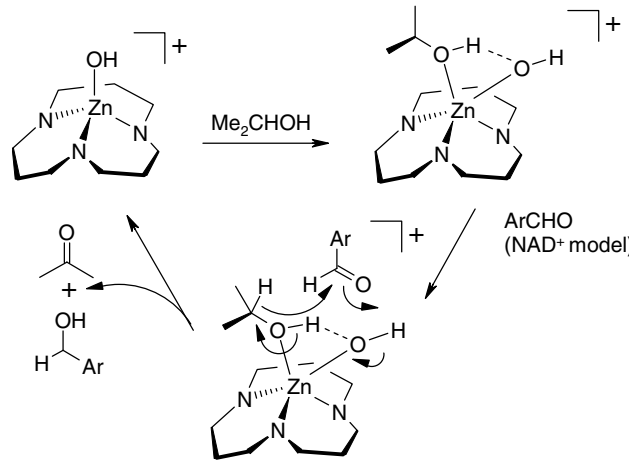


**Scheme 12.13** A functional alcohol dehydrogenase model.[13]

that convert particular nerve transmitters from aldehydes to acids. The nerve transmitters that accumulate can react with the acetaldehyde to form compounds which bear a strong resemblance to morphine-type drugs. Hydride transfer in functional alcohol dehydrogenase mimics from 2-propanol to model $NAD^+$ hydrogen acceptors has been realised by Kimura's group. The reaction scheme is shown in Scheme 12.13.[13]

## 12.6 Haem Analogues

### 12.6.1 Models of Oxygen Uptake and Transport

Collman, J. P. and Zhang, X., 'Functional analogues of the oxygen binding and activating haem proteins', in *Comprehensive Supramolecular Chemistry*, Atwood, J. L., Davies, J. E. D., MacNicol, D. D. and Vögtle, F. (eds), Pergamon: Oxford, 1996, 1–32.

The unique cooperative mechanism by which oxygen is bound and transported by the iron protoporphyrin IX-based haemoglobin has been described in detail in Section 2.5. The striking properties of this system have stimulated a number of attempts to produce small-molecule mimics in order to aid the understanding of the natural system and to develop new forms of chemical reactivity, transport and catalysis. The haemoglobin system is an especially appealing one to supramolecular chemists because, conceptually, it is relatively simple (compared to enzymes for example). The $O_2$ complexation essentially amounts to a thermodynamically controlled binding of a neutral guest species, without the guest undergoing any kind of chemical transformation. In model systems, therefore, there is no need to design the more complex features associated with kinetic selectivity along a reaction pathway. This simple view of $O_2$ binding, however, belies the fact that $O_2$ is a highly non-innocent guest and is chemically very reactive. It is the more sophisticated properties of haemoglobin—such as the prevention of oxide or $\mu$-oxo dimer formation, binding and release under physiological conditions (such as the $O_2$ partial pressures found in areas such as the lungs and muscle tissue) and the control of the Fe(II) redox potential necessary to reduce $O_2$ to superoxide—that make haemoglobin an interesting target for the construction of artificial mimics.

An obvious choice for the construction of artificial oxygen binding mimics is the use of oxidisible transition metal (particularly iron) complexes of porphyrin ligands such as **12.23**, as in the natural system. In such cases, the $O_2$ affinity is governed essentially by the reduction potential of the metal centre ($E_1^0$) as in the reaction: $M^{(n+1)+} + e^- = M^{n+}$. Iron(II) and cobalt(II) are particularly favourable in this regard. These two metal ions are also useful because, when bound to a porphyrin ligand, they have vacant axial coordination sites available for $O_2$ binding. This feature arises because of their preference for an octahedral coordination geometry. Unfortunately, in order to mimic the properties of the natural system closely, only one axial coordination site is required for oxygen binding. Hence one other axial ligand is required in order to fill up the metal coordination sphere. In the natural system, this is a proximal histidine residue. However, in the case of Fe(II), which is a $d^6$ metal ion, there is a strong driving force towards complexation of a second axial ligand because the resulting octahedral ligand field is sufficient to cause a cross-over from high-spin (total spin quantum number, $S = 2$) to low-spin ($S = 0$) behaviour, with accompanying gains in ligand field stabilisation energy (*cf.* Box 10.1). In general, the ratio of equilibrium constants $K_{12}/K_{11} \simeq 15$ (Equations 12.2 and 12.3 – por = porphyrin). In the natural system, the rigidity imposed by the protein tertiary structure prevents the approach of the distal histidine residue to the vacant axial coordination site. This avoids competition by the protein for the $O_2$ binding site. Such competition for the $O_2$ binding site by other axial ligands is not such a factor with the $d^7$ Co(II) because no such spin cross-over occurs.

$$[Fe(por)]^{2+} + L = [Fe(por)L_2]^{2+} \qquad K_{11} \tag{12.2}$$

$$[Fe(por)L]^{2+} + L = [Fe(por)L_2]^{2+} \qquad K_{12} \tag{12.3}$$

In Fe(II) model systems, protein tertiary structure is not present, and hence the issue of generating a five-coordinate metal centre must be addressed in a different way. Some of the more successful approaches are detailed below:

1. Use of 2-methylimidazole as the axial ligand (L). The steric hinderance about the donor atom stabilises five-coordinate Fe(II) porphyrin complexes in which the 'doming' of the iron out of the porphyrin plane reduces steric interactions with the methyl group (Figure 12.9). The resulting 2-methyl imidazole (MeIm) complex with tetraphenylporphyrin (**12.23**, R = Ph) is a good structural model for the deoxygenated form of myoglobin (*cf.* Figure 12.10a). Imidazole and its derivatives are good mimics for the protein histidine residue in the biotic system.
2. Covalent attachment of a single axial ligand to the porphyrin framework. This technique can have the disadvantage that at higher concentrations the system dimerises giving one four-coordinate and one six-coordinate metal centre (Figure 12.11).
3. The most elegant, though synthetically less accessible, technique is to fit one side of the porphyrin ligand with a molecular cage, allowing binding of imidazole axial ligands only to the accessible face of the porphyrin.

A crucial question, however, is the prevention of the decomposition of small-molecule model metalloporphyrin $O_2$ complexes either by irreversible breaking of the O=O bond (*cf.* Scheme 2.4a) or by protonation of the coordinated $O_2$ to give the highly unstable hydroperoxyl radical, $HO_2$. Disassociation of $HO_2$ from the iron centre gives an inactive Fe(III) porphyrin complex and free $HO_2$, which disproportionates rapidly to $O_2$ and $H_2O_2$. Indeed, if the natural system is mutated to give acidic amino acid residues such as tyrosine in the distal site (the oxygen binding pocket), the haem remains in the inactive Fe(III) state, while in model compounds, binding of water has a similar effect.

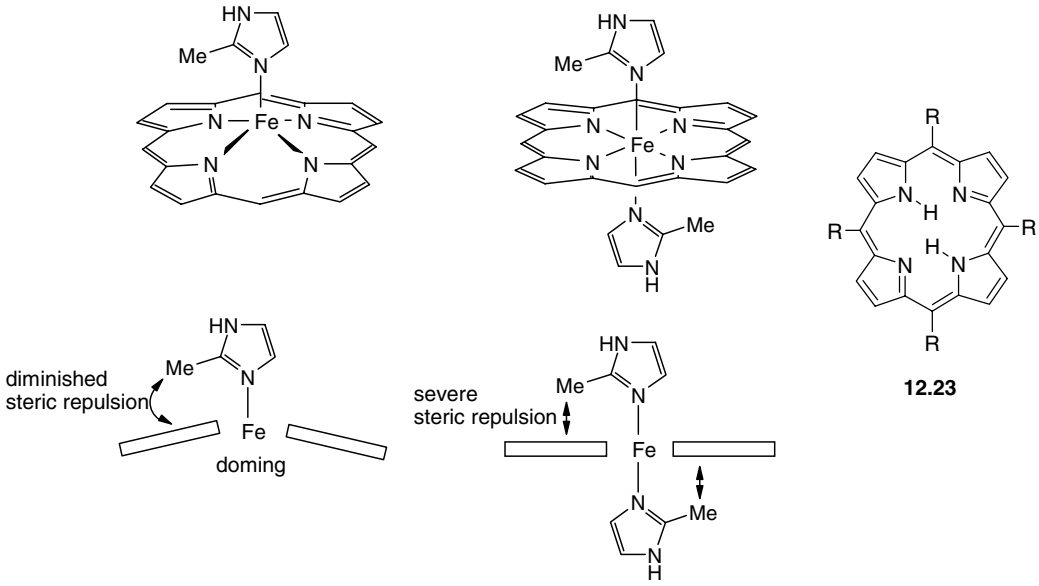


**Figure 12.9** Structural model for deoxymyoglobin based on the formation of a five-coordinate iron complex of tetraphenylporphyrin (**12.23**, R = Ph), stabilised by 2-methyl imidazole.

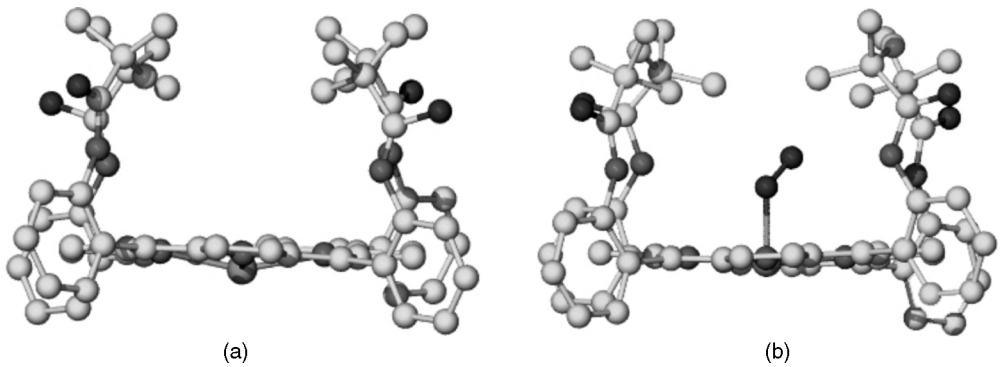


**Figure 12.10** (a) X-ray crystal structure of [Fe(**12.25**)(MeIm)] showing the doming of the five-coordinate iron,[14] (b) X-ray structure of six coordinate [Fe($O_2$)(**12.25**)(MeIm)] (MeIm ligands not shown).[15]

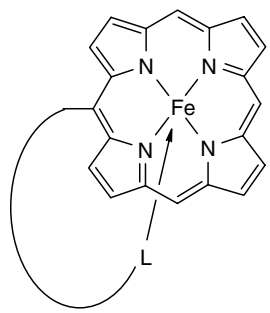


**Figure 12.11** Covalent attachment of one axial ligand.

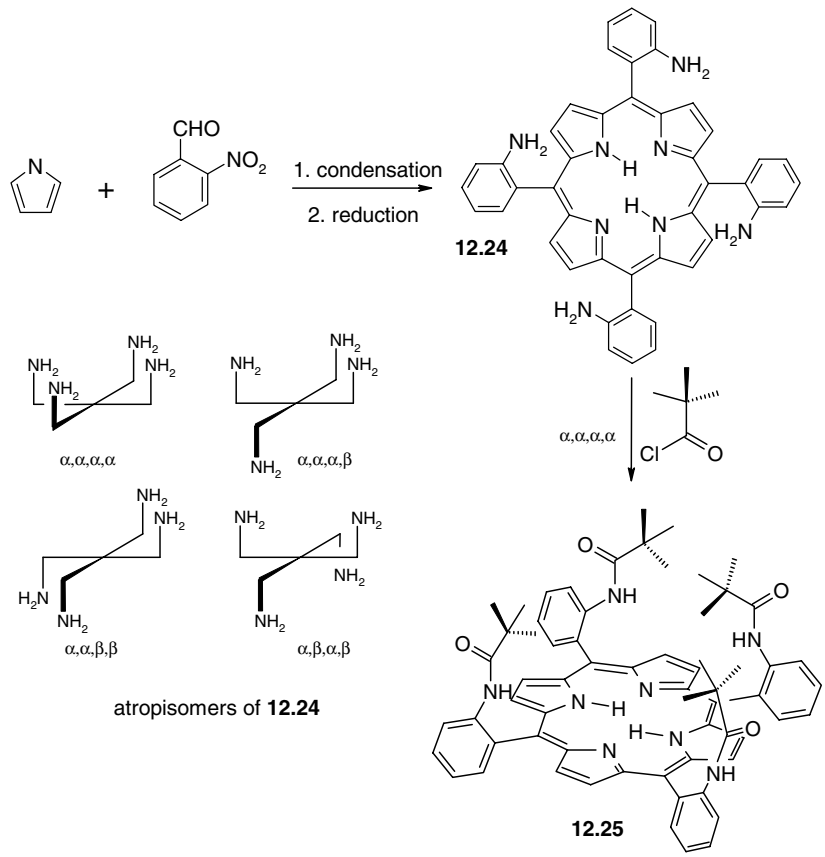


**Scheme 12.14** Synthesis of 'picket fence' porphyrins.

These undesirable decomposition pathways are all prevented in natural myoglobin by the protein tertiary structure, which encloses the $O_2$ binding site within a hydrophobic pocket, preventing dimerisation and denying access to acidic groups. One of the first series of successful haem mimics that model this feature were the 'picket fence' porphyrins.[16] These complexes rely upon the appending of bulky hydrophobic substituents to the porphyrin core to form an upright 'fence' around the iron binding site (Scheme 12.14). Synthesis of these sterically protected species involves the initial condensation of a nitro substituted benzaldehyde with pyrrole, followed by reduction of the $NO_2$ groups to $NH_2$. This gives a porphyrin that exists as a series of isomers (termed *atropisomers*) according to the relative orientations of the $NH_2$ substituents above and below the porphyrin plane. These are non-interconvertable below 80°C and may be separated by chromatography. It is the $\alpha,\alpha,\alpha,\alpha$ isomer (all substituents on the same face of the porphyrin) that is used to form the picket fence porphyrin **12.25**. Unwanted isomers may be equilibrated by warming to above 80°C followed by chromatographic separation to give more product. Similarly, a series of 'pocket' porphyrins such as **12.26** may be prepared by capping three of the four amine substituents, while 'picnic basket' porphyrins (*e.g.* **12.27**) arise from capping all of the amine groups. Similarly, reactions with the $\alpha,\beta,\alpha,\beta$ isomer can give species with caps on both sides of the porphyrin. Different axial substituents on the central metal may be favoured by making these caps chemically different, as in **12.28**.

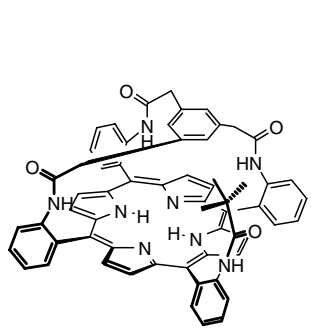

**12.26**

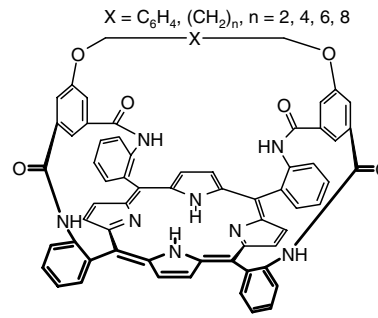


**12.27**

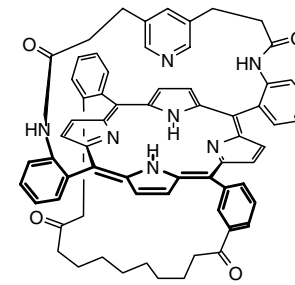

**12.28**

The Fe(II) complex of **12.25**, when reacted with $O_2$, proves to be an excellent model for oxygenated myoglobin. The $O_2$ molecule is bound into the cavity defined by the picket fence substituents, while the unhindered axial site is occupied by a range of nitrogen bases such as imiazole and its *N*-methyl and 2-methyl derivatives. In the case of non-sterically hindered bases, however, oxygen binding by [Fe(**12.25**)] suffers from the competition with the axial ligands since the picket fence does not significantly aid $O_2$ selectivity over these species. However, it is found experimentally that $O_2$ is able to compete to a significant extent, and $O_2$ complexes have been isolated. Furthermore the 'picket fence' substituents prevent decomposition by oxo-dimer formation and complexes of type [Fe($O_2$)(**12.25**)L] (L = 1-MeIm, 2-MeIm) are stable in solution at room temperature for several hours. The X-ray structure of the complex with 1-MeIm shows the desired angular binding in the Fe—$O_2$ unit with the Fe—O—O angle being 128°, as well as demonstrating short Fe—O bond distances of 1.75 Å (Figure 12.10b).[15] The spectroscopic properties match closely those of the natural system (which had not been structurally characterised at the time), *e.g.* $\nu(O_2^-)$ = 1159 $cm^{-1}$.

The more sophisticated 'pocket' and 'picnic basket' porphyrins are also capable of mimicking properties such as $O_2$/CO binding selectivity in which the (normally high) CO affinity is reduced because of steric interactions between the CO molecule (which adopts a linear Fe−C=O conformation) and the capping or strapping moiety. Selectivity for small molecules such as $O_2$ is also enhanced, relative to larger bases.

Attempts have also been made to model the cooperativity observed in the natural system between the four myoglobin units that make up the whole haemoglobin protein. This cooperativity is vital to the functioning of the transport protein over the correct concentration range and takes the form of a synergic enhancement of the affinity of unbound haem units upon interaction of any one of them with $O_2$ (Section 2.5). Thus, binding of $O_2$ to the first haem unit causes a protein-mediated conformational change in the remaining three from the low-affinity T-state to a higher affinity R-state. The key to understanding the difference between the R- and T-states is demonstrated readily using the picket-fence model compounds. It is found that the $O_2$ (and CO) affinity of [Fe(**12.25**)L] is lowered significantly (by a factor of 10–100) when L = 2-MeIm, compared to the unhindered case when L = *N*-MeIm or imidazole itself. Thus, in its deoxygenated state, [Fe(**12.25**)(2MeIm)] is an excellent model for the deoxygenated, low-affinity T-state haem unit within haemoglobin. The reduced oxygen affinity is a result of the unfavourable steric interactions between 2-MeIm and the porphyrin, which are increased on $O_2$ binding because the transition from a five- to a six-coordinate iron centre is accompanied by a significant reduction in the 'doming' of the porphyrin ring plane (Figure 12.12).

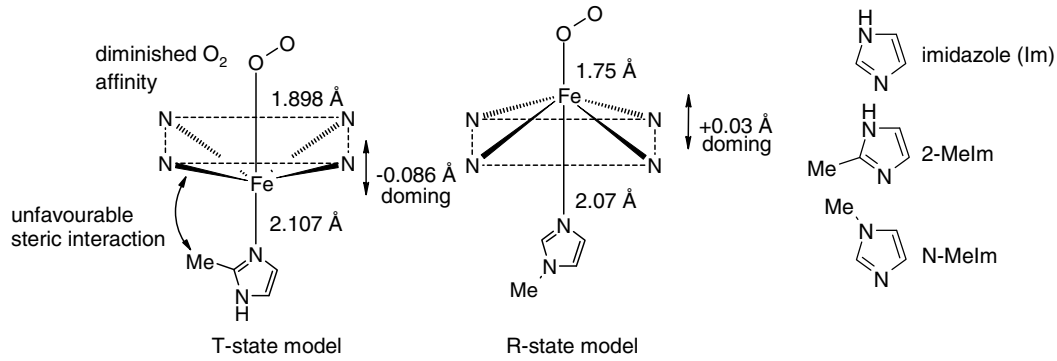


**Figure 12.12** Effects of axial ligands on $O_2$ affinity as a model for protein-mediated cooperativity within the haemoglobin tetramer.

## 12.6.2 Cytochrome P-450 Models

Feiters, M. C., Rowan, A. E., Nolte, R. J. M., 'From simple to supramolecular cytochrome P450 mimics', *Chem. Soc. Rev.* 2000, **29**, 375–384.

Cyrochrome P-450 is a large family of enzymes that use oxygen as their substrate (oxygenases). The P-450 designation represents the fact that the compounds are pigments absorbing visible light at 450 nm. They are found in plants, microorganisms and in most mammalian organs, particularly the liver, and catalyse reactions such as hydroxylation of alkanes (Equation 12.4) or the epoxidation of alkenes. In effect they are one of Nature's workhorses with a major role in detoxification and have been extensively studied over the past 40 years.

$$RH + O_2 \rightarrow ROH + H_2O \tag{12.4}$$

Like myoglobin, cytochrome P-450 enzymes contain an oxygen-binding haem unit; however, a cysteine thiolate residue replaces the axial histidine found in myoglobin. The enzyme is used in both primary metabolism (*e.g.* multiple oxidation of cholesterol) and in the catabolism of hydrophobic xenobiotics (*e.g.* degradation of drugs in the liver). Unlike myoglobin, the function of cytochrome P-450 depends on the breaking of the O=O bond and hence the haem protein environment is quite different. The catalytic cycle for the oxygenase activity of the enzymes is shown in Scheme 12.15. The initial Fe(III) complex is reduced to an $O_2$-binding Fe(II) state using electrons from the reduced form of nicotinamide adenine dinucleotide (NADH—the biological electron transporter). Further reduction and protonation allows cleavage of the O—O bond to give water and an Fe(V) oxo complex ($O_2 \rightarrow O_2^- \rightarrow O_2^{2-}$). Note the absence of $\mu$-oxo dimer formation, which is irreversible and would result in inactivation of the enzyme. This highly reactive high-oxidation-state species is sufficiently oxidising to oxidise organic substrates bound within the enzyme cavity to give the product and regenerate the enzyme in the initial Fe(III) state.

Structural model systems are difficult to construct for cytochrome P-450 because thiolates do not bind strongly to Fe(III) porphyrin units, and oxidation of the thiolate to disulfides accompanied by reduction to Fe(II) is common (Equation 12.5). A range of models for the Fe(III) resting state have been prepared using open iron(III) porphyrins with alkyl or aryl thiolates, however.

$$2[\,Fe^{III}(por)(SR)] \rightarrow 2[\,Fe^{II}(por)] + RSSR \tag{12.5}$$

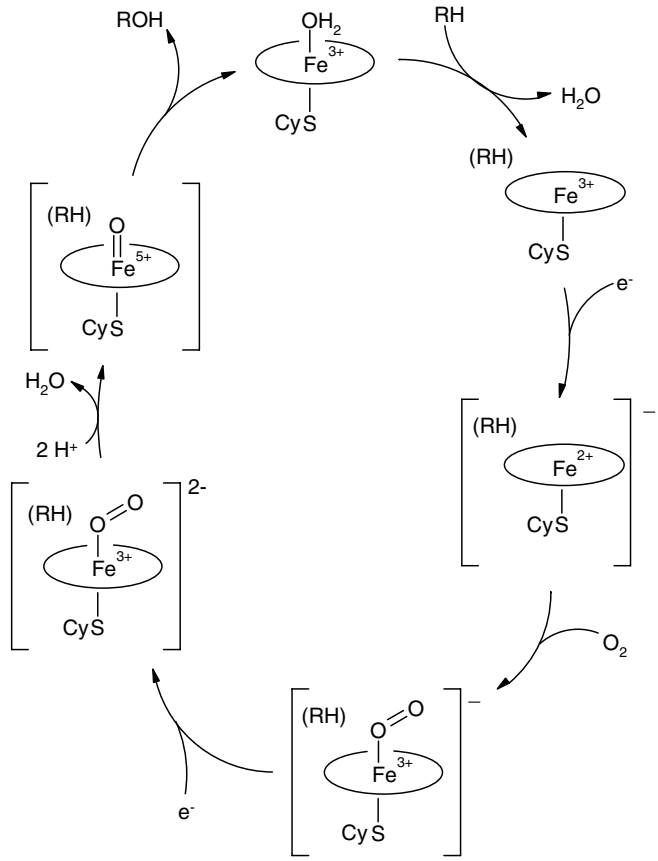


**Scheme 12.15** Catalytic reactivity cycle for cytochrome P-450.

An Fe(II) complex with a tethered axial thiolate has also been prepared (**12.29**) as the CO adduct. This complex exhibits UV–visible and magnetic circular dichroism spectra similar to the analogous CO complexes of the iron P-450 family.

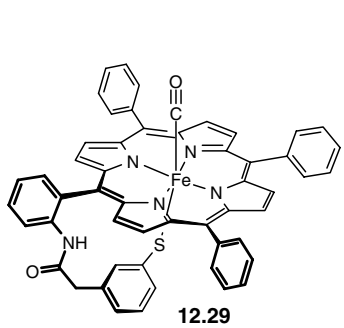


**12.29**

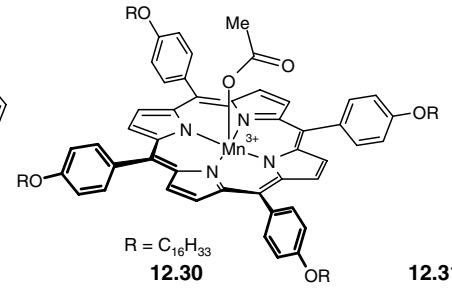


**12.30**

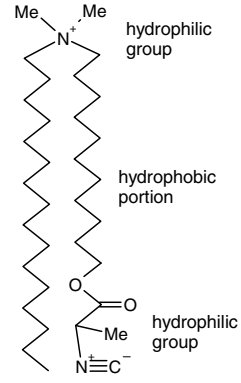


**12.31**

A significant amount of success has also been achieved with the construction of functional model systems exhibiting oxidase activity, including systems that are not based on iron. One example, compound **12.30**[17] incorporates a number of features of the natural enzyme:

1. Membrane-bound metalloporphyrin.
2. Axial ligand.
3. Electron donor (*cf.* NADH).
4. Electron carrier.
5. A membrane system that holds components within its bilayer or within its aqueous compartment.

The metalloporphyrin component is a manganese acetate compound with long, lipophilic tentacles that serve to anchor it within a hydrophobic membrane, much as the protein portion of the natural system holds it within the lipophilic portion of the biological phospholipid cell membrane. The system incorporates an artificial membrane composed of a polymerised isocyanato surfactant (**12.31**), which forms bilayer vesicles in aqueous solution (Section 13.2.1). These vesicles have an inner aqueous region, separated from the bulk aqueous solution by the bilayer surfactant membrane. The inner portion of the vesicle is filled with a colloidal dispersion of platinum metal by reduction of aqueous Pt(II) with molecular hydrogen. The platinum metal acts as the electron source and is gradually reoxidised to Pt(II). The system epoxidises alkenes that are insoluble in water (and therefore are incorporated within the vesicle wall), such as styrene, *and* water-soluble species, such as 2,5-dihydrofuran. The redox-active dye, methylene blue (originally used by Paul Erlich to stain cells, compound **1.5**), has been used as an electron carrier (Scheme 12.16). The 2,5-dihydrofuran gave both 3,4-epoxytetrahydrofuran and a ring-opened product. Only ring-opened products were detected for styrene. Catalytic turnover numbers proved to be very small (8 and 1.3, respectively, for the two substrates) but the system gives a remarkable insight into the translation of biological processes to abiotic molecular devices.

Cyclodextrins have also been used as cytochrome P-450 mimics, in which the cyclodextrin cavity is linked covalently to an iron porphyrinato core, as in **12.32**. Binding of hydrophobic substrates, such as

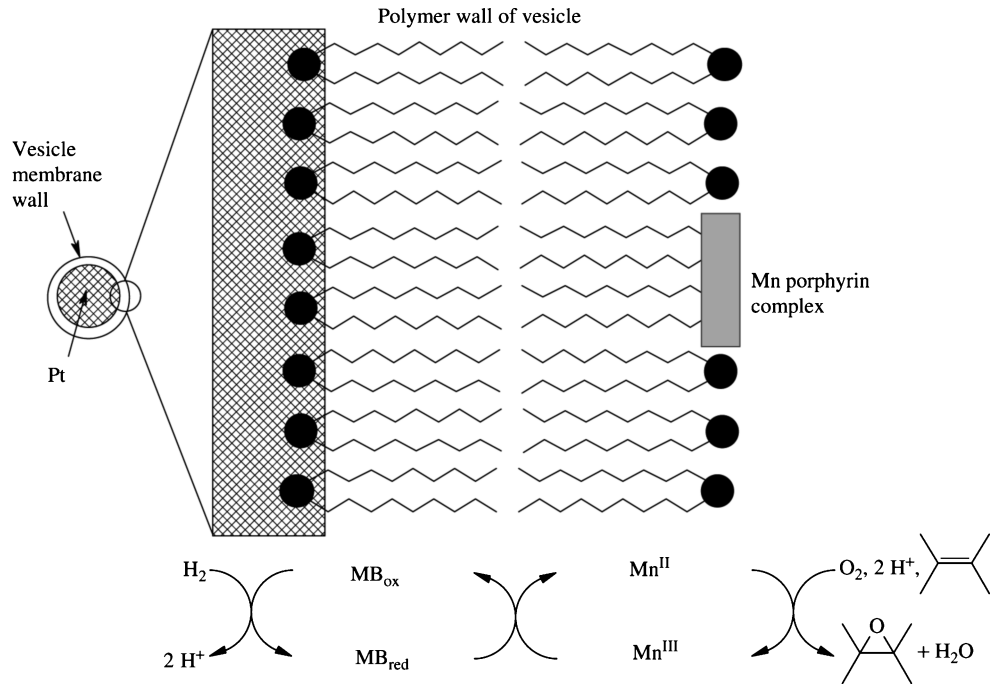


**Scheme 12.16** Cytochrome P-450-mimic microreactor based on a Pt-filled vesicle. ($MB_{ox/red}$ = methylene blue electron carrier, oxidised and reduced forms, respectively.)

cyclohexene, within the cyclodextrin cavity leads to their selective epoxidation using iodosylbenzene as the oxygen source. The reaction hardly occurs at all in the presence of iron porphyrin complexes lacking the cyclodextrin cavity.

Studies on a water soluble iron(III) porphyrin compound, [mesotetrakis(sulfonatomesityl)porphyrinato]iron(III) ([Fe(tmps)], **12.33**) with a variety of oxidants such as *m*-chloroperoxybenzoic acid, iodosylbenzene (PhIO) and $H_2O_2$ using stopped-flow UV-Vis spectroscopy has revealed the dependence of the reaction on pH and on the nature of the oxidation product on the axial ligands. The oxidation product changed from the two electron oxidised oxo–iron(IV)–porphyrin π-cation radical [$Fe^{IV}$(tmps$^{\bullet+}$)(O)] at pH below 5.5 to the one electron oxidised oxo–iron(IV)–porphyrin [$Fe^{IV}$(tmps)(O)] at pH above 7.5. A mixture of both species is produced in the intermediate pH range. The reactivity pattern of the compound correlates with the pH dependence in the electrode potentials of the Fe(III)/Fe(IV) couples and porphyrin oxidation. Using literature data a correlation can be built up for a range of porphyrins (P) with the ability of the axial ligand (X) to stabilise the Fe(IV) form. These model compounds of type [$Fe^{III}$(P)(X)]/ROOH are thus efficient catalysts for the hydroxylation and epoxidation of organic substrates, as long as the two-electron (enzyme-mimetic) oxygenations by [$Fe^{IV}$(P$^{\bullet+}$)(O)(X)] is favoured by careful selection of the of reaction pH and choice of X such that the standard oxidation potential ($E^o$) for the Fe(IV)/Fe(III) couple is close to or slightly greater than $E^o$ for the porphyrin couple P$^{\bullet+}$/P. Under these conditions, heterolytic O=O bond cleavage in the iron-porphyrin-bound peroxide is favoured and [$Fe^{IV}$ (P$^{\bullet+}$)(O)(X)] is the thermodynamically stable oxidised form of [$Fe^{III}$(P)(X)].[18]

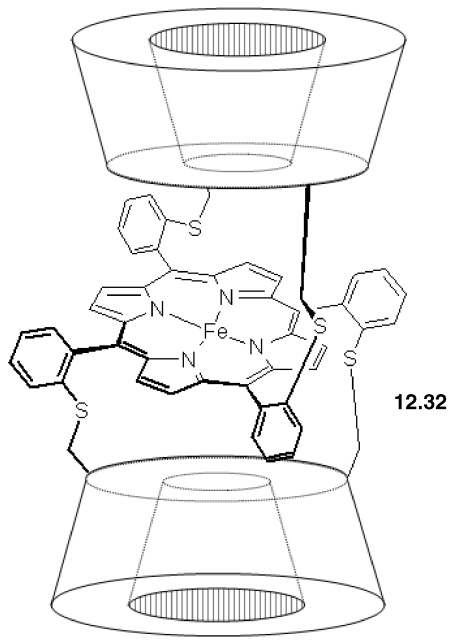


**12.32**

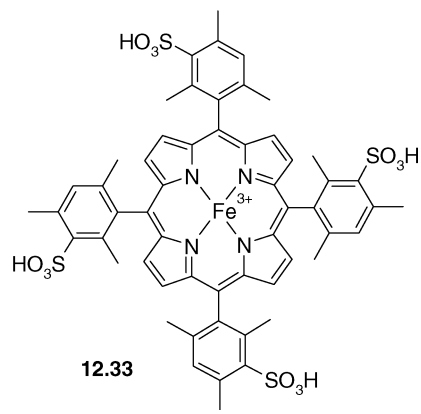


**12.33**

Clearly, while porphyrin complexes are obvious candidates for modelling these kinds of biomimetic oxidations, a range of non-heme iron complexes based on macrocyclic and podand ligand have also proved to be successful structural and functional mimics.[19] To take one example, Figure 12.13 shows the X-ray structure of the iron (IV) tetramethylcyclam (tmc) oxo complex [$Fe^{IV}$(tmc)(O)(MeCN)]$^{2+}$

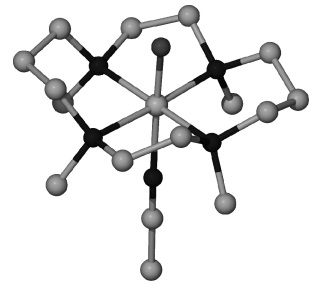

**Figure 12.13** X-ray structure of $[Fe^{IV}(tmc)(O)(MeCN)]^{2+}$ (**12.34**), an oxidation structural model with a low spin Fe(IV) centre and Fe=O 1.646 Å.[20]

(**12.34**) generated by PhIO oxidation of an Fe(II) precursor.[20] This is one of a range of such structural models for these kinds of iron oxidation products.

## 12.6.3 Cytochrome c Oxidase Models

Collman, J. P., Devaraj, N. K., Decreau, R. A., *et al.*, 'A cytochrome c oxidase model catalyzes oxygen to water reduction under rate-limiting electron flux', *Science* 2007, **315**, 1565–1568.

Another crucial heme-based oxidation enzyme is cytochrome c oxidase which catalyses the four-electron reduction of $O_2$ to $H_2O$ during the final stages of respiration. The natural enzyme also contains a copper centre positioned near the heme at the active site. It is vital that highly toxic, partially reduced oxygen species such as the hydroxide radical are not released during this process. The way in which this is accomplished is still a mystery, however, since it is difficult to study the enzyme under conditions where the electron flow is limited (as in the natural system) and hence the reaction stops at these partially reduced species. In 2007, however, a model system was developed by James Collman's group at Stanford (USA) that does just that. Their model system (**12.35**) includes three redox sites – an iron heme unit similar to myoglobin, a copper centre situated some 5 Å above the heme, and a phenolic group that mimics a tyrosine residue in the natural system. The electron flow is controlled by fastening the system onto a gold electrode coated with a self-assembled monolayer. By protecting each of the redox sites in turn Collman's group showed that all three redox centres are necessary to carry out the four-electron reduction and prevent the release of partially reduced products.

A related model also possessing all three redox groups was prepared by Naruta's group in Kyushu, Japan in 2005.[21] These workers showed using spectroscopic data the transformation of a heme–μ-peroxo–Cu(II) intermediate into a heme–superoxo–Cu(I) species during the oxidation process. The researchers proposed a process involving initial binding of the copper ion to $O_2$ before the formation of the peroxo species. The model study implies that during $O_2$ the copper centre is involved in stabilising the heme–superoxide intermediate as well as playing a redox role. They also proposed that the phenolic hydroxy group plays the major role in the generation of the superoxide. The model implies that after one-electron reduction of the oxyheme unit in the natural enzyme under physiological conditions a heme–hydroperoxy unit could be involved in O=O bond breaking rather than a rather than a heme–peroxo–Cu complex.

Very sophisticated model compounds such as the examples detailed here shed tremendous light on these complex natural enzymes because they allow chemists to control and understand the systems in detail. However, the difficulty in constructing these models cannot be overstated – Collman's compound takes 32 convergent synthetic steps to prepare!

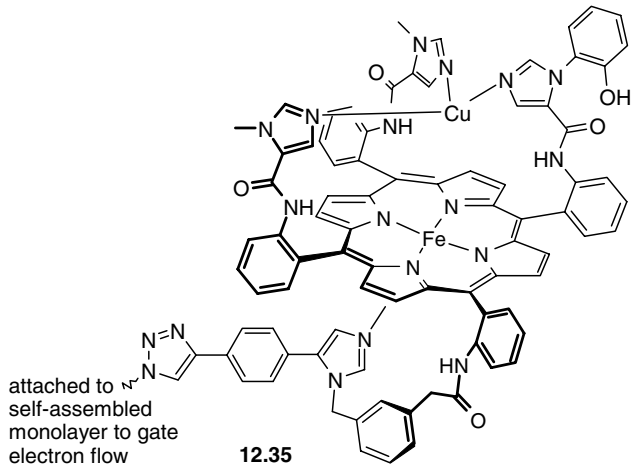


**12.35**

## 12.7 Vitamin $B_{12}$ Models

Toraya, T., 'Enzymatic radical catalysis: Coenzyme B-12-dependent diol dehydratase', *Chemical Record* 2002, **2**, 352–366.

Vitamin $B_{12}$ and its active form coenzyme, $B_{12}$ (5′-deoxyadenosylcobalamin), are tetrapyrrole-based cobalt-containing macrocyclic complexes containing the 15-membered corrin ring. They act in concert with an apoenzyme (a large protein that binds simultaneously the $B_{12}$ cofactor and the substrate in order to carry out a variety of mutase enzymatic transformations, generally involving radical-based 1,2-shifts (Section 2.6.4)). Much of the interest around $B_{12}$ model systems has concerned the role played by the large apoenzyme in directing the course of the radical reactions, which can often be difficult to control. The first coenzyme $B_{12}$ mimic was prepared by Flohr *et al*. in 1976,[22] who synthesised various cobaloximes linked by an intramolecular hydrogen bond and a long diester bridge designed to mimic the stereochemical conditions imposed by the apoenzyme within one of the most important coenzyme $B_{12}$-dependent systems, methylmalonyl-CoA mutase. As hoped for, a rearrangement reaction occurs as in the natural enzyme in an excellent yield of 82 % (Scheme 12.17). This excellent stereochemical control is highly reminiscent of the role played by the protein apoenzyme within the system.

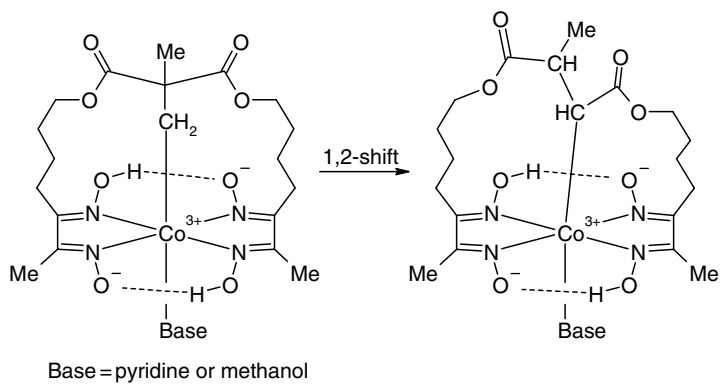


**Scheme 12.17** An early model for the role of the apoenzyme in coenzyme $B_{12}$-dependent mutase activity.[22]

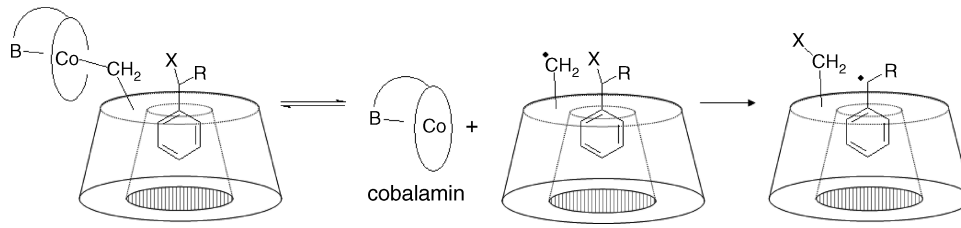


**Scheme 12.18** Simultaneous binding of a cobalamin coenzyme and a substrate by $\beta$-cyclodextrin.

Later work by Breslow *et al*. showed mimicry of the simultaneous binding of a cobalamin and a substrate within a $\beta$-cyclodextrin cavity, which served the purpose of the apoenzyme.[23] The cyclodextrin-bound substrate undergoes a selective, radical-induced transfer of a substituent group (X) to the cyclodextrin. Even though the system does not complete the reaction by transferring the migrating group back to a different site of the substrate, the key reaction step is clear (Scheme 12.18). Coenzyme $B_{12}$ has proved a popular target for enzyme modelling, and a number of very ingenious systems have been devised (*e.g.* based on octopus cyclophanes), including some incorporating vesicle-based model membranes.[24] In recent years there has been interesting results showing that different coenzyme $B_{12}$ dependent enzymes manipulate their axial ligands different ways. One model study designed to investigate the effect of axial ligation was reported in 2004 by Brown *et al*.[25] The advantage of coenzyme $B_{12}$ is that it is already a relatively small molecule and thus Brown's group were able to compare a naturally occurring system which has a bulky 5,6-dimethylbenzimidazole base ligating the cobalt (Figure 2.23), with a less sterically hindered imidazole analogue. They concluded that the steric bulk of the axial ligand in fact has very little influence on the coenzyme reactivity.

## 12.8 Ion Channel Mimics

Gokel, G. W. and Carasel, I. A., 'Biologically active, synthetic ion transporters', *Chem. Soc. Rev.* 2007, **36**, 378–389.

The movement of simple ion such as $K^+$ and $Cl^-$ through biological ion channels is a process that is vital to a range of biochemical processes including the preservation of trans-membrane ionic balance and electrical potential, and in signalling and triggering processes as described in Section 2.2 Indeed a great deal of early interest in supramolecular chemistry stemmed from the ability of artificial cation hosts such as the crown ethers to mimic the ion transport ability of small molecule ionophores such as valinomycin and nonactin. Ionophore-mediated ion transport involves small molecules, however, and it is a much greater challenge to mimic the ion transport ability of transmembrane ion channels of the type described in Section 2.2 which have relative molecular masses often of several hundred thousand Daltons. Model system have the potential, however, to address key questions in ion channel structure and function, particularly how the systems exhibit ion flow rectification (the one-way flow of ions) and how the ions are bound or solvated as they pass through the channel. One of the earliest models for true ion channels was the antibiotic gramicidin (Section 10.8.8) which forms a helical structure suitable to pass alkali metal cations through it. The helix is only half of the *ca.* 5 nm length of the phospholipid cell membrane, but it can dimerise in order to span the distance. Among successful examples of entirely artificial ion channels is the crown-ether based 'hydraphile' family, exemplified by the general structure

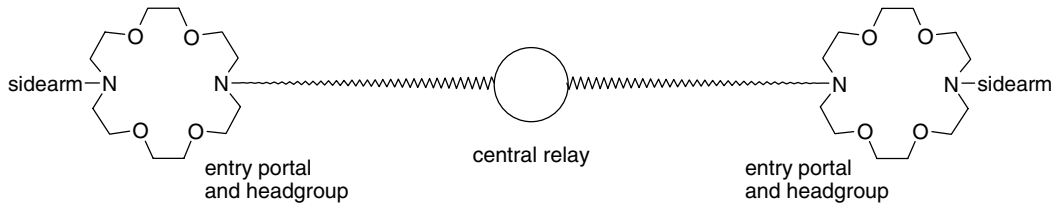


**Figure 12.14** Schematic diagram of the 'hydraphile' family of ion channel mimics.

shown in Figure 12.14. The target length of the hydraphiles is *ca*. 3–3.5 nm, the typical width of the insulator region of a phospholipid bilayer membrane. The crown ethers play the role of ion-binding and concentrating head groups while the 'central relay' is both an organising scaffold and a polar moiety stabilising ions in the least polar central region of the bilayer membrane. The first hydraphiles used an addition diaza[18]crown-6 group as the central relay with $-(CH_2)_{12}-$ spacer chains. Appending fluorescent side-arms allows the conformation of the hydraphile within the bilayer membrane to be deduced. The fluorescence data shows that the side arms experience a relatively polar environment and are buried at the base of the phospholipid groups, separated by the expected 3 nm, Figure 12.15. Related hydraphiles have used both cone and 1,3-alternate calix[4]arenes as central relays while retaining the crown ether entry portals. While the 1,3-alternate calixarene compound also proved effective as an ion channel mimic, the cone compound has all four crown ether groups on one side of the central relay and therefore cannot span the membrane. This expectation was confirmed using plane bilayer conductance data with the cone compound being inactive while the 1,3-alternate isomer showed 'bursting' behaviour with sudden bursts of ion conductance as channels open up.

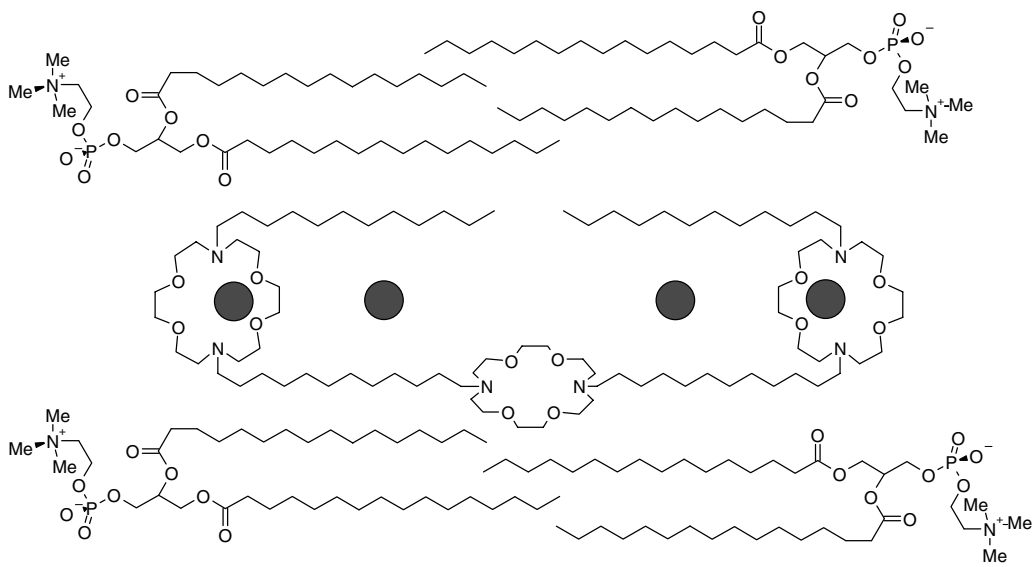

**Figure 12.15** Conformation adopted by the hydraphiles based on dizaz[18]crown-6 within a bilayer membrane such as phosphatidyl choline deduced from experimental evidence (circles represent alkali metal cations).

The efficacy of ion channel mimics is often assessed using an electrophysiology technique termed the single cell patch clamp method. In this technique the current passing across the bilayer membrane of a cell (*e.g.* from hamster brain) through a single ion channel is monitored. The technique traditionally uses a glass pipette with a *ca.* 1 μm diameter open tip which forms a smooth contact with the surface of the cell. The pipette is filled with an electrolyte solution and current monitored by a metal electrode immersed in the solution which transmits a reading to an amplifier. The seal between the pipette and the cell membrane needs to be very tight and is referred to as a *gigaohm seal* since its resistance is at least a gigaohm. The patch clamp recording uses a single electrode to voltage clamp a cell and so the voltage is held constant while changes in current are monitored. A variation is the planar patch clamp method. Instead of positioning a pipette on a cell, a cell suspension or purified phospholipid is pipetted onto a chip or teflon disk containing a microstructured aperture separating two chambers, one of which is filled with the ions under study. The phospholipids spontaneously fill the aperture with a self-assembled bilayer, effectively blocking any current flow from one side of the disk to the other. Addition of an ionophore or channel allows ions to flow between the two chambers. Using these kinds of technique small currents can be measured so sensitively that it is perfectly feasible to measure the open and closing of a single ion channel.

Another way to assess ion channel conductance is to use artificial phospholipid vesicles (liposomes) as cell models. These structures (described in more detail in the next chapter) are commonly used to transport vaccines, drugs, enzymes, or other substances to target cells or organs. The vesicles, which are several hundred nanometres in diameter, do not suffer from interference from residual natural ion channel peptides or ionophores, unlike purified natural cells. A liposome model was used to test the ion transport behaviour of the redox-active hydraphile **12.36**. The compound transports $Na^+$ and the process can also be monitored using $^{23}Na$ NMR spectroscopy.[26] The presence of the ferrocene-derived group in the central relay allows the ion transport to be redox-controlled – oxidation to ferrocinium completely prevents $Na^+$ transport for electrostatic reasons. Some representative data from a planar bilayer measurement is shown for hydraphile **12.36** in Figure 12.16.

Another type of effective ion channel model, this time for anions, are the synthetic heptapeptides **12.37** which form pores that promote chloride efflux in vesicle models. Transmembrane chloride transport is another goal of particular importance because of its role in the genetic disease cystic fibrosis. Cystic fibrosis is the most common lethal genetic defect in Caucasian populations. It arises through mutations in the cystic fibrosis transmembrane conductance regulator (CFTR) protein which acts both as a transmembrane chloride channel and as a regulator of other ion channels. The most common defect, accounting for some 75 % of mutant CFTR alleles, involves the ΔF508 mutation where three nucleotides are deleted from the gene causing the transcribed protein to lack phenylalanine

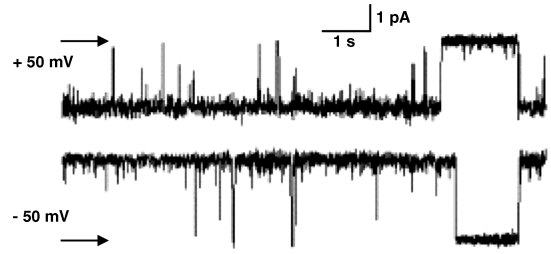


**Figure 12.16** Typical planar bilayer $Na^+$ conductance traces for 10 pmol **12.36** at +50 mV (top trace) and –50 mV (bottom trace) in aqueous buffer using symmetrical KCl conditions. The arrows at the left hand side of the traces indicates the current level of the *closed* state. Peaks indicate the opening of individual ion channels (reproduced by permission of The Royal Society of Chemistry).

at position 508 in its primary structure. This mutation, in common with many others, reduces the ability of affected cells, predominantly epithelial cells lining the lung and other mucosal surfaces, to transport chloride effectively with consequences for fluid transport. Defective fluid transport leads to an underhydration of secretion which obstructs organ passages and causes the widespread and serious organ malfunction associated with the disease

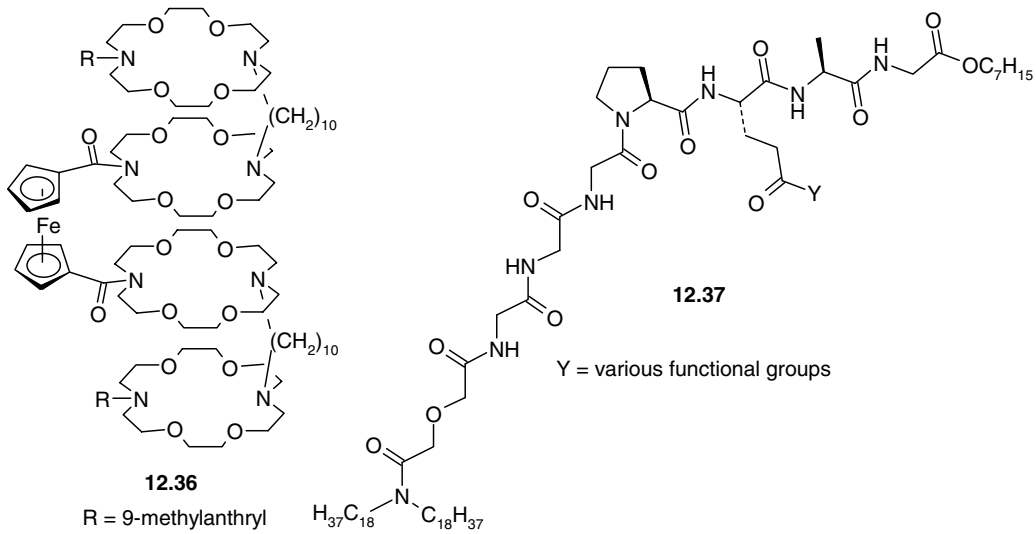


Work by Stefan Matile in Geneva, Switzerland, has resulted in a number of interesting $\beta$-barrel mimetic anion transporting pores such as **12.38** (Figure 12.17).[27] A $\beta$-barrel is a kind of natural protein that forms a rigid channel by self-assembly of peptides into a $\beta$-sheet type of secondary structure. The peptide backbone is mimicked by the rigid octaphenyl backbone which is *ca.* 3.4 nm long and hence spans

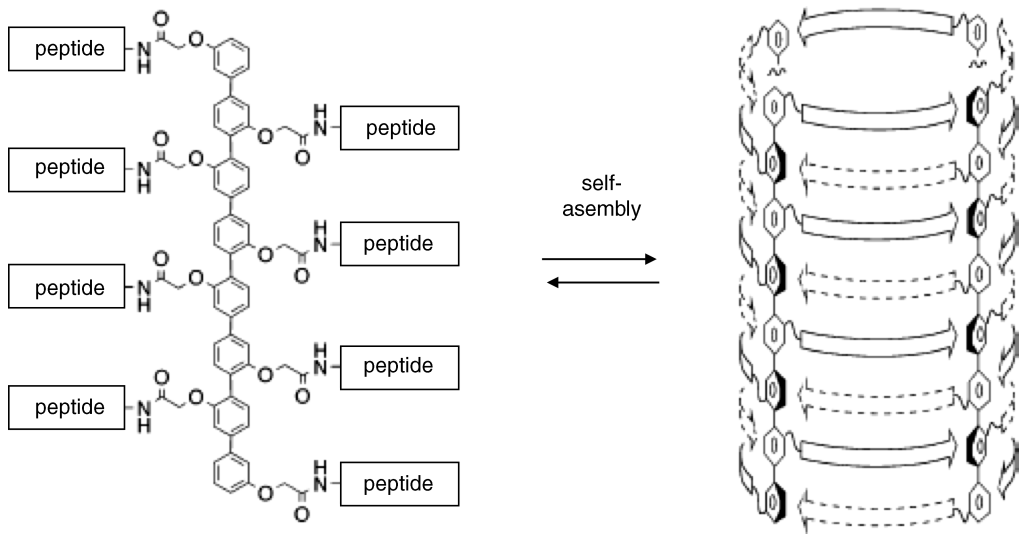


**Figure 12.17** Artificial $\beta$-barrel ion channels formed by self-assembly (reproduced with permission from [27] © 2005 American Chemical Society).

the hydrophobic region of the membrane. A wide range of groups can be appended onto the periphery of the artificial $\beta$-barrels and thus their ion transport ability can be tuned. Generally anionic functionality is suitable for transporting cations and vice versa. Voltage-gated chloride transport was achieved using the polar **12.38** which aligns in the membrane such that all of the sulfonyl groups are pointing in the same direction under the influence of an applied electric field. Reversing the field polarity closes the pores.

Overall the field of ion transport is perhaps one of the most active and interesting in biomimetic supramolecular chemistry and there is a myriad of diverse and interesting systems being produced. The field looks set to evolve rapidly over the next few years.

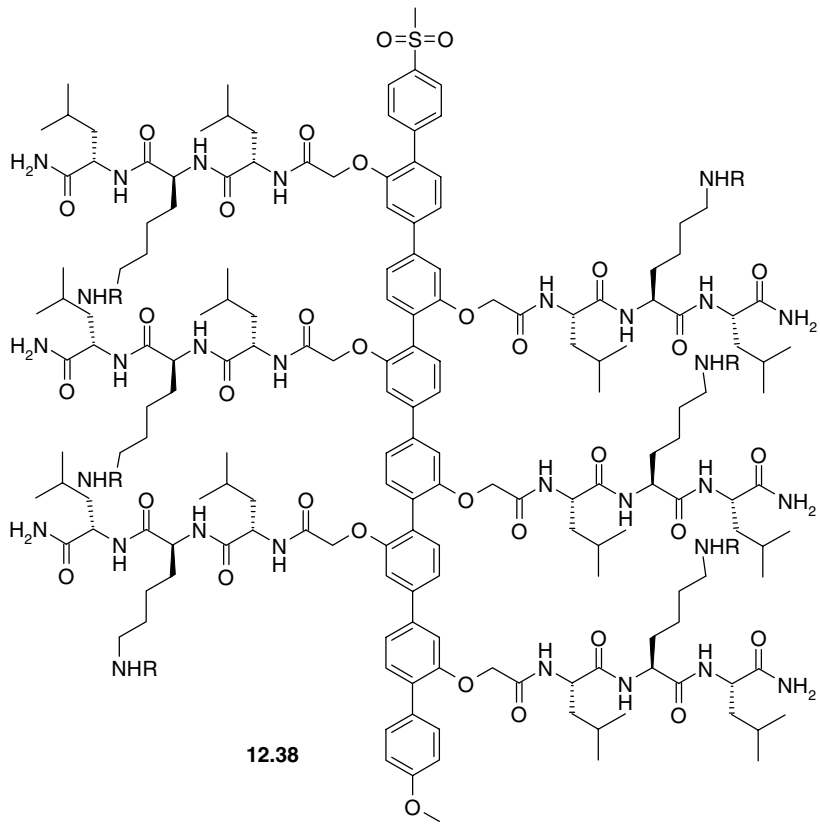

**12.38**

## 12.9 Supramolecular Catalysis

### 12.9.1 Abiotic Supramolecular Catalysis

Schreiner, P. R., 'Metal-free organocatalysis through explicit hydrogen bonding interactions', *Chem. Soc. Rev.* 2003, **32**, 289–296.

In addition to the mimicking of natural enzymes, a fascinating goal in supramolecular chemistry is the development of entirely artificial catalysts. While both heterogeneous and homogeneous catalysts based in particular on coordination of ligands to transition metals are common, supramolecular catalysts use either exclusively, or in addition, some aspect of molecular recognition and non-covalent

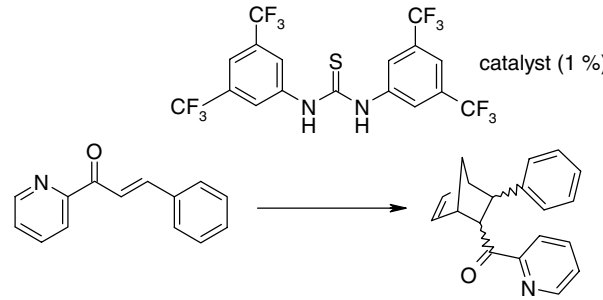


**Scheme 12.19** Organocatalysis with an activated thiourea derivative ($k_{cat}/k_{uncat}$ = 8 at 1 mole % in $CHCl_3$).

bond formation either to enhance the reaction rate or to guide the selectivity. We have seen examples of in-cavity catalysis in earlier sections, as in Rebek's softballs (Section 10.6.1) and Raymond's capsules that include catalytically active metal complexes (Scheme 10.6). Purely metal-free abiotic catalysis is part of the currently highly topical field of *organocatalysis*. This is a vast area and we will highlight examples here that are particularly supramolecular in nature showing how directional, multiple supramolecular interactions either by themselves, or as part of a controlled reaction environment, can bring about interesting, catalytic reactivity.

A simple example based on an activated diaryl thiourea is the catalysis of Diels-Alder reactions such as the example shown in Scheme 12.19. The strongly hydrogen bonding urea acts as a mild Lewis acid, activating the dienophile by hydrogen bonding to the carbonyl group in a classic $R_2^1(6)$ urea hydrogen bonded ring. A number of hydrogen bond donors such as amidinium and guanidinium salts will catalyse this reaction at around 1 mole % with rate enhancement factors of up to 1000-fold. Thioureas are particularly useful, however, because they are easy to prepare from thiophosgene which is relatively easy to handle compared to the oxygen analogue. They are neutral so have a wide range of solubility in non-polar media and the thiocarbonyl group is a relatively poor hydrogen bond acceptor. Moreover, the system exhibits relatively little product inhibition because the affinity for the starting material carbonyl is stronger than the product.

Looking more at host-guest type systems, the cucurbiturils are often very efficient catalysts in cases where they simultaneously bind two guests, thus increasing effective concentration and changing a bimolecular reaction into a *quasi*-unimolecular one. To take one recent example, cucurbit[6]uril (Section 6.2.4) proves to be a very efficient catalyst for the 'click' 1,3-dipolar cycloaddition reaction of an azide with an alkyne, particularly where the substrates are suitable guests for the cavity, as in Scheme 12.20. Cucurbituril binds very effectively to ammonium ions and addition of a small amount

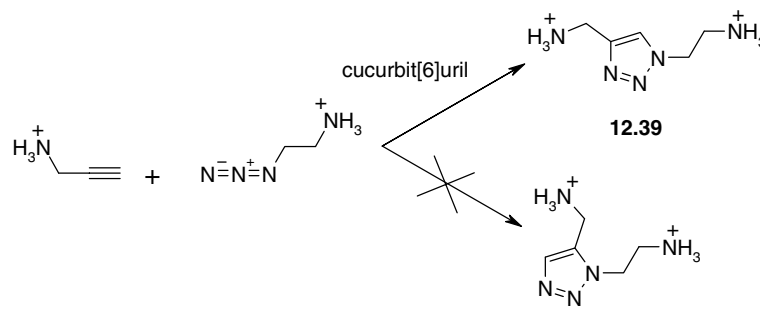


**Scheme 12.20** Over $10^4$ fold rate acceleration of the 'click' reaction by cucurbit[6]uril.[28]

of cucurbit[6]uril to the reaction shown in Scheme 12.20 results in a remarkable 5.5 x $10^4$ fold enhancement in rate and complete regioselectivity; compound **12.39** is the only product! The extremely high efficiency is attributed to the overcoming of entropic constraints and strain activation of the bound substrates.[28]

Supramolecular catalysis may also involve the combination of a host cavity and a metal active site as in the bis(diphenylphosphino)calix[4]arene nickel(II) complex **12.40** which acts as an efficient catalyst for ethylene and propylene polymerisation, and in tandem with zirconocene dichloride, for the formation of linear low-density polyethylene. In the latter case the complex gives very little branching – a significant advantage. The key to the effectiveness of the catalyst involves calixarene-induced changes in the bite angle at the Ni(II) centre, which is square planar in the active form of the catalyst.[29]

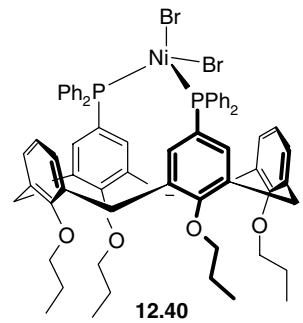


**12.40**

An early example of how 'designer' supramolecular catalysis might be achieved (with systems much smaller than natural enzymes) is shown in Scheme 12.21.[30] The symmetrical catalyst (termed a 'bisubstrate reaction template') is able to bind simultaneously both reactants in order to form a ternary (three-component) complex *via* multiple hydrogen bonds. In the ternary complex, the two reactants are brought into close proximity, resulting in a six-fold acceleration of the nucleophilic attack of the primary amine group on the bromoalkane substituent. While simple and ingenious, this first-generation system suffers from a number of drawbacks that must be considered in catalyst design. Firstly, the binary product complex is almost certainly more stable than the crucial ternary complex, thus immediately poisoning or inhibiting the catalysis. This is ameliorated to some extent by the precipitation of the product as the hydrobromide salt, otherwise hardly any catalysis would be observed. In addition, the identical nature of the two substrate binding sites means that many ternary complexes that do not give rise to the desired reaction may be formed, *e.g.* between the catalyst and two molecules of the same substrate. This problem has been addressed by the preparation of an unsymmetrical second-generation system, which favours the recognition of the correct substrate pair, resulting in a 12-fold rate enhancement.

Bob Crabtree (Yale, USA) has identified a number of different approaches[31] to modifying the selectivity in catalysis that have some claim to being supramolecular, Figure 12.18. These range from simple inclusion and encapsulation (as in catalysis by self-assembled capsules such as Rebek's soft balls, Section 10.6.1) all of which use essentially repulsive steric interactions to shape the binding pocket and hence catalyst selectivity (Figure 12.18a–c) to a full molecular recognition strategy (Figure 12.18e) of the type described in Scheme 12.21 that uses attractive supramolecular interactions to align the substrate precisely with the catalyst active site (*e.g.* metal centre). Alternatively the 'chelate control' strategy (Figure 12.18d) allows chemical reaction adjacent to a pre-existing binding site. Even the full molecular recognition strategy suffers from a number of potential problems if the design and selectivity is not

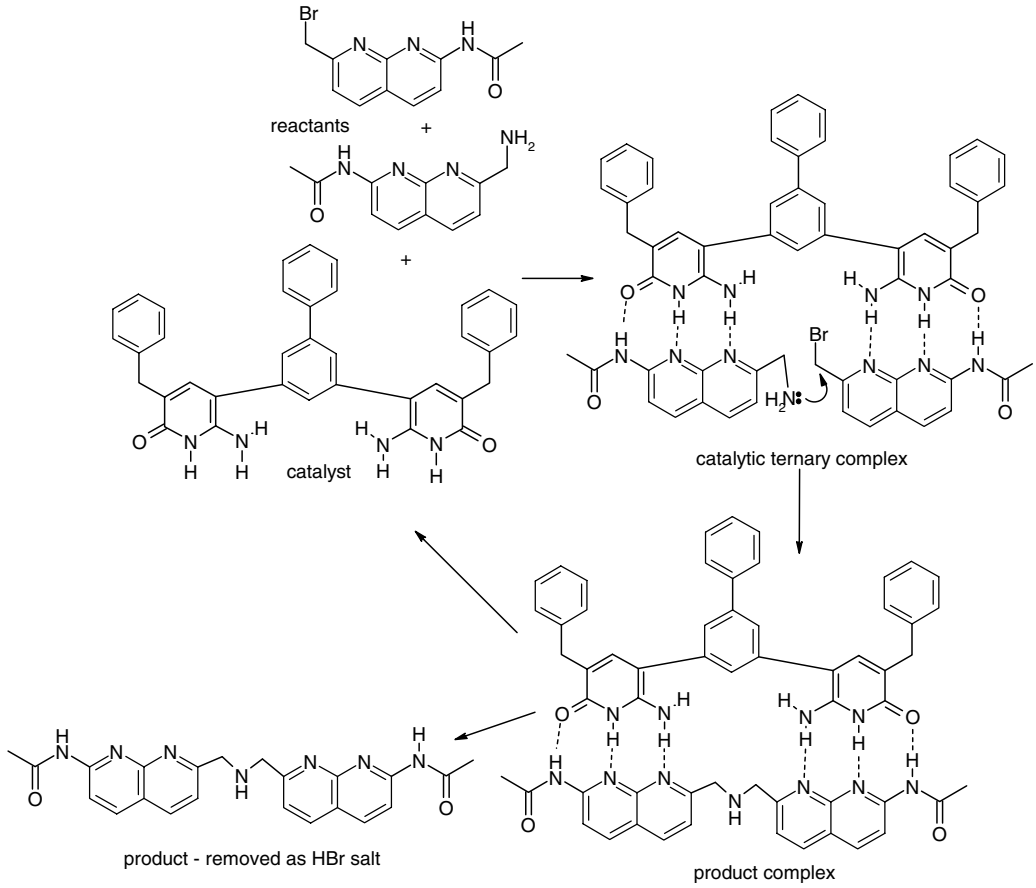


**Scheme 12.21** Self-assembling catalysis *via* a ternary complex involving a bisubstrate reaction template.[30]

perfect; these are illustrated schematically in Figure 12.19. However, using such a molecular recognition strategy, Crabtree's group were able to design (and thoroughly study with appropriate controls lacking molecular recognition functionality) a remarkable C–H bond hydroxylation catalyst. The compound oxidises substrates such as ibuprofen with over 98 % selectivity, Figure 12.20.

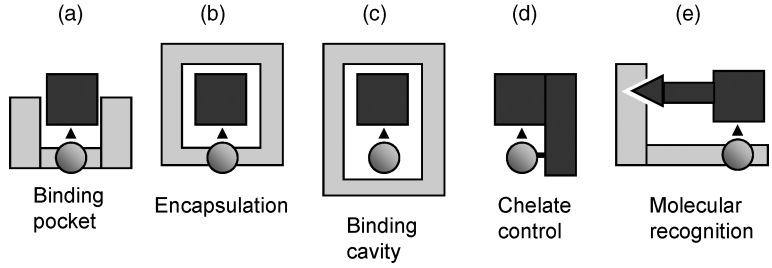


**Figure 12.18** Strategies for modifying selectivity in catalysis – the sphere represents the catalyst active site (*e.g.* metal centre).[31]

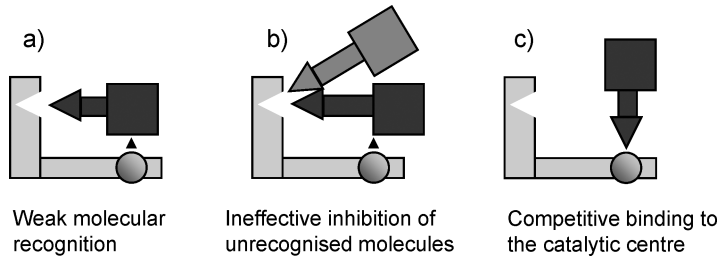


**Figure 12.19** Potential problems with a molecular recognition strategy for supramolecular catalysis.[31]

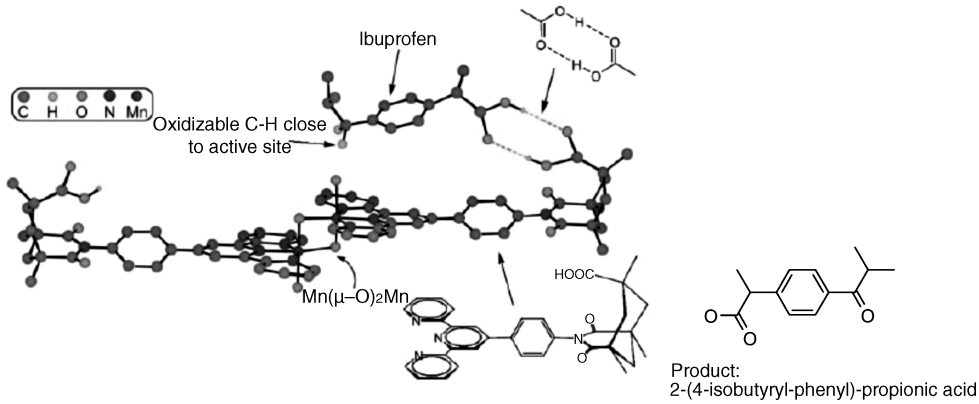


**Figure 12.20** A designer C–H oxidation catalyst the positions the reactive CH-bond over the catalyst active site using molecular recognition. The ibuprofen substrate is oxidised to the 2-(4-Isobutyryl-phenyl)-propionic acid product in > 98 % selectivity (reproduced by permission of The Royal Society of Chemistry).

## 12.9.2 Dynamic Combinatorial Libraries

Philp, D. and Greig, L. M., 'Applying biological principles to the assembly and selection of synthetic superstructures', *Chem. Soc. Rev.* 2001, **30**, 287–302.

In Section 3.9.1 we discussed the thermodynamic template effect – a synthetic method in macrocyclic chemistry whereby the metal ion selects out the ligand most complementary to it from an equilibrating mixture. Thermodynamically controlled reactions such as Schiff base formation are particularly important in this regard. Recently there has been increasing emphasis on this kind of phenomenon which, in general can be thought of as *dynamic combinatorial chemistry*. Combinatorial chemistry ('combichem') is an important field in drug discovery. It uses *irreversible* covalent bond formation and automated (robotic) synthesis methods to generate a library of many compounds (hundreds or thousands) that are then screened for activity against a particular protein target or disease model. In effect it is a 'shotgun approach' to drug discovery, but no less powerful for that. *Dynamic* combinatorial chemistry is the embodiment of the combinatorial philosophy in situations where the library of compounds is in dynamic equilibrium, *i.e.* are all mutually interconverting on a meaningful timescale. The library may include *virtual* compounds that are not present in measurable quantities under standard conditions but may become stabilised and therefore form in significant amount upon the addition of a suitable target, template or binding partner. Covalent post-modification can then fix the resulting stable product. Dynamic combinatorial chemistry can thus be used to discover a

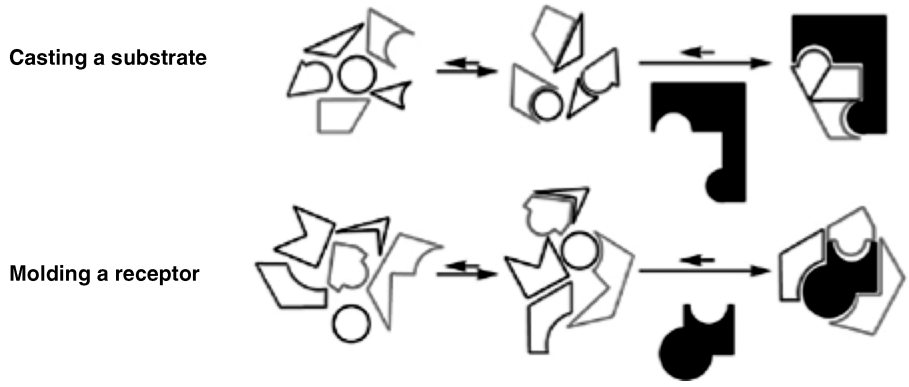


**Figure 12.21** The moulding and casting approaches to dynamical combinatorial chemistry (reproduced by permission of The Royal Society of Chemistry.)

particularly good receptor of a target substrate (the 'moulding' approach) or discover an effective substrate / blocking agent for a particular receptor (the 'casting' approach), Figure 12.21.

A practical application for the casting approach was demonstrated in 1997 by Lehn and Huc, who developed an inhibitor for carbonic anhydrase II (a zinc-based metalloenzyme responsible for the conversion of $CO_2$ to $HCO_3^-$ and $H^+$, *cf.* Section 11.3.2). The process is based on the Schiff base imine forming reaction of an aldehyde and an amine, a process which is reversible under physiological

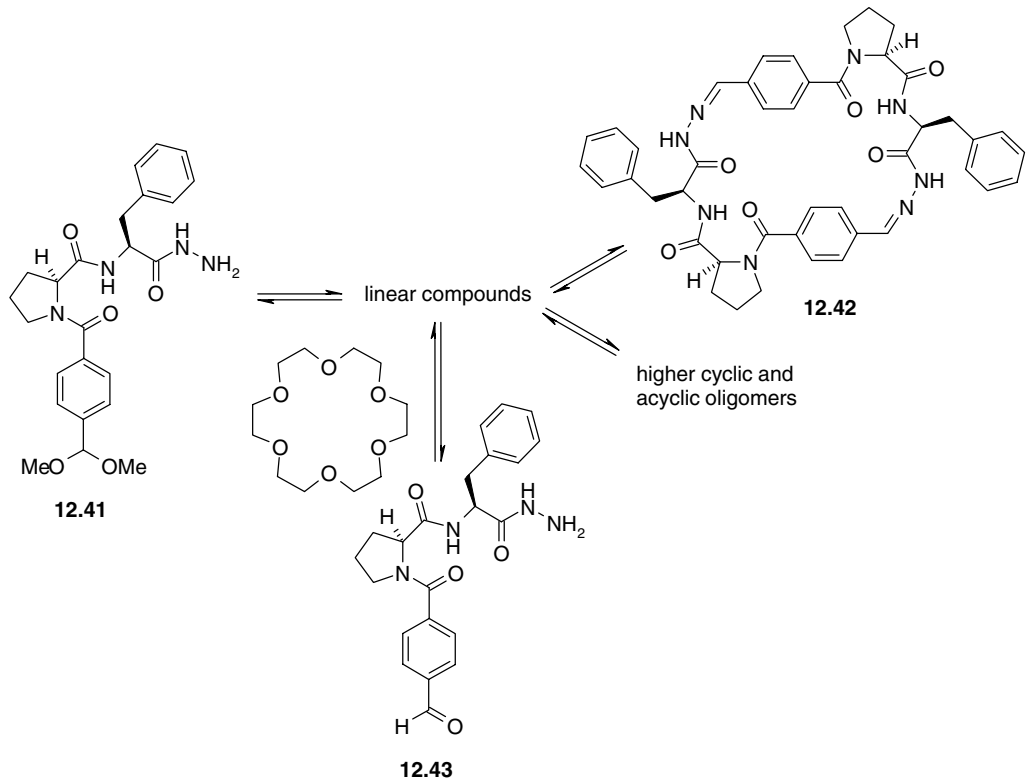


**Scheme 12.22** Amplification of the aldehyde **12.43** by [18]crown-6 within a pseudo-peptide hydrazone dynamic combinatorial library.[33]

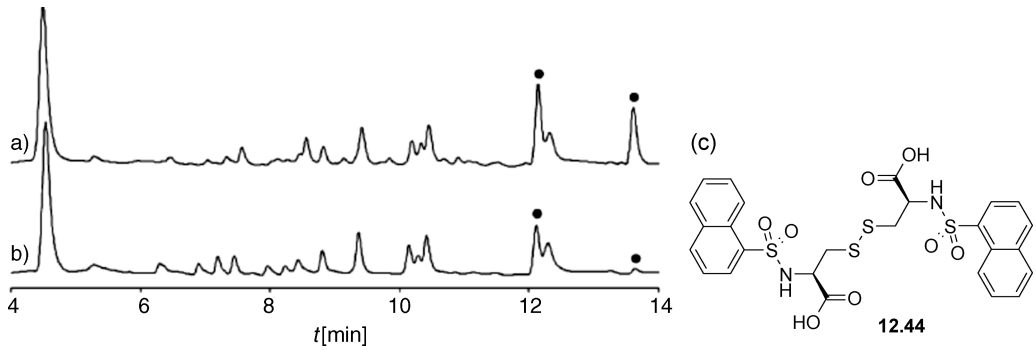


**Figure 12.22** HPLC trace of a disulfide dynamic combinatorial library (a) with and (b) without addition of calmodulin. Dots indicate the peaks enhanced by the protein (Copyright Wiley-VCH Verlag GmbH & Co. KGaA. Reproduced by permission) (c) the chemical structure of the amplified ligand.

conditions, but with a product that can be fixed by reduction to an amine with $NaBH_3CN$. In the absence of the enzyme the mixture produces 15 reduction products and 4 starting amines. However, addition of the enzyme biases the library in favour of the products that have the highest affinity for the carbonic anhydrase zinc(II) based active site.[32]

Work by Jeremy Sanders of the University of Cambridge, UK, has shown the power of the Dynamic Combinatorial approach to amplify the amount of trace products. For example with trifluoroacetic acid as a catalyst the acetal **12.41** gives a pseudo-peptide hydrazone dynamic combinatorial library comprising at least ten cyclic oligomers such as **12.42** that must interconvert *via* at least ten undetected linear components. Addition of [18]crown-6, however, results in the strong stabilisation of the aldehyde **12.43** which cannot be detected otherwise (Scheme 12.22). The amounts of the higher molecular weight macrocycles is significantly diminished.[33]

More recent work by Chris Hunter (Sheffield, UK) has used disulfide bond formation *via* dynamic combinatorial chemistry to generate effective ligands (inhibitors) for the calcium binding and triggering protein calmodulin. Calmodulin has two independently mobile domains and individually the thiol components have low affinity for the target. However a disulfide can potentially bind to both domains giving cooperative enhancement to the binding. Addition of calmodulin to a dynamic combinatorial library of some 15 disulfides significantly amplifies the formation of one particular bifunctional disulfide ligand (compound **12.44**, Figure 12.22) which proves to have a binding constant for the protein *ca.* two orders of magnitude higher than that of the corresponding monofunctional thiol.[34] Control experiments with apocalmodulin (*i.e.* calmodulin without bound $Ca^{2+}$) do not result in enhancement of any particular library member, confirming that specific recognition is taking place.

## 12.9.3 Self-Replicating Systems

Kassianidis, E. and Philp, D., 'Design and implementation of a highly selective minimal self-replicating system', *Angew. Chem., Int. Ed.* 2006, **45**, 6344–6348.

In the system shown in Scheme 12.21, the catalyst is essentially unrelated to the substrate and product molecules. This is analogous to biological enzymatic catalysis. However, if the catalyst is itself the reaction product, then the system becomes *self-replicating*, *i.e.* a synthetic analogue of DNA (although technically DNA does not directly self-replicate – it templates the formation of a complementary strand; you can think of the DNA double helix as self-replicating, but even then only as part of a biological system aided by enzymes). If artificial self-replicating systems can be produced, then chemists will be

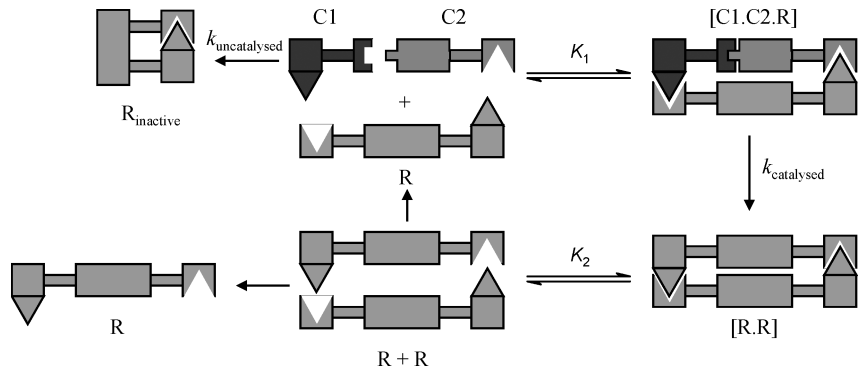


**Scheme 12.23** Minimal self-replication model. The synthesis of replicator R is accelerated by the binding of components C1 and C2 to form a ternary complex [C1·C2·R].

closer to obtaining a clearer understanding of the origins of life itself since the ability to self replicate (along with the ability to undergo Darwinian evolution) is a basic criterion for life.

A minimal model for self-replication is shown in Scheme 12.23. The replicator (R) must be able to recognise and bind at least two different precursor components (C1 and C2) in a ternary (three component) complex, and to accelerate their chemical reaction with each other to produce a product that is a copy of the original R. Such a simple system will always be in competition with the uncatalysed binary reaction of C1 and C2.

A minimal self-replicating systems along the lines illustrated in Scheme 12.23 has been prepared from a Schiff base condensation of aldehyde **12.45** with primary amine **12.46**. The reaction is catalysed by its own product (**12.47**) *via* the ternary complex [**12.45**·**12.46**·**12.47**]. The most noteworthy feature of this system is that kinetic data suggest that the ternary complex [**12.45**·**12.46**·**12.47**] is more stable than the product dimer [**12.47**]$_2$. This factor means that once a single catalyst turnover has been achieved, then the new product is displaced spontaneously from its templating partner by two new reactant molecules, suggesting that exponential autocatalysis may be possible in this system. Such an observation is contrary to expectation on entropic grounds, and must be an enthalpic effect, perhaps arising from the relative strength of the salt bridges.[35]

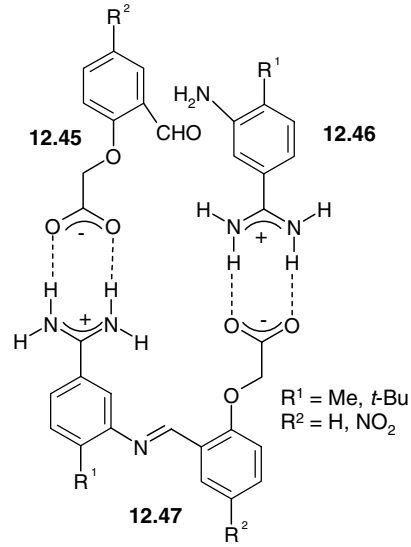

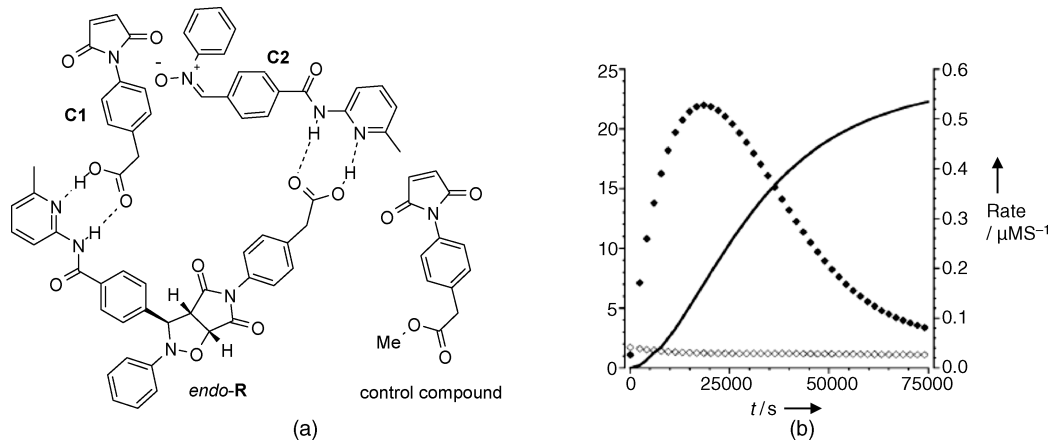


**Figure 12.23** (a) The ternary complex of type [C1·C2·R] designed by Philp and co-workers base on computational investigation of the transition state geometry.[36] (b) Variation of reaction rate for the formation of endo-R (♦, right axis) with time. The formation of the endo diastereoisomer in the control reaction between C2 and the control ester is shown for comparison (◊, right axis). Experimental concentration–time data for endo-R (solid line, left axis, mM) is also shown for comparison (Copyright Wiley-VCH Verlag GmbH & Co. KGaA. Reproduced by permission).

The three key features for the success of a minimal self-replicating model are (1) minimisation of product inhibition arising from a stable [R·R] complex (2) the suppression of the reaction through C1·C2 to form any catalytically inactive (intramolecular self-complementary) isomer of R ($R_{inactive}$) and (3) a high catalytic efficiency within the key ternary complex [C1·C2·R]. Work by Doug Philp (St. Andrews, Scotland) has focussed on a computational approach to the product inhibition problem.[36] Using DFT calculations Philp and co-workers designed the ternary complex shown in Figure 12.23a. The calculations showed that while the *exo* isomer is inactive the *endo* isomer of the replicator has an open structure that should be capable of forming *via* a Diels-Alder reaction from a [C1·C2·R] type ternary complex, while the geometry is unsuitable for a bimolecular reaction *via* [C1·C2]. The calculated structure was prepared experimentally and indeed proves to be an efficient self-replicator exhibiting a sigmoidal growth in the concentration of the *endo* product (Figure 12.23b). This kind of sigmoidal behaviour is characteristic of autocatalysis. The kinetic profile for the ester control compound analogue of C1 that can undergo Diels-Alder reaction but not take part in the ternary complex formation shows no such autocatalysis.

A more sophisticated (although controversial) self-replicating system has been designed by Rebek.[37] The autocatalytic assembly is based on the Kemp's triacid derivative **12.48**, which has its substituents locked axially. Interaction of **12.48** with amine **12.49** gives a self-assembled binary complex **12.50**, in which the amine lone pair is ideally situated to attack the pentafluorophenyl ester substituent on **12.48**. Complex **12.50** is held together by an ingenious combination of a complementary hydrogen bond pair and highly organising face-to-face π–π stacking interactions between the electron-rich naphthalene derivative and the electron-poor heterocyclic ring system in **12.49**. Nucleophilic displacement of the $C_6F_5O$ substituent within the binary complex **12.50** gives the *cis*-amide **12.51**. The key to the initiation of the autocatalytic system comes in the instability of the *cis*-amide linkage, which isomerises rapidly to the more stable *trans* form. This process opens up the product to reveal two new binding sites (A and B), capable of interacting with two new molecules of **12.48** (site A) and **12.49** (site B). In effect, the product, *trans*-**12.51**, is capable of forming a ternary complex **12.52** as seen in the previous catalytic and autocatalytic systems, which brings about the organisation of the two precursors to itself. Reaction of the bound **12.48** and **12.49** generates a further molecule of *trans*-**12.51**, resulting in self-replication. Unfortunately, the resulting (*trans*-**12.51**)$_2$ dimer is self-complementary with an association constant

of 80 000 $M^{-1}$, and so further catalysis is inhibited as a consequence of the need for this product binary complex to break up so that each product molecule may go on to produce two new ternary complexes. At 25 % completion, this means that the equilibrium concentration of **12.52** is only 3 %. Despite this problem, its presence increases the rate of product formation two-fold. Moreover, the catalysis exhibits a sigmoidal rate profile characteristic of a self-replicating pathway. These kinetic measurements suggest that, while the autocatalysis is not dramatic, it is the dominant pathway.[38]

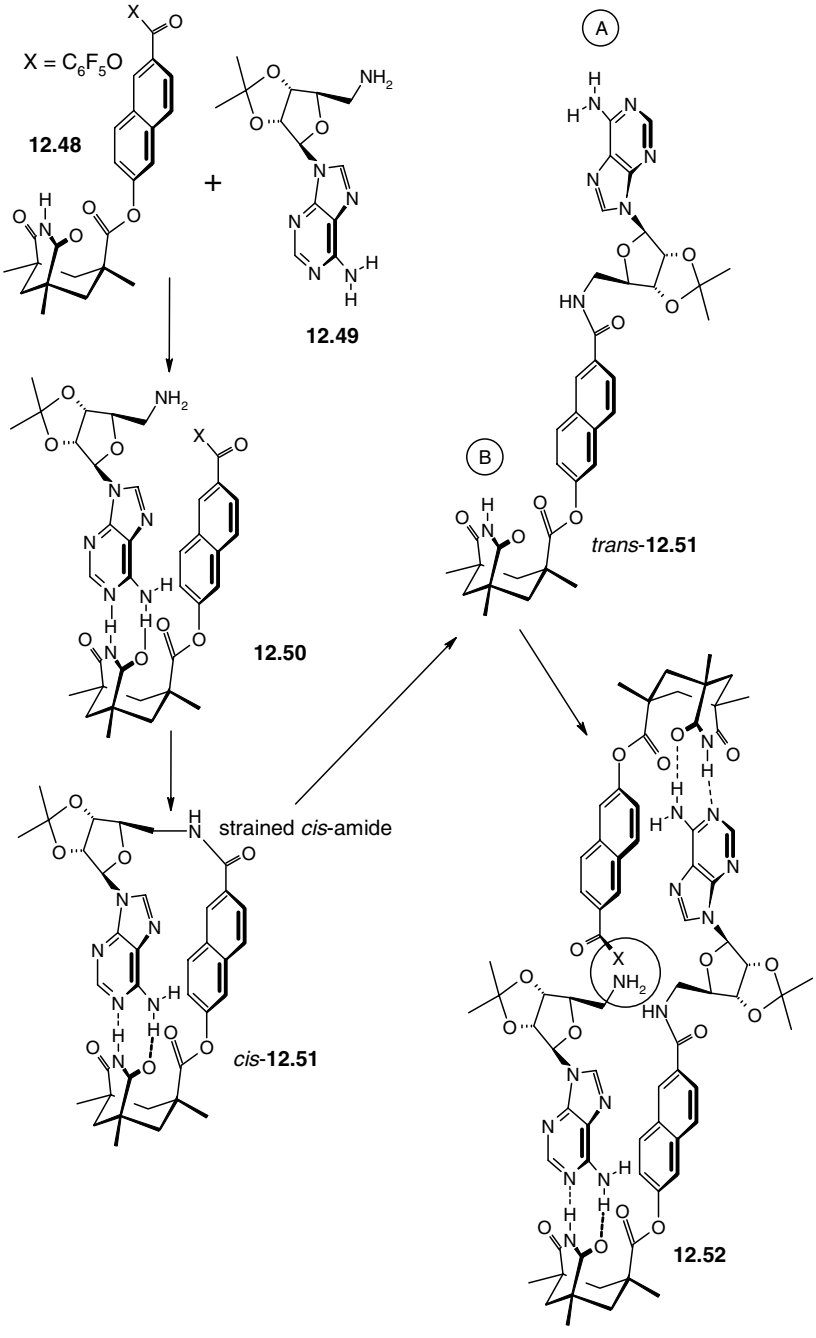

The self-poisoning exhibited by Rebek's self-replicating system is a ubiquitous problem in attempts to make self-replicating molecules; however in 2002 work by Gerald Joyce at Scripps (California, USA) resulted in the isolation of a self-replicating ligase ribozyme (*i.e.* an RNA molecule that catalyses a chemical reaction, from **ribo**nucleic acid en**zyme**) that exhibits efficient catalytic turnover, to some extent overcoming the self-poisoning problem.[39] The R3C ligase ribozyme is a catalytic form of RNA that catalyzes the formation of a 3′,5′-phosphodiester linkage between two RNA molecules. Joyce's group redesigned the ribozyme so that it would bind to two substrates to generate an exact copy of itself. The copy could then go on to catalyse the production of further copies. The system exhibits a linear dependence between the initial rate of formation of new copies and the starting concentration of ribozyme which is consistent with exponential growth in ribozyme concentration and hence autocatalysis.

## 12.9.4 Emergence of Life

Thordarson, P., 'Emergence of Life', in *Encyclopedia of Supramolecular Chemistry*, Atwood, J. L. and Steed, J. W. (eds), Dekker: New York, 2004, vol. 1, *pp.* 528–533.

The current NASA definition of a living system states that 'Life is a self-sustained chemical system capable of undergoing Darwinian evolution.' There is thus more to life than the simple self-replication outlined in the previous section. Living systems do not just self-replicate, they evolve. Clearly while chemists have been moderately successful in developing self-replicating systems it is a further challenge to develop chemical models for living systems that might just help us understand the fundamental questions that surround the prebiotic origins of life. The sorts of approaches that might be adopted may combine aspects of chemical self-replicators and dynamic combinatorial chemistry of the kind outlined in Section 12.9.2. This fusion has been nicely summed up by Joyce whose work we looked at above:

> *Reconciling self-replication and Darwinian evolution requires either bringing the fundamental biological principle of heritable genetic information to a chemical self-replicating system or instilling the chemistry of autocatalysis in a Darwinian system. Such an accommodation would bring history to chemistry and material continuity to biology. Rather than focus on the extreme versions of the two approaches outlined above, it may be fruitful to explore a middle ground in which self-replicating molecules direct the assembly of new copies of themselves from a modest assortment of component modules. Competition for utilisation of these components might provide the basis for Darwinian evolution, while the threshold for achieving self-replication would be greatly lowered compared with that required for residue-by-residue copying of a long polymer.'*[39]

As yet this 'middle ground' remains an unrealised challenge; however, there is a tremendous amount of interest in the study of the chemistry behind the emergence of life and clearly self-replicating, evolving chemical systems such as viruses are very much a real part of the living world. We will finish this chapter, therefore, by looking very briefly at some theories of prebiotic chemistry – the chemical 'bottom up' approach to the emergence of life.

The timeline for the emergence of life is given in Figure 12.24. Some time after the intense bombardment of the Earth by meteorites some 3.9–4.1 billion years ago but before the occurrence of the oldest fossils (*ca.* 3.6 billion years old) life must have emerged from the prebiotic 'soup' in a relatively short time window of no longer than *ca.* 200 million years. We use a strong form of the word 'emerge' here in the context of the time-resolved increase in complexity (chemical 'bootstrapping') discussed in Section 1.10.2. What form did that early life take?

Modern life forms are based on DNA which is located within the cell nucleus and only self-replicates with the aid of enzymes that are synthesised based on instructions coded into the DNA and mediated by RNA. There is thus a 'chicken and egg' paradox – which came first the DNA or the enzymes?

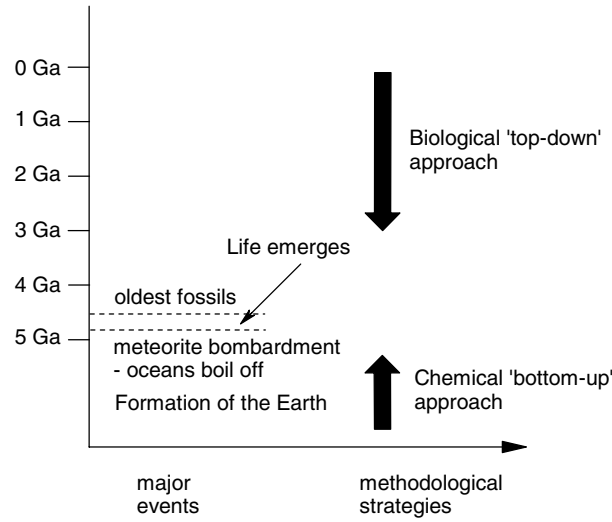


**Figure 12.24** Proposed timescale for the emergence of life along with methodological approaches to its understanding according to Lahav.[40]

Many researchers have postulated that the precursor to the DNA/enzyme system was based on RNA – this is the so-called 'RNA-world hypothesis'. Unlike DNA, RNA can function as both catalysts (as in ribozymes such as the one we saw in the previous section) and as carriers of genetic information (as in retroviruses – viruses belonging to the viral family *Retroviridae*; enveloped viruses with an RNA genome that replicate *via* a host's DNA intermediate). Strong evidence in favour of the RNA-world hypothesis comes from the 2000 demonstration that the peptidyl transferase centre of the ribosome is a ribozyme and hence all protein synthesis is RNA powered. It is postulated that this system is a molecular fossil of the RNA world.[41] In 2001 came evidence for the self-replication of RNA while more recently the crystal structure of an RNA-based ligase with a catalytic $Mg^{2+}$ ion at the centre of three RNA stems has been solved. While this minimal ligase only catalyses its own cyclisation it gives a startling glimpse into the mechanism of such RNA-based replicators that probably became extinct around 3.5 million years ago.[42] An alternative to the RNA-world is the postulate that simple proteins or peptides were the first self-replicating molecules. Self-replicating peptides have been prepared artificially[43] and are capable of exhibiting key features such as chiroselective amplification and dynamic error correction. All of the basic ingredients to form DNA, RNA and proteins (*e.g.* purines, pyrimidines, amino acids and sugars) can be shown to form from simple feedstocks such as HCN, MeCN and formaldehyde that should have been available on the early Earth assuming a reducing atmosphere ($CH_4$, $NH_3$, $H_2$ and $H_2O$). It is also possible to demonstrate the formation of building blocks such as lipids and riboflavins under these conditions, although the field it highly controversial.[40] The delivery of organic carbon by meteorites may also be a significant source.

Theories for even earlier forms of mutateable transmission of genetic information have involved clay minerals. Montmorillonite clay particles have been demonstrated to catalyse the condensation of nucleotides and we discussed in Section 8.2.8 the Cairns-Smith hypothesis of how crystal dislocations could transmit some form of genetic information. Most hypotheses about clays have yet to be demonstrated experimentally, however.

Among the hot debate between theories concerning either a gradual change from RNA self-replication to RNA-coded protein synthesis as in the RNA-world, or a merger of systems involving 'co-evolved' RNA and catalytic peptides, another type of molecule – lipids – have until recently been overlooked.

As we will see in the next chapter lipids, and amphiphiles in general can self-assemble into complex structures such as micelles and vesicles (which could have acted as envelopes for proto-cells). Lipid bilayers form the basis for cell membranes in modern organisms where their function is primarily one of compartmentalisation and hence the production of dynamic gradients such as the $Na^+/K^+$ gradient we discussed in Section 2.2. Lipids do, however, also play a vital role in metabolism, respiration and photosynthesis and the 'lipid-world' theory suggests that they may even have played an early role in genetic information transfer.[44] Micelles are capable of a kind of self-reproduction since the fatty acids within micelles are able to catalyse the hydrolysis of fatty acid esters to give more fatty acids, ultimately resulting in the expansion and splitting of the micelle. Here we use the term 'reproduction' implying the formation of copies of (spherical) geometric structures rather than linear molecular structures.

Whatever form life originally took and how it evolved, it is clear that even simple organisms such as the 'last universal common ancestor' are highly complex systems and hence must rely heavily on the kind of time-resolved hierarchical assembly we discussed in the introduction to Chapter 10 where the lifetime of higher order self-assembled structures increases with their complexity. We are thus just beginning to develop a conceptual framework that may lead us from the simple chemistry of non-covalent interactions all the way to complex, living biological systems. Such a framework in principle transcends the chemical identity of the component parts and may have occurred frequently in different ways in different parts of the universe. Indeed, as the popular evolutionary biologist Richard Dawkins explains, the modern concept of emergent Darwinian evolution is of such tremendous power that we should perhaps not be surprised that emergence of life occurred rapidly and hence may well be commonplace in the universe.[45]

## Summary

- Biological enzymes are a key inspiration for and the archetypal example of supramolecular catalysis.
- Abiotic supramolecular systems can be used as models for biological catalysis and as catalysts for other reactions that are not of biological origin.
- There are two basic kinds of chemical models: structural and functional. Functional models are harder to design and may not physically resemble the system they are designed to mimic (*e.g.* hydraphiles) but do make use of the same concepts. Was can also distinguish *confirmatory* and *speculative* models depending on whether the model is based on a known biological structure or not.
- Supramolecular catalysis can involve 'passive' effects such as the confining of two reactive molecules within a cavity and 'active' effects where the catalyst interacts with the substrate *via* an active site. The active site may be metal-based as in other kinds of homogeneous catalyst based on transition metals or Lewis acids, or my involve interactions such as hydrogen bonding to bring about both polarisation of the reactants and their mutual spatial organisation.
- Supramolecular catalysis can be used to design abiotic self-replicating systems and, in conjunction with the concepts of emergence, hierarchical self-assembly and Darwinian evolution is beginning to give insights into the origins of life.

## Study Problems

12.1 From your reading of Chapters 2 and 12, suggest desirable characteristics that might be exhibited by (a) a structural model and (b) a functional model for haemoglobin.

12.2 Distinguish between the primary, secondary and tertiary structure of proteins. Which is usually responsible for the geometry and properties of the substrate binding site? How are the properties of the binding site reflected by the 'induced fit model'?

12.3 Discuss the implications of Pauling's 1948 statement that 'Enzymes are molecules that are complementary in structure to the transition states of the reactions they catalyse.' Include in your answer a discussion of the selectivity of enzymatic catalysis.

12.4 Why do you think corand **4.12** ([24]ane$N_6O_2$) is such an effective ATPase mimic given the discussion of the relatively low affinity for guest species such as alkali metal cations and halide anions set out in Chapters 3 and 4? Similarly, why was a hemispherand chosen as the central cation-binding core of enzyme mimic **12.16** as opposed to a spherand?

12.5 Discuss the origins and implications of 'doming' in porphyrin and polypyrrole macrocycles. Why is this factor of only limited relevance to more flexible corand-type hosts?

## Thought Experiment

Suggest reasons why the cyclodextrins in particular have proved so popular in attempts to prepare artificial enzyme mimics. How might you adapt other core host systems to act as enzyme mimics for some of the reactions catalysed by cyclodextrin derivatives?

## References


1. Diederich, F., On the way to enzyme models. *Chem. Unserer Zeit* 1983, **17**, 105–119.
2. Yajima, H., Sumaoka, J., Miyama, S., Komiyama, M., Lanthanide ions for the first nonenzymatic formation of adenosine 3',5'-cyclic-monophosphate from adenosine-triphosphate under physiological conditions. *J. Biochem.* 1994, **115**, 1038–1039.
3. Breslow, R., Overman, L. E., 'Artificial enzyme' combining a metal catalytic group and a hydrophobic binding cavity. *J. Am. Chem. Soc.* 1970, **92**, 1075–1077.
4. Fragoso, A., Cao, R., Banos, M., Esterase activity of cyclodextrin dithiocarbamates. *Tetrahedron Lett.* 2004, **45**, 4069–4071.
5. Chao, Y., Weisman, G. R., Sogah, G. D. Y., Cram, D. J., Host-guest complexation .21. Catalysis and chiral recognition through designed complexation of transition-states in transacylations of amino ester salts. *J. Am. Chem. Soc.* 1979, **101**, 4948–4958.
6. Bailey, N. A., Fenton, D. E., Moody, R., *et al*., Complexes of ligands providing endogenous bridges .4. copper(II) complexes of macrocyclic Schiff-bases derived from 2,6-diacetylpyridine and 1,N-diamino-N'-hydroxyalkanes (N,N' = 3,2 – 4,2 – and 5,3) – synthesis, properties, and structures. *J. Chem. Soc., Dalton Trans.* 1987, 2519–2529.
7. Kitajima, N., Tolman, W. B., Coordination chemistry with sterically hindered hydrotris(pyrazolyl)borate ligands – organometallic and bioinorganic perspectives, in *Progr. Inorg. Chem.,* 1995, Vol. 43, *pp.* 419–531.
8. Takano, Y., Yamaguchi, K., Hybrid density functional study of ligand coordination effects on the magnetic couplings and the Dioxygen binding of the models of hemocyanin. *Int. J. Quantum Chem.* 2007, **107**, 3103–3119.
9. Becker, M., Schindler, S., Karlin, K. D., *et al*., Intramolecular ligand hydroxylation: Mechanistic high-pressure studies on the reaction of a dinuclear copper(I) complex with dioxygen. *Inorg. Chem.* 1999, **38**, 1989–1995.
10. Kimura, E., Koike, T., Shionoya, M., Shiro, M., A versatile macrocyclic [12]ane$N_3$ for interconversion of tetrahedral and trigonal bipyramidal zinc(II) complexes - relevance to 4-coordinate ↔ 5-coordinate geometries of zinc(II) in carbonic-anhydrase. *Chemistry Letters* 1992, 787–790.
11. Cronin, L., Foxon, S. P., Lusby, P. J., Walton, P. H., Syntheses and structures of M(L)(X)B$Ph_4$ complexes {M=Co(II), Zn(II), L=cis-1,3,5-tris[3-(2-furyl)prop-2-enylideneamino]cyclohexane, X=0Ac, N0$_3$}: structural models of the active site of carbonic anhydrase. *J. Biol. Inorg. Chem.* 2001, **6**, 367–377.
12. Kaminskaia, N. V., Spingler, B., Lippard, S. J., Hydrolysis of beta-lactam antibiotics catalyzed by dinuclear zinc(II) complexes: Functional mimics of metallo-beta-lactamases. *J. Am. Chem. Soc.* 2000, **122**, 6411–6422.
13. Kimura, E., Shionoya, M., Hoshino, A., Ikeda, T., Yamada, Y., A model for catalytically active zinc(II) ion in liver alcohol-dehydrogenase – a novel hydride transfer-reaction catalyzed by zinc(II)-macrocyclic polyamine complexes. *J. Am. Chem. Soc.* 1992, **114**, 10134–10137.

14. Jameson, G. B., Ibers, J. A., Structure of the free-base capped porphyrin, 5,10,15,20-[pyrromellitoyl(tetrakis-ortho-oxyet hoxyphenyl)]porphyrin. *J. Am. Chem. Soc.* 1980, **102**, 2823–2831.
15. Jameson, G. B., Molinaro, F. S., Ibers, *et al*., Models for the active-site of oxygen-binding hemoproteins - dioxygen binding-properties and the structures of (2-methylimidazole)-meso-tetra (α,α,α,α-ortho-pivalamidophenyl)porphyrinatoiron(II)-ethanol and its dioxygen adduct. *J. Am. Chem. Soc.* 1980, **102**, 3224–3237.
16. Collman, J. P., Gagne, R. R., Halbert, T. R., Marchon, J. C., Reed, C. A., Reversible oxygen adduct formation in ferrous complexes derived from a picket fence porphyrin – model for oxymyoglobin. *J. Am. Chem. Soc.* 1973, **95**, 7868–7870.
17. Schenning, A., Hubert, D. H. W., Vanesch, J. H., Feiters, M. C., Nolte, R. J. M., Novel bimetallic model system for cytochrome-P-450 - effect of membrane environment on the catalytic-oxidation. *Angew. Chem., Int. Ed.* 1994, **33**, 2468–2470.
18. Wolak, M., van Eldik, R., Mechanistic studies on peroxide activation by a water-soluble iron(III)porphyrin: Implications for O-O bond activation in aqueous and nonaqueous solvents. *Chem. Eur. J.* 2007, **13**, 4873–4883.
19. Nam, W., High-valent iron(IV)-oxo complexes of heme and non-heme ligands in oxygenation reactions. *Acc. Chem. Res.* 2007, **40**, 522–531.
20. Rohde, J. U., In, J. H., Lim, M. H., *et al*., Crystallographic and spectroscopic characterization of a nonheme Fe(IV)=O complex. *Science* 2003, **299**, 1037–1039.
21. Liu, J. G., Naruta, Y., Tani, F., A functional model of the cytochrome c oxidase active site: Unique conversion of a heme-mu-peroxo-Cu-II intermediate into heme-superoxo/Cu-I. *Angew. Chem., Int. Ed.* 2005, **44**, 1836–1840.
22. Flohr, H., Pannhorst, W., Retey, J., Synthesis, structure determination, and rearrangement of a model for active-site of methylmalonylcoa mutase with incorporated substrate. *Angew. Chem., Int. Ed. Engl.* 1976, **15**, 561–562.
23. Breslow, R., Duggan, P. J., Light, J. P., Cyclodextrin-B12, a potential enzyme coenzyme mimic. *J. Am. Chem. Soc.* 1992, **114**, 3982–3983.
24. Murakami, Y., Kikuchi, J., Hisaeda, Y., Hayashida, O., Artificial enzymes. *Chem. Rev.* 1996, **96**, 721–758.
25. Brown, K. L., Zou, X., Banka, R. R., Perry, C. B., Marques, H. M., Solution structure and thermolysis of Co beta-5 '-deoxyadenosylimidazolylcobamide, a coenzyme B-12 analogue with an imidazole axial nucleoside. *Inorg. Chem.* 2004, **43**, 8130–8142.
26. Hall, A. C., Suarez, C., Hom-Choudhury, A., *et al*., Cation transport by a redox-active synthetic ion channel. *Org. Biomol. Chem.* 2003, **1**, 2973–2982.
27. Sakai, N., Mareda, J., Matile, S., Rigid-rod molecules in biomembrane models: From hydrogen-bonded chains to synthetic multifunctional pores. *Acc. Chem. Res.* 2005, **38**, 79–87.
28. Carlqvist, P., Maseras, F., A theoretical analysis of a classic example of supramolecular catalysis. *Chem. Commun.* 2007, 748–750.
29. Sémeril, D., Lejeune, M., Matt, D., Calix[4]arene-derived nickel diphosphine complexes for LLDPE synthesis *via* orthogonal tandem and one-pot catalysis. *New J. Chem.* 2007, **31**, 502–505.
30. Kelly, T. R., Zhao, C., Bridger, G. J., A Bisubstrate Reaction Template. *J. Am. Chem. Soc.* 1989, **111**, 3744–3745.
31. Das, S., Brudvig, G. W., Crabtree, R. H., Molecular recognition in homogeneous transition metal catalysis: a biomimetic strategy for high selectivity. *Chem. Commun.* 2008, 413–424.
32. Huc, I., Lehn, J. M., Virtual combinatorial libraries: Dynamic generation of molecular and supramolecular diversity by self-assembly. *Proc. Natl. Acad. Sci. U. S. A.* 1997, **94**, 2106–2110.
33. Furlan, R. L. E., Cousins, G. R. L., Sanders, J. K. M., Molecular amplification in a dynamic combinatorial library using non-covalent interactions. *Chem. Commun.* 2000, 1761–1762.
34. Milanesi, L., Hunter, C. A., Sedelnikova, S. E., Waltho, J. P., Amplification of bifunctional ligands for calmodulin from a dynamic combinatorial library. *Chem. Eur. J.* 2006, **12**, 1081–1087.
35. Philp, D., Stoddart, J. F., Self-assembly in natural and unnatural systems. *Angew. Chem., Int. Ed. Engl.* 1996, **35**, 1155–1196.
36. Kassianidis, E., Philp, D., Design and implementation of a highly selective minimal self-replicating system. *Angew. Chem., Int. Ed.* 2006, **45**, 6344–6348.
37. Tjivikua, T., Ballester, P., Rebek, J., A Self-Replicating System. *J. Am. Chem. Soc.* 1990, **112**, 1249–1250.
38. Rotello, V., Hong, J. I., Rebek, J., Sigmoidal Growth in a self-replicating system. *J. Am. Chem. Soc.* 1991, **113**, 9422–9423.
39. Paul, N., Joyce, G. F., A self-replicating ligase ribozyme. *Proc. Natl. Acad. Sci. U. S. A.* 2002, **99**, 12733–12740.
40. Lahav, N., *Theories of Life's Origin*. Oxford University Press: Oxford, 1999,
41. Nissen, P., Hansen, J., Ban, N., Moore, P. B., Steitz, T. A., The structural basis of ribosome activity in peptide bond synthesis. *Science* 2000, **289**, 920–930.
42. Robertson, M. P., Scott, W. G., The structural basis of ribozyme-catalyzed RNA assembly. *Science* 2007, **315**, 1549–1553.
43. Lee, D. H., Granja, J. R., Martinez, J. A., Severin, K., Ghadiri, M. R., A self-replicating peptide. *Nature* 1996, **382**, 525–528.
44. Segre, D., Ben-Eli, D., Deamer, D. W., Lancet, D., The lipid world. *Orig. Life Evol. Biosph.* 2001, **31**, 119–145.
45. Dawkins, R., *Climbing Mount Improbable*. Norton: New York, 1996.

# 13 Interfaces and Liquid Assemblies

*'One may not doubt that, somehow, good*
*Shall come of water and of mud;*
*And, sure, the reverent eye must see*
*A purpose in liquidity.'*

Rupert Brooke (1887–1915), *Heaven*

## 13.1 Order in Liquids

Fuhrhop, J. -H. and Köning, J., *Membranes and Molecular Assemblies, The Synkinetic Approach*, Royal Society of Chemistry: Cambridge, 1994.

Most of this book has been concerned with long-range order in solids (*e.g.* crystals) and only very short-range order in liquid phases, as in stoichiometic host–guest inclusion compounds. Indeed, the liquid phase is generally thought of as comprising a largely disordered collection of molecular species and solutes in rapid motion. While the same kinds of 'supramolecular' interactions should occur in both the solid and liquid phases, the strengths of these interactions in all but especially designed host–guest compounds is small compared with the molecules' thermal energy in isotropic liquids, especially at high temperatures and/or when small, weakly interacting components are present. Comparing the liquid and gas phases, however, it is clear that intermolecular interactions in liquids must be significant in order to maintain the condensed liquid phase. Indeed, the complementary hydrogen bonds in water keep it a liquid at atmospheric pressure at temperatures up to 100 °C (373 K). The much weaker hydrogen bonds in $H_2S$ result in its boiling at −61 °C (112 K), despite the higher molecular mass. There is evidence for significant order in liquid water from X-ray diffraction studies that reveal a radial distribution function of O···O distances of the form shown in Figure 13.1.[1] The sharp peak at around 3 Å corresponds to hydrogen bonding from water molecule to another, however there are further peaks at around 4.5 and 6.5 Å indicating that each water molecule has ordered second and third coordination spheres.

Dissolution of alkali metal cations such as $Cs^+$ results in short-range liquid order in water as a primary solvation shell of about eight water molecules is established about the metal cation. Lithium, however, exerts a much greater polarising power and is capable of organising a first- and second-coordination sphere of about 12 water molecules about itself, resulting in a much larger hydrated radius for the ion and hence decreased ionic mobility.

While only transient, these examples show that, under the correct circumstances, liquid-phase molecules can exhibit ordering, in terms of enduring zones in which molecules exhibit well-defined spatial relationships to one another of greater range than just a single host guest complex. In fact, ordered and semi-ordered liquids in which the molecules have significant supramolecular interactions between them are enormously important, perhaps even more so than solids, from a biochemical standpoint at least. They are significantly more difficult to study than solids, however. One of the most important examples of liquid ordering is the formation of biological cell membranes. Biological membranes are bulky phospholipids that are forced to order themselves in water by combination of hydrophobic effects and interactions between the solvent and the hydrophilic head group, forming capsule-like vesicles (cells) vital to living processes. The cell membrane must exist in the liquid phase to allow rapid biochemical transport and solution chemistry. At the same time, solid-like long-term structure is needed to preserve membrane potentials, control cellular signalling and protect sensitive intracellular enzymes. The cell membrane must also be sufficiently ordered to anchor transmembrane proteins such as ATPases, and is vital to vectorial excitation transfer in photosynthetic membranes. Liquid ordering is also of enormous importance in modern technological devices, such as liquid crystal displays (LCDs). The very term 'liquid crystal' implies the fast kinetics exhibited by liquids but some degree of crystal-like ordering.

This chapter attempts to summarise briefly the role of supramolecular chemistry and supramolecular interactions in the formation and uses of structured liquid phases. Subjects such as liquid crystalline

*Supramolecular Chemistry, 2nd edition* J. W. Steed and J. L. Atwood
© 2009 John Wiley & Sons, Ltd ISBN: 978-0-470-51233-3

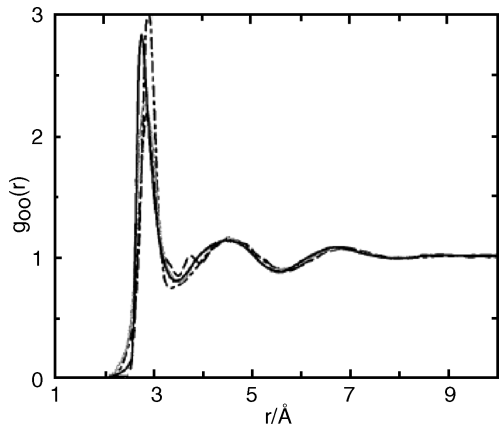


**Figure 13.1** Oxygen···oxygen radial distribution function, $g_{OO}(r)$, in liquid water determined by various X-ray scattering experiments (reproduced with permission from [1] copyright American Institute of Physics).

materials especially are vast and only a brief overview is presented by way of an introduction to the concepts of relevance to supramolecular chemists. As always, relevant of literature is cited for the interested reader.

## 13.2 Surfactants and Interfacial Ordering

Zana, R. (ed.), *Dynamics of Surfactant Self-Assemblies: Micelles, Microemulsions, Vesicles and Lyotropic Phases*. CRC: New York, 2005.

### 13.2.1 Surfactants, Micelles and Vesicles

Hoffmann, H. and Ebert, G., 'Surfactants, Micelles and Fascinating Phenomena', *Angew. Chem., Int. Ed. Engl.*, 1988, **27**, 902–912.

In 1774 Benjamin Franklin recounted his first experiences with surfactants to the British Royal Society.

> *At length at Clapman where there is, on the common, a large pond, which I observed to be one day very rough with the wind, I fetched out a cruet of oil, and dropped a little of it on the water. I saw it spread itself with surprising swiftness upon the surface. the oil, though not more than a teaspoonful, produced an instant calm over a space several yards square, which spread amazingly and extended itself gradually until it reached the leeside, making all that quarter of the pond, perhaps half an acre, as smooth as a looking glass.*

Franklin did not really understand what he was seeing and it was not until 100 years later that Lord Rayleigh speculated that the film was a monolayer, a single molecule thick. However, it was the work of a German, Agnes Pockles at the end of the nineteenth century that resulted in the first quantification of these phenomena. Pockels constructed a basic surface balance and used her kitchen sink to determine the water contamination of surfaces as a function of area for different oils. This work was later published in *Nature* in 1891 and was used by Irwing Langmuir, whose name is now linked to the technique of forming these surfactant monolayer films (Langmuir films) and their transfer to various substrates using the Langmuir-Blodgett technique.

A surfactant is a molecule that has two distinct zones with very different solubilities. The *hydrophilic* zone is highly water-soluble, while the *lipophilic* portion of the molecule is soluble in organic media and is highly hydrophobic. Because of this dual behaviour, surfactants are often referred to as *amphiphiles*. Surfactants are everyday substances, their most obvious applications being in soap (sodium dodecyl sulfate, **13.1**) and shampoo (sodium laureth sulfate and sodium lauryl sulfate). Phospholipids such as phosphatidyl choline (**13.2**), which are involved in biological cell membrane formation, fatty acids, and various other lipids also belong to this category. The lipophilic portion of the molecule can be made from aliphatic hydrocarbon and fluorocarbon chains, aryl rings or a range of other nonpolar organic groups. The hydrophilic regions tend to be highly hydrated groups such as sulfonate, phosphonate, carboxylates, ammonium ions *etc.* Four classes of surfactant can be distinguished based on the nature of their hydrophilic functionality:

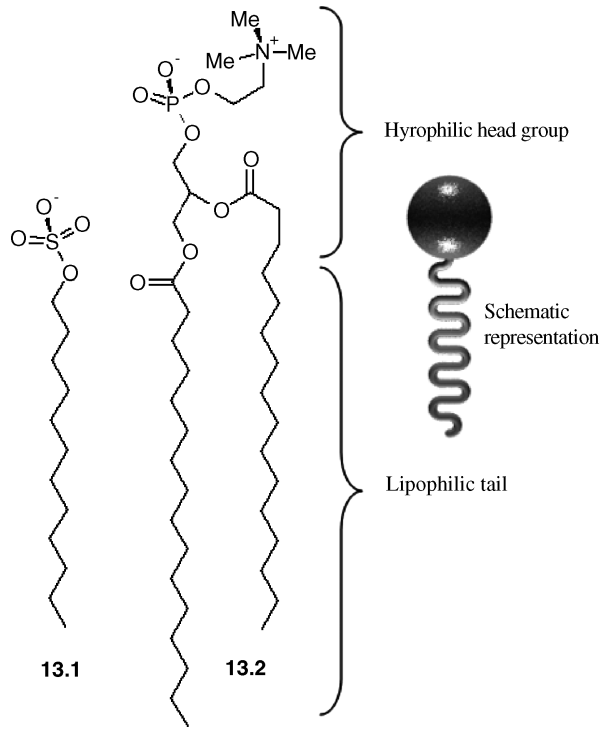


- anionic (phospholipids, soaps)
- cationic (quaternary ammonium salts)
- amphoteric (zwitterionic betaines)
- nonionic (fatty acids).

The hydrophobic effects involving the lipophilic portion of the amphiphile results in aggregation of the molecules at surfaces and interfaces such as the air/water interface. The hydrophilic portions point into the aqueous layer, while the lipophilic tails point up into the gas phase. Such effects are known as monolayer formation (*i.e.* a layer of amphiphiles one molecule thick) and are generally studied by means of a Langmuir trough; Langmuir's refinement of Pockels original equipment. A Langmuir trough is simply a sunken rectangular water bath with a movable barrier for altering its surface area and a sensor for measuring surface pressure. Small, carefully weighed amounts of the amphiphile in

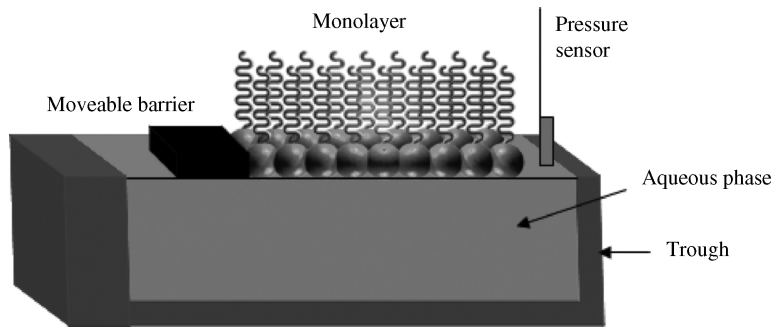


**Figure 13.2** Surface assembly of monolayers in a Langmuir trough.

an organic solvent are added to the surface of the aqueous medium. The organic solvent is allowed to evaporate and the amphiphiles packed into a condensed monolayer by moving the barrier until resistance is encountered. The force applied to the barrier may be measured and correlated with the surface tension ($\gamma$) and hence the surface area of the monolayer coverage. This process results in an ordered monolayer in which all of the hydrophobic tails of the surfactant molecules project vertically from the aqueous surface (Figure 13.2). The surface tension of a clean water surface at room temperature is $\gamma_{water} = 72.4$ mN m$^{-1}$. Surface active molecules reduce the surface tension and the difference $\Pi = \gamma_{water} - \gamma$ is termed the *lateral pressure*. Repulsion between the amphiphilic molecules decreases the surface tension as the area per molecule decreases, resulting in an increase in the lateral pressure. Thus the Langmuir trough measures isotherms in a plot of pressure *vs.* area in order to characterise the thermodynamics of the amphiphile aggregation behaviour. An example plot is shown in Figure 13.3.

Phase transitions of the system such as chain ordering transitions of lipids, appear in the isotherm as regions of constant pressure in the case of first order phase transitions involving the coexistence of two phases, or as a kink in the isotherm corresponding to a second order phase transition. These kinds of surface measurements are highly sensitive to impurities and must be carried out using very pure water and sample materials.

Self-assembled monolayers prepared in this way can be transferred on to various surfaces (silicon, metals, metal oxides *etc.*) for further study and in the construction of monolayer-based devices *etc.* The substrate is dipped into the trough and then withdrawn at a constant rate leading to the monolayer adhering to the active surface, Figure 13.4. A second layer can then be applied by touching the coated surface to a fresh monolayer. Thus a hydrophilic substrate will initially be coated with a monolayer in which the hydrophobic ends point outwards. The second application leads to a bilayer coating. This technique was pioneered by Langmuir's co-worker Katherine Blodgett and allows the careful construction of ordered

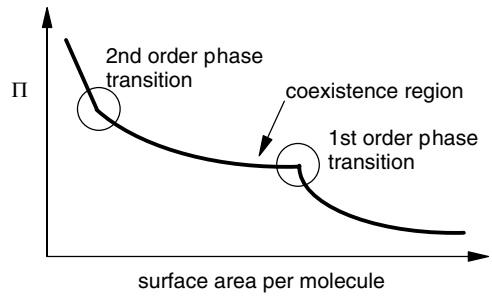


**Figure 13.3** Schematic of a Langmuir isotherm.

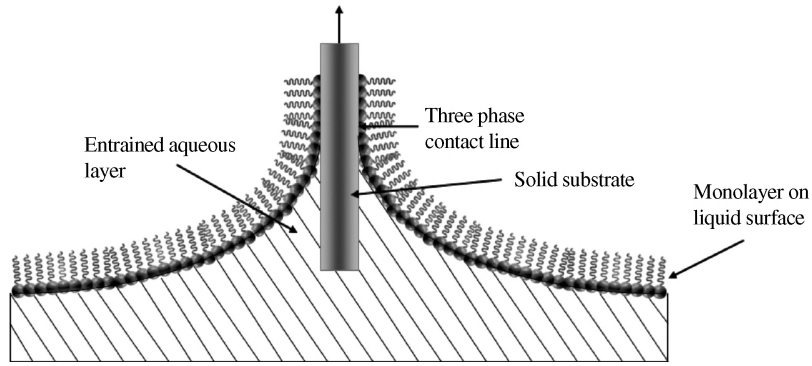


**Figure 13.4** Transfer of a monolayer from an aqueous surface to a solid substrate *via* the Langmuir-Blodgett technique.

layer structures at a molecular level and hence this Langmuir-Blodgett technique is therefore a way to arrange molecules in organised assemblies with uniform thickness and laminar structure.

This type of surface activation provides a kind of connection between aqueous and lipophilic phases, resulting in a variety of phenomena such as a lowering of the surface tension of the aqueous layer, since the hydrophobic interactions between the amphiphiles are not as strong as the interactions between water molecules. Other effects include spreading, wetting, dispersion and emulsion formation, solubilisation and frothing, and this kind of bridging behaviour is the basis for the mode of action of soaps, which promote the dissolution of organic oils in water.

Monolayer formation is not the only kind of behaviour known for aqueous surfactants. Other possibilities include micelle, bilayer and vesicle formation (Figure 13.5). The mode of amphiphile behaviour depends strongly on conditions and concentration. If the surfactant concentration is raised somewhat above that required for monolayer formation, then amphiphiles may close in on themselves to form spherical aggregates termed micelles. In a micelle, all of the lipophilic portions of the molecules are directed inwards towards a common centre, while the hydrophilic groups point outwards. Numerous micelles can be formed suspended in an aqueous solution and their dimensions are dependent on the length of the organic group. The centre of the micelle comprises an organic core with a typical diameter of about 1–3 nm. It is noteworthy that this core is filled with the organic portions of the amphiphiles and so cannot contain guest molecules. In addition to the hydrophobic core, anionic surfactant micelles

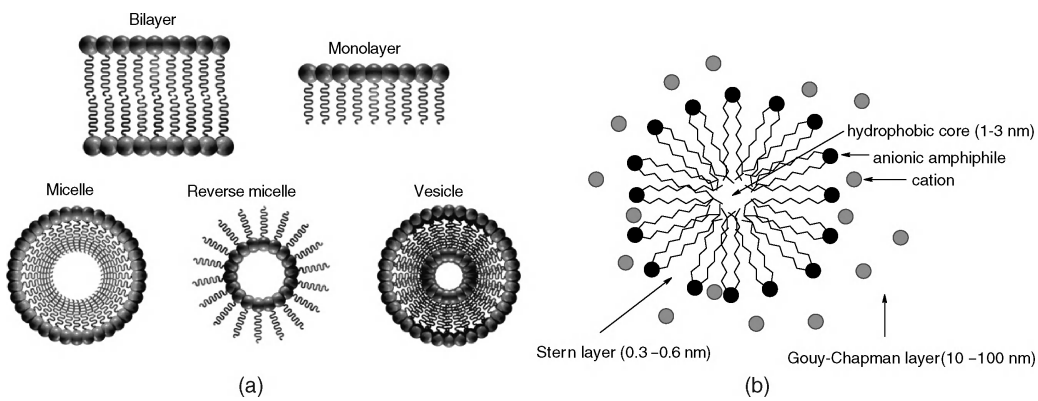


**Figure 13.5** (a) Ordered surfactant structures in aqueous solution. (b) Detail of a spherical anionic micelle with counter-cations.

also possess a hydrophilic Stern layer 0.3–0.6 nm thick, which contains the anionic head groups and some adventitious counter-cations. The micelle is surrounded by a cation and solvent sheath termed the Gouy–Chapman layer, which may be anywhere from 10 to 100 nm thick. Overall the micelle resembles a tiny drop of oil in water.

The concentration at which micelle formation begins is termed the *critical micelle concentration* (cmc) and is related conceptually to the critical self-assembly concentration (csac) discussed in Section 10.4.2. This parameter may be measured with some precision because properties of the water–amphiphile mixture, such as density, conductivity, surface tension and osmometric pressure, display a sudden change as micelles form. The cmc is affected strongly by the nature of the organic group. Branched organic groups tend to increase the cmc, since they have difficulty packing together at the micelle core, while longer alkyl or aryl chains decrease the cmc because of enhanced hydrophobic interactions. For sodium dodecyl sulfate **13.1**, the cmc in water at 20 ºC is rather high (8.1 mol $dm^{-3}$) with micelles containing about 62 monomer units on average. In contrast, long-chain materials such as $Me(CH_2)_{11}(OCH_2CH_2)_6OH$ exhibit a cmc of just 0.1 mol $dm^{-3}$, with 400 monomer units needed on average to present a closed outer surface to the aqueous medium. Micelle formation is especially favoured in non-ionic surfactants of this type because there is no unfavourable electrostatic repulsion in the Stern layer by charged head groups. In some respects, micelles resemble dendritic structures (discussed in the next chapter); however, the micelle is not branched, and the density is not expected to increase further away from the core.

Micelles may go through several changes in structure as the concentration is increased, each with its own particular cmc. At a concentration significantly above the first cmc, a transition from spherical to elongated cylindrical structures is observed, while beyond a third cmc, these structures begin to associate, displaying solution order with respect to one another as a result of their large size (which may be detected by visible light diffraction). This change results in lyotropic liquid crystalline behaviour (Section 13.3), generally of nematic (rod-like) type. Structures formed by surfactants are also dependent on the molecular shape of the individual amphiphiles. The propensity towards various assemblies is governed by the volume ($V$) of the hydrophobic chain of the surfactant, the area ($a$) of the hydrophilic head group, and the length ($l$) of the hydrocarbon chain. Hydrocarbon chains tend to associate with each other in water thus minimising their contact with the aqueous phase. This behaviour results in the formation of micelles if $V/al$ is small. A small $V/al$ corresponds to a cone-shaped amphiphile with a small hydrophobic chain and thus the micelle curvature increases the packing density of the hydrocarbon chains. As $V/al$ increases the behaviour changes to the formation of hexagonal rod-like structures and then to lamellar bilayers where the amphiphile is approximately cylindrical. We saw the use of these hexagonal structures in the templation of M41S zeolites in Section 9.2.1 (see Figure 9.9). Where $V/al$ becomes large reverse hexagonal phases and ultimately reverse micelles predominate, Figure 13.6.

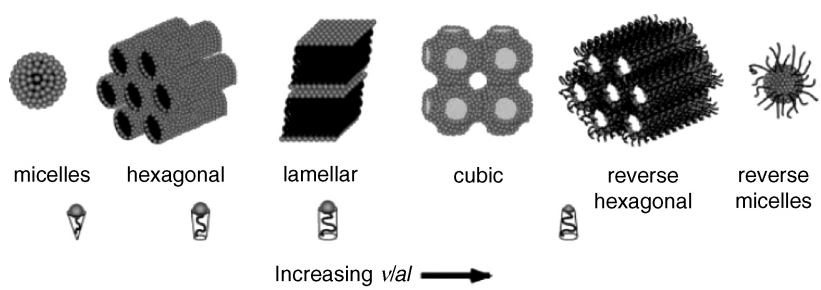


**Figure 13.6** Changes in surfactant microstructures with changing shape parameters (reproduced by permission of The Royal Society of Chemistry).

In lipophilic organic solvents with a greater affinity for the hydrophobic portions of amphiphiles, reversed micelles are particularly favoured. The species have their polar groups pointing inwards towards encapsulated traces of water, which are necessary for the reverse-micelle to form in order to solvate the polar head groups. The organic tails point outwards into the solvent medium. These species resemble tiny drops of water in oil. Increasing the proportion of water present destroys the reverse micelles, giving an emulsion phase, and finally conventional micelle behaviour.

Perhaps of most interest in surfactant chemistry is the formation of bilayers and vesicles. Bilayers are a kind of extended, sheet-like micelle (Figure 13.5). On agitation (*e.g.* by stirring, ultrasound *etc*.), these species can form vesicles in which a bilayer encloses an inner aqueous phase from the outer phase. This situation is strongly reminiscent of biological cells formed by phospholipid bilayers. Extreme agitation can even result in multiple folding to give multiply layered vesicles, rather like an onion skin. It is tempting to view this kind of behaviour as a possible source of the origin of the first biological cells. Dissolution of simple gases in the oceans would be followed by chemical reactions catalysed by the action of heat, UV or cosmic radiation resulting in the formation of simple amphiphilic materials that would form monolayers on the ocean surface. Agitation of the water–air interface would close the monolayers into bilayers and vesicles, trapping other chemical species, particularly amino acids inside. Such a structure could be construed as a protocell, although hardly a living one. The process by which this cell evolved into a growing, replicating organism and learned to cooperate with other such cells to produce multicellular entities is a matter for some rather more extended speculation and forms part of the argument concerning life's origins discussed in Section 12.9.4.

It is important to recognise that biological cells themselves are much more than simple vesicles. In addition to the external bilayer membrane, the cell also contains many transmembrane- and membrane-bound proteins and enzymes. Within the cell, further membranes exist, defining the cell's organelles. A simple vesicle model is unable to explain living cells' diffusional permittivity characteristics. Over the last 40 years, the model that best describes the cell and has come to be widely accepted is the 'fluid mosaic' model, which presents the cell membrane as an extremely fluid structure (it is a liquid after all). The cell is subject to random fluctuation causing some porosity and its properties are a result of time-averaged equilibria and pumped mechanisms rather than absolute differentiation. Proteins are anchored in the cell membrane or transfix it, depending on the length and nature of the lipophilic peptide anchor groups and may be regarded as 'islands' in a lipid 'sea' (Figure 13.7). The model has been verified by techniques such as freeze-fracture electron microscopy, and fluorescence studies.

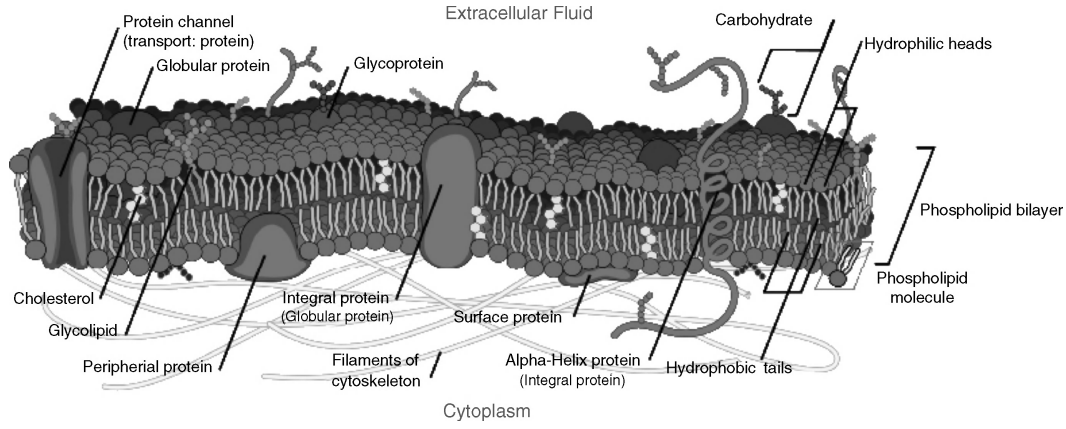


**Figure 13.7** The fluid mosaic model of biological cells. (image courtesy of www.wikipedia.org). See plate section for colour version of this image.

## 13.2.2 Surface Self-Assembled Monolayers

Ulman, A., 'Formation and structure of self-assembled monolayers', *Chem. Rev.* 1996, **96**, 1533–1554.

As we saw in the Langmuir-Blodgett technique, self-assembled monolayers (SAMs) can be transferred to solid surfaces as well as existing at the air-water interface. SAMs can also be prepared directly on a surface simply by immersing a clean substrate into a solution of an amphiphile or related coating molecule and allowing time (minutes to days) for the formation of an ordered structure to self-assemble. The concepts of self-assembly that we looked at in Chapter 10 are relevant in this two-dimensional context because molecules are generally very mobile on surfaces and hence, with sufficient time and material, a densely packed, ordered low energy two dimensional structure (rather like a 2D crystal) will result because such a gap-free arrangement maximises intermolecular interactions. The archetypal example of this process is the assembly of alkane thiols on a cleaned metallic gold surface. The interaction energy of gold and a thiol is about the same strength as a hydrogen bond and hence gold-thiolate bonds form highly reversibly allowing facile self-assembly. Gold-thiolate monolayers are ubiquitous in microscale assembly where they are used in microfabrication, electrode coatings, nanoparticle stabilisation *etc.* Formally the reaction between thiol (RSH) and gold can be thought of as an oxidative addition of the SH bond to Au(0) to give Au(I)–SR and $H_2$. Surface SAMs are characterised by a layer thickness which is determined mainly by the length of the molecule and by a contact angle that the axis of the molecule forms with the surface. The layer thickness ($d$) and number of molecules that can fit on a surface also depend on the contact angle ($\theta$), Figure 13.8.

The process by which an alkane thiol adsorbs onto a gold surface (commonly a well-orientated crystalline Au(111) surface is used) reveal two distinct steps to the thiol adsorption – a fast step taking only minutes at $10^{-3}$ M concentration which results in a thickness of *ca.* 80–90 % of its maximum and contact angles close to limiting values, and a slow step, which takes a number of hours, during which the final thickness and contact angle values are reached. The first step involves diffusion-controlled Langmuir adsorption and depends on the concentration of the thiol. The second step is a ordering or surface crystallisation process involving the rearrangement of the alkyl chains to give a two-dimensional crystal. The kinetics of the first step depend on the interaction of the thiol head group with the gold while the second step depends on the interactions between the organic chains (*e.g.* dipolar and van der Waals interactions and the degree of disorder such as gauche defects *etc.*). Interestingly the process is faster for longer chains apparently because of the increased van der Waals interactions.

There is a vast range of chemistry of functionalised thiols that act as sensitiser electrode coatings in sensing. To take just one example, a ferrocene derived thiol receptor containing amide functional groups

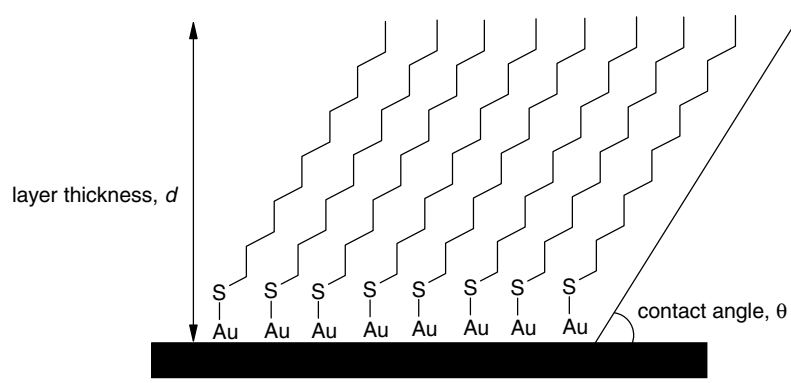


**Figure 13.8** Characteristics of a gold-thiolate monolayer.

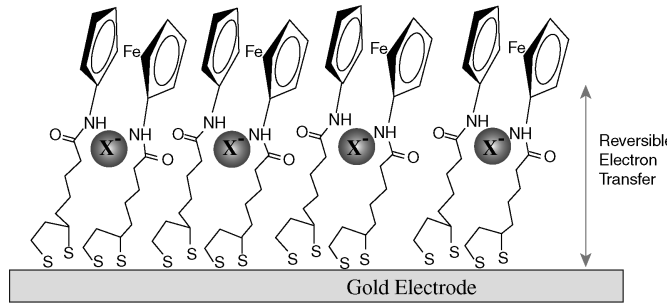


**Figure 13.9** Electrochemical anion sensing by a dithiol SAM. Anion binding results in predictable cathodic perturbation of the SAM voltammetry. Anion binding affinities associated with such SAMs are, in some cases, orders of magnitude greater than those associated with the same receptors free in solution (reproduced by permission of The Royal Society of Chemistry).

has been attached to a gold surface, Figure 13.9. The recognition of an anion perturbs the electron transfer process between the ferrocene-derived reported group and the gold electrode surface either by through space or through bond interaction, resulting in redox sensing.[3] Surface attachment dramatically increases the preorganisation of such receptors resulting in dramatic increases in affinity in some cases.

Gold thiolates are not the only kinds of SAM – indeed there are many different combinations, *e.g.* the deposition of fatty acids onto AgO or alumina surfaces. Another common example is the reaction of trichlorosilanes with silica surfaces. The driving force is the hydrolysis of the silane by trace amounts of water to give solution oligomers that react with surface hydroxyl groups. Too much water, however, will give solution polymers and poor monolayer coverage. A particularly interesting and versatile example is the formation of organic monolayers by reaction of alkenes with hydrogen-terminated silicon surfaces. By way of example this versatile strategy has been used by Ben Horrocks (Newcastle, UK) to produce a range of functional silicon surfaces for use in sensing and device applications. Scheme 13.1 shows the attachment of magnetic polyoxometalate clusters

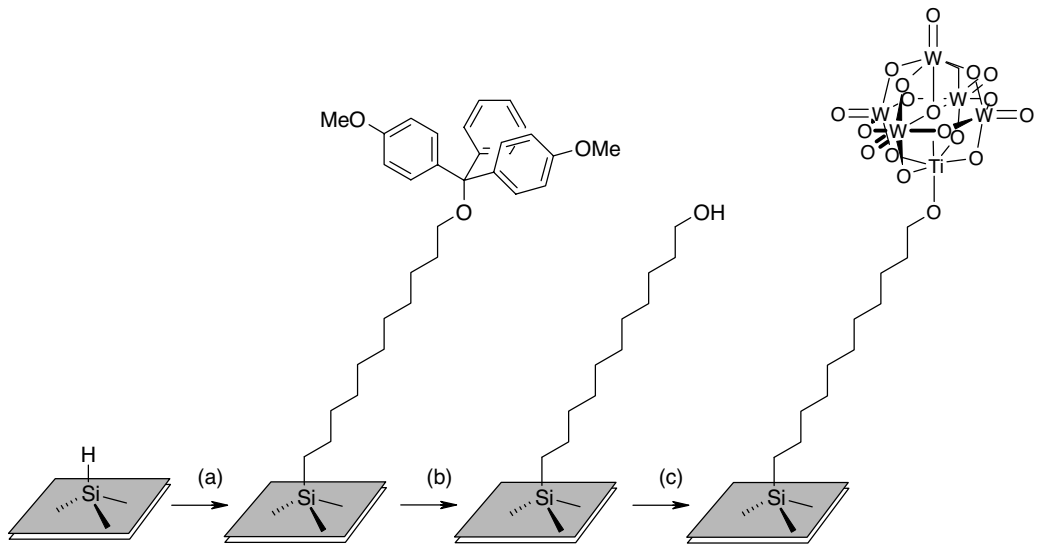


**Scheme 13.1** Reaction of a hydrogen terminated surface with an alkene to generate surface monolayers (a) monolayer formation by reaction of silicon with $H_2C{=}CH(CH_2)_9OPh(C_6H_4OMe)_2$, (b, c) monolayer derivatisation to give a surface layer of tethered magnetic $TiW_5$ polyoxometalate clusters.[4]

to a silicon surface.[4] The approach has also been used to surface tether oligonucleotides, allowing automated surface synthesis of DNA. The semiconductor properties of silicon and absence of an intervening oxide layer allow the process to be monitored electrochemically.[5] These two very different examples show the diverse range of surface chemistry that can be achieved using SAMs based on simple surface reactions.

## 13.3 Liquid Crystals

Collings, P. J., *Liquid Crystals: Nature's Delicate Phase of Matter*, 2nd ed.; Princeton University Press: Princeton, NJ, USA, 2001.

### 13.3.1 Nature and Structure

True long-range order in liquids is referred to as *mesomorphic* or *liquid crystalline* behaviour. The term 'liquid crystal' is highly evocative of the true state of the substance that possesses some of the bulk order of the crystalline state and the facile deformability and dynamics of the liquid phase. In fact, liquid crystals represent an intermediate phase between liquid and solid (or, indeed, a series of liquid phases in some cases). The origin of this anisotropic behaviour is mainly a function of molecular shape. Liquid crystal-forming molecules, termed *mesogens*, are generally either long and cylindrical (rodlike), such as 4′-*n*-pentyl-4-cyanobiphenyl (**13.3**) and cholesteryl nonanoate (**13.4**), or flat and circular (disclike), as in *hexakis*((4-octylphenyl)ethynyl)benzene (**13.5**) and *bis*(3,4-nonyloxybenzoyl)methanato copper(II) (**13.6**). Mesogens can even be polymers or aggregates such as elongated micelles (Section 13.2.1). Even the alkyl-chain-substituted hydrogen-bonded 2,6-diaminopyridine-uracil (PU) system developed by Lehn (Section 10.8.8) shows mesogenic behaviour. The highly anisotropic shape of mesogens causes them to line up with one another in various ordered ways, partly as a result of intermolecular interactions, and partly because the molecules are bulky and the liquid phase is relatively viscous. However, tiny perturbations such as dust particles, or surface inhomogeneities, can cause differential orientation of one zone of mesogens with respect to its neighbours. The result is a fluid material with macroscopic domains of aligned molecules, usually visible to the naked eye as scattering light to give bright, iridescent colours. The liquid order is clearly apparent under a polarising microscope (Figure 13.10), in which each domain

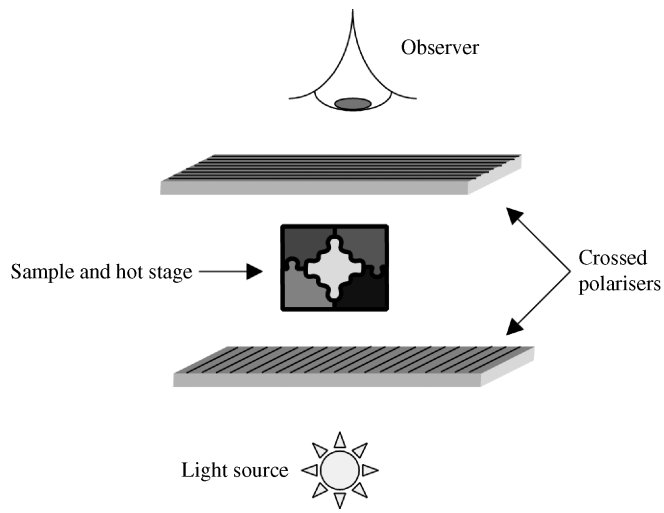


**Figure 13.10** Operation of a polarising hot-stage microscope.

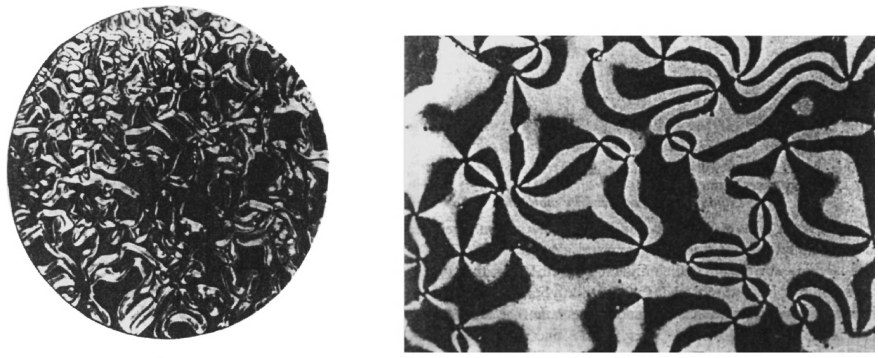


**Figure 13.11** (a) Thread-like domains in a nematic liquid crystal of thickness 100 μm viewed under crossed polarisers. (b) Schlieren texture in a nematic film of thickness 10 μm (reproduced with permission from [6]).

rotates plane-polarised light as in a solid-state crystal, giving light and dark patterns according to whether the polarised light is able to pass through the analyser (Figure 13.11).

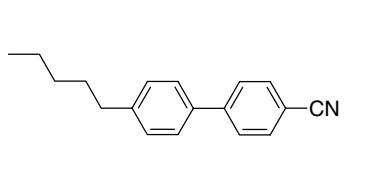


**13.3**

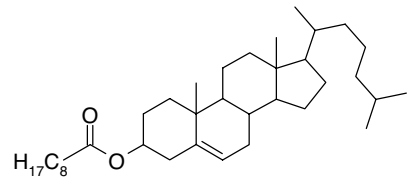


**13.4**

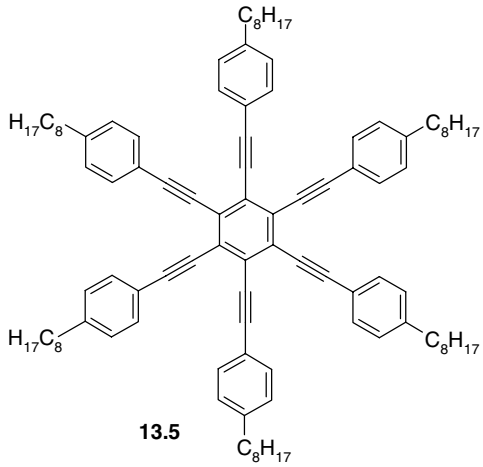


**13.5**

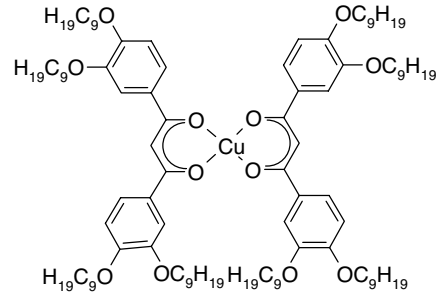


**13.6**

The fact that mesogens are highly fluid, and domains may be deformed very easily, suggests that liquid crystalline behaviour should be highly temperature-dependent, and this is indeed the case. Liquid crystalline behaviour occurs above the melting point of the pure solid material at temperatures low enough such the molecular motion is slow and the energies of intermolecular interactions are strong compared with thermal energies. As the temperature is increased, so molecular motion increases and the liquid crystal may undergo further phase changes, often to less ordered mesophases,

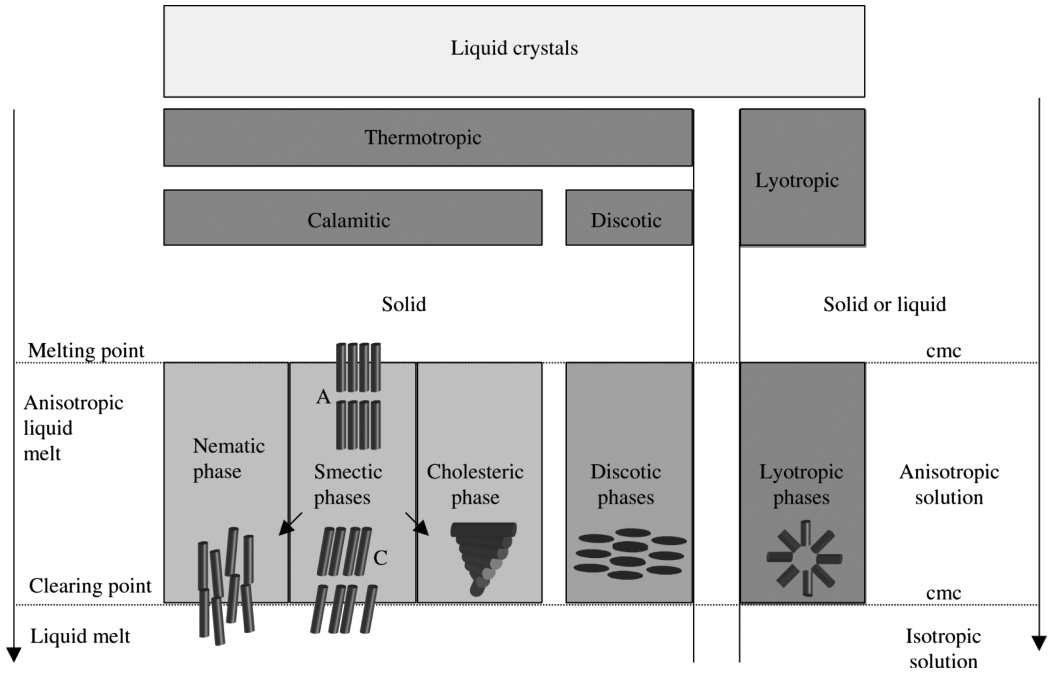


**Figure 13.12** Fundamental classes of liquid crystalline behaviour (temperature increases downwards).

before finally melting into an isotropic liquid once thermal energy is sufficient to induce rapid motion of one molecule with respect to its neighbours. The thermal behaviour is the basis for the first fundamental distinction in liquid crystals. Substances that form mesophases as a function of temperature are termed *thermotropic*, whereas those that require the influence of a solvent or medium (*e.g.* micelles) are termed *lyotropic* (Figure 13.12). Thermotropic phases arise from the gradual melting of a crystalline solid. As the temperature increases, so the molecular vibrations increase until, at the melting point, intermolecular (supramolecular) bonds are broken and a liquid results. In about 5 % of organic molecules, not all intermolecular interactions are broken at once and a liquid crystalline phase results in which the solid order has broken down, but varying degrees of crystalline order are still apparent. As the temperature increases, the various intermolecular interactions are broken one by one, resulting in less and less ordered liquid crystalline phases, until an isotropic melt is finally achieved. In addition to melting, the other way to break down a solid lattice is to dissolve it in a solvent. As with melting, it is possible that, depending on concentration, not all of the crystal is broken up at once and degrees of solute order may exist within the solution. This is a lyotropic phase.

Thermotropic liquid crystals come in two types: *calamitic* and *discotic*. Calamitic phases (from the Greek for 'tube') are all those that are caused by rod-like mesogens. The more recently characterised discotic phases are caused by disc-like species. Calamitic phases may be either *nematic* (from the Greek for 'thread'), *smectic* (from the Greek for 'soap') or *cholesteric* (named after the cholesterol derivatives such as **13.4**, which exhibit this behaviour).

The nematic phase (Figure 13.13a) is characterised by a high degree of long-range orientational order of the molecules but no long-range translational order. In other words, the mesogens all point in the same direction but are disordered with respect to slippage along the rod axis; it is this ready slippage that gives the nematic phase a high degree of fluidity. The nematic phase represents the least ordered of all calamitic phases and, in systems that possess more than one mesophase, the nematic

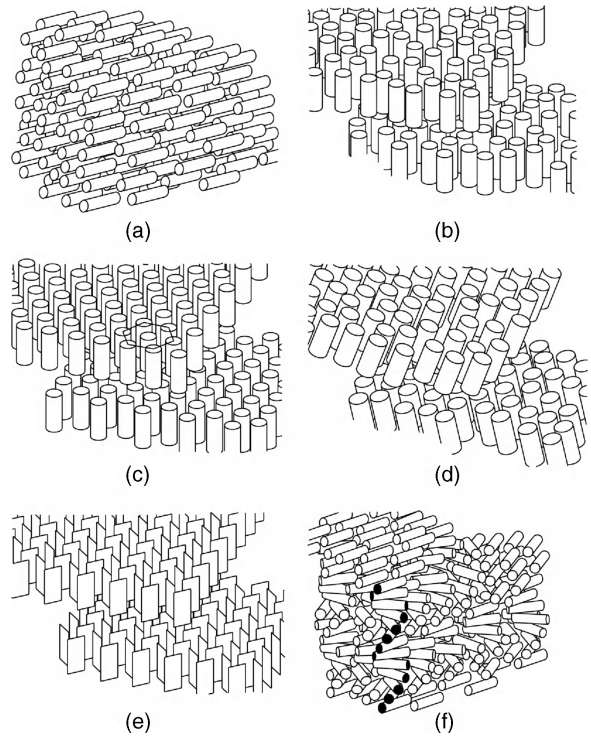


**Figure 13.13** Schematic representation of calamitic liquid crystalline phases: (a) nematic, (b) smectic A, (c) smectic B, (d) smectic C, (e) smectic E and (f) cholesteric (reproduced with permission from [7]).

phase is usually the last to occur before isotropic melting. The degree of order in a nematic phase is quantified by a parameter, *S* (Figure 13.14), which represents the amount of rotational freedom the rod-like molecule has perpendicular to its rod axis. An *S* of 1 represents an ideally organised nematic phase, while an isotropic liquid has $S = 0$. Nematic phases are characterised by brightly coloured, rapidly moving spots, visible to the naked eye or under a microscope, and by the schlieren (centred) texture (Figure 13.11b). This property arises from line singularities perpendicular to the mesophase layer and are analogous to disolocations in crystals. They are termed *disclinations*, and are a form of defect where two regions of different order meet.

Smectic phases represent a higher degree of order then nematic. Smectic phases are based on two-dimensionally ordered layer arrangements in which the layer thickness is approximately equal to the length of the molecular rods. Interactions between layers are limited, allowing one layer to slip easily with respect to the others. Within a layer, less ordered smectic phases such as A and C (Figure 13.13b and Figure 13.13d) exhibit a liquid-like, statistical distribution of mesogens. Increasing order is observed with hexagonal arrangements between rods (smectic B) and a herringbone arrangement of flatter rods such as **13.8** allowing no rotation about the rod axis (smectic E). A total of at least 12 different smectic phases have been characterised (labelled $S_A$–$S_L$), with the most ordered exhibiting a high degree of viscosity. The smectic D phase has a rather unusual cubic structure, and is an exception to the layered rule. Generally, on warming, ordered phases shift to less ordered forms in an order such as $S_E/S_G \rightarrow S_B \rightarrow S_F \rightarrow S_C \rightarrow S_D \rightarrow S_A$. For example, the *n*-octyl derivative of compound **13.3** undergoes a total of three phase transitions. Initially, it melts as 24ºC to give a smectic A phase (enthaply of fusion 25.5 kJ $mol^{-1}$). At 34 ºC, this is transformed into a nematic

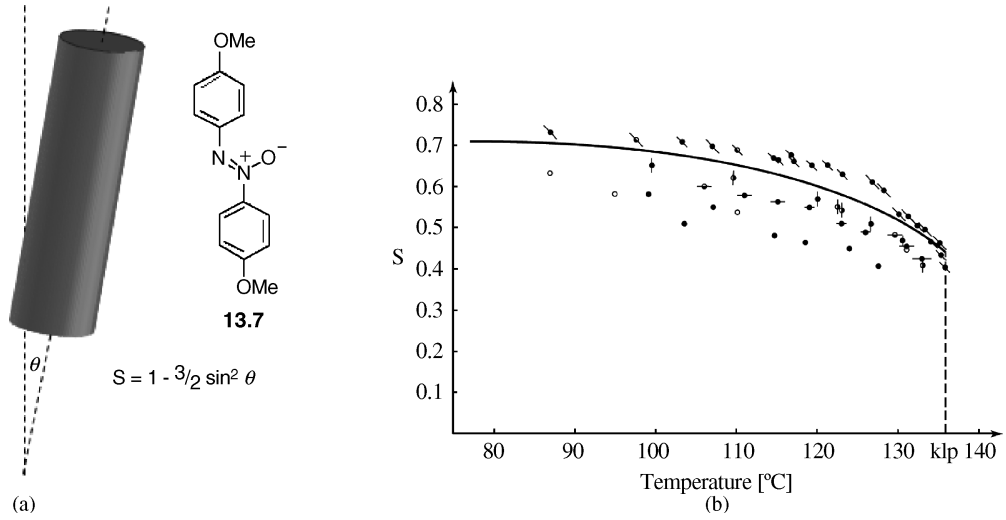


**Figure 13.14** (a) Degree of order, *S*, in a nematic phase. (b) Variation of *S* with temperature for 4,4′-dimethoxyazoxybenzene (**13.7**) (reproduced with permission from [7]).

phase (0.13 kJ mol$^{-1}$), before decomposing finally to an isotropic melt at 42.6 ºC (0.97 kJ mol$^{-1}$). This kind of phase behaviour of such systems is best studied by a polarised hot-stage microscope, in which the sample may be examined visually for characteristic optical patterns as a function of temperature (Box. 13.1).

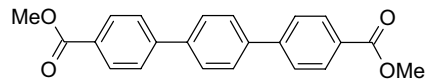


**13.8**

**Box 13.1** Characterisation of Mesophases

There are three main techniques used in characterisation of mesophases: polarised optical hot-stage microscopy, differential scanning calorimetry (*cf.* Box 9.1) and small-angle X-ray scattering.

*Polarised Optical Hot-Stage Microscopy*

This technique, shown diagrammatically in Figure 13.10, is the easiest way to characterise a mesophase, and is generally the first to be employed. The sample (typically $< 1$ mg) is sandwiched between two transparent microscope cover slips and placed on a hot stage that has a precise temperature control. The sample is examined visually through a microscope as it is heated in a slow and controlled manner. Incident light on the sample is first plane-polarised with a polariser between light source and sample. The observer looks through a second polariser at 90 degrees to the first. In the absence of sample, or in the case of an isotropic sample, no light passes and the microscope field is dark. Because of the birefringence of liquid crystals, however, the plane of the polarised light passing through the sample is altered (it becomes elliptically polarised), allowing it to pass through the second polariser to the observer. The textures observed are characteristic of a given mesophase and are best observed during sample cooling.

(*Continued*)

**Box 13.1** (*Continued*)

*Differential Scanning Calorimetry*

The DSC experiment is described in Box 9.1. DSC is strictly complementary to optical microscopy in liquid crystal work. DSC gives information about the enthalpy change during a phase transition. Generally, this change is large during melting and much smaller during a transition between mesophases. DSC results are useful because they enable the operator to be sure that changes in optical appearance observed by microscopy correspond with a phase change, and to identify phase changes that do not give rise to very different appearances.

*Small Angle X-ray Scattering*

Mesomorphic phases are ordered and display a regular periodicity that results in diffraction. The diffraction drops off strongly with angle because the order is often not very long-range and hence measurements are carried out at small scattering angles. The X-ray diffraction pattern of a liquid crystal can give an enormous amount of information about the characteristics of the mesophase and may represent the only way to it definitively characterise. In a smectic phase, for example, diffraction lines that identify both the interlayer and intralayer periodicity can be observed. Correlation with calculated molecular lengths can give information on tilt angle. If the sample is aligned in a magnetic field, the technique gives further information about mesogen orientation.

Cholesteric phases are a kind of helical nematic phase with a helical pitch (length of a single helical turn; *cf.* helicates, Section 10.8) in the region of 200–2000 nm. Instead of lining up in parallel, the rod-like molecules change their orientation with respect to one another in an ordered fashion (Figure 13.13f). The cholesteric mesogens are optically active (indeed, cholesteric phases may be generated by adding nonmesogenic chiral molecules to an ordinary nematic phase, since the energy of twist forms only a very small part of the total energy associated with the molecular order). Cholesteric phases have very interesting optical properties, such as the selective reflection of circularly polarised light, circular dichroism and extremely high degrees of optical rotation in the region of 18 000° $mm^{-1}$ compared to a few tens of degrees for molecular chirality, or some hundreds for chiral fullerenes such as $C_{82}$. As a result, cholesteric mesophases exhibit attractive, iridescent colours. These colours were first brought to the attention of Austrian botanist, Reinitzer, who discovered the liquid crystal phenomenon in 1888 while studying the acetate and benzoate derivatives of cholesterol. Helical cholesteric phases of pitch less than about 500 nm exhibit 'blue phases' (named because of their colour), which generally exist only over a very narrow temperature range (about 1 °C), just before the formation of the isotropic melt. This variable phase behaviour for cholesterol nonanoate **(10.4)** is illustrated in Scheme 13.2.

Blue phases have been known since the early days of liquid crystalline substances. Reinitzer, in a letter to his physicist collaborator, Lehmann, wrote of them in 1888:

> *On cooling [the liquid phase of cholesteryl benzoate] a violet and blue phenomenon appears, which then quickly disappears leaving the substance cloudy but still liquid.*

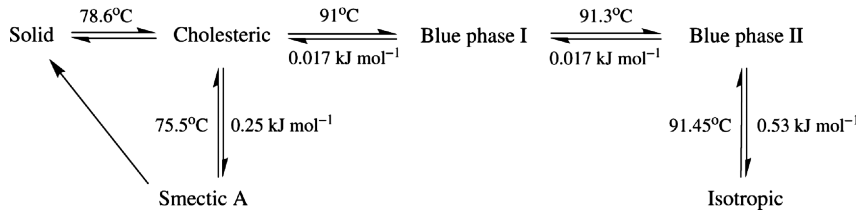


**Scheme 13.2** Phase behaviour of cholesterol nonanoate showing the occurrence of 'blue phases'.

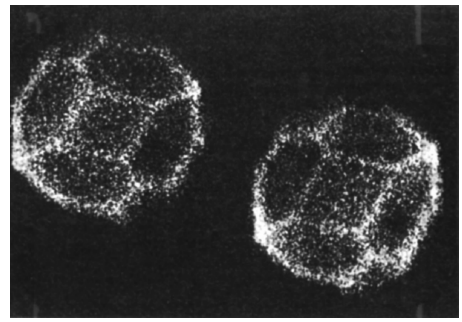

**Figure 13.15** Single crystals of BP I in equilibrium with the isotropic melt (from 58 % weight mixture of cyano-4-methylbutylbiphenyl in Merck nematic ZLI 1840). (Reproduced with permission from [8]).

It was not until the 1970s that blue phases became accepted as thermodynamically distinct phases, but they have since become a main point of interest in condensed matter physics. Three distinct blue phases exist (which are not always blue), known as BP I, II and III, occurring in order of increasing temperature. The phases are due to the formation of tiny single crystals of cubic symmetry: body-centred for BP I and simple cubic for BP II; BP III is quasicrystalline. The crystals exhibit optical Bragg diffraction and small samples up to a few hundred microns in diameter have even been isolated (Figure 13.15). The colour arises from light scattering by the tiny crystallites. Interestingly, it is not possible to distort a helical structure continuously in order to fit a cubic structure, and as a result crystals of BP I and BP II contain defect lines, or disclinations, which contain isotropic liquid, running throughout the lattice.

Discotic phases have been characterised definitively only since 1977, although their existence was postulated by Vorländer in 1923. They fall into two distinct types: a nematic phase and a columnar phase (Figure 13.16). The columnar phase consists of discs stacked one on top of another aperiodically to form liquid-like columns. Order exists between the columns to give a two-dimensional lattice. The columns can form various arrangements such as hexagonal, rectangular, tilted *etc.* Columnar mesophases may also be formed by replacing the flat core of a discotic mesogen by a conical one, as in the cyclotricatechylene hexaester **13.9**. Columnar mesophases that are hollow in the middle are formed by corand derivatives such as hexa(*p*-*n*-dodecyloxybenzoyl)hexacyclen (**13.10**). These are referred to as *tubular mesophases* and are of potential interest as models for ion-channel proteins (*cf.* Section 12.9). The nematic phase is less ordered, with discs showing orientational order without any translational order.

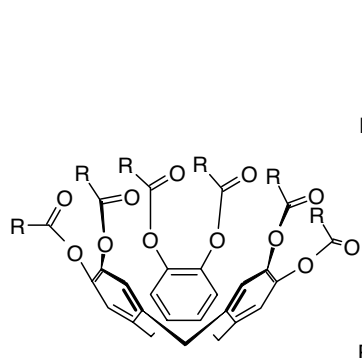
R
O
O
O

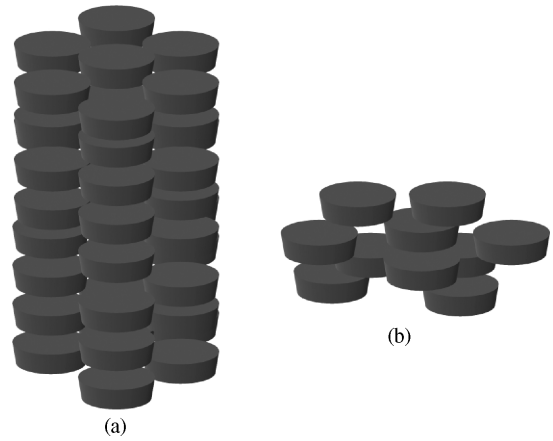


**Figure 13.16** (a) Columnar and (b) nematic discotic phases.

Lyotropic liquid crystal phases are made up of two or more components, one of which is generally an amphiphile (a molecule with hydrophilic and hydrophobic portions, Section 13.2) and the other water or, occasionally, another solvent. Various mesophases are obtained depending on amphiphile concentration. Mesophase formation requires reasonably high amphiphile concentrations in order to bring about interactions between amphiphile aggregates. These liquid crystalline aggregates may be of the lamellar bilayer, micelle or cylindrical type. Lamellar, or 'neat' phases consist of flat bilayers with water sandwiched in between in contact with their hydrophilic groups (*cf.* Figure 13.6). The order comes from the common orientation of the bilayers. These layers may also bend to form micellular or vesicle-based (*cf.* Figure 13.5) *cubic* or *viscous isotropic* phases in which spherical aggregates form a body-centred cubic arrangement. A *hexagonal* phase may also form in which rod-like micellular cylinders are organised parallel to one another in an array rather like the columnar discotic phase (Figure 13.6).

### 13.3.2 Design of Liquid Crystalline Materials

A great deal of work has gone into systematic studies designed to elucidate the molecular properties that give rise to liquid crystalline behaviour. An understanding of these principles has enabled the design of a large range of liquid crystalline materials with very interesting properties. The conventional wisdom may be summarised as follows:

- The molecular shape should be relatively thin or flat, especially within rigid molecular frameworks.
- The molecular length should be at least 1.3 nm (13 Å), consistent with the presence of long alkyl groups on many room-temperature liquid crystals.
- The structure should not be branched or angular (but see recent developments in supramolecular liquid crystals in the next section).
- A highly anisotropic polarisability is required in order to enhance intermolecular dispersive interactions. This is favoured by the presence of easily polarisable groups and permanent dipoles.
- A low melting point is preferable in order to avoid metastable, monotropic liquid crystalline phases. Low-temperature mesoporphic behaviour in general is technologically more useful, and alkyl terminal groups promote this.

An extended, structurally rigid, highly anisotropic shape seems to be the main criterion for liquid crystalline behaviour, and, as a result, many liquid crystalline materials are based on substituted

(particularly *p*-disubstituted) benzene rings. The *para* arrangement lends itself to a long, extended shape, as in stilbene and Schiff's base derivatives such as **13.11** and **13.12**. The *trans* conformation of the central double bond in these compounds is a much more efficient promoter of liquid crystalline behaviour than the analogous *cis* isomers because of the resultant elongated molecular shape. The Schiff's base motif can be problematic, however, as a result of hydrolytic cleavage. It is unnecessary, however, for the central unit to be an aromatic ring, and compounds based on saturated cyclohexyl derivatives also exhibit liquid crystallinity, supporting the notion that it is the structural rigidity (imparted by the ring system), rather than the dispersive, interactions with the aryl ring that are the most important. Polar groups to enhance the intermolecular interactions may be placed anywhere on the molecule. Traditionally they have been situated in the centre of the mesogen (as in **13.7**) with surrounding alkyl chains, but terminal functionalities such as CN, ester or carboxylic acid groups are equally effective, and are often used in modern technologically important liquid crystalline materials, *e.g.* **13.3**. The size and shape dependence is highlighted by non-molecular mesogens such as the hydrogen-bonded carboxylic acid dimer **13.13**. The hydrogen-bonding interactions allow the molecular pair to achieve the necessary length and are strong enough to give the dimer a long enough lifetime for mesophase formation.

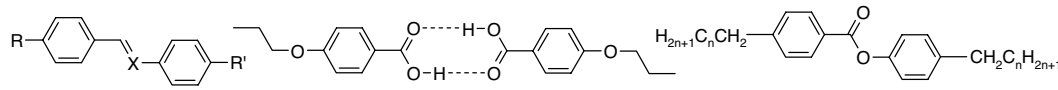


**13.11** X = CH
**13.12** X = N

**13.13**

**13.14**

Alkyl chains lower the melting/clearing point ($T_c$ – temperature of the isotropic phase transition) of the molecule and increase its molecular polarisability. Interesting variations in clearing-point temperature are observed with increasing alkyl chain length, with clearing point alternating with even and odd numbers of carbon atoms, as in **13.14** (Figure 13.17). This results from the effect of the substituent on the polarisation anisotropy of the molecule. The long molecular axis corresponds to the direction of highest polarisability. Addition of a carbon atom along this direction increases the polarisability along this axis more then at right angles to it. Conversely, adding another —$CH_2$—group at 109º to the previous one has the opposite effect, mostly increasing the polarisability perpendicular to the main axis. The liquid crystal clearing point is related closely to the difference between the longitudinal and

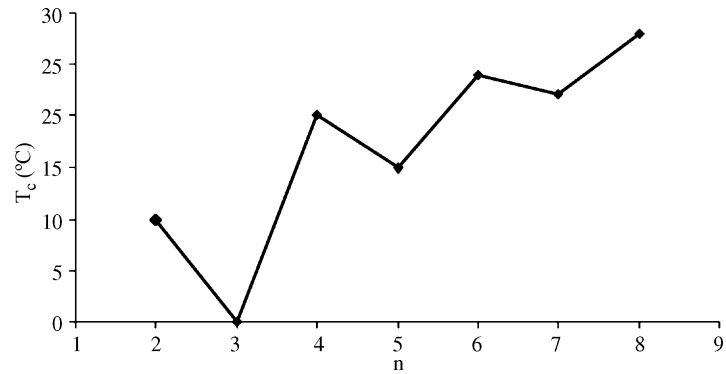


**Figure 13.17** Alternation of clearing point temperature (ºC) with alkyl chain length (*n*) for compounds of type **13.14**.

cross-polarisation, and hence the $T_c$ alternates, with the effect gradually tailing off as chain length and flexibility increases.

## 13.3.3 Supramolecular Liquid Crystals

Paleos, C. M., Tsiourvas, D., 'Supramolecular hydrogen-bonded liquid crystals', *Liquid Crystals* 2001, **28**, 1127–1161.

The carboxylic acid dimer **13.13** along with Lehn's 2,6-diaminopyridine-uracil system (Section 10.8.8) are examples of the use of supramolecular interactions to assemble mesogens. A similar system is the system formed by hydrogen-bonding interactions between 4-butoxybenzoic acid (**13.15**) and *trans*-[4-ethoxy(benzyol)oxyl]-4'-stilbazole (**13.16**) which gives mesogenic rod like structures.[9] Neither molecule is mesogenic by itself, however the heteromolecular hydrogen bonding interaction between the carboxylic acid and the pyridine groups results in a thermally stable rigid rod-like assembly which displays nematic phases up to 214°C.

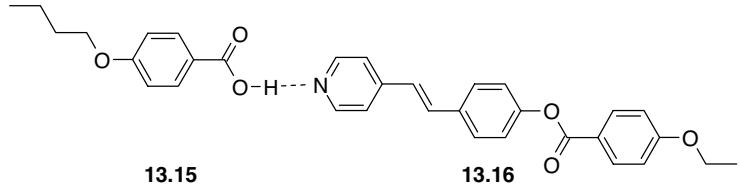


**13.15** **13.16**

Since this 1989 report there have been numerous examples of complex supramolecular liquid crystal systems. Supramolecular chemistry has played a significant role in the move away from traditional disc or rodlike molecules and the past 25 years has seen a whole raft of new liquid crystals based on dendrimers (Section 14.1), bent or bowl-shaped cores, non-covalent bonding, metal coordination or that rely on microphase separation to drive mesophase formation. For example, Figure 13.18 shows a liquid crystal system based on the common guanosine quartet assembly that changes from a smectic (rod-shaped) to hexagonal columnar (disc-shaped) phase on the addition of sodium ions, which template the quartet formation. The oxygen atoms chelate to the metal ions and the liquid crystal reorganises into a circular geometry.[10]

Metal ion coordination in general is an excellent way to generate large, rigid mesogens. Figure 13.19 shows the X-ray structure of a palladium(II) linked metallomesogen in which the palladium coordination links the two pyridyl ligands into an extended dumbbell like structure[11] Depending on the length of the alkyl chains this kind of mesogen forms a number of columnar liquid crystalline phases. These columnar phases were studied by X-ray diffraction of single, ordered liquid crystalline domains. The sample is prepared using uncovered droplets of the mesophase. The compound is deposited onto a glass surface and heated into the isotropic phase. The melt is the slow-cooled, favouring the nucleation of liquid crystal domains with specific orientations at the interfaces with both the glass and the air. In the case of these columnar phases the columns lie horizontally to the glass slide. The X-ray diffraction patterns for the decyloxy analogue of the compound shown in Figure 13.19 are shown in Figure 13.20 at temperature of 104 °C and 82 °C. The lower symmetry evident in the second image corresponds to transition from a columnar hexagonal phase to a columnar rectangular phase on cooling.

Supramolecular liquid crystals have also been reported based on more unusual supramolecular interactions such as halogen bonding (Section 1.8.9).[12] Neither of the components in **13.17** are mesomorphic by themselves but the presence of the highly activated iodine atom in pentafluoroiodobenzene results in a strong N···I interaction (N···I distance 2.81 Å by X-ray crystallography). These

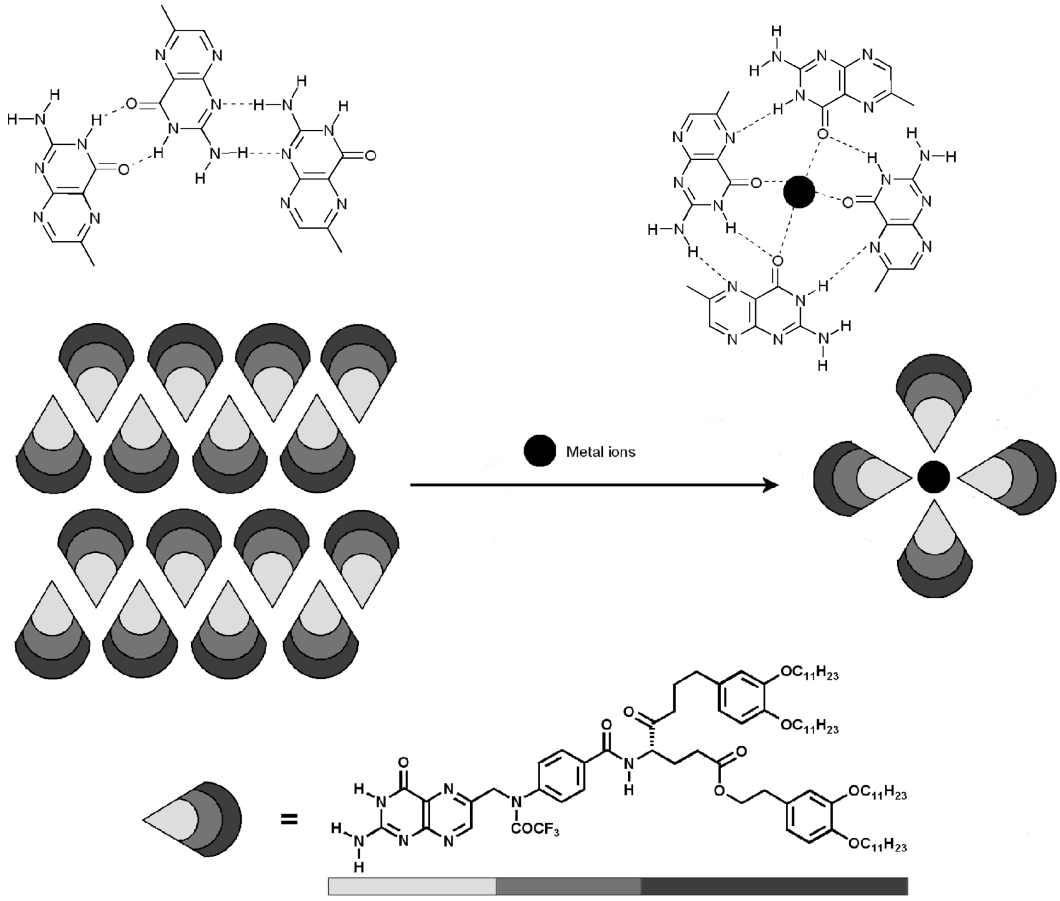


**Figure 13.18** A ribbon structure of a folic acid derivative self-assembles into a disc-like tetramer based on a G-quartet motif showing liquid crystalline behaviour on the addition of a metal ion such as $Na^+$.

interactions are of comparable strength to hydrogen bonds and result in the formation of a smectic A liquid crystalline phase upon cooling the melt to 84 °C. The transition temperature is something of a measure of the strength of the interactions holding the supramolecular mesogen together and this transition temperature compares well with related hydrogen bonded systems.

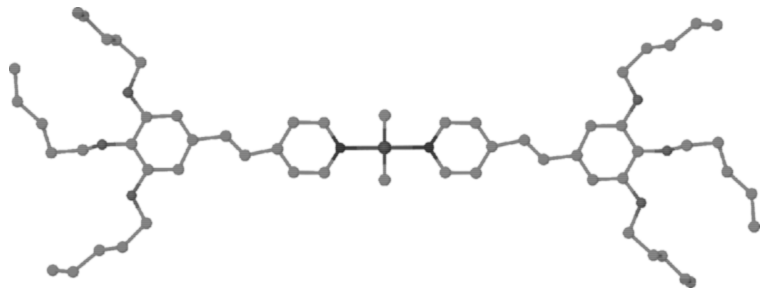

**Figure 13.19** X-ray molecular structure of a metallomesogen based on square planar *trans*-$PdCl_2$ linkers.[11]

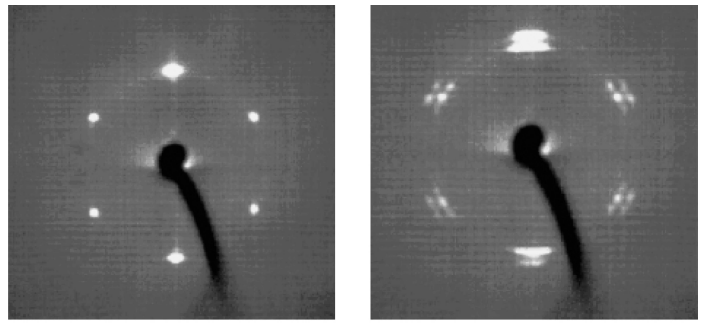


**Figure 13.20** Orientated monodomain X-ray diffraction images from the dodecyloxy analogue of the compound shown in Figure 13.19 at (a) 104 °C and (b) 82 °C corresponding to hexagonal and rectangular columnar phases respectively (reprinted with permission from [11] © 2004 American Chemical Society).

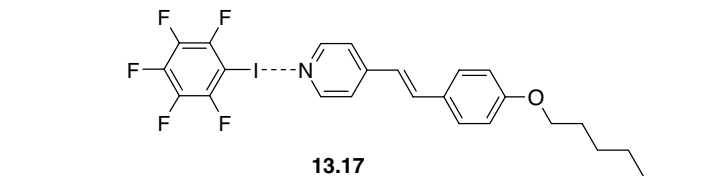

**13.17**

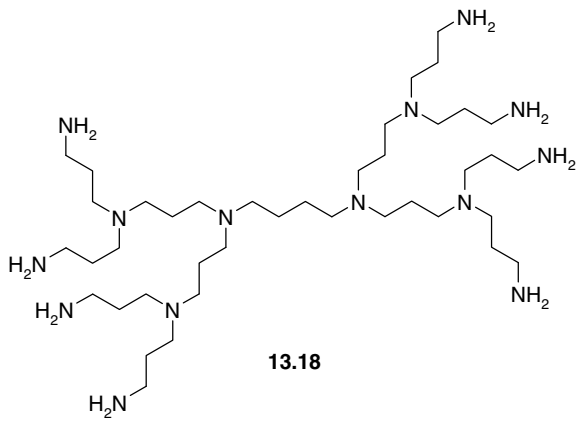

**13.18**

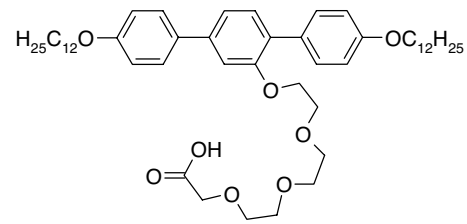

**13.19**

Two component hydrogen bonded mixtures of dendrimers and T-shaped branched amphiphiles are also a rich source of mesophases. Figure 13.21 shows a polarised optical microscope image of the contact region between the dendrimer **13.18** and the T-shaped amphiphile **13.19**. A wide variety of mesophases co-exist as one component diffuses into another. The majority of these have been identified and studied.[13]

Finally an interesting new class of liquid crystals has recently been reported based on the surfactant templating of low-melting *inorganic* salts like $ZnCl_2$. The inorganic component easily forms glasses with strands comprising linked tetrahedra. Addition of amphiphiles gives new hybrid liquid crystalline phases depending on the inorganic-organic composition ratio and the temperature. This class of materials has been named *metallotropic*.[14]

Liquid crystals remain an active and vigorous research area with many technological applications. We will look at one of these applications in the next section. We also return to liquid crystals made up of polymers in chapter 14.

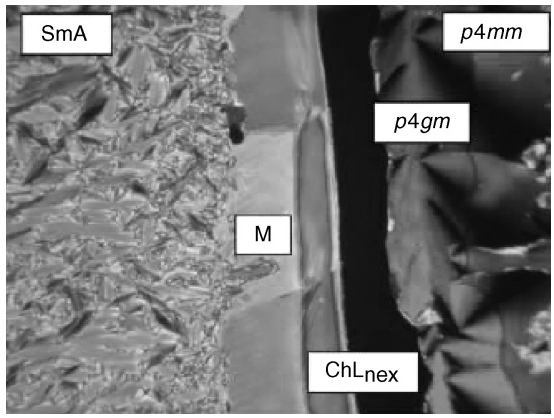


**Figure 13.21** Contact region at 78 °C showing the phase sequence smectic-A (fan texture), M (unidentified mesophase), hexagonal channelled layer phase (ChLhex), square columnar phases p4gm and p4mm (from left to right) upon increasing concentration of **13.18** (reproduced by permission of The Royal Society of Chemistry). See plate section for colour version of this image.

### 13.3.4 Liquid Crystal Displays

Liquid crystals have a number of technologically important applications. They are used in precise temperature measurement, where the liquid crystalline phase changes can give temperature resolution of up to 0.007 K in a 1 K range. On a less precise level, temperatures of between –20 °C and +250 °C can be measured on liquid crystalline thermometers. They are cheap and toxicologically harmless and, as a result, are found in areas as diverse as medicine and even as wall thermometers in 'give away' advertising gimmicks. Liquid crystals are also found in various areas of analytical chemistry, and in any situation where it is important to measure direction- or orientation-dependent properties. Dissolution of the sample in a liquid crystalline nematic phase results in the orientation of the sample molecules in a precise and regular manner, facilitating measurement of anisotropic properties, such as circular dichroism phenomena, by IR and UV–visible spectroscopy. Liquid crystals are also used as stationary phases in the chromatographic separation of closely related isomers (*e.g.* dihaloarenes), which may often have very different solubilities in liquid crystalline phases. A range of NMR applications also exist.

By far the most important application of liquid crystals is in liquid crystal displays (LCD). These made their first appearances in wristwatches and pocket calculators, with the familiar seven-segment display (resembling a number '8' with square edges). Modern LCDs are now used in full-colour computer monitor displays (with the aid of dyes) based on twisted nematic cells (TNC), first outlined by Schadt and Helfrich in 1971. LCDs work on the principle that an applied electric field will alter the molecular orientations and result in changes in the optical behaviour. In a TNC, a thin layer (10–15 μm) of nematic liquid crystal is sandwiched between two transparent glass plates. The glass plates are pretreated with a director that has an orientating effect on the liquid crystalline phase, much like the mesogen orientates itself by interactions with its neighbours. If the two plates are rotated at 90 degrees to each another, a helical twist in the nematic phase is produced, with twist angle of 90° from one side to the other (Figure 13.22). The polarisation of plane-polarised light passing through the layer follows this 90-degree twist. The orientated liquid crystalline layer is placed between crossed polarisers, resulting in a display that is transparent to light at rest in the absence of an electric field. Application of a voltage produces a homeotropic rearrangement of the nematic phase and the twist is lost, resulting in no rotation of the plane-polarised light, no light transmission, and hence a darkened

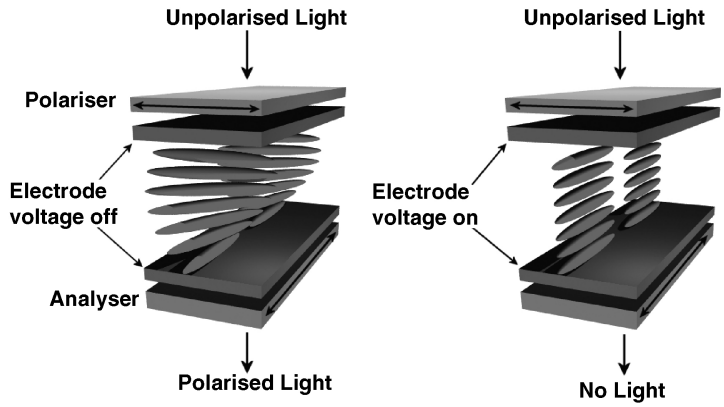


**Figure 13.22** Operation of a twisted nematic cell. In the absence of an applied electric field, the twisted nematic rotates the plane of polarised light from one side of the cell to the other allowing light to pass through. An applied potential renders it opaque.

display. Because a voltage is required only to darken portions of the display when in use, the power consumption is extremely small, making the TNC ideal for use in portable applications such as watches, portable computers *etc.* The displays are also flat and compact, and their readability increases with ambient luminosity. Disadvantages are that the displays cannot be read in the dark (unless backlit), nor at an extreme viewing angle and their response time is slow (about 50 μs) compared with cathode ray tubes (10 μs), limiting their application in television sets, for example. The latest generation of flat panel displays get round some of these problems by using a patterned vertical alignment (PVA) method. In a conventional PVA a vertically aligned liquid crystal (LC) director tilts down in four directions making 45° with respect to crossed polarisers to give a wide viewing angle. The parallel geometry reduces the lag time while molecules reorientate when the voltage is turned off because the twisting occurs when the voltage is switched on.

More modern, much faster responding liquid crystalline displays use ferroelectric liquid crystals such as *p*-decyloxybenzylidine-*p′*-amine-2-methylbutylcinnamate, which can be switched between two stable states by application of an external field. Such properties may also be useful in optical data storage.

## 13.4 Ionic Liquids

Rogers, R. D., Seddon, K. R., 'Ionic liquids – solvents of the future?', *Science* 2003, **302**, 792–793.

An ionic liquid (IL) is literally an ionic compound (a salt) that is a liquid. Of most current interest are salts that are liquids at room temperature (RTILs), or at least below 100 °C. There is a range of compounds that form room temperature ionic liquids dating back to ethanolammonium nitrate, $(EtNH_3)^+(NO_3)^-$ (m.p. 14 °C), synthesised by Walden in 1914. Perhaps the most popular and well-studied are those based on the 1-butyl-3-methylimidazolium (bmim) cation, such as $bmim^+ PF_6^-$ (**13.20**) and $bmim^+BF_4^-$ which melts at *ca.* –80 °C. The imidazolium ionic liquids were initially used as their halogenoaluminate salts but they have a major drawback in that they are highly moisture sensitive.

In 1992, Zaworotko used weakly coordinating anions such as hexafluorophosphate and tetrafluoroborate, greatly expanded the range of ionic liquids available.[15] Modern ionic liquids that are air- and moisture stable based on non-coordinating anions has meant that the field has attracted tremendous

interest in recent years. Ionic liquids have a range of properties that make them highly attractive as solvents, electrolytes and reaction media. Chiefly these are:

- tuneable melting point, viscosity and acidity by variation of the alkyl substituents;
- non-volatility, meaning they do not have an odour nor contribute volatile organic compounds (VOCs) to the atmosphere and can thus lay claim to be 'Green' solvents (although they are certainly toxic and therefore not environmentally benign[16]);
- very high polarity meaning they catalyse some reactions (*e.g.* Diels-Alder) extremely effectively and interact extremely strongly with microwaves (useful in microwave heating[17]), for example;
- Excellent thermal stability and low combustibility.

These properties have resulted in a veritable explosion of research into the synthesis, properties and uses of ionic liquids over the past decade, Figure 13.23. Recently, traditional non-coordinating anions like $PF_6^-$ and $BF_4^-$ are being abandoned as ILs enter mainstream applications, because of their toxicity. Non-toxic replacements include anions such as bis(trifyl)imide $(CF_3SO_2)_2N^-$. Other, less toxic cations are also increasingly popular, *e.g.* choline salts.

In terms of supramolecular chemistry, imidazolium type ionic liquids are interesting because they are excellent C–H hydrogen bond donors. The X-ray crystal structure of bmim $Cl^-$ shown this property clearly with C···Cl = 3.39 Å, Figure 13.24. Interestingly, two different polymorphic forms of this material are known depending on whether it is crystallised from the molten ionic liquid for from solution,

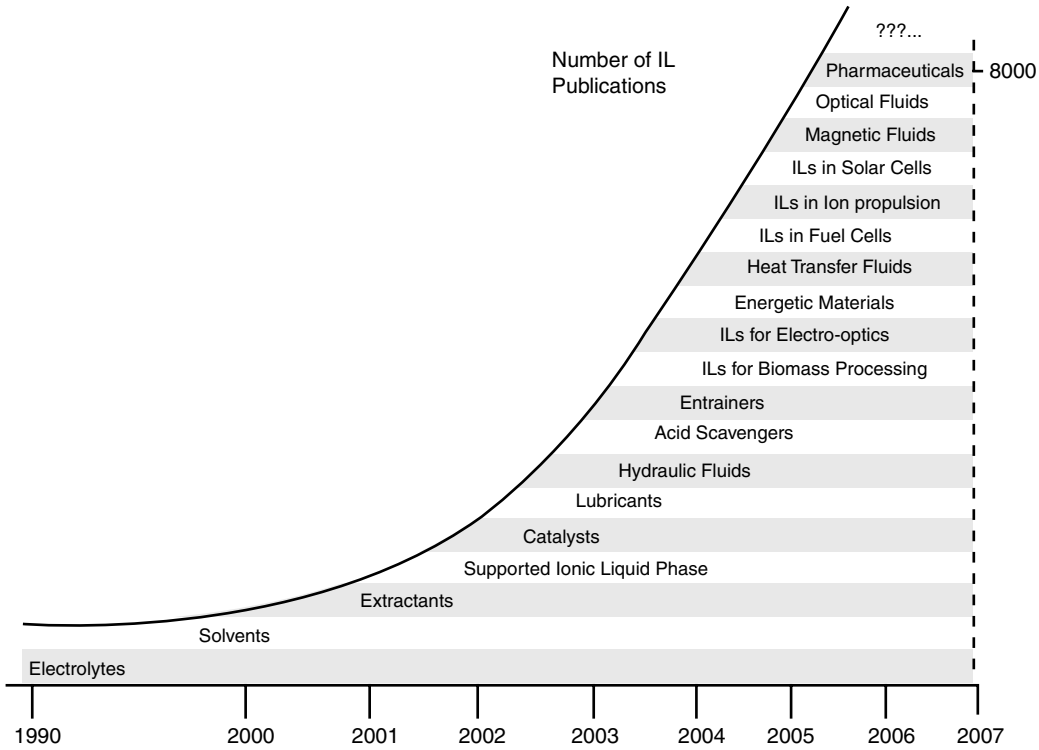


**Figure 13.23** Research activity in ionic liquids as measured by number of publication (reprinted with permission from [18] © 2007 American Chemical Society).

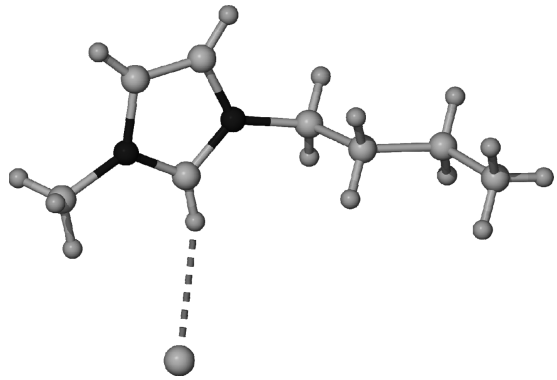

**Figure 13.24** X-ray crystal structure of bmim$^+$Cl$^-$ showing the CH···Cl$^-$ hydrogen bond, C···Cl = 3.39 Å.[21]

differing only in the rotations of the alkyl group. This factor sheds light on the low melting points of ionic liquids which may act as supercooled solutions, crystallising sluggishly as a result of multiple conformational minima for the flexible subsistent.[19] These kinds of hydrogen bonds are implicated in much of the interactions of ILs with their solutes. A study of the Diels-Alder cycloaddition reaction between methyl acrylate and cyclopentadiene in a number of ionic liquids used the *exo/endo* ratio of the products to probe the nature of the solvent. The results showed that hydrogen bonding between the cation of the ionic liquid and the methyl acrylate is the principal interacting controlling the product selectivity.[20]

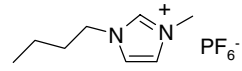


**13.20** bmim$^+$PF$_6^-$

## 13.5 Liquid Clathrates

Spear, S. K., Holbrey, J. D. and Rogers, R. D., 'Liquid clathrates', in *Encyclopedia of Supramolecular Chemistry*, Atwood, J. L. and Steed, J. W. (eds), Dekker: New York, 2004, vol. 1, 804–808.

The term 'liquid clathrate' was coined in 1969 by Jerry Atwood, then of the University of Alabama, USA, to describe the discovery of novel biphasic behaviour of a range of salt solutions in aromatic solvents such as benzene and toluene. It is something of a contradiction, since clathrates are, by definition, solid-state compounds (Section 1.2). The concept of trapping a guest within a host matrix as a result of geometrical and topological (as opposed to chemical) considerations is equally applicable to both the solid and liquid phases, however, and there are close parallels between what might be termed, more rigorously, 'nonstoichiometric liquid inclusion compounds' and conventional solid-state clathrates. Much of the chemistry of liquid clathrates is still poorly understood, but liquid clathrates share several key properties:

- They are formed from a salt of a non-coordinating anion.
- There are special geometrical requirements for both cation and anion.
- Formation of small, closed units of association (*e.g.* dimers, trimers *etc.*) is not permitted.
- Liquid clathrates are useful in a number of selective organic separations.

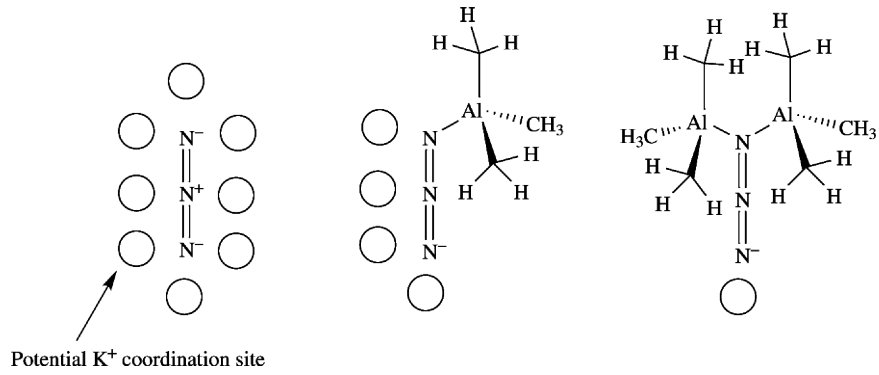


**Figure 13.25** Favourable $K^+$ interaction sites in $[Al_2Me_6N_3]^-$ (the anion in **13.21**), $[AlMe_3N_3]^-$ and $N_3^-$ showing the difficulty experienced by the cations in approaching the anion as its bulk increases. This leads to the creation of regions of solvent-filled space (clathration) even in the liquid phase, which is the basis for liquid clathrate behaviour.

The first liquid clathrates resulted from reaction of $KN_3$ with the highly air- and moisture-sensitive $AlMe_3$ to give solid $K[Al_2Me_6N_3]$ **13.21**. This solid was accidentally mixed with toluene, in which it was thought to be insoluble. In fact, the white solid was observed to dissolve rapidly, forming two immiscible liquid layers consisting of a lower fraction of $K[Al_2Me_6N_3]\cdot 3.8C_6H_5Me$ and an upper layer of pure toluene. The ratio of alkyl aluminium salt to toluene in the lower layer was found to be reproducible, regardless of the amount of toluene added (as long as it was over a certain critical value), and is referred to as the A/A number (aromatic to anion ratio). Similarly, **13.21** forms a liquid clathrate with six molecules of benzene; however, no liquid clathrate formation is observed with the monoaluminium species $K[AlMe_3N_3]$, nor with $KN_3$ itself. This different behaviour is attributed to the bulky shape of the alkyl aluminium anion in the liquid clathrate, which effectively blocks access to the most favourable $K^+$ coordination sites near the X—$N_3^-$ portion of the anion. In contrast, the $N_3^-$ unit is much more exposed in $[AlMe_3N_3]^-$ than the azide anion ($N_3^-$) itself (Figure 13.25). This leads to the conclusion that the size and shape of the anion is highly important in liquid clathrate formation. Anions with little opportunity for multiple close interactions with cations will be likely to display liquid clathrate behaviour. A large number of liquid clathrates have been described based on alkyl aluminium complexes in conjunction with aromatic solvents with anywhere between 1.3 and 42.2 molecules of solvent, although compositions with more than about four aromatic molecules are common.

The model of the solution behaviour of liquid clathrates that appears to best fit the observations is depicted in Figure 13.26. Large regions of liquid order exist in which cations and anions interact strongly with one another. This prevents simple dissolution, but association into aggregates such as dimers and trimers (possibly leading to crystal nucleation) is also prevented by the steric properties of the anions and/or cations. The role of the aromatic solvent is to support the structure and stabilise

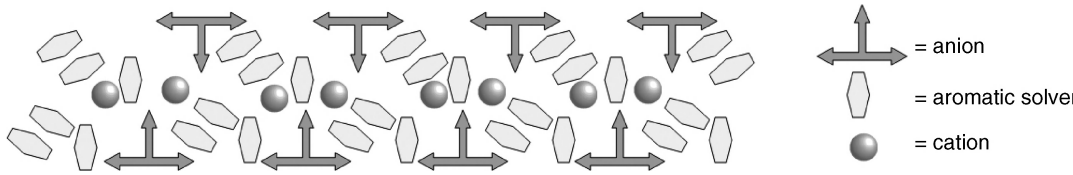


**Figure 13.26** Two-dimensional model of liquid clathrate behaviour.

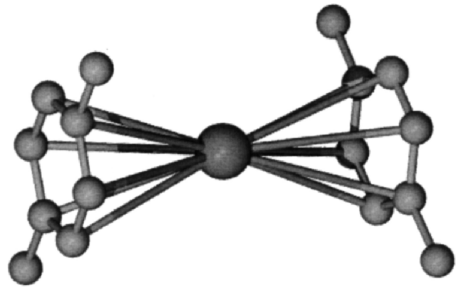

**Figure 13.27** X-ray crystal structure of $Cs[Al_2Me_6N_3]\cdot 2(p\text{-xylene})$ showing the cation–$\pi$ interactions.

the cation and anion charge by extensive $\pi$-stacking and cation–$\pi$ interactions involving the aromatic ring quadrupole (Sections 1.8.5 and 1.8.7). The aromatic solvent also acts as a guest molecule, as in a solid-state clathrate, filling the voids in the structure, hence the origin of the term liquid *clathrate*. The kind of cation–$\pi$ interaction that is taking place in solution may well be represented by the solid-state structure of $Cs[Al_2Me_6N_3]\cdot 2(p\text{-xylene})$, in which the $Cs^+$ cation is sandwiched between the two included aromatic guests (Figure 13.27). Great care must be taken, however, in comparing solid-state and solution results, especially in non-rigid systems such as these.

Considering the process of liquid clathrate formation, solid-state liquid clathrate forming materials such as **13.21** are subject to a dissolution equilibrium or liquefying phase change upon exposure to aromatic solvents (Equation 13.1).

$$MX + nS = M.X \cdot S_n \tag{13.1}$$

This equilibrium is highly temperature-dependent. For example, in the case of **13.21** at 20 ºC, the equilibrium lies entirely to the left, while at 30ºC it is entirely to the right. The limiting (maximum) value of n represents the A/A number. Liquid clathrates can form, however, even when the amount of solvent present is less than the A/A number. For **13.21**, for example, a minimum threshold value of n of about 2.5 in the case of S = benzene is required to initiate liquid clathrate formation. The resulting material is described as a 'hungry' liquid clathrate and gives the appearance of a single homogeneous solution phase. This solution will continue to absorb solvent until it has reached its A/A value (6 in this case) at which point the formation of a pure solvent phase in addition to the liquid clathrate is observed. The A/A value is apparently temperature independent. It is governed by three main factors:

- For a given anion and aromatic, the larger the cation the larger the A/A.
- For a given cation and aromatic, the larger the anion the larger the A/A.
- For a given cation and anion, the larger the aromatic, the smaller the A/A.

The A/A values have been found to correlate extremely well with aromatic molecules' van der Waals volumes, suggesting that the liquid cavity model in which the aromatic is a space filler is an accurate one. The constancy of the A/A value suggests that the cation–anion association produces fairly well-defined solution voids with a volume that is invariant with change of solvent.

The majority of the interest in liquid clathrates has centred around their potential applications in separation science, particularly in the separation of closely related species such as benzene and toluene, or xylene isomers (*cf.* zeolite-based methods, Section 9.2). Separation occurs as a result of the greater ability of one organic solvent over another to stabilise the liquid clathrate phase. Hence, in a

mixed-solvent medium, the relative proportion of two solvent components ($S^1$ and $S^2$) in the liquid clathrate and bulk solvent phases will be different. This difference may be quantified by a selectivity parameter, α, which is defined in Equation 13.2.

$$\alpha = \frac{[S^1]_{LC}/[S^2]_{LC}}{[S^1]_{Bulk}/[S^2]_{Bulk}} \tag{13.2}$$

where $[S^1]_{LC}$ is the concentration of solvent $S^1$ in the liquid clathrate phase and $[S^1]_{Bulk}$ is the concentration of $S^1$ in the bulk solvent phase.

Liquid clathrates offer a great advantage over solid-state separations (*e.g.* by formation of Hoffman-type inclusion compounds, Section 9.4) because of the extremely fast mixing kinetics, the avoidance of the need to wait for crystallisation to occur and the easy separation of the two liquid phases. It should also prove possible to run liquid clathrate separations in a continuous extraction manner. The $\alpha$ values of a number of liquid clathrate-based separations have been reported and are summarised in Table 13.1.

Clearly significant separations can be effected, especially between aromatics and aliphatics. The size basis for the effect is clear in the comparison of hexane and hexene results: the presence of the 1-hexene double bond does not seem to enhance its inclusion into the liquid clathrate phase greatly. Also clear is the strong dependence on the dimensions of the anion, with the smaller, more compact materials giving better separations.

One particularly interesting application of liquid clathrates that has been explored is in coal liquefaction. Coal contains a large number of low-to medium-molecular-weight aromatic hydrocarbons and, while toluene is extremely inefficient at extracting these materials, contact of coal with a toluene-based liquid clathrate at 50 ºC results in the rapid partitioning of 23 % of the coal mass into the liquid clathrate phase. No chemical reaction occurs between the coal and liquid clathrate solution and the liquid clathrate-forming salt may be recovered simply by lowering the temperature. Such a process, which has been patented, may well prove to be of general utility in the production of chemical feed stocks and fuels if there are substantial changes in the relative prices of crude oil and coal.

A great deal of more recent research has concerned liquid clathrates formed from strong acids such as HCl in aromatic solvents in which oxonium ions such as $H_3O^+$ are stabilised by crown ethers and play the role of the cation. This has allowed the isolation of a range of interesting oxonium salts, as discussed in Section 3.11.1.

The fact that liquid clathrates are thus liquids based on ionic compounds means that they are somewhat related in terms of their properties to ionic liquids (Section 13.4), but they are fundamentally a two or more component phase instead of a pure compound. A recent report has shown, however, that bmim

**Table 13.1** Liquid clathrate-based separations of 1:1 feed mixtures.

| Parent compound | Separation | $\alpha$ |
|---|---|---|
| $[NMe_4][Al_2Me_6Cl]$ | Benzene/hexane | 24 |
| $[NMe_4][Al_2Me_6NO_3]$ | Benzene/hexane | 12 |
| $[NMe_4][Al_2Et_6NO_3]$ | Benzene/hexane | 5.0 |
| $[NPr_4][Al_2Me_6I]$ | Benzene/1-hexene | 8.8 |
| $[NMe_4][Al_2Me_6Cl]$ | Benzene/1,5-cyclooctadiene | 4.0 |
| $[NPr_4][Al_2Me_6I]$ | Benzene/dicyclopentadiene | 2.8 |
| $[NMe_4][Al_2Me_6NO_3]$ | Benzene/mesitylene | 1.8 |
| $[NMe_4][Al_2Et_6NO_3]$ | Benzene/mesitylene | 1.6 |

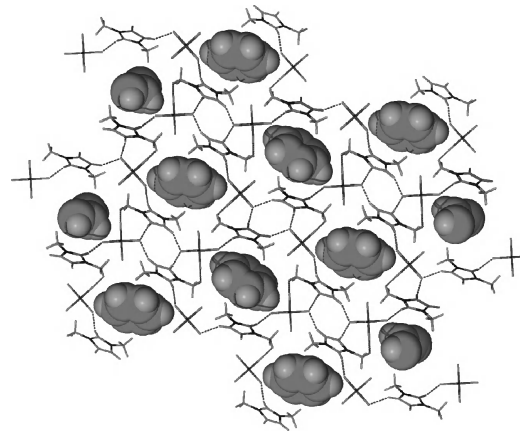

**Figure 13.28** X-ray crystal structure of the liquid-clathrate-derived inclusion compound *N,N′*-dimethylimidazolium$^{+}$($PF_6^{-}$)·0.5$C_6H_6$ showing the stacking of the benzene guest with the imidazolium cations.[22]

type ionic liquids with hexafluorophosphate, bis(trifyl)imide, tetrafluoroborate, and chloride anions also form liquid clathrate phases including up to 3.5 moles of benzene. In some cases crystalline solids can be isolated from such mixtures as in *N,N′*-dimethylimidazolium($PF_6^{-}$)·0.5$C_6H_6$ (Figure 13.28). The ability of ionic liquids to include amounts of aromatic organics may have significant bearing on their applications in chemistry involving such compounds.[22]

## Summary

- While lacking the long-range order of solids liquids exhibit significant supramolecular interactions that are able to weld together large aggregates.
- The significance of these interactions rises as molecules become larger, leading to greater interaction surface area and shape-dependent phenomena.
- Liquid assemblies such as lipid bilayers are of fundamental importance as biological membranes.
- Self-assembled monolayers on solid substrates have significant technological applications as coatings and sensors and in nanofabrication.
- Liquid crystals are highly technologically important materials exhibiting varying degrees of order depending on temperature and molecular shape. They are subject to supramolecular design and mesogens can be assembled using non-covalent interactions.
- Recent work in supramolecular chemistry has dramatically increased the range of available mesogens from the early rigid rod type molecule to dendrimers, those with bent or bowl-shaped cores, non-covalently bonded systems, metal coordinated species and those involving microphase separation
- Ionic liquids are potentially ‘Green’ solvents and offer interesting properties as designer solvents and can act as liquid clathrates, including neutral guest molecules.

## Study Problems

13.1 From your understanding of the non-covalent interactions outlined in Chapter 1, discuss the driving force behind the formation of surface monolayers, micelles and other forms of liquid order.

How does this relate to the formation of hydrophobic molecular host–guest complexes by cyclophanes (Chapter 6)?

13.2 An ammonium ion-based amphiphile has a cross-sectional area of 5 Å$^2$. Calculate the surface area occupied by $2 \times 10^{-5}$ moles of this material. How many moles would be required to form an ordered monolayer on a Langmuir trough of surface area 10 cm$^2$? Suggest how the system might behave if (a) double that quantity of amphiphile were present and (b) 100 times that quantity were present.

13.3 Explain why it is possible to observe more than one liquid crystalline phase within a given system. As a system is heated, why are nematic phases usually the final phases observed before the formation of an isotropic melt?

## References


1. Sorenson, J. M., Hura, G., Glaeser, R. M., Head-Gordon, T., What can x-ray scattering tell us about the radial distribution functions of water? *J. Chem. Phys.* 2000, **113**, 9149–9161.
2. Ward, M. D., Horner, M. J., Structure and order in soft matter: symmetry transcending length scale. *CrystEngComm* 2004, **6**, 401–407.
3. Davis, J. J., Interfacial sensing: surface assembled molecular receptors. *Chem. Commun.* 2005, 3509–3513.
4. Errington, R. J., Petkar, S. S., Horrocks, B. R., Houlton, A., Lie, L. H., Patole, S. N., Covalent immobilization of a TiW5 polyoxometalate on derivatized silicon surfaces. *Angew. Chem., Int. Ed.* 2005, **44**, 1254–1257.
5. Lie, L. H., Patole, S. N., Pike, A. R., Ryder, L. C., *et al.*, Immobilisation and synthesis of DNA on Si(111), nanocrystalline porous silicon and silicon nanoparticles. *Faraday Discussions* 2004, **125**, 235–249.
6. Sackmann, H., Demus, D., Problems of polymorphism in liquid-crystals. *Mol. Cryst. Liquid Cryst.* 1973, **21**, 239–273.
7. Vogtle, F., *Supramolecular Chemistry*. John Wiley & Sons, Ltd: Chichester, 1991,
8. Cladis, P. E., Pieranski, P., Joanicot, M., Elasticity of blue phase-I of cholesteric liquid-crystals. *Phys. Rev. Lett.* 1984, **52**, 542–545.
9. Kato, T., Frechet, J. M. J., New approach to mesophase stabilization through hydrogen-bonding molecular-interactions in binary-mixtures. *J. Am. Chem. Soc.* 1989, **111**, 8533–8534.
10. Pieraccini, S., Gottarelli, G., Mariani, P., Masiero, S., Saturni, L., Spada, G. P., Columnar lyomesophases formed in hydrocarbon solvents by chiral lipophilic guanosine-alkali metal complexes. *Chirality* 2001, **13**, 7–12.
11. Donnio, B., Heinrich, B., Allouchi, H., *et al.*, Generalized model for the molecular arrangement in the columnar mesophases of polycatenar mesogens. Crystal and molecular structure of two hexacatenar mesogens. *J. Am. Chem. Soc.* 2004, **126**, 15258–15268.
12. Nguyen, H. L., Horton, P. N., Hursthouse, M. B., Legon, A. C., Bruce, D. W., Halogen bonding: A new interaction for liquid crystal formation. *J. Am. Chem. Soc.* 2004, **126**, 16–17.
13. Cook, A. G., Baumeister, U., Tschierske, C., Supramolecular dendrimers: Unusual mesophases of ionic liquid crystals derived from protonation of DAB dendrimers with facial amphiphilic carboxylic acids. *J. Mater. Chem.* 2005, **15**, 1708–1721.
14. Martin, J. D., Keary, C. L., Thornton, T. A., Novotnak, M. P., Knutson, J. W., Folmer, J. C. W., Metallotropic liquid crystals formed by surfactant templating of molten metal halides. *Nature Materials* 2006, **5**, 271–275.
15. Wilkes, J. S., Zaworotko, M. J., Air and water stable 1-ethyl-3-methylimidazolium based ionic liquids. *J. Chem. Soc., Chem. Commun.* 1992, 965–967.
16. Zhao, D., Liao, Y., Zhang, Z., Toxicity of Ionic Liquids. *CLEAN - Soil, Air, Water* 2007, **35**, 42–48.
17. Leadbeater, N. E., Torenius, H. M., A study of the ionic liquid mediated microwave heating of organic solvents. *J. Org. Chem.* 2002, **67**, 3145–3148.
18. Smiglak, M., Metlen, A., Rogers, R. D., The second evolution of ionic liquids: From solvents and separations to advanced materials-energetic examples from the ionic liquid cookbook. *Acc. Chem. Res.* 2007, **40**, 1182–1192.
19. Rogers, R. D., Seddon, K. R., Ionic liquids - Solvents of the future? *Science* 2003, **302**, 792–793.
20. Sethi, A. R., Welton, T., Dynamic supramolecular chemistry: The role of hydrogen bonding in controlling the selectivity of Diels-Alder reactions in room-temperature ionic liquids, *Ionic Liquids*, 2002, **818**, 41–246.
21. Holbrey, J. D., Reichert, W. M., Nieuwenhuyzen, M., Johnston, S., Seddon, K. R., Rogers, R. D., Crystal polymorphism in 1-butyl-3-methylimidazolium halides: supporting ionic liquid formation by inhibition of crystallization. *Chem. Commun.* 2003, 1636–1637.
22. Holbrey, J. D., Reichert, W. M., Nieuwenhuyzen, M., Sheppard, O., Hardacre, C., Rogers, R. D., Liquid clathrate formation in ionic liquid-aromatic mixtures. *Chem. Commun.* 2003, 476–477.

# 14 Supramolecular Polymers, Gels and Fibres

*'Each outcry of the hunted hare*
*A fibre from the brain does tear.'*

William Blake (1757–1827), *Auguries of Innocence.*

## 14.1 Introduction

Ciferri, A. (ed.) *Supramolecular Polymers*, Dekker: New York, 2000.

The chemistry of covalent polymers linked together by the chemical union of bifunctional monomers was pioneered by Staudinger in the early 1920s. Covalent polymers such as natural rubber, polystyrene and polyethylene are materials of tremendous practical and technological importance. There is a parallel emerging field of supramolecular polymer chemistry involving non-covalent linkages between bi- or multifunctional monomer units. Such supramolecular polymers can form large aggregates with high degrees of polymerisation (DP; the number of monomer units in the polymer chain) such as fibrin, actin filaments, amyloids, supramolecular gels or as we saw in the last chapter, liquid crystals. Supramolecular chemistry is also concerned with the secondary and tertiary structure in covalent polymers, particularly versatile, tunable materials such as amphiphilic block co-polymers – polymers made up of large regions of different covalently linked monomers with different solubility characteristics. Supramolecular polymer chemistry also extends to the interaction of one polymer strand with another, as in DNA, and the non-covalent binding of many small molecules to a polymer chain. Of particular recent interest is the chemistry of both molecular and supramolecular dendrimers – branching polymers that form discrete, globular assemblies with unique properties. It is these compounds, that in some way bridge the gap between well-defined small molecules, and polymers with their varying DP and molecular weight distribution, that we being this chapter with.

## 14.2 Dendrimers

Newkome, G. R., Moorefield, C. N., Vögtle, F., *Dendrimers and Dendrons: Concepts, Syntheses, Applications.* Wiley-VCH: Weinheim, 2001.

### 14.2.1 Structure and Nomenclature

Friedhofen, J. H., Vögtle, F., Detailed nomenclature for dendritic molecules, *New J. Chem.* 2006, **30**, 32–43.

One of the most amazing classes of macromolecular compounds to become topical in recent years, from synthetic, structural and functional points of view is the dendrimers (from the Greek *dendron* meaning 'tree'; in physiology, a dendrite or dendron is a tree-like branched extension of a nerve cell). Dendrimers, or *cascade molecules*, are, ideally, monodisperse macromolecules with a highly branched, three-dimensional architecture. A dendrimer may be regarded as a many-component compound that has grown from a central core in a tree-like fashion. Thus, structurally, and often synthetically, a dendrimer begins with a multifunctional root or core. From each core functional group springs another multifunctional repeat unit (often the same chemical entity as the core itself) to give an oligomer with a central core and a number of functionalised pendant arms. This is the *first generation* dendrimer. If a second iteration of monomer units are added to the functional groups of the first generation material, a much larger, more highly branched *second generation* dendrimer results. In principle, this iterative process may be repeated indefinitely, ultimately resulting in a well-defined, three-dimensional polymer with each polymeric molecule being of identical molecular weight to all the others if each reaction step has been carried out perfectly. This concept is summarised in Scheme 14.1 and examples of common,

*Supramolecular Chemistry, 2nd edition* J. W. Steed and J. L. Atwood
© 2009 John Wiley & Sons, Ltd ISBN: 978-0-470-51233-3

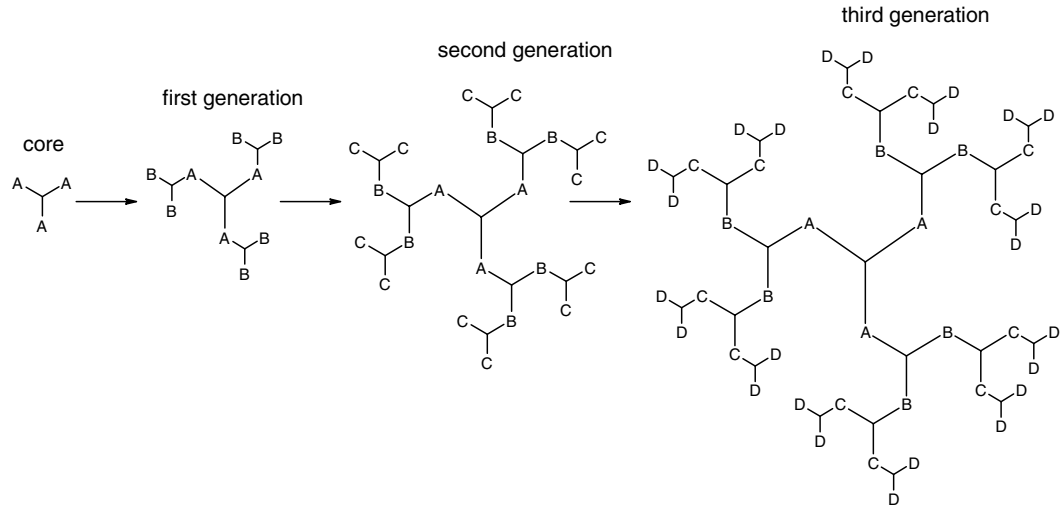


**Scheme 14.1** Schematic diagram showing the iterative preparation of dendrimers.

commercially available dendrimers showing the various generations are shown in Figure 14.1. In the case of poly(amido amine) (PAMAM) dendrimers the intermediate compounds with carboxylate surface groups are given half-integer generation names.

Dendrimers are of interest in a variety of contexts, such as host–guest chemistry and catalysis in which the dendritic core region, which is often highly porous, can exhibit interesting host behaviour, while the densely packed outer layer acts to shield the interior region from the surrounding medium. This suggests applications in mimicking the hydrophobic pocket regions in enzymes. In medicine, the feature of an outer surface comprising multiple identical binding sites is potentially pharamcologically important because of amplified substrate binding. Dendrimers could also be important in the context of drug delivery or functional materials, as in the construction of structured molecular devices of applications in fields such as light-harvesting technology. In addition, the well-defined structural relationship of one layer to another, and the narrow molecular weight range (monodispersity), of well-designed dendrimers make their behaviour easier to characterise than polymeric materials, even though they may reach very high molecular weights and display bulk properties.

Dendrimers may be molecular in which they are made up entirely of covalent bonds and thus the molecule is a well-defined, large single molecule. This molecule may display interesting properties of interest to the supramolecular chemist, *e.g.* arising from the increasing density of linkages towards the edge of the molecule and the creation of void space in the interior. Alternatively they may be supramolecular with, for example, a number of dendritic 'arms' linked *via* non-covalent interactions to a common core.

Like many polymers, the fluidity or flow (rheological) properties of denrimers are of interest (Box 14.1). Dendrimers behave like soft, spherical particles, surrounded by a hard surface shell and hence are often described as 'core-shell' type bodies. Hence the interior of dendrimers can be deformed according to the type of linkage and building blocks and my contain voids suitable for encapsulating guest species.[2]

Friedhofen and Vögtle have recently outlined a detailed nomenclature for dendrimers which is discussed in the Section Key Reference. In brief, a dendrimer is defined as comprising a series of self-resembling units, termed *dendrons*, linked by a common core. The dendrons are referred to as *cascadyl*-substituents or, if there is more than one identical dendron, the molecule is termed a *cascadane*.

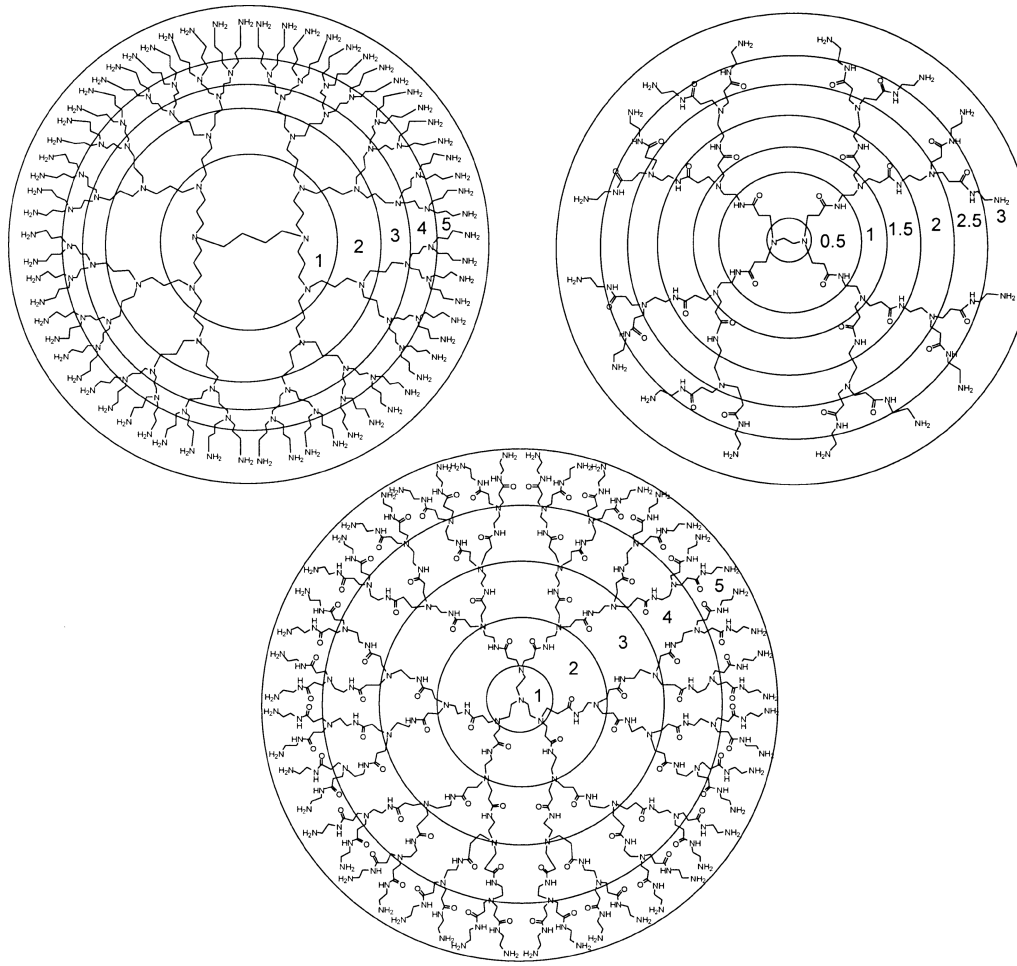


**Figure 14.1** Common commercially available dendrimers. Top left: Poly(propylene imine) dendrimer (G5). Top right: Poly(amido amine) dendrimer (G3). Bottom: Poly(amido amine) ('Starburst™') dendrimer (G5). Each generation is marked with a circle (reproduced by permission of The Royal Society of Chemistry).

The new nomenclature system allows specific naming and numbering of the dendrimer substituents and thus unambiguous naming even for complex structures.

**Box 14.1** Rheological Measurements on Supramolecular Compounds

Mezger, T. G., *The Rheology Handbook*. 2nd ed.; William Andrew Publishing: Norwich, NY, USA, 2006.

Rheology is the study of the deformation and flow of matter under the influence of an applied stress. Commonly a sample such as a polymer or gel is placed between two flat plates or between two concentric cylinders and the stress is applied by moving one plate or cylinder relative to the other while the resulting strain is measured using a pressure transducer. We can define a number of categories of rheological behaviour as a

function of the applied stress on the material. If we apply a continuous weak stress and the material, after some deformation, eventually resists further deformation, then it is a solid. If the material eventually flows, it is a liquid. There are certain intermediate classes of behaviour that fall in between these two extremes over a short timescale. If the *amount of deformation* of the material is proportional to applied force or stress, then the material is said to be *elastic* (like a rubber band). However, if it is the *deformation rate* that is proportional to the force or stress, then the material is said to be *viscous* (like honey). *Viscoelastic materials* exhibit some of both characteristics. While elasticity is generally the result of bond stretching along crystallographic planes in an ordered solid, viscoelasticity arises from the diffusion of molecules in an amorphous material. Many supramolecular polymer and gel phase materials are viscoelastic. Liquid, solid, viscous and elastic behaviour are recognisable under weak applied stresses. However, under high stress, a solid may begin to flow. Such materials are said to be *plastic* and have an associated *yield stress* or *plasticity threshold* beyond which the material flows.

In a rheomety experiment the two plates or cylinders are moved back and forth relative to one another in an oscillating fashion. The elastic storage modulus ($G'$ - The contribution of elastic, *i.e.* solid-like behaviour to the complex dynamic modulus) and elastic loss modulus ($G''$ - The contribution of viscous, *i.e.* liquid-like behaviour to the complex modulus) which have units of Pascals are measured as a function of applied stress or oscillation frequency. For purely elastic materials the stress and strain are in phase and hence there is an immediate stress response to the applied strain. In contrast, for purely viscous materials, the strain follows stress by a 90 degree phase lag. For viscoelastic materials the behaviour is somewhere in between and the strain lag is not zero but less than 90 degrees. The complex dynamic modulus ($G$) is used to describe the stress-strain relationship (equation 14.1; $i$ is the imaginary number square root of –1).

$$G = G' + i\,G'' \tag{14.1}$$

The moduli are related to the quantities $\sigma_0$ and $\varepsilon_0$, the amplitudes of stress and strain, respectively, and $\delta$ – the phase shift between them. We can thus obtain $G'$ and $G''$ from equations 14.2 and 14.3.

$$G' = \frac{\sigma_0}{\varepsilon_0}\cos\delta \tag{14.2}$$

$$G'' = \frac{\sigma_0}{\varepsilon_0}\sin\delta \tag{14.3}$$

The behaviour and magnitude of the storage and loss moduli and yield stress as a function of applied stress or oscillatory frequency and concentration can be modelled mathematically and leads to conclusions about the structure of the material.[3] For supramolecular gels, for example, their structure is not simple and may be described as cellular solids, fractal/colloidal systems or soft glassy materials. In order to be considered as gels (which are solid-like) the elastic modulus ($G'$) should be invariant with frequency up to a particular yield point, and should exceed $G''$ by at least an order of magnitude (Figure 14.2).

The rheology of PAMAM dendrimers has also been studied in highly concentrated solution. The solutions show a shear stress that is proportional to the shear rate and hence are typical Newtonian fluids. There is also no sudden change in the molecular weight dependence of the shear viscosity. That means that the dendrimers form the kinds of entanglements that are typical of linear or randomly branched polymers and also do not stick together. This behaviour is attributed to the hard, dense, closed outer shells of dendrimers. The Newtonian flow behaviour and the lack of an sudden change of slope in the zero-shear viscosity *vs.* molecular weight relationships are taken to be characteristic fingerprint properties for dendrimers and distinguish them all other classes of macromolecular architecture.[2]

(*continued*)

**Box 14.1** (*Continued*)

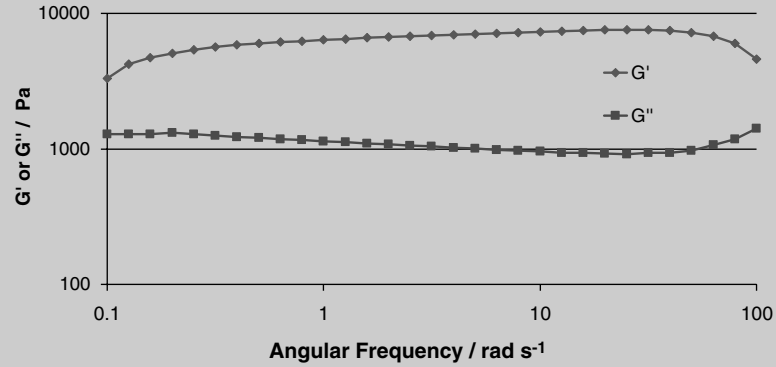


**Figure 14.2** Frequency sweep rheometry data for a supramolecular gel. $G'$ is invariant with frequency up to the yield point and *ca.* one order of magnitude greater than $G''$.

## 14.2.2 Preparation and Properties of Molecular Dendrimers

Bosman, A. W., Janssen, H. M. and Meijer, E. W 'About dendrimers: structure, physical properties and applications', *Chem. Rev.*, 1999, **99**, 1665–1688.

A key issue in traditional covalent dendrimer synthesis is the question of the purity of higher generation dendrimers. This issue is related intimately to the way in which a dendrimer is made. There are two main routes to dendrimer synthesis: the *divergent approach*, as illustrated in Scheme 14.2, in which successive generations are added in an iterative manner, and the *convergent approach*, in which the dendrimer is constructed from the outer surface inwards but with successive coupling of small fragments of the final structure. In the divergent approach, numerous reactions have to be performed on the same molecule. The addition of each generation requires at least a coupling and a deprotection step so that growth occurs one generation at a time rather than by uncontrolled polymerisation. Thus in the case of PAMAM dendrimers a BOC (*t*BuC=O) protected carboxylate is coupled to the growing core. The BOC groups are then removed with $CF_3CO_2H$ to give an intermediate carboxylic acid with is then coupled with the amine of the next generation. Each reaction must proceed in extremely high yield and with excellent selectivity if the introduction of errors or defects is to be avoided. For example, in the synthesis of poly(propylene imine) dendrimers (Scheme 14.2), a fifth-generation material would require 248 reactions to be performed upon 64 amine end groups. If each reaction were to be 99.5 % selective, then the proportion of defect free dendrimer would be $0.995^{248} = 29$ %. If this selectivity drops to 99 %, the result is only 8.3 % pure dendrimer product. Possible side reactions resulting in chain termination are shown in Scheme 14.2. In some cases, final dendrimer purity is governed by statistics because the dendrimer cannot practically be purified at each stage of its growth. Purity can be even less than statistical expectation because of the inaccessibility of reactive sites in later generations as dendrimers become more crowded. However, purification does depend on the system and many workers are able to carry out conventional purification procedures on at least lower-generation dendrimers.

In the convergent approach to dendrimer synthesis, fragments are built up separately and linked to a common core in the final step, thus minimising the number of individual reaction steps that have to take place on a single molecule. As a result, many of the difficulties encountered in the divergent strategy are overcome. A constant and low number of reaction sites is employed in each reaction step, minimising the occurrence of defects and rendering it possible to purify at least early generation materials and molecular weights remain relatively low right up until the last step. The convergent

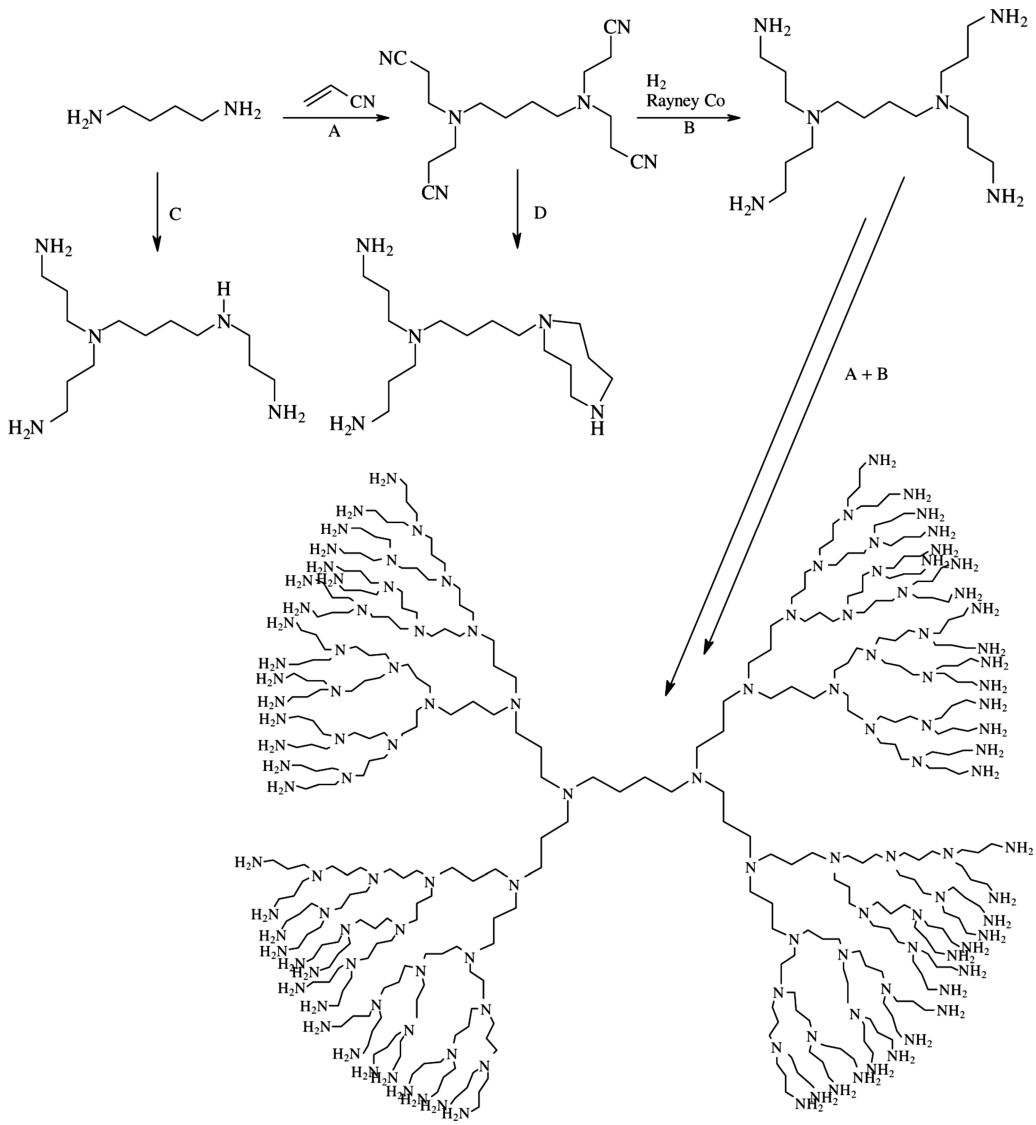


**Scheme 14.2** Divergent synthesis of poly(propylene imine) dendrimers (A and B) and possible side reactions resulting in defects and chain termination (C: missed Michael additions; D: cyclisation).

approach was pioneered by J. M. J. Fréchet and co-workers (Cornell University, USA) in the early 1990s, particularly using the system shown in Figure 14.3 which is often referred to as a Fréchet-type dendrimer.[4] Recently another important new approach to high-yield dendrimer synthesis has been reported. As a dendron is built up either in the divergent approach, or for use in the final steps of the convergent approach, the addition of each new generation generally requires two chemical steps; deprotection followed by coupling, for examples reactions B and A, respectively in Scheme 14.2. However if the deprotection step can be replaced by a kind of reaction that adds a dendrimer generation then the total number of reaction steps is halved. This goal has been realised by the group of Michael Malkoch (Stockholm, Sweden).[5] The researchers used two different dendrons '$AB_2$' and '$CD_2$' with a core and were able to construct a fourth generation Fréchet type dendrimer of type

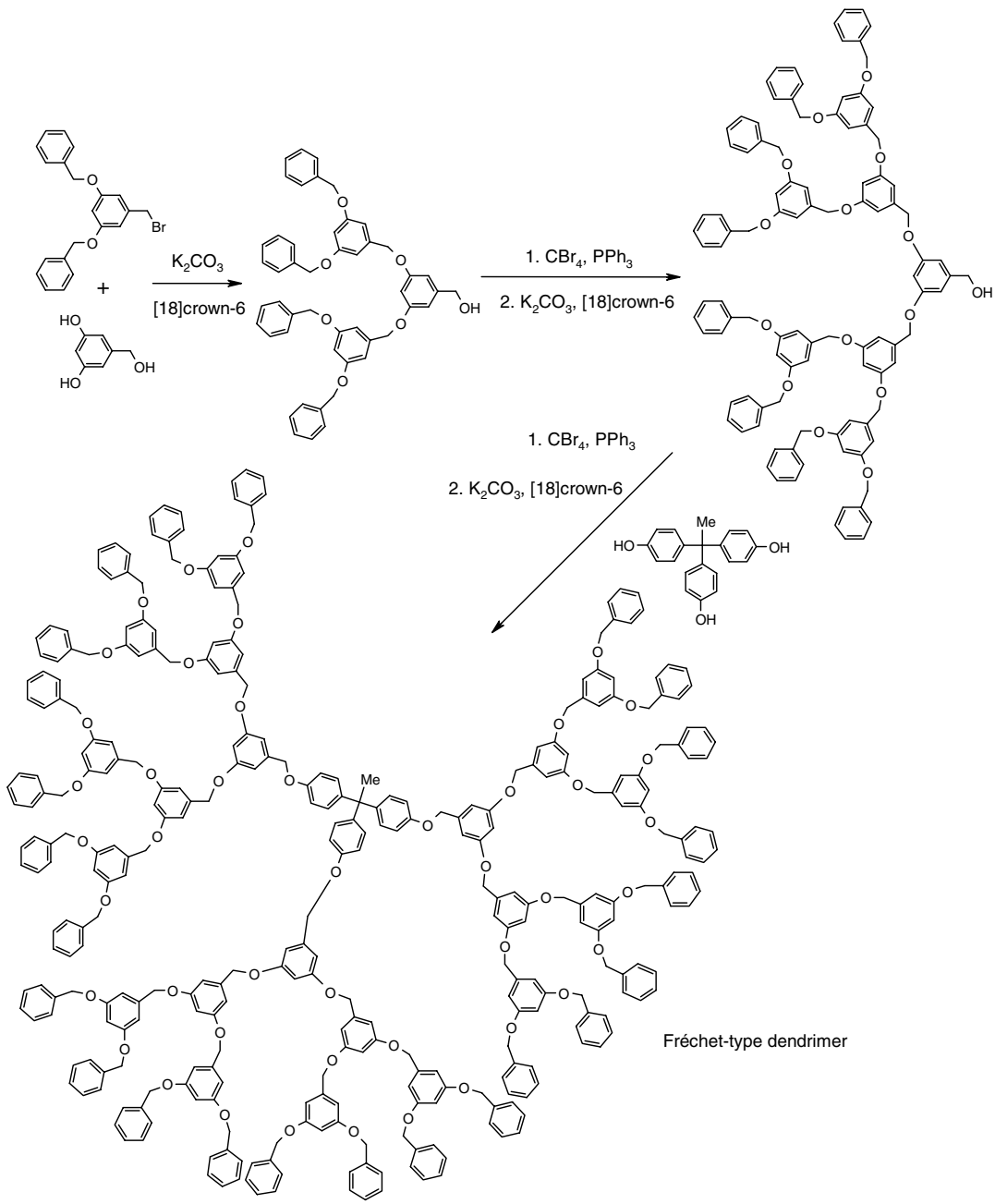


**Figure 14.3** Convergent synthesis pioneered by Fréchet and co-workers. This example shows a core with three third-generation branches. The strategy works well for generations up to at least six, giving a molecular weight of over 13,000 amu for each dendron 'arm'.[4]

'Core-$AB_2CD_2AB_2CD_2$' in just four steps by alternating the conventional reaction of an hydroxyl group with a benzyl bromide, and click chemistry.

Characterisation of dendrimers, especially determination of the dendritic purity (percentage of defect free dendrimer), is difficult because of their large size and high symmetry. Techniques such as NMR

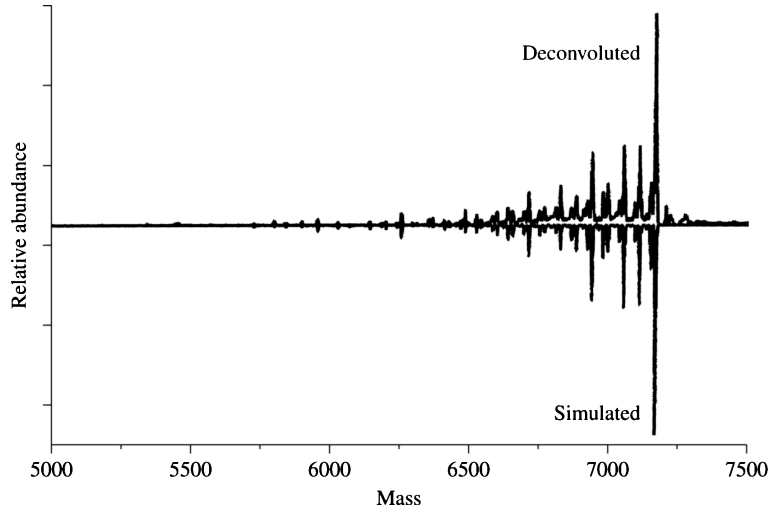


**Figure 14.4** Experimental and calculated ESI–MS spectra for poly(propylene imine) dendrimers. (Reproduced with permission from Section Key Reference © 1999 American Chemical Society).

spectroscopy, elemental analysis and chromatography (*e.g.* HPLC) are used, but cannot reliably reveal small amounts of impurities in higher-generation dendrimers. The best method is generally mass spectrometry, using modern ionisation techniques such as electrospray ionisation (ESI) and matrix-assisted laser desorption ionisation (MALDI). The ESI–MS spectrum of the fifth-generation poly(propylene imine) dendrimers is shown in Figure 14.4. From knowledge of the mass spectra of all of the previous generations of the dendrimer, the dendritic purity at each stage may be calculated by an iterative procedure. The simulated spectrum, which agrees well with experiment, gives a polydispersity of 1.002 ($= M_w/M_n$; the ratio of observed versus theoretical molecular weight) and a dendritic purity of 23 %.

In terms of physical properties, dendrimers are highly variable depending on the nature of the component groups and the interactions between them. Most dendrimers undergo some degree of back-folding, which can reduce their surface density and the number of available surface functional groups. Indeed, there is an entropic penalty in adopting an open, extended and porous structure. At high molecular weights, dendrimers differ significantly from linear macromolecules in their solution properties. The volume occupied by a dendrimer increases cubically with generation, whereas its molecular weight increases exponentially. This means that dendimer viscosity, for example, does not increase with molecular mass, but reaches a maximum at a certain limiting generation. Properties such as size are also highly solvent-dependent, with dendrimers adopting a more open structure in solvents for which they have a high affinity.

### 14.2.3 Dendrimer Host–Guest Chemistry

The dense outer sheath of a dendrimer of any type can result in two interesting kinds of host–guest behaviour: site isolation and guest inclusion. Site isolation involves construction of the dendrimer from a functional core, which becomes, to a large extent, shielded from the external medium as the dendrimer grows. This results in the ability to study the behaviour of the core in isolation from the effects of solvation and self-association interactions. For example, construction of a dendrimer comprising polyethylene glycol arms from an iron(III) porphyrin core gives an isolated, water-soluble haem analogue (**14.1**, Figure 14.5).[6] Comparison of the first- and second- generation dendrimers reveals a +420 mV shift in the reduction potential of the Fe(III) centre as a result of dendrimer inclusion. Similarly, inclusion of an $Fe_4S_4$ core within a tetrahedrally disposed array of poly(aromatic

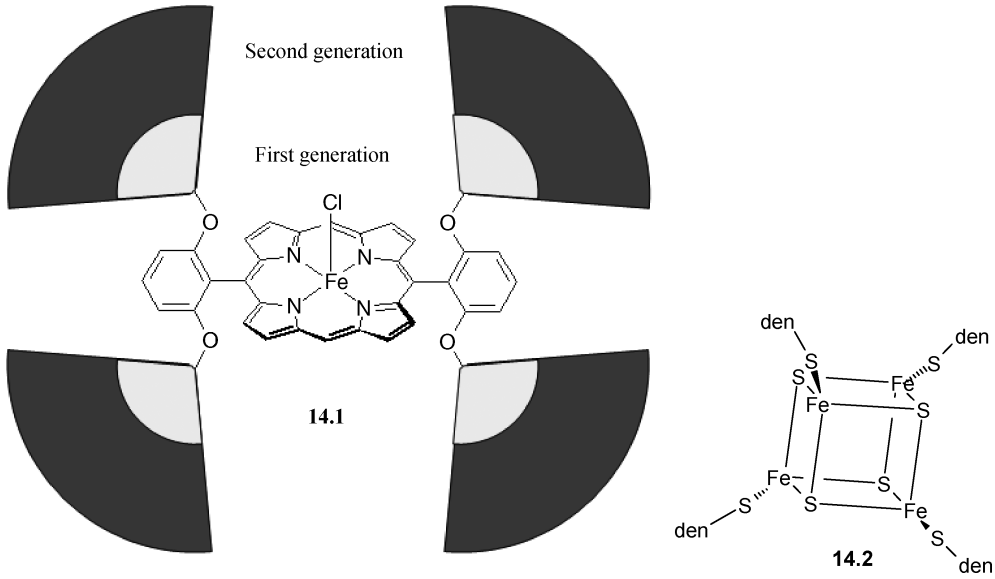


**Figure 14.5** Shielding of an iron porphyrin and thiolate cluster cores within dendrimers.

ether) Fréchet-type dendrimers linked to the iron centres *via* thiolate ligands (**14.2**) interferes with both the kinetics and thermodynamics of reduction of the cluster, which exhibits a more negative reduction potential and increased splitting in the cyclic voltammogram with each successive dendrimer generation.

In addition to covalent core inclusion chemistry, the low density in the core region of many dendrimers can also result in non-covalent guest molecule inclusion and consequent isolation from the external medium. This phenomenon is termed *topological trapping*. Guest encapsulation is irreversible if the outer layer of the dendrimer is functionalised with bulky groups, causing it to become rigid and impermeable. An excellent example is the reaction of the fourth-generation poly(propylene imine) dendrimer DAB-*dendr*-$(NH_2)_{64}$ (DAB = 1,4-diaminobutane) with an activated ester of *N*-*t*-BOC-L-Phe (the chiral amino acid, L-phenylalanine, protected with a *t*-butyl ester group) in the presence of guest molecules such as the fluorescent dye rose Bengal that have some affinity for the tertiary amine groups in the interior of the dendrimer. This reaction gives the rigid shell dendrimer DAB-*dendr*-(NH-*t*-BOC-L-Phe)$_{64}$, with between one and four included molecules of rose Bengal. The encapsulated dye shows strong fluorescence at 600 nm, whereas the free chromophore is quenched at this wavelength. Remarkably, the dendrimer also induces chirality in the achiral dye. In the case of a single trapped molecule, the circular dichroism (CD) spectrum resembles the UV–visible spectrum. When four molecules are trapped, CD spectra consistent with four chromophores in close proximity and well-defined relative orientations are observed. It is clear that, while the dendritic capsules themselves are not chiral, the cavities in the core region have retained chiral features.[7] These kinds of 'dendritic boxes' in which molecules are irreversibly trapped have analogies with the carcerands discussed in Section 6.7. Guest removal is possible however by making a hole in the outer surface of the dendritic box by chemically removing the BOC protecting groups with formic acid. Under these circumstances shape-selective removal of guests occurs. In mixed guest dendrimers this means that removal of the smaller guests is possible while retaining the larger ones.[8]

A novel approach to guest inclusion by dendrimers is the use of 'molecular imprinting'. We will look at molecular imprinted polymers in more detail in Section 14.3. Generally the imprinting technique involves assembly of a covalent polymer – in this case dendrimer – about the target guest which acts

as a template. Subsequent guest removal creates a cavity tailored for that particular template. Work by Steve Zimmerman (Illinois, USA) has applied this concept to dendrimer imprinting by a porphyrin scaffold.[9] With a functional porphyrin as a strating point, Zimmerman's group used a convergent approach to synthesise the alkene-terminated dendrimer shown in Figure 14.6. The dendrimer is then

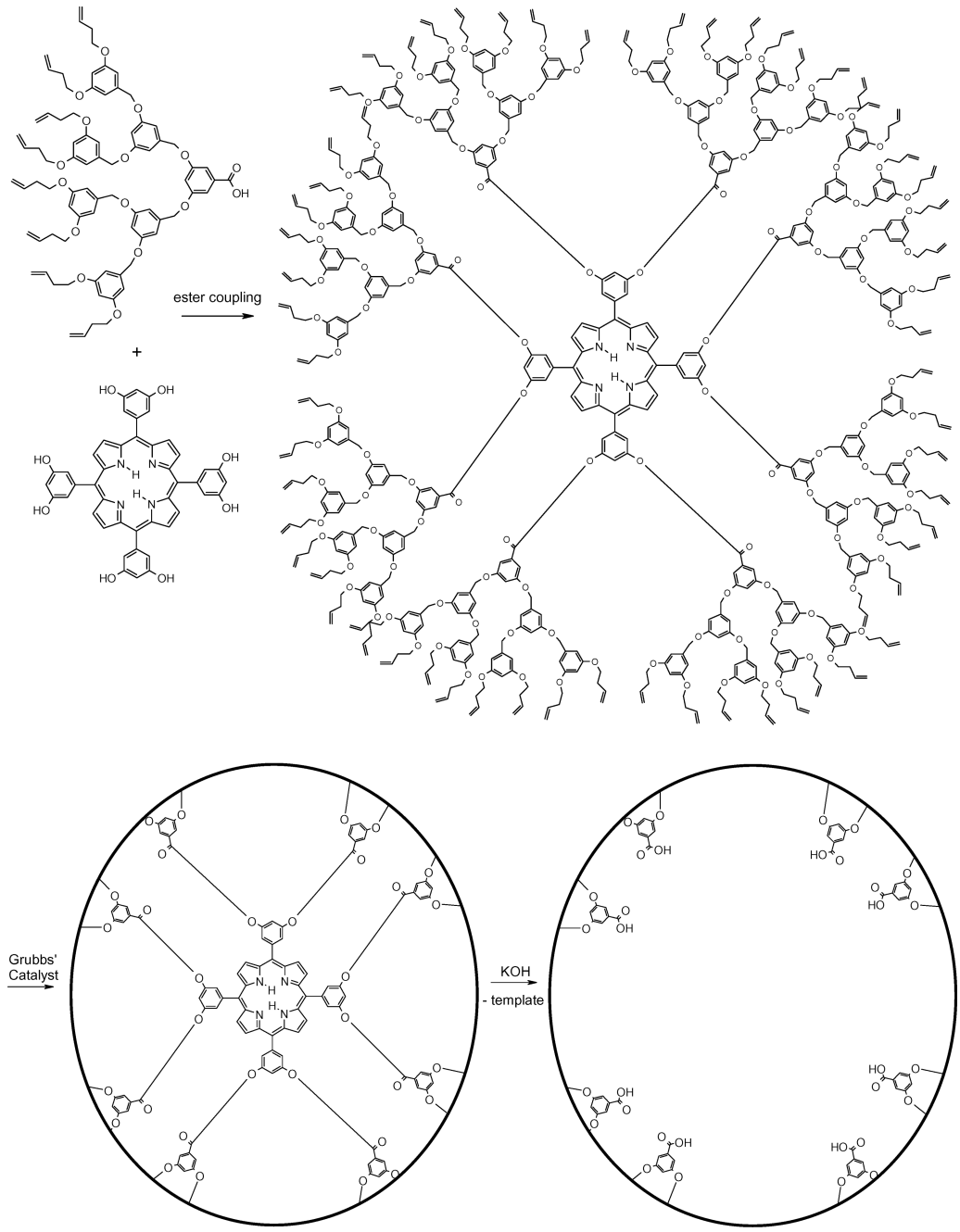


**Figure 14.6** Molecular imprinting in a dendrimer.[9]

rigidified by cross-coupling the alkene functionalities using Grubbs' catalyst. The porphyrin template can then be removed by base hydrolysis of the ester groups, creating a porphyrin-imprinted covalent dendrimer. Similarly, recent work using 'click' chemistry on a poly alkyne amide that forms a self-assembled micelle allows the azide functionalisation and cross-linking of the micelle to give a rigid functionalised shell, cross-linked polymer nanoparticle. Further functionality can be added to the azide groups by additional 'click' chemistry.[10]

Dendrimer host-guest compounds have been studied extensively in the context of drug delivery, where their tuneable solubility allows the solubilisation of otherwise insoluble or readily hydrolysed drug molecules.[1] In this regard dendrimers can act rather like cyclodextrins (Section 6.3.4), although some dendrimers do have significant toxicity issues, for example, destabilisation of cell membranes resulting in cell lysis (chemical-induced cell destruction). Particularly interesting in this regard is the development of dendrophanes (described in Section 6.5.6) that can act as hosts for large biologically active molecules such as steroids.

### 14.2.4 Supramolecular Dendrimer Assemblies

Smith, D. K., 'Dendritic supermolecules – towards controllable nanomaterials', *Chem. Commun.* 2006, 34–44.

In addition to covalent bonds, dendrimers can also be assembled non-covalently. Striking results in this field have been achieved using a Fréchet type dendrimer appended to a double isophthalic acid functionalised molecular cleft.[11] Isophthalic acid is self-complementary, forming a hexagonal assembly of six units (Figure 14.7). The presence of two such hexagonal units and their insulation from the surrounding medium by the dendrimer portion gives the assembly high stability. Fréchet-type dendrimers have also been used as ligands for lanthanide(III) ions in a novel variation of the convergent strategy using focal point functionalised dendrons as in **14.3**. The focal point is a carboxylate moiety; an excellent ligand for the oxophilic lanthanides. The resulting isolation of the lanthanide ion and the antenna effects of the dendrons results in significantly enhanced lanthanide fluorescence.[12] These kinds of species are reminiscent of the light harvesting and conversion devices we looked at in Chapter 11 and indeed the

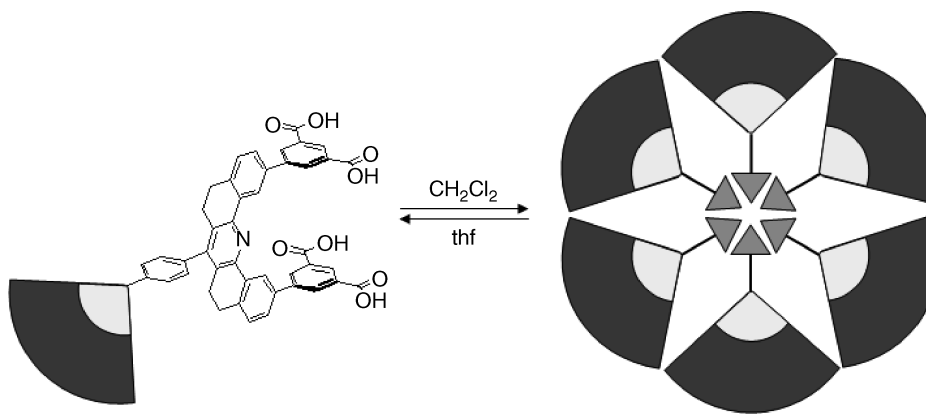


**Figure 14.7** Hexameric assembly of dendrons by isophthalic acid hydrogen bonding interactions.[11]

'complexes-as-metals, complexes-as-ligands' strategy (Section 11.2.5) is an excellent way to prepare metallodendrimers.

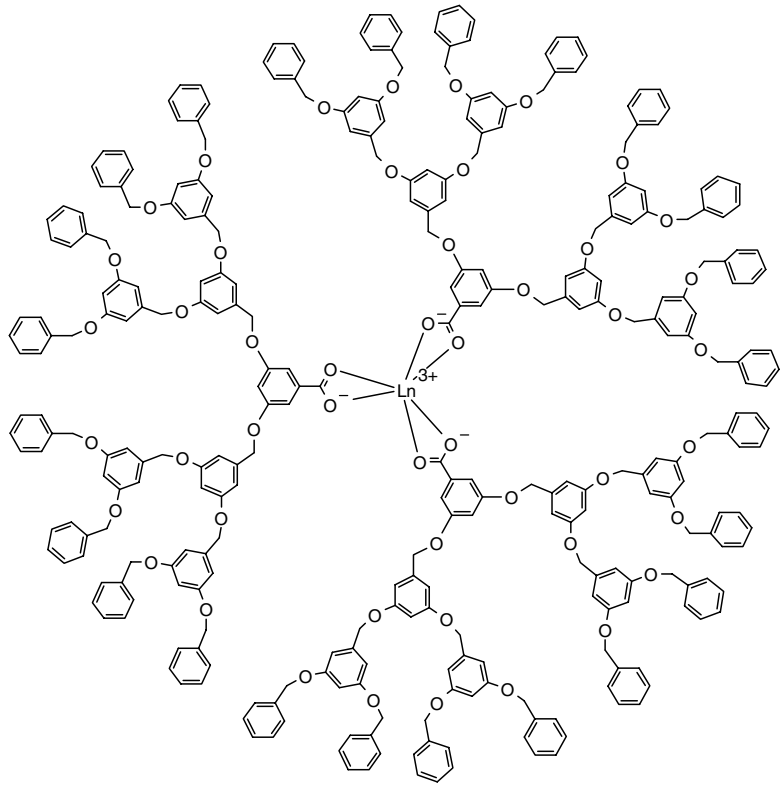


**14.3**

Work by the group of David Reinhoudt (Twente, Netherlands) has resulted in perhaps the only truly reversible, metal-coordination based dendrimer assembly strategy. Starting with the dendron core **14.4** Reinhoudt's group removed the chloride ligands with $AgBF_4$ and coordinated the pyridyl functionality of **14.5** to the resulting vacant sites, giving a first generation metallodendrimer. This first generation material, in turn, can be actived by more $AgBF_4$ allowing growth of stable dendrimers up to generation 5.[13]

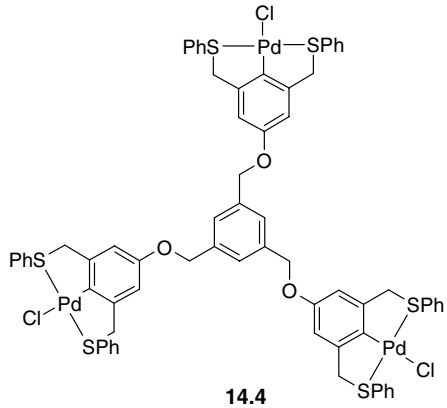


**14.4**

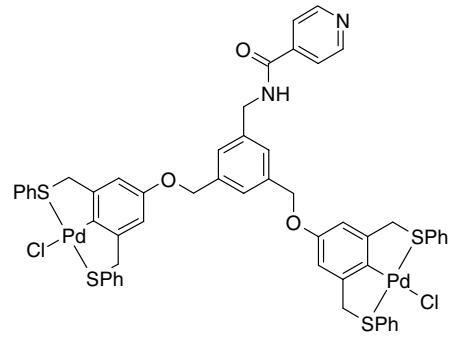


**14.5**

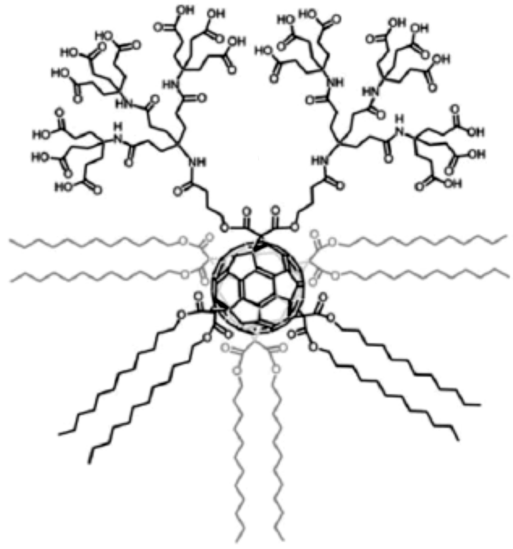

**Figure 14.8** Amphiphilic fullerene and calixarene derivatives with dendritic branches that form long-lived micelles (Copyright Wiley-VCH Verlag GmbH & Co. KGaA. Reproduced by permission).

A range of amphiphilic dendrimers have been reported based on fullerene $C_{60}$ or a calix[4]arene core with dendritic branches on one side and long aliphatic tails on the other, Figure 14.8. The amphiphiles self-assemble into micelles with the aliphatic chains buried in the micelle core and the more hydrophilic dendritic portion facing out.[14]

Work by David Smith, in York, UK, has resulted in an extremely versatile series of multicomponent dendrimer assemblies based on the hydrogen bonding of a linker core to functionalised dendrons. An example is shown in Figure 14.9a. These systems go on to undergo hierarchical assembly producing interesting functional materials able to bind biomolecules, for example. The simple diamine core compounds shown in Figure 14.9b in the presence of L-lysine dendrons forms two-component supramolecular gels whose properties are highly tunable. We will return to the highly topical subject of gels in Section 14.7.

## 14.2.5 Dendritic Nanodevices

De Schryver, F. C., Vosch, T., Cotlet, M., van der Auweraer, M., Mullen, K. and Hofkens, J., 'Energy dissipation in multichromophoric single dendrimers', *Acc. Chem. Res.* 2005, **38**, 514–522.

We have already seen in Chapter 11 dendritic cascade type coordination complexes in which light energy is transferred from the outside of an inorganic dendrimer to a core chromophore. This kind of process is one of the major interests in dendrimer chemistry because it mimics the energy transfer cascade in natural photosynthesis (Section 2.4). Organic dendrimers such as the 'nanostar' dendrimer **14.6** also exhibit light-harvesting and energy transfer properties, particularly because of their fully delocalised nature which allows orbital overlap and hence Dexter-type excitation transfer (Section 11.2.2).[15] The emission intensity of **14.6**, which is based on a perylene chromophore, is 400 times greater than that of the control molecule 1-ethynylperylene. Irradiation at 312 nm generates a $\pi$–electron-hole pair (exciton) that is localised due to the *m*-phenylene joints involved. This exciton moves to the core in a directional, multistep manner giving directional energy transfer from the periphery to the centre of the fourth-generation nanostar.

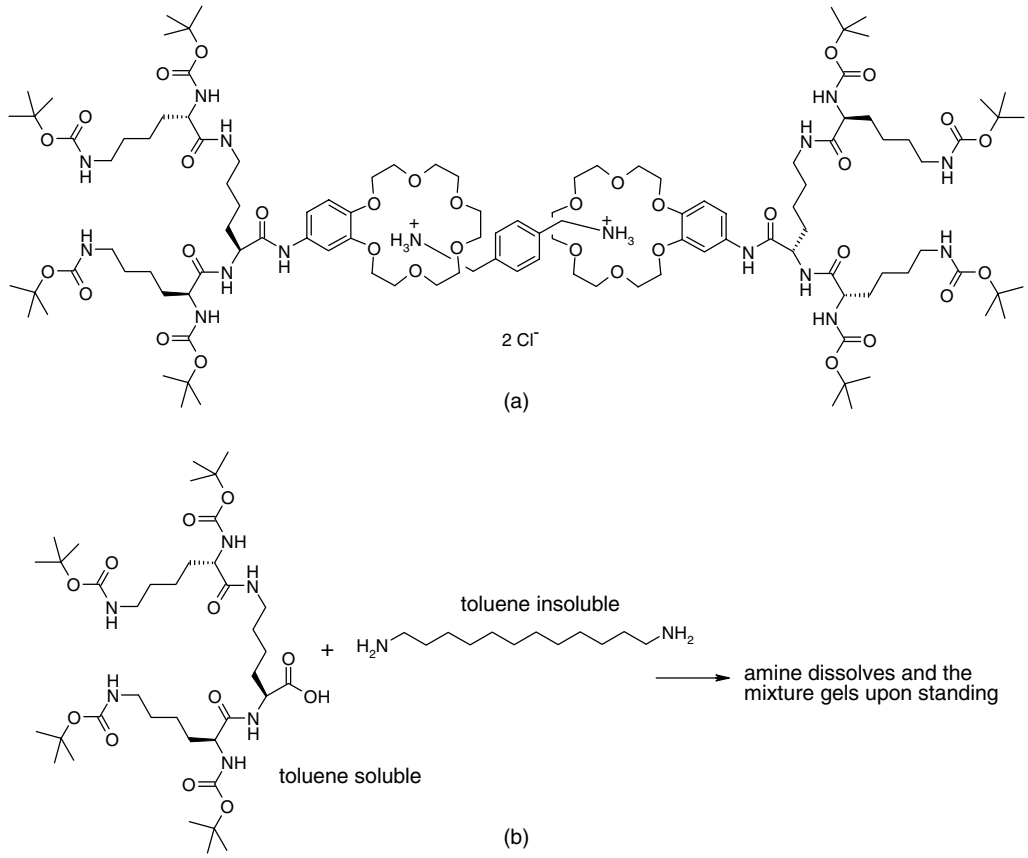


**Figure 14.9** (a) Supramolecular dendrimer based on L-lysine derived dendrons assembled by an ammonium-crown ether interaction, (b) a dendrimer-based two component gel.

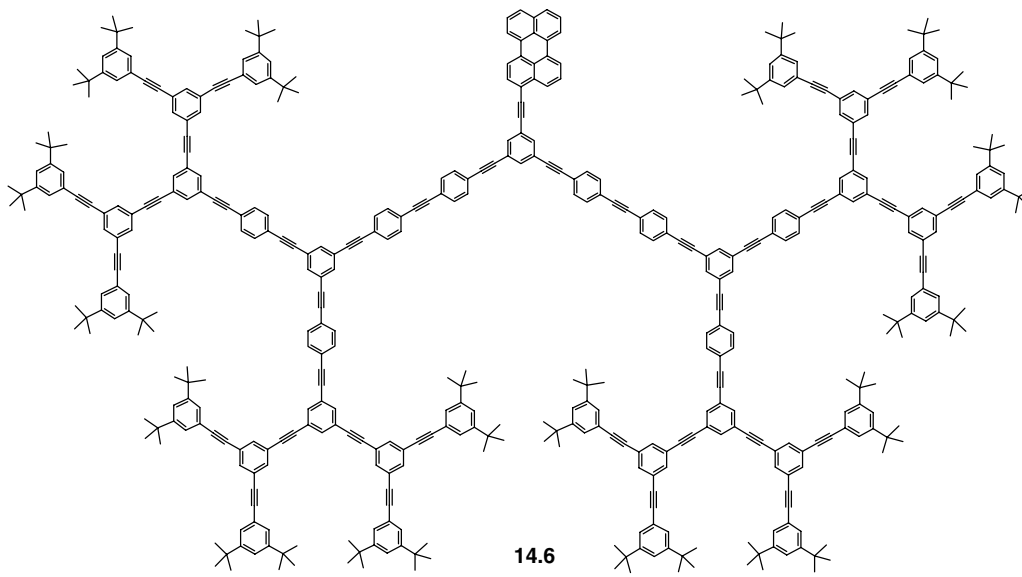

**14.6**

Dendrimer devices have also found applications in magnetic resonance imaging (MRI).[16] The dendrimers act as carriers for paramagnetic Gd(III) ions, a large number of which can be bound per dendrimer. The large size of the dendrimer increases the residence time of the dendrimer-lanthanide conjugate in the bloodstream allowing longer, more detailed imaging studies. Moreover the relaxation properties of the Gd(III) ions are dramatically enhanced compared to small-molecule analogues. Tailoring the exterior surface of the dendrimer also allows a significant degree of biological recognition between the contrast agent and a target site. Other biological applications of dendritic nanodevices include dendrimer-linked antibody assays. The regular spacing between antibody and solid support introduced by replacing a secondary antibody spacer with a dendrimer reduces non-specific interactions between immobilised antibody and analyte and improves manufacturing properties. Dendrimers have also been used as vectors for carrying genetic material into cells and as anti-cancer agents in conjunction with platinum-based anti-cancer drugs such as cisplatin. The cancer cells are more permeable to the large dendrimers than normal cells. A key feature of dendrimers is their high density of surface functionality, allowing 'multivalent' interactions between dendrimer functionality and biomolecules. This feature has been used in the bonding of dendrimer-saccharide conjugates to proteins such as lectins. The multiple interactions and hence strong bonding results in enhanced viral inhibition.

## 14.3 Covalent Polymers with Supramolecular Properties

### 14.3.1 Amphiphilic Block Copolymers

Klok, H. A. and Lecommandoux, S., 'Supramolecular materials *via* block copolymer self-assembly', *Adv. Mater.* 2001, **13**, 1217–1229.

A block co-polymer is a covalent polymer made up of more than one type of monomer unit. The polymer contains large domains comprising a single type of monomer followed by a link to a domain of different monomers. Typically block co-polymers are assembled by a living polymerisation mechanism in which the first monomer is polymerised until the reaction is finished and the feedstock has been used up, at which point the second monomer is added and the chain continues growing by incorporating the new monomer, in which way a high degree of control over the 1D structure of the co-polymer can be obtained. Because the different monomer units may have very different properties (*e.g.* different solubilities arising from a hydrophilic and a hydrophobic monomer resulting in an *amphiphilic block co-polymer*) materials with interesting self-assembled designer properties can result depending on the mutual enthalpic interactions between different segments in block co-polymers, as quantified by the Flory-Huggins-Staverman parameter $\chi$ (a positive value indicates repulsion while a negative value corresponds to attraction). Supramolecular chemists are interested in the folding of the co-polymer chains and in how individual co-polymer strands interact with one another, giving rise to properties such as liquid crystalline behaviour, micelle formation and assembly, and compartmental self-assembly. Block co-polymers are also of interest as templates for the formation of microstructured inorganic materials, as hosts for catalysts, templates for nanoparticle synthesis and as light harvesting devices or other kinds of molecular optoelectronic components. We have already looked at one example of a block co-polymer that acts as a molecular wire in Section 11.4.2. The different chemical nature of the monomers allows vectorial energy transfer along the polymer chain.

The supramolecular structure of block co-polymers allows the design of useful materials properties such as polarity leading to potential applications as second-order nonlinear optical materials, as well as piezo-, pyro-, and ferroelectricity. It is possible to prepare polar superlattices by mixing (blending) a 1:1 ratio of a poly(styrene)-*b*-poly(butadiene)-*b*-poly-(tert-butyl methacrylate) triblock copolymer (**SBT**) and a poly(styrene)-*b*-poly(tert-butyl methacrylate) diblock copolymer (**st**). The result is a polar, lamellar material with a domain spacing of about 60 nm, Figure 14.10.

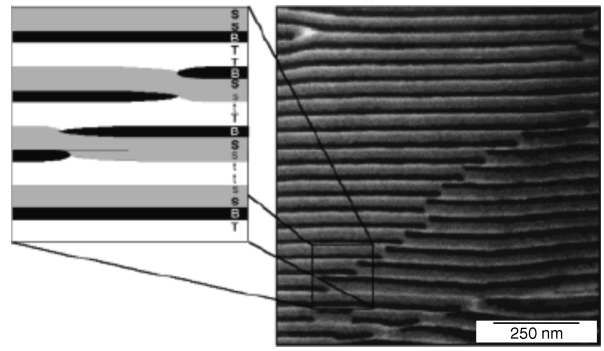


**Figure 14.10** TEM image of blend containing 75 wt. % of a **SBT** triblock copolymer and 25 wt. % **st** diblock co-polymer. The non-centrosymmetric supramolecular structure of this blend is schematically illustrated in the diagram that assigns the different phases observed in the marked part of the micrograph (Copyright Wiley-VCH Verlag GmbH & Co. KGaA. Reproduced by permission).

A particularly interesting block co-polymer assembly is that shown in Figure 14.11, which involves a 'rod-coil' co-polymer. The assembly follows a two-stage hierarchial process in which mushroom-shaped units comprising some 100 molecules are initially formed. The regular size and shape of these nanostructures arises from a delicate balance between the rigid, crystalline nature of the rod portion and the flexible, amorphous nature of the coil. The mushrooms then assemble into macroscopic thin films in which they exhibit a regular, polar head-to-tail arrangement that minimises free volume. Due

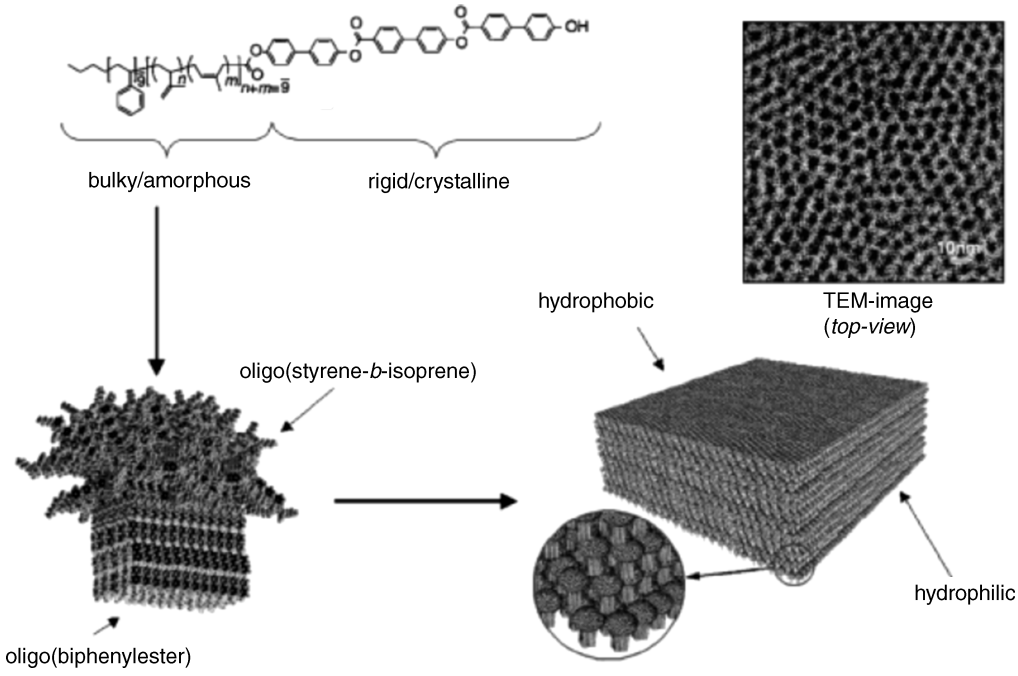


**Figure 14.11** Two-step self-assembly process of rod-coil oligomer *via* mushroom shaped nanostructures into polar supramolecular films. The TEM image represents a top view of such a supramolecular film (Copyright Wiley-VCH Verlag GmbH & Co. KGaA. Reproduced by permission).

to their polar order, these films have the potential to exhibit a number of interesting properties, such as opposite non-adhesive/hydrophobic and sticky/hydrophilic surfaces. Such surfaces are of significant in the development of useful adhesives such as 'Post-it™' notes and in the mimicry of biological phenomena such as the remarkable adhesion of gecko's feet to apparently smooth surfaces.

Extensive work by the group of Roeland Nolte (Nijmegen, Netherlands) has focussed on rod–coil diblock copolymers, consisting of a flexible and a rigid block. These materials are a special type of co-polymer in which a rigid scaffold can be used to organise a more flexible segment. Nolte's group have used polyisocyanopeptides as the rigid component in these materials. These isocyanide based polymers have a very high *persistence length* of around 76 nm because of the well-defined helical β-sheet structure adopted by the side chains of the polymer. The persistence length can be thought of as the length over which the polymer remains rigid. For comparison DNA has a persistence length of 50 nm. The polyisocyanopeptides has been used to organise a wide variety of other components. For example appending dye molecules gives non-linear optical materials with enormous β-values (Section 11.6.1).[17] One of the most remarkable examples of this type of co-polymer is a diblock co-polymer derived from styrene and an isocyanoamino acid containing a thiophene group. The amphiphilic diblock co-polymer, dubbed *PS-PIAT*, is comprised of 40 styrene and 50 3-(isocyano-l-alanyl-amino-ethyl)-thiophene units. The thiophene rings offer the interesting possibility of being covalently polymerisable after the aggregation of polymer nanostructures. PS-PIAT self-assembles to form remarkable hollow vesicle-like structures in chloroform and water that the researchers called *polymersomes*. The separation of the two polymer blocks results in a rigid polyisocyanopeptide group and a more flexible polystyrene chain (Figure 14.12) each of which has slightly different solubilities, with the polyisocyanopeptide being relatively chloroform insoluble. The average diameter is 7 microns with the thickness of the wall being some 27 nm, suggesting a PS-PIAT bilayer arrangement, Figure 14.13.[18] The novel polymersomes have been used in a variety of interesting applications, including the inclusion and study of single enzyme molecules, and production of silver nanoarrays. The concept has been extended to the synthesis of biohybrid triblock copolymers comprising a synthetic diblock, polystyrene-*b*-polyethylene glycol, and a hemeprotein such as myoglobin or horse radish peroxidase. These amphiphilic materials self-assemble in water to give a large variety of interesting aggregates that are strongly influenced by the protein and the polystyrene block length. Structures including micellar rods, vesicles, toroids, figure eight structures, octopus structures, and spheres with a lamellar surface are the result.[19]

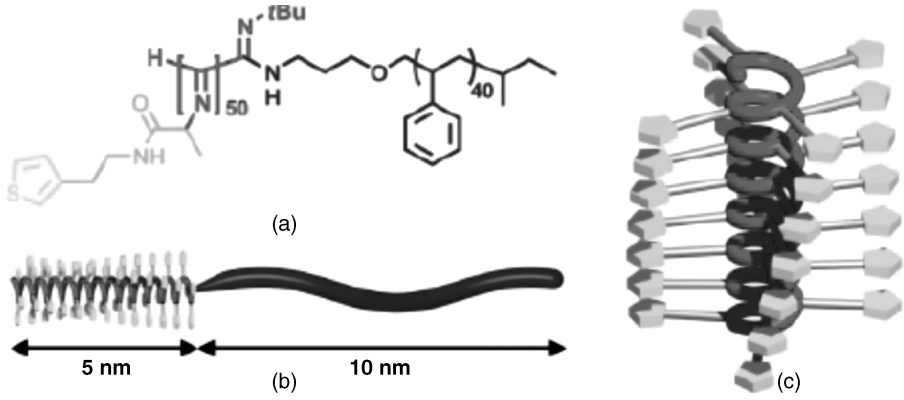


**Figure 14.12** (a) Chemical structure of PS-PIAT; (b) schematic representation of PS-PIAT; (c) schematic representation of the PIAT block showing the stacks of thiophene groups (Copyright Wiley-VCH Verlag GmbH & Co. KGaA. Reproduced by permission).

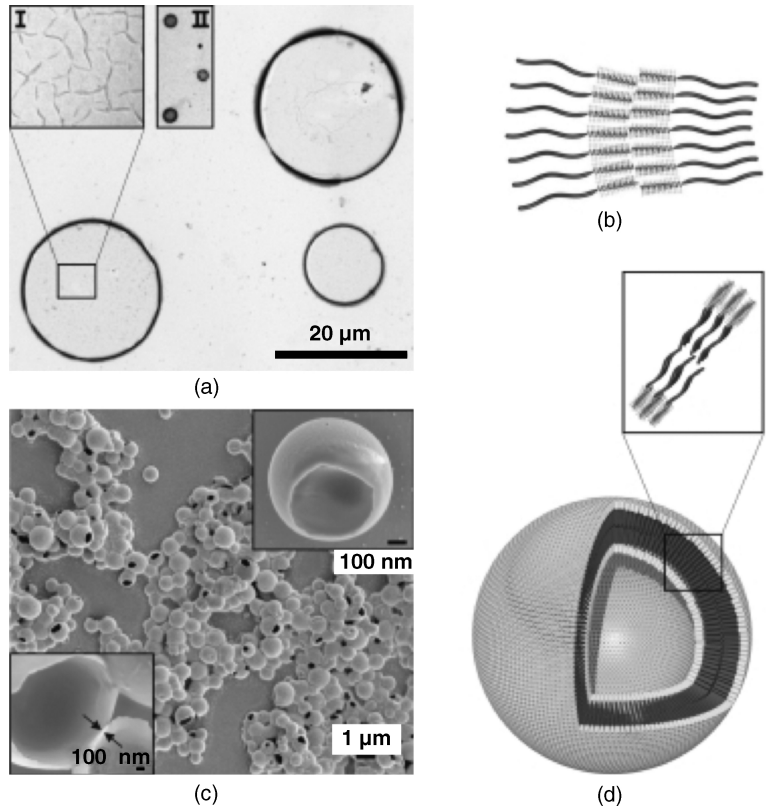


**Figure 14.13** (a) Transmission electron micrograph of PS-PIAT vesicles formed in chloroform and dried. The inset I shows the middle section of the collapsed vesicles and inset II shows vesicles containing $FeCl_3$. (b) Schematic representation of the vesicle wall. (c) Scanning electron micrograph of PS-PIAT vesicles formed in THF/water. (d) Schematic representation of a PS-PIAT vesicle formed in water with a close-up of the vesicle membrane showing the proposed bilayer structure (Copyright Wiley-VCH Verlag GmbH & Co. KGaA. Reproduced by permission).

## 14.3.2 Molecular Imprinted Polymers

Hall, A. J., Emgenbroich, M., Sellergren, B., 'Imprinted polymers', *Top. Curr. Chem.* 2005, **249**, 317–349.

Molecular imprinted polymers (MIPs) are formed by the covalent formation of a highly cross-linked polymer around a small-molecule template. The template is then removed, in principle leaving behind a cavity that is complementary to the templating molecule in terms of size, shape and binding functionality, and may thus be used to bind and/or sense close analogues of the templating species. The cross-linking is necessary to rigidify the polymer so that the imprint of the template is retained after its removal and not lost by random movements of the polymer chains. This kind of imprinting is a relatively new process and remains very topical. A good example of the use of MIPs is a recently reported eight-channel sensor array for discriminating biologically important amines. A series of MIPs based on copolymers of ethylene glycol dimethacrylate and methacrylic acid (80 : 20) were prepared in the presence of templating amine such as ephedrine and analogous aromatic amines. The amine template is washed out and the polymers tested as an array for amine discrimination. While no particular polymer is completely selective for a particular amine the templated polymer tends to bind the templating amine more

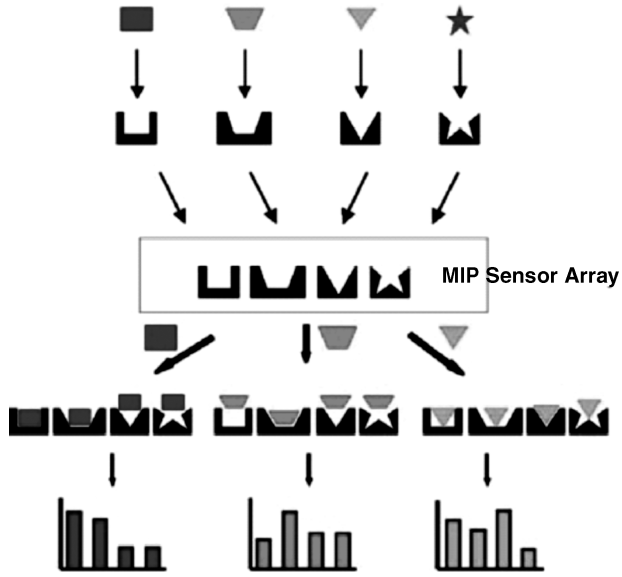


**Figure 14.14** Four imprinted polymers tested in an array against three different analytes to produce different patterns of recognition (reproduced by permission of The Royal Society of Chemistry).

strongly than the other analytes and thus a differential recognition pattern can be built up in an analogous fashion to that described in Section 11.3.4 (Figure 14.14). The binding affinity between different amine analytes is measured by taking constant mass of the polymer and adding it to the same concentration of each amine. The response is measured as a ratio of absorbances before and after equilibration of the eight different polymers added as a powder to solutions of the six different analytes. Visible absorption arises from an indicator of similar structure to the analytes that is displaced from the polymer by analyte binding (an indicator displacement assay). Linear discriminate analysis (LDA) can be used to give a two-dimensional plot that clearly shows binding patterns specific to particular amine analytes.[20]

## 14.4 Self-Assembled Supramolecular Polymers

Rieth, S., Baddeley, C. and Badjic, J. D., 'Prospects in controlling morphology, dynamics and responsiveness of supramolecular polymers', *Soft Matter*, 2007, **3**, 137–154.

We have already examined in Section 10.8.8 the formation of helical hydrogen bonded supramolecular polymers exhibiting liquid crystalline behaviour based on a triple hydrogen bonded recognition motif between 2,6-diaminopyridine and uracil (**10.128**). Apart from interesting properties such as liquid crystallinity, one of the attractions of supramolecular polymers is their synthesis using self-assembly as a facile alternative to covalent polymerisation, and the reversibility of the interactions between monomers, leading to potentially interesting, tunable viscoelastic or adaptive rheological properties (*cf.* Box 14.1). For the formation of stable hydrogen bonded polymers in solution a simple empirical rule is that for each backbone connection there should be at least four hydrogen bonds per backbone unit. It is estimated that each hydrogen bond results in a stabilisation of around 8 kJ $mol^{-1}$ while each secondary diagonal interaction (see Figure 1.17) adds or subtracts *ca.* 3 kJ $mol^{-1}$ depending on whether it is attractive or repulsive.[21] Balancing these considerations against synthetic accessibility, Meijer and co-workers have prepared a series of hydrogen bonded polymers based on the 2-ureido-4[1*H*]pyrimidone moiety, which forms a DDAA array of four hydrogen bonds, **14.7**, for which the

dimerisation constant, $K_{dim} = 5.9 \times 10^8$ in toluene solution. Tethering two of these units together with an hexamethylene spacer as in **14.8** gives strongly associated hydrogen bonded polymers that form highly viscous solutions with an average assembly weight of *ca.* $10^5$ g mol$^{-1}$ for a 40 mM solution in chloroform. Molecular weight distribution and hence viscosity can be tailored by adding some **14.7** monomer to terminate the chain. In a similar way, earlier work on the two-component assembly **14.9** results in long, rigid-rod assemblies that exhibit lyotropic liquid crystalline behaviour.[22]

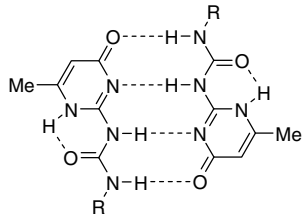

**(14.7)$_2$**

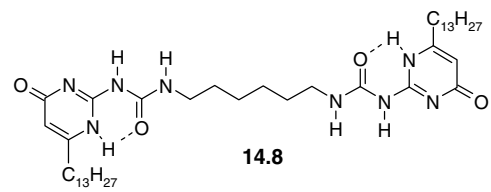

**14.8**

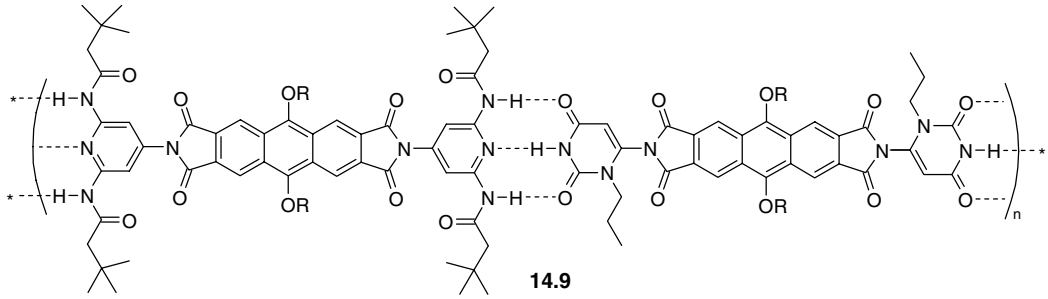

**14.9**

A fascinating class of biologically inspired supramolecular polymer are the very versatile peptide nanotubes prepared by M. Reza Ghadiri (Scripps, USA). The nanotubes form by the self-assembly of flat, cyclic, eight amino acid residue D,L-α-peptides that form β-sheet-like tubular, open-ended cylindrical structures stable in solution, Figure 14.15.[23] The properties of the tube interior and outer surfaces can be greatly varied and tuned by changing the amino acid sequence. The tubes are membrane active and can destroy bacterial cells by piercing a hole in their cell membranes, allowing the contents to leak out through large pores formed by nanotube bundles. The peptides have proved to be effective *in vivo* in mouse studies against aggressive bacterial infections such as methicillin-resistant *Staphylococcus aureus* (MRSA).

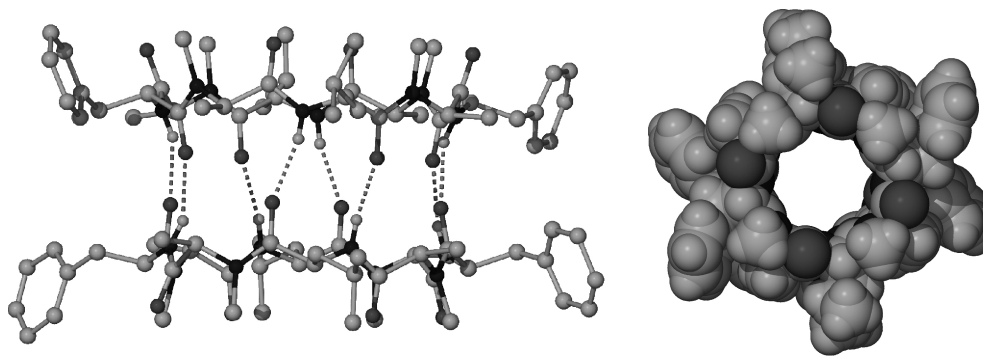


**Figure 14.15** (a) X-ray structure of a model dimer repeat unit of peptide nanotubes made up from the self-assembly of cyclic octapeptides in a β-sheet-like fashion; (b) space filling view showing the central pore.[23]

The self-assembly of amphiphile **14.10** is interesting because the morphology of the resulting supramolecular polymers it is highly dependent on solvent. In thf solvent the amphiphiles assemble into artificial carbon nanotubes with the hydrophobic dodecyl groups on the inside and the wider, more hydrophilic portion on the outside. Addition of water modifies the morphology to give a helical coiled morphology as the triethyleneglycol chains are more highly solvated, Figure 14.16. The nanotubes are thermally stable until the formation of liquid crystalline phases at 203 °C. Interestingly, addition of electron accepting trinitrofluorenone groups to the end of

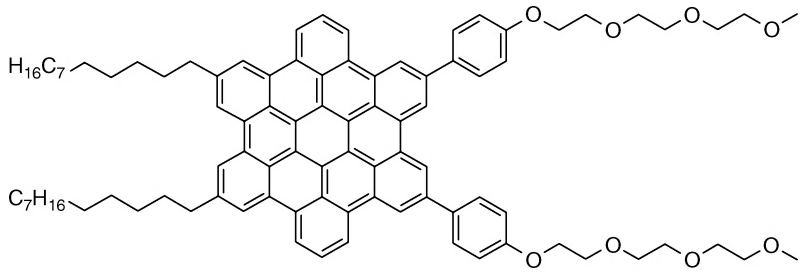


**14.10**

(a)

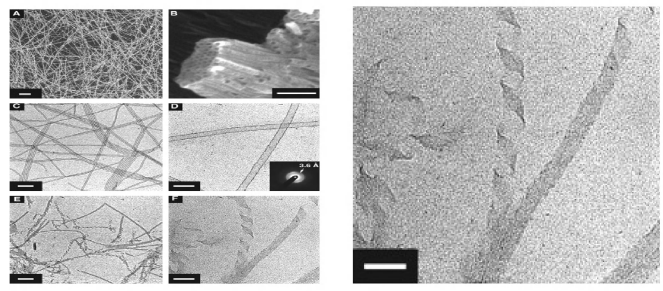

(b) (c)

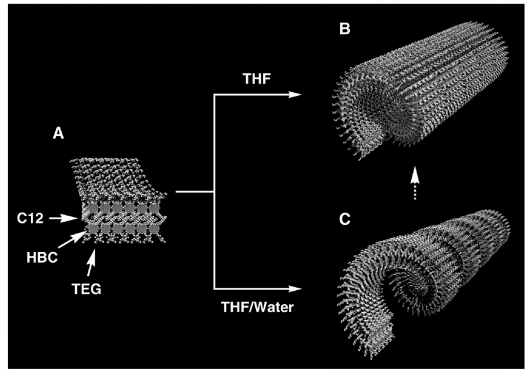


(d)

**Figure 14.16** (a) Structure of amphiphile **14.10** (b and c) SEM images of self-assembled nanotubes of **14.10** under various conditions (scale bars 100 and 50 nm, respectively), (d) proposed mechanism for the assembly process (reproduced from [24] with permission from AAAS).

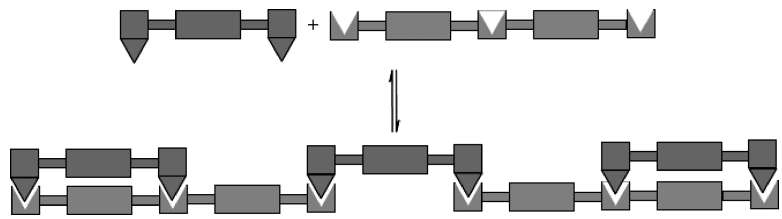

**Figure 14.17** The Vernier mechanism for controlling supramolecular oligomerisation. An *n*-mer plus a complementary *m*-mer gives an assembly ($n \times m$) in length.[25]

the hydrophilic chains results in analogous nanotubes that are strong photoconductors (*i.e.* conduct electricity on irradiation). The key to this interesting property is the nanotube structure that involved a segregated hexabenzocoronene layer sandwiched between two layers of trinitrofluorenone.

Like many polymerisation processes the degree of polymerisation (*i.e.* final number of monomers in each polymer strand) in many supramolecular polymer assemblies, is variable and a range of assembly weights is obtained. An ingenious answer to this problem that uses the principles of thermodynamic self-assembly is the 'Vernier' mechanism, named after the Vernier scale found on a variety of traditional measuring devices. To read a Vernier scale one looks at the point where the tick marks line up. Figure 14.17 shows how this analogy is transferred to molecular assembly. If two different oligomer strands are constructed such that their mutually complementary binding sites line up but the two components are of different length ($n$ and $m$) then a polymer will form of length equal to $n \times m$. This particular polymer is the most stable because it is the only one that does not involve unfilled binding sites. This design process has been realised in the construction of a Sn(IV) bis(porphyrin) with axial isonicotinic acid ligands that can bind to a complementary Zn(II) tris(porphyrin). The mismatch between the $n = 2$ tin compound and $m = 3$ zinc compound results in a polymer containing $2 \times 3 = 6$ such components and hence a total of 12 metalloporphyrin units.[25] There is a clear analogy to the self-assembly of cyclic oligomers of similar metalloporphyrins described in Section 10.4.2.

## 14.5 Polycatenanes and Polyrotaxanes

Raymo, F. M. and Stoddart, J. F., 'Polymers with intertwined superstructures and interlocked structures', in *Supramolecular Polymers*, Ciferri, A. (Ed.), Dekker: New York, 2000.

A particularly appealing way to attempt to make a supramolecular polymer is to use entirely mechanical linkages to produce a daisy-chain like polymer (which would be a polyrotaxane) or a series of mechanically interlinked rings like children's paper chains (a polycatenane). A series of many rings on a single polymeric chain would also be an alternative approach, giving a different kind of polyrotaxane. While a linear poly[2]catenane directly analogous to the paper chain remains elusive, a number of catenane polymers have been prepared based on the strategies outlined in Scheme 14.3.[26] To take one example of the approach shown in Scheme 14.3a, self-templated macrocyclisation of a bis(amide) analogous to the catenanes discussed in Section 10.7.4 with an aryl bromide based diacid chloride gives a bromo[2]catenane in 9 % yield. The catenane can then undergo a tin-based aryl-alkyne coupling reaction to give a poly[2]catenane in 84 % yield. The molecular weight of the resulting material was assessed by gel permeation chromatography to give a weight average molecular weight

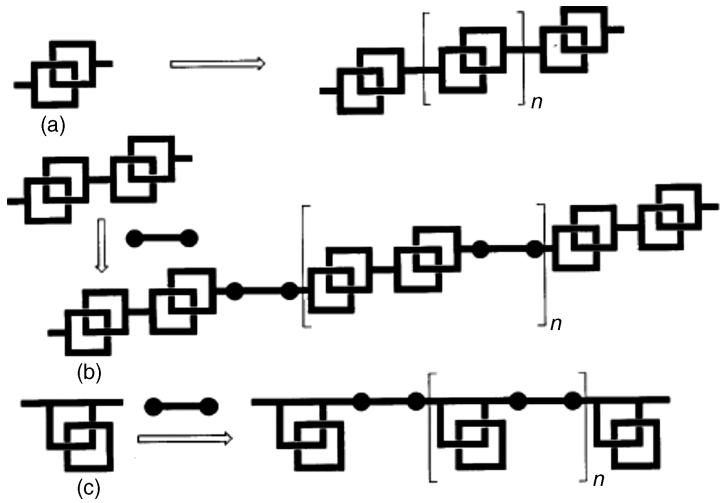


**Scheme 14.3** Synthetic approaches to (a) a main-chain poly([2]catenane), (b) a main-chain poly(bis[2]catenane), and (c) a pendant poly([2]catenane) (reproduced with permission from Reference 26).

of 3600 – *i.e.* a relatively short oligomer.[27] The materials do display broad, polymer-like $^1$H NMR spectra and exhibit a glass transition at 245 °C by DSC scan (a glass transition occurs when a polymer goes from a high temperature rubbery, viscous state to a low temperature crystalline, brittle state in which the polymer chains are no longer free to move with respect to one another – *e.g.* immersing a rubber tube in liquid nitrogen cools it to below its glass transition temperature and it will shatter if banged against a wall).

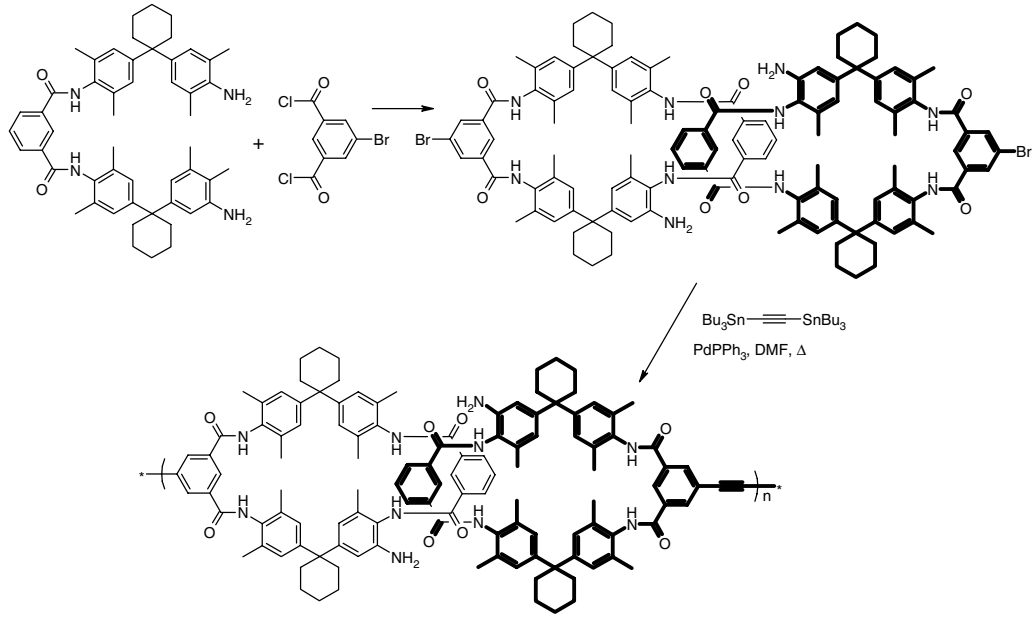


**Scheme 14.4** Synthesis of a main chain poly[2]catenane based on an aryl coupling reaction.[27]

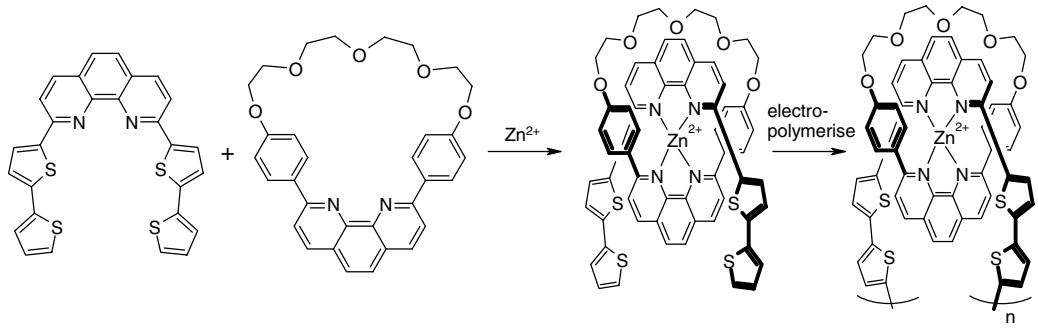


**Scheme 14.5** Synthesis of the metallopolyrotaxane by electropolymerisation of a pseudorotaxane precursor.[29]

Polyrotaxanes have been prepared by threading multiple α-cyclodextrin units onto a bulky benzimidazole-based linear chain polymer with an aliphatic spacer where the cyclodextrin resides. The rotaxane forms as the cyclodextrin-bound precursor amine is polymerised. Compared to the polymer in the absence of the cyclodextrins, the glass transition temperature is raised by some 20 °C even though only *ca.* 16 % of the aliphatic spacers in the polymer are rotaxanated.[28] A novel approach to polyrotaxanes involved the use of a metal ion such as $Zn^{2+}$ to thread a phenanthroline-based macrocycle onto a thiophene-based complementary monomer. The resulting pseudorotaxane can then be electropolymerised and the $Zn^{2+}$ ions removed to give a polyrotaxane, Scheme 14.5. The redox and conductivity properties of the polymer are very much dependent on whether a metal ion is bound or not.[29]

## 14.6 Biological Self-Assembled Fibres and Layers

### 14.6.1 Amyloids, Actins and Fibrin

Sipe, J. D. and Cohen, A. S., 'Review: history of the amyloid fibril', *J. Struct. Biol.* 2000, **130**, 88–98.

There is a range of biological self-assembled polymer fibres such as amyloids, actins and fibrin that have important positive and negative roles in biochemistry. These biopolymers act as an inspiration for supramolecular design and share many features in common with their abiotic analogues. We will mention them briefly here in the context of supramolecular polymers.

Amyloids are highly topical supramolecular fibres that involve insoluble aggregates of proteins.[30] The accumulation of amyloid fibres leads to neurodegenerative diseases such as Alzheimer's disease and prion-based conditions such as Bovine spongiform encephalopathy (BSE) and the human equivalent, Creutzfeldt-Jakob disease (CJD). Amyloids are also involved in more useful contexts such as some forms of spider silk. Amyloid fibres are generally (but not exclusively) extracellular, protein-based insoluble deposits that have a cross β-sheet structure. They arise due to the mis-folding of unstable proteins. The cross β-sheet has two characteristic scattering diffraction maxima in its X-ray diffraction pattern at 4.7 and 10 Å which arise from the inter-strand and stacking distances in the β-sheets. These β-sheet stacks are short and propagate across the width of the amyloid fibril (*i.e.* bundle of filaments) while the long axis comprises aligned strands, Figure 14.18a and b. Figure 14.18c shows the NMR structure of a prion in its amyloid form. The central region is comprised of β-sheets type structures that form a solenoid with a triangular hydrophobic core.[31]

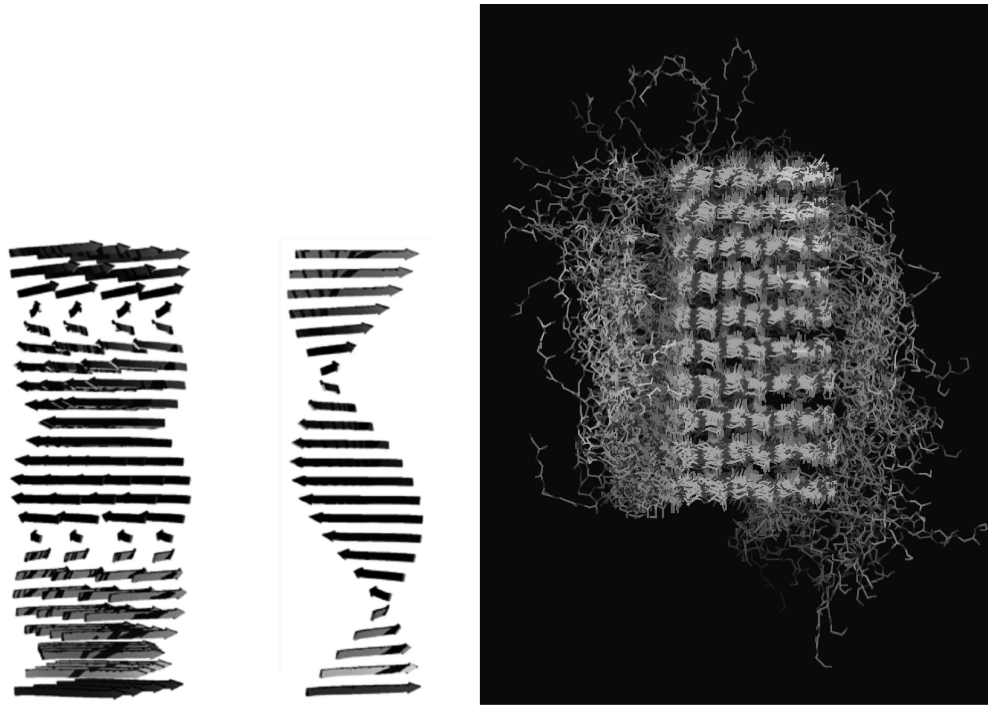


**Figure 14.18** Structure of an amyloid fibril (a) and individual fibre (b) formed from insoluble protein aggregates; the arrows represent β-sheet units; (c) Structure of The HET-s(218-289) prion in its amyloid form obtained by solid-state NMR spectroscopy.[31]

Actin filaments are ubiquitous components of eucaryotic cells. The protein is present in high concentration and its sequence is highly conserved – it differs by no more than 20 % in organisms as diverse as humans and algae! Actin itself (g-actin) is a globular protein of molecular mass *ca.* 42 kDa and is the monomeric component of long, self-assembled helical microfilaments of pitch 36 nm (f-actin)[32] which comprise one of the three major components of the cytoskeleton. It is also a component of thin filaments that are involved in muscle contraction. Actin filaments are bound by a protein termed myosin that acts a motor, travelling along the actin filament powered by ATP. Myosin molecules repeatedly hydrolyse ATP cycling between different nucleotide binding states with different actin-binding affinities. Myosin-ATP and myosin-ADP-Pi (Pi = $H_2PO_4^-$) bind weakly to actin filaments while myosin-ADP and myosin itself bind strongly. Changes in myosin nucleotide binding state involve large rotations in the position of the light chain binding domain that serves as a lever arm resulting in muscle contraction. Generally actin has a major role in a huge range of cellular functions such as muscle contraction, cell motility and division, cellular signalling and in maintaining the shape of cells.[33]

Another important biopolymer fibre is fibrin, a protein involved in blood clotting. The protein is made by from fibrinogen monomer, a soluble glycoprotein synthesised by the liver that is present in blood at about 7 μM concentration. At a wound site the coagulation cascade results in the conversion of fibrinogen to fibrin monomer. The fibrin is then polymerised by factor XIII to produce a mesh that catches blood platelets, forming a clot that prevents indefinite bleeding. Fibrinogen itself is a hexameric protein comprising three different chains dubbed α, β, and γ that are linked by disulfide bonds. The cross-linking of the chains involves cysteine residues (that can form covalent disulfide bonds) from the

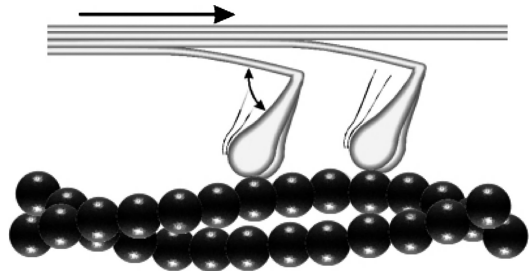

**Figure 14.19** Lever mechanism of myosin moving along an actin filament. The spheres represent globular actin monomers.

*N*-terminal sections of these three chains, which are close in evolutionary terms. The α and β chains are terminated by a short peptide sequence called a fibrinopeptide that ordinarily prevents the spontaneous polymerisation of fibrinogen.

## 14.6.2 Bacterial S-Layers

Sleytr, U. B. and Beveridge, T. J., 'Bacterial S-layers', *Trends Microbiol.* 1999, **7**, 253–260.

Bacteria and archaea* contain a crystalline single protein or glycoprotein species around their exteriors called S-layers (surface laters). They exhibit either an oblique, square, or hexaganol lattice ranging in crystallographic unit cell dimensions from 3 – 30 nm with an S-layer thickness of 5–10 nm and pores that are evenly spaced every 2–8 nm, *e.g.* Figure 14.20. The S-layer is a self-assembled single molecule layer made up of identical proteins or glycoproteins and encloses the whole cell surface. As a result the S-layer protein coat can form up to 15% of the whole cell protein content. In the case of many bacteria the S-layer represents the outermost interaction zone with the organism's environment and its functions are very diverse and species dependent. For Gram-negative archaea the S-layer is the only component of the cell wall and hence it is used for mechanical stability. In addition S-layers are used for protection against viruses (bacteriophages), resistance to pH changes, as mechanical barriers to the entry of high molecular weight substances such as enzymes, as surface adhesives (in the case of glycoprotein-based S-layers), and membrane stabilisation.

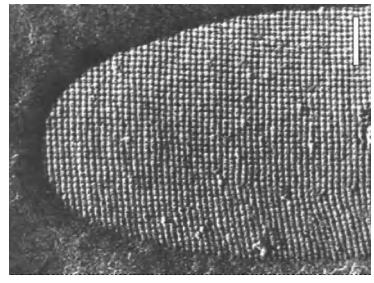

**Figure 14.20** TEM image of a freeze-etching preparation of a bacterial cell exhibiting an S-layer with square (*P*4) lattice symmetry (scale bar = 100 nm) (reproduced by permission of Blackwell Publishing Ltd).

* Archaea comprise one of the three-domains that separate all forms of life; the other two are bacteria and eukarytoa.

Bacterial S-layers are very useful surfaces for artificial bionanotechnological applications.[34] For example their use of as superstructures for artificial arrays where their underlying, crystalline order on the nanoscale allows facile formation of nanoscale components that can adhere to proteins. The S-layer is chemically removed from the bacterium and divided into individual subunits. A key feature of isolated S-layers is their ability to self-assemble into two-dimensional arrays, either in solution or on a solid support, such as a silicon wafer, metal surface, lipid film or liposome. Binding an enzyme such as glucose oxidase to an S-layer surface attached to an electrode and measuring the current passing through electrode as the oxidase reacts with the glucose makes a useful glucose sensor, for example. In another application, self-assembled S-layers can be exposed to metal-salt solutions followed by slow reaction with a reducing agent, such as hydrogen sulfide. This procedure gives nanoparticle superlattices that match the lattice spacing and symmetry of the underlying S-layer. Because the precipitation of the metal complexes is confined to the pores of the S-layer, the nanoparticles take on the pore morphology. This procedure has been used to make CdS quantum dots for example. We will return to the interesting properties of nanoparticles and quantum dots in the final chapter.

## 14.7 Supramolecular Gels

Smith, D. K., 'Molecular gels – nanostructured soft materials', in *Organic Nanostructures*, Atwood, J. L. and Steed, J. W. (eds), Wiley-VCH: Weinheim, 2008.

Gels are a colloidal state of matter that are commonplace in everyday life, *e.g.* jelly (or jell-o), toothpaste, contact lenses, hair gel, meat jelly *etc*. Fundamentally a gel is characterised by the following properties.[35]

- A two (or more) component system, comprising a fibrous solid-like phase (typically *ca*. 1 % by weight) immobilising a much larger liquid volume.
- A continuous structure with macroscopic dimensions that is permanent on the timescale of an analytical experiment
- Solid-like in its rheological behaviour (Box 14.1)

Gels also typically exhibit a melting point, $T_{gel}$, a temperature above which the gel converts to an isotropic solution and a typical way of preparing gels is to dissolve the gelator in the warm solution and allow to cool below the $T_{gel}$. Thus for example the geminal bis(urea) gelators of type **14.11** form thermoreversible gels at concentrations of less than 3 mM that are stable at temperatures over 100 °C.[36] There have also been recent reports of gels induced by sonication (as in metallogelator **14.12**)[37] or photochemical rearrangements (as in **14.13** which changes from a microsphere to gel morphology upon irradiation).[38] In the case of a *hydrogel* the liquid component is water, while for an *organogel* it is an organic solvent. An *aerogel* has a gas as the fluid phase instead of a liquid while *metallogels* are gels in which the fibre components are linked together in some way by metal ions. A particularly striking aerogel is formed by **14.14** which can gel supercritical $CO_2$. Careful depressurisation to remove the $CO_2$ gives an aerogel without collapse of the gel matrix because the outgassing $CO_2$ as no surface tension.[39] A nice example of a metallogel comes from the reaction of $LaCl_3$ with 1H-5-(2-pyridyl)tetrazole (**14.15**) which gels reversibly when treated with an excess of triethylamine in ethanol. Addition of a mixture of ethanol and isopropanol gives crystals of $[La(\mathbf{14.15}\text{-H})_3(H_2O)_3]\cdot 4H_2O$.

On the macroscale gels do not flow and hence a simple test for a gel is to invert its container – if it lands on the floor with a splash it is probably not a gel! On the microscale the solid-like component generally comprises fibrillar bundles of high aspect ratio and in the case of chiral gelators can adopt

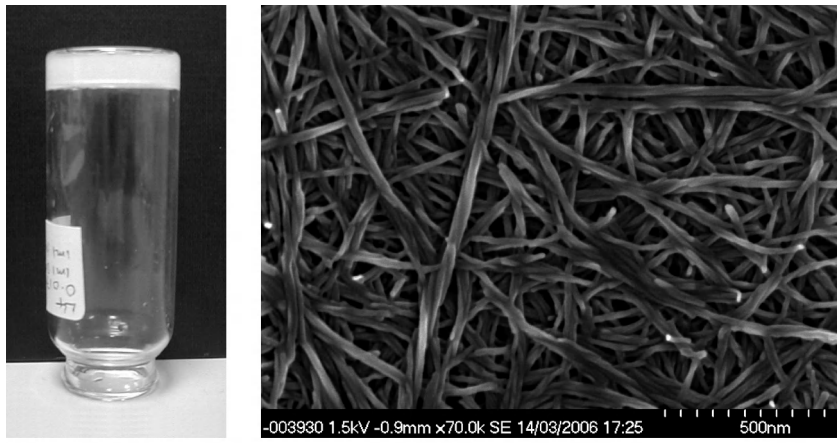


**Figure 14.21** (a) a typical gel passing the 'inversion test', (b) SEM micrograph of a dried gel (xerogel) made from a chiral gelator showing helical fibrils.[3]

a helical morphology, Figure 14.21. Some gels also exhibit *thixotropy*, they flow when shaken but re-form on standing. The mechanical forces involved in shaking are enough to temporarily break the bonds holding the gel fibres together.

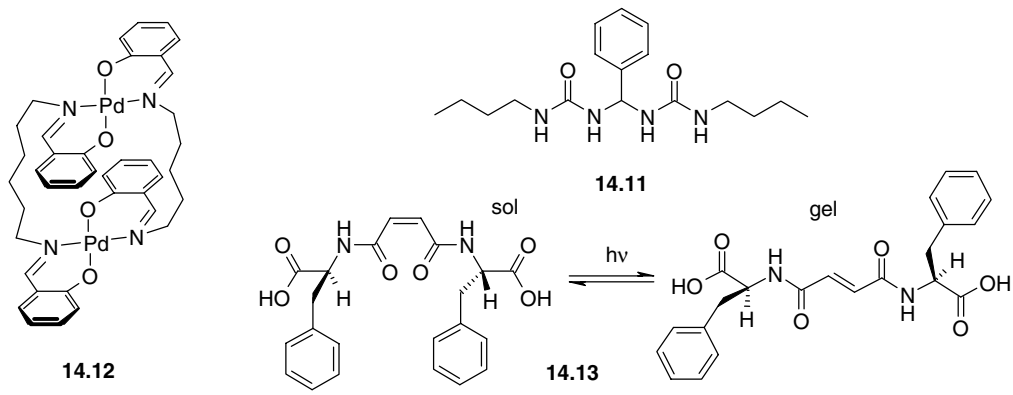


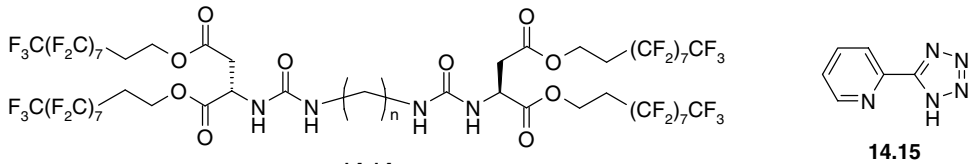


Despite their solid appearance, within the gel the liquid component is mobile and is only held by capillary forces. The solid network can be either a covalent polymer or a supramolecular assembly of small molecules. The latter class of compound, termed *low molecular weight gelators* (LMWG) of which **14.11**–**14.15** are examples, is perhaps of most interest to supramolecular chemists. Perhaps the most well known gels are metal oxide based polymeric materials produced by the sol-gel process. The sol-gel process involves the hydrolysis and polycondensation of monomeric metal salts such as early transition

metal or silicon alkoxides to produce a mixture of colloidal particles *ca.* 2–200 nm in size dispersed in a solvent in solution (a *sol*). The sol matures, forming longer, more highly cross-linked chains involving M–O–M or M–OH–M bridges to give a continuous inorganic network containing the liquid phase – the *gel*. The liquid is then removed by drying leaving a rigid, highly porous material (*an aerogel*). The process is typically employed in the ceramics industry, where the sol phase allows dopants such as colours to be readily added. The aerogel can also be fired at high temperatures for increased mechanical strength. Materials made by the sol-gel process, often in the presence of a cast or a template have a broad range of technological applications in optics, electronics, energy, space, sensing and biosensing, controlled drug release and chromatography. The classic sol-gel reaction is the acid hydrolysis of tetraethyl orthosilicate leading to the formation of fibrous or monolithic $SiO_2$; a process known since the 1880s.

In addition to these 'inorganic' polymers, organic polymeric materials such as gelatin (a hydrolysed form of collagen) and abiotic covalent polymers also form gels. The gels arise from the mutual entanglement of the polymer chains. Thus in order to form similar supramolecular gels, LMWG compounds must aggregate to produce long supramolecular polymers that can in turn associate laterally and cross-link to produce analogous fibrillar structures. Clearly the formation of such long-lived aggregates from solutions of small molecules is very much akin to the process of crystallisation and indeed gelation has been described as a kind of arrested crystallisation, or 'crystallisation gone wrong'. Unlike crystallisation, however, gelation is directional with rapid growth occurring in only one direction along the strand axis. Thus LMWG are commonly compounds that for strong interactions such as hydrogen bonds in one direction while forming only weaker (*e.g.* van der Waals) interactions in the other two. Typical examples of LMWG include strong hydrogen bond donor/acceptors such as bis(ureas), amides, fatty acids, steroids and nucleobases.

The mechanism of aggregation of LMWG in water is generally dominated by hydrophobic interactions, whereas in organic solvents hydrogen bonding dominates. Like the formation of many supramolecular polymeric structures, gel aggregation is hierarchial. Figure 14.23 shows a schematic diagram of a proposed mechanism for the assembly of rod-like chiral peptides into helical fibres in water. The dark surfaces are hydrophobic while light surfaces are hydrophilic and are therefore exposed to the medium. The difference in these surface energies leads to the helical shape. In organic media hydrogen bonding as in the classic urea α-tape motif (Figure 14.22a) becomes

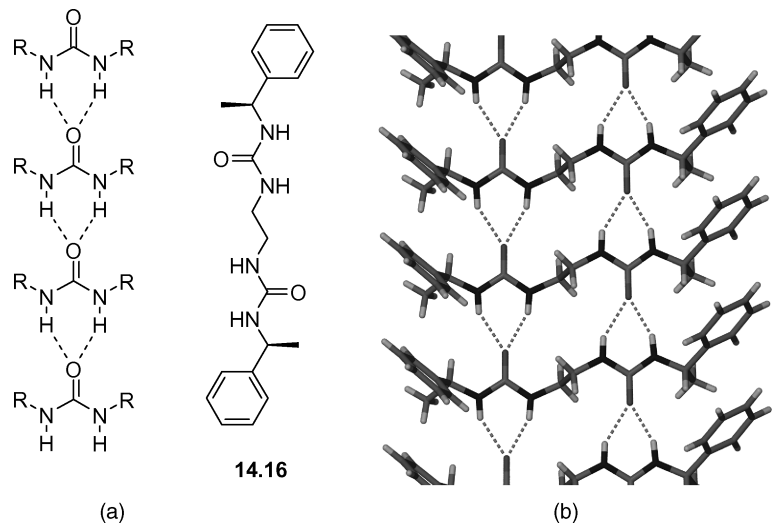


**Figure 14.22** (a) Urea α-tape motif and (b) X-ray crystal structure of **14.16** showing the urea tape hydrogen bonding. PXRD studies confirm that the crystal structure is the same phase as the xerogel.[40]

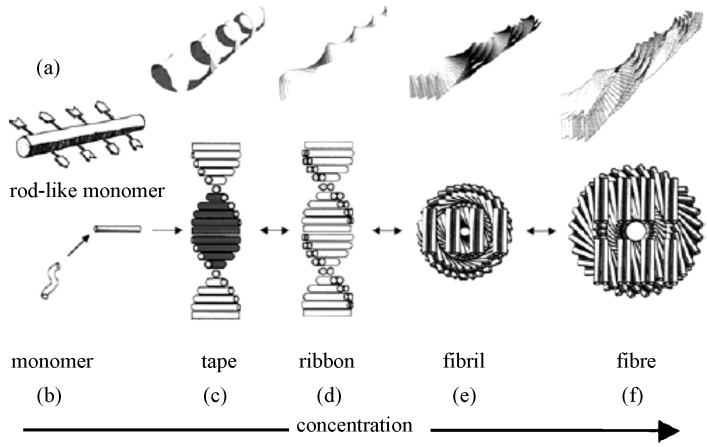


**Figure 14.23** Schematic model for the assembly of rod-like chiral peptides into helical fibres of the type found in gels (reproduced with permission from [41]).

more important. Figure 14.22b shows the X-ray crystal structure of the chiral bis(urea)gelator **14.16** which forms an anti-parallel arrangement of urea tape hydrogen bonds.[40] X-ray powder diffraction measurements confirm that the structure of the single crystal and the xerogel are the same. We have seen this kind of urea self-association in Section 10.6.1 in the context of the formation of molecular capsules; the process is the same here except that an infinite polymer is formed instead of a closed hydrogen bonded ring. Ureas are also excellent anion-binding functional groups and indeed addition of *ca.* 10 mole % of tetrabutylammonium salts of anions such as $Cl^-$ or $OAc^-$ to gels of **14.16** disrupts the urea tape hydrogen bonding resulting in gels with lower $G'$ and lower yield stresses. In contrast, anions such as $BF_4^-$ that are only weakly bound have much less effect.

One of the potentially most interesting properties of LMWG systems is the reversibility of the supramolecular interactions between the gelator molecules, suggesting the possibility of dynamic behaviour such as self-healing or slow release. Supramolecular gels are highly topical but much of the research in the field remains serendipitous. Some of the possible and actual uses (and abuses) of supramolecular gels are listed below.

- Lithium greases, a well characterised blend of mineral oil and the lithium salt of 12-hydroxystearic acid that exhibits a fibrillar self-assembled structure
- Napalm – an infamous gel originally made up of the aluminium salts of napthelenic and palmitic acids mixed with petrol. Used widely by the military from the second world war onwards, burning napalm sticks to its victim causing severe burns and rapid local deoxygenation. Moden napalm uses a polymer additive to achieve gelation.
- Tissue engineering – gels can act as a form of nanoscaffolding encouraging the growth of slow growing tissue such as nerves through peptide based gels.
- Drug delivery – many drugs are already formulated as polymer gels for oral delivery. Small molecule based gels offer the possibility if slow release or a sudden burst of drug from a chemically triggered get-sol transition.
- Templating or transcribing self-assembled morphology – gels have been used extensively as growth regulators for the preparation of metallic nanoparticles or as templates for the formation of porous polymers. Soft gel structures have also been transcribed into hard inorganic morphologies

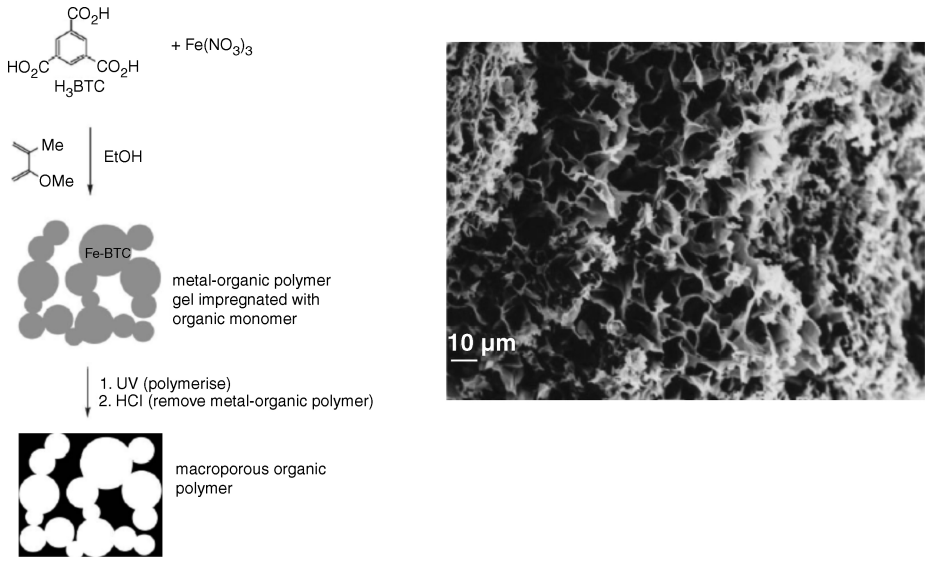


**Figure 14.24** Templation of a covalent polymer (PMMA) by a supramolecular metallogel of iron(III) benzene tricarboxylate (BTC) (reproduced by permission of The Royal Society of Chemistry).

such as CdS 'nanohelices'. An interesting report describes the formation of the covalent polymer polymethylmethacrylate (PMMA) from an ethanol solution of the metallogel formed from $Fe(NO_3)_3$ and trimesic acid (benzene 1,3,5-tricarboxylic acid). After washing away the gel (taking advantage of its supramolecular nature) a spongy covalent polymer is left where the pores may reflect the solvent pockets within the gel phase, Figure 14.24.[42]

- Molecular electronics – the long, fibrillar nature of gels strongly suggests that they might find applications in the construction of molecular wires.
- Sensing – compound **14.17** is a poor gelator in itself but undergoes a reaction with β-lactamase enzyme to produce **14.18** which is a good gelator. β-Lactamase catalysed hydrolysis of a β-lactam

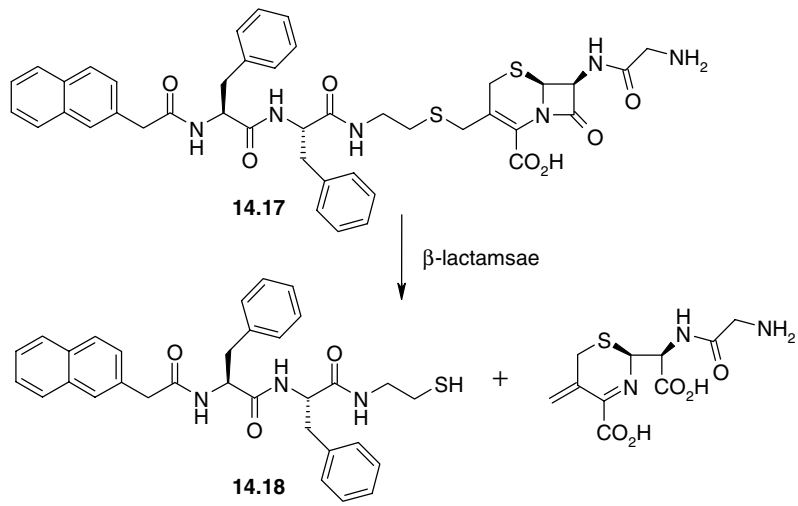

ring in penicillin type drugs is a significant cause of bacterial drug resistance and hence the formation of a gel from **14.17** *via* **14.18** is a way of sensing the presence of penicillin-resistant bacteria.[43]

## 14.8 Polymeric Liquid Crystals

Tschierske, C., 'Liquid crystal engineering – new complex mesophase structures and their relations to polymer morphologies, nanoscale patterning and crystal engineering', *Chem. Soc. Rev.* 2007, **36**, 1930–1970.

A growing trend in liquid crystal research has been the synthesis of dendritic and polymeric liquid crystalline compounds. These may be of the type where either the polymer backbone itself includes the mesogen (termed main chain liquid crystalline polymers), or the mesogenic moieties are appended to the polymer like pendants on a chain (side chain). The advantage offered by the polymer is the further restriction of molecular mobility; however, it is very important that the spacers that separate one mesogenic unit from another are sufficiently flexible to allow the mesogens to orientate themselves in the way required to manifest liquid crystalline behaviour. In such cases, liquid crystalline polymers behave in much the same way as their low-molecular-weight analogues, in which the mesogens are not chemically tethered together. Polymers based on rod-shaped mesogens such as **14.19** or **14.20** give mesophases similar to the nematic, cholesteric and smectic types (Figure 14.25). For discotic mesogenic moieties, some new structural types have been found. A polyester with the disc-shaped triphenylene as the repeating unit (**14.21**), separated by flexible spacers, forms a hexagonal, columnar structure (Figure 14.26a). Discotic groups as part of a rigid main chain polymer, on the other hand, give rise to a new phase termed 'sandic' (board-like) nematic. The boards stack parallel to one another as in Figure 14.26b.

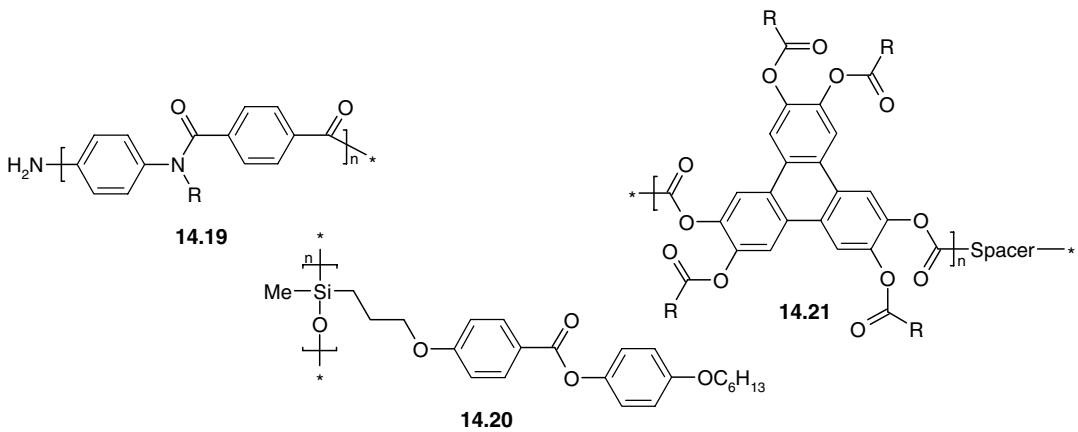


Coatings derived from cholesteric liquid crystalline polymers are used commercially as reflective sheets and polarisers. The liquid crystal is cooled below the vitrification temperature resulting in a solid polymer that is amorphous but contains large regions of 'frozen' liquid crystalline order. Such structures are also found in nature in the iridescent, almost metallic colours of beetles and other insects, which result from helical cholesteric structures in the outer layer of the carapace.

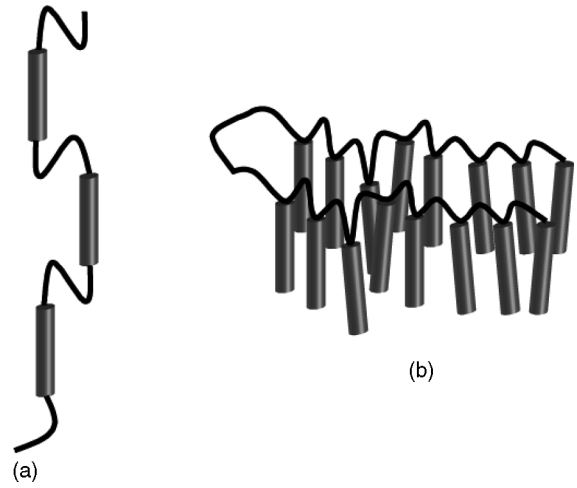


**Figure 14.25** Mesogenic polymers. The mesogenic groups may (a) form part of the main chain or (b) be attached as side chains.

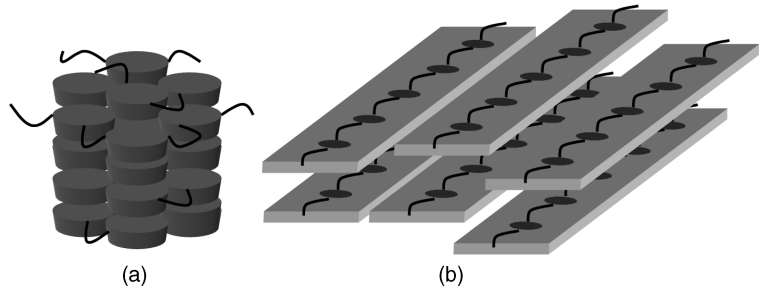


**Figure 14.26** Discotic polymeric mesogens: (a) columnar hexagonal; (b) sandic nematic.

## Summary

- Self-assembled supramolecular polymers and fibres based on proteins are ubiquitous biological building blocks
- Highly controlled, branching polymers called *dendrimers* represent an intermediate between conventional polymers and small-molecule synthesis. They have unique rheology compared to other polymers based on a rigid shell and soft core. They can act as hosts for guests such as as drug molecules and are capable of strong interactions with surfaces and biomolecules because of their high degree of surface functionality leading to cooperative multiple interactions – *multivalency.*
- Covalent polymers can be imprinted with patterns from small guest molecules at the time of synthesis. These *molecular imprinted polymers* (MIPs) are useful in sensing applications.
- Covalent polymers comprising regions of more than one type of monomer (*block co-polymers*) have interesting, designer conformational characteristics leading to their assembly into useful nanoscale morphologies with novel interfacial properties.
- Non-covalent interactions can result in the formation of supramolecular polymers even from small organic molecules. Typically multiple, strong directional interactions are involved and interesting materials with liquid crystalline, viscoelastic or gel-type behaviour are observed.

- Rheology is an important technique for looking at polymer properties and association characteristics. Gels are characterised by their solid-like rheology even though they comprise *ca*. 99 % immobilised liquid material.
- Supramolecular chemistry allows novel kinds of polymer linkages such as the mechanical links found in polycatenanes and polyrotaxanes.

## Study Problems

14.1 A dendrimer is prepared from a tetrafunctional core, which may be regarded as a sphere of radius 5.0 Å. With each successive dendrimer generation, each added dendron has a radius of 5.0 Å and presents three new binding sites for ensuing growth. Assuming the entire dendrimer adopts an approximately spherical shape with maximum extension, calculate the volume of empty space within the dendrimer with each successive generation, and hence predict how many generations may feasibly be added before the dendrimer runs out of space. (Volume of a sphere $= \frac{4}{3}\pi.r^3$.)

14.2 The same dendrimer discussed in question 14.1 is formed in a yield of 98.5 % for each unit reaction (the addition of each spherical component). What will be the yield of pure dendrimer at each generation? Do you think it would be feasible to construct a dendrimer along these lines, which reaches enough generations to isolate the dendrimer core from the external medium entirely?

14.3 According to Schneider[21] every attractive hydrogen bond contributes 7.87 kJ $mol^{-1}$ in polymer stabilisation, while diagonal secondary interactions contribute ± 2.93 kJ $mol^{-1}$ depending on whether they are attractive or repulsive. According to the data given in Section 14.4 the dimer $(\mathbf{14.7})_2$ has a dimerisation constant of $K_{dim} = 5.9 \times 10^8\ M^{-1}$ in toluene solution. How well does this compare with the value calculated from Schneider's predictions? Can you explain any differences? How would you expect the experimental value to change if wet chloroform is used as the solvent instead of toluene (see Sections 1.9.2 and 6.5.7). ($R = 8.314\ J\ K^{-1}\ mol^{-1}$, $T = 298$ K.)

## References


1. Boas, U., Heegaard, P. M. H., Dendrimers in drug research. *Chem. Soc. Rev.* 2004, **33**, 43–63.
2. Uppuluri, S., Keinath, S. E., Tomalia, D. A., Dvornic, P. R., Rheology of dendrimers. I. Newtonian flow behavior of medium and highly concentrated solutions of polyamidoamine (PAMAM) dendrimers in ethylenediamine (EDA) solvent. *Macromolecules* 1998, **31**, 4498–4510.
3. Stanley, C. E., Clarke, N., Anderson, K. M., Lenthall, J. P., Steed, J. W., Anion binding inhibition of the formation of a helical hydrogel. *Chem. Commun.* 2006, 3199–3201.
4. Grayson, S. M., Frechet, J. M. J., Convergent dendrons and dendrimers: from synthesis to applications. *Chem. Rev.* 2001, **101**, 3819–3867.
5. Antoni, P., Nystrom, D., Hawker, C. J., Hult, A., Malkoch, M., A chemoselective approach for the accelerated synthesis of well-defined dendritic architectures. *Chem. Commun.* 2007, 2249–2251.
6. Dandliker, P. J., Diederich, F., Gisselbrecht, J. P., Louati, A., Gross, M., Water-soluble dendritic iron porphyrins: Synthetic models of globular heme proteins. *Angew. Chem., Int. Ed. Engl.* 1996, **34**, 2725–2728.
7. Jansen, J., Debrabandervandenberg, E. M. M., Meijer, E. W., Induced chirality of guest molecules encapsulated into a dendritic box. *Recueil Des Travaux Chimiques Des Pays-Bas-Journal of the Royal Netherlands Chemical Society* 1995, **114**, 225–230.
8. Jansen, J., Meijer, E. W., Debrabandervandenberg, E. M. M., The dendritic box - shape-selective liberation of encapsulated guests. *J. Am. Chem. Soc.* 1995, **117**, 4417–4418.
9. Zimmerman, S. C., Wendland, M. S., Rakow, N. A., Zharov, I., Suslick, K. S., Synthetic hosts by monomolecular imprinting inside dendrimers. *Nature* 2002, **418**, 399–403.
10. Joralemon, M. J., O'Reilly, R. K., Hawker, C. J., Wooley, K. L., Shell Click-crosslinked (SCC) nanoparticles: A new methodology for synthesis and orthogonal functionalization. *J. Am. Chem. Soc.* 2005, **127**, 16892–16899.

11. Zimmerman, S. C., Zeng, F. W., Reichert, D. E. C., Kolotuchin, S. V., Self-assembling dendrimers. *Science* 1996, **271**, 1095–1098.
12. Kawa, M., Frechet, J. M. J., Self-assembled lanthanide-cored dendrimer complexes: Enhancement of the luminescence properties of lanthanide ions through site-isolation and antenna effects. *Chem. Mat.* 1998, **10**, 286–296.
13. Huck, W. T. S., Prins, L. J., Fokkens, R. H., Nibbering, N. M. M., van Veggel, F., Reinhoudt, D. N., Convergent and divergent noncovalent synthesis of metallodendrimers. *J. Am. Chem. Soc.* 1998, **120**, 6240–6246.
14. Burghardt, S., Hirsch, A., Schade, B., Ludwig, K., Bottcher, C., Switchable supramolecular organization of structurally defined micelles based on an amphiphilic fullerene. *Angew. Chem., Int. Ed.* 2005, **44**, 2976–2979.
15. Tada, T., Nozaki, D., Kondo, M., Yoshizawa, K., Molecular orbital interactions in the nanostar dendrimer. *J. Phys. Chem. B* 2003, **107**, 14204–14210.
16. Stiriba, S. E., Frey, H., Haag, R., Dendritic polymers in biomedical applications: From potential to clinical use in diagnostics and therapy. *Angew. Chem., Int. Ed.* 2002, **41**, 1329–1334.
17. Kauranen, M., Verbiest, T., Boutton, C., *et al.*, Supramolecular 2nd-order nonlinearity of polymers with orientationally correlated chromophores. *Science* 1995, **270**, 966–969.
18. Vriezema, D. M., Hoogboom, J., Velonia, K., *et al*., Vesicles and polymerized vesicles from thiophene-containing rod-coil block copolymers. *Angew. Chem., Int. Ed.* 2003, **42**, 772–776.
19. Reynhout, I. C., Cornelissen, J., Nolte, R. J. M., Self-assembled architectures from biohybrid triblock copolymers. *J. Am. Chem. Soc.* 2007, **129**, 2327–2332.
20. Greene, N. T., Morgan, S. L., Shimizu, K. D., Molecularly imprinted polymer sensor arrays. *Chem. Commun.* 2004, 1172–1173.
21. Sartorius, J., Schneider, H. J., A general scheme based on empirical increments for the prediction of hydrogen-bond associations of nucleobases and of synthetic host-guest complexes. *Chem. Eur. J.* 1996, **2**, 1446–1452.
22. Kotera, M., Lehn, J. M., Vigneron, J. P., Self-assembled supramolecular rigid rods. *J. Chem. Soc., Chem. Commun.* 1994, 197–199.
23. Bong, D. T., Clark, T. D., Granja, J. R., Ghadiri, M. R., Self-assembling organic nanotubes. *Angew. Chem., Int. Ed.* 2001, **40**, 988–1011.
24. Hill, J. P., Jin, W. S., Kosaka, A., *et al*., Self-assembled hexa-peri-hexabenzocoronene graphitic nanotube. *Science* 2004, **304**, 1481–1483.
25. Hunter, C. A., Tomas, S., Accurate length control of supramolecular oligomerization: Vernier assemblies. *J. Am. Chem. Soc.* 2006, **128**, 8975–8979.
26. Hamers, C., Raymo, F. M., Stoddart, J. F., Molecular meccano, 42 – Main-chain and pendant poly([2]catenane)s incorporating complementary $\pi$-electron-rich and -deficient components. *Eur. J. Org. Chem.* 1998, 2109–2117.
27. Geerts, Y., Muscat, D., Mullen, K., Synthesis of Oligo[2]Catenanes. *Macromolecular Chemistry and Physics* 1995, **196**, 3425–3435.
28. Yamaguchi, I., Osakada, K., Yamamoto, T., Polyrotaxane containing a blocking group in every structural unit of the polymer chain. Direct synthesis of poly(alkylenebenzimidazole) rotaxane from Ru complex-catalyzed reaction of 1,12-dodecanediol and 3,3'-diaminobenzidine in the presence of cyclodextrin. *J. Am. Chem. Soc.* 1996, **118**, 1811–1812.
29. Zhu, S. S., Swager, T. M., Conducting polymetallorotaxanes: Metal ion mediated enhancements in conductivity and charge localization. *J. Am. Chem. Soc.* 1997, **119**, 12568–12577.
30. Sipe, J. D., Cohen, A. S., Review: history of the amyloid fibril. *J. Struct. Biol.* 2000, **130**, 88–98.
31. Wasmer, C., Lange, A., Van Melckebeke, H., Siemer, A. B., Riek, R., Meier, B. H., Amyloid fibrils of the HET-s(218-289) prion form a beta solenoid with a triangular hydrophobic core. *Science* 2008, **319**, 1523–1526.
32. Holmes, K. C., Popp, D., Gebhard, W., Kabsch, W., Atomic Model of the Actin Filament. *Nature* 1990, **347**, 44–49.
33. Kinbara, K., Aida, T., Toward intelligent molecular machines: Directed motions of biological and artificial molecules and assemblies. *Chem. Rev.* 2005, **105**, 1377–1400.
34. Sleytr, U. B., Huber, C., Ilk, N., Pum, D., Schuster, B., Egelseer, E. M., S-layers as a tool kit for nanobiotechnological applications. *Fems Microbiology Letters* 2007, **267**, 131–144.
35. Terech, P., Weiss, R. G., Low molecular mass gelators of organic liquids and the properties of their gels. *Chem. Rev.* 1997, **97**, 3133–3160.
36. Schoonbeek, F. S., van Esch, J. H., Hulst, R., Kellogg, R. M., Feringa, B. L., Geminal bis-ureas as gelators for organic solvents: Gelation properties and structural studies in solution and in the gel state. *Chem. Eur. J.* 2000, **6**, 2633–2643.
37. Naota, T., Koori, H., Molecules that assemble by sound: an application to the instant gelation of stable organic fluids. *J. Am. Chem. Soc.* 2005, **127**, 9324–9325.
38. Frkanec, L., Jokic, M., Makarevic, J., Wolsperger, K., Zinic, M., Bis(PheOH) maleic acid amide-fumaric acid amide photoizomerization induces microsphere-to-gel fiber morphological transition: The photoinduced gelation system. *J. Am. Chem. Soc.* 2002, **124**, 9716–9717.
39. Shi, C., Huang, Z., Kilic, S., *et al*., The gelation of CO2: A sustainable route to the creation of microcellular materials. *Science* 1999, **286**, 1540–1543.

40. Piepenbrock, M.-O. M., Lloyd, G. O., Clarke, N., Steed, J. W., Gelation is crucially dependent on functional group orientation and may be tuned by anion binding. *Chem. Commun.* 2008, 2644.
41. Aggeli, A., Nyrkova, I. A., Bell, M., *et al*., Hierarchical self-assembly of chiral rod-like molecules as a model for peptide beta-sheet tapes, ribbons, fibrils, and fibers. *Proc. Natl. Acad. Sci. U. S. A.* 2001, **98**, 11857–11862.
42. Wei, Q., James, S. L., A metal-organic gel used as a template for a porous organic polymer. *Chem. Commun.* 2005, 1555–1556.
43. Yang, Z. M., Ho, P. L., Liang, G. L., *et al*., Using beta-lactamase to trigger supramolecular hydrogelation. *J. Am. Chem. Soc.* 2007, **129**, 266–267.

# 15 Nanochemistry

*'To you then, tenants of life's middle state,*
*Securely placed between the small and great,*
*Whose character, yet undebauch'd, retains*
*Two thirds of all the virtue that remains.'*

William Cowper (1731–1800), *Tirocinium*

## 15.1 When Is Nano Really Nano?

Ozin, G. and Arsenault, A. *Nanochemistry*, Royal Society of Chemistry: Cambridge, 2005.

In this final chapter we turn to the frontiers of chemistry as chemists explore ever further upwards in size, not just synthesising but understanding and controlling objects and devices on the multi-nanometre scale. We left our discussion of nanochemistry with some scene-setting comments in Section 1.10.3. Since then we have seen how an atomic and molecular level understanding of non-covalent interactions both within and between molecules and in 'soft' materials can gradually build up a full picture of simple binding events in solution, through to self-assembly, the functioning of molecular electronic components, materials structure and properties, and the complex assembly and viscoelastic properties of polymeric systems. We discussed in Section 1.10.3 the strict definition of nanochemistry as not just a molecular approach to objects of dimensions on the 2–200 nm scale but to systems whose properties scale with size (as in the surface plasmon resonance of metallic nanoparticles, Section 15.7.2). Taking such a definition of nanoscience as the science of materials whose properties scale with size is a nice one from a materials stand point. From that point of view nanochemistry stands apart from well-defined molecular assemblies and machines, which albeit of multi-nanometre size, do not fit into such a definition... but what if you combine two or more of them? On a more pedestrian level there is a case for describing nanochemistry simply as the chemistry of multi-nanometre scale molecules and indeed this sheer size regime, giant by the standards of molecular characterisation but small in comparison to the conventional macroscopic world, carries with it particular challenges for the chemist. Taking on board the ideas of hierarchial self-assembly that we have seen particularly in Chapters 10 and 14, however, it is clear that there are certain properties and features that emerge according to the length scale on which a system assembles, and indeed on which it is studied. Bearing in mind all of the detailed information we have learned about intermolecular interactions and properties we now look at how those characteristics scale up into the nanoworld and along the way examine the frontiers and future of supramolecular chemistry, as direct microscopic imaging and manipulation on the multi-nanometre scale become increasingly technologically feasible. We will also see the influence on chemistry of the powerful concept of *emergence* – the 'arising of novel and coherent structures, patterns and properties during the process of self-organisation in complex systems'.[1]

## 15.2 Nanotechnology: The 'Top Down' and 'Bottom Up' Approaches

Foster, L. E., *Nanotechnology: Science, Innovation, and Opportunity*, Prentice Hall: Upper Saddle River, NJ, USA, 2005.

The term *nanotechnology* is quite broadly interpreted and can be considered to be a field of applied science and technology based on the control, manipulation and fabrication of matter on the size scale approaching that of atoms and molecules. Of particular interest to nanotechnologists is the fabrication of devices with critical dimensions (*i.e.* the dimensions of the smallest functional components) that lie within the 2–200 nm size range. As currently practised, nanotechnology is highly multidisciplinary and draws on techniques and knowledge from applied physics, materials science, interface and colloid science, device physics, chemical and biological engineering and of course supramolecular chemistry. The archetypical image in nanotechnology is that of Don Eigler's quantum corrals in which an electron is confined on a copper(111) surface

*Supramolecular Chemistry, 2nd edition* J. W. Steed and J. L. Atwood
© 2009 John Wiley & Sons, Ltd ISBN: 978-0-470-51233-3

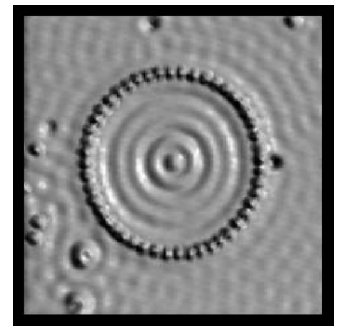

**Figure 15.1** Assembly of a circular corral on a copper(111) surface of radius 71.3 Å constructed out of 48 iron adatoms. The corral provides evidence for size quantisation and is consistent with an electron trapped in a round two-dimensional box (reproduced from [2] with permission from AAAS).

within closed structures defined by barriers built from individual surface adsorbed iron atoms (*adatoms*), positioned with the tip of a scanning tunnelling microscope (STM) at 4 $K^2$, Figure 15.1.

Much of the early progress in nanotechnology, and certainly the vast majority of current practical nanodevices, has relied on the *top-down approach* in which the nanoscale components of interest are fabricated by cutting down larger precursors, *e.g.* by some kind of *lithographic* (literally 'stone writing') technique. For example, lithographic etching of silicon semiconductor is used in the construction of modern computer chips. Current chip components have features around 90 nm in size as compared to 500 nm a decade ago. Approaches based on nanotechnology are needed to produce components on the 30 nm scale and below in order to postpone the inevitable limits of Moore's law, which has become a major industrial driving force.* At this size materials stop behaving as bulk solids and instead start to show quantum effects in which the individual component can be regarded as having its own set of discrete energy levels rather than a continuous band of orbitals. There are also tremendous problems of heat dissipation. So, below the 30 nm size regime an entirely new paradigm in integrated circuits may be required. Of particular appeal to chemists is the *bottom up*, or *synthesising up* approach to nanotechnology. This methodology involves using (broadly) chemical or at least molecular techniques to assemble multi-nanoscale devices. We have already seen in Section 11.4.6 some of the remarkable but nascent recent progress in molecular electronics towards this goal. The fact that a molecular approach is possible is elegantly demonstrated by Nature which synthesises up molecular machinery such as motors, self-replicators and nanostructures of breathtaking complexity. The evolution of such sophisticated molecular machinery is difficult to comprehend but is *inter alia* an illustration *par excellence* of the power of the modern concept of Darwinian evolution which shows that such structures and devices arise not by chance, but *emerge* under the extremely directing pressure of natural selection.[3] Reassuringly for the chemist, however, Nature may not be perfect. Darwinian evolution can never go downhill and undo an inefficient system in order to take advantage of a potentially better one. As a result there are evolutionary 'dead ends' and with the increasing arsenal of abiotic chemistry some nanoscale devices that improve on Nature may yet be designed or discovered. Chemists are also beginning to harness and hybridise natural structures giving rise to *nanobiology* – the extension of nanotechnology to biology. Nanobiology encompasses nanotechnological solutions to biological problems such as diagnosis and monitoring, the

* In 1965, Gordon. E. Moore, one of the co-founders of Intel, observed that the number of transistors per square inch on an integrated circuit had doubled since the integrated circuit was first produced. From his initial observations, Moore then went on to predict that every 18 months the 'complexity' of an integrated circuit (generally taken to be proportional to the number of transistors) would double.

study of nanoscale biological systems and phenomena, the use of biological components in nanotechnological applications and the synthesis or construction of nanometre scale mimics of biological entities.[4] Examples include the use of DNA for molecular computing,[5] or as a nanoscale structural scaffold,[6] and the templation of nanostructures using bacterial S-layers (Section 14.6.2). With these ideas in mind we turn first to templated morphosynthesis; the chemical synthesis of nanoscale morphologies that often mimic complex structures found in the Natural world.

## 15.3 Templated and Biomimetic Morphosynthesis

Colfen, H. and Mann, S., 'Higher-order organization by mesoscale self-assembly and transformation of hybrid nanostructures', *Angew. Chem., Int. Ed.* 2003, **42**, 2350–2365.

The idea of morphosynthesis, literally the synthesis of form or shape, draws considerable inspiration from the beautiful structures of natural diatoms and radiolaria – single-celled algae, which have a delicate and elaborate mineral exoskeleton. The study of these elegant and exotic organisms goes back to 1887 and the work of German biologist and philosopher Ernst Haeckel who, amongst his many accomplishments, was responsible for popularising Charles Darwin's work on evolution, in Germany, Figure 15.2.

The kinds of structures adopted by these microorganisms as well as other mineral morphologies, are the subject of increasing study as chemists look at 'soft' templated routes to nanoscale objects. Early work in the 1990s by a team at Mobile used supramolecular micelles, lamellae and bicontinuous phases[†] formed by amphiphiles, to assemble inorganic materials, particularly silica and alumina. A range of new

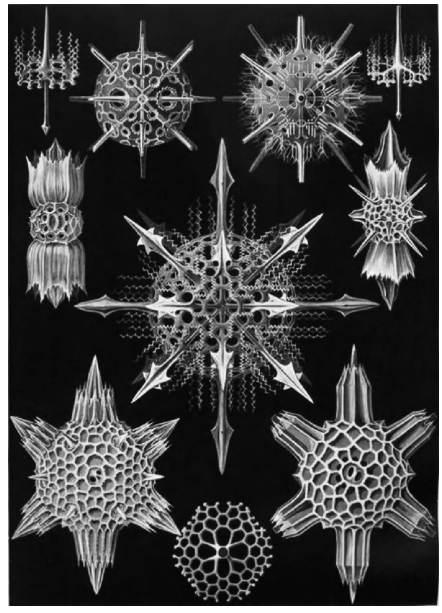

**Figure 15.2** Plate from Ernst Haeckel's *Kunstformen der Natur* (1904), depicting (perhaps slightly exaggerated) radiolarians classified as *Acanthophracta*.

[†] A bicontinuous or 'sponge' phase occurs when the amount of water and oil in an emulsion are approximately equal and form a continuous phase. The analogy with a sponge demonstrates the principle: as a liquid is pored into a sponge it contains a continuous phase of the liquid, in the same way the material that the sponge is made from also forms a continuous phase.

materials resulted, with interesting abiotic microscale shapes and patterns mimicking the microskeletal structures of diatoms and radiolaria. The shapes arise from the templating behaviour of surfactant-cosurfactant-based supramolecular assemblies. The chemical basis for the templation is a mixture of different ratios of tetraethylene glycol (TEG) and an amphilic alkylamine ($C_{10}H_{21}NH_2$) with phosphoric acid – a mixture that immediately gels. The mixture can be identified by X-ray crystallography as a crystalline mesolamellar alkylammonium dihydrogen phosphate phase, $(C_{10}H_{21}NH_3)^+(H_2PO_4)^-$, linked by an extensive hydrogen bonding array. Addition of alumina results in phase separation to give (TEG)Al(III) ionophores throughout the vesicle structure. A proposed mechanism for the templating is shown in Figure 15.3 and is based on the ionophore complexes assembling to give the surface patterning.[7] The resulting biomimetic structures have only a passing resemblance to the natural forms, but they do shed light onto how the natural system may create their remarkable complexity.

The templating of mesoporous silica ($SiO_2$) structures has been extensively investigated.[8] The uncharged nature of the silica framework means that it is tolerant of a very wide range of templating molecules and salts, particularly complex patterns arising from surfactant assemblies that act as supramolecular templates. Importantly this kind of morphosynthesis must proceed under unstirred aqueous acidic conditions in which the small differences in surface interfacial energies can be expressed in the final, robust morphology. The building blocks are delivered under diffusion control and so there is no mechanical disruption of fluid solution assemblies. For example, using cetyltrimethylammonium chloride (CTACl) as the surfactant template, and the classic tetraethylorthosilicate (TEOS) as the silica source, a diverse range of silica forms and topologies are revealed by SEM imaging of the products, Figure 15.4. These forms are *emergent*, because they are not predictable and evolve as a function of time and length scale. Interestingly a recent report has shown that natural silica structures such as those that form radiolarian exoskeletons can be reduced to elemental silicon without losing their intricate morphology. The silica structure is sealed in a steel ampoule with magnesium and reduced at 650 °C – hot enough to generate magnesium gas but cool enough that the silicon remains non-volatile.

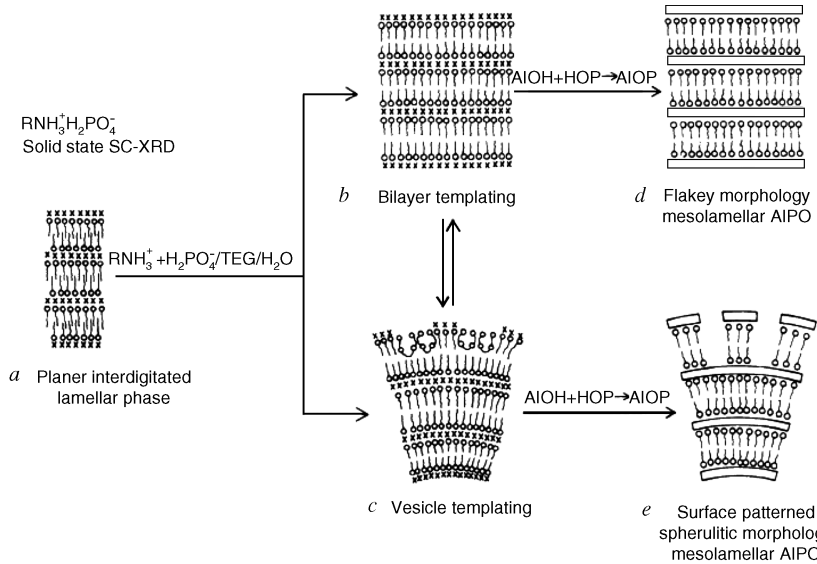


**Figure 15.3** The proposed template patterning mechanism in the formation of biomimetic microskeletal structures. The circles with tails represent the cation surfactant, the crosses the anionic dihydrogen phosphate counterions and the connected circles represent the tetraethylene glycol molecules (TEG) (reproduced by permission from Macmillan Publishers Ltd).

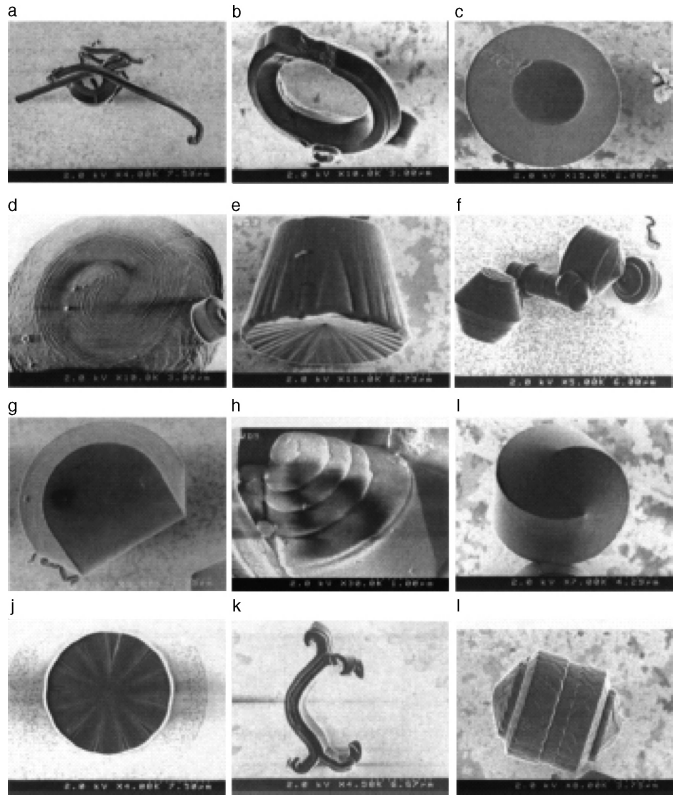


**Figure 15.4** SEM images showing diverse mesoporous silica shapes and patterns produced by surfactant templating; (a) rope, (b) toroid, (c) discoid, (d) pinwheel, (e) wheel, (f) gyroid, (g) bagel, (h) shell, (i) knot, (j) clock, (k) eccentric 1 and ( l) eccentric (reproduced by permission from Macmillan Publishers Ltd).

An acid wash removes excess magnesium, leaving the silicon nanostructures behind. By implication the process could be used for artificial structures as well and the versatile semiconductor properties of silicon mean that some interesting nanofabricated devices could result.[9]

Work by Steve Mann (Bristol, UK) has focused on the deposition of ordered arrays of nanocrystals of the highly insoluble $BaSO_4$ or $BaCrO_4$. Taking an unstirred solution of isooctane containing a mixture of $Ba(AOT)_2$ (AOT = *bis*(2-ethylhexyl)sulfosuccinate) and water-in-oil microemulsion droplets (reverse micelles) prepared from NaAOT and aqueous chromate or sulfate anions it is possible to bring about the controlled deposition of the inorganic crystalline solid as the reverse micelle encapsulated anions slowly interact with the $Ba^{2+}$ cations. At a $Ba^{2+} : CrO_4^{2-}$ ratio of 1:1 the result is spontaneous assembly of linear chains of crystallographically aligned, prismatic $BaCrO_4$ nanoparticles spaced at a distance of 2 nm from each other (Figure 15.5). This precise spacing and alignment is an emergent property of a mesophase transition in which the disordered pendent AOT molecules become organised into a bilayer that is interdigitated between adjacent nanoparticles. Related work has resulted in the preparation of curved nanofilaments and trumpet-like structures that exhibit fractal features with critical discontinuities in their growth resulting in the repetition of similar morphologies across various length scales.

In general, a wide range of nanocomposite polymer materials are already finding real world applications. Traditional nanocomposites are based on (1) copolymerisation of functional macroorganosilanes and metal alkoxides, (2) the encapsulation of organic components within sol–gel derived silica or metallic

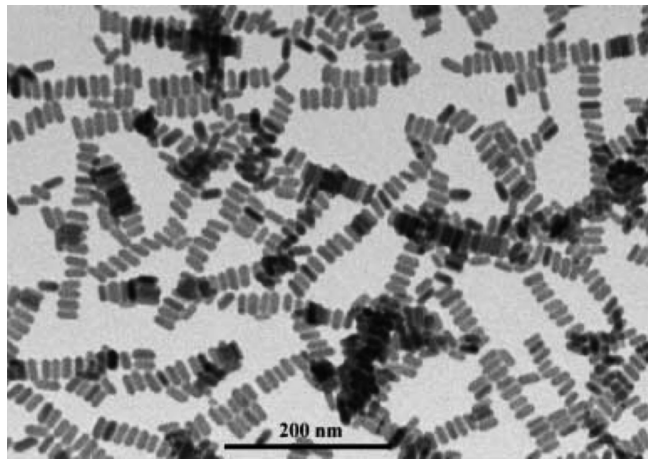


**Figure 15.5** TEM image showing ordered chains of prismatic $BaCrO_4$ nanoparticles prepared in AOT microemulsions (Copyright Wiley-VCH Verlag GmbH & Co. KGaA. Reproduced by permission).

oxides and (3) the organic functionalisation of nanofillers, nanoclays or other compounds with lamellar structures, *etc.* New chemical strategies to nanomaterials based on self-assembly type approaches offer new possibilities for a next generation of intelligent, vectorial assembly of structurally well-defined nano objects with hierarchial structure and function.[11]

## 15.4 Nanoscale Photonics

Another interesting materials area that involves 'bottom up' templation is the production of micro-structured *inverse opals.* These materials have a high dielectric constant and periodicity of the order of the wavelength of visible light making them the optical analogues of semiconductors and hence they are referred to as *photonic crystals.* Such materials are projected to have a major impact on the optical computers of tomorrow. Opal itself is a mineraloid with generally little crystallinity. It has a characteristic shimmering appearance that can range in colour from a milky white, through blue, green red all the way to black (Figure 15.6a). The colour is caused by the presence of spheres of opal ($SiO_2 \cdot nH_2O$) of a size of the order of the wavelength of visible light that cause the interference colours.

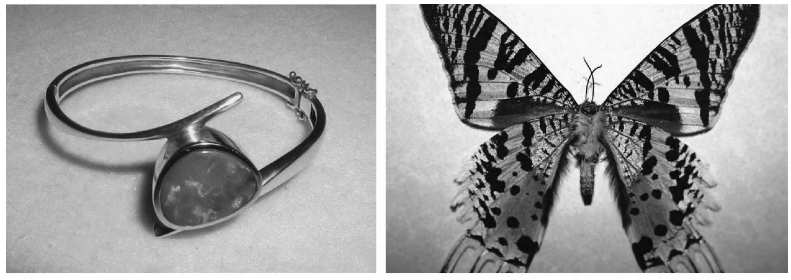

(a) (b)

**Figure 15.6** (a) an opal bracelet and (b) the iridescent colours of the Madagascan sunset moth. The colouration in both come from light interference patterns caused by nanostructured materials. See plate section for colour version of this image.

An opal is thus an aggregate of hydrated silica nanospheres. These kinds of interference colours are found throughout Nature, for example in the iridescent colours of the Madagascan sunset moth (*Chrysiridia rhipheus* – Figure 15.6b) or the colours of a peacock's plumage – all arising from light scattering by micro- or nanostructured materials rather than pigments. The theoretical description of these phenomena in 1987 by Yablonovitch[12] and John[13] has generated intense interest in the field of artificial photonics.

Inverse opals are formed by the use of micro- or nanospheres to template a structure containing spherical cavities. One way of doing this is to use monodisperse latex spheres. These latex spheres are prepared by slow addition of an aqueous precursor solution into a reservoir of hydrophobic silicone liquid, forming emulsion droplets. The size of the droplets is controlled by the concentration of the aqueous latex, the speed at which the suspension is stirred and ratio between the silicone liquid and latex. Polymerisation results in latex spheres of well defined size of the order of a few hundred nanometers, and spherical shape. As the concentration of the latex spheres increases to its critical concentration *i.e.* the concentration at which the colloidal spheres start to order themselves into a close-packed structure, the balls are filtered off and are dried to give an artificial opal. Aqueous colloids of latex spheres can also be induced to form artificial opals by centrifugation and careful evaporation of the water. These relatively fragile artificial opals can then act as templates for an inorganic matrix that fills in the gaps between the spheres and hardens to give inverse opals, Figure 15.7. For example, $TiO_2$ inverse opals can be prepared by anaerobic infusion of titanium(IV) propoxide solution into the latex opals followed by exposure of the mixture to air to allow atmospheric moisture to hydrolyse the alkoxide to $TiO_2$. The resulting aggregate is then calcined by careful heating up to 450 °C to burn away the organic component. These kinds of nanosphere templated materials have applications as photonic materials, in high density magnetic data storage, microchip reactors and as biosensors.[14]

Latex spheres have also been used to template biocompatible inverse opals using biopolymers such as silk fibres. Infusion of a regenerated (redissolved) silk-fibroin solution into a latex opal allows in situ transformation to a crystalline β-sheet state to give a macroporous silk inverse opal. The inverse opal retains the elasticity of the silk fibres and the inverse opals are capable of spreading load evenly by a reversible pore deformation process making them tough biocompatible materials with significant load-bearing capability. The inverse opal architecture of the reconstituted silk monoliths also significantly reduces their surface wettability and so they are effective barriers to water penetration and should exhibit self-cleaning properties.[15]

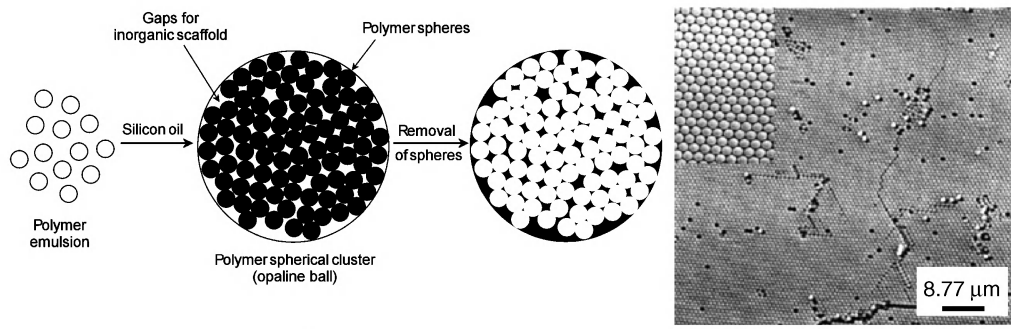


**Figure 15.7** (a) The preparation of inverse opal photonic balls using polymer spheres and an inorganic scaffold; (b) SEM image of the polymer template using balls of radius 463 ± 2 nm. The spheres form a crystalline hexagonal array (reprinted with permission from [14] © 2003 American Chemical Society).

## 15.5 Microfabrication, Nanofabrication and Soft Lithography

del Campo, A. and Arzt, E., 'Fabrication approaches for generating complex micro- and nanopatterns on polymeric surfaces', *Chem. Rev.* 2008, **108**, 911–945.

Microfabrication is the collective term used to describe modern manufacturing processes that involve the production of materials or devices with features on the micrometer scale or smaller.[16] Application areas of microfabrication include the manufacture of integrated circuits ('microchips'), Microelectromechanical systems (MEMS), Micro-opto-electromechanical systems (MOEMS – devices that involve sensing or manipulating optical signals on a micrometre size scale using integrated mechanical and electrical systems), microfluidic devices such as ink jet print heads, laser diodes, flat panel displays, microsensor or biosensor arrays, and fuel cells. Microfabrication has traditionally been a 'top down' approach involving some kind of *lithography* in which the desired features are cut or etched onto the surface of a hard substrate such as silicon (in the case of microchips) or transparent materials such as glass or quartz (in the case of flat panel displays). Typically microfabrication is a multi-step process with many steps that are carried out in sequence. The usual procedure involves depositing a film, patterning the film with the desired micro-scale features, and removing (or *etching*) portions of the film. To take the classic example of memory microchips there are around 30 lithography steps, 10 oxidation steps, 20 etching steps and 10 doping steps along with a number of other stages. The complexity of a microfabrication process is often described by its *mask count* – the number of different pattern layers that constitute the final device.

Commonly this patterning process is carried out using UV radiation as a pattern source (*photolithography*). The UV light results in a chemical reaction of a photoactive organic polymer coating (a *photoresist*), changing its solubility. In the case of a positive image the UV irradiation makes the polymer more soluble and the irradiated region is dissolved allowing removal of the underlying silicon (or other substrate) layer, *e.g.* by acid etching. The remaining silicon is protected by the insoluble, non-irradiated polymer and forms the basis for an integrated circuit for use in processors or memory chips. The process can also be used the other way round in which the irradiation of a negative image makes the irradiated resist *less* soluble. The non-irradiated resist is then removed allowing the etching of the material below the non-irradiated region (or indeed the deposition of fresh material according to the pattern defined by the irradiation, Figure 15.8.

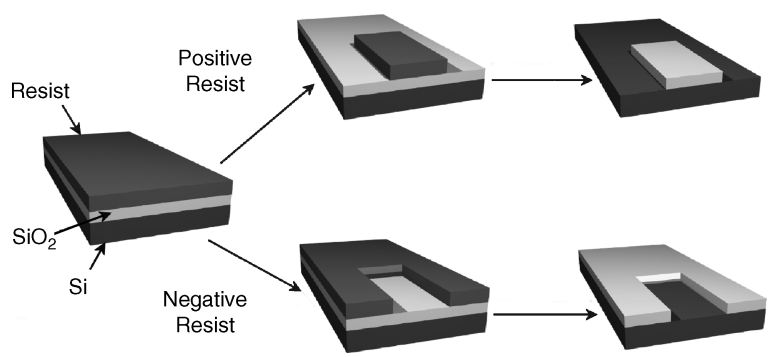


**Figure 15.8** Microfabrication – irradiation alters the solubility of a polymer film and treatment with a solvent produces a positive or negative image by dissolution of the more soluble portion of the resist layer and the underlying material.

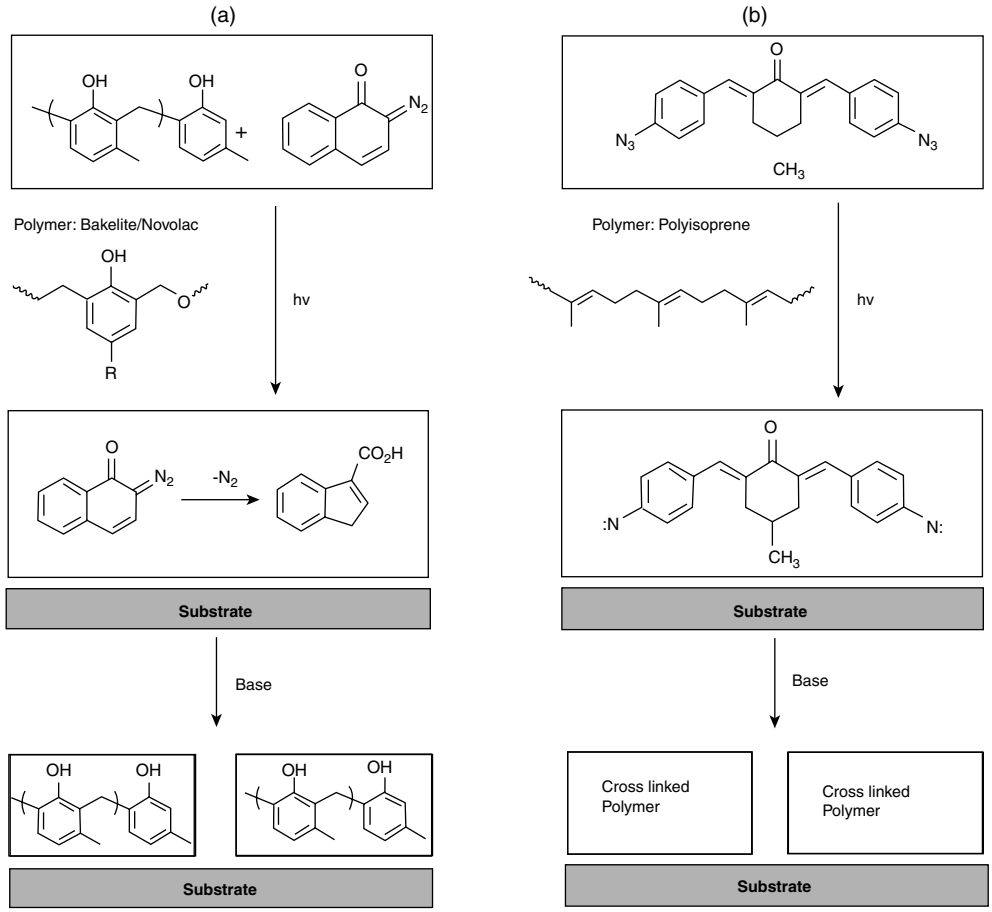


**Figure 15.9** The photochemistry of optical lithography using (a) positive and (b) negative resists based on Bakelite or polyisoprene polymers, respectively. The rectangles around the structures represent regions of polymer (chemical structure shown within the rectangles).

Examples of this photochemical patterning are shown in Figure 15.9. In Figure 15.9a a Bakelite-type phenol-formaldehyde resin doped with diazonaphthoquinone (DNQ) is used to as a positive resist. The polymer acts as a *dissolution inhibitor* but when it is irradiated by a mercury arc UV lamp according to a pre-defined pattern the irradiated polymer reacts with with the DNQ, transforming the hydrophobic DNQ into a hydrophilic indenecarboxylic acid, *via* a Wolff re-arrangement. This soluble product can be dissolved in aqueous tetramethylammonium hydroxide exposing the underlying substrate in a pattern that is a positive copy of the irradiation pattern. The approach is limited by the wavelength of the UV light (diazo compounds such as DNQ absorb at about 350 nm) and hence the smallest features on the image that is obtained are about 0.5 μm. Shorter wavelengths can give higher resolution and photochemistry using *ca.* 200 nm radiation is a current frontier area in optical lithography. A good example of a negative resist is the hydrophobic polyisoprene (synthetic rubber) containing a photoactive cross-linking agent. UV irradiation cross links the polymer making it more insoluble effectively protecting the region below the irradiated areas. When the non-irradiated polymer is washed away the areas that were masked from the UV light are exposed in a pattern that is like the photographic negative of the original mask.

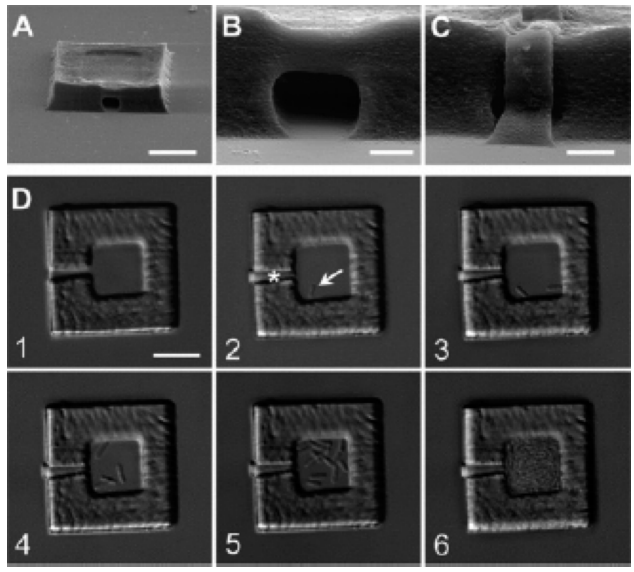


**Figure 15.10** Biocompatible microfabrication allows trapping of a single bacterium. (A, B) SEM images of a bovine serum albumin microcontainer. (C) SEM of a container after the entrance was plugged with a bacterium inside. (D) Sequence showing the container before (1) and immediately after (2) fabrication of a plug to trap the bacterium (arrow; scale bar, 10 μm.). Cell division eventually fills the trap with no loss of bacteria (3-6) (reprinted with permission from [17] © 2007 American Chemical Society).

A recent trend in microfabrication is two-photon mask-based lithography. This process can be used in a matter of minutes to produce a huge range of 3D shapes on the micrometer scale. A focused laser beam is directed through a confocal microscope to a single spot in a protein solution. The irradiation promotes the cross-linking of proteins producing a solid localised to the site of the irradiation. To create 3D objects the fine focus of the microscope is adjusted and the object is built up in planes. Obvious potential applications are in the creation of artificial biological tissues.[17] The technique has been used to produce a 3D house from bovine serum albumin in which a single *E. coli* bacterium is trapped by sealing the entrance. The trap is eventually filled by bacterial cell division with no escapes, Figure 15.10!

As technology demands the fabrication of ever smaller features in microfabricated devices, the key research area is in *nanofabrication* – pushing the fabrication size regime down to the nanoscale and it is here that 'bottom up' chemistry can play a role. Optical lithography, is capable of producing features smaller than 100 nm with the use of very short wavelengths (currently 193 nm) but is predicted not to be cost effective below 30 nm. X-ray lithographic techniques may allow access to features of around 15 nm, using wavelengths of around 1 nm. In contrast, bottom up techniques are not wavelength limited and a particularly important development is soft lithography, introduced by George Whitesides (Harvard, USA). Soft lithography involves the use of elastomeric 'stamps' and moulds by various techniques for surface patterning on the nanoscale. A transparent elastomeric polydimethylsiloxane (PDMS) stamp with a patterned relief on the surface is used to transfer a self-assembled monolayer (SAM; Section 13.2.2) of an alkane thiol to a gold substrate in a particular localised pattern. It is the soft, flexible nature of these monolayers that gives the technique its name.[18] Typically, the stamp employed is created by casting prepolymers against a master patterned by conventional lithographic techniques. This stamp is then used to create a number of replica moulds by pressing it repeatedly into the siloxane surface. A variety of methods are used to imprint a pattern into the SAM. The most

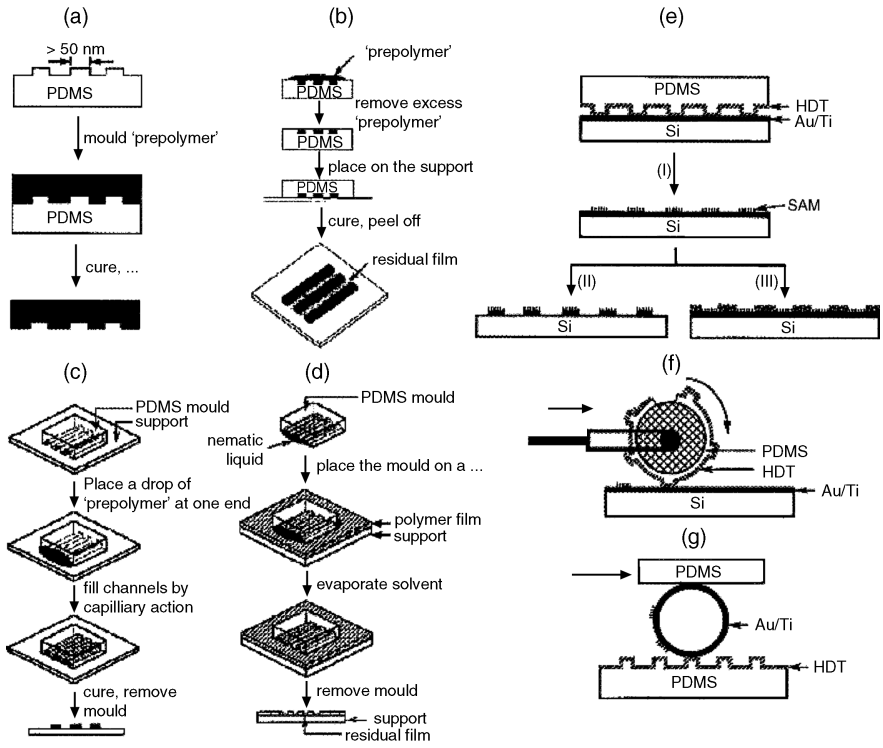


**Figure 15.11** Soft lithographic methods: (a) replica moulding; (b) microtransfer moulding; (c) micromoulding in capillaries; and (d) solvent assisted micromoulding. (e) Three examples of microcontact printing: printing on a planar surface with a planar stamp (I), printing of the SAM (II) etching and (III) deposition. (f) Printing on a planar surface with a rolling stamp and (g) Printing on a non-planar surface with a rolling stamp (Copyright Wiley-VCH Verlag GmbH & Co. KGaA. Reproduced by permission).

common are microcontact printing (mCP) and replica moulding. Other techniques such as microtransfer moulding (mTM), micromoulding in capillaries (MIMIC), and solvent-assisted micromoulding (SAMIM) are also used. These techniques are illustrated diagrammatically in Figure 15.11 and described briefly below.

- *Microcontact Printing.* An 'ink' of alkanethiols is spread on a patterned PDMS stamp. The stamp is then brought into contact with the substrate, which can range from coinage metals to oxide layers. The thiol ink is transferred to the substrate where it forms a self-assembled monolayer that can act as a resist against etching.
- *Replica Moulding.* A PDMS stamp is cast against a conventionally patterned master. Polyurethane is then moulded against the secondary PDMS master. In this way, multiple copies can be made without damaging the original master.
- *Microtransfer Moulding.* A PDMS stamp is filled with a prepolymer or ceramic precursor and placed on a substrate. The material is cured and the stamp is removed. The technique generates features as small as 250 nm and is able to generate multilayer systems.
- *Micromoulding in Capillaries.* Continuous channels are formed when a PDMS stamp is brought into conformal contact with a solid substrate. Capillary action fills the channels with a polymer precursor. The polymer is cured and the stamp is removed.

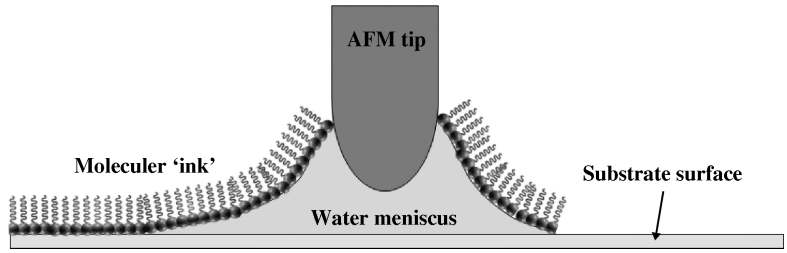


**Figure 15.12** Principle behind DPN.

- *Solvent-assisted Microcontact Moulding.* A small amount of solvent is spread on a patterned PDMS stamp and the stamp is placed on a polymer, such as a photoresist. The solvent swells the polymer and causes it to expand to fill the surface relief of the stamp.

Soft lithography has a number of advantages compared to traditional microfabrication methods. The fact that it uses molecular self-assembly on a surface means that it is very tolerant of some surface defects. It is also relatively cheap and hence defective products are readily discarded. The process is truly nanoscale. Initial work on soft lithography focussed on features above 100 nm, however, with modern enhancements to limit size such as mould size reduction, filler extraction or solvent swelling, features down to 30 nm can be achieved since the technique is not diffraction limited. Moreover, a range of different surface types can be used employed that differ in size and topology. Disadvantages include possible deformations of the stamp patterns particularly on repeated usage. It still remains to be seen whether components produced by soft lithography are compatible with other integrated-circuit processes.

Another way to produce features on the scale of a few tens of nanometres using these kinds of soft techniques is *dip pen nanolithography* (DPN). The method works under ambient laboratory conditions and involves using the tip of a scanning probe microscope (such as an AFM, Box 15.1) to deliver a tiny fragment of alkane thiol monolayer from the probe tip to the substrate *via* a water meniscus, Figure 15.12. The method is not limited to thiols and gold substrates and by adapting the molecule to the surface characteristics of the substrate it is possible to write patterns as fine as 10 nm across with a variety of molecules such as polymers or biomolecules onto metals, semiconductors and dielectric surfaces.

**Box 15.1** Scanning Tunnelling Microscopy and Atomic Force Microscopy

The remarkable ability of modern scanning probe microscopic techniques to relatively routinely image small molecules and self-assembled arrays directly on the nanoscale is becoming an increasingly common and important technique in nanoscale supramolecular chemistry and will lead to a raft of interesting new developments in the near future as chemists increasing move to directly observing processes on the molecular scale. The STM (scanning tunneling microscopy) and AFM (atomic force microscopy) approaches are perhaps the most commonly utilised techniques.

STM was developed in the early 1980s[19] and operates on a truly atomic scale because of the very localised nature of the probing. In an STM experiment a very thin layer of the compound (typically a monolayer) is deposited onto a conducting substrate such as a metallic surface or graphite. For very high resolution experiments a highly ordered surface such as Ag(111) or highly ordered pyrolytic graphite (HOPG – a layered structure of carbon atoms arranged in a honeycomb lattice) is required and the sample environment can be a very high vacuum, air or solution making the technique very versatile. A voltage is applied between the microscope tip (typically a very sharp metal wire) and the substrate giving rise to a

(*continued*)

**Box 15.1** (*Continued*)

tunnelling current. The distance between tip and substrate can be controlled very finely (atomic level) by tuning this current (which has an exponential dependence on the distance between tip and substrate). The current is attenuated by any intervening material and so the probe can be used to scan across the surface and a map of the resulting tunnelling current developed. The technique is also sensitive to the chemical nature of the target with atoms with high electron density showing up more clearly than lighter atoms. The STM tip can also be used to manipulate molecules by moving them around the surface and to carry out chemistry, particularly redox chemistry, involving the tunnelling current.

Atomic force microscopy complements STM in some ways. The AFM instrument consists of a cantilever containing a sharp tip, typically made from silicon nitride with nanometre scale dimensions. The tip is brought into close proximity to the surface to be studied. van der Waals interactions between the tip and surface features result in deflections of the cantilever which are measured by a laser, Figure 15.13. The tip is continuously scanned across the sample surface to give a three-dimensional map of the sample topography. AFM is highly versatile and can be used at ambient temperatures and in a liquid environment making it particularly suitable to biological samples, for example. It also does not require a conducting substrate and so much thicker samples can be measured compared to STM. While the vertical resolution is on the nanoscale, lateral resolution is generally less than in an STM experiment. The tip of an AFM can be modified with a variety of chemical derivatives with a particular (receptor substrate type) affinity for the target material leading to chemically specific imaging. Very recent work has also shown that the force between an AFM tip and different elements is slightly different and hence it is possible using very careful measurements to produce a chemical as well as topological map of a surface.[20]

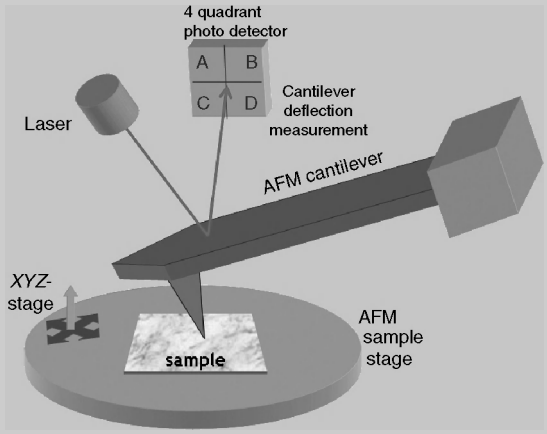


**Figure 15.13** Schematic diagram of an atomic force microscope (image courtesy of the *Opensource Handbook of Nanoscience and Nanotechnology*).

## 15.6 Assembly and Manipulation on the Nanoscale

### 15.6.1 Chemistry with a Microscope Tip

Wouters, D. and Schubert, U. S., 'Nanolithography and Nanochemistry: Probe-Related Patterning Techniques and Chemical Modification for Nanometer-Sized Devices', *Angew. Chem. Int. Ed.* 2004, **43**, 2480–2495.

The advent of high resolution electron and scanning probe microscopic techniques have resulted in tremendous progress in our ability to image and manipulate objects on the scale of molecules, moving

molecular science firmly from traditional 'pot boiling' techniques ever closer to the ability to directly grasp, position, join and fragment individual molecules. Ultimately it is beginning to be possible to envisage a kind of single molecule chemistry in which molecules are modified and studied conceptually in the same way that macroscale objects are, and the process of a chemical reaction at the molecular level followed like a movie in real time. From a supramolecular perspective this approach could involve building up supramolecular assemblies by direct manipulation rather than self-assembly. While this kind of chemistry is a long way off we will look in this section at ways in which individual molecules can be studied as they undergo chemical and supramolecular transformations and assembly.

Moving and grasping individual molecules on the nanoscale is termed *nanomanipulation* – in practice a very difficult task. The only thing small enough to hold a molecule is another molecule and thus there is a fundamental difficulty bridging the gap between the human and molecular scale. However, scanning probe microscope tips are now just a few nanometres across and can image and manipulate large molecule such as DNA even though it is difficult to apply the necessary force to move such fragile molecules about on such a small scale. Use of an AFM, however, means that molecules can be addressed in a liquid environment on a dielectric surface without damaging currents and so manipulations of single molecular such as strands of DNA are becoming relatively commonplace. For example, an AFM tip has been used to move DNA around a mica surface to give various regular patterns at the will of the operator and even write the letters 'DNA' with single DNA strands, Figure 15.14.[21]

A number of other approaches have been developed to bridge the human-molecule size gap and allow molecules to be manipulated directly. Particularly novel is the use of optical or magnetic tweezers. In this approach a large molecule such as DNA is derivatised with either a magnetic nanoparticle or dielectric bead to form a magnetic or optical 'handle'. Optical tweezers and traps exploit the restoring force that can be exerted on a dielectric microbead by the electric-field gradients at the focus of a laser beam. In the case of magnetic tweezers a magnetic nanoparticle is manipulated between magnetic poles. Glass micro fibres can also be used to directly manipulate large molecules. Work by Colin Bain (Durham, UK) has shown that micron-sized emulsion droplets of solutions of low surface tension such as heptane as can be manipulated using optical tweezers. The droplets can be deformed from spherical to triangular or square and can be pulled apart and joined together. As the droplets are pulled apart a tiny thread of molecules can be seen to link the droplets together.[22] Microscale droplets are not single molecules of course, so let's move down the length scale and look at some individual small molecule chemistry.

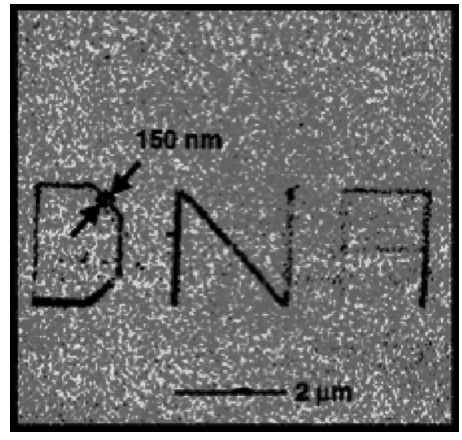


**Figure 15.14** 'DNA' has been spelled out on a surface with DNA strands using atomic force microscopy (reproduced from [21] with permission from AAAS).

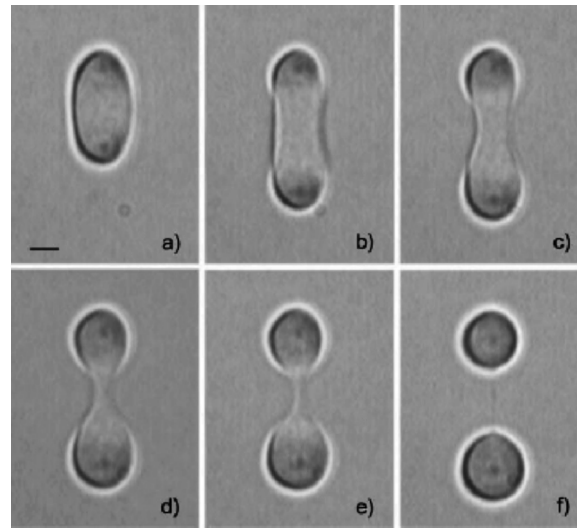


**Figure 15.15** Manipulation of heptane droplets using optical tweezers. The droplets form dumbbell shapes on extension and can be separated and rejoined. Time elapsed between each image a – f is 1 second. Careful inspection of image (f) reveals that a thin thread connects the separated droplets (reproduced by permission of The Royal Society of Chemistry).

Scanning tunnelling microscopy (STM) is an extremely high resolution and powerful technique not just for imaging at the molecular level but also, through use of the tunnelling current, for manipulating molecules. STM has been used to carry out an example of single molecule chemistry analogous to the well known Ullman reaction[23] – the copper-catalysed coupling of iodobenzene to produce biphenyl ($H_5C_6$–$C_6H_5$), first reported in 1904. The current from a tungsten STM tip is used to bring about the electron-induced breaking of the C–I bonds in two individual iodobenzene molecules. The abstracted iodine atoms can be parked on a nearby terrace on the Cu(111) surface. The STM tip can then laterally manipulate the two resulting phenyl residues into close proximity, bringing about their electron-induced chemical coupling to give biphenyl. The newly formed molecule can then be pulled along with the STM tip as a single entity confirming its single molecule nature, Figure 15.16.

## 15.6.2 Self-Assembly on Surfaces

de Feyter, S. and de Schryver, F. C., 'Two-dimensional supramolecular self-assembly probed by scanning tunneling microscopy', *Chem. Soc. Rev.* 2003, **32**, 139–150.

We saw in Chapter 8 how the principles of crystal engineering, particularly the use of robust supramolecular synthons, can be used to design somewhat predictable crystalline supramolecular assemblies whose structure can be determined using X-ray diffraction techniques. However, it is now becoming possible to use high resolution microscopy, particularly scanning tunnelling microscopy (STM) to visualise the formation of these kinds of crystalline supramolecular assemblies directly, providing unprecedented detail about the assembly process, since microscopy is not limited by the averaging across billions of unit cells that results from diffraction studies. Thus it is possible to study molecular manipulation using direct self-assembly principles. One group that has made the transition from crystal engineering to nanoscale engineering is that of Neil Champness (Nottingham, UK). Champness' group

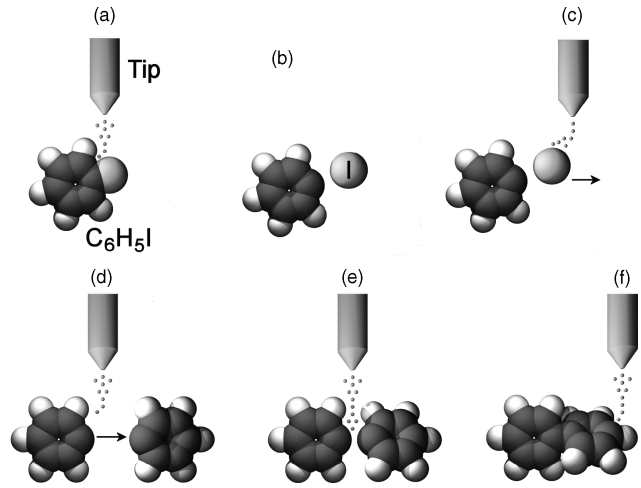


**Figure 15.16** Schematic illustration of the STM tip-induced synthesis steps of a molecule of biphenyl (a),(b) Electron-induced selective abstraction of iodine from iodobenzene, (c) removal of the iodine atom to a terrace site by lateral manipulation, (d) bringing together two phenyls by lateral manipulation, (e) electron-induced chemical association of the phenyl couple to biphenyl and (f) pulling the synthesised molecule by its front end with the STM tip to confirm the association.[23]

studied a two-dimensional hydrogen-bonding motif involving the triple hydrogen bonded interaction between perylene tetra-carboxylic acid diimide (**15.1**) and melamine (**15.2**). These tectons are known from crystallographic studies to form a honeycomb motif. Champness's group showed the spontaneous self-assembly of the honeycomb network (**15.3**) on a silver surface under vacuum, Scheme 15.1.[24] Interestingly the workers were able to observe the migration of molecules across the surface by looking at the interface between regions of pure melamine and pure diimide. The honeycomb forms in the interfacial region, gradually expanding and molecules diffuse together.

The honeycomb lattice contains very large hexagonal cavities which, in a 3D crystal under ambient conditions would be filled by guest molecules. The same principles can be applied on the nanoscale but with less reliance of the crystallisation lottery. Once the 2D lattice is formed on the silver surface, Fullerene $C_{60}$ can be sublimed onto the hexagonal network. The STM image shows that discrete heptamers of $C_{60}$ assemble in the pores of the honeycomb network, Figure 15.17. Seven $C_{60}$ molecules are just the right size to fill the hexagonal cavity. It has been proposed that such self-assembled networks could be used as nanoscale containers for the arrangement or synthesis of a variety of nanoscale assemblies.

The formation and dissolution of coordination polymer networks has also been studied on surfaces. The two coordination polymers shown in Figure 15.18 are based on the same mixed pyridyl / terpyridyl tecton. Both form coordination polymers that can be imaged on a graphite surface (highly ordered pyrolytic graphite – HOPG) but in the case of the $CoCl_2$ based complex the overall strand is neutral and forms laterally uncorrelated 1D strands that dissolve over a period of minutes to give fragments of nanostructures. If Pd(II) is used as the linker instead then the metal forms a charged, square planar node. The charge is balanced by $BF_4^-$ counter ions that effectively form an electrostatic link between the 1D chains resulting in a regular 2D array, Figure 15.18. The STM images give quantitative detail about that dimensions of the structures and spacing of the metal atoms (which show up as dark spots because of their high electron density). Thus the presence of the $BF_4^-$ anions in Figure 15.18b can be inferred from the cross-sectional area of the 2D unit cell of the layer of 8 $nm^2$ (black rectangle in Figure 15.18b).

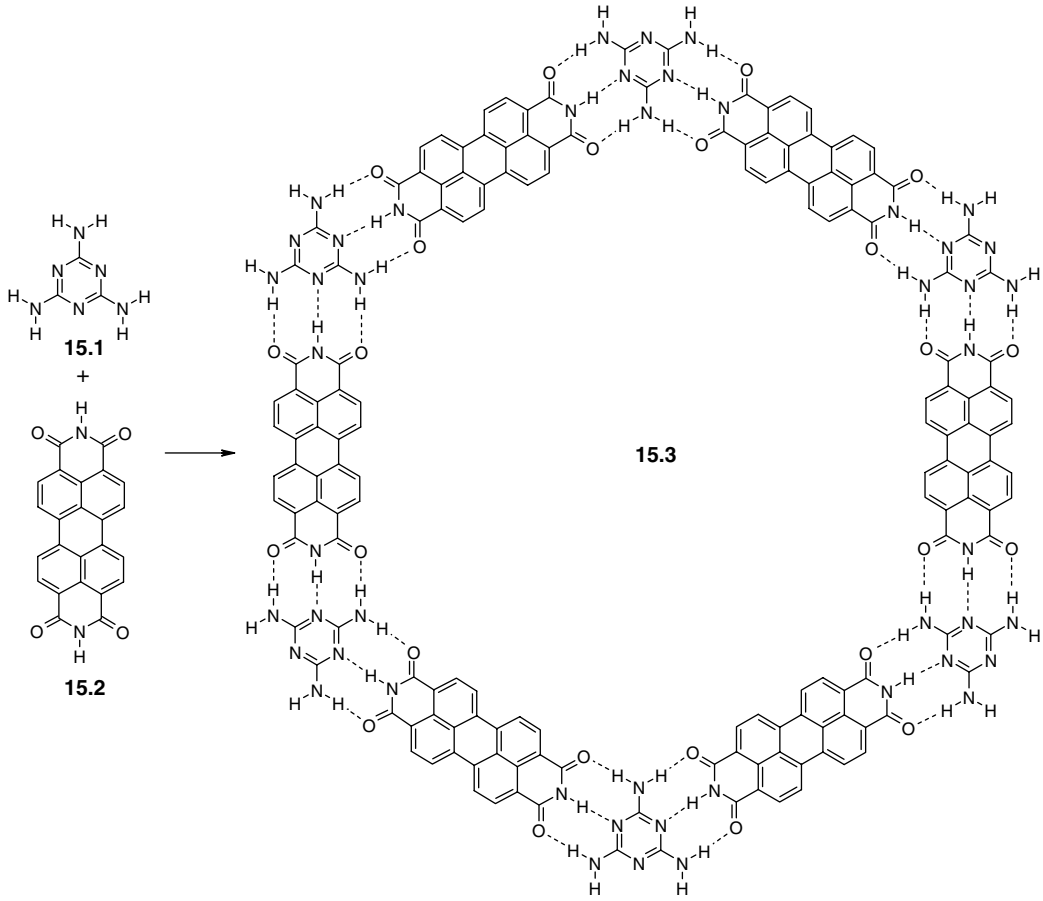


**Scheme 15.1** The honeycomb self-assembled network formed between tetra-carboxylic acid diimide **15.1** and melamine (**15.2**).

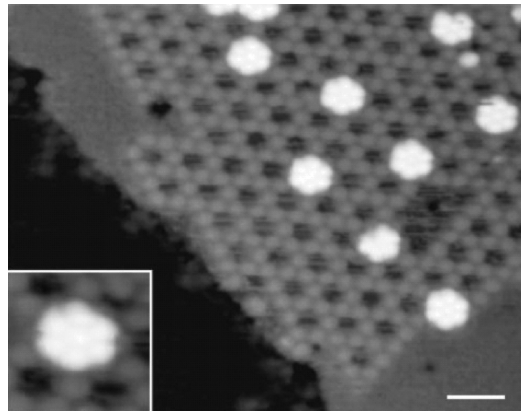

**Figure 15.17** STM image of a honeycomb organic network showing Fullerene $C_{60}$ heptamers residing in the cavities (reprinted by permission from Macmillan Publishing Ltd).

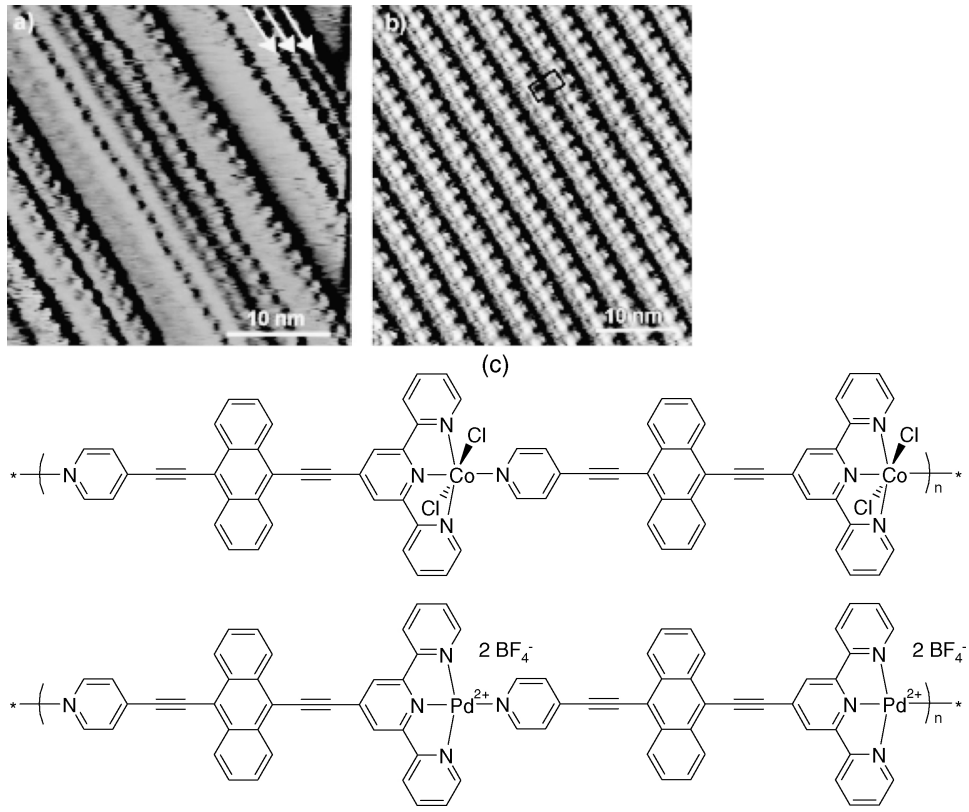


**Figure 15.18** (a) STM images of the network generated upon combining the ligand shown in (c) with (a) $CoCl_2$ and (b) $Pd^{2+}$. Image (a) shows the formation of laterally uncorrelated 1D nanostructures, while (b) displays the parallel packing of 1D networks that leads to the generation of a 2D nanoscale array. (c) The chemical structures of the 1D coordination polymers involving the same pyridyl / terpyridyl tecton and either an overall neutral octahedral $CoCl_2$ linker or a cationic $Pd^{2+}$ ion with tetrafluoroborate counter ions (Copyright Wiley-VCH Verlag GmbH & Co. KGaA. Reproduced by permission).

It is possible to study not just the structure of materials in nanoscale arrays such as this (including 2D chirality) but also to look at chemical reactivity, induced either by irradiation or by the current of the STM probe itself. A particularly interesting possibility of the use of the surface (*e.g.* the underlying periodicity of the substrate) to orientate and preorganise molecules for a chemical reaction that they would not ordinarily undergo. An example is the 'topochemical' (Section 8.2.9) reaction of a dialkyne to give a dialkyne polymer on a HOPG surface. This surface reaction has been realised in the light-induced polymerisation of a diacetylene containing isophthalic acid derivative, Figure 15.19.[26] The STM image clearly shows the acetylene moieties lined up in a fashion such that they are in close mutual proximity in accordance with the topochemical postulate.

It is also possible to study the self-assembly of individual molecules as well as networks such as **15.3**. The V-shaped zinc(II) bis(porphyrin) shown in Figure 15.20a self-assembles into decaporphyrin pentagonic and dodecaporphyrin hexagonic assemblies. The assemblies can be fixed by alkene metathesis using Grubbs' catalyst. This process represents self-assembly followed by covalent modification as described in Section 10.3.2. The assemblies can be directly imaged by high resolution STM (HRSTM)

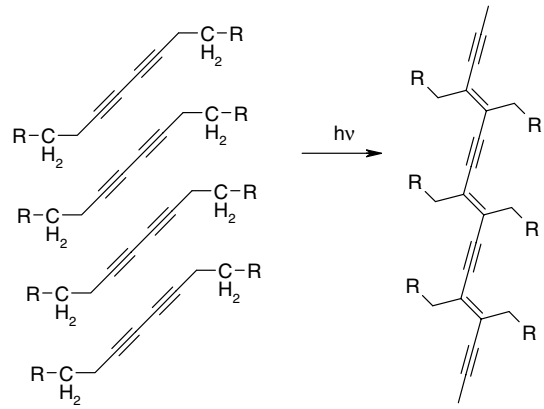


**Figure 15.19** Light induced topochemical polymerisation of a diacetlyene self-assembled layer on HOPG.[26]

on a gold surface – the HRSTM image of a single decanuclear porphyrin pentagonic array is shown in Figure 15.20b.[27]

## 15.6.3 Addressing Single Molecules

Ruben, M., Lehn, J.- M. and Muller, P., 'Addressing metal centres in supramolecular assemblies', *Chem. Soc. Rev.* 2006, **35**, 1056–1067.

Supramolecular grid type assemblies of the type described in Section 10.5.4 are very interesting in terms of nanoelectronics because, if it were possible to address each individual metal centre (as a kind of atomic quantum dot) then read and write processes of these individual *ion-dots* might be possible giving rise to the ultimate in miniaturisation in the quantum computers of tomorrow. Such molecular grid assemblies can be deposited from very dilute solutions (*ca.* $10^{-9}$ M in MeCN) onto substrates suitable for use in STM experiments such as HOPG (Box 15.1). For example the [2 × 2] $Co^{II}_4$ grid involving ligand **15.4** exhibits 2D assemblies of grids, 1D lines and isolated molecules of the [2 × 2] grid. At very low loading a regular pattern of isolated [2 × 2] grids is observed. At this very small size the topography map of the complex appears as a single spot about 1.7 nm wide, in agreement with the 1.65 nm size derived from X-ray crystallography, Figure 15.21a. However, thermal fluctuations mean that no further detail is discernible. The STM image contains a combination of topographical and electronic information and it is possible to use several techniques to deconvolute the electronic and topographic signals and hence obtain finer detail. Of particular interest in this context are scanning tunnelling spectroscopy (STS) which can be used to probe electronic states of the molecules studied as a function of energy within the range of a few eV around the Fermi level (*i.e.* energy of the highest occupied molecule orbital), and current imaging tunnelling spectroscopy (CITS). In CITS, both topography and current–voltage characteristic (I–V) data of are recorded simultaneously and hence the technique gives information about the electronic properties of supramolecular assemblies on surfaces. Each pixel of the STM topography image is recorded with constant tunnelling current, I. In a CITS experiment the current control is released and the I–V characteristics at the particular pixel are recorded. This added information represents a three-dimensional data set of current-voltage characteristics as a function of the *x*, *y* spatial position on the image and can be displayed as a 3D map of current at a particular location at a particular voltage. At certain bias voltages, the current

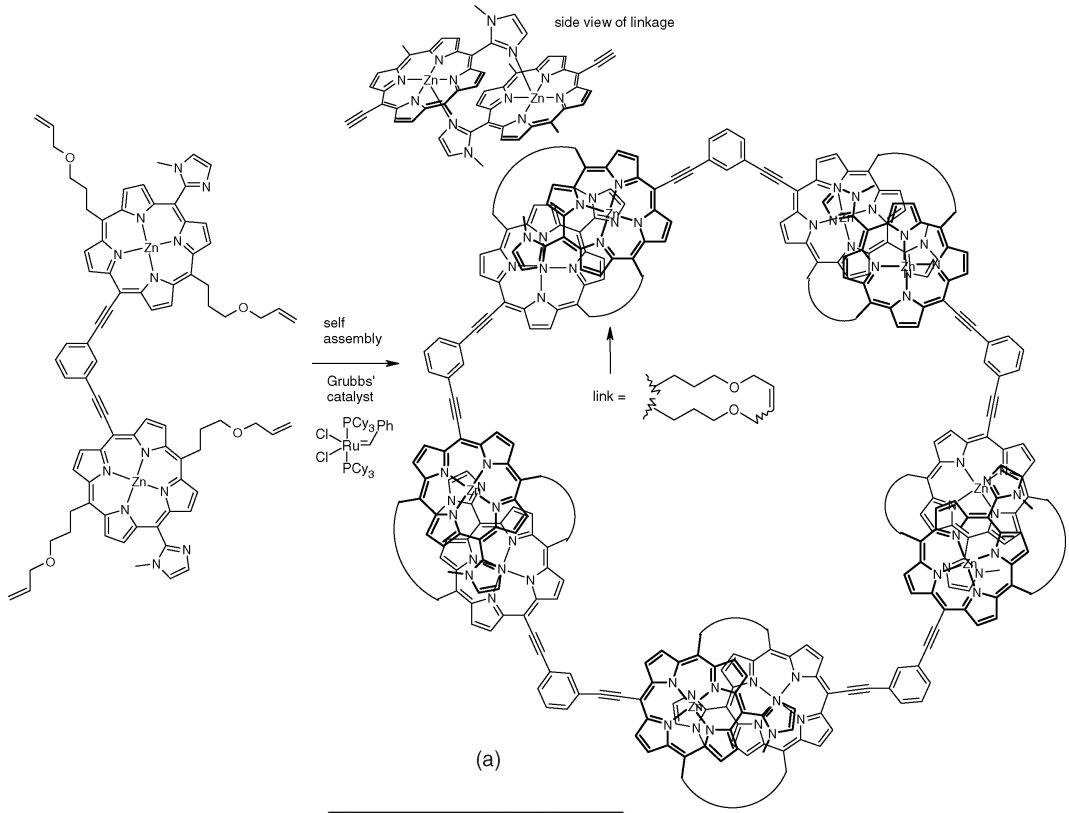


**Figure 15.20** (a) Pentagonic and hexagonic assemblies based on self-assembly followed by covalent modification (b) HRSTM image of one of the pentagonal structures (scale bar = 2 nm) (reproduced by permission of The Royal Society of Chemistry).

and hence image contrast is markedly affected when new molecular energy levels are encountered such as those found in a metal ion.

The CITS map of the [2 × 2] grid of $[\{Co(\mathbf{15.4})\}_4]^{8+}$ at –0.94 V is shown in Figure 15.21b. The image reveals four bright spots separated by 0.7 nm, in good agreement with the experimental Co–Co distance obtained by X-ray crystallography. The electronic characteristics of the metal centres make them stand out clearly from the organic ligands in the CITS map. The observed CITS pattern can also be correlated with the results of DFT electronic structure calculations. A particular advantage of CITS

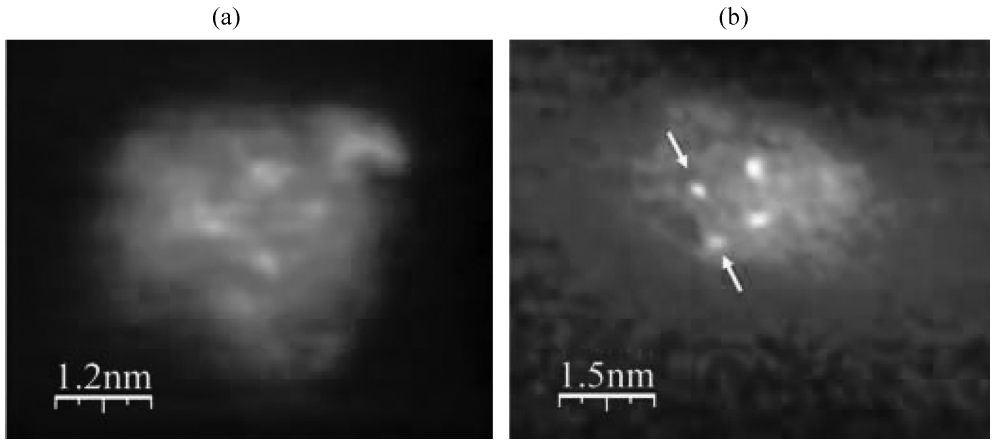


**Figure 15.21** (a) Experimental topography map of an individual [2 × 2] grid of $[\{Co(\mathbf{15.4})\}_4]^{8+}$ and (b) CITS map showing the positions of the Co(II) ions as bright spots indicated by arrows (reproduced by permission of The Royal Society of Chemistry).

is that it works under ambient conditions where supramolecular assemblies are stable as opposed to the ultra high vacuum of traditional high resolution electron microscopy methods.

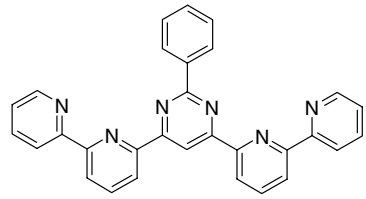

**15.4**

## 15.6.4 Atomic-Level Assembly of Materials

Yan L, Niu H, Bridges C. A., Marshall P. A., *et al.*, 'Unit-cell-level assembly of metastable transition-metal oxides by pulsed-laser deposition', *Angew. Chem. Int. Ed.* 2007, **46**, 4539–4542.

In addition to imaging and addressing objects and assemblies on the nanoscale it would be very useful to be able to fabricate or assemble them with atomic or molecular resolution and thus achieve true sub-nanoscale control over materials composition and properties. We saw in Section 15.5 the latest progress toward bottom up nanofabrication techniques in which self-assembly methods contribute to the fabrication of materials with nanoscale features. What about genuinely atomic-level materials synthesis with the kind of individual control exemplified by the STM synthesis of biphenyl described in Figure 15.16? This kind of atomic manipulation is still very much in its infancy but has been achieved for metal oxide type compounds by the related techniques of molecular beam epitaxy (MBE) and pulsed laser deposition (PLD). The traditional synthesis of inorganic oxide materials involves the diffusion of atoms in micron-scale powder grains at elevated temperatures, often resulting in thermodynamically controlled products. To access more designed materials a kinetic approach based on stepwise addition of each component is needed. Here we will look at a recent report by

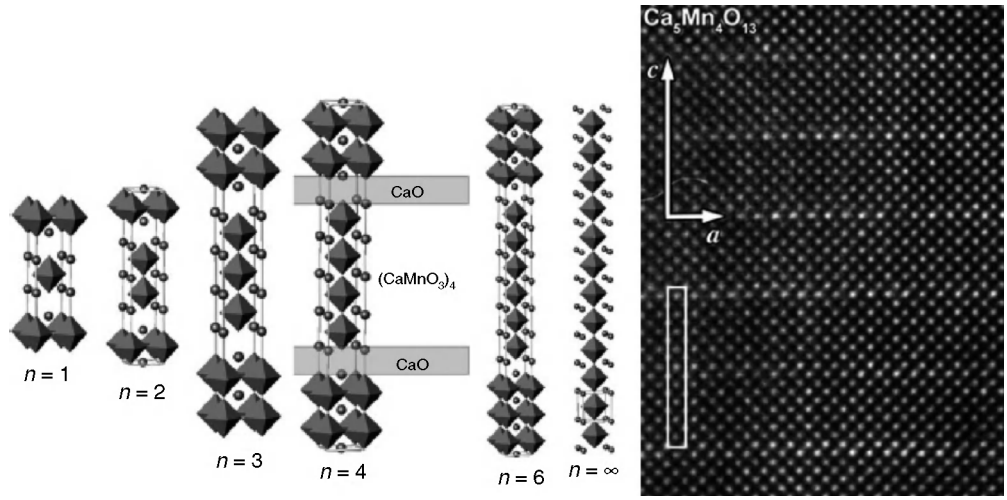


**Figure 15.22** (a) The Ruddlesden–Popper (RP) series $A_{n+1}B_nO_{3n+1}$ can be viewed as an assembly of AO rock-salt and $ABO_3$ perovskite layers. The unit cells of the n = 1 – 6 and infinity members of the $Ca_{n+1}Mn_nO_{3n+1}$ (or $CaO(CaMnO_3)_n$) RP family are shown. The $MnO_6$ octahedra are shown as polyhedra and the $Ca^{2+}$ ions as spheres. (b) Cross-sectional HRTEM image of the epitaxially grown RP phase $Ca_5Mn_4O_{13}$ ($n = 4$) the unit cell is outlined in white (Copyright Wiley-VCH Verlag GmbH & Co. KGaA. Reproduced by permission).

the group of Matt Rosseinsky in Liverpool, UK, of the designed synthesis of the $n = 4$, 5, and 6 members of the $Ca_{n+1}Mn_nO_{3n+1}$ ions – the so-called Ruddlesden–Popper (RP) series, Figure 15.22a. Typical ceramic synthesis yields $n = 3$ as the maximum value but the higher members of the series are of interest as 'natural spin valves' for applications in tunnelling magnetoresistance. Rosseinsky and coworkers adopted a layer-by-layer assembly approach for the higher RP structure from by using PLD deposition of individual unit cells of $CaMnO_3$ and CaO from two separate targets. The build up of unit cells is monitored by reflection high-energy electron diffraction (RHEED) and allows the structure to be built up atom-by atom and hence precise control of the number of $CaMnO_3$ repeat units, Figure 15.22b.

## 15.7 Nanoparticles

### 15.7.1 Nanoparticles and Colloids: Definition and Description

Moores, A. and Goettmann, F. 'The plasmon band in noble metal nanoparticles: an introduction to theory and applications', *New J. Chem.*, 2006, **30**, 1121–1132.

Perhaps nothing typifies the emerging, multidisciplinary science of nanochemistry more than nanoparticles. On the face of it the concept of a nanoparticle is relatively simple. Nanoparticles are simply very small usually approximately spherical fragments of material of radius in the approximate range 2–100 nm. In principle a nanoparticle can be made of any material, although metallic nanoparticles, *e.g.* of gold or silver, catalytic metals such as rhodium or palladium, or of semiconductor materials such as CdSe or ZnS are particularly commonly studied. Strictly the term nanoparticle is a general one and can encompass both crystalline and amorphous solid particles. Nanoscale single crystals with

regular, faceted structures comprising ordered arrays of perhaps a few thousands of atoms are termed *nanocrystals*, while the term *quantum dots* is often applied to semiconductor nanoparticles that have interesting properties such as fluorescence. Sometimes the term *nanocluster* is also used to refer to a nanoparticle 1 –10 nm in size. In general nanoparticles are relatively monodisperse with a size distribution of less than 15 per cent.

Nanoparticles are frequently used as a suspension in some kind of solvent. This is a two phase mixture of suspended solid and liquid solvent and is thus an example of a *colloid*. The solid doesn't separate out as a precipitate partially because the nanoparticles are so small and partially because they are stabilised by coating groups that prevent their aggregation into a precipitate and enhance their solubility. Colloidal gold, which has a typical red colour for particles of less than 100 nm, has been known since ancient times as a means of staining glass. Colloid science is a mature discipline that is much wider than the relatively recent field of nanoparticle research. Strictly a colloid can be defined as a stable system of small particles dispersed in a different medium. It represents a multi-phase system in which one dimension of a dispersed phase is of colloidal size. Thus, for example, a *foam* is a gas dispersed in a liquid or solid. A *liquid aerosol* is a liquid dispersed in gas, whereas a *solid aerosol* (or smoke) is a solid dispersed in a gas. An *emulsion* is a liquid dispersed in a liquid, a *gel* is liquid dispersed in a solid and a *sol* is a solid dispersed in a liquid or solid. We saw in Section 14.7 the distinction between sol and gel in the sol gel process.

## 15.7.2 Gold Nanoparticles

Daniel, M. C., Astruc, D., 'Gold nanoparticles: Assembly, supramolecular chemistry, quantum-size-related properties, and applications toward biology, catalysis, and nanotechnology', *Chem. Rev.* 2004, **104**, 293–346.

What makes nanoparticles interesting is the fact that their *physical properties depend on their size*. In other words the fact that they are nanoscale has a huge effect on their absorption and emission of electromagnetic radiation, their binding and aggregation characteristics, their electronic structure and energy levels, their solubility and tuneability, and their interactions with biological systems. Nanoparticles thus have a rapidly increasing and extremely wide ranging portfolio of applications in biology, medicine, sensing, labelling and molecular electronics. The obvious place to start is the red colour of colloidal gold. Metallic gold is a yellow colour so why should it turn red in particles of less than 100 nm? The answer lies in the collective movement of free electrons around the surface of the nanoparticle. This process gives rise to a strong absorption in the visible region of the electromagnetic spectrum termed a *surface plasmon resonance* (SPR) absorption. The exact wavelength of the SPR band depends on the size of the nanoparticle. The most famous example is the Lycurgus cup (British Museum, London, UK). This fourth-century Roman chalice (shown on the front cover of this book) appears green in reflected light but is red if illuminated from inside. The colour arises from mixed Au–Ag particles of *ca.* 70 nm diameter embedded within the glass. The properties of the alloy are crucial to the bright scarlet colour. The wavelength, band shape and extinction coefficient of the surface plasmon band is highly dependent on the dielectric constant of the surrounding medium, the electronic interactions of the nanoparticle with the surface stabilising ligands (and hence the electron density inside the nanoparticle) and the size, shape and monodispersity of the nanoparticles. It is this size dependence that makes SPR truly a nanoscale phenomenon.

Coinage metal nanoparticles (Au, Ag and Cu) have been particularly popular in nanoparticle research because of their easy synthesis, the high intensity of their surface plasmon band and the ease of functionalising the metal surface with ligands such as thiolates. Gold nanoparticles are prepared

by two main methods, both based on arrested nucleation and growth. The earlier method, first developed by J. Turkevich *et al.* in 1951 with refinements by G. Frens in 1970s, is simple and produces fairly monodisperse spherical gold nanoparticles of *ca.* 10–20 nm diameter suspended in water. The method involves the reduction of aqueous tetrachloroaurate(III) with sodium citrate. The citrate acts as a reducing and stabilising agent, preventing growth and aggregation of the nanoparticles as well as imparting good water affinity. The solution goes from tallow, to clear to purple and eventually deep red. The purple colour arises from gold nanowires formed as transient intermediates.[28]

Gold nanoparticles soluble in organic solvents can be produced by a method developed by Brust and Schiffrin in early 1990s. The procedure again involves reduction of $[AuCl_4]^-$ this time with $NaBH_4$ in the presence of tetraoctylammonium bromide which acts as a surfactant and phase transfer agent, solubilising the gold(III) salt in an organic solvent such as toluene. The resulting gold nanoparticles can be isolated and their monodispersity improved by centrifugation to give particles of *ca.* 5–6 nm diameter. The tetraoctylammonium bromide coats the nanoparticles in a lipophilic sheath imparting organic solubility but the layer is not strongly bound and thus is readily replaced by alkane thiolates, for example, that bind gold more strongly. The thiol can also be added directly during synthesis.[29]

Other metal nanoparticles can also be produced by citrate reduction, for example Ag, from $AgNO_3$, Pd from $H_2[PdCl_4]$ and Pt from $H_2[PtCl_6]$. Noble metal nanoparticles such as these can act as effective catalysts[30] for example in hydrogenation or hydrogen atom splitting in hydrogen storage (termed *spillover*[31]) because of their high surface area. It is also feasible to prepare mixed nanoparticle systems, known as composite materials, alloys or mixed-grain nanoparticles such as magnetic FePt nanoparticles.[32] Elaborate composite nanoparticles can be prepared by depositing metals in layers around colloidal nanoparticle nuclei or *seeds*, for example the coating of gold nanoparticles with silver (as in the Lycurgus cup!). While careful choice of conditions can control nanoparticle size and growth, size control can also be achieved by immobilisation of the nanoparticle on particular substrates. Functionalised nanoparticles can be prepared by using a wide range of thiols with various end functionalities. The thiol then acts to stabilise and solubilise the nanoparticle as well as allow selective chemistry or recognition on its outer surface. For example, reduction of $H[AuCl_4]$ with $NaBH_4$ in the presence of (γ-mercaptopropyl)-trimethoxysilane to produce a nanoparticle containing a silane functionality, Scheme 15.2. This methodology has been employed to attach many functional groups onto other metal nanoparticles including amines and carboxylic acid groups.[33] In addition dendritic thiolate stabilised gold nanoparticles have also been produced by cleavage of a disulfide containing dendritic L-lysine groups during the gold(III) reduction process (see Section 14.2 for a discussion of dendrimer chemistry).

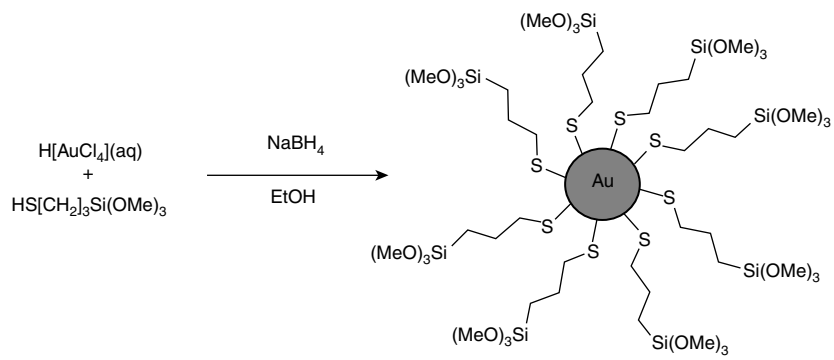


**Scheme 15.2** Synthesis of functionalised gold nanoparticles *via* the *in situ* reduction of Au(III) in the presence of a functionalised thiol.[33]

This system represents gold nanoparticles with a biocompatible stabilising L-lysine based shell. The dendritic generation of the stabilising ligand has a significant influence on the size of the gold nanoparticles produced in this way with nanoparticle radius decreasing from 2.9 to 1.8 nm from generations 1–3.[34] Dendritic ferrocenyl amide-derived nanoparticles have been used as chemiresistor sensors for the detection of volatile organic compounds.

Functionalised thiols are beginning to be used to develop supramolecular sensors based on nanoparticles in which an analyte binding group is anchored to the nanoparticle surface *via* a gold-thiol interaction. Work by Paul Beer and Jason Davis (Oxford, UK) has resulted in an anion-binding porphyrin derivatised with four disulfide arms derived from the readily available thioctic acid (**15.5**). On binding to a gold nanoparticle the disulfide bond is broken to give a dithiol, Figure 15.23. This two point interaction is much stronger than a single gold-sulfur bond and of course the whole porphyrin derivative has four such anchors so forms a particularly robust linkage able to displace some of the nanoparticle's original dodecanethiolate coating. Beer and Davies used the nanoparticle-anchored porphyrin as a sensor for anions such as halides. Binding to the nanoparticle markedly enhances the preorganisation of the porphyrin for guest binding resulting in a chloride affinity in DMSO solution of log $K_a$ of less than 2 for the free receptor **15.5** and a value of 4.3 for the nanoparticle-bound system.[35] In this case the concentration of the bound porphyrin and the halide affinity were assessed by changes in the strong absorption of the porphyrin chromophore which masks the nanoparticle surface plasmon band, however other systems have used the surface plasmon absorption itself as a sensing mechanism. For example an efficient way of visually detecting copper(II) using L-cysteine functionalised gold nanoparticles in water has been described.[36] Copper binding causes the nanoparticle solution to change from red to blue in colour as the nanoparticles aggregate in response to the formation of a 2:1 cysteine:$Cu^{2+}$ surface complex. The method allows sensitive copper detection down to $10^{-5}$ M. The surface plasmon band can be highly sensitive to the adsorption of molecules on the nanoparticle surface in this way. It has been demonstrated using

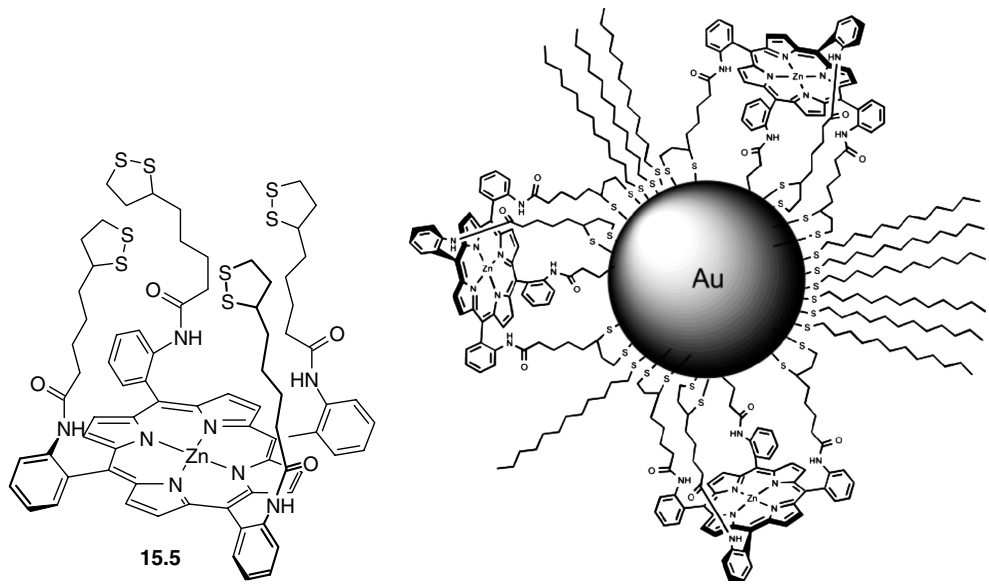


**15.5**

**Figure 15.23** Zinc(II) porphyrin-derived anion sensor **15.5** and the mixed nanoparticle derived from it (reproduced by permission of The Royal Society of Chemistry).

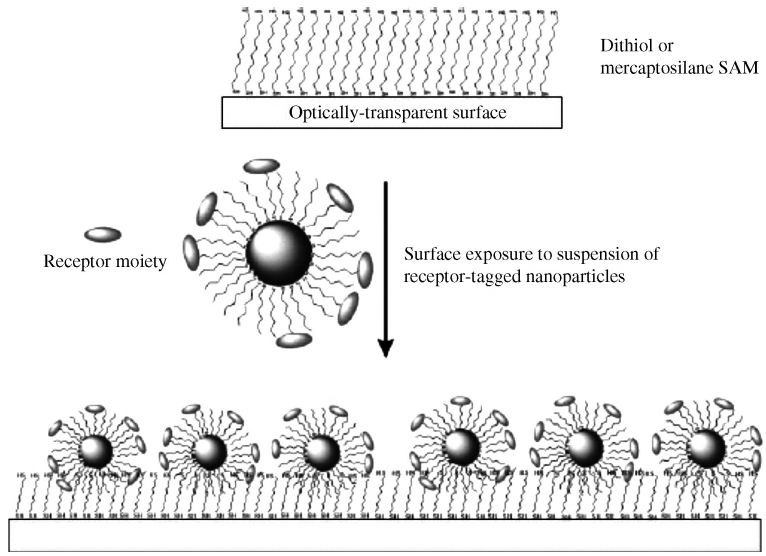


**Figure 15.24** A schematic hightlighting that multiple funtionalised nanoparticles can be attached to a large surface to fabricate a nanoparticle derived sensor device (reproduced by permission of The Royal Society of Chemistry).

dark-field optical microscopy that the adsorption of fewer than 60 000 1-hexadecanethiol molecules (a zeptomolar amount!) on to an individual silver nanoparticle results in a localised shift of the surface plasmon resonance band of 40.7 nm. Moreover the kinetics of the response are as fast as other real-time sensor technologies.[37]

The high affinity of sulfur for metallic surfaces such as gold may form the basis for fabricating such nanoparticle sensors into sensitive sensing nanodevcies by combining the 3D gold thiol coating of the nanoparticle with a 2D SAM on an optically transparent surface such as indium tin oxide. The result is a hierarchical nanoscale assembly involving the binding of functionalised nanoparticles containing receptor groups to an electrode surface, Figure 15.24.[38] It is possible that enhanced sensitivity will be achieved in this way due to the large surface area of binding sites.

## 15.7.3 Quantum Dots

Trindade, T., O'Brien, P. and Pickett, N. L., 'Nanocrystalline semiconductors: Synthesis, properties, and perspectives', *Chem. Mat.* 2001, **13**, 3843–3858.

A *quantum dot* is a semiconductor material such as CdS, CdSe or ZnS with electron-hole pairs (*excitons*) that are confined in three dimensions. Hence quantum dots have size-dependent properties and behaviour intermediate between bulk semiconductors and discrete molecules. Quantum dots are of intense current interest in transistors, solar cells, light emitting diodes and as fluorescent tags or labels in medical imaging. In a quantum dot electrons are excited by absorption of a photon from the valence band to the conduction band of the nanoparticle leaving behind a 'hole' of opposite charge. The electron-hole pair is then mutually attracted to one another electrostatically. The exciton results from the binding of the electron with the hole. This bound electron-hole pair gives rise to the most fascinating attribute of the

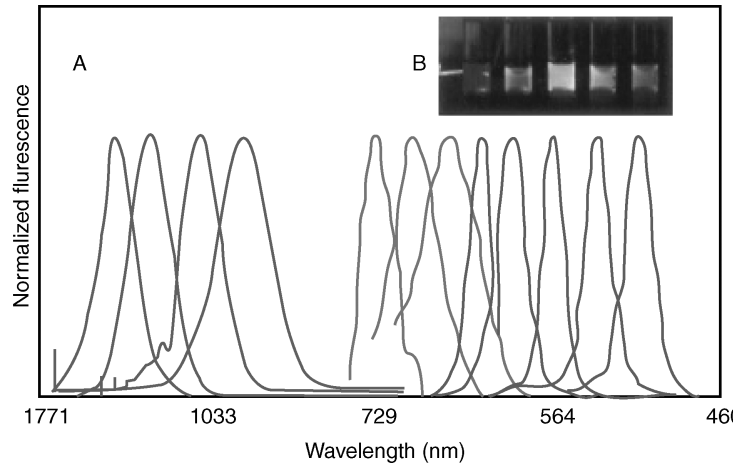


**Figure 15.25** (a) Size- and material-dependent emission spectra of several surfactant-coated semiconductor nanocrystals (quantum dots) in a variety of sizes. The blue series (right) represents different sizes of CdSe nanocrystals with diameters of 2.1, 2.4, 3.1, 3.6 and 4.6 nm (from right to left). The green series (centre) is of InP nanocrystals with diameters of 3.0, 3.5 and 4.6 nm. The red series (left) is of InAs nanocrystals with diameters of 2.8, 3.6, 4.6, and 6.0 nm. (b) A true-colour image of the fluorescence of a series of silica-coated core (CdSe)-shell (ZnS or CdS) nanocrystals (reproduced from [39] with permission from AAAS). See plate section for colour version of this image.

quantum size effect in nanoparticles – their optical features. The UV-visible absorption and fluorescence properties of quantum dots exhibit a characteristic wavelength for the individual particle that depend not only on the material from which it is made but also upon its size. The wavelength of the absorption band *hypsochromically* shifts (*i.e.*, moves to higher energy or is *blue shifted*) as the particle size decreases, Figure 15.25.

CdSe quantum dots have been used extensively in sensing and tagging applications. To take one supramolecular example, CdSe nanocrystals derivatised with simple aromatic groups at the cluster surface have been shown to bind and intercalate organic cations allowing them to penetrate near to the cluster core with consequent effects on the cluster photoluminescence, particularly quenching *via* π–π interactions.[40]

While CdS and CeSe quantum dots are particularly luminescent and have been used extensively, there are concerns over their application in medical imaging in particular because of the potential toxicity associated with cadmium. As a result the syntenthesis of alternative luminescent nanoparticles based on less toxic materials such as $Zn_3P_2$ stabilised by tri-*n*-octylphosphine oxide is an active area of endeavour.[41]

As we saw with gold nanoparticles, the surface immobilisation of quantum dots is a desirable goal in the fabrication of luminescent nanoscale devices. For example, a bilayer of CdTe nanocrystals has been assembled in a stepwise fashion using a mercaptopropyltrimethoxysilane-derivatised glass substrate. The thiolated glass is first treated with red-emitting CdTe nanocrystals in toluene solution creating a luminescent CdTe monolayer. Subsequent addition of a dithiol allows the tethering of a second layer of smaller (3.2 nm green emitting) nanocrystals on top of the first. Interestingly no green emission is observed from the second layer. Instead the addition of the second layer significantly enhances the lower energy red emission intensity of the first layer *via* a FRET process (see Section 11.2.2 for an explanation of FRET), Figure 15.26.[42]

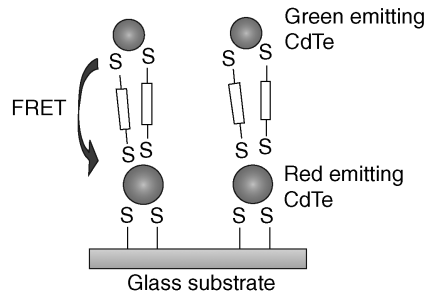


**Figure 15.26** Microfabricated CdTe fluorescent bilayer showing FRET enhancement of the long wavelength emission of the lower layer of nanocrystals by FRET from the upper layer.[42]

### 15.7.4 Non-Spherical Nanoparticles

While spherical nanoparticles are the most common, recent work has resulted in a plethora of nanoobjects such as nanorods, nanorings and nanostars. Each is made by a templation or arrested growth mechanism involving materials such as surfactants and the objects' size and shape can have marked effect on their optical and materials properties. For example gold nanorods terminated with polystyrene polymer caps ('pom-poms') and stabilised at the sides by cetyl trimethylammonium bromide have been reported that exhibit supramolecular organisation into higher order strutures involving side-by side and end-to-end assembly. The result is bundles, chains, rings, and bundled chains of nanorods. Like their spherical gold nanoparticle cousins, nanorods exhibit size-dependent longitudinal surface plasmon bands that in this case depend on their assembly mode. The formation of end-to-end chain-like structures suggests applications in plasmon waveguides.[43]

Crystalline nanorings, literally closed circular nanoparticles with a hollow centre, were first prepared from zinc oxide in 2004 by a spontaneous self-coiling process from polar nanobelts.[44] Semiconductor nanorings and indeed interestingly shaped nanoobjects in general, promise much in the way of applications as tools to probe fundamental physical phenomena and as nanoscale sensors, transducers, and resonators.

Another interesting development is the imparting of valency to nanoparticles to make them behave like single atoms. Work by Francesco Stellacci (MIT, USA) has allowed the selective functionalisation of the axial polar positions of a gold nanoparticles with carboxylate-terminated thiols. This turns the nanoparticle into effectively a divalent 'superatom'. Condensation of the carboxylic acid groups with 1,6-diaminocyclohexane gives 1D polymeric strands of nanoparticles up to 20 nm long.[45]

## 15.8 Endohedral Fullerenes, Nanotubes and Graphene

Delgado, J. L., Herranz, M. A. and Martin, N., 'The nano-forms of carbon', *J. Mater. Chem.* 2008, **18**, 1417–1426.

We reviewed the history of the discovery of the Fullerenes, closed hollow clusters made up only of carbon atoms, in Box 7.1 and looked at their purification and role as guests in supramolecular systems in Section 7.8.2. The Fullerenes and their relatives, particularly carbon nanotubes and graphene (a flat single atom thick graphite sheet conceptually derived from opening out a carbon nanotube onto a flat surface) are highly topical in nanochemistry because of their interesting structures inclusion properties and electronic characteristics. They represent just a few of the increasing plethora of the nanoforms of carbon that also includes cup-stacked nanotubes, nanohorns, nanotori, nanobuds, nano-onions (Fullerenes

included within Fullerenes), diamond nanorods and such materials as carbon nanofoams *etc.* We will take a brief look at the ability of the closed Fullerenes to act as supramolecular hosts and then move up the nanoscale to nanotubes and the highly topical subject of nanofabrication of graphene into the computers of tomorrow.

## 15.8.1 Fullerenes as Hosts

Diederich, F. and Gomez-Lopez, M. 'Supramolecular fullerene chemistry', *Chem. Soc. Rev.*, 1999, **28**, 263–277.

Since their discovery the aesthetic elegance of the Fullerenes, particularly $C_{60}$, has resulted in a tremendous amount of activity in the chemical[46] and supramolecular derivatisation. For example, the fullerenes are known to form a number of organometallic complexes, such as $[\{Pt(PEt_3)_2\}_6(C_{60})]$, in which fullerenes $C_{60}$, $C_{70}$ and $C_{82}$ act as essentially monodentate ligands for each transition metal centre. The metal centre bonds to the outer surface of the fullerene through a single fullerene C=C bond situated at the more electron-rich '6–6' ring junction rather than the longer '6–5' bond (Figure 15.27). In general, such compounds are outside the scope of this book, although one particular iridium complex has been used to produce a self-complementary $C_{60}$-based host in an imaginative way.[47] The complex $[Ir(\eta^2\text{-}C_{60})(CO)Cl(L)_2]$ (L = $Ph_2PCH_2C_6H_4OCH_2Ph$, **15.6**), projects two electron-rich benzylether 'arms', which envelop adjacent $C_{60}$ ligands (Figure 15.28).

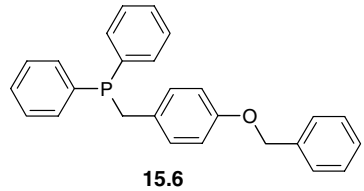


**15.6**

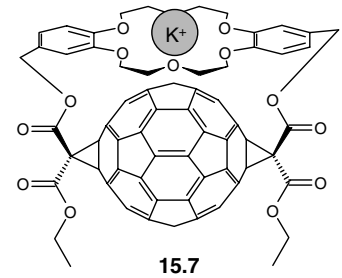


**15.7**

Remarkable work by François Diederich of the ETH lab in Zürich has resulted in the buckminsterfullerene-based redox sensing device **15.7**. This novel sensor, which is produced in yields of up to 50 per cent, holds a dibenzo[18]crown-6 cavity in enforced close contact with the fullerene surface. Binding of $K^+$ within the crown ether cavity results in relatively large anodic shifts of 90 mV of the first fullerene reduction ($C_{60\rightarrow}C_{60}^{\bullet -}$). The implication is that the proximity of the potassium cation to the fullerene

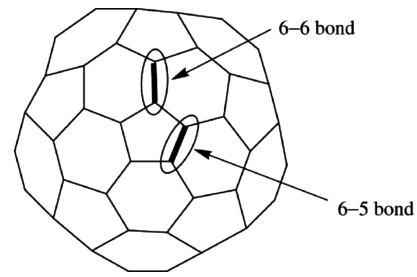


**Figure 15.27** Projection of one $C_{60}$ hemisphere showing '6–6' and '6–5' bonds.

renders it significantly easier to reduce to the monoanion. The binding of $K^+$ within the crown cavity, near the external surface of the fullerene, has been confirmed by X-ray crystallography.

The Fullerenes form particularly strong complexes with porphyrins as exemplified by the X-ray crystal structure of the covalent Fullerene-porphyrin conjugate **15.8** (Figure 15.29).[48] This property allows fullerenes and porphyrins to form extended supramolecular arrays (even when not covalently linked) and has been used to engineer host-guest complexes in which a Fullerene is sandwiched in between a pair of porphyrins, and ordered arrays involving interleaved porphyrins and Fullerenes. Applications include the use of porphyrin solid phases in the chromatographic separation of Fullerenes and potential applications in porous frameworks and photovoltaic devices.[49]

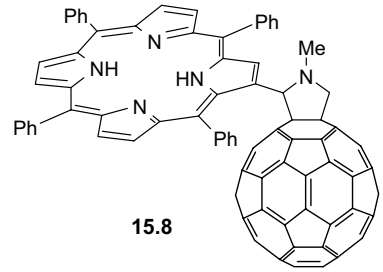


**15.8**

The possibility of complexing metal cations and neutral atoms to the inside of the fullerene cavities to produce a 'trapped' metal atom is of active interest to supramolecular chemists. The cavity in $C_{60}$ is about 7 Å across, and is clearly large enough to include at least monatomic guests. Larger fullerenes such as $C_{70}$ and $C_{82}$ might be expected to include more then one atom, or even small molecule guests. Clearly, the closed structure of molecules like $C_{60}$ containing five- and six-membered rings does not possess an aperture large enough to admit even a single atom under the normal conditions of a chemical reaction and therefore alternative strategies are needed. In fact, a range of fullerene inclusion compounds, designated M@$C_x$ (where M is the guest species, normally a metal atom, and $C_x$ is the fullerene, $x$ = 60, 70, 74, 82 *etc.*), have been produced either by cage closure during fullerene synthesis in the presence of metal atom vapour, or by high-energy bimolecular collision.[50] Almost at the same time as the discovery of the fullerenes, Smalley was able to produce M@$C_{60}$ (M = La, Ni, Na, K, Rb, Cs) as well as a variety of other lanthanum complexes of $C_{70}$, $C_{74}$ and $C_{82}$. Evidence for the inclusion of the metal atom within the fullerene cavity comes from the fact that the compounds, which contain normally very strongly reducing metals, are inert to $O_2$, $NH_3$ and water. The metal is protected by the surrounding cage. Macroscopic amounts of La@$C_{82}$ have been isolated and shown by X-ray photoelectron spectroscopy to comprise a $La^{3+}$ ion (the most stable oxidation state of La), a $C_{82}^{2-}$ anion in which the

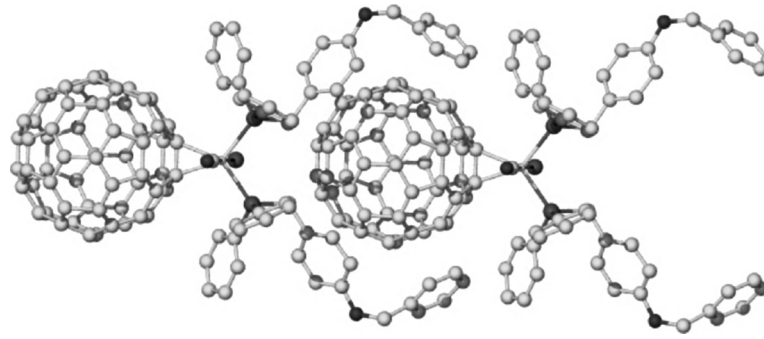

**Figure 15.28** X-ray crystal structure of [Ir($\eta^2$-$C_{60}$)(CO)Cl(**15.6**)$_2$] showing self-inclusion.[47]

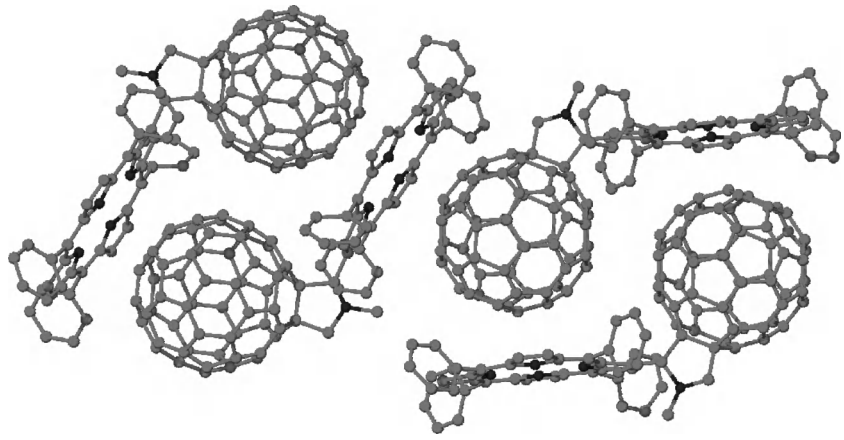

**Figure 15.29** X-ray crystal structure of **15.8** showing the porphyrin-fullerene stacking. In this case the fullerene and porphyrin regions are linked covalently, however non-covalent stacking of this type is common in two-component systems as well.[48]

fullerene has been reduced by the metal (the fullerenes have a very rich electrochemistry, and $C_{82}^{2-}$ is thought to be particularly stable), and a 'free' electron also occupying the cavity. The compound is thus a very unusual electride (*cf.* Section 3.13). Bimetallic complexes $M_2@C_{80}$ (M = La, Y) have also been prepared and it has been suggested that these may prove to be superconducting metallofullerenes. The 1999 work by Dorn *et al*. resulted in the landmark synthesis of $Sc_3N@C_{80}$ *via* a trimetallic nitride template method. This breakthrough allows the relatively straightforward synthesis of macroscopic amounts of endohedral metallofullerenes. Definitive proof for the endohedral nature of these remarkable structures comes from the X-ray crystal structure of a benzoether Diels-Alder adduct of $Sc_3N@C_{80}$ which shows a triangle of scandium ions linked by a nitride anion, Figure 15.30.[51]

A fascinating strategy in the encapsulation of guests within Fullerenes is the *molecular surgery* approach in which a Fullerene is chemically opened and a guest inserted in a controlled way, followed by chemical closure to regenerate the original fullerene with the included addition. This is a fiendishly difficult process and has only relatively recently been accomplished. The initial publication in the area in 1995 was entitled 'There is a hole in my bucky' and reported the work of F. Wudl *et al*. (University of California, Santa Barbara) who created an 11-membered ring orifice on the surface of $C_{60}$.[52] but it proved difficult to include even an atom as small as helium through this aperture. The original molecular

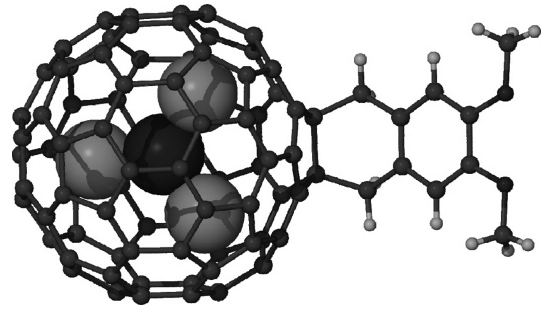

**Figure 15.30** X-ray crystal structure of a derivative of the endohedral fullerene complex $Sc_3N@C_{80}$ (Sc and N atoms shown as large spheres).[51]

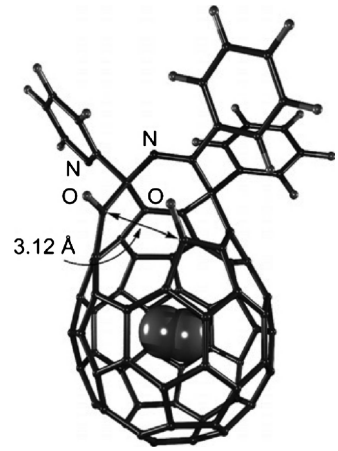


**Figure 15.31** Optimised structure of the $C_{60}$ derivative with a 13-membered ring that incorporates $H_2$ in a 100 per cent yield (reprinted with permission from [54] © 2006 American Chemical Society).

surgery operation was performed in 1999 by Rubin and co-workers who opened a 15-membered ring in $C_{60}$ capped by a cobalt(III) ion. Rubin's group also prepared a lactam derivative with a 14-membered ring and were successful in including a mixture of He and $H_2$, albeit in only *ca.* 5 per cent of the cages. Molecular surgery finally came into its own in 2005 with the 100 per cent yield encapsulation of molecular hydrogen within $C_{60}$ by the group of Komatsu (Kyoto, Japan).[53] These researchers prepared a derivative of Buckminsterfullerene with a 13-membered ring orifice by heating it with a derivative of 1,2,4-triazine (Figure 15.31). With the hydrogen inside, the aperture was closed by a further four chemical steps to give about 100 mg of the novel endohedral fullerene, $H_2@C_{60}$ which shows a $^1H$ NMR spectroscopic signal for the included hydrogen at –1.45 ppm consistent with the shielding nature of the cavity. This endohedral host-guest complex (a kind of carceplex) is formally a hydrocarbon!

Fullerene complexes have some fascinating materials properties. Of particular interest are a number of superconducting fullerene intercalates with alkali metal ions on the *outside* of the Fullerene cage that display superconductivity at temperatures as high as 33 K (for $Cs_2RbC_{60}$), although this is not particularly impressive when compared to inorganic superconductors of the ceramic type (*e.g.* yttrium barium copper oxide), which superconduct well above liquid nitrogen temperatures (up to 123 K) it is very interesting in a carbon-based material. Rather like graphite, fullerenes are readily reduced by alkali metals to give species such as $M_xC_{60}$ (M = Na, K, Rb, Cs, Ba, Ca *etc.*, $x = 1, 2, 3, 4, 6$), of which $K_3C_{60}$, and $K_6C_{60}$, which adopt face-centred cubic and body-centred cubic structures respectively, are two of the best known. The compounds are prepared by reaction of a reducing agent such as $NaBH_4$ with $C_{60}$ and may be considered as comprising fullerene anions with alkali metal cations occupying both tetrahedral and octahedral sites within the fullerene lattice.[55]

## 15.8.2 Carbon Nanotubes

*The Nanotube Site* (http://www.pa.msu.edu/cmp/csc/NTSite/nanopage.html) accessed April 2008; Niyogi, S., Hamon, M. A., Hu, H., *et al.*, 'Chemistry of single-walled carbon nanotubes', *Acc. Chem. Res.*, 2002, **35**, 1105–1113.

Carbon nanotubes are rolled up tubes of carbon made up of a graphitic hexagonal structure. They can either be open or capped at the end by carbon pentagons which give all Fullerenes their closed curvature.

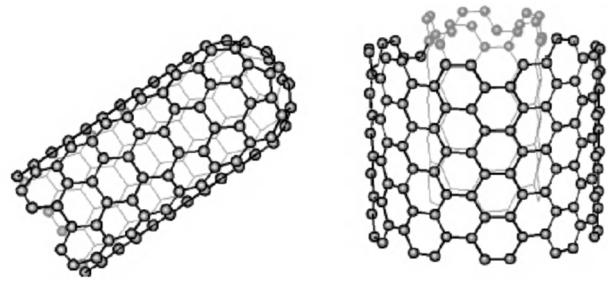


**Figure 15.32** (a) Single walled carbon nanotube (SWCNT) with capped end (b) multi-walled carbon nanotube (MWCNT).

Broadly there are two kinds of carbon nanotube; single-walled carbon nanotubes (SWCNT) and multi-walled carbon nanotubes (MWCNT) which are coaxial bundles of SWCNT, one inside the next, Figure 15.32. MWCNT were the first to be discovered in 1991 (although earlier reports in the Russian literature date back to the 1950s). SWCNT are closely related to fullerenes and have very uniform diameters. The formation of Fullerenes, SWCNT or MWCNT by the arc-discharge method, laser ablation or chemical vapour deposition are all highly dependent on conditions (temperature, pressure, presence of an inert gas such as helium *etc*.) and empirical research over the past 15 years has allowed reasonable yields of nanotubes to be produced, albeit often in low purity and as part of mixtures of carbon products. Crude nanotubes often contain impurities like polyhedral carbon particles, metal catalysts, amorphous carbon and fullerenes. Further purification strategies to produce nanotubes of uniform width, free of impurities include oxidation (which 'burns away' more reactive forms of carbon without closed ends), acid treatment, annealing, ultrasonication, microfiltration, ferromagnetic separation, chemical functionalisation and chromatography.

Since their discovery in 1991 carbon nanotubes have become one of the hottest areas in science, particularly in nanotechnology. A brief timeline highlights just some of the astonishing developments in their chemistry in recent years, Figure 15.33.

The high strength of the C-C bond in graphitic structures and the delocalised π-system gives carbon nanotubes unique electronic and mechanical properties. Carbon nanotubes have very high tensile strength and stiffness (Young's modulus *ca.* 1 TPa and maximum tensile strength *ca.* 30 GPa). For example a microfabricated tensile strength measurement device has recorded a tensile strength some 220 times that of steel. Nanotubes are also highly elastic along their axis and hence they are appropriate for uses in composite materials with anisotropic properties. The thermal and electrical conductivity of carbon nanotubes is similar to graphite meaning they can conduct electricity while being exceptionally chemically resistant. Their electrical conductivity is highly diameter-dependent because nanotube diameter influences the size of the band gap and hence nanotubes are either semi-conducting or metallic depending on size. Carbon nanotubes also have some interesting properties that are relatively unique to them such as helicity. They have a large surface area which has suggested absorption type applications such as hydrogen storage and of course their hollow interior and the structure of MWCNT immediately suggests that they may have a role in including guest species. The chemical reactivity of carbon nanotubes is related to the π-orbital mismatch caused by their curvature. Smaller nanotubes are more tightly curved and hence are more chemically reactive than flat graphitic sheets. As a result nanotubes have a versatile chemistry in which either the side walls or the more reactive end caps can be selectively modified and derivatised to produce hybrid materials and of course this reactivity is useful in

1991 Discovery of multi-wall carbon nanotubes
1992 Conductivity of carbon nanotubes
1993 Structural rigidity of carbon nanotubes
1993 Synthesis of single-wall nanotubes
1995 Nanotubes as field emitters
1996 Ropes of single-wall nanotubes
1997 Quantum conductance of carbon nanotubes
1997 Hydrogen storage in nanotubes
1998 Chemical Vapor Deposition synthesis of aligned nanotube films
1998 Synthesis of nanotube peapods in which a nanotube includes a row of $C_{60}$ molecules
2000 Thermal conductivity of nanotubes
2000 Macroscopically aligned nanotubes
2001 Integration of carbon nanotubes for logic circuits and intrinsic superconductivity of carbon nanotubes
2003 Ballistic carbon nanotube field-effect transistors with zero or slightly negative Schottky barriers
2003 Super-tough carbon nanotube fibres
2003 Non-covalent functionalised carbon nanotubes as highly specific electronic biosensors
2004 Transparent, conductive carbon nanotube films
2005 Exciton model for optical resonances in carbon nanotubes
2006 Fast mass transport through sub-2-nanometer carbon nanotubes
2007 Single molecule motion within a carbon nanotube

**Figure 15.33** A subjective timeline showing some of the key developments in carbon nanotube research.

their purification. A particularly interesting potential application of carbon nanotubes is their use as probes in scanning probe microscopes. Their elasticity means that they are not readily damaged by impact with the target surface and their chemical properties could give rise to interesting contrast variations.

It is perhaps the inclusion properties of carbon nanotubes that most resonate with supramolecular chemists and nanotubes have proved to be a rich template for the formation of all kinds of 1D wires of various materials. *Quasi* one-dimensional crystals of metals such as gold and silver and salts such as KI have been prepared by incorporating them into SWCNT, Figure 15.34. The lattice spacing in the included KI is substantially different from that in pure KI crystals. Measurements on a number of different samples of varying size shows that the amount of strain in the KI, and hence its physical properties, is related to the SWCNT diameter due to the reduced coordination of the surface atoms and proximity of the nanotube wall.[56] A particularly striking feat is the inclusion of a row of $C_{60}$ molecules into a SWCNT in a 'peapod' fashion, Figure 15.35.[57] This was achieved by vacuum heating of open ended SWCNTs at around 500 $^{o}$C in the presence of $C_{60}$. Higher temperatures up to 1200 $^{o}$C resulted in the coalescence of the $C_{60}$ molecules to produce double walled carbon nanotubes.

A lovely recent result is the confinement of a carborane derivative bearing two long alkyl chains within a SWCNT, Figure 15.36.[59] The vapourised carborane was allowed to diffuse into the nanotube in a vacuum. Using TEM the molecular motions of the included molecule can be followed in breathtaking

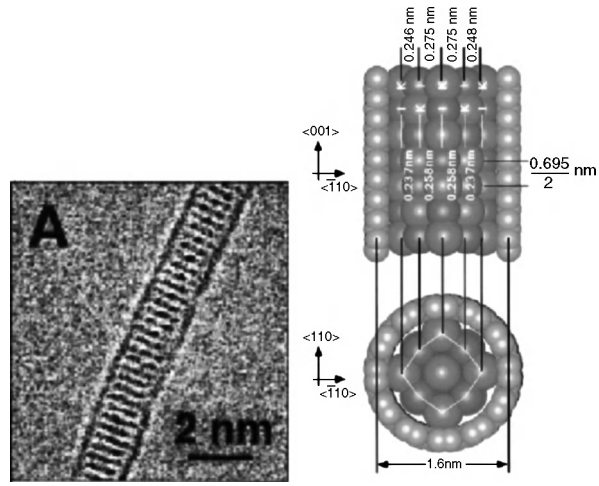


**Figure 15.34** High resolution TEM image (A) and structural model of a single crystal of KI incorporated within a 1.6 nm wide SWCNT (reproduced with permission from Reference 56).

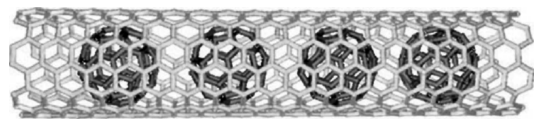

**Figure 15.35** Inclusion of $C_{60}$ within a SWCNT (reproduced with permission from Reference 58).

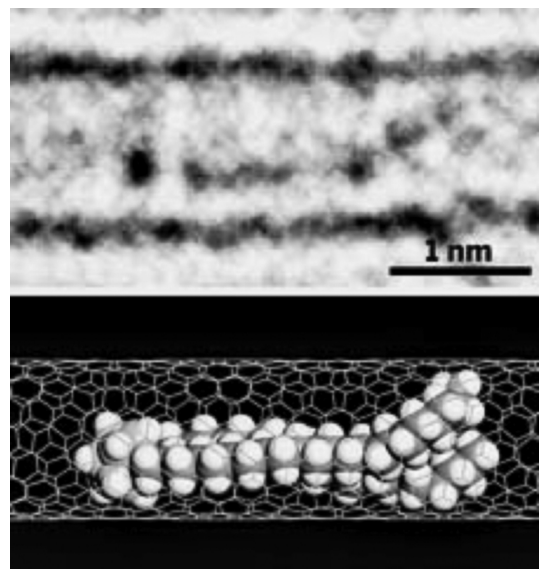


**Figure 15.36** A dialkyl carborane trapped and moving within a SWCNT some 1.2 nm in diameter (reproduced with permission from Reference 59).

detail (a video of the process is available at http://pubs.acs.org/cen/news/85/i09/8509notw4.html – accessed April 2008). Nanotube encapsulation slows down the thermal movement which is normally too fast to observed in a vacuum, and protects the molecule from decomposition by the electron beam.

### 15.8.3 Graphene

Geim, A. K. and Novoselov, K. S., 'The rise of graphene', *Nature Materials* 2007, **6**, 183–191.

Unrolling an open SWCNT into a flat sheet gives graphene – a chicken wire mesh of carbon atoms that is a single atom thick. Graphene is very difficult to isolate because it tends to curl up, but in 2004 André Geim's group in Manchester, UK, found a method of isolating individual graphene flakes by simply cleaving graphite with sticky tape. As a nanomaterial graphene has tremendous potential. Its defect-free structure makes it an extremely effective electrical conductor which, coupled with its small size, holds out tremendous promise for a new breed of computer chips. Applications in other areas such as batteries, solar cell coatings and LCD displays are also talked about. Lithographic etching of such a thin material is extremely challenging, although use of extremely thin (5–10 nm wide) strips may aid the process, however, the first graphene transistors have already been produced either based on an electric field used to control current flow through a graphene sheet or by surrounding a graphene quantum dot with two graphene ribbons to restrict the passage of electrons, Figure 15.37. One problem with graphene is that it is such a good conductor that leakage of current through such devices can occur even when the device is supposed to be 'off'.

### 15.8.4 Afterword – Damascus Steel

Reibold, M., Paufler, P., Levin, A. A., Kochmann, W., Patzke, N. and Meyer, D. C., 'Carbon nanotubes in an ancient Damascus sabre', *Nature* 2006, **444**, 286–286.

Finally, we finish this chapter, and indeed this book, with a reminder that 'there is nothing new under the sun'. Way before the era of modern nanotechnology the Crusaders came across a material called

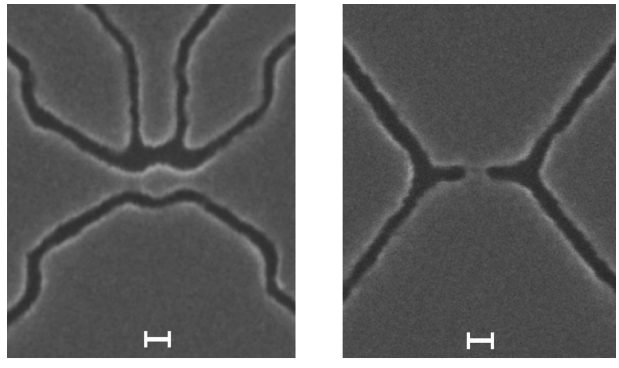

(a) (b)

**Figure 15.37** SEM images of (a) a graphene quantum dot device and (b) a graphene nanoconstriction (scale bars 20 nm, images courtesy of the University of Manchester).

**Figure 15.38** Section of a blade of Damascus steel showing the characteristic damask or 'watering pattern.

Damascus steel used against them by their Muslim adversaries to devastating effect. Swords made of this amazing material were extremely strong, but flexible enough to bend from hilt to tip. Legend has it that they were so sharp that they could cleave a silk scarf while it floated to the ground and of course they could slice through an enemy's protective clothing and even armour. Damascus steel was a very high carbon form of steel produced from the very high temperature heating of high carbon steel (termed 'wootz') and iron fragments in a ceramic crucible to fuse them together. The material has a very high carbon content (usually above 2% - most steels used have less than 1% carbon) and hence contains a great deal of carbide material, which precipitates out, forming characteristic 'watering' lines (termed a *damask* pattern) on the surface of the steel, Figure 15.38. A recent study has looked at the steel from a seventeenth-century Damascus saber. The iron metal was dissolved away using hydrochloric acid and the residue analysed by SEM. The microscope images reveal the presence of multi-wall carbon nanotubes and nanowires of iron carbide, $Fe_3C$. The results suggest that such nanowires, templated by nanotubes, might have played a role in the properties of these ancient high-tech materials.

## Summary

- Nanochemistry is the science of materials with key features on the 2–200 nm scale whose properties often scale with size. More broadly nanochemistry encompasses the visualisation and manipulation of nanoscale objects including molecules.
- Advances in nanochemistry have been fuelled by advances in instrumentation for visualisation and manipulation on the nanoscale, particularly scanning probe microscopic techniques such as STM and AFM, and observing and manipulating the chemistry of single molecules is now a reality.
- While nanotechnology is predominantly focussed on 'top-down' lithographic type techniques for fabricating nanoscale objects and devices, chemistry has a major part to play in 'bottom-up' nanotechnology, often inspired by natural molecular machinery found in biology.
- Nanoscale objects have unique properties part way between the quantum and macroscopic worlds that result in unexpected properties such as light scattering.
- Important techniques for 'bottom-up' nanofabrication include *soft lithography* and surface self-assembly. Also the use of containers such as carbon nanotubes to confine molecular scale objects in one dimension is a useful tool.
- Metallic and semiconductor nanoparticles are of increasing interest in sensing and imaging applications because of their interesting optical properties and are among the first commonly available fruits of chemical nanotechnology.
- Nanoscale structures such as *inverse opals* have fascinating photonic properties related to Natural nanostructures with potential applications in optical computing.

## Thought Experiment

How might you use carbon nanotubes to produce photonic crystals? For inspiration see Pokropivnyi, V. V., 'Two-dimensional nanocomposites: Photonic crystals and nanomembranes (review). I. Types and preparation', *Powder Metallurgy and Metal Ceramics* 2002, **41**, 264–272.

## References


1. Goldstein, J., Emergence as a Construct: History and Issues. *Emergence: Complexity and Organization* 1999, **1**, 49–72.
2. Crommie, M. F., Lutz, C. P., Eigler, D. M., Confinement of electrons to quantum corrals on a metal-surface. *Science* 1993, **262**, 218–220.
3. Dawkins, R., *Climbing Mount Improbable*. Norton: New York, 1996,
4. LaVan, D. A., Lynn, D. M., Langer, R., Moving smaller in drug discovery and delivery. *Nature Reviews Drug Discovery* 2002, **1**, 77–84.
5. Adleman, L. M., Molecular computation of solutions to combinatorial problems. *Science* 1994, **266**, 1021–1024.
6. Seeman, N. C., An overview of structural DNA Nanotechnology. *Molecular Biotechnology* 2007, **37**, 246–257.
7. Oliver, S., Kuperman, A., Coombs, N., Lough, A., Ozin, G. A., Lamellar aluminophosphates with surface patterns that mimic diatom and radiolarian microskeletons. *Nature* 1995, **378**, 47–50.
8. Sayari, A., 'Mesoporous silica and silica-organic hybrids'. in *Encyclopedia of Supramolecular Chemistry*, Atwood, J. L., Steed, J. W., eds. Dekker: New York, 2004, Vol. 1, *pp.* 852–860.
9. Bao, Z. H., Weatherspoon, M. R., Shian, S., *et al*., Chemical reduction of three-dimensional silica micro-assemblies into microporous silicon replicas. *Nature* 2007, **446**, 172–175.
10. Yang, H., Coombs, N., Ozin, G. A., Morphogenesis of shapes and surface patterns in mesoporous silica. *Nature* 1997, **386**, 692–695.
11. Sanchez, C., Julian, B., Belleville, P., Popall, M., Applications of hybrid organic-inorganic nanocomposites. *J. Mater. Chem.* 2005, **15**, 3559–3592.
12. Yablonovitch, E., Inhibited spontaneous emission in solid-state physics and electronics. *Phys. Rev. Lett.* 1987, **58**, 2059–2062.
13. John, S., Strong localization of photons in certain disordered dielectric superlattices. *Phys. Rev. Lett.* 1987, **58**, 2486–2489.
14. Wijnhoven, J., Bechger, L., Vos, W. L., Fabrication and characterization of large macroporous photonic crystals in titania. *Chem. Mat.* 2001, **13**, 4486–4499.
15. Swinerd, V. M., Collins, A. M., Skaer, N. J. V., Gheysens, T., Mann, S., Silk inverse opals from template-directed beta-sheet transformation of regenerated silk fibroin. *Soft Matter* 2007, **3**, 1377–1380.
16. Franssila, S., *Introduction to Microfabrication*. John Wiley & Sons, Inc.: New York, 2004.
17. Kaehr, B., Shear, J. B., Mask-directed multiphoton lithography. *J. Am. Chem. Soc.* 2007, **129**, 1904–1905.
18. Y. Xia, Whitesides, G. M., Soft Lithography. *Angew. Chem. Int. Ed* 1998, **37**, 550–575.
19. Binning, G., Rohrer, H., Gerber, C., Weibel, E., Surface studies by scanning tunneling microscopy. *Phys. Rev. Lett.* 1982, **49**, 57–61.
20. Sugimoto, Y., Pou, P., Abe, M., *et al*., Chemical identification of individual surface atoms by atomic force microscopy. *Nature* 2007, **446**, 64–67.
21. Demers, L. M., Ginger, D. S., Park, S. J., Li, Z., Chung, S. W., Mirkin, C. A., Direct patterning of modified oligonucleotides on metals and insulators by dip-pen nanolithography. *Science* 2002, **296**, 1836–1838.
22. Ward, A. D., Berry, M. G., Mellor, C. D., Bain, C. D., Optical sculpture: controlled deformation of emulsion droplets with ultralow interfacial tensions using optical tweezers. *Chem. Commun.* 2006, 4515–4517.
23. Hla, S. W., Bartels, L., Meyer, G., Rieder, K. H., Inducing all steps of a chemical reaction with the scanning tunneling microscope tip: Towards single molecule engineering. *Phys. Rev. Lett.* 2000, **85**, 2777–2780.
24. Theobald, J. A., Oxtoby, N. S., Phillips, M. A., Champness, N. R., Beton, P. H., Controlling molecular deposition and layer structure with supramolecular surface assemblies. *Nature* 2003, **424**, 1029–1031.
25. Surin, M., Samori, P., Jouaiti, A., Kyritsakas, N., Hosseini, M. W., Molecular tectonics on surfaces: Bottom-up fabrication of 1D coordination networks that form 1D and 2D arrays on graphite. *Angew. Chem., Int. Ed.* 2007, **46**, 245–249.

26. Grim, P. C. M., De Feyter, S., Gesquiere, A., *et al*., Submolecularly resolved polymerization of diacetylene molecules on the graphite surface observed with scanning tunneling microscopy. *Angew. Chem., Int. Ed.* 1997, **36**, 2601–2603.
27. Satake, A., Tanaka, H., Hajjaj, F., Kawai, T., Kobuke, Y., Single molecular observation of penta- and hexagonic assembly of bisporphyrin on a gold surface. *Chem. Commun.* 2006, 2542–2543.
28. Pong, B. K., Elim, H. I., Chong, J. X., Ji, W., Trout, B. L., Lee, J. Y., New insights on the nanoparticle growth mechanism in the citrate reduction of Gold(III) salt: Formation of the au nanowire intermediate and its nonlinear optical properties. *Journal of Physical Chemistry C* 2007, **111**, 6281–6287.
29. Brust, M., Walker, M., Bethell, D., Schiffrin, D. J., Whyman, R., Synthesis of Thiol-derivatized gold nanoparticles in a 2-phase liquid-liquid system. *J. Chem. Soc., Chem. Commun.* 1994, 801–802.
30. Lee, H. Y., Ryu, S., Kang, H., Jun, Y. W., Cheon, J., Selective catalytic activity of ball-shaped Pd@MCM-48 nanocatalysts. *Chem. Commun.* 2006, 1325–1327.
31. Holscher, M., Increased hydrogen storage capacity in metal-organic frameworks by designed use of spillover. *Green Chemistry* 2006, **8**, 675–676.
32. Howard, L. E. M., Nguyen, H. L., Giblin, S. R., *et al.*, A synthetic route to size-controlled fcc and fct FePt nanoparticles. *J. Am. Chem. Soc.* 2005, **127**, 10140–10141.
33. Schmittel, M., Kalsanl, V., Kienle, L., Simple and supramolecular copper complexes as precursors in the HRTEM induced formation of crystalline copper nanoparticles. *Chem. Commun.* 2004, 1534–1535.
34. Love, C. S., Chechik, V., Smith, D. K., Brennan, C., Dendron-stabilised gold nanoparticles: generation dependence of core size and thermal stability. *J. Mater. Chem.* 2004, **14**, 919–923.
35. Beer, P. D., Cormode, D. P., Davis, J. J., Zinc metalloporphyrin-functionalised nanoparticle anion sensors. *Chem. Commun.* 2004, 414–415.
36. Yang, W. R., Gooding, J. J., He, Z. C., Li, Q., Chen, G. N., Fast colorimetric detection of copper ions using L-cysteine functionalized gold nanoparticles. *J. Nanosci. Nanotech.* 2007, **7**, 712–716.
37. McFarland, A. D., Van Duyne, R. P., Single silver nanoparticles as real-time optical sensors with zeptomole sensitivity. *Nano Letters* 2003, **3**, 1057–1062.
38. Davis, J. J., Interfacial sensing: surface assembled molecular receptors. *Chem. Commun.* 2005, 3509–3513.
39. Bruchez Jr., M., Moronne, M., Gin, P., Weiss, S., Alivisatos, A. P., Semiconductor Nanocrystals as Fluorescent Biological Labels. *Science* 1998, **281**, 2013–2016.
40. Hiratani, T., Konishi, K., Surface-cap-mediated host-guest chemistry of semiconductor CdS: Intercalative cation accumulation around a phenyl-capped CdS cluster and its notable effects on the cluster photoluminescence. *Angew. Chem., Int. Ed.* 2004, **43**, 5943–5946.
41. Green, M., O'Brien, P., A novel metalorganic route to nanocrystallites of zinc phosphide. *Chem. Mat.* 2001, **13**, 4500–4505.
42. Tsuruoka, T., Takahashi, R., Nakamura, T., Fuji, M., Akamatsu, K., Nawafune, H., Highly luminescent mono- and multilayers of immobilized CdTe nanocrystals: controlling optical properties through post chemical surface modification. *Chem. Commun.* 2008, 1641–1643.
43. Nie, Z. H., Fava, D., Rubinstein, M., Kumacheva, E., 'Supramolecular' assembly of gold nanorods end-terminated with polymer 'Pom-Poms': Effect of pom-pom structure on the association modes. *J. Am. Chem. Soc.* 2008, **130**, 3683–3689.
44. Kong, X. Y., Ding, Y., Yang, R., Wang, Z. L., Single-crystal nanorings formed by epitaxial self-coiling of polar nanobelts. *Science* 2004, **303**, 1348–1351.
45. DeVries, G. A., Brunnbauer, M., Hu, Y., *et al*., Divalent metal nanoparticles. *Science* 2007, **315**, 358–361.
46. Schwarz, H., C60-Fullerene – a playground for chemical manipulations on curved surfaces and in cavities. *Angew. Chem., Int. Ed.* 1992, **31**, 293–298.
47. Balch, A. L., Catalano, V. J., Lee, J. W., Olmstead, M. M., Supramolecular aggregation of an $\eta^2$-$C_{60}$ iridium complex involving phenyl chelation of the fullerene. *J. Am. Chem. Soc.* 1992, **114**, 5455–5457.
48. Sun, Y. P., Drovetskaya, T., Bolskar, R. D., Bau, R., Boyd, P. D. W., Reed, C. A., Fullerides of pyrrolidine-functionalized C-60. *J. Org. Chem.* 1997, **62**, 3642–3649.
49. Boyd, P. D. W., Reed, C. A., Fullerene-porphyrin constructs. *Acc. Chem. Res.* 2005, **38**, 235–242.
50. Shinohara, H., Endohedral metallofullerenes. *Reports on Progress in Physics* 2000, **63**, 843–892.
51. Lee, H. M., Olmstead, M. M., Iezzi, E., Duchamp, J. C., Dorn, H. C., Balch, A. L., Crystallographic characterization and structural analysis of the first organic functionalization product of the endohedral fullerene $Sc_3N@C_{80}$. *J. Am. Chem. Soc.* 2002, **124**, 3494–3495.
52. Hummelen, J. C., Prato, M., Wudl, F., There is a hole in my bucky. *J. Am. Chem. Soc.* 1995, **117**, 7003–7004.
53. Komatsu, K., Murata, M., Murata, Y., Encapsulation of molecular hydrogen in fullerene $C_{60}$ by organic synthesis. *Science* 2005, **307**, 238–240.
54. Murata, M., Murata, Y., Komatsu, K., Synthesis and properties of endohedral C-60 encapsulating molecular hydrogen. *J. Am. Chem. Soc.* 2006, **128**, 8024–8033.

55. Okino, F., Touhara, H., 'Graphite and Fullerene Intercalation Compounds'. in *Comprehensive Supramolecular Chemistry*, Atwood, J. L., Davies, J. E. D., MacNicol, D. D., Vögtle, F., eds. Pergamon: Oxford, 1996, Vol. 7, *pp.* 25–76.
56. Meyer, R. R., Sloan, J., Dunin-Borkowski, *et al.*, Discrete atom imaging of one-dimensional crystals formed within single-walled carbon nanotubes. *Science* 2000, **289**, 1324–1326.
57. Smith, B. W., Monthioux, M., Luzzi, D. E., Encapsulated C-60 in carbon nanotubes. *Nature* 1998, **396**, 323–324.
58. Delgado, J. L., Herranz, M. A., Martin, N., The nano-forms of carbon. *J. Mater. Chem.* 2008, **18**, 1417–1426.
59. Koshino, M., Tanaka, T., Solin, N., Suenaga, K., Isobe, H., Nakamura, E., Imaging of single organic molecules in motion. *Science* 2007, **316**, 853–853.

# Index

Note: Figures, Schemes, structures and Tables are indicated by *italic page numbers*, Boxes by **emboldened numbers**, and footnotes by suffix 'n'


abiotic supramolecular catalysis 813–17
absolute structure determination 112
acetaldehyde
  formation from ethanol 797
  physiological effects 797–8
acetyl phosphate, as phosphorylating cofactor 787
acetylcholine *52*, 84
  fluorescent indicator displacement assay 740
acetylene, absorption of
  by metallomacrocycles 436, *437*
  in metal-organic frameworks 582
*N*-acetyltryptophan 249
actin filaments, movement of myosin along 886, *887*
actins 886
activation energy, factors comprising **636**
active pharmaceutical ingredient (API) 487–8, 493
active site of enzyme 75
  cascade receptor as model 289
activity coefficient 11
acyclics 118
  *see also* podands
'Adam effect' 458
adamantane-1,3,5,7-tetracarboxylic acid, diamondoid network 527–8
adamantoid cages 527
  interpenetration in diamondoid structure *527*
adatoms 901
addressable molecular devices 760–2
adenine, extraction by molecular tweezers 339
adenine–thymine interactions (in DNA) 91
adenine–uracil interactions (in RNA) 91, 602
adenosine-based coenzymes 80
adenosine monophosphate (AMP) 41
  3′,5′-cyclic (cAMP) 782, *783*
adenosine triphosphate (ATP) 50–1, 80, *81*
  hydrolysis by protonated corands 786–7
  synthesis of 70, 787–8
adenosine triphosphate (ATP) anions, electrochemical detection of 743
adenylate cyclase, cyclodextrins as mimics 782, *783*
adhesives, rod-coil co-polymer-based 878
aerogels 888, 890
aerosols 922
$^{109}$Ag NMR spectroscopy 638
agostic bonding 514–15
Agre, Peter *5*, 497
air–liquid interfaces, crystal growth at 456–8
$[Al_2Me_6N_3]^-$ anion, effect of solvents 523, 855
alanine **89**, *228*
alcohol dehydrogenase 797–8
  functional model for 798
alcohols, as supramolecular synthons 507, 508–9, *508*
alicyclic diols, channel structures formed by 401–2
alizarin *739*, 740
alkali metal cations
  in biochemistry 50–61
  properties **160**, *226*
  selective binding of **160**
alkali metal picrates 144, *145–6*
alkalide salts 114, 196–7
alkanes, hydroxylation of 803
alkanones and alkanediones, urea inclusion compounds 396–8
alkene metathesis reaction 344
  applications 658–60, 667, 917, *919*
alkenes, epoxidisation of 803, 805
*p*-alkylcalixarenes 314
alkyne coupling, copper-catalysed 342, *343*
allosteric effect 19–20, 74, 626
allotropy 487
allyl lariat ethers, complexation with cations 209
Alzheimer's disease 885
amide-based receptors 253–5
amide cryptands, fluoride binding 255
amide dimers, as supramolecular synthons *446*, 507
amides, as hydrogen-bond donors 230–1, 507
amidopyrrole, imidazole-functionalised 258, 296
amidothiourea-based metallacages 302–3
amine–aldehyde condensation
  cyclophanes synthesised by 342
  *see also* Schiff base condensation reactions
amine-recognition MIP array 879–80
amines, basicity 164–5, 177
$\alpha$-amino acid, synthesis by transamination 785
amino acids **88–90**
  intermolecular condensation reaction **89**
  listed **89**
  synthesis **89**



*Supramolecular Chemistry, 2nd edition* J. W. Steed and J. L. Atwood


© 2009 John Wiley & Sons, Ltd


ISBN: 978-0-470-51233-3

amino acids (*Continued*)
zwitterionic structure *287*
aminotransferase-catalysed amino acid synthesis **90**, 227
aminotransferases **89**
ammonium cations
binding by 3D hosts 183–4
binding by corands 181–3
ammonium-based podands 239–40
amphiphiles 53, 825, 832, 834
nanotubes 882–3
T-shaped, hydrogen-bonded mixtures with dendrimers 850
amphiphilic block co-polymers 876–8
amphiphilic receptors 193–4
amyloids 598, *599*, 885, *886*
analytical chemistry applications, cyclodextrins 336
AND gate, molecular logic 758
Anfinsen, Christian 595, 596n
8-anilino-1-naphthalenesulfonate (ANS) 14, 247, 309, 347, *348*
anion activation by macrocyles 150
examples 151–2
anion-based helices 687
anion binding 42, 223–84
anion binding proteins 228–9
anion extractants 297–8
anion host design 232–5
coordination number considerations 235
entropic considerations 233–4
Lewis basicity considerations 235
negative-charge considerations 234
pH effects 236–47
polarisability considerations 235
preorganisation in 232–3
shape selectivity 238–9
solvation considerations 235
anion hosts
amide-based receptors 253–5
biological receptors 227–32
cyclophanes 246–7
guanidinium-based receptors 248–51
inert metal-containing receptors 259–76
neutral receptors 251–9
peptide-based 258–9
pyrrole derivatives 257–8
urea and thiourea derivatives 255–7
zwitterions 253
anion–$\pi$ interactions 33
anion sensors 733, 734, 735, 838, 924
anion templating 300–2
anions
biological applications 224–5
properties 225–6
anisodynmic motions 185
anomalous dispersion 112
antenna dendrimers 721, 723–4
anthracene-based derivatives
fluorescence detection by 732
in logic gates 758, 759
photodimerisation of 759
antibiotics 57, 97, 688, 797
antibody assays, dendrimer-linked 876
anticancer agents/drugs 93–4, 97, 876
anticrowns 235, 271–6
mercury-containing 272–3
tin(IV)-containing 274, *275*
anticryptands, tin(IV)-containing 274–5
anti-Hofmeister selectivity 239
antiport mechanism 51, 245, 294, 296
apoenzyme 79–80
model for 808
apohost 386
aqua regia 175
aquaporins 497
arginine **89**, *229*
as anion binding site 229–30
arginine fork motif 229
aromatic interactions 519–22, 519–24
arsphenamine 8
artificial biological cells 563–4
aryl embraces *446*, 522–3
aryl sulfonates, in hourglass inclusions 464, 465
asparagine **89**
aspartic acid **89**
assembly number 619
assembly tree 618, *618*
assisted self-assembly 596
atom–atom potential method 503–4
atomic force microscopy (AFM) 45, 473, **912**
nanomanipulation using 913
atomic-level assembly 920–1
ATP *see* adenosine triphosphate
ATPases (enzymes) 50, 51
corands as mimics 785–8
mechanism of action *60*
atropisomers 801
attractive *gauche* effect 131
aurophilic interactions 36, 37
autocatalysis 820, 821, 822, 823
auxiliary linkage approach, synthesis of catenanes and rotaxanes 669–77, 692
azacorands 128, 240–3
ADP- and ATP-binding ability 243, 785–8
anion coordination behaviour 240–2
binding of $NH_4^+$ cations by 181
azacrowns *120*, 122
proton binding by 176
selectivity for α, ω-dicarboxylic acids 244
synthesis 158
*see also* diaza[18]crown-6
azacyclophanes 341
NMR spectra 179
synthesis 344–5
azamacrocycles
basicity effects 164–5
*see also* cyclam

β-barrel ion channels 812–13
back bonding **169**
bacterial S-layers 887–8
bacteriochlorophylls 63, *64*, 66, *67*
bacteriopheophytin 66, *67*
Bakelite (phenol–formaldehyde polymer) **198**
ball mills 470, *471*
barbiturates
  calixarene receptors for 317
  chiral resolution of 336
  cyclophane hosts for 353, *354*
barium chromate nanoparticles 904, *905*
barium sulfate nanoparticles 904
base pairing (in DNA) 90–1
  in DNA self-assembly 91
'basic zinc acetate' building unit *579*, 584
benzamide, polymorphs 487, 491
benzene
  herringbone packing motif 34, 520
  Kekulé's structure *340*
benzene-1,4-dithiol, in molecular electronics 761–2
benzene-1,3,5-tricarboxylate trianion 256–7
benzene-1,3,5-tricarboxylic acid *see* trimesic acid
benzo[15]crown-5
  'naked' carbide complex formation using 153
  in sandwich complexes 292
benzo[18]crown-6, synthesis 155–6
benzoic acid *529*
*p*-benzoquinone, binding by cyclophane hosts 355–6
5-benzyl-2-benzylidene-cyclopentanone, photodimerisation of 473
benzyne 377–8
Bermuda Triangle phenomenon 392
bibracchial lariat ethers (BiBLEs) 121, *128*
  with amide side-arms 141–2
  binding constants for alkali metal complexes 141
  cation–π interactions 209–10
bicyclic guanidinium derivatives 249–50
bilayers *834*, 836
bimolecular reactions, compared with intramolecular reactions 78, *79*
binding constants 9–17
  definition and use 9–11
  listed
    alkali metal–macrocyle complexes 9, *10*, *25*, *120*, *135*, *140–1*, *143*
    ionophores *57*
    quinone receptor, with various hydrogen-bonding guests *356*
    siderophores 214, 215, *216*
    sulfonated [4]resorcarenes, with various alcohol guests *316*
  measurement of 11–17
    by calorimetric titration 15, *16*
    by continuous-variation (Job plots) method 12–13, *14*
    by extraction experiments 16–17
    by fluorescence titration 13–14
    by nuclear magnetic resonance titration 12, *13*
    by potentiometric titration 11–12
    by UV-Vis spectrophotometric titration 15
  solvation effects 39, *40*, 235
  stepwise formation of supercomplexes 242, *243*
binding selectivity 16, 26, 740, 778–9
biochemical self-assembly 99–102, 600–4
biological anion receptors 227–32
biological cell imaging, lanthanide-based probes for 735, *736*
biological cell membranes 830
biological enzymes, features *779*, 780
biological mimics 777–813
biological models
  characteristics 779–80
  metal-containing sites in 792
biological self-assembled polymer fibres 885–7
biological systems, supramolecular chemistry in 49–104
biomimetic morphosynthesis 902–5
biphenyl, STM tip induced synthesis 914, *915*
2,2′-bipyridine, in photochemical devices 716–18
4,4′-bipyridinium tetrachloroplatinate(II) *511*
2,2′-bipyridyl-type light-harvesting devices 718–24
4,4′-bipyridyl 'blue box' 357
  in molecular electronic memory device 760, *761*
  pseudorotaxanes constructed with 657
  in [2]rotaxane-based molecular shuttle 754, *755*
4,4′-bipyridyl ligands and expanded analogues *570*, *573*, *576*
  porous networks based on 576–7
  in supramolecular cube *622*, 623
Birch reduction 195
bis(benzene)chromium 521
  charge-transfer complex, $Cr(C_6H_6)_2.C_6F_6$ 521, *522*
bis(2,2′-bipyridine) bridging ligand, mixed-valence compounds based on 719–20
bis(bipyridinium) cyclophane 357
  electrochemistry 662
  in synthesis of [2]catenanes 660
  *see also* paraquat
bis(bora)-*p*-*tert*-butylcalix[4]arene derivative 270, *271*
bis(calixarenes) 206, *207*
bis[2]catenanes, synthesis 665–6
bis(cobaltocenium) receptors 261–2
1,8-bis(dimethylamino)naphthalene 268, *269*
bis(diphenylphosphino)calix[4]arene nickel(II) complex 815
bis(guanidinium) receptors 249–50
  bicyclic guanidinium derivatives incorporated 250
*N*,*N*′-bis(pentafluorophenylethyl)diaza[18]crown-6 210
*N*,*N*'-bis(phenylethyl)diaza[18]crown-6, cation–π interactions 210
*trans*-1,2-bis(4-pyridyl)ethylene, photocyclisation of 473
bis([4]resorcarene), propan-2-ol linked 647
bis(tren) cryptates 238
bisubstrate reaction template 815, *819*
bis(urea) gelator *890*, 891
Bjerrum model 310

block co-polymers 876–8
electron transfer through 747–8
molecular wires based on 747–8
'blue box' cyclophane 357, 657
blue phases (liquid crystals) 844–5
bombykol (pheromone) 85, *86*, 778
bond stretch isomerism 464, **466–7**
*Book of Kells* lettering 691
Boolean logic operations 758
boronic acid derivatives, as anion hosts 254, 270, *271*
Borromean networks/weaves 574, 700
Borromean rings *574*, *691*, 697–9
Borromeates 698–9
bottom-up approach 593, 901, 907
bovine serum albumin microcontainer 909
bovine spongiform encephalophy (BSE) 885
'bow-tie' shaped intermediate 618
Bragg–Brentano method **474–5**
'brick wall' network topology 540, 566
bridging cyanide ligands 568–9, 624
Brookhaven Protein Data Bank (PDB) 484
Brownian machines 764–5
Brownian motion 764
Brunauer–Emmett–Teller (BET) analysis 430, 435
Buchner, Eduard 76
buckminsterfullerene ($C_{60}$)
in hydroquinone clathrates 407
purification of 423
redox sensor based on 928
in [4]resorcarene-based capsules 647
in solid-state CTV inclusion complexes 359, 416
structure **425**, 649
*p-t*-butylcalix[4]arene 35, 197, *198*
in colorimetric sensors 739
conformers **199**
gas sorption by 431–3
inclusion compounds (types listed) *421*
Mo(VI) derivative of tetraanion 313
solid-state phase behaviour *422*
tetramethyl ether 200–1
in van der Waals inclusion complex 35, *36*
*p-t*-butylcalix[4]arene·toluene complexes 35, *36*, 312, 419, 420–1, *422*
effect of heating 421–2
*p-t*-butylcalix[6]arene·$(C_{60})_2$ complex 423, *424*
*p-t*-butylcalix[8]arene·$C_{60}$ complex 423
*p-t*-butylcalix[n]arenes, phase transport equilibria 204–5

C–H bond, as hydrogen bond acid 517–19
C–H···$\pi$–$\pi$ interactions 518–19
cadmium selenide (CdSe) quantum dots 926
cadmium telluride (CdTe) nanocrystals 926, *927*
caesium, coordination by calixarenes 204–5
caesium effect 155, 344–5
caesium-137, extraction in nuclear industry 297, 299
cage-type structures
cyclodextrin complexes 334
tri-*o*-thymotide complexes 411, 413
Cahn–Ingold–Prelog notation 110–11, 680
Cairns-Smith crystals-as-genes hypothesis 469–70, 824
calamitic liquid crystal phases 841–3, 844–5
calcium sensors 744
calix crater vase 197, *198*
calixarene-based ion pair receptors 295
calix[4]arene amidinium derivative, in heterodimer capsule 646
calix[4]arene-based sensor 733
calix[4]arene-bis-crown-5 203, *204*
(calix[5]arene)$_4$·$(C_{60})_5$·(toluene)$_2$ complex 423, *424*
calix[6]arene thiourea derivative 256
calix[n]arene sulfonates 315, 426–9
calixarenes 197–208
with adamantyl terminal groups, anchored to immobilised cyclodextrins 320, *321*
1,2-alternate conformation *199*, 300
1,3-alternate conformation *199*, 201, 202–3
amphiphilic dendrimers based on 874
in anion binding hosts 262–5
calix[4]arenes
$Ag^+$ complex 202, *203*
1,3-alternate conformer 202–3, 733
anatomy in cone conformation *200*
conformational aspects of cation inclusion 201, *202*
gas sorption by 433–4
guest exchange dynamics 321–2
intramolecular hydrogen-bonding interactions *312*
in ion channel mimics 810
structure (cone conformation) *200*, *311*
upper-rim bridged 206
calix[5]arenes 313, 420
calix[6]arenes 313
calix[8]arenes **200**, 313
carbohydrate-derived 319
cation complexation by 198–204
cone conformation **199**, 201
conformations **199**, 312
cyanuric acid derivatives 651–2
diethylbarbituric acid derivatives 317
as enzyme mimics **200**
fullerenes separation using 423
gas sorption by 431–4
in heterodimeric capsules 646
history of chemistry **198–200**
hybrid calixarenes, cation complexation by 206–8
inclusion compounds 419–29
in non-aqueous solution 314
organic-soluble 419–22
organometallic derivatives 33
partial cone conformation *199*, 201
phase transport equilibria 204–6
solid-state inclusion compounds 314, 419–29
with fullerenes 314, 423–4
water-soluble 426–9
*see also p-t*-butylcalix[4]arene; *p*-sulfonatocalix[4]arene
calixcrowns 203, *204*, 207–8
calix[4]pyrroles 15, *16*, 257

calmodulin 231, 819
calorimetric titration 15, *16*
Calvin cycle 67
Cambridge Crystallographic Data Centre (CCDC) 484
  crystal structure prediction blind tests 504–5
Cambridge Structural Database (CSD) 484–7, 500
  biological recognition of phosphate and sulfate 229
  crystallographic space groups **462**
  high-$Z'$ structures 499
  hydrate structures 498
  hydrogen bonding interactions 29, 450, 484, *485*, 505–6, 517
  intermolecular C···O distances in carbonyls 513, *514*
  interpenetrated structures 572
  polymorphs 488
  powder X-ray diffraction patterns and **475**
canted-spin antiferromagnetism 569
cappedophanes *345*, 346
capsids (virus coatings) 101
capsular complexes 148, 183, **189**, 320, 427
  design of self-assembling structures *621*
carbamazepine–saccharin co-crystal 496–7
carbide complex, formation using macrocycles 152–3
carbon monoxide, binding to haemoglobin 73
carbon monoxide ligands
  coordination modes *513*
  hydrogen bonds to 512–13
carbon nanotubes 553, 927, 931–5
  applications 932, 933, 936
  in Damascus steel 936
  development timeline *933*
  electrical properties 932
  inclusion properties 933–5
  mechanical properties 932
  synthesis 933
  *see also* multi-walled carbon nanotubes; single-walled carbon nanotubes
carbonic anhydrase (CA) 737, 795
  inhibitor 818–19
  mechanism of action 796
  structural model for 796, *797*
carbonyls, dipole–dipole interactions in 28
carboplatin 94
*o*-carborane, in solid-state CTV inclusion complexes 359, 416, *417*
carboxylic acid co-crystals with 2-aminopyrimidine, Etter's rules for hydrogen bonding 480
carboxylic acid dimers 29
  as supramolecular synthons *446*, 506, *529*
carboxypeptidase A 230
carceplexes 370, *371*
carcerands 4, 370–9
  definition 370
  with giant covalent cavities 379–80
  synthesis *370*, 371, *372*
    template effects 373
carcerism 375–6, 644
caroviologens 747, *748*
cascadanes 863
cascade complexes/receptors 286, *287*, 289–91
  di-copper(II) complexes 289, 291
  di-manganese(II) complexes 290
  di-vanadyl complex 290
cascadyl-substituents 863
Catalan solids 648
catalysis
  by metal-organic frameworks 583
  enzymatic 77–9
  photochemical molecular devices for 720–1
  strategies for modifying selectivity 815, *816*
  supramolecular 813–23
  in various environments *779*
catalytic spillover (splitting of $H_2$ into hydrogen atoms) 585
catechol 216
  in siderophores *213*, 214, 215
catechol-derived binding sites 627–8
catenands 653, *654*, 674
catenanes 45, 195, 596, 605, *606*, 653–78
  [2]catenanes
    amide-based 666, *667*
    doubly interlocked *655*, 696
    electrochemically controlled translational isomerism 756, *757*
    electrochemistry 661–2
    properties 660–1
    synthesis 625–6, 660, 666, *667*
    triply interlocked *696*
    X-ray crystal structure *661*
  [3]catenanes
    synthesis 662–3, 671
    translational isomers *671*
  [5]catenanes, synthesis 664–5
  [7]catenanes, synthesis 665
  hydrocarbon catenanes, synthesis 669, *670*, 672, *673*
  hydrogen-bonded 666–7
  metal-backbone catenanes 625–6
  nomenclature 653, *654*
  synthesis 653–4
    anion-templated 676–7
    auxiliary linkage approaches 669–77, 692
    directed approaches 660–6
    metal-ion-templated 672–6
    statistical approaches 655–6
    statistical then directed approach 672, *673*
  as topological isomers 654, *655*, 691
  *see also* polycatenanes
catenates 653, *654*, 674–6
cation-binding hosts 42, 105–222
  alkalide salts 114, 196–7
  calixarenes 197–8
  crown ethers 114–17, 135–9
  cryptands 122–4, 142–4
  electride salts 114, 195–7
  lariat ethers 120–1, 140–2
  nomenclature 127–9
  podands 118–20
  proton binding hosts 173–80

cation-binding hosts (*Continued*)
siderophores 213–17
solution behaviour 149–53
spherands 125–7
synthesis methods 153–9
as transacylase mimics 788–92
*see also* crown ethers; cryptands; lariat ethers; podands; spherands
cation carriers 149
cation complexation
selectivity 129–49
factors affecting 129–30
cation extractants 297
cation–$\pi$ interactions 32, 523
in calixarenes and derivatives 202–3
with hydrocarbon hosts 211–13
with mixed C–heteroatom hosts 209–11
cation receptors 149
cation sensors 732, 734, 736–8, 745
cavitands
chiral 192–3
examples *7*
guest binding by 310–17
meaning of term 6, 308, 310
range of structural types *311*
cavitates 6, 310
examples *7*
guest-exchange dynamics 320–2
cavity-containing assembly 627
cavity occupancy factor, cryptophane complexes *365*, 366
$CdSO_4$ framework *541*
cell division 97–8, 593
cell membranes 830
fluid mosaic model 836
cellulose 331
central discrimination 182, *183*
channel hosts
cyclodextrin complexes 334–5
gas sorption by 434–5
trimesic acid complexes 399–401
tri-*o*-thymotide clathrates 411, *412*
tubular structures 401–2
urea clathrates 393, 395–6, 435
channel-mediated ion transport 53, *54*
chaperones 596, 598
charge compression 486
charge transfer *712*, 713
charge-coupled device X-ray diffractometer **56**
charge-transfer complexes 310, 314, 413, 521–2
charge-transfer cyclophanes 357–8
chelate control strategy (in catalysis) 815, *816*
chelate effect 17–22, *24*
kinetic effects 18
ring size dependence of stabilisation 18–19
thermodynamic effects 18
chelate ring size effects 134
chelation-enhanced fluorescence (CHEF) effect 240, 737–8
chemically modified ISFETs (CHEMFETs) 745–6
chemistry of life 49–104
chemotherapy 8
'chicken wire' structures
graphite and graphene 520, 551, 935
saturated hydrogen-bonded co-crystals 494
trimesic acid inclusion complexes 400, 401
chiral barrier hosts 190, 789
chiral chromatography 191, 336
chiral corands 190
as transacylase mimics 788–90
chiral guest recognition 185, 190–3
chiral molecules 110–12
chiral recognition factors 190
chirality
amplification 413
catenanes *655*
double helicates 680, *681*
helices 679
transfer by inclusion reaction 413
chloride channels 58–9, 227, 811
chloride sensors 733
chloride transport 58–9, 811, 813
chlorine hydrate *5*, 386
chlorophylls 61, 63, *64*
absorption spectra *64*
coordinated $Mg^{2+}$ ion in 65
cholapods 278–81
cholesteric liquid crystal phases 841, 844–5
cholesterol framework *279*
cholic acid 278, *279*, *311*
*p*-toluenesulfonamide 279
chromium carbonyl, $Cr(CO)_6$, crystal deconstruction for 481, *482*
chromoionophore 119
chromophores 710, 712, 726
chromophoric molecular switches 756, *757*
chronology, supramolecular chemistry development *5*
chymotrypsin
mimic compounds 790–2
structure 790, *791*
circular dichroism 112
induced 192
circular dichroism (CD) spectroscopy **368–9**
cisplatin 93–4, 95
citrate, binding with guanidinium-based receptors 250–1
citrate sensors 735
clamp proteins 98, 99
clathrands 6
clathrate chemistry 4
clathrate hydrates 387–92
applications 391–2
formation of 387–8
hydrogen storage applications 392, 430
properties 390–1
structure 388–90
clathrates
examples *7*, 393–406
term first introduced 6, 386

clathration, compared with sorption 538
clay minerals *426*, *551*
clearing-point temperature (liquid crystals) 847–8
cleft hosts 228
clefts 228
  as active sites in enzymatic catalysis 75
'click' chemistry 872
'click' reaction, catalysis by cucurbit[6]uril 814–15
closed shell bonding 36–7, 524
coal liquefaction 857
coalescence method **187**
  application 661
cobalamin coenzymes 61, 83
  models 809
cobaloximes 808
cobaltocenium-based hosts, redox potential shifts 261, 262–3, 742–3
cobaltocenium cation, DOSY spectrum **189**
co-crystals 386, 493–8
  CTV–carborane 418, *419*
  designer co-crystals 494–7
  hydrates 497–8
  meaning of term 493–4
coelenterands 210–11
coenzyme A 80, *81*
coenzyme $B_{12}$ and derivatives 80–3, 497
  mimics/models for 808–9
  mutase activity 83, *84*
coenzyme F450 62, 80
coenzymes 79–80
  examples 62, 80–3, 785
coinage metal nanoparticles 922
  *see also* gold nanoparticles
collagen, biosynthesis of 596
colloidal gold 44, 922
colloids 44, 922
colorimetric reporters 259, *260*, 278
colorimetric sensors 738–9
colorimetry, Fe(III)-specific *216*, 217
columnar discotic liquid crystal phase 845, *846*
columnar hexagonal discotic polymeric mesogens 893, *894*
columnar mesophases 845, *846*
combinatorial chemistry 741, 817
commensurate structures 396, 397
complementarity 25
  combined with preorganisation 25–6
complexes-as-metals/complexes-as-ligands strategy 718–19
  dendrimers assembled using 721, *722*, 873
computer applications, nanomaterials proposed 901, 905, 918, 935
concomitant polymorphs *490*, 491
conformational polymorphs *490*, 491
constrictive binding 265, 373
constrictive binding energy 266, 373, *374*
contact ion pair receptors 286, 287–8
convergent binding sites (in host–guest chemistry) 3, 620
convergent process, self-assembly as 43, 595
cooperative binding of substrate to enzyme 78
cooperativity 17–22, 308
  myoglobin units in haemoglobin 802
  in self–assembled complexes 610
  in site binding model 612, 614, *615*
coordination chemistry 8, 106–13
  basic concepts 106–12
  chelate effect 17–22
  noncovalent anion coordination chemistry 224
  optical isomerism 110–12
coordination complexes
  bonding in 107–8
  gas sorption by 435–7
  kinetic and thermodynamic stability **636–7**
  nomenclature 108–9
  synthesis 109
coordination number 108
coordination polymer networks 567
  formation and dissolution on surfaces 915, *917*
coordination polymers 561–86
  design factors 567
  interpenetrated structures 571–4
  magnetism 568–70
  negative thermal expansion 570–1
  porous and cavity-containing structures 575–8
  terminology 561–2
  three-dimensional networks 567
  two-dimensional grids/nets 566
  zero-dimensional clusters 562–4
coordinato-clathate approach to crystal engineering 483
copper production 297, *298*
  historical processes 297n
corands 22, 23, *24*, 127
  as ATPase mimics 785–8
  binding of ammonium cations by 181–3
  chiral 190
  *see also* crown ethers
coraplexes 129
corates 129
Corey, Elias James 443n
Corey–Pauling–Koltun (CPK) space-filling molecular models 125, 370, 790
corrin ring system 61, *62*
  cobalt(III) complexes 61, 81, *82*
corroborative models 793
corynebactin *213*, 215
coulombic energy transfer mechanism 713, *714*
'Coup du Roi' 680
covalent polymers 862
  with supramolecular properties 876–80
covalent template synthesis 604–5
Cram, Donald 3, 4, *5*, 25, 125, 370, 778
Creutz–Taube cation 715
Creutzfeldt–Jakob disease (CJD) 885
critical aggregation concentration (cac) 350
critical micelle concentration (cmc) 835
critical self-assembly concentration (csac) 608–9
Crowfoot-Hodgkin, Dorothy *5*, 83

crown–anthracene system, fluorescence detection by 732
crown ethers 114–17
acyclic analogues 118
*see also* podands
anion activation using 150–1, 152–3
benzo[15]crown-5, 'naked' carbide complex formation using *153*
benzo[18]crown-6, synthesis 155–6
with boronate centre 291
cation binding by 135–9
cavity sizes *137*, 162
common examples *116*
conformational characteristics 130–1, 144
[12]crown-4 *136*, *137*, 162, 163
[15]crown-5 *136*, *137*, 162
[18]crown-6
binding constant of $K^+$ complex 9, *10*, *25*, *120*, *135*
cation binding to 135, *136*, *161*, 162, *163*
cavity size *137*, 162
conformational rearrangement in K1 complex 130–1, 144
donor group orientation 133–4
oxonium ion binding by 174–5
phase transfer catalysis involving 149–50, *151*
solution behaviour 149, *150*
synthesis 116, 154
thermodynamic contributions to stability of $K^+$ complex *135*
[21]crown-7 137, 138
cylohexyl crown ethers *136*
diaza[18]crown-6 *25*, *120*, *143*
dibenzo[18]crown-6
properties 114-15
synthesis 114, *115*, 153–4
dibenzo[24]crown-8 138, *140*
dibenzo[30]crown-10 138, *140*
binding to Pt(II) complex 194
and herbicide receptors 194, 195
$K^+$ complex 138, 194
selectivity of cation complexation 138, 139
dicyclohexano[18]crown-6 116, *117*, 152, 299
discovery and scope 114–16
electride complexes 196
nitrogen analogues *25*, *120*, *143*, 160–2
nomenclature 127
oxonium ion binding by 174–6
pyridine-based
as chiral host(s) 191, *192*
interaction with nitromethane 30, *31*
solubility behaviour 149, *150*
sulfur analogues 161, 162–3
synthesis methods 114, *115*, 116, *117*, 153–7
tribenzo[21]crown-7 138, *139*
cryptands 4, 23, *24*, 33, 122–4, 127
binding free energies for alkali-metal picrates *145*, *146*
cation binding by 142–4
[1.1.1]cryptand, as proton binding host 180
[2.1.1]cryptand 143, 144
[2.2.1]cryptand 122, 143, 144
synthesis *122*
[2.2.2]cryptand 122
binding constant of $K^+$ complex 9, *10*, *25*, *135*, 143
cation binding to 143, 144, *164*
conformational rearrangement in $K^+$ complex 144, *147*
electride complexes 196–7
synthesis *122*
thermodynamic contributions to stability of $K^+$ complex *135*
electride complexes 196–7
nitrogen analogues 163–4
nomenclature 129
proton binding by 176
synthesis methods 122–3, *158*, 159
cryptaspherands 126, *127*
binding free energies for alkali-metal picrates *145*
binding of $NH_4^+$ by 183
cryptaspheraplexes 183
cryptates 129
mixed 168
cryptophanes 359–60
in anion binding hosts 265–6
competition with solvent 363–4
complexes with
alkyl ammonium ions 364
halocarbons 361–3, *365*, 366
with metal cations 364–5
methane 365–6
xenon 366
$^1H$ NMR spectra *361*
'imploding' 366–7
synthesis 360, *361*
*see also* hemicryptophanes
crystal allotropy 487
crystal close packing 36
crystal deconstruction 481–2
crystal engineering 441–536
concepts 442–53
design strategies 482–4
diamondoid arrays 526–30
nonlinear optical materials 445, *446*, 526, 765
crystal growth, at air–liquid interfaces 456–8
crystal interfaces, dyeing 462–4
crystal nucleation
chirality induction 458–60
NMR spectroscopy as probe tool 455–6
theory 453–5
crystal self-assembly 442
crystal structure calculation 501–4
cluster method 501–3
procedure flowchart *502*
crystal structure prediction 500–5
CCDC blind tests 504–5
soft vs hard predictions 500–1
techniques used *501*, 504

crystal structures, understanding 476–84
crystal symmetry **461–2**
crystallographic space groups **461–2**
crystals-as-genes hypothesis 469–70, 824
cubanes 527, 528
cubeoctahedron, self-assembly of 630, *631*
cubes, supramolecular 621–4, 648
cubic liquid crystal phases 846
cucurbituril 324
  guest exchange dynamics 325
  structure *323*
  synthesis 324
cucurbit[n]uril family 324
  cucurbit[6]uril *325*, 325
    as catalyst for 1,3-dipolar cycloaddition 814–15
    in molecular necklaces 677–8
  cucurbit[10]uril 324, *325*
  dimensions *325*
  inverted cucurbit[n]urils 324, *325*
cucurbit[10]uril·cucurbit[5]uril inclusion complex 325
cumulene **424**, **425**
Curl, Robert F. 423
current imaging tunnelling spectroscopy (CITS) 918–20
cyanometallates, hydrogen bonds to 511–12
cyanopolyynes **425**
cyanosilylation reaction, MOF-catalysed 583
cyclam 128, 133
  basicity effects 165, *178*
  conformers *165*, 166
  derivatives 166–7, 293–4
  synthesis 165, 166
cyclen ([12]aneN$_4$) binding site, affinity for $Zn^{2+}$ 737–8
cyclic bis[2]catenane 666, *667*
cyclic helicates 686, *687*
cyclic voltammetry **266–8**
  applications 261, *263*, **267–8**, 288, 661–2, 675–6
  auxiliary electrode **267**
  reference electrode **267**
  working electrode **267**
cyclobutadiene 377
cyclococondensation reactions 159
cyclodextrin anion 781
  acetylation of 781, *782*
cyclodextrin hydrates 330–1
cyclodextrins 327–36
  anatomy 328–9
  characteristics *329*, 781
  $\alpha$-cyclodextrin
    anatomy *329*
    binding constants for various guests *333*
    characteristics *329*
    structure *311*, *328*
  $\beta$-cyclodextrin
    anatomy *329*
    anion *781*
    binding of cobalamin and substrate 809
    characteristics *329*
    ester hydrolysis by 782, *783*
    structure *328*
  as cytochrome P-450 mimics 805–6
  as enzyme mimics 780–5
  as esterase mimics 782, *783*
  functionalised 783–5
  guest sizes *329*, 332
  immobilised on gold surface 320, *321*
  inclusion chemistry 331–5, 424
  industrial applications 327–8, 335–6, 493
  preparation of 331
  structure(s) *311*, *328*
  water solubility *329*, 330
1,2,4,6-cycloheptatriene 378
cyclohexane imine-based carbonic anhydrase mimics 796, *797*
cyclohexanedione·benzene cycla-6-mer 447
cyclohexyl crown ethers, binding constant as function of cation radius *136*
cyclooctatetraene 377
cyclopentadienyl-arene iron(II) cations, CTV inclusion complexes with 417
cyclophane-based dendrimers 350–2
cyclophanes 4, 310, 340–58
  as anion binding hosts 246–7
  binding of $NH^{4+}$ by 183–4
  charge-transfer cyclophanes 357–8
  as chiral hosts 191–2
  diphenylmethane-derived 211–12
  guest inclusion by hydrogen bonding 353–7
  hydrophobic effects 38–9
  meaning of term 340
  [2.2]metacyclophane 341
  [1.1.1]metacyclophanes, substituted 197, 341
  nomenclature 341–2
  [2.2]paracyclophane 211, *212*, 341, 345
    $Cr^+$ complex 213
    synthesis 342, *343*
  [2.2.2]paracyclophane 211, *212*, *341*
  [3.3]paracyclophane 211, *212*, *341*, 345
    $Cr^+$ complex *212*, 213
  [8.8]paracyclophane 346, *347*
  synthesis 342–5
  ultrashort nonbonded contacts in 345–6
  *see also* calixarenes; resorcarenes
cyclo[8]pyrrole *244*, 246
cyclotetramethylenetetranitramine, co-crystal with ammonium perchlorate 495
cyclotricatechylene hexaester 845
cyclotriveratrylene (CTV) 193, 358–9, 414–19
  in anion binding host 264–5
  cavitands based on 359
  inclusion chemistry 416–17
  network structures 418–19
  properties 414
  structure *311*, *414*
  synthesis 414–15

cypovirus 101
cysteine **89**, *228*
cystic fibrosis 811–12
  treatment of 280
cystic fibrosis transmembrane conductance regulator (CFTR) protein 59, 225, 811
cytochrome c oxidase 807
  models for 807, *808*
cytochrome P-450 enzymes 803
  catalytic reactivity cycle for 803, *804*
  features 805
  models for 803–7

Damascus steel 935–6
dansylamide, effect of carbonic anhydrase on fluorescence 737
dansylamidoethylcyclen 737
Darwinian evolution 820, 823, 901
  and self-replicating systems 823
data storage applications, molecular switches used 753–4
daughter crystals/phases 469, 500–1
Daumas–Hérold model 551, *552*, 553
Davy, Sir Humphry *5*, 195, 386, 388
Dawkins, Richard 825
Debye–Scherrer rings **474**
decamethylcucurbit[5]uril 324
decoration, meaning of term 561, 562
definitions, supramolecular chemistry 2–3
degeneracy parameter, in site binding model 612, 613
degree of order, liquid crystal phases 842, *843*
dendrimers 862–76
  characterisation of 868–9
  commercially available *864*
  cyclophane-based 350–2
  Fréchet-type dendrimers 867, *868*
  host–guest chemistry 869–72
  hydrogen-bonded mixtures with T-shaped amphiphiles 850
  iterative preparation of 862, *863*, 866
  light-harvesting assembly 721–2
  molecular imprinting in 870–2
  nomenclature 863–4
  physical properties 869
  rheological properties 863, **865–6**
  structure 862–3
  synthesis
    convergent approach 866–8
    divergent approach 862, *863*, 866, *867*
dendritic boxes 870
dendritic nanodevices 874–6
dendrons 863
dendrophanes 350–2, 872
density functional theory (DFT) calculations 504
denticity of ligands 107
deoxymyoglobin, structural model for 799, *800*
deoxyribonucleic acid (DNA) 86–99
  binding to 93–7
  calix[4]arene derivative binding to 319–20
  double helix 87
    base pairs in 32, 90–1
    self-assembly of 601–2, 678
    unwinding of 97–8, 593–4
  hydrogen bonding in 32
  knot-forming tendencies *692*, 696–7, *698*
  platinum binding to 93–5
derived crystal packing model 500–1
designer co-crystals 494–7
desolvation, enzymatic catalysis affected by 79
Dewar–Chatt–Duncanson bonding model **169**
Dexter electron-exchange mechanism 713, *714*, 874
dextrins 331
  *see also* cyclodextrins
diacetylene-containing isophthalic acid derivative, light-induced polymerisation of 917, *918*
dialkyne diol, channel structures formed by 402–3
1,2-diaminoethane chelate complex 18
2,6-diaminopyridine–uracil system 688–9, 839, 880
  mesogens formed from 848
diamond, properties 526–7
diamondoid networks 526–30, 541, 567
  with interpenetration 526, 527, 572–3
Dianin's compound *406*, 407
  cavity dimensions *407*
  clathrates 407–8, 430, 431, 507
  inclusion of morpholine by 409
  modifications *408*
  structure *407*
  thiol analogue 408
diarylureas, Etter's rules for hydrogen bonding 479, 481
diastereoisomerism, catenanes *655*
diatoms, structural mimics 902–3
1,11-diazabicyclo[9.9.9]nonacosane, chloride complex *225*
1,4-diazabicyclo[2.2.2]octane (DABCO), co-crystal with ferrocene dicarboxylic acid 471, *472*
diaza[18]crown-6
  in ion channel mimics 810
  K+ binding constants *25*, *120*, *143*
  in synthesis of cryptands 122–3
diaza[3.3]metacyclophane *341*
dibenzo[18]crown-6 114, 127
  properties 114–15
  in reaction of anions with benzyl derivatives *152*
  synthesis 114, *115*
dibenzo[24]crown-8 138, *140*
dibenzo[30]crown-10 138, *140*
  binding to Pt(II) complex 194
  and herbicide receptors 194, 195
  $K^+$ complex 138, 194
  selectivity of cation complexation 138, 139
1,2-dicarbadodecaborane(12) *see o*-carborane
$\alpha,\omega$-dicarboxylic acids, recognition by azacrowns 244
dicarboxylic acids, redox sensor for 354
dichroic filters 398
di-copper(I) model compound, dioxygen binding by 795

dicopper tetraacetate *575*, 585
  interaction with bipyridylpropane 577, *578*
dicyanamide complexes 569, *570*
dicyclohexano[18]crown-6 116, *152*, *299*
  isomers 116, *117*
dicyclohexano[18]crown-6/*N*,*N*'-diphenylthiourea dual-host system 299
*p*-didecylbenzene, in urea-based inclusion compound 395–6
dideoxykohnkene 326–7
Diels–Alder addition reaction
  in ionic liquids 854
  kohnkene synthesis *326*
  'softball' host-catalysed 643, *644*
  thiourea-catalysed 814
diethyl phosphoramidates, *N*-alkylation of 344
*trans*-1,4-diethynylcyclohexane-1,4-diol, conformers 491
differential scanning calorimetry (DSC) **560**
  liquid crystals studied by **844**
differential thermal analysis (DTA) **560–1**
diffusion ordered spectroscopy (DOSY - NMR technique) **188–9**
diffusion selectivity in zeolites 549
dihaloalkane derivatives 525–6
$\alpha,\omega$-dihaloperfluoroalkanes 525–6
dihydrogen bonds 516
dihydrogen phosphate anions
  electrochemical recognition of 743–4
  *see also* potassium dihydrogen phosphate (KDP)
1,4-dihydroquinoxaline-2,3-dione-based hosts 498
2,10-dihydroxynaphthalene *348*
  binding in cyclophane complex 348
dimeric capsules 294–5
4,4′-dimethoxyazoxybenzene, nematic liquid crystal phase *843*
1,2-dimethoxyethane, donor group orientation for 133
4-(*N*,*N*′-dimethylamino)benzoic acid, co-crystal with 4-nitrobenzoic acid 517
4-(4-dimethylaminophenylazo)-1-methylpyridinium $[MnCr(oxalate)_3]\cdot$ 0.6MeCn, powder X-ray diffraction pattern **476**
*N*,*N*′-dimethyl-4,4′-bipyridinium *see* paraquat
*N*,*N*-dimethylformamide (DMF), methyl exchange mechanism **188**
dip pen nanolithography (DPN) 911
diphenylglycoluril 323
diphenylmethane *311*, *348*
  as spacer in cyclophanes 246–7, 347–52
dipole–dipole interactions 28
  hydrogen bonds as 29
diquat 194–5, 656
directed self-assembly 596
'disappearing polymorphs' 488, 491–2
disclinations, in nematic liquid crystal phase 842
discotic liquid crystal phases 841, 845, *846*
discotic polymeric mesogens 893, *894*
discrimination 740
  inter-guest 26
dissociation constant 9
distamycin A, binding to DNA 97
1,2-dithienylethene switchable unit 752–3
ditopic ligands 639
ditopic receptors 184–5, 286, *287*, 292–5
  in sensors 732, 733
ditopic supramolecular coupling reagent 495–6
divergent binding sites (in host–guest chemistry) 3, 620
DNA *see* deoxyribonucleic acid
DNA clamp protein 98, 99
DNA helicase (enzyme) 98
DNA helicase RepA sulfate complex 228
DNA intercalators 95–6
DNA knots *692*, 696–7, *698*
DNA ligase 99
DNA polymerase 76, 92, 97–9
DNA primase 98, 99
DNA replication fork 98
1,12-dodecanedinitrile, silver(I) complexes 572–3
dodecyl phosphocholine (DPC) complex with [4]resorcarenes 318
donor group orientation, in cation-binding hosts 132–4
DOPA, resolution of 358
double-helicate complexes 682, 683
double helicates, chirality 680, *681*
double helices, DNA 60–2, 87, 678
double mutant cycles 615–16
double quantum filtering 430
double-shell complexes, halogen bonding in 526
drug delivery
  cyclodextrins used 336, 493
  dendrimer host–guest compounds used 872
  supramolecular gels used 891
dual-host salt extraction 298–9
durene (1,2,4,5-tetramethylbenzene) 347, *348*
  binding in cyclophane complex 347, *348*
dye displacement assay *see* indicator displacement assay
dyeing of crystal interfaces 462–4
dynamic combinatorial chemistry 817–19
  casting-of-substrate approach 818
  moulding-of-receptor approach 818
dynamical effects, in enzymatic catalysis 78

edge-to-face $\pi$–$\pi$ interactions 34, 310, 519
  assessment of strength 616, *617*
effective molarity, self-assembly of coordination complexes 608, 609, 611
egg-shaped carcerand 375, *376*
Ehrlich, Paul *5*, 7, 8, 805
elastic materials **865**
electric-field-induced second harmonic generation (EFISH) experiment 768
electrides 114, 195–7, 930
electrochemical sensors 742–6, 838
electron-exchange mechanism 713, *714*
electron transfer, photoinduced *714*, 720, 724, 726
electronic design, supermolecules as basis 593

'electronic nose' 742
'electronic tongue' 277, 742
electronics, molecule-based 746–62
electrophoretic mobility shift assay 319
electrophotoswitchable systems 754
electrostatic interactions 310
electroswitchable systems 753
1,6-elimination reactions, cyclophanes synthesised by 342, *343*
emergence of life 823–5
  timescale *824*
emergence of self-organised system 43, 595
emergent structures 43
emulsions 922
enantioenterobactin 214
enantiomer-resolving machine 190–1
enantiotropic polymorphism 489
endo-acidic cyclophanes 356–7
endohedral metallofullerenes 929–30
endo-templated synthesis 156
energy level diagrams, photoinduced electron transfer *720*
energy transfer, after photoexcitation 711, 722, *723*
energy-transfer mechanisms 713–15
'engineering down' approach 593, 901, 907
enniatins 57
entanglement structures *see* Borromean rings; knots; ravels
entatic state 73, 75
enterobactin *213*, 214–15
enthalpic hydrophobic effect 38
entropic contribution to anion binding 233–4
entropic hydrophobic effect 38
entropy-driven encapsulation mechanism 643
enzymatic catalysis, mechanisms 77–9
enzyme active sites 75
  cascade receptors as models 289
enzyme mimics
  calixarenes as **200**
  cyclodextrins as 780–5
enzyme–substrate binding 7–8
enzymes 74–83
  characteristics 74–6
  nomenclature 76
  structures 75–6
epitaxial growth of crystals 467–8
equilibrium constants 9
  self-assembly of coordination complexes 607–8
  successive addition of ligands 10–11, 20–1
  *see also* binding constants
Ercolani's site binding model 611–14
*Escherichia coli*, enterobactin 214, 215
esterase mimics, cyclodextrins as 782, *783*
etching (in microfabrication) 907
ethanol, acetaldehyde produced from 797
ethanolammonium nitrate (ionic liquid) 852
ethyl chlorophyllide 65, *66*
ethylenediamine, donor group orientation for 133
ethylenediamine palladium(II) moiety 617, 619
  *see also* $Pd(en)^{2+}$
ethylenediaminetetraacetate ($EDTA^{4-}$) 112–13
  siderophores compared with 214, *216*
2-ethylyladamantan-2-ol 517, *518*
Etter's rules 478–81
  carboxylic acid co-crystals with 2-aminopyrimidine 480
  diarylureas 479, 481
  nitroanilines 479
  nucleotide base co-crystals 480
Euler, Leonhard 539, 540
Euler's Law **425**
europium complexes, in biological cell imaging 735, *736*
europium cryptates, in light-conversion devices 725
europium triple helicate complex, self-assembly of 614–15
eutrophication 224–5
excimers 711, *712*
exciplexes 711, *712*
excitation transfer 713, *714*
excitons 925
exfoliated graphite 553–4
expanded porphyrins 244–5, 304
extended site binding model 610, 613–15
extraction experiments 16–17
Eyring equation **187**

face-to-face charge-transfer $\pi$-stacking 357, 522
face-to-face $\pi$–$\pi$ interactions 34, 310, 519, 520–2
faujasite (FAU) zeolites *544*, *545*, 546, 550
ferredoxin, iron–sulfur anions in 231
ferritin 100–1
ferrocene 32
  $\alpha$-cyclodextrin complex *335*
  DOSY spectrum **189**
  polymorphic forms 521
ferrocene-based electrochemical sensors 743–4
ferrocene-derived anion receptors 259, *260*, *303*, 304
ferrocene dicarboxylic acid, co-crystal with 1,4-diazabicyclo [2.2.2]octane 471, *472*
ferroelastic materials 397–8
ferroelectric liquid crystals 852
ferromagnetism 569
fibrinopeptide 887
figure-of-eight DNA knot *698*
first-generation dendrimers 862, *863*
Fischer, Emil *5*, 7
flexible hosts, guest exchange dynamics 321–2
fluid mosaic model (of cell membrane) 836
fluorescence 710, *711*
fluorescence titration 13–14
fluorochlorobromomethane, separation of enantiomers 363
foam 922
foldamers 599–600
food industry applications, cyclodextrins 335–6
force-field methods for crystal structure calculation 504
formula units 498
  *see also* high-$Z'$ structures

Förster resonance energy transfer (FRET) mechanism 713, *714*
  applications 729–30
Franck–Condon principle *711*
Franklin, Benjamin 831
Fréchet-type dendrimers 867, *868*
free energy changes, in course of chemical reaction **636**
Fuller, Richard Buckminister **425**
fullerenes 927–35
  amphiphilic dendrimers based on 874
  applications 929
  in calixarene inclusion complexes 314, 423–4
  discovery of 423, **424–5**
  as guests 314, 359, 407, 423–4
  as hosts 423, 928–31
  in hydroquinone clathrates 407
  inclusion compounds 929–31
  intercalates 931
  molecular surgery approach to guest-encapsulation 930–1
  organometallic complexes 928
  purification/separation of 423
  self-assembly and 595
  in solid-state CTV inclusion complexes 359
  synthesis 932
  *see also* buckminsterfullerene
fused-ring aromatic hydrocarbons (FAHs), structures 520–1

G-quartet (guanosine tetramer) motif 295, *296*, 848, *849*
gadolinium(III) ions, dendrimers as carriers 876
$\gamma$-aminobutyric acid (GABA) *303*, 304
gas sorption 429–32
  by calixarenes 431–4
  by channel hosts 434–5
  by coordination complexes 435–7
gas sorption isotherm 430, *431*
gate functions (in pump storage model), 52
*gauche* conformation *130*
*gauche* interactions
  [4]resorcarenes 319
  *see also* attractive *gauche* effect; repulsive *gauche* effect
gelatin 890
gels 888–93
  characteristic properties 888
  meaning of term 888, 922
genetic code *88*
  transformation from DNA to ribosome 90
genetic engineering 91–2
genetic information, as imperfections in minerals 469–70
giant self-assembling capsules 646–51
Gibbs equation 11
gigaohm seal 811
glass transition temperature 471n
global warming 392
glucose sensors 888
glutamate **90**
glutamate dehydrogenase **89**
glutamic acid **89**
glutamine **89**
glycine **89**, *228*, *457*
  polymorphs 492
$\alpha$-glycine
  crystal growth at air–liquid interfaces 456–8
  graph set assignments 477–8
glycoluril *311*, 323
glycoluril-based hosts 323–5, 641, 642, 728
glycoside cluster effect 319
glyoxalases, cyclodextrin derivatives as mimics 784
gold nanoparticles 44, 922–5
  preparation of 922–3
gold(I) phosphine macrocycles, self-assembly of 302
gold–thiolate monolayers 837
Gouy–Chapman layer 835
gramicidins 688, *689*, 809
graph set analysis 476–8
graph set descriptor(s) 477
  dimer synthons *506*
  illustrative examples *477*
graphene 935
graphite 34, 520, 551–2
graphite foams 554
graphite foils 554
graphite intercalcates 552, 553–4
'green' hydrogen fuel cells 429, 584
'green' solvents 853
greenhouse gases 392
grid structures 566, *637*, 638–9
grinding-induced crystal engineering 470–3, 577
Grubbs' catalyst 658, 872, 917, *919*
guanidine group in arginine, hydrogen bonding involving 229
guanidinium-based receptors 248–51, 303–4
  chiral derivatives 249
guanidinium sulfonates 554–6
guanidinocarbonyl pyrroles 251
guanine–cytosine interactions (in DNA) 91
guest, definition 3, 232, 620
guest-determining step (GDS), in carcerand synthesis 373
guest discrimination 26
guest exchange dynamics
  cavitates 320–2, 325
  NMR spectroscopy **187–8**

Haeckel, Ernst 902
haem analogues 798–807
haem complexes 62, 70
haemocyanin(s) 289, 793
  dioxygen binding by 289, *290*, 793
  models 289, 793–5
  structure of active site 793–4
haemoglobin
  oxygen saturation curves *74*
  structure 70, 598, 802, *803*
  uptake and transport of oxygen by 70–4, 798
halide coordination geometries, in anion hosts 236

haloalkanes
encapsulation by cryptophanes 361–3, *365*, 366
encapsulation by 'tennis ball' hosts 642
halogen bonding 36, *37*, *446*, 524–6
in metallomesogens 848–9
halogens, hydrogen bonds to 510–11
hapten, meaning of term 779n
hard ions and ligands 109, 110
hard and soft acids and bases (HSAB) principle 109–10
helical bimetallic complexes 301
helical foldamer *690*, 691
helical structures 565
helical tubuland hosts 401–2, 525
helicates 678–91
cyclic 686, *687*
[4 + 4]helicates 682–3
[6 + 6]helicates 683–4
positive cooperativity in formation 685, *686*
self-recognition in 684–5
synthetic considerations 681–2
helices
anion-based 687
double helices of DNA 60–2, 87, 678
hydrogen-bonded 687–91
hemicarcerands 370
coordination capsules 634–5
inclusion reactions 376–9
self-assembly of 647, 648
synthesis *372*
*see also* cryptophanes
hemicryptophanes 367–8, *369*
CD spectra *369*
synthesis *368*
hemispherands 126, *127*
binding free energies for alkali-metal picrates *146*
binding of $NH_4^+$ by 183
*t*-butylammonium complex 148, 790
heptafoil knots 696
heptapeptides, in ion channel model 811, *812*
herbicide receptors 194–5
Herman–Maugin notation **461**
herringbone packing motif 34, 520, *521*
heterodimeric capsules 646
heterogeneous dilution 344
*see also* high-dilution synthesis
heteronuclei, crystal nucleation affected by 492
heterosynthons 496–7
hexacyanoferrate(II) anion, in complexes with azacorands 241–2, *243*
hexacyclen 128, 240–1
hexa(*p*-*n*-dodecyloxybenzoyal)hexacyclen 845
hexagonal array of sixfold phenyl embraces (HA6PE) 530
hexagonal structures 835
liquid crystal phases 846
M41S zeolites *547*
hexahedron, self-assembly of 629–30
hexahost strategy 409, *410*, 483, 507
hexameric carcerand 379–80
hexametallic cage, self-assembly of 617–19, *618*
hexamethyl(Dewar)benzene **466**
*O*-hexyl-*p*-*t*-butylcalix[4]arene, $NO^+$ complex 314
hierarchial self-assembly 598, 825, 900
high-dilution synthesis methods 122, 157–9, 344, 673
high-resolution scanning tunnelling microscopy (HRSTM), application 917–18, *919*
high-$Z'$ structures 498–500
highly ordered pyrolytic graphite (HOPG) **911**
Hill coefficient/equation/plot 21, *22*, 610
histidine **89**
Hoffman's benzene clathrate 556, *557*
Hoffman-type inclusion compounds 556, 857
Hofmeister series 226–7, 239
holoenzymes 80
homeomorphic structures 654
homooxocalixarenes 203–4
honeycomb self-assembled network 915, *916*
fullerene $C_{60}$ heptamers assembled in 915, *916*
Hoogstein base pairing 91, *92*
hormones 83, 85
host, definition 3, 232, 233, 620
host design 41–2
anion hosts 232–5
host–guest chemistry 3–4
host–guest compounds, classification 6, *7*
host–guest interactions, cyclodextrin inclusion complexes 332–3
host–guest relationship, definition 3
'host within a host' 646
hourglass inclusions 464–5
Hückel rule 62
Human Genome (HUGO) project 92
human immunodeficiency virus 1 (HIV-1) protease 101
hydraphile family of ion channel mimics 809–10
hydrate growth inhibitors 391, 455
hydrated proton *see* oxonium ion
hydrates
in co-crystals 497–8
*see also* clathrate hydrates
hydride sponge 268, *269*
hydrocarbon catenanes, synthesis 669, *670*, 672, *673*
hydrocarbon hosts 211–13
hydrogels 888
hydrogen bond synthons 505–19
hydrogen-bonded catenanes 666–7
hydrogen-bonded rings, as supramolecular synthons 505–9
hydrogen-bonded rotaxanes 667–9
hydrogen-bonded supramolecular synthons 445, 505–19
hydrogen bonding 28–32, 310
acidity and basicity 30, 452–3
bond energies 29, 447
C—H donor hydrogen bonds 517–19
to carbon monoxide ligands 512–14
categories 29–30
conic correction factor 29, 451

to cyanometallates 511–12
as dipole–dipole interaction 29
geometries 30, *31*
guest inclusion in cyclophanes 353–7
to halogens 510–11
to metal hydrides 515–16
in metallomesogens 848, 850
to metals 514–15
moderate/medium-strength hydrogen bonds *30*, 450–1
in organometallic chemistry 514–16
properties *30*
self-assembly of closed complexes by 641–52
special role in supramolecular chemistry 29, 447–51, 505
strong hydrogen bonds *30*, 449–50
as templating factor 606, 821, 890
water molecules in clathrate hydrates *389*
weak hydrogen bonds *30*, 451
hydrogen bridge 447
hydrogen production 429, 430
hydrogen storage applications 392, 407, 430, 583–6
hydrophobic effect 38–9, 308, 309, 332, 349
contributions 38, 309, 332, 519
hydroquinone
clathrates 406–7
solid-state forms 406
hydrotris(3,5-diisopropylpyrazolyl)borate-based model 794
$\omega$-hydroxy acids, conversion into lactones 342, *343*
hyperpolarisability 767
hypervalent compounds 268

ibuprofen 816, *817*
ice
diamondoid network *527*
properties 388, 527
*see also* water
imidazole-functionalised amidopyrrole 258
imidazoline and derivatives, in haem analogues 799, *801*
imidazoline-derived metallomacrocycles 436
imidazoline receptor 277
imidazolium ionic liquids 852, 853–4
inclusion chemistry 4
calixarenes 419–29
cyclodextrin complexes 331–5
cyclotriveratrylene clathrates 416–17
factors affecting 332
hemicarcerands 376–9
inclusion compounds
methods to study **559–61**
solid-state 385–440
urea clathrates 398
incommensurate symmetry interactions 597
indicator displacement assay (IDA) 112, 739
applications 250–1, 277, 740–1
indigo, efffect on crystal growth 463–4
induced circular dichroism (ICD) effects 192
induced dipolar interactions 310
induced fit model
enzyme–substrate binding *8*, 9, 779
examples 78, 230, 247, 626
induced polarisation, as function of time 766
inert complexes, meaning of term **636**
inert metal-containing receptors 259–76
general considerations 259–60
inert metal ion, definition 286
innate curvature of cavitands 310–11, 648
insulin, biosynthesis of 602–3, *604*
intercalates 551–2
applications 552, 553
fullerene intercalates 931
graphite intercalates 552, 553–4
intercalators, binding to DNA 95–6
interdigitated cavities 409
intermolecular multicentre hetero-acceptor (IMH) hydrogen bonds *514*, 515
intermolecular pseudo-agostic (IPA) bonding interactions *514*, 515
International Union of Pure and Applied Chemistry (IUPAC) nomenclature
coordination/inorganic chemistry 108–9
cyclophanes 341–2
zeolites 543
interpenetrated structures 539, 562
coordination polymers 571–4
diamondoid networks 526, 527
metal-organic frameworks 580–1, 582
inter-ribbon puckering angle 555
intersystem crossing after photoexcitation 710, *711*
intramolecular reactions, compared with bimolecular reactions 78, *79*
intrinsically curved molecular building blocks 310–11, 648
inverse crown compounds 275–6
inverse opals 905, 906
inverted cucurbit[n]urils 324, *325*
4-iodo-4′-nitrobiphenyl 445, 446, 484
ion channel conductance, measurement of 811
ion-channel proteins, mimics 809–13, 845
ion channels 53, *54*
ion–dipole interactions 27–8, 107
ion-dots 918
ion–ion interactions 27
ion pair receptors 285–306
types 286, *287*
cascade complexes 286, *287*, 289–91
ditopic receptors 286, *287*, 292–5
zwitterion receptors 286, *287*, 303–4
ion pairs, types 286
ion-selective electrodes 208, 273
ion-selective field-effect transistors (ISFETs) 745, *746*
ion transport across cell membranes 53–60, 809
ionic liquids (ILs) 852–4
characteristics 853
research publications *853*
ionic radii, listed for various anions and cations **160**, *226*
ionic strength, meaning of term 177n

ionophores 53, *54*, 57, 207–8, 809
  binding constants *57*
iridescent colours *905*, 906
iridium(III)-based antenna array 723–4
iridium(III) dihydride, bonding in 516
IRMOF-6 579–80
iron, biochemical role 213
'iron maidens' 180, 345–6
iron(III) porphyrin compound 806
iron(IV) tetramethylcyclam oxo complex 806–7
irreversible self-assembly 596
2-(4-isobutyryl-phenyl)-propionic acid 817
isochratic (chromatographic) technique 257n
isocyanato surfactant *804*, 805
isocyanide-based polymers 878
isoleucine **89**
isomeric constellations *645*, 646
isomorphous crystals 467n
isophthalamide, effect of attaching $Cr(CO)_3$ groups 263
isophthalic acid hydrogen bonding interactions, dendrimer assembly by 872
*p*-isopropylcalix[4]arene 312–13
isoreticular expansion 561
isoreticular metal-organic frameworks (IRMOFs) 561, 562, 579–80
isosbestic point 15
isoskeletal structures 402
IsoStar scatterplots 485
isostructural crystals 467n
isothermal titration calorimetry (ITC) 15, *16*, 233
isotopic structures 654
IUPAC *see* International Union of Pure and Applied Chemistry

'jam'/'jelly' doughnut molecule 644, *645*
jasmine oil 86
Job plots 12–13, *14*
Johnson solid 648
junk DNA 99

Kagan's ether, molecular tweezers containing 339
katapinands 224, *225*
  as anion hosts 233
  conformational change on anion binding 233
Kemp's triacid *311*, *338*
  molecular clips derived from 338–9
Kemp's triacid derivative, in self-replicating system 821, *822*
kinesin 763
kinetic effects, chelate effect and 18
kinetic selectivity 26, 227
kinetic stability, coordination complexes **636**
kinetic template effect 121, 155–6, 604, 626
kinetic template synthesis approach 155, 604, 626, 672
knots
  DNA knots *692*, 696–7, *698*
  molecular knots 596, 692–700
    as topological isomers 692
    prime knots *692*
    topology 691–2
kohnkene 326–7
  X-ray structure *327*
Kohnkene precursor *311*, *326*
koilands 313
koilates 313
Kondo resonance 761
Koopman's theorem 717
Kroto, Harold W. 423, **424**, **425**
Kryptofix® products 122, *146*, 147

labile complexes, meaning of term **636**
labile coordination compounds, as anion hosts 260, 299–303
$\beta$-lactamase 892
  functional model for 797
lactase 76
ladder structures 494, 565, 637, *638*, 639
ladderanes *473*, 474
lamellar liquid crystal phases 846
Langmuir–Blodgett technique 831, 833–4
Langmuir isotherm 833
Langmuir monolayer films 831, 833
  nonlinear optical materials in 768, *769*
Langmuir trough 832–3
lantern structures *575*, 577, *579*
lanthanide-based networks 567
lanthanide cations
  binding of 108
  dendrimers as ligands for 872, *873*
lanthanide(III) complexes
  in logic gates 758–9
  in sensors 734–5
lanthanide cryptates, in light-conversion devices 725–6
lanthanide helicates 614–15
lanthanides/lanthanoids *see* europium; gadolinium; terbium
lanthanum complexes of fullerenes 929
lariat ethers 120–1, *128*
  ammonium binding to 141, *142*
  bibracchial lariat ethers 121, *128*, 141–2
  binding constants for alkali metal complexes *25*, *120*, *140–1*
  binding free energies for alkali-metal picrates *146*
  cation binding by 140–2
  cation–$\pi$ interactions 209–10
lateral discrimination 182, *183*
lateral pressure (monolayer films) 833
lattice energy minimisation procedures 502–3
layer-type cyclodextrin complexes *334*
layered solids
  characteristics 550–3
  classes *551*
  controlling 554–6
Le Chatelier's Principle 605
Leden–Chatt triangle 110
Lehn, Jean-Marie 2, 4, *5*, 122, 594
leucine **89**

Lewis acid chelates 268–71
Lewis bases 107, 235
librational shortening of covalent bonds 449
life
  definitions 820, 823
  emergence of 823–5
ligand bite angle 137
ligand-exchange reactions **636–7**
ligand field activation energy (LFAE) **637**
ligand field stabilisation energy (LFSE) **636**
ligands 107
ligase ribozymes, in self-replicating system 823, 824
light-conversion devices 725–6
light-harvesting antenna arrays and pigments 63, *65*, 721, 723–4
light-harvesting devices 718–24
light-harvesting pigments 61, 63, *65*
light-powered molecular shuttle 763, *764*
Linde type A (LTA) zeolites *544*, *545*, 546
linear dichroism (LD) spectroscopy 747 & n
linear molecular recognition 184–5
lipid bilayers 825, 836
lipid-world theory 825
lipids, self-assembly into complex structures 825, 834
liposomes 811
liquid aerosol 922
liquid clathrates 854–8
  A/A number 855
    factors affecting 856
  advantages over solid-state separations 857
  key properties 854
  solution-behaviour model 855–6
  term first coined 854
liquid crystal displays (LCDs) 830, 851–2
liquid crystalline materials, design of 846–8
liquid crystals 839–52
  applications 851–2
  polymeric 893–4
  supramolecular 848–51
liquid ordering 830–1
lithium greases 891
lithography 901, 907
  *see also* soft lithography
living system, definition 823
localised molecular orbital approximation 712
lock-and-key interactions
  enzyme–substrate binding 7–8, 778
  in ferritin molecule 101
  modifications 8–9
logic gates 756, 758
London dispersion forces 35
low-molecular-weight gelators (LMWGs) 889, 890
  properties 891
lucigenin (dye), quenching of fluorescence *280*, 281
luminescence 710
  *see also* fluorescence; phosphorescence
Lycurgus cup (Roman chalice) 922
lyotropic liquid crystal phases 835, 841, 846
lyotropic series 226–7
lysine **89**

$\mu$–$\eta^2$:$\eta^2$ bridging mode of peroxide ligand 794
machine(s)
  definition 708
  molecular analogues 762–5
MacKinnon, Roderick *5*, 58, 227
macrobicycles
  contact ion pair receptors 287–8
  tin-containing 274–5
  *see also* cryptands; katapinands
macrobicyclic amides 255
macrobicyclic effect 23
  chelate effect and *24*
macrocyclic amides 254
macrocyclic effect 22, 135
  chelate effect and *24*
macroporous materials 430
macrotricycles 41
Maddox, J., on crystal structure prediction 500
magnesium tetrapyrrole macrocycles, in photosynthesis 61, 63–7
magnetic resonance imaging (MRI) 876
magnetic spin crossover 569–70
magnetic tweezers 913
magnetism, coordination polymers 568–70
manganese, suitability as oxidation catalyst 69–70
manganese catalase enzyme 290
manganese-catalysed oxidation of water to oxygen 68–70
manganese cubane 527, 528
Mannich reaction 294
Markov growth model 405
mass spectrometry
  catenands 675
  catenanes 669, 671
Maxwell's Demon 764
MCM zeolites 545, 547
MECAM 215
mechanical machines, molecular analogues 762–5
mechanochemistry 460, 470–3, 577
melamine·cyanuric acid derivatives 651–2, *653*
  rosette motifs 651, *652*
  tape motifs 651, *652*
melamine·tetracarboxylic acid diimide network 915, *916*
membrane ionophores, in CHEMFETs 745–6
membrane potentials 50–3
membrane transport 53–60
menaquinone 66, *67*, *81*
[9]mercuracarborand-3 273
[12]mercuracarborand-4 273
  chloride inclusion within 273, *274*
mercury crown compounds 272–3
mesogenic polymers 893, *894*
mesogens 839

mesomorphic behaviour 839
*see also* liquid crystalline behaviour
mesophases, characterisation of **843–4**
mesoporous materials 430, 545, 547
mesoporous silica structures, templating of 903–4
[mesotetrakis(sulfonatomesityl)porphyrinato]iron(III) 806
metacyclophanes
*in*-[$3^{4,10}$][7]metacyclophane 180, 345
[1.1.1]metacyclophanes, substituted *see* calixarenes
metal–acetylide polymers 749
metal-atom ligand-vapour synthesis 213
metal-backbone catenanes 625–6
metal extraction processes 297–8
metal hydrides, hydrogen bonds to 515–16
metal-ion-templated synthesis 604
catenanes 672-6
metal-organic frameworks (MOFs) 538, 561, 562, 578–83
catalysis by 583
hydrogen storage by 583–6
MOF-5 579, 585, 586
MOF-9 580–1
MOF-177 584, *585*
pyrazene-based 582
*see also* isorecticular metal-organic frameworks
metal–$\pi$ interactions 523–4
metal salt symport 297–8
metal-to-ligand charge transfer (MLCT) *712*, 713
metallobiosites 792–8
metallocene derivatives
in electrochemical sensors 742–4
nonlinear optical properties 770
*see also* cobaltocinium; ferrocene
metallogels 888
metallohemicarcerands 634–5
metallomesogens 848
metallophilic interactions 36, 37, 525
metalloporphyrin $O_2$ complexes 799–800
metalloproteins 70–4, 792
metallotropic materials 850
metals, hydrogen bonds to 514–15
metastable polymorphs 488, 491–2
methane
absorption by IRMOF-6 579–80
encapsulation by ‘tennis ball’ hosts 642
environmental impacts 392
steam reforming reaction 429, 430
methane hydrate 392
methionine **89**
methyl jasmonate 86
*p*-methylcalix[4]arene, synthesis **199**
methylene blue (dye) 8, 805
methylmalonyl-CoA mutase *83*
model for 808
5-methyl-2-[(nitrophenyl)amino]-3-thiophenecarbonitrile 488
micelles 834–5
self-replication of 825
Michael addition 293, *294*
Michaelis constant 77
Michaelis–Menten model 77
exceptions 78
microcontact moulding, solvent-assisted 911
microcontact printing 910
microfabrication 907–9
micromoulding in capillaries 910
microporous materials 430
microscale machines 708
microtransfer moulding 910
Miller indices 456
minimal self-replicating model 820
examples 820, 821
factors affecting success 821
MIP sensor arrays 879–80
Mitsonobu reaction 342, *343*
mixed C–heteroatom hosts 209–11
mixed cryptates 168
mixed-valence devices 715–16
$Mn_{12}$-acetate 562, *563*
models 778, 779
*see also* biological models; corroborative models; functional models; speculative models; structural models
MOFs *see* metal-organic frameworks
molecular baskets 323
molecular beam epitaxy (MBE) technique 921
molecular biology 50
molecular chaperones 596, 598
molecular chemistry, compared with supramolecular chemistry 2
molecular clips 323, 338–9
molecular containers 617–19, 620–35
molecular devices and machines 707–75
principles 708
molecular electronics 746, 892
molecular elevator 762–3
molecular ‘extension cable’ 729
molecular graph 654
molecular guests, in solution 307–84
molecular imprinted polymers (MIPs) 879–80
molecular imprinting in dendrimers 870–2
molecular ‘iron maidens’ 180, 345–6
molecular knots 596, 691–700
molecular lock method, platinum catenane synthesis by 626
molecular logic 756–60
molecular loops 635
molecular machines 762–5
molecular memory devices 760–1
molecular motors 763, 886, *887*
molecular ‘muscles’ 762
molecular necklaces 325, 677–8
molecular orbital (MO) diagram, octahedral transition metal complex *712*
molecular panelling 617–18, 629–33

molecular ratchets 764–5
molecular reaction vessels
  hemicarcerands as 376–7
  'softball' and 'tennis ball' hosts as 643–4
molecular recognition between host and guest 8, 709
molecular recognition strategy (in catalysis) 815, *816*
  example of application 816, *817*
  potential problems 815–16, *817*
molecular rectifiers 750–2
molecular rosettes 651–2
molecular scaffolding 624–9
molecular self-assembly, compared with supramolecular self-assembly 594
molecular sensors
  basis 730
  construction criteria 731
molecular sieves, zeolites as 545
molecular squares and boxes 624–35
  coordination capsules 634–5
  molecular panelling approach 629–33
  molecular scaffolding approach 619, *619*, 624–9
molecular surgery approach to guest-encapsulation in fullerenes 930–1
molecular switch tunnel junction (MSTJ) 760
molecular switches 752–6
molecular symmetry operations **460**
molecular 'syringe' 208
molecular transistor 761
molecular tweezers 336–8, 339–40
  chiral 339–40
  progression to cyclophanes 346–7
molecular wires 713, 746–9, *750*, 892
molecular zippers 616, *617*
molybdenum blues 563
molybdenum carbide complex, formation using macrocycles 152–3
monodisperse latex spheres 906
monolayers, formation of 832, 833
monotropic polymorphism 489
montmorillonite *551*
montmorillonite clay particles, condensation of nucleotides catalysed by 469, 824
$Mo(O)Cl_2(PMe_2Ph)_3$ **466**
Moore's law 901 & n
morpholine *48*
  inclusion by Dianin's compound 409
morphosynthesis 902–5
motif 477
Mukaiyama-aldol reaction 583
Mülliken correlation 33
Mullis, Kary B. 91, 594
multi-component molecular crystals 493
  *see also* co-crystals
multimediated multiple interaction self-assembly 597
multiple interaction self-assembly 597
multistorey self-assembled structures 639, *640*
multi-walled carbon nanotubes (MWCNTs) 933, 936
murexide indicator 112, 739
muscle contraction 886
muscle mimics 762–3
mycobactin 213, 214
myoglobin, oxygen saturation curve *74*
myosin 763, 886, *887*

NaCl lattice *27*, 233
$Na^+/K^+$-ATPase enzyme 50, 51, 76, 785
  crystal structure 59–60
  *see also* ATPase
'naked anion' effect 150–1, 286
  example 152–3
NAND gate, molecular logic 758–9
nanobelts 927
nanobiology 901–2
nanochemistry 44–5, 899–938
nanoclusters 922
nanocomposites 904–5
nanocrystals 44, 922
  *see also* quantum dots
nanofabrication 909–11
nanomaterials 44
nanoparticle-based sensors 924–5
nanoparticles 44, 921–7
  definition 921–2
  gold nanoparticles 44, 922–5
  non-spherical nanoparticles 927
nanorings 927
nanorods 927
nanoscale containers 909, 915, *916*
nanoscale machines 708
nanoscale photonics 905-6
nanoscience, meaning of term 900
nanoscratching 472–3
nanosphere templated materials 906
'nanostar' dendrimer 874, *875*
nanotechnology 44, 900–2
  bottom-up/synthesising up approach 593, 901, 909
  top-down/engineering-down approach 593, 901, 907
nanotubes 553, 881–3, 927
  *see also* carbon nanotubes; peptide nanotubes
napalm 891
naphthalene, crystal structure calculation for 503–4
naphthalene-2-sulfonate, binding in diphenylene-based host **352**
natural gas hydrates 392
NbO framework 541, *567*
negative cooperativity 17, 610
negative thermal expansion (NTE), coordination polymers 570–1
nematic liquid crystal phase *840*, 841–2
  degree of order 842, *843*
  in LCD applications 851–2
nerve cells, signal transduction in *52*
nerve gas agents, colorimetric detection of 738
nesting complexes 148, 183

nests 230–1
netropsin, binding to DNA 97
network solids 537–89
  classification 538–9
  concepts 538
network topology 539–41
  (6,3) net 540
  (10,3)-a nets 541, *542*
  notation 540–1
neurodegenerative diseases 885
neurotransmitters 83–4
neutral anion receptors 251–9
neutron diffraction 175, **448**
nicotinamide adenine dinucleotide 797
  reduced form (NADH) 80, 803
nicotine 84
nicotinic acetylcholine receptor protein 84–5
nitro/iodo supramolecular sython 445, *446*
nitroanilines, Etter's rules for hydrogen bonding 479
nitrocefin, hydrolysis of 797
nitrogen analogues
  crown ethers *25*, *120*, *143*, 160–2
  cryptands 163–4
nitrogen dioxide, calixarene binding 314
NMR spectroscopy *see* nuclear magnetic resonance (NMR) spectroscopy
noble metal nanoparticles 923
  *see also* gold nanoparticles
nomenclature
  cation-binding macrocycles 127–9
  coordination complexes 108–9
  enzymes 76
nonactin 53, 57
  binding to DNA 97
non-covalent anion coordination chemistry 224
non-covalent interactions 27–37, 445–6
nonlinear optical (NLO) effects 765
  origins 765–8
nonlinear optical (NLO) materials 765–71
  crystal engineering 445, *446*, 526, 765
  data for metallocene derivatives *770*
  second-order 768–71
  third harmonic generation materials 771
non-spherical nanoparticles 927
non-vitamin coenzymes *81*
NOT gate 758
nuclear fuel industry applications 225, 292, 297, 299
nuclear magnetic resonance (NMR) spectroscopy **186–9**
  aromatic ring current effects **186**
  azacyclophanes 179
  chiral shift agents 681
  complexation-induced shifts (CIS) **352**
  crystal nucleation analysed by 455–6
  guest exchange dynamics **187–8**
  solution structures analysed by **352–3**
  spin–spin coupling **187**
nuclear magnetic resonance (NMR) titration 12, *13*, **186**
  examples 252
nuclear Overhauser enhancement (NOE) effects **186–7, 352**
  calix[4]arenes 201–2
nucleobases 87, *88*
  hydrogen bonding interactions between 90–1
nucleotide base co-crystals, Etter's rules for hydrogen bonding 480
nucleotides 87, *88*

octahedral iridium(III) compounds, energy-transfer processes in 723–4
octahedron, self-assembly of 630–2, *631*
octaphyrin, diprotonated, $SO_4^+$ binding by *245*, 246
octaporphyrin nanocyle 632, *634*
octazacryptand *238*, 247
'office block' structures 639
oil and gas industry
  hydrate-formation problems and ways of addressing 391–2
  *see also* petroleum industry
Okazaki fragments *98*, 99
olympiadane 665
one-dimensional chains/ladders/strands *529*, 538, *539*, 565
opal 905–6
optical isomerism 110–12
optical lithography 907–9
  photochemistry 908
optical tweezers, nanomanipulation using 913, *914*
OR gate, molecular logic 759
order in liquids 830–1
organic cations, complexation of 180–95
organic zeolites 434–5, 528–30, 558, 575
organocatalysis 814
organogels 888
organometallic materials, nonlinear optical properties 770
organometallic receptors 261–6
Ostwald's step rule 488
oxidation states 107
oxonium ion crown ether complexes 174–6
oxygen-evolving complex (OEC) 68
oxygen uptake and transport
  by haemoglobin 70–4, 798
  by mimics/models 798–803
oxyhaemocyanin, X-ray crystal structure 794

$\pi$-acid ligands, complexes stabilised by **169**, 208–13
$\pi$–$\pi$ interactions 33–5, 310, 519–22
  edge-to-face interactions 34, 310, 519, 616, *617*
  face-to-face interactions 34, 310, 519, 520–2
  in molecular tweezers 337
  in photochemical devices 728
  synthesis of catenanes involving 660–6
  synthesis of pseudorotaxanes involving 656–7
  synthesis of rotaxanes involving 657–60
P-loop 231
$^{31}$P NMR spectroscopy, ATP hydrolysis by azacorand *786*
'paddle' structures *575*, 577, *579*

paracetamol, crystallisation of 453–4
paracyclophanes
[2.2]paracyclophane 211, *212*
$Cr^+$ complex 213
[3.3]paracyclophane 211, *212*
$Cr^+$ complex *212*, 213
[2.2.2]paracyclophane 211, *212*
paraquat 194, 195, 656, 657
charge-transfer complexes 195, 357
Pauling, Linus, on enzymes 78
Pauling model (for binding of oxygen to haemoglobin) 71, *72,* 78
$Pd(en)^{2+}$ moiety 617, 619
in molecular panels 632, *633*
in molecular squares *619*, 625, 626
peak selectivity (of cryptands) 142–3
Pedersen, Charles *5*, 114, 195, 224
pencillin-resistant bacteria, sensor for 892–3
pentaethyleneglycoldimethylether *25*
pentafoil knots 696
pentagon-based topology 566
peptide-based anion receptors 258–9
peptide links **88–9**
peptide nanotubes 881
perching complexes 148, 181
perching geometry 241, 257, 273
perhydrotriphenylene (PHTP) inclusion compounds 403–6
3-periodic network topologies 541
peripheral crowding, rosette formation by 651, *652*
pernicious anaemia, treatment of 82
persistence length (of polymers) 878
pertechnetate anion, binding of 292
perylenyl chromphore 729, *730*, 874
petroleum industry
separation of hydrocarbons 394–5
zeolites in 548–50
*see also* oil and gas industry
pH-activated molecular 'elevator' 762–3
pH measurements 177
pH sensors 734, 745
pharmaceutical industry applications
co-crystallising agents 496
cyclodextrins 336, 493
effects of hydrate formation 497
polymorphism 487–8
phase problem (in X-ray crystallography) **55**
phase transfer catalysis 149–50, *151*, 204
phenanthroline and derivatives
in catenate synthesis 673–4, 676
in helicate synthesis 679, 693
in photochemical devices 717
phenylacetic acid, retrosynthetic analysis 444–5
phenylalanine **89**, *250*
*m*-phenylene diamide anion binding group 287–8
*o*-phenylenedimercurial receptor
adducts/complexes with chloride anion 271
oxo-bridged analogue 272
pheromones 85, 778
phloroglucinol *see* 1,3,5-trihydroxybenzene
phosphate binding protein (PBP) 228, 235
phosphodiesterase, cyclodextrins as mimics 782, *783*
phospholipid biomembrane *53*
ion transport across *54*
molecular conductivity through 747, *748*
phosphorescence 710, *711*
phosphorus-containing macrocycles 167–8
photochemistry *see* supramolecular photochemistry
photo-excitation, radiative events following 710–11
photo-induced electron collection and storage system 720
photo-induced electron transfer *714*, 715, 720
mediation by $\pi$-stacking interactions 728
photo-induced electron transfer (PET) sensors 732, 733
photolithography 907
photonic crystals 905–6
photonic devices, in biological systems 60–1
photophysical fundamentals of supramolecular photochemical 710–13
photophysical sensing and imaging 731–8
photoresist 907
photoswitchable systems 753, 755
photosynthesis 63–70, 720
photosynthetic systems
key components 65, 726
mimics 720–4, 726
photosystems PSI and PSII 68
phthalocyanines 172
'picket fence' porphyrins 73, 801
'picnic basket' porphyrins 801, 802
picrates, alkali-metal 144, *145–6*, 150, *151*
piedfort unit 409, *410*
pillared clays 552–3
mimics 555
PIXEL method 503
plastic materials **865**
plateau selectivity (of crown ethers) 135, 136, 137
platinum anticancer drugs 93–4
platinum(II) ethylenediamine complexes 625–6
in molecular necklaces 677–8
*see also* $Pt(en)^{2+}$ moiety
platinum(II) polyalkyne molecular wire *747*
Platonic solids 427, 648, *649*
occurrence in natural forms *444*
'plug-and-socket' system 728, *729*
molecular 'extension cable' as part of 729
Pockels surface balance 831
'pocket' porphyrins 801, 802
podands 19, 22, *24*, 118–20, 127
ammonium-based 239–40
binding constant of $K^+$ complex *25*, *120*, *135*
binding free energies for alkali-metal picrates *146*
rigid end group concept 119–20, 346
podates 129
polar flattening effect *486*, 487
polar superlattices 876, *877*

polarisability 766
factors affecting 767
polarised optical hot-stage microscopy, liquid crystals viewed in 839–40, **843**
poliovirus, assembly of protein capsid 593
$\alpha$-polonium ($\alpha$-Po) network 541, 568
polyacetylene **424**, **425**
polyamides, in protein backbones 230
poly(amido amine) (PAMAM) dendrimers 863
rheology **865**
polyamines
basicity 177, *178*
location of protonation site 179
polycatenanes 883–4
polymer surfaces, crystal nucleation affected by 492
polymerase chain reaction (PCR) 92–3, *94*, 594
polymeric liquid crystals 893–4
polymersomes 878
polymorph screening 492
polymorphism 487–92
controlling 492
first described 487
importance 487–8
types 489–92
polyoxomolybdate nanoclusters 562–3
polypeptide-based materials, electron-transfer characteristics 748
polypeptide chains 75
poly(propylene imine) dendrimers
divergent approach to synthesis *867*
ESI-MS spectra 869
polyrotaxanes 883, 885
nets *678*
poly(styrene)-*b*-poly(butadiene)-*b*-poly(*t*-butyl methacrylate) triblock co-polymer 876, *877*
polytopic receptors 184
porosity of solids, factors affecting 542–3
porous materials
classification by pore size 430, 543
coordination polymers 575–8
without pores 436, 542–3
porphobilinogen deaminase 231
dipyrromethane-based cofactor in *232*
porphyrin-based molecular wire 749
porphyrin chromophores
magnesium-containing 63, *64*, 65
zinc-containing 726–7, 728
porphyrin-imprinted covalent dendrimer *871*, 872
porphyrins 61–2
'doming' in 71, *72*, 799, *800*, *803*
expanded 244–5
iron-containing 806
zinc-containing 606–10, 646, 726
*see also* expanded porphyrins; 'picket fence' porphyrins; 'picnic basket' porphyrins; 'pocket' porphyrins
positive cooperativity 17, 610
in helicate formation 685, *686*
postmodification, self-assembly with 596, 602–3, *604*, 632, *634*
potassium channels 58, 227
potassium dihydrogen phosphate (KDP) *454*, 526
diamondoid networks 526, 527
uses 527, 765, 767
potassium hydrogen phthalate crystals 469
potassium ion ($K^+$), biochemical distribution *51*
potassium permanganate, oxidation of organic substrates by 151, *152*
potassium sulfate, hourglass inclusion compounds 465
potentiometric titration 11–12, 240
powder X-ray diffraction (PXRD) 471, **474–6**
compared with single-crystal method **474**
structure solution model **475**
Powell, H. M. 6, 386
prebiotic chemistry 823
precursor preprocessing 602, *603*
precursors, modification followed by self-assembly 596
preinsulin 603, *604*
preorganisation 22–5
anion hosts 232–3
combined with complementarity 25–6
for herbicide receptors 195
kinetic and dynamic effects 147–9
rosette formation by 651, *652*
thermodynamic effects 144–7, 604
preprogramming 592
pretzelane 666, *667*
primary charge separation 66, *67*, 710
primary hydrogen-bond interactions 30
principal component analysis (PCA) 742
prion-based diseases 885
prions 598, *886*
processive catalysis 99
prodigiosins 232
mimics 257, 258, 296
proinsulin 603, *604*
proline **89**
*O*-propyl-*p*-*t*-butylcalix[4]arene, $NO^+$ complex *314*
propylene diamine, donor group orientation for 133
protein amino acids **88–90**
protein self-assembly 100–10
protein tyrosine phosphatases (PTPases) 229
proteins
diffusion into 432
folding of 596
main-chain anion binding sites 230–1
quaternary structures *75*, 598
secondary structures *75*, 598
self-assembly of 598
tertiary structures *75*, 598
X-ray crystallography **56**
protocells 825, 836
proton binding hosts 173–80

proton complexes
  solution chemistry 177–80
  *see also* pH
proton NMR spectroscopy
  cryptophanes binding to halocarbons *361*
  crystal nucleation studied by 455–6
  solution structures analysed by **352–3**
'proton sponge' 268, *269*
  complexes 449
protoporphyrin IX *62*, 231
Prussian blue 568–71
  bridging cyanides in 568–9, 624
PS-PIAT block co-polymer 878
  vesicles formed by 878, *879*
pseudopolymorphism 489, *490*
pseudorotaxane-based chromophoric switch 756, *757*
pseudorotaxane-based XOR gate 759–60
pseudorotaxanes 641, 653–4
  polyrotaxanes synthesised from 885
  synthesis
    directed approach 656–7
    statistical approach 656
$Pt(en)^{2+}$ moiety, in molecular squares 625–6
PtS network 541
pulsed laser deposition (PLD) technique 920, 921
pump storage model 51–2
purines (in DNA) 87, *88*
push–pull polyenes 768, *769*
pyrazene carceplex
  relative stability *374*
  X-ray crystal structure *375*
pyrazole ligands 301
pyrene butyric acid 650, *651*
pyrene excimer 711, *712*
pyridoxamine cofactor 785
pyridyl/terpyridyl tecton, coordination polymers based on 915, *917*
pyridylpyrazne-based assemblies 627
pyrimidines (in DNA) 87, *88*
pyrogallo[4]arene *647*
  hexameric assembly 650
pyrrole-based anion receptors 257–8
pyrrole-based biomolecules *62*, 231–2
pyrrole-based macrocycles 245–6

quantum corrals 900–1
quantum dots 922, 925–6
quaterpyridine, in helicates *680*, 681–2, 682–3
quencher 726
quinone receptors 355–6, 507
quinquepyridine, in helicates 682

racemic crystals 493–4
rack structures, self-assembled *637*, *640*, 641
radiolaria, structural mimics 902–3
ranitidine hydrochloride 488
ratchet movement 764
ravels 697, *698*
reaction vessels *see* molecular reaction vessels
receptor–substrate binding, enzymes 7–8
receptors
  term first introduced 7
  *see also* anion receptors; cation receptors; ion pair receptors; neutral receptors
rectifiers 750
redox potential
  environmental factors affecting **267**
  estimation by cyclic voltammetry **266**
redox sensors 254, 354, 742–3, 928
redox-switchable rotaxanes 755
reflection high-energy electron diffraction (RHEED) 921
replica moulding 910
reporter dye(s) 650
repulsive *gauche* effect 131
resorcarene-based carcerands 370–5
  [5]resorcarene-based carcerand 379, *380*
resorcarene-based ion pair receptors 294, *295*
[4]resorcarene–calix[4]arene hybrid carcerands 375–6
resorcarene hexamers 635
[4]resorcarene tetracarboxylic acid, in hydrogen-bonded capsules *648*
resorcarene trimers 635
resorcarenes
  conformations 312
  dithiocarbamate-functionalised 635
[4]resorcarenes
  dimethylsilyl derivative 316, *317*
  dodecyl phosphocholine complex 318
  hexamers, fluorescence detection by 729–30
  intramolecular hydrogen-bonding interactions *312*
  in molecular containers 647–8
  multiply bridged 316, *317*
  with rigid upper rim 322
  structure *311*, 312, *647*
  sulfonated derivatives 315–16
  synthesis 311, *312*
  tetrametallic complexes 276
reticular synthesis 561
retina (of human eye)
  cone cells 61
  rod cells 60–1
retrosynthesis 443
  example 444–5
retroviruses 824
reverse micelles *834*, 835
rhenium–alkyne oligomers 748–9
rheology **864–5**
  dendrimers **865–6**
rhinovirus 101
  topology 650
*Rhodopseudomonas viridis* photosynthetic reaction centre 65–6
  charge separation at *67*
rhodopsin 60–1

rhombicubeoctahedron 427
ribbon structures 445, *446*, 511, 517, 525
ribonuclease 100
ribonucleic acid (RNA) 90, 824
ribozymes 823, 824
Richman–Atkins cyclisation reaction 158, *159*, 344
Rietveld refinement method 471, **476**
rigid end group concept, in podands 119–20, 346
rigid group principle 345
ring-opening metathesis polymerisation (ROMP) 748
ritonavir 488
RNA-world hypothesis 824
rod-coil co-polymers 877–8
rose Bengal (dye) 870
rosettes 651–2
rotavirus 101–2
[2]rotaxane-based switchable molecular shuttle 754–5
rotaxanes 325, 605, *606*, 653–78
  hydrogen-bonded 667–9
  in molecular necklaces *678*
  nomenclature 653–4, *654*
  [2]rotaxane 658
  [3]rotaxane 658, *659*
  [4]rotaxane 658, *659*
  synthesis 653–4
    alkene metathesis approach 658
    auxiliary linkage approach 676, 677
    'clipping' procedure 658
    directed approaches 657–60
    'slipping' procedure 658
    statistical approach 656, 672, *673*
    'threading' procedure 657, *658*
  *see also* polyrotaxanes
ROY 488
[Ru([9]ane-S3)(4,4'-bipyridyl)3]21 (supramolecular cube) *622*, 623–4
$[Ru(bpy)_3]^{2+}$
  electrochemical properties 717
  phosphorescence spectrum 717
Ruddlesden–Popper (RP) series 921
'Russian doll' complex 335
ruthenium(II) biimidazole complexes, hydrogen bonding from 511–12
ruthenium(II) calix[4]arene host *252*, 264
ruthenium(II) chelate complexes 259–60
ruthenium(II) complexes
  in nonlinear optical devices 770–1
  in photochemical devices 717
ruthenium(II)/iridium(III) photochemical device *720*, 721
rutile network 541, *568*, 569

saccharin
  co-crystal with carbamazepine 496–7
  crystallisation of 462–4
salen-based receptor 292
salicylaldoxime 298
*Salmonella typhimurium*
  binding-protein/sulfate interactons 228
  chloride channel 58
  enterobactin 214
sandic nematic liquid crystal phase 893, *894*
sandwich polymers *272*, 273
sapphyrin
  diprotonated 244
    complex with fluoride 245
sarcophagenes 123–4, 128
saturated hydrogen-bonded (SHB) co-crystals 494
scaffolds 276–81
  cholapods 278–81
  trialkylbenzene-based 251, 277–8
scanning probe microscopies
  carbon nanotubes as probes 933
  *see also* atomic force microscopy; scanning tunnelling microscopy
scanning tunnelling microscopy (STM) 45, **911–12**
  high-resolution 917–18, *919*
  nanomanipulation using 45, 913, 914, *915*
  visualisation by 914, *916*, *917*, *919*
scanning tunnelling spectroscopy (STS) 918
Scatchard equation/plot 21, *22*, 610
Schiff base condensation reactions 4, 170–1, 342
Schiff base macrocycles
  in cascade complexes 289–90
  example of use 171–2
  first to be synthesised *170*
Schiff bases 170–2
Schläfli symbols 540
second-generation dendrimers 862, *863*
second harmonic generation (SHG) 767
second harmonic generation (SHG) nonlinear optical materials 765, 768–71
secondary bonding 37, 525
secondary building units (SBUs) 540, 546, 561, 562
secondary charge separation 66, *67*
secondary hydrogen-bond interactions 30–1
Seebeck effect 761
selectivity 16, 26, 740, 778–9
selenium-containing macrocycles 163
self-assembled monolayers (SAMs) 837–9
  cyclodextrins 320, *321*
  on silicon surface 838–9
  thiol-based 837–8
self-assembled supramolecular polymers 880–3
self-assembled viruses 101
self-assembling catalysis 815, *819*
self-assembling coordination compounds 620–41
  design 620, *621*
  grid/ladder/rack arrays 637–41
  molecular squares and boxes 624–35
  notation 621, *622*
  supramolecular cubes 621–4
self-assembly 3, *7*, 42, 43, 591–706
  anion templating 300–3
  assisted 596

biochemical 99–102, 600–4
catenanes and rotaxanes 655–77
classification 595–7
closed complexes 641–53
concepts 594–5
cooperativity in 610–15
with covalent modification 596, 602–3, 632, *634*
crystallisation as 442
definition 592
directed 596, 626
DNA 91, 99–100
extended-site binding model 611, 613–15
helicates 681–91
hydrogen bonding in 641–53
with intermittent processing 596
irreversible 596
labile complexes 300, 301–2
ligands with anion and cation binding functionality 260
metal arrays 637–41
panelling approach 617–18, 629–36
with postmodification 596, 602–3, *604*, 632, *634*
precursor modification followed by 596, 602, *603*
probability 616–19
scope and goals 592–4
strict 595–6, 600–2
on surfaces 914–18
template effects 604–6
thermodynamic model 606–10
time-resolved 594
self-complementary assemblies 641–6
self-complementary building blocks 527, *528*, 606
self-organisation 43, 595
self-recognition, helicates 684–5
self-replicating peptides/proteins 824
self-replicating systems 606, 819–23
self-poisoning in 821–2, 823
*see also* minimal self-replicating model
self-replication 593–4
and Darwinian evolution 823
minimal model for 820
semiconductor nanocrystals 926
*see also* quantum dots
semiochemistry
biological 85–6
meaning of term 85, 730
supramolecular 730–1
sensing arrays 740, 741
sensing and signalling 85, 730
sensitised lanthanide(III) complexes, as sensors 734–5
sephulchrates 123, *124*, 128
serine **89**, *228*
serine proteases, oxyanion hole in 231
'seven bridges of Könisberg' problem, Euler' solution 539–40
sexipyridine 683, *684*, 716
sheathed rack structures *640*, 641
'ship-in-a-bottle' structure, in octahedral capsule 630, *632*
siderands 217
siderophores 213–17
naturally occurring 213–15
synthetic 215–17, 604
silicon-containing Lewis acid chelates 270
silicon surfaces, self-assembled monolayers on 838–9
silk inverse opal 906
simultaneous anion and cation binding 286–99
single cell patch clamp method 811
single-crystal neutron diffraction **448**
single-crystal X-ray crystallography **55–6**
compared with powder X-ray diffraction **474**
single-interaction self-assembly 597
single-molecule chemistry 913–14, *915*, 918–20
single-molecule magnet 562, *563*
single-molecule wire 749, *750*
single-walled carbon nanotubes (SWCNTs) 933
buckminsterfullerence molecules as inclusions 933, *934*
carborane derivative confined in 933, *934*, 935
single crystals encapsulated in 933, *934*
site binding model 610
Ercolani's model 611–13
extended 611, 613–15
site-directed mutagenesis 91–2, *93*
sixfold aryl embrace (6AE) *446*, 522, *523*
small-angle X-ray scattering, liquid crystals studied by **844**
Smalley, Richard E. 423, **425**
smectic liquid crystal phases 841, 842–3
degree of order 842
Smith, Michael 91
snub cube, [4]resorcarene-based 649–50
soaps 832, 834
'soccer ball' cryptand *123*, 129, 236, *237*
tetrahedral recognition of $NH_4^+$ by 180, *181*
'soccer ball' cryptates 237
social isomerism 644, *645*, 646
sodalite (SOD) zeolites *544*, *545*, 546
sodium chlorate, magnetically stirred crystallisation of 459
sodium chloride (NaCl) lattice 27
sodium dodecyl sulfate (SDS) 318
sodium ion ($Na^+$), biochemical distribution *51*
sodium ion channel *54*
soft ions and ligands 110
soft ligands for soft metal ions 160–73
soft lithography 909–11
advantages and disadvantages 911
'softball'-shaped hosts 642–3, 814, 815
sol 890, 922
sol–gel process 889–90, 922
solid aerosol 922
solid solutions 493
solid-state cyclodextrin hydrates 330–1
solid-state cyclodextrin inclusion complexes 333–5
solid-state host–guest compounds 6, 386–7
*see also* clathrates

solid-state inclusion complexes
calix[4]arene-based 313
[4]resorcarene-based 313
solid-state inclusion compounds 385–440
solid-state inclusion polymer(s), silicon-containing 313
solid-state separation, liquid clathrate based separation compared with 857
Solomon knot 699
solution, molecular guests in 307–84
solution self-assembly 442
solvating reagents, in metals extraction processes 297
solvation effects 39–41
in anion binding 234
solvation free energies, listed for various anions and cations *226*
solvation shell 830
solvatomorphism 489
solvent-assisted micromoulding 911
solvent-separated ion pairs 286
solvophobic effects, guest encapsulation affected by 643
sonic spray ionisation mass spectrometry (SSI-MS) 635
sorption, compared with clathration 538
spatiotemporal theory 79
speciation maps, $Pd(en)^{2+}$/4,4′-dipyridine mixtures 619, *620*
specific rotation **369**
speculative models 793
speleands 193
speleates 193
spherands 4, 125–6, 127
binding constants *25*
binding free energies for alkali-metal picrates *145*
binding of $NH_4^+$ by 183
conformational rearrangement in $Li^+$ spheraplex *147*
hybrid hosts 126, *127*
synthesis 126
spheraplexes *126*, 129, 144, *147*
spillover (hydrogen molecule splitting) 585, 923
square brackets 9n, 106, 197, 341
square grid topology *539*, 566
square planar Pd(II) and Pt(II) complexes 95, 112, 162
in metallomesogen 848, *849*
transformation to square pyramidal adduct 436–7
squarine-based siderophore *216*, 217
$SrAl_2$ framework *541*
$SrSi_2$ framework 541
stannacycles 274–5
starch 331
steel swords 935–6
stepwise binding constants 10
formation of supercomplexes 242, *243*
steric compression, in cyclophanes 345–6
sterically directed synthesis of catenanes 669, *670*, 671
Stern layer *834*, 835
steroids, binding in dendrophanes 351
sterol framework, in cholapods 278, *279*
stilbite 545
*Streptomyces lividans*, potassium channel 58
strict self-assembly 595–6
examples 600–2
structural isomerism, bipyridyl and terpyridyl complexes 717, *718*
structural models 792
structure correlation principle 484
sulfamerizine 455–6
sulfate binding protein (SBP) 228
sulfonated [4]resorcarenes 315–16
binding constants with various alcohol guests *316*
*p*-sulfonatocalix[4]arene 426–9
in heterodimeric capsules 646
spherical assemblies 427, *428*, *429*
structure compared with vermiculite *426*
tubular assemblies 427, *428*, *429*
*p*-sulfonatocalix[n]arenes 315, 426
sulfur analogues
crown ethers 161, 162–3
cryptands 163
sulfur dioxide, absorption by coordination compounds 436–7
sulfur extrusion reactions, cyclophanes synthesised by 342, *343*
superanion complexes 427
superatoms 927
supercomplexes 241
superexchange mechanism 715
superlubricity of graphite 34, 520, 551–2
supersaturated solutions, crystal growth in 454
supersecondary structure 598
superstring theory 691
super-wurtzite structure 495
supported liquid membrane (SLM) 297
supramolecular catalysis 813–23
supramolecular chemistry
compared with molecular chemistry 2
definitions 2–3, 708
development 4–6
supramolecular chemistry of life 49–104
supramolecular cubes 621–4, 648
supramolecular dendrimer assemblies 872–4
supramolecular design 41–5
supramolecular devices, definition 709–10
supramolecular gels 888–93
applications 891–3
rheological properties **865**, **866**
supramolecular grid-type assemblies 637–41, 919, *920*
supramolecular interactions 27, 308
types 27–37, 309–10
anion–$\pi$ interactions 33
cation–$\pi$ interactions 32
closed shell interactions 36–7
crystal close packing 36
dipole–dipole interactions 28, 308
electrostatic interactions 310
hydrogen bonding 28–32, 308, 310

hydrophobic binding 38–9, 309
induced dipolar interactions 310
ion–dipole interactions 27–8, 308
ion–ion interactions 27
$\pi$–$\pi$ interactions 33–5, 310
van der Waals interactions 35, 235
supramolecular isomerism 492, 555, 562
supramolecular liquid crystals 848–51
supramolecular photochemistry 710–30
energy/electron-transfer mechanisms 713–15
light-conversion devices 725–6
light-harvesting devices 718–24
mixed-valence devices 715–16
non-covalently bonded systems 726–30
photophysical fundamentals 710–13
pyridyls as device components 716–18
supramolecular 'plug-and-socket' system 728, *729*
supramolecular polymers, self-assembled 880–3
supramolecular self-assembly 3, *7*, 42, 43, 591–706
compared with molecular self-assembly 594–5
supramolecular semiochemistry 730–1
supramolecular synthons 443–4, 445, *446*
supramolecular tectons 42, 445, 594
surface adhesives 887
surface interactions 309
surface plasmon resonance (SPR) absorption 44, 922
surface tension 833
surfaces, self-assembly on 914–18
surfactants 831–2
types 832
Suzuki–Miyaura cross-coupling reaction 344
switchable molecular devices 752–6
switchable nonlinear optical devices 770–1
symport 59, 286, 295–6
examples 245, *246*, 258, 296–8
synergic effect **169–70**
'synthesising up' approach 593
synthons 443–4, *446*
'syringe' action of calixarenes 208

'tailbiter' foldamer 600
tape structures 445, *446*, 511, 517, 525, 651, *652*, 749, 890–1
tartaric acid derivatives, in hydrogen-bonded helices 688–9
Taube, Henry 286n, **636**
tectons 42, 445, 594
tellurium-containing macrocycles 163
template effect 122, 153–7, 594
in self-assembly 604–6
template patterning mechanism for biomimetic structures 903
template positioning, for solid-state topochemical photocyclisation 473
template ratios, carcerand synthesis 373, *374*
template reactions/synthesis 43, 109, 153–7
benzo[18]crown-6 155–6
carcerands 373
catenanes 660
clathrate hydrates 388–9
enterobactin *214*
metal-ion-templated 604, 672–6
metalloid-templated 604–5
phthalocyanines 172
tetraazamacrocycles *156*, *166*
triphosphine macrocycle *168*
zeolites 547, *548*
templation, self-assembly based on 43, 594, 891–2
tennis ball-shaped hosts 641–2, 648
terbium complexes
in logic gates 758–9
in sensors 734
terephthalic acid *529*
termite mound 43
terpyridine, in photochemical devices 716, 717–18
testosterone *351*
binding in dendrophanes 351
1,4,7,10-tetraazacyclododecane, synthesis *159*
1,4,8,11-tetraazacyclotetradecane
synthesis 165, 166
*see also* cyclam
1,6,20,25-tetraaza[6.1.6.1]paracyclophane 347, *348*
durene complex 347, *348*
1,1,2,2-tetrachloroethane, effect on binding constant of host 39, *40*
tetra-*N*-cyclam
basicity *178*
binding with transition metals *165*
tetrahedral receptors 236–7
tetrahedral tetrametallic self-assembled clusters 628–9
tetra(hydroxypropyl)cyclam 293–4
tetra-1-naphthoid *412*, 413
tetranuclear complexes, energy-transfer processes in *723*
tetrapyrrole macrocycles 61–2, 80–1, 244
in photosynthesis 61, 63–7
tetrathiafulvalene (TTF) 358
cyclophane based on 358
redox chemistry *358*
tetrathiafulvalene (TTF) derivatives
in addressable molecular electronic devices 760–1
in electrochemical sensors 745
tetrathiafulvalene-derived dipyridophenazine (TTF-dppz) ligands, in photochemical devices 724
tetrazamacrocycles, synthesis 156
thermal conductivity, inclusion compounds 390, 408
thermal expansion, negative 570–1
thermodynamic anion templating 300–2
thermodynamic effects, chelate effect and 18
thermodynamic selectivity 26, 227
thermodynamic stability, coordination complexes **636**
thermodynamic template effect 156, 605
thermodynamic template synthesis
of Schiff base macrocycles 170–1
of tetrazamacrocycles 156
thermoelectric effect 761–2

thermogravimetric analysis (TGA) **559–60**
examples 366–7, 558, **559**, **561**
thermometers, liquid crystalline 851
thermotropic liquid crystal phases 841–3, 844–5
thiacalixarenes, water binding in 434
thiacrowns 131
thiohydantoin, nanoscratching of *472*, 473
thiols, functionalised 837, 923, 924
thiourea-based receptors 256–7
thiourea clathrates 255–6, 393
1-bromoadamantane-based 398
thiourea derivatives, organocatalysis with 814
third-generation dendrimers 862, *863*
third harmonic generation 767
third harmonic generation nonlinear optical materials 771
thixotropy 889
threaded rotaxane-type compounds 669
three-dimensional hosts, binding of ammonium cations by 183–4
three-dimensional networks 526–30, 539, 567
*see also* diamondoid networks
three point rule (in chiral recognition) 189–90
threonine **89**
$ThSi_2$ framework *541*
time-resolved self-assembly 594
timeline, supramolecular chemistry development *5*
tissue engineering 891
titanium dioxide nanoparticle, in photon acceptor 727, *728*
tobacco mosaic virus (TMV) 101, 600–1
6(*p*-toluidino)naphthalene-2-sulfonate 352
top-down approach 593, 901, 907
topochemistry 443, 470, 473–4, 917, *918*
topoisomerase 98
topological isomers
catenanes as 654, *655*, 691
knots as 692
topological trapping by dendrimers 870
topology 539–40
knots 691–3
torands 173
trace products, amplification of *818*, 819
*trans*/*anti* conformation 130, 319
transacylases
cation-binding hosts as mimics 788–92
functional mimics 788–90
structural mimics 790–2
*see also* chymotrypsin
transamination, $\alpha$-amino acid synthesis by 785
transduction between receptor and signalling units 731
transesterification reactions, catalysts for 249
transition metal ion pair receptors 293–4
transition state selectivity in zeolites 550
transition state stabilisation, in enzymatic catalysis 78
translational isomerism, catenanes *671*, 756, *757*
translational symmetry operators **461**
transmembrane current flow 51–2
transmembrane enzymes 51
trefoil knots
DNA knots 697, *698*
synthesis 671, *672*, 693–5
as topological enantiomers *655*, *698*
tren (2,2′,2″-tris(aminoethyl)amine) and derivatives 239, 254
trialkylbenzene-based cores/scaffolds 251, 254, *255*, 277–8
1,5,9-triazacyclododecane, synthesis 156
tribenzo[21]crown-7 138, *139*
tricatecholate mesitylene derivative 215
1,3,5-tricyanobenzene, co-crystal with hexamethylbenzene 451, *452*
triethylbenzene-derived anion hosts 254, *255*, 277
triethylbenzene ‘pinwheel’ structure *277*, *311*, 740, 741
triflate (trifluoromethane sulfonate) anion 211
trigger mechanism 71
1,3,5-trihydroxybenzene (THB), hydrogen bonding to cyclophanes 356–7
trilactone rings, in siderophores 214, 215
trimeric carcerand 379
trimesic acid (TMA) 399, *579*
channel clathrates 399–401
layered coordination polymer based on 578, *579*
as two-dimensional sheet *529*
4,4′-trimethylenedipyridine, co-crystal with 4,4′-sulfonyldiphenol 573
*N*,*N*′,*N*″-trimethyltriazacyclononane, copper(II) complexes 468
triphenylmethane and derivatives *311*
triphosphine macrocycle, synthesis 167–8
triple-helicate complexes 683, *684*
triple helices 689, *690*
triply interlocked structures
synthesis 671, *672*
*see also* trefoil knots
tripyridyltriazine-based complex 541, *542*
tripyridyltriazine-based ‘molecular panels’ 617, *619*
trischelate unit(s), in ammonium-based podands 240
tris(diazabicyclooctane) 27
tris(guanidinium) receptors 250
trislactams 412
tri-*o*-thymotide (TOT) *410*
applications 413
conformations 410–11
derivatives 412–13
inclusion chemistry 410–12
synthesis 412
tritopic receptors 184
Tröger’s base *311*
in cyclophanes 349
truth table, for Boolean operations *758*
tryptophan **89**, *250*
TSQ 736
tubular mesophases 845
twisted nematic cells (TNCs) 851–2
two-dimensional hosts 240–6

two-dimensional nets/grids/honeycombs/sheets *529*, 538, *539*, 566
tyrosine **89**

U-tube model membranes, transport across 245, *246*, 304
ubiquinone 66, *67*
Ullman reaction, single-molecule analogue 914, *915*
2,10-undecanedione, urea inclusion compound 397–8
UNI atom–atom potential method 503–4
unimediated multiple interaction self-assembly 597
unitary graph set 477
unobstructed cross-sectional area (UCA), helical tubulands 402
unsaturated hydrocarbon macrocycle 211
uranyl cation
  extraction in nuclear industry 297
  in Schiff base macrocycle 171–2
uranyl-centred ditopic receptors 292
  phosphate complexes 292, *293*
uranyl complex, co-crystal with [15]crown-5 499–500
urea-based gels 890–1
urea-based receptors 256, 257
urea clathrates 255, 393–8
  applications 398
  guest order and disorder in 394–8
  structure 393–4, *435*
ureases 792–3
2-ureido-4[1*H*]pyrimidone-based polymers 880–1
urotropin, ammonium tetrafluoroborate complex 495
US Department of Energy (DOE), hydrogen storage materials targets 430, 584
UV-Vis spectrophotometric titration 15

valine **89**
valinomycin 53, 57
  $K^+$ complex *54*
van der Waals interactions 34, 35, 235
  in layered solids 550
van der Waals radii 448
van t'Hoff plots 340, 362
vancomycin, drug–receptor complex 19
Vaska's compound 70, *71*
vermiculite *551*
  structure compared with *p*-sulfonatocalix[4]arene *426*
Vernier mechanism for controlling supramolecular oligomerisation 883
vesicle-directed biomimetic mineralisation 596
vesicle walls
  with bilayer surfactant membranes 805
  molecular conductivity through 747, *748*
vesicles *834*, 836
  chloride efflux from 296
  cholapods in 280–1
viologens (*N*,*N*′-disubstituted 4,4′-bipyridyl derivatives) 194, 310, 357
  ditopic receptors based on *277*, 278
  redox chemistry *358*
  *see also* paraquat
viral capsids, self-assembly of 101, 593
'virtual porosity' 543
virtual products (in dynamic combinatorial chemistry) 817
viscoelastic materials **865**
viscous materials **865**
vitamin $B_{12}$ 61
  X-ray crystal structure *82*, 83
vitamin coenzymes 80–3, 808
voltage-gated chloride transport 813

water
  in co-crystals 497–8
  hydrogen bonding in 830
  molecular structure *527*
  oxidation to oxygen 65, 68–70
  oxygen–oxygen radial distribution function 830, *831*
  *see also* ice
water–gas shift reaction 429, 430
water molecules, structure in clathrate hydrates 389
water motifs, classification scheme 497–8
Watson–Crick base pairs 90–1
Weiss model (for binding of oxygen to haemoglobin) 71, *72*
Wells notation 540
Werner, Alfred *5*, 8, 106
Werner clathrates 556, 557–8
'wheel-and-axle' concept 402–3
'whisky tumbler' shape, resorcarene derivative 322
Wilkinson's compound 2
Williamson ether synthesis 116
Wurtz coupling 342, *343*

X-ray crystallography **55–6**, 112
X-ray dichroic filters 398
xenon, absorption in clathrates 430, *431*
xerogels *889*
XOR gate, molecular logic 759–60

*Yersinia* protein tyrosine phosphatase 229

Zeise's salt 32
zeolites 543–50
  applications 543, 548–50
  composition 543, *544*
  organic mimics 434–5, 528–30, 558, 575
  primary building units 544
  secondary building units 546
  structure 544–7, *544*
  synthesis 547–8
  *see also* aluminosilicate zeolites; organic zeolites
zero-dimensional clusters/molecules/points *529*, 538, 562–4
zig-zag chains 565
zinc, biological roles 736, 795

zinc(II) bis(porphyrin), pentagonic assembly 917, *919*
zinc-containing enzymes 737, 795–8
zinc porphyrin complexes
  in heterodimeric capsules 646
  in photochemical devices 726
  self-assembly of 606–10
zinc(II) porphyrin-derived anion sensor 917, 924
zinc sensors 736–8
Zinke reaction **198**
Zinquin (fluorophore) 736
zipper complexes 616, *617*
'zipping up' of double helices 602, 685
ZSM zeolites 545, 546
zwitterionic receptors 253
zwitterionic structure of amino acid 286, *287*
zwitterions, receptors for 286, *287*, 303–4